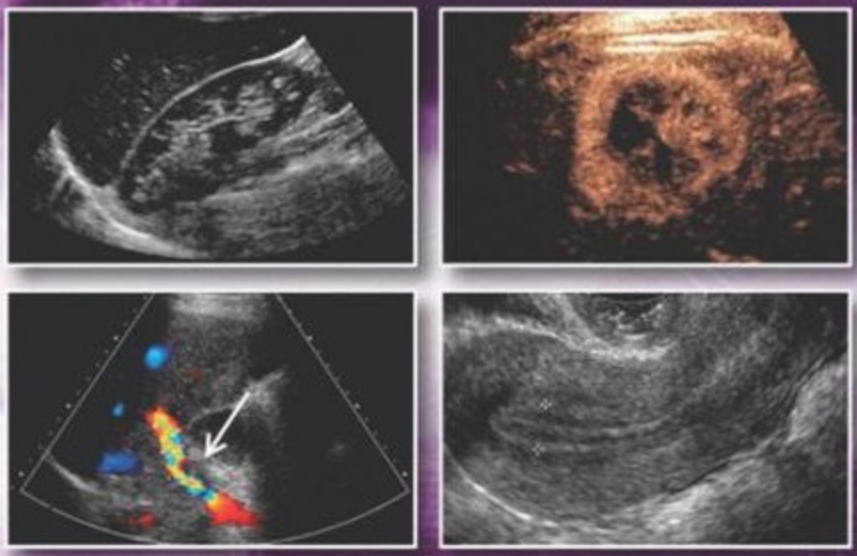
Expert CONSULT Activate at expertconsult.com Searchable Full Text Online

CLINICAL ULTRASOUND

PAUL L. ALLAN • GRANT M. BAXTER • MICHAEL J. WESTON

VOLUME ONE



THIRD EDITION

CHURCHILL LIVINGSTONE ELSEVIER

Copyrighted Material

CLINICAL ULTRASOUND

Commissioning Editor: Michael Houston
Development Editor: Ben Davie
Editorial Assistant: Rachael Harrison/Kirsten Lowson
Project Manager: Elouise Ball
Design: Charles Gray
Illustration Manager: Gillian Richards
Illustrator: Amanda Williams
Marketing Manager (UK/USA): Gaynor Jones/Tracie Pasker

CLINICAL ULTRASOUND

THIRD EDITION

Edited by

Paul L. Allan BSc MBChB DMRD FRCR FRCPE
Consultant Radiologist
Department of Radiology
Royal Infirmary
Edinburgh, UK

Grant M. Baxter MBChB FRCR
Consultant Radiologist
Department of Radiology
Western Infirmary
Glasgow, UK

Michael J. Weston MBChB MRCP FRCR
Consultant Radiologist
Department of Radiology
St James's University Hospital
Leeds, UK

Section Editors

Ian Beggs MBChB FRCR
Consultant Musculoskeletal Radiologist
Department of Radiology
The Royal Infirmary of Edinburgh
Edinburgh, UK

Norman McDicken BSc PhD FIPEM
Emeritus Professor
Medical Physics
Edinburgh University
Edinburgh, UK

David W. Pilling MBChB DCH DMRD FRCR FRCPCH
Consultant Paediatric Radiologist
Department of Radiology
Royal Liverpool Children's Hospital Alder Hey
Liverpool, UK

CHURCHILL LIVINGSTONE
ELSEVIER

CHURCHILL
LIVINGSTONE
ELSEVIER
© 2011, Elsevier Limited. All rights reserved.

First edition 1993
Second edition 2001
Third edition 2011

The right of Paul L. Allan, Grant M. Baxter and Michael J. Weston to be identified as authors of this work has been asserted by them in accordance with the Copyright, Designs and Patents Act 1988.

No part of this publication may be reproduced or transmitted in any form or by any means, electronic or mechanical, including photocopying, recording, or any information storage and retrieval system, without permission in writing from the publisher. Details on how to seek permission, further information about the Publisher's permissions policies and our arrangements with organizations such as the Copyright Clearance Center and the Copyright Licensing Agency, can be found at our website: **www.elsevier.com/permissions.**

Notices
Knowledge and best practice in this field are constantly changing. As new research and experience broaden our understanding, changes in research methods, professional practices, or medical treatment may become necessary. Practitioners and researchers must always rely on their own experience and knowledge in evaluating and using any information, methods, compounds, or experiments described herein. In using such information or methods they should be mindful of their own safety and the safety of others, including parties for whom they have a professional responsibility.

With respect to any drug or pharmaceutical products identified, readers are advised to check the most current information provided (i) on procedures featured or (ii) by the manufacturer of each product to be administered, to verify the recommended dose or formula, the method and duration of administration, and contraindications. It is the responsibility of practitioners, relying on their own experience and knowledge of their patients, to make diagnoses, to determine dosages and the best treatment for each individual patient, and to take all appropriate safety precautions.

To the fullest extent of the law, neither the Publisher nor the authors, contributors, or editors, assume any liability for any injury and/or damage to persons or property as a matter of products liability, negligence or otherwise, or from any use or operation of any methods, products, instructions, or ideas contained in the material herein.

ISBN: 978-0-7020-3131-1

British Library Cataloguing in Publication Data
A catalogue record for this book is available from the British Library

Library of Congress Cataloging in Publication Data
A catalog record for this book is available from the Library of Congress

ELSEVIER your source for books, journals and multimedia in the health sciences
www.elsevierhealth.com

Working together to grow libraries in developing countries
www.elsevier.com | www.bookaid.org | www.sabre.org
ELSEVIER BOOK AID International Sabre Foundation

The publisher's policy is to use **paper manufactured from sustainable forests**

Printed in China
Last digit is the print number: 9 8 7 6 5 4 3 2 1

PREFACE

Ultrasound remains one of the most frequently used and valuable modalities for imaging and guiding interventional procedures. The number of ultrasound examinations carried out world-wide continues to increase and the global sales of ultrasound equipment, both new and refurbished, is increasing at some 3-5% each year. The flexibility, ease of use, range of applications and relatively low cost of the equipment make ultrasound an important investigative imaging tool.

The first and second editions of this book, edited by David Cosgrove, Keith Dewbury, Hylton Meire and Pat Farrant, were a great success, providing information and advice across the full range of diagnostic ultrasound. They were essential reading for those training in ultrasound and a source of information for many sonographers and sonologists across the world.

Techniques, hardware and data processing have all evolved and progressed at a rapid rate since the second edition of this book was published in 2001. As a result of these developments, ultrasound equipment is now available in more sizes, specifications and complexity than ever before and this has enabled many different types of clinician to use ultrasound in particular niche areas, in addition to the more general imaging function that it has always provided.

The chapters in the two volumes of this book cover all aspects of general ultrasound, as well as more specialised areas such as peripheral vascular and ophthalmic ultrasound. Some areas, such as musculoskeletal ultrasound, have developed into major applications of ultrasound and this is now essential to the management of patients with a wide variety of muscle and joint disorders. There has therefore been a significant enhancement of the coverage of these areas in this new edition.

Conversely, detailed fetal and maternal obstetric scanning in the mid and final trimesters has followed cardiac echography into a separate sphere of expertise. There are many excellent text books dealing with these aspects, therefore, the editors felt that a comprehensive review of obstetric scanning was best left to these volumes. However, first trimester problems will still be seen by sonographers undertaking general scanning so an account of these is included in this book.

The potential applications of echo enhancing agents, or microbubbles, have developed and changed significantly since the publication of the second edition of this book. Originally developed to rescue inadequate Doppler examinations, interesting properties of these agents have led to potential uses delivering drugs and genes.

The editors of the third edition of Clinical Ultrasound are extremely grateful to the many experts in their particular fields of ultrasound who have contributed the authoritative, comprehensive and informative chapters that make up this book. In particular, our thanks go to Ian Beggs, David Pilling and Norman McDicken, who were responsible for coordinating the musculoskeletal, paediatric and physics sections of the book. We are also very grateful to Michael Houston, Ben Davie and all the other staff at Elsevier who have worked on the many aspects of publication between the first outline discussions and the final published product.

Paul Allan
Grant Baxter
Michael Weston

Volume 1

1. Physics and Basic Principles 1

1. Basic physics of medical ultrasound 3
W.N. McDicken and T. Anderson

2. Basic equipment, components and image production 16
Kevin Martin

3. Practical ultrasound – using scanners and optimising ultrasound images 31
Colin R. Deane

4. Safety 51
Hazel C. Starritt and Francis A. Duck

5. Artefacts in B-mode scanning 61
David O. Cosgrove

6. Ultrasonic contrast agents 77
Carmel M. Moran

2. Abdomen 91

7. Liver: anatomy and scanning techniques 93
Simon Elliott

8. Diffuse parenchymal liver disease 104
James M. Pilcher

9. Liver: infections and inflammations 120
James M. Pilcher

10. Focal liver lesions/echo enhancing agents and the liver 138
Gavin Low and Edward Leen

11. Biopsy technique and RF ablation 167
Riccardo Lencioni, Clotilde Della Pina, Dania Cioni and Laura Crocetti

12. Vascular disorders of the liver 179
Christopher J. Harvey and Adrian K.P. Lim

13. Liver transplantation 199
Suzanne M. Ryan, Maria E.K. Sellars and Paul S. Sidhu

3. Gallbladder and Bile Ducts 225

14. Gallbladder and biliary tree 227
Jane A. Smith

15. Intraoperative ultrasound 273
Steven Kennish and Jane A. Smith

4. Pancreas and Spleen 283

16. Pancreas 285
Zahir Amin

17. Spleen 324
Simon J. Freeman

5. Gastrointestinal Tract 349

18. Oesophagus and stomach 351
John N. Plevris and Scott Inglis

19. Small intestine 369
Peter M. Rodgers

20. Appendix, colon and rectum 388
Rakesh Sinha

6. Kidneys and Urinary System 411

21. Kidneys: anatomy and technique 413
Paul L. Allan

22. Pelvi-ureteric dilatation 428
Tze M. Wah

23. Medical diseases of the kidney 445
Paul L. Allan

24. Infectious diseases of the kidney 460
Paul L. Allan

25. Vascular disorders of the kidney 467
Dennis L. Cochlin

26. Renal cystic disorders 486
Michael J. Weston

27. Solid renal masses 505
Michael J. Weston and Tze M. Wah

28. Renal transplantation 528
Grant M. Baxter

29. Ultrasound of the bladder 550
Jonathan L. Richenberg

30. The prostate and seminal vesicles 572
Uday Patel

31. Diseases of the testis and epididymis 593
Paul S. Sidhu

32. Ultrasound of the penis 621
Anthony J. Edey, C. Jason Wilkins and Paul S. Sidhu

33. Adrenals 632
Keith Dewbury and Elizabeth E. Rutherford

7. Gynaecology 643

34. Pelvic anatomy and scanning techniques 645
Tracey Hughes

35. Ovaries 660
Diane DeFriend

36. Uterus and vagina 686
Michael J. Weston

37. Gynaecological intervention techniques 720
Michael J. Weston

38. Ultrasound assessment of fertility 730
Stephen R. Killick

39. The first trimester, gynaecological aspects 740
Anne Marie Coady

Volume 2

8. Other Abdominal Applications 771

40. The abdominal aorta and inferior vena cava 773
Tim Hartshorne

41. The abdominal wall, peritoneum and retroperitoneum 798
Michael J. Bradley and David O. Cosgrove

42. Abdominal trauma 828
Orlando Catalano

43. Interventional ultrasound in the abdomen 847
Elizabeth E. Rutherford, Brian Stedman and David J. Breen

9. Head and Neck 865

44. Thyroid and parathyroid 867
Neil Cozens

45. Ultrasound of the neck 890
Rhian Rhys

46. Cervical lymph nodes 920
Rhian Rhys

47. The eye and orbit 938
John A. Fielding

48. Carotids, vertebrals and TCD (transcranial Doppler) 965
Paul L. Allan and Joanna M. Wardlaw

10. Chest and Breast 985

49. Breast 987
Jonathan J. James and Andrew J. Evans

50. Lung, pleura and chest wall 1005
Najib M. Rahman and Fergus V. Gleeson

11. Musculoskeletal System 1023

51. Muscular ultrasound – introduction 1025
Ian Beggs

52. Ultrasound of the shoulder 1030
Simon Ostlere

53. Ultrasound of the elbow 1043
James Teh

54. Ultrasound of the wrist and hand 1055
Carlo Martinoli, Alberto Tagliafico and Gerd Bodner

55. Musculoskeletal ultrasound of the adult hip and groin 1069
Philip Robinson

56. Ultrasound of the knee 1084
Ian Beggs

57. Ultrasound of the ankle and foot 1093
David Wilson and Gina Allen

58. Ultrasound of soft tissue masses 1109
Rob Campbell

59. Ultrasound imaging in rheumatological disease 1126
Andrew J. Grainger and Philip O'Connor

60. Sonography of muscle injury 1137
Justin C. Lee and Jeremiah C. Healy

61. Ultrasound of the peripheral nerves 1158
Stefano Bianchi, Ferdinando Draghi and Ian Beggs

62. Interventional musculoskeletal ultrasound 1168
Catherine L. McCarthy and Eugene G. McNally

12. Peripheral Arteries and Veins 1195

63. Peripheral arteries 1197
Colin R. Deane and David E. Goss

64. Peripheral veins 1227
Grant M. Baxter and David E. Goss

13. Paediatric Aspects 1251

65. The neonatal brain 1253
Rob Dineen and Tim Jaspan

66. Head and neck masses in children 1294
Laurence Abernethy

67. The infant spine 1315
Tim Jaspan and Rob Dineen

68. Paediatric chest 1337
Edward Y. Lee and Marilyn J. Siegel

69. Paediatric liver and bile ducts, gallbladder, spleen and pancreas 1356
Helen Williams

70. Paediatric bowel and mesentery 1383
Marilyn J. Siegel and Edward Y. Lee

71. The paediatric renal tract and adrenal gland 1406
Guraleep S. Mann

72. The paediatric uterus, ovaries and testes 1468
Guraleep S. Mann, Maria E.K. Sellars and Paul S. Sidhu

73. Paediatric musculoskeletal imaging 1497
Caren J. Landes

Index I-1

LIST OF CONTRIBUTORS

Laurence J. Abernethy MD FRCR
Consultant Paediatric Radiologist
Department of Radiology
Royal Liverpool Children's Hospital,
Alder Hey
Liverpool, UK

Paul L. Allan BSc MBChB DMRD FRCR FRCPE
Consultant Radiologist
Department of Radiology
Royal Infirmary
Edinburgh, UK

Georgina M. Allen BM MRCGP DCH MFSEM MRCP FRCR
Consultant Radiologist
Radiology Department
University Hospitals Birmingham
Birmingham University
Birmingham, UK

Zahir Amin MBBS MRCP MD FRCR
Consultant Radiologist
Department of Radiology
University College London Hospitals
London, UK

Tom Anderson MSc
Senior Research Fellow
Medical Physics
University of Edinburgh
Edinburgh, UK

Grant M. Baxter MBChB FRCR
Consultant Radiologist
Department of Radiology
Western Infirmary
Glasgow, UK

Ian Beggs FRCR
Consultant Musculoskeletal Radiologist
Department of Radiology
The Royal Infirmary of Edinburgh
Edinburgh, UK

Stefano Bianchi MD
Director
CIM SA
Cabinet Imagerie Médicale
Geneva, Switzerland

Gerd Bodner MD
Professor of Radiology
Specialist Medical Centre
Gibraltar

Michael J. Bradley MBChB DMRD FRCR
Honorary Clinical Lecturer, Bristol University
Lecturer, University of the West of England
Consultant Radiologist
Department of Radiology
Southmead
Westbury-on-Trym, Bristol, UK

David J. Breen MRCP FRCR
Consultant Abdominal Radiologist
Department of Radiology
Southampton University Hospitals
Southampton, UK

Robert S.D. Campbell MBChB DMRD FRCR
Consultant in Musculoskeletal Radiology
Department of Radiology
Royal Liverpool University Hospital
Liverpool, UK

Orlando Catalano MD
Assistant
Department of Radiology
Pascale Institute
Naples, Italy

Dania Cioni MD
Assistant Professor of Radiology
Division of Diagnostic Imaging and Intervention
Department of Liver Transplantation, Hepatology, and Infectious Diseases
University of Pisa
Pisa, Italy

Anne Marie Coady MRCP FRCR
Consultant Radiologist
Head of Obstetric and Gynecologic Ultrasound
Ultrasound Department
Hull and East Yorkshire Women and Children's Hospital
Hull, UK

Dennis L. Cochlin MBBCh FRCR
Consultant Radiologist
Division of Radiology
University Hospital of Wales
Cardiff, UK

David O. Cosgrove MA MSc FRCP FRCR
Emeritus Professor
Imaging Sciences Department
Hammersmith Hospital
Imperial College
London, UK

Neil J.A. Cozens MBChB DMRD FRCR
Consultant Radiologist
Derby Hospitals NHS Foundation Trust
Derbyshire Royal Infirmary
Derby, UK

Laura Crocetti MD PhD
Assistant Professor of Radiology
Division of Diagnostic Imaging and Intervention
Department of Liver Transplantation, Hepatology, and Infectious Diseases
University of Pisa
Pisa, Italy

Colin R. Deane PhD MIPEM
Clinical Scientist
Vascular Laboratory
Department of Medical Engineering and Physics
King's College Hospital
London, UK

Diane DeFriend BSc MBChB FRCR
Consultant Radiologist
Imaging Directorate
Derriford Hospital
Plymouth, UK

Clotilde Della Pina MD PhD
Consultant Radiologist
Division of Diagnostic Imaging and Intervention
Department of Liver Transplantation, Hepatology, and Infectious Diseases
University of Pisa
Pisa, Italy

Keith Dewbury BSc MBBS FRCR
Consultant Radiologist and Senior Lecturer
Department of Clinical Radiology (Ultrasound)
Southampton General Hospital
University of Southampton
Southampton, UK

Rob Dineen MRCP FRCR PhD
Clinical Associate Professor
Honorary Consultant Neuroradiologist
Academic Radiology
University of Nottingham
Nottingham, UK

Ferdinando Draghi
Fondazione IRCCS Policlinico S. Matteo
Università degli Studi Istituto di Radiologia
Pavia, Italy

Francis A. Duck PhD DSc
Medical Physicist
Department of Medical Physics and Bioengineering
Royal United Hospital
Bath, UK

Anthony J. Edey BMedSci MRCP FRCR
Specialist Registrar
Department of Radiology
King's College Hospital
London, UK

Simon T. Elliott MBChB FRCR
Consultant Radiologist
Radiology Department
Freeman Hospital
Newcastle-upon-Tyne, UK

Andrew J. Evans MRCP FRCR
Professor of Breast Imaging
Centre for Oncology & Molecular Medicine
Division of Medical Sciences
University of Dundee
Ninewells Hospital & Medical School
Dundee

John A. Fielding MD FRCR FRCP(Edin)
Consultant Radiologist
Department of Radiology
Royal Shrewsbury Hospital NHS Trust
Shrewsbury, UK

Simon J. Freeman MBBS MRCP FRCR
Consultant Radiologist
Department of Radiology
Derriford Hospital
Plymouth, UK

Fergus V. Gleeson MBBS FRCR
Consultant Radiologist
Department of Radiology
The Churchill Hospital
Headington, Oxford, UK

David E. Goss PhD MIPEM
Clinical Scientist
Vascular Laboratory
Department of Medical Engineering and Physics
King's College Hospital
London, UK

Andrew J. Grainger MRCP FRCR
Consultant Musculoskeletal Radiologist
Department of Radiology
Leeds Teaching Hospitals
Leeds, UK

Timothy Hartshorne AVS
Vascular Technologist
Department of Surgery
Leicester Royal Infirmary
Leicester, UK

Christopher J. Harvey BSc(Hons) MBBS MRCP FRCR
Consultant Radiologist
Honorary Senior Lecturer, Imperial College
Department of Imaging
Hammersmith Hospital
London, UK

Jeremiah C. Healy MA MB BChir MRCP FRCR
Consultant Musculoskeletal Radiologist
Honorary Senior Lecturer, Imperial College
Department of Radiology
Chelsea and Westminster Hospital
London, UK

Tracey Hughes MB, BCh, BAO, BA, MRCP, FRCR
Consultant Radiologist
Radiology Department
Queen Elizabeth Hospital
Gateshead, UK

Scott Inglis BSc MSc PhD MIPEM CSci
Senior Clinical Scientist
Department of Medical Physics
NHS Lothian / University of Edinburgh
The Royal Infirmary of Edinburgh
Edinburgh, UK

Jonathan J. James FRCR
Consultant Radiologist
Nottingham Breast Institute
Nottingham City Hospital
Nottingham, UK

Tim Jaspan MBChB BSc FRCR FRCP
Consultant Paediatric Neuroradiologist
Imaging Centre
University Hospital
Queen's Medical Centre
Nottingham, UK

Steven J. Kennish MBChB, MRCS(Ed) FRCR
Specialist Registrar in Radiology
St James University Hospital
Leeds, UK

Stephen R. Killick MD FRCOG FFSRH
Professor of Reproductive Medicine and Surgery
University of Hull and Hull York Medical School (HYMS)
Women and Children's Hospital
Hull, UK

Caren J. Landes MBChB MRCPCH FRCR
Consultant Paediatric Radiologist
Radiology Department
Alder Hey Children's NHS Foundation Trust
Liverpool, UK

Edward Y. Lee MD MPH
Assistant Professor of Radiology
Department of Radiology and
Department of Medicine
Pulmonary Division
Children's Hospital Boston and Harvard Medical School
Boston, MA, USA

Justin C. Lee BSc MBBS MRCS FRCR
Consultant Musculoskeletal Radiologist
Department of Radiology
Chelsea and Westminster Hospital
London, UK

Edward Leen MB MD FRCR
Professor of Radiology
MRC Clinical Sciences Centre
Faculty of Medicine
Imperial College London
Hammersmith Hospital
London, UK

Riccardo Lencioni MD
Associate Professor of Radiology
Director, Division of Diagnostic and Intervention
Department of Liver Transplantation, Hepatology, and Infectious Diseases
University of Pisa
Pisa, Italy

Adrian Kuok Pheng Lim MD FRCR
Consultant Radiologist
Honorary Senior Lecturer, Imperial College
Imaging Department
Charing Cross Hospital
London, UK

Gavin Low MBChB MRCS FRCR
Assistant Professor
Department of Radiology & Diagnostic Imaging
University of Alberta Hospital
Edmonton, AB, Canada

Gurdeep S. Mann MBChB MRCP(UK) FRCR
Consultant Radiologist
Department of Radiology
Royal Liverpool Children's Hospital, Alder Hey
Liverpool, UK

Kevin Martin BSc PhD FIPEM
Consultant Clinical Scientist
Department of Medical Physics
Leicester Royal Infirmary
Leicester, UK

Carlo Martinoli MD
Associate Professor of Radiology
Radiologia – DISC. Università di Genova
Genoa, Italy

Catherine L. McCarthy MBChB FRCR
Consultant Musculoskeletal Radiologist
Department of Radiology
Nuffield Orthopaedic Centre NHS Trust
Headington, Oxford, UK

Norman McDicken BSc PhD
Emeritus Professor
Medical Physics
Edinburgh University
Edinburgh, UK

Eugene G. McNally MB BCh BAO FRCPI FRCR
Consultant Musculoskeletal Radiologist
Department of Radiology
Nuffield Orthopaedic Centre NHS Trust
Headington, Oxford, UK

Carmel M. Moran PhD FIPEM
Reader in Medical Physics
Centre for Cardiovascular Sciences
University of Edinburgh
Queens Medical Research Institute
Edinburgh, UK

Philip J. O'Connor MRCP FRCR
Consultant Musculoskeletal Radiologist
Department of Radiology
Leeds Teaching Hospitals
Leeds, UK

Simon Ostlere FRCR
Consultant Musculoskeletal Radiologist
Department of Radiology
Nuffield Orthopaedic Centre NHS Trust
Headington, Oxford, UK

Uday Patel MBChB MRCP FRCR
Consultant Radiologist
Department of Radiology
St George's Hospital and Medical School
London, UK

James M. Pilcher MSc MRCP FRCR
Consultant Radiologist and Clinical Lead of Adult Ultrasound
Department of Radiology
St George's Hospital
London, UK

David W. Pilling MBChB DCH DMRD FRCR FRCPCH
Consultant Paediatric Radiologist
Department of Radiology
Royal Liverpool Children's Hospital, Alder Hey
Liverpool, UK

John N. Plevris MD DM PhD FRCP(E)
Consultant Gastroenterologist & Reader (hon)
Centre for Liver & Digestive Disorders
The Royal Infirmary of Edinburgh;
University of Edinburgh Medical School
Edinburgh, UK

Najib M. Rahman BM BCh MA(Oxon) MRCP
MRC Training Fellow
Specialist Registrar in Respiratory Medicine
Oxford Centre for Respiratory Medicine
Churchill Hospital
Headington, Oxford, UK

Rhian Rhys MBBCh FRCS(Otol) FRCR
Consultant Radiologist
Department of Radiology
Royal Glamorgan Hospital
Llantrisant, Cardiff, UK

Jonathan L. Richenberg MA MRCP FRCR
Consultant Uroradiologist and Honorary Senior Lecturer
Department of Radiology
Brighton and Sussex University Hospitals NHS Trust
Brighton, East Sussex, UK

Philip Robinson MBChB MRCP FRCR
Consultant Musculoskeletal Radiologist
Department of Radiology
Chapel Allerton Hospital
Leeds Teaching Hospitals
Leeds, UK

Peter Rodgers MBBS FRCR
Consultant Radiologist
Leicester Royal Infirmary
University Hospitals of Leicester NHS Trust
Leicester, UK

Elizabeth E. Rutherford BMedSci MBBS MRCS FRCR
Consultant Radiologist
Department of Ultrasound
Southampton General Hospital
Southampton, UK

Suzanne M. Ryan MD MRCP(Ireland) FRCR
Consultant Radiologist
Department of Radiology
King's College Hospital
London, UK

Maria E.K. Sellars
King's College Hospital
London, UK

Paul S. Sidhu BSc MBBS MRCP FRCR DTMBH
Consultant Radiologist and Senior Lecturer
Department of Radiology
King's College Hospital
London, UK

Marilyn J. Siegel MD
Professor of Radiology and Pediatrics
Mallinckrodt Institute of Radiology
Washington University School of Medicine
St Louis, MO, USA

Rakesh Sinha MBBS MD FRCR FICR
Consultant Radiologist and Assistant Professor
Department of Clinical Radiology
Warwick Hospital Foundation Trust and Warwick Medical School
Warwick, UK

Jane A. Smith MPhil DMU DCRR
Consultant Sonographer
Ultrasound Department
St James's University Hospital
Leeds, UK

Hazel C. Starritt PhD FIPEM
Medical Physicist
Medical Physics and Bioengineering
Royal United Hospital
Bath, UK

Brian Stedman BSc FRCR FRCS
Consultant Abdominal and Interventional Radiologist
Department of Radiology
Southampton University Hospitals NHS Trust
Southampton, UK

Alberto Tagliafico MD
Staff Radiologist
Department of Radiology
University of Genoa
Genoa, Italy

James Teh BSc MBBS MRCP FRCR
Consultant Musculoskeletal Radiologist
Department of Radiology
Nuffield Orthopaedic Centre NHS Trust
Headington, Oxford, UK

Tze Min Wah MBChB FRCR
Consultant Radiologist and Lead for Percutaneous Tumour Ablation Program
Department of Radiology
Leeds Teaching Hospital NHS Trust
Leeds, UK

Joanna M. Wardlaw MB ChB (Hons) FRCP FRCR MD FMedSci
Professor of Applied Neuroimaging and Honorary Consultant Neuroradiologist
University of Edinburgh and NHS Lothian
Director, Scottish Imaging Network, A Platform for Scientific Excellence (SINAPSE) Collaboration
Division of Clinical Neurosciences
Western General Hospital
Edinburgh, UK

Michael J. Weston MBChB MRCP FRCR
Consultant Radiologist
Department of Radiology
St James's University Hospital
Leeds, UK

C. Jason Wilkins MA MRCP FRCR
Consultant Radiologist
Department of Radiology
King's College Hospital
London, UK

Helen Williams MRCP FRCR
Consultant Paediatric Radiologist
Radiology Department
Birmingham Children's Hospital
Birmingham, UK

David J. Wilson MBBS BSc FRSEM FRCP FRCR
Consultant Musculoskeletal Radiologist
Department of Radiology
Nuffield Orthopaedic Centre NHS Trust
Headington, Oxford, UK

CHAPTER

1 Basic physics of medical ultrasound

W.N. McDicken and T. Anderson

PRODUCTION OF ULTRASOUND 3
INTENSITY AND POWER 5
DIFFRACTION AND INTERFERENCE 5
IMAGE SPECKLE 6
FOURIER COMPONENTS 7
STANDING WAVES AND RESONANCE 7
REFLECTION 9
SCATTERING 9
REFRACTION 10
LENSES AND MIRRORS 10
ABSORPTION AND ATTENUATION 11
NON-LINEAR PROPAGATION 11
TISSUE CHARACTERISATION AND ELASTOGRAPHY 12
DOPPLER EFFECT 13
RESOLUTION 14
APPENDIX 15
Continuous wave ultrasound 15
Pulsed wave ultrasound 15

In this chapter the physics of medical ultrasound will be discussed at an introductory level for users of the technology. Several texts exist which readers can consult to deepen their understanding.[1–5] Discussed later in this chapter are parameters related to ultrasound in tissue such as speed of ultrasound, attenuation and acoustic impedance. Values of these parameters for commonly encountered tissues and materials are quoted (for more values see Duck[6] and Hill et al.[7]). The clinical user is not required to have a detailed knowledge of these values but some knowledge helps in the production and interpretation of ultrasound images and Doppler blood flow measurements. Basic physics is also of central importance in considerations of safety.

PRODUCTION OF ULTRASOUND

Ultrasound vibrations (or waves) are produced by a very small but rapid push–pull action of a probe (transducer) held against a material (medium) such as tissue. Virtually all types of vibration are referred to as acoustic, whereas those of too high a pitch for the human ear to detect are also called ultrasonic. Vibrations at rates of less than about 20 000 push–pull cycles/s are audible sound, above this the term ultrasonic is employed. In medical ultrasound, vibrations in the range 20 000 to 50 000 000 cycles/s are used. The term frequency is employed rather than rate of vibration and the unit hertz (Hz) rather than cycles/s. We therefore use frequencies in the range 20 kilohertz (20 kHz) to 50 megahertz (50 MHz).

We most commonly encounter audible acoustic waves produced by the action of a vibrating source on air (vocal cords, loudspeaker, musical instruments, machinery). In medical ultrasound the source is a piezoelectric crystal, or several, mounted in a hand-held case and driven to vibrate by an applied fluctuating voltage. Conversely, when ultrasound waves strike a piezoelectric crystal causing it to vibrate, electrical voltages are generated across the crystal, hence the ultrasound is said to be detected. The hand-held devices containing piezoelectric crystals and probably some electronics are called transducers since they convert electrical to mechanical energy and vice versa. They are fragile and expensive, about the same price as a motor car. Transducers are discussed more fully in Chapter 2. The great majority of medical ultrasound machines generate short bursts or pulses of vibration, e.g. each three or four cycles in duration; a few basic fetal heart or blood flow Doppler units transmit continuously. Figure 1.1 illustrates the generation of pulsed and continuous ultrasound. For a continuous wave an alternating (oscillating) voltage is applied continuously whereas for a pulsed wave it is applied for a short time. The basic data for most ultrasound techniques is obtained by detecting the echoes which are generated by reflection or scattering of the transmitted ultrasound at changes in tissue structure within the body.

The push–pull action of the transducer causes regions of compression and rarefaction to pass out from the transducer face into the tissue. These regions have increased or decreased tissue density. A waveform can be drawn to represent these regions of increased and decreased pressure and we say that the transducer has generated an ultrasound wave (Fig. 1.2). The distance between equivalent points on the waveform is called the wavelength and the maximum pressure fluctuation is the wave amplitude (Fig. 1.3). If ultrasound is generated by a transducer with a flat face, regions of equal compression or rarefaction will lie in planes as the vibration passes through the medium. Plane waves or wavefronts are said to have been generated. Similarly if the transducer face is convex or concave the wavefront will be convex or concave. The latter can be used to provide a focused region at a specified distance from the transducer face. In tissue if we could look closely at a particular point, we would see that the tissue is oscillating rapidly back and forward about its rest position. As noted above, the number of oscillations per second is the frequency of the wave. The speed with which the wave passes through the tissue is very high close to 1540 m/s for most soft tissue, i.e. several times the speed of most passenger jet planes. We will see in the discussion of imaging techniques that this is very important since it means that pulses can be transmitted and echoes collected very rapidly, enabling images to be built up in a fraction of a second. The speed of sound, c, is simply related to the frequency, f, and the wavelength, λ, by the formula:

$$c = f\lambda$$

In the acoustic waves just described the oscillations of the particles of the medium are in the same direction as the wave travel. This type of wave is called a longitudinal wave or compressional wave since it gives rise to regions of increased and decreased

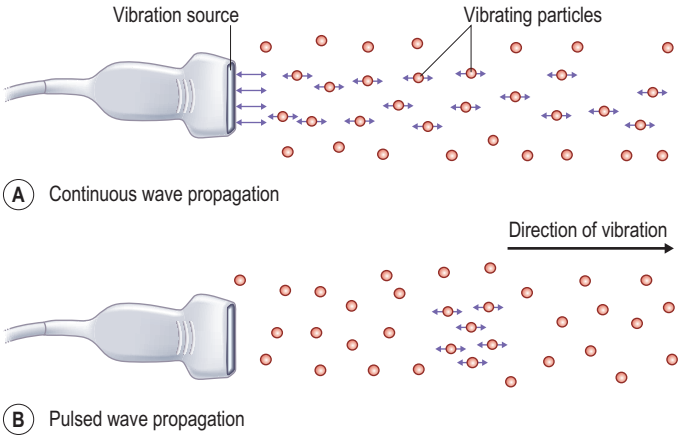


Figure 1.1 The generation of continuous and pulsed wave ultrasound by a vibrating source in contact with the propagating medium.

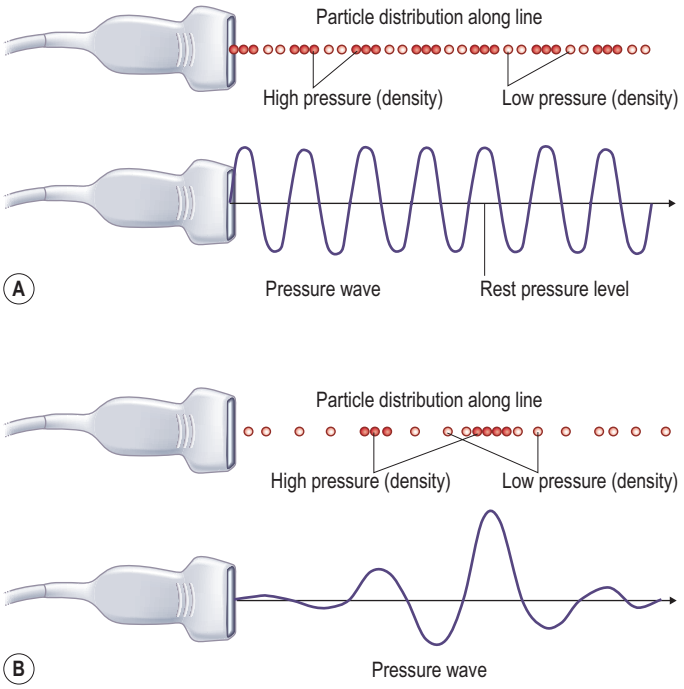


Figure 1.2 The waveform description of ultrasound pressure fluctuations. A: Continuous wave. **B:** Pulsed wave.

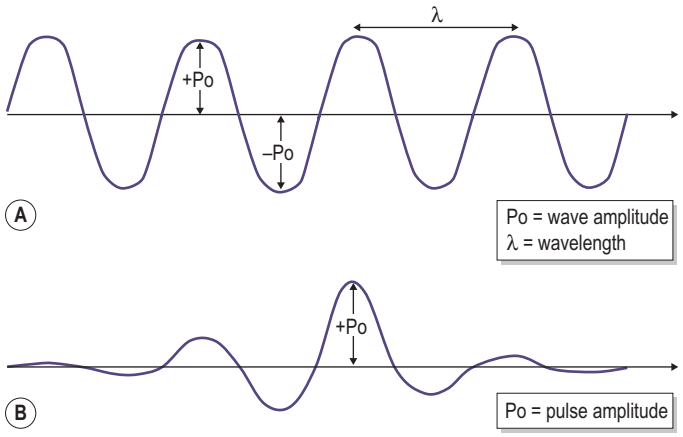


Figure 1.3 Ultrasound wavelength and wave amplitude. A: Continuous wave. **B:** Pulsed wave.

Table 1.1 Speed of ultrasound and acoustic impedance

Material	Speed (m/s)	Acoustic impedance (g/cm^2 s)
Water (20°C)	1480	1.48×10^5
Blood	1570	1.61×10^5
Bone	3500	7.80×10^5
Fat	1450	1.38×10^5
Liver	1550	1.65×10^5
Muscle	1580	1.70×10^5
Polythene	2000	1.84×10^5
Air	330	0.0004×10^5
Soft tissue (average)	1540	1.63×10^5

Basic ultrasound concepts

- Ultrasound is high-frequency vibration that travels through tissue at high speed, close to 1540 m/s.
- In medical ultrasound, the frequency range used is 1 to 50 MHz.
- Ultrasound vibration travels as a pressure waveform.
- Ultrasound can be generated and detected by piezoelectric crystals contained in small hand-held transducers.
- Echoes produced by transmitted ultrasound pulses at tissue interfaces are the basic source of information in diagnostic ultrasound.

pressure. In another type of wave the oscillations are perpendicular to the direction of wave travel, like ripples on a pond, and they are called transverse or shear waves. At MHz frequencies the latter are attenuated rapidly in tissues and fluids and hence are not encountered at present in diagnostic ultrasound. Ongoing developments at lower frequencies aim to utilise them in elastography (see later in this chapter). Transmitted energy, power and pressure amplitude are discussed more quantitatively in Chapter 4 on safety.

The speed of ultrasound in soft tissue depends on its rigidity and density (Table 1.1), the more rigid a material, the higher the speed. From the table we can see that the speed in soft tissues is fairly closely clustered around an average value of 1540 m/s. Virtually all diagnostic instruments measure the time of echo return after the instant of pulsed ultrasound transmission and then use the speed in tissue to convert this time into the tissue depth of the reflecting structure. For a mixture of soft tissues along the pulse path, an accurate measure of depth is obtained by the assumption of an average speed of 1540 m/s for conversion of time into depth. The high speed in bone can cause severe problems as will be seen later when refraction of the ultrasound is considered. Unless bone is thin it is best avoided during ultrasound examinations. The speed of ultrasound in soft tissue is independent of frequency over the diagnostic range, i.e. 1 to 50 MHz. The very high value of the speed of sound in tissue means that echo data can be collected very rapidly; e.g. for a particular beam direction echoes might be collected in less than 0.2 millisecond. This rapid collection could allow a single image (frame) to be produced in 20 milliseconds. In a later section it will be seen that the speed of sound in blood is also used in the Doppler equation when the velocity of blood is calculated.

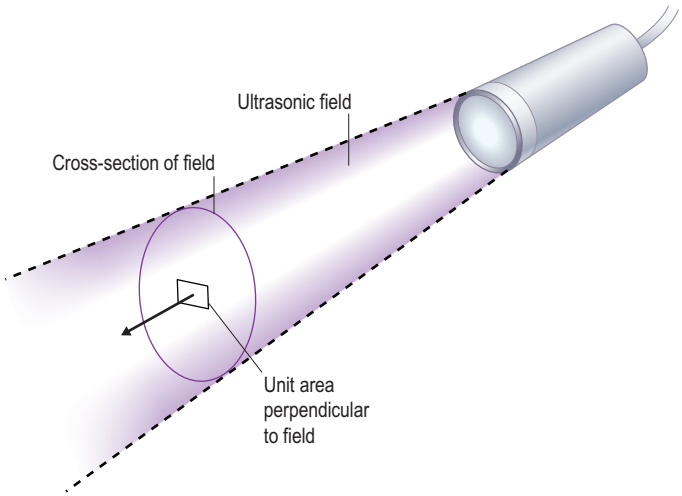


Figure 1.4 **Intensity at a point** – rate of flow of energy through unit area in an ultrasound beam. Power – rate of flow of energy through whole cross-section of ultrasound beam.

Ultrasound beams and power

- The vibration produced by the transducer is a flow of energy through the tissue.
- Intensity and power are related but different physical quantities that are measures of the flow of energy and are of particular interest with regard to safety.
- The ultrasound field or beam is the region in front of the transducer that is affected by the transmitted vibration.
- The decibel notation can be employed to label the controls of intensity, power and amplifier gain. Decibel labelling of a control is not absolute but refers each setting of the control to a reference level.
- Radiation force is experienced when the transmitted energy strikes a target and is reflected or absorbed.

INTENSITY AND POWER

When a transducer is excited by an electrical voltage, vibrations pass into the tissue, i.e. energy passes from the transducer to the tissue. The intensity at a point in the tissue is the rate of flow of energy through unit area at that point (Fig. 1.4). For example, the intensity may be 100 milliwatts per square centimetre (100 mW/cm^2). The intensity is related to the square of the pressure wave amplitude.

The region of tissue in front of the transducer subjected to the vibrations is referred to as the ultrasound field or beam. Intensity is often measured at the focus of the field or within 1 or 2 cm of the transducer face. Transducer designers will often measure the pressure amplitude or intensity over the full depth range for which the transducer will be used.

For safety studies, intensity is often defined precisely to ensure validity in the conclusions drawn; for example, I_{spta} is the intensity at the spatial peak (often the focus) averaged over time. Each definition gives rise to an intensity relevant to that definition. These intensities are not used in routine scanning but it is useful to know their origins when the safety literature is being studied (see Appendix at the end of this chapter). It will be seen in Chapter 4 that from a clinical application point of view, the two quantities of interest to optimise safety are thermal index (TI) and mechanical index (MI).

The power of an ultrasonic beam is the rate of flow of energy through the cross-sectional area of the beam (Fig. 1.4). This is a quantity that is often quoted since it gives a feeling for the total output and is relatively easy to measure.

Power and intensity controls on ultrasonic scanners are sometimes labelled using the decibel notation. This occurs less frequently on new machines. Although not essential for the operation of machines, familiarity with this labelling removes its mystique and can be helpful when reading the literature. The manipulation of machine controls is covered in Chapter 3, where it is demonstrated that logical operation can be readily achieved. The decibel notation basically relates the current value of intensity or power to a reference value. For example, taking the maximum intensity position of the control as giving the reference output value I_o, other values of intensity I, corresponding to other control positions, are calibrated relative to I_o as:

$$\text{Output intensity in decibels (dB)} = 10\log(I/I_o)$$

This output in dB is therefore the ratio of two intensities and is not an absolute unit like cm or watt. Output power controls can also be labelled in terms of dB:

$$\text{Output power in decibels (dB)} = 10\log(P/P_o)$$

The dB notation was employed in the past when it was fairly difficult to measure absolute values of intensity and power in units of mW/cm^2 or mW respectively and also since separate calibration is required for each transducer. This notation is essentially an historical hangover and is of no value in machines designed for clinical application. More recently the outputs of machines have been related to possible biological effects, in particular heating and cavitation. Cavitation is the violent response of bubbles when subjected to the pressure fluctuations of an ultrasound wave (Chapter 4). Thermal (TI) and mechanical indices (MI) relate to these phenomena and are displayed onscreen (Chapter 4).

The decibel notation is also found applied to the gain of a receiver amplifier:

$$\text{Gain} = \text{Output volts/Input volts}$$

Or:

$$\text{Gain in decibels} = 20\log(V_{out}/V_{in})$$

Another application relates to differences in pressure amplitude of an ultrasound wave:

$$\text{Acoustic pressure difference in decibels} = 20\log(p_1/p_2)$$

Absolute values of ultrasonic intensity are normally measured with a hydrophone, which takes the form of a small probe with a piezoelectric element at its tip.

Absolute values of ultrasonic power are measured with a radiation power balance which is based on the following. There is a flow of energy in an ultrasonic field from the transducer as the vibrations pass into water. Associated with the flow of energy in a beam there is a flow of momentum. Due to this momentum a force is experienced by an object placed in the field, the force being directly related to the power of the field. These small forces can be measured by placing the object under water on the pan of a sensitive chemical balance, hence the name power balance.

For a beam of power P incident perpendicularly on a totally reflecting flat surface:

$$\text{Radiation force} = 2P/c$$

The force experienced is 0.135 mg per milliwatt. Power levels down to 0.1 mW can be measured with balances. For an object that totally absorbs the beam, the force is half that of the reflection case.

DIFFRACTION AND INTERFERENCE

Diffraction describes the spreading out of a wave as it passes from its source through a medium. The pattern of spread is highly dependent on the shape and size of the source relative to the

wavelength of the sound. To produce an approximately parallel-sided beam, the diameter of the crystal face is typically 10 to 20 times that of the ultrasound wavelength. The diffraction pattern of a disc-shaped crystal as found in basic medical ultrasound transducers is approximately cylindrical for a short distance, after which it diverges at a small angle (Fig. 1.5). The diffraction pattern from a small transducer is divergent at a larger angle from close to the transducer (Fig. 1.6A). Within a diffraction pattern there may be fluctuations in intensity, particularly close to the transducer. Diffraction also occurs beyond an obstacle such as a slit aperture or an array of slits which partially blocks the wavefront (Fig. 1.6B). The narrowness of a beam or the sharpness of a focus is ultimately determined by diffraction. The submillimetre wavelengths associated with the high frequencies of medical ultrasound permit the generation of well-focused beams, one of the most important facts in medical ultrasound technology. The higher the frequency, the narrower the beam can be made and hence the finer the image detail. Unfortunately, we will see later that absorption also increases with frequency, which puts an upper limit on the frequency that can be employed in any particular application.

Interference of waves occurs when two or more overlap as they pass through the propagating medium. The resultant wave pressure amplitude at any point is determined by adding the pressure amplitudes from each wave at the point (Fig. 1.7A). When the waveforms are in step, they add constructively (constructive interference) to give an increase in amplitude. Out of step they add destructively (destructive interference), resulting in a lower pressure amplitude (Fig. 1.7B). This 'principle of superposition' is widely used to predict ultrasound field shapes using mathematical models. In such modelling the shape of the transducer field is calculated by considering the crystal face to be subdivided into many small elements. The diffraction pattern for each element is calculated and the effect of them overlapping and interfering gives the resultant ultrasound field shape. Interference and diffraction are rarely considered in detail since, as techniques stand at present, ultrasound beams and fields are not tightly defined.

The terms 'ultrasound field' and 'ultrasound beam' tend to get used interchangeably. It would probably be better if we restricted 'field' to label the transmitted ultrasound pattern in front of the transducer and 'beam' to a combination of the transmitted field and the reception sensitivity pattern in front of the transducer. For a single crystal transducer the two patterns are the same but for array transducers they are probably always different. For example, the transmission focusing and the reception focusing are usually different (Chapter 2). It is the shape of the beam, i.e. the combination of transmission and reception, that plays an important part in determining the detail in an image. The loose usage of 'field' and 'beam' is not usually serious, but it is worth remembering that both transmit power and receiver gain influence the lateral resolution in an image. Image detail (resolution) is discussed later in this chapter.

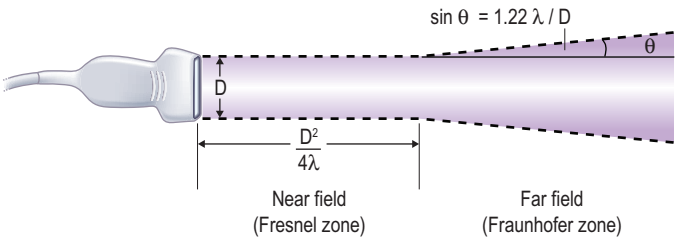


Figure 1.5 Schematic diffraction pattern for a disc-shaped crystal generating a continuous wave beam.

IMAGE SPECKLE

When an ultrasound pulse passes through tissue the very large number of small discontinuities generate small echoes which travel back to the transducer and are detected. These small echoes overlap and interfere both constructively and destructively to produce a fluctuating resultant signal (Fig. 1.8). The related electronic fluctuating signal produced by the transducer is presented along each scan line in the display as fine fluctuations in the grey shades. The whole image appears as a speckle pattern. In practice the speckle is often a combination of the true speckle from very small tissue structures

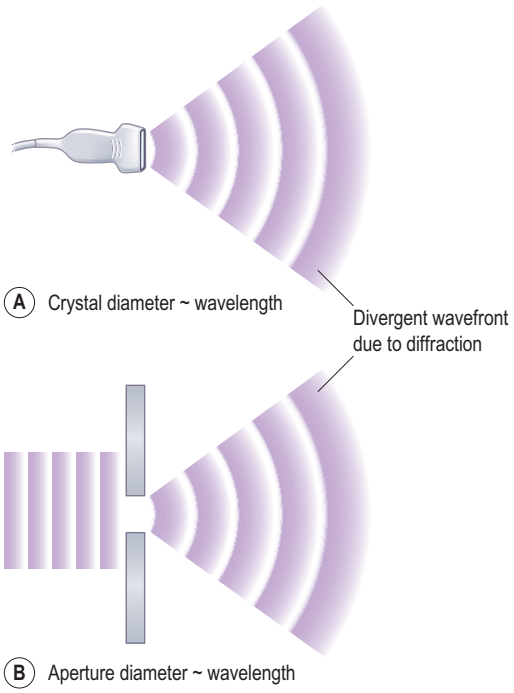


Figure 1.6 Diffraction pattern. A: For a small transducer. **B:** For a small aperture.

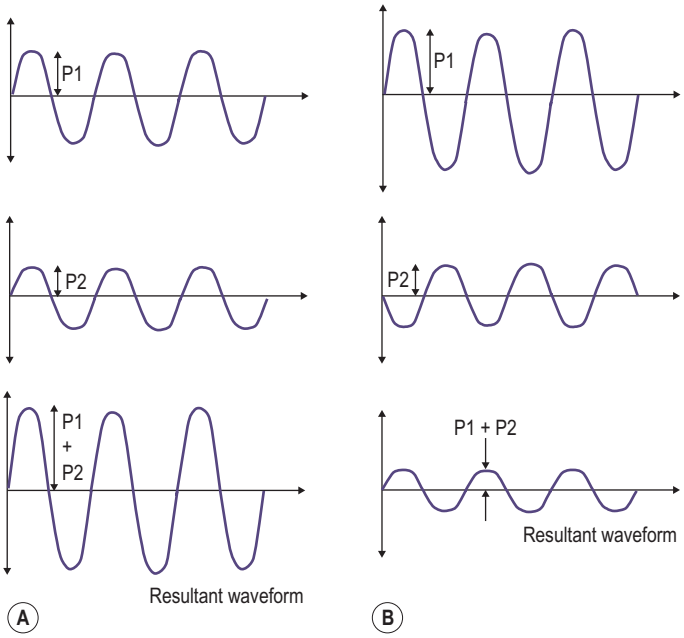


Figure 1.7 A: Constructive interference of two waves. **B:** Destructive interference of two waves.

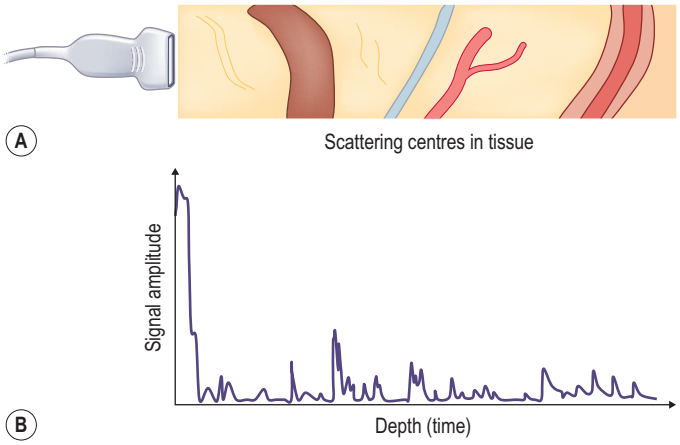


Figure 1.8 Fluctuating echo signals resulting from constructive and destructive interference of echoes from structures lying along one beam direction through tissue. **A:** Transducer transmitting ultrasound along one beam direction into complex tissue. **B:** Echo signals received from one beam direction into tissue.

and some slightly bigger echoes from structures such as blood vessels or muscle fibres. The true speckle does not depict the very small tissue structures but the overall result of their echoes interfering. These tissue structures are smaller than can be imaged by ultrasound in the diagnostic frequency range. The speckle appearance of an image of tissue may help to identify the state of the tissue when the operator has a lot of experience with a particular machine. Comparison of speckle patterns between machines will probably not be valid as transducer design and the electronics influence the speckle appearance. In some applications tissue motion is measured by tracking the speckle pattern, for example in myocardial velocity imaging or elastography. The true speckle does not necessarily follow the tissue exactly but the echoes from the slightly bigger structures do and help to make the technique more robust.

With a sensitive B-mode scanner the speckle image of blood can be observed. The changing pattern relates to the motion of cells or groups of cells. The technique goes by the General Electric trade name of B-Flow.

FOURIER COMPONENTS

In the discussion on interference, it was seen that when two waves or signals overlap the resultant wave pattern has a shape different from either of the two original waves. The simple case of two similar waves was considered giving constructive or destructive interference. However, if two or more waves or signals are considered of different frequencies and in and out of step by varying degrees, complex resultant waveforms can be produced (Fig. 1.9). The resultant waveform is said to be synthesised from the frequency components. The degree to which waves are in or out of step is the phase difference between the waves. Phase is important in the design of technology but it is not a concept that is of direct interest to the clinical user.

The opposite process of breaking a complex waveform down into its frequency components is of more direct interest in medical ultrasound. Then the complex waveform is said to be analysed into its frequency components. This is called frequency or Fourier analysis after its inventor. The more complex the waveform, the more Fourier components it has. A continuous wave of pure sinusoidal shape has one frequency component (Fourier component). A pulse has a range of frequency components. The shorter and sharper the pulse, the larger the range of frequency components; the range is known as the bandwidth of the pulse (Fig. 1.10). Each transducer

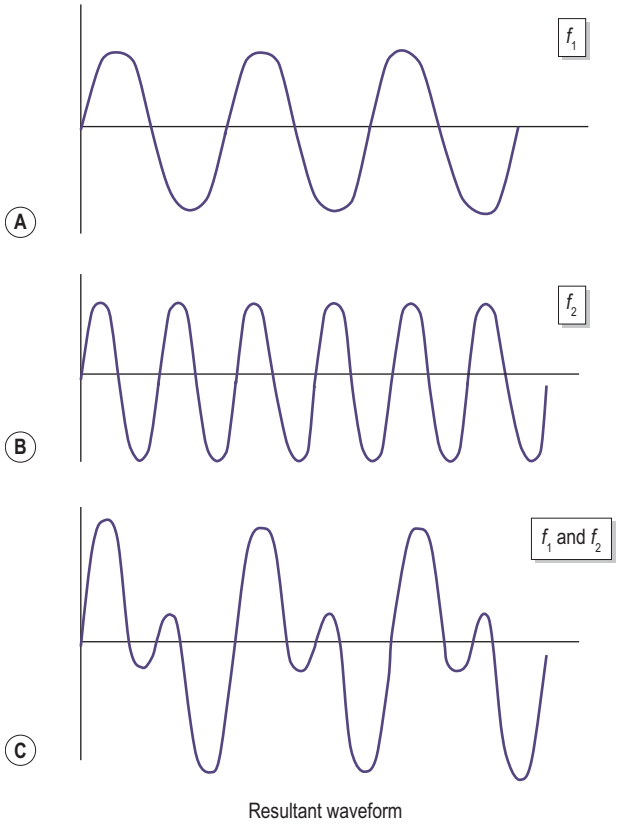


Figure 1.9 Synthesis of a complex waveform by the addition of waves of different frequency. Frequency analysis of a complex waveform is the reverse process which reveals frequency components.

can only handle a specific range of frequencies, known as the bandwidth of the transducer. Ultrasound frequencies outside this range are attenuated and hence are lost to further processing. In Doppler blood flow techniques the complex Doppler signal is often analysed into its frequencies since they relate directly to the velocities of the blood cells at the site interrogated.

Some processes may remove frequencies from a waveform, e.g. absorption may remove the higher-frequency components of the signal. Other processes may add frequencies above or below the initial bandwidth of the transmitted ultrasound pulse, e.g. non-linear propagation or scattering at microbubbles. The frequencies that are added are often referred to as harmonics (above the upper bandwidth limit) or subharmonics (below the lower bandwidth limit) of the original signal.

STANDING WAVES AND RESONANCE

When two waves of the same frequency travelling in opposite directions interfere, standing waves are formed. Examination of the wave pressure variations show alternate regions of high and low pressure amplitude oscillations that are not moving through the medium, i.e. a pattern of stationary nodes and anti-nodes has been formed (Fig. 1.11A). When a sound wave is reflected back and forth between two flat parallel surfaces in such a way that the sound travelling in opposite directions overlaps, standing waves are formed. If the separation of the surfaces is a whole number of half wavelengths, a marked increase in the pressure amplitude is observed (Fig. 1.11B). This is due to the waves adding constructively to give a resonance. When the separation of the surfaces is

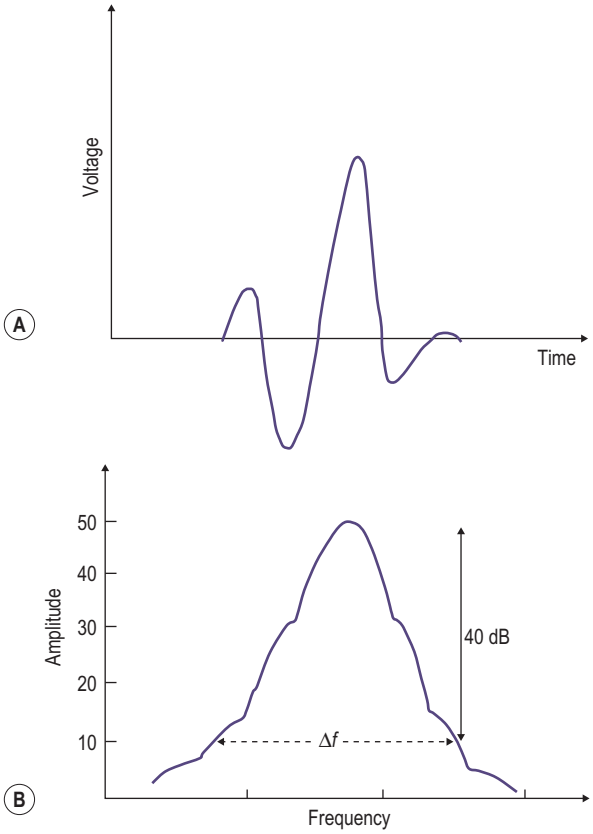


Figure 1.10 The frequency spectrum of a pulsed signal. A: An echo pulse detected by a transducer. **B:** A plot of the amplitude (size) of the frequency components in the pulse after Fourier analysis.

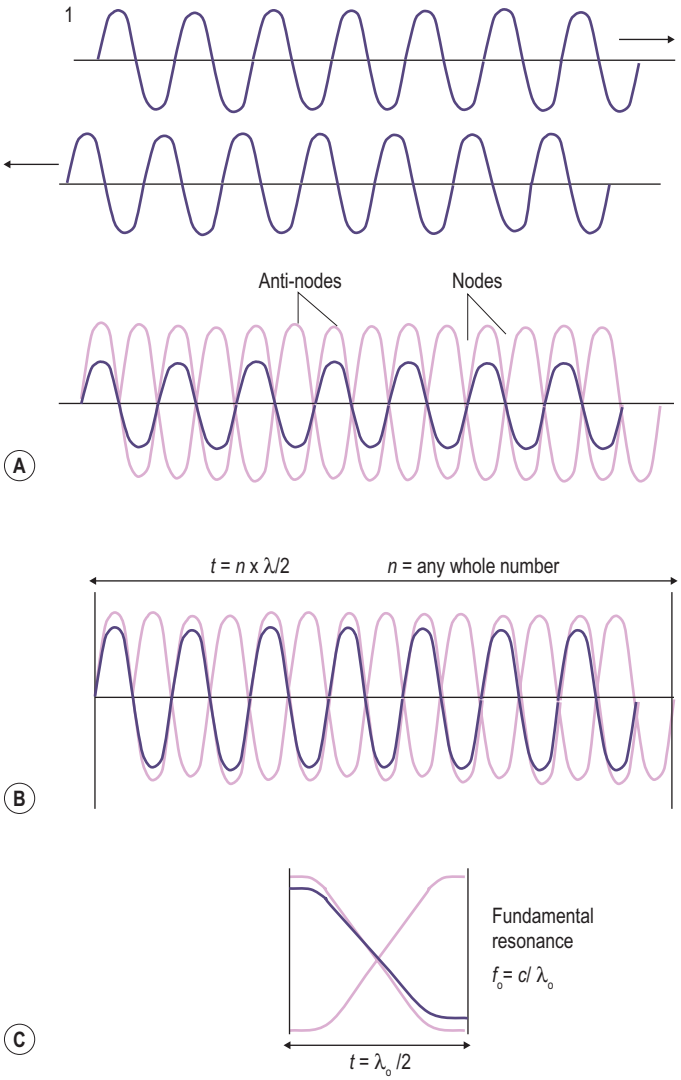


Figure 1.11 A: The generation of a standing-wave pattern by two overlapping waves travelling in opposite directions. **B:** Standing waves produced by waves reflected within parallel surfaces. **C:** Fundamental resonance for surfaces separated by one half-wavelength.

one half-wavelength, a strong resonance occurs, known as the fundamental resonance (Fig. 1.11C).

At other separations equal to multiples of the half wavelength, other weaker resonances are known as harmonics. Conversely harmonics can also be seen when the separation is fixed and the wavelength is varied. These harmonics occur when the wavelength equals some multiple of the separation.

Piezoelectric transducer elements are made equal in thickness to one-half of the wavelength corresponding to their desired operating frequency to give efficient generation and detection of ultrasound. Continuous wave Doppler transducers have little or no damping and resonate at their operating frequency. Imaging and pulsed wave Doppler transducers have some damping which absorbs energy and spreads their sensitivity over a frequency range; i.e. they have a wider frequency response (bandwidth), which can be desirable though the damping reduces their sensitivity. When the size of an object has a special numerical relationship to the wavelength, a resonance will occur. An interesting example of resonance is exhibited when microbubbles of a particular size resonate in an ultrasound field. This resonance is exploited to improve the detection of these bubbles when they are injected into the bloodstream to act as imaging contrast agents (Chapter 6). By coincidence microbubbles, the size of red blood cells, resonate in the same MHz ultrasound frequency range as used in tissue imaging.

Standing waves and interference are of interest to the designer of transducers. They are two of the phenomena that contribute to the overall performance of a transducer and provide some insight into its complex operation. Given this complexity and scope for variation, it is always worth thoroughly assessing the performance of each transducer in clinical use.

Interference, frequencies and resonance

- Waves diffract and interfere.
- At high frequencies, and hence small wavelengths, diffraction can be controlled to produce directional beams.
- High frequencies produce narrow beams.
- Image speckle is produced by interference of echoes from small-scale structures within tissue. The speckle pattern is related to the structure but does not represent the actual structure.
- Complex waveforms (ultrasonic or electronic) can be broken down into frequency components. Frequency analysis is a very powerful technique for characterising signals.
- The frequency spectrum of a signal is important when 'harmonic imaging' and also Doppler blood flow detection are employed.
- Resonance can occur when ultrasound is reflected internally in a structure in which the dimensions of the structure are some multiple of the wavelength.
- Resonance is commonly encountered in transducer crystals and microbubbles.

REFLECTION

Ultrasound is reflected when it strikes the boundary between two media where there is a change in density or compressibility or both. To be more exact, reflection occurs where there is a difference of acoustic impedance (Z) between the media (Fig. 1.12A). The impedance is a measure of how readily tissue particles move under the influence of the wave pressure. The acoustic impedance of a medium equals the ratio of the pressure acting on the particles of the medium divided by the resulting velocity of motion of the particles. Therefore for tissues of different impedance a passing wave of particular pressure produces different velocities in each tissue. Note, the velocity of particle motion about the rest position is not the same as the velocity (speed) of the ultrasound waveform through the medium. For a wave in which the peaks and troughs of pressure lie in flat planes, plane waves, the acoustic impedance of a medium is equal to the density (ρ) times the speed of sound in the medium, i.e. $Z = \rho c$. It is not surprising that reflection depends on quantities such as density and speed of sound, since the latter depends on the rigidity of the medium. In practice when imaging, echo size is often related roughly to the change in acoustic impedance at tissue boundaries. An approximate knowledge of tissue impedances is helpful in this respect (Table 1.1). Note that it is the change that is important – it does not matter whether there is an increase or decrease in impedance. The large changes in acoustic impedance at bone/soft tissue and gas/soft tissue boundaries are problematic since the transmitted pulse is then greatly reduced or even totally blocked in the case of gas by reflection at the boundary. The size of the echo in an image (i.e. the shade of grey) relates to the change in acoustic impedance at the interface producing it. Shades of grey are therefore related to the properties of tissues though signal processing in the scanner also plays an important part.

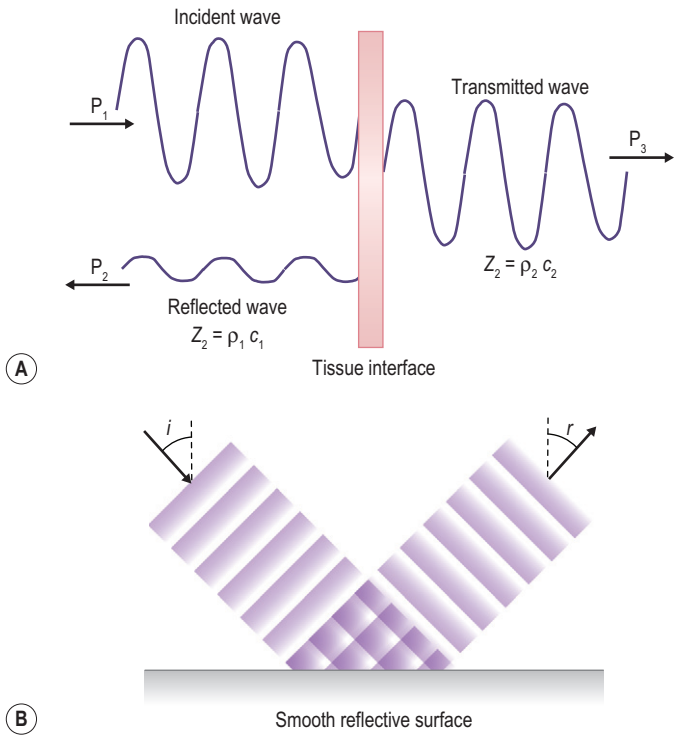


Figure 1.12 Reflection. A: Reflection at change in acoustic impedance between two media. **B:** Reflection at a smooth interface.

The unit of acoustic impedance is the Rayl, where 1 Rayl = 1 kg/m^{2}s (units are often named after individuals, e.g. hertz, watt, pascal, rayleigh). As noted above, impedance is referred to in a semi-quantitative way; numerical values with units are rarely quoted except in some scientific studies, for example where attempts are made to characterise the ultrasonic properties of tissues. As can be seen from Table 1.1, the higher the density or stiffness of a material, the higher is its acoustic impedance.

It is instructive to consider the simple case of reflection of an incident ultrasound wave at a flat boundary between two media of impedances $\rho_1 c_1$ and $\rho_2 c_2$. The magnitude of the echo amplitude is calculated using:

$$\text{Reflected amplitude} = \text{Incident amplitude} \times (\rho_1 c_1 - \rho_2 c_2)/(\rho_1 c_1 + \rho_2 c_2)$$

Table 1.2 gives a rough appreciation of echo sizes produced at different boundaries. Since properties of tissue are usually not accurately known and are highly dependent on the state of the tissue, significant differences from these values may exist in particular cases.

Reflection of ultrasound at a smooth surface is similar to light reflecting at a mirror and is sometimes referred to as specular reflection (Fig. 1.12B). Here it can be seen that the angle of incidence, i, is equal to the angle of reflection, r.

SCATTERING

As an ultrasound wave travels through tissue it will probably interact with small tissue structures whose dimensions are similar to or less than a wavelength and whose impedances exhibit small variations. Some of the wave energy is then scattered in many directions (Fig. 1.13). Scattering is the process that provides most of the echo signals for both echo imaging and Doppler blood flow techniques. The closely packed scattering structures are very large in number and have a random distribution. Computer models of a wave interacting with such structures can predict a scattered wave with properties like those observed in practice. We noted earlier that the fluctuations in echo signals explain the fine speckled patterns detected from organ parenchyma and blood. Red cells in blood, singly or in the groups, are the scattering structures which produce the signals used in Doppler techniques. Reflection at a flat boundary, as discussed above, is a special case of scattering which occurs at smooth surfaces on which the irregularities are very much smaller than a wavelength. When the irregularities are comparable to the wavelength, they can no longer be ignored. This scattering at a non-smooth tissue interface enables it be imaged more easily since echoes are detectable over a wide range of angles of incidence of the beam at the interface.

The ratio of the total ultrasound power, S, scattered in all directions by a target to the incident intensity, I, of the ultrasound beam is called the total scattering cross-section of the target. This ratio is used to compare the scattering powers of different tissues. Table 1.3

Table 1.2 Percentage of incident energy reflected at tissue interfaces (perpendicular incidence at flat interface)

Fat/muscle	1.08
Muscle/blood	0.07
Bone/fat	48.91
Fat/kidney	0.64
Lens/aqueous humour	1.04
Soft tissue/water	0.23
Soft tissue/air	99.90

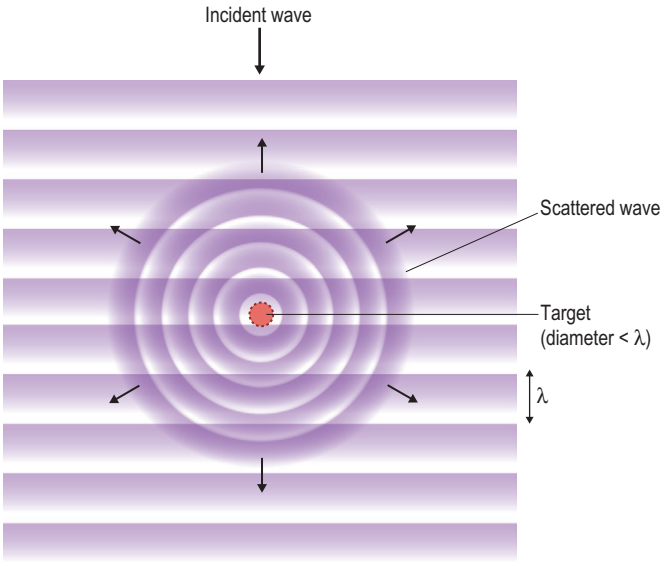


Figure 1.13 Wave scattering at a target of dimensions much less than the wavelength.

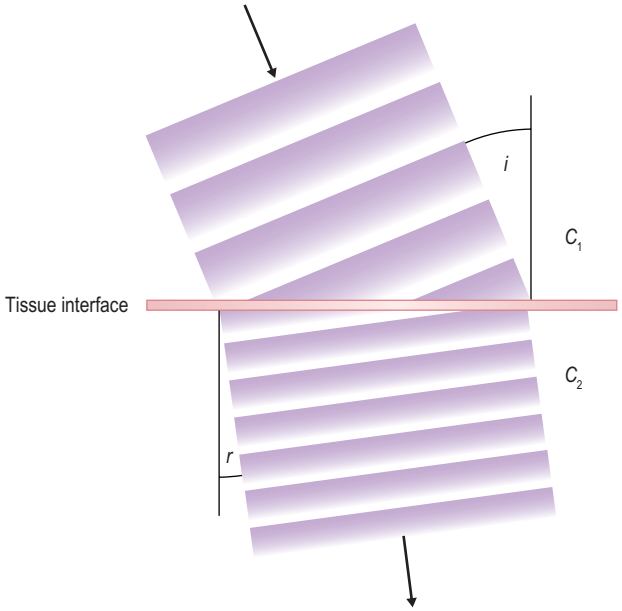


Figure 1.14 Deviation of an ultrasound beam on striking at an angle the interface between two media of differing speed of sound.

Table 1.3 Scattering within organs. Scattered signal level compared to typical soft tissue boundary (fat/muscle) echo level

Reference boundary (fat/muscle)	Echo level	1.0
Liver parenchyma	Scatter level	0.032
Placenta	Scatter level	0.1
Kidney	Scatter level	0.01
Blood	Scatter level	0.001
Water	Scatter level	0.000

provides an idea of the scattering powers of some common tissues. The use of such scattering measurements has not been sufficiently discriminatory for tissue characterisation. However, the depiction of different levels of scattered echo signals in an image provides much of the information in the image.

REFRACTION

The change in direction of a beam when it crosses a boundary between two media in which the speeds of sound are different is called 'refraction' (Fig. 1.14). If the angle of incidence is 90° there is no beam bending but at all other angles there is a change in direction. Refraction of light waves in optical components such as lenses and prisms is a common example. For an angle of incidence *i*, the new angle of the beam to the boundary on passing through it (the angle of refraction *r*) is easily calculated using Snell's law:

$$\sin i / \sin r = c_1 / c_2 = \mu$$

where μ is the refractive index.

Table 1.4 shows that deviations of a few degrees can occur at soft tissue boundaries. The results in ultrasonic imaging allow us to conclude that refraction is not a severe problem at soft tissue interfaces. An exception is at soft tissue/bone boundaries, where it can be a severe problem due to the big differences in speed of ultrasound between soft tissue and bone.

Table 1.4 Beam deviation due to refraction at typical soft/tissue boundaries (angle of incidence 30°)

Bone/Soft tissue	19°
Muscle/Fat	2.5°
Muscle/Blood	0.5°
Muscle/Water	1°
Lens/Aqueous humour	2°

Reflection, refraction and scattering

- An echo is generated at a change in acoustic impedance. The bigger the change, the bigger the echo. It does not matter if the change is an increase or decrease.
- The acoustic impedance of a tissue is related to the density and rigidity of the tissue.
- Bone and gas have acoustic impedances that are markedly different from those of soft tissue.
- Reflection is said to occur at surfaces of dimensions greater than the ultrasound wavelength and for smooth surfaces is analogous to light reflecting from a mirror or glass surface.
- Scattering occurs at small structures of acoustic impedance different from that of the surrounding medium. Scattering redirects the incident ultrasound over a wide range of angles, possibly through all angles in 3D.
- Very small tissue structures and blood cells are scattering centres of interest.
- Refraction occurs at a tissue interface where the velocity of ultrasound changes and the angle of incidence is not 90°.

LENSES AND MIRRORS

We often think of ultrasound behaving in a manner similar to that of light. This is not surprising since both are wave phenomena. As for light, lenses and mirrors can be constructed for ultrasound by exploiting reflection and refraction (Fig. 1.15). Lenses are designed by selecting material in which the velocity of ultrasound is different

Table 1.5 Tissue thickness (in cm) to half intensity of ultrasound beam (–3 dB) for common clinical frequencies and materials

	1 MHz	3 MHz	5 MHz	10 MHz	20 MHz
Blood	17	8.5	3	2	1
Fat	5	2.5	1	0.5	0.25
Liver	3	1.5	0.5	–	–
Muscle	1.5	0.75	0.3	0.15	–
Bone	0.2	0.1	0.04	–	–
Polythene	0.6	0.3	0.12	0.6	0.03
Water	1360	340	54	14	3.4
Soft tissue (average)	4.3	2.1	0.86	0.43	0.21

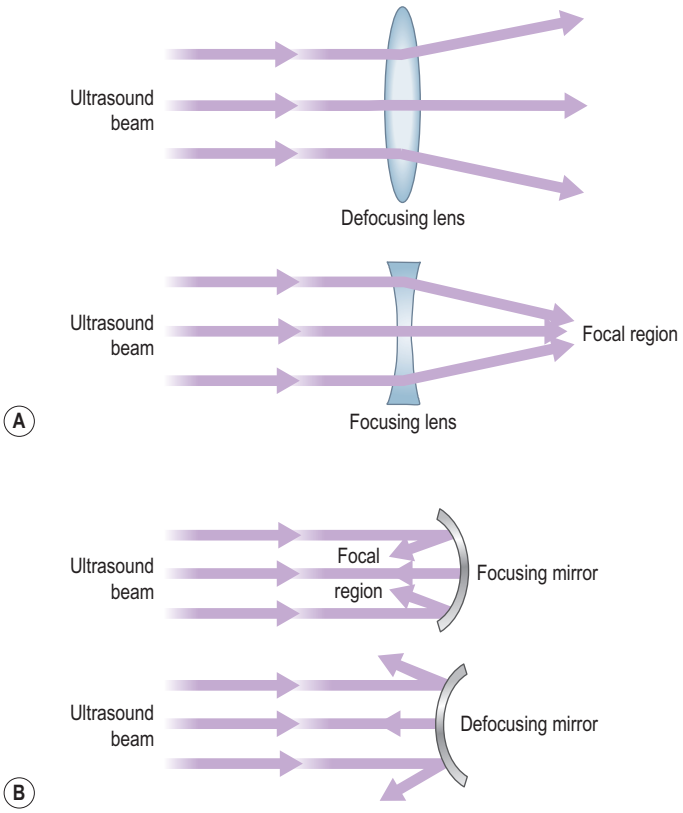


Figure 1.15 Lenses (A) and mirrors (B) for ultrasound.

from that of water or tissue. Mirror material has an acoustic impedance markedly different from water or tissue and hence results in very strong reflection. Lenses are most commonly found on the front face of transducers. Mirrors are rarely used.

ABSORPTION AND ATTENUATION

As an ultrasound wave passes through tissue, its orderly vibrational energy is converted into random vibrational heat energy and hence the wave pressure amplitude reduces with distance travelled. This process is known as absorption. The higher the ultrasound frequency, the more rapidly is the amplitude reduced. Absorption rate also depends on the tissue involved.

In addition to absorption, other effects contribute to the total attenuation of the wave amplitude. These effects are reflection, scattering and beam divergence. The last two are frequency dependent, hence attenuation in tissue is highly dependent on frequency. Attenuation rises quickly over the diagnostic frequency range. Scanning equipment uses several techniques to compensate for attenuation and the operator should ensure that the appropriate controls have been optimised. This is further discussed in Chapter 3.

Table 1.5 presents attenuation for commonly encountered tissues. In the laboratory, attenuation is measured by noting the decrease in pressure amplitude as a wave passes through a known thickness of tissue. By taking the ratio of the input and output pressure amplitudes at either side of the slab of tissue, the drop in pressure amplitude can be quoted in dB/cm (attenuation coefficient). It is common practice to quote attenuation coefficients in dB/cm when imaging techniques are being considered, though in clinical application this would only be with special techniques related to tissue characterisation.

From Table 1.5 it can be seen that the attenuation in most soft tissues is similar and therefore an average value of 0.7 dB/cm/MHz can be used to compensate roughly for it (e.g. 2.1 dB/cm for 3 MHz ultrasound). The high attenuation of bone and calcified tissue is a particular problem. Later, in Chapter 3, controls will be discussed for attenuation compensation. It will be seen that compensation is applied by creating an image in which the average echo amplitude is made similar over the depth of tissue penetration. It will also be noted that some machines leave the compensation to a computer which assesses average signal level and applies compensation automatically (adaptively). This approach makes a lot of sense since it is in fact difficult to compensate for attenuation when the tissues being scanned are changing either due to their own motion or that of the scanning action of the transducer.

NON-LINEAR PROPAGATION

Attenuation, discussed above, reduces the amplitude of ultrasound as it passes through tissue. It also reduces the high-frequency components in a pulse more than the lower ones and hence alters the shape of the pulse. This effect is rarely considered in clinical application. However, another phenomenon which alters the shape of a pulse and which is routinely exploited is called non-linear propagation. It is not significant for low-amplitude waves (e.g. 50 kPa) but important for high amplitude ones (e.g. 1 MPa). For waves of large pressure amplitude, the speed of sound is higher in regions where the pressure amplitude is positive than it is in the regions where the pressure is negative. The speed is different in the regions experiencing positive half-cycles than in negative half-cycles because the density of the medium changes with pressure. The effect is such that as the waveform passes through the tissue, the positive half-cycles catch up on the negative half-cycles resulting in distortion of

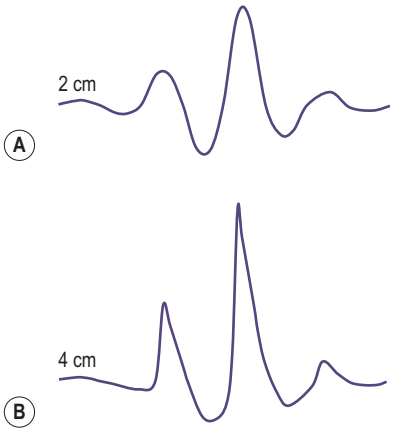


Figure 1.16 A and B: Change of waveform shape due to non-linear propagation in tissue. Note the high-frequency spikes indicating the production of harmonic frequencies.

the waveform (Fig. 1.16). The greater the path travelled by the wave, the greater the distortion. The wave may become considerably distorted and have sharp discontinuities in its shape. The sinusoidal shape seen close to the transducer has then been replaced by a more saw-toothed shape, and the positive half-cycles can become particularly spiked.

The amount of non-linear distortion that occurs depends on the nature of the propagating medium as well as the wave parameters such as frequency and pressure amplitude. The amount of non-linear distortion is related to the molecular and structural properties of the medium in a complex way. However, the phenomenon has been very successively exploited without the requirement to consider the differences between tissues. It is employed to produce narrower ultrasound beams rather than to provide information on the tissues through which the ultrasound passes.

Non-linear distortion is significant in the ultrasound methods used in medicine and has been exploited to improve images. The distortion is generated where the pressure is high, i.e. along the central axis of the ultrasound beam. Distortion is less in the weaker fringes or side-lobes of the beam, i.e. away from the central axis. By only using echoes produced by the non-linear transmitted pulse near the central axis, the scanning beam is effectively narrowed. It is possible to filter out these echoes since their shock-wave shape means that they contain a range of harmonic frequencies over and above those in the original transmitted pulse. It has been noted in the section on Fourier components that the shorter and sharper the shape, the bigger is the range of frequencies. These extra frequencies, which are generated as non-linear propagation distorts the pulse, are called harmonics. The technique utilising harmonics to produce narrower beams is known as harmonic imaging. The narrower beam improves the lateral resolution in the image. Harmonic imaging is very extensively used, indeed it is often the default mode which the machine is automatically programmed to activate when first switched on.

TISSUE CHARACTERISATION AND ELASTOGRAPHY

When echo signals are collected there is often interest in saying more about the characteristics of the tissues that produced them. The most obvious characterisation would be to distinguish benign from malignant, but other distinctions may be attempted such as fatty from fibrotic liver or degree of calcification of arterial plaque. Parameters related to the phenomena described in previous sections may be measured to attempt tissue characterisation, e.g. speed

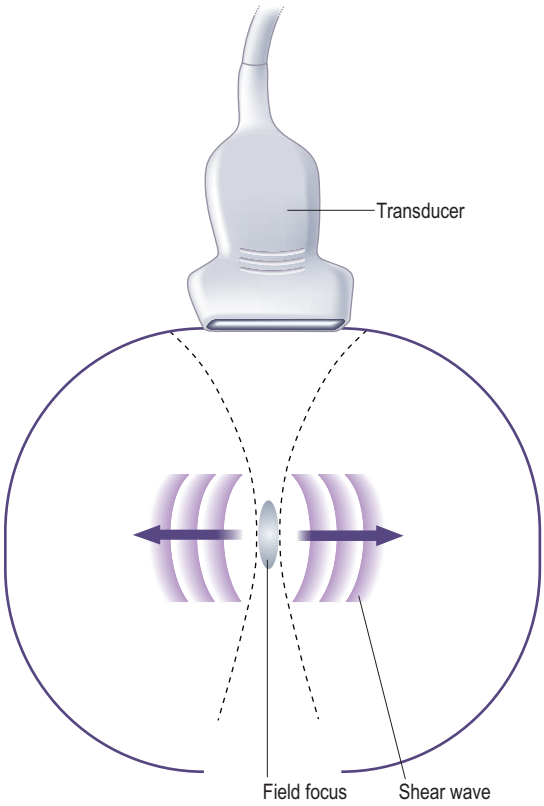


Figure 1.17 The generation of shear waves by the force at the focus of an ultrasound beam.

of sound, attenuation coefficient and scattering coefficient. Characterisation of tissue is often made difficult by the degradation of the ultrasound beam by fat and muscle between the transducer and the site of interest. Invasive imaging reduces this problem, for example by the use of catheter-based scanners to characterise blood vessel walls which are examined with a short beam path through blood. The problems are also reduced if there is a well-specified path between the transducer and the tissue of interest, e.g. through the eye to the retina or through a water-bath to skin lesions.

There is substantial development at the moment in the measurement of tissue elasticity by ultrasonic means. When a tissue is compressed by an external force, changes in its shape and size can be measured from the changes in position of the echo speckle pattern. From the size of the force and the tissue distortion, quantities can be calculated that relate to the elasticity of the tissue. This is analogous to palpation though the aim is to develop techniques that are more quantitative and can be applied to tissues deep within the body. It is known that the hardness of a mass can often be related to its pathology. Several different methods may be employed to apply a force to tissue, ranging from simply pushing the scanning transducer to using the beam radiation force to generate shear waves which spread out around the focus of a normal ultrasound beam. It was noted earlier that when the momentum of an ultrasound beam is interrupted by reflection or absorption at a target, the target experiences a radiation force. In the arrangement shown in Figure 1.17, a target tissue at the focus of the beam will experience a force impulse when subjected to an ultrasonic pulse. The resulting motion of the tissue produces a shear wave which travels sideways from the direction of the ultrasound beam, not unlike the ripple on a pond when a small pebble is dropped in. If several focal points are targeted at successive depths by successive transmitted pulses, the shear waves produced interfere with each other as they travel sideways and produce two plane shear waves travelling in opposite

directions at an angle to each other. This 'V'-shaped shear wave pattern resembles the sonic boom pressure wave generated by a jet aircraft travelling at the speed of sound. Labels such as 'radiation force' or 'supersonic' are used for these techniques.

Shear waves of MHz frequencies are attenuated very strongly in tissue and have not found application. However, shear waves of a few hundred Hz travel well through tissue and are the basis of the supersonic approach. The frequencies of the shear wave are determined by the pulsing rate of the ultrasound transducer. The speed of the shear waves and the wavelength are also very different from typical ultrasound waves as normally employed in ultrasound imaging (e.g. speed 1500 m/s and wavelength 0.5 mm for normal compression wave ultrasound and speed 1 m/s and wavelength 1 mm for shear waves in tissue). As the shear waves travel out from the focus (the shear wave source), the tissue moves under its influence, e.g. back and forth over typically 50 microns. The ultrasound scanner operating at a very high frame rate can image these small motions using signal processing methods similar to those used in colour Doppler imaging. From this image the speed of the shear wave at each point can be calculated. This speed depends on the elasticity (stiffness) of the tissue and hence can be used for diagnostic purposes. The results may be quoted in terms of the shear modulus in units of the pascal (Pa). Shear modulus is a scientific measure of the stiffness of the tissue. Considerable computation is required to provide the ultra-fast imaging and the elasticity images in real-time. Shear wave techniques are at quite an advanced state of development, and the first clinical machines are now available. Biological and clinical studies are in progress to establish their efficacy. The acoustic exposure of the patients is within FDA guidelines. In addition to elasticity, in the future measures of viscosity of tissue may be provided.

This field is normally called elastography or sonoelastography. It is a field that has been developed over the past 20 years and given the complex response of tissue to physical forces, this will continue both in terms of technological and clinical studies. That said, commercial equipment is now available for clinical evaluation.

Attenuation, propagation and harmonics

- Absorption occurs as ultrasound energy is converted into heat. It is highly frequency and tissue dependent.
- Attenuation is the reduction of beam intensity as it passes through tissue. It is the total effect of absorption, scattering, reflection, refraction and diffraction. It is highly frequency dependent. To obtain adequate echo signals from deep in tissue, the operator manipulates gain controls to compensate for attenuation.
- Non-linear propagation occurs as the wave pressure alters the properties of the tissue as it passes through it. It distorts the waveform which then contains additional frequency components – harmonics and subharmonics.
- Non-linear propagation occurs most near the axis of the beam where the wave amplitude is high relative to the sides of the beam. By only detecting the harmonics the beam is effectively made narrower, which gives better lateral resolution.
- Harmonics and subharmonics frequencies are also generated when ultrasound interacts with contrast microbubbles. Detection of these frequencies is exploited in the location of the bubbles in vivo.
- Many operators use harmonic imaging as the method of choice.
- Many attempts have been made to identify tissue types by measuring the acoustic properties of the tissue, e.g. attenuation, scattering and speed of sound. Some success has been achieved where there is well-defined anatomy but difficulties often arise where the ultrasound beam is distorted by overlying layers of fat and muscle.
- Present research into tissue characterisation seeks to develop elastography.

DOPPLER EFFECT

When an ultrasound source and detector are at rest the frequency detected equals that transmitted provided the waveform is not distorted by the propagating tissue (Fig. 1.18A). The Doppler effect is the change in the observed frequency of a wave due to motion of the source of the wave or the observer. If the observer is moving towards a static source, an increase in frequency is observed since more wave cycles per second are encountered (Fig. 1.18B). Conversely for motion away from the source, fewer wave cycles are encountered per second and a decreased frequency is detected (Fig. 1.18C). The size of the Doppler shift is directly related to the size of the velocity. In another situation the source may move toward a static observer, the wavelengths are compressed as the source follows the wave and hence there is an increase in frequency (Fig. 1.18D). Motion of the source away from the observer stretches the wavelength and gives a decrease in frequency (Fig. 1.18E). Both of these cases of motion which give rise to changes in the observed frequency are in fact slightly different effects since in the first the wave is not altered and in the second it is compressed or stretched.

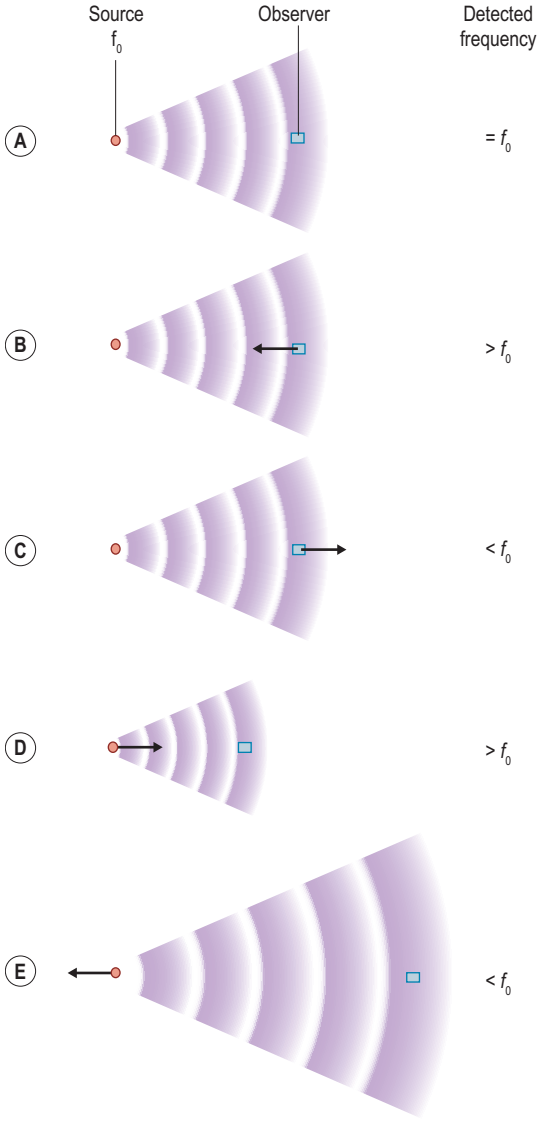


Figure 1.18 A–E: The Doppler effect in different situations relating to the relative motion of the source and observer.

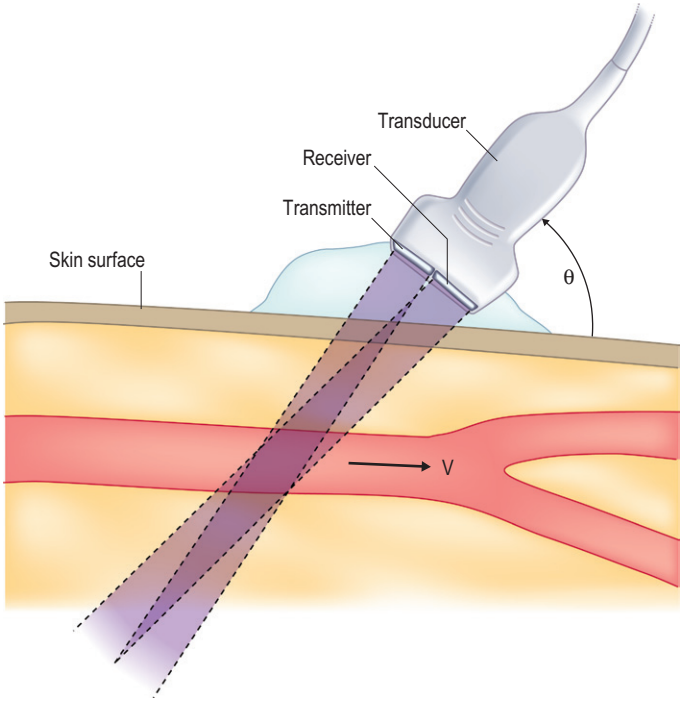


Figure 1.19 Examination of a blood vessel with a continuous wave Doppler transducer.

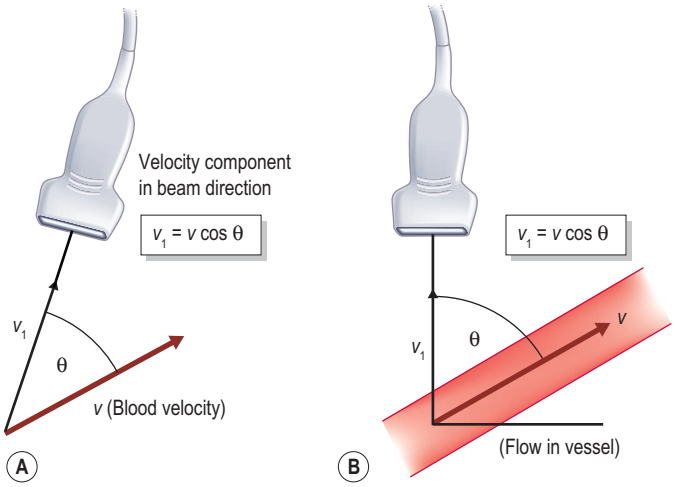


Figure 1.20 A: Velocity component for angle between beam and motion directions. **B:** Measurement of velocity in a blood vessel.

Doppler techniques

- The Doppler effect is a very sensitive and accurate detector of motion. It is mostly used to study blood flow but it can also be employed to measure tissue motion.
- Users of Doppler techniques should be aware of the large effect of beam/motion angle on the velocity measurement.
- Most Doppler devices measure the velocity component along the ultrasound beam axis.
- Processes such as absorption, attenuation, scattering, refraction and non-linear propagation discussed for pulse-echo imaging also apply to Doppler methods.
- Doppler images and spectrograms are produced in real-time, making them very useful for the study of physiological function.

In medical ultrasound, a beam from an effectively static transducer is scattered back from tissues to produce echo signals (Fig. 1.19). The process of sending echoes back to the transducer is often called 'backscatter'. Weak signals from blood are detected in this way and since the blood is moving the ultrasound has experienced a Doppler shift. In this situation if cells are moving towards the transducer, the total Doppler effect is produced by the cells moving through the waves plus the cells moving after the reflected ultrasound and hence compressing the echo signals. Motion of the cells towards the transducer produces an increase in ultrasound frequency due to this 'double Doppler' effect. Likewise, a reduction in frequency is produced by cells moving away from the transducer.

If the direction of the beam is at an angle to the direction of motion, it is the velocity component along the beam axis (v_1) that is the relevant velocity when the Doppler effect is considered (Fig. 1.20A). Very often a simplified picture of blood flow is assumed in which the direction of flow is parallel to the walls of the blood vessel (Fig. 1.20B). This enables the beam/flow angle to be measured from an ultrasound image and hence the velocity to be calculated from the Doppler shift frequency.

A simple but useful Doppler equation links the Doppler shift, the transmitted frequency, the velocity and the angle between directions of sound propagation and motion:

$$f_d = 2vf_t \cos\theta/c \text{ or } v = f_d c/2f_t \cos\theta$$

where f_d is the Doppler shift, f_t is the transmitted frequency, v is the velocity, θ is the angle and c is the speed of ultrasound.

So far we have discussed blood cells moving with the same velocity giving rise to one Doppler shift frequency. Obviously in blood flow there can be many moving groups of cells with different velocities in a limited region in the beam. The limited region, which might typically be a few millimetres in diameter, is called the sample volume. Each group of cells gives rise to an echo signal with a particular Doppler shift and all of these signals combine to produce a complex Doppler signal from the blood. This complex signal can be analysed into a spectrum of frequencies by Fourier techniques. The frequency components in the spectrum can then be converted to velocities in the blood using the Doppler equation.

It is instructive to consider some numerical evaluations of this formula for values encountered in medical ultrasound. For example, if $v = 20$ cm/s, $c = 154\,000$ cm/s, $\theta = 0°$ ($\cos\theta = 1$), $f_t = 2 \times 10^6$ Hz, then the Doppler shift equals 519 Hz.

If the machine measures the Doppler shift and the beam angle, the velocity can be calculated and presented automatically on the screen. The Doppler shift is seen to be small, around one part in 1000, but electronics can measure it. The Doppler shift frequencies are also in the audible range, which means they can easily be studied simply by listening with earphones as well as using the spectral Doppler feature of machines.

It will be seen in Chapter 3 that the Doppler effect is exploited in various ways to present information on blood flow and tissue motion. A spectrum of velocities from a sample volume at a site of interest or colour images of velocities can be produced. Doppler methods probably provide the greatest amount of velocity information among all blood flow detection techniques.

RESOLUTION

The detail that can be observed in ultrasound images or traces depends on the smallest change that can be presented by the ultrasound systems. The detail in a particular presentation usually is said to depend on one or more resolution. These resolutions depend on the shape of the ultrasound beam, the ultrasound pulse shape and the way they are transmitted. They are now listed since they apply to techniques described in later chapters.

Axial resolution in a pulse-echo image is the smallest separation of two targets lying along the beam axis for which individual echoes can be seen. Axial resolution depends on the length of the transmitted ultrasound pulse. Shorter pulses can be generated at higher ultrasound frequencies so higher (better) resolution is achievable at high frequencies.

In-plane (lateral) resolution is the smallest separation of two targets, placed side-by-side, for which separate echo spots are presented in an image. As the ultrasound beam sweeps across the scan plane, the echoes from the targets are detected one after the other if the targets are separated by more than the beam width. If the separation is less than the beam width, the echoes are detected simultaneously and they cannot be presented separately. The use of high frequencies and focusing enable generation of narrower beams and hence higher resolution is achieved. It is unfortunate that attenuation increases with frequency, limiting the upper values that can be used.

Out-of-plane (elevational, azimuthal) resolution is the minimum separation of two targets in the out-of-plane direction for which separate echoes can be detected. It is determined by the width of the ultrasound beam in the out-of-plane direction. This width is not always the same as the in-plane width. It is worth remembering when viewing an ultrasound image that the echoes have been collected from a tissue slice of finite width. Out-of-plane resolution is sometimes called slice-thickness resolution.

Contrast resolution is the smallest change in echo signal level that can be detected between regions in an image. This is most likely to be considered in terms of changes in shades of grey. Contrast resolution depends on the noise in the echo signal. The random fluctuations of noise may be from electronic sources in the scanner or from speckle resulting from the interference of echoes from small scattering structures in tissue. Averaging over a number of images can reduce noise, i.e. improve contrast resolution, but it slows up the imaging process. Contrast resolution is a somewhat neglected quantity but it is of major significance with regard to image quality.

Temporal resolution is the smallest separation in time for which two events can be identified separately. It depends on how quickly the information is refreshed. In imaging, temporal resolution depends on the rate at which images are produced, i.e. the frame rate. With physiological traces as encountered in Doppler techniques, the temporal resolution is related to the fast changes in the signal. We have seen earlier that the faster the changes occur in a trace, the greater is the range of frequency components in the trace. In other words, the greater the frequency bandwidth, the higher is the temporal resolution.

In Doppler imaging, different velocities are presented as different colours. The velocity resolution is the smallest change in velocity that can be detected. Likewise in a Doppler spectrogram, the velocity resolution is the smallest change in velocity that can be measured.

APPENDIX

Continuous wave ultrasound

- **Intensity spatial peak (I_{sp}):** For a continuous wave beam, the intensity may be measured at the location of the maximum intensity in the beam (the spatial peak) to give the spatial peak intensity (I_{sp}).
- **Intensity spatial average (I_{sa}):** For a continuous wave beam, the intensity may be averaged across the beam to give the spatial average intensity (I_{sa}).

Pulsed wave ultrasound

For pulsed wave ultrasound, the intensity may be also averaged over the pulse length or the duration of the exposure time, i.e. temporal averaging may be carried out as well as spatial averaging.

- **Intensity spatial peak temporal average (I_{spta}):** For a pulsed wave beam, the spatial peak intensity may be averaged over the duration of a sequence of several pulses to give the spatial peak, temporal average intensity (I_{spta}).
- **Intensity spatial peak pulse average (I_{sppa}):** For a pulsed wave beam, the spatial peak may be averaged over the pulse to give the spatial peak, pulse average intensity (I_{sppa}).

REFERENCES

1. McDicken WN. Diagnostic ultrasonics: principles and use of instruments. 3rd edn. Edinburgh: Churchill Livingstone; 1991.
2. Hoskins PR, Thrush A, Martin K, Whittingham TA. Diagnostic ultrasound: physics and equipment. London: Greenwich Medical Media; 2003.
3. Oates C. Cardiovascular haemodynamics and Doppler waveforms explained. London: Greenwich Medical Media; 2001.
4. Allan PL, Dubbins PA, Pozniak MA, McDicken WN. Clinical Doppler ultrasound. 2nd edn. Edinburgh: Churchill Livingstone; 2006.
5. Kremkau FW. Diagnostic ultrasound: principles, instrumentation and exercises. 7th edn. Philadelphia: Saunder; 2006.
6. Duck FA. Physical properties of tissue – a comprehensive reference book. London: Academic Press; 1990.
7. Hill CR, Bamber JC, ter Haar GR. Physical principles of medical ultrasonics. Chichester: Wiley; 2004.

CHAPTER

2

Basic equipment, components and image production

Kevin Martin

INTRODUCTION 16

PRINCIPLES OF B-MODE IMAGE FORMATION 17

TRANSDUCERS AND BEAM FORMING 18
Transducer construction 18
Image formats 18
The stepped array 20
The steered array 20
Other beam steering applications 20
Electronic focusing 21
Aperture control 21
The beam former 21
Elevation focusing 21
3/4D transducers 21
Mechanical transducers 22

IMAGE PROCESSING 23
Time gain compensation (TGC) 23
Dynamic range 23
Harmonic imaging 24
Pulse coding 25
Demodulation 25
Image memory 25
Field of view and zoom 25
Post processing 26

DOPPLER ULTRASOUND 26
Continuous wave Doppler (CW) 26
Pulsed wave Doppler (PW) 26
High pass filtering 28
Aliasing 28
Doppler frequency estimation and display 28
Colour flow imaging 28
Limitations of colour flow imaging 29
Power Doppler 30

INTRODUCTION

The clinical use of ultrasound is an interactive process, which requires the user to manipulate the ultrasound transducer in contact with the patient's skin surface, while viewing and interpreting the image in real-time. Before the examination, the user must select the transducer, operating mode and system settings most relevant to the investigation and thereafter make regular adjustments to the system controls to optimise the diagnostic quality of the image. To make informed choices of system components and settings, it is essential to have an understanding of their function and how making changes is likely to affect the resulting image. This chapter describes the main components of the ultrasound imaging system and explains how they operate to produce ultrasound images and other useful diagnostic information. The aim of the chapter is to provide a basic understanding of system function, which will help users to produce optimum quality diagnostic information when scanning. The intention is that these explanations should be accessible to all without any detailed knowledge of physics or technology.

Figure 2.1 shows a typical general purpose ultrasound imaging system being used to acquire images of anatomical features within a patient's abdomen. The transducer is held by the operator in contact with the skin surface. The transducer produces short bursts, or pulses of ultrasound, which travel into the abdomen and are reflected from the abdominal tissues and organs back to the transducer. These returned echoes are converted into electrical signals by the transducer and used to produce an image of echo-producing features within the patient. From information such as the direction of travel of the pulse, the time of arrival of the echoes and the strength of the reflection, the system processor forms scaled images of these internal anatomical features. The operator uses the controls available on the console to optimise the system operation for different anatomical targets and moves the transducer around the skin surface to interrogate different areas within the abdomen. The ultrasound images are viewed continuously as they are formed on the display monitor and may be recorded as hard copy still images or cine clips or stored remotely in a picture archiving system (PACS).

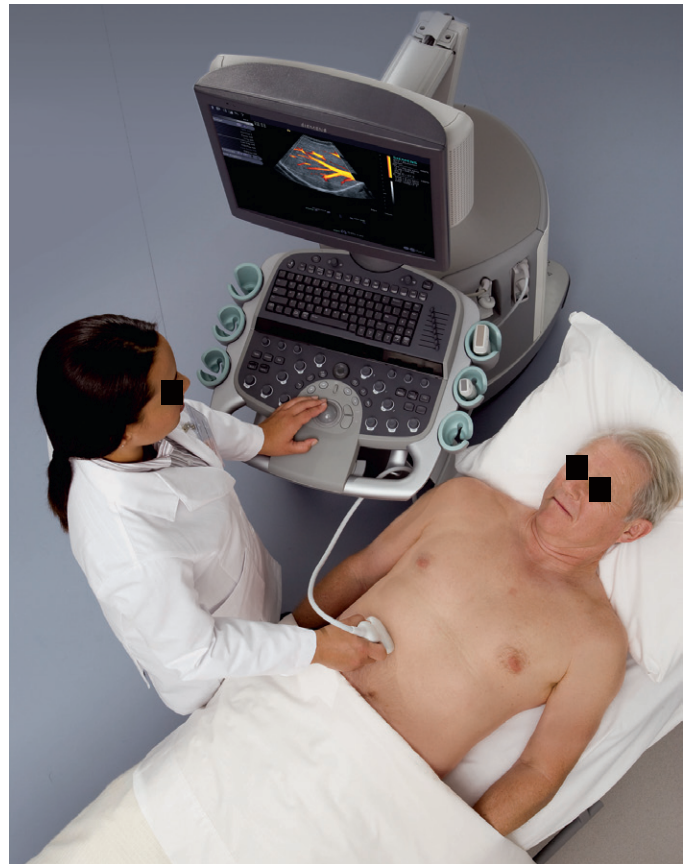


Figure 2.1 An ultrasound imaging system in use. (Courtesy of Siemens Healthcare.)

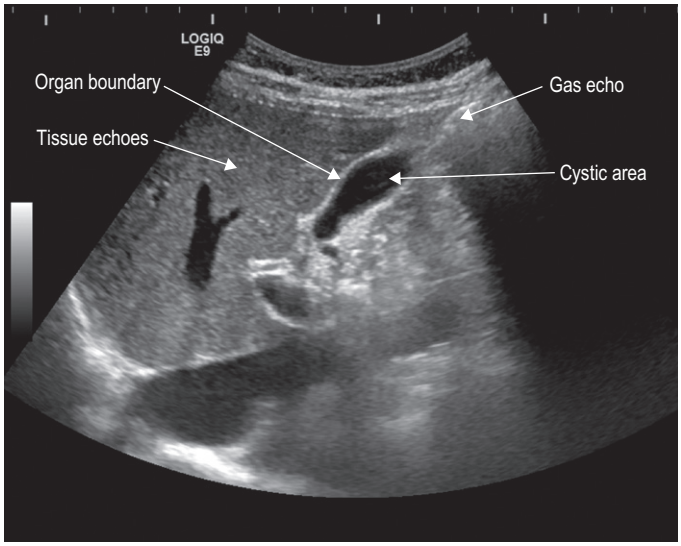


Figure 2.2 **A B-mode image using a curvilinear array transducer.**

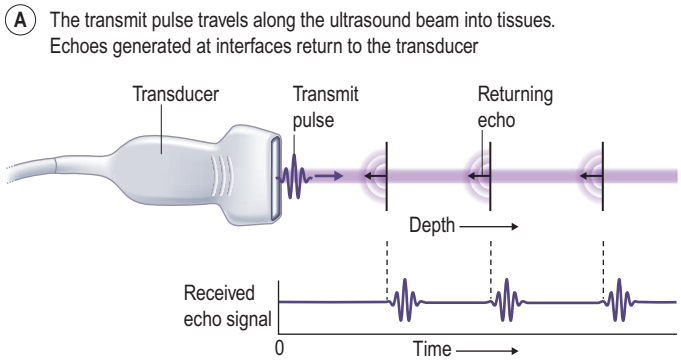
Figure 2.2 shows a typical ultrasound image from within the upper abdomen. As the ultrasound beams, which are used to interrogate the anatomy, are all constrained by the transducer to lie in the same plane, the resulting image is a two-dimensional cross-sectional image. The upper, curved edge of the image corresponds to the surface of the skin, which has been deformed to the shape of the curved transducer face. Distance down the image from this surface corresponds to increasing depth within the patient. The ultrasound beams from this transducer are transmitted at right angles to its curved surface resulting in a sector-shaped image.

The image is a greyscale image. As the ultrasound pulse travels into the tissues, some of its energy is reflected, whenever it encounters a change in acoustic impedance, as described in Chapter 1. Relatively strong reflections are produced at organ and tissue boundaries, which appear as bright features in the image. Much weaker echoes are produced by scattering from small-scale features within organ tissues, e.g. liver parenchyma, which are displayed as a darker shade of grey. Cystic regions contain no changes in acoustic properties and so generate no echoes. These appear as black in the image. As described in Chapter 1, an interface between tissue and gas will reflect so strongly that the ultrasound pulse is unable to travel any further. With a tissue–bone interface there will also be a strong reflection, and high attenuation in the bone. Such interfaces will be displayed as a very bright echo with a black shadow behind it. The greyscale image is also known as a B-mode image (B for brightness) as the strength of the echo is displayed in terms of image brightness.

To allow fine detail and closely spaced targets to be resolved in the image, it is essential that the ultrasound beam is narrow and the ultrasound pulse short. Better resolution is achieved by transmitting higher ultrasound frequencies. Unfortunately, higher frequencies are attenuated more rapidly, as explained in Chapter 1, leading to reduced depth of penetration of the ultrasound pulse into tissues. It is this phenomenon that determines the maximum depth from which ultrasound echoes can be received and displayed in the image.

PRINCIPLES OF B-MODE IMAGE FORMATION

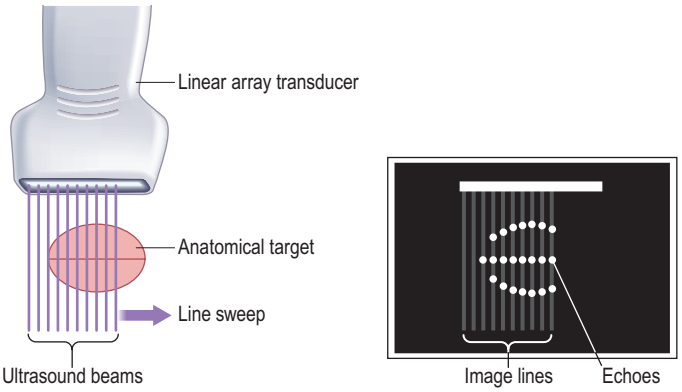
The two-dimensional (2D) B-mode image is composed of a large number of individual, adjacent B-mode lines. In the simplest image forming process, each line is formed by a single pulse-echo cycle as illustrated in Figure 2.3.



(A) The transmit pulse travels along the ultrasound beam into tissues. Echoes generated at interfaces return to the transducer

(B) The time of arrival of echoes after transmission increases with the depth of the reflector

Figure 2.3 **The pulse-echo cycle.**



(A) Pulse-echo cycles are initiated at a series of adjacent beam positions along the transducer face

(B) The line of echoes produced by each cycle is used to form a B-mode line in the image

Figure 2.4 **B-mode image formation from a sequence of lines.**

The transducer produces a pulse of ultrasound, consisting of a few cycles at the selected transmit frequency, e.g. 5 MHz. The pulse propagates through the tissues along a beam-shaped corridor at the speed of sound c for the particular tissue. Upon reaching a reflecting interface, an echo is produced, which travels back to the transducer, also at speed c. Meanwhile, the pulse has travelled on to deeper interfaces, generating further echoes, which also travel back to the transducer, but arrive at later times. The total time after transmission of the pulse for each echo to arrive back at the transducer is called the 'go and return' time, which is simply twice the depth (go and return) divided by the speed c, i.e. $2d/c$. As described in Chapter 1, the speeds of sound in the soft tissues of the body are all (excluding fat) within 5% of the average value of 1540 m/s. The image processor assumes this value to calculate the depth of origin of each echo-producing feature from the time of arrival.

In real tissues, there is an almost continuous series of interfaces and scatterers along the ultrasound beam, which generate a continuous series of echoes, following transmission of the pulse. The line of echoes is used to form a B-mode line in the image, with echo strength displayed in terms of image brightness at each point on the line and time of arrival of the echo by distance down the line. Once echoes have been received from the maximum depth, another pulse-echo cycle is initiated along a beam in an adjacent position to the first, generating an adjacent B-mode line in the image (Fig. 2.4). By repeating this process along the entire length of the transducer face, a large number of adjacent image lines (typically 256) are formed, resulting in a 2D B-mode image.

Once the last line in the image has been formed, the process is repeated to form a continuous series of images or frames. The

B-mode image formation

- The 2D B-mode image is formed from a set (>100) of B-mode lines.
- Each line is formed from one pulse-echo cycle.
- The pulse travels along a beam-shaped corridor.
- Echoes received are displayed along the line according to their time of arrival.
- The strength of the echo is displayed in terms of brightness.

ultrasound images are displayed as they are formed, resulting in a real-time display of moving images.

The finite travel time of the ultrasound pulses and echoes to and from the reflecting target results in a fundamental limitation of ultrasound imaging systems. The time to form each image line is the 'go and return' time to the maximum depth. Large imaging depths result in long line times. When coupled with a large number of image lines, this leads to a long frame time and low image repeat rate or frame rate. If a high frame rate is needed to image a rapidly moving target, e.g. the heart, it may be necessary to restrict the imaged depth and/or the width of the image.

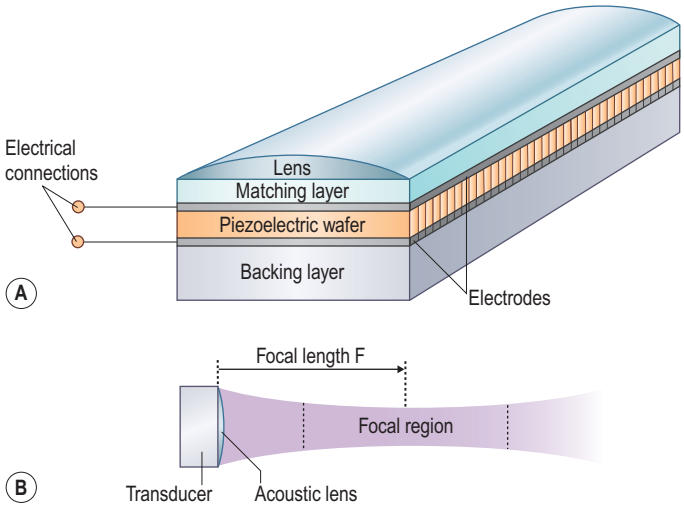


Figure 2.5 Transducer construction. A: A cross-section through an ultrasound transducer. **B:** The beam can be focused by adding an acoustic lens to the transducer face, resulting in a narrower beam in the focal region.

TRANSDUCERS AND BEAM FORMING

Transducer construction

Ultrasound transducer construction

- Ultrasound pulses of the required frequency are produced by the transducer using the piezoelectric effect.
- The piezoelectric element within the transducer is a thin wafer of PZT.
- A matching layer must be used to improve transmission of ultrasound into soft tissue.
- A backing layer is used to reduce ringing in the PZT wafer and give a short pulse.
- Transducer bandwidth can be improved by reducing the acoustic impedance of the PZT wafer.
- A lens on the front face of the transducer focuses the beam to make it narrower.

The transducer is one of the most important components of the ultrasound system and its performance is critical to the quality of the ultrasound image.

Ultrasound pulses are produced by the transducer, which converts the electrical signal supplied by the processor into a corresponding ultrasound wave. At the heart of the transducer is a thin wafer of piezoelectric material with metal electrodes on each side of it as illustrated in Figure 2.5A. The piezoelectric material is normally a ceramic made from lead zirconate titanate (PZT). A fluctuating electrical voltage applied to the electrodes causes a corresponding change in the thickness of the element, generating a sound wave in the adjacent medium. When an echo is received back at the transducer, the thickness changes induced by the sound wave are converted back into an electrical signal at the electrodes.

A major challenge in the design of the ultrasound transducer is that of transmitting the ultrasound energy from the PZT element into the soft tissues of the body. As described in Chapter 1, when a travelling ultrasound wave encounters an interface where there is a large change in acoustic impedance, most of the energy is reflected back and little is transmitted into the next medium. As the mismatch between the impedance of the PZT (approximately 3000 rayls) and soft tissue (about 1.5 rayls) is very large, a matching layer must be used between the two, which has an intermediate value of acoustic impedance. If the thickness of this layer is also equal to one quarter of the wavelength of the ultrasound wave, transmission efficiency is further improved. Normally, several matching layers are used to optimise transmission over a range of frequencies. Such improvements in coupling to tissue convert electrical energy more efficiently into transmitted ultrasound energy and improve the sensitivity of the transducer to weak returned echoes.

The range of frequencies that a transducer can respond to efficiently is referred to as its bandwidth. A short ultrasound pulse, as required for imaging, contains a relatively wide range of ultrasound frequencies above and below the nominal transmit frequency (approximately ±20%) and the transducer must be able to respond to these to maintain a short pulse. When stimulated by an electrical signal, the piezoelectric wafer has a tendency to resonate or ring like a bell at its natural frequency, giving a narrow bandwidth and a long ultrasound pulse. To maintain a short pulse, suitable for imaging purposes, a backing layer (also called a damping layer) is added to the wafer, which absorbs some of the vibrational energy and causes any resonance to die out quickly. Modern transducers extend this process by employing more effective techniques for transmitting ultrasound energy through the front face of the transducer into the tissues. For example, by cutting a cross hatch of slots through the PZT wafer and filling them with materials of low acoustic impedance, the overall acoustic impedance of the wafer can be reduced, reducing the mismatch to the soft tissues. By extracting more acoustic energy from the transducer into the tissues, the tendency to resonate is reduced and the bandwidth is increased. Modern transducers can have bandwidths that extend to ±70% of the centre frequency. Wide bandwidth transducers can be driven at a range of frequencies selected by the user (multi-frequency transducers) and make techniques such as harmonic imaging possible (see 'Image processing' section, below).

The width of the ultrasound beam that is produced by the transducer can be reduced by focusing. In a simple transducer as in Figure 2.5A, this can be achieved by adding an acoustic lens to the front surface. This acts like an optical lens, forming a focal region about a specific focal length *F* (Fig. 2.5B) in which the beam is narrower than an equivalent unfocused beam. The reduction in the width of the ultrasound beam gives improved resolution of small, adjacent targets.

Image formats

To form a 2D ultrasound image, the ultrasound beam produced by the transducer must be moved in sequence, to a large number of

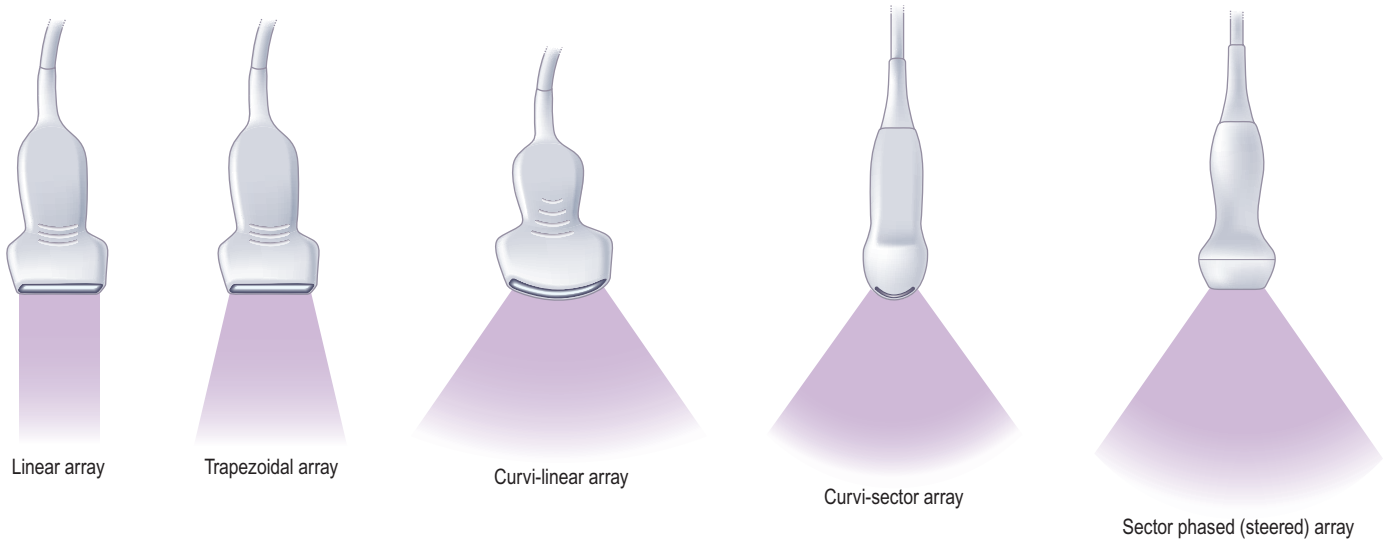


Figure 2.6 **Common types of array transducer shape and image format.**







Figure 2.7 **Endo-cavity transducers. A:** An 8–4 MHz curved array endo-vaginal transducer. (Courtesy of Siemens Healthcare.) **B:** A 7–3 MHz trans-oesophageal phased array transducer, which can be rotated to acquire a 3D data set. (Courtesy of Siemens Healthcare.) **C:** An endo-anal transducer for urological studies. (Courtesy of BK Medical.)

adjacent positions within the tissues, as described earlier. For most applications, this movement is achieved electronically using a transducer, which has an array of elements (typically 128 or 256). Array transducers are available in a variety of shapes, giving a choice of image formats for different applications. Figure 2.6 shows a range of common types of array transducers for transcutaneous imaging. Sector transducers are used where access to the target tissues is through a narrow acoustic window, e.g. approaching the heart through an intercostal space between the ribs. Linear and curved array transducers are used where a wide anterior field of view is needed and access is not limited by regions of bone or gas, e.g. in the upper abdomen, neck or peripheral vasculature. Endocavity transducers use small transducer arrays mounted on a suitable stem for insertion into body cavities as shown in Figure 2.7. These can bring the transducer into closer proximity to the target, allowing the use of higher frequencies and avoiding intervening obstructions such as gas or bone.

All array transducers make use of one or both of two methods to scan the beam through the tissues. The beam can be electronically stepped to different positions along the array or steered in different directions.

The stepped array

Figure 2.8 illustrates the stepped array principle for a linear array transducer. As explained in Chapter 1, in order to produce a relatively parallel-sided ultrasound beam, the active transducer width or aperture must be at least 10 times the wavelength of the ultrasound wave. As each element in a typical array is only about 1 wavelength wide, the electrical pulse waveform is applied simultaneously to a group of say 10 adjacent elements, e.g. elements 1–10. The echo signals received back at these elements can be added together also to form the first B-mode line. When this first pulse-echo cycle is complete, the beam position is stepped along the array by applying the pulse to elements 2–11 and adding the returned echoes from these. By continuing this process, the beam can be stepped along the whole array to form a large number of closely spaced B-mode lines.

The stepped array process is used with linear array transducers and with curved array transducers, which are simply an array of elements mounted onto a curved surface to give a curved field of view.

The steered array

In the steered array transducer (also known as the phased array transducer), the beam is steered in adjacent directions rather than stepped to adjacent positions. The array elements are very narrow, so the total length of the array is only 1.5–2 cm. The electrical transmission pulse is applied to all elements on each pulse-echo cycle and the beam direction is controlled by staggering the times at which the electrical pulse is applied to each element.

As the array elements are less than a wavelength wide, when excited by the electrical pulse waveform, they produce a wave that is roughly circular in shape (in the image plane). If the electrical pulse is applied to all elements simultaneously, as illustrated in Figure 2.9A, the circular waves merge to form a flat wavefront and a collimated beam in the straight ahead direction. If element 1 is fired first, followed after a very short delay by element 2, then element 3 and so on, by the time the last element is fired, the circular waves from the others have travelled various distances into the tissue and they merge to form a wavefront that propagates at an angle to the straight ahead direction (Fig. 2.9B).

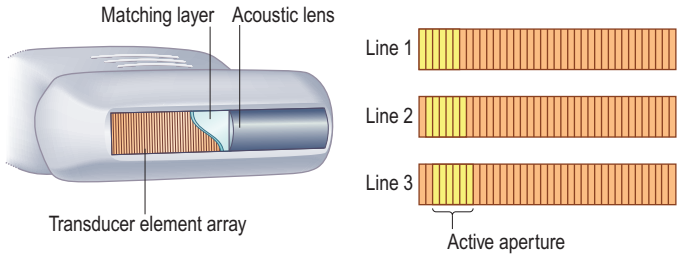
When the echoes are received, similar delays are applied before they are added together. By steadily increasing the delay between elements on each successive pulse-echo cycle, the beam is steered further away from the straight ahead position. Angles of up to ±45° can be achieved by this technique.

Other beam steering applications

Beam steering is used with some linear arrays to form a trapezoidal field of view (Fig. 2.6). Here, a half sector is added to each side of the normal rectangular field of view using beam steering with a group of elements at each end of the array.

Beam steering is used by some manufacturers with linear array transducers to generate images of a target from a number of different directions. The direction of the beams from the linear array may be steered in up to nine different directions on successive image frames, giving a so-called compound image. This technique helps to give more complete images of curved organ or lesion boundaries and helps to average out image speckle. However, the frame rate is reduced, as each complete compound image takes longer to form.

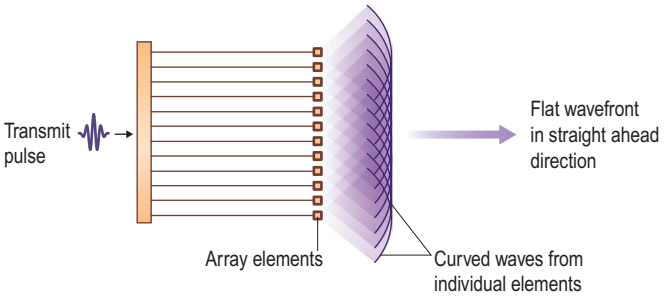
Beam steering is used with pulsed Doppler systems (see 'Doppler ultrasound' section, below) to improve the angle at which the Doppler beam interrogates vessels that lie parallel to the skin surface.



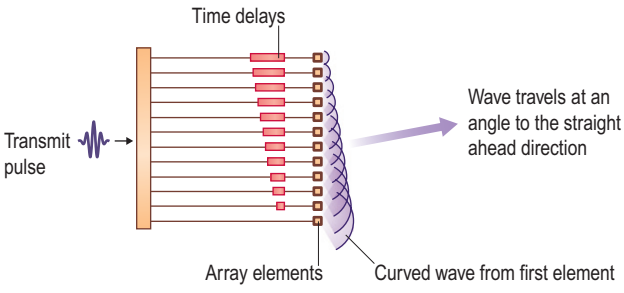
(A) Cut-away of a linear array transducer, showing array elements, matching layer and cylindrical lens

(B) The active aperture is stepped along the array on each pulse–echo cycle

Figure 2.8 The linear, stepped array transducer.

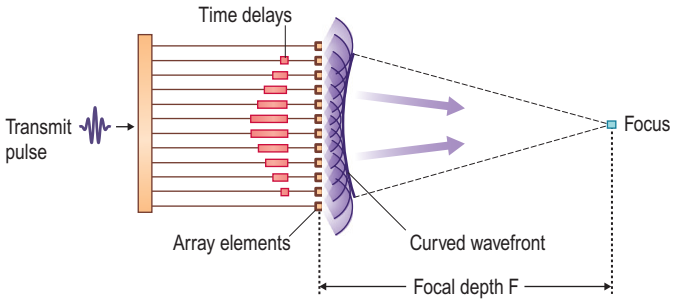


(A) When the electrical pulse is applied to all elements simultaneously, the circular waves from each merge to form a flat wavefront and a collimated beam in the straight ahead direction

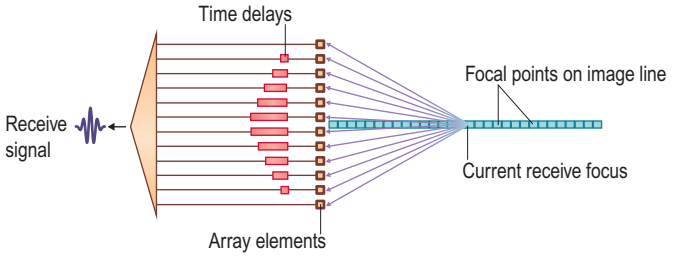


(B) If each element is fired in turn after a short delay, a wave is formed which propagates at an angle to the straight ahead direction

Figure 2.9 The steered array principle.



(A) Transmit focus: if the outer elements are fired first with increasing delays towards the central elements, a converging wavefront is formed which produces a focused transmit beam



(B) Receive focus: in reception, delays are applied to the signals received at each element before they are added together. The delays are calculated for each target depth so that the receive focus tracks the current receive depth, producing a much narrower receive beam

Figure 2.10 **Electronic focusing.**

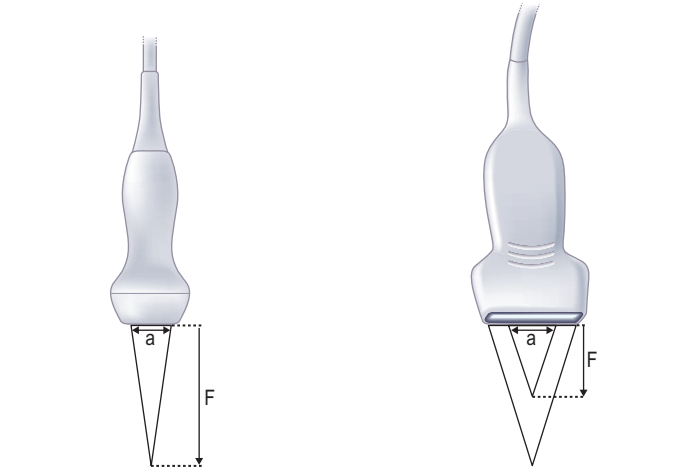
Electronic focusing

Focusing of the beam in the scan plane can be achieved in both stepped and steered arrays by controlling the timing of signals to and from the active elements. In Figure 2.10A, the outer elements of the active area are fired first, followed after small delays by consecutive element pairs towards the centre. The circular waves from the individual elements add together to form a concave wavefront, which converges to a focus, reducing the width of the beam. Increasing the delay time between elements reduces the distance of the focus from the transducer.

The transmitted pulse is normally focused to a depth chosen by the user via the machine console and has a single value for each transmission. In reception, as the depth from which echoes are being received is known from the time after transmission, dynamic control of the echo delays is applied so that the receive focus effectively tracks the echo source. Focusing is applied for each point along the line by calculating the travel time to each receive element and then aligning the received signals in time before adding them together. The resulting receive beam is much narrower than the transmit beam (Fig. 2.10B).

Aperture control

Focusing is most effective when the aperture width, i.e. the active length of the transducer, is similar to the focal depth. If the focal depth is much greater than the aperture width, then the focusing effect is weak. As the depth of the focus is increased by the user, the active aperture width would normally be increased to maintain effective focusing. For linear array transducers, the aperture can be increased potentially to the full length of the array, maintaining an effective focus to large depths (Fig. 2.11). For curved arrays and phased arrays, the maximum aperture is restricted by the geometry



(A) The ratio of aperture *a* to focal depth *F* is restricted for sector transducers leading to weak focusing

(B) A higher ratio of aperture *a* to focal depth *F* can be maintained in linear arrays by increasing the active aperture at larger depths

Figure 2.11 **Aperture control and focusing.**

of the transducer and so focusing is less effective at large depths, leading to poorer resolution in these regions of the image.

The beam former

In modern ultrasound systems, the beam manipulation techniques described above are all implemented using digital techniques in a component of the ultrasound system known as the beam former.[1] The beam former is programmed to activate a chosen group of elements to transmit a focused pulse. Echo signals are then received by the elements within the active aperture. These are converted into digital format and stored temporarily as a data series for each element. The beam former then uses the stored element data to create B-mode lines by applying the techniques described above. By using more than one beam former, the same stored element signals can be used to form several adjacent B-mode lines at the same time, reducing the time needed to form each image.

Elevation focusing

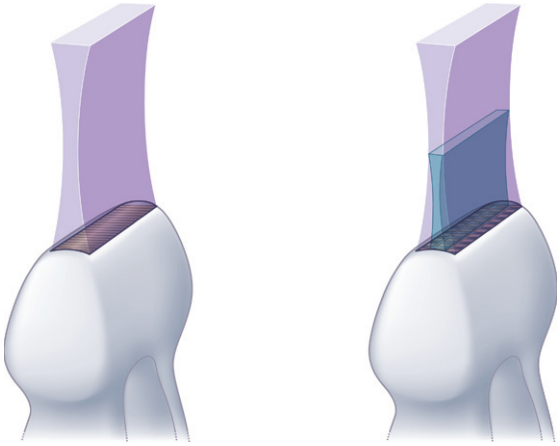
While electronic focusing techniques can be used to produce a beam that is very narrow in the direction along the scan plane, focusing at right angles to the scan plane, the slice thickness direction, often relies simply on a fixed acoustic lens as shown in Figure 2.12A. This fixed and relatively weak focusing results in a slice thickness that is much greater than the in-plane beam width. A large slice thickness can result in poor visualisation of small cysts and blood vessels. Slice thickness can be reduced near to the transducer by the use of arrays containing several parallel rows of elements rather than just one. These are referred to as 1.25D, 1.5D, 1.75D, 2D multi-row or matrix transducers according to the level of technology employed (and manufacturer terminology). In a 1.25D array, the multiple rows are used simply to give aperture control, reducing the number of rows used for superficial targets (Fig. 2.12B). The 1.5D array also employs electronically controlled focusing in elevation but the rows are paired to give symmetric delays. The 1.75D array has independent control of delays to each row.

3/4D transducers

The beam manipulation techniques described so far result in a real-time, cross-sectional image, which allows the anatomy to be examined, slice by slice, as the transducer is moved by the operator. The

3D transducer is used to acquire image data from a 3D volume of tissue. Here, the transducer is held in a fixed position by the operator as the image plane is swept sideways automatically through the target volume and a set of 2D images stored.

Two types of transducer designs are available to carry out 3D volume acquisitions. The most common type contains a curvilinear array mounted on a swivel within a small water bath in the transducer head (Fig. 2.13A). To acquire a 3D volume, the array is rotated slowly by an electric motor, sweeping the image plane sideways through the tissues. The orientation of the scan plane is measured by an angle sensor coupled to the motor. The operator holds the transducer assembly steady as a set of 2D curvilinear images is acquired.



(A) The slice profile for a linear array transducer with a single row of elements

(B) The slice thickness can be reduced near to the transducer in the 1.25D array by using only the middle row of elements for superficial targets

Figure 2.12 Elevation focusing and slice thickness.

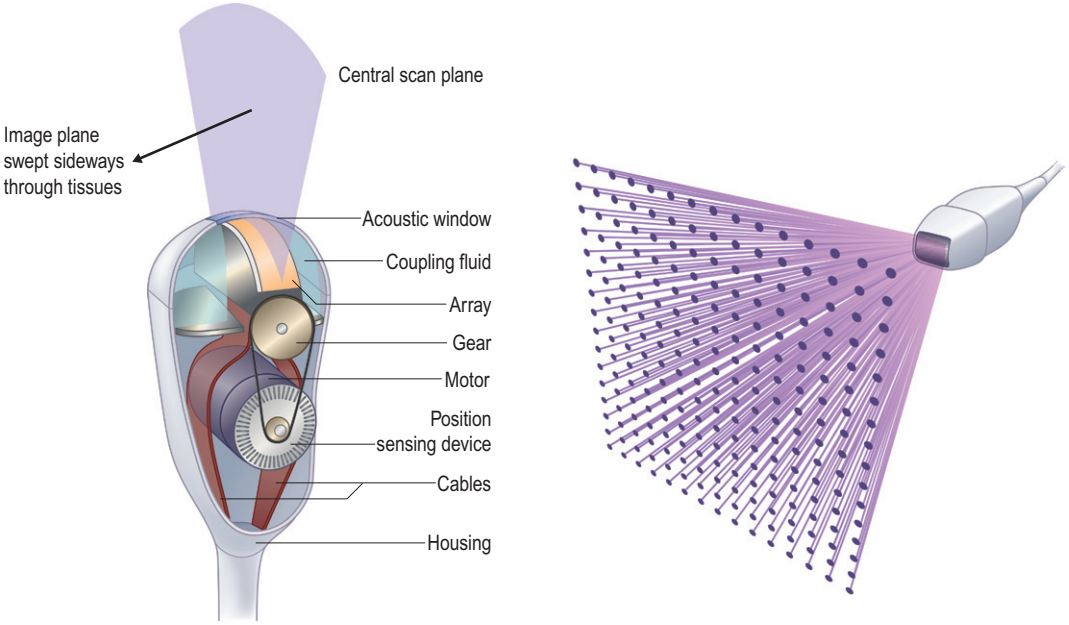
The alternative type of transducer that can be used for 3D acquisition is the square array transducer, which uses a square matrix of transducer elements, e.g. 128×128 (Fig. 2.13B). This type of transducer can be used in phased array mode to produce a sector image in one plane as described earlier. Using beam steering in the orthogonal plane, the sector image can then be swept sideways on each successive frame to interrogate a pyramid-shaped 3D volume of tissue.

Both types of transducer can be used to produce continuously updated volume data sets by repeating the volume acquisition process. The repeat rate of the resulting 4D images may be quite low due to the time required to form a set of 2D images. By restricting the depth of the images and the angle of the acquired pyramid of data, image update rates of up to 30 per second can be achieved using a square array transducer.

Perhaps the most widely useful application of 3D transducers is in the acquisition of a single volume data set from the target tissues in the form of multiple adjacent planes. If the 3D volume data set is stored, it can be interrogated and displayed in several ways. The set of 2D views of the original scan plane being swept through the tissues can be reviewed. Similar views can be displayed of a set of sections orthogonal to the original 2D plane. 2D images can also be created at a range of depths in a plane parallel to the transducer face (C-scan). This plane is one that is not normally accessible with a standard 2D transducer. The 3D data set can also be processed for display in various viewing modes including see through view and surface rendering, where a 3D surface corresponding to the skin surface, for example, is segmented from the data and displayed.[2] Surface rendering is most effective where the surface of interest is adjacent to a region of fluid (e.g. in obstetrics), so that the surface echo can be detected automatically by the system processor.

Mechanical transducers

The 2D transducers described so far have all used multi-element arrays, which stepped or steered the beam position by manipulating the active aperture or the timing of the transmit waveforms and



(A) A 3D volume can be imaged using a 2D curvilinear transducer which is rotated by an electric motor

(B) The square array transducer has a square matrix of elements, which can steer the beam to image a pyramidal volume

Figure 2.13 3/4D transducers.

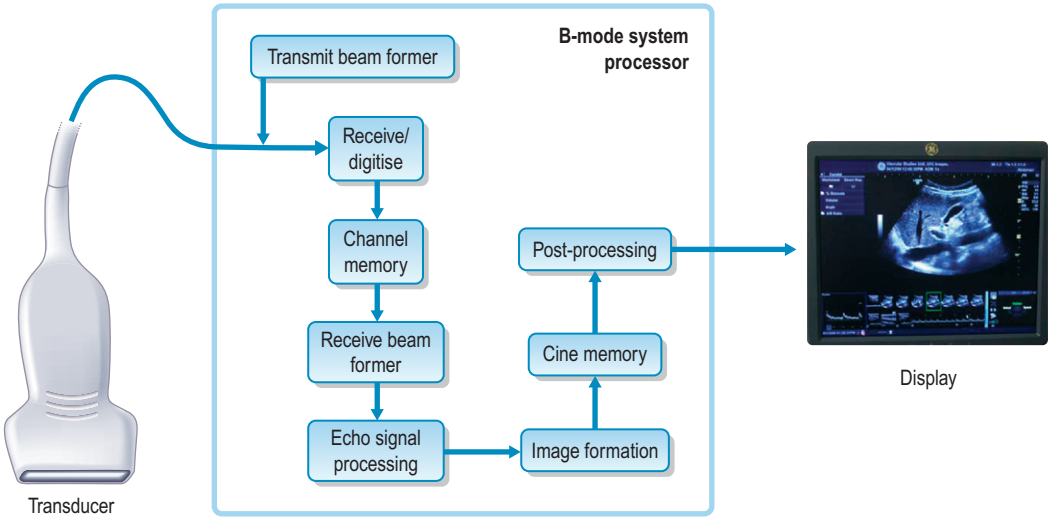


Figure 2.14 **B-mode system block diagram.**

Array transducers and beam formation

- The transducer contains an array (>100) of elements, which are used to move the beam electronically.
- The beam may be manipulated to form sector, rectangular or trapezoidal fields of view.
- The beam may be stepped along the array by moving the active aperture.
- The beam may be steered in different directions by phasing the signals to and from each element.
- Electronic focusing is achieved by varying the signal timing across the active aperture.
- The transmit beam is focused electronically to a depth selected by the user.
- In receive, focusing tracks the depth of the target.

received echoes to and from the elements. The earliest real-time scanners used single element transducers, which were physically moved to sweep the ultrasound beam through the target tissues. This technique is now confined to less common applications such as intravascular ultrasound scanning and specialist applications such as high-frequency (40–60 MHz) imaging of the skin or small laboratory animals. The fabrication of arrays to work at high frequencies is difficult, but the small size and weight of high-frequency transducers makes them suitable for intravascular work and linear mechanical scanning at high frame rates. For intravascular applications, a single element transducer mounted on a catheter tip is rotated with the beam at 90° to the axis of rotation, as for the beam from a lighthouse, sweeping out a circular field of view. Miniature cylindrical arrays have also been used for this purpose.

IMAGE PROCESSING

Figure 2.14 is a simplified block diagram of the main components of an ultrasound imaging system. The beam former and transducer produce the sets of B-mode lines required to construct each individual frame as described above. To form a useful B-mode image, the lines of echo signals must be processed in a number of ways before the image is built up and stored in the image memory. Further image processing takes place when the image is read out of the image memory, before it reaches the display screen. Although the diagram implies that the processing steps follow beam formation, some signal conditioning must take place immediately after the transducer elements to prepare the signal for digitising. All subsequent processing operations, including beam forming, are then carried out using digital techniques.

Time gain compensation (TGC)

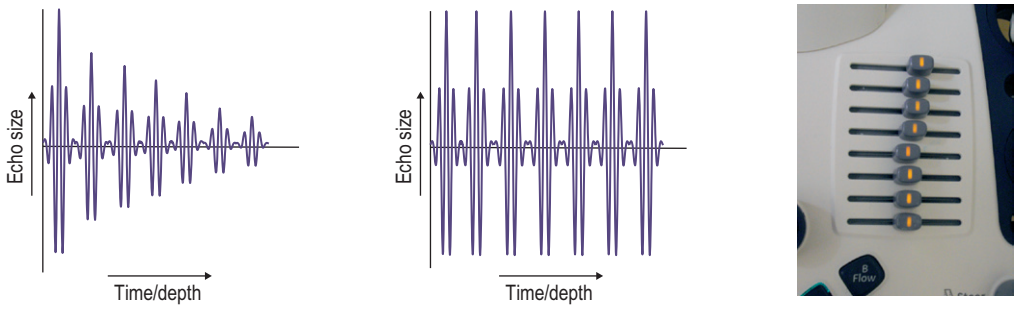
As explained in Chapter 1, ultrasound waves are attenuated as they propagate through tissues. Hence echoes arising from deep targets are weaker than those from similar targets nearer to the transducer (Fig. 2.15A). The B-mode image is required to display similar targets with the same brightness regardless of their depths. As the target depth is known to increase with time of arrival of the echo, attenuation can be compensated for by increasing the amplification or gain applied to the echoes with increasing time of arrival after transmission (Fig. 2.15B). The technique is called time gain compensation (TGC). The machine normally applies a base level of TGC appropriate to the frequency of the transducer, but the operator can make further adjustments to the gain level applied to each depth via controls (usually slide controls) on the console as shown in Figure 2.15C. The operator can also adjust the overall brightness of the displayed echoes via an overall gain control.

Dynamic range

Echoes received at the transducer may arise from a range of possible target types giving rise to a wide range of echo strengths. An interface between tissue and gas reflects almost 100% of the pulse energy and gives rise to a very strong echo (assuming it is directed back to the transducer). A tissue/tissue interface, e.g. liver/kidney, can reflect up to 1% of the energy and is still considered to be a relatively strong reflector. Most of the echoes that form the image are due to scattering from small structural details within tissues.[3] These are very much weaker than interface echoes (by a factor of about 1 million), but still contain important diagnostic information (Fig. 2.16A).

Echoes from large interfaces, such as organ boundaries, show anatomical structure and organ size and shape, while scattered echoes from organ parenchyma can show internal pathology or lesions. For effective ultrasound diagnosis, it is necessary to display both types of information at the same time.

Echo strengths are normally expressed in decibels (dB) with respect to a reference level rather than a percentage or factor. The dB simply expresses a ratio on a logarithmic scale, allowing the numbers to be added rather than multiplied, as for factors and percentages. A factor of 10 (in energy or intensity) is equivalent to

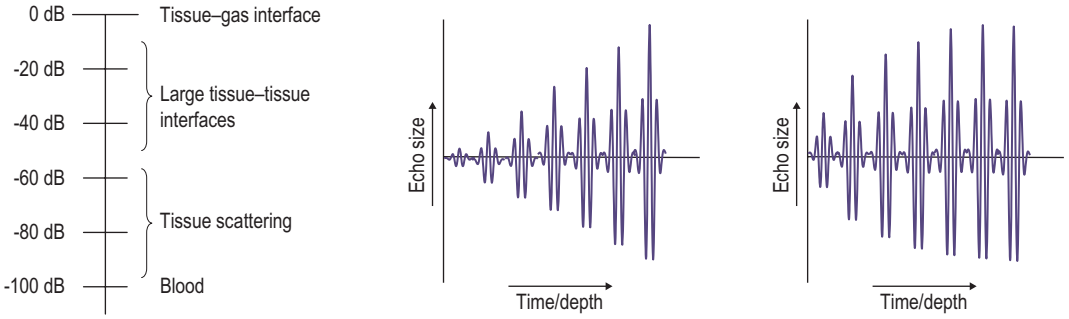


(A) Echo signals received at the transducer become weaker with increasing depth/time of arrival due to attenuation

(B) TGC is used to compensate for attenuation so that echoes from similar targets are the same size regardless of target depth

(C) The user can adjust the TGC via slide controls on the console

Figure 2.15 **Time gain compensation (TGC).**



(A) Echo sizes from different target types. A 60 dB range of echo strengths must be displayed to include tissue interfaces and scattering

(B) Echo signals before compression

(C) Echo signals after compression

Figure 2.16 **Dynamic range (compression).**

10 dB and a factor of 100 (=10×10) to 20 dB (=10+10) and so on. A factor of 1 million in pulse energy equates to 60 dB.

To be able to display large interface echoes at the same time as scattered internal echoes, the system must be able to display a 60 dB range of echo strengths as brightness variations on the display screen. However, this is far greater than the typical maximum range of brightness levels (about 30 dB) that can be displayed by a typical modern flat screen display. The dynamic range of received echo signals must be compressed by the system processor to fit into the available dynamic range of the display. This is achieved by amplifying the weak echoes more than the large echoes (Fig. 2.16B and C). The user is able to alter the dynamic range of echoes displayed (sometimes labelled compression) for different applications via the machine controls.

Harmonic imaging

The processing described so far has assumed that the transmitted pulse consists of a few cycles of the chosen transmit frequency, e.g. 5 MHz, and that the returned echoes are simply miniature versions of the same thing. However, at the relatively high pulse amplitudes transmitted by modern ultrasound imaging systems, propagation through soft tissues is non-linear and the transmitted pulse becomes distorted as it travels into the tissue. The effect is strongest in the centre of the ultrasound beam where the amplitude is highest. Distortion of the waveform is associated with the generation of harmonics or multiples of the original fundamental frequency that was transmitted.

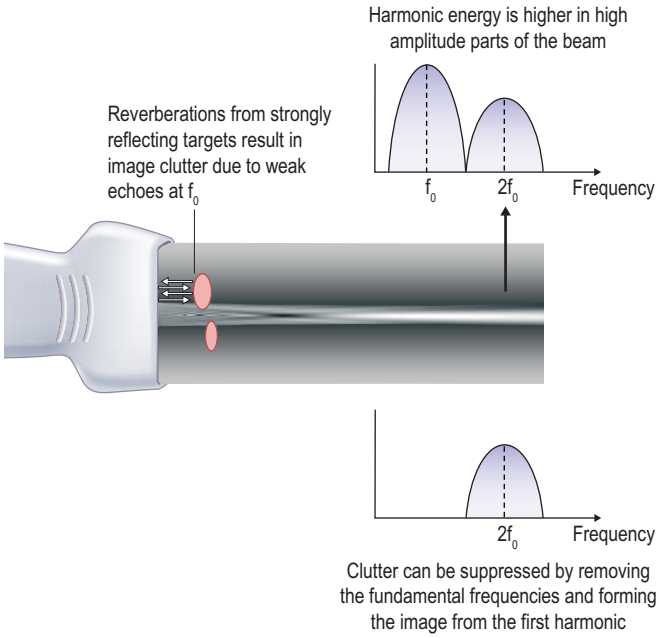


Figure 2.17 **Harmonic imaging.**

When an image is formed from the original fundamental frequency that was transmitted, it may contain clutter due to weak echoes from beam side lobes or multiple reflections (reverberation) of the pulse between strongly reflecting features (Fig. 2.17). As harmonic generation is only significant where the pulse amplitude is high, the clutter can be reduced by removing the fundamental

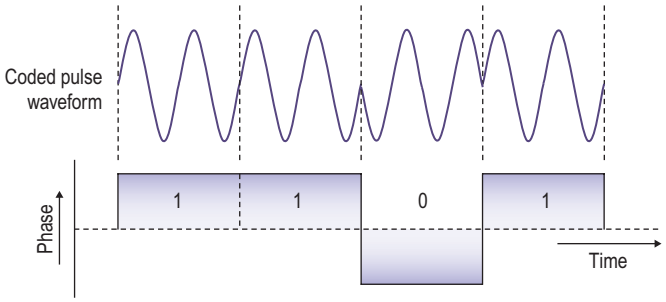


Figure 2.18 Pulse coding. The phase of the elongated transmit pulse is alternated according to a chosen digital code. The same code is embedded in a digital filter applied to returned echoes to pinpoint their time of arrival.

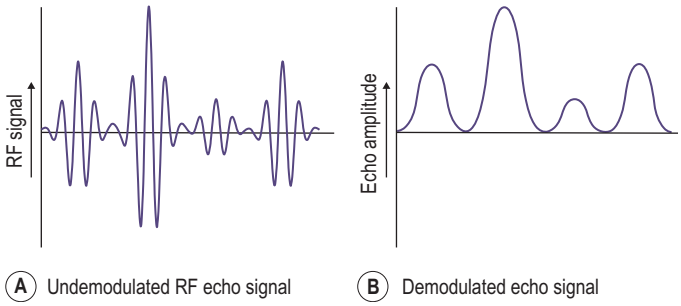


Figure 2.19 Demodulation.

frequency from the returned echoes and forming an image from the harmonic frequency. This is known as harmonic imaging.[4] As the energy at the harmonic frequency is always less than that at the fundamental, the system penetration may be reduced to some extent when operating in harmonic mode.

To form a harmonic image, the transducer must be able to transmit the fundamental frequency, but also receive the second harmonic (twice the fundamental). Hence a transducer with a wide frequency response is required. The harmonic image can be formed by applying a frequency-selective filter to the returned echoes, which rejects the fundamental frequency but allows through the harmonic frequency.[5]

Harmonic images can also be produced using a method called pulse inversion. In this method, two pulse-echo cycles are used to form each B-mode line. In the first cycle, a short imaging pulse is transmitted and echoes received as normal and stored. Then a second pulse, which is an inverted version of the first, is transmitted along the same path and echoes received. The second line of echoes is subtracted from the first. In low amplitude parts of the beam, where there is little distortion of the transmitted pulse, the lines of echoes cancel out. In the high-amplitude regions, the lines of echoes generated from the distorted normal and inverted pulses contain energy at the fundamental and second harmonic frequencies. The fundamental parts cancel out leaving the second harmonic parts to form the image.

Pulse coding

The maximum depth from which echoes can be received is determined by the attenuation of the pulse and returning echoes by the tissues they pass through. Higher frequencies give improved image resolution but suffer more rapid attenuation and hence reduced penetration of tissues. For a given frequency, penetration can be improved by using a longer transmitted pulse, making its echoes easier to detect. However, the increased pulse length degrades the axial resolution of the system. Pulse coding techniques allow the use of long transmit pulses while maintaining good axial resolution.[6]

The long transmit pulse is divided into time segments in which the phase of the wave is alternated according to a predetermined code (Fig. 2.18). When the echoes are received, they are passed through a digital filter which is programmed to search for the code. When a match is detected, the time at which it occurs gives the effective time of arrival of the echo, restoring the axial resolution. Pulse coding allows greater penetration to be achieved at higher frequencies.

Demodulation

All of the processing steps described so far have been applied to signals that contain the original ultrasound transmit frequency or its harmonics. This is referred to as the radio-frequency or RF signal. The brightness value that is displayed at each point in the image is related to the amplitude or envelope of the RF signal. The final processing step in forming the B-mode image is to remove the radio-frequency element of the signal to leave the envelope signal. This process is referred to as demodulation (Fig. 2.19).

B-mode instrumentation and processing

- Time gain compensation (TGC) is used to compensate for increasing attenuation of echoes with depth.
- The dynamic range of echoes must be compressed to display reflected and scattered echoes simultaneously.
- Harmonic imaging may be used to reduce reverberations and clutter in the image.
- Pulse coding may be used to increase penetration for a given frequency.
- Echoes must be demodulated to remove the transmit frequency before image formation.
- Post-processing is applied as the image is read out from the image memory.

Image memory

Following the various processing steps described above, the B-mode lines are written into the image memory to form the image as an array of pixels similar to an image in a digital camera. The dimensions of the image in the memory array are typically 1200 × 1200 pixels, with each pixel capable of storing up to 256 different grey levels (8 bits). As for a digital camera, the system is capable of storing many images (over 2000 for some models) and successive frames are stored in a cine memory until the memory is full. The first image stored is then overwritten so that the last frames are always stored. The chosen image is read out from the image memory in a raster pattern which is synchronised to that of the display monitor.

The image can be written to the image memory and read out in a number of different ways. If the image memory is being constantly updated with new images and the last image to be formed is always read out to the display, a real-time, moving image is displayed. In freeze mode, new images are not written into the memory and the last image stored is read out repeatedly to the display monitor. In cine loop mode, the writing process is again frozen but the whole sequence of stored images is read out in a repeated cycle showing the last 30 seconds or so of the real-time image.

Field of view and zoom

When images are written to the image memory, they are scaled to match the field of view, chosen by the operator, to the memory

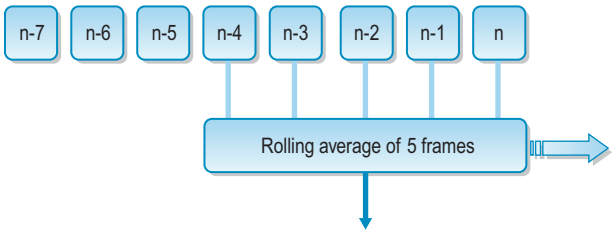


Figure 2.20 Frame averaging (persistence).

dimensions. A specific region of interest within the image can also be chosen by the operator to fill the memory space, leading to the storage of a zoomed-in image (write zoom), rather like using a telephoto lens with a camera. A similar process can be applied when the image is read out. Here a region of the stored image can be chosen to be read out and fill the display screen. This is referred to as read zoom. The zoomed area can be moved around the stored image but may appear pixelated at large magnifications.

Post processing

When images are read out from the image memory, a number of further processing steps may be applied before they are sent to the display. These steps are referred to as post processing as they take place after image storage.

Persistence is used to suppress fluctuating noise patterns in the image. As described earlier, the echo signals received by the transducer from scattering within tissues, especially those from large depths, are very weak and may be contaminated by random electronic noise produced in the processing electronics. The pattern of noise signals stored within each image is different and can be distracting as it fluctuates when images are displayed in real-time mode. The random noise patterns can be suppressed by frame averaging, also known as persistence. This is achieved by displaying an average of the last four or five images stored in the image memory (Fig. 2.20). Instead of displaying a given image pixel from the last frame, the average of the corresponding pixels from the last four or five frames is sent to the display. Random image noise is suppressed but moving targets may be smeared in the image if too many frames are averaged. The degree of persistence may be chosen by the operator.

The gamma curve (also referred to as the grey map) is a form of post processing chosen by the user to emphasise particular ranges of echo amplitudes in the image. The amplitude values stored in the pixels of the image memory are represented in the image in terms of displayed image brightness or grey level. The way that the displayed grey levels relate to the stored values is controlled by the gamma curve. Different curves are available for the user to choose from according to the clinical application (Fig. 2.21). For example, a curve that assigns more grey levels to the lower amplitude signals (Fig. 2.21B) may be more suited to imaging of the liver where the most useful information is obtained from weak echoes scattered from the liver parenchyma.

Various other post-processing techniques have been employed by manufacturers to enhance the displayed image. These include smoothing to reduce noise and speckle and edge enhancement to emphasise boundaries such as vessel walls. Adaptive processing techniques analyse the image to identify features such as boundaries. These can then be enhanced by smoothing along the boundary. Other areas are smoothed to reduce noise and speckle.

DOPPLER ULTRASOUND

The ultrasound imaging techniques described so far have all been based on the assumption that during the formation of each image,

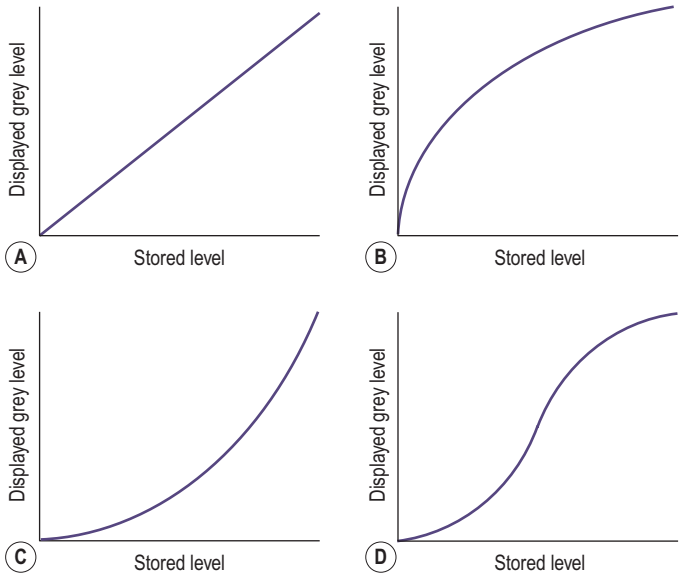


Figure 2.21 Post-processing gamma curves. A: Linear. **B:** Enhancement of weak echoes. **C:** Enhancement of higher level echoes. **D:** Enhancement of mid-range echoes (s-curve).

the reflecting or scattering targets remain stationary. The rapid succession of images, which forms the real-time display, shows tissue movements, e.g. the heart wall, as a progressive change in position through consecutive frames. Ultrasound is an important diagnostic tool in the study of blood flow in arteries and veins but, due to the homogeneous nature of blood and its weak scattering, makes use of the Doppler effect to detect movement.

Continuous wave Doppler (CW)

As explained Chapter 1, when a transmitted continuous wave of ultrasound is scattered by flowing blood, the frequency of the received echo signal is shifted due to the Doppler effect, by an amount related to the velocity of the blood. The Doppler shift frequency f_D can be used to measure and monitor the blood flow velocity. In the simplest Doppler ultrasound system, a dual element transducer is used with one element transmitting continuously and the other receiving, as shown in Figure 2.22A. Blood movement can be detected in vessels that pass through the region where transmit and receive beams overlap. To extract the Doppler shift frequency, the received echo signal (at frequency f_R) is mixed with a sample of the transmit frequency (f_T). The resulting signal contains components at frequencies f_T+f_R (at several MHz) and f_T-f_R (at several kHz), which is the Doppler shift frequency f_D. The MHz components are then filtered out to leave the Doppler shift frequency, as shown in Figure 2.22B. As this frequency is in the audible range, the observer can listen to it via headphones or a loudspeaker. Continuous wave Doppler is used widely to monitor blood flow in superficial arteries, which can be located without image guidance, or in vessels with very high flow velocities, such as the ascending aorta. However, it cannot separate signals from multiple blood vessels which fall within the beam overlap region. Locating deeper vessels is also difficult with CW Doppler.

Pulsed wave Doppler (PW)

Pulsed wave Doppler is used in conjunction with a B-mode image, facilitating the location and identification of vessels. This is referred to as duplex imaging. The pulsed wave method also allows spatial separation of signals from adjacent vessels. In pulsed Doppler systems, a relatively long pulse of ultrasound (say 10 cycles) is transmitted. As for B-mode imaging, a continuous series of echoes

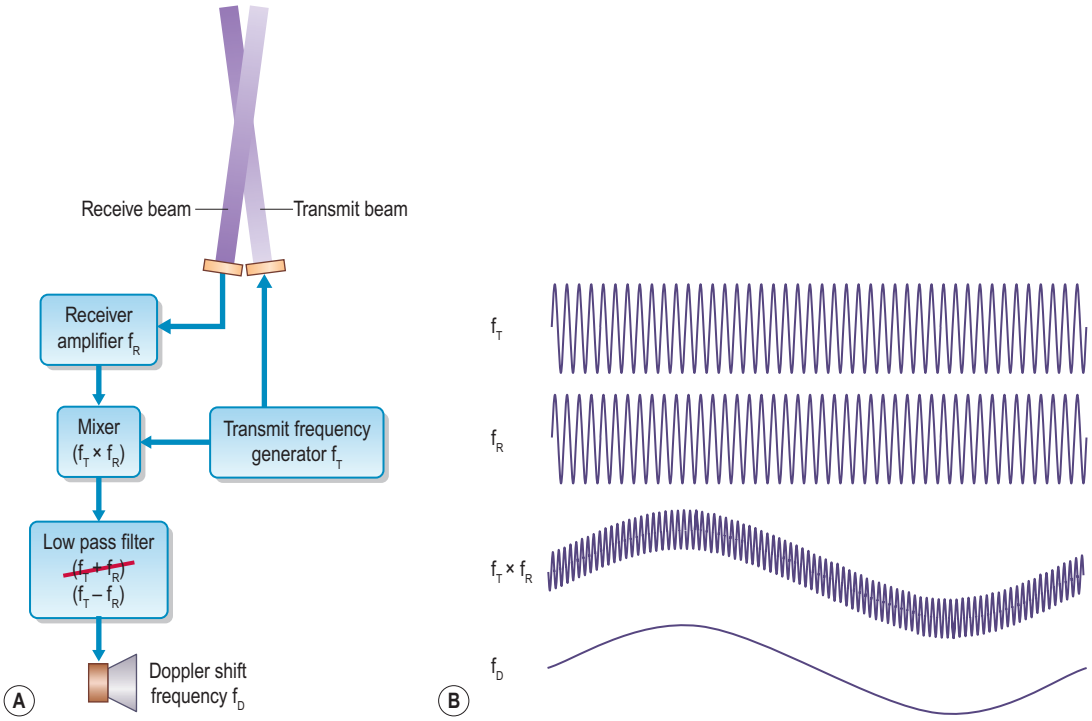


Figure 2.22 Continuous wave Doppler. A: System block diagram. **B:** The demodulation process.

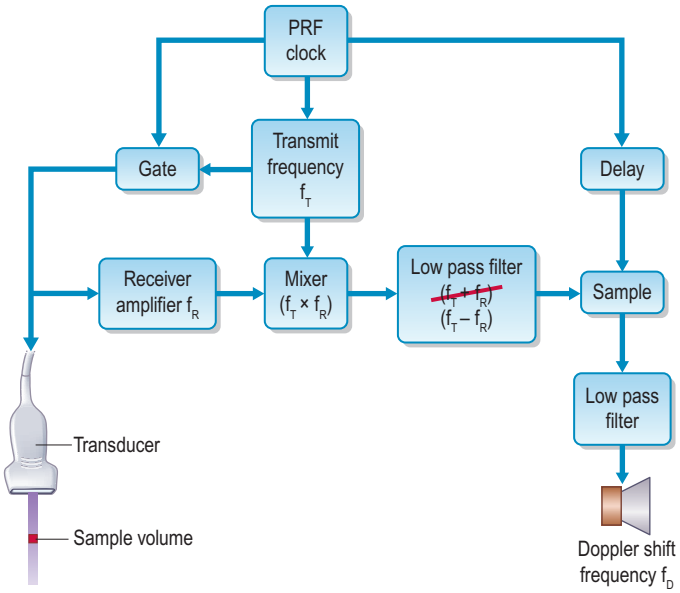


Figure 2.23 A pulsed wave Doppler system block diagram. PRF, pulse repetition frequency.

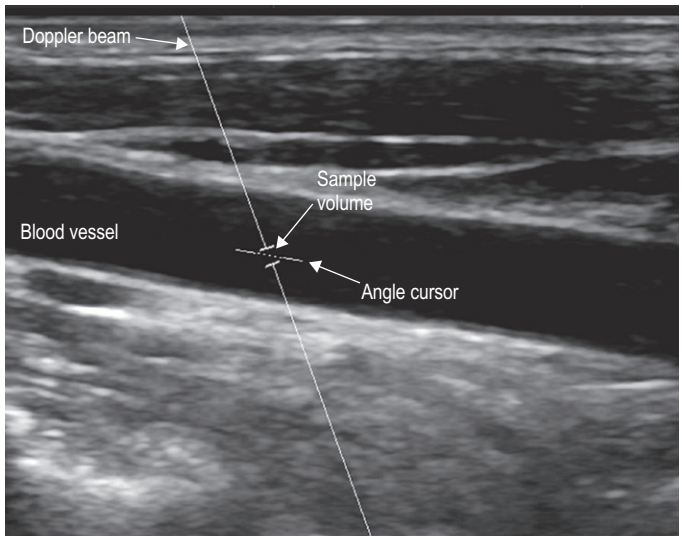


Figure 2.24 The pulsed Doppler sample volume and angle cursor are adjusted by the operator to align with the vessel of interest.

of the pulse is then received from increasing depths, following each transmission. The returned signals are processed as for CW Doppler to extract the Doppler shift frequencies. Doppler signals from a specified blood vessel are then isolated for further processing by the use of a time gate, which allows through only those signals corresponding to the depth of interest (Fig. 2.23). The position of the time gate (the sample volume) is indicated on the B-mode image by cursors (Fig. 2.24). The user adjusts the position of the Doppler beam and the depth (or range) of the sample volume along it, so that the sample volume is located over the vessel of interest. As this is a pulse-echo technique, the same transducer or active aperture can be used to transmit and receive. The user also adjusts the angle of a cursor in the centre of the sample volume to indicate the direction of blood flow to the system.

The process for extracting the Doppler shift frequency is similar in principle to that used for CW Doppler. However, the received signal now consists of one brief sample of the Doppler frequency from the depth corresponding to the target vessel, for each transmitted pulse (Fig. 2.25). These can be thought of as a set of samples of the equivalent CW Doppler shift frequency. The value of each sample is determined by the phase relationship between the corresponding f_R sample and the reference transmit frequency f_T. The continuous Doppler shift frequency signal is constructed from the samples by low pass filtering.[7]

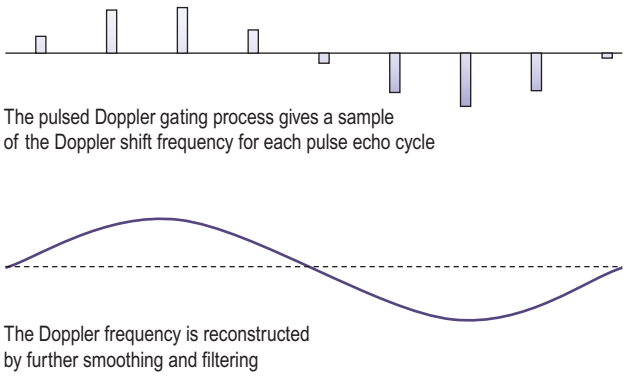


Figure 2.25 Pulsed Doppler demodulation.

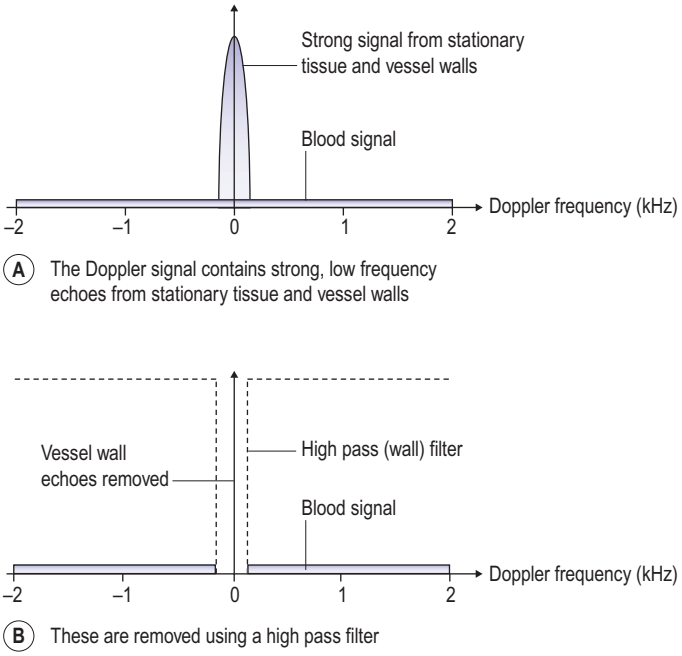


Figure 2.26 High pass filtering of the Doppler signal.

For both CW and pulsed Doppler, further signal mixing and processing is then used to separate signals from flow towards the transducer and flow away from the transducer.

High pass filtering

The Doppler shift signal in CW and pulsed Doppler systems contains several components as illustrated in Figure 2.26. The strongest signal components are those due to reflection and scattering from stationary or slowly moving tissues and tissue boundaries. These are associated with low Doppler shift frequencies. Blood flow velocities can range from zero (during parts of the cardiac cycle) to several metres per second, giving rise to Doppler shift frequencies up to several kHz. The signal due to scattering from blood is much weaker than that from tissue, however. A particular problem in arterial signals is the large signal from the slowly moving arterial wall which gives rise to a 'wall thump' in the audio signal. Such large signals from slowly moving tissues must be removed by filtering to allow the smaller blood signal to be analysed. This is done using a high pass filter, also known as a wall thump filter, which rejects the low-frequency Doppler shift signals. The cut-off frequency of this filter may be selected by the operator to reject the arterial wall signal with minimum loss of blood signal.[8]

Aliasing

The sampled nature of the reconstructed pulsed Doppler signal leads to a major limitation of pulsed Doppler systems at high blood flow velocities. Each transmitted pulse leads to one sample of the Doppler shift signal. Hence the number of samples produced per second, the sample rate, is the same as the number of Doppler pulses transmitted per second, the pulse repetition frequency (PRF). To reconstruct a sine wave of a given frequency, it is necessary to have at least two samples for each cycle of the wave, i.e. the PRF must be at least $2f_D$. If the Doppler frequency for flow towards the transducer (forward flow) increases to the point where the PRF is too low, it will appear instead as an aliased, reverse flow frequency, shifted downwards by an amount equal to the PRF.

Aliasing is most likely to be a problem when the Doppler shift frequency is high (high blood flow rates and high transmit frequency) and the PRF is low (due to large target depth).

Doppler frequency estimation and display

Doppler signals can be observed by listening via headphones or loudspeakers, and the expert user can infer much about blood flow and disease states in blood vessels using this approach. However, objective assessments of many disease states can only be made by quantifying the blood flow velocity and other flow characteristics. This is done via the sonogram, which is a time varying display of the flow velocities within the Doppler sample volume (Fig. 2.27A).

To generate the sonogram, the continuous Doppler signal is divided into a set of fixed time intervals, typically 10 ms in duration. Each 10 ms section is then analysed, using digital Fourier transform methods, to create a distribution or histogram of Doppler frequencies. The distribution is displayed as a vertical line with the power of the signal at each frequency represented on a greyscale (Fig. 2.27B). Using the Doppler angle set by the user and the Doppler equation (Chapter 1), the system converts the Doppler frequencies to a velocity scale. Light grey or white areas in the display indicate velocities at which there are many blood cells flowing and dark grey areas where there are few. As consecutive 10 ms intervals are analysed, they are displayed as adjacent vertical lines creating a time-varying display of blood flow velocities and their distribution.

The user can adjust the velocity and time scales of the display. As the precision of the frequency estimate is given by the inverse of the time interval (e.g. 100 Hz for a 10 ms sampling interval), slow sweep speeds (which use longer time intervals) give greater frequency (velocity) precision and vice versa.

Doppler ultrasound instrumentation

- The frequency of ultrasound scattered from moving blood is shifted due to the Doppler effect.
- For typical transmit frequencies and blood velocities, the Doppler shift frequency is in the audible range.
- Continuous wave Doppler may be used to study blood flow in superficial vessels.
- Pulsed Doppler uses time gating to isolate Doppler signals from deeper vessels using B-mode image guidance.
- High-amplitude low-frequency signals from slowly moving tissues and vessel walls must be filtered out using a wall thump filter.
- The PRF used in pulsed Doppler systems must be at least twice the Doppler shift frequency to avoid aliasing.
- The sonogram is used to display the time varying distribution of flow velocities within the Doppler sample volume.

Colour flow imaging

Pulsed Doppler systems, in conjunction with a sonogram display, are widely used to make detailed studies of flow velocities and their

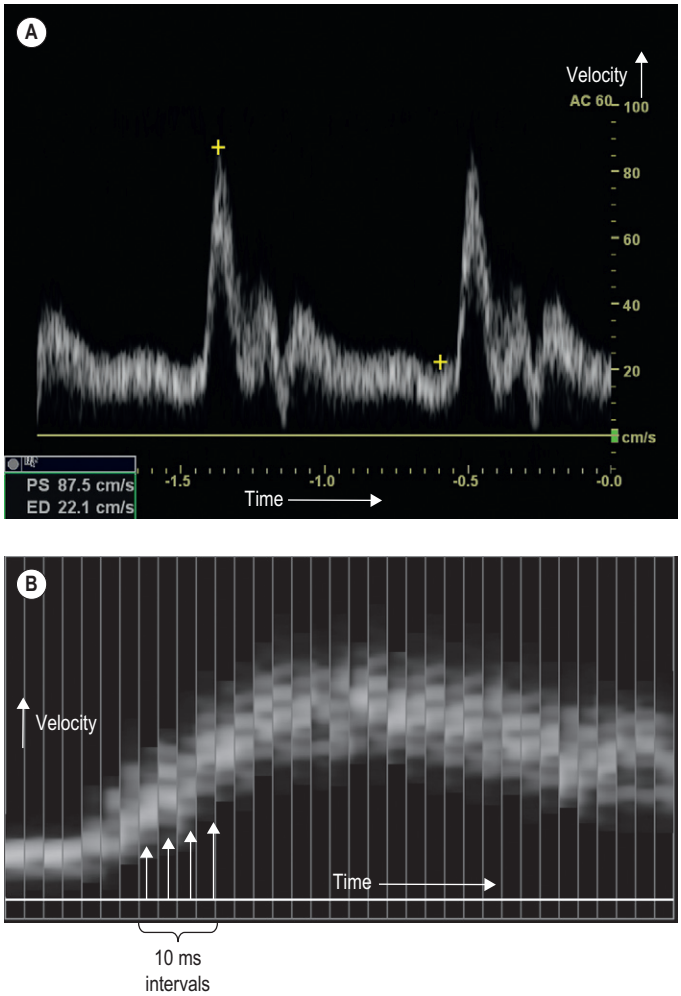


Figure 2.27 **A:** A sonogram from the carotid artery. **B:** To construct the sonogram, the velocity distributions in consecutive 10 or 20 ms samples are displayed as adjacent vertical lines. The amount of blood flowing at each velocity is represented on a greyscale.

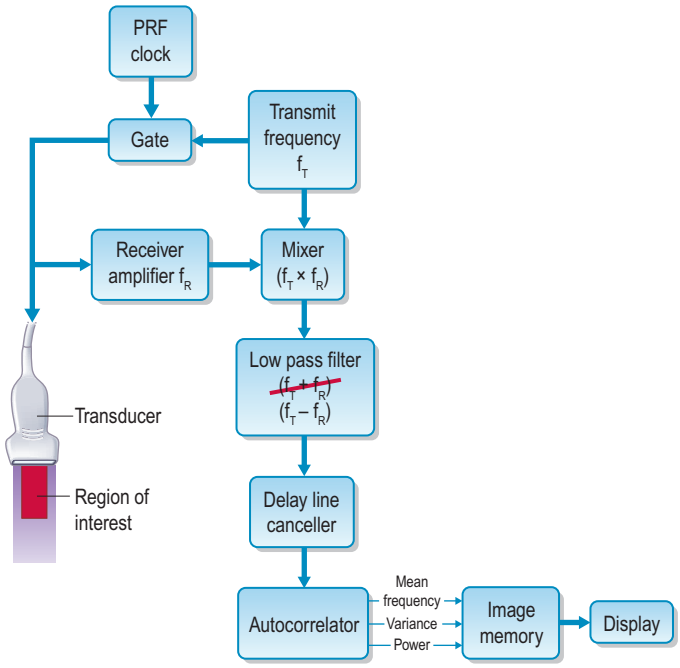


Figure 2.28 **Colour flow imaging system block diagram.** PRF, pulse repetition frequency.

distribution within a stationary sample volume placed within a blood vessel. Colour flow imaging systems give a real-time 2D image of blood flow patterns in blood vessels as a colour overlay on a B-mode image. Here the colour of the display, at each point in the image, represents the mean blood flow velocity at a given time.

Colour flow imaging systems can be seen as an extension of the time gating approach from a single sample volume to multiple adjacent sample volumes along the Doppler beam. The beam is also swept through the region of interest as in B-mode image formation, to form a 2D colour map. However, the time restrictions imposed by real-time 2D image formation require different techniques to be used for removal of stationary tissue echoes and for Doppler frequency estimation. Whereas frequency analysis in the sonogram is performed on a 10 or 20 ms sample of the Doppler signal, each line in the colour flow map must be formed in about 1 ms to allow real-time display.

For each line in the colour flow image, the beam is held in the same position for a number of pulse-echo cycles (typically eight). The number of pulses transmitted in this sequence is referred to as the ensemble length. As illustrated in Figure 2.28, the received echoes are mixed with the transmit frequency and filtered to extract the Doppler shift frequency as for CW and pulsed Doppler systems. No gating is applied as Doppler signals are required from all depths along the line. To remove the large echoes from stationary and slowly moving tissues, a technique called delay line cancellation is then used rather than filtering. Each line of echoes in the ensemble is stored digitally and compared with the next one by subtracting one from the other. This removes echoes from stationary targets, which do not change, while preserving signals from those that are moving, as they do not cancel out. Modern systems use more elaborate versions of this technique to give enhanced separation of stationary echoes.

Estimation of the Doppler shift frequency is most commonly carried out by a technique called autocorrelation.[7] In essence, each line of Doppler signals generated by each pulse-echo cycle in the ensemble is compared with the one before it. The rate at which the phase of the signal, at each point along the line, changes in the interval between one line in the ensemble and the next leads to an estimate of the Doppler frequency at that point in the line. By extending this process over the ensemble of pulses, an estimate of the mean frequency is obtained for each point along the line. Mean frequency is represented in the image on a colour scale, commonly using red for flow towards the transducer and blue for flow away (Fig. 2.29). Low frequencies are displayed as dark shades of red or blue leading, with increasing frequency, to lighter shades through to white. The display normally includes a colour wedge showing the range of available shades of red and blue next to a corresponding velocity scale. The velocity scale indicates the component of blood flow velocity in the direction of the Doppler beam (i.e. not corrected for Doppler angle).

The autocorrelator can also give an estimate of the variability of the Doppler frequency during the ensemble for each point along the line. This is expressed in terms of the variance of the signal and is used to display an alternative form of colour map which can indicate the degree of disturbance in the blood flow in the vessel.

Limitations of colour flow imaging

As the mean frequency values displayed in each line of the colour flow image are estimated from the set of samples obtained from

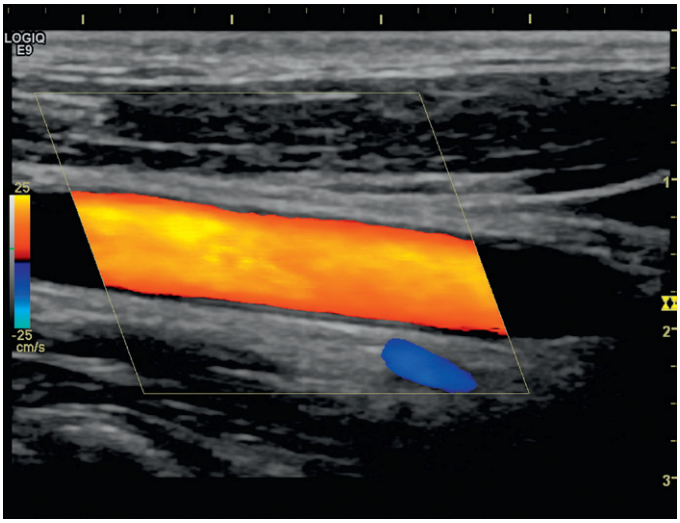


Figure 2.29 A colour Doppler display, showing blood flow in the carotid artery. Mean velocity with respect to the angle of the Doppler beam is shown on a colour scale.

each ensemble, colour flow images are also affected by aliasing. Aliasing of the red channel shows as a sudden inversion to dark blue and vice versa. As for pulsed Doppler, aliasing occurs at high flow velocity, high transmit frequency and low PRF. The colour flow overlay is usually restricted to a region of interest to minimise line/image formation time and maximise the PRF.

At the other end of the frequency scale, the precision of the frequency estimate and sensitivity of the system to low velocities is determined by the total sample time, which is the duration of the ensemble. Expanding the velocity scale will ensure that these parameters are optimised for detecting low frequencies (velocities).

Power Doppler

Colour flow imaging systems are very effective at showing variations in flow velocity at different points and times in a blood vessel. Early systems had poor sensitivity to signals from small vessels, especially at low flow velocities. In cases where the requirement was simply to demonstrate the presence or absence of flow in small vessels, power Doppler was more effective. To create a power Doppler image, the autocorrelator module carries out a different calculation on the signals to give the power of the Doppler signal at each point along the line, rather than the mean velocity. The colour at each point is then related to the amount of blood flowing through the Doppler beam and not to its velocity. The power Doppler signal is less susceptible to noise and so can detect weaker flow signals. As it is not related to Doppler shift frequency, it is not affected by aliasing or by the Doppler angle.

Colour Doppler instrumentation and processing

- Colour flow imaging systems give a real-time 2D image of blood flow patterns in blood vessels as a colour overlay on a B-mode image.
- The colour of the display at each point represents the current value of mean flow velocity.
- Large echoes from slowly moving tissues and vessel walls are removed by delay line cancellation.
- Mean frequency at each point in the image is estimated by comparing the phase of the Doppler signal on each line with the previous one.
- Colour flow images are also affected by aliasing.
- Power Doppler gives a real-time 2D image of the amount of blood flowing in a blood vessel.

REFERENCES

1. Thomenius KE. Evolution of ultrasound beamformers. IEEE Ultrasonics Symposium Proceedings 1996;2:1615–1622.
2. Fenster A, Downey DB, Cardinal HN. Three dimensional ultrasound images. Phys Med Biol 2001;46:R67–99.
3. Kossof G, Garrett WJ, Carpenter DA, et al. Principles and classification of soft tissues by grey scale echography. Ultrasound Med Biol 1976;2:89–105.
4. Desser TS, Jedrzejewicz MS, Bradley C. Native tissue harmonic imaging: basic principles and clinical applications. Ultrasound Q 2000;16:40–48.
5. Tranquart F, Grenier N, Eder V, Pourcelot L. Clinical use of ultrasound tissue harmonic imaging. Ultrasound Med Biol 1999;25:889–894.
6. Eckersley RJ, Tang M, Chetty K, Hajnal J. Microbubble contrast agent detection using binary coded pulses. Ultrasound Med Biol 2007;33:1787–1795.
7. Evans DE, McDicken WN. Doppler ultrasound – physics, instrumentation and signal processing. Chichester: John Wiley; 2000.
8. Hoskins P, Thrush A, Martin K. Diagnostic ultrasound: physics and equipment. London: Greenwich Medical Media; 2003.

CHAPTER

3 Practical ultrasound – using scanners and optimising ultrasound images

Colin R. Deane

INTRODUCTION 31

VARIATION IN ULTRASOUND SCANNERS – CONTROLS AND NOMENCLATURE 31
General controls and keys 32
B-mode 32
Colour flow imaging (CFI) and power Doppler imaging 32
Pulsed wave spectral Doppler (PW) 32

TRANSDUCERS 32

APPLICATION SET-UPS 33
Patient type/frequency 33
Output power 34

B-MODE PARAMETERS 34
Gain 34
Time gain control/depth gain control 35
Dynamic range 36
Depth 36
Frequency 36
Focus 36
Zoom 36
Harmonics 37
Spatial and frequency compounding 37
Adaptive processing 38

COLOUR FLOW IMAGING 40
Power 40
Gain 40
Scale/pulse repetition frequency (PRF) 40
Invert 41
Frequency/patient type 41
Colour flow imaging box/area size 42
Focus 42
Beam steering in linear arrays 42
Filter, space/time, post-processing, persistence, priority 42
Flow settings – combination controls 44

PULSED WAVE SPECTRAL DOPPLER (PW) 44
Basic rules – beam/flow angle and angle correction 45
Power 46
Gain 46
Invert – baseline 46
Scale and HPRF 46
Sample volume/gate/range gate 48
Other parameters – filter/sweep 49
Angle correction errors 49

INTRODUCTION

Ultrasound images are dependent on two main factors:

1. the scanning approach and manipulation of the transducer
2. the transducer and ultrasound scanner combination used, its settings and the display.

The quality of an ultrasound image may be varied significantly by altering either; learning good ultrasound scanning and image interpretation requires an understanding of both.

Ultrasound users tend to prefer to hold the transducer with their dominant hand. The dexterity required and proprioception are important in understanding what is displayed on the screen as the user builds up a three-dimensional (3D) appreciation of the structures under investigation from a large series of 2D images obtained from many views and in many planes. Practical manipulation of the transducer can only be effectively taught and learned by live scanning; books, although they can show the basic scanning approaches, are limited in teaching these skills.

Ultrasound science texts tend naturally to concentrate on scanner setting, to explain, for example, the effect that gain, frequency or colour scale has on the image. These are important although the sheer number of parameters in some current scanners can be daunting. This chapter will concentrate on the most important factors and changes that affect image quality. It is important that the main controls and their effect are rapidly learned. To use an analogy, many learner drivers spend a lot of time and effort worrying about the basic controls of the car, effective use of the brakes, clutch, gears and how best to employ them in three-point turns or hill starts. They can become fixated on learning special manoeuvres. Good driving is, however, dependent on awareness of what is going on in the road and driving safely to suit the conditions and environment. In order to get to that point, the controls and their use should become second nature. So it is with ultrasound. Look at an experienced sonographer and you'll notice her hand flicking at gain, TGC, frequency, harmonics, scale controls without looking at the keyboard, her eyes focused on the image and her mind concentrated on the information within it.

The chapter will cover the major controls of ultrasound scanners, showing their effect on images and measurements obtained from them. Suggestions are made as to how to optimise specific controls and settings.

VARIATION IN ULTRASOUND SCANNERS – CONTROLS AND NOMENCLATURE

There are currently a wide range of ultrasound scanners available, from small portable scanners with a minimum of user-controls to sophisticated 'flagship' models with menus and sub-menus of commands to effect a range of options for 2D, 3D and other modalities. There is considerable variation in the layout of the controls (Fig. 3.1) and even how they are described. There is a similar lack of consistency in how, if and where settings are displayed on the screen. Ultrasound practitioners coming to a new machine are often confronted by difficulty in finding out how to use it well, in some cases, even how to switch it on. In a hospital where there may be several ultrasound scanners, the disparate functionality can be a source of difficulty and can lead to wasted time and suboptimal image quality. Practitioners using a machine for the first time should ensure that they are familiar with the main controls and their particular operation. It is to be hoped that there will be a gradual standardisation of controls and their layout but there is no imperative to achieve this and the protective use of trade names used for marketing only adds to the confusion in nomenclature.



Presets	1
Gain	2
TGC/DGC	3
Depth	4
Frequency/ patient type	5
Focus	6
Zoom	7
Freeze	8
Callipers	9



Presets	1
Gain	2
TGC/DGC	3
Depth	4
Frequency/ patient type	5
Zoom	6
Freeze	7
Callipers	8

Figure 3.1 A and B: Control panels for two ultrasound scanners. Although there are a large number of keys and controls knobs, it is essential to know the location and function of a few important controls before starting to scan. The main controls for B-mode imaging are shown for these two scanners. TGC/DGC, time gain compensation/depth gain compensation.

What follows is a description of the main factors for B-mode, colour flow imaging and pulsed wave spectral Doppler. Some of the minor controls and their effects will be discussed, but it is possible that particular controls, perhaps used by individual manufacturers, will not be covered.

A fairly full list of controls and a brief description of their function is given in the summary boxes which follow later in the chapter, for B-mode, colour flow imaging and spectral Doppler. The lists are not comprehensive but an experienced practitioner should know why they might need to be altered and how to achieve this. For this chapter, the main controls chosen are those that it is important to use in everyday scanning. It is also a guide for those using an unfamiliar scanner for the first time. The following is a list of essential controls necessary for an operator to manipulate to achieve the optimum performance from the scanner.

General controls and keys

- Change/choose/switch the transducer
- Enter patient data
- Application selection (for example abdominal/thyroid/leg veins/first trimester)
- Freeze the image
- Store images
- Review images.

B-mode

- Frequency/patient or exam type
- Power
- Gain
- TGC
- Dynamic range
- Depth
- Focus (if the system has this)
- Harmonics
- Zoom function
- Compounding/adaptive processing (if the system has this)
- Measurements (callipers).

Colour flow imaging (CFI) and power Doppler imaging

- Power
- Gain
- Scale
- Colour scale invert (not applicable to all power Doppler systems)
- Focus (if the system has this)
- Frequency/patient type
- Area selected for CFI
- For linear arrays – beam steering.

Combination controls may be available that select several parameters to optimise settings for particular applications (e.g. slow flow, fast flow).

Pulsed wave spectral Doppler (PW)

- Power
- Gain
- Scale
- Baseline
- Invert
- For linear arrays – beam steering
- Angle correction
- Sample volume/gate size
- Measurements.

TRANSDUCERS

There are a wide range of transducers available for most scanners. When choosing a transducer, the main considerations are:

- transducer type, e.g. curvilinear/phased/linear array, endocavity
- the frequency range
- the size of the array: for example small linear array for paediatric and perioperative work

- additional features, for example matrix arrays for dynamic focusing in the slice thickness/elevation plane.

In recent years large frequency ranges have been quoted for some transducers and it is tempting to believe that a single transducer will have good performance over a wide range of depths. Transducers are limited by physical constraints, in particular for focusing in the elevation plane. For example, a linear array optimised for superficial work will tend to have a narrower width in the elevation plane for more precise beam control in the near field. A linear array suitable for investigation of deep vein thrombosis will have to have good performance from 1.5 to 5 cm depth; the width of the elements in the elevation plane is greater allowing better control of focusing here through a larger aperture but with reduced precision in the near field. Much depends on the standard of investigation required, but for optimum performance, a range of transducers is required.

Figure 3.2 shows the range of transducers for one scanner for work in our vascular laboratory. In particular, we find it useful to have low-frequency curvilinear and phased arrays for abdominal vascular work. While the small aperture of the phased array leads to B-mode images that have poorer spatial resolution than the curvilinear array, the phased array has good colour sensitivity and is useful when overlying ribs restrict access of the curvilinear array.

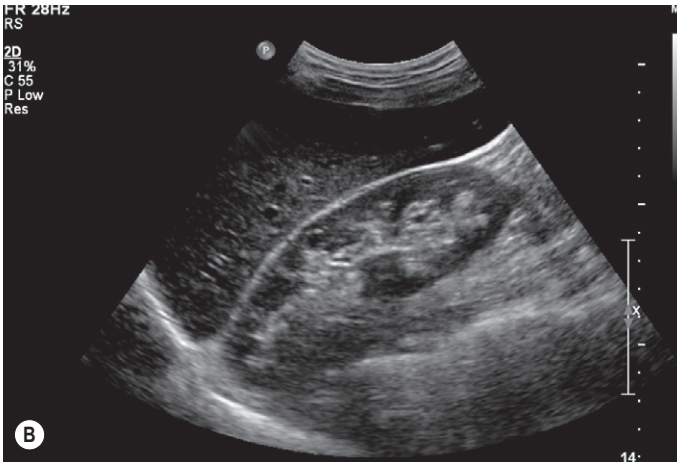
APPLICATION SET-UPS

Different applications require different scanning parameters. For example, imaging a thyroid setting may use a high degree of frame averaging and multiple transmit focal zones to reduce speckle and provide a uniform image of tissue that is static. Such a setting would be less than optimum for the carotid artery next to it, where frame averaging and the slow frame rate resulting from multiple transmit pulses leads to blurring of the pulsatile wall. Applications keys set a large number of parameters for B-mode, colour flow and spectral Doppler to produce images appropriate for the particular application. As a first step they are useful; in most systems, users can modify these to produce their own preferred image appearance. The difference can be marked, as shown in Figure 3.3 where the aorta is shown with an abdominal setting and abdominal vascular setting.

Patient type/frequency

In some systems, further modifications can be made by altering a 'patient type' or similar control. In one system, the type is easy, medium or difficult, in another the terms resolution or penetration are used. For difficult patients, a lower frequency or harmonics are used but other parameters are also altered. This is also a useful first step to improving images but the consequences for measurements may be unpredictable. As an example, the use of a difficult setting in the measurement of nuchal translucency may produce longer echoes from interfaces and a slightly smaller measurement. In a system where the frequency can be selected independently, the reasons for this are obvious and measures can be undertaken to standardise this. In controls and keys where manufacturers alter several parameters to improve the appearance of the image, it may not be obvious what the parameters are and how measurements or detectability are affected. As an example, images of a kidney with resolution and penetration settings are shown in Figure 3.4.





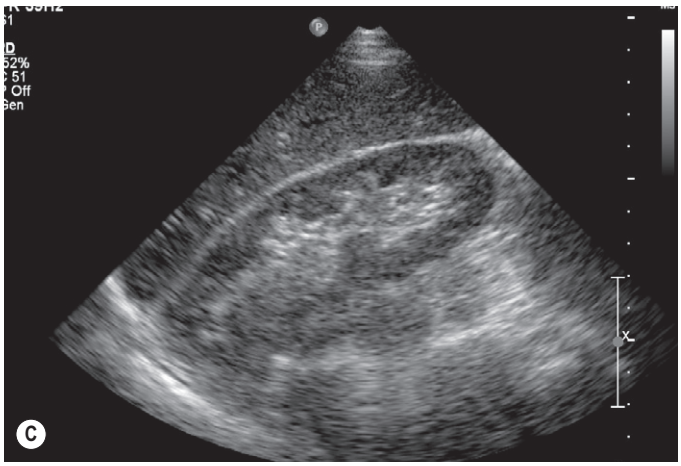


Figure 3.2 Transducers used for vascular imaging. A: In the top row are a range of linear arrays with different frequency ranges and apertures for a range of paediatric and adult peripheral vascular applications. The middle row has three different curvilinear arrays with frequency ranges from 1 to 8 MHz. The two phased arrays have different transducer face formats, one for deep abdominal vascular applications and the other for transcranial Doppler imaging. There is some overlap between transducers but by having a range of transducers, optimal imaging can be achieved for the full range of applications. **B and C:** Longitudinal image of a kidney with a curvilinear transducer **(B)** and phased array transducer **(C)**. Spatial and contrast resolution is better with the curvilinear array in this case. The phased array may be useful if there is restricted access; it also has good performance in colour flow and spectral Doppler imaging.

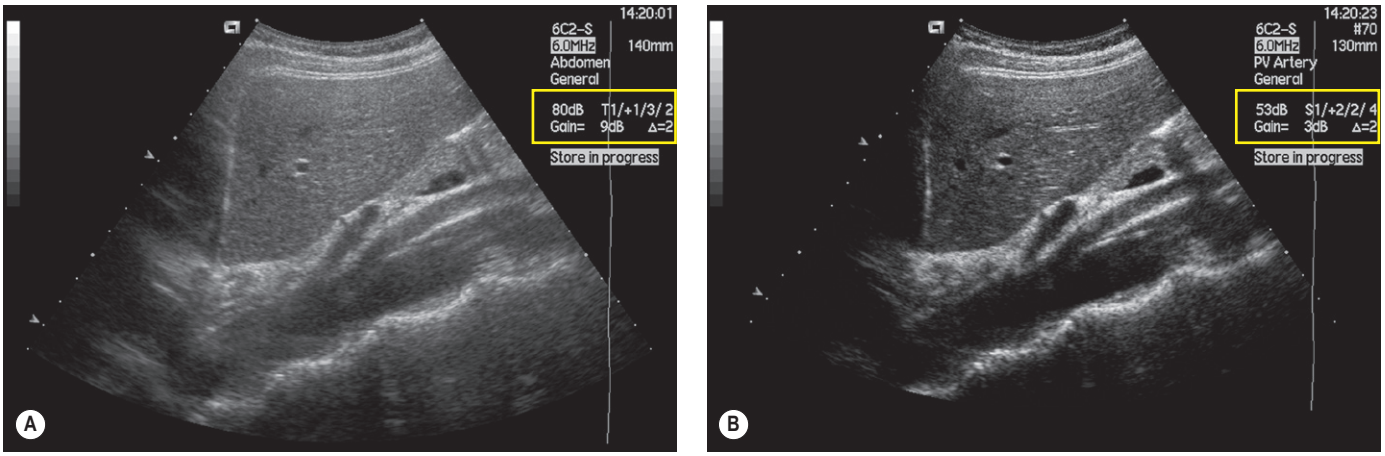


Figure 3.3 **Longitudinal image of an aorta** with an abdominal setting **(A)** and abdominal vascular setting **(B)**. Many parameters – indicated in the yellow box – are different, for example dynamic range, gain and persistence. The vascular setting has higher contrast as a result.

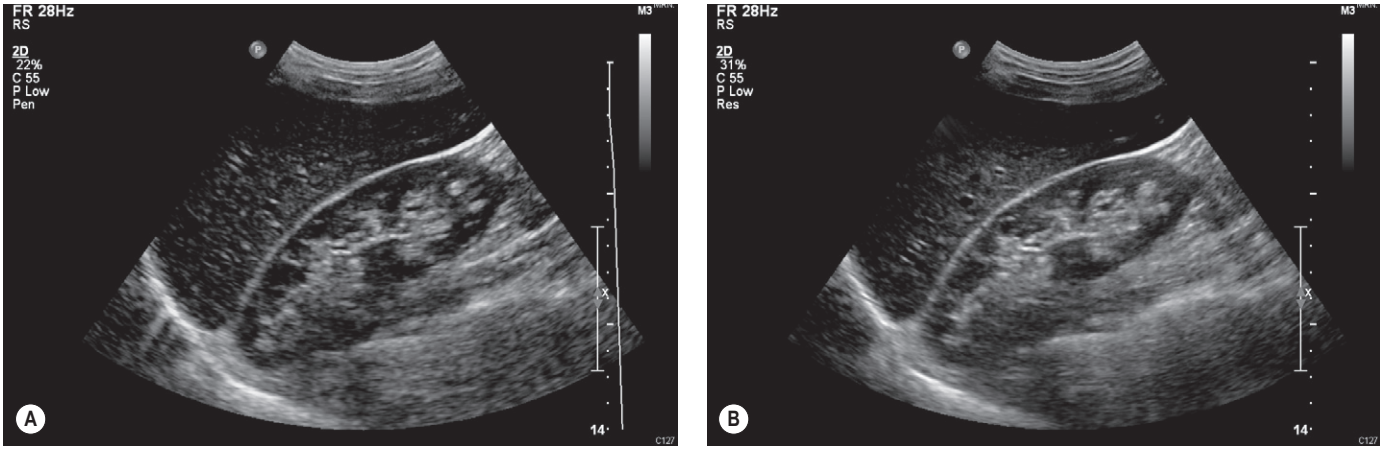


Figure 3.4 **Longitudinal image of a kidney** with a penetration setting **(A)** and resolution setting **(B)**. Subtle differences in spatial resolution, image smoothness and contrast at depths are evident. Several parameters are altered including the transmitted frequencies.

Output power

Output power is the main scanner parameter affecting heating of tissue and other non-heating effects on tissue including streaming of fluid. In some scanners, there is no separate power output control, but in many scanners, especially high end scanners, the operator has control of the output power level used. A representation of the level of power is given by the thermal index (TI) and mechanical index (MI) on the display (Chapter 4). For many applications, output levels are of limited safety concern since there is little possible risk from the low heating that occurs and it is more important to obtain the best image. However, for some applications, including ophthalmic imaging and fetal imaging in the first trimester, there are recommendations as to the maximum levels used or the time over which these levels are used. Lower outputs in B-mode result in decreased penetration and reduced contrast, especially in harmonic imaging (Fig. 3.5). Similarly, low power in colour flow imaging and power Doppler reduces the amount of colour signal and in pulsed wave spectral Doppler, a reduction in sonogram intensity. However, once a power setting for an application is chosen, it is not usually altered during the scan and so is not included in the individual settings listed below.

B-MODE PARAMETERS

Gain

The gain control alters the amplification of all received echoes in the image. By changing the gain, the brightness of the overall image is decreased or increased. Too low a gain will result in a dark image, too high a gain in a bright image. In either case, the range of grey-scales available is not used to best advantage. A common error for new users is to increase the overall gain to detect weak echoes. This also increases weak echoes from noise and boosts medium level echoes so that they appear brighter. The effect is to reduce contrast between strong echoes and lower amplitude echoes (Fig. 3.6). This can be a particular problem when ultrasound scanners are used in a brightly lit room when the tendency is to increase image brightness.

In some scanners, gain is automatically altered to compensate for changes in output power. The effect is to keep the grey levels at a similar level. Penetration and contrast at depth may be reduced if output power is lowered.

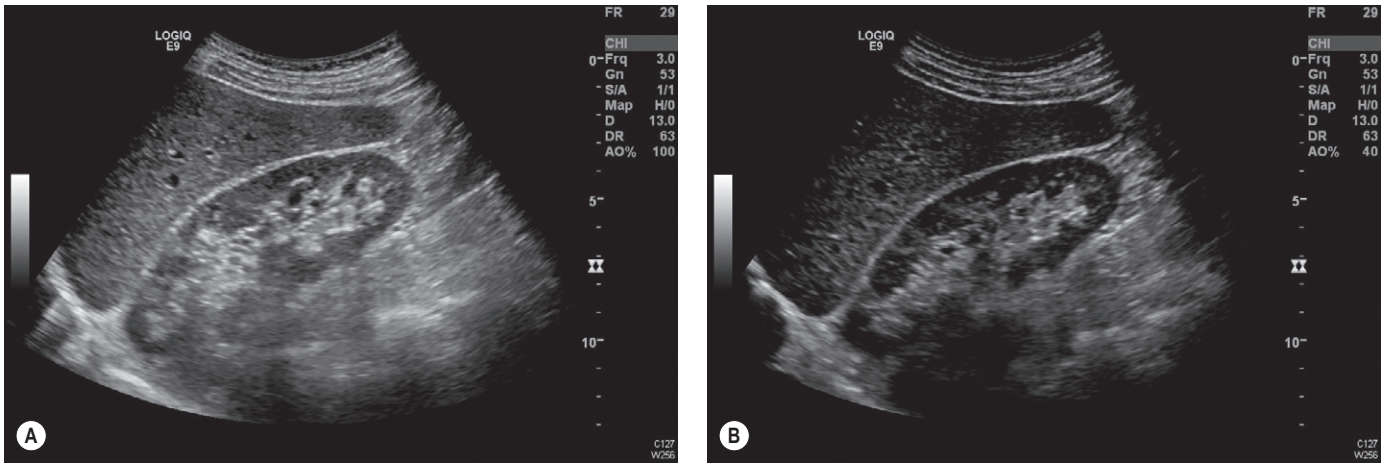


Figure 3.5 Harmonic imaging of a kidney at full **(A)** and reduced **(B)** power. Thermal index (TI) and mechanical index (MI) are lower at reduced power but in this example there is a general marked lowering of echo levels.

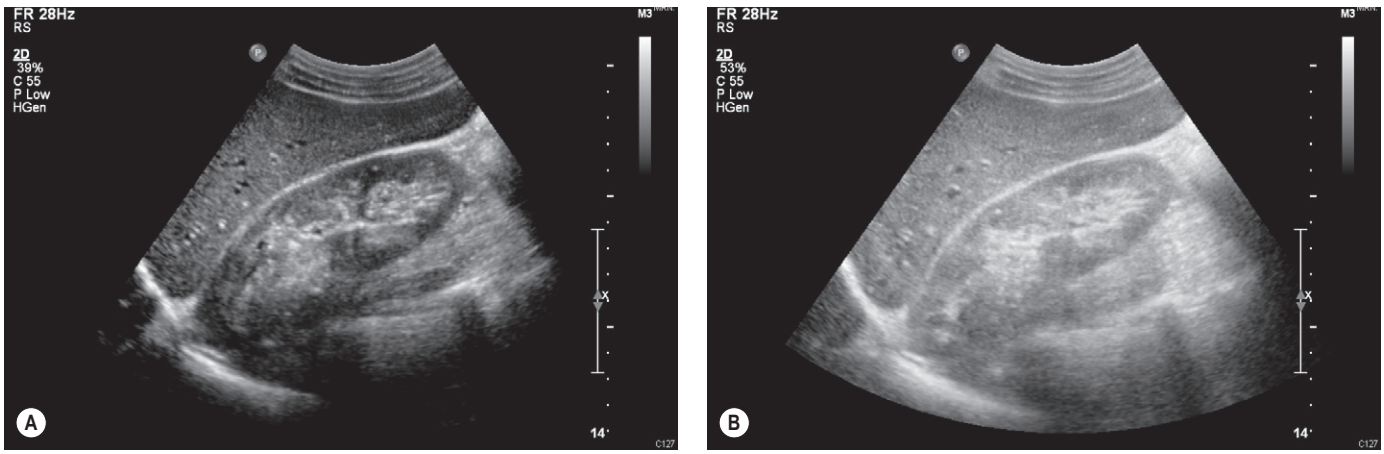


Figure 3.6 Effect of increased gain in an image of a kidney. With the normal setting **(A)**, a wide range of greyscales from black to white are used. With increased gain **(B)**, the image is brighter, more echo levels are depicted as white and contrast between adjacent structures is reduced.

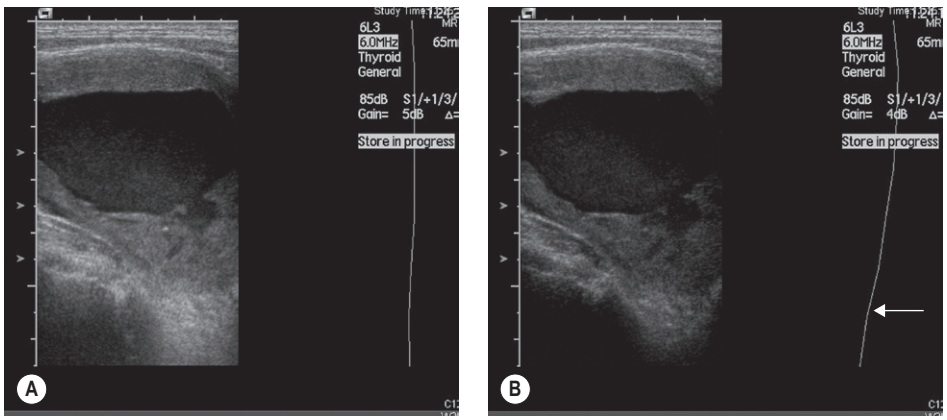


Figure 3.7 The image is of a large cyst in a thyroid gland. There is low attenuation through the fluid and deep structures appear brighter because of overcompensation for attenuation **(A)**. With the TGC/DGC set to reduce gain at depth (arrow), a more uniform image is displayed **(B)**.

Time gain control/depth gain control

The scanner automatically compensates for attenuation as the transmitted and received pulses travel through the tissue. Echoes from deeper tissue are amplified on the assumption of a uniform attenuation to provide uniform greyscales from similar tissue interfaces at different depths.

The operator can usually modify this by manual control of the amount of amplification at different depths using a set of sliders or rotational controls (Fig. 3.1). This control is usually described as DGC (depth gain compensation) or TGC (time gain compensation) since echoes from deeper tissue take longer to return. This is useful if there is abnormally low attenuation in the image, for example through fluid in ascites, the bladder, cysts or amniotic fluid, or if there is high attenuation. In Figure 3.7 low attenuation through a cyst in a thyroid causes tissue deep to the cyst to appear bright. By reducing gain at depth through the DGC/TGC, a more uniform image is obtained. The DGC/TGC settings can be displayed as a line which reflects the shape of the slider controls.

Dynamic range

The dynamic range control dictates the range of echoes displayed on the greyscale. Usually expressed in decibels, the value displayed shows the ratio between the largest echo amplitude that does not cause saturation to the smallest that can be distinguished from echoes displayed as black.

With a high dynamic range, a large range of echoes is displayed on the greyscale and there is less contrast between different echo levels. With a lower dynamic range there is more contrast between different echo levels but more low amplitude echoes are displayed as black, which may cause weak echoes to be missed and higher level echoes to be displayed as white. Dynamic range is set by the application key to suit the application and may not need to be changed during an investigation. For general imaging in the abdomen, thyroid and breast, high dynamic ranges tend to be used; for vascular and cardiac applications lower dynamic ranges are common (Fig. 3.8).

As an example of the advantages and disadvantages for vascular imaging, low dynamic range has the advantage that the vessel lumen appears dark and there is high contrast with surrounding tissue. Weak echoes from artefacts are suppressed. It has the disadvantage that weak echoes from echo-poor thrombus or plaque may be also be suppressed and that pathological findings may be missed. An example is shown in Figure 3.9 where plaque is difficult to image but becomes more evident when dynamic range or gain is increased.

Depth

It almost goes without saying that the depth and consequent field of view should be appropriate to the tissue under investigation. This is especially significant for ultrasound where increased image depth requires a longer time for echoes to be received from deeper tissue. As a consequence frame rate may be reduced and image quality may deteriorate as compromises in line density, focusing and signal processing are made on the larger image.

Using an inappropriately large depth is a common error for those new to ultrasound imaging. Large depths have the advantage that surrounding anatomy can be viewed and the effects of some artefacts, notably speckle, may be less apparent, but the image of the target is suboptimal (Fig. 3.10).

Frequency

The effect of frequency has been discussed in Chapter 2 and in the section on patient type/frequency above where frequency or a frequency range is selected to suit the application. It is worth repeating that changes in frequency affect penetration and resolution and that this control can be altered during scanning to improve the spatial and contrast resolution.

Focus

On most systems the focal zone or focus optimises the transmit beam focus to suit a particular depth or range of depths. By focusing the transmit beam, beam width and intensity are optimised with improvements in lateral resolution and contrast resolution at the chosen depth (Fig. 3.11). In many scanners multiple transmit focal zones can be selected. This extends the range over which the focus is optimised but may lead to a deterioration in frame rate if more transmit pulses are required to achieve this. For tissue with little movement this may be useful, but for tissue where there is movement this may lead to blurring of the image.

Some smaller scanners dispense with a focus control and others use processing techniques whereby transmit focus is less important to the overall image than in conventional scanners. Most scanners use sophisticated automatic focusing on reception to optimise lateral resolution throughout the image.

Zoom

The zoom function is used to magnify a region of the image on the screen. Depending on the way in which zoom is implemented, the image in this region may be improved as the scanner alters the scanning parameters in the selected area, for example increasing line density. In other implementations zoom is a simple magnification of a portion of the scanned image in which case the resolution of the image will be similar to the original.

Zoom is useful if measurements are to be made of small distances and areas since the precision may change to suit the change in scale of the image shown. Accurate location of the callipers may be enhanced (Fig. 3.12).

The zoom or res key/control is one for which manufacturers have used considerable imagination and originality. Both the area and size of the enlarged area can usually be adjusted prior to the zoom

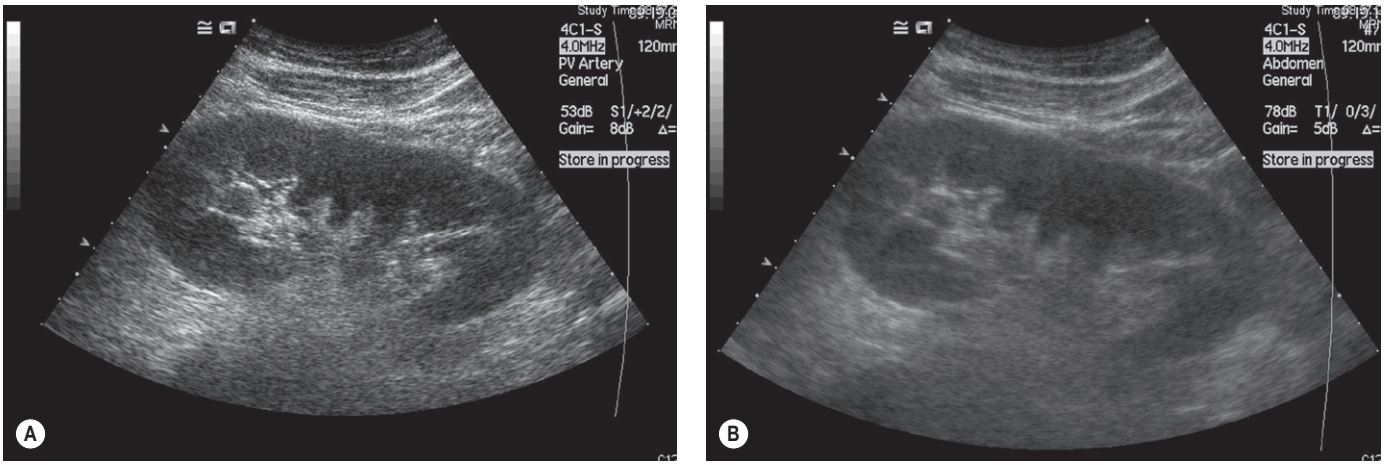


Figure 3.8 Image of a kidney transplant with low dynamic range (A) and high dynamic range (B). With a low dynamic range there is increased contrast between the medulla/cortex and surrounding tissue but speckle is more obvious and detail in the cortex/medulla may be lost.

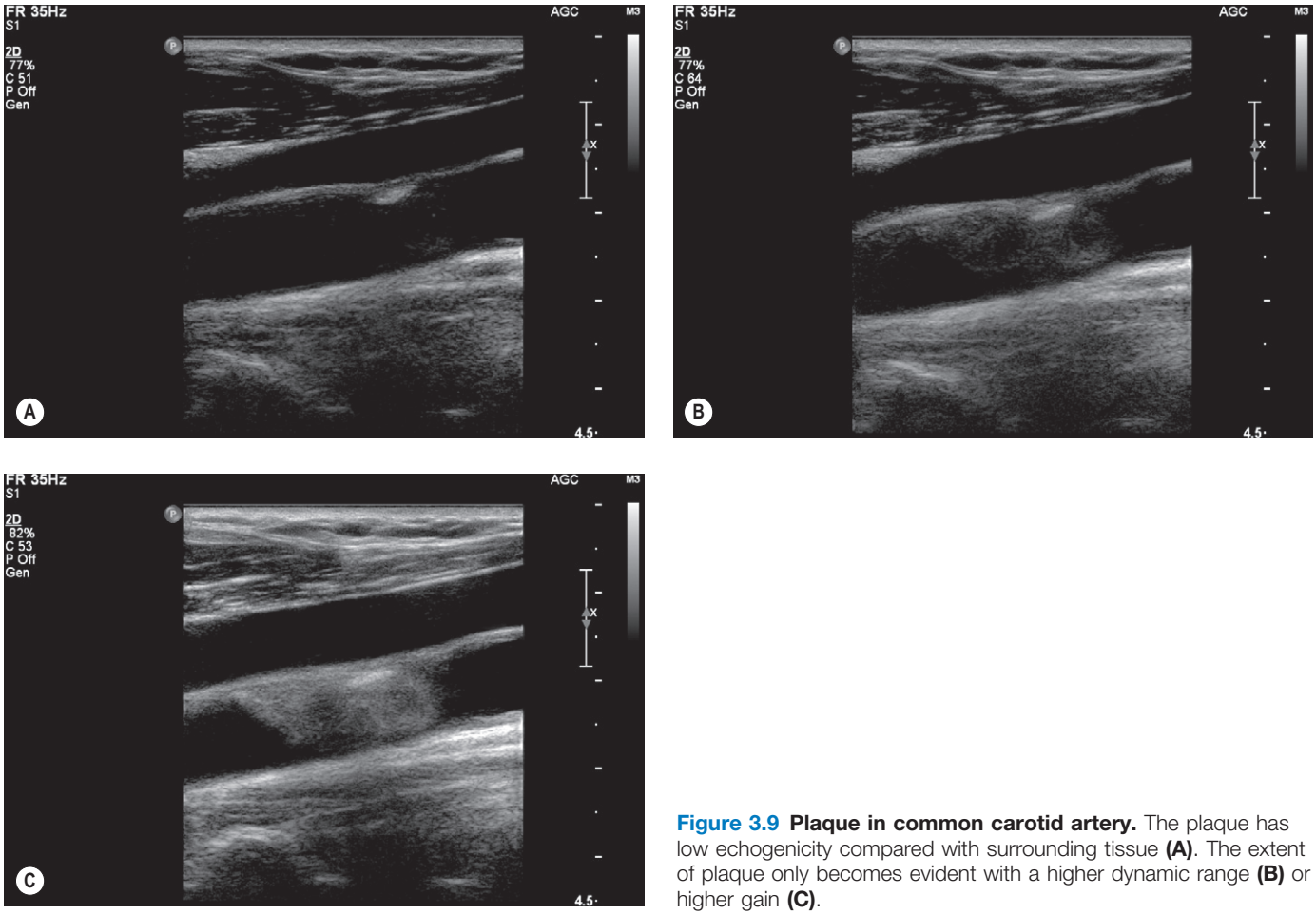


Figure 3.9 Plaque in common carotid artery. The plaque has low echogenicity compared with surrounding tissue **(A)**. The extent of plaque only becomes evident with a higher dynamic range **(B)** or higher gain **(C)**.

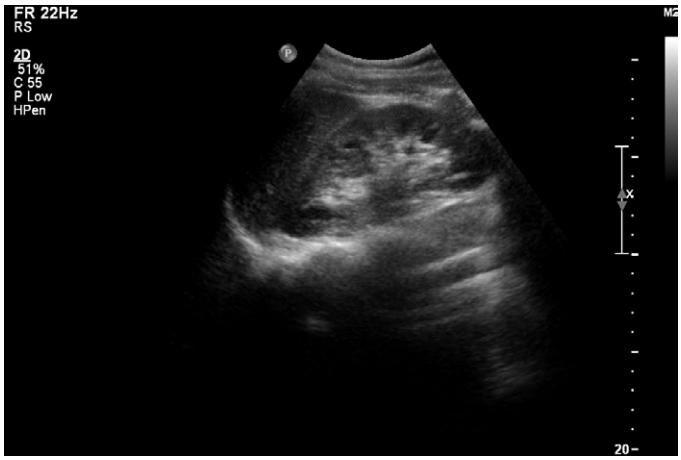


Figure 3.10 Inappropriate depth setting. The deep image is redundant, no information is displayed and the kidney is not displayed to best advantage. The frame rate also suffers because of the need for long pulse-echo times.

key being activated but there are a variety of means to do this and the user might like to try out the various permutations before they begin scanning clinically.

Harmonics

Native tissue harmonics are now commonplace in scanners from small portable devices to flagship models. The benefits of reduced artefact from the near field, a theoretical tighter beam in the transverse and elevation plane and an inherently reduced dynamic range all combine to produce images that often demonstrate improvements in resolution over fundamental images (Fig. 3.13).

The development of harmonics has continued since their introduction in the mid 1990s. Originally thought to be mainly applicable to low-frequency imaging for abdominal and cardiac applications, harmonic imaging now finds itself the default application for many manufacturer presets including high-frequency scanning for musculoskeletal applications. Since harmonics are generated by passage of the ultrasound pulse through tissue, the images that result appear to combine harmonics and non-harmonic components. Harmonics are also used in conjunction with spatial and frequency compounding (see below) and adaptive processing (see below) so that there may be several combinations from these three parameters alone.

Spatial and frequency compounding

Several versions and implementations of compounding are marketed. One method of spatial compounding uses transmit beam steering to produce echoes from several different transmit beam angles. This has the effect of providing strong echoes from interfaces over a wider range of angles than in conventional imaging. The images from different transmit beam directions have variations in speckle distribution; compounding images averages this and reduces its effect on the final image (Fig. 3.14). Spatial compounding requires more time to complete a compounded image.

Frequency compounding is offered in some scanners. The speckle pattern in images is frequency dependent; by combining images obtained from several transmitted frequencies, the effect of speckle is reduced.

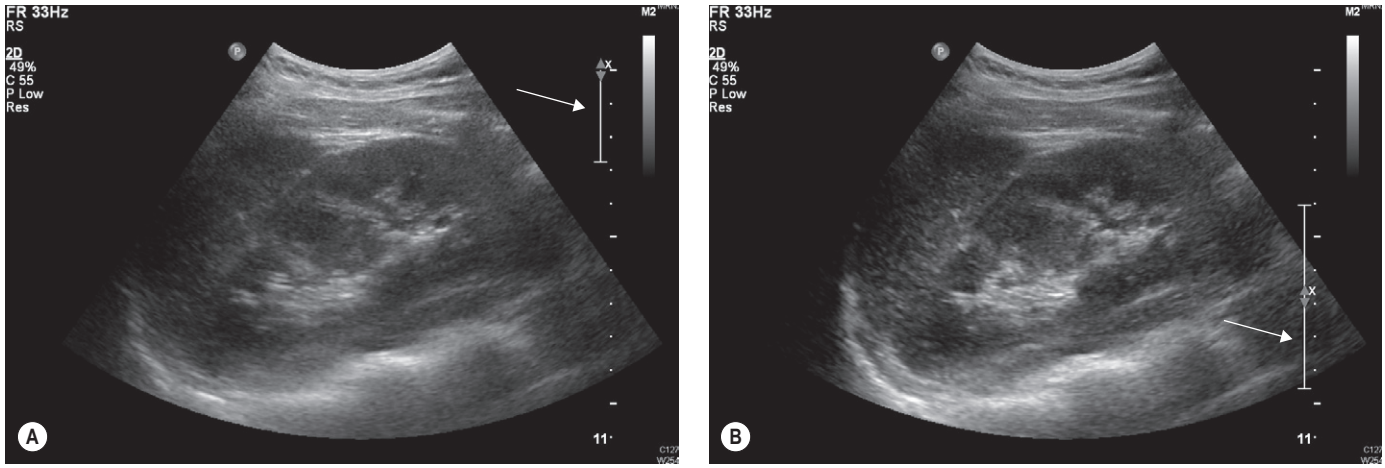


Figure 3.11 Influence of transmit focus. With the focus set for superficial tissue (**A**, arrow) the upper pole of the kidney is not displayed as clearly as it is when the focal depth is set to the appropriate depth **(B)**.

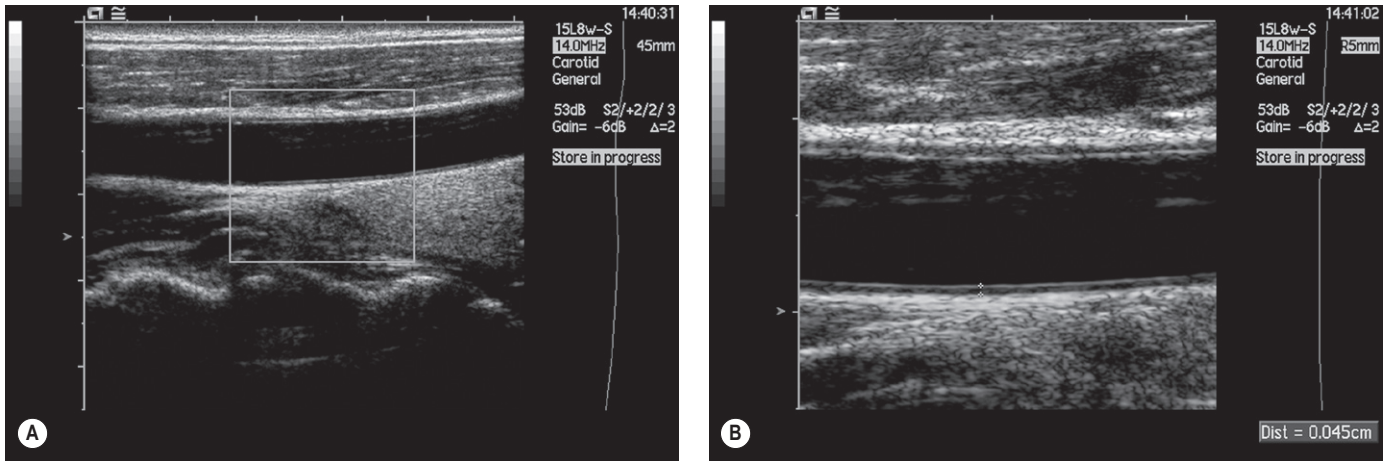


Figure 3.12 Zoom function. In a measurement of intima–media thickness, an area of the image is selected for investigation **(A)**. Scanning parameters are optimised for this area and the image allows more precise measurements **(B)**.

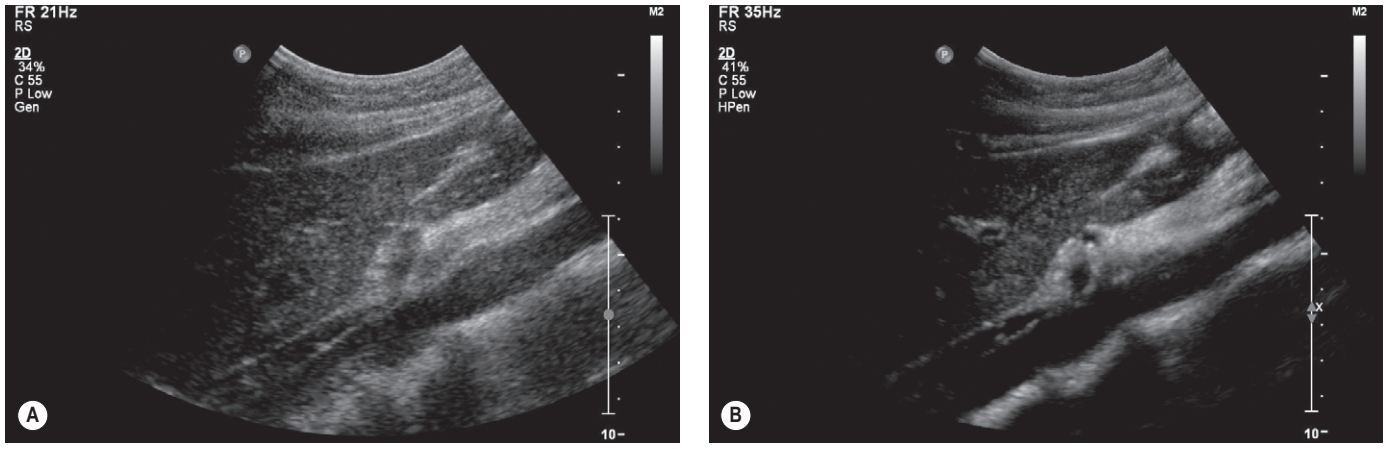


Figure 3.13 Longitudinal image of an aorta with fundamental (A) and harmonic (B) imaging. Reduced echo levels in the aorta increases contrast in the harmonic image.

When colour flow is deployed, compounding is often switched off automatically since the increased time required for colour flow imaging reduces the time available for the multiple direction transmit beams necessary for the compounded B-mode image.

Adaptive processing

The availability of increasingly fast computing power has allowed ever more complex processing of images. The term adaptive processing in ultrasound covers a wide range of techniques

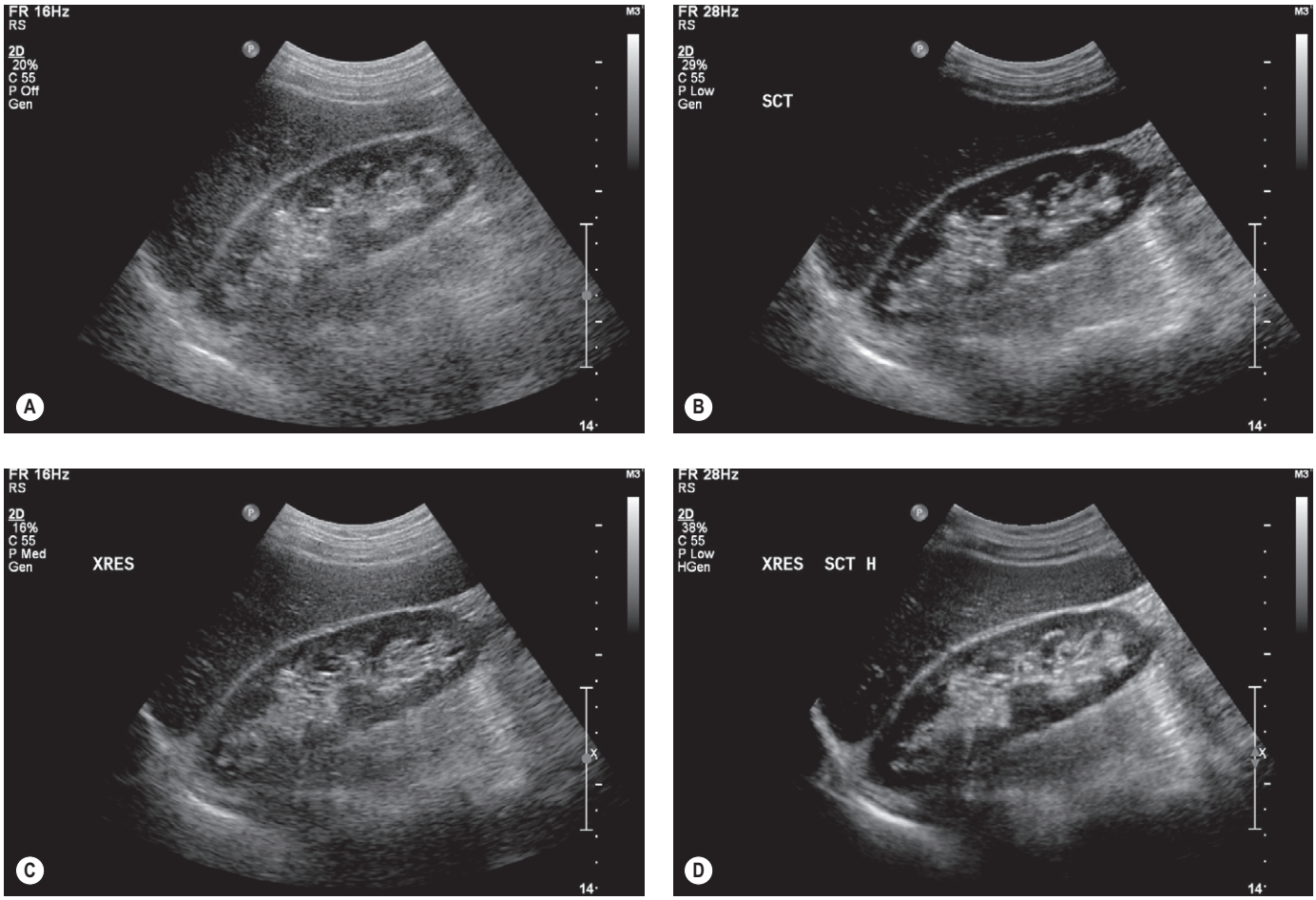


Figure 3.14 Longitudinal image of a kidney. The four images show a standard image **(A)**, use of spatial compounding **(B)**, use of adaptive processing **(C)** and a combination of spatial compounding, adaptive processing and harmonics **(D)**.

B-mode parameters

- **Power:** Alters the output power. This is usually set to a maximum but is reduced for specific applications, for example imaging through the eye. Some scanners do not have a separate output control.
- **Gain:** Alters the amplification of the overall received signal. Increasing gain boosts the signals and makes the overall image brighter.
- **Time gain control/depth gain control/swept gain:** Alters the gain at a specific depth range. Compensates for variation in attenuation.
- **Frequency/Patient type:** Trades resolution for penetration.
- **Focus:** Transmit focus improves lateral resolution and image quality at a specific depth. Multiple transmit focal zones may be used which may reduce frame rate.
- **Dynamic range:** Selects the range of echoes to display on the greyscale. A low dynamic range produces high contrast in the image.
- **Harmonics:** Harmonic images have a lower dynamic range, are less prone to artefacts, especially near-field artefacts. They tend to produce a higher contrast image. Axial and lateral resolution may be altered.
- **Compounding:** Many scanners now offer spatial or frequency compounding where images are reconstructed from several images obtained with different beam steering or transmit frequencies. Tissue structures are common to each individual image, artefacts – especially speckle – are random and the effect of speckle is reduced.
- **Depth:** Alters the depth of the image. Greater depths require more time, resulting in a decreased frame rate.
- **Zoom/Res:** Magnifies an area of the image. The zoom can magnify an area of the scanned image or can be used to image a reduced area.
- **Adaptive processing:** Many variations of these are marketed and aim to reduce the effect of speckle and accentuate true differences in the acoustic properties within tissue.
- **Temporal/spatial controls:** The image may be optimised for high temporal resolution, for example by using a lower line density and reducing lateral resolution. High spatial resolution may be chosen at the expense of frame rate.
- **Persistence/frame averaging:** Successive frames may be combined to produce a 'smoother image' with less speckle. Moving structures may appear blurred. For fast moving structures, low persistence may be used.
- **Edge enhancement:** Large changes in amplitude may be accentuated to display shaper edges. This may aid calliper placement but makes speckle appear more prominent.
- **Post-processing:** Allocates a greyscale to the range of echoes. Colour maps are possible but are not commonly used.
- **Measurements:** Linear and area measurements may be made from the frozen image.

designed to enhance the ultrasound signals from tissue features while reducing artefactual signals in the image, particularly those from speckle. Adaptive processing algorithms permit changes in response to local changes in time and space and may be based on the statistical analysis of signals. Manufacturers of commercial scanners use proprietary descriptive terms, for example Dynamic Tissue Contrast Enhancement – TCE (Siemens), Delta function (Acuson), XRES (Philips), SRI – Speckle Reduction Imaging (GE) for their own implementation of processing. Different levels of processing may be offered. Images may appear smoother and detail of 'tissue structure or texture' may appear freer of speckle (Fig. 3.14C). The difference in algorithms between systems may lead to differences in image appearance which may in turn be disconcerting to those comparing clinical images.

Spatial compounding may be used in combination adaptive processing and harmonic imaging (Fig. 3.14D). The utility of each or in combination is the subject of objective study and subjective preference.

COLOUR FLOW IMAGING

All the following factors, with the exception of colour scale invert, also apply to power Doppler (also called energy Doppler/amplitude Doppler).

Power

Colour flow imaging uses several pulses along each scan line to obtain the information necessary to give a colour map of velocity vectors. Blood is a weak scatterer and higher amplitude pulses with a longer pulse length may be employed to provide adequate signals for processing. As a consequence, outputs from colour flow imaging are often higher than for B-mode. Where there are issues of safety, particularly in first and second trimester scanning and imaging through the eye, particular consideration should be given to output limits and, in those scanners where output power is adjustable, operators should be aware of its effect on image quality and indicated output through the output display standards of MI and TI (Chapter 4).

Gain

By increasing gain, the colour flow image is more sensitive to moving echoes. However, increasing gain may lead to artefacts from moving tissue with colour 'bleeding' into surrounding tissue (Fig. 3.15). Inadequate gain leads to poor sensitivity to blood flow. The gain is usually set by the application key at a new patient investigation but in some systems the gain last set is retained. The gain value can be expressed in decibels (dB) or as a percentage. There is inconsistency between manufacturers as to the default settings; in our own department one scanner has a default setting of 50%, another is optimised at between 60% and 75% and yet another has a value of 25 with no units listed.

Scale/pulse repetition frequency (PRF)

Perhaps the most important control for CFI is the scale setting. Changing the scale alters the rate at which pulses are transmitted, the pulse repetition frequency (PRF). For slow flows, scale/PRF is set low to detect the small movement between pulses. This can lead to problems of aliasing for high velocities since PRF may not be sufficient for unambiguous measurement of the Doppler frequency. For high velocities, a high scale uses high PRFs to depict the resulting Doppler shifts unambiguously although very high velocities may lead to aliasing. The effect is shown in an image of arterial and venous flow (Fig. 3.16). Scale settings are shown on the colour bar in the image; the number at the extremity of the scale represents

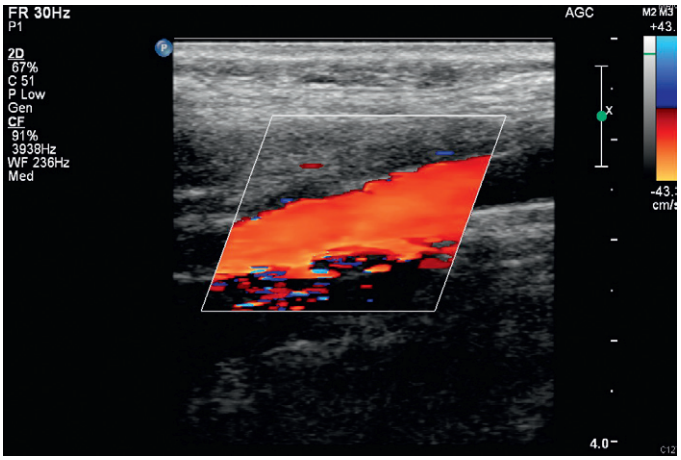


Figure 3.15 The colour flow gain is too high; there is overwriting (bleeding) of colour flow signals extending beyond the vessel under examination.

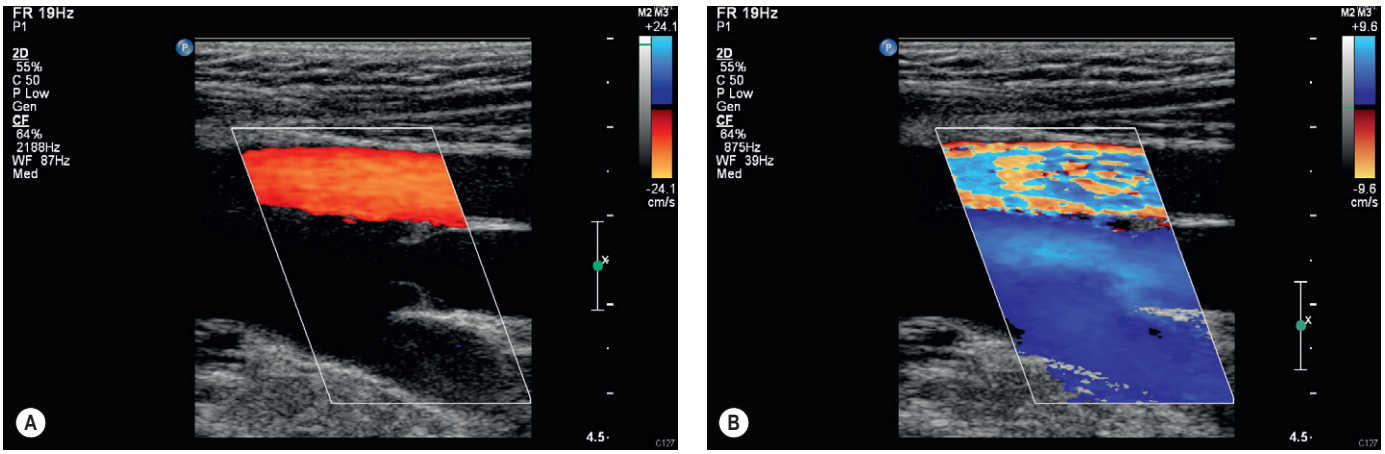


Figure 3.16 Images of a femoral artery and the confluence of the deep and superficial veins. With a high scale setting **(A)** indicated by a scale of ±24.1 cm/s, flow in the artery is displayed but venous velocities are too low for the high pulse repetition frequency. By lowering the scale to ±9.6 cm/s **(B)**, flow in the veins is now displayed. There is aliasing in the artery because the PRF is too low for the high arterial Doppler shifts.

the velocity vector corresponding to that colour. More importantly, since colour is seldom used to quantify velocities, the number represents a range of velocities shown so that a scale value of 0.03 m/s or 3 cm/s is appropriate for low velocities, a scale value of, for example 0.4 m/s or 40 cm/s is appropriate for arterial flow. Both m/s and cm/s values are used by manufacturers, who seem unable to agree a standard.

The maximum scale is dependent on the maximum PRF possible due to the depth of the image, and is also dependent on the transmitted frequency used. Users may find that the maximum scale changes automatically as depth is changed in an investigation.

The appropriate scale is selected when an application is chosen. For arterial flow, the colour image will vary throughout the cardiac cycle since systolic velocities are higher than diastolic. In investigations of arterial disease, aliasing is invaluable to identify areas of high velocities at sites of narrowing (Fig. 3.17).

Invert

The colour scale shows the direction of flow relative to the ultrasound beam. This varies depending on the course of the vessels and the beam direction, which in turn is dependent on the transducer type and, in linear arrays, beam steering. There is no established standard for allocating colour to direction. For curvilinear and phased arrays, users tend to choose red as flow towards the transducer (e.g. Fig. 3.20). For linear arrays, where the beam direction is changed to improve insonation of vessels lying parallel to the skin, users may choose to invert the colour scale to suit their preference for a particular application or anatomy (Fig. 3.18), for example showing flow in carotid arteries as red.

Frequency/patient type

As in B-mode, low frequencies give better penetration into tissue and can improve sensitivity to flow in deep tissue. Low frequencies also give higher aliasing limits at depth since the resulting Doppler frequencies are lower, allowing a lower maximum PRF. In some systems the frequency can be altered as a separate control. In others the frequency is one of several parameters altered to improve penetration (Fig. 3.19).

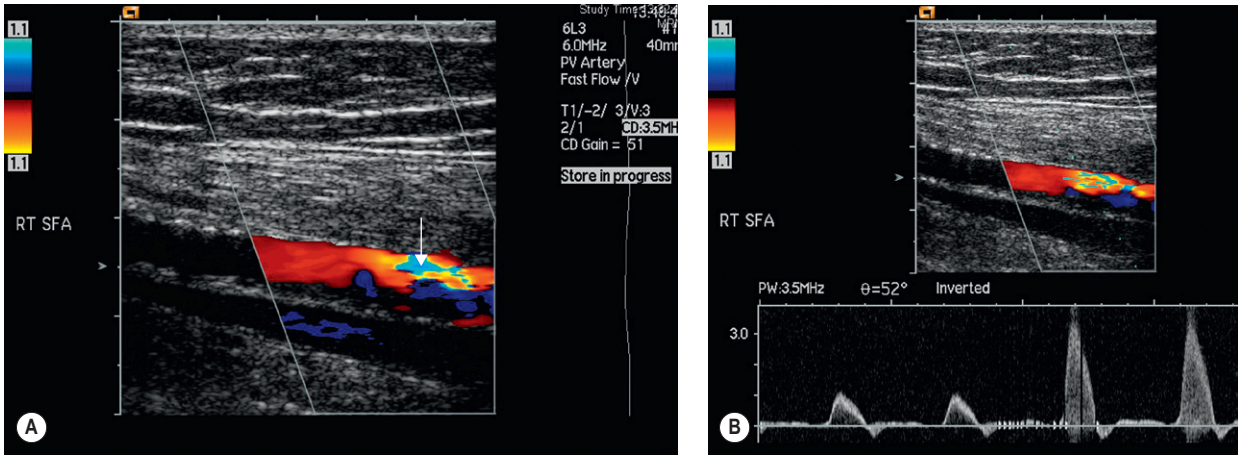


Figure 3.17 Using aliasing in arterial investigation. The colour flow image of a femoral artery shows a small length of aliasing (arrow) indicating raised velocities at this point **(A)**. Spectral Doppler images **(B)** show a change of velocity as the cursor is moved into the area of colour aliasing indicating severe arterial narrowing.

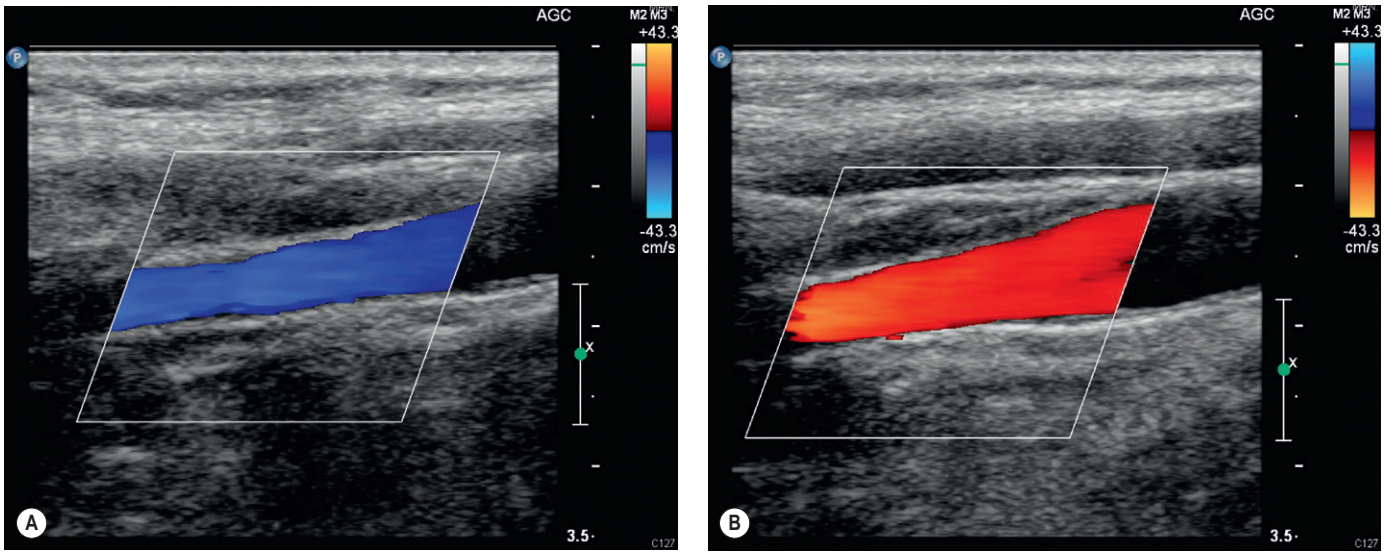


Figure 3.18 Colour flow invert. Flow in an internal carotid artery is from right to left in image **A**. The colour scale shows blue as Doppler shifts away from the beam direction. By inverting the scale the image can display this flow as red **(B)**. In some systems this can be done after the image is frozen.

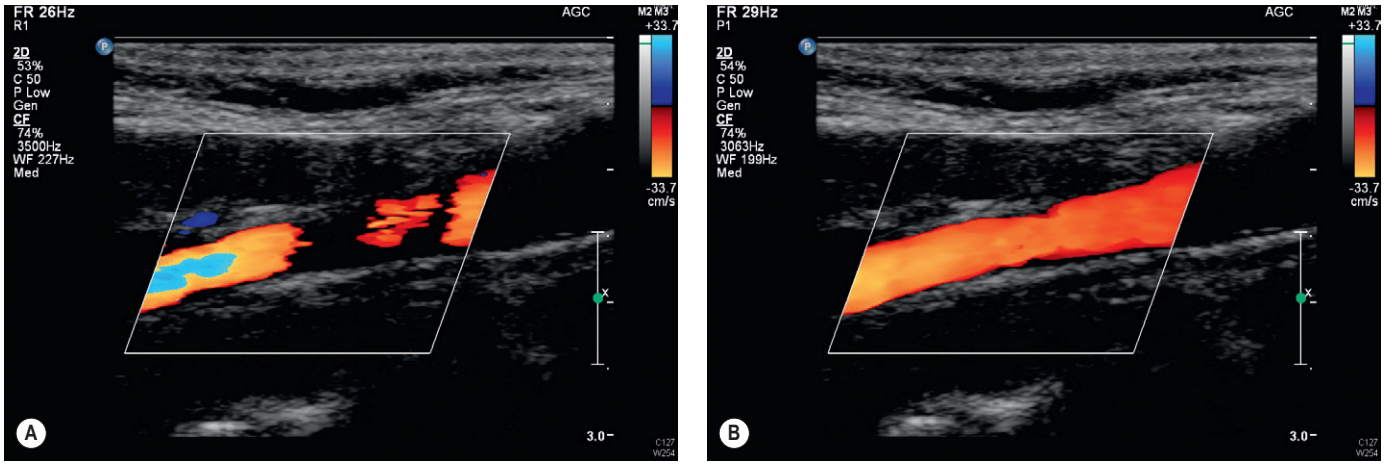


Figure 3.19 In image **A** there is an area within the artery where colour flow signals are poor. By changing the setting to improve penetration **(B)**, colour filling is improved. In other scanners this can be achieved by lowering transmit frequency.

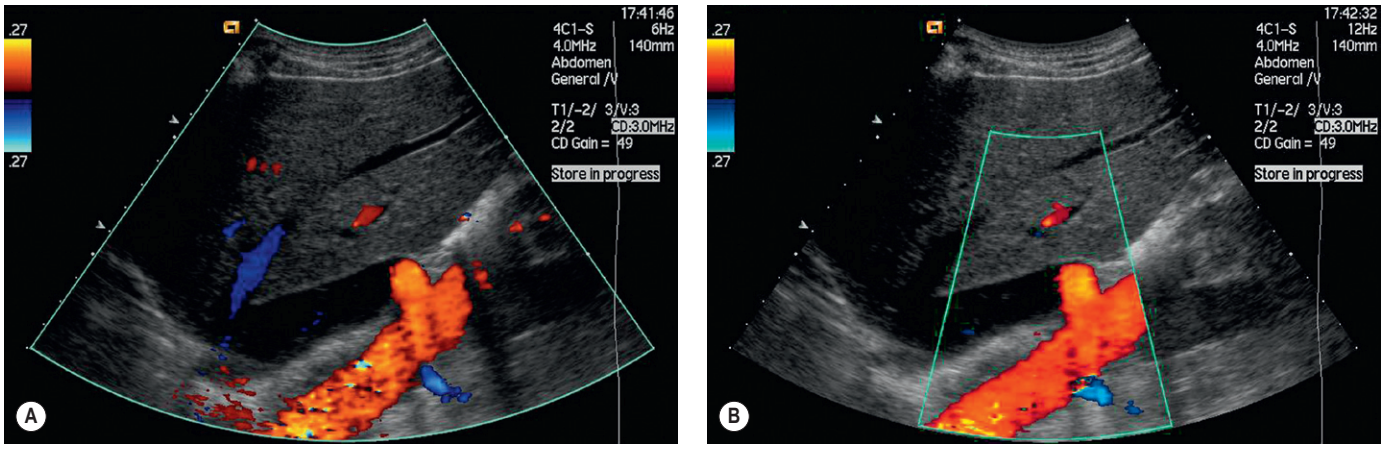


Figure 3.20 Colour box size. By setting the colour box area across the entire image **(A)** there are large demands on time to obtain flow information. Indicated frame rate is 6 fps and the quality of the colour image is limited, possibly because line density and ensemble length is restricted. By reducing the area of colour investigation **(B)**, the CF image of aorta and renal artery origins shows improved colour quality. Frame rate is doubled.

Colour flow imaging box/area size

In most colour flow scans, a particular area of the B-mode image is selected for CFI investigation. CFI requires several pulses for each line of the image to detect the movement between pulses. This is comparatively time-intensive and many compromises are made to ensure an acceptable frame rate in the combined CFI/B-mode image. Engineers adjust line density, the number of pulses used for each line of colour and the use of advanced B-mode techniques to ensure a satisfactory image appearance. Improvements in frame rate, colour sensitivity and spatial resolution can often be seen if a small area of colour flow is selected. Examples of improvements in spatial resolution and frame rate are shown in Figure 3.20.

Focus

In systems where focus can be altered, it is beneficial to move the transmit focal point to the depth of investigation. This improves colour sensitivity and spatial resolution (Fig. 3.21).

Beam steering in linear arrays

Linear arrays are used extensively in peripheral vascular investigations where arteries and veins often lie parallel or nearly parallel to the skin surface. This poses problems for Doppler ultrasound where beam/flow angles close to 90° lead to confusing images. In transverse imaging, adequate Doppler angles are obtained by tilting the transducer. In longitudinal section there is limited scope to do this. Beam steering produces an offset colour, and spectral Doppler, beam direction so that unambiguous colour flow images may be obtained by reducing the beam/flow angle (Fig. 3.22). The amount of steering available depends on the transducer and the frequencies used; lower frequencies tend to have a larger range of steering angles. It is not always advantageous to steer the colour 'box'; unsteered colour areas sometimes have better sensitivity (Fig. 3.23), especially in images of vertebral arteries where the vertebral processes can 'shield' the arteries from the steered beam.

Filter, space/time, post-processing, persistence, priority

There are several other controls that affect the performance and appearance of the colour flow imaging system. These are listed in the following box with their main effects. Again, not all features are applicable to all scanners and there may be differences in nomenclature.

These factors are not all described in detail here because they are set by the application key to be appropriate for the specific examination type and may not require modification during the examination. They can, however, make a considerable difference to the

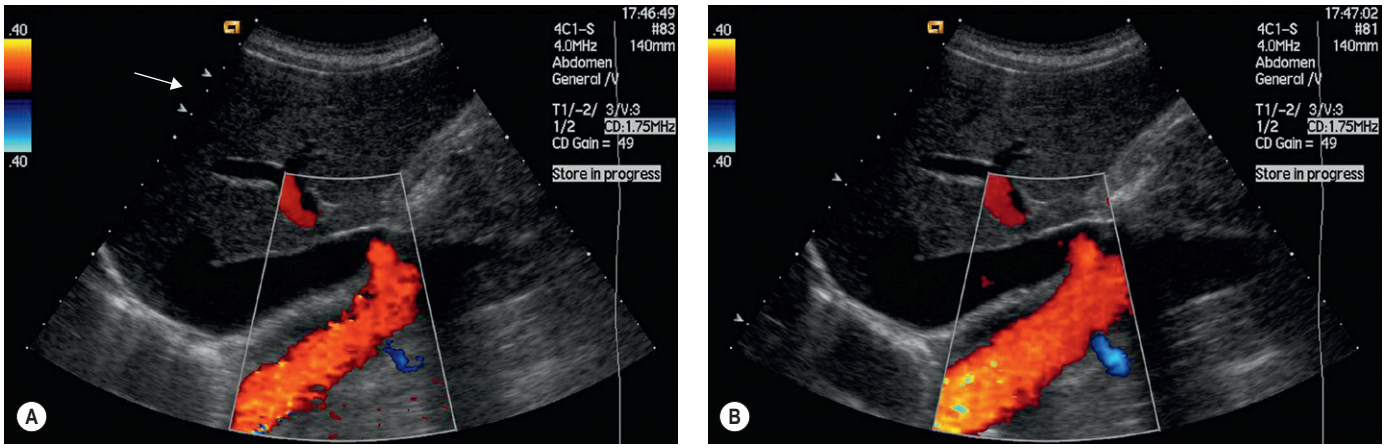


Figure 3.21 **Transmit focus. A:** With a focus set for superficial tissue (arrow), the colour flow image of the aorta and renal artery flow at depth is suboptimal. With the focus set for deeper tissue **(B)**, the image is improved.

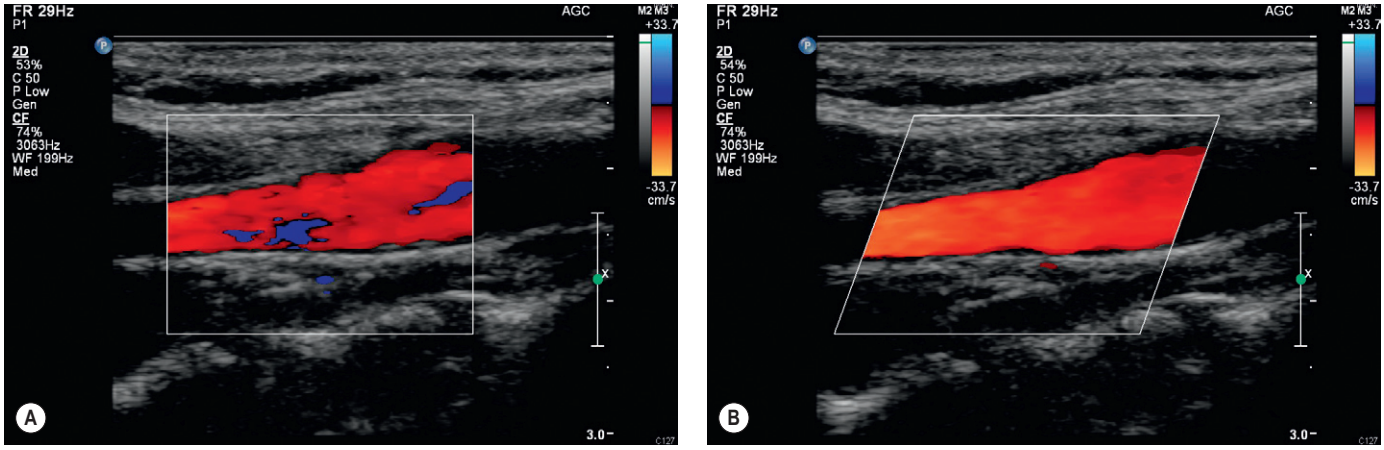


Figure 3.22 **Beam steering in linear arrays – I.** In this image of the carotid bulb **(A)**, flow is predominantly from right to left. The flow vectors are close to 90° from the beam direction and variations in the artery lead to flow away from (red) and towards (blue) the beam. By angling the colour box, the transmit beam is steered so that flow is consistently away from the beam with a uniformly red image of flow **(B)**.

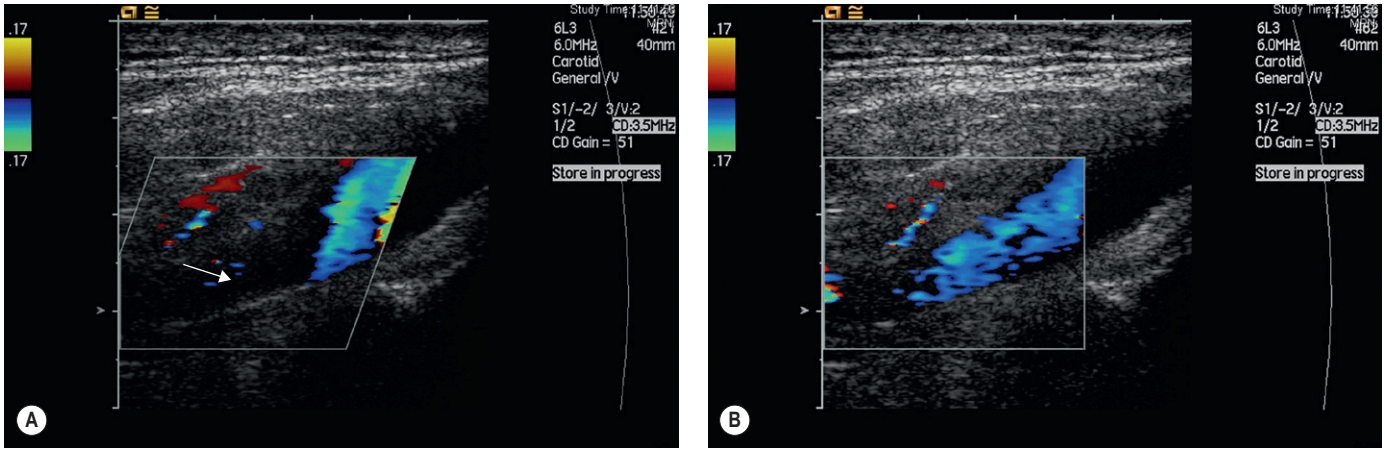


Figure 3.23 **Beam steering in linear arrays – II.** Beam steering doesn't always give the best colour image in linear arrays. In this image of an internal carotid artery **(A)**, there is a void in the colour image (arrowed), possibly due to the long path length and refraction lowering the intensity of the transmitted and scattered signal. In this case, slightly contrary to expectations, the colour flow image is improved with no steering **(B)**, despite poorer beam/flow angles.

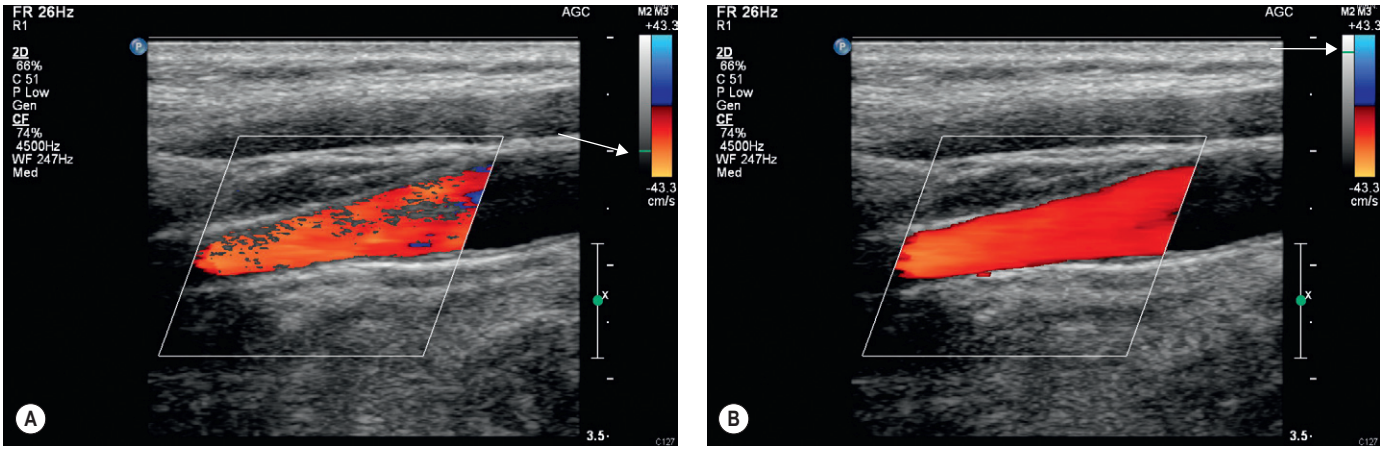


Figure 3.24 Mixing B-mode and colour images – priority. A colour flow image is a superimposition of colour flow information on a B-mode image. Colour may overwrite B-mode levels and vice versa. The extent to which one mode has priority over the other is variable as shown in these two images where colour overwriting of B-mode images is suppressed **(A)** and is maximum **(B)**. The level of priority is shown on the colour scale (arrow).

Colour flow imaging parameters (most also apply to power Doppler)

- **Power:** Alters the output power. Not all scanners have this control. High powers may be a concern where there is a risk of causing temperature increase, for example in colour flow imaging in the first trimester.
- **Gain:** Alters the sensitivity of colour flow to moving targets.
- **Scale/PRF:** Alters the rate at which pulses are transmitted. This affects sensitivity to low velocities and aliasing.
- **For linear arrays – beam steering:** Offset beam steering is used to provide a better and more consistent beam/flow angle in arteries and veins parallel to the skin surface.
- **Baseline:** Alters the range of each direction, compressing the flow scale in one direction and expanding it in the other. This is not commonly altered in clinical practice.
- **Invert:** Inverts the colour maps used to show the direction of flow relative to the ultrasound beam.
- **Focus:** As for B-mode, sensitivity and performance are optimised at the depth selected for transmit focus.
- **Colour flow area/box size:** A smaller colour flow area may allow a higher frame rate, better spatial resolution or sensitivity to flow.
- **Post processing:** Changes the colours of the colour flow map to suit the application.
- **Frequency/patient type:** Lower frequencies penetrate better into tissue but sensitivity to low velocities may be reduced and resolution may be reduced.
- **Filter:** Reduces signal from low-velocity moving targets. Especially useful where there is high-amplitude low-velocity movement, for example in the abdomen from transmit pulsations from the aorta.
- **B-mode/colour balance priority:** Selects how much the B-mode image shows through the colour map of movement. In some scanners this markedly affects the appearance of colour images.
- **Packet size/ensemble length:** A few scanners allow change of the number of pulses sent for each line of colour flow image. You have to be verging on the obsessive to alter this in everyday scanning but an increased ensemble length does improve the colour image at the expense of frame rate or line density.
- **Temporal/spatial controls:** The image may be optimised for high temporal resolution, for example by using a lower line density and reducing lateral resolution. Higher spatial resolution may be chosen at the expense of frame rate.
- **Persistence:** Colour frames may be combined to improve apparent sensitivity to flow and a more consistent image of colour flow. High persistence settings blur the dynamic appearance of rapidly changing flow and are typically used in low-velocity flow states, particularly venous flow.

appearance, and an experienced operator may wish to change individual parameters to optimise a particular scan. An example of changes in the priority setting is shown in Figure 3.24 where the emphasis of the colour and B-mode images relative to each other is altered.

One control and concept that does require further explanation is the space/time balance of a colour image. Because a colour flow image requires several pulses for each line to obtain measurement of movement, it imposes limits on the frame rate. Several compromises are made to ensure acceptable images, such as removing multi-beam B-mode options, reducing frame rate or reducing the spatial resolution of the colour image, for example by using a lower line density.

Many scanners offer user-modification of the colour image in terms of improved temporal resolution with a reduction in spatial resolution or improved spatial detail with a lower frame rate (Fig. 3.25). The controls to do this are variously described and implementations include pre-processing, space/time controls or colour line density.

Flow settings – combination controls

Many scanners offer settings for different flow states, for example slow flow or fast/high flows which optimise several parameters to suit the flow conditions. For fast flows, high PRFs, low persistence, low ensemble lengths and high filters may be employed. For slow flows, parameters will be selected to best show colour flow images in these vessels. The controls and the way in which they are implemented are specific to manufacturers and individual scanners; an example of the effect of these controls is shown in Figure 3.26.

PULSED WAVE SPECTRAL DOPPLER (PW)

There are several controls that affect the appearance of the spectral Doppler sonogram. Just as importantly, many of these controls also affect the accuracy of measurements made from the sonogram. Doppler measurements of velocity and, for appropriate

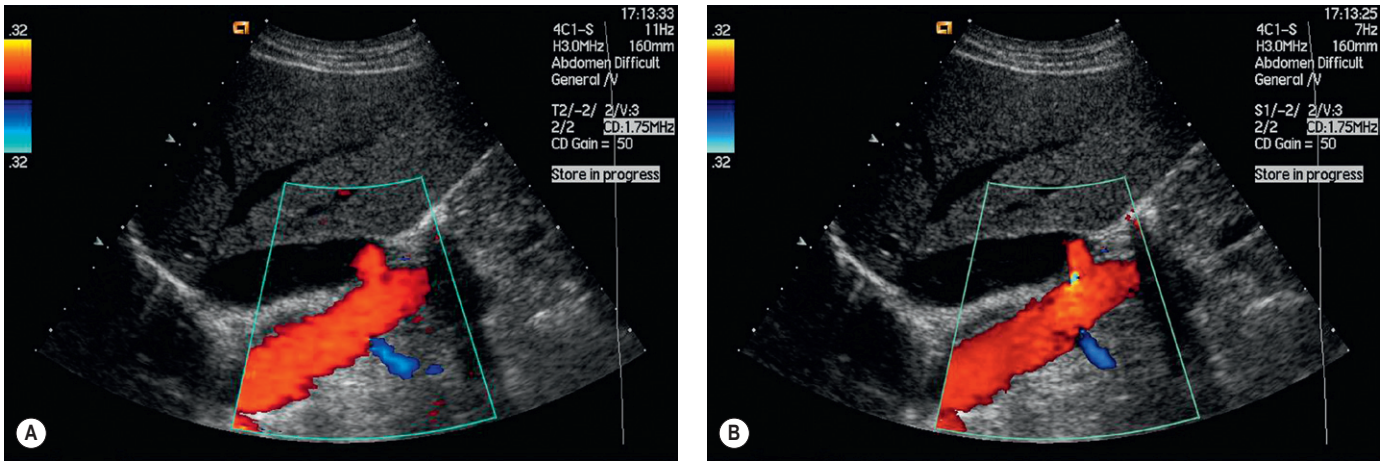


Figure 3.25 **Space/time priority.** With temporal priority **(A)**, frame rate (11 Hz) is improved but the spatial resolution of the image is degraded. With a higher spatial setting **(B)**, frame rate is reduced but the colour image appears to have improved spatial resolution.

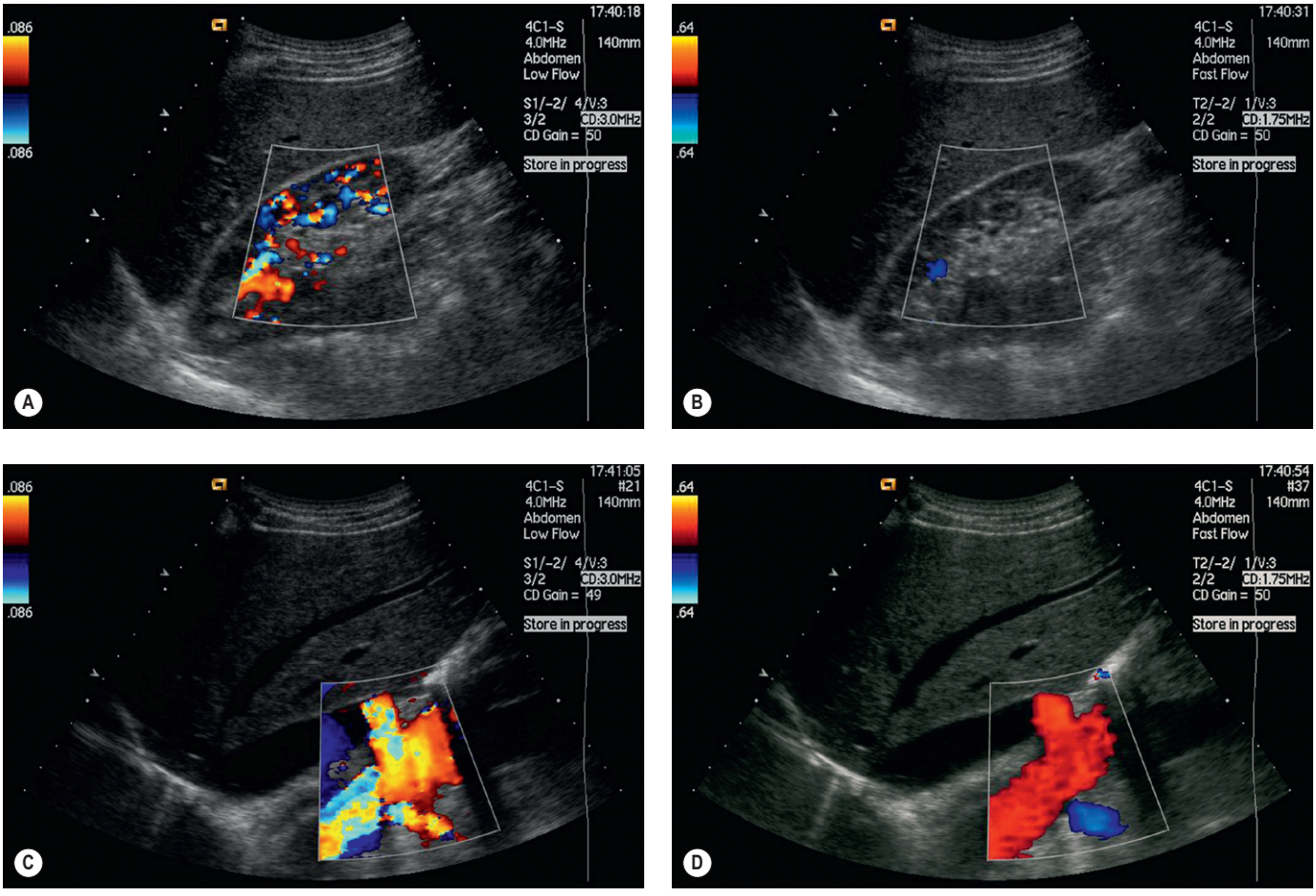


Figure 3.26 **Low flow/fast flow settings.** In this scanner, several parameters are altered to suit a particular flow state. A low flow setting is good to display flow within a kidney **(A)** but leads to aliasing at the renal artery bifurcation **(C)**. A fast flow settings barely displays any flow in the kidney **(B)** but is appropriate for the renal artery bifurcation **(D)**. Factors changed include transmit frequency and scale/PRF.

investigations, volume flow are highly susceptible to errors in scanning technique and manipulation of controls. Velocity measurement errors of over 10% are commonplace in clinical practice. Volume flow errors can exceed 20% even in ideal circumstances. The fact that these values are frequently displayed to four significant figures is a testament to the optimism and sense of humour of the engineers. However, the seemingly high degree of precision can lead the unwary to assume that this reflects the accuracy of the measurements made.

Basic rules – beam/flow angle and angle correction

There are two basic rules for spectral Doppler investigation.

1. Obtain a good sonogram by aligning the Doppler beam so that there is a good (typically <60–70° depending on the investigation) beam/flow angle to obtain adequate Doppler shifts. This is done by moving the transducer so that there is

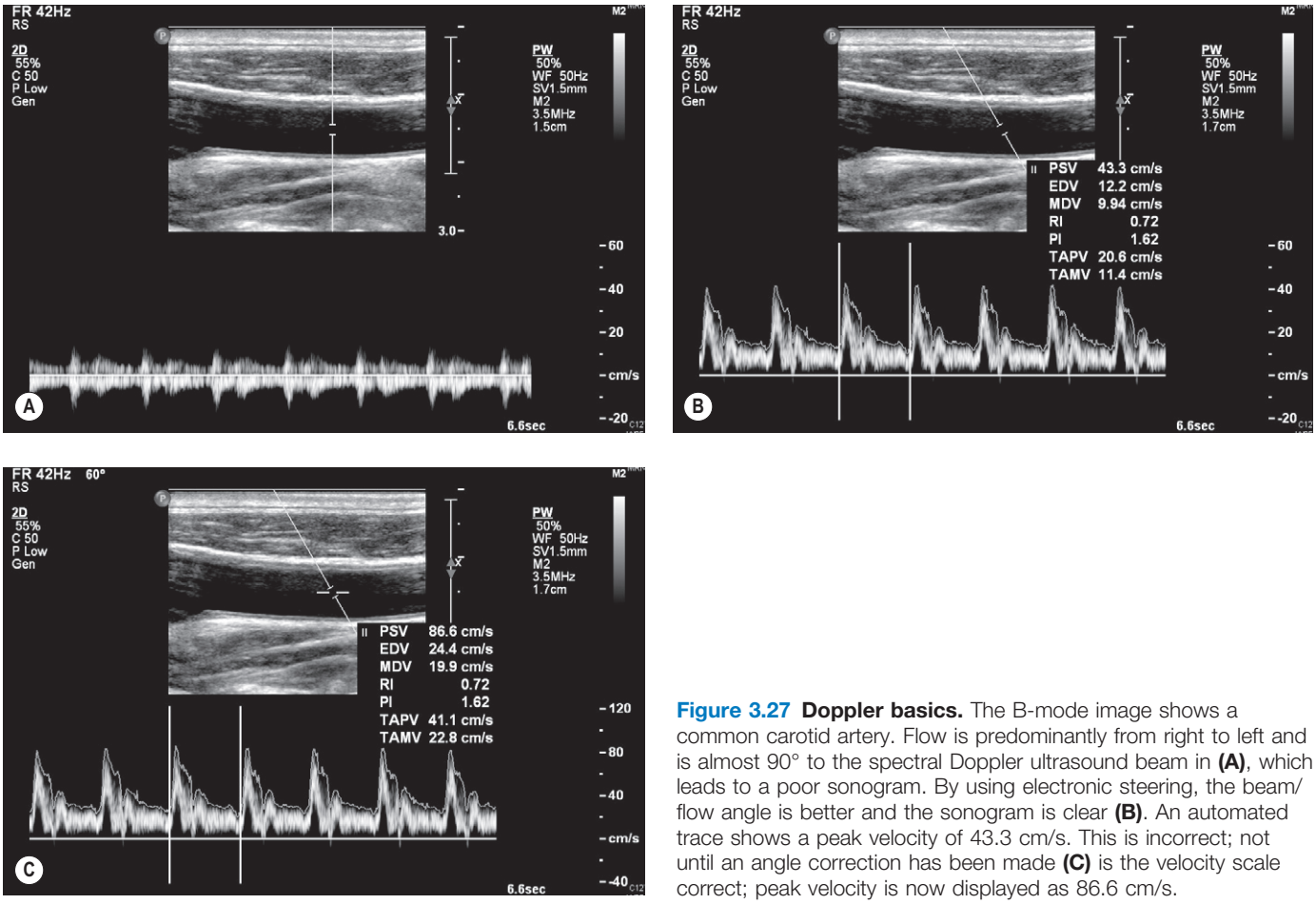


Figure 3.27 Doppler basics. The B-mode image shows a common carotid artery. Flow is predominantly from right to left and is almost 90° to the spectral Doppler ultrasound beam in **(A)**, which leads to a poor sonogram. By using electronic steering, the beam/flow angle is better and the sonogram is clear **(B)**. An automated trace shows a peak velocity of 43.3 cm/s. This is incorrect; not until an angle correction has been made **(C)** is the velocity scale correct; peak velocity is now displayed as 86.6 cm/s.

an adequate beam/flow angle. For linear arrays, beam steering may be used. Alter the scale so that the sonogram is clearly displayed.

2. If measurements of velocity are required, alter the Doppler cursor angle correction so that it is aligned with the direction of flow. Without this correction, the velocity scale and measurements made from it are incorrect (unless the beam and flow direction are very closely aligned).

These principles are shown in Figure 3.27 for measurements of velocity in a carotid artery.

If velocities are not required then rule 2 is not appropriate and it may be sufficient to obtain a good sonogram and make qualitative assessment of flow or measurements of non-dimensional indices such as resistance/resistive index and pulsatility index for which angle correction is not required.

Power

Intensities for spectral Doppler are generally higher than for B-mode. For applications where there is risk from higher output levels (see section above on application set-ups), the operator should ensure that recommendations are followed and that the output display guidelines are observed, monitored and used to ensure good practice.

Gain

Increasing the gain increases sensitivity to weak scatterers by amplifying the received signal. In general, venous flow provides stronger backscattered signals than do arteries and this can lead to suboptimal sonogram images if the gain is set incorrectly for the vessel under investigation. If gain is too high then cross-talk can appear in the Doppler sonogram with apparent flow in the opposite direction (Fig. 3.28). In general, low gains reduce the brightness of the sonogram display and some frequencies may not be displayed. Conversely, high gains amplify weaker Doppler frequencies in the sonogram and can lead to apparently higher velocities being displayed and measured (Fig. 3.29). High gains may also increase the noise, confusing automatic measurements.

Invert – baseline

The direction of flow is indicated by whether the sonogram appears above or below the baseline. The sonogram scale can be inverted when necessary so that the flow display appears above the baseline. This tends to make flow waveforms easier to understand. There is an indication on the sonogram as to whether this is inverted or not (Fig. 3.30). If flow is predominantly in one direction then the position of the baseline in the sonogram can be set so that the sonogram can be shown to best advantage (Fig. 3.30B, C).

Scale and HPRF

The scale alters the pulse repetition frequency for spectral Doppler and has a similar function to the scale control for colour flow imaging (see section above on scale/pulse repetition frequency). Typically, low scales are used for venous flow and for flow in small vessels. Flow in large arteries is faster and requires a high scale. If too low a scale is used, aliasing may occur (Fig. 3.31);

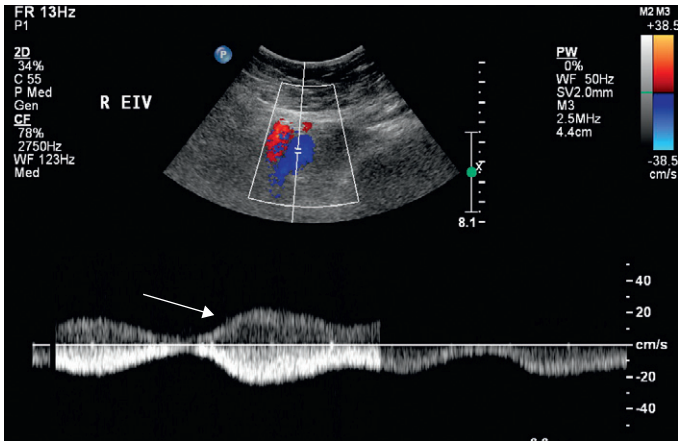


Figure 3.28 Gain in the spectral Doppler. The sonogram shows flow in a vein. If gain is too high as in the left of the sonogram image, cross-talk may be displayed (arrow). By reducing gain a better quality sonogram is seen (right of image).

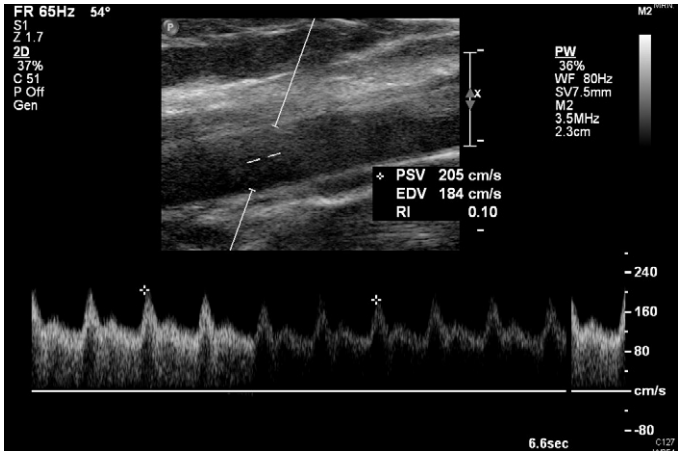
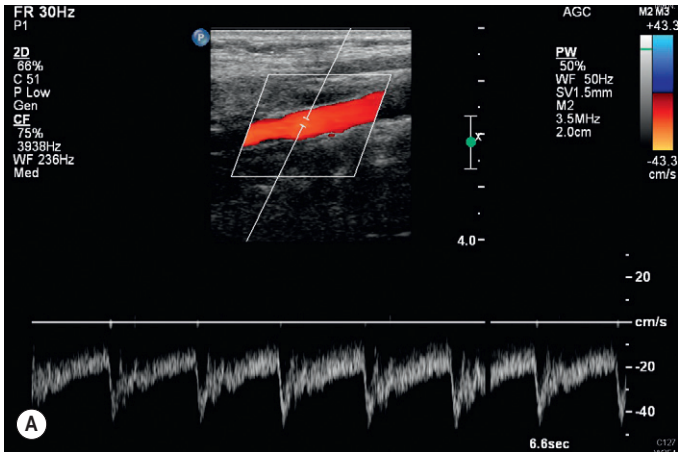
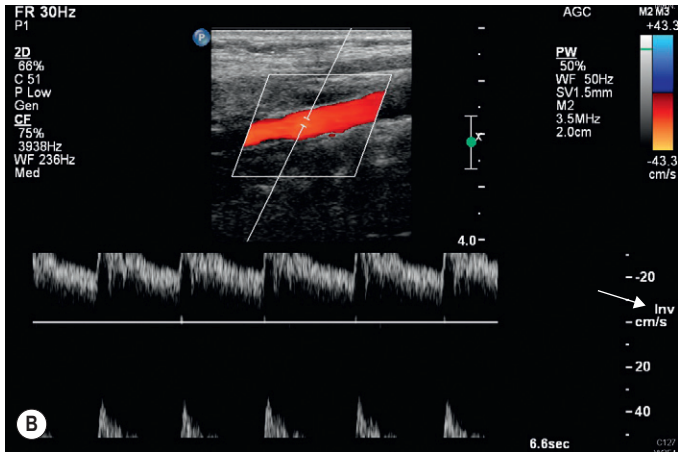


Figure 3.29 Effect of gain on measurements made from a sonogram. The spectral Doppler trace from flow in a dialysis fistula shows the effect of change in peak velocity as gain is reduced in the right of the sonogram. Peak velocity falls from 205 to 184 cm/s.





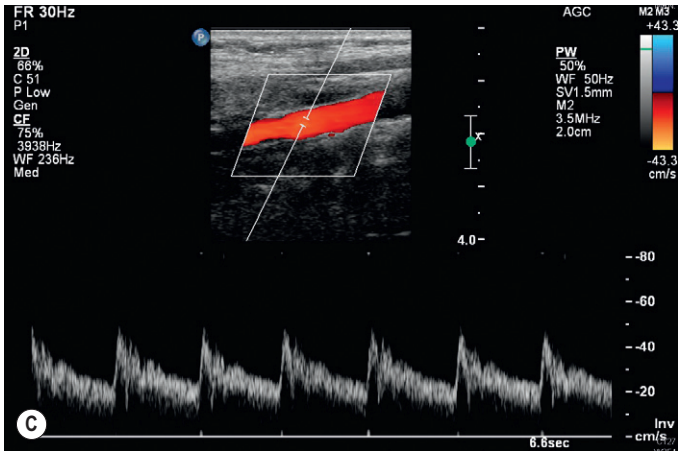


Figure 3.30 Invert – baseline. A: Flow is away from the beam and the sonogram appears under the baseline. By inverting the sonogram display, the sonogram now appears above the baseline although peak velocities show evidence of aliasing **(B)**. There is on-screen indication of Doppler invert (arrow). By lowering the baseline **(C)** the entire sonogram can be displayed clearly.

if too high a scale is used, the sonogram shape may not be clear (Fig. 3.32).

A major limitation of pulsed wave Doppler ultrasound is that the scale is limited by the depth of investigation. Conventionally, the scale is limited by the need for pulses from the sample volume to return before the next pulse is transmitted. This leads to difficulties for high velocities in deep tissue, for example in renal artery stenosis where the high Doppler frequencies that result are often too high to be measured unambiguously. In some systems the limits can be extended by choosing a low transmit frequency (typically 2 MHz) which in turn leads to lower Doppler frequencies, thereby allowing lower PRFs for the same velocity.

In order to circumvent this, many ultrasound systems offer an option whereby the PRF limit can be overridden and a second pulse sent out before the first has returned. This setting, usually referred to as HPRF – high pulse repetition frequency, leads to an additional

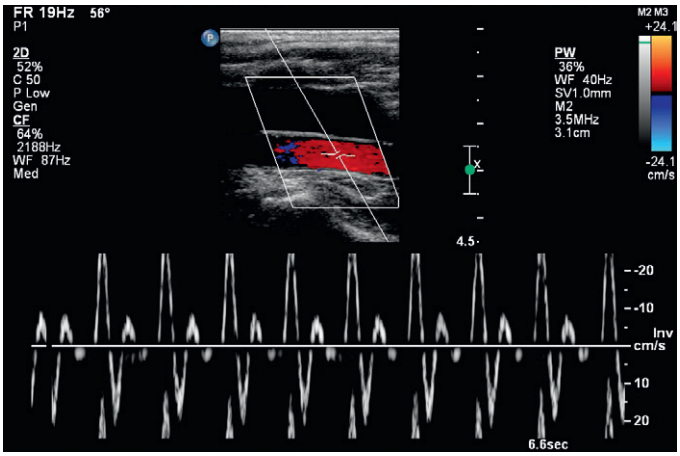


Figure 3.31 **With a scale set too low,** there is aliasing in the sonogram. The peaks of this femoral artery waveform appear as negative velocities. The wraparound cannot be overcome by moving the baseline in this case – the scale must be increased.

superficial sample volume which adds to noise in the sonogram but allows an extended velocity range (Fig. 3.33) from the deeper sample volume.

Sample volume/gate/range gate

The size of the sample volume can be altered to interrogate various distances along the beam from typically 1 mm to >8 mm. If flow information from a very specific position in the vessel is required or the vessel itself is small, then a small sample volume may be required. A larger sample volume is used when measuring volume flow in arteries or veins, since a measurement of mean velocity must encompass the full range of velocities in the vessel as best it can. Large sample volumes may also be useful in improving sensitivity to flow, although there is a risk that the sonogram also shows flow information from adjacent vessels. The influence of change in sample volume in large vessels is illustrated in Figure 3.34.

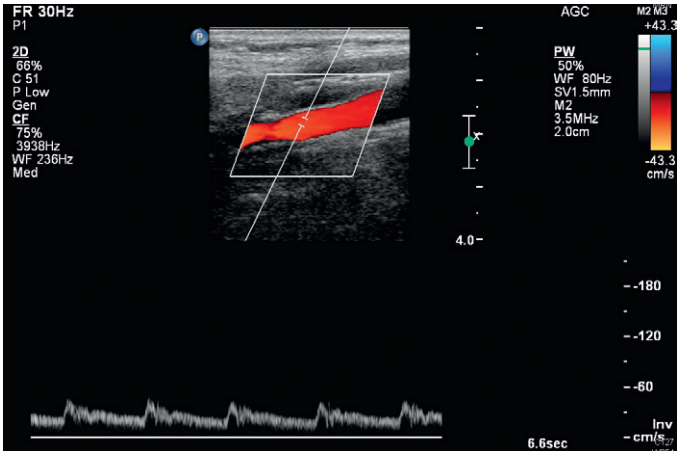


Figure 3.32 **With too high a scale,** the shape of the flow waveform is unclear and measurements are difficult.

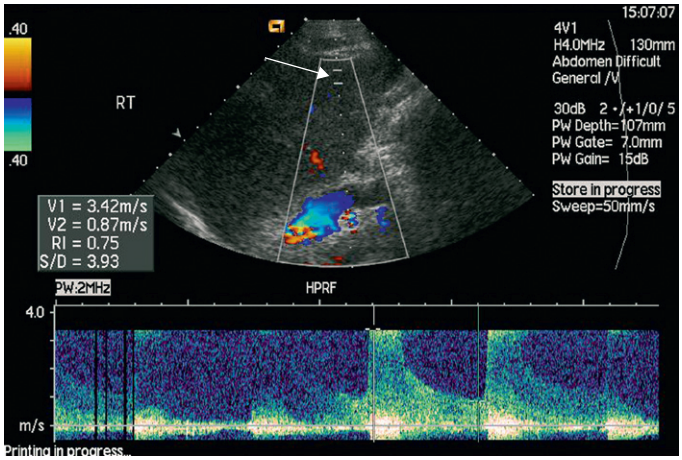


Figure 3.33 **Investigation of high velocities in deep arteries may require high pulse repetition frequencies (HPRF)** whereby a second pulse is transmitted before the first returns. An additional superficial sample volume appears in the image (arrow) and the sonogram has more background noise.

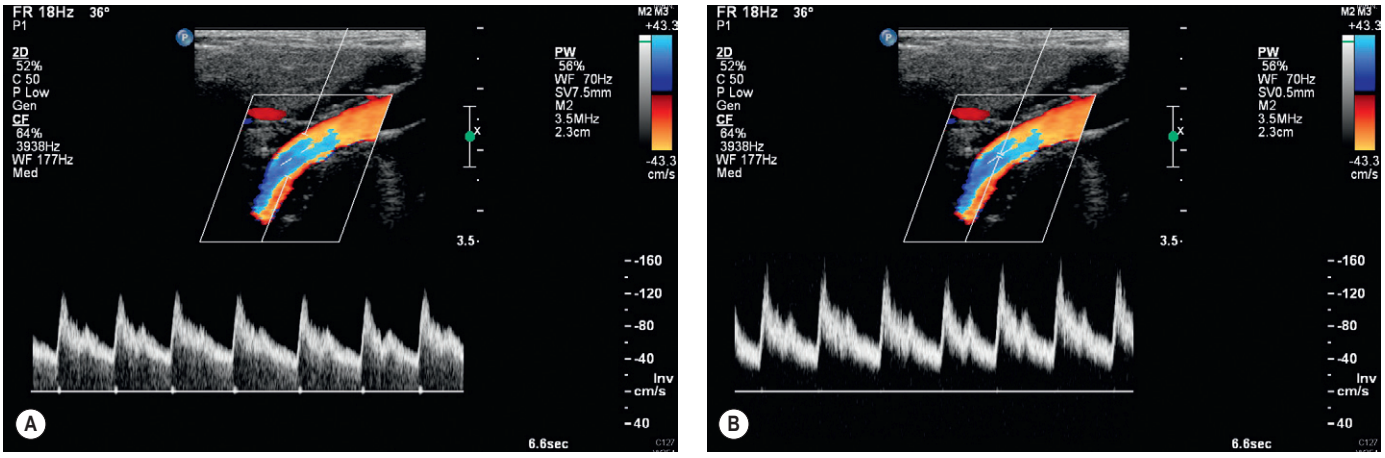


Figure 3.34 **Sample volume/gate size.** With a larger sample volume **(A)**, the sonogram shows low velocities from flow near the vessel wall. With a sample volume limited to the centre of vessel **(B)**, the sonogram does not show the low velocities near the wall.

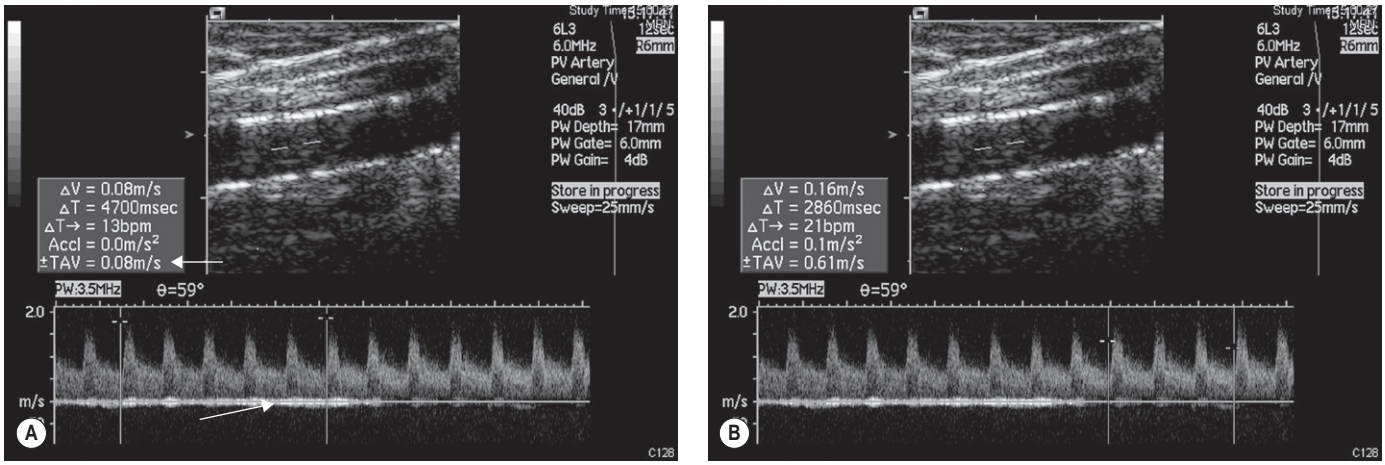


Figure 3.35 Wall filter. In the sonogram the wall filter is increased to remove the low velocities from wall movement in the left of the sonogram (arrow). This has a profound effect on the measurement of time-averaged velocity. With the filter allowing strong echoes from wall movement **(A)**, the mean velocity (short arrow) measured is 8 cm/s. When the filter removes low-velocity echoes, the measurement of mean velocity is now 61 cm/s **(B)**.

Other parameters – filter/sweep

The Doppler filter or wall filter removes low-frequency echoes from the sonogram. The range of low frequencies removed can be altered to suit particular applications; for low-velocity flow in stationary tissue a low filter setting is appropriate. For arterial flow in the abdomen, a high filter setting removes noise from abdominal tissue movement. Filter settings are important if time-averaged mean velocity is to be measured, for example in volume flow calculations. High filters remove the low velocities near the vessel wall, artificially raising measured mean velocity. Low filters risk including wall noise. This is illustrated in Figure 3.35 where the change of filter setting leads to a large change in measured mean velocity caused by high-intensity low-frequency noise.

Sweep speed can be changed to show a long or short timescale. This alters the appearance of flow waveforms but can be useful in looking at variation in arterial waveforms not evident over shorter periods (Fig. 3.36).

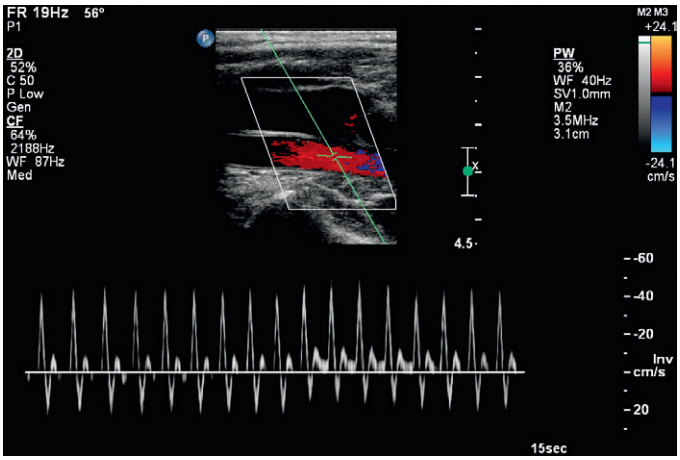


Figure 3.36 Sweep speed. A slow sweep speed permits investigation of longer-term trends in flow waveforms.

Angle correction errors

As described above ('Basic rules – beam/flow angle and angle correction'), angle correction must be made to obtain accurate velocities from the sonogram. The accuracy of the measurements made is dependent on accurate alignment of the cursor with the flow direction. It is inevitable that slight errors are made in clinical practice; even where the direction of flow is clear, errors of greater than 5° are possible. Where the flow direction is less clear, much larger errors are possible. The effect on measured velocities is highly dependent on the angle between the beam and flow. At low angles, the velocity is comparatively unaffected by changes in angle correction. At higher angles, velocities change significantly (Fig. 3.37). There is no cut-off above which errors suddenly become worse but as a general rule, angles over 60° should not be used if absolute measurements of velocity are required, for example in internal carotid artery stenosis.

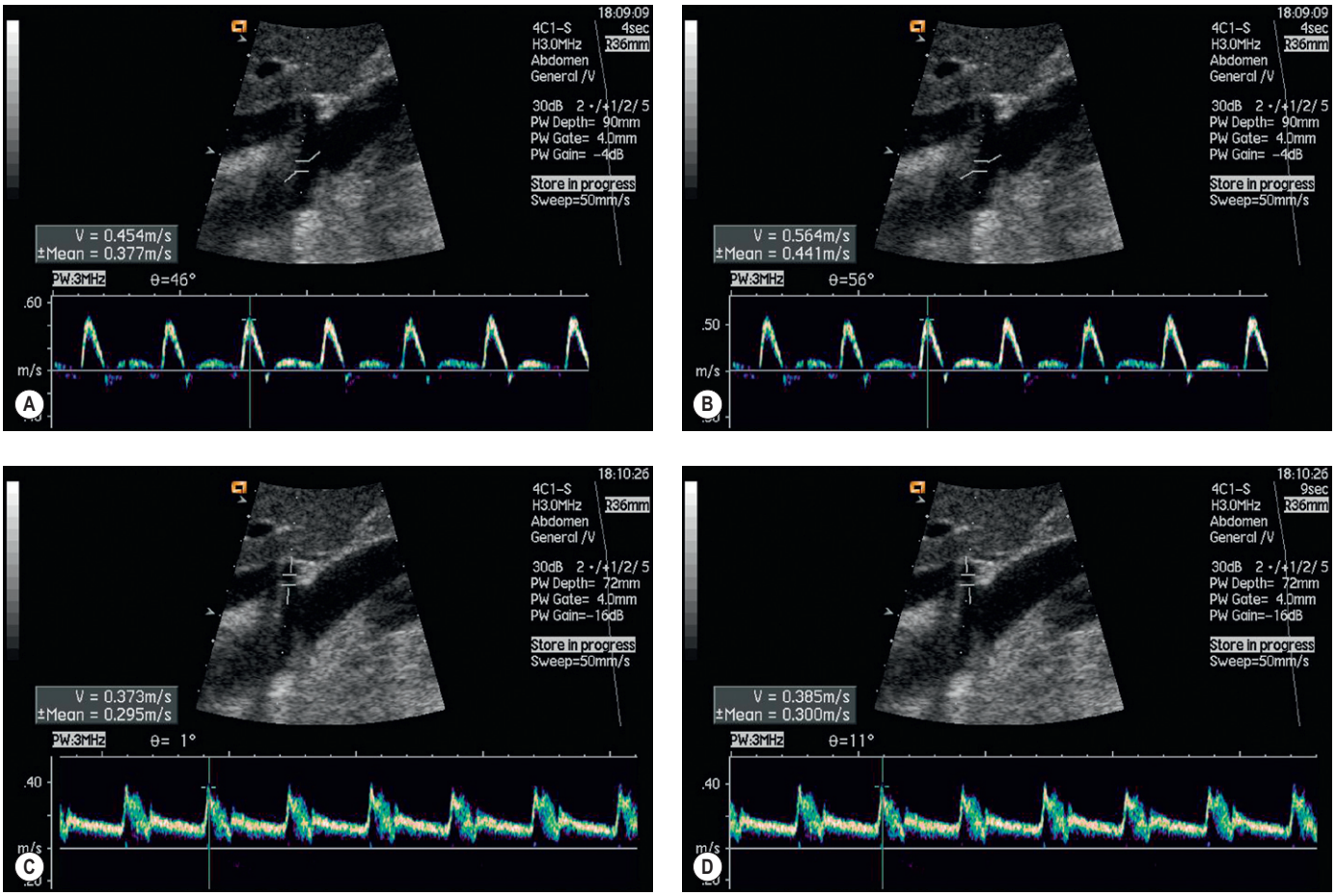


Figure 3.37 **Errors in velocity** arising from a 10° change in beam/flow correction angle. In images **A** and **B**, the peak velocities in the aorta change from 45 to 56 cm/s when the angle correction is changed from 46° to 56° (the image and sonogram are identical, only the angle correction is changed). In images **C** and **D** the peak velocity in the renal artery changes only slightly from 37 to 38 cm/s with a change from 1° to 11°. The images demonstrate that velocity measurements are increasingly prone to error as the beam/flow angle increases.

Pulsed wave/spectral Doppler parameters

- **Power:** Alters the output power. Not all scanners have this control. Power should be reduced where there is concern over the use of high output levels, for example imaging through the eye.
- **Gain:** Alters the sensitivity of the spectrum to blood flow and the brightness of the spectrum and noise in the spectrum.
- **PRF/Scale:** Alters the range of frequencies/velocities displayed on the sonogram. The scale should be adjusted to show the velocities under investigation clearly.
- **Baseline:** The baseline can be adjusted to increase the range of velocities displayed in one direction and reduce it in the other.
- **Invert:** Inverts the velocity scale – used when appropriate for the direction of flow under investigation.
- **Volume** of the Doppler signal. Self-explanatory. Low volumes can be difficult to hear, high volumes can cause alarm to patients and staff.
- **For linear arrays – beam steering:** Offset beam steering is used to provide a better and more consistent beam/flow angle in arteries and veins parallel to the skin surface.
- **Angle correction:** Tells the scanner the direction of flow relative to the ultrasound beam so that velocity measurements can be made.
- **Frequency:** Some scanners allow changes of transmit frequency in PW mode. This can be useful to improve penetration and signal strength at depth.
- **Sample volume/gate size:** A large gate may be used to insonate flow across a vessel. A small gate is used if a very precise location for velocities is required.
- **Filter:** Reduces signal from low-velocity moving targets. Useful where there is high-amplitude low-velocity movement but high filters may remove low-velocity flows from the sonogram.
- **Sweep speed:** Alters the timescale of the sonogram. Slow sweep speeds can show longer-term changes, high sweep speeds allow more detailed examination of changes in a cardiac cycle.
- **Post-processing:** Different brightness ranges or colour hues of the sonogram.
- **Measurements:** Automatic and manual measurements from sonograms. Major parameters are discussed in the text.

CHAPTER

4 Safety

Hazel C. Starritt and Francis A. Duck

INTRODUCTION 51

THERMAL EFFECTS AND TI 52
Heating mechanisms 52
Physical factors 52
Biological factors 52
Experimental investigation of heating 52
Heating due to tissue absorption 52
Transducer heating 53
Implications of heating 53
Hazard indication – thermal index (TI) 54
Use of TI during ultrasound examination 54

CAVITATION AND GAS BODY EFFECTS 54
What do we mean by acoustic cavitation? 54
Hazards from gas bubble activity and cavitation 55
Review of experimental work associated with cavitation and gas body activity 55
Modelling 55
In-vivo animal and human effects 55
Factors affecting incidence of cavitation and gas body activity 55
Physical factors 55
Biological factors 55
Definition of MI 56
Mechanical index in clinical practice 56
Situations of potentially higher risk 56
Reduction of MI during scanning 56
Surveys of MI values in clinical practice 56

EPIDEMIOLOGY 56
Review of epidemiological studies 56
Childhood cancer 56
Birth weight 56
Dyslexia 56
Handedness 57
Conclusion 57

REGULATIONS AND GUIDELINES 57
Food and Drug Administration (FDA) 57
BMUS guidelines 57
General guidelines 57
Specific guidance for use of thermal and mechanical Indices 57
EFSUMB 58
Ultrasound during pregnancy 58
Other sensitive organs 58
Contrast agents 58
WFUMB 58
Recommendations on thermal effects 58
Recommendations on non-thermal effects 58
Recommendations on contrast agents 58

INTRODUCTION

In recent years ultrasound imaging equipment has been required to display safety indices in appropriate circumstances. This chapter will consider the reasons for this requirement and give guidance on the meaning and usefulness of the specific indicators. It is important to state at the outset that ultrasound is a relatively safe imaging modality. Unlike X-ray imaging it does not involve the use of ionising radiation which has well-known risks. In comparison with narrow-bore MRI scanning, it does not require injection of toxic contrast materials, nor are there the hazards associated with very high magnetic fields.

Ultrasound scanning is widely used throughout the world. One of the major areas of application is in obstetric scanning and almost every woman in the developed world will undergo as a minimum a routine dating scan during pregnancy. Other applications of ultrasound in medicine are wide ranging; it is used in cardiology, mammography and general abdominal imaging, for eye scanning and fetal heart monitoring and for investigations of peripheral vascularity. In 2008/09 over 7.4 million ultrasound scans were carried out in NHS Trusts in England and of these 2.4 million were obstetric/gynaecological scans. The use of ultrasound is increasing, the fastest growth being in non-obstetric scanning where a 70% increase has occurred over the last ten years. In spite of the large number of examinations carried out each year there have been no confirmed reports of ill effects following ultrasound examination. It remains the case that probably the greatest risk arising from the use of ultrasound in obstetrics is the risk of misdiagnosis.

The acoustic output from ultrasound equipment is well controlled by the manufacturers in line with regulatory requirements. The USA Food and Drug Administration (FDA)[1] require the maximum available ultrasound intensity to be limited and compliance with AIUM/NEMA Output Display Standards (ODS).[2] These restrictions apply to all equipment manufactured or sold in the USA; in effect all the major worldwide manufacturers are included. The FDA limits are set out later in this chapter in the section on guidelines and regulations.

There are certain clinical situations in which extra care should be taken to ensure that the exposure is no greater than necessary. In these situations the on-screen safety indices are of great value to the operator since they allow an immediate assessment of potential risk to be made for specific exposure conditions. In general, well-perfused tissue is less susceptible to thermal effects than is less well-perfused tissue, and cells are more susceptible to external influence during periods of rapid division. For both these reasons the fetus may be considered to be at some risk and operators should attempt to ensure that the exposure is well managed. There is a common misconception that vaginal scanning is more risky than external scanning; this is not true since vaginal transducers operate within the same regulatory limits on in-situ exposure as do other transducers. The greatest risk from vaginal scanning may arise from transducer self-heating. Neonatal scanning is carried out at a stage in life where cells are rapidly turning over and this also requires careful management. In eye scanning using ultrasound there is a concern that thermal effects may be induced due to poor perfusion, with the consequent risk of cataract formation. Experimental evidence for cataract formation is available for high temperatures only; nevertheless proper management of ultrasound exposures in eye scanning is prudent, a view endorsed by the FDA in setting lower mandatory limits for ophthalmological equipment.[1]

Scanning of a soft tissue–gas interface will increase the risk of ultrasound-induced effects and the areas which may be vulnerable are the lungs and the intestinal tract. The use of contrast materials, where gas bubbles are deliberately introduced into the body, carries

a degree of risk and this is discussed further in the section on cavitation and gas body effects, later in this chapter.

To ensure that the likelihood of any ultrasound-induced effects is minimised, safety indices relating to thermal effects and gas-bubble activity have been developed. The current advice on managing ultrasound exposure is based on the use of these displayed safety indices. The safety indices are based on two known biophysical mechanisms of ultrasound, which are thermal effects and mechanical effects associated with gas bubbles. This chapter focuses on these well-established mechanisms. The likelihood of other potential mechanisms, for example radiation force effects, is not predicted by the safety indices.[3]

THERMAL EFFECTS AND TI

A thermal index (TI) has been developed to allow the user to assess the tissue heating that may occur for a particular transducer and particular equipment settings. The index displayed is the ratio between the actual acoustic power and the acoustic power required to produce a worst-case, maximum, steady-state temperature rise of 1°C in tissue.

Heating mechanisms

Whenever an ultrasonic beam passes through tissue there will be a transfer of energy from the acoustic wave to the tissue. The process is known as acoustic absorption. This will cause an increase in the temperature of the tissue and, if sufficient energy is transferred, this increase will have physiological effect. A biologically significant temperature rise will induce changes within the cells of the tissue and the evidence for such effects is covered in the section on experimental investigation of heating, below. The amount of tissue heating produced will depend on a range of physical and biological factors.

Physical factors

Physical factors influencing the potential for heating are listed here and the effect produced by varying each factor in turn is described:

1. Acoustic power (watts) and intensity (watts per square centimetre): an increase in the power or intensity in the acoustic beam will result in an increased potential for tissue heating.
2. Acoustic frequency: absorption of acoustic energy in tissue is dependent on frequency, with higher acoustic frequency waves being absorbed more strongly. This also affects the penetration depth of the beam; the highest frequency beams will only have the potential to produce heating in superficial tissue.
3. Beam cross-sectional area: a larger exposed area has the potential to result in a greater temperature rise in tissue, for a given spatial-peak temporal-average intensity, *I*(spta). This is due to slower conduction of heat away from the affected area because of its volume.
4. Dwell time: increasing the time that any particular region is exposed to an ultrasound beam may increase the temperature rise produced; this will also depend on the rate of heat conduction away from the area and on the effects of blood perfusion.
5. Other machine settings: scan mode, focusing, frame rate, line density and zoom are secondary factors which affect heating through their effect on the acoustic power or the beam area. It is not possible to predict easily the effects produced by varying these factors due to differences in equipment design.

Biological factors

The two primary biological factors affecting the potential for heating to occur in an acoustic beam are tissue absorption and blood perfusion. Attenuation coefficients have been measured for a range of tissues in humans and in animal studies and are available in the literature. (Attenuation includes the small additional contribution from scattering of an ultrasound beam by tissue.) Bone has the potential to absorb most strongly and body fluids least strongly with soft tissues in between. Table 4.1 gives representative values of ultrasound attenuation coefficients of selected tissues[4] at 1 MHz, and attenuation coefficients at other frequencies can be estimated by scaling these values linearly with frequency.

There has been no systematic approach taken to the measurement of attenuation coefficient in vivo and much of the work on absorption has been carried out on animals and on tissues in vitro, resulting in large gaps in the knowledge base. Ethical considerations mean that it is now very difficult to make measurements such as these on human tissue.

Table 4.1 Attenuation coefficients[4] at 1 MHz in dB/cm

Tissue	Attenuation coefficient: dB/cm at 1 MHz
Blood	0.20
Liver	0.50
Brain	0.60
Muscle	0.74
Breast	0.75
Average fatty soft tissue	0.40
Average non-fatty soft tissue	0.60
Skin (range)	2.3–4.7
Cortical bone (range)	14–20

Absorption of acoustic energy

- Acoustic energy is absorbed from an ultrasound wave into tissue.
- The absorbed energy causes tissue heating.
- The amount of heating depends on the acoustic beam shape and power, and on the tissue type.

Experimental investigation of heating

Heating due to tissue absorption

Although it is well established that ultrasound can produce heating in tissue, only limited measurements of temperature increases induced by diagnostic exposures have been made. Barnett[5] offers a useful review of these. A small number of studies investigated heating in tissue specimens or tissue-mimicking materials. None of these studies attempted to simulate the cooling effect of blood flow and so the temperature increases were likely to be higher than in perfused tissue. In addition, some live animal studies have been carried out. There have been no significant temperature increases observed with ultrasound equipment operated in pulse-echo mode but temperature increases have been measured in unperfused tissue specimens exposed at pulsed Doppler output levels using commercial ultrasound equipment or equivalent laboratory systems.

For soft tissue exposed in pulsed Doppler mode, a maximum temperature of 1.9°C was measured after 2 minutes (*I*(spta) 2.0 W cm^{-2}; 5 MHz) using a sample of porcine liver;[6] and in excised sheep brain an increase of 2.5°C occurred after 5 minutes at a similar exposure level. In a simulated pulsed Doppler beam, excised guinea-pig brain showed an increase in temperature of 2.5°C after 2 minutes.[7]

Greater temperature increases have been reported where bone is located in the path of the acoustic beam. For example, at the bone/brain interface in the skull of guinea-pig fetuses a maximum temperature rise of 5.2°C was measured adjacent to the parietal bone (260 mW, 3.2 MHz).[7] In a separate study the degree of heating was found to increase with fetal gestational age as the bone became denser.[8] A similar effect was observed with human fetal femurs.[9] Doody et al.[10] reported temperature measurements on the surface of unperfused human fetal vertebrae. The maximum temperature reached in this bone, exposed in vitro to a simulated, medium-power, Doppler ultrasound beam (50 mW), increased from 0.6°C to 1.8°C with increasing gestational age from 13 weeks to 39 weeks.

Heat generated at the bone/brain interface is of particular concern for obstetric scanning because of the risk of damage to the developing brain and central nervous system. In anaesthetised mice, a maximum temperature elevation in the mouse skull of 5°C was recorded after 90 s exposure (I(spta) 1.5 W cm^{-2}).[11] Temperature elevations were 10% higher when repeated after the animals had been killed, showing that the effect of blood perfusion on temperature elevation in the mouse skull was small. Other studies have reported differences in the ultrasound-induced temperature elevation in guinea-pig fetuses depending on gestational age. Horder et al.[12] reported a 12% reduction in the temperature increase in guinea-pig fetuses near to full term due to a better developed vascular system. Investigations have also been carried out on fetal sheep brain in utero.[13] A temperature increase of 1.7°C in 120 s was measured in soft tissue adjacent to the parietal skull bone which was approximately 40% lower than the unperfused value measured postmortem (spatial-average temporal-average intensity, I(sata) 0.3 W cm^{-2}). Different responses to changes in perfusion have been associated with different beam areas, with heating in the smaller focal regions of diagnostic beams being less affected by altered perfusion.[14]

Heating in tissue

- More heating occurs in bone than in soft tissue.
- The fetal brain may be at greater risk of heating as the skull ossifies during gestation.
- Temperature rises measured in vitro from diagnostic ultrasound exposure are small.

Transducer heating

Until now we have been considering heating effects in tissue resulting from direct transfer of energy from the ultrasound beam to the tissue. A separate mechanism for heating tissue has been identified and occurs when the temperature of the ultrasonic transducer increases due to inefficient energy conversion. Pulsed transducers in particular are often inefficient in converting electrical energy into acoustic energy. Heat generated within the transducer is conducted from the front face of the transducer into adjacent soft tissues. This is the dominant source of heat for tissue in contact with the surface of the transducer and exceeds that arising from the absorption of ultrasound by tissue.[15]

If uncontrolled, transducer heating could result in thermal damage to surrounding tissues. Transvaginal scanning has been a situation of particular concern due to the proximity of the transducer to fetal tissue. Calvert et al.[16] investigated the heating depth-profile in a tissue-mimicking material (TMM) for two transvaginal transducers operated at output conditions close to maximum. The greatest temperature increase was found to always occur at the interface between the transducer and TMM and to reduce to 10% of the surface value at about 1 cm depth. Temperature increases were higher when the transducers were operated in colour flow and pulsed Doppler modes than for pulse-echo mode.

In the past there has been experimental evidence demonstrating that the surface temperature of ultrasound transducers could increase excessively if operated in air under maximum output conditions.[17] An upper limit for the permitted temperature of the transducer face has now been set by the IEC;[18] when coupled to tissue the temperature is limited to 43°C after 30 minutes, i.e. an increase of 6°C, and if operated in air prior to scanning the temperature must not exceed 50°C. In general transducer heating is now well managed and transducers are designed to operate with the constraint imposed by the IEC limits.

Implications of heating

Current ultrasound equipment has the potential to cause heating in tissue and to raise the temperature locally due to absorption when operated towards the upper end of available powers and intensities. The greatest temperature increase due to ultrasound absorption occurs at the surface of ossified bone; in soft tissues it is very unlikely that the temperature would be increased above 2°C due to absorption. Uncalcified bone does not absorb ultrasound strongly. The potential for heating resulting from obstetric applications is of concern because hyperthermia is known to be a teratogen in animals. In obstetric examinations the developing brain is within the ultrasound beam and in close proximity to the skull.

Animal studies have shown that abortion or reabsorption may occur in early embryos and that developmental effects are most likely when hyperthermia occurs during organogenesis, with the central nervous system being most at risk. In the following studies the core temperature of pregnant animals was elevated by immersion in water in order to investigate the effect of heat on fetal development. In studies investigating brain development following whole body heating of pregnant rats[19,20] it was found that the threshold temperature for abnormalities was 4°C increase in maternal core temperature maintained for 5 minutes. The majority of abnormalities involved encephaloceles and microphthalmia. A 5°C increase in maternal temperature resulted in developmental abnormalities in the fetal rat brain when maintained for less than 1 minute. In mice a threshold for exencephaly has been reported at a temperature increase of 4.5°C above normal body temperature, maintained for 5 minutes[21] and in mice and rats at 3.5°C maintained for 10 minutes[22] following whole body hyperthermia. Abnormalities in proliferating bone marrow cells were found in guinea-pigs heated in a hot air incubator[23] and similar effects were observed when an equivalent temperature elevation was produced by ultrasound.

In summary, there is a large body of evidence demonstrating that heat induces developmental abnormalities in a range of animal species. The sensitivity varies with stage of gestation and peaks during neurogenesis. At this stage, a sustained temperature elevation of about 2.0°C above maternal body temperature results in developmental defects such as micrencephaly, microphthalmia and retarded brain development in a wide range of animals. The same types of developmental defects were observed following heating for shorter periods where the temperatures were higher. Thus, the risk depends on both the temperature elevation and the time for which that temperature elevation is maintained. The time to cause any particular biological effect becomes shorter as the temperature elevation increases. At high temperatures (above about 43°C), the time is halved for each additional 1°C.

For these reasons it is important to consider how the changes in the absorption coefficient of human embryonic and fetal tissues will affect local heating. Ossification only commences towards the end of the first trimester, starting with the cranial and jaw bones. Until this stage in gestation, the absorption coefficient of embryonic tissue is thought to be at the lower end of soft tissue absorption and significant heating is unlikely to occur. Later in pregnancy, as the fetal skeleton develops, absorption is greater and heating is more likely. During the third trimester, it is possible for a stationary Doppler beam to heat fetal bones lying approximately at the focus of the beam, especially when a large proportion of the acoustic path is though amniotic fluid.

For adult scanning, transcranial pulsed Doppler studies have been judged to carry the greatest risk of localised heating.[3] This is due to the relatively high acoustic output used and because the transducer is held in a fixed position and orientation for extended periods. Bone is exposed, with no overlying tissue attenuation and conducted heat from any transducer self-heating will add to the heat generated by absorption of ultrasound in bone.

Risks associated with tissue heating

- Sustained heating of the embryo is known to cause developmental abnormalities in animals.
- In the adult, the greatest risk of localised heating arises during transcranial Doppler studies.

Hazard indication – thermal index (TI)

The user could be forgiven for thinking that the evidence for heating by ultrasound in vivo is unclear, suggesting that heating may or may not occur and if it does occur it may be to a greater or lesser extent. Primarily this is because of the wide range of variables that need to be considered in each situation. One of the most important aspects is the ultrasound mode, for example the potential for heating may increase in moving from pulse-echo to colour flow imaging. The acoustic output power and the beam properties determine the acoustic energy available, whilst the tissue absorption and perfusion determine the temperature rise generated by absorption of acoustic energy. Ideally, a user would need to give due consideration to each of these factors for each ultrasound examination in order to assess the risk and act accordingly. However, this is not practical and a simplified approach has been adopted by displaying the thermal safety index (TI) on the ultrasound scanner.[1,2]

The display of TI on many modern scanners allows the operator to identify scanner operating conditions most likely to cause tissue heating in a range of situations and, if necessary, to make adjustments to minimise the heating caused by ultrasound absorption. At present, the display does not include information about surface temperature caused by transducer self-heating.

The thermal index (TI) is defined as the ratio W/W_{deg}, where W is the acoustic power emitted by the transducer at any time, and W_{deg} is the power required to cause a maximum temperature rise of 1°C anywhere in the beam, contributed by ultrasound absorption alone.[24] It is assumed that a steady state is reached and hence would require that the beam remains stationary with respect to the tissue for several minutes. Three simple physical models are assumed for the computational programs that generate the TI values displayed on ultrasound scanners. These are:

1. *Soft tissue thermal index (TIS).* The soft tissue model assumes a uniform homogeneous tissue-mimicking material with an absorption coefficient somewhat lower than soft tissue to allow for fluid pathways, and makes some allowance for heat loss from blood perfusion.
2. *Bone-at-focus thermal index (TIB).* This model includes a layer of strongly absorbing material (bone mimic) within the soft tissue model at the depth that maximises temperature rise.
3. *Cranial bone thermal index (TIC).* The third tissue model omits soft tissue, and considers the absorption of ultrasound in a bone-equivalent layer coupled directly to the transducer.

These three models can be used to estimate TI in scanned beams (pulse-echo B-mode, and Doppler imaging/colour flow) and unscanned beams (M-mode and pulsed Doppler).

Use of TI during ultrasound examination

Most scanners now display TI values calculated from these models and this provides a clear and simple indication of thermal hazard to the user. Occasionally differences between the actual worst-case temperature rise in situ and that inferred from the displayed TI have been reported. These are most probably due to differences between the assumed tissue models and the actual tissue structure, but may also reflect real differences in individual transducer performance. In addition it must be stressed that displayed TI is not the actual temperature increase in degrees Celsius generated in tissue while scanning. TI is, however, the best indication of thermal hazard available to the user and allows risk to be quickly assessed during an ultrasound examination.

There are a number of ways in which the operator can adjust scan conditions in order to reduce TI and to minimise risk when necessary. In all operating modes and all clinical applications, reducing the acoustic output power will reduce TI. Using a lower acoustic frequency may result in lower TI due to less local absorption. Reducing the frame rate or increasing the sector width may again reduce TI. If the transducer dwell time is short, the risk of heating will be reduced. This will not, however, be reflected in the displayed value of TI because the model assumes that the transducer is stationary for a sufficient time for a steady state to be reached.

In 2008 a survey of TI displayed during a range of scans in clinical practice was carried out in the United Kingdom by the Safety Committee of the British Medical Ultrasound Society.[25] The results showed that the greatest range of TI values (0.1 to 2.5) and the average of the highest TI values (0.98) were displayed during obstetric examinations. The average examination time (15.4 ± 0.7minutes) was also longest for obstetric examinations. The highest TI values were associated with pulsed Doppler examinations. Deane and Lees[26] also found TI to be highest during pulsed Doppler examination. A similar study in the USA[27] concentrated on obstetric scanning. The conclusion was that while acoustic power levels, as expressed by TI and MI, were generally low, TI >1.5 could be reached during colour Doppler examination and accounted for a small proportion of the total examination time.

The success of TI as a safety indicator depends on the extent to which it is understood and used by the user. There is some evidence[24,28] that obstetric ultrasound users do not, in general, use the indices and are not confident of their meaning, in spite of extensive training opportunities.

The thermal index (TI)

- TI is the thermal safety index.
- It is displayed to guide users in assessing the likelihood of heating.
- It should be kept to a value minimum consistent with diagnostic quality.

CAVITATION AND GAS BODY EFFECTS

In addition to the thermal safety index (TI), a mechanical safety index (MI) is displayed on many ultrasound scanners. This index is intended to warn the user about the hazard arising from inertial cavitation due to the behaviour of bubbles or gas bodies in the acoustic beam. Although MI relates to inertial cavitation, gas body activity can produce a range of effects which need to be considered in the context of patient safety.

What do we mean by acoustic cavitation?

Acoustic cavitation is a term used to refer to the behaviour of a gas bubble contained in a liquid, in an acoustic beam. The bubble experiences variations in pressure due to the acoustic wave. It expands in size during the period of decreased pressure and contracts during compression to an extent dependent on the acoustic pressure. At low acoustic pressure, these oscillations in bubble size occur broadly in step with variations in acoustic pressure in a stable fashion. This is known as non-inertial, or stable, cavitation.

However, if the peak acoustic pressure increases, different motions may be induced until finally the bubble becomes unstable and collapses under the inertia of the surrounding liquid. This is known as 'inertial cavitation' or collapse cavitation. The term acoustic cavitation also refers to the generation of bubbles in a liquid by a sound wave. For this to occur pre-existing nucleation sites such as microscopic impurities are required.

Hazards from gas bubble activity and cavitation

Inertial cavitation, in which very rapid bubble collapse occurs, results in the generation of extremely high instantaneous temperatures and pressures within the bubble cavity. The temperature can increase by thousands of degrees. This is sufficient for highly chemically reactive free radicals to be formed which are known to be potentially damaging to molecules in the body.

A different hazard is posed by the complex mechanical forces associated with bubble activity. For example, the shear forces exerted at the bubble surface by a pulsating bubble can generate a small steady flow of fluid via a process known as microstreaming.[29] The variation of this flow with distance from the bubble creates extremely high shear stresses near the bubble surface, which have been associated with cell destruction (haemolysis), and temporary alteration in permeability (sonophoresis).[30] These mechanical forces occur with both non-inertial and inertial cavitation, but are significantly higher in the latter case. Furthermore, additional heating of the surrounding medium may result.[31]

Review of experimental work associated with cavitation and gas body activity

Modelling

Cavitation has been investigated theoretically using mathematical modelling.[32,33] Maximum collapse pressures and temperatures within bubble cavities and collapse speeds of the cavities were calculated for a range of nucleus sizes.[33] Further work gave evidence that cavitation could, in theory, occur in the type of pulsed acoustic beams employed in diagnostic ultrasound. Holland and Apfel[34] predicted the threshold acoustic pressure required for cavitation to occur at different frequencies, and this analysis was used as the basis for MI. In practice pre-existing gas bubbles are required for cavitation and these are unlikely to occur naturally in the body. Church[35] has published perhaps the most relevant theoretical paper for diagnostic ultrasound. He examined the likelihood that cavitation nuclei could give rise to acoustic cavitation within soft tissue, under diagnostic conditions. He determined that the threshold acoustic pressure for such events lay above those used in current practice, and that even at slightly higher acoustic pressures, viscous and other forces within the tissue made the likelihood of cavitation events vanishingly small.

In-vivo animal and human effects

Biological effects attributed to cavitation and other gas body effects have been observed in association with the use of ultrasound in extra-corporeal shock-wave lithotripsy (ESWL) where bruising may sometimes be observed on the skin on the exit beam side of the patient. There is evidence that the destruction of gallstones and renal calculi is due to cavitation effects.[36] In ESWL the peak acoustic pressure is typically 20 MPa compared to approximately 2 MPa for diagnostic ultrasound and the acoustic frequency of ESWL pulses is much lower than diagnostic pulses. These factors make cavitation more likely to occur.

Lung tissue is vulnerable to damage from diagnostic ultrasound because of the presence of air. Damage has been demonstrated in mammals, and acoustic pressure thresholds for haemorrhage in mouse lung have been determined experimentally[37,38] to be 1.4 MPa for pulsed ultrasound in the frequency range 1–4 MHz, with a dependence on pulse length. Typically damage included extravasation of blood cells into the alveolar spaces suggesting ruptured capillaries. The exact mechanism remains unclear, since it is difficult to explain all the experimental results on the basis of ultrasound-induced cavitation occurring in the alveolar spaces.[39] Thresholds for lung damage have been determined for monkey,[40] rat[41] and rabbit lung,[42] for neonatal pig[43] and mouse.[44] Gas in the intestine has been associated with damage to the intestinal wall in mice[45,46] on exposure to ultrasound.

The injection of microbubbles into the circulation as contrast agents causes effects that do not occur under normal conditions. There is evidence that ultrasound and microbubbles can lead to increased permeability of the blood–brain barrier.[47] It may be possible to use this effect to assist the delivery of macromolecular agents to the brain. It has been shown that the blood–brain-barrier can be transiently opened using focused ultrasound and introduced microbubbles without acute neuronal damage.[48] However, there is insufficient evidence to conclude that there is no damage to the barrier as a result of the effects of ultrasound and microbubbles.

To date there has been one experimental study reporting an observed bioeffect associated with ultrasound which is not easily explained by any of the accepted mechanisms. Ang et al.[49] reported increased migration of neurons in fetal mice with exposure to diagnostic ultrasound. The mechanism is unclear and the need for further research is indicated.

Factors affecting incidence of cavitation and gas body activity

Physical factors

Before cavitation can occur, gas bubbles or nucleation sites within the fluid or tissue are required. Once this condition is met, the likelihood and amount of cavitational activity will depend on two physical properties of the acoustic beam. Firstly it depends on the acoustic frequency and is more likely at lower frequencies. Secondly there is a threshold level of the peak acoustic pressure in the decompression phase of the acoustic wave, below which inertial cavitation will not occur. Bubble activity is influenced by surface tension and viscosity.

Biological factors

The use of contrast materials, which introduce gas bubbles into an acoustic field, significantly increases the potential for cavitation during clinical ultrasound examinations. Contrast agents consist of stabilised bubbles, 1–10 μm in diameter, typically surrounded by a lipid or polymeric shell. When activated by high acoustic pressures, these shells may become damaged, allowing the release of free gas bubbles. Demonstrable harm can result when tissues containing gas-filled contrast agents are exposed to ultrasound under so-called 'high MI' conditions. Capillary rupture can occur, with leakage of blood contents into the surrounding extravascular space.[50,51] In addition, ventricular extra-systolic contractions can be induced during cardiac scanning.[52] Without the addition of contrast materials other gas body activity of the type outlined above may occur at any gas/tissue interfaces within the body for example in the lung or intestinal tract.

Cavitation and tissue

- Inertial cavitation is potentially damaging to tissue.
- The use of contrast agents enhances the likelihood of ultrasound-induced cavitation.
- In the absence of contrast agents there is no evidence of cavitation occurring in vivo at current diagnostic exposures.

Definition of MI

A safety index displayed on a scanner allows a user to manage acoustic exposure in such a way that the risk of cavitation effects is minimised. The mechanical index, (MI) is formally a predictor of inertial cavitation and was derived from a theoretical analysis which predicts the onset of inertial cavitation in water or blood, given the existence of available bubbles. The index is related to acoustic pressure and frequency according to the equation:

$$MI = p_r / \sqrt{f}$$

where p_r is the in-situ rarefaction pressure and f is the acoustic frequency.

Mechanical index in clinical practice

Situations of potentially higher risk

In the following situations tissue is particularly vulnerable to gas bubble activity and/or acoustic cavitation in an acoustic beam and exposures should be well managed:

1. Echocardiography in premature infants, particularly in combination with lung surfactant therapy.
2. Any clinical application of ultrasound involving contrast materials (further discussed in Chapter 6) or saline for endometrial evaluation.
3. The incidental exposure of any tissue/air interfaces such as lung and intestine.
4. Mechanical effects are equally likely to occur in pulsed Doppler beams and in B-mode imaging beams, since a very similar range of acoustic pressures is used in each mode.

Reduction of MI during scanning

To reduce the MI, the acoustic pressure may be decreased by reducing the acoustic output power using the transmit control. It is not possible to predict the outcome of altering the acoustic frequency, because any frequency change will also change the acoustic pressure.

Reducing the risk of cavitation

- The threshold for cavitation depends on the peak negative acoustic pressure and on the acoustic frequency.
- The likelihood of cavitation occurring can be reduced by reducing the acoustic pressure if possible.
- On most systems, MI may be reduced by using the acoustic output control.

Surveys of MI values in clinical practice

A UK survey of ultrasound exposure conditions investigated displayed values of MI.[25] The greatest range of values occurred during abdominal examinations (0.4 to 1.6) and the average of the highest values (0.97) was also associated with this examination. MI values for obstetric and transvaginal applications had lower average maxima (0.74 and 0.7 respectively). Sheiner et al.[27] carried out a survey of MI during obstetric ultrasound examinations in the USA. The average MI was greatest during third trimester examinations where the average displayed value was 1.06 (range 0.2 to 1.5). MI is limited to 1.9 by FDA regulation.

EPIDEMIOLOGY

Epidemiology studies allow the effects of prenatal diagnostic ultrasound on the exposed population to be studied directly. Necessarily such studies lag behind changes in practice and technology; much of the current evidence from epidemiology is based on examinations carried out 10 or more years in the past. During that time many changes have occurred. Equipment operating at higher maximum acoustic pressures and intensities is much more widely used; also transvaginal transducers, harmonic imaging, pulsed Doppler and contrast materials have all become available and are commonly employed. Hence epidemiological evidence can never be used to prove that current ultrasound practice is risk free.

There are a number of issues surrounding the design of epidemiology studies. First of these is the need to find a matched unexposed control group. Since its introduction into clinical practice 40 years ago the use of ultrasound in fetal scanning has increased dramatically. It is now very unusual in the developed world for a fetus not to be scanned routinely with ultrasound. This makes it impossible to design new, large randomised studies which have unexposed control groups.

Very commonly, ultrasound exposures are poorly documented, often including no record of acoustic power settings or duration of exposure, so making it impossible to demonstrate any relationship between effect and acoustic exposure. In any epidemiological study the selected outcomes are likely to be influenced by additional factors other than ultrasound exposure. Any clinical reason for additional or extensive ultrasound examination in utero may be associated with outcomes that are unrelated to the acoustic exposure. In order to produce statistically valid results, studies require very large groups of participants because, if there are ultrasound-induced effects, they would appear to be subtle and to occur with very low probability.

None of this negates the importance of epidemiology studies; developments in ultrasound technology and increased acoustic power levels[53,54] make it essential that further epidemiological research into possible adverse effects of ultrasound on the developing brain continues.[55]

Review of epidemiological studies

An excellent review[56] of epidemiological studies which focuses on several key biological endpoints is summarised here.

Childhood cancer

In five well-designed studies no association was found between exposure to ultrasound in utero and childhood malignancy.

Birth weight

Many epidemiological studies have studied human birth weight in relation to ultrasound exposure and only one has given cause for concern.[57] This was a randomised controlled trial of 2834 pregnant women, a group of whom were offered continuous wave Doppler examinations during the third trimester of pregnancy. The outcome showed a small (statistically insignificant) reduction in birth weight in the babies exposed to Doppler ultrasound in utero. No other randomised trials have demonstrated an association between diagnostic imaging examination and low birth weight. There is an expert consensus that ultrasound exposure during pregnancy does not result in reduced birth weight.

Dyslexia

One study of childhood development gave some cause for concern[58] since the authors reported a significant proportion of children

exposed to ultrasound in utero to be dyslexic. This prompted careful follow-up studies designed to look at effects of ultrasound on the developing fetal brain. No associations were found between ultrasound and dyslexia, poor performance at school, poor vision or hearing or delayed neurological development.[59]

Handedness

An association has been found between ultrasound exposure and non-right-handedness.[60] This was of borderline statistical significance and was restricted to boys. It was confirmed by the findings of an independent study.[61] This finding is not substantiated in studies where the sexes are not analysed separately.[62] A statistical association between ultrasound exposure and left-handedness is not indicative of harm to the developing brain.

Conclusion

Epidemiology studies to date show no association between ultrasound exposure during pregnancy and childhood malignancies, reduced birth weight, dyslexia, or abnormal neurological development. It is impossible, however, to rule out an association between ultrasound and left-handedness among males. Further research is essential to ensure the continuing safety of ultrasound for obstetric examination.

Evidence from epidemiology

- Epidemiology provides direct information on human population exposed to ultrasound.
- To date studies show no effect from prenatal ultrasound on birth weight, dyslexia, childhood cancer or neurological development.

REGULATIONS AND GUIDELINES

A number of statements have been issued by national and international organisations concerning the safe use of medical ultrasound. What follows is a summary of the main points of these guidelines and is not complete. Ultrasound practitioners are advised of the need to be familiar with the full guideline recommendations.

Food and Drug Administration (FDA)

Two alternative routes exist by which manufacturers can obtain Food and Drug Administration (FDA) approval in the USA for the manufacture and sale of ultrasound scanners,[1,2] The original requirement was for application-specific limited acoustic output and is rarely applied now. Currently the more commonly adopted route permits all equipment, except ophthalmology scanners, to operate to the maximum limit previously applied only for vascular scanning (so-called 'Track 3'). This route also requires on-screen displays indicating to the user the likelihood of thermal and mechanical effects. Current limits for this option are shown in Table 4.2.

The following requirements apply to the display of safety indices:[18]

1. Not all ultrasound equipment is required to display on-screen safety indices. Only those systems capable of reaching an MI or TI of 1.0 are required to display that index, beginning at a value of 0.4 and increasing to the maximum in increments of no less than 0.2.
2. Only one thermal index will be displayed (TIS, TIB or TIC) but the equipment must allow the user to retrieve the other two.

Table 4.2 USA FDA[1] threshold exposures for diagnostic ultrasound equipment. All are estimated in-situ quantities, so-called 'derated' values

	I(spta), mW cm^{-2}	*I*(sppa), W cm^{-2}	MI	TI
All except ophthalmology	720	190	1.9	6.0*
Ophthalmology	50	Not specified	0.23	1.0

**The limit of 6.0 on TI is not absolute, but exposures in excess of this require justification.*
I(spta), spatial-peak temporal-average intensity; I(sppa), spatial-peak pulse-average intensity.

3. TIC must be displayed for adult or neonatal transcranial applications.

When TIs are sufficiently low for display not to be required, some manufacturers display the value, some do not. This may be advantageous for reasons not associated with safety, for example in the use of MI to control the behaviour of contrast agents.

BMUS guidelines

In the UK guidance on the safe use of ultrasound equipment is provided by the British Medical Ultrasound Society (BMUS). The information in this section is taken from the current guidelines available on the BMUS website.[63]

General guidelines

1. Medical ultrasound imaging should only be used for medical diagnosis.
2. Ultrasound equipment should only be used by people who are fully trained in its safe and proper operation. This requires:
   - an appreciation of the potential thermal and mechanical bio effects of ultrasound
   - a full awareness of equipment settings
   - an understanding of the effect of machine settings on power levels.
3. Examination times should be kept as short as is necessary to produce a useful diagnostic result.
4. Output levels should be kept as low as is reasonably achievable whilst producing a useful diagnostic result.
5. The operator should aim to stay within the BMUS recommended scan times (especially for obstetric examinations).
6. Scans in pregnancy should not be carried out for the sole purpose of producing souvenir videos or photographs.

Specific guidance for use of thermal and mechanical Indices

Obstetric examination

- TIS should be monitored for scans during the first 10 weeks after LMP.
- TIB should be monitored for scans following 10 weeks after LMP.
- TI up to 0.7: no time restriction, but observe ALARA.
- TI up to 1.0: maximum exposure time of an embryo or fetus should be restricted to no more than 60 minutes.

- TI up to 1.5: maximum exposure time of an embryo or fetus should be restricted to no more than 30 minutes.
- TI up to 2.0: maximum exposure time of an embryo or fetus should be restricted to no more than 15 minutes.
- TI up to 2.5: maximum exposure time of an embryo or fetus should be restricted to no more than 4 minutes.
- TI up to 3.0: maximum exposure time of an embryo or fetus should be restricted to no more than 1 minute.
- TI >3.0: scanning of embryo or fetus is not recommended, however briefly.

Neonatal scanning

- MI >0.3: possibility of minor damage to neonatal lung or intestine. Restrict exposure time as much as possible.
- TI: use TIS for all transcranial and spinal scanning using the time limits given for obstetrics.

Abdominal, peripheral vascular and other scanning

- Use TIB with less restrictive time limits than those for obstetric scanning; for example unrestricted time limit with ALARA for TIB <1.0: TIB >6.0 is not recommended.

Fetal heart monitoring

- This modality is not contraindicated on safety grounds even when used for extended periods due to low acoustic power levels.

Eye scanning

- TI >1.0: eye scanning is not recommended other than as part of a fetal scan.

Transcranial ultrasound examinations

- TIC should be monitored.
- TIC >3.0 is not recommended.

Use of contrast agents

- MI >0.7: risk of cavitation exists if a contrast agent containing microspheres is used and there is a theoretical risk of cavitation without the use of contrast agent. The risks increase with MI above this threshold.

EFSUMB

The European Committee of Medical Ultrasound Safety (ECMUS) within the Federation of Societies of Ultrasound in Medicine and Biology (EFSUMB) has published a revised Clinical Safety Statement for Diagnostic Ultrasound.[64] This states that ultrasound produces heating, pressure changes and mechanical disturbances in tissue, and ultrasound at diagnostic levels can produce temperature rises that are hazardous to sensitive organs and to the embryo/fetus. Users are advised to check TI and MI during scanning and to adjust the machine controls to keep them as low as reasonably achievable without compromising the diagnostic quality of the examination. Where this is not possible, examination times should be as short as possible.

ECMUS highlights that spectral pulse wave Doppler and Doppler imaging modes can produce higher TI values, indicating more likelihood of heating, than can B-mode imaging. Tissue harmonic imaging can also sometimes involve high MI values. 4D (real-time 3D) scanning involves continuous exposure and users should avoid prolonging the examination by attempting to improve the image sequence beyond what is required for diagnostic purposes.

Ultrasound during pregnancy

Care should be taken to limit the exposure time and the TI and MI to the minimum commensurate with an acceptable clinical assessment. There is no reason to withhold diagnostic ultrasound scanning during pregnancy provided it is medically indicated and used prudently by fully trained operators. Fetal heart monitoring is not contraindicated on safety grounds when used for extended periods of time.

Other sensitive organs

Particular care should be taken to reduce the risk of thermal and non-thermal effects during investigations of the eye and when carrying out neonatal cardiac and cranial investigations.

Contrast agents

Situations in which damage to microvasculature could have serious implications should be treated cautiously, for example in the brain, the eye and the neonate. MI and TI should be continually monitored and kept as low as possible. Users should be aware that it is possible to produce premature ventricular contractions in contrast-enhanced echocardiography with high MI and take appropriate precautions and avoid cardiac examinations in patients with recent acute coronary syndrome or unstable ischaemic heart disease.

WFUMB

Recommendations of the World Federation for Ultrasound in Medicine and Biology (WFUMB) followed a symposium on the safety of ultrasound in medicine in 1997.[65] These make no reference to TI and MI because they predate their widespread introduction. More recently, WFUMB has published further recommendations for the safe use of ultrasound contrast agents.[66]

Recommendations on thermal effects

A diagnostic exposure that produces a maximum temperature increase of no more than 1.5°C may be used without reservation on thermal grounds.

A diagnostic exposure that elevates embryonic and fetal in-situ temperature to 41°C for 5 minutes or more should be considered potentially hazardous.

Recommendations on non-thermal effects

Currently available data indicate that it is prudent to reduce ultrasound exposure of the human lung to the minimum necessary to obtain the required diagnostic information. Gas bodies introduced by a contrast agent increase the probability of cavitation. When tissue/gas interfaces or contrast agents are not present the use of B-mode imaging need not be withheld because of concern for ultrasound safety. When tissue/gas interfaces or contrast agents are present, ultrasound exposure levels and duration should be reduced to the minimum level necessary to obtain the required diagnostic information.

Recommendations on contrast agents

Clinical users should balance the expected clinical benefit from ultrasound contrast agents against the possibility of associated bioeffects. Caution should be exercised in the use of microbubble ultrasound in tissues where damage to microvasculature could be dangerous. Some areas of concern include the brain, the eye, the fetus and the neonate. Clinical users of contrast echocardiography should be alert to the possibility of cardiac rhythm disturbances. Electrocardiograms should be monitored during these procedures.

The mechanical index (MI) is a useful but imperfect guide for safety and no absolute threshold can be defined. Bioeffects have been observed in small animals in ultrasound contrast agent studies with MI as low as 0.4; the clinical implications are yet to be determined.

Strategies that reduce the likelihood of bioeffects include:

1. scanning at lower MI
2. scanning at higher frequencies
3. reducing total acoustic exposure time
4. reducing contrast agent dose
5. adjusting the timing of cardiac triggering (end-systole being, in general, the most vulnerable phase for triggering ventricular arrhythmias).

The use of contrast agents in a diagnostic ultrasound study should be avoided 24 hours before lithotripsy procedures.

REFERENCES

1. FDA. Information for manufacturers seeking marketing clearance of diagnostic ultrasound systems and transducers. US Department of Health and Human Services: Food and Drug Administration; 2008. www.fda.gov/cdrh/ode/guidance/560.pdf.
2. IUM/NEMA 1992: revision 2 2004. Standard for real-time display of thermal and mechanical acoustic output indices on diagnostic ultrasound equipment. UD 3-2004. American Institute for Ultrasound in Medicine/National Electrical Manufacturers Association, USA.
3. Duck F. Hazards, risks and safety of diagnostic ultrasound. Med Eng Phys 2008;30:1338–1348.
4. ICRU. Tissue substitutes, phantoms and computational modelling in medical ultrasound. ICRU Report 61. Bethesda, MD: International Commission on Radiation Units and Measurements; 1998.
5. Barnett SB. Can ultrasound heat tissue and cause biological effects? In: Barnett SB, Kossoff G, editors. Safety of diagnostic ultrasound. New York: Parthenon Publishing Group; 1998. p. 27–38.
6. ter Haar G, Duck FA, Starritt HC, Daniels S. Biophysical characterisation of diagnostic ultrasound equipment – preliminary results. Phys Med Biol 1989;34:1533–1542.
7. Bosward KL, Barnett SB, Wood AKW, et al. Heating of the guinea-pig fetal brain during exposure to pulsed ultrasound. Ultrasound Med Biol 1993;19:415–424.
8. Horder MM, Barnett SB, Edwards, MJ, Kossoff G. In utero measurements of ultrasound-induced heating in guinea-pig fetal brain (Abstr. 2300). In: Proceedings of the 41st Annual Convention of AIUM. San Diego, USA; 1997:22.
9. Drewniak JL, Carnes KI, Dunn F. In-vitro ultrasound heating of fetal bone. J Acoust Soc Am 1989;88:26–34.
10. Doody C, Porter H, Duck FA, Humphrey VF. In-vitro heating of human fetal vertebra by pulsed diagnostic ultrasound. Ultrasound Med Biol 1999;8:1289–1294.
11. Carstensen EL, Child, SZ, Norton S, Nyborg W. Ultrasonic heating of the skull. J Acoust Soc Am 1990;87:1310–1317.
12. Horder MM, Barnett SB, Edwards MJ, Kossoff G. In-vivo temperature rise in the fetus from duplex Doppler ultrasound (Abstr). In: Proceedings of the 23rd Annual Conference of the Australasian Society of Ultrasound in Medicine. September 1993;Australia.
13. Duggan PM, Liggins GC, Barnett SB. Ultrasound heating of the brain of fetal sheep in utero. Ultrasound Med Biol 1995;21:553–560.
14. Vella GJ, Humphrey VF, Duck FA, Barnett SB. Ultrasound-induced heating in a foetal skull bone phantom and its dependence on beam width and perfusion. Ultrasound Med Biol 2003;29:779–788.
15. Thomenius KE. Estimation of the potential for bioeffects. In: Ziskin MC, Lewin PA, editors. Ultrasonic exposimetry. Boca Raton, FL: CRC Press; 1992. p. 371–407.
16. Calvert J, Duck F, Clift S, Azaime H. Surface heating by transvaginal transducers. Ultrasound Obstet Gynecol 2007;29:427–432.
17. Duck FA Starritt HC, ter Haar GR, Lunt MJ. Surface heating of diagnostic ultrasound transducers. Br J Radiol 1989;67:1005–1013.
18. IEC, 2005. IEC 60601 part 2–37: Medical Electrical Equipment: Particular requirements for the safety of ultrasound diagnostic and monitoring equipment 2001 & Amendment 1 2005. International Electrotechnical Commission, Geneva.
19. Germain MA, Webster WS, Edwards MJ. Hyperthermia as a teratogen: parameters determining hyperthermia-induced head defects in the rat. Teratology 1985;31:265–272.
20. Sasaki J, Yamaguchi A, Nabeshima Y, et al. Exercise at high temperature causes maternal hyperthermia and fetal anomalies in rat. Teratology 1995;51:233–236.
21. Shiota K. Induction of neural tube defects and skeletal malformations in mice following brief hyperthermia in utero. Biol Neonate 1988;53:86–97.
22. Edwards MJ, Shiota K, Smith MSR, Walsh DA. Hyperthermia and birth defects. Reprod Toxicol 1995;9:411–442.
23. Edwards MJ, Penny RHC. Effects of hyperthermia on the myelograms of adult and fetal guinea-pigs. Br J Radiol 1985;59:93–101.
24. Abbott JG. Rationale and derivation of MI and TI – a review. Ultrasound Med Biol 1999;25:431–441.
25. ter Haar G. Results of a survey of exposure conditions used in ultrasound scans in the UK, February 2007. BMUS Bulletin 2008;16:110–113.
26. Deane C, Lees C. Doppler obstetric ultrasound: a graphical display of temporal changes in safety indices. Ultrasound Obstet Gynecol 2000;15:418–423.
27. Sheiner E, Freeman J, Abramowicz J. Acoustic output as measured by mechanical and thermal indices during routine obstetric ultrasound examinations. J Ultrasound Med 2005;24:1665–1670.
28. Maršál K. The output display standard: has it missed its target? Ultrasound Obstet Gynecol 2005;25:211–214.
29. Nyborg WL. Acoustic streaming. In: Hamilton MF, Blackstock DT, editors. Nonlinear acoustics. New York: Academic Press; 1998. p. 207–231.
30. Wu J, Ross JP, Chiu J-F. Reparable sonoporation generated by microstreaming. J Acoust Soc Am 2002;111:1460–1464.
31. Holt RG, Roy RA. Measurements of bubble-enhanced heating from focused, MHz-frequency ultrasound in a tissue-mimicking material. Ultrasound Med Biol 2001;27:1399–1412.
32. Flynn HG. Cavitation dynamics. II. Free pulsation and models for cavitation bubbles. J Acoust Soc Am 1975;58:1160–1170.
33. Apfel RE. Acoustic cavitation: a possible consequence of biomedical uses of ultrasound. Br J Cancer 1982;45:140–146.
34. Holland CK, Apfel RE. An improved theory for the prediction of microcavitation thresholds. IEEE Trans UFFC 1989;36: 204–208.
35. Church CC. Spontaneous, homogeneous nucleation, inertial cavitation and the safety of diagnostic ultrasound. Ultrasound Med Biol 2002;28:1349–1364.
36. Coleman AJ, Saunders JE, Crum LA, Dyso M. Acoustic cavitation generated by an extracorporeal shockwave lithotripter. Ultrasound Med Biol 1987;15:213–227.
37. Penney DP, Schenk EA, Maltby K, et al. Morphological effects of pulsed ultrasound in the lung. Ultrasound Med Biol 1993;19: 127–135.
38. Child SZ, Hartman CL, Schery LA, Carstensen EL. Lung damage from exposure to pulsed ultrasound. Ultrasound Med Biol 1990;16:817–825.
39. O'Brien WD Jr. Ultrasound – biophysics mechanisms. Prog Biophys Molec Biol 2007;93:212–255.
40. Tarantal AF, Cranfield DR. Ultrasound-induced lung hemorrhage in the monkey. Ultrasound Med Biol 1994;20:65–72.
41. Holland CK, Zheng X, Apfel RE, et al. Direct evidence of cavitation in-vivo from diagnostic ultrasound. Ultrasound Med Biol 1996;22:917–925.
42. Delecki D, Child SZ, Raeman CH, et al. Ultrasonically induced lung haemorrhage in young swine. Ultrasound Med Biol 1997;23: 777–781.
43. Baggs R, Penney DP, Cox C, et al. Thresholds for ultrasonically induced lung haemorrhage in neonatal swine. Ultrasound Med Biol 1996;22:119–128.
44. Frizzell LA, Chen E, Chong L. Effects of pulsed ultrasound on the mouse neonate: hind limb paralysis and lung hemorrhage. Ultrasound Med Biol 1994;20:53–63.
45. Miller DL, Thomas RM. Thresholds for haemorrhages in mouse skin and intestine induced by lithotripter shock waves. Ultrasound Med Biol 1995;21:249–257.
46. Delecki D, Raeman CH, Child SZ, Carstensen EL. Intestinal haemorrhage from exposure to pulsed ultrasound. Ultrasound Med Biol 1995;21:1067–1072.
47. Taniyama Y, Tachibana K, Hiraoka K, et al. Local delivery of plasmid DNA into rat carotid artery using ultrasound. Circulation 2002;105:1233–1239.
48. Hynynen K, McDannold N, Vykhodtseva N, Jolesz FA. Non-invasive MR imaging-guided focal opening of the blood-brain-barrier in rabbit. Radiology 2001;220:640–646.

49. Ang E, Gluncic V, Duque A, et al. Prenatal exposure to ultrasound waves impacts neuronal migration in mice. Proc Natl Acad Sci USA 2006;103:12903–12910.
50. Skyba DM, Price RJ, Link AZ, et al. Direct in vivo visualization of intravascular destruction of microbubbles by ultrasound and its local effects on tissue. Circulation 1998;98:290–293.
51. Miller DL, Quddus J. Diagnostic ultrasound activation of contrast agent gas bodies induces capillary rupture in mice. Proc Natl Acad Sci USA 2000;97:10179–10184.
52. Van der Wouw PA, Brauns AC, et al. Premature ventricular contractions during triggered imaging with ultrasound contrast. J Am Soc Echocardiogr 2000;13:288–294.
53. Duck FA, Martin K. Trends in diagnostic ultrasound exposure. Phys Med Biol 1991;38:1423–1432.
54. Henderson J, Whittingham TA, Dunn T. A review of the acoustic output of modern diagnostic equipment. BMUS Bull 1997;November:10–14.
55. Keiler H. Epidemiological studies on adverse effects of prenatal ultrasound – what are the challenges? Prog Biophys Mol Biol 2007;93: 301–308.
56. Salvesen KA. Epidemiological prenatal ultrasound studies. Prog Biophys Mol Biol 2007;93:295–300.
57. Newnham J, Evans S, Machael C, et al. Effects of frequent ultrasound during pregnancy: a randomized controlled trial. Lancet 1993;342:887–891.
58. Stark C, Orleans M, Haverkamp A, Murphey J. Short and long term risks after exposure to diagnostic ultrasound in utero. Obstet Gynecol 1984;63:194–200.
59. Salvesen KA, Bakketeig LS, Eik-Nes SH, et al. Routine ultrasonography in utero and school performance at age 8–9 years. Lancet 1992;339:85–89.
60. Salvesen KA, Vatten LJ, Eik-Nes SH, et al. Routine ultrasonography in utero and subsequent handedess and neurological development. BMJ 1993;307:159–164.
61. Keiler H. Epidemiological studies on adverse effects of prenatal ultrasound – what are the challenges? Prog Biophys Mol Biol 2007;93:301–308.
62. Neilson JP. Ultrasound for fetal assessment in early pregnancy. Cochrane Database Syst Rev 1998;4: Art. No. CD000182/
63. BMUS. Guidelines for the safe use of diagnostic ultrasound equipment. 2009. www.bmus.org
64. EFSUMB. European Committee of Medical Ultrasound Safety. Clinical Safety Statement for Diagnostic Ultrasound – 2008 (www.efsumb.org).
65. Barnett SB, ed. Conclusions and recommendations on thermal and non-thermal mechanisms for biological effects of ultrasound. In: World Federation for Ultrasound in Medicine and Biology Symposium on Safety of Ultrasound in Medicine. Ultrasound Med Biol 1998;SI 24:1–55.
66. Barnett SB, Duck F, Ziskin M. Recommendations on the safe use of ultrasound contrast agents. Ultrasound Med Biol 2007;33:173–174.

CHAPTER

5 Artefacts in B-mode scanning

David O. Cosgrove

INTRODUCTION 61
NOISE 61
SCATTERING AND SPECULAR INTERFACES 61
SHADOWING AND INCREASED SOUND TRANSMISSION 64
MULTIPLE ECHOES 65
VELOCITY ERRORS 68
BEAM WIDTH 72
TIME SAMPLING PROBLEMS 74
ARTEFACTS IN THREE-DIMENSIONAL SCANNING 75

INTRODUCTION

Strictly, an artefact is any man-made object; in radiology the term is used in a looser sense to describe unwanted information generated in the process of image formation.[1,2] Most artefacts interfere with interpretation, though there are occasional 'friendly artefacts' which contain diagnostically useful clues (e.g. acoustic shadowing). Ultrasound is particularly prone to artefacts: their recognition and avoidance form a major part of the skill and art of sonography.[3]

NOISE

Two types of noise beset all imaging systems: random and structured. All electrical components produce random voltage changes at low level; when these are amplified they appear as a fluctuating, moving pattern of fine grey spots resembling a snowstorm. Since the scanner's electronic components are designed to keep such noise at low levels, it is only seen when high degrees of amplification are applied and so is usually most obvious in the deeper parts of the image where the time gain control (TGC) amplifier adds most to the overall receiver gain (Fig. 5.1). Noise is also produced by tissue where it arises from random vibrations of molecules. Noise sets the limit to the maximum depth that can be reached at a given transducer frequency. Because this type of noise is random in time, its effects can be reduced by temporal smoothing (the scanner controls for this are labelled 'frame averaging' or 'persistence' on some machines). With this technique the information in two or more images is added together. The 'real' information is reinforced while the random noise tends to cancel out. Another way to reduce the impact of noise is to encode the transmitted pulses so that the corresponding echoes can be picked out from the noise by recognising the encoded signature in the receive circuitry. This approach has been implemented in high-end scanners and allows the use of higher-frequency transducers, thus improving the spatial resolution of the images.

Noise

- May be random, producing a snowstorm pattern.
- May be structured, producing bands or stripes recognised by their non-anatomical appearance.

Random noise may also be produced by electrical interference but in this case it usually forms patterned signals such as flashes or bars in the image; structured noise such as this is known as clutter (Fig. 5.2). It is caused by pick-up of extraneous signals in the radio-frequency band, the transducer acting as an antenna, or by electrical pulses breaking through into the mains or interconnecting cables to attachments such as recorders. The noise they produce is usually obviously artefactual, the interference appearing randomly or intermittently, sometimes coinciding with the switching of a nearby motor or diathermy unit. Transient pulses can also wreak havoc with the digital circuitry of the scanner computer, causing it to lock up or otherwise misbehave. Mains filters or even shielding of the scanning room may be required in severe cases.

Structured noise can also be caused by body or probe movements. In practice these are usually too low in amplitude to produce detectable signals in B-mode but they are important as motion artefacts in Doppler. However, in phase inversion harmonics, used either in the tissue harmonic mode or with microbubbles, motion artefact can be apparent as flashes of grey highlights when the probe is swept across a structure.[4] This arises because the system is sensitive to differences between sequential pulses (see Chapter 6).

There are numerous other sources of noise such as interference from the scan-head motor and faulty connections and soldered joints which may affect ultrasound scanners, but they are uncommon and generally not diagnostically confusing, though rectification requires specialist service engineers. Structured noise due to multiple reflections and side lobes is discussed in the section on multiple echoes later in the chapter.

SCATTERING AND SPECULAR INTERFACES

Two distinct types of ultrasound echo formation are recognised and each produces important artefacts. Echoes arising from small regions[5] (around the ultrasound wavelength, say 0.1–1 mm) where there is a change in impedance are known as scattered echoes because they are sent out more or less uniformly in all directions.[6] It follows that the amount of ultrasound energy returning to the transducer from each scattering structure is extremely low (e.g. if the scattering is truly omnidirectional, then only some 0.25% is received by the transducer, depending on its diameter and on the depth of the scatterer); generally this signal will be too weak to be detected. However, when a group of such weak scatterers lies in the beam (this is the usual situation when, for example, they are the surfaces related to liver lobules or renal tubules), the echoes combine to form an interference pattern, cancelling out in some directions but summing in others to produce signals strong enough to be detected (Fig. 5.3). The near-random pattern that results is known as speckle: it is the acoustic equivalent of the speckled texture seen

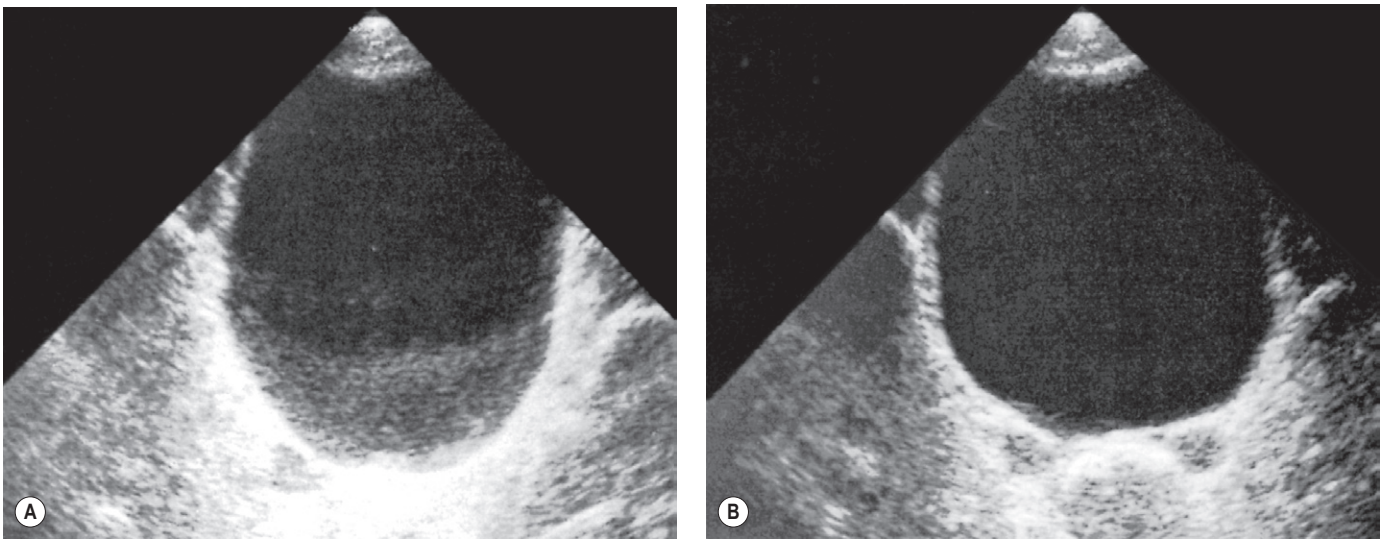


Figure 5.1 Gain-related noise. A: The combination of high overall gain and the high TGC amplification at depth may produce random noise in the image. Though this is present throughout the deeper parts of the image, because it is masked by the echoes from tissue structure, the noise is most obtrusive in echo-free regions such as within the urinary bladder. **B:** In this case, correction of the excessive gains removed the noise but this cannot always be achieved without also darkening the structure whose display is required.

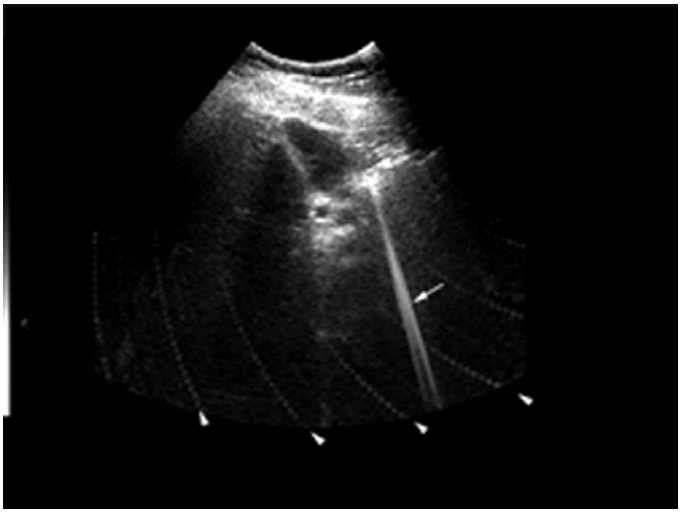


Figure 5.2 Structured noise. Persistent oblique bars (arrowheads) on these images were found to be due to electrical interference to the scanner by a nearby diathermy apparatus. Similar effects can be produced by radio transmitters and by stray fields from poorly shielded television monitors and video recorders. CB radio transmitters are particularly troublesome offenders. Note also the comet-tail artefact (arrow) (see also Fig. 5.15).

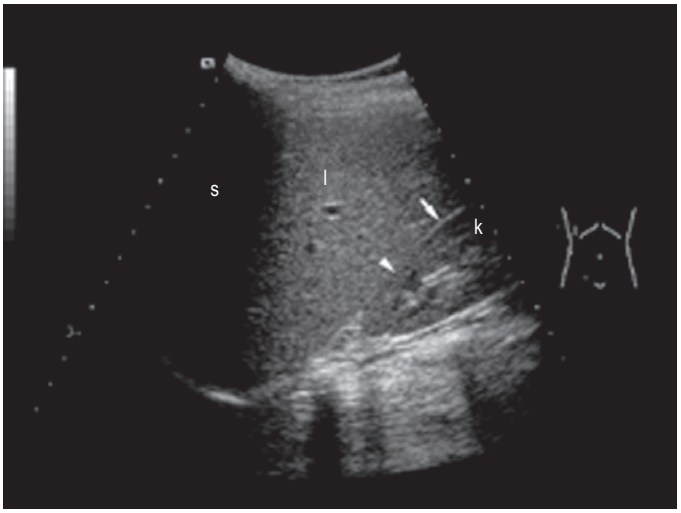


Figure 5.3 Specular and scattered echoes. Scattered signals account for the low-intensity parenchymal echoes from the liver (l) and kidney (k). Their appearance is independent of the direction of the ultrasound beam. Specular echoes arise from the flatter structures of the peritoneal and fascial layers separating the liver from the kidney. These echoes are strongly dependent on the angle between the beam and the surface, being intense when the surface is aligned at 90° (arrow) but weak or even completely absent when the beam runs along the interface (arrowhead). Note also the rib shadow (s).

under laser light, for example in a hologram. The ultrasound pattern, though isotropic (i.e. uniform regardless of scanning direction), is only indirectly related to the real tissue structure: the displayed texture is actually a convolution of the real structure by the ultrasound pulse shape. Thus a pixel on the ultrasound image of the parenchyma of, say, the liver cannot be expected to correspond to a histological interface in the organ. Because the speckle pattern is as much produced by the transducer as by the tissue, the same organ will produce a different texture with different transducers and tissues with different histological structures may have indistinguishable appearances on ultrasound – an example is the near-identical texture of liver and spleen.

When the reflecting surface is flat (relative to the ultrasound wavelength), it behaves like a mirror so that the direction of reflection equals the angle of incidence. Since the focused beam of ultrasound is not dispersed, all of the reflected energy can be picked up by the transducer so that the signals are much stronger than for scatterers. However, they are intensely directional and thus are only detected when the transducer is correctly directed, i.e. when the surface is at right angles to the beam in standard pulse-echo imaging. As the surface is tilted away from the right angle, the signal intensity falls off rapidly; in fact, were it not for the tolerance afforded by the beam width and the fact that real biological surfaces are rarely mirror-smooth, any tilting of the surface from 90° would cause the echo to be lost and this constraint would apply in both the scanned and orthogonal planes. In practice most interfaces are

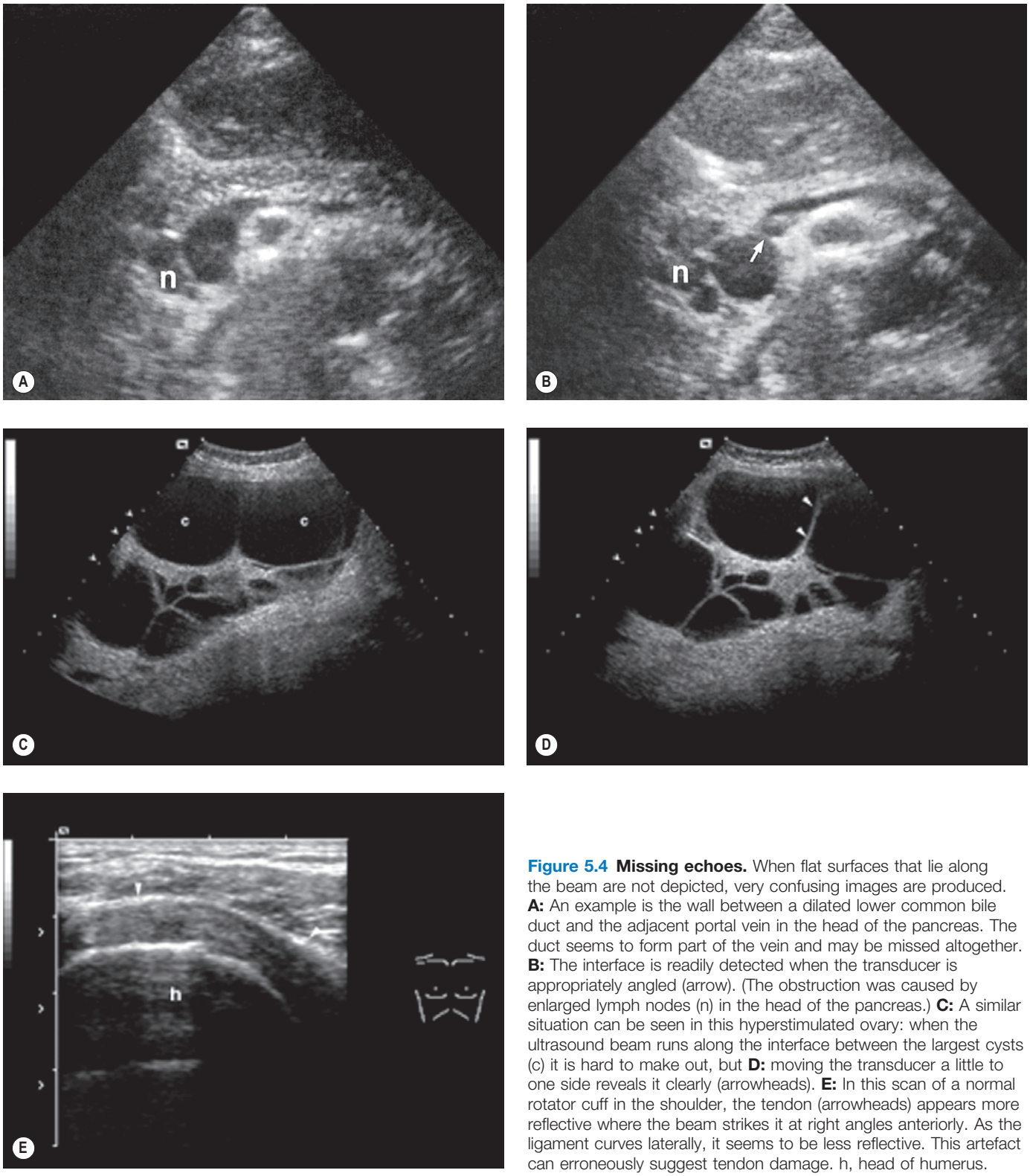


Figure 5.4 Missing echoes. When flat surfaces that lie along the beam are not depicted, very confusing images are produced. **A:** An example is the wall between a dilated lower common bile duct and the adjacent portal vein in the head of the pancreas. The duct seems to form part of the vein and may be missed altogether. **B:** The interface is readily detected when the transducer is appropriately angled (arrow). (The obstruction was caused by enlarged lymph nodes (n) in the head of the pancreas.) **C:** A similar situation can be seen in this hyperstimulated ovary: when the ultrasound beam runs along the interface between the largest cysts (c) it is hard to make out, but **D:** moving the transducer a little to one side reveals it clearly (arrowheads). **E:** In this scan of a normal rotator cuff in the shoulder, the tendon (arrowheads) appears more reflective where the beam strikes it at right angles anteriorly. As the ligament curves laterally, it seems to be less reflective. This artefact can erroneously suggest tendon damage. h, head of humerus.

detectable up to angles of more than 60°, albeit with diminished intensity, depending on the particular structures involved (Fig. 5.3). A situation where this may cause confusion is in scanning tendons, whose fibrillar structure gives strong echoes when they lie at right angles to the beam but at oblique angles appear as relatively echo-poor, simulating a tear or tendinosis.[7,8]

However, beyond some limiting angle, flat surfaces are not imaged and this can be confusing (Fig. 5.4). It accounts for the apparent communication sometimes seen between the inferior vena cava and the aorta when these lie close together, for the failure to image the sides of the globe of the eye, and for the invisibility of the superior surface of the urinary bladder in ascites scanned from certain angles. Such 'missing' surfaces can be demonstrated by scanning from other angles: the sonographer needs to be aware of the problem to avoid serious diagnostic errors.

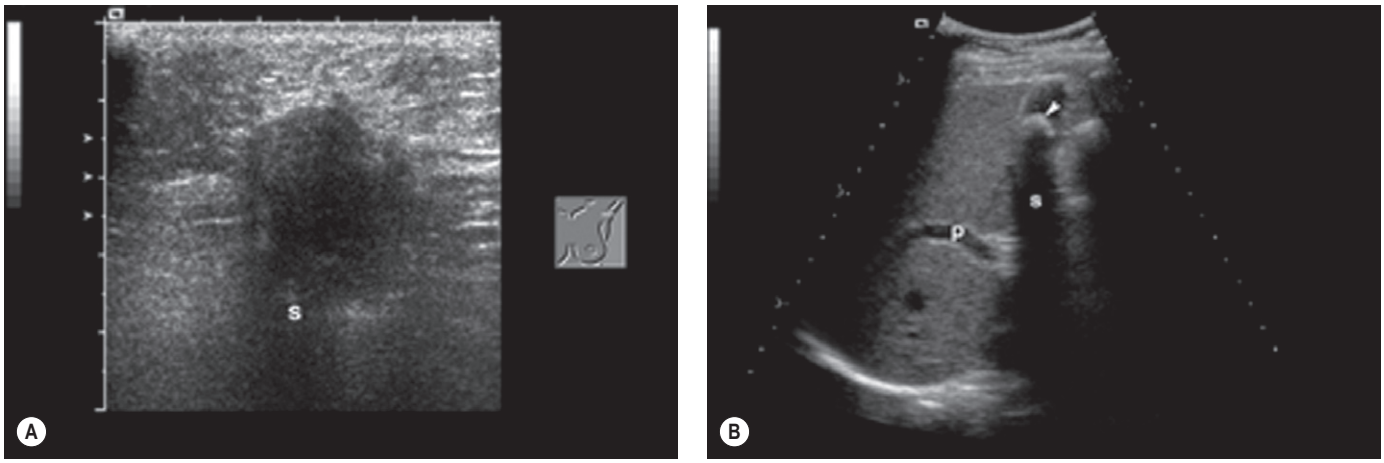


Figure 5.5 Acoustic shadowing. When a structure absorbs more sound energy than its surroundings, the TGC correction is inadequate for that region and the deeper structures appear darker: this is known as acoustic or distal shadowing. **A:** Produced by fibrosis in a breast surgery scar and **B:** by gallstones in the gallbladder (arrowhead). p, portal vein; s, shadowing.

Table 5.1 Types of shadowing

Type	Source
Attenuation	Attenuation higher than TGC compensation
Reflective	Near-total reflection
Edge	From curved surfaces

Interfaces

- Speckle is often misinterpreted as information.
- Loss of signal from specular interfaces beyond a critical angle leads to confusing gaps in the image.
- Mirror artefacts can be very confusing, especially from pelvic bowel gas.

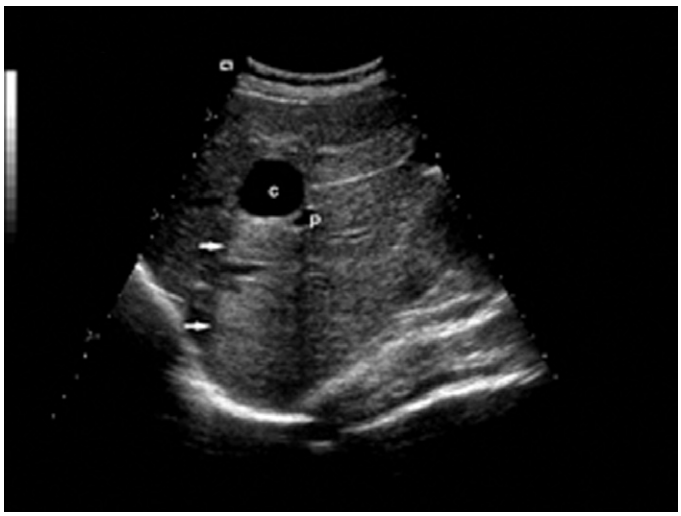


Figure 5.6 Increased through transmission. The fluid in a cyst absorbs very little of the sound energy passing through it so that the TGC, which has been adjusted to correct for attenuation in the surrounding tissues (here, the liver) is locally excessive. The deeper tissues are depicted as being more reflective giving a lighter band (arrows) known as distal or acoustic enhancement. c, cyst; p, portal vein.

SHADOWING AND INCREASED SOUND TRANSMISSION

The commonest form of shadowing (and its counterpart, increased through transmission of sound) are perhaps not true artefacts and their presence provides important diagnostic information about the attenuation of the tissues responsible for them (Table 5.1).[9,10] Shadowing occurs when a region of the tissue has a higher attenuation coefficient than the majority of the tissue in the scan; since the TGC (which corrects for the attenuation with depth) can only be set for an average value, an inadequate correction will be applied to this region so that both it and the tissues deep to it are depicted as less reflective than they actually are (Fig. 5.5). The dark band is referred to as an acoustic or distal shadow. Conversely, if a region of tissue attenuates less than its surroundings, echoes from it and the deeper tissue are overcorrected and appear as a bright band known as 'enhancement' but, in view of the enhancing effects of microbubble contrast agents (see Chapter 6), it is perhaps better termed 'increased through transmission' or 'distal bright-up' (Fig. 5.6). The degree of shadowing and increased sound transmission is determined by the difference in attenuation from the surrounding structures as well as the path length through the anomalous region. Thus these effects provide clues to the attenuation of the tissue regions responsible – they can be thought of as 'friendly artefacts'. Ways to reduce shadowing and increased through transmission have been developed and promise to facilitate correct setting of the TGC.[3]

Since shadowing is simply loss of acoustic signal for a tissue region, it can also be produced by an extremely efficient reflector (Fig. 5.7).[11] Gas bubbles or regions of calcification, for example, where 99% and 80% of the incident sound beam is reflected back respectively, cast acoustic shadows because very little of the sound energy penetrates to insonate the deeper tissues (in addition, any echoes from them would probably not cross the reflective layer on the return journey since they would be re-reflected distally).

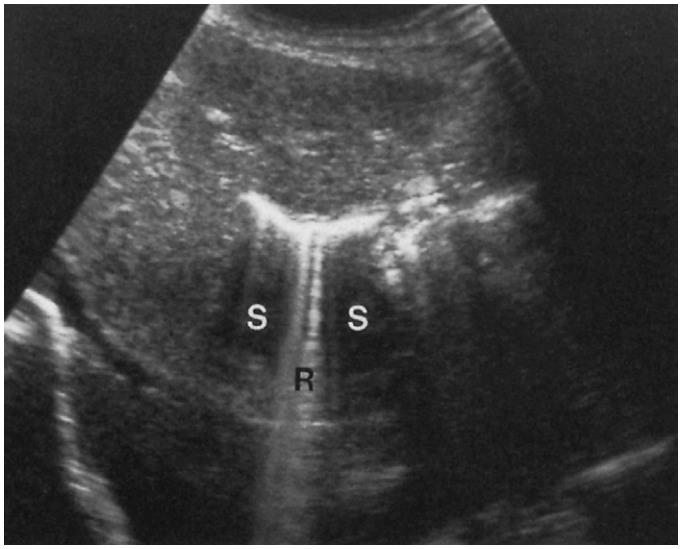


Figure 5.7 Reflective shadowing. When an interface reflects all or almost all of the incident sound energy, a situation that is typical of gas (here, gas in the common bile duct), so little penetrates that a band of distal shadowing (S) results. Though the effect is the same as with absorptive shadowing (compare with Fig. 5.5), the mechanism is different. The intense flat reflector that the gas forms often leads to reverberation artefacts (R) that partially fill the shadow (compare with Fig. 5.14).

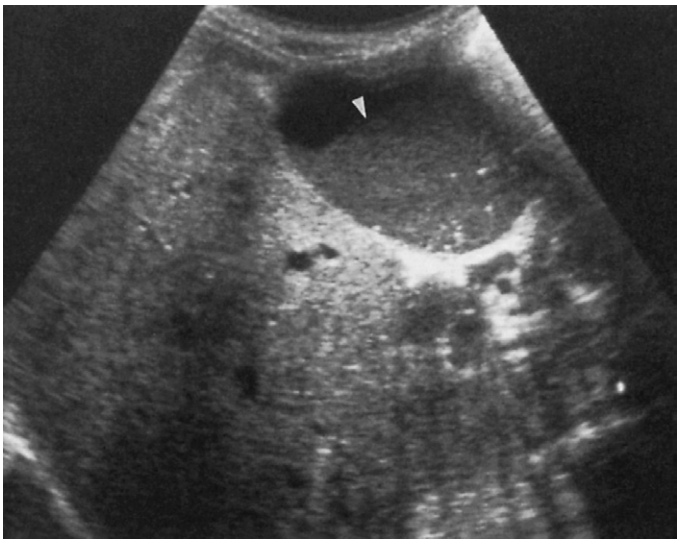


Figure 5.8 Echogenic fluid. Since in many real situations only a small amount of energy is removed from the beam by reflection, it is quite possible to encounter debris-containing fluids that are accompanied by enhancement. In this example echogenic bile (arrowhead) partly fills the gallbladder.

Sound transmission

- May be 'friendly', as increases behind cysts.
- Intense shadowing deletes information.
- 'Enhancement' suggests an effect of microbubble contrast agents, so 'increased sound transmission' is preferred.

However, it should be noted that, for most soft tissues, only a small proportion of the loss of energy from the beam (i.e. the attenuation) is due to reflection (in fact only between 1% and 20%) so that echogenicity does not correlate closely with attenuation. Echogenic fluids (e.g. crystalline bile or a pyonephrosis) are examples where strong echoes are associated with increased through transmission (Fig. 5.8).

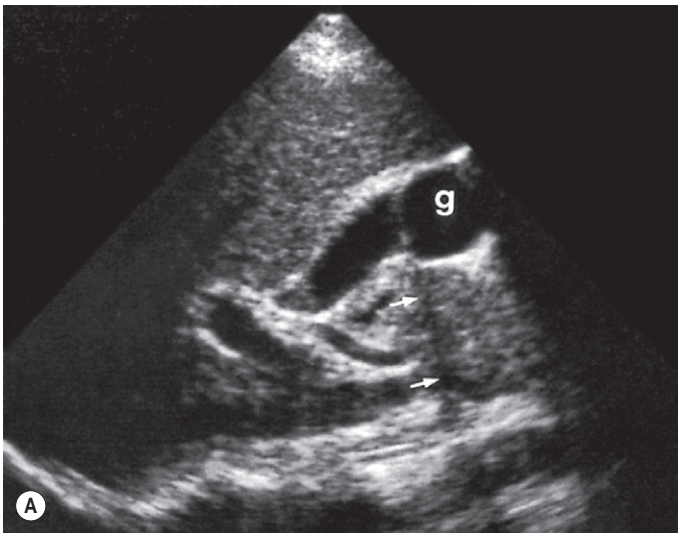
An interesting and sometimes confusing form of shadowing occurs deep to the edges of strongly curved surfaces such as vessels, cyst walls and fetal skull (Fig. 5.9). Fine, dark lines are seen extending distal to such edges; in the case of a cyst, they are striking by contrast with the increased through transmission behind the cyst itself. Two explanations have been offered (Fig. 5.10). In the refractive model, the ultrasound beam is dispersed as it is reflected from the curved edge because the leading edge of the ultrasound beam strikes it at a different angle than the trailing edge. Thus the ultrasound energy is spread through a larger tissue region and so the returning echoes are weaker, resulting in a 'shadow'; at the same time, the velocity differences may focus the beam in the region immediately deep to the structure, increasing the signals here.[12] Simple geometric reflection, as from a flat surface, would not have the same effect, for a mirror image of the tissues it strikes will be superimposed on the band immediately behind the edge; this is the mirror image artefact (see below). The other explanation presumes that the tissue of the wall of the curved structure has a higher attenuation than the surrounding tissue; the ultrasound beam passing along the edge must pass through three to four times as much of this tissue than that crossing at the diameter and therefore will be attenuated more. The effect is familiar to those who have used a hacksaw in plumbing: cutting a pipe is difficult at first, becoming easier towards the centre of the pipe before becoming more difficult again as the full thickness of the other side is cut. In this model the edge shadows are a form of attenuation, but only of the wall material, not of the contents. The two mechanisms could coexist in different situations.

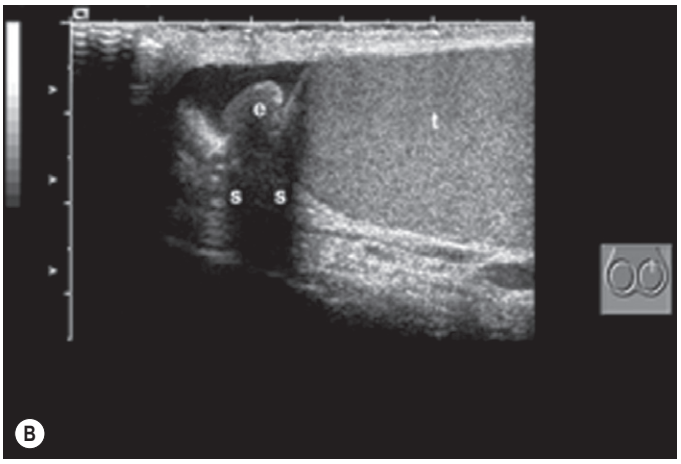
Edge or refractive shadows do not have the same diagnostic significance as bulk shadowing. Unfortunately, edge shadows commonly occur in situations where shadowing suggests calcification (e.g. in the kidney, arising from vessel walls in the renal sinus) or malignancy (e.g. in the breast, where they arise from Cooper's ligaments); they must be recognised for what they are and dismissed.

MULTIPLE ECHOES

A basic and critical assumption in pulse-echo ultrasound is that the ultrasound beam returns directly to the transducer after a single reflection.[13] Where the geometry allows multiple reflections to occur, multiple images are formed, and sometimes these are confusing. Repeat echoes are more likely to occur where the reflections are strong and this implies flat surfaces giving specular echoes. Since the path lengths for multiples are longer, the corresponding images are depicted as lying deeper in the body and they are weakened as the ultrasound is attenuated. Therefore, multiple echoes are more likely to be observed when the surfaces are close together and when the intervening tissue is of low attenuation, for example when it is a fluid.

An example of a single echo is the mirror image artefact where a repeat of a structure is depicted on the 'other side' of a specular reflector and equidistant from it.[14,15] This effect is readily demonstrated for the diaphragm: imaged from below through the liver, echoes commonly appear above the diaphragm and sometimes discrete structures in the normal liver or focal lesions can be recognised there (Fig. 5.11). This is not the appearance of lung (which is seen as an intensely reflective band when imaged intercostally) and is





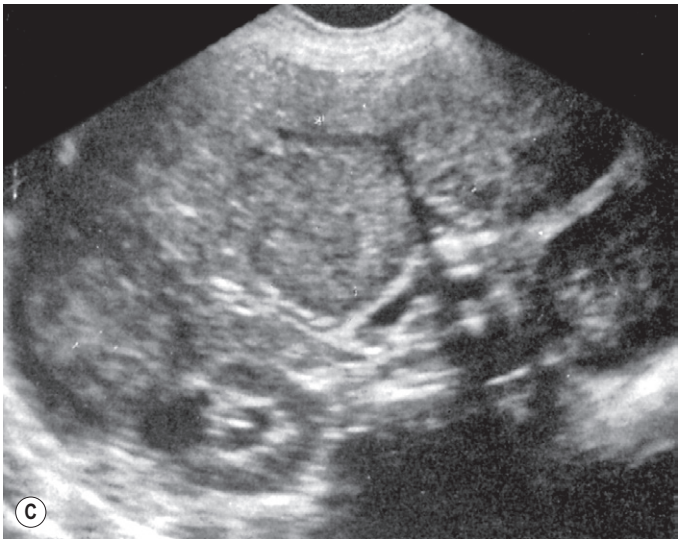


Figure 5.9 Edge shadows. Edge or refractive shadows (s) are commonly produced by smooth curved surfaces. In **A** such a shadow (arrows) is seen beyond a fold within the gallbladder (g), while in **B** the upper pole of a normal testis (t) and the surface of the head of the epididymis (e) have had the same effect. In **C** metastasis in the liver has produced an edge shadow from one margin.

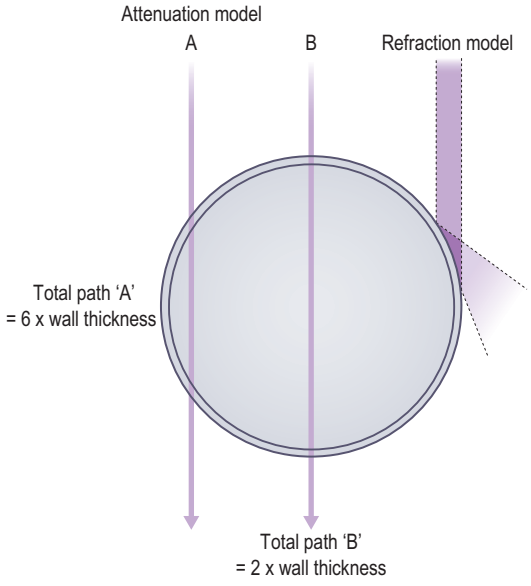


Figure 5.10 Mechanisms of edge shadows. Edge shadows are fine echo-poor lines extending deep to the edges of strongly curved structures. Two possible mechanisms are illustrated. On the left is the attenuation model, which proposes that the wall is more attenuating than the surrounding tissue; since the beam traversing the edge of the wall 'A' must traverse three times the thickness of the wall as the beam 'B' passing through the diameter of the curved structure, it is more heavily attenuated. On the right is the refractive model, which proposes that the beam is dispersed as it reflects from the curved edge which is struck at more than the critical angle; the returning echoes from the spreading beam have less energy than echoes from a confined beam, so that, even though they are reflected from the interfaces they encounter, their intensity is reduced. In either case the shadows should not be construed as signifying high attenuation, as would ordinarily be the case.

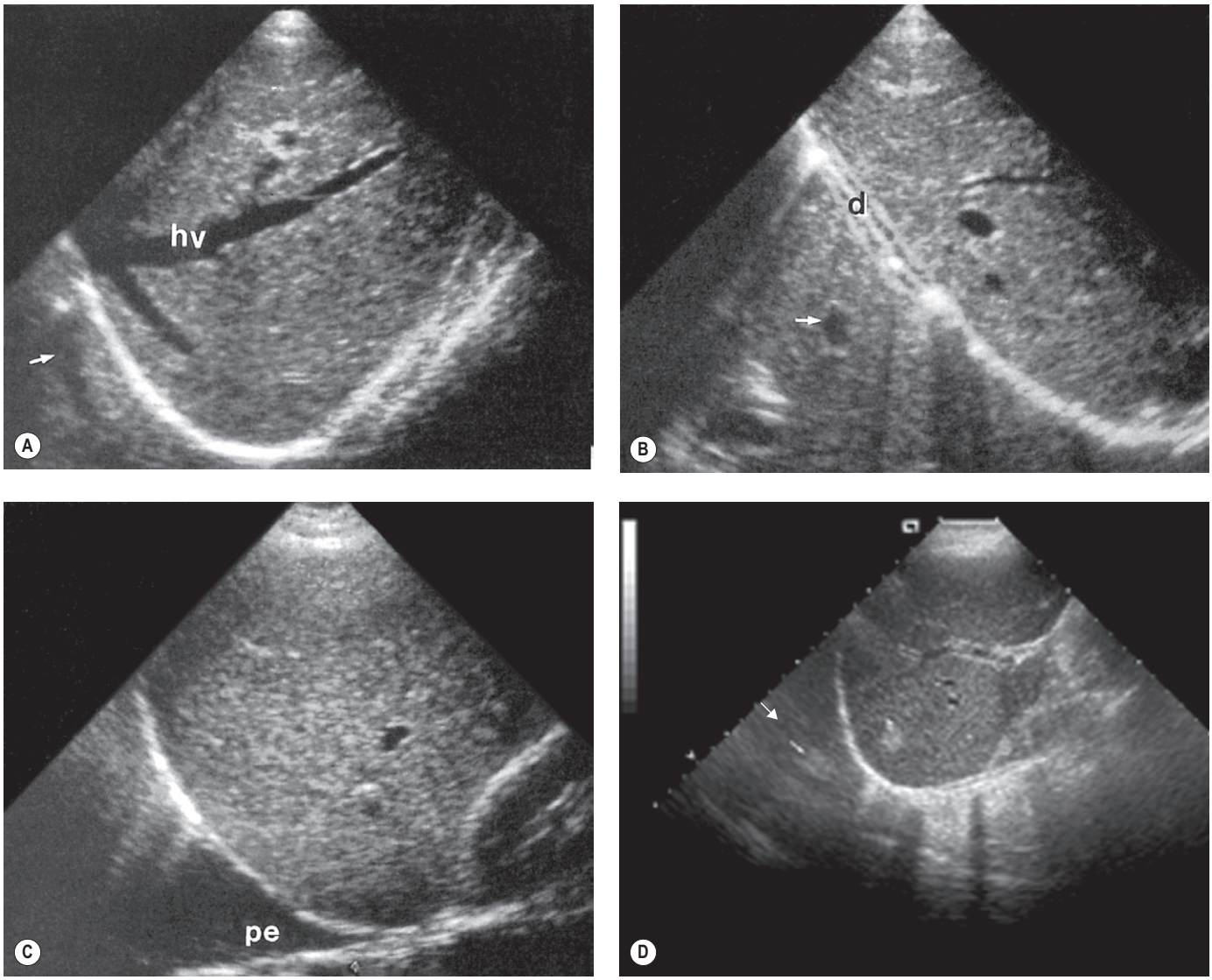


Figure 5.11 **Mirror image artefacts.** The apparent tissue normally visualised above the diaphragm in the right lower zone of the chest is actually artefactual, being produced by the air–pleura interface acting as an acoustic mirror. Sometimes recognisable structures feature in the artefact, forming 'ghost images'. An example **(A)** is a branch of the right hepatic vein (arrow), while in **B** a blood vessel (arrow) is cut in cross-section. In this image the diaphragm appears as a triple-layered structure: probably this is a mirror image of thickening of the diaphragmatic peritoneum. **C:** Since the artefact depends on reflection from the air surface, where this is replaced, such as by consolidation or a pleural effusion (pe), the artefact no longer occurs. **D:** Pathological changes may appear as 'ghost lesions'; an example is the haemangioma in the upper part of the right lobe of the liver. It has its mirrored counterpart (arrow), seemingly within the chest. d, diaphragm; hv, hepatic vein.

attributable to the beam reflecting back into the liver from the diaphragm.[16] Actually the reflecting surface is probably the air–pleura interface since the muscle of the diaphragm itself would be expected to act as a scatterer rather than a specular reflector.

Generally this artefact is not a diagnostic problem and on rare occasions it may actually be useful, for example when it reveals increased sound transmission beyond a peripheral liver cyst where it would otherwise be invisible as it falls onto the diaphragm; since this is already shown as a full white on the screen no further increase in intensity can be depicted. In other situations the mirror artefact is confusing; in the pelvis, for example, a repeat echo of the bladder or of structures immediately posterior to it (the rectum or sigmoid) may appear as a deeper line marking the back of an echo-poor mass (Figs 5.12 and 5.13). In fact the echo-poor region is the mirror image of the bladder. The typical position should arouse suspicion that it is artefactual and the back wall of the 'mass' often lies beyond the position of the sacrum and so is anatomical nonsense. A further clue is the weak superior and inferior walls compared to the strong anterior and posterior walls.

Multiple repeat echoes are known as reverberations. They are produced when two strong reflectors lie parallel to each other. By far the commonest example of this is when a flat surface such as a gas pocket or a stone is parallel to the skin surface where the skin–transducer interface forms the second reflector (Fig. 5.14). Ultrasound reflected from the gas travels back to the transducer in the usual way to generate a correctly placed image, but a proportion of the echo is re-reflected back into the tissue, retracing its path. On its second reflection from the gas surface it produces a second image at twice the depth of the real image. Sequential repeat echoes are depicted deeper behind the first ('real') echo. A striped pattern results, with the deeper multiple echoes becoming weaker because of loss of sound energy due to incomplete reflection at the surfaces and to attenuation by the intervening tissues. Since weaker echoes appear to be narrower than stronger ones, the reverberating bands

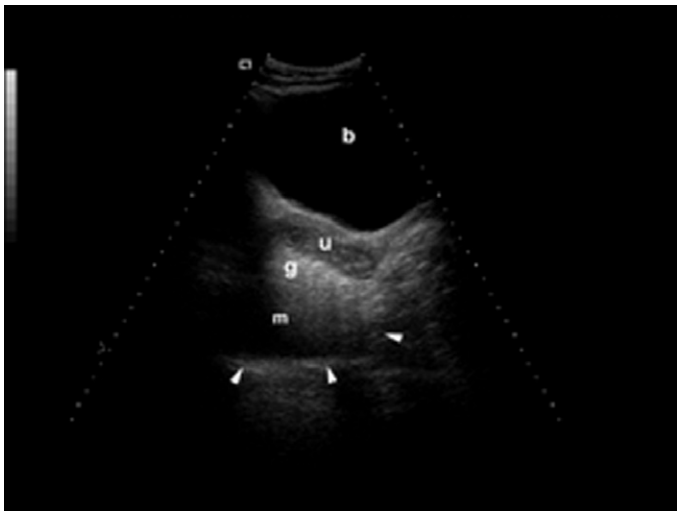


Figure 5.12 False pelvic mass. Ultrasound reflecting from the gas surfaces in pelvic bowel loops may be re-reflected into the tissues and produce a second-time-around echo depicted at twice the depth of the gas surface (arrowheads). Here it may simulate a deep interface forming the back wall of a pseudomass which is nothing more than a mirror artefact. The typical geometry, the anatomical impossibility of a mass lying so far posteriorly and the lack of superior and inferior walls are clues to its artefactual nature. b, bladder; g, gas in bowel; m, mass; u, uterus.

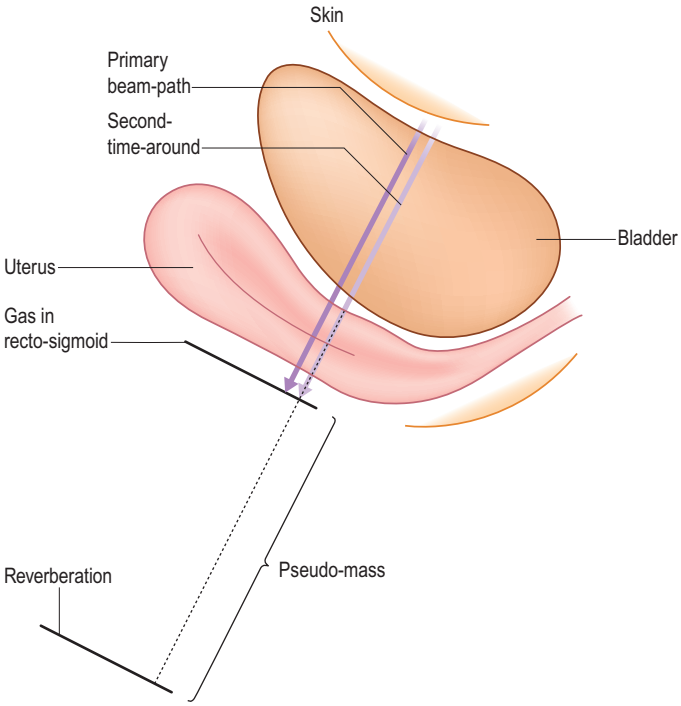


Figure 5.13 Mechanism of the false pelvic mass. The strong interface of bowel gas immediately posterior to the bladder acts as a mirror, reflecting the sound beam back to the transducer from which a proportion is re-reflected into the tissues to give a repeat or second-time-around image that simulates the back wall of a large pelvic mass.

Reverberation

- Multipath signals can be very confusing.
- Vigilance is required to avoid misinterpretation.
- Reverberations in cysts are especially troublesome.
- Sometimes helpful as 'comet tails' behind gas and metallic bodies.

become shorter as well as less intense with depth. The spacing between the bands depends on the distance between the reflectors; if they are very close together the echoes may merge to form a reflective band in which the individual components cannot be discerned (Fig. 5.15). A bright streak appears on the display, forming a tail distal to the image of the causal structure, itself usually strongly reflective. The whole complex looks rather like a comet with its bright tail.[17,18]

This 'comet-tail' artefact is commonly seen deep to calcifications[19] and foreign bodies such as surgical clips, implants (including IUCDs) and catheters. Bullets and shrapnel may also cause the comet-tail effect, as may small fluid cavities such as the Aschoff–Rokitansky sinuses in the wall of the gallbladder in adenomyosis. Presumably here the sound reverberates within each fluid space, echoing repeatedly from its walls. The same phenomenon probably accounts for the comet tail commonly seen distal to frothy or foamy collections of gas bubbles, the sound reflecting repeatedly from the outer surfaces of the gas bubbles in all directions within the intervening fluid so that a continuous stream of sound escapes, some of which returns to the receiving transducer. The effect is often observed from gas within the duodenal cap and is transient as a peristaltic wave moves the gas on.

VELOCITY ERRORS

An important assumption of the pulse-echo technique used in ultrasound imaging is that the velocity of ultrasound in soft tissues is constant. In fact this is not quite true, fat, for example, conducting ultrasound some 15% more slowly than most other soft tissues (Table 5.2).[20–23] Prosthetic materials show more marked deviations; for example, silicone used for breast augmentation and testicular implants has a sound speed of about half that of soft tissue.

The average velocity of 1540 m/s used to calibrate scanners corresponds to a delay-to-depth conversion constant and the scanner is calibrated so that every 13 μs delay in the echoes after the transmit pulse corresponds to 1 cm depth on the final image. Where a tissue conducts more slowly the echoes from deeper structures are further delayed and are therefore depicted as originating from deeper in the body (Fig. 5.16A).[23,24] This geometric distortion does not affect lateral dimensions of the image since this is set by the scanning action of the transducer rather than by the speed of sound. For the most part, velocity errors are too small to be clinically important, though, especially for silicone implants, the effects may be surprisingly marked. However, in ophthalmic measurements, where great precision is required, the distortion caused by the significantly higher velocity in the lens can be important. The speed of sound in the lens of the eye is 1620 m/s; regions of the retina imaged through it appear closer than the parts imaged through the sclera so that a shelf-like anterior distortion is produced (known as Baum's bumps after the sonologist who first described them; Fig. 5.16B).[25]

Changes in velocity also produce refractive artefacts: the ultrasound beam deviates from its straight line path when it crosses obliquely between two tissues of different velocities (Fig. 5.17). The beam is bent towards the 90° line when entering a 'slower tissue' and vice versa. The scanner, of course, continues to operate on the assumption that the beam follows a straight line so that reflectors distant to the surface are incorrectly plotted to the side of their true

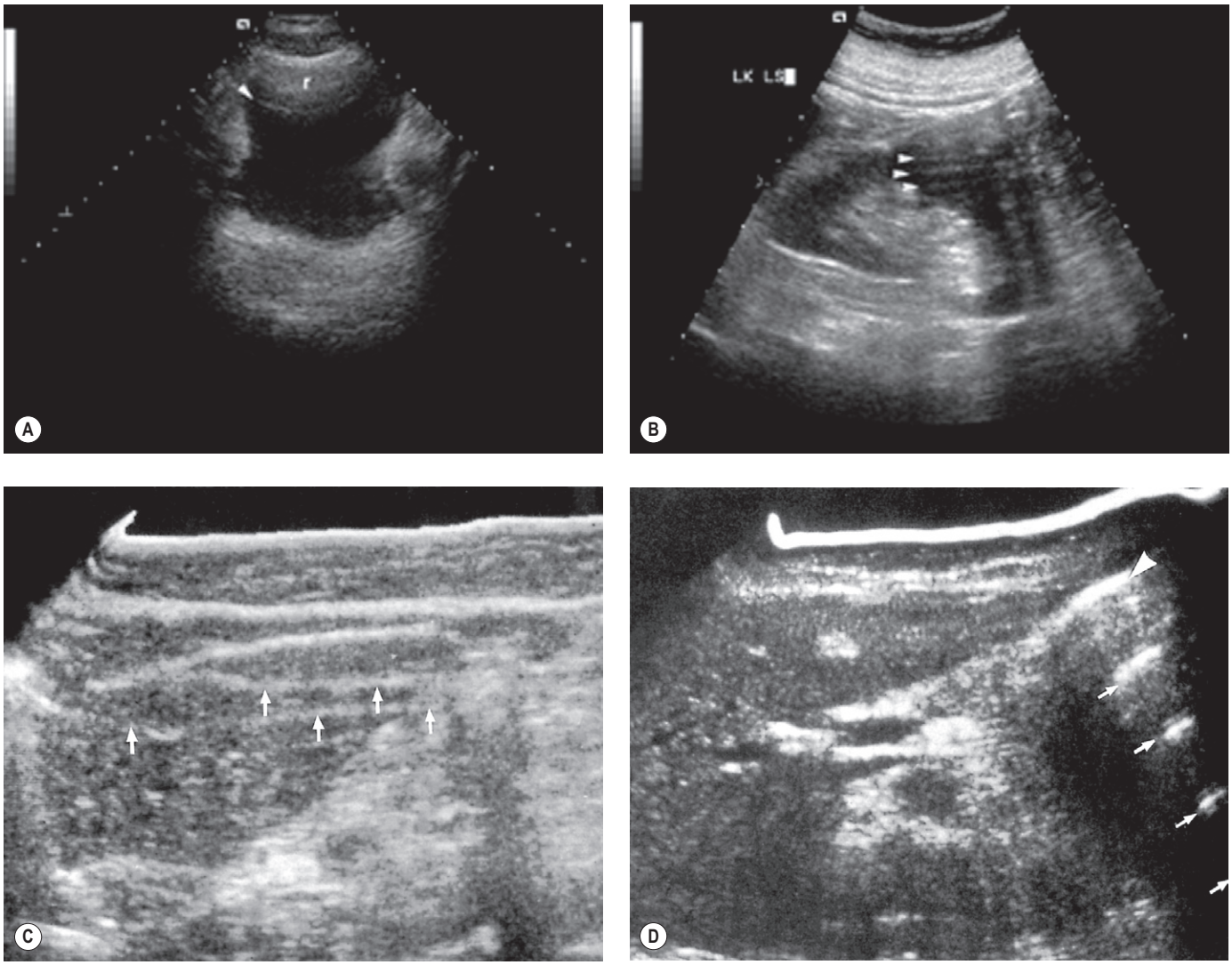


Figure 5.14 **Reverberation artefacts. A:** A second-time-around signal occurs when a strong reflector, in this example the anterior surface of the bladder, lies parallel to the skin-transducer surface so that some of the received signal is re-reflected into the tissue to be received as a false surface (arrowhead) at twice the depth of the real surface. The mechanism is the same as for the false pelvic mass (see Fig. 5.13) There are also complex reverberations (r) giving an impression of noise in the anterior part of the bladder. **B:** The same effect occurs in solid tissue, here across a kidney (arrowheads), though here it is often masked by the tissue echoes themselves.

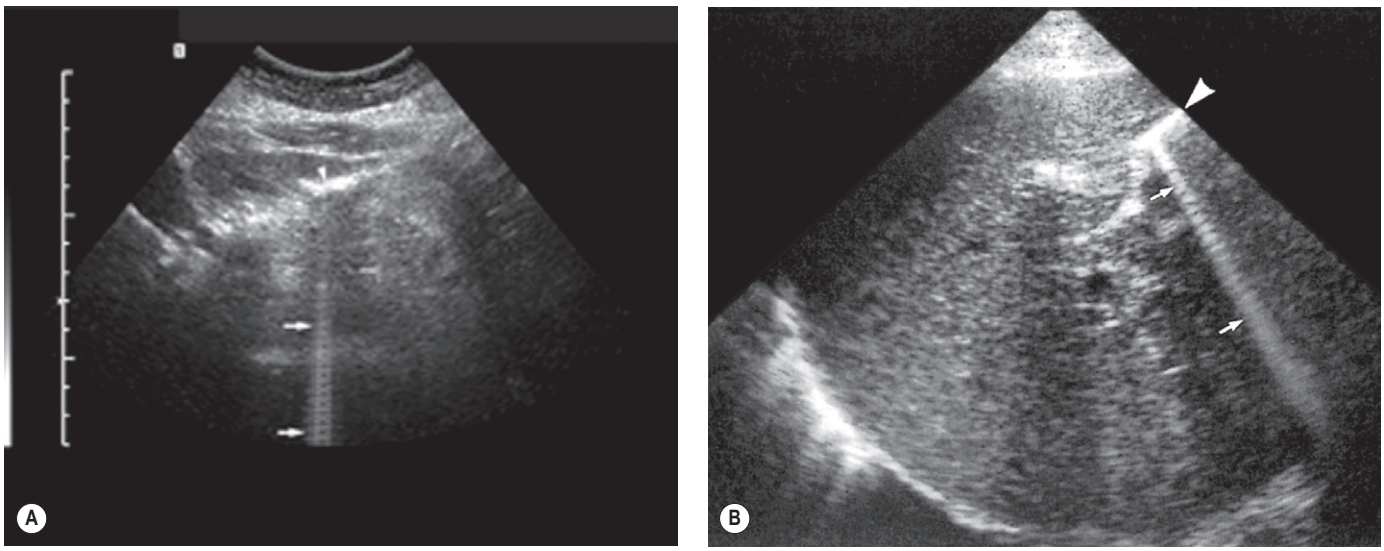


Figure 5.15 **Comet-tail artefact (A and B):** When a pocket of gas forms a foam, there is the possibility for multiple, almost random reflection paths between the bubbles to produce trains of echoes. They are seen as intensely reflective lines (arrows) extending deep to the gas. This is most commonly seen from the duodenum (arrowheads).

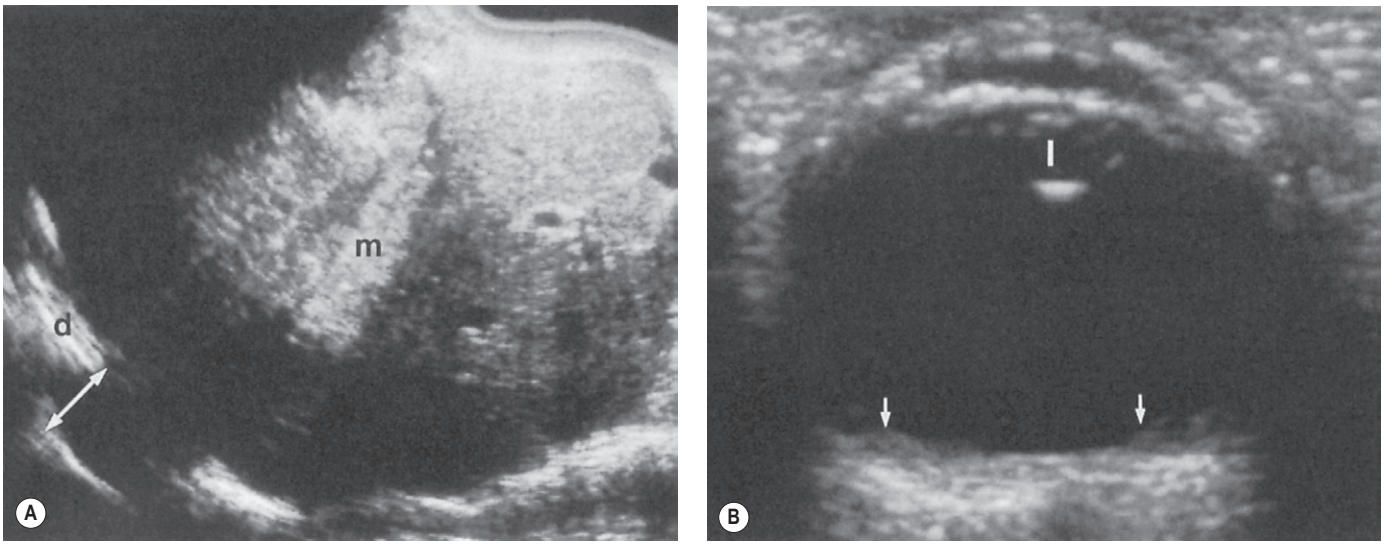


Figure 5.16 Velocity errors. When traversing a region where it is conducted slowly, the sound beam takes longer to complete the go-and-return pathway, so that echoes from beyond it are depicted deeper in the image than their real positions. **A:** In this example, a fatty metastasis (m) in the liver has slowed the sound beam so that the diaphragm (d) appears to have a shelf (arrow). **B:** The reverse situation, where a high-velocity region is traversed, as is the case for the lens (l) of the eye, moves the portion imaged through it closer. The resulting distortion, known as Baum's bumps (arrows), can cause serious errors in eye diameter measurements.

Table 5.2 Velocity of ultrasound in biologically important materials (from Wells,[20] Goss et al.[21] and Bamber[22])

Tissue type	Velocity (m/s)
Air	330
Fat	1450
Water (20°C)	1480
Amniotic fluid	1510
Brain	1565
Blood	1570
Kidney	1560
Muscle	1580
Liver	1600
Uterus	1630
Skin	1700
Lens of eye	1650
Fascia	1750
Perspex	2680
Bone	3500
Soft tissue average	**1540**

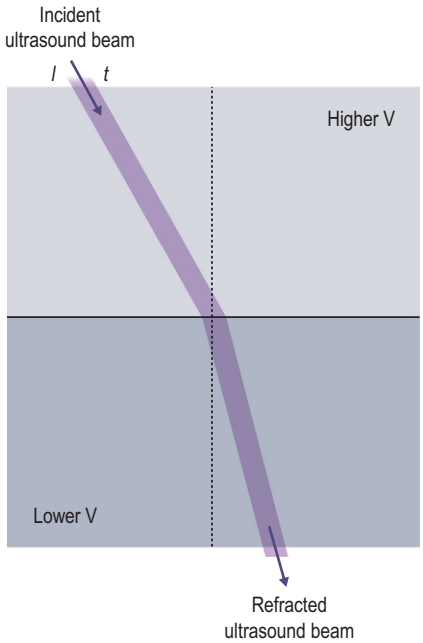


Figure 5.17 Refraction of ultrasound. When the ultrasound beam crosses obliquely between two tissues of differing velocities, the beam is refracted to emerge in a new direction. The situation is exactly the same as the refraction of a light beam. The diagram illustrates the effect of crossing into a material that conducts the ultrasound more slowly: the sound in the leading edge of the beam (*l*) is slowed first, while sound towards the trailing edge (*t*) is affected later. This results in the entire beam being refracted towards the 90° direction. The converse occurs when the deeper medium conducts faster.

position. The degree of displacement depends both on the speed of sound difference and on the distance of the object from the surface. A particular situation where this lateral distortion is important clinically is in transabdominal pelvic scans. The beam crossing the wedge-shaped fat space around the rectus muscles is refracted so that deep pelvic structures (e.g. the uterus or prostate) can appear stretched laterally (Figs 5.18 and 5.19).[26,27] A transverse obstetric measurement made under these circumstances may be in serious error. In extreme cases the object, for example a gestational sac, may seem to be duplicated giving rise to the false appearance of twins – this is one reason for the phenomenon of the 'vanishing twin' noted when ultrasound was first used in early pregnancy. The distortion disappears when the transducer is moved so as to image the pelvis through the centre of the muscle and this allows the appearance to be recognised as artefactual. It is also less common in longitudinal scans (because the alignment of the fat–muscle interface is changed) and in the epigastrium (presumably because there is less fat here).

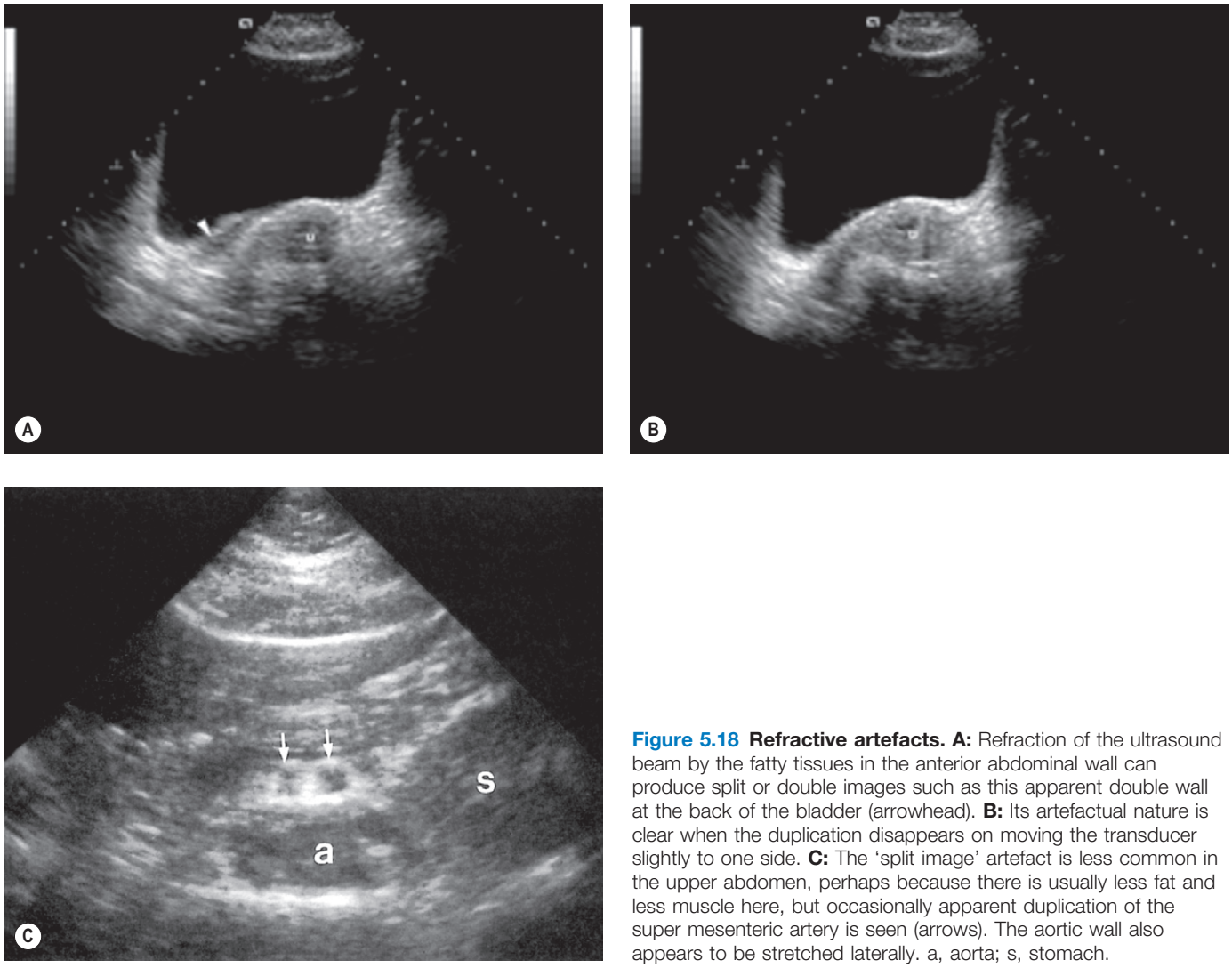


Figure 5.18 Refractive artefacts. A: Refraction of the ultrasound beam by the fatty tissues in the anterior abdominal wall can produce split or double images such as this apparent double wall at the back of the bladder (arrowhead). **B:** Its artefactual nature is clear when the duplication disappears on moving the transducer slightly to one side. **C:** The 'split image' artefact is less common in the upper abdomen, perhaps because there is usually less fat and less muscle here, but occasionally apparent duplication of the super mesenteric artery is seen (arrows). The aortic wall also appears to be stretched laterally. a, aorta; s, stomach.

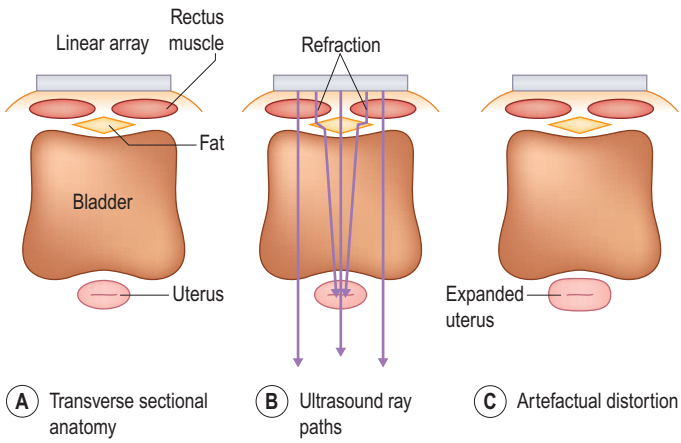


Figure 5.19 Double images in the pelvis. (A) When the ultrasound beam strikes the slower-conducting layer of fat, it is bent towards the midline so that medial structures are displayed lateral to their true position **(B)**. They therefore appear laterally stretched **(C)** or even duplicated, leading to confusing or even serious diagnostic errors.

Velocity errors

- Refraction errors produce stretched or even double images.
- Fat prism behind the linea alba is a common cause.
- Possible cause of 'lost twins' in early pregnancy.

The mechanism by which the ultrasound beam is focused depends on the compression and rarefaction waves of which it is composed coinciding in their proper phase at the focal zone and, in the same way, at the transducer surface during receive focusing. If the velocity in the intervening tissue is different from the calibrated value, the focal zone is shifted and, when the intervening tissue has heterogeneous velocities, defocusing will occur because the waves no longer coincide precisely, some arriving early when the propagation path includes tissues of a high velocity, others arriving late when the path includes fat, for example. The beam is thus defocused, degrading the lateral resolution. This effect partly accounts for the marked variation in ultrasound image quality from patient to patient, despite which the quality of images from obese subjects is sometimes surprisingly good. The larger the transducer aperture used, the worse the effect; this is probably why

sophisticated systems such as high-resolution linear arrays in which 500 or more elements are used to form each ultrasound line give such exquisite images in 'easy' subjects, but perform badly with 'difficult' subjects, in whom images from smaller, simple transducers may be less degraded.

BEAM WIDTH

Unfortunately the real ultrasound beam shape falls far short of the desired uniformly narrow laser-like configuration that would be optimal.[28] A typical actual focused beam (Fig. 5.20) consists of a disturbed region immediately in front of the transducer surface, then a near field that progressively narrows to the focus, after which it spreads rapidly in the far field. In addition to this main beam there are side lobes, low-energy beams directed at angles away from the centre line.

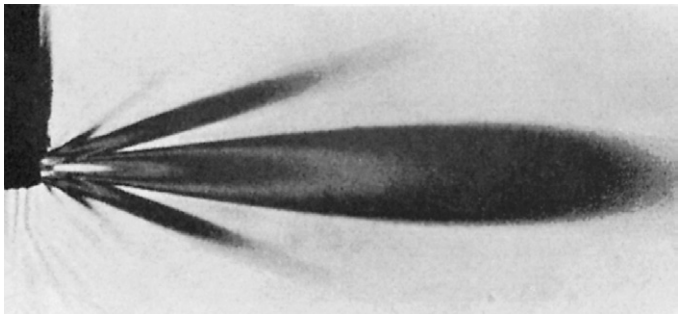


Figure 5.20 Ultrasound beam shape. In this Schlieren tank photograph of the ultrasound field from an unfocused disc transducer, the main beam is accompanied by several side lobes emitted at angles from the central axis. The width of the main beam limits resolution in the transverse direction. The side lobes cause falsely positioned images. (Taken by Hiedemann E and Osterhammel K; discussed in Hiedemann E and Osterhammel K, Optische Untersuchung der Richtcharakteristik von Ultraschallquellen. Z Phys 1937;107:272-282, Hiedemann E and Osterhammel K: Untersuchung von Schallamplitudenfeldern mittels einer Methode der Isochromaten. Proc Ind Acad 1938;8:275-80 and 1938;8:23, and Osterhammel K, Optische Untersuchung der Schallfelder kobenförmig schwingender Quarze. Akust Z 1941;6:78-86).

Axial resolution depends on the pulse length, which is mainly determined by the wavelength; typically this might be 0.3 mm for a 5 MHz transducer and it does not change greatly with depth. In contrast, the width of the main beam defines the lateral resolution of the ultrasound image because adjacent objects can only be resolved separately if the beam is narrower than the distance between them.[29] If the beam is wider, they are depicted as one larger object on the screen. Because of the complex shape of the typical practical ultrasound beam, lateral resolution varies with depth, being best at the focal zone and deteriorating rapidly beyond it.

The edges of the beam are not sharply defined; the ultrasound energy is concentrated on the centre line of the beam and falls off progressively from the centre line with a Gaussian distribution. This means that a strong reflector will continue to give detectable echoes further from the central axis than a weak reflector. In clinical terms this means that the resolution of ultrasound is better for weak reflectors. Strong reflectors tend to blur laterally and are therefore seen as cigar-shaped smears or streaks so that their width is exaggerated. This is the 'beam width artefact' (Fig. 5.21), and is most obvious when the smearing overlaps an echo-free structure, often encountered when a gassy or bony structure lies adjacent to a fluid space.[30] However, it also leads to the general tendency to fill in small echo-free regions, such as ducts, and in part for the discrepancy between the ultrasound and X-ray measurements of the calibre of the bile and pancreatic ducts (the remaining discrepancy being attributable to the magnification on X-ray and to duct dilatation caused by contrast agents).

Beam width artefacts also occur in the orthogonal plane, i.e. in the slice thickness. With circular transducers (either the simple disc type or annular arrays) the beam is symmetrical in all planes but, for linear and phased arrays, the beam is wider in the orthogonal plane. These artefacts are exactly the same as the slice thickness artefact in CT except that the ultrasound beam is not uniform with depth; low-level information derived from signals in adjacent planes is spuriously depicted in the image plane.[31,32] Typically, bands or lines are noted within echo-free spaces (Fig. 5.22). They

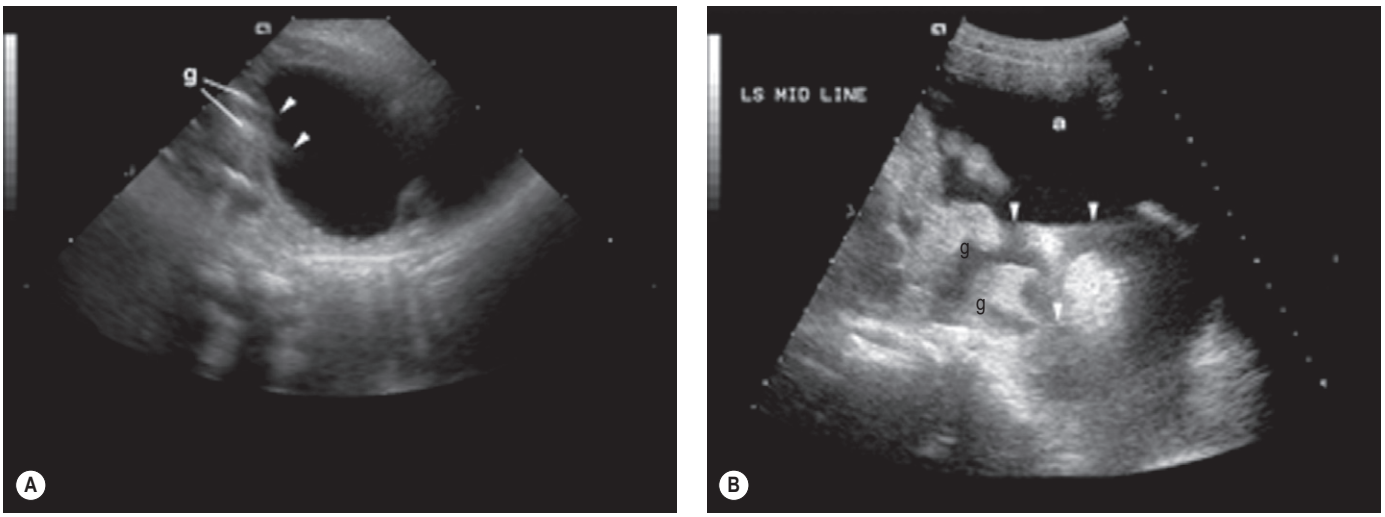


Figure 5.21 Beam width artefact. Echoes arising from structures at the edge of the ultrasound beam, which has a finite width, are depicted as lying in the centre line of the beam. The more intense the reflection, the further off-axis its echoes will be received. **A:** In this example the strong echoes from a pocket of gas in pelvic gut loops (g) smear across the bladder (arrowheads). **B:** A beam spread artefact misplaces echoes from the reflective gas in gut loops (g) spread across the ascitic fluid (arrowheads). As is often the case with artefacts, they are more obvious when the false signal overlies an echo-free region but, in fact, are present everywhere to a greater or lesser extent, depending on the beam shape (mainly determined by focusing) and the reflectivity of the off-axis interfaces. a, ascites.

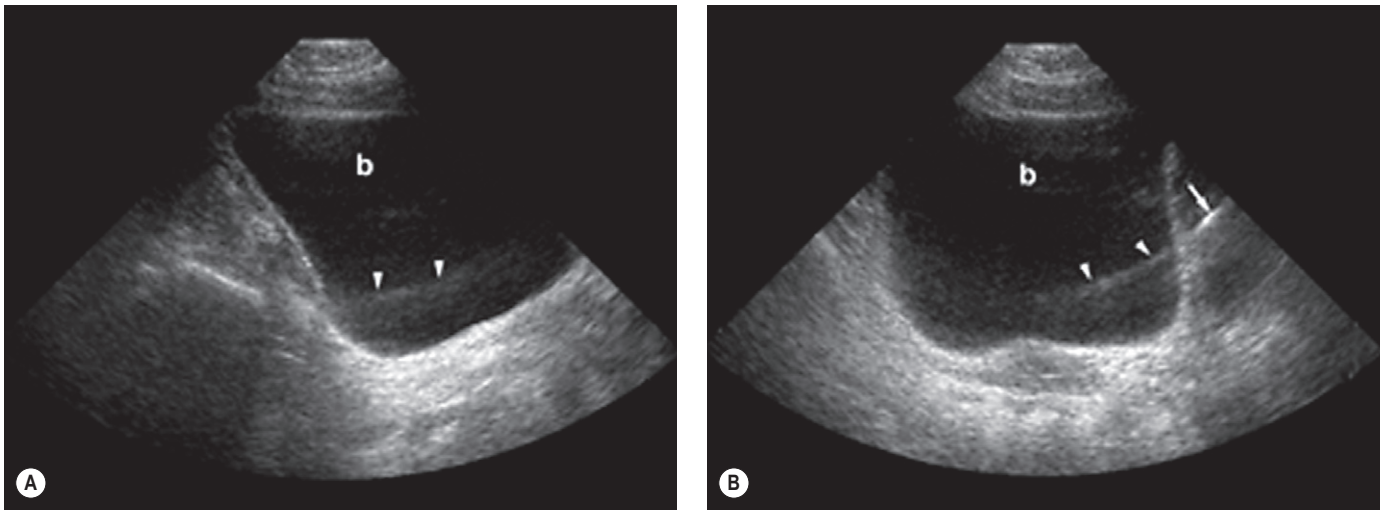


Figure 5.22 Orthogonal beam width artefact. A: The low-level echoes (arrowheads) within this longitudinal section of the bladder are not due to debris or echogenic urine but are a beam width artefact arising from gas in adjacent bowel loops seen in **B**, the transverse section (arrow); because the artefact arises out of the plane of the tomogram, this variant of the beam width artefact is more difficult to recognise. b, bladder.

may mislead the operator into thinking that the fluid contains debris. Because the 'offending' reflector is not visualised within the image, the orthogonal beam width artefact is more difficult to recognise than the same artefact occurring within the scanned plane.

Unfortunately, even this rather complex description of the shape of the ultrasound beam is incomplete because the profile is even further complicated by the inevitable presence of side lobes and, for array transducers, of grating lobes also.[33–35] Both these are misdirected, aberrant lines of ultrasound energy transmitted alongside the main beam. They have their exact counterpart in off-axis regions of sensitivity when the transducer is in the receive mode. Side lobes are generated as part of the beam focusing mechanism, whether by applied lenses or by curving of the transducer face, and consist of ill-defined beams, the first some 20° away from the main beam and much weaker than it (by about 40 dB). For a disc transducer they form a series of rings, while in the case of linear arrays they are asymmetrical, being differently positioned in the two planes.

Grating lobes are similar but are produced by array transducers of all types; however, they tend to be more discrete and powerful. Grating lobes are less marked when the elements are small and numerous because the array then approximates more closely to a continuous transducer. Because they are weaker than the main beam, only strong reflectors cause serious side and grating lobe artefacts in clinical practice but if a gas bubble or bone surface happens to lie at the position of a side lobe then its grating lobe echo will be depicted in the line of the main beam (Fig. 5.23). The result is a convex-shaped streak that has been dubbed the 'Chinese hat artefact' (Fig. 5.24). Because these artefacts may appear consistently on rescanning the same region, they may be rather confusing. Often the cause can be visualised within the image, but side lobes can extend beyond the imaged area and do also occur in the orthogonal plane. Because the same focusing mechanisms are used in Doppler, the same misregistration of signals may occur and be quite difficult to recognise.

The introduction of tissue harmonic modes has reduced some of these artefacts and produces cleaner images, especially in 'difficult' subjects.[36] They operate by exploiting the fact that harmonics are only generated at relatively high acoustic powers and so the lower powers that occur in side and grating lobes and in reverberations do not excite harmonics and therefore echoes are not detected (Fig. 5.25). Such harmonic signals are generated because tissue resists compression more than it resists expansion so that an ultrasound pulse that begins as a symmetrical sine wave becomes asymmetrical as it propagates through the tissue. The harmonics are represented by the asymmetry, and are much more strongly formed with higher sound pressures. There are two ways to exploit the phenomenon. In one, the receiver circuitry is tuned to accept echoes at twice the frequency of the transmitted sound. In another approach, the phase inversion mode, each image line is formed from the sum of the echoes from a pair of pulses sent in the same direction, the second of which is inverted with respect to the first. Where the sound is conducted in a linear fashion, the echoes are out of phase and cancel out, but asymmetries caused by non-linear conduction result in differences that do not cancel and these are used to form the image.

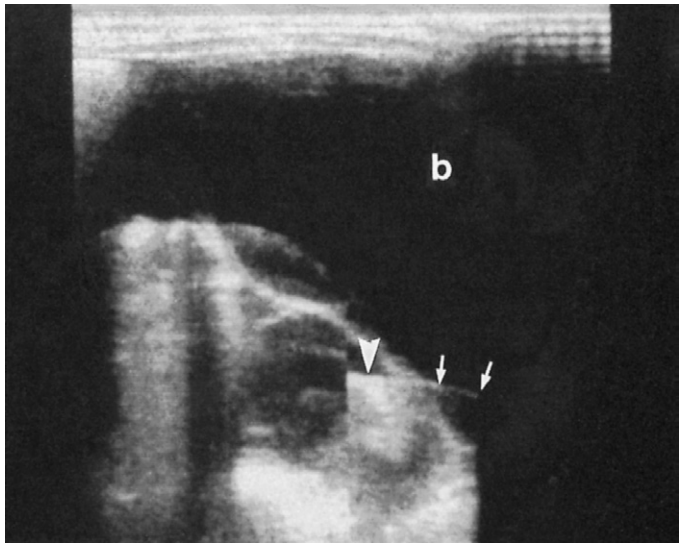


Figure 5.23 Grating lobe artefact. Grating lobe artefacts have essentially the same effects as simple beam spread artefacts but are more severe and only occur with array transducers. They often have a convex shape (arrows). This example arose from a gas-containing pelvic gut loop (arrowhead). b, bladder.

Beam width

- May produce lateral smearing of strong signals in the scan plane.
- Can exaggerate fetal measurements.
- Produce slice thickness effects in the z plane.
- Also occur with Doppler.

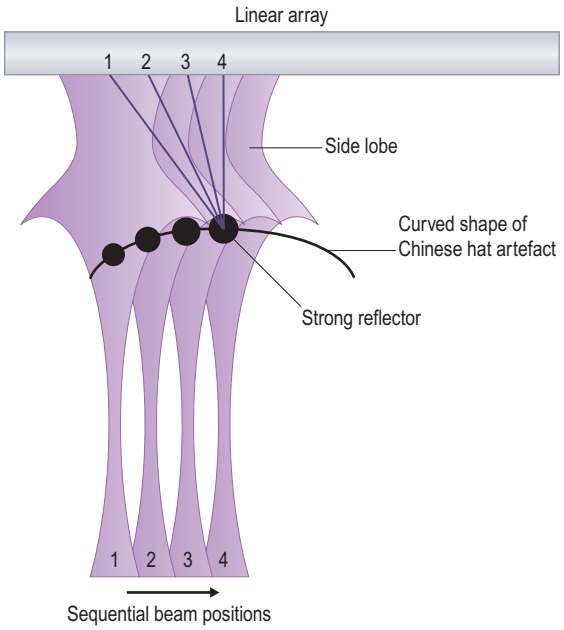


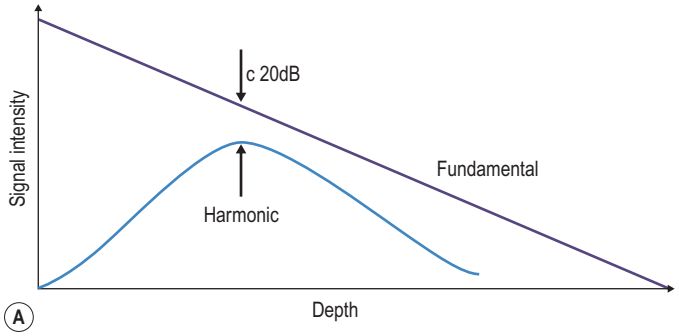
Figure 5.24 Mechanism of the Chinese hat artefact. When a side or grating lobe strikes a strongly reflective target (1), a weak signal will be received and registered as originating slightly deeper than the real target depth because the oblique line of sight takes longer for the beam to traverse than the direct line that results when the beam is correctly centred on the target (4). The result is a cigar-shaped artefact whose ends are depicted as lying deeper than the centre, recalling the shape of a Chinese hat.

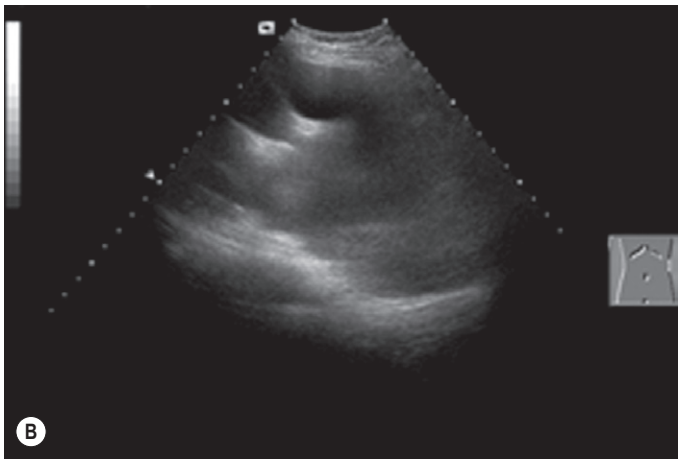
Both modes give cleaner images with less clutter; the phase inversion mode images have half the frame rate, while dual frequency harmonics have some compromise in spatial resolution because they use longer narrower band pulses. Both have limited depth penetration because the high powers that are critical to the generation of the harmonics are attenuated at depths greater about 10–15 cm.

TIME SAMPLING PROBLEMS

Some interesting and important artefacts arise from the fact that there is an upper limit for the rate at which ultrasound pulses can be repeated. This is set by the speed of sound in tissue and the depth penetration required. If the next pulse is sent before the deepest echoes from the first have faded away, then these late echoes will be received soon after transmission of the second pulse. The scanner has no means of identifying which pulse is responsible and wrongly plots these deep echoes as nearby reflectors from the second pulse (Fig. 5.26). The process is repeated for subsequent pulses. Thus a distant structure is imaged as though it lies close to the transducer. Flickering 'objects' are seen in the near field and their depth can be altered by changing the pulse repetition frequency (PRF).[37] Since the PRF is usually linked to the depth of field, they move with a change in scale. Properly adjusted scanners should not allow this effect to occur, though the constraints affecting duplex Doppler (both pulsed and colour) may force a compromise in this respect.

The limited frame rate can also obscure the motion of fast-moving structures such as heart valves, because their position is not being sampled sufficiently frequently for a true rendition of their movement to be displayed. Generally this results in a jerky, cartoon-like rendition of the movement, but in some cases the movement can seem to be slowed or even reversed in direction.[33]





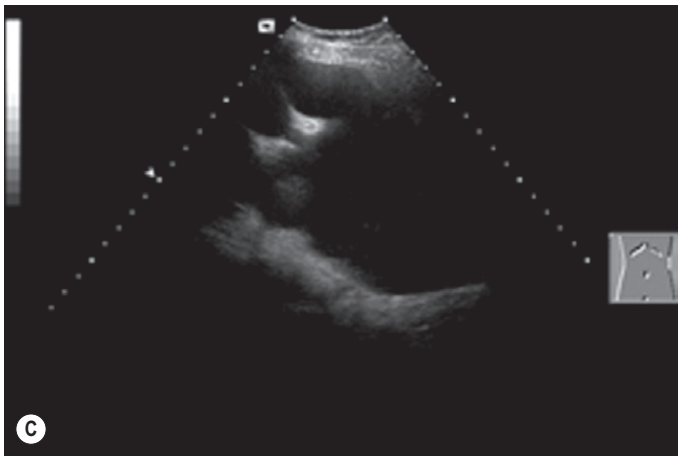


Figure 5.25 Tissue harmonics. A: Because their generation depends on the amount of acoustic pressure applied to the tissue, harmonics are always weaker than the fundamental echoes and fade off more with depth. They take a few centimetres to develop and so are less obvious in superficial tissues. Their effect is to improve contrast in the tissue because there are fewer reverberant and beam width artefacts since these both require higher energy levels than are seen in the reflections and in the side/grating lobes. **B:** In this example of a hydronephrosis, marked reverberant and beam width artefacts partly fill the pelvis with artefactual echoes; **C:** in the dual frequency harmonic image they have been greatly reduced and the image has been 'cleaned up'.

Time sampling

- 'Second-time-around' artefacts place objects falsely close to the skin.
- Occur when high PRFs are used.
- Especially common in Doppler of renal artery stenosis.

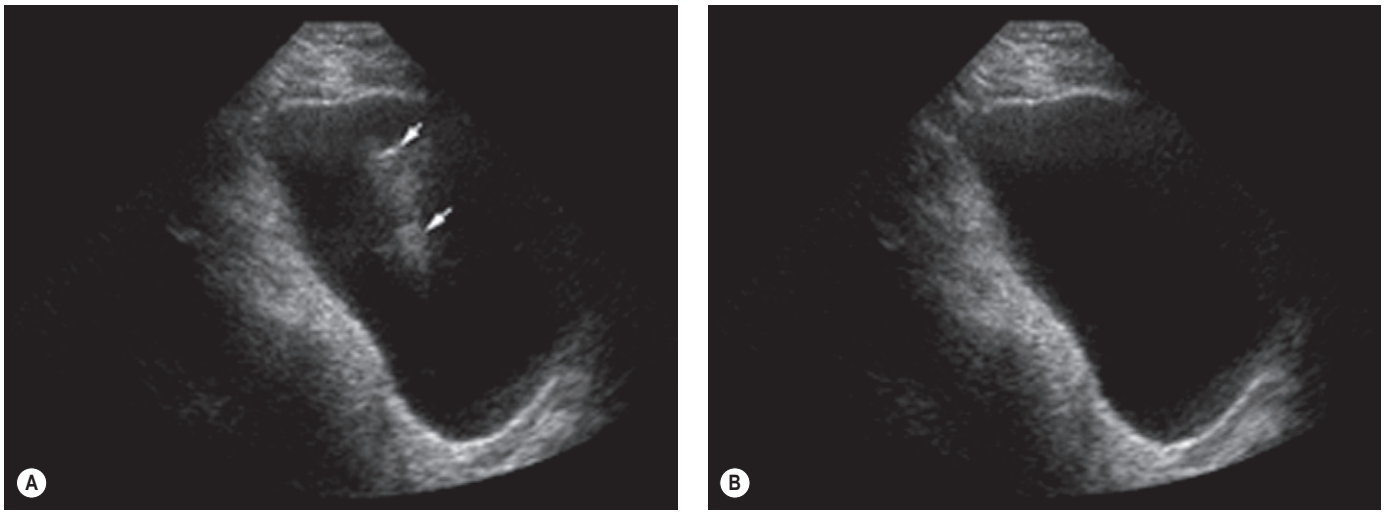


Figure 5.26 Ranging artefact. If the manufacturer exceeds the limit in the pulse repetition frequency – in an attempt to increase the frame rate – late echoes from pulse 1 overlap early echoes from pulse 2, etc. and signals are falsely depicted in the near field. **A:** The phenomenon is most obvious when a fluid path is traversed and so is well seen in transabdominal pelvic scanning, as in this example (arrows). **B:** Reducing the PRF eliminates this range overlap or 'wraparound' artefact.

This phenomenon, known as aliasing, is rare in real-time imaging but is important in Doppler.

ARTEFACTS IN THREE-DIMENSIONAL SCANNING

Some artefacts are only encountered in three-dimensional (3D) ultrasound.[38] They may stem from errors in the data collection process, for example movements of the probe that are too rapid result in gaps in the final image that may be depicted as such in registered 3D but when the data are collected freehand (where no correction is made for the *z*-plane movement), they produce errors in the geometry of this axis that are not necessarily apparent in the image: this is why measurements from this type of unregistered 3D scan are unreliable.[39] Obviously errors in the system that generated the spatial coordinates of the raw images distort the final rendered image.

Speckle in the ultrasound data also produces defects in the final image and they are particularly obvious in surface-rendered displays where they show as serpiginous holes.[40] Though unaesthetic, they do not affect the validity of the image; speckle reduction techniques can be used to mitigate the problem.

If the rendering algorithm does not interpolate adequately for missing slices, a 'gappy' rendered image results giving a toothcomb appearance when the three-dimensional set is rotated to align the *z*-axis.

If the structure being imaged moves during the data collection, the final rendered set will be distorted. This is particularly a problem with an active fetus and produces bizarrely distorted three-dimensional images. It is also a problem with vascular three-dimensional imaging because of vessel pulsations.

REFERENCES

1. Robinson DE, Kossoff G, Garrett WJ. Artefacts in ultrasonic echoscopic visualisation. Ultrasonics 1966;14:186–194.
2. Laing FC. Commonly encountered artifacts in clinical ultrasound. Semin Ultrasound 1983;4:1–25.
3. Sanders RC. Atlas of ultrasonographic artifacts and variants. In: Year book of ultrasound. Chicago: Mosby; 1986.
4. Hope-Simpson D, Burns PN. Pulse inversion Doppler: a new method for detecting nonlinear echoes from microbubble contrast agents. IEEE Ultrasound Symposium 1999.
5. Wells PNT, Halliwell M. Speckle in ultrasonographic imaging. Ultrasonics 1981;19:225–232.
6. Burchard CB. Speckle in ultrasound B-scan. IEEE Trans Son Ultrason 1978;SU-25:1–6.
7. Grechenig W, Clement HG, Fellinger M, et al. Value of ultrasound imaging of the Achilles tendon in traumatology. Radiologe 1997;37:322–329.
8. Bachmann GF, Melzer C, Heinrichs CM, et al. Diagnosis of rotator cuff lesions: comparison of US and MRI on 38 joint specimens. Eur Radiol 1997;7:192–197.
9. Suramo I, Paivanslo M, Vuoria P. Shadowing and reverberation artifacts in abdominal ultrasonography. Eur J Radiol 1985;5:147–151.
10. Robinson DE, Wilson LS, Kossoff G. Shadowing and enhancement in ultrasonic echograms by reflection and refraction. J Clin Ultrasound 1981;9:181–188.
11. Sommer FG, Taylor KJ. Differentiation of acoustic shadowing due to calculi and gas collections. Radiology 1980;135:399–403.
12. Ziskin MC, LaFollette PS, Blathras K, et al. Effect of scan format on refraction artefacts. Ultrasound Med Biol 1990;16:183–191.
13. Bly SH, Foster FS, Patterson US, et al. Artefactual echoes in B-mode images due to multiple scattering. Ultrasound Med Biol 1985;11:99–111.
14. Cosgrove DO, Garbutt P, Hill CR. Echoes across the diaphragm. Ultrasound Med Biol 1978;3:388–392.
15. Gardner FJ, Clark RN, Kozlowski R. A model of a hepatic mirror image artifact. Med Ultrasound 1980;4:18–21.
16. Fried AM, Cosgrove DO, Nassiri DK, et al. The diaphragmatic echo complex: an in vitro study. Invest Radiol 1985;20:62–67.
17. Thickman DI, Ziskin MC, Goldenburg NJ, et al. Clinical manifestations of the comet tail artifact. J Ultrasound Med 1983;2:225–230.
18. Lichtenstein D, Meziere G, Biderman P, et al. The comet-tail artifact: an ultrasound sign ruling out pneumothorax. Intensive Care Med 1999;25:383–388.
19. Ahuja A, Chick W, King W, et al. Clinical significance of the comet-tail artifact in thyroid ultrasound. J Clin Ultrasound 1996;24:129–133.
20. Wells P. Physical principles of ultrasonic diagnosis. London: Academic Press; 1969.
21. Goss SA, Johnstone RL, Dunn F. Comprehensive compilation of empirical ultrasound properties of mammalian tissues. J Acoust Soc Am 1978;64(2):423–457.
22. Bamber JC. Attenuation and absorption. In: Hill CR, editor. Physical principles of medical ultrasonics. Chichester: Ellis Horwood; 1986.
23. Pierce G, Golding RH, Cooperberg PL. The effects of tissue velocity changes on acoustical interfaces. J Ultrasound Med 1982;1:185–187.

24. Richman TS, Taylor KJW, Kremkau FW. Propagation speed artefact in a fatty tumour (myelolipoma). J Ultrasound Med 1983;2:45–47.
25. Baum G. Ultrasonography in clinical ophthalmology. Trans Am Acad Ophthalmol Otolaryngol 1964;68:265–276.
26. Müller N, Cooperberg PL, Rowley VA, et al. Ultrasonic refraction by the rectus abdominis muscles: the double image artefact. J Ultrasound Med 1984;3:515–520.
27. Sauerbrei EE. The split image artefact in pelvic ultrasonography: anatomy and physics. J Ultrasound Med 1985;4:29–34.
28. Goldstein A, Parks JA, Osborne B. Visualization of B-scan transducer transverse cross-sectional beam patterns. J Ultrasound Med 1982;1:23–35.
29. Jaffe CC, Taylor KJ. The clinical impact of ultrasonic beam focusing patterns. Radiology 1979;131:469–472.
30. Finet G, Cachard C, Delachartre P, et al. Artifacts in intravascular ultrasound imaging during coronary artery stent implantation. Ultrasound Med Biol 1998;24:793–802.
31. Fiske OE, Filly RA. Pseudo-sludge. Radiology 1982;144:631–632.
32. Goldstein A, Madrazo BL. Slice-thickness artifacts in gray-scale ultrasound. J Clin Ultrasound 1981;9:365–375.
33. Laing FC, Kurtz AB. The importance of ultrasonic side-lobe artifacts. Radiology 1982;145:763–768.
34. McKeighen RE. The influence of grating lobes on image quality using real-time linear arrays. J Ultrasound Med 1982;1(S):83.
35. Balthez PY, Leveille R, Scrivani PV. Side lobes and grating lobes artifacts in ultrasound imaging. Vet Radiol Ultrasound 1997;38:387–393.
36. Tranquart F, Grenier N, Eder V, Pourcelot L. Clinical use of ultrasound tissue harmonic imaging. Ultrasound Med Biol 1999;25:889–894.
37. Goldstein R, Downey DB, Pretorius DH. Three dimensional ultrasound. Philadelphia: Lippincott; 1999.
38. Eckersley RJ, Goldberg BB, Cosgrove DO, et al. Vessel beading in normal vessels using three dimensional ultrasound imaging. Radiology 1999;213:396.
39. Tong S, Cardinal HN, Downey DB, et al. Analysis of linear, area and volume distortion in 3D ultrasound imaging. Ultrasound Med Biol 1998;24:355–373.
40. Rohling R, Gee A, Berman L. Three-dimensional spatial compounding of ultrasound images. Med Image Anal 1997;1:177–193.

CHAPTER

6 Ultrasonic contrast agents

Carmel M. Moran

HISTORY AND DEVELOPMENT 77

MICROBUBBLE DYNAMICS 78

TYPES OF CONTRAST AGENTS 78
Lipid-stabilised contrast microbubbles 79
SonoVue 79
Definity 79
Sonazoid 80
Imavist 80
Albumin-coated microbubbles 80
Optison 80
PESDA 80
Polymer-coated microbubbles 80
CARDIOsphere 80
Imagify (AI-700) 81
Other types of agents 81
Levovist 81

IMAGING OF CONTRAST MICROBUBBLES 81
Fundamental imaging 81
Second harmonic imaging 81
Low MI techniques 82
Pulse inversion imaging/phase inversion imaging (PI) 82
Amplitude modulation/power modulation (PM/AM) 82
Power-modulated pulse inversion (PIAM) 82
High MI techniques 82
Flash contrast imaging; triggered imaging; destruction-replenishment 82
Newer imaging techniques 84
Subharmonic imaging 84
Coded excitation 84
Radial modulation imaging 84

CLINICAL APPLICATIONS OF CONTRAST IMAGING 84
Radiology applications 84
Liver 84
Renal 84
Spleen and pancreas 85
Transcranial 85
Urology 85
Cardiology 85

OTHER POTENTIAL USES OF CONTRAST MICROBUBBLES 86
Targeted contrast microbubbles 86
Drug and gene delivery 87

SAFETY OF CONTRAST MICROBUBBLES 87

IMAGING ARTEFACTS 88
Propagation artefacts 88
Doppler artefact 88

HISTORY AND DEVELOPMENT

Ultrasound signal enhancement using a contrast agent was first reported in the 1960s and initial experiments were performed by Joyner (unpublished) using physiological saline as an ultrasound contrast agent in the anatomical identification of the mitral valve echo. The same phenomena were subsequently observed using dextrose and indeed the patient's own blood in the assessment of cardiac anatomy and function.[1] Over the next 20 years contrast agents were used mainly to determine the presence of cardiac shunts and to validate cardiac anatomy. Indeed the use of agitated saline is still routinely used in cardiac studies today for the assessment of a patent foramen ovale (PFO) (Fig. 6.1). Such free (unencapsulated) bubble contrast agents were initially made by agitating the carrier liquids; however, the range of bubble size was large. By a process called 'sonication' in which a low-frequency sonic field (20 kHz) is applied to liquids, small cavitation bubbles of a more limited size range (<10 μm) were created.[2] Various in-vivo experiments using early contrast agents including colloidal suspensions, aqueous solutions, emulsions and encapsulated microbubbles have been reviewed[3] and it is evident from this review and subsequent work that agents working on the principle of scattering from microbubbles were most likely to be successful in clinical applications. In the mid-1980s clinical interest re-emerged with rapid commercial development of a large range of contrast agents, many of which were the precursors of those now commercially available. By 1987 bubbles smaller than 5 μm were produced by sonicating albumin at high intensity and low frequency.[4] The encapsulating shell consisted of the denatured albumin protein. Another practical approach to making small encapsulated microbubbles was to support the small bubbles in a saccharide crystal structure with the addition of palmitic acid as a surfactant to stabilise the bubbles.[5] These breakthroughs in the production of stable encapsulated bubbles which could be injected intravenously and survive passage through the pulmonary circulation opened up the possibility of a wide range of clinical applications. In addition, there existed an increasing clinical demand for the development of an ultrasonic technique that was capable of measuring myocardial perfusion. A longer-term interest in microbubbles is related to their potential use as carriers of pharmaceuticals or genes to targeted sites where the microbubbles would be destroyed, once attached, by an ultrasound beam, releasing the contents of the microbubbles in situ. Some types of contrast agents are discussed in this chapter; they should be considered as examples of different formulations and not an exhaustive list. In addition, although different methods of imaging contrast agents are discussed, this is an area of continuing commercial sensitivity for ultrasonic scanner manufacturers so only an overview of different approaches to contrast imaging details are given.

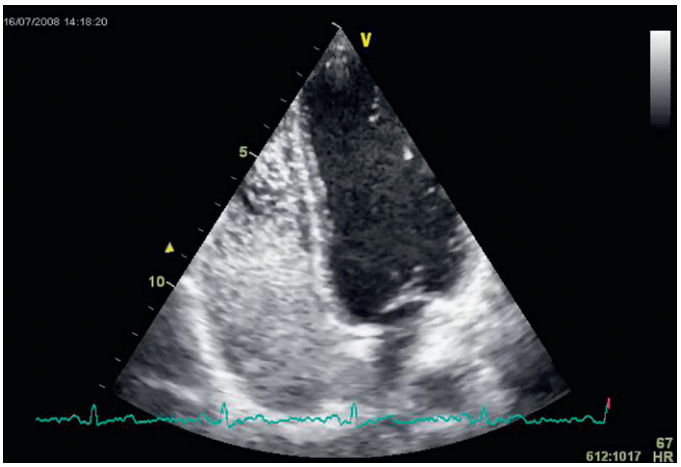


Figure 6.1 Four-chamber view of the heart after injection of agitated saline in the clinical assessment of PFO. Right atrium and right ventricle are filled with agitated saline. There is no evidence of bubbles in the left atrium or the left ventricle indicating that there is no PFO. (Image courtesy of Audrey White, Western General Hospital, Edinburgh, Scotland.)

Microbubble dynamics

- Microbubbles oscillate in response to the ultrasound beam.
- It is the compressibility of the gas within the microbubbles that makes them such efficient scatterers.
- The resonant frequency of commercial microbubbles lies in the diagnostic frequency range of ultrasound scanners.
- The ultrasound beam may force the microbubbles to oscillate in a non-linear manner, resulting in the generation of harmonics.
- At high acoustic pressures, the microbubbles can be forced to collapse or fragment, releasing free gas bubbles which diffuse rapidly in the blood.

MICROBUBBLE DYNAMICS

The equations which govern the dynamics of the motion of gas bubbles in an acoustic field were derived by Rayleigh[6] and Plesset[7] and consider the response of a spherical, unencapsulated bubble to a time-varying pressure field in an incompressible fluid. This model was extended to consider the effect of an elastic thin layer encapsulating a gas-filled microbubble.[8] It was demonstrated that the addition of a thin shell significantly increased the damping of the bubble oscillations and reduced the acoustic response of the microbubble in comparison to free microbubbles. However, the resonant oscillation was shown to still add significantly to the magnitude of the backscattered intensity.

It is serendipity that microbubbles of a size similar to red blood cells resonate at low megahertz frequencies, similar to those used routinely in diagnostic clinical ultrasound. Theoretical and experimental determination of the resonance frequency of free and encapsulated gas bubbles is an active area of research.[9] The equation below describes a derived approximation of the resonance frequency, f_0, of a free air bubble in water:

$$f_0 = 3.3/R_0$$

where R_0 is the bubble radius in microns. Substituting appropriate values into this formula shows that free bubbles with radii between 1 and 3 μm have resonances which lie approximately in the range of 5 to 1 MHz. Addition of an outer shell, such as albumin, shifts this resonant frequency higher. A more detailed review of the theory which governs the interaction of ultrasound with both free and encapsulated microbubbles in water may be found elsewhere.[10] However, although such theory is useful to describe the resonant behaviour of the microbubbles, the interaction of encapsulated microbubbles with an insonating acoustic field in a biological system is complex. This is particularly true as the acoustic pressure incident on the microbubbles increases. At low acoustic pressures, theory predicts that the acoustic wave incident on a contrast microbubble with an elastic shell causes the microbubble to oscillate, expanding when the pressure is negative (rarefaction) and contracting when the pressure is positive (compression). This results in minimal destruction of the microbubbles but may cause microstreaming in the fluid in the vicinity of the microbubbles. As the acoustic pressure increases the bubble cannot contract as much as it can expand, due to the gas within the microbubble. This results in asymmetric motion of the microbubbles and the resultant scattered wave is consequently distorted and contains frequency components that are multiples (harmonics) of the incident (fundamental) frequency. As the acoustic pressure increases further, the microbubble can expand and then violently implode. Such an event is known as inertial (transient) cavitation and can produce extremely large, highly localised temperatures, free radicals and high-velocity jets. The manner in which the microbubbles collapse is dependent on a range of insonating conditions including pressure amplitude, pulsing regime and ultrasound frequency.[11] Also important are microbubble parameters such as composition of the encapsulating shell, size of the microbubbles and proximity of the microbubbles to other structures (including other microbubbles and cell walls). The shells of the microbubbles have been observed to buckle, fragment and crack, allowing the gas to leak from the shells over successive incident ultrasound pulses.[12] The range of phenomena that can be induced at different acoustic pressures are discussed elsewhere.[13]

On commercial scanners, an indication of the acoustic pressure is given by the mechanical index (MI), defined as:

$$\mathrm{MI} = P_{-\mathrm{ve}} / \sqrt{f}$$

where $P_{-\mathrm{ve}}$ is the peak derated negative (rarefaction) acoustic pressure and f is the ultrasonic frequency (see Chapter 4). This parameter is an on-screen index designed to give an indication of the likelihood of mechanical bioeffects. Although defined and used as a safety index, the mechanical index is often used as an indicator of microbubble behaviour for a particular scanner set-up and contrast agent. In general for low MI imaging, the number of contrast microbubbles collapsing as a result of the insonating pressure pulse will be minimal. However, as the MI increases, the likelihood of inertial cavitation increases as the contrast microbubbles can be forced to collapse releasing free gas bubbles. Clinical contrast imaging techniques utilise both low MI and high MI applications.

TYPES OF CONTRAST AGENTS

Commercially available ultrasonic contrast agents are gas-filled microbubbles which are generally coated with a lipid, protein or polymer shell. Although free gas bubbles scatter ultrasound much more effectively than encapsulated microbubbles, they dissolve quickly in the blood, generally in the order of milliseconds, due to surface tension and diffusion effects. The encapsulation is required to lengthen the lifetime of the bubbles within the blood, by providing an elastic membrane surrounding a gaseous interior. The gas contained within commercially available clinical microbubbles is generally a perfluorocarbon as these gases diffuse less readily than air within blood. Microbubble diameters generally lie within the 1–5 μm range although production of smaller microbubbles of a

Table 6.1 Examples of commercially developed ultrasonic contrast agents. Early-generation agents that encapsulated air have been omitted

Contrast agent	Manufacturer	Capsule/ Shell	Gas	Bubble diameter	Charge	Status
CARDIOsphere (PB 127)	Point Biomedical Corp	Polylactide/ Albumin	Nitrogen	4 μm	Slight negative	Not available
Imagify (AI 700)	Acusphere Inc	Poly(L-lactide-co-glycolide)	Decafluorobutane	NA	Negative	Awaiting approval in USA
Definity (USA/ Canada) Luminity (EU)	Lantheus Medical Imaging	Lipids: DPPA, DPPC, MPEG5000, DPPE	Octafluoropropane	98% <10 μm	Negative	USA approved CA approved LVO, EBD
Imavist/ AF0150	Imcor Pharmaceuticals Inc	Lipid: DMPC	Perfluorohexane/ Nitrogen	99.8% <10 μm	Neutral	USA approved LVO, EBD
Sonazoid/ NC100100	GE Healthcare	Lipid: HEPS	Perfluorobutane	Median 2.6 μm 99.9% <7 μm	Negative	Japan approved, focal liver lesions
SonoVue (BR1)	Bracco	Lipids: Macrogol 4000, DSPC, DPPG, palmitic acid	SF_6	99% <11 μm	Negative	EU approved LVO, EBD Doppler (non-cardiac studies)
Optison/FS069	GE Healthcare/ Amersham	Albumin	Octafluoropropane	93% <10 μm	Slight negative	EU, USA approved, EBD, LVO

HEPS, hydrogenated egg phosphatidyl serine; DMPC, dimyristoylphosphatidylcholine; DPPC, dipalmitoyl glycerophosphocholine; DPPA, dipalmitoyl glycerophosphate; DPPE, dipalmitoyl glycerophosphoethanolamine; DSPC, distearoyl glycerophosphocholine; DPPG, dipalmitoyl glycerophosphoglycerol.

well-defined radius (mono-disperse) and usually polymer-encapsulated is becoming more common. The number of microbubbles in commercial products tends to range from 10^8 to 10^{10} mL^{-1} with typical injection doses ranging from 0.1 mL to 1 mL, although larger or multiple doses may be administered dependent on specific manufacturers' recommendations. Contrast agent injections are given intravenously, generally as a bolus injection, but infusions are possible and in some instances necessary for clinical studies such as in the assessment of cardiac perfusion.

When reviewed historically, ultrasonic contrast agents are often subdivided into 'generations'. First-generation contrast agents are non-transpulmonary contrast agents including free gas bubbles and Echovist, an agent developed by Schering and still used for hysterosalpingo-contrast-sonography for the assessment of Fallopian tube patency. Second-generation agents are those that are transpulmonary but have a relatively short half-life (several minutes) and can be seen in the vascular bed. These microbubbles generally encapsulate air within their structure. Third-generation agents are also transpulmonary vascular agents but tend to have a longer half-life and encapsulate fluorocarbons. One exception to this is SonoVue, which incorporates sulphur hexafluoride.

Table 6.1 gives a listing of different types of contrast microbubbles that have been developed over recent years – some of these are commercially available, others are currently undergoing clinical trials. The majority of the commercially available agents are licensed for left ventricular opacification (LVO) and endocardial border definition (EBD). In certain countries, the use of contrast agents for the assessment of focal liver lesions is also included. The use of contrast agents in the assessment of myocardial perfusion has not yet been licensed but at least one manufacturer has an agent currently submitted to the FDA in the USA for approval for this application. A more extensive list of contrast agent properties can be found elsewhere.[14]

Lipid-stabilised contrast microbubbles

The majority of commercially available contrast agents fall into this category with a mono- or bi-lipid layer providing the stabilising layer required for the microbubbles to pass into the systemic system. Phospholipid layers tend to vary in thickness from 10 to 200 nm. These microbubbles are distinct from echogenic multilamellar liposomes which have been developed principally for research applications and for which the echogenicity is achieved by encapsulation of gas within the lamellar structure.[15]

SonoVue

SonoVue (Bracco) consists of sulphur hexafluoride gas bubbles encapsulated in a lipid monolayer. The size distribution of the microbubbles is such that 99% of the microbubbles are less than 11 μm in diameter. A typical concentration is 2×10^8 mL^{-1}. The agent is presented in an integral kit which enables 5 mL of saline to be injected into 25 mg of the dry lyophilised powder in an atmosphere of sulphur hexafluoride (Fig. 6.2). The agent does not require refrigeration and is currently licensed in the European Union (EU) for cardiac applications (including endocardial border enhancement (EBD) in the chambers of the heart and left ventricular opacification (LVO). It is also used for Doppler exams of both cardiac and non-cardiac microvasculature. This agent can be administered both as a bolus and as an infusion.

Definity

Definity (acquired in 2008 from Bristol-Myers Squibb by Lantheus Imaging) is also known as Luminity in the majority of EU countries.



Figure 6.2 Preparation kit for SonoVue.



Figure 6.3 Vialmix with inset of Definity/Luminity vial.

It is a lipid bi-layer microbubble encapsulating octafluoropropane. The size distribution of the microbubbles is such that 98% are less than 10 μm in diameter. A typical concentration is 10^9 mL^{-1}. The agent is supplied in vials as a clear liquid with a head-space of octafluoropropane. To form the bubbles, the vial must be agitated in a mechanical shaker (Vialmix) for 45 seconds prior to withdrawal of the milky solution (Fig. 6.3). The vial is vented using a needle prior to withdrawal of the solution. The agent must be refrigerated prior to use. Luminity is licensed in the EU but is not currently marketed there. In the USA and Canada the agent is licensed for LVO and EBD.

Sonazoid

Sonazoid (GE Healthcare) is a lipid (hydrogenated egg phosphatidyl serine) encapsulated perfluorobutane microbubble. The agent is reconstituted using 2 mL of water and manually mixed for 1 min to produce a milky solution. A typical concentration is 1.2×10^9 mL^{-1} with a median size of 2.6 μm.[16] This agent is currently not available in the EU and USA but is licensed in Japan for the assessment of focal liver lesions.

Imavist

Imavist (IMCOR Pharmaceuticals Inc) is a lipid-encapsulated, perfluorohexane and nitrogen encapsulated microbubble. The size distribution of the microbubbles is such that 99.8% are less than 10 μm in diameter. The agent is approved in the USA for EBD and LVO.

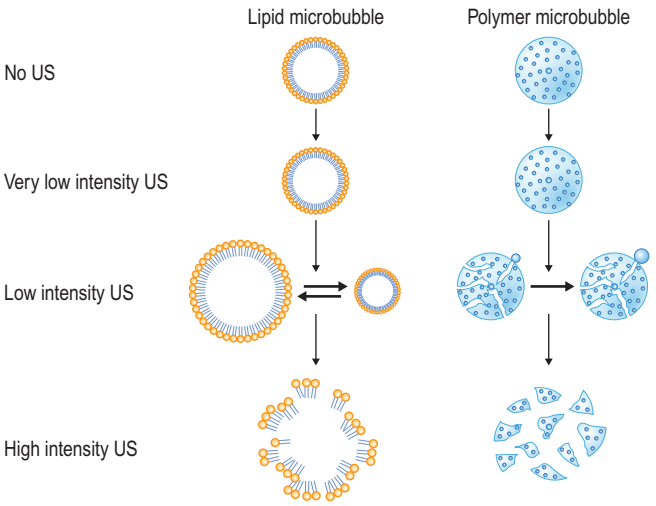


Figure 6.4 Schematic representation of lipid (left column) and polymer (right column) microbubble interaction with ultrasound of increasing intensity (top to bottom). (Reprinted from Advanced Drug Delivery Reviews, Vol 60, Hernot S, Klibanov AL. Microbubbles in ultrasound-triggered drug and gene delivery. 1153–1166.Copyright (2008) with permission of Elsevier.)

Albumin-coated microbubbles

Optison

Optison (GE Healthcare) microbubbles are a development from the first-generation contrast agent Albunex, which was one of the first commercially available agents to demonstrate EBD. In Optison, octafluoropropane has replaced the air that was encapsulated in Albunex. The shell of Optison microbubbles is of denatured human serum albumin and the size distribution is such that 93% are less than 10 μm in diameter. A typical concentration is 5×10^8 mL^{-1}. The agent is supplied in vials that must be refrigerated prior to use. The agent is hand agitated to produce a milky solution prior to withdrawal of the agent from the vial. Optison is licensed for EBD and LVO in the USA and EU.

PESDA

PESDA (perfluorocarbon exposed dextrose albumin) comprises sonicated dextrose albumin microbubbles containing decafluorobutane gas. It has been developed by Porter et al. exclusively for research use.[17] The mean size of the microbubbles is 5.1 μm and the concentration is 3.1×10^9 mL^{-1}.

Polymer-coated microbubbles

Polymer-coated microbubbles have a much stiffer shell than lipid- or albumin-encapsulated microbubbles. As a result these microbubbles do not oscillate (expand and contract) in the ultrasound field at low acoustic pressures.[18] However, as the acoustic pressure increases, the polymer shell can buckle and crack, releasing free gas (Fig. 6.4).

CARDIOsphere

CARDIOsphere microbubbles (POINT Biomedical Corp) are manufactured using a technique described as BiSphere technology in

Contrast agents

- Ultrasonic contrast agents are micron-sized encapsulated bubbles.
- The shells of the microbubbles are generally either lipid or polymer.
- The gases within current contrast microbubbles are perfluorocarbons.
- There are approximately 10^9 microbubbles/mL of contrast agent solution.
- Contrast agents are generally injected into the femoral vein as either a bolus or infusion.

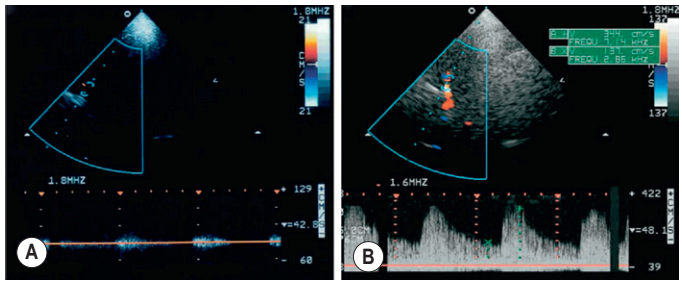


Figure 6.5 **A:** Suspected middle cerebral artery (MCA) stenosis on unenhanced transcranial colour-coded duplex sonography. In the Doppler frequency spectrum only suspicious low-frequency bidirectional signals can be obtained. In colour mode the MCA is barely visible. **B:** Improvement of the Doppler frequency spectrum and the colour mode depiction of the MCA after application of an ultrasound contrast agent. Flow velocities >300 cm/s ascertain the presence of a high-grade MCA stenosis. (Reprinted from Seminars in Cerebrovascular Diseases and Stroke, Vol 5, Stolz EP and Kaps M, Ultrasound contrast agents and imaging of cerebrovascular disease 111–131.Copyright (2005) with permission from Elsevier.)

which microbubbles are produced comprising an outer layer of a biocompatible material (albumin) and an inner polymer layer. The microbubbles are filled with air and have been developed for myocardial perfusion studies. Their mean diameter is 4.0 µm. Using BiSphere technology, smaller sub-micron microbubbles have also been manufactured for lymphatic imaging.

Imagify (AI-700)

Imagify (Acusphere Inc) consists of a synthetic polymer poly(L-lactide co-glycolide) shell and a phospholipid layer encapsulating a perfluorobutane gas. The agent is made using a spray drying technique to produce microbubbles. The mean size of the microbubbles is 2.0 µm. FDA approval is currently being sought for this agent for myocardial contrast perfusion imaging.

Other types of agents

Levovist

Levovist (Schering, Germany) is a first-generation agent and one of the first agents to undergo clinical trials and be commercially available. Unlike the majority of commercial agents, Levovist is an air-filled microbubble. The microbubbles are formed within a galactose microstructure which controls the size of microbubbles formed and the microbubbles are stabilised by the addition of palmitic acid. The diameter of the microbubbles lies between 3 and 5 µm. The agent is supplied in vials containing 4 g of dry galactose granules and 0.1% palmitic acid. Sterile water is injected into the vials, the quantity of water determining the concentration of the agent. Recommended concentrations are 200 mg mL^{-1} (17 mL injection of water into vial), 300 mg mL^{-1} (11 mL injection of water into vial) or 400 mg mL^{-1} (8 mL injection of water into vial). Once the water is injected, the granules are vigorously shaken for 5–10 seconds and then allowed to stand for a further 2 minutes prior to injection into the patient. By this stage the solution is milky white. Care must be taken to avoid excessive increases in temperature caused by holding the vials tightly in hand or strong negative pressure when drawing up the solution.

IMAGING OF CONTRAST MICROBUBBLES

The development of imaging techniques to detect contrast microbubbles continues to be an exciting and active area of research. Such techniques aim to isolate and differentiate the acoustic signatures from tissue and contrast. Current approaches adopted by commercial ultrasound scanner manufacturers include utilising the different frequency components of the scattered ultrasound signal (fundamental, harmonics, subharmonics), and the different acoustic amplitude responses of the microbubbles. Indeed several manufacturers utilise both frequency and amplitude components of the scattered wave to provide sensitive contrast imaging techniques. Current contrast imaging techniques can be divided into either low MI imaging techniques which minimise destruction of the microbubbles or high MI techniques which maximise microbubble destruction.

Fundamental imaging

Initial clinical imaging of the first commercial ultrasound contrast agents was performed in the fundamental imaging mode: ultrasound transducers emitting and receiving the ultrasound signal over the same bandwidth of the transducer. In these early years, the use of the term contrast agent was clearly a misnomer as although the agent provided transient enhancement of the blood pool, the relative backscatter of tissue to blood was reduced. In some cases, the quantity of contrast agent injected in order to achieve enhancement was such that significant and long-lasting acoustical shadowing in distal regions of the image made diagnosis difficult. It was in 'rescuing' Doppler studies that the first clear indications of benefit were seen using contrast in studies where the blood signal was too small to be picked up (Fig. 6.5). Fundamental imaging of contrast agents has now been completely replaced by contrast-specific imaging techniques.

Second harmonic imaging

When the radius of a microbubble changes its size in direct proportion to the pressure variations of the ultrasonic wave it is said to be responding in a linear fashion. In this case the frequency of the scattered wave is the same as that of the incident wave. However, for larger pressure fluctuations the change in radius is not in proportion and the bubble is said to be responding in a non-linear way. When a bubble responds in a non-linear manner, the scattered ultrasound wave is distorted and contains additional frequency components above and below the frequency of the incident wave. These additional components are called harmonics and there is particular interest in the second harmonic which can be as strong as the ultrasound scattered from the microbubbles at the incident frequency, i.e. the first harmonic (fundamental frequency). Second harmonic imaging relies upon detecting and displaying only this second harmonic signal from the scattered ultrasound. Although at low acoustic pressures (low MI), second harmonic imaging significantly improves the contrast-to-tissue ratio (CTR), at higher

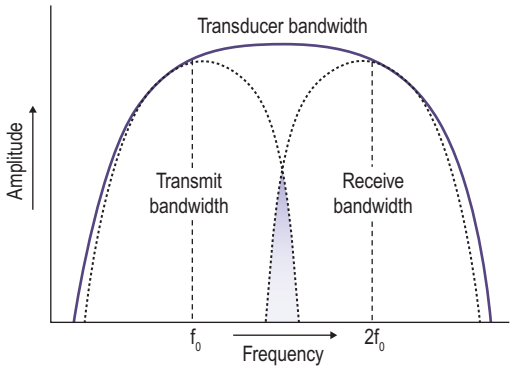


Figure 6.6 Schematic diagram illustrating the overlap in the transmit and receive bandwidths with second harmonic imaging, where f_0 is the central transmit frequency.

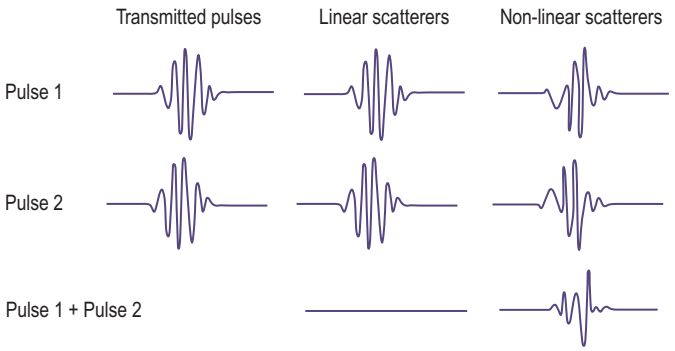


Figure 6.7 Schematic diagram illustrating the principle of the pulse inversion imaging technique. Two pulses are transmitted down each line, the second pulse the inverse of the first. The sum of the scattered pulses from linear scatterers will sum to zero, while the sum from non-linear scatterers will not equal zero.

acoustic pressures (high MI) non-linear propagation through tissue and the generation of tissue harmonics[23] results in a reduction of CTR compared to low MI. There is thus an inherent limitation to the potential increase in the CTR using second harmonic imaging. In addition, second harmonic imaging requires broad bandwidth transducers to enable separate transmit frequencies and receive frequencies (at twice the transmit frequency). This requirement in the transmitted and received bandwidths can result in a reduction in axial resolution (Fig. 6.6).

The advent of second harmonic imaging marked the beginning of an exciting period of development in both contrast agent manufacture and contrast-specific imaging techniques to further capitalise on the non-linear properties.

Low MI techniques

Pulse inversion imaging/phase inversion imaging (PI)

The specific algorithms and bandwidth filters used within commercial scanners to separate microbubble and tissue echoes are not known, but pulse/phase inversion techniques have the potential to overcome the bandwidth limitations of second harmonic imaging.[19] In this technique, two consecutive pulses are sent down each transmit line such that the second pulse is identical but inverted with respect to the first pulse (180° out of phase). The detection and summation of the two scattered echoes from linear scatterers will equate to zero. However, scattering from non-linear targets, such as microbubbles, will result in non-identical pulses. Summation of the two pulses will predominantly cancel out the fundamental part of the signal. The image is formed from the remaining signal (Fig. 6.7).

Pulse/Phase inversion is a low MI imaging technique which does not destroy the microbubbles in situ. One limiting factor of this technique is a reduction in the frame rate since it is necessary to send two pulses down each transmit line rather than one.

Amplitude modulation/power modulation (PM/AM)

In amplitude/power modulation two, or more usually three, pulses of identical phase but different magnitude are sent along each transmit line. The amplitude of the pulses is often in a sequence where the first and third pulses are half the magnitude of the second pulse. Upon reception the signals are combined such that the sum of the response from the half amplitude transmit pulses is subtracted from the response from the full amplitude pulse. Lower-amplitude transmit pulses will generate less harmonics than high-amplitude pulses,

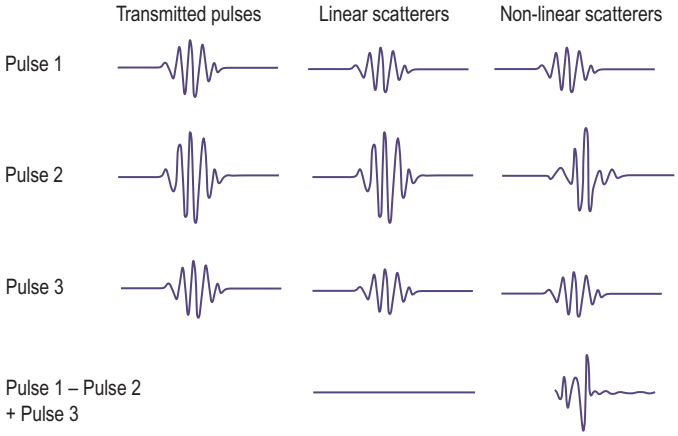


Figure 6.8 Schematic diagram illustrating the principle of amplitude modulation imaging techniques. In this technique, three pulses are emitted, all of them in phase with one another. The first and third pulses are half the amplitude of the second pulse. Upon reception, summation of the scattered signals from linear scatterers will sum to zero, those from non-linear scatterers will not.

therefore the difference in the received pulses is due to the non-linear response of the target (Fig. 6.8).

Power-modulated pulse inversion (PIAM)

This technique combines the two techniques described previously. In this case the two pulses that are sent down each scan line vary in both amplitude and phase. This results in a more sensitive detection of non-linear signals.[20]

High MI techniques

Flash contrast imaging; triggered imaging; destruction-replenishment

The contrast-specific imaging modes that have been discussed to date are predominantly used at low acoustic outputs where the

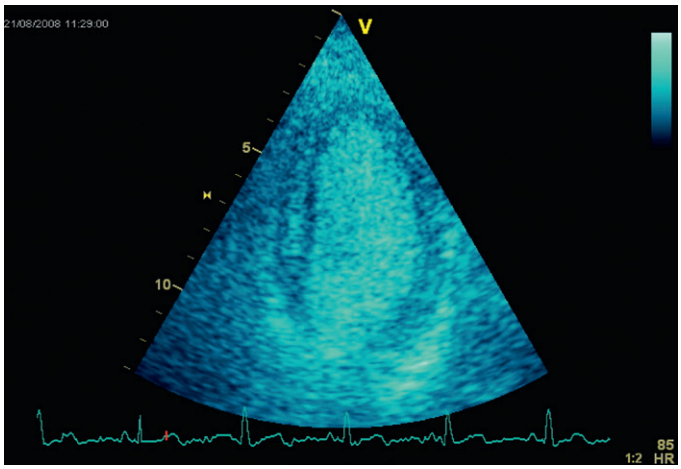


Figure 6.9 A 'flash frame' acquired during a perfusion study. A high mechanical index frame disrupts SonoVue microbubbles within the myocardium and ventricle.

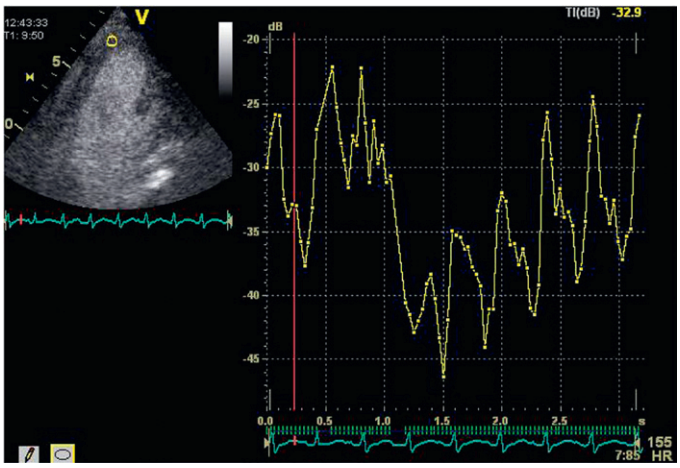


Figure 6.10 Contrast perfusion study using infusion of SonoVue with graphical display illustrating variation in backscatter signal in selected ROI within the myocardium. A pulse inversion imaging technique is used to image reperfusion of the myocardium following application of a high MI pulse. (Image courtesy of Dr Stephen Glen, Stirling Royal Infirmary, Scotland.)

majority of the microbubbles are not destroyed. In some instances, however, destruction of the microbubbles in situ by one or several high pressure frames (flash frames) can be used to assess blood flow within an organ. Formerly for an assessment of flow within the myocardium, this technique involved varying the interval between successive high MI frames triggered from the ECG and not scanning between the high MI frames.[21] More recently this technique has been developed further such that low MI imaging is performed between the high MI destruction frames. In such cases the microbubbles can be viewed initially using a low MI imaging technique. Once a constant enhancement has been established by infusion, application of a single, or several, high MI frames causes rupture of the microbubble shells. Upon rupture the microbubbles release free gas bubbles which rapidly diffuse into the blood and are therefore generally only visualised in one frame (Fig. 6.9). On return to continuous low MI imaging, new contrast microbubbles may be visualised entering the scan plane and replenishing the destroyed contrast. The time taken for the contrast to refill the scan-plane is an indicator of myocardial blood flow[22] (Fig. 6.10) and can be studied using refill kinetics theory. In this approach it is assumed that the enhancement of the ultrasound backscatter signal within the scan-plane is proportional to the microbubble concentration in the tissue, the infusion rate of the contrast and the pulse interval between successive high MI destruction pulses. When intensity measurements are made with increasing pulse intervals, a graph can be plotted of intensity, $I(t)$, as a function of t, the time pulse interval between successive high MI destruction pulses (Fig. 6.11). The ultrasound intensity, $I(t)$, is given by:

$$I(t) = I_0(1 - e^{-\beta t})$$

where I_0 is the ultrasound intensity of the plateau and β is a time constant. From this graph, β and I_0 can be calculated. The former is related to the blood flow velocity, and the latter to the vascular volume.

High MI destruction techniques are also used in other organs, e.g. liver and spleen.[23] Early techniques called loss-of-correlation imaging (LOC) or stimulated acoustic emission (SAE) imaging used colour Doppler to display the rapid collapse of the microbubbles as a chaotic colour Doppler region within the image. These imaging techniques have largely been replaced by contrast-specific imaging techniques such as maximum intensity projection or microbubble trace imaging, which are similar techniques that use the interplay of high and low MI techniques to study the path of moving bubbles to trace out the vascular structure.[24] In these techniques, a high MI pulse is applied to the organ to destroy the microbubbles, and then a low MI pulse inversion technique is used to image the organ as new individual microbubbles enter the field of view. The images are processed so that the echoes from the

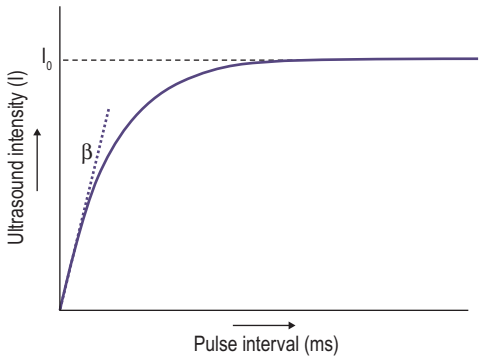


Figure 6.11 Schematic example of intensity–time curve. I_0 is the plateau intensity (related to vascular volume) and β is a time constant (related to the blood flow velocity).

Imaging techniques

- Contrast microbubbles can be imaged using a variety of techniques.
- Harmonic imaging filters out the harmonic component of the signal.
- Pulse inversion separates the fundamental and harmonic components by subtraction technique rather than filtering so can utilise wider bandwidths.
- Pulse inversion and amplitude modulation imaging techniques are low MI imaging techniques and take advantage of the non-linear properties of contrast agents.
- At MI values of 0.1 or less, contrast microbubbles are not significantly destroyed.
- Destruction-replenishment imaging involves switching between high MI and low MI techniques is often used in cardiology.

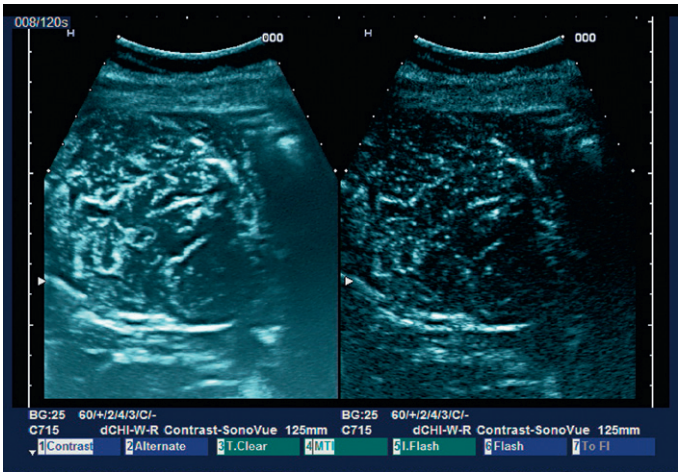


Figure 6.12 Image of a benign splenic lesion showing the pulse inversion harmonic image on the right side (about 15 seconds after injection of SonoVue), and the microbubble trace image on the left side. (Courtesy of Christoph Dietrich.)

microbubbles are summated over time, thus showing the path of the microbubbles through the vascular bed. In addition, the echoes are weighted such that the intensity decreases with elapsed time so that the direction of movement of the microbubbles can be studied (Fig. 6.12). Early studies have indicated that these techniques can illustrate arterial structure but the diagnostic benefit is as yet undetermined.

Newer imaging techniques

Subharmonic imaging

Subharmonic imaging is based upon the principle that contrast microbubbles when scattering non-linearly not only generate harmonics higher than the fundamental but also generate subharmonics. In addition, tissue does not generate subharmonics and therefore at subharmonic frequencies the contrast-to-tissue ratio is generally higher than that achieved at second harmonic frequencies. Much of the work associated with subharmonic imaging has been performed at frequencies normally associated with intravascular ultrasound imaging (30 MHz). An improvement of contrast-to-tissue ratio of 30 dB at the subharmonic (15 MHz) in comparison to the fundamental (30 MHz) has previously been achieved, highlighting the potential of using subharmonic imaging for vasa vasorum imaging.[25]

Coded excitation

Coded excitation involves the transmission of a high energy long transmit pulse with limited peak amplitude and is well known as a means of improving signal-to-noise ratio in ultrasound B-mode imaging. Recovery of axial resolution is achieved by the receive electronics examining the signals and picking out the echoes of similar shape to the transmitted pulse. Use of coded excitation in combination with phase and amplitude modulation techniques has been shown to improve sensitivity to non-linear signals from microbubbles at relatively low signal to noise but with limited benefit at high signal-to-noise levels. A review of coded excitation techniques is given elsewhere.[26]

Radial modulation imaging

Radial modulation imaging is based upon the premise that contrast microbubbles respond differently to an incident acoustic imaging pulse dependent upon their current oscillatory state. By insonating the microbubbles with a low-amplitude, low-frequency pulse (modulation pulse), the microbubbles are initially forced to oscillate. While the bubbles are oscillating, they are then insonated with two consecutive higher-frequency imaging pulses. Because of the lower-frequency modulation pulse, the bubbles will be in different stages of their expansion and contraction cycle when they are insonated by these higher-frequency imaging pulses and consequently the response of the microbubbles will be different. In comparison the response from the tissue should not vary.[27] The potential benefits of using this technique have yet to be proven but initial in-vitro results look very promising.

CLINICAL APPLICATIONS OF CONTRAST IMAGING

One of the most significant advantages of the use of contrast agents is the real-time nature of contrast enhancement and the resultant real-time diagnostic potential. In addition, the ability provided by some commercial ultrasound manufacturers to view the B-mode image and the contrast image simultaneously using a split-screen function (Fig. 6.12) enables visualisation of the organ of interest on one half of the screen, while simultaneously visualising the uptake of contrast on the other half. The conventional B-mode image is acquired at low MI to avoid disruption of the microbubbles.

The number of applications for which contrast agents are now used has increased significantly over the past 5 years and has been reviewed by the European Federation of Societies for Ultrasound in Medicine and Biology (EFSUMB).[28] In this review the guidelines for each contrast procedure and recommendations for good clinical practice are presented. Some of these applications are not currently licensed (e.g. myocardial perfusion, renal applications) but the diagnostic benefits that clinicians have observed using contrast agents for applications other than those for which the agent is licensed (off-label applications) merit a mention in this chapter and elsewhere in this book.

Radiology applications

The initial use of ultrasonic contrast agents was primarily focused on 'rescuing' colour Doppler studies where the signal from blood was too small to be detected. Injection of contrast microbubbles increased these low signals so that they could be detected and displayed (Fig. 6.5).[35]

Liver

The organ in which contrast agents have provided substantial diagnostic impact is in the liver for the characterisation of focal liver lesions. There is now substantial evidence to suggest that ultrasonic contrast agent imaging using low MI techniques (during the arterial, portal venous and late phases) is an effective diagnostic tool for the characterisation of focal liver lesions[29] (Fig. 6.13). Maximum diagnostic potential from these studies is achieved when the pre-contrast image is such that there is little tissue structure visible and only major anatomical markers such as the diaphragm are presented. This relies upon interplay of both the gain and MI controls.

Renal

No contrast agents have currently been licensed for the assessment of renal lesions. However, there has been substantial documentation of the benefits of using contrast microbubbles in the assessment of complex cystic lesions (Fig. 6.14), vascular diseases and transplanted kidneys.[30] For the assessment of renal lesions, contrast is injected as a bolus and low MI imaging techniques are used.

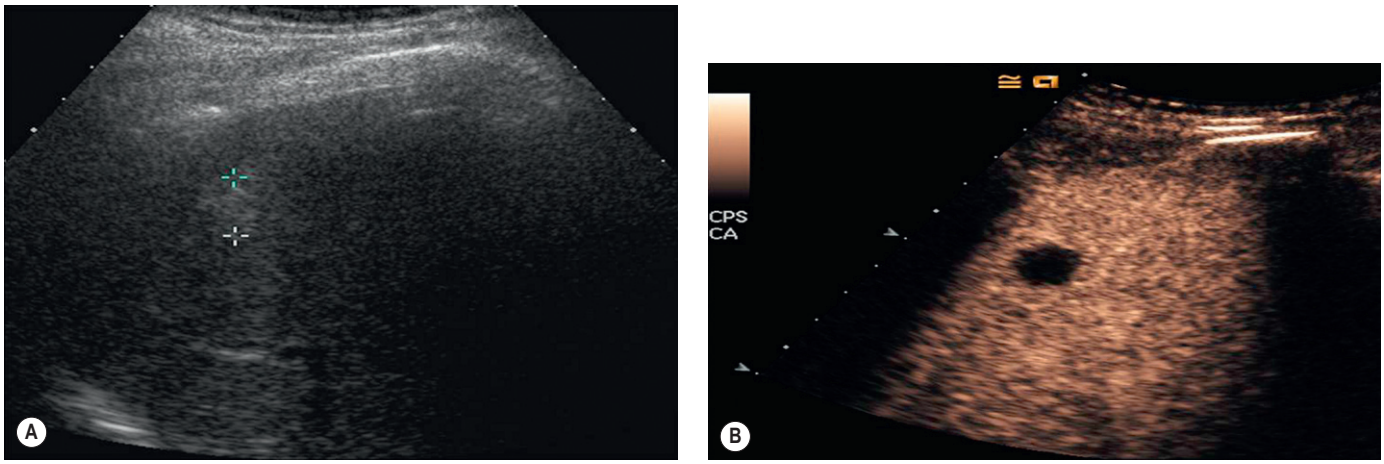


Figure 6.13 **A:** Image of an echogenic liver metastasis (between callipers) acquired in fundamental imaging. **B:** Image acquired 1 minute and 24 seconds after bolus injection of SonoVue (portal-venous stage). Low reflective area in the contrast-enhanced image is indicative of malignancy. (Images courtesy of Dr Paul Sidhu, King's College Hospital, London, UK.)

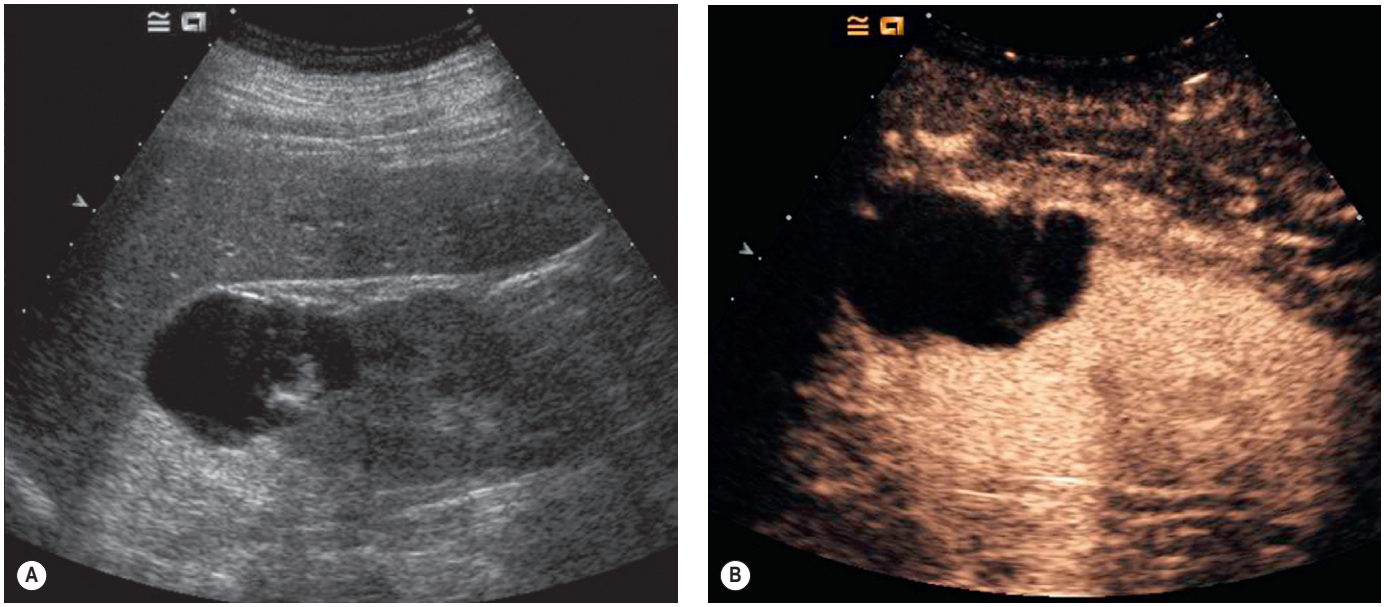


Figure 6.14 **A:** Image acquired in fundamental mode and suggestive of a complex renal cyst. **B:** Image acquired after a bolus injection of SonoVue using a low MI imaging technique. No septation enhancement evident, therefore lesion unlikely to be malignant. (Images courtesy of Dr Paul Sidhu, King's College Hospital, London, UK.)

Spleen and pancreas

No current contrast agents have been licensed for the assessment of splenic and pancreatic lesions. However, contrast agents have been used to depict and characterise lesions (Fig. 6.15).

Transcranial

No contrast agents have currently been licensed for the assessment of perfusion in transcranial studies. For the assessment of cerebral arteries, contrast is injected as a bolus to enhance either duplex sonography or colour Doppler imaging. It is used to enhance the Doppler signals in regions where the skull significantly attenuates the Doppler signal or the blood volume is too low.[31]

Urology

Contrast microbubbles can also be injected into body cavities rather than intravenously. Vesicoureteric reflux can be demonstrated after contrast has been placed in the bladder. The kidneys and bladder can then be scanned and refluxing microbubbles observed.[32]

Cardiology

The majority of commercially available contrast agents have been licensed for cardiac applications and in particular for enhancement of endocardial border and left ventricular opacification. The ability to be able to identify the endocardial border is of importance in cardiac patients undergoing either a pharmacological or physical

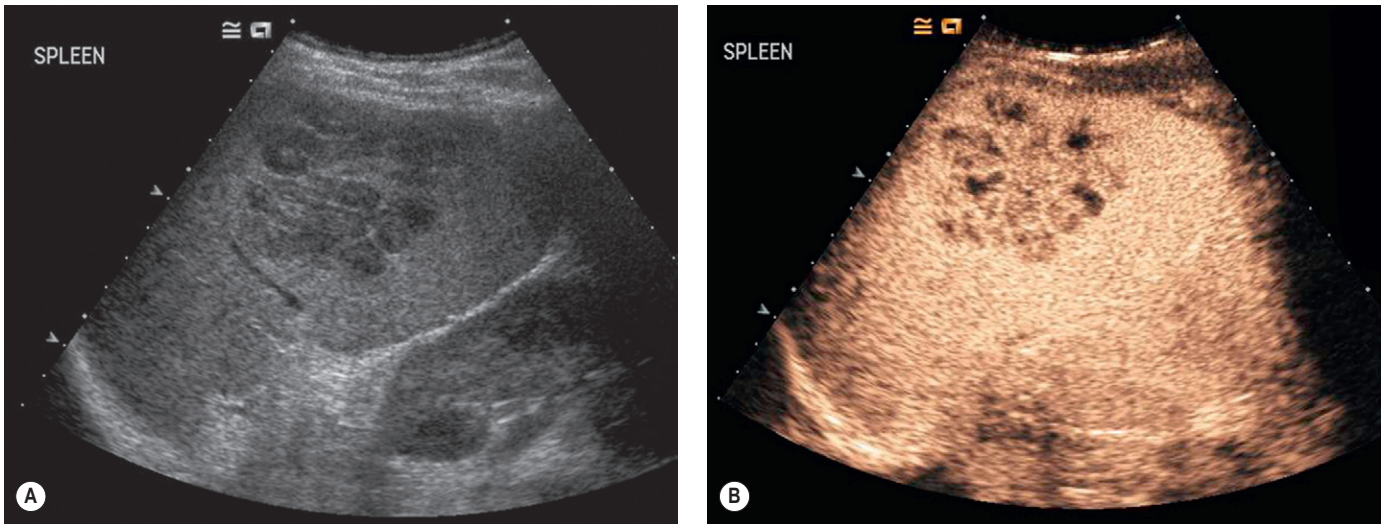


Figure 6.15 **A:** Image acquired in fundamental mode and suggestive of a possible splenic cyst. **B:** Image acquired after a bolus injection of SonoVue and using a low MI technique to image the spleen. Honeycomb pattern suggestive of a spleen abscess. (Images courtesy of Dr Paul Sidhu, King's College Hospital, London, UK.)

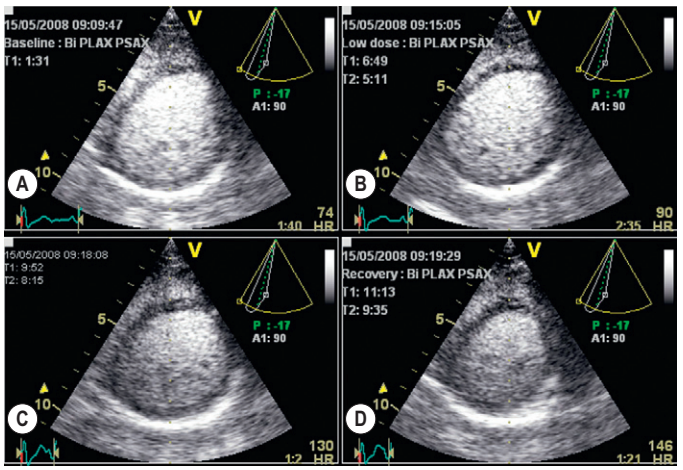


Figure 6.16 **Cardiac parasternal short-axis view of the heart** during a pharmacologically stressed cardiac stress-echo study. A low MI imaging technique is used. Images acquired at baseline **(A)**, low dose stress **(B)**, high dose stress **(C)** and recovery **(D)**. (Images courtesy of Dr Stephen Glen, Stirling Royal Infirmary, Scotland.)

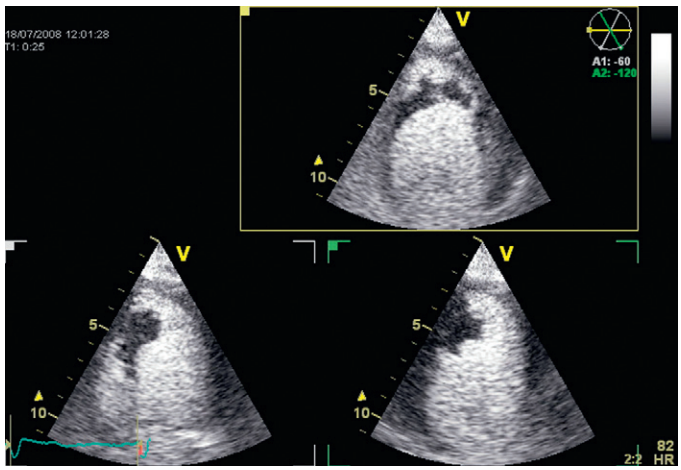


Figure 6.17 **Contrast-enhanced images of a cardiac thrombus** obtained in three imaging planes. (Images courtesy of Dr Stephen Glen, Stirling Royal Infirmary, Scotland.)

diagnostic stress test, where regions of the myocardium are individually assessed for movement under rest, stress and recovery conditions. Such studies are normally undertaken at low MI, ensuring that the complete ventricular endocardial border can be visualised without microbubble disruption and associated shadowing effects (Fig. 6.16).[33]

There are currently no ultrasonic contrast agents that are licensed to aid in the assessment of myocardial flow and hence perfusion. As described previously, when microbubbles are administered as an infusion and a consistent level of enhancement is achieved, it is possible to destroy the microbubbles in the scan-plane using a single or several high MI pulses. By then returning to low MI imaging, the time required for segments within the myocardium to become enhanced can be measured. Since this value is related to myocardial blood flow, areas of the myocardium that have a reduced blood flow take longer to enhance.

Ultrasonic contrast agents can also be used to assess other abnormalities such as LV apical thrombus many of which are difficult to image without the use of contrast microbubbles (Fig. 6.17). A comprehensive review of clinical applications of ultrasonic contrast agents in echocardiography is given in a recent American Society of Echocardiography Statement.[34]

OTHER POTENTIAL USES OF CONTRAST MICROBUBBLES

Targeted contrast microbubbles

One of the most exciting areas of progress in contrast agent development has been that of selective targeting of the microbubbles to

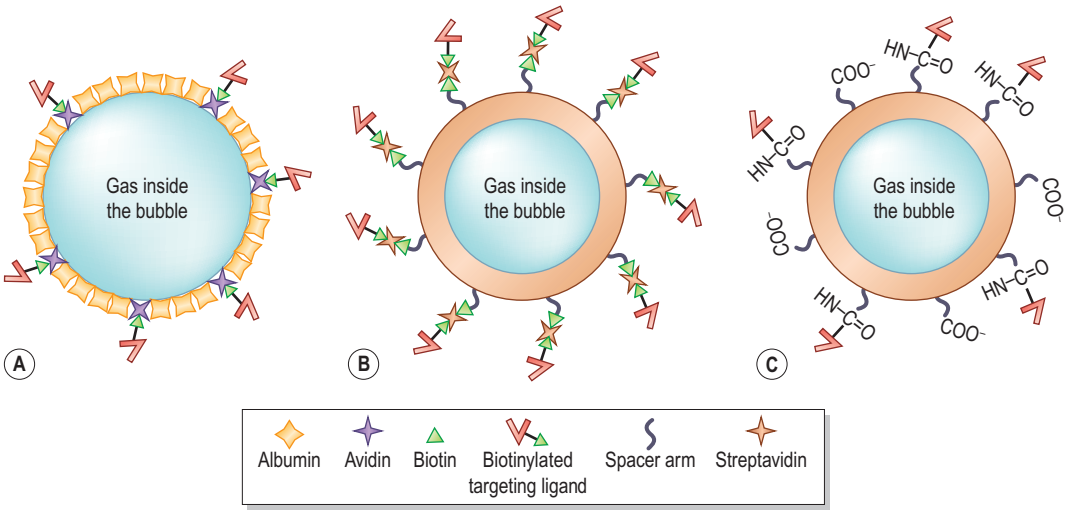


Figure 6.18 Methods to attach targeting ligands to microbubble shell. A: Non-covalent method, where avidin is embedded in the shell during bubble formation. **B:** Biotinylated bubble is coated with streptavidin and then biotinylated ligand. **C:** Ligand is covalently attached to the bubble shell by a peptide bond. (Reprinted from Klibanov AL. Ultrasound molecular imaging with targeted microbubble contrast agents. J Nucl Cardiol 2007;14:876–884.)

particular sites within the body, enabling acoustic visualisation of localised biological markers expressed in disease processes.

However, the proportion of microbubbles that bind to the surface is dependent on many factors including the number of receptor sites available for binding and the shear stress exerted on the microbubbles at the receptor sites.[35] Initial in-vitro studies demonstrated encouraging results under well-controlled flow dynamics[36] and a review of this field is given elsewhere.[37] Figure 6.18 illustrates schematically the potential methods of attaching ligands onto the surface of lipid- or albumin-coated microbubbles. Most commonly the binding for liposomal agents is achieved by formulating the liposome using a biotinylated lipid and using streptavidin as the linking mechanism between the biotinylated liposome and a biotinylated ligand. The antibody-loaded microbubble when injected into the body is then targeted to biological markers in which the receptor antigens are expressed. Increases in attachment can also be achieved using the radiation force of an ultrasound beam to push the targeted microbubbles towards the cell receptors by applying the ultrasound beam perpendicularly to blood flow.[38] Although this has been shown to be useful for in-vitro applications, it is difficult to assess how controllable this would be in clinical situations.

Early results in this area have shown promise with applications that include targeting of microbubbles to atherosclerosis, intravascular thrombi[39] and sites of angiogenesis and tissue inflammation.[40]

Drug and gene delivery

Although targeting mechanisms enable the microbubbles to become attached to particular biological markers, it is the ability of ultrasound in the presence of the microbubbles to cause transient poration of the cell wall that enables the microbubbles, their contents or other localised extracellular materials to pass into the cell. This transient permeability of the cell wall is known as sonoporation. To date, it is unclear from the literature the exact range of phenomena that are responsible for sonoporation. Although early research suggested that inertial cavitation was the source, more recent work using high speed cameras suggests that micro-streaming associated with non-inertial cavitation may also be associated with sonoporation.[41] Alternatively, the generation of extremely high temperatures associated with inertial cavitation may result in an increase in the fluidity of the phospholipid membranes thus allowing the microbubble to fuse with the cell membrane. However, from the literature it appears that many factors affect the size and permanency of the opening in the cell wall not least the relative closeness of the microbubble to the cell wall.[42]

Once sonoporation has occurred, extracellular molecules, such as drugs or genes, either incorporated within the microbubbles or injected near the site of sonoporation, may then enter the cells during this period of permeability thus enhancing the payload of the drugs or genes to the cell.[43] Comprehensive reviews of this topic are available.[44]

SAFETY OF CONTRAST MICROBUBBLES

The main area of concern over the safety of ultrasonic contrast agents is based around the likelihood of acoustic cavitation taking place under routine clinical scanning conditions. The potential hazards and risks of diagnostic ultrasound with and without contrast agents have recently been addressed.[45] In summary, since acoustic cavitation is extremely unlikely to occur in a conventional scan due to the lack of pre-existing gas bubbles within the body, the probability of harm is extremely low. If contrast is introduced the risk of acoustic cavitation and the severity of harm induced by it are considered higher.

The safety of two contrast agents (Definity and Optison) has recently been assessed retrospectively in a large multicentre clinical study. The conclusions of the study indicated that the agents had a good safety profile in both cardiac and abdominal ultrasound applications and the incidence of severe adverse reactions is less than that associated with other contrast agents used with other imaging modalities.[46]

The World Federation for Ultrasound in Medicine and Biology (WFUMB) published a series of articles as a result of a safety symposium dedicated to the use of ultrasonic contrast agents in diagnostic applications. This series of articles comprehensively addresses clinical applications and safety concerns for contrast agents,[47] in-vitro bioeffects,[48] in-vivo bioeffects,[49] exposures from diagnostic ultrasound equipment[50] and mechanisms for the interaction of ultrasound.[51] As a result of this symposium, recommendations for reducing the likelihood of bioeffects when using ultrasound contrast agents included: (i) scanning at low MI, (ii) scanning at higher

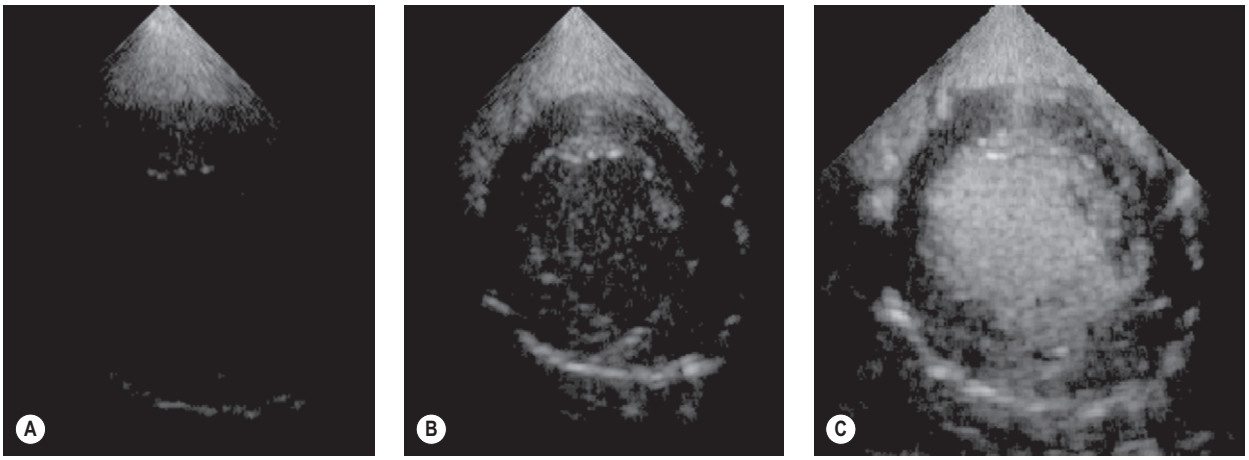


Figure 6.19 Example of acoustic shadowing during a cardiac study after a bolus injection of contrast. A: complete shadowing of left ventricle by contrast in right ventricle. **B:** contrast begins to clear from right ventricle, shadowing reduces. **C:** complete left ventricular opacification is now visualised.

Clinical applications and safety

- Ultrasound contrast microbubbles can be targeted to sites within the body.
- They are currently being investigated as drug delivery agents.
- WFUMB recommendations for the safe use of ultrasound include:
  - scanning at low MI
  - scanning at higher frequencies
  - reducing total acoustic exposure time
  - reducing contrast dose
  - adjusting cardiac triggering to avoid end-systole triggering.

frequencies, (iii) reducing total acoustic exposure time, (iv) reducing contrast agent dose and (v) adjusting the timing of cardiac triggering to avoid systole where most ventricular arrhythmias have been shown to occur.[52] The safety of ultrasound is discussed more fully in Chapter 4.

IMAGING ARTEFACTS

There are several artefacts that must be taken into consideration when making clinical ultrasound measurements after the injection of a bolus of contrast. These may be subdivided into propagation artefacts and Doppler artefacts.

Propagation artefacts

When contrast is injected into the body, although it scatters ultrasound strongly it also strongly attenuates and consequently as the bolus of contrast passes through a vessel or through the heart, organs distal to the vessels will temporarily disappear from the screen until the bolus clears through the system. This is readily observed in cardiac scanning where a large amount of the contrast agent can build up within the ventricles and obscure the posterior walls (Fig. 6.19). Shadow artefacts are commonly helpful in making a diagnosis in ultrasonic imaging; however, those created by contrast agents have not been used in that way.

Although a single bubble can be detected as a single spot in an image, when there are a large number of bubbles the spots in the image cannot be directly related to individual bubbles. The echo signals from bubbles in this situation interfere to form a speckle pattern, just as in the familiar case of echoes from the scattering centres in the parenchyma of organs. It is worth noting that the motion of the speckle pattern does not necessarily relate directly to the motion of the bubbles.

Where strong scatterers are present, such as gas bubbles, the echo signals may not travel directly back to the transducer; instead the path may involve multiple scatters. The multiple scattering delays the return time of an echo and hence it is depicted deeper than the actual position of the original source of the echo. The distal aspect of the region containing bubbles may therefore be displayed beyond its true boundary.

Doppler artefact

After the injection of a bolus of contrast agent, an artefact known as colour blooming may be observed during colour Doppler studies. When contrast agent enters a vessel the magnitude of the signal scattered from within the vessel increases, giving a corresponding increase in the Doppler signal. This effectively broadens the width of the scanning beam, allowing flow to be detected in the weaker regions of the beam. The resulting degradation of the lateral resolution causes the colour-coded flow region in the image to expand, i.e. 'bloom'. The effect is similar to having the Doppler gain too high and may be compensated by reducing the gain.

REFERENCES

1. Gramiak R, Shah P, Kramer D. Ultrasound cardiography: contrast study in anatomy and function. Radiology 1969;92:939–948.
2. Feinstein SB, ten Cate FJ, Zwehl W, et al. Two-dimensional contrast echocardiography. I. In vitro development and quantitative analysis of echo contrast agents. J Am Coll Cardiol 1984;3(1):14–20.
3. Ophir J, Parker KJ. Contrast agents in diagnostic ultrasound. Ultrasound Med Biol 1989;15(4):319–333.
4. Keller M, Feinstein SB, Watson DD. Successful left ventricular opacification following peripheral venous injection of sonicated contrast agent: an experimental evaluation. Am Heart J 1987;114: 570–575.
5. Schlief R, Schurmann R, Balzer T, et al. Saccharide based contrast agents. In: Nanda C, Schlief R, eds. Advances in echo imaging using contrast enhancement. Dordrecht: Kluwer Academic Publishers; 1993.
6. Rayleigh L. On the pressure developed in a liquid during the collapse of a spherical cavity. Philosophy Magazine 1917;6:94–98.

7. Plesset MS. The dynamics of cavitation bubbles. J Appl Mech 1949;16:272–282.
8. de Jong N. Acoustic properties of ultrasound contrast agents. PhD thesis, Erasmus University, Rotterdam, 1993.
9. Doinikov AA, Haac JF, Dayton PA. Resonance frequencies of lipid-shelled microbubbles in the regime of non-linear oscillations. Ultrasonics 2009;49:263–268.
10. Sboros V. Response of contrast agents to ultrasound. Adv Drug Deliv Rev 2008;60:1117–1136.
11. Chomas JE, Dayton PA, May D, et al. Optical observation of contrast agent destruction. Appl Phys Lett 2000;77:1056–1058.
12. Boukaz A, Versluis M, de Jong N. High speed optical observations of contrast agent destruction. Ultrasound Med Biol 2005;31:391–399.
13. Stride E, Saffari N. Microbubble ultrasound contrast agents: a review. Proc Inst Mech J Eng Med H 2003;217:429–447.
14. Boukaz A, de Jong N. WFUMB safety symposium on echo-contrast agents: nature and types of ultrasound contrast agents. Ultrasound Med Biol 2007;33(2):187–196.
15. Huang S-L, Hamilton AJ, Pozharski E, et al. Physical correlates of the ultrasonic reflectivity of lipid dispersions suitable as diagnostic contrast agents. Ultrasound Med Biol 2002;28:339–348.
16. Sontum PC. Physiochemical characteristics of Sonazoid™, a new contrast agent for ultrasound imaging. Ultrasound Med Biol 2008;34:824–833.
17. Porter TR, Xie F, Kilzer K. Intravenous perfluoropropane-exposed sonicated dextrose albumin produces myocardial contrast which correlates with coronary blood flow. J Am Soc Echocardiogr 1995;8:710–718.
18. Bloch SH, Dayton PA, Wan M, Ferrara KW. Optical observation of lipid- and polymer-shelled ultrasound microbubble contrast agents. Appl Phys Lett 2004;84:631–633.
19. Hope Simpson D, Chin CT, Burns P. Pulse inversion Doppler: a new method for detecting nonlinear echoes from microbubble contrast agents. IEEE Trans Ultrason Ferroelectr Freq Control 1999;46:372–382.
20. Eckersley RJ, Chin CT, Burns PN. Optimising phase and amplitude modulation schemes for imaging microbubble contrast agents at low acoustic power. Ultrasound Med Biol 2005;31:213–219.
21. Wei K, Jayaweera AR, Froozan S, et al. Quantification of myocardial blood flow with ultrasound-induced destruction of microbubbles administered as a constant venous infusion. Circulation 1998;97: 473–483.
22. Tiemann K, Lohmeier S, Kuntz S, et al. Real-time contrast echo assessment of myocardial perfusion at low emission power: first experimental and clinical results using power pulse inversion imaging. Echocardiography 1999;16:799–809.
23. Blomley MJK, Albrecht T, Cosgrove DO, et al. Stimulated acoustic emission in the liver parenchyma with the ultrasound contrast agent Levovist. Lancet 1998b;351:568.
24. Wilson SR, Jang H-J, Kim TK, et al. Real-time temporal maximum-intensity-projection imaging of hepatic lesions with contrast-enhanced sonography. Am J Roentgenol 2008;190:691–695.
25. Goertz DE, Frijlink ME, Tempel D, et al. Subharmonic contrast intravascular ultrasound for vasa vasorum imaging. Ultrasound Med Biol 2007;33:1859–1872.
26. Eckersley RJ, Tang M-X, Chetty K, Hajnal JV. Microbubble contrast agent detection using binary coded pulses. Ultrasound Med Biol 2007;33:1787–1795.
27. Cherin E, Brown J, Masoy S-E, et al. Radial modulation imaging of microbubble contrast agents at high frequency. Ultrasound Med Biol 2008;34:949–962.
28. EFUSMB study group. Guidelines and good clinical practice recommendations for contrast enhanced ultrasound (CEUS) – Update 2008. Ultraschall Med 2008;29:28–44.
29. Tranquart F, Le Gouge A, Correas JM, et al. Role of contrast enhanced ultrasound in the blinded assessment of focal liver lesions in comparison with MDCT and CEMRI: results from a multicentre study. EJC Suppl 2008;6:9–15.
30. Jiang J, Chen Y, Zhou Y, Zhang H. Clear cell renal carcinoma: contrast-enhanced ultrasound features relation to tumor size. Eur J Radiol 2010;73:162–167.
31. Droste DW, Jurgens R, Weber S, et al. Benefit of echocontrast-enhanced transcranial color-coded duplex ultrasound in the assessment of intracranial collateral pathways. Stroke 2000;31: 920–933.
32. Darge K. Contrast-enhanced voiding urosonography for diagnosis of vesicoureteral reflux in children. Pediatr Radiol 2007;38:40–63.
33. Mathias W Jr, Arruda AL, Andrade JL, et al. Endocardial border delineation during dobutamine infusion using contrast echocardiography. Echocardiography 2002;19:109–114.
34. Mulvagh SL, Rakowski H, Vannan MA, et al. American Society of Echocardiography consensus statement on the clinical applications of ultrasonic contrast agents in echocardiography. J Am Soc Echocardiogr 2008;21:1179–1201.
35. Butler MB, Moran CM, Anderson T, et al. Laser Doppler anemometry measurements of the shear stresses on ultrasonic contrast agent microbubbles attached to agar. Ultrasound Med Biol 2005;31:545–552.
36. Takalkar AM, Klibanov AL, Rychak JJ, et al. Binding and detachment dynamics of microbubbles targeted to P-selectin under controlled shear flow. J Control Release 2004;96:473–482.
37. Klibanov AL. Ultrasound molecular imaging with targeted microbubble contrast agents. J Nucl Cardiol 2007;14:876–884.
38. Rychak JJ, Klibanov AL, Ley KF, Hossack JA. Enhanced targeting of ultrasound contrast agents using acoustic radiation force. Ultrasound Med Biol 2007;33:1132–1139.
39. Lanza GM, Wallace KD, Scott MJ, et al. A novel site-targeted ultrasonic contrast agent with broad biomedical application. Circulation 1996;94:3334–3340.
40. Linder JR, Song J, Xu F, et al. Noninvasive ultrasound imaging of inflammation using microbubbles targeted to activated leukocytes. Circulation 2000;102(22):2745–2750.
41. Wu J, Ross JP, Chiu JF. Reparable sonoporation generated by microstreaming. J Acoust Soc Am 2002;111:1460–1464.
42. Prentice P, Cuschieri A, Dholakia K, Prausnitz M, Campbell P. Membrane disruption by optically controlled microbubble cavitation. Nature Phys 2005;1:107–110.
43. Van Wamel A, Kooiman K, Harteveld M, et al. Vibrating microbubbles poking individual cells: drug transfer into cells via sonoporation. J Control Rel 2006;112:149–155.
44. Hernot S, Klibanov AL. Microbubbles in ultrasound-triggered drug and gene delivery. Adv Drug Deliv Rev 2008;60:1117–1136.
45. Duck FA. Hazards, risks and safety of diagnostic ultrasound. Med Eng Phys 2008;30:1338–1348.
46. Wei K, Mulvagh SL, Carson L, et al. The safety of Definity and Optison for ultrasound image enhancement: a retrospective analysis of 78,383 administered contrast doses. J Am Soc Echocardiogr 2008;21: 1202–1206.
47. Blomley M, Claudon M, Cosgrove D. WFUMB safety symposium on echo-contrast agents: clinical applications and safety concerns. Ultrasound Med Biol 2007;33(2):180–186.
48. Miller DL. WFUMB safety symposium on echo-contrast agents: in vitro bioeffects. Ultrasound Med Biol 2007;33(2):197–204.
49. Dalecki D. WFUMB safety symposium on echo-contrast agents: bioeffects of ultrasound contrast agents in vivo. Ultrasound Med Biol 2007;33(2):205–213.
50. Whittingham TA. WFUMB safety symposium on echo-contrast agents: exposure from diagnostic ultrasound equipment relating to cavitation risk. Ultrasound Med Biol 2007;33(2):214–223.
51. Nyborg W. WFUMB safety symposium on echo-contrast agents: mechanisms for the interaction of ultrasound. Ultrasound Med Biol 2007;33(2):224–232.
52. Barnett SB, Duck F, Ziskin M. WFUMB symposium on safety of ultrasound in medicine: Recommendations on the safe use of ultrasound contrast agents. Ultrasound Med Biol 2007;33(2): 173–174.

CHAPTER

7 Liver: anatomy and scanning techniques

Simon Elliott

INTRODUCTION 93

ANATOMY 93

VASCULAR AND BILIARY ARCHITECTURE 94

SEGMENTAL ANATOMY OF THE LIVER 95

VARIATIONS IN ANATOMY AND DEVELOPMENT 96

SCANNING TECHNIQUES 98
Segmental approach 98
Liver parenchyma 100
Liver surface 101
Liver size 101
Vascular and ductal morphology 102

INTRODUCTION

The liver is the largest organ in the human abdomen. Due to its size, position and architecture, it has a special place in abdominal ultrasound, often influencing both the selection and set-up of ultrasound scanners. Knowledge of the normal anatomy and appearances is essential, in view of developments in hepatic surgical and interventional techniques, and the worldwide increase in chronic liver diseases.

ANATOMY

The normal liver lies mostly in the right upper abdomen, protected by the lower right rib cage; only its thin left part lies to the left of midline. It is a solid organ, weighing approximately 1.5 kg.[1] It shows a basic wedge shape, rounded on the right and tapering to the left. The domed superior surface fits smoothly under the cupola of the right diaphragm and adjacent right ribs; the flatter inferior surface is tilted such that it faces posteriorly and to the left, and is described as the visceral surface due to its contact with a number of other abdominal structures (Fig. 7.1).

Whereas the superior surface is smooth, the visceral surface is more complex, and most significantly contains the hilum, or porta hepatis. Organs in contact with the visceral surface include, from right to left: right kidney, gallbladder, duodenum and stomach. The generally smooth surface of the liver is indented anteroinferiorly by the gallbladder and ligamentum teres.

The liver is clothed in adherent peritoneum, apart from the fossae for the inferior vena cava and the gallbladder, and the so-called 'bare area' posteriorly. At certain points, however, the peritoneum is reflected off the surface of the liver to form complex folds which connect with neighbouring structures; the coronary ligament, and right and left triangular ligaments are situated posteriorly, related to the bare area, and are not seen in abdominal scans. However, the two other peritoneal folds may be seen clearly in the presence of ascites. The falciform ligament is a long triangular fold that lies between the liver and the anterior parietal peritoneum, attached anteriorly from the diaphragm down to the umbilicus, and posteriorly to the liver from the upper end of the ligamentum teres and along its anterior surface. It shows a third, free edge extending from the inferior argin of the liver to the umbilicus, enclosing the ligamentum teres.

The lesser omentum is an important anatomical landmark in the abdomen, but also is usually only seen when surrounded by fluid. It is a double layer of peritoneum that extends as a sheet from the lesser curve of the stomach to the liver and is also known as the hepatogastric ligament. It attaches in the fissure for the ligamentum venosum and from there folds back on itself to continue as the peritoneal layer covering the liver itself. At the oesophagogastric region the anterior layer continues over the diaphragm as the parietal peritoneum while the posterior layer is reflected over the posterior abdominal wall (mainly covering the body and tail regions of the pancreas) as the posterior wall of the lesser sac. On the right the two layers separate to enfold the hepatic pedicle (comprising the portal vein, the hepatic artery and the bile duct), fusing lateral to them to form a free border that stretches up from the first part of the duodenum to the lateral part of the porta hepatis where the layers again continue into the peritoneum covering the liver. Thus a foramen is formed immediately posterior to the porta hepatis where the general peritoneum communicates with the recess (the lesser sac); it is known as the 'foramen of Winslow' and its posterior margin overlies the inferior vena cava. The other walls of the lesser sac are formed by the posterior wall of the stomach and the peritoneum over the upper retroperitoneal structures so that part of the pancreas lies immediately posterior to it. On the left it extends up to the splenic hilum. Most of the caudate lobe lies within it.

The coronary ligaments over the diaphragmatic surface of the liver divide the subphrenic peritoneal space into anterior and posterior portions which are more completely separated on the right where the ligament is more extensive. The posterior subphrenic space continues into the hepatorenal space ('Morison's pouch'). These spaces delimit regions in which ascitic fluid and infective collections are confined.

The ligamentum teres and ligamentum venosum are remnants of the fetal circulation (Fig. 7.2) which appear as fibrous, reflective bands on ultrasound. Ligamentum venosum (fetal ductus venosus) extends from the left portal vein branch, upwards and to the right of the caudate lobe to join the vena cava at the orifice of the left hepatic vein. Ligamentum teres (fetal umbilical vein) runs in the liver from the anteroinferior fissure of the left lobe to join the left portal vein branch. Small, normally invisible vessels run along it: the hepatic branch of the superior epigastric artery, and small veins connecting portal vein to the umbilicus (the latter may dilate markedly in portal hypertension to form the paraumbilical vein and subcutaneous periumbilical collaterals – 'caput Medusae').

The liver is traditionally divided into left and right lobes, and currently the most widely accepted segmental classification is that described by Couinaud (see below), which is based on the vascular architecture of the liver.[2]

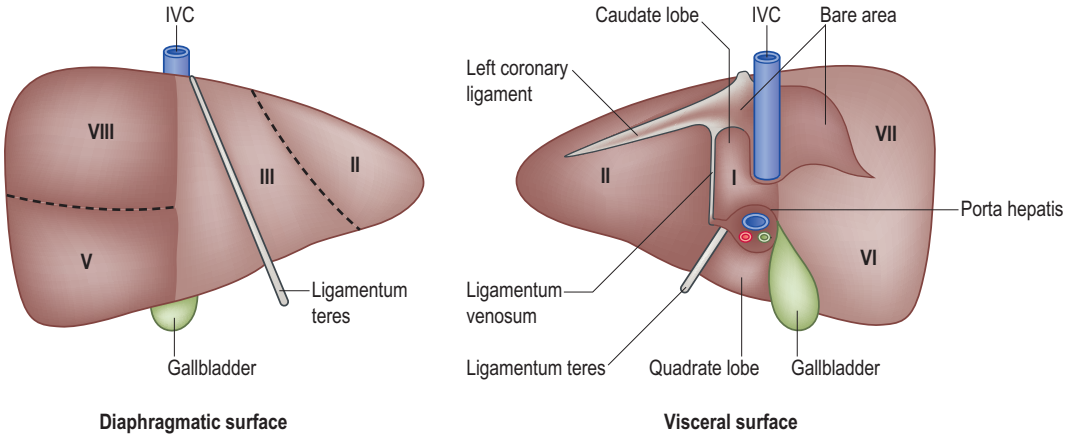


Figure 7.1 Anatomy of the liver. Two views of the liver are shown in diagrammatic form. The diaphragmatic surface is much simpler than the visceral surface which contains the porta hepatis. Note that in vivo the visceral surface is tilted to face inferomedially. Couinaud's segmental numbering system is indicated. IVC, inferior vena cava.

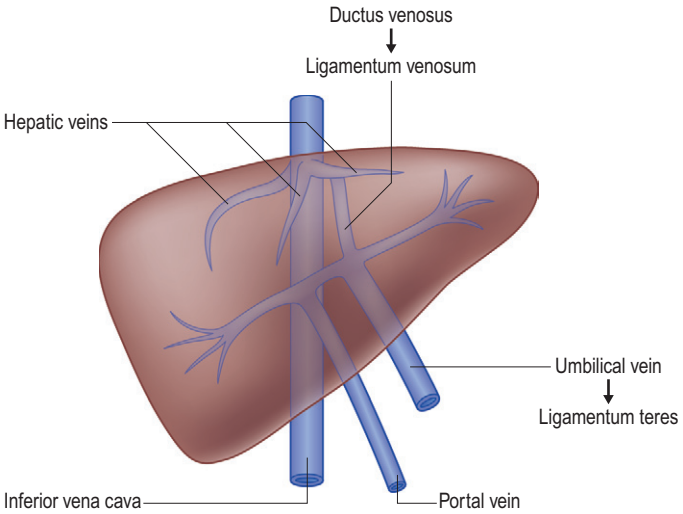


Figure 7.2 Fetal circulation through the liver. The venous bypass in the fetus takes blood returning from the placenta via the umbilical vein to the left portal vein and thence directly to the left hepatic vein and on into the inferior vena cava. The temporary vessels that carry this blood (the umbilical vein and the ductus venosus) undergo vasospasm at birth and they subsequently thrombose to form the ligamentum teres and ligamentum venosum, respectively. If the spasm extends into the left portal vein itself, lateral parts of the left lobe of the liver become ischaemic. This may account for the marked variability in size of this segment.

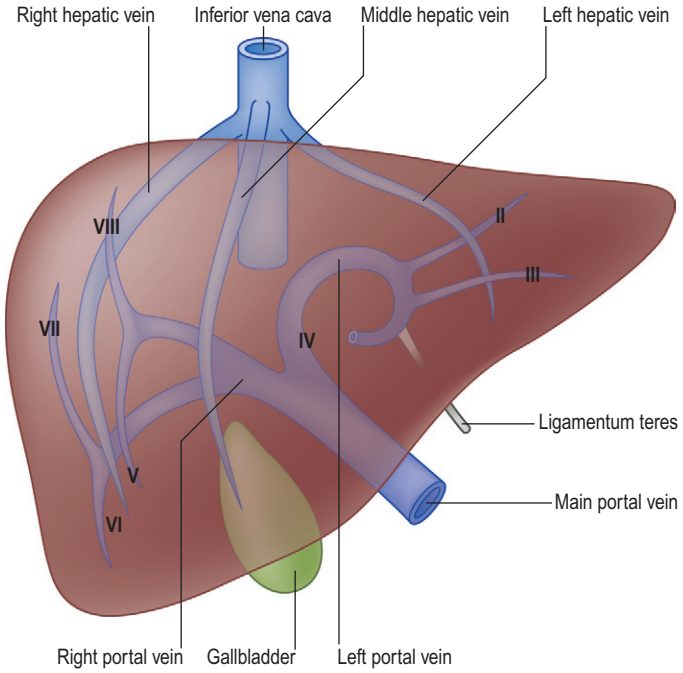


Figure 7.3 Blood vessels of the liver. The main branches of the portal vein and the way they interdigitate with the three main hepatic veins are illustrated. Couinaud's segmental divisions are indicated in Roman numerals.

VASCULAR AND BILIARY ARCHITECTURE

The generally smooth liver parenchyma is traversed by several vascular structures: the portal veins, hepatic veins, hepatic arteries and the bile ducts. The liver is unique in receiving two blood supplies: the hepatic artery provides approximately 25% of the inflow at rest, in the form of oxygenated blood direct from the systemic arterial system; the portal vein provides partially deoxygenated blood (75%) via the bowel, spleen and other viscera. Both pass through the porta hepatis, along with the bile duct. Venous drainage occurs via the hepatic veins, directly into the upper inferior vena cava to the right atrium of the heart (Fig. 7.3).

The common hepatic artery is normally a branch of the coeliac axis, and divides into left and right branches at or somewhere before the porta hepatis. In around 50% of people variations in its origin occur,[3] including separate left and right supplies from the coeliac axis and superior mesenteric artery (SMA), or common supply from the SMA alone. Identification of these vessels is important in preoperative assessment of liver transplant recipients. The diameter of the normal common hepatic artery is 5 mm or less. On ultrasound images, the artery is roughly parallel with the portal vein at the porta, but is more tortuous, and is seen coming in and out of the scan plane.

The portal vein originates as the confluence of the splenic and superior mesenteric veins, and enters the liver at the porta hepatis. It runs roughly transversely in the right upper abdomen, angled superiorly and to the right, and always lies posterior to the hepatic artery and bile duct. The main portal vein is a short trunk, a few centimetres in length and around 1 cm in diameter, which divides as it enters the liver into left and right branches. The left branch curves anteriorly before dividing further into segmental branches.

The right portal vein passes transversely for a few centimetres before dividing into anterior and posterior branches, then further subdividing into segmental veins. Within the liver parenchyma the hepatic arteries follow the same course.

The hepatic veins comprise three main veins – left, middle and right. The left vein is relatively short, and lies approximately in the midline sagittal plane; the middle vein courses from the line of the gallbladder fossa towards the inferior vena cava, usually joining with the left vein to form a short trunk before draining into the inferior vena cava (Fig. 7.4). The right vein lies in the coronal plane and empties directly into the vena cava. In addition to this normal arrangement of the three major veins, some liver segments which lie in direct contact with the vena cava are drained directly by the short inferior hepatic veins; these segments include the caudate lobe and the superomedial part of the right lobe (Fig. 7.5).

The bile ducts drain bile from the liver into the duodenum. The intrahepatic arrangement of the ducts is similar to that of the portal venous system, with the small segmental ducts joining to form left and right ducts, which normally lie anterior to their companion portal vein branches. Close to the porta hepatis, the right hepatic duct passes over the right portal vein, usually with the hepatic artery in between. The confluence of the left and right ducts lies just outside the liver parenchyma, forming the common hepatic duct. At a variable point along its length, the common hepatic duct is joined by the cystic duct (which drains the gallbladder) to form the common bile duct. Since this point cannot always be identified with transabdominal ultrasound, the extrahepatic duct is often referred to simply as the 'common duct'. From the liver, the common duct passes down anterolateral to the portal vein, then posterior to the first part of duodenum, through the posterior border of the head of pancreas, and turns sharply and transversely to the right to empty into the second part of duodenum at the ampulla of Vater. The common duct does not lie perfectly parallel with the main portal vein, but sits in a very slightly more sagittal plane, so that it appears to cross the portal vein as it passes inferomedially to the duodenum. This difference in duct/vein plane may become more pronounced in older patients.

The liver also possesses a lymphatic system. The network of lymph vessels lies predominantly within the portal tracts, and like elsewhere in the body is not seen with ultrasound. However, their distribution can be revealed in the presence of lymphoedema (for instance in some forms of cirrhosis or after liver transplantation), when low reflectivity cuffing may be seen surrounding the portal tracts.[4]

Microscopically, the anatomy of the liver is still a matter of interesting debate.[5] Functional units within the liver structure have been described since 1833, in the form of Kiernan's 'classic lobule' – a hexagonal lobule made up of the sinusoids, with portal tracts (including portal vein, hepatic artery and bile ducts) at the six corners and a draining hepatic vein at the centre. Later models include the 'portal lobule' – portal tract at the centre and hepatic venules at the periphery – and the 'liver acinus'. Current concepts favour primary and secondary lobules, with 'vascular septa' as the basis for the lobular architecture. It should be noted that the microanatomy of the liver differs across species, both between animal species and between animals and humans. Also, that these relationships apply only to the adult liver; the arterial and biliary systems are immature at birth, and in humans the hepatic arterial system may only proliferate to reach the adult state at 15 years of age, suggesting that the portal blood supply may be more important than the arterial in establishing the lobular architecture.[5]



Figure 7.4 Venous drainage of the liver. Transverse section. Arrow points to the short trunk forming the confluence of left and middle hepatic veins before entering inferior vena cava. The right hepatic vein enters the cava separately.

Overview of liver

- The liver is the largest organ in the abdomen.
- Knowledge of its complex three-dimensional structure is essential for localisation and surgical planning.
- Peritoneal folds, other ligaments and vascular structures are important landmarks.
- The liver receives a dual blood supply: 25% from hepatic artery, 75% from portal vein.

SEGMENTAL ANATOMY OF THE LIVER

An understanding of the segmental anatomy is now an essential part of the ultrasound examination of the liver. The most widely used classification is that described by Claude Couinaud, a French surgeon. The common usage of the Couinaud nomenclature allows for more accurate surgical planning and improved, consistent

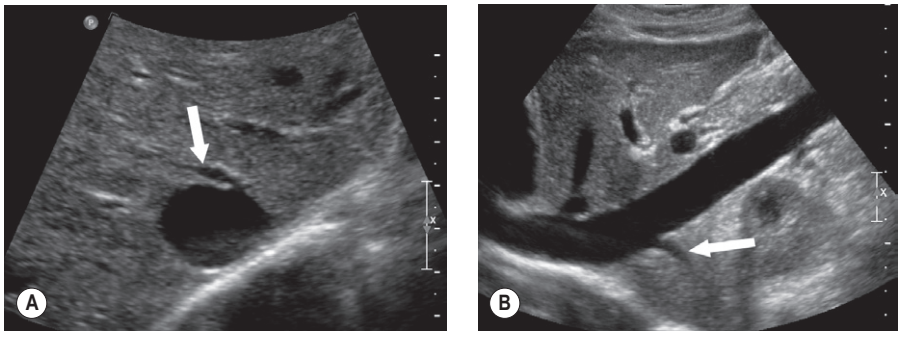


Figure 7.5 Inferior hepatic veins. A: Vein draining direct from the caudate lobe into vena cava. **B:** Vein draining directly from right lobe.

Segmental anatomy of the liver

- Couinaud nomenclature is the most widely accepted classification of liver segments.
- Classification is based mainly on portal and hepatic vein relationships.
- Each half of the liver contains four segments.
- Caudate lobe (I), left lobe (II, III, IV), right lobe (V, VI, VII, VIII).
- Variations on this basic arrangement do occur.

communication of the ultrasound findings to referring clinicians and radiological colleagues. The Couinaud system is based on the vascular architecture, specifically the anatomical relationships of the portal and hepatic venous systems.

Firstly, the liver is divided into left and right lobes along a virtual line (or main hepatic fissure), which extends from the gallbladder inferiorly to the left side of the inferior vena cava superiorly. This line passes through the porta hepatis and demarcates the equal sized parts of the liver which are supplied by the left and right portal veins and hepatic arteries, and which are drained by the left and right bile ducts. Note that the middle hepatic vein lies in this plane.

According to Couinaud, each half of the liver contains four segments (usually but not essentially using Roman numerals): segments I (caudate lobe) to IV on the left, and V to VIII on the right.

Each segment basically has a portal vein branch at its centre and a hepatic vein at its margin. The importance of the hepatic veins is that these borders form the resection planes for focal liver surgery. Variations in the basic arrangement do occur, particularly in the right lobe; these variations and the basis of the normal sonographic appearances of liver segments are well described from studies of cadavers and living subjects.[6]

Segment I, the caudate lobe, begins as an extension of the upper posterior part of the right lobe. This caudate process passes to the left across the subdiaphragmatic section of the inferior vena cava, and expands to form the caudate lobe, lying immediately posterior to the left lobe, from which it is separated by a fibrous fissure. The caudate lobe differs in that it may receive portal flow from the left and right portal veins.

Segments II and III form the left and right portions of the lateral part of the left lobe, respectively.

Segment IV (the quadrate lobe) is separated from II and III by the ligamentum teres and falciform ligament. It may be further subdivided into IVa superiorly and IVb inferiorly, such that IVb lies adjacent to the gallbladder. To the right it is separated from V and VIII by the middle hepatic vein and the main hepatic fissure.

Segments V and VIII form the anterior part of the right lobe, with V inferiorly and VIII superiorly. Segment V is bordered medially by the gallbladder.

Segments VI and VII form the posterior part of the right lobe, with VI inferiorly and VII superiorly. Segment VI is the segment closest to the right kidney.

Segments VI and VII are separated from V and VIII by the right hepatic vein.

Further details on the practical segmental anatomy are discussed in the later section on scanning techniques.

VARIATIONS IN ANATOMY AND DEVELOPMENT

Variations in shape of the liver may occur as simple changes or as true developmental anomalies. The left lobe is commonly affected by changes in shape: it may be lengthened supero-inferiorly as a thin sheet extending well below the costal margin, which is rarely clinically palpable (Fig. 7.6), or it may extend far to the left of the abdomen and be in contact with the left cupola of the diaphragm

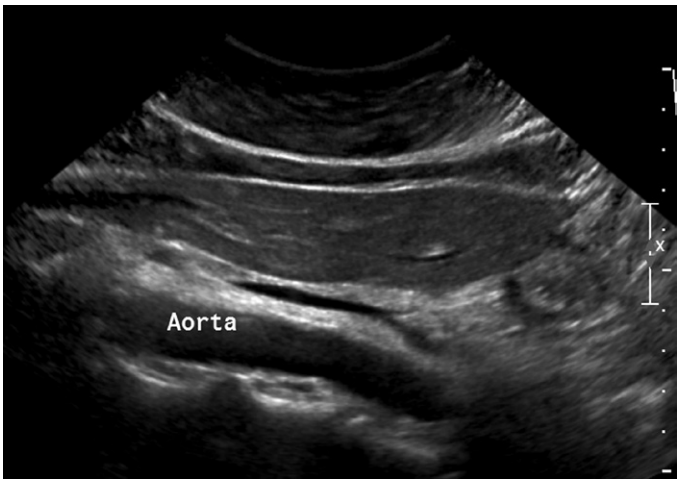


Figure 7.6 Left lobe variation. Sagittal section. A remarkably long, thin extension of the left lobe, the inferior tip of which lies in the lower abdomen anterior to the first sacral segment.



Figure 7.7 Left lobe variation. Left intercostal view. Lateral extension of the left lobe appearing as a low reflectivity region between spleen and diaphragm. This can give the appearance of a 'two-tone spleen', or suggest a subphrenic collection.

and upper pole of the spleen. This gives rise to a very misleading appearance – the 'two-tone spleen' – which can be misinterpreted as a left subphrenic collection, the liver being of lower reflectivity than the spleen (Fig. 7.7).

Riedel's lobe is a common anomaly, seen as a tongue-like elongation of the right lobe extending inferiorly, and lying anterior to the right kidney (Fig. 7.8). A Riedel's lobe may extend well into the right iliac fossa, and may appear to be almost pedunculated. True pedunculated accessory lobes are rare, and may cause clinical and imaging confusion as they can be found in any position in the abdomen;[7] they may also be affected by focal masses or torsion.

The caudate lobe may vary markedly in shape and size, from very small to extending below the free inferior border of the left lobe (Fig. 7.9). In transverse section an enlarged or partly pedunculated caudate lobe can be mistaken for a pre-aortic mass or abnormal lymph node (Fig. 7.10).

Sitting snugly in the upper abdomen, the soft liver surface can easily be indented by firmer adjacent structures. Thus the diaphragmatic surfaces of the liver are often indented by a series of curved grooves from ribs and muscular leaflets, which can produce a confusing picture in almost any plane (Fig. 7.11). These are particularly



Figure 7.8 Riedel's lobe. Sagittal section. A large Riedel's lobe extending well below the right kidney into the right iliac fossa.



Figure 7.9 Caudate lobe. Sagittal section. In this individual the caudate lobe (arrow) is slightly elongated and projects inferiorly.



Figure 7.10 Caudate lobe. Transverse section. A pedunculated caudate lobe can appear almost separate from the liver and may suggest an extrahepatic mass.

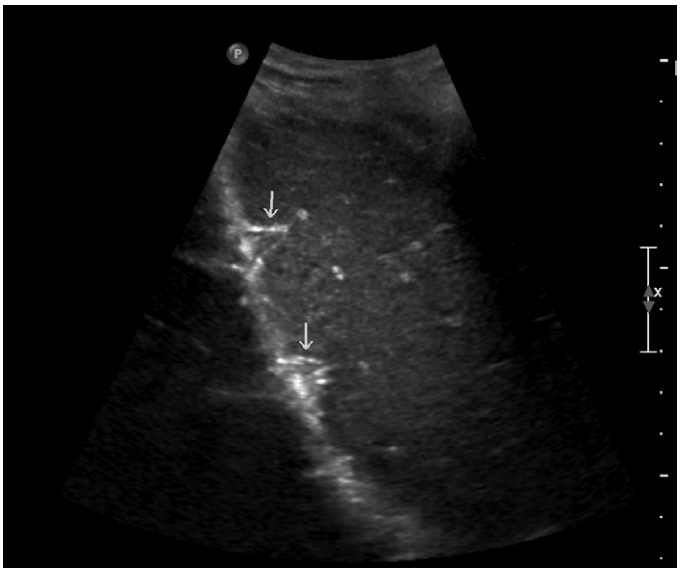


Figure 7.11 Diaphragmatic slips. Oblique section. These slips are most noticeable in thin individuals and can appear as angular grooves on the normally smooth upper and right surfaces of the liver.

noticeable in thin subjects. Deep peritoneal folds also may produce accessory fissures from the diaphragmatic surface.

True congenital anomalies of the liver are rare, and in the case of segmental fusion may not be detected with cross-sectional imaging. For instance, a study of 54 cadavers[8] showed normal lobar development in 54%, the most frequent variations from normal being various segmental fusions (30%), with lobar absence comprising left 2%, caudate 7% and quadrate 4%; whereas a review of 383 CT scans identified around 95% as normal, with lobar absence comprising left 3%, right 0.3%, other segments 2%.

Failure of development most commonly affects the left lobe – segments II and III – with subsequent compensatory hypertrophy of segment IV and the right lobe. This failure may be the result of true hypoplasia, or due to ischaemia resulting from excessive spasm of the left portal vein branch associated with closure of the placental-hepatic bypass at birth. Occasionally this condition is associated with defective development of the diaphragm, which may give rise to gastric volvulus. Absence of the right lobe is rare, and may also be associated with diaphragmatic defects.

Adult polycystic liver disease (APLD) is an inherited disorder which affects approximately 50% of patients with autosomal dominant polycystic kidney disease (ADPKD).[9] The cysts tend to appear from puberty onwards, and increase with age; thus they are found in around 20% of patients in their third decade and 75% in the seventh decade; they are more common in women. The cysts result from an overgrowth of biliary epithelium and supportive connective tissue, and range in size from microscopic to several centimetres in diameter. A severely affected liver may be hugely enlarged and occupy most of the abdominal cavity. Cysts may also be found in the pancreas and spleen.

ADPKD and APLD present problems for ultrasound imaging. The large numbers of cysts produce multiple reflecting surfaces and through transmissions, resulting in a 'hall of mirrors' effect (Fig. 7.12). Although the near field cysts may be seen well, the ultrasound image often degrades rapidly with depth, so that searching for the common symptomatic complications of these conditions (e.g. haemorrhage and infection) can be difficult if not impossible. Tissue harmonic imaging should be used to reduce noise and improve contrast, along with appropriate adaptation of time gain compensation. If both the liver and the kidneys are severely affected, it can be difficult to identify the organs separately using cross-sectional imaging (Fig. 7.13); in this situation real-time ultrasound

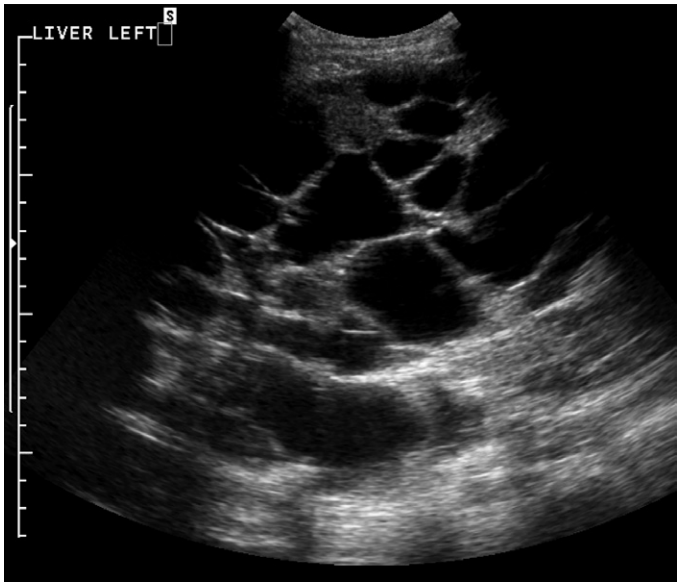


Figure 7.12 Adult polycystic liver. The left lobe almost completely occupied by cysts of varying size. The near field detail is crisp, but the image degrades with depth – the 'hall of mirrors' effect.



Figure 7.13 Adult polycystic liver and kidney. The polycystic liver in the near field is difficult to differentiate from the polycystic right kidney in the far field. In real time, visceral slide can be used to identify the planes of tissue separation.

has an advantage, in that by observing 'visceral slide' between the two during respiration, it is usually possible to identify their plane of separation.

SCANNING TECHNIQUES

The liver is a large, complex three-dimensional structure, so it is important that the ultrasound practitioner develops a steady, systematic approach to the assessment of each component of the examination. These components should include:

- segmental approach
- parenchyma
  - reflectivity
  - attenuation
  - uniformity
  - texture
- surface
- size
- vascular and ductal morphology.

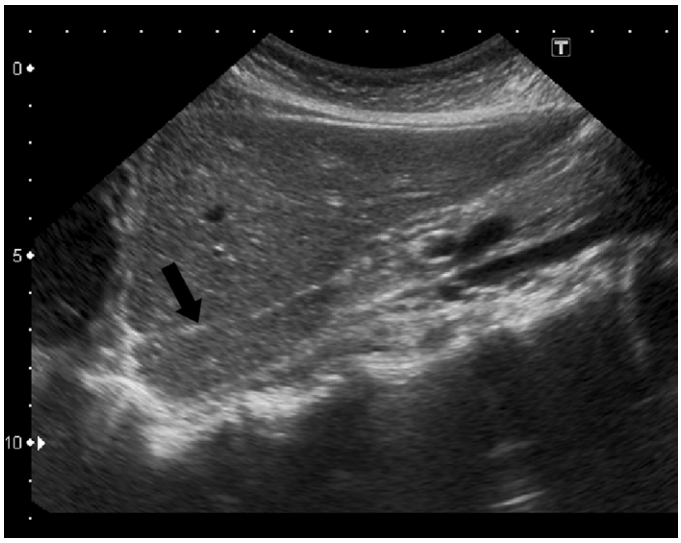


Figure 7.14 Normal left lobe. Sagittal section. Normal configuration of left lobe with sharp anteroinferior margin and thin caudate lobe (arrow).

Segmental approach

The examination is ideally based upon mentally following the segmental anatomy, e.g. from I to VIII, so that no part of the organ is overlooked. The Couinaud segments can be followed by a sequence of simple and easily identifiable landmarks: the central portal veins, the caudate lobe itself, ligamentum teres, the gallbladder, right kidney, middle and right hepatic veins.

Each segment or group of segments should be examined by sweeps in two orthogonal planes, e.g. sagittal and transverse, wherever possible. Sweeps should extend beyond the liver capsule, to identify exophytic liver lesions or adjacent extrahepatic pathology.

Starting in the midline sagittal plane with the transducer positioned just below the xiphisternum, the normal left lobe shows a triangular shape with a sharp anteroinferior border (Fig. 7.14). The caudate lobe can be seen deep to the left lobe, separated by the reflective fissure line. This view also allows identification of other epigastric structures, notably the pancreas, stomach, aorta, mesenteric artery origins and adjacent lymph nodes.

Note that in thin subjects, in deep inspiration, the crura of the diaphragm may also appear as a pre-aortic wedge-shaped structure of varying reflectivity (Fig. 7.15).

Rotate the transducer anticlockwise into the transverse plane; in this plane, the segments I to IV are arranged anticlockwise, so identify the caudate lobe (I) again, then the segmental portal vein branches supplying segments II (posterior) and III (anterior), and sweep through the segments accordingly (Fig. 7.16). The ligamentum teres appears as a highly reflective fibrous band passing down from the anterior surface of the liver towards the left portal vein (Fig. 7.17). It is often dense enough to cast a significant acoustic shadow. The inferior margin of the ligament and the left portal vein are important landmarks for identifying, using colour Doppler, the presence of a patent para-umbilical vein in portal hypertension. In the presence of ascites, the falciform ligament can be seen extending from the ligamentum teres to the anterior parietal peritoneum.

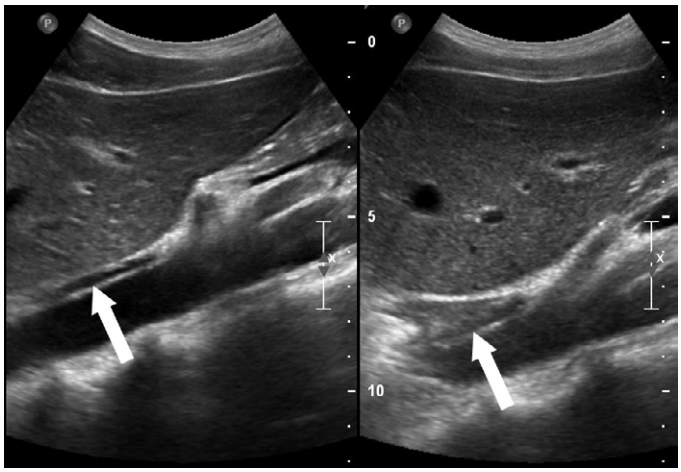


Figure 7.15 Crura of the diaphragm. Sagittal section. The crura (arrowed) are seen as pre-aortic structures in expiration (left) and inspiration (right). In inspiration these can appear as a surprisingly large structure, with similar reflectivity to adjadcent liver.

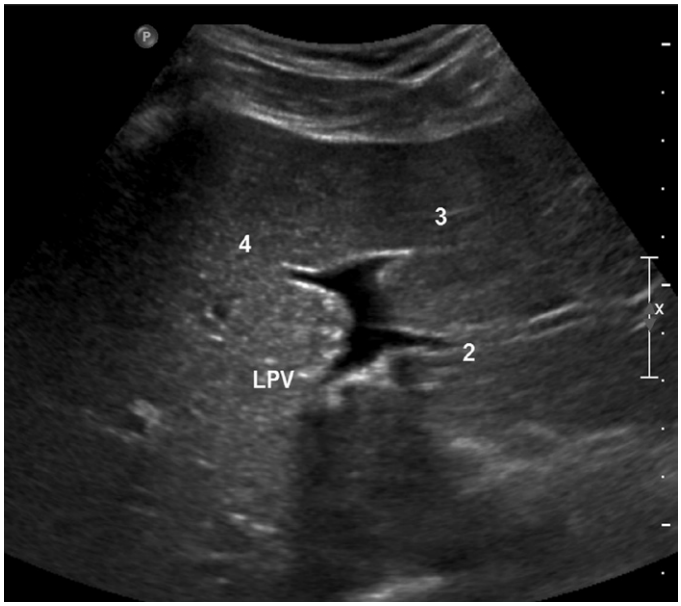


Figure 7.16 Left portal vein branches. Transverse section. Classical 'H' on its side appearance of the main left portal vein (LPV) branches to segments II, III and IV (2, 3 and 4).

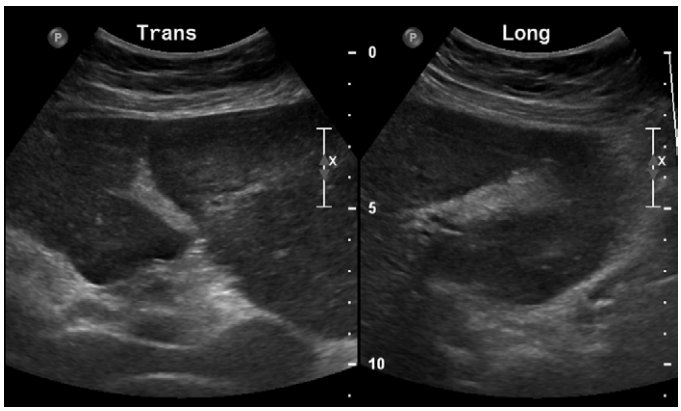


Figure 7.17 Ligamentum teres. Transverse (left image) and sagittal (right) sections. The ligamentum teres appears as a highly reflective band which is usually linear in transverse section and may be triangular or sheet-like in sagittal. It often cast a dense acoustic shadow.

Continuing along the anticlockwise path, segment IV must lie to the right of the landmark formed by the ligamentum teres, with IVb adjacent to gallbladder.

In a patient with the appropriate body shape and on deep inspiration, it should be possible to place the transducer in a transverse oblique plane, just to the right of midline below the costal margin, and angle superolaterally to view segment IV and most of the right lobe (Fig. 7.18). This is particularly important in order to cover the potential 'blind' area of the upper right lobe segments which occurs from the intercostal window (Fig. 7.19).

Most of the right lobe, the porta hepatis and the major hepatic vessels are best assessed from an intercostal window in the right anterior axillary line (Fig. 7.20). This approach also provides reliable access to these important structures in postoperative patients, when much of the abdominal surface may be inaccessible due to wounds, drains and dressings.

Segment V lies anteriorly and is bordered medially by the gallbladder and middle hepatic vein.

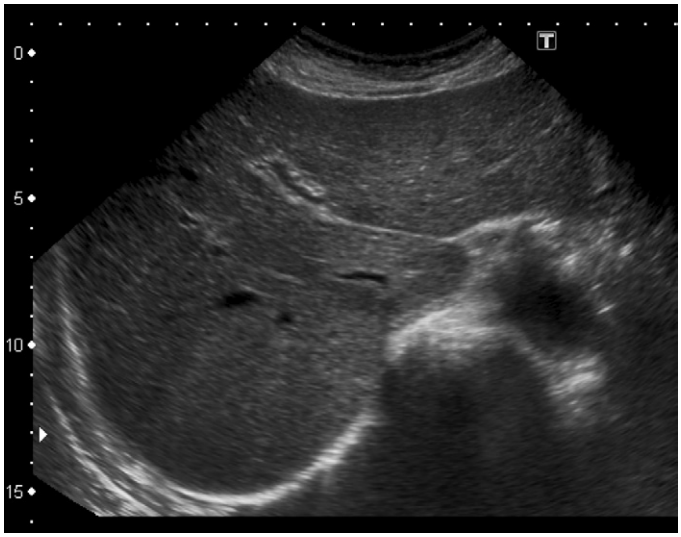


Figure 7.18 Subcostal transverse view of liver. This view is very useful, demonstrating much of the liver, but can be obtained only in some individuals, being very dependent on body shape and bowel gas.

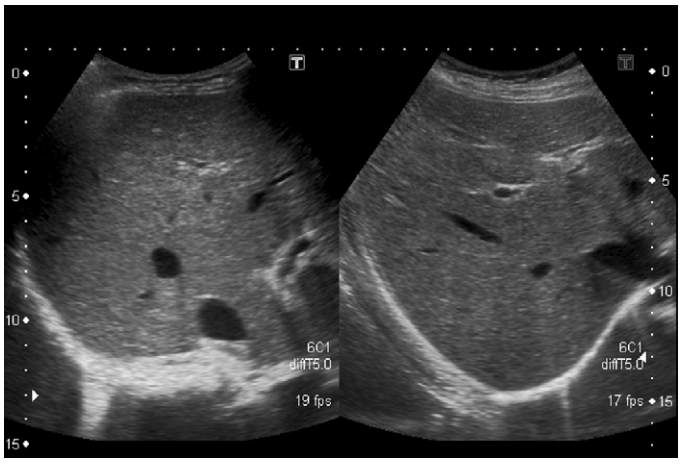


Figure 7.19 Right lobe – the 'blind area'. The intercostal section (left image) shows lack of information in the upper segments close to dome of diaphragm, usually due to overlying rib or aerated lung. These segments may be seen by taking a right subcostal approach in deep inspiration, with cephalad angulation of the transducer (right image).



Figure 7.20 Right intercostal view. Classical access window to the right lobe of liver and porta hepatis, with gallbladder on the right.

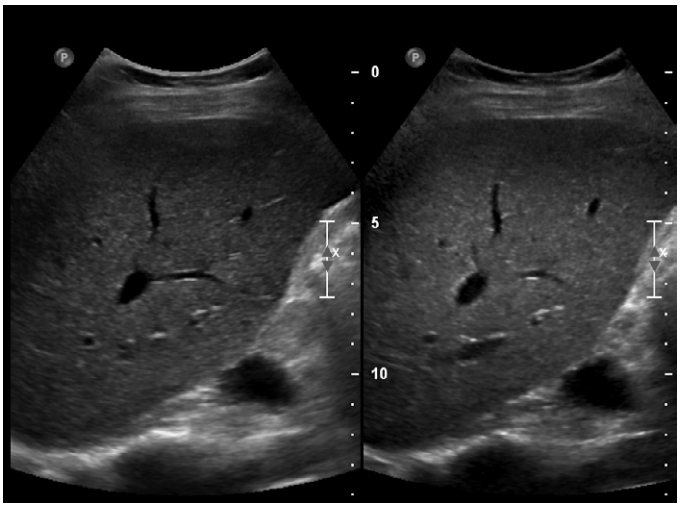


Figure 7.21 Liver parenchyma. Fundamental imaging (left) with a broadband 1–5 MHz transducer. Tissue harmonic imaging (right) with same transducer, showing subtle changes in representation of the liver parenchyma.

Segment VI is the closest segment to the right kidney.

Segment VII lies superior to VI, and segment VIII superior to V, but defining these upper segments can be difficult in practice, sometimes impossible. It is common, across all cross-sectional imaging modalities, to see liver pathology described as lying in 'segments VI/VII' or 'V/VIII'.

Liver parenchyma

The 'ideal' ultrasound image of the normal liver is very much a matter of personal preference, and can be a major influence on purchasing decisions. The assessment of liver parenchymal texture is notoriously subjective, and can give rise to a confusing range of reporting terminology in both normal and abnormal situations. Some users prefer to see a smooth texture with minimum speckle pattern, others prefer a sharper, more 'speckly' image. Modern ultrasound scanners possess a vast range of beam-forming and image processing techniques, each of which can significantly alter the perceived 'echotexture' of the liver; just changing transducers on the same scanner can markedly affect interpretation, and it may take several scanning sessions to get a feel for normal liver texture for each individual transducer/scanner combination. The aim in every department should be to develop agreed standards, both for imaging technique and reporting terminology.

The key to ultrasound examination of liver parenchyma is image optimisation. Firstly, depth should be adjusted to include only the section of liver down to its deepest surface, followed by optimisation of 2D gain. Time gain compensation should be adjusted to produce an image that is as uniform as possible from near to far field. Focus depth is generally positioned at the area of interest, but may be placed in the far field to improve penetration. An increasing number of systems provide semi-automated optimisation controls, which alter several parameters simultaneously; these are remarkably effective and can be used for rapid image optimisation. Tissue harmonic imaging may be used for baseline scanning or activated when increased tissue contrast is required – this again is a matter of personal preference depending on the system used (Fig. 7.21). High-resolution or 'read' zoom should be used to interrogate areas of interest.

Normal liver has a uniform reflectivity that is the same or is slightly increased compared to the adjacent normal right renal cortex (Fig. 7.22). The parenchymal texture should be homogeneous. Since the time gain compensation curves of most scanners are set up using the right lobe of liver as a reference, there should be little or no appreciable attenuation of echoes when progressing from near to far field in normal circumstances.

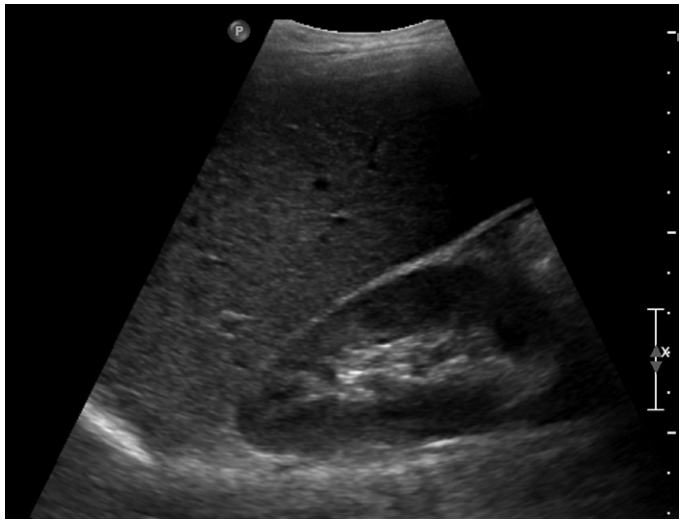


Figure 7.22 Liver reflectivity. The normal liver texture is uniform and shows slightly increased reflectivity compared with adjacent normal renal cortex.

Liver assessment

- Scanning technique should be systematic and segmental.
- Perception of liver texture is highly subjective.
- Parenchymal appearances can be markedly changed using different systems and imaging parameters.
- Accurate assessment of liver size is difficult.
- Assessment of the liver surface is an important component of the examination.

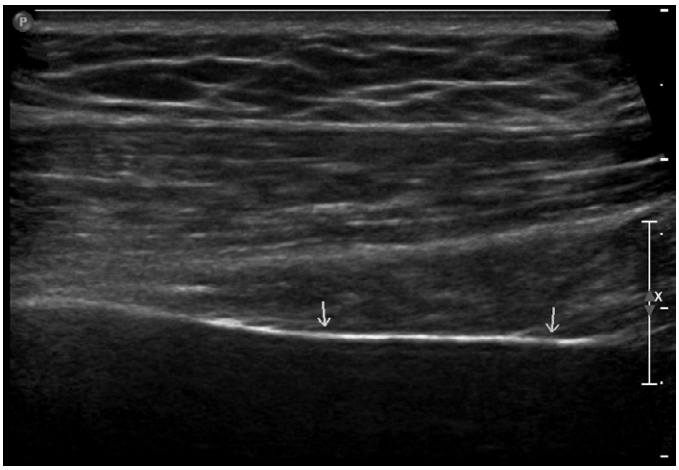


Figure 7.23 Liver surface. Sagittal section of left lobe using a linear 5–17 MHz transducer with spatial compound imaging. Normal linear appearance (arrows) with no irregularity.

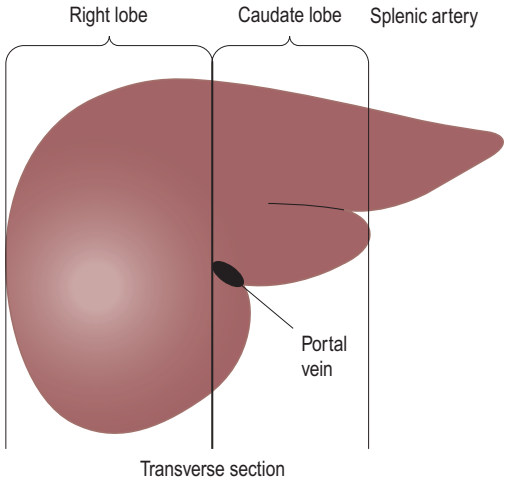


Figure 7.24 Measurement of the caudate lobe. The position for measurement of the caudate lobe in the transverse plane is shown. The normal caudate is less than two-thirds the transverse diameter of the right lobe.

Table 7.1 Dimensions of the normal liver[3]

Diameter	Mean ± SD (cm)
Midclavicular longitudinal	10.5 ± 1.5
Midclavicular anteroposterior	8.1 ± 1.9
Midline longitudinal	8.3 ± 1.7
Midline anteroposterior	5.7 ± 1.5

Liver surface

The surface of the normal liver presents as a very smooth reflective interface. Identification of a change to an irregular or nodular surface is extremely important in the assessment of diffuse chronic liver disease, e.g. cirrhosis, so an ultrasound examination of the liver should include a high-resolution image of its surface. This is best obtained from a 'free' edge (usually the anterior border of the left lobe, as the right lobe intercostal surface may be compressed by the adjacent chest wall) using a high-frequency linear transducer (Fig. 7.23). Spatial compound imaging assists in improving the edge definition of the liver surface, allowing detection of subtle variations. Systems are also increasingly able to provide improved edge definition at depth, e.g. of the free inferior (visceral) surfaces of both left and right hepatic lobes.

Liver size

Clinical hepatomegaly is defined by palpation of the liver edge below the costal margin, but this evaluation is notoriously unreliable.[10,11] For example, a normal size liver may be displaced inferiorly by overinflated lungs or by an enlarged heart, or a Riedel's lobe may be present. One advantage of ultrasound is that the inferior border of the liver can rapidly be located in relation to the clinical marker of the costal margin, so that a clinical diagnosis of hepatomegaly can be correlated directly with normal or abnormal ultrasound findings.

Wide variations in the configuration of the liver make any assessment of its overall size difficult, and like so many aspects of liver ultrasound, this evaluation is subjective. Ultrasound assessment of liver size is possible, using linear measurements in standard positions, and these may be useful in specific circumstances.[12] For reference, longitudinal (maximum supero-inferior span) measurements of the left lobe in the midline and right lobe in midclavicular line from 1000 healthy subjects are listed in Table 7.1.

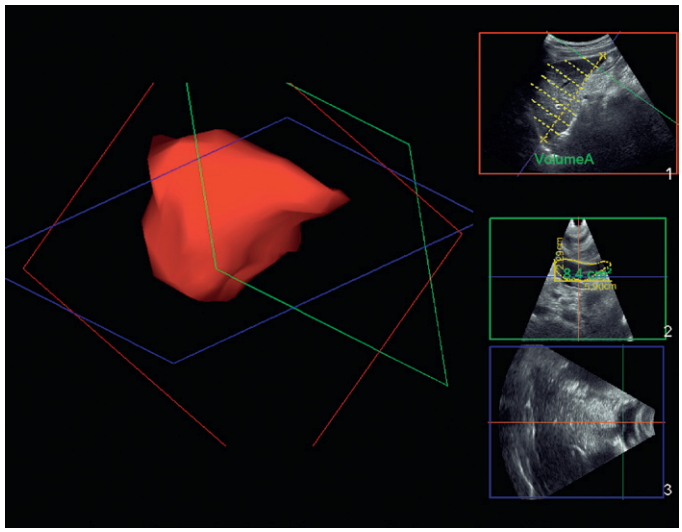


Figure 7.25 Volume ultrasound. Volume acquisition of the left lobe of liver (segments II and III) using a 2–6 MHz mechanically swept curvilinear transducer, 3 second scan time. Multiplanar images (right) have been measured using a stacked contour technique, to produce a surface-rendered representation of this part of the left lobe. Volume calculation 250 mL.

However, the size of the caudate lobe is relatively easily assessed using linear ultrasound measurements, and this may be helpful in confirming enlargement in conditions such as cirrhosis or hepatic vein occlusion (Budd–Chiari syndrome). The transverse diameter can be obtained as shown in Figure 7.24, where this diameter at the level of the porta can be compared with that of the right lobe. The normal caudate lobe should be less than two-thirds the diameter of the right lobe.[13] The anteroposterior diameter of the caudate lobe can also be measured and compared with that of the adjacent left lobe; the normal caudate diameter should be less than half that of the left lobe.

Recent and ongoing developments in volume acquisition ultrasound, using mechanical and true matrix transducers, provide for more accurate volumetric analysis, but the size of the normal liver is too great for their current acquisition range. However, these techniques can be used for measuring the volume of specific parts of the liver, e.g. left lobe (Fig. 7.25), and are increasingly being used to

assess more accurately the size and progress of neoplastic masses in the liver. Since assessment of overall liver size is now achievable using rapid MR or CT sequences, these may be the method of choice.

Vascular and ductal morphology

These structures can be imaged at the porta hepatis, and in their intrahepatic and extrahepatic portions.

The porta hepatis is usually assessed from the right intercostal approach. This approach also provides an optimal incident angle (around 30°) for Doppler studies. The portal vein should be identified as the largest vessel at the porta, and the scan plane oriented such that it is seen lengthways (Fig. 7.20). With slight variations from this plane, the common duct will be seen as a smaller vascular structure lying above the portal vein. Closer to the hilum of the liver, the right and left ducts, and the right and left portal veins, may be traced as separate structures. At the hilum, the hepatic artery, more likely the right branch of the hepatic artery, may be identified in cross-section lying between the duct and portal vein. The relationship of the hepatic artery and common duct shows variations along their lengths, but the pair almost without exception lie above the portal vein on this projection.

In transverse section, the portal vein appears as the largest vascular 'ring', with the hepatic artery and common duct lying immediately anteriorly.

The portal vein can be traced from the porta into left and right branches. Each of these generally divides in 'H' form, with the 'H' appearing to lie on its side, to supply the lobar segments[6] (Fig. 7.16).

The intrahepatic portal and hepatic veins can be differentiated by their anatomical orientation, rather like the interlocking fingers of two hands, and to some extent by their structural appearances. Portal veins tend to have thicker, more reflective walls, whereas hepatic veins may appear to have no walls at all (Fig. 7.26). The portal vein wall borders are enhanced by the accompanying bundle of hepatic artery, bile duct and associated connective tissue. However, this is a very variable difference, and depends markedly on the incident angle of the ultrasound beam. Thus normal hepatic veins lying perpendicular to the beam may show a reflective wall, which disappears when approached from a different, more acute angle (Fig. 7.27). In addition, modern adaptive image processing techniques can markedly alter the appearances of both liver texture and linear structures within the liver – another case for learning the capabilities of, and variations produced by, individual systems. It should be noted that a number of diffuse liver diseases are more likely to show changes around the portal tracts than around the hepatic veins.

As well as developments in image processing, progressive improvements in spatial resolution are making it possible routinely to identify the components within the portal tracts (vein, artery and duct) as discrete vessels, down to at least segmental level (Fig. 7.28). For quantification and surveillance purposes, a transverse view of the left lobe should be recorded with the portal tracts of segments 2 and/or 3 seen lengthways, i.e. perpendicular to the beam. Although clearly there may be asymmetry of these structures between left and right lobes, in diffuse disease these tracts are more easily assessed than those in the right lobe.

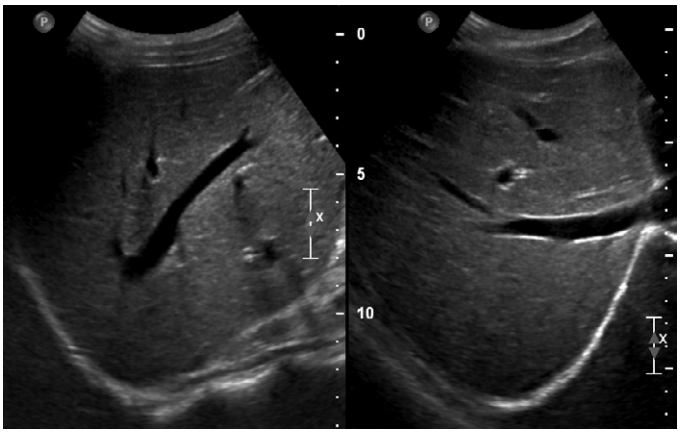


Figure 7.27 Hepatic vein walls. The effect of incident beam angle on wall reflectivity (right hepatic vein). With an acute angle of approach (left) the hepatic vein shows little or no wall reflectivity. The same vein imaged with a perpendicular approach (right) shows highly reflective walls, similar to a normal intrahepatic portal vein.



Figure 7.26 Hepatic and portal vein walls. Section of right lobe. The portal veins in cross-section show highly reflective walls compared with the interposed hepatic vein.

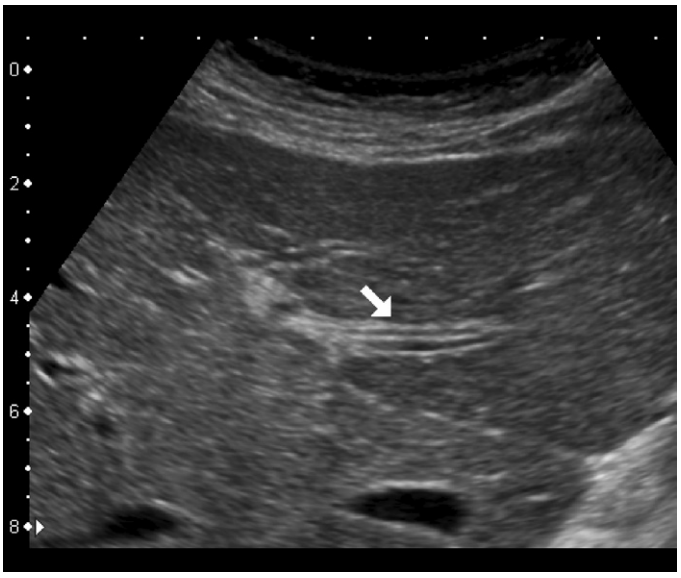


Figure 7.28 Left lobe portal tract: segment II. Recent developments in spatial resolution allow routine visualisation of vascular detail in the portal tracts. In this image of the segment II tract, the portal vein is the largest vascular structure, with normal bile duct and hepatic artery anteriorly.

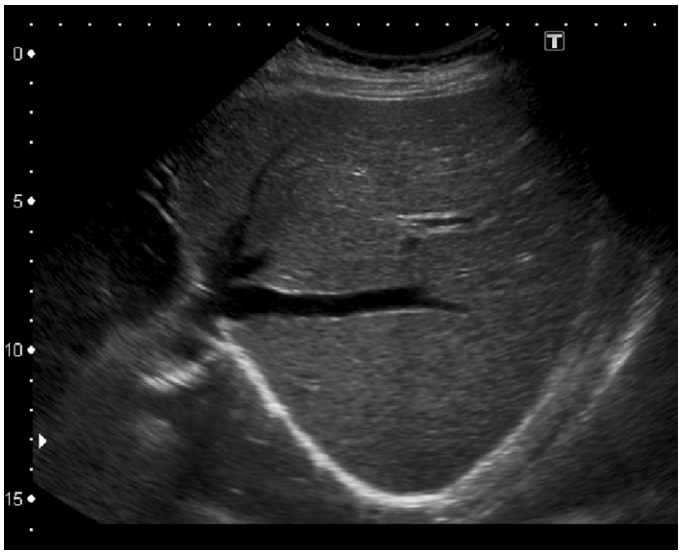


Figure 7.29 Right hepatic vein. Intercostal coronal oblique showing right hepatic vein entering inferior vena cava.

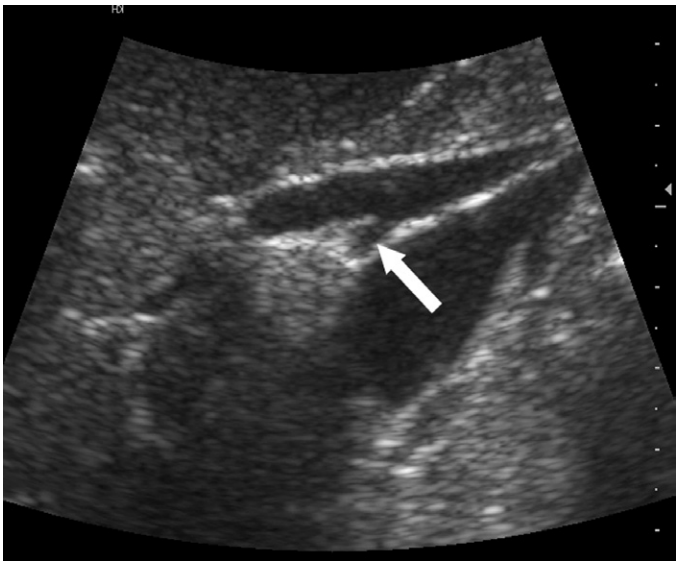


Figure 7.31 Cystic duct insertion. Subcostal oblique section. The cystic duct (arrow) is seen entering the deep wall of the common hepatic duct, combining to form the common bile duct. Note the slight dilatation of the common duct at this point.

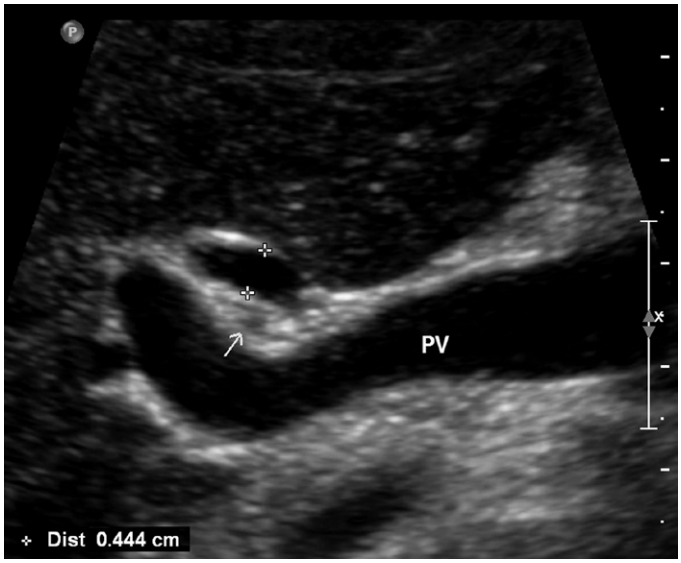


Figure 7.30 Common hepatic duct measurement. Intercostal view of porta hepatis. The common duct is measured (callipers) at the point where it crosses the hepatic artery (arrow) in cross-section. PV, portal vein.

The three main hepatic veins can sometimes be seen at once in subxiphoid high transverse sections of the liver as they converge towards the inferior vena cava. More often, several different planes are required to image them individually. The right hepatic vein can be seen in a coronal oblique plane from the intercostal window, and traced directly into the vena cava (Fig. 7.29). Left and middle hepatic veins can be seen converging into their common trunk from a transverse plane with some cephalad angulation (Fig. 7.4).

The common duct is conventionally measured at the porta hepatis, around the point where the triad of vein, duct and artery are seen, and the artery is in cross-section (Fig. 7.30). Taking an average adult diameter of 4 mm, and an upper limit of normal as around 6 mm, a useful formula to remember is to add 1 mm per decade of life (i.e. 7 mm at 70 years of age would be within normal limits). On occasion, the normal cystic duct draining the gallbladder may be seen entering the common duct, usually into its deeper aspect (Fig. 7.31) and around this level the common duct may show some slight natural dilatation of a millimetre or two. Difficulties in choosing the right level for measurement can also occur in older patients, when the duct may show some fusiform dilatation.

REFERENCES

1. Gelfand DW. Anatomy of the liver. Radiol Clin North Am 1980;18:187–194.
2. Couinaud C. Le foie; études anatomiques et chirurgicales. Paris: Masson; 1957.
3. Sidhu PS, Chong WK. Measurement in ultrasound: a practical handbook. London: Arnold; 2004.
4. Worthy SA, Elliott ST, Bennett MK. Low-reflectivity periportal collar on hepatic ultrasound. Br J Radiol 1994;67:1050–1051.
5. Saxena R, Theise ND, Crawford J. Microanatomy of the human liver – exploring the hidden interfaces. Hepatology 1999;30:1339–1346.
6. LaFortune M, Madore F, Patriquin H, Breton G. Segmental anatomy of the liver: a sonographic approach to the Couinaud nomenclature. Radiology 1991;181:443–448.
7. Massaro M, Valencia MP, Guzman M, Mejia J. Accessory hepatic lobe mimicking an intra-abdominal tumor. J Comput Assist Tomogr 2007;31:572–573.
8. Aktan ZA, Savas R, Pinar Y, Arslan O. Lobe and segment anomalies of the liver. J Anat Soc India 2001;50:15–16.
9. Torra R. Polycystic kidney disease. http://emedicine.medscape.com/article/244907-overview. 2008.
10. Naftalis J, Leevy CM. Clinical estimation of liver size. Am J Dig Dis 1963;8:236–243.
11. Sullivan S, Krasner N, Williams R. The clinical estimation of liver size. BMJ 1976;2:1042–1043.
12. Niederau C, Sonnenberg A, Müller JE, et al. Sonographic measurements of the normal liver, spleen, pancreas and portal vein. Radiology 1983;149:537–540.
13. Harbin WP, Robert NJ, Ferrucci JT. Diagnosis of cirrhosis based on regional changes in hepatic morphology: a radiological and pathological analysis. Radiology 1980;135:273–283.

CHAPTER

8

Diffuse parenchymal liver disease

James M. Pilcher

INTRODUCTION 104

LIVER REFLECTIVITY AND ATTENUATION 104

LIVER ECHO PATTERN 104

FATTY LIVER 105
Focal fatty change 107
Focal fatty sparing 108
NAFLD/NASH 110

FIBROSIS 111

CIRRHOSIS 111
Biliary cirrhosis 115
Screening in cirrhosis 115

GLYCOGEN STORAGE DISEASES (GSDS) 116

NODULAR REGENERATIVE HYPERPLASIA (NRH) 116

CONGENITAL GENERALISED LIPODYSTROPHY (CGL) 116

AMYLOID 117

HAEMOCHROMATOSIS 117

WILSON'S DISEASE 117

CYSTIC FIBROSIS 117

INTRODUCTION

Ultrasound is usually the first imaging modality employed in patients with repeatedly altered liver function tests or clinically suspected diffuse liver disease. As well as being able to exclude other conditions such as biliary obstruction, there are a number of recognised patterns of altered liver echotexture, contour and shape that are indicative of certain diffuse liver conditions. These changes, however, are often subtle or even non-detectable; therefore the operator needs to be extremely familiar with the appearance of normal liver on the particular ultrasound system they are using.

When assessing the liver parenchyma, both a standard curvilinear abdominal transducer and ideally a high-resolution (8–12 MHz) linear or curvilinear array should be used. The latter enables a detailed assessment of the liver surface, parenchymal echotexture and contour of the peripheral portal tracts and hepatic veins. Although not covered in this chapter, Doppler interrogation of the hepatic artery, veins and portal vein offers valuable information with respect to the altered haemodynamics associated with certain liver conditions.

Recently the use of microbubble contrast agents has been shown to assist both in the assessment of altered hepatic blood flow[1,2] and in the characterisation of focal nodules seen in chronic liver disease.[3,4] Novel applications of pulse-echo technology can now be applied to measure the speed of a generated elastic shear wave through the liver,[5] or the extent of tissue displacement following a short acoustic radiation force.[6] Both of these techniques produce an objective measurement of liver stiffness and can therefore potentially identify fibrosis before it is visibly detectable on conventional B-mode imaging.

LIVER REFLECTIVITY AND ATTENUATION

Assessment of the liver's parenchymal reflectivity and attenuation is usually made by direct comparison to adjacent organs and to internal reflective interfaces, namely the portal tracts. Care must be taken with respect to the overall gain setting, time gain compensation, and on more recent scanners the use of tissue harmonics and 'auto-optimisation' controls, all of which may alter the operator's perception of both relative reflectivity and attenuation (Fig. 8.1A–C).

Normal liver parenchyma has a reflectivity similar or slightly higher to that of the right kidney. Misinterpretation of altered liver reflectivity may therefore occur in the presence of certain renal pathologies, due to an increase or reduction in renal parenchymal echotexture. Liver parenchyma is less reflective than that of the spleen and this is potentially a more reliable comparison than using the right kidney; however, it is not always easy to make if the left lobe is small.

In the normal liver the portal tracts are strongly reflective, appearing as white lines outlining the portal veins. Any increase in parenchymal reflectivity will reduce this differential in reflectivity with a resulting loss of portal vein wall clarity.[7] Likewise conditions resulting in periportal oedema or inflammation may increase the apparent reflectivity of the portal tracts.

Normal liver attenuates the ultrasound beam at around 1 dB/MHz/cm of depth and diffuse liver disease may either increase or decrease this. With the correct TGC settings, the normal liver has relatively uniform echo amplitude throughout its depth and the interface with the diaphragm is clearly seen. Broadband tissue harmonic imaging can improve tissue penetration in the liver[8] and may therefore potentially mask an early increase in liver attenuation: likewise a similar situation may occur with the use of auto-optimisation controls.

A number of studies have sought to objectively measure the attenuation of liver parenchyma using the amplitude of the raw RF data within the returning echo in order to distinguish between various diffuse parenchymal processes.[9,10] Although this has shown promise, to date, these techniques have not been adopted into routine clinical practice.

LIVER ECHO PATTERN

The spatial distribution and amplitude of the interleaving echoes returning from the liver parenchyma determine the perceived echotexture of the liver. This will change in various pathologies, becoming finer, coarser or more irregular in distribution depending upon the underlying process. However, it should be remembered that there is little correlation between perceived echotexture and any

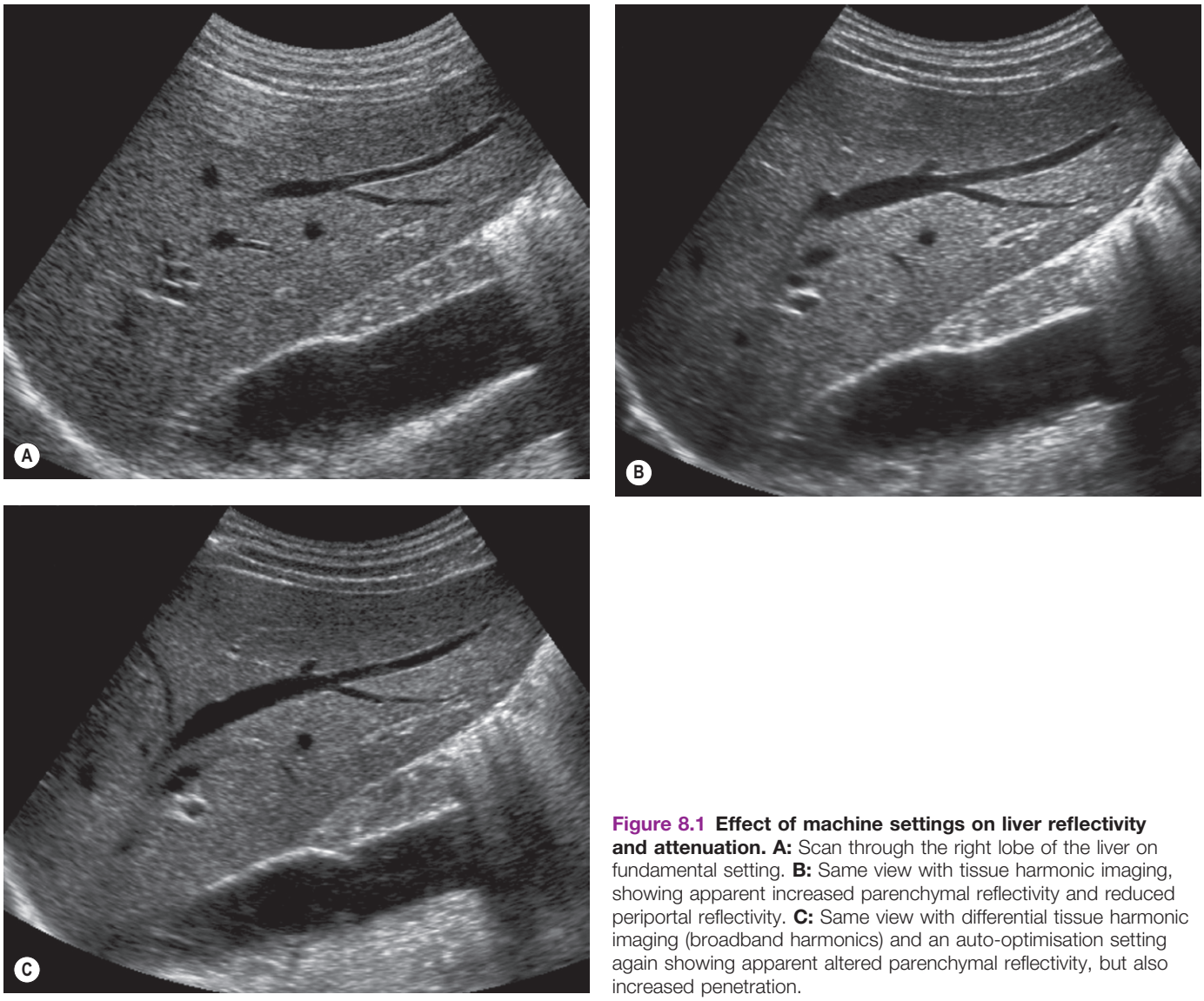


Figure 8.1 Effect of machine settings on liver reflectivity and attenuation. A: Scan through the right lobe of the liver on fundamental setting. **B:** Same view with tissue harmonic imaging, showing apparent increased parenchymal reflectivity and reduced periportal reflectivity. **C:** Same view with differential tissue harmonic imaging (broadband harmonics) and an auto-optimisation setting again showing apparent altered parenchymal reflectivity, but also increased penetration.

Sonographic features of normal liver

- Liver reflectivity ≥ right kidney
- Liver reflectivity < spleen
- Defined reflective periportal tracts
- Visible diaphragmatic interface
- Uniform parenchymal speckle pattern

true anatomical structure, with a significant contribution towards the altering echo amplitude arising from scatter. Echotexture is also dependent upon technical factors within the ultrasound scanner and therefore speckle reduction techniques such as spatial or frequency compounding can dramatically alter the apparent liver texture (Fig. 8.2A and B).

FATTY LIVER

Fatty liver is one of the commonest abnormal findings on an abdominal ultrasound and its incidence across Western countries is increasing. It represents the reversible accumulation of triglycerides within the cytoplasm of hepatocytes as a result of disruption to normal lipid metabolic pathways, predominantly those of free fatty acids.[11] Initially hepatocyte accumulation of lipid is centrilobular (around the hepatic vein) in distribution, but with increasing severity this extends out towards the portal tracts (Fig. 8.3A and B).

Worldwide the commonest two causes of a fatty liver are alcohol and non-alcoholic fatty liver disease (NAFLD).[11,12] Other important secondary causes include obesity, diabetes mellitus, hyperlipidaemia, pregnancy, starvation, drugs (especially steroids), severe hepatitis, gastrointestinal bypass surgery, cystic fibrosis and glycogen storage disease (Table 8.1). As the process behind fatty liver is dynamic any correction of the primary cause will frequently result in its rapid reversal (Fig. 8.4A and B).[13]

On ultrasound the presence of multiple fat interfaces throughout the liver causes a diffuse increase in parenchymal reflectivity, making it greater than that of the adjacent normal right kidney, or more reliably the spleen. Unlike other causes of a 'bright liver' (Table 8.2), the echo pattern is fine and uniform, and with increasing fat deposition there is attenuation of the ultrasound beam, through both absorption and scatter.[11,14,15]

Diffuse fatty liver can be described as: 'mild' when there is minimal increase in parenchymal reflectivity, 'moderate' when

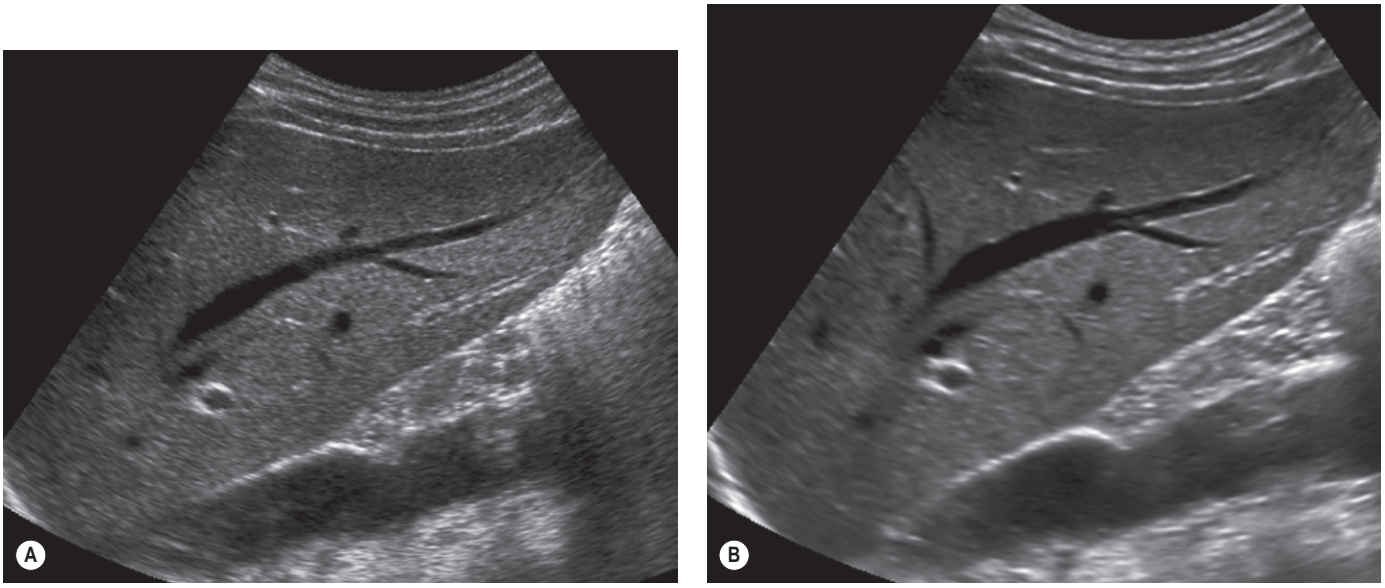


Figure 8.2 Alteration of liver echotexture with machine settings. A: Identical view to Figure 8.1 with spatial compounding showing a fine interleaving echo pattern from the liver parenchyma. **B:** Same view with frequency compounding switched on resulting in a much more uniform echotexture.

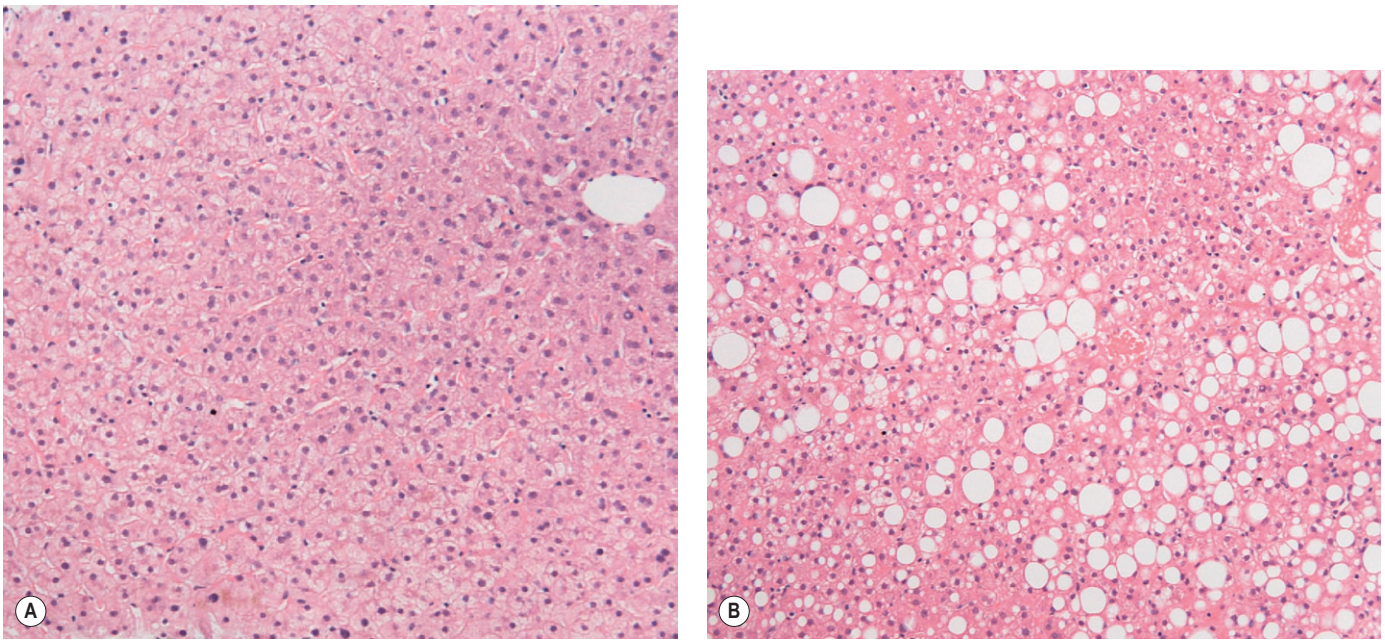


Figure 8.3 Fatty liver histology. A: Normal liver biopsy (H&E stain, ×100 magnification), demonstrating uniformity of hepatocyte distribution, interrupted by sinusoidal spaces. **B:** Liver biopsy (H&E stain, ×100 magnification) showing moderate diffuse fatty change; at ultrasound the fat globules act as multiple acoustic interfaces hence increasing the parenchymal reflectivity.

there is loss of intrahepatic vessel wall definition with impaired visualisation of the diaphragm, and 'severe' when there is poor penetration of the posterior aspect of the right lobe of the liver with very poor or non-visualisation of the hepatic vessels and diaphragm.[16] With increasing severity there is often a degree of hepatomegaly (Fig. 8.5A–C).

The reported sensitivity and specificity for ultrasound in assessing the presence of fatty liver depends upon the degree of severity and is therefore variable at 60–100% and 77–95%, respectively.[17,18] The lower specificity may well be due to the coexistence of fibrosis in a number of the conditions associated with fatty liver. Despite its apparent sensitivity, the detection of fatty liver at ultrasound can be highly subjective, with only moderate inter-observer agreement reported.[19] In acute fatty liver of pregnancy the liver most often appears normal on ultrasound.[20]

As well as the greyscale changes, increasing hepatic steatosis can cause dampening of the normal hepatic vein spectral Doppler triphasic waveform, resulting in a biphasic or monophasic pattern. A reduction in the hepatic artery resistive index has also been reported.[21]

Table 8.1 Conditions associated with fatty liver

Common	Rare	Congenital
Alcohol NAFLD Obesity Hyperlipidaemia Hepatitis B and C **Drugs:** Steroids Chemotherapeutic agents Amiodarone Valproic acid	Pregnancy Starvation Rapid weight loss Total parenteral nutrition Jejunal-ileal bypass Radiation therapy	**Metabolic disorders:** Organic aciduria Aminoacidopathy **Storage diseases:** Glycogen storage disorders α1-Antitrypsin deficiency Wilson's disease Haemochromatosis **Other:** Cystic fibrosis

NAFLD, non-alcoholic fatty liver disease.

Table 8.2 Causes of increased liver reflectivity

Fatty infiltration
Cirrhosis
Chronic hepatitis
Alcoholic hepatitis
Granulomatous hepatitis
Miliary tuberculosis
Recurrent cholangitis
Periportal fibrosis, e.g. schistosomiasis
Congestive cardiac failure

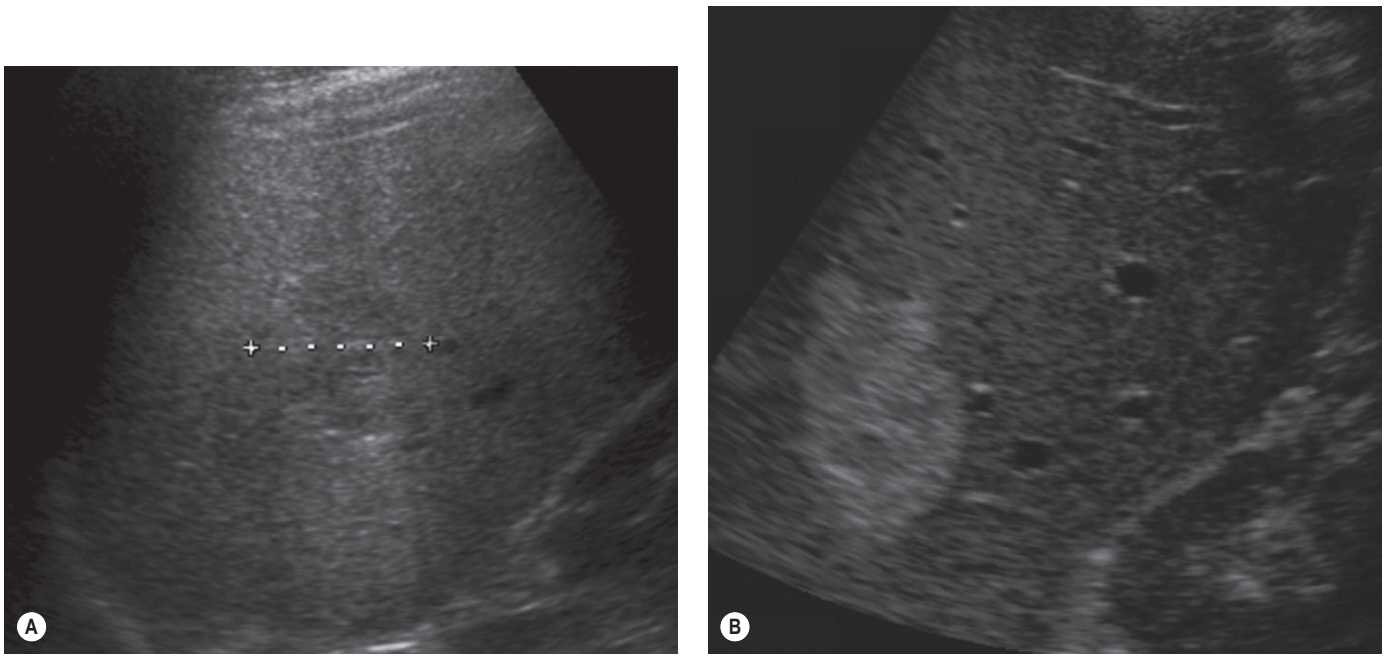


Figure 8.4 Temporal changes in fatty infiltration. A: Moderate fatty liver with a focal heterogeneous mass in a patient with high alcohol consumption. **B:** Repeat scan 16 days later shows complete resolution of fatty infiltration revealing a typical haemangioma.

Focal fatty change

Although fatty infiltration is usually a diffuse process, it may sometimes affect only one lobe, segment or subsegment of the liver. In these cases it usually has a fairly characteristic geographic pattern, with relatively well-defined, straight or angulated margins between areas of differing reflectivity: less frequently an interdigitating pattern has been described.[14,22,23] When subsegmental, preferred locations for this distribution include the porta hepatis, gallbladder fossa and areas adjacent to the falciform ligament[21–23] (Fig. 8.6A–C).

Focal fatty infiltration can sometimes be more rounded in appearance and may also be multifocal in distribution, so that on ultrasound it can potentially be mistaken for haemangiomas or echogenic metastases.[24] Careful ultrasound examination will show that these areas lack any mass effect and do not alter the course of regional vessels.[21] An interval scan may also reveal a rapid change in size or shape of these areas. If there is still concern, contrast-enhanced ultrasound should demonstrate iso-enhancement of the focal area in comparison to the adjacent normal liver. Liver MRI with in and out of phase gradient echo sequencing can also confirm the presence of focal fat.[11]

Subcapsular fatty infiltration in diabetic patients receiving intraperitoneal insulin, and perivascular infiltration (predominantly affecting the hepatic veins) in high alcohol consumers are more unusual patterns that have been described on CT and MRI.[11,25] The latter has a rather non-specific distribution on ultrasound.

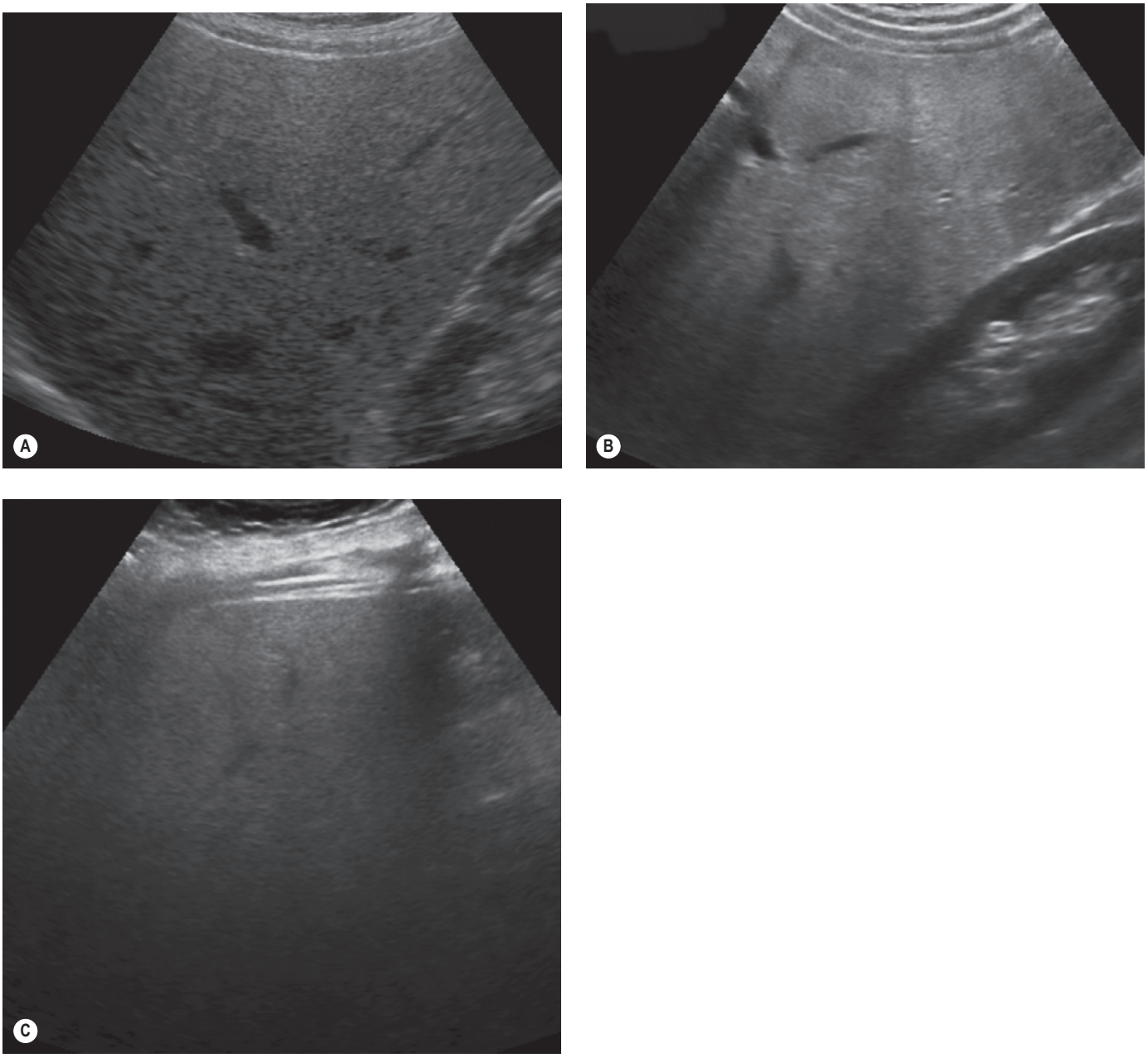


Figure 8.5 Differing degrees of diffuse fatty infiltration. A: Mild, with diffuse increased reflectivity, but good vessel visualisation and penetration. **B:** Moderate, with indistinct vessel walls and reduced penetration. **C:** Severe, with poor vessel visualisation and very limited penetration.

Focal fatty sparing

Within a diffusely fatty liver there may be focal areas of relatively normal liver parenchyma. At ultrasound these appear as low reflective focal lesions, which can be misinterpreted as discrete hepatic masses. The common locations for this appearance are similar to those of focal fatty change, namely the gallbladder fossa, periportal region and around the falciform ligament, where they typically demonstrate a geographic pattern (Fig. 8.7A and B).[11,14,26] Focal 'nodular like' areas in segment II of the liver have also been described (Fig. 8.8A).

These focal areas of fatty sparing are thought to be due to regional reduction in portal vein perfusion, most often as a result of aberrant splanchnic veins or divisions of normal (non-portal) veins draining directly into the liver.[11] A number of studies have now described this phenomenon using colour Doppler, contrast ultrasound and CT angiography to demonstrate the aberrant vessels.[27–30]

On the whole the location and contour of fatty sparing is usually characteristic enough on ultrasound, to recognise it for what it is. However, as with focal fatty infiltration, it can have a more nodular appearance so that, on occasion, further assessment is required. Contrast ultrasound will show a uniform enhancement pattern identical to background liver (Fig. 8.8B) throughout all phases.[31] As with focal fatty infiltration, liver MRI with in and out of phase gradient echo will confirm the altered fat content.[32]

Areas of focal fatty sparing may also be seen around benign and malignant focal liver lesions, including: haemangiomas, focal nodular hyperplasia, hepatocellular carcinoma and metastases. In these cases compression of adjacent hepatocytes by the focal tumour

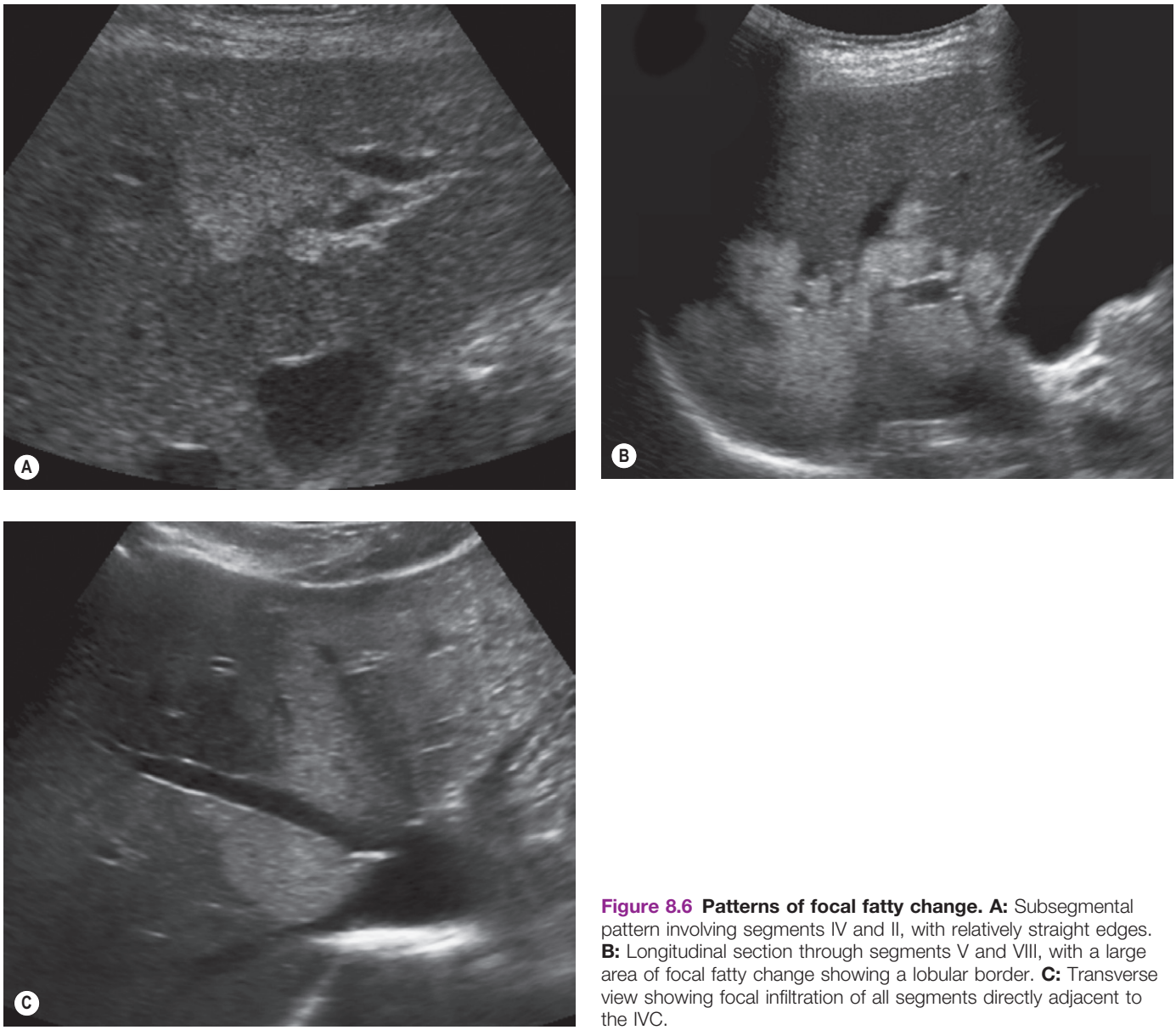


Figure 8.6 **Patterns of focal fatty change. A:** Subsegmental pattern involving segments IV and II, with relatively straight edges. **B:** Longitudinal section through segments V and VIII, with a large area of focal fatty change showing a lobular border. **C:** Transverse view showing focal infiltration of all segments directly adjacent to the IVC.

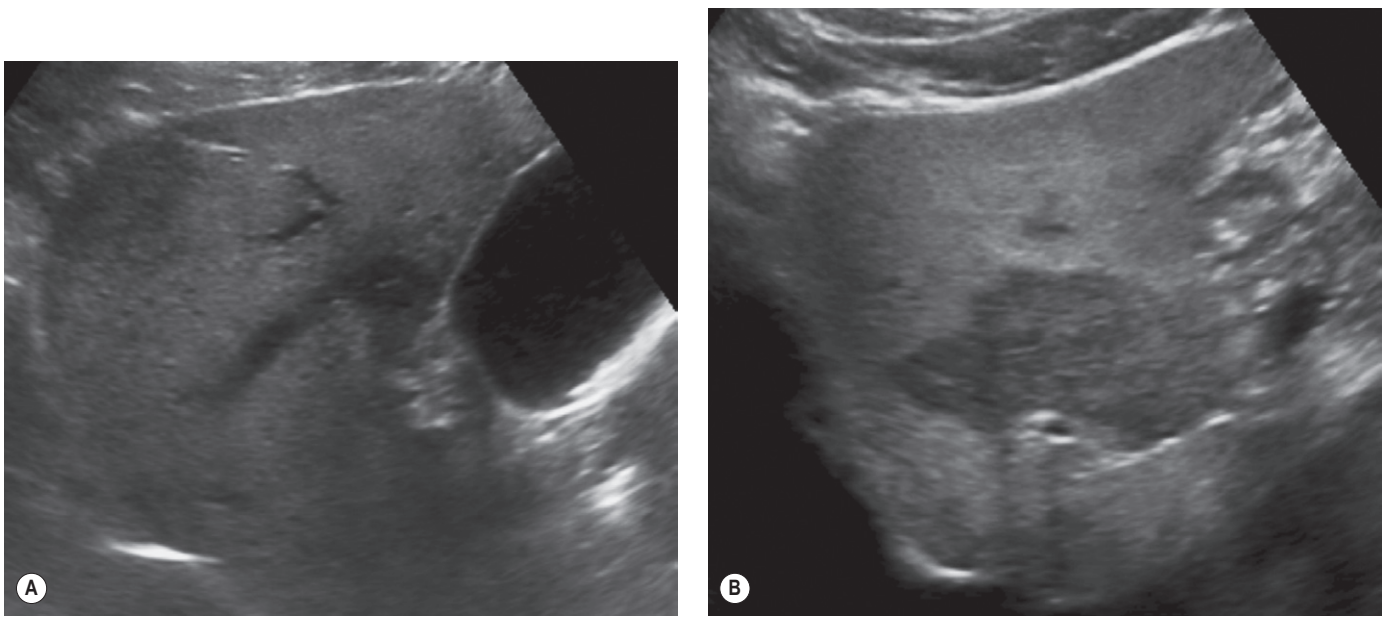


Figure 8.7 **Patterns of focal fatty sparing. A:** Fatty liver, with a typical wedge-shaped area of focal sparing adjacent to the gallbladder. **B:** More extensive area of fatty sparing in segments II and III of the liver, again showing a geographical pattern.

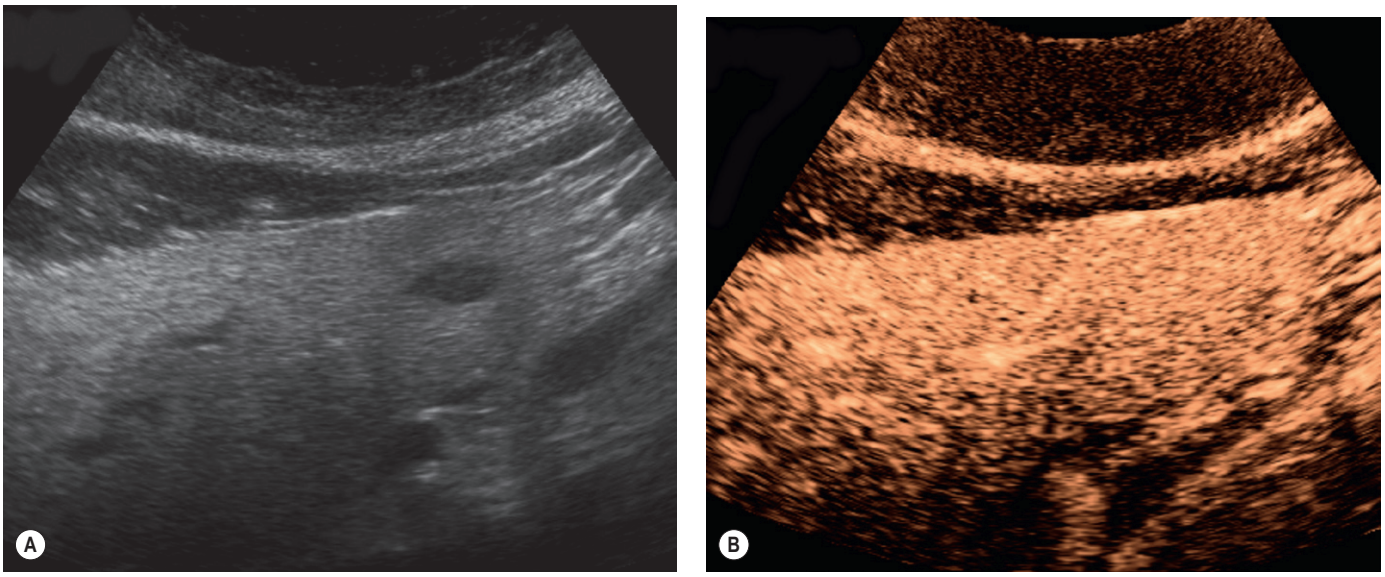


Figure 8.8 Patterns of focal fatty sparing. A: Oval shaped area of focal sparing in segment II with moderate background fatty change. **B:** CEUS confirms iso-enhancement of the area with respect to the background liver consistent with focal fatty sparing.

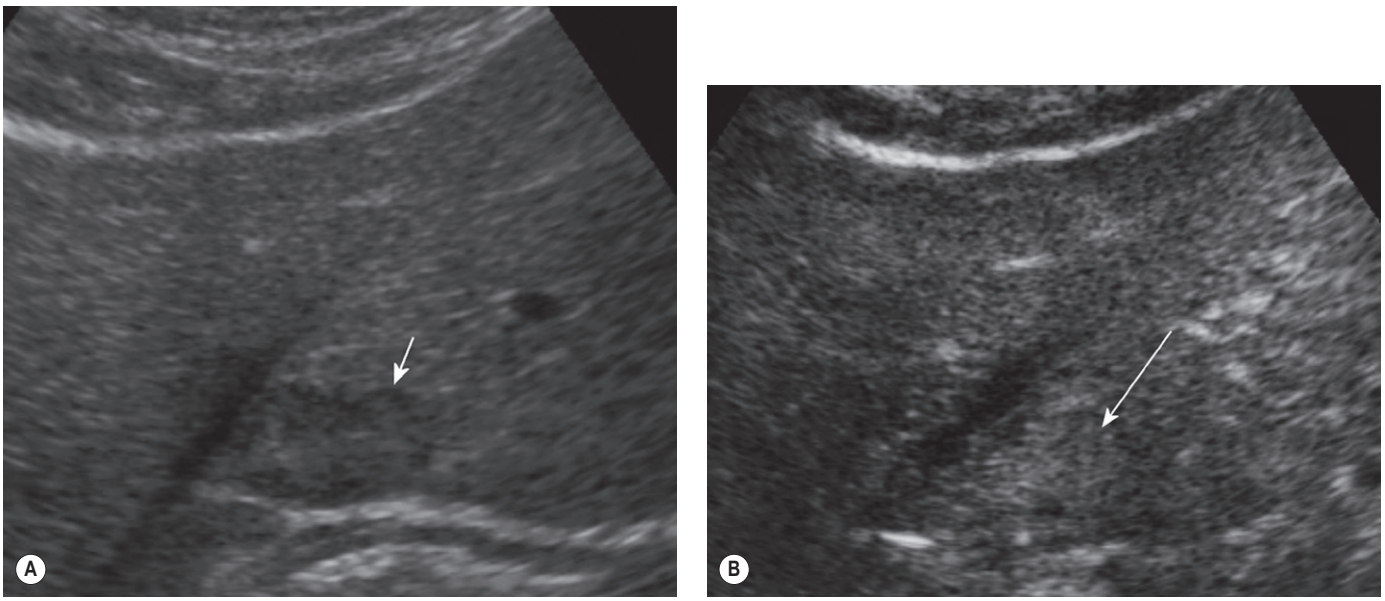


Figure 8.9 Perilesional focal fatty sparing. A: Mild-moderate fatty liver with focal lesion in left lobe (arrow) showing a peripheral low reflective halo (perilesional fatty sparing) suggestive of a metastasis. **B:** Post contrast the lesion shows early arterial enhancement of the central component (arrow), becoming isoechoic with background liver and apparent 'halo' during the parenchymal phase: biopsy confirmed focal nodular hyperplasia.

Sonographic features of focal fatty change/sparing

- No distortion of liver contour
- No displacement of hepatic vessels
- Geographic pattern (may be nodular/interdigitating)
- May demonstrate rapid change
- Classic location: portal bifurcation, gallbladder fossa, falciform ligament
- Contrast ultrasound: uniform enhancement with background liver

may account for the change in fat distribution. On ultrasound it can produce a misleading appearance, such as a low reflective halo surrounding an echogenic haemangioma.[21] Again in these cases, contrast ultrasound can help in confirming the underlying benign nature of the lesion[28] (Fig. 8.9).

NAFLD/NASH

Non-alcoholic fatty liver disease (NAFLD) is an increasingly prevalent condition throughout the world's population. It encompasses a spectrum of hepatic disorders, arising from hepatocyte accumulation of lipid in the absence of significant alcohol intake, and ranges from simple hepatic steatosis, through steatohepatitis (NASH), to advanced fibrosis and cirrhosis.[33] There is increasing evidence that NAFLD represents the hepatic component of a metabolic syndrome characterised by obesity (particularly central obesity), hyperinsulinaemia, peripheral insulin resistance, diabetes, hypertriglyceridaemia and hypertension.[33–35] What exactly triggers the progression of simple steatosis on to inflammation and fibrosis remains unclear, but there is a close association with insulin resistance.[33] About a third of patients who develop NASH will show progressive hepatic

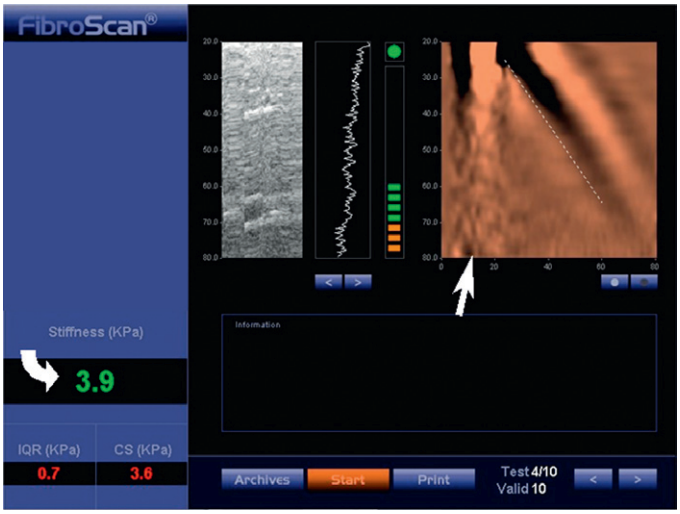


Figure 8.10 Shear wave display: acquisition display from a Fibroscan® showing the generated strain rate image (arrow) from a normal liver following a mechanical shear wave. The overlaid line indicates the speed of propagation which relates to parenchymal stiffness, displayed in kPa (curved arrow). (Courtesy of C. Guiducci, Echosens, Paris, France.)

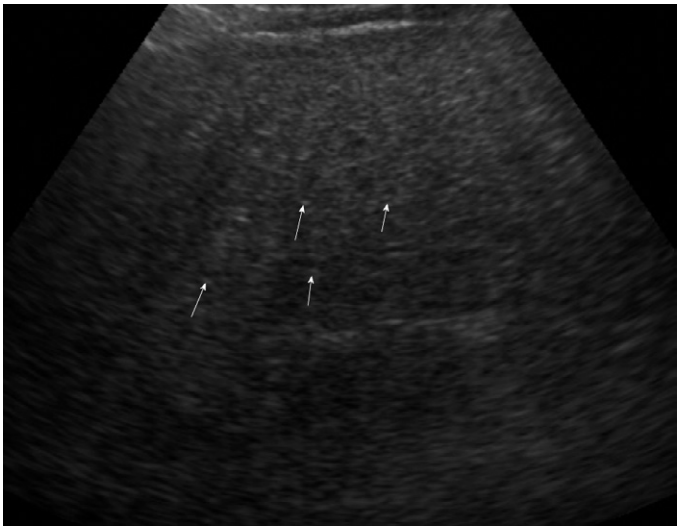


Figure 8.11 Fat and fibrosis. Moderate fatty liver with coexistent fibrosis, demonstrated by bright focal bright pinpoint echoes (arrows).

fibrosis at repeated liver biopsy, with 5–20% of them continuing on to established cirrhosis.[36,37] Although there is an observed association between NASH and the development of hepatocellular carcinoma, as yet it remains unclear whether the former is causal.[38]

The role of ultrasound in NAFLD is currently confined to the detection and grading of fatty liver. As with CT and MRI, ultrasound is unable to distinguish between NAFLD and NASH, which remains a biopsy diagnosis. The use of ultrasound contrast agents that demonstrate hepatic sinusoidal uptake is currently being explored to see if the rate of enhancement in NASH is different from other causes of fatty liver.[39]

The longitudinal monitoring of NASH patients for progression of fibrosis is currently not feasible with conventional ultrasound, but the pulse-echo technology of ultrasound can be used to measure the speed of propagation of an elastic shear wave through the liver. The shear wave may be produced by a mechanical vibrator that is placed against the skin overlying the right lobe of the liver. There is a direct relationship between liver stiffness and the measured speed of the shear wave[5,40] (Fig. 8.10). An alternative technique utilises the ultrasound transducer to generate an acoustic pressure wave through the liver, immediately followed by a series of standard imaging pulses. The RF data from these pulses is then used to track tissue displacement which correlates with tissue stiffness.[6] There is now increasing interest in the employment of these techniques in the follow-up of patients with potential fibrotic chronic liver diseases such as NAFLD/NASH. Unfortunately patient obesity can cause problems in obtaining reliable measurements with the elastic shear wave technique.[35]

FIBROSIS

Hepatic fibrosis is the common outcome of a number of chronic liver disorders, frequently progressing on to frank cirrhosis. However, it can often be difficult to distinguish on ultrasound due to the coexistence of associated parenchymal processes, such as fatty infiltration or chronic inflammatory change (Fig. 8.11). The quoted sensitivity of ultrasound for the detection of fibrosis is therefore highly variable, with values as low as 35%.[41]

When it is appreciated, fibrosis produces a coarsening of the normal parenchymal echo pattern. This can appear as multiple bright 'pin-head' echoes that with increasing severity take on a more coarse linear type interface.[15] Irregular thickening of the periportal tracts is a well-described feature, which is more striking in certain aetiologies. Loss of the gallbladder wall's smooth contour has also been described.[42] The use of a high-resolution transducer to assess the peripheral liver parenchyma in more detail is often very helpful.[43] As already mentioned above, some ultrasound systems are now able to measure the mechanical properties of tissue thus increasing their diagnostic accuracy for fibrosis.[5]

With progressive hepatic fibrosis, secondary haemodynamic changes occur within the liver including portal hypertension: these findings are discussed in Chapter 12.

CIRRHOSIS

Cirrhosis is the final common (currently believed irreversible) histological outcome for a number of chronic liver diseases. It is increasing in incidence and is one of the leading causes of death internationally. It is defined as a diffuse process characterised by fibrosis and the conversion of normal liver into structurally abnormal nodules, the underlying pathological processes being, cell necrosis, fibrosis and regeneration.[44] Cirrhosis is typically classified by its morphology, aetiology or a combination of the two as a number of causal agents will result in the same morphology and likewise a single agent can lead to a variety of morphological outcomes. Micronodular describes a histological pattern where the regenerating nodules are <3 mm in size, with a macronodular pattern the majority of nodules are >3 mm, while in a mixed nodular pattern the distribution is about equal.[45]

In the West, the most common causes of cirrhosis are alcohol, which tends to produce a micronodular pattern of disease, and chronic viral hepatitis, namely hepatitis C, which is typically macronodular.[46] NAFLD/NASH is now emerging as an important aetiology, probably accounting for a large percentage of patients previously labelled as having cryptogenic cirrhosis.[34] Other causes produce a mixture of morphological patterns and include: autoimmune hepatitis, biliary cirrhosis (primary and secondary), Wilson's disease, chronic venous congestion, parasitic diseases and haemochromatosis[44,45] (Table 8.3).

The clinical picture can be variable for patients, with approximately only 60% presenting with symptoms or signs of liver disease: lethargy, hepatomegaly, jaundice and ascites.[47] Progressive disease,

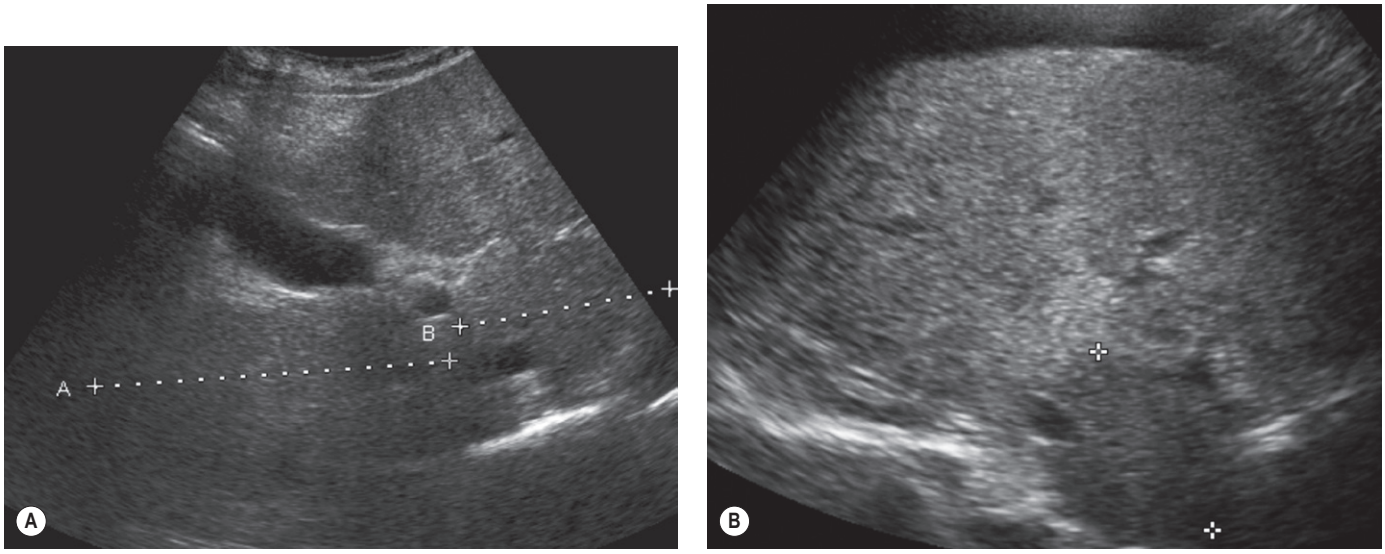


Figure 8.12 Cirrhotic liver morphology. A: Transverse measurements of caudate (6 cm) and right lobe (9 cm) in a patient with established cirrhosis. **B:** Enlarged caudate lobe in a cirrhotic liver giving a pseudo-mass appearance.

Table 8.3 Aetiology of cirrhosis

Alcohol
Viral hepatitis
NASH
Autoimmune hepatitis
Biliary cirrhosis
Sclerosing cholangitis
Hepatic venous congestion
Schistosomiasis
Metabolic disorders (e.g. haemochromatosis, Wilson's disease, α1-antitrypsin deficiency, galactosaemia)
Drugs and toxins (e.g. methotrexate, alkaloids)
Gastric bypass surgery
Cryptogenic

however, will result in hepatocellular failure, portal hypertension with its associated risks of haemorrhage, and an increased incidence of hepatocellular carcinoma: particularly in cirrhosis with a viral aetiology.[48]

Although liver biopsy remains the gold standard for the diagnosis of cirrhosis, it has an attached potential morbidity and mortality, and is not without false negative results. Therefore there is great interest in the ability of cross-sectional imaging in detecting cirrhosis, with ultrasound being the most frequently used modality. There are a number of described sonographic patterns associated with cirrhosis:

- *Liver morphology.* In early cirrhosis the liver may be slightly enlarged, but with progressive disease it tends to shrink. There can be a differential reduction in size of the right lobe with respect to the left and caudate, which both may show regenerative hypertrophy. On a transverse ultrasound image, just inferior to the portal vein bifurcation, the ratio of the width of the caudate lobe to that of the right lobe (C/RL) can be measured, with a value ≥0.65 seen as indicative of cirrhosis (Fig. 8.12A and B). Although the C/RL ratio has a quoted sensitivity of 43–84% and specificity of 100%,[49,50] it is somewhat dependent upon the aetiology of the cirrhosis: more likely in post-hepatic and primary biliary cirrhosis. The original studies describing this ratio excluded conditions such as Budd–Chiari, which would almost certainly upset the high specificity.

  Other described comparative measurements are the sagittal length of the right lobe in the midclavicular line, divided by the left in the midline (<1.3 in cirrhosis),[51] and the width of the left main portal vein compared to that of the right.[52] Both these ratios reflect relative hypertrophy of the left lobe and are again most sensitive in hepatic cirrhosis. It would seem however that not all the left lobe hypertrophies in cirrhosis. Selective atrophy of segment IV has been described at ultrasound and CT and is probably a result of portal venous hypoperfusion.
- *Echotexture.* Liver reflectivity is highly variable in cirrhosis dependent upon aetiology. Although there is the description of a 'bright liver' in fibrosis/cirrhosis, this probably reflects the more heterogeneous echo pattern of fibrotic tissue, with loss of portal vein wall definition and focal coarse reflective foci.[53] Typically there is no attenuation of sound unless there is concomitant fatty infiltration, such as in alcoholic liver disease. Then it can be difficult to distinguish fibrosis from the typically fine background pattern of fatty change.[54] A nodular pattern has also been described, predominantly in hepatic cirrhosis, with poorly defined low reflectivity nodules measuring <6 mm, not necessarily associated with liver surface irregularity[55] (Fig. 8.13A–C).
- *Surface nodularity.* In established cirrhosis the combination of fibrosis and regenerating nodules produces a surface nodularity often detectable using a low-frequency abdominal transducer.[56] The presence of ascites will increase the detection of this sign, particularly if the pattern is micronodular (Fig. 8.14A and B). In the absence of ascites high-resolution zoom of one of the hepatic vein contours may be helpful, or assessment of the contour of the deeper liver surface against the gallbladder wall or right kidney (Fig. 8.15A and B). The use of modern high-frequency transducers has significantly increased the detection of liver contour irregularity, although there is a recognised overlap between severe fibrosis and established cirrhosis[57,58] (Fig. 8.16). Liver surface irregularity has also been described in patients with fulminant hepatic failure and multiple liver metastases.

Regenerating nodules in cirrhosis are localised areas of hepatocyte hyperplasia, most measuring between 2 mm and 2 cm. They lack the normal lobular architecture and are surrounded by fibrous

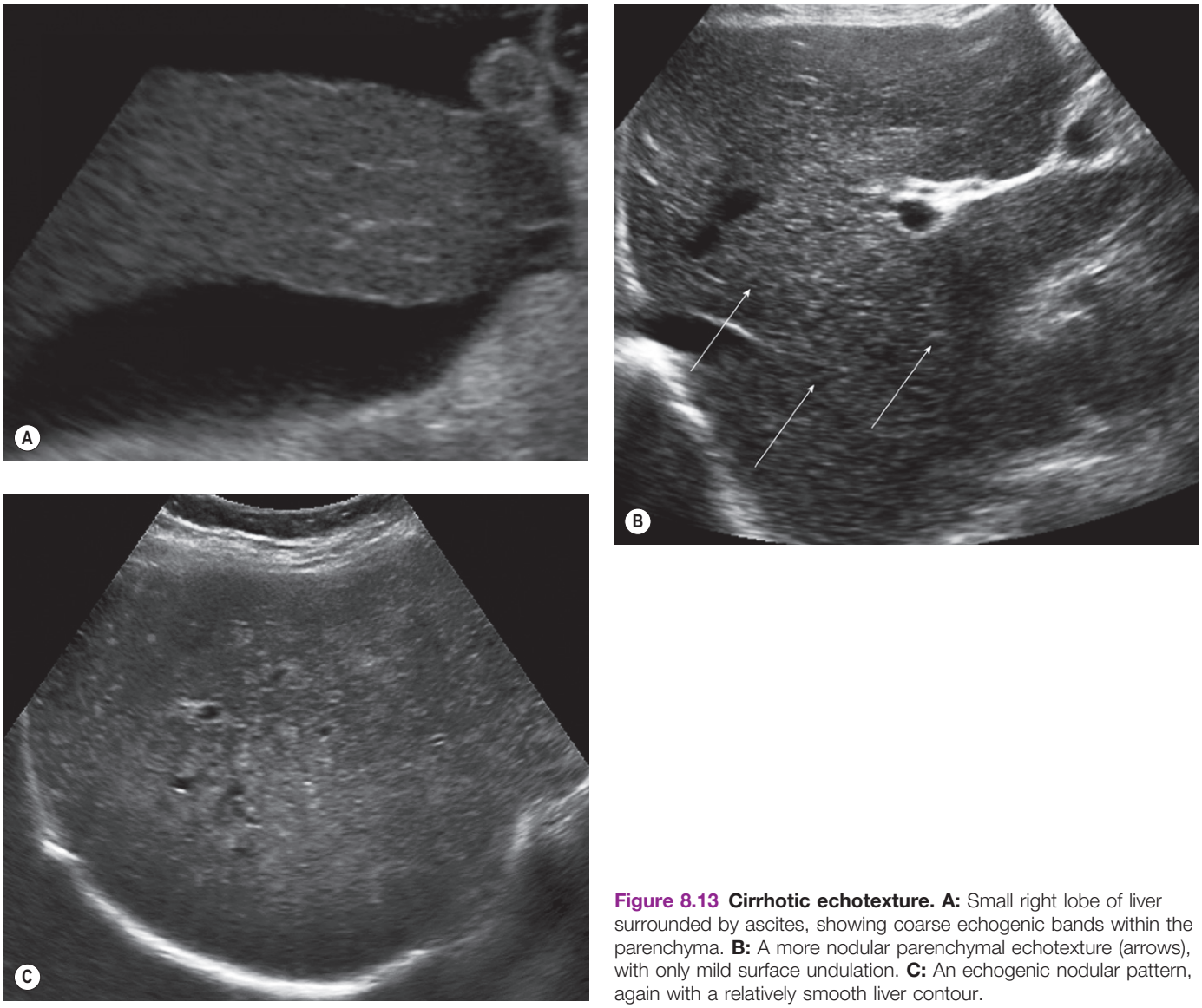


Figure 8.13 **Cirrhotic echotexture. A:** Small right lobe of liver surrounded by ascites, showing coarse echogenic bands within the parenchyma. **B:** A more nodular parenchymal echotexture (arrows), with only mild surface undulation. **C:** An echogenic nodular pattern, again with a relatively smooth liver contour.

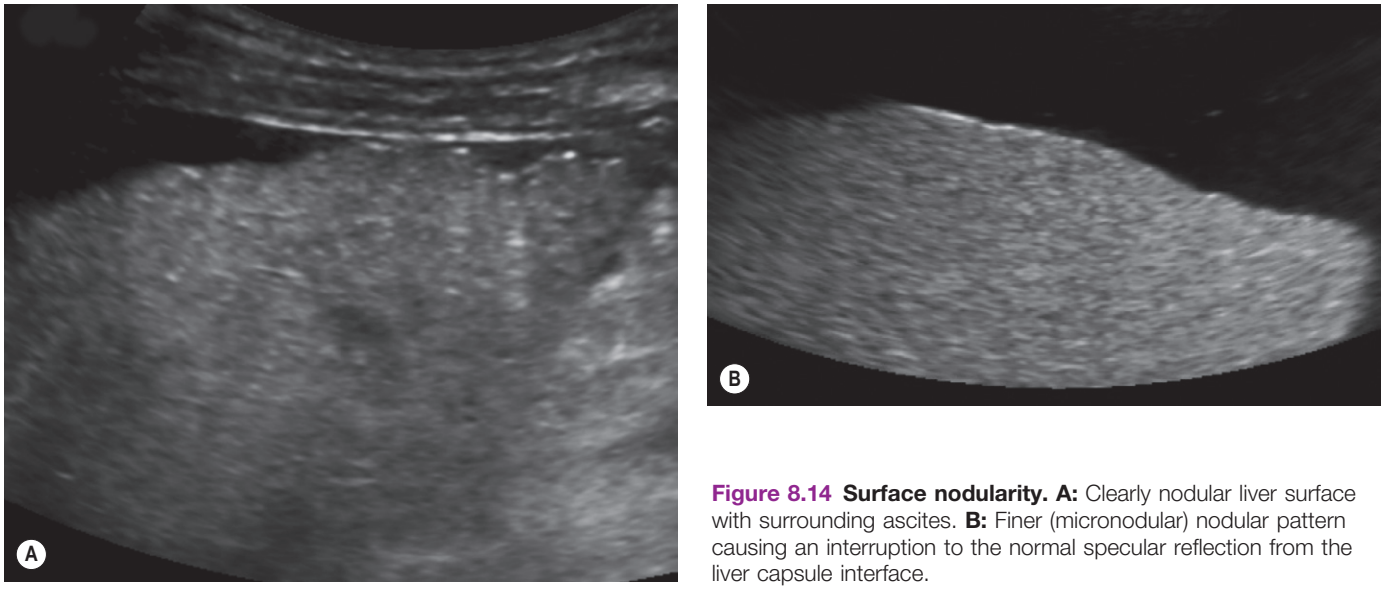


Figure 8.14 **Surface nodularity. A:** Clearly nodular liver surface with surrounding ascites. **B:** Finer (micronodular) nodular pattern causing an interruption to the normal specular reflection from the liver capsule interface.

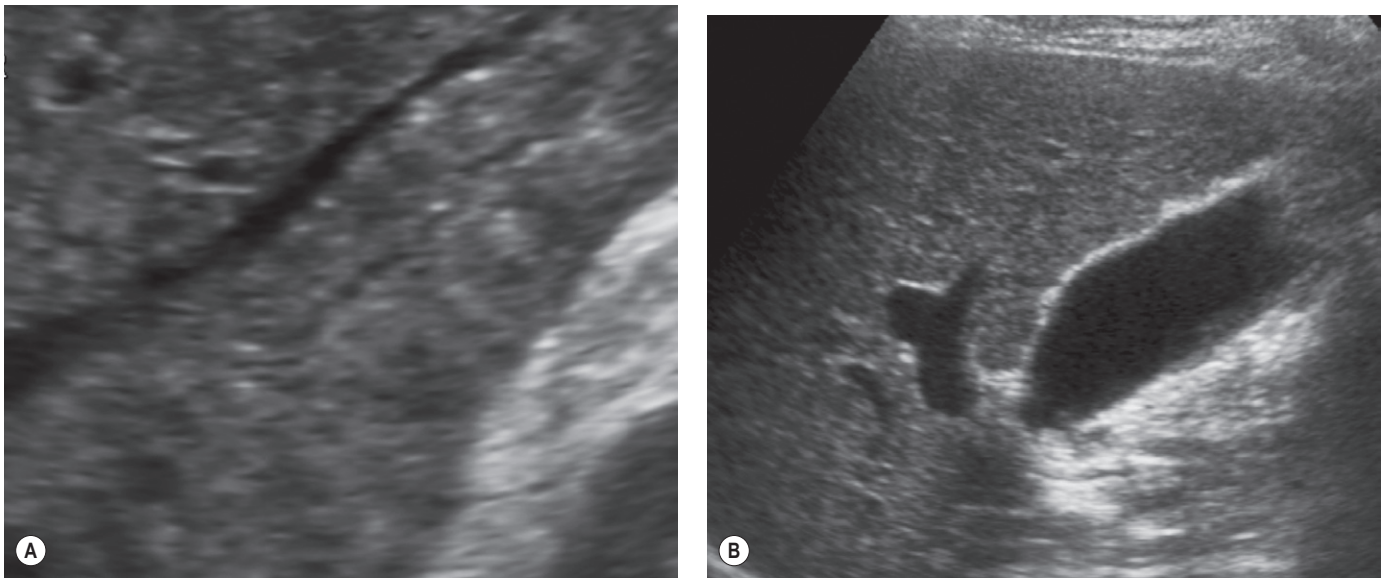


Figure 8.15 Surface nodularity. A: In the absence of ascites high-resolution ultrasound of a hepatic vein contour can help demonstrate surface nodularity. **B:** Irregular liver surface demonstrated against the gallbladder wall.

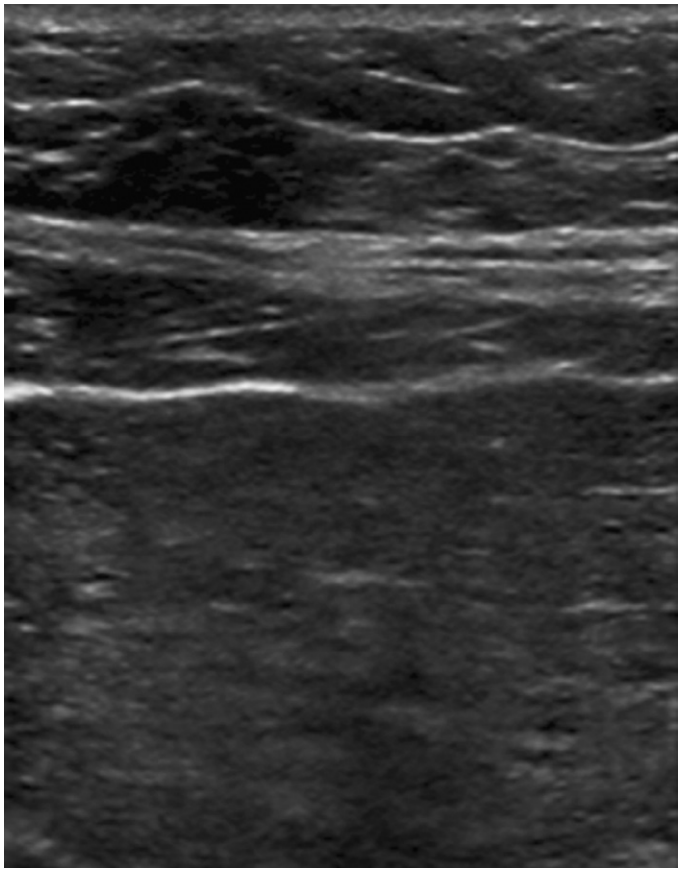


Figure 8.16 Surface nodularity. High-resolution image of liver surface demonstrating irregular contour and a coarsened echotexture in the peripheral parenchyma.

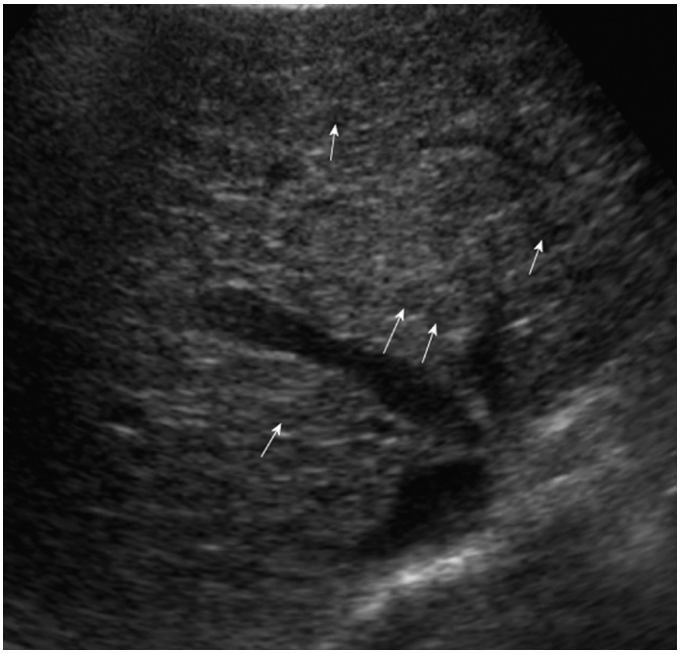


Figure 8.17 Regenerating nodules. Cirrhotic liver with distinct low reflective regenerating nodules (arrows), most showing a fine reflective (fibrotic) halo.

connective tissue. Some nodules contain portal tracts although their relationship to any efferent veins is abnormal.[45] Their detection at ultrasound is variable as not surprisingly they are often isoechoic to background liver texture, but they can appear as low reflective nodules, with an echogenic border[56] (Fig. 8.17). Use of a high-frequency transducer may improve their detection, particularly when surveying the liver surface as described above. Occasionally regenerating nodules can be much larger (5–15 cm) and have a heterogeneous echotexture, making distinction from hepatocellular carcinoma (HCC) difficult.[59] They may also appear as multiple echogenic masses mimicking metastatic liver disease.[60] Contrast-enhanced ultrasound can be helpful in these situations as regenerating nodules enhance in an identical fashion to the background parenchyma, as opposed to the recognised malignant enhancement patterns.[61] Liver MR combined with liver-specific contrast agents is also increasingly being used to characterise liver nodules in cirrhosis.[62]

Dysplastic nodules tend to be larger than regenerative nodules and are considered premalignant, the hepatocytes showing histological features of atypical growth. With increasing dysplasia angiogenic pathways are activated leading to the development of a predominantly arterial supply.[45,63] On contrast-enhanced ultrasound (CEUS) low-grade dysplastic nodules tend to have an identical enhancement pattern to that of regenerating nodules; however, increasingly high-grade dysplastic nodules will begin to show arterial phase enhancement[64] (Fig. 8.18).

Sonographic features of cirrhosis

- Relative enlargement of left lobe and caudate
- Coarse echotexture
- Surface irregularity
- Focal nodules (hypo/hyperechoic)
- Splenomegaly, ascites and visceral congestion
- Damped hepatic vein spectral traces.
- Reduced liver transit times with CEUS
- Increased tissue stiffness on sonoelastography

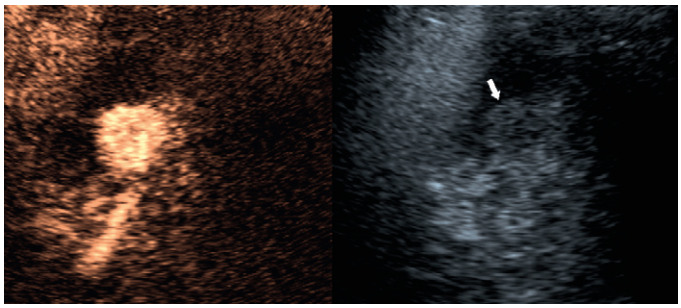


Figure 8.18 Dysplastic nodule. CEUS with simultaneous greyscale image showing avid arterial enhancement in a discrete nodule in a patient under surveillance for cirrhosis. Lack of subsequent washout on this study and subsequent MRI suggests dysplastic nodule as most likely diagnosis.

Other greyscale findings in cirrhosis reflect the altered haemodynamics associated with portal hypertension, including splenomegaly, enlarged venous collaterals and intrahepatic arterial branches, gallbladder and stomach wall thickening and the presence of ascites (Fig. 8.19A and B). All of these are covered in more detail in Chapter 12. The altered haemodynamics seen in cirrhosis can also be demonstrated using functional imaging methods with ultrasound contrast agents. There is a significant reduction in the transit time of these intravascular agents through the liver in cirrhosis, which can be detected using either spectral Doppler or contrast harmonic imaging.[1,2,65] The details of this technique are described in Chapter 10.

Biliary cirrhosis

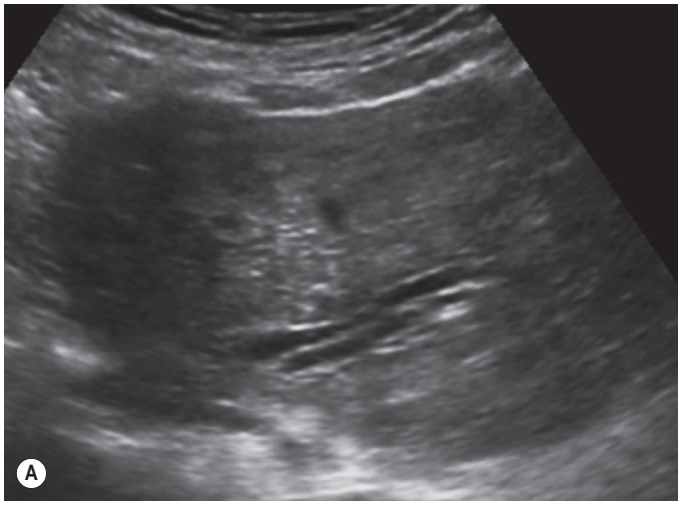
Primary biliary cirrhosis (PBC) is a slowly progressive autoimmune disease of the liver that primarily affects women in the fifth decade of life. Histopathologically there is periportal inflammation with immune-mediated destruction of the intrahepatic bile ducts, leading to accumulation of toxic substances and further hepatic damage with fibrosis and finally cirrhosis.[66] Serologically anti-mitochondrial antibodies are present in the majority of patients.[66]

In early stages the liver is usually normal or slightly enlarged, with no textural changes: a pattern of periportal low reflectivity has been described; however, this is a non-specific finding.[67] With progressive disease the liver tends to appears nodular, and shows coarse thickening of the periportal tracts (Fig. 8.20A). The coexistence of gallstones is a common finding and a significant number of patients will have enlarged periportal, gastro-hepatic ligament or upper retroperitoneal lymph nodes (Fig. 8.20B). Enlarged perihepatic lymph nodes are also a common described finding in hepatitis C and autoimmune hepatitis.[68,69]

Secondary biliary cirrhosis is a result of longstanding biliary obstruction, often with only minor visible bile duct dilatation. Underlying conditions include sclerosing cholangitis, choledochal cyst, bile duct strictures or atresias. The subsequent cirrhotic changes have no particular features.

Screening in cirrhosis

Ultrasound is currently used alongside serum α-fetoprotein (AFP) in surveillance programmes (six-monthly or annual) for the early detection of HCC in patients with cirrhosis.[70] The risk of developing



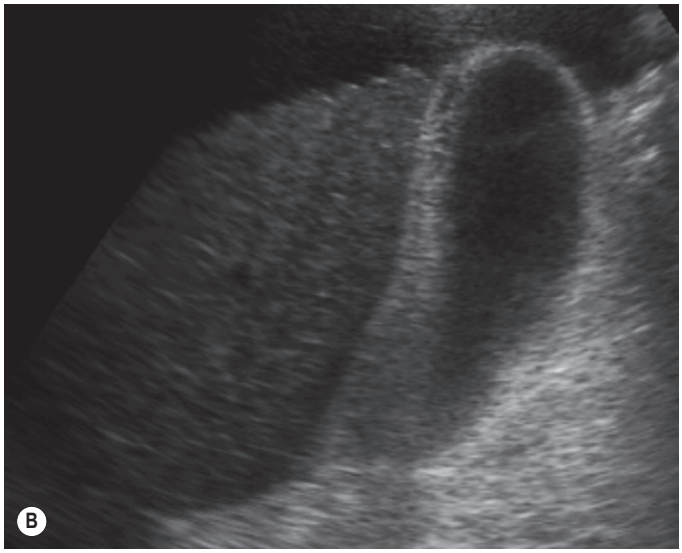


Figure 8.19 Associated findings in cirrhosis. A: Enlarged segmental hepatic artery due to portal hypertension, which may be mistaken for intrahepatic bile duct dilatation. **B:** Congestive cholecystopathy in cirrhotic portal hypertension causing moderate gallbladder wall oedema.

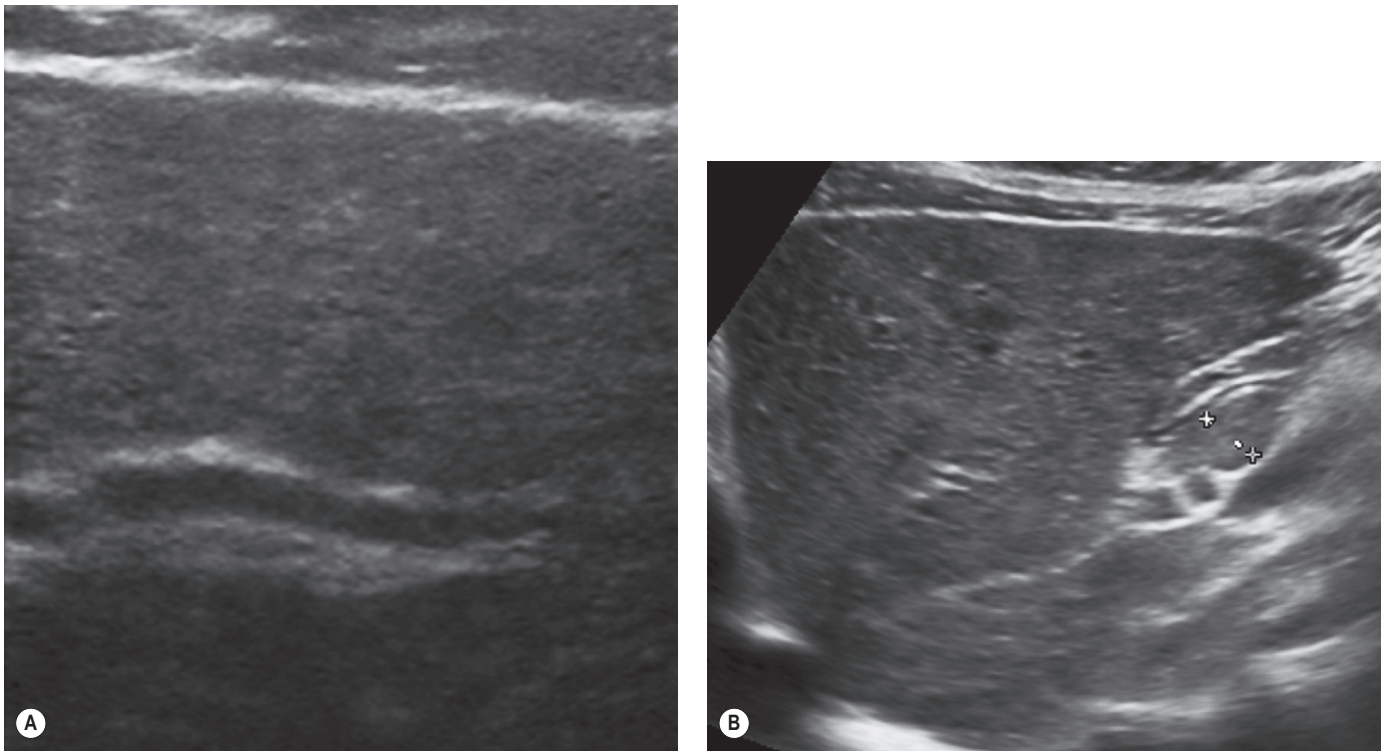


Figure 8.20 Primary biliary cirrhosis. A: High-resolution scan through the left lobe showing marked periportal echogenic thickening. **B:** Longitudinal scan showing enlarged lymph nodes in the hepatoduodenal ligament in a patient with PBC.

HCC in cirrhosis is very much dependent upon its aetiology, with a higher percentage in hepatitis B and C and a very low incidence in primary biliary cirrhosis. At present observational data suggests that the combination of ultrasound and AFP results in the detection of HCC at an earlier stage in these patients, and hence it is more likely to be treatable. Although there are some studies confirming the possibility of curative treatment, there is currently a lack of suitably large randomised controlled trials demonstrating a true survival benefit from this practice.[71,72]

GLYCOGEN STORAGE DISEASES (GSDS)

The glycogen storage diseases are a heterogeneous group of inherited disorders of glycogen metabolism, typed 0–XIII, which predominantly affect either the liver or skeletal muscle.[73]

The hepatic GSDs (I, III, VI and IX) are characterised by excessive storage of glycogen within the hepatocytes and in type I (von Gierke's disease) the proximal convoluted tubules of the kidneys. They have a variable clinical picture, most commonly hepatomegaly, growth retardation and fasting hypoglycaemia.[74] Dietary therapy has greatly improved the prognosis in some of the GSDs although there are recognised long-term complications.[73]

Liver ultrasound in the hepatic GSDs shows variable degrees of increased reflectivity, indistinguishable from diffuse fatty liver. GSD-I tends to show the most severe changes and is associated with the development of hepatic adenomas (GSD-III to a lesser extent).[74] These typically appear as uniformly reflective masses, which are often multiple, but they may look hypoechoic due to the increased background parenchymal reflectivity.[75] They sometimes contain foci of reduced reflectivity indicating areas of necrosis or haemorrhage. Malignant transformation can occur in the absence of cirrhosis and on ultrasound may be indicated by rapid growth and loss of lesion definition.[75]

NODULAR REGENERATIVE HYPERPLASIA (NRH)

Nodular regenerative hyperplasia is a relatively rare diffuse liver condition characterised by hyperplastic nodules containing normal hepatocytes, including portal radicals.[76] The lack of any significant surrounding fibrosis distinguishes this condition from cirrhosis and it is frequently asymptomatic; however, it can lead to non-cirrhotic portal hypertension.[77] The pathophysiology of NRH is not clearly understood, but is thought to be a regenerative response to a microvascular occlusive process and is associated with a number of rheumatological and haematological conditions, and also certain drugs.[77]

Liver ultrasound in NRH has a variable appearance and may be normal. Multiple small low reflective nodules suggestive of cirrhosis are a recognised finding, but occasionally more coalescing nodules can mimic a primary liver tumour or metastases with low reflective haloes due to sinusoidal ectasia.[76,78] A more unusual ultrasound finding is that of diffuse low reflective periportal cuffing (Fig. 8.21), which although described,[78] is a non-specific pattern and has a recognised differential (Table 8.4).

CONGENITAL GENERALISED LIPODYSTROPHY (CGL)

Berardinelli–Seip syndrome is a rare metabolic syndrome characterised by the near total lack of adipose tissue from birth. Patients with CGL have severe insulin resistance, hypertriglyceridaemia and marked fat deposition in the liver and skeletal muscle. Liver ultrasound shows an enlarged echogenic liver typical of fatty infiltration: of note the image quality tends to be excellent, due to the lack of surrounding adipose tissue.[79]

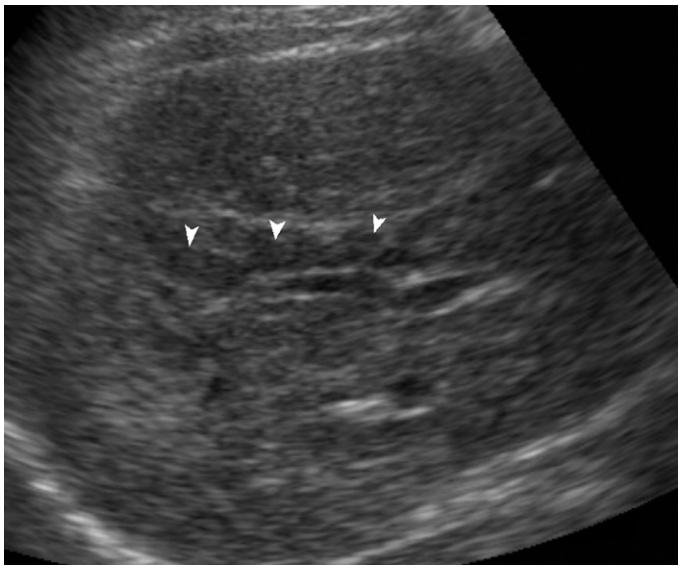


Figure 8.21 Nodular regenerative hyperplasia. Heterogeneous liver echotexture in a patient with unexplained portal hypertension. There is nodular low reflective 'cuffing' surrounding the portal vessels (arrowheads). Biopsy confirmed NRH.

Table 8.4 Causes of low reflectivity periportal cuffing

Malignant portal lymphadenopathy
Sclerosing cholangitis
Pre-cirrhotic primary biliary cirrhosis
Nodular regenerative hyperplasia

AMYLOID

Primary systemic amyloidosis is a rare disorder characterised by the deposition of amyloid protein within the vascular walls of various organs ultimately resulting in their failure. It commonly involves the liver although this is often subclinical. Deposits of the amyloid protein occur along the hepatic sinusoids and if extensive will compress the adjacent hepatocytes causing them to atrophy.[80] There are only limited reports of liver ultrasound in amyloid showing a non-specific heterogeneous reflectivity throughout the liver.[80] It may, however, have a role in guiding diagnostic liver biopsy.[81]

HAEMOCHROMATOSIS

Haemochromatosis is characterised by the progressive increase in total body iron stores resulting in abnormal iron deposition in a number of organs. It is either a primary autosomal recessive genetic disorder or secondary to other causes of increased body iron, most commonly haemolytic anaemias. In the primary disorder the liver is the main organ of iron deposition which leads to periportal fibrosis and eventually cirrhosis, with a significantly high risk of developing hepatocellular carcinoma. Liver ultrasound will show the features of fibrosis and cirrhosis if this is present, but the increased parenchymal iron does not affect the liver reflectivity.[82] The diagnostic imaging test of choice is liver MRI where the paramagnetic effect of the increased iron content causes a marked reduction in liver signal on T2-weighted gradient echo sequences.[82]

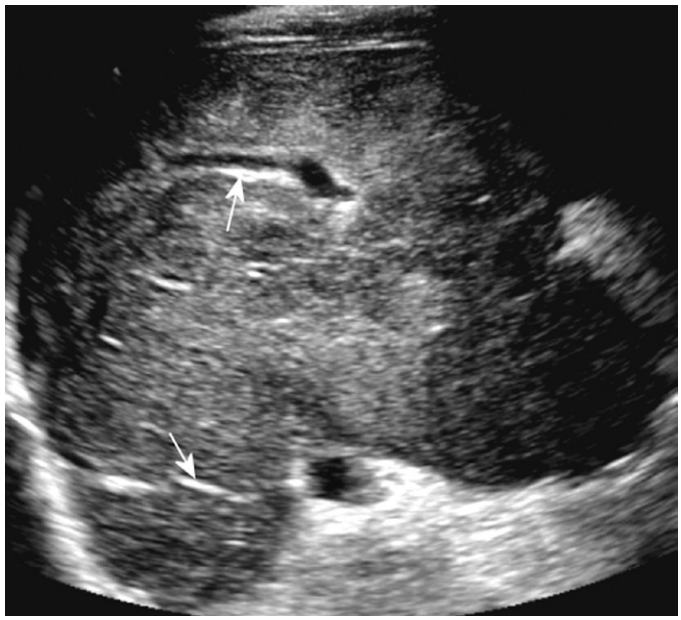


Figure 8.22 Cystic fibrosis. Right lobe of liver in CF. There is patchy altered reflectivity consistent with differential fatty infiltration, periportal thickening and a lobular contour to the liver. (Courtesy of Dr H. Massouh, Frimley Park Hospital, Surrey, UK.)

WILSON'S DISEASE

Wilson's disease is a rare autosomal recessive inherited disorder of copper metabolism, characterised by the accumulation of copper within hepatocytes and extrahepatic organs including the brain and cornea. Depending upon the severity of the disease at diagnosis liver ultrasound will show: an echogenic fatty liver, fibrotic periportal thickening or frank nodular cirrhotic change.

In cirrhosis secondary to Wilson's disease the ratio of the right lobe to caudate is often normal.[83] The nodular parenchymal pattern can be a mixture of high and low reflective nodules, resembling metastatic[84] disease, and an increased thickness in the perihepatic fat layer has also been described.[85] While none of these features are pathognomonic for Wilson's disease, the combination of these findings in a young patient with cirrhosis should suggest it as a possible cause.

CYSTIC FIBROSIS

Cystic fibrosis (CF) is the most common genetically inherited disorder affecting exocrine gland function. Within the liver, the failure of normal transmembrane conductance within the biliary epithelium is thought to cause delayed excretion of bile salts, resulting in damage of the biliary tree. Subsequent hepatocyte injury leads to the formation of regenerating nodules, and finally diffuse cirrhosis with portal hypertension.[86]

The improved survival in CF patients has resulted in an increased incidence of liver disease, although the exact percentage is unclear, with estimates of 1.4–72%: the incidence increasing with age. Clinical diagnosis can be difficult, with liver function tests tricky to interpret. The patchy nature of the disease can also result in false negative liver biopsy.[86,87]

A variety of appearances can be seen on ultrasound with diffuse increased reflectivity representing fatty infiltration the most common. The fat accumulation can have a regional distribution, producing a more geographic pattern of increased reflectivity (Fig. 8.22). With the onset of focal biliary cirrhosis there is increased

periportal tract reflectivity and thickening, with a generalised coarsening of the parenchymal texture.[86–89] Surface irregularity, with regenerating nodules 2–3 cm in size, is seen in diffuse cirrhosis along with atrophy of the right lobe and possibly signs of portal hypertension. The coexistence of a micro-gallbladder in CF patients is a well-described feature.[89]

REFERENCES

1. Albrecht T, Blomley MJ, Cosgrove DO, et al. Non-invasive diagnosis of hepatic cirrhosis by transit-time analysis of an ultrasound contrast agent. Lancet 1999;353:1579–1583.
2. Lim AK, Taylor-Robinson SD, Patel N, et al. Hepatic vein transit times using a microbubble agent can predict disease severity non-invasively in patients with hepatitis C. Gut 2005;54:128–133.
3. Forner A, Vilana R, Ayuso C, et al. Diagnosis of hepatic nodules 20 mm or smaller in cirrhosis: prospective validation of the noninvasive diagnostic criteria for hepatocellular carcinoma. Hepatology 2008;47:97–104.
4. Jang H-J, Kim TK, Wilson SR. Small nodules (1–2 cm) in liver cirrhosis: characterization with contrast-enhanced ultrasound. Eur J Radiol 2008 Sep 30; Epub 2008 Sep 30.
5. Friedrich-Rust M, Ong MF, Herrmann E, et al. Real-time elastography for noninvasive assessment of liver fibrosis in chronic viral hepatitis. AJR Am J Roentgenol 2007;188:758–764.
6. Dahl JJ, Pinton GF, Mark L, et al. A parallel tracking method for acoustic radiation force impulse imaging. IEEE Trans Ultrason Ferroelectr Freq Control 2007;54:301–312.
7. Kurtz AB, Dubbins PA, Rubin CS, et al. Echogenicity: analysis, significance, and masking. AJR Am J Roentgenol 1981;137: 471–476.
8. Chiou S-Y, Forsberg F, Fox TB, Needleman L. Comparing differential tissue harmonic imaging with tissue harmonic and fundamental gray scale imaging of the liver. J Ultrasound Med 2007; 26:1557–1563.
9. Garra BS, Insana MF, Shawker TH, Russell MA. Quantitative estimation of liver attenuation and echogenicity: normal state versus diffuse liver disease. Radiology 1987;162:61–67.
10. Oosterveld BJ, Thijssen JM, Hartman PC, et al. Ultrasound attenuation and texture analysis of diffuse liver disease: methods and preliminary results. Phys Med Biol 1991;36:1039–1064.
11. Hamer OW, Aguirre DA, Casola G, et al. Fatty liver: imaging patterns and pitfalls. Radiographics 2006;26:1637–1653.
12. Farrell GC, Larter CZ. Nonalcoholic fatty liver disease: from steatosis to cirrhosis. Hepatology 2006;43:S99–S112.
13. Clain JE, Stephens DH, Charboneau JW. Ultrasonography and computed tomography in focal fatty liver. Report of two cases with special emphasis on changing appearances over time. Gastroenterology 1984;87:948–952.
14. Tchelepi H, Ralls PW, Radin R, Grant E. Sonography of diffuse liver disease. J Ultrasound Med 2002;21:1023–1032.
15. Joseph AE, Saverymuttu SH, al-Sam S, et al. Comparison of liver histology with ultrasonography in assessing diffuse parenchymal liver disease. Clin Radiol 1991;43:26–31.
16. Scatarige JC, Scott WE, Donovan PJ, et al. Fatty infiltration of the liver: ultrasonographic and computed tomographic correlation. J Ultrasound Med 1984;3:9–14.
17. Joy D, Thava VR, Scott BB. Diagnosis of fatty liver disease: is biopsy necessary? Eur J Gastroenterol Hepatol 2003;15:539–543.
18. Saadeh S, Younossi ZM, Remer EM, et al. The utility of radiological imaging in nonalcoholic fatty liver disease. Gastroenterology 2002;123:745–750.
19. Strauss S, Gavish E, Gottlieb P, Katsnelson L. Interobserver and intraobserver variability in the sonographic assessment of fatty liver. AJR Am J Roentgenol 2007;189:W320–W323.
20. Van Le L, Podrasky A. Computed tomographic and ultrasonographic findings in women with acute fatty liver of pregnancy. J Reprod Med 1990;35:815–817.
21. Karcaaltincaba M, Akhan O. Imaging of hepatic steatosis and fatty sparing. Eur J Radiol 2007;61:33–43.
22. Quinn SF, Gosink BB. Characteristic sonographic signs of hepatic fatty infiltration. AJR Am J Roentgenol 1985;145:753–755.
23. Jain KA, McGahan JP. Spectrum of CT and sonographic appearance of fatty infiltration of the liver. Clin Imaging 1993;17:162–168.
24. Kroncke TJ, Taupitz M, Kivelitz D, et al. Multifocal nodular fatty infiltration of the liver mimicking metastatic disease on CT: imaging findings and diagnosis using MR imaging. Eur Radiol 2000;10:1095–1100.
25. Hamer OW, Aguirre DA, Casola G, Sirlin CB. Imaging features of perivascular fatty infiltration of the liver: initial observations. Radiology 2005;237:159–169.
26. Sauerbrei EE, Lopez M. Pseudotumor of the quadrate lobe in hepatic sonography: a sign of generalized fatty infiltration. AJR Am J Roentgenol 1986;147:923–927.
27. Tochio H, Kudo M, Okabe Y, et al. Association between a focal spared area in the fatty liver and intrahepatic efferent blood flow from the gallbladder wall: evaluation with colour Doppler sonography. AJR Am J Roentgenol 1999;172:1249–1253.
28. Liu LP, Dong BW, Yu XL, et al. Analysis of focal spared areas in fatty liver using color Doppler imaging and contrast-enhanced microvessel display sonography. J Ultrasound Med 2008;27:387–394.
29. Gabata T, Matsui O, Kadoya M, et al. Aberrant gastric venous drainage in a focal spared area of segment IV in fatty liver: demonstration with colour Doppler sonography. Radiology 1997;203:461–463.
30. Matsui O, Takahashi S, Kadoya M, et al. Pseudolesion in segment IV of the liver at CT during arterial portography: correlation with aberrant gastric venous drainage. Radiology 1994;193:31–35.
31. Bleuzen A, Tranquart F. Incidental liver lesions: diagnostic value of cadence contrast pulse sequencing (CPS) and SonoVue. Eur Radiol 2004;14(Suppl 8):P53–62.
32. Tom WW, Yeh BM, Cheng JC, et al. Hepatic pseudotumor due to nodular fatty sparing: the diagnostic role of opposed-phase MRI. AJR Am J Roentgenol 2004;183:721–724.
33. Duvnjak M, Leroti I, Barši N, et al. Pathogenesis and management issues for non-alcoholic fatty liver disease. World J Gastroenterol 2007;13:4539–4550.
34. Angulo P. Non-alcoholic fatty liver disease. N Engl J Med 2002;346:1221–1231.
35. Farrell GC, Larter CZ. Nonalcoholic fatty liver disease: from steatosis to cirrhosis. Hepatology 2006;43:S99–S112.
36. Powell EE, Cooksley WGE, Hanson R, et al. The natural history of nonalcoholic steatohepatitis: a follow-up study of forty-two patients for up to 21 years. Hepatology 1990;11:74–80.
37. Hui JM, Kench JG, Chitturi S, et al. Longterm outcomes of cirrhosis in nonalcoholic steatohepatitis compared with hepatitis C. Hepatology 2003;38:420–427.
38. Charlton M, Kasparova P, Weston S, et al. Frequency of nonalcoholic steatohepatitis as a cause of advanced liver disease. Liver Transpl 2001;7:608–614.
39. Moriyasu F, Iijima H, Tsuchiya K, et al. Diagnosis of NASH using delayed parenchymal imaging of contrast ultrasound. Hepatol Res 2005;33:97–99.
40. Friedrich-Rust M, Ong M-F, Martens S, et al. Performance of transient elastography for the staging of liver fibrosis: a meta-analysis. Gastroenterology 2008;134:960–974.
41. Saverymuttu SH, Joseph AEA, Maxwell JD. Ultrasound scanning in the detection of fibrosis and steatosis. BMJ 1986;292:13–15.
42. Zheng R-Q, Wang Q-H, Lu M-D, et al. Liver fibrosis in chronic viral hepatitis: an ultrasonographic study. World J Gastroenterol 2003;9:2484–2489.
43. Nishiura T, Watanabe H, Ito M, et al. Ultrasound evaluation of the fibrosis stage in chronic liver disease by the simultaneous use of low and high frequency probes. Br J Radiol 2005;78:189–197.
44. Wolf DC. Cirrhosis. emedicine [ONLINE] 2008 Aug [update 22 Dec 2009]. Available from: http://emedicine.medscape.com/article/185856-overview.
45. Anthony PP, Ishak KG, Nayak NC, et al. The morphology of cirrhosis. J Clin Pathol 1978;31:395–414.
46. MacSween RNM, Anthony PP, Scheuer PJ. Pathology of the liver. 2nd edn. New York: Churchill Livingstone; 1987:342–363.
47. Rumack CM, Wilson S, Charboneau JW. Diagnostic Ultrasound. 3rd edn. Missouri: Mosby; 2004.
48. Zaman SN, Melia WM, Johnson RD, et al. Risk factors in development of hepatocellular carcinoma in cirrhosis: prospective study of 613 patients. Lancet 1985;1:1357–1360.
49. Harbin WP, Robert NJ, Ferrucci JT. Diagnosis of cirrhosis based on regional changes in hepatic morphology. Radiology 1980;135:273.
50. Giorgio A, Amoroso P, Lettiri G, et al. Cirrhosis: value of caudate to right lobe ratio in diagnosis with ultrasound. Radiology 1986;161:443.
51. Goyal AK, Pokharna DS, Sharma SK. Ultrasonic diagnosis of cirrhosis: reference of quantitative measurements of hepatic dimensions. Gastrointest Radiol 1990;15:32.

52. Paruleker SG, Bree RL. Liver. In: McGahan JP, Goldberg BB, editors. Diagnostic ultrasound. 2nd edn. New York: CRC Press; 2008. p. 339–426.
53. Martínez-Noguera A, Calonge E, Coscojuela P, et al. Chronic liver disease: comparison of ultrasound patterns with laparoscopy and biopsy. J Clin Ultrasound 1993;21:325–330.
54. Taylor KJW, Gorelick FS, Rosenfield AT, Riely CA. Ultrasonography of alcoholic liver disease with histological correlation. Radiology 1981;141:157–161.
55. Caturelli E, Castellano L, Fusilli S, et al. Coarse nodular US pattern in hepatic cirrhosis: risk for hepatocellular carcinoma. Radiology 2003;226:691–697.
56. Freeman MP, Whitley Vick C, Taylor KJW, et al. Regenerating nodules in cirrhosis: sonographic appearance with anatomic correlation. AJR Am J Roentgenol 1986;146:533–536.
57. Simonovsky V. The diagnosis of cirrhosis by high resolution ultrasound of the liver surface. Br J Radiol 1999;72:29–34.
58. Colli A, Fraquelli M, Andreoletti M, et al. Severe liver fibrosis or cirrhosis: accuracy of US for detection-analysis of 300 cases. Radiology 2003;227:89–94.
59. Laing FC, Jeffrey RB, Federle MP, et al. Noninvasive imaging of unusual regenerating nodules in the cirrhotic liver. Gastrointest Radiol 1992;7:245.
60. Kraus GJ, Schedlbauer P, Lax S, et al. The reverse target sign in liver disease: a potential ultrasound feature in cirrhotic liver nodules characterization. Br J Radiol 2005;78:355–357.
61. Solbiati L, Martegani A, Leen E, et al. Contrast-enhanced ultrasound of liver diseases. Milan: Springer-Verlag; 2003.
62. Lencioni R, Crocetti L, Della Pina MC, Cioni D. Guidelines for imaging focal lesions in liver cirrhosis. Expert Rev Gastroenterol Hepatol 2008;2:697–703.
63. Ueda K, Terada T, Nakanuma Y, Matsui O. Vascular supply in adenomatous hyperplasia of the liver and hepatocellular carcinoma: a morphometric study. Hum Pathol 1992;23:619–626.
64. Nicolau C, Vilana R, Catalá V, et al. Importance of evaluating all vascular phases on contrast-enhanced sonography in the differentiation of benign from malignant focal liver lesions. AJR Am J Roentgenol 2006;186:158–167.
65. Bang N, Nielsen MB, Rasmussen AN, et al. Hepatic vein transit time of an ultrasound contrast agent: simplified procedure using pulse inversion imaging. Br J Radiol 2001;74:752–755.
66. Kaplan MM, Gershwin ME. Primary biliary cirrhosis. N Engl J Med 2005;353:1261–1273.
67. Worthy SA, Elliott ST, Bennett MK. Low-reflectivity periportal collar on hepatic ultrasound. Br J Radiol 1994;67:1050–1051.
68. Soresi M, Bonfissuto G, Magliarisi C, et al. Ultrasound detection of abdominal lymph nodes in chronic liver diseases. A retrospective analysis. Clin Radiol 2003;58:372–377.
69. Del Olmo J-A, Esteban J-M, Maldonado L, et al. Clinical significance of abdominal lymphadenopathy in chronic liver disease. Ultrasound Med Biol 2002;28:297–301.
70. Thompson Coon J, Rogers G, Hewson P, et al. Surveillance of cirrhosis for hepatocellular carcinoma: systematic review and economic analysis. Health Technol Assess 2007;11(34):1–206.
71. Larcos G, Sorokopud H, Berry G, Farrell GC. Sonographic screening for hepatocellular carcinoma in patients with chronic hepatitis or cirrhosis: an evaluation. AJR Am J Roentgenol 1998;171:433–435.
72. Wun YT, Dickinson JA. Alpha-fetoprotein and/or liver ultrasonography for liver cancer screening in patients with chronic hepatitis B (Review). Cochrane Database of Systematic Reviews 2003, Issue 2. Art. No.: CD002799. DOI: 10.1002/14651858.CD002799.
73. Ozen H. Glycogen storage diseases: new perspectives. World J Gastroenterol 2007;13:2541–2553.
74. Lee P, Mather S, Owens C, et al. Hepatic ultrasound findings in glycogen storage diseases. Br J Radiol 1994;67:1062–1066.
75. Grossman H, Ram P, Coleman R, et al. Hepatic ultrasonography in type I glycogen storage disease (von Gierke disease): detection of hepatic adenoma and carcinoma. Radiology 1981;141:753–756.
76. Dachman A, Ros P, Goodman Z, et al. Nodular regenerative hyperplasia of the liver: clinical and radiologic observations. AJR Am J Roentgenol 1987;148:717–722.
77. Leung V, Ng W-L, Luk I, et al. Unique hepatic imaging features in a patient with nodular regenerative hyperplasia of the liver associating with systemic lupus erythematosus. Lupus 2007;16:205–208.
78. Clouet M, Boulay I, Boudiaf M, et al. Imaging features of nodular regenerative hyperplasia of the liver mimicking hepatic metastases. Abdom Imaging 1999;24:258–261.
79. Smevik B, Swensen T, Kolbenstvedt A, Trygstad O. Computed tomography and ultrasonography of the abdomen in congenital generalized lipodystrophy. Radiology 1982;142:687–689.
80. Monzawa S, Tsukamoto T, Omata K, et al. A case with primary amyloidosis of the liver and spleen: radiologic findings. Eur J Radiol 2002;41:237–241.
81. Kim S, Han J, Lee K, et al. Abdominal amyloidosis: spectrum of radiological findings. Clin Radiol 2003;58:610–620.
82. Mergo P, Ros P, Buetow P, Buck J. Diffuse disease of the liver: radiologic-pathologic correlation. Radiographics 1994;14:1291–1307.
83. Vogel W, Kathrein H, Dietze O, Judmaier G. Sonography of the liver in Wilson's disease. Sonographic studies of the liver in Wilson's disease – significance for assessing prognosis? Ultraschall Med 1988;9:270–273.
84. Akpinar E, Akhan O. Liver imaging findings of Wilson's disease. Eur J Radiol 2007;61:25–32.
85. Akhan O, Akpinar E, Oto A, et al. Unusual imaging findings in Wilson's disease. Eur Radiol 2002;12:S66–S69.
86. Stewart L. The role of abdominal ultrasound in the diagnosis, staging and management of cystic fibrosis liver disease. J R Soc Med 2005;98(Suppl. 45):17–27.
87. Ling S, Wilkinson J, Hollman A, et al. The evolution of liver disease in cystic fibrosis. Arch Dis Child 1999;81:129–132.
88. Graham N, Manhire A, Stead R, et al. Cystic fibrosis: ultrasonographic findings in the pancreas and hepatobiliary system correlated with clinical data and pathology. Clin Radiol 1985;36:199–203.
89. Fields T, Michel S, Butler C, et al. Abdominal manifestations of cystic fibrosis in older children and adults. AJR Am J Roentgenol 2006;187:1199–1203.

CHAPTER

9

Liver: infections and inflammations

James M. Pilcher

HEPATITIS 120
Acute hepatitis 120
Viral 120
Alcoholic 121
Chronic hepatitis 122

LIVER ABSCESS 124
Bacterial 124
Brucellar abscess 126
Amoebic abscess 126

FUNGAL INFECTION 127
Candidiasis 127

SCHISTOSOMIASIS 128

TOXOCARIASIS 129

ECHINOCOCCAL INFECTION 129
Echinococcal cyst (hydatid disease) 129
Hepatic alveolar echinococcosis 130

ACUTE FASCIOLIASIS 131

INFLAMMATORY PSEUDO-TUMOUR 131

HIV/AIDS 131
***Pneumocystis carinii* 132**
***Mycobacterium avium* complex 132**
Cytomegalovirus 132

GRANULOMATOUS HEPATITIS 132
Sarcoid 132
Tuberculosis 132

CHRONIC GRANULOMATOUS DISEASE 133

CAT SCRATCH FEVER 133

HYPEREOSINOPHILIC SYNDROME 134

HEPATIC CALCIFICATION 134

Ultrasound plays a pivotal role in the management of hepatic infections and inflammatory processes, often being the first imaging investigation for patients with pyrexia of unknown aetiology. However, although it is relatively sensitive in the detection of a large number of these conditions, it often lacks specificity, particularly in necrotic infections which can mimic a hepatic cyst or necrotic tumour. In these cases computed tomography (CT) or magnetic resonance imaging (MRI) has often been employed to obtain further information: the increasing use of microbubble contrast agents in ultrasound may see these modalities being required less frequently. As with diffuse parenchymal disease, some of the changes in the inflamed/infected liver are either subtle or have a fine pattern; therefore high-frequency curvilinear or linear arrays need to be employed when making an assessment of the liver. Access to the relevant clinical details such as age, sex, presenting history, symptoms and immune status is also key to achieving a more accurate presumptive diagnosis. In a number of conditions, despite cross-sectional imaging, aspiration or biopsy is still required to obtain the final diagnosis, and ultrasound is the ideal modality to guide this process. It may also be employed in the subsequent management, such as the insertion of a drainage catheter.

HEPATITIS

Hepatitis is any inflammatory process affecting the liver leading to hepatocyte injury. This may be an acute, self-limiting event or chronically progressive leading to scarring and ultimately cirrhosis, with the associated risk of hepatocellular carcinoma.

Acute hepatitis

Viral

The most common cause of an acute hepatitis is viral, usually by one of the distinct group of six hepatitis viruses A–E and G (Table 9.1). A number of other viral infections may also cause a hepatitis (Table 9.2), although it tends not to be a dominant feature of their presentation.[1] With acute hepatitis the clinical picture can vary from a mild self-limiting condition, as seen in the majority of hepatitis A cases, through to fulminant hepatic failure with deep jaundice, encephalopathy and deranged clotting, requiring urgent liver transplant. Pathologically there is diffuse hepatocellular injury with necrosis of hepatocytes, proliferation of Kuppfer cells and portal inflammatory infiltrate. Hepatocyte regeneration is seen in the recovery phase, but in more severe cases confluent necrosis is seen to extend between the portal tracts and central veins.[2] On the whole, patients are relatively asymptomatic, but may present with malaise, mild fever, right upper quadrant pain and after a few days become jaundiced. Liver function tests are elevated, particularly the aminotransferases, and the diagnosis can be confirmed with serological markers (HAV-IgM, HBsAg and HEV-IgM).

Although the main role of ultrasound is to exclude a surgical cause of obstructive jaundice, the diagnosis of viral hepatitis can be suggested by the finding of an enlarged liver showing a diffuse reduction in parenchymal reflectivity and a relative increase in reflectivity of the portal triads[3] (Fig. 9.1). The latter finding is thought to be due to hydropic swelling of the surrounding hepatocytes and is referred to as the 'starry-sky' appearance; however, it is rather non-specific and has been described in a number of other circumstances (Fig. 9.2), including normal individuals.[4] Echogenic periportal thickening is a more marked type of inflammatory change that has also been described.[3] Gallbladder wall thickening is a very common reported finding in viral hepatitis[4,5] and may be striking with pericholecystic oedema: this is sometimes associated with reduced luminal volume and echogenic sludge (Fig. 9.3). Endoscopic ultrasound has demonstrated that it is the muscular and serosal layers that are mainly affected, with the degree of

Table 9.1 The hepatitis viruses

Virus	Transmission	Chronicity	Diagnostic serology	Specific features
HAV	Faecal–Oral	No	HAV-IgM	Younger patients affected. Mortality rate 0.1%, usually fulminant hepatitis
HBV	Percutaneous/ Venereal	Yes Majority vertical infection	HBsAg	HBsAg may be seen in acute of chronic infection. HBeAg detected with active viral replication, i.e. highly infective
HCV	Percutaneous	Yes (75%)	Anti-HCV	Majority of acute cases clinically mild. Histology unable to distinguish progressive disease
HDV	Percutaneous	Yes Majority superinfection	Anti-HDV	Requires the presence of HBsAg for its expression. Either simultaneous co-infection of subsequent superinfection
HEV	Faecal Oral	No	Anti-HEV	Leading cause of infective hepatitis in a number of developing countries. High mortality in pregnancy
HGV	Percutaneous	Yes (mild)	Research tool	Association with hepatocellular carcinoma remains unclear

HBsAg, hepatitis B surface antigen.

Table 9.2 Causes of acute hepatitis

Viral: Hepatitis A–E and G
- Herpes Simplex
- Cytomegalovirus
- Epstein–Barr
- Adenoviruses
- Coxsackie

Alcohol

Toxins

Drugs: Paracetamol
- Isoniazid
- Statins
- Methotrexate

Ischaemia

Metabolic: Wilson's disease

Pregnancy

Autoimmune: Systemic lupus erythematosus

Differential diagnosis for 'starry–sky' appearance

Diagnosis	Supportive findings at ultrasound
Acute viral hepatitis	Gallbladder wall thickening Regional lymphadenopathy
Infectious mononucleosis	Splenomegaly Mesenteric lymphadenopathy
Toxic shock syndrome	
Congestive cardiac failure	Hepatic vein enlargement Altered hepatic vein Dopplers Ascites
Periportal fibrosis	Heterogeneous hepatic parenchyma Regional lymphadenopathy
Cholangitis	Thickened common bile duct
Radiation injury	Regional pattern of change
Inflammatory bowel diseases	Bowel wall thickening Hyperaemia on power Doppler
Schistosomiasis (mansoni)	
Burkitt's lymphoma	
Normals	

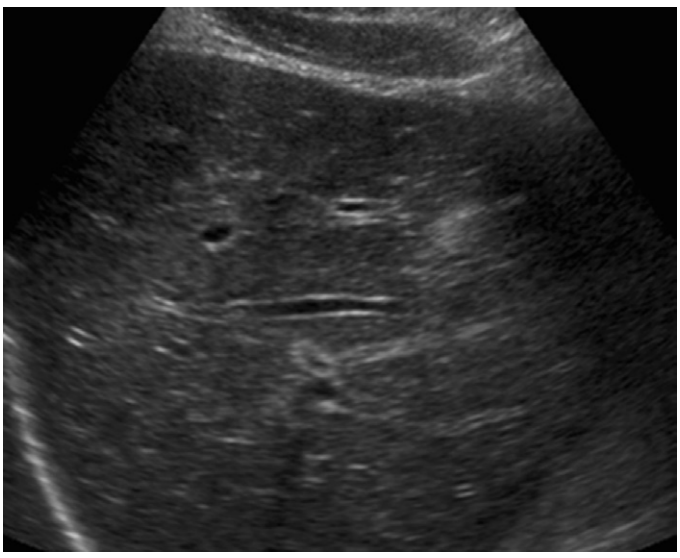


Figure 9.1 Hepatitic liver. Adult male with recent history of influenza-like illness and right upper quadrant pain now presenting with jaundice. The liver shows apparent reduction in parenchymal reflectivity and increased periportal reflectivity.

thickening relating to the level of enzyme elevation.[6] However, the pathogenesis for this thickening remains uncertain. Portal lymphadenopathy is another finding typically seen with hepatitis C infection, but also hepatitis A and non-viral causes of hepatitis (Fig. 9.4).

Alcoholic

Acute alcoholic hepatitis is a defined clinicopathological condition of varying severity, which can present both in long-term alcohol abusers and in moderate drinkers following a short-term alcohol binge.[7] At histology there is neutrophilic infiltration with centrilobular ballooning and necrosis of hepatocytes with Mallory hyaline inclusions: fatty infiltration and cirrhosis may also be seen in more chronic cases.

The clinical features are fever, right upper quadrant pain and jaundice, with a neutrophilia, hyperbilirubinaemia, elevated aspartate aminotransferase and prothrombin time. In its most severe form the mortality rate can approach 50%.[8] At ultrasound the liver is often enlarged, with diffuse increased reflectivity as a result of fatty infiltration or fibrosis[8] (Fig. 9.5). A described ultrasound feature in acute alcoholic hepatitis is the 'pseudo-parallel' channel

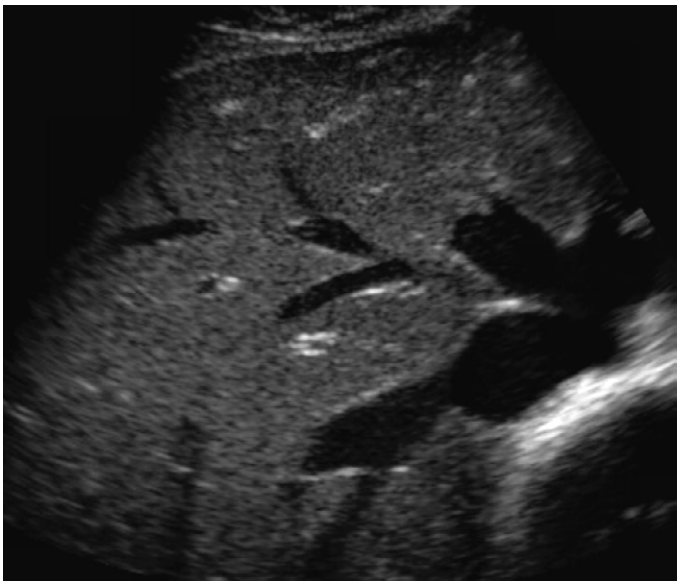


Figure 9.2 Differential for 'starry sky' pattern in the liver. Male patient with hepatic venous congestion secondary to cardiomyopathy. There is increased periportal reflectivity and enlarged hepatic veins.

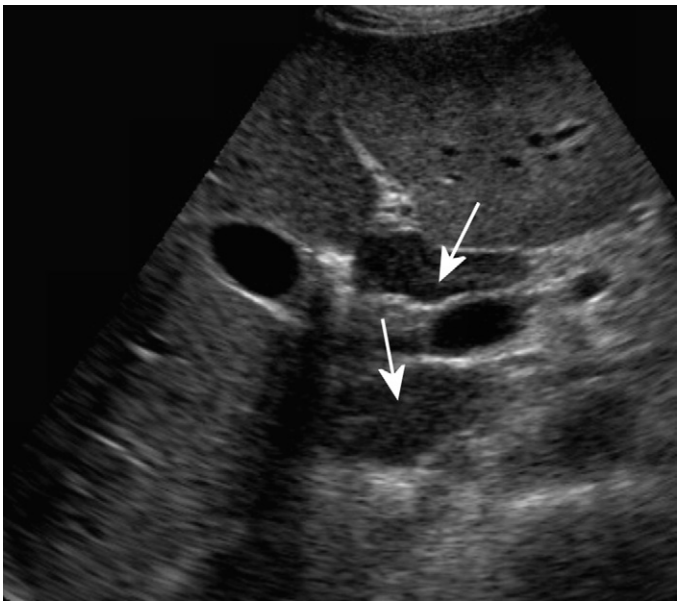


Figure 9.4 Regional lymphadenopathy in hepatitis C. Pre-liver biopsy ultrasound in a patient with known hepatitis C showing enlarged periportal lymph nodes (arrows).

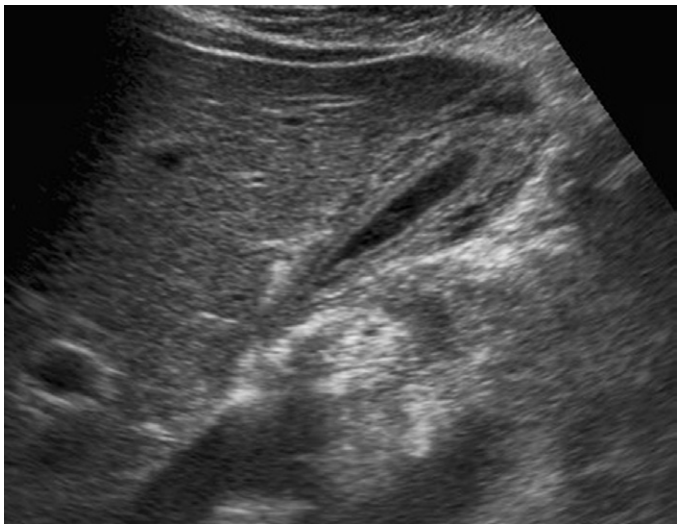


Figure 9.3 Gallbladder wall changes in hepatitis. Male patient with confirmed acute hepatitis A showing a non-distended, striated thick-walled gallbladder. (Courtesy of Dr E. Rutherford.)



Figure 9.5 Alcoholic hepatitis patient with right upper quadrant pain and abnormal liver function tests following heavy alcohol intake, showing enlarged fatty liver with underlying early fibrosis (arrows).

sign representing a dilated hepatic artery adjacent to a portal venous branch.[9] Peak systolic velocity measurements in the right hepatic artery are also elevated compared to normal subjects.[10] Both findings are thought to reflect increased arterial flow to the liver to compensate reduced portal venous flow as a result of rising sinusoidal resistance.

Chronic hepatitis

Chronic hepatitis (CH) is defined as continued disease activity beyond 6 months, detectable by persistent elevation of liver enzymes, and has a number of aetiologies: most commonly viral (hepatitis B, C, D and G), but also metabolic (Wilson's disease, alpha-1-antitrypsin deficiency, and haemochromatosis), autoimmune and drugs. Histologically there is infiltration of the portal tracts by predominantly mononuclear cells, which when confined to the portal triads is defined as mild. In moderate CH there is increasing extension of inflammatory infiltrate into the adjacent parenchyma and it becomes severe when there is confluent necrosis between portal triads and/or the central veins, the latter being much more likely to progress to cirrhosis.[11]

The main role of ultrasound in patients with CH is in monitoring for evidence of developing cirrhosis, portal hypertension and hepatocellular carcinoma. There are no diagnostic ultrasound features for CH and the liver often appears normal, with adenopathy in the

hepatoduodenal ligament sometimes the only finding. The liver can also appear enlarged with diffuse increased reflectivity and loss of portal vein wall definition, identical to fatty infiltration. With progression of CH the liver may appear more heterogeneous in texture due to increasing fibrosis and eventually cirrhosis, with regenerating nodules (Fig. 9.6). In patients with hepatitis C, ultrasound has been used to try and stage its severity, both through the detection of focal fatty sparing at the portal bifurcation and by measuring the hepatic vein arrival time of intravenous microbubble contrast agents.[12,13]

Causes of multiple low reflective hepatic nodules

- Metastases
- Lymphoma
- Cirrhosis
- Nodular regenerative hyperplasia
- Fungal infection
- Granulomatous hepatitis
- Hypereosinophilic syndrome

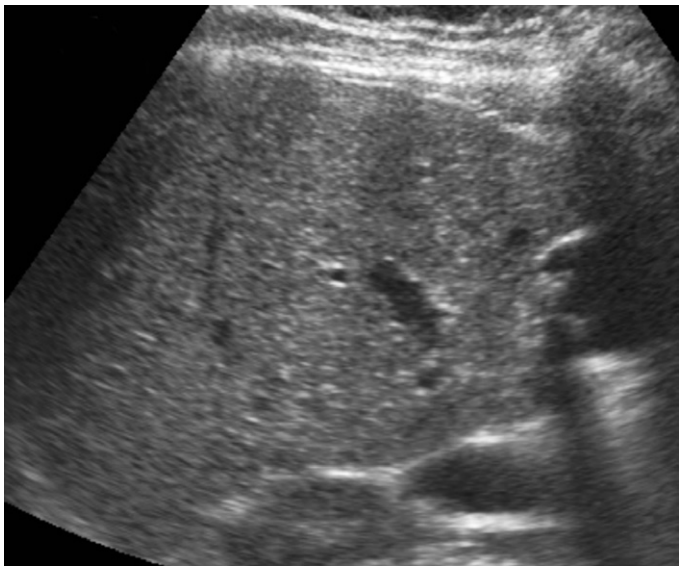
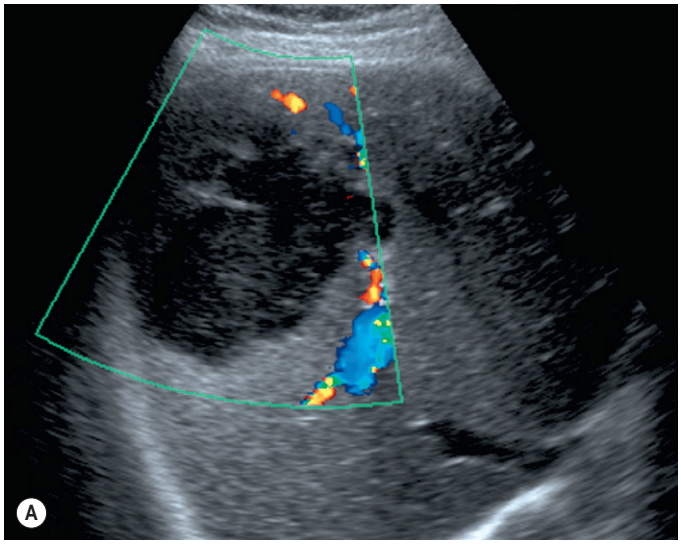
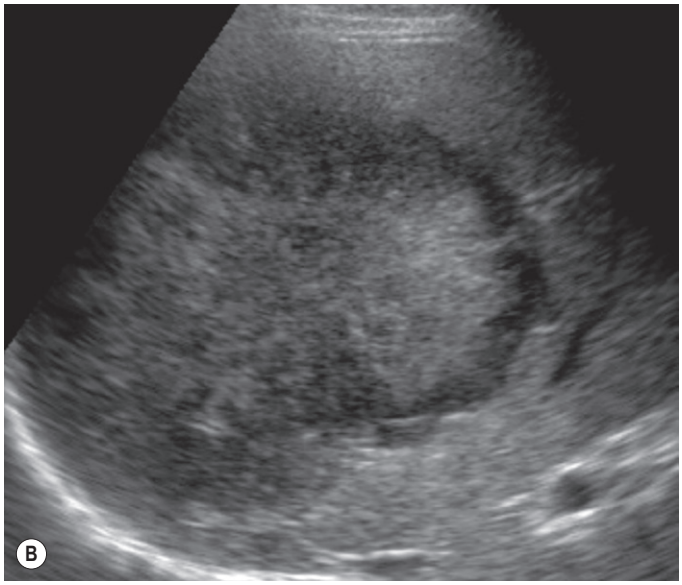


Figure 9.6 Chronic hepatitis. Surveillance ultrasound in a female patient with chronic hepatitis B. The liver parenchyma shows multiple fine echogenic linear foci, with mild irregular thickening of the portal tracts, indicative of developing fibrosis.





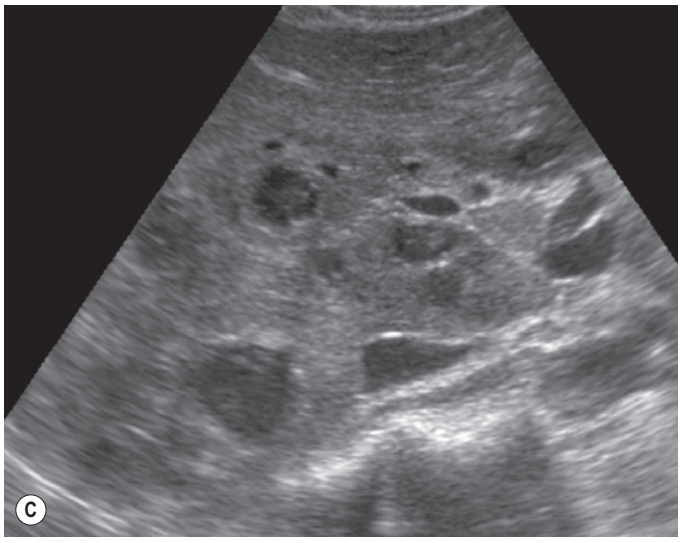


Figure 9.7 Variable appearance of pyogenic liver abscess. Liver abscesses may appear predominantly cystic **(A)**; solid: mimicking a focal mass lesion **(B)**; or in some cases multifocal, mimicking metastases **(C)**.

LIVER ABSCESS

Necrotic infection within the liver can be caused by a number of bacterial, fungal and parasitic organisms. Ultrasound plays an important role in the diagnosis, management and follow-up of these infections, although frequently the appearances can be non-specific or frankly misleading. Access to epidemiological and clinical information, including the patient's immune status, is therefore vital in order to enable a more accurate presumptive diagnosis.

Bacterial

The aetiology of pyogenic liver abscess formation from bacterial spread to the liver has changed significantly in the past twenty years. Currently the most common source of infection is direct extension from the biliary tract in patients with suppurative cholangitis or cholecystitis.[14] Direct extension may also sometimes come from the lung, kidney or colon. Other sources include: portal venous spread from appendicitis, diverticulitis or other inflammatory bowel disease; hepatic artery spread from distant infection such as subacute bacterial endocarditis or osteomyelitis; and penetrating injury from trauma, surgical intervention and more recently minimally invasive ablative techniques.[15]

Escherichia coli has traditionally been the most common organism isolated from pyogenic liver abscesses, with *Staphylococcus aureus*, *Streptococcus milleri* and the anaerobes *Clostridia* and *Bacteroides* also being found: the latter two are likely to have been significantly under-reported in the past due to inadequate culture techniques.[16] Recent case reviews, however, have identified *Klebsiella pneumoniae* as an increasingly important pathogen, particularly amongst Asians and people with diabetes.[17–19] The clinical presentation for all these infections is variable, and can be non-specific, such as fever, malaise and anorexia. More specific features include right upper quadrant pain, pleuritic pain, vomiting and jaundice. At laboratory analysis, most patients will have a leukocytosis and marked elevation of the alkaline phophatase.[17] In patients with a *K. pneumoniae* liver abscess, bacteraemia is extremely common with end-organ seeding and distant abscess formation well reported.[19,20]

The main treatment approach for a pyogenic liver abscess is systemic antibiotics and percutaneous drainage/aspiration (see below); however, despite this approach mortality rates can still reach 6–14%.[21]

On ultrasound pyogenic liver abscesses are highly variable in appearance and can range from resembling a simple cyst to a solid echogenic mass, or multiple low reflective nodules suggestive of metastatic disease (Fig. 9.7A–C). Appearances are closely related to the pathological process, with early suppuration prior to hepatocyte necrosis appearing as a solid mass with altered, usually reduced, reflectivity and frequently demonstrating distal acoustic accentuation.[22] With necrosis and liquefaction abscesses become increasingly heterogeneous in reflectivity and eventually demonstrate central cystic change, which may contain septations or echogenic debris. With gas-forming organisms, the abscess may contain highly reflective foci demonstrating reverberation artefact, and if more extensive, strong linear echoes with acoustic shadowing (Fig. 9.8). The fibrous walls of the abscess can vary in appearance from irregular and indistinct to well defined and, less frequently, irregular and thick.[23] In patients with *Klebsiella pneumoniae* infection abscesses tend to have a predominantly solid appearance, with lack of through-transmission of sound,[24] while with *Staphylococcus aureus* infection a pattern of multiple micro-abscesses (<2 cm) mimicking fungal infection has been described.[25]

The sensitivity of ultrasound for liver abscess detection is up to 97%.[26] However, there is a differential for the varied appearance including a haemorrhagic simple cyst, focal haematoma or malignant tumour. Contrast-enhanced ultrasound (CEUS), may help make the distinction, with the most common enhancement pattern for a confirmed abscess showing early peripheral parenchymal enhancement, followed by arterial rim enhancement and septations (if present) (Fig. 9.9A–C). There tends to be lesion washout in the portal venous phase or late phase of imaging.[12]

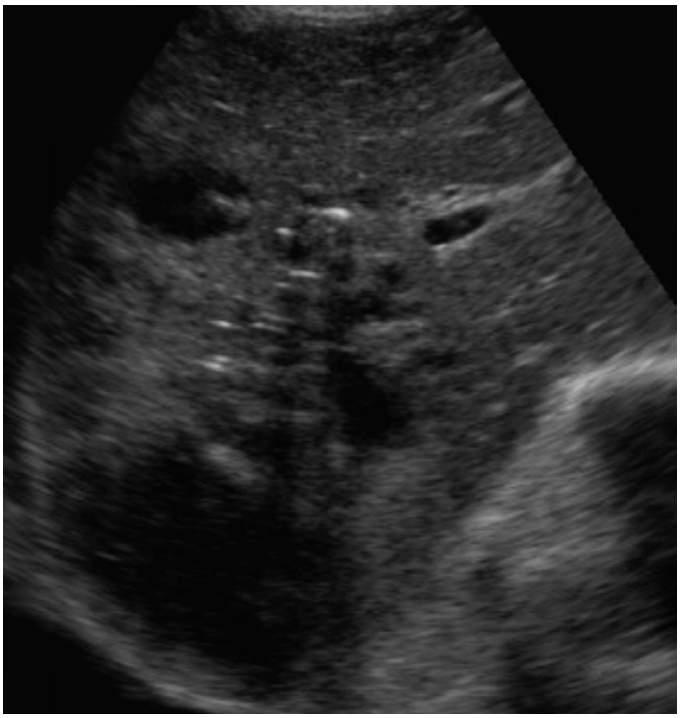


Figure 9.8 Liver abscess containing gas. Focal liver abscess with cystic and solid components. There are several strongly echogenic linear areas, some with acoustic shadowing, representing air within the abscess.

The traditional management approach of surgical drainage for pyogenic liver abscess has long been superseded by percutaneous aspiration or drainage under image guidance combined with parenteral broad-spectrum antibiotics.[21,27–31] Ultrasound is frequently employed to guide needle placement within the abscess and the majority of reported series have used a freehand approach in order to allow adjustment to its trajectory. For percutaneous aspiration a 22-18-gauge trocar needle is used depending upon the size of the liver abscess (Fig. 9.10).[28] If there are multiple abscesses, the deepest one is targeted first to avoid overlying artefact from gas bubbles. Repeated aspirations may be required if the patient has persistent fever, leukocytosis or the abscess cavity remains significant on ultrasound follow-up: this appears to be unrelated to the initial size of the abscess.[28,29] Percutaneous drainage is performed either as a single-stick procedure,[30] or using the Seldinger technique,[31] with an 8–10F pigtail catheter being introduced into the abscess (Fig. 9.11). This is fixed to the skin and left on free drainage until the patient shows clinical improvement or there is a fall in catheter output to <10 mL/24 h.[31] Both procedures appear to be tolerated well by the patient, although there is a recognised risk of post-procedure sepsis following catheter drainage.[32] There is a continuing debate amongst centres as to whether aspiration or drainage should be the first-line approach to liver abscess management. It has been suggested that for abscesses less than 5 cm in size, aspiration is a reasonable first-line approach, with drainage reserved for larger abscesses or complex loculated abscesses. With regard to aspiration, abscesses secondary to *Klebsiella pneumoniae* infection appear to aspirate poorly compared to other pyogenic abscesses, with only a couple of millilitres of pus being obtained in many cases.[24]

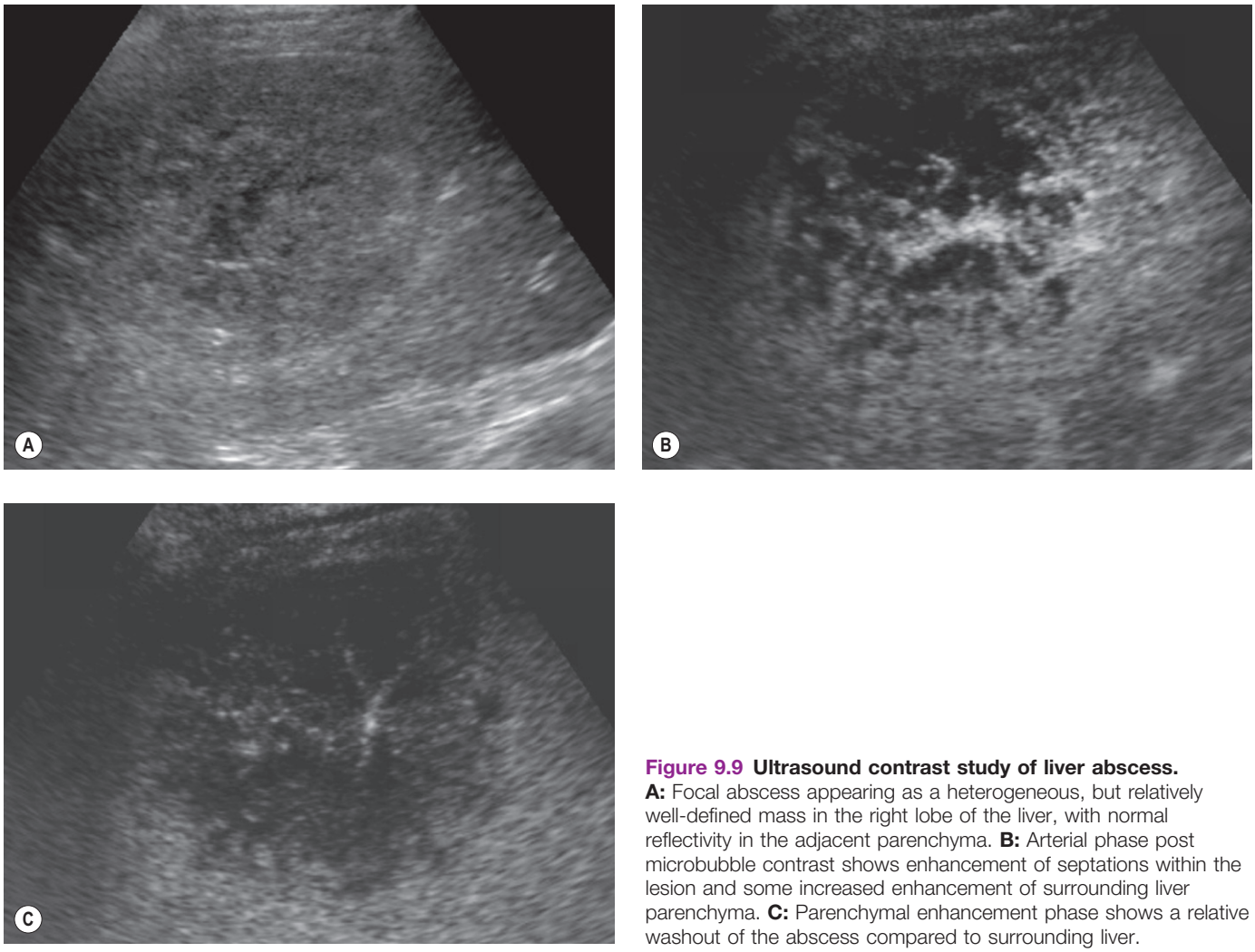


Figure 9.9 Ultrasound contrast study of liver abscess. **A:** Focal abscess appearing as a heterogeneous, but relatively well-defined mass in the right lobe of the liver, with normal reflectivity in the adjacent parenchyma. **B:** Arterial phase post microbubble contrast shows enhancement of septations within the lesion and some increased enhancement of surrounding liver parenchyma. **C:** Parenchymal enhancement phase shows a relative washout of the abscess compared to surrounding liver.

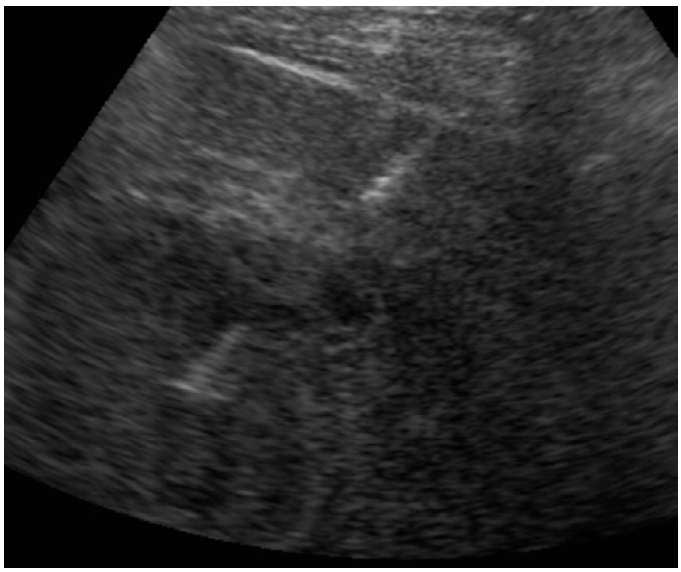


Figure 9.10 Needle aspiration of liver abscess. Diagnostic aspiration of pseudo-solid liver abscess, with the needle tip from a 20G spinal needle clearly seen on ultrasound.

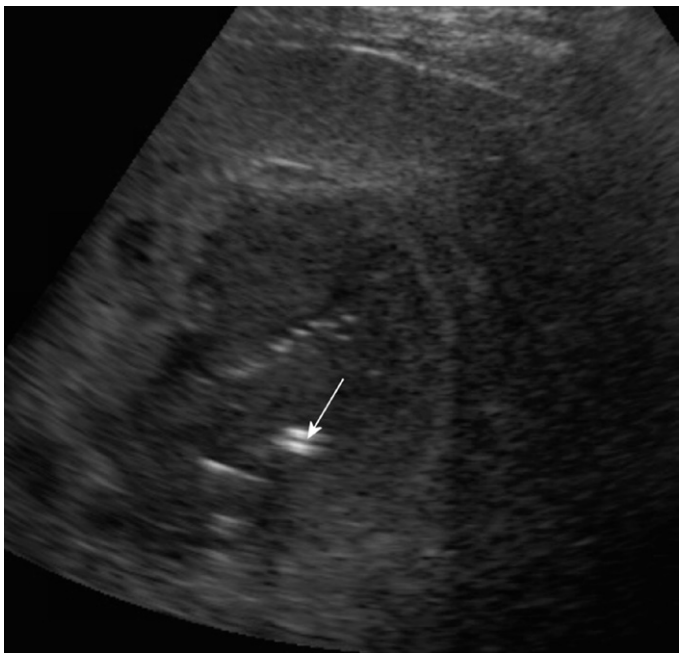


Figure 9.11 Drainage catheter seen in liver abscess. Following successful placement the tubing from an 8F pigtail drain is clearly visualised within the abscess (arrow): the smaller reflective foci anterior to this represent air that has been introduced during the procedure.

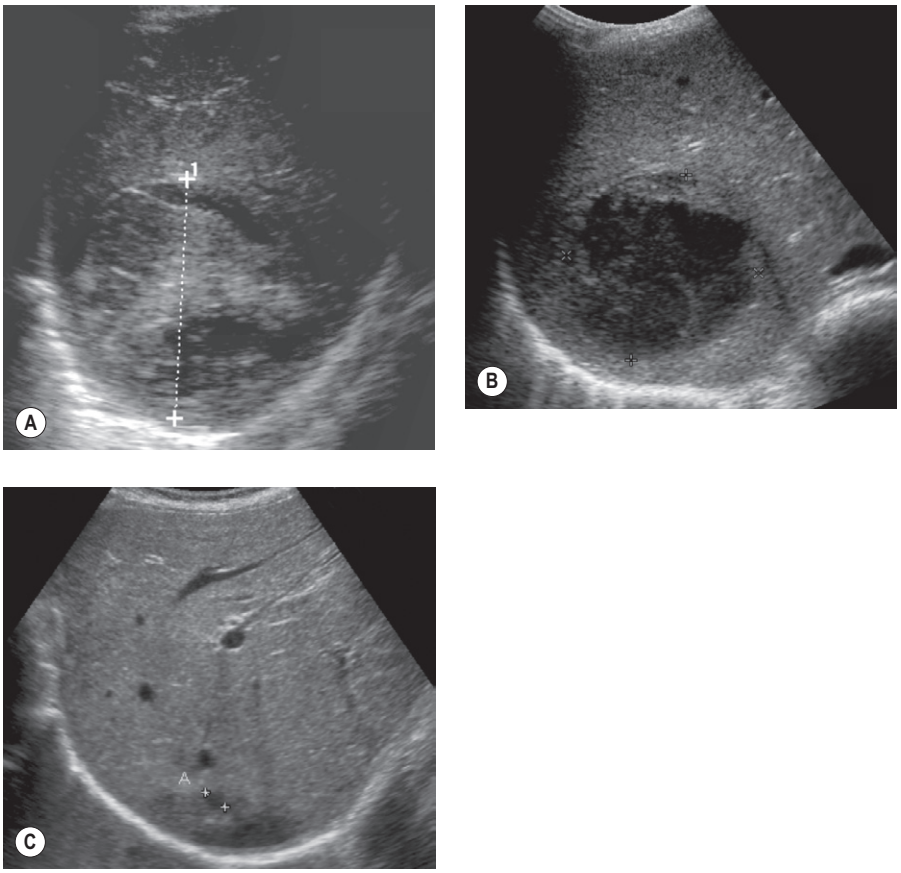


Figure 9.12 Follow-up of liver abscess to resolution. A: Large right lobe liver abscess with mixed reflectivity, which was treated with antibiotics alone. **B:** Repeat scan at one month shows a smaller, more homogeneous low reflective collection. **C:** At 10 months there is a very small residual cyst-like focus.

Ultrasound follow-up of treated pyogenic abscesses shows a resolution time that lags significantly behind the clinical findings. The majority will resolve to sonographically normal parenchyma (Fig. 9.12A–C), but a few will continue to show a persisting cystic cavity, even at 2 years, or focal areas of calcification.[33]

Brucellar abscess

Brucellosis is a worldwide zoonosis, which is endemic in parts of the Mediterranean, India, Mexico and Central America. Infection can involve any organ of the body and in the liver this usually manifests as a granulomatous hepatitis.[34] A brucellar abscess is far less common (0.2–1.6%). On ultrasound these appear as low reflective hepatic masses, with central areas of liquefaction and one or more areas of focal calcification (65% of reported cases).[35] A recent report describes its appearance on CEUS as a thick enhancing rim of inflammatory tissue surrounding a non-enhancing central area with subsequent washout.[35] These findings, however, are not totally specific and need to be combined with positive serology or blood cultures.

Amoebic abscess

Liver abscess is the commonest extraintestinal manifestation (1–25%) of infection by the protozoan parasite *Entamoeba histolytica*[36] and outside the Western world is far more common than bacterial sources of focal liver infection. Transmission is by the faecal–oral route, with ingestion of the cysts through contaminated food or water. These excystate in the small bowel to release the trophozoites that adhere to – and sometimes invade – the colonic mucosa.[37] Amoebic colitis may then develop, although infection can often be asymptomatic.[37] Invasion of the colonic mucosa into the mesenteric venules allows the amoebae to reach the liver via the portal vein, where they lodge in the peripheral capillaries leading to hepatocyte necrosis, with little leukocytic response or fibrotic reaction.[38] Abscess formation is most commonly seen in the posterior right hepatic lobe, typically measuring 4–10 cm in size although in 20–25% of cases they can be small and multiple.[38] For some unknown reason males are affected four times more frequently than females.[39]

Patients present with fever and right upper quadrant pain, but frequently lack any associated gastrointestinal symptoms (65–90%).[37] There is often a leukocytosis and serology for anti-amoebic antibodies will be positive in 70–80% in the acute phase, increasing to over 90% after a week and remaining positive long term in about 10%.[37] More recently introduced highly specific diagnostic tests involve the detection of protein antigens in serum or faeces using monoclonal antibodies.[40]

At ultrasound the typical described features of an amoebic abscess are[36,38,39,41]:

- an absence of significant wall echoes
- oval or round shape
- reduced reflectivity to background liver with fine internal echoes
- mild distal acoustic enhancement that increases with treatment
- subcapsular location.

All of these features may also be seen in pyogenic abscesses, however, and there is significant overlap. A blinded comparison between these two types of liver abscess found that a rounded shape and low reflectivity with fine internal echoes were features more prevalent in an amoebic abscess, yet this was not sufficient to make a distinction between the two (Fig. 9.13).[39] Ultrasound findings need to be combined with relevant clinical history and serological testing to reach the correct diagnosis. In about 5% of cases amoebic abscesses will be echogenic in appearance and can be mistaken for solid masses.[38] Other less typical findings are: thick echogenic walls which tend to resolve with treatment, mural nodules and septations.[36–39,41,42]

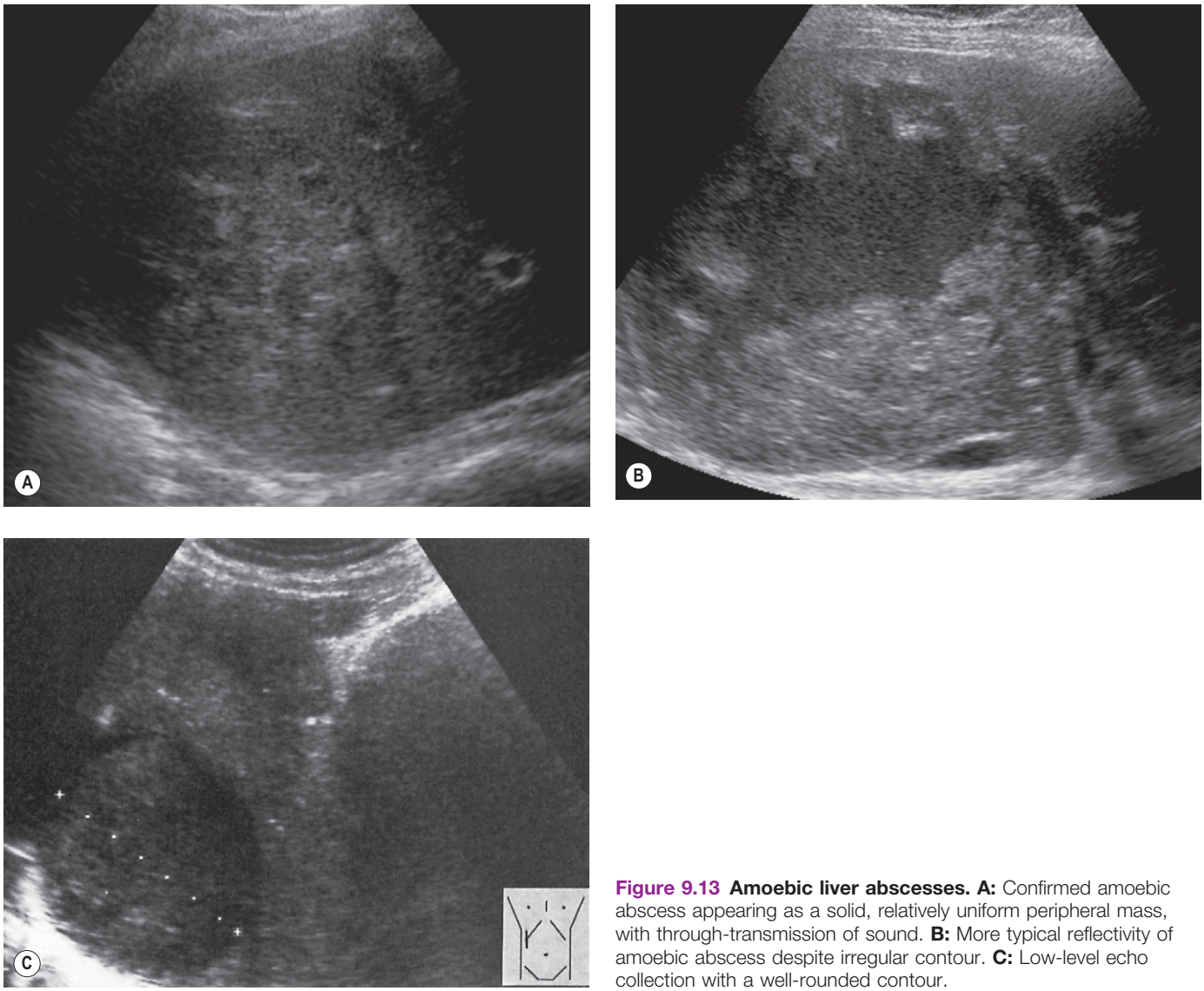


Figure 9.13 **Amoebic liver abscesses. A:** Confirmed amoebic abscess appearing as a solid, relatively uniform peripheral mass, with through-transmission of sound. **B:** More typical reflectivity of amoebic abscess despite irregular contour. **C:** Low-level echo collection with a well-rounded contour.

Following diagnosis and the commencement of appropriate antibiotic therapy, namely metronidazole, patient symptoms usually resolve rapidly over 48 hours, with the liver abscess tending to become more sonolucent and reducing in size.[38] For uncomplicated amoebic liver abscess there is no convincing evidence to support percutaneous aspiration or drainage over standard medical treatment.[43] There are, however, a limited number of indications for percutaneous drainage, namely: continuing diagnostic uncertainty, lack of response to drug therapy, a left lobe abscess close to the pericardium, or pregnancy.[42] Potential complications include rupture of the abscess into the pleural cavity, pericardium or peritoneal cavity or compression of the inferior vena cava.

With successful treatment the majority of abscesses disappear sonographically within 5–23 weeks. In a number of cases resolution of the abscess cavity may take over a year and in a minority of patients a residual focus resembling a hepatic cyst may persist (Fig. 9.14).[40]

FUNGAL INFECTION

Disseminated fungal infection involving the liver primarily affects patients with prolonged or recurrent neutropenia: in particular patients with leukaemia, patients undergoing chemotherapy for lymphoproliferative disorders and recipients of organ transplants. Systemic candidiasis is the commonest underlying organism and should be suspected in any patients with a resolving neutropenia and a fever unresponsive to antibiotic treatment. Other recognised hepatic fungal infections include cryptococcosis, histoplasmosis, murcomycosis and occasionally aspergillosis.

Candidiasis

Diagnosis of systemic candidiasis can be challenging. Targeted aspiration of the focal liver lesions may be falsely negative[44] or aspiration is contraindicated due to impaired coagulation. Imaging therefore plays a key diagnostic role, with MRI seen as the most sensitive modality for detection of focal fungal disease.[44] However, ultrasound is often used as the first-line investigation.

On ultrasound hepatic candidiasis has four described appearances, which are believed to relate both to the timing of the infection and to the extent of the patient's neutropenia.[45] In the absence of an inflammatory response there may be nothing focal to see. Type I is seen early in the disease and is described as a 'wheel within a wheel' appearance, with a low reflective or anechoic central nidus centred in an echogenic ring, surrounded by a low reflective halo. Histologically this has been shown to represent a central area of necrosis with fungal elements, surrounded by inflammatory cells and a ring of

fibrosis. Type II is the 'bull's eye' lesion, appearing later when the neutrophil count has recovered and measuring 1–4 cm in size. The echogenic centre with a low reflective halo can potentially mimic metastatic disease, but here the centre contains inflammatory cells (Fig. 9.15A, B). Type III is the most common appearance reported: seen with healing of the lesions, these uniformly hypoechoic nodules represent fibrosis. Type IV is echogenic foci, sometimes with acoustic shadowing representing focal calcification as a result of scarring.[44,46]

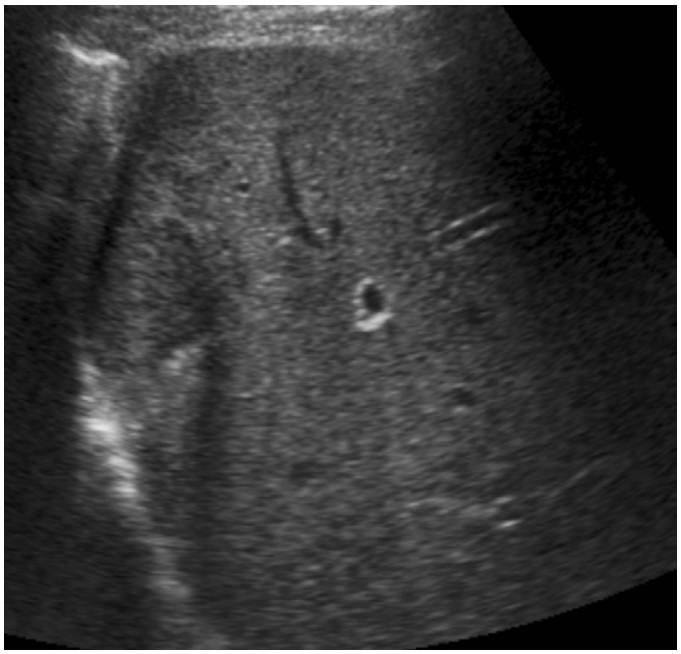


Figure 9.14 Resolving amoebic abscess. Four-month follow-up on patient seen in Figure 9.13A showing significant reduction in size of abscess cavity with more uniform, reduced reflectivity and through-transmission.

SCHISTOSOMIASIS

Schistosomiasis is one of the most common parasitic infections in humans, affecting around 200 million people worldwide. Hepatic/intestinal schistosomiasis is caused by the trematodes *Schistosoma mansoni*, *S. japonicum* and less commonly *S. mekongi* and *S. intercalatum*.[47] Infection occurs through contact with contaminated water, with the cercaria penetrating the skin/mucosa and migrating first to the lungs and then to the venules of the mesentery.[48] Here the mature flukes release eggs into the venules which enter the portal venous system, lodging in the periportal spaces and along the liver capsule. The resulting chronic granulomatous inflammation leads to periportal fibrosis – described by Symmers as 'clay-pipestem' – in the healing stage, with the development of portal hypertension without frank cirrhosis.[48,49]

In the acute stage of infection patients may complain of fever, itching and diarrhoea, with an eosinophilia found on full blood count and positive serology to schistosome antigen. There are no reliable imaging features at this stage, although low reflective nodules scattered throughout the liver of uncertain aetiology have been described.[50] The more chronic changes are somewhat dependent upon the trematode present:

- *Schistosoma mansoni* causes a more central periportal fibrosis, with marked echogenic thickening of the portal tracts (up to 2 cm) seen on ultrasound, predominantly around the porta hepatis. Left lobe hypertrophy, portal vein enlargement with venous collaterals, echogenic thickening of the gallbladder wall and splenomegaly are other typical findings (Fig. 9.16).[48,49]
- *Schistosoma japonicum* has a more peripheral pattern of portal tract fibrosis giving a reticular pattern/'fish-scale network' to the appearance of the liver on ultrasound, with relatively normal appearing parenchyma between these echogenic septa that extend out to a thickened liver capsule.[48,51] Doppler studies of the portal vein in these patients tend to be within normal limits.[51]

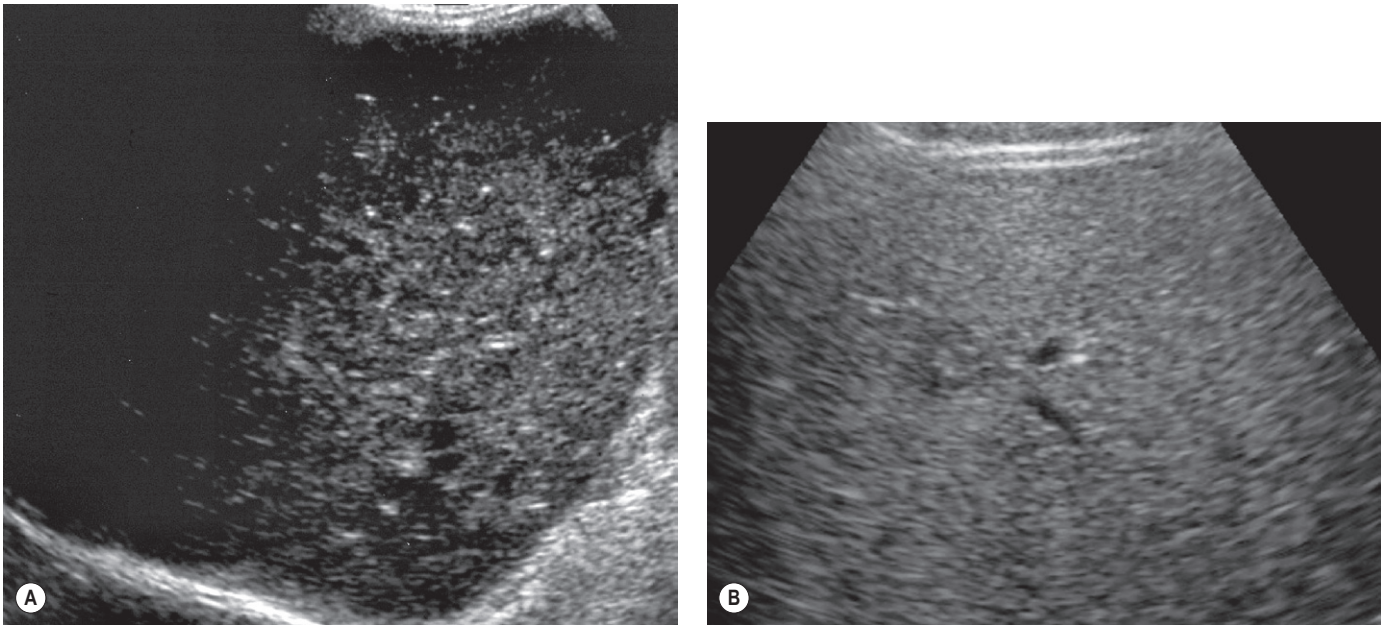


Figure 9.15 Hepatic candidiasis. A and B: Hepatic candidiasis in two immunocompromised patients, both showing a type II pattern, i.e. discrete low reflective focal lesions with an echogenic central nidus.

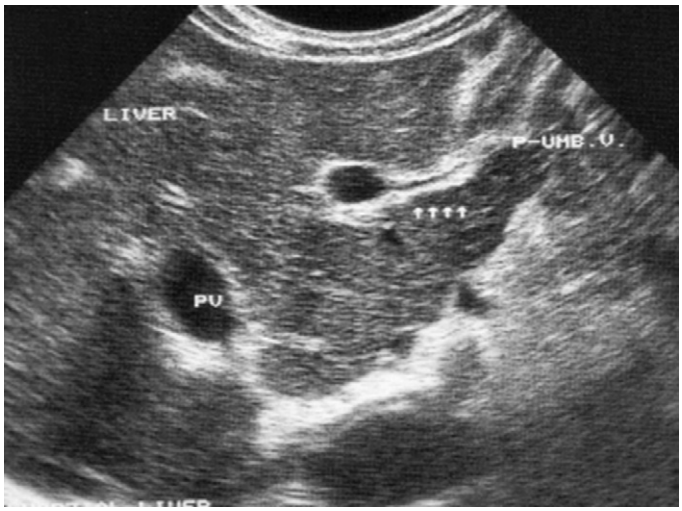


Figure 9.16 Periportal fibrosis seen with *schistosomiasis mansoni***.** Marked echogenic periportal thickening in a patient with schistosomiasis mansoni. (Courtesy of Dr N. Arafa.)

TOXOCARIASIS

Toxocariasis is caused by the human ingestion of eggs from the faeces of dogs and cats infected with the nematodes *Toxocara canis* and *T. catis*. The larvae are liberated in the intestine and burrow through the wall to reach the liver, but may migrate on to involve a number of organs. The migrating larvae stimulate a localised eosinophilic infiltration leading to granuloma or eosinophilic abscess formation.[52,53] On ultrasound the liver is seen to contain multiple oval shaped or elongated, low reflective lesions with poorly defined margins usually measuring <2 cm in size. Follow-up ultrasound may see resolution of these focal areas, or a change in location thought to indicate migration of the larvae.[54]

ECHINOCOCCAL INFECTION

Echinococcal cyst (hydatid disease)

There are two types of *Echinococcus* infection causing hydatid disease in humans. By far the most common is that by the larval stage of the cestode (tapeworm) *Echinococcus granulosus*, resulting in the formation of hydatid cysts in the liver or other organs.

Traditionally *E. granulosus* is prevalent in sheep- and cattle-raising countries, being endemic throughout the Middle East, South America, Australia and parts of the Mediterranean. Increasing travel and tourism, however, means it can now potentially be seen anywhere in the world.[55] The adult tapeworm usually resides in the intestine of dogs or another carnivore (the definitive host) and its eggs are excreted in their faeces. These are then ingested by the intermediate host, namely sheep, cattle, goats and sometimes humans. The eggs hatch in the intestine and the freed larvae permeate the intestinal mucosa to enter the portal venous system. The majority become trapped in the hepatic capillary system, where they either die or encyst and grow slowly (approximately 2–3 cm per year depending upon host immunity).[56] Some will, however, pass through the liver to reach the lungs and other organs.[55]

The right lobe of the liver is most commonly affected and the wall of the developing hydatid cyst is made of three layers: The outer pericyst represents the inflammatory response by the host and is predominantly dense connective tissue, sometimes containing biliary radicals: this will often partially calcify. The endocyst is the inner germinal layer; this gives rise to brood capsules which in turn form infectious scolices, both of which may precipitate within the cyst to form hydatid sand. Between these is a thin laminated acellular membranous layer known as the ectocyst that allows the passage of nutrients to the cyst. The cyst fluid is clear or pale yellow in colour, may contain scolices and is antigenic, with a risk of anaphylaxis if the cyst ruptures.[56] In certain circumstances, not clearly understood, daughter cysts develop within the mother cyst which are an exact replica of the mother cyst, but lack a pericyst.

At ultrasound hydatid cysts may be single or multiple and have a number of described appearances, largely dependent upon the stage of the disease[56,57]:

- Initially they can appear as simple cysts. Distinguishing features include a double linear echo to the cyst wall, fine echogenic debris (hydatid sand) within the cyst, which can be accentuated by moving the patient and there may be evidence of cyst wall calcification.
- A cyst showing detachment of the endocyst from the pericyst, which may be due to falling cyst pressure, host response, trauma or treatment. This results in the 'ultrasound water lily sign' seen as an undulating series of echogenic linear interfaces that appear to float in relatively anechoic fluid. Ultrasound is the most sensitive modality for the detection of membranes, septa and hydatid sand.
- Multivesicular cysts represent the presence of multiple daughter cysts, sometimes separated by echogenic matrix material (cyst fluid containing scolices, broken brood capsules). The appearance is a characteristic 'cartwheel' or 'honeycomb' cyst. Large amounts of matrix material can result in a pseudo-solid echogenic mass.
- Calcification of the cyst wall can be partial or complete and dense, with the latter producing a strong acoustic shadow. Partial calcification does not always indicate death of the cyst (Fig. 9.17).

Ultrasound has a >90% sensitivity for the diagnosis of hydatid cyst, based on its sonographic features, which can be confirmed on antibody titres to hydatid antigen using counter immunoelecrophoresis.[55]

The main complication of hepatic hydatid is cyst rupture (50–90%), which can be contained, communicating or direct. In contained rupture the endocyst ruptures, but the pericyst remains intact. The collapsed floating membranes are seen on ultrasound as serpiginous linear echoes: this may occur as a result of cyst degeneration, medical treatment or following trauma. Communicating rupture into the biliary system, via biliary radicles within the pericyst, can lead to cholangitis and death of the parasite due to an influx of bile into the cyst. Biliary obstruction is more often seen with a wide neck rupture into a main biliary branch due to the extrusion of daughter cysts, membrane debris and hydatid sand into the central bile ducts. The cyst becomes increasingly echogenic and layering of echogenic hydatid sand or linear membranous material has been described in the dilated biliary system, in up to 77% of cases. Biliary dilatation can sometimes be seen proximal to the cyst simply due to pressure effect rather than obstruction secondary to rupture. Direct rupture into the peritoneal cavity or transdiaphragmatic rupture into the pleural space can carry serious consequences, with seeding throughout the abdomen and a high risk of anaphylaxis.[58] Biliary–bronchial fistulas can sometimes arise when a transdiaphragmatic rupture involves the lung. In direct ruptures ultrasound can demonstrate the wall defect as well as track the passage of cyst content.

Cyst infection only occurs following rupture and can result in abscess formation, which on ultrasound is indistinct from other types of liver abscess, and may have a pseudo-solid appearance on ultrasound, with or without air–fluid levels.[56] Traditionally contrast-enhanced CT has been decreed as the investigation of choice to assess infection, yet there may now be a role for CEUS.

Medical treatment for hydatid with mebendazole or albendazole has a variable success rate and should be monitored with

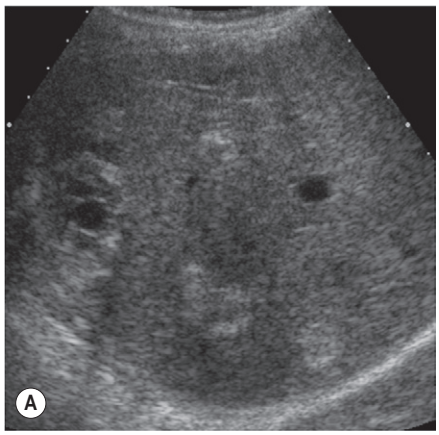
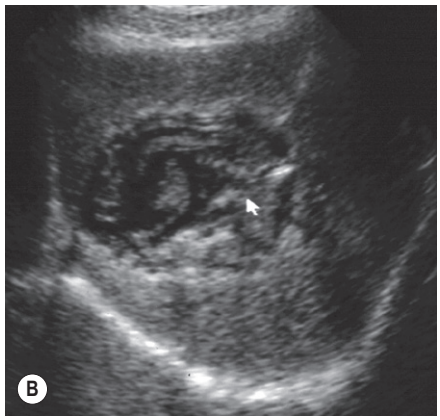
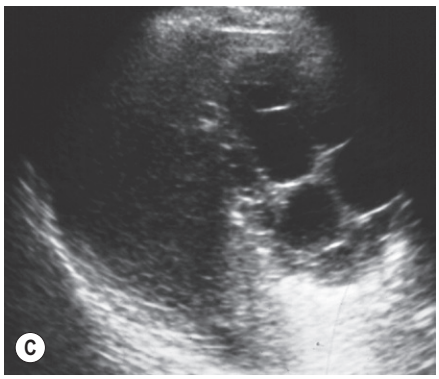




Figure 9.17 Various appearances of hydatid cyst. A: Multifocal hydatid cysts; some are seen as echogenic thick-walled structures. (Courtesy of Dr P. Sidhu.) **B:** Detachment of endocyst, with an undulating echogenic interface. **C:** Typical honeycomb appearance of daughter cysts, with echogenic content. (**B** and **C** courtesy of Dr M. Haddad.)

ultrasound. A good response is confirmed by a reduction in cyst dimensions, detachment of the endocyst from the pericyst, sometimes with the development of calcification, and an alteration in cyst content echotexture towards a more uniform echogenic 'pseudo-solid' lesion.[59] Doubts over its clinical efficacy, however, mean that medical treatment tends to be reserved for disseminated disease or cases where intervention/surgery is contraindicated.[55]

Although surgery is still seen by some groups as the definitive treatment for intrahepatic hydatid disease,[55] there is increasing evidence that percutaneous aspiration/drainage procedures are not only safe but offer a highly effective treatment alternative. The technique known as PAIR (percutaneous aspiration injection and re-aspiration) involves the insertion of a fine needle (e.g.19G) into the hydatid cyst under ultrasound guidance followed by the aspiration of half the cyst volume. Hypertonic saline is then injected into the cyst, left for a period and then the entire cyst content is aspirated.[60] A variation of this technique describes repeated injection and aspiration until the endocyst is seen to separate from the pericyst on ultrasound.[61] For larger cysts (>6 cm) a drainage catheter is inserted at the end of the procedure and left in situ for 24 hours. Other groups have tried injecting alcohol as a scolicidal agent with good results (Fig. 9.18A, B),[62] although care must be taken to ensure there is no fistulous communication with the biliary tree. The reported complication rate for this procedure is around 8%, with liver abscess formation being the most significant. The concern over severe anaphylaxis from leakage of cyst content would appear to be unjustified, but prophylactic mebendazole is often administered to reduce the risk of dissemination. Following successful treatment ultrasound shows a gradual reduction in cyst size, eventually concluding with a small residual cyst, an echogenic focus in the liver parenchyma or complete resolution[62] (Fig. 9.19). Persistence of a round anechoic cyst is seen as an indication of treatment failure.

Hepatic alveolar echinococcosis

Hepatic alveolar echinococcosis (HAE) is a rare disease caused by larvae of *Echinococcus multilocularis*, which behaves in a very different way from the more common hydatid disease. The primary host is the fox, with humans becoming infected either through direct contact or indirectly from contaminated water of plant life in the wild. It is endemic in parts of the USA, Canada, Japan and Central Europe.[63]

The liver is involved in 90% of infections, with *E. multilocularis* producing multiple alveolar cysts, each containing a germinal layer, that grow by exogenous proliferation, aggressively invading host tissue. As the multicystic masses expand they are highly prone to central necrosis, leaving a surround of viable metacestoidal vesicles.

At ultrasound the typical described finding is a 'hailstorm' pattern made up of multiple poorly defined echogenic nodules due to numerous cyst wall interfaces and microcalcification, interspaced by areas of necrosis.[64] Large areas of central necrosis appear similar to pyogenic abscesses although they tend to have thick, irregular, echogenic margins. With progressive disease, coarse peripheral calcification can be seen to surround areas of necrosis. The latter can mimic a calcified liver cyst, and if suspected, serology for HAE antibodies can help make the distinction.

Complications from HAE arise from hilar infiltration of the biliary tree, leading to intrahepatic duct dilatation, and invasion of the portal and hepatic veins resulting in ischaemic atrophy of liver segments, both of which can be identified at ultrasound.

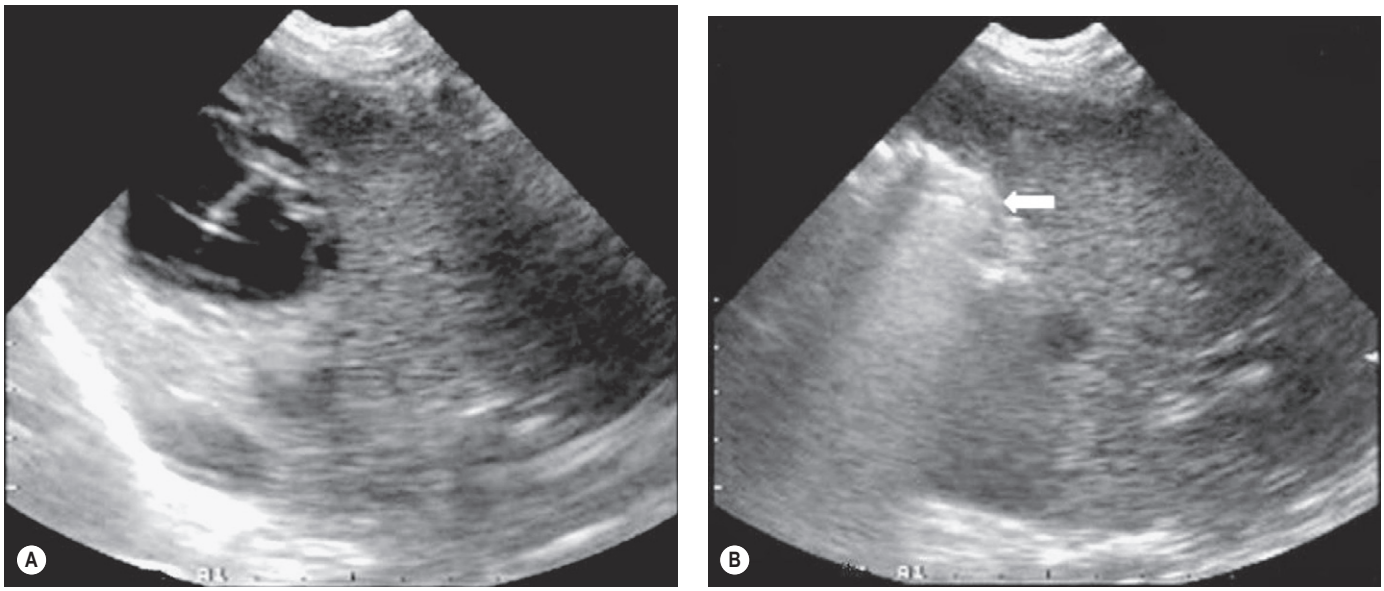


Figure 9.18 Ethanol injection of hydatid. A: Ultrasound-guided needle puncture of a hydatid cyst. **B:** Following aspiration of cyst content, 95% alcohol is injected into the cyst cavity causing a strongly echogenic focus (arrow). (From Giorgio A et al. Clinical and sonographic management of viable hydatid liver cysts. Journal of Ultrasound 2008;11:107–112.)



Figure 9.19 Old hydatid. Calcified rounded focus in the right lobe of the liver, in a patient previously treated for hydatid.

ACUTE FASCIOLIASIS

Fasciola hepatica is a trematode that commonly infests sheep or cattle. Human infestation occurs through the consumption of contaminated aquatic vegetables and has an acute, latent and chronic phase. In the acute phase the larvae penetrate the small intestine entering the peritoneal cavity and then pass through Glisson's capsule to migrate through the liver towards the bile ducts. Patients typically experience fever, upper abdominal pain and have a marked eosinophilia. Anti-fluke antibody serology becomes positive in the first few weeks of infection, with the detection of eggs in stool samples occurring a few months later.[65] In the acute phase liver ultrasound findings can be variable, but may show low reflective tunnel-like branching lesions in a subcapsular distribution caused by the parasites' migration through the liver.[66] More commonly the pattern is of rounded or nodular lesions of varying reflectivity and size, but again tending to a peripheral location in the liver, occurring more frequently in the right lobe.[66] In the chronic phase the ultrasound findings reflect the biliary involvement and can mimic sclerosing cholangitis.

INFLAMMATORY PSEUDO-TUMOUR

Inflammatory pseudo-tumour (IPT) of the liver is a rare condition of uncertain aetiology producing a chronic inflammatory mass in the liver consisting of collagenous tissue infiltrated with plasma cells and other inflammatory cells. More common in young men, it tends to present with fever, weight loss, abdominal pain and general malaise.[67] Although the imaging findings can be concerning, the prognosis for IPT is good and therefore needs to be considered, to avoid unnecessary surgical intervention.

At ultrasound the findings can be concerning, with a well or poorly defined mass of either increased or decreased reflectivity, sometimes showing through-transmission of sound. CEUS gives a variable pattern, with either increased or reduced enhancement in the arterial phase, but all lesions showing reduced enhancement during the portal venous phase, suspicious for a malignant focal liver lesion.[27] CT or MRI may demonstrate a delayed enhancement pattern suggestive of IPT.[68]

HIV/AIDS

Throughout the clinical course of the human immunodeficiency virus, from the initial infection through to early symptomatic disease and finally late stage AIDS, the liver is affected by a wide range of pathologies and frequently appears abnormal on ultrasound examination. At the time of primary infection the liver may show features of associated infections, namely acute or chronic

Table 9.3 Focal liver lesions in HIV/AIDS patients

Infective: Tuberculoma
Mycobacterium avium complex (rare)
CMV
Toxoplasmosis
Metabolic: Focal fatty infiltration
Vascular: Peliosis hepatis
Malignant: Lymphoma
Kaposi's sarcoma
Spindle cell tumour
Hepatocellular carcinoma
Drug reaction: Trimethoprim/sulfamethoxazole

active viral hepatitis. As the disease evolves, hepatomegaly is the commonest finding, often with fatty infiltration, of variable aetiology, but often due to patient malnutrition. When the absolute CD4+ lymphocyte count begins to fall, bacterial infections including *Mycobacterium tuberculosis* may be seen, the latter producing a granulomatous hepatitis. Increasing immune compromise sees the occurrence of diffuse fungal infections leading to multiple hepatic micro-abscesses. At the end stage of the disease, infection with *Mycobacterium avium* complex and/or cytomegalovirus becomes commonplace.

In addition to infections, drug reactions may cause fatty infiltration of the liver or a granulomatous hepatitis and focal liver lesions can arise from AIDS-associated tumours (Table 9.3).

Pneumocystis carinii

Prior to the HIV epidemic in the 1980s pneumonic infection with the unicellular fungus *Pneumocystis carinii* (now called *Pneumocystis jiroveci*) was uncommon and extrapulmonary *P. carinii* was extremely rare. During the 1980s *P. carinii* pneumonia (PCP) rapidly became recognised as an AIDS-defining illness and remains the most common opportunistic infection in HIV patients today. Other patients at risk of *P. carinii* infection include those with a primary immune deficiency syndrome, patients on immune suppression for solid organ or bone marrow transplant, haematological malignancies and those suffering severe malnutrition.

Extrapulmonary *P. carinii* was increasingly reported in the early 1990s in HIV patients, with some series linking it to the use of aerosolised pentamidine as a prophylaxis against PCP. Since the move to systemic prophylaxis, there has been a significant reduction in the number of cases, although it is still reported.[69] It can affect numerous organ sites simultaneously – liver, spleen, renal cortex, thyroid, pancreas – and when associated with HIV infection tends to present with clinical symptoms relating to the affected organ.[69]

On ultrasound hepatic involvement is seen as multiple tiny non-shadowing strongly echogenic foci diffusely dispersed throughout the liver. This strongly reflective interface may be caused by the fibrinous exudate seen on histology surrounding the pneumocystis.[70] Larger echogenic clumps with acoustic shadowing representing calcific foci are seen later in the infection and can also be demonstrated on CT.[71] Although highly characteristic, this sonographic pattern has a recognised differential including hepatic infection by *Mycobacterium avium-intracellulare* and cytomegalovirus.[72]

Mycobacterium avium complex

Mycobacterium avium complex is the commonest opportunistic infection found at liver biopsy in HIV patients, when it is usually widely disseminated throughout the abdomen. Liver function tests are often abnormal, in particular the alkaline phosphatase, probably due to granulomatous obstruction of the biliary radicals.[72] The commonest described finding on ultrasound is hepatomegaly, often with diffuse increased reflectivity as a result of fatty infiltration, most likely a reflection of the underlying HIV virus.[73] Multifocal pinpoint echoes, identical to those seen in extrapulmonary PCP infection, have been described in a number of cases.[74]

Table 9.4 Causes of granulomatous hepatitis

Bacterial: *Mycobacterium*
Brucellosis
Actinomycosis
Q fever
Fungal: Histoplasmosis
Blastomycosis
Cryptococcosis
Parasitic: Schistosomiasis
Toxoplasmosis
Viral: Infectious mononucleosis
Cytomegalovirus
Drugs: Allopurinol
Phenytoin
Idiopathic: Sarcoid

Cytomegalovirus

Cytomegalovirus (CMV) infection of the gastrointestinal tract is a relatively common infection in patients with AIDS. CMV hepatitis, however, is much less common, affecting around 5% of patients,[75] and often coexisting with other opportunistic infections such as cryptosporidia. Findings at ultrasound may be totally non-specific, with simply a heterogeneous echotexture and mild hepatomegaly. Multifocal echogenic nodules mimicking haemangiomas or echogenic metastases have, however, been described. Histologically these represent areas of focal fatty infiltration, with an inflammatory cell infiltrate and intranuclear CMV inclusions.[76]

GRANULOMATOUS HEPATITIS

Granulomatous hepatitis is not a distinct disease but a pathological reaction from a number of stimuli (Table 9.4). Histologically it is characterised by the accumulation of epithelioid macrophages and histiocytes, typically surrounded by small lymphocytes, with the former coalescing to form multinucleated giant cells. The granulomas themselves tend not to incite hepatocellular dysfunction, unless they are part of a more widespread inflammatory process and therefore the clinical presentation is very much dependent on the underlying cause. There may be no signs of primary liver disease, hepatomegaly is often absent or mild and the liver function tests are usually only mildly deranged. Although liver biopsy may provide histological evidence for a specific aetiology, the appearance is frequently non-specific and in case series a significant percentage remain labelled as idiopathic.[77]

At ultrasound hepatic granulomas have been identified as discrete echogenic nodules of 3–5 mm with a low reflective halo[78] or hypoechoic nodules of varying size (usually <10 mm) and shape.[32,79] Both of these patterns can potentially be mistaken for metastatic liver disease.

Sarcoid

Hepatosplenic involvement is frequently seen in systemic sarcoidosis (50–70%), but is usually clinically silent. On the whole liver ultrasound is usually unhelpful or non-specific, with hepatomegaly, increased parenchymal reflectivity, coarsening of the parenchymal echotexture and focal calcifications reported as findings.[80] If focal nodules are seen, these are either low reflective or demonstrate mixed reflectivity, measuring between 0.5–1.5 cm (Fig. 9.20). On CEUS it would seem that these focal granulomatous nodules do not enhance[81] (Fig. 9.21).

Tuberculosis

Liver involvement in tuberculosis is categorised as either miliary, local or biliary. Hepatic involvement in diffuse miliary tuberculosis is reported to be >80%. However, the fine miliary pattern is not



Figure 9.20 Diffuse sarcoid liver. Multiple low reflective nodules on a background of a mildly coarsened liver parenchyma, in a patient with known sarcoidosis.

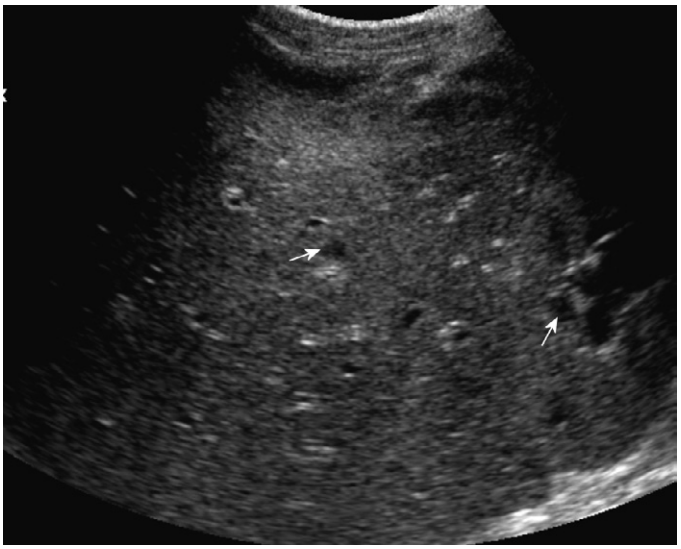


Figure 9.22 Small hepatic tuberculomas. Small multifocal low reflective lesions (arrows) in the liver in a patient with HIV and confirmed tuberculosis.

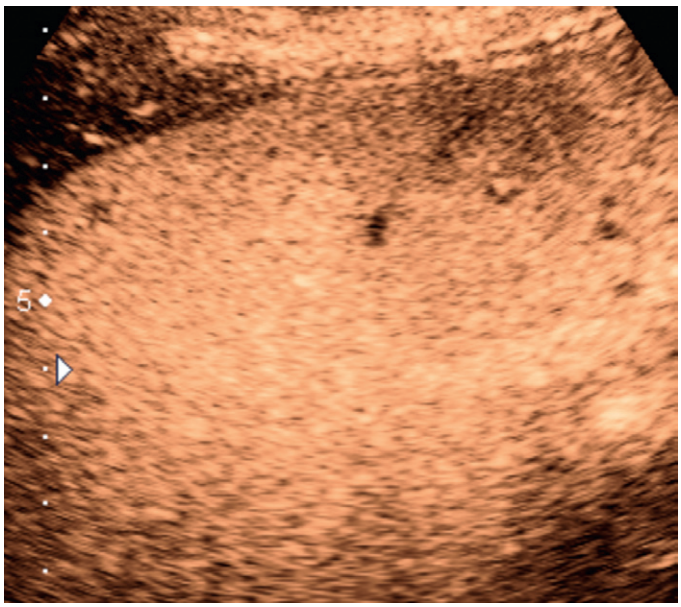


Figure 9.21 Post-contrast sarcoid. Contrast ultrasound in a patient with known sarcoid and multiple poorly defined, mildly echogenic nodules which are seen as non-enhancing foci.

usually resolvable on imaging and hepatomegaly is usually the only ultrasound finding, with or without a heterogeneous parenchymal texture.

Local nodular hepatic disease without pulmonary tuberculosis is relatively rare, but is more often seen in immunocompromised individuals, especially HIV patients. It has a non-specific presentation with fever, abdominal pain, weight loss, and variable liver biochemistry.[82] Ultrasound may show multiple low reflective nodules (0.5–2 cm) scattered throughout the liver, which can easily be mistaken for metastatic disease (Fig. 9.22).[83] Occasionally the nodules can be echogenic, some showing partial calcification, and there may also be coexisting portal and retroperitoneal lymphadenopathy. With CEUS focal tuberculomas show arterial phase enhancement, with subsequent washout in the portal venous and parenchymal phase, again unfortunately mimicking liver malignancy[81] (Fig. 9.23A, B). Occasionally hepatic tuberculomas are limited in number but are significantly larger in size. Sonographically macronodular disease appears as either low reflective or echogenic focal masses, sometimes demonstrating acoustic shadowing due to partial calcification.[84] As with nodular disease, there is a differential for this appearance, but additional ultrasound findings such as ascites, lymphadenopathy and coexisting splenic lesions may help make the distinction.

Rarely primary infection of the liver results in an isolated tuberculous abscess, which can easily be mistaken for a pyogenic abscess or primary liver tumour. The two described patterns at ultrasound are: poorly defined low reflective masses, made up of coalescing tubercles, or a low reflective mass with an echogenic halo. More complex mass-like structures have also been described. Diagnostic aspiration can be guided by ultrasound and some groups have advocated percutaneous drainage of these abscesses combined with quadruple therapy.

CHRONIC GRANULOMATOUS DISEASE

Chronic granulomatous disease is a group of familial disorders resulting in a congenital defect in neutrophil function rendering them unable to destroy certain phagocytosed bacteria. Children with this condition suffer recurrent infections and granuloma formation in various organs, including the liver. On ultrasound multiple poorly defined low reflective lesions, with no through-transmission of sound, are seen within the liver representing clumps of granulomatous tissue. Focal pyogenic abscesses or fungal micro-abscesses may also be seen.[85]

CAT SCRATCH FEVER

The Gram-negative bacillus *Bartonella hensellae* typically causes a localised lymphadenitis proximal to its inoculation site: usually the result of a cat scratch. In 5–10%, however, a disseminated infection

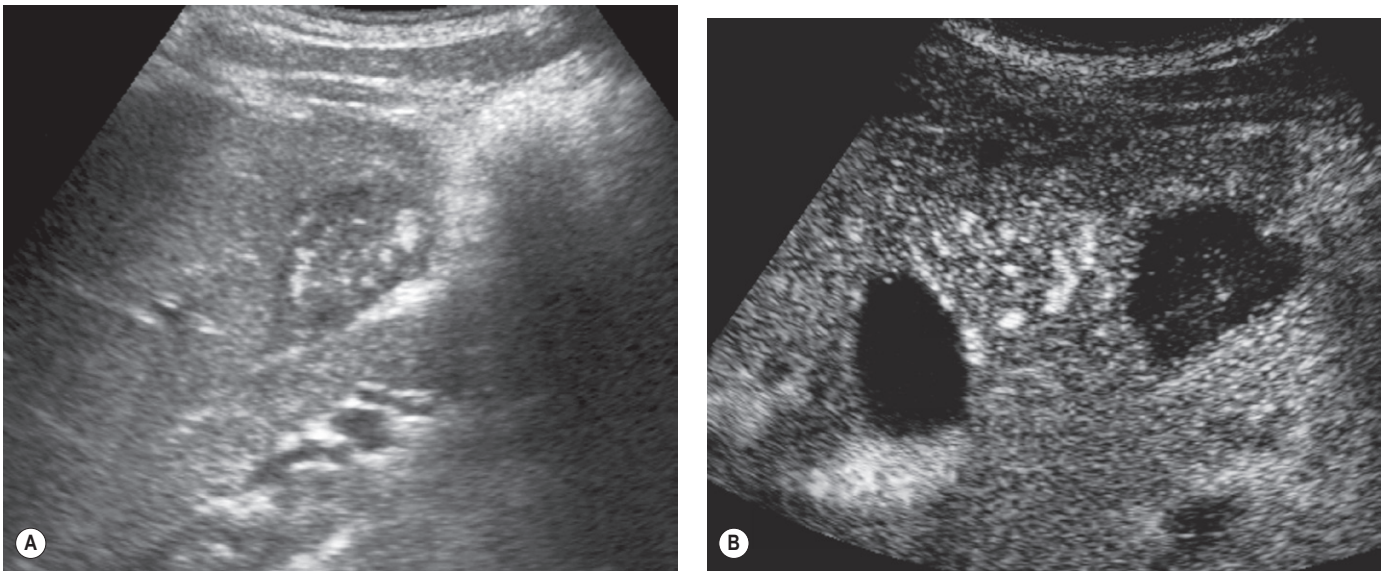


Figure 9.23 Large tuberculoma pre- and post-contrast scan. A: Left lobe 3 cm heterogeneous mass in a patient with confirmed hepatic tuberculosis. **B:** Post contrast there was no convincing enhancement even in the arterial phase.

can occur with the development of multiple necrotising hepatic granulomas appearing as well or poorly defined low reflective or heterogeneous nodules on ultrasound.[86] Peliosis hepatis can also found in the liver with this infection and its appearance on ultrasound has been covered in Chapters 10 and 12.

HYPEREOSINOPHILIC SYNDROME

Hypereosinophilic syndrome is a group of related conditions varying from a localised benign form (Loeffler syndrome), to a disseminated form producing a marked eosinophilic leukocytosis and organ dysfunction as a result of infiltration by mature eosinophils.[87] The latter condition typically affects middle-aged men, and is characterised by a persistent eosinophilia in the absence of parasitic infection or allergy. A number of organ systems are involved, most importantly the heart and nervous system, with periportal infiltration of the liver seen in 50–90% of cases.[88,89]

At ultrasound three patterns of hepatic involvement have been described[87–89]:

1. Multiple rounded/oval low reflective foci measuring 1–2 cm scattered throughout the liver. These often have poorly defined margins and can sometimes fluctuate in location.
2. One or two larger (3–4 cm) low-reflective, geographic shaped, masses: both this and the above pattern can be mistaken for metastatic disease and may require biopsy.
3. Diffuse hepatomegaly with a non-specific coarsened echotexture.

With the focal infiltrative patterns, the number of lesions and extent of liver involvement seen, both on CT and ultrasound, appears to correspond to the degree of eosinophilia.[88,89] Resolution or reduction in size and number of these nodules occurs with corticosteroid and antihistamine treatment.

HEPATIC CALCIFICATION

The incidental finding of hepatic parenchymal calcification on ultrasound is relatively uncommon, yet it has a wide variety of causes (Table 9.5): most commonly calcified granulomas and hydatid cysts followed by calcification associated with hepatic neoplasms.[90] In general hepatic calcification appears as elsewhere on ultrasound, with a strong reflection and a variable straight-edged acoustic shadow: the latter can be enhanced by scanning with a higher-frequency probe . The size and the morphology may offer some indication as to the aetiology, with curvilinear echoes suggesting a cyst wall, dense nodular masses seen in granulomas and amorphous type calcification often found within soft tissue tumours (Fig. 9.24). Sometimes a distinction needs to be made between calcification from other sources, namely vascular calcification and intrahepatic ductal calculi, the latter may be associated with bile duct dilatation. CT may be required on occasion to assess large, densely calcified masses.

In a large number of cases parenchymal calcification can be taken to represent a sign of decreased disease activity or a residual of previous treatment, but careful scrutiny is required if there is any associated soft tissue component or in the case of hydatid, where partial calcification can be seen with ongoing parasitic infection.[91]

Table 9.5 Causes of hepatic calcification

Infections:	**Malignant:**
Tuberculosis	Fibrolamellar carcinoma
Histoplasmosis	Hepatocellular carcinoma
Brucellosis	Cholangiocarcinoma
Old calcified abscess	Hepatoblastoma
Vascular:	**Metastases:**
Haematoma	Mucinous carcinomas
Portal vein thrombosis	Melanoma
Aneurysm	Thyroid
Benign tumour:	Osteosarcoma
Haemangioma (rare)	Carcinoid
Adenoma	**Biliary:**
Regenerating nodule	Calculus (usually not calcified)
Cyst	Ascariasis, clonorchiasis

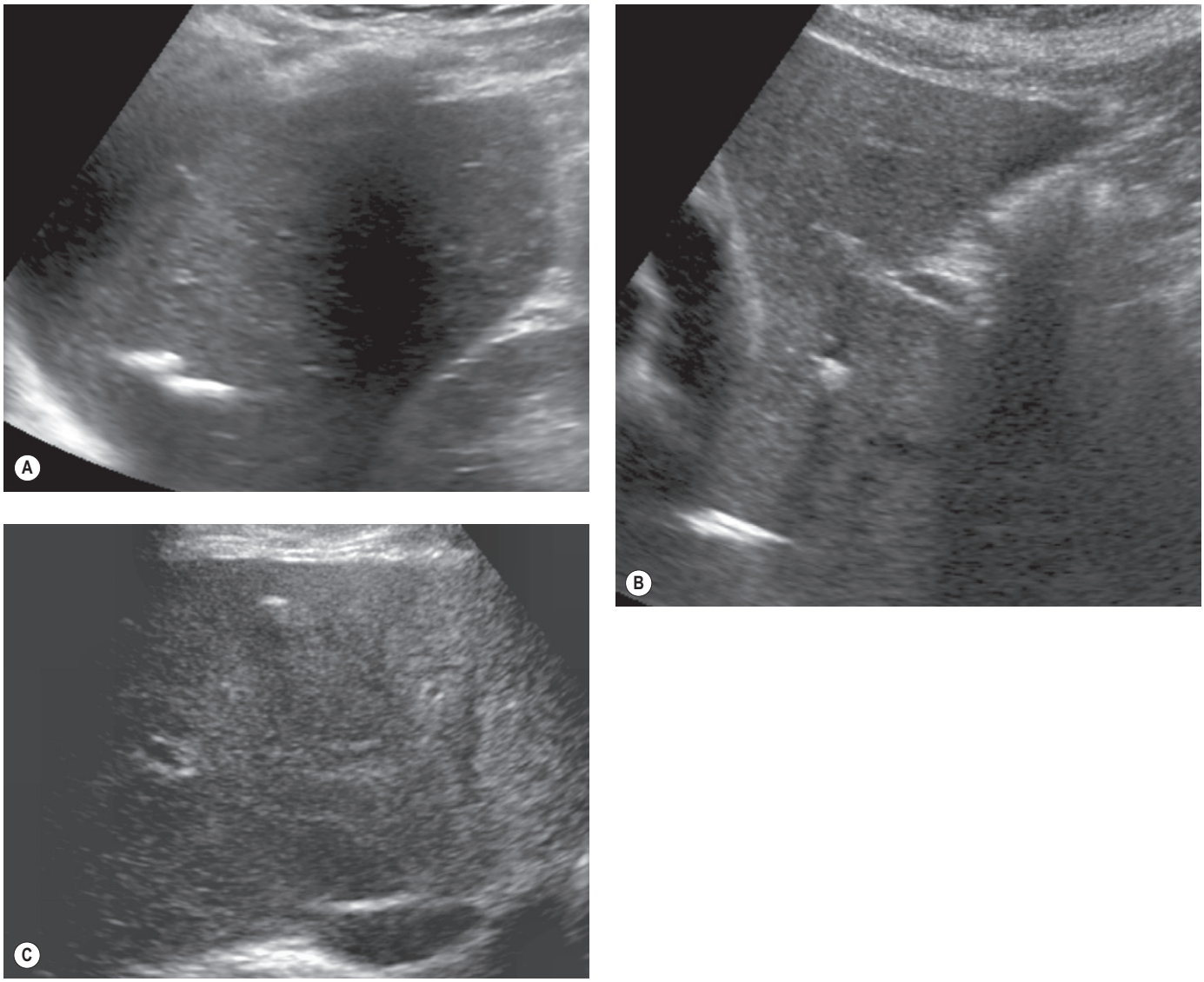


Figure 9.24 **Examples of incidental hepatic calcification,** with varying degrees of acoustic shadowing. The linear calcification in **A** was thought to be a result of previous trauma, while in **B** and **C** the most likely cause is granulomatous.

REFERENCES

1. Mortele KJ, Segatto E, Ros PR. The infected liver: radiologic-pathologic correlation. Radiographics 2004;24:937–955.
2. Bain VG, Ma M. Acute viral hepatitis. In: Thomson ABR, Shaffer EA, eds. first principles of gastroenterology: the basis of disease and an approach to management. 3rd edn. Toronto: Astra Pharma; 1997:479–491.
3. Kurtz AB, Rubin CS, Cooper HC, et al. Ultrasound findings in hepatitis. Radiology 1980;136:717–723.
4. Giorgio A, Amoroso P, P. Fico P, et al. Ultrasound evaluation of uncomplicated and complicated acute viral hepatitis. J Clin Ultrasound 1986;14:675–679.
5. Jüttner HU, Ralls PW, Quinn MF, Jenney JM. Thickening of the gallbladder wall in acute hepatitis: ultrasound demonstration. Radiology 1982;142:465–466.
6. Kim MY, Baik SK, Choi YJ, et al. Endoscopic sonographic evaluation of the thickened gallbladder wall in patients with acute hepatitis. J Clin Ultrasound 2003;31:245–249.
7. Ceccanti M, Attili A, Balducci G, et al. Acute alcoholic hepatitis. J Clin Gastroenterol 2006;40:833–841.
8. Taylor KJW, Gorelick FS, Rosenfield AT, Riely C. Ultrasonography of alcoholic liver disease with histological correlation. Radiology 1981;141:157–161.
9. Sumino Y, Kravetz D, Kanel GC, et al. Ultrasonographic diagnosis of acute alcoholic hepatitis 'pseudoparallel channel sign' of intrahepatic artery dilatation. Gastroenterology 1993;105:1477–1482.
10. Han SH, Rice S, Cohen SM, et al. Duplex Doppler ultrasound of the hepatic artery in patients with acute alcoholic hepatitis. J Clin Gastroenterol 2002;34:573–577.
11. Bain VG, Ma M. Chronic hepatitis. In: Thomson ABR, Shaffer EA, eds. First principles of gastroenterology: the basis of disease and an approach to management. 3rd ed. Toronto: Astra Pharma; 1997:492–502.
12. Hirche TO, Ignee A, Hirche H, et al. Evaluation of hepatic steatosis by ultrasound in patients with chronic hepatitis C virus infection. Liver Int 2007;27:748–757.
13. Grier S, Lim AK, Patel N, et al. Role of microbubble ultrasound contrast agents in the non-invasive assessment of chronic hepatitis C-related liver disease. World J Gastroenterol 2006;12:3461–3465.
14. Lee KT, Wong SR, Sheen PC. Pyogenic liver abscess: an audit of 10 years' experience and an analysis of risk factors. Dig Surg 2000;18:459–466.
15. Rhim H, Dodd GD 3rd, Chintapalli KN, et al. Radiofrequency thermal ablation of abdominal tumors: lessons learned from complications. Radiographics 2004;24:41–52.
16. Yu SCH, Lo RHG, Kan PS, Metreweli C. Pyogenic liver abscess: treatment with needle aspiration. Clin Radiol 1997;52:912–916.

17. Lederman ER, Crum NF. Pyogenic liver abscess with a focus on *Klebsiella pneumoniae* as a primary pathogen: an emerging disease with unique clinical characteristics. Am J Gastroenterol 2005;100:330–332.
18. Rahimian J, Wilson T, Oram V, Holzman RS. Pyogenic liver abscess: recent trends in etiology and mortality. Clin Infect Dis 2004;39:1654–1659.
19. Wang JH, Liu YC, Lee SS, et al. Primary liver abscess due to *Klebsiella pneumoniae* in Taiwan. Clin Infect Dis 1998;26:1434–1438.
20. Cheng DL, Liu YC, Yen MY, et al. Pyogenic liver abscess: clinical manifestations and value of percutaneous catheter drainage treatment. J Formos Med Assoc 1990;89:571–576.
21. Yu SC, Ho SS, Lau WY, et al. Treatment of pyogenic liver abscess: prospective randomized comparison of catheter drainage and needle aspiration. Hepatology 2004;39:932–938
22. Terrier F, Backer CD, Triller JK. Morphologic aspects of hepatic abscesses at computed tomography and ultrasound. Acta Radiol 1983;24:129–137.
23. Kuligowska E, Connors SK, Shapiro JH. Liver abscess: sonography in diagnosis and treatment. AJR Am J Roentgenol 1982;138:253–257.
24. Hui JY, Yang MK, Cho DH, et al. Pyogenic liver abscesses caused by *Klebsiella pneumoniae:* US appearance and aspiration findings. Radiology 2007;242:769–776.
25. Verbanck J, Ponette J, Verbanck M, et al. Sonographic detection of multiple Staphylococcus aureus hepatic microabscesses mimicking Candida abscesses. J Clin Ultrasound 1999;27:478–481.
26. Vassiliades VG, Bree RL, Korobkin M. Focal and diffuse benign hepatic disease: correlative imaging. Semin Ultrasound CT MR 1992;13:313–335.
27. Liu GJ, Lu MD, Xie XY, et al. Real-time contrast-enhanced ultrasound imaging of infected focal liver lesions. J Ultrasound Med 2008;27:657–666.
28. Giorgio A, Stefano G, Di Sarno A, et al. Percutaneous needle aspiration of multiple pyogenic abscesses of the liver: 13-year single-centre experience. AJR Am J Roentgenol 2006;187: 1585–1590.
29. Ch Yu S, Hg Lo R, Kan PS, Metreweli C. Pyogenic liver abscess: treatment with needle aspiration. Clin Radiol 1997;52:912–916.
30. Zerem E, Hadzic A. Sonographically guided percutaneous catheter drainage versus needle aspiration in the management of pyogenic liver abscess. AJR Am J Roentgenol 2007;189:W138–W142.
31. Rajak CL, Gupta S, Jain S, et al. Percutaneous treatment of liver abscess: needle aspiration versus catheter drainage. AJR Am J Roentgenol 1998;170:1035–1039.
32. Thomas J, Turner SR, Nelson RC, Paulson EK. Postprocedure sepsis in image guided percutaneous hepatic abscess drainage: how often does it occur? AJR Am J Roentgenol 2006;186:1419–1422.
33. Sudhamshu KC, Sharma D. Long-term follow-up of pyogenic liver abscess by ultrasound. Eur J Radiol 2009; doi:10.1016/j. ejrad.2009.01.017.
34. Pappas G, Akritidis N, Bosilkovski M, Tsianos E. Brucellosis. N Engl J Med 2005;352:2325–2336.
35. Meloni MF, Andreano A, Laeseke PF, et al. Contrast-enhanced ultrasonographic findings in a Brucellar hepatic abscess. J Ultrasound Med 2008;27:1511–1515.
36. Ralls PW, Colletti PM, Quinn MF, Halls J. Sonographic findings in hepatic amebic abscess. Radiology 1982;145:123–126.
37. Haque R, Huston CD, Hughes M, et al. Amebiasis. N Engl J Med 2003;348:1565–1573.
38. Stoopen ME, Kimura-Fujikami K, Quiroz y Ferrari FA, Barios-Boullard V. Ultrasound imaging of hepatic amebic abscess. Ultrasound Q 1999;15:189–200.
39. Shamsi K, De Schepper A, Deckers F, et al. Role of ultrasound in the diagnosis and treatment follow-up of amoebic abscess. Eur Radiol 1993;3:434–438.
40. Sharma MP, Ahuja V. Amoebic liver abscess. JIACM 2003;4:107–111.
41. Ralls PW, Barnes PF, Radin DR, et al. Sonographic features of amebic and pyogenic liver abscesses: a blinded comparison. AJR Am J Roentgenol 1987;149:499–501.
42. Berry M, Bazaz R, Bhargava S. Amebic liver abscess: sonographic diagnosis and management. J Clin Ultrasound 1986;14:239.
43. Chavez-Tapia NC, Hernandez-Calleros J, Tellez-Avila FI, et al. Image-guided percutaneous procedure plus metronidazole versus metronidazole alone for uncomplicated amoebic liver abscess. Cochrane Database of Systematic Reviews 2009, Issue 1. Art. No.: CD004886. DOI: 10.1002/14651858.CD004886.pub2.
44. Semelka RC, Kelekis NL, Sallah S, et al. Hepatosplenic fungal disease: diagnostic accuracy and spectrum of appearances on MR imaging. AJR Am J Roentgenol 1997;169:1311–1316.
45. Pastakia B, Shawker TH, Thaler M, et al. Hepatosplenic candidiasis: wheels within wheels. Radiology 1988;166:417–421
46. Miller JH, Greenfield LD, Wald BR. Candidiasis of the liver and spleen in childhood. Radiology 1982;142:375–380.
47. Chiavaroli R, Grima P, Grima P. Detection of early liver fibrosis in patients with intestinal schistosomiasis: sonographic and histologic findings in Schistosoma mansoni infection. Infection 2008;36:585–589.
48. Manzella A, Ohtomo K, Monzawa S, Lim JH. Schistosomiasis of the liver. Abdom Imaging 2008;33:144–150.
49. Cerri GG, Alves VAF, Magalhaes A. Hepatosplenic schistosomiasis mansoni: ultrasound manifestations. Radiology 1984;153:777–780.
50. Cesmeli E, Vogelaers D, Voet D, et al. Br J Radiol 1997;70:758–760.
51. Chou Y-H, Chiou H-J, Tiu C-M, et al. Duplex Doppler ultrasound of hepatic schistosomiasis japonica: a study of 47 patients. Am J Trop Med Hyg 2003;68:18–23.
52. Clarke HM, Hinde FRJ, Manns RA. Case report: hepatic ultrasound findings in a case of toxacariasis. Clin Radiol 1992;45:135–136.
53. Chan S, Lim JH, Choi D, et al. Hepatic visceral larva migrans of Toxocara canis: CT and sonographic findings. AJR Am J Roentgenol 2006;187:W622–W629.
54. Lim JH. Toxocariasis of the liver: visceral larvae migrans. Abdom Imaging 2007;33:151–156.
55. Safioleas MC, Misiakos EP, Kouvaraki M, et al. Hydatid disease of the liver. A continuing surgical problem. Arch Surg 2006;141: 1101–1108.
56. Pedrosa I, Saiz A, Arrazola J, et al. Hydatid disease: radiologic and pathologic features and complications. Radiographics 2000;20: 795–817.
57. Lewall DB, McCorkell SJ. Hepatic echinococcal cysts: sonographic appearances and classification. Radiology 1985;155:773–775.
58. Lewall DB. Hydatid disease: biology, pathology, imaging and classification. Clin Radiol 1998;53:863–874.
59. Bezzi M, Teggi A, De Rosa F, et al. Abdominal hydatid disease: US findings during medical treatment. Radiology 1987;162:91–95.
60. Ustünsöz B, Akhan O, Kamiloğlu MA, et al. Percutaneous treatment of hydatid cysts of the liver: long-term results. AJR Am J Roentgenol 1999;172:91–96.
61. Akhan O, Ozmen MN, Dinçer A, et al. Liver hydatid disease: long-term results of percutaneous treatment. Radiology 1996;198:259–264.
62. Giorgio A, Di Sarno A, de Stefano G, et al. Sonography and clinical outcome of viable hydatid liver cysts treated with double percutaneous aspiration and ethanol injection as first-line therapy: efficacy and long-term follow-up. AJR Am J Roentgenol 2009;193:W186–W192.
63. Didier D, Weiler S, Rohmer P, et al. Hepatic alveolar echinococcosis: correlative US and CT study. Radiology 1985;154:179–186.
64. Czermack BV, Unsinn KM, Gotwald T, et al. Echinococcus multilocularis revisited. AJR Am J Roentgenol 2001;176:1207–1212.
65. Andresen B, Blum J, Weymarn AV, et al. Hepatic fascioliasis: report of two cases. Eur Radiol 2000;10:1713–1715.
66. Cosme A, Ojeda E, Poch M, et al. Sonographic findings of hepatic lesions in human fascioliasis. J Clin Ultrasound 2003;31:358–363.
67. Soudack M, Shechter A, Malkin L, et al. Inflammatory pseudotumor of the liver: sonographic and computed tomographic features with complete regression. J Ultrasound Med 2000;19:501–504.
68. Yan FH, Zhou KR, Jiang YP, Shi WB. Inflammatory pseudotumor of the liver: 13 cases of MRI findings. World J Gastroenterol 2001;7:422–424.
69. Ng VL, Yajko DM, Hadley WK. Extrapulmonary pneumocystis. Clin Microbiol Rev 1997;10:401–418.
70. Keane MA, Finlayson C, Joseph AE. A histological basis for the 'sonographic snowstorm' in opportunistic infection of the liver and spleen. Clin Radiol 1995;50:220–222.
71. Spouge AR, Wilson SR, Gopinath N, et al. Extrapulmonary *Pneumocystis carinii* in a patient with AIDS: sonographic findings. AJR Am J Roentgenol 1990;155:76–78.
72. Reeders JWAJ, Yee J, Gore RM, et al. Gastrointestinal infection in the immunocompromised (AIDS) patient. Eur Radiol 2004;14:E84–E102.
73. Wetton CW, McCarty M, Tomlinson D, et al. Ultrasound findings in hepatic mycobacterial infections in patients with acquired immune deficiency syndrome (AIDS). Clin Radiol 1993;47:36–38.
74. Bray HJ, Lail VJ, Cooperberg PL. Tiny echogenic foci in the liver and kidney in patients with AIDS: not always due to disseminated *Pneumocystis carinii*. AJR Am J Roentgenol 1992;158:81–82.
75. Glasgow BJ, Anders K, Layfield K, et al. Clinical and pathologic findings of the liver in the acquired immunodeficiency syndrome (AIDS). Am J Clin Pathol 1985;83:582–588.

76. Vieco PT, Rochon L, Lisbona A. Multifocal cytomegalovirus-associated hepatic lesions simulating metastases in AIDS. Radiology 1990;176:123–124.
77. Gaya DR, Thorburn D, Oien KA, et al. Hepatic granulomas: a 10 year single centre experience. J Clin Pathol 2003;56:850–853.
78. Mills P, Saverymuttu S, Fallowfield M, et al. Ultrasound in the diagnosis of granulomatous liver disease. Clin Radiol 1990;41:113–115.
79. Monill-Serra JM, Martinez-Noguera A, Montserrat E, et al. Abdominal ultrasound findings of disseminated tuberculosis in AIDS. J Clin Ultrasound 1998;25:1–6.
80. Kessler A, Mitchell DG, Israel HL, Goldberg BB. Hepatic and splenic sarcoidosis: ultrasound and MR imaging. Abdom Imaging 1993;18:159–163.
81. Xu HX, Xie XY, Lu MD, et al. Unusual benign focal liver lesions: findings on real-time contrast-enhanced sonography. J Ultrasound Med 2008;27:243–254.
82. Huang W-T, Wang C-C, Chen W-J, et al. The nodular form of hepatic tuberculosis: a review with five additional new cases. J Clin Pathol 2003;56; 835–839.
83. Blangy S, Cornud F, Sibert A, et al. Hepatitis tuberculosis presenting as tumoral disease on ultrasonography. Gastrointest Radiol 1988;13:52–54.
84. Akhan O, Pringot J. Imaging of abdominal tuberculosis. Eur Radiol 2002;12:312–323.
85. Garel LA, Pariente DM, Nezelof C, et al. Liver involvement in chronic granulomatous disease: the role of ultrasound in diagnosis and treatment. Radiology 1984;153:117–121.
86. Larsen CE, Patrick LE. Abdominal (liver, spleen) and bone manifestations of cat-scratch disease. Pediatr Radiol 1992;22:353–355.
87. Kim GB, Kwon JH, Kang DS. Hypereosinophilic syndrome: imaging findings in patients with hepatic involvement. AJR Am J Roentgenol 1993;161:577–580.
88. Nam K-J, Jung W-J, Choi J-C, et al. Hepatic involvement in hypereosinophilia: sonographic findings. J Ultrasound Med 1999;18:475–479.
89. Lee WJ, Lim HK, Lim JH, et al. Foci of eosinophil related necrosis in the liver: imaging findings and correlation with eosinophilia. AJR Am J Roentgenol 1999;172:1255–1261.
90. Reeder MM. Gamut: liver calcification. Semin Roentgenol 1975;10:171.
91. Stoupis C, Taylor HM, Paley MR, et al. The rocky liver: radiologic-pathologic correlation of calcified hepatic masses. Radiographics 1998;18:675–685.

CHAPTER

10

Focal liver lesions/echo enhancing agents and the liver

Gavin Low and Edward Leen

INTRODUCTION 138

CONTRAST AGENTS FOR LIVER IMAGING 139

CONTRAST AGENT KINETIC DISTRIBUTION 139

OPTIMISATION AND SCANNING STRATEGY FOR DETECTION AND CHARACTERISATION 139

BENIGN FOCAL LIVER LESIONS 140
Cavernous haemangioma 140
Fibronodular hyperplasia 142
Hepatic adenoma 143
Hepatic abscess 145
Hepatic steatosis 146
Focal fat sparing 147
Focal steatosis 147
Multifocal steatosis 147
Liver haematoma 148
Rare benign lesions 148
Hepatic angiomyolipoma 149
Hepatic lipoma 149
Intrahepatic biliary cystadenoma 149
Biliary epithelial dysplasia of the intrahepatic bile duct 150
Hepatic inflammatory pseudo-tumour 150
Peliosis hepatis 150
Hepatic sarcoidosis 150
Solitary necrotic hepatic nodule 150

MALIGNANT FOCAL LIVER LESIONS 150
Liver metastasis 150
Improved detection of liver metastases with contrast-enhanced intraoperative US (CE-IOUS) 152
Hepatocellular carcinoma 153
Incidence 153
Screening and surveillance of HCC 153
Regenerating nodules, dysplastic nodules and HCC 154
Cholangiocarcinoma 156
Hepatic lymphoma 160
Rare malignant lesions 160
Fibrolamellar hepatocellular carcinoma 160
Epithelioid haemangioendothelioma 160
Biliary cystadenocarcinoma 161

INTRODUCTION

Conventional ultrasound (US) is the first-line imaging investigation for assessing the liver as it is non-invasive, widely available, and inexpensive with an excellent safety profile. Focal liver lesions are encountered on US in a wide variety of different clinical scenarios such as (a) an incidental finding during an abdominal survey performed for a separate clinical indication; (b) in patients with clinical (jaundice) or biochemical (deranged liver function tests) suspicion of liver disease; (c) in those with medical conditions that predispose to development of focal liver disease, e.g. hepatitis virus, cirrhosis, haemochromatosis, Wilson's disease and glycogen storage disorders, etc.; (d) in the work-up of newly diagnosed oncology patients where the identification of a focal liver lesion and its accurate characterisation has implications for staging, treatment options and prognosis; and (e) in cancer patients with known liver metastases undergoing neoadjuvant or local ablative therapy where US assessment of disease burden determines the treatment efficacy and directs clinical management.

It is important that the sonographer be familiar with the spectrum of common pathologies that can present as focal liver lesions and the sonographic features that enable accurate lesion characterisation. US can assess if a lesion is solid or cystic or a combination of the two. It can confidently confirm a simple cyst even when it is sub-centimetre in diameter and in this respect it is superior to CT. However, for the majority of solid focal masses, accurate lesion characterisation by US is limited when based on morphological features such as size, shape, echogenicity or colour Doppler findings because of a broad overlap in the imaging appearance of various pathologies.[1–3]

The intravenous (IV) administration of contrast agent as part of the routine protocol for CT and MRI has shown that focal liver lesions can be accurately characterised based on their dynamic enhancement pattern with respect to the background liver.[4,5] Conventional US is limited in the detection of solid focal liver masses compared to contrast-enhanced CT and MRI.[6] However, it is inappropriate to compare conventional US with contrast-enhanced CT and MRI as without contrast the performance of the latter modalities may be equal or even inferior to that of US. Traditionally, patients who are detected with indeterminate liver lesions on conventional ultrasound are referred for further imaging studies such as contrast-enhanced CT or MRI for lesion characterisation. These limitations have been overcome with the advent of contrast-enhanced US (CEUS), which enables improved liver lesion detection and characterisation.[1,7–11] Furthermore, with the newer generation of agents, CEUS permits real-time dynamic imaging, unlike contrast-enhanced CT or MRI where the images are acquired at 'snap-shots' in time and where imaging at an inappropriate time delay will lead to a suboptimal examination. Liver lesions detected for the first time on ultrasound can be characterised at the same sitting through the use of a US contrast agent, thus shortening the diagnostic pathway, obviating the need for further tests such as CT, MRI or biopsy and potentially improving patient satisfaction. In a prospective multicentre trial comparing CEUS to conventional US involving 127 patients with 134 focal liver lesions, CEUS reduced the number of indeterminate diagnoses by 51–67% and improved the sensitivity and specificity to 90.2–95.4% and 80.8–89.8% respectively, and reduced the need for further imaging from 90.4% to 23.7% of cases.[11] The reduction in the overall per-patient costs, due to elimination of further imaging, may help control the escalating cost of a health care system with limited resources. A cost analysis study involving 398 patients with 408 indeterminate benign focal liver lesions discovered on conventional US showed that use of CEUS also provided significant cost savings, compared with contrast-enhanced CT, for lesion characterisation.[12]

In this chapter, the use of ultrasound contrast agents for liver imaging, their kinetic distribution, optimisation and optimal scanning strategy for detection and characterisation of focal liver lesions are described; the spectrum of both benign and malignant focal

solid liver pathologies that may be encountered in clinical practice and the sonographic findings on both conventional and contrast-enhanced US that enable lesion characterisation are discussed.

CONTRAST AGENTS FOR LIVER IMAGING

Based on evidence from clinical trials, expert committee reports and consensus, the European Federation of Societies of Ultrasound in Medicine and Biology (EFSUMB) has already issued guidelines on use of ultrasound contrast agents (USCAs) in clinical practice.[13]

For liver imaging, it is more appropriate to classify USCAs according to their specificity for normal hepatic parenchymal uptake (Tables 10.1 and 10.2). Earlier agents were primarily designed to be blood pool agents to salvage conventional Doppler examinations and have been shown to be highly effective in enhancing the macrovasculature on spectral/colour/power Doppler modes lasting for up to 7 minutes following a bolus intravenous administration. Agents such as NC100100 (GE Healthcare, Oslo), SHU 508A and SHU 563A (Bayer AG, Berlin) have additional tissue-specific properties; they are selectively taken up by the Kupffer cells of the reticuloendothelial system after the vascular phase and enhance the normal hepatic parenchyma for up to an hour with non-linear imaging modes depending on the dosage used. The advantage of such agents is that lesions, which are deficient of Kupffer cells or associated with Kupffer cell dysfunction, do not retain the agents, thereby improving the lesion to tissue contrast ratio resulting in higher sensitivity for detection as well as specificity in tissue characterisation. Other agents such as SonoVue (Bracco SPA, Milan) or Definity (BMS, Billerica, USA), which were also primarily designed to be blood pool agents, are known to be trapped or slowed in the hepatic sinusoids, thereby demonstrating late phase uptake, which may last for up to 6 minutes.[14] This characteristic confers similar advantage clinically to those Kupffer cell targeted agents.

CONTRAST AGENT KINETIC DISTRIBUTION

In order to optimise the use of USCAs in the detection and characterisation of focal liver tumours, it is important to understand their kinetic distribution following a bolus intravenous injection. In that respect there are some similarities to the haemodynamic profiles observed during CT or MR examinations, except for the volumes of the agents required and their transit times. A very small volume (0.2 to 2.4 mL) of USCA is sufficient in enhancing the liver parenchyma as a result of the higher sensitivity of the US non-linear modes compared with CT or MR imaging; the intensity–time curves of USCA are shifted by 10–15 seconds earlier. In the late phase the tumour to liver contrast ratio is increased sevenfold.[15] This may enable the detection of very small liver metastases. In addition, imaging with USCA is in real-time with the added advantage that USCA is truly intravascular, which may be particularly useful for more accurate perfusion quantification.[16]

Primary and secondary neoplasms of the liver demonstrate wide variability in their vascularity, which is dependent on their size and growth rate. When the tumour is small (about 1 mm) its main blood supply is via the portal vein and as it grows, a new arterial system develops and becomes the predominant or exclusive blood supply.[17] However only 20–25% of the blood supply to the normal liver originates from the hepatic artery and the remainder is from the portal vein. After a bolus intravenous injection of USCA, hypervascular tumours show hyper-enhancement compared with the adjacent liver in the arterial phase, which ranges between 15 and 25 seconds from the time of the injection. As blood with the higher volume of USCA is then delivered to the liver via the portal vein, the echogenicity of the liver rises rapidly; in contrast within malignant tumours, USCA washout is observed during that period. The reversal in the enhancement between the liver and the tumour is accentuated during this phase and peaks from 35 to 90 seconds. All contrast agents will display such arterial and portal phases. Therefore optimal scanning for detection of hyper- and hypovascular malignant tumours is during the hepatic arterial and portal venous phases respectively. However, beyond the vascular phases, some agents such as Optison clear out of the circulation fairly rapidly whilst other agents such SonoVue or Definity are held in the sinusoids for up to 5–6 minutes from the time of the bolus injection and this phase can be called the 'late phase'.[10,18] On the other hand, with USCAs, which are taken up by the Kupffer cells, liver parenchymal enhancement continues beyond the 5 minutes and may last for up to an hour depending on the dose use.[19] Optimal imaging for malignant tumours for detection and characterisation is during this late phase.

Table 10.1 Ultrasound contrast: liver-specific uptake

Licensee	Trade name	Code name
Bayer AG	Levovist	SHU 508A
Bayer AG	Sonavist	SHU 563A
Bracco Spa		BR14
Bracco Spa	SonoVue	BR1
Lantheus	Definity	MRX-115
GE Healthcare	Sonazoid	NC 100100

Table 10.2 Ultrasound contrast agents: no liver-specific uptake as yet confirmed

Licensee	Trade name	Code name
Acusphere	A1700	
Point Biomedical	BiSphere	PB127
GE Healthcare	Optison	FS069
Bayer AG	Imavist	AFO-150

OPTIMISATION AND SCANNING STRATEGY FOR DETECTION AND CHARACTERISATION

Non-linear mode is essential for any USCA imaging and in particular low output power (MI: mechanical index) is required to enable real-time scanning in the detection and characterisation of liver tumours. The MI and receiver gain can be adjusted according to the patient's body habitus but the MI should be kept as low as possible (0.07–0.12). The use of dual screens with simultaneous non-linear and fundamental modes side by side is advised to ensure scanning over the region of interest to assess the relative distribution of contrast between pathology and normal liver. The focal zone should be set low down the screen to enable homogeneity of the enhancement. Persistence setting, which refers to the temporal smoothing that the scanner performs in displaying images, should be minimised. There are other parameters such as dynamic range/compression and line density, which would also affect microbubble destruction and contrast display sensitivity, but these would already have been optimised by the equipment manufacturer and the user is best advised to adopt the default setting for the specific contrast agent.

For detection, standardisation of the scanning protocol is important to ensure coverage of the whole liver. In our unit, each hepatic lobe is scanned axially followed by sagittal sweeps. Oblique sweeps through the three right intercostal spaces are also performed to complete the examination. This sequence of scanning is repeated

systematically throughout the hepatic arterial, portal venous and late phases. The whole examination should be recorded digitally and archived for further review. The hepatic arterial phase may be too short to complete a full liver coverage to specifically detect all the hypervascular malignant tumours; however, the contrast washout is usually rapid for these lesions and the portal and late phases are long enough for them to be depicted. Irrespective of the tumour vascularity, the vast majority of malignant lesions are detectable using the standardised protocol described. For the purpose of characterisation it is important to understand the temporal changes in the lesional enhancement during the three phases. Agents with late phase uptake have the advantage that there is sufficient scanning time and are ideally suited for both detection and characterisation.

In the characterisation of focal liver tumours, a standardised scanning protocol is also useful to evaluate the tumoral vascular morphology during the hepatic arterial, portal venous and the late phase by observing the relative contrast entrapment/uptake within the tumour compared to the surrounding normal liver parenchyma in. Following the administration of the contrast agent, gentle sweeps to cover the whole lesion are recommended instead of maintaining the same scanning plane continuously; although there is minimal destruction when scanning at low MI, microbubble destruction still occurs if the probe is kept constantly at the same scan plane. In addition, when sweeping through the lesion, a three-dimensional perspective of the lesional vascular morphology and geometry is obtained. These sweeps can be repeated over the whole vascular phase and into the late phase. However, for suspected benign haemangiomas the protocol needs to be tailored to demonstrate the centripetal progression of the peripheral nodular enhancement by progressively increasing the delays between sweeps thereby minimising microbubble destruction, to allow for the accumulation of agent throughout the lesion.

However, the equipment settings and scanning protocols are different for agents such as Levovist and Sonavist as they are best displayed using non-linear imaging modes set at high MI (over 1.0). The scanning protocol for detection is as follows: the left lobe and then the right lobe is scanned axially or sagittally at 4–5 minutes post Levovist or Sonavist injection. Oblique scans at the intercostal spaces can also be performed to complete the right lobe examination. As this is a destructive mode, the contrast display with Levovist is transient; the first sweep through each lobe will provide the best and possibly the only chance to visualise tissue enhancement. Pre-contrast scan planning is therefore essential to ensure complete coverage of the whole liver. If the examination is incomplete after the first injection, repeated contrast administration is possible. With the transience of the contrast display, biopsy of newly identified lesions is difficult with this agent. For characterisation, single sweeps through the lesion can be performed at the hepatic arterial (15–20 seconds) and portal venous (60–90 seconds) phases at high MI to demonstrate the lesion vascular morphology and then in the late phase to demonstrate the amount of contrast uptake within the lesion. During the vascular phase following Levovist administration, the number of sweeps over the lesion should be minimised, as it may spoil the late phase imaging. However, with Sonavist, despite the destructive high MI mode being used, repeated sweeps are possible to complete the liver examination in the vascular and late phases; this is most likely because of the much higher dose of Sonavist used.[20]

BENIGN FOCAL LIVER LESIONS

Cavernous haemangioma

Cavernous haemangioma is a common benign liver tumour with a prevalence of 0.5–20% in the general population[21] and it is often detected as an incidental finding on abdominal imaging.[22] It is most frequently detected in the 30- to 40-year-old age group and has a 2–5 times higher incidence in females than males.[23] Haemangioma is often solitary but can be multiple in 10–50% of cases.[24,25] It may occur anywhere in the liver but has a predilection for peripheral and subcapsular locations and is most frequently found in the posterior segment of the right lobe.[26] Due to their benign nature, haemangiomas are predominantly asymptomatic although complications can occur, particularly in large haemangiomas. The incidence of complications occurring in haemangiomas >5 cm in size is 5–20%.[27] Potential complications include inflammation, Kasabach–Merritt syndrome, intra-tumoral haemorrhage, volvulus and compression of adjacent structures.[21] An inflammatory process of uncertain aetiology has been reported in large haemangiomas, which may lead to rapid tumour growth, and non-specific clinical findings such as fever, weight loss and abdominal pain. Kasabach–Merritt syndrome is a coagulopathy consisting of intravascular coagulation, clotting and fibrinolysis within the haemangioma that can lead to systemic thrombocytopenia. Intra-tumoral haemorrhage is a rare complication in large haemangiomas and can occur spontaneously or following anticoagulation therapy. Rarely, large haemangiomas may present as pedunculated masses and there are two case reports of these masses having undergone volvulus.[28,29] A large haemangioma can exert local compressive effects on adjacent biliary (particularly for those situated at liver hilum) and hepatic vascular structures or on neighbouring organs such as the kidney or a loop of bowel.

Haemangiomas are composed of blood-filled cavernous spaces lined with a single layer of flat endothelial cells and separated by fibrous septa. At microscopy, they have a honeycomb appearance. On US, haemangiomas are typically well-defined, round or lobulated lesions, measuring ≤3 cm in size, and have a uniformly hyperechoic appearance with or without posterior acoustic enhancement. The increased echogenicity on US is due to the multiple interfaces between the walls of the cavernous spaces and the blood within them.[30] The posterior acoustic enhancement reflects the low acoustic impedance of blood-filled spaces and tends to occur in lesions ≥2.5 cm in size.[31] Colour Doppler US is limited in assessment of haemangiomas as it is not sensitive enough to detect the slow flow in the cavernous spaces of these focal lesions, particularly in small lesions and lesions located deep within the liver.[32,33] Power Doppler has a higher sensitivity in detecting slow flow compared with colour Doppler but suffers from being more sensitive to motion artefact thus limiting its value.[34]

In patients where a confident diagnosis of cavernous haemangioma can be made based on typical US findings, no further confirmatory imaging test is required except perhaps for a routine follow-up ultrasound to determine interval stability consistent with a benign aetiology. However, haemangiomas can present with atypical US findings in 20–40% of cases with potential for misdiagnosis.[35] In a retrospective study of 29 proven atypical haemangiomas in 29 patients, Moody and Wilson observed a number of sonographic features that suggest a haemangioma.[35] The most useful feature is an echogenic border around a solid tumour while other suggestive features include a partially hypoechoic internal echo pattern and a curvilinear outline, which may be scalloped. The hypoechoic internal echo pattern is postulated to be secondary to degenerative changes in a haemangioma such as haemorrhage, necrosis, fibrosis or myxomatous change. Less frequently, atypical haemangiomas may rapidly enlarge in size, calcify, present as a cystic/ multilocular lesion, contain fluid–fluid levels or become hyalinised.[21] Growth in haemangiomas is thought to be due to vascular ectasia. Some haemangiomas have oestrogen receptors and rapid growth has been observed during oestrogen influence during puberty, pregnancy, oral contraceptive use and hormonal treatment.[36] Fluid–fluid levels in a haemangioma are thought to represent stagnant or slow-flowing blood with red blood cell sedimentation on the dependent portion of the tumour. Hyalinisation is believed to represent the end-stage involution of a haemangioma with replacement of the vascular spaces by hyalinised fibrotic tissue leading to loss of the typical morphological appearance and enhancement pattern of

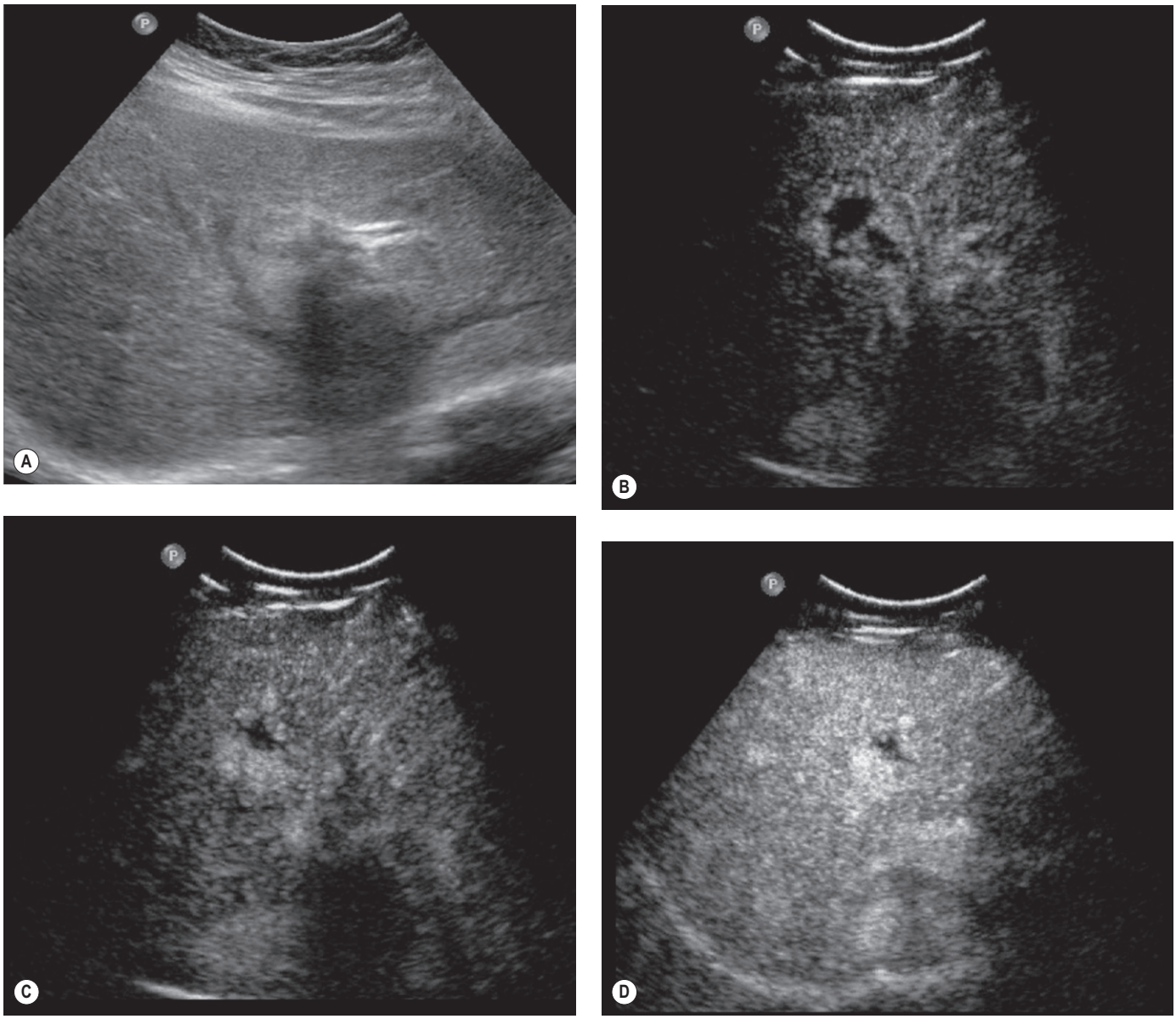


Figure 10.1 Haemangioma. A: Baseline scan showing central lesion with mixed echoes almost isoechoic to adjacent liver. **B:** Arterial phase scan showing peripheral rim enhancement with nodular outline. **C:** Portal phase scan shows centripetal filling-in with more prominent peripheral globular enhancement. **D:** Late phase scan shows further centripetal filling-in of the peripheral globular enhancement.

a haemangioma. In addition, haemangiomas occurring in a background of diffuse hepatic steatosis may have variable echogenicity, making pattern recognition difficult. Haemangiomas may appear slightly hypoechoic, isoechoic or hyperechoic compared to the steatotic liver but usually maintain their posterior acoustic enhancement (which may be the only clue to their aetiology).[37] High flow haemangiomas are reported to have a tendency for a hypoechoic appearance compared to the typically seen hyperechoic appearance in most slow flow haemangiomas, and may be associated with an arterio-portal shunt.[38]

Cavernous haemangiomas, even those with atypical appearances on conventional US, can be confidently diagnosed based on their enhancement pattern on CEUS[36,39,40] (Fig. 10.1). Peripheral nodular enhancement in the arterial phase with centripetal filling on the portal venous and late vascular phases is a typical feature seen on CEUS, and resembles the pattern seen on contrast-enhanced CT and MRI. A study of the CEUS enhancement pattern of histologically proven haemangiomas in 58 patients[36] found that the sensitivity for detecting haemangiomas based on peripheral nodular enhancement was 74% (95% confidence interval, 61–85%); for complete portal or late phase filling it was 78% (65–88%); and for the combination of both, it was 98% (91–100%) (Fig. 10.2). In 22% of cases, haemangiomas demonstrated incomplete centripetal filling in the portal or late vascular phases. Quaia et al.[40] also noted this similar finding in a study of atypical haemangiomas on CEUS and showed that in these cases of incomplete centripetal filling (Fig. 10.3), a thrombotic or fibrosclerotic pattern was proven at histology. In general, this pattern is seen in larger haemangiomas >4 cm.[41] In small haemangiomas (usually <1 cm in size) an immediate homogeneous enhancement pattern may be seen in the arterial phase, due to rapid filling within these haemangiomas. These 'flash filling' haemangiomas account for about 16% of all cases.[36] Rarely, a centrifugal (inside out) enhancement pattern has been described on CEUS whereby there is a central enhancing focus in the arterial phase followed by centrifugal enhancement in the portal and late vascular phases.[41] Assessment of lesion enhancement in the portal and late vascular phases is also important to determine whether a liver tumour is benign or malignant. Consistent with other benign tumours, haemangiomas are hyperechoic or isoechoic compared with the background liver during these phases, whilst malignant

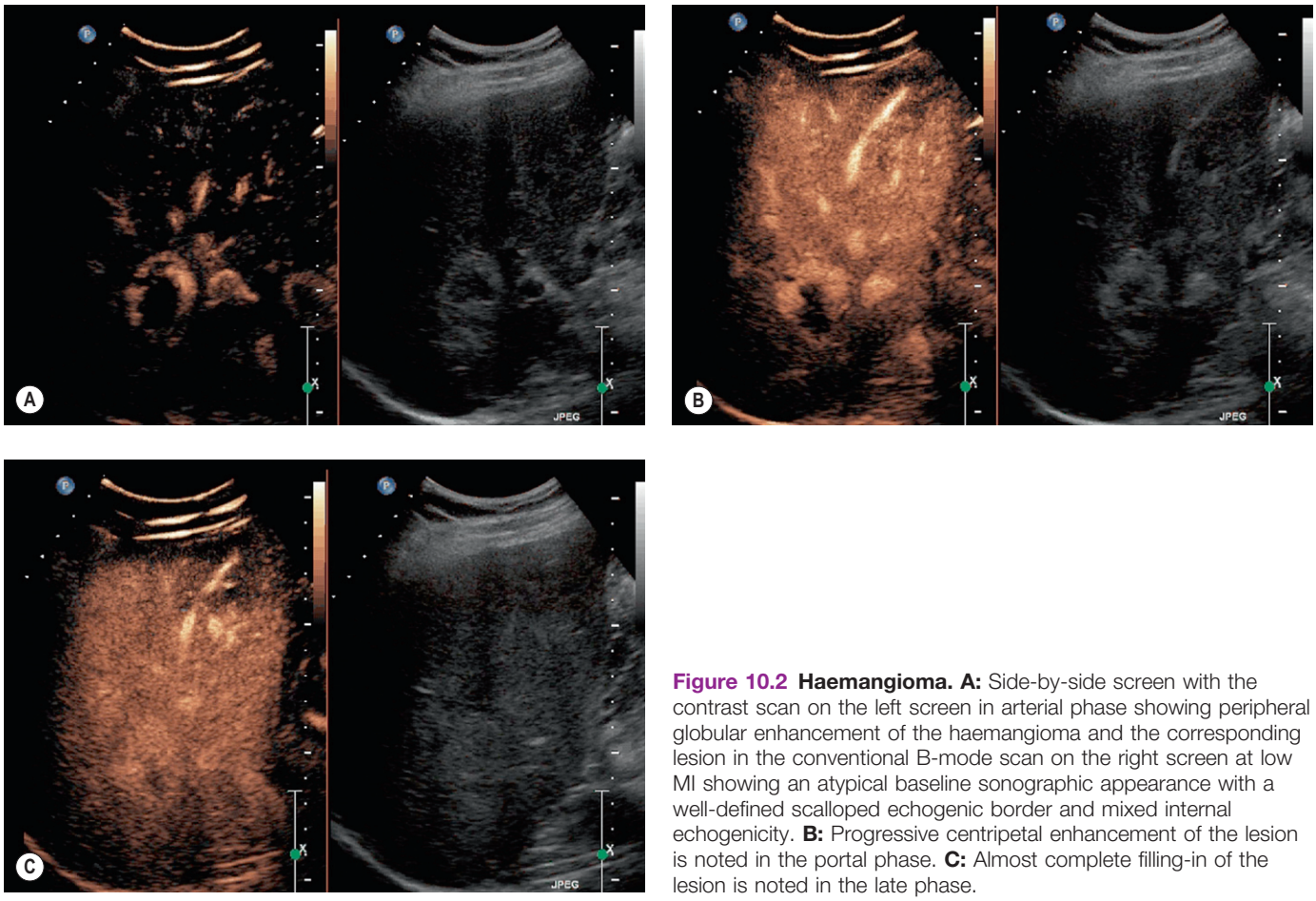


Figure 10.2 **Haemangioma. A:** Side-by-side screen with the contrast scan on the left screen in arterial phase showing peripheral globular enhancement of the haemangioma and the corresponding lesion in the conventional B-mode scan on the right screen at low MI showing an atypical baseline sonographic appearance with a well-defined scalloped echogenic border and mixed internal echogenicity. **B:** Progressive centripetal enhancement of the lesion is noted in the portal phase. **C:** Almost complete filling-in of the lesion is noted in the late phase.

tumours show contrast washout and are therefore typically hypoechoic.

Fibronodular hyperplasia

Fibronodular hyperplasia (FNH) is another common benign liver tumour representing 8% of all liver tumours.[42] It has a prevalence of 3–5% in the general population, a female to male ratio of 8:1 and occurs most frequently in the 20–50-year-old age group.[42] When occurring in men, atypical presentation is more common with lesions usually detected at a smaller size and at an older age.[43] FNH is usually a solitary lesion <5 cm in size but can be multiple in up to 20% of cases. An FNH syndrome of simultaneous occurrence of multiple FNHs and haemangiomas has been recognised.[44] FNH is usually diagnosed incidentally on imaging but may be symptomatic in up to 20% of cases, mainly in patients with larger lesions where the mass effect causes abdominal pain and distension.[45]

The aetiology of FNH is uncertain but dominant theories include a hyperplastic response to a pre-existing vascular malformation or a response to ischaemia due to an occult vascular occlusion. On pathological examination, FNH is composed of circumscribed nodules of hyperplastic parenchyma surrounded by radiating fibrotic septa originating from a central scar, which contains fibrous connective tissue and malformed vascular structures. The arterial vessels in FNH are most prominent in the central scar but are also present along the septa, which extend from the centre to the periphery of the lesion with a recognised centrifugal flow pattern. FNH contains normal hepatocytes and Kupffer cells and proliferating malformed bile ducts with absence of portal triads and central veins.[46] FNH is divided into two types: classic (80%) and non-classic (20%). Classic FNH contains all components, including an abnormal nodular architecture, malformed vessels, and bile duct proliferation. The non-classic type contains two of the three components but always shows bile duct proliferation.

FNH is typically not well visualised on conventional US as the lesion is usually of similar echogenicity to the surrounding liver. Detection is challenging for this 'stealth lesion' with displacement of adjacent intrahepatic vessels by mass effect occasionally being the only clue to its presence.[47] FNH is usually a well-defined and homogeneous lesion with sharp margins and may be slightly hypoechoic (85% of cases), isoechoic or hyperechoic relative to normal liver. A peri-lesional hypoechoic halo simulating a pseudo-capsule has been observed which is thought to represent compressed liver tissue or vessels around the liver. The central scar and the septa are often difficult to appreciate on US but occasionally when apparent, they are usually hyperechoic in appearance. The addition of colour and power Doppler[48,49] to conventional US interrogation has been shown to be useful for FNH characterisation showing a spoke wheel arterial pattern of vessels, radiating from the central feeding artery to the periphery of the lesion. However, colour and power Doppler US have limitations, particularly in detection of slow flow in intra-tumoral vessels and particularly in small lesions deep within the liver parenchyma.

USCAs can improve the demonstration of tumoral microvascularity in FNH thereby facilitating its diagnosis. USCAs enable the

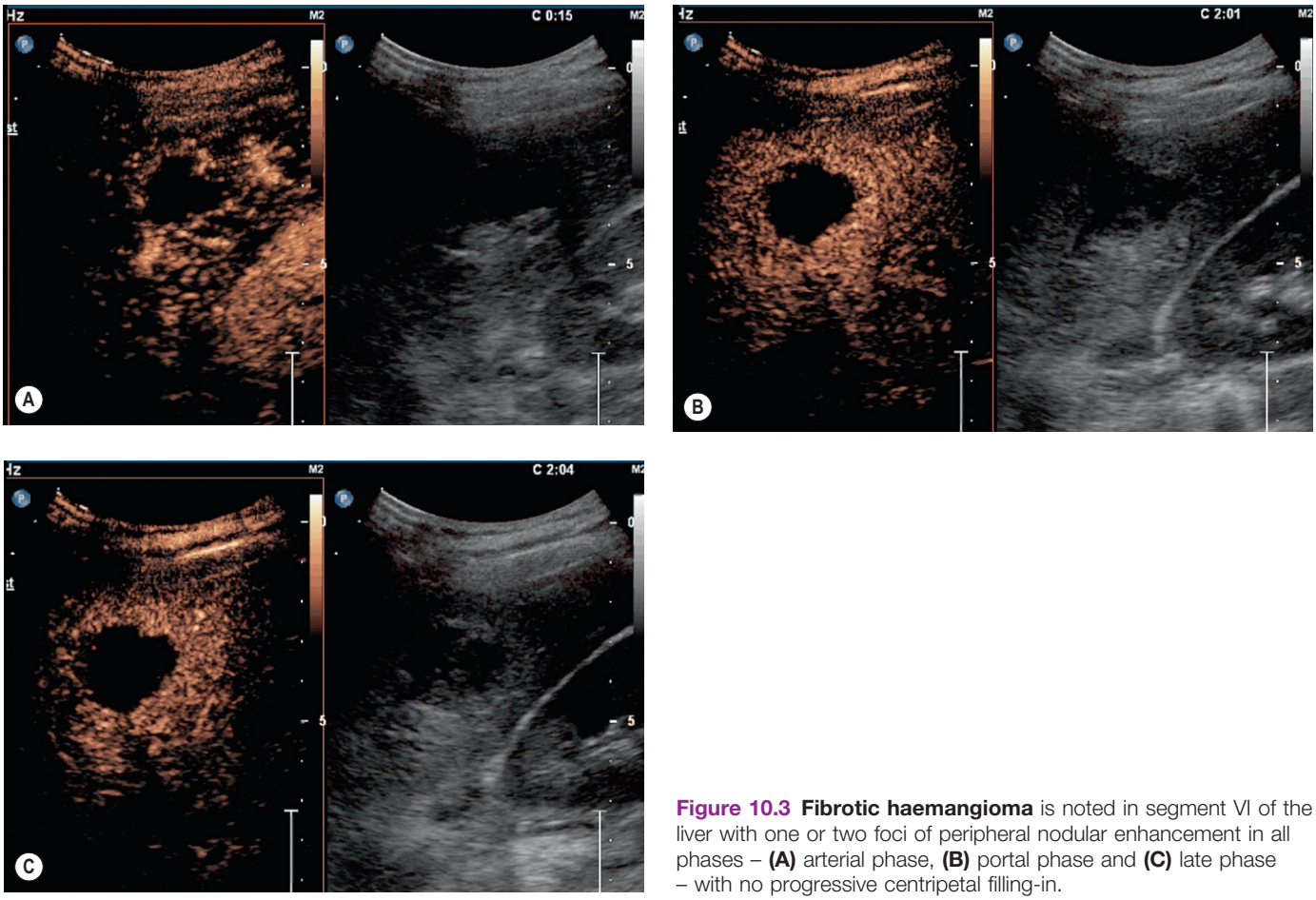


Figure 10.3 **Fibrotic haemangioma** is noted in segment VI of the liver with one or two foci of peripheral nodular enhancement in all phases – **(A)** arterial phase, **(B)** portal phase and **(C)** late phase – with no progressive centripetal filling-in.

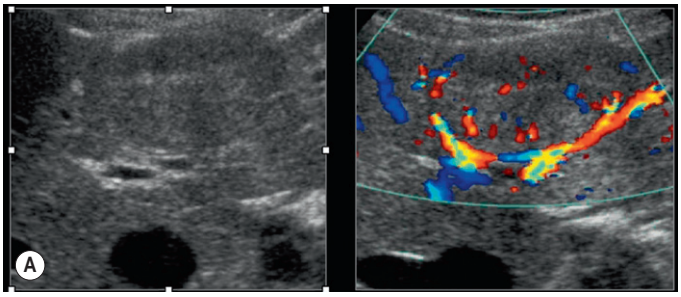
detection of low-velocity blood flow because they increase the signal to noise ratio so improve display of vascular pattern[50] (Figs 10.4 and 10.5). The central feeding vessel with the FNH scar and the communicating network of surrounding arteries is displayed as a centrifugal 'spoke wheel' pattern of enhancement[51] (Fig. 10.5). Central scar is present in 35% of lesions <3 cm and in 65% of lesions >3 cm.[52] On CEUS, it has been reported in 31–56% of cases.[1,11,53,54] CEUS compares favourably with other modalities for detecting the characteristic vascular pattern and central scar in FNH[55,56] (Fig. 10.6). In a study of 34 histologically proven FNHs, Yen et al.[55] found that CEUS had the highest sensitivity (97.1%) in detection of the spoke wheel enhancement or central scar compared with colour Doppler US/power Doppler US (40%), contrast-enhanced CT or MRI (40%), hepatic angiography (50%) and liver scintigraphy (0%). Janica et al.[56] observed that the spoke wheel sign was detected by CEUS in 100% of FNHs in a study of 26 patients. CEUS is therefore an important diagnostic tool for detecting and confirming the presence of FNH with performance at least on par or even superior to other available imaging options.

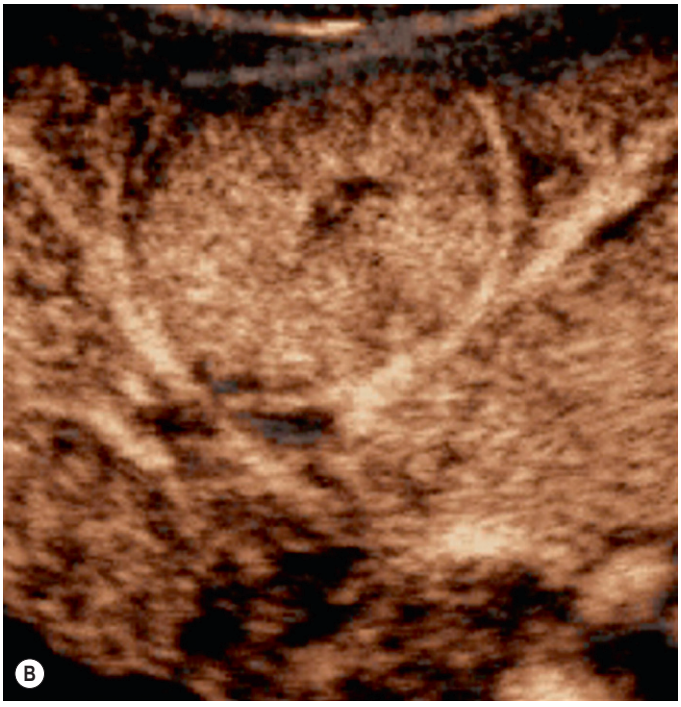
Hepatic adenoma

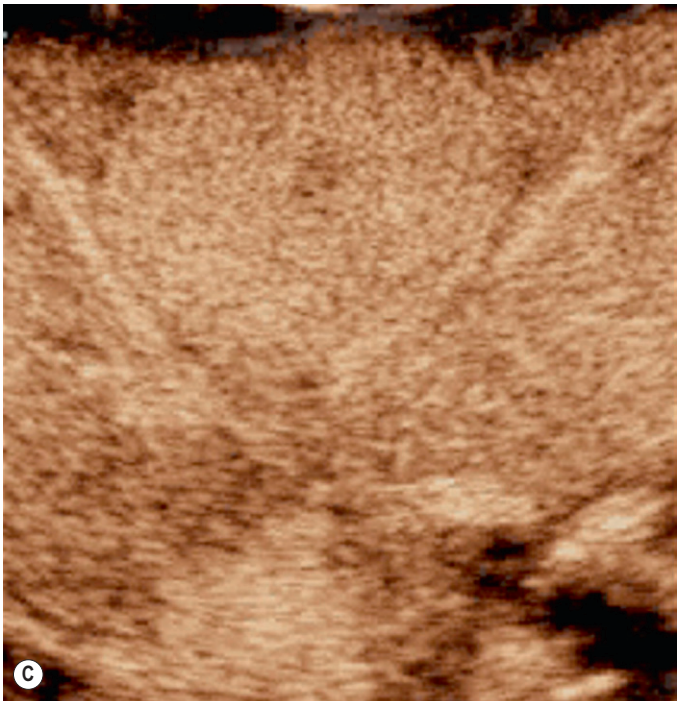
Adenoma is a benign hepatic tumour with an annual incidence of 3–4 per 100 000 adult patients and is most commonly encountered in young women on the oral contraceptive pill.[57] It has an overwhelming female preponderance with a female to male ratio of 10:1 and occurs most frequently in the 20–30-year-old age group.[58] It is a solitary lesion in 70–80% of cases and has an average size of 8–10 cm.[59] Adenomas are typically found in a subcapsular location in the right lobe of liver (75% of cases) but may be intraparenchymal or pedunculated (10% of cases).[59]

Long-term oral contraceptive usage is linked with development of adenomas with only a few cases of this disease being recorded prior to introduction of the contraceptive pill in the 1960s.[60] An extensive epidemiological study[61] showed a 25 times higher incidence of hepatic adenoma in women on long-term oral contraceptives compared to those who had either never used oral contraception or had used it for less than 24 months. Adenomas rarely occur in men, and when present, are usually found in men with predisposing risk factors such as anabolic steroid usage, diabetes or type 1 glycogen storage disorders.

Pathologically, hepatic adenoma is a well-circumscribed mass composed of sheets of cells that closely resemble hepatocytes that are arranged in plates separated by sinusoids.[62] Bile ducts and portal tracts are absent and Kupffer cells if present are reduced both in number and functionality. Large tortuous arteries and dilated thin-walled veins are often present, which denotes the hypervascular nature of the tumour. Poor connective tissue support predisposes adenomas to haemorrhage. As a tumour capsule is often absent or incomplete, haemorrhage may lead to spread into the liver or rupture into the peritoneal cavity. The risk of haemorrhage is related to the size of the adenoma and is present in about 40–50% of tumours.[63] Macroscopic fat deposition may occur in adenomas as the cells accumulate lipid and glycogen. Adenomas also calcify in about 5–15% of cases. Rarely, malignant transformation into hepatocellular carcinoma has been reported in adenomas, mainly in larger tumours >10 cm in size.[59] Surgical resection is recommended, particularly for larger adenomas, due to the risk of haemorrhage and malignant transformation.[63]







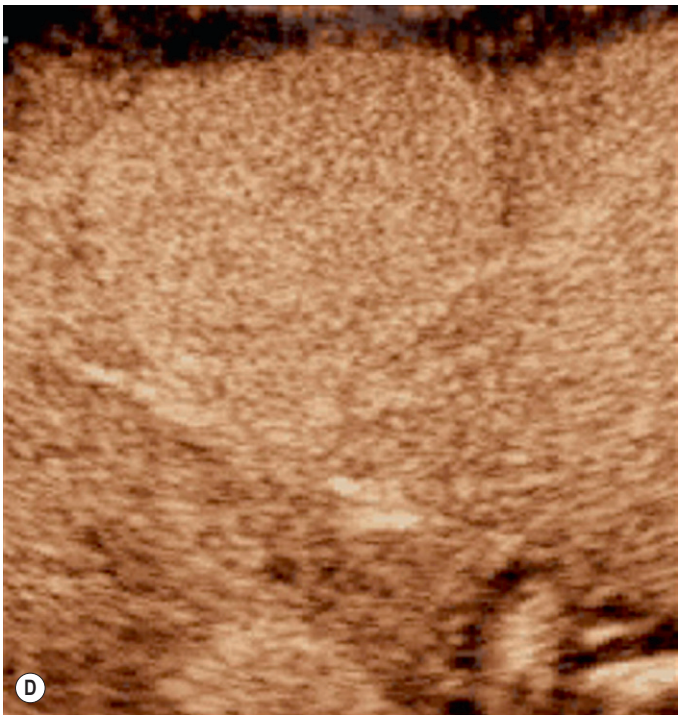


Figure 10.4 Focal nodular hyperplasia. A lesion is noted in segment IV **(A)** at baseline with greyscale and colour Doppler scans showing isoechoic vascular lesion with no central scar, **(B)** at arterial phase showing central scar and central artery and displacement of surrounding normal vessels; and showing as an iso-enhancing lesion in the portal **(C)** and late **(D)** phase with visualisation of the central scar.

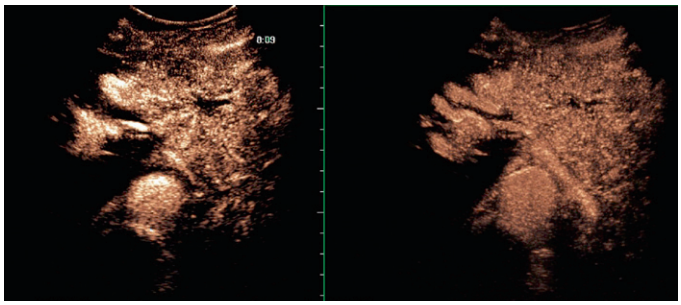


Figure 10.5 Focal nodular hyperplasia using microvascular imaging technique (MVI) in the right screen in the arterial phase; note the depiction of the central artery and spoke wheel distribution of the feeding vessels.

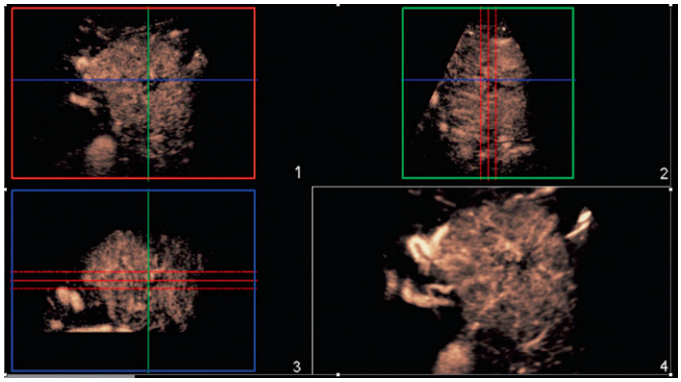


Figure 10.6 Focal nodular hyperplasia in 3D CEUS in the three orthogonal planes (1, 2 and 3) and the 3D reconstruction demonstrating the characteristics of the FNH (4).

The sonographic appearance of hepatic adenoma is non-specific as it may be hyperechoic, isoechoic, hypoechoic or of mixed echogenicity.[62] Uncomplicated adenomas may have a homogeneous appearance while presence of fat, intra-tumoral haemorrhage or necrosis will lead to a heterogeneous internal appearance. In general, increased echogenicity is seen in tumours with fat or intra-tumoral haemorrhage and posterior acoustic shadowing is detected in calcified lesion. Colour and power Doppler US may demonstrate peripheral peri-tumoral and intra-tumoral vessels. Several authors have demonstrated a continuous venous waveform in adenomas, which may potentially aid in differentiation from malignant tumours such as hepatocellular carcinoma (HCC), which show a pulsatile waveform pattern.[64,65] However, these studies were done on larger lesions with a mean diameter of >5 cm. In smaller lesions, the utility of colour and power Doppler US is limited due to technical difficulties in obtaining reproducible signals.

On CEUS, hepatic adenoma is typically hyper-enhancing in the arterial phase and may be iso-enhancing with respect to the background liver on the portal venous and late phase[66,67] (Fig. 10.7). Atypical of a benign hepatic tumour, some adenomas may also show portal phase non-enhancement or washout.[68,69] Persistent focal non-enhancement on all vascular phases is also seen in areas of intra-tumoral haemorrhage or necrosis. Clinically, distinction of adenoma from FNH is important as these pathologies generally occur in the same patient cohort, i.e. young women of reproductive age, and whilst FNHs are typically 'leave alone' lesions, adenomas should be treated more aggressively. In a CEUS study of 62 patients with 43 FNHs and 19 adenomas, Kim et al.[68] found that FNH is predicted on the basis of arterial phase centrifugal filling and stellate vascularity while adenomas were less reliably predicted on the basis of centripetal or mixed filling without stellate vascularity. The

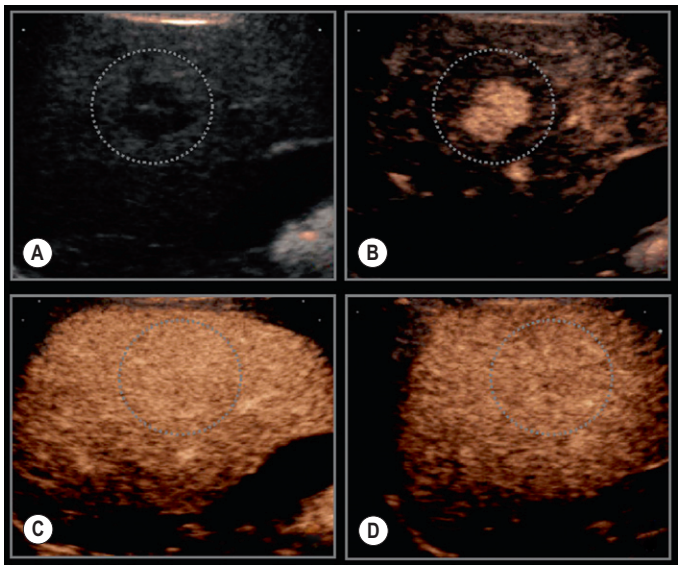


Figure 10.7 Adenoma at baseline **(A)** as a hypoechoic lesion, hyper-enhancing in the arterial phase **(B)** and iso-enhancing in the portal **(C)** and late **(D)** phases.

study also found that sustained portal phase enhancement is more common in FNH than in adenomas but less contributory to the diagnosis.

Hepatic abscess

Pyogenic and amoebic abscess represent the majority of hepatic abscesses detected worldwide. Both diseases have an excellent prognosis if treated early but are potentially fatal if left undiagnosed. US is the first-line imaging investigation for infected patients who may present with non-specific clinical and laboratory findings. Familiarity with the disease process and pertinent sonographic findings facilitates prompt diagnosis and treatment.

Pyogenic abscess is a localised collection of pus with destruction of involved hepatic parenchyma and stroma, caused by a bacterial pathogen.[69] At histopathology, the abscess cavity shows multiple locules, usually filled with thick purulent material and lined by a fibrous tissue wall.[70] Depending on the evolutionary stage of the abscess, there may be suppuration, liquefaction or fibrosis and the edges of the cavity are lined by a chronic inflammatory infiltrate. The most common organisms responsible are *Escherichia coli* and *Klebsiella pneumoniae*, although there is a polymicrobial source in more than 50% of infected patients. The usual route of bacterial seeding is by haematogenous dissemination (via the portal vein or hepatic artery) or via the biliary tract from ascending cholangitis. Infection can also occur by direct extension from adjacent organs. Common clinical conditions that predispose to pyogenic abscess include acute appendicitis, acute diverticulitis, trauma and surgery.

Amoebic abscess is caused by the protozoan *Entamoeba histolytica* and the usual mode of transmission is via the faecal–oral route. The liver is the most common extraintestinal organ involved (in 8.5% of cases) with spread to the liver from the gastrointestinal tract via the portal vein.[70] Amoebic abscess is most prevalent in the developing world where it is endemic in parts of Africa, the Far East, and in Central and South America. Worldwide it affects about 10% of the population.[70] Histologically, there is scant inflammatory reaction at the margins and a shaggy fibrin layer. Haemorrhage into the abscess can lead to a pasty material known as 'anchovy paste'. The abscess may be purulent if involved by secondary bacterial infection.

The clinical presentation for both these abscess types is highly variable. The classic triad of right upper quadrant pain, fever and

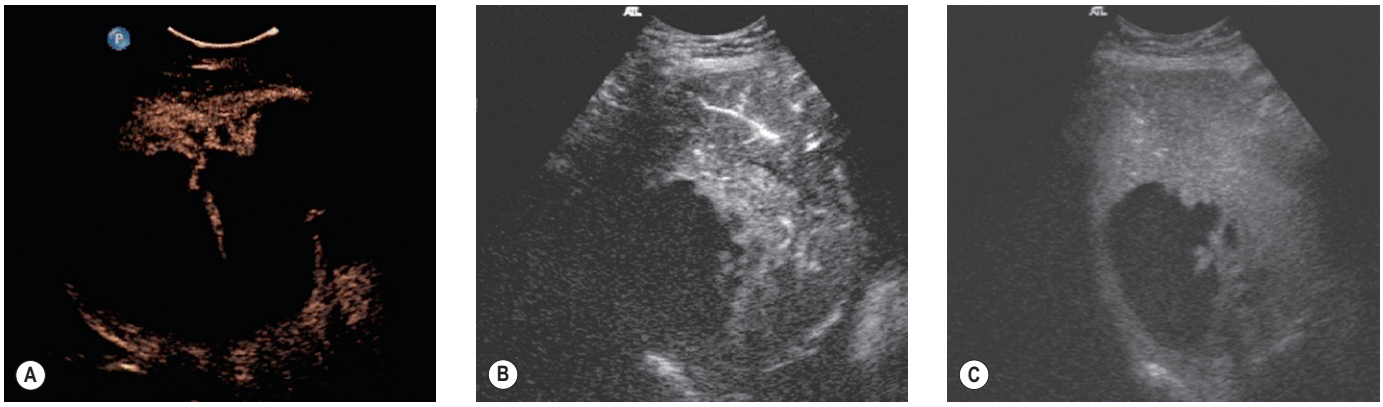


Figure 10.8 Abscess. Large non-enhancing lesion in the right lobe in the late phase with enhancing septum **(A)**; another abscess with enhancing pseudo-capsule and segmental normal liver parenchymal hyperperfusion in the arterial phase **(B)** and non-enhancement of the bulk of the abscess in the late phase **(C)**.

jaundice may be present in some patients. However, many patients present with non-specific clinical findings such as nausea, vomiting, diarrhoea, malaise and weight loss. In general, patients with amoebic abscess tend to be more acutely unwell than those with pyogenic abscess. Laboratory markers such as white cell count and liver functions tests (e.g. serum bilirubin, transaminases, alkaline phosphatase) are usually deranged in hepatic abscess. Blood cultures are positive in patients with pyogenic abscess in only 50% of cases. Immunoassays are positive in amoebiasis in over 90% of cases but may be normal in the early stage of infection (within the first week) before an appreciable immunological response can be mounted.[70] Definitive diagnosis requires US-guided abscess aspiration and culture of the infected contents. Standard treatment involves abscess drainage by US-guided percutaneous catheter placement and a course of appropriate antimicrobial therapy.

The sonographic appearance of pyogenic abscess is highly variable and depends on the pathological stage of the infection.[71,72] The abscess can appear solid in the early stage prior to the onset of parenchymal necrosis.[72] At this stage, sonographic features may overlap with those of other focal hepatic pathologies such as liver tumours.[73] As the evolutionary stage progresses, liquefaction occurs and the abscess will appear increasingly fluid with a mixed echogenic appearance seen.[72] At a later stage, as the abscess matures with central liquefaction, it will appear predominantly cystic. Histologically, at this stage, most abscesses are multiloculated with locules communicating with each other.[72] As the majority of infected patients present at this late stage, pyogenic abscess is most frequently detected as multiloculated cystic hepatic lesions. Due to the cystic contents, posterior acoustic enhancement may be detected on sonography. Internal echoes are frequently seen within the cystic contents as a result of internal debris from necrosis. The abscess typically has well-defined but irregularly shaped thin walls.[71] Gas-containing abscesses (such as those caused by *K. pneumoniae* and *Clostridium*) may demonstrate intense internal echogenicity with posterior reverberation artefact. Colour Doppler interrogation may show flow around the periphery of the abscess and within its parenchymal septations. The majority of pyogenic abscesses resolve to normal parenchyma within 18 weeks following treatment.[74] In a small proportion of cases, residues remain which may calcify.

Typical sonographic features of amoebic abscess are: (1) absence of significant wall echoes, (2) round or oval shape, (3) lower echogenicity than normal liver with fine homogeneous low level internal echoes at high US gain setting, (4) contiguity with the liver capsule[75] and (5) posterior acoustic enhancement. Studies have shown that amoebic and pyogenic abscess cannot be reliably distinguished based on sonographic appearances alone.[76,77] However, Ralls et al.[76] found that two sonographic signs – (1) round or oval shape and (2) hypoechoic appearance with fine homogeneous echoes at high US gain – were more prevalent in hepatic abscesses to a statistically significant degree. Oleszczuk-Raszke et al.[77] found that (1) pyogenic abscess was more likely to have an irregular 'honeycomb' content and ill-defined margins while amoebic abscess was more likely to be a sharper defined lesion with a peripheral halo; (2) both abscess types may contain central liquefaction but this was more common in amoebiasis; (3) multiplicity was more common in amoebic abscess and when present this was likely to be contiguous; and (4) amoebic abscess was slower to heal than pyogenic abscess and more likely to develop echogenic changes. Sonographic findings in patients undergoing treatment for amoebic abscess can be confusing and may worsen (lesions may increase in number and/or size) even when the patient is improving clinically.[71,78] Treated lesions can become anechoic or calcified or persist as cystic appearing foci.[71,78,79] Clinical management should be tailored according to the clinical status of the patient rather than the imaging findings.[71,79]

CEUS contributes to the imaging analysis of hepatic abscess by increasing lesion conspicuity and so improving detection and characterisation (Fig. 10.8). An abscess is typically detected as a lesion with an enhancing rim and a persistent hypoechoic central component.[80] Pulsatile vessels may be seen in the rim or along the internal septa. In comparison to conventional US, the abscess geometry is better appreciated on CEUS with sharper boundaries seen between the normal liver parenchyma and the outer wall of the abscess; and between the inner wall of the abscess and the liquefactive/necrotic center[80] (Fig. 10.9). CEUS can also detect changes in the adjacent liver parenchyma that may not be visualised on conventional US. Transient arterial hypervascularity due to reactive hyperaemia, a peripheral hypovascular area due to oedema or defective venous perfusion, and flow reversal in the adjacent portal vein have been reported.[80–82]

CEUS can be used to differentiate liver abscess from hepatic malignancy. Kim et al.[83] studied the morphological characteristics of pyogenic hepatic abscesses and hypovascular liver malignancies in 24 patients with 16 abscesses and 22 neoplasms. The study found that distinguishing features suggesting pyogenic abscess include a coalescent appearance, a sharp boundary to the necrotic cavity, and lack of internal enhancement. Conversely, the study found that malignant neoplasms generally had ill-defined borders, a variable degree of internal tumour enhancement, and were typically less complex morphologically.

Hepatic steatosis

Hepatic steatosis is commonly seen in the Western world, affecting about 10–15% of the general population.[84] It is characterised by elevated triglyceride accumulation within the liver, as a result of a

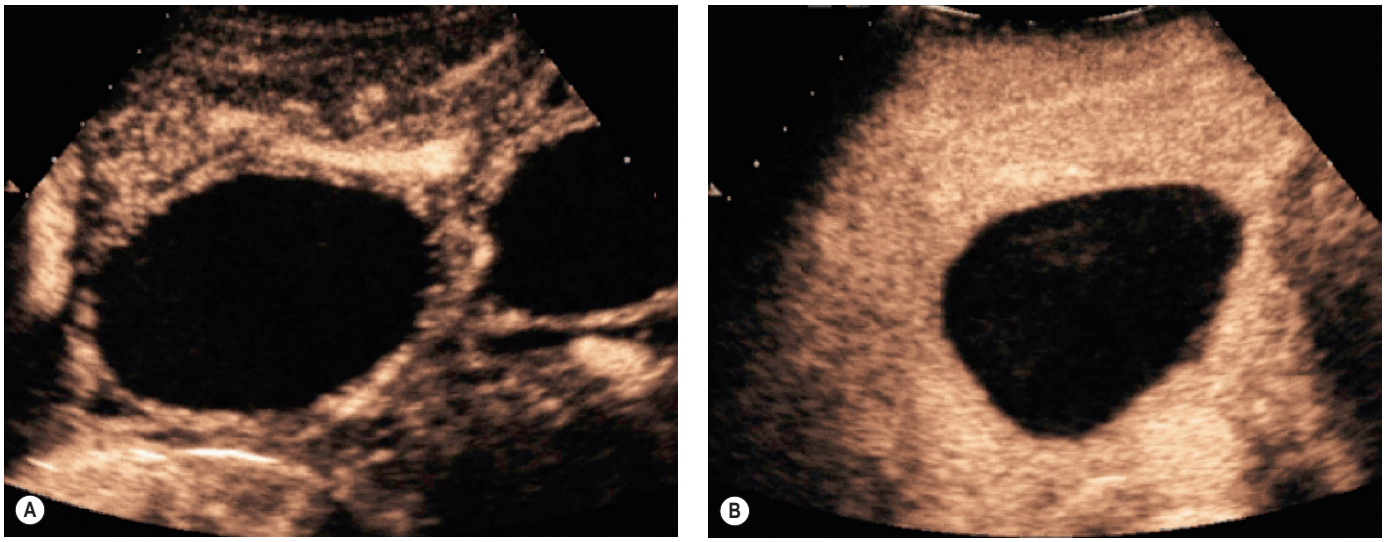


Figure 10.9 **Abscess** in the arterial **(A)** and portal phase **(B)** showing enhancement of capsule with non-enhancement of the fluid content.

variety of predisposing factors.[85–87] The most common aetiological factors associated with development of hepatic steatosis are excessive alcohol consumption, diabetes, obesity and hyperlipidaemia. Less often, hepatic steatosis is secondary to viral hepatitis, drugs (e.g. steroids and chemotherapy agents) and nutritional and dietary abnormalities. Triglyceride accumulation within hepatocytes occurs as a result of defects in hepatocellular lipid metabolism. Macroscopically, the steatotic liver has a yellowish coloration and may be enlarged.[88] Microscopically, lipid vacuoles are seen within involved hepatocytes and this enables the severity of steatosis to be quantified based on the proportion of hepatocytes that contain fat inclusions (mild <30%, moderate 30–60%, severe >60%).[88] Lipid accumulation is non-uniform in the early stage and has a geographic bias with hepatoctyes situated close to central veins more susceptible than those situated close to portal triads.[84] At an advanced stage, a more uniform liver involvement is typically seen. Generalised hepatic steatosis is visualised sonographically as a homogeneous increase in liver echogenicity, which exceeds that of renal cortex and spleen. Poor depth penetration leading to reduced appreciation of hepatic architecture is also typically present as a result of the increased attenuation of US waves in hepatic steatosis compared to normal hepatic parenchyma. Steatosis, particularly when there is non-uniform liver involvement, dramatically increases the complexity of conventional sonographic interpretation.[89–91] Lesions that conform to a nodular shape can be misdiagnosed as neoplasms.[89,90] Detection and characterisation of other pathologies can be compromised as a consequence of loss of typical sonographic features that enable pattern recognition, due to image distortion from the steatotic background.[91,92]

Several patterns of non-uniform hepatic steatosis have been recognised on imaging.[93,94] These include: (1) focal fat sparing in a generalised fatty liver, (2) focal steatosis, (3) multifocal steatosis, (4) lobar or segmental steatosis and (5) perivascular steatosis. Focal fat sparing and focal/multifocal steatosis can mimic other focal liver pathologies on imaging, and are discussed below.

Focal fat sparing

The pathogenesis of this condition is uncertain, but a disturbance in portal flow has been suggested.[88,94] As lipid delivery to the liver from the gastrointestinal tract is via the portal venous system, a geographic reduction of portal flow (due to third hepatic inflow from aberrant venous supply) to part of the liver is hypothesised to spare hepatocytes in that area from steatosis.[88] Typically locations for focal fat sparing include segment IV around the gallbladder fossa, adjacent to the left portal vein, the porta hepatis, adjacent to the falciform ligament and in subcapsular areas. On conventional US, areas of focal fat sparing appear hypoechoic against the echogenic background of hepatic steatotic. A geographic margin (abruptly angled) and absence of mass effect on adjacent liver parenchyma and vessels is typical. Colour Doppler ultrasound may be useful in demonstrating a normal vascular distribution in affected areas with no evidence of vessel displacement. On CEUS, focal fat sparing is isoechoic to the rest of the liver parenchyma on all vascular phases (arterial/portal/late phase)[95,96] (Fig. 10.10).

Focal steatosis

This is less common than focal fatty sparing. The pathogenesis is uncertain but abnormal accumulation of fat may occur as a result of ischaemia due to decreased portal venous blood flow or decreased delivery of unknown substances via the portal vein.[88] A key factor is related to increased insulin load in portal blood. Focal steatosis occurs in similar locations to focal fat sparing such as the gallbladder fossa, adjacent to the falciform ligament, the porta hepatis and subcapsular locations. This is because both conditions are related to venous anomalies in those areas of the liver. Focal steatosis is hyperechoic to the background liver and typically has a geographic outline. Focal steatosis does not exhibit mass effect on the adjacent liver parenchyma or vessels. On CEUS, focal fat is isoechoic to the rest of the liver parenchyma on all vascular phases (arterial/portal/late phase). A study by Liu et al.[94] found that contrary to the norm, the enhancement pattern of focal steatosis may exhibit hypoenhancement in the arterial phase (in 11 of 25 lesions in the study), which may reflect unusual blood supply and/or histological changes.

Multifocal steatosis

This is a rare presentation of focal fatty infiltration, which can mimic metastatic disease particularly when it has a nodular configuration.[97] Correct diagnosis is challenging, especially in patients with known malignancy. Multifocal steatosis appears as multifocal areas of increased echogenicity compared to the background liver. Clues to its presence include lack of mass effect, and stability over time. On CEUS, multifocal steatosis is isoechoic to the rest of the liver parenchyma on all phases (arterial/portal/late phase).

In all these cases of non-uniform hepatic steatosis, a confident diagnosis can be made on CEUS based on an enhancement pattern

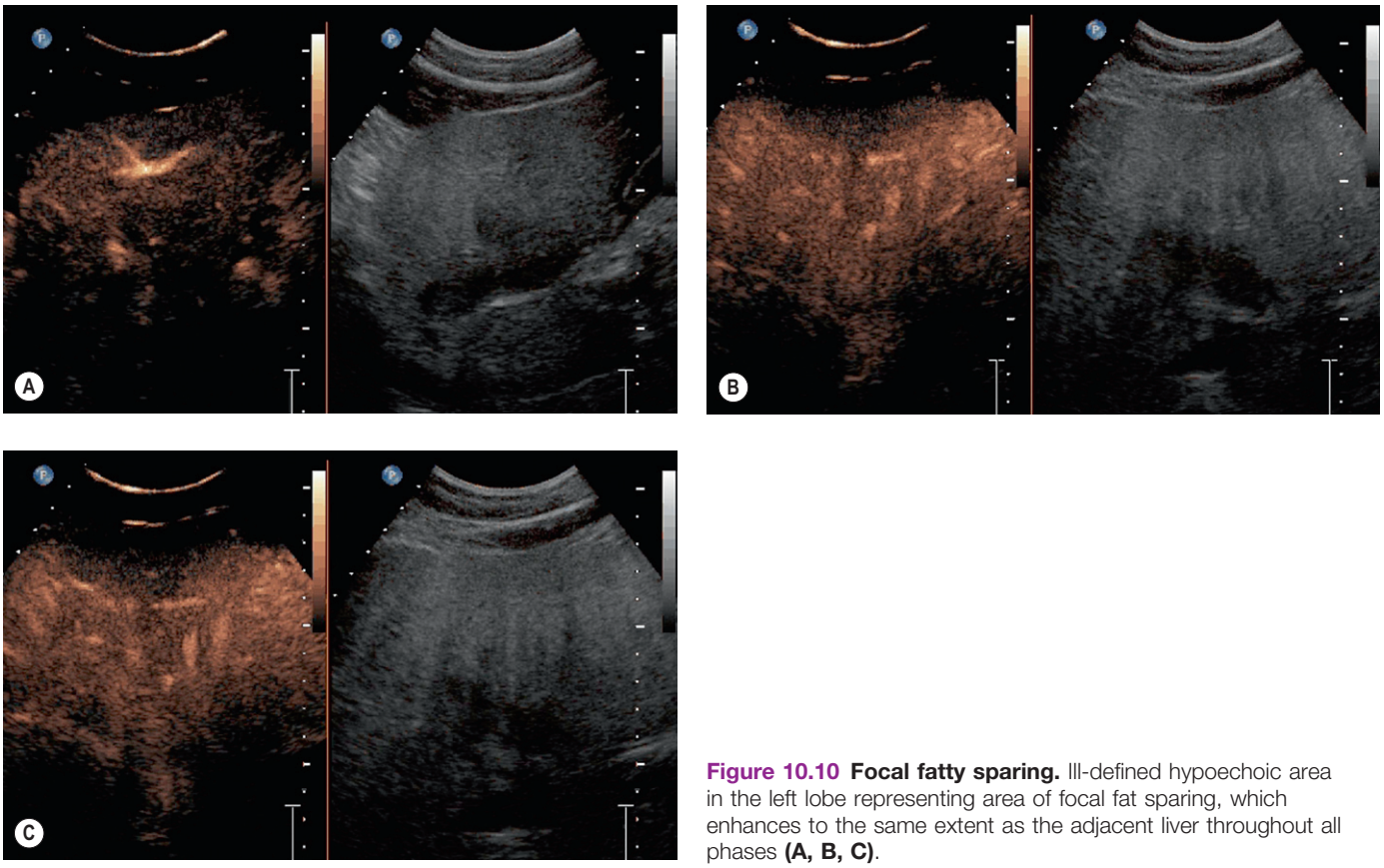


Figure 10.10 Focal fatty sparing. Ill-defined hypoechoic area in the left lobe representing area of focal fat sparing, which enhances to the same extent as the adjacent liver throughout all phases **(A, B, C)**.

which is identical to that of background liver. CEUS also improves the detection and characterisation of liver neoplasms that coexist in the steatotic liver as these lesions may be diagnosed based on recognised enhancement patterns, which remain unaltered.[92,95]

Liver haematoma

Liver haematoma is most commonly caused by blunt abdominal trauma, with the liver being the second frequent abdominal organ injured during blunt trauma (after the spleen). The liver is susceptible to trauma due to its large size (the largest intra-abdominal organ), its relatively fixed position in the abdomen and its proximity to bony structures such as ribs and spine. Other predisposing causes for liver haematoma include surgery, liver biopsy, coagulopathy, intra-tumoral haemorrhage and pregnancy. Hepatic haematomas are also frequently found in newborns at perinatal autopsy, but are usually small, subcapsular in location and clinically silent.[98] It is postulated that the delicate hepatic capsule and its connections to the collagen along the sinusoids provide the pathogenesis of these haematomas in neonates.[98]

Haematomas may have variable shapes and echogenicity. Subcapsular haematomas typically have a lentiform shape which conforms to the outer contour of the liver capsule. Intraparenchymal haematomas are typically spherical with irregular walls but may also follow given anatomical structures resulting in a more starlike configuration.[99] The ultrasound appearance of haematoma depends on the severity of the bleed and the timing of the scan relative to the onset of bleeding.[100] Acute and subacute haematomas appear homogeneous and hyperechoic (due to multiple acoustic interfaces as a result of the fibrin and erythrocytes in the haematoma), whereas in chronic cases, the haematoma appears more cystic with internal echoes due to clot liquefaction.[100] Fluid–fluid levels can be seen in haematomas due to the haematocrit effect. Internal septations, which float freely during real-time scanning and which do not show vascularity on colour Doppler US interrogation, are a recognised finding. Serial US will show a change in size and appearance of the haematoma with time. Eventually, over a period of months, the haematoma will resolve due to regeneration of liver tissue, but a residual scar or cystic space may persist. On CEUS, haematoma is hypoechoic on all vascular phases. Haematomas secondary to intratumoral haemorrhage in a pre-existing hepatic neoplasm will show avascularity of the haematoma juxtaposed with the vascular pattern of the underlying tumour. CEUS is a useful supplement to conventional US in the assessment of trauma patients, with studies showing superior detection of solid organ injuries with CEUS compared to conventional US.[101,102] Liver lacerations typically appear as well-defined hypoechoic linear or branched areas while contusions appears as ill-defined hypoechoic areas without clearly defined margins – these are best appreciated on the portal venous phase[103] (Fig. 10.11). Active haemorrhage is identified as an extravasation of microbubbles into the haematoma and suggests a more clinically significant injury. Performance of CEUS may almost approach that of contrast CT in the assessment of trauma patients, and CEUS may have a role in the triage of trauma patients who cannot undergo CT due to haemodynamic instability but who could have a bedside ultrasound examination in the emergency unit.[101] In addition, CEUS could be used in the follow-up of hospitalised patients with known solid organ injuries who are managed conservatively and who cannot be easily moved to the CT suite.[101]

Rare benign lesions

The findings on conventional US and CEUS of several documented rare focal liver lesions are discussed.

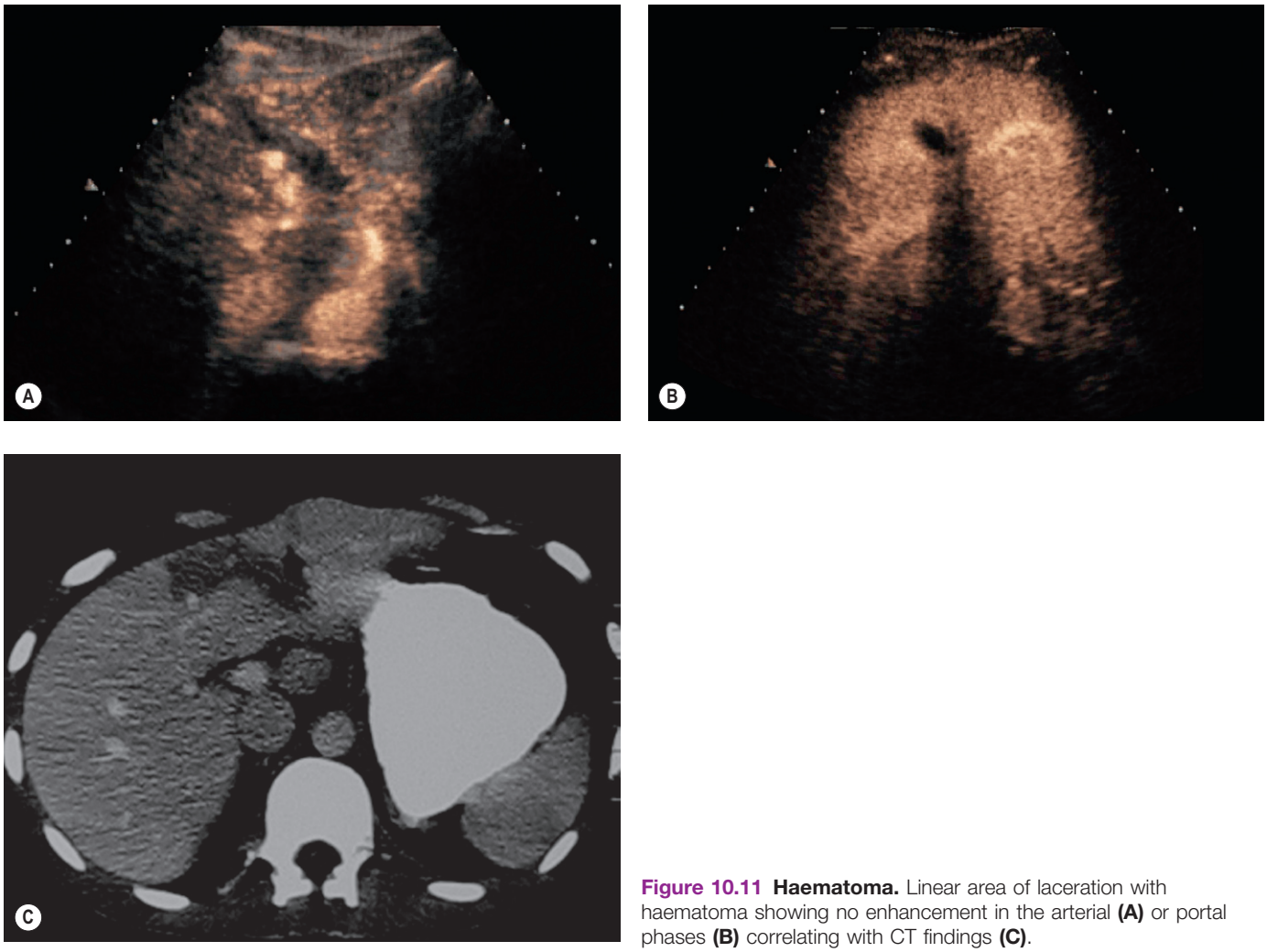


Figure 10.11 Haematoma. Linear area of laceration with haematoma showing no enhancement in the arterial **(A)** or portal phases **(B)** correlating with CT findings **(C)**.

Hepatic angiomyolipoma

Angiomyolipoma (AML) is a mesenchymal tumour containing varying proportions of three elements – mature adipose tissue, smooth muscle and thick-walled blood vessels. It is classified histologically into mixed, lipomatous, myomatous and angiomatous types.[104,105] It is an extremely rare tumour of the liver and is usually diagnosed postoperatively or by autopsy. Hepatic angiomyolipoma can be diagnosed preoperatively according to the following findings: (1) hypervascular nature on imaging suggestive of vascular proliferation within the tumour, (2) imaging findings of intratumoral fat and (3) positive actin and HMB-45 stains on biopsy specimens which confirms smooth muscle component.[106–109] On conventional US, AML may show increased echogenicity secondary to presence of intra-tumoral fat. However, the fat content within AMLs varies ranging from 5% to 90% and can lead to atypical imaging appearances.[106] Fat-poor AMLs can therefore appear as hypo- or isoechoic lesions. In these cases, evaluation of the haemodynamic characteristics of the hypervascular tumour is more useful for diagnosis. Colour Doppler imaging can reveal avid tumour vascularity and pulsatile flow.[110] In a study of 2209 focal liver lesions using CEUS, Xu et al.[111] reported the enhancement pattern of four biopsy-proven hepatic AMLs. All lesions showed rapid heterogeneous ($n = 1$) or homogeneous ($n = 3$) hyper-enhancement during the arterial phase with enhancement commencing 10–16 seconds after contrast injection. Intra-lesional and peri-lesional arteries were present in all cases. During the portal phase, half the cases showed slight hyper-enhancement and the other half showed iso-enhancement. In the late phase, all lesions showed iso-enhancement. Zheng and Kudo[106] demonstrated on CEUS that the efferent vessel in two cases of hepatic AML was the hepatic vein, confirmed by conventional angiography and CT angiography. The authors postulated that this haemodynamic finding may be an important characteristic of hepatic AMLs and may facilitate the differential diagnosis from other focal hepatic tumours such as HCC where the main drainage vessel is the portal vein.

Hepatic lipoma

Histologically this lesion is composed of mature adipose tissue.[104,105] On conventional US, hepatic lipomas appear as well-defined uniformly hyperechoic lesions.[112] These lesions may or may not show acoustic shadowing on US. Xu et al.[111] found a liver lipoma that showed inhomogeneous hyper-enhancement in the arterial phase with iso-enhancement on the portal venous and late phases.

Intrahepatic biliary cystadenoma

Biliary cystadenoma is a rare cystic neoplasm of the liver and accounts for less than 5% of all cystic lesions of the liver, with fewer than 200 cases reported globally.[113] Histologically, the tumour is a multiloculated cystic lesion lined by mucus-secreting cuboidal or columnar epithelium with an accompanying dense cellular 'ovarian like' stroma.[114] The tumour usually presents in middle-aged women with a mean age of 50 years and with a great variability in size

ranging from 1.5 to 30 cm.[115] The majority of patients are asymptomatic but large tumours can present with a palpable mass and cause symptoms. The tumour is slow growing but is postulated to be premalignant with risk of malignant transformation as high as 30%.[116] Biliary cystadenoma has a tendency to recur following surgical excision. On conventional US, cystadenoma appears as a well-defined anechoic cystic mass with echogenic septations and/or papillary infoldings.[104,111] Xu et al.[111] reported a case of cystadenoma that showed hyper-enhancement of the cystic wall, internal septations and an intracystic solid portion during the arterial phase with contrast washout in these areas during the portal and late phases. Lin et al.,[117] in a blinded reader study on the diagnostic performance of CEUS for complex cystic focal lesions, found two cases of histologically proven cystadenomas; they appeared as a well-defined unilocular or multilocular cystic mass which rarely contained mural or septal nodules. On CEUS, the tumour showed septal enhancement in the arterial phase and hypo-enhancement during the portal venous and late phases.

Biliary epithelial dysplasia of the intrahepatic bile duct

This is a premalignant lesion that arises from the epithelium of the intrahepatic bile duct.[118] Xu et al.[111] found one histologically proven lesion which was slightly hyperechoic and located within a dilated bile duct on conventional US; on CEUS, the lesion showed homogeneous enhancement during the arterial phase with washout in the portal venous and late phases. Sonographically, the lesion is difficult to separate from an intrahepatic cholangiocarcinoma.

Hepatic inflammatory pseudo-tumour

Inflammatory pseudo-tumour is a benign hepatic mass consisting of inflammatory cells and fibrous stroma on histological examination.[119] The aetiology is unclear but it is postulated to be secondary to an inciting hepatic infection.[120] The lesion may have variable non-specific appearances on imaging studies. The mass may be well defined or poorly defined, have variable echogenicity (hypo- or hyperechoic or mixed), may contain multiple septa, and can have posterior acoustic enhancement.[121,122] Inflammatory pseudo-tumour can be hypo- or hypervascular. Ding et al.[123] found that all four lesions in their study showed hypo-enhancement throughout all phases on CEUS. Xu et al.[111] had seven lesions in their study, which showed a mixture of hyper-, iso- or hypo-enhancement, either homogeneous or heterogeneous in the arterial phase with all lesions showing hypo-enhancement in the portal venous and late phases. Due to non-specific imaging appearances, diagnosis of inflammatory pseudo-tumour can be difficult and may require biopsy.

Peliosis hepatis

This is a rare benign vascular lesion characterised by sinusoidal dilatation and blood-filled hepatic spaces. Various aetiological factors have been described including infectious agents such as *Bartonella* and HIV, malignancies such as HCC, renal and cardiac transplantation, diabetes, drugs such as steroids and oral contraceptives and toxins such as arsenic and polyvinyl chloride.[124] It is idiopathic in 50% of cases. The pathogenesis is unknown but possible causes include increased sinusoidal pressure, disappearance of normal parenchyma by hepatocyte necrosis, and sinusoidal wall weakening.[111,125] On conventional US, peliosis hepatis demonstrates variable echogenicity relative to the surrounding liver and may have internal vascularity on colour Doppler US imaging.[126,127] The lesion is typically hyperechoic but can show iso-, hypo- or mixed echogenicity due to the variety of its possible histological features as well as the possibility of additional haemorrhage. Perinodular and intranodular vascularity can be seen on colour Doppler US imaging. Two histologically proven lesions had previously been reported, which showed homogeneous hyper-enhancement in one lesion and iso-enhancement in the other lesion during the arterial phase, associated with washout in both lesions during the portal and late phases.[111]

Hepatic sarcoidosis

Hepatic or splenic sarcoid granulomas are found in 40–70% of patients with sarcoidosis.[128] Liver involvement is usually not appreciable on imaging but when identified the most commonly observed pattern is non-specific textural heterogeneity and hepatomegaly.[129] Conventional US may demonstrate normal or increased liver echogenicity, hepatomegaly, coarsening of liver texture with or without discrete nodules (which can be of variable echogenicity), focal calcifications and contour irregularities.[111,128,130] Hepatic sarcoidosis showed hypo-enhancement on CEUS in all phases.[111]

Solitary necrotic hepatic nodule

This is a very rare benign lesion of uncertain aetiology. The pathogenesis is probably multifactorial and could be related to pathologies such as parasitic infection, trauma or sclerosing haemangiomas.[131] Histologically, the mass shows a uniform complete necrotic core with a dense hyalinised fibrous capsule containing elastin fibres with inflammatory cells.[132] On conventional US, the solitary necrotic nodule is usually hypoechoic or a 'target' lesion with a hyperechoic centre.[111] No enhancement is seen on CEUS on all vascular phases.[111,133]

MALIGNANT FOCAL LIVER LESIONS

Liver metastasis

The liver is a frequent site for metastasis from the gastrointestinal tract cancers and is one of the most common clinical requests for abdominal US imaging. Metastatic disease of the liver is about 20 times more common than any of the primary hepatic neoplasms. It is a sign of advanced tumour stage and implies a very poor prognosis. In the Western world, colorectal cancer accounts for 14–16% of cancer deaths in men and women respectively with approximately 25% of patients having liver involvement at the time of initial presentation and up to 50% will develop hepatic metastases during the course of their disease.[134,135] For patients with colorectal hepatic metastases, surgical resection is the treatment of choice with 10–20% of patients being candidates for potentially curative resection; resection is indicated if there is no unresectable extrahepatic disease, if liver deposits can be resected with a free clearance margin of 1 cm and if there is adequate liver reserve. The 5-year survival rates vary from 25 to 40%.[136,137] Seventy-five per cent of those who undergo liver resection will develop recurrence and of these, the liver is involved in 50%. For metastases from other primary malignancies such as pancreatic cancer, hepatic involvement signifies poor prognosis and only palliative treatment can be offered.

Hepatic metastases typically appear as multiple focal discrete lesions in 90% of cases, but solitary lesions may also occur.[100] Diffuse infiltrative hepatic involvement may be seen in breast cancer or lymphoma. On conventional ultrasound, a metastasis may appear hypoechoic, hyperechoic or of mixed echogenicity and some look like target lesions.[138] These appearances are non-specific in determining the primary tumour. CEUS appearance of metastasis is variable depending on the size and vascularity of the tumour and the degree of necrosis. Metastases of the same cellular type (e.g. colon) may vary in their enhancement characteristics and metastases of different cellular types (breast and colon) may produce identical appearances.[139,140] Hepatic metastases from colon and lung carcinomas had previously been described as being hypovascular. However, on continuous scanning at low MI using non-linear imaging modes, these lesions usually show some peri-tumoral

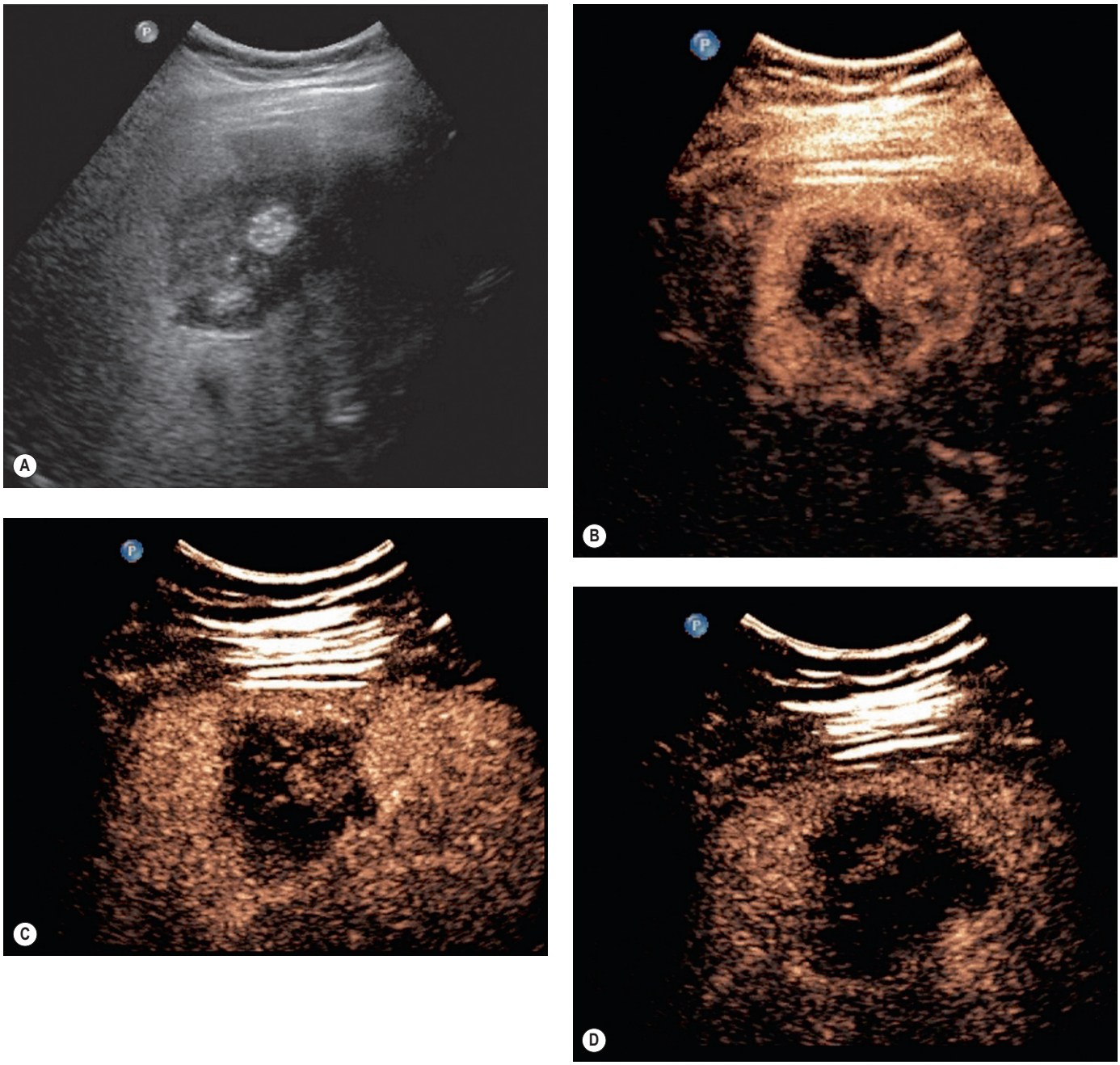


Figure 10.12 Metastasis. Mixed echogenic tumour at baseline **(A)** showing rim enhancement in the arterial **(B)** and portal **(C)** phases and complete filling defect in the late phase **(D)**.

vessels with central necrosis or homogeneous enhancement during the arterial phase; during the portal phase, they typically appear as hypoechoic filling defects surrounded by a brighter liver parenchyma and rim enhancement (Fig. 10.12).[13] For lesions that are hyperechoic at baseline, there is a characteristic reversal of the echogenicity to become hypoechoic in the portal and late phases. Smaller colorectal liver metastases may show a more uniform display of the intra-lesional vessels during the arterial phase; however, during the portal phase, the liver parenchyma enhances and the metastases may appear as echo-poor filling defects with or without rim enhancement. In contrast, hypervascular metastases (such as the carcinoids, islet cell, melanoma, breast, renal or thyroid malignancies) become markedly hyperechoic during the arterial phase. In the portal phase, these hypervascular lesions may become isoechoic to adjacent liver parenchyma and the contrast agent washes out of the lesions gradually to become hypoechoic to the surrounding liver with improved delineation[13] (Fig. 10.13). In the case of breast and colonic metastases, there may be a combination of both hyper- and hypovascular lesions; some of the hypervascular lesions may become isoechoic to surrounding liver parenchyma during the arterial phase but can still be recognised by virtue of the microbubbles' haphazard movement within the hypervascular lesions. During delayed imaging with sinusoidal/liver-specific agents, both hyper- and hypovascular metastases characteristically appear as hypoechoic lesions with or without rim enhancement in a background of echogenic liver.[13]

Conventional US is particularly poor for detecting metastases that are small (especially <1 cm in size) or isoechoic compared to surrounding liver parenchyma.[141] CEUS has improved detection of liver metastases compared to conventional US based on published literature.[142–146] In a study comparing conventional versus CEUS in the detection of liver metastases, the average number of confirmed

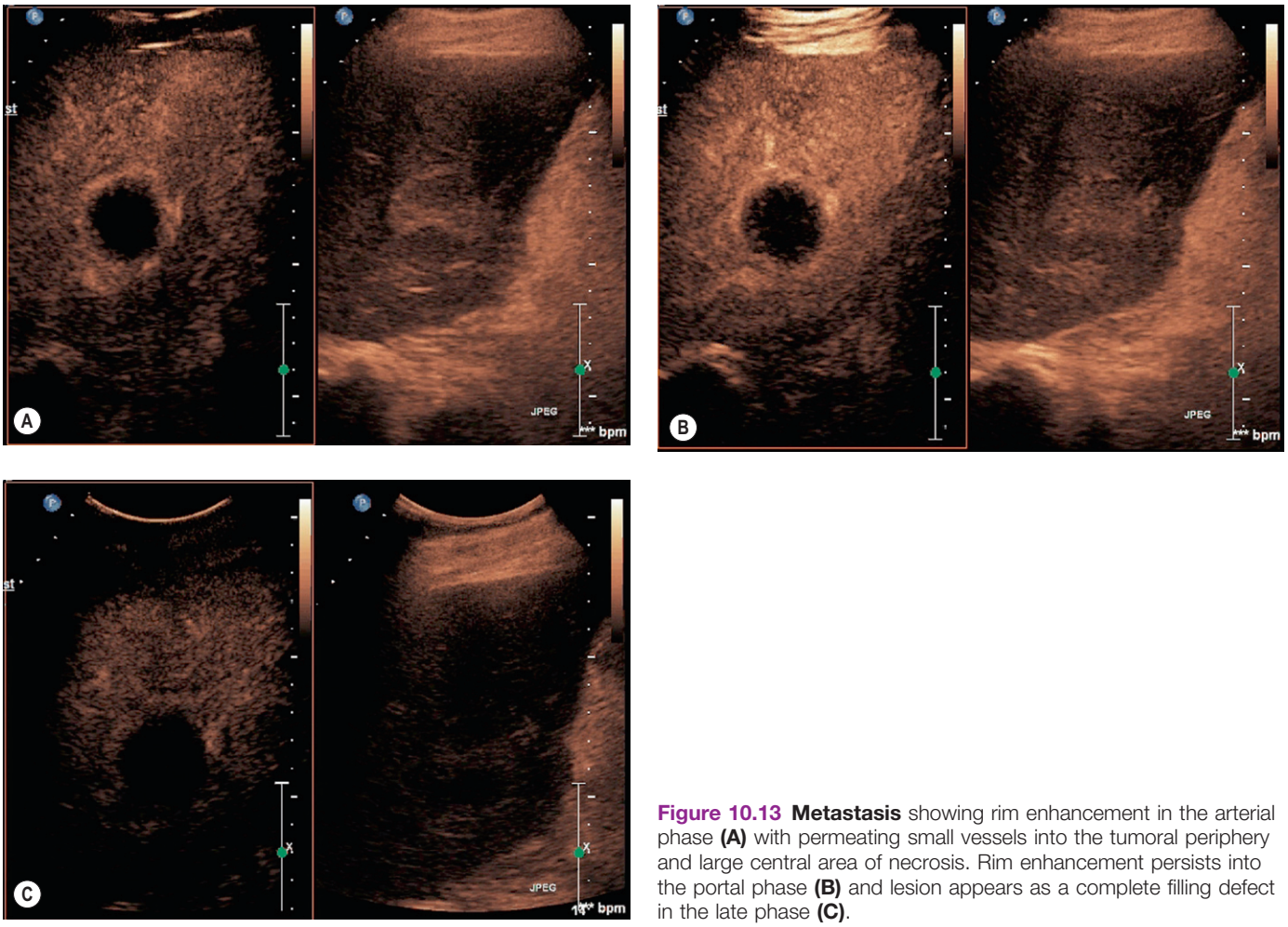


Figure 10.13 **Metastasis** showing rim enhancement in the arterial phase **(A)** with permeating small vessels into the tumoral periphery and large central area of necrosis. Rim enhancement persists into the portal phase **(B)** and lesion appears as a complete filling defect in the late phase **(C)**.

metastases increased from 3.06 to 5.42 following contrast administration; the sensitivity for detecting individual metastases significantly improved from 63% to 91%. More importantly sub-centimetre lesions were identified in over 92% of confirmed cases following contrast compared with 54% at baseline.[147] In a multicentre study of 123 patients evaluating conventional US versus CEUS for the detection of liver metastases, similar results were observed with the sensitivity for detection of individual lesions improving significantly from 71% to 87% following contrast administration. Furthermore the specificity also improved significantly from 60% to 88%; in a small subgroup of patients CEUS also showed more metastases in 32% of patients than did contrast-enhanced CT.[143] In a subsequent multicentre study of 157 patients, off-site blinded readers showed improved sensitivity for detection of individual lesions from 38% to 67% following contrast injection, and the characterisation of the lesions was also improved with none of the metastases showing contrast uptake in the late phase.[148] Compared with contrast-enhanced helical CT scan, CEUS was shown to detect more metastases in 12%, equal number in 74% and fewer in 14% of the 83 patients presenting with fewer than five lesions.[149] There was no significant difference in the accuracy between contrast-enhanced helical CT and CEUS. More recently Konopke and colleagues showed that CEUS significantly improved the sensitivity of US from 56.3% to 83.8% in the detection of liver lesions in a prospective study of 108 patients suspected of having liver metastases using histology and intraoperative US as the reference standard.[150] CEUS led to the improved detection of sub-centimetre lesions, subcapsular lesions and lesions adjacent to the ligamentum teres in patients who had had adjuvant chemotherapy.

Improved detection of liver metastases with contrast-enhanced intraoperative US (CE-IOUS)

More recently, we assessed the value of CE-IOUS in 60 consecutive patients undergoing liver resection of metastases. The technique for IOUS and CE-IOUS is as described above.[144] Metastases identified on CT and/or MR, IOUS and CE-IOUS were counted, sized and mapped according to the Couinaud classification on a liver schematic chart for each modality and in real-time for all the sonographic examinations. Benign cysts were not included in the counts. The excised liver segments or lobes were sectioned at pathology to obtain a true pathologic gold standard of the lesions. Correlation with resection/biopsy histopathology findings was also carried out. Changes in surgical management following CE-IOUS compared with those made after IOUS were documented (e.g. abandoned resection, more extensive resection, limited resection or combined resection with radio-frequency ablation, etc.).

A total of 107 lesions were identified on histopathology findings of biopsies and resected tissues and of these 103 were confirmed metastases and 4 haemangiomas. The number of correctly identified metastases on CT/MRI combined, IOUS and CE-IOUS was 79,

84 and 101, respectively. There was a statistically significant increase in the number of detected metastases on CE-IOUS compared with IOUS and also with combined CT/MRI ($p = 0.029$ and $p = 0.047$, respectively). No statistical difference was observed in the number of metastases detected between IOUS and combined CT/MRI ($p = 0.53$). For CT/MRI, IOUS and CE-IOUS, the sensitivity was 76.7%, 81.5% and 96.3%, respectively; accuracy was 73.8%, 78.5% and 96.3%, respectively; the positive predictive value was 95.2%, 95.5% and 98.0%, respectively. The mean (±SD) size of the lesions identified on CT/MRI/IOUS combined and CE-IOUS was 2.73 (±1.46) cm and 1.71 (±1.57) cm, respectively. The median size of the additional lesions identified on CE-IOUS was 0.8 cm. The smallest metastasis identified was 4 mm in diameter. Of the 60 patients, CE-IOUS was not performed in 3 patients, 2 patients had peritoneal metastases at exploration, and 1 patient had widespread metastases in a background of fatty liver on the basis of IOUS. In 40 of the remaining 57 patients, there was no alteration in the surgical management; CE-IOUS detected no additional lesion in 37 patients; in 2 cases there were additional lesions but they did not entail any extended resection or adjunctive surgical manoeuvres; in another patient, one of the lesions was wrongly diagnosed on IOUS and CT as metastasis and was accurately identified as a benign haemangioma on CE-IOUS. In contrast, new information identified on CE-IOUS alone altered the surgical plan in the remaining 17 of 57 patients (29.8%); additional hepatic metastases were detected in 11 cases (19.3%), which extended to a tri-segmentectomy in 3 cases, additional non-segmental wedge resection in 2 patients and radio-frequency ablations of the additional lesions in 6 cases, as an adjunct to the planned hepatic lobectomy. Prior to radio-frequency ablation all additional lesions were biopsied and confirmed as metastasis; all biopsies and radio-frequency ablations were performed using CE-IOUS guidance. In 2 patients (3.5%) there were fewer lesions than identified on preoperative imaging scans and could not be confidently excluded on IOUS alone, which resulted in alteration in the original surgical plan from right hepatectomy to excision of three segments in one and removal of segment VII/VIII plus a metastasectomy in the other. CE-IOUS also confirmed presence of an arteriovenous malformation in one patient (1.8%), which was not identified on IOUS and was previously diagnosed as apparent solitary metastasis on CT; CE-IOUS also accurately diagnosed a solitary benign haemangioma with characteristic peripheral nodular enhancement with progressive filling-in over the vascular and late phases in 2 patients (3.5%) which were wrongly identified as metastasis on CT and IOUS. Previously planned resections were therefore not carried out. In one case the tumour margin could only be clearly visualised on CE-IOUS to be too close to the inferior vena cava for resection and it was ablated instead. New findings on CE-IOUS alone also altered IOUS/CT/MRI hepatic staging in 35.1% (20 of 57) of patients.

In many centres, hepatic ultrasonography remains the primary imaging modality of choice in imaging the liver for suspected metastases from primary tumours such as: breast, melanoma, oesophagus, stomach, pancreas and lung. This practice is merely historical, readily available and cheap (compared to CT or MR) and is usually triggered by the patients' abnormal liver function tests or raised tumour markers; the identification of liver metastasis is also used as a prognostic indicator of poor outcome. For these tumour types, in contrast to colorectal cancer, 'global detection' of hepatic metastasis, i.e. whether metastasis is present or not, is the primary goal rather than 'the actual number and localisation' of the metastasis as liver resection is usually not an option. In that context, CEUS should be implemented for improved detection.[151] The recommendations of the European Federation of Societies for Ultrasound in Medicine and Biology (EFSUMB) regarding use of CEUS for liver metastases are:[13]

1. CEUS should be performed to rule out liver metastasis unless conventional US shows clear evidence of the lesions.
2. CEUS should be used in selected cases, when clinically relevant for treatment planning, to assess the number and location of liver metastases as a complement to contrast-enhanced CT and/or MRI.
3. CEUS should be used routinely in the surveillance of oncology patients.

Hepatocellular carcinoma

Incidence

Hepatocellular carcinoma (HCC) is a malignant neoplasm composed of cells with hepatocellular differentiation.[152] It is the most common primary liver malignancy, the fifth most frequent cancer type and third most frequent cause of cancer-related deaths globally.[153] More than half a million new cases are diagnosed yearly with an age-adjusted worldwide prevalence of 5.5–14.9 per 100 000 population.[154] In some parts of Asia, HCC is the leading cause of death from cancer. In the developed world, the incidence of HCC has increased in the past two decades largely attributable to hepatitis C virus infection.[155] In the United States, the average annual age-adjusted incidence of HCC increased from 1.3 per 100 000 in 1981–1983 to 3 per 100 000 in 1996–1998 with a 25% increase between 1993 and 1998.[156] In more than 80% of cases, HCC occurs in the cirrhotic liver, and in these patients HCC constitutes the leading cause of death.[154] HCC is up to 16 times more common in patients with cirrhosis than in those without cirrhosis (annual incidence 2–6.6% in cirrhotics and 0.4% in non-cirrhotics).[154] In patients with cirrhosis, the incidence of HCC at 5 years may exceed 25%.[157]

Screening and surveillance of HCC

Early tumour detection while it is still at a low grade and is amenable to curative treatment is the hallmark of a successful screening programme. Screening and surveillance for HCC remains a clinical challenge. Despite the lack of concrete evidence of any true survival benefit or cost-effectiveness, it is now becoming widely accepted among hepatologists and endorsed by the World Health Organization that it should be routine in the management of patients with end-stage liver disease. Nevertheless some of the rationales for screening and surveillance are compelling.

The worldwide incidence of HCC is increasing but more noticeably in North America and Europe; it is now believed that the rise in the latter continents, which is progressively affecting younger patients, is mainly due to the rise in hepatitis C viral infection, whilst the rates associated with alcoholic cirrhosis and hepatitis B virus infection have remained stable.[158] The disease is extremely lethal, with median survival rates of untreated symptomatic cases ranging between 4 and 6 months. Even for patients with small tumours there is a significant mortality as less than 50% will survive 5 years despite undergoing apparently curative resection.

The target population for screening and surveillance for HCC is readily identifiable. Chronic hepatitis B and C virus infections are well recognised to increase the risk of HCC. In Europe, approximately 28% of liver cancer has been attributed to chronic hepatitis B virus infection and 21% to hepatitis C virus infection,[159] but the risk is greatest in the presence of co-infection with both hepatitis B and C virus; male sex and alcohol abuse are also significant risk factors.[160] Cirrhosis is another major risk factor irrespective of the aetiology. The annual risk of developing HCC in cirrhosis ranges between 1% and 6%.[161,162] The risk is higher in patients with cirrhosis caused by viral infection compared with non-viral causes. However, patients with cirrhosis as a result of genetic haemochromatosis also have high rates of HCC. In a prospective study of 152 patients with haemochromatosis (homozygotes) by Fargion et al.,[163] of those with liver cirrhosis 29% developed HCC whilst none of those without cirrhosis developed HCC; age over 55 years, presence of HBsAg and alcohol abuse increased the relative risk of HCC by 13.3-, 4.9- and 2.3-fold, respectively.

In contrast, the estimated incidence of HCC in patients with primary biliary cirrhosis is 2.4%.[164] The development of HCC appears to be restricted to patients with stage III/IV disease and the incidence is 5.9% in that category. The male sex has a significant impact on disease outcome; the incidence of HCC in female patients is low compared to male patients (4.1% versus 20%). In the presence of advanced disease the incidence for male compared to female patients is even higher (45.4% versus 8.3%). The reason for the increased risk of HCC development in male compared to female cirrhotic patients with primary biliary cirrhosis is unclear. It has been suggested that this may be the result of increased incidence of underlying risk aetiologies such as alcohol abuse and chronic hepatitis B carriage in males. However, in the study report of Jones et al.,[164] such confounding aetiological factors including hepatitis B and C, alcoholic liver disease and haemochromatosis have been excluded, which therefore confirms that the risk for HCC is truly increased in males. The incidence of hereditary causes of cirrhosis such as Wilson's disease, alpha-1-antitypsin deficiency, galactosaemia, type IV glycogen storage disease, tyrosinaemia, Osler–Weber–Rendu syndrome and familial cirrhosis and autoimmune cirrhosis is not clearly established but is presumably much lower than the above-mentioned well-recognised aetiologies.

Whilst cirrhosis is a major risk factor irrespective of aetiology, up to 56% of patients presenting with HCC have previously undiagnosed cirrhosis.[165] Cirrhosis may be easily diagnosed by any cross-sectional imaging modality if characteristic features such as nodular hepatic contour, ascites and/or varices are present. Conventional US has a sensitivity of 43–87.7% and a specificity of 79.9–100% for diagnosing cirrhosis, with the most widely accepted signs of disease being (1) enlargement of the caudate lobe with an increased caudate to right lobe ratio, (2) superficial nodularity – best appreciated on high-frequency US probes and (3) a coarse parenchymal echo pattern.[166] However, in the early stages of the disease, it may be impossible to differentiate between stage III fibrosis and cirrhosis. If the presence of cirrhosis alone were to be used to define the target population, these patients would not have been recruited into the screening or surveillance programme. Zaman et al.[165] also showed that those patients with occult cirrhosis were predominantly HBsAg-seropositive. Therefore patients with chronic viral hepatitis as well as those with overt cirrhosis have to be included in any screening or surveillance programme.

Serum alpha-fetoprotein levels (AFP) and conventional ultrasonography have been the most commonly used screening tests for HCC. The ideal screening tests should also have high sensitivity and specificity. The performance of AFP has been poor in that respect with a sensitivity of 39–64%, a specificity of 76–91% and a positive predictive value of 9–32%.[167–169] In addition, rise in levels of AFP is not specific for HCC and it may also increase transiently, persistently or intermittently with flares of active hepatitis. In contrast, within the context of screening healthy HBsAg carriers as well as cirrhotic patients, ultrasound has been shown to have a sensitivity of 71% and 78%, respectively, specificity of 93% but with a positive predictive value of 14% and 73%, respectively.[167,169] These could be improved further with the administration of a USCA.

Previous reported surveillance intervals ranged between 3- and 12-month intervals and it is now generally accepted that the intervals should be 6 months taking into account reported median tumour doubling time, which is about 117 days.[170] There are as yet no studies to determine the best recall policy; however, at the consensus meeting of the European Association for the Study of Liver in Barcelona in 2000,[171] it had been suggested that cirrhotic patients should undergo 6-monthly ultrasound and AFP levels assessment; patients who have no nodule on US but have increasing AFP levels should have spiral CT of their liver performed; for those patients with a nodule of less than 1 cm, 3-monthly ultrasound is recommended on the basis that these lesions are far too small to characterise accurately and at least 50% of these sub-centimetre lesions will not be HCC; patients with a nodule of over 2 cm should have AFP levels over 400 ng/mL and CT, MRI or angiography evidence of lesion hypervascularity before HCC can be confirmed.[171] If the nodule is less than 2 cm, diagnosis can be made using non-invasive criteria (if biopsy is not an option), which have been defined as: (a) radiological criteria: two coincidental imaging techniques showing arterial hypervascularisation for lesions over 2 cm; (b) combined criteria: one imaging modality showing arterial hypervascularisation associated with AFP levels over 400 ng/mL. Biopsy may be another option in some centres, but remains controversial; in some North American and European centres, biopsy would prelude hepatic resection or transplant because of risk of tumour seeding along the needle track. Furthermore a negative biopsy of a lesion visible on imaging techniques in a cirrhotic liver does not necessarily rule out malignancy completely. Therefore within the context of the cirrhotic patient, HCC can be diagnosed non-invasively using the above-mentioned criteria. Ultrasound is widely accepted to be adequate in screening for hepatomas. Clearly there are several stages in this algorithm whereby the use of USCAs might be more effective namely (a) in the 6-monthly recalls to improve detection, (b) the characterisation of the lesions measuring less than 2 cm and (c) as the second modality in demonstrating the hypervascularity of the lesion in the non-invasive diagnosis of HCC.

Regenerating nodules, dysplastic nodules and HCC

Cirrhosis is characterised by destruction of normal hepatic architecture, which is replaced by fibrosis and a spectrum of nodules ranging from benign regenerative nodules to HCC.[172,173] The development of HCC is postulated to be due to a multistep process of carcinogenesis.[174,175] This involves progression from regenerative nodule to low-grade dysplastic nodule to high-grade dysplastic nodule to dysplastic nodule with foci of HCC to overt HCC. Progression along this path is characterised by cytological and architectural changes. These entities show overlap in imaging appearances on conventional US, making accurate differentiation almost impossible. A study by Bennett et al.[176] of 200 patients with cirrhosis who underwent conventional US followed by liver transplantation within 90 days concluded that sonography has poor sensitivity for detecting dysplastic nodules (patient sensitivity 4.8% and lesion sensitivity 1.6%) and HCC (patient sensitivity 29.6% and lesion sensitivity 20.5%).

CEUS has an important role in characterising nodules in the cirrhotic liver, as the vascular supply to the nodule and thus its enhancement pattern may allow the differentiation of HCC from other focal lesions. As part of the stepwise progression of carcinogenesis in a cirrhotic nodule, there is progressive loss of portal venous supply and development of new arterial vessels, which become the dominant supply in overt HCC.[177] This arterial neoangiogenesis is the hallmark of HCC and the key to imaging diagnosis.[178,179] In general, non-neoplastic nodules have a predominantly portal venous supply while HCC has a predominantly hepatic arterial supply. HCC typically demonstrates washout in the portal venous or late phase due to decreased or absent portal venous in-flow.

Regenerative nodule

This is defined histologically as a hepatocellular nodule containing portal tracts surrounded by fibrous septa in a liver involved by cirrhosis or other severe disease.[172] These nodules may be micronodular (≤3 mm), macronodular (>3 mm) or mixed type. Rarely, regenerating nodules can measure several centimetres in size and mimic a neoplasm.[172] The blood supply to the regenerative nodule is predominantly from the portal vein, with minimal contribution from the hepatic artery. These nodules typically appear hypoechoic on conventional US. On CEUS, these nodules show hypo- or iso-enhancement in the arterial phase and iso-enhancement in the portal venous and late phases compared to the background liver[180] (Fig. 10.14).

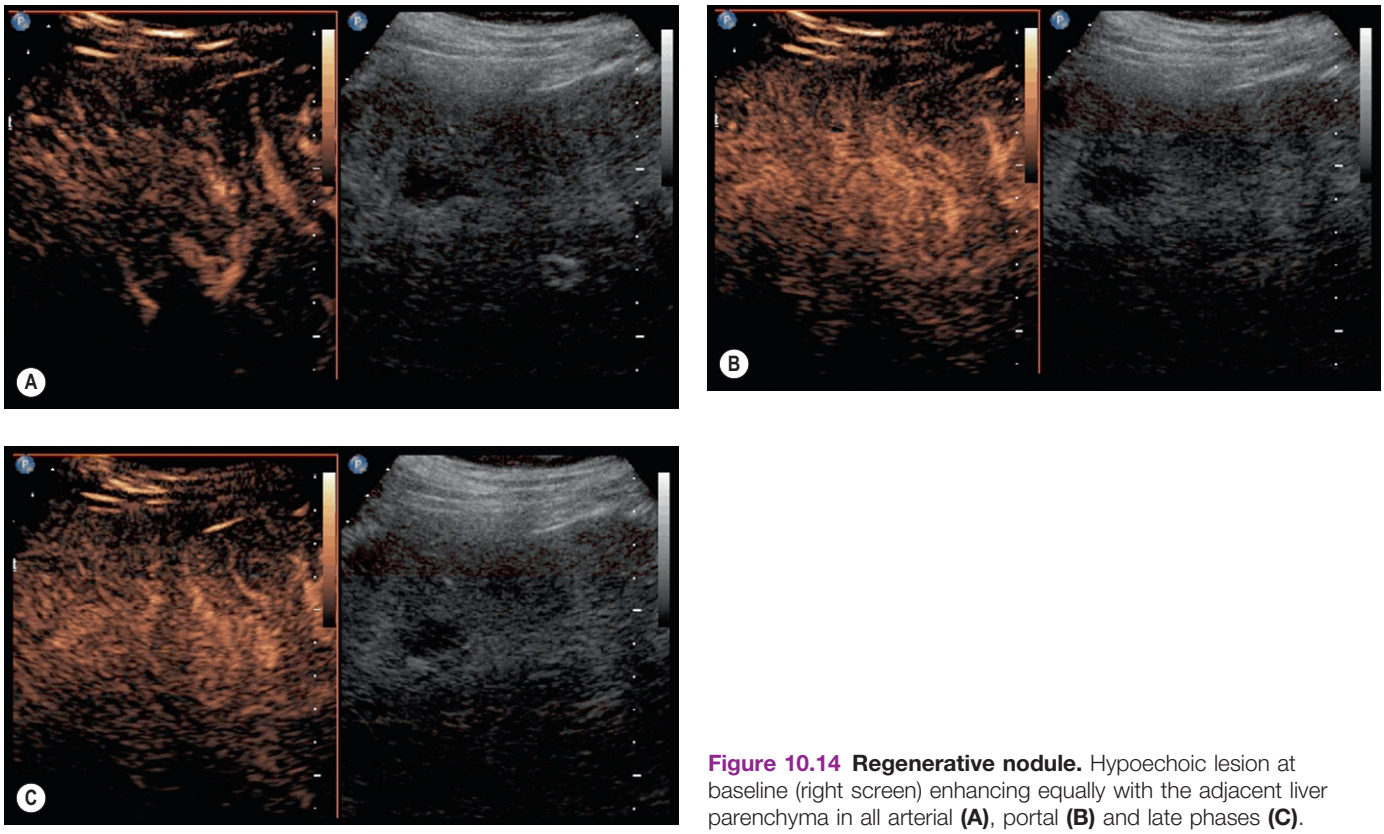


Figure 10.14 Regenerative nodule. Hypoechoic lesion at baseline (right screen) enhancing equally with the adjacent liver parenchyma in all arterial **(A)**, portal **(B)** and late phases **(C)**.

Dysplastic nodules

These are considered premalignant nodules and are found in 15–25% of cirrhotic livers.[181] They are defined histologically as nodules of hepatocellular origin that are ≥1 mm in diameter with dysplasia but no histological criteria of malignancy.[182] These nodules may be of low or high grade depending on the degree of cellular atypia and mitosis. On conventional US, dysplastic nodules are typically hypoechoic and cannot be reliably differentiated from other cirrhotic nodules. Occasionally they can be greater than 2 cm in size.[182] Progression to HCC has been reported within as little as 4 months, with a 'nodule within a nodule' appearance sometimes seen – referring to the presence of a focus of HCC within a dysplastic nodule.[183] On CEUS, most dysplastic nodules show hypo- to iso-enhancement in the arterial phase and iso-enhancement on the portal venous and late phases compared to background liver due to predominant portal venous supply similar to regenerating nodules[180] (Fig. 10.15). High-grade dysplastic nodules and those with focus of HCC have an increasing supply from the hepatic artery and may show arterial hypervascularity on CEUS.[180]

HCC

There are three recognised morphological presentations of HCC.[184]

1. Massive – refers to a single large mass with or without satellite nodules.
2. Nodular – refers to multiple fairly discrete nodules throughout the liver.
3. Diffuse – refers to multiple indistinct minute nodules throughout the liver.

On conventional US, HCC has a variable echogenicity and can be hypo-, iso- or hyperechoic or mixed pattern. Small HCCs (<2 cm in size) tend to be hypoechoic while larger HCCs tend to be inhomogeneous and complex with areas of internal echogenicity (seen in 50% of large HCCs) secondary to fibrosis, haemorrhage or necrosis.[185] Ebara et al.[186] correlated the US pattern of HCC with their size and demonstrated that with increasing nodule size there was a tendency to progress from a hypoechoic appearance to one with a hypoechoic periphery with echogenic centre to finally a lesion with larger areas of intra-tumoral echogenicity. Certain morphological features are suggestive of HCC and may aid in the differentiation from other focal liver lesions. These include the presence of a pseudo-capsule, intra-tumoral septa, daughter/satellite nodules and tumour thrombus in the adjacent portal or hepatic veins.[187] The pseudo-capsule around an HCC is composed of thick fibrous tissue and is caused by compression of normal hepatic parenchyma by expansile tumour growth.[188] The encapsulated type of HCC is usually well differentiated histologically and is slower growing with lower propensity to form daughter nodules or tumour thrombi.[188,189] It has a generally better prognosis than non-encapsulated HCC. Malignant portal venous invasion is reported to occur in association with HCC in 5–44% of cases.[190] Distinction from non-tumour thrombus, which occurs in 0.65–15.8% of cirrhotic patients,[191] is important as tumoral vascular invasion substantially worsens the prognosis and may result in exclusion of patients from surgery. Features that favour malignant tumour thrombus include contiguity with the parenchymal tumour, vein expansion in malignant thrombus compared to near normal vein calibre in bland thrombus, and presence of thrombus neovascularity which may be detected on colour Doppler imaging or CEUS.[172,192] The arterial supply to the tumour thrombus is retrograde down the vein from the parenchymal tumour so the arterial flow within the tumour thrombus is usually away from the liver, opposite to that of the hepatic artery.[100]

Arterial neo-angiogenesis is the hallmark of HCC and the key to imaging diagnosis.[178,179] On colour Doppler imaging, approximately 75% of HCCs show a fine peripheral network of vessels, surrounding and penetrating the lesion (the so-called 'basket pattern').[193]

Flow within HCC is typically high velocity on Doppler and the flow may have low resistance due to arterial-venous shunting within the tumour.[100] On CEUS, the enhancement pattern of HCC is related to the degree of the histological differentiation[194] (Fig. 10.16). Jang et al.[194] performed a retrospective study of 112 consecutive patients with 112 histologically proven HCCs (23 well differentiated, 77 moderately differentiated, and 12 poorly differentiated) comparing the arterial and portal venous phase enhancement patterns on CEUS with the degree of histological differentiation. The authors found that moderately differentiated HCC, which accounted for the majority of cases, showed a classic enhancement pattern of heterogeneous arterial hypervascularity (74 of 77 lesions, 96%) and portal venous phase washout (72 of 74, 97%). On continuous low MI scanning with contrast-enhanced pulse inversion harmonic (PIH) imaging, chaotic peri-tumoral and intra-lesional tortuous 'corkscrew'/'s' shaped vessels may be clearly depicted in the arterial phase when the lesions become hyperechoic (Fig. 10.17). The authors depicted dysmorphic intra-tumoral arteries in the majority of HCCs (81 of 112, 72%). In contrast, well-differentiated and poorly differentiated HCCs may give atypical appearances on CEUS (Figs 10.18, 10.19 and 10.20). In their study Jang et al.[194] found that some well-differentiated HCCs demonstrated arterial phase iso- or hypovascularity (9 of 23 lesions, 39%) and iso-vascularity throughout the portal phase (9 of 9, 100%), postulated to reflect decreased normal hepatic arterial flow without significant development of neoplastic arteries and with preservation of portal venous flow. In poorly differentiated HCCs, the authors found early washout (7 of 9 lesions, 78%) within 90 seconds. A possible explanation for early washout of poorly differentiated HCCs may derive from its total lack of similarity to normal hepatocytes and its architecture. While the majority of HCCs in the study demonstrated washout in the portal venous or late phase (up to 5 minutes post contrast injection), 9% demonstrated no washout and of these 78% (7 of 9 lesions) were well-differentiated HCCs.

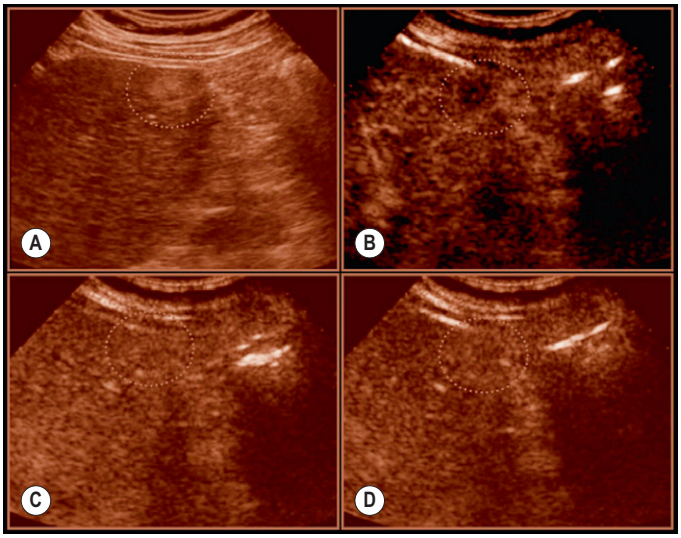


Figure 10.15 Dysplastic nodule. Hyperechoic lesion at baseline **(A)** which is hypo-enhancing in the arterial phase **(B)**, and iso-enhancing in both portal **(C)** and late **(D)** phases.

Cholangiocarcinoma

Cholangiocarcinoma (CC) is the second most common primary hepatic cancer, representing 30% of all primary hepatic neoplasms,[195] and accounts for about 3% of all gastrointestinal cancers globally.[196] It has an incidence of 1–2 cases per 100 000 population[197] with the peak prevalence in the seventh decade of life and a slight male preponderance.[198] CCs arise from bile duct epithelium and are adenocarcinomas in 90–95% of cases.[199] Histologically, tumours are usually associated with extensive intra-lesional fibrosis. Sixty to seventy per cent of CCs arise at the bifurcation of the hepatic ducts (Klatskin tumours), 20–30% at the distal common bile duct, while 5–10% are peripheral (occurring distal to the second order bile duct branches) and arise from intrahepatic ducts of the liver

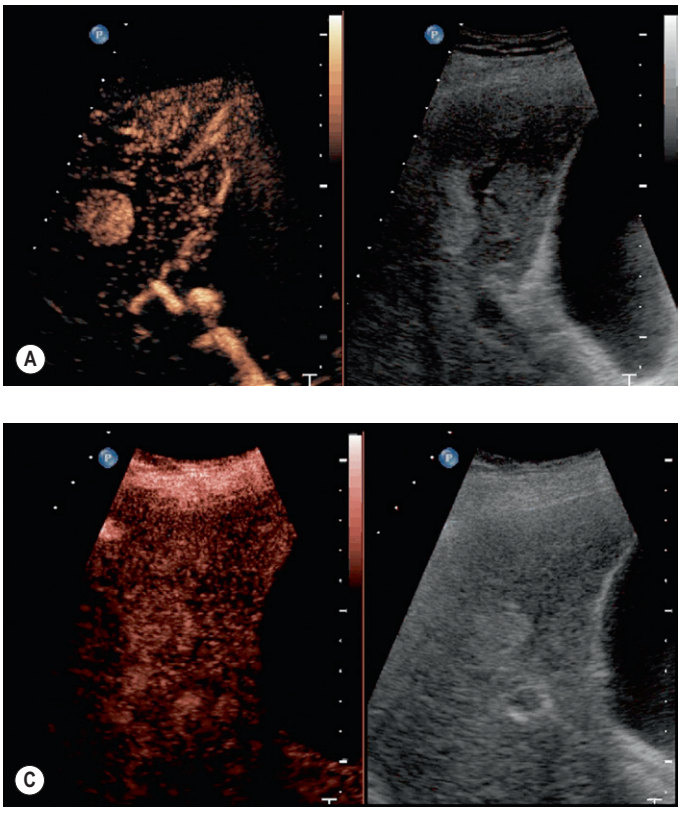


Figure 10.16 Well-differentiated hepatocellular carcinoma. Large hyperechoic lesion at baseline which enhances homogeneously in the arterial phase **(A)** associated with pseudo-capsule which is hypo-enhancing, and on portal phase **(B)** the lesion is iso-enhancing whilst the pseudo-capsule enhances; in late phase both are iso-enhancing **(C)**.

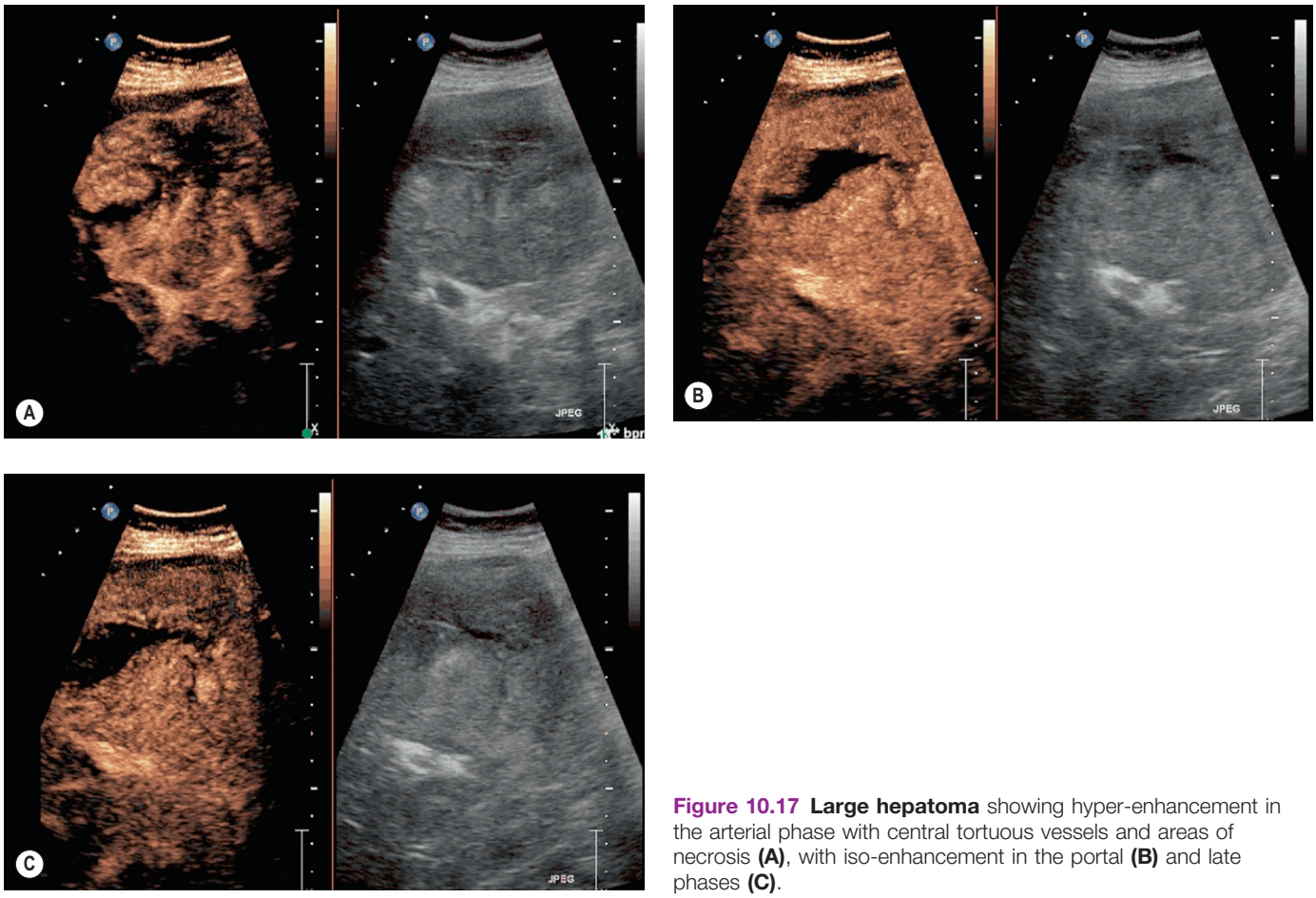


Figure 10.17 **Large hepatoma** showing hyper-enhancement in the arterial phase with central tortuous vessels and areas of necrosis **(A)**, with iso-enhancement in the portal **(B)** and late phases **(C)**.

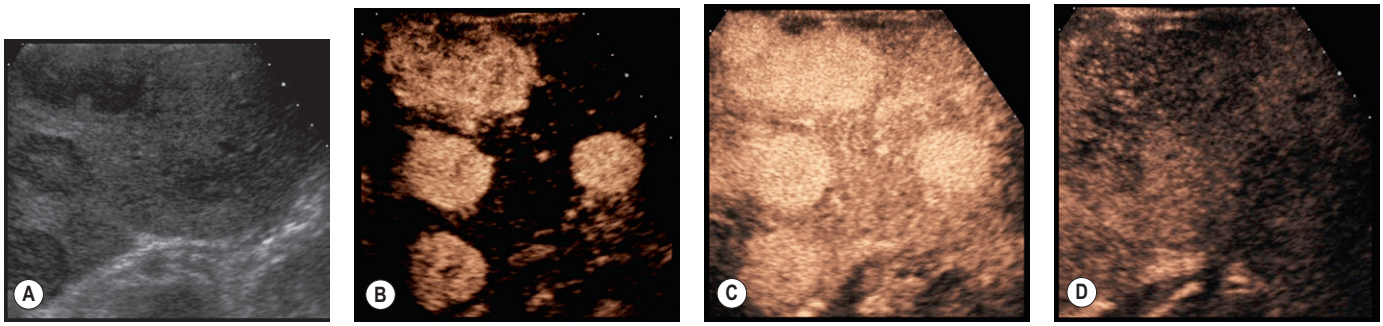


Figure 10.18 **Multiple small hepatomas**, which are hypoechoic at baseline **(A)** showing hyper-enhancement in the arterial phase **(B)**, iso-enhancement in the portal venous phase **(C)** and washout in the late phase **(D)**.

parenchyma.[200,201] Intrahepatic CCs such as hilar and peripheral forms can be classified according to their growth characteristics as periductal-infiltrating (most common), intraductal or mass-forming types.[202]

Conventional US is the first-line imaging modality in this patient cohort as patients usually present at a late stage when signs and symptoms suggestive of biliary obstruction such as jaundice or deranged liver function tests trigger an imaging investigation. US is highly sensitive for confirming bile duct dilatation, localising the site of obstruction and excluding gallstones as a potential cause.[203] On US, dilatation of the intrahepatic bile ducts that converge on the liver hilum is the most common finding in patients with Klatskin tumours. Other findings depend on the growth characteristics of the CC type. Periductal infiltrating CCs are difficult to detect sonographically due to small size as well as perceptual difficulties as they can appear isoechoic or show only mild textural inhomogeneity compared to the surrounding liver. Mural and periductal soft tissue thickening or focal irregularities of the bile ducts may occasionally be appreciated.[204] In longstanding cases due to obstruction, lobar atrophy and resultant crowding of bile ducts and blood vessels is seen.[205] Due to the propensity for local invasion, these tumours may infiltrate adjacent vessels, with portal venous involvement detected on conventional US with colour Doppler imaging in 50% of cases.[206] Intraductal tumours may show wall thickening or resemble polypoidal masses but are difficult to appreciate on imaging due to small size. Mass-forming CCs appear as a solid

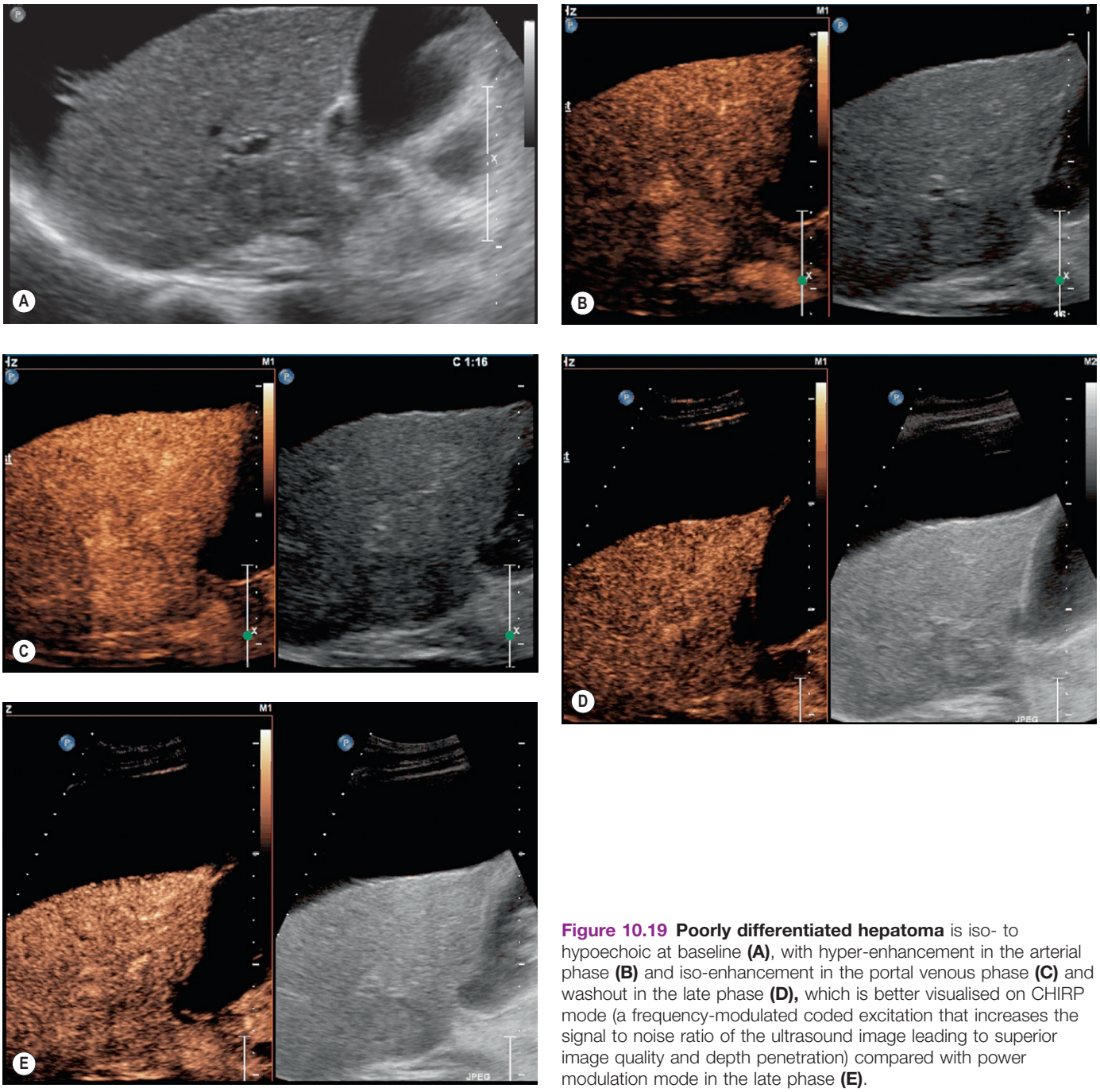


Figure 10.19 Poorly differentiated hepatoma is iso- to hypoechoic at baseline **(A)**, with hyper-enhancement in the arterial phase **(B)** and iso-enhancement in the portal venous phase **(C)** and washout in the late phase **(D),** which is better visualised on CHIRP mode (a frequency-modulated coded excitation that increases the signal to noise ratio of the ultrasound image leading to superior image quality and depth penetration) compared with power modulation mode in the late phase **(E)**.

mass with irregular borders and variable echogenicity on conventional US with no specific imaging features. Small CCs often appear hypo- or isoechoic while larger CCs are generally inhomogeneous with mixed echogenicity.[100] Small satellite nodules neighbouring the primary tumour are a recognised finding. Ancillary findings that may aid diagnosis if present include peri-lesional bile duct dilatation (seen in up to 30% of cases) and capsular retraction.[207]

Khalili et al.[208] found that detection and staging of hilar CCs were improved by the use of a first-generation US contrast agent (Levovist) in the post-vascular phase of US compared with conventional US. Similar data using second-generation USCAs with low MI technique are lacking although it is reasonable to assume similar if not superior results as more information can be obtained by real-time interrogation of the tumour in the various vascular phases. On low MI CEUS, intrahepatic CCs typically demonstrate peripheral irregular rim-like enhancement during the arterial phase and hypo-enhancement during the late phase.[13,53,209–211] Three other reported patterns of arterial enhancement are also seen on CEUS for intrahepatic CCs.[209] Chen et al.[209] retrospectively studied 40 pathologically proven intrahepatic CCs in 40 patients who underwent both CEUS and triphasic CT. The authors found that in the arterial phase, intrahepatic CCs demonstrated (i) peripheral irregular rim-like enhancement (47.5%), (ii) diffuse heterogeneous hyper-enhancement (22.5%), (iii) diffuse homogeneous hyper-enhancement (12.5%) and (iv) diffuse heterogeneous hypo-enhancement (17.5%). The arterial phase patterns on CEUS

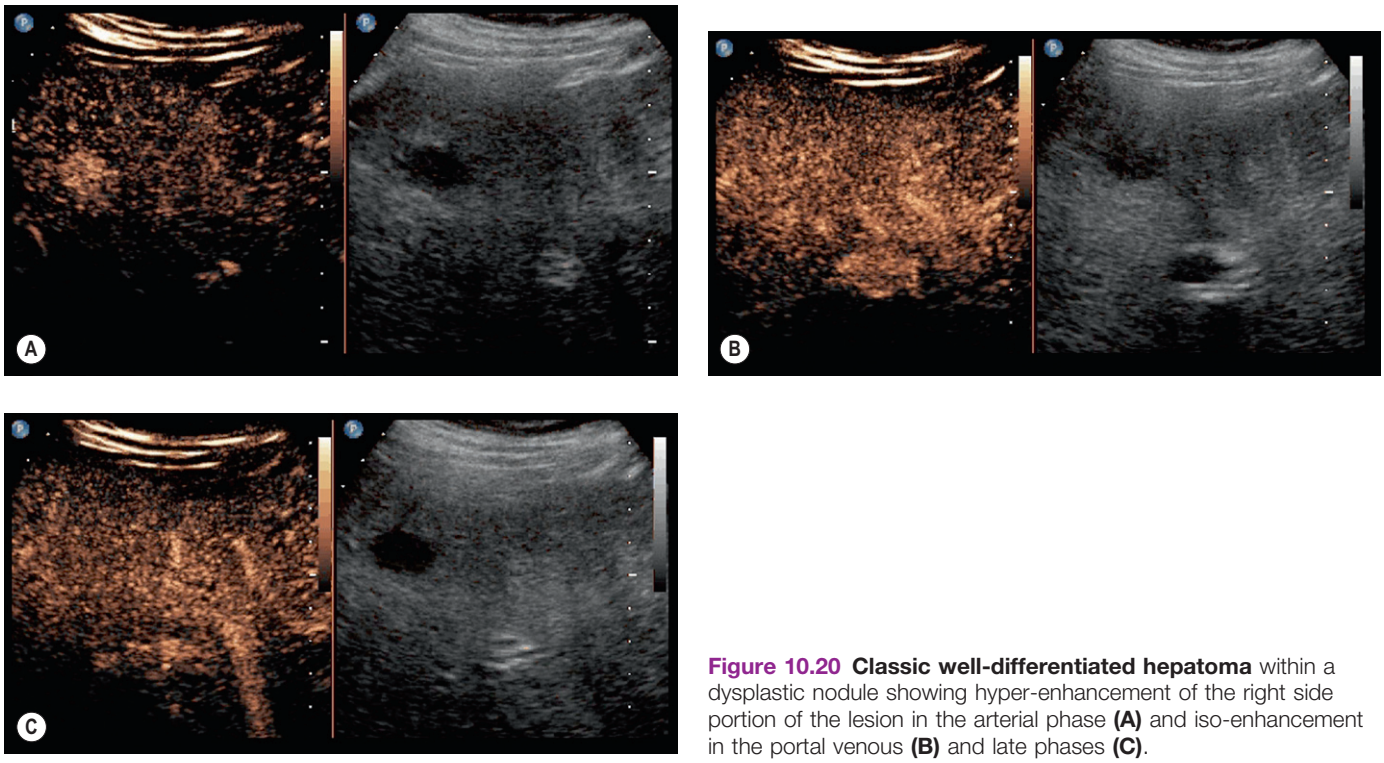


Figure 10.20 **Classic well-differentiated hepatoma** within a dysplastic nodule showing hyper-enhancement of the right side portion of the lesion in the arterial phase **(A)** and iso-enhancement in the portal venous **(B)** and late phases **(C)**.

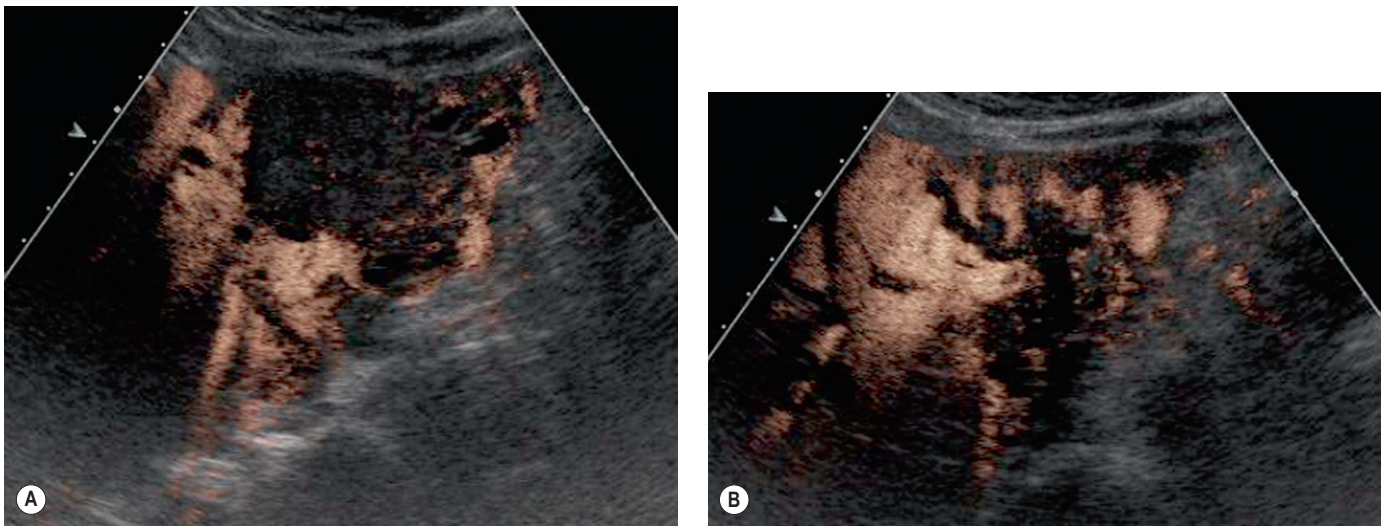


Figure 10.21 **Cholangiocarcinoma**, which appears as a filling defect in the portal venous **(A)** and late phases **(B)** associated with biliary dilatation.

correlated well with those on contrast-enhanced CT. The authors postulated that the different enhancement patterns may relate to different pathological components in the tumour.[209,212] Concentration of tumour cells in the lesion periphery with fibrosis in the lesion centre may give rise to the peripheral rim-like enhancement pattern seen in the majority of intrahepatic CCs. Tumour may show diffuse enhancement if the major component is tumour cells and there is no central fibrosis. When there is abundant fibrous stroma, the tumour may show arterial hypo-enhancement. The authors also found that the enhancement pattern correlated with tumour size – smaller lesions had a trend towards homogeneous hyper-enhancement while larger tumours showed variable enhancement patterns. This finding may relate to pathological changes that occur as the tumour increases in size such as compression of central vessels resulting in central hypovascularity or necrosis.[213]

On portal venous and late phase scanning, the vast majority of intrahepatic CCs demonstrate washout on CEUS[13,53,209–211] (Fig. 10.21). These findings are discordant with contrast-enhanced CT, which generally shows tumour iso- to hyper-enhancement in the late phase.[209,210] This difference may be explained by considering the different properties of the CT and US contrast media. USCAs are purely intravascular agents with no flow outside the vascular bed whereas CT contrast agents have both an intra- and extravascular distribution with flow into the interstitium to reach an

equilibrium state.[214,215] Therefore, in the late post-contrast phase, the fibrous component of the tumour will appear hypo-enhancing on CEUS and hyper-enhancing on contrast-enhanced CT.

The enhancement pattern of intrahepatic CCs may overlap those of HCC and metastases with potential for misdiagnosis. Diffuse hyper-enhancement in the arterial phase followed by portal venous and late phase washout can be seen in both HCC and intrahepatic CCs. Hypovascular metastases, especially from adenocarcinomas of the gastrointestinal tract, may show peripheral rim-like enhancement similar to that of intrahepatic CCs.[216,217] In these cases, the background clinical history (such as the presence of underlying primary malignancy, hepatitis virus infection, etc.), relevant laboratory data (such as elevation of serum AFP and other serum tumour markers), pertinent additional imaging findings (such as evidence of metastatic disease elsewhere in the body, morphological evidence of cirrhosis or associated peri-lesional biliary dilatation) may be useful discriminating factors.

Hepatic lymphoma

Liver involvement by lymphoma usually occurs in the context of the presence of lymphomatous tissue elsewhere in the body (secondary hepatic lymphoma). Primary hepatic lymphoma is very rare, with approximately 100 cases reported worldwide. In comparison, secondary hepatic lymphoma is not uncommon. It occurs in approximately 3–14% of newly diagnosed cases, whereas at autopsy; it is found in 50–80% of patients with Hodgkin's or non-Hodgkin's lymphoma.[218,219] Conditions associated with an increased risk for development of lymphoma include HIV/AIDS, hepatitis C, organ transplantation and immunosuppression. Liver involvement in patients with AIDS-related non-Hodgkin's lymphoma has been reported to occur in 26–45% of cases.[220–222] A recent meta-analysis revealed that hepatitis C virus (HCV) prevalence in patients with non-Hodgkin's lymphoma was 15%, as opposed to 1.5% in the general population and 2.9% in patients with other haematological malignancies, implying a causative role of HCV in non-Hodgkin's lymphoma.[223] Post-transplant lymphoproliferative disorder (PTLD) is a serious condition that occurs in 2–10% of all organ transplant recipients as a result of chronic immunosuppression,[224] which leads to an unregulated expansion of lymphoid proliferation. The disorder ranges from plasma cell hyperplasia through premalignant polymorphic B cell proliferation to malignant monoclonal lymphoma.[225] In most cases, the disorder results from Ebstein–Barr virus induced B-cell lymphoproliferation unopposed by the host's pharmacologically suppressed T-cell system. The abdomen is the most common site involved by PTLD (may be the only site involved in up to 50% of cases) and the liver the most common abdominal organ affected.[226,227]

There are three established morphological patterns of hepatic lymphoma involvement: (i) solitary hepatic mass, (ii) multifocal nodules, and (iii) diffuse infiltrative disease.[228] Primary hepatic lymphoma (usually non-Hodgkin type) most commonly presents as a solitary mass in 55–60% of cases.[229] Secondary hepatic lymphoma most commonly presents with multiple nodular liver masses in the context of lymphadenopathy elsewhere in the body. Diffuse infiltrative involvement is the most infrequent of the three types and has the worst prognosis. A fourth type of extremely rare hepatic lymphoma involvement has also been reported. There are three case reports of lymphoma presenting as a periportal mass tracking into the liver; two cases were identified on contrast-enhanced CT[218,230] and one case on CEUS.[231] On conventional US, hepatic lesions are typically hypoechoic, which is thought to be related to the uniform cellularity of lymphoma without significant background stroma.[232] Posterior acoustic enhancement, typically less than that of a cyst, may also be seen due to the uniformity of the tumour.[100] Lesions may also appear almost anechoic and septated and mimic abscesses, appear nearly isoechoic relative to hepatic parenchyma, or be hypoechoic with a central echogenic focus and mimic metastatic disease.[233] On CEUS, liver infiltrates of lymphoma behave like hypovascular metastases showing some degree of mild peripheral rim-like arterial enhancement with rapid washout and subsequent hypoechogenicity in the portal venous and late phases with progressive increase in lesion conspicuity[234] (Fig. 10.22).

Rare malignant lesions

Fibrolamellar hepatocellular carcinoma

Fibrolamellar HCC is a rare primary hepatic malignancy first described by Edmonson in 1956.[235] Clinical, pathological and imaging studies have established it as a distinct entity from conventional HCC by its morphology and biological behaviour.[236,237] Clinically, fibrolamellar HCC occurs in young patients while the majority of cases of conventional HCC are diagnosed in patients older than 40 years of age. The disease has a unimodal distribution, beginning in late adolescence, with a peak incidence at 24.8 ± 13 years.[238] It has no sex bias but is more common in white people. The typical risk factors for conventional HCC such as cirrhosis, viral hepatitis, excessive alcohol consumption and metabolic disease are generally absent in patients with fibrolamellar HCC. Serum tumour markers such as AFP are typically not elevated. Histologically, the disease is composed of well-differentiated malignant hepatocytes with deeply eosinophilic and granular cytoplasm due to the presence of numerous mitochondria associated with thick fibrous lamellae throughout the tumour.[239] Prognosis is better for fibrolamellar HCC than conventional HCC with increased length of survival observed, even after adjusting for age of cancer diagnosis and other demographic data.[240]

On imaging fibrolamellar HCC usually appears as a solitary well-defined lobulated mass (in 80–90% of cases) with an average size of 9–12 cm (ranges from 5–20 cm).[241] It has a central scar in 20–71% of cases, which is typically large and may be broad or stellate, eccentric or central.[241] Calcifications are typical and occur in 35–68% of cases and may be punctate, nodular or stellate and are usually located near the tumour centre.[241] Unlike FNH, calcification within the central scar of a fibrolamellar HCC is a relatively common finding. On conventional US, the tumour has a variable echotexture with mixed echogenicity found in 60% of cases with predominance of hyperechoic or isoechoic components.[242] On US the central scar is typically hyperechoic but US is less successful in demonstrating central scars, with 33–60% of scars detected at US compared to CT and pathological analysis.[243] The central scar in FNH is typically hypervascular while in fibrolamellar HCC it is typically hypovascular but may show mild gradual contrast enhancement in the late phase. Fan et al.[244] described a case of fibrolamellar HCC imaged with CEUS. This demonstrated rapid tumour enhancement in the arterial phase with abnormal vessels of septum distribution seen followed by washout in the portal venous phase. The rarity of this tumour and paucity of cases studied by CEUS does not permit more detailed evaluation of its enhancement features on CEUS.

Epithelioid haemangioendothelioma

This is a rare malignant vascular hepatic tumour characterised by the epithelioid appearance of its neoplastic cells, which accounts for its name.[245] It originates from vascular endothelial cells and spindle cells. It should not be confused with infantile haemangioendothelioma, which is a separate entity and is histologically benign and occurs exclusively in infants and young children and resolves spontaneously in many cases. Prognosis in epithelioid haemangioendothelioma is variable and unpredictable. While 20% of patients die within the first 2 years after presentation, another 20% have extended survival of 5–28 years, regardless of whether they undergo treatment. Metastatic disease does not preclude a long survival.[246]

Epithelioid haemangioendotheliomas are often multiple and peripherally located and can cause capsular retraction secondary to tumour desmoplasia.[233] The lesions may coalesce over time. Lesions

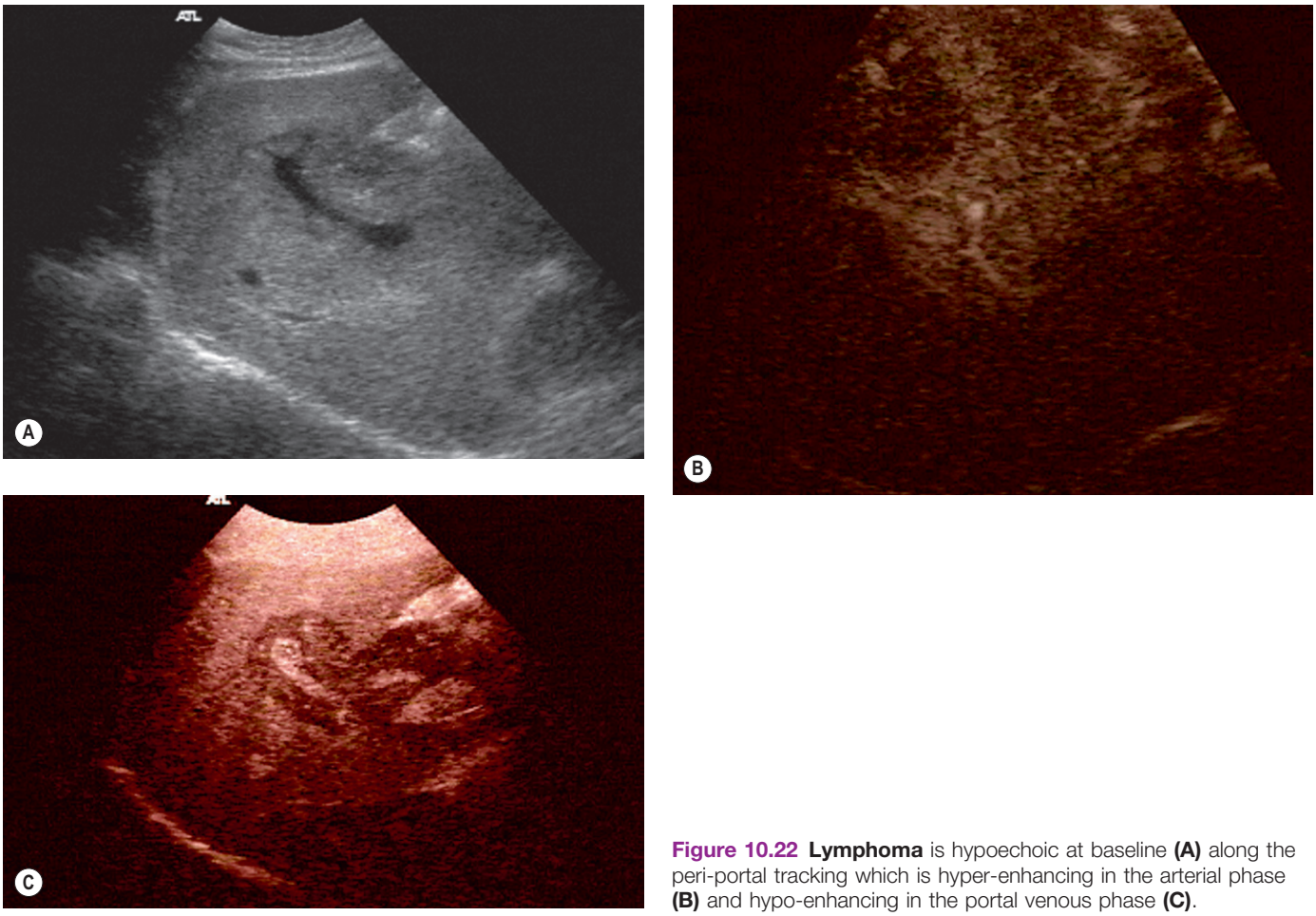


Figure 10.22 **Lymphoma** is hypoechoic at baseline **(A)** along the peri-portal tracking which is hyper-enhancing in the arterial phase **(B)** and hypo-enhancing in the portal venous phase **(C)**.

are typically hypoechoic, which correlates with the central core of myxoid stroma. The combination of hypoechoic coalescent peripheral hepatic masses with capsular retraction is highly suggestive of diagnosis.[232] On CEUS, the mass typically shows irregular intratumoral vessels and diffuse or peripheral hypervascularity during the arterial phase and rapid washout in the portal venous phase, especially in the peripheral zone compared to the central zone.[233] The entire lesion shows washout eventually on CEUS whereas on CT or MRI, the peripheral zone enhancement persists or enlarges gradually over time. Similar to cholangiocarcinoma, this tumour has a rich fibrous stroma and the discordance between findings on CEUS and contrast-enhanced CT and MRI can be attributed to the different properties of the contrast media. Quaia et al.[1] found a case of a histologically proven low-grade malignant epithelioid haemangioendothelioma, which had an atypical enhancement pattern suggestive of a benign lesion. On conventional US and colour Doppler imaging, the tumour appeared hypoechoic with a peripheral vessel. On CEUS, there was homogeneous tumour contrast enhancement during the arterial and portal venous phases with persisting enhancement present in the late phase. The two reviewers in the study erroneously categorised this lesion as being benign.

Biliary cystadenocarcinoma

Biliary cystadenoma is a rare malignant cystic neoplasm that may arise de novo or be the end product of malignant degeneration in a benign biliary cystadenoma. It cannot be confidently separated from biliary cystadenoma on imaging due to overlap of imaging findings and so surgical excision is generally recommended for both pathologies. On US, biliary cystadenoma usually presents as a multiloculated cystic mass. Mural nodularity within the wall or septations of the cystic lesion and thick coarse calcifications are suggestive of cystadenocarcinoma as these are rare in cystadenoma.[247] CEUS may reveal wall and septal enhancement during the arterial phase, with mural or septal nodule enhancement. During the portal and late phases, contrast washout is seen.[117]

REFERENCES

1. Quaia E, Calliada F, Bertolotto M, et al. Characterization of focal liver lesions with contrast specific US modes and a sulfur hexafluoride-filled microbubble contrast agent: diagnostic performance and confidence. Radiology 2004;232(2):420–430.
2. Reinhold C, Hammers L, Taylor CR, et al. Characterization of focal hepatic lesions with duplex sonography: findings in 198 patients. AJR Am J Roentgenol 1995;164:1131–1135.
3. Lee MG, Auh YH, Cho KS, et al. Color Doppler flow imaging of hepatocellular carcinomas: comparison with metastatic tumours and hemangiomas by three step grading colour hues. Clin Imaging 1996;20:199–203.
4. Van Leeuwen MS, Noordzij J, Feldberg MA, et al. Focal liver lesions: characterization with triphasic CT. Radiology 1996;201:327–336.
5. Balci NC, Semelka RC. Contrast agents for MR imaging of the liver. Radiol Clin North Am 2005;43(5):887–898.
6. Lencioni R. Impact of European Federation of Societies for Ultrasound in Medicine and Biology (EFSUMB) guidelines on the use of contrast agents in liver ultrasound. Eur Radiol 2006;16:1610.
7. Albrecht T, Hohmann J, Oldenburg A, et al. Detection and characterization of liver metastases. Eur Radiol 2004;14(Suppl 8): 25–33.
8. Leen E, Moug S, Horgan PG. Potential impact and utilization of ultrasound contrast media. Eur Radiol 2004;14(Suppl 8):16–24.
9. Brannigan M, Burns P, Wilson S. Blood flow patterns in focal liver lesions at microbubble enhanced US. Radiographics 2004;24:921–935.

10. Leen E, Angerson WJ, Yarmenitis S, et al. Multi-centre clinical study evaluating the efficacy of SonoVue (BR1), a new ultrasound contrast agent in Doppler investigation of focal hepatic lesions. Eur J Radiol 2002;41(3):200–206.
11. Leen E, Ceccotti P, Kalogeropoulou C, et al. Prospective multicentric trial evaluating a novel method of characterizing focal liver lesions using contrast enhanced sonography. AJR Am J Roentgenol 2006;186(6):1551–1559.
12. Faccioli N, D'Onofrio M, Comai A, Cugini C. Contrast enhanced ultrasonography in the characterization of benign focal liver lesions: activity-based cost analysis. Radiol Med 2007;112(6):810–820.
13. Albrecht T, Blomley M, Bolondi L, et al. Guidelines for the use of contrast agents in ultrasound. January 2004. Ultraschall Med. 2004;25(4):249–256.
14. Kono Y, Steinbach GC, Peterson T, et al. Mechanism of parenchymal enhancement of the liver with a microbubble based US contrast medium. Radiology 2002;224:253–257.
15. Becher H, Burns PN. A handbook of contrast echocardiography. Heidelberg: Springer; 2000.
16. Blomley MJ, Eckersley RJ. Functional ultrasound methods in oncological imaging. Eur J Cancer 2002;38(16):2108–2115.
17. Ackerman NB. The blood supply of experimental liver metastases. IV. Changes in vascularity with increasing tumour growth. Surgery 1974;75(4):589–596.
18. Wilson SR, Burns PN. Microbubble contrast for radiological imaging: 2. Applications. Ultrasound Q 2006;22(1):15–18.
19. Ramnarine KV, Kyriakopoulou K, Gordon P, et al. Improved characterization of focal liver tumours: dynamic power Doppler imaging using NC100100 echo-enhancer. Eur J Ultrasound 2000;11(2):95–104.
20. Bauer A, Blomley M, Leen E, et al. Liver-specific imaging with SHU 563A: diagnostic potential of a new class of ultrasound contrast media. Eur Radiol. 1999;9(Suppl 3):S349–352.
21. Vilgrain V, Boulos L, Vullierme MP, et al. Imaging of atypical hemangiomas of the liver with pathological correlation. Radiographics 2000;20(2):379–397.
22. Ros PR. Computed tomography–pathologic correlations in hepatic tumors. In: Ferrucci JT, Mathiew DG, editors. Advances in hepatobiliary radiology. St Louis: CV Mosby; 1990:75–108.
23. Mergo PJ, Ros PR. Benign lesions of the liver. Radiol Clin North Am 1998;36:319–331.
24. Gandolfi L, Leo P, Solmi L, et al. Natural history of hepatic haemangiomas: clinical and ultrasound study. Gut 1991;32:677–680.
25. Takayasu K, Makuuchi M, Takayama T. Computed tomography of a rapidly growing hepatic hemangioma. J Comput Assist Tomogr 1990;14:143–145.
26. Gibbs JF, Litwin AM, Kahlenberg MS. Contemporary management of benign liver tumors. Surg Clin North Am 2004;84(2):463–480.
27. Caseiro-Alves F, Brito J, Araujo AE, et al. Liver haemangioma: common and uncommon findings and how to improve the differential diagnosis. Eur Radiol 2007;17:1544–1554.
28. Blondet A, Ridereau- Zins C, Michalak S, et al. Multiple pedunculated liver hemangiomas presenting with volvulus. J Radiol 2007;88(6):891–894.
29. Tran-Minh VA, Gindre T, Pracros JP, et al. Volvulus in a pedunculated hemangioma of the liver. AJR Am J Roentgenol 1991;156(4):866–867.
30. Gibney RG, Hendin AP, Cooperberg PL. Sonographically detected hepatic hemangiomas: absence of change over time. AJR Am J Roentgenol 1987;149:953–957.
31. Taboury J, Porcel A, Tubiana JM, Monnier JP. Cavernous hemangiomas of the liver studied by ultrasound: enhancement posterior to a hyperechoic mass as a sign of hypervascularity. Radiology 1983;149:781–785.
32. Hosten N, Puls R, Bechstein WO, Felix R. Focal liver lesions: Doppler ultrasound. Eur Radiol 1999;9:428–435.
33. Perkins AB, Imam K, Smith WJ, Cronan JJ. Colour and power Doppler sonography of liver hemangiomas: a dream unfulfilled? J Clin Ultrasound 2000;28:159–165.
34. Kim TK, Han JK, Kim AY, et al. Hepatic hemangiomas using a sonographic contrast agent (Levovist) and power Doppler ultrasonography. J Ultrasound Med 1999;18:737–743.
35. Moody AR, Wilson SR. Atypical hepatic hemangioma: a suggestive sonographic morphology. Radiology 1993;188:413–417.
36. Dietrich CF, Mertens JC, Braden B, et al. Contrast enhanced ultrasound of histologically proven liver hemangiomas. Hepatology 2007;45:1139–1145.
37. Marsh JI, Gibney RG, Li DK. Hepatic hemangioma in the presence of fatty infiltration: an atypical sonographic appearance. Gastrointest Radiol 1989;14:262–264.
38. Kim KW, Kim AY, Kim TK, et al. Hepatic hemangiomas with arterio-portal shunts: sonographic appearances with CT and MRI correlation. AJR Am J Roentgenol 2006;187(4):406–414.
39. Kim KW, Kim TK, Han JK, et al. Hepatic hemangiomas: spectrum of US appearances on grey scale, power Doppler, and contrast enhanced US. Korean J Radiol 2000;1:191–197.
40. Quaia E, Bartolotta TV, Midiri M, et al. Analysis of different contrast enhancement patterns after microbubble based contrast agent injection in liver hemangiomas with atypical appearance on baseline scan. Abdom Imaging 2006;31:59–64.
41. Bartolotta TV, Taibbi A, Galia M, et al. Centrifugal (inside out) enhancement of liver hemangiomas: A possible atypical appearance on contrast enhanced US. Eur J Radiol 2007;64:447–455.
42. Ungermann L, Elias P, Zizka J, et al. Focal nodular hyperplasia: spoke wheel arterial pattern and other signs on dynamic contrast enhanced ultrasonography. Eur J Radiol 2007;63:290–294.
43. Luciani A, Kobeiter H, Maison P, et al. Focal nodular hyperplasia of the liver in men: is presentation the same in men and women? Gut 2002;50:877–880.
44. Nguyen BN, Flejou JF, Terris B, et al. Focal nodular hyperplasia of the liver: a comprehensive pathologic study of 305 lesions and recognition of new histologic forms. Am J Surg Pathol 1999;23: 1441–1454.
45. Kuo YH, Wang JH, Lu SN, et al. Natural course of hepatic focal nodular hyperplasia: a long term follow up study with sonography. J Clin Ultrasound 2009;37:132–137.
46. Wanless IA, Mawdsley C, Adams R. On the pathogenesis of focal nodular hyperplasia of the liver. Hepatology 1985;5(6): 1194–1200.
47. Buetow PC, Pantongrag-Brown L, Buck JL, et al. Focal nodular hyperplasia of the liver: radiologic–pathologic correlation. Radiographics 1996;16:369–388.
48. Wang LY, Wang JH, Lin ZY, et al. Hepatic focal nodular hyperplasia: findings on colour doppler ultrasound. Abdom Imaging 1997;22: 178–181.
49. Uggowitzer M, Kugler C, Machan L, et al. Power doppler imaging and evaluation of the resistive index in focal nodular hyperplasia of the liver. Abdom Imaging 1997;22:268–273.
50. Goldberg BB, Hilpert PL, Burns PN, et al. Hepatic tumours: signal enhancement at Doppler US after injection of a contrast agent. Radiology 1990;177:713–717.
51. Numata K, Tanaka K, Mitsui K, et al. Flow characteristics of hepatic tumours at colour Doppler sonography: correlation with arteriographic findings. Am J Roentgenol 1993;160: 515–521.
52. Kamal IR, Liapi E, Fishman EK. Focal nodular hyperplasia: lesion evaluation using 16 MDCT and 3D CT angiography. AJR Am J Roentgenol 2006;186:1587–1596.
53. Xu HX, Liu GJ, Lu MD, et al. Characterization of focal liver lesions using contrast enhanced sonography with a low mechanical index mode and a sulfur hexafluoride filled microbubble contrast agent. J Clin Ultrasound 2006;34:261–272.
54. Dietrich CF, Schuessler G, Trojan J, et al. Differentiation of focal nodular hyperplasia and hepatocellular adenoma by contrast enhanced ultrasound. Br J Radiol 2005;78:704–707.
55. Yen YH, Wang JH, Lu SN, et al. Contrast enhanced ultrasonographic spoke wheel sign in hepatic focal nodular hyperplasia. Eur J Radiol 2006;60:439–444.
56. Janica J, Wojciech S, Dolorzycki S, et al. Contrast enhanced, wide band phase inversion power Doppler imaging of hepatic focal nodular hyperplasia. Hepato-Gastroenterology 2004;51: 705–708.
57. Reddy KR, Schiff ER. Approach to a liver mass. Semin Liver Dis 1993;13:423–435.
58. Faria SC, Iyer RB, Rashid A, Whitman GJ. Hepatic adenoma. AJR Am J Roentgenol 2004;182:1520.
59. Federle MP, Jeffrey RB, Desser TS, et al. Diagnostic imaging: abdomen. Salt Lake City, UT: Amirsys, 2004;110–112.
60. Baum JK, Bookstein JJ, Holtz F, Klein EW. Possible association between benign hepatomas and oral contraceptives. Lancet 1973;2:926–929.
61. Edmondson HA, Henderson B, Benton B. Liver cell adenomas associated with use of oral contraceptives. N Engl J Med 1976;294:470–472.
62. Hussain SM, van den Bos IC, Dwarkasing RS, et al. Hepatocellular

adenoma: findings at state of the art magnetic resonance imaging, ultrasound, computed tomography and pathologic analysis. Eur Radiol 2006;16:1873–1886.
63. Leese T, Farges O, Bismuth H. Liver cell adenomas: A 12 year surgical experience from a specialist hepato-biliary unit. Ann Surg 1988;208:558–564.
64. Numata K, Tanaka K, Mitsui K, et al. Flow characteristics of hepatic tumours at colour Doppler sonography: correlation with arteriographic findings. AJR Am J Roentgenol 1993;160: 515–521.
65. Bartolozzi C, Lencioni R, Paolicchi A, et al. Differentiation of hepatocellular adenoma and focal nodular hyperplasia of the liver: comparison of power Doppler imaging and conventional colour Doppler sonography. Eur Radiol 1997;7:1410–1415.
66. Dietrich CF, Ignee A, Trojan J, et al. Improved characterization of histologically proven liver tumours by contrast enhanced ultrasonography during the portal venous and specific late phases of SHU 508A. Gut 2004;53:401–405.
67. Wilson SR, Burns PN. An algorithm for the diagnosis of focal liver masses using microbubble contrast enhanced pulse inversion sonography. AJR Am J Roentgenol 2006;186:1401–1412.
68. Kim TK, Jang HJ, Burns PN, et al. Focal nodular hyperplasia and hepatic adenoma: differentiation with low mechanical index contrast enhanced sonography. AJR Am J Roentgenol 2008;190:58–66.
69. Barreda R, Ros PR. Diagnostic imaging of liver abscesses. Crit Rev Diagn Imaging 1992;33:29–58.
70. Mortele KJ, Segatto E, Ros PR. The infected liver: radiologic-pathologic correlation. Radiographics 2004;24:937–955.
71. Benedetti NJ, Desser TS, Brooke Jeffrey R. Imaging of hepatic infections. Ultrasound Q 2008;24:267–278.
72. Hui JYH, Yang MKW, Cho DHY, et al. Pyogenic liver abscesses caused by Klebsiella pneumoniae: US appearances and aspiration findings. Radiology 2007;242(3):769–776.
73. Ryan RS, Al-Hashimi H, Lee MJ. Hepatic abscesses in elderly patients mimicking metastatic disease. Ir J Med Sci 2001;170:251–253.
74. Sudhamshu KC, Sharma D. Long term follow up of pyogenic liver abscess by ultrasound. Eur J Radiol 2009, doi:10.1016/j.ejrad.2009.01.017 (in press).
75. Ralls PW, Meyers HI, Lapin SA, et al. Grey scale ultrasonography of hepatic amoebic abscess. Radiology 1979;132:125–129.
76. Ralls PW, Barnes PF, Radin DR, et al. Sonographic features of amebic and pyogenic abscesses: A blinded comparison. AJR Am J Roentgenol 1987;149:499–501.
77. Oleszczuk-Raszke K, Cremin BJ, Fisher RM, et al. Ultrasonic features of pyogenic and amoebic hepatic abscesses. Pediatr Radiol 1989;19:230–233.
78. Landay MJ, Setiawan H, Hirsch G, et al. Hepatic and thoracic amoebiasis. AJR Am J Roentgenol 1980;135(3):449–454.
79. Ralls PW, Quinn MF, Boswell WD Jr, et al. Patterns of resolution in successfully treated hepatic amoebic abscess: sonographic evaluation. Radiology 1983;149(2):541–543.
80. Catalano O, Sandomenico F, Raso MM, Siani A. Low mechanical index contrast enhanced sonographic findings of pyogenic hepatic abscesses. AJR Am J Roentgenol 2004;182:447–450.
81. Mendez RJ, Schiebler ML, Outwater EK, Kressel HY. Hepatic abscesses: MR imaging findings. Radiology 1994;190:431–436.
82. Miller MA, Balfe DM, Middleton WD. Peripheral portal venous blood flow alterations induced by hepatic masses: evaluation with color and pulsed Doppler sonography. J Ultrasound Med 1996;15:707–713.
83. Kim KW, Choi BI, Park SH, et al. Pyogenic hepatic abscesses: distinctive features from hypovascular hepatic malignancies on contrast enhanced ultrasound with SH U 508A; early experience. Ultrasound Med Biol 2004;30(6):725–733.
84. Hamer OW, Aguirre DA, Casola G, et al. Fatty liver: imaging patterns and pitfalls. Radiographics 2006;26:1637–1653.
85. Karcaaltincaba M, Akhan O. Imaging of hepatic steatosis and fatty sparing. Eur J Radiol 2007;61:33.
86. Siegelman ES, Rosen MA. Imaging of hepatic steatosis. Semin Liver Dis 2001;21:71.
87. Danet IM, Semelka RC, Braga L. MR imaging of diffuse liver disease. Radiol Clin North Am 2003;41:67.
88. Valls C, Iannacconne R, Alba E, et al. Fat in the liver: diagnosis and characterization. Eur Radiol 2006;16:2292–2308.
89. Zezos P, Tatsi P, Nakos A, et al. Focal fatty liver sparing lesion presenting as a 'pseudotumour': case report. Acta Gastroenterol Belg 2006;69:323–326.
90. Palakow J, Ladny JR, Krejza J. Focal solitary hypoechoic area in hepatic fatty infiltration: a cause of hepatic pseudomass in ultrasound examination. Rocz Akad Med Bialyms 1996;41:499–504.
91. Kim KW, Kim MJ, Lee SS, et al. Sparing of fatty infiltration around focal hepatic lesions in patients with hepatic steatosis: sonographic appearance with CT and MRI correlation. AJR Am J Roentgenol 2008;190:1018–1027.
92. Bartolotta TV, Taibbi A, Galia M, et al. Characterization of hypoechoic focal hepatic lesions in patients with fatty liver: diagnostic performance and confidence of contrast enhanced ultrasound. Eur Radiol 2007;17:650–661.
93. Dong BW, Chen MH, Li JG, et al. Further study on sonographic patterns of non uniform fatty liver. Chin J Ultrasonogr 1993;2:62.
94. Liu LP, Dong BW, Yu XL, et al. Evaluation of focal fatty infiltration of the liver using color doppler and contrast enhanced sonography. J Clin Ultrasound 2008;36:560–566.
95. Wang ZL, Tang J, Weskott HP, et al. Undetermined focal liver lesions on grey scale ultrasound in patients with fatty liver: characterization with contrast enhanced ultrasound. J Gastroenterol Hepatol 2008;23:1511–1519.
96. Nicolau C, Vilana R, Catala V, et al. Importance of evaluating all vascular phases on contrast enhanced sonography in the differentiation of benign from malignant focal liver lesions. AJR Am J Roentgenol 2006;186:158.
97. Kroncke TJ, Taupitz M, Kivelitz D, et al. Multifocal nodular fatty infiltration of the liver mimicking metastatic disease on CT: imaging findings and diagnosis using MR imaging. Eur Radiol 2000;10: 1095–1100.
98. Singer D, Neave C, Oyer C, et al. Hepatic subcapsular hematomas in fetuses and neonatal infants. Pediatr Dev Pathol 1999;2:215–220.
99. Scholmerich J, Volk BA. Differential diagnosis of anechoic/hypoechoic lesions in the abdomen detected by ultrasound. J Clin Ultrasound 1986;14:339–353.
100. Li D, Hann LE. A practical approach to analyzing focal lesions in the liver. Ultrasound Q 2005;21(3):187–200.
101. McGahan JP, Horton S, Gerscovich EO, et al. Appearances of solid organ injury with contrast enhanced sonography in blunt abdominal trauma: preliminary experience. AJR Am J Roentgenol 2006;187: 658–666.
102. Valentino M, Serra C, Zironi G, et al. Blunt abdominal trauma: emergency contrast enhanced sonography for detection of solid organ injuries. AJR Am J Roentgenol 2006;186:1361–1367.
103. Valentino M, Serra C, Pavlica P, Barozzi L. Contrast enhanced ultrasound for blunt abdominal trauma. Semin Ultrasound CT MRI 2007;28(2):130–140.
104. Horton KM, Bluemke DA, Hruban RH, et al. CT and MR imaging of benign hepatic and biliary tumours. Radiographics 1999;19: 431–451.
105. Prasad SR, Wang H, Rosas H, et al. Fat containing lesions of the liver: radiologic-pathologic correlation. Radiographics 2005;25:321–331.
106. Zheng RQ, Kudo M. Hepatic angiomyolipoma: identification of an efferent vessel to be hepatic vein by contrast enhanced harmonic ultrasound. Br J Radiol 2005;78:956–960.
107. Kudo M, Okuno T, Tomita S, et al. Hepatic angiomyolipoma preoperatively diagnosed by imaging. J Gastroenterol Hepatol 1993;8:483–488.
108. Chang JC, Lee YW, Kim HJ. Preoperative diagnosis of angiomyolipoma of the liver. Abdom Imaging 1994;19:546–548.
109. Ahmadi T, Itai Y, Takahashi M, et al. Angiomyolipoma of the liver: significance of CT and MR dynamic study. Abdom Imaging 1998;23:520–526.
110. Yen YH, Wang JH, Lu SN, Changchien CS. Contrast enhanced ultrasonography in hepatic angiomyolipoma. J Ultrasound Med 2005;24:855–859.
111. Xu HX, Xie XY, Lu MD, et al. Unusual benign focal liver lesions. Findings on real time contrast enhanced sonography. J Ultrasound Med 2008;27:243–254.
112. Sonsuz A, Ozdemir S, Akdogan M, et al. Lipoma of the liver. Z Gastroenterol 1994;32:348–350.
113. Teoh AYB, Ng SSM, Lee KF, Lai PBS. Biliary cystadenoma and other complicated cystic lesions of the liver: diagnostic and therapeutic challenges. World J Surg 2006;30:1560–1566.
114. Edmondson HA. Tumours of the liver and intrahepatic bile ducts. In: Atlas of tumour pathology, fasc. 25, first series. Washington DC: Armed Forces Institute of Pathology; 1958.
115. Del Poggio P, Buonocore M. Cystic tumours of the liver: a practical approach. World J Gastroenterol 2008;14(23):3616–3620.
116. Devaney K, Goodman ZD, Ishak KG. Hepatobiliary cystadenoma

and cystadenocarcinoma: a light microscopic and immunohistochemical study of 70 patients. Am J Surg Pathol 1994;18:1078–1091.
117. Lin MX, Xu HX, Lu MD, et al. Diagnostic performance of contrast enhanced ultrasound for complex cystic focal liver lesions: blinded reader study. Eur Radiol 2009;19:358–369.
118. Shimonishi T, Sasaki M, Nakanuma Y. Precancerous lesions of intrahepatic cholangiocarcinoma. J Hepatobiliary Pancreat Surg 2000;7:542–550.
119. Anthony PP, Telesinghe PU. Inflammatory pseudotumour of the liver. J Clin Pathol 1986;39(7):761–768.
120. Horiuchi R, Uchida T, Kojima T, Shikata T. Inflammatory pseudotumour of the liver: clinicopathologic study and review of the literature. Cancer 1990;65(7):1583–1590.
121. Nam KJ, Kang HK, Lim JH. Inflammatory pseudotumour of the liver: CT and sonographic findings. AJR Am J Roentgenol 1996;167(2): 485–487.
122. Celik H, Ozdemir H, Yucel C, et al. Characterization of hyperechoic focal liver lesions: quantitative evaluation with pulse inversion harmonic imaging in the late phase of Levovist. J Ultrasound Med 2005;24(1):39–47.
123. Ding H, Wang WP, Huang BJ, et al. Imaging of focal liver lesions: low mechanical index real time ultrasonography with SonoVue. J Ultrasound Med 2005;24:285–297.
124. Anderson SW, Kruskal JB, Kane RA. Benign hepatis tumours and iatrogenic pseudotumours. Radiographics 2009;29:211–229.
125. Berzigotti A, Magalotti D, Zappoli P, et al. Peliosis hepatis as an early histological finding in idiopathic portal hypertension: a case report. World J Gastroenterol 2006;12:3612–3615.
126. Iannaccone R, Federle MP, Brancatelli G, et al. Peliosis hepatis: spectrum of imaging findings. AJR Am J Roentgenol 2006;187(1): 43–52.
127. Kim SH, Lee JM, Kim WH, et al. Focal peliosis hepatis as a mimicker of hepatic tumours: radiological-pathological correlation. J Comput Assist Tomogr 2007;31(1):79–85.
128. Sartori S, Galeotti R, Calia N, et al. Sonographically guided biopsy and sonographic monitoring in the diagnosis and follow up of 2 cases of sarcoidosis with hepatic nodules and inconclusive thoracic findings. J Ultrasound Med 2002;21:1035–1039.
129. Folz SJ, Johnson CD, Swensen SJ. Abdominal manifestations of sarcoidosis in CT studies. J Comput Assist Tomogr 1995;19: 573–579.
130. Kessler A, Mitchell DG, Israel HL, Goldberg BB. Hepatic and splenic sarcoidosis: ultrasound and MR imaging. Abdom Imaging 1993;18:159–163.
131. Zhou YM, Li B, Xu F, et al. Clinical features of solitary necrotic nodule of the liver. Hepatobiliary Pancreat Dis Int 2008;7(5): 485–489.
132. Shepherd NA, Lee G. Solitary necrotic nodule of the liver simulating hepatic metastasis. J Clin Pathol 1983;36:1181–1183.
133. Wang Y, Yu X, Tang, et al. Solitary necrotic nodule of the liver: contrast enhanced sonography. J Clin Ultrasound 2007;35: 177–181.
134. O'Brien MJ. Cancer of the colon and rectum: current concepts of etiology and pathogenesis. Br J Med Sci 1988;157:5–15.
135. McArdle CS, Hole D, Hansell D, et al. A prospective study of colorectal cancer in the West of Scotland: a ten year follow up. Br J Surg 1990;77:206–208.
136. Scheele J, Strang R, Altendorf-Hofmann A, Paul M. Resection of colorectal liver metastases. World J Surg 1995;19:59–71
137. Fong Y, Cohen AM, Fortner JG, et al. Liver resection for colorectal metastases. J Clin Oncol 1997;15:938–946.
138. Leen E. The role of contrast enhanced ultrasound in the characterization of focal liver lesions. Eur Radiol 2001;11(Suppl 3):E27–E34.
139. Green B, Bree RL, Goldstein HM, Stanley C. Grey scale ultrasound evaluation of hepatic neoplasms: patterns and correlations. Radiology 1977;124:203–208.
140. Hillman BJ, Smith EH, Gammelgaard J, Holm HH. Ultrasonographic-pathologic correlation of malignant hepatic masses. Gastrointest Radiol 1979;4:361–365.
141. Oldenburg A, Hohmann J, Foert E, et al. Detection of hepatic metastases with low MI real time contrast enhanced sonography and SonoVue. Ultraschall Med 2005;26:277–284.
142. Beissert M, Delorme S, Mutze S, et al. Comparison of B mode and conventional colour/power Doppler ultrasound, contrast enhanced Doppler ultrasound and spiral CT in the diagnosis of focal lesions of the liver. Results of a multicentric study. Ultraschall Med 2002;23(4): 245–250.
143. Albrecht T, Blomley MJ, Burns PN, et al. Improved detection of hepatic metastases with pulse-inversion US during the liver-specific phase of SHU 508A: multicenter study. Radiology 2003;227(2): 361–370.
144. Leen E, Ceccotti P, Moug SJ, et al. Potential value of contrast-enhanced intraoperative ultrasonography during partial hepatectomy for metastases: an essential investigation before resection? Ann Surg 2006;243(2):236–240.
145. Harvey CJ, Blomley MJ, Eckersley RJ, et al. Hepatic malignancies: improved detection with pulse inversion US in late phase of enhancement with SH U 508A – early experience. Radiology 2000;216(3):903–908.
146. Larsen LP, Rosenkilde M, Christensen H, et al. The value of contrast enhanced ultrasonography in detection of liver metastases from colorectal cancer: a prospective double blinded study. Eur J Radiol 2007;62(2):302–307.
147. Albrecht T, Hoffmann CW, Schmitz SA, et al. Phase-inversion sonography during the liver-specific late phase of contrast enhancement: improved detection of liver metastases. AJR Am J Roentgenol 2001;176(5):1191–1198.
148. Leen E, Correas JM, Needleman L, et al. Multi-centre study of Sonazoid enhanced sonography of patients with known primary cancer: improved detection of liver metastases. Radiology 2002 (RSNA abstract).
149. Quaia E, Bertolotto M, Forgács B, et al. Detection of liver metastases by pulse inversion harmonic imaging during Levovist late phase: comparison with conventional ultrasound and helical CT in 160 patients. Eur Radiol 2003;13(3):475–483.
150. Konopke R, Kersting S, Bergert H, et al. Contrast-enhanced ultrasonography to detect liver metastases: a prospective trial to compare transcutaneous unenhanced and contrast-enhanced ultrasonography in patients undergoing laparotomy. Int J Colorect Dis 2007;22(2):201–207.
151. Dietrich CF, Kratzer W, Strobe D, et al. Assessment of metastatic liver disease in patients with primary extrahepatic tumors by contrast-enhanced sonography versus CT and MRI. World J Gastroenterol 2006;12(11):1699–1705.
152. Baron RL, Peterson MS. Screening the cirrhotic liver for hepatocellular carcinoma with CT and MR imaging: opportunities and pitfalls. Radiographics 2001;21:S117–132.
153. Parkins DM, Bray F, Ferlay J, Pisani P. Estimating the world cancer burden. GLOBOCAN 2000. Int J Cancer 2001;351:214–215.
154. Llovet JM, Burroughs A, Bruix J. Hepatocellular carcinoma. Lancet 2003;362:1907–1917.
155. El-Serag HB, Mason AC. Rising incidence of hepatocellular carcinoma in the United States. N Engl J Med 1999;340(10):745–750.
156. Davila JA, Morgan RO, Shaib Y, et al. Hepatitis C infection and the increasing incidence of hepatocellular carcinoma: a population based study. Gastroenterology 2004;127(5):1372–1380.
157. Forner A, Vilana R, Ayuso C, et al. Diagnosis of hepatic nodules 20mm or smaller in cirrhosis: Prospective validation of the non invasive diagnostic criteria for hepatocellular carcinoma. Hepatology 2008;47(1):97–104.
158. El-Serag HB, Mason AC. Risk factors for the rising rates of primary liver cancer in the United States. Arch Intern Med 2000;160(21): 3227–3230.
159. Bosch FX, Ribes J. Epidemiology of liver cancer in Europe. Can J Gastroenterol 2000;14(7):621–630.
160. Benvegu L, Fattovich G, Noventa F, et al. Concurrent hepatitis B and C virus infection and risk of hepatocellular carcinoma in cirrhosis. A prospective study. Cancer 1994;74:2442–2448.
161. Colombo M, De Franchis R, Del Ninno E, et al. Hepatocellular carcinoma in Italian patients with cirrhosis. Lancet 1991;325: 675–680.
162. Zoli M, Magolotti D, Bianchi G, et al. Efficacy of surveillance program for early detection of hepatocellular carcinoma. Cancer 1996;78:977–985.
163. Fargion S, Fracanzani AL, Piperno A, et al. Prognostic factors for hepatocellular carcinoma in genetic haemochromatosis. Hepatology 1994;10:1426–1431.
164. Jones DE, Metcalf JV, Collier JD, et al. Hepatocellular carcinoma in primary biliary cirrhosis and its impact on outcomes. Hepatology 1997;26:1138–1142.
165. Zaman SN, Johnson PJ, Williams R. Silent cirrhosis in patients with hepatocellular carcinoma. Implications for screening in high incidence and low incidence areas. Cancer 1990;65:1607–1610.
166. Caturelli E, Castellano L, Fusilli S, et al. Coarse nodular US pattern in

hepatic cirrhosis: risk for hepatocellular carcinoma. Radiology 2003;226:691–697.
167. Pateron D, Ganne N, Trinchet JC, et al. Prospective study of screening for hepatocellular carcinoma in Caucasian patients with cirrhosis. J Hepatol 1994;20:65–71.
168. Oka H, Tamori A, Kuroki T, et al. Prospective study of alpha-fetoprotein in cirrhotic patients monitored for development of hepatocellular carcinoma. Hepatology 1994;19:61–66.
169. Sherman M, Peltekian, KM, Lee C. Screening for hepatocellular carcinoma in chronic carriers of hepatitis B virus: incidence and prevalence of hepatocellular carcinoma in a North American urban population. Hepatology 1995;22:432–438.
170. Sheu JC, Chen DS, Sung JL, et al. Hepatocellular carcinoma in the early stage. Radiology 1985;155:463–467.
171. Bruix J, Sherman M, Llovet JM, et al. Clinical management of hepatocellular carcinoma. Conclusions of the Barcelona 2000 EASL Conference. J Hepatol 2001;35:421–430.
172. Willatt JM, Hussain HK, Adusumilli S, Marrero JA. MR imaging of hepatocellular carcinoma in the cirrhotic liver: challenges and controversies. Radiology 2008;247(2):311–330.
173. Ito K, Mitchell DG. Imaging diagnosis of cirrhosis and chronic hepatitis. Intervirology 2004;47(3–5):134–143.
174. Coleman WB. Mechanisms of human hepatocarcinogenesis. Curr Mol Med 2003;3(6):573–588.
175. Efremidis SC, Hytiroglou P. The multistep process of hepatocarcinogenesis in cirrhosis with imaging correlation. Eur Radiol 2002;12(4):753–764.
176. Bennett GL, Krinsky GA, Abitbol RJ, et al. Sonographic detection of hepatocellular carcinoma and dysplastic nodules in cirrhosis: correlation of pretransplantation sonography and liver explant pathology in 200 patients. AJR Am J Roentgenol 2002;179:75–80.
177. Matsui O. Imaging of multistep human hepatocarcinogenesis by CT during intraarterial contrast injection. Intervirology 2004;47(3–5):438–447.
178. Marrero JA, Hussain HK, Nghiem HV, et al. Improving the prediction of hepatocellular carcinoma in cirrhotic patients with an arterially enhancing liver mass. Liver Transpl 2005;11(3):281–289.
179. Torimura T, Ueno T, Kin M, et al. Overexpression of angiopoietin 1 and angiopoietin 2 in hepatocellular carcinoma. J Hepatol 2004;40(5):799–807.
180. Quaia E, D'Onofrio M, Cabassa P, et al. Diagnostic value of hepatocellular nodule vascularity after microbubble injection for characterizing malignancy in patients with cirrhosis. AJR Am J Roentgenol 2007;189:1474–1483.
181. Theise ND, Schwartz M, Miller C, Thung SN. Macroregenerative nodules and hepatocellular carcinoma in 44 sequential adult liver explants with cirrhosis. Hepatology 1992;16(4):949–955.
182. Krinsky GA, Lee VS. MR imaging of cirrhotic nodules. Abdom Imaging 2000;25(5):471–482.
183. Mitchell DG, Rubin R, Siegelman ES, et al. Hepatocellular carcinoma within siderotic regenerative nodules: appearances as a nodule within a nodule on MR images. Radiology 1991;178(1):101–103.
184. Hepatocelullar carcinoma. In: Ishak KG, Goodman ZD, Stocker JT. Atlas of tumour pathology: tumours of the liver and intrahepatic bile ducts. Third series, fascicle 31. Armed Forces Institute of Pathology 2001:199–230.
185. Harvey CJ, Albrecht T. Ultrasound of focal liver lesions. Eur Radiol 2001;11:1578–1593.
186. Ebara M, Ohto M, Shinagawa T, et al. Natural history of minute hepatocellular carcinoma smaller than three centimeters complicating cirrhosis. A study in 22 patients. Gastroenterology 1986;90:289–298.
187. Itoh K, Nishimura K, Togashi K, et al. Hepatocellular carcinoma: MR imaging. Radiology 1987;164:21–25.
188. Okabe M. Patho-morphological studies on hepatocellular carcinoma: a study on a mechanism of capsule formation and septum formation of tumour nodule. Acta Hepatol Jpn 1979;20:144–156.
189. Okuda K, Musha H, Nakashima Y, et al. Clinicopathological features of encapsulated hepatocellular carcinoma: a study of 26 cases. Cancer 1977;40:1240–1245.
190. Takayasu K, Arii S, Ikai I, et al. Prospective cohort study of transarterial chemoembolization for unresectable hepatocellular carcinoma in 8510 patients. Gastroenterology 2006;131(2):461–469.
191. Amitrano L, Guardascione MA, Brancaccio V, et al. Risk factors and clinical presentations of portal vein thrombosis in patients with cirrhosis. J Hepatol 2004;40(5):736–741.
192. Tarantino L, Francica G, Sordelli I, et al. Diagnosis of benign and malignant portal vein thrombosis in cirrhotic patients with hepatocellular carcinoma: colour Doppler US, contrast enhanced US, and fine needle biopsy. Abdom Imaging 2006;31:537–544.
193. Morin SHX, Lim AKP, Cobbold JFL, Taylor-Robinson SD. Use of second generation contrast enhanced ultrasound in the assessment of focal liver lesions. World J Gastroenterol 2007;13(45):5963–5970.
194. Jang HJ, Kim TK, Burns PN, Wilson SR. Enhancement patterns of hepatocellular carcinoma at contrast US: comparison with histologic differentiation. Radiology 2007;244(3):898–906.
195. Khalili K, Wilson SR. The biliary tree and gallbladder. In: Rumack CM, Wilson SR, Charboneau JW, Johnson JM, editors. Diagnostic ultrasound. 3rd edn. St Louis: Elsevier Mosby; 2005:171–212.
196. Vauthey JN, Blumgart LH. Recent advances in the management of cholangiocarcinomas. Semin Liver Dis 1994;14:109–114.
197. Shaib YH, El-Serag HB, Davila JA, et al. Risk factors of intrahepatic cholangiocarcinoma in the United States: a case control study. Gastroenterology 2005;128:620–626.
198. Shaib Y, El-Sherag HB. The epidemiology of cholangiocarcinoma. Semin Liver Dis 2004;24:115–125.
199. Ishak KG, Anthony PP, Sobin LH. Histological typing of tumours of the liver. WHO International Histological Classification of Tumours. Berlin: Springer Verlag; 1994.
200. Nakeeb A, Pitt HA, Sohn TA, et al. Cholangiocarcinoma: a spectrum of intrahepatic, perihilar and distal tumours. Ann Surg 1996;224: 463–473.
201. Khan SA, Thomas HC, Davidson BR, Taylor-Robinson SD. Cholangiocarcinoma. Lancet 2005;366:1303–1314.
202. Liver Cancer Study Group of Japan. The general rules for the clinical and pathological study of primary liver cancer. 4th edn. Tokyo: Kanehra; 2000.
203. Saini S. Imaging of the hepatobiliary tract. N Engl J Med 1997;336:1889–1894.
204. Choi JY, Kim MJ, Lee JM, et al. Hilar cholangiocarcinoma: role of preoperative imaging with sonography, MDCT, MRI, and direct cholangiography. AJR Am J Roentgenol 2008;191:1448–1457.
205. Bloom CM, Langer B, Wilson SR. Role of US in the detection, characterization and staging of cholangiocarcinoma. Radiographics 1999;19:1199–1218.
206. Hann L, Greatrex KC, Bach AM, et al. Cholangiocarcinoma at the hepatic hilum: sonographic findings. AJR Am J Roentgenol 1997;168:985–989.
207. Chen MF. Peripheral cholangiocarcinoma (cholangiocellular carcinoma): clinical features, diagnosis and treatment. J Gastroenterol Hepatol 1999;14:1144–1149.
208. Khalili K, Metser U, Wilson SR. Hilar biliary obstruction: preliminary results with Levovist enhanced sonography. AJR Am J Roentgenol 2003;180:687–693.
209. Chen LD, Xu HX, Xie XY, et al. Enhancement patterns of intrahepatic cholangiocarcinoma: comparison between contrast enhanced ultrasound and contrast enhanced CT. Br J Radiol 2008;81:881–889.
210. D'Onofrio M, Vecchiato F, Cantisani V, et al. Intrahepatic peripheral cholangiocarcinoma (IPCC): comparison between perfusion ultrasound and CT imaging. Radiol Med 2008;113:76–86.
211. Li R, Guo Y, Hua X, et al. Characterization of focal liver lesions: comparison of pulse inversion harmonic contrast enhanced sonography with contrast enhanced CT. J Clin Ultrasound 2007;35(3):109–117.
212. Ros PR, Buck JL, Goodman ZD, et al. Intrahepatic cholangiocarcinoma: radiologic-pathologic correlation. Radiology 1988;167:689–693.
213. Zhang Y, Uchida M, Abe T, et al. Intrahepatic peripheral cholangiocarcinoma: comparison of dynamic CT and dynamic MRI. J Comput Assist Tomogr 1999;23:670–677.
214. D'Onofrio M, Rozzanigo U, Masinielli BM, et al. Hypoechoic focal liver lesions: characterization with contrast enhanced ultrasonography. J Clin Ultrasound 2005;33:164–172.
215. Burns PN, Wilson SR. Focal liver masses: enhancement patterns on contrast enhanced images – concordance of US scans with CT scans and MR images. Radiology 2006;242:162–174.
216. Dietrich CF. Characterization of focal liver lesions with contrast enhanced ultrasonography. Eur J Radiol 2004;51(Suppl): S9–17.
217. Furuse J, Nagase M, Ishii H, Yoshino M. Contrast enhancement patterns of hepatic tumours during the vascular phase using coded harmonic imaging and Levovist to differentiate hepatocellular carcinoma from other focal lesions. Br J Radiol 2003;76:385–392.
218. Coakley FV, O'Reily EM, Schwartz LH, et al. Non-Hodgkin lymphoma as a cause of intra-hepatic periportal low attenuation on CT. J Comput Assist Tomogr 1997;21:726–728.
219. Soyer P, Beers BV, France TT, et al. Hodgkin's and non-Hodgkin's

hepatic lymphoma: sonographic findings. Abdom Imaging 1993;18:339–343.
220. Townsend RR, Laing FC, Jeffrey RB Jr, Bottles K. Abdominal lymphoma in AIDS: evaluation with US. Radiology 1989;171(3): 719–724.
221. Radin DR, Esplin JA, Levine AM, Ralls PW. AIDS related non-Hodgkin's lymphoma: abdominal CT findings in 112 patients. AJR Am J Roentgenol 1993;160(5):1133–1139.
222. Nyberg DA, Jeffrey RB Jr, Federle MP, et al. AIDS related lymphomas: evaluation by abdominal CT. Radiology 1986;159(1): 59–63.
223. Gisbert JP, Garcia-Buey L, Pajares JM, Moreno-Otero R. Prevalence of hepatitis C virus infection in B-cell non-Hodgkin's lymphoma: systematic review and meta-analysis. Gastroenterology 2003;125: 1723–1732.
224. Burney K, Bradley M, Buckley A, et al. Post transplant lymphoproliferative disorder: a pictorial review. Australas Radiol 2006;50:412–418.
225. Nalesnik MA. The diverse pathology of post-transplant lymphoproliferative disorders: the importance of a standardized approach. Transpl Infect Dis 2001;3:88–96.
226. Pickhardt PJ, Siegel MJ. Abdominal manifestations of post transplantation lymphoproliferative disorder. AJR Am J Roentgenol 1998;171:1007–1013.
227. Pickhardt PJ, Siegel MJ. Posttransplantation lymphoproliferative disorder of the abdomen: CT evaluation in 51 patients. Radiology 1999;213:73–78.
228. Gazelle GS, Lee MJ, Hahn PF, et al. US, CT, and MRI of primary and secondary liver lymphoma. J Comput Assist Tomogr 1994;18: 412–415.
229. Noronha V, Shafi NQ, Obando JA, Kummar S. Primary non-Hodgkin's lymphoma of the liver. Crit Rev Oncol/Hematol 2005;53:199–207.
230. Park KY, Yu JS, Yoon SW, et al. Burkitt's lymphoma representing periportal infiltrating mass on CT. Yonsei Med J 2004;45:723–726.
231. Low G, Leen E. Diagnosis of periportal hepatic lymphoma with contrast-enhanced ultrasonography. J Ultrasound Med 2006;25: 1059–1062.
232. Wilson SR. The liver. In: Rumack CM, Wilson SR, Charboneau JW, editors. Diagnostic ultrasound. 3rd edn. St Louis, MO: Elsevier Mosby; 2005:126–135.
233. Jang HJ, Kim TK, Wilson SR. Imaging of malignant liver masses: Characterization and detection. Ultrasound Q 2006;22:19–29.
234. Catalano O, Nunziata A, Lobianco R, Siani A. Real-time harmonic contrast material-specific US of focal liver lesions. Radiographics 2005;25:333–349.
235. Edmonson HA. Differential diagnosis of tumours and tumour like lesions in infancy and childhood. AMA J Dis Child 1956;91(2): 168–186.
236. Criag JR, Peters RL, Edmondson HA, Omata M. Fibrolamellar carcinoma of the liver: a tumour of adolescents and young adults with distinctive clinico-pathologic features. Cancer 1980;46:372–379.
237. Vecchio FM. Fibrolamellar hepatocellular carcinoma of the liver: a distinct entity within hepatocellular tumours – a review. Appl Pathol 1988;6:139–148.
238. Torbenson M. Review of the clinicopathological features of fibrolamellar carcinoma. Adv Anat Pathol 2007;14(3):217–223.
239. Craig JR. Fibrolamellar carcinoma: clinical and pathologic features. In: Okuda K, Tabor E, eds. Liver cancer. New York: Churchill Livingstone; 1997:255–262.
240. El-Serag HB, Davila JA. Is fibrolamellar carcinoma different from hepatocellular carcinoma? A US population based study. Hepatology 2004;39(3):798–803.
241. Blachar A, Federle MP, Ferris JV, et al. Radiologists' performance in the diagnosis of liver tumours with central scars by using specific CT criteria. Radiology 2002;223:532–539.
242. Friedman AC, Lichtenstein JE, Goodman ZD, et al. Fibrolamellar hepatocellular carcinoma. Radiology 1985;157:583–587.
243. McLarney JK, Rucker PT, Bender GN, et al. Fibrolamellar carcinoma of the liver: radiologic-pathologic correlation. Radiographics 1999;19:453–471.
244. Fan ZH, Chen MH, Dai Y, et al. Evaluation of primary malignancies of the liver using contrast enhanced sonography: correlation with pathology. AJR Am J Roentgenol 2006;186:1512–1519.
245. Weiss SW, Enzinger FM. Epithelioid hemangioendothelioma: a vascular tumour often mistaken for a carcinoma. Cancer 1982;50: 970–981.
246. Buetow PC, Buck JL, Ros PR, Goodman ZD. Malignant vascular tumours of the liver: radiologic-pathologic correlation. Radiographics 1994;14:53–166.
247. Korobkin M, Stephens DH, Lee JKT, et al. Biliary cystadenoma and cystadenocarcinoma: CT and sonographic findings. AJR Am J Roentgenol 1989;153:507–511.

CHAPTER

11 Biopsy technique and RF ablation

Riccardo Lencioni, Clotilde Della Pina, Dania Cioni and Laura Crocetti

LIVER BIOPSY 167
Technique 167
Percussion–palpation approach 167
Image-guided approach 167
Type of needle 168
The quality of the specimen 168
Indications 169
Diagnosis 169
Prognosis 169
Treatment 169
Patient management 170
Complications 170

RADIOFREQUENCY ABLATION 171
Technique 171
Principles 171
The role of imaging 172
Indications 172
Complications 174
Clinical results 174
Treatment of hepatocellular carcinoma 174
Treatment of colorectal hepatic metastases 175

LIVER BIOPSY

Liver biopsy (LB), and thus histological assessment of the liver, has been used as a method for diagnosing parenchymal liver diseases since the mid-1940s, well before the development of the sophisticated imaging techniques and sensitive blood tests now routinely used to improve diagnostic accuracy.[1] Although these non-invasive techniques have in many instances replaced liver histology, LB remains an essential tool in the diagnosis and management of parenchymal liver diseases.[2] Moreover, the use of LB is increasing with the advent of liver transplantation and the progress being made in antiviral therapeutic agents. While blind percutaneous needle biopsy is the traditional technique, the use of ultrasound (US) guidance has increased considerably. Histological assessment can be performed even on a focal liver lesion, when a patient's overall clinical picture, together with imaging features, are not sufficient to establish a diagnosis. Image guidance is needed whenever biopsy has to be performed on a focal liver lesion.[2] All LB techniques require specific training to ensure appropriate-sized specimen retrieval and the lowest rate of complications.

Technique

Currently, there are three techniques for performing an LB: percutaneous, transjugular and laparoscopic. The percutaneous LB can be performed blind, US guided or US assisted[2–4] (Table 11.1).

Percussion–palpation approach

The percussion–palpation approach is sometimes referred to as the blind approach. Percutaneous LB is usually performed with the patient in the supine position, close and parallel to the edge of the bed, with the patient's right hand positioned behind the head.[5] Caudal percussion is helpful in selecting the site for the biopsy over the hemithorax between the anterior and midaxillary lines, until an intercostal space is reached where dullness is maximal at the end of expiration. The intercostal space below this point is used. Local infiltration with lidocaine 1–2% (without adrenaline) is usually performed to ensure that this area is well anaesthetised. The total length of time required to pass the biopsy needle into and then remove it from the liver is usually 2–3 seconds. The specimen is then discharged from the needle into a 10% formaldehyde solution.[5]

Image-guided approach

The LB can be performed under imaging control or guidance using US, computed tomography or magnetic resonance imaging. US is the most common imaging modality used because it is readily and widely available, simple, the least costly and does not expose the patient to radiation. When US is used in obtaining the LB, it is done either immediately before (site marking) or throughout the entire procedure (real-time).[2,3] Local infiltration with lidocaine 1–2% (without adrenaline), as mentioned above, is usually performed. Prebiopsy US helps to detect focal hepatic tumours (benign or malignant), cysts, ascites, intrahepatic biliary dilatation or hepatic anatomical variation. For focal hepatic lesions, it is an accepted standard of practice that image guidance is used in order to guide and direct the LB.[6,7] Although right lobe biopsy is the usual biopsy site in patients with diffuse disease, the choice of where to biopsy the liver using imaging guidance varies according to the operator. The intercostal approach does not usually require an extreme breath hold. This approach is associated with a small risk of intercostal artery puncture, which can be minimised by inserting the needle over the cephalad rather than the caudad aspect of the rib. Although the intercostal approach is typically closer to the costophrenic sulci, the lung can be easily avoided because it is readily visible as an echogenic structure on US.[2]

- *Ultrasound-assisted approach.* This approach is sometimes also referred to as site marking. The US is performed immediately before the LB, an optimal site is identified on the skin, and the distance from the skin to any large hepatic vessels or ducts is measured. In this way, a reasonably precise measurement of the depth needed to be reached by the biopsy needle is determined[2,3] (Fig. 11.1).
- *Ultrasound-guided approach.* Under real-time US guidance, the liver and biopsy needle are imaged throughout the procedure. This is usually achieved by utilising an automated biopsy device that can be operated with one hand while the US probe is held with the other hand.[3,8] US-guided approach is

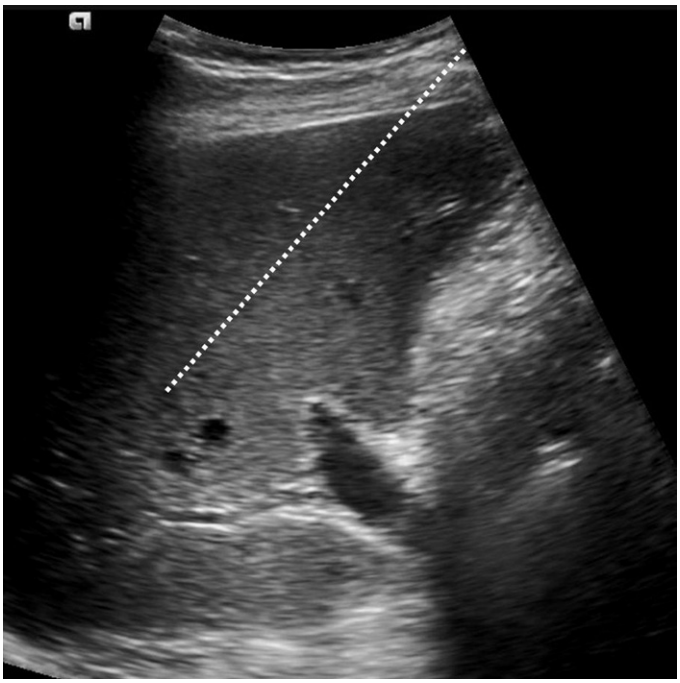


Figure 11.1 US-assisted liver biopsy. The right liver lobe is visualised with US with an intercostal approach. A peripheral portion of the liver, not including major vessels, is chosen to perform US-assisted liver biopsy and the needle path is planned (dotted line).



Figure 11.2 US-guided liver biopsy. The focal liver lesion in segment VII is visualised at US, with an intercostal approach. A 20-gauge spring-loaded automated cutting needle in placed within the lesions under US guidance.

Table 11.1 Techniques for performing liver biopsy

Percutaneous	
1. Percussion–palpation guided or blind	The most appropriate biopsy site is determined on the basis of clinical examination
2. Image guided:	Liver biopsy site is performed under imaging (US, computed tomography, magnetic resonance) guidance
US guided	The most appropriate biopsy site is determined by US before the biopsy
US assisted	The most appropriate biopsy site is determined by US and US is used in real-time for tissue procurement
Transjugular or transvenous	Biopsy is accomplished through a jugular or femoral venous approach under fluoroscopic guidance
Laparoscopic	Biopsy is accomplished through a laparoscopic approach under direct vision

US, ultrasound.

needed whenever a mass lesion biopsy has to be performed (Fig. 11.2). Manolakopoulos et al., in a retrospective study, showed that the US-assisted approach is as safe as US-guided approach and both obtained adequate specimens for histological diagnosis.[9]

Type of needle

The LB devices used most widely today for diagnosis and management of patients with parenchymal liver disease are the core-aspiration needles (Menghini, Jamshidi or Klatskin) and sheathed cutting needles (either manual or spring-loaded, often referred to as a 'Tru-cut style' in reference to one of the earliest cutting devices). Newer automated versions of this latter type have recently emerged, allowing variable pitch and specimen length. The cutting needle devices generally pass into the liver parenchyma using a troughed needle before an outer sheath or hood slides over this to secure a core of tissue. Usually the choice of the biopsy instrument/needle is based on operator preference, instrument availability and clinical scenario.[2,10] Tru-cut needles are superior to aspiration-type needles in patients with fibrosis or cirrhosis.[11] The average length of the tissue specimen is greater when obtained with an automatic cutting biopsy needle compared with the Tru-cut needle.[12,13] The risk of bleeding was reported to be higher when the cutting-type needle was used,[14,15] while in a prospective study this risk was not affected by the type of needle used.[16] Spring-loaded automated guns are used with greater ease and a shorter intrahepatic phase, and accomplish biopsies without the 'jabbing motion' associated with non-automated needles. Nowadays, in clinical practice, spring-loaded devices are the most widely used needles.[3]

The quality of the specimen

The quality of LB specimen is usually determined by length, width, fragmentation and complete portal tracts (CPTs).[17] The concept of the quality of an LB specimen has recently emerged as a critical factor in the assessment of the grade and stage of the liver disease in patients with chronic viral hepatitis. Nowadays, the number of CPTs is considered to be crucial for reliable grading and staging, and it is generally accepted that an optimal LB specimen is defined as being 20–25 mm long and/or containing more than 11 CPTs.[18–20]

Large-needle biopsy (>19-gauge needles) is used for diffuse liver disease, whereas fine-needle biopsy (FNB) (20-gauge needles or smaller) is used for the investigation of focal liver lesions.[21] The biopsy size influences the histological grading and staging of chronic viral hepatitis, as FNB carries a higher risk of inadequate tissue specimen, and according to some authors would underestimate the grade and stage.[19,21,22] In contrast, Petz et al. concluded that the grading and staging of chronic hepatitis is feasible also with FNB.[23] In fibrosis and cirrhosis, automated biopsy needle devices provide better quality tissue compared with aspiration-type needles. Hence, clinicians should be encouraged to use automated needles once advanced fibrosis or cirrhosis is suspected.[13]

Experimental studies showed that the larger the calibre of the needle, the greater the absolute blood loss after LB in a porcine model.[24,25] However, because more tissue can be recovered and because fewer passes are necessary, the chance of complications is reduced despite the greater amount of blood loss and therefore the use of larger-calibre needles is considered more efficient. Other studies concerning the size of the needle in connection with the rate of haemorrhagic complications, performed in humans, did not show any difference.[26] It has been demonstrated that taking more than one biopsy can increase the diagnostic value, but may have an effect on morbidity.[27–31] However, in a study performed by Riley on 165 patients, multiple passes were necessary in only 1.8% of cases (noting that a low multiple pass rate was observed when applying ultrasound guidance).[29] From a practical point of view, the visual inspection of the hepatic fragment obtained by LB represents the guarantee that enough histological material was obtained. If the size of the specimen is considered inadequate, another hepatic pass in the same session should be performed, rather than take a new biopsy later.

After the collection, the specimen should be fixed in 10% neutral buffered formalin or other fixative preferred by the local laboratory, because this will usually allow the full range of stains, both routine histochemical (haematoxylin and eosin and Masson trichrome) and immunohistochemical.[2]

Indications

LB has currently three major roles: (a) for diagnosis of diffuse or focal disease and mass lesions, (b) for assessment of prognosis and (c) to assist in making therapeutic management decisions.[2]

Diagnosis

Liver histology, in conjunction with the full gamut of clinical and laboratory data, is considered to establish a diagnosis in multiple parenchymal liver diseases (acute and chronic hepatitis, cholestatic disorders, fatty liver disease, vascular diseases, infiltrative or storage diseases, etc.). Moreover it plays a fundamental role in the management of the patient with a diagnostic dilemma. This includes the patient with abnormal liver tests of unknown aetiology, or the patient in whom a specific liver disease has been considered but has not yet been confirmed.[2]

The use of LB for evaluation of focal liver disease (i.e. a lesion detected by imaging) is highly variable. However, almost always it depends on the specific clinical scenario.[2] For example, evaluation of mass lesions requires consideration of whether the patient has any known underlying liver disease or whether the patient has a known parenchymal liver process. In patients with underlying liver disease, especially cirrhosis, the overriding concern is with hepatocellular carcinoma (HCC). This diagnosis can be made in patients with a typical lesion (usually >1 cm in size, with a typical vascular pattern seen with dynamic imaging techniques).[32] In lesions with atypical behaviour, liver biopsy is advised. In patients without underlying liver disease, focal liver lesions are usually represented by benign lesions, most often solitary, but on occasion multiple. For the most part, these should have sufficient distinguishing characteristics on high quality imaging modalities such that liver biopsy is unnecessary. When a patient's overall clinical picture together with imaging features are not sufficient to establish a diagnosis, liver biopsy is advised.[2]

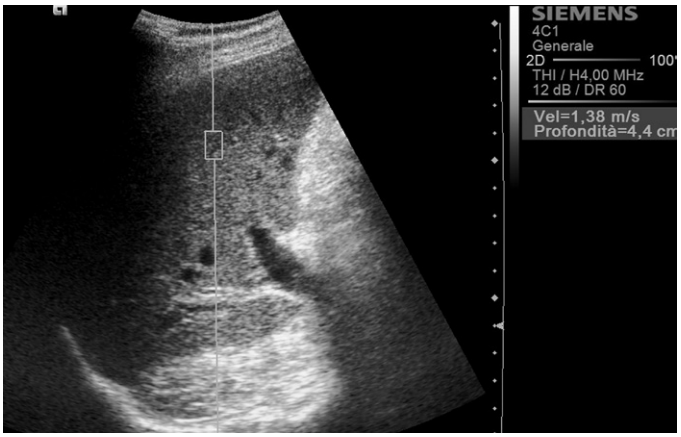


Figure 11.3 Non-invasive evaluation of liver fibrosis by means of elastography. Elastography of a portion of the liver is performed under US guidance by means of acoustic radiation force-based imaging (ARFI). The velocity value of 1.38 indicates moderate fibrosis.

Indications

Diagnosis
- Parenchymal disease.
- Focal lesion – not always needed.

Prognosis
- Severity of disease.

Treatment
- Treatment planning and prognosis of diffuse liver disease.
- Management of patients post liver transplantation.

Prognosis

A further important use of liver biopsy is in assessing disease severity, notably fibrosis, which is strongly related to prognosis.[2]

Treatment

Currently, LB is used more than ever to develop treatment strategies. This has evolved because of the many new therapies available for patients with a variety of liver disease. Not only can a treatment plan be instituted in a patient after a specific diagnosis is made, but among those with established liver disease, treatment may be predicated on the specific histological lesion.[33–35]

Assessment of liver histology can be also an essential component of management of patients following liver transplantation. It is often important to make a specific diagnosis in the setting of liver test abnormalities early after transplantation to investigate allograft rejection, preservation or reperfusion injury, drug-induced liver injury (usually recurrent) viral infection, or bile duct injury.[2] LB is also often helpful in the setting of late allograft dysfunction, including investigating the possibility of recurrence of the original disease.[36,37]

It is important to emphasise that the role of histological analysis of the liver in the management of patient with liver disease is likely to evolve over time, particularly as non-invasive modalities for assessment of liver fibrosis, such as transient elastography (Fibroscan) and acoustic radiation force impulse (ARFI) imaging, are positioned more in the mainstream.[38,39] (Fig. 11.3).

Patient management

Currently, LB is typically undertaken on an outpatient or 'same day' basis. Indications for, benefits, risks and alternatives of LB have to be discussed with the patient. Written informed consent should be obtained prior to LB.[2]

Pre-biopsy testing includes measurement of the complete blood count, including platelet count, prothrombin time (PT)/international normalised ratio (INR). In some institutions the activated partial thromboplastin time and/or cutaneous bleeding time at a suitable juncture prior to the biopsy are requested. A prothrombin time ratio (normal time/patient's time) >50% and a platelet count higher than 50000/μL are required to keep the risk of bleeding at an acceptably low level.[2]

Usual daily activities may be undertaken up until the day preceding liver biopsy. Following the procedure, patients are encouraged to rest quietly. Many physicians recommend that patients who live more than 1 hour travelling distance by car from the centre remain close by that evening, in case of potential late complication. However, in the absence of an evident complication or significant pain that necessitates use of potent analgesia, there should be no restriction upon return to work the following day. Patients are discouraged from lifting weights for a minimum of 24 hours, because this may increase intra-abdominal pressure and in theory could facilitate bleeding from the puncture site.[2]

An important issue surrounds management of antiplatelet (i.e. aspirin, ticlodipine, clopidogrel, IIb/IIIa receptor antagonists, non-steroidal anti-inflammatory drugs) and/or anticoagulant drugs (i.e., warfarin) before and after the time of liver biopsy. According to the American Association for the Study of Liver Diseases antiplatelet medications should be discontinued several to 10 days before liver biopsy. Antiplatelet therapy may be restarted 48–72 hours after liver biopsy. Even anticoagulant medications should be discontinued prior to liver biopsy. Warfarin should generally be discontinued at least 5 days prior to liver biopsy. Heparin and related products should be discontinued 12–24 hours prior to biopsy. Warfarin may be restarted the day following liver biopsy.[2,40,41]

Routine placement of an intravenous cannula prior to the procedure is practised in many facilities as a precaution should there be significant pain and/or bleeding after the procedure.[2]

Once liver biopsy has been accomplished, the patient then rests quietly and is carefully observed by experienced nursing staff. The patient is often placed in the right lateral decubitus position (to allow the liver to rest against the lateral abdominal wall and thereby limit bleeding), although this is largely performed as a result of longstanding clinical practice.[42] The risk of bleeding is greatest immediately after liver biopsy; thus, it is recommended that patients be observed carefully over the first 2–3 hours after biopsy.[31,43]

Complications

The reported complications range from minor (pain and transient hypotension) to major, including (a) haemorrhage (intraperitoneal, intrahepatic, haemothorax); (b) perforation of the gallbladder or the colon; (c) pneumothorax; and (d) intrahepatic arteriovenous fistula. Significant bleeding and bile peritonitis are serious complications and may lead to mortality. Severe bleeding (requiring hospitalisation, the likelihood of transfusion, or even radiological intervention or surgery) has been estimated to occur in between 1 in 2500 and 1 in 10000 biopsies after an intercostal percutaneous approach for diffuse, non-focal, liver disease. Less severe bleeding, defined as that sufficient to cause pain or reduced blood pressure or tachycardia, but not requiring transfusion or intervention, occurs in approximately 1 in 500 biopsies. Mortality after LB is usually related to haemorrhage. Despite a wide variation in the literature, the most commonly quoted mortality rate is less than or equal to 1 in 10000 liver biopsies.[14,15,17,28,31,44–48]

A large retrospective multicentric study demonstrated that 61% of the complications appeared in the first 2 hours after the biopsy, 82% in the first 10 hours and 96% in the first 24 hours after biopsy.[14] Some studies showed that the rate of complications is similar in outpatients and inpatients.[15,49]

Differences in complication rates, either minor or major, have been reported between the blind and US-guided LB. The mortality rate from blind LB is 0.01–0.1%.[14,15,44] The use of US guidance can prevent inadvertent puncture of other organs or large intrahepatic vessels. US may also reduce the incidence of major complications such as haemorrhage, bile peritonitis, pneumothorax, etc. Caturelli et al. have shown that, when compared with a historical control group from within their institution, there was an overall statistically significant decrease in complications when US was used (0.53% versus 2.1% in the historical control group, $p < 0.05$).[50] Moreover, it has been demonstrated that US-guided LB causes significantly less biopsy pain and significantly less pain-related morbidity.[50,51]

The relationship between LB complications and the number of needle passes is well documented.[15] The frequency of complications increases with the number of passes performed at a rate of 26.4%, with one pass versus 68% with two or more passes ($p < 0.001$).[28]

A recent meta-analysis of best available evidence concludes that the use of US-guided biopsy is superior to blind needle biopsy. The odds ratios of the controlled studies showed that blind needle biopsy carried a higher risk for major complications, post-biopsy pain and biopsy failure.[3]

When a malignant focal liver lesion is biopsied, the procedure is associated with a risk of tumour spread usually along the biopsy track.[52,53] Although potentially a devastating complication, especially in transplant candidates where immunosuppression may predispose to seeded tumour growth, this risk is almost certainly overstated in earlier literature. For example, in a recent retrospective study of patients undergoing image-guided biopsy of a lesion suspicious for HCC, HCC was diagnosed by biopsy in 74 (63%) of 118 cases, and an additional 10 were found to have HCC on follow-up; no patient developed evidence of tumour spread along the needle track.[54] Biopsy and/or aspiration of infectious lesions is generally safe. It has been suggested that the presence of an echinococcal cyst (hydatid disease) represents an absolute contraindication to biopsy because it is known that piercing of an echinococcal cyst may be associated with fatal anaphylaxis. However, available data suggest that careful aspiration of these lesions with 19-gauge to 22-gauge needles is relatively safe. Nevertheless, if suspected, some consideration and preparation for possible anaphylaxis is warranted.[55]

Pre-biopsy testing

- Blood count, including a platelet count.
- Prothrombin time.
- Antiplatelet medications stopped for several to 10 days prior to biopsy.
- Warfarin stopped for 5 days prior to biopsy.
- Heparin stopped for 12–24 hours prior to biopsy.
- Corrective measures may be needed if a biopsy is urgent.

Complications of liver biopsy

- Bleeding – peritoneal, intraparenchymal and thoracic.
- Bile peritonitis.
- Damage to colon or gallbladder.
- Pneumothorax.
- Arteriovenous fistula.
- Mortality related to bleeding 1:10000.
- Overall complication rate 0.5–2.0% depending on technique.
- Ultrasound-guided biopsy causes less pain and has the lowest complication rate.

RADIOFREQUENCY ABLATION

The development of image-guided percutaneous techniques for local tumour ablation has been one of the major advances in the treatment of liver malignancies. Among these methods, radiofrequency (RF) ablation is currently established as the primary ablative modality at most institutions. RF ablation is accepted as the best therapeutic choice for patients with early-stage HCC when liver transplantation or surgical resection are not suitable options.[56,57] In addition, RF ablation is considered as a viable alternative to surgery for inoperable patients with limited hepatic metastatic disease, especially from colorectal cancer, in patients deemed ineligible for surgical resection, because of extent and location of the disease or concurrent medical conditions.[56,58]

Technique

Principles

The goal of RF ablation is to induce thermal injury to the tissue through electromagnetic energy deposition. In RF ablation, the patient is part of a closed-loop circuit that includes an RF generator, an electrode needle and a large dispersive electrode (ground pads). An alternating electric field is created within the tissue of the patient. Because of the relatively high electrical resistance of tissue in comparison with the metal electrodes, there is marked agitation of the ions present in the target tissue that surrounds the electrode, since the tissue ions attempt to follow the changes in direction of alternating electric current. The agitation results in frictional heat around the electrode. The discrepancy between the small surface area of the needle electrode and the large area of the ground pads causes the generated heat to be focused and concentrated around the needle electrode.[59] The thermal damage caused by RF heating is dependent on both the tissue temperature achieved and the duration of heating. Heating of tissue at 50–55°C for 4–6 minutes produces irreversible cellular damage. At temperatures between 60 and 100°C near immediate coagulation of tissue is induced, with irreversible damage to mitochondrial and cytosolic enzymes of the cells. At more than 100–110°C, tissue vaporises and carbonises.

For adequate destruction of tumour tissue, the entire target volume must be subjected to cytotoxic temperatures. Thus, an essential objective of ablative therapy is achievement and maintenance of a 50–100°C temperature throughout the entire target volume for at least 4–6 minutes. However, the relatively slow thermal conduction from the electrode surface through the tissues increases the duration of application to 10–20 minutes. On the other hand, the tissue temperature should not be increased over these values to avoid carbonisation around the tip of the electrode due to excessive heating. Another important factor that affects the success of RF thermal ablation is the ability to ablate all viable tumour tissue and an adequate tumour-free margin. The most important difference between surgical resection and RF ablation of hepatic tumours is the surgeon's insistence on a 1 cm wide tumour-free zone along the resection margin. To achieve rates of local tumour recurrence with RF ablation that are comparable to those obtained with hepatic resection, physicians should produce a 360°, 1 cm thick tumour-free margin around each tumour.[60] This cuff will assure that all microscopic invasions around the periphery of a tumour have been eradicated. Thus, the target diameter of an ablation should ideally be 2 cm larger than the diameter of the tumour that undergoes treatment.[60]

Heat efficacy is defined as the difference between the amount of heat produced and the amount of heat lost. Therefore, effective ablation can be achieved by optimising heat production and minimising heat loss within the area to be ablated. The relationship between these factors has been characterised as the bio-heat equation. The bio-heat equation governing RF-induced heat transfer through tissue has been described by Pennes[61] and subsequently simplified to a first approximation by Goldberg and colleagues[59] as follows:

$$\text{Coagulation} = \text{energy deposited} \times \text{local tissue interactions} - \text{heat loss}.$$

Heat production is correlated with the intensity and duration of the RF energy deposited. Tissues cannot be heated to greater than 100–110°C without vaporising, and this process produces significant gas that both serves as an insulator and retards the ability to effectively establish an RF field. On the other hand, heat conduction or diffusion is usually explained as a factor of heat loss in regard to the electrode tip. Heat is lost mainly through convection by means of blood circulation. These processes, together with the rapid decrease in heating at a distance from the electrode, essentially limit the extent of induced coagulation from a single, unmodified monopolar electrode to no greater than 1.6 cm in diameter. Therefore, most investigators devoted their attention to strategies that increase the energy deposited into the tissues and several corporations have manufactured new RF ablation devices based on technologic advances that increase heating efficacy. To accomplish this increase, the RF output of all commercially available generators has been increased to 150–250 W, which may potentially increase the intensity of the RF current deposited at the tissue. Multiple or multitined expandable electrodes permit the deposition of this energy over a larger volume and ensure more uniform heating that relies less on heat conduction over a large distance. Internally cooled electrodes have been designed to minimise carbonisation and gas formation around the needle tip by eliminating excess heat near the electrode. Moreover multi-tined micro-perfused electrodes have been introduced: administration of saline solution – at a very low rate – during the application of RF current increases tissue conductivity and thereby allows greater deposition of RF current and increased tissue heating and coagulation.[62]

Inadequate coagulation can be the result of the other two elements of the 'bio-heat equation': (a) heterogeneity of tissue composition, by which differences in tumour tissue density, including fibrosis and calcification, alter electrical and thermal conductance; and (b) blood flow, by which perfusion-mediated tissue cooling (vascular flow) reduces the extent of thermally induced coagulation. These limitations have led investigators to the study of manoeuvres or adjuvant therapies in an attempt to improve RF ablation, either in conjunction with or as an alternative to multiple ablations of a given tumour. In particular, several strategies for reducing blood flow during ablation therapy have been proposed. Total portal inflow occlusion (Pringle manoeuvre) has been used at open laparotomy and at laparoscopy. Angiographic balloon catheter occlusion of the hepatic artery or embolisation of the tumour feeding artery has also been shown to be useful in hypervascularised tumours.[63] In the setting of HCC, combining thermal ablation with other therapies such as chemoembolisation or transarterial administration of drug-eluting beads has shown very promising results in early clinical investigation.[64,65] The findings of experimental studies suggested that adjuvant chemotherapy may increase the ablation volume compared with RF ablation therapy alone in different tumour types.[66,67] Further research to determine optimal methods of combining chemotherapeutic regimens (both agent and route of administration) with RF ablation is ongoing.

Radiofrequency ablation

- Heating tissue to cause cell death.
- Heating rapidly decreases with distance from the electrode – so need multiple or expandable electrodes to increase area of ablation.
- Cooling by blood flow. Additional manoeuvres to limit blood flow at operation or angiographically can be employed.
- Aim to ablate an area 1 cm wider than the tumour (2 cm greater diameter) to produce a tumour-free margin around the lesion.

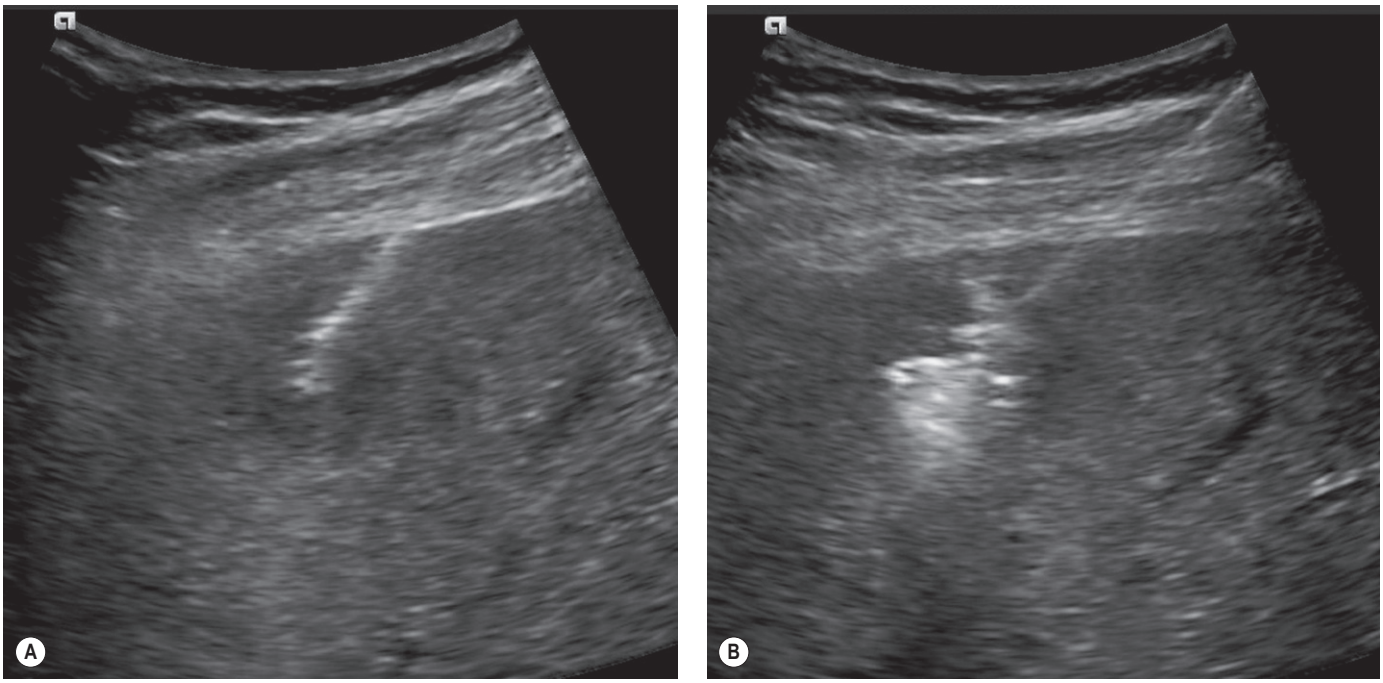


Figure 11.4 US-guided RF ablation. A: A multi-tined expandable needle is inserted and deployed within an HCC nodule. **B:** Following the activation of the RF generator, a hyperechoic cloud appears at the site of treatment.

The role of imaging

Targeting of the lesion can be performed with US, computed tomography, or magnetic resonance imaging (Fig. 11.4). The guidance system is chosen largely on the basis of operator preference and local availability of dedicated equipment such as computed tomography fluoroscopy or open magnetic resonance systems. During the procedure, important aspects to be monitored include how well the tumour is being covered and whether any adjacent normal structures are being affected at the same time. While the transient hyperechoic zone that is seen at ultrasound within and surrounding a tumour during and immediately after RF ablation can be used as a rough guide to the extent of tumour destruction, magnetic resonance is currently the only imaging modality with validated techniques for real-time temperature monitoring. After activation the generators are run by automated programs, designed to modulate the released power relying on direct temperature measurement or on electrical measurement of tissue impedance, to avoid overheating and carbonisation. At the end of the procedure, coagulation of the needle track is performed, to prevent tumour seeding.

Contrast-enhanced US performed after the end of the procedure may allow an initial evaluation of treatment effects (Fig. 11.5). However, contrast-enhanced computed tomography and magnetic resonance imaging are recognised as the standard modalities to assess treatment outcome. Computed tomography and magnetic resonance images obtained after treatment show successful ablation as a non-enhancing area with or without peripheral enhancing rim. The enhancing rim that may be observed along the periphery of the ablation zone appears a relatively concentric, symmetric and uniform process in an area with smooth inner margins. This is a transient finding that represents a benign physiological response to thermal injury (initially, reactive hyperaemia; subsequently, fibrosis and giant cell reaction). Benign periablational enhancement needs to be differentiated from irregular peripheral enhancement due to residual tumour that occurs at the treatment margin. In contrast to benign periablational enhancement, residual unablated tumour often grows in scattered, nodular or eccentric patterns.[67] Later follow-up imaging studies should be aimed at detecting the recurrence of the treated lesion (i.e. local tumour progression), the development of new hepatic lesions, or the emergence of extrahepatic disease. Evaluation of tumour response should be performed following criteria recently developed by a panel of experts of the American Association for the Study of Liver Diseases.[68]

Table 11.2 BCLC classification in patients diagnosed with HCC

Very early stage	PS 0, Child–Pugh A, single HCC <2 cm
Early stage	PS 0, Child–Pugh A–B, single HCC or 3 nodules <3 cm
Intermediate stage	PS 0, Child–Pugh A–B, multinodular HCC
Advanced stage	PS 1–2, Child–Pugh A–B, portal neoplastic invasion, nodal metastases, distant metastases
Terminal stage	PS >2, Child–Pugh C

PS, performance status.

Indications

RF ablation is the therapy of choice in very early and early HCC according to the Barcelona Clinic Liver Cancer (BCLC) classification (Table 11.2) when patients are not candidates for either liver resection or transplantation.[32,57] Patients are required to have a single tumour or as many as three nodules smaller than 3 cm each, no evidence of vascular invasion or extrahepatic spread, performance status test of 0, and liver cirrhosis in Child–Pugh class A or B.

In the setting of metastatic disease, RF ablation is generally indicated for non-surgical patients with colorectal cancer oligometastases isolated to the liver.[69,70] Selected patients with limited hepatic and pulmonary colorectal metastatic disease, however, may qualify for percutaneous treatment.[71,72] In patients with hepatic metastases

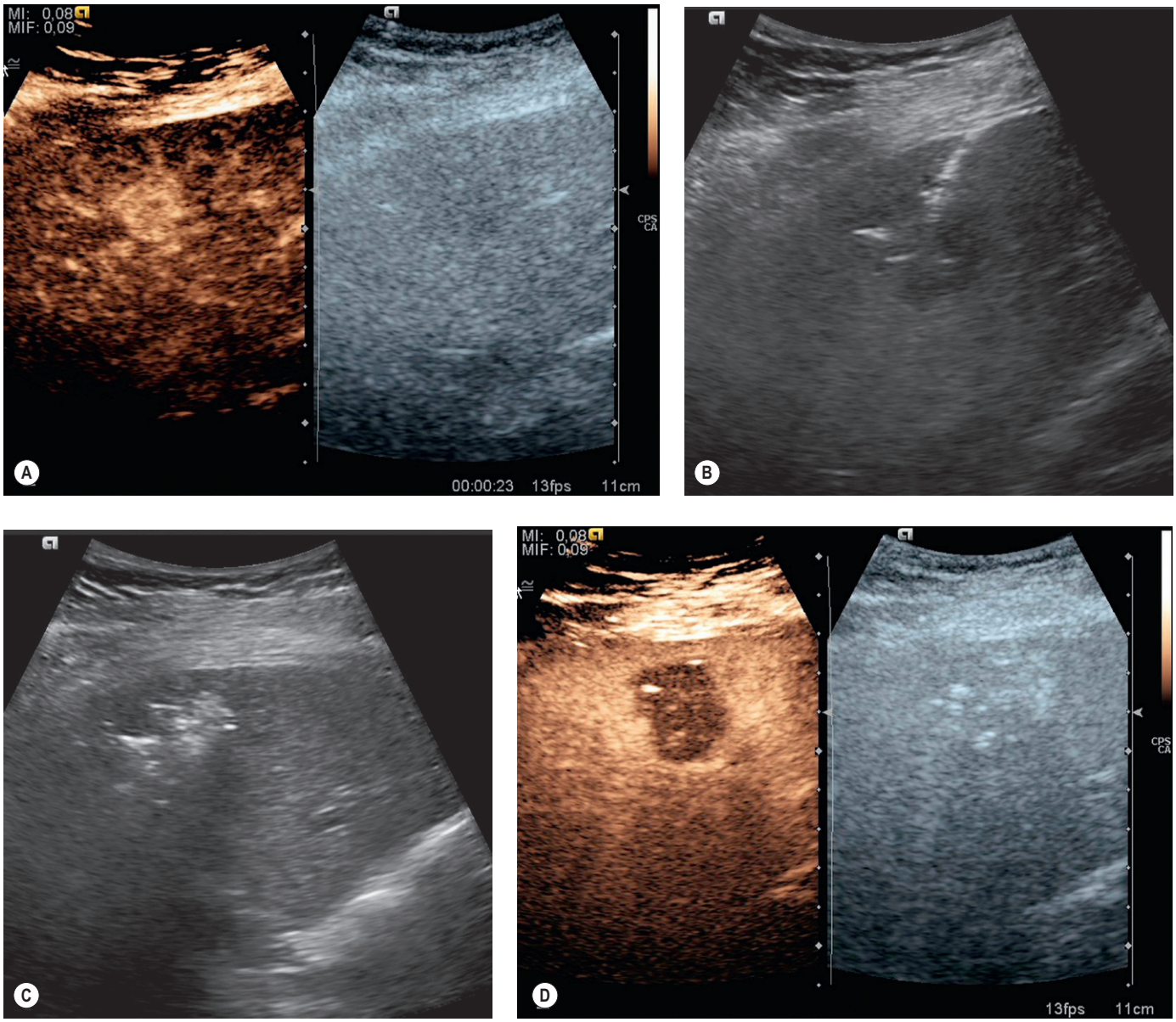


Figure 11.5 Initial evaluation of tumour response to RF ablation with contrast-enhanced US. A: Pre-treatment contrast-enhanced US obtained in the arterial phase shows the small HCC lesion as a hypervascular nodule. B-mode low-mechanical index image is shown in the right side of the image; the contrast-specific mode during the arterial phase is shown in the left side. **B:** The tumour is treated with RF ablation under US guidance. **C:** At the end of the procedure, a hyperechoic cloud covering the tumour as well as a cuff of surrounding liver parenchyma is seen on US. **D:** Contrast-enhanced US study performed at the end of the procedure shows the ablation zone as a non-enhancing area completely covering the tumour. Periablation enhancement is also seen, representing reactive hyperaemia.

from other primary cancers, promising initial results have been reported in the treatment of breast and endocrine tumours. The number of lesions should not be considered an absolute contraindication to RF ablation if successful treatment of all metastatic deposits can be accomplished. Nevertheless, most centres preferentially treat patients with four or fewer lesions. Tumour size is of utmost importance to predict the outcome of RF ablation. Imaging studies underestimate the size of metastatic deposits. Therefore, the target tumour should not exceed 3 cm in longest axis to ensure complete ablation with most of the currently available devices.[56]

A careful clinical, laboratory and imaging assessment has to be performed in each individual patient by a multidisciplinary team to evaluate eligibility for percutaneous ablation. Laboratory tests should include measurement of serum tumour markers, such as alpha-fetoprotein for HCC and carcinoembryonic antigen for colorectal metastases, as well as a full evaluation of the patient's coagulation status. A prothrombin time ratio (normal time/patient's time) >50% and a platelet count higher than 50 000/μL are required to keep the risk of bleeding at an acceptably low level. The tumour staging protocol must be tailored to the kind of malignancy. In patients with HCC, the detection of the nodule by ultrasound is usually followed by multidetector spiral computed tomography or dynamic magnetic resonance, following the recommendations of the American Association for the Study of Liver Diseases.[32] In patients with liver metastases tumour staging protocol should include abdominal US and spiral computed tomography or dynamic magnetic resonance imaging of the abdomen. Chest computed tomography and positron emission tomography (or positron emission tomography – computed tomography) may be required to exclude or confirm extrahepatic locations of metastatic disease.[56]

Pre-treatment imaging must carefully define the location of each lesion with respect to surrounding structures. Lesions located along

the surface of the liver can be considered for RF ablation, although their treatment requires adequate expertise and may be associated with a higher risk of complications. Thermal ablation of superficial lesions that are adjacent to any part of the gastrointestinal tract must be avoided because of the risk of thermal injury to the gastric or bowel wall. The colon appears to be at greater risk than the stomach or small bowel for thermally mediated perforation. Gastric complications are rare, probably owing to the relatively greater wall thickness of the stomach or the rarity of surgical adhesions along the gastrohepatic ligament. The mobility of the small bowel may also provide it with greater protection compared with the relatively fixed colon. The use of special techniques – such as intraperitoneal injection of dextrose to displace the bowel – can be considered in such instances.[73] Treatment of lesions adjacent to the hepatic hilum carries a risk of thermal injury to the biliary tract. This tumour location represents a relative contraindication to RF ablation. In experienced hands, thermal ablation of tumours located in the vicinity of the gallbladder was shown to be feasible, although associated in most cases with self-limited iatrogenic cholecystitis.[74] Thermal ablation of lesions adjacent to hepatic vessels is possible, since flowing blood usually protects the vascular wall from thermal injury: in these cases, however, the risk of incomplete treatment of the neoplastic tissue close to the vessel may increase because of the heat loss by convection.[62]

Complications

Early major complications associated with RF ablation occur in 2.2–3.1% of patients and include intraperitoneal bleeding, liver abscess, intestinal perforation, pneumo/haemothorax and bile duct stenosis and tumour seeding (0.5%); the procedure mortality rate is 0.1–0.5%.[75–77] The minor complication rate ranges from 5% to 8.9%. The most common causes of death are sepsis, hepatic failure, colon perforation and portal vein thrombosis (particularly in patients submitted to RF ablation with a surgical approach and Pringle manoeuvre), while the most common complications are intraperitoneal bleeding, hepatic abscess, bile duct injury, hepatic decompensation and grounding pad burns. Minor complications and side effects are usually transient and self-limiting.[75–77] An uncommon late complication of RF ablation can be tumour seeding along the needle track. In patients with HCC, tumour seeding occurred in 8 (0.5%) of 1610 cases in a multicentre survey[75] and in 1 (0.5%) of 187 cases in a single-institution series.[78] Lesions with subcapsular location and an invasive tumoral pattern, as shown by a poor differentiation degree, seem to be at higher risk for such a complication.[79]

Clinical results

Most early clinical research with RF ablation was conducted in the framework of feasibility studies, aimed at demonstrating the local effect and the safety of the procedure.[80–82] More recently, the clinical efficacy of RF ablation has been evaluated in the treatment of HCC and colorectal hepatic metastases.

Treatment of hepatocellular carcinoma

The therapeutic effect of RF ablation in HCC has been assessed by studies that evaluated the outcome of treatment at the histological level and by randomised or cohort studies that investigated the long-term survival outcomes of treated patients. Histological data from explanted liver specimens in patients who underwent RF ablation showed that tumour size and presence of large (3 mm or more) abutting vessels significantly affect local treatment effect. Complete tumour necrosis was pathologically shown in 83% of tumours <3 cm and 88% of tumours in a non-perivascular location.[83] Comparison with percutaneous ethanol injection (PEI) in five randomised trials[84–88] has shown that RF ablation had higher local anticancer effect than PEI, leading to a better local control of the disease (Table 11.3). The two European trials failed to show a statistically significant difference in overall survival between patients who received RF ablation and those treated with PEI.[84,88] However, survival advantages were identified in three Asian studies.[85–87] These data were recently pooled in two independent meta-analyses and the survival benefit for patients with small HCC submitted to RF ablation was confirmed.[89,90] Therefore, RF ablation appears as the preferred percutaneous treatment for patients with early-stage HCC on the basis of a more consistent local tumour control and better survival outcomes.

Recently, the long-term survival outcomes of RF ablation-treated patients were reported (Table 11.4) and were useful to elucidate factors influencing patient prognosis.[78,91–95] The severity of the underlying cirrhosis and occurrence of new lesions represent the

Table 11.3 Randomised studies comparing RF ablation and PEI in the treatment of early-stage HCC

Author	No. of patients	Tumour size	Complete ablation (%)	Treatment failure (%)[a]	3-year overall survival	*p*
Lencioni et al.[84]						
RF	52	1 HCC <5 cm or 3 <3 cm	91	8	81	>0.05
PEI	50		82	34	73	
Lin et al.[85]						
RF	52	1–3 HCC <4 cm	96	17	74	0.014
PEI	52		88	45	50	
Shiina et al.[86]						
RF	118	1–3 HCC <3 cm	100	2	80	0.02
PEI	114		100	11	63	
Lin et al.[87]						
RF	62	1–3 HCC <3 cm	97	16	74	0.031
PEI	62		89	42	51	
Brunello et al.[88]						
RF	70	1–3 HCC <3 cm	96	34	59	>0.05
PEI	69		66	64	57	

[a]*Includes initial treatment failure (incomplete response) and late treatment failure (local recurrence/progression).*

Table 11.4 Studies reporting long-term survival outcomes of patients with early-stage HCC who underwent percutaneous RF ablation

		SURVIVAL (%)		
Author	**No. of patients**	**1 year**	**3 years**	**5 years**
Lencioni et al.[78]				
Child A, 1 HCC <5 cm or 3 <3 cm	144	100	76	51
1 HCC <5 cm	116	100	89	61
Child B, 1 HCC <5 cm or 3 <3 cm	43	89	46	31
Tateishi et al.[91]				
Naive patients[a]	319	95	78	54
Non-naive patients[b]	345	92	62	38
Cabassa et al.[92]	59	94	65	43
Choi et al.[93]				
Child A, 1 HCC <5 cm or 3 <3 cm	359	NA	78	64
Child B, 1 HCC <5 cm or 3 <3 cm	160	NA	49	38
Takahashi et al.[94]				
Child A, 1 HCC <5 cm or 3 <3 cm	171	99	91	77
Hiraoka et al.[95]				
Child–Pugh A–B	105	NA	88	59

[a]*Patients who received RF ablation as primary treatment.*
[b]*Patients who received RF ablation for recurrent tumour after previous treatment including resection, ethanol injection, microwave ablation and transarterial embolisation.*
NA, not available.

most important prognostic factors. Patients with early stage HCC in Child–Pugh class A had a 5-year survival rate of 51–77% while patients in Child–Pugh class B had a 5-year survival rate of 31–38%. The incidence of new HCC lesions in cirrhotic liver is very high as it approaches 80% at 5 years after the first treatment.[78] This limitation is true of all local treatments, including surgical resection. It has been demonstrated that new lesions occurring within 2 years of treatment are related to occult dissemination of the original tumour, while lesions occurring in later periods are often true 'de novo' tumours. Only in very early HCCs, with diameter <2 cm, are there optimal conditions for radical local therapies, as the probability of microvascular invasion and microsatellites is very low. In patients with very early HCC the complete response rate approaches 97%, with 5-year survival rates of 68%.[96] In such small tumours, therefore, RF ablation seems to challenge the role of surgical resection and in many centres RF ablation is offered even in operable patients. However, there is not robust evidence that supports the use of RF ablation as a first-line therapy. In the only randomised trial comparing RF ablation with surgical resection in patients with solitary HCC <5 cm in diameter, no differences in overall survival rates and cumulative recurrence-free survival rates were observed.[97]

Despite the many published reports some questions concerning image-guided RF ablation in HCC treatment are still unanswered. Some authors have reported that RF ablation may be a safe and effective bridge to liver transplantation.[83] However, randomised studies would be needed to determine advantages and disadvantages of RF ablation with respect to chemoembolisation for HCC patients awaiting transplantation. Recent studies have reported encouraging results in the treatment of intermediate-size (3–7 cm) HCC lesions with a combination of transcatheter chemoembolisation and RF ablation.[64] Innovative experimental approaches for tumour >3 cm include the intra-arterial administration of doxorubicin-eluting beads after RF ablation and the intravenous injection of thermally sensitive liposomes uploaded with doxorubicin. These strategies are aimed at reaching a high drug concentration at the periphery of the ablation volume to determine an additive cytotoxic effect on tumoral tissue that was exposed to sublethal temperatures.

Table 11.5 Studies reporting long-term survival outcomes of patients with colorectal hepatic metastases who underwent percutaneous RF ablation

		SURVIVAL (%)		
Author	**No. of patients**	**1 year**	**3 years**	**5 years**
Solbiati et al.[101]	117	93	46	NA
Lencioni et al.[69]	423	86	47	24
Gillams et al.[70]	73	91	28	25
Machi et al.[102]	100	90	42	30
Jackobs et al.[103]	68	96	68	NA
Sorensen et al.[104]	102	87	46	26[a]
Veltri et al.[105]	122	79	38	22

[a]*Four-year survival.*
NA, not available.

Treatment of colorectal hepatic metastases

Many studies have investigated the use of RF ablation in the treatment of limited colorectal cancer hepatic metastatic disease in patients who were excluded from surgery. Two early studies reported rates of complete response that did not exceed 60–70%.[80,98] Subsequently, owing to the advances in RF technique and probably to the treatment of smaller tumours, reported rates of successful local tumour control following RF treatment substantially increased. In two series, RF ablation allowed eradication of 91% of 100 metastases and 97% of 74 metastases, respectively.[99,100]

Recently, data on long-term survival of non-surgical patients with hepatic colorectal metastases who underwent RF ablation have

been reported (Table 11.5).[69,70,101–105] In particular, in three series including patients with five or fewer lesions, each 5 cm or less in diameter, the 5-year survival rate ranged from 24% to 44% at 5 years.[69,101,103] When RF ablation was performed in patients with small (<4 cm), solitary hepatic colorectal metastases, 40% 5-year survival rate was demonstrated.[106] These figures are substantially higher than those obtained with any chemotherapy regimens and provide indirect evidence that RF ablation therapy improves survival in patients with limited hepatic metastatic disease. This conclusion is supported by the interim analysis of a randomised controlled trial comparing chemotherapy plus RF ablation to chemotherapy alone in colorectal cancer metastatic to the liver.

Recent studies analysed the role of RF ablation with respect to surgical resection. In one study, patients with colorectal metastases isolated to the liver were treated with hepatic resection, RF ablation plus resection, RF ablation only, or chemotherapy only. Overall survival for patients treated with RF ablation plus resection or RF ablation only was greater than for those who received chemotherapy only. However, overall survival was highest after resection: 4-year survival rates after resection, RF ablation plus resection, and RF ablation only were 65%, 36%, and 22%, respectively.[107] In another paper, the outcome of patients with solitary colorectal liver metastasis treated by surgery or by RF ablation did not differ: the survival rate at 3 years was 55% for patients treated with surgery and 52% for those who underwent RF ablation.[108] Other authors used RF ablation instead of repeated resection for the treatment of liver tumour recurrence after partial hepatectomy.[109] The potential role of performing RF ablation during the interval between diagnosis and resection as part of a 'test-of-time' management approach was investigated.[110] Eighty-eight consecutive patients with colorectal liver metastases who were potential candidates for surgery were treated with RF ablation. Among the 53 patients in whom complete tumour ablation was achieved after RF treatment, 98% were spared surgical resection because they remained free of disease or because they developed additional metastases leading to unresectability. No patient in whom RF treatment did not achieve complete tumour ablation became unresectable due to the growth of the treated metastases.

REFERENCES

1. Sherlock S. Aspiration liver biopsy, technique and diagnostic application. Lancet 1945;2:397–401.
2. Rockey DC, Caldwell SH, Goodman ZD, et al. Liver biopsy. Hepatology 2009;49:1017–1044.
3. Al Knawy B, Shiffman F. Percutaneous liver biopsy in clinical practice. Liver Int 2007;27:1166–1173.
4. Grant A, Neuberger J. Guidelines on the use of liver biopsy in clinical practice. British Society of Gastroenterology. Gut 1999;45(Suppl. 4):IV1–IV11.
5. Hegarty JE, Williams R. Liver biopsy: techniques, clinical applications, and complications. Br Med J 1984;288:1254–1256.
6. Buscarini L, Fornari F, Bolondi L, et al. Ultrasound-guided fine-needle biopsy of focal liver lesions: techniques, diagnostic accuracy and complications. A retrospective study on 2091 biopsies. J Hepatol 1990;11:344–348.
7. Sbolli G, Fornari F, Civardi G, et al. Role of ultrasound guided fine needle aspiration biopsy in the diagnosis of hepatocellular carcinoma. Gut 1990;31:1303–1305.
8. Nazarian LN, Feld RI, Herrine SK, et al. Safety and efficacy of sonographically guided random core biopsy for diffuse liver disease. J Ultrasound Med 2000;19:537–541.
9. Manolakopoulos S, Triantos C, Bethanis S, et al. Ultrasound-guided liver biopsy in real life: comparison of same-day pre-biopsy versus real-time ultrasound approach. J Gastroenterol Hepatol 2007;22:1490–1493.
10. Adams T, Lewis JH. Percutaneous liver biopsy. Clin Perspectives Gastroenterol 2002;2:117–121.
11. Colombo M, Del Ninno E, de Franchis R, et al. Ultrasound assisted percutaneous liver biopsy: superiority of the Tru-Cut over the Menghini needle for diagnosis of cirrhosis. Gastroenterology 1988;95:487–489.
12. Lindor KD, Bru C, Jorgensen RA, et al. The role of ultrasonography and automatic-needle biopsy in outpatient percutaneous liver biopsy. Hepatology 1996;23:1079–1083.
13. Sherman K, Goodman Z, Sullivan S, Farris-Young S. Liver biopsy in cirrhotic patients. Am J Gastroenterol 2007;102:789–793.
14. Piccinino F, Sagnelli E, Pasquale G, Giusti G. Complications following percutaneous liver biopsy. A multicentre retrospective study on 68,276 biopsies. J Hepatol 1986;2:165–173.
15. McGill DB, Rakela J, Zinsmeister AR, Ott BJ. A 21-year experience with major haemorrhage after percutaneous liver biopsy. Gastroenterology 1990;99:1396–4000.
16. Forssell PL, Bonkowsky HL, Anderson PB, Howell DA. Intrahepatic hematoma after aspiration liver biopsy. A prospective randomized trial using two different needles. Dig Dis Sci 1981;26:631–635.
17. Bravo AA, Sheth SG, Chopra S. Liver biopsy. N Engl J Med 2001;344:495–500.
18. Bedosa P, Dargere D, Paradis V. Sampling variability of liver fibrosis in chronic hepatitis C. Hepatology 2003;38:1449–1457.
19. Colloredo G, Guido M, Sonzogni A, Leandro G. Impact of liver biopsy size on histological evaluation of chronic viral hepatitis: the smaller the sample, the milder the disease. J Hepatol 2003;39:239–244.
20. Cholongitas E, Senzolo M, Standish RA, et al. A systemic review of the quality of liver biopsy specimens. Am J Clin Pathol 2006;125:710–721.
21. Demetris AJ, Ruppert K. Pathologist's perspective on liver needle biopsy size. J Hepatol 2003;39:275–277.
22. Rocken C, Meier H, Klauck S, et al. Large-needle biopsy versus thin-needle biopsy in diagnostic pathology of liver diseases. Liver 2001;21:391–397.
23. Petz D, Klauck S, Rohl FW, et al. Feasibility of histological grading and staging of chronic viral hepatitis using specimens obtained by thin needle biopsy. Virchows Arch 2003;442:238–244.
24. Gazelle GS, Haaga JR, Rowland DY. Effect of needle gauge, level of anticoagulation, and target organ on bleeding associated with aspiration biopsy. Work in progress. Radiology 1992;183: 509–513.
25. Plecha DM, Goodwin DW, Rowland DY, et al. Liver biopsy: effects of biopsy needle caliber on bleeding and tissue recovery. Radiology 1997;204:101–104.
26. Farrell RJ, Smiddy PF, Pilkington RM, et al. Guided versus blind liver biopsy for chronic hepatitis C: clinical benefits and costs. J Hepatol 1999;30:580–587.
27. Cadranel JF, Rufat P, Degos F. Practices of transcutaneous liver biopsies in France. Results of a retrospective nationwide study. Gastroenterol Clin Biol 2001;25:77–80.
28. Cadranel JF, Rufat P, Degos F. Practices of liver biopsy in France: results of a prospective nationwide survey. For the Group of Epidemiology of the French Association for the Study of the Liver (AFEF). Hepatology 2000;32:477–481.
29. Riley 3rd TR. How often does ultrasound marking change the liver biopsy site? Am J Gastroenterol. 1999;94:3320–3322.
30. Maharaj B, Bhoora IG. Complications associated with percutaneous needle biopsy of the liver when one, two or three specimens are taken. Postgrad Med J 1992;68:964–967.
31. Firpi RJ, Soldevila-Pico C, Abdelmalek MF, et al. Short recovery time after percutaneous liver biopsy: should we change our current practices? Clin Gastroenterol Hepatol 2005;3:926–929.
32. Bruix J, Sherman M. Management of hepatocellular carcinoma. Hepatology 2005;42:1208–1236.
33. Strader DB, Wright T, Thomas DL, Seeff LB. Diagnosis, management, and treatment of hepatitis C. Hepatology 2004;39:1147–1171.
34. Lok AS, McMahon BJ. Chronic hepatitis B. Hepatology 2007;47:507–539.
35. Heathcote EJ. Management of primary biliary cirrhosis. The American Association for the Study of Liver Diseases practice guidelines. Hepatology 2000;31:1005–1013.
36. Smith AD. Recurrence of the original liver disease. In: Killenberg PG, Clavien PA, editors. Medical care of the liver transplant patient. 3rd edn. Oxford: Blackwell; 2006. p. 419–438.
37. Demetris AJ, Adeyi O, Bellamy CO, et al. Liver biopsy interpretation for causes of late liver allograft dysfunction. Hepatology 2006;44:489–501.
38. Rockey DC. Non-invasive assessment of liver fibrosis and portal hypertension with transient elastography. Gastroenterology 2008;134:8–14.
39. Takahashi H, Ono N, Eguchi Y, et al. Evaluation of acoustic radiation force impulse elastography for fibrosis staging of chronic liver disease: a pilot study. Liver Int 2009 Oct 27. [Epub ahead of print]

40. Eisen GM, Baron TH, Dominitz JA, et al. Guideline on the management of anticoagulation and antiplatelet therapy for endoscopic procedures. Gastrointest Endosc 2002;55:775–779.
41. Madura JA, Rookstool M, Wease G. The management of patients on chronic coumadin therapy undergoing subsequent surgical procedures. Am Surg 1994;60:542–546.
42. Hyun CB, Beutel VJ. Prospective randomized trial of post-liver biopsy recovery positions: does positioning really matter? J Clin Gastroenterol 2005;39:328–332.
43. Beddy P, Lyburn I, Geoghegan T, et al. Outpatient liver biopsy: a prospective evaluation of 500 cases. Gut 2007;56:307.
44. Perrault J, McGill DB, Ott BJ, Taylor WF. Liver biopsy: complications in 1000 inpatients and outpatients. Gastroenterology 1978;74: 103–106.
45. Stone MA, Mayberry JF. An audit of ultrasound guided liver biopsies: a need for evidence-based practice. Hepatogastroenterology 1996;43:432–434.
46. Janes CH, Lindor KD. Outcome of patients hospitalized for complications after outpatient liver biopsy. Ann Intern Med 1993;118:96–98.
47. Myers RP, Fong A, Shaheen AA. Utilization rates, complications and costs of percutaneous liver biopsy: a population-based study including 4275 biopsies. Liver Int 2008;28:705–712.
48. Knauer CM. Percutaneous biopsy of the liver as a procedure for outpatients. Gastroenterology 1978;74:101–102.
49. Douds AC, Joseph AE, Finlayson C, Maxwell JD. Is day case liver biopsy underutilised? Gut 1995;37:574–575.
50. Caturelli E, Giacobbe A, Facciorusso D, et al. Percutaneous biopsy in diffuse liver disease: increasing diagnostic yield and decreasing complication rate by routine ultrasound assessment of puncture site. Am J Gastroenterol 1996;91:1318–1321.
51. Pasha T, Gabriel S, Therneau T, et al. Cost-effectiveness of ultrasound-guided liver biopsy. Hepatology 1998;27:1220–1226.
52. Durand F, Regimbeau JM, Belghiti J, et al. Assessment of the benefits and risks of percutaneous biopsy before surgical resection of hepatocellular carcinoma. J Hepatol 2001;35:254–258.
53. Liu YW, Chen CL, Chen YS, et al. Needle tract implantation of hepatocellular carcinoma after fine needle biopsy. Dig Dis Sci 2007;52:228–231.
54. Bialecki ES, Ezenekwe AM, Brunt EM, et al. Comparison of liver biopsy and noninvasive methods for diagnosis of hepatocellular carcinoma. Clin Gastroenterol Hepatol 2006;4:361–368.
55. Khuroo MS, Wani NA, Javid G, et al. Percutaneous drainage compared with surgery for hepatic hydatid cysts. N Engl J Med 1997;337:881–887.
56. Crocetti L, DeBaere T, Lencioni R. Quality improvement guidelines for radiofrequency ablation of liver tumours. Cardiovasc Intervent Radiol 2009 [Epub ahead of print].
57. Bruix J, Sherman M, Llovet JM, et al. EASL Panel of Experts on HCC. Clinical management of hepatocellular carcinoma. Conclusions of theBarcelona-2000 EASL conference. European Association for the Study of the Liver. J Hepatol 2001;35:421–430.
58. Stang A, Fischbach R, Teichmann W, et al. A systematic review on the clinical benefit and role of radiofrequency ablation as treatment of colorectal liver metastases. Eur J Cancer 2009 [Epub ahead of print].
59. Goldberg SN, Gazelle GS, Mueller PR. Thermal ablation therapy for focal malignancies: a unified approach to underlying principles, techniques, and diagnostic imaging guidance. ALR Am J Roentgenol 2000;174:323–331.
60. Dodd III GD, Frank MS, Aribandi M, et al. Radiofrequency thermal ablation: computer analysis of the size of the thermal injury created by overlapping ablations. AJR Am J Roentgenol 2001;177:777–782.
61. Pennes HH. Analysis of tissue and arterial blood temperatures in the resting human forearm. J Appl Physiol 1948;1:93–122.
62. Lencioni R, Crocetti L, Pina MC, Cioni D. Percutaneous image-guided radiofrequency ablation of liver tumours. Abdom Imaging 2009 34:547–556.
63. Rossi S, Garbagnati F, Lencioni R, et al. Percutaneous radio-frequency thermal ablation of nonresectable hepatocellular carcinoma after occlusion of tumour blood supply. Radiology 2000;217:119–126.
64. Lencioni R, Crocetti L, Petruzzi P, et al. Doxorubicin-eluting bead-enhanced radiofrequency ablation of hepatocellular carcinoma: a pilot clinical study. J Hepatol 2008;49:217–222.
65. Goldberg SN, Saldinger PF, Gazelle GS, et al. Percutaneous tumour ablation: increased necrosis with combined radio-frequency ablation and intratumoral doxorubicin injection in a rat breast tumour model. Radiology 2001;220:420–427.
66. Ahmed M, Liu Z, Lukyanov AN, et al. Combination radiofrequency ablation with intratumoral liposomal doxorubicin: effect on drug accumulation and coagulation in multiple tissues and tumour types in animals. Radiology 2005;235:469–477.
67. Goldberg SN, Charboneau JW, Dodd III GD, et al. Image-guided tumour ablation: proposal for standardization of terms and reporting criteria. Radiology 2003;228:335–345.
68. Llovet JM, Di Bisceglie AM, Bruix J, et al; Panel of Experts in HCC-Design Clinical Trials. Design and endpoints of clinical trials in hepatocellular carcinoma. J Natl Cancer Inst 2008;100: 698–711.
69. Lencioni R, Crocetti L, Cioni D, et al. Percutaneous radiofrequency ablation of hepatic colorectal metastases. Technique, indications, results, and new promises. Invest Radiol 2004;39:599–689.
70. Gillams AR, Lees WR. Radio-frequency ablation of colorectal liver metastases in 167 patients. Eur Radiol 2004;4:2261–2267.
71. Lencioni R, Crocetti L, Cioni R, et al. Response to radiofrequency ablation of pulmonary tumours: a prospective, intention-to-treat, multicentre clinical trial (the RAPTURE study). Lancet Oncol 2008;9:621–628.
72. Berber E, Pelley R, Siperstein AE. Predictors of survival after radiofrequency thermal ablation of colorectal cancer metastases to the liver: a prospective study. J Clin Oncol 2005;23:1358–1364.
73. Rhim H, Dodd III GD, Chintapalli KN, et al. Radiofrequency thermal ablation of abdominal tumours: lessons learned from complications. Radiographics 2004;24:41–45.
74. Chopra S, Dodd III GD, Chanin MP, Chintapalli KN. Radiofrequency ablation of hepatic tumours adjacent to the gallbladder: feasibility and safety. AJR Am J Roentgenol 2003;180:697–701.
75. Livraghi T, Solbiati L, Meloni MF, et al. Treatment of focal liver tumours with percutaneous radio-frequency ablation: complications encountered in a multicentre study. Radiology 2003;26:441–451.
76. De Baere T, Risse O, Kuoch V, et al. Adverse events during radiofrequency treatment of 582 hepatic tumours. AJR Am J Roentgenol 2003;181:695–700.
77. Bleicher RJ, Allegra DP, Nora DT, et al. Radiofrequency ablation in 447 complex unresectable liver tumours: lessons learned. Ann Surg Oncol 2003;10:52–58.
78. Lencioni R, Cioni D, Crocetti L, et al. Early-stage hepatocellular carcinoma in cirrhosis: long-term results of percutaneous image-guided radiofrequency ablation. Radiology 2005;234:961–967.
79. Llovet JM, Vilana R, Bru C, et al. Barcelona Clinic Liver Cancer (BCLC) Group. Increased risk of tumour seeding after percutaneous radiofrequency ablation for single hepatocellular carcinoma. Hepatology 2001;33:1124–1129.
80. Lencioni R, Goletti O, Armillotta N, et al. Radiofrequency thermal ablation of liver metastases with a cooled-tip electrode needle: results of a pilot clinical trial. Eur Radiol 1998;8:1205–1211.
81. Curley SA, Izzo F, Delrio P, et al. Radiofrequency ablation of unresectable primary and metastatic malignancies: results in 123 patients. Ann Surg 1999;230:1–8.
82. Wood TF, Rose DM, Chung M, et al. Radiofrequency ablation of 231 unresectable hepatic tumours: indications, limitations, and complications. Ann Surg Oncol 2000;7:593–600.
83. Lu DS, Yu NC, Raman SS, et al. Radiofrequency ablation of hepatocellular carcinoma: treatment success as defined by histologic examination of the explanted liver. Radiology 2005;234:954–960.
84. Lencioni R, Allgaier HP, Cioni D, et al. Small hepatocellular carcinoma in cirrhosis: randomized comparison of radiofrequency thermal ablation versus percutaneous ethanol injection. Radiology 2003;228:235–240.
85. Lin SM, Lin CJ, Lin CC, et al. Radiofrequency ablation improves prognosis compared with ethanol injection for hepatocellular carcinoma < or =4 cm. Gastroenterology 2004;127:1714–1723.
86. Shiina S, Teratani T, Obi S, et al. A randomized controlled trial of radiofrequency ablation versus ethanol injection for small hepatocellular carcinoma. Gastroenterology 2005;129:122–130.
87. Lin SM, Lin CJ, Lin CC, et al. Randomised controlled trial comparing percutaneous radiofrequency thermal ablation, percutaneous ethanol injection, and percutaneous acetic acid injection to treat hepatocellular carcinoma of 3 cm or less. Gut 2005;54:1151–1156.
88. Brunello F, Veltri A, Carucci P, et al. Radiofrequency ablation versus ethanol injection for early hepatocellular carcinoma: a randomized controlled trial. Scand J Gastroenterol 2008;43:727–735.
89. Orlando A, Leandro G, Olivo M, et al. Radiofrequency thermal ablation vs. percutaneous ethanol injection for small hepatocellular carcinoma in cirrhosis: meta-analysis of randomized controlled trials. Am J Gastroenterol 2009;104:514–524.

90. Cho YK, Kim JK, Kim MY, et al. Systematic review of randomized trials for hepatocellular carcinoma treated with percutaneous ablation therapies. Hepatology 2009;49:453–459.
91. Tateishi R, Shiina S, Teratani T, et al. Percutaneous radiofrequency ablation for hepatocellular carcinoma. Cancer 2005;103:1201–1209.
92. Cabassa P, Donato F, Simeone F, et al. Radiofrequency ablation of hepatocellular carcinoma: long-term experience with expandable needle electrodes. AJR Am J Roentgenol 2006;185:S316–S321.
93. Choi D, Lim HK, Rhim H, et al. Percutaneous radiofrequency ablation for early-stage hepatocellular carcinoma as a first- line treatment: long-term results and prognostic factors in a large single-institution series. Eur Radiol 2007;17:684–692.
94. Takahashi S, Kudo M, Chung H, et al. Initial treatment response is essential to improve survival in patients with hepatocellular carcinoma who underwent curative radiofrequency ablation therapy. Oncology 2007;72:S98–S103.
95. Hiraoka A, Horiike N, Yamashita Y, et al. Efficacy of radiofrequency ablation therapy compared to surgical resection in 164 patients in Japan with single hepatocellular carcinoma smaller than 3 cm, along with report of complications. Hepatogastroenterology 2008;55:2171–2174.
96. Livraghi T, Meloni F, Di Stasi M, et al. Sustained complete response and complications rates after radiofrequency ablation of very early hepatocellular carcinoma in cirrhosis: is resection still the treatment of choice? Hepatology 2008;47:82–89.
97. Chen MS, Li JQ, Zheng Y, et al. A prospective randomized trial comparing percutaneous local ablative therapy and partial hepatectomy for small hepatocellular carcinoma. Ann Surg 2006;243:321–328.
98. Solbiati L, Goldberg SN, Ierace T, et al. Hepatic metastases: percutaneous radio-frequency ablation with cooled-tip electrodes. Radiology 1997;205:367–373.
99. De Baere T, Elias D, Dromain C, et al. Radiofrequency ablation of 100 hepatic metastases with a mean follow-up of more than 1 year. AJR Am J Roentgenol 2000;75:1619–1625.
100. Helmberger T, Holzknecht N, Schopf U, et al. Radiofrequency ablation of liver metastases. Technique and initial results. Radiologe 2001;41:69–76.
101. Solbiati L, Livraghi T, Goldberg SN, et al. Percutaneous radio-frequency ablation of hepatic metastases from colorectal cancer: long-term results in 117 patients. Radiology 2001;221:159–166.
102. Machi J, Oishi AJ, Sumida K, et al. Long-term outcome of radiofrequency ablation for unresectable liver metastases from colorectal cancer: evaluation of prognostic factors and effectiveness in first- and second-line management. Cancer J 2006;12:318–326.
103. Jackobs TF, Hoffmann RT, Trumm C, et al. Radiofrequency ablation of colorectal liver metastases: mid-term results in 68 patients. Anticancer Res 2006;26:671–680.
104. Sorensen SM, Mortensen FV, Nielsen DT. Radiofrequency ablation of colorectal liver metastases: long-term survival. Acta Radiol 2007;48:253–258.
105. Veltri A, Sacchetto P, Tosetti I, et al. Radiofrequency ablation of colorectal liver metastases: small size favorably predicts technique effectiveness and survival. Cardiovasc Intervent Radiol 2008;31:948–956.
106. Gillams AR, Lees WR. Five-year survival following radiofrequency ablation of small, solitary, hepatic colorectal metastases. J Vasc Interv Radiol 2008;19:712–717.
107. Abdalla EK, Vauthey JN, Ellis LM, et al. Recurrence and outcomes following hepatic resection, radiofrequency ablation, and combined resection/ablation for colorectal liver metastases. Ann Surg 2004;239:818–825.
108. Oshowo A, Gillams A, Harrison E, et al. Comparison of resection and radiofrequency ablation for treatment of solitary colorectal liver metastases. Br J Surg 2003;90:1240–1243.
109. Elias D, De Baere T, Smayra T, et al. Percutaneous radiofrequency thermoablation as an alternative to surgery for treatment of liver tumour recurrence after hepatectomy. Br J Surg 2002;89:752–756.
110. Livraghi T, Solbiati L, Meloni F, et al. Percutaneous radiofrequency ablation of liver metastases in potential candidates for resection: the 'test-of-time approach'. Cancer 2003;97:3027–3035.

CHAPTER

12 Vascular disorders of the liver

Christopher J. Harvey and Adrian K.P. Lim

PORTAL VEIN 179
Anatomy and scanning techniques 179
Normal findings 179
Portal hypertension 180
Pathophysiology 180
Ultrasound findings in portal hypertension 181
Portal vein flow changes 181
Change in portal vein calibre 182
Splenomegaly 182
Changes in hepatic arterial flow in portal hypertension 182
Portosystemic collaterals (varices) 182
Management of portal hypertension 185
Surgical portosystemic shunts 185
Transjugular intrahepatic portosystemic shunt (TIPS) 186
Portal vein occlusion 188
Portal vein aneurysm 189
Portal vein gas 189

HEPATIC ARTERY 189
Anatomy and scanning techniques 189
Normal findings 189
Hepatic artery aneurysms 192
Hereditary haemorrhagic telangiectasia (HHT) 192

HEPATIC VEINS 192
Anatomy and scanning technique 192
Normal anatomical variations 193
Hepatic venous waveforms 194
Hepatic venous outflow obstruction 194
Hepatic veno-occlusive disease 195
Hepatic venous waveforms in cardiac and pulmonary disease 195
Hepatic vein transit times 197
Peliosis hepatis 197

PORTAL VEIN

Anatomy and scanning techniques

The portal vein provides approximately 70% of the liver's blood supply. The portal vein is formed at the confluence of the splenic vein and superior mesenteric vein posterior to the neck of the pancreas. It then passes posterior to the pancreatic head and first part of duodenum to the liver hilum via the hepatoduodenal ligament. The main portal vein enters the liver at the porta hepatis (liver hilum) lying posterior to the hepatic artery and bile duct (the bile duct lying anterolaterally and the hepatic artery lying anteromedially). It divides into the main right and left branches before penetrating the liver, although there is some variation in this. The right branch passes transversely in the liver substance for a few centimetres before dividing into anterior and posterior branches. The left portal vein curves anteriorly giving off branches as it traverses the liver. The hepatic arteries and bile ducts follow the same pattern. The left main portal vein is joined by the ligamentum teres (obliterated umbilical vein) and ligamentum venosum (obliterated ductus venosum) as it enters the left lobe.

A 'principal plane' divides the liver into right and left lobes of almost equal size. On the visceral surface of the liver this plane is denoted by a line that runs from the gallbladder fossa through the porta hepatis to the inferior vena cava. The right lobe (Couinaud segments V, VI, VII and VIII) is supplied by the right portal vein and the left lobe (segments II, III and IV) is supplied by the left portal vein (Fig. 12.1). Segment I (caudate lobe) receives supply from both left and right portal venous branches.[1]

A curved array 3.5–6 MHz probe is suitable for imaging the liver and portal vein supplemented with colour and spectral Doppler. The portal vein can be imaged subcostally pointing posterocephalad or by a right intercostal approach pointing medially. These approaches give good views of the portal vein, hepatic artery and common bile duct. The left lateral decubitus position provides good views of the portal vein at the porta hepatis. In this position a longitudinal oblique section demonstrates the portal vein and its relationship to the hepatic artery and common bile duct.

Colour and spectral Doppler is used to document normal hepatopetal flow (towards the liver). Any reversal of flow away from the liver (hepatofugal) is pathological. The main, right and left portal vein branches can be best imaged by using a right oblique approach through the ribs, so that the course of the vein is towards the probe and an angle of less than 60° with the beam is obtained, providing a good Doppler signal.

At the porta the hepatic artery crosses anterior to the main portal vein with the bile duct anteriorly (Fig. 12.2). A common normal variant (10–15%) is seen when the artery lies anterior to the duct (Fig. 12.3).

Normal findings

The diameter of the portal vein is variable and is usually about 10 mm. The portal vein diameter is measured as it passes anterior to the inferior vena cava (IVC). The diameter increases with deep inspiration, postprandially and with posture. A diameter of greater than 13 mm in the supine position during quiet respiration is taken as abnormal.

The mean velocity in the portal vein is 12–20 cm/s but there is wide variation due to prandial state, position, exercise, respiration and cardiac activity. When discussing portal and hepatic venous flow the term 'periodicity' refers to velocity variation due to cardiac activity and 'phasicity' refers to respiratory induced changes. The term 'pulsatility' should only be reserved for arterial flow. Portal venous flow velocity is usually uniform. Minor phasicity may be seen due to respiration as well as mild periodicity due to retrograde transmission of the A wave from the right atrium via the hepatic veins or due to hepatic arterial systolic inflow (Fig. 12.4). These rises in pressure result in transient decreases in the antegrade portal venous flow, which were present in up to 64% of a normal study group in one series.[2,3] The velocity is reduced in portal hypertension and may be increased in anastomotic stenoses, e.g. liver transplant patients.

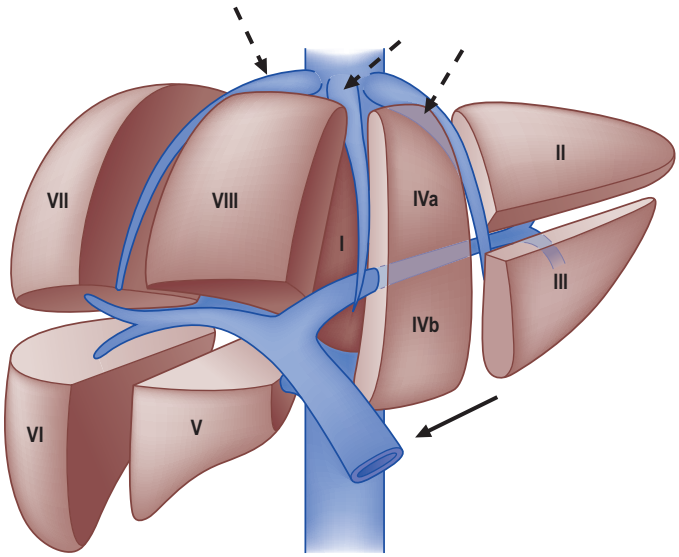


Figure 12.1 Drawing of Couinaud's classification demonstrating how the liver is divided into the eight segments by the portal vein (arrow) and hepatic veins (broken arrow). (Modified from Szklaruk J, Silverman PM and Charnsangavej C. Imaging in the Diagnosis, Staging, Treatment, and Surveillance of Hepatocellular Carcinoma. Am J Roentgenol 2003;180(2):441. Image located at http://www.ajronline.org/cgi/content-nw/full/180/2/441/FIG10, accessed 03/15/2010.)

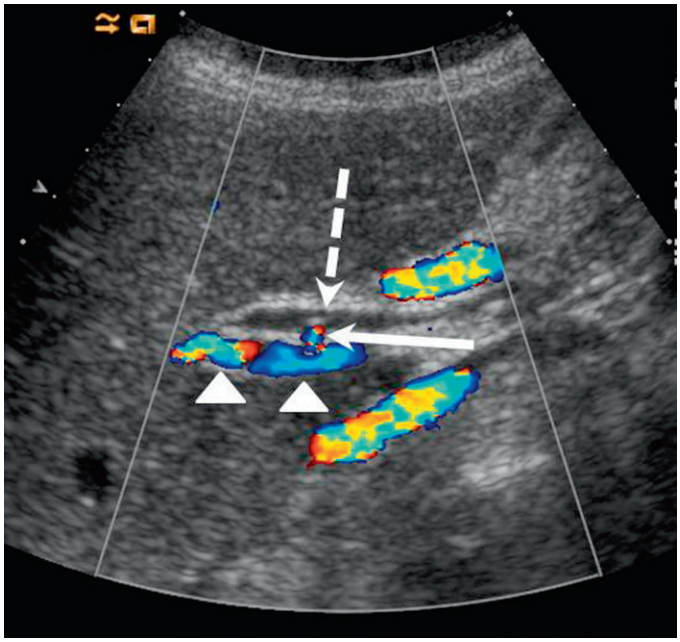


Figure 12.2 Colour Doppler image of the portal triad showing the portal vein (arrowheads) and hepatic artery (straight arrow). The correct site to measure the bile duct diameter, as it crosses the hepatic artery, is indicated (broken arrow).

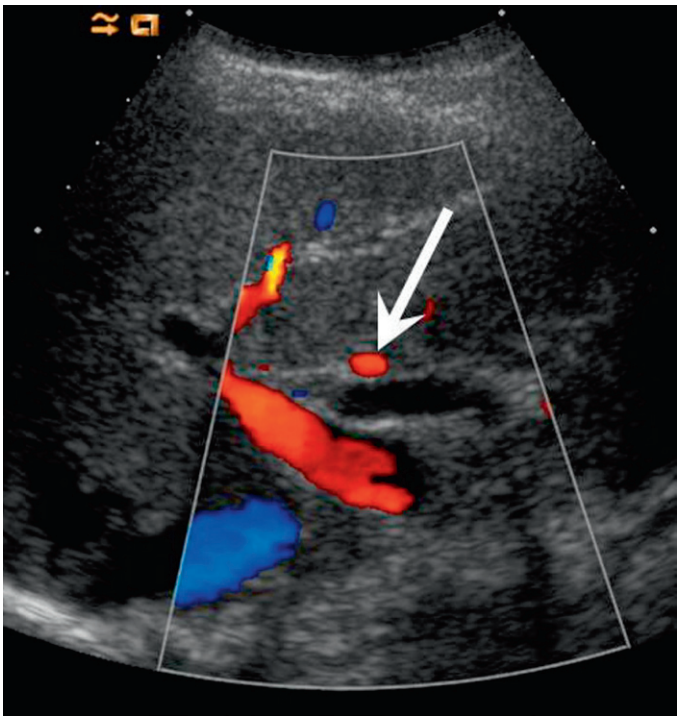


Figure 12.3 A common normal variant (10–15%) is seen with the hepatic artery (arrow) lying anterior to the bile duct.

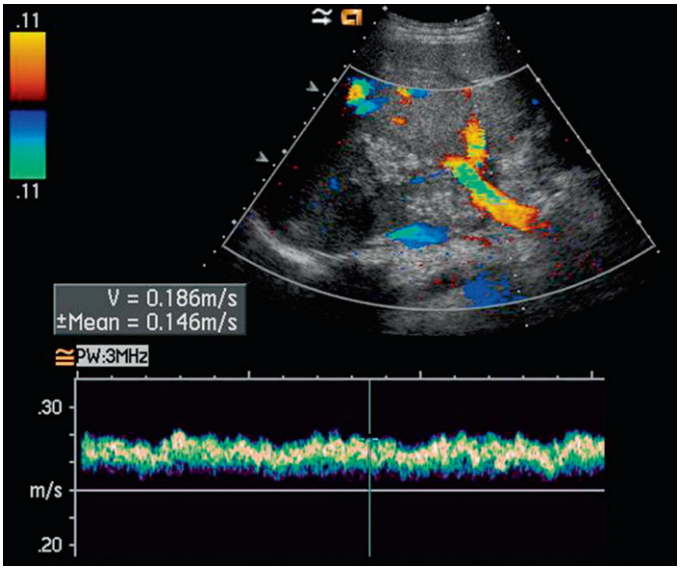


Figure 12.4 Normal portal venous flow with a velocity of 18 cm/s demonstrating hepatopetal direction and undulating waveform due to cardiac pulsation and respiration. Note the multiple liver metastases.

Portal hypertension

Portal hypertension is defined as portal venous pressure exceeding 10 mmHg. More specifically it means that there is a pressure gradient from the portal vein to the hepatic veins or IVC of 10 mmHg or greater. Because direct measurement of portal venous pressure is difficult it may be estimated indirectly by measurement of the corrected sinusoidal pressure. This is calculated by taking the hepatic wedge pressure and subtracting the free hepatic venous pressure. The causes of portal hypertension may be divided into hepatic, pre- and post-hepatic. The most common cause is cirrhosis in which diffuse destruction and regeneration of liver parenchyma results in fibrosis and distortion of liver architecture. This results in obstruction and increased resistance to portal flow that leads to an increase in the portal venous pressure.

Pathophysiology

As well as obstruction and increased resistance leading to portal hypertension ('backward flow' theory) experimental evidence has shown that increased portal blood flow (hyperkinetic portal

Main causes of portal hypertension

Prehepatic
- Portal vein thrombosis
- Portal vein compression (tumour, trauma, lymphadenopathy)

Intrahepatic
- *Pre-sinusoidal:* This is usually due to disease affecting the porta hepatis such as congenital hepatic fibrosis, sarcoidosis, lymphoma, schistosomiasis, primary biliary cirrhosis, toxic fibrosis secondary to arsenic, copper and polyvinyl chloride (PVC)
- *Sinusoidal:* Due to hepatitis, sickle cell anaemia or fatty infiltration
- *Post-sinusoidal:* Alcoholic cirrhosis (commonest); veno-occlusive disease

Post-hepatic
- Budd–Chiari syndrome
- Veno-occlusive disease
- Right heart failure
- Constrictive pericarditis

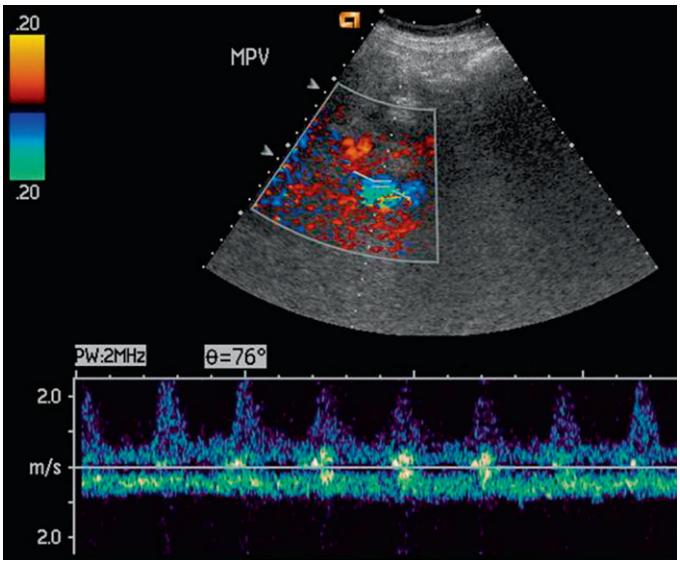


Figure 12.5 Spectral Doppler interrogation over the porta hepatis demonstrates reverse flow in the portal vein and increased velocity in the hepatic artery (>2 m/s) due to arterialisation of the liver blood supply in portal hypertension.

hypertension) plays an important role ('forward flow' theory).[4–7] In patients with liver cirrhosis a characteristic finding is splanchnic and systemic vasodilatation due to a reduced vascular resistance and tone. This results in increased blood flow in the systemic and splanchnic circulation accompanied by an increase in cardiac output, such that patients with cirrhosis have warm peripheries and bounding pulses. The increased flow through the portal venous system (>15 mL/min/kg) is a major contributing factor in the maintenance of portal hypertension. In addition it was thought that the raised intrahepatic resistance of cirrhosis was solely due to fibrosis, scarring and distortion of liver parenchyma. Recent evidence supports an additional role of sinusoidal and endothelial cells in accentuating vascular resistance. Under the influence of mediators (e.g. nitrous oxide, NO) and endothelin, the contractile effects of these cells potentiate the increased intrahepatic resistance.

It is now generally accepted that increased intrahepatic vascular resistance and a hyperdynamic splanchnic blood flow are the main contributing factors to portal hypertension.

Hyperkinetic portal hypertension is seen in congenital and acquired arteriovenous fistulae in the intrahepatic or extrahepatic portal venous circulation. Congenital fistulae are seen in hereditary haemorrhagic telangiectasia (HHT; Osler–Weber–Rendu disease), which is discussed below.

Ultrasound findings in portal hypertension

An increase in portal venous pressure by 5–10 mmHg leads to changes in haemodynamics with alteration in direction of flow, velocity and waveforms, increase in spleen size, formation of ascites, change in the response of the portal, splenic and superior mesenteric veins to respiration, enlargement of portal veins and diversion of blood flow through low resistance portosystemic collaterals. Ultrasound can demonstrate all these findings and is the modality of choice in the initial assessment of suspected portal hypertension. The sonographic findings are now discussed.

Portal vein flow changes

Doppler interrogation allows an assessment of the presence, direction and characteristics of blood flow. Portal venous flow is dependent on numerous factors including posture, exercise, prandial state and cardiac output.[8] The flow varies widely both in patients with cirrhosis and in normal subjects.[9] A 'congestion index' may be applied to help diagnose portal hypertension. The index is the ratio of portal vein cross-sectional area (cm^2) divided by the mean portal flow velocity (cm/s).[10] The ratio is normally less than 0.7.

Sonographic findings in portal hypertension

- Portal vein diameter >13 mm is abnormal. This is specific but not sensitive.
- <20% increase in SMV and splenic vein diameter from quiet respiration to full inspiration.
- Liver cirrhosis (micro- or macronodular change).
- Reversed flow in the portal vein, splenic vein or SMV.
- Absence of portal vein respiratory phasic variability.
- Slow portal venous flow or to-and-fro flow on Doppler.
- Portosystemic collateral vessels.
- Portal or splenic vein aneurysm.

In portal hypertension a number of changes may be seen in the portal venous flow. The flow may be normal in direction and velocity. There may be reduction in velocity (<10 cm/s) with damping of the normal respiratory variation. In worsening liver disease blood entering via the hepatic artery follows the path of least resistance and instead of passing through the hepatic sinusoids to the hepatic veins, blood is shunted through the portal vein via the vasa vasorum or arteriovenous shunts resulting in reversed hepatofugal blood flow (Fig. 12.5).[11] In one series of 228 cirrhotic patients the prevalence of hepatofugal flow was 8.3%.[12] Hepatofugal flow has been shown to be associated with a significant decrease in portal venous calibre and reversed flow in the splenic vein correlates with hepatic encephalopathy due to splenorenal collaterals.[13]

Prior to reversal the flow may be 'balanced', in which forward and reverse low velocity flow to-and-fro pattern is seen (Fig. 12.6). This state may also be a prelude to thrombosis.

Marked periodicity may be seen superimposed on the hepatofugal flow waveform due to hepatic arterial systole as the hepatic arterial flow increases in response to the decrease in portal venous flow.

Marked periodicity may be seen in the portal venous waveform independent of hepatic arterial systole secondary to cardiac disease. This occurs in raised right atrial pressure or in tricuspid regurgitation, producing a giant 'CV' wave or a reversed 'S' wave in the hepatic veins which is transmitted back through the sinusoids to the portal vein (Fig. 12.7).

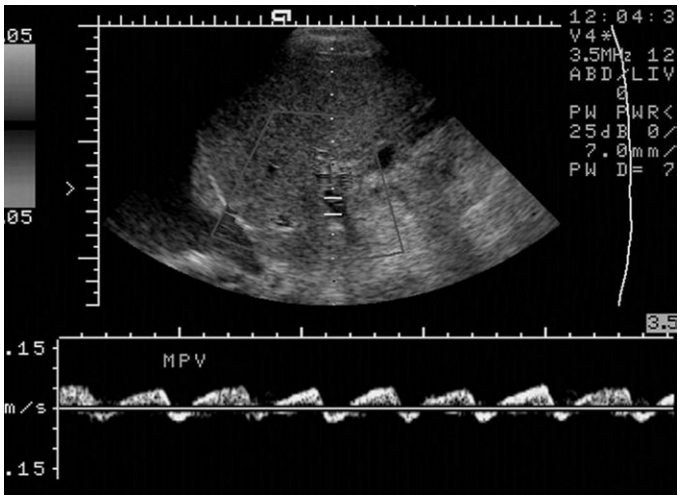


Figure 12.6 **Balanced to-and-fro low velocity flow** is seen in the portal vein in a case of cirrhosis. (Courtesy of Professor David Cosgrove.)

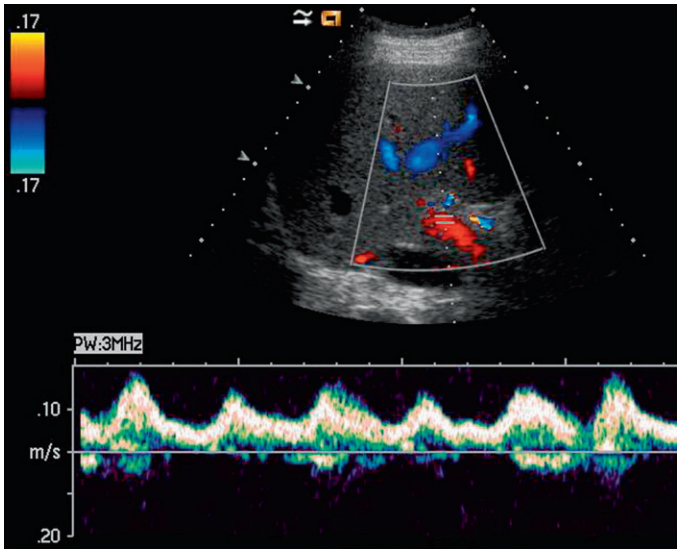


Figure 12.7 **Spectral Doppler of the portal vein** in a patient with tricuspid regurgitation due to right ventricular failure. Marked periodicity is present in the waveform.

Change in portal vein calibre

The diameter of the portal vein is variable but should not be greater than 13 mm (Fig. 12.8). The diameter increases with deep inspiration, postprandially and with posture. A diameter of greater than 13 mm in the fasting state, supine position and during quiet respiration is taken as abnormal. This gives an almost 100% specificity but is less sensitive (56%).[14,15] A calibre of over 17 mm has been shown to be 100% predictive for large oesophageal varices.[16] However, a normal calibre portal vein does not exclude portal hypertension. Dilatation of the splenic and superior mesenteric veins also occurs in portal hypertension with the upper limit of normal ranging from 10 to 12 mm for these vessels. Dilatation of the splenic vein is associated with splenomegaly but it may be difficult to distinguish between portal hypertension and increased splenic blood flow (due to the hyperdynamic splanchnic circulation) as aetiologies for the dilatation.



Figure 12.8 **Dilated portal vein** (14 mm) in a patient with portal hypertension secondary to extensive metastatic liver disease.

Another interesting sign is the lack of change of calibre in the portal vein, splenic vein and superior mesenteric vein in response to deep inspiration. In normal individuals the portal vein and splanchnic vessel diameters should increase by 70–100% from quiet respiration to deep inspiration but in portal hypertension there is a lack of variation due to the presence of already dilated vessels. This sign has an 80% sensitivity and a high specificity.[15]

Splenomegaly

Splenomegaly is an important sign of portal hypertension. The spleen is best measured in the coronal plane with a maximum cephalocaudal measurement of 13 cm reliably indicating enlargement. Splenic size does not correlate well with portal pressure and splenomegaly can be seen in chronic liver disease independent of portal hypertension. However, splenomegaly is commonly seen in portal hypertension and is useful in follow-up in patients with chronic liver disease.

Changes in hepatic arterial flow in portal hypertension

Normally the liver receives 70% of its blood supply via the portal vein and 30% from the hepatic artery. In portal hypertension due to cirrhosis arterialisation occurs in response to a decrease in portal venous flow (Fig. 12.5). The hepatic artery becomes dilated and is easily seen on colour Doppler with spectral Doppler demonstrating a significant increase in flow both in the main hepatic artery as well as the intrahepatic branches. In addition, arteriovenous shunts form at the sinusoidal level shunting blood from the hepatic arteries to the portal vein, resulting in arterialised portal venous blood.

Portosystemic collaterals (varices)

With rising portal venous pressure (>15 mmHg), anastomoses between the high-pressure portal circulation and the lower-pressure systemic system form to shunt blood away from the portal system. The collateral vessels formed are thin walled and prone to rupture. The presence of collaterals is highly indicative of portal hypertension except in isolated splenic or mesenteric vein occlusion.

Ultrasound underestimates the extent of portosystemic collaterals, reportedly visualising 65–90% of varices.[17–19] However, the vast

majority of described collaterals have been imaged by ultrasound[9,17] but only a few groups are regularly identified.

The potential of large portosystemic collateral vessels to decompress the portal venous system and decrease gastrointestinal haemorrhage is controversial. The presence of a large splenorenal shunt has been linked with a reduction in bleeding from gastric varices[20] whilst other studies have not demonstrated a clear protective effect.[21] The pattern of collateral development can influence direction of flow in the portal vein. Flow may be reversed in the presence of a large splenorenal shunt. However, if decompression is mainly due to a large umbilical vein then flow will be hepatopetal. In this situation flow may be reversed in the right portal vein and normal direction in the left portal vein since the recanalised umbilical vein arises from the left portal vein.

The common portosystemic anastomotic sites (Fig. 12.9) are:

- *Gastric and lower oesophagus.* Left gastric varices (also known as coronary vein varices) run from the portal/splenic vein to the lesser gastric curve and may be seen through the left lobe of liver (Fig. 12.10). Short gastric varices run between the spleen and the greater gastric curvature and can be seen on ultrasound using the spleen as a window. Both groups of varices converge at the gastro-oesophageal junction and can extend cranially via oesophageal varices to anastomose with the azygos vein and systemic circulation. Oesophageal varices are prone to bleeding and therefore numerous manoeuvres are available to prevent haemorrhage at this site as discussed below.
- *Umbilical vein.* In utero the umbilical vein carries oxygenated blood from the placenta to the left portal vein. This involutes after birth, forming the ligamentum teres in the falciform ligament. In portal hypertension a paraumbilical vein can dilate and carry blood from the left portal vein to the umbilical region where it anastomoses with systemic veins (superior and inferior epigastric veins) to form a 'caput medusae'. The enlarged umbilical vein is readily seen on ultrasound, carrying blood away from the liver, as it courses deep to the anterior abdominal wall musculature (Figs 12.11 and 12.12). It should be noted that a patent umbilical vein may be seen in normal subjects but it is less than 2 mm in diameter and its velocity is not greater than 5 cm/s.
- *Splenorenal.* These are seen as large tortuous vessels coursing between the splenic hilum, upper pole of the left kidney and left renal vein (Fig. 12.13).
- *Pericholecystic.* These varices occur in the gallbladder wall especially in portal vein thrombosis, bypassing the thrombosed vessel communicating with the intrahepatic portal branches. They can also communicate via subhepatic collaterals to subcostal veins.
- *Pancreatico-duodenal.* These varices are difficult to visualise on ultrasound. They communicate with superior and inferior mesenteric veins as well as the left gastroepiploic veins.
- *Porta hepatis.* Varices may be seen around the portal vein especially if it is thrombosed.

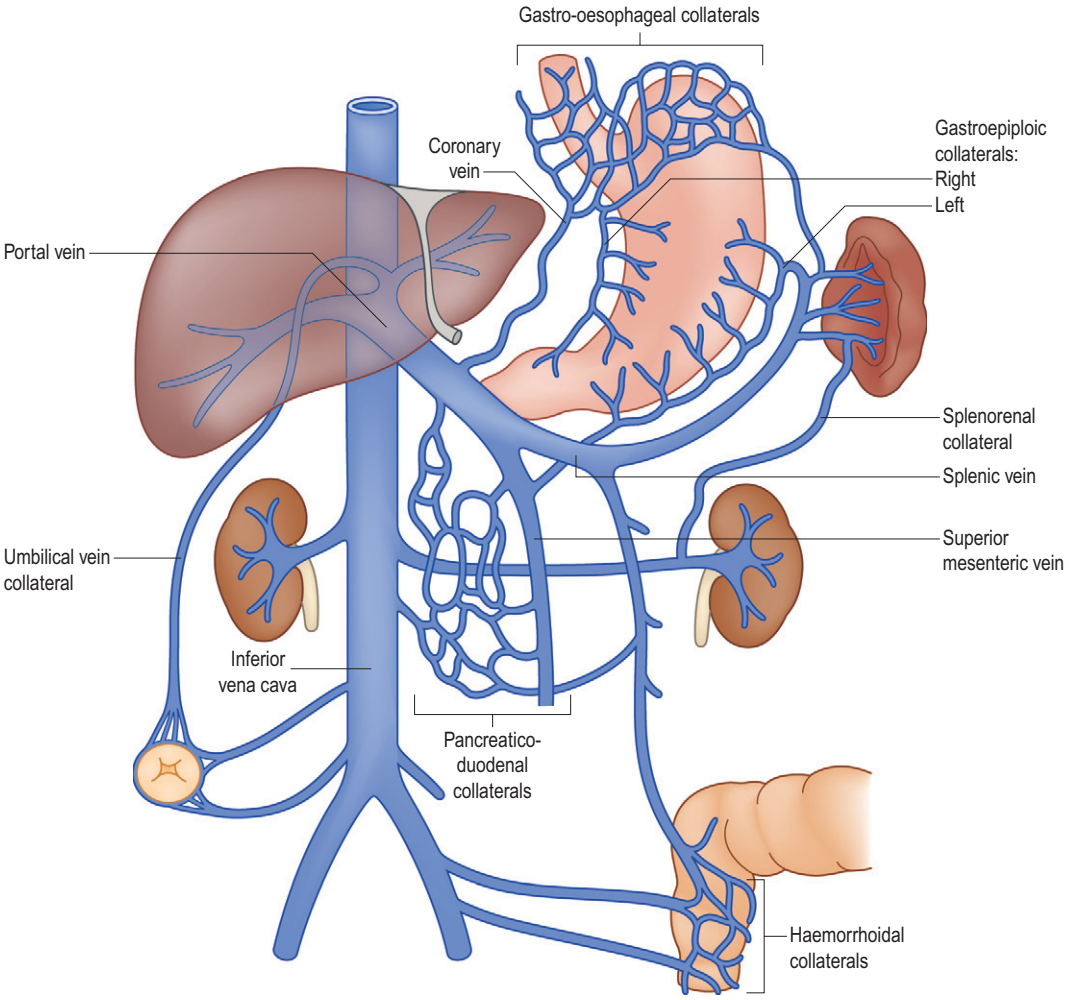
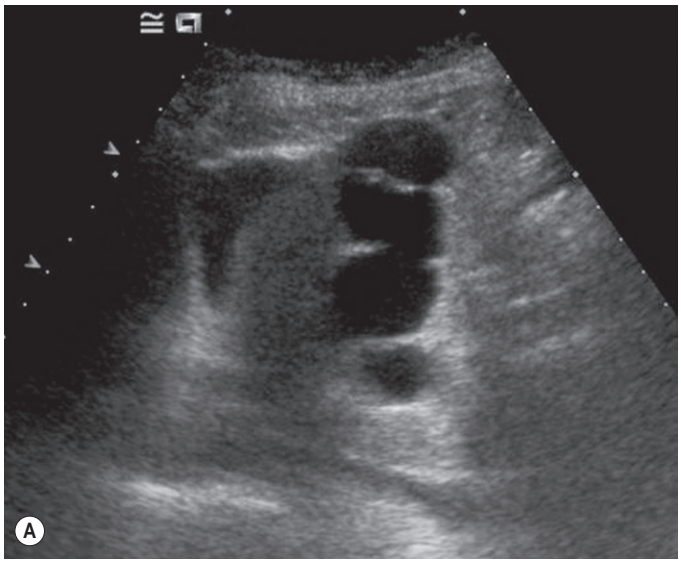
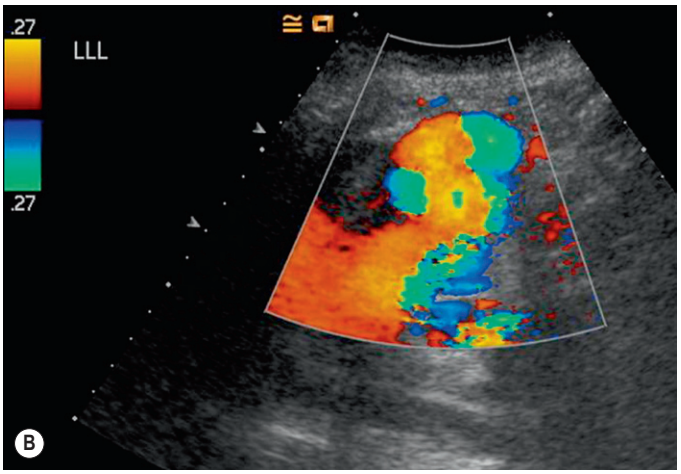


Figure 12.9 Major portosystemic collaterals. (Redrawn from Zwiebel WJ, Pellerito JS. Introduction to Vascular Ultrasonography, 5th edn. Elsevier Saunders, Philadelphia, 2004.)





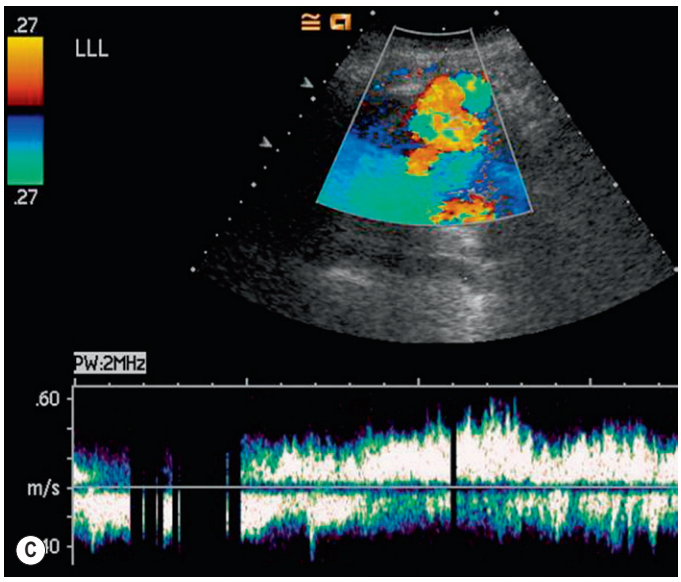
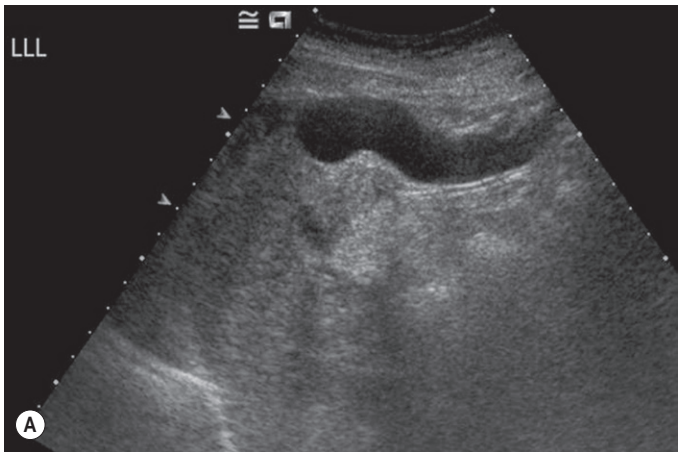


Figure 12.10 **Longitudinal section through the left lobe of liver showing gastric varices. A:** Greyscale shows multiple tortuous serpiginous vessels. **B:** Colour Doppler demonstrates turbulent flow in the varices. **C:** Spectral Doppler confirms venous flow in the varices.



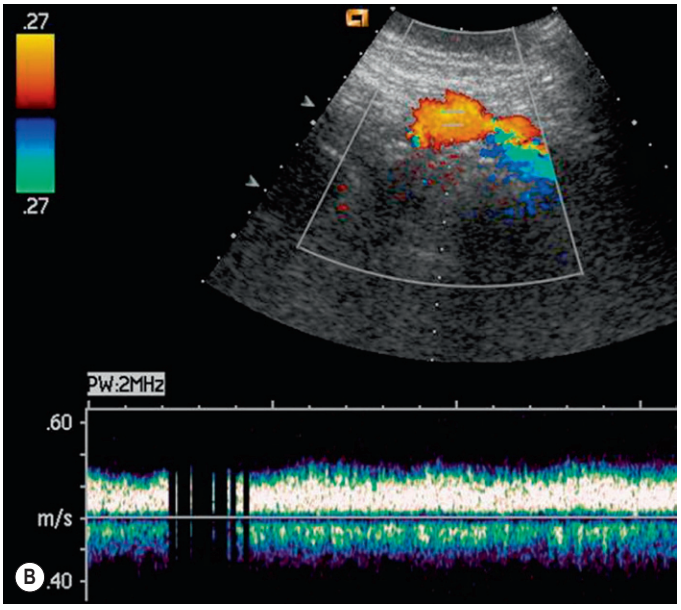


Figure 12.11 **Recanalised umbilical vein in a patient with cirrhosis. A:** B-mode shows a large vessel below the left lobe of liver. **B:** Doppler shows venous blood flow towards the transducer and away from the liver.

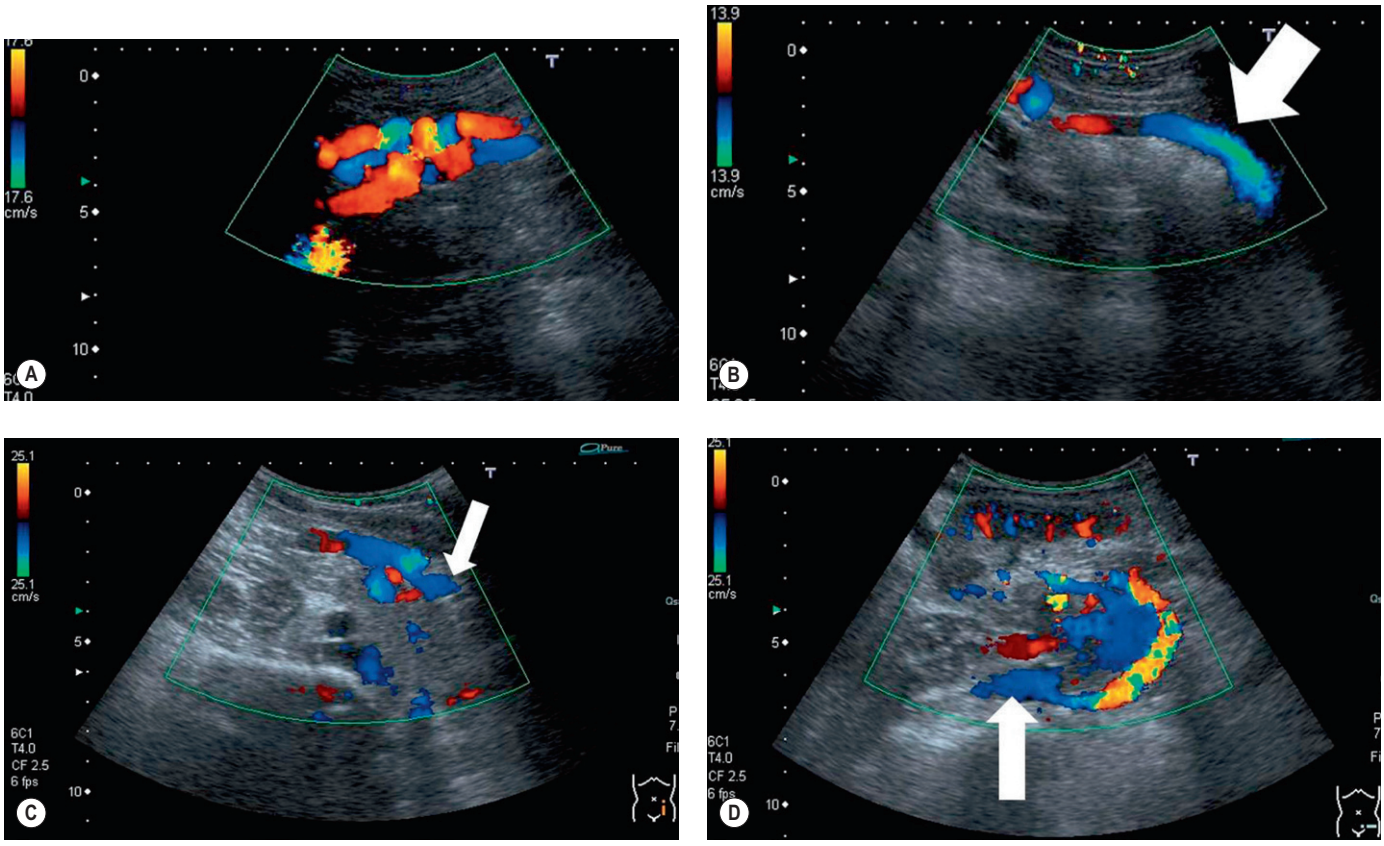


Figure 12.12 Liver cirrhosis and varices in a 26-year-old woman with cystic fibrosis. **A:** Colour Doppler shows varices in the left upper quadrant which, when followed caudally, continued **(B)** as a vessel (arrow) with flow away from the transducer. This vessel bypassed the umbilicus. **C:** In the pelvis the vessel joins the inferior epigastric vein (arrow), which **(D)** joins the external iliac vein (arrow). There was no umbilical collateral vessel or 'caput medusae' in this patient. (Courtesy of Professor David Cosgrove.)

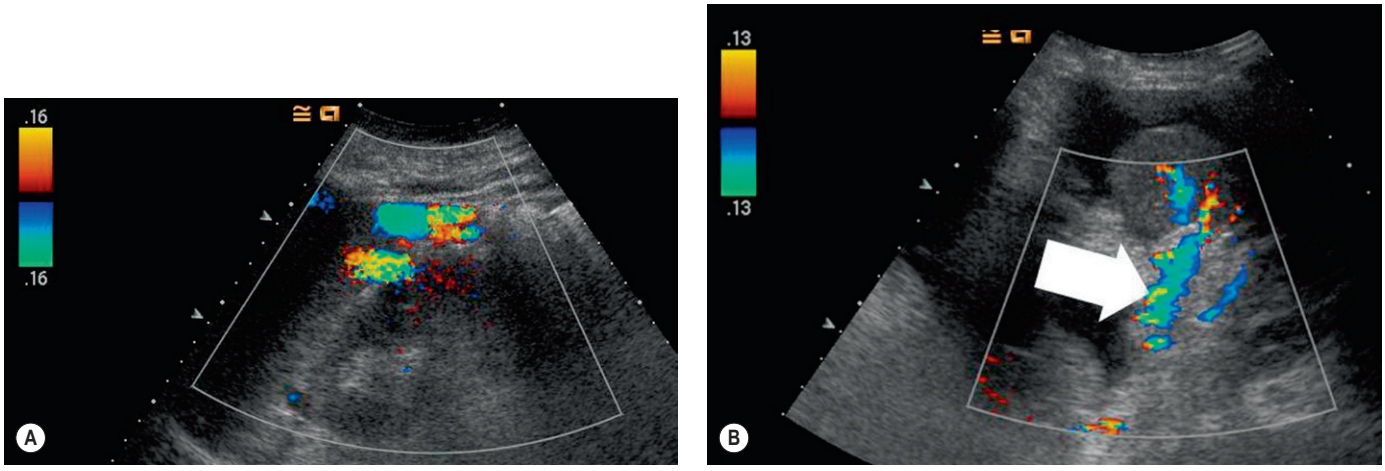


Figure 12.13 Splenorenal varices. A: Varices are seen between the spleen and left kidney. **B:** A large collateral vessel (arrow) is seen carrying blood away from the probe towards the left renal vein.

Other less common portosystemic anastomotic sites are haemorrhoidal, gonadal, iliolumbar and retrosternal.

Management of portal hypertension

One of the major life-threatening problems in portal hypertension is bleeding varices. There are a variety of options available to manage this problem. Management options consist of medical therapy, endoscopic techniques (injection sclerotherapy or banding of oesophageal varices), compression of actively bleeding varices with a Sengstaken tube, surgical or transjugular intrahepatic portosystemic shunts (TIPS).

Surgical portosystemic shunts

The objective of all shunts is to decompress the portal system to minimise the risk of variceal bleeding. There are numerous types

of surgical shunts including portacaval, proximal and distal splenorenal (Warren shunt), mesocaval and mesoatrial shunts.

Non-selective shunts divert all the portal blood flow into the systemic circulation resulting in decompression of the entire portal system and therefore varices. One of the simplest procedures to perform is the portacaval end-to-side shunt in which the portal vein is transected at the liver hilum and anastomosed to the inferior vena cava. These shunts produce immediate protection from variceal bleeding but they have a high rate of encephalopathy and may worsen liver function.

With selective shunts, such as the Warren shunt, liver encephalopathy is less common. The Warren shunt consists of anastomosing the splenic vein to the left renal vein. The left gastric vein, umbilical vein, right gastroepiploic vein, pancreatic branches and other collateral vessels are ligated. This approach selectively decompresses the gastro-oesophageal varices and excludes the gastrosplenic circulation from the rest of the portal system.

When there is portal vein thrombosis, surgical shunts cannot be performed. In these cases the Sugiura procedure may be performed. This consists of splenectomy, devascularisation of the stomach and lower oesophagus along with oesophageal transection to stop flow to the gastro-oesophageal varices and is very effective in preventing haemorrhage from these varices.

The surgical shunt itself is usually difficult to directly visualise because of its retroperitoneal location and therefore Doppler is extremely useful in documenting the secondary changes in portal flow. Preoperative assessment of the portal venous system is essential to assess the haemodynamic consequences of the shunt on portal flow and also to look for shunt stenosis and thrombosis in the follow-up period. Surgical shunts are now rarely performed and have been largely replaced by transjugular intrahepatic portosystemic shunt (TIPS).

Transjugular intrahepatic portosystemic shunt (TIPS)

This minimally invasive procedure was first performed in 1969 but only became a widespread clinical application in the 1980s following the introduction of metallic stents (Fig. 12.14). These uncovered stents were prone to occlusion and stenosis. The use of covered stents in the late 1990s brought with them lower complication rates.[22] TIPS may be regarded as a palliative procedure in end-stage liver disease. The technique involves connecting the portal system to the right hepatic vein via an expandable stent. It avoids surgery and is safe in severe liver failure. Indications include refractory ascites and varices and it has been shown to significantly reduce rebleeding compared to endoscopic management but at a cost of an increased rate of encephalopathy.[23,24] The majority of variceal bleeds can be managed by endoscopic and medical treatment and TIPS is reserved for those who do not respond. It can also be employed prior to liver transplantation or if the patient is a poor surgical risk. The procedure is extremely effective in preventing haemorrhage from gastro-oesophageal varices, reducing ascites and improving the quality of life in end-stage cirrhosis. Complications include precipitation of encephalopathy and worsening liver function as the stent results in diversion of blood away from the liver. Other complications include haemorrhage (Fig. 12.15) (serious intraperitoneal haemorrhage due to laceration of the portal vein or hepatic artery or puncture of the liver capsule) 1–2%, death (5%) and infection (1–2%).[25] Ultrasound has an important role in the evaluation of the hepatic and portal veins pre-procedure as well as the post-procedure assessment of shunt function and patency.

The procedure is performed under fluoroscopic guidance. A catheter is passed via the internal jugular vein to the inferior vena cava and into the right/middle hepatic vein. A tract is then formed across the liver connecting the right portal vein with the hepatic vein. A metal stent is sited to keep the shunt open. This results in immediate decompression of varices and improvement of the sequelae of portal hypertension.

The main problems with TIPS are stent occlusion and stenosis. Occlusion or stenosis within the first few weeks is usually due to technical problems with the procedure. Late occlusion or stenosis is related to neointimal hyperplasia (Fig. 12.16).

Direct portography with portosystemic gradient measurement is still the gold standard in the assessment of TIPS function but this is invasive and utilises ionising radiation and iodinated contrast. Therefore regular surveillance with ultrasound is used to detect problems earlier to allow interventions such as angioplasty and thrombolysis. The 1-year stent patency is approximately 85% with these interventions, a figure that falls to approximately 50% in their absence. Despite its widespread use in screening for TIPS

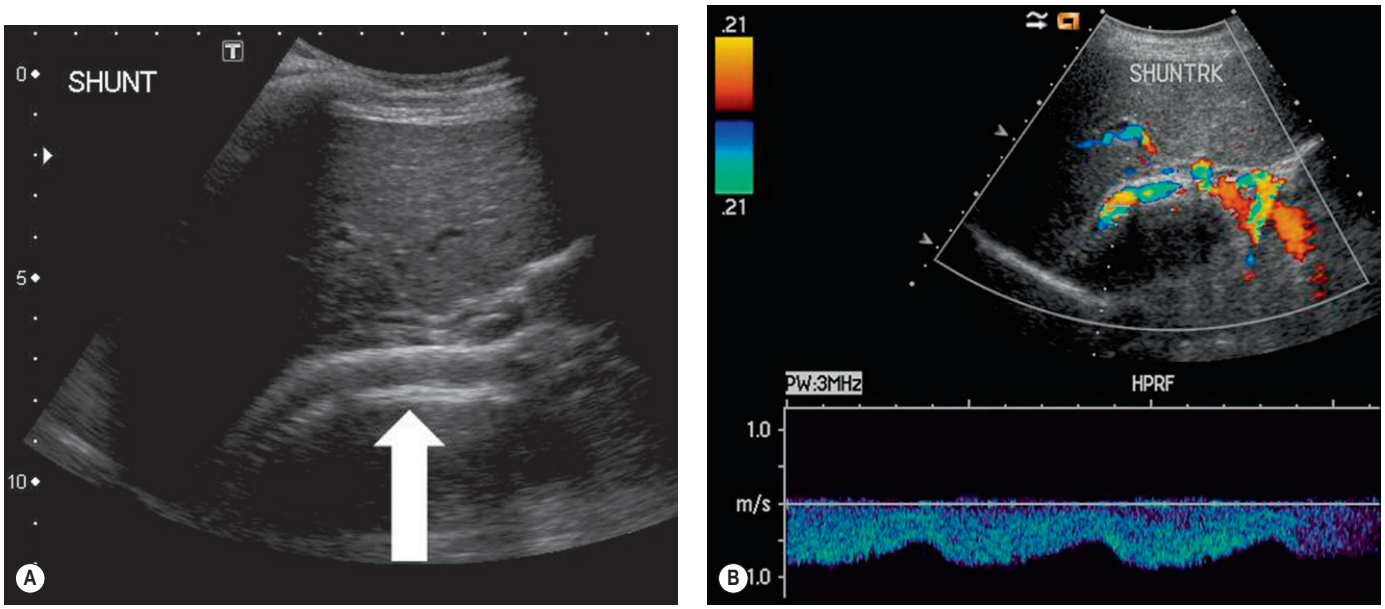


Figure 12.14 Normal transjugular intrahepatic portosystemic shunt (TIPS). A: B-mode shows a normally sited metallic TIPS stent (arrow). **B:** Doppler shows a normal pulsatile waveform indicative of a widely patent stent.

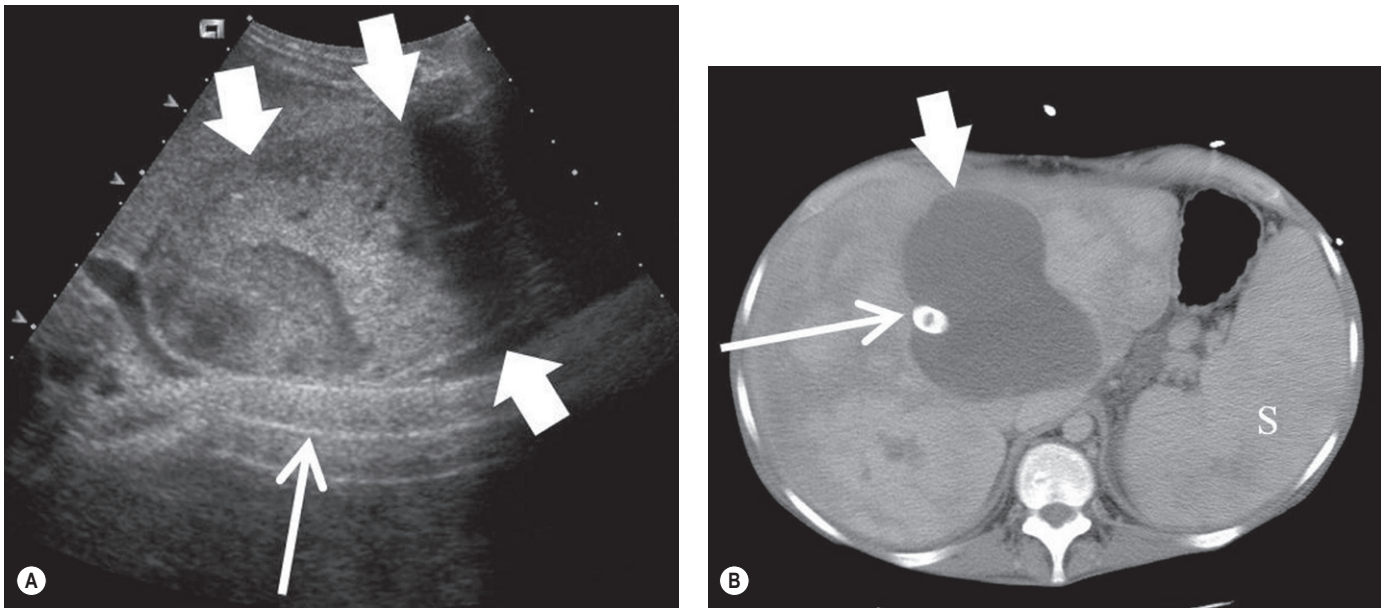


Figure 12.15 Transjugular intrahepatic portosystemic shunt (TIPS) in a patient with Budd–Chiari syndrome. **A:** The ultrasound shows a large haematoma (thick arrows) adjacent to the stent (thin arrow). **B:** Computed tomography shows the extent of the haematoma (thick arrow) adjacent to the stent (thin arrow). Note the heterogeneous liver attenuation and splenomegaly (S) due to Budd–Chiari syndrome.

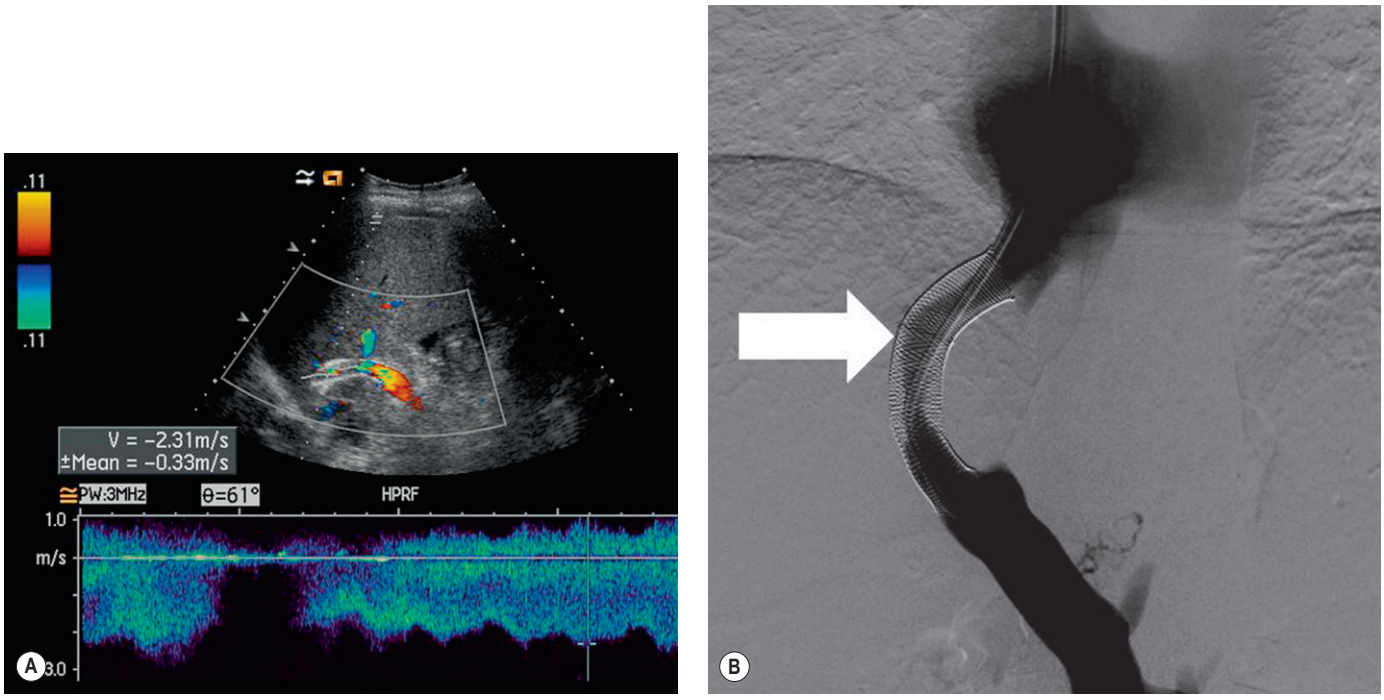


Figure 12.16 Transjugular intrahepatic portosystemic shunt (TIPS) stenosis. A: Spectral Doppler shows marked elevated (2.3 m/s) turbulent flow in the stent which had been normal several months earlier after insertion. **B:** Direct portography showed a mid-stent stenosis (arrow) presumably due to neointimal hyperplasia. The portosystemic gradient was 21 mmHg, which following dilatation reduced to 14 mmHg with a good angiographic result (not shown).

dysfunction, Doppler data are inconsistent and its role in surveillance is controversial. The sensitivity and specificity vary widely in the ultrasound detection of shunt dysfunction.[26–29]

Assuming a right portal vein to right hepatic vein TIPS, Doppler measurements (velocity, direction of flow and waveform) should routinely be performed at the portal venous end, midpoint and hepatic venous end of the shunt as well as the hepatic vein, main portal vein and left portal vein. Several haemodynamic changes occur immediately after TIPS placement; both portal vein diameter and mean velocity may increase, resulting in a marked increase in portal vein flow volume. Blood flow in the main portal vein is hepatopetal but flow within the intrahepatic portal veins may be hepatofugal. Knowledge of the wide spectrum of normal findings following TIPS is essential.

The most common site for stent stenosis is at the junction of the stent with the hepatic vein. There are several Doppler parameters

Normal Doppler indices following transjugular intrahepatic portosystemic shunt (TIPS) (adapted from Zwiebel WJ, Pellerito JS. Introduction to Vascular Ultrasonography, 5th edn. Elsevier Saunders, Philadelphia, 2004)

1. Pulsatile turbulent flow in the shunt
2. Peak systolic velocity in the shunt of at least 50–60 cm/s (range 90–120 cm/s). Mean velocity ranging from 100 cm/s to >200 cm/s
3. Similar velocity at the portal and hepatic venous ends of the shunt
4. Hepatopetal flow in the portal and splenic vein
5. Portal vein velocity:
   significantly greater then preshunt value
   at least 30 cm/s (range 20–50 cm/s)
6. Increase in portal vein diameter which along with the increase in velocity results in a marked increase in portal vein flow volume
7. Hepatofugal flow may occur in intrahepatic portal vein branches

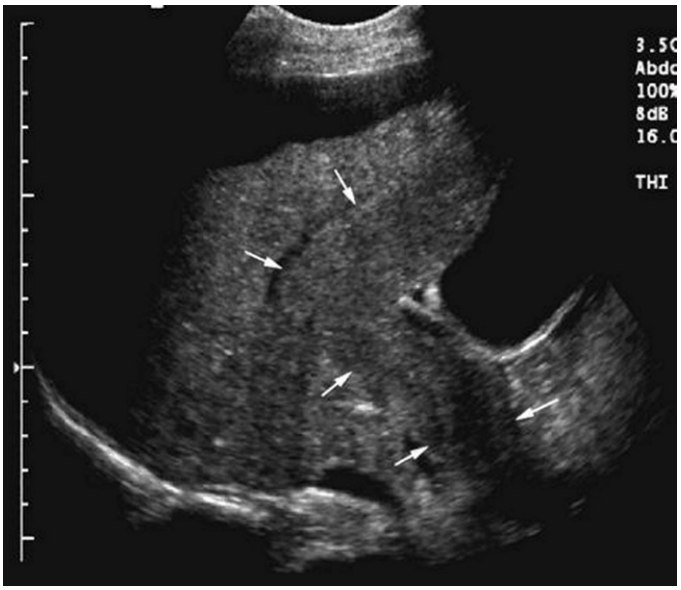


Figure 12.17 Subtle echo-poor complete portal vein thrombosis (arrows) in a patient with cirrhosis.

Abnormal clinical features and Doppler indices for transjugular intrahepatic portosystemic shunt (TIPS) (adapted from Zwiebel WJ, Pellerito JS. Introduction to Vascular Ultrasonography, 5th edn. Elsevier Saunders, Philadelphia, 2004)

1. Localised high velocity (>220 cm/s) with post-stenotic turbulent flow
2. Change in velocity of >100 cm/s across the stent
3. Visible narrowing with or without high velocity
4. Diffuse low velocity throughout the stent (<50 cm/s)
5. Continuous non-pulsatile flow in the stent
6. Decrease in portal vein velocity compared to pre-procedure values
7. Portal vein velocity <30 cm/s
8. Development of hepatofugal or to-and-fro main portal or splenic vein flow
9. Development of hepatopetal flow in the intrahepatic portal vein branches
10. Absent flow in stent
11. Recurrence of variceal gastrointestinal bleeding
12. Development of ascites and splenomegaly

Causes of portal vein thrombosis

1. Chronic liver disease and portal hypertension, especially cirrhosis
2. Malignancy: hepatocellular carcinoma, cholangiocarcinoma, pancreatic and gastric cancer
3. Inflammatory:
   pancreatitis
   acute cholecystitis
   ascending cholangitis
   abdominal sepsis
   ischaemic bowel
4. Coagulopathies:
   associated with Budd–Chiari syndrome
   dehydration
   oestrogen therapy
   complication of splenectomy especially in myeloproliferative disorders
5. Trauma: umbilical vein catheterisation

which can be helpful in diagnosing stent stenosis but comparison with the pre-procedure indices is essential. No one Doppler parameter is sufficiently sensitive to be used in isolation to diagnose stenosis but use of several indices may be more helpful.[30] Ultrasound contrast agents have been shown to improve sensitivity and specificity in the diagnosis of shunt dysfunction.[31,32]

A shunt velocity of less than 50 cm/s is highly suggestive of stenosis. Also local high-velocity flow or areas of turbulence or a change in velocity of greater than 100 cm/s across the stent are suspicious of stenosis.

Stent occlusion is reliably diagnosed by Doppler with a high sensitivity and specificity. However, trickle flow may be missed by ultrasound and ultrasound contrast agents or formal portography is essential to confirm this.

Portal vein occlusion

The main causes of portal vein occlusion are due to thrombosis or tumour invasion. The occlusion may be complete or partial and only affect a branch. The most common cause is portal hypertension due to cirrhosis.

In patients with cirrhosis, the reported incidence of portal vein thrombosis (PVT) is 5–20%.[33–35] With more advanced stages of cirrhosis there is a higher risk of PVT than in patients with compensated liver disease.[36] Doppler is the most sensitive technique to detect PVT in cirrhosis, with the prevalence of partial and complete thrombosis being 1.8% and 4.4%, respectively, in one series.[12] The accuracy is less for branch PVT. PVT is not uncommonly a chance finding in cirrhosis and Amitrano et al.[36] showed that only 57% of cirrhotic patients with PVT were symptomatic. The presence of symptoms depends on whether the thrombus is complete or partial as well as rate of thrombus development. Clinical presentations of PVT include variceal bleeding due to collaterals, refractory ascites and small bowel ischaemia/infarction.[36] In acute thrombosis the thrombus may be anechoic and it may be difficult to differentiate from a patent vessel, especially in an attenuating cirrhotic liver (Fig. 12.17). The ultrasound settings should be optimised, with the Doppler sensitivity set to pick up low flow and the vein axis made less than 60° to the transducer before diagnosing portal vein thrombosis. A Valsalva manoeuvre may induce hepatofugal flow in a low flow system by transiently increasing portal venous resistance. The addition of ultrasound contrast agents or the use of other imaging modalities may resolve the problem. The thrombus may dilate the

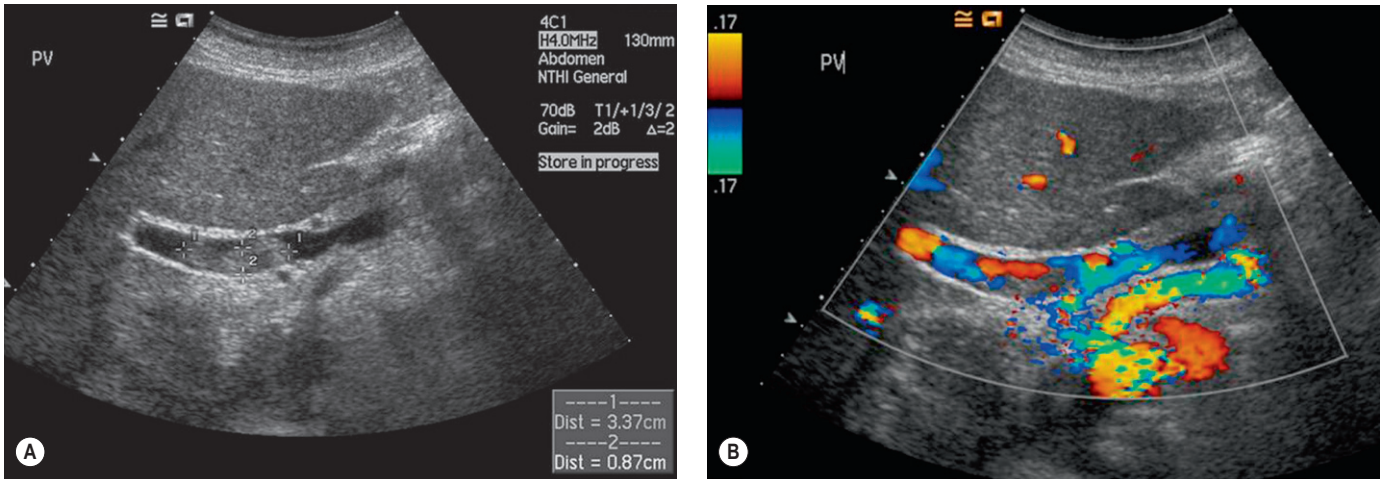


Figure 12.18 Recanalisation of an old main portal vein thrombosis. A: B-mode shows an echogenic thrombus measured by callipers. **B:** Colour Doppler shows flow around the thrombus.

vein. The superior mesenteric and splenic veins should be interrogated to establish the extent of the thrombus. If these vessels are not involved with thrombus they are usually dilated and exhibit slow or reversed flow. As the thrombus matures it becomes more echogenic and retracts resulting in partial recanalisation (Fig. 12.18). More frequently cavernous transformation occurs (see below).

False positives occur on ultrasound due to inadequate technique or insensitive equipment, low velocity to-and-fro portal flow, which is difficult to detect with Doppler, and failure to use Doppler in acute anechoic thrombus. False negatives may be due to the detection of flow within collateral vessels erroneously mistaken for the main portal vein.

In chronic portal vein thrombosis a network of collateral vessels (cavernous transformation) may develop within a few weeks around the thrombosed portal vein (Fig. 12.19). Spectral Doppler demonstrates portal flow in the vessels of the cavernoma. Portosystemic and intrahepatic collateral vessels may form in chronic portal vein thrombosis.

In malignancies such as hepatocellular carcinoma it is very important to differentiate tumour thrombus from bland thrombus. Massive dilatation of the portal vein (>20 mm) is suggestive of tumour but this is not specific. Tumour thrombus can be differentiated from bland thrombus by the presence of an arterial spectral waveform in the thrombosis (Fig. 12.20). This is important as the presence of tumour thrombus carries a grave prognosis and renders the tumour unresectable. Tumour may extrinsically compress the portal vein, resulting in stenosis (Fig. 12.21).

Portal vein aneurysm

Aneurysm of the portal vein is very rare. It may be seen in portal hypertension and infective aetiologies. It is important to differentiate it from a hepatic artery aneurysm, which carries a worse prognosis.

Portal vein gas

Portal venous gas is seen in bowel ischaemia/infarction, ulceration, gastrointestinal sepsis and bowel obstruction. In these conditions it has a poor prognosis. However, more recently improved imaging techniques have demonstrated it in more benign conditions such as pneumatosis coli, obstructive airways disease, iatrogenic enema administration, colonoscopy and gastrostomy tubes. Tiny echogenic foci are seen in the portal vein. Spectral Doppler demonstrates spikes of high signal superimposed on the background portal vein trace (Fig. 12.22).

HEPATIC ARTERY

Anatomy and scanning techniques

The common hepatic artery arises from the coeliac axis; after the origin of the gastroduodenal artery, it becomes the hepatic artery proper. It enters the liver adjacent to the portal vein and then divides into right and left hepatic branches supplying the respective liver lobes. The artery accompanies the portal vein, which together with the bile duct forms the portal triad and these terminate at the acinus. The hepatic artery crosses posterior to the common bile duct (CBD) and anterior to the portal vein at the level of the porta hepatis and provides an important reference point for measuring the CBD (Fig. 12.2). Usually the hepatic artery has divided and so the right hepatic artery branch is most often imaged as it passes between the bile duct and portal vein. The hepatic artery always lies medial to the common bile duct throughout its course and similar to the right portal vein, the right branch traverses the liver substance for a few centimetres before dividing into the anterior and posterior branches, while the left branch curves anteriorly, dividing into segmental branches of the parts of the liver it supplies.

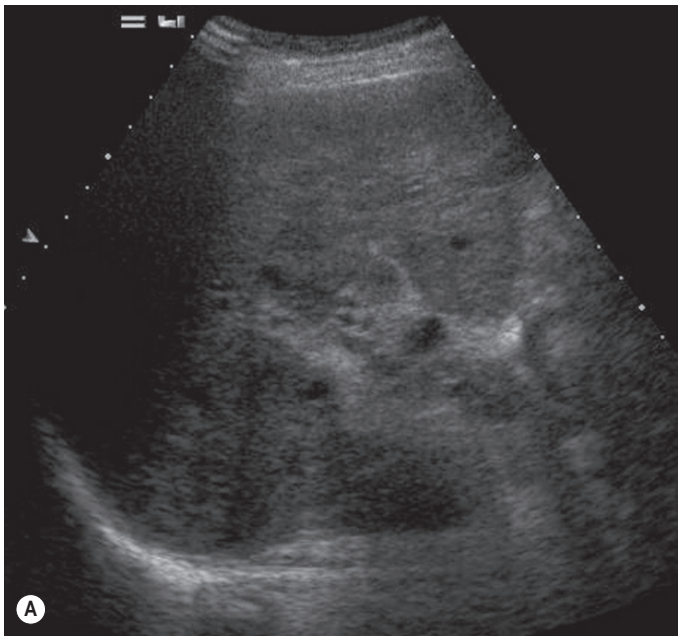
There are numerous vascular anomalies that can occur; the common hepatic artery can aberrantly arise from the superior mesenteric artery (SMA) in approximately 3% of normal variants or alternatively the right hepatic artery may arise from the SMA in 11% or the left hepatic artery is replaced with a branch from the left gastric artery.[37]

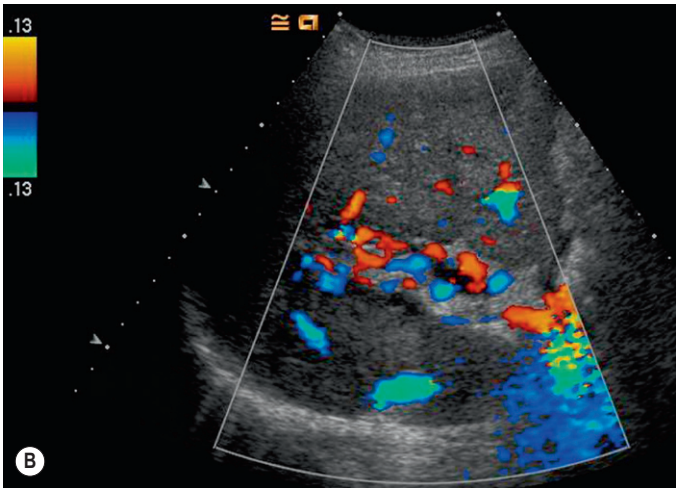
The hepatic artery only contributes to 25% of the blood supply of the liver where it is predominantly supplied by the portal vein.[38] This dual supply explains the relatively low prevalence of hepatic infarction.

The hepatic artery can be traced from the coeliac axis and is easily visualised in the mid-clavicular line just beneath the costal margin in a longitudinal oblique plane. It is at the porta hepatis where the hepatic artery crosses between the common bile duct and portal vein that the artery is commonly assessed, particularly with respect to Doppler indices.

Normal findings

Doppler ultrasound can provide a quantitative measure of blood flow to the liver. The hepatic artery commonly demonstrates a splanchnic waveform on Doppler studies and normal main hepatic artery peak velocities are variable partly because of the angle of insonation (Doppler angle) which should be between 45° and 60°.





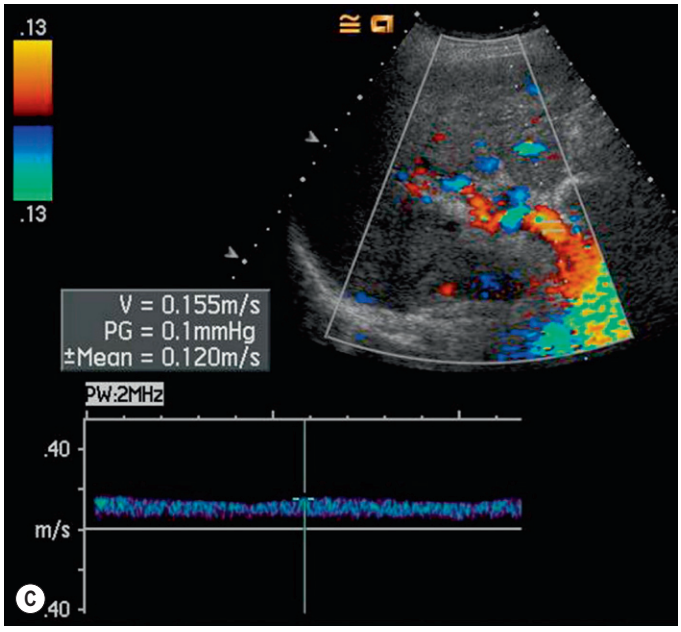


Figure 12.19 Cavernous transformation of a portal vein thrombosis. A: B-mode shows absence of the characteristic anechoic normal portal vein at the porta. **B:** Colour Doppler shows collaterals around an old thrombosed portal vein. **C:** Spectral Doppler reveals venous flow in these collaterals.

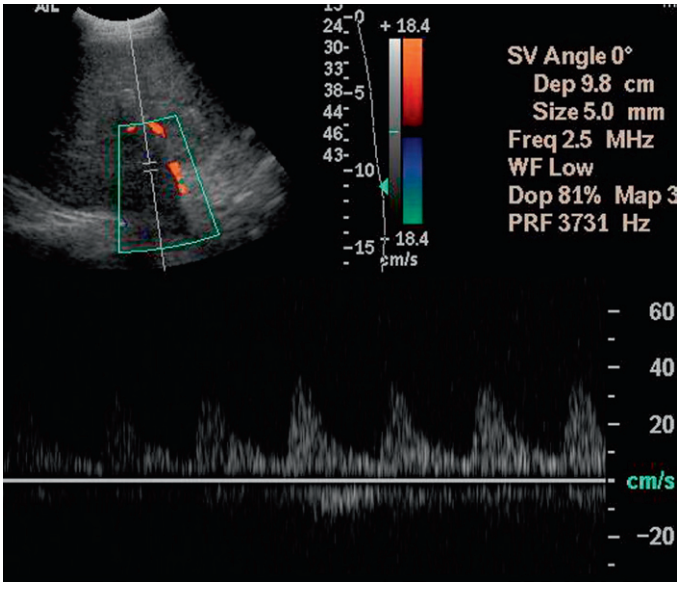


Figure 12.20 Arterial flow pattern is obtained from a thrombosed portal vein in a patient with hepatocellular carcinoma confirming tumour thrombus.

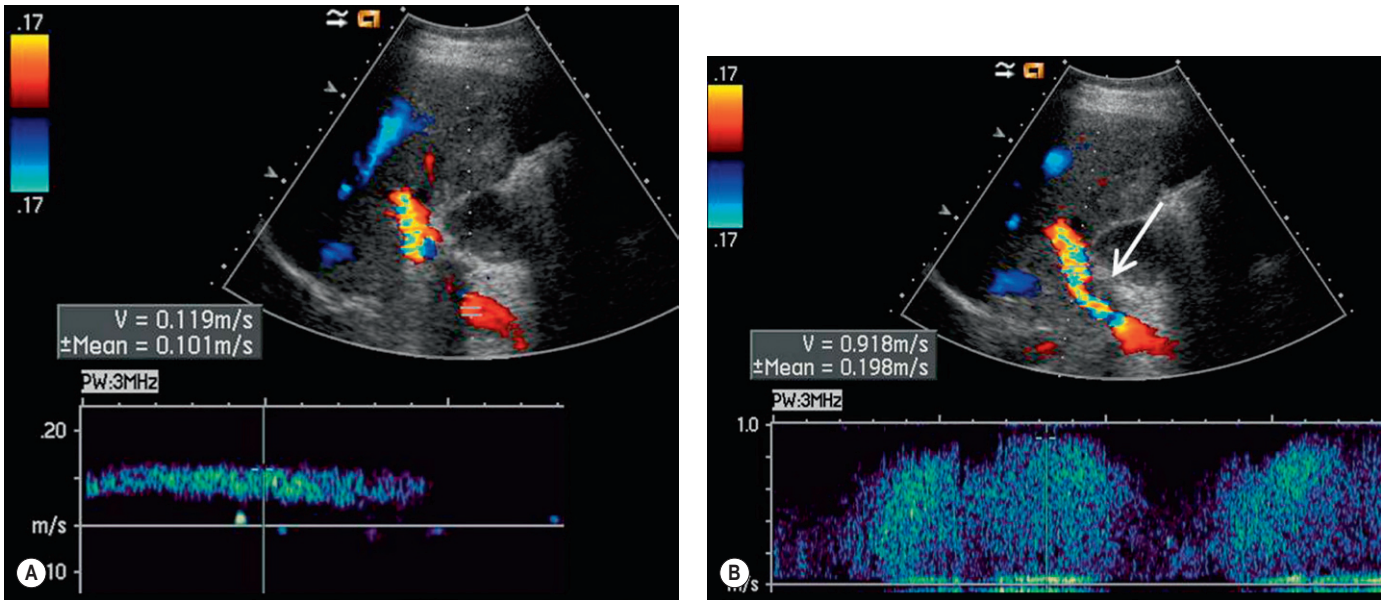


Figure 12.21 **Portal vein stenosis in a case of pancreatic carcinoma. A:** Doppler from the prehepatic portal vein (proximal to a stenosis) shows a normal flow pattern. **B:** A tumour mass (arrow) is seen compressing the portal vein. The peak velocity distal to this site is elevated (91 cm/s) with spectral broadening.

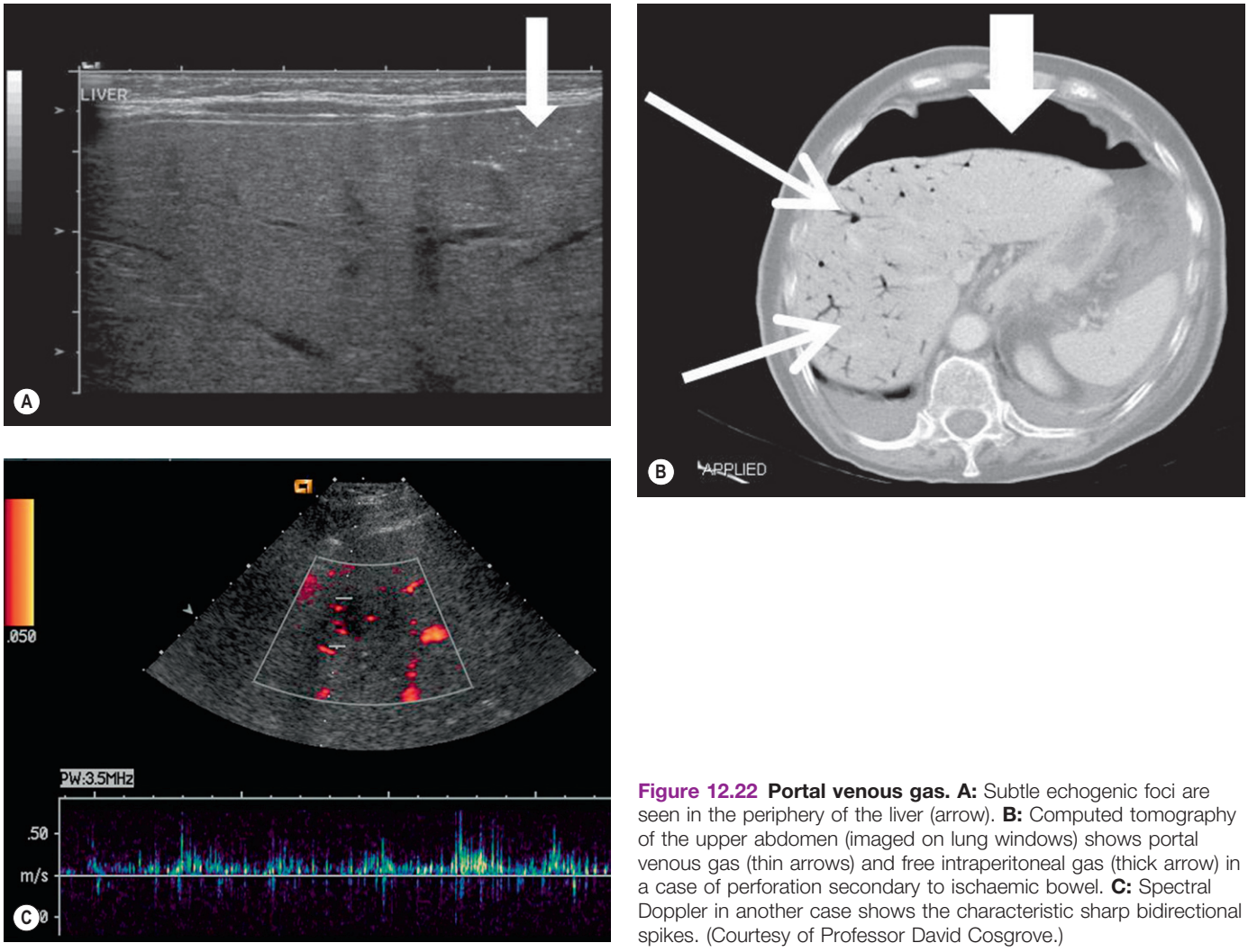


Figure 12.22 **Portal venous gas. A:** Subtle echogenic foci are seen in the periphery of the liver (arrow). **B:** Computed tomography of the upper abdomen (imaged on lung windows) shows portal venous gas (thin arrows) and free intraperitoneal gas (thick arrow) in a case of perforation secondary to ischaemic bowel. **C:** Spectral Doppler in another case shows the characteristic sharp bidirectional spikes. (Courtesy of Professor David Cosgrove.)

In the fasting state the hepatic artery has a low resistance flow pattern with a peak systolic velocity of 30–40 cm/s and a diastolic flow of 10–15 cm/s.[39]

It is widely accepted that changes in the haemodynamic circulation of the liver occur with chronic liver disease where there is an increase in hepatic arterial velocity with increasing fibrosis and progression to cirrhosis. Owing to the variation in using the velocity measurement on its own, many research studies have used the resistive index (RI) and being a ratio, it is independent of the Doppler angle. Hepatic artery resistive index (RI) is calculated as (Peak systolic velocity – End diastolic velocity)/Peak systolic velocity. Typical values range between 0.7 and 0.8.

Previous studies in patients with chronic liver disease have demonstrated an increase in hepatic artery RI in chronic liver disease, which has been thought to be related to the architectural derangement that occurs within the liver with increasing severity of disease.[40–43] The reproducibility of such data, however, has been shown to be unreliable, with varying reports of success from different research groups. This is predominantly owing to the fact that the RI is affected by many variables such as age and heart rate and most studies have shown no correlation with histology.[44]

Hepatic artery aneurysms

The common sites of arterial aneurysms in following order are infrarenal aorta, iliac arteries, splenic artery followed by the common hepatic artery. Ultrasonic findings demonstrate a hypoechoic mass which shows marked turbulent flow on colour Doppler (Fig. 12.23). The commonest cause is iatrogenic (following biopsy) but other causes include trauma, liver transplantation, transarterial chemo-embolisation, vasculitides (polyarteritis nodosa), sepsis and they have been reported in chronic pancreatitis.[45] These aneurysms commonly rupture (up to 80%) with catastrophic consequences and therefore should be treated urgently.

Hereditary haemorrhagic telangiectasia (HHT)

This is an autosomal dominant condition characterised by multiple small aneurysmal telangiectases affecting the skin, mucous membranes, gastrointestinal tract, brain, liver and lungs. These vessels are fragile with an increased propensity to haemorrhage. In the liver, ultrasound can demonstrate vascular malformations. Anatomically, three different patterns of abnormal vascular communications can occur in liver: portal vein to hepatic vein (portovenous), hepatic artery to hepatic vein (arteriovenous) and hepatic artery to portal vein (arterioportal), with the most common being arteriovenous (Fig. 12.24). Only 5–8% of patients with these vascular malformations are symptomatic. When symptomatic, patients present with high-output cardiac failure, biliary ischaemia (which, when severe, can progress to biliary and hepatic necrosis and lead to acute liver failure), or portal hypertension.[46–52]

Acquired arteriovenous fistulae are most commonly traumatic secondary to liver biopsy, transhepatic biliary drainage procedures, surgery, neoplasms or rupture of a hepatic, superior mesenteric or splenic artery aneurysm.

HEPATIC VEINS

Anatomy and scanning technique

The blood from the sinusoids of the liver parenchyma enter the hepatic terminal venules where these unite to form larger veins, which can vary in number and position although typically in the majority of the population there are three major veins: the right, middle and left hepatic veins which empty into the superior part of the inferior vena cava (IVC). They are best imaged in the transverse plane. They are larger in calibre than the portal veins and can be differentiated from them by their relatively thin anechoic walls compared to the brighter thicker walls of the portal triads (containing the portal vein, bile duct and hepatic artery) that are encased by echogenic fibrous walls (extension of Glisson's capsule). The hepatic veins do not have valves. The veins run superiorly and posteriorly, curving towards the IVC, and the vessel calibre increases as they approach the IVC.

The right hepatic vein lies in the coronal plane and empties separately into the IVC 1 cm below the diaphragm/right atrium. The middle hepatic vein passes from the position of the gallbladder fossa and joins the left to form a short common trunk and both empty into the anterolateral aspect of the IVC but enter separately in 15–35%.

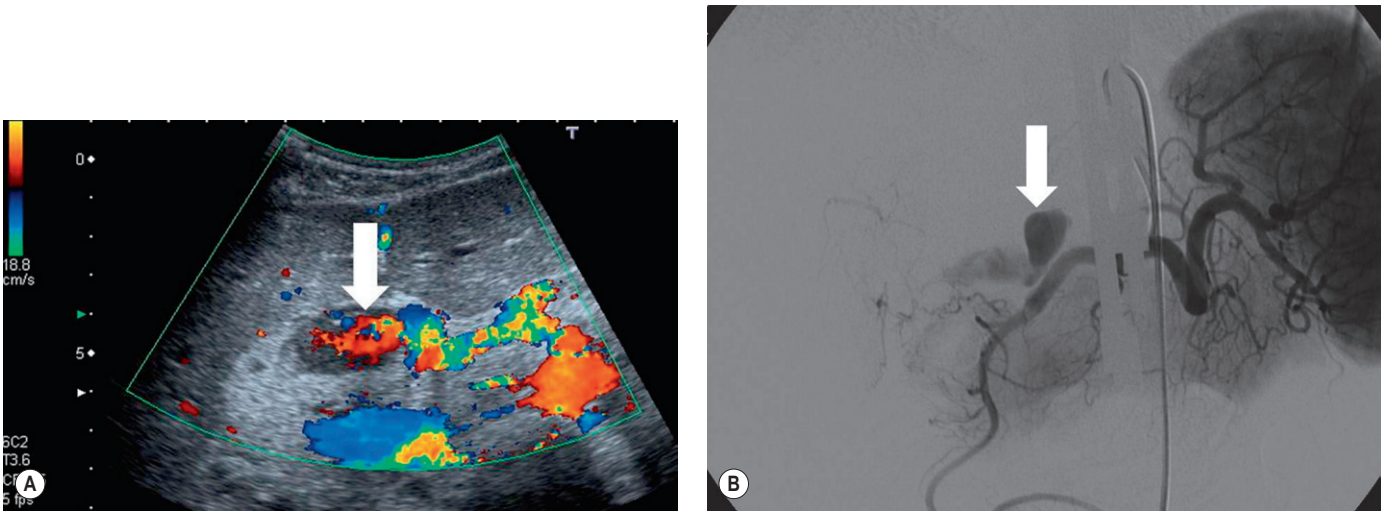


Figure 12.23 Hepatic artery pseudoaneurysm secondary to endocarditis. A: Colour Doppler shows an aneurysm arising from the hepatic artery with turbulent flow in it (arrow). **B:** A selective coeliac axis angiogram revealed a bilobed pseudoaneurysm (arrow) arising from the left hepatic artery which was successfully embolised.

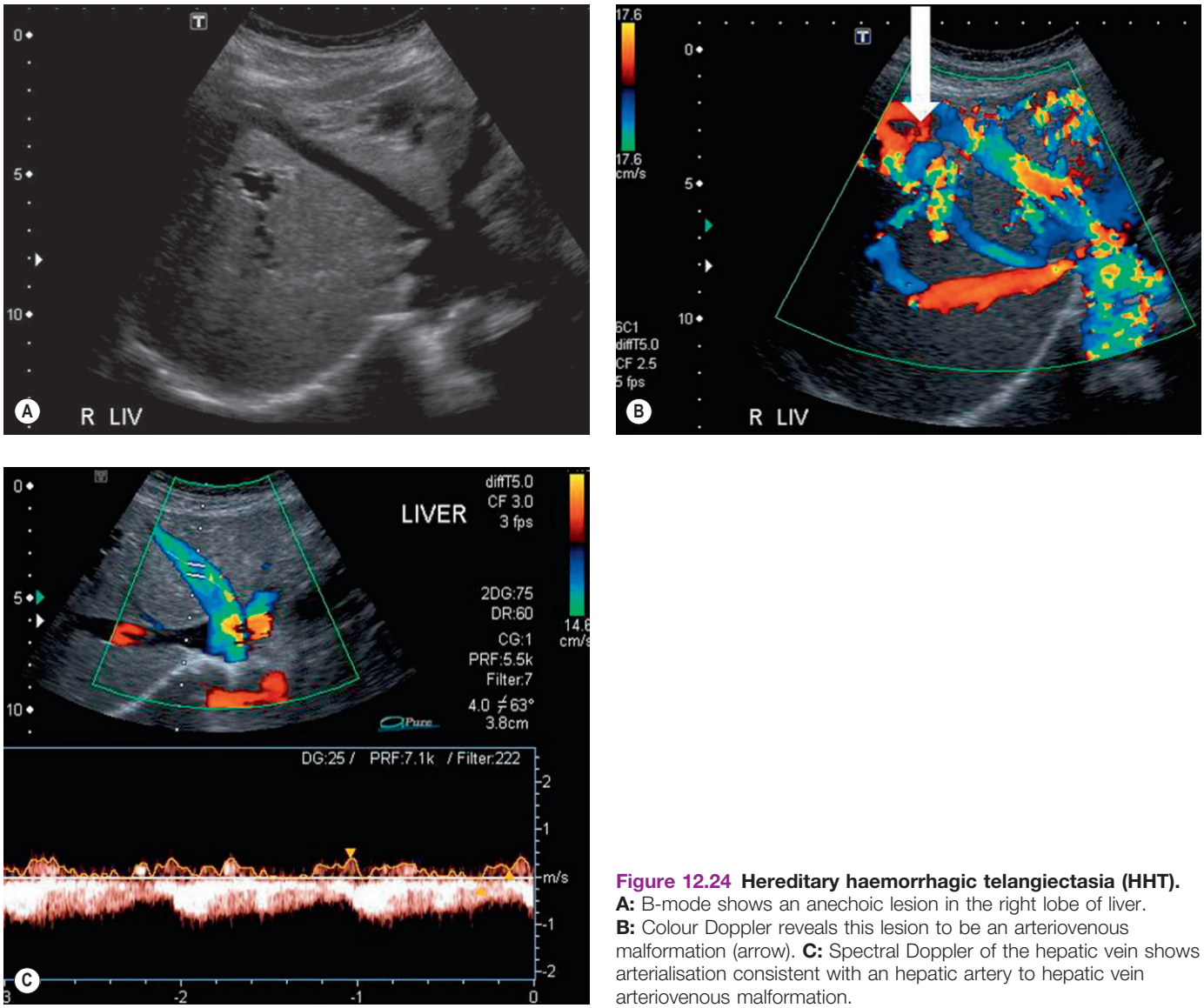


Figure 12.24 Hereditary haemorrhagic telangiectasia (HHT). **A:** B-mode shows an anechoic lesion in the right lobe of liver. **B:** Colour Doppler reveals this lesion to be an arteriovenous malformation (arrow). **C:** Spectral Doppler of the hepatic vein shows arterialisation consistent with an hepatic artery to hepatic vein arteriovenous malformation.

Understanding the portal and venous anatomy is essential in understanding how the liver is divided into segments based on the Couinaud's classification.[1] This system has become widely accepted and is particularly useful when a precise description of the position of a lesion is required, particularly with respect to planning surgery. This system based on the anatomy of the portal and hepatic veins is considered more accurate than a biliary segmental approach. The major hepatic veins course between the lobes and segments and all drain cephalically at confluence with the inferior vena cava (IVC) as described above. The middle hepatic vein runs within the main lobar fissure dividing the liver into two main lobes (right and left), thereby separating segments I–IV from segments V–VIII (Fig. 12.25). The left hepatic vein (LHV) on the other hand runs within the left intersegmental fissure dividing the left lobe into medial and lateral segments, i.e. separating segments II and III from segment IV. Lastly, the right hepatic vein runs in the right intersegmental fissure dividing the right lobe of the liver into anterior and posterior segments, separating segments V and VIII from segments VI and VII, respectively (Fig. 12.26). The portal vein, on the other hand, separates the superior and inferior segments of the liver, i.e. segments II from III, segments IVa from IVb and segments V and VIII from segments VI and VII. Therefore in general, the portal vein divides the segments superiorly and inferiorly while the hepatic veins separate the anterior from the posterior segments (Fig. 12.1).

The hepatic veins are generally easily visualised intercostally or subcostally. The left and middle hepatic veins are best assessed in a transverse oblique plane at the xiphisternum while the right hepatic vein is best assessed intercostally. Sometimes owing to the cardiac pulsations, the middle hepatic vein can be assessed in the intercostal plane but should be carefully distinguished from the right hepatic vein.

Normal anatomical variations

The variation in branching and presence of accessory veins of the hepatic venous system are relatively common. The most common accessory vein drains the anterosuperior segment of the right lobe (segment VIII) and is present in approximately 30% of the population. This accessory vein drains either into the middle or right hepatic vein, the former being more common.[53] Small inferior veins drain from the caudate and medial aspect of the right lobe directly into the IVC. This drainage pattern explains the behaviour of the caudate lobe in cirrhosis and the characteristic computed tomography (CT) enhancement pattern seen in Budd–Chiari syndrome. Another venous anomaly is a large accessory right hepatic vein entering the IVC several centimetres inferior to the main venous confluence in 6–10% of people. Smaller accessory veins of the LHV



Figure 12.25 In this transverse oblique section, the middle hepatic vein is demonstrated (arrow) and divides the right from the left lobe of the liver. Segment IV lies in between the middle hepatic vein and the left hepatic vein (arrowhead).

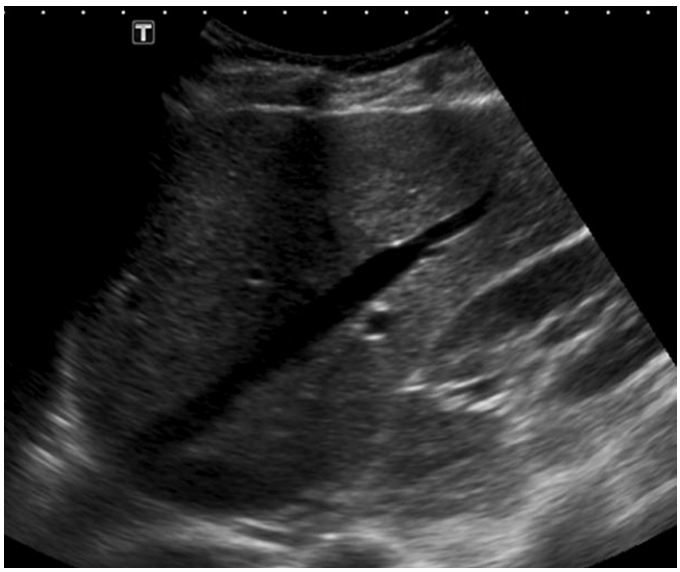


Figure 12.26 The right hepatic vein seen in this longitudinal section dividing the anterior and posterior segments of the right lobe of the liver.

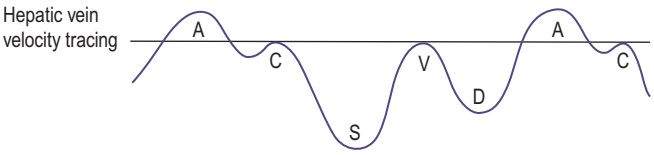


Figure 12.27 Line drawing of a normal hepatic venous spectral Doppler waveform demonstrating the A, C, S, V and D waves. See text for full explanation. (From Allan PL, Dubbins PA, Pozniak MA, McDicken WN. Clinical Doppler Ultrasound. Churchill Livingstone, Edinburgh, 2001.)

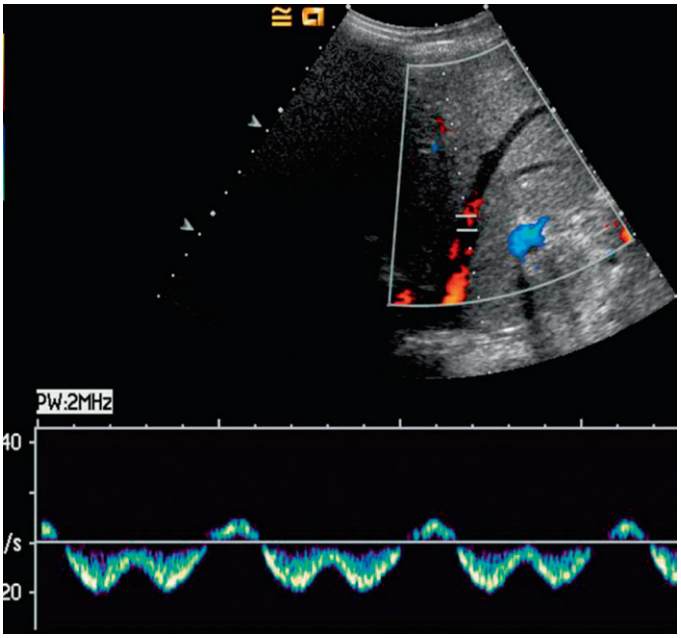


Figure 12.28 Normal triphasic waveform of a hepatic vein.

and RHV have also been documented, the former being more common and seen in 12% of the population while only 3% have a right marginal vein. Absence of one of the three main hepatic veins is relatively uncommon and seen in less than 10% of people, although typically when this is the case variations of accessory veins draining the respective lobes are found.

Hepatic venous waveforms

The hepatic veins normally demonstrate a triphasic waveform pattern reflecting pressure from the right atrium owing to the thin venous walls and varying also with the respiratory cycle. The spectral waveform in the normal hepatic vein is similar to that seen in the internal jugular vein, being triphasic. There is a retrograde 'A' wave due to right atrial contraction that results in retrograde flow down the IVC into the hepatic veins. At the end of right atrial contraction, at the beginning of ventricular systole, the tricuspid valve closes, producing the 'C' wave. During ventricular systole the right atrium continues to fill, producing the 'S' wave with antegrade flow towards the heart. At the end of atrial filling antegrade flow decreases and can briefly reverse, resulting in a 'V' wave. During ventricular diastole the tricuspid valve opens and both the right atrium and ventricle fill, resulting in antegrade flow towards the heart seen as a 'D' wave (Figs 12.27 and 12.28). The cycle is then repeated. However, there is a large amount of variability in the hepatic venous trace depending on cardiac status, heart rate, liver disease, hydration and distance from the right atrium.[54]

It has been documented that this waveform changes with chronic liver disease, where the increased liver fibrosis reduces the elasticity of the liver, thereby damping the triphasic waveform and resulting in either a biphasic or monophasic wave pattern (Figs 12.29 and 12.30).

Studies have shown that the progression from a triphasic to a monophasic waveform is associated with increasing severity of liver fibrosis. However, this was not specific and overlap was found between the mild, moderate and severe fibrosis groups. It can therefore only be inferred that an abnormal trace is likely to be associated with more severe chronic liver disease.[40,55,56]

Hepatic venous outflow obstruction

Thrombosis of the hepatic veins is a relatively rare occurrence known as Budd–Chiari syndrome which is characterised by

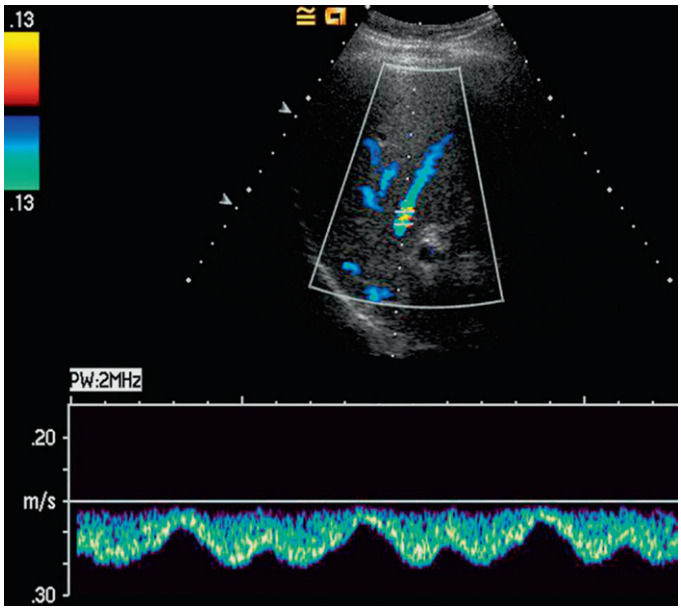


Figure 12.29 Damping of the normal waveform in a patient with chronic liver disease; this is depicted as a biphasic waveform pattern.

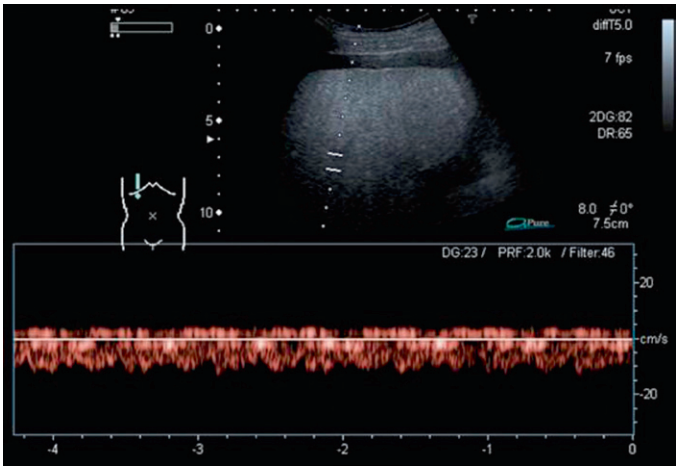


Figure 12.30 Further damping of the normal triphasic waveform in a patient with moderately severe fibrosis secondary to hepatitis C virus related liver disease; there is now only a monophasic trace.

occlusion of the lumina of the hepatic veins with or without involvement of the IVC.

Budd–Chiari syndrome can be either primary or secondary; the primary type is caused by thrombosis or intrinsic luminal web, and the secondary type is caused by tumour invasion or extraluminal compression.

The aetiology of Budd–Chiari syndrome varies and is most commonly idiopathic (66%) although there is an increased risk with blood coagulopathies, such as polycythaemia rubra vera, chronic leukaemia, anaemia and paroxysmal nocturnal haemoglobinuria. Other benign causes include the oral contraceptive pill, pregnancy and congenital abnormalities, particularly with obstructing membranes. Extension of tumours into the hepatic veins can also be caused by tumour extension typically seen with hepatocellular carcinoma (HCC), renal cell carcinoma and adrenocortical carcinoma.

Membranous obstruction of the suprahepatic IVC (IVC diaphragm) is a common cause of Budd–Chiari syndrome in the Indian subcontinent, Asia and southern Africa.

In the acute phase sonographic assessment demonstrates a large, swollen and heterogeneous liver, and ascites is invariably present. Haemorrhagic infarction may occur, leading to a region of altered echotexture. The caudate lobe typically appears normal and is spared owing to its direct venous drainage into the IVC from emissary veins. However, in the chronic phase it may become enlarged owing to the increased blood flow.

The hepatic veins may be partially or completely occluded by thrombus, or demonstrate stenosis with proximal dilatation (Fig. 12.31). These occluded hepatic veins also cause intrahepatic collateral channels to open up, which appear as tubular anechoic structures extending from the hepatic vein to other hepatic or portal venous branches or to the liver surface where they anastomose with the systemic capsular vessels giving a 'spider's web' appearance.[57] Colour and spectral Doppler sonography is useful in determining whether there is complete occlusion, and in cases of incomplete obstruction there will be alteration in the phasicity of the hepatic venous waveform towards a monophasic pattern. Reversed flow in one or more of the hepatic veins is pathognomonic. Turbulent flow or to-and-fro pattern has also been documented.[58,59] Portal venous flow may be slowed, reversed or absent in thrombosis. The IVC is often involved in Budd–Chiari syndrome and may show reversed flow in its lower portion or normal antegrade flow with loss of phasic oscillation.

Ultrasound contrast agents may be useful in assessing venous patency in difficult cases.

Chronically the affected areas of the liver in Budd–Chiari syndrome atrophy due to extensive fibrosis, increasing in echogenicity, as progression to cirrhosis occurs with the development of signs of portal hypertension. There is accompanying enlargement of the caudate lobe and adjacent part of the central part of the right lobe and medial segment of the left lobe.

Hepatic veno-occlusive disease

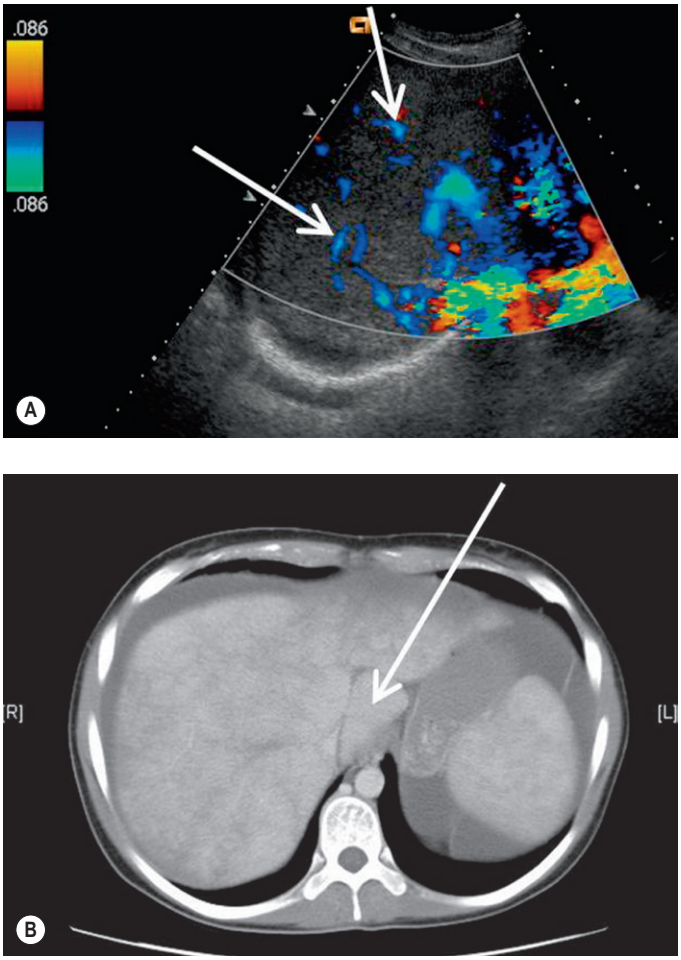
This is a disease that is caused by progressive occlusion of the small hepatic venules at the sinusoidal level. It is commonly caused iatrogenically by hepatic irradiation and chemotherapy, especially in patients undergoing bone marrow transplantation.[60] These patients demonstrate clinical symptoms that are indistinguishable from Budd–Chiari syndrome. However, in these cases, Doppler sonography shows normal appearing hepatic veins and IVC with antegrade flow. It is the portal vein that may demonstrate an abnormality where the flow may be reversed (Fig. 12.32) or show phases of antegrade and retrograde flow ('to and fro'). This can also be suggested by a reduction in the flow/velocity of the portal vein. However, owing to the variation of portal vein flow, a baseline measurement needs to be performed in each individual.

Hepatic venous waveforms in cardiac and pulmonary disease

Alteration of the hepatic venous waveform occurs in many cardiac and pulmonary diseases.

Dilatation of the hepatic veins is a common finding in both conditions with increase in the retrograde flow which is most commonly due to tricuspid regurgitation (TR) (Fig. 12.33). In mild TR there is increase in the V wave with attenuation of the S wave. In severe TR there is fusion of the S and V waves with systolic reversal of the S wave.

In right ventricular dysfunction, due to pulmonary and cardiac disease, the A wave amplitude may be increased due to right atrial hypertrophy, which with further deterioration is accompanied by attenuation of the S wave followed by tricuspid regurgitative changes.



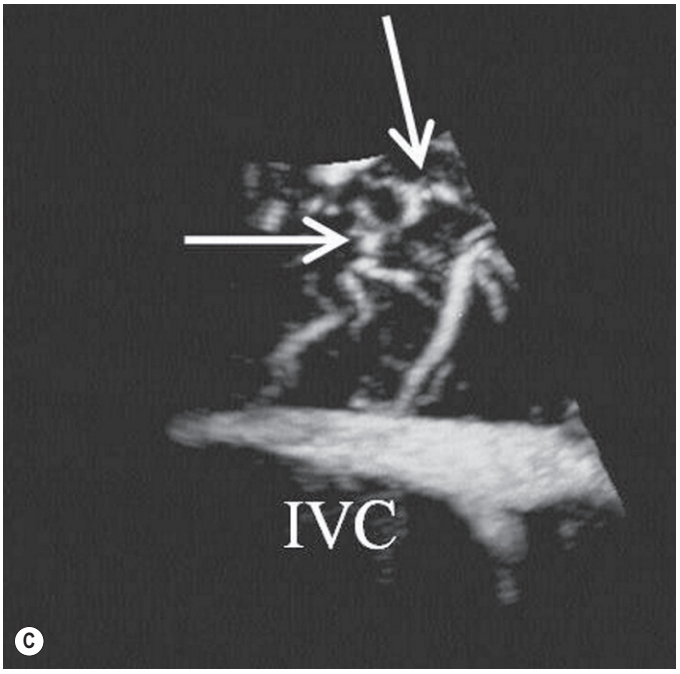
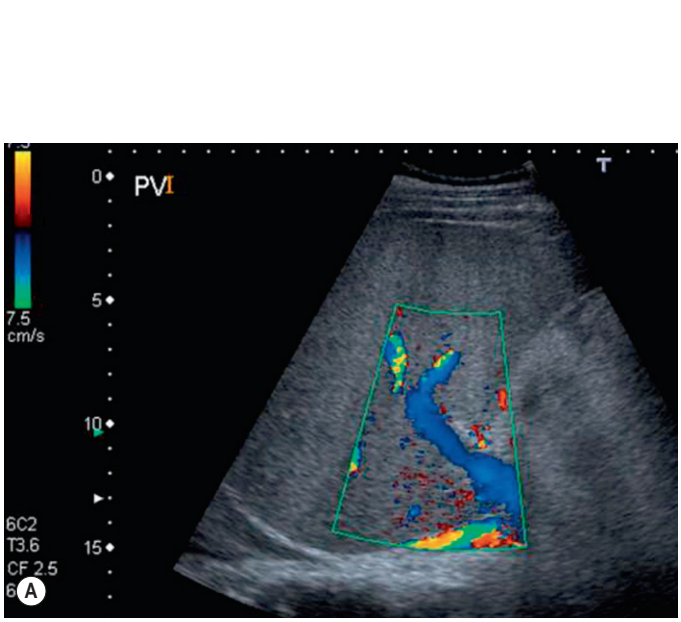


Figure 12.31 **Budd–Chiari syndrome. A:** A 'spider's web' of collateral vessels (arrows) is seen in the right lobe of the liver. **B:** Computed tomography shows heterogeneous enhancement of the liver with no patent hepatic veins seen. The caudate lobe (arrow) enhances normally due to its venous drainage directly into the inferior vena cava. **C:** In another patient 3D reconstruction of the collateral veins has been performed following intravenous ultrasound microbubbles. This shows multiple intrahepatic collateral vessels (arrows) which drain into the inferior vena cava (IVC).



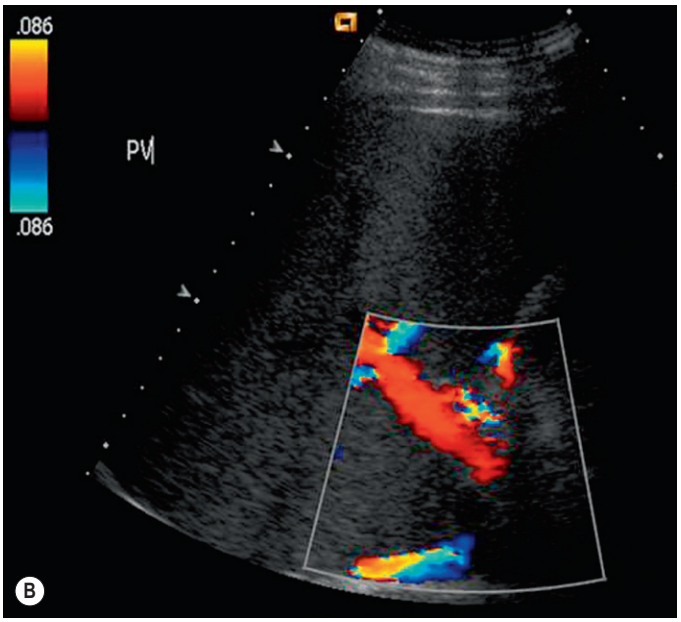


Figure 12.32 **Veno-occlusive disease following bone marrow transplantation. A:** The main portal vein is patent but shows reverse flow. All three main hepatic veins were also patent (not shown). **B:** Following treatment the portal venous flow normalises in direction.

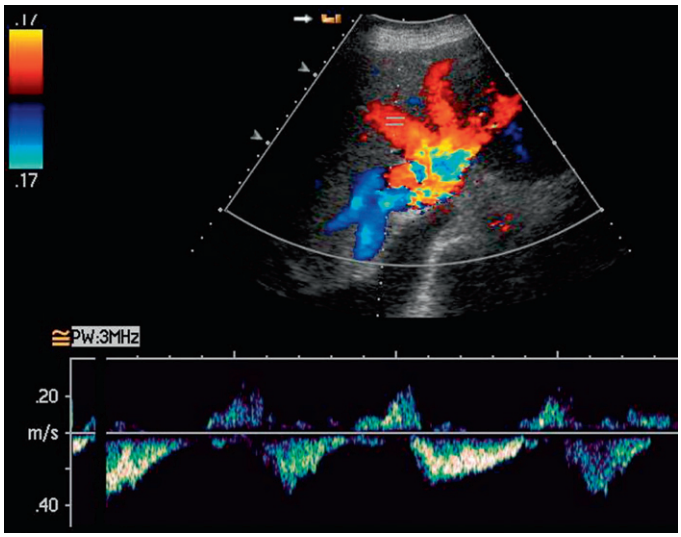


Figure 12.33 Doppler trace showing tricuspid regurgitation.

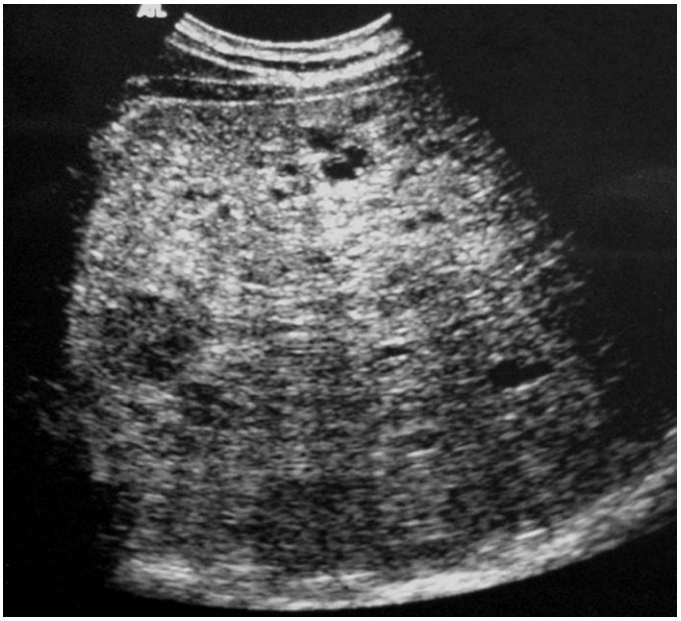


Figure 12.34 Multiple hypoechoic and hyperechoic rounded lesions within the liver with minimal vascularity. These features are non-specific but biopsy revealed peliosis hepatis. (Courtesy of Dr Pilcher.)

'Cannon' A waves are seen in atrioventricular dissociation (complete heart block) due to atrial systole against a closed tricuspid valve. In atrial fibrillation the A wave is lost.

Hepatic vein transit times

The advent of contrast ultrasound has allowed functional assessment of the vascularity of the liver. These microbubbles can be used as a tracer and the theory is that in the presence of chronic liver disease or when there is alteration of the blood flow through the liver, for example in patients with metastases, this causes arteriovenous shunting. Therefore, the time taken for a contrast agent to travel through the liver parenchyma and 'arrive' in the hepatic vein will be shortened in contrast to normal healthy individuals. There has been much research into utilising this technique, particularly with staging and grading chronic liver disease as well as detecting micrometastases not visible ultrasonically.[61–63] These studies have shown a significant decrease in hepatic vein transit time (HVTT) in patient with cirrhosis and there is also an appreciable decrease in distinguishing patients with mild from moderately severe hepatitis and fibrosis. It has been documented that different microbubble agents, however, demonstrate differing HVTT and limits of normality need to be individualised according to the agent used.[64] An earlier arrival time has also been shown to occur in patients with metastases.[65]

Peliosis hepatis

This is a rare disorder where blood-filled cavities of varying sizes (mm to cm) develop within the liver. It is different from haemangiomas where there are portal tracts and stroma within these blood-filled spaces. The diagnosis can only be confirmed histologically. There is an association with immunosuppressed patients and those taking anabolic steroids. Doppler sonography is non-specific and may show single or multiple masses of varying and heterogeneous echogenicity[66] (Fig. 12.34). The assessment with contrast ultrasound has not been fully described and anecdotally the lesion can demonstrate mild enhancement but appears bland.

REFERENCES

1. Couinaud C. Liver anatomy: portal (and suprahepatic) or biliary segmentation. Dig Surg 1999;16(6):459–467.
2. Hosoki T, Arisawa J, Marukawa T, et al. Portal blood flow in congestive heart failure: pulsed duplex sonographic findings. Radiology 1990;17:733–736.
3. Wachsberg R, Needleman L, Wilson DJ. Portal vein pulsatility in normal and cirrhotic adults without cardiac disease. J Clin Ultrasound 1995;23:3–15.
4. Freeny PC. Portal hypertension and hepatic veno-occlusive disease. Radiology 1986;4:1–10.
5. Vorobioff J, Bredfeldt JE, Groszmann RJ. Increased blood flow through the portal system in cirrhotic rats. Gastroenterology 1984;87:1120–1126.
6. Benoit JN, Womack WA, Hernandez L, Granger DN. 'Forward' and 'backward' flow mechanisms of portal hypertension. Relative contribution in the rat model of portal vein stenosis. Gastroenterology 1985;89:1092–1096.
7. Sikuler E, Groszmann RJ. Interaction of flow and resistance in maintenance of portal hypertension in a rat model. Am J Physiol 1986;250:205–212.
8. Gorg C, Riera-Knorrenschild J, Dietrich J. Pictorial review: colour Doppler ultrasound flow patterns in the portal venous system. Br J Radiol 2002;75:919–929.
9. Zweibel WJ. Sonographic diagnosis of hepatic vascular disorders. Semin Ultrasound CT MRI 1995;16:34–48.
10. Moriyasu F, Nishida O, Ban N, et al. Congestion index of the portal vein. AJR Am J Roentgenol 1986;146:735–739.
11. Rector WG, Hoefs JC, Hossack KF, Everson GT. Hepatofugal flow in cirrhosis: observations on hepatic haemodynamics and the nature of arterioportal communications. Hepatology 1988;8:16–20.
12. Gaiani S, Bolondi L, Li Bassi S, et al. Prevalence of spontaneous hepatofugal portal flow in liver cirrhosis. Clinical and endoscopic correlation in 228 patients. Gastroenterology 1991;100:160–167.
13. Ohnishi K, Saito M, Sato S, et al. Direction of splenic venous flow assessed by pulsed Doppler flowmetry in patients with a large splenorenal shunt. Relation to spontaneous hepatic encephalopathy. Gastroenterology 1985;89:180–185.
14. Bolondi L, Gandolfi L, Arienti V, et al. Ultrasonography in the diagnosis of portal hypertension: diminished response of portal vessels to respiration. Radiology 1982;142:167–172.
15. Bolondi L, Mazziotti A, Arienti V, et al. Ultrasonographic study of portal venous system in portal hypertension and other portosystemic shunt operation. Surgery 1984;95:261–269.
16. Cottone M, Sciarrino E, Marceno MP, et al. Ultrasound in the screening of patients with cirrhosis with large varices. BMJ 1983;533:287.
17. Lafortune M, Patriquin H, Pomier G, et al. Haemodynamic changes in portal circulation after portosystemic shunts: use of duplex sonography in 43 patients. AJR Am J Roentgenol 1987 149:701–706.
18. Subramanyam B, Balthazar E, Madamba M, et al. Sonography of

portosystemic collaterals in portal hypertension. Radiology 1983;146:161–166.
19. Subramanyam B, Balthazar E, Raghavenadra B, Lefleur R. Sonographic evaluation of patients with portal hypertension. Am J Gastroenterol 1983;78:369–373.
20. Takayasu K, Moriyama N, Shima Y, et al. Sonographic detection of large spontaneous shunts and its clinical significance. Br J Radiol 1984;57:565–570.
21. Schmassmann A, Zuber M, Livers M, et al. Recurrent bleeding after variceal haemorrhage: Predictive value of portal venous duplex sonography. AJR Am J Roentgenol 1993;160:41–47.
22. Owen A, Stanley A, Vijayananthan A, Moss J. The transjugular intrahepatic portosystemic shunt (TIPS). Clin Radiol 2009;64:664–674.
23. Khan S, Tudur S, Williamson P, et al. Portosystemic shunts versus endoscopic therapy for variceal bleeding in patients with cirrhosis. Cochrane Database Syst Rev 2006; CD000553.
24. Saab S, Nieto J, Ly D, et al. TIPS versus paracentesis for cirrhotic patients with refractory ascites. Cochrane Database Syst Rev 2004; CD004889.
25. Tripathi D, Helmy A, Macbeth K, et al. Ten years' follow-up of 472 patients following transjugular intrahepatic portosystemic stent-shunt insertion at a single centre. Eur J Gastroenterol Hepatol 2004;16:9–18.
26. Kanterman R, Darcy M, Middleton W, et al. Doppler sonography findings associated with trans-jugular intrahepatic portosystemic shunt malfunction. AJR Am J Roentgenol 1997;168:467–472.
27. Surratt R, Middleton W, Darcy M, et al. Morphological and hemodynamic findings at sonography before and after creation of a trans-jugular intrahepatic portosystemic shunt. AJR Am J Roentgenol 1993;160:627–630.
28. Dodd G III, Zajko A, Orons P, et al. Detection of trans-jugular intrahepatic portosystemic shunt dysfunction: value of duplex Doppler sonography. AJR Am J Roentgenol 1995;164:1119–1124.
29. Carr C, Tuite C, Soulen M et al. Role of ultrasound surveillance of trans-jugular intrahepatic portosystemic shunts in the covered stent era. J Vasc Interv Radiol 2006;17:1297–1305.
30. Middleton W, Teefey S, Darcy M. Doppler evaluation of trans-jugular intrahepatic portosystemic shunts. Ultrasound Q 2003;19:56–70.
31. Uggowitzer MM, Kugler C, Machan L, et al. Value of echo-enhanced Doppler sonography in evaluation of transjugular intrahepatic portosystemic shunts. AJR Am J Roentgenol 1998;170:1041–1046.
32. Furst G, Maims J, Heyer T, et al. Transjugular intrahepatic portosystemic shunts: improved evaluation with echo-enhanced color Doppler sonography, power Doppler sonography, and spectral duplex sonography. AJR Am J Roentgenol 1998;170:1047–1054.
33. Belli L, Romani F, Sansalone CV, et al. Portal vein thrombosis in cirrhotics. A retrospective analysis. Ann Surg 1986;203:286–291.
34. Monarca A, Natangelo R, Tavani E, Azzolini V. Cirrhosis and portal vein thrombosis. Gastroenterology 1986;90:509.
35. Nonami T, Yokoyama I, Iwatsuki S, Starzi TE. The incidence of portal vein thrombosis at liver transplantation. Hepatology 1992;16: 1195–1198.
36. Amitrano L, Guardascione MA, Brancaccio V, et al. Risk factors and clinical presentation of portal vein thrombosis in patients with liver cirrhosis. J Hepatol 2004;40:736–741.
37. Hiatt J, Gabbay J, Busuttil R. Surgical anatomy of the hepatic arteries in 1000 cases. Ann Surg 1994;220(1):50–52.
38. Rygaard H, Forrest M, Mygind T, Baden H. Anatomic variants of the hepatic arteries. Acta Radiol Diagn (Stockh) 1986;27(4):425–427.
39. Sudhamashu KC, Matsutani S, Maruyama H, et al. Doppler study of hepatic veins in cirrhotic patients. Correlation with liver dysfunction and hepatic haemodynamics. World J Gastroenterol 2006;12:5853–5858.
40. Lim AK, Patel N, Eckersley RJ, et al. Can Doppler ultrasonography assess the severity of chronic liver disease? Am J Roentgenol 2005;184:1848–1853.
41. Piscaglia F, Gaiani S, Calderoni D, et al. Influence of liver fibrosis on hepatic artery Doppler resistance index in chronic hepatitis of viral origin. Scand J Gastroenterol 2001;36:647–652.
42. Walsh KM, Leen E, MacSween RN, Morris AJ. Hepatic blood flow changes in chronic hepatitis C measured by duplex Doppler color sonography: relationship to histological features. Dig Dis Sci 1998;43:2584–2590.
43. Piscaglia F, Gaiani S, Zironi G, et al. Intra- and extrahepatic arterial resistances in chronic hepatitis and liver cirrhosis. Ultrasound Med Biol 1997;23:675–682.
44. Mostbeck GH, Gossinger HD, Mallek R, et al. Effect of heart rate on Doppler measurements of resistive index in renal arteries. Radiology 1990;175:511–513.
45. Falkoff GE, Taylor KJ, Morse S. Hepatic artery pseudo-aneurysm. Diagnosis with real-time and pulsed Doppler ultrasound. Radiology 1986;158:55–56.
46. Khalid SK, Garcia-Tsao G. Hepatic vascular malformations in hereditary haemorrhagic telangiectasia. Semin Liver Dis 2008;28:247–258.
47. Garcia-Tsao G. Liver involvement in hereditary haemorrhagic telangiectasia (HHT). J Hepatol 2007 46:499–507.
48. Sabbà C, Pompili M. Review article: the hepatic manifestations of hereditary haemorrhagic telangiectasia. Aliment Pharmacol Ther 2008;28(5):523–533.
49. Buscarini E, Manfredi G, Zambelli A. Doppler ultrasonography for the diagnosis of liver vascular malformations in hereditary hemorrhagic telangiectasia. J Hepatol 2008;49:658–659.
50. Ocran K, Rickes S, Heukamp I, Wermke W. Sonographic findings in hepatic involvement of hereditary haemorrhagic telangiectasia. Ultraschall Med 2004;25:191–194.
51. Caselitz M, Bahr MJ, Bleck JS, et al. Sonographic criteria for the diagnosis of hepatic involvement in hereditary haemorrhagic telangiectasia (HHT). Hepatology 2003;37:1139–1146.
52. Buonamico P, Suppressa P, Lenato GM, et al. Liver involvement in a large cohort of patients with hereditary haemorrhagic telangiectasia: echo-color-Doppler vs multislice computed tomography study. J Hepatol 2008;48:811–820.
53. Cosgrove DO, Arger PH, Coleman BG. Ultrasonic anatomy of hepatic veins. J Clin Ultrasound 1987;15:231–235.
54. Shapiro RS, Winsberg F, Maldjian C, Stancato-Pasik A. Variability of hepatic vein Doppler tracings in normal subjects. J Ultrasound Med 1993;12:701–703.
55. Bolondi L, Li Bassi S, Gaiani S, et al. Liver cirrhosis: changes of Doppler waveform of hepatic veins. Radiology 1991;178:513–516.
56. Colli A, Cocciolo M, Riva C, et al. Abnormalities of Doppler waveform of the hepatic veins in patients with chronic liver disease: correlation with histologic findings. AJR Am J Roentgenol 1994;162:833–837.
57. Menu Y, Alison D, Lorphelin J-M, et al. Budd-Chiari syndrome: Ultrasound evaluation. Radiology 1985:157:761–764.
58. Hosoki T, Kuroda C, Tokunaga K, et al. Hepatic venous outflow obstruction: evaluation with pulsed Duplex sonography. Radiology 1989;170:733–737.
59. Millener P, Grant EG, Rose S, et al. Color Doppler imaging findings in patients with Budd Chiari syndrome. Correlation with venographic findings. AJR Am J Roentgenol 1993;161:307–312.
60. Brown BP, Abu-Youssef M, Farner R, et al. Doppler sonography: a non-invasive method for evaluation of hepatic veno-occlusive disease. AJR Am J Roentgenol 1990;154:721–724.
61. Lim AK, Taylor-Robinson SD, Patel N, et al. Hepatic vein transit times of an ultrasound microbubble can predict disease severity non-invasively in patients with hepatitis C. Gut 2005;54:128–133.
62. Blomley MJ, Lim AK, Harvey CJ, et al. Liver microbubble transit time compared with histology in diffuse liver disease: a cross-sectional study. Gut 2003;52:1188–1193.
63. Harvey CJ, Blomley M. Imaging of liver haemodynamics in patients at risk for hepatic metastatic disease. Br J Radiol 2005;78:103–104.
64. Lim AK, Patel N, Eckersley RJ, et al. Hepatic vein transit times using SonoVue: a comparative study with Levovist. Radiology 2006;240:130–135.
65. Blomley M, Albrecht T, Cosgrove DO, et al. Liver vascular transit time analyzed with dynamic hepatic venography with bolus injections of an US contrast agent: early experience in seven patients with metastases. Radiology 1998;209:862–866.
66. Lloyd RL, Lyons EA, Levi CS, et al. The sonographic appearance of peliosis hepatis. J Ultrasound Med 1982;1:293.

CHAPTER

13 Liver transplantation

Suzanne M. Ryan, Maria E.K. Sellars and Paul S. Sidhu

INTRODUCTION 199

INDICATIONS FOR LIVER TRANSPLANTATION 199

PRE-TRANSPLANT ULTRASOUND 199
Acute liver failure 199
Chronic liver disease 200
Liver parenchyma 200
Hepatocellular carcinoma (HCC) 200
Other malignancies 201
Preoperative vascular assessment 201
Portal vein 201
Hepatic veins 202
Hepatic artery 202
Portal-venous shunts 203
Assessment of living related donors 203
Liver volume assessment 203

SURGICAL TECHNIQUES 204

EARLY POSTOPERATIVE ULTRASOUND 204
Normal postoperative ultrasound 205
Abnormal postoperative ultrasound 205
Vascular complications 205
Non-vascular complications 211
Miscellaneous complications 213
Complications of split liver transplantation 213

ROLE OF ULTRASOUND IN LONG-TERM FOLLOW-UP 213
Non-vascular complications 213
Post-transplant lymphoproliferative disease (PTLD) 213
Renal complications 214
Graft versus host disease 215
Rejection 215
Infection 215
Budd–Chiari syndrome 215
Disease recurrence 215

PAEDIATRIC LIVER TRANSPLANTATION 216
Introduction 216
Clinical indications for paediatric liver transplantation 216
Chronic liver disease 216
Acute liver failure (ALF) 217
Metabolic liver disease 217
Portal hypertension (PHT) 217
Liver tumours 217
Surgical techniques for paediatric liver transplantation 217
Auxiliary liver transplantation 217
Reduced liver transplantation 217
Split liver transplantation 217
Ultrasound evaluation of the paediatric transplant liver 217
Ultrasound of complications of paediatric liver transplantation 219
Vascular complications 219
Biliary complications 220
Diaphragmatic function 221
Small bowel complications 221
General surgical complications 221
Post-transplant lymphoproliferative disease 221
Recurrent disease in children 221
Hepatoblastoma 221
Hepatocellular carcinoma 222

INTRODUCTION

Liver transplantation is an effective treatment for a variety of irreversible acute and chronic liver diseases. With advances in perioperative techniques, immunosuppressive agents, and postoperative care, liver transplantation has 1-year survival figures in excess of 85%.[1] Liver transplantation is offered for a wider range of diseases and to older patients than previously. Imaging and in particular ultrasound has transformed the care of patients undergoing transplantation, with the ready availability of bedside ultrasound imaging providing an instant answer to an often non-specific clinical scenario. The advent of colour Doppler ultrasound (CDUS) in particular has considerably aided the management of vascular abnormalities associated with liver transplantation. The addition of microbubble contrast agents has further strengthened the usefulness of ultrasound.[2]

This chapter will illustrate the role of ultrasound in the pre-transplant and short- and long-term postoperative imaging of the liver in the adult patient. In addition, aspects of ultrasound in relation to paediatric liver transplantation will be discussed.

INDICATIONS FOR LIVER TRANSPLANTATION

The indications for liver transplantation include end-stage acute liver failure, advanced chronic liver disease, inherited metabolic disorders (where function of the native liver is inadequate), and primary hepatic malignancy confined to the liver, incurable by any other treatment (Table 13.1). End-stage chronic liver disease accounts for approximately 70% of all liver transplant activity in Europe and North America but the indications for transplantation have changed over the past ten years, with alcohol-related and viral-related cirrhosis, predominantly hepatitis C, presenting an expanding indication.[3] Patients with early-stage hepatocellular carcinoma (HCC) are accepted for transplantation if they meet the Milan criteria of no lesion greater than 5 cm in diameter and no more than three lesions greater than 3 cm in diameter.[4] Often the bulk of the HCC is down-sized with local chemo-embolisation therapy prior to transplantation.

PRE-TRANSPLANT ULTRASOUND

Pre-transplant imaging plays an important role in identifying contraindications to transplantation, anatomical abnormalities and variants that may alter the surgical approach.

Acute liver failure

Patients presenting with acute liver failure may have a normal liver on ultrasound, or may present with a small or rapidly shrinking

Table 13.1 Indications for liver transplantation in adults

Chronic liver disease	Metabolic	Neoplastic	Acute liver failure	Congenital
• Primary biliary cirrhosis • Primary sclerosing cholangitis • Secondary biliary cirrhosis • Alcohol • Autoimmune hepatitis • Viral hepatitis (HCV, HBV, HDV) • Budd–Chiari syndrome	• Wilson's disease • Haemochromatosis • α_1-Antitrypsin deficiency • Familial hypercholesterolaemia • Familial amyloid polyneuropathy • Primary hyperoxaluria • Cystic fibrosis	• Hepatocellular carcinoma • APUDomas • Epitheloid haemangioendothelioma	• Drugs/toxins • Viral (HAV, HBV) • Wilson's disease	• Polycystic disease • Caroli's disease

liver. Monitoring the size of the liver by ultrasound is a guide to prognosis. Patients presenting with acute liver failure will lack the sequelae of chronic liver disease and portal hypertension: ascites, heterogeneous liver parenchyma, irregular liver margin and an enlarged spleen. Ultrasound serves as a 'screening' tool to exclude unsuspected disease without contributing to the management of the liver failure, to confirm the patency of the portal vein and to exclude extensive liver malignancy. The assessment of the hepatic artery resistive index (RI), a measure of the 'stiffness' of the failing liver, can predict the need for transplantation, as with improved medical management of acute liver failure, recovery without the need for transplantation can be achieved.[5]

Chronic liver disease

The majority of patients referred for liver transplant assessment will have chronic liver disease, the cause of which will already be established. The emphasis in investigating these patients is in recognizing the sequelae of chronic disease and to exclude any contraindications to transplantation.

Liver parenchyma

Cirrhosis can be defined as macronodular, with nodules >3 mm in size, more commonly seen in chronic viral hepatitis, Wilson's disease and α_1-antitrypsin deficiency, or micronodular, with nodules <3 mm in size, as seen in alcoholic cirrhosis, biliary obstruction, haemochromatosis and Budd–Chiari syndrome.[6] However, there is considerable overlap between the two groups, and a mixed pattern is often present. Signs of cirrhosis on ultrasound include a coarse, heterogeneous echotexture with increased reflectivity (Fig. 13.1). There is often relative atrophy of segments IV–VIII, with hypertrophy of the caudate (segment I) and left lateral lobes (segments II and III). The gallbladder wall is often thickened (Fig. 13.2).

The caudate lobe can become enlarged surrounding the inferior vena cava (IVC), which is of relevance in living donor transplantation where the recipient IVC is preserved. Cirrhosis may cause narrowing of the hepatic veins with loss of the normal phasic waveform. Intrahepatic vessels may be indistinct.[7]

Hepatocellular carcinoma (HCC)

Ultrasound is often used to screen for HCC in a high-risk population, and will be used to assess patients waiting for a transplant. Cirrhotic nodules can progress to regenerative, then dysplastic nodules and then on to frank hepatocellular carcinoma, with 80% of hepatocellular lesions arising from this process. The reflectivity of hepatic nodules reflects their histological composition, whereas their detectability on ultrasound depends on the difference in reflectivity between the nodule and the normal liver parenchyma. Nodules can be hyperechoic, isoechoic or hypoechoic on

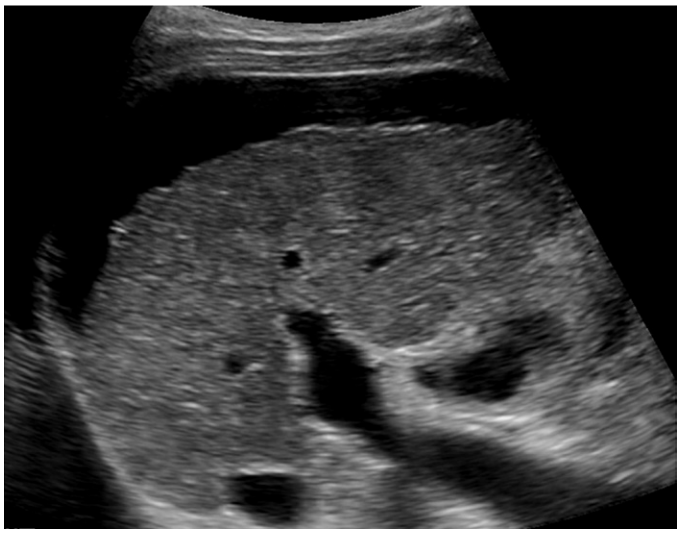


Figure 13.1 Advanced cirrhosis. The liver is surrounded by fluid, the texture is heterogeneous and the surface is irregular.

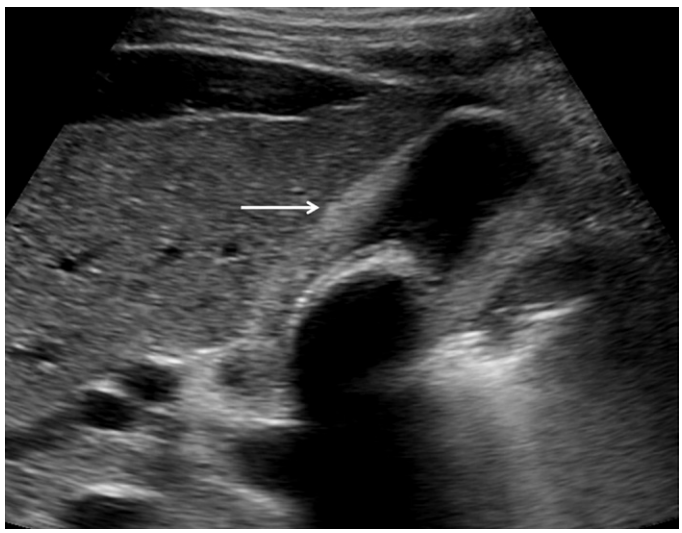


Figure 13.2 Gallbladder wall thickening. The gallbladder wall is markedly thickened (arrow) and there is a large gallstone present in a patient with advanced cirrhosis.

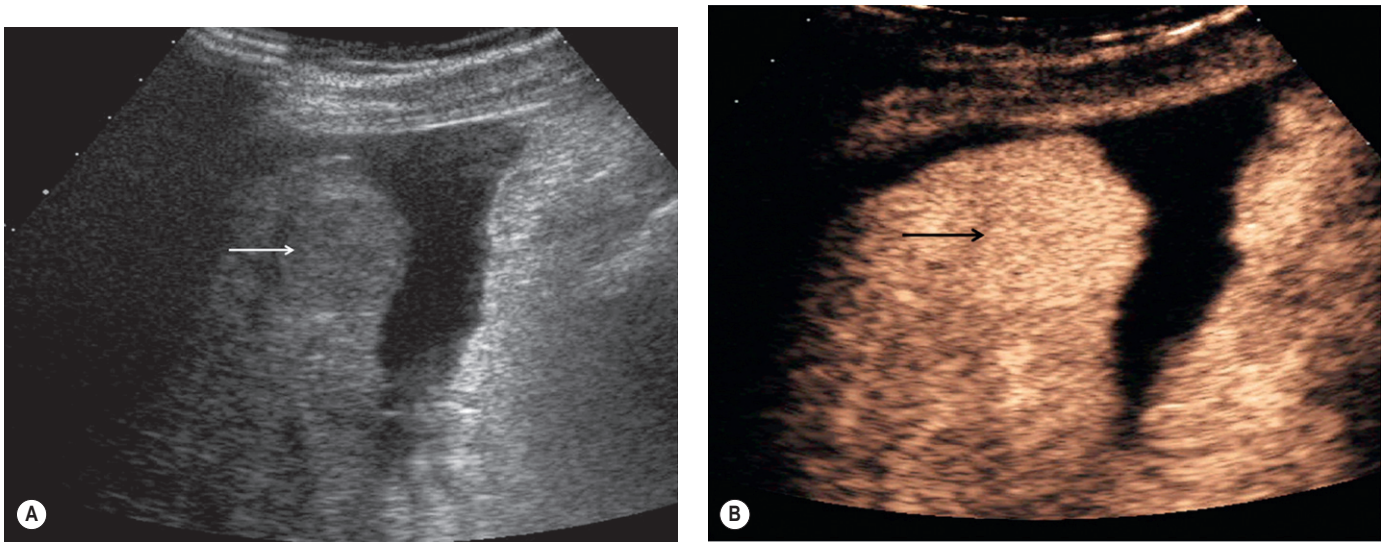


Figure 13.3 Nodule in cirrhosis. A: A 'new' focal lesion of low reflectivity (arrow) is seen in this patient with cirrhosis. **B:** A microbubble contrast-enhanced ultrasound demonstrates that this is a benign regenerative nodule (arrow).

ultrasound, making a definite diagnosis of a de-novo hepatocellular carcinoma on routine B-mode imaging ultrasound unreliable.[8] Hence any new nodule in a patient under surveillance for chronic liver disease should be viewed with suspicion (Fig. 13.3). Ultrasound for early detection of hepatocellular carcinoma in a screening population has sensitivities of 85–100%, specificities of 81–98%, and positive predictive values of 54–78%.[8] The use of contrast-enhanced ultrasound (CEUS) may help to further characterise the lesions.[9,10] The sensitivity and specificity of CEUS in the diagnosis of HCC have been found to be similar to that of contrast-enhanced computed tomography (CECT), with enhancement on the arterial phase, and washout on the portal venous phase, taken as diagnostic for HCC.[11] As many as 25% of lesions <2 cm with arterial enhancement but without venous washout in cirrhotic liver remain stable or regress over time and are not HCC.[12]

Other malignancies

Cholangiocarcinoma is seen most commonly as a consequence of primary sclerosing cholangitis, seen on ultrasound as a hyper- to hypoechoic ill-defined mass, usually in the region of the liver hilum, giving rise to dilated intrahepatic ducts. Proven cholangiocarcinoma is a contraindication to transplantation. Fibrolamellar hepatocellular carcinoma (FLHCC) is a subtype of HCC, has distinct radiographic features and a better prognosis. FLHCC occurs primarily in young adults, without any associated cirrhosis or elevation of alpha-fetoprotein and is relatively slow growing. On ultrasound, FLHCC usually presents as a large solitary mixed reflective mass within a non-cirrhotic liver. Surface lobulations, punctate calcification and a central fibrous scar, similar to that seen in focal nodular hyperplasia, are evident in the majority of patients.[13] These patients may be candidates for either resection or transplantation even with large tumours. The detection of an extrahepatic tumour with or without hepatic metastases excludes the patient from transplantation.

Preoperative vascular assessment

Portal vein

The main portal vein usually bifurcates into the right and left portal veins, readily demonstrated by CDUS. The main portal vein may trifurcate with an early branching pattern in the right hepatic lobe. Ultrasound is not reliable in the delineation of more complex anatomy of the portal vein. Portal venous spectral Doppler ultrasound in normal patients should give a continuous, undulating hepatopetal trace, although there is considerable variation in flow velocity. In the cirrhotic liver, portal hypertension develops, with the increase in pressure accounting for the ensuing complications. Portal velocity and portal venous flow vary inversely with the hepatic venous pressure gradient.[14] Portal hypertension may also result in splenomegaly, which may be readily assessed by ultrasound and monitored over time. Recanalisation of the umbilical vein in the ligamentum teres may be seen, inferring patency of the portal vein with antegrade flow.

Portal venous thrombosis is a common complication of chronic liver disease, occurring in 5–10% of patients with end-stage cirrhosis.[15] Although not an absolute contraindication to transplantation,[16] preoperative detection is vital as the full extent of any thrombus needs to be demonstrated for optimal surgical planning.[17] B-mode imaging of thrombus may show the presence of hyper-reflective material lying within the portal vein, seen as either complete occlusion or a tongue of thrombus with some surrounding flow. Ultrasound is both sensitive and specific in the detection of portal venous thrombosis, with the small proportion of inaccurate investigations attributed to a diminished flow rate.[18] Although CDUS of the portal vein has a reported sensitivity of 87.5–94.0% compared to indirect portography, the use of CEUS improves colour and spectral Doppler signal in difficult cases.[19] Ultrasound is sufficiently accurate, as compared to CECT, in predicting portal venous patency for it to be advocated as the sole means of assessment in patients with no prior surgery.[20] Low flow or reversal of flow in the portal vein may be better documented with CEUS, a reliable indicator of flow direction (Fig. 13.4).[21] Microbubble contrast is reported to improve portal vein visualisation in up to 94% of patients with a suboptimal baseline CDUS examination.[19] In equivocal cases either magnetic resonance venography (MRV) or alternatively indirect portography should be performed, but should rarely be needed with the availability of microbubble contrast enhancement. In patients with HCC, malignant thrombus can be inferred by the presence of enhancement within the thrombus with CEUS whereas absence is more likely in benign thrombus.[22] A venous conduit may be fashioned from the patent superior mesenteric vein (SMV) to the donor graft; demonstration of SMV patency is required when portal vein thrombus is seen. However, this is difficult to achieve even with the use of microbubble enhancement, and indirect portography, CECT or MRV may be necessary.

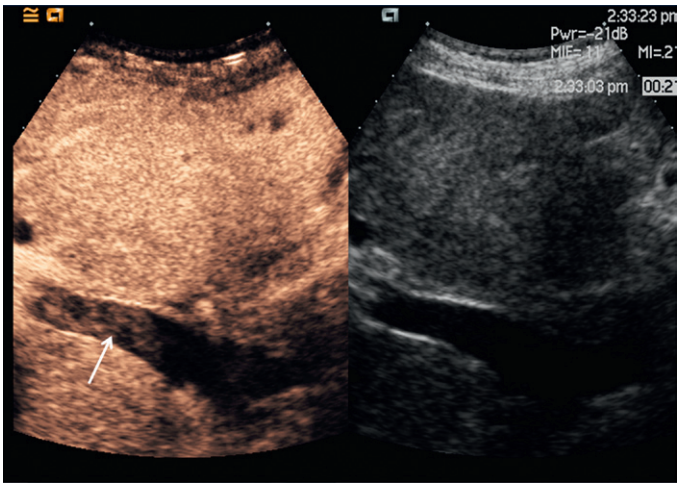


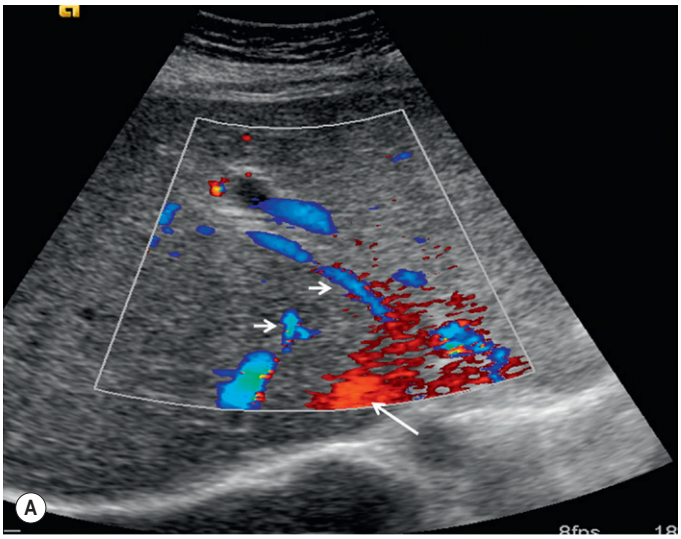
Figure 13.4 Flow reversal in the portal vein. On the baseline colour Doppler ultrasound examination, no flow was seen in the portal vein. With contrast-enhanced ultrasound, contrast is seen to fill the portal vein (arrow) late and flow in a reversed direction. This confirms portal vein patency, important preoperative information.

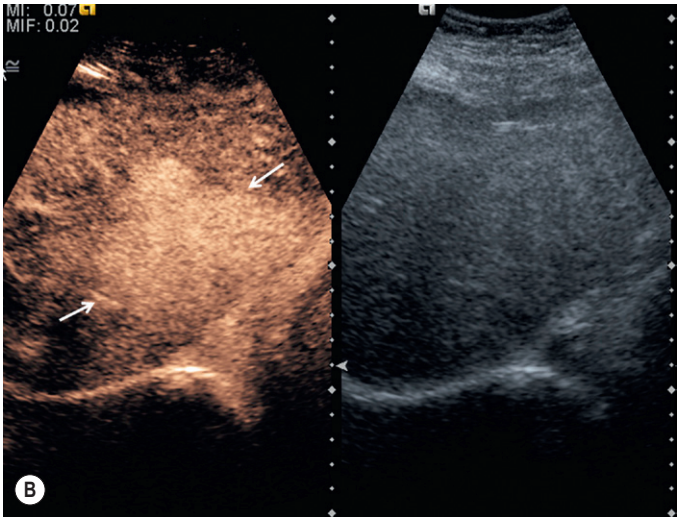
Hepatic veins

The main branches of the hepatic vein drain into the IVC. Accessory right hepatic veins occur in 6% of people and can cause increased bleeding if unrecognised before surgery. The normal hepatic venous waveform is triphasic but loss of pulsatility and damping occurs in conditions of decreased liver compliance (such as cirrhosis) as well as other causes of raised intra-abdominal pressure such as ascites.[23] Occlusion of the venous flow may occur at the level of the post-sinusoidal vein to the IVC and right atrium in Budd–Chiari syndrome, with CDUS assessment of hepatic venous patency usually definite in the normal patient.[24] Non-visualisation of the veins is not diagnostic of occlusion and use of microbubble contrast is reported to improve operator confidence (Fig. 13.5).[16] Hepatic venography remains the reference standard used in diagnosis of hepatic vein occlusion, demonstrating a spider web appearance due to occlusion of the hepatic veins.

Hepatic artery

The spectral waveform pattern of the hepatic artery may give indirect clues to ongoing disease changes. For example, in the presence of cirrhosis, there is a hyper-dynamic hepatic arterial circulation





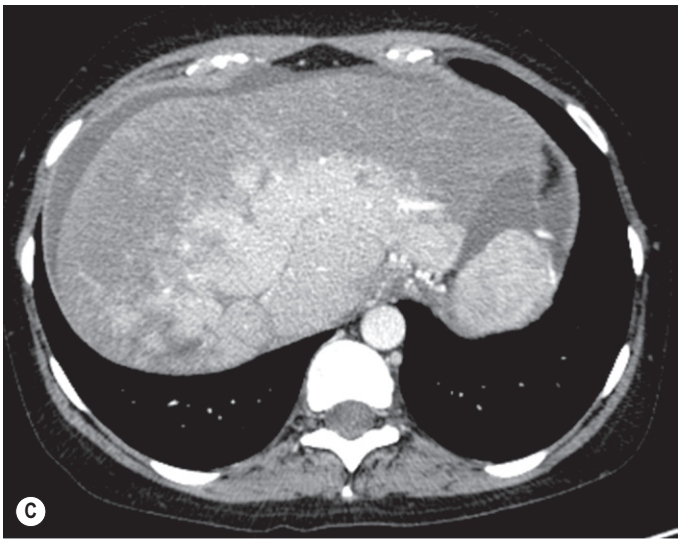


Figure 13.5 Budd–Chiari syndrome. A: The inferior vena cava (long arrow) receives tributaries (short arrows) from the caudate lobe in the patient with Budd–Chiari syndrome. **B:** Contrast-enhanced ultrasound demonstrates the enhancement of the hypertrophied caudate lobe (arrows) with relative poor enhancement of the remainder of the liver. **C:** The equivalent CT image demonstrating poor perfusion of the liver outside the caudate lobe.

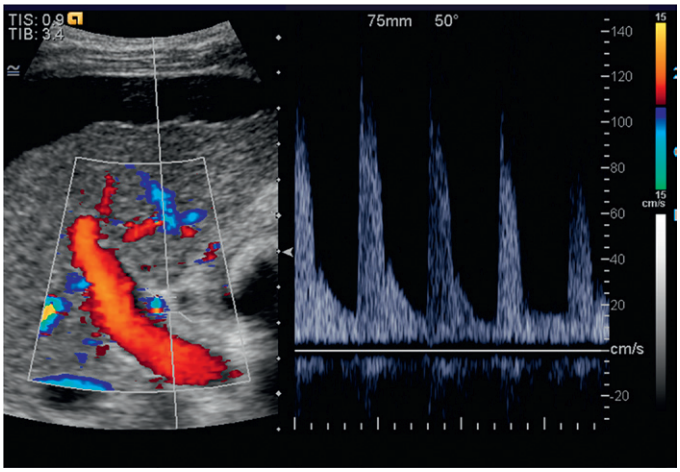


Figure 13.6. Hepatic artery in cirrhosis. The configuration of the spectral Doppler waveform in the hepatic artery of a patient with advanced liver cirrhosis, and a patent portal vein, demonstrates a high resistive index reflecting the increased stiffness of the liver.

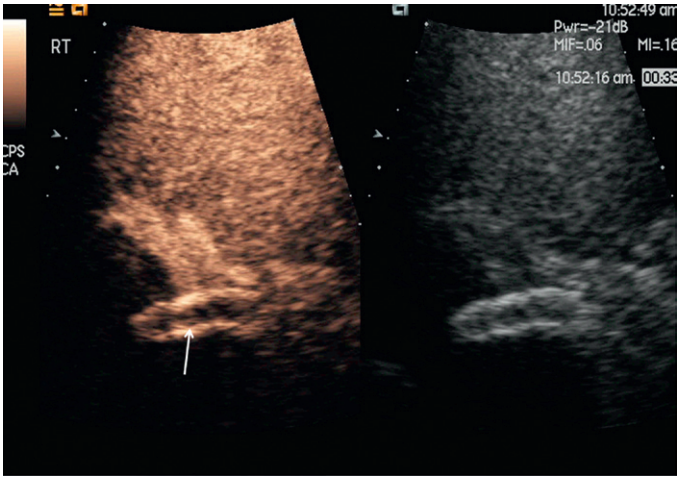


Figure 13.7 Occluded transjugular intrahepatic portosystemic shunt. The reflective walls of the stent are seen with no enhancement of the lumen (arrow) following administration of microbubble contrast.

with a high RI, manifest by low-velocity forward flow in diastole (Fig. 13.6). The RI falls with the development of a portal vein thrombosis. An RI <0.5 is reported to be 100% specific but only 44% sensitive for the development of a portal vein thrombus.[25] With fulminant hepatic failure the RI of the hepatic artery is elevated and mirrors the decline in hepatic function, and may be used as a further parameter to indicate the need for transplantation.[5]

Portal-venous shunts

Transjugular intrahepatic portosystemic (TIPS) shunt, the creation of a shunt between the portal and hepatic venous systems, is a common procedure in the management of variceal haemorrhage and intractable ascites secondary to portal hypertension. This is often a holding measure whilst awaiting transplantation. Unfortunately TIPS stents have a significant rate of stenosis and occlusion and require frequent monitoring. Clearly therefore, non-invasive imaging is preferable in this group of patients.[26] B-mode imaging of the TIPS stent will demonstrate a highly echogenic grid pattern, representing the wall of the stent, through which the internal lumen often cannot be adequately visualised. The exact range of 'normal' flow velocity is disputed. Flow velocities in excess of 200cm/sec should be regarded as suspicious for a narrow stent.[27] Contrast-enhanced ultrasound confirms patency of the TIPS stent and will identify narrowing (Fig. 13.7).[28] A suspected TIPS stenosis by any criteria should be referred for further imaging, either with MRV or transjugular venography. End-to-side portacaval shunts may be demonstrated with some difficulty by ultrasound, but there are no data published regarding the accuracy in comparison with direct venography (Fig. 13.8).[29]

Assessment of living related donors

Ultrasound of the abdomen is routinely performed as part of the radiological work-up of living related donors, with visualisation of all of the solid organs, in order to confirm their normality, and to exclude liver parenchyma changes and unsuspected lesions. The focus of the examination, however, is the hepatic vasculature, with particular attention paid to the anatomy of the hepatic veins, as this has an influence on choice of resection. In addition to ultrasound, donors will routinely undergo dual phase CECT of the liver (portal and hepatic venous phases), thus giving the surgeon the maximum possible information with which to plan surgery.

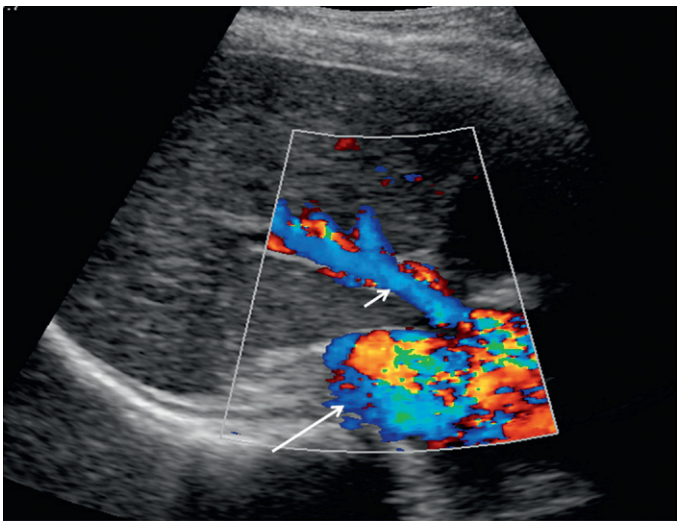


Figure 13.8 Portal vein to inferior vena cava shunt. There is flow reversal in the portal vein (short arrow) with an enlarged inferior vena cava with turbulent flow note (long arrow) in a patient with a surgical portosystemic shunt.

Liver volume assessment

Of critical importance in determining the successful outcome of transplantation, particularly with the advent of split liver grafts in the fields of paediatric and living related donor transplantation, is the size of the graft used. A donor liver should be no less than 50% of the size of the replaced native liver, since below this there is a risk of hepatic failure postoperatively. Conversely, a graft may be up to 20% larger than the explanted liver. Grafts above this size may cause compression of the adjacent vascular structures and be poorly perfused. In all cases, mismatches lead to problems in performing the vascular and biliary anastomoses.[30,31] Ultrasound determination of volume can be performed by measuring the cross-sectional area of the liver as seen on consecutive scans in the sagittal plane at 1 cm intervals and adding these together, a technique that has been shown to be both accurate and reproducible.[32] However, this is a time-consuming procedure and has now been superseded

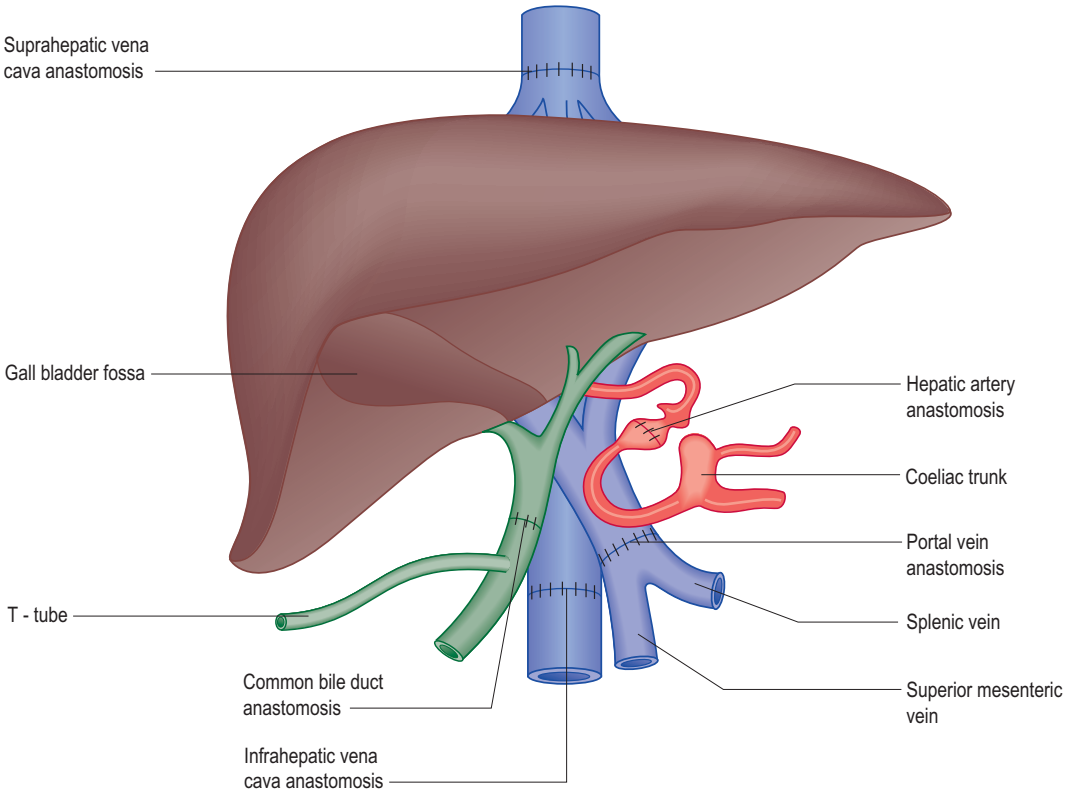


Figure 13.9 Conventional liver transplantation. Donor-recipient sites for vascular and biliary anastomoses. The gallbladder is normally removed. (Modified from Sidhu PS and Baxter GM (eds), Ultrasound of Abdominal Transplantation. Thieme, Stuttgart, 2006.)

by CECT, which is accurate and has the additional capability of calculating segmental volumes.[33]

SURGICAL TECHNIQUES

Prior to performing an ultrasound examination in the post-transplant patient, it is important to know the type of surgical procedure performed, as variations exist, from transplant of the whole liver, transplant of a single liver lobe, or segmental liver transplantation.[34]

In adults the usual procedure is to explant the native liver and replace with a cadaveric allograft, termed orthotopic liver transplantation (OLT). Revascularisation of the allograft requires anastomoses of the hepatic artery, portal vein and IVC, with biliary tract reconstruction performed to establish bile drainage; the gallbladder is normally removed (Fig. 13.9). Many different anastomoses may be performed according to the preference of the surgeon, the anatomy of the donor and recipient vessels, and the underlying disease. Traditionally the anastomoses are 'end-to-end' except with the IVC where a modified technique preserves a stump of the donor IVC and an anastomosis is fashioned with the three hepatic veins ('piggy-back' technique). This technique avoids clamping the IVC during surgery (Fig. 13.10).

The term liver reduction is used when a liver is cut down to the required size for the recipient and the remaining segments are discarded. The technique of liver splitting is an extension of liver reduction and enables a donor liver to be used to transplant two recipients rather than one, the liver usually being split into an extended right lobe and the left lateral segment.[35]

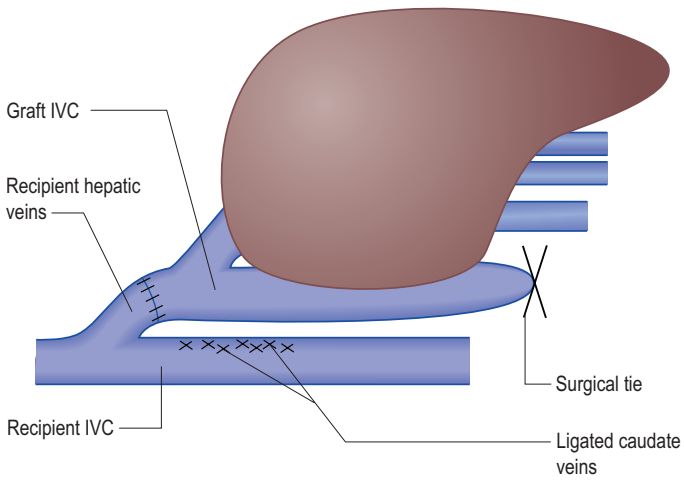


Figure 13.10 'Piggy-back' implantation in liver transplantation. The sagittal section demonstrates the various anastomoses. (Modified from Sidhu PS and Baxter GM (eds), Ultrasound of Abdominal Transplantation. Thieme, Stuttgart, 2006.)

EARLY POSTOPERATIVE ULTRASOUND

Following liver transplantation patients are susceptible to a wide variety of complications that can threaten both allograft and patient survival. Some complications are those seen in any patient who has undergone a major surgical procedure or is receiving



Figure 13.11 Fluid in the falciform ligament. Fluid surrounds the falciform ligament (arrow) in this patient following transplantation.

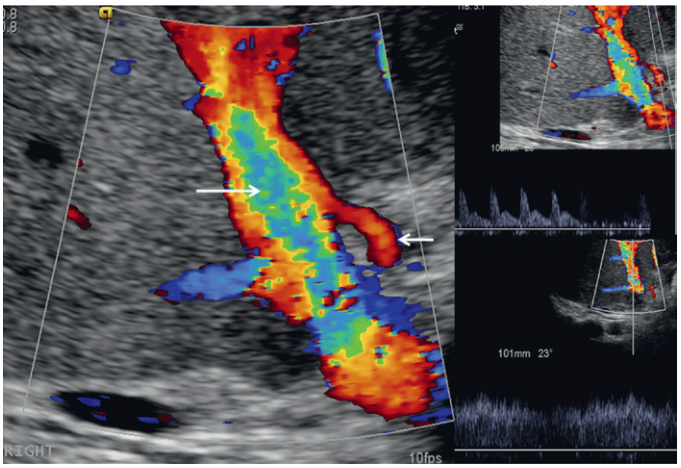


Figure 13.12 Normal post-transplant hepatic artery and portal vein. The normal hepatic artery (short arrow) should return a low resistance spectral pattern with high forward velocity in end diastole with a resistive index of between 0.5 and 0.8. The portal vein (long arrow) should demonstrate a continuous hepatopetal flow with minor respiratory modulation.

immunosuppressive drug therapy, but other complications are unique to the surgical transplantation procedure performed. The main postoperative complications may be grouped into vascular and non-vascular abnormalities.[36,37] Clinical and laboratory findings are often non-specific, making the clinical diagnosis and management of these complications difficult. Ultrasound is normally the first line of evaluation in the post-transplant phase, used when there is clinical evidence of graft dysfunction, or routinely for the early detection of complications before any clinical suspicion of abnormality.

Normal postoperative ultrasound

Following transplantation the liver appears of normal smooth homogeneous reflectivity as would a normal liver in any patient. Often during the procedure haemorrhage occurs or residual ascites may be present, with small amounts of free fluid seen, occasionally tracking along the falciform ligament (Fig. 13.11). The biliary tree is normal, although areobilia may be encountered in patients with a fashioned choledochojejunostomy (Roux-en-Y loop). All the vessels (hepatic artery, portal vein, IVC and hepatic veins) should be patent (Fig. 13.12). Colour and spectral Doppler imaging of the vessels will confirm patency, with interrogation of the main, left and right hepatic artery of importance. The normal hepatic artery should return a low resistance spectral pattern with high forward velocity in end diastole. The RI of a normal hepatic artery is 0.5–0.8. The normal acceleration time (from end diastole to the first systolic peak) is less than 0.08 second. The portal vein should demonstrate a continuous hepatopetal flow with minor respiratory modulation, with the hepatic waveform demonstrating variation during the cardiac cycle.

Abnormal postoperative ultrasound

Vascular complications

Hepatic artery

In the first 2 weeks following liver transplantation, routine colour and spectral Doppler ultrasound plays an important role in the detection of both clinically evident and clinically unsuspected vascular complications, particularly hepatic artery thrombosis (HAT). There is evidence to suggest that routine ultrasound of all the hepatic vessels on the first day following liver transplantation and, subsequently, every 3 days in the early postoperative phase is beneficial.[38] Any clinical change would also prompt immediate ultrasound of the hepatic artery as after transplantation the donor biliary system is entirely dependent on hepatic arterial blood supply, in particular the right hepatic artery.[39] In the early postoperative period, the spectral Doppler waveform can be quite variable, from the presence of high forward diastolic flow to the absence of any flow at all in diastole. Absence or reversal of flow in diastole does not appear to indicate a predisposition for thrombosis in the immediate postoperative period.[40] While absence of any colour or spectral Doppler flow in the hepatic artery can be suggestive of thrombosis in the immediate post-transplant period, other factors may contribute to an undetectable hepatic artery signal.[16] Reperfusion oedema may occur within the graft for up to 72 hours post transplant, leading to an increased RI, and diminished Doppler arterial signal. Furthermore, any cause of oedema or inflammation in the transplant may produce a similar result; viral hepatitis or rejection can cause severe oedema that can markedly damp the hepatic artery waveform.[41]

Hepatic artery thrombosis

The quoted incidence of HAT is 5% of adults and 9–18% of children.[42] HAT is a serious complication with mortality of 50–58%; re-transplantation is often required and even following re-transplantation mortality remains high at 27–30%. Risk factors for HAT include a significant difference in hepatic artery calibre between the donor and recipient, an arterial conduit, excessive cold ischaemia time, ABO blood type incompatibility, cytomegalovirus infection, acute rejection, and previous stenotic lesion of the coeliac axis.[42] Clinically, impending or complete occlusion of the hepatic artery is often indicated by generalised non-specific deterioration of the liver function tests or a biliary leak.[39] If the biliary tree survives the initial ischaemic event, then biliary strictures may develop, particularly at the hilum of the left and right ducts.[43] This in turn may lead to infective complications such as cholangitis and biliary abscess formation. Hepatic abscess formation is also more common with chronic ischaemia.[44]

The normal Doppler waveform in the hepatic artery is of a broad systolic peak, high diastolic velocity and low resistive index. Any

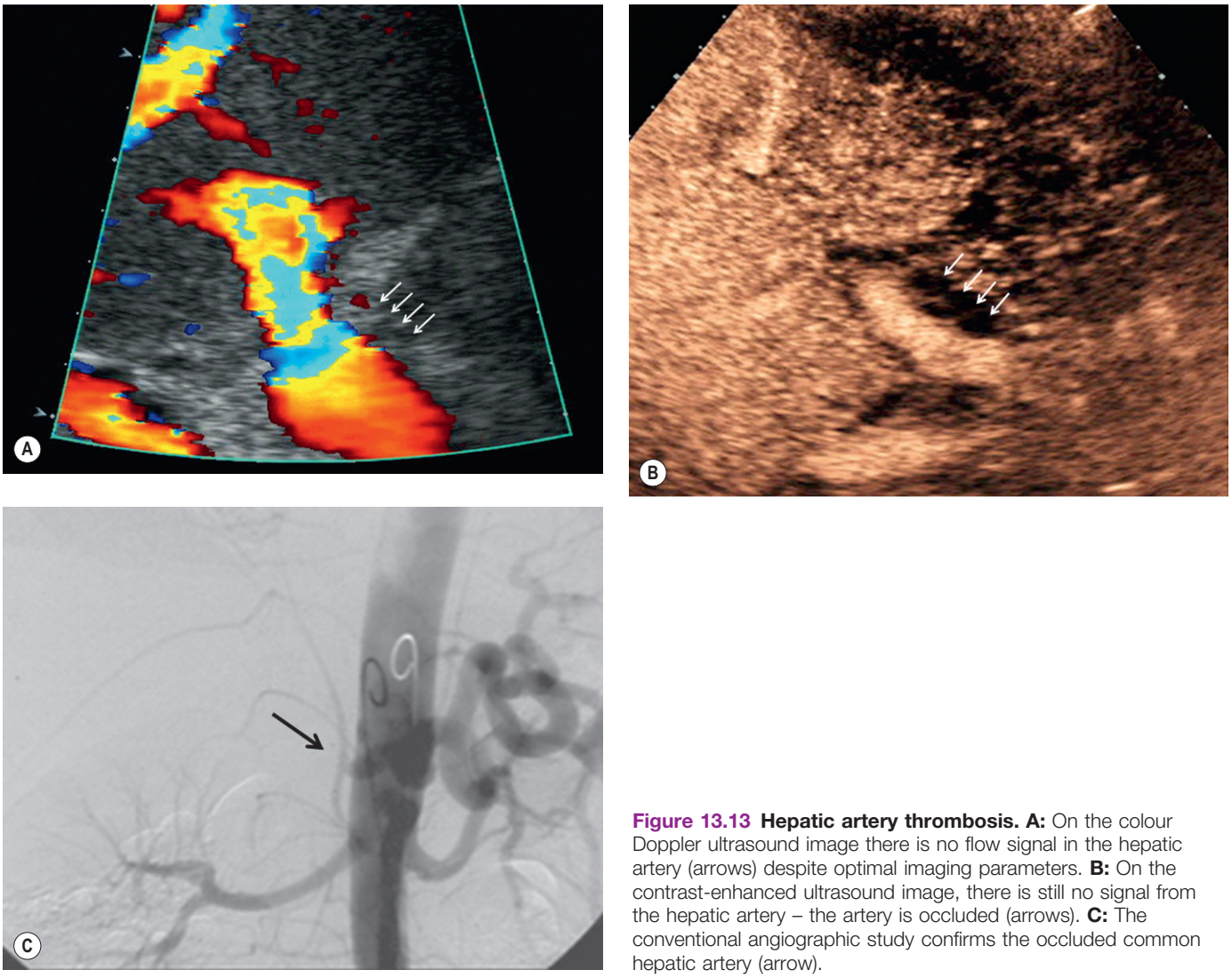


Figure 13.13 Hepatic artery thrombosis. A: On the colour Doppler ultrasound image there is no flow signal in the hepatic artery (arrows) despite optimal imaging parameters. **B:** On the contrast-enhanced ultrasound image, there is still no signal from the hepatic artery – the artery is occluded (arrows). **C:** The conventional angiographic study confirms the occluded common hepatic artery (arrow).

deviation from this pattern must be carefully watched and followed up with serial spectral Doppler ultrasound, with a low threshold to proceeding to CECT angiography or conventional angiography, the gold standard in evaluation of hepatic artery patency.[45] Although the hepatic arterial waveform in the immediate postoperative period varies, impending thrombosis is suggested when a previously normal Doppler waveform proceeds to absent diastolic flow with damping of the systolic peak. This is thought to occur prior to progression to complete loss of the hepatic arterial signal.[46]

The ultrasound features of HAT include an absence of colour and spectral Doppler flow, with a wall 'thump' on Doppler ultrasound. Ultrasound microbubble contrast media, by markedly increasing the intensity of the Doppler signal, may help to prevent false positive diagnosis of HAT (Fig. 13.13).[2,16,46] HAT is most common in the first 6 weeks following transplantation but can arise distant from the time of transplantation. Collateral vessel formation with recruitment of vessels from the jejunal vascular arcade in patients with a choledochojejunostomy rarely occurs in adults, and takes at least 3 weeks to become apparent, but is more common in children (Fig. 13.14).[47] B-mode ultrasound will demonstrate ischaemia as areas of heterogeneity and decreased reflectivity, but this is a late development and revascularisation will not save the graft. Ischaemic lesions tend to liquefy and may become infected, acting as a source of intermittent or recurrent sepsis (Fig. 13.15). CDUS has quoted

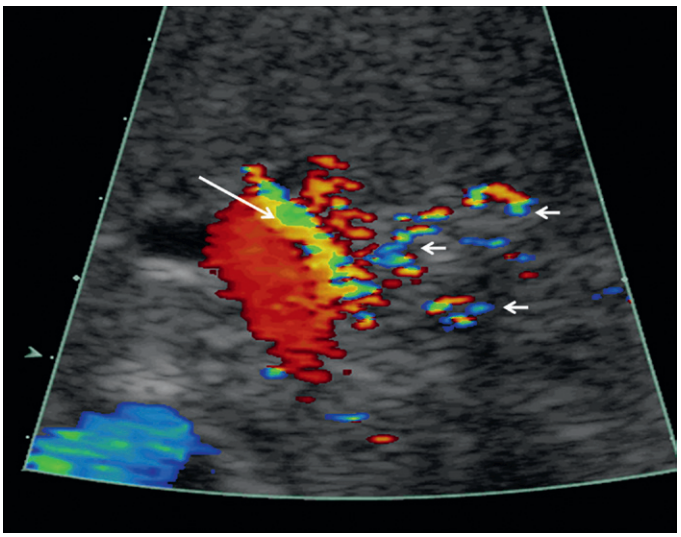


Figure 13.14 Collateral vessel formation. In this adult patient with hepatic artery thrombosis, collateral vessels (short arrows) have arisen to re-form the intrahepatic artery (long arrow).

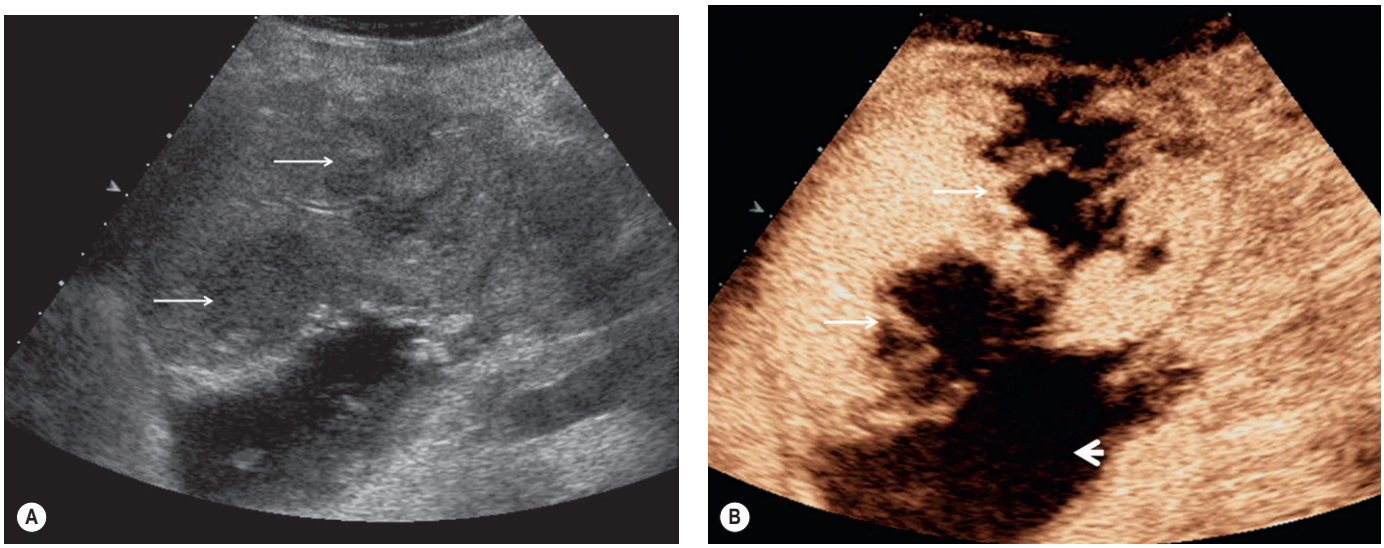


Figure 13.15 Liver ischaemia and infarction with hepatic artery thrombosis. A: There are area of altered reflectivity (arrows) in the liver of this patient with hepatic artery thrombosis (same patient as in Fig. 13.13), suggesting areas of ischaemia and infarction. **B:** On contrast-enhanced ultrasound these areas (arrows) are more obvious and likely to be areas of infarction. The liver graft is not viable and re-transplantation is necessary. The arrowhead points to a subhepatic fluid collection.

sensitivities of 82–92% in the diagnosis of HAT.[36,48] Our experience suggests that colour Doppler ultrasound of the HA will visualise 96% of hepatic arteries post transplant, and further interrogation of the non-visualised hepatic artery using CEUS improves detection to 98.7%.[46] Using microbubble contrast has the advantage of reinforcing the signal from the hepatic artery in patients with diminished but present hepatic arterial flow; and precludes the need for more cumbersome and invasive imaging with CECT or angiography. False negative findings may result from the presence of periportal arterial collateral vessels in chronic thrombosis. Collateral vessel flow causes damped (tardus parvus) hepatic artery waveform similar to that distal to a significant hepatic artery stenosis (HAS), with a prolonged acceleration time and low RI (Fig. 13.16). Patients who still demonstrate absent flow following CEUS undergo CECT angiography of the liver. The excellent spatial resolution and rapid scan times allow CECT angiography to depict small vessels for evaluation of both patency and stenosis.[49] Ultrasound will, however, continue to provide first-line imaging assessment of the post-transplant hepatic artery.

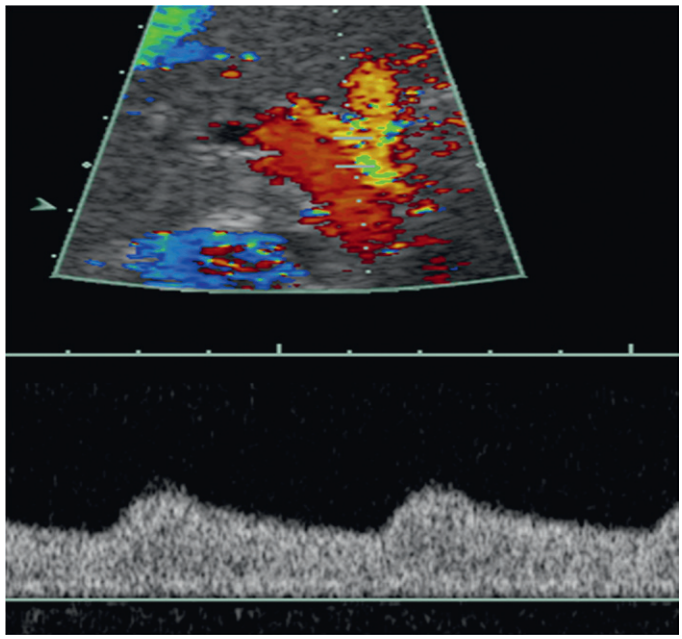


Figure 13.16 Chronic hepatic artery thrombosis. Collateral vessel flow causes damped hepatic artery waveform similar to that distal to a significant hepatic artery stenosis with a prolonged acceleration time and low resistive index (same patient as Fig. 13.14).

Hepatic artery stenosis

Stenosis of the hepatic artery has been reported to occur in up to 5% of hepatic transplant recipients,[50] but in our experience the incidence is close to 3%.[51] Hepatic artery stenosis commonly occurs in the early postoperative period but may occur several years after transplantation; occurring most often at the site of the surgical anastomosis. If untreated, severe HAS can lead to allograft rejection and progress further to the development of all the complications associated with HAT.[50] Hepatic artery stenosis may be attributed to inadequate surgical technique, surgical clamp injury, allograft rejection, microvascular injury associated with disrupted vasa vasorum, underlying liver disease, and preservation injury. Hepatic artery stenosis produces an intrahepatic spectral Doppler tardus parvus waveform, which is defined as a reduced RI of less than 0.5, and a prolonged systolic acceleration time (SAT) of greater than or equal to 0.08 seconds (Fig. 13.17).[51] The SAT is defined as the time from the onset of the systolic upstroke to the first systolic peak. Based on the tardus parvus waveform, sensitivity of between 85% and 97% for CDUS detection of the presence of HAS has been quoted.[41,50] However, if only one of the defining parameters – reduced RI or prolonged SAT – is present, the frequency of finding hepatic artery stenosis is decreased.[41] The tardus parvus spectral waveform is non-specific for stenosis and similar patterns may be seen in severe aorto-coeliac atherosclerotic disease, arteriovenous fistula, arteriobiliary fistula formation and in long-standing thrombosis with collateral development. Therefore the primary Doppler ultrasound criterion of arterial stenosis in any location of the body, a marked focal increase in peak systolic velocity (>2 m/s) at the site of the stenosis, should be sought and is dependent on the direct evaluation of the site of the stenosis (Fig. 13.18). Difficult ultrasound evaluation of the vessels, particularly in the subhepatic space, markedly

reduces the possibility of detecting a raised peak systolic velocity. The use of CEUS may be beneficial in patients with HAS, making it easier to accurately identify the exact site of the stenosis and to identify collateral vessel formation, if present.[51]

There are two situations where the diagnosis of HAS should be made with caution: during surgery using intraoperative Doppler ultrasound, and in the early (<48 hours) postoperative period. Frequently the postoperative low RI will over time return to normal. Therefore follow-up ultrasound is recommended when a low RI is detected in the HA in the presence of normal hepatic function in the postoperative period. If clinical suspicion for HAS remains high, a normal ultrasound examination should not prevent CECT angiography, as HAS may not manifest the tardus parvus Doppler ultrasound abnormality.[49] However, in the absence of a tardus parvus waveform the HAS is less severe, but nevertheless important to identify, in order that appropriate clinical management is instituted. A normal hepatic artery spectral Doppler waveform on serial examinations accurately excludes significant hepatic artery disease. The diagnosis of HAS may be inferred using ultrasound if serial hepatic arterial spectral Doppler waveforms show a progressive reduction in arterial velocity proximal to the site of the stenosis and the development of the tardus parvus waveform in the absence of parenchyma abnormality.

Hepatic artery stenosis and occlusion over a long period may have less devastating consequences to the liver graft. If the hepatic artery narrows and subsequently becomes occluded graft function may be preserved due to the formation of a number of arterial collaterals. Furthermore, when a choledochojejunostomy is fashioned in children or adults replacing a recipient common bile duct, the highly vascular jejunal bed allows rapid collateralisation and protects the graft from acute ischaemic complications. In the presence of a good collateral supply an entirely normal intrahepatic spectral Doppler waveform may be demonstrated even in the presence of complete main hepatic artery occlusion. A more common finding is the damping of the intrahepatic systolic arterial spectral Doppler waveform with the maintenance of high diastolic spectral Doppler waveform. Hence the presence of hepatic arterial flow within the graft must be taken in the clinical context of graft function. Although late arterial occlusion may be clinically silent, the majority of patients suffer one or more complications.[42]

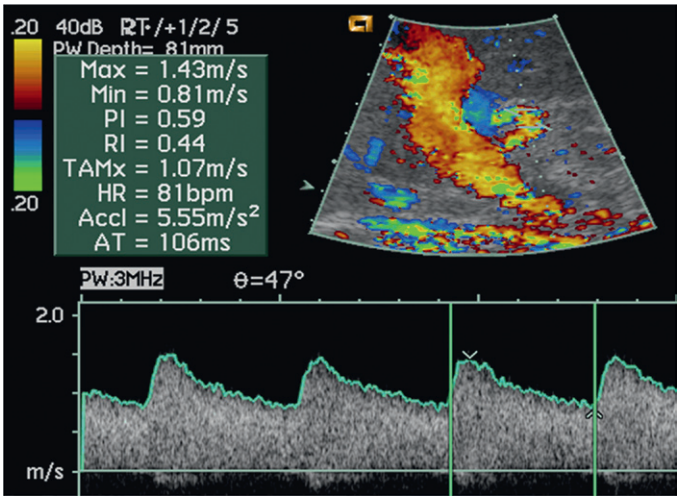
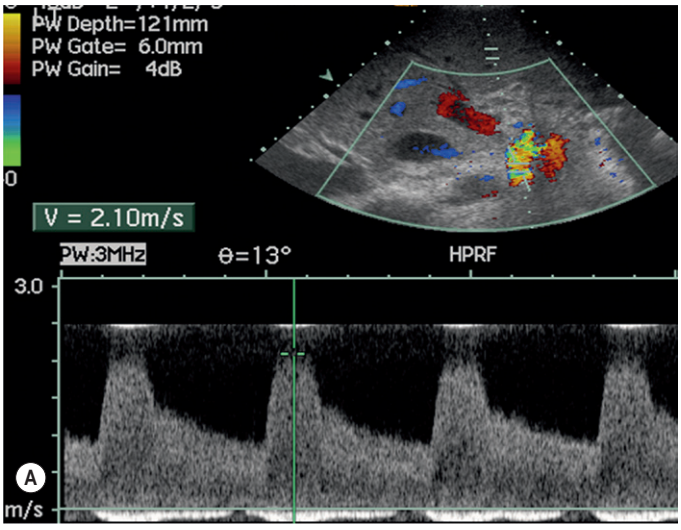


Figure 13.17 Hepatic artery stenosis – intrahepatic waveform. Hepatic artery stenosis produces an intrahepatic spectral Doppler tardus parvus waveform, in this patient with a resistive index of 0.44, and a prolonged systolic acceleration time of 0.106 seconds.

Hepatic artery pseudo-aneurysm (HAP)

Hepatic artery pseudo-aneurysm formation following liver transplantation is an uncommon vascular complication with an estimated occurrence of 1%.[52] Hepatic artery pseudo-aneurysm may be caused by defective vascular reconstruction or infection, and usually occurs at the site of the anastomosis. When seen in an intrahepatic site, percutaneous needle biopsy is usually responsible. The potential for rupture, followed by fatal haemorrhage, makes early diagnosis and treatment important. Diagnosis of HAP requires a high degree of suspicion, as it is often asymptomatic. Any low reflective collection in the vicinity of the hepatic artery anastomosis must be evaluated with colour Doppler ultrasound. Biopsy-related intrahepatic pseudo-aneurysms may be small and may not be seen with ultrasound or CECT, with arteriography the gold standard for detection.[52] Pseudo-aneurysm formation must be considered in any patient with haemobilia, gastrointestinal bleeding beyond the second part of the duodenum without an endoscopically visible source, and also in those with enlarging intrahepatic haematomas



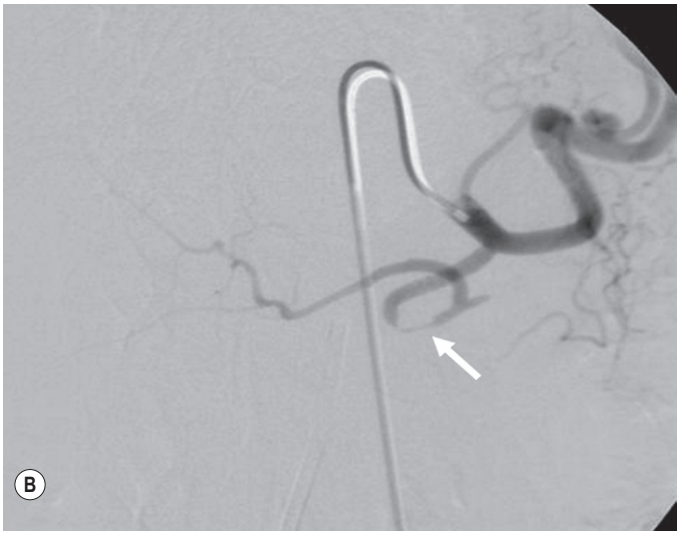


Figure 13.18 Hepatic artery stenosis – direct visualisation. A: The primary Doppler ultrasound criterion of arterial stenosis in any location of the body is a marked focal increase in peak systolic velocity by direct evaluation of the site of the stenosis. In this case a velocity of 2.10 m/s is seen in the transplant hepatic artery in the subhepatic space. **B:** The angiographic study demonstrates the stenosis of the hepatic artery (arrow) as seen on the ultrasound examination.

on ultrasound. Mortality from an extrahepatic HAP approaches 70%; re-transplantation is often required, with trans-arterial embolisation a temporary holding manoeuvre. On CDUS, a HAP appears as a cystic structure, usually near the course of the hepatic artery; its interior is colour filled, demonstrating a turbulent arterial flow (Fig. 13.19).

Post-transplant hepatic artery/portal vein

- A normal hepatic artery spectral Doppler waveform on serial ultrasound examinations accurately excludes significant hepatic artery disease.
- Hepatic artery occlusion and stenosis over a long period may have a less devastating consequence on liver graft function; hepatic abscess formation is more common.
- A peak velocity of greater than 100 cm/s or a three- to fourfold step-up in velocity across the narrowed portal vein is suggestive of stenosis.

Portal vein stenosis

The flow characteristics in the transplanted portal vein are often abnormal owing to a degree of infolding at the portal anastomosis. This leads to flow disturbances beyond the anastomosis, manifest by colour turbulence on CDUS. Portal vein stenosis has an incidence of 1% after liver transplantation.[53] If found in the immediate postoperative period, serial CDUS imaging is helpful as the portal vein stenosis may resolve over time.[54] Signs of portal vein stenosis include post-stenotic dilatation and portal hypertension demonstrated by an increase in the size and the number of collateral vessels. On CDUS focal colour aliasing occurs in the presence of an increase in flow velocity at the site of stenosis relative to flow velocity in the pre-stenotic segment (Fig. 13.20). Assessment of the splenic length in many post-transplant patients shows a small reduction in spleen size; a significant increase suggests portal hypertension. A peak velocity of greater than 100 cm/s or a three- to fourfold step-up in velocity across the narrowed portal vein is suggestive of stenosis.[54] Transhepatic portal vein cannulation and measurement of venous pressures across the anastomosis may

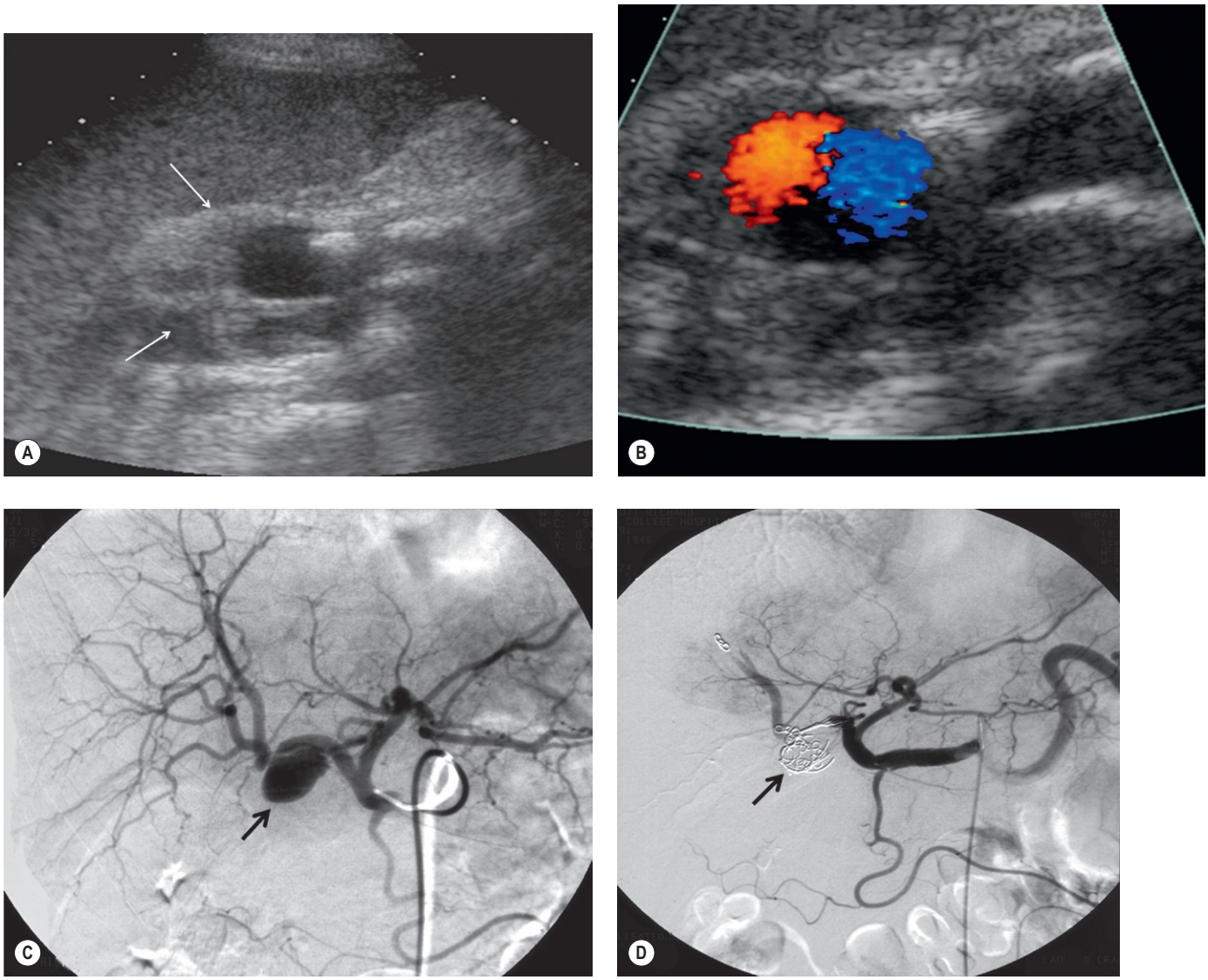


Figure 13.19 Hepatic artery pseudo-aneurysm. A: A cystic structure with surrounding soft tissue changes (arrows) close to the site of the surgical anastomoses in the transplant patient. **B:** There is colour filling of the central cystic aspect demonstrating the classical 'ying–yang' sign of a pseudo-aneurysm caused by turbulent arterial flow. **C:** The pseudo-aneurysm (arrow) is identified on the selective angiographic study. **D:** The pseudo-aneurysm has been treated successfully with coil embolisation (arrow).

document portal vein stenosis in the absence of any thrombus.[55] Percutaneous transhepatic dilatation of the portal vein stenosis may be successful.[56] However, if this technique fails, patients should be treated by portosystemic shunt or revision of the portal vein anastomosis. If adequate collateralisation occurs, with both portal vein stenosis and portal vein thrombosis, graft survival may be unaffected.

Portal vein occlusion

Portal vein occlusion following liver transplant is uncommon, occurring in less than 2% of patients, more often in children.[36,42,53] Portal vein thrombosis is invariably related to technical difficulties: malalignment with a redundant length of portal vein, leading to kinking and stricturing. Other predisposing factors include previous portal vein shunt surgery, previous portal vein thrombosis and sclerosis, vessel trauma from a portal cannula and underlying prothrombotic state. Acute rejection with diminished portal venous flow has been proposed as a cause of portal vein thrombosis and may be an important factor in small children with full size liver grafts.[55] Portal vein thrombus may be demonstrated on ultrasound as internal echoes within the portal vein, expansion of the portal vein and loss of colour Doppler signal. Reduction in the hepatic artery RI accompanies portal vein thrombosis and may be a helpful secondary sign for the determination of portal vein thrombosis (Fig. 13.21). A hepatic artery RI of 0.50 or less, together with an equivocal finding at portal venous CDUS, is reported to have a specificity of 100% and a sensitivity of 44% for portal vein thrombosis.[57] Eventually, an acute thrombus becomes anechoic; CDUS may show lack of portal venous flow and CEUS may be used to increase the confidence in diagnosis.[2,15]

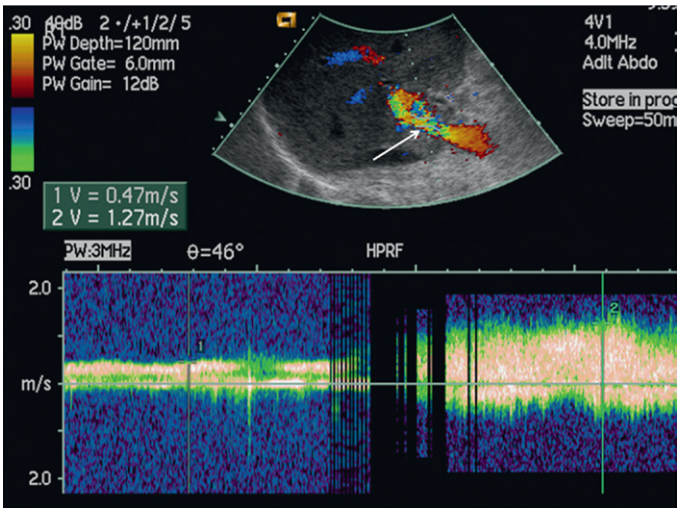


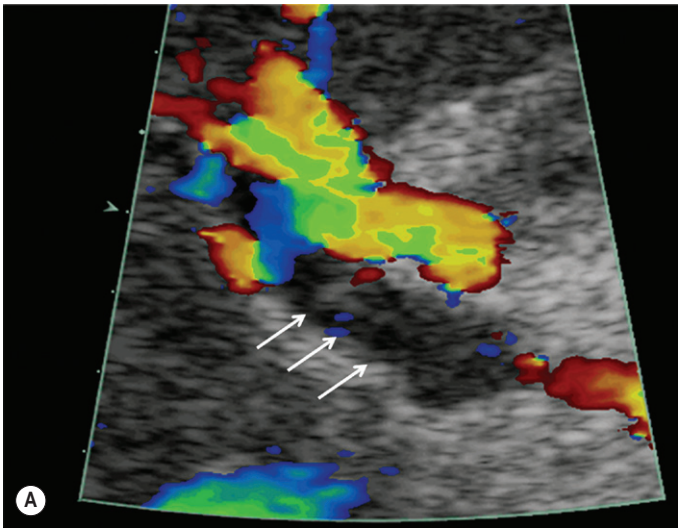
Figure 13.20 Portal vein stenosis. A focal area of narrowing and colour turbulence is observed in the portal vein (arrow). A peak velocity of 127 cm/s and a step-up in velocity across the narrowed portal vein is suggestive of a portal vein stenosis.

Portal vein gas

Intraportal venous gas is occasionally seen as echogenic shadowing within the portal vein, and is a more common finding than previously recognised. While it may be secondary to necrotic bowel, or intra-abdominal sepsis, it can also be an incidental finding post liver transplantation without any long-term consequences.[58]

Hepatic veins

Occlusion or stenosis of the IVC anastomosis is rare, occurring in less than 1% of recipients, usually due to technical surgical problems or as a consequence of compression by a fluid collection.[59] Suprahepatic stenosis presents with a clinical picture of acute or chronic Budd–Chiari syndrome with ascites, peripheral oedema, portal hypertension and biopsy evidence of hepatic venous congestion. Infrahepatic stenosis may cause only lower extremity swelling. A reduction in the calibre of the IVC or hepatic vein, with impaired flow and resultant pre-stenotic dilatation of the hepatic veins, is an indirect diagnostic finding of stenosis at CDUS. Direct signs of stenosis include a focal stricture on B-mode images and turbulent flow with increased velocity on spectral Doppler ultrasound (Fig. 13.22). Thrombosis of the hepatic vein or IVC may be depicted as intraluminal echogenic thrombus with no flow on Doppler images. Distension of the hepatic veins and IVC may also be demonstrated. A persistent monophasic waveform is a sensitive finding of stenosis at spectral Doppler ultrasound, but it is not specific for a substantial hepatic vein stenosis. Any pathological process that changes liver



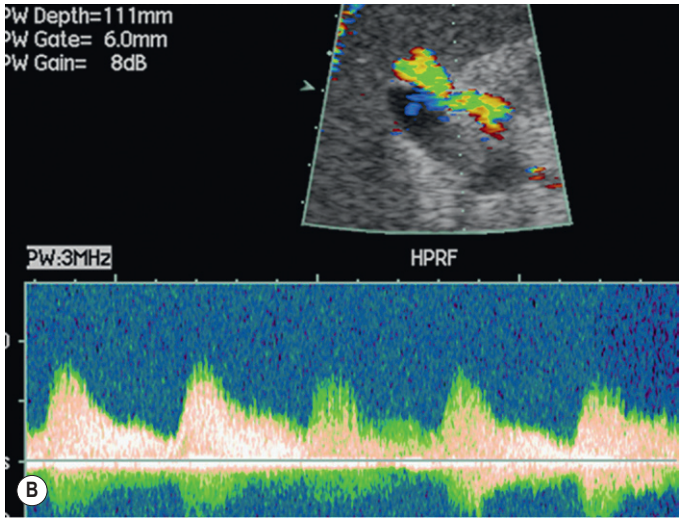


Figure 13.21 Portal vein thrombosis. A: The portal vein (arrows) demonstrates no colour Doppler flow with an echo-poor thrombus-filled lumen. The colour Doppler signal is present in the patent hepatic artery. **B:** The spectral Doppler waveform in the transplant hepatic artery demonstrates high forward flow in diastole in the same patient as in part **A**.

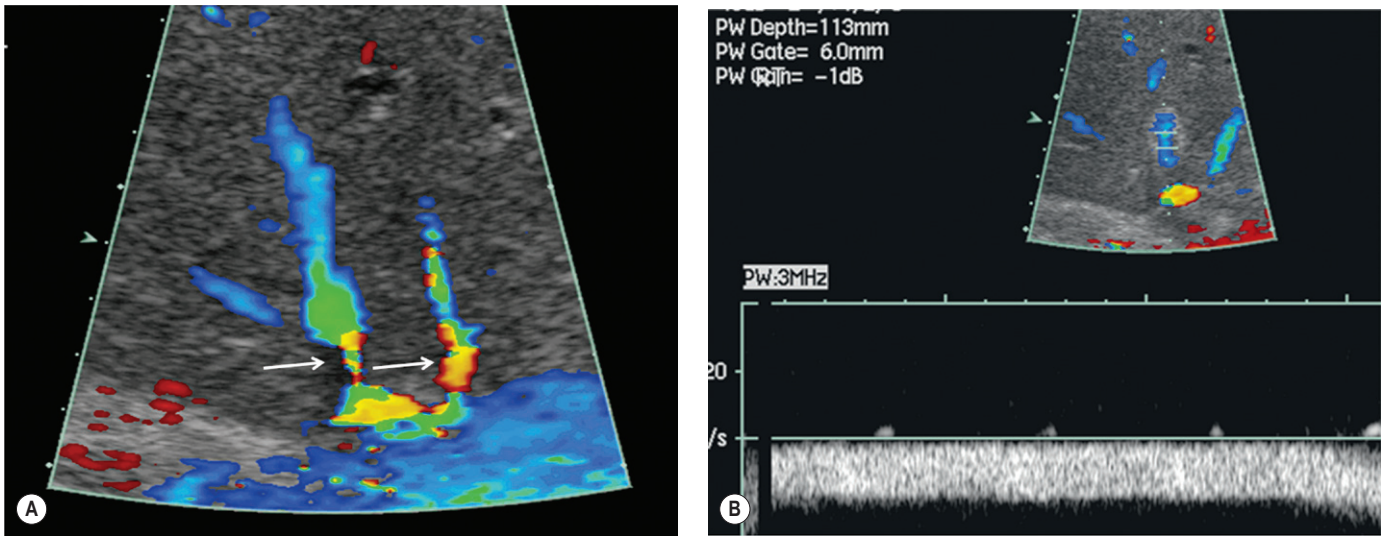


Figure 13.22 Hepatic vein stenosis. A: There are areas of narrowing and increase in colour Doppler flow (arrows) in two hepatic veins post-liver transplantation with the 'piggy-back' technique. **B:** There is complete loss of the normal pulsatility in the hepatic vein as a consequence of the hepatic vein stenosis.

compliance will alter hepatic vein pulsatility.[60] Perioperative ischaemia, vascular catastrophe, rejection and cholangitis may all cause damping of the spectral Doppler trace. Although ultrasound can be diagnostic, inferior vena cavography and pressure studies are required for the definitive diagnosis. Hepatic vein thrombosis is rare, as the hepatic veins are not directly involved in a surgical anastomosis. Hepatic vein thrombosis may be seen in those recipients who have had a transplant for Budd–Chiari syndrome, when the underlying abnormality recurs.[61]

A common variation of caval replacement is the 'piggy-back' technique. The three hepatic veins are joined together to form a single large orifice. The blind inferior end of the donor IVC often thromboses and this thrombus may be seen in the blind end of the donor IVC on routine ultrasound. Some sources have found the piggy-back technique to be prone to the Budd–Chiari syndrome, or haemorrhage, but this has not been the experience at our institution.[53]

Non-vascular complications

Rejection

Following hepatic transplantation, acute rejection is the most common serious complication affecting allograft survival, and occurs in more than 30% of patients.[62] Treatment, which is usually successful, involves manipulation of immunosuppressive drug therapy. Acute rejection is due to an inflammatory cellular infiltrate and does not significantly affect the peripheral hepatic vasculature.[63] In chronic rejection there is deposition of subintimal foam cells, myo-intimal foam cells, myo-intimal hyperplasia, and intimal sclerosis, resulting in progressive arterial narrowing and slow flow with subsequent thrombosis.[64] Non-anastomotic vascular stenosis, as well as diffuse intrahepatic arterial narrowing, is a feature in patients with chronic transplant rejection.

Ultrasound presents a non-specific profile in acute rejection; there is no correlation between the RI and acute rejection[64] and no correlation between loss of hepatic artery diastolic flow and acute rejection.[63] Changes in hepatic arterial and venous velocity profiles reflect alteration in hepatic vascular resistance, which is not specific to rejection; occurring with preservation injury, sepsis and non-thrombotic graft infarction.[60] An area of decreased reflectivity and attenuation has also been described in the periportal region with ultrasound and CECT, respectively, but this has a low sensitivity and specificity in the diagnosis of rejection.[65] There is no reliable non-invasive diagnostic examination modality to detect liver allograft rejection, with the main role of radiology to exclude other complications prior to a histological diagnosis with liver biopsy.

Biliary system

Biliary complications are an important cause of postoperative morbidity and mortality in liver transplantation.[37] The main complications after liver transplantation are biliary obstruction and bile leakage. The reported incidence of complications has decreased from 50% with mortality as high as 30% in early series to a current complication rate of less than 20% and a mortality of less than 5%.[66] The current surgical practice for biliary reconstruction is end-to-end anastomosis, where the recipient bile duct may be utilised. However, if the recipient has an underlying biliary abnormality with an insufficient length of a common bile duct, such as in biliary atresia or sclerosing cholangitis, or when a cut-down graft is transplanted, it will be necessary to construct a choledochojejunostomy.

Strictures of the bile duct anastomosis are more common after duct-to-duct reconstruction, occurring in 5–14% of cases (Fig. 13.23).[43,67] Non-anastomotic strictures carry a worse prognosis, representing a diffuse biliary injury occurring with HAT, prolonged cold ischaemia and ABO incompatible donors (Fig. 13.24).[68] It is important that CDUS confirms patency of the hepatic artery when non-anastomotic strictures are present.

Bile duct dilatation is unusual in the early postoperative transplant period.[69] In non-transplant patients, ultrasound is the accepted method for detecting biliary duct dilatation.[70] However, the sensitivity is lower in liver transplant patients, with a sensitivity of 38–46%, and a specificity of 98%.[71] Dilatation of the intrahepatic ducts has a higher predictive value for diagnosis of biliary obstruction than common bile duct diameter. If bile duct dilatation is suspected clinically, ultrasound nonetheless remains the investigation of choice, providing evidence to support the need to proceed to further imaging.

On ultrasound, in the early postoperative period it is practice to measure the common, left and right bile ducts to confirm non-dilatation and record the baseline measurement. This is particularly important in cut-down grafts in children, where intrahepatic bile duct dimensions are those of adult proportions and early measurement will avoid an erroneous call of bile duct dilatation. If the bile ducts increase in size along with biochemical changes or biliary dilation is persistent for more than 3 months after transplantation, a biliary system abnormality is invariably present.

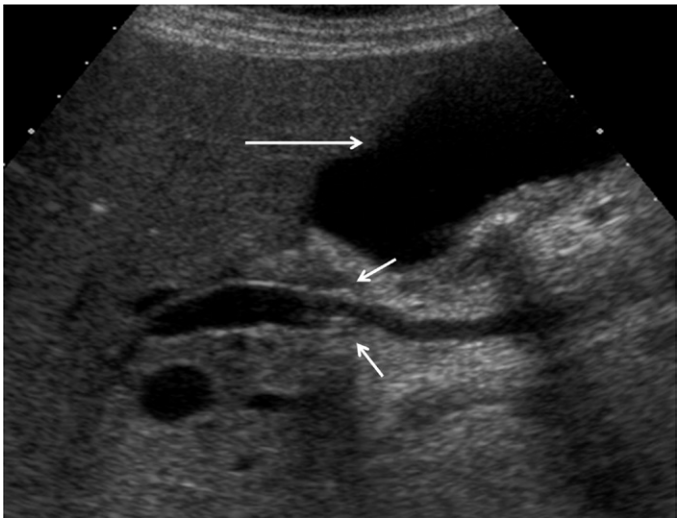


Figure 13.23 Common bile duct anastomosis. A subhepatic fluid collection (long arrow) allows clear visualisation of the common bile duct, demonstrating a change in calibre at the site of the anastomosis (short arrows).

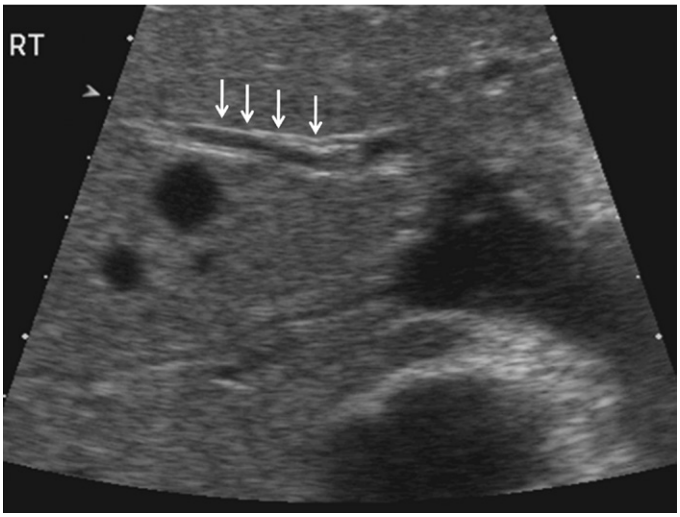


Figure 13.24 Non-anastomotic bile duct strictures. There are focal areas of bile duct dilatation (arrows) in the transplant liver of a patient with hepatic artery thrombosis, indicating areas of focal ischaemic strictures.

Bile leaks are usually secondary to anastomotic complications. In a review of biliary complications in 1792 patients following liver transplant, 50% of bile leaks were due to anastomotic complications and the remaining leaks were due to HAT (17.2%), leaks at the T-tube site (31%), and leaks from aberrant ducts.[69] The majority of bile leaks occur early, within the first thirty days of liver transplantation or at the time of removal of the T-tube, if in position. Diagnosis of a biliary leak is often difficult without cholangiography. Ultrasound can readily detect intra- and extrahepatic bilomas that occur as a result of post-transplantation bile leaks. However, their appearance may be indistinguishable from other collections of fluid in the upper abdomen such as ascites, seroma or haematoma (Fig. 13.25). Subhepatic collections are common in the early post-transplant period. Ultrasound-guided fine-needle aspiration may confirm the nature of the fluid. Drainage of bile leaks may promote healing of the bile ducts and may save the liver graft.[72]

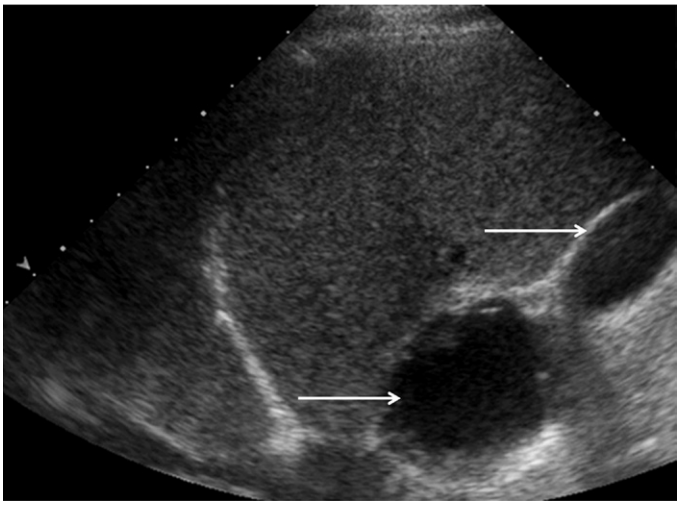


Figure 13.25 Subhepatic collections. Two subhepatic collections (arrows) are present; the nature cannot be ascertained from the ultrasound appearances and may be either haematomas or bile collections.

Non-vascular complications of liver transplantation

- There are no reliable ultrasound criteria for the diagnosis of rejection and liver biopsy is the definitive investigation, safely guided by ultrasound.
- Non-anastomotic bile duct strictures carry a worse prognosis than anastomotic strictures, as these are representative of diffuse biliary injury.
- There are no distinguishing ultrasound features of fluid collections in the upper abdomen and these may be bilomas, ascites, serum or haematomas.
- Abscess formation occurs in 10% of liver transplant patients most often in the sub-phrenic or sub-hepatic spaces.

Anastomotic strictures arise secondary to operative difficulties and respond to transhepatic balloon dilatation.[73] In a small group of patients with postoperative biliary system obstruction, extensive epithelial casts form within the biliary tree. These patients usually have a patent hepatic artery, suggesting that the lesions are unlikely to be vascular in origin. It is possible that this is a late manifestation of preservation injury affecting the harvested liver leading to epithelial sloughing within the biliary system. Most patients with this condition require re-transplantation.

Fluid collections

Abscess formation occurs in approximately 10% of liver transplants postoperatively, most of which occur in subphrenic or subhepatic spaces.[74] Ultrasound guidance will allow drainage of any fluid collection. Occasionally, fluid collections may be completely obscured by bowel gas on ultrasound, with CECT providing the conclusive imaging modality. Haematoma formation may be seen in the immediate postoperative period and is usually secondary to extensive intraoperative abdominal bleeding from varices. Haematomas may be present at any site, again most commonly in the subphrenic and subhepatic space.[37] In the first 3 weeks following liver transplant the majority of haematomas are composed of clotted blood and aspiration is neither necessary nor possible. The development of new collections in the late postoperative period raises the possibility of bile leak as a consequence of HAT, or loculated ascites as a consequence of portal vein or IVC flow abnormalities.[37]

Post transplantation abdominal bleeding occurs in less than 10% of patients and may be due to HAP, breakdown of a vascular

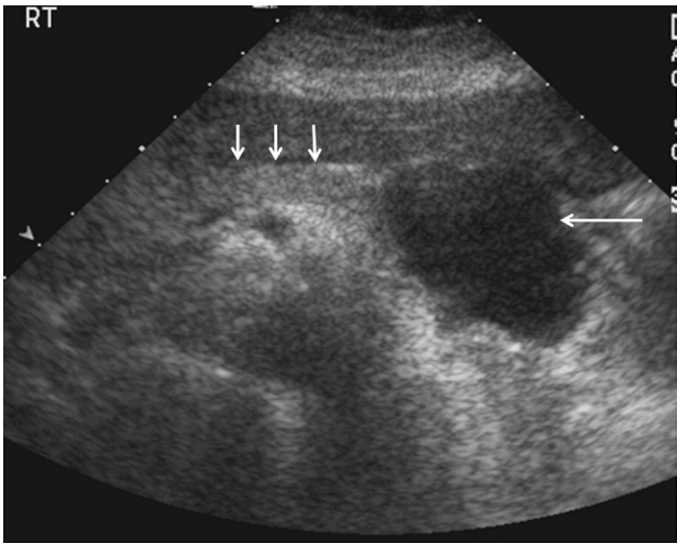


Figure 13.26 Pancreatic collection. A collection of fluid (long arrow) is present adjacent to the pancreas (short arrows) in a patient with pancreatitis following liver transplantation.

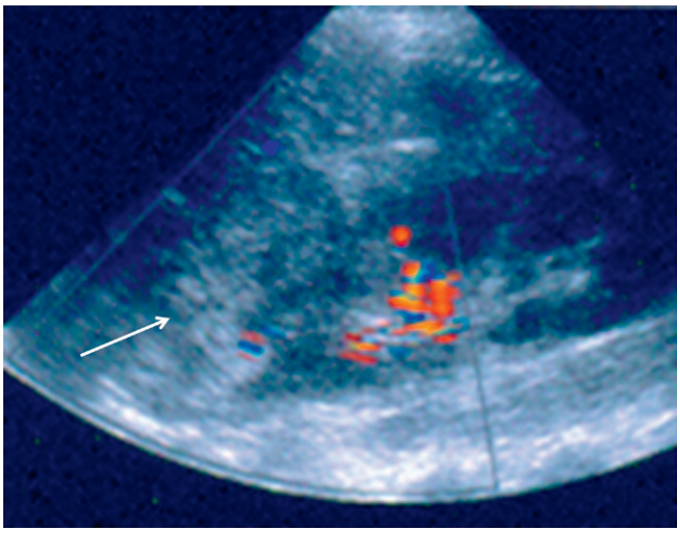


Figure 13.27 Adrenal infarction and haemorrhage. A mixed reflective area (arrow) lies in the region of the right adrenal gland in this liver transplant patient with an adrenal infarction.

anastomosis, infection or haemobilia.[75] Radiological investigation may only serve to delay treatment in the unstable patient where surgery is required. However, if the patient is stable, ultrasound-guided aspiration of fluid may help to confirm the presence of free intra-abdominal blood.

Miscellaneous complications

Infrequently seen complications include pancreatitis and adrenal haemorrhage, both of which may be identified by ultrasound. Enlargement of the pancreas may be seen in uncomplicated pancreatitis and fluid collections may be detected (Fig. 13.26). Adrenal infarction, which may be haemorrhagic, occurs on the right side and is caused by inadvertent ligation of the adrenal vein at the time of transplantation. On ultrasound this may appear as a suprarenal mass of mixed reflectivity (Fig. 13.27). Pleural effusions, which are sympathetic in nature, are commonly seen on the right side. These can be drained under ultrasound guidance if causing respiratory compromise.[3]

Complications of split liver transplantation

While no difference in the frequency of primary graft non-function or arterial thrombosis in split grafts as compared with full size grafts has been noted, the collective European experience suggests an 18.5% incidence of postoperative haemorrhage, 11% incidence of HAT, 4% incidence of portal vein thrombosis, and a 20% biliary complication rate. Biliary complications include anastomotic and cut surface leaks and anastomotic and non-anastomotic stricture formation.[34]

ROLE OF ULTRASOUND IN LONG-TERM FOLLOW-UP

Ultrasound plays a vital role in the long-term follow-up of liver transplant patients with emphasis on the long-term complications of immunosuppression. All post-transplant patients should have an ultrasound examination prior to clinical follow-up with results available to the consulting physician. Vascular complications have the same presentation as in the early postoperative phase but are less common. In particular HAT may be an incidental and unexpected finding but still carrying the same poor prognosis in the long term in the adult patient. Non-vascular complications are more likely to occur, and disease recurrence should be a particular consideration that requires imaging awareness.

Non-vascular complications

Post-transplant lymphoproliferative disease (PTLD)

Post-transplant lymphoproliferative disease is a B-cell proliferation in lymph nodes and solid organs associated with the Epstein–Barr virus (EBV), typically developing within the first year after solid organ transplantation.[76] The reported incidence of PTLD increases with decreasing age of liver transplant patient and is associated with potent immunosuppression agents.[77] The incidence of PTLD ranges from 2% to 10% in adults[78] and 2.9% to 18.9% in children.[76] Children are more at risk for the development of PTLD primarily because they are likely to be seronegative for EBV before transplantation and acquire primary infection post transplantation.[76,77] PTLD has a broad clinical spectrum, ranging from an infectious mononucleosis-like syndrome to manifestations of frank lymphoma.[79] Recognised characteristics of PTLD include a tendency toward extranodal involvement and a variable response to treatment. The aim of imaging is initial detection, and then staging and finally post-treatment follow-up of the disease. Once an abnormality is demonstrated, imaging may be used to guide biopsy for histological confirmation. CECT is the imaging modality of choice for staging and assessing the bulk of disease and follow-up of treatment response. The abdomen is the commonest site of involvement with PTLD and up to 50% of patients present with isolated abdominal disease.[80] Extranodal abdominal disease is three to four times more frequent than nodal disease; 88% of liver transplant recipients assessed with CECT in one series had extranodal abdominal PTLD.[81]

Three distinct patterns of hepatic PTLD may be seen at ultrasound. The most common is focal areas of low reflectivity measuring 1–4 cm, followed by a diffuse parenchymal involvement with no discrete lesions resulting in hepatomegaly and progressing to liver failure (Fig. 13.28).[80] The third pattern involves the porta hepatis, which may result in biliary obstruction and is postulated to originate within the biliary tree (Fig. 13.29).[82] Rarely fulminant disease may present as a consequence of PTLD causing extensive graft necrosis.[83]

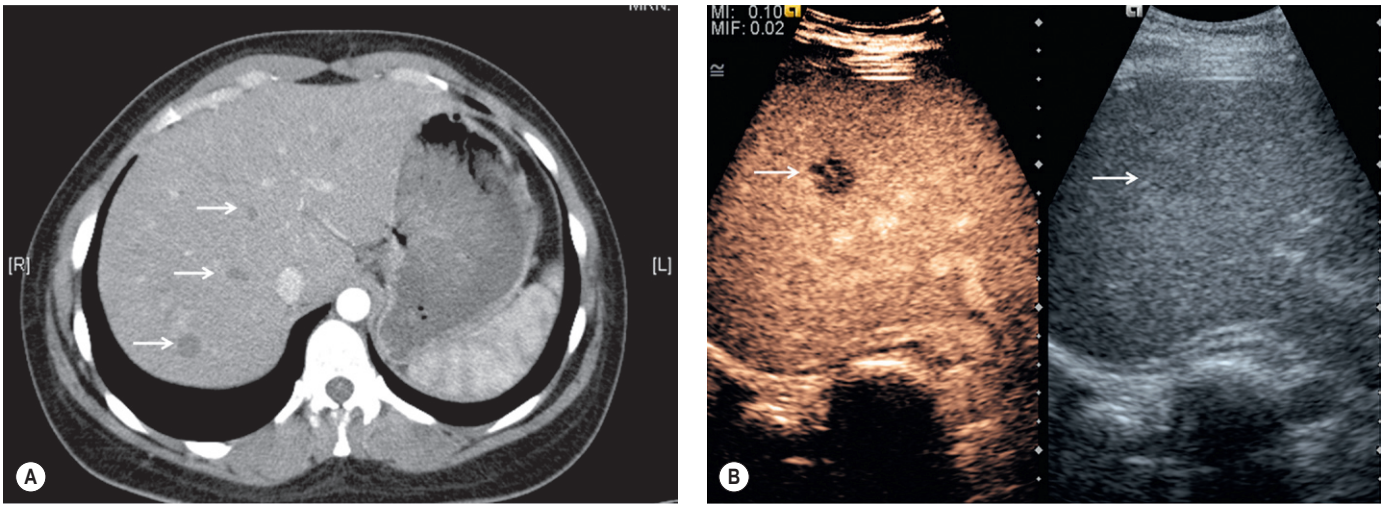


Figure 13.28 Focal hepatic post-transplant lymphoproliferative disease. A: In this post-transplant patient several focal low attenuation lesions (arrows) are seen on the arterial phase of the CECT examination. **B:** On the post-contrast ultrasound a single subtle low reflective lesion (arrow) demonstrates washout in the late phase but still has some intralesional vascularity identified.

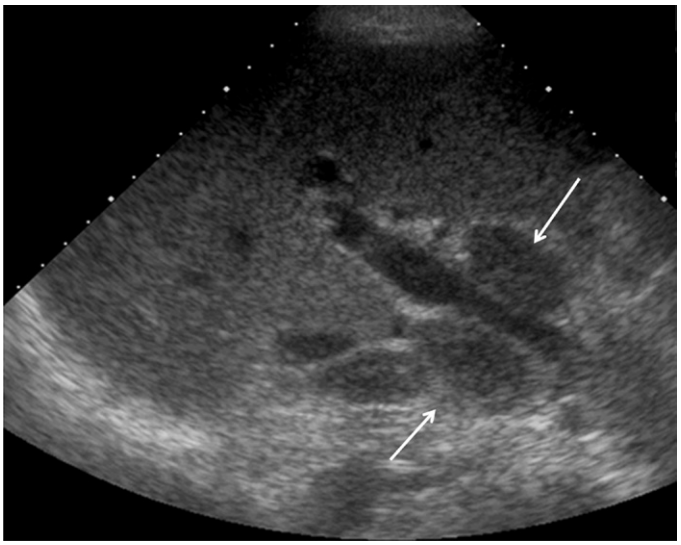


Figure 13.29 Porta hepatis post-transplant lymphoproliferative disease. Low reflective focal lesions (arrows) surround the portal vein in this patient with porta hepatis post-transplant lymphoproliferative disease.

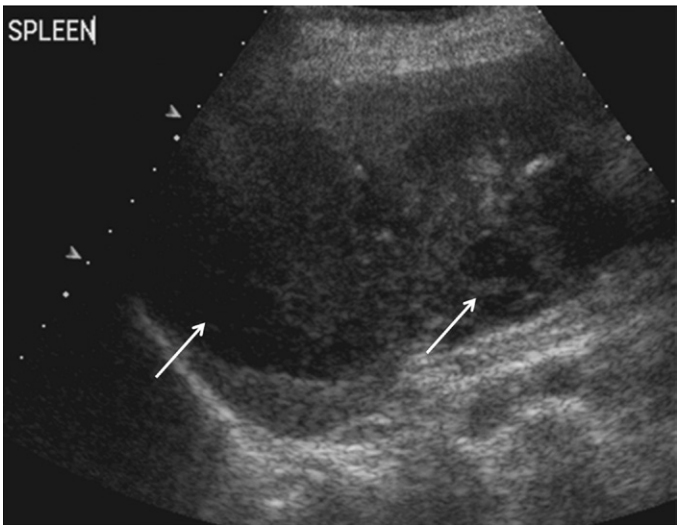


Figure 13.30 Splenic post-transplant lymphoproliferative disease. Two large low reflective (arrows) lesions with pockets of high reflectivity in a liver transplant patient with post-transplant lymphoproliferative disease.

Other extranodal manifestations of abdominal PTLD include involvement of the gastrointestinal tract (approximately 30%) with the small bowel most frequently involved, splenic involvement in 28% of cases manifesting as focal low-reflectivity lesions, splenomegaly or both, and renal involvement which occurs in less than 20% of patients (Fig. 13.30).[80] Unlike renal lymphoma that arises in the non-transplant patient, PTLD kidney involvement tends to be unilateral and unifocal. A solitary round low echogenic lesion without renal enlargement is the most common manifestation, while diffuse renal enlargement, which may extend beyond the capsule, occurs less commonly. Abdominal lymph node involvement, seen in about 20% of patients, appears as non-specific nodal enlargement. These involved nodes are typically 2–3 cm in diameter but may coalesce to form larger masses with central low attenuating areas from necrosis being an uncommon finding. Any combination of peritoneal, retroperitoneal and extraperitoneal lymph nodes may be enlarged. Omental and mesenteric involvement by PTLD is less common, seen in about 10% of patients with abdominal disease and manifesting as an 'extranodal mass'. These may be well circumscribed or infiltrative, representing either primary tumour involvement or direct extension from an abdominal organ.

Renal complications

Renal insufficiency due to the nephrotoxic effects of the immunosuppressive therapy is a common complication and has been reported in up to 25% of paediatric recipients.[84] Ultrasound may be used to exclude obstruction in patients with deteriorating renal function and give information regarding the size and reflectivity of the kidneys.

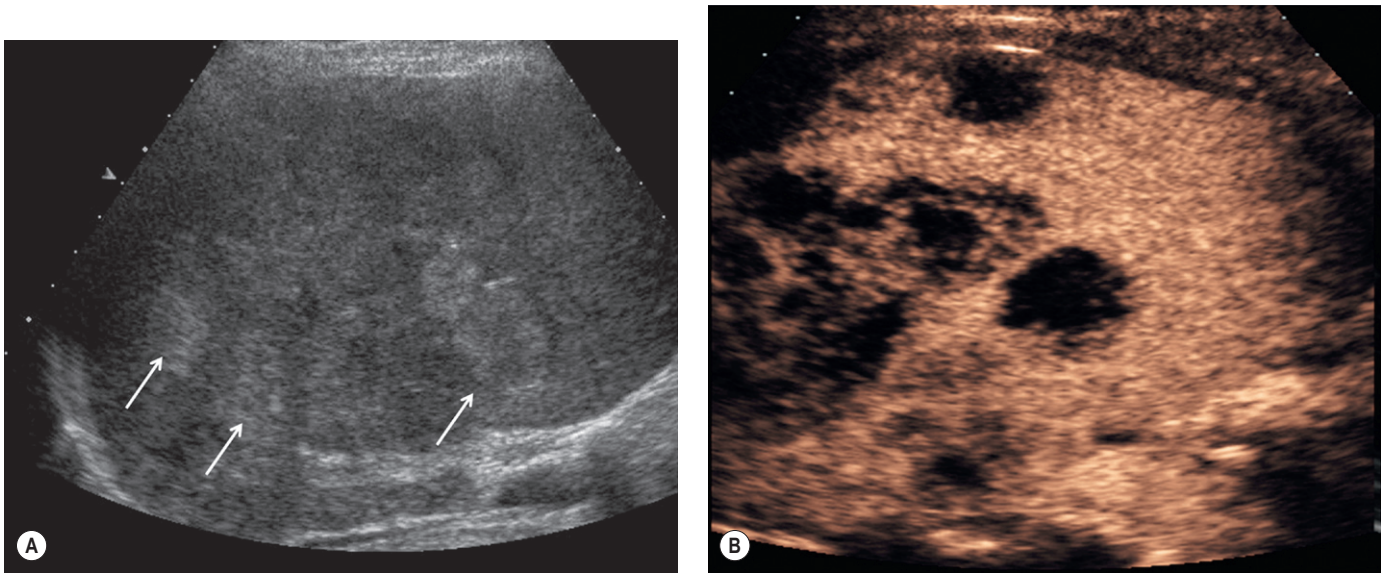


Figure 13.31 Post-transplant liver abscess. A: Multiple areas of mixed reflectivity (arrows) in a liver transplant patient. **B:** On the contrast-enhanced images these areas are seen to be avascular, with irregular borders and septations in keeping with multiple abscesses.

Long-term complications of liver transplantation

- Biopsy evidence of recurrence of hepatitis C is seen in 87% and hepatitis B in 90% of liver transplants.
- Post-transplant lymphoproliferative disease is a B-cell proliferation in lymph nodes and solid organs associated with the Epstein–Barr virus developing after solid organ transplantation.
- Children are more at risk of the development of post-transplant lymphoproliferative disease.
- Three patterns of post-transplant lymphoproliferative disease are seen in the transplant liver on ultrasound: focal lesion, diffuse parenchymal abnormality, and involvement of the porta hepatis causing biliary obstruction.

Graft versus host disease

This is a common complication following bone marrow transplantation and is becoming increasingly recognised following solid organ transplantation.[85] This entity has serious consequences and may be fatal. Imaging has no role in the assessment of graft versus host disease other than to exclude structural abnormalities of the graft.

Rejection

Rejection is common in liver transplant recipients but imaging is neither sensitive nor specific for rejection.[86] Ultrasound is used to exclude structural abnormalities in the graft that may present in a clinical fashion similar to rejection. The diagnosis of rejection is made on histology following liver biopsy.

Infection

Infection is the most common complication of liver transplantation, with immunosuppressive therapy the major risk factor.[87] In the presence of a structural abnormality of the graft, such as HAT or a biliary stricture, infection may be localised to the graft. Hepatic abscess formation may be readily visualised with ultrasound and treated by ultrasound-guided drainage (Fig. 13.31). Abscesses may be visualised as areas of either increased or decreased reflectivity. A retrospective review of adult liver transplantation over a 9-year period demonstrated an incidence of hepatic abscess of 3.9%. Eighty-five per cent were bacterial in origin, 15% fungal and both were found to contribute to eventual graft failure.[88]

Budd–Chiari syndrome

Liver transplantation in Budd–Chiari syndrome represents a viable treatment option with a favorable long-term survival.[89] However, depending on the initial cause of the Budd–Chiari thromboembolic phenomena, the syndrome may recur not only in the hepatic veins but also in the portal vein and hepatic artery.[90] This contributes significantly to the postoperative morbidity and mortality. Patients are placed on long-term full anticoagulation to prevent recurrent thrombosis. A CDUS examination of all hepatic vessels at follow-up is mandatory to exclude recurrent disease.

Disease recurrence

The initial indication for liver transplantation should be considered when surveillance ultrasound is performed in the post-transplant phase to allow for the possibility of disease recurrence.

Viral infection

Viral infection can recur in the transplant liver. Biopsy evidence of recurrence of hepatitis C is seen in 87% of transplants and tends to occur within 2 years of transplantation.[91] Early recurrence is associated with a higher incidence of rejection and cirrhosis leading to eventual graft loss. The role of ultrasound is limited to the exclusion of other complications when the biochemical parameters become abnormal. Ultrasound is useful to monitor complications of recurrent infection such as cirrhosis, and portal hypertension and for surveillance for the development of focal liver lesions. The recurrence rate for hepatitis B is also high at 90%.[92] This reinfection leads to early graft loss, estimated at 41% at 14 months. Recurrent hepatitis B virus (HBV) infection in a transplant patient is more aggressive than in the pre-transplant patient; furthermore, patients transplanted for chronic HBV may develop end-stage liver disease in a number of months.[93] This poor outcome of chronic HBV infection was initially considered a contraindication to transplantation; however, now the aim of treatment in the post-transplant period is

to prevent reinfection with immunoprophylaxis and antiviral therapy.

Hepatocellular carcinoma (HCC)

The histological pattern and degree of differentiation of HCC give no indication as to the subsequent course of disease, as it is the preoperative staging of the tumour which indicates the recurrence rate. The lowest recurrence rates occur in small tumours of less than 5 cm without evidence of disease spread.[94] Tumour recurrence rate of 7% is seen with tumours less than 5 cm and 62% when tumours are greater than 5 cm in size.[95] Furthermore, infiltration of regional lymph nodes or the presence of gross or microscopic vascular invasion by tumour at the time of transplantation significantly influences the prognosis.[96] A combination of ultrasound, CECT and magnetic resonance imaging is accurate at detecting HCC recurrences in the liver transplant. Imaging features for HCC in the post-transplant liver are similar to those in the pre-transplant liver. Overall, children who have received a liver transplant for primary hepatic malignancy have a better prognosis than adults. The quoted 10-year survival rate is 21% in adults and 50% in children.[97] The recurrence of HCC in a non-cirrhotic liver transplant should be readily detected on ultrasound but there are no available published data to confirm this.

Fibrolamellar HCC

The recurrence rate for fibrolamellar hepatocellular carcinoma following transplantation is unexpectedly high for a tumour that is slower growing and has a higher resectability rate than classic HCC.[98] This may in part be due to the late presentation of these tumours generally with a large bulk of tumour. The survival rate at 5 years following transplantation is 50%.[94]

Alcoholic liver disease

Survival after transplantation for alcoholic liver disease is similar to that of other forms of chronic liver disease.[99] Abstinence prior to transplantation is required but relapse following surgery occurs and cirrhosis recurs.

Cholangiocarcinoma and metastatic disease

The rate of recurrence of cholangiocarcinoma is higher than HCC; the finding of lymphatic involvement is a contraindication to transplantation. Early lymphatic spread is the normal finding and in essence transplantation for cholangiocarcinoma is rarely performed.[100] In metastatic disease recurrence is so high that transplantation is contraindicated.

Primary biliary cirrhosis (PBC)

The most accurate method of determining the possibility of recurrence is based on histology, as the presence of pruritus, antimitochondral antibodies and an elevated IgM in the post-transplant patient are non-specific. The rate of recurrence increases with time, so that by 10 years recurrence may be seen in up to 30–50% of liver biopsy specimens.[101] In the medium term recurrence of PBC has little clinical impact and ultrasound has no role in the detection of recurrence but only to exclude structural abnormalities that may present in a similar fashion.

Primary sclerosing cholangitis (PSC)

Ultrasound has limited use in the assessment of PSC recurrence, since as with the pre-transplant condition the ultrasound may be entirely normal.[102] The presence of bile duct dilatation in the transplant graft invariably indicates a newly developed biliary abnormality for which recurrence of PSC must be considered. Most patients transplanted for PSC will have a choledochojejunostomy as a consequence of abnormal recipient extrahepatic ducts, which is prone to a higher incidence of cholangitis and biliary strictures leading to a cholangiopathy similar to PSC. This presents difficulty both on cholangiographic and histological methods in determining absolute PSC recurrence. Furthermore, patients transplanted for PSC are known to have a higher incidence of biliary complications, again reflecting the use of a choledochojejunostomy reconstruction.

PAEDIATRIC LIVER TRANSPLANTATION

Introduction

Paediatric liver transplantation is a well-established and effective treatment option for children with acute or chronic liver disease. In the United Kingdom approximately 100 children undergo liver transplantation annually either as an elective procedure (approximately 85% 5-year survival rate) or as an emergency in the acute setting. Paediatric liver donors are rare and therefore various surgical techniques have been developed to facilitate transplantation in this group of patients, leading to improved survival and quality of life.

Clinical indications for paediatric liver transplantation

Chronic liver disease

Congenital extrahepatic biliary atresia (1:10000 live births), is the commonest cause of chronic liver disease in infants and young children. An early porto-enterostomy (modified Kasai procedure) before 8 weeks of age can alleviate the symptoms of jaundice but is rarely curative and cannot reverse the ongoing liver damage leading to progressive secondary biliary cirrhosis.[103] Patients with severe progressive liver failure secondary to a failed Kasai procedure or undiagnosed biliary atresia constitute an important group in whom liver transplantation offers survival. In these children ultrasound assessment is technically difficult as a result of several factors, including previous surgery, associated congenital anomalies, ascites, heterogeneous and highly reflective liver and a lack of patient cooperation. Patients with biliary atresia have an increased incidence of congenital anomalies, including situs inversus abdominis, situs ambiguus, malrotation of the gut, abnormalities of the hepatic artery, portal vein and IVC and polysplenia or asplenia. It is important that as many of these as possible are identified or excluded on the preoperative investigations, so that the surgeon can be warned of their existence.[104] In particular, the hepatic artery anatomy is frequently abnormal, with multiple arteries and/or an anomalous extrahepatic course. Rarely the portal vein may drain directly into the vena cava, or may lie in a pre-duodenal position. The IVC may be absent, left-sided, or subject to a number of other anomalies, the commonest of which is IVC interruption with azygos vein continuation.

Hypoplasia of the intrahepatic bile ducts leads to severe cholestasis. This can be seen in Alagille's syndrome, post infection, associated with trisomy 18 and 21 and with metabolic disorders such as cystic fibrosis (5% of children develop liver disease) and Zellweger's syndrome.[105] Progressive familial intrahepatic cholestasis begins in infancy and progresses to cirrhosis within the first decade of life.[106]

Other causes of chronic liver disease in infancy and childhood include neonatal hepatitis syndrome, short gut associated liver disease, the glycogen storage diseases, tyrosinaemia, autoimmune hepatitis, sclerosing cholangitis, congenital hepatic fibrosis in

association with infantile polycystic kidney disease and Langerhans cell histiocytosis.

Acute liver failure (ALF)

Usually secondary to infection, ALF is defined by the presence of hepatic encephalopathy and coagulopathy within 8 weeks of the onset of liver disease. Over half of cases are due to non-A-E hepatitis.[107] Other causes include paracetamol overdose, mushroom poisoning, autoimmune liver failure and metabolic diseases such as neonatal haemochromatosis, tyrosinaemia and Wilson's disease.

Metabolic liver disease

Liver transplantation for metabolic diseases is divided into that performed for end-stage liver disease or premalignant change (including α_1-antitrypsin deficiency, Wilson's disease, galactosaemia, protoporphyria, glycogen storage diseases) and that performed for major extrahepatic features (including Crigler–Najjar syndrome, primary familial amyloidosis, homozygous hypercholesterolaemia).

Portal hypertension (PHT)

PHT follows obstruction of the paediatric intra- or extrahepatic portal venous system. This can be at a hepatic level secondary to liver cirrhosis, prehepatic due to thrombosis or rarely posthepatic following obstruction to venous outflow or IVC obstruction.[106]

Liver tumours

Transplantation is offered to those children presenting with irresectable benign or isolated malignant tumours with no evidence of extrahepatic spread. These tumours include epithelioid haemangioendothelioma, hepatoblastoma and fibrolamellar carcinoma.

Surgical techniques for paediatric liver transplantation

Historically paediatric patients needing liver transplantation had high morbidity and mortality rates due to incompatible size-matched cadaveric organs. A better understanding of liver anatomy revolutionised surgical techniques of liver transplantation in the paediatric population. In 1984, Bismuth first reported on the orthotopic transplantation of a reduced sized graft from a deceased adult.[108] Five years later the first successful living donor liver transplantation in a child was performed using a left lateral segment (segments II and III) graft.[109] Various techniques have been developed to provide suitable organs for paediatric recipients; these are reduced, split and living related liver transplantation.[108,110] These techniques have the potential to overcome discrepancies between donor and recipient weights of up to 10:1. Split liver transplantation results in the liver being shared between an adult (extended right lobe) and a child (left lateral segment). If a liver becomes available from a paediatric organ donor and is implanted into a similar sized recipient then the technical principles of the transplant operation are very similar to those of the adult operation. However, the majority of biliary anastomoses in children are hepatico-jejunostomies rather than duct-to-duct anastomoses because the recipient duct is usually either absent (in extrahepatic biliary atresia) or very small.[34] Paediatric organ donors are much less common, with the inevitable consequence that children have to wait longer for a suitable liver to become available for transplantation.

Auxiliary liver transplantation

Auxiliary liver transplantation is performed on children with acute liver failure and to correct liver-based metabolic disorders. In this situation, instead of removing the whole of the diseased liver, only part of it is resected. A donor reduced or split lobe is used to replace the resected lobe. In acute liver failure, once the native right liver recovers and regenerates, withdrawal of immunosuppression will cause the atrophy of the transplanted segments.[111]

Reduced liver transplantation

The term 'liver reduction' is used when a liver is cut down to the required size of recipient and the remaining segments are discarded.[112] The left lobe (segments I to IV) can be removed, leaving the right lobe (segments V to VIII) for transplantation, or the right lobe can be removed and the left lobe transplanted. In both these cases the IVC is retained with the transplanted lobe, so either caval replacement or 'piggy-back' techniques can be used. A liver can also be reduced to a left lateral segment (segments II and III) by removing the extended right lobe (segments I and IV to VIII); this allows an adult liver to be used for a small paediatric recipient. In this case, the IVC of the donor liver cannot be retained with the left lateral segment and the 'piggy-back' technique has to be used, joining the left hepatic vein of the donor liver to the confluence of the hepatic veins on the anterior wall of the IVC of the recipient. A left lateral segment reduction is rarely performed these days as the right lobe can be used for another recipient, resulting in what is described as a split liver transplant in which one organ is used for two recipients. Following transplantation, the principal difference between a reduced graft and a whole organ is that there is a relatively flat cut surface which has the potential to bleed or leak bile (Fig. 13.32).

Split liver transplantation

The technique of liver splitting is an extension of liver reduction and enables a donor liver to be used to transplant two recipients rather than just one.[113] The liver is usually split into an extended right lobe and the left lateral segment. Segment IV is sometimes excised from the right lobe and discarded. The IVC is retained with the right lobe. The main portal trunk and hepatic artery are assigned to one or other side of the split (not necessarily the same side). This inevitably results in anastomoses closer to the hilum than usual on the grafts with a short portal vein or hepatic artery. An exception to this arises if there is a replaced right or left hepatic artery, in which case both sides of the split liver graft can have a good length of artery (Fig. 13.33).

Ultrasound evaluation of the paediatric transplant liver

Ultrasound is the primary imaging modality in the follow-up of paediatric liver transplantation. Knowledge of the surgical technique prior to performing the ultrasound is vital to ensure thorough visualisation of the graft, vessels and biliary system. Auxiliary transplants require examination of both the native and auxiliary liver, whilst left lateral segmental grafts are best examined from a transverse epigastric approach (Fig. 13.34).

Normal hepatic parenchyma is homogeneous on greyscale imaging with a non-dilated bile duct system and often an increased periportal reflectivity secondary to liver parenchyma oedema. The hepatic artery and portal vein are best examined at the porta hepatis and the hepatic veins at the level of the venous confluence. The normal hepatic arterial waveform demonstrates a rapid systolic upstroke with a peak systole of >20 cm/s, with antegrade diastolic flow with an RI of between 0.5 and 0.8. A tardus parvus waveform is normal in the first 72 hours due to oedema at the level of the anastomosis, and low or absent diastolic flow may be seen particularly in the presence of an arterial conduit. The portal vein should demonstrate a continuous antegrade waveform although velocity variations are seen with respiration. The hepatic veins and IVC

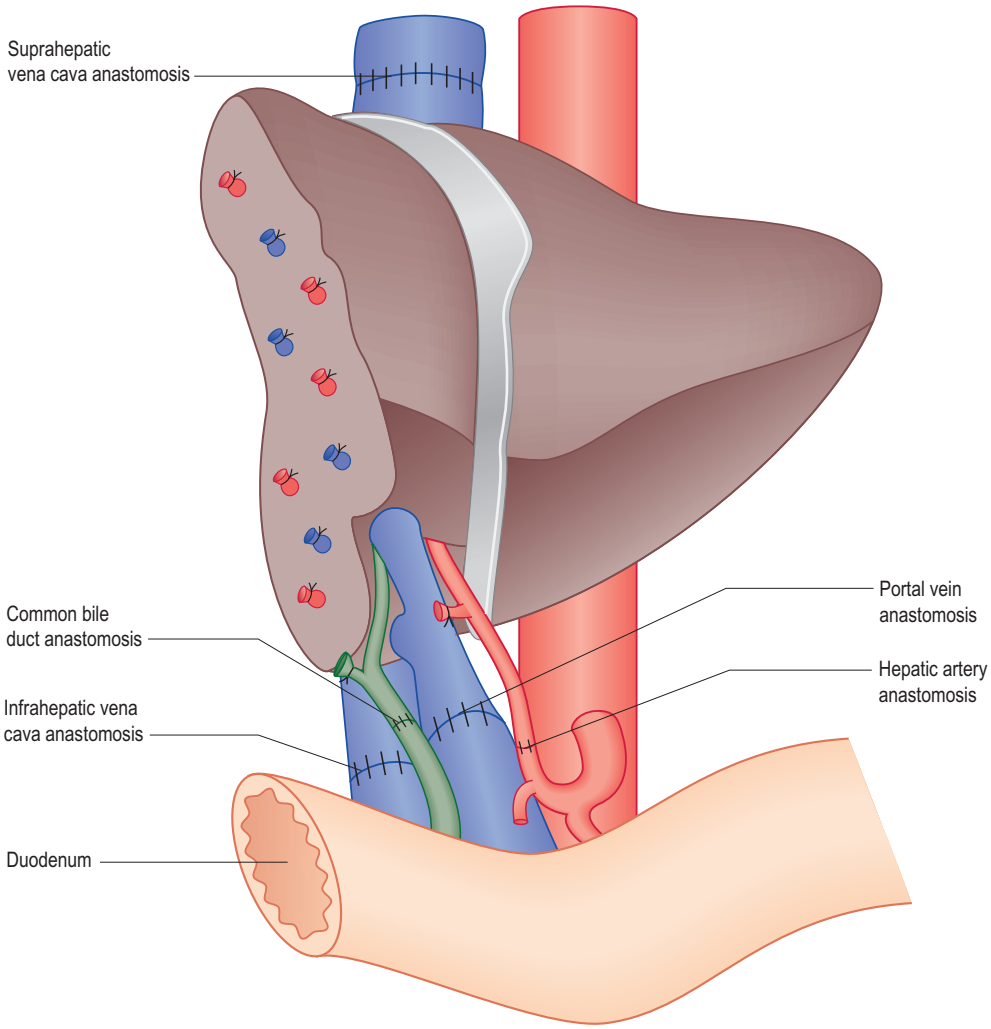


Figure 13.32 Paediatric left lobe transplantation. (Modified from Sidhu PS and Baxter GM (eds), Ultrasound of Abdominal Transplantation. Thieme, Stuttgart, 2006.)

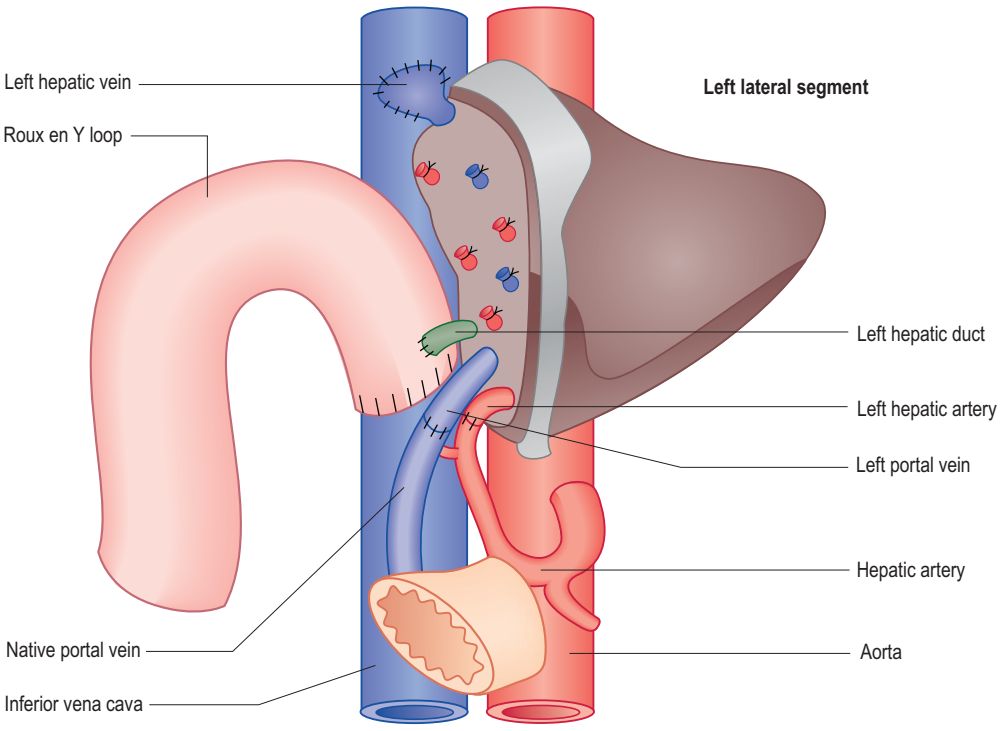


Figure 13.33 Paediatric left lateral segment transplantation. (Modified from Sidhu PS and Baxter GM (eds), Ultrasound of Abdominal Transplantation. Thieme, Stuttgart, 2006.)

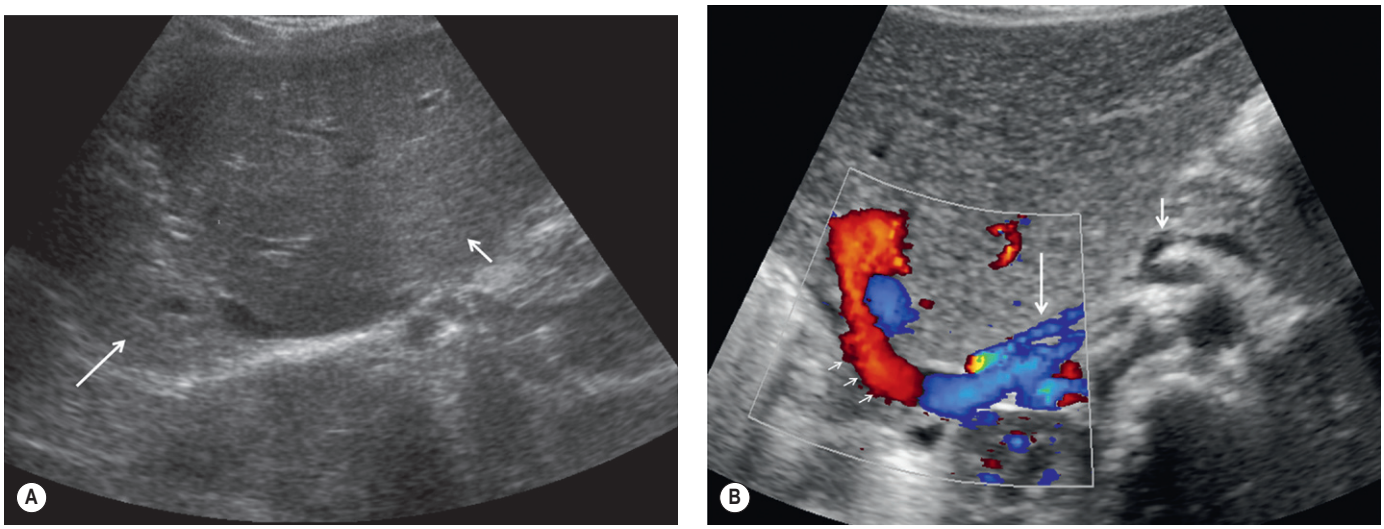


Figure 13.34 Normal ultrasound appearances in the paediatric patient post liver transplantation. A: The native liver (long arrow) is slightly more echogenic in comparison with the transplanted auxiliary liver graft (short arrow), which is not always as distinct on the ultrasound examination. **B:** The splenic artery (short arrow) is seen arising from the coeliac axis with the patent hepatic artery (long arrow) coursing towards the 'split liver' transplant in an 18-month-old child. The portal vein (small arrows) is patent.

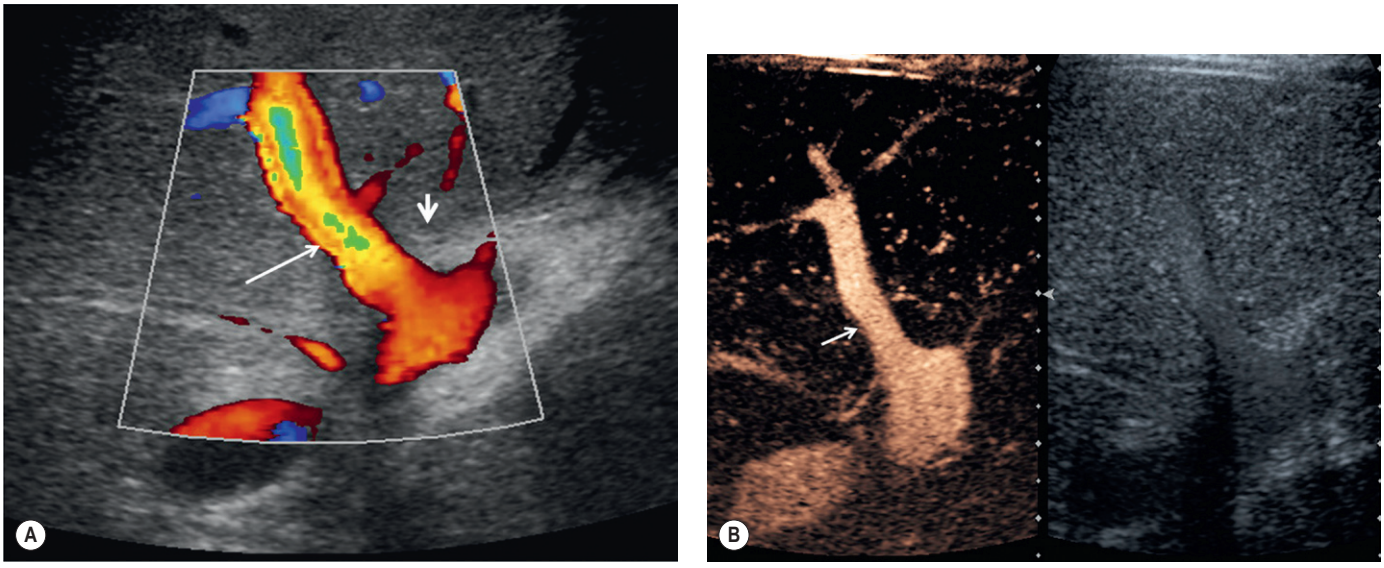


Figure 13.35 Paediatric hepatic artery thrombosis. A: The portal vein is patent on colour Doppler ultrasound (arrow) but no colour Doppler signal is present at the site of the hepatic artery (arrowhead) in this patient with a split liver graft. **B:** Following contrast-enhanced ultrasound, the occlusion of the hepatic artery is confirmed by absence of any enhancement in the hepatic artery, but with enhancement seen in the portal vein (arrow).

show a bi- or triphasic waveform pattern due to transmitted cardiac pulsations.[114,115] Variable volumes of free fluid may be seen in the abdomen and pelvis and haematoma at the cut surface of a reduced sized graft is common. Spleen length is important in the assessment of portal vein flow and the development of portal hypertension.

Ultrasound of complications of paediatric liver transplantation

Post-surgical vascular and biliary complications are more common in children than in adults primarily due to discrepancies in the size of the donor and recipient vessels and use of vascular conduits. It is therefore important for the observer to have an understanding of the surgical techniques used which determine the vascular and biliary anatomy. Clinical manifestations of early complications are varied and there may be no alteration in the liver biochemistry. Post-surgical surveillance ultrasound is therefore important for the detection of 'silent' complications and ultimately graft salvage.[36,114,116] Routinely at our institution uncomplicated paediatric liver transplant patients are imaged with ultrasound on day 1, day 5 and prior to discharge (usually after 10–14 days) with follow-up at 1 month, 3 months, 6 months and then annually thereafter.

Vascular complications

Vascular complications usually occur early, the commonest being hepatic artery thrombosis, which can occur in up to 18% of paediatric patients[117](Fig. 13.35). Ultrasound may demonstrate no arterial

spectral or colour Doppler signal although some intrahepatic Doppler signal may be detected due to collateralisation from the adjacent vascular choledochojejunostomy. These arterial collaterals may exhibit a normal or tardus parvus waveform with an RI of <0.5 and can go undetected due to the speed at which they develop in the absence of any altered hepatic biochemistry.[47] The graft may later demonstrate changes secondary to infarction and bile duct ischaemia with biliary dilatation.

Hepatic artery stenosis is reported to occur in up to 14% of children leading to rejection, biliary ischaemia and hepatic failure.[116] This usually occurs at the anastomotic site. Spectral Doppler waveform demonstrates an accelerated velocity (>200 cm/s) with turbulent colour Doppler in the portion of the vessel immediately distal to the stenosis.[36]

Portal vein thrombosis commonly occurs in the extrahepatic segment. There is a spectrum of change ranging from non-occlusive filling defects on greyscale imaging to absent flow with reverse flow in the intrahepatic portal vein branches (Fig. 13.36).

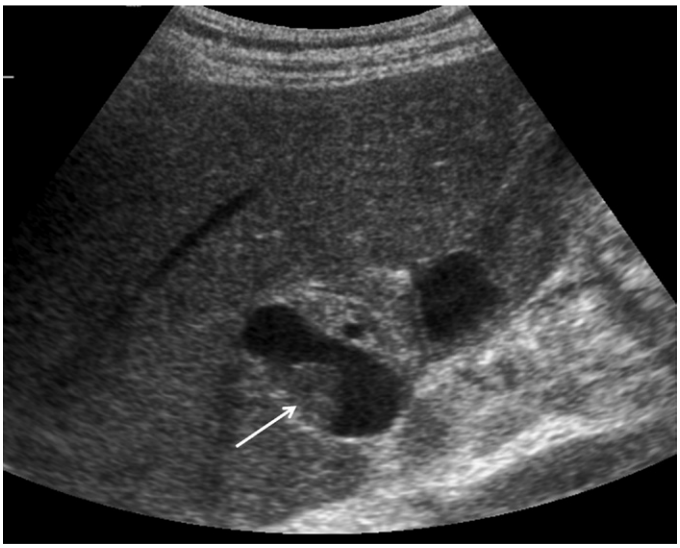


Figure 13.36 Paediatric portal vein thrombosis. Non-occlusive thrombus is present in the portal vein (arrow) following a split liver transplantation.

Portal vein stenosis is rare and usually occurs at the anastomosis site. This may be detected on routine follow-up with high-velocity turbulent flow in the dilated post-stenotic segment and a decrease in the vessel lumen of >50%. A post-stenotic jet with a velocity of >100 cm/s is usually pathognomonic[36,114] (Fig. 13.37).

Inferior vena cava and hepatic vein complications are rare (<1%). These are often suspected clinically as patients present with hepatomegaly, ascites, oedema and pleural effusions and are usually related to surgical problems at the site of the anastomosis.[36]

Biliary complications

These are more common than vascular complications, occurring in up to 30% of patients. Patients who have received a 'cut-down' liver may be at increased risk of biliary anastomotic complications, and the altered anatomy makes imaging of these livers difficult (Fig. 13.38). This group of patients deserves particularly careful monitoring of the intrahepatic duct diameters because in paediatric patients receiving a left lobe graft from an adult donor, the diameter of the bile duct will be appropriate for an adult and may be unusually large for a child. It is therefore important to record the size of the bile duct in such cases during the early postoperative phase, and to monitor for any subsequent dilatation. Failure to do this may give rise to an erroneous diagnosis of biliary dilatation in this group of patients.

Paediatric liver transplantation

- Early post-transplant complications in children may not be clinically suspected; ultrasound surveillance is therefore paramount in detecting 'silent' complications.
- Anastomotic bile duct leaks are the commonest complication following liver transplantation in children.
- Hepatic artery thrombosis, the commonest vascular complication in children, usually leads to early collateralisation of the graft from the highly vascular choledochojejunostomy without graft loss.
- Congenital extrahepatic biliary atresia is the commonest cause of chronic liver disease in infants and young children.
- Non-A-E hepatitis accounts for >50% of causes of acute liver failure in the paediatric population.

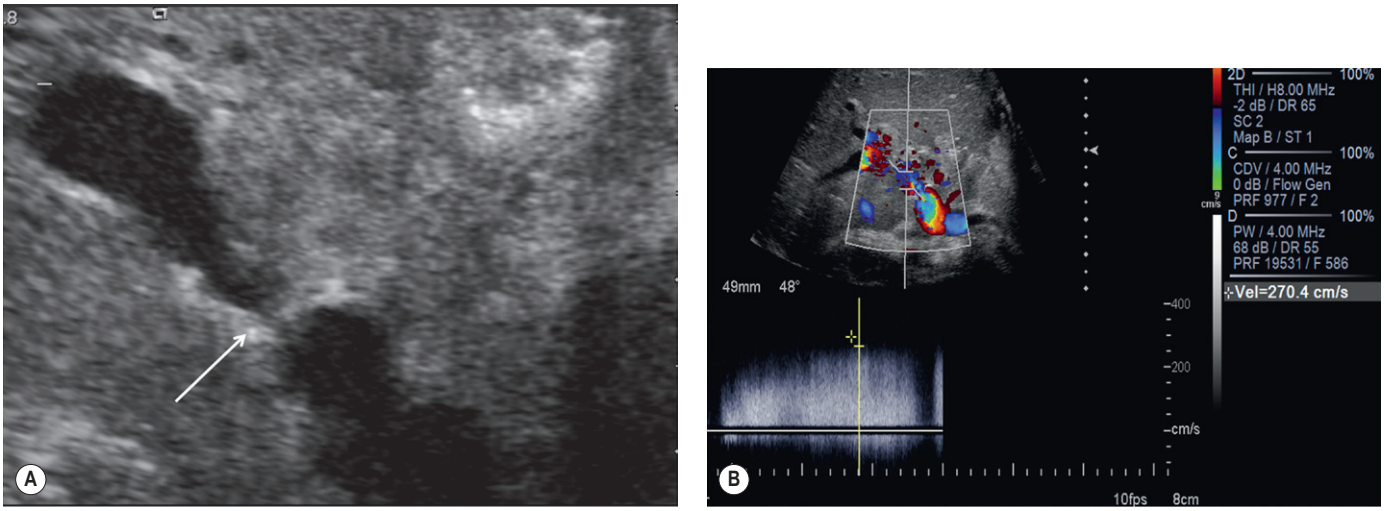


Figure 13.37 Paediatric portal vein stenosis. A: There is an echogenic area of narrowing (arrow) at the site of the portal vein stenosis in a split liver transplant. **B:** The spectral Doppler gate is placed at the site of maximum colour Doppler turbulence and the velocity is measured at 270.4 cm/s, in keeping with a pronounced portal vein stenosis.

Anastomotic bile leaks are the commonest complication but strictures following vascular problems, cut surface bile leaks and obstruction due to debris and stones also occur. Intraparenchymal bilomas, cholangitis and cystic duct remnant mucoceles are rarely reported.[118,119] Ultrasound typically demonstrates bile duct dilatation, perihepatic or cut surface collections in the case of bile leaks which are usually amenable to ultrasound-guided drainage (Fig. 13.39). Fluid in the choledochojejunostomy may masquerade as a pathological fluid collection, and care needs to be taken to identify this.[115]

Diaphragmatic function

Diaphragmatic paralysis with consequent respiratory compromise has been identified in a minority of young children following liver transplantation.[120] Ultrasound is valuable in these patients to establish the diagnosis by observing the diaphragm movement during spontaneous respiration. The condition is probably caused by damage to the phrenic nerve during clamping of the suprahepatic vena cava.

Small bowel complications

These typically involve the choledochojejunostomy and include 'Roux' loop torsion, stasis, intussusception and infarction.[121]

General surgical complications

These include bleeding and haematoma formation, right-sided pleural effusions and ascites, small bowel perforation and right diaphragmatic injury. Hepatic infarcts and a heterogeneous parenchyma may be seen in the presence of rejection.



Figure 13.38 Paediatric bile duct dilatation. Central bile duct dilatation (between cursors) in a child with a left lateral segment graft who developed a liver hilar anastomotic stricture following portal vein stenosis.

Post-transplant lymphoproliferative disease

This occurs in 3% of patients in the presence of the EBV and high levels of immunosuppression and is usually non-Hodgkin's in origin.[122] Typically it involves the abdominal nodes and small bowel, and ultrasound may detect lymphadenopathy at the porta and thickened small bowel. Chest manifestation includes nodules, adenopathy, effusions and consolidation, and periventricular white matter change can be seen on head CT.

Recurrent disease in children

Hepatoblastoma

Hepatoblastoma is the commonest primary liver tumour in children under 5 years of age for which transplantation is a recognised treatment. Factors associated with a poor prognosis and disease recurrence include previous resection, portal vein invasion by tumour, multifocal disease, other vascular invasion and the presence of extrahepatic disease. Unifocal disease, irrespective of tumour size, with fetal epithelium on histology is associated with a better outcome whilst the presence of anaplastic cell type has been associated with a poor prognosis.[123]

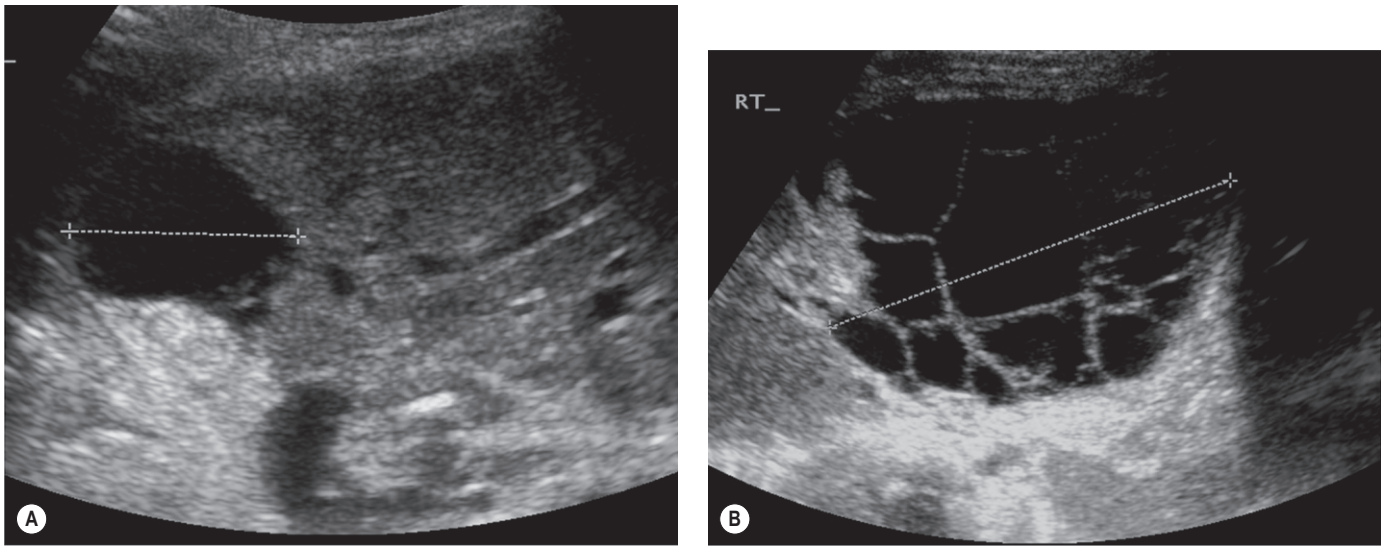


Figure 13.39 Paediatric abdominal collections. A: Anechoic fluid collection (between cursors) adjacent to the cut surface of a left lateral segment graft. **B:** Complex septated collection (between cursors) in the upper abdomen representing bilomas or haematoma.

Hepatocellular carcinoma

The common age range for HCC is between 5 and 15 years but is less common than hepatoblastoma. Any pre-existing conditions that lead to cirrhosis will predispose to HCC development. This includes biliary atresia, Fanconi's syndrome and metabolic diseases such as tyrosinaemia. HCC in children has a worse prognosis than hepatoblastoma as it often presents late with evidence of metastatic disease. Children with the worst survival were those transplanted for HCC with pre-existing underlying liver disease. Children with tyrosinaemia are transplanted to prevent the development of HCC; the incidence of HCC increases with age in these patients.[124]

REFERENCES

1. Norris S. Chronic liver diseases: indications for liver transplantation. In: Sidhu PS, Baxter GM, editors. Ultrasound of abdominal transplantation. Stuttgart: Thieme; 2002. p. 61–68.
2. Berry JD, Sidhu PS. Microbubble contrast-enhanced ultrasound in liver transplantation. Eur Radiol 2004;14:P96–P103.
3. Shaw AS, Ryan SM, Beese RC, et al. Liver transplantation. Imaging 2002;14:314–328.
4. Mazzaferro V, Regalia E, Doci R, et al. Liver transplantation for the treatment of small hepatocellular carcinomas in patients with cirrhosis. N Engl J Med 1996;334:693–699.
5. Deasy NP, Wendon J, Meire HB, Sidhu PS. The value of serial Doppler ultrasound as a predictor of clinical outcome and the need for transplantation in fulminant and severe acute liver failure. Br J Radiol 1999;72:134–143.
6. Kim MJ, Lim JH, Lee SJ, et al. Correlation between the echogenicity of dysplastic nodules and their histopathologically determined fat content. J Ultrasound Med 2003;22:327–334.
7. Farrant P, Meire HB. Hepatic vein pulsatility assessment on spectral Doppler ultrasound. Br J Radiol 1997;70:829–832.
8. Mok TSK, Yu SCH, Lee C, et al. False-negative rate of abdominal sonography for detecting hepatocellular carcinoma in patients with hepatitis B and elevated serum α-fetoprotein levels. AJR Am J Roentgenol 2004;183:453–458.
9. Nicolau C, Vilana R, Bru C. The use of contrast-enhanced ultrasound in the management of the cirrhotic patient and for the detection of HCC. Eur Radiol 2004;14:P63–P71.
10. Nicolau C, Catala V, Vilana R, et al. Evaluation of hepatocellular carcinoma using SonoVue, a second generation ultrasound contrast agent: correlation with cellular differentiation. Eur Radiol 2004;14:1092–1099.
11. Quaia E, D'Onofrio M, Cabassa P, et al. Diagnostic value of hepatocellular nodule vascularity after microbubble injection for characterizing malignancy in patients with cirrhosis. AJR Am J Roentgenol 2007;189:1474–1483.
12. Forner A, Vilana R, Ayuso C, et al. Diagnosis of hepatic nodules 20 mm or smaller in cirrhosis: Prospective validation of the noninvasive diagnostic criteria for hepatocellular carcinoma. Hepatology 2008;47:97–104.
13. Ichikawa T, Federle MP, Grazioli L, et al. Fibrolamellar hepatocellular carcinoma: imaging and pathologic findings in 31 recent cases. Radiology 1999;213:352–361.
14. Tessler FN, Gehring BJ, Gomes AS, et al. Diagnosis of portal vein thrombosis: value of color Doppler imaging. AJR Am J Roentgenol 1991;157:293–296.
15. Marshall MM, Beese RC, Muiesan P, et al. Assessment of portal venous patency in the liver transplant candidate: a prospective study comparing ultrasound, microbubble-enhanced colour Doppler ultrasound with arteriography and surgery. Clin Radiol 2002;57:377–383.
16. Sidhu PS, Marshall MM, Ryan SM, Ellis SM. Clinical use of Levovist, an ultrasound contrast agent, in the imaging of liver transplantation: assessment of the pre and post transplant patient. Eur Radiol 2000;10:1114–1126.
17. Devlin J, O'Grady J. Indications for referral and assessment in adult liver transplantation: a clinical guideline. Gut 1999;45(Suppl 6): VI1–VI22.
18. Kolmannskog F, Jakobsen JA, Schrumpf E, Bergan A. Duplex Doppler sonography and angiography in the evaluation for liver transplantation. Acta Radiol 1994;35:1–5.
19. Sellars ME, Sidhu PS, Heneghan M, et al. Infusions of microbubbles are more cost effective than bolus injections in Doppler studies of the portal vein: a quantitative comparison of normal volunteers and patients with cirrhosis. Radiology 2000;217(P):636.
20. Bach AM, Hann LE, Brown KT, et al. Portal vein evaluation with US: comparison to angiography combined with CT arterial portography. Radiology 1996;201:149–154.
21. Alpern MB, Rubin JM, Williams DM, Capek P. Porta hepatis: duplex Doppler US with angiographic correlation. Radiology 1987;162:53–56.
22. Ueno N, Kawamura H, Takahashi H, et al. Characterization of portal vein thrombus with the use of contrast-enhanced sonography. J Ultrasound Med 2006;25:1147–1152.
23. Colli A, Cocciolo M, Riva C, et al. Abnormalities of Doppler waveform of the hepatic veins in patients with chronic liver disease: correlation with histologic findings. AJR Am J Roentgenol 1994;162:833–837.
24. Millener P, Grant EG, Rose S, et al. Color Doppler imaging findings in patients with Budd-Chiari syndrome: correlation with venographic findings. AJR Am J Roentgenol 1993;161:307–312.
25. Iwao T, Toyonaga A, Shigemori H, et al. Hepatic artery hemodynamic responsiveness to altered portal blood flow in normal and cirrhotic livers. Radiology 1996;200:793–798.
26. Owens CA, Bartolone C, Warner DL, et al. The inaccuracy of duplex ultrasonography in predicting patency of transjugular intrahepatic portosystemic shunts. Gastroenterology 1998;114:1433–1434.
27. Haskal ZJ, Pentecost MJ, Soulen MC, et al. Transjugular intrahepatic portosystemic shunt stenosis and revision: early and mid term results. AJR Am J Roentgenol 1994;163:439–444.
28. Furst G, Malms J, Heyer T, et al. Transjugular intrahepatic portasystemic shunts: improved evaluation with echo-enhanced color Doppler sonography, power Doppler and spectral duplex sonography. AJR Am J Roentgenol 1998;170:1047–1054.
29. Ralls PW, Lee KP, Mayekawa DS, et al. Color Doppler sonography of portocaval shunts. J Clin Ultrasound 1990;18:379–381.
30. Kawasaki S, Makuuchi M, Matsunami H, et al. Preoperative measurement of segmental liver volume of donors for living related liver transplantation. Hepatology 1993;18:1115–1120.
31. Redvanly RD, Nelson RC, Stieber AC, Dodd GD. Imaging in the preoperative evaluation of adult liver-transplant candidates: goals, merits of various procedures, and recommendations. AJR Am J Roentgenol 1995;164:611–617.
32. Van Thiel DH, Hagler NG, Schade RR, et al. In vivo hepatic volume determination using sonography and computed tomography. Validation and a comparison of the two techniques. Gastroenterology 1985;88:1812–1817.
33. Schiano TD, Bodian C, Schwartz ME, et al. Accuracy and significance of computed tomographic scan assessment of hepatic volume in patients undergoing liver transplantation. Transplantation 2000;69:545–550.
34. Heaton ND, Corbally MT, Rela M, Tan KC. Surgical techniques of segmental reduction. Split and auxillary liver transplantation. In: Williams R, Portmann B, Tan KC, editors. The practice of liver transplantation. London: Churchill Livingstone; 1995. p. 143–151.
35. Bowles M, Rela M. Liver transplantation: surgical techniques. In: Sidhu PS, Baxter GM, editors. Ultrasound of abdominal transplantation. Stuttgart: Thieme; 2002:69–75.
36. Glockner JF, Forauer AR. Vascular or ischemic complications after liver transplantation. AJR Am J Roentgenol 1999;173:1055–1059.
37. Shaw AS, Ryan SM, Beese RC, Sidhu PS. Ultrasound of non-vascular complications in the post-transplant patient. Clin Radiol 2003;58:672–680.
38. Nolten A, Sproat IA. Hepatic artery thrombosis after transplantation; temporal accuracy of diagnosis with duplex ultrasound and the syndrome of impending thrombosis. Radiology 1996;198:553–559.
39. Tzakis A, Gordon R, Shaw B, et al. Clinical presentation of hepatic artery thrombosis after liver transplantation in the cyclosporine era. Transplantation 1985;40:667–671.
40. Propeck PA, Scanlan KA. Reversed or absent hepatic arterial diastolic flow in liver transplants shown by duplex sonography: a poor predictor of subsequent hepatic artery thrombosis. AJR Am J Roentgenol 1992;159:1199–1201.
41. Dodd GD, Memel DS, Zajko AB, et al. Hepatic artery stenosis and thrombosis in transplant recipients: Doppler diagnosis with resistive index and systolic acceleration time. Radiology 1994;192:657–661.
42. Wozney P, Zajko AB, Bron KM, et al. Vascular complications after liver transplantation: a five-year experience. AJR Am J Roentgenol 1986;147:657–663.
43. Stratta RJ, Wood RP, Langnas AN, et al. Diagnosis and treatment of biliary tract complications after orthoptic liver transplant. Surgery 1989;106:675–684.

44. Balan V, Abu-Elmagd K, Demetris AJ. Autoimmune liver diseases. Recurrence after liver transplantation. Surg Clin North Am 1999;79:147–152.
45. Katyal S, Oliver JH, Buck DG, Federle MP. Detection of vascular complications after liver transplantation: early experience in multislice CT angiography with volume rendering. AJR Am J Roentgenol 2000;175:1735–1739.
46. Sidhu PS, Shaw AS, Ellis SM, et al. Microbubble ultrasound contrast in the assessment of hepatic artery patency following liver transplantation: role in reducing frequency of hepatic artery arteriography. Eur Radiol 2004;14:21–30.
47. Hall TR, Diarmid SV, Grant EG, et al. False-negative duplex Doppler studies in children with hepatic artery thrombosis after liver transplantation. AJR Am J Roentgenol 1990;154:573–575.
48. Flint EW, Sumkin JH, Zajko AB, Bowen A. Duplex sonography of hepatic artery thrombosis after liver transplantation in the cyclosporin era. AJR Am J Roentgenol 1988;151:481–483.
49. Ryan SM, Sidhu PS. CT of liver transplantation. Appl Radiol 2006;35:10–21.
50. Abbasoglu O, Levy MF, Vodapally MS, et al. Hepatic artery stenosis after liver transplantation – incidence, presentation, treatment, and long term outcome. Transplantation 1997;27:250–255.
51. Sidhu PS, Ellis SM, Karani JB, Ryan SM. Hepatic artery stenosis following liver transplantation: significance of the tardus parvus waveform and the role of microbubble contrast media in the detection of a focal stenosis. Clin Radiol 2002;57:789–799.
52. Marshall MM, Muiesan P, Srinivasan P, et al. Hepatic artery pseudoaneurysms following liver transplantation: incidence, presenting features and management. Clin Radiol 2001;56:579–587.
53. Lerut J, Tzakis A, Bron KM, et al. Complications of venous reconstruction in human orthotopic liver transplantation. Ann Surg 1987;205:404–414.
54. Hamady M, Rela M, Sidhu PS. Spontaneous resolution of a portal vein stenosis over a 21-month period in a "split-liver" transplant: demonstration by colour Doppler ultrasound, catheter angiography and splenic pulp pressures. Eur Radiol 2002;12:2280–2283.
55. Samuel D, Gillet D, Reynes M, Bismuth H. Portal and arterial thrombosis in liver transplantation: a frequent event in severe rejection. Transplantation Proc 1989;21:2225–2227.
56. Raby N, Karani JB, Thomas S, et al. Stenoses of vascular anastomoses after hepatic transplantation: treatment with balloon angioplasty. AJR Am J Roentgenol 1991;157:167–171.
57. Platt JF, Rubin JM, Ellis JH. Hepatic artery resistance changes in portal vein thrombosis. Radiology 1995;196:95–98.
58. Chezmar JL, Nelson RC, Bernardino ME. Portal venous gas after hepatic transplantation; sonographic detection and clinical significance. AJR Am J Roentgenol 1989;153:1203–1205.
59. Rossi AR, Pozniak MA, Zarvan NP. Upper inferior vena caval anastomotic stenosis in liver transplant recipients: Doppler US diagnosis. Radiology 1993;187:387–389.
60. Coulden RA, Britton PD, Farman P, Noble-Jamieson G, Wright DGD. Preliminary report: hepatic vein Doppler in the early diagnosis of acute liver transplant rejection. Lancet 1990;336:273–275.
61. Ruckert JC, Ruckert RI, Rudolph B, Muller JM. Recurrence of the Budd–Chiari syndrome after orthotopic liver transplantation. Hepatogastroenterology 1999;46:867–871.
62. Demetris JA, Slasky S, Van Thiel DH, et al. Pathology of hepatic transplantation; a review of 62 adult allograft recipients immunosuppressed with a cyclosporine/steroid regimen. Am J Pathol 1985;118:151–161.
63. Longley DG, Skolnick ML, Sheahan DG. Acute allograft rejection in liver transplant recipients: lack of correlation with loss of hepatic artery diastolic flow. Radiology 1988;169:417–420.
64. Marder DM, De Marino GB, Sumkin JH, Sheahan DG. Liver transplant rejection: value of the resistive index in Doppler US of hepatic arteries. Radiology 1989;173:127–129.
65. Kaplan SB, Sumkin J, Campbell WL, et al. Periportal low attenuation areas on CT; value as evidence of liver transplant rejection. AJR Am J Roentgenol 1989;152:285–287.
66. Klein AS, Savador S, Burdick JF, et al. Reduction of morbidity and mortality from biliary complications after liver transplantation. Hepatology 1991;14:818–823.
67. Lerut J, Gordon RD, Iwatsuki S, et al. Biliary tract complications in human orthoptic liver transplantation. Transplantation 1987;43: 47–51.
68. Lopez RR, Bennar KG, Ivanceu K, et al. Management of biliary complications after liver transplantation. Am J Surg 1992;163: 519–524.
69. Greif F, Bronsther OL, Van Thiel DH, et al. The incidence, timing and management of biliary tract complications after liver transplantation. Ann Surg 1994;219:40–45.
70. Neimin HL, Mintzer RA. Accuracy of biliary duct ultrasound; conparison with cholangiography. AJR Am J Roentgenol 1977;129: 979–982.
71. Kok T, Van der Sluis A, Klein JP, et al. Ultrasound and cholangiography for the diagnosis of biliary complications after orthoptic liver transplantation; a comparative study. J Clin Ultrasound 1996;24:103–115.
72. Kaplan S, Zajko AB, Koneru B. Hepatic bilomas due to hepatic artery thrombosis in liver transplant recipients: percutaneous drainage and clinical outcome. Radiology 1990;174:1031–1035.
73. Evans RA, Raby ND, O'Grady J, et al. Biliary complications following orthoptic liver transplantation. Clin Radiol 1990;41:190–194.
74. Woods RP, Shaw BW, Starzl TE. Extrahepatic complications of liver transplantation. Semin Liver Disease 1985;5:377–384.
75. Caiado AHM, Blasbalg R, Marcelino ASZ, et al. Complications of liver transplantation: multimodality imaging approach. Radiographics 2007;27:1401–1417.
76. Cox KL, Lawerence-Miyasaki LS, Garcia-Kennedy R, et al. An increased incidence of Epstein-Barr virus infection and lymphoproliferative disorders in young children on FK506 after liver transplantation. Transplantation 1995;59:524–529.
77. Younes BS, McDiarmid MG, Martin JH, et al. The effect of immunosuppression on post-transplant lymphoproliferative disease in pediatric liver transplant patients. Transplantation 2000;70:94–97.
78. McCarthy M, Ramage JK, McNair A, et al. The clinical diversity and role of chemotherapy in lymphoproliferative disorder in liver transplantation recipients. J Hepatol 1997;27:1015–1021.
79. Morrison VA, Dunn DL, Manivel JC, et al. Clinical characteristics of post-transplant lymphoproliferative disorders. Am J Med 1994;97: 14–24.
80. Pickhardt PJ, Siegel MJ. Abdominal manifestations of post transplantation lymphoproliferative disorder. AJR Am J Roentgenol 1998; 171:1007–1013.
81. Pickhardt PJ, Siegel MJ. Post transplantation lymphoproliferative disorder of the abdomen: CT evaluation in 51 patients. Radiology 1999;213:73–78.
82. Navarro F, Pyda P, Pageaux GP, et al. Lymphoproliferative disease after liver transplantation: primary biliary location. Transplant Proc 1998;30:1486–1488.
83. Bowen A, Hungate RG, Kaye RD, et al. Imaging in liver transplantation. Pediatr Gastrointest Radiol 1996;34:757–778.
84. McDiarmid SV, Busuttil RW, Ascher NL, et al. FK506 (Tacrolimus) compared with cyclosporine for primary immunosuppression after paediatric liver transplantation: results from the US multicenter trial. Transplantation 2001;59:530–536.
85. Cattral MS, Langas AN, Wisecarver JL, et al. Survival of graft versus host disease in a liver transplant recipient. Transplantation 1994;57:1271–1274.
86. Holbert BL, Campbell WL, Skolnick ML. Evaluation of the transplanted liver and postoperative complications. Radiol Clin North Am 1998;33:521–540.
87. Nicholson V, Johnson PC. Infectious complications in solid organ transplant recipients. Surg Clin North Am 1994; 74:1223–1245.
88. Desai SR, Beese RC, Karani JB. Intrahepatic abscess formation following adult orthoptic liver transplantation. Br J Radiol 1996;96:200.
89. Jamieson NV, Williams R, Calne RY. Liver transplantation for Budd Chiari syndrome 1976–1990. Ann Chir 1991; 45:362–365.
90. Hulff G, Todo S, Tzakis AG, et al. Liver transplantation for Budd Chiari syndrome. Ann Surg 1990;211:43–49.
91. Testa G, Crippin JS, Netto GJ, et al. Liver transplantation for hepatitis C: recurrence and disease progression in 300 patients. Liver Transpl 2000;6:553–561.
92. O'Grady JG, Smith HM, Davies SE, et al. Hepatitis B reinfection after orthoptic liver transplantation. Serological and clinical implications. J Hepatol 1992;14:104–111.
93. Davern TJ, Lake JR. Recurrent disease after liver transplantation. Semin Gastrointest Dis 1998;9:86–109.
94. McPeake JR, O'Grady J, Zaman S, et al. Liver transplantation for primary hepatocellular carcinoma: tumor size and number determine outcome. J Hepatol 1993;18:226–234.
95. Imatsuki S, Gordon RD, Shaw BJ, Starzl TE. Role of liver transplantation in cancer therapy. Ann Surg 1985;202:401–407.
96. Ismail T, Angrisani L, Gunson BK, et al. Primary hepatic malignancy: the role of liver transplantation. Br J Surg 1990;77:983–987.

97. Migliazza L, Lopez Santamaria M, Murcia J, et al. Long-term survival expectancy after liver transplantation in children. J Pediatr Surg 2000;35:5–7.
98. El-Gazzaz G, Wong W, El-Hadary MK, et al. Outcome of liver resection and transplantation for fibrolamellar hepatocellular carcinoma. Transpl Int 2000;13:S406–S409.
99. Mackie J, Groves K, Hoyle A, et al. Orthoptic liver transplantation for alcoholic liver disease: a retrospective analysis of survival and risk factors predisposing to recidivision. Liver Transpl 2001;7:418–427.
100. O'Grady JG, Polson RJ, Rolles K, et al. Liver transplantation for malignant disease. Results in 93 consecutive patients. Ann Surg 1988;207:373–379.
101. Garcia RF, Garcia CE, McMaster P, Neuberger J. Transplantation for primary biliary cirrhosis: retrospective analysis of 400 patients in a single center. Hepatology 2001;33:22–27.
102. Gow PJ, Chapman RW. Liver transplantation for primary sclerosing cholangitis. Liver 2000;20:97–103.
103. Kelly DA. Current results and evolving indications for liver transplantation in children. J Pediatr Gastroenterol Nutr 1998;27:214–221.
104. Bisset GS, Strife J, Balistreri WF. Evaluation of children for transplantation; value of MR imaging and sonography. AJR Am J Roentgenol 1990;155:351–356.
105. Colombo C, Russo MC, Zazzeron L, Romano G. Liver disease in cystic fibrosis. J Pediatr Gastroenterol Nutr 2006;43:S49–S55.
106. Engelmann G, Schmidt J, Oh J, et al. Indications for paediatric liver transplantation. Data from the Heidelberg paediatric liver transplantation program. Nephrol Dial Transplant 2007;22:823–828.
107. Lee WS, McKieman P, Kelly DA. Etiology, outcome and prognostic indicators of childhood fulminant hepatic failure in the United Kingdom. J Pediatr Gastroenterol Nutr 2005;40:1160–1172.
108. Bismuth H, Houssin D. Reduced-sized orthotopic liver graft in hepatic transplantation in children. Surgery 1984;95:367–370.
109. Strong R, Lynch S, Ong T, et al. Successful liver transplantation from a living donor to her son. N Engl J Med 2010;322:1505–1507.
110. Strong RW, Ong TH, Pillay P, et al. A new method of segmental orthotopic liver transplantation in children. Surgery 1988;104:104–107.
111. Bartlett A, Rela M. Progress in surgical techniques in paediatric liver transplantation. Paediatr Transplant 2009;14:33–40.
112. de Hemptinne B, Salizzoni M, Tan KC, Otte JB. The technique of liver reduction in orthotopic liver transplantation. Transplant Proc 1988;20:508–511.
113. Rela M, Vougas V, Muiesan P, et al. Split liver transplantation. Kings College Hospital experience. Ann Surg 1998;227:282–288.
114. Crossin JD, Muradali D, Wilson SR. US of liver transplants: normal and abnormal. Radiographics 2003;23:1093–1114.
115. Caron KH, Strife JL, Babock DS, Ryckman FC. Left-lobe hepatic transplants: spectrum of normal imaging findings. AJR Am J Roentgenol 1992;159:497–501.
116. Berrocal T, Parron M, Alvarez-Luque A, et al. Pediatric liver transplantation: a pictorial essay of early and late complications. Radiographics 2006;26:1187–1209.
117. Karani JB, Heaton ND. Review. Imaging in liver transplantation. Clin Radiol 1998;53:317–322.
118. Lorenz JM, Funaki B, Leef JA, et al. Percutaneous transhepatic cholangiography and biliary drainage in paediatric liver transplant patients. AJR Am J Roentgenol 2001;176:761–765.
119. O'Loughlin EV, Stromon MO, Shun A, et al. Biliary strictures and hepatic artery flow abnormalities in split liver transplants. Pediatr Transpl 2010;14:121–125.
120. Smyrniotis V, Andreani P, Muiesan P, et al. Diaphragmatic nerve palsy in young children following liver transplantation. Successful treatment by plication of the diaphragm. Transpl Int 1998;11:281–283.
121. Gimson AES, Karani JB, Heaton ND. Major biliary tract and vascular complications. In: Williams R, Portmann B, Tan KC, editors. The practice of liver transplantation. London: Churchill Livingstone; 1995. p. 199–209.
122. Wilde EW, Moore DJ, Bellah RD. Posttransplantation lymphoproliferative disorder in pediatric recipients of solid organ transplants: timing and location of disease. AJR Am J Roentgenol 2005;285:1335–1341.
123. Koneru B, Flye MW, Busuttil RW, et al. Liver transplantation for hepatoblastoma. The American experience. Ann Surg 1991;213: 118–121.
124. Ryckman FC, Alonso MH, Busuttil RW, Klintmalm GBG. Transplantation for primary hepatic malignancy in children. In: Transplantation of the liver. Philadelphia: WB Saunders; 1996. p. 216–226.

CHAPTER

14 Gallbladder and biliary tree

Jane A. Smith

NORMAL ANATOMY OF THE BILIARY TREE 227
Gallbladder 227
Cystic duct 227

NORMAL ANATOMICAL VARIANTS 227
Ducts 227
Gallbladder 228
Hepatic artery 228

TECHNIQUE AND ULTRASOUND APPEARANCE 228
Measurement of the common duct 234
Function studies 236

ENDOSCOPIC ULTRASOUND 236

LAPAROSCOPIC ULTRASOUND 236

PATHOLOGY OF THE GALLBLADDER 236
Stones 237
Classic appearances 237
Contracted gallbladder 238
Movement/layering/floating of stones 239
Microlithiasis/biliary sludge 240
Gallbladder wall thickening 241
Acute cholecystitis 243
Chronic cholecystitis 246
Hyperplastic cholecystoses 247
Polyps 247
Carcinoma 249
Worms 250
Ascariasis 250
Clonorchiasis 251
Fascioliasis 251
Hydrops 251
Microgallbladder 251

BILE DUCT PATHOLOGY 253
Jaundice 253
Bile duct dilatation 254
Obstruction without dilatation 255
Dilatation without jaundice 255
Rapid changes in duct diameter 255
Gallbladder distension 256
Choledocholithiasis 258
Bile duct neoplasms 261
Other tumours obstructing the bile ducts 263
Choledochal cysts 263
Caroli's disease 264
Oriental cholangiohepatitis 265
Biliary ascariasis 266
Sclerosing cholangitis 267

NORMAL ANATOMY OF THE BILIARY TREE

The intrahepatic bile ducts run in the portal tracts alongside the portal vein radicles and hepatic artery branches. At the porta hepatis, the right and left hepatic ducts join to form the common hepatic duct, which passes inferiorly for approximately 3 cm before being joined by the cystic duct to form the common bile duct.

The common bile duct continues caudally for approximately 7 cm, lying anterior to the right margin of the portal vein and lateral to the hepatic artery (Figs 14.1 and 14.2). It runs parallel with both vessels for a short distance before passing behind the first part of the duodenum. Distally, the common duct lies in a deep groove on the posterior aspect of the head of the pancreas, often completely surrounded by pancreatic tissue.

Within the posterolateral part of the pancreatic head, the distal end of the common bile duct passes laterally, accompanying the pancreatic duct into the second part of the duodenum.

Gallbladder

The gallbladder serves as a reservoir for bile secreted by the liver; thus its size varies according to digestive requirements throughout the day.

The gallbladder lies in a fossa on the undersurface of the right lobe of the liver. It has a thin smooth wall, up to 2 mm in thickness (Fig. 14.3),[1] composed of an outer serosal layer, a middle fibromuscular layer and inner mucosa. The bulbous distal portion of the gallbladder, the fundus, is generally in the most caudal and anterior position, often projecting below the inferior margin of the liver. The fundus tapers into the body and finally into the neck, which curves posterocaudally before becoming continuous with the cystic duct (Fig. 14.4).

The wall of the gallbladder is at its thickest in the region of the neck– normally up to 2 mm (Fig. 14.5). A small pouch may be seen projecting caudally and posteriorly – Hartmann's pouch, which often becomes more marked in cases of gallbladder dilatation.

Cystic duct

The cystic duct, 3 to 4 cm in length, is lined by mucosal folds which project into the lumen in a spiral arrangement – hence the term 'spiral valve'. It is not in fact a true valve, and bile can flow in both directions through the duct determined by differences in pressure between the gallbladder and common bile duct. Its importance to the sonographer is that there may be an acoustic shadow beyond the valve, falsely suggesting a stone in the cystic duct (Fig. 14.6).[2]

NORMAL ANATOMICAL VARIANTS

Ducts

Normal variations in the anatomy of the ducts are common. The point at which the cystic duct joins the common hepatic duct is particularly variable; usually the ducts unite just beyond the porta hepatis, but the cystic duct may join the right hepatic duct or the join may be much lower – occasionally within the head of the



Figure 14.1 Right hepatic duct. The normal calibre right hepatic duct (arrows) is seen anterior to the right branch of the portal vein.

pancreas itself. The cystic duct may pass medially either posteriorly or anteriorly to the common hepatic duct, then curving laterally to join its medial border.

On ultrasound scans it is not usually possible to recognise the exact point of union of the cystic and common hepatic ducts, and it has therefore become accepted convention to refer to the extrahepatic bile duct as 'the common duct'.[3]

Gallbladder

The shape, size and position of the gallbladder are highly variable. In some cases the gallbladder fossa lies deep within the liver so the gallbladder appears to be surrounded by hepatic tissue – the so-called 'intrahepatic gallbladder'. At the other end of the spectrum, the gallbladder may be attached to the porta only at the neck, forming a very mobile structure which may be found in the right iliac fossa or even in the pelvic region, depending upon patient position.

In some subjects the fundus of the gallbladder is folded over – the 'Phrygian cap' – which can make examination of the lumen difficult.[4] Turning the patient onto his/her left side, or even partially prone, can unfold the gallbladder, making it more accessible to full ultrasound interrogation (Figs 14.7 and 14.8). Not infrequently the neck of the gallbladder may be elongated, and turned back on itself. This may be mistaken for a duct or vessel, or may even be missed altogether. The sonographer must be aware of this anatomical shape in order to reliably exclude gallstones (Fig. 14.8C).

Folding of the gallbladder is a common variation which may mimic septation. True septa are uncommon, and can be distinguished from folding of the gallbladder by scanning in both longitudinal and transverse planes with the patient supine and in the left decubitus position. Septae can lead to errors in diagnosis when the sonographer reports one portion of the gallbladder as free of stones and misses a stone in the distal portion (Fig. 14.9).[5] Although not usually considered clinically significant, there is some evidence that gallbladder septae or folds may delay gallbladder emptying, particularly from the distal segment, and that this may be associated with abdominal pain.[6]

The gallbladder may be totally absent, or there may be double or even triple gallbladders with either a single cystic duct or with multiple separate cystic ducts – these anomalies are extremely rare.[7]

Hepatic artery

Usually, the hepatic artery arises from the coeliac axis and runs for a short distance to the right before turning superiorly. At this point the artery lies anterior to the portal vein with the common duct to the right. Just proximal to the porta hepatis the artery branches, and the right hepatic artery crosses to the right, posterior to the common hepatic duct before entering the substance of the liver (Fig. 14.10).

In about 15% of subjects, the right hepatic artery passes anteriorly to the common hepatic duct, and in a smaller proportion (approximately 5%), the right hepatic artery originates from the superior mesenteric artery – the replaced right hepatic artery – and passes posteriorly to the superior mesenteric vein before turning anteriorly to the portal vein.[8] Colour Doppler ultrasound may be useful in sorting out the anatomy in these cases,[9] although it is usually possible to identify the vessels by tracing them back to their point of origin (Fig. 14.11).

TECHNIQUE AND ULTRASOUND APPEARANCE

The biliary system should be examined after the patient has fasted – not only does this distend the gallbladder with bile to allow investigation of its lumen, but it helps to reduce the contents of the stomach and duodenum, which may obscure the common duct and pancreas.

In some patients, the posterior wall of the gallbladder is closely adjacent to the duodenum and distal acoustic shadowing from the latter may simulate gallbladder pathology (Fig. 14.12). In such cases, giving the patient a drink of water usually helps to outline the duodenum and display the gallbladder wall more clearly.

The normal gallbladder in the non-fasted state is contracted and thick walled (Fig. 14.13). This may be indistinguishable from pathological contraction and care should always be taken to ensure that the patient has adhered to the correct preparation if the gallbladder is small or not visualised on ultrasound.[10]

The equipment of choice for examination of the gallbladder and biliary tree is a curved array transducer, which allows good acoustic access both subcostally and intercostally, with an adequate near field to accommodate superficial gallbladders. A frequency of 5–6 MHz, with a focal zone set at the appropriate depth, generally provides sufficiently good resolution to detect even small stones within the gallbladder. The penetration at this frequency may, however, not be adequate in large or obese patients, in whom a lower frequency (3–4 MHz) may be necessary. With the lower frequency the width of the beam is greater and small stones may not be demonstrated due to lack of acoustic shadowing.[11] Similarly, if the stone is outside the focal zone of the transducer, in the near or far fields, acoustic shadowing from a stone may be lost because the beam is wider (see Figs 14.23 and 14.24).[12]

A comprehensive examination of the biliary system naturally includes the demonstration of both liver and pancreas. The normal intrahepatic bile ducts are rarely visualised during routine scans but it is not uncommon to display the main right and left hepatic ducts as thin tubular structures running parallel to the main branches of the portal vein (Fig. 14.1).[13]

An initial survey of the gallbladder with the patient supine, along with the liver and pancreas, is usual. In the majority of patients, the gallbladder is best imaged with the patient decubitus, as the gallbladder flops medially, allowing the sonographer access through the acoustic window of the liver, and unfolding the gallbladder. In addition, the improved access allows the sonographer to position the transducer perpendicular to the long axis of the gallbladder, allowing a more thorough and confident interrogation. It is helpful to align the transducer along the long axis of the gallbladder, to include neck and fundus, then angling laterally and medially so that the entire volume of the gallbladder is examined. A subcostal approach may often be possible using suspended deep inspiration

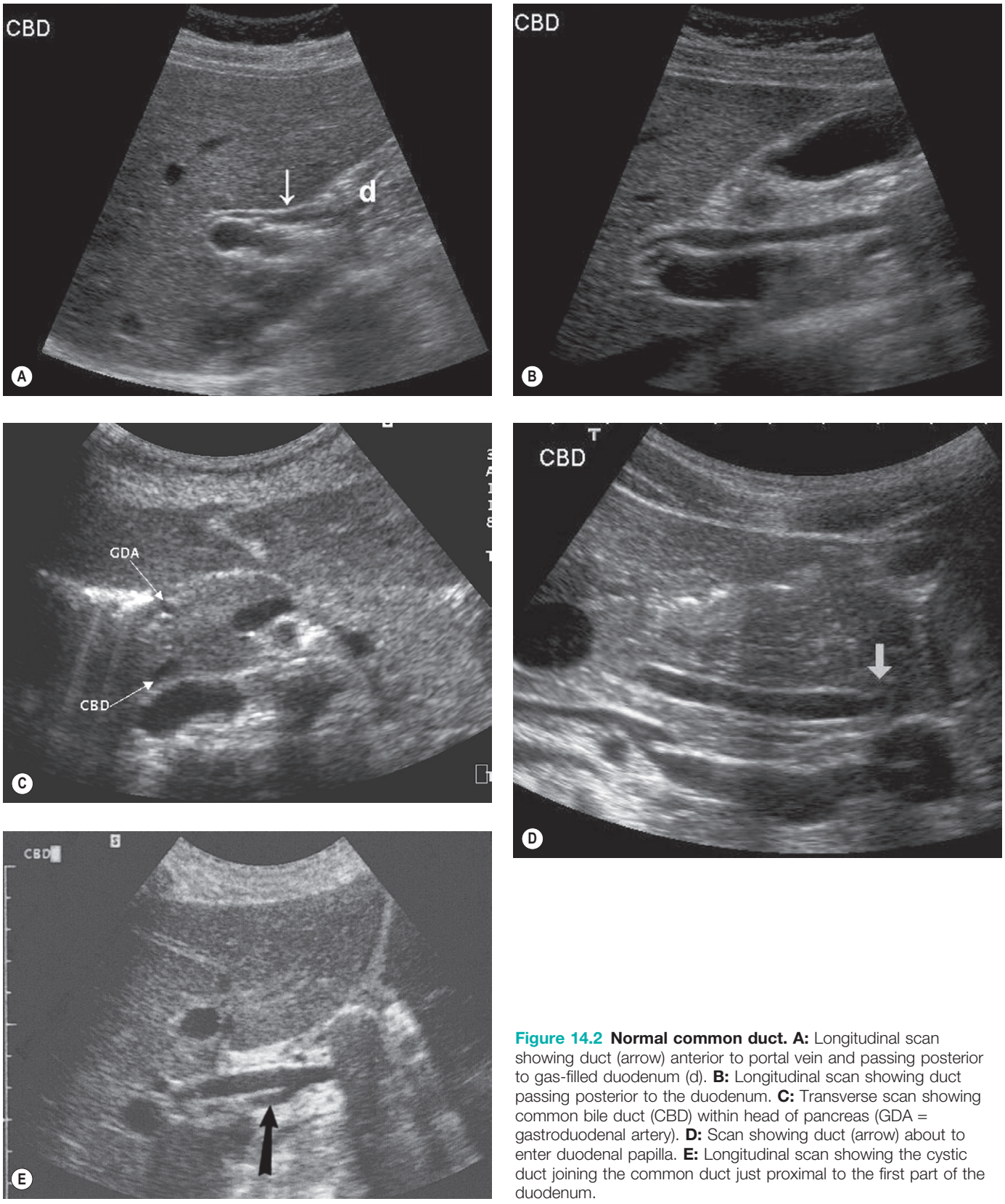


Figure 14.2 **Normal common duct. A:** Longitudinal scan showing duct (arrow) anterior to portal vein and passing posterior to gas-filled duodenum (d). **B:** Longitudinal scan showing duct passing posterior to the duodenum. **C:** Transverse scan showing common bile duct (CBD) within head of pancreas (GDA = gastroduodenal artery). **D:** Scan showing duct (arrow) about to enter duodenal papilla. **E:** Longitudinal scan showing the cystic duct joining the common duct just proximal to the first part of the duodenum.



Figure 14.3 **Gallbladder.** Normal, thin gallbladder wall.

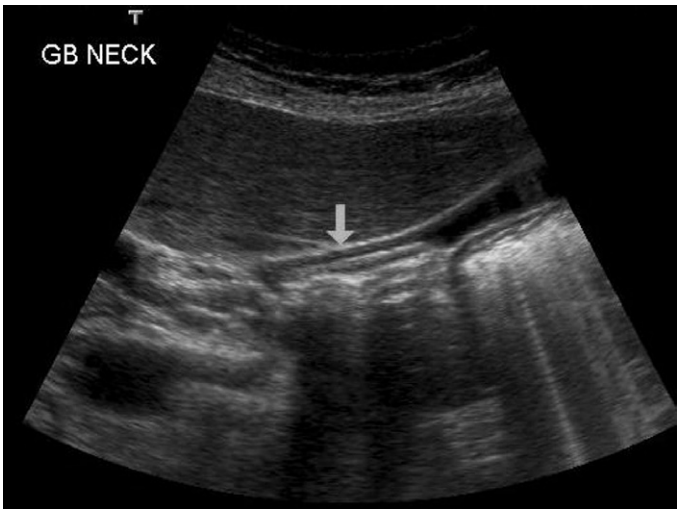
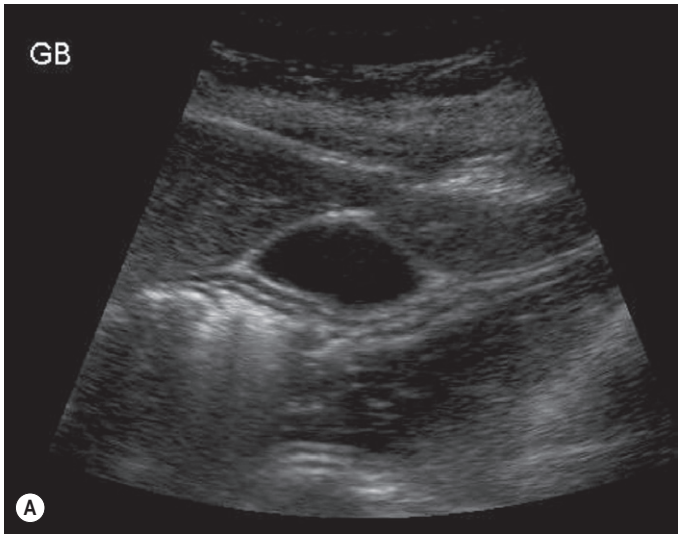
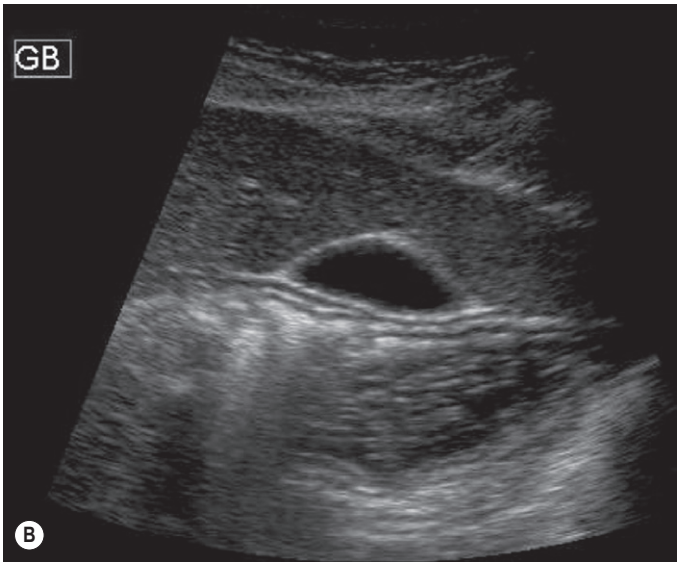


Figure 14.4 **Neck of gallbladder.** Body of gallbladder tapers down to neck (arrow).





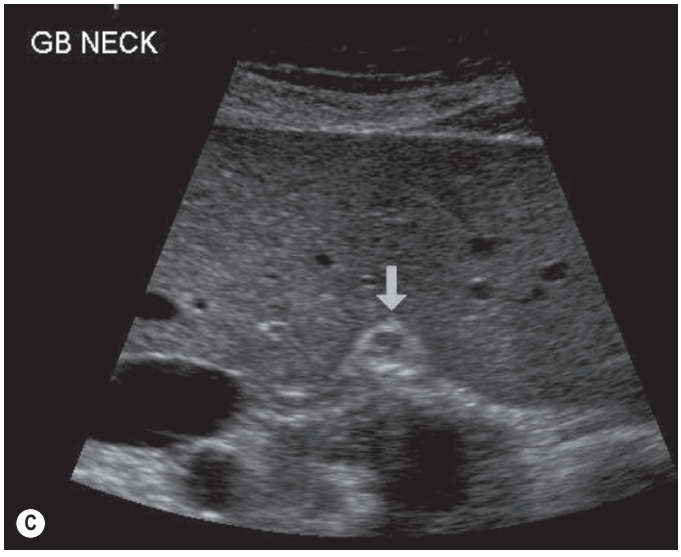


Figure 14.5 **Neck of gallbladder.** Transverse scans through gallbladder showing how the wall becomes thicker in the neck. **A:** Fundus. **B:** Body. **C:** Neck.

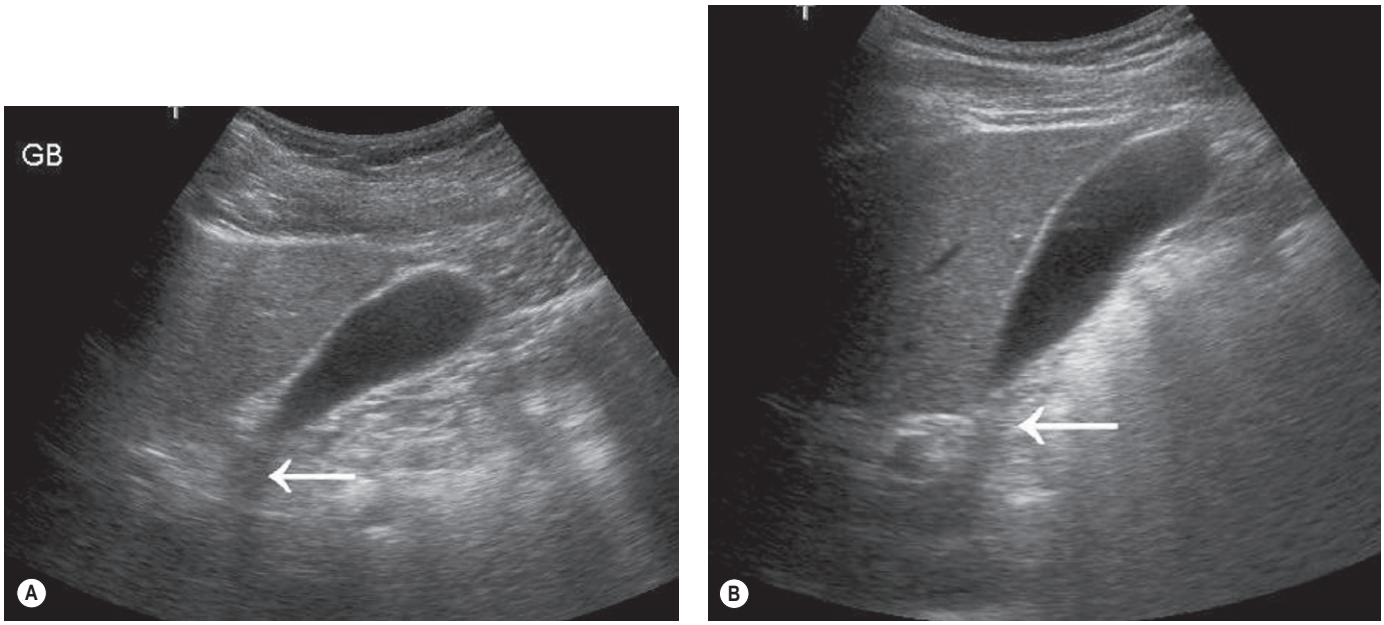


Figure 14.6 **Shadow from neck of gallbladder**. **A:** Acoustic shadow from normal neck of gallbladder. **B:** Because the gallbladder neck is parallel (rather than perpendicular) to the beam, sound is attenuated more by the neck wall, causing a shadow.

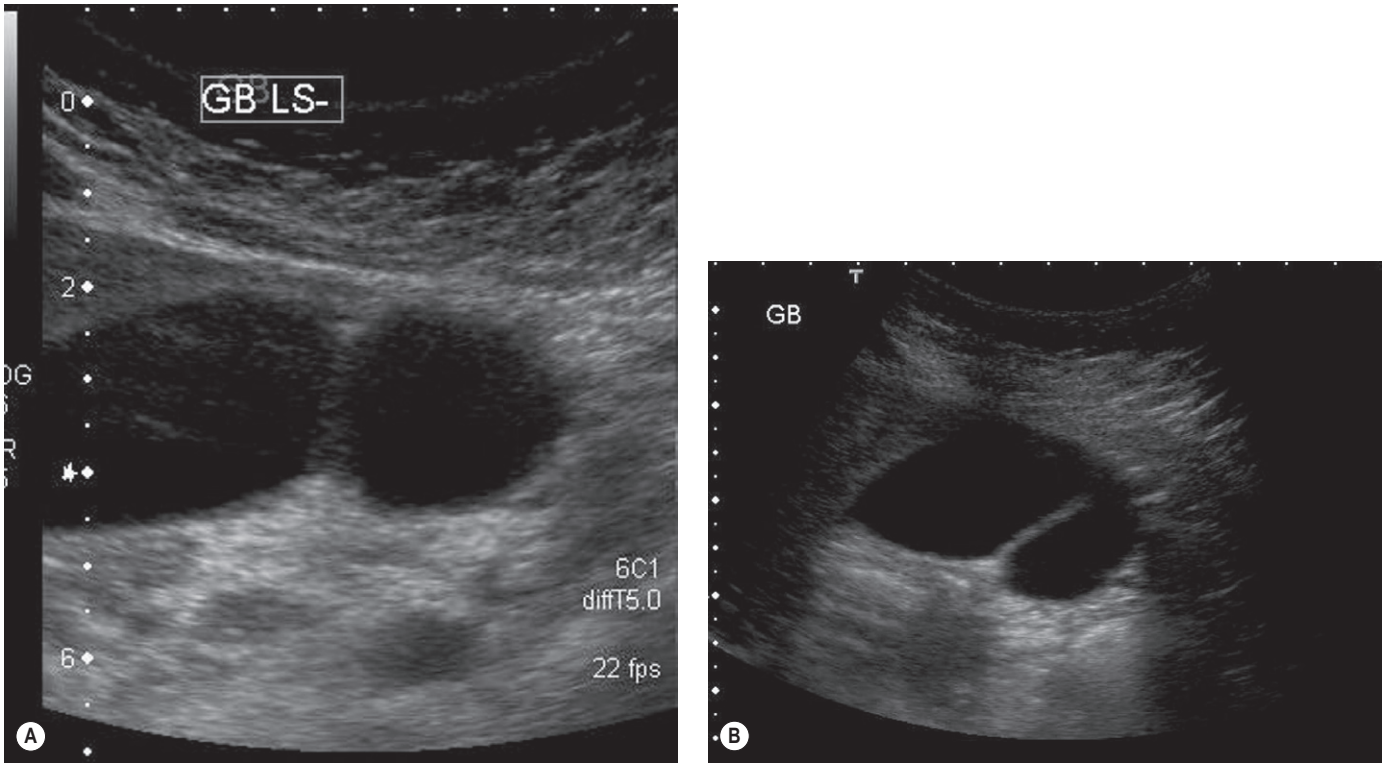
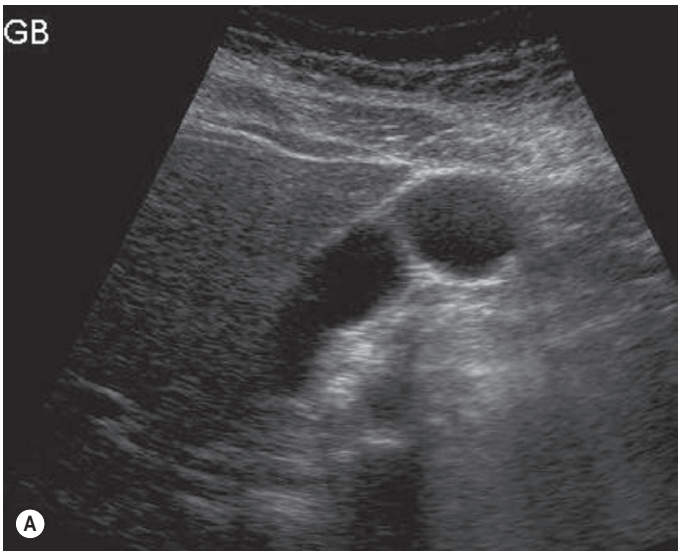
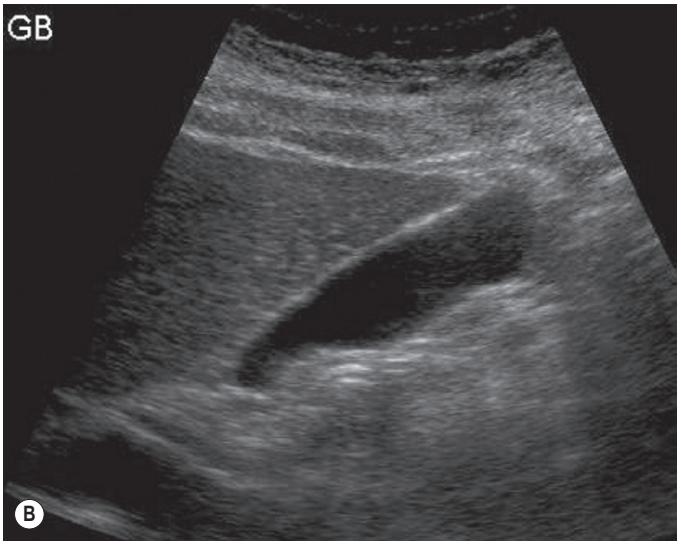


Figure 14.7 **Phrygian cap. A:** Patient supine. **B:** Patient right side raised.





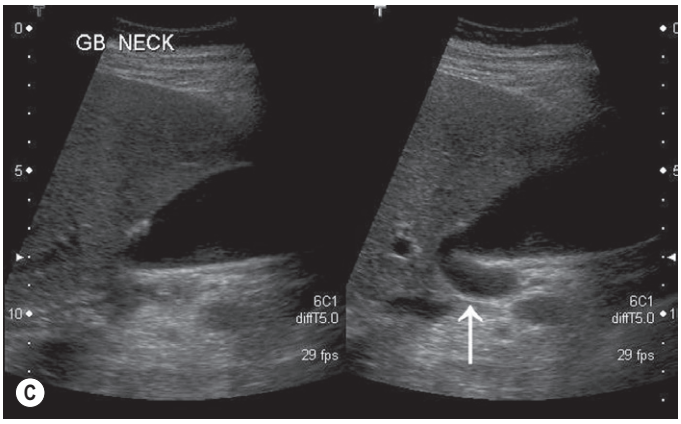


Figure 14.8 **Folded gallbladder. A:** Patient supine. **B:** Patient right side raised, demonstrating the unfolded gallbladder. **C:** The left-hand image fails to demonstrate the GB neck when the patient is supine – the right-hand image shows the full extent of the GB neck, which is folded back, when the patient is turned.

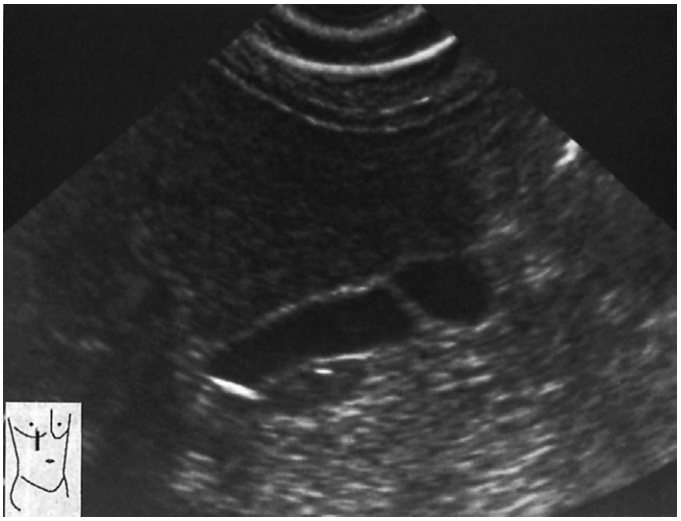


Figure 14.9 **Septated gallbladder.** Longitudinal scan.

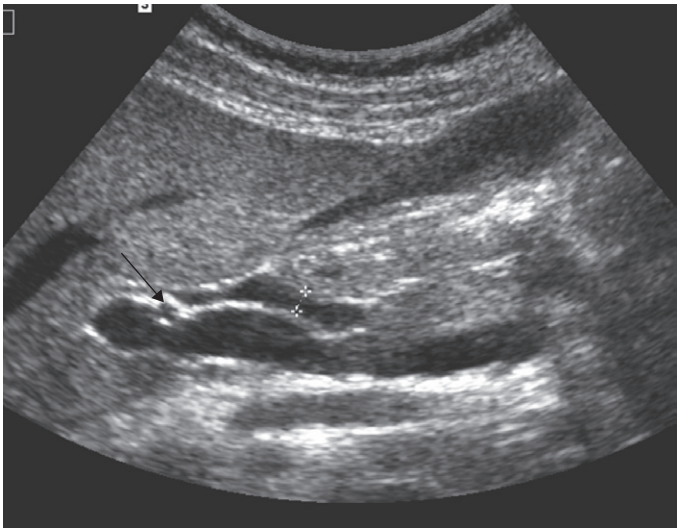


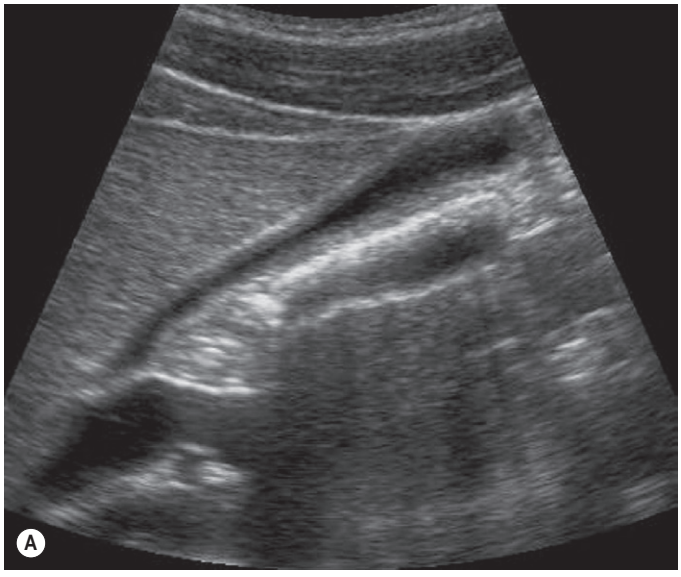
Figure 14.10 **Normal hepatic artery** (arrow) crossing between common duct (callipers) and portal vein.



Figure 14.11 **Anomalous hepatic artery** crossing anterior to common duct.



Figure 14.12 **Bowel indenting posterior wall of gallbladder** with intraluminal gas casting an acoustic shadow.



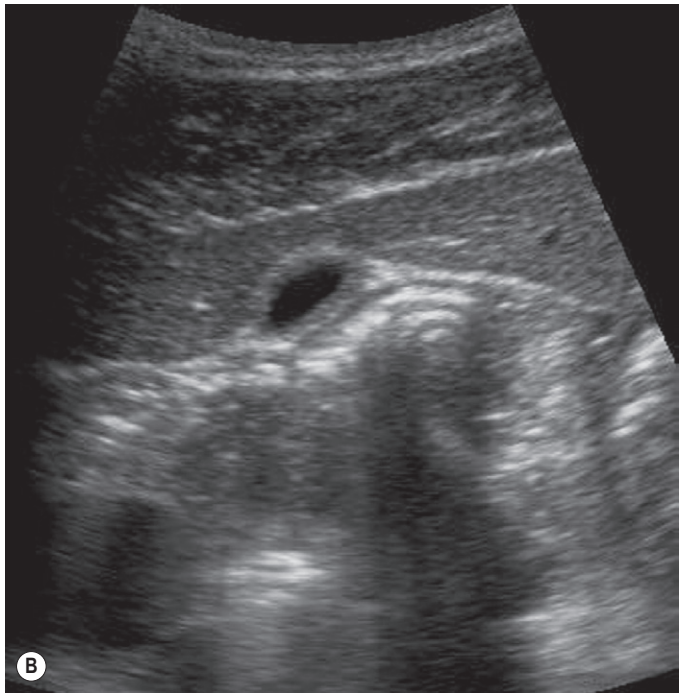


Figure 14.13 **Normal contracted gallbladder.** Normal wall thickness of physiologically contracted (postprandial) gallbladder **A:** Longitudinal scan. **B:** Transverse scan.

to bring the liver down to provide an acoustic window. However, an intercostal approach is the most successful technique in the majority of patients, allowing the gallbladder to be imaged through the right lobe of the liver in quiet respiration, with the minimum of artefact due to scattering and reverberation from adjacent bowel.

The normal gallbladder has an echo-free lumen and is surrounded by a smooth, moderately reflective wall. Since there is little attenuation of the ultrasound beam, the time gain compensation used appropriately for the adjacent liver will result in acoustic enhancement behind the gallbladder. However, this may not be apparent if gas-filled bowel lies immediately posteriorly (Fig. 14.14). In transverse scans, the gallbladder appears circular, increasing in diameter towards the fundus. If possible, the transducer should be maintained at right angles to the long axis, as an oblique section may give a spurious impression of gallbladder wall thickening (Fig. 14.15).[14]

The gallbladder must be examined with the patient in at least two different positions if small mobile stones or non-mobile polyps are

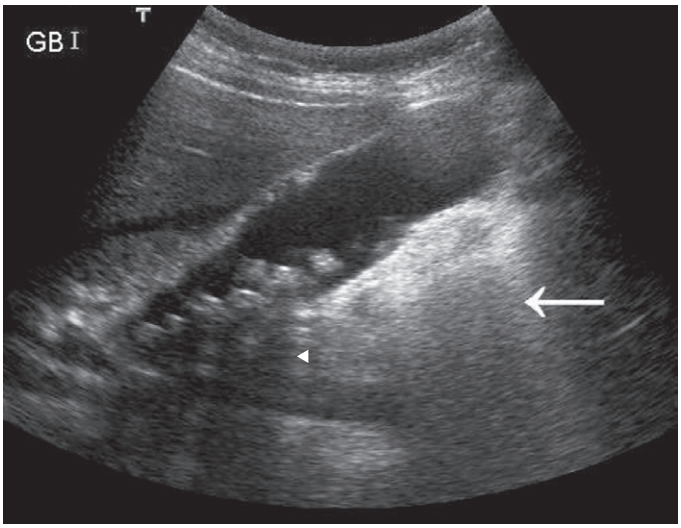


Figure 14.14 Shadowing – stone versus gas. Posterior to the gallbladder neck there is 'clean' shadowing beyond a row of stones (arrowhead). The bowel loop located behind the body and fundus of the gallbladder (arrow) transmits a more reverberative 'dirty' shadow. Posterior enhancement behind the fluid-filled gallbladder may not be apparent if bowel gas lies against the gallbladder.



Figure 14.15 Spurious gallbladder wall thickening due to angulation of the beam, which is not perpendicular to the GB wall, and artefact due to lateral resolution.

to be correctly diagnosed. Following initial scans in the supine position, the patient is turned into the left decubitus position, and other positions may sometimes be necessary, for example erect scans with the patient either sitting or standing.

The common bile duct (CBD) is usually most successfully seen in the left decubitus position, as this displaces the liver slightly medially and creates an acoustic window avoiding the hepatic flexure (Fig. 14.16). The duct can then be traced distally, running from the porta hepatis to the head of the pancreas as an immediate anterior



Figure 14.16 Normal common duct anterior to portal vein. Note how the duct widens as it travels in the free edge of the lesser omentum.

relation of the portal vein.[15] The lower end of the duct is best demonstrated on transverse scans through the head of the pancreas (Fig. 14.17).

A water load may be helpful in allowing visualisation of the lower end of the common duct by displacing gas from the gastric antrum and duodenum in the left anterior oblique position, and it may also act as an acoustic window.

Measurement of the common duct

The ability of ultrasound to discriminate between a normal and a dilated common duct is vital in the management of the jaundiced patient. This facility for the distinction between obstructive ('surgical') and non-obstructive ('medical') causes of jaundice depends on knowing the upper limit of normal for the duct diameter. A clear value dividing normal from abnormal is not attainable, and in a normal population the values for the diameter of the common duct will be distributed around a mean,[3] with some overlap as some normals will fall outside the normal range, and conversely, some abnormals will fall within it.

In the case of the ultrasound-derived measurement of common duct diameter, there are particular factors to be considered:

1. Level of the measurement – the duct is most consistently demonstrated in its proximal portion via the right anterior oblique longitudinal view and measurements are most often made just caudal to the porta hepatis.[15,16] Nevertheless this may not represent the point of widest diameter of the duct, as the duct usually widens slightly as it passes caudally in the free edge of the lesser omentum and after it receives the cystic duct (Fig. 14.16).
2. The walls of the duct are highly reflective, and 'blooming' of the echoes from the walls may reduce the apparent duct lumen.[13,17] The gain controls should be optimally adjusted to minimise this artefact (Fig. 14.18B).
3. The cross-sectional shape of the duct is oval rather than circular, and thus measurements may differ according to which diameter is demonstrated on a particular scan plane. Measuring the duct in transverse plane, as on the right-hand image in Figure 14.19, is inadvisable, as the section is frequently oblique and will overestimate the true diameter.[15]

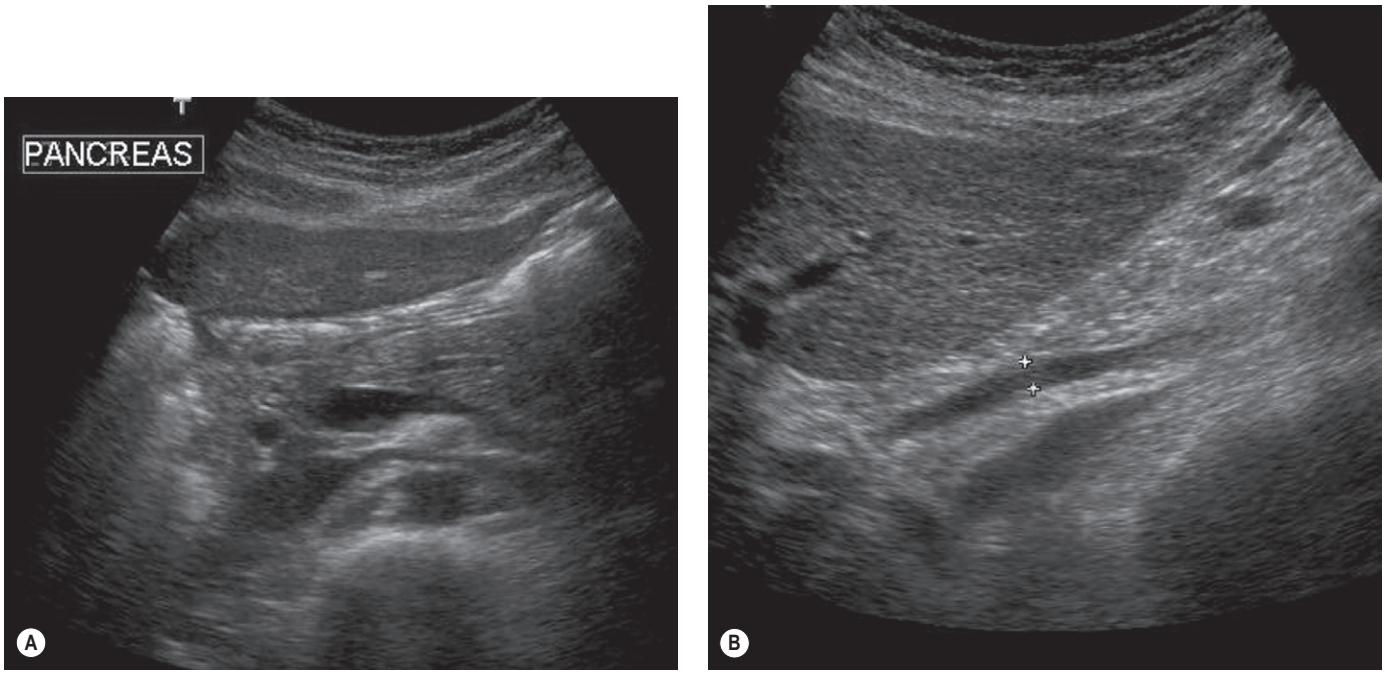


Figure 14.17 **Normal common duct in head of pancreas on transverse scans. A:** Duct seen within pancreatic head in transverse scan. **B:** Duct (callipers) entering the duodenal papilla.

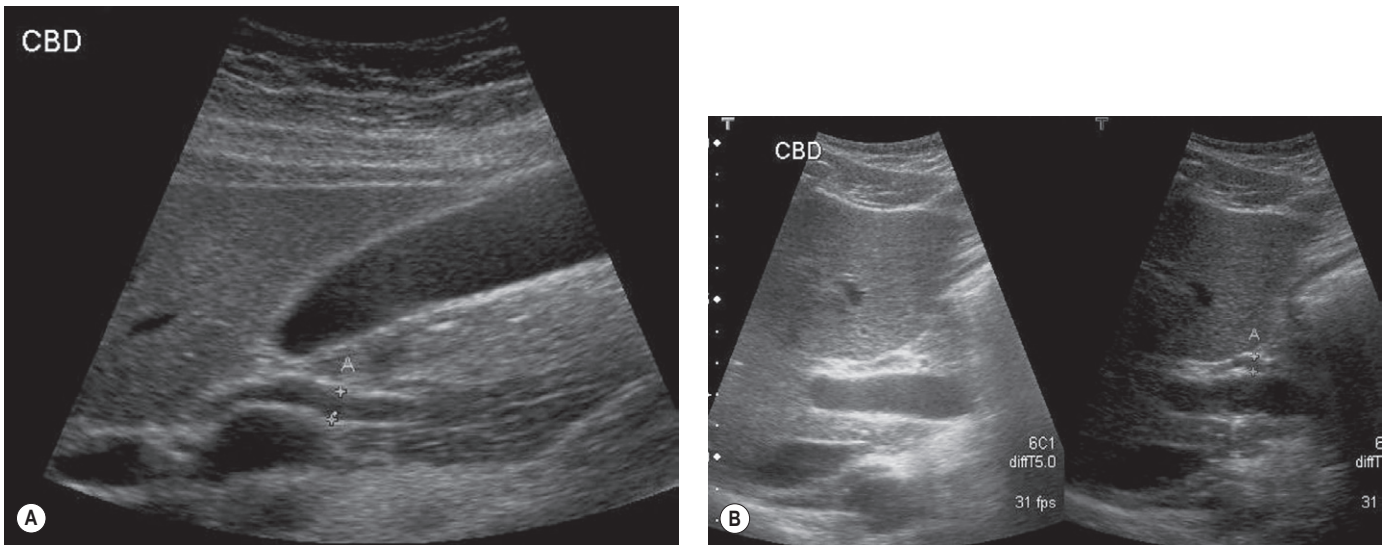


Figure 14.18 **Measurement of the common duct. A:** Callipers across the walls of a normal calibre common duct. **B:** Left-hand image demonstrates over-amplification (too much gain) causing blooming of the echoes in the walls of the duct. This could give rise to inaccurate measurements. The right-hand image illustrates an accurate duct measurement with the correct gain settings.

4. In the elderly there is a generalised loss of elasticity of the tissues and the normal duct diameter increases with advancing age.[18]
5. The diameter of the duct is often increased in patients who have had a cholecystectomy. Ducts that were normal preoperatively tend to remain normal postoperatively, while ducts that were acutely obstructed usually decrease in size postoperatively following stone removal or drainage procedure. However, ducts that were chronically dilated or in which there has been chronic infection often remain permanently dilated after surgery or non-operative drainage, or may even increase slightly in diameter.[18–21] Inflammation presumably reduces the elasticity of the duct wall so that it becomes incapable of recoiling back down, and the resultant floppy duct will distend with minimal pressure or volume increases as the duct assumes some of the original gallbladder reservoir function.[22,23]

Bearing all the above in mind, a useful working rule is that the diameter of the normal common duct as measured on ultrasound

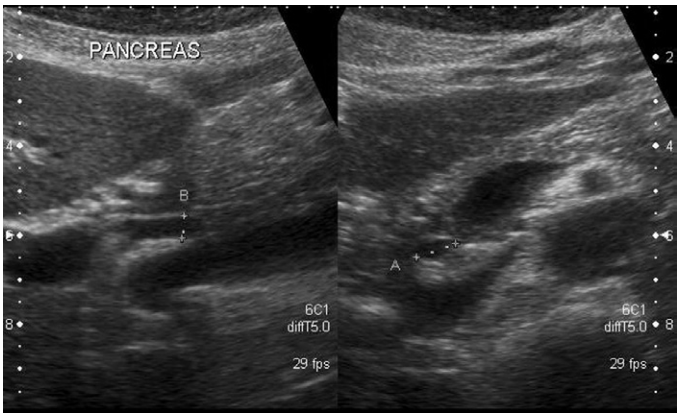


Figure 14.19 Oval shape of common duct. A normal duct (callipers B, left-hand image) can be falsely overestimated if measured in the head of pancreas (callipers A, right-hand image) due to an oblique section through the duct in the head of pancreas.

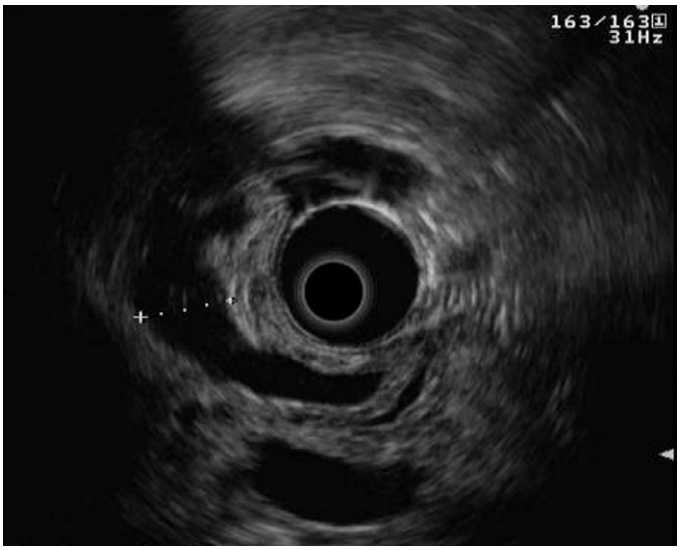


Figure 14.20 Endoscopic US showing the normal common duct (callipers) entering the papilla.

scans is less than 5 mm in its upper portion, although this figure can be increased to 6 mm for a measurement at its lower end, 8 mm in the elderly, and 1 cm in patients who have had a cholecystectomy.

Using the 'less than 5 mm' limit, the sensitivity of ultrasound for the diagnosis of extrahepatic obstruction has been shown to be 99% with a specificity of 87%,[24] while moving the limit to 5 mm would have decreased the sensitivity to 94% without significantly altering the specificity.

Function studies

While ultrasound scanning displays excellent structural detail of the gallbladder, the images give little functional information. Impaired gallbladder emptying is associated with stone formation, although in patients who have stones, efficient gallbladder motility is more likely to result in symptoms, while those with sluggish motility are less likely to suffer from biliary pain and obstruction.[25] Ultrasound has been used in combination with various pharmacological agents, such as cholecystokinin, to investigate the dynamics of gallbladder filling and emptying in health and disease.[26,27] Potential uses for this include investigation of patients at risk of gallbladder stasis (and thus, stones) and in patients who may benefit from dissolution therapy.

Gallbladder emptying dynamics have been studied in smokers,[28] in pregnancy,[29] in patients with coeliac disease[30] and spinal cord injuries,[31] and in response to various drugs.

Functional ultrasound to determine gallbladder motility remains essentially a research tool, as accurate measurement of the gallbladder volume is fraught with errors. Three-dimensional ultrasound may offer potential in this regard.[32,33]

The response of the diameter of the common duct to a fatty meal has also provided considerable material for study. The fatty meal causes release of cholecystokinin from the duodenal mucosa and this promotes gallbladder contraction, relaxation of the sphincter of Oddi and an increase in the flow of bile from the liver. In a normal subject the bile duct diameter will either reduce or remain unchanged, but if there is partial or complete obstruction, the diameter will usually increase, though occasionally it remains unchanged.[34–37]

ENDOSCOPIC ULTRASOUND

Endoscopic ultrasound (EUS) enables a high-frequency transducer to be placed in close proximity to the lower end of the bile duct (Fig 14.20) and thus gives more detailed visualisation of lesions in this vicinity,[38] which are difficult to evaluate using conventional transabdominal ultrasound. A high-frequency ultrasound transducer is incorporated into a fully functional fibreoptic endoscope with both light and optical bundles and air/water channels together with controllable tip movement.

Endosonography has been shown to be significantly more sensitive, accurate and effective than either CT or transabdominal ultrasound in the evaluation of local spread of neoplastic obstructions. Magnetic resonance cholangiopancreatography (MRCP) is the imaging of choice for diagnosing and staging cholangiocarcinomas, but EUS can provide increased specificity in some cases, as well as allowing cytology to be obtained for a definitive diagnosis.[39] EUS outperforms both MRCP[40] and endoscopic retrograde cholangiopancreatography (ERCP)[41]in the diagnosis of ductal calculi. It also has a much lower complication rate than ERCP, although its invasive nature means that its role is often secondary to MRCP in cases of a negative MRCP with continued clinical probability.

LAPAROSCOPIC ULTRASOUND

The majority of elective cholecystectomy operations are now performed laparoscopically. The trend towards increasing laparoscopic surgery for a range of surgical techniques has influenced the development of adjunctive laparoscopic ultrasound. Like endosonography, this is a difficult technique to master and requires a specialised, flexible, high-frequency laparoscopic probe to evaluate the biliary anatomy, and in particular to examine the common duct for stones. Once learned, laparoscopic ultrasound has been shown to be highly sensitive and specific in evaluating the biliary tree,[42] and has the advantage of avoiding unnecessary radiation dose. It has now largely replaced fluoroscopy for routine cases in many centres.

PATHOLOGY OF THE GALLBLADDER

Ultrasound has been firmly established for many years as the primary imaging investigation in all cases of suspected gallbladder disease.[43]

In patients who present with acute right upper quadrant pain, ultrasound has the ability not only to demonstrate lesions of the gallbladder, but to show other causes for the patient's pain.

Stones

The prevalence of gallstones in developed societies is approximately 10%, and as many as two-thirds of gallstone carriers are asymptomatic.[44,45] But, since the probability of developing biliary symptoms for subjects with silent stones has been shown to be only 15–25% in 10 years,[46] the increasing use of ultrasound in patients with symptoms that suggest the presence of gallstones will unmask many previously undiagnosed stones and thus create both ethical and economic dilemmas for physicians and health care planners.[47] Only around 30% of patients with asymptomatic gallstones eventually require surgery.

The standard management for symptomatic gallstones is laparoscopic cholecystectomy, with open surgery being reserved for more complex cases. Previous experience with medical (dissolution) therapies has been disappointing, as despite its excellent safety record there is a high incidence of stone recurrence (up to 60%) and slow response to treatment.[48]

Cholescintigraphy, using a ^{99m}Tc-labelled derivative of iminodiacetic acid, is useful as a second-line test for confirmation of cystic duct obstruction, either when ultrasound has failed to show stones, or when the origin of the symptoms remains in doubt in the presence of stones.

The composition, size, shape and number of stones vary widely from patient to patient, presenting a wide range of ultrasound appearances.

Classic appearances

The most commonly encountered ultrasound appearance of a stone in the gallbladder is that of a highly reflective intraluminal structure which is gravity-dependent and casts an acoustic shadow (Fig. 14.21). When all these features are present, the diagnostic accuracy is 100%.[49] It is useful to analyse each of these ultrasound features more closely so that the limitations of the method are appreciated, thus enabling scan technique and machine settings to be adjusted appropriately.

The size of a structure that can produce an echo from within the gallbladder lumen is not a limitation since it has been shown that particles as small as 5 to 10 μm will produce echoes within bile.[50] Such tiny particles are not considered to be 'stones', and do not fulfil the diagnostic criteria given above since they do not produce acoustic shadows.

The production of an acoustic shadow beyond a reflecting structure depends upon both the absorption and reflection of sound by the structure, and the resulting shadow should be sharp and 'clean' (Fig. 14.22). This is in contradistinction to the shadowing beyond bowel gas, which is caused purely by reflection of sound and is therefore usually less well defined and 'dirty' due to reverberation artefacts[51] – a useful practical point in sorting out whether shadows are due to gallstones or to bowel gas. Shadowing beyond a stone is not affected by the chemical composition of the stone, the presence of calcium within the stone, or the shape and surface characteristics of the stone,[52] but is dependent on the geometric relationship between the ultrasound beam and the stone.[53] The beam width needs to be as small as possible since shadowing will not occur unless the stone occupies the full width of the beam (Fig. 14.23). Beam width is reduced by focusing and by using transducers of higher frequency.

A further practical consideration concerning the demonstration of stones in the gallbladder relates to signal processing methods.[54]

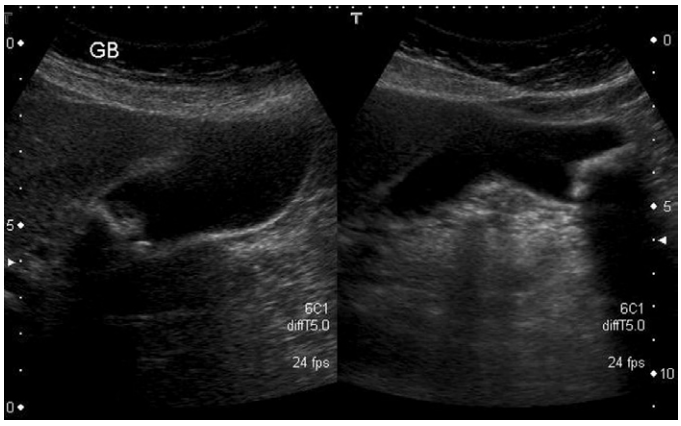


Figure 14.21 Gallstones. Left image: the patient is supine, with shadowing from stones at the gallbladder neck. Right image: with the patient erect, the stones drop with gravity to the gallbladder fundus. Note the reverberative shadowing from bowel distal to the body of the gallbladder, as distinct from the stronger shadows from the stones.



Figure 14.22 Gallstone shadowing. Transverse scan of gallbladder; 'clean' shadowing from two small stones, which is free from reverberation. Compare with the reverberation from the bowel behind the gallbladder to the left of the stones.

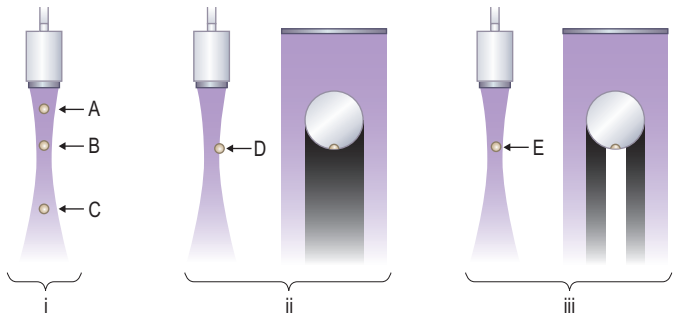


Figure 14.23 Beam width and shadowing. Diagram to show the effect of beam width and incidence on the production of an acoustic shadow beyond a stone. **(i)** Stone B is in the focal zone of the beam and will give rise to an acoustic shadow, while stones A and C in the near and far fields of the beam are less likely to shadow (after Jaffe and Taylor[54]). **(ii)** and **(iii)** Diagrams to show the effect of positioning of a stone in relation to the beam; a linear array is viewed end-on on the left and in the scanning plane on the right. Stone D (ii) at the periphery of the beam will not occupy a sufficient proportion of the beam width to cast a shadow, while the same size stone E (iii) at the centre of the beam will shadow. (Redrawn with permission from Filly et al.[53].)

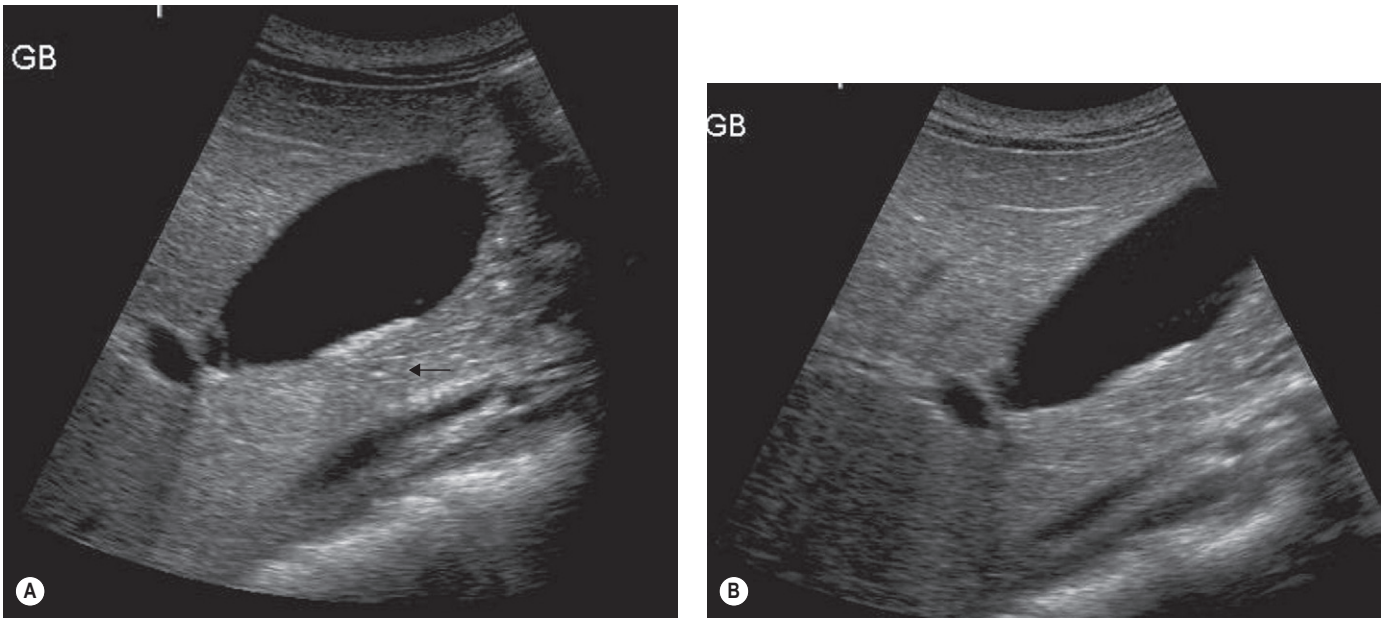


Figure 14.24 Tiny stones with acoustic shadowing. A: Longitudinal scan demonstrating the shadow from a row of tiny stones (arrow). **B:** The same case with the focal zone set anterior to the stones; note how the shadowing is no longer apparent as the beam is wider at this level.



Figure 14.25 Contracted gallbladder full of stones, longitudinal scan demonstrating distal acoustic shadowing.

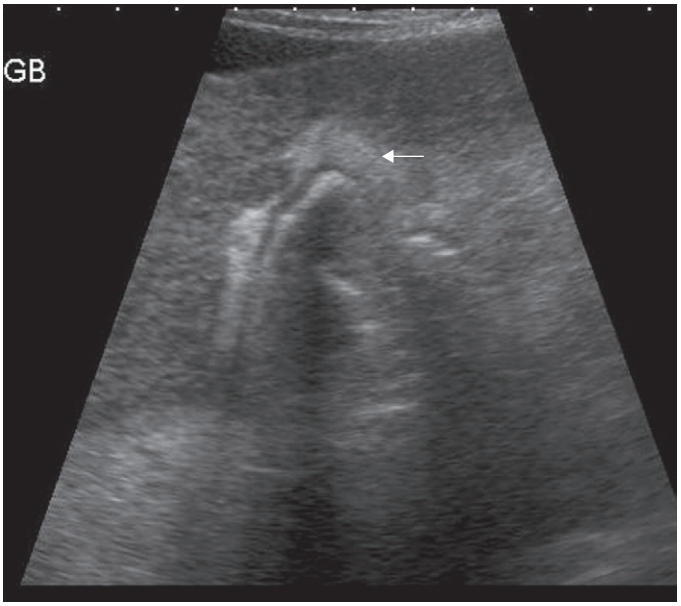


Figure 14.26 Double-arc shadow sign. The gallbladder fossa in transverse section demonstrates echoes from the anterior gallbladder wall (arrow), behind which is a strong band of reflective echoes from the stones within the gallbladder, casting a distal acoustic shadow. Detection of an echo-poor anterior rim improves diagnostic specificity.

TV display monitors have limited dynamic range and this necessitates the use of compression amplification. When this is combined with the use of time gain compensation curves, the distinction between acoustic shadow and surrounding tissues may be imperceptible.[55] This may be the most important limiting factor in real-life scanning, but good quality modern equipment is capable of demonstrating tiny, sub-millimetre stones in the gallbladder, although it is imperative that optimal settings, such as correctly placed focal zone, are used (Fig. 14.24).

Contracted gallbladder

In the description of the 'classic' appearances of stones in the gallbladder, it will be appreciated that the gallbladder lumen contains fluid bile within which the echoes reflected by the stone or stones can be detected. In situations where the lumen is totally filled by stones, or where the gallbladder wall has been chronically inflamed and become fibrotic, or where the cystic duct has been obstructed, there may be no fluid bile within the lumen.

These 'contracted' or 'sclero-atrophic' gallbladders are reliably recognised with modern equipment. In cases when the gallbladder lumen cannot be visualised, distal acoustic shadowing may often be seen to emanate from the gallbladder fossa, representing the stone-filled lumen.[49] The ability to locate the gallbladder fossa in different scan planes is crucial (Fig. 14.25).[56]

Refinement of scanning technique can further improve the accuracy rates (to almost 99%), using movement of the patient during the study[57] to observe differences in movement between bowel gas in the duodenum or hepatic flexure and a contracted gallbladder full of stones. Diagnostic specificity is also aided by the observation of the wall–echo–shadow (WES) triad,[58] otherwise known as the 'double-arc-shadow sign'.[59] This complex consists of the reflective anterior wall of the gallbladder separated by a thin echo-poor rim (representing either a small amount of residual bile or an echo-poor portion of the thickened gallbladder wall) from the reflective anterior surface of the stone, which casts a complete acoustic shadow (Fig. 14.26).

Persistent acoustic shadowing emanating from the gallbladder fossa may also be produced by a porcelain gallbladder, which is the term given to calcification of the gallbladder wall.[60] Wall calcification may be the end-result of chronic infection and inflammatory reaction. This condition is associated with gallstones in over 95% of cases, but its particular importance lies in the increased incidence of both gallbladder carcinoma and cholangiocarcinoma (in 10% to 20% of cases), and prophylactic cholecystectomy is usually advised (see section on gallbladder carcinoma).

Movement/layering/floating of stones

Gravity dependence of stones can be demonstrated by moving the patient during the ultrasound examination. Usually this is achieved by turning the patient into the left decubitus or right anterior oblique positions, but erect scans with the patient sitting or standing may also be performed. In this way, previously hidden stones lying in the neck of the gallbladder may come into view and the distinction between polyps and stones is facilitated (Figs 14.27 and 14.28).

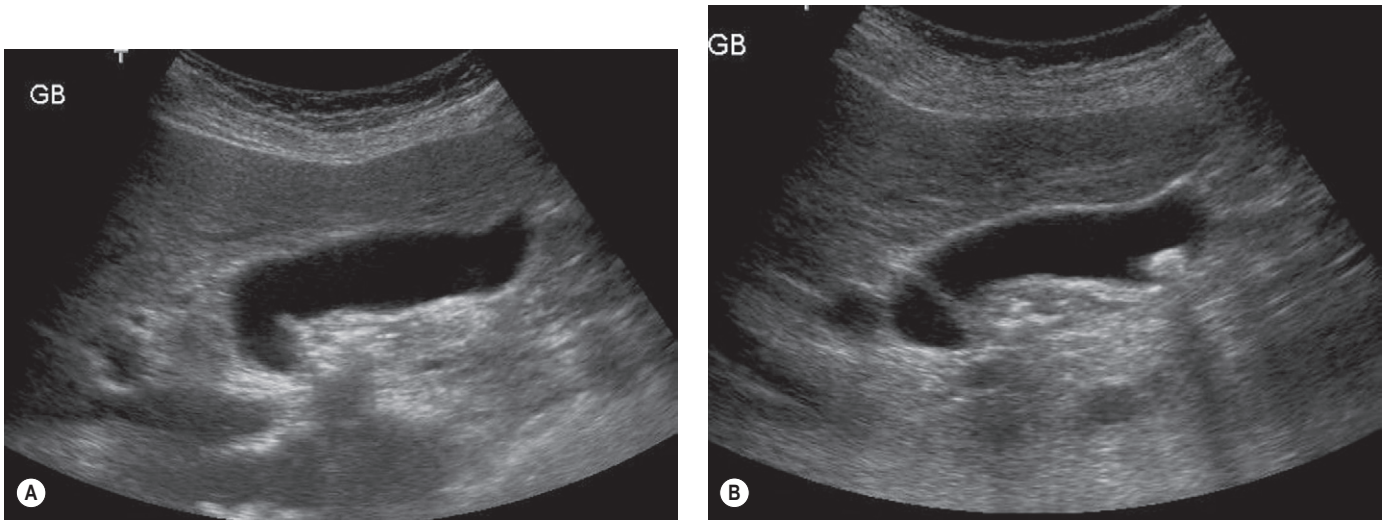


Figure 14.27 Stone in the gallbladder. A: With the patient supine there is no evidence of any stone. **B:** A stone comes into view when the patient is turned right side up.

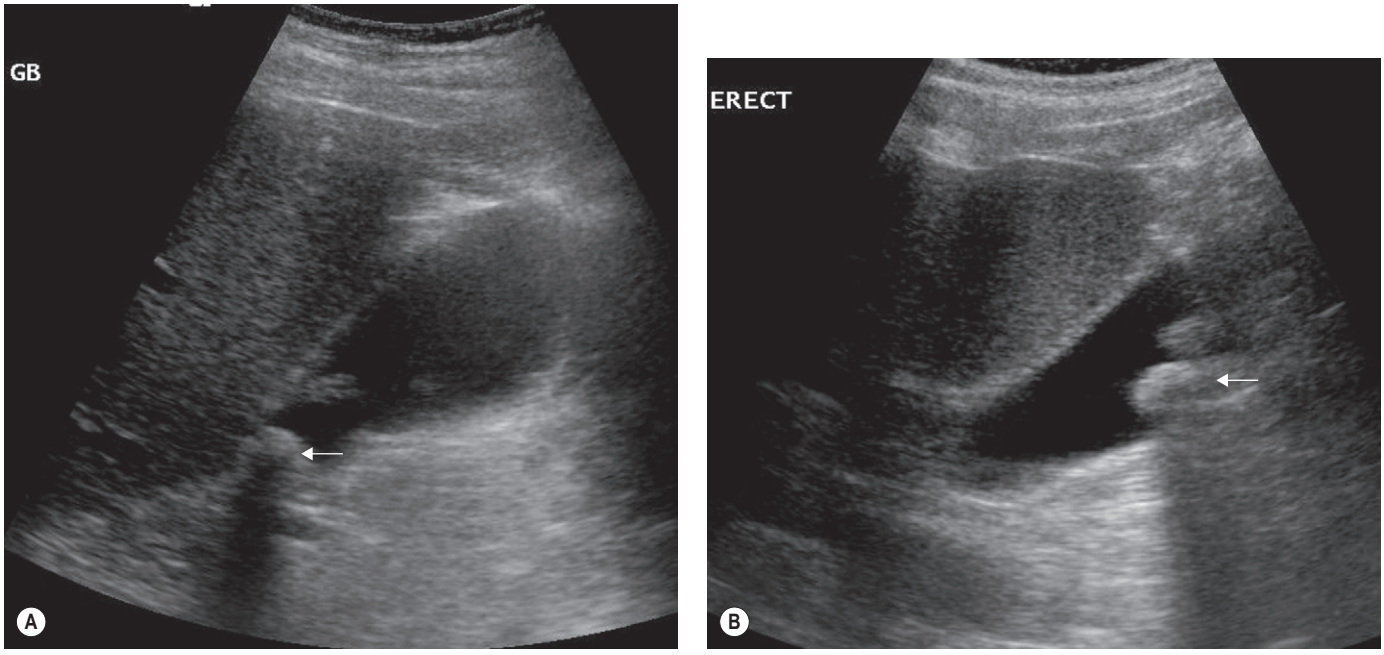


Figure 14.28 Stone in the fundus. The stone in the gallbladder neck (**A**, supine) is clearly seen in the fundus of the gallbladder when the patient is scanned in the erect position **(B)**.

Movement may also help when there are small stones from which it is proving difficult to demonstrate acoustic shadowing. If these stones can be collected into a group then the shadow may become more readily visible.[61]

Similarly, if small stones form a thin layer on the posterior wall of the gallbladder, the echoes from the stones may be erroneously ascribed to the wall itself. Shadowing from small stones lying on the posterior wall of the gallbladder may be obscured by the high reflectivity of the wall itself or of the immediately adjacent bowel gas, causing a 'blooming' effect (Fig. 14.29). If such stones can be encouraged either to float across the gallbladder lumen or to clump together, the shadowing becomes obvious. Good technique, including the correct use of frequency, focal zone and gain settings, is essential in the diagnosis of tiny stones (Fig. 14.30).

Difficulties can sometimes arise when stones float up to the anterior wall so that the gallbladder lumen is not visualised, but once again, movement of the patient is crucial in avoiding this pitfall (Fig. 14.31).

Milk of calcium bile (sometimes known as 'limy bile'), where the bile becomes a thick paste-like material, is another instance where gravity dependence is an aid to ultrasound diagnosis. The appearances here are predominantly those of echoes and shadowing from the gallbladder fossa, but layering out of the milk of calcium will be evident on the erect scans.[62,63]

Microlithiasis/biliary sludge

Non-shadowing, gravity-dependent echoes within the gallbladder are variously referred to as 'biliary sludge' or 'echogenic bile'. Several different pathological and physiological entities can result in these ultrasound appearances and, since neither of the above terms specifies a particular cause, there is considerable confusion about the significance of these findings. Most commonly the echoes represent particles (calcium salts) that have precipitated from the bile. In-vitro studies have shown that the echoes in 'biliary sludge' are caused by particles 5 to 10 μm in size, and chemical analysis revealed that these were mainly calcium bilirubinate granules together with some cholesterol crystals.[53]

Echogenic bile may also be due to pus or blood in the bile as a result of infection or trauma, or it may be seen in association with obvious stones in the gallbladder (Fig. 14.32).[64] In these cases, the appearances are incontrovertibly pathological, and when taken in



Figure 14.29 Layered stones. A layer of small stones on the posterior wall is difficult to separate from the wall echoes, but note the band of distal shadowing.

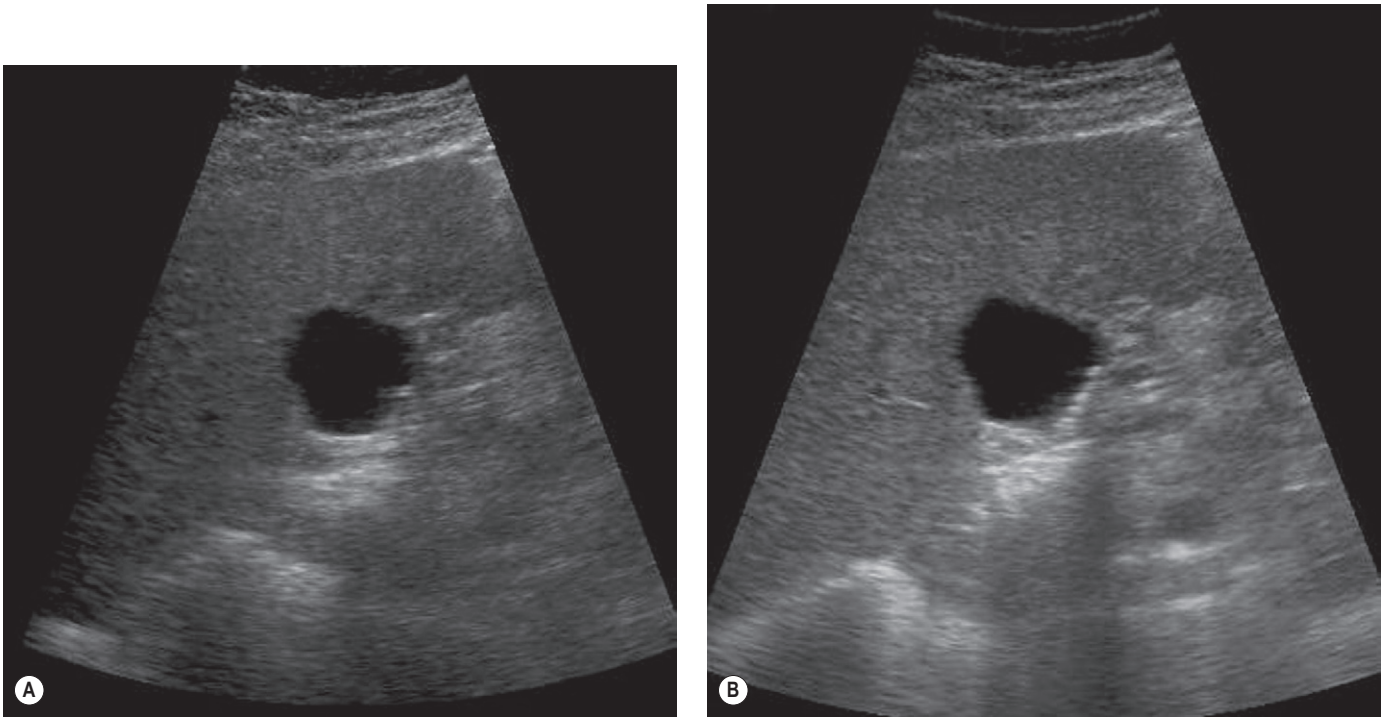


Figure 14.30 Technique for small stones: transverse scan of the gallbladder. **A:** Line density has been increased by reducing the area of scan, and the frequency has been increased from the normal liver setting. **B:** The focal zone has been moved alongside the gallbladder to display the small stones.

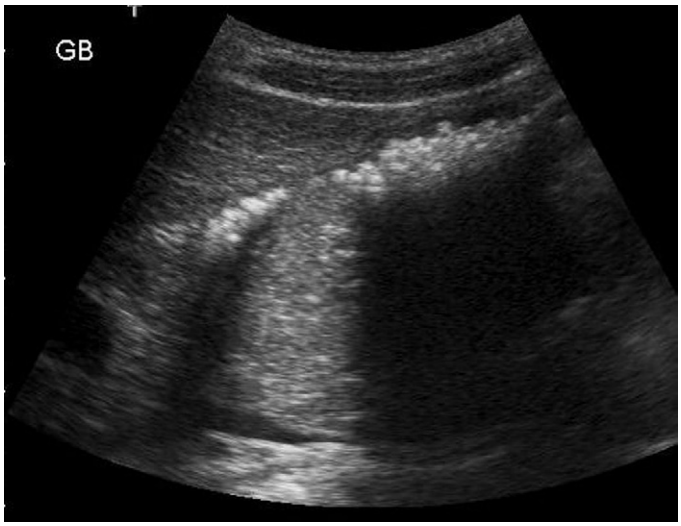
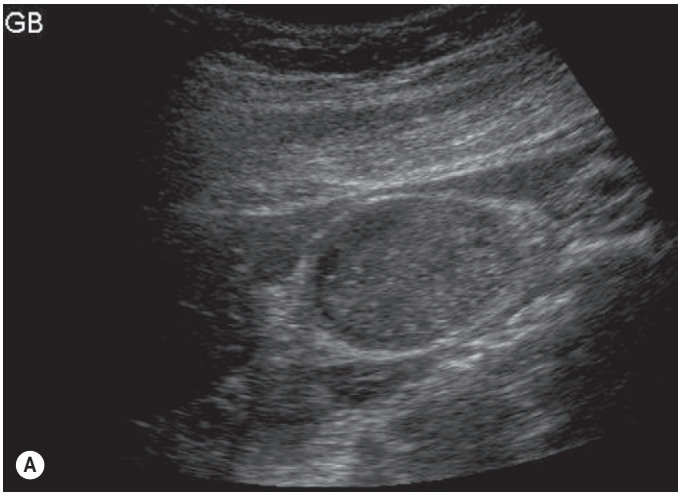


Figure 14.31 Floating stones. The gallbladder lumen may be masked by the shadow from stones which float up to the anterior wall.



Figure 14.32 Stones and echogenic bile. Stones in the neck of the gallbladder (shadowing) with inspissated bile, or biliary sludge, filling the gallbladder lumen.



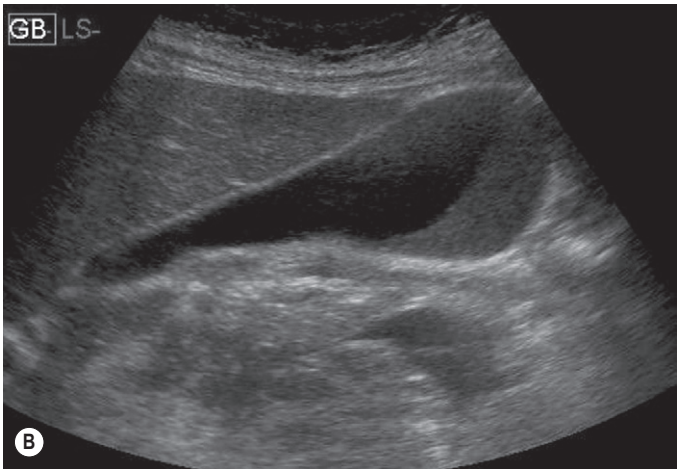


Figure 14.33 Echogenic bile. A: Transverse scan through a gallbladder containing non-shadowing echogenic material in a patient who had been on intravenous feeding. **B:** Layering gallbladder sludge in a fasting patient.

conjunction with the patient's history, physical signs and other ultrasound features, the diagnosis can be quite specific.

However, echogenic bile may also be seen when there is bile stasis in the absence of stone disease, and several clinical conditions have been associated with this including pregnancy, rapid weight loss, parenteral nutrition (Fig. 14.33), octreotide therapy and bone marrow transplant.[65]

Microlithiasis may also be due to pathological biliary obstruction or physiological factors, such as gallbladder dysmotility, and can be associated with biliary colic, acute cholecystitis and, in a minority of cases, recurrent acute pancreatitis.[66] The larger particles are an intermediary step towards the formation of gallstones[67] (although this result is by no means inevitable if biliary sludge is demonstrated).

It has been pointed out that some non-shadowing echoes within the gallbladder are due to slice thickness artefacts. Clues that should alert the sonographer to this possibility include non-dependence on receiver gain and lack of change in height of debris between scans performed in transverse and longitudinal planes (Fig. 14.34).[68]

Occasionally non-shadowing echoes within the gallbladder may clump together, giving the so-called 'sludge balls' or 'tumefactive sludge' (Fig. 14.35). This may give rise to a diagnostic dilemma since the appearances may mimic a soft tissue mass projecting into the gallbladder lumen, resulting in a false diagnosis of gallbladder tumour or polyp (Fig. 14.36).[69] Movement of the echoes with gravity should be the key to differentiating these conditions, but the bile in these cases may be thick and viscid so that movement of the echoes may be imperceptibly slow. A repeat scan with a normal diet in the interim should reveal the true nature of the problem.[70]

Gallbladder wall thickening

In the fasting state, the normal gallbladder is distended and has a wall thickness of less than 3 mm.[71] The normal anterior wall appears as a single smooth well-defined reflecting structure and its thickness can be measured accurately, while the posterior wall can be more difficult to measure because this wall is frequently in contact with air-containing bowel and the end-point is indistinct (Fig. 14.37).

When the gallbladder contracts in response to a fat-containing meal or injection of cholecystokinin, the wall becomes thicker[72] and

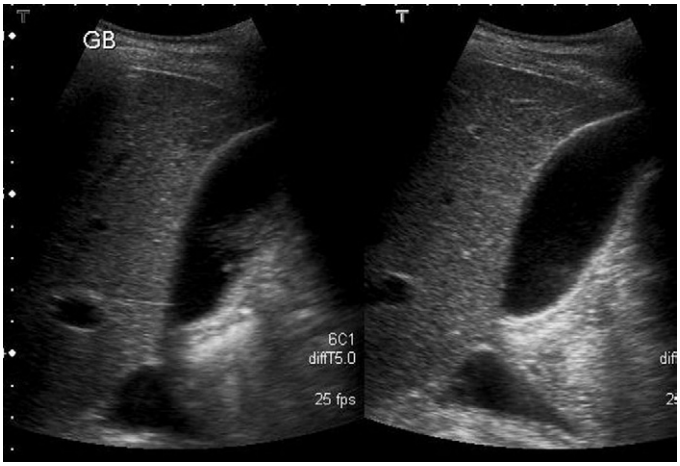


Figure 14.34 False echogenic bile. Slice thickness artefact causing echoes within the gallbladder on the left-hand image. The bile is echo-free after slight readjustment of transducer angulation on the right-hand image.



Figure 14.35 Tumefactive sludge in the gallbladder neck.



Figure 14.36 Lumpy bile. Sludge gives the impression of a soft tissue mass. This can potentially lead to an erroneous diagnosis of gallbladder carcinoma.



Figure 14.37 Non-fasting gallbladder. Normal non-fasting gallbladder wall. Longitudinal scan.



Figure 14.38 Gallbladder in ascites. Thickened gallbladder wall in the presence of ascites.

three distinct zones can then be identified – a strongly reflecting outer contour, a reflecting inner contour, and an echo-poor layer between the reflecting structures (Fig. 14.38).[73]

The method of measurement of gallbladder wall thickness is an important consideration since the ultrasound beam should be perpendicular to the wall so that measurements are truly axial. This may mean that measurements of both anterior and posterior wall thicknesses cannot be made on the same scan section. Wall thickness should be measured with the gallbladder in a longitudinal (not transverse) section, where the callipers can be reliably placed perpendicular to the wall, as it has been shown that minor angulation or decentring of the beam can cause 'pseudothickening' of the gallbladder wall[74] (Fig. 14.15).

Gallbladder wall thickening is also related to non-biliary disease, such as hepatic disease, ascites, heart and renal failure, AIDS and sepsis.[75] It had been observed that the gallbladder wall appeared to be thickened in the presence of ascites (Fig. 14.38)[76] and this was thought to be due to oedema of the gallbladder wall. It had also been shown that chronic alcoholics with hypoalbuminaemia had thickened gallbladder walls (Fig. 14.39), and in the majority of the cases under study there was no ascites in contact with the gallbladder.[77] It was therefore suggested that gallbladder wall thickening in



Figure 14.39 Gallbladder wall in hypoalbuminaemia. Thickened gallbladder wall in a patient with hypoalbuminaemia but no ascites.

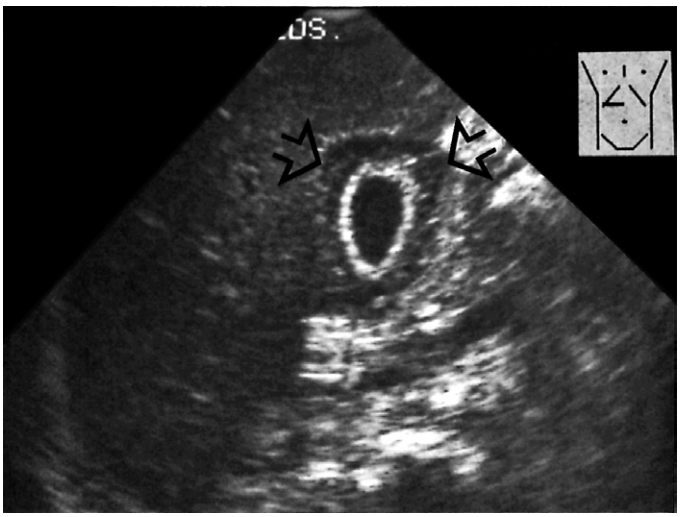


Figure 14.40 Gallbladder in leukaemia. Grossly thickened gallbladder wall (arrows) in leukaemia.

Table 14.1 Causes of gallbladder wall thickening

Physiological:
Postprandial
Inflammatory disease of the gallbladder:
Acute cholecystitis
Chronic cholecystitis
Sclerosing cholangitis[85]
AIDS[86]
Crohn's disease[87]
Non-inflammatory disease of the gallbladder:
Adenomyomatosis
Carcinoma of gallbladder
Leukaemia
Multiple myeloma
Oedema of the gallbladder wall:
Ascites
Hypoalbuminaemia
Heart failure
Portal hypertension
Renal disease
Malignant lymphatic obstruction[88]/lymphoma
Adjacent inflammatory disease:
Acute viral hepatitis
Alcoholic hepatitis[89]
Acute pancreatitis
Pericholecystic abscesses
Hepatobiliary schistosomiasis[90]

the presence of ascites was due to the underlying hypoalbuminaemia with shift of fluid from the intravascular to extravascular space. Patients with *non*-portal hypertension ascites, due to malignancy, are more frequently found to have normal gallbladder wall thickness.[78,79]

Gallbladder wall thickening can be seen in the presence of ascites even when the serum albumin level is normal and care is taken over transducer angulation,[80] and in these cases the wall thickening is caused by ascites per se, presumably due to passive diffusion of fluid. A further twist to the tale has been provided by the observation that in patients with cirrhosis of the liver, portal hypertension can give rise to thickening of the gallbladder wall – 'congestive cholecystopathy' due to venous dilatation – in the absence of either hypoalbuminaemia or ascites,[81] and colour or power Doppler can assist in identifying varices of this nature.

The gallbladder wall thickens in response to a wide range of pathological processes (Fig. 14.40) (see Table 14.1) and is thus a very non-specific sign when used in isolation.[82] However, several of the conditions listed in Table 14.1 result in other ultrasound findings; the detection of gallbladder wall thickening may then provide useful contributory or confirmatory evidence.

Ultrasound signs may, of course, have uses other than purely diagnostic. In acute viral hepatitis, gallbladder wall thickening has not only been observed,[83] but has also been shown to correlate well with the degree of liver cell necrosis[84] and thus carries prognostic implications (Fig. 14.41).

Acute cholecystitis

Most patients presenting with acute cholecystitis undergo laparoscopic cholecystectomy, following analgesia, within the first week of the onset of symptoms.[91] This trend for urgent cholecystectomy demands that the diagnosis is made quickly, and therefore for patients who present with acute right upper quadrant pain, ultrasound is the initial imaging procedure of choice, also enabling a search to be made for other causes of the patient's pain.[43]

There is no single ultrasound sign that is specific for the diagnosis of acute cholecystitis; rather there is a range of findings which are conveniently discussed as either 'major' or 'minor' signs (Table 14.2).

Most studies have indicated that the sensitivity for a major sign of acute cholecystitis is 81–86%, and the specificity is 94–98%. The addition of a minor sign increases the sensitivity of ultrasound to 90–98%.[92] Not reflected in these figures for sensitivity and specificity is the ability to diagnose non-biliary sources of right upper quadrant pain – in as many as 35% of the patients without gall disease.[93]

Increased thickness of the gallbladder wall (Fig. 14.42) is well documented in acute cholecystitis,[94,95] but as discussed above, it is found in many other conditions, and is thus a minor sign. However,



Figure 14.41 Gallbladder in hepatitis. Thickened gallbladder wall in acute viral hepatitis. Stones are also present.

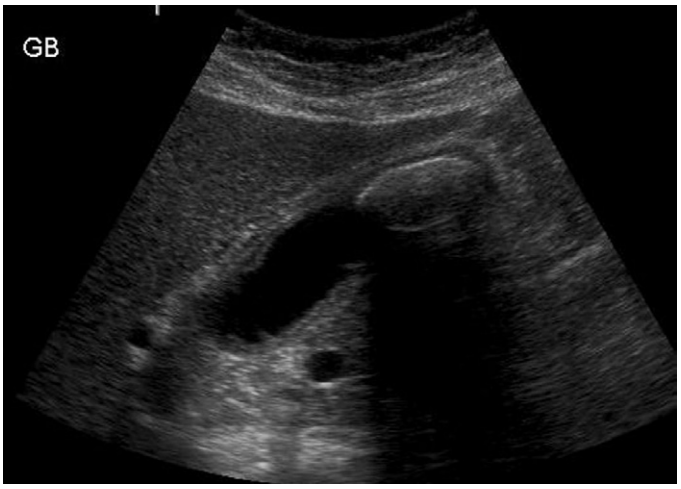


Figure 14.42 Acute cholecystitis. Thickened gallbladder wall with a hypoechoic central zone due to acute cholecystitis, tender on scanning. Note the large stone in the fundus.

Table 14.2 Ultrasound signs of acute cholecystitis

Major	Minor
Stones in the gallbladder	Pericholecystic fluid
Oedema of gallbladder wall	Thickening of gallbladder wall
Gas in gallbladder wall	Intraluminal changes
+ve Murphy's sign	Over-distended gallbladder

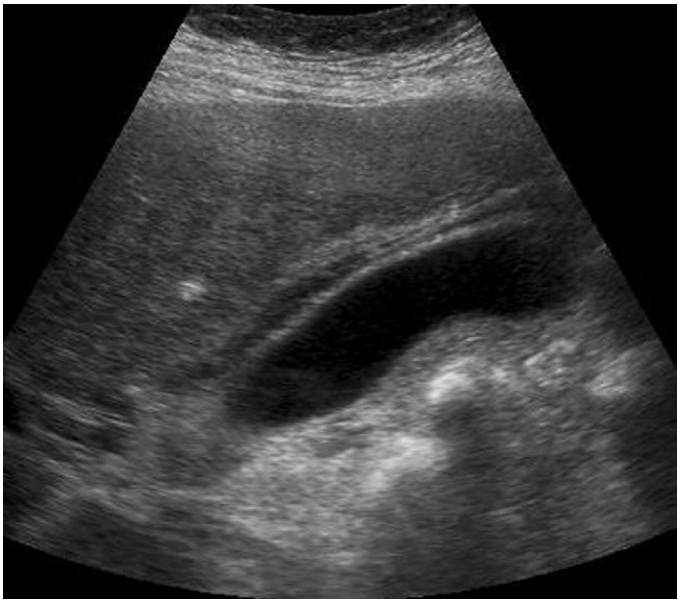


Figure 14.43 Acute cholecystitis. Thickened gallbladder wall with an echo-poor 'halo' due to acute cholecystitis.

more obvious oedema of the gallbladder wall, which is recognisable by either a continuous echo-poor rim around the gallbladder or by a focal echo-poor zone in the wall, is a major sign of acute cholecystitis, providing that other causes of gallbladder wall oedema such as hypoalbuminaemia, heart failure, and other local inflammation have been excluded (Fig. 14.43). The echo-poor zones probably represent accumulation of oedema, inflammatory exudate and/or haemorrhage. The echo-poor 'halo' is most easily demonstrated between the liver and the anterior wall of the gallbladder since the echo-poor bowel wall that is often adjacent to the posterior gallbladder wall may give a false positive 'halo sign'.[96]

Gallbladder tenderness is popularly known as the 'ultrasonic Murphy's sign',[97] but it does differ significantly from the clinical sign described by Murphy and modified by Moynihan.[98] In the clinical sign, the left hand of the examiner is placed on the costal margin in such a manner that the thumb lies over the fundus of the gallbladder. The thumb exerts moderate pressure and the patient is asked to take a deep breath. The sign is positive if the patient 'catches their breath' when the descending diaphragm causes the inflamed gallbladder to impinge on the thumb. A positive ultrasonic Murphy's sign is present when the tenderness is maximal over the ultrasonically localised gallbladder,[99] thus ensuring that the pain is elicited only during image-verified deformation of the gallbladder.[72] The combination of stones in the gallbladder and a positive ultrasound Murphy's sign are highly specific for acute cholecystitis (92%).[100] There is some evidence that colour Doppler of the gallbladder wall is useful in indicating the degree of inflammation in cholecystitis,[101] although this is rarely necessary in clinical practice.

It is important to recognise complications of acute cholecystitis, as this can lead more readily to open surgery and carries increased risk for the patient.[102] Acute cholecystitis may progress to gangrenous cholecystitis, which may perforate, resulting in a pericholecystic abscess (Figs 14.44 and 14.45) or peritonitis. The morbidity and mortality associated with this condition are considerably higher than with uncomplicated acute cholecystitis and it is important to look for ultrasound signs that may expedite diagnosis and emergency surgery. Marked irregularity or asymmetrical thickening of the gallbladder wall reflect the pathological changes of ulceration, haemorrhage, necrosis and intramural micro-abscesses.[103] Strands of fibrinous exudate and infected debris, due to sloughing of the gallbladder wall, may be present in the gallbladder lumen (Fig. 14.46).[104] Ultrasound may often detect perforation of the gallbladder wall, although CT is also a valuable adjunct in difficult cases.[105]

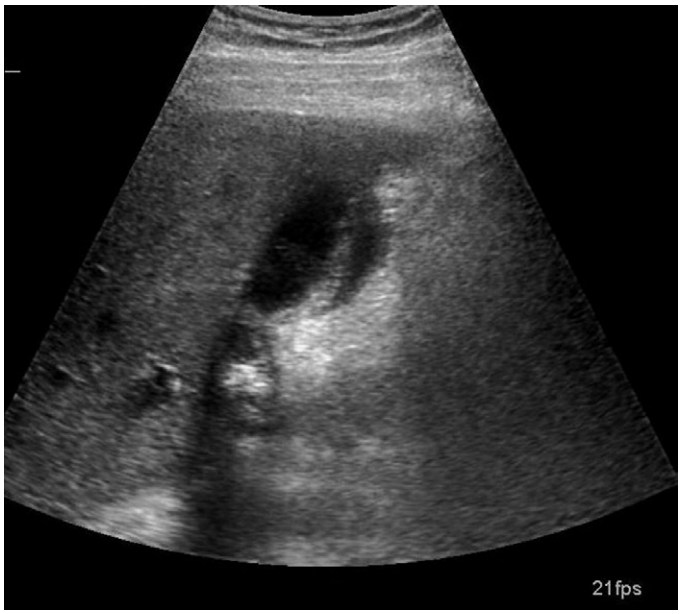


Figure 14.44 Gangrene. Gangrenous gallbladder wall with small pericholecystic leak.

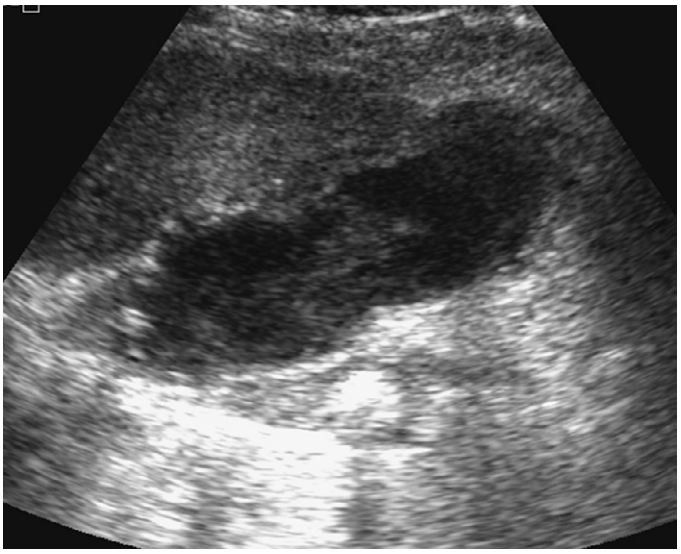


Figure 14.46 Gangrenous cholecystitis. Gangrenous gallbladder wall and typical intraluminal membranes representing desquamated mucosa.



Figure 14.45 Pericholecystic collection. The fluid within a pericholecystic leak (arrow) near the gallbladder fundus contains echoes due to pus. The gallbladder has a thickened, tender wall and contains stones.



Figure 14.47 Empyema of the gallbladder. Thickened, irregular wall with echogenic material, representing pus, filling the lumen.

Interestingly, only 33% of patients with gangrenous gallbladders are said to have a positive ultrasonic Murphy's sign[106] compared with the 95% prevalence in patients with acute non-gangrenous cholecystitis.[99] Perhaps the lack of pain is due to necrosis of the nerves in the muscular and serosal layers of the gallbladder.

Empyema of the gallbladder is difficult to recognise on ultrasound because the typical finding of sludge (non-shadowing gravity-dependent echoes) may be caused by many processes other than debris or pus (Fig. 14.47).[107,108]

Pericholecystic fluid collections may be due to localised peritonitis or to leaks from perforation of the gallbladder wall. These latter may vary in size and complexity from a small bile collection as a result of a microperforation to a true pericholecystic abscess (Fig. 14.48).[109] The ultrasound appearances of such abscesses can be quite variable, ranging from predominantly echo-free to predominantly highly reflective, although increased through transmission of sound should remain apparent.[110]

Gas in the gallbladder wall, the hallmark of emphysematous cholecystitis, is due to gas-forming organisms in the bile, and is one of the major ultrasound signs of acute cholecystitis. It may be recognised by highly reflective areas within a thickened and oedematous gallbladder wall with shadowing and reverberations distally (Fig. 14.49).[111–113] There may also be gas within the gallbladder lumen, which may make it difficult to distinguish the gallbladder from a loop of bowel. Repositioning the patient may help, and it has been documented that the gas in the gallbladder wall may shift with gravity,[114] and that the gas in the lumen may be seen to 'effervesce' on real-time observation.[115] Although this is a rare condition, it is important to recognise because of its strong association with gangrene and perforation of the gallbladder.[116] Due to the

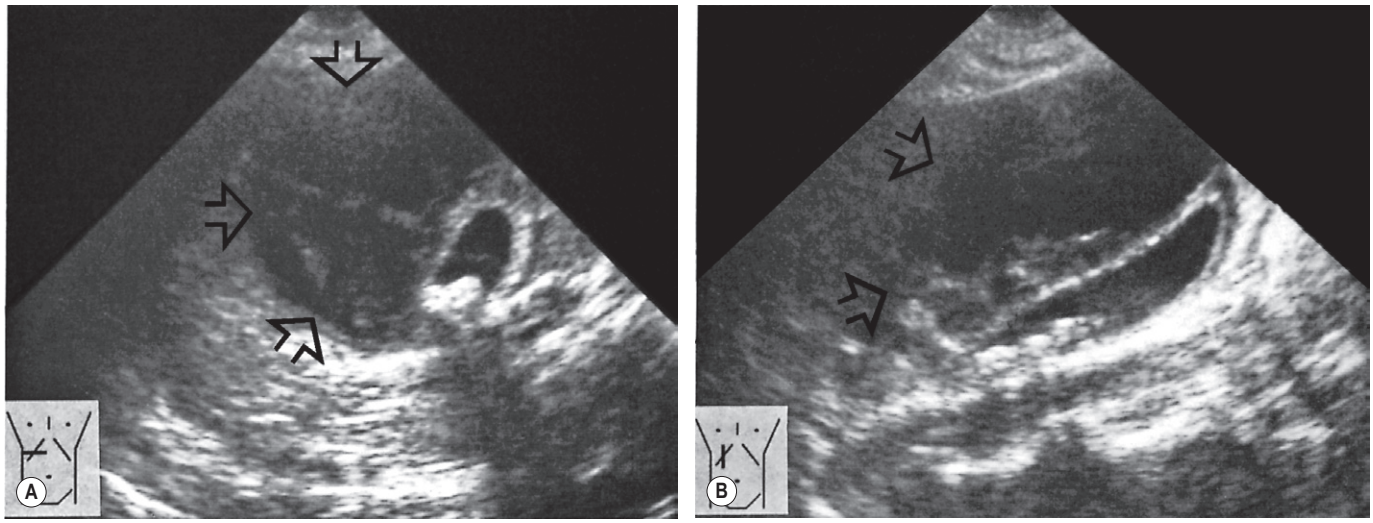


Figure 14.48 Large pericholecystic abscess (arrows) extending into the liver from the thick-walled gallbladder which is seen to contain stones. **A:** Longitudinal scan. **B:** Transverse scan.

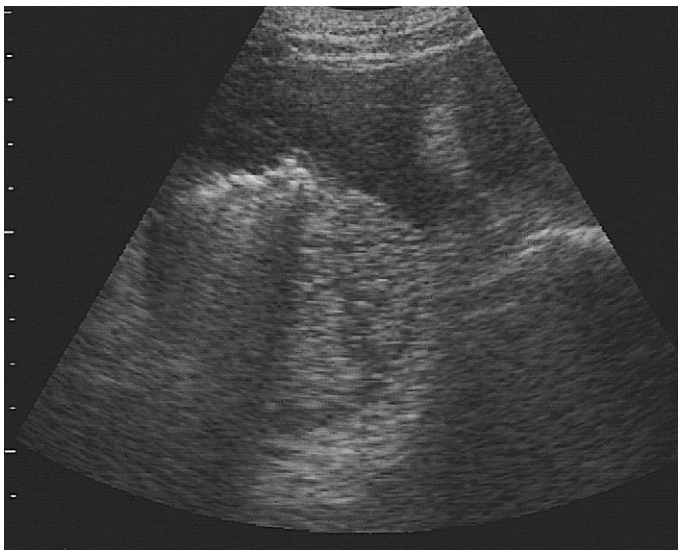


Figure 14.49 Emphysematous cholecystitis. Thickened gallbladder wall containing an area of high reflectivity with distal shadowing due to gas.



Figure 14.50 Acalculous cholecystitis. Thickened gallbladder wall in acalculous cholecystitis.

increasing use of high-resolution ultrasound in suspected biliary disease, however, the condition is being diagnosed with increasing frequency and a spectrum of severity is now recognised whereby conservative treatment may be considered in a proportion of patients.[117] Emphysematous cholecystitis may occur in the absence of gallstones – usually in diabetics – it is postulated that ischaemia of the gallbladder wall may be a primary factor in these cases.

Acute cholecystitis is acalculous in approximately 5–10% of all patients with acute cholecystitis.[118] It frequently occurs as a complication of a prolonged or severe illness such as recent major surgery, burns, sepsis, prolonged hypotension, general debility and diabetes.[119] Histologically, the changes in the gallbladder wall are similar to calculous cholecystitis, although gangrene and perforation are more common in the acalculous variety – presumably because of delayed diagnosis and treatment. The lack of stones and the inability to elicit the ultrasonic Murphy's sign in a comatose patient contribute to the diagnostic difficulty, although thickening of the gallbladder wall in association with a lack of response of the gallbladder to cholecystokinin, distension of the gallbladder and the presence of sludge are helpful signs (Fig. 14.50).[120] Diagnostic specificity may be improved by ultrasound-guided percutaneous aspiration of the gallbladder so that bacteria and/or leukocytes can be detected in the bile,[121] but initial enthusiasm for the technique has become tempered by the limitation that a negative result does not exclude acute cholecystitis.[122] This is only to be expected when it is remembered that in patients coming to surgery for acute cholecystitis, only approximately half have infected bile from which aerobic or anaerobic organisms may be cultured.

In patients with acute cholecystitis who are unsuitable for surgery, and in whom antibiotics have not been effective, percutaneous gallbladder drainage under ultrasound guidance represents an effective, bedside treatment,[123] with aspiration being preferred over cholecystostomy due to its lower complication rate.[124]

Chronic cholecystitis

Chronic cholecystitis, which is associated with recurrent right upper quadrant pain, is almost always found in association with gallstones although the exact aetiology is unclear and the classic

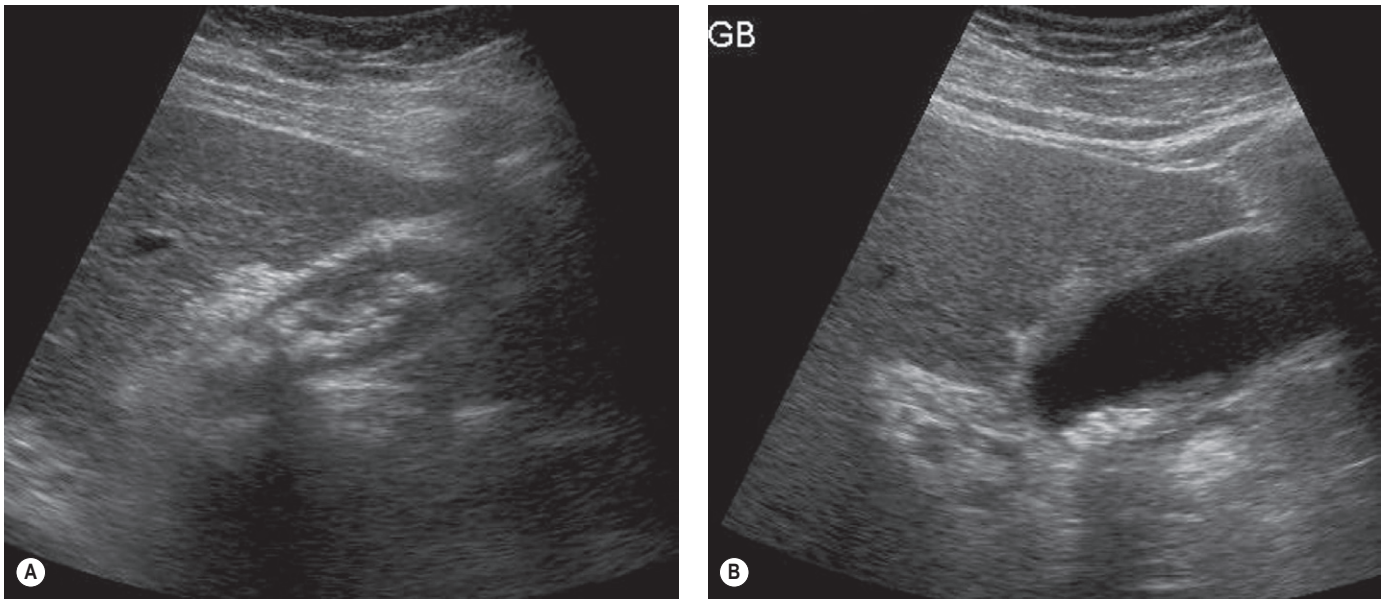


Figure 14.51 Chronic cholecystitis. A: Contracted, thick-walled gallbladder containing stones. **B:** Irregularly thickened, hyperechoic gallbladder wall, with stones.

'chicken and egg' debate continues to rage. Chronic inflammation of the wall is likely to be associated with repeated episodes of (sometimes) subclinical acute cholecystitis, together with mechanical abrasion of the gallbladder wall from stones.

In association with the stones there is a chronic inflammatory cell infiltrate throughout all the layers of the wall which becomes thickened with fibrosis in both the subserosal and muscular layers, resulting in overall shrinkage of the viscus and reduction of the lumen. In this clinical context, the ultrasonic demonstration of stones in the gallbladder, with or without thickening of the gallbladder wall, is usually taken to be diagnostic (Fig. 14.51).

If the presence of ultrasonically demonstrated gallstones is taken as an indicator of chronic gallbladder disease as defined by surgery, then ultrasound has been found to have a sensitivity ranging from 90% to 98%, with specificity consistently in the 94–98% range.[92]

If clinical suspicion persists in the case of a normal ultrasound, MRCP is useful in identifying stones in the common duct in addition to demonstrating possible biliary duct anomalies.[125]

Hyperplastic cholecystoses

In some cases of chronic cholecystitis, the lining epithelium of the gallbladder extends between the muscle bundles, giving rise to deeply situated gland-like structures, known as Rokitansky–Aschoff sinuses. When extensive, these diverticula form numerous gland-like spaces lined by epithelial cells that extend throughout the gallbladder wall. A focal increase in wall thickness may result in localised narrowing of the gallbladder lumen, giving rise to the appearance of a stricture. The term 'cholecystitis glandularis proliferans' has been applied to such a condition.

However, these 'hyperplastic' changes in the gallbladder wall may occur in the absence of either gallstones or inflammatory infiltrates, when the condition is known as adenomyomatosis.[126] Adenomyomatosis is thought to be present in up to 5% of the adult population,[127] and has also been recorded in the paediatric population. It is distinct from chronic cholecystitis, and although excessive intraluminal pressure has been suggested as the cause, the exact aetiology remains unclear.

The ultrasound features of adenomyomatosis are well recognised.[128] There is diffuse or segmental thickening of the gallbladder wall, with intramural diverticula which may be echo-free if they contain fluid bile, or highly reflective if they contain bile concretions. Segmental and eccentric wall thickening may produce mid-cavity strictures, and the high-amplitude periluminal foci (due to aggregates of solid bile elements in the Rokitansky–Aschoff sinuses) give a typical 'diamond ring' appearance on transverse sections of the gallbladder (Fig. 14.52).[129]

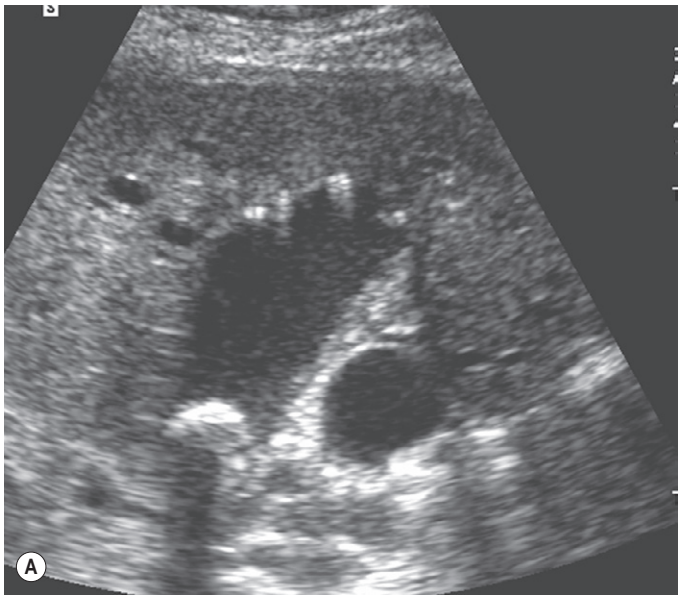
The clinical significance of adenomyomatosis of the gallbladder is controversial since it is found in both symptomatic and asymptomatic individuals. However, a significant proportion of patients with adenomyomatosis do improve after cholecystectomy, especially if the symptoms were more suggestive of biliary colic than of vague dyspepsia, or if gallstones are found in association with the adenomyomatosis. Segmental adenomyomatosis, in which the gallbladder is effectively divided by a stricture into two compartments, predisposes to cholecystolithiasis, particularly in the fundal compartment, due to bile stasis.[130]

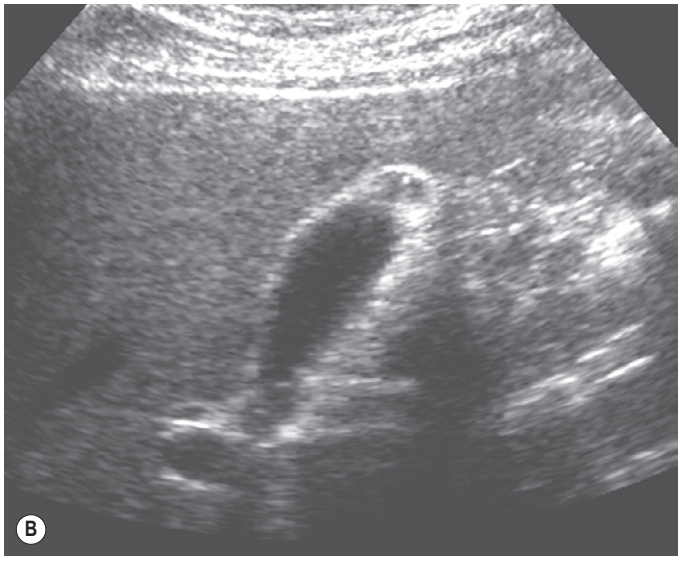
The 'strawberry gallbladder' of cholesterolosis, another non-inflammatory condition of the gallbladder, is the result of the accumulation of lipids in the mucosa of the gallbladder wall. The resulting surface nodules are usually less than 1 mm in diameter, which may be difficult to demonstrate on ultrasound, but larger polypoid excrescences forming cholesterol polyps may also develop. These are displayed as small reflective foci attached to the wall of the gallbladder which do not exhibit posterior shadowing or mobility with patient movement (Fig. 14.53).[131]

The aetiology of cholesterolosis is not fully understood. It is suggested that the mucosal changes might arise simply because of increased cholesterol uptake from bile containing extra cholesterol, and a correlation with high serum cholesterol has been demonstrated,[132] but this remains controversial and the exact causes are complex and likely to be multifactorial.[133] Whilst cholecystectomy is unlikely to benefit patients with vague dyspeptic symptoms, it is likely to help patients in whom the history suggests biliary colic, or when there are associated gallstones.[134]

Polyps

Polyps of the gallbladder include pseudo-tumours such as inflammatory polyps, cholesterol polyps and adenomyomas, the localised form of adenomyomatosis. They are common, and in the absence





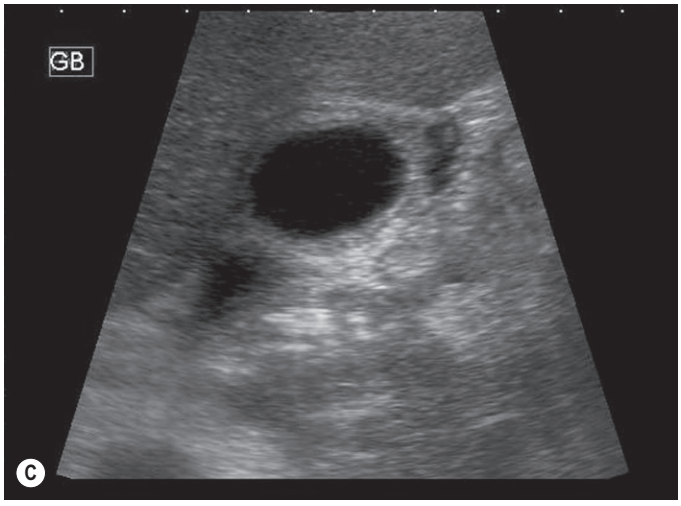


Figure 14.52 Adenomyomatosis. **A:** Adenomyomatosis at the gallbladder fundus showing the typical comet-tail artefacts. Note the solitary large gallstone. **B:** Adenomyomatosis at the fundus in a different patient, demonstrating the 'diamond ring' appearance with concretions in a dilated sinus, longitudinal scan. **C:** Transverse scan of the patient shown in **B**.



Figure 14.53 Multiple cholesterol polyps. Transverse scan through the body of the gallbladder demonstrating multiple small polyps projecting into the lumen.

of accompanying gallstones are probably not clinically significant if small.

The commonest type of true benign neoplasm is the adenoma, which can be either sessile or papillary and is usually solitary.[135] Adenomatous gallbladder polyps have been described in Peutz–Jeghers syndrome;[136] 10% are multiple, and 10% show evidence of carcinoma in situ.[137] Intestinal metaplasia can be found in large adenomas and may be a premalignant change[138] and, as in the intestinal tract, it is probably the larger adenomas that undergo malignant transformation. Adenomas are usually incidental findings, but they can cause biliary colic.

The typical ultrasound appearance is of a soft tissue mass projecting into the gallbladder lumen (Figs 14.54 and 14.55). It remains fixed to the gallbladder wall despite movement of the patient and does not cast an acoustic shadow (Fig. 14.56). Because of the probability of an adenoma/carcinoma sequence, cholecystectomy is advisable if the polyp is 10 mm or larger, even for asymptomatic polyps.[139] Other risk factors for malignancy include a wide-based, or sessile polyp, irregularity of the surface, solitary lesions and age over 50.[140] Polyps that show a tendency to enlarge are also at higher risk of malignant transformation, and may be monitored with ultrasound. CT is useful in identifying early signs of malignancy in large polyps prior to surgery.

Contrast-enhanced ultrasound has been used in helping to differentiate gallbladder polyps and carcinomas from sludge balls[141] but as vascularity in the form of contrast uptake is demonstrable in the majority of larger lesions,[142] and also occurs in different types of polyps, its clinical usefulness is limited (Fig. 14.57).

There are other benign neoplasms of the gallbladder including fibroma, lipoma, myoma, carcinoid and haemangioma, but they are all extremely rare.[143]

Carcinoma

Carcinoma of the gallbladder is a highly malignant tumour characterised by early metastases and a 5-year survival rate of less than 5%.[144] although this can be improved in cases of early detection.[145] It is the fifth most common malignancy of the gastrointestinal tract, and the most common cancer of the biliary tract worldwide, comprising 1–3% of all cancers. It affects females four times as commonly as males, and its prevalence increases with age. There is a

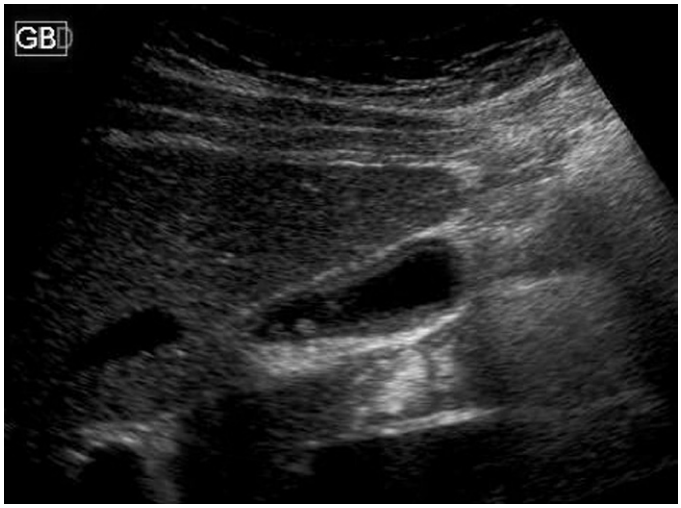


Figure 14.54 **Hyperplastic gallbladder polyps** in the gallbladder.



Figure 14.56 **Broad-based, adenomatous polyp** in the gallbladder.



Figure 14.55 **Two hyperplastic polyps** within the same gallbladder.



Figure 14.57 **Contrast ultrasound of gallbladder polyps** shows take-up of contrast in the polyps.

high correlation with gallstones (80–90%) and chronic cholecystitis, suggesting that chronic inflammation of the gallbladder mucosa may result in a dysplasia which goes on to neoplastic transformation. Up to 1.5% of patients undergoing cholecystectomy for stones turn out to have gallbladder carcinoma.[146]

Early diagnosis of this tumour is difficult, and frequently not made until local spread and metastases have occurred, but the ultrasound detection of gallbladder wall irregularities,[147] or of a complex reflective mass obliterating the gallbladder lumen,[148] may enable the diagnosis to be made preoperatively.

The various ultrasonic appearances of gallbladder carcinoma[149–152] have been well described. The most common finding is of a large solid mass filling the gallbladder bed (Fig. 14.58). This appearance is non-specific, the underlying nature of the mass being implied by the lack of visualisation of a separate gallbladder lumen or the presence of stones within the mass. The tumour may also be detected as an irregular polypoid mass within the gallbladder lumen, or as irregular thickening of the gallbladder wall which may be focal or diffuse, or as a combination of the two. In patients with gallbladder polyps, the risk of malignant transformation is increased in polyps of 10 mm or over, and in patients aged over 50.[153] For this reason, cholecystectomy is advised in such cases.

Local extension of the tumour into the adjacent liver is also readily identifiable with ultrasound.[154] However, CT is still the method of choice for staging purposes, particularly in the detection of lymphatic and peritoneal spread.

Approximately 25% of patients with a porcelain gallbladder (calcification of the gallbladder wall) will have associated carcinoma, and the lesion may be obscured by the acoustic shadow arising from the calcified anterior wall. Differentiating a porcelain gallbladder from a gallbladder full of stones is important because of this high risk of malignancy. With careful scanning, the non-calcified anterior wall of the gallbladder can be seen in the case of stones,[58,59] while the calcified posterior wall of a porcelain gallbladder may be seen, giving diagnostic appearances of a biconvex curvilinear reflective structure (Fig. 14.59).[60] The development of a carcinoma within a porcelain gallbladder can be detected if there is local or diffuse thickening of the gallbladder wall external to the calcified portion, an eccentric mass arising from the gallbladder wall, or if there is evidence of biliary obstruction, porta hepatis or peripancreatic lymphadenopathy, or liver metastases.[96]

Although the overall prognosis for this tumour remains bleak with a mean survival of less than 5 months from the time of diagnosis, ultrasound may facilitate treatment of early and curable carcinomas by the fortuitous detection of tumours in patients who are asymptomatic or who have symptoms attributable to the coexistent stones.[155] In countries where the rate of cholecystectomy for cholelithiasis has increased, there has been a corresponding decrease in the mortality from gallbladder carcinoma.[156]

As with any other abdominal viscus, blood-borne metastases may find their way to the gallbladder, albeit rarely, and asymmetrical wall thickening or polypoid intraluminal masses may be indistinguishable from primary gallbladder cancer (Fig. 14.60).[157] Malignant melanoma is the most common source of gallbladder metastases although this is rare, and associated with an extremely poor prognosis.[158]

Worms

Parasitic infections are common in tropical countries, and may find their way into the gallbladder and/or bile ducts, causing biliary obstruction, cholangitis or even cholangiocarcinoma. They are increasingly recognised on ultrasound as worldwide travel exposes individuals in non-endemic areas to parasites, with a consequent improvement in the understanding of the imaging features of infestation.

Ascariasis

The *Ascaris lumbricoides* roundworm is the most common parasitic infestation of the gastrointestinal tract worldwide, and is endemic in the Far East, countries of the former Soviet Union, Latin America and Africa. Worldwide it is probably second only to gallstones as a cause of acute biliary symptoms. The adult worm is 15–50 cm long and some 5 mm thick, and lives mainly in the jejunum. It has a propensity to migrate up into the common bile duct from where it may enter the gallbladder or intrahepatic bile ducts. It may then

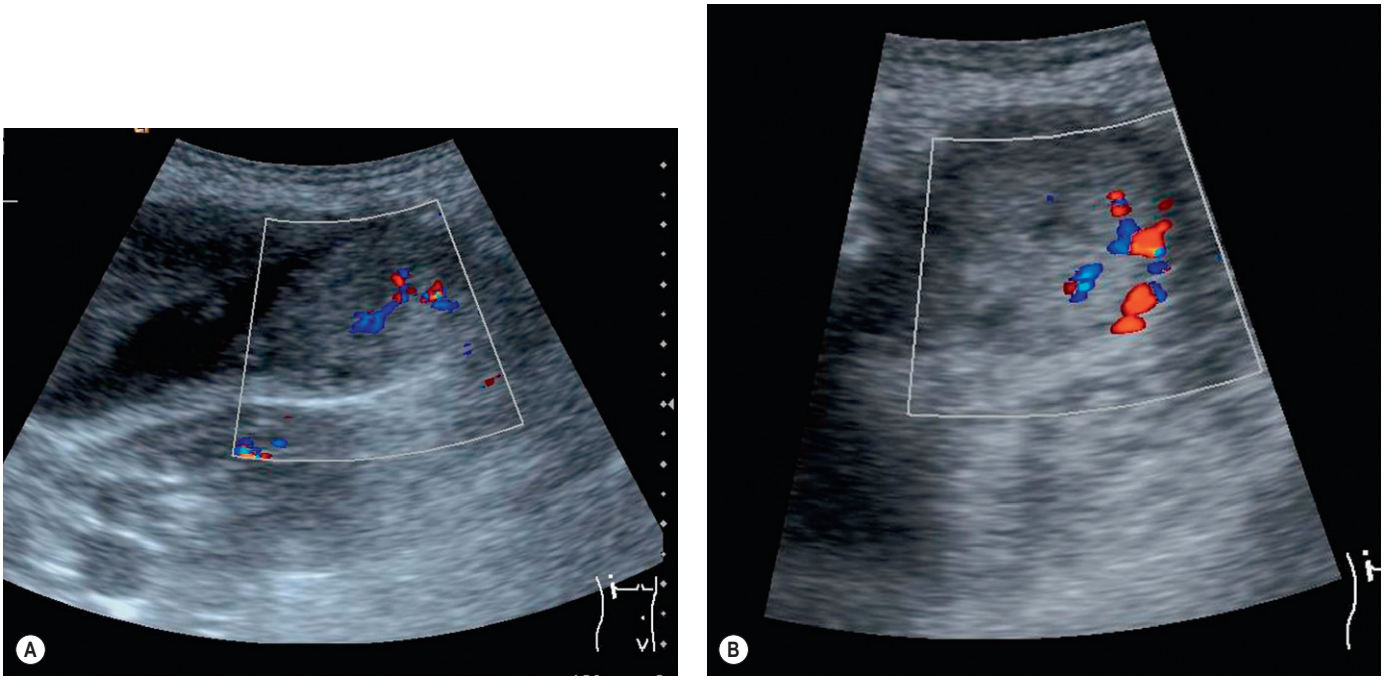


Figure 14.58 Carcinoma of the gallbladder producing a large, ill-defined solid mass in the gallbladder fossa – note the colour flow within the mass. **A:** Longitudinal scan. **B:** Transverse scan.

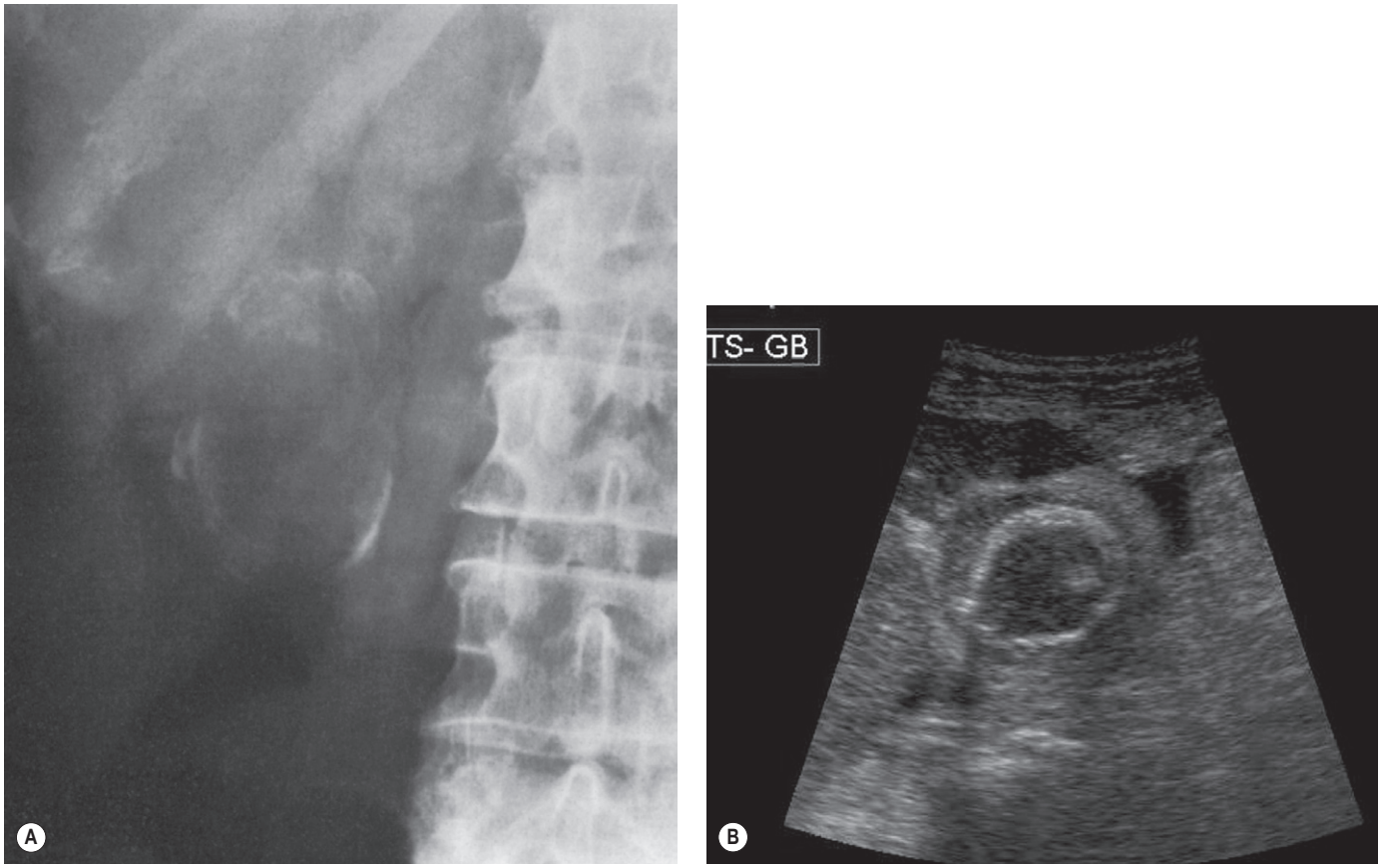


Figure 14.59 Porcelain gallbladder. A: X-ray showing typical gallbladder wall calcification. **B:** Transverse scan through the gallbladder demonstrating calcification of the inner wall.

cause biliary colic, acute cholecystitis, liver abscess or biliary obstruction.[159,160] Ultrasound scans will demonstrate the worms in the common duct or gallbladder as single strips, multiple strips, coils, or as amorphous fragments (Fig. 14.61). The writhing movements of the living worm are striking on real-time scanning.

Clonorchiasis

People ingest the *Clonorchis sinensis* liver fluke by eating raw freshwater fish, and the disease is endemic in the Far East. The adult worms are some 5 mm in length and tend to reside in the peripheral intrahepatic bile ducts, causing regional peripheral dilatation and chronic inflammation with ductal wall thickening. Usually the main ducts remain undilated, but occasionally the worms migrate to the extrahepatic ducts and gallbladder. Intrahepatic duct dilatation and cholangitis are the main features of the disease, but the parasites can be demonstrated in the gallbladder, where they cause floating or dependent, discrete, non-shadowing, intraluminal reflective foci, which are fusiform in shape and measure 3–6 mm. Spontaneous movements of these structures have been observed on ultrasound, representing movement of living worms. Infestation can cause various complications including gallstones, intrahepatic stones, cholangitis, abscess formation, cirrhosis and, occasionally, cholagiocarcinoma.[161,162]

Fascioliasis

Fasciola hepatica is a cattle fluke which may occasionally infect the human liver and biliary tract. Adult *Fasciola* worms may be demonstrated in the gallbladder and biliary ducts as intraluminal, reflective flat structures 20–30 mm long.[161]

Biliary complications can also be seen with *Opisthorchis viverrini*, *O. felineus* and *Dicrocoelium dendriticum*, which are closely related to *Clonorchis sinensis*.[162]

Hydrops

The term refers to distension of the gallbladder, usually in the absence of stones, as a result of cystic duct blockage, or mucocele. The appearance tends to be a rounded, tense gallbladder with increased intraluminal pressure (Fig. 14.62). Enlargement of the gallbladder is a subjective judgement as the range of normal variation precludes precise ranges for the normal dimensions. The long axis measurement should not exceed 10 cm and the short axis 5 cm, but these figures are only a rough guide as many abnormally distended gallbladders will be smaller than these sizes, and some normal gallbladders will be larger.

Numerous conditions are associated with gallbladder distension, such as diabetes, pregnancy[163] and in response to some drugs.[164] Longstanding gallbladder outflow obstruction produces an overdistended organ in which the bile pigments become absorbed and the fluid within turns sterile and watery or mucoid (white). The wall may or may not be thickened.

In children, acute non-inflammatory hydrops may result from a variety of causes, such as Kawasaki syndrome (mucocutaneous lymph node syndrome),[165] typhoid, leptospirosis,[166] hepatitis, nephritic syndrome and Sjögren's disease.[167]

Chronic dilatation may be due to stones in Hartmann's pouch or the cystic duct, giving rise to a mucocele of the gallbladder (Fig. 14.63).

Microgallbladder

A small, often thick-walled gallbladder in the fasting state, which does not fill or empty normally, is classified as a microgallbladder and this occurs in approximately 25% of patients with cystic fibrosis.[168] The gallbladder usually contains colourless viscid mucus – 'white bile' – and the cystic duct may be atrophic or occluded with mucus.

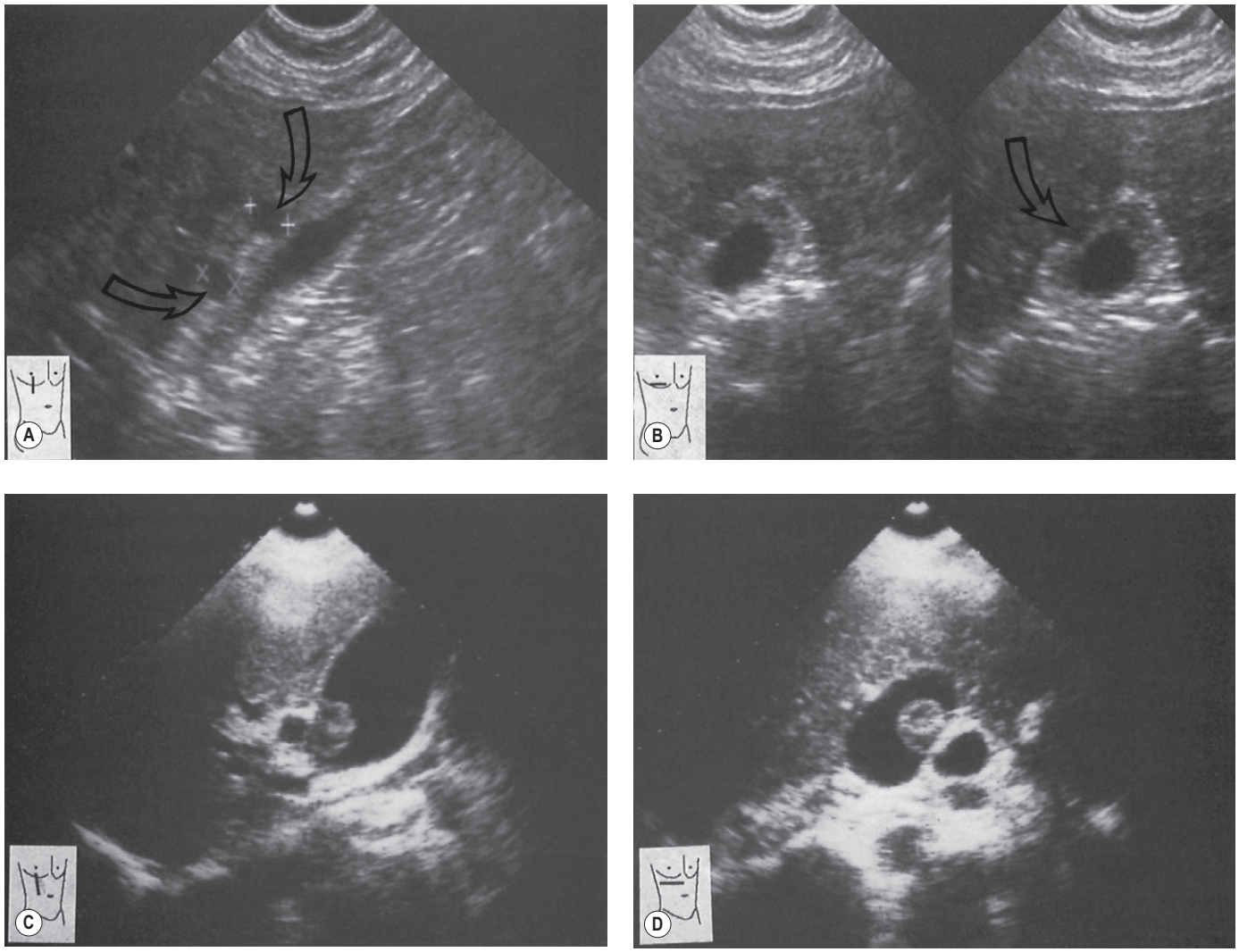


Figure 14.60 **Metastatic deposits (**arrows) from an anaplastic lung primary are seen in the gallbladder wall as echo-poor nodules. **A:** Longitudinal scan. **B:** Transverse scans. **C:** Metastases from malignant melanoma giving rise to a clearly defined, slightly heterogeneous soft tissue lesion arising from the gallbladder wall, oblique scan and **D:** transverse scan.

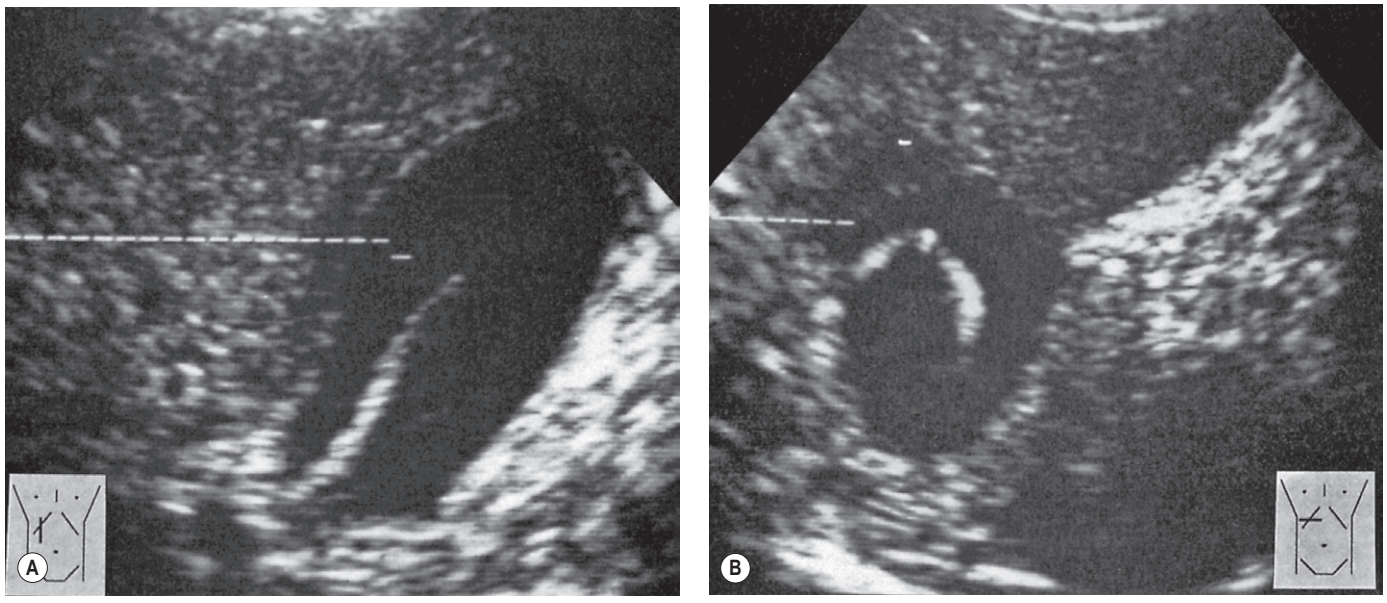


Figure 14.61 **Worms in gallbladder.** Longitudinal scan **(A)** and transverse scan **(B)** showing curved worm in the gallbladder lumen.

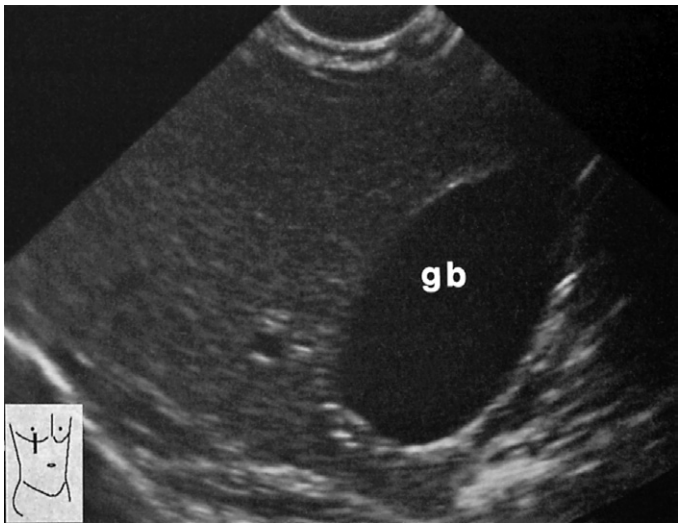


Figure 14.62 Hydrops of the gallbladder due to mucocutaneous lymph node (Kawasaki syndrome) in a child aged 3 months.

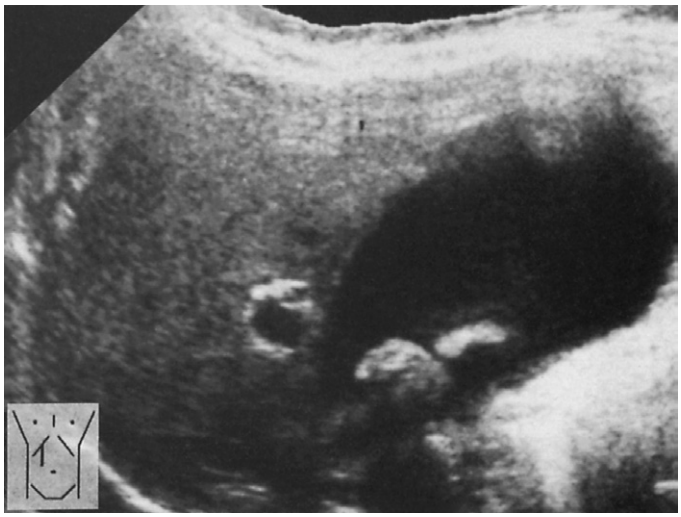


Figure 14.63 Mucocele of the gallbladder. The gallbladder is distended, thin walled and contains stones.

There is an increased incidence of gallstones in cystic fibrosis due to a combination of factors, which include loss of bile salts because of malabsorption, increased biliary lipid composition and bile stasis, with consequent obstruction of smaller bile ducts leading to obstructive cirrhosis. Thickening of the gallbladder wall may develop if secondary cholecystitis occurs (Fig. 14.64).[169]

BILE DUCT PATHOLOGY

Jaundice

Jaundice is due to an increase in the serum bilirubin level above the normal range of 1 to 15 mg/L (1.7 to 25 µmol/L). When the increase is mild its presence may only be detected on biochemical analysis of the blood, but when the bilirubin level rises sufficiently there is clinically detectable yellow discoloration of the skin, sclerae and mucous membranes.

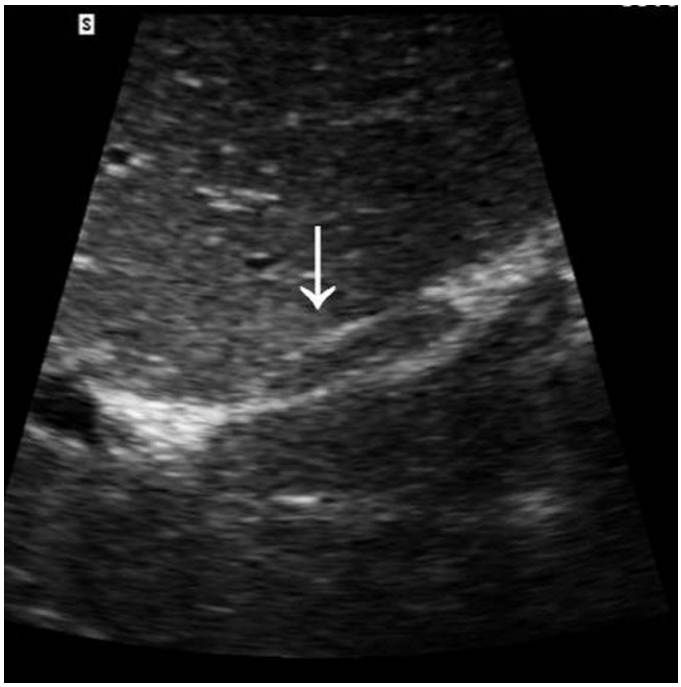


Figure 14.64 Microgallbladder (arrow) in a fasted patient with cystic fibrosis.

The pathological mechanisms that give rise to jaundice can be classified into three main groups: haemolytic (or prehepatic), hepatocellular (or hepatic), and obstructive.

The haemolytic nature of jaundice is readily apparent from haematological and biochemical blood tests, and imaging has little part to play in diagnosis or management.

There are many causes of hepatocellular jaundice, most of which will be diagnosed on biochemical, serological or histological examinations of the blood or liver, but some will cause structural changes in the liver which may be detectable on ultrasound scans. The ultrasound features of parenchymal liver diseases such as the various types of hepatitis and cirrhosis, of primary and secondary malignant disease of the liver, and of inflammatory processes such as pyogenic liver abscesses, are discussed in Chapters 8 and 10. Ultrasound may suggest the cause of hepatocellular jaundice and it can be used to guide a needle for a diagnostic aspiration or biopsy (see Chapter 11).

Obstructive jaundice is strictly defined as due to a block in the pathway between the site of conjugation of bile in the liver cells and the entry of bile into the duodenum through the ampulla. The block may be intrahepatic, at the biochemical, cellular or canalicular level, or extrahepatic in the bile ducts. It is this latter group of causes of extrahepatic obstructions that are referred to as *surgical* jaundice, to simplify their distinction from all other causes of jaundice which are then referred to as *medical*.

Although the cause can often be diagnosed on the basis of a careful history and examination, the differing managements of medical and surgical jaundice make early differential diagnosis essential. Conventional blood testing will usually confirm the presence of cholestasis but provides little or even misleading information about the site of obstruction and its cause. A variety of techniques for visualising the biliary tree are now available and it is important that patients are subjected to a diagnostic pathway most appropriate for their particular needs and clinical presentation, as there are inherent risks involved in some diagnostic tests, such as endoscopic procedures or contrast injection. Ultrasound scores highly on grounds of safety, simplicity, cost and accuracy, and has therefore come to be universally regarded as the best initial imaging procedure.[170]

Ultrasound has been shown to be highly accurate in diagnosing surgical jaundice, detecting dilatation of the intrahepatic or extrahepatic biliary tree in 85–95% of patients with proven obstruction,[171–177] and has a high positive predictive value for obstruction with an incidence of false positive findings of less than 5%. Ultrasound is also highly accurate at defining the level of obstruction, although the actual cause may be diagnosed in only about a third of patients.

Obstruction may occur without duct dilatation (see below) and thus there is a false negative rate although, more recently, the reported sensitivity for the detection of choledocholithiasis has increased to over 80%.[178,179] These results are attributable to improvements in equipment and meticulous scanning technique. Furthermore, the introduction of endoscopic ultrasound has demonstrated sensitivities of up to 97% in the detection of CBD stones[180] and, although invasive, has the advantage of improved sensitivity for stone detection. In cases of biliary duct dilatation, EUS is also accurate in diagnosing the cause of obstruction[181,182] in cases of stricture, neoplasm and other, extra-ductal causes of obstruction relating to the ampulla and head of pancreas. EUS is considered a safe and useful technique for selecting patients for therapeutic ERCP, allowing many patients to avoid the potential complications of a purely diagnostic ERCP.[183]

Bile duct dilatation

The ultrasound diagnosis of obstructive (surgical) jaundice depends upon the detection of bile duct dilatation.

Within the liver, the normal non-dilated small bile ducts are difficult to visualise on ultrasound. The larger main right and left bile ducts can be identified as tubular structures running anterior to and parallel with the right and left branches of the portal vein and measure up to 2 mm in diameter in the non-dilated system (Fig. 14.65).[184,185] The diameter of the normal common duct at the porta hepatis should be less than 5 mm,[186,187] increasing slightly (less than 6 mm) as the duct runs caudally in the free edge of the lesser omentum[188] and within the head of the pancreas.

The diameter of the non-obstructed duct does increase with age[189] or if there has been previous obstruction.[190] The dilated preoperative duct returns to a normal diameter in 75% of patients following removal of the stone, but may remain 'baggy' and mildly dilated in around 25% of cases.[191]

Dilatation of the intrahepatic bile ducts is usually most apparent near the porta hepatis if the obstruction is in the common duct, with dilatation of the left hepatic ducts often being more noticeable than those in the right lobe in the early stages of obstruction. The ultrasound appearances of dilated ducts have been variously described as the 'parallel channel'[192] and 'double-barrelled shot-gun'[193] signs, which depend upon the bile ducts dilating to become equal to or greater than the diameter of the adjacent portal vein branch. (When scanned along their long axes, these structures are seen as two parallel channels, while in cross-section the appearance is apparently reminiscent of looking into a double-barrelled shot-gun) (Fig. 14.66). When the parallel channels occur in a fatty liver the outer walls may be masked by the high reflectivity of the liver parenchyma. In this case all that is seen is the interface between the vein and duct, giving rise to the 'stylet' sign (Fig. 14.66B).[194] Care should be taken, however, not to confuse biliary duct dilatation with the 'double channel' of a thrombosed portal vein in portal hypertension, and consequent increased diameter of the hepatic artery. Careful examination of the main portal vein should establish if it is thrombosed, and whether the artery is dilated. Colour Doppler will differentiate the main artery from the portal vein, but will not, of course, distinguish a thrombosed portal vein and a dilated bile duct, neither of which demonstrates flow.

When scanning a patient with dilated intrahepatic ducts, there is often an immediate overall impression of 'too many tubes' in the liver. These tubes do not correspond to hepatic arteries or portal veins, and must be bile ducts (Fig. 14.67).[195] The nature of the branching pattern of the intrahepatic bile duct system is such that when dilated, the ducts are seen to converge together, giving a characteristic 'stellate pattern'. This is in contradistinction to the branching pattern of the portal veins which have a more orderly arrangement whereby the peripheral branches all take origin from the main right and left branches (Fig. 14.68).[196]

Finally, the fluid in the dilated bile ducts is clear bile and ultrasound is transmitted without attenuation. When, as is usual, the time gain compensation is set to compensate for the liver's attenuation, there will be increased through transmission of sound (enhancement) beyond dilated ducts (Fig. 14.69). This is

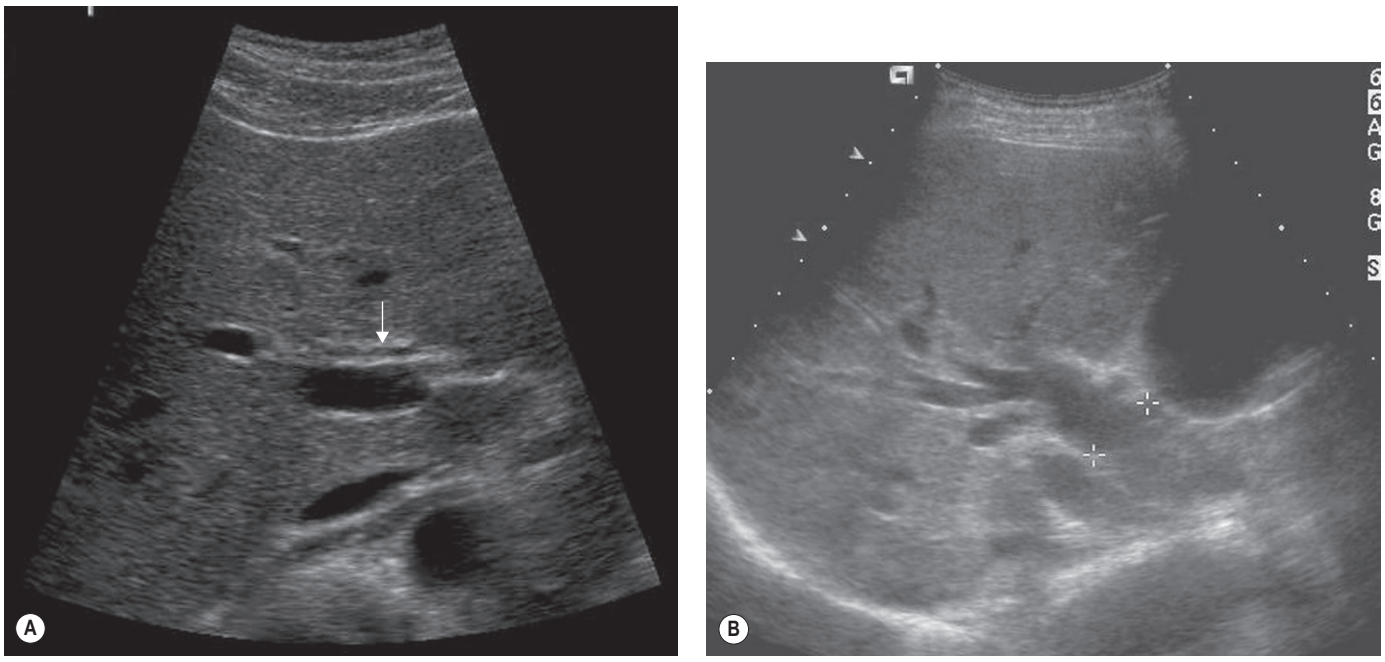


Figure 14.65 **A:** Normal intrahepatic bile duct. Right hepatic duct (arrow) seen running anterior to right branch of portal vein. **B:** A different case demonstrating a dilated CBD (callipers) with branching dilated intrahepatic ducts.

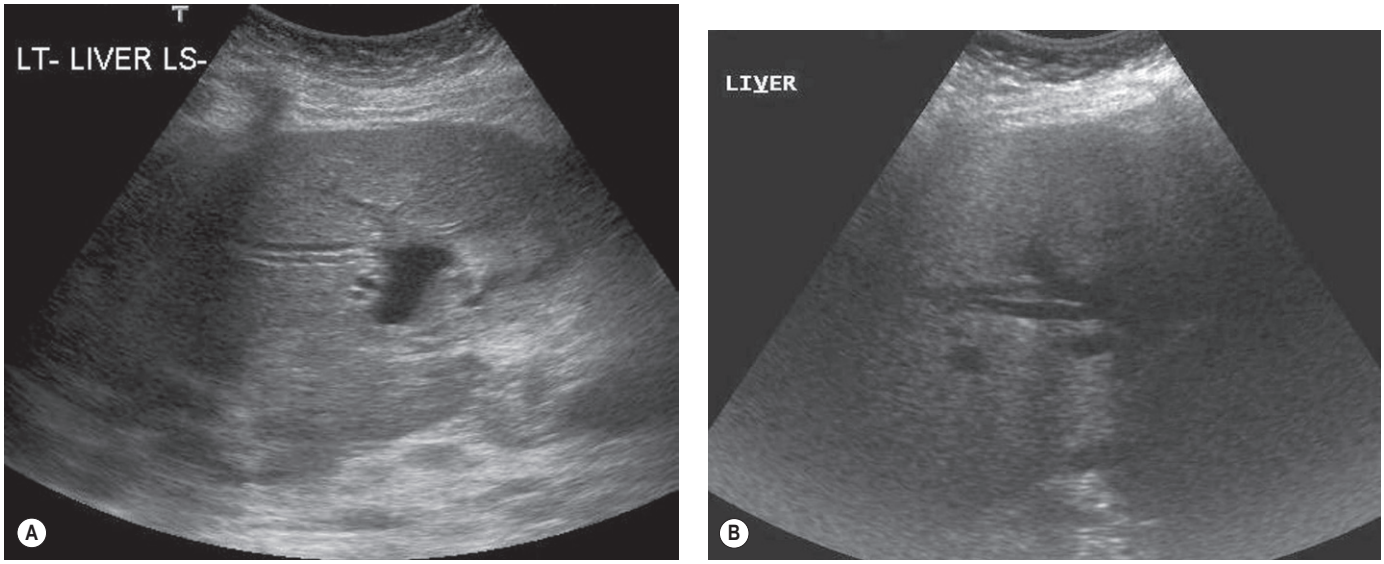


Figure 14.66 **Dilated intrahepatic bile duct. A:** 'Parallel channel' or 'double-barrelled shot-gun' sign of dilated ducts. **B:** Stylet sign; the linear echo represents the interface between the vein and dilated duct.



Figure 14.67 **Dilated intrahepatic bile ducts** – 'too many tubes' within the liver.

often disadvantageous in the clinical situation when the patchy enhancement beyond the dilated bile ducts so disturbs the normally uniform echo pattern of the liver parenchyma that it becomes impossible to diagnose small metastatic lesions with confidence.

Obstruction without dilatation

Unfortunately, complete reliance upon the ultrasound detection of duct dilatation to detect obstruction will lead to a false negative diagnosis in some cases since it has been well documented that obstruction may occur without dilatation.[197–200]

If the obstruction is of recent onset, the ducts may not have had time to dilate despite the onset of jaundice.[201] Rescanning after an interval of a couple of days may well detect these cases, and is recommended if the ultrasound findings do not fit with the clinical impression.

It is possible to detect stones in non-dilated ducts on ultrasound, but a negative scan in suspicious clinical circumstances should lead to further investigations such as CT scanning or direct cholangiography via the percutaneous transhepatic or endoscopic retrograde routes.[179]

Other causes of obstruction without dilatation are encasement of the common duct by tumour[199] or fibrosis of the duct wall as in sclerosing cholangitis,[172,202] and in cases of chronic hepatitis or cirrhosis dilatation of intrahepatic ducts may be impossible due to rigidity of the surrounding liver parenchyma.

MRCP (Fig. 14.70) is a reliable, accurate and relatively non-invasive method of evaluating the biliary tree and can demonstrate biliary strictures in patients with undilated ducts on ultrasound.[203,204]

Dilatation without jaundice

Ultrasound detection of biliary dilatation may precede the onset of clinically detectable jaundice.[205,206] This situation may occur in several different clinical settings: (a) when segments of the intrahepatic biliary tree are obstructed by tumour while other parts remain unobstructed; (b) when there are stones in the common duct causing a ball-valve effect, the intermittent relief of obstruction allows clearance of the bile so that jaundice may not develop; (c) in chronic incomplete or slowly progressive obstruction such as may be caused by tumour in the head of pancreas or chronic pancreatitis, the wider extrahepatic portions of the biliary tree dilate more, in keeping with Laplace's law.

These pathological conditions must be differentiated from the non-pathological dilatation of the common duct with increasing age[207] and from post-cholecystectomy dilatation. However, it should also be noted that while the serum bilirubin may not be elevated, so that the patient remains anicteric, the serum level of alkaline phosphatase is more sensitive and will almost always be raised if the duct dilatation is pathological, and this finding should aid the decision to proceed to CT scan or MRCP.

Rapid changes in duct diameter

The diameter of the common duct may respond rapidly to both physiological and pathological changes in intraductal pressure[207–209] and thus the ultrasound measurement of duct calibre at any one moment of time may not convey the entire picture. The walls of the extrahepatic ducts are composed mainly of elastic fibres and connective tissue with little or no smooth muscle.[210] The stretch potential of the elastic fibres permits duct dilatation while the elastic recoil of the fibres is responsible for return of the duct to normal size after relief of an obstruction.

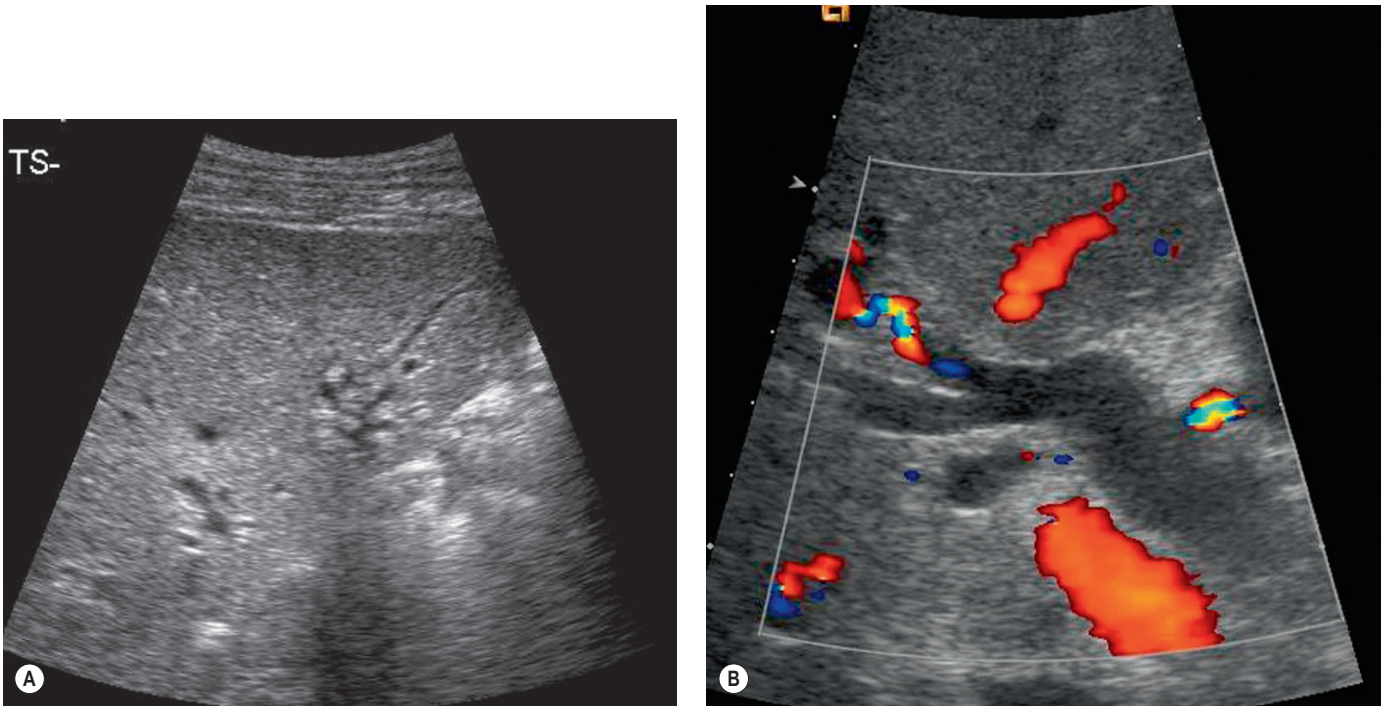


Figure 14.68 **A: Dilated intrahepatic bile ducts** near the periphery of the liver form a 'stellate branching pattern'. **B:** Colour Doppler demonstrating the dilated duct (no flow) next to the normal portal vein (in red.).

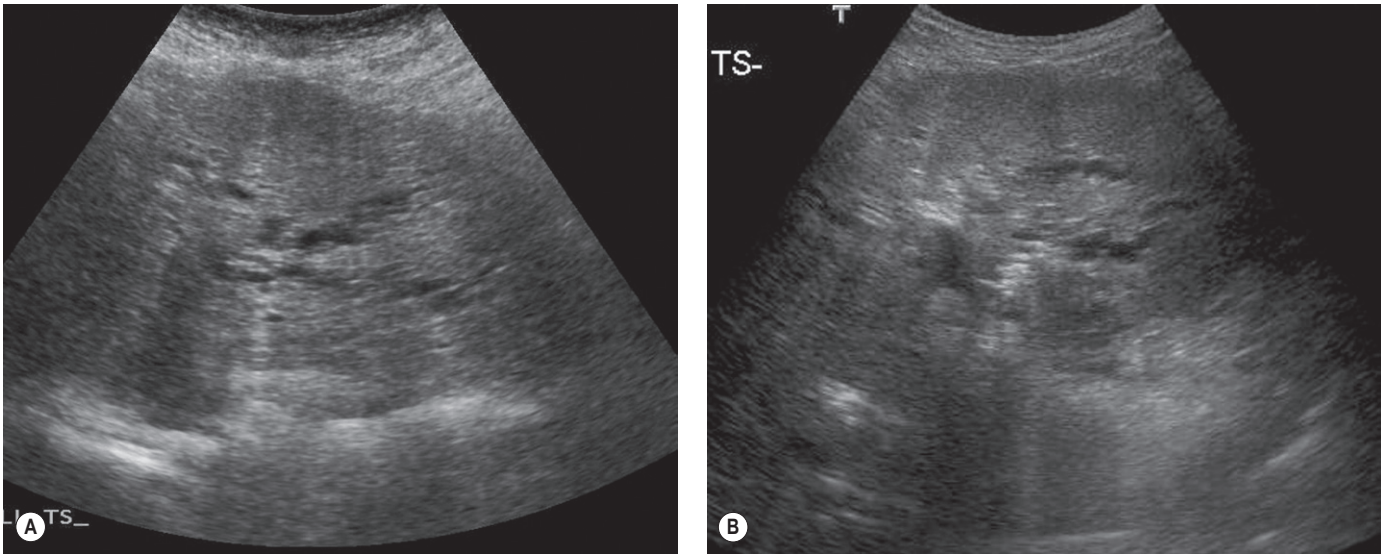


Figure 14.69 **Dilated intrahepatic bile ducts. A:** 'Enhancement beyond dilated ducts'. **B:** Duct dilatation with posterior enhancement results in a 'patchy' echotexture within liver which can be difficult to interpret.

An increase in the volume of bile within the biliary system will result in increased intraductal pressure and the common duct will dilate.[211] The bile volume is controlled by the balance between bile production (choleresis) and bile outflow, which is itself controlled in health by the tone of the sphincter of Oddi and the reservoir function of the gallbladder.

After cholecystectomy, a choleresis may so stress the capacity of the common duct that marked dilatation may result. This would be particularly liable to occur in 'floppy' ducts which have been subject to previous obstruction and dilatation.

It is also apparent that an abrupt increase in bile duct volume caused by the injection of contrast medium into the bile duct at cholangiography may result in transient dilatation, and an assessment of duct diameter that is significantly discrepant from the preceding ultrasound scan.[209,212]

Gallbladder distension

Courvoisier's law states that, 'if in a jaundiced patient the gallbladder is enlarged, it is not a case of stone impacted in the common duct, for previous cholecystitis which existed when the stone was in the gallbladder, must have rendered the gallbladder fibrotic and incapable of dilatation'.[213] We now know that, as with all rules in medicine, there are many exceptions to this law. Stones can form de novo in the common duct, leaving the gallbladder wall in pristine condition, there may be double impaction of stones when the stone in the cystic duct causes a distended gallbladder and the stone in the common duct causes jaundice (Fig. 14.71), or there may be a pancreatic calculus impacted at the ampulla obstructing both bile and pancreatic ducts.

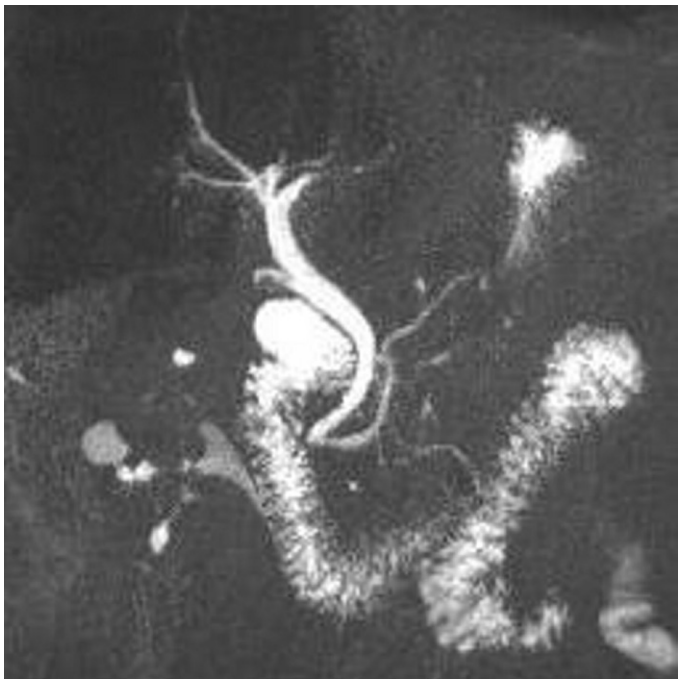
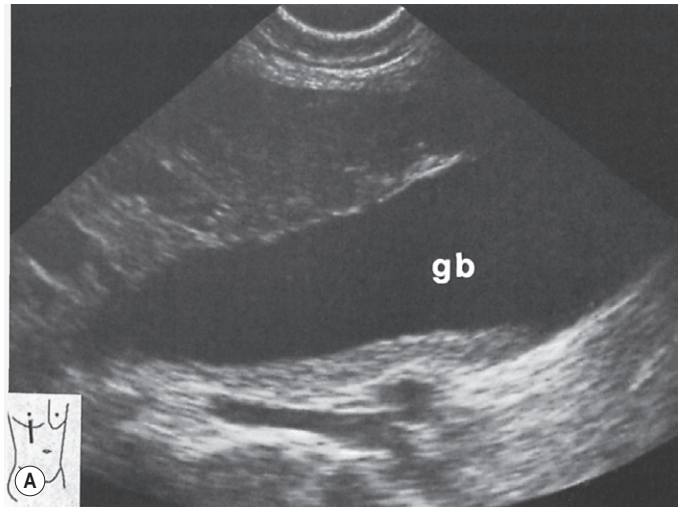
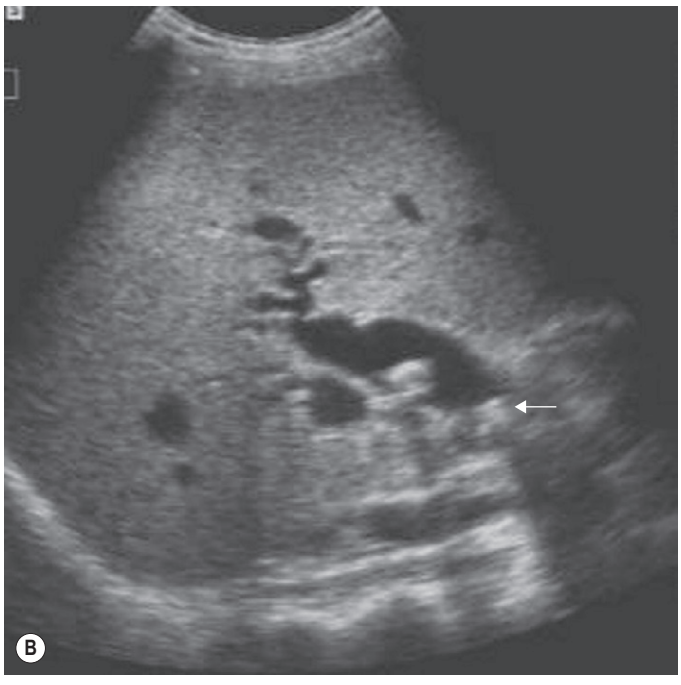


Figure 14.70 MRCP showing a normal CBD and pancreatic duct.





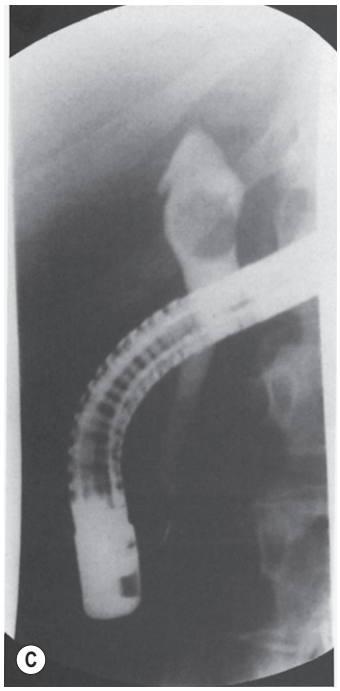


Figure 14.71
Choledocholithiasis. A: Distended gallbladder (gb) due to **(B)** a stone obstructing the common duct (CBD) (arrow). **C:** Confirmed on ERCP prior to stone removal.

However, whenever duct dilatation is encountered, it is useful to assess the degree of distension of the gallbladder as this may offer a clue to the level of the obstructing lesion. A distended gallbladder suggests a low common duct obstruction, while a contracted gallbladder is consistent with obstruction above the level of the cystic duct insertion. But the possibility of dual pathology must always be considered, and the gallbladder findings must be regarded as supportive rather than of primary importance.

Choledocholithiasis

Sensitivity rates for the detection of stones in the bile duct are around 75–82%,[214–216] with careful percutaneous scanning techniques and good equipment resolution. This is increased up to 94% with EUS.[183]

Choledocholithiasis occurs in approximately 15% of patients with stones in the gallbladder,[217] but may also occur in the absence of cholelithiasis, and may be found in as many as 4% of post-cholecystectomy cases,[218] many of whom will present with abdominal symptoms without jaundice.[190]

The classic clinical presentations of choledocholithiasis include biliary colic, jaundice and fluctuating fever – Charcot's triad. However, one or more of these components is often absent, the clinical features depending upon the varying degrees of bile duct obstruction, inflammation and infection present in any individual case.

There are several explanations for the persistently lower sensitivity of ultrasound in the diagnosis of choledocholithiasis:

1. Gas in the first and second parts of the duodenum may obscure the common duct, which accounts for the finding that stones in the proximal portion of the duct are very much more often detected than stones in the distal portion (Fig. 14.72).[214]
2. Lack of dilatation of common ducts that contain stones, even in the presence of obstruction is now well recognised[199,200] and may occur in as many as 25% of acutely obstructed ducts (Fig. 14.73).[219] Explanations for this phenomenon include the so-called 'ball-valve effect' whereby the intermittent nature of the obstruction prevents the intraductal pressure from rising sufficiently to cause duct dilatation, and the 'temporal lag' between onset of obstruction and onset of dilatation.[201]
3. The absence of a bile pool around stones in the duct impairs the ability of the ultrasonographer to spot the stones. The contrast between the reflectivity of solid stone and the echo-free nature of fluid bile that is so useful in the diagnosis of stones in the gallbladder is not present when the stones are in direct contact with the highly reflective walls of the duct and the adjacent gas-containing bowel. A particularly embarrassing situation can arise when the duct is absolutely

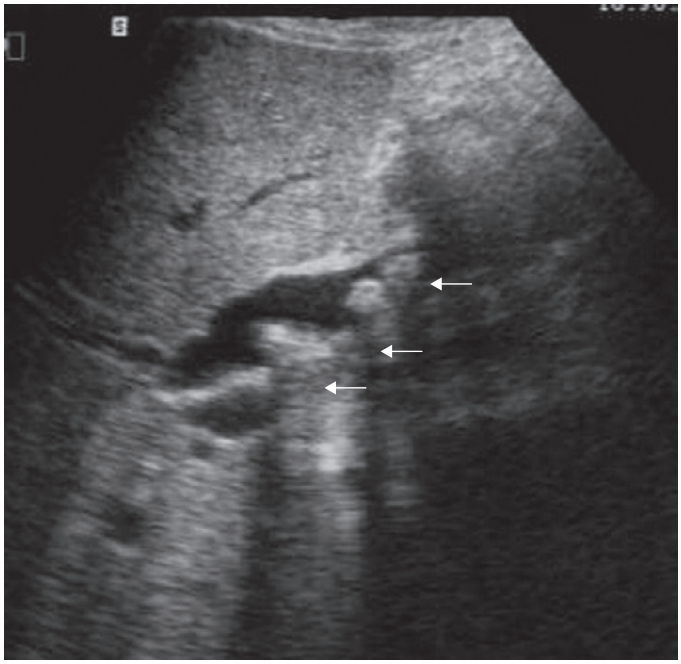


Figure 14.72 Choledocholithiasis. Stones in the dilated common duct casting acoustic shadows (arrows).

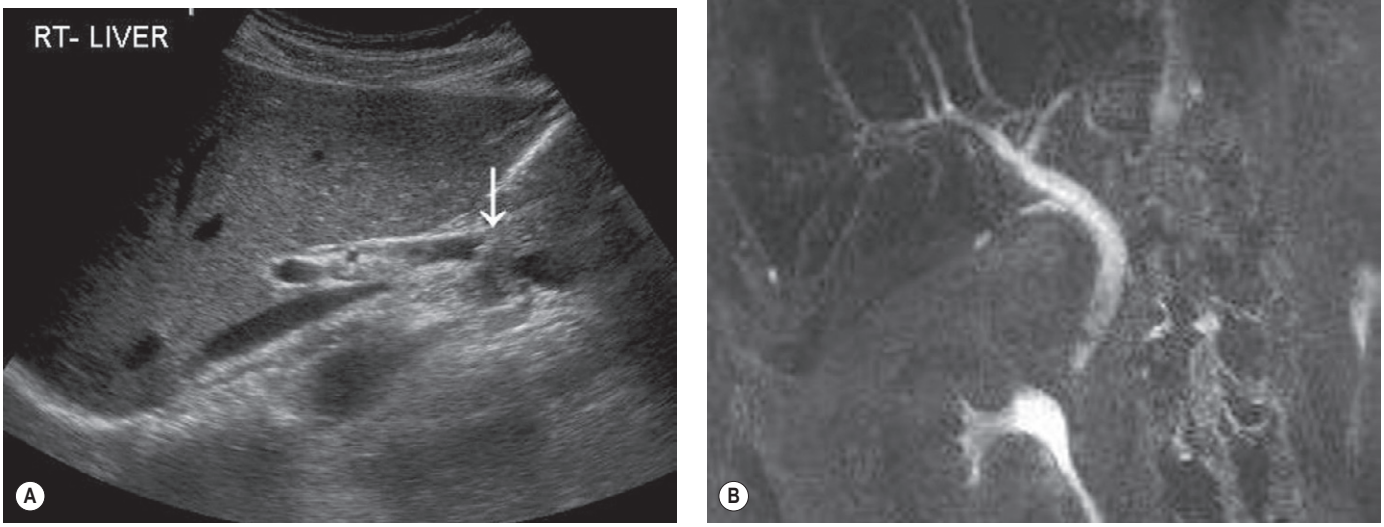


Figure 14.73 Stone in non-dilated duct. A: A stone is present at the lower end of the normal calibre CBD. Note the shadowing from the stone is difficult to recognise due to the close proximity of bowel. **B:** MRCP of the same case demonstrating the stone in the non-dilated duct.

full of stones, giving rise to a highly reflective structure with distal acoustic shadowing which is misdiagnosed as bowel gas (Fig. 14.74).

4. As many as 10% of common duct stones may lack a distal acoustic shadow,[220,221] especially when the stones are at the lower end of the duct (Fig. 14.75). This phenomenon may be due to the differing composition of common duct stones (as compared to gallbladder stones), and indeed some are merely conglomerations of soft sludge, or to technical factors such as gain settings, transducer frequency and focusing, and reflection/refraction of sound by the curved walls of the duct. Non-shadowing stones in the duct cannot be distinguished from other intraluminal pathology such as blood clot, tumour or parasitic infection.
5. Gas in the bile duct may give ultrasound appearances identical to those of stones, i.e. high reflectivity and acoustic shadowing emanating from within the duct lumen (Fig. 14.76), and may obscure the presence of stones. The gas is usually widely distributed throughout the intrahepatic biliary ducts and thus the nature of the problem should be apparent to the sonographer. However, the increasing incidence of endoscopic sphincterotomy severely restricts the usefulness of ultrasound in searching for retained stones after surgical or endoscopic procedures.

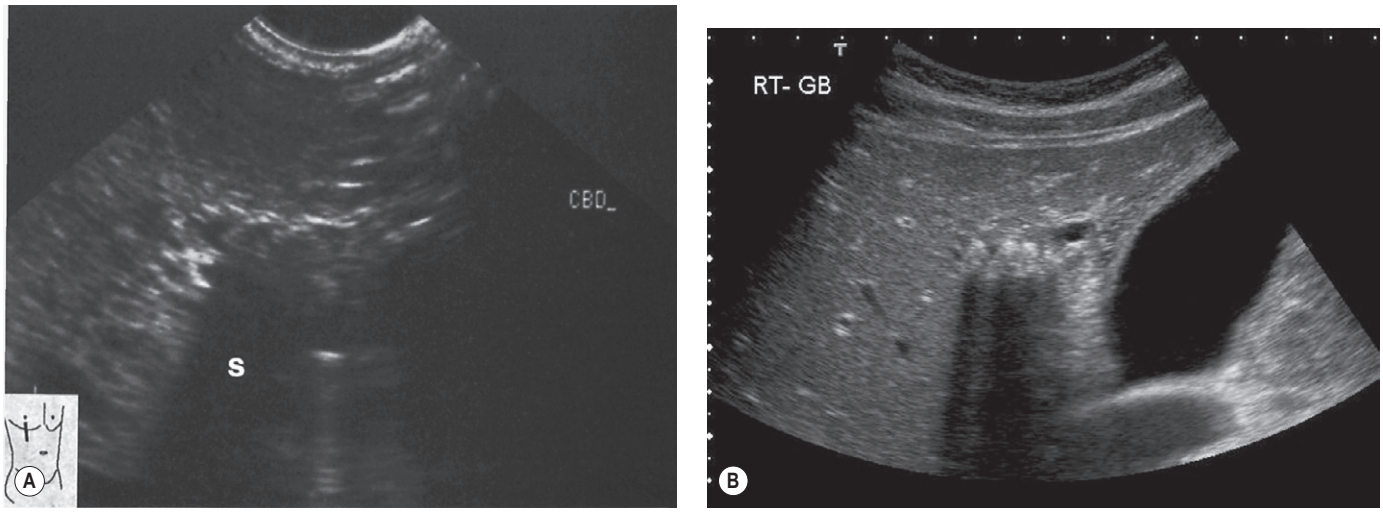


Figure 14.74 Stones filling the lumen of the common duct (A) casting a posterior acoustic shadow(s). **B:** Shadows from a row of stones within the right intrahepatic bile duct.

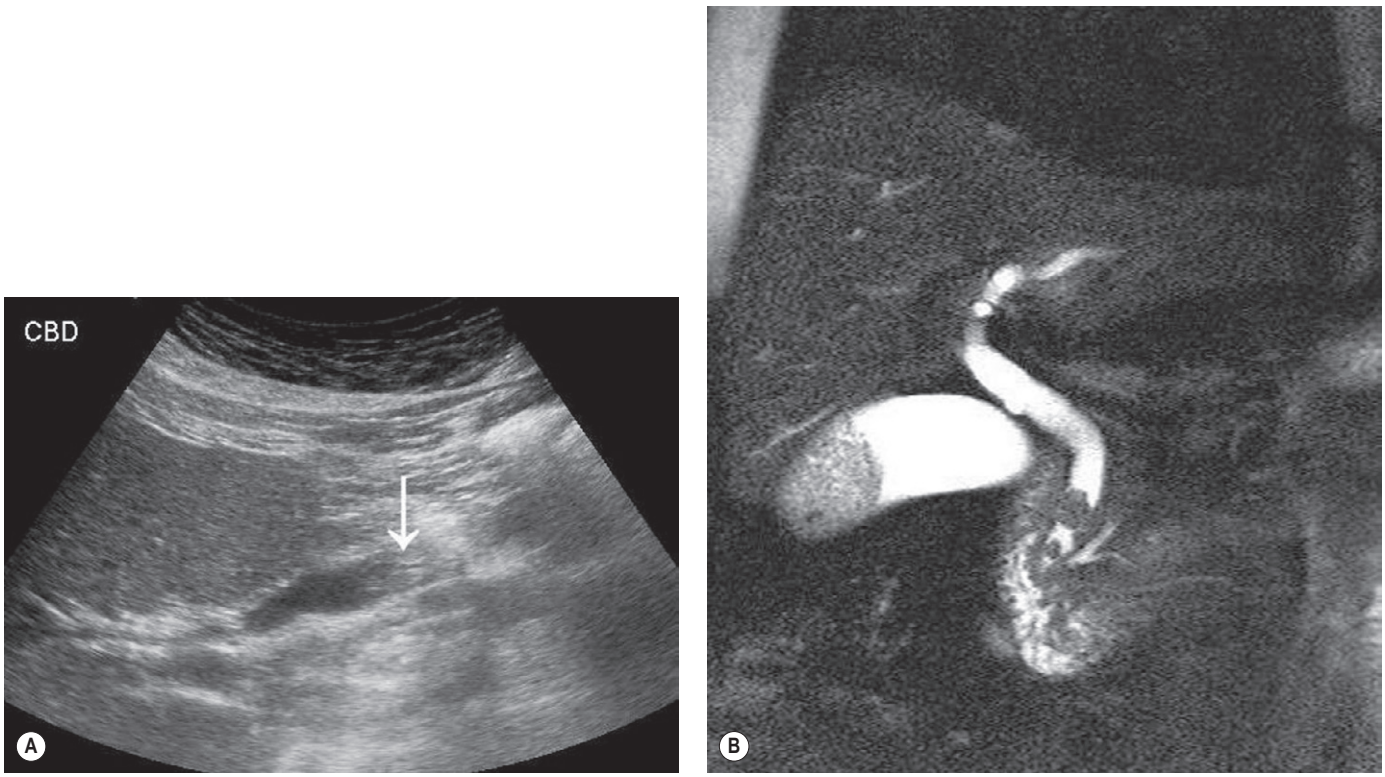


Figure 14.75 No shadowing from stones within the common duct. A: Stone (arrow) in the lower duct. **B:** MRCP of patient in **A**, confirming stones at the lower end of the duct.

Developments in equipment and transducer technology do permit the demonstration of small stones within minimally dilated, or even normal calibre ducts, as long as meticulous scanning technique is employed. It is important to scan the common duct in both longitudinal and transverse scan planes (Fig. 14.77), to be prepared to employ various patient positions, including decubitus with right side raised (Fig. 14.78), as well as upright and semi-upright positions, and to use water in the stomach and duodenum, all in an effort to demonstrate pathology in the common duct. An important clue to a calculous aetiology of biliary obstruction is the disproportionate dilatation of the extrahepatic biliary tree in comparison to the intrahepatic ducts. When this is noted, the search for a calculus should be even more diligent. However, despite all these efforts, approximately 30% of common duct stones will be missed – mainly due to impaction in the lower end of the common duct where they are hidden by the duodenum (Fig. 14.79). MRCP and EUS are helpful in demonstrating ductal stones in the presence of a negative percutaneous ultrasound and continuing clinical suspicion.[222]

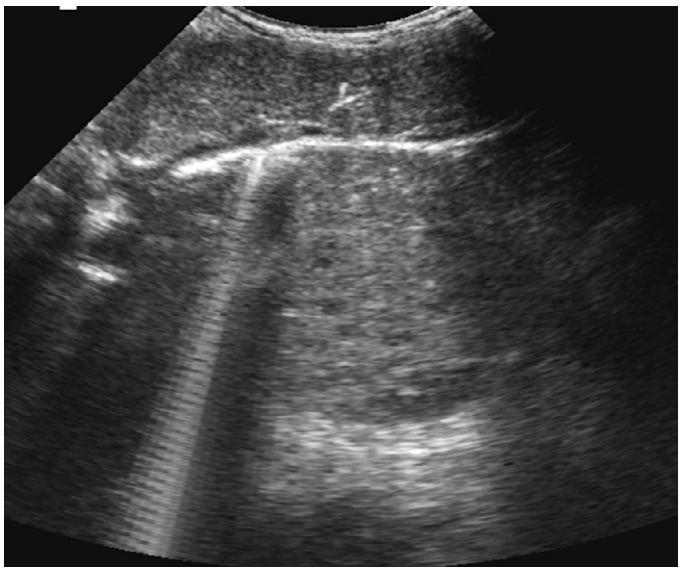


Figure 14.76 Gas in the intrahepatic bile ducts showing highly reflective echoes coinciding with the course of the bile duct, with reverberative shadowing posteriorly.



Figure 14.78 Stone in the common bile duct. Stone seen in duct obscured by duodenum supine, but demonstrated with the patient right side raised.

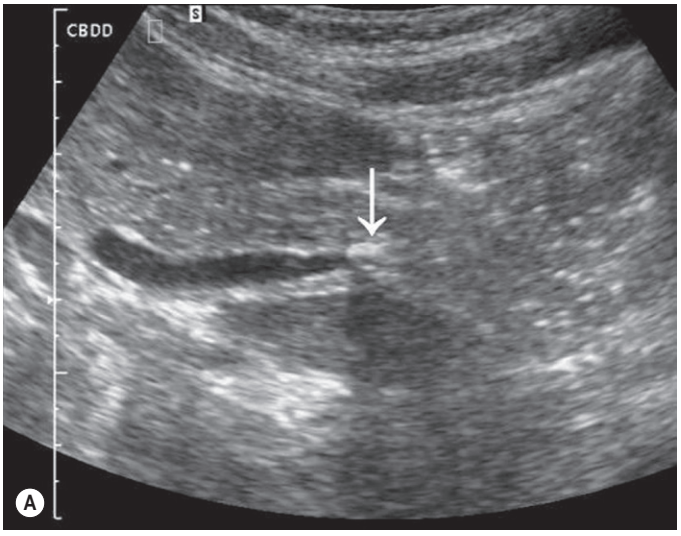




Figure 14.77 Stone in the lower end of the common bile duct. A: Stone (with posterior shadowing identified) within the lower end of common duct. **B:** Confirmed on MRCP.



Figure 14.79 Stone in the common bile duct. Stone (callipers) impacted within the lower end of the common duct, just above the level of the duodenum.

The importance of a good quality scan in trained hands is emphasised, as this may increase the sensitivity of percutaneous ultrasound to 82%.[216]

Bile duct neoplasms

Benign tumours of the bile ducts are all extremely rare, and include papillomas, adenomas, cystadenomas and granular cell myoblastomas.[220,223–226] Papillomas and solid adenomas appear as solid, non-shadowing intraluminal masses, while cystadenomas are multiloculated cystic masses which usually occur in young females. These latter originate from the bile duct epithelium but usually do not communicate with the biliary tree. The differential diagnosis includes echinococcal cysts, cystic metastases, abscesses, partially liquefied haematomas and hepatic artery aneurysms.

Primary malignant tumours of the bile ducts – cholangiocarcinomas – are much more common than benign tumours and their incidence is increasing[227,228] particularly in cases of chronic, cholestatic diseases[229] which contribute to the rise in incidence in the Western world. They may develop at any level within the biliary tree, and when they involve the confluence of the left and right hepatic ducts at the porta hepatis they are referred to as Klatskin tumours, following his original description in 1965.[230]

The ultrasound features of cholangiocarcinomas have been well documented,[231–238] although the frequency with which these signs are detected varies greatly depending upon the site and size of the tumour. Intrahepatic tumours are frequently isoechoic with the background liver, making them difficult to locate unless accompanied by focal intrahepatic duct dilatation. Dilatation of the biliary tree can be followed down to the point of obstruction where it may be possible to detect a solid poorly reflective mass, which, if large enough, can be seen to have a heterogeneous internal echo pattern and ill-defined margins (Fig. 14.80).

Occasionally an intraluminal mass is detected (Fig. 14.81), while in other cases thickening of the walls of the bile duct may be the only evidence of a tumour (Fig. 14.82). These ultrasound signs are a direct representation of the gross pathology since these tumours can vary from large solid masses to lesions that infiltrate the submucosa with a thickness of only a few millimetres, when they may be undetectable to both palpation by the surgeon and naked eye

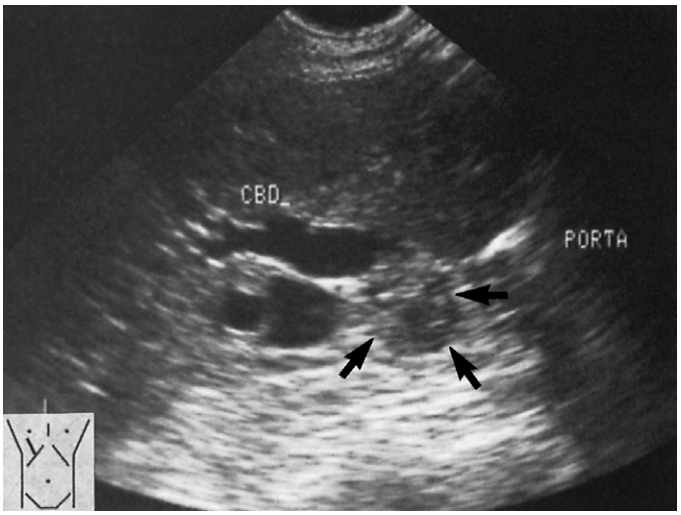


Figure 14.80 Klatskin tumour (arrows) obstructing the common duct.



Figure 14.81 Cholangiocarcinoma – intraluminal mass (callipers) at the lower end of the dilated common duct.

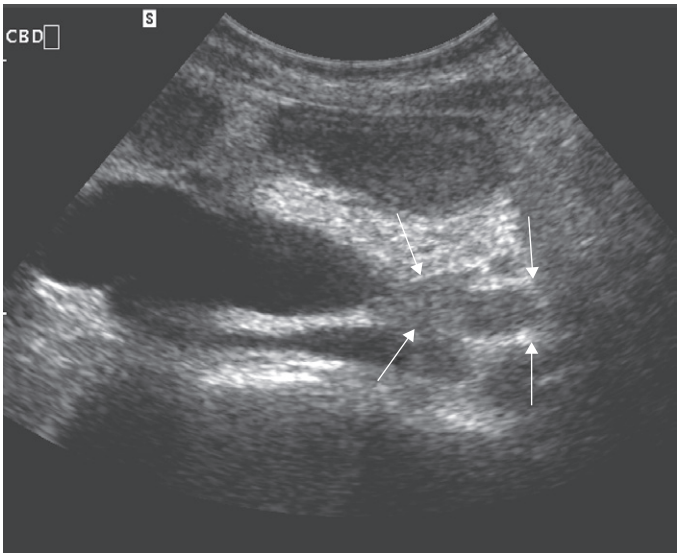


Figure 14.82 Cholangiocarcinoma – a stricture caused by tumour at the lower end of the common duct (arrows).

inspection by the pathologist. It is this latter form of cholangiocarcinoma that presents on ultrasound as biliary dilatation without a detectable mass, possibly with some increased reflectivity and thickening of the duct wall, and is thus extremely difficult to diagnose.

The ultrasound visibility of these tumours may increase after a biliary stent has been inserted (percutaneous or endoscopic) (Fig. 14.83), and it is often then possible to visualise the lesion sufficiently well to permit ultrasound-guided confirmatory biopsy. However, cholangiocarcinomas have a fibrous nature making it difficult to

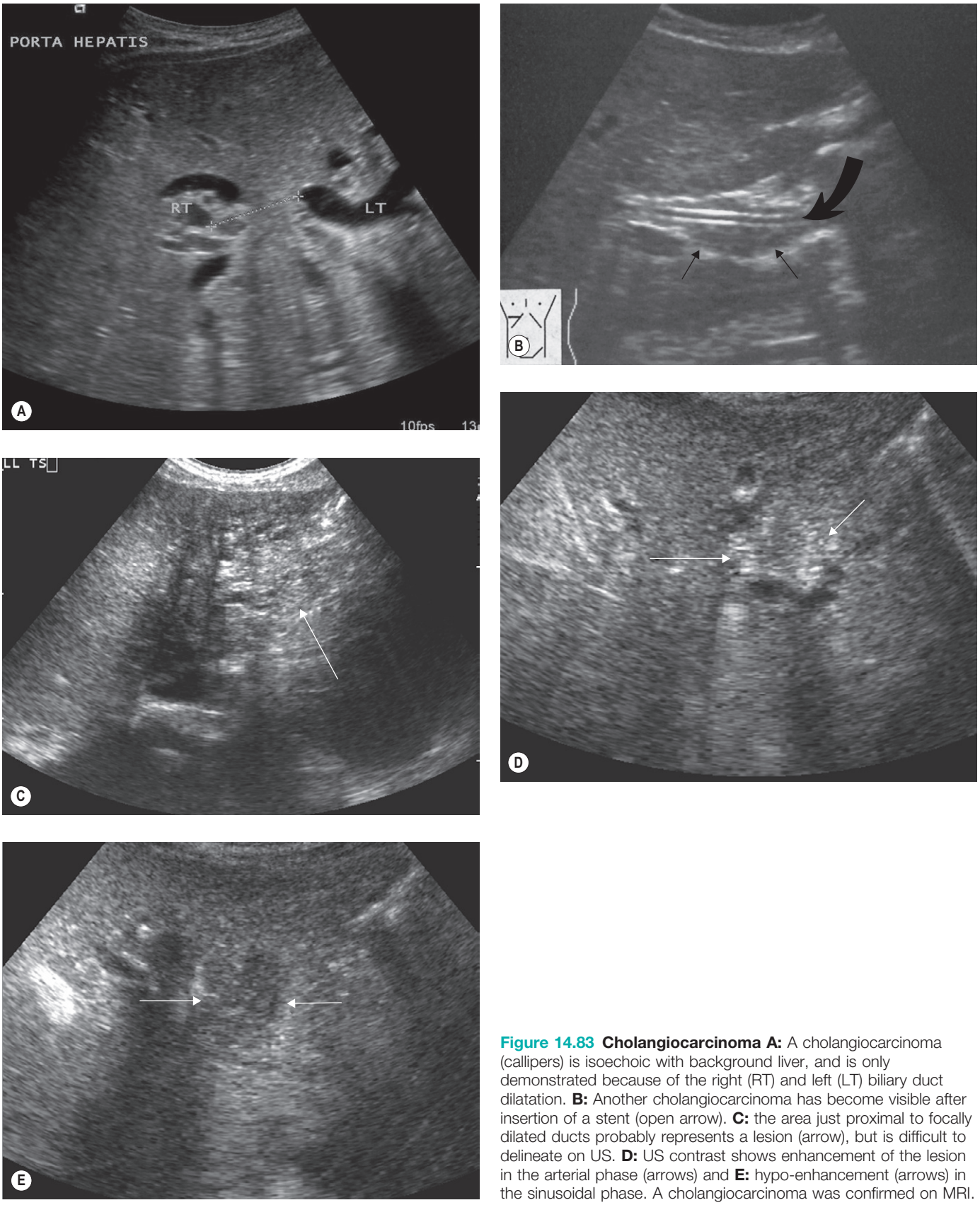


Figure 14.83 **Cholangiocarcinoma A:** A cholangiocarcinoma (callipers) is isoechoic with background liver, and is only demonstrated because of the right (RT) and left (LT) biliary duct dilatation. **B:** Another cholangiocarcinoma has become visible after insertion of a stent (open arrow). **C:** the area just proximal to focally dilated ducts probably represents a lesion (arrow), but is difficult to delineate on US. **D:** US contrast shows enhancement of the lesion in the arterial phase (arrows) and **E:** hypo-enhancement (arrows) in the sinusoidal phase. A cholangiocarcinoma was confirmed on MRI.

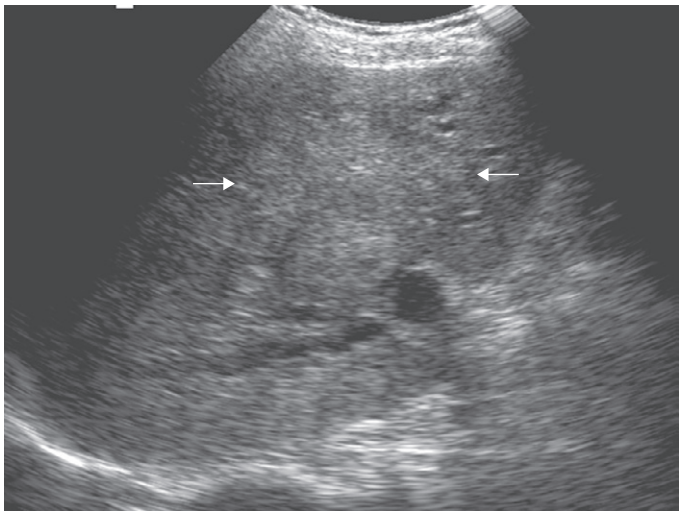


Figure 14.84 **Cholangiocarcinoma**. An intrahepatic cholangiocarcinoma occupying segment IV of the liver (arrows). This large lesion is almost isoechoic with the background liver, demonstrating a subtle alteration in echotexture and some dilatation of the intrahepatic ducts to the right of the tumour margin.

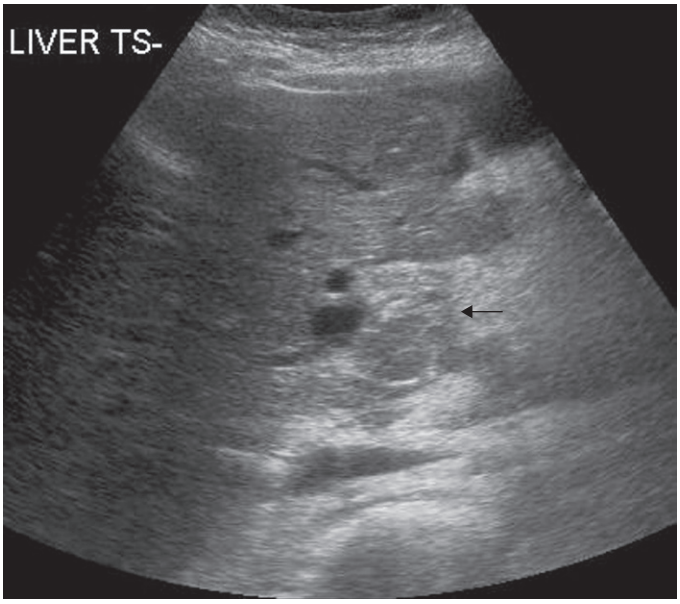


Figure 14.85 **Lymph node mass** at porta hepatis (Hodgkin's disease).

obtain samples adequate for cytological confirmation via fine-needle aspiration, so that a cutting biopsy for a histological sample is often necessary.

Ultrasound may provide additional information in the diagnosis of cholangiocarcinomas, although it tends to under-diagnose the extent of large lesions. Contrast ultrasound can provide a more accurate picture of the extent and potential operability of the lesion (Fig. 14.83C–E). Direct invasion to involve surrounding structures such as the portal vein, hepatic artery and liver substance, as well as metastatic spread to regional lymph nodes, are all demonstrable on ultrasound (Fig. 14.84). However, the demonstration of extrahepatic spread is limited with ultrasound, and helical CT, MRCP and, more recently, PET-CT, can improve the accuracy of staging in patients with cholangiocarcinoma prior to surgery.[239]

As well as metastasising to the liver, cholangiocarcinomas may be multifocal and may be indistinguishable from hepatic metastatic disease on ultrasound, and from sclerosing cholangitis on cholangiography due to the multiple strictures in the biliary tree.

Other tumours obstructing the bile ducts

Biliary ducts may be obstructed by intrahepatic tumour, enlarged lymph nodes at the porta hepatis, carcinoma of the head of the pancreas and ampullary tumours.

The lymph nodes at the porta hepatis are not usually demonstrable on ultrasound scans unless enlarged. Because of their proximity to the confluence of the right and left hepatic ducts and their distribution along the length of the common duct, the bile ducts may be compressed and obstructed by lymphomatous or metastatic disease in the nodes. The nodal nature of a mass at the porta hepatis is usually obvious on ultrasound by carefully observing the interfaces that indicate that the tumour is composed of several discrete masses and, whilst it is true that lymphoma usually results in large nodes that are particularly poorly reflective, biopsy is required for accurate distinction between lymphoma and metastases (most frequently from colon, stomach, pancreas and breast) (Fig. 14.85).

Enlargement of the head of the pancreas, whether due to inflammation or malignancy, may compress the lower end of the common duct as it traverses the gland prior to entering the duodenal papilla. Acute pancreatitis may cause transient extrahepatic duct dilatation but usually does not result in intrahepatic duct dilatation (Fig. 14.86), whereas the fibrous stricturing of the common duct of chronic pancreatitis may be indistinguishable from malignant disease both on ultrasound and at surgery. Carcinomas of the head of the pancreas are characteristically hypoechoic, solid masses into which the dilated common duct can be followed (Fig. 14.87). Detection of coexistent pancreatic duct dilatation provides useful confirmatory evidence of pancreatic pathology, and 'ultrasonic double duct dilatation' may be caused by chronic pancreatitis, impacted pancreatic and biliary calculi, and ampullary carcinoma, as well as by pancreatic carcinoma. Ultrasound is highly sensitive for duct dilatation but has less specificity than the ERCP sign of 'double duct obstruction', which is almost invariably due to pancreatic carcinoma (Fig. 14.88).

Ampullary carcinoma is difficult to identify on ultrasound. The findings of dilatation of the common duct with a normal head of pancreas should raise the suspicion of this tumour, especially if pancreatic duct dilatation is also detected. The diagnosis must be made endoscopically, and it is important that it is not overlooked, since these tumours often present early with jaundice (due to their strategic location) and radical surgery may offer a good chance of cure.

Choledochal cysts

Choledochal cysts usually present in children or young adults, and are discussed more fully in Chapter 69. The ultrasound appearances are usually of massive cystic dilatation of the extrahepatic common duct, although the main intrahepatic ducts may be affected.[240–243] The underlying anomaly is thought to be an abnormal insertion of the common duct into the distal pancreatic duct, resulting in reflux of pancreatic secretions into the common duct that cause fibrotic structuring and obstruction to the biliary tree.[244,245] The condition is more common in females and East Asians and presents with jaundice, fever and pain (due to cholangitis) with a palpable right upper quadrant mass (Fig. 14.89). As well as recurrent cholangitis, complications include stone formation with progression to biliary cirrhosis and portal hypertension

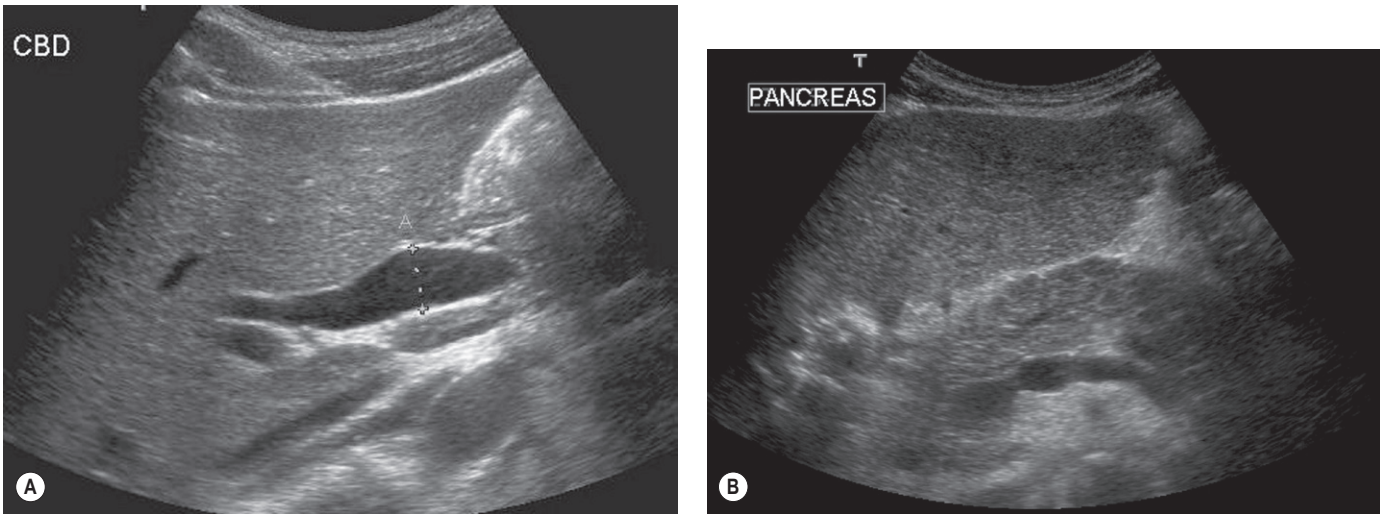


Figure 14.86 Dilated common duct due to acute pancreatitis. A: Longitudinal scan. **B:** Transverse scan showing the oedematous, inflamed pancreas.

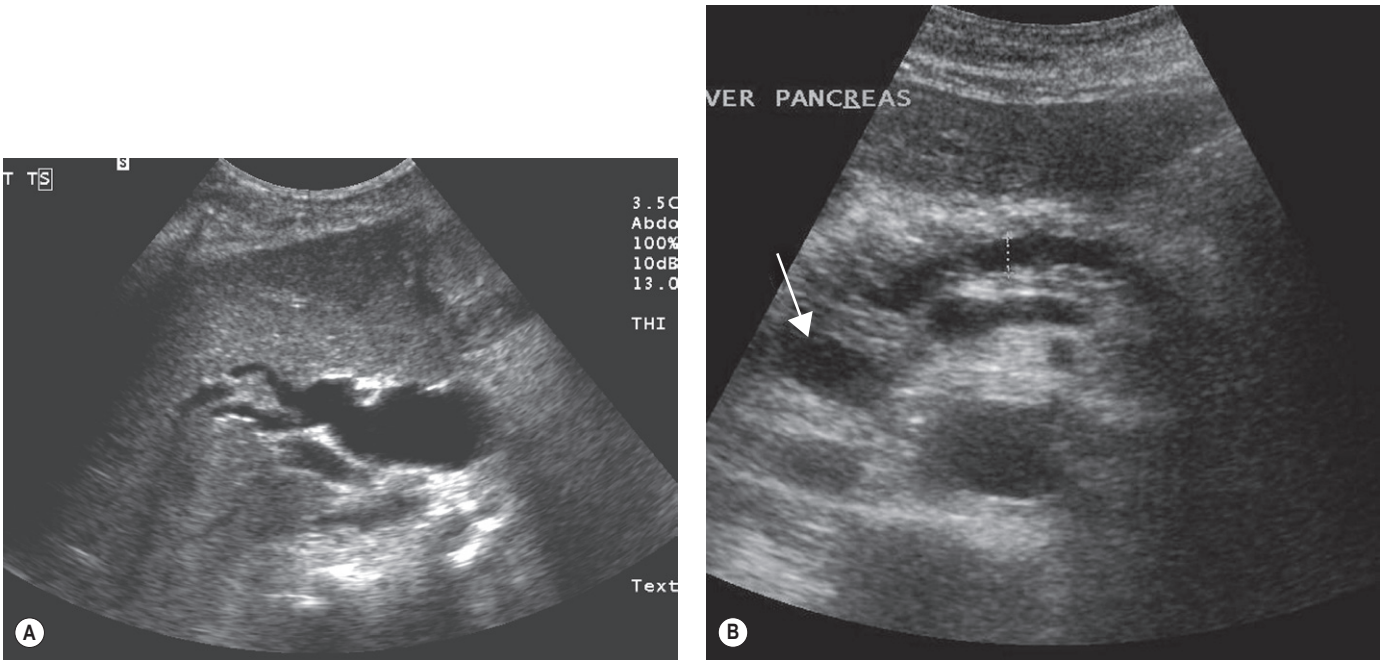


Figure 14.87 Dilated common duct due to pancreatic carcinoma. A: Longitudinal scan showing dilated common and hepatic ducts. **B:** Transverse scan showing the dilated CBD (arrow) in the head of pancreas with a dilated pancreatic duct (callipers).

and an increased incidence of cholangiocarcinoma. The differential diagnosis includes other fluid-filled masses such as hepatic cyst, pancreatic pseudocyst, enteric duplication, hepatic artery aneurysm[246] and echinococcal disease (Fig. 14.90). Confirmation of the diagnosis may be obtained from ^{99m}Tc-HIDA scintigraphy, when excretion of radioactivity into the cyst will confirm its continuity with the biliary system.

Caroli's disease

Caroli's disease – congenital dilatation of the intrahepatic bile ducts,[247] otherwise known as communicating cavernous ectasia of the intrahepatic ducts[248] – is an autosomal recessive disorder in which ultrasound scanning reveals multiple cystic spaces throughout the liver substance (Fig. 14.91).[249–250] These 'cysts' represent non-obstructive saccular dilatation of the intrahepatic biliary tree,[251] which can be demonstrated on CT, percutaneous cholangiography, ERCP or MRCP. The extrahepatic bile ducts are usually unaffected. Stones may form within the cysts or dilated ducts, giving rise to cholangitis which may progress to the formation of pyogenic liver abscesses. There may be an association with renal tubular ectasia or other forms of cystic disease of the kidney, and there is a rather uncertain relationship to congenital hepatic fibrosis in which there is bile duct proliferation and multiple strictures with proximal cystic dilatation[252] – also in association with renal cystic disease, usually of the infantile polycystic type. Caroli himself classified the condition into two types: the pure form without hepatic fibrosis or portal hypertension, and a second type associated with congenital hepatic fibrosis.[253]

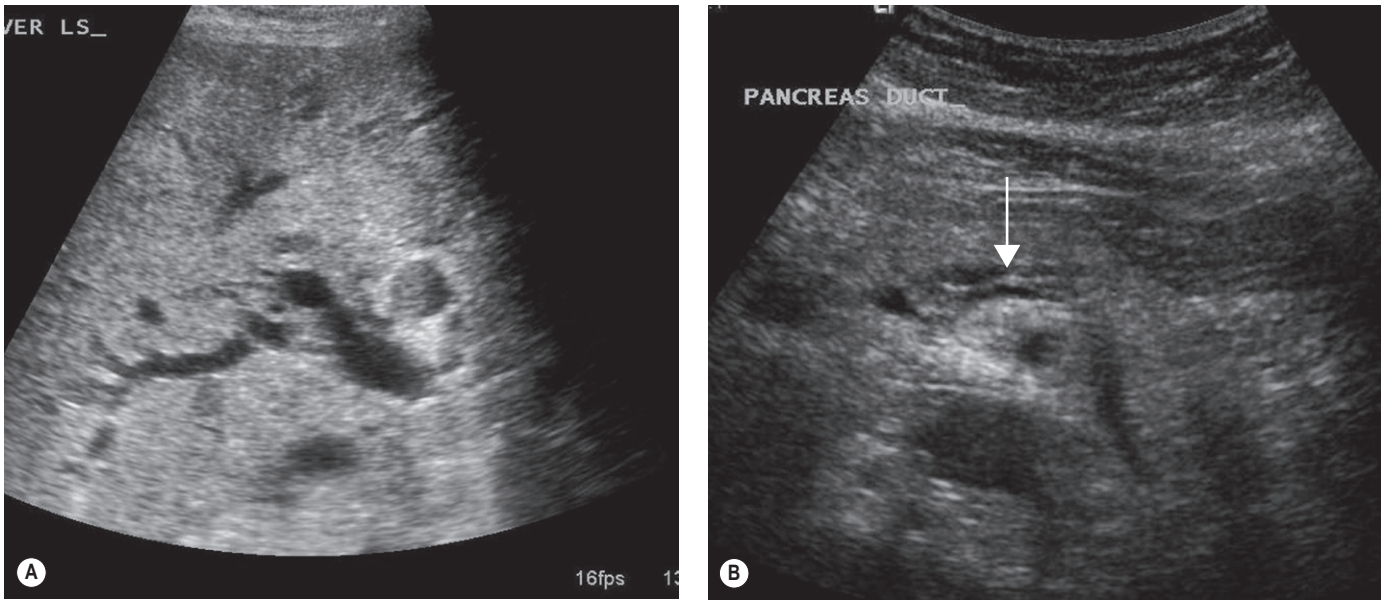


Figure 14.88 **Double duct obstruction due to pancreatic carcinoma. A:** Dilatation of the common bile duct in the liver. **B:** Dilatation of the pancreatic duct (arrow).

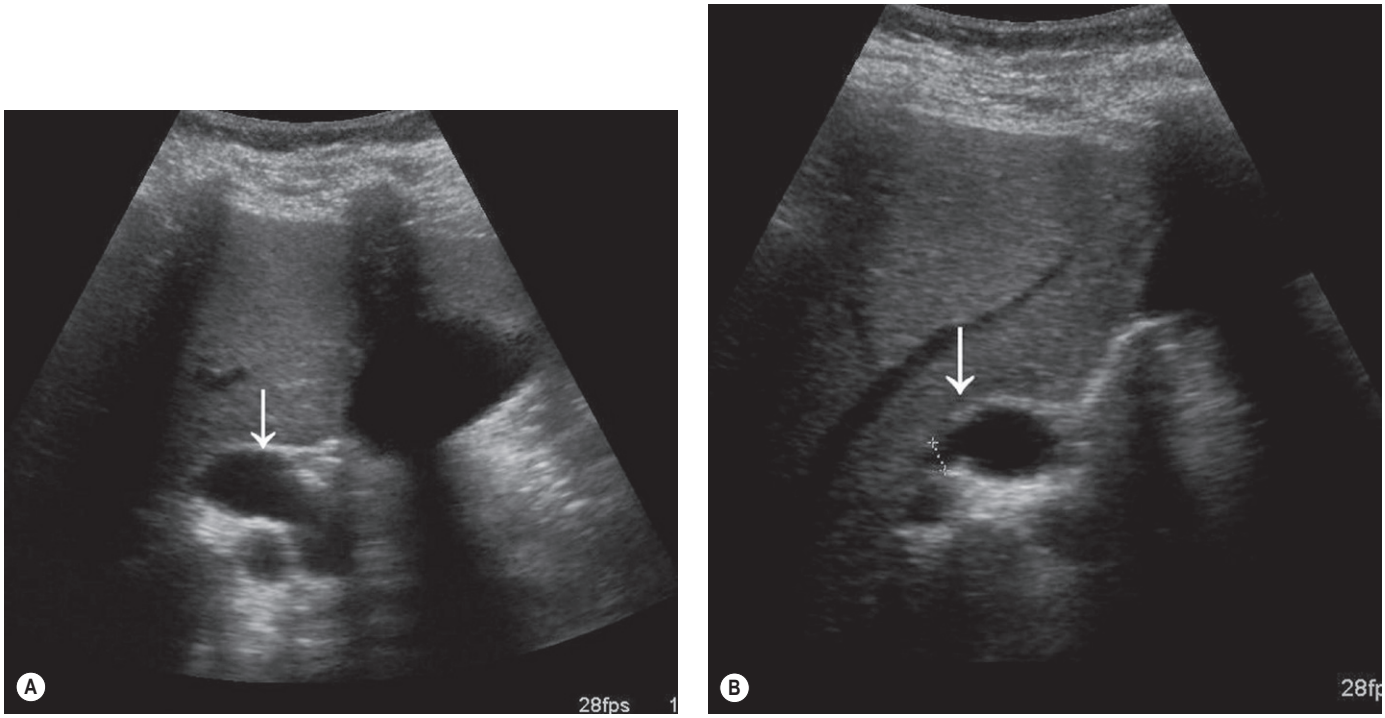


Figure 14.89 **Choledochal cyst. A:** Longitudinal scan (arrow). **B:** Transverse scan showing aneurysmally dilated common duct with no intrahepatic duct dilatation. Callipers are shown across the normal calibre proximal duct, leading into the choledochal cyst.

The differential diagnosis includes severe biliary dilatation due to any of the other causes of biliary obstruction, polycystic disease of the liver (in which the cysts do not communicate with the bile ducts or each other) and congenital hepatic fibrosis. Other non-invasive imaging tests, such as ^{99m}Tc-HIDA scanning, may help in diagnosis,[254] but, as alluded to above, it has been speculated that Caroli's disease, polycystic disease and congenital hepatic fibrosis are all parts of the same spectrum,[255] and hence MRCP or CT may be needed for a specific diagnosis. The condition may sometimes be lobar, affecting only part of the liver, in which case surgical resection is appropriate, but in cases of the diffuse form, transplantation may be considered curative.

Oriental cholangiohepatitis

Recurrent pyogenic cholangitis, also known as oriental cholangiohepatitis, is endemic in southeast Asia but now occasionally recognised in Western societies, particularly amongst the Asian

population.[256] It is characterised by recurrent attacks of cholangitis, due to peribiliary fibrosis which causes biliary duct strictures, and is caused by the adult worms of the *Clonorchis sinensis* liver fluke which are ingested by humans in raw freshwater fish. However, the parasites are not found in all patients with the clinical condition, and some authorities question the causal relationship.

The ultrasound features consist of massively dilated bile ducts with multiple strictures, the common duct being most frequently involved, followed by left, then right hepatic ducts. The parasites may be identified within the ducts[255] and also within the gallbladder.[257] There are often bilirubinate stones within the ducts; these are often soft and sludge-like. In most patients there is secondary bacterial infection with *E. coli* in the bile. Gas-forming organisms may result in pneumobilia and there is an increased incidence of cholangiocarcinoma – presumably as a result of chronic irritation leading to dysplasia. As the disease progresses, with recurrent attacks of cholangitis, biliary cirrhosis with portal hypertension may result.[256] All these pathological processes result in a complex ultrasonographic picture,[257–259] and although ultrasound may be of considerable value in screening for the disease and in suggesting the diagnosis, further imaging including MRCP, CT or cholangiography may be needed for full evaluation.

Biliary ascariasis

The *Ascaris lumbricoides* roundworm is an extremely common cause of biliary pathology worldwide. The worms infest the small bowel but can migrate up the common bile duct and may enter the gallbladder and the intrahepatic ducts. Biliary colic is common, while jaundice, ascending cholangitis and parasitic liver abscesses occur occasionally.

The characteristic ultrasound appearance is of single or multiple reflective, linear or curved intraductal structures, usually non-shadowing. These may produce a spaghetti-like appearance due to the central echo-free digestive tract of the worm.[260,261] Movements of the worms in the common duct and gallbladder may be observed using real-time ultrasound (Fig. 14.92).[262] The diagnosis is confirmed by isolating the worms or their eggs from the stool, and medical treatment is usually effective in eradicating the infestation.

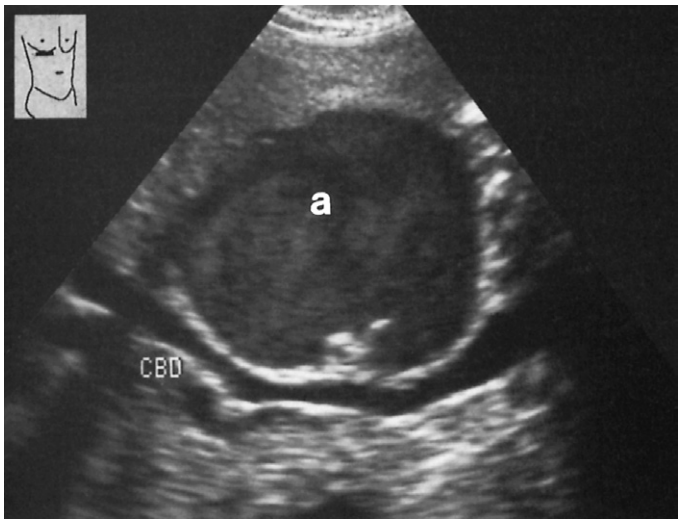


Figure 14.90 Hepatic artery aneurysm (a) obstructing the common bile duct (CBD). Transverse scan. Note the low level echoes within the aneurysm due to blood clot in this case.

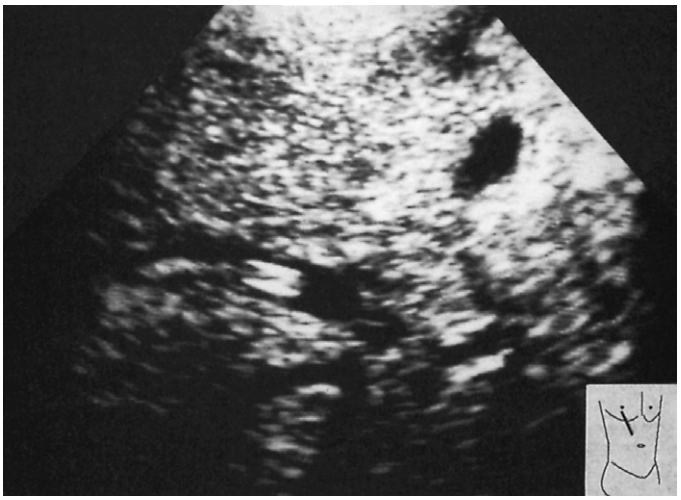


Figure 14.92 *Ascaris* worm in biliary tract. Oblique view of common hepatic duct showing the typical 'tramline' appearance of *Ascaris* in the duct.

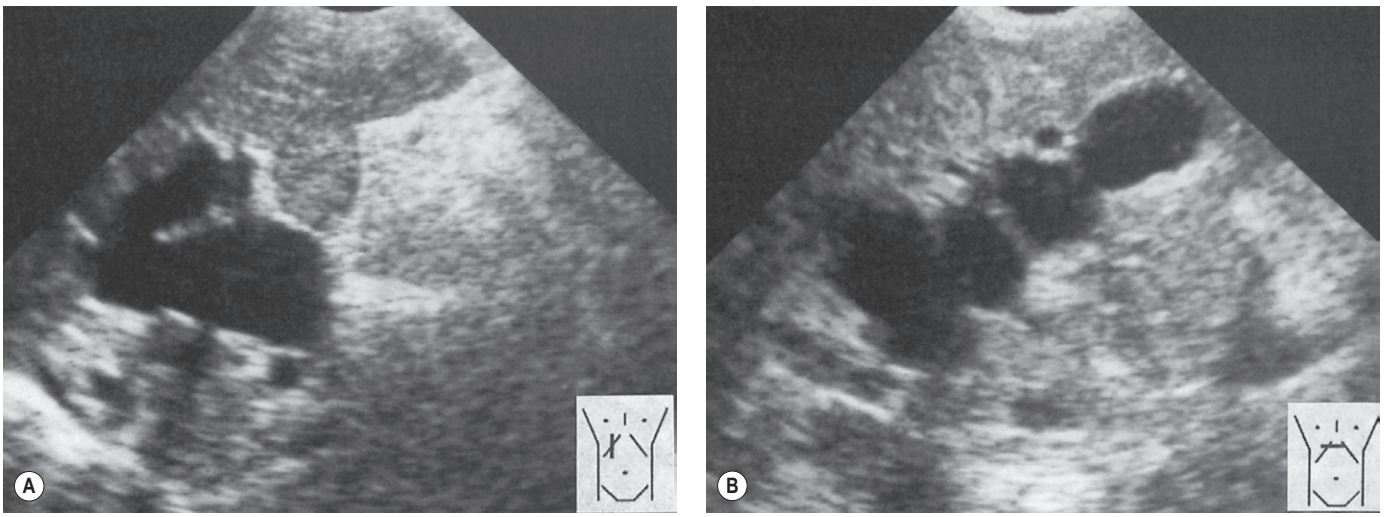


Figure 14.91 Caroli's disease. A and B: Cystic dilatation of the biliary tree in a child, subsequently shown to be Caroli's disease.

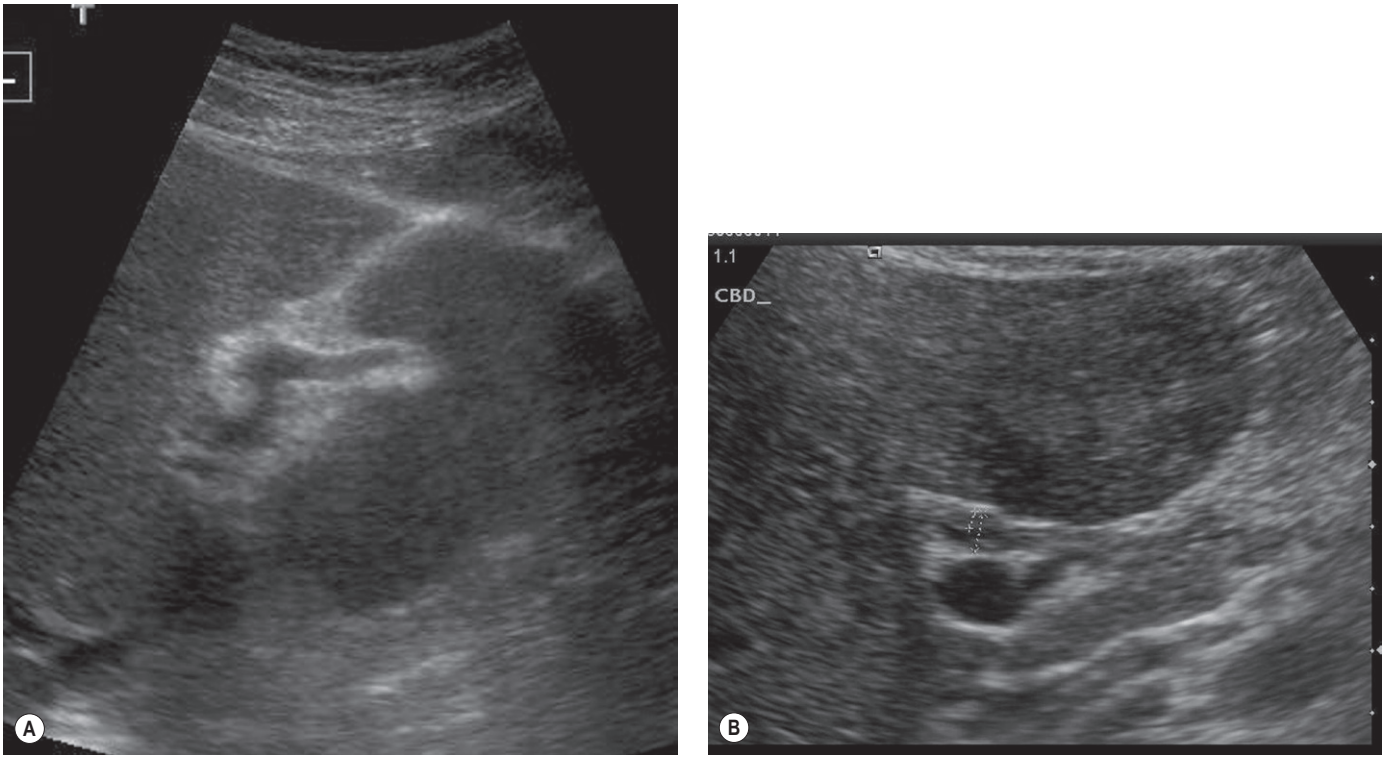


Figure 14.93 **Sclerosing cholangitis. A:** Increased reflectivity of intrahepatic portal tracts. **B** There is irregular mucosal thickening in the common duct.

Sclerosing cholangitis

Sclerosing cholangitis is a progressive, cholestatic disease which can lead to hepatic cirrhosis. It predominantly affects young men and it may be idiopathic or associated with inflammatory bowel disease. Histologically there is non-specific inflammation of bile duct walls. Ultrasound findings may demonstrate dilatation of the intrahepatic bile ducts which may be confined to one or more segments or lobes, depending on the anatomical location of the strictures[263] but this is not invariable, due to the stricturing of the ducts, preventing dilatation. The extent of intrahepatic biliary strictures can be more comprehensively demonstrated on MRCP. Mural thickening of the common duct,[202] and increased reflectivity of the portal tracts are also ultrasound features associated with cholangitis, although these are non-specific for sclerosing cholangitis (Fig. 14.93). There is an increased incidence of cholangiocarcinoma, especially in the advanced stages of the disease, and care should be taken to examine the proximal region of any focal duct dilatation for an obstructing mass.

REFERENCES

1. Finberg HJ, Birnholz JC. Ultrasound evaluation of the gallbladder wall. Radiology 1979;133:693–698.
2. Taylor KJW, Carpenter DA. The anatomy and pathology of the porta hepatis demonstrated by gray scale ultrasound. J Clin Ultrasound 1975;3:117–119.
3. Parulekar SG. Evaluation of common bile duct size. Radiology 1979;133:703–707.
4. Edell S. A comparison of the 'Phrygian cap' deformity with 'bistable and gray scale ultrasound. J Clin Ultrasound 1978;6:34–35.
5. Cooperberg PL, Gibney RG. Imaging of the gallbladder, 1987. Radiology 1987;163:605–613.
6. Krishnamurthy GT, Krishnamurthy S, Milleson T, et al. Segmentation of the gallbladder: effect on bile entry and exit and its clinical relevance in a patient with abdominal pain. Nucl Med Commun 2007;28(2):109–115.
7. Safioleas MC, Papavassiliou VG, Moulakakis KG, et al. Congenital duplication of the gallbladder. Am Surg 2006;72(3):217–220.
8. Marchal G, Kint E, Nijssens M, Baert AL. Variability of the hepatic arterial anatomy: a sonographic demonstration. J Clin Ultrasound 1981;9:377–381.
9. Berland LL, Lawson TL, Foley WD. Porta hepatis: sonographic discrimination of bile ducts from arteries with pulsed Doppler with new anatomic criteria. AJR Am J Roentgenol 1982;138:833–840.
10. Marchal G, Van de Voorde P, Van Dooren W, et al. Ultrasonic appearance of the filled and contracted normal gallbladder. J Clin Ultrasound 1980;8:439–442.
11. Filly RA, Moss AA, Way LW. In vitro investigation of gallstone shadowing with ultrasound tomography. J Clin Ultrasound 1979;7:255–262.
12. Jaffe CC, Taylor KJW. The clinical impact of ultrasonic beam focussing patterns. Radiology 1979;131:469–472.
13. Dewbury KC. Visualisation of normal biliary ducts with ultrasound. Br J Radiol 1980;53:774–780.
14. Lewandowski BJ, Winsberg F. Gallbladder wall thickness distortion by ascites. AJR Am J Roentgenol 1981;137:519–521.
15. Behan M, Kazam E. Sonography of the common bile duct: value of the right anterior oblique view. AJR Am J Roentgenol 1978;130:701–709.
16. Laing FC, Jeffrey RB, Wing VW, Nyberg DA. Biliary dilatation: defining the level and cause by real time ultrasound. Radiology 1986;160:39–42.
17. Sauerbrei EE, Cooperberg PL, Gordon P, et al. The discrepancy between radiographic and sonographic bile duct measurements. Radiology 1980;137:751–755.
18. Daradkeh S, Tarawneh E, Al-Hadidy A. Factors affecting common bile duct diameter. Hepatogastroenterology 2005;52(66):1659–1661.
19. Majeed AW, Ross B, Johnson AG. The preoperatively normal bile duct does not dilate after cholecystectomy: results of a five year study. Gut 1999;45(5):741–743.
20. Mueller PR, Ferrucci JT Jr, Simeone JF, et al. Post-cholecystectomy bile duct dilatation: myth or reality? AJR Am J Roentgenol 1981;136:355.
21. Wedmann B, Borsch G, Coenen C, Paassen A. Effect of cholecystectomy on common bile duct diameters; a longitudinal prospective ultrasonographic study. J Clin Ultrasound 1988;16:619–624.

22. Glazer GM, Filly RA, Laing FC. Rapid change in caliber of the non-obstructed common duct. Radiology 1981;140:161–162.
23. Mueller PR, Ferrucci JT, Simeone JF, et al. Observations on the distensibility of the common bile duct. Radiology 1982;142:467–472.
24. Cooperberg PL, Li D, Wong P, et al. Accuracy of common duct size in the evaluation of extrahepatic biliary obstruction. Radiology 1980;135:141–144.
25. Colecchia A, Sandri L, Bacchi-Reggiani ML, et al. Is it possible to predict the clinical course of gallstone disease? Usefulness of gallbladder motility evaluation in a clinical setting. Am J Gastroenterol 2006;101(11):2576–2581; quiz 2672.
26. Portincasa P, Moschetta A, Colecchia A, et al. Measurements of gallbladder motor function by ultrasonography: towards standardization. Dig Liver Dis 2003;35(Suppl 3):S56–61.
27. Pallotta N. Ultrasonography in the assessment of gallbladder motor activity. Dig Liver Dis 2003;35(Suppl 3):S67–69.
28. Degirmenci B, Albayrak R, Haktanir A, et al. Acute effect of smoking on gallbladder emptying and refilling in chronic smokers and nonsmokers: a sonographic study. World J Gastroenterol 2006;12(34):5540–5543.
29. Braverman DZ, Johnson ML, Kern F. Effects of pregnancy and contraceptive steroids on gallbladder function. N Engl J Med 1980;302:362–364.
30. Delamarre J, Capron J-P, Joly J-P, et al. Gallbladder inertia in celiac disease: ultrasonographic demonstration. Dig Dis Sci 1984;29: 876–877.
31. Nino-Murcia M, Burton M, Chang P, et al. Gallbladder contractility in patients with spinal cord injuries: a sonographic investigation. AJR Am J Roentgenol 1990;154:521–524.
32. Stads S, Venneman NG, Scheffer RC, et al. Evaluation of gallbladder motility: comparison of two-dimensional and three-dimensional ultrasonography. Ann Hepatol 2007;6(3):164–169.
33. Yoon HJ, Kim PN, Kim AY, Lee MG. Three-dimensional sonographic evaluation of gallbladder contractility: comparison with cholescintigraphy. J Clin Ultrasound 2006;34(3):123–127.
34. Fisher RS, Thistle J, Lembo A, et al. Tegaserod does not alter fasting or meal-induced biliary tract motility. Am J Gastroenterol 2004;99(7):1342–1349.
35. Wilson SA, Gosink BB, van Sonnenberg E. Unchanged size of a dilated common bile duct after a fatty meal: results and significance. Radiology 1986;160:29–31.
36. Simeone JF, Butch RJ, Mueller PR, et al. The bile ducts after a fatty meal: further sonographic observations. Radiology 1985;154:763–768.
37. Darweesh RMA, Dodds WJ, Hogan WJ, et al. Fatty meal sonography for evaluating patients with suspected partial common duct obstruction. AJR Am J Roentgenol 1988;151:63–68.
38. Amouzal P, Palazzo L, Amouzal G, et al. Endosonography: promising method for diagnosis of extrahepatic cholestasis. Lancet 1989;ii:1195–1198.
39. McMahon CJ. The relative roles of magnetic resonance cholangiopancreatography (MRCP) and endoscopic ultrasound in diagnosis of malignant common bile duct strictures: a critically appraised topic. Abdom Imaging 2008;33(1):10–13.
40. McMahon CJ. The relative roles of magnetic resonance cholangiopancreatography (MRCP) and endoscopic ultrasound in diagnosis of common bile duct calculi: a critically appraised topic. Abdom Imaging 2008;33(1):6–9.
41. Sgouros SN, Bergele C. Endoscopic ultrasonography versus other diagnostic modalities in the diagnosis of choledocholithiasis. Dig Dis Sci 2006;51(12):2280–2286.
42. Perry KA, Myers JA, Deziel DJ. Laparoscopic ultrasound as the primary method for bile duct imaging during cholecystectomy. Surg Endosc 2008;22(1):208–213.
43. Health and Policy Committee, American College of Physicians. How to study the gallbladder. Ann Intern Med 1988;109:752–754.
44. Barbara L. Epidemiology of gallstone disease: the 'Sirmione Study'. In: Capocaccia L, Ricci G, Angelico F, et al, editors. Epidemiology and prevention of gallstone disease. Lancaster: MTP Press; 1984, p. 23–25.
45. GREPCO. Prevalence of gallstone disease in an Italian adult female population. Am J Epidemiol 1984;119:796–805.
46. Gupta SK, Shukla VK. Silent gallstones: a therapeutic dilemma. Trop Gastroenterol 2004;25(2):65–68.
47. Dowling RH. Epidemiology and medical treatment of cholesterol gallstones: recurrence, post-dissolution management and the future. In: Capocaccia L, Ricci G, Angelico F, et al, editors. Epidemiology and prevention of gallstone disease. Lancaster: MTP Press; 1984, p. 116–128.
48. Konikoff FM. Gallstones – approach to medical management. Med Gen Med 2003;5(4):8.
49. Crade M, Taylor KJW, Rosenfield AT, et al. Surgical and pathologic correlation of cholecystosonography and cholecystography. AJR Am J Roentgenol 1978;131:227–229.
50. Filly RA, Allen B, Minton MJ, et al. In vitro investigation of the origin of echoes within biliary sludge. J Clin Ultrasound 1980;8:193–200.
51. Sommer FG, Taylor KJW. Differentiation of acoustic shadowing due to calculi and gas collections. Radiology 1980;135:399.
52. Carroll BA. Gallstones: in vitro comparison of physical, radiographic and ultrasonic characteristics. AJR Am J Roentgenol 1978;131: 223–226.
53. Filly RA, Moss AA, Way LW. In vitro investigation of gallstone shadowing with ultrasonic tomography. J Clin Ultrasound 1979;7: 255.
54. Jaffe CC, Taylor KJW. The clinical impact of ultrasonic beam focussing patterns. Radiology 1979;131:469–472.
55. Taylor KJW, Jacobson P, Jaffe CC. Lack of an acoustic shadow on scans of gallstones: a possible artefact. Radiology 1979;131:463–464.
56. Callen PW, Filly RA. Ultrasonographic localisation of the gallbladder. Radiology 1979;133:693–698.
57. Conrad MR, Leonard J, Landay MJ. Left lateral decubitus sonography of gallstones in the contracted gallbladder. AJR Am J Roentgenol 1980;134:141–144.
58. MacDonald FR, Cooperberg PL, Cohen MM. The WES triad – a specific sign of gallstones in the contracted gallbladder. Gastrointest Radiol 1981;6:39–41.
59. Ratpopoulos V, D'Orsi C, Smith E, et al. Dynamic cholecystosonography of the contracted gallbladder: the double-arc-shadow sign. AJR Am J Roentgenol 1982;138:275–278.
60. Kane RA, Jacobs R, Katz J, Costello P. Porcelain gallbladder: ultrasound and CT appearance. Radiology 1984;152:137–141.
61. Crow HC, Bartrum RJ, Foote SR. Expanded criteria for the ultrasonic diagnosis of gallstones. J Clin Ultrasound 1976;4:289.
62. Love MB. Sonographic features of milk of calcium bile. J Ultrasound Med 1982;1:325–327.
63. Chun GH, Deutsch AL, Scheible W. Sonographic findings in milk of calcium bile. Gastrointest Radiol 1982;7:371–373.
64. Conrad MR, Janes JO, Dietchy J. Significance of low level echoes within the gallbladder. AJR Am J Roentgenol 1979;132:967–972.
65. Pazzi P, Gamberini S, Buldrini P, Gullini S. Biliary sludge: the sluggish gallbladder. Dig Liver Dis 2003;35(Suppl 3): S39–45.
66. Garg PK, Tandon RK, Madan K. Is biliary microlithiasis a significant cause of idiopathic recurrent acute pancreatitis? A long-term follow-up study. Clin Gastroenterol Hepatol 2007;5(1):75–79.
67. Jüngst C, Kullak-Ublick GA, Jüngst D. Gallstone disease: Microlithiasis and sludge. Best Pract Res Clin Gastroenterol 2006;20(6):1053–1062.
68. Goldstein A, Madrazo BL. Slice thickness artefacts in gray scale ultrasound. J Clin Ultrasound 1981;9:365–375.
69. Anastasi B, Sutherland GR. Biliary sludge ultrasonic appearance simulating neoplasm. Br J Radiol 1981;54:679–681.
70. Fakhry J. Sonography of tumefactive biliary sludge. AJR Am J Roentgenol 1982;139:717–719.
71. Engel JM, Deitch EA, Sikkema W. Gallbladder wall thickness: sonographic accuracy and relation to disease. AJR Am J Roentgenol 1979;134:907–909.
72. Finberg HJ, Birnholtz J. Ultrasound evaluation of the gallbladder wall. Radiology 1979;133:693–698.
73. Marchal G, Van de Voorde P, Van Dooren W, et al. Ultrasonic appearance of the filled and contracted normal gallbladder. J Clin Ultrasound 1980;8:439–442.
74. Lewandowski BJ, Winsberg F. Gallbladder wall thickness distortion by ascites. AJR Am J Roentgenol 1981;137:519–521.
75. Laing FC. Gall bladder and bile ducts. In: Rumack CM, Wilson SR, Charboneau JW, editors. Diagnostic ultrasound. St Louis: Mosby; 1998, p. 175–219.
76. Sanders RC. The significance of sonographic gallbladder wall thickening. J Clin Ultrasound 1980;8:143–146.
77. Fiske CE, Laing FC, Brown TW. Ultrasonographic evidence of gallbladder wall thickening in association with hypoalbuminemia. Radiology 1980;135:713–716.
78. Dayananda L, Moorthy S, Prabhu NK, et al. Diagnostic value of gall bladder wall thickness in patients with ascites. Ind J Gastroenterol 2006;25:44–45.
79. Tsujimoto F, Miyamoto T, Tada S. Differentiation of benign from malignant ascites by sonographic evaluation of gallbladder wall. Radiology 1985:157:503–504.

80. Ralls PW, Quinn MF, Juttner HU, et al. Gallbladder wall thickening: patients without intrinsic gallbladder disease. AJR Am J Roentgenol 1981;137:65–68.
81. Saverymuttu SH, Grammatopoulos A, Meanock CI, et al. Gallbladder wall thickening (congestive cholecystopathy) in chronic liver disease: a sign of portal hypertension. Br J Radiol 1990;63:922–925.
82. Shlaer WJ, Leopold GR, Scheible FW. Sonography of thickened gallbladder wall: a non-specific finding. AJR Am J Roentgenol 1981;136:337–339.
83. Maudgal DP, Wansborough Jones MH, Joseph AEA. Gallbladder abnormalities in acute infectious hepatitis. Dig Dis Sci 1984;29:257–260.
84. Juttner H-U, Ralls PW, Quinn MF, Jenney JM. Thickening of gallbladder wall in acute hepatitis: ultrasound demonstration. Radiology 1982;142:465–466.
85. Brandt DJ, MacCarty RL, Charbonneau JW, et al. Gallbladder disease in patients with primary sclerosing cholangitis. AJR Am J Roentgenol 1988;150:571–574.
86. Romano AJ, van Sonnenberg E, Casola G, et al. Gallbladder and bile duct abnormalities in AIDS: sonographic findings in eight patients. AJR Am J Roentgenol 1988;150:123–127.
87. McClure J, Banerjee SS, Schofield PS. Crohn's disease of the gallbladder. J Clin Pathol 1984;37:516–518.
88. Carroll BA. Gallbladder wall thickening secondary to focal lymphatic obstruction. J Ultrasound Med 1983;2:89–91.
89. Laudanna AA, Ferreyra NP, Cerri GG, Bettarello A. Thickening of the gallbladder wall in alcoholic hepatitis verified by ultrasonographic examination. Scand J Gastroenterol 1987;22: 521–524.
90. Cerri GG, Alves V, Magalhaes A. Sonography in hepatobiliary schistosomiasis. Radiology 1984;153:777.
91. Johansson M, Thune A, Blomqvist A, et al. Impact of choice of therapeutic strategy for acute cholecystitis on patient's health-related quality of life. Results of a randomized, controlled clinical trial. Dig Surg 2004;21:359–362.
92. Marton KI, Doubilet P. How to image the gallbladder in suspected cholecystitis. Ann Intern Med 1988;109:722–729.
93. Laing FC, Federle MP, Jeffrey RB, Brown TW. Ultrasonic evaluation of patients with acute right upper quadrant pain. Radiology 1981;190:449–455.
94. Handler SJ. Ultrasound of gallbladder wall thickening and its relation to cholecystitis. AJR Am J Roentgenol 1979;132:581–585.
95. Marchal GJF, Casaer M, Baert AL, et al. Gallbladder wall sonolucency in acute cholecystitis. Radiology 1979;133:429–433.
96. Kane RA. The biliary system. In: Kurtz AB, Goldberg BB, editors. Gastrointestinal ultrasonography. New York: Churchill Livingstone; 1988, p. 75–137.
97. Sherman M, Ralls PW, Quinn M, et al. Intravenous cholangiography and sonography in acute cholecystitis: prospective evaluation. AJR Am J Roentgenol 1980;135:311–313.
98. Clain A. Hamilton Bailey's physical signs in clinical surgery. 14th ed. Bristol: Wright; 1967.
99. Ralls PW, Halls J, Lapin SA, et al. Prospective evaluation of the sonographic Murphy sign in suspected acute cholecystitis. J Clin Ultrasound 1982;10:113–115.
100. Ralls PW, Colletti PM, Lapin SM, et al. Real time sonography in suspected acute cholecystitis. Radiology 1985;155:767.
101. Yamashita H, Hachisuka Y, Kotegawa H, et al. The blood flow velocity in the wall of the gallbladder is an indicator of the degree of inflammation in acute cholecystitis. Hepatogastroenterology 2006;53(72):819–822.
102. Dinkel HP, Kraus S, Heimbucher J, et al. Sonography for selecting candidates for laparoscopic cholecystectomy, a prospective study. AJR Am J Roentgenol 2000;174:1433–1439.
103. Jeffrey RB, Laing FC, Wong W, Callen PW. Gangrenous cholecystitis: diagnosis by ultrasound. Radiology 1983;148:219–221.
104. Wales LR. Desquamated gallbladder mucosa: unusual sign of cholecystitis. AJR Am J Roentgenol 1982;139:810–811.
105. Sood BP, Kalra N, Gupta S, et al. Role of sonography in the diagnosis of gallbladder perforation. J Clin Ultrasound 2002;30(5):270–274.
106. Simeone JF, Brink JA, Mueller PR, et al. The sonographic diagnosis of acute gangrenous cholecystitis: importance of the Murphy sign. AJR Am J Roentgenol 1989;152:289–290.
107. Kane RA. Ultrasonographic diagnosis of gangrenous cholecystitis and empyema of the gallbladder. Radiology 1980;134:191–194.
108. Jenkins M, Golding RH, Cooperberg PL. Sonography and computed tomography of haemorrhagic cholecystitis. AJR Am J Roentgenol 1983;140:1197–1198.
109. Bergman AB, Neiman HL, Kraut B. Ultrasonographic evaluation of pericholecystic abscesses. AJR Am J Roentgenol 1979;132:201–203.
110. Madrazo BL, Francis I, Hricak H, et al. Sonographic findings in perforation of the gallbladder. AJR Am J Roentgenol 1982;139: 491–496.
111. Hunter ND, Macintosh PK. Acute emphysematous cholecystitis: an ultrasonic diagnosis. AJR Am J Roentgenol 1980;134:592–593.
112. Blaquiere RM, Dewbury KC. The ultrasound diagnosis of emphysematous cholecystitis. Br J Radiol 1982;55:114–116.
113. Parulekar SG. Sonographic findings in acute emphysematous cholecystitis. Radiology 1982;145:117–119.
114. Bloom RA, Fisher A, Pode D, Asaf Y. Shifting intramural gas: a new ultrasound sign of emphysematous cholecystitis. J Clin Ultrasound 1984;12:40–42.
115. Nemcek AA, Gore RM, Vogelzang RL, Grant M. The effervescent gallbladder: a sonographic sign of emphysematous cholecystitis. AJR Am J Roentgenol 1988;150:575–577.
116. Bloom RA, Libson E, Lebensart PD, et al. The ultrasound spectrum of emphysematous cholecystitis. J Clin Ultrasound 1989;17:251–256.
117. Gill KS, Chapman AH, Weston MJ. The changing face of emphysematous cholecystitis. BJR 1997;70:986–991.
118. Deitch EA, Engel JM. Acute acalculous cholecystitis: an ultrasonic diagnosis. Am J Surg 1981;142:290–292.
119. Shuman WP, Rogers JV, Ruydd TG, et al. Low sensitivity of sonography and cholescintigraphy in acalculous cholecystitis. AJR Am J Roentgenol 1984;142:531–534.
120. Mirvis SE, Vainright JR, Nelson AW, et al. The diagnosis of acute acalculous cholecystitis: a comparison of sonography, scintigraphy, and CT. AJR Am J Roentgenol 1986;147:1171–1175.
121. McGahan JP, Walter JR. Diagnostic percutaneous aspiration of the gallbladder. Radiology 1985;155:619–622.
122. McGahan JP, Lindfors KK. Acute cholecystitis: diagnostic accuracy of percutaneous aspiration of the gallbladder. Radiology 1988;167: 669–671.
123. Tsutsui K, Uchida N, Hirabayashi S, et al. Usefulness of single and repetitive percutaneous transhepatic gallbladder aspiration for the treatment of acute cholecystitis. J Gastroenterol 2007;42(7): 583–588.
124. Chopra S, Dodd GD 3rd, Mumbower AL, et al. Treatment of acute cholecystitis in non-critically ill patients at high surgical risk: comparison of clinical outcomes after gallbladder aspiration and after percutaneous cholecystostomy. AJR Am J Roentgenol 2001;176(4): 1025–1031.
125. De Waele E, Op de Beeck B, De Waele B, Delvaux G. Magnetic resonance cholangiopancreatography in the preoperative assessment of patients with biliary pancreatitis. Pancreatology 2007;7(4): 347–351.
126. Berk RN, van der Vegt JH, Lichtenstein JE. The hyperplastic cholecystoses: cholesterolosis and adenomyomatosis. Radiology 1983;146:595–601.
127. Stunell H, Buckley O, Geoghegan T, et al. Imaging of adenomyomatosis of the gall bladder. J Med Imaging Radiat Oncol 2008;52(2):109–117.
128. Raghavendra BN, Subramanyam BR, Balthazar EJ, et al. Sonography of adenomyomatosis of the gallbladder: radiologic-pathologic correlation. Radiology 1983;146:747–752.
129. Fowler RC, Reid WA. Ultrasound diagnosis of adenomyomatosis of the gallbladder: ultrasonic and pathological correlation. Clin Radiol 1988;39:402–406.
130. Nishimura A, Shirai Y, Hatakeyama K. Segmental adenomyomatosis of the gallbladder predisposes to cholecystolithiasis. J Hepatobiliary Pancreat Surg 2004;11(5):342–347.
131. Price RJ, Stewart ET, Foley WD, Dodds WJ. Sonography of polypoid cholesterolosis. AJR Am J Roentgenol 1982;139:1197.
132. Khairy GA, Guraya SY, Murshid KR. Cholesterolosis. Incidence, correlation with serum cholesterol level and the role of laparoscopic cholecystectomy. Saudi Med J 2004;25(9):1226–1228.
133. Strömsten A, von Bahr S, Bringman S, et al. Studies on the mechanism of accumulation of cholesterol in the gallbladder mucosa. Evidence that sterol 27-hydroxylase is not a pathogenetic factor. J Hepatol 2004;40(1):8–13.
134. Planells Roig M, Bueno Lledó J, Sanahuja Santafé A, García Espinosa R. Quality of life (GIQLI) and laparoscopic cholecystectomy usefulness in patients with gallbladder dysfunction or chronic non-lithiasic biliary pain (chronic acalculous cholecystitis). Rev Esp Enferm Dig 2004;96(7):442–446, 446–451.
135. Carter SJ, Rutledge J, Hirsch JH. Papillary adenoma of the gallbladder: ultrasonic demonstration. J Clin Ultrasound 1978;6:433.

136. Foster DR, Foster DBE. Gallbladder polyps in Peutz-Jeghers syndrome. Postgrad Med J 1980;56:373–376.
137. Niv Y, Kosakov K, Shcolnik B. Fragile papilloma (papillary adenoma) of the gallbladder. A cause of recurrent biliary colic. Gastroenterology 1986;91:999–1001.
138. Kozuka S, Kurashina M, Tsubone M, et al. Significance of intestinal metaplasia for the evolution of cancer in the biliary tract. Cancer 1984;54:2277–2285.
139. Sun XJ, Shi JS, Han Y, et al. Diagnosis and treatment of polypoid lesions of the gallbladder: report of 194 cases. Hepatobiliary Pancreat Dis Int 2004;3(4):591–594.
140. Myers RP, Shaffer EA, Beck PL. Gallbladder polyps: epidemiology, natural history and management. Can J Gastroenterol 2002;16(3): 187–194.
141. Numata K, Oka H, Morimoto M, et al. Differential diagnosis of gallbladder diseases with contrast-enhanced harmonic gray scale ultrasonography. J Ultrasound Med 2007;26(6):763–774.
142. Inoue T, Kitano M, Kudo M, et al. Diagnosis of gallbladder diseases by contrast-enhanced phase-inversion harmonic ultrasonography. Ultrasound Med Biol 2007;33(3):353–361.
143. Majeski JA. Polyps of the gallbladder. J Surg Oncol 1986;32:16–18.
144. Lai CH, Lau WY. Gallbladder cancer – a comprehensive review. Surgeon 2008;6(2):101–110.
145. Misra MC, Guleria S. Management of cancer gallbladder found as a surprise on a resected gallbladder specimen. J Surg Oncol 2006;93(8):690–698.
146. Lai CH, Lau WY. Gallbladder cancer – a comprehensive review. Surgeon 2008;6(2):101–110.
147. Olken SM, Bledsoe R, Newmark H. The ultrasonic diagnosis of primary carcinoma of the gallbladder. Radiology 1978;129:481–482.
148. Crade M, Taylor KJW, Rosenfield AT, et al. The varied ultrasonic character of gallbladder tumour. JAMA 1979;241:2195–2196.
149. Yeh H-C. Ultrasonography and computed tomography of carcinoma of the gallbladder. Radiology 1979;133:167–173.
150. Dalla Palma L, Rizzatto G, Pozzi-Mucelli RS, Bazzocchi M. Grey scale ultrasonography in the evaluation of carcinoma of the gallbladder. Br J Radiol 1980;53:662–667.
151. Yum HY, Fink AH. Sonographic findings in primary carcinoma of the gallbladder. Radiology 1980;134:693–696.
152. Ruiz R, Teyssou H, Fernandez N, et al. Ultrasonic diagnosis of primary carcinoma of the gallbladder: a review of 16 cases. J Clin Ultrasound 1980;8:489–495.
153. Lee KF, Wong J, Li JC, Lai PB. Polypoid lesions of the gallbladder. Am J Surg 2004;188(2):186–190.
154. Bach AM, Loring LA, Hann LE, et al. Gallbladder cancer: can ultrasonography evaluate extent of disease? J Ultrasound Med 1998;17:303–309.
155. Koga A, Yamauchi S, Izumi Y, Hamanaka N. Ultrasonographic detection of early and curable carcinoma of the gallbladder. Br J Surg 1985;72:728–730.
156. Diehl AK, Beral V. Cholecystectomy and changing mortality from gallbladder cancer. Lancet 1981;ii:187–189.
157. Phillips G, Pochaczevsky R, Goodman J, et al. Ultrasound patterns of metastatic tumours in the gallbladder. J Clin Ultrasound 1982; 10:379.
158. Marone U, Caracò C, Losito S, et al. Laparoscopic cholecystectomy for melanoma metastatic to the gallbladder: is it an adequate surgical procedure? Report of a case and review of the literature. World J Surg Oncol 2007;5:141.
159. Lim JH. Parasitic diseases in the abdomen: imaging findings. Abdom Imaging 2008;33(2):130–132.
160. Das CJ, Kumar J, Debnath J, Chaudhry A. Imaging of ascariasis. Australas Radiol 2007;51(6):500–506.
161. Lim JH, Mairiang E, Ahn GH. Biliary parasitic diseases including clonorchiasis, opisthorchiasis and fascioliasis. Abdom Imaging 2008;33(2):157–165.
162. Rana SS, Bhasin DK, Nanda M, Singh K. Parasitic infestations of the biliary tract. Curr Gastroenterol Rep 2007;9(2):156–164.
163. Braverman DZ, Johnson ML, Kern F Jr. Effects of pregnancy and contraceptive steroids on gallbladder function. N Engl J Med 1980;302:362.
164. Kane RA. Ultrasonographic evaluation of the gallbladder. Crit Rev Diagn Imaging 1982;17:107.
165. Singh S, Kansra S. Kawasaki disease. Natl Med J India 2005;18(1): 20–24.
166. Mateen MA, Saleem S, Rao PC, et al. Ultrasound in the diagnosis of typhoid fever. Indian J Pediatr 2006;73(8):681–685.
167. Tanaka K, Shimada M, Hattori M, et al. Sjogren's syndrome with abnormal manifestations of the gallbladder and central nervous system. J Pediatr Gastroenterol Nutr 1985;4:148–151.
168. Dietrich CF, Chichakli M, Hirche TO, et al. Sonographic findings of the hepatobiliary-pancreatic system in adult patients with cystic fibrosis. J Ultrasound Med 2002;21(4):409–416.
169. Chaudry G, Navarro OM, Levine DS, Oudjhane K. Abdominal manifestations of cystic fibrosis in children. Pediatr Radiol 2006;36(3):233–240.
170. Lunderquist A. The radiology of jaundice. Clin Gastroenterol 1989;3:387–406.
171. Taylor KJW, Rosenfield AT. Grey scale ultrasonography in the differential diagnosis of jaundice. Arch Surg 1977;112:820–825.
172. Sample WF, Sarti DA, Goldstein LI, et al. Gray-scale ultrasonography of the jaundiced patient. Radiology 1978;128:719–725.
173. Vallon AG, Lees WR, Cotton PB. Gray-scale ultrasonography in obstructive jaundice. Gut 1979;20:51–54.
174. Koenigsberg M, Wiener SN, Walzer A. Accuracy of sonography in the differential diagnosis of obstructive jaundice: a comparison with cholangiography. Radiology 1979;133:157–165.
175. Dewbury KC, Joseph AEA, Hayes S, Murray C. Ultrasound in the evaluation and diagnosis of jaundice. Br J Radiol 1979;52: 276–280.
176. Wild SR, Cruikshank JG, Fraser GGM, et al. Grey-scale ultrasonography and percutaneous transhepatic cholangiography in biliary tract disease. BMJ 1980;281:1524–1526.
177. Haubek A, Pedersen JH, Buscharth F, et al. Dynamic sonography in the evaluation of jaundice. AJR Am J Roentgenol 1981;136: 1071–1074.
178. Caddy GR, Tham TC. Gallstone disease: symptoms, diagnosis and endoscopic management of common bile duct stones. Best Pract Res Clin Gastroenterol 2006;20(6):1085–1101.
179. Lindsell DRM. Ultrasound imaging of pancreas and biliary tract. Lancet 1990;335:390–393.
180. Ney MV, Maluf-Filho F, Sakai P, et al. Echo-endoscopy versus endoscopic retrograde cholangiography for the diagnosis of choledocholithiasis: the influence of the size of the stone and diameter of the common bile duct. Arq Gastroenterol 2005;42(4): 239–243.
181. Songür Y, Temuçin G, Sahin B. Endoscopic ultrasonography in the evaluation of dilated common bile duct. J Clin Gastroenterol 2001;33(4):302–305.
182. Garrow D, Miller S, Sinha D, et al. Endoscopic ultrasound: a meta-analysis of test performance in suspected biliary obstruction. Clin Gastroenterol Hepatol 2007;5(5):616–623.
183. Tse F, Liu L, Barkun AN, et al. EUS: a meta-analysis of test performance in suspected choledocholithiasis. Gastrointest Endosc 2008;67(2):235–244.
184. Dewbury KC. Visualisation of normal biliary ducts with ultrasound. Br J Radiol 1980;53:774–780.
185. Bressler EL, Rubin JM, McCracken S. Sonographic parallel channel sign: a reappraisal. Radiology 1987;164:343–346.
186. Cooperberg PL. High resolution real time ultrasound in the evaluation of the normal and obstructed biliary tract. Radiology 1978;129:477–480.
187. Cooperberg PL, Li D, Wong P, et al. Accuracy of common hepatic duct size in the evaluation of extrahepatic biliary obstruction. Radiology 1980;135:141–144.
188. Parulekar SG. Evaluation of common bile duct size. Radiology 1979;133:703–707.
189. Wu C-C, Ho Y-H, Chen C-Y. Effect of ageing on common bile duct diameter: a real time sonographic study. J Clin Ultrasound 1984;12:473.
190. Ruddell WSJ, Ashton MG, Lintott DJ, Axon ATR. Endoscopic retrograde cholangiography and pancreatography in investigation of post-cholecystectomy patients. Lancet 1980;i:444–447.
191. Csendes A, Csendes P, Burdiles P, et al. Behavior of the common bile duct diameter before and 12 years after choledochostomy for cholecystolithiasis and choledocholithiasis. A prospective study. J Gastrointest Surg 2007;11(10):1294–1297.
192. Weill F, Eisencher A, Zeltner F. Ultrasonic study of the normal and dilated biliary tree: 'shot-gun sign'. Radiology 1978;127:221.
193. Conrad MR, Landay MJ, Janes JO. Sonographic 'parallel channel' sign of biliary tree enlargement in mild to moderate obstructive jaundice. AJR Am J Roentgenol 1978;130:279.
194. Ingram C, Joseph AEA. The stilette sign: the appearance of dilated ducts in the fatty liver. Clin Radiol 1989;40:257–258.

195. Laing FC, London LA, Filly RA. Ultrasonographic identification of dilated intrahepatic bile ducts and their differentiation from portal venous structures. J Clin Ultrasound 1978;6:90.
196. Taylor KJW, Rosenfield AT, De Graaff CS. Anatomy and pathology of the biliary tree as demonstrated by ultrasound. In: Taylor KJW, editor. Diagnostic ultrasound in gastrointestinal disease. Clinics in diagnostic ultrasound. Edinburgh: Churchill Livingstone; 1979, p. 103–121.
197. Muhletaler CA, Gerlock AJ, Fleischer AC, James AE. Diagnosis of obstructive jaundice with non-dilated bile ducts. AJR Am J Roentgenol 1980;134:1149–1152.
198. Thomas JL, Zornoza J. Obstructive jaundice in the absence of sonographic biliary dilatation. Gastrointest Radiol 1980;5:357–360.
199. Beinart C, Efremidis S, Cohen B, Mitty HA. Obstruction without dilatation. JAMA 1981;245:353–356.
200. Greenwald RA, Pereiras R, Morris SJ, Schiff ER. Jaundice, choledocholithiasis, and a non-dilated common duct. JAMA 1978;240:1983–1984.
201. Fried AM, Bell RM, Bivins BA. Biliary obstruction in a canine model: sequential study of the sonographic threshold. Invest Radiol 1981;16:317–319.
202. Carroll BA, Oppenheimer DA. Sclerosing cholangitis: sonographic demonstration of bile duct wall thickening. AJR Am J Roentgenol 1982;139:1016.
203. Vaishali MD, Agarwal AK, Upadhyaya DN, et al. Magnetic resonance cholangiopancreatography in obstructive jaundice. J Clin Gastroenterol 2004;38(10):887–890.
204. Filippone A, Ambrosini R, Fuschi M, et al. Clinical impact of MR cholangiopancreatography in patients with biliary disease. Radiol Med (Torino) 2003;105(1–2):27–35.
205. Weinstein DP, Weinstein BJ, Brodmerkel GJ. Ultrasonography of biliary tract dilatation without jaundice. AJR Am J Roentgenol 1979;132:729–734.
206. Weinstein BJ, Weinstein DP. Biliary tract dilatation in the non-jaundiced patient. AJR Am J Roentgenol 1980;134:899.
207. Glazer GM, Filly RA, Laing FC. Rapid change in calibre of the non-obstructed common duct. Radiology 1980;140:161–162.
208. Scheske GA, Cooperberg PL, Cohen MM, et al. Dynamic changes in the caliber of the major bile ducts, related to obstruction. Radiology 1980;135:215–216.
209. Mueller PR, Ferrucci JT Jr, Simeone JF. Observations on the distensibility of the common bile duct. Radiology 1982;142:467–472.
210. Mahour GH, Wakim KG, Soule EH, et al. Structure of the common bile duct in man. Ann Surg 1967;166:91–94.
211. Schein CF, Beneventano TC. Choledochal dynamics in man. Surg Gynecol Obstet 1968;126:591–596.
212. Sauerbrei EE, Cooperberg PL, Gordon P, et al. The discrepancy between radiographic and sonographic bile duct measurements. Radiology 1980;137:751–755.
213. Clain A. Hamilton Bailey's physical signs in clinical surgery. 14th ed. Bristol: Wright. 1967.
214. Laing FC, Jeffrey RB, Wing VW. Improved visualisation of choledocholithiasis by sonography. AJR Am J Roentgenol 1984;143:949–952.
215. Dong B, Chen M. Improved sonographic visualisation of choledocholithiasis. J Clin Ultrasound 1987;15:185–190.
216. Rickes S, Treiber G, Mönkemüller K, et al. Impact of the operator's experience on value of high-resolution transabdominal ultrasound in the diagnosis of choledocholithiasis: a prospective comparison using endoscopic retrograde cholangiography as the gold standard. Scand J Gastroenterol 2006;41(7):838–843.
217. Way LW, Sleisenger MH. Biliary obstruction, cholangitis, and choledocholithiasis. In: Sleisenger MH, Fordtran JS, editors. Gastrointestinal disease. Philadelphia: WB Saunders; 1983, p. 1389–1403.
218. Glenn F. Postcholecystectomy choledocholithiasis. Surg Gynecol Obstet 1972;134:249–252.
219. Laing FC, Jeffrey RB. Choledocholithiasis and cystic duct obstruction: difficult ultrasonographic diagnosis. Radiology 1983;146:475–479.
220. Kane RA. The biliary system. In: Kurtz AB, Goldberg BB, editors. Gastrointestinal ultrasonography. Clinics in diagnostic ultrasound. Edinburgh: Churchill Livingstone; 1988, p. 75–137.
221. Dewbury KC, Smith CL. The misdiagnosis of common bile duct stones with ultrasound. Br J Radiol 1983;56:625–630.
222. Ledro-Cano D. Suspected choledocholithiasis: endoscopic ultrasound or magnetic resonance cholangio-pancreatography? A systematic review. Eur J Gastroenterol Hepatol 2007;19(11):1007–1011.
223. Carroll BA. Biliary cystadenoma and cystadenocarcinoma: gray scale ultrasound appearance. J Clin Ultrasound 1978;6:337–340.
224. Bondstam S, Kivilaakse EO, Standetskjold-Nordenstam C-GM, et al. Sonographic diagnosis of a bile duct polyp. AJR Am J Roentgenol 1980;135:610–611.
225. Stanley J, Vujic I, Schabel SI, et al. Evaluation of biliary cystadenoma and cystadenocarcinoma. Gastrointest Radiol 1983;8:245–258.
226. Marchal G, Gelin J, Van Steenbergen WV, et al. Sonographic diagnosis of intraluminal bile duct neoplasm; a report of 3 cases. Gastrointest Radiol 1984;9:329–333.
227. Patel T. Worldwide trends in mortality from biliary tract malignancies. BMC Cancer 2002;2:10.
228. Davila JA, El-Serag HB. Cholangiocarcinoma: the 'other' liver cancer on the rise. Am J Gastroenterol 2002;97:3199–3200.
229. Wise C, Pilanthananond M, Perry BF, et al. Mechanisms of biliary carcinogenesis and growth. World J Gastroenterol 2008;14(19): 2986–2989.
230. Klatskin G. Adenocarcinoma of the hepatic duct at its bifurcation within the porta hepatis. Am J Med 1965;38:241–256.
231. Dillon E, Peel ALG, Parkin GJS. The diagnosis of primary bile duct carcinoma (cholangiocarcinoma) in the jaundiced patient. Clin Radiol 1981;32:311–317.
232. Meyer DG, Weinstein BJ. Klatskin tumors of the bile ducts: sonographic appearance. Radiology 1983;148:803–804.
233. Subramanyam BR, Raghavendra BN, Balthazar EJ, et al. Ultrasonic features of cholangiocarcinoma. J Ultrasound Med 1984;3:405.
234. Marchan L, Muller NL, Cooperberg PL. Sonographic diagnosis of Klatskin tumors. AJR Am J Roentgenol 1986;147:509.
235. Gibson RN, Yeung E, Thompson JN, et al. Bile duct obstruction; radiologic evaluation of level, cause and tumour resectability. Radiology 1986;160:43–47.
236. Karstrup S. Ultrasound diagnosis of cholangiocarcinoma at the confluence of the hepatic ducts (Klatskin tumours). Br J Radiol 1988;61:987–990.
237. Yeung EYC, McCarthy P, Gompertz RH, et al. The ultrasonographic appearances of hilar cholangiocarcinoma (Klatskin tumours). Br J Radiol 1988;61:991–995.
238. Kruskal JB, Kane RA. Correlative imaging of malignant liver tumors. Semin Ultrasound CT MR 1992;13(5):336–354.
239. Kim JY, Kim MH, Lee TY, et al. Clinical role of 18F-FDG PET-CT in suspected and potentially operable cholangiocarcinoma: a prospective study compared with conventional imaging. Am J Gastroenterol 2008;103(5):1145–1151.
240. Filly RA, Carlsen EN. Choledochal cyst: report of a case with specific ultrasonographic findings. J Clin Ultrasound 1979;4:7–10.
241. Reuter K, Raptopoulos VD, Cantelmo N, et al. The diagnosis of a choledochal cyst by ultrasound. Radiology 1980;136:437–438.
242. Han BK, Babcock DS, Gelfand MH. Choledochal cyst with bile duct dilatation; sonography and 99mTc IDA cholescintigraphy. AJR Am J Roentgenol 1981;136:1075–1079.
243. Kangarloo H, Sarti DA, Sample WF, et al. Ultrasonographic spectrum of choledochal cysts in children. Pediatr Radiol 1980;9:15.
244. Kimura K, Ohto M, Ono T, et al. Congenital cystic dilatation of the common bile duct: relationship to anomalous pancreaticobiliary ductal union. AJR Am J Roentgenol 1977;128:571–577.
245. Jona JZ, Babitt DP, Starshak RJ, et al. Anatomic observations and etiologic and surgical considerations in choledochal cyst. J Pediatr Surg 1979;14:315–320.
246. Filly RA, Freimanis AK. Thrombosed hepatic artery aneurysm – report of a case diagnosed echographically. Radiology 1970;97:629–630.
247. Caroli J, Spoupaut R, Kossakowski J, et al. La dilatation polykistique congenitale des voies biliaires interhepatiques: essai de classification. Sem Hop 1958;34:488–495.
248. Mujahed Z, Glenn F, Evans J. Communicating cavernous ectasia of the intrahepatic bile ducts (Caroli's disease). AJR Am J Roentgenol 1971;113:21–26.
249. Bass EM, Funston MR, Shaff MI. Caroli's disease: an ultrasound diagnosis. Br J Radiol 1977;50:366–369.
250. Mittelstaedt CA, Volberg FM, Fischer GJ, et al. Caroli's disease: sonographic findings. AJR Am J Roentgenol 1980;134:585–587.
251. Yonem O, Bayraktar Y. Clinical characteristics of Caroli's disease. World J Gastroenterol 2007;13(13):1930–1933.
252. Rosenfield AT, Siegel NJ, Kappelman NB, Taylor KJW. Gray scale ultrasonography in medullary cystic disease of the kidney and congenital hepatic fibrosis with tubular ectasia: new observations. AJR Am J Roentgenol 1977;129:297–303.

253. Caroli J. Diseases of intrahepatic bile ducts. Isr J Med Sci 1968;4:213–215.
254. Imai Y, Watanabe MD, Kondo Y, Nakanishi MD. Caroli's disease: its diagnosis with non-invasive methods. Br J Radiol 1981;54:526–528.
255. Morikawa P, Ishida H, Niizawa M, et al. Sonographic features of biliary clonorchiasis. J Clin Ultrasound 1988;16:655–658.
256. Mori T, Sugiyama M, Atomi Y. Gallstone disease: management of intrahepatic stones. Best Pract Res Clin Gastroenterol 2006;20(6): 1117–1137.
257. Lim JH, Ko YT, Lee DH, Kim SY. Clonorchiasis: sonographic findings in 59 proved cases. AJR Am J Roentgenol 1989;152:761–764.
258. Ralls PW, Colletti PM, Quinn MF, et al. Sonography in recurrent oriental pyogenic cholangitis. AJR Am J Roentgenol 1981;136:1010.
259. Federle MP, Cello JP, Laing FC, Jeffrey RB. Recurrent pyogenic cholangitis in Asian immigrants. Radiology 1982;143:151.
260. Schulman A, Loxton AJ, Heydenrych JJ, Abdurahman KE. Sonographic diagnosis of biliary ascariasis. AJR Am J Roentgenol 1982;139:485–489.
261. Al Absi M, Qais AM, Al Katta M, et al. Biliary ascariasis: the value of ultrasound in the diagnosis and management. Ann Saudi Med 2007;27(3):161–165.
262. Cerri GC, Leite GJ, Simoes JB, et al. Ultrasonographic evaluation of ascaris in the biliary tract. Radiology 1983;146:753–754.
263. Doyle TCA, Roberts-Thomson IC. Radiological features of sclerosing cholangitis. Australas Radiol 1983;27:163.

CHAPTER

15 Intraoperative ultrasound

Steven Kennish and Jane A. Smith

INTRODUCTION 273

EQUIPMENT AND TECHNIQUES 273
Equipment 273
Technique 274

CLINICAL APPLICATIONS 275
Liver 275
Pancreas 279
Biliary tree 279
Urology 280

INTRODUCTION

Intraoperative ultrasound (IOUS) provides dynamic real-time imaging with an immediate impact on the surgical approach to predominantly oncological solid organ disease. The liver, bile ducts, pancreas, adrenal glands and kidneys are all particularly suited to intraoperative ultrasonic interrogation. Improved disease staging can be made with a view to resection and/or ablation, at the same sitting.

The diagnostic superiority and superb anatomical demonstration provided by IOUS is facilitated by direct transducer contact with the organ of interest. The lack of subcutaneous tissue reduces artefact and attenuation, and the subsequent decreased need for penetration affords the use of a much higher frequency than that used for percutaneous scanning, resulting in very high-resolution imaging (Fig. 15.1).

IOUS is established as the gold standard imaging for assessing the liver during planned resections for primary malignancy and metastatic disease.[1] Its dominance is based on an improved detection rate over preoperative imaging for focal liver lesions, and demonstration of essential real-time anatomy for the operating surgeon.[2,3] These factors are said to modify the surgical approach in up to 51% of planned liver resection cases.[4]

Despite this impressive pedigree, these figures are based on somewhat historical evidence. With improved preoperative imaging modalities and techniques such as contrast-enhanced magnetic resonance imaging (MRI), the improved lesion detection rate of IOUS is undoubtedly diminished.[5] Nevertheless intraoperative hepatic vascular anatomical demonstration with depiction of suitable dissection planes remains an unquestionable advantage.

Technological developments in ultrasound continue to improve the diagnostic potential of surgical ultrasound, and to widen its applications. Laparoscopic ultrasound has traditionally been associated with biliary surgery, in particular the imaging of the common bile duct during cholecystectomy. It is also now established as an essential adjunct to minimally invasive surgery of the liver with promising results[6] and is starting to play an increasing role in renal surgery. Further groundbreaking developments include the intraoperative use of ultrasound contrast agents. Remarkable early results have shown improved IOUS lesion detection for metastatic disease, and better characterisation of focal lesions in the cirrhotic patient undergoing resection for hepatocellular carcinoma.[7,8]

Intraoperative imaging is arguably the most exciting and challenging utilisation of sonography. Direct benefits to patient care include improved disease staging and guidance for surgery, immediate assessment of resection margins and specimens, reduced blood loss and shortened operating times.

Special considerations must, however, be given to the modified equipment and techniques needed to safely maximise the inherent advantages of direct contact transducer imaging.

EQUIPMENT AND TECHNIQUES

Radiologists and sonographers have not universally taken up the challenge of IOUS provision. Reasons cited include too much time away from the radiology department and the unpredictable timing of surgical cases.

Many centres rely on the acquired expertise of the operating surgeon. There is no doubt that surgeons can become proficient at scanning organs within their field of interest, with suitable training and practice. They often, however, do not have the familiarity or experience with sonography that enables their radiological colleagues to fully optimise the imaging potential of the available equipment[9] and in centres where surgery can be planned and organised with radiology support, there are advantages to a radiology-based service due to comprehensive ultrasound training, image optimisation and interpretation.

Discussion in the literature of standard presets for depth of field, location of focal zones, scan orientation and image zoom settings for surgeon-led image acquisition suggests that there is indeed still an important role for the sonologist.[10]

Practical steps to assist the sonologist to minimise time away from the radiology department have been proposed. Pre-booking IOUS cases, advanced notice of a case on the day, sonologists wearing surgical attire in preparation, and having an ultrasound machine already set up in theatre have been advocated.[11]

Equipment

In the past, surgical ultrasound machines, which must be small and mobile, have suffered from inferior imaging capabilities. This was largely mitigated by the use of high-frequency probes. However, technological developments have enabled smaller machines to offer imaging of much higher quality, with consequent benefits to intraoperative imaging.

The choice of ultrasound transducer is important. Transducer frequencies for IOUS are typically higher than those chosen for percutaneous scanning. Modern broadband probes operate at frequencies of around 6–8 MHz, which gives good resolution with adequate penetration through most livers.[9]

The transducer shape is due to individual choice and depends on the work predominantly performed. Both curvilinear and linear arrays are commercially available. The linear probe is frequently

used to scan organs such as the pancreas and bile ducts, when good line density can be achieved throughout the field. Curved arrays are particularly useful for liver scanning when a wider field of view is required. Many electronic linear arrays have a beam steering facility which allows the field of view to be converted into a 'trapezoid' shape for hepatic imaging.

T-shaped or side-fire probes are specifically designed for scanning organs such as the liver where access to the dome may be limited even after surgical mobilisation. Ergonomic design allows a comfortable grip between the fingers (Fig. 15.2). End-fire probes can also be used when more space is available within the abdominal cavity, or when larger resection specimens are removed and scanned separately. Doppler imaging functions are also now routinely available in IOUS transducers, enabling vascular patency to be established during transplant and resection, and allowing thrombus to be located during surgical resection procedures.

Transducers with pulse inversion harmonic imaging capability are required for contrast-enhanced IOUS (CE-IOUS).

The design of a laparoscopic ultrasound probe is constrained by the 10–11 mm diameter of a standard laparoscopic port, through which access to the abdominal cavity is gained (Fig. 15.3). Nevertheless, laparoscopic probes have benefited from the technological improvements that have allowed the miniaturisation of established high performance linear and curved array transducers. A penalty is paid in terms of a reduced field of view, but longer crystal lengths (up to 4 cm) help reduce the scanning times of larger organs.[12] As with standard transducers, broadband probes which operate at 5–7 MHz are useful for organs such as the liver, and probes of 7.5–10 MHz are suited to imaging the common bile duct, pancreas and kidneys. Modern laparoscopic probes are designed to be flexible to assist with maintenance of good organ surface contact.

Technique

Scanning technique is tailored to the target organ and the individual patient, and it is always advisable to review preoperative imaging,

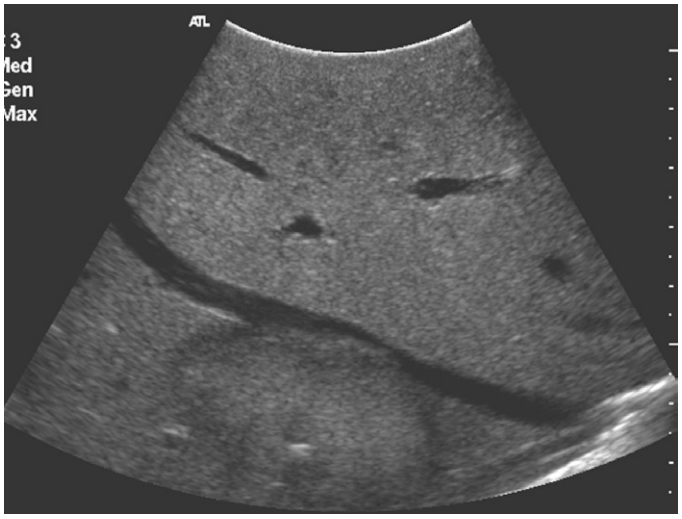


Figure 15.1 IOUS using a curved array high-frequency transducer. The liver with the middle hepatic vein is demonstrated. A metastasis is breaching the vein wall.



Figure 15.3 A laparoscopic US probe with a linear array configuration. The probe is flexible in two planes by manipulating the control at the handle.

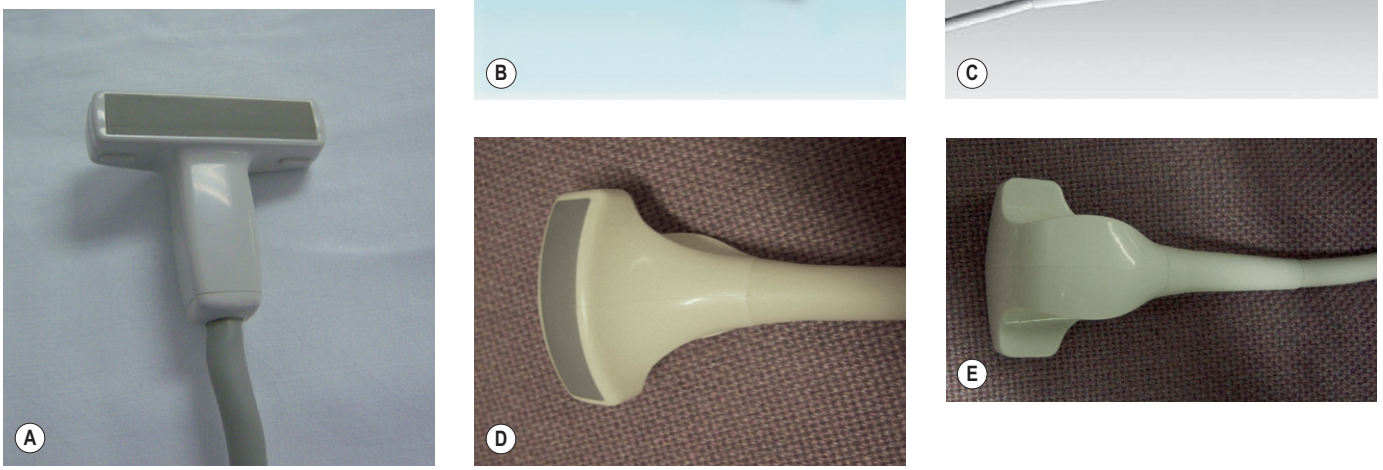


Figure 15.2 IOUS probes. A: T probe. **B:** 'I' shaped array. **C:** an end-firing array. **D:** A curved array – particularly useful for hepatic scanning with access to the dome of the liver. **E**: The back of the curved array is shaped to take the sonographer's fingers.

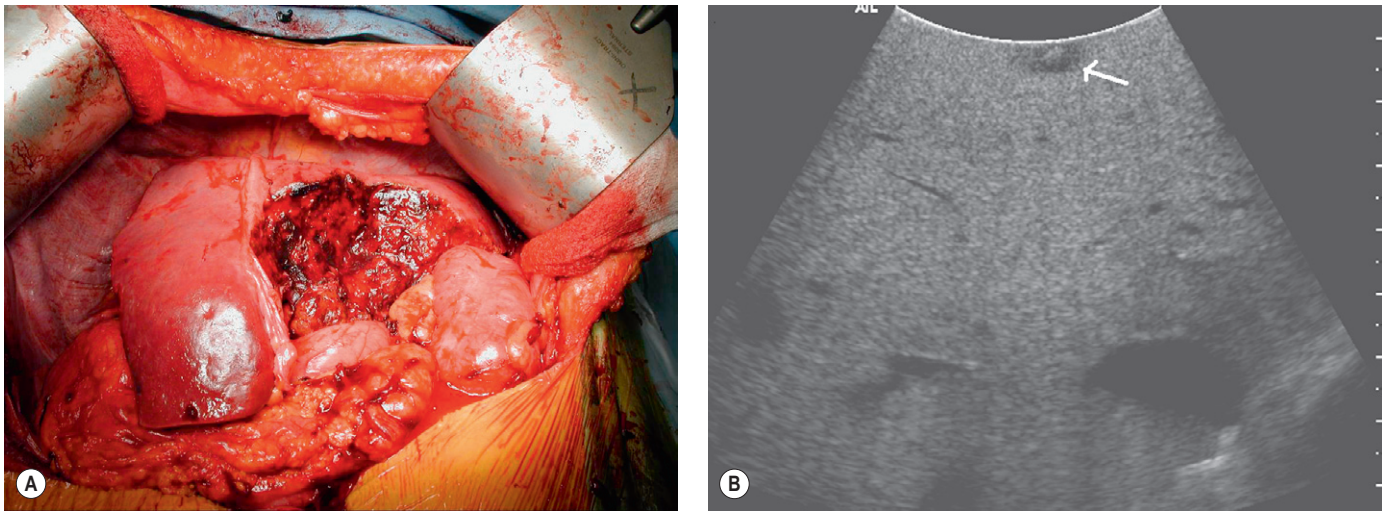


Figure 15.4 IOUS, liver. A: The surface moisture of the organs enables the IOUS probe to be placed directly onto the surface of the liver. **B:** A small surface metastasis, not demonstrated preoperatively, is palpated and demonstrated on IOUS.

or have it available on a viewing screen within theatre. It is important to have easily accessible, suitable preset programmes in the machine, which incorporate all the basic image optimisation functions, as once scrubbed up, it may be difficult to optimise the image unless a second ultrasound colleague is present.

For most open surgical IOUS procedures it is sufficient to put a sterile probe cover over the clean probe. Sterile gel should be put inside the cover first, and the probe placed into the cover taking care to smooth any air bubbles from the probe face. As most probe covers tend to be relatively short, a second, sterile laparoscopic-style cover, which is longer and open at both ends, can be placed over the whole, allowing the cable to be covered and keeping the area sterile.

The whole organ or region in question must be adequately imaged. A methodical approach is recommended with a slow sweeping motion over the organ surface in a controlled manner. It is sensible to overlap areas with scanning sweeps and to image both in sagittal and transverse planes.[1,10] Specific attention can be given to any lesions encountered, and image capture may be used for documentation and audit purposes. Contrast administration and/or biopsy may be used to assist diagnosis, and ablation is among the options available for treatment. Specific reference to vascular anatomy is vital for the operating surgeon, and the Couinaud classification for liver segmentation is used.

IOUS can be seen as an extension of the bimanual examination of the organ, especially when considering the liver and pancreas (Fig. 15.4). Indeed studies have demonstrated that palpation alone can identify surface lesions missed by IOUS.[3,13] This results from a recognised limitation, whereby near-field lesions just below the liver capsule surface are inadequately imaged due to compression by the probe, or poor near-field focusing. Bathing the organ surface with sterile degassed saline can overcome this problem by utilising the water standoff principle.[1] However, the natural moisture found coating the abdominal organs is usually sufficient to provide acoustic coupling (Fig. 15.4) and modern probes with good near-field focusing have improved the demonstration of near-field lesions. In cases when a tiny lesion can be palpated but not adequately visualised on IOUS, scanning from underneath the liver whilst identifying the lesion with a finger is useful. This can bring the lesion into the focal zone of the transducer, making location more successful.

Laparoscopic ultrasound lacks the advantage of direct organ palpation, compounded by a lack of tactile stimulus feedback from the laparoscopic probe, and relies solely on imaging. The planes of scan are limited by the laparoscopic port and the flexibility of the probe. For small structures, such as ducts or superficial pancreatic nodules, a water standoff may be beneficial for assessing the near field.

A split-screen viewing system with laparoscopic ultrasound images side by side laparoscopic camera views of the intra-abdominal probe position is advised. This is said to help prevent iatrogenic organ damage from overzealous probe manipulation.[12]

A methodical approach to scanning with a laparoscopic probe consists of numerous arching sweeps with the pivot fixed at the port site. This can be time-consuming compared to conventional open IOUS, but the benefits of an overall shorter operation time and faster patient recovery must be borne in mind. Laparoscopic ultrasound is perhaps an area where the surgeon is at an advantage over his or her radiological colleague. Competent laparoscopic instrument manipulation necessitates an operator learning curve. The surgeon will be comfortable with this technique, but a number of training simulators and courses are available to the enthusiastic sonologist.[14]

A further consideration with laparoscopic ultrasound is the necessity for probe sterilisation, as unlike IOUS, the probe comes into direct contact with the patient. A number of sterilisation agents are discussed in the literature, including ethylene oxide gas, low-temperature hydrogen peroxide gas and glutaraldehyde solution.[1,8] A suitable 'bath' long enough to accommodate the probe and cable is required, and care should be taken to avoid contact between the plug and cleaning fluid.

CLINICAL APPLICATIONS

Liver

IOUS is most commonly performed to assess the liver during planned resection for primary or metastatic disease. It has a useful role in allowing targeted biopsy guidance if questionable lesions are encountered, and guiding thermal ablation procedures as part of treatment. It is also used to assess adult living–related donor liver, and is invaluable for providing vascular anatomical information to provide an operative roadmap for the surgical team (Fig. 15.5).

Colorectal cancer is the third most common malignancy after breast and lung cancer, in the United Kingdom, a picture that mirrors much of the Western world.[15] Surgical resection is the only current hope of cure, with 5-year survival in up to 45% of patients.[16] Only 10–20% of patients with colorectal metastases to the liver will be suitable for resection, although newer surgical techniques and chemotherapeutic regimes have helped increase the numbers of

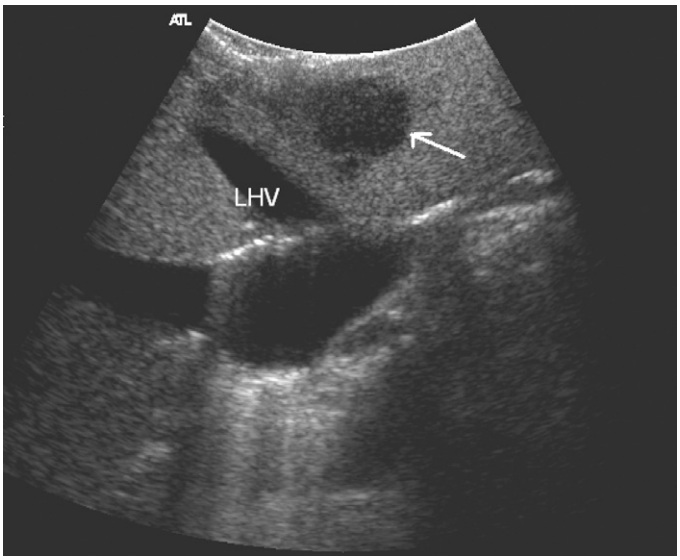


Figure 15.5 The relationship of a metastasis (arrow) to the left hepatic vein (LHV) is demonstrated on IOUS prior to resection.

those eligible.[17] It is imperative that every effort is made to identify all suspicious liver lesions in patients who are put through the considerable morbidity of major hepatic surgery. The prognosis and chance of curative resection is clearly better in patients with a low bulk of disease and/or lesions that are confined to a relatively small number of segments. This enables a less complex procedure to be carried out and reduces postoperative morbidity. In patients with more widespread disease, a combination of resection and ablation may be necessary in order to render the liver disease free (Fig. 15.6).

IOUS became established in the late 1980s and early 1990s as the gold standard imaging modality for assessing primary and metastatic disease of the liver with a view to resection. It had been consistently demonstrated that additional lesions could be identified in up to 25–38% of patients, with a significant impact on surgical planning.[2–4] New lesions do not always necessitate alteration to the surgical plan, however, especially if they lie within segments of the liver already marked down for resection. Nevertheless, demonstration of vascular anatomy was, and still is, deemed invaluable for identifying surgical dissection planes. Even recent papers have suggested that IOUS provides a considerable pick-up rate for lesions missed on preoperative imaging. These studies often have percutaneous ultrasound or thicker slice single-phase computed tomography (CT) imaging as a preoperative baseline, rather than state-of-the-art imaging modalities and techniques.[18,19] It is also

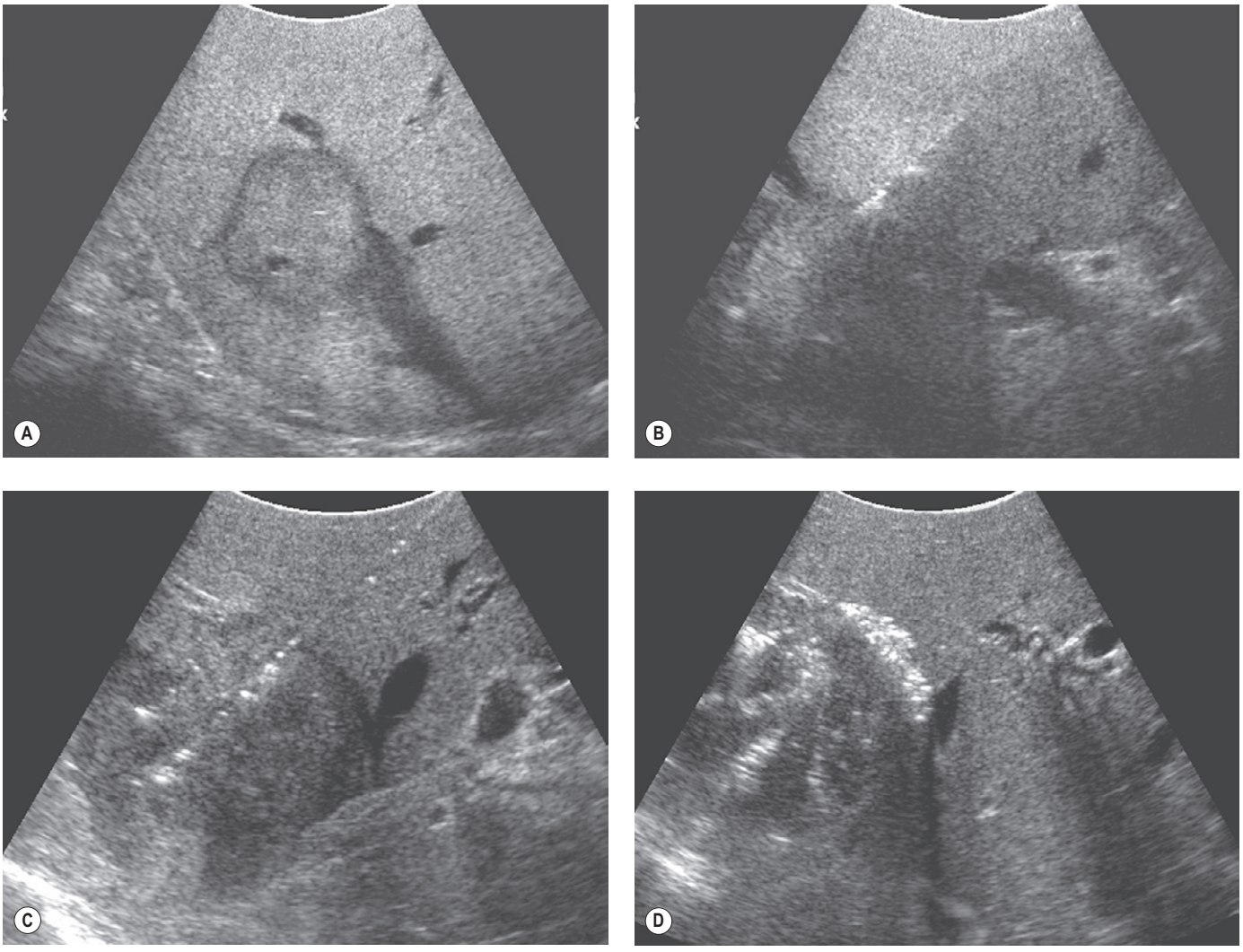


Figure 15.6 A: A metastasis close to the hepatic vein is planned for ablation. **B:** The ablation probe is guided to the lesion using IOUS. **C:** The tines of the RF ablation probe are deployed in the lesion. **D:** Small reflective air bubbles are discharged during the ablation process.

worth considering the delay between preoperative imaging and IOUS. Gaps of over 6 weeks are not unusual in some studies.[19] It may be that this delay accounts for the 'emergence' of some of the smaller lesions, rather than a true superiority of IOUS over preoperative imaging. Nevertheless, this makes an important case for the use of IOUS in cases where delays between preoperative imaging and surgery cannot be avoided.

Surgical planning is clearly dependent on preoperative imaging, and the emphasis on improving preoperative imaging is motivated by the desire to avoid offering patients a laparotomy, only to discover that the volume of hepatic or extrahepatic disease encountered precludes an attempt at curative resection. The evolution of laparoscopic assessment does not solve this problem, as a general anaesthetic and procedure is still obviously best avoided if unnecessary. Significant progress has been made with improved lesion detection for both CT and MRI over the past 20 years.

CT during arterial portography (CTAP) has been demonstrated to have a liver metastasis pick-up rate comparable to IOUS, with a sensitivity rate between 80 and 97%.[20–22] However, it is relatively invasive, with recognised risks of arterial dissection, groin haematoma and pseudoaneurysm formation. It also suffers from a high false positive rate, which has the potential to overstage disease and potentially deny a patient a curative resection, and it has now been largely replaced by improvements in MRI techniques and hardware.

MRI is easy to perform, does not involve radiation and is non-invasive, if you discount the peripheral intravenous injection of contrast medium. It has been shown to be as good at detecting liver metastases as CTAP with a lower false positive rate.[22] There has been some interest as to whether (with improved MRI scanner hardware and techniques) the improved detection of lesions with IOUS still holds true. A relatively recent paper acknowledging improved preoperative MRI indicated that IOUS still provided additional useful information for 47% of patients undergoing hepatic resection.[17] Surgical strategy was altered in 18% of patients based on IOUS findings alone. Identification of sub-centimetre metastatic lesions, lesion characterisation and demonstration of vascular anatomy are cited as major areas to which IOUS contributes. Other groups comparing preoperative MRI and IOUS have shown less impressive differences, with IOUS changing the surgical plan in just 4–11.5% of patients.[5,23] However, many studies fail to take into account the operator and training dependence of ultrasound, and the possible differences in ultrasound detection rates of different qualities and ages of ultrasound equipment, all of which have a potential impact on the accuracy of IOUS. Nevertheless, almost all comparative imaging studies conclude by advocating IOUS as the ultimate determinant of liver lesion quantity, characteristics and anatomical location.

It is foreseeable that with continued improvements to MRI, the now minimal to moderate improved detection rate of IOUS over preoperative imaging will diminish further. The danger, however, is that this will become a self-fulfilling prophecy, with non-sonologists using IOUS with the sole purpose of identifying MRI-detected lesions, for characterisation and demonstration of anatomical relations. To prevent this scenario a dedicated complete survey of the liver by an experienced sonologist is advocated for every case.

Almost all liver lesions missed on preoperative imaging are less than 1.5 cm in diameter.[20] High-resolution IOUS improves the detection rate at this range, but is by no means perfect. Substantial recurrence rates after partial resection indicate that small metastases are still missed by IOUS.[24] When considering the sensitivity and specificity of various imaging modalities, careful consideration must be given to the reference standard. This should be a detailed histopathological examination of the resected specimen. It will often be apparent, however, that resection specimens are laminated transversally in slices of 5 mm thickness for microscopic examination.[24] Lesions smaller than 5 mm in diameter may still be missed by histopathological examination.

Recently, ultrasound contrast agents have been found to improve the detection rate of metastases intraoperatively, in particular sub-centimetre lesions.

Exciting early results have shown CE-IOUS to be significantly more sensitive (96.1%) than CT/MRI (76.7%) and conventional IOUS (81.5%) in detecting liver metastases with histopathology as a reference standard.[7] Ultrasound contrast agents are microbubbles of air or low solubility gas such as perfluorocarbons and sulphur hexafluoride. Metastases show variable contrast take-up in the arterial phase of contrast injection, but are universally hypo-enhancing in the sinusoidal phase (Fig. 15.7). Persistent

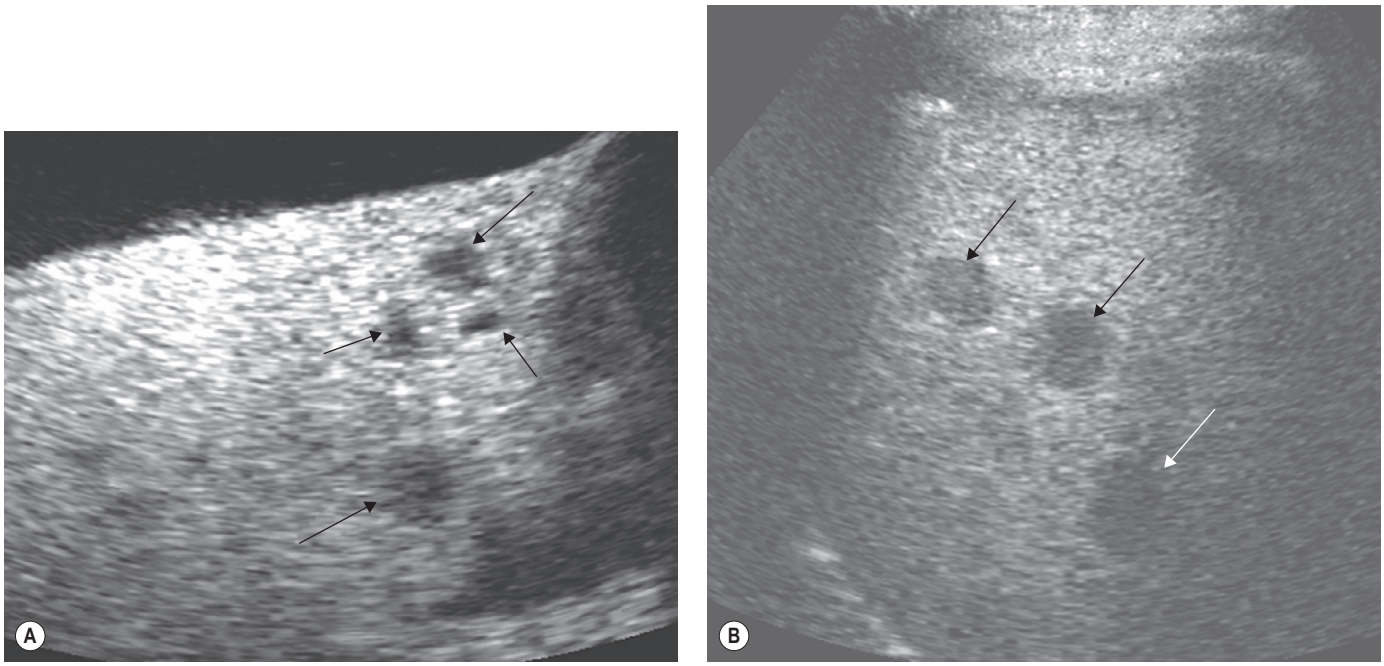


Figure 15.7 **A:** Contrast-enhanced US demonstrates the hypo-enhancing nature of a metastasis during the sinusoidal phase of injection. Small, sub-centimetre lesions can now be seen (arrows). **B:** The normal background liver parenchyma has taken up contrast to become hyperechoic, increasing the contrast resolution between the three metastases (arrows) and normal liver.

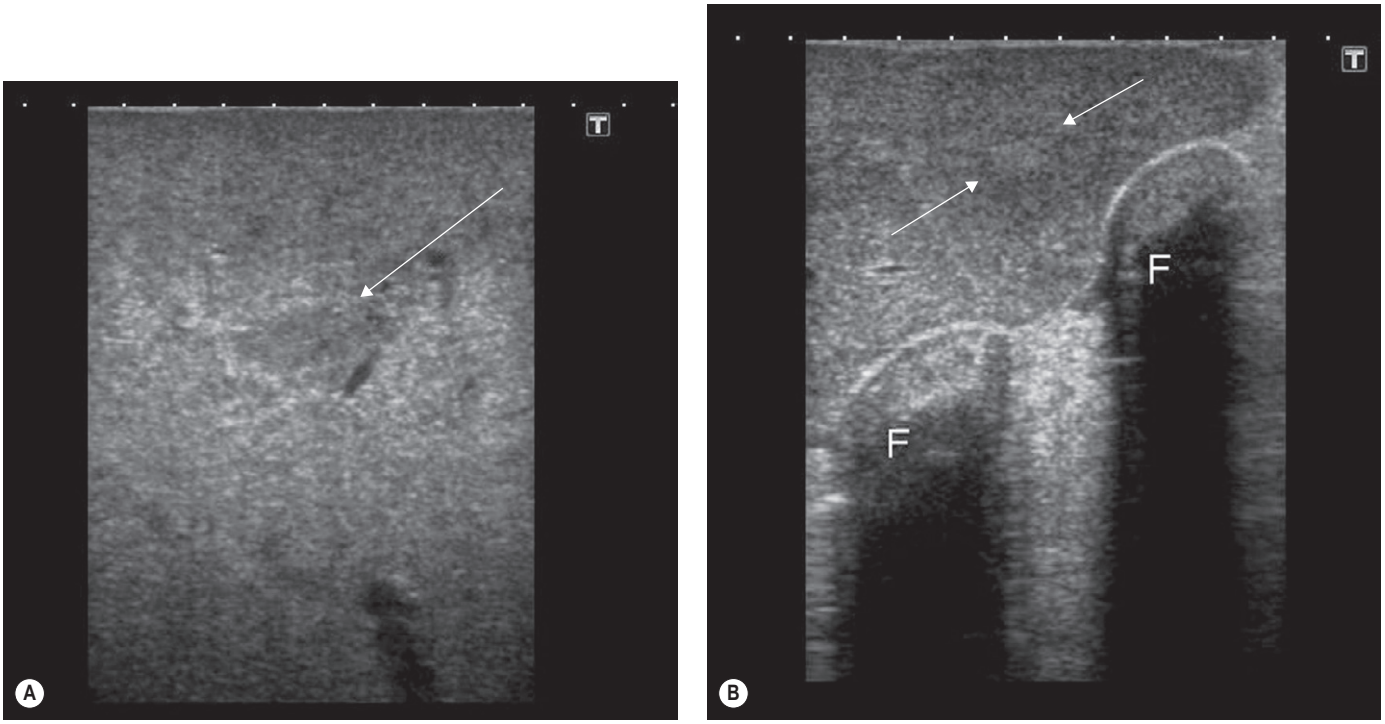


Figure 15.8 **A:** A small metastasis (arrow) is almost isoechoic with the background liver. **B:** The sonographer's fingers (F) palpate a small isoechoic metastasis (arrows) to locate it prior to guided open ablation.

enhancement of the normal liver parenchyma in the late sinusoidal phase can last for several minutes with careful scanning, allowing a comprehensive sonographic survey to be performed.[7,25] Additional lesions detected with CE-IOUS have been shown to have a median diameter of 0.8 cm.[7]

Size is not the only factor when considering liver metastases occult to traditional IOUS. Lesions that are isoechoic with background liver are naturally more difficult to demonstrate (Fig. 15.8). Studies have shown that most liver metastases are hypoechoic, with a minority demonstrating isoechoic features.[10] It may simply be that small isoechoic lesions are not seen with conventional IOUS. Indeed it is estimated that half of all lesions less than 1 cm in size remain undetected with IOUS.[26] CE-IOUS allows for the detection of at least some of these problem lesions, because hypo-enhancement in the portal phase makes them stand out from the background liver. Further evidence is awaited, however. More recent data suggests that although new metastatic lesions can be identified, CE-IOUS has little added value in terms of lesion characterisation over CT and conventional IOUS.[24]

CE-IOUS has been shown to be of benefit for characterising liver nodules in the cirrhotic patient undergoing resection for hepatocellular carcinoma (HCC). The dilemma for the surgeon in these circumstances is that a number of nodules may be present, with the majority representing regenerative nodules rather than dysplastic or HCC nodules. With CEUS, most HCCs exhibit rapid arterialisation followed by sinusoidal hypo-enhancement. However, others may be relatively hypovascular with only minimal sinusoidal hypo-enhancement, and experience shows that variable contrast take-up patterns, together with the often subtle nature of late phase hypo-enhancement, can make it difficult to confidently characterise sub-centimetre lesions. However, characterisation of nodules with CE-IOUS has been shown to be useful, with histopathology confirming that the majority of nodules with different enhancement patterns to background liver parenchyma (particularly arterial hyper-enhancement and early washout) were HCC nodules.[8,27] Studies with longer-term follow-up of the regenerative nodules are required and further studies with demonstration of reproducibility by different centres would support such a classification system.

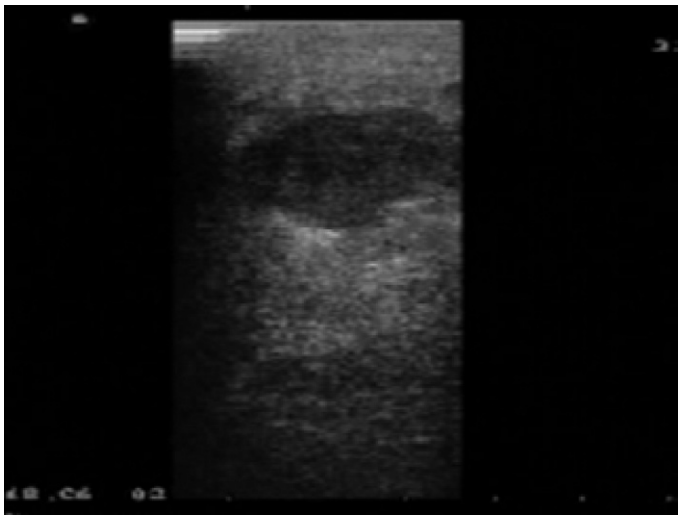


Figure 15.9 **A laparoscopic US image of an HCC**, prior to US-guided ablation.

Demonstration of a significant improvement over the information provided by preoperative imaging would also be needed to justify the potential but remote risks of the contrast agent.

Hepatic resection surgery has seen success with minimally invasive techniques in large centres.[6,28,29] Laparoscopic US enhances initial laparoscopic disease staging, allows for laparoscopic targeted lesion biopsy, facilitates laparoscopic guided radio-frequency ablation (RFA) (Fig. 15.9) and guides minimally invasive liver resection depending on disease volume and location. Further specific roles include demarcation of surgical resection margins, vascular anatomy demonstration and of course, identification of occult lesions. Large studies have demonstrated the benefits of minimally invasive liver resection, achieving reduced overall operating time, reduced blood loss and transfusion requirements, reduced length of hospital stay and reduced complication rates compared to

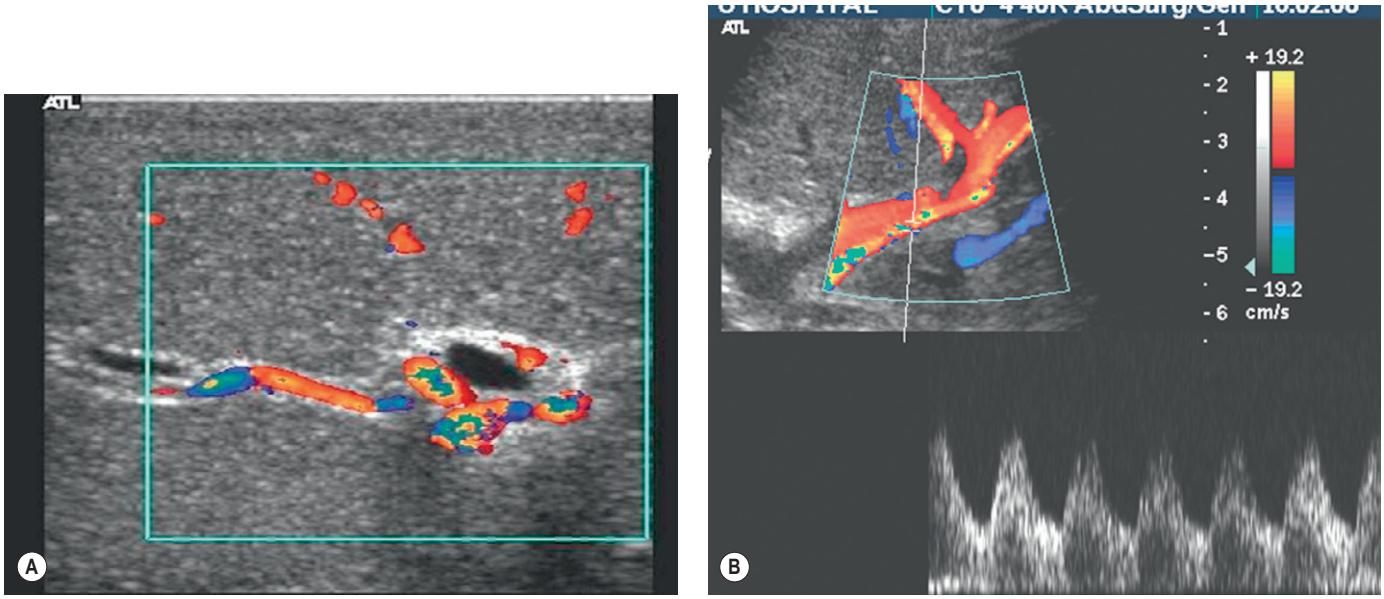


Figure 15.10 **A:** During liver transplant, the main hepatic artery is established as patent with colour Doppler following anastomosis. **B:** Spectral trace of the artery demonstrating normal flow.

equivalent open techniques.[6,28] Inability to bimanually palpate the liver probably places more emphasis on careful laparoscopic US technique, and longer-term follow-up results are awaited.

IOUS is rarely required during liver transplantation, but still has a role in confirming the patency of vascular structures, such as the hepatic artery, following a difficult surgical procedure or when a level of doubt exists (Fig. 15.10).

Pancreas

Islet cell tumours with endocrine activity can present with profound clinical features when tumour volume is still very small. Insulinomas with recurrent episodes of hypoglycaemia and gastrinomas with refractory peptic ulcer disease are prime examples. Small tumours may be radiologically occult, with up to 50% of insulinomas and gastrinomas not showing up on preoperative imaging.[30] Even recent studies have demonstrated a disappointing sensitivity of 63.9% for insulinoma location with modern multislice CT.[31] Once again, IOUS has been advocated as an extension of bimanual palpation at open surgery (Fig. 15.11), and successful location of tumours in up to 96.7% of patients has been demonstrated.[31] Most islet cell tumours are hypoechoic with respect to surrounding pancreatic tissue. Their hypervascular nature allows power and colour Doppler imaging to assist in localisation.[9] IOUS also allows for the detailed assessment of peripancreatic tissues and regional lymph nodes for metastatic disease. A comprehensive survey is required because islet cell tumours are frequently multiple.

Results for laparoscopic US localisation of islet cell tumours have not been as promising, and conversion to open procedures has been deemed necessary for a significant minority of cases. This probably emphasises the benefits of careful bimanual palpation of the pancreas and surrounding duodenum, and also perhaps the inherent difficulty of laparoscopic pancreatic surgery.

Endoscopic ultrasound (EUS) has been shown to have an islet cell tumour detection rate of up to 88%, outperforming CT and MRI as preoperative imaging.[32] Lesions within the body and tail of the pancreas are naturally more difficult to detect with EUS than those in the head of the gland. Conventional open IOUS is still the gold standard imaging modality because pancreatic head lesions are still better dealt with by open surgery, and real-time imaging is invaluable to the surgeon.

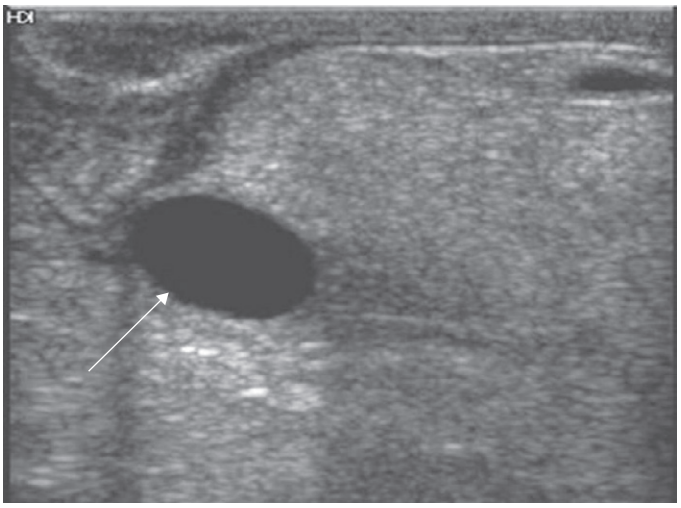


Figure 15.11 **The normal head of pancreas during open surgery**, with the normal common bile duct (arrow).

Biliary tree

Enthusiasts of laparoscopic US suggest that its use to visualise the extrahepatic biliary tree can exclude common bile duct stones and prevent iatrogenic duct injury (Fig. 15.12).[33] Bile duct injury was a particular concern with the original learning curve for laparoscopic cholecystectomy seen in the 1990s, when an increase in this particularly troublesome complication was seen. Laparoscopic US is useful as, apart from the lack of radiation involved, it allows anatomical delineation prior to tissue dissection. However, most surgeons still seem more comfortable with on-table cholangiography (OTC). An OTC requires visual identification of anatomy based on the camera view alone, and considerable tissue dissection is required to get to the point of cystic duct cannulation and fluoroscopy. It is possible for a bile duct injury to occur during this period of pre-OTC laparoscopic dissection.

Certainly, avoiding ionising radiation is sensible, and colour Doppler imaging may be useful in identifying the cystic artery. The

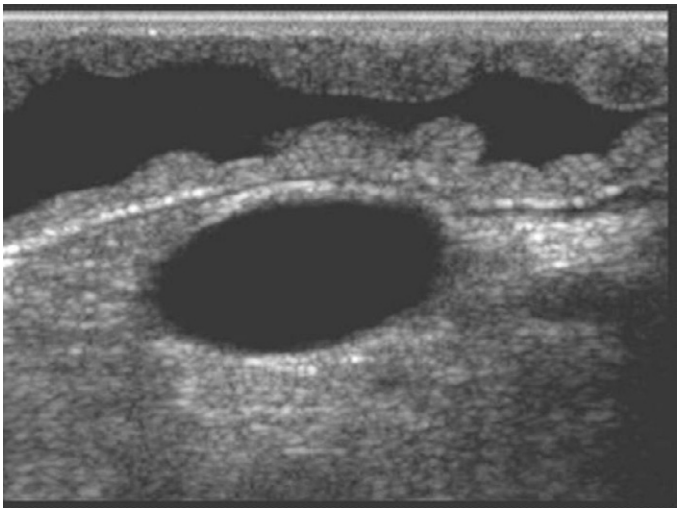


Figure 15.12 Laparoscopic US of the common bile duct seen through a fluid-filled duodenum.

Intraoperative ultrasound

- IOUS provides dynamic real-time imaging for the assessment of predominantly solid-organ oncological disease.
- Direct transducer contact with the organ/s of interest allows higher-frequency scanning than used for percutaneous ultrasound, and produces high-resolution images.
- IOUS is the gold-standard imaging modality for assessing the liver during resection for primary cancer and metastatic disease.
- IOUS demonstrates greater sensitivity than preoperative imaging modalities for detecting small lesions.
- Improvements in preoperative computed tomography and magnetic resonance imaging have reduced the impact of IOUS on surgical planning, although IOUS still retains an improved detection rate.
- IOUS facilitates the real-time assessment of vascular anatomy and surgical dissection planes.
- Laparoscopic IOUS is used to image the liver and other organs as an adjunct to minimally invasive surgery.
- Contrast-enhanced IOUS has shown some early promise of improved liver lesion detection over conventional IOUS.

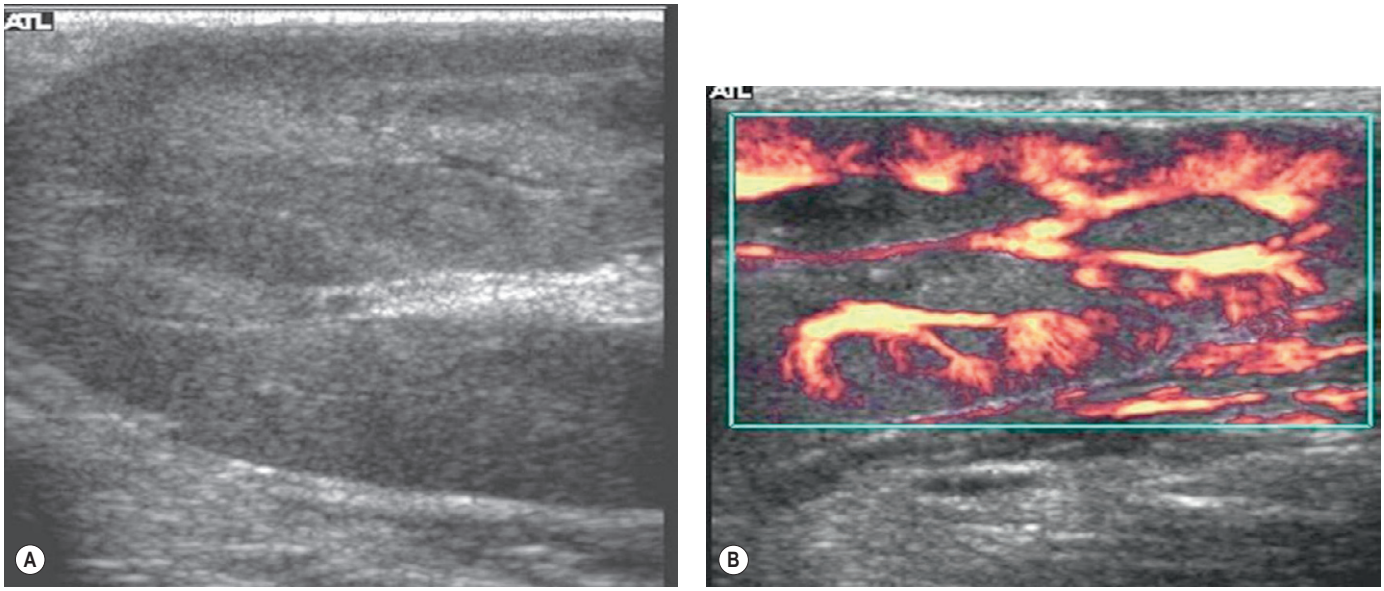


Figure 15.13 A: Transplant kidney on IOUS. **B:** Power Doppler demonstrates good perfusion of the kidney.

learning curve for laparoscopic US of the bile ducts is admittedly slow, however, and it has been shown that this technique cannot completely replace OTC. Unclear visualisation of the bile duct, equivocal determination of bile duct stones, poor anatomical demonstration and technical difficulties with the equipment have all been cited as reasons to proceed to OTC.[33]

Most patients with a clinical or biochemical suspicion of intraductal stones will have had preoperative magnetic resonance cholangiopancreatography (MRCP) or endoscopic retrograde cholangiography (ERCP), where stones can be removed or a sphincterotomy can be performed. Some surgeons still advocate OTC or laparoscopic US, however, especially if there has been a delay between MRCP or ERCP and surgery.

Urology

Surgeons are becoming ever more willing to embrace laparoscopic US, particularly because it is seen as a compensation (at least in part) for the loss of opportunity to palpate organs of interest as traditionally open procedures become laparoscopic. There is already evidence to support the use of conventional IOUS for open nephron-sparing surgery for smaller hereditary renal cancers.[34] The impact of CT-guided RFA on this kind of work is perhaps becoming apparent. Partial adrenalectomy and nephrectomy are guided by laparoscopic US.[35,36] Conventional IOUS with colour Doppler imaging is useful for assessing the vasculature of transplant kidneys (Fig. 15.13).

REFERENCES

1. Kruskal JB, Kane RA. Intraoperative US of the liver: techniques and clinical applications. Radiographics 2006;26:1067–1084.
2. Clarke MP, Kane RA, Steele Jr G, et al. Prospective comparison of preoperative imaging and intraoperative ultrasonography in the detection of liver tumours. Surgery 1989;106:849–855.
3. Boutkan H, Luth W, Meyer S, et al. The impact of intraoperative ultrasonography of the liver on the surgical strategy of patients with

gastrointestinal malignancies and hepatic metastases. Eur J Surg Oncol 1992;18:342–346.
4. Kane RA, Hughes LA, Cua EJ, et al. The impact of intraoperative ultrasonography on surgery for liver neoplasms. J Ultrasound Med 1994;13(1):1–6.
5. Sahani DV, Kalva SP, Tanabe KK, et al. Intraoperative US in patients undergoing surgery for liver neoplasms: comparison with MR imaging. Radiology 2004;232:810–814.
6. Koffron AJ, Auffenberg G, Kung R, Abecassis M. Evaluation of 300 minimally invasive liver resections at a single institution, less is more. Ann Surg 2007;246:385–394.
7. Leen E, Ceccotti P, Moug SJ, et al. Potential value of contrast-enhanced intraoperative ultrasonography during partial hepatectomy for metastases, an essential investigation before resection? Ann Surg 2006;243:236–240.
8. Torzilli G, Palmisano A, Del Fabbro D, et al. Contrast-enhanced intraoperative ultrasonography during surgery for hepatocellular carcinoma in liver cirrhosis: is it useful or useless? A prospective cohort study of our experience. Ann Surg Oncol 2007;14(4): 1347–1355.
9. Kane RA. Intra-operative ultrasound. In: Cosgrove DO, editor. Clinical ultrasound: abdominal and general. 2nd ed. Edinburgh: Churchill Livingstone; 2000. p. 143–164.
10. Coti MA, Kaloma F, de Oliveira ML, et al. Patient variability in intraoperative ultrasonographic characteristics of colorectal liver metastases. Arch Surg 2008;143(1):29–34.
11. Silas AM, Kruskal JB, Kane RA. Intraoperative ultrasound. Radiol Clin North Am 2001;39(3):429–448.
12. Ganguli S, Kruskal JB, Brennan DD, Kane RA. Intraoperative laparoscopic ultrasound. Radiol Clin North Am 2006;44(6):925–935.
13. Jarnagin WR, Bach AM, Winston CB, et al. What is the yield of intraoperative ultrasonography during partial hepatectomy for malignant disease? J Am Coll Surg 2001;192(5):577–583.
14. Gurusamy KS, Aggarwal R, Palanivelu L, Davidson BR. Virtual reality training for surgical trainees in laparoscopic surgery. Cochrane Database Syst Rev 2009;21(1):CD006575.
15. UK Bowel Cancer Incidence Statistics. Cancer Research UK. http://info.cancerresearchuk.org/cancerstats/types/bowel/incidence/
16. Malik HZ, Prasad KR, Halarzun KJ, et al. Preoperative prognostic score for predicting survival after hepatic resection for colorectal liver metastases. Ann Surg 2007;246(5):806–814.
17. Conlon R, Jacobs M, Dasgupta D, Lodge JPA. The value of intraoperative ultrasound during hepatic resection compared with improved preoperative magnetic resonance imaging. Eur J Ultrasound 2003;16:211–216.
18. Gaitini D, Kopelman D, Soudak M, et al. Impact of intraoperative sonography on resection and cryoablation of liver tumours. J Clin Ultrasound 2001;29(5):265–272.
19. Guimaraes CM, Correia MM, Baldisserotto M, et al. Intraoperative ultrasonography of the liver in patients with abdominal tumors. Journal of Ultrasound Med 2004;23:1549–1555.
20. Soyer P, Levesque M, Elias D, et al. Detection of liver metastases from colorectal cancer: comparison of intraoperative US and CT during arterial portography. Abdom Gastrointest Radiol 1992;183:541–544.
21. Nomura K, Kadoya M, Ueda K, et al. Detection of hepatic metastases from colorectal carcinoma: comparison of histopathologic features of anatomically resected liver with results of preoperative imaging. J Clin Gastroenterol 2007;41(8):789–995.
22. Vogl TJ, Schwarz W, Blume S, et al. Preoperative evaluation of malignant liver tumours: comparison of unenhanced and SPIO (Resovist)-enhanced MR imaging with biphasic CTAP and intraoperative US. Eur Radiol 2003;13:262–272.
23. Cerwenka H, Raith J, Bacher H, et al. Is intraoperative ultrasonography during partial hepatectomy still necessary in the age of magnetic resonance imaging? Hepatogastroenterology 2003;50(53): 1539–1541.
24. Fioole B, de Haas RJ, Wicherts DA, et al. Additional value of contrast enhanced intraoperative ultrasound for colorectal liver metastases. Eur J Radiol 2008;67:169–176.
25. Albrecht T, Hohmann J, Oldenburg A, et al. Detection and characterisation of liver metastases. Eur Radiol Suppl 2004;14(8): 25–33.
26. Siosteen AK, Elvin A. Intra-operative uses of contrast-enhanced ultrasound. Eur Radiol Suppl 2004;14(8):87–95.
27. Torzilli G, Olivari N, Moroni E, et al. Contrast-enhanced intraoperative ultrasonography in surgery for hepatocellular carcinoma in cirrhosis. Liver Transpl 2004;10(2–1):34–38.
28. Buell JF, Thomas MT, Rudich S, et al. Experience with more than 500 minimally invasive hepatic procedures. Ann Surg 2008;248(3): 475–486.
29. Lai EC, Tang CN, Ha JP, et al. The evolving influence of laparoscopy and laparoscopic ultrasonography on patients with hepatocellular carcinoma. Am J Surg 2008;196(5):736–740.
30. Zeiger MA, Shawker TH, Norton JA. Use of intraoperative ultrasonography to localize islet cell tumors. World J Surg 1993;17: 448–454.
31. Roland CL, Lo CY, Miller BS, et al. Surgical approach and perioperative complications determine short-term outcomes in patients with insulinoma: results of a bi-institutional study. Ann Surg Oncol 2008;15(12):3532–3537.
32. Liu H, Peng C, Zhang S, et al. Strategy for the surgical management of insulinomas: analysis of 52 cases. Dig Surg 2007;24:463–470.
33. Machi J, Johnson JO, Deziel DJ, et al. The routine use of laparoscopic ultrasound decreases bile duct injury: a multicenter study. Surg Endosc 2009;23(2):384–388.
34. Choyke PL, Pavlovich CP, Daryanan KD, et al. Intraoperative ultrasound during renal parenchymal sparing surgery for hereditary renal cancers: a 10-year experience. J Urol 2001;165:397–400.
35. Ukimura O, Okihara K, Kamoi K, et al. Intraoperative ultrasonography in an era of minimally invasive urology. Int J Urol 2008;15:673–680.
36. Cheng SP, Saunders BD, Gauger PG, Doherty GM. Laparoscopic partial adrenalectomy for bilateral pheochromocytomas. Ann Surg Oncol 2008;15(9):2506–2508.

CHAPTER

16 Pancreas

Zahir Amin

INTRODUCTION 285

ANATOMY 285

SCANNING TECHNIQUE 286
Transabdominal ultrasound 286
Endoscopic ultrasound (EUS) 288
Intraoperative ultrasound 291

NORMAL APPEARANCES 293

ACUTE PANCREATITIS 293
General considerations 293
Aetiology 294
Pathophysiology 294
Clinical features 295
Role of ultrasound 295
Appearances on ultrasound 297
Mild pancreatitis 297
Severe pancreatitis 297
Complications 298
Pancreatic necrosis 298
Pseudocyst 299
Pancreatic phlegmon 299
Infection 299
Portal venous thrombosis 299
Arterial bleeding and pseudoaneurysm 299
Biliary obstruction 299
Gastrointestinal tract obstruction and renal obstruction 300
Intervention 300
Pseudocyst aspiration/drainage 300
Infected necrosis 300
Thrombin injection of pseudoaneurysm 301

CHRONIC PANCREATITIS 301
Imaging 301
Ultrasound and EUS 302

AUTOIMMUNE PANCREATOPATHY 305

PANCREATIC TUMOURS 306
Imaging 306
Differential diagnosis 306
Adenocarcinoma 306
Ultrasound features 306
Cystic neoplasms 311
Serous cystadenoma 311
Mucinous cystic neoplasm 312
Intraductal papillary mucinous neoplasms (IPMN) 312
Solid pseudopapillary neoplasm 312
Management of cystic pancreatic lesion 312
Neuroendocrine tumours (NETs) 313
Imaging NETs 314
Ultrasound 314
Miscellaneous tumours 315
Lymphoma 315
Metastases 315

PANCREATIC BIOPSY 318
Indications 318
Techniques 318
Results 318
Complications 318

PANCREATIC TRANSPLANTATION 319

INTRODUCTION

Major technological advances in all of the imaging modalities have changed their roles in pancreatic imaging.[1–3] Computed tomography (CT) and magnetic resonance imaging (MRI) are the principal modalities used to evaluate pancreatic pathology.[3,4] If clinical suspicion for pancreatic pathology is high, then CT is often the initial test requested rather than ultrasound, because of a significant false negative rate for detecting pancreatic pathology with ultrasound. However, transabdominal ultrasound is still frequently the first imaging modality to detect or infer (if dilated common bile duct) pancreatic pathology. Although the deep posterior position of the pancreas can result in poor or suboptimal ultrasound views because of overlying bowel gas or in large patients,[5] when the pancreas is well seen ultrasound can be a powerful imaging tool for detecting and characterising pancreatic pathology.[6] With modern ultrasound machines, high quality images of the pancreas can be acquired, ultrasound contrast medium is available for enhancement,[7,8] and the image detail may be comparable or superior to CT or MRI.[9] Endoscopic ultrasound is being increasingly used and usually gives very high quality and detailed images of the pancreas – although a relatively invasive test, there is greater availability and expertise, and it now has a useful role for problem-solving and guided aspirations and biopsies.[3,10,11] Therefore, ultrasound still has an important complementary role in evaluating pancreatic pathology.

ANATOMY (Figs 16.1, 16.2)[12,13]

The pancreas is a retroperitoneal organ in the anterior pararenal space, and develops embryologically from the fusion of dorsal and ventral buds. It usually lies in a slightly oblique transverse position at around the level of the first or second lumbar vertebra, but its exact position and size are variable. It is divided into a head, neck, body and tail region.

The head of the pancreas lies most caudally and sits just anterior to the inferior vena cava and inferior to the portal vein. It lies adjacent to the duodenal loop, with the first part of duodenum lying superolaterally, the second part laterally and third part inferiorly. The uncinate process extends from the medial, inferior and posterior part of the head of pancreas and lies posterior to the superior mesenteric vessels. The neck of the pancreas is usually thinner than the rest of the gland and lies anterolateral to the portal vein/superior mesenteric vein (SMV) confluence, and just posterior to the

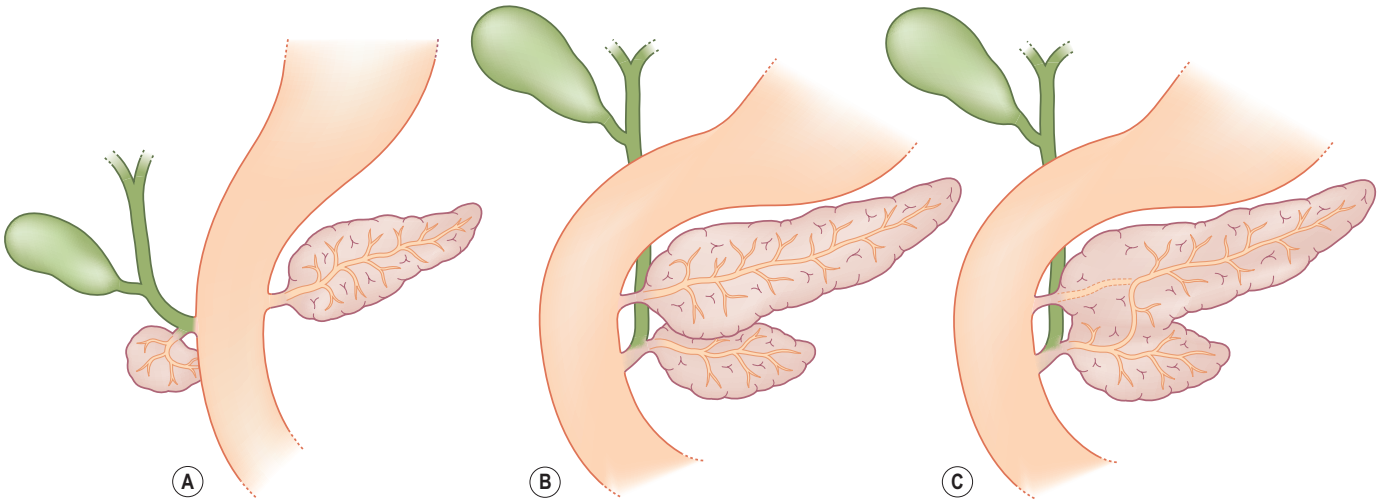


Figure 16.1 Embryological development of the pancreas. A: The dorsal and ventral buds of the pancreas are initially separate. **B:** In the 5-week embryo the ventral bud has migrated around the duodenum to lie close to the dorsal bud. **C:** By week 6, the two buds fuse. The main pancreatic duct is derived from the distal part of the dorsal bud and the proximal part of the ventral bud. The duct connecting the dorsal bud to the duodenum usually degenerates.

Pancreatic imaging

- Pancreatic imaging has improved along with major technological advances.
- CT and MRI are the principal imaging modalities for assessing the pancreas.
- Conventional US still has a significant false negative rate for detecting pancreatic pathology because of its deep posterior position.
- However, when the pancreas is well seen, US may give better detail than CT and MRI.
- Endoscopic US is increasingly available and provides very high quality and detailed pancreatic images.
- US has an important complementary role in evaluating pancreatic pathology.

pylorus; the groove for the gastroduodenal artery separates the head and neck of the pancreas. The body of the pancreas lies in the midline posterior to the gastric antrum/body or left lobe of liver and anterior to the splenic vein. The tail of the pancreas extends laterally to the splenic hilum, anterior to the splenic vein, which is a main anatomical landmark.

The gastroduodenal artery arises from the common hepatic artery and runs along the anterior lateral margin of the neck and head of the pancreas. The common bile duct crosses the anterior surface of the portal vein to the right of the hepatic artery, and passes behind the first part of duodenum to run inferiorly and posteriorly within the head of pancreas. The right hepatic artery may arise from the superior mesenteric artery, and so may be seen passing close to the undersurface of the head of pancreas – this is an important variant for the surgeon planning a resection of the pancreatic head. The splenic artery is very tortuous and runs along the superior margin of the body and tail of the pancreas.

The main pancreatic duct (Wirsung) runs along the length of the gland from the ampulla and tapers towards the pancreatic tail. In 40–50% of cases an accessory duct (Santorini) may be present, passing laterally from the main duct in the head of pancreas to an accessory papilla in the duodenum just above the level of the ampulla. In 5–10% of the population the dorsal and ventral parts of the pancreas fail to completely fuse, resulting in complete or incomplete pancreas divisum with a small ventral duct in the separate head of pancreas and a larger main dorsal duct extending from the accessory papilla to the pancreatic tail[14,15] – in incomplete pancreas divisum a thin branch just connects dorsal and ventral ducts.[15] Most patients with pancreas divisum are asymptomatic but some patients may have stenosis and partial obstruction at the accessory papilla, resulting in poor drainage which may cause acute or chronic pancreatitis or pancreatic type pain.[16] Annular pancreas can also occur with failure of dorsal/ventral fusion, and the ventral pancreas then partially encases and narrows the second part of duodenum.[17]

SCANNING TECHNIQUE

These include conventional transabdominal ultrasound, endoscopic ultrasound and intraoperative/laparoscopic ultrasound. With all these techniques, the texture, size and contour of the pancreas should be evaluated, and the pancreatic duct, distal common bile duct, splenic/superior mesenteric/portal veins, and the coeliac axis/superior mesenteric artery identified.

Transabdominal ultrasound

Although the image of the pancreas that can be obtained has improved considerably over recent years with improvements in machine and transducer technology, the technique, skill and persistence of the ultrasonographer is the most important aspect of good pancreatic ultrasound. This will also depend on patient size, depth of the pancreas and overlying bowel gas. However, even in large patients, it can be worthwhile trying to image the pancreas since with transducer pressure, good views of the pancreas are still possible with ultrasound (Fig. 16.3).

Patient fasting prior to abdominal ultrasound ensures an empty stomach, allowing compression and apposition of the walls of the gastric antrum and visualisation of the body and neck of the pancreas (Fig. 16.2A). Water or a solution containing cellulose particles or simethicone can be given to the patient to fill the stomach and provide an acoustic window to the pancreas[18] (Fig. 16.4). A gradual increase in transducer pressure may displace gas-filled bowel loops, with the image nearly always improving during the ultrasound examination (Fig. 16.5).

Optimising ultrasound views of the pancreas varies between patients but includes transverse, longitudinal and angled oblique scans. Techniques to further improve the images include scanning

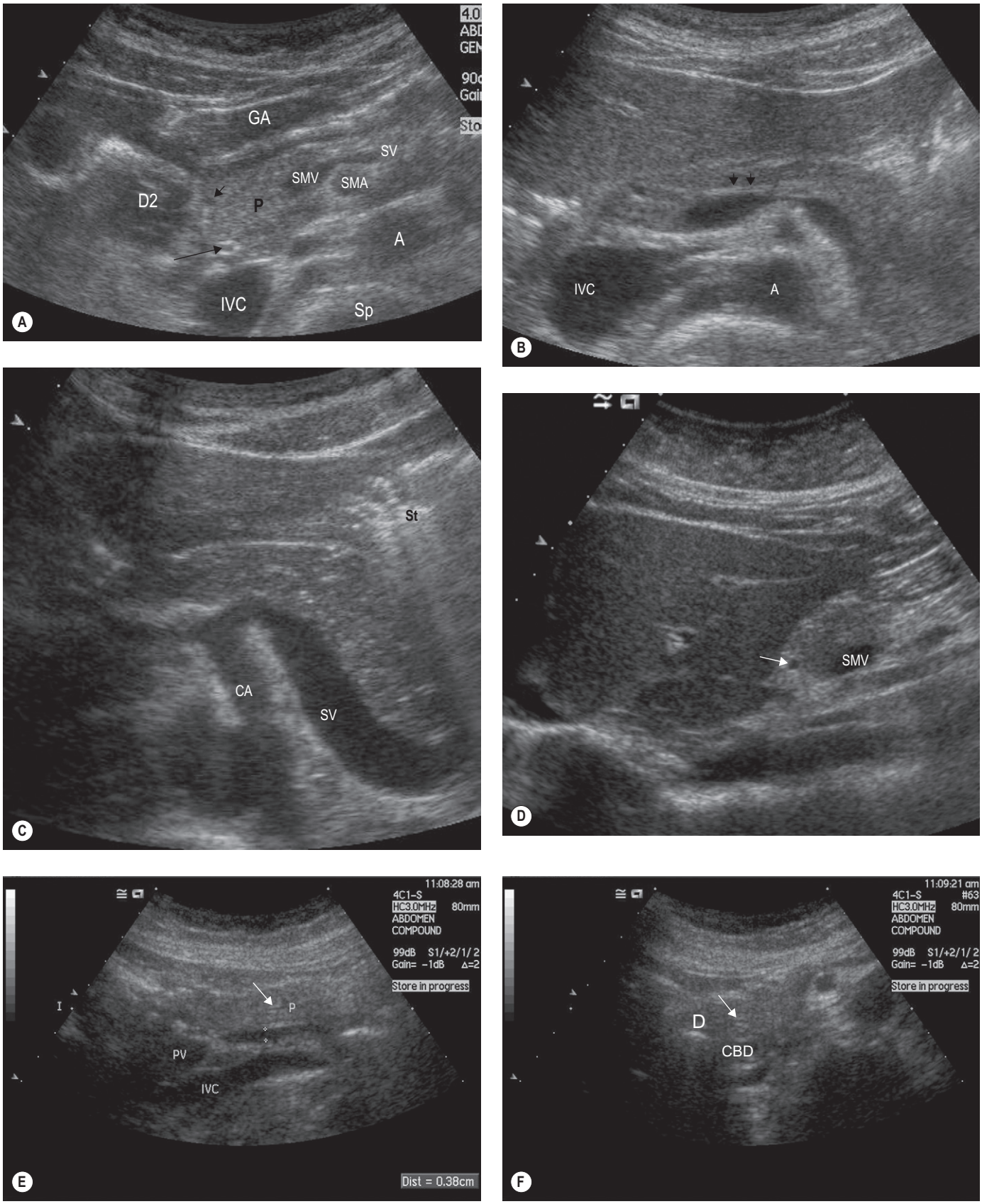


Figure 16.2 **Normal pancreas. A:** The pancreatic head (P) lies anterior to the inferior vena cava (IVC), posterior to the gastric antrum (GA) and medial to the second part of duodenum (D2). Both the gastroduodenal artery (short arrow) and common bile duct are shown (long arrow). **B:** More superior view showing the neck, body and part of the tail of pancreas posterior to the left lobe of liver with a normal thin pancreatic duct just visible (arrows). **C:** The pancreatic tail is seen lying anterior to the splenic vein (SV). **D:** Sagittal view of the body of pancreas posterior to the liver and anterior to the SMV. The hepatic artery is seen (arrow). **E:** More lateral oblique sagittal view of the head of pancreas (P), showing the CBD, portal vein (PV) and also the pancreatic duct (arrow). **F:** Inferior head of pancreas close to the ampulla. The pancreatic duct (arrow) is anterior to the CBD, close to the duodenum (D), appearances suggestive of pancreas divisum. A, aorta; IVC, inferior vena cava; SMV, superior mesenteric vein; SV, splenic vein; SMA, superior mesenteric artery; CA, coeliac axis; Sp, spine, St, stomach.

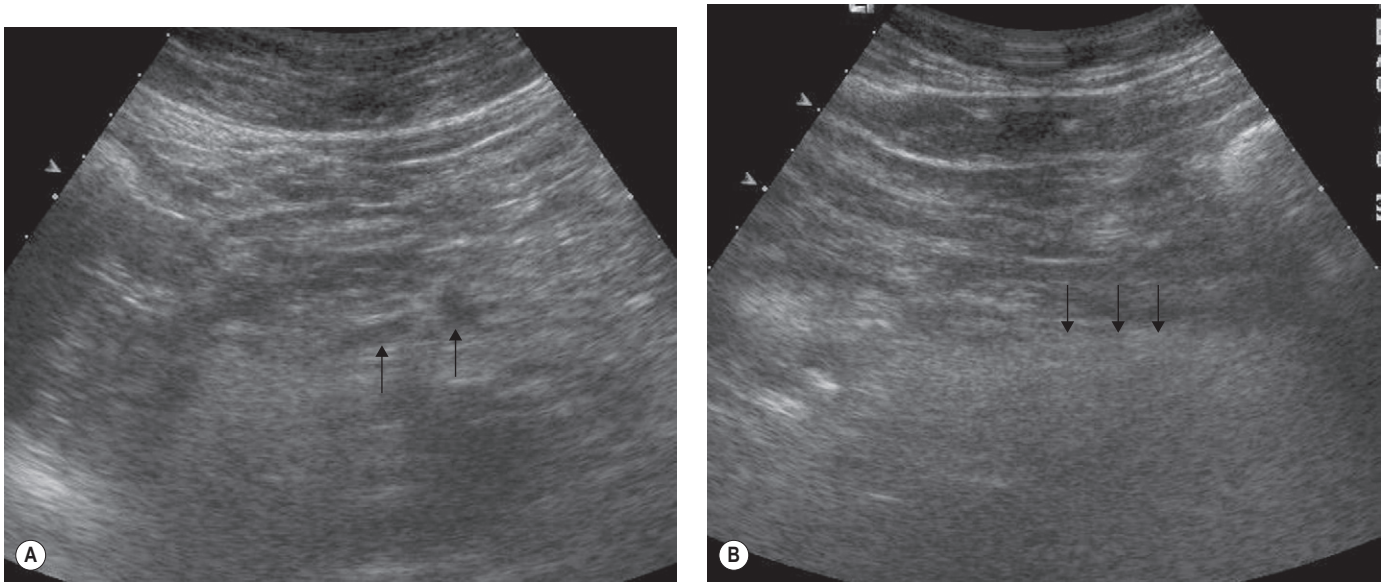


Figure 16.3 Large patient. A: Head of pancreas seen as a deep echogenic structure just lateral to the mesenteric vessels (arrows). **B:** More superiorly the echogenic body of pancreas is outlined (arrows).



Figure 16.4 Water in gastric antrum. Optimum imaging of the neck of pancreas with water providing a good acoustic window between the liver and pancreas.

during suspended inspiration or expiration, and changing the patient's position to left or right decubitus, and sometimes standing.

The head/uncinate, neck, body and tail of pancreas should be identified (Fig. 16.2). The pancreatic tail may be well seen through the spleen (Fig. 16.6), usually in thin patients, and part of the tail may be seen anteriorly through gastric body/fundus (Fig. 16.2C). In larger patients the margins of the pancreas can be difficult to locate and define, but using the mesenteric vessels as landmarks can help define the head of the pancreas, after which the neck, body and tail may become easier to visualise (Fig. 16.3).

Multifrequency transducers are now routinely available with modern machines and allow the pancreas to be imaged with the correct frequency for any depth.

Image quality can be improved with a variety of new techniques mostly requiring a single push of a button on the ultrasound (US) machine – compound and harmonic imaging reduce acoustic noise and result in improved spatial/contrast resolution and border detection;[19] in pancreatic imaging these techniques result in better lesion conspicuity and fluid–solid differentiation (Fig. 16.7). Other techniques such as panoramic US, photopic US and 3D/4D US also improve image display, but their role in pancreatic imaging is not yet clear.[6,19]

Colour Doppler evaluation is an integral part of ultrasound of the pancreas, and can be useful in assessing vascular involvement by pancreatic masses, or occluded veins as a result of pancreatitis[20] (Fig. 16.8).

Contrast-enhancement with SonoVue is not widely used for assessing pancreatic pathology, but several recent publications suggest a useful role in characterising pancreatic tumours by differentiating hypervascular neuroendocrine tumours from hypovascular adenocarcinoma (Fig. 16.9), and also in assessing vessels and parenchymal necrosis in pancreatitis.[7,8] However, in practice CT and MRI are preferred imaging modalities for these indications, and obtaining good quality ultrasound images in patients with pancreatitis is likely to be limited by abdominal tenderness and presence of a small bowel ileus.

Ultrasound elastography has recently been reported – this assesses tissue rigidity by tracking tissue movement during compression or in response to external vibration; initial reports have suggested it may have a role in the differential diagnosis of a focal pancreatic mass, especially focal pancreatitis versus pancreatic cancer.[21]

Endoscopic ultrasound (EUS)

Ultrasound transducers incorporated into the tip of endoscopes allow high quality ultrasound images of the gut wall and adjacent structures. This technique has been available since the 1980s, but has been more widely used over the past decade.[22–24] Two main types of echo-endoscopes are available – radial mechanical (360° image perpendicular to endoscope), or electronic with the option of a radial 270° image probe or a linear array probe (image along line of endoscope).[25,26] The electronic radial and linear array probes

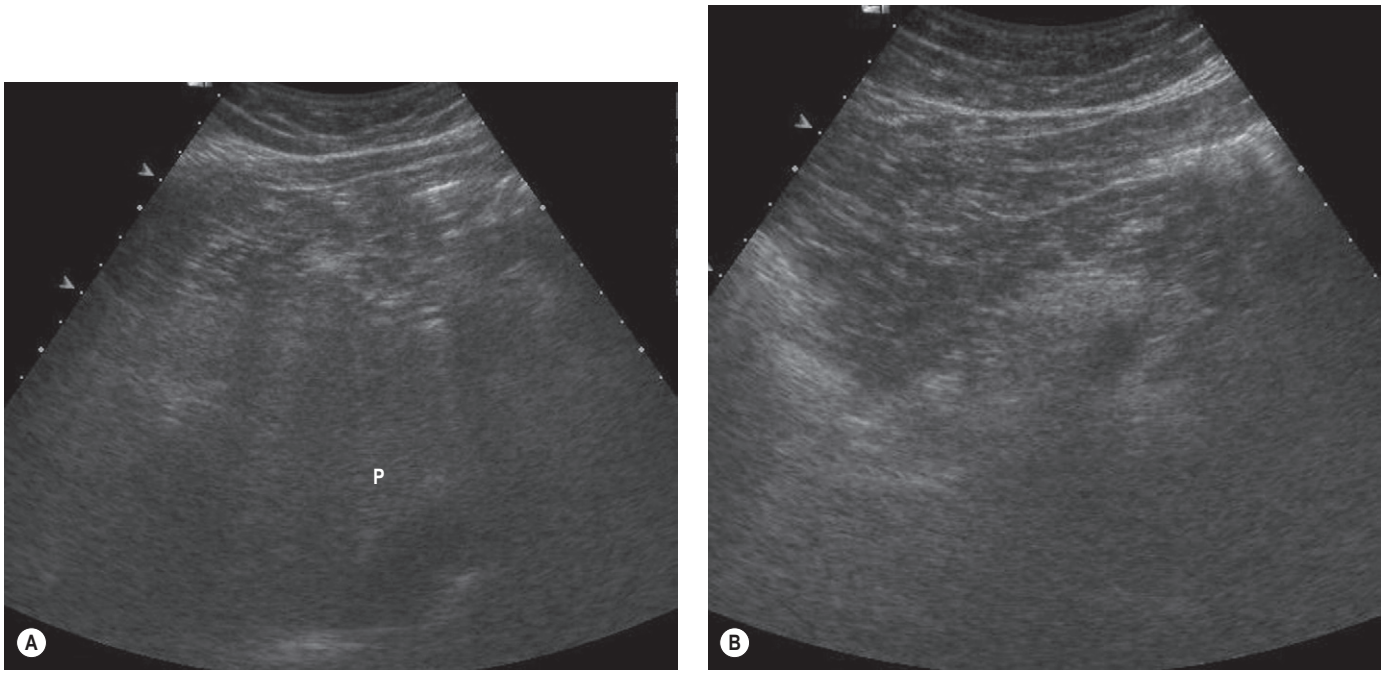


Figure 16.5 **Compression ultrasound. A:** Poor view of head of pancreas (P) before transducer pressure. **B:** Improved image of pancreatic head after transducer pressure.

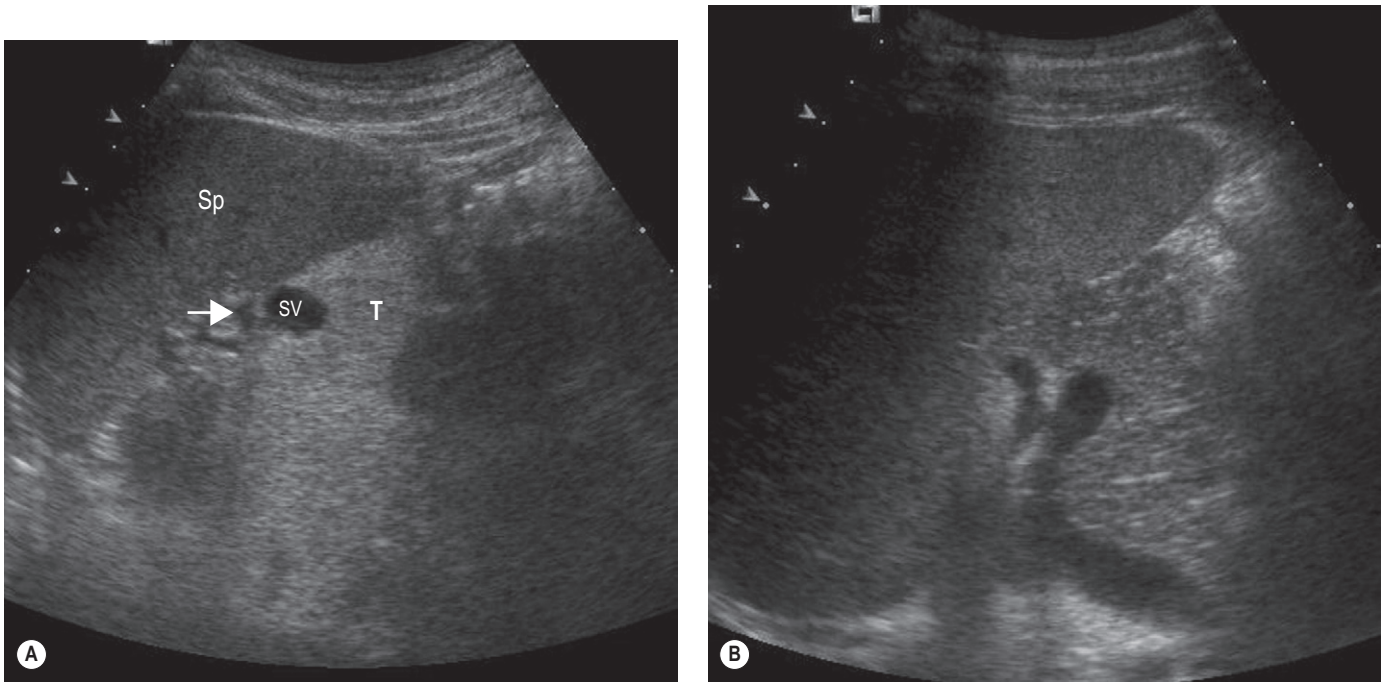


Figure 16.6 **Pancreatic tail. A:** Pancreatic tail (T) seen through the spleen (Sp), lying anterior to the splenic vein (SV) and artery (arrow). **B:** In a younger patient the tail appears more hypoechoic.

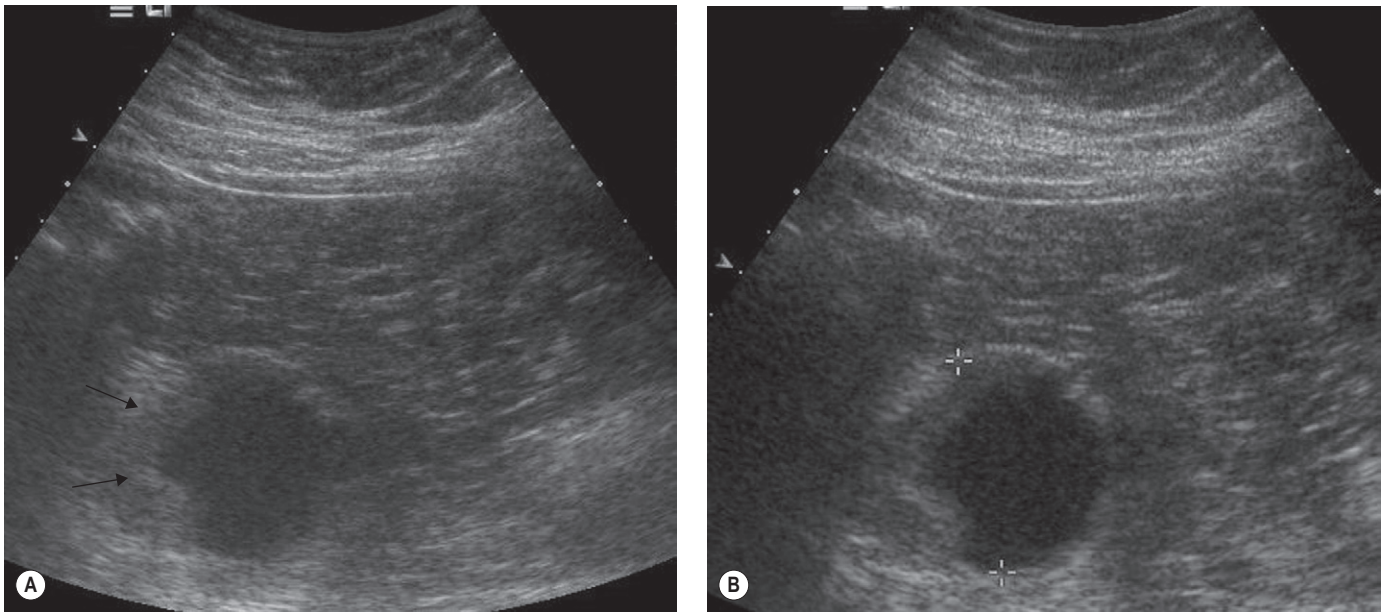


Figure 16.7 Harmonic imaging. A: Mucinous cystic neoplasm in tail of pancreas with eccentric wall thickening (arrows). **B:** With harmonic imaging there is reduced noise and a sharper image, with clearer solid/fluid differentiation.

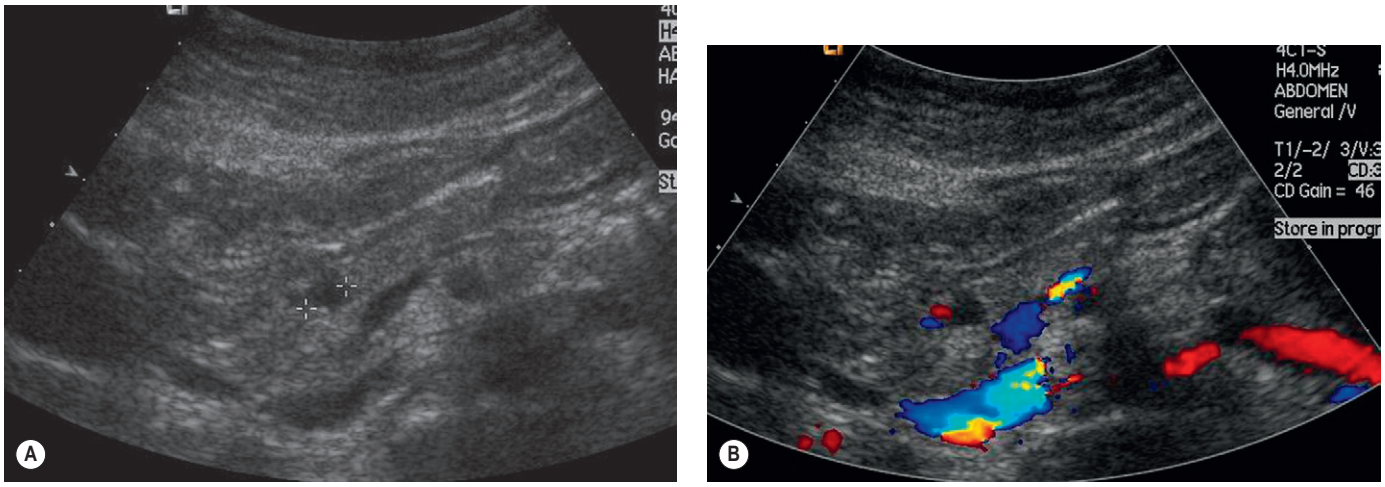


Figure 16.8 Colour Doppler. A: Small cyst in the neck of pancreas (between cursors) of similar echogenicity to adjacent vessels. **B:** Colour Doppler allows differentiation of cyst and vessels.

allow colour Doppler to differentiate vessels from cystic lesions. The linear array probe allows needle-guided aspirations and biopsies (Fig. 16.10). A balloon over the transducer tip can be distended with water to improve acoustic contact between transducer and gut wall. The close proximity between pancreas and stomach/duodenal wall means that high frequencies can be used to get detailed high-resolution images of the pancreas and pancreatic duct down to under 1 mm (Fig. 16.11). The range of frequencies available are usually 5–12 MHz, the lower frequency allowing greater depth of imaging away from the gut wall, up to about 7 cm.

After passing the echo-endoscope into the stomach and duodenum, the air is removed during slow withdrawal. Gentle tip angulation and rotation is used to optimise views of the pancreas. The uncinate process is seen from the third part of the duodenum; most of the head of pancreas from the second part of the duodenum and the body and tail of pancreas can be visualised through the stomach (Fig. 16.11).

Although occasionally used as a primary diagnostic/assessment, EUS is best used for targeted problem-solving or for EUS fine-needle aspiration (FNA)/biopsy after the patient has been imaged less invasively by CT or MRI[10,27] (Fig. 16.12). Since EUS is often performed at more specialist referral centres, a common problem is that CT or MRI is not available at the time of the EUS, and this inevitably makes the test less useful. EUS is best viewed as complementary to CT and/or MRI.[27,28] There are still limited training centres for EUS, and learning pancreatic EUS is considerably more difficult and demanding compared to oesophageal EUS.[22,29]

Increasingly, with high quality US/CT/MRI, EUS is used as an interventional tool for biopsy of lesions adjacent to the oesophagus, stomach and duodenum, or for guided drainage of adjacent collections such as pseudocysts, or for coeliac axis block.[10,26,27] Although very high sensitivities have been reported for EUS FNA, the number of false negatives and inadequate samples can be relatively high, resulting in the biopsy being repeated either by EUS or under US or CT guidance.[30]

Miniprobes are also available – these are tiny transducers fixed to the tip of thin 2–4 mm diameter catheters. They are not very

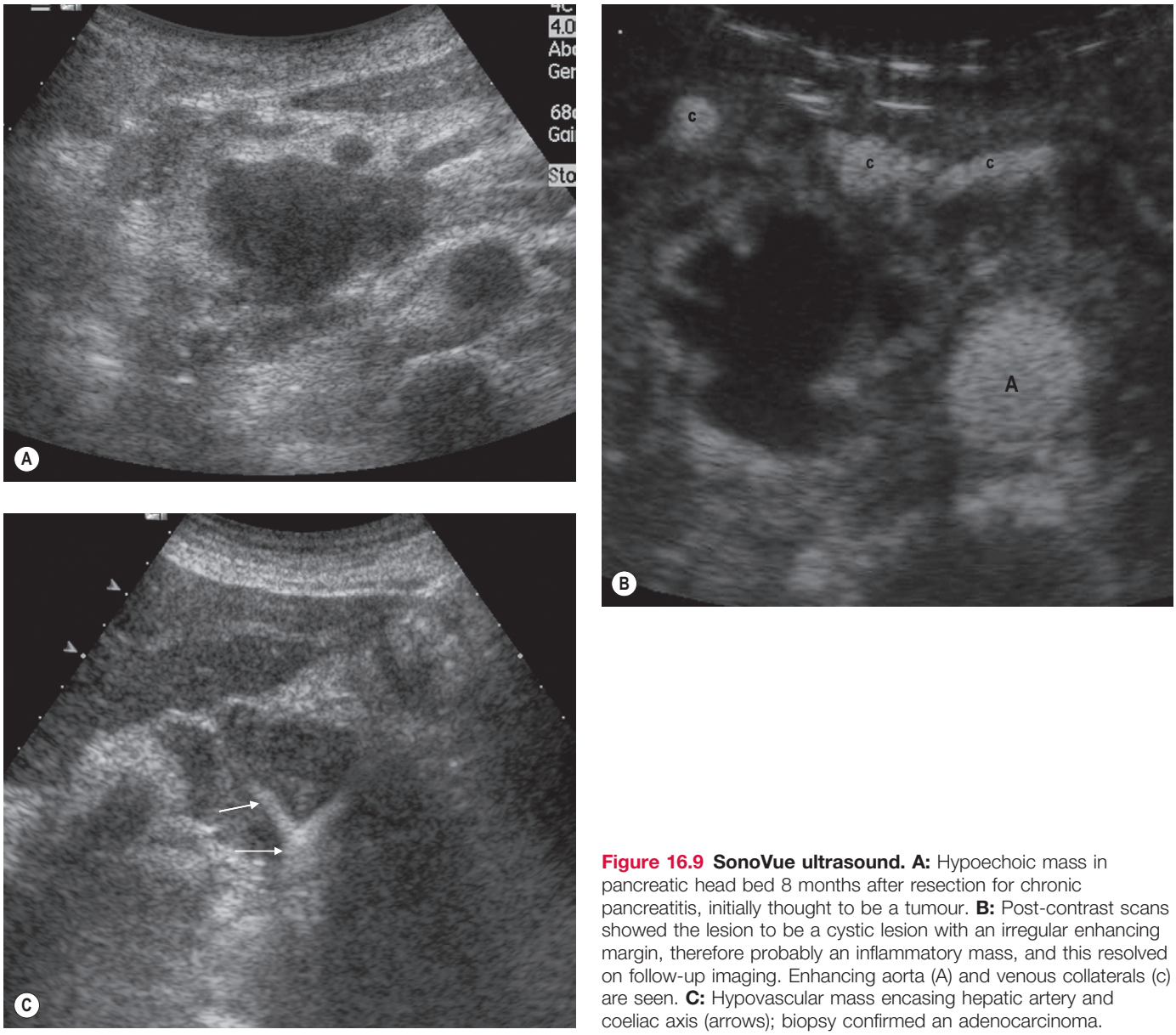


Figure 16.9 **SonoVue ultrasound. A:** Hypoechoic mass in pancreatic head bed 8 months after resection for chronic pancreatitis, initially thought to be a tumour. **B:** Post-contrast scans showed the lesion to be a cystic lesion with an irregular enhancing margin, therefore probably an inflammatory mass, and this resolved on follow-up imaging. Enhancing aorta (A) and venous collaterals (c) are seen. **C:** Hypovascular mass encasing hepatic artery and coeliac axis (arrows); biopsy confirmed an adenocarcinoma.

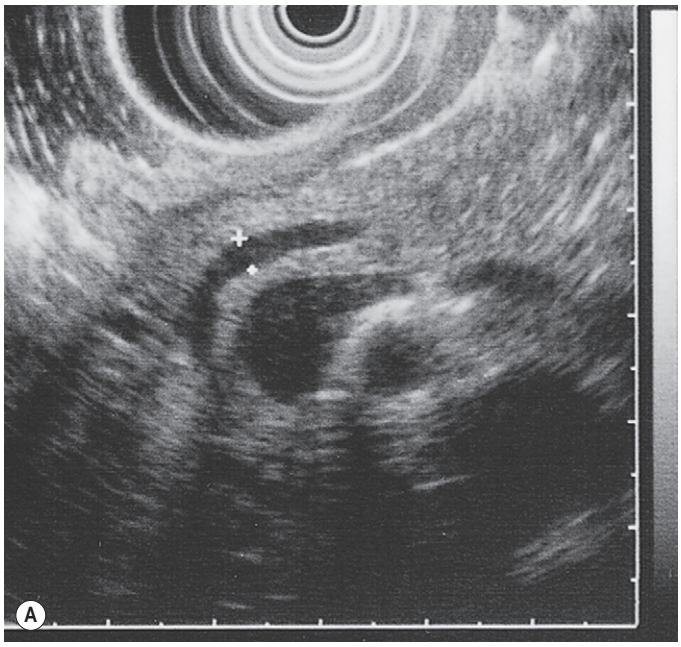


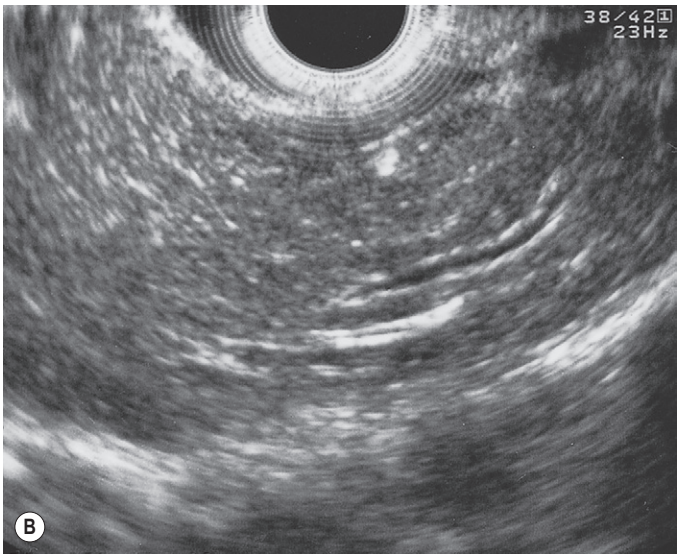
Figure 16.10 **EUS.** Linear array probe with balloon over the tip of the transducer and aspiration needle shown through the working channel of the echo-endoscope.

robust, but can be passed down the working channel of endoscopes and then into the bile duct or pancreatic duct to give detailed morphology within a few millimetres of the transducer using very high frequencies of about 20 MHz – they may have a role in differentiating intraductal stones from tumour masses, but their practical use is very limited.[31]

Intraoperative ultrasound

High-frequency linear array probes (7.5–10 MHz), covered with a sterile plastic sheath and held against the pancreas at laparotomy, provide very good images of the pancreas and pancreatic duct.[32] Transducers at the tip of laparoscopes are also being increasingly used to provide high quality images[33] (Fig. 16.13). Filling the lesser sac with fluid may improve more superficial resolution. The need for the presence of a radiologist during intraoperative scanning is diminishing, since many surgeons using these techniques have been trained in their use.





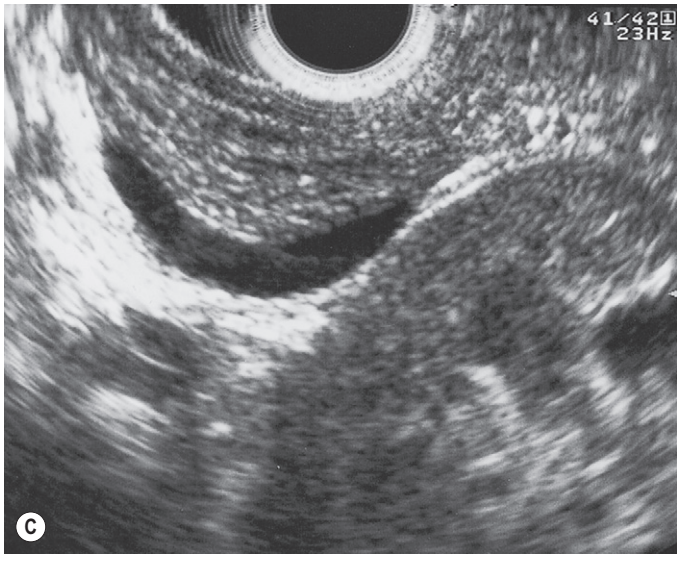
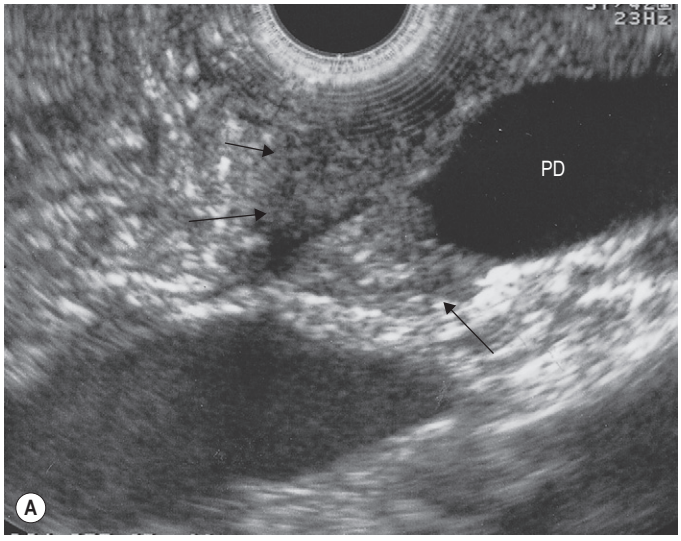


Figure 16.11 EUS normal pancreas. A: Neck of pancreas with a slightly dilated pancreatic duct. **B:** Body of pancreas with a normal pancreatic duct. **C:** Pancreatic tail close to the left kidney.



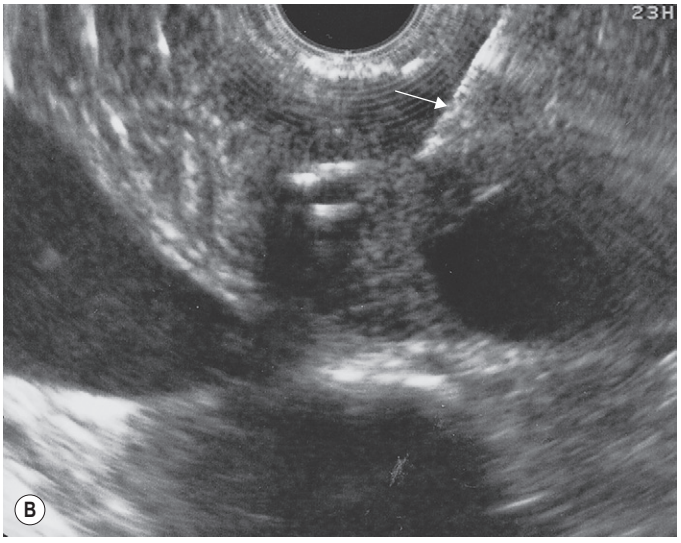


Figure 16.12 EUS ampullary mass. A: Small mass (arrows) at the ampulla not seen on CT, blocking and dilating the pancreatic duct (PD). **B:** Needle (arrow) inserted into the mass between the bile duct stent and blocked pancreatic duct, for aspiration cytology.

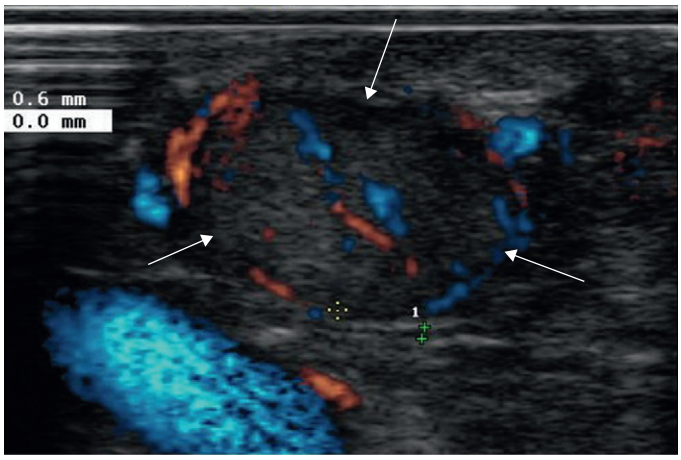


Figure 16.13 Laparoscopic ultrasound. Small insulinoma (arrows) with increased vascularity on colour Doppler lying just adjacent to a normal pancreatic duct (between small cursors). (Courtesy of Dr Adrian Lim.)



Figure 16.14 Normal pancreatic tail. Appears prominent but normal.

Scanning techniques

- US assessment of the pancreas should include its parenchymal texture, size and contour, the pancreatic and bile ducts, the coeliac axis, portal vein and superior mesenteric vessels.
- Good technique, experience and persistence of the ultrasonographer all contribute in the assessment of the pancreas with US.
- Even in large patients, transducer compression can result in good US views of the pancreas.
- Pancreatic US views can be improved by filling the stomach with water, alterations in patient breathing and position, harmonic imaging, and colour Doppler to define the vessels.
- Contrast-enhanced US has a limited role in pancreatic US – it may be useful in characterising the nature of a pancreatic mass if well seen.

The main indications for intraoperative scanning are detection of small insulinomas and intraductal papillary mucinous tumours, and defining the anatomy and position of the pancreatic duct during duct drainage procedures.[34,35]

NORMAL APPEARANCES

The normal size of the pancreas is variable, and measurements are not usually made; more important than actual size of the pancreas is any focal or diffuse change in echogenicity or duct calibre. However, the presence of parenchymal atrophy is important. The maximum measurement of the head of pancreas is about 2.5 cm, the neck <1 cm, the body 1.5 cm, and the tail 3.5 cm. The normal tail of pancreas can appear focally enlarged and is not infrequently called abnormal if well seen on ultrasound (Fig. 16.14).

The pancreas is typically homogeneous, and slightly more echogenic than liver.[36] The echogenicity is related to the degree of fat deposition[37] and is variable; younger patients tend to have a hypoechoic pancreas and older patients have a hyperechoic pancreas with increased fat replacement[38] (Figs 16.6 and 16.15); the latter also occurs in obesity, with steroid ingestion, in Cushing's syndrome and with cystic fibrosis.[39,40] The pancreas can be as echogenic as retroperitoneal fat in up to 35% of cases.[41] The parenchyma may be heterogeneous with hyperechoic stranding (Fig. 16.16), especially in older patients.[42] The margins of the pancreas are usually well defined but lobulated.

If the pancreas is well seen on ultrasound then the main pancreatic duct is usually visible in the neck/body region (Figs 16.11A and 16.17). The size of the duct increases with age, up to a maximum of 3 mm;[43]; up to age 30 years the mean duct diameter has been reported as 1.5 mm, and in those over 80 years the mean diameter is 2.3 mm.[44] However, duct diameters of up to 5 mm may be seen in elderly people.[41]

Ultrasound assessment of the pancreatic duct following secretin (1 iu/kg) stimulation has been reported.[44,45] In one study, younger patients' duct increased from 1.6 mm to 3.1 mm, and older patients' from 1.9 mm to 3.5 mm.[44] A suboptimal response suggests pancreatic insufficiency and a greater duct dilatation suggests obstruction of the duct. However, ultrasound assessment after secretin stimulation will only be used occasionally in most centres if the patient is unable to have secretin-stimulated magnetic resonance cholangiopancreatography (MRCP) or even CT, since these tests will usually give better and more consistent images of the pancreatic duct as well as duodenal secretions.

Pancreas divisum is usually a difficult diagnosis to make on ultrasound but may be suggested if the pancreatic duct is dilated and can be followed from the body/neck to its insertion into the duodenum separate from the common bile duct (CBD), cranial and ventral to the ampulla (where CBD inserts). However, the often thin communication between dorsal and ventral pancreatic ducts will not be seen on ultrasound, so the diagnosis of divisum can only be suggested rather than confirmed (Fig. 16.2F).

A relatively common normal variant is a hypoechoic posterior head/uncinate process of pancreas, due to focal fatty sparing of the ventral pancreas[46] (Fig. 16.18). Although it can mimic a mass, there is no duct dilatation or real mass effect and the diagnosis can usually be made on ultrasound. It has been reported to be present in 30–40% of patients having abdominal US,[47] and up to 75% of patients undergoing EUS.[48]

ACUTE PANCREATITIS

General considerations

Acute pancreatitis is acute inflammation of the pancreas with acute abdominal pain and raised serum amylase or lipase, the latter

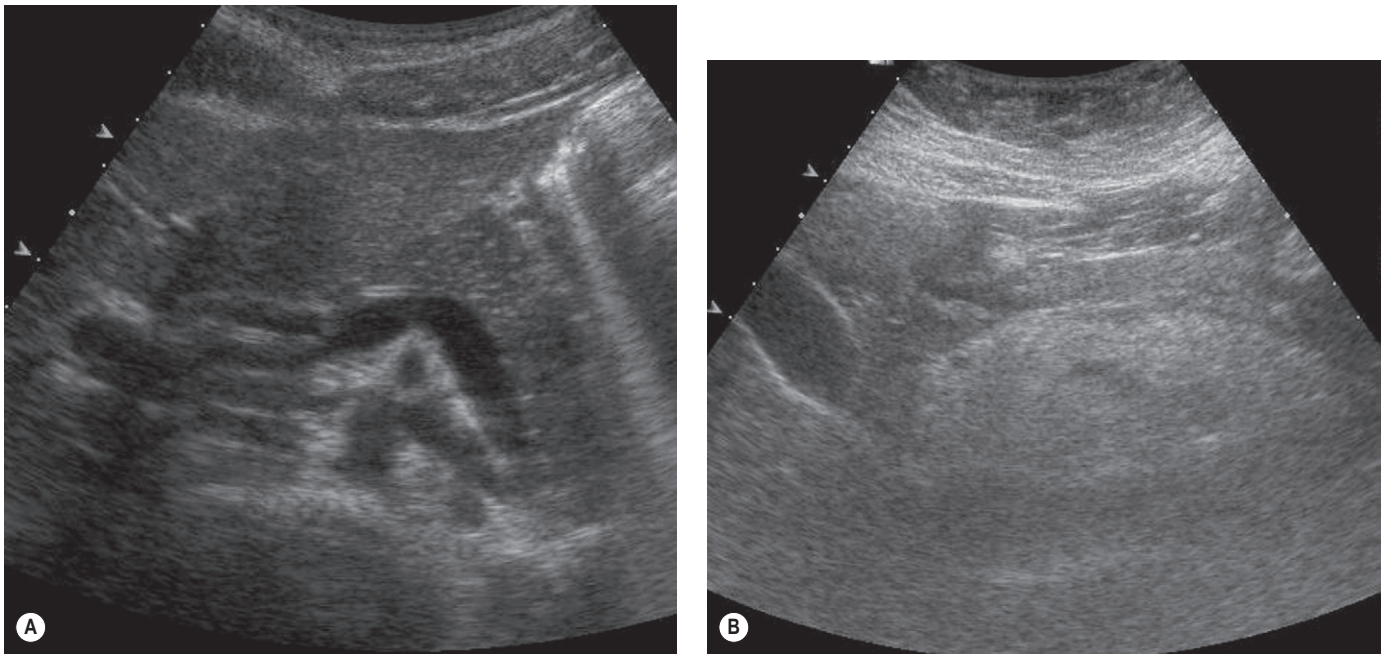


Figure 16.15 Pancreas. A: Normal hypoechoic pancreatic body/tail. **B:** Normal echogenic pancreas.



Figure 16.16 Hyperechoic stranding. Thin pancreatic duct between cursors, and the adjacent parenchyma of the body of pancreas has several prominent and short linear echoes.

(lipase) being more specific for pancreatic inflammation and persisting for longer.[49,50] There is oedema, necrosis and haemorrhage of pancreatic and peripancreatic tissue, with variable involvement of other regional and remote tissues. This may be mild with interstitial pancreatic oedema, or severe with local necrosis, fluid collections and systemic complications.[51]

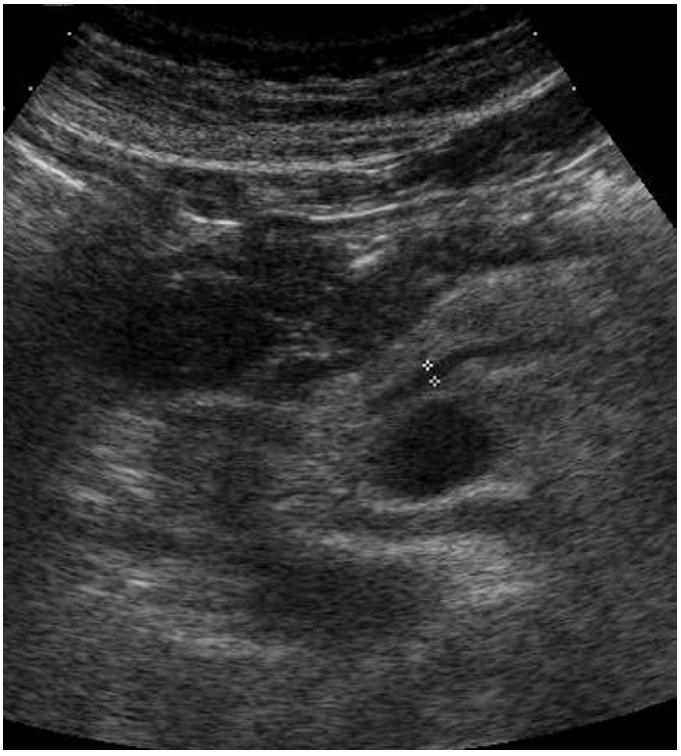


Figure 16.17 Pancreatic duct. This is thin and lies between the cursors in the neck and body of pancreas.

Aetiology

Gallstones are the commonest cause (in about 50% of cases), including occult stones, microlithiasis and sludge.[49] Alcohol is the second commonest cause, in 20–25% of cases.[52,53] Other causes include raised lipids, hypercalcaemia, endoscopic retrograde cholangiopancreatography (ERCP), trauma, viral infections, and various drugs.[49,52] In 20–25% of cases no cause is found and these are labelled 'idiopathic'.[52]

Pathophysiology

This is not clearly understood, but several factors initiate inflammation.[54] These include overdistension of the pancreatic duct (by obstruction or reflux of bile/duodenal contents), alcohol (protein plugs form in ducts) and other toxins, hypertriglyceridaemia and hypercalcaemia.[55] The end result is a release of activated and destructive pancreatic enzymes into the pancreas and surrounding tissues. This may lead to changes ranging from mild interstitial

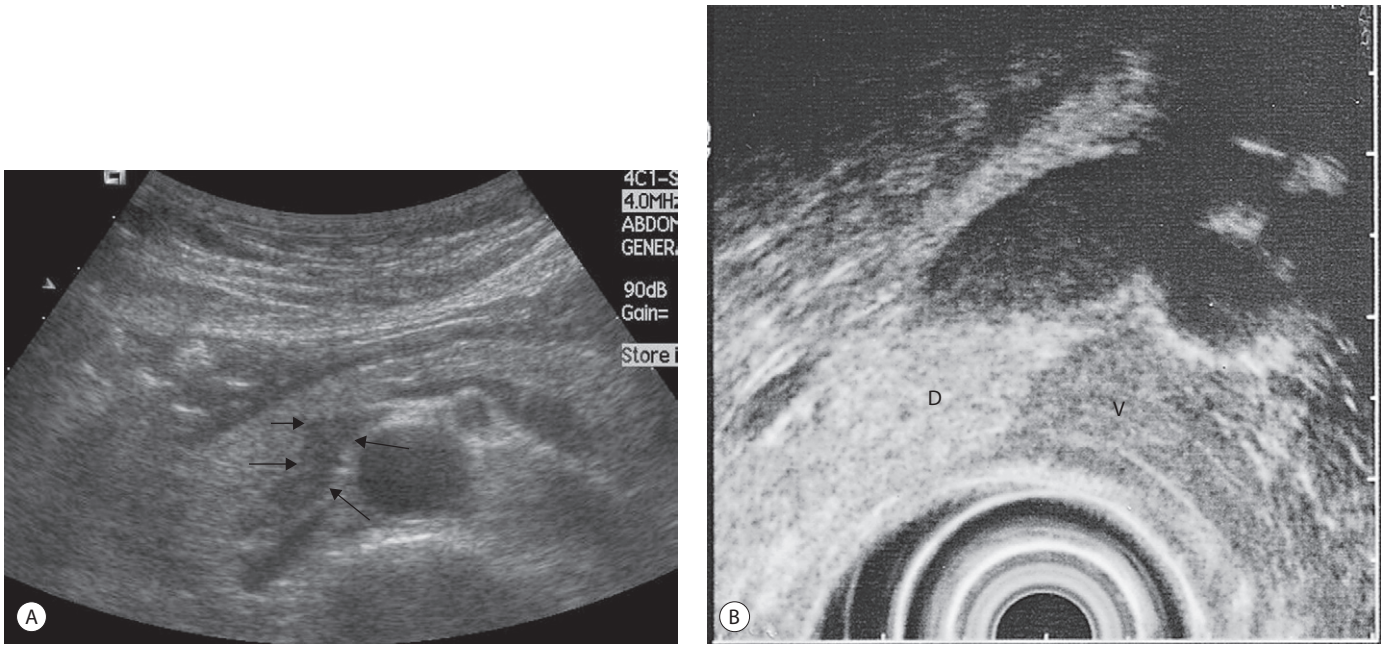


Figure 16.18 **Ventral pancreas. A:** Hypoechoic ventral pancreas (arrows) in the posterior head of pancreas. **B:** EUS from the third part of the duodenum showing a hypoechoic ventral pancreas (V) posterior to the superior mesenteric artery and an echogenic dorsal head of pancreas (D).

Normal appearances

- The normal size of the pancreas is variable, any alteration in echogenicity or duct dilatation being more important in assessing pathology.
- The echogenicity of the pancreas increases with age, with increased fat replacement.
- The pancreatic duct diameter also increases with age – mean diameter 1.5 mm in patients under 30 years, and 2.3 mm in patients over 80 years. Duct diameters up to 5 mm have been reported in elderly patients without associated pancreatic pathology.
- Pancreas divisum occurs in 5–10% of the population and may be suggested on US if the dorsal duct is dilated and followed to the duodenum with a separate insertion from the bile duct, cranial and ventral to the ampulla.
- A hypoechoic posterior head/uncinate process of pancreas occurs due to focal fatty sparing of the ventral pancreas, may mimic a mass, and is reported in 30–40% of patients having abdominal US and in as many as 75% of patients undergoing EUS.

pancreatitis to severe pancreatic or peripancreatic necrosis, as well as release of toxins into the systemic circulation.[55] Pancreatic parenchymal necrosis is maximal at 2–3 days after the acute onset of attack. Vascular damage occurs by direct effect of pancreatic enzymes, necrosis and infection, and can lead to venous thrombosis, acute arterial or venous haemorrhage, or pseudoaneurysm formation.

In patients with pancreas divisum, gallstone pancreatitis affects only the relatively small ventral pancreas. Drainage via the accessory papilla may be impaired and so this may predispose to pancreatitis in patients with divisum, but this is controversial.[49]

Traumatic pancreatitis usually results in duct disruption and a parenchymal defect, and a large pseudocyst often forms.[56] Penetrating injuries can result in disruption at any point, and may be associated with traumatic necrosis, abscess and fistulas.[57] Blunt abdominal injuries result in disruption in the vulnerable neck of pancreas region, with the duct tearing where it is compressed against the aorta and spine – this is the commonest cause of pancreatitis in children, and distal pancreatectomy is usually required if there is complete duct disruption.[58]

Clinical features

Typical presentation is with acute epigastric pain and elevated pancreatic enzymes. Mild pancreatitis occurs in 70–80% of cases and causes minimal organ dysfunction with rapid resolution of symptoms.[59] Severe pancreatitis occurs in 20–30% and is associated with severe systemic disturbance and an early toxic phase and later septic complications. The serum amylase rise may be transient and unrecorded, and the diagnosis may be unclear even if there is severe pancreatitis. Various clinical scoring systems can be used to predict severity of an episode of acute pancreatitis, although there is still a need for a more objective early measure of severity.[49,52] A C-reactive protein of greater than 150 mg/L at 48 hours also predicts a severe attack.[52,60]

Around 20–35% of patients with gallstone pancreatitis will have gallstone-related morbidity within 6 months,[61,62] so early cholecystectomy is indicated; if the patient is unfit for surgery endoscopic sphincterotomy is indicated.[52]

Mortality rates after acute pancreatitis are dependent on intensive care and radiological monitoring with active treatment of complications, most serious of which are infected necrosis and arterial bleeding/pseudoaneurysm formation. In patients with pancreatic necrosis, mortality is about 10% with sterile necrosis and 25% with infected necrosis.[63]

Role of ultrasound

CT is the technique of choice in evaluating patients with suspected or established acute pancreatitis. However, US is often the initial test in patients presenting with abdominal pain – it may be possible to assess the abnormal pancreas and any fluid collections, but views may be limited with ileus and pain/tenderness (Fig. 16.19).[3]

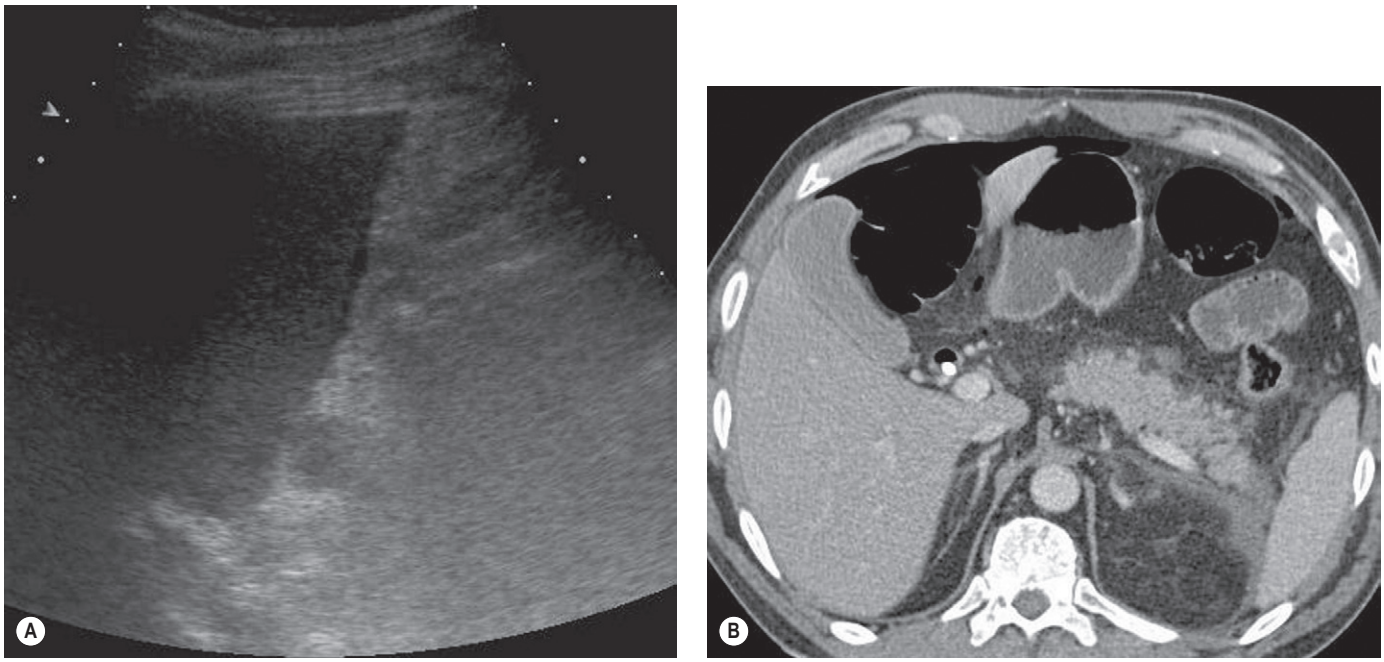


Figure 16.19 Acute pancreatitis. A: Pain and extensive bowel gas because of an ileus limited US views of the pancreas but a small amount of free fluid was seen adjacent to the liver, supporting some acute intra-abdominal inflammation. **B:** CT in the same patient shows some fluid and stranding around the pancreatic tail. Note the distended air-filled bowel anteriorly, highlighting the reason for the poor US views.

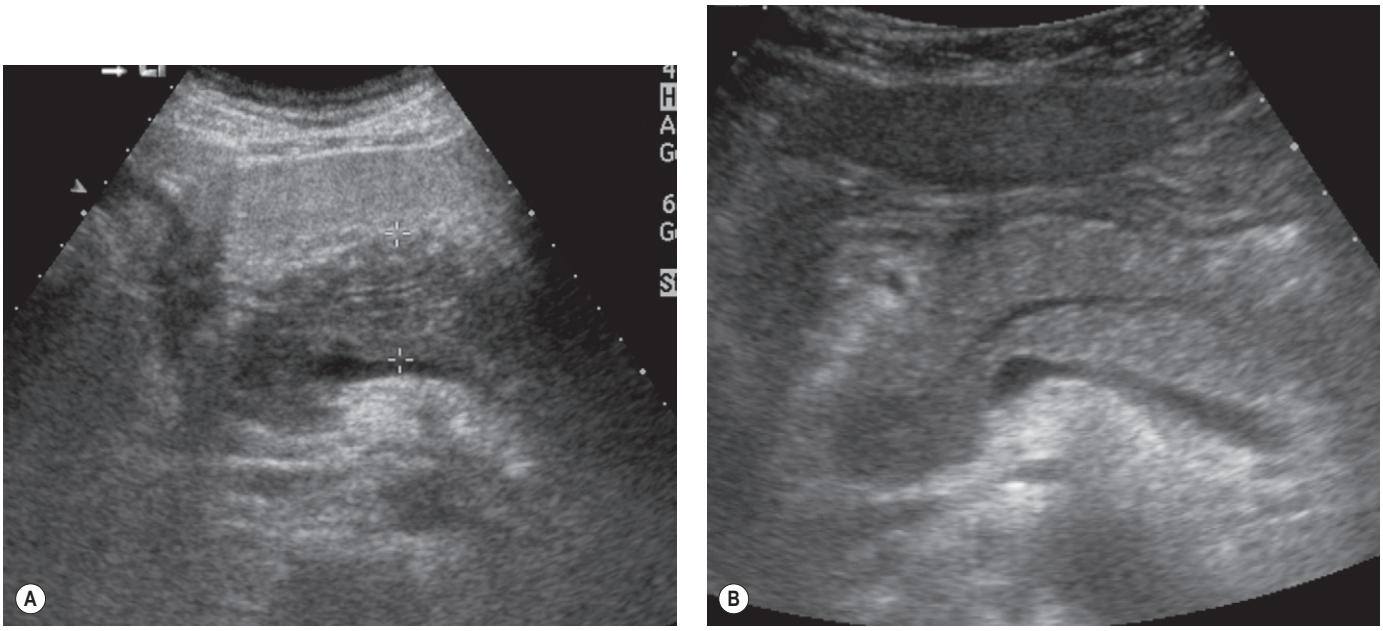


Figure 16.20 Mild acute pancreatitis. A: Slightly enlarged, oedematous and hypoechoic body of pancreas. **B:** Focal pancreatitis with an ill-defined hypoechoic mass in the head of pancreas and slight dilatation of the pancreatic duct.

Therefore CT is indicated if there is still clinical concern and US unhelpful. US has a critical role in detecting gallstones, and should be repeated if no stones are initially detected.[52] Biliary dilatation will be seen on US if the distal CBD is obstructed, and CBD stones may be visible with US.

EUS may detect tiny stones or microlithiasis as a cause of acute pancreatitis.[64] Although some authors suggest EUS after the first attack of acute pancreatitis,[65] there is not enough evidence to support this. However, patients with recurrent 'idiopathic' pancreatitis should have EUS.[52] EUS is as accurate as and safer than ERCP for the detection of CBD stones.[52]

Once the diagnosis of acute pancreatitis is established, any deterioration is imaged with CT (or MRI), but US can be used intermittently and may allow adequate views and assessment of collections.

A very useful and underused role of US is in assessing how much fluid or solid component is present within a pseudocyst, allowing a decision on whether further drainage of any liquid component is needed.[66]

US or EUS can be used prior to endoscopic cystgastrostomy to assess the gut/pseudocyst wall thickness and the presence of any intervening blood vessels, particularly venous collaterals.[66]

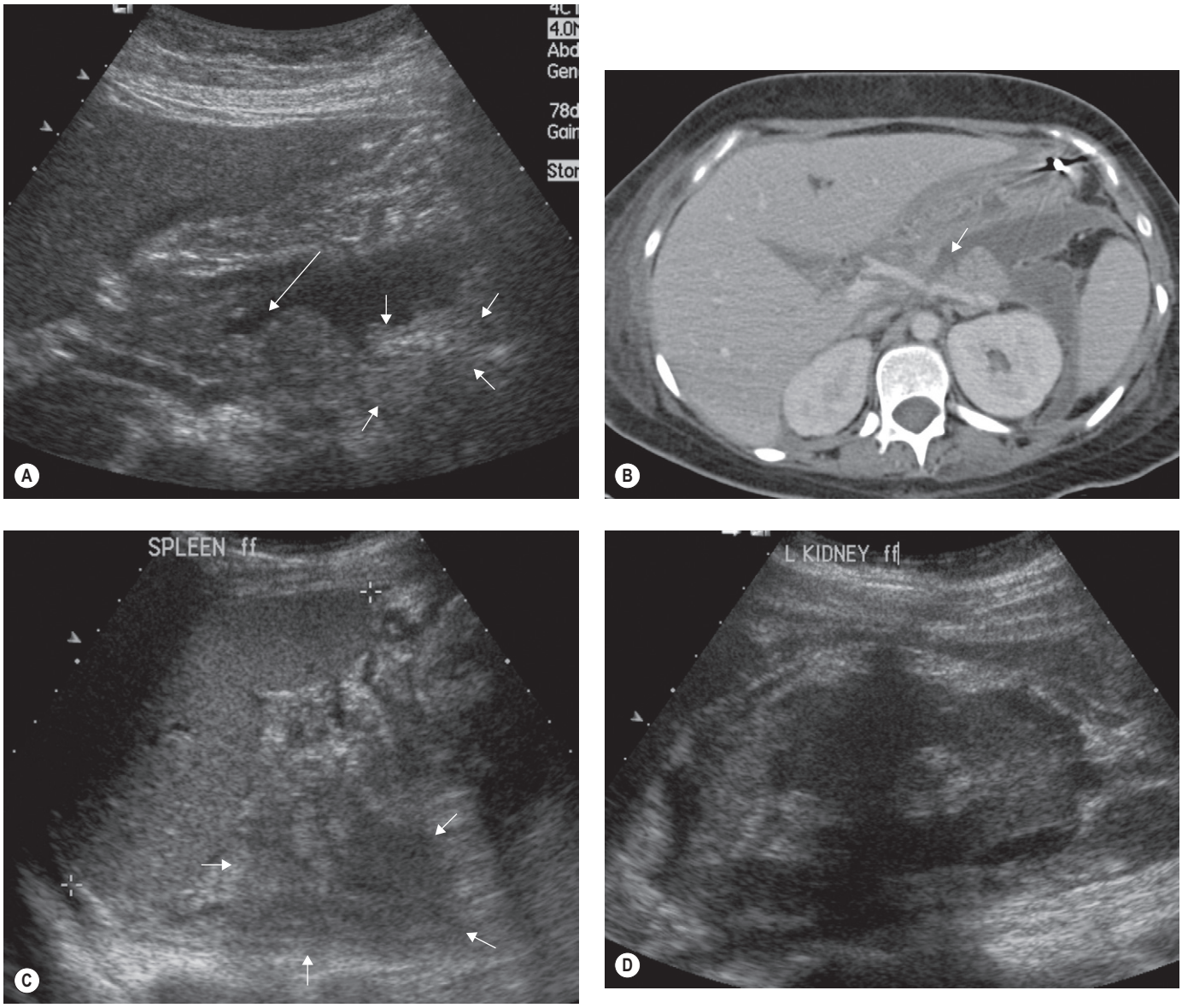


Figure 16.21 **Severe acute pancreatitis. A:** Disruption of pancreatic parenchyma in the body/tail of pancreas (long arrow), adjacent fluid and solid necrosis (short arrows). **B:** Corresponding CT showing the disrupted pancreas (arrow) and the peripancreatic necrosis tracking around the pancreatic tail, spleen and left kidney. **C:** Enlarged, disorganised pancreatic tail (arrows) with tiny pockets of fluid/oedema and variable echogenicity of fat necrosis. **D:** Similar findings around the left kidney.

Contrast-enhanced US has been reported to be useful in patients with acute pancreatitis,[67] but there are problems with consistently imaging the whole pancreas in these patients, which is a significant drawback to its practical value in this situation.[3]

Appearances on ultrasound

Mild pancreatitis

The pancreas may appear normal, enlarged, hypoechoic (less than liver echogenicity) and oedematous (Fig. 16.20). Reduction in parenchymal echogenicity results in increased visibility of duct wall, and thin septations separating lobules may also be seen. There may be oedema/fluid around pancreas and/or around the liver and spleen and in the flanks. CT is less sensitive at showing subtle changes within the pancreas, but much more sensitive at defining change in the peripancreatic fat (Fig. 16.19B).

Hypoechoic change may be diffuse or focal, the latter mimicking a tumour mass (Fig. 16.20B). The pancreatic duct is usually compressed and thin, and may not be visible, but if there is a focal mass, there may be some mass effect resulting in slight dilatation of the duct beyond the mass.

Severe pancreatitis

Ultrasound views are likely to be more limited because of increased tenderness and ileus. Views of the head and tail of pancreas are sometimes possible from the flanks. The abnormalities that may be seen include free fluid, a hypoechoic bulky gland, and possible parenchymal disruption. Peripancreatic fluid/collections accumulate in the lesser sac and/or track down the flanks. Fat necrosis and solid inflammatory change are common findings on CT, but are difficult to see well on ultrasound and usually appear as solid areas of increased and decreased echogenicity and associated with tiny pockets of fluid echogenicity (Fig. 16.21).

Complications

These may be detected with US, but CT assessment is nearly always indicated.

Most are minor and transient clinical problems and resolve without intervention.

Pancreatic necrosis

Pancreatic necrosis occurs in about 20% of patients with acute pancreatitis,[68] with focal or diffuse areas of non-viable pancreatic parenchyma, usually with peripancreatic fat necrosis. Necrosis develops early in severe pancreatitis, the full extent occurring 4 or more days after its onset.[52] Pancreatic necrosis is best detected and defined by dynamic contrast-enhanced CT. US has little role in assessing pancreatic necrosis and is unable to detect it. However, some recent articles suggest that contrast-enhanced US can define the necrosis similar to CT,[67] but this is unlikely to be widely used because of difficulty in achieving good US views of the whole pancreas in these patients, who are usually very unwell and tender.

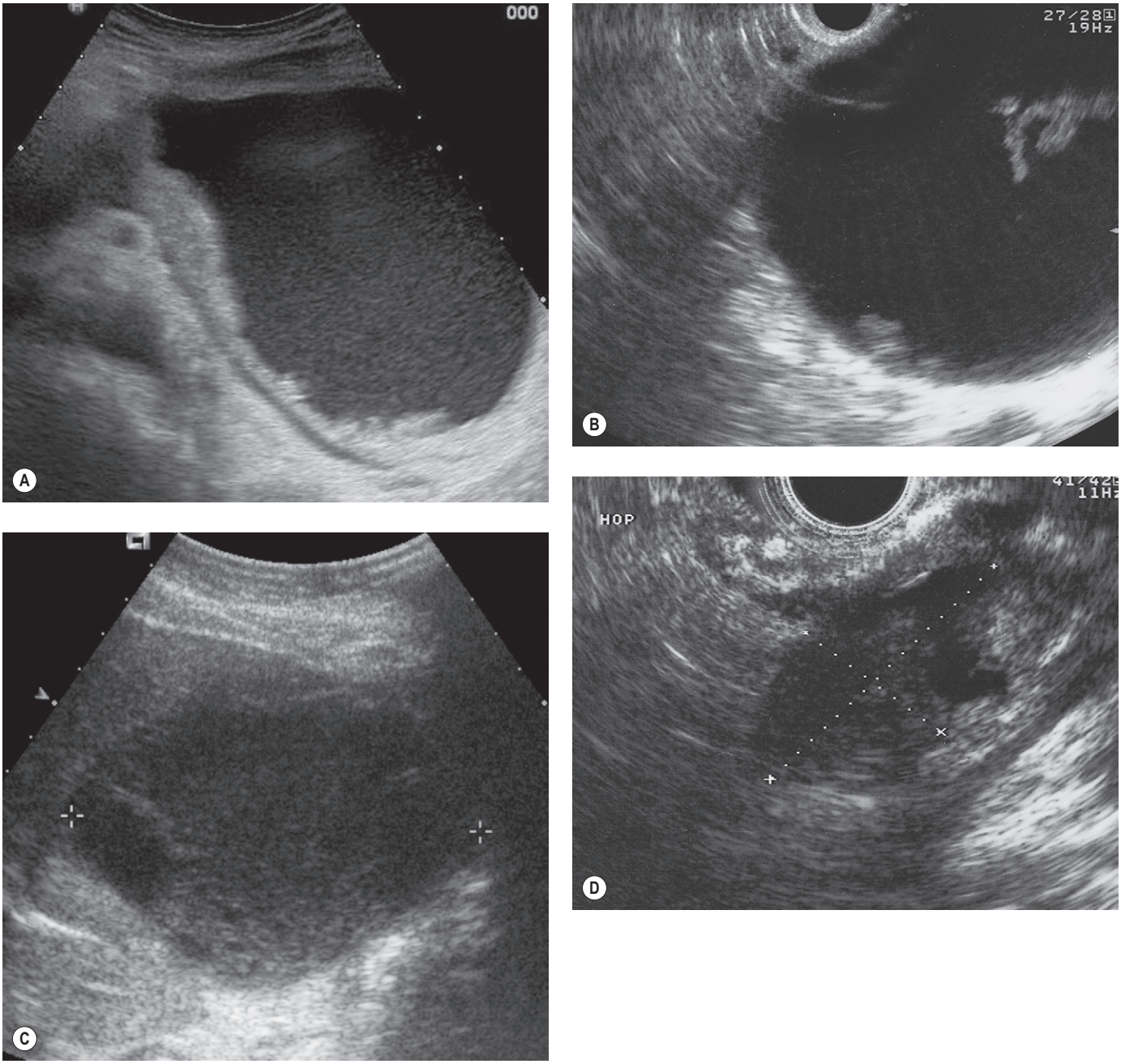


Figure 16.22 Pseudocysts. A: Large pseudocyst arising from the pancreatic tail, some internal echoes and a slightly irregular and thick margin. **B:** EUS of a large pseudocyst with thick nodular septa and nodules attached to the wall. The main differential diagnosis was of a mucinous cystic neoplasm, but analysis of aspirated fluid showed absence of mucin, high amylase and low tumour markers, making a pseudocyst much more likely. **C:** Although this pseudocyst appeared cystic on CT, US showed it was mainly solid with small cystic components – a drain was inserted but very little fluid aspirated as suggested by the US appearance. **D:** In another patient, a pseudocyst was drained and follow-up CT suggested a residual cyst, but EUS showed there was mainly solid material within it.

Pseudocyst

Pseudocysts are collections of pancreatic fluid with a non-epithelialised wall of fibrous or granulation tissue – they may initially be ill-defined in outline, but gradually become better defined with thicker walls. They are usually round or oval, and develop in about 50% of patients 4 weeks after a severe attack. They may occur even after a mild attack; therefore follow-up imaging (usually with CT) on one occasion has been suggested before discharging patients from hospital.[52,69] Pseudocysts often communicate with the main pancreatic duct, but more than 50% resolve spontaneously.

Pseudocysts are usually easy to see on US, and may have internal echoes, septations and solid debris, and so can mimic a cystic tumour on imaging appearance alone. A significant advantage of US over CT is the ability to differentiate liquid and solid components (Fig. 16.22).

Pseudocysts are usually located close to the pancreas but may occur distant from the pancreas via tracts dissecting through tissues. They can cause mass effect with gastrointestinal tract or biliary obstruction. Pseudocysts may also rupture, resulting in an acute abdomen and pancreatic ascites.

Pancreatic phlegmon

This term is often misused, but is still sometimes used to indicate the presence of solid inflammatory tissue due to fat/tissue necrosis and fluid/haemorrhage (Fig. 16.23, and also Figs 16.21, 16.22D).

Infection

Causes of infection after acute pancreatitis include infected pseudocyst/abscess, infected pancreatic necrosis and infected peripancreatic necrosis (Fig. 16.24). An abscess occurs 2–4 weeks after onset of acute pancreatitis and is typically well defined with a thick wall, hypo- or anechoic centre and often containing bright echoes which may indicate pus, air or necrotic tissue debris. Necrosis may become infected in about 10% of patients with acute pancreatitis, but in up to 80% with severe necrotising pancreatitis;[68] this peaks at 3 weeks and is associated with a high mortality. A discrete abscess is relatively easy to define on US, but infected solid or semi-solid necrotic fat/tissue is very difficult to assess; the presence of air may be detected on ultrasound, and usually indicates infection. However, CT is crucial in the septic patient with acute pancreatitis. An abscess requires drainage under CT or US guidance, and infected necrosis may require surgical debridement.

Portal venous thrombosis

Acute thrombus in the portal/splenic veins may occasionally be seen, but often the veins (most commonly splenic vein) are found to be occluded on imaging, with formation of venous collaterals.

Arterial bleeding and pseudoaneurysm

Pseudoaneurysms usually occur 2–3 weeks after severe pancreatitis, and are detected on post-contrast arterial phase thin collimation CT (Fig. 16.25). A fatal haemorrhage can occur, and if arterial bleeding or pseudoaneurysm is detected angiographic intervention is needed. Arterial wall breakdown can result in irregularity and direct bleed, or initial pseudoaneurysm formation, which is at high risk of bleeding. Pseudoaneurysms may rarely be detected on US, but follow-up scans after diagnosis of severe acute pancreatitis are nearly always CT. US may show a focal area of reduced echogenicity with heterogeneous or layered internal echoes, and blood flow on colour Doppler.

Biliary obstruction

US should easily detect any biliary dilatation, and if gallstones are present or suspected, urgent ERCP is indicated. Transient swelling of the pancreatic head can lead to an oedematous CBD stricture, but this can later lead to a more fibrotic stricture. There is a risk of cholangitis, so if the liver function tests are obstructive then biliary stenting is appropriate.

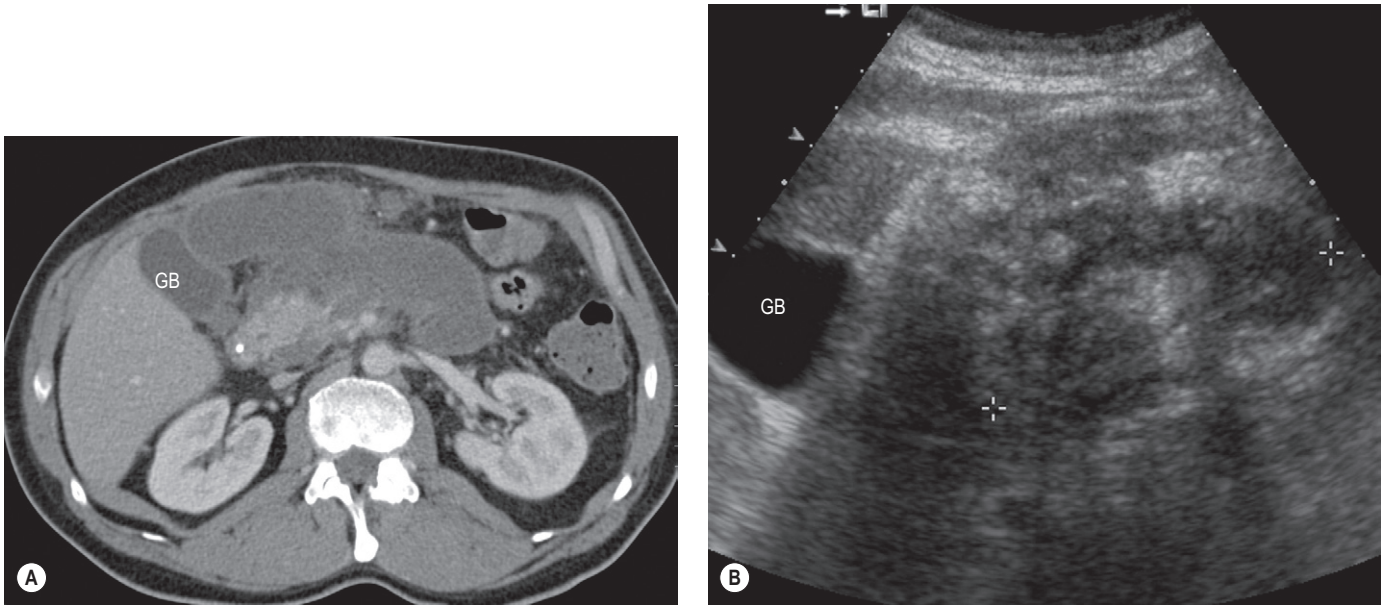


Figure 16.23 Phlegmon. A: CT showing large low-density collection anterior to the head of pancreas, thought to be cystic, but of slightly increased density compared to the adjacent gallbladder. **B:** US showed this to be a solid heterogeneous inflammatory mass. GB, gallbladder.

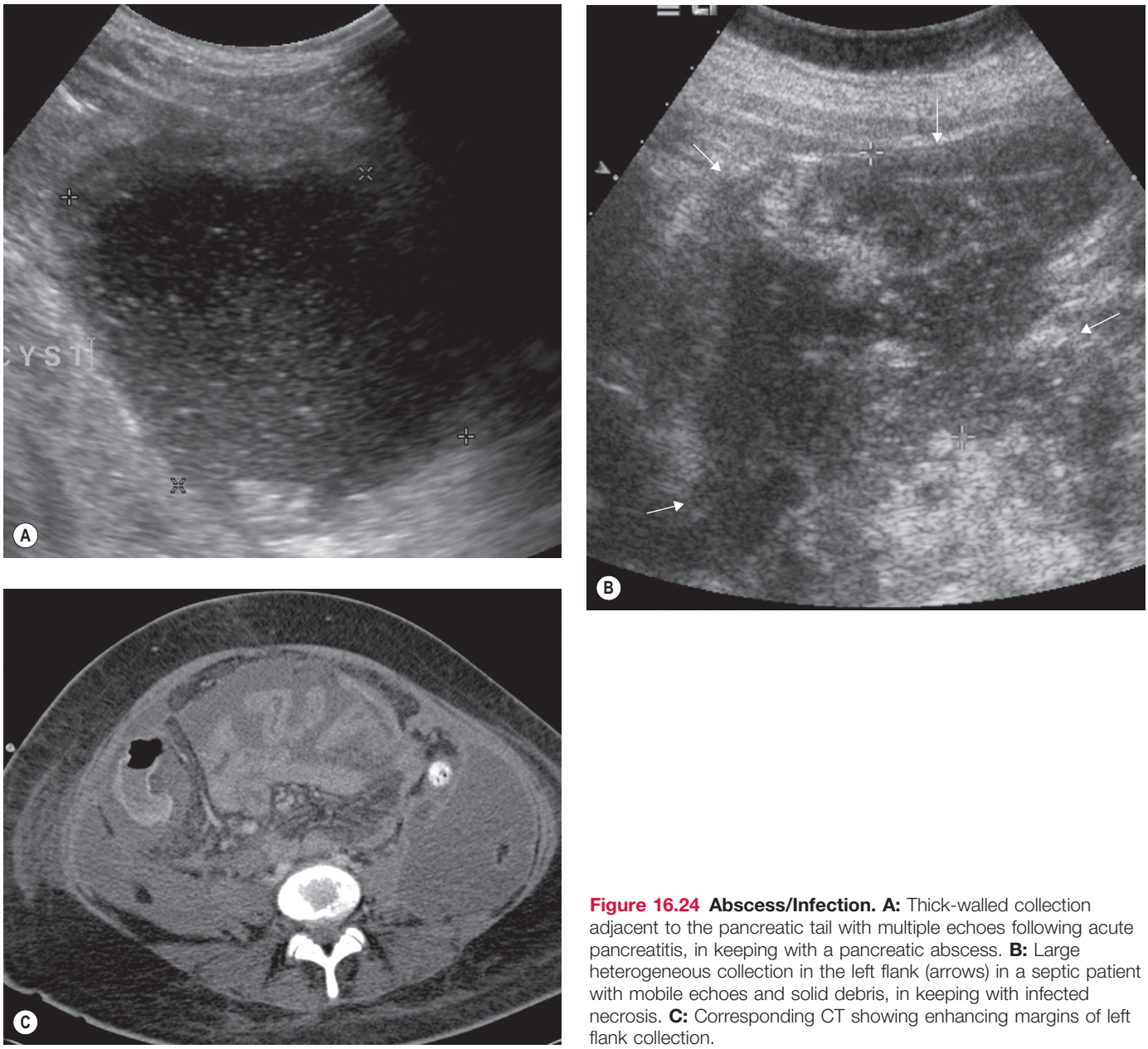


Figure 16.24 **Abscess/Infection. A:** Thick-walled collection adjacent to the pancreatic tail with multiple echoes following acute pancreatitis, in keeping with a pancreatic abscess. **B:** Large heterogeneous collection in the left flank (arrows) in a septic patient with mobile echoes and solid debris, in keeping with infected necrosis. **C:** Corresponding CT showing enhancing margins of left flank collection.

Gastrointestinal tract obstruction and renal obstruction

These may be seen as sequelae of acute pancreatitis; they usually resolve with time and without intervention.

Intervention

Pseudocyst aspiration/drainage

This can be performed by direct puncture, or by a transgastric approach with US and/or fluoroscopic guidance (Fig. 16.26). EUS guidance can also be used for endoscopic transgastric aspiration and drainage. Drainage is indicated if the patient is symptomatic or the cyst is infected or enlarging. Continued drainage after the initial procedure implies a significant persistent communication with the main pancreatic duct. ERCP and pancreatic stent is indicated initially, and surgery may need to be considered.

Infected necrosis

Suspected infected necrosis should be aspirated for culture.[70] If pus is aspirated, then a radiological drain usually follows. However, consideration should be given to necrosectomy, although this is not mandatory as previously reported.[52]

A common scenario in practice is that some (varying proportion) solid necrosis that does not initially drain becomes more infected after the drain has been inserted and then liquefies and drains very slowly (may be weeks to months) – usually requiring further drains, changes and upsizing. The infected cavity may evacuate from the drain, or fistulation occurs into adjacent gastrointestinal (GI) tract.

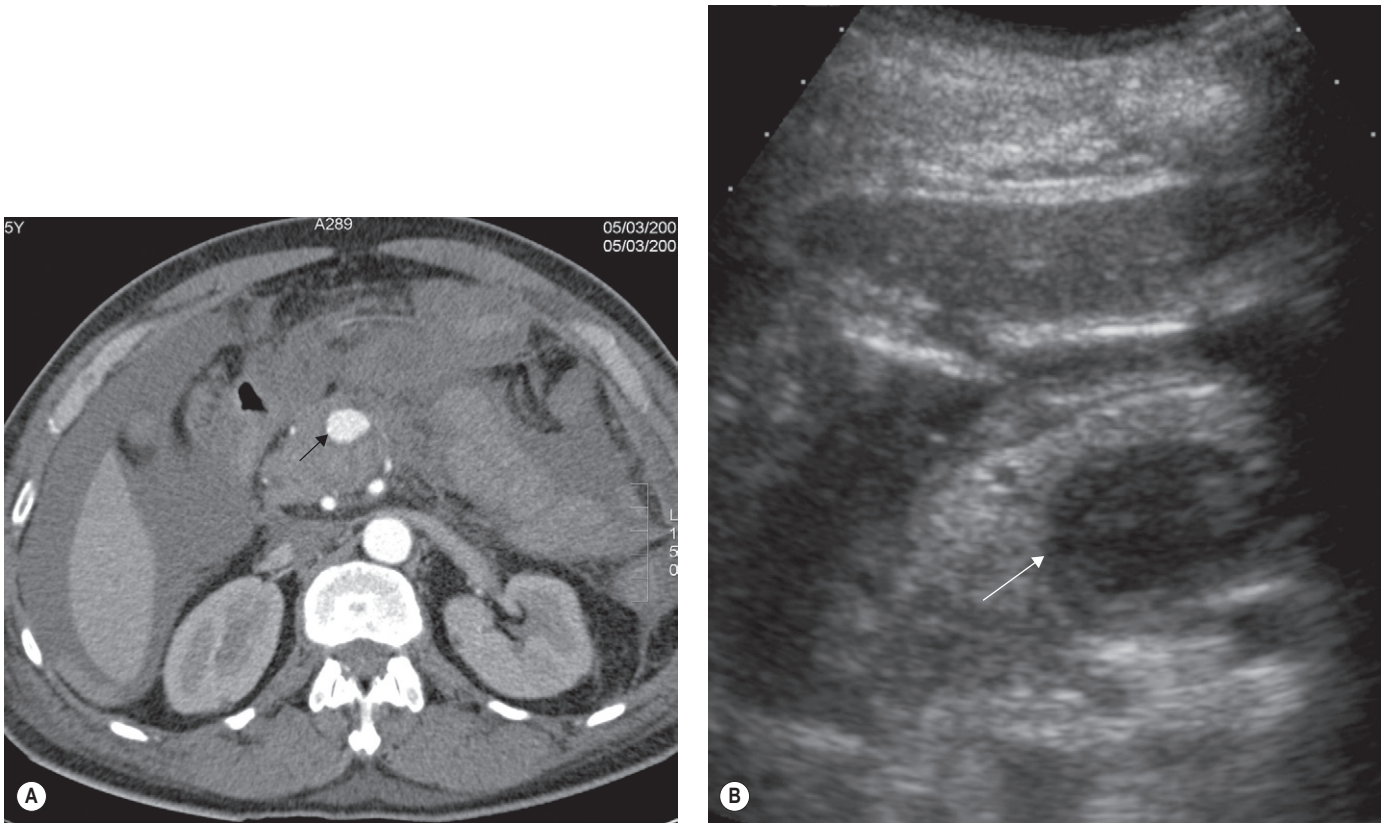


Figure 16.25 **Pseudoaneurysm. A:** Arterial phase CT showing pseudoaneurysm (arrow) surrounded by thrombus in the head of pancreas, not initially recognised. **B:** US 1 week later showed an echo-poor and heterogeneous corresponding focal area, but no colour Doppler flow (arrow). The pseudoaneurysm had spontaneously thrombosed, confirmed on repeat CT.

Acute pancreatitis

- Acute pancreatitis is caused by gallstones or alcohol in over 70% of cases.
- US has an important role for detecting gallbladder stones, and should be repeated if initially negative in a patient with acute pancreatitis.
- US in mild pancreatitis may show the pancreas to be normal, or enlarged with decreased echogenicity.
- In severe pancreatitis, there is usually also peripancreatic free fluid. Contrast-enhanced CT is necessary to assess pancreatic necrosis and other complications.
- US has a limited role in further imaging of patients with severe pancreatitis. However, it may be useful in monitoring collections, differentiating solid from liquid low-density collections identified on CT, and may detect CBD stones, pseudoaneurysms, venous thrombosis, or abscesses.
- US can be useful for guided drainage of collections.
- EUS has a role in patients with recurrent acute pancreatitis of unknown aetiology, to look for gallbladder microlithiasis or sludge.

US is not usually adequate to assess these collections with mainly solid infected tissue and air. Percutaneous necrosectomy can be performed, ideally through a retroperitoneal tract.[71]

Thrombin injection of pseudoaneurysm

This can be performed under US guidance, but does risk rupture of the aneurysm and if considered should be done in the angiography suite, so that angiography and embolisation can be performed if necessary.[72]

CHRONIC PANCREATITIS

Chronic pancreatitis is a continuing inflammatory disease of the pancreas, characterised by irregular sclerosis of the pancreatic parenchyma and replacement of glandular elements of the pancreas by fibrous tissue, resulting in progressive and permanent loss of exocrine and endocrine pancreatic function.[73]

In developed countries, alcohol is the commonest cause (60–70%), and 30–40% of cases are idiopathic. Although relatively uncommon, its incidence is increasing, probably as a result of increasing alcohol consumption. Alcohol may cause direct parenchymal damage or precipitate protein secretions resulting in blocked ducts. Scarring leads to strictures of the main pancreatic duct as well as the side branches. Intraductal protein plugs often calcify as the disease progresses.

The diagnosis of chronic pancreatitis is based on a combination of clinical findings, endocrine and exocrine pancreatic function tests, and imaging findings. However, the diagnosis can be difficult, especially in early disease since there is no gold standard test[74] and histological diagnosis is also difficult.[75] Differentiating early chronic pancreatitis (lobular fibrosis) from acute or recurrent acute pancreatitis (focal necrosis/autodigestion) is also difficult.[3]

Imaging

In advanced chronic pancreatitis there is good correlation between the various imaging modalities and tests of pancreatic function, but there is no reliable test for diagnosing early chronic pancreatitis and differentiating this from other causes of abdominal pain.[3]

CT is again the principal imaging modality in chronic pancreatitis, and the main features are gland calcification, parenchymal atrophy and duct dilatation. There may be acute on chronic

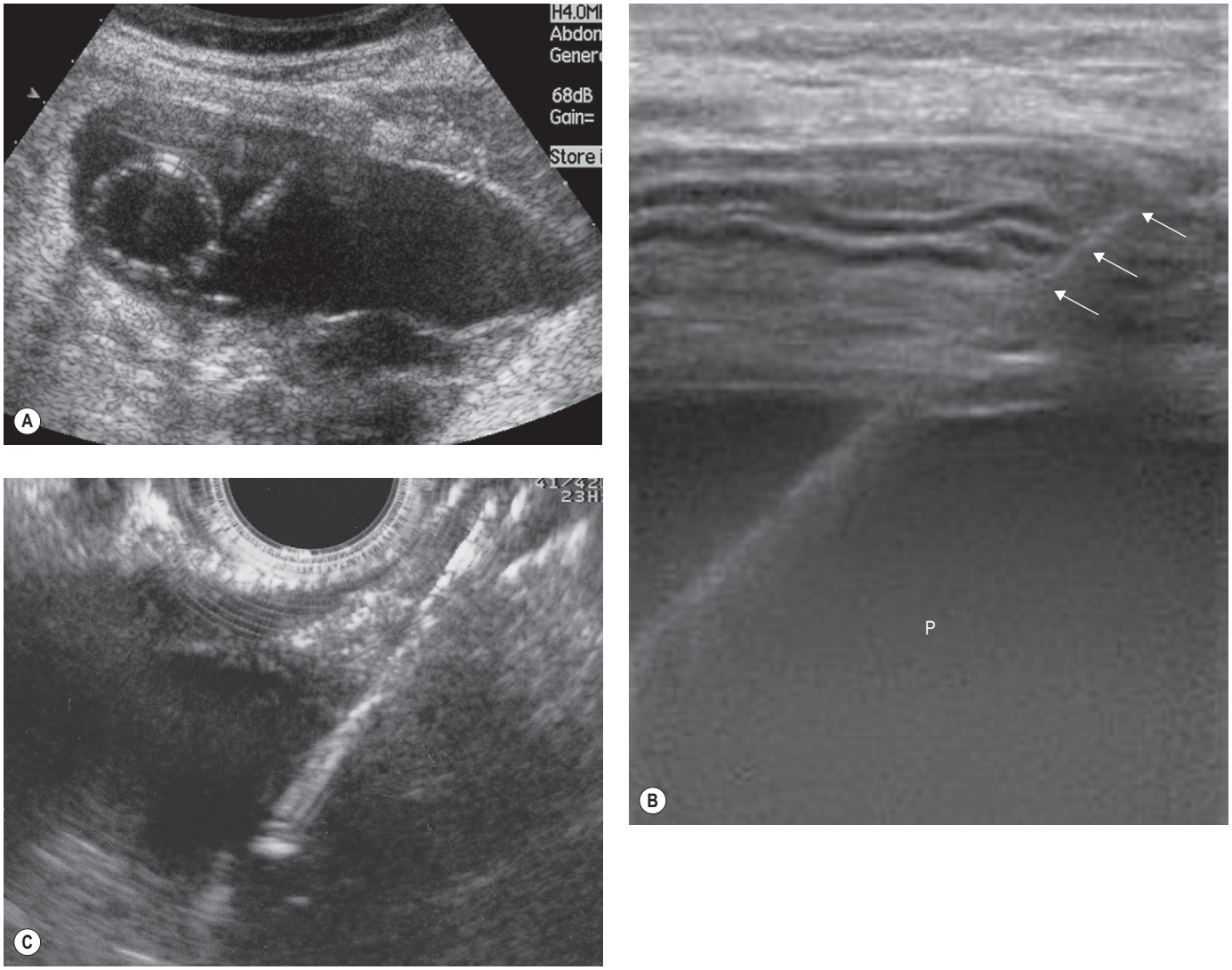


Figure 16.26 Drainage of pseudocyst. A: US-guided insertion of a pigtail catheter into a pseudocyst. **B:** High-frequency US used to guide a needle through the gastric antrum (arrows) into a pseudocyst (P). The tract is then dilated before insertion of a pigtail catheter. The drain can be cut within the stomach at a later date to allow continued internal drainage. **C:** EUS-guided aspiration of a pseudocyst posterior to the gastric wall.

inflammatory change, low density fibrosis within and around the pancreas, pseudocysts, bile duct or duodenal strictures, portal vein thrombosis/venous collaterals, and pseudoaneurysm formation.

ERCP also has an important role in diagnosis of chronic pancreatitis, especially early change – it may be the only test to show subtle main duct stricturing and side branch ectasia.[76] Non-invasive imaging with secretin-stimulated MRCP is being increasingly used, giving almost comparable ductal information to ERCP, as well as some functional information through quantification of pancreatic fluid output after secretin stimulation.[77]

Changes of chronic pancreatitis may be focal, and when confined to the part of the pancreas between bile duct and duodenum are called 'groove' pancreatitis. This may result in dilatation of the main pancreatic duct and small cysts in a thickened duodenal wall.[78] Focal pancreatitis occurs in about 20% of cases, and usually involves the head of pancreas, and may mimic a pancreatic tumour (Fig. 16.27).[79]

Ultrasound and EUS

Ultrasound has the advantage over CT of allowing detailed views of the pancreatic parenchyma when it is visualised, and many

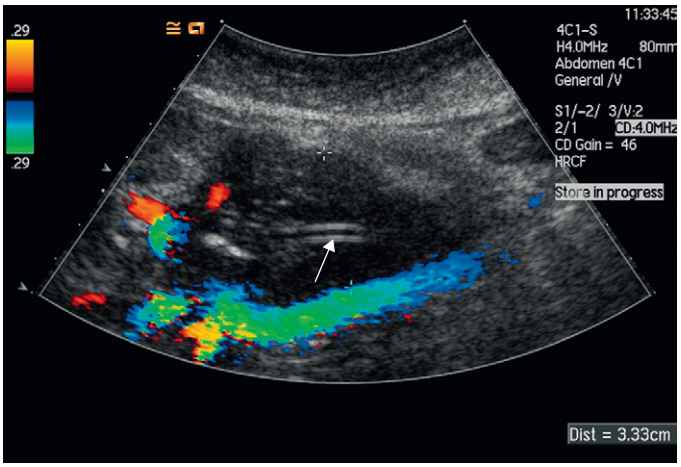


Figure 16.27 Focal chronic pancreatitis. Hypoechoic mass in the head of pancreas, around a bile duct stent (arrow), in a patient known to have chronic pancreatitis. Several biopsies from this mass revealed fibrosis only, and no progression on follow-up CT scans.

papers have been written about the changes in the echotexture of the pancreatic parenchyma in chronic pancreatitis.[3,80–82] A normal echotexture may be seen in up to 40% of patients with chronic pancreatitis, mainly in the early stages. However, the echogenicity of the pancreas usually increases in chronic pancreatitis due to a combination of increased fat and fibrosis, but this is also seen in obese and older patients.[6,38,41–42] Therefore, on its own this ultrasound change is not helpful. Similarly, volume assessment is difficult and subjective, and parenchymal atrophy is non-specific. Foci of increased and decreased gland echogenicity are said to be more specific for chronic pancreatitis,[83] but again this is more reliable as a supportive sign.

Ultrasound detection of pancreatic intraductal calcification is highly suggestive of chronic pancreatitis[6,84] (Fig. 16.28), although any focal cluster of calcification associated with a mass may be due to tumour calcification (Fig. 16.29). Intraductal calculi are protein aggregates with calcium carbonate deposits, and their echogenicity increases with increasing calcium content. Non-calcified intraductal protein plugs are usually not detectable, but may be seen on high-frequency US and/or with harmonic imaging as echogenic foci without acoustic shadowing (Fig. 16.30).

The presence of duct dilatation and irregularity may also be seen on ultrasound of patients with chronic pancreatitis. Any pseudocysts detected further support a diagnosis of chronic pancreatitis.

A pancreatic duct diameter of greater than 3 mm is considered pathological.[83] It is the most easily identified US sign in chronic pancreatitis with a sensitivity of 60–70% and specificity 80–90%.[6] However, it may be normal, especially in the early stages of chronic pancreatitis, and duct dilatation may be secondary to an obstructing lesion, or an intraductal papillary mucinous neoplasm (IPMN).

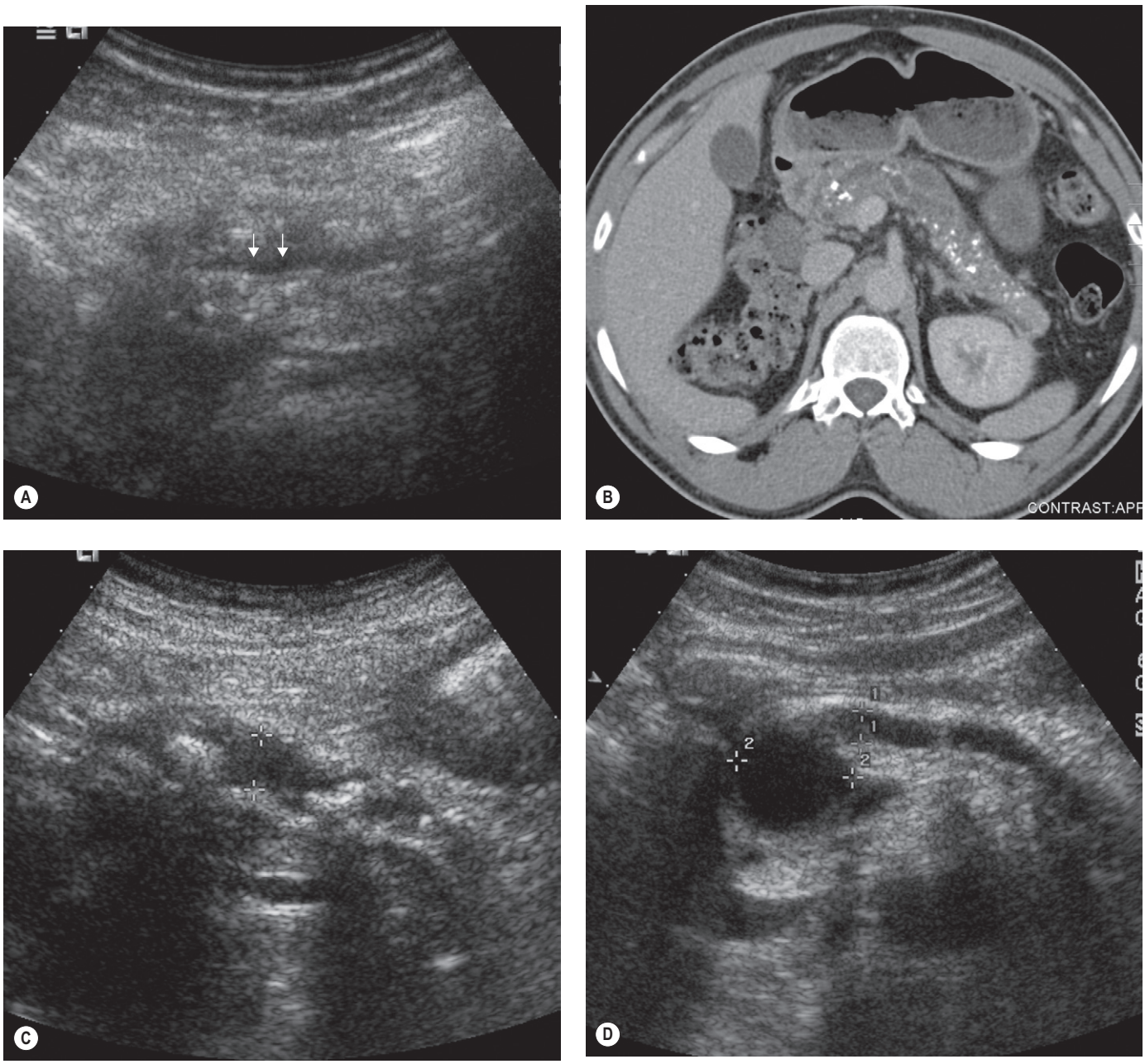


Figure 16.28 Chronic pancreatitis. A: Small echogenic foci in the body of pancreas around a slightly dilated pancreatic duct (arrows). **B:** Corresponding CT showing numerous small calcifications and an irregular and dilated pancreatic duct. **C:** Dilated pancreatic duct containing large stones, and marked parenchymal atrophy. **D:** Cyst in the head of pancreas, dilated pancreatic duct and parenchymal atrophy in a patient with longstanding chronic pancreatitis.

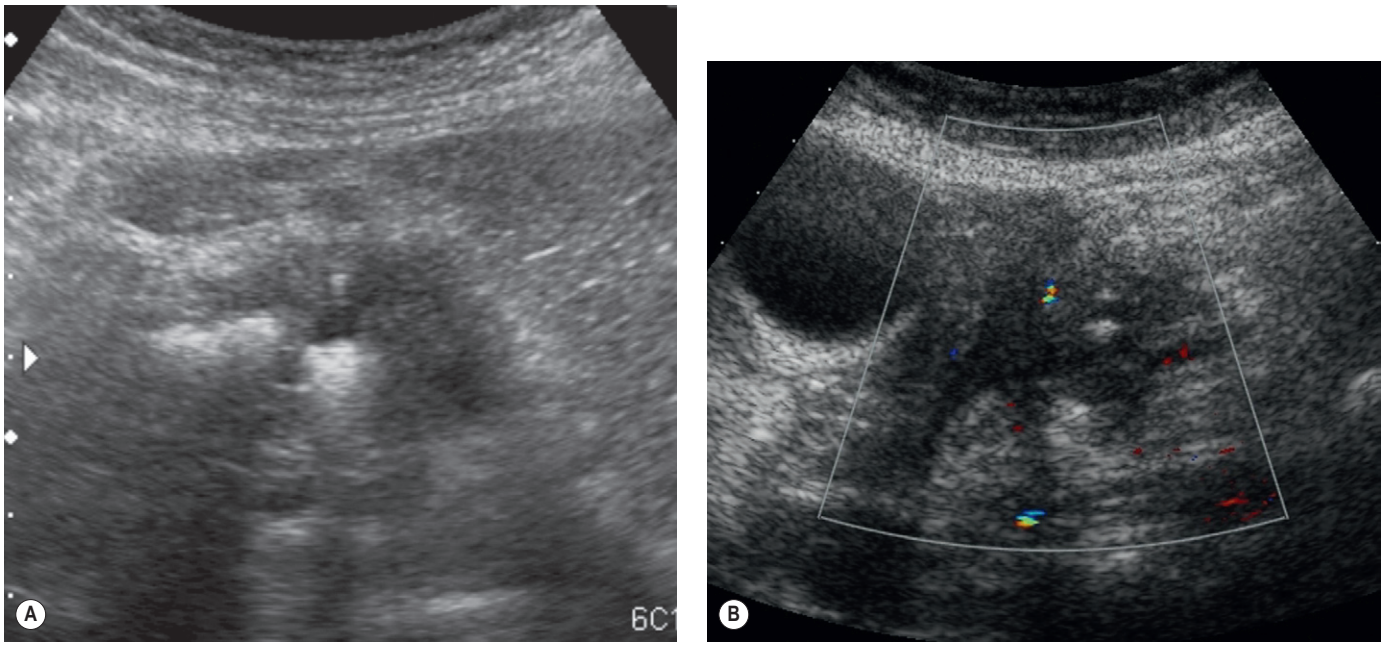


Figure 16.29 Chronic pancreatitis mass. A and B: Hypoechoic masses around calcifications in patients with known chronic pancreatitis; in **A** biopsy and follow-up were in keeping with benign change, but in **B** biopsy showed adenocarcinoma.

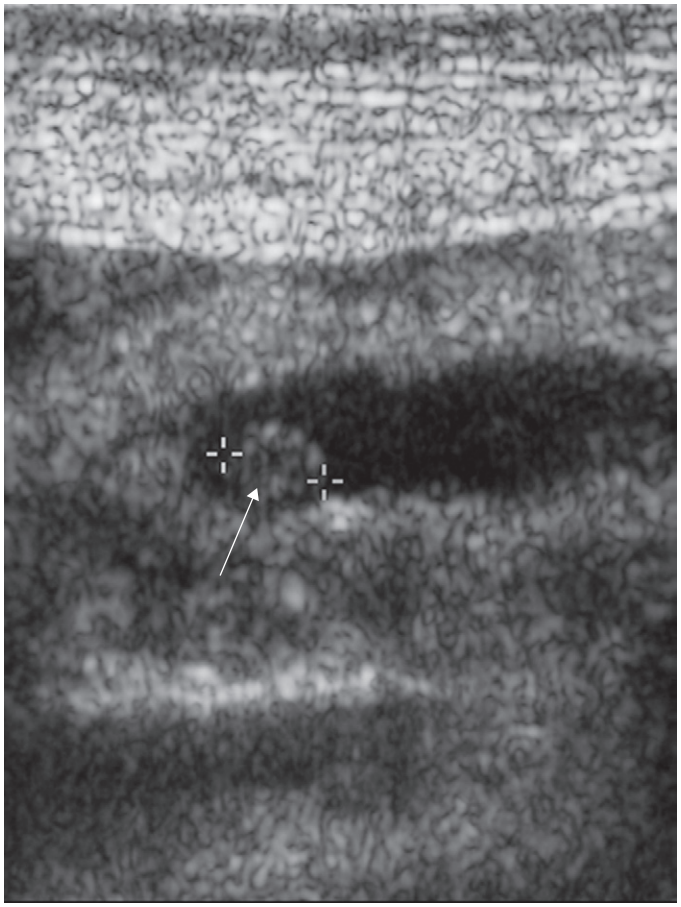


Figure 16.30 Protein plug. Patient with chronic pancreatitis, dilated duct, parenchymal atrophy and presumed protein plug (arrow).

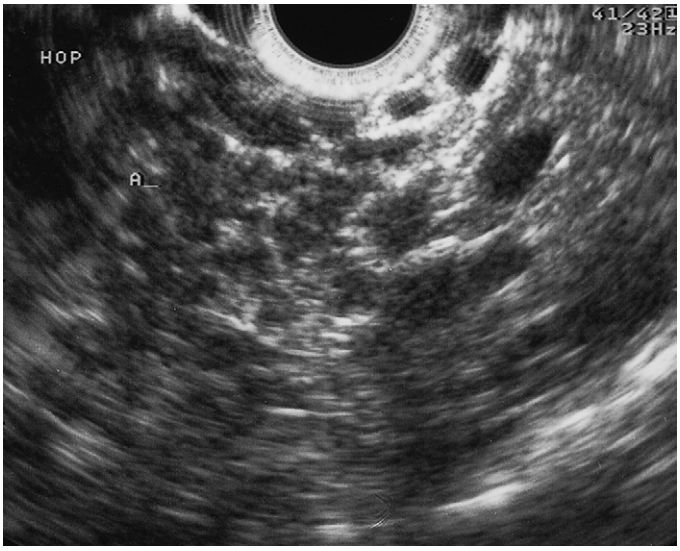


Figure 16.31 EUS chronic pancreatitis. Lobulated parenchyma, suggestive of chronic pancreatitis.

Secretin-stimulated ultrasound of the pancreas has been reported to be useful in diagnosing chronic pancreatitis by correlating changes in the pancreatic duct to exocrine pancreatic function, a suboptimal dilatation associated with pancreatic insufficiency.[45] However, this test is only likely to be used if the more objective MRCP with secretin stimulation cannot be performed.

EUS gives more detailed and consistent views of the pancreas compared to transabdominal US. Features seen on EUS in chronic pancreatitis, not well seen by other imaging modalities, include hyperechoic duct wall, lobulation of parenchyma, small cystic change, and side branch ectasia[3,77,81] (Fig. 16.31). However, EUS may be oversensitive, since some of these changes can be seen in older patients without clinical evidence of chronic pancreatitis.[42]

AUTOIMMUNE PANCREATOPATHY

This is being increasingly recognised as a type of chronic pancreatic dysfunction caused by an autoimmune mechanism and is often associated with a cholangiopathy resembling sclerosing cholangitis.[85–87] This condition has become established as an important diagnosis over the past 10 years, not least because it can mimic pancreatic cancer clinically and radiologically.[86] Early and accurate diagnosis is crucial, since it can be treated with corticosteroids, which can rapidly reverse the changes produced.[86] It is estimated to be present in about 5% of patients diagnosed with chronic pancreatitis, and typically presents with painless jaundice, weight loss and variable abdominal pain.[86]

The most important imaging features are an enlarged pancreas and a narrow main pancreatic duct. There should also be raised serum autoantibodies (or IgG/IgG4) and/or pancreatic biopsy showing fibrosis and periductal infiltration by lymphocytes and plasma cells.[87]

The pancreas is initially increased in volume, diffusely enlarged with sharp margins and a rim of low density typically seen on CT – the appearance described as a 'sausage' shaped pancreas. The pancreatic duct is compressed, and seen as thin and irregular at ERCP. Extra-pancreatic disease (especially lung and kidney) is well recognised and due to IgG4-positive plasma cell infiltrate.[88]

On US the pancreas appears focally or more usually diffusely enlarged and hypoechoic, without calcification, duct dilatation or surrounding fluid (Fig. 16.32). It is important to consider and exclude malignancy. The evolution of changes over several months

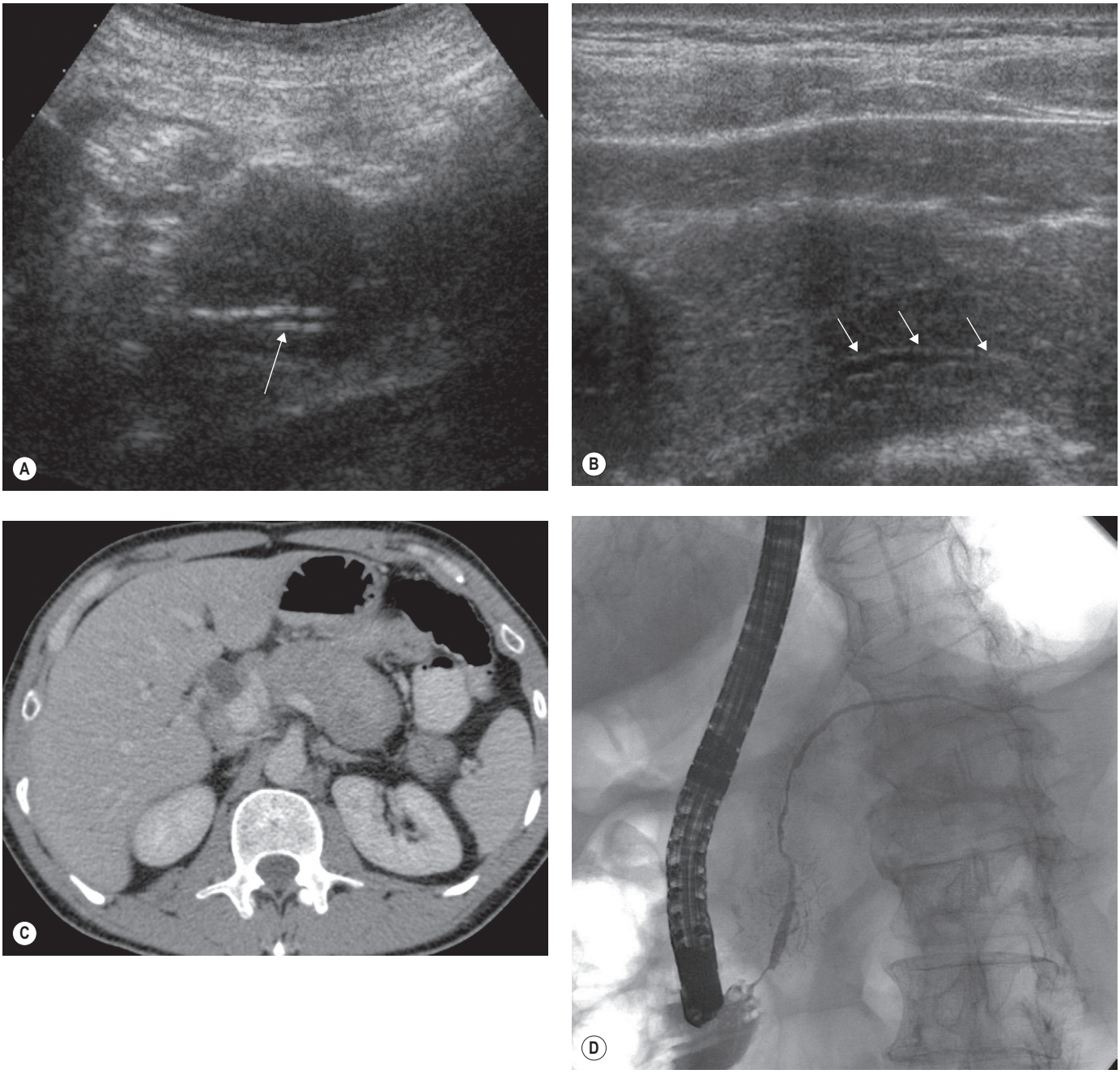


Figure 16.32 Autoimmune pancreatopathy. A: Enlarged hypoechoic head of pancreas with a plastic bile duct stent (arrows). **B:** Enlarged body of pancreas with a slightly irregular duct (arrows). **C:** CT showing typical enlarged pancreatic tail with a rim of low density fibrosis. **D:** ERCP showing typical appearance of an irregular pancreatic duct.

Chronic pancreatitis

- US features of chronic pancreatitis include calcification, dilated duct or side branches, parenchymal atrophy, and pseudocysts.
- Focal pancreatitis may mimic a tumour, and often occurs between the duodenum and head of pancreas – 'groove' pancreatitis, and this may be associated with a dilated pancreatic duct and small cysts in a thickened duodenal wall.
- Autoimmune pancreatopathy is being increasingly recognised – the pancreas is usually diffusely enlarged and hypoechoic, and the pancreatic duct is thin and irregular. The biliary tree is often affected, with appearances of sclerosing cholangitis. There is usually a good response to steroids, and the pancreas undergoes parenchymal atrophy on follow-up imaging.

is to a small atrophic pancreas. Duct dilatation and calcification are unusual.

The principal role of US and especially EUS is for guided pancreatic biopsy so that histological assessment can support the diagnosis and exclude cancer.

PANCREATIC TUMOURS

The majority of pancreatic tumours (about 90%) are ductal adenocarcinoma, but with improved imaging cystic tumours are being increasingly recognised.[3]

Pancreatic cancer has a relatively low incidence but poor prognosis, so that it ranks eighth in a world listing of cancer mortality.[89] At presentation, less than 20% of patients are suitable for curative resection.[3] It is more common with increasing age and so its incidence is increasing in most Western countries whose population is ageing.[89]

There are no specific aetiological agents but reported risk factors include smoking, diabetes, chronic pancreatitis, familial adenomatosis polyposis, and a family history of pancreatic cancer.[89]

Clinical presentation is usually with weight loss, abdominal pain (often radiating to the back), and jaundice if the bile duct is involved, but cystic and neuroendocrine tumours (NET) may be asymptomatic or have few symptoms.[3] Tumours in the head of pancreas are usually smaller at presentation because local mass effect on bile duct and/or duodenum leads to earlier symptoms such as jaundice and vomiting, whereas tumours in the tail of pancreas are more often much larger and may be metastatic at presentation.

The presence of metastases and arterial involvement by tumour are usually a contraindication to resection, but local portal venous involvement no longer excludes the surgical option since vein grafts are now being undertaken.[90] However, the extent of venous involvement is important in making the decision whether to try to operate with venous grafting. Unresectable tumours may be treated with chemotherapy, sometimes chemoradiotherapy with a view to downstaging before reconsidering surgical resection.[91] Surgical intervention has become more aggressive in the past decade with improvements in surgical technique and more specialist surgeons, but the long-term outcome has not yet been assessed.[92] Laparotomy with a view to resection is still frequently being converted to biliary and gastric bypass since the tumour is found to be too advanced; preoperative imaging, although improved considerably, is still missing small peritoneal and liver metastases.[93]

Overall 5-year survival for pancreatic cancer is only 1–2%, increased to 10% if resected, but the prognosis for rarer tumours is better.

Imaging

Imaging is used for detection, characterisation and staging of pancreatic tumours, with assessment of local extension, vascular invasion and metastases.

The key imaging modality is multislice CT dedicated to the pancreas for assessment of the tumour and including the chest for complete staging.

Ultrasound is frequently the initial imaging test in evaluating patients with abdominal pain/weight loss and/or jaundice. Although US does not allow consistently good images in all patients, it can provide very useful information for diagnosis and staging of pancreatic masses if time and care is taken during the examination and when used by experienced and skilled operators. US should also be considered as a problem-solving tool and repeated after CT if necessary; for example, if a mass is not identified on CT it may be shown on repeat US, or if there is contact between portal vein and tumour on CT, US may show invasion into the wall. Endoscopic US is often used in these circumstances and can give excellent images, but sometimes the problem can be resolved with transabdominal US.

Differential diagnosis

The detection of a focal pancreatic mass on imaging could be due to a variety of benign and malignant causes. The commonest causes of a solid mass are pancreatic adenocarcinoma and focal pancreatitis. Other causes include neuroendocrine tumours, metastases and lymphoma. All of these masses are usually hypoechoic, so difficult to differentiate on US. The presence of cystic change and calcification supports chronic pancreatitis. However, a cystic element to the mass may be due to a cystic NET, mucinous cystic neoplasm, serous cystadenoma, or a cystadenocarcinoma. A dilated main pancreatic duct (MPD) with or without an associated cystic lesion is suggestive of an IPMN. Non-neoplastic causes of cystic lesions should also be considered, and these include pseudocysts, hydatid cysts and true congenital cysts. Contrast-enhanced ultrasound defines the tumour vascularity and so can be useful in differentiating between more vascular (NETs, serous cystadenomas and focal pancreatitis) and less vascular (adenocarcinoma) masses.[7,8]

Adenocarcinoma

Pancreatic adenocarcinomas are most common in the head of pancreas, often resulting in bile duct compression and jaundice, and usually larger in the tail of pancreas. Tumours in the head and neck of pancreas cause dilatation of the MPD and CBD ('double duct' sign, highly suggestive of adenocarcinoma). CBD dilatation does not always occur with pancreatic head tumours, and also if the main tumour mass is located in the uncinate process, body/tail of pancreas. Adenocarcinomas typically lead to perineural and perivascular invasion, and early metastases in the liver, nodes peritoneum are common.

Ultrasound features

As with CT and MRI, ultrasound is best performed before any bile duct stenting, since following a dilated duct down to the level of obstruction makes it far easier to identify and localise any mass. A dilated CBD and MPD are usually easily detected (Fig. 16.33). Even in the absence of a visible mass, the dilated ducts are strongly suggestive of a pancreatic head neoplasm. There is usually parenchymal atrophy associated with the dilated MPD (Fig. 16.33). However, the double duct sign is not exclusive to cancers, since any focal mass or inflammation can cause this. Pancreatic adenocarcinoma masses are typically hypoechoic, fairly homogeneous solid masses, and often with a well-defined but irregular margin (Fig. 16.34). Occasionally the tumours are of heterogeneous echotexture with small foci of increased echogenicity, but it is rare for adenocarcinoma to be hyperechoic (Fig. 16.34). Any associated acute or chronic pancreatitis makes US detection and staging of the tumour more difficult. If the surrounding parenchyma is echogenic, then the tumour margins are usually easy to define on US. However, if the rest of the pancreas is hypoechoic, then detecting and defining the tumour

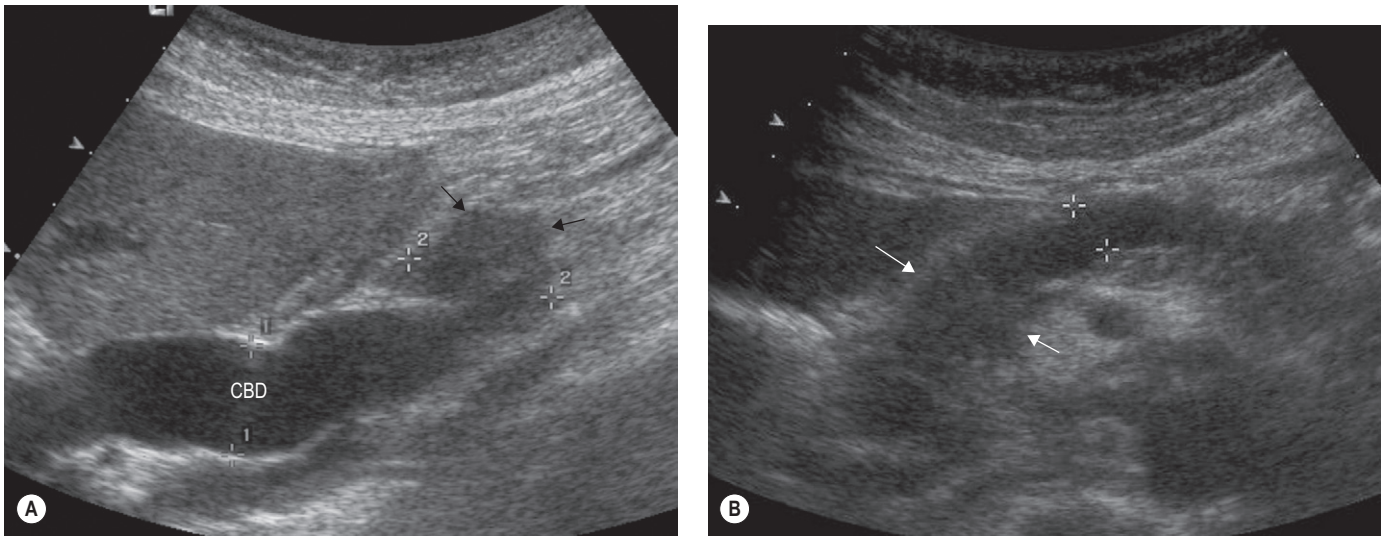


Figure 16.33 **Cancer-dilated ducts. A:** Dilated CBD down to a small obstructing mass (arrows). **B:** Dilated pancreatic duct and parenchymal atrophy secondary to an obstructing mass (arrows).

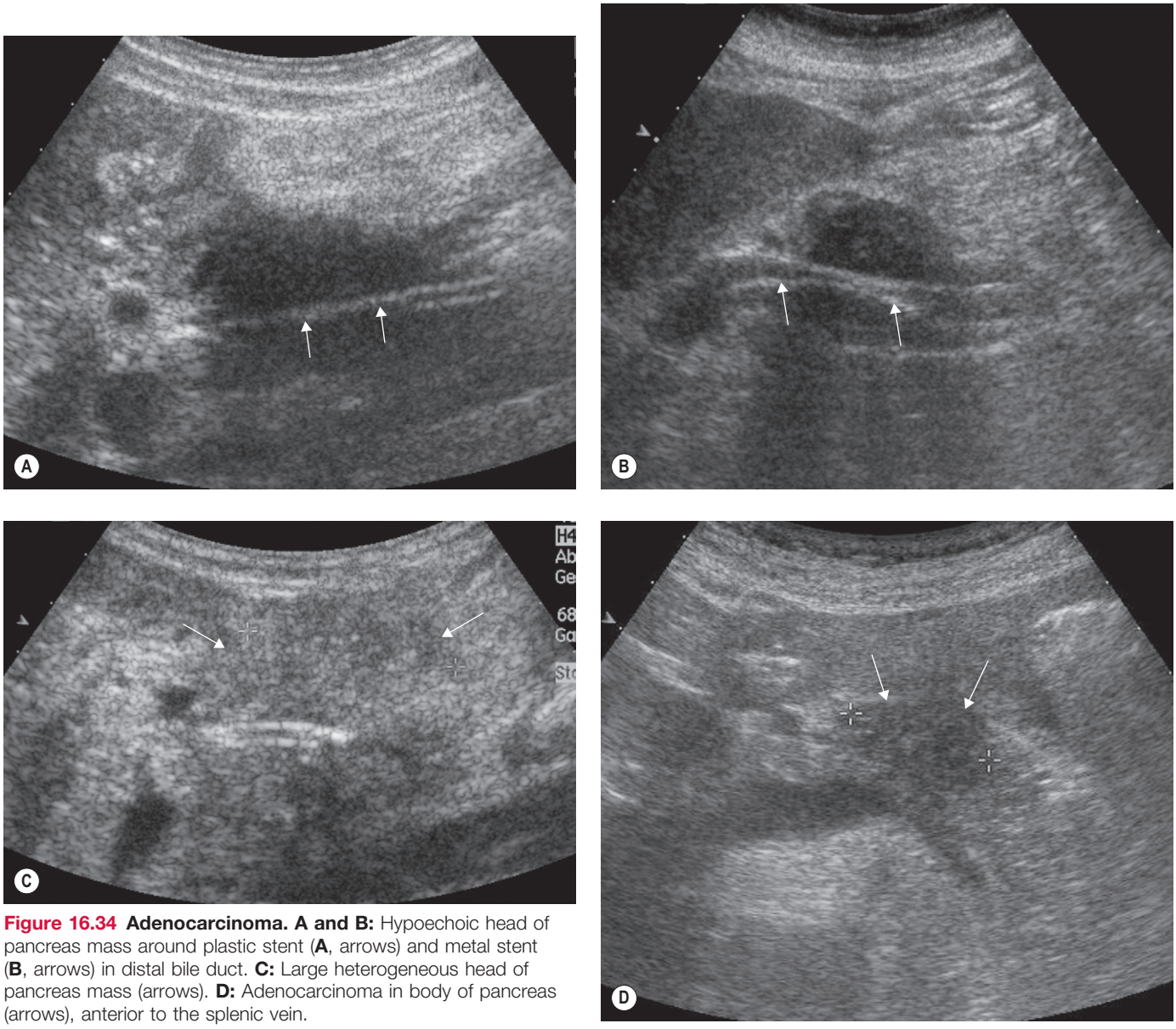


Figure 16.34 **Adenocarcinoma. A and B:** Hypoechoic head of pancreas mass around plastic stent (**A**, arrows) and metal stent (**B**, arrows) in distal bile duct. **C:** Large heterogeneous head of pancreas mass (arrows). **D:** Adenocarcinoma in body of pancreas (arrows), anterior to the splenic vein.

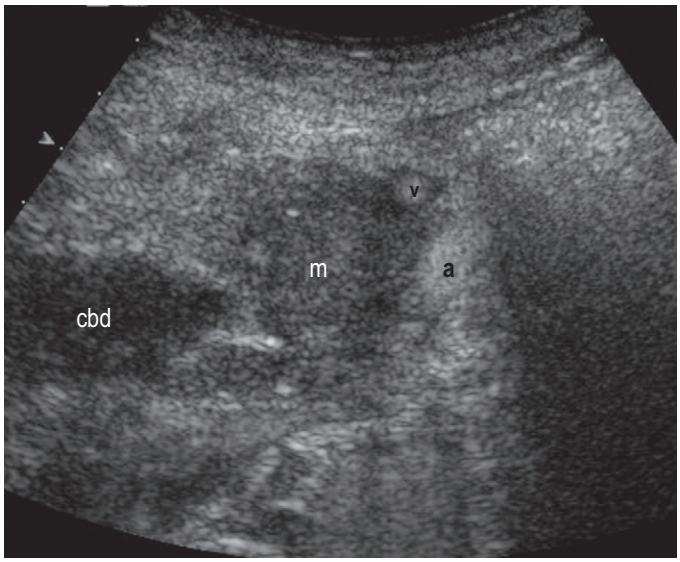
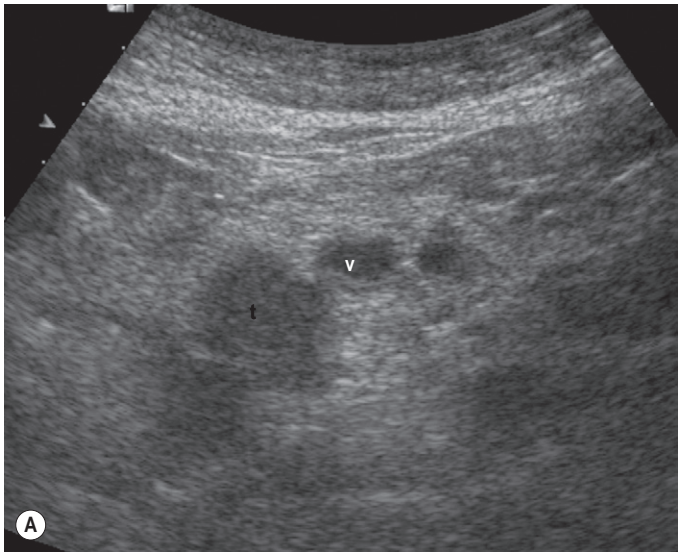
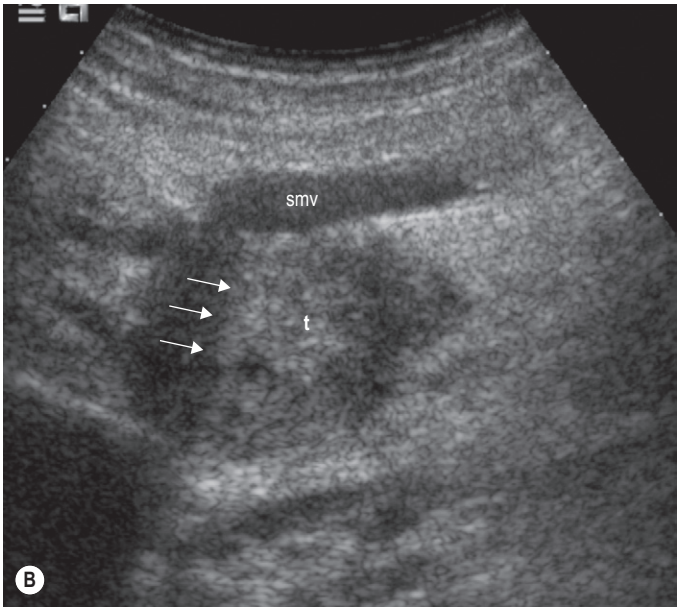
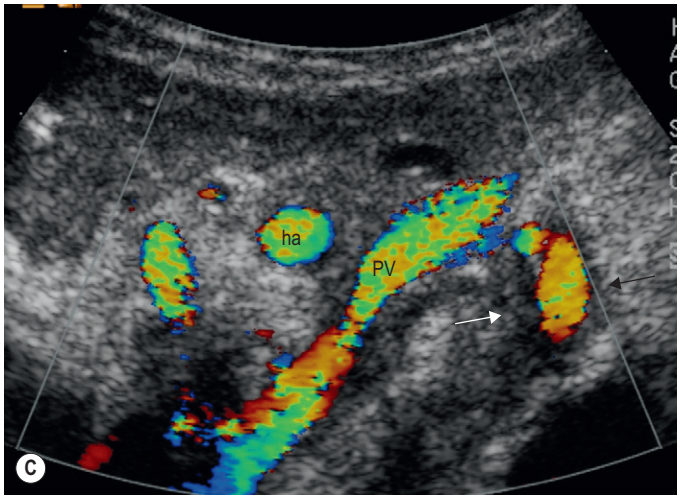


Figure 16.35 SonoVue cancer. Hypovascular mass (m) obstructing distal bile duct (cbd), encasing SMV (v) and touching SMA (a).







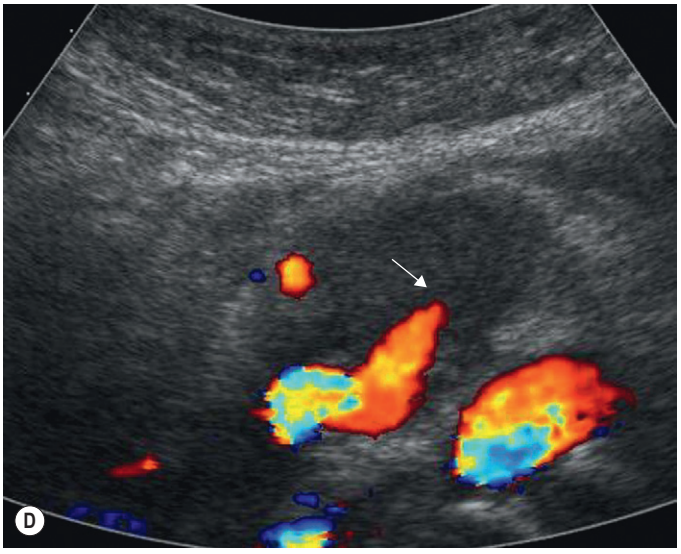


Figure 16.36 Venous involvement. A: Tumour (t) just touching SMV (v) but echogenicity around vessel preserved. **B:** Sagittal US showing loss of echogenicity between tumour (t) and portal vein superiorly (arrows), although this is preserved with the SMV (smv) anteriorly. **C:** Colour Doppler showing tumour encasing and narrowing the portal vein (PV), partially encasing the hepatic artery (ha), and further tumour encasing the SMA (arrows). **D:** Colour Doppler demonstrating complete occlusion of the portal vein (arrow).

extent may be impossible on US since the mass is then almost isoechoic to normal pancreas. Ultrasound contrast media may be helpful in this situation, and the tumour may be better shown as a hypovascular mass than on post-contrast CT scans[6,94] (Figs 16.9C and 16.35). The sensitivity of US tumour detection is 72–98%, and specificity greater than 90%.[6] However, overall contrast-enhanced CT is more sensitive than contrast-enhanced US in tumour detection,[6] and CT is also more objective with consistently better images.

Tumour size is important to record since it may have prognostic value; masses under 2 cm not surprisingly have a more favourable outlook.[95]

Assessment of the local extent of the tumour should be made, and whether there is invasion into the stomach and duodenum – gastric distension with fluid suggests gastroduodenal stricturing. Posterior extension into retroperitoneal fat occurs early and tumour tracks along perineural sheaths and lymphatics. The mesenteric vessels, portal vein and main arterial branches should be assessed for any vessel encroachment, encasement or occlusion by tumour. If the tumour is in contact with the portal vein or SMV it is not necessarily invading these structures – any loss of echogenicity of the vessel wall suggests invasion (Fig. 16.36). Any tumour contact with the hepatic artery, superior mesenteric artery (SMA) and coeliac axis suggests vessel involvement (Fig. 16.37). More obvious signs of vascular involvement are direct tumour extension into vessel lumen, complete encasement, vessel distortion and narrowing, and vessel occlusion. Colour flow US can be very helpful in defining the vessels, and more clearly showing a strictured segment. Acute vascular thrombosis may be difficult to diagnose on greyscale US if the thrombus is very hypoechoic, and so colour flow US can also be useful in clarifying this. Doppler US may show high velocity jets through strictured segments and turbulent flow beyond this, but in practice the greyscale and colour flow information allows adequate vascular assessment. Lymphadenopathy may occur, and this is seen usually around the pancreaticoduodenal region, hepatoduodenal region and around the coeliac axis. Slightly enlarged reactive nodes are common after bile duct stent insertion, but significantly enlarged abdominal nodes are likely to be involved (Fig. 16.38). The liver should be carefully assessed for any metastases; these are often small (Fig. 16.38) and better seen on CT than US. The presence of ascites suggests peritoneal metastases, the latter occasionally seen on ultrasound.

Endoscopic ultrasound detects smaller lesions not seen on US, and also gives better staging/assessment of portal vein/SMV involvement[2,3] (Fig. 16.39). Much has been written comparing EUS with CT and other imaging modalities for detection and staging of pancreatic masses, but many of these studies are heavily biased in favour of EUS. EUS performs best as a complementary technique for problem-solving after the operator has studied the cross-sectional images – it is an invasive technique which should not be used on its own for evaluating pancreatic tumours since it does not perform well if the operator is blinded to the results of other imaging studies.[96]

Pancreatic tumours – adenocarcinoma

- 90% of pancreatic tumours are ductal adenocarcinomas with a poor prognosis due to metastases and local vascular invasion.
- The differential diagnosis of a solid focal pancreatic mass also includes focal pancreatitis, NET, lymphoma and metastases.
- Contrast-enhanced US may differentiate between vascular and non-vascular masses, but gives similar information to contrast-enhanced CT and MRI.
- US or EUS may detect a pancreatic mass if none is seen on CT or MRI, so can be useful for problem-solving in suspected pancreatic neoplasms.
- Surgery for pancreatic cancer has become more aggressive, and although metastases and arterial encasement precludes surgery, portal venous involvement can be dealt with by venous grafts.
- US or EUS may define the extent of portal venous involvement if CT/MRI are inconclusive.

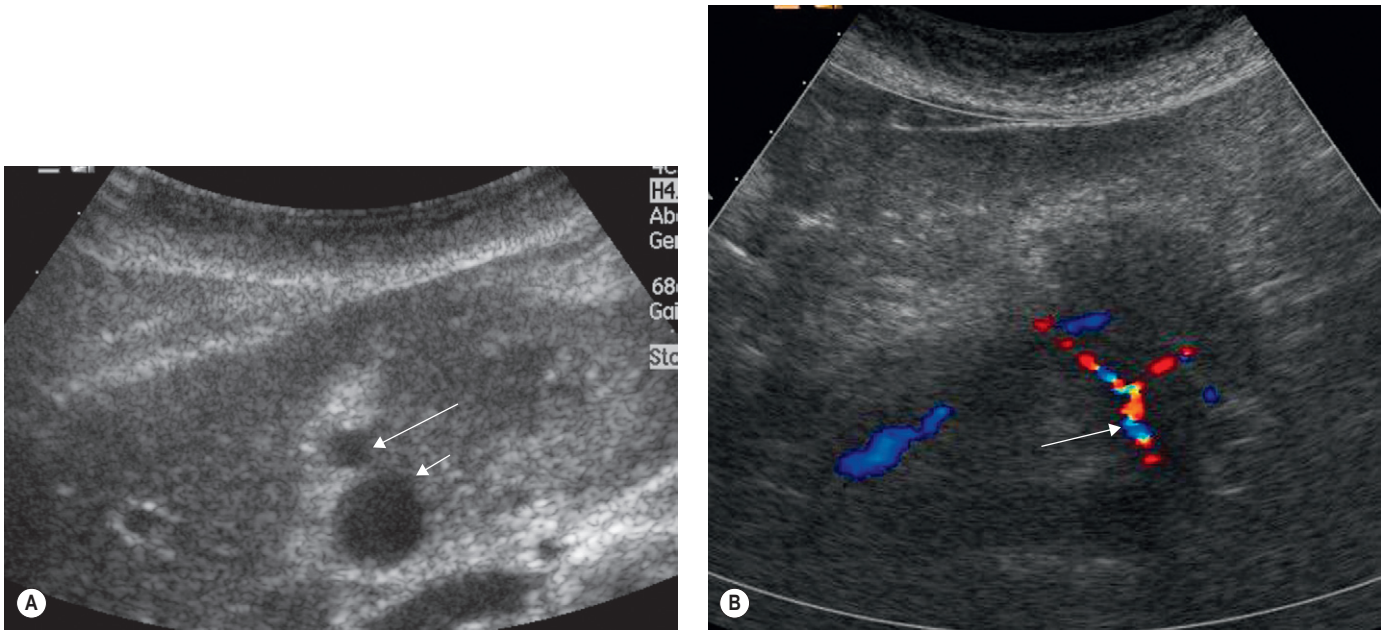


Figure 16.37 Arterial involvement. A: Sagittal view of a pancreatic tumour involving the inferior margin of the hepatic artery (long arrow) and the anterior inferior wall of the portal vein (short arrow). **B:** Encasement and narrowing of the coeliac axis (arrow) and its main branches by a large pancreatic body tumour, the narrowed vessels well seen with colour Doppler.

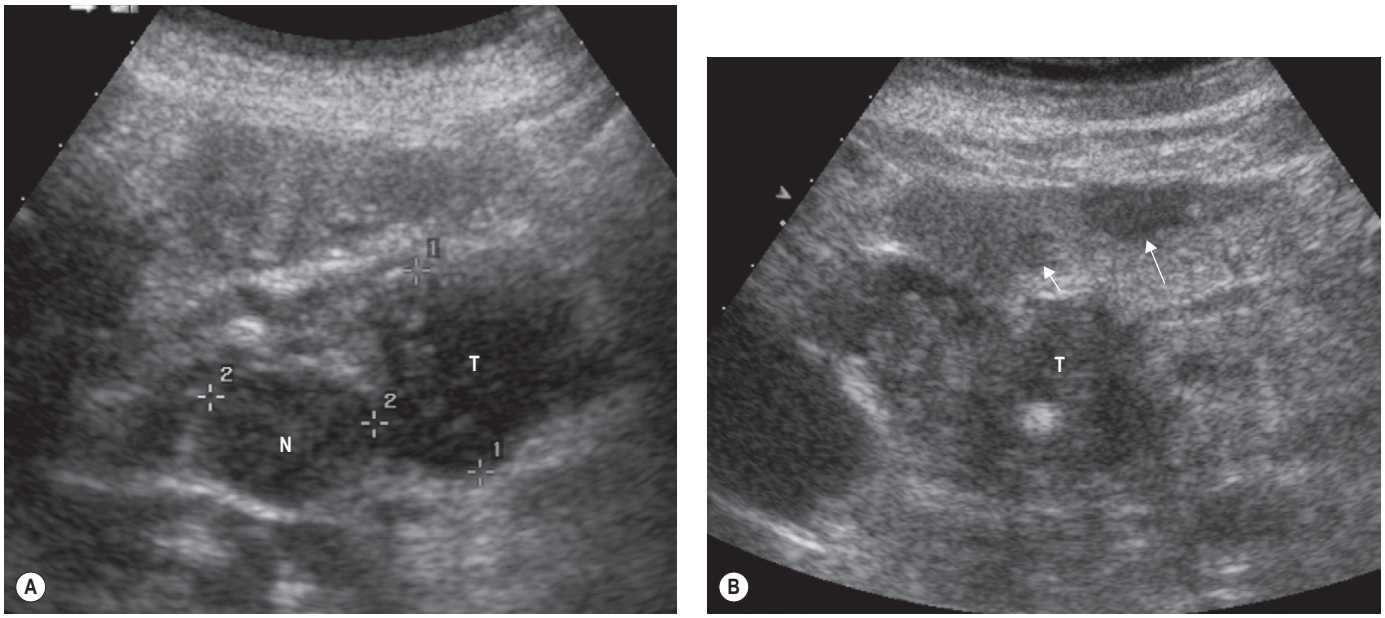
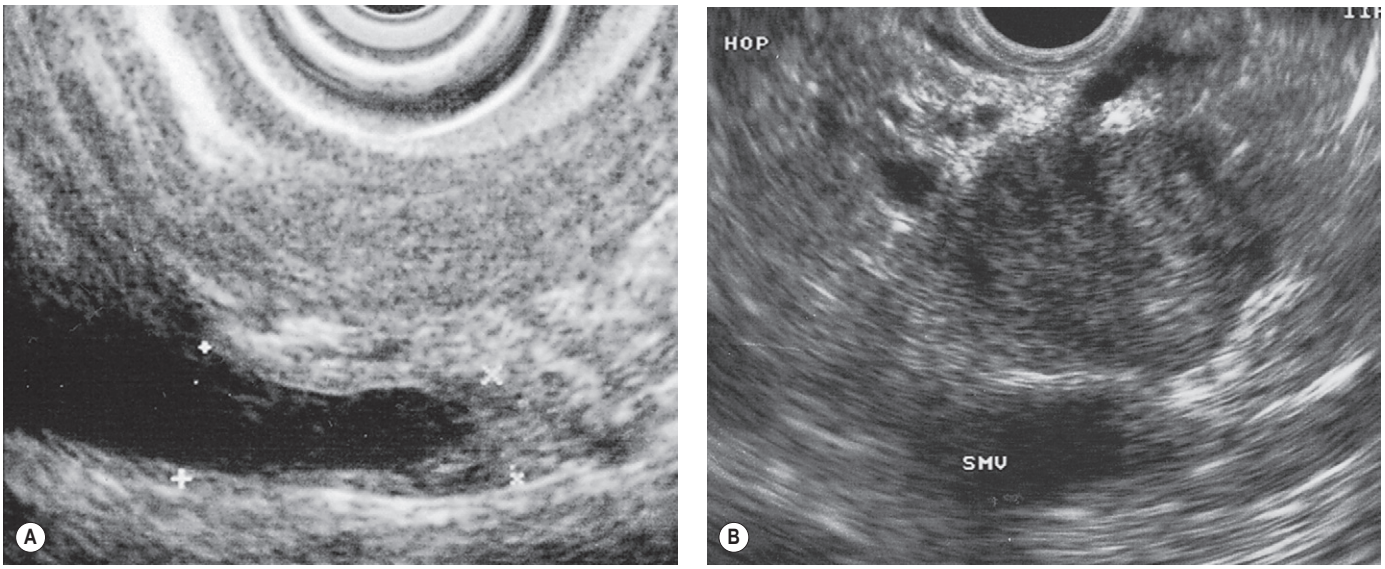


Figure 16.38 **Nodes and liver metastases. A:** Pancreatic head tumour (T) with a large adjacent lymph node (N). **B:** Pancreatic tumour (T) surrounding a biliary stent, and two metastases at the edge of the adjacent left lobe of liver (arrows).



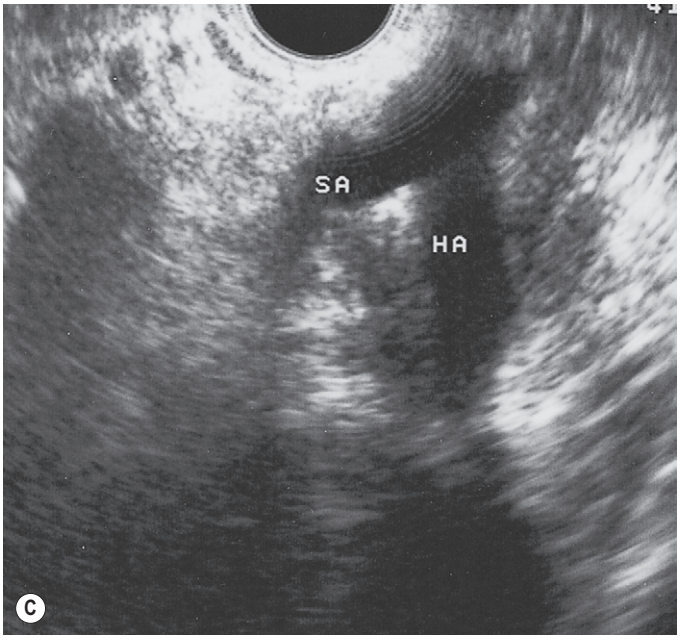


Figure 16.39 **EUS staging. A:** Small mass in distal CBD, not shown on CT or regular US. **B:** Small pancreatic head tumour lying close to SMV but not invading wall. **C:** Small volume tumour infiltration around the hepatic artery (HA). SA, splenic artery.

Cystic neoplasms

Cystic pancreatic neoplasms are uncommon and represent 10–15% of all pancreatic neoplasms. Some cystic pancreatic lesions have specific imaging features allowing differentiation. The more common cystic neoplasms include serous cystadenomas, mucinous cystic neoplasms and IPMN. Less common causes of cystic pancreatic neoplasms include cystic endocrine tumours and cystic metastases.[97] Other causes of cystic pancreatic lesions include pseudocysts, hydatid cysts and true congenital cysts.

Because of the dramatic improvement in imaging quality and also use, small cystic pancreatic lesions are being increasingly detected in asymptomatic individuals.[98]

Serous cystadenoma

Previously called microcystic adenoma, this is a benign lesion, usually found in women above 50 years. It usually occurs in the head of pancreas. It is a well-defined tumour consisting of multiple small cysts (<2 cm) (Fig. 16.40). Cysts contain glycogen-rich serous fluid separated by a vascular fibrous stroma with numerous thin septa. In up to 15% of cases there is a central scar which may calcify. If cysts are tiny (<2 mm), the lesion is seen on US as a well-defined echogenic mass (shows enhancement on contrast-enhanced US). It can have some mass effect and larger lesions can compress adjacent structures. The cysts do not communicate with the MPD, but the duct may be compressed and dilate distal to this. This lesion is non-malignant, and so biopsy/resection is not necessary if typical

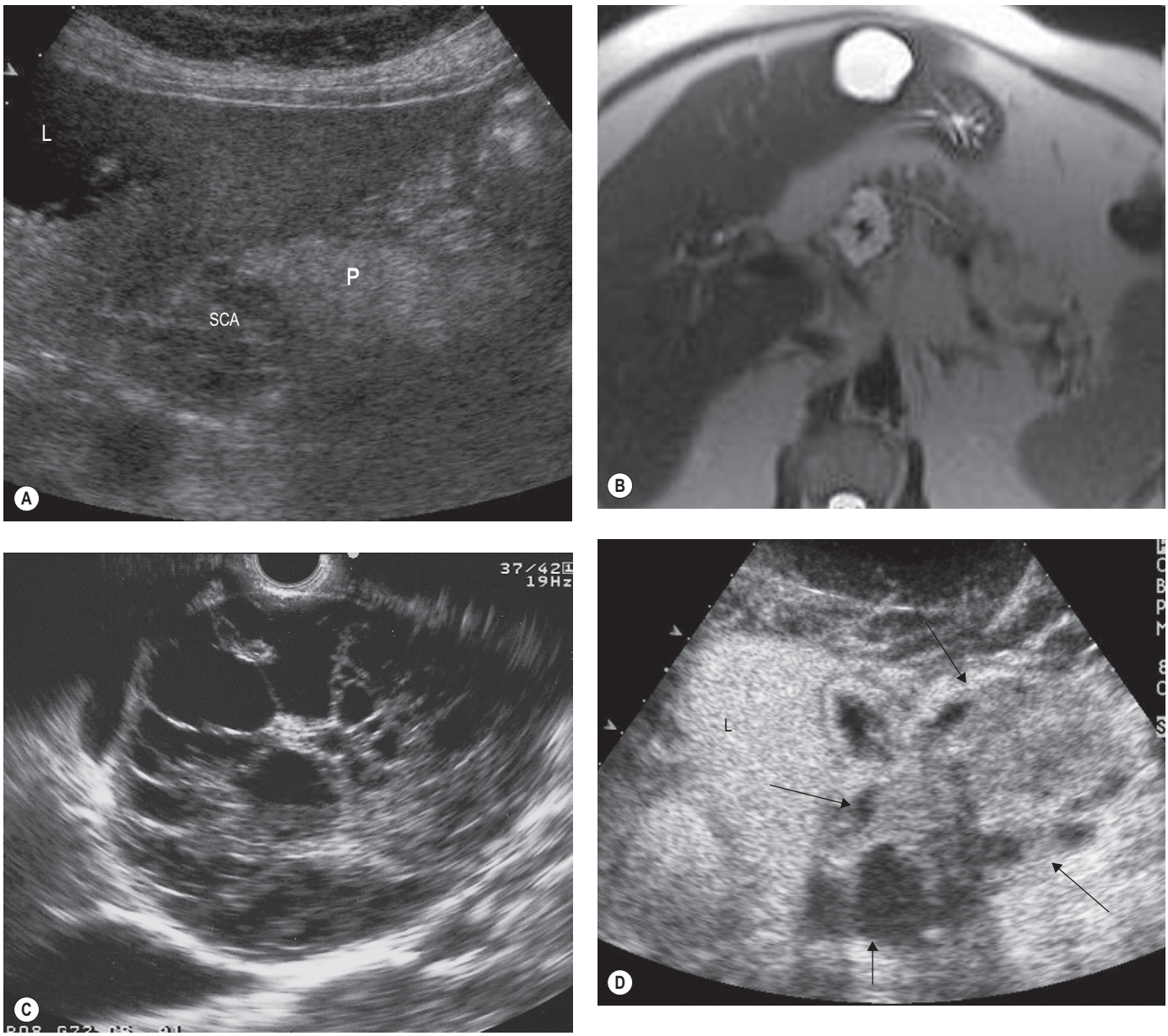


Figure 16.40 Serous cystadenoma. A: Well-defined, heterogeneous and mainly solid-looking mass (SCA) in the pancreatic head and neck with a few tiny cysts. The pancreatic body (P) was echogenic. Large cyst (L) is seen in the liver. **B:** Corresponding T2-weighted MR image with a bright T2 lesion indicating it is cystic, with a central signal void in keeping with a scar. **C:** Cystadenoma seen on EUS with detailed view of small cysts of variable size and an echogenic stroma. **D:** Following microbubble contrast enhancement, a larger cystadenoma (arrows) shows moderate enhancement, some calcification and larger cysts. Enhancing liver (L) is also seen.

imaging features are present. The decision to biopsy or resect is made based on the ultrasound/CT/MR features: only typical serous cystadenomas are observed on follow-up imaging; others are resected or followed up usually after biopsy confirmation of the diagnosis.[99–101]

Mucinous cystic neoplasm

This was previously called macrocystic adenoma. It may be malignant or have a high risk of malignant change, and so is resected if the diagnosis is made or suspected. It usually occurs in women aged 30–50 years, mostly in the margin of the body/tail of pancreas. It may be unilocular or multilocular and the cysts are typically >2 cm. The cysts are lined by columnar epithelium and contain mucin, which may result in fine echoes on US. There may be nodular or papillary projections and septations on US; the wall is usually thick and may be calcified (Fig. 16.7 and 16.41). When there is malignant change, there may be metastases to the nodes and liver.

This neoplasm has a much better prognosis than ductal adenocarcinoma following surgical resection.[102]

Intraductal papillary mucinous neoplasms (IPMN)

These are characterised by proliferation of pancreatic ductal epithelium and excessive production of mucin. They may be main duct type, branch duct type, or a combined type. They are benign or low-grade malignant neoplasms, but foci of aggressive cancer may form and become invasive.[103]

There is usually very dilated, non-strictured MPD containing mucin (may be reflective on ultrasound) (Fig. 16.42A,B). ERCP typically shows a patulous papilla with mucin extruding, and this is diagnostic; there may be filling defects on a pancreatogram due to mucin or mural nodules. The branch type is due to cystic ectasia of a side branch and is seen as a cyst communicating with the MPD, which is not usually dilated (main differential diagnosis is pseudocyst) (Fig. 16.42C,D). There is a good prognosis with long-term survival after pancreatectomy. Resection is usually performed for main duct IPMN, but is more controversial for branch duct type, which can usually be managed with follow-up imaging and resected if they cause symptoms, become >3 cm in size, associated with dilatation of the main pancreatic duct, or if they contain mural nodules.[104]

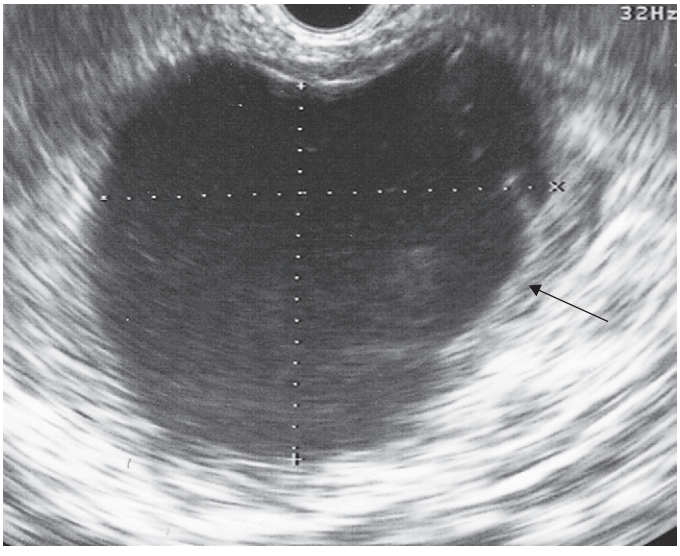


Figure 16.41 Mucinous cystic neoplasm. EUS showed a large cyst with a slightly irregular and thickened wall (arrow).

Solid pseudopapillary neoplasm

This is a rare low-grade malignant tumour, usually occurring in young women.[105,106] It occurs more frequently in the head of pancreas, and appears on imaging as a large well-defined heterogeneous mass with solid and cystic elements – there are typically finger-like projections of pseudopapillary excrescences. It may be completely cystic if there is extensive necrosis of haemorrhage. Fluid–fluid debris may be seen, and there may be calcification in the periphery of the mass. It is generally hypovascular following contrast medium injection, but any solid tissue within it does enhance. It may appear solid on ultrasound.

Cystic neoplasms

- Cystic pancreatic neoplasms include serous cystadenomas, mucinous cystic neoplasm, IPMN, solid pseudopapillary neoplasm, cystic NETs and cystic metastases.
- Serous cystadenomas are benign lesions with multiple <2 cm cysts, and may appear as an echogenic mass if the cysts are tiny (<2 mm).
- Mucinous cystic neoplasms may be uni- or multilocular, and the cysts are typically >2 cm. Nodular projections or septations may be seen on US.
- IPMNs produce mucin which distends the duct and the papilla. They may be main duct type or branch duct type, the latter presenting as a cystic mass without significant main duct dilatation.
- Small incidental pancreatic cysts are being increasingly detected, and may be due to a small pseudocyst, serous cystadenoma, mucinous cystic neoplasm, or IPMN. If the cyst is <3 cm, unilocular and asymptomatic, then it is very likely to be benign and can be followed up on imaging. Septations or solid components warrant further investigation such as EUS FNA for tumour markers and cytology.

Management of cystic pancreatic lesion

This is an increasingly common problem in view of improved imaging resulting in a greater number of cystic pancreatic lesions being detected (Fig. 16.43).

The commonest causes to consider are pseudocyst, serous cystadenoma, mucinous cystic neoplasm and IPMN.

If there is a clear history of pancreatitis and the imaging features are consistent with a pseudocyst, then it is usually reasonable to manage as such, with either follow-up or drainage. However, consideration should be given to the possibility of pancreatitis occurring secondary to a cystic neoplasm. If there is a cluster of tiny cysts in an echogenic stroma, then it may be reasonable to treat as a serous cystadenoma and follow up with imaging unless the patient is symptomatic.

All patients with pancreatic cysts should be assessed clinically, serum tumour markers measured, and then considered for detailed thin section multislice CT, MRI with MRCP (to look for any obvious communication with duct), and EUS with cyst fluid analysis.[100]

Assessment should be of cyst size, septations, calcification, mural/intracystic nodules and communication with the pancreatic duct.[107]

EUS morphology is of limited use in view of significant inter- and intra-observer variability.[108] However, fluid viscosity (?mucin) and a raised CEA (or CA19.9) are useful in predicting a premalignant or malignant cyst; abnormal cytology is rarely seen.[107,109]

Cysts which are symptomatic, multilocular (solid components and thick wall), with raised tumour markers or mucin, or abnormal cytology, should be considered for surgical resection.[107,109] Small unilocular cysts are nearly always benign, but the presence of

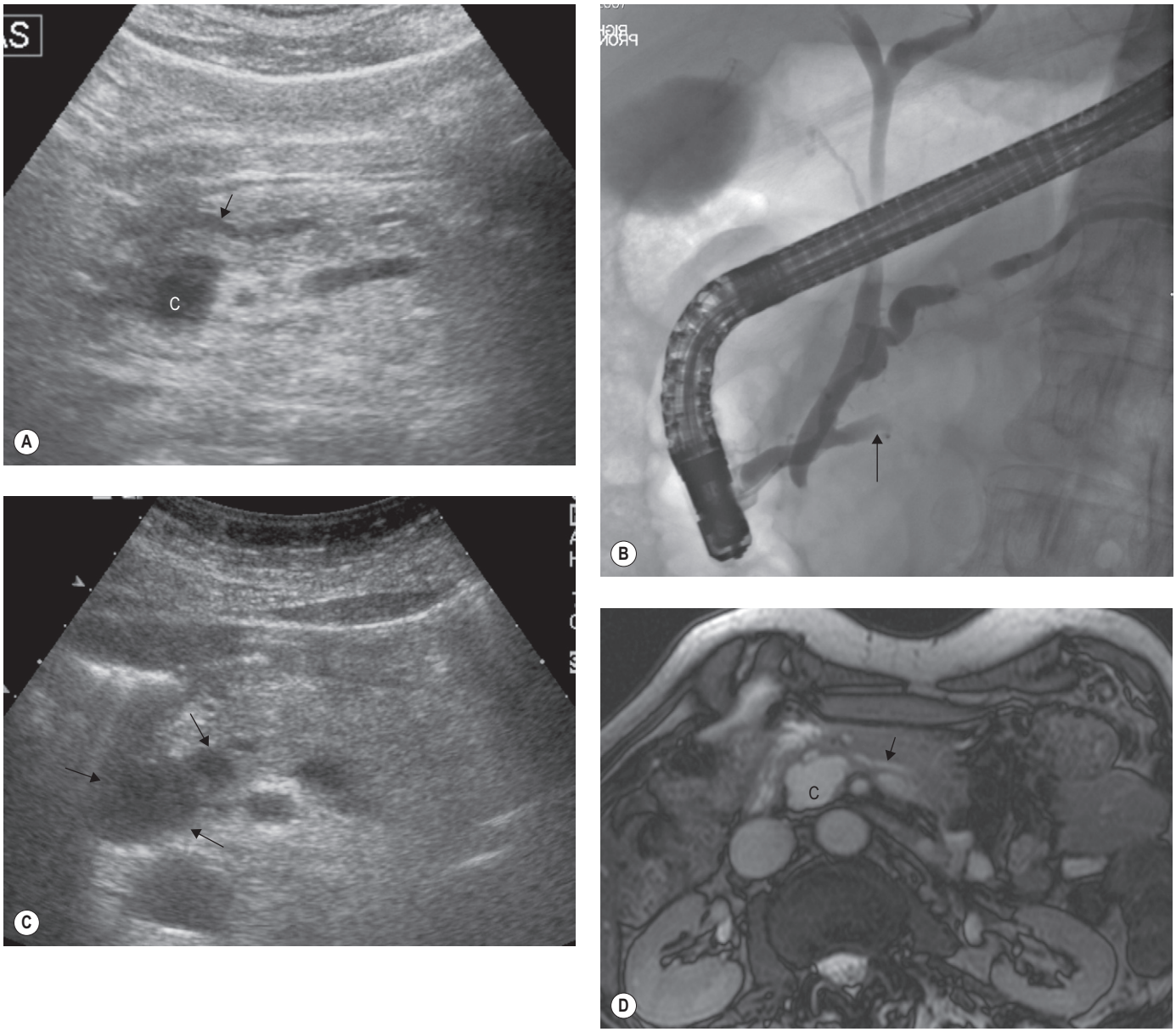


Figure 16.42 **IPMN. A:** Dilated pancreatic duct (arrow) and cyst (c) in head of pancreas. **B:** Corresponding ERCP, this patient had pancreas divisum and the accessory papilla was open and had mucus extruding from it, which is diagnostic of an IPMN. Opacification showed mobile filling defects (arrow) in large branch connecting to main duct, in keeping with mucus. **C:** Lobulated cyst (arrows) in pancreatic head without main duct dilatation. **D:** Corresponding MRI (T2-weighted sequence) with cyst (c) and non-dilated pancreatic duct (arrow).

septations, although not diagnostic of malignancy, is associated with borderline or in-situ malignancy in 20% of cases.[110]

Small asymptomatic cysts, <3 cm, with no suspicious features on imaging or EUS aspirate, may be followed up. These will be the majority of incidental pancreatic cysts. Follow-up of these lesions has not been clearly defined, but suggested to be for at least 4 years since the growth rate of small cystic neoplasms is usually very slow;[109,111] a repeat FNA should be considered if there is change in cyst morphology/size or clinical circumstances.[109] Size criteria alone are insufficient, since a significant number of cysts <3 cm are malignant or mucinous.[112]

Neuroendocrine tumours (NETs)

Pancreatic neuroendocrine tumours arise from the islet cells, and may be functioning (85%) or non-functioning (15%) depending on whether they secrete excess hormones leading to specific clinical syndromes.[113,114] Most solitary tumours occur sporadically, but multiple NETs usually occur in familial multiple endocrine neoplasia (MEN) type 1.[115] The commonest functioning tumours are insulinomas (50–60%) and gastrinomas (20%), and because of the symptoms caused they present early and are usually small. Most (90%) insulinomas are benign, single, intrapancreatic and <2 cm at presentation.[113] Malignant insulinomas (about 10%) are usually >3 cm and about a third have metastases at time of diagnosis.[6] Gastrinomas are often small (40% are <1 cm) and multiple and about 60% are malignant – they produce excessive gastrin, resulting in increased gastric acid and peptic ulcers (Zollinger–Ellison syndrome).[110,112] They are more difficult to localise than insulinomas, and are more often extra-pancreatic. They are typically located in the gastrinoma triangle, a region defined by the junction of the cystic duct/CBD, junction of the second and third portions of the duodenum, and junction of head/neck of pancreas. About 25–30% of NETs of the

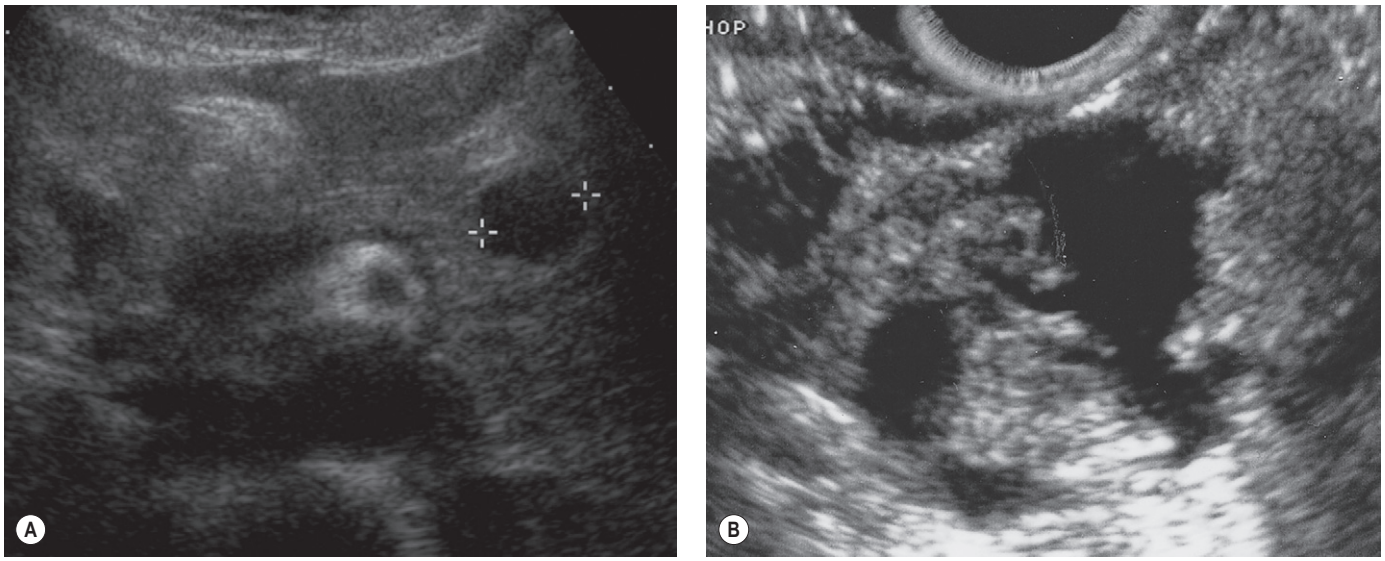


Figure 16.43 Incidental cysts. A: Thin-walled 1.6 cm cyst at junction of body/tail of pancreas. EUS aspirate showed clear fluid with low tumour markers. **B:** 2 cm cyst identified on CT, but EUS showed irregular outline and solid components, and aspiration revealed mucin and raised tumour markers. Pathology after resection showed an IPMN.

pancreas are non-functioning neuroendocrine tumours, and have variable size at diagnosis, 1–20 cm.[6] They are increasingly detected incidentally as small masses during multislice CT, sometimes picked up on routine abdominal ultrasound. When symptomatic, they are large or metastatic (up to 90%) – symptoms are non-specific and related to mass effect on adjacent organs. At presentation they are often malignant, but less aggressive than adenocarcinomas.

Imaging NETs

The diagnosis of functioning NETs is usually based on clinical presentation and abnormal biochemistry.

Imaging is used to localise the tumour, define its relationships in particular to vessels and the pancreatic duct to allow surgical planning for enucleation or partial pancreatectomy, and for the detection of metastases.[114,116] Localisation of the primary tumour is often difficult, but detecting and resecting a benign insulinoma usually leads to a cure.[113] No single imaging test is clearly superior, and most patients have several different imaging studies. Arterial and venous phase thin collimation CT is almost routinely used, the tumours often strongly enhancing on the early phase; sensitivity for detection with CT is up to 80%, depending on tumour size.[116] MRI should be used if CT is negative, and has similar sensitivity but may detect some lesions not seen on CT.[113,116] Somatostatin receptor scintigraphy with radiolabelled octreotide is also a very useful test for imaging the primary tumour and any metastases, since about 80% of NETs have a high concentration of somatostatin receptors.[117] Transhepatic portal venous sampling and selective arterial calcium stimulation with hepatic venous sampling may also be used in some centres.[113]

Ultrasound

NETs are typically round, well-defined and hypoechoic masses, and they may have a hypoechoic halo. They may be detected on transabdominal US despite a negative CT and MRI. Functioning NETs are usually small, but non-functioning ones are typically large if symptomatic. Small NETs are usually easy to identify if the surrounding pancreas is echogenic, but in young patients a hypoechoic NET can be difficult to define within a relatively hypoechoic pancreas (Fig. 16.44). Calcification or cystic change may be present.

Neuroendocrine tumours (NETs)

- NETs arise from islet cells and are functioning in 85% of cases – insulinomas and gastrinomas are the most common.
- Insulinomas are usually benign (90%), single, intra-pancreatic, and <2 cm.
- Gastrinomas are often multiple and small (40% are <1 cm), and 60% are malignant. They are often extra-pancreatic.
- 25–30% of NETs are non-functioning, and if symptomatic are usually large or metastatic. However, they are being increasingly detected as small incidental pancreatic masses on CT or US.
- Localisation of a small functioning NET can be difficult, and EUS and IOUS have very useful roles in the imaging work-up of these cases.
- US contrast enhancement can be useful, but of only occasional practical value since the majority of these patients will have contrast-enhanced CT and/or MRI.

The sensitivity of transabdominal US for detecting NETs has wide variation in the literature, 20–86%, increasing with tumour size;[116] use of harmonic imaging increases the definition and sensitivity for detecting these tumours.[19] Contrast-enhanced US also improves the sensitivity (reported to be greater than 90%) of detecting these lesions, which are usually vascular.[7] US can be a very powerful imaging tool, especially in experienced hands, but will remain of limited value in very large patients.

Endoscopic ultrasound has been reported to have the highest preoperative sensitivity of over 90%,[113,118] and is particularly useful for detecting small lesions (Figs 16.44, 16.45). In expert hands tiny gastrinomas may be detected in the gastroduodenal wall. Tumours adjacent to the pancreas can be difficult to differentiate from a benign lymph node, and so EUS FNA can be used to help establish the diagnosis with sensitivities >85% for a correct histological diagnosis.[119] Intraoperative ultrasound (IOUS) can be very helpful. If not detected preoperatively, the surgeon can sometimes feel the tumour at laparotomy. IOUS combined with surgical palpation has a very high sensitivity of nearly 100%, but does require very experienced operators and complete exposure and assessment of the whole pancreas.[113] Laparoscopic US can also be used and has been reported to have high sensitivity of

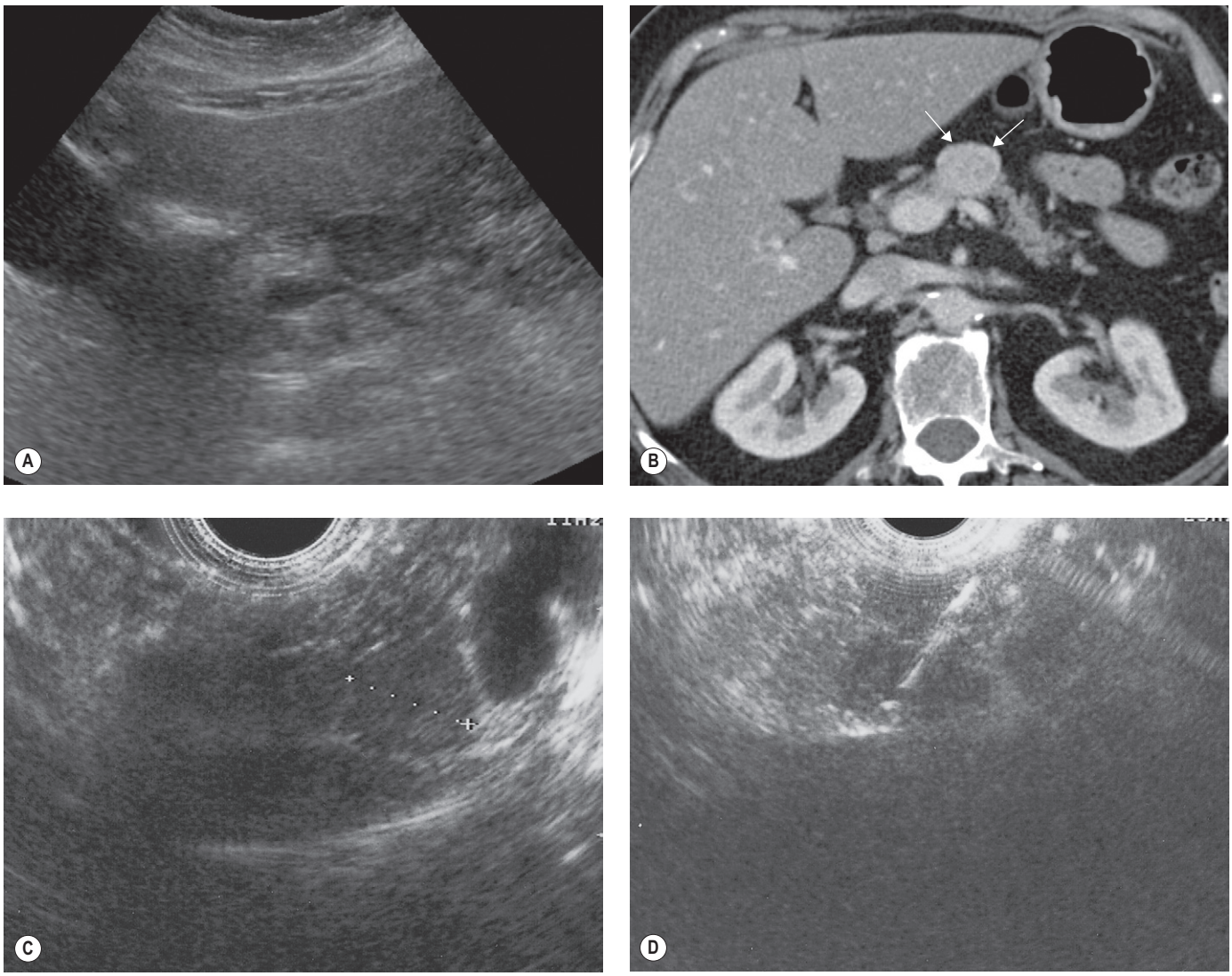


Figure 16.44 Neuroendocrine tumours. A: Incidental hypoechoic NET extending anterior to an echogenic pancreas, surrounded by some hypoechoic intra-abdominal fat and against the undersurface of an echogenic liver. **B:** Corresponding CT showing marked arterial phase enhancement of tumour (arrows). **C:** EUS showing a hypoechoic nodule just visible within a hypoechoic pancreatic tail. **D:** EUS FNA confirmed a NET.

80–90% for detecting small NETs (Fig. 16.13), which may then be possible to resect laparoscopically.[120]

Non-functioning NETs are well defined on US and usually easy to see because of their size at presentation. They often have areas of necrosis, haemorrhage or calcification, and so are heterogeneous on US (Fig. 16.46). Larger lesions may show cystic degeneration. An irregular or ill-defined margin is suggestive of malignancy.[116]

Miscellaneous tumours

Lymphoma

Pancreatic lymphoma is rare. Primary pancreatic lymphoma may be large and multifocal and there may be enlarged peripancreatic nodes, but it is not usually associated with significant lymphadenopathy elsewhere.[121] Secondary involvement of the pancreas may occur, usually with widespread lymphadenopathy and often hepatosplenomegaly. On US pancreatic lymphoma appears as hypoechoic focal or diffuse pancreatic enlargement (Fig. 16.47). Features that should increase suspicion for pancreatic lymphoma include: pancreatic duct not significantly dilated despite the presence of a large mass; no significant parenchymal atrophy; and enlarged nodes below the level of the renal hilum.[122] Biopsy is important if pancreatic lymphoma is suspected since most cases respond well to chemotherapy.[123]

Metastases

These can occur from lung, GI tract, breast, kidney or melanoma,[124] and may be seen as focal or multifocal masses or diffuse pancreatic enlargement. The commonest primary tumour to metastasise to the pancreas reported in surgical resection series is renal cell cancer.[125] The tumours may be solid or cystic, and are usually hypoechoic on US (Fig. 16.48).

Many cases detected present late after the original diagnosis or surgical resection of the primary cancer, and surgical resection has been reported with good survival rates.[126]

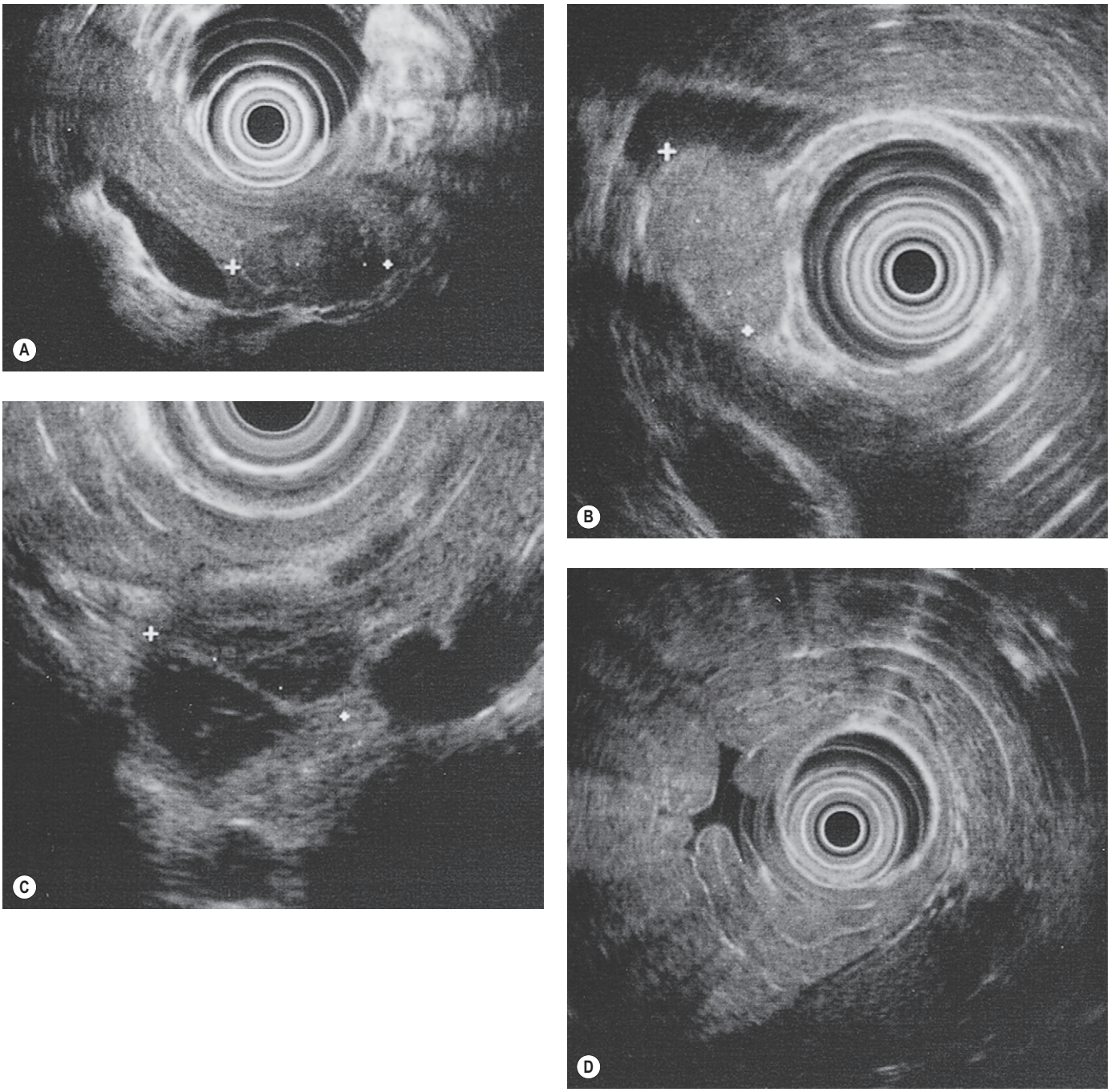


Figure 16.45 **NETs on EUS. A:** Hypoechoic insulinoma. **B:** Extra-pancreatic gastrinoma, relatively echogenic. **C:** Cystic extra-pancreatic gastrinoma. **D:** Corresponding EUS views of thickened gastric folds, in keeping with hypergastrinaemia.

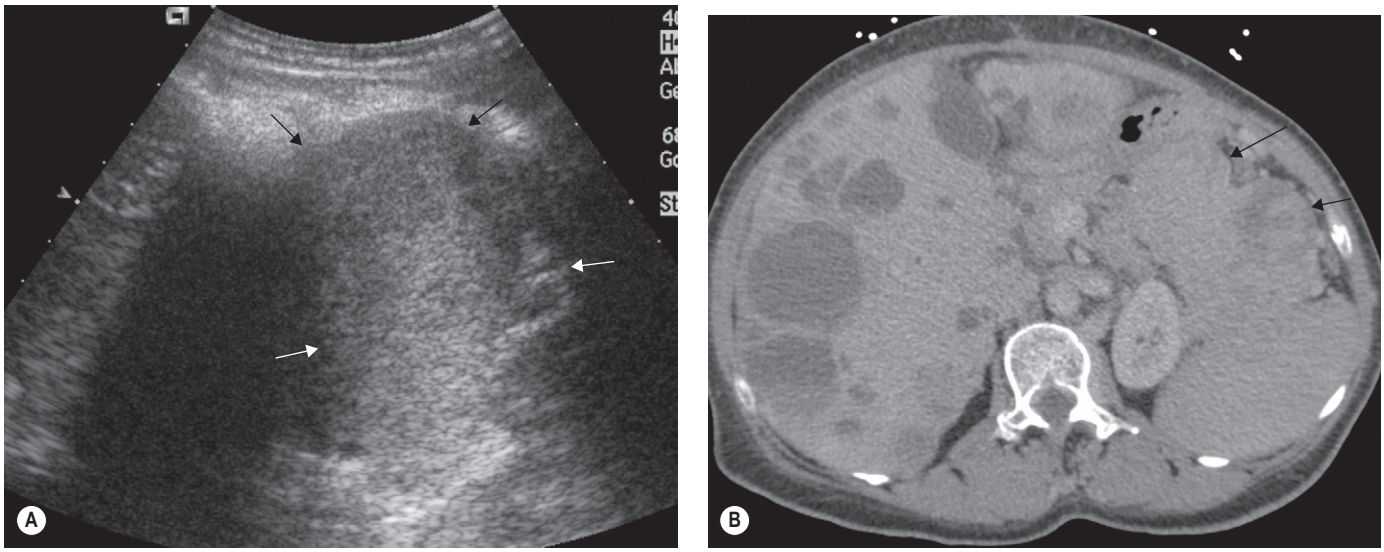


Figure 16.46 **Large NET. A:** Large mass arising from tail of pancreas (arrow). **B:** Corresponding CT with pancreatic tail mass (arrow) and numerous cystic liver metastases.

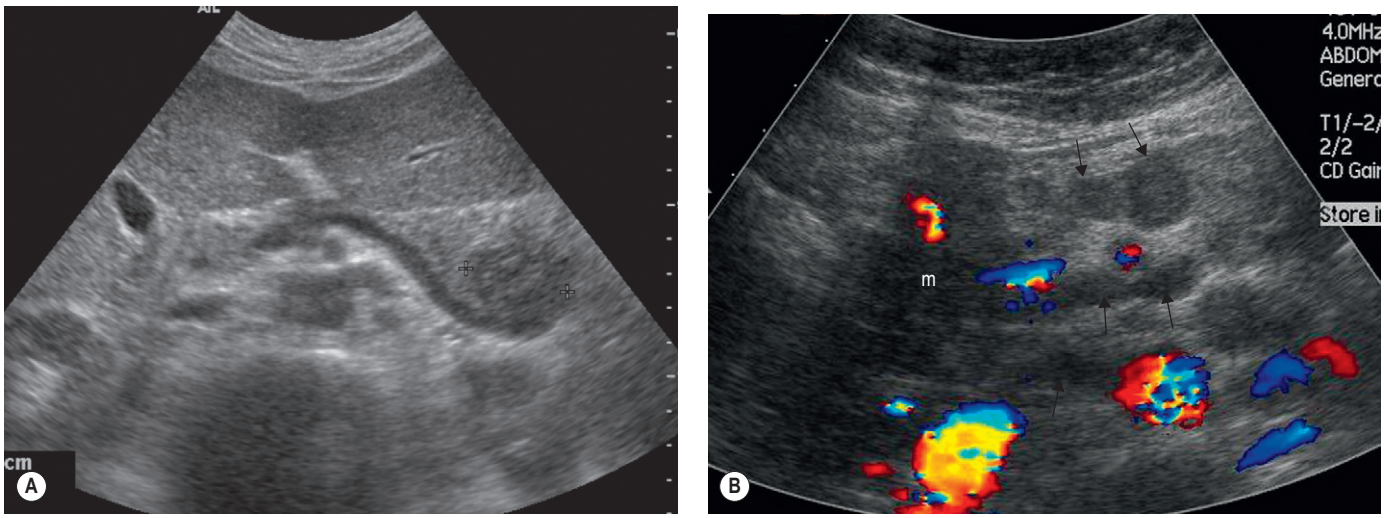


Figure 16.47 **Lymphoma. A:** Focal mass in pancreatic tail in HIV-positive patient; biopsy showed this to be lymphoma. **B:** Large mass in head of pancreas (m) with multiple adjacent enlarged nodes (arrows).

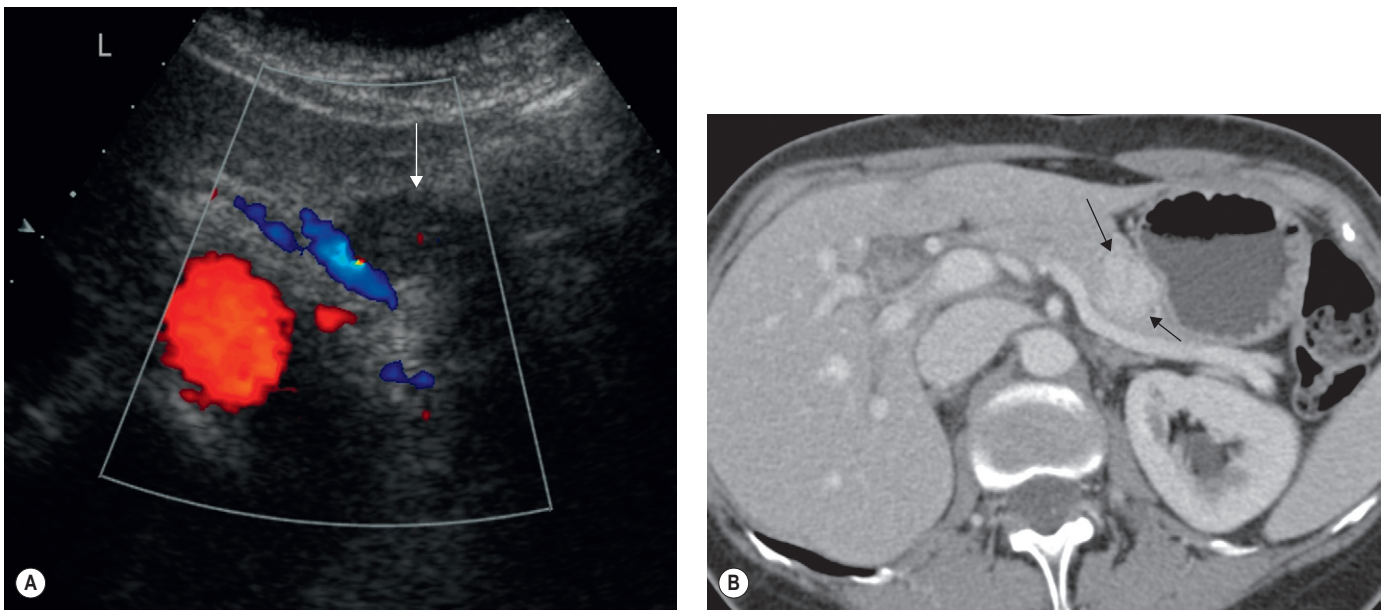


Figure 16.48 **Metastases. A and B:** Focal hypervascular mass (arrows) in pancreatic tail several years after resection of a renal cancer. EUS FNA confirmed a renal cancer metastasis.

PANCREATIC BIOPSY

Indications

Although certain imaging findings suggest specific causes of pancreatic masses, the imaging features do overlap. Patients found to have a potentially resectable pancreatic mass generally should not have a biopsy for confirmation – these patients are worked up for surgical resection.[127] A small proportion of patients who have had resections will have benign pathology on histology, most commonly focal pancreatitis mimicking pancreatic cancer. Patients who are thought to be surgically resectable should only proceed to biopsy if they are not suitable for surgery for other reasons. In these patients and in others who have extensive inoperable local or metastatic pancreatic tumours, tissue confirmation of the diagnosis is appropriate to allow any alternative treatment such as chemotherapy and for prognostic purposes. Another group of patients in whom biopsy is appropriate is patients whose imaging and clinical presentation is atypical for pancreatic cancer, and the possibility exists of diagnoses such as lymphoma or a benign mass, which would require different management strategies. There may be an argument for not subjecting some patients to a biopsy if there is a typical imaging appearance of adenocarcinoma and no further management change is likely based on the results.[128] Such patients may include very elderly or frail patients in whom chemotherapy may not be appropriate.

Techniques

Percutaneous biopsy is performed with CT or US guidance, and an increasingly used alternative is EUS-guided FNA or core biopsy (Figs 16.12B, 16.44D, 16.49). Although CT guidance is often preferred for FNA or Tru-cut biopsy of pancreatic masses, US guidance has significant advantages if the mass is well seen. Sometimes a mass may be easier to see with US than with CT. Smaller masses are more effectively biopsied using US since the mass can be fixed and held down by the US transducer and the biopsy needle-tip guided into the mass, and the position of the needle-tip confirmed immediately after biopsy. US-guided pancreatic biopsy is generally a quicker technique than CT-guided biopsy. For difficult cases a combination of US and CT guidance can be used. EUS-guided biopsy is the safest technique since the mass is seen up against the duodenal or gastric wall, and so the needle only has to take a short track to reach the mass. EUS FNA of pancreatic masses using a 19–21G needle has been widely performed and reported (recommended number of passes: seven), and more recently EUS-guided core biopsy has been reported.[127] The main advantage of using EUS is the easier targeting of smaller pancreatic masses, combined with the likelihood of fewer complications. The presence of a cytotopathologist during EUS FNA has been shown to improve sensitivity significantly and reduces the number of unnecessary passes once adequate diagnostic tissue is obtained.[127]

Percutaneous US-guided biopsy is performed after the patient has fasted for 6 hours, and any coagulopathy or low platelet count excluded. Sedation is not generally used, but should be considered for difficult cases or repeat biopsies. For head of pancreas masses a longitudinal US transducer position is ideal, allowing the mass to be targeted from an inferior position, angling the needle caudocranially. An attempt is made to avoid transverse colon and any major vessels, although it is likely that any small venous collaterals become compressed during transducer pressure and can be difficult to avoid – however, the risk of significant bleeding from these vessels is low. Also, it is unlikely that traversing the transverse colon results in any significant complications.[129]

The advantage of obtaining a core biopsy over an FNA is that a better tissue sample is usually obtained for histological evaluation and immunohistochemical staining, allowing more reliable diagnosis of NETs and lymphoma.[130]

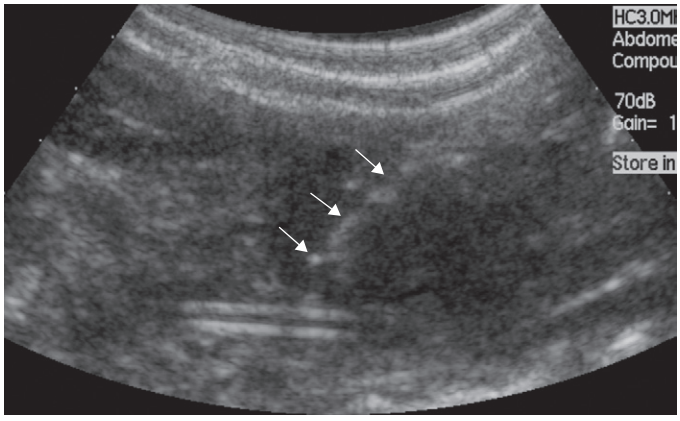


Figure 16.49 Biopsy. Echogenic needle tract (arrows) through pancreatic head mass close to plastic stent.

Results

Reported studies with all techniques have shown very good sensitivities and specificities.

Most reported studies on percutaneous techniques have used CT- or US-guided fine-needle aspiration (FNA). Percutaneous core biopsy reports have been small series with variable techniques and wide variations in reported sensitivities of 45–91%.[128] One large multicentre study reported US-guided fine-needle cytology and histology sensitivities of 87% and 94%, respectively.[131] Another large series reported the accuracy of US-guided biopsy to be 95%, compared to 86% for CT-guided biopsy.[119]

A study comparing EUS biopsy and CT/US biopsy showed similar accuracies of 76% and 81%, respectively,[132] with EUS being used mainly for smaller and more difficult lesions. There have been numerous publications of the results of EUS FNA of pancreatic masses, with sensitivities of 85–90%, and specificities of almost 100%.[127,133] The results depend on operator experience, the presence of a cytopathologist, and the nature of the pancreatic mass.[134,135] Well-differentiated adenocarcinoma, necrotic or cystic tumours, or associated chronic pancreatitis/desmoplastic reaction all contribute to difficulty in obtaining a reliable pathological diagnosis, and a 19G EUS Tru-cut core biopsy needle has been developed for better tissue samples.[136] However, experience with the EUS Tru-cut needle has not been good compared to EUS FNA in terms of diagnostic samples obtained, although combining FNA and Tru-cut EUS biopsies has given better results than FNA alone, 96% versus 87%.[133]

Repeating an initially negative biopsy is appropriate in most cases; sometimes multiple biopsies are required to make a diagnosis.[128] However, obtaining a false negative biopsy may delay diagnosis and treatment, and should not prevent surgery if there is a high clinical and radiological suspicion of pancreatic malignancy – in these circumstances a biopsy is not indicated.[137] If the mass is not thought to be surgically resectable, or the patient is unfit for surgery, then repeating an initially negative biopsy is usually appropriate to guide further management.[128]

Complications

The complication rate for pancreatic biopsy is low, theoretically greater for percutaneous targeted biopsies compared to EUS guidance.

For percutaneous biopsies, the minor complication rate is up to 5%, mainly post-procedure pain, and the major complication rate is about 1% including bleeding, duodenal perforation and abscess.[128,129,131]

With EUS-guided biopsies, the reported complication rate is 1–3%, the most frequent being self-limiting pain or mild pancreatitis; others include a small haematoma and very rarely duodenal perforation.[127,133,138]

Although the risk of peritoneal seeding with percutaneous biopsy of tumours is unclear, it is theoretically reduced with EUS-guided biopsy.[127,139]

False positive biopsies are rare, but can occur and are usually due to misinterpretation by the cytopathologist.[140]

Miscellaneous tumours; pancreatic biopsy

- Pancreatic lymphoma should be considered as a cause of a pancreatic mass if there are significantly enlarged adjacent lymph nodes, or a large mass without biliary or pancreatic duct dilatation.
- Pancreatic metastases can occur from renal cancer and melanoma, as well as cancers of the breast, lung and GI tract. Cases may present late after the diagnosis of the primary cancer.
- Biopsy is not indicated if a pancreatic mass is potentially resectable and likely to be a cancer.
- If the mass is inoperable, or there are atypical clinical or imaging features, then biopsy should be considered. This is often with CT or US guidance, but EUS-guided FNA and core biopsies are being increasingly performed.
- Complication rates from pancreatic biopsies are low, and EUS-guided biopsies are probably the safest.

PANCREATIC TRANSPLANTATION

Pancreatic transplantation is being increasingly performed throughout the world, with more than 15 000 transplantations reported to the International Pancreas Transplant Registry as of October 2000.[141] It can result in very good glucose control in diabetics and potentially reverse some of the complications. There has been a significant improvement in surgical technique, resulting in low mortality and 1-year graft function rates of up to 84%.[141] Pancreatic transplant is often combined with renal transplant in diabetic patients with end-stage nephropathy.

The most frequent operation involves transplanting the whole pancreas and duodenum onto the bladder with a duodenovesical anastomosis, the donor coeliac axis and superior mesenteric artery connected to the recipient common or external iliac artery, and the donor portal vein anastomosed to the recipient common or external iliac vein (Fig. 16.50A). Although this has a technically low complication rate, problems occur with venous outflow from the pancreas into the systemic circulation rather than the portal venous system, resulting in hyperinsulinism and early atherosclerosis. Also, exocrine secretions into the bladder can cause recurrent urinary tract infections, and graft pancreatitis can occur secondary to reflux.

To try to avoid these problems, grafts are increasingly being performed with portal-enteric drainage, so that the donor duodenum is anastomosed to jejunum and pancreatic venous outflow is drained into recipient superior mesenteric vein (Fig. 16.50B).

Postoperative complications include graft rejection, infection, pancreatitis, fluid collections, anastomotic leaks, vascular thrombosis and haemorrhage. The graft rejection rate is 7–9% after 1 year.[142] There are often no symptoms to suggest graft dysfunction, and so

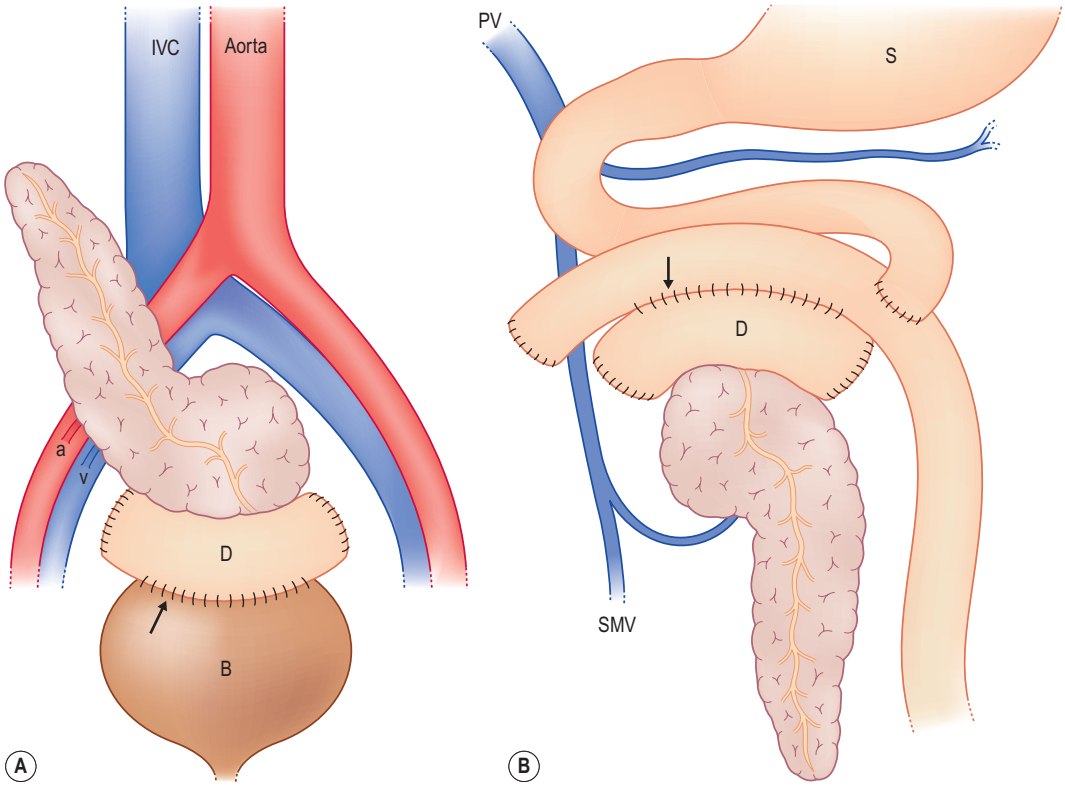


Figure 16.50 Pancreatic transplant. A: Diagram showing duodenovesical anastomosis (arrow). The donor aortic segment (a) containing the coeliac axis and SMA is attached to the recipient common iliac artery, and the donor portal vein (v) is attached to the common iliac vein. **B:** Diagram showing duodeno-jejunal anastomosis (arrow) with venous drainage into the recipient SMV. B, bladder; D, donor duodenum attached to pancreas; IVC, inferior vena cava; PV, portal vein; S, stomach; SMV, superior mesenteric vein.

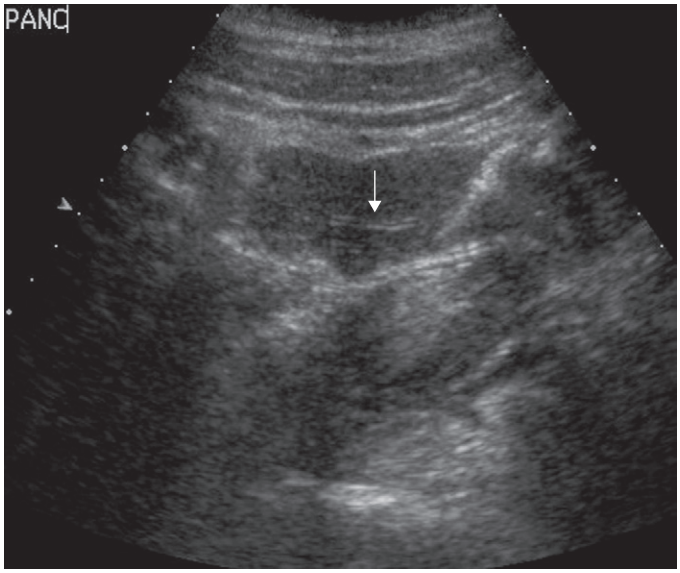


Figure 16.51 **Pancreatic transplant.** Normal post-transplant pancreas just deep to the abdominal wall, with a normal pancreatic duct (arrow). (Courtesy of Dr Paul Tait.)

Pancreatic transplantation

- Pancreatic transplantations are being increasingly performed with low mortality and 1-year graft function rates of up to 84%.
- Pancreatic and renal transplants are often combined in diabetic patients with end-stage nephropathy.
- The preferred technique is the donor duodenum (with pancreas) anastomosed to the recipient jejunum and venous flow to the SMV, rather than duodenum to bladder and venous flow to iliac vein as was originally done. This reduces complications.
- Graft dysfunction is often asymptomatic, and so regular monitoring is needed. Biochemical markers and US features of rejection are non-specific, and surveillance US-guided biopsy of the graft is often used.
- US is the main modality in the initial imaging assessment of pancreatic transplants, and may show collections or vascular problems.
- US views of the pancreatic transplant may be poor because of adjacent bowel gas and/or a small transplant. CT or MRI may be needed for further evaluation.

regular postoperative monitoring of biochemical markers is undertaken. Serum creatinine can be useful if a renal transplant has also been performed (since rejection usually involves both grafts), but otherwise assessment for rejection is difficult since biochemical markers such as amylase are not sensitive or specific, and surveillance US-guided biopsy of the pancreas is often used.[142]

US is the main initial imaging modality in assessing pancreatic transplants and detecting postoperative complications.[143] However, good visualisation of the transplanted pancreas is not always possible; it may be quite difficult to detect but any surrounding fluid collection makes it easier to define. The normal pancreatic transplant has soft tissue echogenicity surrounded by more echogenic omental and peritoneal fat (Fig. 16.51). Fluid collections are easy to see on US but non-specific and may be due to blood, urine, ascites or infection. Pancreatic necrosis may occur secondary to infection, and any air within the pancreas warrants CT to confirm infected necrosis.

The US findings of rejection and pancreatitis can be subtle and non-specific, making them difficult to diagnose and differentiate with US alone, and interpretation must be in conjunction with clinical and biochemical findings. US may show gland enlargement, poor definition of the margins and increased/heterogeneous echotexture in rejection and pancreatitis.[144]

Colour Doppler evaluation of the vessels may be very useful if CT cannot be used because of a high serum creatinine. Complications such as thrombosis, strictures and pseudoaneurysms may be detected. Echogenic thrombus can be detected, but if there is fresh thrombus it can appear very hypoechoic and confirmation of absent flow should be made with colour flow and Doppler analysis. Strictures should be suspected if there is high velocity or turbulent flow at anastomoses.

Percutaneous biopsy performed with US guidance is used for evaluating the graft if the biochemical markers and sonographic findings suggest an abnormality, or as part of surveillance for graft rejection.[145] An 18-gauge core biopsy needle is inserted directly into the pancreas under US guidance and usually two samples are taken, the success rate being as high as 96%.[145] The complication rate is low and includes intra-abdominal bleeding, haematuria, pancreatitis and pain, occurring in approximately 2–3% of cases.[141,142] Poor visualisation of the transplant because of adjacent bowel or a small transplant can result in technical failure.

The limitations of US should be recognised and consideration given to other imaging modalities to answer any further specific questions. CT may define deeper collections more precisely, and CT angiography can give excellent detail of the vessels. MRI is being increasingly used in evaluating such patients, giving cross-sectional imaging information and allowing MR angiography for evaluating vascular anatomy.

ACKNOWLEDGEMENTS

I thank Anita Patel for help with the figures.

REFERENCES

1. Kinney TP, Freeman ML. Recent advances and novel methods in pancreatic imaging. Minerva Gastroenterol Dietol 2008;54(1):85–95.
2. Miura F, Takada T, Amano H, et al. Diagnosis of pancreatic cancer. HPB (Oxford) 2006;8(5):337–342.
3. Nichols MT, Russ PD, Chen YK. Pancreatic imaging: current and emerging technologies. Pancreas 2006;33(3):211–220.
4. Kalra MK, Maher MM, Mueller PR, Saini S. State of the art imaging of pancreatic neoplasms. Br J Radiol 2003;76(912):857–865.
5. Shmulewitz A, Teefey SA, Robinson BS. Factors affecting image quality and diagnostic efficacy in abdominal sonography: a prospective study of 140 patients. J Clin Ultrasound 1993;21:623–630.
6. Martinez-Noguera A, D'Onofrio M. Ultrasonography of the pancreas. 1. Conventional imaging. Abdom Imaging 2007;32(2):136–149.
7. Rickes S, Monkemuller K, Malfertheiner P. Contrast-enhanced ultrasound in the diagnosis of pancreatic tumours. JOP 2006;7(6):584–592.
8. Rickes S, Rauh P, Uhle C, et al. Contrast-enhanced sonography in pancreatic diseases. Eur J Radiol 2007;64(2):183–188.
9. Kwon RS, Scheiman JM. New advances in pancreatic imaging. Curr Opin Gastroenterol 2006;22(5):512–519.
10. Levy MJ. Endoscopic ultrasound-guided trucut biopsy of the pancreas: prospects and problems. Pancreatology 2007;7(2–3): 163–166.
11. Chaya CT, Bhutani MS. Ultrasonography of the pancreas. 6. Endoscopic imaging. Abdom Imaging 2007;32(2):191–199.
12. Standing S, editor. Gray's anatomy: the anatomical basis of clinical practice. 40th Rev edn. Chapter 70, Pancreas. Edinburgh: Elsevier Health Sciences; 2008.
13. Hoff FL, Gabriel H, Hammond N, Gore RM. Pancreas: normal anatomy and examination techniques. In: Gore M, Levine M, editors. Textbook of gastrointestinal radiology. 3rd ed. Philadelphia: Saunders; 2008.

14. Quest L, Lombard M. Pancreas divisum: opinio divisa. Gut 2000;47(3):317–319.
15. Kamisawa T, Tu Y, Egawa N, et al. Clinical implications of incomplete pancreas divisum. JOP 2006;7(6):625–630.
16. Kamisawa T, Tu Y, Egawa N, et al. Pancreas divisum in pancreaticobiliary maljunction. Hepatogastroenterology 2008;55(81):249–253.
17. Zyromski NJ, Sandoval JA, Pitt HA, et al. Annular pancreas: dramatic differences between children and adults. J Am Coll Surg 2008;206(5):1019–1025.
18. Abu-Yousef MM, El-Zein Y. Improved US visualization of the pancreatic tail with simethicone, water, and patient rotation. Radiology 2000;217:780–785.
19. Hohl C, Schmidt T, Honnef D, et al. Ultrasonography of the pancreas 2. Harmonic imaging. Abdominal Imaging 2007;32:150–160.
20. Bertolotto M, D'Onofrio M, Martone E, et al. Ultrasonography of the pancreas 3. Doppler imaging. Abdominal Imaging 2007;32:161–170.
21. Uomo G. Ultrasound elastography. A possible improvement of the paraphernalia of pancreatic imaging. JOP 2008;9(5):666–667.
22. Das A, Mourad W, Lightdale CJ, et al. An international survey of the clinical practice of EUS. Gastrointest Endosc 2004;60(5):765–770.
23. Lennon AM, Penman ID. Endoscopic ultrasound in cancer staging. Br Med Bull 2007;84:81–98.
24. Kahl S, Malfertheiner P. Role of endoscopic ultrasound in the diagnosis of patients with solid pancreatic masses. Dig Dis 2004;22:26–31.
25. Rossi FT. Endoscopic ultrasound. Minn Med 2008;91(6):38–41.
26. Boujaoude J. Role of endoscopic ultrasound in diagnosis and therapy of pancreatic adenocarcinoma. World J Gastroenterol 2007;13(27):3662–3666.
27. Agarwal B, Krishna NB, Labundy JL, et al. EUS and/or EUS-guided FNA in patients with CT and/or magnetic resonance imaging findings of enlarged pancreatic head or dilated pancreatic duct with or without a dilated common bile duct. Gastrointest Endosc 2008;68(2):237–242.
28. Meining A, Dittler HJ, Wolf A, et al. You get what you expect? A critical appraisal of imaging methodology in endosonographic cancer staging. Gut 2002;50:599–603.
29. Keafalides PT, Gress F. Simulator training for endoscopic ultrasound. Gastrointest Endosc Clin N Am 2006;16(3):543–552.
30. Miura F, Takada T, Amano H, et al. Diagnosis of pancreatic cancer. HPB (Oxford) 2006;8:337–342.
31. De Angelis C, Martini M, Repici A, et al. Instruments and accessories for diagnostic endoscopic ultrasound (radial scanning and miniprobes). Minerva Med 2007;98(4):253–260.
32. D'Onofrio M, Vecchiato F, Faccioli N, et al. Ultrasonography of the pancreas 7. Intraoperative imaging. Abdom Imaging 2007;32(2): 200–206.
33. Jakimowicz JJ. Intraoperative ultrasonography in open and laparoscopic abdominal surgery: an overview. Surg Endosc 2006;20(Suppl 2):S425–435.
34. Falconi M, Bettini R, Boninsegna L, et al. Surgical strategy in the treatment of pancreatic neuroendocrine tumors. JOP 2006;7(1): 150–156.
35. Hayashibe A, Sakamoto K, Shinbo M, et al. A resected case of multiple intraductal papillary mucinous tumors of the pancreas with US guided ductal branch oriented partial pancreatectomy. Pancreatology 2005;5:462–465.
36. Wiersema MJ, Wiersema LM. Endosonography of the pancreas: normal variation versus changes of early chronic pancreatitis. Gastrointest Endosc Clin N Am 1995;5:487–496.
37. Marks V, Filly R, Callen P. Ultrasonic evaluation of normal pancreatic echogenicity and its relation to fat deposition. Radiology 1980;137:457–459.
38. Glaser J, Stienecker K. Pancreas and aging: a study using ultrasonography. Gerontology 2000;46(2):93–96.
39. Gupta A, Arenson A, Mckee J. Effect of steroid ingestion on pancreatic echogenicity. J Clin Ultrasound 1987;15:171–174.
40. Haber HP. Cystic fibrosis in children and young adults: findings on routine abdominal sonography. AJR Am J Roentgenol 2007;189(1): 89–99.
41. Martinez-Noguera A, Montserrat E, Torrubia S, et al. Ultrasound of the pancreas: update and controversies. Eur Radiol 2001;11: 1594–1606
42. Rajan E, Clain JE, Levy MJ, et al. Age-related changes in the pancreas identified by EUS: a prospective evaluation. Gastrointest Endosc 2005;61(3):401–406.
43. Ikeda M, Sato T, Morozumi A, et al. Morphologic changes in the pancreas detected by screening ultrasonography in a mass survey, with special reference to main duct dilatation, cyst formation and calcification. Pancreas 1994;9:508–512.
44. Glaser J, Stienecker K. Does aging influence pancreatic response in the ultrasound secretin test by impairing hydrokinetic exocrine function or sphincter of Oddi motor function. Dig Liver Dis 2000;32(1):25–28.
45. Osawa S, Kataoka K, Sakagami J, et al. Relation between morphologic changes in the main pancreatic duct and exocrine pancreatic function after a secretin test. Pancreas 2002;25(1):12–19.
46. Atri M, Nazarnia S, Mehio A, et al. Hypoechogenic embryologic ventral aspect of the head and uncinate process of the pancreas: in vitro correlation of US with histopathologic findings. Radiology 1994;190(2):441–444.
47. Coulier B. Hypoechogenic aspects of the ventral embryonic cephalic pancreas: a large prospective clinical study. J Belge Radiol 1996;79(3):120–124.
48. Savides TJ, Gress FG, Zaidi SA, et al. Detection of embryologic ventral pancreatic parenchyma with endoscopic ultrasound. Gastrointest Endosc 1996;43(1):14–19.
49. Kingsnorth A, O'Reilly D. Acute pancreatitis. BMJ 2006;332:1072–1076.
50. Srivastava R, Fraser C, Gentleman D, et al. Hyperamylasaemia: not the usual suspects. BMJ 2005;331:890–891.
51. Beger HG, Rau BM. Severe acute pancreatitis: clinical course and management. World J Gastroenterol 2007;13(38):5043–5051.
52. British Society of Gastroenterology. UK guidelines for the management of acute pancreatitis. Gut 2005;54(Suppl III):S1–9.
53. Gullo L, Migliori M, Pezzilli R, et al. An update on recurrent acute pancreatitis: data from five European countries. Am J Gastroenterol 2002;97:1959–1962.
54. Bhatia M, Wong FL, Cao Y, et al. Pathophysiology of acute pancreatitis. Pancreatology 2005;5(2–3):132–144.
55. Steinberg W, Tenner S. Acute pancreatitis. N Engl J Med 1994;330(17):1198–1210.
56. Kao LS, Bulger EM, Parks DL, et al. Predictors of morbidity after traumatic pancreatic injury. J Trauma 2003;55(5) 898–905.
57. Vasquez JC, Coimbra R, Hoyt DB, Fortlage D. Management of penetrating pancreatic trauma: an 11-year experience of a level-1 trauma center. Injury 2001;32(10):753–759.
58. Mattix KD, Tataria M, Holmes J, et al. Pediatric pancreatic trauma: predictors of nonoperative management failure and associated outcomes. J Pediatr Surg 2007;42(2):340–344.
59. Beger HG, Rau B, Mayer J, Pralle U. Natural course of acute pancreatitis. World J Surg 1997;21(2):130–135.
60. Dervenis C, Johnson CD, Bassi C, et al. Diagnosis, objective assessment of severity, and management of acute pancreatitis: Santorini consensus conference. Int J Pancreatol 1999;25:195–210.
61. McCullough LK, Sutherland FR, Preshaw R, Kim S. Gallstone pancreatitis: does discharge and readmission for cholecystectomy affect outcome? HPB (Oxford) 2003;5(2):96–99.
62. Gurusamy KS, Samraj K, Fusai G, Davidson BR. Early versus delayed laparoscopic cholecystectomy for biliary colic. Cochrane Database Syst Rev 2008 Oct 8;(4): CD007196.
63. Dervenis C. Assessments of severity and management of acute pancreatitis based on the Santorini Consensus Conference report. JOP 2000;1:178–182.
64. Al-Haddad M, Wallace MB. Diagnostic approach to patients with acute idiopathic and recurrent pancreatitis, what should be done? World J Gastroenterol 2008;14(7):1007–1010.
65. Yusoff IF, Raymond G, Sahai AV. A prospective comparison of the yield of EUS in primary vs. recurrent idiopathic acute pancreatitis. Gastrointest Endosc 2004;60:673–678.
66. Baron T. Treatment of pancreatic pseudocysts, pancreatic necrosis, and pancreatic duct leaks. Gastrointest Endosc Clin N Am 2007;17(3):550–579.
67. Rickes S, Uhle C, Kahl S, et al. Echo-enhanced ultrasound: a new valid initial imaging approach for severe acute pancreatitis. Gut 2006;55(1):74–78.
68. Al Mofleh IA. Severe acute pancreatitis: pathogenetic aspects and prognostic factors. World J Gastroenterol 2008;14(5):675–684.
69. Toouli J, Brooke-Smith M, Bassi C, et al. Guidelines for the management of acute pancreatitis. J Gastroenterol Hepatol 2002;17(suppl):S15–39.
70. Rau B, Pralle U, Mayer JM, Beger HG. Role of ultrasonographically guided fine-needle aspiration cytology in the diagnosis of infected pancreatic necrosis. Br J Surg 1998;85:179–184.

71. Carter CR, McKay CJ, Imrie CW. Percutaneous necrosectomy and sinus tract endoscopy in the management of infected pancreatic necrosis: an initial experience. Ann Surg 2000;232:175–180.
72. McErlean A, Looby S, Lee MJ. Percutaneous ultrasound-guided thrombin injection as first-line treatment of pancreatic pseudoaneurysm. Cardiovasc Intervent Radiol 2007;30:526–528.
73. Siddiqi AJ, Miller F. Chronic pancreatitis: ultrasound, computed tomography, and magnetic resonance imaging features. Semin Ultrasound CT MR 2007;28(5):384–394.
74. Forsmark CE. The diagnosis of chronic pancreatitis. Gastrointest Endosc 2000;52:293–298.
75. Walsh TN, Rode J, Theis BA, Russell RC. Minimal change chronic pancreatitis. Gut 1992;33:1566–1571.
76. Glasbrenner B, Kahl S, Malfertheiner P. Modern diagnostics of chronic pancreatitis. Eur J Gastroenterol Hepatol 2002;14(9): 935–941.
77. Wallace MB. Imaging the pancreas: into the deep. Gastroenterology 2007;132:484–487.
78. Balakrishnan V, Chatni S, Radhakrishnan L, et al. Groove pancreatitis: a case report and review of the literature. JOP 2007;8(5):592–597.
79. Lee H, Lee JK, Kang SS, et al. Is there any clinical or radiologic feature as a preoperative marker for differentiating mass-forming pancreatitis from early-stage pancreatic adenocarcinoma? Hepatogastroenterology 2007;54(79):2134–2140.
80. Raimondo M, Wallace MB. Diagnosis of early chronic pancreatitis by endoscopic ultrasound. Are we there yet? JOP 2004;5(1):1–7.
81. Wallace MB, Hawes RH, Durkalski V, et al. The reliability of EUS for the diagnosis of chronic pancreatitis: interobserver agreement among experienced endosonographers. Gastrointest Endosc 2001;53:294–299.
82. Kahl S, Glasbrenner B, Leodolter A, et al. EUS in the diagnosis of early chronic pancreatitis: a prospective follow-up study. Gastrointest Endosc 2002;55(4):507–511.
83. Remer EM, Baker MB. Imaging of chronic pancreatitis. Radiol Clin North Am 2002;40:1229–1242.
84. Homma T, Harada H, Koizumi M. Diagnostic criteria for chronic pancreatitis by the Japan Pancreas Society. Pancreas 1997;15: 14–15.
85. Sahani DV, Kalva SP, Farrell J, et al. Autoimmune pancreatitis: imaging features. Radiology 2004;233(2):345–352.
86. Zandieh I, Byrne MF. Autoimmune pancreatitis: a review. World J Gastroenterol 2007;13(47):6327–6332.
87. Okazaki K, Uchida K, Matsushita M, Takaoka M. How to diagnose autoimmune pancreatitis by the revised Japanese clinical criteria. J Gastroenterol 2007;42(Suppl 18):32–38.
88. Deshpande V, Chiocca S, Finkelberg D, et al. Autoimmune pancreatitis: a systemic immune complex mediated disease. Am J Surg Pathol 2006;30:1537–1545.
89. Lowenfels AB, Maisonneuve P. Epidemiology and risk factors for pancreatic cancer. Best Pract Res Clin Gastroenterol 2006;20(2): 197–209.
90. Adham M, Mirza DF, Chapuis F, et al. Results of vascular resections during pancreatectomy from two European centres: an analysis of survival and disease-free survival explicative factors. HPB (Oxford) 2006;8(6):465–473.
91. Lind PA, Isaksson B, Almstrom M, et al. Efficacy of preoperative radiochemotherapy in patients with locally advanced pancreatic carcinoma. Acta Oncol 2008;47(3):413–420.
92. Loos M, Kleeff J, Friess H, Buchler MW. Surgical treatment of pancreatic cancer. Ann NY Acad Sci 2008;1138:169–180.
93. White R, Winston C, Gonen M, et al. Current utility of staging laparoscopy for pancreatic and peripancreatic neoplasms. J Am Coll Surg 2008;206(3):445–450.
94. Minniti S, Bruno C, Biasiutti C, et al. Sonography versus helical CT in identification and staging of pancreatic ductal adenocarcinoma. J Clin Ultrasound 2003;31(4):175–182.
95. Birk D, Fortnagel G, Formentini A, Beger HG. Small carcinoma of the pancreas. Factors of prognostic relevance. Hepatobiliary Pancreatic Surg 1998;5:450–454
96. Rosch T, Dittler HJ, Strobel K, et al. Endoscopic ultrasound criteria for vascular invasion in the staging of cancer of the head of the pancreas: a blind re-evaluation of videotapes. Gastrointest Endosc 2000;52(4):469–477.
97. Sidden CR, Mortele KJ. Cystic tumors of the pancreas: ultrasound, computed tomography, and magnetic resonance imaging features. Semin Ultrasound CT MR 2007;28(5):339–356.
98. Brugge WR, Lauwers GY, Sahani D, et al. Cystic neoplasms of the pancreas. N Engl J Med 2004;351(12):1218–1226.
99. Hung JS, Yang CY, Hu RH, et al. Surgical treatment of pancreatic serous cystadenoma: aggressive for operations but limited resections. Pancreas 2007;35(4):358–360.
100. Scheiman JM. Management of cystic lesions of the pancreas. J Gastrointest Surg 2008;12(3):405–407.
101. Belsley NA, Pittman MB, Lauwers GY, et al. Serous cystadenoma of the pancreas: limitations and pitfalls of endoscopic ultrasound-guided fine-needle aspiration biopsy. Cancer 2008;114(2):102–110.
102. Fernandez-del Castillo C. Mucinous cystic neoplasms. J Gastrointest Surg 2008;12(3):411–413.
103. Burdick JS. Intraductal papillary mucinous neoplasms. Gastrointest Endosc Clin N Am 2008;18(3):523–533.
104. Waters JA, Schmidt CM. Intraductal papillary mucinous neoplasm – when to resect? Adv Surg 2008;42:87–108.
105. Huang H-L, Shih S-C, Chang W-H, et al. Solid-pseudopapillary tumor of the pancreas: clinical experience and literature review. World J Gastroenterol 2005;11(9):1403–1409.
106. Choi J-Y, Kim M-J, Kim JH, et al. Solid pseudopapillary tumor of the pancreas: typical and atypical manifestations. AJR Am J Roentgenol 2006;187:W178–W186.
107. Edirimanne S, Connor SJ. Incidental pancreatic cystic lesions. World J Surg 2008;32(9):2028–2037.
108. Ahmad NA, Kochman ML, Brensinger C, et al. Interobserver agreement among endosonographers for the diagnosis of neoplastic versus non-neoplastic pancreatic cystic lesions. Gastrointest Endosc 2003;58:59–64.
109. Garcea G, Ong SL, Rajesh A, et al. Cystic lesions of the pancreas. A diagnostic and management dilemma. Pancreatology 2008;8(3):236–251.
110. Sahani DV, Saokar A, Hahn PF, et al. Pancreatic cysts 3 cm or smaller: how aggressive should treatment be? Radiology 2006;238:912–919.
111. Das A, Wells CD, Nguyen CC. Incidental cystic neoplasms of pancreas: what is the optimal interval imaging surveillance? Am J Gastroenterol 2008;103(7):1657–1662.
112. Walsh RM, Vogt DP, Henderson JM, et al. Management of suspected pancreatic neoplasms based on cyst size. Surgery 2008;144(4):677–684.
113. Abboud B, Boujaoude J. Occult sporadic insulinoma: localization and surgical strategy. World J Gastroenterol 2008;14(5):657–665.
114. Jani N, Moser AJ, Khalid A. Pancreatic endocrine tumors. Gastroenterol Clin North Am 2007;36:431–439.
115. Scarsbrook AF, Thakker RV, Wass JAH, et al. Multiple endocrine neoplasia: spectrum of radiologic appearances and discussion of a multitechnique imaging approach. Radiographics 2006;26(2):433–451.
116. Power N, Reznek RH. Imaging pancreatic islet cell tumours. Imaging 2002;14:147–159.
117. Intenzo CM, Jabbour S, Lin HC, et al. Scintigraphic imaging of body neuroendocrine tumors. Radiographics 2007;27(5):1355–1369.
118. Anderson MA, Carpenter S, Thompson NW, et al. Endoscopic ultrasound is highly accurate and directs management in patients with neuroendocrine tumors of the pancreas. Am J Gastroenterol 2000;95(9):2271–2277.
119. Ardengh JC, de Paulo GA, Ferrari AP. EUS-guided FNA in the diagnosis of pancreatic neuroendocrine tumors before surgery. Gastrointest Endosc 2004;60(3):378–384.
120. Jaroszewski DE, Schlinkert RT, Thompson GB, Schlinkert DK. Laparoscopic localization and resection of insulinomas. Arch Surg 2004;139:270–274.
121. Liakakos T, Misiakos EP, Tsapralis D, et al. A role for surgery in primary pancreatic B-cell lymphoma: a case report. J Med Case Reports 2008;2:167.
122. Leite NP, Kased N, Hanna RF, et al. Cross-sectional imaging of extranodal involvement in abdominopelvic lymphoproliferative malignancies. Radiographics 2007;27:1613–1634.
123. Saif MW, Khubchandani S, Walczak M. Secondary pancreatic involvement by a diffuse large B-cell lymphoma presenting as acute pancreatitis. World J Gastroenterol 2007;13(36):4909–4911.
124. Adsay NV, Andea A, Basturk O, et al. Secondary tumors of the pancreas: an analysis of a surgical and autopsy database and review of the literature. Virchows Arch 2004;444:527–535.
125. David AW, Samuel R, Eapen A, et al. Pancreatic metastasis from renal cell carcinoma 16 years after nephrectomy: a case report and review of the literature. Trop Gastroenterol 2006;27(4):175–176.
126. Bachmann J, Michalski CW, Bergmann F, et al. Metastasis of rectal adenocarcinoma to the pancreas. Two case reports and a review of the literature. JOP 2007;8(2):214–222.
127. Brugge WR. Pancreatic fine needle aspiration: to do or not to do? JOP 2004;5(4):282–288.

128. Amin Z, Theis B, Russell RC, et al. Diagnosing pancreatic cancer: the role of percutaneous biopsy and CT. Clin Radiol 2006;61(12): 996–1002.
129. Brandt KR, Charboneau JW, Stephens DH, et al. CT- and US-guided biopsy of the pancreas. Radiology 1993;187:99–104.
130. Ihse I, Axelson J, Dawiskiba S, Hansson L. Pancreatic biopsy: Why? When? How? World J Surg 1999;23:896–900.
131. Di Stasi M, Lencioni R, Solmi L, et al. Ultrasound-guided fine needle biopsy of pancreatic masses: results of a multicenter study. Am J Gastroenterol 1998;93:1329–1333.
132. Mallery JS, Centeno BA, Hahn PF, et al. Pancreatic tissue sampling guided by EUS, CT/US, and surgery: a comparison of sensitivity and specificity. Gastrointest Endosc 2002;56:218–224.
133. Shah SM, Ribeiro A, Levi J, et al. EUS-guided fine needle aspiration with and without Trucut biopsy of pancreatic masses. JOP 2008;9(4):422–430.
134. Erickson RA, Sayage-Rabie L, Beissner RS. Factors predicting the number of EUS-guided fine-needle passes for diagnosis of pancreatic malignancies. Gastrointest Endosc 2000;51:184–190.
135. Eloubeidi MA, Tamhane A. EUS-guided FNA of solid pancreatic masses: a learning curve with 300 consecutive procedures. Gastrointest Endosc 2005;61:700–708.
136. Wiersema MJ, Levy MJ, Harewood GC, et al. Initial experience with EUS-guided trucut needle biopsies of perigastric organs. Gastrointest Endosc 2002;56:275–278.
137. Nakamura R, Machado R, Amikura K, et al. Role of fine needle aspiration cytology and endoscopic biopsy in the preoperative assessment of pancreatic and peripancreatic malignancies. Int J Pancreatol 1994;16:17–21.
138. Eloubeidi MA, Chen VK, Eltoum IA, et al. Endoscopic ultrasound-guided fine needle aspiration biopsy of patients with suspected pancreatic cancer: diagnostic accuracy and acute and 30-day complications. Am J Gastroenterol 2003;98:2663–2668.
139. Micames C, Jowell PS, White R, et al. Lower frequency of peritoneal carcinomatosis in patients with pancreatic cancer diagnosed by EUS-guided FNA vs. percutaneous FNA. Gastrointest Endosc 2003;58:690–695.
140. Schwartz DA, Unni KK, Levy MJ, et al. The rate of false-positive results with EUS-guided fine-needle aspiration. Gastrointest Endosc 2002;56:868–872.
141. Gruessner AC, Sutherland DE. Pancreas transplant outcomes for United States (US) cases reported to the United Network for Organ Sharing (UNOS) and non-US cases reported to the International Pancreas Transplant Registry (IPTR) as of October, 2000. Clin Transpl 2002;45–72.
142. Gruessner AC, Sutherland DER. Report for the International Pancreas Transplant Registry-2000. Transplant Proc 2001;33:1643–1646.
143. Nikolaidis P, Amin RS, Hwang CM, et al. Role of sonography in pancreatic transplantation. Radiographics 2003;23:939–949.
144. Wong JJ, Krebs TL, Klassen DK, et al. Sonographic evaluation of acute pancreatic transplant rejection: morphology – Doppler analysis versus guided percutaneous biopsy. AJR Am J Roentgenol 1996;166:803–807.
145. Atwell TD, Gorman B, Larson TS, et al. Pancreas transplants: experience with 232 percutaneous US-guided biopsy procedures in 88 patients. Radiology 2004;231:845–849.

CHAPTER

17

Spleen

Simon J. Freeman

INTRODUCTION 324

FUNCTION 324

EMBRYOLOGY, ANATOMY AND MICROSTRUCTURE 324

EXAMINATION TECHNIQUE 325

NORMAL ULTRASOUND FINDINGS 326
Splenic size 327

NORMAL VARIANTS AND CONGENITAL ABNORMALITIES OF THE SPLEEN 327
Septation, clefts and notches 327
Accessory spleens/splenunculi and splenosis 328
Wandering spleen 329
Heterotaxy syndrome: polysplenia and asplenia 330

SPLENOMEGALY 331

FOCAL LESIONS OF THE SPLEEN 331
Splenic tumours 331
Lymphoma 331
Splenic metastases 334
Primary malignant splenic tumours 334
Benign tumours of the spleen 334
Cystic lesions of the spleen 337
Congenital splenic cysts 338
Splenic pseudocysts 338
Infection and splenic abscess 338
Other cystic splenic masses 340
Vascular lesions of the spleen 340
Splenic infarction 340
Splenic vascular aneurysms 342
Splenic vein thrombosis and portal hypertension 342
Miscellaneous conditions of the spleen 343
Sarcoidosis 343
Spontaneous rupture of the spleen 343
Splenic calcifications 343
The spleen in AIDS 343

DIFFERENTIAL DIAGNOSIS OF FOCAL SPLENIC LESIONS 343

ULTRASOUND INTERVENTIONS IN THE SPLEEN 345

INTRODUCTION

Splenic pathology is uncommon and frequently clinically silent; for this reason the spleen has been named 'the forgotten organ'.[1] A great many different conditions may, however, affect the spleen, recognition of which will frequently be clinically relevant. There are also many congenital abnormalities of the spleen that must be recognised in order to avoid diagnostic error.

The spleen is readily accessible to sonographic examination. All general abdominal ultrasound studies should include evaluation of the spleen. Ultrasound is also ideally suited for the initial assessment of patients presenting with symptoms or signs of splenic disease; abnormalities will thus be regularly encountered by most ultrasound practitioners. Whilst ultrasound is not always able to provide a definitive diagnosis, when combined with clinical, laboratory and other imaging information a specific or short differential diagnosis is usually possible.

FUNCTION

The spleen has a number of important functions including: (1) haemopoiesis, (2) storage, (3) filtration and (4) participation in the immune response.[2] In the fetus it is a major source of red blood cell production and haemopoiesis can be reactivated in adult life in conditions of severe anaemia. The spleen stores red blood cells and platelets and acts as a filter, removing damaged red blood cells, bacteria and other particulate matter. It performs an important role in immune function stimulating antibody production and is a major reservoir of lymphocytes. Splenectomy or functional hyposplenia is associated with an increased risk of severe infection, particularly in children. Splenectomy also appears to result in an increased risk of pulmonary embolism.[3]

EMBRYOLOGY, ANATOMY AND MICROSTRUCTURE

The spleen begins to develop in the fifth week of fetal life from mesenchymal cells in the dorsal mesogastrium arising from multiple lobules which fuse before birth. As development proceeds, the stomach rotates around its long axis, swinging the dorsal mesogastrium to the left creating the lesser peritoneal sac and splenorenal ligament.[4,5] The dorsal mesentery between the spleen and stomach forms the gastrosplenic ligament and there is a further attachment with the diaphragm and splenic flexure of the colon (phrenicocolic ligament). The spleen is thus intraperitoneal apart from a small bare area, which can be helpful in distinguishing ascitic from pleural fluid on imaging studies.[6]

The spleen lies in the left upper quadrant of the abdomen with its long axis in the line of the tenth rib. It has a curved wedge or 'domed tetrahedral' shape with superolateral and inferomedial surfaces.[7] The superolateral surface is smooth and in contact with the left hemidiaphragm. The inferomedial surface is convex and has impressions from the adjacent stomach, kidney, pancreas and splenic flexure of the colon (Fig. 17.1). The splenic hilum, in the inferomedial surface, transmits branches of the splenic artery, vein, lymphatics and nerves. The splenic artery is usually a branch of the coeliac axis; it has a tortuous course passing superolaterally initially above and then behind the pancreas before entering the splenorenal ligament and dividing as it approaches the splenic hilum. It gives off branches to the pancreas, the left gastroepiploic and short gastric arteries which pass into the gastrosplenic ligament. The splenic vein is formed from two to six splenic tributaries and receives the short gastric, left gastroepiploic, pancreatic veins and the inferior mesenteric vein. It runs below the artery, posterior to the pancreas,

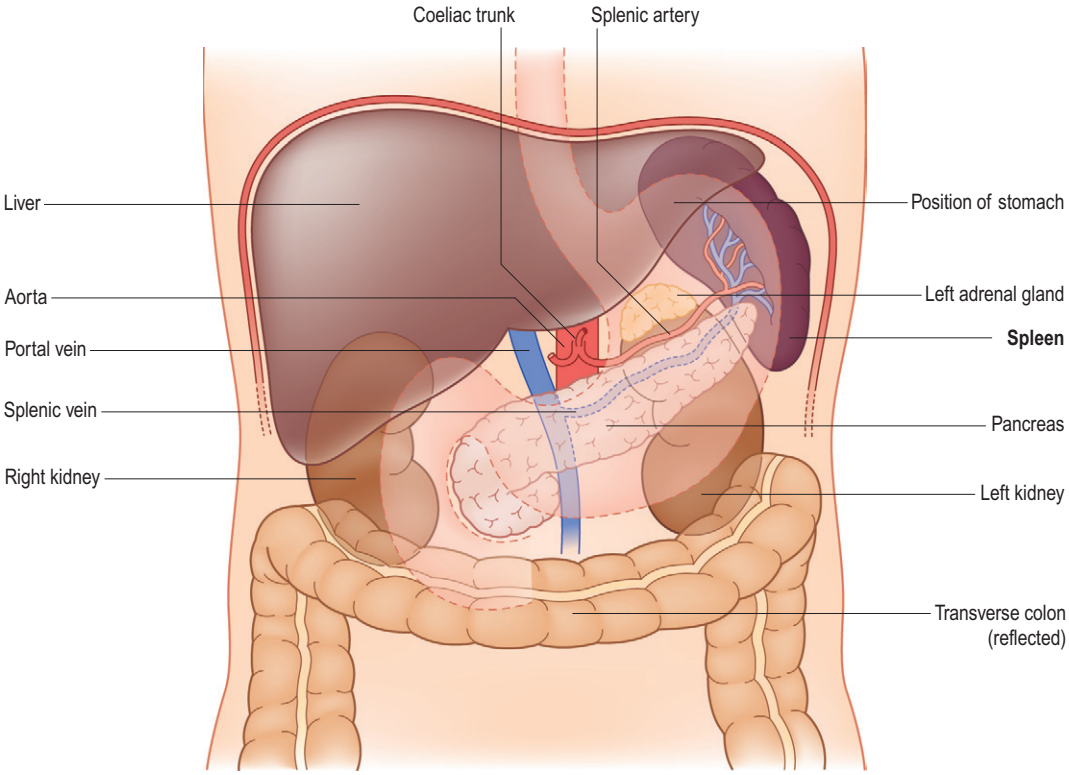


Figure 17.1 Diagrammatic representation of the anatomical relations of the spleen (stomach removed and position indicated by the dotted lines).

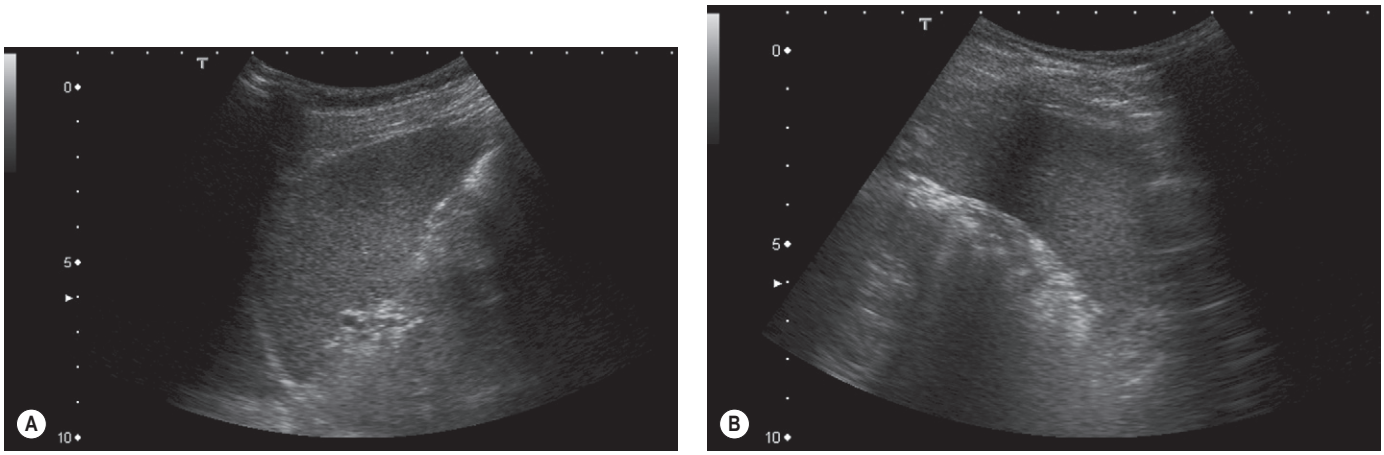


Figure 17.2 Normal spleen. A: Longitudinal view. **B:** Transverse view.

terminating at its confluence with the superior mesenteric vein to form the portal vein. The lymphatic drainage of the spleen runs adjacent to the splenic vessels to nodes around the coeliac axis. The spleen is innervated mainly from sympathetic nerves; referred pain from the spleen is usually localised to the epigastrium and left upper quadrant.

Microscopically the spleen has two major components: the red and white pulps, supported by a fibrous trabecular framework. The white pulp consists of sheaths of lymphoid cells around splenic arterioles; in many areas these sheaths are focally enlarged, forming lymphoid follicles. The red pulp makes up most of the splenic volume and consists of venous sinusoids and splenic cords. Arterioles that have passed through the white pulp divide into capillaries which then terminate either directly into the splenic sinusoids (closed circulation) or alternatively into macrophage-rich cord space between the sinusoids (open circulation). Transit times through the spleen are much faster for blood passing through the closed system than the open system.

EXAMINATION TECHNIQUE

A coronal (longitudinal) view of the spleen can usually be obtained with the patient supine or lying in the right lateral decubitus position with the transducer in the mid-axillary line; it is often helpful to raise the patient's left arm. The spleen is examined in its entirety through the intercostal spaces in longitudinal and transverse planes (Fig. 17.2). Scans are performed in suspended respiration and it is frequently necessary to try different phases of respiration to achieve

complete visualisation. Subcostal, anterior and posterior approaches are not usually helpful unless the spleen is enlarged. The spleen can also be examined with endoscopic ultrasound (Fig. 17.3).

The spleen is ideally suited to examination with ultrasound microbubble contrast agents. Contrast-enhanced ultrasound (CEUS) examinations are performed in real-time following intravenous injection of second-generation ultrasound contrast media. Contrast-specific low acoustic power machine presets are required which result in almost complete suppression of tissue echoes from the splenic parenchyma. Indications for CEUS include:[8]

1. focal splenic or perisplenic lesions (particularly splenunculi)
2. diffuse inhomogeneity of the splenic parenchyma
3. assessment of splenic trauma.

Almost all focal splenic pathology is hypovascular relative to normal splenic tissue; thus abnormalities are evident as echo-poor defects. CEUS often greatly increases the conspicuity of focal splenic lesions (Fig. 17.4).[9] However, its ability to characterise splenic masses is less well established.

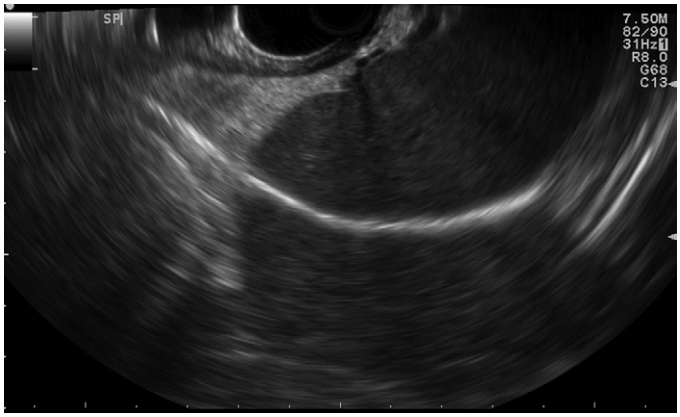


Figure 17.3 Endoscopic ultrasound image of a normal spleen.

NORMAL ULTRASOUND FINDINGS

The spleen has a uniform echotexture that is similar to liver parenchyma; the capsule usually cannot be appreciated sonographically. Normal echogenicity is greater than that of liver and kidney; in some patients the left lobe of the liver may extend into the left hypochondrium, allowing a direct comparison of the relative echogenicity of spleen, liver and kidney (Fig. 17.5). In patients with fatty infiltration of the liver, the normal difference in echogenicity may be reversed. The splenic vessels can usually be identified entering and leaving the spleen at the hilum (Fig. 17.6) before passing

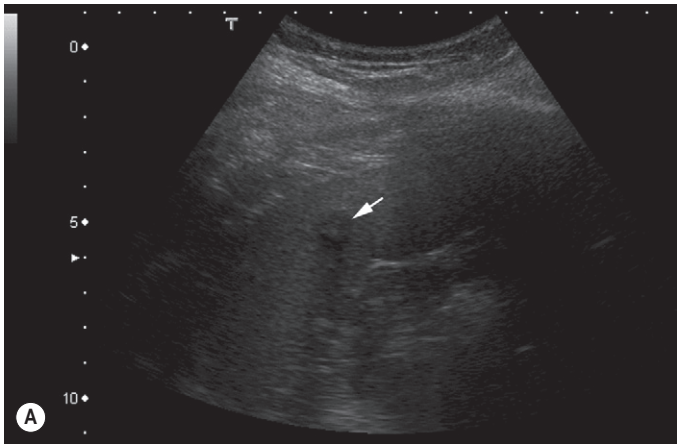


Figure 17.4 A small echo-poor splenic mass that is poorly appreciated on conventional greyscale ultrasound (**A**, arrow) but is easily seen with CEUS **(B)**.

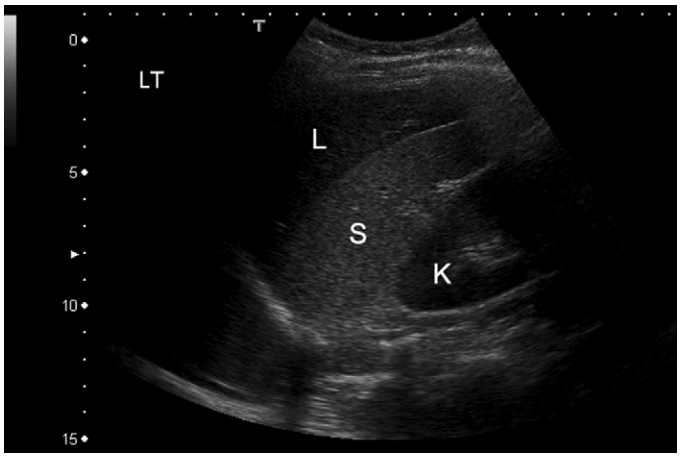


Figure 17.5 The left lobe of the liver extends above the spleen in this patient, allowing direct comparison of the (normal) differences in echogenicity between spleen (S), liver (L) and kidney (K).

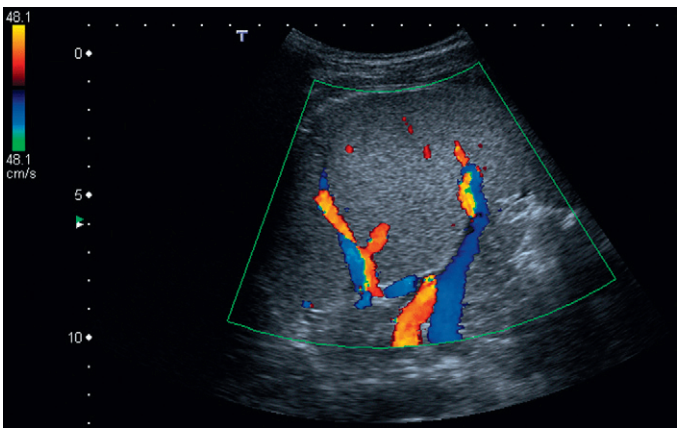


Figure 17.6 Colour Doppler image demonstrating the splenic artery and vein dividing at the splenic hilum to enter the splenic parenchyma.

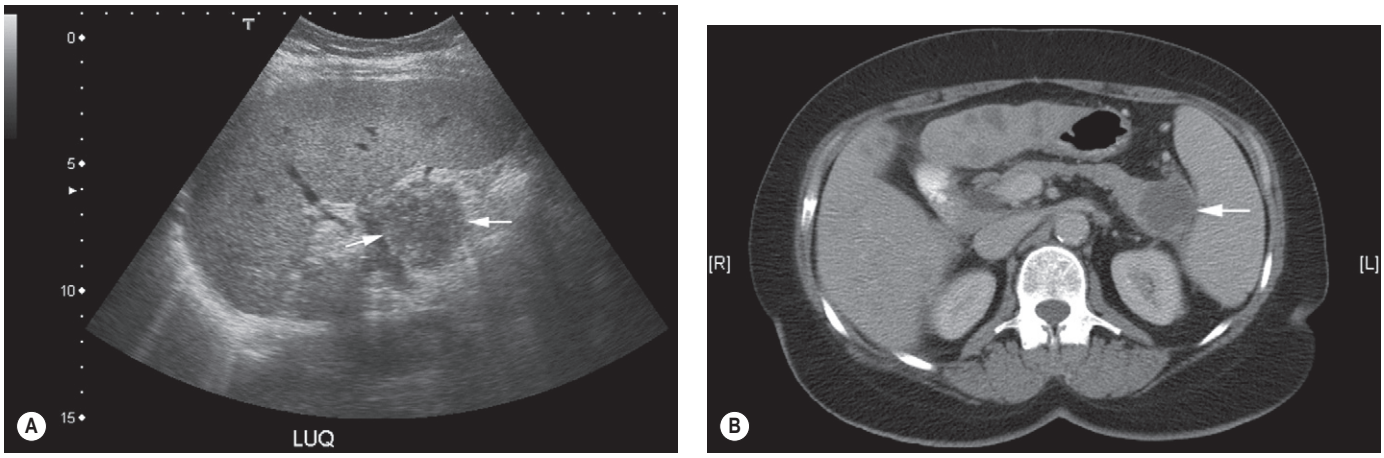


Figure 17.7 **A:** Tumour in the pancreatic tail (arrow) visualised using the spleen as an acoustic window. **B:** corresponding CT image.

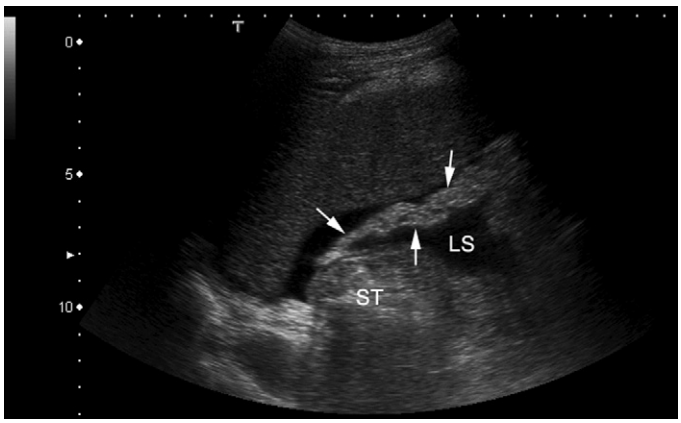


Figure 17.8 **In this patient with ascites the gastrosplenic ligament** is outlined by ascitic fluid (arrows); the position of the lesser sac (LS) and stomach (ST) are shown.

posterior to the pancreas. The pancreatic tail often lies in the splenorenal ligament and can sometimes be well seen using the spleen as an acoustic window (Fig. 17.7). In some patients with ascites the gastrosplenic ligament may be visualised (Fig. 17.8).

CEUS studies show avid splenic parenchymal enhancement approximately 15 seconds after injection. Initially (arterial phase) enhancement is inhomogeneous due to differential flow rates through the open and closed splenic circulation, analogous to the appearances of normal arterial phase CT. After 30–60 seconds (late phase) enhancement becomes homogeneous and persists for 5–7 minutes, well beyond blood-pool enhancement, due to microbubble accumulation in the spleen (Fig. 17.9).[10]

Splenic size

Physical examination only has 56–82% sensitivity for identifying splenomegaly in comparison with imaging studies.[11] Ultrasound is a simple and reliable method for measuring splenic size. Size is usually assessed by a single longitudinal length measurement. This has been shown to have good correlation to actual splenic length, volume and weight on cadaveric studies and to in-vivo calculations of splenic volume.[12,13] Area and volume calculations based on 2D and 3D ultrasound have also been proposed but these more complex measurements are not used in routine clinical practice.[14–16]

The spleen reaches maximum size soon after puberty but there are conflicting data regarding the normal size of the adult spleen. One large study found 95% of subjects had a splenic length of less than 11 cm, breadth less than 7 cm and thickness less than 5 cm.[17] Another study found that a length of over 12 cm was two standard deviations above the mean.[18] However, a study of normal college athletes found that 7% had a spleen length of greater than 13 cm.[19] The weight of the spleen is greater in males, increases with increasing body weight, height and surface area and declines with age after early adulthood.[20] It is difficult therefore to give a single measurement for the upper limit of splenic size that is applicable to all patients and the sonologist will need to make a judgement based on the patient's age, sex and body habitus. As a guide it is often considered that a measurement less than 12 cm is normal, 12–13 cm indeterminate and more than 13 cm enlarged.

Splenic size

- Clinical examination is imprecise in detecting splenomegaly.
- A single longitudinal ultrasound measurement of the spleen accurately correlates with splenic size.
- Assessment of splenic size must pay due regard to the patient's age, sex and body habitus.
- The spleen increases in size during normal pregnancy.
- A small and hypovascular spleen may indicate functional hyposplenia.

The spleen shows a linear increase in size in healthy women throughout pregnancy[21,22] and changes in size of the spleen have also been documented following abdominal trauma[23] and as an adaptation to high altitude.[24]

Small splenic size (length ≤7 cm, width ≤3 cm) may indicate functional hyposplenia, particularly if accompanied by absent or reduced parenchymal blood flow on colour Doppler or CEUS examination.[1,25] This is a potentially important finding in view of the association with overwhelming infection.

NORMAL VARIANTS AND CONGENITAL ABNORMALITIES OF THE SPLEEN

Septation, clefts and notches

Incomplete fusion of the splenic lobules may result in clefts or notches in the normally smooth superolateral surface (Fig. 17.10); these can occasionally be misinterpreted as lacerations in the setting of abdominal trauma.[26] Echogenic septation is sometimes seen between splenic lobules (Fig. 17.11).

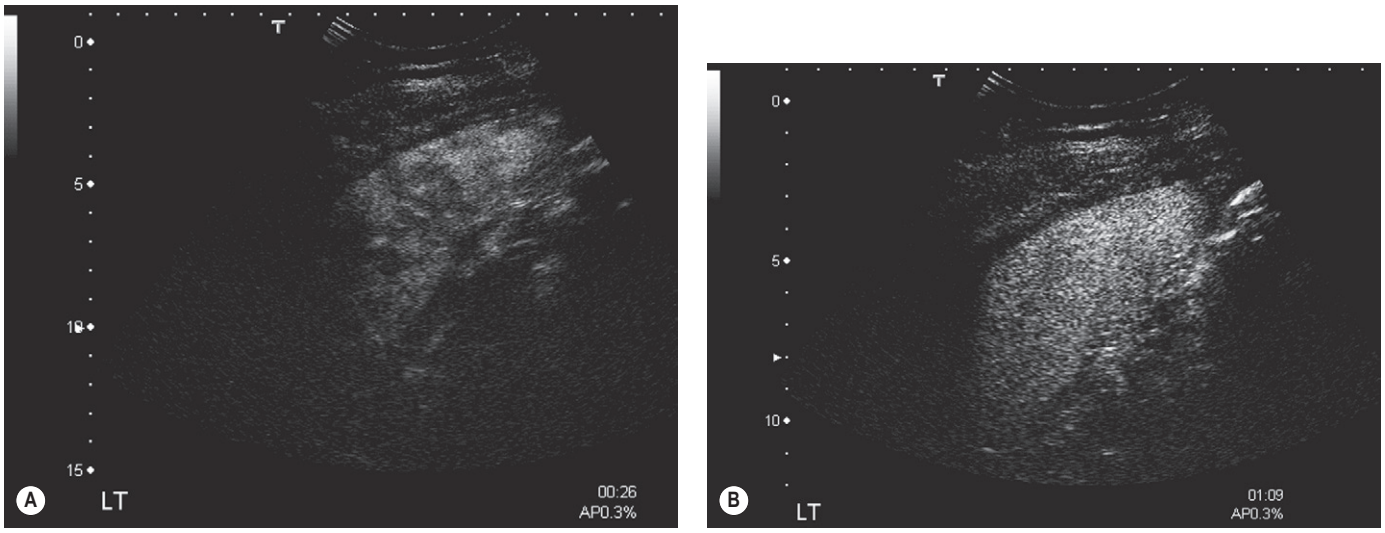


Figure 17.9 Normal appearance of the spleen following ultrasound contrast medium injection. A: In the early (arterial) phase there is inhomogeneous enhancement due to differential circulation in the open and closed systems. **B:** In the same patient in the late phase there is uniform enhancement.



Figure 17.10 Large cleft in the superolateral surface of the spleen (arrows).

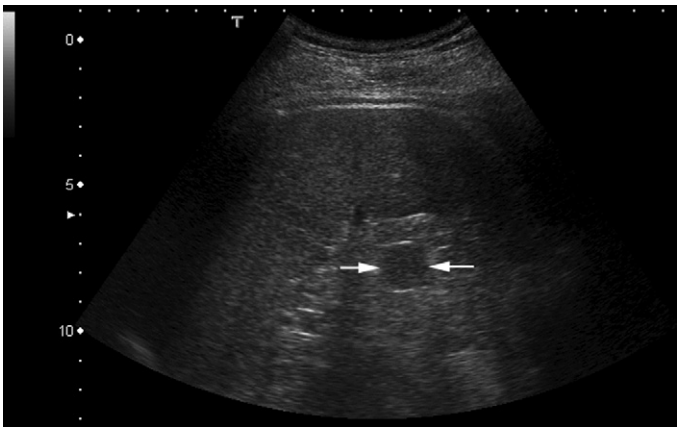


Figure 17.12 Accessory spleen (arrows) in a typical location medial to the spleen.

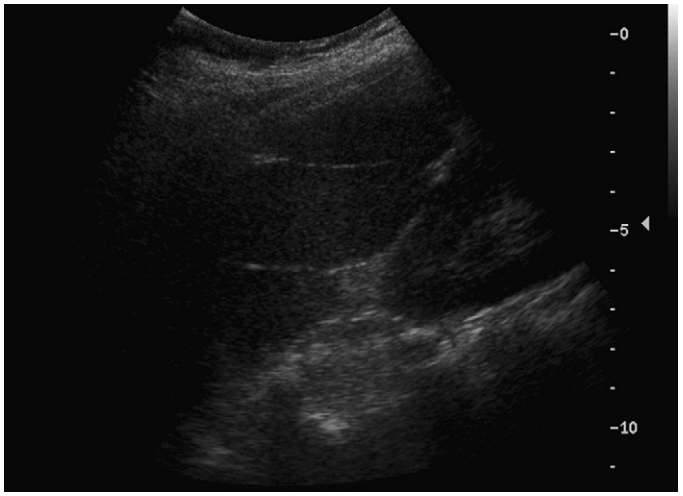


Figure 17.11 Echogenic septation running through the splenic parenchyma. (Courtesy of Dr P Allan, Royal Infirmary, Edinburgh, UK.)

Accessory spleens/splenunculi and splenosis

Accessory spleens (splenunculi) arise due to failure of fusion of one or more of the splenic lobules. They occur in 10–30% of patients on postmortem studies[26] and in approximately 2% more than one may be present.[27] Accessory spleens are most commonly located medial to the splenic hilum, adjacent to or within the pancreatic tail or below the spleen (in the splenorenal ligament). Rarely they may be located elsewhere in the abdomen.[28]

Sonographically accessory spleens are usually homogeneous, round, smaller than 2 cm in diameter and identical in echogenicity to the spleen (Fig. 17.12).[27] The presence of a vascular pedicle and vascular supply from the main splenic vessels can frequently be demonstrated with Doppler ultrasound and are helpful diagnostic features.[29,30] Diagnosis is not usually difficult but errors may arise, particularly:

1. post splenectomy[31]
2. when the accessory spleen is located in the pancreatic tail where it may mimic a pancreatic mass[32,33]
3. when the accessory spleen is unusually located

4. in patients with a history of malignancy where it may resemble tumour recurrence or lymphadenopathy.[34]

In difficult cases CEUS can be helpful; the vascular hilum is demonstrated in the early arterial phase followed by uniform parenchymal uptake identical in appearance and timing to the normal spleen.[1,9] Persistent delayed enhancement allows differentiation from pathological masses. If accessory spleens are not recognised and removed at splenectomy for haematological or neoplastic disease, they can form a site for disease relapse (Fig. 17.13); conversely, if preserved at splenectomy for trauma, they may preserve immune function.[35]

Splenosis refers to the autotransplantation of splenic tissue following trauma or surgery. In one ultrasound study it could be identified in approximately a third of patients post splenectomy.[36] Splenosis most commonly occurs in the abdomen but may also be seen in the thorax.[35] The masses are rounded and uniform and may be found anywhere in the abdomen or pelvis (Fig. 17.14); they do not have a pathognomonic ultrasound appearance and can be wrongly interpreted as pathological masses or tumour recurrence.[37–40] Post-splenectomy status should alert the sonologist to the possibility of this condition; scintigraphy using labelled heat-damaged red blood cells can provide a definitive diagnosis.[41]

Wandering spleen

Wandering spleen is a rare condition in which the spleen is excessively mobile and migrates from its expected position to ectopic sites in the abdomen or pelvis (Fig. 17.15). It is most commonly congenital in origin due to underdevelopment or elongation of the supporting ligaments. Excessive splenic mobility may also be acquired in conditions such as pregnancy, abdominal wall laxity or splenomegaly.[42,43] Diagnostic errors where the spleen is misinterpreted as a pathological mass can occur, particularly when absence of the spleen from the splenic fossa has not been appreciated. A wandering accessory spleen has also been reported.[44]

The wandering spleen is usually asymptomatic but patients may present with abdominal pain due to torsion. This complication should be considered when ultrasound shows an abnormally located spleen with low echogenicity and when colour flow cannot be identified in the splenic parenchyma or pedicle.[45] Sonographic diagnosis of torsion of a wandering spleen that remains in the left upper quadrant is more difficult but a splenic hilar mass, representing the torted splenic pedicle, may be seen.[46] The tail of the pancreas can be involved in the torsion and result in acute pancreatitis.[47,48]

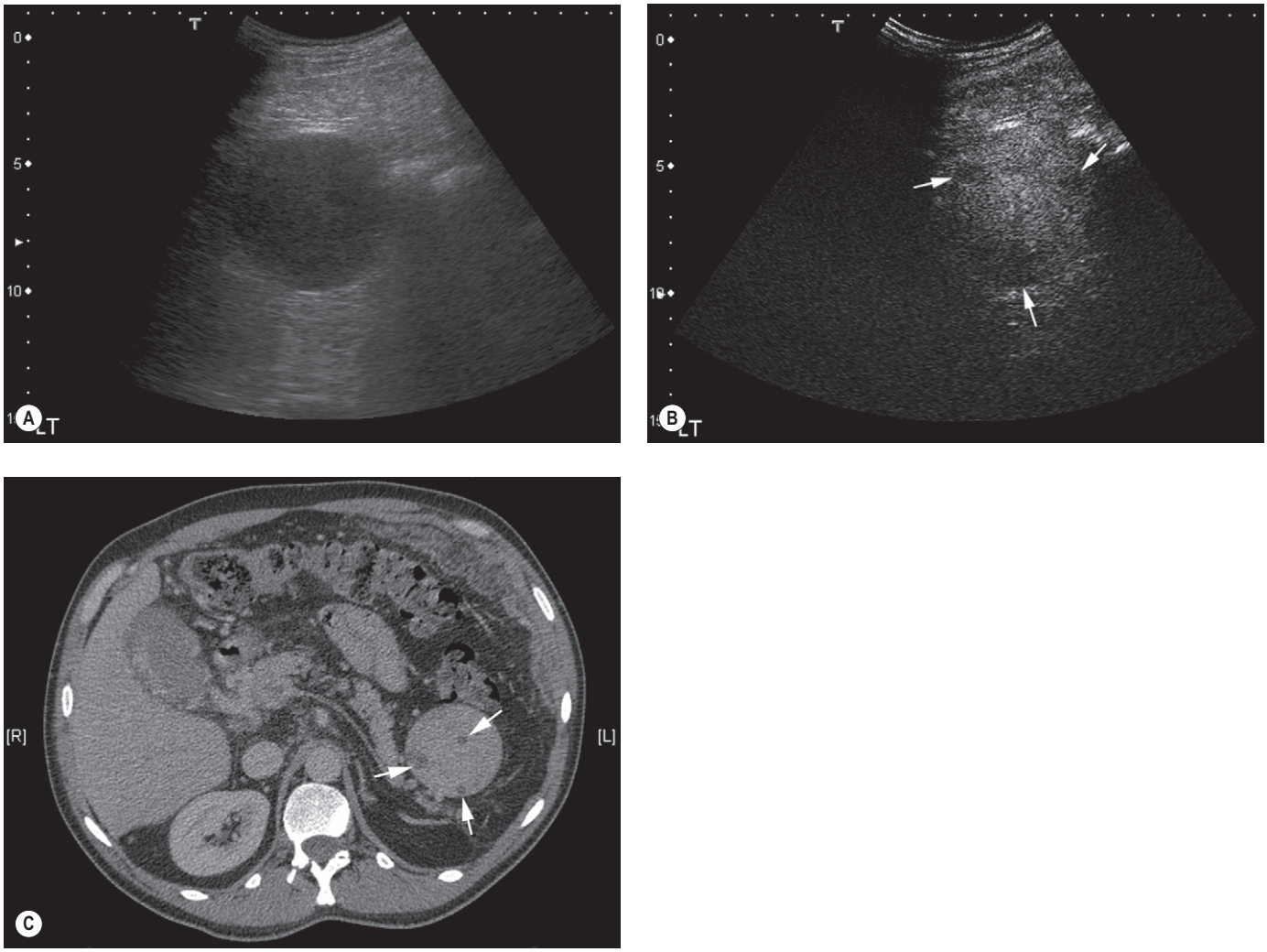


Figure 17.13 Recurrent littoral cell angioma in an accessory spleen post splenectomy. A: Greyscale image showing a soft tissue mass in the splenic bed representing a accessory spleen. **B:** CEUS demonstrates a number of ill-defined hypovascular nodules within the accessory spleen in the late phase of enhancement (arrows). **C:** Corresponding CT image showing recurrent nodules of littoral cell angioma (arrows).

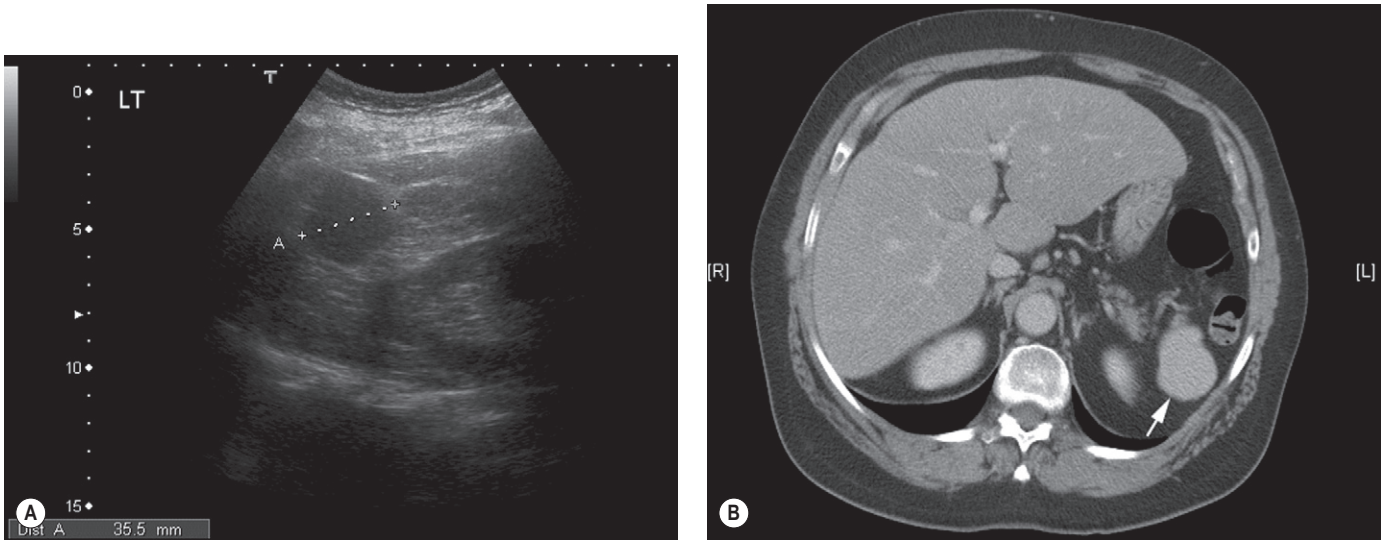


Figure 17.14 Splenosis following splenectomy. A: Ultrasound. **B:** CT appearances showing a soft tissue nodule adjacent to the left kidney representing splenosis (arrow).

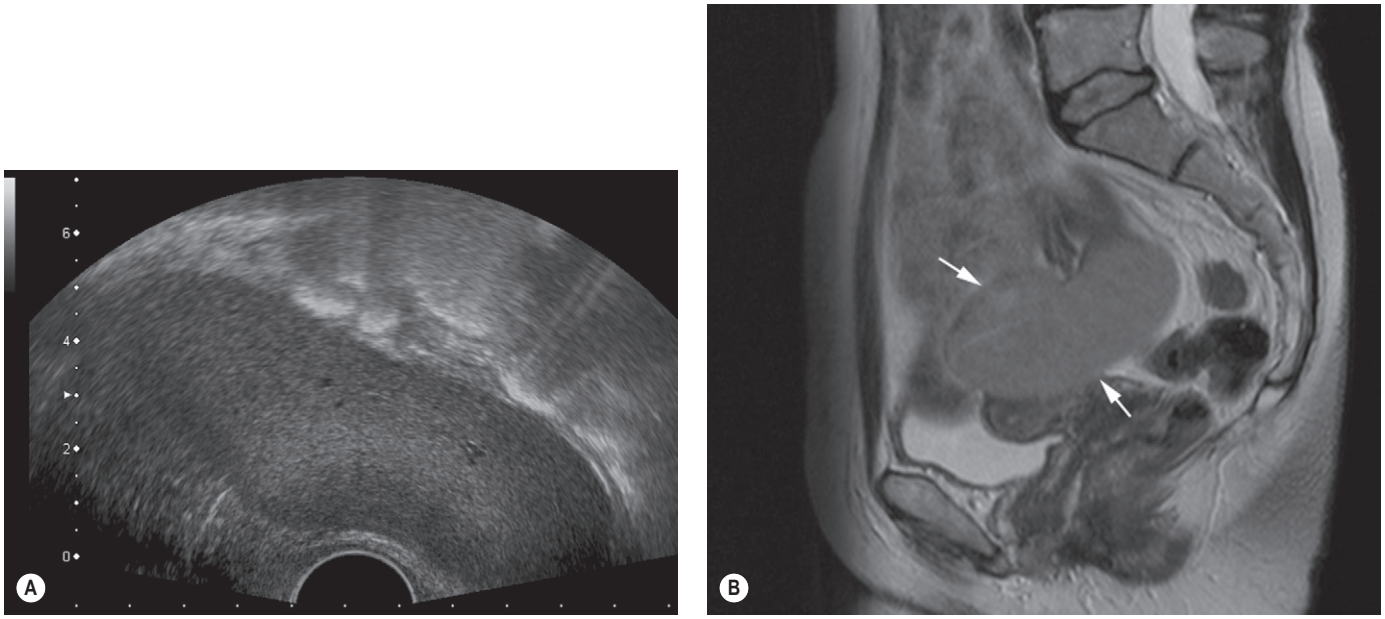


Figure 17.15 Wandering spleen in the pelvis mimicking a pathological pelvic mass. A: Transvaginal ultrasound image. **B:** Corresponding T2-weighted sagittal MRI image showing the ectopic spleen (arrows) above the uterus. (Courtesy of Dr H. Andrews, Bristol Royal Infirmary, UK.)

Heterotaxy syndrome: polysplenia and asplenia

The normal asymmetrical arrangement of the heart and viscera is referred to as situs solitus and the mirror image situs inversus. Heterotaxy syndromes are present when the arrangement of the organs is abnormally symmetrical and different from situs solitus or inversus. There is a strong association with congenital heart disease (50–100%) and intestinal malrotation (predisposing to volvulus).[49,50] There are two major groups of heterotaxy: (1) asplenia (bilateral right-sidedness) and (2) polysplenia (bilateral left-sidedness), although there is a wide spectrum lying between the two extremes.[49] Abnormalities include midline position of the liver, indeterminate position of the stomach, left-sided position or interruption of the inferior vena cava, malrotation of the small intestine and symmetry of the cardiac atria and lungs. In asplenia the spleen is absent; in polysplenia patients typically have multiple spleens located along the greater curve of the stomach (Fig. 17.16). Death occurs in the first year of life in 60% (polysplenia) to 80% (asplenia) of patients.

Ultrasound is a valuable imaging modality in these patients to evaluate the presence, number and position of spleens and the appearance of the great vessels. It is usually combined with chest radiography, echocardiography and barium studies to fully define the anatomy. Occasionally heterotaxy will be discovered as an incidental finding in an adult patient without congenital heart disease on an abdominal ultrasound study.

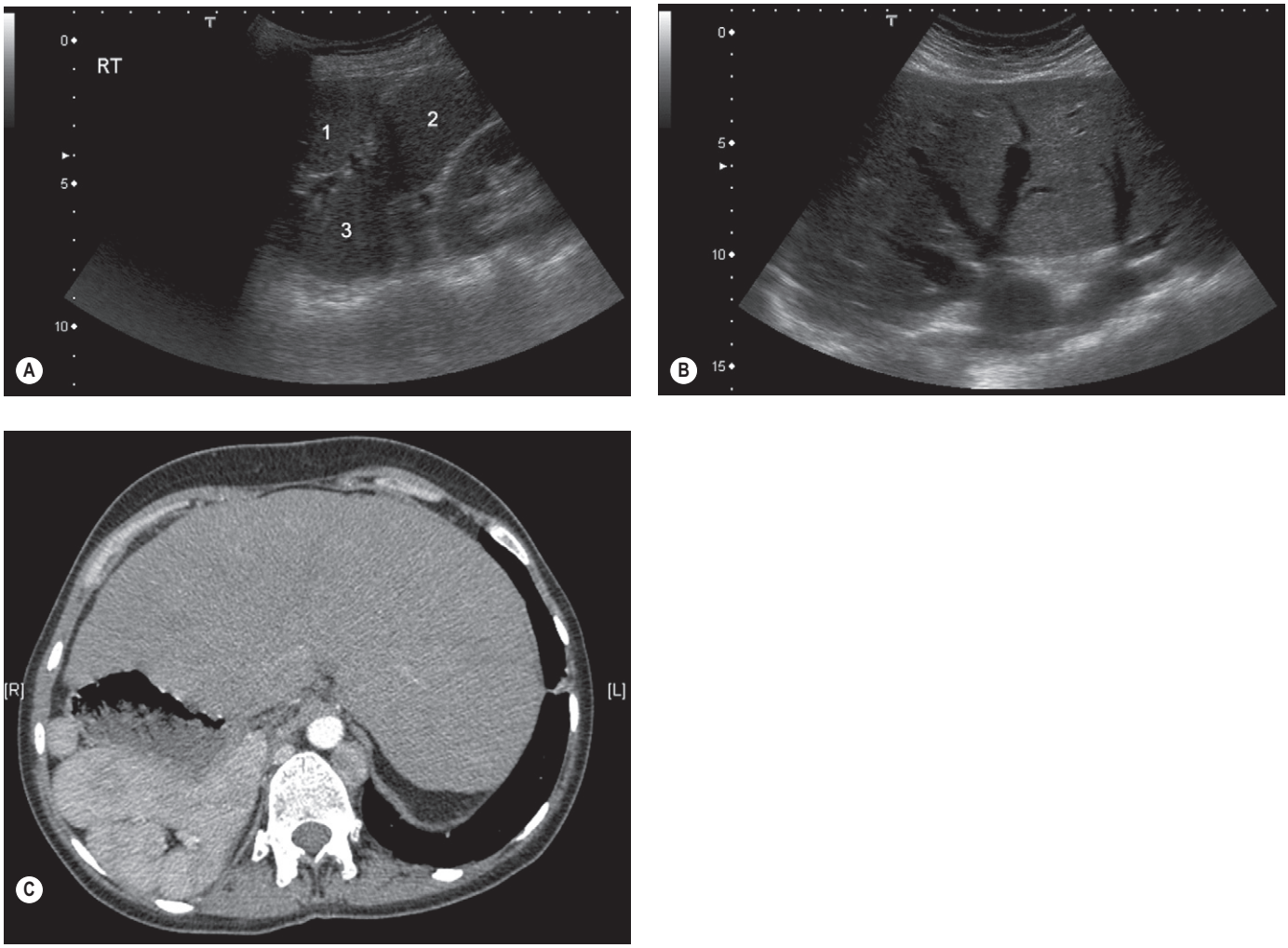


Figure 17.16 Heterotaxy syndrome (polysplenia). In this asymptomatic patient ultrasound demonstrates **A:** three splenic masses on the right side of the abdomen, **B:** midline liver with anomalous drainage of the hepatic veins above the diaphragm. **C:** Corresponding CT image.

SPLENOMEGALY

There are a great many causes of splenomegaly which can be divided into several categories (Table 17.1).[51] In Western Europe and the USA viral infection, portal hypertension and haematological causes are most prevalent, in tropical areas protozoal infection and haemolytic anaemias predominate.

Correct identification of the cause of an enlarged spleen is frequently impossible by ultrasound alone. Correlation with clinical and laboratory findings is usually necessary to make the correct diagnosis. Ultrasound can, however, confirm that splenomegaly is present and quantify it. Sometimes the spleen is so large that accurate measurement is not possible within the ultrasound sector; in this situation extended field of view imaging can be helpful (Fig. 17.17). Ultrasound can also identify and characterise focal splenic lesions and recognise ancillary findings that may point to the cause of splenic enlargement; a specific search should be made for features of portal hypertension and chronic liver disease (Fig. 17.18) and for abdominal lymphadenopathy which may indicate lymphoma (Fig. 17.19).

FOCAL LESIONS OF THE SPLEEN

Focal lesions of the spleen are relatively rare, being present in only 0.2–1% of all abdominal ultrasound examinations.[9] The majority are hypoechoic relative to normal splenic parenchyma; benign lesions are slightly more common than malignant.[52]

Splenic tumours

Lymphoma

Lymphoma accounts for 4–6% of adult tumours in the UK and USA and is the most common malignancy affecting the spleen.[53–55] Primary splenic lymphoma is rare and the vast majority of splenic lymphoma occurs as part of secondary disease in which 10–40% of patients have splenic involvement at presentation.[53,55,56] Hodgkin's disease (HD) has a bimodal incidence with peaks in the third and fifth decades of life. Non-Hodgkin's lymphoma (NHL) increases in

Table 17.1 Some causes of splenic enlargement

Category	Type	Example
Infection	Acute viral and bacterial infections	Infectious mononucleosis, bacterial endocarditis
	Chronic bacterial infections	Brucellosis, tuberculosis
	Chronic viral infections	AIDS
	Protozoal infections*	Malaria, leishmaniasis, schistosomiasis
	Tropical splenomegaly	
Congestive	Posthepatic	Budd–Chiari syndrome, right heart failure
	Hepatic	Cirrhosis
	Prehepatic	Portal/splenic vein thrombosis or compression
Lymphohaematological, non-neoplastic	Haemolytic anaemia	Sickle cell disease, thalassaemia, hereditary spherocytosis
	Idiopathic thrombocytopenic purpura	
	Myeloproliferative disorders	Myelofibrosis*, polycythaemia vera
Lymphohaematological, neoplastic	Lymphoma	Hodgkin's disease, non-Hodgkin's lymphoma
	Leukaemia	Chronic myeloid leukaemia*, chronic lymphocytic leukaemia
Immunological/ Inflammatory		Rheumatoid arthritis, systemic lupus erythematosus
Storage diseases*		Gaucher's disease, Niemann–Pick disease, mucopolysaccharidoses
Miscellaneous		Amyloid, sarcoidosis, focal splenic masses

**Commonly causes massive splenomegaly.*

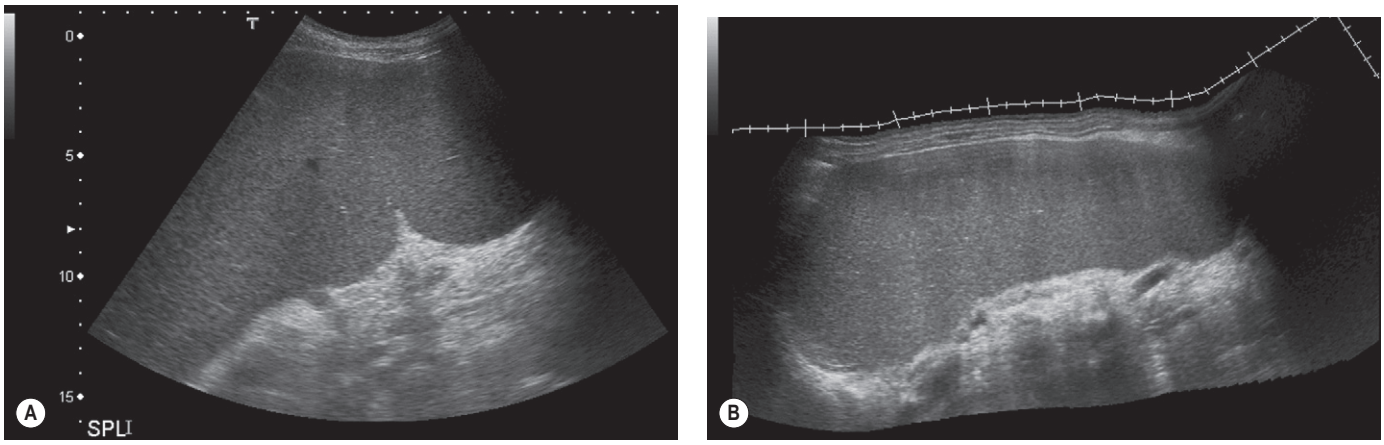


Figure 17.17 Massive splenomegaly due to myelofibrosis. A: On a standard ultrasound image the spleen is too large for measurement within the ultrasound sector. **B:** Extended field of view imaging allows the entirety of the spleen to be imaged and measured.



Figure 17.18 Splenomegaly due to liver cirrhosis: large splenorenal varices are seen medial to the lower third of the spleen.

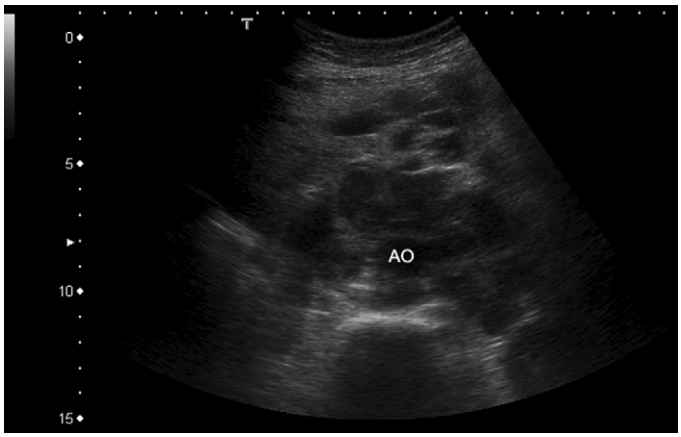


Figure 17.19 Extensive echo-poor retroperitoneal lymphadenopathy encasing the aorta (AO) in a patient with lymphoma and splenomegaly.

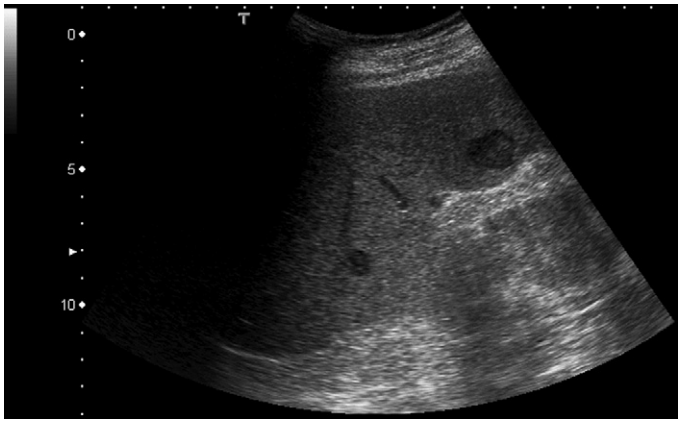


Figure 17.20 Low-grade NHL showing sparse small echo-poor nodules.



Figure 17.21 NHL with a large nodular deposit.

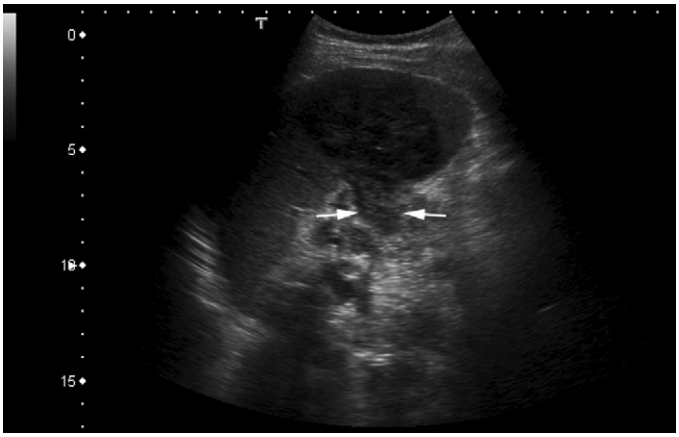


Figure 17.22 NHL with bulky disease and infiltration of the pancreatic tail (arrows).

incidence from the fifth decade and represents a diverse group of lymphatic malignancies. NHL is more likely to affect extranodal sites (including the spleen) than HD,[54] generally carries a worse prognosis and can be broadly divided into low-grade and high-grade groups. Low-grade NHL is usually widely disseminated at presentation and is a slowly progressive disease; high-grade NHL more often presents with rapidly progressing localised disease. Accurate anatomical staging of disease is important, particularly in HD, to select appropriate treatment regimens with a minimum of toxicity. CT and MRI, rather than ultrasound, are the mainstays of staging although positron emission tomography CT (PET-CT) is now becoming increasingly important.

Standard imaging techniques (ultrasound, CT and MRI) have a low sensitivity in detecting lymphomatous infiltration of the spleen although PET-CT may perform better.[57,58] Historically this resulted in the need for staging laparotomy and splenectomy in many patients with HD.[59,60] Fortunately modern treatment regimens mean that surgery is no longer recommended and failure to detect splenic involvement does not adversely affect prognosis.[55]

The size of the spleen is not a reliable predictor of lymphomatous involvement. In up to one-third of patients the spleen will appear normal in size despite infiltration being present. Conversely reactive splenomegaly is a common finding; mild to moderate splenic enlargement without infiltration occurs in approximately 30% of patients with HD and 70% of patients with NHL.[55] Massive splenomegaly, however, almost always indicates infiltration.

A number of parenchymal sonographic abnormalities have been described in the lymphomatous spleen; in one study approximately 15% of lymphoma patients had an abnormal ultrasound appearance of the splenic parenchyma.[61] Discrete focal lesions may be single or multiple and are invariably echo-poor relative to normal spleen;[61,62] echogenic, calcified or cystic lesions are exceptionally uncommon. Patterns include:

1. diffuse alteration of splenic echotexture. This is most commonly seen in HD and low-grade NHL and is often difficult to appreciate although ultrasound appears to be superior to CT in identifying this subtle type of involvement.[60,63] CEUS may help accentuate this heterogenicity[9,64,65]
2. small nodules (<3 cm) are most commonly seen in HD and low-grade NHL (Fig. 17.20)
3. large nodules (>3 cm) are usually a feature of high-grade NHL (Fig. 17.21)
4. bulky disease, which may extend outside the spleen to involve adjacent organs, is seen in high-grade NHL (Fig. 17.22).

In view of the rarity of other splenic masses, detection of a hypoechoic rounded mass in the spleen of a patient with known lymphoma can be regarded as evidence of involvement without the need for biopsy[61] although infarction (see below), which is common in patients with lymphoma, should be considered when typical lesions are identified. In many patients ultrasound will also be able to demonstrate intra-abdominal lymphadenopathy, nodes at the splenic hilum indicating splenic involvement (Fig. 17.23).[55]

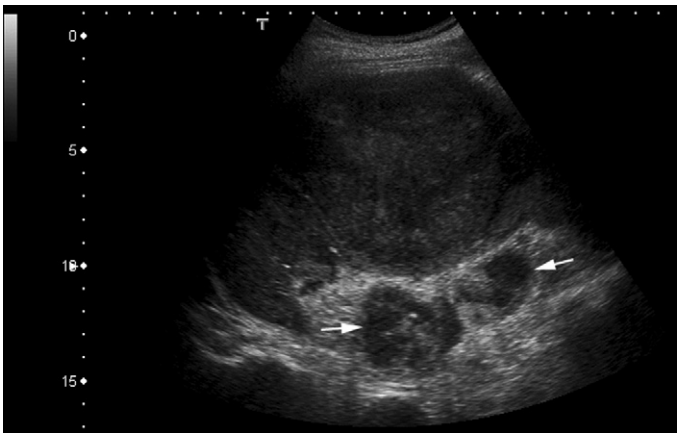


Figure 17.23 Splenic hilar lymphadenopathy in NHL (arrows).



Figure 17.24 Post-transplant lymphoproliferative disease affecting the spleen: multiple ill-defined echo-poor nodules are demonstrated. (Courtesy of Dr P. Sidhu, King's College Hospital, London, UK.)

Lymphoma

- Lymphoma is the most common malignancy affecting the spleen.
- 10–40% of patients with lymphoma have involvement of the spleen at presentation.
- All standard imaging techniques have limited accuracy in detecting lymphomatous infiltration of the spleen.
- Reactive splenomegaly is common in patients with lymphoma.
- Almost all focal lymphoma deposits are hypoechoic relative to splenic parenchyma.

The incidence of NHL is increased in immunocompromised patients, particularly those with acquired immune deficiency syndrome (AIDS) or patients receiving immunosuppression following organ transplantation (Fig. 17.24). AIDS-related lymphoma tends to present with high-grade and widespread disease with a greater incidence of extranodal involvement than in the general lymphoma population and it carries a poor prognosis.[66]

Splenic metastases

The spleen is an uncommon site for non-lymphoid metastases; theories that may account for this are related to the tortuosity of the splenic artery, absence of afferent lymphatic supply and anti-neoplastic immune nature of the spleen. When present, metastases are rarely isolated and are usually found in patients with disseminated malignancy and a poor prognosis.[67] The most common metastatic lesions to the spleen arise from lung, cutaneous malignant melanoma and breast cancers.[68]

There are a variety of patterns of splenic metastasis. Lesions may be single or multiple, may occur in the parenchyma of the spleen or, in the case of ovarian cancer, may be distributed along the peritoneal surface reflecting the trans-coelomic method of spread of this tumour. Splenic metastases are usually hypoechoic relative to adjacent spleen parenchyma but may occasionally be cystic (particularly in melanoma due to necrosis, or in tumours producing mucin) or hyperechoic. A hypoechoic halo is occasionally seen but this is less common than in liver metastases (Fig. 17.25).[69,70] On CEUS metastases appear hypoechoic relative to splenic parenchyma in the late phase, facilitating their detection (Fig. 17.26).[8,10,65]

Primary malignant splenic tumours

All primary non-lymphomatous malignant splenic tumours are exceptionally rare. The least uncommon is angiosarcoma, a highly malignant tumour with a very poor prognosis. Patients usually present with abdominal pain, fever, weight loss and/or a splenic mass but may also present with metastatic disease (most commonly to the liver) or haemoperitoneum due to splenic rupture. Sonographically most patients will have splenomegaly and a focal splenic mass or multiple nodules that usually have a heterogeneous appearance and often contain cystic spaces due to haemorrhage or necrosis. Other features include increased peripheral blood flow on Doppler examination, sonographic evidence of intra-abdominal metastases or haemoperitoneum (Fig. 17.27).[71,72]

Other rare malignant tumours of the spleen include fibrosarcoma, malignant fibrous histiocytoma, leiomyosarcoma and malignant teratoma. Littoral cell angioma (Fig. 17.13), haemangioendothelioma and haemangiopericytoma have a variable malignant potential. No pathognomonic imaging features of these tumours have been identified.[71]

Benign tumours of the spleen

The most common benign splenic tumour is the haemangioma, which has cavernous and capillary types. Reported in 0.03–14% of patients on postmortem studies, they are less frequently seen on imaging investigations.[74] Haemangiomas are usually solitary, asymptomatic and an incidental finding; occasionally, however, they may be large and present with pain, mass, bleeding/rupture or the triad of anaemia, thrombocytopenia and coagulopathy (Kasabach–Merritt syndrome). Occasionally haemangiomas may be multiple and very rarely diffuse splenic angiomatosis may be encountered as an isolated finding or as part of a generalised angiomatosis such as Klippel–Trénaunay syndrome (Fig. 17.28).[73]

The typical sonographic appearance of a splenic haemangioma is that of a well-circumscribed echogenic mass, sometimes with posterior acoustic enhancement, measuring less than 2 cm in diameter (Fig. 17.29); as an incidental finding this appearance can be assumed to be benign.[69] Atypical features include a hypoechoic appearance, internal cystic spaces, and calcifications (Fig. 17.30).[75] For hypoechoic lesions CEUS can be used; small capillary haemangiomas may show pronounced arterial phase enhancement (Fig. 17.31).[65] Many haemangiomas show persistent late phase enhancement, appearing

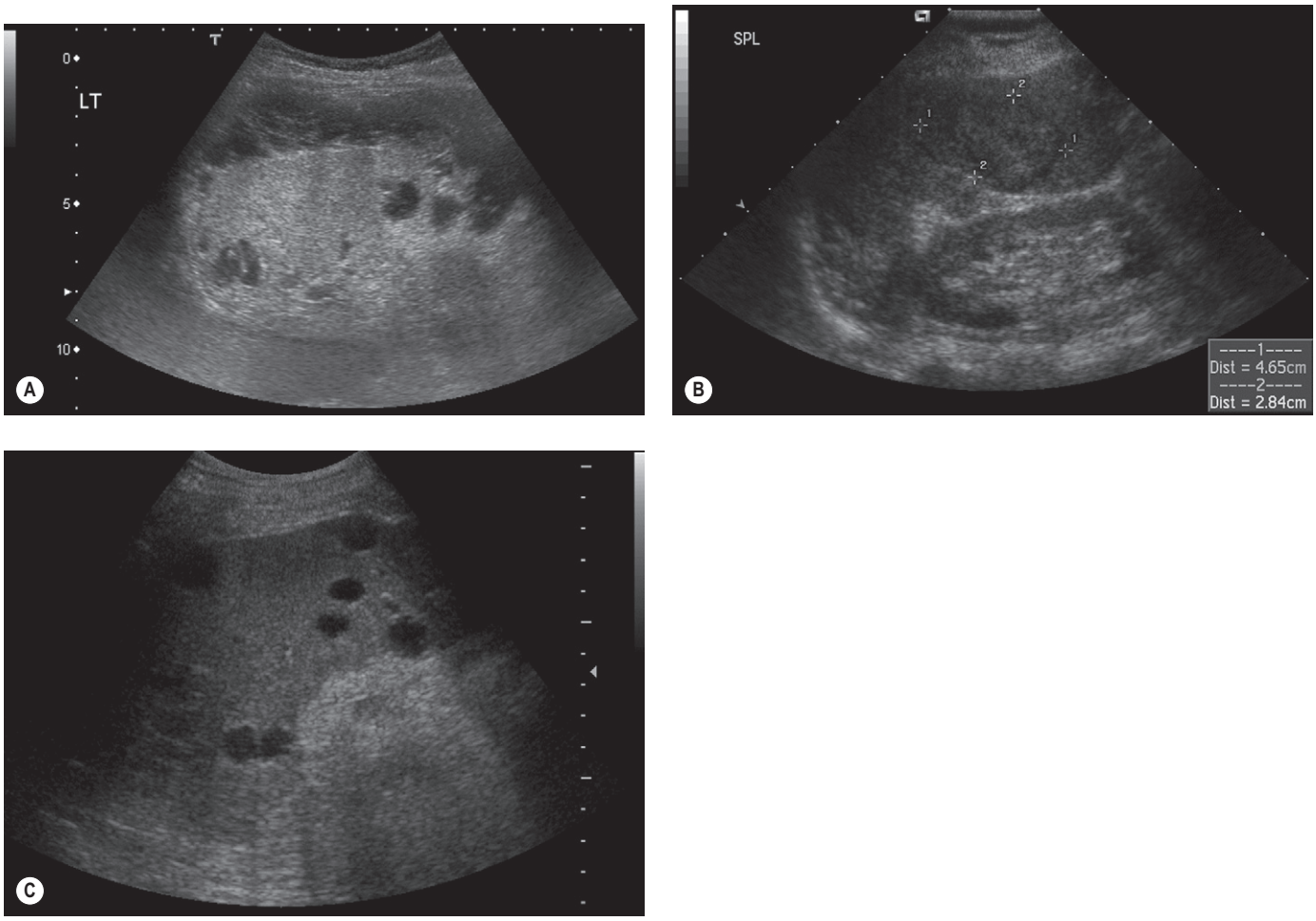


Figure 17.25 **Splenic metastases. A:** Echo-poor metastases secondary to ovarian cancer; the complex fluid lateral to the spleen is secondary to pseudomyxoma peritonei. **B:** Isoechoic metastasis with an echo-poor halo secondary to breast cancer. **C:** Cystic metastases secondary to melanoma. (Part C courtesy of Dr P. Allan, Royal Infirmary, Edinburgh UK).

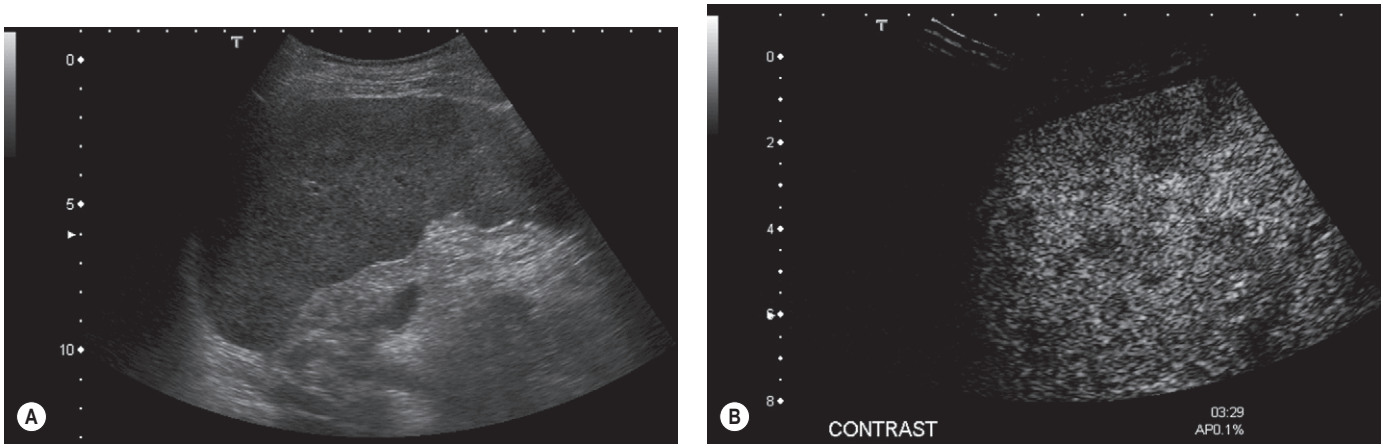


Figure 17.26 **Breast metastases. A:** Greyscale imaging demonstrates an inhomogeneous splenic parenchyma with an abnormal surface contour. **B:** Following ultrasound contrast microbubble administration the metastases are more easily identified.

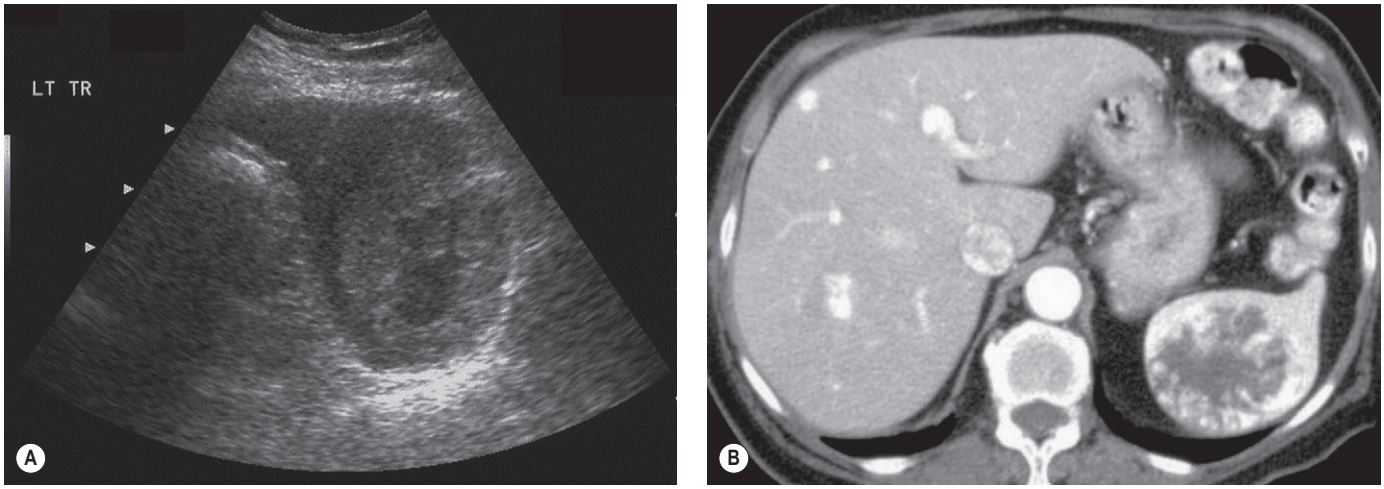


Figure 17.27 Splenic angiosarcoma. A: Ultrasound image shows a splenic mass that is predominantly echogenic but with a central cystic/necrotic component. **B:** Corresponding CT image showing the splenic mass and hypervascular liver metastases. (Reproduced from Abbott RM, Levy AD, Aguilera NS, Gorospe L, Thompson WM. Primary vascular neoplasms of the spleen: Radiologic-pathologic correlation. RadioGraphics 2004;24:1137-1163, provided courtesy of the Armed Forces Institute of Pathology, Washington, DC.)

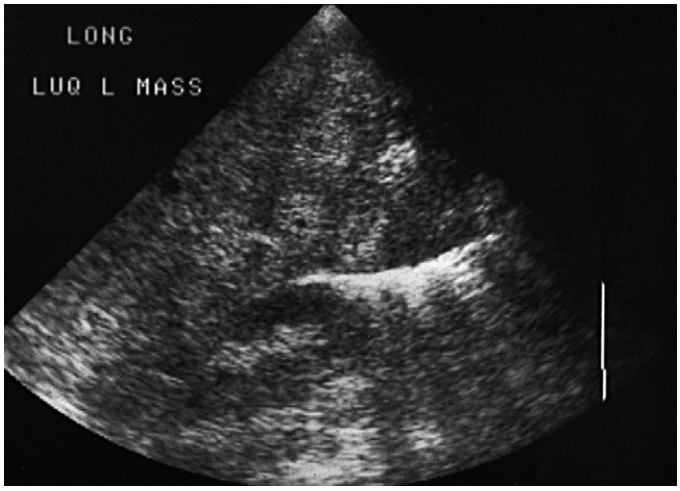


Figure 17.28 Splenic haemangiomatosis in Klippel–Trénaunay syndrome. Multiple small echogenic nodules are present throughout the splenic parenchyma. (Reproduced from Abbott RM, Levy AD, Aguilera NS, Gorospe L, Thompson WM. Primary vascular neoplasms of the spleen: Radiologic-pathologic correlation. RadioGraphics 2004;24:1137-1163, provided courtesy of the Armed Forces Institute of Pathology, Washington, DC.)

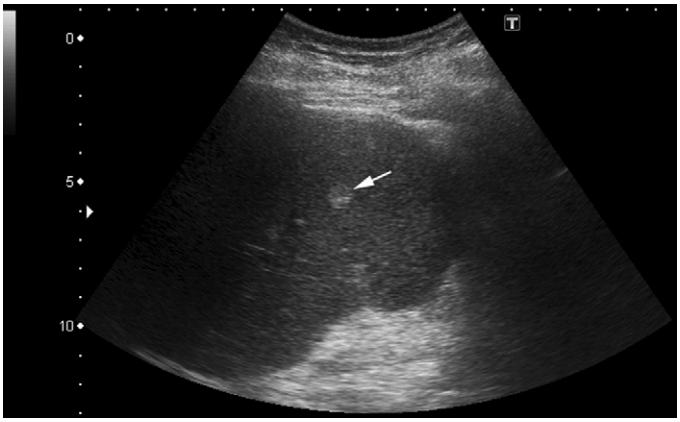
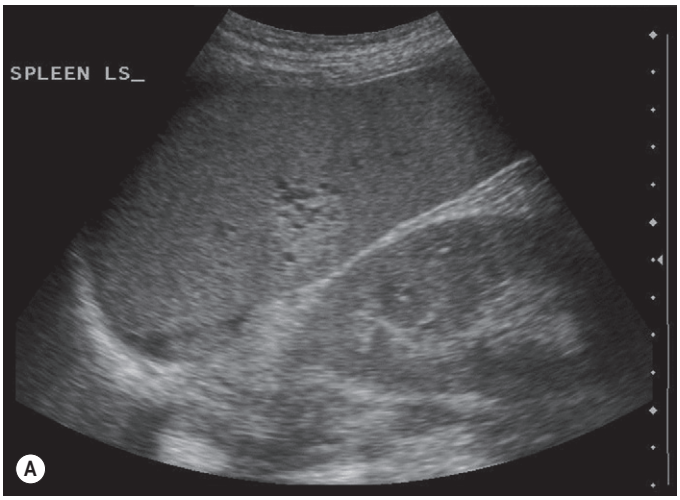


Figure 17.29 Small echogenic splenic nodule (arrow) typical of a splenic haemangioma.



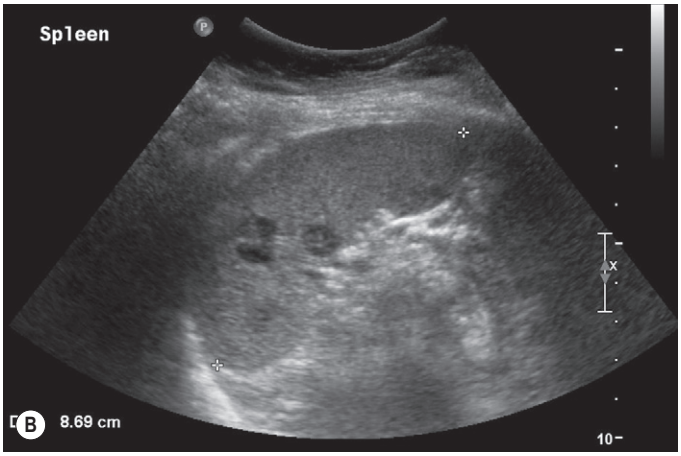


Figure 17.30 Atypical haemangioma. A: Containing small cystic spaces (courtesy of Mrs J. Bates, St James University Hospital, Leeds, UK). **B:** Echo-poor haemangiomas (courtesy of Dr S. Elliot. Freeman Hospital, Newcastle, UK).

isoechoic in comparison with the normal spleen (Fig. 17.32).[8] Other lesions may be hypoechoic in the late phase and therefore impossible to differentiate from many other splenic lesions.[1,9] The typical nodular peripheral enhancement pattern with centripetal filling seen in liver haemangiomas appears to be uncommon.[9] For lesions with atypical features correlative CT, MRI or red-cell scintigraphy may be required.

Splenic hamartomas are rare benign tumours composed of malformed normal splenic tissue; it is uncertain whether they are developmental or neoplastic in nature. Hamartomas are usually solitary and asymptomatic; however, large lesions may present with a palpable mass or thrombocytopenia/anaemia. Multiple lesions may be associated with tuberous sclerosis and Wiskott–Aldrich syndrome.[73] Sonographically the lesions are usually solid, well circumscribed of varying but usually increased echogenicity, sometimes with internal blood flow on colour Doppler examination (Fig. 17.33).[71,73,76] Cystic spaces and calcifications are occasionally present.

Splenic lymphangiomas are rare benign tumours composed of lymph-filled cystic spaces and are most commonly seen in children. They are usually asymptomatic unless large in size, when they may present with symptoms due to compression. Rarely they may be part of a generalised lymphangiomatosis involving multiple sites in the body. Sonographically the spleen may be normal in size or enlarged, containing one or more well-defined cystic masses that may contain fine septa, small calcifications and low level echoes within the cyst fluid (Fig. 17.34).[70,73] Demonstration of intrasplenic arteries and veins running along the walls of the cysts with colour Doppler may be a helpful diagnostic feature.[77]

Other rare benign splenic masses include inflammatory pseudotumours, lipomas, angiomyolipomas and fibromas.

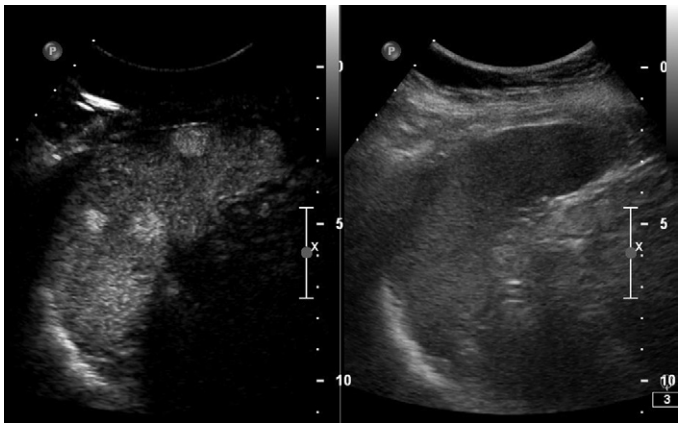


Figure 17.31 Composite greyscale and CEUS image showing hypervascularity of multiple splenic haemangiomas in the arterial phase. (Courtesy of Dr S. Elliot, Freeman Hospital, Newcastle, UK.)

Cystic lesions of the spleen

Cystic masses are rarely encountered in the spleen. However, many different disease processes may produce appearances ranging from simple cysts to solid masses with cystic components. Cystic splenic masses may be broadly categorised into congenital cysts,

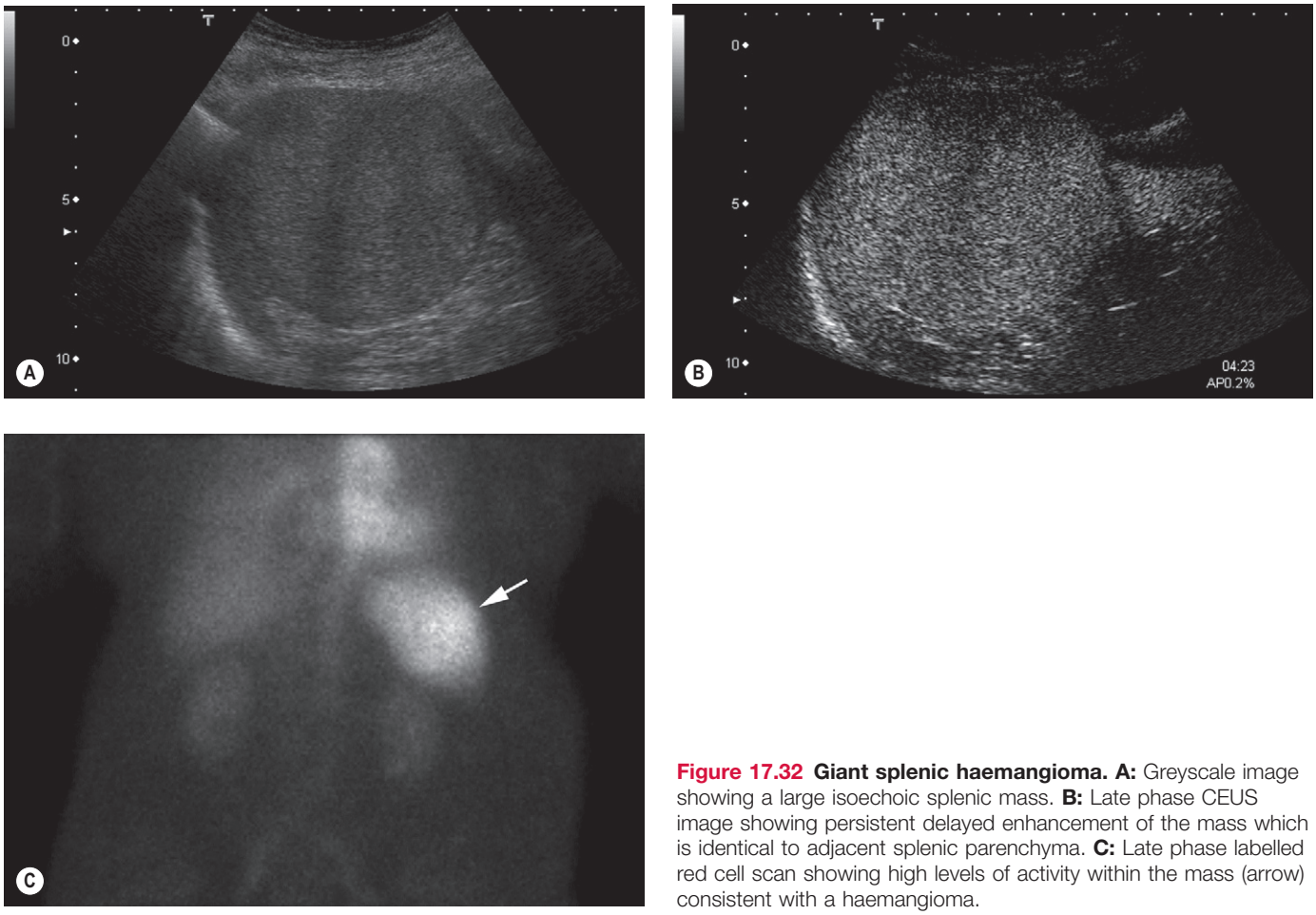


Figure 17.32 Giant splenic haemangioma. A: Greyscale image showing a large isoechoic splenic mass. **B:** Late phase CEUS image showing persistent delayed enhancement of the mass which is identical to adjacent splenic parenchyma. **C:** Late phase labelled red cell scan showing high levels of activity within the mass (arrow) consistent with a haemangioma.

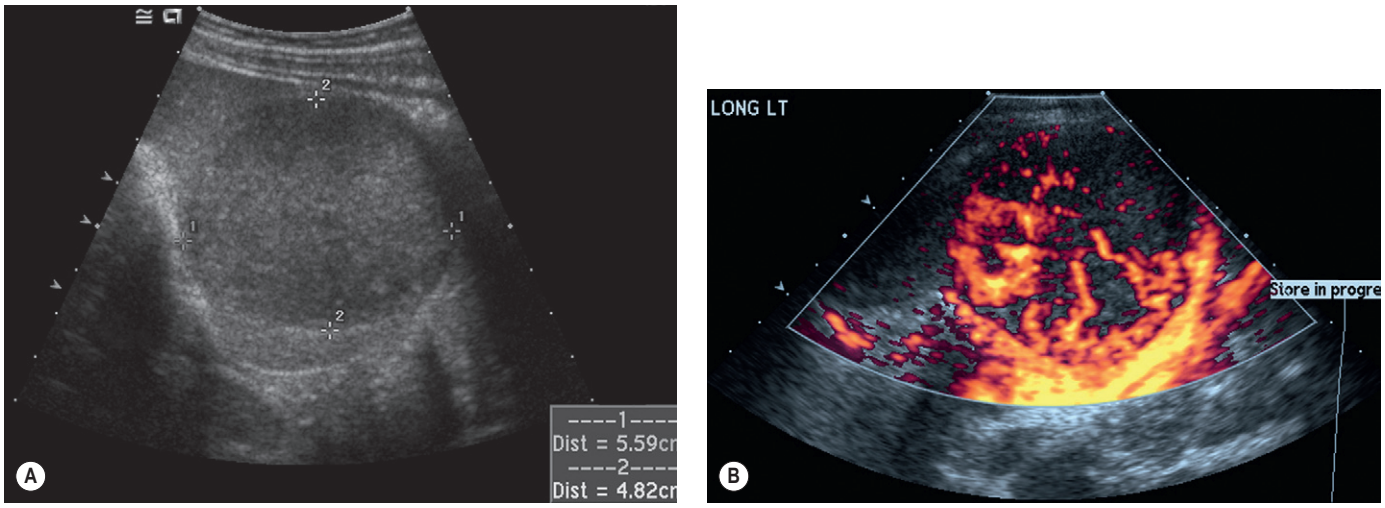


Figure 17.33 Splenic hamartoma. Greyscale **(A)** and power Doppler **(B)** images showing a hypervascular hypoechoic solid splenic mass. (Reproduced from Abbott RM, Levy AD, Aguilera NS, Gorospe L, Thompson WM. Primary vascular neoplasms of the spleen: Radiologic-pathologic correlation. RadioGraphics 2004;24:1137-1163, provided courtesy of the Armed Forces Institute of Pathology, Washington, DC.)

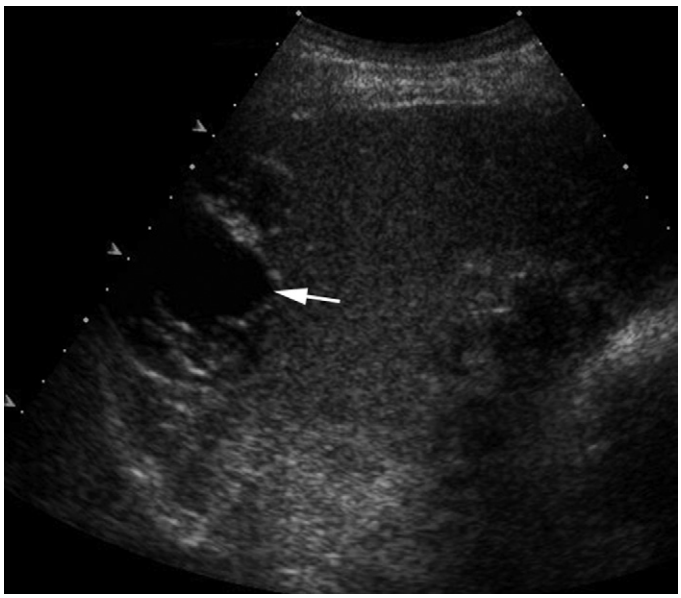


Figure 17.34 Splenic lymphangioma. There is a complex cystic mass in the superior aspect of the spleen (arrow). (Courtesy of Dr P. Sidhu, King's College Hospital, London, UK.)

Table 17.2 Classification of cystic splenic masses

Pathogenesis	Types	Example
Congenital	Epidermoid	
	Mesothelial	
Pseudocyst	Traumatic (infarction, infection)	
Infective	Parasitic	Echinococcal
	Bacterial	
	Fungal	*Candida*
	Mycobacterial	
Neoplastic	Benign	Lymphangioma, haemangioma
	Malignant	Metastasis
Other	Pancreatic pseudocyst	

pseudocysts and cystic masses secondary to infection or neoplasia (Table 17.2).

Congenital splenic cysts

Congenital cysts of the spleen are characterised by the presence of an inner endothelial lining thought to arise from infolding or trapping of peritoneal mesothelial cells between splenic lobules.[78] The epidermoid cyst accounts for 90% of cases but it is still a rare lesion representing only 10% of benign non-parasitic splenic cysts.[79,80] Such cysts are often an incidental finding but, when large, may present with pain or a palpable mass; spontaneous rupture is a rare complication.[81] Large lesions may elevate serum tumour markers (CA19–9, CA125 and CEA).[71,79] Sonographically the cysts are usually solitary, well defined and unilocular although septations have been described; calcification is unusual.[71] Cyst contents may be anechoic but echoes may be present due to cholesterol crystals or haemorrhage; posterior acoustic enhancement indicates the cystic nature of the mass (Fig. 17.35).[80]

Splenic pseudocysts

Splenic pseudocysts lack an epithelial lining and are therefore false cysts. They are usually post-traumatic in aetiology although 30% of patients are unable to recall a relevant history.[79] Pseudocysts account for up to 75–80% of all splenic cysts in areas where echinococcal disease (see below) is non-endemic.[70] Pseudocysts cannot be reliably distinguished from congenital cysts by their sonographic appearance,[82] although a history of trauma, age above the fourth decade and wall calcification favour a diagnosis of pseudocyst (Fig. 17.36).[70,71,82]

Infection and splenic abscess

Splenic infection may be due to bacterial (including mycobacteria), protozoal or fungal agents. Splenic abscess is rare but clinical presentation can be non-specific, and delayed diagnosis is associated with a high mortality rate, particularly if there is rupture into the peritoneum.

Bacterial splenic abscess is caused by haematogenous spread of infection in 75% of cases,[70] but can also arise following trauma,

direct spread from an adjacent organ or within an area of pre-existing infarction. Presentation is usually with one or more of fever, pain and leukocytosis although symptoms may be lacking, particularly in immunocompromised patients.[83] Sonographically pyogenic abscesses may be single or multiple and have a variety of appearances according to their state of evolution (Fig. 17.37). Typically they are echo-poor, round or oval but irregular in shape, poorly defined with variable posterior acoustic enhancement and absence of internal blood flow on colour Doppler examination (Fig. 17.38). CEUS may demonstrate rim or septal enhancement in the late phase.[8] Wedge-shaped abscesses may be seen in patients with septic emboli. Occasionally gas locules may be demonstrated. This is a diagnostic feature but most abscesses do not contain gas and the ultrasound appearances must be correlated with the patient's clinical presentation. Ultrasound-guided percutaneous aspiration for smaller abscesses (<3–3.5 cm) or catheter drainage for larger abscesses, combined with antibiotic therapy, has replaced splenectomy and is now the treatment of choice for most patients.[84]

Involvement of the spleen in *Mycobacterium tuberculosis* infection (MTB) is rare in non-endemic countries but rising due to the increased prevalence of AIDS. The most common ultrasound abnormality is multiple hypoechoic nodules, although abscess formation or isolated splenomegaly is also reported (Fig. 17.39).[85] Associated features of abdominal tuberculosis such as lymph node enlargement, intestinal wall thickening and ascites may help to suggest the diagnosis; ultrasound-guided fine-needle aspiration biopsy (FNAB) of the spleen or enlarged lymph nodes is usually diagnostic.[86,87]

Fungal infection of the spleen does not usually occur in the absence of immune compromise. *Candida albicans* is the most common pathogen and typically produces multiple small (<2 cm) abscesses.[70] Four sonographic patterns of hepatosplenic candidiasis are described:[88]

1. 'wheel within a wheel' pattern comprising a peripheral hypoechoic rim encasing an echogenic zone with a central echo-poor nidus
2. 'bulls-eye' lesion comprising an echo-poor rim and echogenic central area (Fig. 17.40)
3. uniformly hypoechoic nodules
4. multiple small echogenic foci with variable degrees of posterior acoustic shadowing representing calcifications late in the course of the disease.

The type 1 and type 2 patterns appear to be most specific for candidiasis but are only found in patients who are not neutropenic.

Parasitic splenic abscesses are usually due to hydatid disease and of these 95% of cases are caused by *Echinococcus granulosus*. Splenic

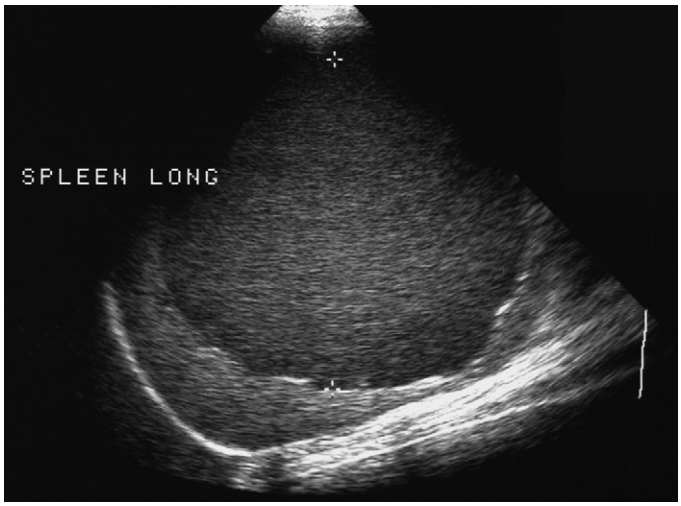
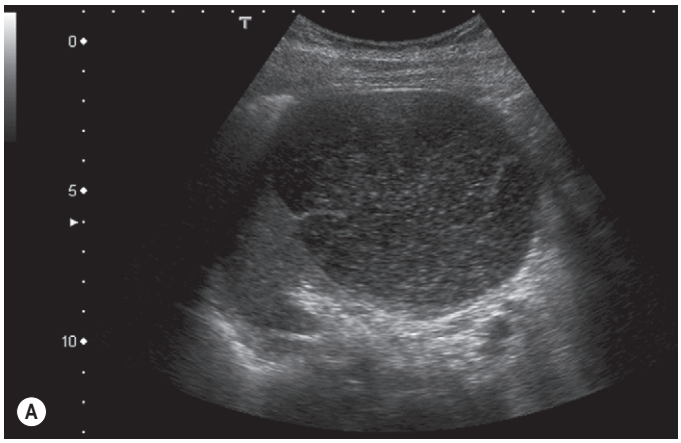


Figure 17.35 Epidermoid cyst. The presence of internal echoes is likely to represent blood or cholesterol crystals. (Courtesy of Dr S. Thorogood, Treliske Hospital, Truro, UK.)



Figure 17.37 Pyogenic splenic abscess (arrows).



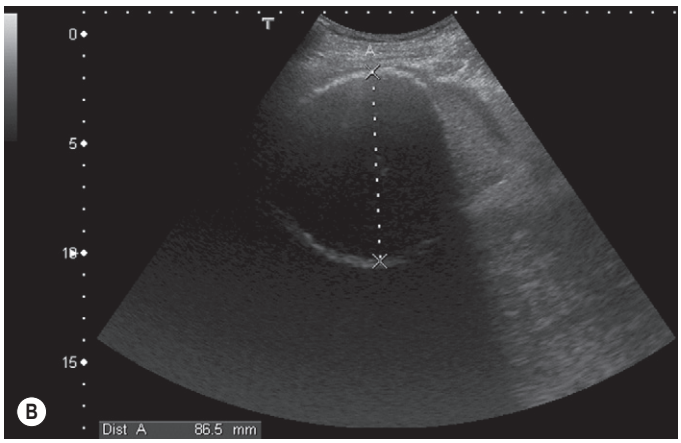


Figure 17.36 Presumed pseudocysts; incidental finding of two cystic lesions in asymptomatic patients. **A:** Cyst containing internal debris. **B:** Cyst with wall calcification.

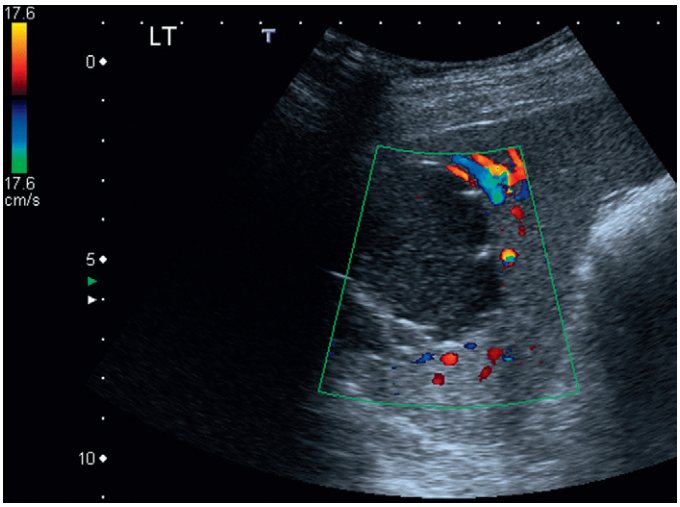


Figure 17.38 Pyogenic abscess showing peripheral, but not central, flow on colour Doppler examination.

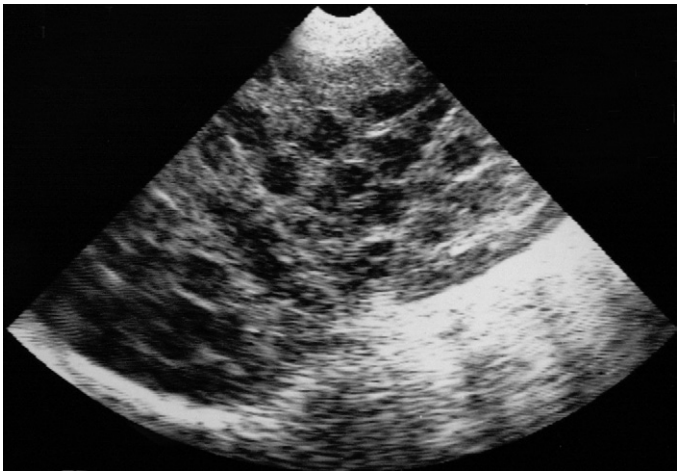


Figure 17.40 Splenic *Candida* microabscesses. Many of the echo-poor nodules have a 'bulls-eye' appearance comprising an echo-poor periphery and echogenic centre.

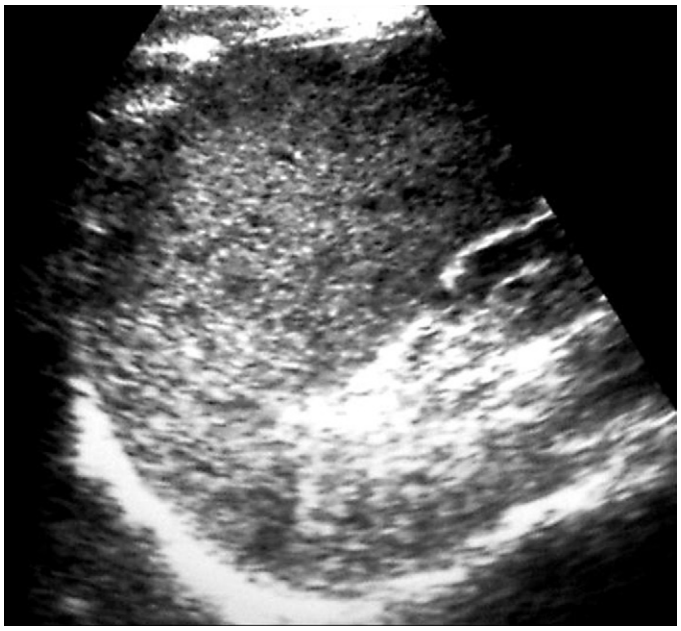


Figure 17.39 Splenic tuberculosis in a patient with AIDS. The spleen contains numerous small, poorly defined nodules. (Reproduced with permission from Kawooya MG, Muyinda Z, Byanyima R, Malwadde EK. Abdominal ultrasound findings in HIV patients: A pictorial review. Ultrasound 2008; 16:62–72.)

Splenic cysts

- Congenital splenic cysts are rare; most incidentally discovered cysts are post-traumatic pseudocysts.
- Splenic abscess may be sonographically indistinguishable from other splenic cysts; diagnostic aspiration is indicated where there is clinical suspicion of infection.
- Ultrasound-guided aspiration or catheter drainage is the treatment of choice for most pyogenic splenic abscesses.
- *Mycobacterium tuberculosis* is the most common cause of hypoechoic splenic nodules in AIDS patients.
- Echinococcal splenic cysts and *Candida* microabscesses may show a pathognomonic ultrasound appearance.

involvement is only present in 0.9–8% of patients and is much less common than involvement of the liver (70%) or lung (15–20%).[89] Patients are generally asymptomatic but, unless treated, the cysts grow slowly and may eventually cause pain due to pressure. Rarely cysts may become secondarily infected or rupture into the peritoneum with the risk of anaphylactic shock. A variety of sonographic patterns of hydatid cysts have been described. The World Health Organization (WHO) classification is based on the natural history of the disease and comprises five categories: types CE1 and CE2 are active cysts, type CE3 are transitional and types CE4 and CE5 inactive.[90] The CE2 and CE3 patterns have a pathognomonic appearance showing floating membranes (water-lily sign) and the presence of daughter cysts (multiple cysts within a larger cyst) (Fig. 17.41).[90,91] Percutaneous drainage of active cysts with injection of sclerosing agents is now regarded by many as the treatment of choice.[92]

Other cystic splenic masses

A number of other splenic lesions may have a partially cystic appearance on ultrasound examination including haematoma, metastases and primary vascular splenic tumours. Peliosis of the spleen is a very rare entity of uncertain aetiology characterised by multiple blood-filled spaces in the spleen usually associated with liver involvement. Sonographically it appears as multiple poorly defined hypoechoic cystic lesions.[93] Acute pancreatitis involving the pancreatic tail may extend into the splenic parenchyma, resulting in an intra-splenic pseudocyst.

Vascular lesions of the spleen

Splenic infarction

The splenic artery is an end artery and occlusion of the main artery or its branches will usually result in splenic infarction, which may be global or, more commonly, segmental in distribution. Venous infarction may also occur secondary to splenic or portal vein thrombosis. There are many recognised causes of splenic infarction (Table 17.3).[94] In young patients (under 40 years old) haematological disorders predominate; in older patients emboli (particularly from cardiac causes) are more common.[95] Infarction may be asymptomatic or may produce left upper quadrant pain. Sonographically changes may not be visible until 24 hours or more after infarction. Typically there is a well-defined wedge-shaped low echogenicity lesion with the base at the splenic capsule and apex directed towards the hilum (Fig. 17.42).[96] Blood flow is absent on colour Doppler examination and visualisation can be greatly facilitated

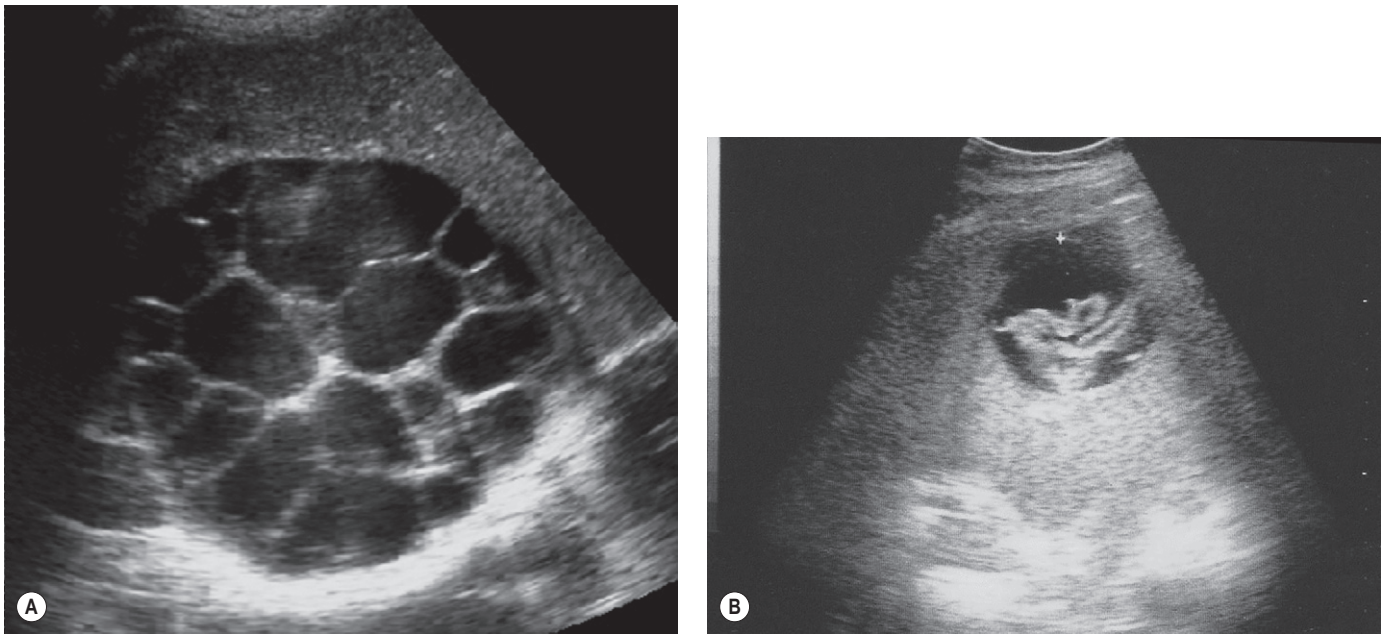


Figure 17.41 Hydatid disease. A: Type CE2 hydatid cyst containing multiple daughter cysts completely filling the mother cyst (courtesy of Professor Okan Akhan, Hacettepe University, Ankara, Turkey). **B:** Splenic hydatid cyst showing detached floating membranes (water-lily sign) (courtesy of Professor N. Örmeci, Ankara University Medical School, Ankara, Turkey).

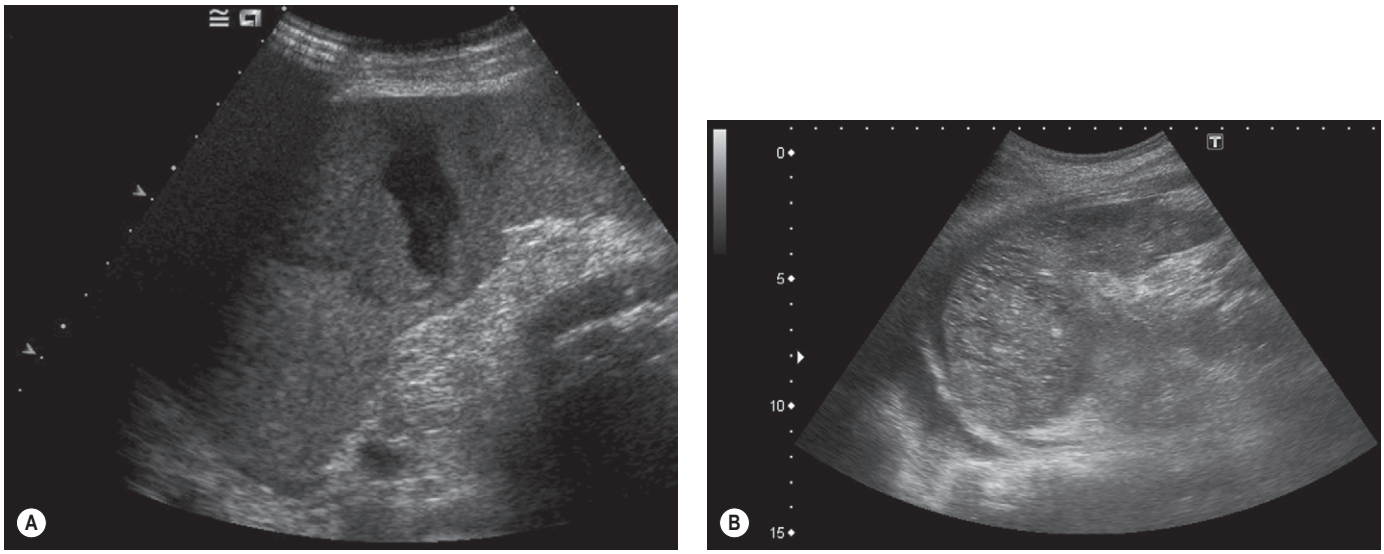


Figure 17.42 Examples of focal splenic infarction. A: Cystic appearing infarct (courtesy of Dr P. Sidhu, King's College Hospital, London, UK). **B:** Extensive splenic infarction secondary to hypovolaemic cardiac arrest.

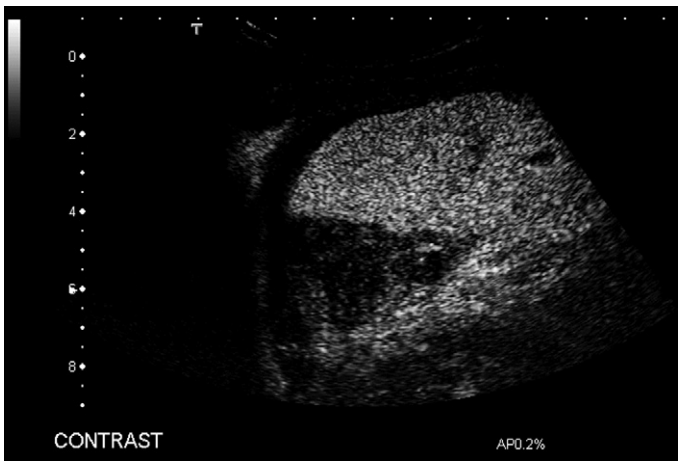


Figure 17.43 CEUS image of splenic infarction showing a large wedge-shaped area of non-perfusion secondary to trauma.

with CEUS (Fig. 17.43). Infarction may, however, also appear as round or oval lesions indistinguishable from other focal splenic masses.[97] With time the area of infarction reduces in size and increases in echogenicity or may disappear completely. Infarction may be complicated by secondary infection, haemorrhage or rupture. Chronic (recurring) splenic infarction is particularly seen in patients with myeloproliferative and sickle cell disease,[98] in the latter condition this frequently results in splenic atrophy (autosplenectomy).

Table 17.3 Aetiology of splenic infarction[93–95]

Haematological	Haemoglobinopathies* (esp. sickle cell disease)
	Lymphoproliferative diseases
	Lymphoma/Leukaemia
	Myelofibrosis
	Gaucher's disease
	Paroxysmal nocturnal haemoglobinopathy
	Polycythaemia vera
Embolic	Cardiac (endocarditis*, infarction, valvular disease, atrial fibrillation*, LV aneurysm)
	Pancreatic disease (pancreatitis, cancer)
Vascular	Splenic artery aneurysm
	Atherosclerosis*
	Aortic dissection
	Splenic vein thrombosis
	Portal hypertension
Autoimmune	Vasculitis (Kawasaki disease, Wegener's granulomatosis, polyarteritis nodosa)
	SLE/Connective tissue disease
Infection	Meningococcal
	Infectious mononucleosis
	Kala-azar
	Salmonella
	Malaria
Mechanical	Splenic torsion
	Wandering spleen
Miscellaneous	Amyloidosis
	Sarcoidosis
	Iatrogenic (liver transplant, catheter embolisation, cardiac surgery)

Denotes the most common causes.

Splenic vascular aneurysms

The splenic artery is the most common site for visceral arterial aneurysms. The incidence varies from 0.16% to 10.4% in various series, and splenic artery aneurysms are more common in women.[99] Most are asymptomatic but rarely rupture may occur, which carries a high mortality, particularly in pregnant patients. Sonographically the aneurysm appears as an anechoic mass along the course of the splenic artery with internal flow on Doppler examination as the diagnostic feature; wall calcification or thrombus may be present (Fig. 17.44). Treatment is usually recommended if the aneurysm is greater then 2 cm in diameter, particularly if increasing in size; catheter embolisation is now preferred to surgery.[100] Pseudoaneurysms of the splenic artery may be seen following trauma or pancreatitis. Splenic vein aneurysms are very rare lesions and are usually an incidental discovery.[93]

Splenic vein thrombosis and portal hypertension

Isolated thrombosis of the splenic vein (without thrombosis of the main portal vein) is usually due to pancreatic pathology (pancreatitis or carcinoma).[101] Patients may present with splenomegaly or gastrointestinal bleeding from isolated gastric varices. Ultrasound may directly demonstrate thrombus within a dilated splenic vein, with absent flow or incomplete luminal filling on colour Doppler examination indicating complete or partial thrombosis (Fig. 17.45).[78,93] When transabdominal ultrasound is non-diagnostic endoscopic ultrasound is often able to make the diagnosis.[102]

In patients with portal hypertension ultrasound is frequently able to demonstrate portosystemic varices (oesophageal, short gastric and splenorenal) in the perisplenic area (Fig. 17.46).

Vascular lesions of the spleen

- Splenic infarction is usually due to haematological disorders in younger patients and embolic causes in older patients.
- Infarction is a common cause of a focal splenic mass.
- Splenic infarction typically appears as a low echogenicity 'wedge-shaped' lesion with absent Doppler colour flow.
- The splenic artery is the most common site for visceral arterial aneurysms.

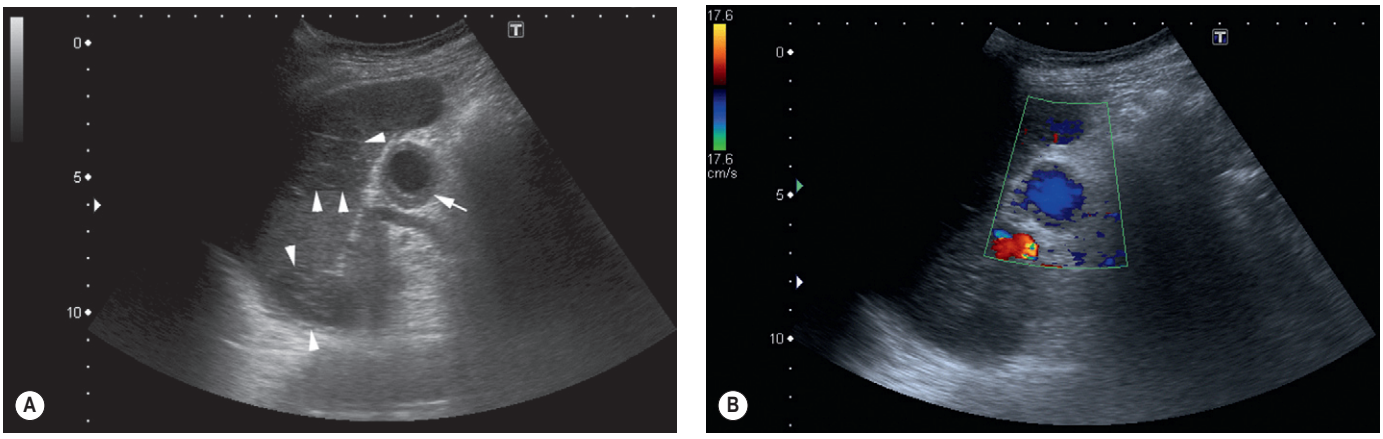


Figure 17.44 Splenic artery aneurysm. Greyscale **(A)** and colour Doppler **(B)** images of an aneurysm arising from the distal splenic artery (arrow); note the large areas of low attenuation in the spleen (arrowheads) representing splenic infarction.

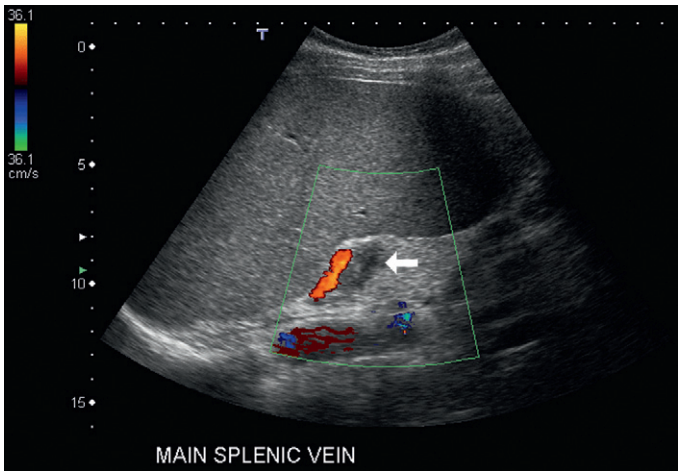


Figure 17.45 Splenomegaly due to splenic vein thrombosis. The dilated splenic vein (arrow) can be identified at the hilum (adjacent to the artery) containing echogenic thrombus and showing absence of colour flow.

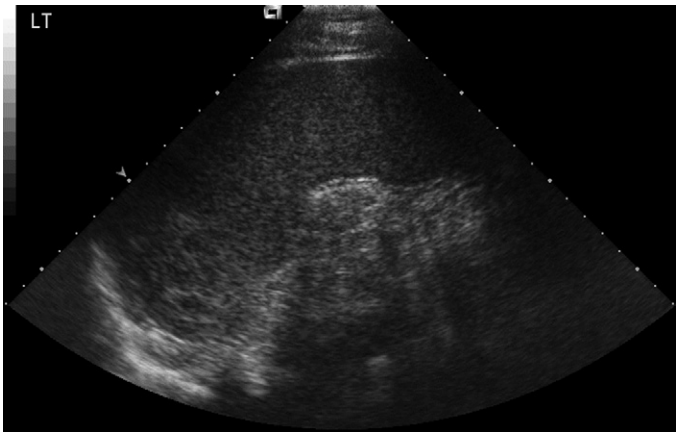


Figure 17.47 Splenic sarcoidosis. The spleen has a diffusely coarsened and inhomogeneous parenchyma; biopsy was performed, which revealed sarcoid infiltration.

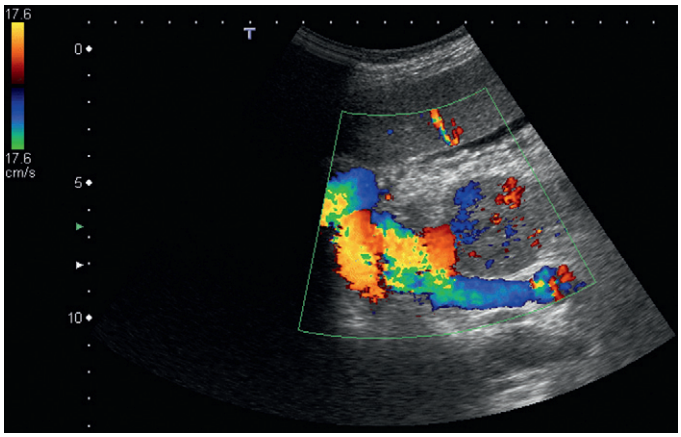


Figure 17.46 Colour Doppler image showing large splenorenal varices extending from the splenic hilum towards the left kidney.

Miscellaneous conditions of the spleen

Sarcoidosis

Sarcoidosis is a generalised non-caseating granulomatous disease of unknown aetiology. Although virtually any organ may be involved, the lungs and thoracic lymph nodes are the most commonly affected sites. Involvement of the spleen is usually asymptomatic but splenic enlargement is present in approximately one-third of patients on imaging studies.[103] Ultrasound may also show a diffusely inhomogeneous splenic echotexture or multiple small hypoechoic splenic nodules.[104] There is a wide differential diagnosis for this appearance, particularly as there appears to be a poor relationship between splenic involvement and chest radiograph abnormalities (Fig. 17.47).[103]

Spontaneous rupture of the spleen

Splenic rupture is usually due to trauma but occasionally atraumatic rupture may occur and the diagnosis may be delayed. Usually there is an underlying abnormality of the spleen, most commonly infection (particularly malaria and infectious mononucleosis) or haematological malignancy.[105,106] Ultrasound examination may demonstrate one or more of the following features: (1) intraparenchymal haematoma, (2) subcapsular haematoma (Fig. 17.48), (3) free intraperitoneal fluid (haemoperitoneum), (4) intrasplenic pseudoaneurysm. Splenomegaly is usually, but not universally, present. Splenectomy is the usual treatment; however, in view of the short- and long-term morbidity of surgery, conservative treatment with close clinical and sonographic monitoring can be successfully applied to patients who are haemodynamically stable.

Splenic calcifications

Many diseases may result in splenic calcification (Table 17.4). Although accurate diagnosis is not always possible the type of calcification and presence or absence of an associated mass are helpful features.

Multiple small echogenic foci, with or without acoustic shadowing, are usually the result of calcified granulomatous disease (Fig. 17.49). Linear or curvilinear calcifications may occur in vascular disease (atheroma or splenic artery aneurysm) or in the walls of splenic cysts – particularly pseudocysts (Fig. 17.36B). Focal dystrophic calcification may also arise in old splenic infarction, abscess and haematoma. Some primary and secondary splenic tumours may also contain foci of calcification.

The spleen in AIDS

The spleen is commonly involved in AIDS; sonographically detected splenomegaly is seen in 20–45% of patients and focal lesions are much more common than in the general population.[107,108] Multiple hypoechoic and rounded lesions are the most common pattern, for which the differential diagnosis is wide; tuberculosis is the most common cause but other infections and lymphoma are the main differential consideration.[109,110] If tuberculous infection cannot be confirmed from other sites, fine-needle biopsy may be performed.

DIFFERENTIAL DIAGNOSIS OF FOCAL SPLENIC LESIONS

Focal splenic lesions are frequently difficult to diagnose based purely on their ultrasound appearances. Clinical history including malignancy (lymphoma, metastases), trauma (haematoma, pseudocyst), infection or immunosuppression (abscess), pancreatitis

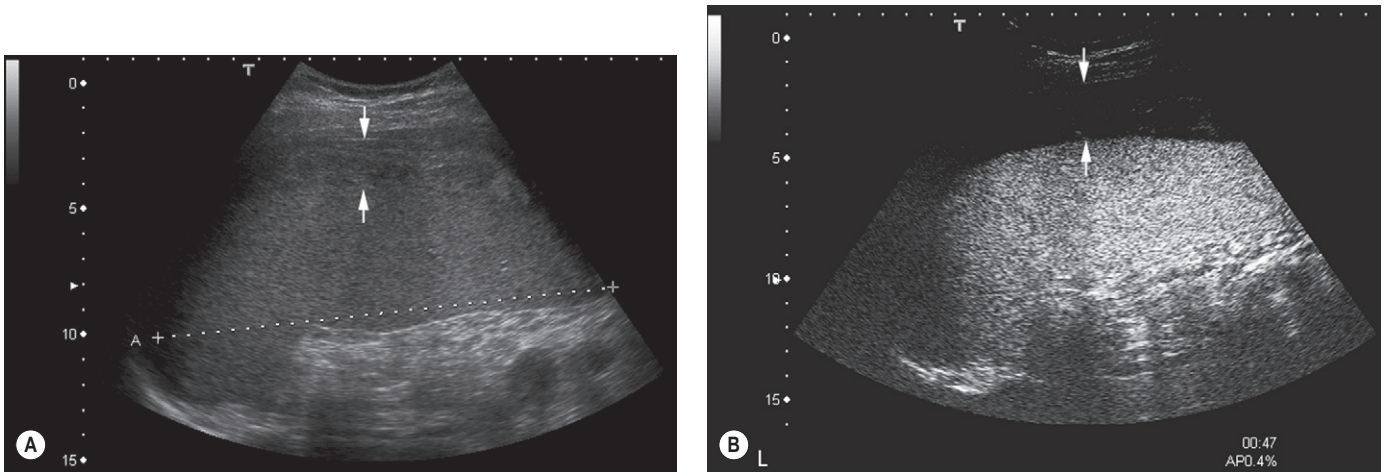


Figure 17.48 Spontaneous splenic rupture in a patient with infectious mononucleosis. The spleen is enlarged and there is a large perisplenic haematoma (arrows). This is almost isoechoic with splenic parenchyma on the greyscale image **(A)**, but easily differentiated following contrast medium administration **(B)**.

Table 17.4 Causes of splenic calcification

Category	Example
Infection	Healed granulomas (TB, histoplasmosis, brucellosis)
	Old abscess
	Hydatid
Vascular	Atherosclerosis
	Old haematoma/pseudocyst
	Aneurysm
	Old infarction
	Phlebolith
Neoplastic	Haemangioma
	Hamartoma
	Lymphangioma
	Metastasis
	Angiosarcoma
Miscellaneous	Sickle cell disease
	Haemosiderosis
	Sarcoidosis
	Amyloid
	Congenital cysts



Figure 17.49 Calcified splenic granulomatous disease. There are multiple small echogenic foci too small to cast an acoustic shadow.

(pseudocyst) and travel to endemic areas (TB, hydatid abscess) combined with laboratory data will often allow a presumptive diagnosis to be made.

Lesions can be broadly divided into those that are cystic, those that are echo-poor and those that are echogenic. Simple cystic lesions are likely to be benign and most will be pseudocysts. Diagnosis is more difficult when internal echoes are present and cyst aspiration should be considered in any patient with signs of infection to exclude abscess formation. Solid, small, well-defined, echogenic splenic masses are usually benign vascular neoplasms (haemangioma or hamartoma); ultrasound surveillance may be appropriate in this group. Large, heterogeneous or ill-defined echogenic masses will require additional imaging or biopsy for diagnosis.

Echo-poor lesions represent the greatest diagnostic challenge. However, a number of generalisations can be made:

1. Almost all malignant secondary splenic tumours (lymphoma and metastasis) are echo-poor.
2. A focal echo-poor mass in a patient with a known diagnosis of lymphoma can be assumed to represent a lymphomatous deposit.
3. Splenic infarction is relatively common and frequently has a characteristic appearance.
4. Increased vascularity within an incidentally discovered well-defined hypoechoic lesion on colour Doppler examination or in the arterial phase of CEUS tends to indicate a benign process.[111]
5. CEUS may increase diagnostic confidence for certain conditions, particularly splenic infarction and some echo-poor haemangiomas.

When a definitive diagnosis cannot be made further alternative imaging techniques may be diagnostic. When there is remaining uncertainty and the clinical situation requires a definitive diagnosis ultrasound guided biopsy is both accurate and safe.

ULTRASOUND INTERVENTIONS IN THE SPLEEN

Ultrasound-guided interventional procedures are infrequently performed in the spleen, probably reflecting the rarity of focal lesions and anxieties regarding the risk of haemorrhage. Procedures can, however, be performed with high levels of accuracy and low rates of complication.

Both fine-needle aspiration biopsy (FNAB) and core biopsy of the spleen are well-established techniques. Prior to biopsy, coagulation is measured and abnormalities corrected if there is significant derangement.[112] A safe route for biopsy must be identified, particularly avoiding the lung, pleura, kidney and colon. Procedures can usually be performed under local anaesthesia during suspended respiration. Following biopsy the patient must be closely observed to detect evidence of complications – particularly bleeding. In a large multicentre study of splenic FNAB and core biopsy overall accuracy was 90.9%, the major complication rate was less than 1% (no deaths or emergency splenectomies) and minor complication rate 5.2%.[113] Both FNAB and core biopsy gave similarly high levels of accuracy in this study except for lymphoma, where core biopsy performed much better. Core biopsy using an 18-gauge needle does not appear to carry a higher complication rate than with smaller needles and has a greater diagnostic accuracy.[114] Unlike targeted biopsy of the liver, the route chosen for splenic biopsy should traverse the minimum amount of normal parenchyma to minimise the risk of bleeding; particular care must be taken with lesions close to the hilum to avoid injury to the major vessels.[115] Despite its relative safety, splenic biopsy does carry a higher risk of bleeding than biopsy of other abdominal organs and therefore should be limited to cases where no suitable alternative exists.[115]

Ultrasound-guided aspiration and drainage is now the initial method of choice for diagnosis and treatment of most patients with pyogenic splenic abscesses, with reported success rates of 60–100% and complication rates of 0–18%.[112,115]

REFERENCES

1. Görg C. The forgotten organ: contrast enhanced sonography of the spleen. Eur J Radiol 2007;64:189–201.
2. Woolf N. The lymphoreticular system. In: Pathology basic and systemic. London: WB Saunders; 1998. p. 941–987.
3. Pimpl W, Dapunt O, Kaindl H, Thalhamer J. Incidence of septic and thromboembolic-related deaths after splenectomy in adults. Br J Surg 1989;76:517–521.
4. Moore KL, Persaud TVN, editors. The digestive system. In: Before we are born. Essentials of embryology and birth defects. 6th ed. Philadelphia: WB Saunders; 2003. p. 202–227.
5. Sherman LS, Potter SS, Scott WJ. Development of the gastrointestinal tract. In: Larson WJ, editor. Human embryology. 3rd ed. Philadelphia: Churchill Livingstone; 2001. p. 235–264.
6. Vibhakar SD, Bellon EM. The bare area of the spleen: a constant CT feature of the ascitic abdomen. AJR Am J Roentgenol 1984;141: 953–955.
7. Standring S, editor in chief. Spleen. In: Gray's anatomy. 39th ed. Edinburgh: Elsevier; 2005. p. 1239–1244.
8. Catalano O, Sandomenico F, Vallone P, et al. Contrast-enhanced sonography of the spleen. Semin Ultrasound CT MRI 2006;27: 426–433.
9. Catalano O, Lobianco R, Sandomenico F, et al. Real-time contrast-enhanced ultrasound of the spleen: examination technique and preliminary clinical experience. Radiol Med 2003;106:338–356.
10. Thorelius L. Contrast-enhanced ultrasound: beyond the liver. Eur Radiol 2003;13(S3):N91–N108.
11. Adamson JW, Longo DL. Anaemia and polycythaemia. In: Kasper DL, Braunwald E, Fauci AS, et al., editors. Harrison's principles of internal medicine. 16th ed. New York: McGraw-Hill; 2005. p. 329–348.
12. Loftus WK, Chow LTC, Metreweli C. Sonographic measurement of splenic length: correlation with measurement at autopsy. J Clin Ultrasound 1999;27:71–74.
13. Lamb PM, Lund A, Kanagasabay RR, et al. Spleen size: how well do linear ultrasound measurements correlate with three-dimensional CT volume assessments? Br J Radiol 2002;75:573–577.
14. Sheth SG, Mani S, Tamhankar H, Mehta PJ. Spleen size in health and disease: a sonographic assessment. J Assoc Phys India 1995;43: 182–184.
15. Ishibashi H, Higuchi N, Shimamura R, et al. Sonographic assessment and grading of spleen size. J Clin Ultrasound 1991;19:21–25.
16. De Odorico I, Spaulding KA, Pretorius DH, et al. Normal splenic volumes estimated using three-dimensional ultrasonography. J Ultrasound Med 1999;18:231–236.
17. Frank K, Linhart P, Kortsik C, Wohlenberg H. Sonographic determination of spleen size: Standard dimensions in the healthy adult. Ultraschall 1986;7:134–137 [Article in German].
18. Loftus WK, Metreweli C. Normal splenic size in a Chinese population. J Ultrasound Med 1997;16:345–347.
19. Hosey RG, Mattacola CG, Kriss V, et al. Ultrasound assessment of spleen size in college athletes. Br J Sport Med 2006;40:251–254.
20. DeLand FH. Normal spleen size. Radiology 1970;97:589–592.
21. Maymon R, Strauss S, Vaknin Z, et al. Normal sonographic values of maternal spleen size throughout pregnancy. Ultrasound Med Biol 2006;12:1827–1831.
22. Maymon R, Zimerman AL, Strauss S, Gayer G. Maternal spleen size throughout normal pregnancy. Semin Ultrasound CT MRI 2007;28: 64–66.
23. Goodman LR, Aprahamian C. Changes in splenic size after abdominal trauma. Radiology 1990;176:629–632.
24. Sonmez G, Ozturk E, Basekim CC, et al. Effects of altitude on splenic volume: sonographic assessment. J Clin Ultrasound 2007;35:182–185.
25. Görg C, Eichkorn M, Zugmaier G. The small spleen: sonographic patterns of functional hyposplenia or asplenia. J Clin Ultrasound 2003;31:152–155.
26. Gayer G, Hertz M, Strauss S, Zissin R. Congenital anomalies of the spleen. Semin Ultrasound CT MRI 2006;27:358–369.
27. Mortelé KJ, Mortelé B, Silverman SG. CT features of the accessory spleen. AJR Am J Roentgenol 2004;183:1653–1657.
28. Wadham BM, Adams PB, Johnson MA. Incidence and location of accessory spleens. N Engl J Med 1981;304:1111 [Letter].
29. Subramanyam BR, Balthazar EJ, Horii SC. Sonography of the accessory spleen. AJR Am J Roentgenol 1984;143:47–49.
30. Bertolotto M, Gioulis E, Ricci C, et al. Ultrasound and Doppler features of accessory spleens and splenic grafts. Br J Radiol 1998;71:595–600.
31. Katz JF, Kane RA. Sonographic appearance of accessory spleen. J Clin Ultrasound 1984;12:163–165.
32. Ota T, Ono S. Intrapancreatic accessory spleen: diagnosis using contrast enhanced ultrasound. Br J Radiol 2004;77:148–149.
33. Barawi M, Bekal P, Gress F. Accessory spleen: a potential cause of misdaignosis at EUS. Gastrointest Endosc 2000;52:769–772.
34. Froehner M, Leike S, Manseck A, et al. Splenunculus mimicking late local recurrence of renal cell carcinoma. Scand J Urol Nephrol 1998;32:418–419.
35. Zissin R, Gutman M, Evan-Sapir E, Gayer G. Anatomic and pathologic computed tomographic findings following splenectomy. Semin Ultrasound CT MRI 2007;28:67–78.
36. Müller U, Röthlin M. Splenic neoformation following trauma-induced splenectomy – diagnosis and function. Swiss Surg 1995;5:230–235 [in German].
37. Delamarre J, Capron J-P, Drouard F, et al. Splenosis: ultrasound and CT findings in a case complicated by an intraperitoneal implant traumatic haematoma. Gastrointest Radiol 1988;13:275–278.
38. Sarraf KM, Abdalla M, Al-Omari O, Sarraf MG. Diagnostic difficulties of pelvic splenosis: case report. Ultrasound Obstet Gynecol 2006;27:220–221.
39. Tasci Y, Kayikcioglu F, Cavusoglu D, Gokcin H. Splenosis mimicking pelvic mass. Obstet Gynecol 2005;106:1167–1169.
40. Dawson C, McCormick C, Menai-Williams R, Malone PR. Splenunculus masquerading as an adrenal mass. Br J Urol 1995;76:404–405.
41. Pumberger W, Wiesbauer P, Leitha T. Splenosis mimicking tumor recurrence in renal cell carcinoma: detection on selective spleen scintigraphy. J Pediatr Surg 2001;36:1089–1091.
42. Kinori I, Rifkin MD. A truly wandering spleen. J Ultrasound Med 1988;7:101–105.
43. Buehner M, Baker MS. The wandering spleen. Surg Gynecol Obstet 1992;175:373–387.
44. Erden A, Karaalp G, Özcan H, Cumhur T. Wandering accessory spleen. Surg Radiol Anat 1995;17:89–91.

45. Yilmaz C, Esen OS, Colak A, et al. Torsion of a wandering spleen associated with portal vein thrombosis. J Ultrasound Med 2005;24:379–382.
46. Kessler A, Miller E, Keidar S, et al. Mass at the splenic hilum: a clue to torsion of a wandering spleen located in a normal left upper quadrant position. J Ultrasound Med 2003;22:527–530.
47. Gilman RS, Thomas RL. Wandering spleen presenting as acute pancreatitis in pregnancy. Obstet Gynecol 2003;101:1100–1102.
48. Karmazyn B, Steinberg R, Gayer G, et al. Wandering spleen – the challenge of ultrasound diagnosis: report of 7 cases. J Clin Ultrasound 2005;33:433–438.
49. Applegate KE, Goske MJ, Pierce G, Murphy D. Situs revisited: imaging of the heterotaxy syndrome. Radiographics 1999;19: 837–852.
50. Ditchfield MR, Hutson JM. Intestinal rotational abnormalities in polysplenia and asplenia syndromes. Pediatr Radiol 1998;28:303–306.
51. Aster JC. Diseases of white blood cells, lymph nodes, spleen and thymus. In: Kumar V, Abbas AK, Fausto N, editors. Robbins and Cotran pathological basis of disease. 7th ed. Philadelphia: Elsevier Saunders; 2005. p. 661–709.
52. Goerg C, Schwerk WB, Goerg K. Sonography of focal lesions of the spleen. AJR Am J Roentgenol 1991;156:949–953.
53. Sandrasegaran K, Robinson PJ, Selby P. Staging of lymphoma in adults. Clin Radiol 1994;49:149–161.
54. Rademaker J. Hodgkin's and non-Hodgkin's lymphomas. Radiol Clin North Am 2007;45:69–83.
55. Bhatia K, Sahdev A, Reznek RH. Lymphoma of the spleen. Semin Ultrasound CT MRI 2007;28:12–20.
56. Spier CM, Kjeldsberg CR, Eyre HJ, Behm FG. Malignant lymphoma with primary presentation in the spleen. Arch Pathol Lab Med 1985;109:1076–1080.
57. Siniluoto T, Päivänsalo M, Alavaikko M. Ultrasonography of spleen and liver in staging Hodgkin's disease. Eur J Radiol 1991;13:181–186.
58. Even-Sapir E, Lievshitz G, Perry C, et al. Fluorine-18 fluorodeoxyglucose PET/CT patterns of extranodal involvement in patients with non-Hodgkin's lymphoma and Hodgkin's disease. Radiol Clin North Am 2007;45:697–709.
59. Castellino RA. Hodgkin disease: practical concepts for the diagnostic radiologist. Radiology 1986;159:305–310.
60. Munker R, Stengel A, Stäbler A, et al. Diagnostic accuracy of ultrasound and computed tomography in the staging of Hodgkin's disease: verification by laparotomy in 100 cases. Cancer 1995;76: 1460–1466.
61. Görg C, Weide R, Schwerk WB. Malignant splenic lymphoma: sonographic patterns, diagnosis and follow-up. Clin Radiol 1997;52:535–540.
62. Goerg C, Schwerk WB, Goerg K, Havemann K. Sonographic patterns of the affected spleen in malignant lymphoma. J Clin Ultrasound 1990;18:569–574.
63. Siniluoto TMJ, Tikkakoski TA, Lähde ST, et al. Ultrasound or CT in splenic diseases? Acta Radiol 1994;35:597–605.
64. Görg C, Graef C, Bert T. Contrast-enhanced sonography for differential diagnosis of an inhomogeneous spleen of unknown cause in patients with pain in the left upper quadrant. J Ultrasound Med 2006;25:729–734.
65. Peddu P, Shah M, Sidhu PS. Splenic abnormalities: a comparative review of ultrasound, microbubble-enhanced ultrasound and computed tomography. Clin Radiol 2004;59:777–792.
66. Townsend RR, Laing FC, Jeffrey Jr RB, Bottles K. Abdominal lymphoma in AIDS: evaluation with US. Radiology 1989;171: 719–724.
67. Lam KY, Tang V. Metastatic tumours to the spleen: a 25-year clinicopathologic study. Arch Pathol Lab Med 2000;124:526–530.
68. Schön CA, Görg C, Ramaswamy A, Barth PJ. Splenic metastases in a large unselected autopsy series. Pathol Res Pract 2006;202:351–356.
69. Goerg C, Schwerk WB, Goerg K. Splenic lesions: sonographic patterns, follow-up, differential diagnosis. Eur J Radiol 1991;13: 59–66.
70. Urrutia M, Mergo PJ, Ros LH, et al. Cystic masses of the spleen: radiologic-pathologic correlation. RadioGraphics 1996;16:107–129.
71. Warshauer DM, Hall HL. Solitary splenic lesions. Semin Ultrasound CT MRI 2006;27:370–388.
72. Thompson WM, Levy AD, Aguilera NS, et al. Angiosarcoma of the spleen: imaging characteristics in 12 patients. Radiology 2005;235: 106–115.
73. Abbott RM, Levy AD, Aguilera NS, et al. Primary vascular neoplasms of the spleen: radiologic-pathologic correlation. RadioGraphics 2004;24:1137–1163.
74. Willcox TM, Speer RW, Schlinkert RT, Sarr MG. Haemangioma of the spleen: presentation, diagnosis and management. J Gastrointest Surg 2000;4:611–613.
75. Andrews MW. Ultrasound of the spleen. World J Surg 2000;24: 183–187.
76. Tang S, Shimizu T, Kikuchi Y, et al. Color Doppler sonographic findings in splenic hamartoma. J Clin Ultrasound 2000;28:249–253.
77. Komatsuda T, Ishida H, Konno K, et al. Splenic lymphangioma: US and CT diagnosis and clinical manifestations. Abdom Imaging 1999;24:414–417.
78. Rolfes RJ, Ros PR. The spleen: an integrated imaging approach. Crit Rev Diagn Imaging 1990;30:41–83.
79. Hansen MB, Moller AC. Splenic cysts. Surg Laparosc Endosc Percutan Tech 2004;14:316–322.
80. Shirkhoda A, Freeman J, Armin AR, et al. Imaging features of splenic epidermoid cyst with pathological correlation. Abdom Imaging 1995;20:449–451.
81. Rathaus V, Zissin R, Goldberg E. Spontaneous rupture of an epidermoid cyst of spleen: Preoperative ultrasonographic diagnosis. J Clin Ultrasound 1991;19:235–237.
82. Dachman AH, Ros PR, Murari PJ, et al. Nonparasitic splenic cysts: a report of 52 cases with radiologic-pathologic correlation. AJR Am J Roentgenol 1986;147:537–542.
83. Ng KK, Lee TY, Wan YL, et al. Splenic abscess: diagnosis and management. Hepatogastroenterology 2002;49:567–571.
84. Chou YH, Tiu M, Chiou HJ, et al. Ultrasound-guided interventional procedures in slpenic abscesses. Eur J Radiol 1998;28:167–170.
85. Sharma SK, Smith-Rohrberg D, Tahir M, et al. Radiological manifestations of splenic tuberculosis: a 23-patient case series from India. Indian J Med Res 2007;125:669–678.
86. Tarantino L, Giorgio A, de Stefano G, et al. Disseminated mycobacterial infection in AIDS patients: abdominal US features and value of fine-needle aspiration biopsy of lymph nodes and spleen. Abdom Imaging 2003;28:602–608.
87. Suri R, Gupta S, Gupta SK, et al. Ultrasound guided fine needle aspiration cytology in abdominal tuberculosis. Br J Radiol 1998;71:723–727.
88. Pastakia B, Shawker TH, Thaler M, et al. Hepatosplenic candidiasis: wheels within wheels. Radiology 1988;166:417–421.
89. Akhan O, Koroglu M. Hydatid disease of the spleen. Semin Ultrasound CT MRI 2007;28:28–34.
90. WHO Informal Working Group. International classification of ultrasound images in cystic echinococcosis for application in clinical and field epidemiological settings. Acta Tropica 2003;85:253–261.
91. Pant CS, Gupta RK. Diagnostic value of ultrasonography in hydatid disease in abdomen and chest. Acta Radiol 1987;28:743–745.
92. Örmeci N, Soykan I, Palabiyikoğlu M, et al. A new therapeutic approach for treatment of hydatid cysts of the spleen. Dig Dis Sci 2002;47:2037–2044.
93. Vanhoenacker FM, de Beeck O, De Schepper AM, et al. Vascular disease of the spleen. Semin Ultrasound CT MRI 2007;28:35–51.
94. Gupta S, Kakar A. Splenic infarct of unusual aetiology. J Ind Acad Clin Med 2004;5:310–314.
95. Jaroch MT, Broughan TA, Hermann RE. The natural history of splenic infarction. Surgery 1986;100:743–748.
96. Weingarten MJ, Fakhry J, McCarthy J, et al. Sonography after splenic embolization: the wedge-shaped acute infarct. AJR Am J Roentgenol 1984;142:957–959.
97. Goerg C, Schwerk WB. Splenic infarction: sonographic patterns, diagnosis, follow-up and complications. Radiology 1990;174:803–807.
98. Görg C, Zugmaier G. Chronic recurring infarction of the spleen: Sonographic patterns and complications. Ultraschall Med 2003;24:245–249.
99. Trastek VF, Pairolero PC, Bernatz PE. Splenic artery aneurysms. World J Surg 1985;9:378–383.
100. McDermott VG, Shlansky-Goldberg R, Cope C. Endovascular management of splenic artery aneurysms and pseudoaneurysms. Cardiovasc Intervent Radiol 1994;17:179–184.
101. Moossa AR, Gadd MA. Isolated splenic vein thrombosis. World J Surg 1985;9:384–390.
102. Wiersema MJ, Chak A, Kopecky KK, Wiersema LM. Duplex Doppler endosonography in the diagnosis of splenic vein, portal vein, and portosystemic shunt thrombosis. Gastrointest Endosc 1995;42:19–26.
103. Warshauer DM. Splenic sarcoidosis. Semin Ultrasound CT MRI 2007;28:21–27.
104. Kessler A, Mitchell DG, Israel HL, Goldberg BB. Hepatic and splenic sarcoidosis: ultrasound and MR imaging. Abdom Imaging 1993;18: 159–163.

105. Sterlacci W, Heiss S, Augustin F, Tzankov A. Splenic rupture, beyond and behind: a histological, morphometric and follow-up study of 254 cases. Pathobiology 2006;73:280–287.
106. Görg C, Cölle J, Görg K, et al. Spontaneous rupture of the spleen: ultrasound patterns, diagnosis and follow-up. Br J Radiol 2003;76:704–711.
107. Gore RM, Miller FH, Yaghmai V. Acquired immunodeficiency syndrome (AIDS) of the abdominal organs: imaging features. Semin Ultrasound CT MRI 1998;19:175–189.
108. Yee JM, Raghavendra BN, Horii SC, Ambrosino M. Abdominal sonography in AIDS: a review. J Ultrasound Med 1989;8:705–714.
109. Porcel-Martin A, Rendon-Unceta P, Bascuñana-Quirell A, et al. Focal splenic lesions in patients with AIDS: sonographic findings. Abdom Imaging 1998;23:196–200.
110. Kawooya MG, Muyinda Z, Byanyima R, Malwadde EK. Abdominal ultrasound findings in HIV patients: a pictorial review. Ultrasound 2008;16:62–72.
111. Görg C, Görg K, Bert T, Barth P. Colour Doppler ultrasound patterns and clinical follow-up of incidentally found hypoechoic, vascular tumours of the spleen: evidence for a benign tumour. Br J Radiol 2006;79:319–325.
112. Lieberman S, Libson E, Sella T, et al. Percutaneous image-guided splenic procedures: update on indications, technique, complications and outcomes. Semin Ultrasound CT MRI 2007;28:57–63.
113. Civardi G, Vallisa D, Bertè R, et al. Ultrasound-guided fine needle biopsy of the spleen: high clinical efficacy and low risk in a multicentre Italian study. Am J Hematol 2001;67:93–99.
114. Liang P, Gao Y, Wang Y, et al. US-guided percutaneous needle biopsy of the spleen using 18-gauge versus 21-gauge needles. J Clin Ultrasound 2007;35:477–482.
115. Kang M, Kalra N, Gulati M, et al. Image guided percutaneous splenic interventions. Eur J Radiol 2007;64:140–146.

CHAPTER

18 Oesophagus and stomach

John N. Plevris and Scott Inglis

INTRODUCTION 351

EUS EQUIPMENT 351

ANATOMICAL STRUCTURE OF UPPER GI TRACT 352

EUS APPEARANCE OF UPPER GI TRACT 352

CLINICAL INDICATIONS FOR EUS IN THE UPPER GI TRACT 353

PRINCIPLES OF EUS CANCER STAGING 353

EUS AND THE OESOPHAGUS 354
Cancer 354
Barrett's oesophagus 356
Submucosal (subepithelial) lesions 358
Benign posterior mediastinal masses 358
Oesophageal varices 359
Achalasia and other dysmotility disorders 359

EUS AND THE STOMACH 360
Cancer 360
Gastric lymphoma 360
Gastric polyps 360
Submucosal lesions and hypertrophic folds 362
Gastric varices 363
Duodenum 365
Peptic ulcer disease 365

EUS IN UPPER GI TRACT: PRESENT AND FUTURE 366

Introduction and general principles

- Endoscopic ultrasound (EUS) refers to the integration of the modalities of white light video endoscopy and ultrasonography.
- Echo-endoscopes are classified by the orientation of the transducer; these are radial and curvilinear. The radial echo-endoscope has a 360° scan plane and is primarily used for diagnosis, while the curvilinear has a 15° scan plane and is mostly used as an interventional device.
- The ultrasonic appearance of the wall of the upper GI tract imaged consists of a number (usually five) of bright (hyperechoic) and dark (hyoechoic) rings.
- One of the most important uses of EUS is staging of upper GI malignancies. EUS is also used to investigate submucosal abnormalities including vascular structures, as well as for therapeutic applications such as fine-needle aspiration or core biopsies.

INTRODUCTION

Ultrasonography has been for a number of years a standard technique in the investigation of intra-abdominal organs. However, conventional transcutaneous ultrasound has limited application for the oesophagus and the stomach. Its main disadvantage is that ultrasound waves are reflected by the air–tissue interface and any organs surrounded by air, as is the oesophagus, are virtually invisible by ultrasonography. Furthermore, the stomach can only be examined by conventional ultrasound if it is fluid filled and the patient is carefully positioned to displace the gas from one part of the stomach to the other. In addition, because penetration of ultrasound waves and resolution of imaging are inversely related, detail is generally less in the posterior aspects of the stomach.

Despite the above caveats, diagnostic ultrasonography has undoubtedly a number of advantages over other imaging modalities as it is non-invasive, can be easily repeated without patient discomfort and non-ionising radiation is used. Ultrasound machines, in general, are compact and can easily be used at the bedside.

It was therefore quite an expected development when in the early 1980s it did become possible to integrate the techniques of endoscopy and ultrasonography[1] under the name endoscopic ultrasound (EUS).

EUS EQUIPMENT

Modern echo-endoscopes are classified by the orientation of the transducer, as radial and curvilinear.[2] The radial echo-endoscope is primarily used for diagnosis, to produce a 360° image of the anatomy. The ultrasound image obtained is easily related to the anatomy of the oesophagus or stomach and reduces the complexity of its interpretation.

The first flexible EUS scopes incorporated a rotating single element piezoelectric crystal transducer attached to the tip of the endoscope, to produce a 360° ultrasound B-mode cross-sectional image of the wall of the gastrointestinal (GI) tract (Fig. 18.1A). Furthermore a blind echo-endoscope was developed for malignant oesophageal strictures that is inserted over a guide wire. (Fig. 18.1B). The recent advent of solid-state electronic radial echo-endoscopes has meant that Doppler, elastography, flow and harmonic imaging are now available (Fig. 18.1C, D). The mechanical and electronic echo-endoscopes operate at frequencies between 5 and 20 MHz, depending upon the transducer. In all cases, acoustic contact with the wall of the GI tract is obtained by a water-filled balloon.[2]

EUS mini-probes are radial devices, incorporating a small mechanical rotating single element piezoelectric ultrasound transducer (Fig. 18.1E). They have been designed to be used within areas that are normally inaccessible to echo-endoscopes (e.g. pancreatobiliary ducts, stenotic lumen) or when a high-frequency study of the oesophageal or gastric wall is needed.[3]

These devices are introduced through the biopsy channel of a standard video endoscope. They tend to be fragile with limited lifespan and suffer from limited penetration although resolution can be excellent if good contact is obtained with the wall of the GI tract.[4]

The curvilinear echo-endoscope (Fig. 18.1F) was introduced clinically in the early 1990s[5,6] and produced an image that was

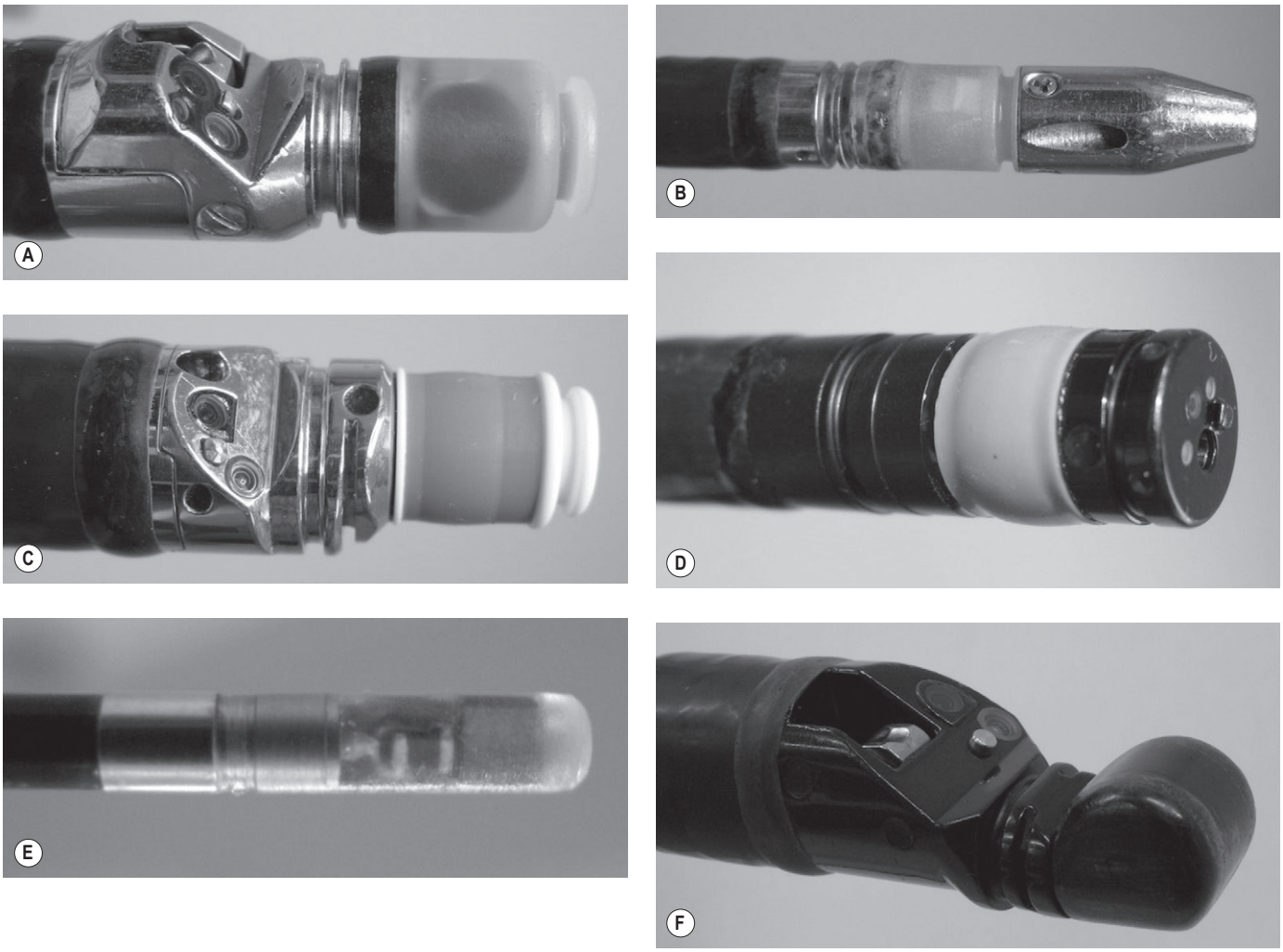


Figure 18.1 Examples of the Olympus and Fujinon echo-endoscopes that are currently available and an example of a mini-probe transducer.
A: The tip of the Olympus GF-UM series radial echo-endoscope. Diameter of scope series ranges between 12.5 and 13.5 mm.
B: The tip of the Olympus MH-908 radial echo-endoscope. Diameter of scope 8.5 mm.
C: The tip of the Olympus GF-UE 260 electronic radial echo-endoscope. Diameter of scope 13.8 mm.
D: The tip of the Fujinon electronic EG-530UR radial echo-endoscope. Diameter of scope 11.5 mm.
E: The tip of the Fujinon 26–12 MHz mini-probe. Diameter of probe ranges between 2 and 2.6 mm.
F: The tip of the Olympus GF-UCT 240 electronic curvilinear echo-endoscope. Diameter of scope 14.6 mm.

longitudinally orientated in relation to the endoscope; it is mostly used as an interventional device and normally operates at a frequency between 5 and 10 MHz.[2,6–8] However, interpretation of the ultrasound images can be more difficult compared with those of radial echo-endoscopes.

ANATOMICAL STRUCTURE OF UPPER GI TRACT

The wall of the oesophagus and stomach is made up of a number of tissue layers of different cellular consistencies. The innermost layer towards lumen, is the mucosa and is made up of a number of sublayers, namely epithelium, lamina propria and muscularis mucosae. The next layer is the submucosa and is composed of dense connective tissue. The muscularis propria of the upper GI tract is a muscular layer composed of both skeletal and smooth muscle fibres. This may be subdivided into sublayers, the inner circumferential fibres and outer longitudinal fibres, dependent upon location; the upper third of the oesophagus is mostly composed of skeletal muscle; the middle third has both skeletal and smooth muscle; and the lowest third is only composed of smooth muscle fibres. The approximate thicknesses of the muscularis propria circular and longitudinal fibre layers are 500 µm and 300 µm, respectively.

The oesophagus is covered by an adventitia until it pierces the diaphragm, after which it is covered by a serosa, which continues throughout the outer lining of stomach.

A detailed cross-section of the anatomy of the wall of the oesophagus is shown in Figure 18.2.

EUS APPEARANCE OF UPPER GI TRACT

As the main operating frequencies of the echo-endoscopes are 5, 7.5, 10, 12 and 20 MHz, the tissue detail and number of boundary reflections observed during imaging of the walls of the oesophagus

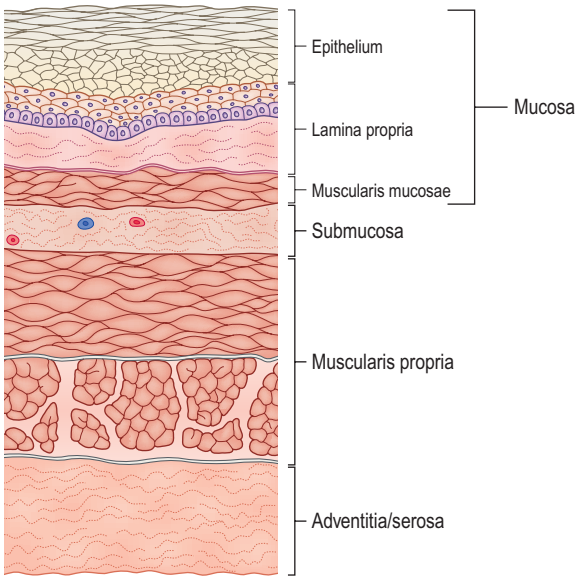


Figure 18.2 Anatomy of the wall of the oesophagus.

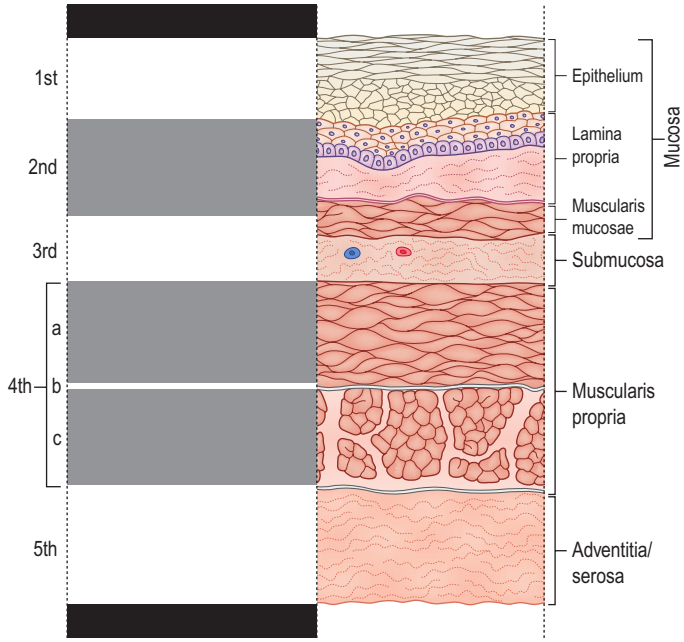


Figure 18.3 Correlation between the standard five EUS layers and histological layers of the normal oesophageal wall. 1st = interface between balloon, fluid in the lumen and the superficial mucosa; 2nd = lamina propria and muscularis mucosae, 3rd = the interfaces between the submucosa and mucosa and muscularis propria; 4th = muscularis propria; (4a) circular, (4c) longitudinal and (4b) thin connective tissue layer, only seen at high frequencies; 5th = interface between muscularis propria and the adventitia. (The histological images were modified from AJCC Cancer Staging Atlas.[12])

and stomach will be dependent upon frequency and the resultant pulse wavelength. For simplicity most endoscopists approximate the boundary reflections as the GI wall layers. The ultrasonic appearance of the wall of the GI tract imaged under EUS consists of a number of bright (hyperechoic) and dark (hypoechoic) rings.

Figure 18.3 illustrates an idealised ultrasound image relating to the anatomical layers of the oesophagus. A water-filled latex balloon is used to maintain contact with the wall of the oesophagus. The balloon is normally filled to the extent where good contact is obtained with the wall, but not to the point where the layers are compressed. When the ultrasound pulse is being transmitted, a reflection will occur producing the first hyperechoic boundary or layer due to the change in acoustical impedance from water to the latex/mucosa. The thickness of the 'layer' or boundary will depend on the ultrasound frequency and its corresponding wavelength. As the mucosa is approximately 500 µm, the remainder of the mucosa will appear hypoechoic and form the second layer. When the pulse reaches the mucosa/submucosa interface, there is a difference in the tissue types and a reflection will occur, producing a hyperechoic boundary and the third layer. This layer can merge with the reflection obtained from the submucosa/muscularis propria interface, resulting in a wide, prominent hyperechoic layer. The remainder of the muscularis propria will form the hypoechoic fourth layer. As the muscularis propria changes consistency in the upper, mid and lower segments of the oesophagus, a hyperechoic layer may be visualised during the mid segment, as it consists of separate layers of circular and longitudinal muscular fibres. The interface between these muscle layers can produce the hyperechoic layer, depending upon the imaging frequency and pathology of the wall. Therefore, the number of visualised layers can change from five to seven layers depending on location and frequency of the transducer. The hyperechoic fifth layer is produced by the ultrasound pulse striking the boundary between the muscularis propria and the adventitia/serosa.

In reality the actual number of visible layers can vary from patient to patient. This depends on the type of EUS device/transducer used, the operating frequency, the orientation of the transducer, the actual thicknesses of the wall layers, the fat content, the presence of abnormal pathology, and the anatomical site under investigation.

Figure 18.4A and B illustrate the layers of the oesophageal wall at 20 MHz and 12 MHz. The ultrasound images were acquired when the transducer was located in the mid oesophagus from two different patients and in both cases seven layers of the oesophagus were observed. Figure 18.4A illustrates normal, mid, oesophageal wall layers imaged at 20 MHz. Figure 18.4B illustrates the effects of abnormal pathology on the oesophageal wall layers. On the left side of the oesophagus, the wall layers were normal, and not visible due to compression by the balloon. However, on the right side of the oesophagus seven layers were visualised. This effect was due to its proximity to abnormal pathology that caused the wall thickness to expand. The first hyperechoic layer observed at 12 MHz was due to the interface of the latex balloon and the mucosa of the oesophageal wall.

CLINICAL INDICATIONS FOR EUS IN THE UPPER GI TRACT

Endoscopic ultrasound (EUS) is a technique that is used to diagnose a variety of gastrointestinal diseases that cannot be reliably imaged by other modalities (CT, MRI) or diagnosed with conventional endoscopy and biopsies. Endoscopic ultrasound is used to investigate (a) luminal GI malignancies,[9] (b) submucosal abnormalities (e.g. lipoma, gastrointestinal stroma tumours (GISTs)),[9] (c) vascular structures (e.g. varices),[10] (d) extraluminal abnormalities identified on other imaging studies (e.g. cyst, normal anatomy imprint) and (e) therapeutic applications (e.g. EUS FNA, cyst drainage, core biopsies).[11]

PRINCIPLES OF EUS CANCER STAGING

One of the most important uses of radial EUS is for cancer staging. Both cancer of the oesophagus and the stomach are classified using

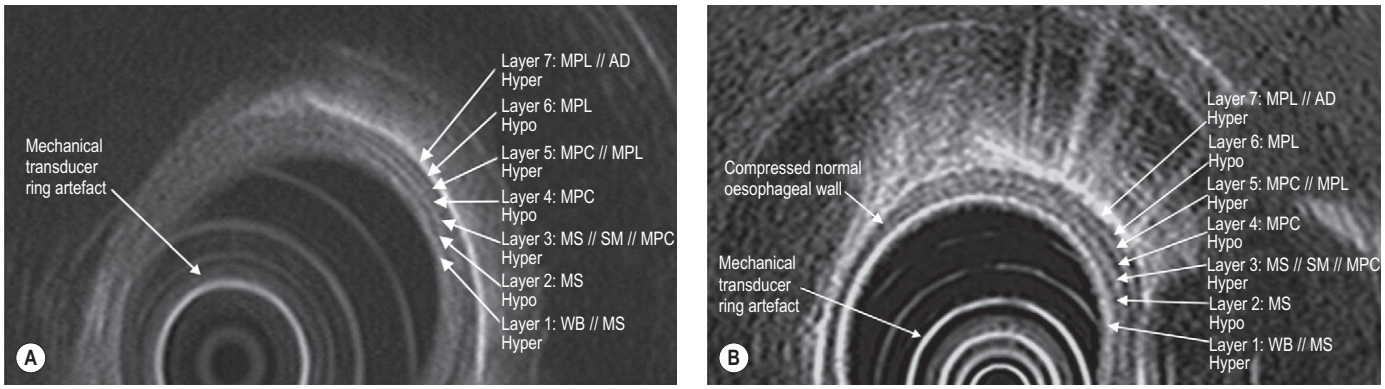


Figure 18.4 Layers of the oesophageal wall. A: Normal oesophageal wall layers imaged at 20 MHz (seven layers were observed). The image was acquired in the mid oesophagus. The wall layers were most prominent when the wall was perpendicular to the transducer. The GF-UM2000 echo-endoscope and EU-M2000 processor was used to acquire the image. **B:** Expanded oesophageal wall layers, preceding an area of abnormal pathology, acquired at 12 MHz (seven layers were observed). The image was acquired in the area of the mid oesophagus. The GF-UM2000 echo-endoscope and EU-M2000 processor were used to acquire the image. WB, water balloon; MS, mucosa; SM, submucosa; MPC, muscularis propria circular; MPL, muscularis propria longitudinal; AD, adventitia; Hyper, hyperechoic layer; Hypo, hypoechoic layer; //, interface.

the TNM staging (primary Tumour, regional Nodes, Metastasis), with some differences that are organ specific (see Tables 18.1 and 18.2). There is close correlation between TNM staging and group staging with 5-year survival probability.

T (primary tumour) is the extent of the tumour and is detailed from T0 to T4. Figure 18.5 illustrates the corresponding idealised EUS images (T1 to T3) to tumour pathology as it invades the oesophageal wall layers and T4 is the invasion of nearby structures. N (regional node) staging signifies the absence or presence and number of lymph nodes metastases and is classified as N0 to N3 for the oesophagus and N0 to N3 for the stomach according to the 2009 IUAC TNM classification.[12,13]

To distinguish between malignant and benign nodes, via radial EUS using frequencies above 7 MHz, the criteria in Table 18.3 were used.[14] A single matching factor signifies a low possible presence of malignancy. However, as the number of matching factors increases, the possibility of the node being malignant also increases, giving over 90% certainty if all four criteria are fulfilled (Fig. 18.6). Unfortunately only 25% of malignant nodes will fulfil all four criteria.[15]

More recently, the modified EUS malignant lymph node criteria have been proposed for the oesophagus that include the four classical criteria plus three additional: localisation of nodes (coeliac region), number of nodes >5, and presence of T3/4 disease.[16] When more than three of the seven criteria were present, the accuracy for the presence of malignant nodes was over 86%.[15]

M (metastasis) refers to the presence or absence of metastasis and is classified as either M0 or M1.[12,17–21] However, EUS only provides locoregional M classification of the disease (e.g. left lobe of the liver, presence coeliac axis lymph nodes). Computed tomography (CT) or positron emission tomography (PET) are far better placed to provide distant metastasis staging.

EUS AND THE OESOPHAGUS

Cancer

Oesophageal cancer is an aggressive malignancy with an overall 5-year survival of 5–10%. Two-thirds of patients have inoperable disease at diagnosis.[22] Accurate staging of oesophageal cancer is important because survival is closely related to tumour, nodal and presence of metastases (TNM) stage. Usually helical-computed tomography (CT) is the first staging investigation once the histological diagnosis is made. Its ability, however, to accurately determine T stage is limited (sensitivity 40–60%) because it cannot reliably delineate the component layers of the oesophageal wall.[23]

Furthermore, helical CT scanning cannot define accurately to proximal and distal margins of oesophageal tumours and has limited accuracy in the detection of lymph nodes measuring <1 cm. With the advent of multi-detector computed tomography (MDCT) there has been an increase in the image resolution and a decrease in the acquisition time compared with helical CT. EUS, however, remains the most accurate modality of oesophageal T staging even compared to MDCT, with accuracies between 71% and 86% for EUS versus accuracies between 42% and 81% for MDCT compared with surgical resection.[24] The accuracy of locoregional nodal staging reported by Sandha et al.[24] was 68% for MDCT, 56% for PET and 81% for EUS.

Furthermore, the development of curvilinear scopes which enable aspiration of tissue through a fine needle (EUS FNA) in order to obtain tissue samples of the nodes has further increased the accuracy of nodal staging (Fig. 18.7). Distal nodal diagnosis around coeliac access and hepatic artery territory is the only area where MDCT is superior to EUS with accuracies in the range 81–92% while it is 65–73% for EUS. Again, the ability of endoscopic ultrasound to obtain tissue of the coeliac axis nodes significantly improves accuracy. There is little doubt that EUS is the investigation of choice in the locoregional staging of oesophageal cancer and selection of patients for oesophageal surgery.

Over the past 5 years there have been several therapeutic developments in the management of oesophageal cancer, particularly of the early disease. In early tumours without nodal involvement the treatment possibilities include endoscopic mucosal resection or endoscopic submucosal dissection, while in more advanced disease with nodal involvement neoadjuvant chemotherapy is used prior to surgery in order to improve outcome.[25] The role of EUS is therefore pivotal in guiding the clinician to select the most appropriate treatment modality. Illustrative examples of oesophageal cancer staging are presented in Figure 18.8A–E.

There are, however, some limitations to the diagnosis using endoscopic ultrasound. The technique is most accurate in the diagnosis of T3 and T4 disease (>90%).[26] Accuracy is reduced in T1 and T2 disease by approximately 10%. There are some caveats in the use of endoscopic ultrasound. The inflammatory reaction around the tumour can result in over-staging while it is sometimes impossible to detect microscopic invasion, resulting in underestimation of staging. An oblique scanning plane may also give rise to overestimation of stage.

Table 18.1 TNM staging with corresponding grouping for oesophageal carcinoma and relative survival[13]

Primary tumour

Stage	Tumour involvement
Tx	Cannot be assessed
Tis	Carcinoma in situ/High-grade dysplasia
T1	Lamina propria or submucosa
A	Lamina propria or muscularis mucosae
B	Submucosa
T2	Muscularis propria
T3	Adventitia
T4	Adjacent structures
A	Pleura, pericardium, diaphragm, or adjacent peritoneum
B	Other adjacent structures, e.g. aorta, vertebral body, trachea

Regional lymph nodes

Stage	Nodal involvement
Nx	Nodes cannot be assessed
N0	No regional node metastasis
N1	1 to 2 regional lymph nodes
N2	3 to 6 regional lymph nodes
N3	>6 regional lymph nodes

Distant metastases

Stage	Presence of distant metastases
Mx	Distant metastases cannot be assessed
M0	No distant metastases
M1	Distant metastases present

Stage group, TNM stage and survival

Stage group	TNM stage			5-year survival
O	Tis	N0	M0	>95%
IA	T1	N0	M0	50–80%
IB	T2	N0	M0	
IIA	T3	N0	M0	30–40%
IIB	T1, T2	N1	M0	10–30%
IIIA	T4A	N0	M0	10–15%
	T3	N1	M0	
	T1, T2	N2	M0	
IIIB	T3	N2	M0	
IIIC	T4A	N1, N2	M0	
	T4B	Any N	M0	
	Any T	N3	M0	
IV	Any T	Any N	M1	0–5%

Table 18.2 TNM staging with corresponding grouping for gastric carcinoma and relative survival[13]

Primary tumour

Stage	Tumour involvement
Tx	Cannot be assessed
T1	Lamina propria, submucosa
A	Lamina propria
B	Submucosa
T2	Muscularis propria
T3	Subserosa
T4 A	Perforates serosa
B	Adjacent structures

Regional lymph nodes

Stage	Nodal involvement
Nx	Nodes cannot be assessed
N0	No regional node metastasis
N1	1 to 2 nodes
N2	3 to 6 nodes
N3A	7 to 15 nodes
N3B	16 or more nodes

Distant metastases

Stage	Presence of distant metastases
Mx	Distant metastases cannot be assessed
M0	No distant metastases
M1	Distant metastases present

Stage group, TNM stage and survival

Stage group	TNM stage			5-year survival
O	Tis	N0	M0	>90%
IA	T1	N0	M0	80%
IB	T2	N0	M0	
	T1	N1	M0	
IIA	T3	N0	M0	56%
	T2	N1	M0	
	T1	N2	M0	
IIB	T4A	N0	M0	
	T3	N1	M0	
	T2	N2	M0	
	T1	N3	M0	
IIIA	T4A	N1	M0	38%
	T3	N2	M0	
	T2	N3	M0	
IIIB	T4B	N0, N1	M0	15%
	T4A	N2	M0	
	T3	N3	M0	
IIIC	T4A	N3	M0	0–5%
	T4B	N2, N3	M0	
IV	Any T	Any N	M1	

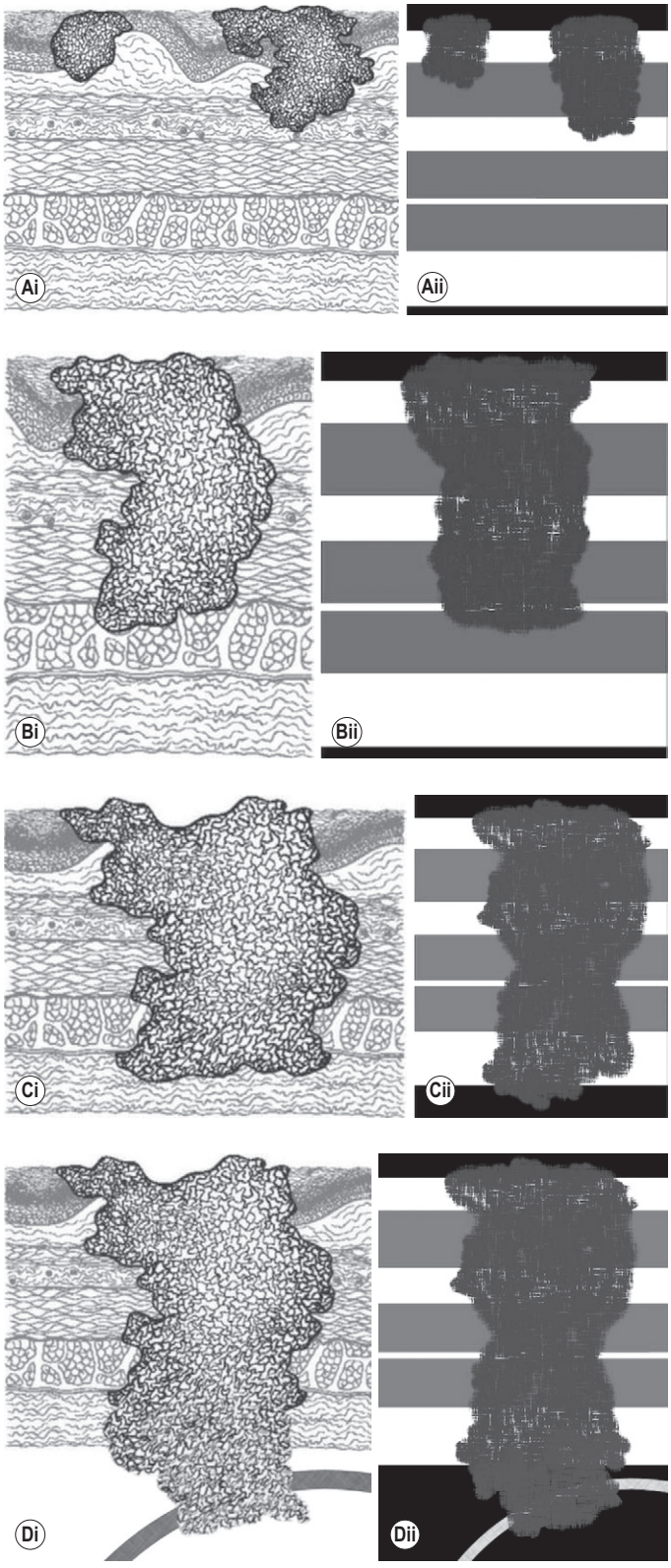


Figure 18.5 The histological T staging of oesophageal cancer and the idealised corresponding EUS image. (The histological images were modified from AJCC Cancer Staging Atlas.[12])

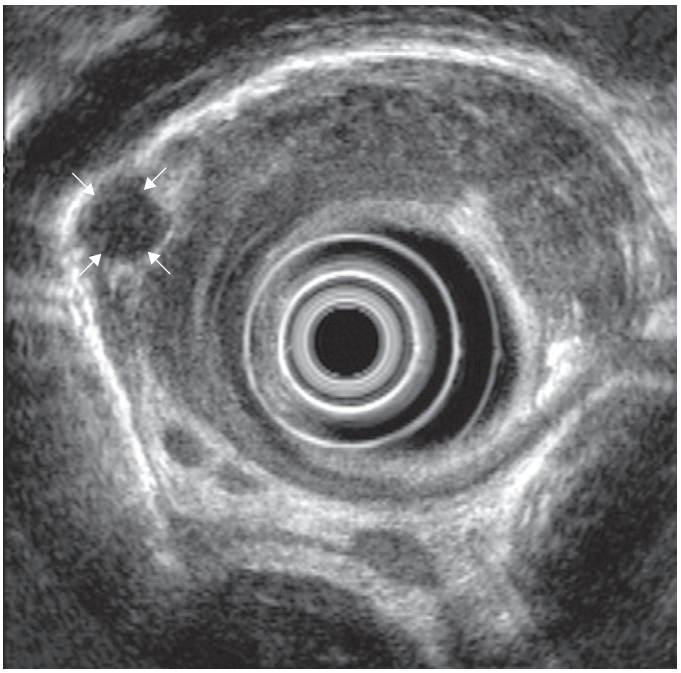


Figure 18.6 Example of malignant lymph nodes in a patient with advanced oesophageal cancer. The nodes appear hypoechoic, well demarcated, round and approach 1 cm in size.

Table 18.3 Classical criteria to differentiate malignant from benign lymph nodes

Characteristics	Malignant	Benign
Boundaries	Well defined	Indistinct
Echogenicity	Hypoechoic Homogeneous	Hyperechoic centre Less homogeneous
Shape	Round	Flat
Size	≥10 mm	Not diagnostic

Luminal narrowing is very common in advanced primary tumours (T3 or T4) and this may limit the ability of endoscopic ultrasound to stage the tumour. In that respect, blind echo-endoscopes (MH908, Olympus Japan) have been developed which can be inserted over the guide wire through a stenotic lesion in order to achieve accurate staging. Alternatively, miniature ultrasound probes (mini-probes) have been used for this purpose (Fig. 18.1E).

EUS also has a role in the detection of postoperative recurrence of tumour although development of fibrosis at the area of the anastomosis may sometimes limit its use. For this reason, endoscopic ultrasound is highly sensitive but has a relatively low specificity.[27] Also following radiation therapy, assessment of tumour recurrence can be difficult because of inflammation due to radiotherapy.

Barrett's oesophagus

EUS is used in the evaluation of cancer complicating Barrett's oesophagus. In general, the echo-endoscopic appearances of Barrett's oesophagus are non-specific and of a thickened oesophageal wall (Fig. 18.9); should there be any suspicion of cancer on Barrett's, biopsy is more sensitive than endoscopic ultrasound in the detection of early cancer. EUS therefore is reserved only for staging of a biopsy-proven early carcinoma.

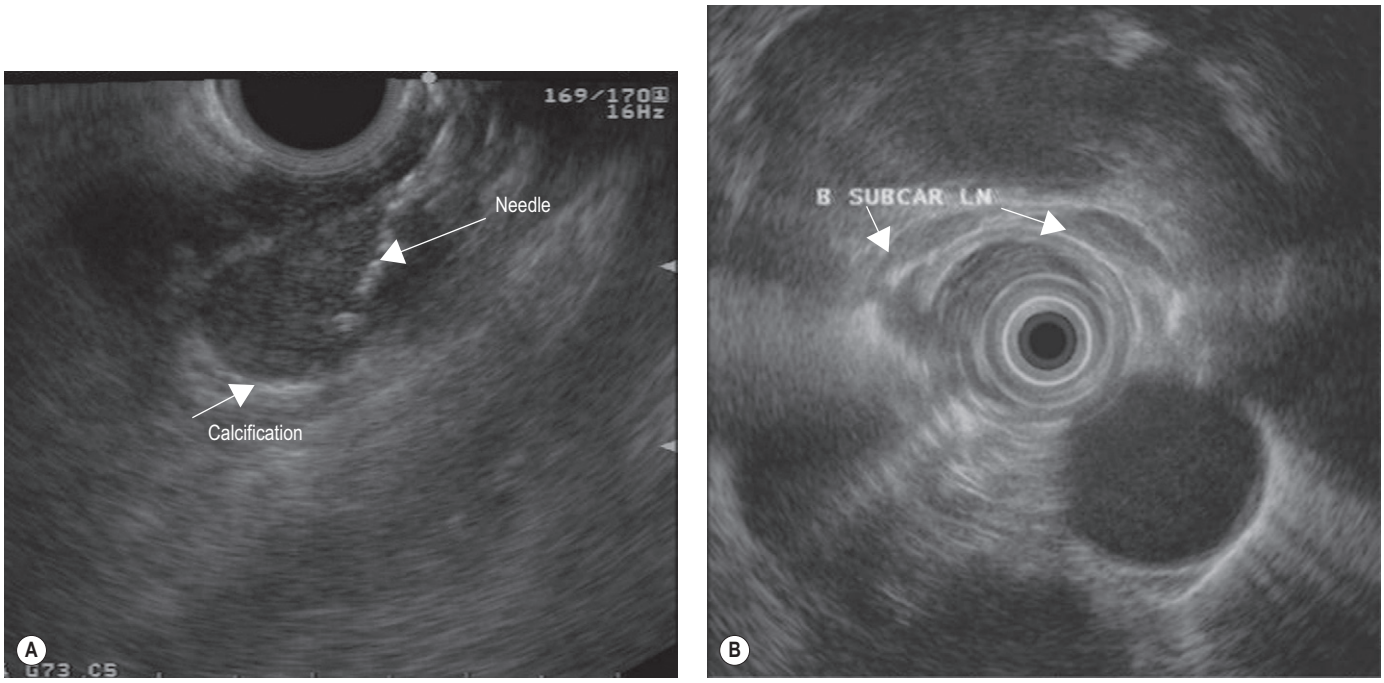


Figure 18.7 Subcarinal nodes. A: EUS-guided FNA from an enlarged subcarinal node. Note the presence of node calcification. **B:** Benign subcarinal nodes are often present in smokers and appear flat with a relatively hyperechoic centre.

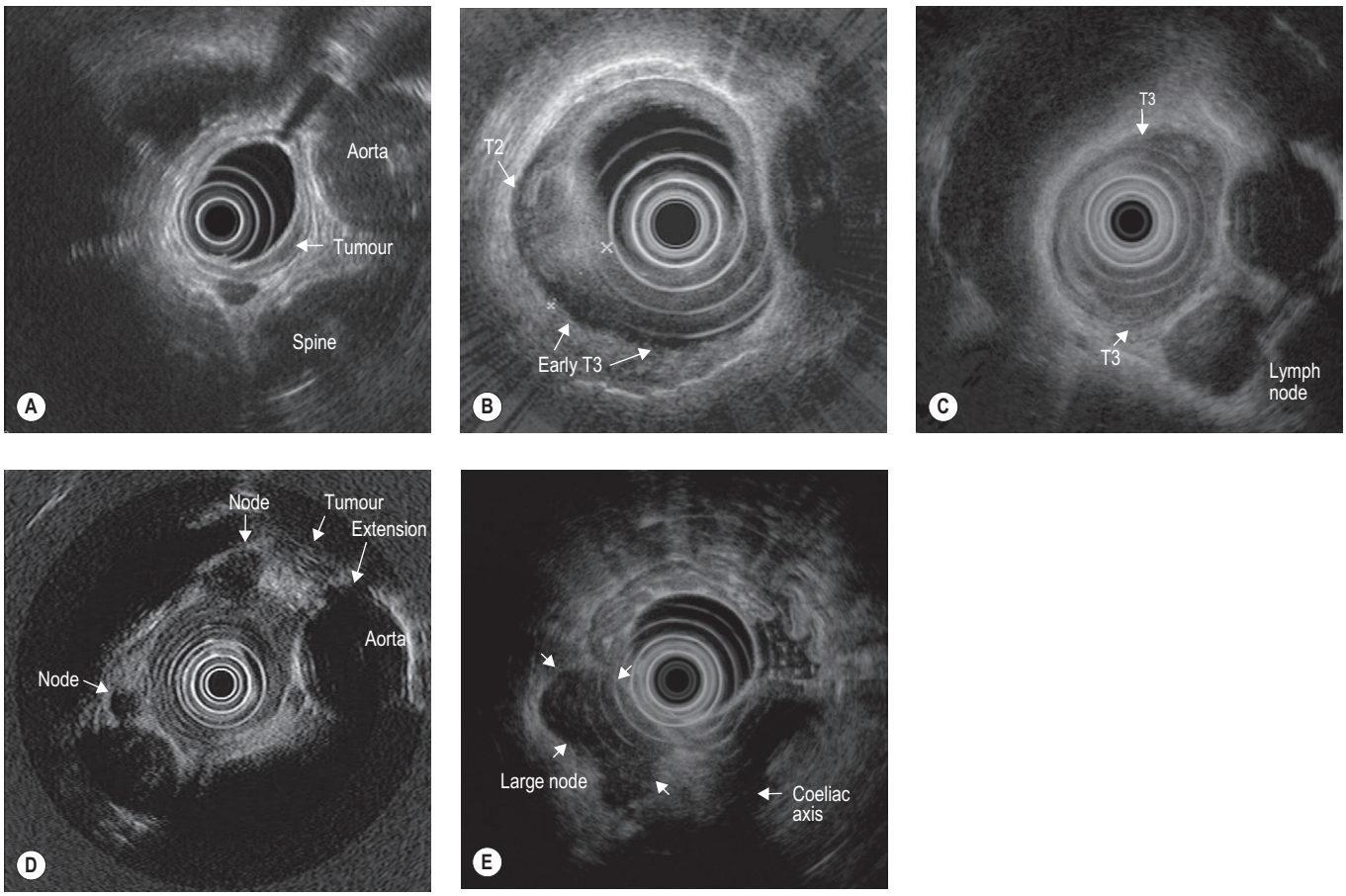


Figure 18.8 Examples of locoregional EUS staging of oesophageal cancer. A: T1 disease confined within the first three layers of the oesophagus (12 MHz). **B:** T2 disease with evidence of infiltration to the muscularis propria. There is a suggestion of early T3 (extension to the adventitia between 6 and 8 o'clock.). **C:** T3 disease with a large malignant looking node (N1). **D:** T4 disease with extension to mediastinum and infiltration of the aorta. Large peritumour nodes are also present. **E:** Coeliac axis lymph node involvement in a patient with advanced adenocarcinoma of the lower oesophagus.

Submucosal (subepithelial) lesions

The ability of EUS to accurately delineate the layers of the gastrointestinal tract has made it an ideal modality to investigate these lesions. Submucosal lesions usually come to clinical attention less frequently than mucosal abnormalities and in many cases they are found incidentally during routine evaluation of the upper gastrointestinal tract, although very occasionally they can ulcerate or bleed.

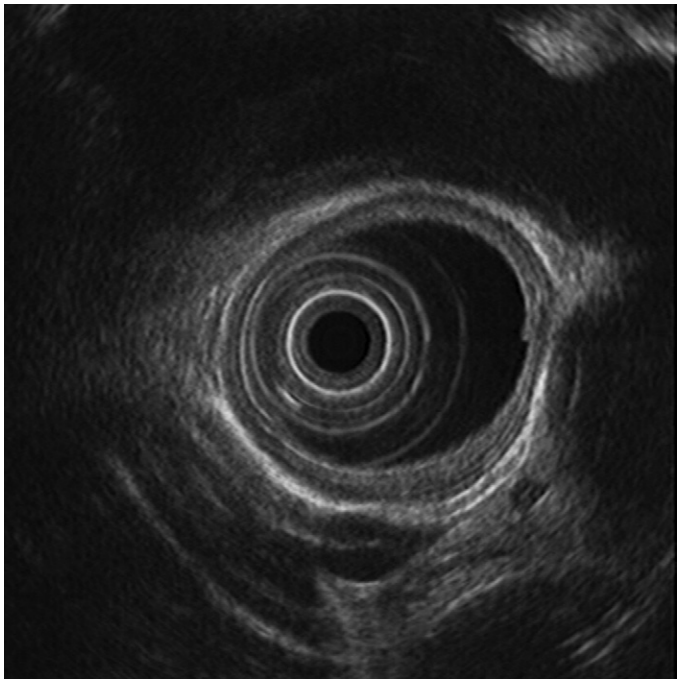


Figure 18.9 EUS appearance of Barrett's oesophagus; the layers of the oesophagus are well preserved but there is thickening of the mucosal/submucosal layer.

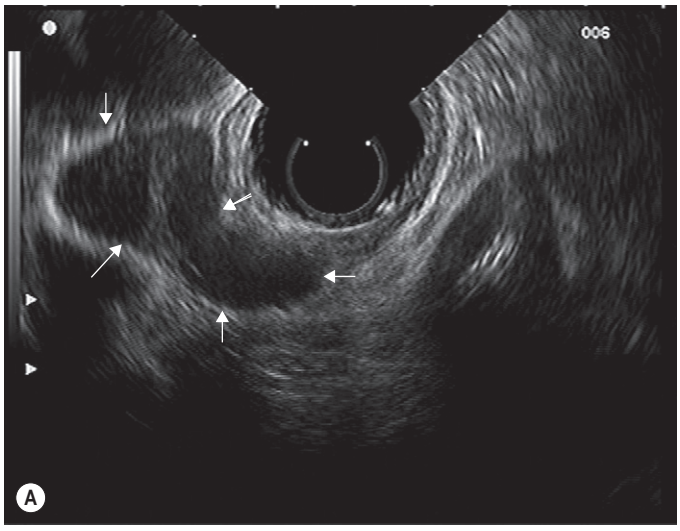
Gastrointestinal stroma tumours (GISTs) are by the far the commonest true submucosal lesions. They account for about 65% of all benign tumours of the oesophagus, although less than 10% of all GISTs are localised in the oesophagus. They are characterised by growth of the smooth muscle of the muscularis propria, although they occasionally rise from the muscularis mucosa. They can have varying mitotic activity and those tumours of size less than 2 cm and very low mitotic activity (mitotic count <5/50 high power fields) are considered of very low risk of malignancy. Under endoscopic ultrasound these lesions appear as homogeneous hypoechoic well-demarcated areas measuring <2 cm in size. GISTs with higher mitotic activity tend to grow larger and the internal echo structure tends to become more heterogeneous with irregular margins and appearance of necrotic areas, septa and presence of calcification.[28] Satellite lymphadenopathy may be present.

Endoscopic ultrasound is useful in the follow-up of these lesions to establish whether they grow larger, and if there are worrying features or size >3 cm surgery is recommended (Fig. 18.10A,B). EUS FNA in most case provides an adequate sample for immunohistochemical staining for c-kit, CD34, CD117 and to determine the degree of mitotic activity. In recent studies the overall accuracy of EUS imaging for the diagnosis of malignant GIST was 78% and was improved to 91% by EUS FNA.[29] Other submucosal lesions include lipomas (Fig. 18.11), cysts, granular cell tumours, fibrovascular polyps as well as ectopic gastric glandular tissue. Lipomas are the second commonest lesion after GISTs. They are benign tumours composed of fat; they are echo bright and appear to arise from the third layer, which corresponds to the submucosa.

Benign posterior mediastinal masses

Benign mediastinal 'masses' which EUS with or without FNA can diagnose with accuracy, in addition to GISTs, include cysts, teratomas and inflammatory masses due to TB, histoplasmosis and sarcoidosis.[30]

Cysts usually appear posteriorly in the submucosal layer of the oesophagus and can be reliably diagnosed by EUS (Fig. 18.12). They account for 10–15% of mediastinal masses.



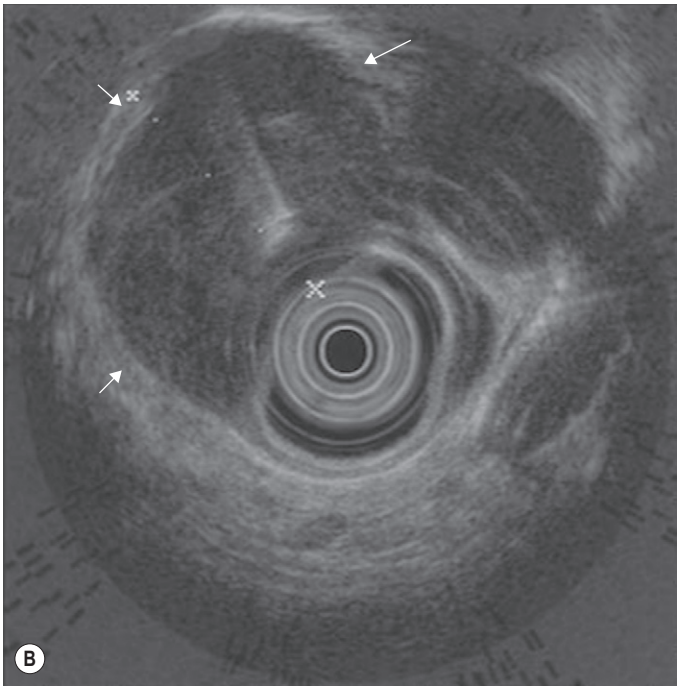


Figure 18.10 GIST in the oesophagus. A: Large multilobular GIST >5 cm arising from the fourth layer of the oesophagus. **B:** GIST in the oesophagus with benign characteristics – homogeneous, hypoechoic with clearly defined borders.

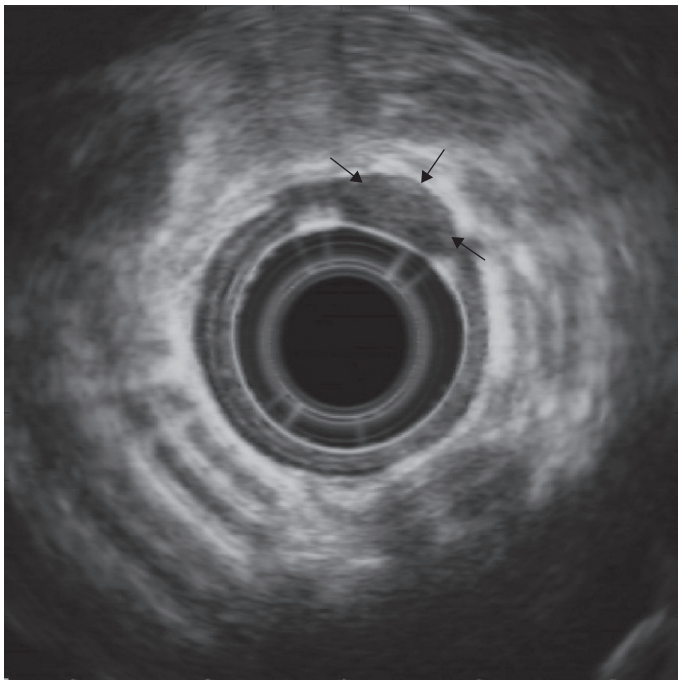


Figure 18.11 A small lipoma seen arising from the third layer of the oesophageal wall.

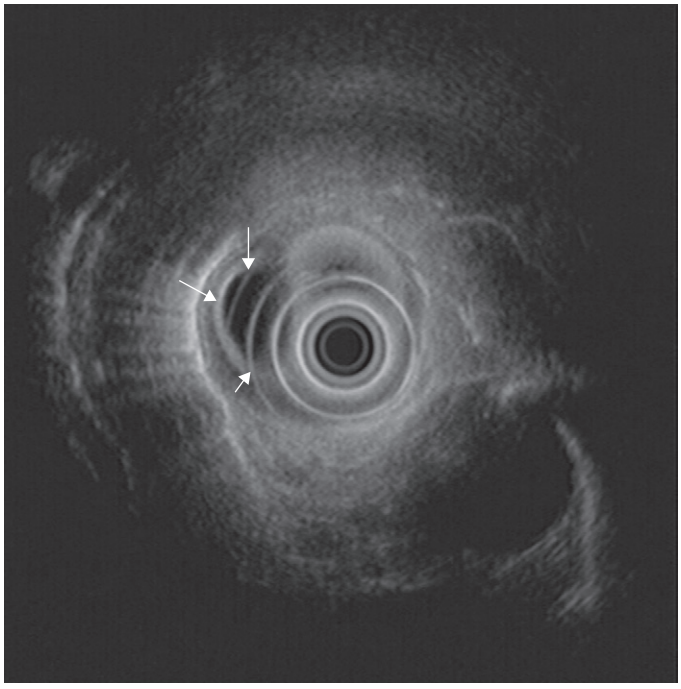


Figure 18.12 EUS of an oesophageal cyst appearing as a hypoechoic well-demarcated area arising from the submucosal (second) layer of the oesophagus.

The two main types are congenital foregut duplication cysts, which are mostly localised but sometimes extend for the whole length of the oesophagus, and acquired mucous retention cysts, which are usually small. Occasionally some cysts arise away from the oesophageal wall and they are more suggestive of bronchogenic cysts. Cysts are generally asymptomatic, although they can give symptoms such as chest pain, dysphagia or dyspnoea. Under CT they appear as contrast non-enhancing lesions but not uncommonly they are mistaken for malignant tumours, particularly those containing thick gelatinous material.

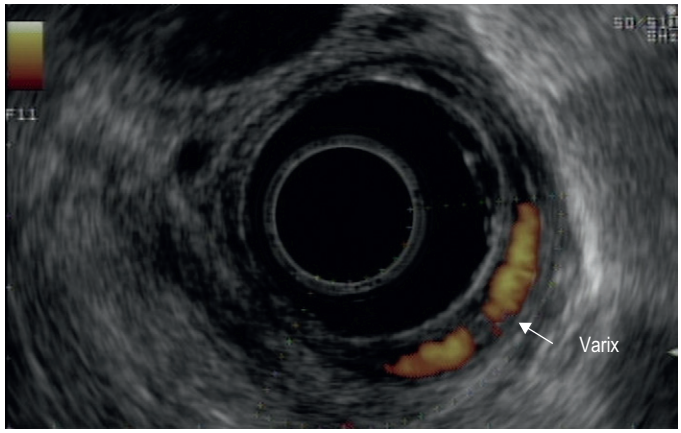


Figure 18.13 Oesophageal varices appear as tortuous intramural vessels in the lower third of the oesophagus with evidence of blood flow under colour power flow EUS.

Cystic lesions under EUS appear as echo-free round or tubular lesions arising from the third layer with some acoustic enhancement.[31]

Cysts are in their vast majority completely benign and clinical observation is recommended unless they become symptomatic. Furthermore it is not recommended to sample these cysts by EUS FNA as this can introduce infection, resulting in mediastinitis. If there is, however, a high suspicion of malignancy and sampling is required, antibiotic prophylaxis should be administered. In the event of the diagnosis of a cyst being made by EUS FNA, it is preferable to completely drain the cyst to minimise infection risk.[32]

Oesophageal varices

Endoscopic ultrasonography is an excellent technique in the diagnosis of oesophago-gastric varices.[33] In general, intramural vessels in the oesophagus are imaged as echo-free structures. These are usually submucosal but also collateral vessels can be visualised. The ability of endoscopic ultrasound to detect oesophageal varices is often operator dependent as the endoscope balloon easily compresses small varices. The newer electronic radial and linear endoscopes equipped with colour flow and Doppler facilities can delineate in great detail the presence of varices and collateral circulation (Fig. 18.13). Furthermore, enlargement of the azygos vein is a good indicator of the presence of portal hypertension.

Injection to obliterate oesophageal varices under EUS guidance has proven to be an effective technique.[34] More recently EUS-guided thrombin injection to control bleeding varices both in the oesophagus and the cardia of the stomach was successfully applied in complex cases where other treatment options had previously failed[35,36] (Fig. 18.14A, B).

Achalasia and other dysmotility disorders

Endoscopic ultrasound is occasionally used to differentiate between true achalasia and extrinsic compression of the lower oesophagus due to a submucosal lesion or cancerous lesion (pseudo-achalasia). Typically in achalasia, the fourth layer under EUS appears concentrically thickened in the area corresponding to the lower oesophageal sphincter. Endoscopic injection of botulinum toxin under EUS guidance has been used to ensure that the botulinum has been injected into the lower oesophageal sphincter in the hope of achieving a more sustained response.[37]

The development of three-dimensional endoscopic ultrasound may increase the use of this technique in the assessment of specific thickened segments in the oesophagus with a view to a

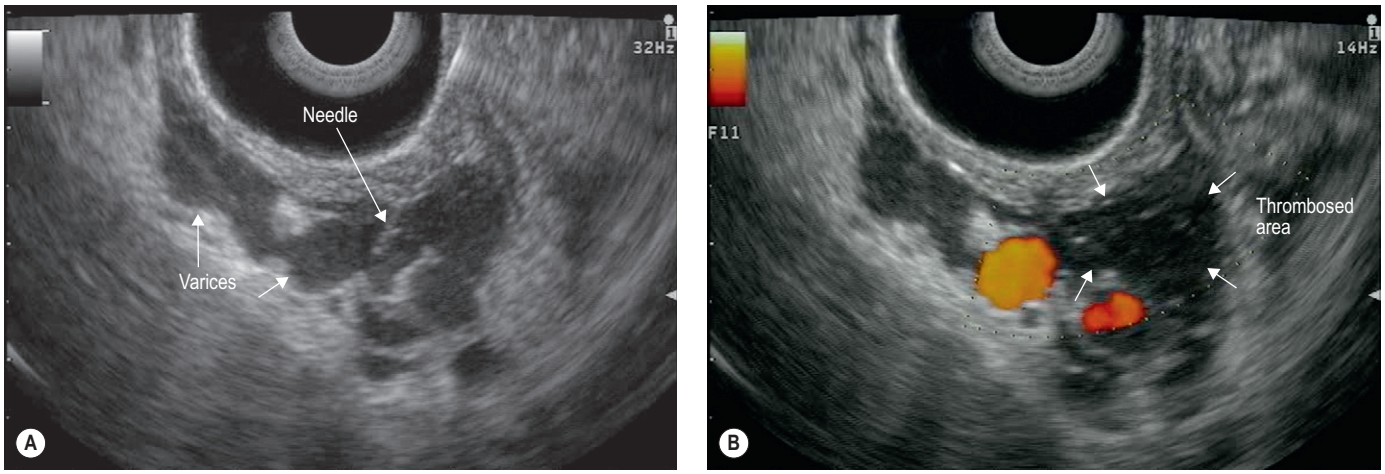


Figure 18.14 EUS-guided thrombin injection. A: Thrombin injection of bleeding oesophageal varices under EUS guidance using the therapeutic (linear) echo-endoscope. The needle is seen within the varix. **B:** Post-thrombin injection: colour power flow EUS shows clot formation as multiple speckled hyperechoic areas with no blood flow within the injected varix.

Oesophagus

- EUS is the most accurate modality of oesophageal cancer staging. EUS provides accurate information on TN staging and locoregional M staging due to presence of coeliac axis lymph nodes.
- The ability of EUS to accurately delineate the layers of the gastrointestinal tract has made it an ideal modality to investigate and characterise oesophageal submucosal lesions such as GISTs depending on the layer they arise from, and their echogenic characteristics.
- Benign mediastinal 'masses' which EUS can diagnose with or without FNA in addition to GISTs include cysts, teratomas and inflammatory masses.
- EUS is an excellent technique in the diagnosis of varices as well as for EUS-guided treatment of difficult cases of bleeding varices.

directed surgical myotomy in other dysmotility syndromes such as oesophageal spasm. We have used this technique as illustrated in Figure 18.15.

EUS AND THE STOMACH

Cancer

EUS is a complementary technique in the investigation and staging of gastric cancer once a biopsy-based diagnosis is made. It provides important information on the depth of cancer invasion, nearby lymph node metastases as well as the presence of ascitic fluid. Although EUS has an important role in the cancer of cardia (junctional), to assess the extension into the oesophagus, it has a relatively more limited role in the decision-making process for surgical resection of gastric cancer involving the body and antrum. This is because the combination of laparoscopy with peritoneal washings and abdominal CT scan can in most cases give adequate information on which to base the decision for surgical treatment.[23]

In the UK over 80% of cases of gastric cancer have associated lymphadenopathy due to late diagnosis, which is in striking contrast with Japan where at least one-third of cancers are diagnosed at an early stage because of screening and, in those cases, <15% have associated lymphadenopathy. In most studies, the accuracy of T staging varies between 88% in T1 and >90% in T3. The lowest accuracy, approximately 55%, is in T2.[38] In early cancer, endoscopic mucosal resection and endoscopic submucosal dissection (ESD) are excellent treatment options but require accurate assessment as to whether a lesion is confined to the mucosa or submucosa; in that respect, endoscopic ultrasound is invaluable to guide endoscopic therapy.[39,40]

Furthermore, endoscopic ultrasound can detect direct liver or pancreatic invasion or presence of ascites, which would exclude surgery (Fig. 18.16).

The most important caveat of endoscopic ultrasound in the staging of gastric cancer is that only lymph nodes adjacent to the stomach can be detected; therefore EUS is complementary to CT scanning for accurate lymph node staging.

EUS is of particular value in the investigation of thickened gastric wall to differentiate gastric linitis plastica from gastric lymphoma or other causes of submucosal lesions including gastric varices. Linitis plastica is often difficult to diagnose on endoscopy and biopsy alone, and endoscopic ultrasound would not only demonstrate heterogeneous hyperechoic thickening but would also enable EUS-assisted full wall thickness biopsy.

Gastric lymphoma

EUS is of important value in the diagnosis of gastric lymphoma (Fig. 18.17). This, in most cases, is a non-Hodgkin's B-cell lymphoma that is often difficult to diagnose because of non-specific endoscopic findings. Under EUS the abnormal area has poorly reflective thickened wall characteristics with associated lymph node enlargement. EUS-assisted FNA of the nearby nodes may provide definitive tissue diagnosis. Endoscopic ultrasonography is very useful in the staging of gastric MALT (mucosa associated lymphoid tissue) lymphoma, which is strongly associated with *Helicobacter pylori* infection. This is one of the few lymphomas that can regress completely following eradication therapy as long as it is restricted to the mucosa and submucosa.[41] EUS is therefore of particular value in planning treatment for these patients.

Gastric polyps

Polypoid lesions are often encountered in the stomach and in most cases they are hyperplastic polyps although on occasions adenomatous polyps are present. The distinction between those polyps can

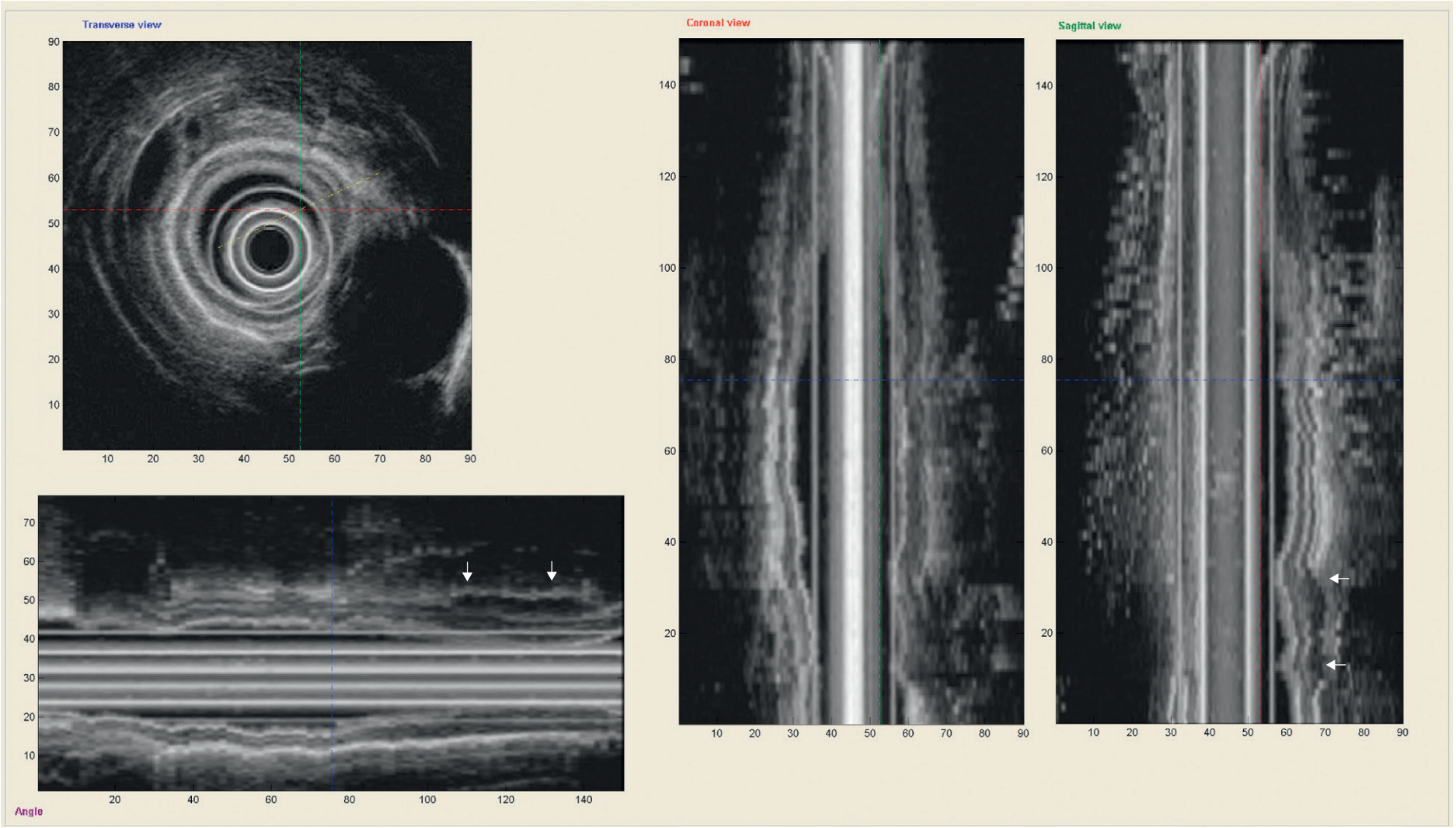


Figure 18.15 Three-dimensional reconstruction of the oesophageal wall of a patient with oesophageal spasm and segmental thickening of the muscularis propria. A targeted myotomy in that segment resulted in marked clinical improvement.

only be made histologically; however, endoscopic ultrasound may be of value prior to attempted endoscopic removal of polyps to assess vascularity and depth of invasion (Fig. 18.18).

Submucosal lesions and hypertrophic folds

The most common submucosal gastric benign tumour is GIST. The stomach is the commonest site of GISTs in the GI tract (Fig. 18.19A, B). GISTs usually arise from the fourth layer (muscularis propria) of the stomach. The principles of diagnosis and management already covered under the oesophageal GISTs section equally apply for the gastric GISTs. In most cases they are asymptomatic and if they are small (<2 cm) no further action is usually necessary, although some centres prefer a repeat EUS or CT scan a year later to ensure no change in size. It is not uncommon for the larger of these gastric GISTs to ulcerate and present with acute upper GI bleeding or pain. The role of endoscopic ultrasound in these cases is limited as surgical excision is usually recommended. In general, surgery for a gastric GIST is technically easier, in contrast to the oesophageal, where oesophagectomy is often required.

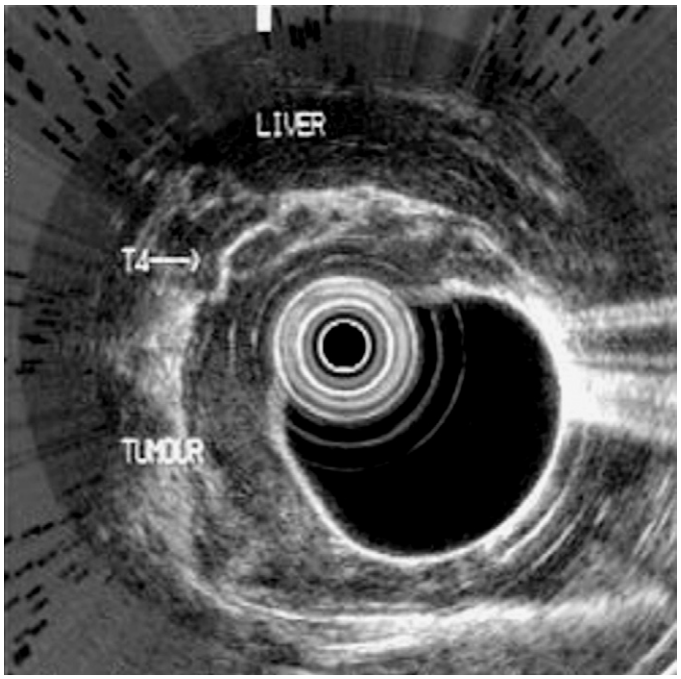


Figure 18.16 Advanced gastric adenocarcinoma with direct invasion of the liver (T4 disease).

In those cases where the decision for surgery is not immediate, EUS-guided FNA of the tumour is of value to clarify the histological diagnosis and determine the degree of mitotic activity. EUS-guided FNA is also useful in cases of extensive GISTs with high mitotic activity, when preoperative chemotherapy with imatinib (Gleevec) is being considered to reduce tumour size, to facilitate surgical excision.

Other subepithelial lesions include lipomas, which are imaged as homogeneous hyperechoic submucosal masses arising from the third layer (Fig. 18.20). Carcinoid tumours present as small relatively hypoechoic tumours arising from the second or third layers (Fig. 18.21). An aberrant pancreas is presented as a hyperechoic mass, usually in the antrum of the stomach with occasional ductal structures present (Fig. 18.22).

Endoscopic ultrasound is often used to differentiate true subepithelial/submucosal lesions from extramural compression (Fig. 18.23). Occasionally, the liver, gallbladder and splenic artery can imprint on the wall of the stomach (Fig. 18.24). Endoscopic ultrasound will visually delineate the anatomy in such cases.

Endoscopic ultrasound is often used to investigate hypertrophic gastric folds from diffuse pathological conditions, such as gastric lymphoma or linitis plastica.[42]

In hypertrophic folds the mucosa and submucosa layers are thickened but the muscularis and serosal layers are well preserved. This is in contrast to diffuse malignant processes where there is fusion of layers and extension depending on the disease stage.

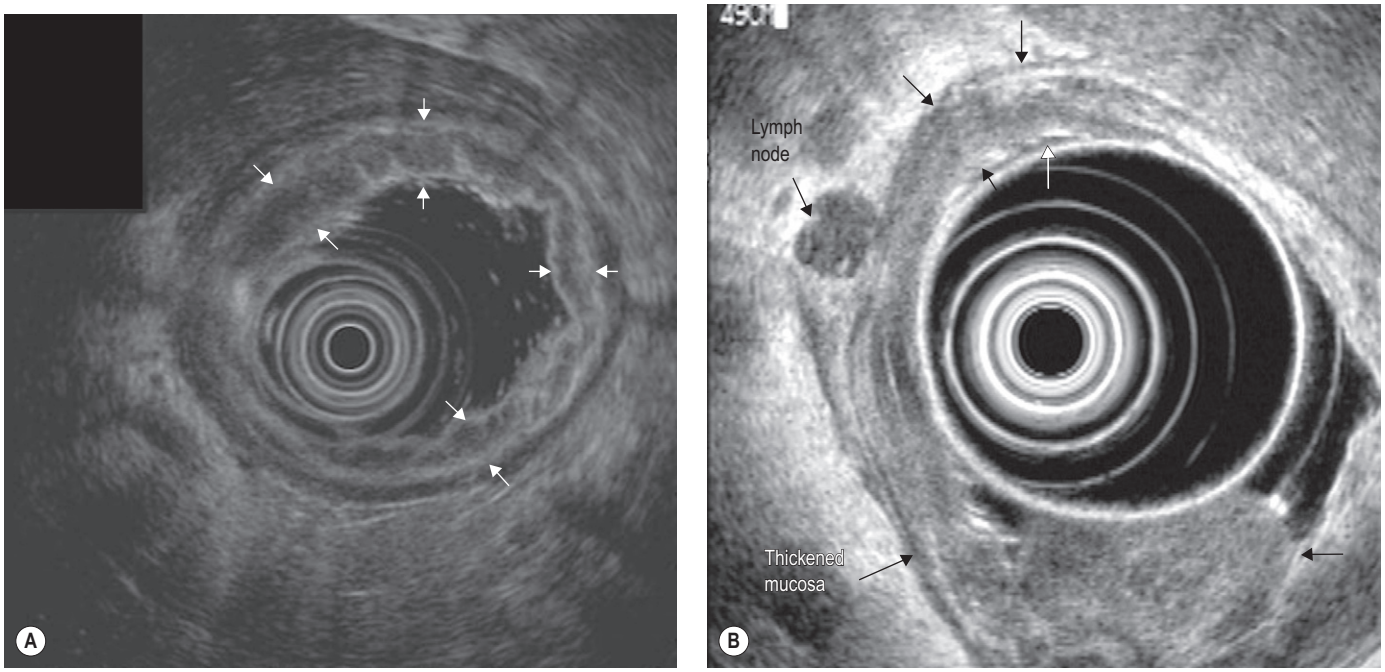


Figure 18.17 Gastric lymphoma. A: EUS appearances of early gastric MALT lymphoma confined to the superficial layers of the stomach. The mucosa is thickened with irregular hypoechoic appearance. **B:** High-grade gastric lymphoma with nearby enlarged lymph nodes.

Gastric varices

EUS performed with the latest generation of electronic scopes with colour flow and Doppler facilities has been particularly useful in the detection of gastric varices; not only in fundal varices but also in cases of ectopic varices, which are often misdiagnosed as polypoid lesions in the stomach. Gastric varices display as multiple rounded echo-free structures beneath the mucosa and submucosa of the fundus with colour flow detection (Fig. 18.25A, B). Furthermore, endoscopic ultrasound can visualise multiple tiny round hypoechoic areas within the submucosa of the stomach, which is a pathognomonic finding of portal hypertensive gastropathy. Examination of the deeper structures in these patients usually reveals dilation of the mesenteric veins with extensive collateral circulation in the perigastric area. With the modern echo-endoscopes with

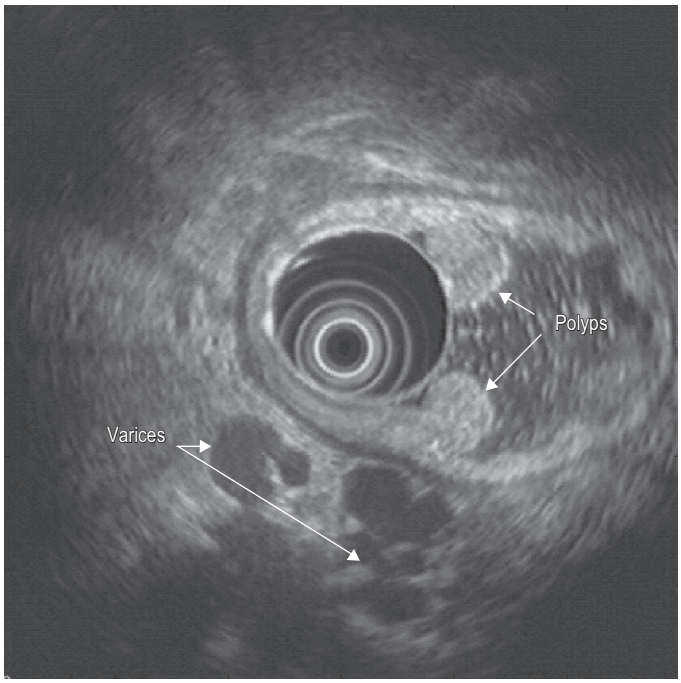


Figure 18.18 Presence of gastric polyps (hyperechoic protruding into lumen lesions) in a patient with portal hypertension and gastric varices (tortuous hypoechoic areas).

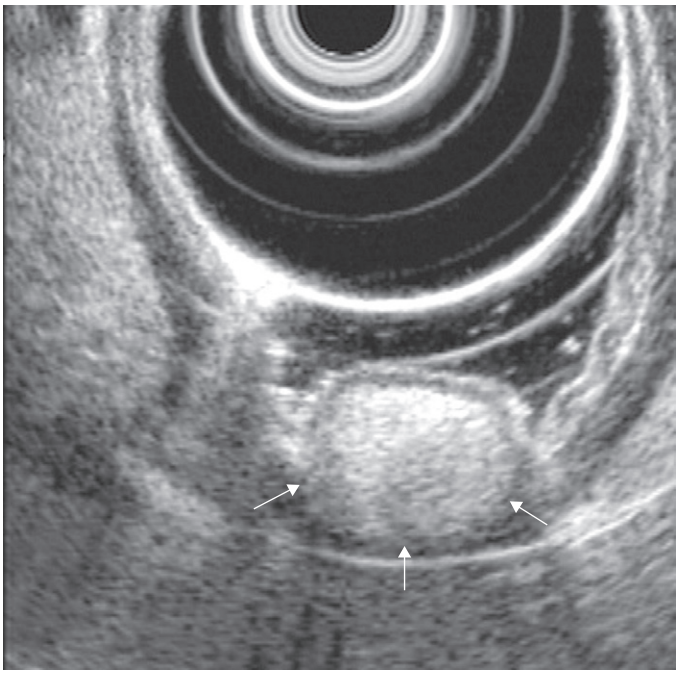
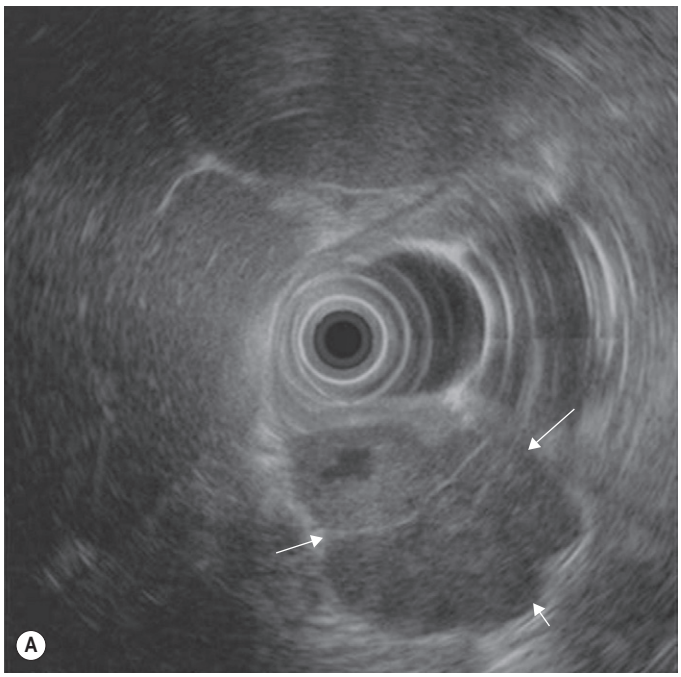


Figure 18.20 Gastric lipoma appears as a hyperechoic lesion arising from the third layer of the stomach.



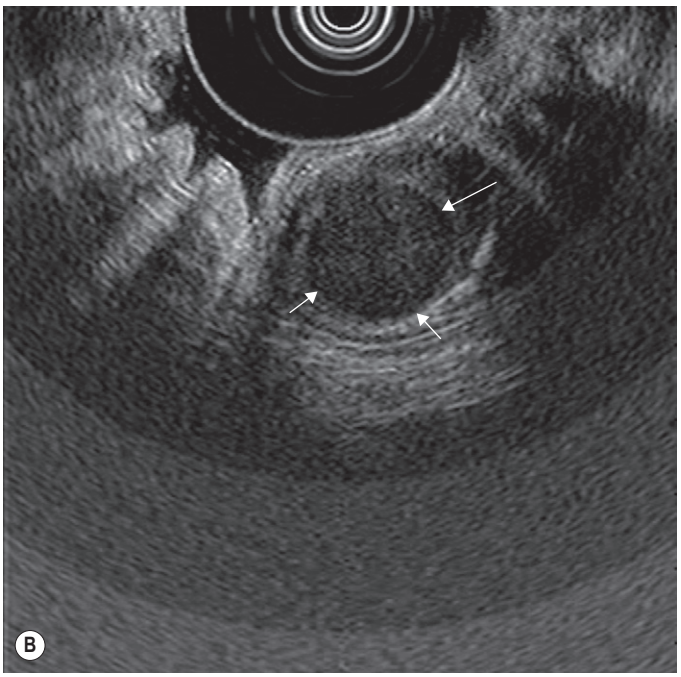


Figure 18.19 GIST in the stomach. A: Malignant GIST arising from the fundus of the stomach infiltrating the left lobe of the liver. The lesion is heterogeneous with necrotic centre in one area and lobular irregular appearance. **B:** Benign GIST (leiomyoma) that appears as a round hypoechoic area arising from the fourth layer of the stomach wall.

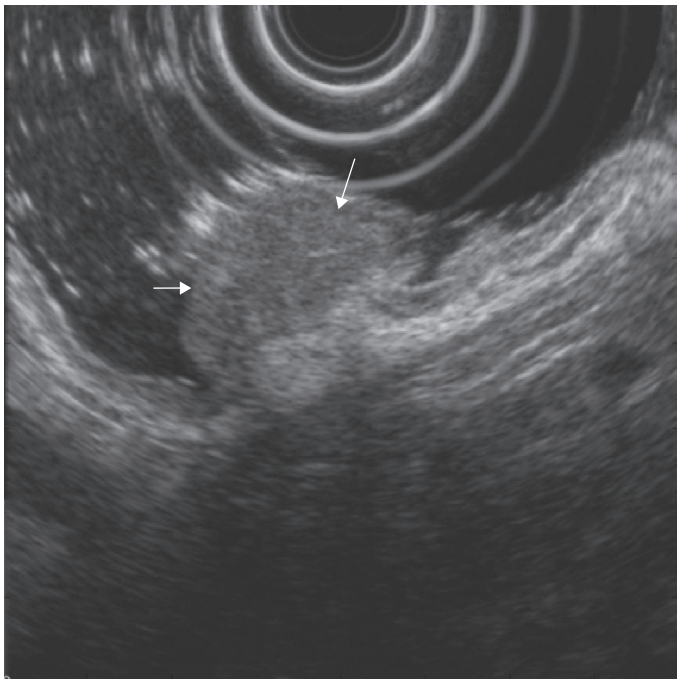


Figure 18.21 EUS appearance of a gastric carcinoid. The lesion appears relatively hypoechoic arising from the second layer of the stomach.

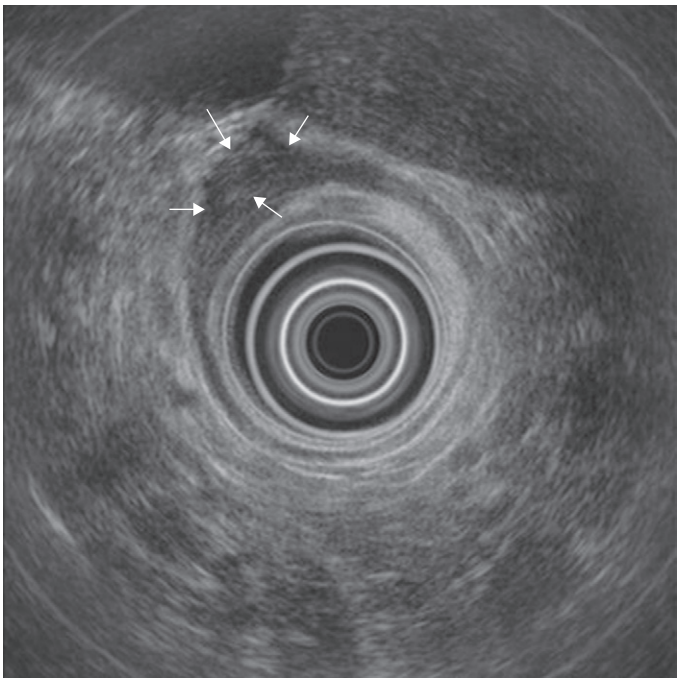


Figure 18.22 Incidental finding of a pancreatic rest in the antrum of the stomach.

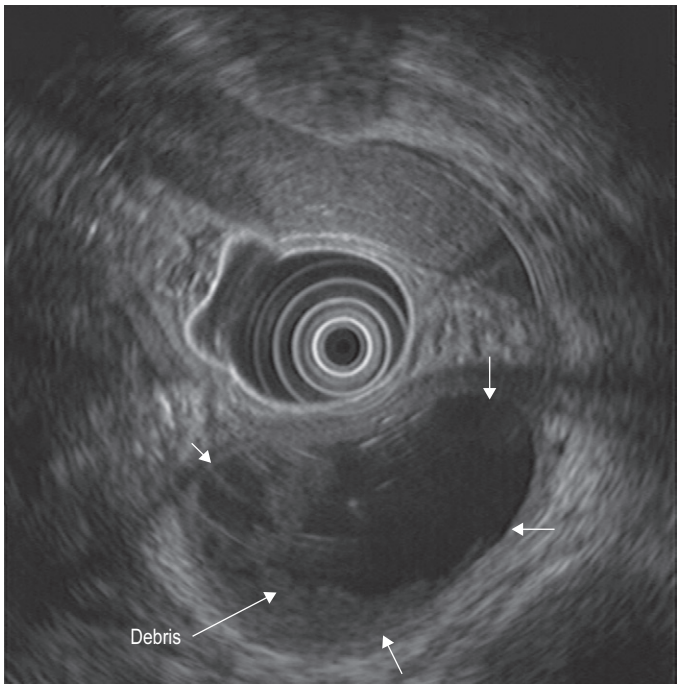


Figure 18.23 Extramural compression of the stomach wall due to a pancreatic pseudocyst. The pseudocyst appears heterogeneous, containing necrotic material.

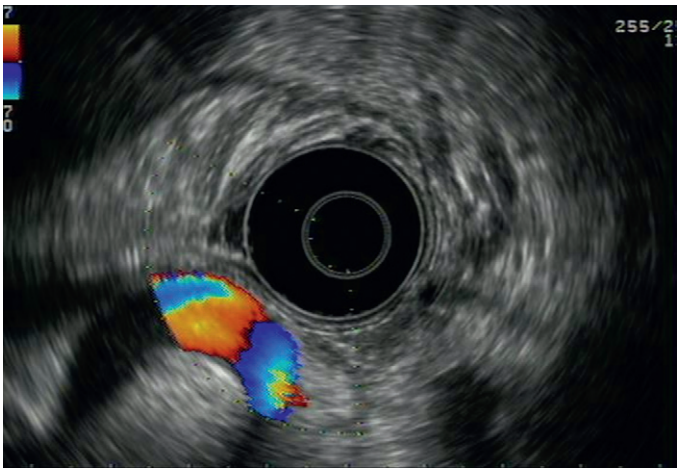


Figure 18.24 Splenic artery imprint at the posterior aspect of the stomach, giving the impression of a submucosal mass, endoscopically.

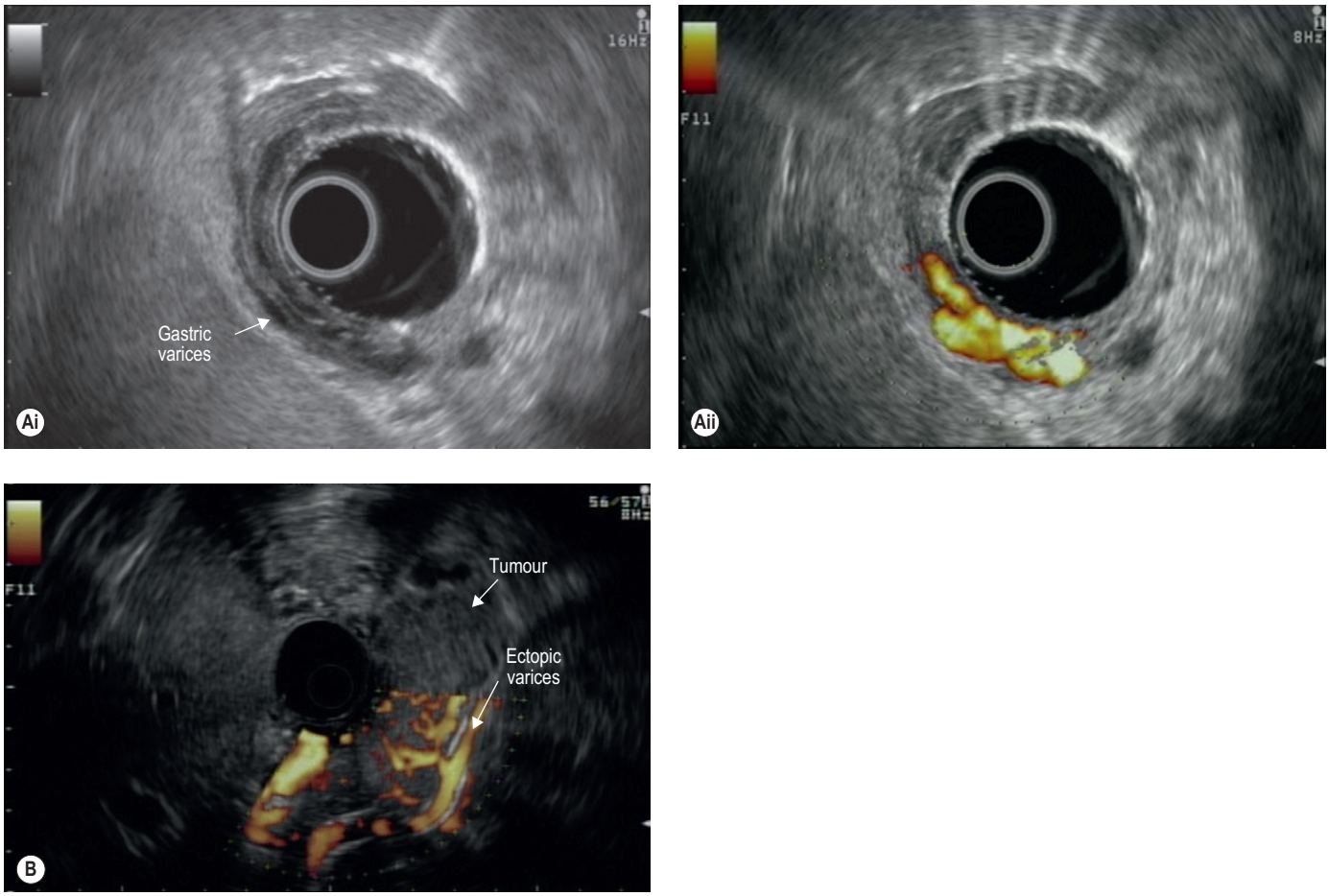


Figure 18.25 **Gastric varices. A:** Gastric fundal varices appear as tortuous hypoechoic areas within the gastric wall with (i) standard B-mode EUS and (ii) under power flow EUS. **B:** Multiple gastric ectopic varices under colour power flow EUS in a patient with splenic vein thrombosis due to neuroendocrine tumour of the tail of pancreas.

Doppler facilities, thrombosis of the portal or splenic vein can also be identified.

More recently, endoscopic ultrasound-guided therapy has been attempted for difficult cases to control gastric variceal bleeding. Cyanoacrylate (superglue) or thrombin has been used real-time to obliterate bleeding gastric varices. Alternative techniques used in our department include the use of a therapeutic endoscope with injection of thrombin under mini-probe guidance (Fig. 18.26). At present the role of endoscopic ultrasound in portal hypertension is still under investigation but this technique appears to be invaluable for complex cases and can be of assistance in the diagnosis and treatment.[35,36]

Duodenum

In general the value of endoscopic ultrasound in the duodenum is limited because of the rarity of malignancy in this area. However, as in the oesophagus and the stomach, it can be of particular value in the assessment of duodenal lymphoma, duodenal carcinoma and benign submucosal tumours (Fig. 18.27).

Peptic ulcer disease

The role of endoscopic ultrasound is limited in the investigation of benign gastroduodenal ulcers. Differentiation between malignancy and benign disease should always be done histologically. The appearances of benign ulcers are those of hypoechoic thickening of the area surrounding the ulceration, while coexisting fibrosis may present as a linear hyperechoic area at the ulcer base.

Stomach

- EUS is a complementary technique in the staging of gastric cancer, particularly in cancer of the cardia (junctional), to assess the extension into the oesophagus, but it has a relatively more limited role in the decision-making for surgical resection of gastric cancer of the body and antrum.
- EUS is of value in the investigation of thickened gastric wall to differentiate gastric linitis plastica from gastric lymphoma or other causes of submucosal lesions including gastric varices.
- EUS performed with colour flow and Doppler facilities is particularly useful in the detection of gastric varices, both fundal varices and ectopic, which are sometimes misdiagnosed as polypoid lesions in the stomach. EUS-guided treatment of difficult cases of bleeding ectopic varices is gaining wider acceptance.

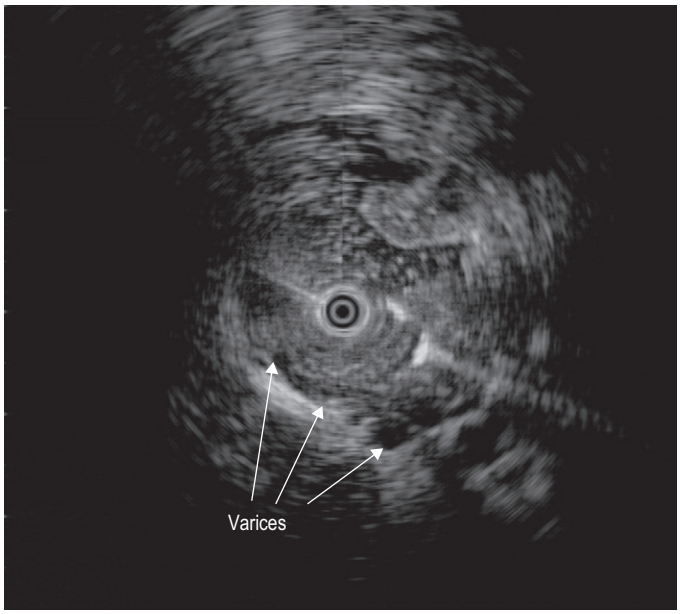


Figure 18.26 Mini-probe EUS used to assess obliteration of gastric varices following thrombin injection. The speckled hyperechoic areas indicate thrombus formation.

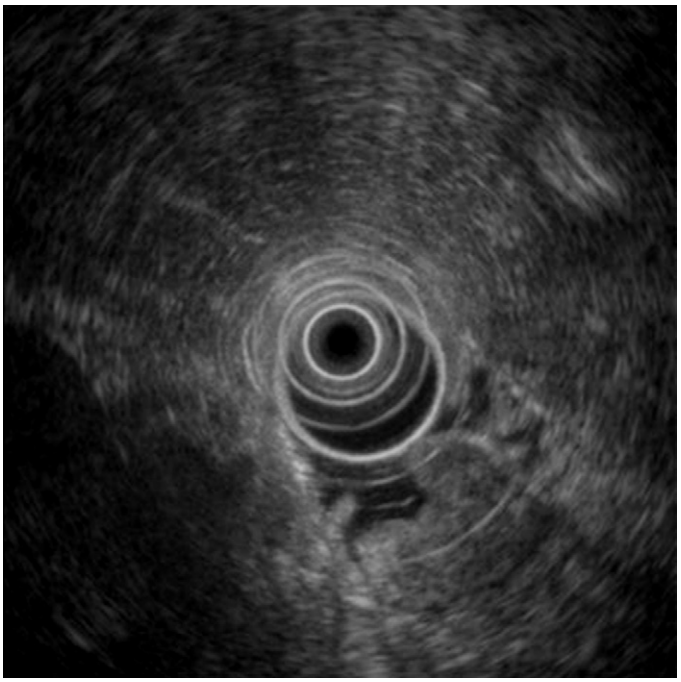


Figure 18.27 Duodenal polyp in a patient with neurofibromatosis type I.

EUS IN UPPER GI TRACT: PRESENT AND FUTURE

With the advent of faster and more powerful computing capabilities as well as technological improvements in the manufacturing of echo-endoscopes, imaging has substantially improved. Furthermore, the latest solid-state electronic echo-endoscopes can now be directly connected to powerful ultrasound scanners, thus making it possible to apply advanced ultrasound imaging techniques such as tissue elastography and harmonic imaging in the differentiation of benign from malignant tissue.[43]

As transducer manufacturing improves, new thinner 360° radial electronic echo-endoscopes are being developed that permit optical forward viewing. They are easier and safer to use to intubate the oesophagus as they allow direct vision. More recently, prototypes of forward viewing therapeutic echo-endoscopes have also been developed for transgastric drainage of pancreatic pseudocysts.[44]

Generic freehand 3D-EUS add-on systems to echo-endoscopes[45] have also been developed in order to further improve cancer staging and provide important information regarding tumour characteristics such as length, depth, volume and distance from reference anatomical structures including the aortic arch and oesophagogastric junction (Fig. 18.28).

Another important development is the very thin echo-endoscope with optics similar to endobronchial ultrasound scopes for staging of stenotic oesophageal lesions.

Finally merging of EUS with CT scanning has been attempted, using position sensors in order to fuse images and facilitate the interpretation of both CT and EUS images to further improve staging for upper GI cancer.

Present and future

- New technological developments, such as forward viewing EUS scopes for diagnosis and therapy, tissue elastography, three-dimensional EUS, and merging of EUS with CT or MRI images for more accurate anatomical correlations, are likely to enhance further the role of EUS in the diagnosis and management of upper GI pathologies.

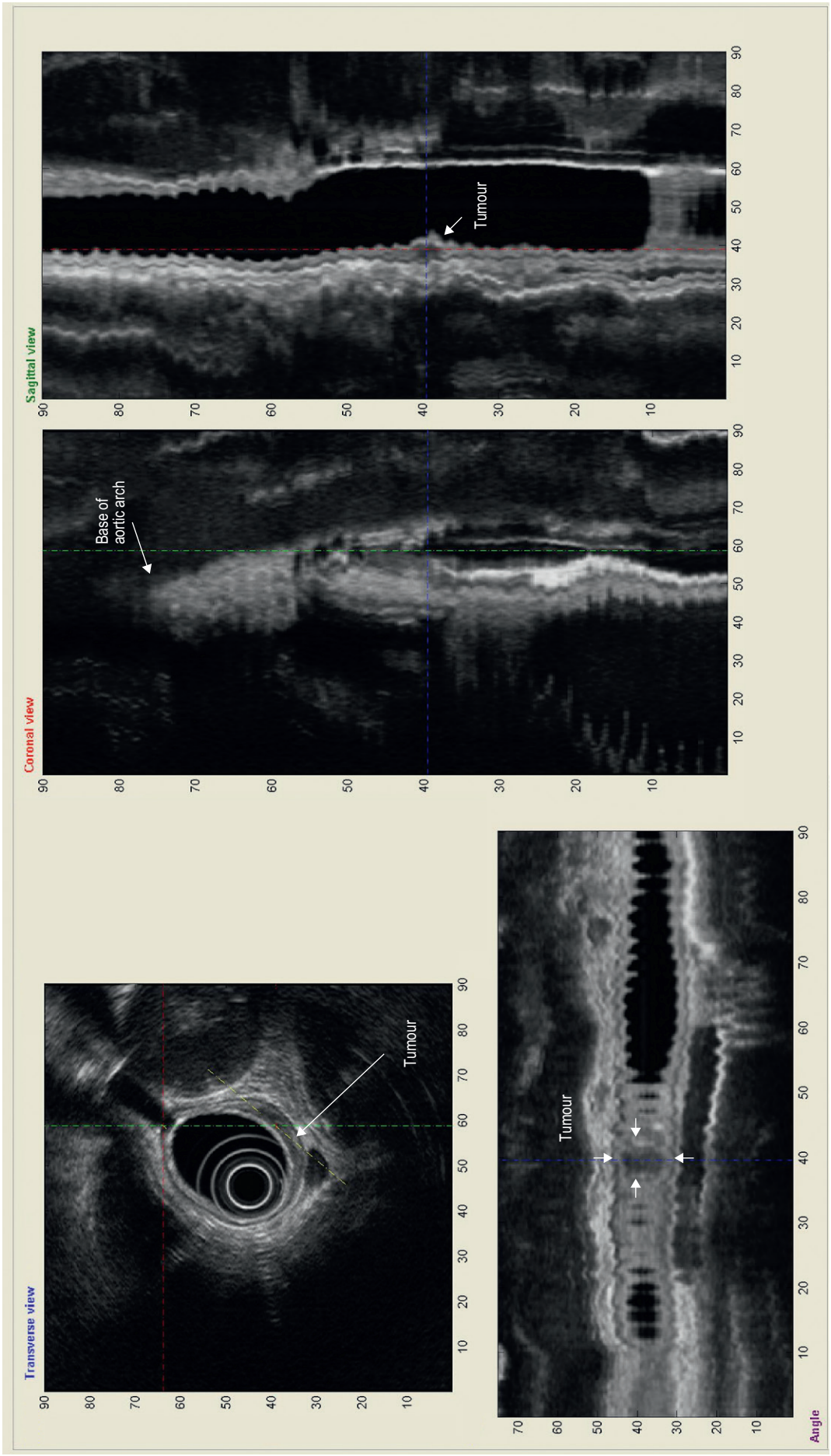


Figure 18.28 Example of a 3D EUS reconstruction in a patient with oesophageal cancer who was treated with radiotherapy.

REFERENCES

1. Dimagno EP, Baxton JL, Regan PT, et al. Ultrasonic endoscope. Lancet 1980;I:629–631.
2. Yusuf TE, Tsutaki S, Wagh MS, et al. The EUS hardware store: state of the art technical review of instruments and equipment. Gastrointest Endosc 2007;66(1):131–143.
3. Cysewska-Sobusiak A, Skrzywanek P, Sowier A. Utilization of miniprobes in modern endoscopic ultrasonography. Sensors Journal, IEEE 2006;6(5):1323–1330.
4. Okamura S, Tsutsui A, Muguruma N, et al. The utility and limitations of an ultrasonic miniprobe in the staging of gastric cancer. J Med Invest 1999;46:49–53.
5. Raj M, Chen RY. Interventional applications of endoscopic ultrasound. J Gastroenterol Hepatol 2006;21(2):348–357.
6. Erickson RA. Linear array endosonography: normal EUS anatomy. In: Gress F, Bhattacharya I, editors. Endoscopic ultrasonography. Oxford: Blackwell Publishing; 2000. p. 58–69.
7. Yong AA, Roberts SA. Interventional endoscopic ultrasound. Clin Radiol 2003;58(1):32–43.
8. Yamao K, Irisawa A, Inoue H, et al. Standard imaging techniques of endoscopic ultrasound-guided fine-needle aspiration using a curved linear array echoendoscope. Dig Endosc 2007;19(s1):S180–S205.
9. ASGE Standards of Practice Committee, Gan SI, Rajan E, Adler DG, et al. Role of EUS. Gastrointest Endosc 2007;66(3):425–434.
10. Irisawa A, Shibukawa G, Obara K, et al. Collateral vessels around the oesophageal wall in patients with portal hypertension: comparison of EUS imaging and microscopic findings at autopsy. Gastrointest Endosc 2002;56(2):249–253.
11. Giovannini M. Ultrasound-guided endoscopic surgery. Best Pract Res Clin Gastroenterol 2004;18(1):183–200.
12. Greene FL, Compton CC, Fritz AG, et al., editors. Esophagus. In: AJCC cancer staging atlas. New York: Springer; 2006. p. 77–88.
13. Sobin LH, Gospodarowicz MK, Wittekind C, editors. TNM classification of malignant tumours. 7th ed. Wiley-Blackwell; 2009. p. 63–81.
14. McLean A, Fairclough P. Endoscopic ultrasound – current applications. Clin Radiol 1996;51:83–98
15. Bhutani MS, Hawes RH, Hoffman BJ. A comparison of the accuracy of echo features during endoscopic ultrasound (EUS), and EUS-guided fine needle aspiration for diagnosis of malignant lymph node invasion. Gastrointest Endosc 2006;63(2):204–211.
16. Vazquez-Sequeiros E, Levy MJ, Clain JE, et al. Routine vs selective EUS-guided FNA approach for preoperative nodal staging of oesophageal carcinoma. Gastrointest Endosc 2006;63(2):204–211.
17. Shimpi RA, George J, Jowell P, Gress FG. Staging of esophageal cancer by EUS: staging accuracy revisited. Gastrointest Endosc 2007;6(3): 475–482.
18. Kelly S, Harris KM, Berry E, et al. A systematic review of the staging performance of endoscopic ultrasound in gastro-oesophageal carcinoma. Gut 2001;49:534–539.
19. Tio TL, Coene PP, Schouwink MH, Tytgat GN. Esophagogastric carcinoma: preoperative TNM classification with endosonography. Radiology 1989;173:411.
20. Kwee RM, Kwee TC. Imaging in local staging of gastric cancer: a systematic review. J Clin Oncol 2007;25(15):2107–2116.
21. Lennon AM, Penman ID. Endoscopic ultrasound in cancer staging. Br Med Bull 2007;84:81–98.
22. Harewood GC, Kumar KS. Assessment of clinical impact of endoscopic ultrasound on oesophageal cancer. J Gastroenterol Hepatol 2004;19:433–439.
23. Wakelin SJ, Deans C, Crofts TJ, et al. A comparison of computerised tomography, laparoscopic ultrasound and endoscopic ultrasound in the preoperative staging of oesophago-gastric carcinoma. Eur J Radiol 2002;41(2):161–167.
24. Sandha GS, Severin D, Postema E, et al. Is positron emission tomography useful in locoregional staging of esophageal cancer? Results of a multidisciplinary initiative comparing CT, positron emission tomography, and EUS. Gastrointest Endosc 2008;67(3): 402–409.
25. Veuillez V, Rougier P, Seitz J-F. Multimodal treatment of oesophageal cancer. Best Pract Res Clin Gastroenterol 2007;21(6):947–963.
26. Rösch T, Classen M. Oesophageal carcinoma. In: Gastroenterologic endosonography. Stuttgart: Thieme; 1992. p. 45.
27. Lightdale CJ, Botet JF, Kelsen DP, et al. Diagnosis of recurrent upper gastrointestinal tract cancer at the surgical anastomosis by endoscopic ultrasound. Gastrointest Endosc 1989;16:149.
28. Tio TL, Tytgat GN, den Hartog Jagar FC. Endoscopic sonography for the evaluation of smooth muscles in the upper gastrointestinal tract and experience with 42 cases. Gastrointest Endosc 1990;36:342–350.
29. Ando N, Goto H, Niwa Y, et al. The diagnosis of GI stromal tumours with EUS-guided fine needle aspiration with immunohistochemical analysis. Gastrointest Endosc 2002;55(1):37–43.
30. Devereaux BM, LeBlanc JK, Yousif E, et al. Clinical utility of EUS-guided fine needle aspiration of mediastinal masses in the absence of known pulmonary malignancy. Gastrointest Endosc 2002;56(3):397–401.
31. Geller A, Wang KK, Di Magno EP. Diagnosis of foregut duplication cysts by endoscopic ultrasonography Gastroenterology 1995;109(3): 838–842.
32. Fazel A, Moezardalan K, Varadarajulu S, et al. The utility and the safety of EUS-guided FNA in the evaluation of duplication cysts. Gastrointest Endosc 2005;62(4):575–580.
33. Lee YT, Chan FK, Ching JY, et al. Diagnosis of gastroesophageal varices and portal collateral venous abnormalities by endosonography in cirrhotic patients. Endoscopy 2002;34:391–398.
34. Lahoti S, Catalano MF, Alcocer E, et al. Obliteration of esophageal varices using EUS-guided sclerotherapy with color Doppler. Gastrointest Endosc 2000;51:331–333.
35. Plevris JN, Inglis S, Lennon AM, et al. Role of endoscopic ultrasound in the management of liver disease patients with ectopic or gastric varices. Gut 2009;58(suppl 1):A17.
36. Romero-Castro R, Pellicer-Bautista FJ, Jimenez-Saenz M, et al. EUS-guided injection of cyanoacrylate in perforating feeding veins in gastric varices: results in 5 cases. Gastrointest Endosc 2007;66(2): 403–406.
37. Maiorana A, Fiorentino E, Genova EG, et al. Echo-guided injection of botulinum toxin in patients with achalasia: initial experience. Endoscopy 1999;31(2):3s–4s.
38. Yasuda K, Nakajima M, Kawai K. Malignant lesions of the gastrointestinal tract. In: Kawai K, editor. Endoscopic ultrasonography in gastroenterology. Tokyo: Igaku-Shoin; 1988. p. 56.
39. Akahoshi K, Chijiiwa Y, Hamada S, et al. Endoscopic ultrasonography: promising method for assessing the prospects of endoscopic mucosal resection in early gastric cancer. Endoscopy 1997;29:614–619.
40. Ohashi S, Segawa K, Okamura S, et al. The utility of endoscopic ultrasonography and endoscopy in the endoscopic mucosal resection of early gastric cancer. Gut 1999;45(4):599–604.
41. Sackmann M, Morgner A, Rudolph B, et al. Regression of gastric MALT lymphoma after eradication of *Helicobacter pylori* is predicted by endosonographic staging. MALT Lymphoma Study Group. Gastroenterology 1997;113(4):1087–1090.
42. Tio TL. Large gastric folds evaluated by endoscopic ultrasonography. Gastrointest Endosc Clin N Am 1995;5(3):683–691.
43. Giovannini M, Botelberge T, Bories E, et al. Endoscopic ultrasound elastography for evaluation of lymph nodes and pancreatic masses: a multicenter study. World J Gastroenterol. 2009;15(13):1587–1593.
44. Voermans R, Eisendrath P, Bruno M, et al. Initial evaluation of a novel prototype forward-viewing US endoscope in transmural drainage of pancreatic pseudocysts (with videos). Gastrointest Endosc 2007;66(5): 1013–1017.
45. Inglis S, Christie D, Plevris JN. Development of a new freehand radial 3D-EUS system for the examination of oesophagus. Gut 2009;58(suppl 1):A8.

CHAPTER 19

Small intestine

Peter M. Rodgers

ULTRASOUND TECHNIQUE 369

THE ULTRASOUND APPEARANCE OF NORMAL SMALL BOWEL WALL 370

THE ULTRASOUND APPEARANCES OF ABNORMAL SMALL BOWEL 371
Bowel wall thickness 371
Bowel wall layers 371
Bowel lumen 371
Bowel plasticity/mobility/peristalsis 371
Altered blood flow 371
Extramural changes 371
Mesenteric lymphadenopathy 371

CROHN'S DISEASE 371
Clinical features of CD 372
Ultrasound features of Crohn's disease 372
Bowel wall thickening 372
Bowel wall layers (mural stratification) 372
Fat wrapping 373
Vascular changes 374
Locoregional lymphadenopathy 374
Local complications of small bowel Crohn's disease 374
Stricture 374
Abscess 374
Fistula 375
Disease activity 375

INTESTINAL INFECTIONS 376
Infectious ileocaecitis 377
Intestinal tuberculosis 377
Anisakiasis 379

SMALL BOWEL ISCHAEMIA 379

SMALL BOWEL VASCULITIS 379

SMALL BOWEL TUMOURS 380
Clinical presentation 380
Malignant small bowel tumours 380
Adenocarcinoma 380
Carcinoid 381
Lymphoma 381
Mesenchymal tumours 381
Secondary intestinal malignancies 381
Benign small bowel tumours 381

INTUSSUSCEPTION 384

SMALL BOWEL OBSTRUCTION 384

COELIAC DISEASE 385

US-GUIDED NEEDLE BIOPSY OF BOWEL LESIONS 385

ULTRASOUND TECHNIQUE

Ultrasound (US) examination of the bowel should be performed together with a general US examination of the abdomen and pelvis. Following the example of clinical palpation of the abdomen, it is advisable to perform the general US first, prior to focusing on the bowel and any areas of specific symptoms or local tenderness. The complications of bowel disease often extend to involve adjacent organs, the mesentery, peritoneal recesses (e.g. subdiaphragmatic and pelvic collections), or spread haematogenously, particularly via the portal vein to the liver. Using a lower-frequency probe, particular attention should be paid to those areas beyond the reach of the high-frequency probes needed for detailed examination of the bowel wall.

The general abdominal probe may also be used to map the layout of the large bowel, identified by its typical haustral pattern, and to examine pelvic small bowel loops.

A higher-frequency probe is needed for detailed examination of the bowel wall, but the improved resolution comes with reduced penetration. Equipment parameters need optimising to maximise the contrast differences in bowel wall layers and to retain sharp images during active peristalsis. Most manufacturers now offer a bowel setting but fine adjustment with an application specialist is advisable.

Graded compression of the abdominal wall with the probe involves the gradual increase of compression whilst scanning, avoiding pain to the patient, and this technique has multiple benefits. Overlying soft tissues are compressed, bringing the probe closer to the bowel; gas is displaced from bowel loops, overlying bowel loops are displaced from those beneath, and the compressibility/rigidity of normal and abnormal bowel loops and mesenteric fat can be assessed.[1]

The right and left iliac fossae are relatively superficial spaces and common sites of bowel pathology. On the left, the colon descends in front of the psoas and iliac vessels before reflecting back up into the lower abdomen as the sigmoid loop (Fig. 19.1). Being larger than small bowel and more easily identified, it is a good starting point for the focused bowel examination and an opportunity to optimise scanning parameters so that the bowel wall layers can be clearly identified.

The relationship between the terminal ileum, caecum and the right iliac fossa is less constant; the terminal ileum should only be specified as such if seen entering the ileocaecal valve. Systematic sweeps of the probe up and down/across the abdomen allows interrogation of the small bowel, with the advantage that abnormal small bowel segments are frequently more obvious than healthy bowel loops. It is often advantageous to re-examine the right iliac fossa with the patient in a left decubitus position, which allows movement of mobile small bowel and caecum into a different

position and often reduces the amount of soft tissue between probe and target loops. In adult female patients transvaginal scanning may give excellent views of pelvis small bowel loops.

If a suspicious bowel segment is identified, it should be specifically examined for bowel thickening and alteration in individual bowel layers (see below). Extraintestinal abnormalities such as thickened mesenteric fat, interloop fluid, exudates, lymphadenopathy etc. should be sought. The vascularity of the abnormal segment should be assessed with colour and power Doppler.

Diseases in the caecum and appendix are dealt with elsewhere, but it is always valuable to record the finding of a normal appendix, and essential to document whether the appendix has been identified or not when other pathology is demonstrated in the right iliac fossa.

Ultrasound technique

- Focused bowel ultrasound should always be accompanied with a general examination of the abdomen and pelvis.
- Lower-frequency probes are essential for examining bowel loops in deeper recesses.
- Higher-frequency probes are essential for detailed analysis of bowel wall changes.
- Graded compression brings bowel loops within reach of the high-frequency probe and displaces bowel gas.
- Specific bowel settings should be defined or optimised (with the application specialist if necessary).

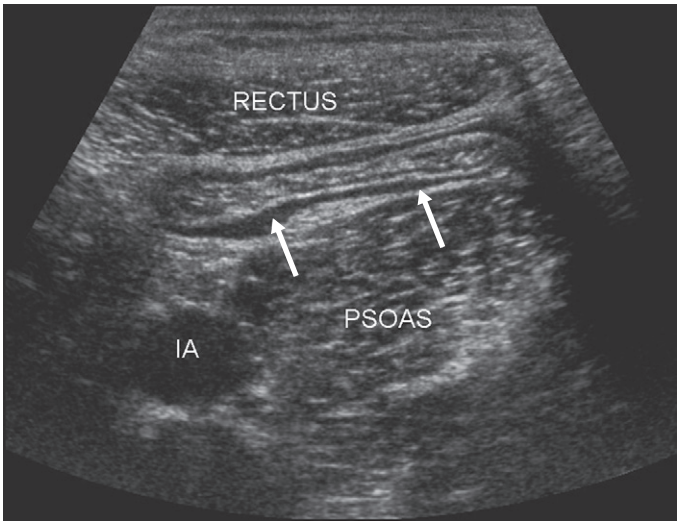


Figure 19.1 Sonogram of a normal left iliac fossa. Anteriorly, rectus muscle; posteriorly, psoas muscle and iliac artery (IA). Empty left colon seen in cross-section in front of the psoas muscle (white arrows).

THE ULTRASOUND APPEARANCE OF NORMAL SMALL BOWEL WALL

At diagnostic transabdominal US frequencies, under favourable conditions, five distinct bowel wall layers can be discerned. Viewed transversely these are appreciated as concentric circles of alternating hyper- and hypoechogenicity. These layers approximate to the histological structures (Fig. 19.2):

1. superficial mucosa (fine bright line)
2. deep mucosa including the lamina propria (grey)
3. submucosa (bright)
4. muscularis propria (dark)
5. serosa (fine bright line)

Comparison of histological measurements with in-vivo and in-vitro ultrasound measurements indicate that strong interface echoes tend to exaggerate the thickness of the submucosa at the expense of the adjacent hypoechoic layers.[2] The visibility of the fine bright interface reflections of the 'serosa/adventitia' and the 'superficial mucosa' is highly dependent on the echogenicity of adjacent structures and is most easily seen where there is fluid in the bowel lumen or ascites between bowel loops.

At lower diagnostic frequencies and less favourable conditions at least the two most prominent layers are evident: the bright submucosa (third layer) and the dark muscularis propria (fourth layer),

Normal small bowel – US features

- Five bowel wall layers may be identified under optimal conditions.
- The most prominent layers are submucosa (bright) and muscularis propria (dark).
- Small bowel wall thickness is less than 3 mm.
- Doppler US does not demonstrate normal bowel wall vascularity.
- Normal small bowel loops are compliant, easily displaced and show peristalsis.

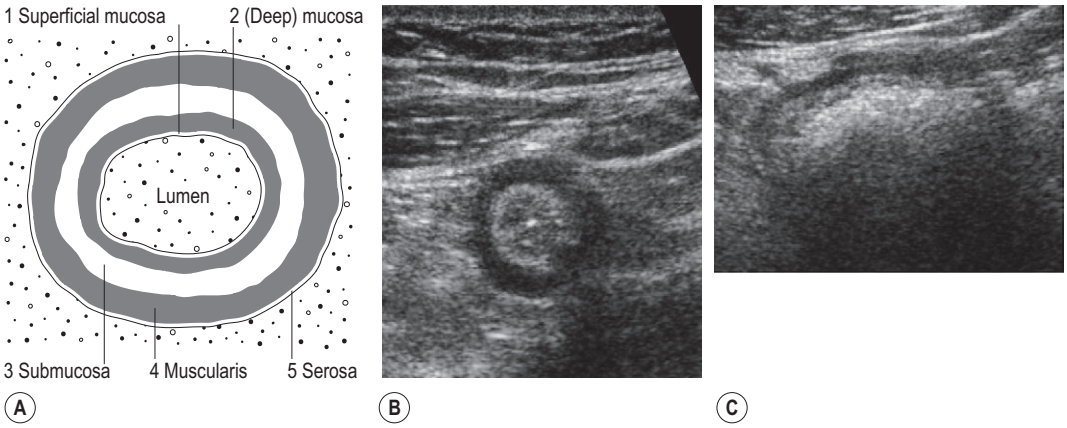


Figure 19.2 Normal small bowel ultrasound. A: Graphic representation of a transverse US view of distal small bowel demonstrating the five-layer structure. **B, C:** Transverse US images of normal distal small bowel in contracted and distended states. Only the bright submucosa and dark muscularis propria are easily discernible.

due to their relative thickness and high contrast. The deep mucosa is of similar thickness but being of intermediate echogenicity is more easily lost against the luminal contents.

The normal small bowel wall is up to 2–3 mm thick,[3,4] varying with the state of contraction/relaxation (Fig. 19.2). Small bowel folds consisting of mucosa and submucosa, but not muscularis propria, extend into the lumen. In the jejunum these folds are taller, slightly thicker and more numerous than in the ileum where folds are absent or sparse; in the collapsed state at fasting US examination, jejunal folds fill the lumen and may be perceived as a 'herring bone pattern'.

Peristaltic waves pass along small bowel segments at a frequency determined by multiple factors, such as gastric distension. As elective US examinations are usually performed after a period of fasting, the intestines are generally observed in a quiescent state but some peristalsis should be seen in healthy bowel segments.

Slung in the peritoneal cavity on a long mesentery, the small bowel is mobile and adjacent loops are easily displaced by compression. Healthy small bowel is easily compressed (note: excessive compression may give false measurements).

The intestinal blood supply runs in the mesentery to the mesenteric border of the bowel and branches (vasa recta) extend around to the antimesenteric border, perforating at intervals to access the bowel wall. In health these bowel wall vessels are barely, if at, all visible on colour or power Doppler.[5]

In optimal conditions, small oval mesenteric lymph nodes may be demonstrated, but if easily seen, numerous or enlarged, these should be considered significant and an intestinal cause sought.

Mesenteric fat within the visceral peritoneum is commonly observed as alternating hypo- and hyperechoic bands, which may cause confusion, mimicking longitudinal sections of bowel loops. This is easily solved by altering the plane of interrogation when the bands persist and are confirmed not to be tubular structures.

THE ULTRASOUND APPEARANCES OF ABNORMAL SMALL BOWEL

Before considering specific diseases of the small bowel it is worth noting the general characteristics altered by pathology that may be observed at US, which form a useful checklist during examinations. These are as follows:

- bowel wall thickness
- bowel wall layers
- bowel lumen
- bowel plasticity/mobility/peristalsis
- altered blood flow
- mesenteric/interloop changes.

Bowel wall thickness

The most common US feature of small intestinal pathology is thickening of the bowel wall, which may be focal or diffuse, circumferential or segmental. Thickening may be due to the presence of oedema, haemorrhage, inflammation, tumour growth or infiltration. Any of these may result in the classic US feature of a hypoechoic circumferential thickening around a strong echogenic centre (lumen),variously referred to as the target sign, ring sign or pseudokidney sign.

Tumours may produce focal expansion towards/into the bowel lumen (endoeccentric) to produce a polyp or polypoid mass, or away from the lumen (exoeccentric) into the peritoneal cavity displacing adjacent bowel loops.

Bowel wall layers

Where bowel wall thickening is observed with high-frequency transducers, the normal bowel layer pattern may be preserved, exaggerated, distorted, diminished or obliterated. The high resolution of US provides a unique opportunity to identify the specific bowel layers affected, to characterise the lesions and diagnose the underlying process.

Bowel lumen

Commonly when the bowel wall is thickened, the bowel lumen is compromised, becoming narrowed or strictured. An uncommon exception to this is aneurysmal dilatation, where the lumen in the diseased segment enlarges; this is a particular feature of intestinal lymphoma and thought to be due to destruction of the autonomic nerve plexus in the bowel wall by infiltrating tumour.[6]

Dilatation of the bowel lumen is seen proximal to the obstructing lesion, where it may initially be accompanied by increased peristalsis. Dilatation with no peristalsis may be due to late stage obstruction or 'paralytic' ileus (most commonly seen after abdominal surgery).

Bowel plasticity/mobility/peristalsis

Most disease processes result in stiffening of the affected bowel segment(s), which is observed at US as more rigid, less compressible, less easily displaced and with reduced or absent peristalsis.

Altered blood flow

Where an abnormal bowel segment or mass is identified, examination with colour or power Doppler may usefully demonstrate an associated alteration in blood flow (e.g. hyperaemia in actively inflamed segments).

Extramural changes

Bowel wall disease may extend out to involve adjacent loops or solid organs, or be the result of external disease involving the bowel loop. Direct or secondary involvement of mesenteric structures may also be seen.

Mesenteric lymphadenopathy

Lymph node size, shape (oval/round), echotexture (hyper/hypoechoic, heterogeneous), smooth or irregular surface, conglomeration/matting, should be documented as these may aid in narrowing the diagnosis.

CROHN'S DISEASE

Crohn's disease (CD) is a lifelong inflammatory gastrointestinal condition of uncertain aetiology characterised by episodes of remission and relapse and the development of serious complications. The disease course may be modified by medical therapy but 90% will require surgery within 10 years of diagnosis.[7] US has a useful role

Abnormal small bowel – US features

- Small bowel wall thickness >3 mm is probably abnormal; > 4 mm is definitely so.
- Bowel wall thickening may be due to oedema, haemorrhage, inflammation/infection or tumour.
- Thickened bowel wall segments should be interrogated for changes in bowel wall layers, altered vascularity, perienteric fluid or fat proliferation.
- If bowel wall is thickened, check lymph nodes and liver.

in diagnosing CD,[8,9] assessing and monitoring disease activity and identifying complications.[10]

CD may involve any part of the gastrointestinal tract and may involve multiple segments at the same or different times. Large bowel disease, ileocolic and terminal ileal disease are the most common patterns with the terminal ileum being involved in up to 75% of cases at presentation. Proximal small bowel CD without terminal ileal involvement is seen in only 3% of cases.[11]

The inflammatory process may extend through all the bowel layers and beyond, resulting in intraperitoneal disease and involvement of adjacent bowel loops and/or organs.

Inflammatory episodes commence in the mucosa with an immune response to the trigger event(s). Through leaky vessels, an initially humoral and subsequently cellular immune response results in thickening of the mucosal layer and damage to the mucosal surface. The submucosa generally thickens in response to the hypervascularity or inflammatory cellular infiltration. But CD is characterised by transmural inflammation that extends out to involve the muscularis propria and serosa, interrupting sonographic layers and blurring or completely obliterating stratification in either a segmental or circumferential fashion.

As the inflammation becomes more chronic, fibrosis may make this exaggeration or loss of stratification permanent. The inflamed segment becomes more rigid and less compressible, with the loss of normal peristaltic activity. Where there is circumferential involvement of the bowel wall, the lumen becomes narrowed and there may be dilatation of the proximal healthy bowel. Asymmetrical involvement of the bowel wall with disease predominantly affecting the mesenteric border may result in ballooning of the antimesenteric wall (pseudo-sacculation).

Clinical features of CD

Patients with CD may present at any age, but most commonly in late teens and early adulthood.

Diarrhoea of more than 6 weeks duration, abdominal pain and weight loss are the most common presenting symptoms. The young patient with right iliac fossa pain and a mass may easily be misdiagnosed as having acute appendicitis. Blood and/or mucus in the stool generally indicate colonic involvement. Perianal fistulas are present in 10% of patients at presentation.[12] Extraintestinal involvement is also common, particularly an associated inflammatory arthropathy.

Ultrasound features of Crohn's disease

Bowel wall thickening

The primary imaging feature of CD is thickening of the bowel wall and US has been shown to identify wall thickening in patients with suspected CD with a sensitivity of 75–94% and a specificity of 67–100%.[13]

Crohn's disease

- Patients are often children or young adults and most commonly have a history of diarrhoea and abdominal pain.
- US is very good at identifying terminal ileal and ileocolic CD.
- Bowel layers may be separately thickened, or bowel layers may be indistinct/blurred or obliterated by hypoechoic transmural inflammation.
- Actively inflamed segments show increased vascularity on power Doppler and associated lymphadenopathy.
- Look for CD complications; stricture, abscess and fistula.

Bowel wall thickening – diagnostic threshold

The earliest changes of mucosal interface interruption and thickening limited to the mucosal layer may be subtle, insensitive and open to inter-observer error. Reliance therefore tends to be placed on absolute measurements of bowel wall thickening. The normal small bowel wall thickness is taken to be up to 3 mm (this varies considerably with peristaltic distension and contraction). The sensitivity and specificity for the diagnosis of CD by wall thickening is determined by the threshold set for defining 'abnormal thickness'. A meta-analysis of studies using US measurements of wall thickening to diagnose CD reported an 88% sensitivity and 93% specificity with a diagnostic threshold of >3 mm, changing to 75% and 97% respectively when the threshold is raised to >4 mm.[14]

Bowel wall layers (mural stratification)

Careful examination of the involved segment may show one of the following patterns:

1. **Isolated thickening of the mucosa** (Figs 19.3, 19.4) which may be accompanied by interruption of the lumen-interface echo (layer 1) due to sloughing of the mucosal surface, and/or tiny bright echoes due to gas in mucosal ulcers.
2. **Thickening of the mucosa and submucosa with clear preservation of the bowel layers** (Fig. 19.5) producing a target sign.
3. **Segmental or circumferential hypoechoic thickening of the full thickness of the bowel wall** with the layers being indistinct or completely absent (Figs 19.6, 19.7). Irregular

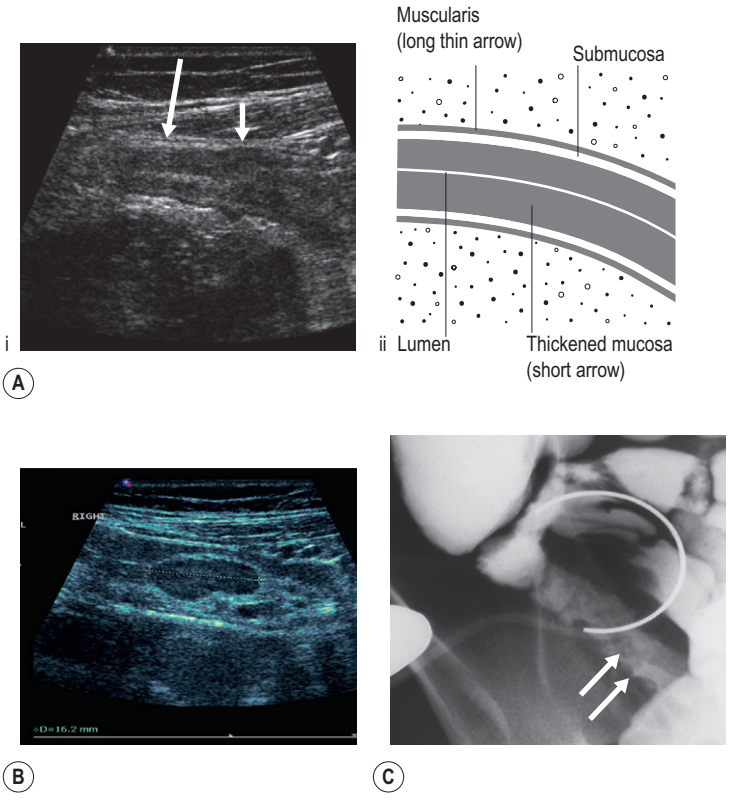


Figure 19.3 Crohn's disease: acute terminal ileitis with mucosal thickening only. A young adult female presented with diarrhoea and weight loss. **A:** Longitudinal US of distal ileum with nodular thickening of mucosa with normal submucosa and muscle layers. **B:** Adjacent mesenteric lymphadenopathy. **C:** Spot image from a concurrent barium study showing aphthous and shallow terminal ileum ulcers (white arrows).

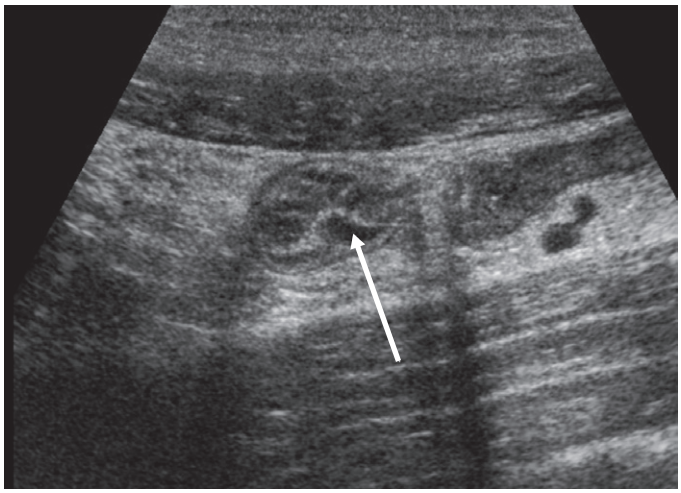


Figure 19.4 Crohn's disease: jejunal fold thickening. Transverse US showing jejunal CD with thickening limited to mucosal folds (arrow).

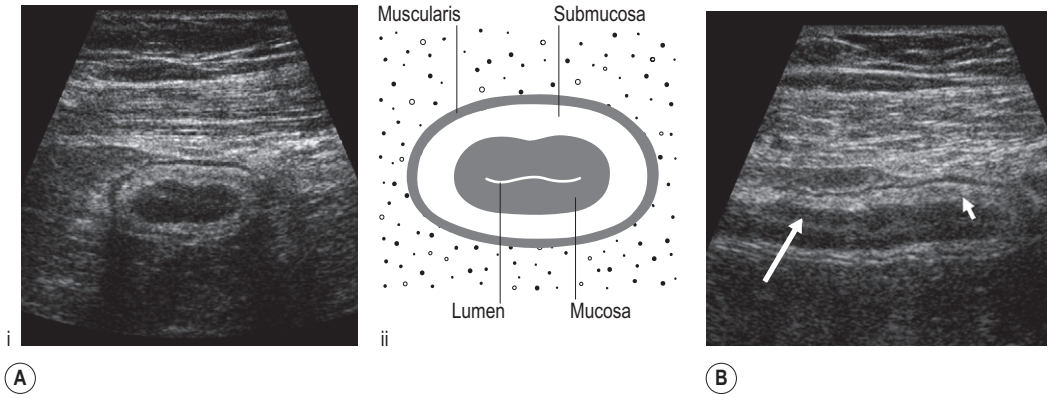


Figure 19.5 Crohn's disease: acute ileitis (preserved layers). Longitudinal **(A)** and transverse **(B)** images of ileum showing thickened mucosa (interrupted long white arrow), thickening submucosa (long solid white arrow) but normal muscle layer (short white arrow) and no peri-intestinal fat wrapping or fluid.

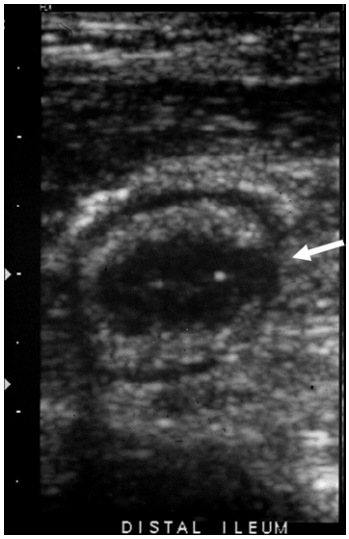


Figure 19.6 Crohn's disease: acute ileitis with segmental transmural inflammation. Transverse scan of distal ileum demonstrating thickening of mucosa and submucosa (pattern 2) with a small segment of transmural inflammation breaching the submucosa (white arrow).

mixed hypoechoic inflammatory exudate may be present on the serosal surface. Deep ulcers may be easily evident if filled with bowel gas. The transmural hypoechoic change may be limited to a section of the bowel circumference.

These patterns indicate the progress of the disease through the bowel wall;[15] pattern 3, indicating transmural inflammation, may be accompanied by complications (see below).

Fat wrapping

Transmural inflammation stimulates proliferation of mesenteric/subserosal fat, which 'creeps' around the inflamed bowel segment, a distinguishing characteristic of transmural CD (Fig. 19.7). Fat wrapping correlates with histological evidence of transmural inflammation and associated complications like fistulation.[16]

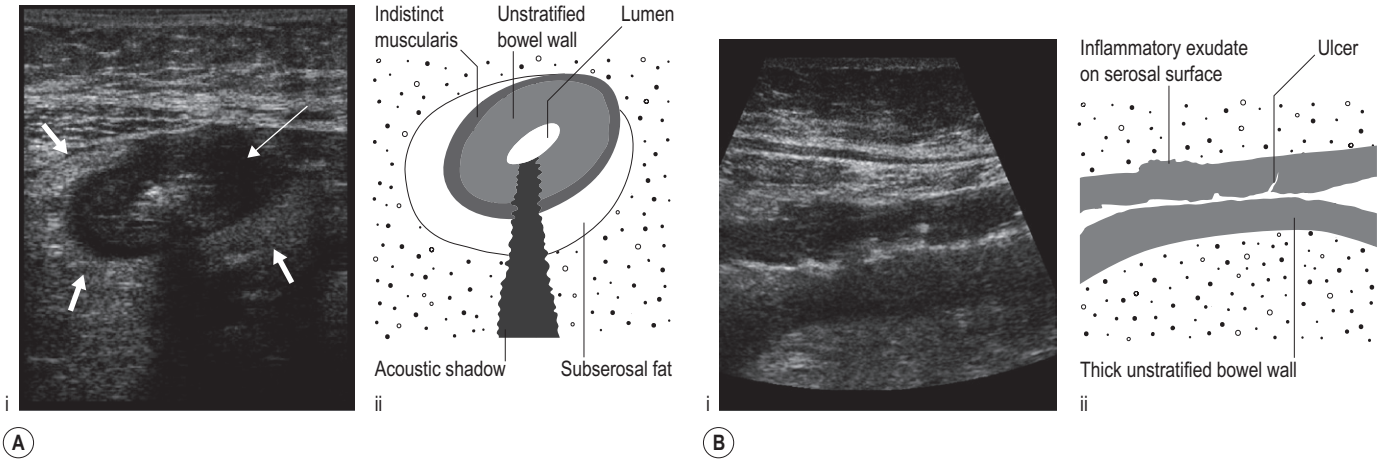


Figure 19.7 Crohn's disease: circumferential transmural inflammation. **A:** Transverse scan of a diseased segment of distal ileum. The inflamed wall is thickened and hypoechoic with loss of layers (long white arrow). The lumen is narrowed. The segment is surrounded by subserosal 'creeping fat' (short white arrows). **B:** Longitudinal scan of the same bowel segment. Transmural hypoechoic thickening with deep ulcers and inflammatory exudate on the serosal surface.

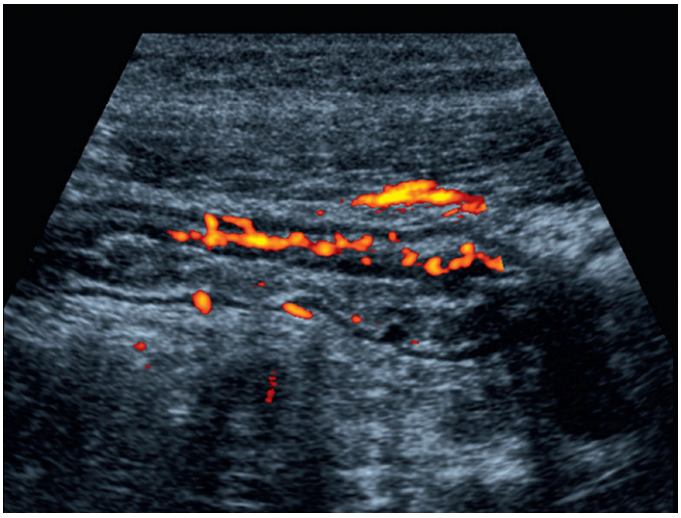


Figure 19.8 Crohn's disease: active inflammation. US ileal bowel loop with mucosal thickening and hyperaemia shown with power Doppler, indicating active inflammation.

Vascular changes

Actively inflamed bowel segments have an increased blood flow which may be demonstrated with colour Doppler or power Doppler imaging (Fig. 19.8). Studies have shown this phenomenon to be helpful in distinguishing active inflammatory lesions from fibrotic strictures, and in monitoring response to medical therapies. The use of US contrast media may further increase the diagnostic confidence by quantifying this phenomenon.[17]

Locoregional lymphadenopathy

Active intestinal CD is usually accompanied by lymphadenopathy in the mesentery.

Local complications of small bowel Crohn's disease

Transmural inflammation is a hallmark of CD and this results in the local complications of stricture, abscess and fistula. US is useful in detecting these complications but may miss enteroenteric fistulas.[18]

Stricture

Narrowing of the bowel lumen sufficient to produce impaired intestinal function and obstructive symptoms may be seen both in active inflammatory segments (hot strictures) and in segments where fibrosis dominates (cold strictures) (Fig. 19.9). Spasm and oedema contribute to the narrowing of active disease segments and may rapidly respond to medical therapy. Persistent symptomatic stricture is the most common indication for surgery. In addition to clinical assessment, laboratory results and endoscopic findings, imaging makes a significant contribution in distinguishing between inflammatory and fibrotic strictures.

Active inflammatory strictures are hyperaemic compared with normal bowel and with fibrotic strictures. Colour and power Doppler barely demonstrates normal vascular activity in healthy bowel wall but both demonstrate the increased flow in inflamed bowel wall and inflammatory masses (see Figs 19.9, 19.12, 19.13). Doppler US assessment of increased superior mesenteric artery blood flow has also been used to assess CD activity.[19]

Abscess

Transmural inflammation extending out to and beyond the serosal bowel surface may be seen at US as irregular mixed low echo inflammatory exudate on the serosal surface, a mixed low echo

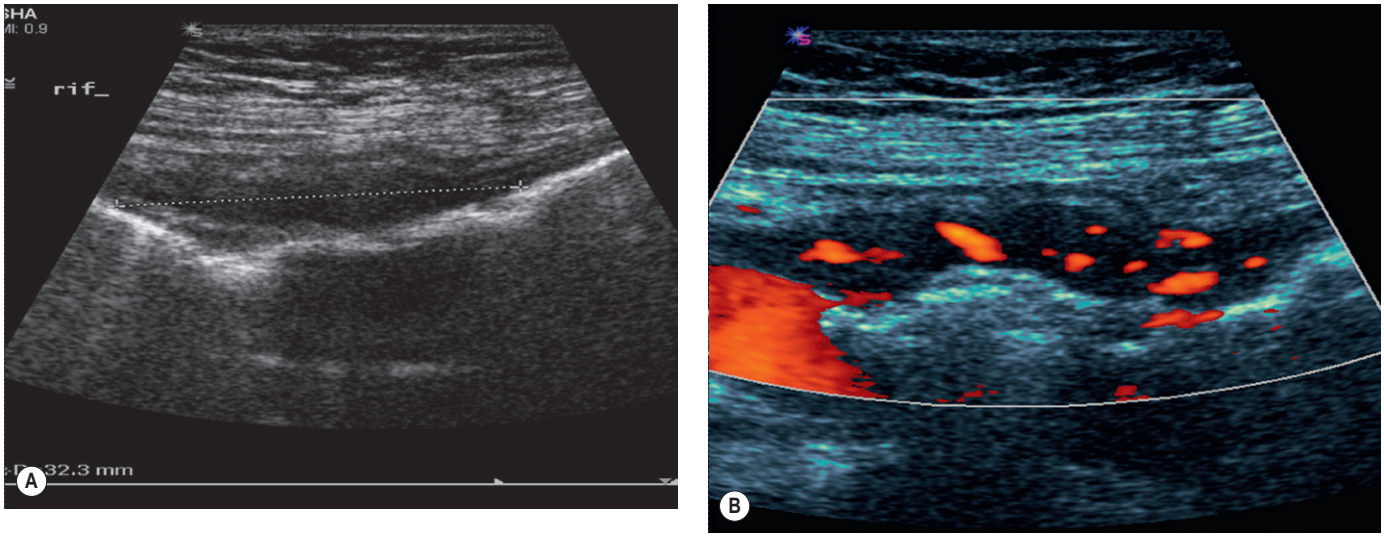


Figure 19.9 Crohn's disease: stricture. **A:** Longitudinal scan of a short ileal stricture with bright gas in the tight lumen. Only the mucosa appears thickened. **B:** Power Doppler shows hyperaemia indicating an inflammatory stricture (suitable for medical therapy). **C:** Another bowel segment in the same patient showing transmural hypoechoic thickening and a deep gas-filled ulcer.

inflammatory mass between bowel loops, or an irregularly thick and walled collection with a liquid centre (abscess). Abscesses may form between bowel loops or in adjacent structures such as the abdominal wall (Fig. 19.10).

Fistula

In up to one-third of patients, penetrating fissures can extend to create an abnormal communication between the lumen of the disease bowel segment and adjacent bowel loops (enteroenteric or enterocolic fistula), the skin (enterocutaneous fistula) or any adjacent hollow organ (uterus, bladder etc.).

The communication between adherent bowel loops may be difficult to identify and underestimated by all imaging modalities. At US fistulas are identified as irregular tubular hypoechoic tracks[20] (Fig. 19.11) and occasionally may demonstrate small hyper-reflective air bubbles within (Fig. 19.13),[21] but the presence of adjacent indrawn, angulated bowel loops connected by mixed hypoechoic inflammatory exudate is highly suspicious of fistula formation (Fig. 19.12).

Disease activity

Management decisions in CD require reliable assessments of disease activity. Clinical assessment and laboratory results are central and scoring systems such as the Crohn's Disease Activity

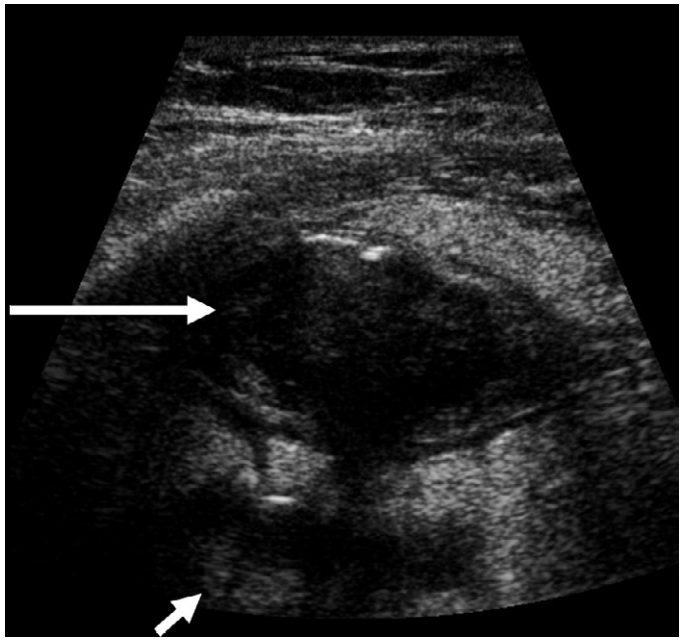


Figure 19.10 Crohn's disease: abscess. A well-circumscribed anterior abdominal wall abscess (long white arrow). Deep to the abscess is a bowel loop showing transmural inflammation (short white arrow).

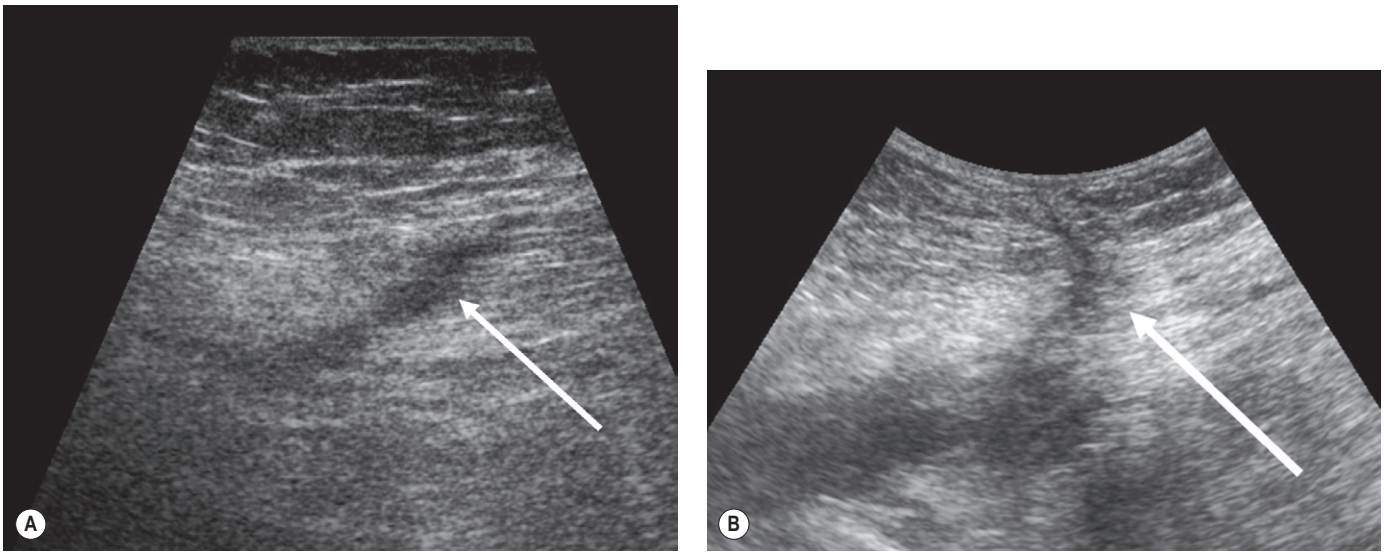


Figure 19.11 Crohn's disease: enterocutaneous fistula. A and B: Irregular hypoechoic fistula (long white arrows) track through the anterior abdominal wall and subcutaneous tissues.

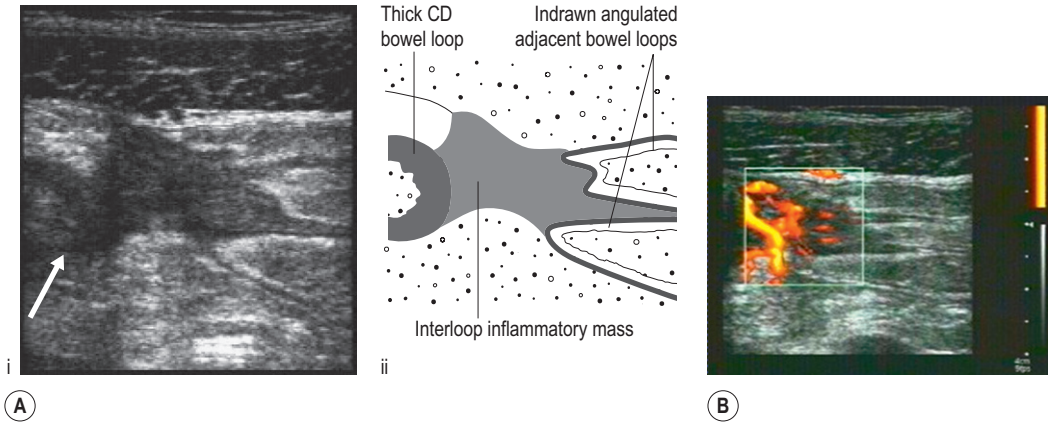


Figure 19.12 Crohn's disease: enteroenteric fistula. A: Interloop inflammatory exudate is seen between the thickened hypoechoic bowel loop (white arrow) and adjacent normal bowel loops. **B:** Power Doppler scan demonstrates hyperaemia in the inflammatory exudate.

Index (CDAI), based on symptoms (e.g. number of loose stools/day), signs (e.g. palpable abdominal mass) and blood test results, are commonly used to monitor therapeutic responses. However, symptoms may be due to factors other than active inflammation (e.g. cold strictures, bacterial overgrowth) and US may usefully contribute to assessment of disease activity by documenting the vascularity of lesions with colour or power Doppler (Figs 19.8, 19.9, 19.12, 19.13) and accuracy may be improved by the use of intravenous contrast agents.[22] Semi-quantitative scoring systems have been devised for comparative assessments; one such, the Limberg score, combines wall thickening (>4 mm with blurred or lost layers) with increasing degrees of vascularity on power Doppler (none, spots, branching vessels, and extent into mesentery), and good correlation with histological assessment of inflammatory activity has been demonstrated.[23]

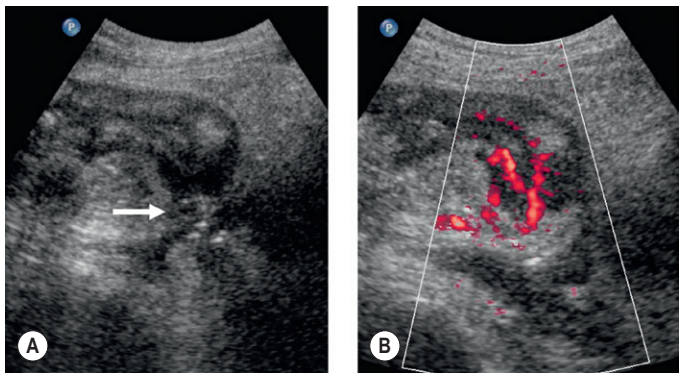


Figure 19.13 Crohn's disease: pelvic fistula. This 43-year-old man presented with a 2-month history of lower abdominal pain, increasing urinary frequency, night sweats and raised inflammatory markers. **A:** US shows a thickened small bowel loop descending into the pelvis with extraintestinal hypoechoic fistula tracks containing hyper-reflective gas bubbles. **B:** Power Doppler confirms the inflammatory hyperaemia.

INTESTINAL INFECTIONS

The small bowel is a common site for infections from viruses, bacteria and parasites (such as *Anisakis* worms from raw fish). Most symptomatic episodes are short, self-limiting and seldom present

for imaging investigations. Exceptions to this are a group of infections that mimic acute appendicitis, and chronic infections, particularly intestinal tuberculosis, that may mimic inflammatory bowel disease.

Infectious ileocaecitis

Yersinia, *Campylobacter* and *Salmonella* bacteria are well-known causes of acute diarrhoeal illnesses, usually self-limiting, diagnosed symptomatically and not intentionally referred for imaging investigations.

Uncommonly, however, these organisms may produce an enteric infection confined to the ileocaecal region, patients presenting with right iliac fossa symptoms of pain and tenderness; diarrhoea may be minimal or absent. The severity of symptoms varies but in more acute cases may result in unnecessary appendectomy, and in more protracted cases may be mistaken for Crohn's disease or appendix mass.

Ultrasound examination reveals a symmetrical thickening of the wall of the terminal ileum and caecum confined to the mucosal and submucosal layers with no extension to the muscularis, serosa or beyond into the mesentery. It has been reported that the extent of caecal/colonic involvement may vary with the specific pathogen.[24] Local mesenteric lymph nodes are usually enlarged. The visualised appendix is normal (Fig. 19.14).

The absence of transmural inflammatory changes/complications and the relatively short course of symptoms help to distinguish acute infectious ileocaecitis from Crohn's disease. Most importantly, this condition is distinguished from acute appendicitis and an unnecessary operation avoided.

Intestinal tuberculosis

In Western countries, where tuberculosis is no longer endemic, this disease has re-emerged particularly in migrant populations and those immunocompromised by HIV/AIDS.

Non-specific symptoms such as abdominal pain, weight loss, anaemia and fever predominate but patients may present with symptoms of intestinal obstruction or palpable abdominal mass.

Though any part of the gastrointestinal tract can be affected, ileocaecal involvement is most common but isolated ileal or jejunal disease does occur and is a particular feature of atypical tuberculosis (e.g. *Mycobacterium avium intracellulare*).

Ultrasound features[25,26] include bowel thickening with luminal narrowing and superficial or deep ulcers. Typically the bowel thickening involves the terminal ileum, ileocaecal valve and caecum (Figs 19.15, 19.16). Lymphadenopathy is common and may form conglomerate (matted) lymph node masses. Bowel loops may be matted together by interloop exudates or abscesses. Extraintestinal disease may produce ascites or peritoneal thickening.

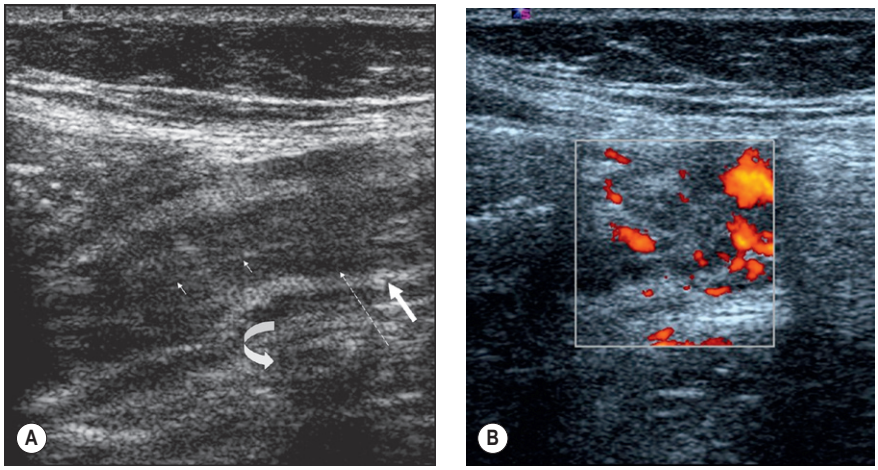


Figure 19.14 Acute infectious ileitis. This 53-year-old woman presented with 3 days of right iliac fossa pain. Appendicitis was suspected. **A:** Longitudinal US of the terminal ileum which thickening of the mucosa (interrupted arrow), thickening and blurring of the submucosa (short white arrow). A fine white line (tiny white arrows) is seen at the meeting of anterior and posterior wall mucosal surfaces. The normal appendix is seen deep to the terminal ileum (curved arrow). **B:** Power Doppler transverse scan of the terminal ileum showing hyperaemia. After conservative management, a repeat US 2 months later showed normal terminal ileum and appendix.

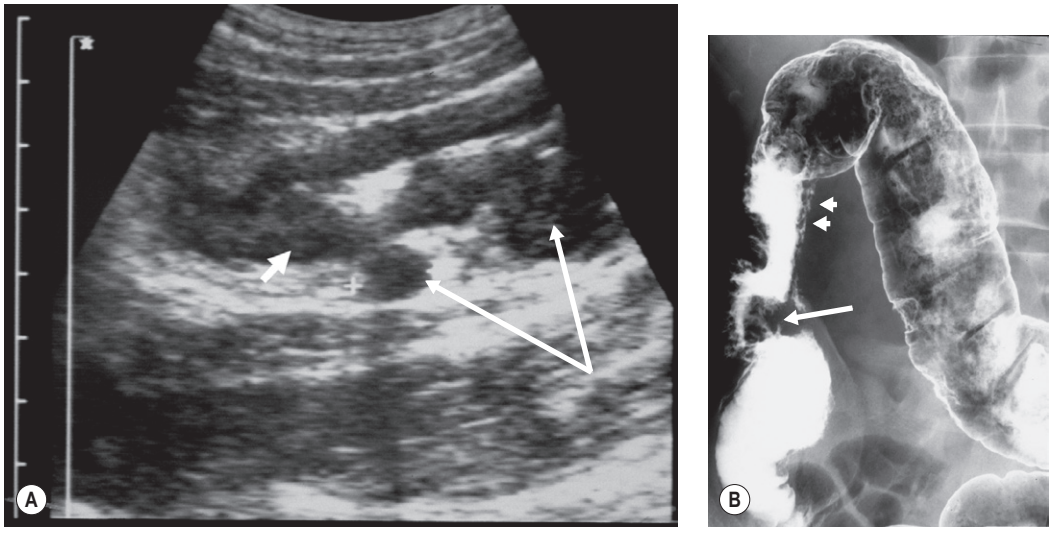


Figure 19.15 Ileocaecal tuberculosis. **A:** US showed a thickened contracted caecum (short white arrow) and enlarged pericaecal lymph nodes (long white arrows). **B:** Spot film of the barium study showing the contracted caecum and superficial ulcerations (white arrowheads) along the ascending colon. The terminal ileum is dilated and there is the distorted ileocaecal valve at an obtuse angle (long white arrow).

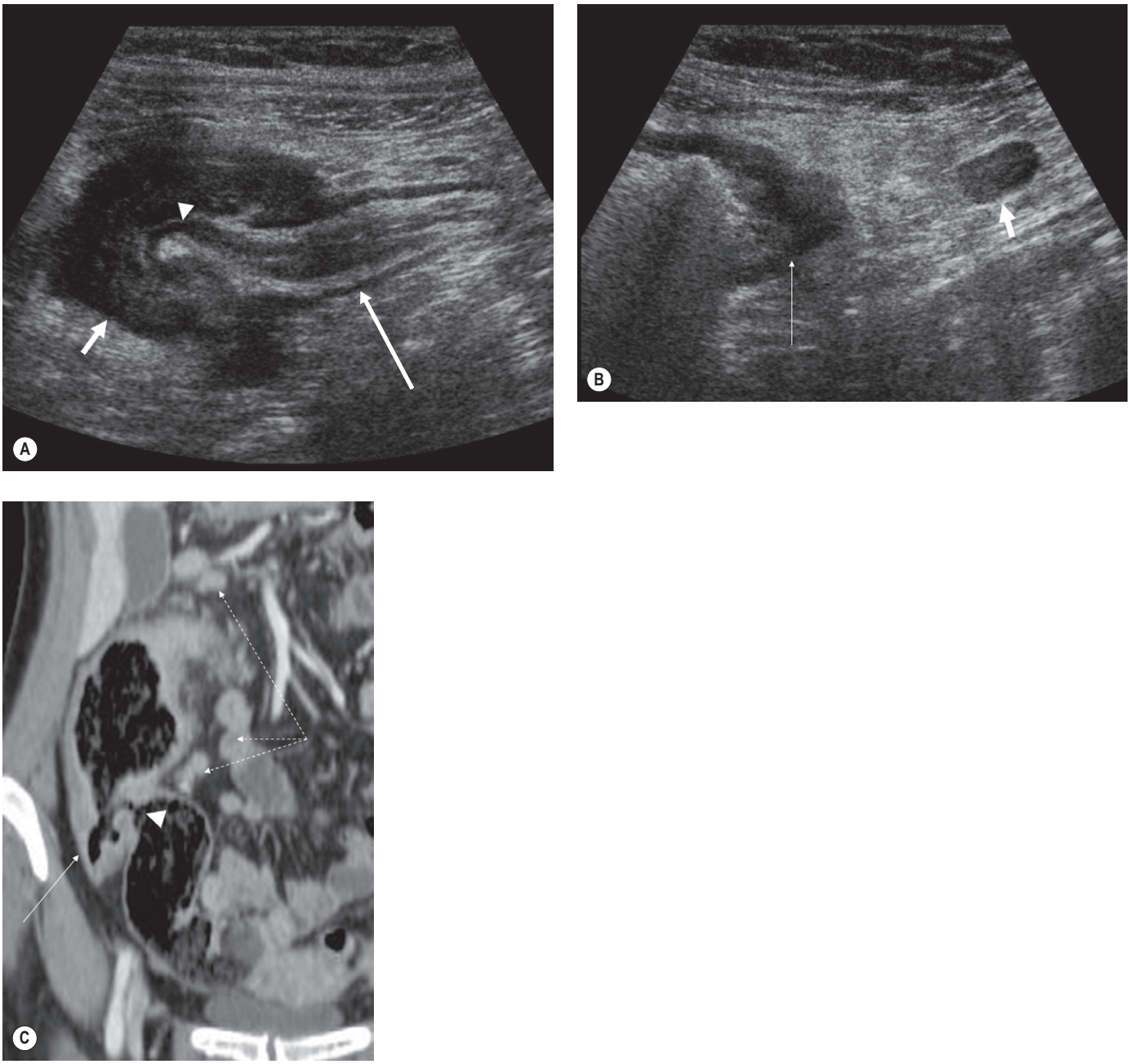


Figure 19.16 Ileocaecal tuberculosis. This 47-year-old Asian woman with previous pulmonary TB presented with weight loss and abdominal pain. **A:** Sonogram showing an irregular, hypoechoic contracted caecum, the ileocaecal valve (arrowhead) and thickened terminal ileum with distorted but preserved stratification. **B:** Doppler US showed no hyperaemia. **C:** An earlier CT scan of the same patient showing the thickened contracted caecum (white arrow), fixed, open ileocaecal valve (arrowhead), a dilated terminal ileum, and multiple enlarged mesenteric lymph nodes (interrupted white arrows).

Anisakiasis

Anisakiasis is a parasitic infection of the gastrointestinal tract due to a worm present in raw or undercooked fish. Patients present within a couple of days of consuming the fish with acute abdominal pain. US may demonstrate 10–40 cm long segments of small bowel thickening due to an eosinophilic granulomatous response, most commonly in the distal ileum, with interloop ascites.[27]

SMALL BOWEL ISCHAEMIA

Interruption or critical reduction in the blood supply to or venous drainage of the bowel may result in ischaemic damage which may be focal or diffuse. The extent and severity of the injury is determined by the level of the interruption, the extent of vascular disease in the mesenteric circulation, and the cardiovascular function. Ischaemic damage may be limited to the mucosa in small vessel disease, but large vessel occlusion may result in full thickness bowel infarction which is frequently fatal (Table 19.1).

The classic clinical presentation of acute mesenteric ischaemia (AMI) is the sudden onset of severe abdominal pain with diarrhoea or vomiting. Patients are typically over 50 years old, or have a high risk factor such as atrial fibrillation if under 50. In the early stage there is little to find on examination, but later bowel infarction or perforation may result in signs of peritonitis and fever, and profound shock may develop.

Computed tomography (CT) scanning is the investigation of choice in AMI. US may be hampered by gas in distended bowel loops (paralytic ileus), but sonographic features include bowel wall thickening (transmural hypoechoic or predominantly submucosal), ascites, and reduced or absent vascularity of the thickened bowel on Doppler scanning.[28,29] Doppler examination may demonstrated the level of obstruction in the mesenteric vessels.

Differential diagnosis

- Not all bowel thickening is due to Crohn's disease; remember ischaemia, infection and malignancy among others.
- Hypoechoic transmural thickening with no increased vascularity suggests a cause other than CD.
- Marked thickening of caecum and terminal ileum may be seen in lymphoma and tuberculosis.
- Acute infectious ileocaecitis and CD may both clinically mimic acute appendicitis.

SMALL BOWEL VASCULITIS

There are a number of uncommon immune-mediated diseases affecting the intestinal blood vessels, producing ischaemia, mural oedema and haemorrhage, and mucosal ulceration. The extent of the ischaemia depends on the size of the vessels affected (Table 19.2). The smallest vessels supply the mucosa and this is the primary site of ischaemic damage; deeper layers may survive due to collateral perfusion. Full thickness infarction is usually only seen with large vessel involvement.

US features are bowel thickening with reduced peristalsis, preserved, exaggerated, indistinct or obliterated layers, and mucosal ulceration. Interloop ascites and other mesenteric changes may be

Table 19.1 Causes of bowel ischaemia

Cause	Mechanism
Mesenteric arterial occlusion	Thrombosis/thromboembolism/embolism (including therapeutic) Atherosclerosis Aortic surgery/stent placement Fibromuscular dysplasia Vasculitis
Mesenteric venous occlusion	Venous thrombosis (primary and secondary) Intramural vein phlebitis
Mechanical	Strangulation (bowel obstruction with vascular compromise) Closed loop obstruction Prolonged bowel dilatation of any cause
Inflammation	Pancreatitis/appendicitis/diverticulitis etc.
Low flow or vasospasm	Shock (haemorrhagic/cardiogenic/septic) Cardiac failure/arrhythmia Dehydration Drug-related (including recreational, e.g. cocaine)
Other	The radiation/trauma/corrosive injury/chemotherapy Adjacent to intestinal tumours (e.g. carcinoid)

Table 19.2 Vasculitis

Type of vasculitis	Affected vessel type/size	Target organs/bowel segments	Bowel lesions/complications
Polyarteritis nodosa	Medium to smaller arteries	Kidneys, liver, intestines	Penetrating ulcers/haemorrhagic infarcts
Rheumatoid vasculitis	Medium sized vessels	Joints/intestines	Segmental infarction/intestinal strictures
Systemic lupus erythematosus	Small vessels	Small intestine	Segmental necrosis/perforation
Henoch–Schönlein purpura	Post-capillary venulitis	Small intestine (distal ileum)	Gastrointestinal bleeding, mucosal/submucosal haemorrhage/ulcers/intussusception
Behçet's syndrome	Small vessels	Skin/joints/CNS intestines (ileocaecal)	Shallow/deep ulcers/perforation
Churg–Strauss syndrome	Large vessels	Lung/skin/intestines (small and large)	Ulcers/necrosis/perforation

Data from Herlinger H, Maglinte DT, Birnbaum BA. Clinical Imaging of the Small Intestine, 2nd Edition, Springer, 2001.

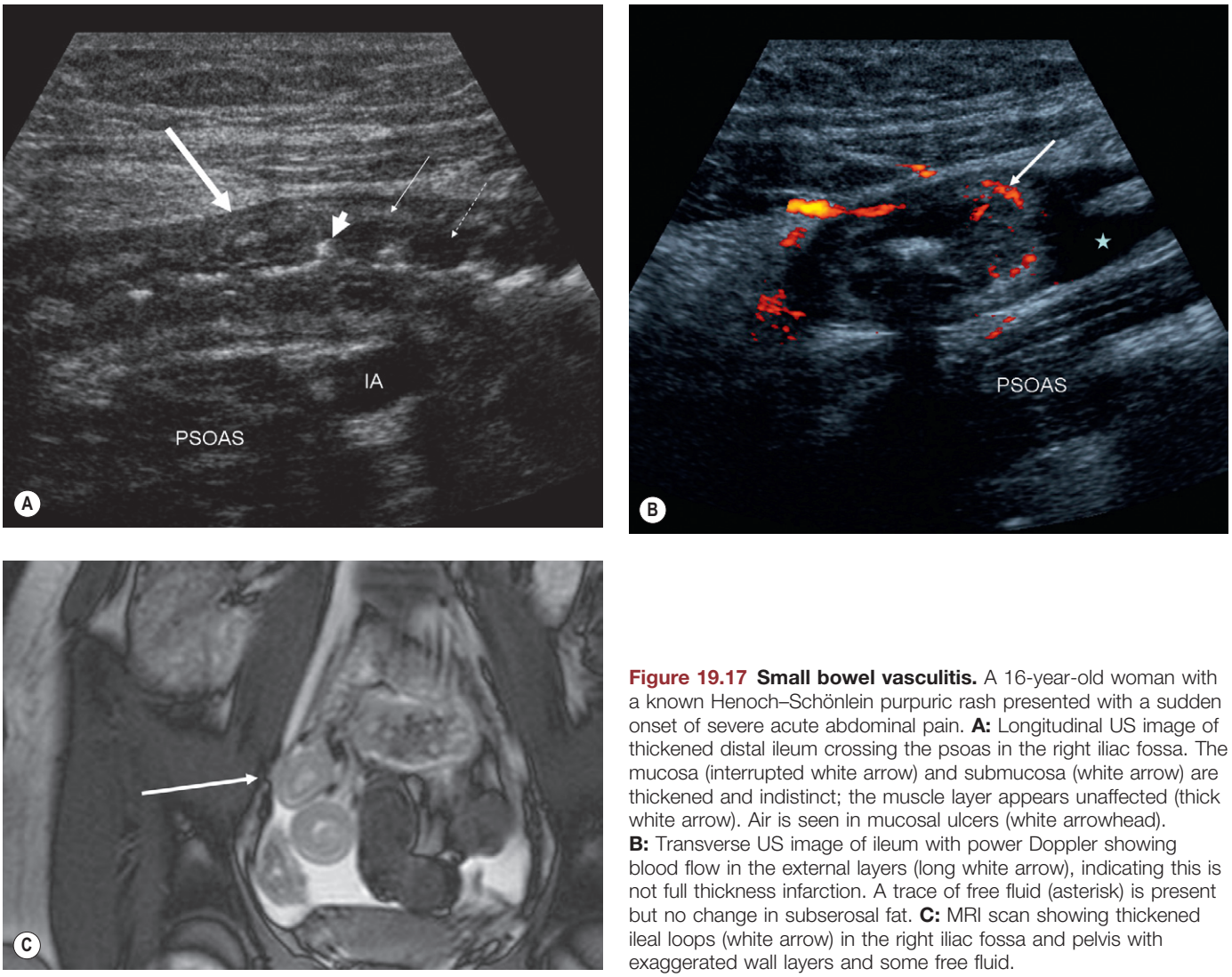


Figure 19.17 Small bowel vasculitis. A 16-year-old woman with a known Henoch–Schönlein purpuric rash presented with a sudden onset of severe acute abdominal pain. **A:** Longitudinal US image of thickened distal ileum crossing the psoas in the right iliac fossa. The mucosa (interrupted white arrow) and submucosa (white arrow) are thickened and indistinct; the muscle layer appears unaffected (thick white arrow). Air is seen in mucosal ulcers (white arrowhead). **B:** Transverse US image of ileum with power Doppler showing blood flow in the external layers (long white arrow), indicating this is not full thickness infarction. A trace of free fluid (asterisk) is present but no change in subserosal fat. **C:** MRI scan showing thickened ileal loops (white arrow) in the right iliac fossa and pelvis with exaggerated wall layers and some free fluid.

seen. Studies differ on distinguishing between inflammation and ischaemia on wall thickening alone[30,31] but US colour/power Doppler may show normal, reduced or absent blood flow in the ischaemic bowel wall in contrast to the hyperaemia of acute inflammatory conditions[32] (Fig. 19.17).

SMALL BOWEL TUMOURS

Primary small bowel tumours are rare. Although the small bowel constitutes 75% of the length and 90% of the surface area of the gastrointestinal tract, it is the site of only 25% of benign and less than 5% of malignant gastrointestinal tract tumours. Large bowel cancer is 60 times more common. Protective factors may include, among others, rapid cell turnover, fast transit times, alkaline intestinal contents and the scarcity of bacteria.[33]

Clinical presentation

Symptomatic lesions, whether benign or malignant, most commonly present with abdominal pain (intermittent or progressing to full-blown obstruction), bleeding (usually non-visual but occasionally as frank haemorrhage), and uncommonly with a palpable mass.

Malignant small bowel tumours

About two-thirds of symptomatic small bowel tumours are malignant and over 95% of these are adenocarcinomas, carcinoids, lymphomas or sarcomas (malignant gastrointestinal stromal tumours or leiomyosarcomas).[30]

Adenocarcinoma

Adenocarcinomas are the most common primary small bowel malignancy and usually develop in the duodenum or proximal jejunum. There is an increased risk of adenocarcinoma in long-standing Crohn's disease and these lesions may occur in the ileum.

Sonographically these tumours may be intraluminal or intramural, annular, polypoid or infiltrative, echogenic masses or target lesions (Fig. 19.18).[34,35] The lesions spread to lymph nodes, liver and peritoneum. Lymphadenopathy is usually less marked than with lymphomas.

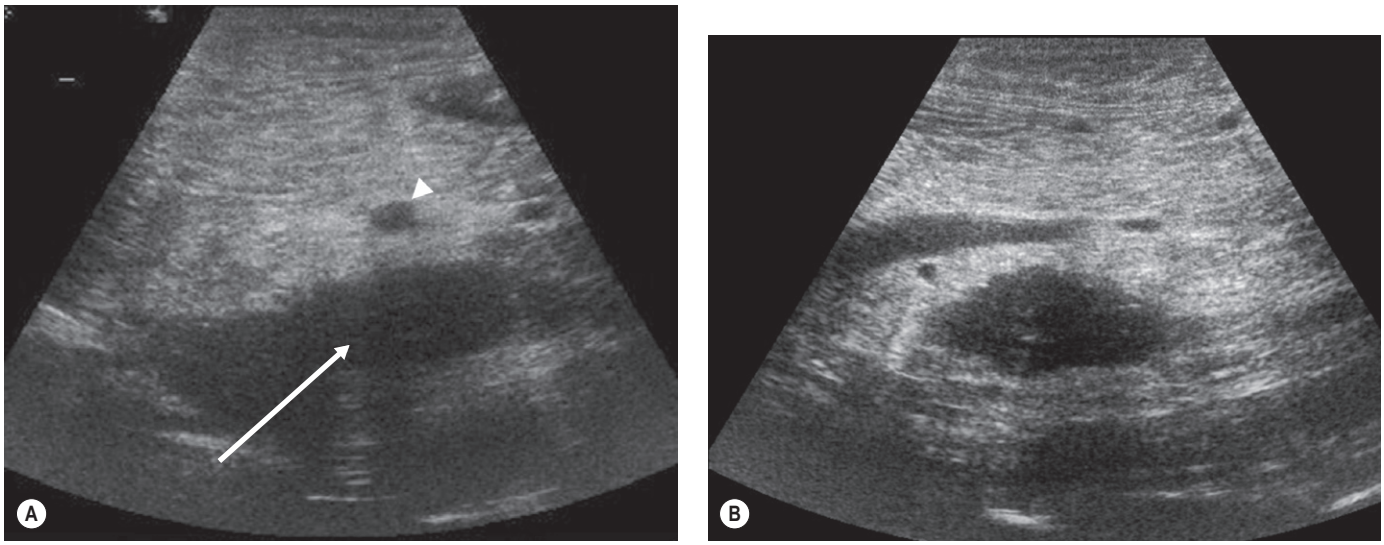


Figure 19.18 Primary intestinal adenocarcinoma. A 53-year-old man presented with abdominal pain and vomiting. **A:** US Long view of an hypoechoic annular tumour (white arrow) with an irregular surface occluding the third part of the duodenum deep to the superior mesenteric artery (arrowhead). **B:** US transverse scan of the tumour beneath the SMA.

Carcinoid

Carcinoid tumours are small, slow-growing, submucosal tumours occurring most commonly in the appendix and the ileum. Malignant potential is related to size and 95% of lesions measuring greater than 2 cm diameter have metastasised.

The sonographic appearance is of a smooth, predominantly intraluminal mass of low homogeneous echogenicity.[36] Doppler may show hypervascularity (Fig. 19.19). Local invasion may be seen as a thickening of the adjacent muscularis propria and serosal transgression with puckering and retraction. Metastatic involvement of local lymph nodes is often accompanied by an intense fibrotic reaction tethering adjacent bowel loops.

Lymphoma

Gastrointestinal lymphoma is an extranodal lymphoma, i.e. the bulk of the disease is in an extranodal site, and the associated lymph node involvement is restricted to the relevant locoregional nodes at presentation. Primary lymphoma of the intestines involves the ileum/ileocaecal region in two-thirds of cases.[37]

The typical US appearance is of a transmural, circumferential, hypoechoic bowel lesion with the lumen forming a bright echogenic centre (the classic 'target' lesion, or in bulkier tumours the 'pseudokidney' lesion) (Figs 19.20, 19.21). Instead of being compressed, the lumen may enlarge within the tumour to a diameter greater than normal small bowel (aneurysmal dilatation). Less common US findings include long segments of involved bowel mimicking inflammatory bowel disease, and diffuse disease limited to the mucosa.[38] Lymphomatous lymph nodes are typically large, round and hypoechoic without enhanced transmission.

Mesenchymal tumours

Gastrointestinal mesenchymal tumours are rare. Until the last decade these were classified as smooth muscle tumours (leiomyoma/leiomyosarcoma), but with the introduction of KIT immunohistochemistry, which identifies a specific protein marker (CD117) produced by the cells, the majority were reclassified as gastrointestinal stromal tumours (GISTs).

The most common locations for GISTs are the stomach (50–60%) and the small intestine (30–40%). The majority of these tumours are benign but up to 20% may be malignant; tumour size >4 cm and histological findings are the main indicators of malignant potential.[39]

GISTs arise in the bowel wall but predominantly grow outwards, displacing adjacent structures, and may become large without causing obstruction; most patients present with non-specific symptoms such as abdominal pain. However, the tumour may erode the bowel mucosa and present with gastrointestinal bleeding.

Sonographically these tumours appear as echo-poor, homogeneous masses but may show areas of central anechoic necrosis.[40] Doppler ultrasound demonstrates the rich vascularity of these tumours (Fig. 19.22). The commonest sites for metastasis are the liver and peritoneal cavity.[41]

Secondary intestinal malignancies

Metastatic involvement of the small bowel is common and usually occurs by seeding across the peritoneal cavity from abdominopelvic primary tumours with deposits onto the bowel serosa and peritoneum (Fig. 19.23), or by haematogenous seeding into the bowel wall, particularly associated with malignant melanoma but also with lung and breast cancers.[32]

Benign small bowel tumours

Benign tumours may arise from any of the mesenchymal cell types in the bowel wall, but leiomyomas, adenomas, lipomas and haemangiomas account for approximately 90%. The leiomyomas and adenomas are more common in the proximal small bowel, lipomas are most frequently found in the ileum.

These tumours are generally small and present as incidental findings, but may cause bowel obstruction due to intussusception (see below) or present with bleeding. Lipomas are sonographically hyperreflective, well circumscribed and may deform on compression.

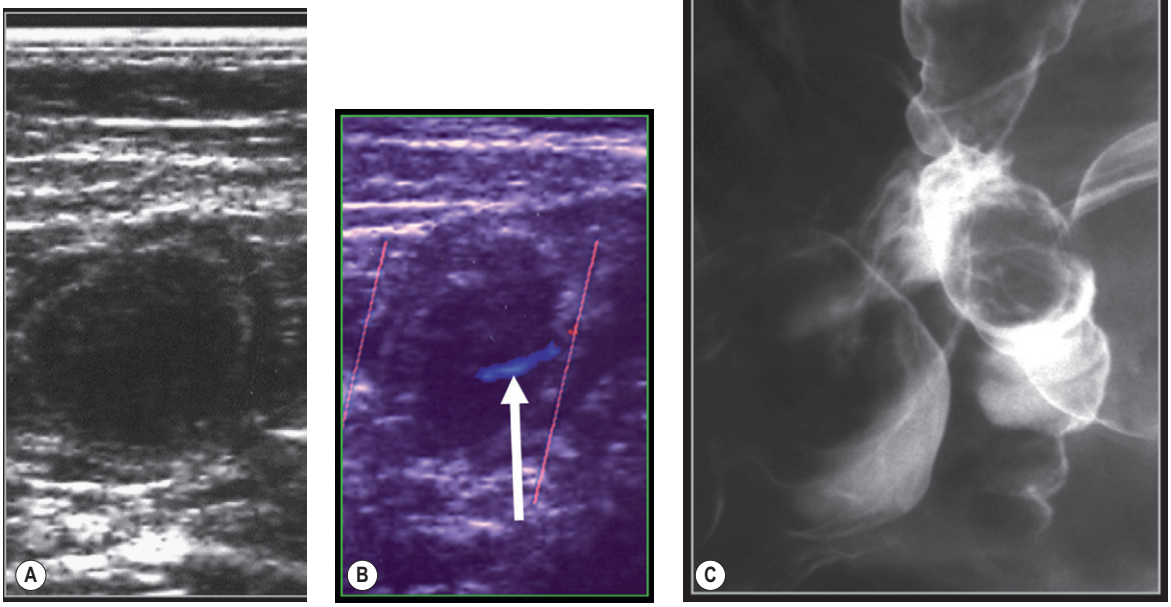


Figure 19.19 Ileal carcinoid tumour. A 60-year-old woman presented with intermittent abdominal pain. **A:** Transverse scan of an 18 mm diameter, non-compressible filling defect in the terminal ileum. **B:** Same lesion with blood supply shown on colour Doppler (white arrow). **C:** Spot barium image confirming a terminal ileal polyp (white arrow). **D:** Resected specimen showing the ileal carcinoid polyp (arrowhead), terminal ileum (white arrow) and appendix orifice (interrupted black arrow).

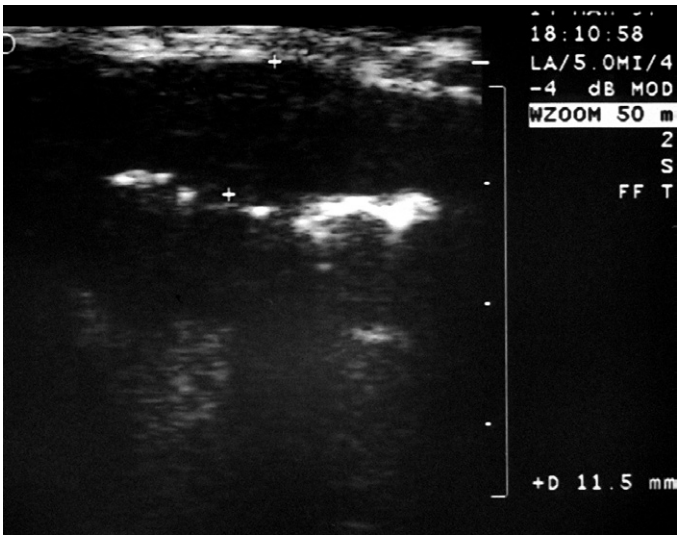


Figure 19.20 Ileal lymphoma. Transverse scan of a short hypoechoic circumferential ileal lesion with bright gas echoes in the compressed lumen (pseudo-kidney appearance).

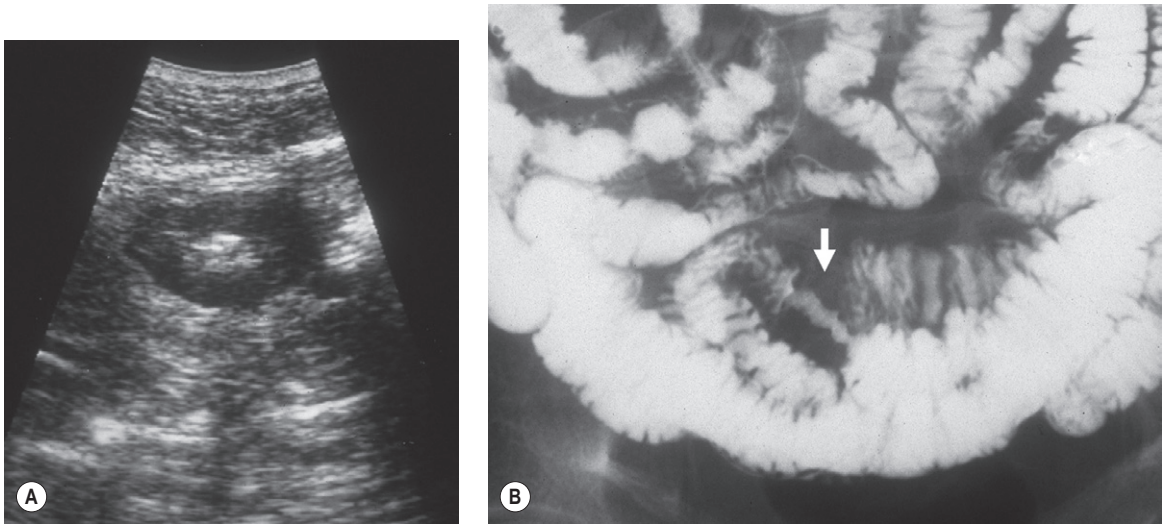


Figure 19.21 Ileal lymphoma. Middle-aged HIV-positive man. **A:** Transverse US scan showing a small bowel lesion with hypoechoic circumferential wall thickening. **B:** Barium study confirming the small circumferential lesion in the ileum (white arrow). Non-Hodgkin's lymphoma was confirmed on US-guided percutaneous needle biopsy.

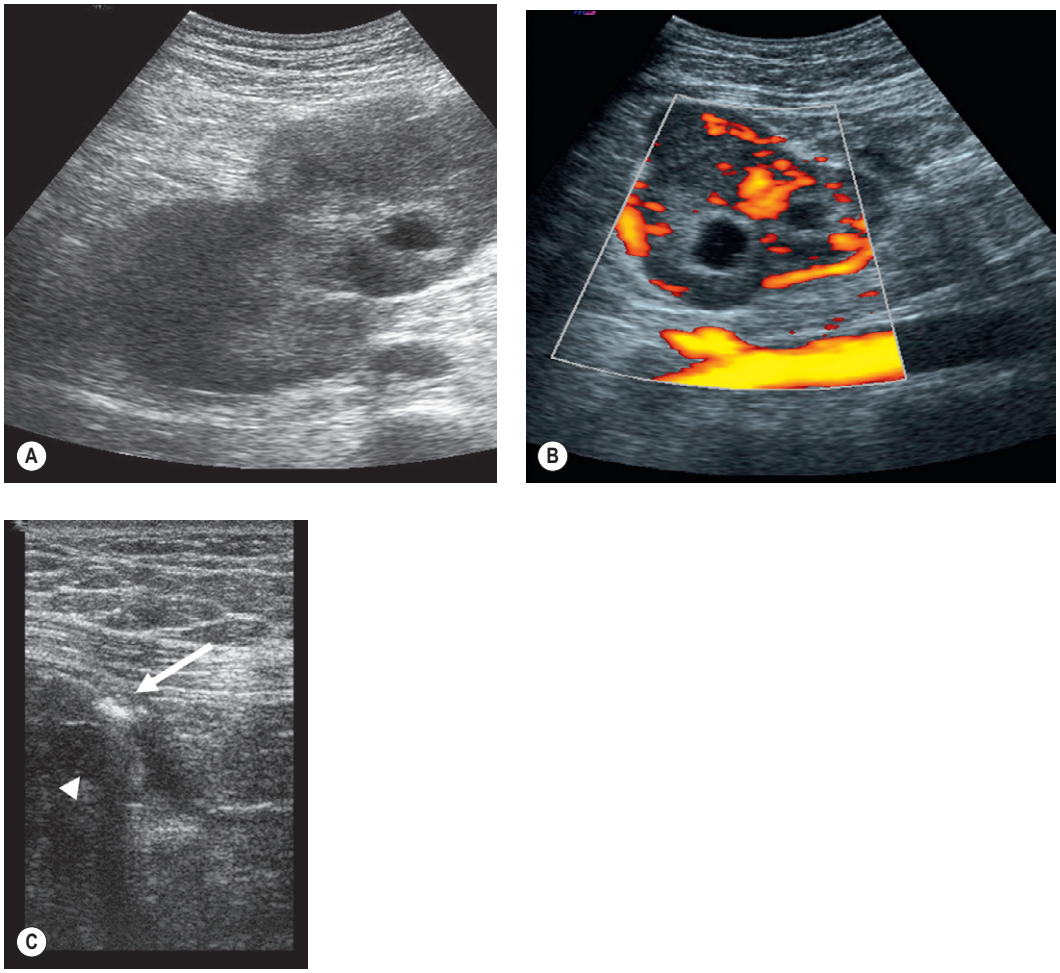


Figure 19.22 Exophytic GIST tumour. A 62-year-old man presented with acute intestinal haemorrhage. RIF US scan shows a large, mixed echogenicity, dumbbell-shaped tumour **(A)** which demonstrates central anechoic necrotic cavities and hypervascularity on Doppler scan **(B)**, and **(C)** a gas-filled ulcer (white arrow) on the surface of the tumour (arrowhead) in the bowel lumen. US-guided needle biopsy confirmed the diagnosis prior to therapy.

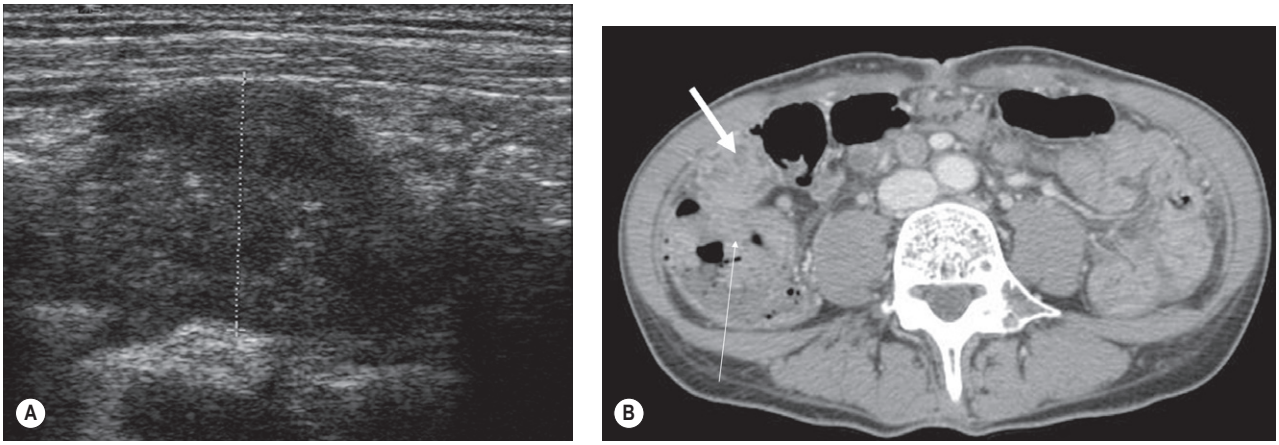


Figure 19.23 Serosal/peritoneal metastatic tumour deposits. A 57-year-old woman had intra-abdominal secondary tumours at the time of presentation with a primary caecal adenocarcinoma. US-guided needle biopsy allowed histological confirmation prior to chemotherapy, avoiding colonoscopy. **A:** Right iliac fossa US scan showed a 2 cm diameter echogenic peritoneal/serosal secondary. **B:** Concurrent CT scan image showing the metastatic deposit (thick white arrow) and the caecal primary tumour beneath (long white arrow).

INTUSSUSCEPTION

Intussusception is the telescoping of one segment of bowel into an adjacent one (Fig. 19.24). It is a common cause of an acute abdomen in children but accounts for less than 5% of mechanical small bowel obstruction in adults. In adults an underlying cause is present in 80% of cases; small bowel intussusception usually being due to benign causes such as lipoma, adenomatous polyp, haemangioma, adhesion, coeliac disease or villous adenoma of the appendix.[42]

At US an intussusception is identified as a complex mass with a variety of appearances from different perspectives due to the combination of the components: three bowel wall layers, indrawn mesentery and, if present, a lead point such as an intraluminal polyp. If oedema or low scan frequency prevent appreciation of the separate bowel wall components, the appearance is of a thick hypoechoic ring surrounding a hyperechoic centre. This has been described as the 'doughnut sign' axially, or the 'crescent in doughnut sign' (Fig. 19.24) when the echogenic mesentery forms a crescent to one side of the intussuceptum.[43] Scanned obliquely, intussusception is yet another cause of the 'pseudo-kidney' sign, and scanned longitudinally the layers of bowel in bowel have been called the 'sandwich sign' (Fig. 19.24); the terms 'hayfork' or 'trident' signs have also been used.[44] Confusingly the term 'sandwich sign' has also been used to describe layers of enlarged lymph nodes and mesentery in abdominal nodal lymphomas.[45]

Because underlying pathology is usually present in adults, intussusception has been taken as an indication for surgery, but transient self-limiting intussusception does occur and may be predicted by the absence of a lead point, a length <3.5 cm, normal wall thickness, normal non-dilated proximal small bowel and normal vascularity on colour Doppler.[46,47]

Tumours and tumour-related US findings

- Primary small bowel tumours are rare (most of these adenocarcinomas, carcinoids, lymphomas or GISTs).
- GISTs and lymphomas may be very large without causing obstruction.
- Involvement of bowel and peritoneum by secondaries is common.
- Intramural tumours may be drawn within distal bowel segment, forming an intussusception.
- Non-obstructing intussusceptions may be seen in coeliac disease.

SMALL BOWEL OBSTRUCTION

Small bowel obstruction is generally suspected from the clinical history and examination, and may be confirmed on plain radiography but with limited sensitivity and specificity. Further imaging is required to identify the definitive cause, the level of obstruction and to predict the necessity for and timing of surgical intervention. CT scanning is currently the investigation of choice to address these issues but US can confirm the diagnosis, identify the level and cause, and should be considered before CT in younger patients, thin patients and those for whom intravenous contrast media is contraindicated (e.g. impaired renal function).

The bowel proximal to the level of obstruction dilates and the abdomen becomes distended. Initially the dilated loops are filled with air and this and the distension, which prevents compression, militate against US, but as the air is progressively replaced by fluid US easily demonstrates the fluid-filled loops and the fold pattern distinguishes the jejunal and ileal loops, aiding assessment of the level of obstruction (Fig. 19.25). Sonographically small bowel obstruction may be confirmed if the bowel loops are dilated above 3 cm diameter, the dilated segment is longer than 10 cm and there is increased peristalsis (to and fro movement of lumen contents). In the absence of peristalsis, paralytic ileus should be considered.[48]

In patients with a previous history of laparotomy, adhesions are the most common cause of obstruction and this is the most likely cause when US finds no obstructing lesion. In older patients and those with no prior laparotomy, malignancy is the most likely diagnosis, but the less common causes should be sought including external hernias and gallstone ileus (look for air in the biliary tree).

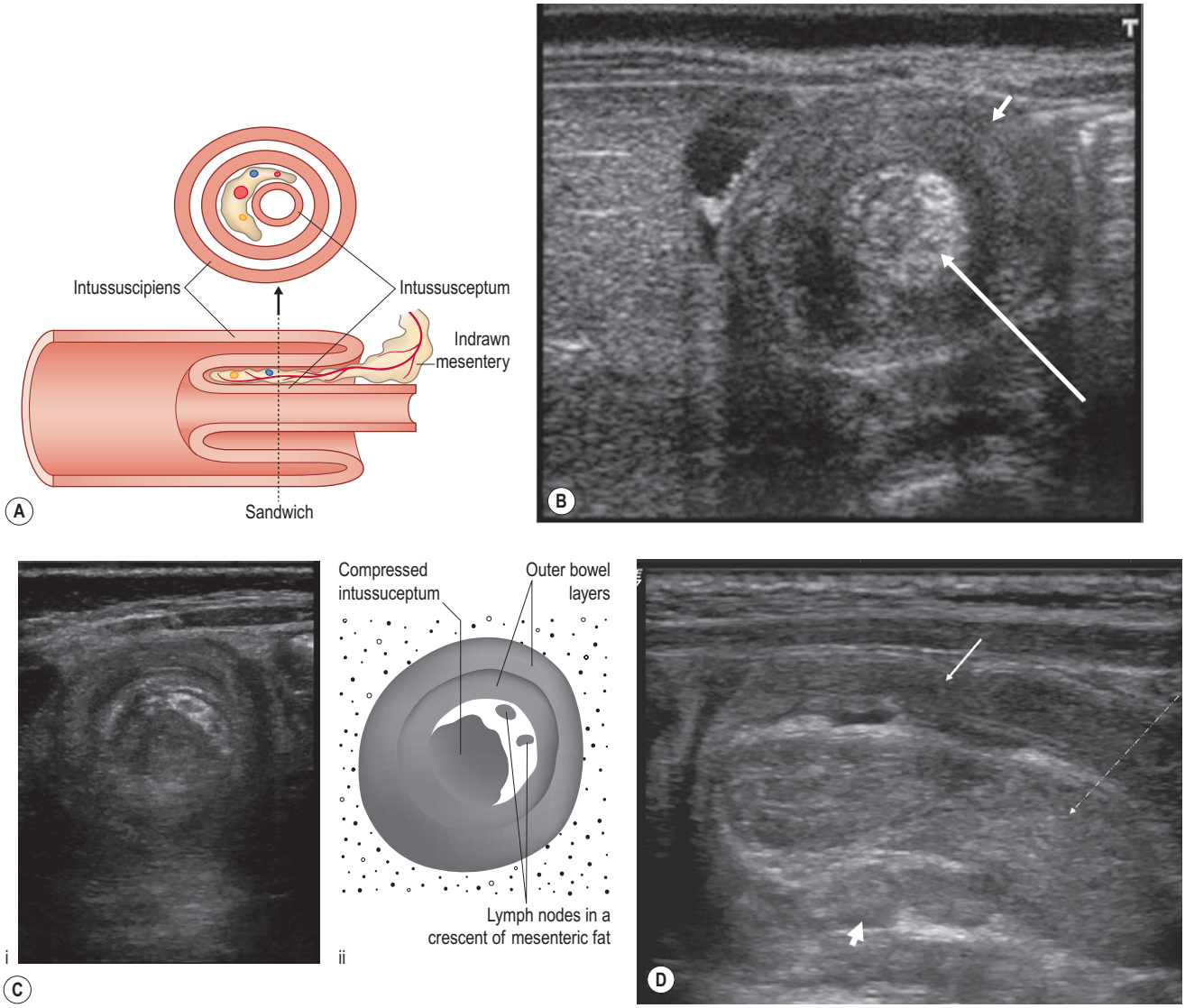


Figure 19.24 **Intussusception. A:** Graphic illustration of an intussusception showing the relationships of indrawn inner bowel segment (intussusceptum) and associated mesentery including vessels and nodes within the outer bowel sleeve (intussuscipiens). **B:** Doughnut sign. Transverse sonogram showing the thick ring of two outer bowel walls (short white arrow) and the bright centre of mesentery and nodes (long white arrow). **C:** Crescent in doughnut sign. Transverse sonogram and accompanying graphic showing the crescent of mesenteric fat and nodes around the collapsed indrawn bowel segment – the intussusceptum. **D:** Sandwich sign. Longitudinal sonogram showing the outer layers (white arrow), the intussuscipiens (interrupted arrow) and mesenteric lymph nodes (white arrowhead).

COELIAC DISEASE

Bowel dilatation with increased luminal fluid and increased peristalsis are features of coeliac disease, an intolerance to gluten producing characteristic damage to intestinal mucosa and resultant malabsorption. Coeliac disease affects 1 in 200 to 300 people and, if suspected, is easily diagnosed by serological testing. However, the diagnosis can be suspected on imaging features. In addition to finding dilated, fluid-filled bowel loops, US may demonstrate thickened bowel folds, reactive mesenteric lymphadenopathy, ascites, and non-obstructing small bowel intussusceptions. A highly specific but insensitive sign is increased gallbladder volume.[49]

US-GUIDED NEEDLE BIOPSY OF BOWEL LESIONS

The facility to identify bowel lesions beyond the reach of endoscopic biopsy, to displace adjacent normal bowel loops, to fix the bowel lesion by compression and perform diagnostic fine-needle aspiration or cutting needle biopsies has been demonstrated to allow histological diagnosis and avoid unnecessary surgery with a low risk of complications; lesions on the serosal surface or peritoneum may similarly be biopsied (Fig. 19.26).[50,51]



Figure 19.25 Small bowel obstruction. A subsequent sonogram of the patient with metastatic peritoneal tumours, as bowel obstruction developed (Fig. 19.23). demonstrating dilated, fluid-filled jejunal loops, characterised by the fold length and frequency. Cine loops capture the typical increased peristalsis with to and fro movement of liquid and more solid contents.

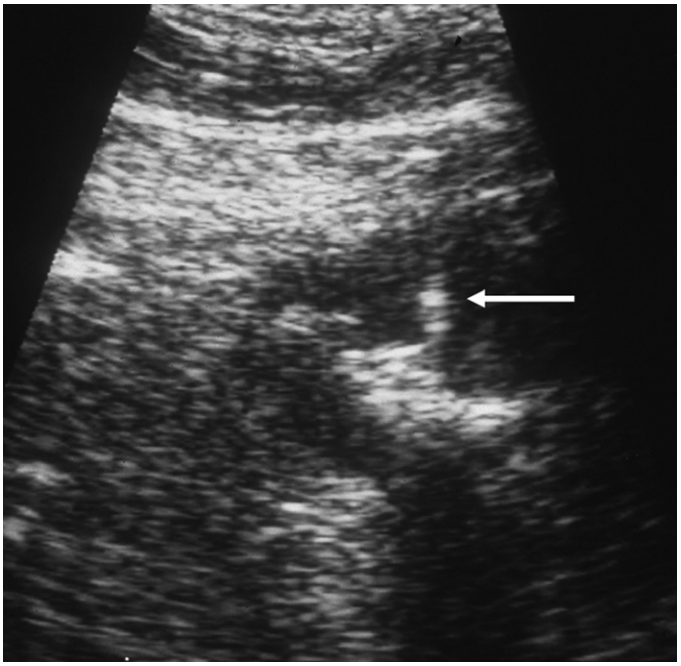


Figure 19.26 US-guided needle biopsy. The linear echogenic cutting needle (white arrow) is shown within the circumferential hypoechoic small bowel lesion.

REFERENCES

1. Puylaert JB. Ultrasound of acute GI tract conditions. Eur Radiol 2001;11:1867–1877.
2. Kimmey MB, Martin RW, Maggitt RC, et al. Histologic correlates of gastrointestinal ultrasound images. Gastroenterology 1989;96: 433–441.
3. Fleicher AC, Muhletaler CA, James AR Jr. Sonographic assessment of the bowel wall. AJR Am J Roentgenol 1981;136:887–891.
4. Hata J, Haruma K, Yamanaka H, et al. Ultrasonographic evaluation of the bowel wall in inflammatory bowel disease: comparison of in vivo and in vitro studies. Abdom Imaging 1994;19:395–399.
5. Esteban JM, Maldonaldo L, Sanchiz V, et al. Activity of Crohn's disease assessed by colour Doppler ultrasound analysis of the affected loops. Eur J Radiol 2001;11(8):1423–1428.
6. O'Malley ME, Wilson SR. US of Gastrointestinal tract abnormalities with CT correlation. Radiographics 2003;23(1):59–72.
7. Gardiner KR, Dasari BV. Operative management of small bowel Crohn's disease. Surg Clin North Am 2007;87:587–610.
8. Sheridan MB, Nicholson DA, Martin DF. Transabdominal sonography as the primary investigation in patients with suspected Crohn's disease or recurrence; a prospective study. Clin Radiol 1993;48:402–404.
9. Parente F, Greco S, Molteni M, et al. Role of early ultrasound in detecting inflammatory intestinal disorders and identifying their anatomical location within the bowel. Aliment Pharmacol Ther 2003;18:1009–1016.
10. Maconi G, Bollani S, Bianchi Porro G. Ultrasonographic detection of intestinal complications in Crohn's disease. Dig Dis Sci 1996;41:1643–1648.
11. Thoreson R, Cullen JJ. Pathophysiology of inflammatory bowel disease. Surg Clin North Am 2007;87:575–585.
12. Stange EF, Travis SP, Vermeire S, et al. European evidence based consensus on the diagnosis and management of Crohn's disease: definitions and diagnosis. CCO Gut 2006;55;i1–i15.
13. Fraquelli M, Colli A, Casazza G, et al. Role of US in detection of Crohn's disease: meta-analysis. Radiology 2005;236:95–101.
14. Fraquelli M, Colli A, Casazza G, et al. Role of US in detection of Crohn disease: meta-analysis. Radiology 2005;236:95–101.
15. Hata J, Haruma K, Suenaga K, et al. Ultrasonographic assessment of inflammatory bowel disease. Am J Gastroenterol 1992;87:443–447.
16. Sheehan AL, Warren BF, Gear MW, et al. Fat-wrapping in Crohn's disease: pathological basis and relevance to surgical practice. Inflamm Bowel Dis 2008;14(11):1555–1561.
17. Kratzer W, Schmidt SA, Mittrach C, et al. Contrast-enhanced wideband harmonic imaging ultrasound (SonoVue®): a new technique for quantifying bowel vascularity in Crohn's disease. Scand J Gastroenterol 2005;40(8):985–991.
18. Maconi G, Bollani S, Bianchi Porro G. Ultrasonographic detection of intestinal complications in Crohn's disease. Dig Dis Sci 1996;41:1643–1648.
19. van Oostayen J, Wasser M, van Hogezand R, et al. Doppler sonography evaluation of superior mesenteric artery flow to assess Crohn's disease activity. AJR Am J Roentgenol 1997;168:429–433.
20. Gasche C, Moser G, Turetschek K, et al. Transabdominal bowel sonography for the detection of intestinal complications in Crohn's disease. Gut 1999;44:112–117.
21. Sarrazin J, Wilson S. Manifestations of Crohn's disease at US. Radiographics 1996;16(3):499–520.
22. Ruess L, Nussbaum Blask AR, Bulas DI, et al. Inflammatory bowel disease in children and young adults: correlation of sonographic and clinical parameters during treatment. AJR Am J Roentgenol 2000;175:79–84.
23. Drews BH, Barth TF, Hänle MM, et al. Comparison of sonographically measured bowel wall vascularity, histology and disease activity in Crohn's disease. Eur Radiol 2009;19:1379–1386.
24. Puylaert JB, Van der Zant FM, Mutsaers JA. Infectious ileocaecitis caused by Yersinia, Campylobacter, and Salmonella: clinical, radiological and US findings. Eur Radiol 1997;7:3–9.
25. Kedar RP, Shah PP, Shivde RS, et al. Sonographic findings in gastrointestinal and peritoneal tuberculosis. Clin Radiol 1994;49: 24–29.
26. Sharma MP, Bhatia V. Abdominal tuberculosis. Indian J Med Res 2004;120:305–315.
27. Shirahama M, Takafumi K, Ishibashi H, et al. Intestinal anisakiasis: US in diagnosis. Radiology 1992;185:789–793.
28. Frisoli JK, Desser TS, Jeffrey RB. Thickened submucosal layer: a sonographic sign of acute gastrointestinal abnormality representing

submucosal edema or hemorrhage. AJR Am J Roentgenol 2000;175:1596–1599.
29. Teefey SA, Roarke MC, Brink JA, et al. Bowel wall thickening: differentiation of inflammation from ischaemia with color Doppler and duplex US. Radiology 1996;198:547–551.
30. Seigel MJ, Friedland JA, Hildebolt CF. Bowel wall thickening in children: differentiation with US. Radiology 1997;203:631–635.
31. Teefey SA, Roarke MC, Brink JA, et al. Bowel wall thickening: differentiation of inflammation from ischaemia with color Doppler and duplex US. Radiology 1996;198:547–551.
32. Shirahama M, Umeno Y, Tomimasu R, et al. The value of colour Doppler ultrasonography for small bowel involvement of adult Henoch-Schönlein purpura. Br J Radiol 1998;71:788–791.
33. Neugut AI, Jacobson JS, Suh S, et al. The epidemiology of cancer of the small bowel. Cancer Epidemiol Biomarkers Prev 1998;7:243–251.
34. Bin W, Jianguo L, Baowei D. Sonographic appearances of small bowel tumours. Clin Radiol 1992;46:30–33.
35. Maglinte DT, Herlinger H. Small bowel neoplasms. In: Herlinger H, Maglinte DD, Birnbaum BA, editors. Clinical imaging of the small intestine. New York: Springer-Verlag; 2001. p. 377–438.
36. Rioux M, Langis P, Naud F. Sonographic appearance of primary small bowel carcinoid tumour. Abdom Imaging 1995;20(1):37–43.
37. Chua SC, Rozalli FI, O'Connor SR. Imaging features of primary extranodal lymphomas. Clin Radiol 2009;64:574–588.
38. Goerg C, Schwerk WB, Goerg K. Gastrointestinal lymphoma: sonographic findings in 54 patients. AJR Am J Roentgenol 1990;155:795–798.
39. Katz SC, DeMatteo RP. Gastrointestinal stromal tumours and leiomyosarcomas. J Surg Oncol 2008;97:350–359.
40. Nylund K, Ødegaard S, Hausken T, et al. Sonography of the small intestine. World J Gastroenterol 2009;15(11):1319–1330.
41. Burkill GJ, Badran M, Al-Muderis, et al. Malignant gastrointestinal stromal tumour: distribution, imaging features, and pattern of metastatic spread. Radiology 2003;226:527–532.
42. Byrne AT, Goeghegan T, Govender P, et al. The imaging of intussusception. Clin Radiol 2005;60:39–46.
43. del-Pozo G, Intussusception: US findings with pathologic correlation – the crescent in doughnut sign. Radiology 1996;199:688–692.
44. Chaubal N, Dighe M, Shah M, et al. Sonography of the gastrointestinal tract. J Ultrasound Med 25:87–97.
45. Hardy SM. The sandwich sign. Radiology 2003;226:651–652.
46. Montali G, Croce F, De Pra L, et al. Intussusception of the bowel: a new sonographic pattern. Br J Radiol 1983;56:621–623.
47. Mateen MA, Saleem S, Chandrasekhar Rao P, et al. Transient small bowel intussusceptions: ultrasound findings and clinical significance. Abdom Imaging 2006;31(4):410–416.
48. Ko YT, Lim JH, Lee DH, et al. Small bowel obstruction: sonographic evaluation. Radiology 1993;188(3):649–653.
49. Castiglione F, Rispo A, Cozzolino A, et al. Bowel sonography in adult celiac disease: diagnostic accuracy and ultrasonographic features. Abdom Imaging 2007;32:73–77.
50. Tudor GR, Rodgers PM, West KP. Bowel lesions: percutaneous US-guided 18-gauge core biopsy – preliminary experience. Radiology 1999;212:594–597.
51. Ledermann HP, Binkert C, Fröhlich E, et al. Diagnosis of symptomatic intestinal metastases using transabdominal sonography and sonographically guided puncture. AJR Am J Roentgenol 2001;176:155–158.

CHAPTER

20

Appendix, colon and rectum

Rakesh Sinha

APPENDIX 388
Anatomy 388
Ultrasound technique 388
Acute appendicitis 389
Pitfalls and differential diagnosis 391
Appendiceal tumours 392
Mucocele 392
Carcinoid tumour 392
Other tumours 393
Miscellaneous disorders 394
Crohn's disease 394
Stump appendicitis 394

COLON 394
Anatomy and scanning technique 394
Congenital abnormalities 395
Diverticulitis 396
Right-sided diverticulitis 397
Inflammatory colitis 397
Crohn's colitis 397
Ulcerative colitis 397
Infective colitis 399
Tuberculous colitis 399
Amoebic colitis 400
Pseudomembranous colitis 400
Typhlitis 401
Other infections 401
Ischaemia 401
Tumours 402
Miscellaneous conditions 402
Endometriosis 402
Intussusception 402
Epiploic appendagitis 402

RECTUM AND ANAL CANAL 405
Ultrasound technique 405
Normal anatomy 406
Anal canal 406
Rectum 407
Anorectal tumours 407
Anal sepsis 408
Anal trauma 408
Miscellaneous conditions 409
Solitary rectal ulcer syndrome 409
Other sphincter abnormalities 409

APPENDIX

Anatomy

The appendix vermiformis is a vestigial, tubular organ that arises from the inferior pole of the caecum. In adults, a normal vermiform appendix varies in length from 5 to 35 cm (average 8 cm). The appendix has its own mesentery that extends from the terminal ileum to the medial aspect of the caecum and appendix. This mesenteric fold contains the appendicular artery. The venous drainage of the appendix is via the ileocolic and the right colic veins into the portal vein.

Ultrasound technique

Although ultrasonography is operator dependent, experienced personnel can identify the appendix in the majority of patients.[1,2] The normal appendix is seen as a blind-ended tubular structure attached to the caecal pole. The position of the appendiceal body and tip is variable; however, its orifice is usually constant in position, situated 2–2.5 cm inferior to the ileocaecal junction. The appendix is commonly located in the retrocaecal or pelvic region (Fig. 20.1).

The normal appendix is easily compressible and is less than 6 mm in external diameter. It has a layered appearance and may contain a small amount of fluid or air within its lumen (Fig. 20.2). The normal appendix usually does not demonstrate any colour flow or Doppler signal.

Optimum assessment of the appendix requires a specific graded compression technique during ultrasonography.[1] In this technique gentle pressure is applied in the right iliac fossa by the ultrasound probe. Care must be taken not to perform intermittent or rapid compression of the abdomen as this may provoke pain due to rebound tenderness (secondary to peritoneal inflammation) and hence limit the ultrasonographic examination. Therefore pressure should be applied gently and then gradually increased. The objective of graded compression is to displace bowel loops, overlying fat and other abdominal structures overlying the appendix and also to bring the psoas and iliacus muscles in close approximation with the anterior abdominal muscles. Displacement of overlying structures and approximation of the abdominal muscles allows interrogation of the anatomical structures in the right iliac fossa by high-frequency transducers. The patient should initially be examined in the supine position and scanning should be done at the region of maximum pain as indicated by the patient. Self-localisation of pain has a high degree of accuracy in locating the appendix and can also expedite the visualisation of the appendix. However, in cases with appendiceal perforation, localisation may not be possible, as the pain may be generalised or vague.

If the appendix is not visualised in the supine position, scanning via the posterolateral approach is essential to assess the retrocaecal region (Fig. 20.3). Patients with retrocaecal appendicitis may not present with typical pain at McBurney's point and the pain may only be elicited on deep palpation. The appendix in such cases is not visualised in the supine position as the gas-filled caecum obscures the retrocaecal region. Scanning patients via the posterolateral approach while the patient is in a left decubitus position can also help in the detection of pneumoperitoneum, as free air collects under the elevated portion of the abdominal wall.

Posterior compression of the right flank should be performed in obese or muscular individuals with poor visualisation of the posterior caecal region.[3] Compression of the posterior right flank is performed using the operator's free hand while simultaneously compressing the anterior abdomen with the transducer.

When the appendix has a deep orientation in the pelvis, patients can present with diarrhoea as the inflamed appendix irritates the rectum. In such cases graded compression with a forced upward sweeping motion of the transducer can be useful. The upward sweep of the transducer helps to move the caecum superiorly on to the psoas muscle and thereby increases the visibility of the entire distal appendix (Fig. 20.3).

Transverse and longitudinal scans of the abdomen should also be performed in order to detect atypical locations of the appendix. In obese individuals, 3–5 MHz probes may be needed. Accurate localisation of the appendix is useful as an atypical location may alter the surgical approach. Once visualised, the appendix needs to be evaluated in its entirety as inflammation may only be located in a small segment such as the appendiceal tip. Visualisation of a normal-sized, compressible appendix has high negative predictive value for acute appendicitis.[4]

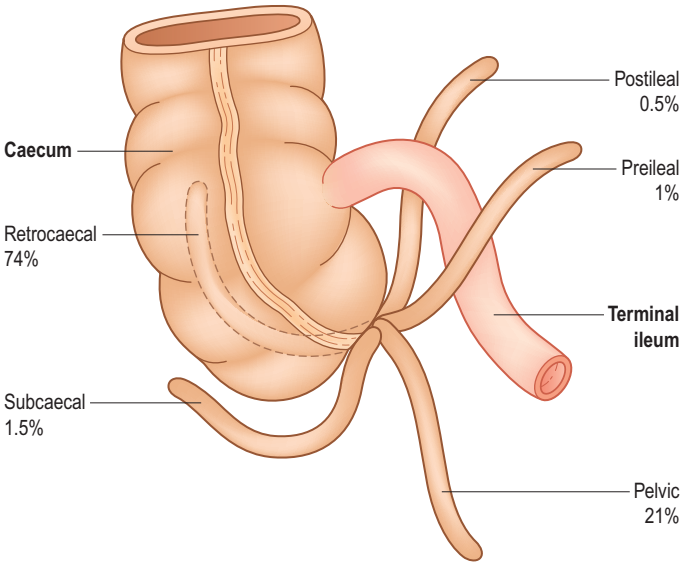


Figure 20.1 Schematic diagram showing locations of the vermiform appendix.

Acute appendicitis

Acute appendicitis is one of the commonest acute abdominal conditions presenting to the emergency department. The highest incidence of appendicitis is in teenagers and young adults and there is a familial tendency to develop appendicitis. The clinical diagnosis of appendicitis may be overlooked and misinterpreted, leading to delay in treatment or unnecessary surgery. Diagnosis of acute appendicitis in children can be particularly difficult as a significant proportion of patients present with atypical symptoms. Diagnosis of appendicitis may also be delayed in infants as they are unable to provide clinical information or localise pain.

Acute appendicitis occurs when the lumen of the appendix is obstructed by a faecalith, mucous plug or fibrosis. Rarely the appendiceal orifice may be obstructed by tumours, infections or foreign bodies. Perforation of the appendiceal wall may occur if there is advanced inflammation and transmural necrosis. In older children and adults the perforation is sealed off by the adjacent omentum and therefore localised abscesses are formed. In younger children, due to the smaller size of the omentum, perforation may lead to widespread peritonitis. Conversely in obese patients, the abundant mesenteric and omentum fat may mask symptoms of appendicitis or perforation.

In children appendicitis is invariably associated with vomiting and aversion to food. Elderly patients have the highest mortality rates as the usual signs and symptoms of appendicitis may be diminished or absent, which leads to a higher rate of perforation and resultant greater morbidity and mortality. Acute appendicitis is also the commonest non-gynaecological acute abdominal condition complicating pregnancy.

Ultrasound plays a valuable role in the diagnosis of acute appendicitis.[1,5–7] Using ultrasound the appendix can be directly visualised, thereby confirming or excluding appendiceal pathology. Furthermore, complications related to appendicitis and alternative diagnoses mimicking appendicitis may also be demonstrated using this modality. Ultrasonography has been shown to have similar accuracy for detection of acute appendicitis as compared to CT examinations.[8]

On ultrasonography the inflamed appendix is seen as a thickened, non-compressible, tubular structure at the site of tenderness (Fig. 20.4). A layered appearance corresponding to the mural

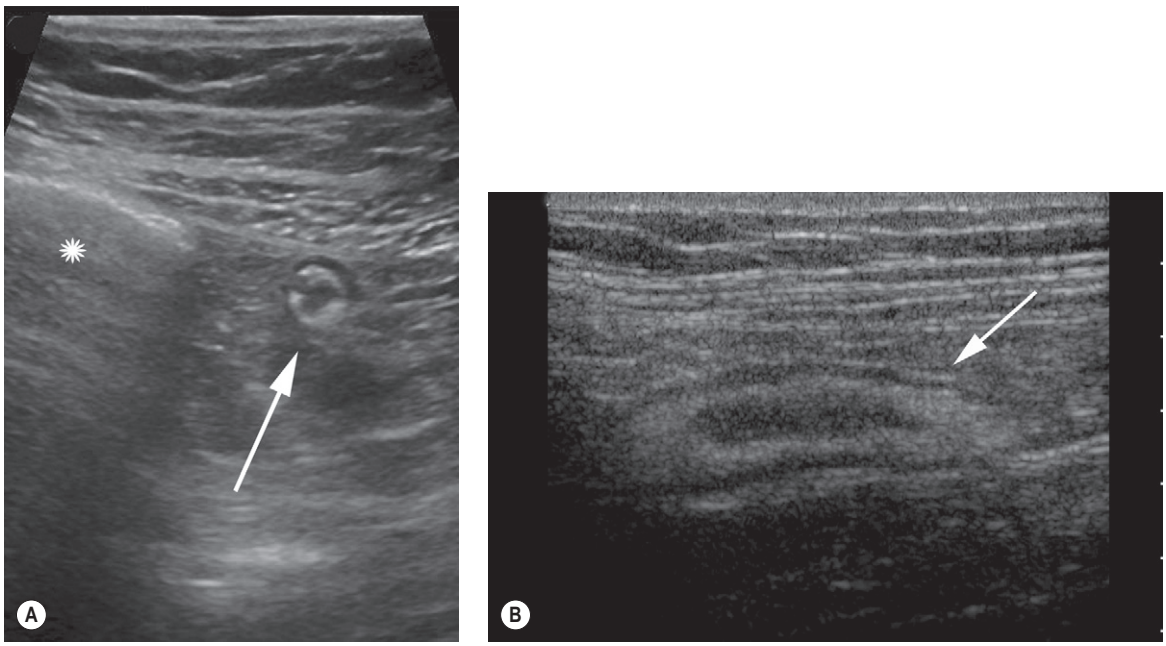


Figure 20.2 Normal appendix. A: Transverse view of the normal appendix (arrow) showing a layered mural pattern. Asterisk = caecum. **B:** Longitudinal view of the normal appendix (arrow) showing a layered mural pattern.

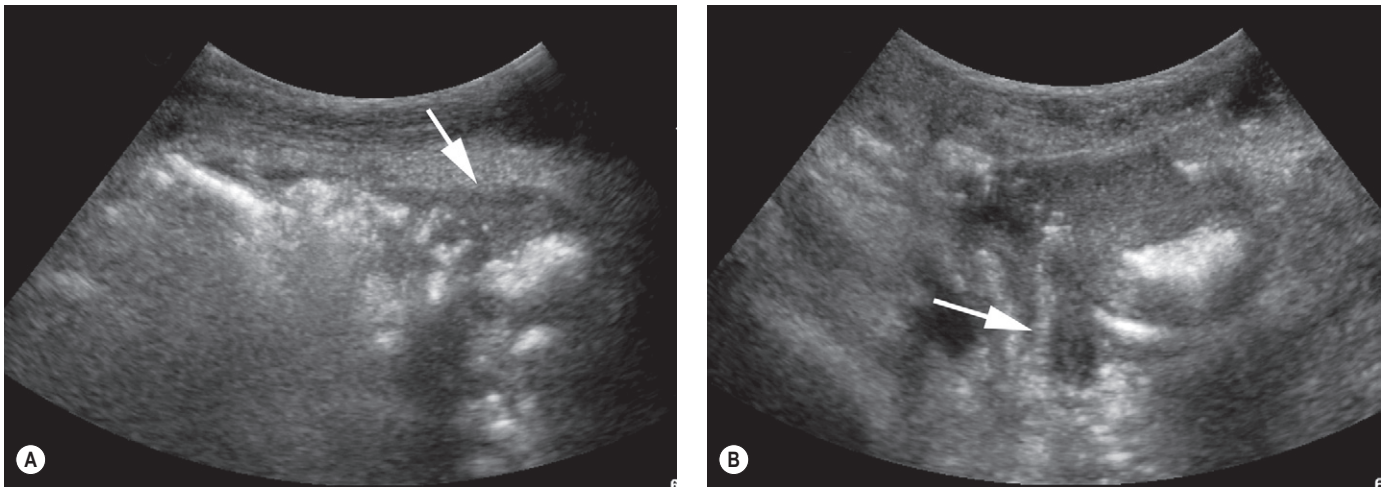


Figure 20.3 Retrocaecal and pelvic appendix. **A:** Ultrasound image shows obscuration of right iliac fossa contents due to acoustic shadowing from the caecal contents (arrow). **B:** Scan performed in the decubitus position with posterior flank compression demonstrates thickened and inflamed retrocaecal appendix (arrow). **C:** Inflamed appendix (arrow) in the pelvic location behind the bladder visualised on graded compression and forced upward sweep of the transducer.

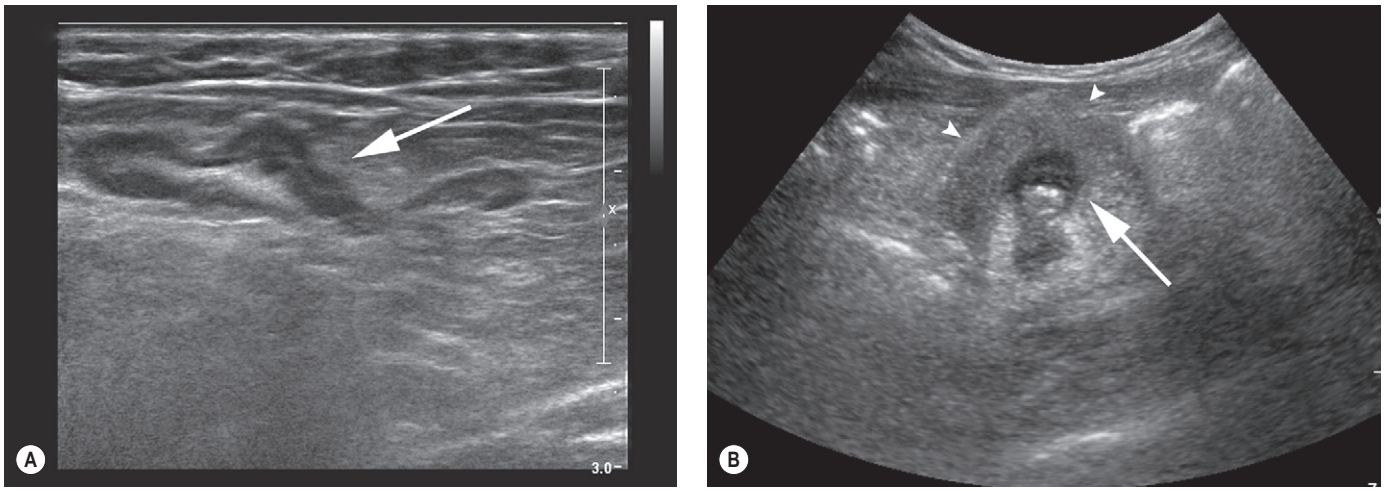


Figure 20.4 Acute appendicitis. **A:** Inflamed appendix seen as a tubular, non-compressible structure (arrow). The layered mural structure is evident. **B:** Inflamed appendix containing an echogenic appendicolith (arrow) with posterior acoustic shadowing. Note inflamed, non-compressible fat overlying the appendix (arrowheads).

structure can also be seen with high-frequency probes. Up to 30% of cases with appendicitis may have an intraluminal appendicolith.[5] Appendicoliths are characteristically seen as highly reflective lesions within the appendiceal lumen with posterior acoustic shadowing (Fig. 20.4). Appendicoliths should be distinguished from air or inspissated faecal matter, which can produce similar acoustic shadowing, although the shadowing seen due to air tends to be heterogeneous with specular artefacts. A non-compressible appendix with an external diameter of greater than 6 mm is the most accurate predictor of acute appendicitis.[6] The finding of a normal appendix measuring less than 6 mm has high negative predictive value (98%) for acute appendicitis.[6]

Inflamed mesentery and omentum surrounding the appendix appear non-compressible and of increased reflectivity. Most patients

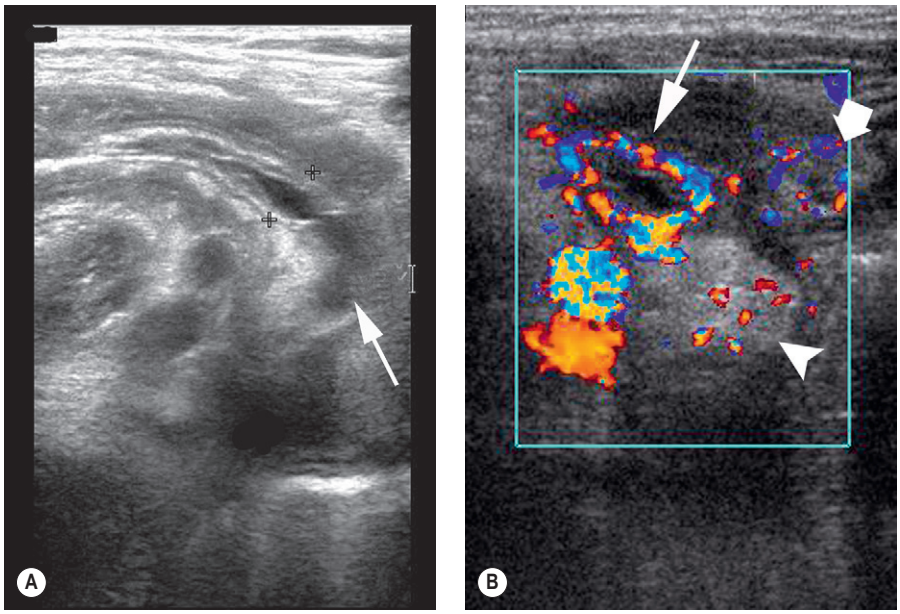


Figure 20.5 Acute appendicitis. **A:** Inflamed appendix (callipers) with mesenteric lymphadenopathy (arrow). **B:** Doppler study demonstrates high colour signal in the appendix (arrow), lymph nodes (thick arrow) and inflamed mesentery (arrowhead).

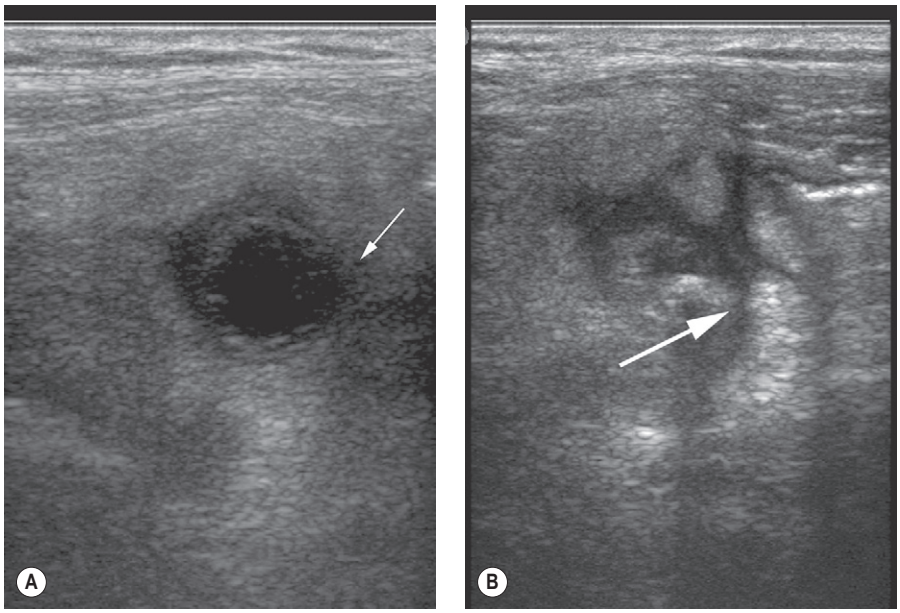


Figure 20.6 Appendiceal perforation. **A:** Irregular thickening of the appendix with loss of mural stratification (arrow) suggestive of a perforation. **B:** Pericaecal echogenicity (arrow) with free fluid. The appendix was not identified. Linear, poorly reflective liponecrotic tracts are seen. Perforated appendix was found at surgery.

with acute appendicitis may also have enlarged mesenteric nodes (Fig. 20.5). Inflammation also leads to hyperaemia and hyperperfusion of the appendix, which manifests as increased colour Doppler signal in the appendix, mesentery and reactive lymph nodes (Fig. 20.5).

An irregular contour or disruption of the layered appearance of the appendix is suggestive of perforation or impending rupture (Fig. 20.6). Other findings that are associated with perforation include asymmetrical wall thickening, fluid collections, ileus and increased pericaecal echogenicity (Fig. 20.6). Two of these findings – loss of the submucosal layer and pericaecal fluid – have been reported to have a significant correlation with appendiceal performation.[9]

Once perforation occurs, there may be generalised peritonitis. However, in the majority of cases, the peritoneal spillage is contained in the right iliac fossa as the mesenteric fat and omentum seal the perforation.

Patients with delayed presentation or with appendiceal perforation may present with a right iliac fossa mass. Such a mass typically consists of the inflamed appendix with adherent omental and mesenteric fat, lymphadenopathy and inflammatory adhesions and is termed an appendiceal phlegmon. Usually these are treated conservatively as surgery can be difficult in such cases. On ultrasonography an appendiceal phlegmon is seen as a non-compressible, poorly-defined mass. The mass is predominantly poorly reflective but may have bright areas due to contained inflamed fat. Poorly defined, linear, low reflective streaks may be seen that correspond to liponecrotic tracks and inflammatory adhesions (Fig. 20.7).

If a circumscribed pus collection is present, the mass is termed an appendiceal abscess. Abscesses are seen as fluid collections with contained air pockets or fluid levels (Fig. 20.7). Most appendiceal abscesses resolve spontaneously; however, if pain and fever persists percutaneous drainage under CT or US guidance may be necessary.

Pitfalls and differential diagnosis

A false positive diagnosis of acute appendicitis may be made in patients with intra-abdominal inflammation. The appendix may be falsely thickened in patients with sigmoid diverticulitis, perforated peptic ulceration or inflammatory bowel disease.[10] Caecal tumours

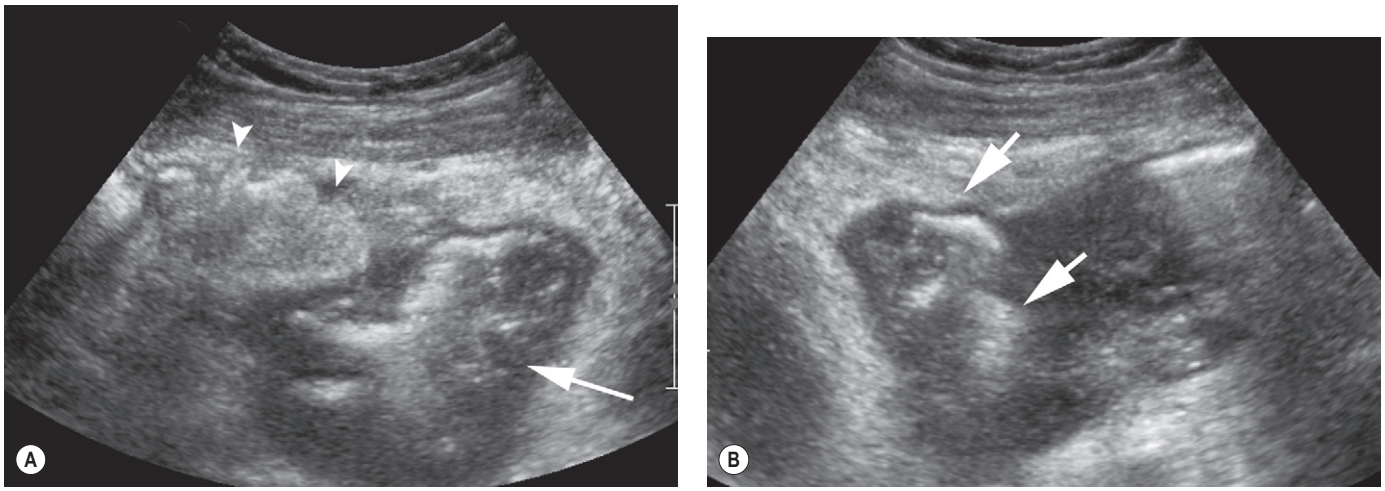


Figure 20.7 Appendiceal phlegmon and abscess. A: Phlegmon is seen as a large poorly reflective mass with internal bright areas (arrow) inferior to the caecum (arrowheads). **B:** Appendiceal abscess with multiple fluid levels and air pockets (arrows).

Ultrasound in acute appendicitis

- Non-compressible, tender appendix with external diameter >6 mm.
- Appendicoliths are present in up to a third of cases.
- Lymphadenopathy is present in up to 50% of cases.
- Free fluid, asymmetric appendiceal thickening, mesenteric inflammation and ileus are strongly suggestive of appendiceal perforation.
- Retrocaecal and pelvic regions should be routinely assessed in the patients with suspected appendicitis.

may obstruct the appendiceal orifice with resultant dilatation leading to an incorrect diagnosis of appendicitis or an appendiceal mass. A distended, non-tender appendix has been reported in amoebic colitis.

The commonest cause of a false negative examination is the inability to visualise the appendix on ultrasonography. Inability to locate the appendix may be due to an atypical location; lack of an adequate ultrasonographic window due to ileus; or generalised peritonitis that limits graded compression. Occasionally the normal proximal appendix is demonstrated whereas the inflamed tip is overlooked, leading to a false negative examination. Furthermore, inflammation and thickening of the terminal ileum secondary to appendicitis may be erroneously labelled as Crohn's disease or infectious ileocolitis.

Many other clinical conditions may mimic appendicitis, and it is important to distinguish between these conditions. These include caecal diverticulitis, infectious ileitis, mesenteric lymphadenitis, ovarian cysts, tubo-ovarian abscesses, urological conditions, epiploic appendagitis, infective ileitis, inflammatory bowel disease and Meckel's diverticulitis.[11,12] The normal appendix may have a diameter of greater than 6 mm in patients who have undergone radiotherapy or those with cystic fibrosis.[13]

Ultrasonography can be useful in distinguishing between these differential diagnoses. In patients with equivocal ultrasound findings and especially in obese patients, CT examinations can be useful.

Appendiceal tumours

Primary tumours of the appendix are rare and are found in only 0.5–1.0% of appendicectomy specimens at pathological examination. Most primary tumours affect individuals in the middle to older age group with the exception of carcinoid tumours. Many primary appendiceal tumours present with symptoms similar to acute appendicitis and most tumours – except for adenocarcinomas and carcinoids larger than 2 cm – are managed by appendicectomy.[14,15] All appendiceal tumours are associated with a high incidence of a synchronous and metachronous colonic tumours.[15]

Mucocele

A primary appendiceal mucocele is relatively rare, with reported incidence of 0.2–0.3%, and is more common in females than males.[16] Most mucoceles are asymptomatic and found incidentally at surgery. Mucoceles are usually benign and are formed due to obstruction of the appendiceal orifice secondary to fibrosis, faecaliths or scarring. The obstruction causes sterile accumulation of mucus within the appendiceal lumen leading to mucocele formation.

Malignant mucoceles occur secondary to mucin-secreting adenocarcinomas. If there is appendiceal perforation due to such a mucocele, there is peritoneal seeding of the malignant cells leading to pseudomyxoma peritonei.

Mucoceles are usually incidental findings on ultrasonography and present as tubular, well-defined structures in the right lower abdomen (Fig. 20.8). A pear-shaped appearance has been described on ultrasonography. The contents may be of variable echogenicity; however, low or intermediate reflectivity is typical and there may be contained septations. Bright, reflective foci within the mass or its wall may also be seen corresponding to dystrophic calcification. Curvilinear mural calcification is a highly suggestive feature on ultrasonography, although this is seen in only 50% of cases (Fig. 20.8).

It may be difficult to differentiate between benign and malignant mucoceles. However, mucoceles resulting from benign obstruction rarely exceed 2 cm in size, and larger mucoceles should be considered to be malignant. Malignant mucoceles may demonstrate irregular thickening of the wall and infiltration of the surrounding mesentery. Rarely, mucoceles may become infected and present with symptoms and ultrasonographic features indistinguishable from acute appendicitis. Fluid levels and air pockets within a mucocele are indicative of a superadded infection. The differential diagnosis of a mucocele includes a tubo-ovarian abscess, hydrosalpinx, enteric duplication cysts and peri-appendiceal abscesses.

Carcinoid tumour

The commonest primary appendiceal neoplasm is a carcinoid tumour and they constitute up to 80% of primary appendiceal

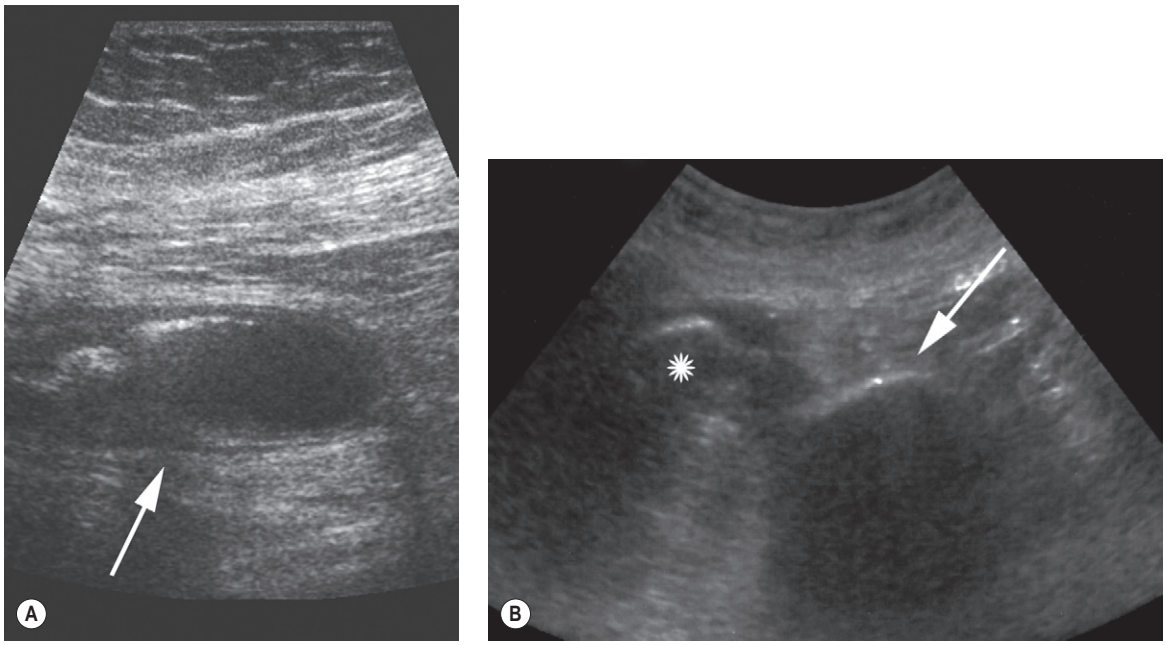


Figure 20.8 Appendiceal mucoceles. A: Incidentally discovered cystic lesion of the appendix with low reflectivity, bright margins and debris (arrow). **B:** Dense, curvilinear calcification with shadowing (arrow) in the right iliac fossa consistent with a calcified mucocele. Asterisk = caecum.

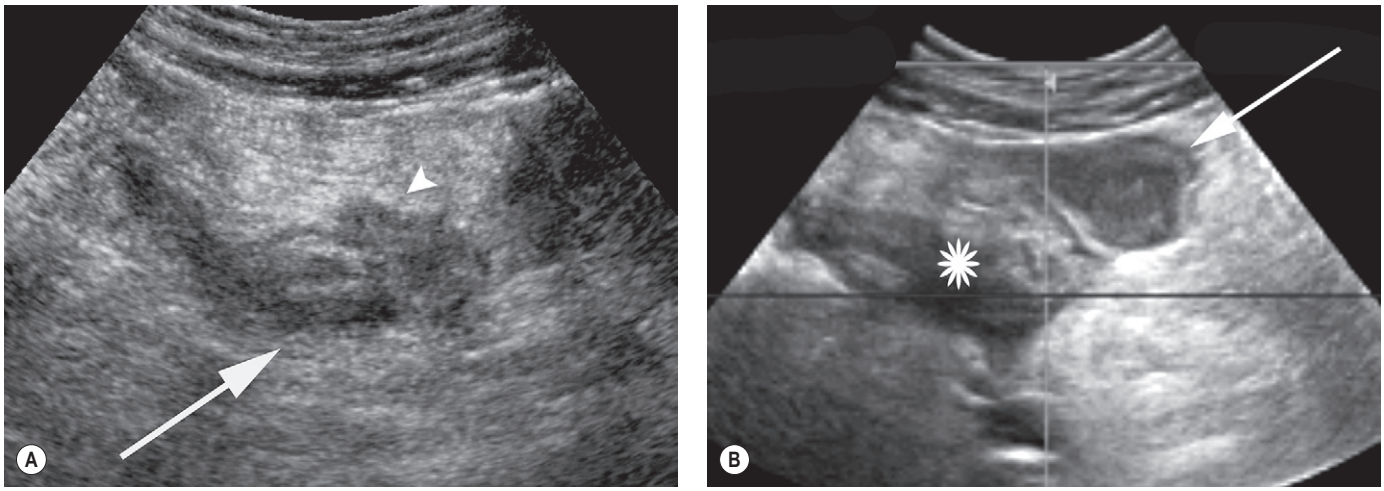


Figure 20.9 Appendiceal tumours. A: Longitudinal image of the right iliac fossa in a patient with suspected appendicitis shows a small appendiceal mass at the tip of the appendix (arrow). Note infiltration of the adjacent mesentery (arrowhead). Carcinoid tumour was found on surgery. **B:** 3D image of the right iliac fossa shows a large mass arising from the appendix (arrow). Adenocarcinoma was identified on histopathology. Asterisk = caecum.

tumours.[16] Most appendiceal carcinoid tumours are only detectable at microscopic level and are incidentally discovered during histological examination of an appendicectomy specimen. Most of these incidentally discovered tumours are less than 1 cm in size.[17] Unlike carcinoids occurring at other gastrointestinal sites, appendiceal carcinoids are seen in younger adults and typically follow an indolent course. Appendicectomy appears to be adequate treatment for such incidentally detected tumours, although for tumours larger than 2 cm a right hemicolectomy may need to be performed.

Carcinoids may present with acute appendicitis. Larger tumours are seen as poorly reflective masses and may show infiltrative and desmoplastic reaction in the surrounding mesentery (Fig. 20.9). Calcification may be present within the mass and there may be hypervascularity on Doppler studies.

Other tumours

Primary adenocarcinomas of the appendix are very rare. Ultrasonographic features of these tumours are that of a diffuse or focal enlargement of the appendix with adjacent lymphadenopathy (Fig. 20.9). Tumours may appear as solid, poorly reflective lesions or solid lesions with internal cystic changes.

Lymphoma of the appendix may manifest as homogeneous thickening of the entire appendiceal wall. Aneurysmal dilatation of the appendix may be present.[18]

Miscellaneous disorders

Crohn's disease

Appendiceal Crohn's disease may mimic acute appendicitis or an appendiceal mass at presentation and it is important to distinguish between the two as the treatment for appendiceal Crohn's disease is medical rather than surgical. The pathological changes in the appendix are similar to those found in other affected segments of the bowel. The appendix may be involved in a significant percentage (up to 20%) of patients with ileocaecal Crohn's disease.[19] The appendix may also be involved due to contiguous spread of inflammation from adjacent bowel segments (peri-appendicitis). Crohn's appendicitis is invariably associated with Crohn's disease of the ileocaecal region.

Isolated granulomatous appendicitis is a rare condition discovered incidentally in patients presenting with acute appendicitis. Previously this condition was thought to be a variant of Crohn's disease limited to the appendix, although now it is thought to be a separate entity and is termed idiopathic granulomatous appendicitis distinct from Crohn's disease.

Occasionally it may be difficult to differentiate appendiceal Crohn's disease from acute appendicitis. However, certain features are helpful in making this distinction. Appendiceal Crohn's disease is almost always associated with disease in the terminal ileum.[19] Other features of Crohn's disease that may be demonstrated are thickening of the submucosal layer of the terminal ileum and fibrofatty proliferation of the mesentery around the inflamed terminal ileum. A normal appearing terminal ileum virtually excludes the diagnosis of appendiceal Crohn's disease. Caecal thickening may be seen in both diseases; however, isolated thickening of the caecum is more specific for acute appendicitis.

Ultrasonographically the appendix appears thickened with preserved stratification and may show increased blood flow of Doppler studies (Fig. 20.10). In advanced disease the stratification may be lost and sinuses or fistulae may be present.

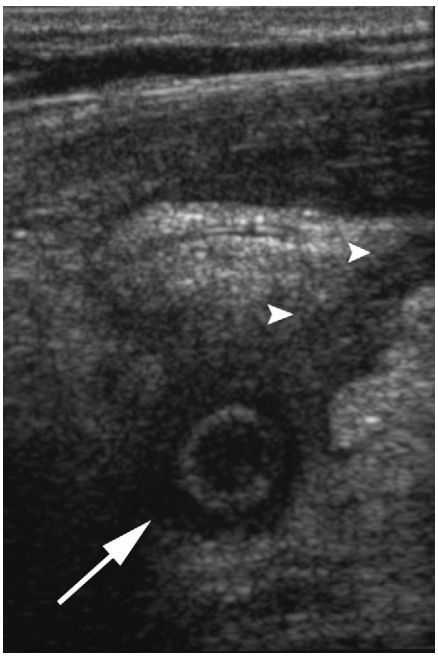


Figure 20.10 Appendiceal Crohn's disease. Transverse image of the right iliac fossa in a patient with known Crohn's disease shows diffuse thickening of the appendix (arrow) with preserved stratification and surrounding fibrofatty proliferation. A fistula is also seen as a linear track (arrowheads).

Stump appendicitis

Inflammation of the appendiceal stump is a rare complication after appendicectomy. The exact rate of incidence and its prevalence are not accurately defined. Failure to resect the appendix at its base is considered to be necessary for stump appendicitis to occur. Previous history of appendicectomy may delay the correct diagnosis of stump appendicitis in a patient presenting with signs and symptoms of right lower quadrant pain and inflammation. Ultrasonography may demonstrate a thickened and oedematous appendiceal stump at the caecal tip and pericaecal inflammation (Fig. 20.11).[20,21]

COLON

Anatomy and scanning technique

Unlike the small bowel, most of the colon is relatively fixed in position and therefore can be assessed using anatomical landmarks. The colon can be differentiated from the small bowel by the presence of haustrations, lack of peristalsis and by location. The ascending and descending colon can be evaluated by scanning both flanks as these structures are retroperitoneal and fixed in position. The caecum may

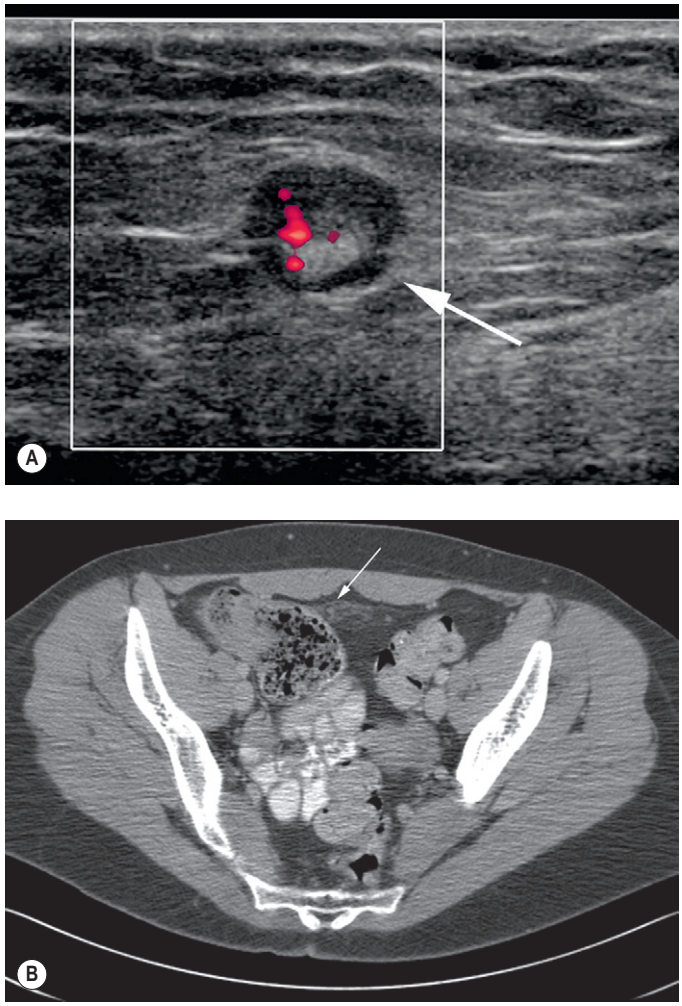


Figure 20.11 Stump appendicitis. Patient with history of appendicectomy. **A:** Transverse image of the right iliac fossa shows a tubular structure with hyperaemia (arrow) at the caecal pole. Presumptive diagnosis of stump appendicitis was made. **B:** Axial CT image confirms inflamed appendiceal stump (arrow).

be identified in the right iliac fossa by tracing down the colon from the hepatic flexure. Gentle compression on the abdomen using the transducer helps to provide better views of the colon. The transverse and sigmoid colon may be variable in position as they are suspended by their respective mesenteries within the peritoneal cavity. The transverse colon can be scanned by following its contour in a transverse direction between the hepatic and splenic flexures. Similarly the sigmoid colon is traced between the distal descending colon and the rectum. In thin individuals and children, high-frequency linear transducers can be used that provide detailed colonic images.

On transabdominal ultrasonography, the colon typically demonstrates a stratified mural pattern. Usually three layers can be identified corresponding to the submucosa, mucularis propria and the mucosa. Haustrations can be identified as indentations in the contour of the bowel (Fig. 20.12). If there is sufficient intraluminal fluid in the colon or ascites, the entire mural structure may be visualised. However, more often than not, there is air within the lumen that obscures the colonic wall distal from the transducer. The normal thickness of the colonic wall is less than 3 mm. If a lesion associated with the colon is found, its true relation or attachment to the colon should be confirmed by observation during deep inspiration and expiration and abdominal compression. Lesions intrinsic to or attached to the colon will move with the bowel during respiration or compression.

Some investigators have advocated using ultrasonography after instillation of a water or saline enema (hydrocolonic ultrasonography) for optimal assessment of the colon.[22–24] In this technique patients need to ingest a large amount of oral electrolyte solution prior to the examination followed by warm water or saline enema. Comparison of hydrocolonic ultrasonography with optical colonoscopy has not been promising.[25] This has been mainly due to problems with adequate bowel preparation, artefacts from faecal matter and the inability to obtain diagnostic images of all segments of the colon in large or obese patients. Furthermore, in view of other more sensitive tests (e.g. CT colonography) being available for evaluation of the colon, the use of this technique has fallen out of favour.

Congenital abnormalities

Most anorectal and colonic congenital anomalies manifest in the paediatric population. In adult patients the congenital anomaly most commonly encountered is a colonic duplication cyst. Usually duplication cysts are asymptomatic, but occasionally they may perforate and cause intussusception or bowel obstruction. Malignancy has also been reported in duplication cysts.[26] Most cases demonstrate a bright, reflective inner mucosal layer and a darker, poorly reflective outer muscular layer on ultrasonography.[27] These layers

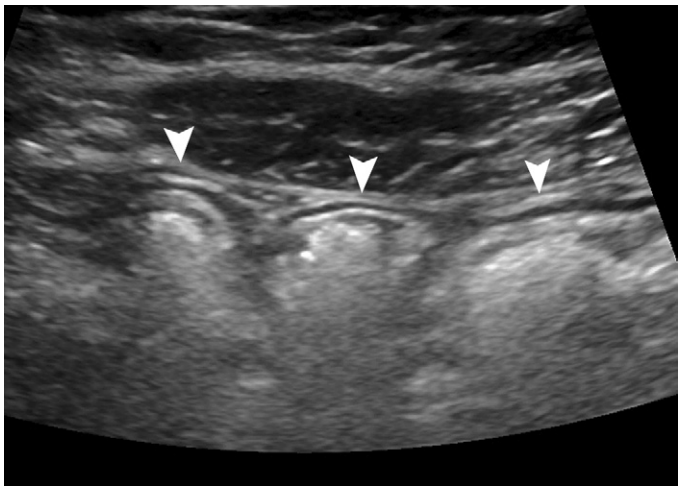


Figure 20.12 Normal colon. Longitudinal scan of the descending colon shows haustrations and a three-layer pattern (arrowheads).

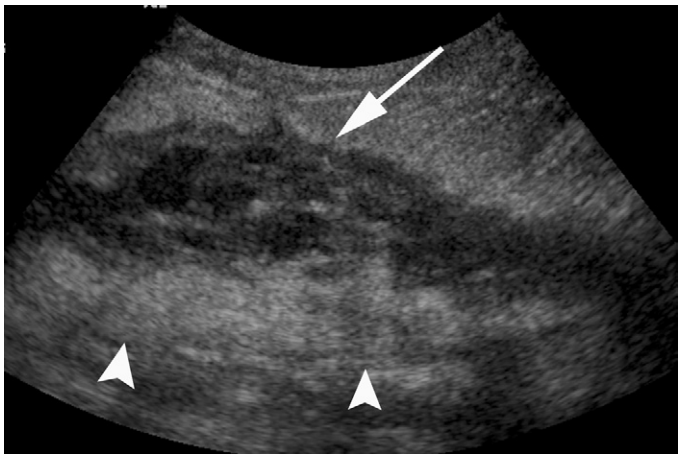


Figure 20.13 Congenital abnormality. Longitudinal scan of the ascending colon (arrowheads) in an asymptomatic patient shows a colonic duplication cyst as a tubular cystic structure with bright mucosal lining and internal debris (arrow).

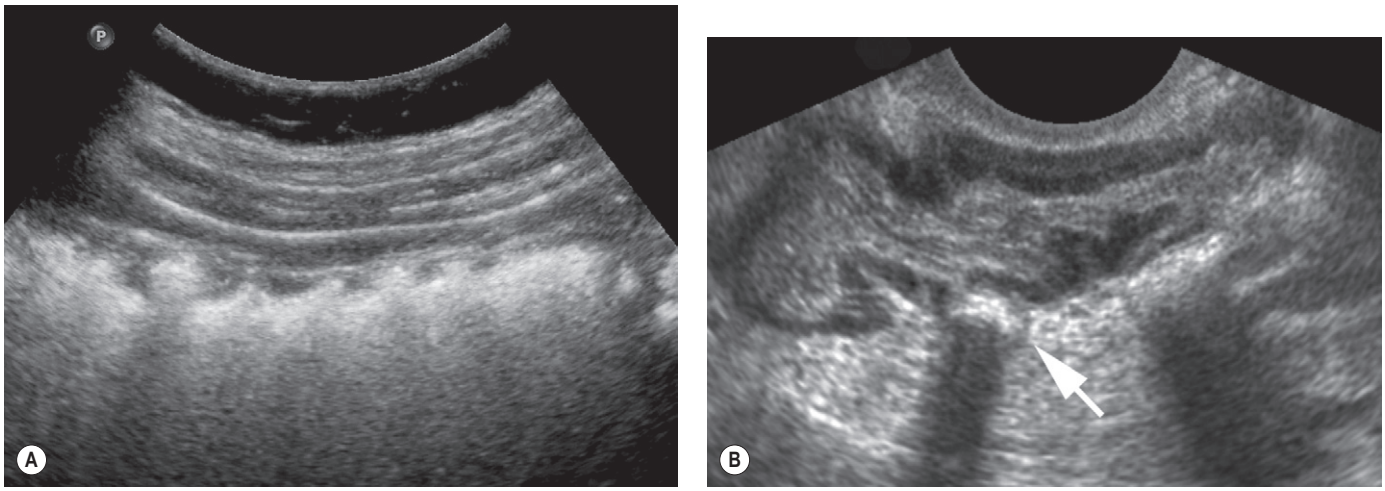


Figure 20.14 Diverticular disease. A: Longitudinal scan of the descending colon showing multiple diverticula as outpouching from the colonic wall. **B:** Transvaginal scan of the distal sigmoid colon shows diverticulum with highly reflective inspissated material causing acoustic shadowing (arrow).

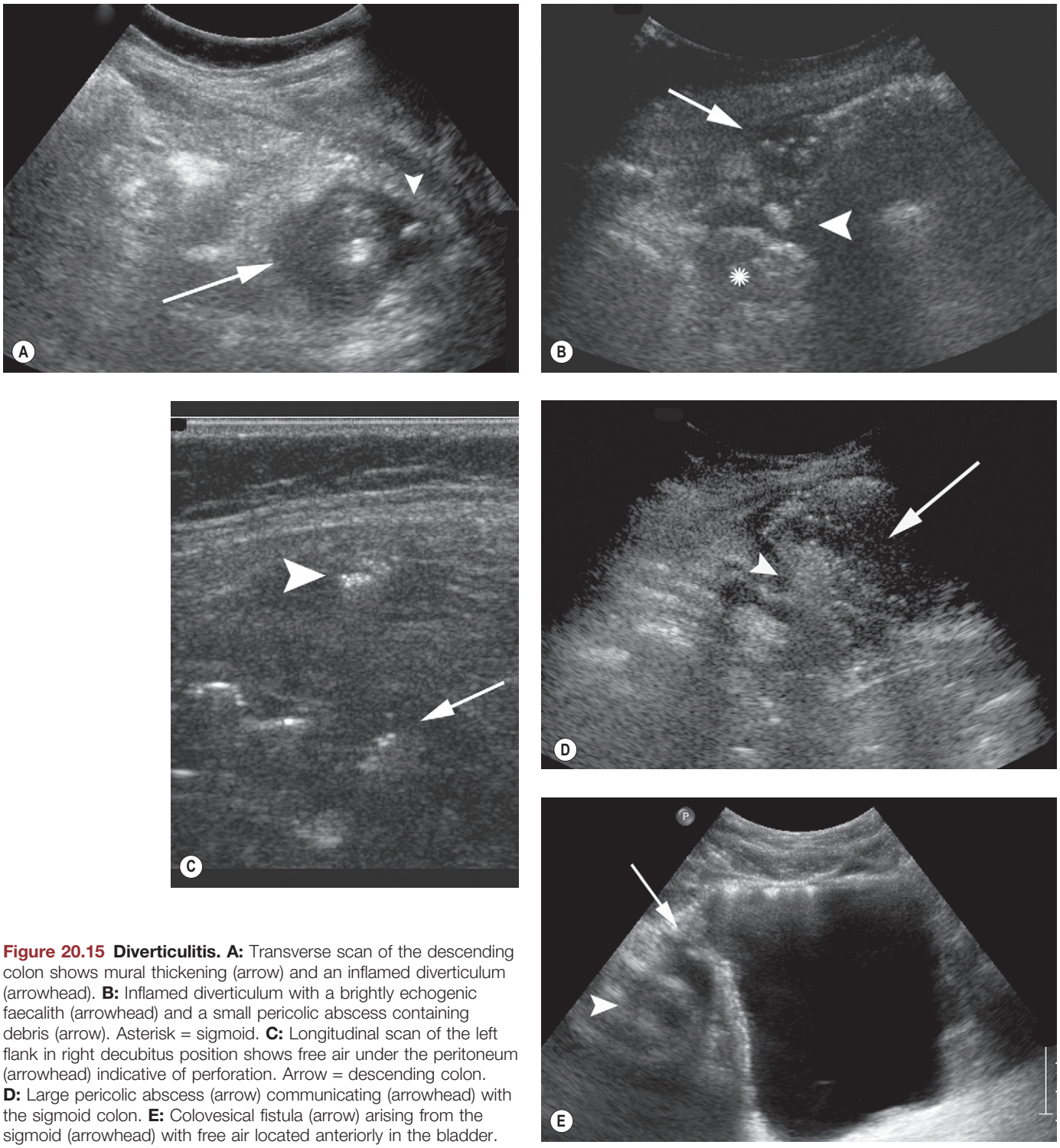


Figure 20.15 **Diverticulitis. A:** Transverse scan of the descending colon shows mural thickening (arrow) and an inflamed diverticulum (arrowhead). **B:** Inflamed diverticulum with a brightly echogenic faecalith (arrowhead) and a small pericolic abscess containing debris (arrow). Asterisk = sigmoid. **C:** Longitudinal scan of the left flank in right decubitus position shows free air under the peritoneum (arrowhead) indicative of perforation. Arrow = descending colon. **D:** Large pericolic abscess (arrow) communicating (arrowhead) with the sigmoid colon. **E:** Colovesical fistula (arrow) arising from the sigmoid (arrowhead) with free air located anteriorly in the bladder.

are often non-uniform in thickness and the cyst may contain internal septa and echogenic debris (Fig. 20.13).

Diverticulitis

Colonic diverticula are formed by herniation of the colonic mucosa through the muscular layer. These herniations occur at weak points in the colonic wall, such as between the longitudinal taenia coli or at the entry point of blood vessels.[28] The sigmoid colon is the area most commonly affected by diverticular disease. Sigmoid diverticula are commonly multiple.

On ultrasonography, diverticula are seen as rounded outpouchings adjacent to the colonic wall. There may be associated circumferential or eccentric mural thickening secondary to hypertrophy of the muscular layer (Fig. 20.14). Inspissated faecal matter or air within the diverticulum may produce acoustic shadowing (Fig. 20.14).

An inflamed diverticulum is usually seen as a poorly reflective structure adjacent to the colonic wall. There is tenderness on direct compression over the lesion and the inflamed diverticulum may be surrounded by echogenic, non-compressible fat.[29–33] The diverticulum often contains a faecalith or inspissated material which is seen as an highly reflective, bright lesion. The colonic segment involved may demonstrate circumferential or eccentric mural thickening and hyperaemia (Fig. 20.15).

Diverticulitis may progress to a pericolic abscess or perforation. Abscesses manifest as anechoic collections adjacent to the colon and

may contain pockets of air or debris (Fig. 20.15).[5] Scanning in a decubitus position may help to establish localised perforation by allowing air to collect under the peritoneum (Fig. 20.15). Complications secondary to diverticulitis such as a fistula can also be demonstrated on ultrasonography. Fistulae are seen as linear, low-echo tracks and a typical colo-vesical fistula may demonstrate air within the bladder.

The accuracy rate of ultrasonography in detecting diverticulitis has been reported to be 80–95%.[33] Ultrasonography can be used to monitor resolution of diverticulitis or a diverticular abscess. Percutaneous ultrasound-guided drainage of diverticular abscesses is an established procedure with excellent follow-up results.

Right-sided diverticulitis

Right-sided diverticulitis occurs more commonly in younger patients, women and persons of Asian ethnicity. Isolated right-sided diverticular disease is uncommon and may be due to a single congenital diverticulum. Congenital right-sided diverticula are true diverticula as they contain all the colonic wall layers. Inflammation of a right-sided diverticulum may mimic appendicitis and it is important to distinguish between these conditions as right-sided diverticulitis is treated conservatively and abscess formation is rare.[34] Ultrasonographic appearances of right-sided diverticulitis are similar to left-sided diverticulitis except for location along the caecum or ascending colon and a normal appendix (Fig. 20.16).

Inflammatory colitis

The two major forms of inflammatory colitis are Crohn's disease (also called Crohn's colitis) and ulcerative colitis. Ultrasonography can be used to assess the extent of colitis and has been shown to have good correlation with disease activity. Typical ultrasonographic features in the inflammatory colitides include mural thickening, loss of haustral pattern, reduced compressibility and lack of peristalsis.[35,36]

Crohn's colitis

Crohn's colitis has a transmural inflammatory progression similar to the disease seen in small bowel. As a result it causes marked colonic wall thickening.[37] In early or superficial ulcerating disease the stratification or layering of the bowel wall is preserved, whereas this pattern is lost in advanced, transmural inflammation (Fig. 20.17). Therefore in early disease, ultrasound shows colonic wall thickening with preserved stratification. More advanced inflammation results in transmural ulcers, which can be detected using high-frequency probes and are seen as low-echo linear streaks in the bowel wall. Distended perforating vessels may be visualised along these deep ulcers. Transmural ulcers eventually penetrate the serosa and cause inflammation in the adjacent mesenteric tissue, leading to formation of small para-intestinal abscesses and sinus tracts (Fig. 20.17). These tiny abscesses start as small inflammatory masses that are seen as ill-defined, low-reflectivity areas adjacent to the inflamed bowel segment. Larger abscesses may contain fluid levels and brightly reflective signals due to contained air bubbles. Sinuses may track through the wall of an adjacent organ and form a fistula. Fistulae typically manifest as linear, poorly reflective tracks on ultrasonography. Larger sinus tracks and fistulae may contain high signal echoes due to contained air or purulent material. Hyperaemia within fistulae on Doppler studies has been shown to correlate with inflammatory activity.[38]

In the inflammatory phase of Crohn's colitis there is associated oedema and fibrofatty proliferation of the surrounding omental and mesenteric fat. This inflamed and oedematous fat around inflamed colon has increased reflectivity and non-compressible appearance. Other ultrasonographic hallmarks of Crohn's disease include involvement of the small bowel and skip lesions. Studies have shown high volume flow in the mesenteric arteries on Doppler sonography in patients with actively inflamed bowel segments. In the chronic phase of the disease there is marked fibrosis and fatty infiltration of the submucosal layer. These pathological changes lead to marked echogenic thickening of the submucosal layer. Strictures may form, which are most commonly seen as low-reflectivity, stenotic lesions with proximal obstruction.

Ulcerative colitis

Ulcerative colitis is mainly a mucosal or superficial ulcerating disease, and therefore the inflammation is limited to the mucosa and submucosa (Fig. 20.18). As a result the colonic thickening is less marked than that in Crohn's disease. The stratified appearance of the bowel is maintained and there is no evidence of fistulae or sinuses. The involvement of the colon is contiguous and there are no skip lesions.

Occasionally it may be difficult to differentiate between ulcerative colitis and Crohn's colitis on ultrasonography; however, the presence of transmural changes, mesenteric abnormalities, skip lesions, small intestinal involvement and marked mural thickening should prompt the diagnosis of Crohn's disease (Table 20.1). On ultrasonography, a thickened colonic wall of greater than 7 mm with loss of stratification has been considered to be typical of Crohn's disease, whereas a thickness of 4–7 mm with preservation of the stratification is more typical in ulcerative colitis.

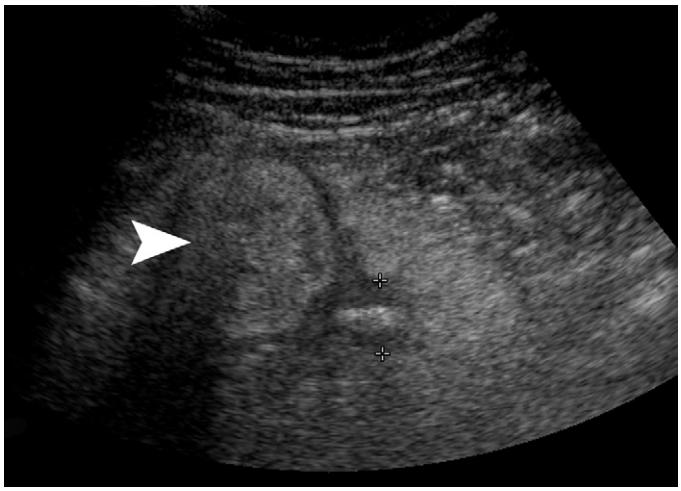


Figure 20.16 Right-sided diverticulitis. Transverse scan reveals an inflamed diverticulum (callipers) medial to the ascending colon (arrowhead). Note increased reflectivity in the inflamed fat around the diverticulum. The appendix was normal and a diagnosis of right-sided diverticulitis was made.

Crohn's colitis versus ulcerative colitis

- Crohn's colitis causes marked mural thickening and mural stratification may be lost.
- Ulcerative colitis causes modest bowel thickening with preserved stratification.
- Involvement of the terminal ileum may be present in Crohn's colitis.
- Fistulae, sinuses and abscesses are seen in Crohn's colitis.
- Crohn's colitis may show discontinuous, skip lesions whereas inflammation in ulcerative colitis is contiguous.

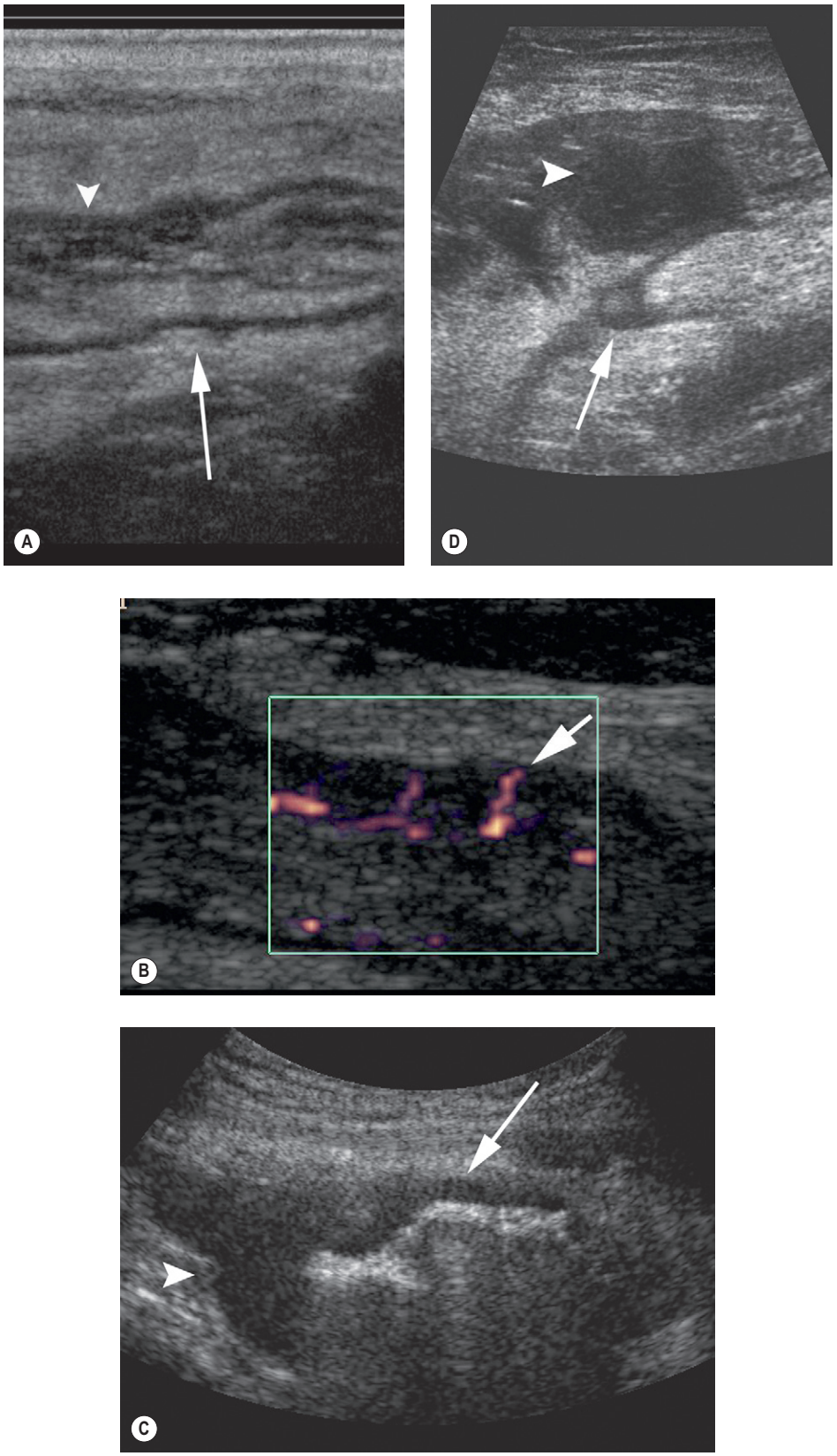


Figure 20.17 Crohn's colitis. A: Longitudinal image of the descending colon (arrow) shows marked mural thickening. There is loss of stratification in one segment (arrowhead) suggestive of transmural inflammation. **B:** Doppler study of the descending colon shows hyperaemia. Corkscrew, transmural vessels are seen indicative of fissuring ulcers (arrow). **C:** Transverse image shows contiguous, diffuse thickening of the caecum (arrowhead) and terminal ileum (arrow). **D:** Entero-colic fistula is seen as a linear, reduced reflectivity track between the ascending colon (arrowhead) and adjacent ileum. A small amount of air (arrow) is present in the fistula indicative of fistula patency.

Table 20.1 Differential diagnosis of common colitides

	Common location	Mural thickening	Doppler findings	Stratification	Pericolonic findings
Crohn's colitis	Ileocaecal	Marked (>7 mm)	Hyperaemia in active phase	Preserved or lost	Fibrofatty proliferation, lymphadenopathy, sinuses, fistula, abscesses
Ulcerative colitis	Rectosigmoid	Moderate (<7 mm)	Hyperaemia in active phase	Preserved	Fibrofatty proliferation
Ischaemic colitis	Splenic flexure	Moderate to marked	Loss of Doppler signal	Preserved or lost	Ascites, pericolic stranding, pneumatosis
Pseudomembranous colitis	Rectosigmoid	Marked with maintained haustral pattern	Hyperaemia	Preserved	Ascites
Tuberculous colitis	Ileocaecal	Moderate	Hyperaemia	Preserved or lost	Ascites, cavitating lymph nodes, thickened omentum and mesentery
Typhlitis	Caecal	Moderate to marked	Normal to mildly hyperaemic	Lost	Ascites and pericolic stranding
Yersinia enterocolitis	Ileocaecal	Minimal	Normal to mildly hyperaemic	Preserved	Lymphadenopathy

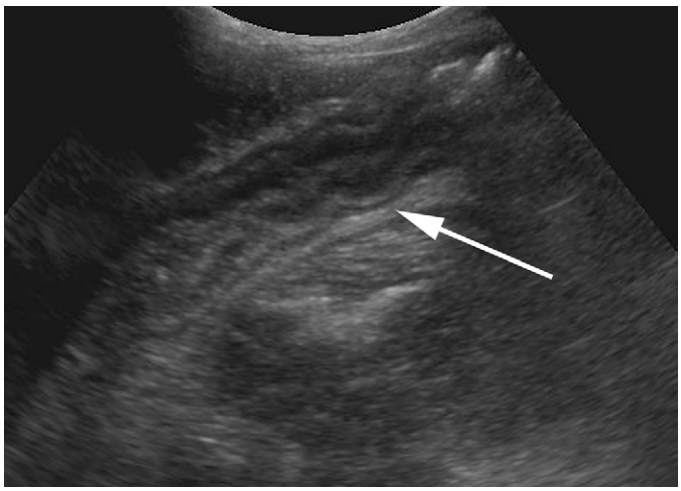


Figure 20.18 Ulcerative colitis. Diffuse, contiguous moderate thickening of the colon (arrow) with preserved stratification is seen.

Infective colitis

Tuberculous colitis

Intestinal tuberculosis typically affects the ileocaecal region. Isolated tuberculous colitis is extremely rare and only affects less than 3% of patients with documented intestinal tuberculosis. The most commonly observed pattern is concentric thickening of the ileum and caecum (Fig. 20.19). There may be associated ascites and mesenteric lymphadenopathy in the majority of patients.[39,40] Although the lymphadenopathy may be discrete, matted and cavitating lymph nodes are more frequent. Cavitating nodes have an anechoic central area. The ascites may be clear or may contain septations and debris.[41,42] Mesenteric and omental thickening is also present in tuberculous ileocolitis. Chronic tuberculous ileocolitis may lead to a cicatrisation and fibrosis of the bowel and patients may present with ileocolic strictures, mesenteric retraction and

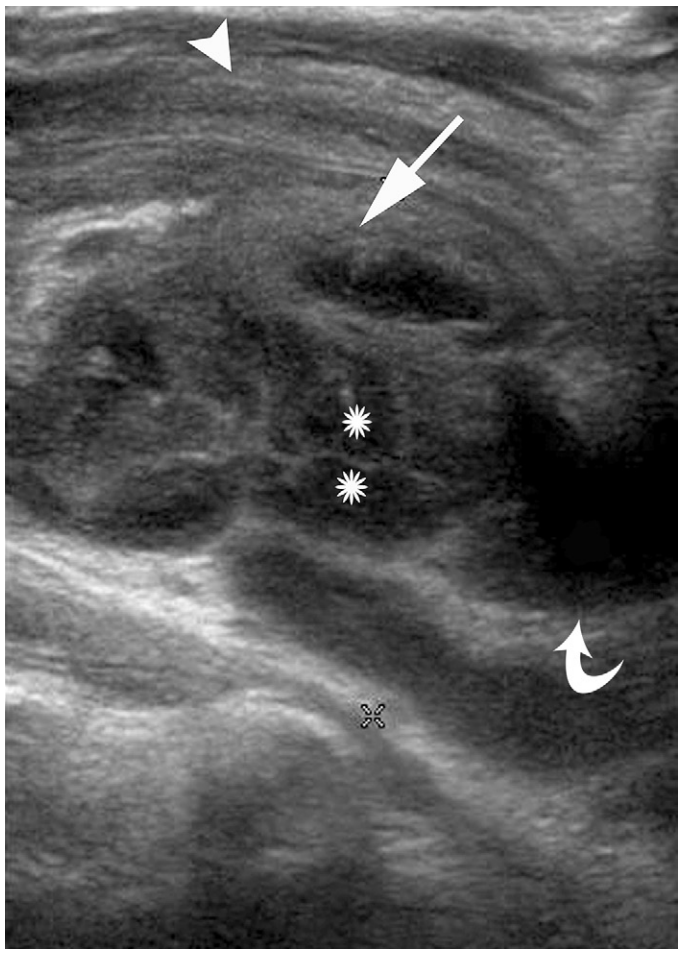


Figure 20.19 Tuberculous ileocolitis. Transverse ultrasound image of the right iliac fossa shows concentric thickening of the terminal ileum (arrow), necrotic, anechoic lymph nodes (asterisk), ascites (curved arrow). Note marked omental thickening (arrowhead). (Figure courtesy of Dr S. Rawat.)

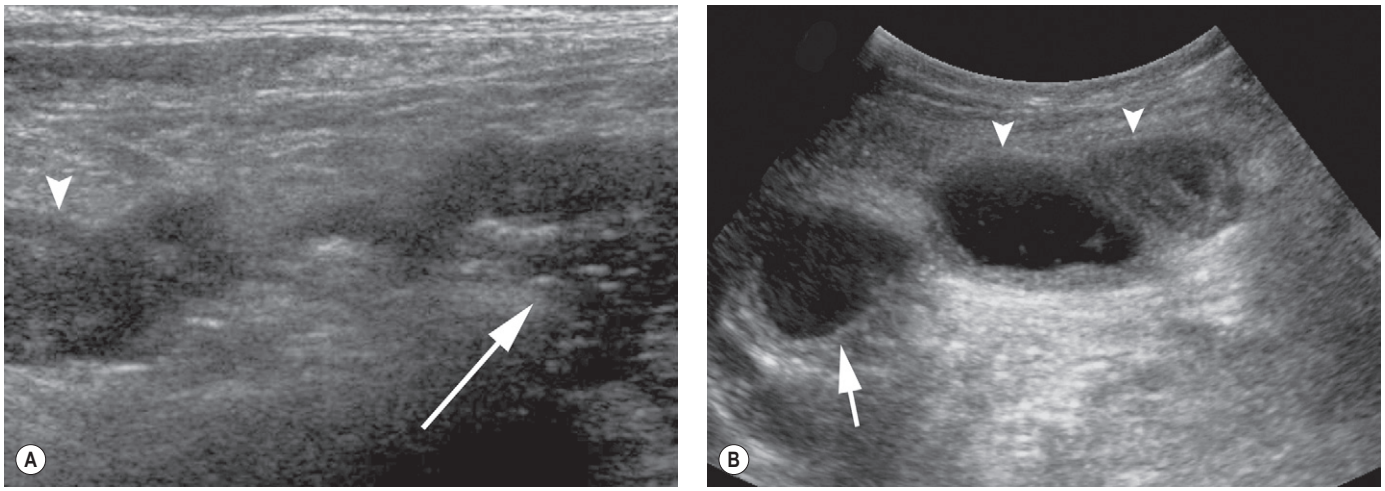


Figure 20.20 Amoebic colitis. A: Longitudinal image shows diffuse thickening of the ascending colon (arrowhead) and mass-like thickening of the caecum (arrow) (image courtesy of Dr S.B. Vijayraghavan). **B:** Thickened, fluid-filled caecum, terminal ileum (arrowheads) and distended non-tender appendix (arrow).

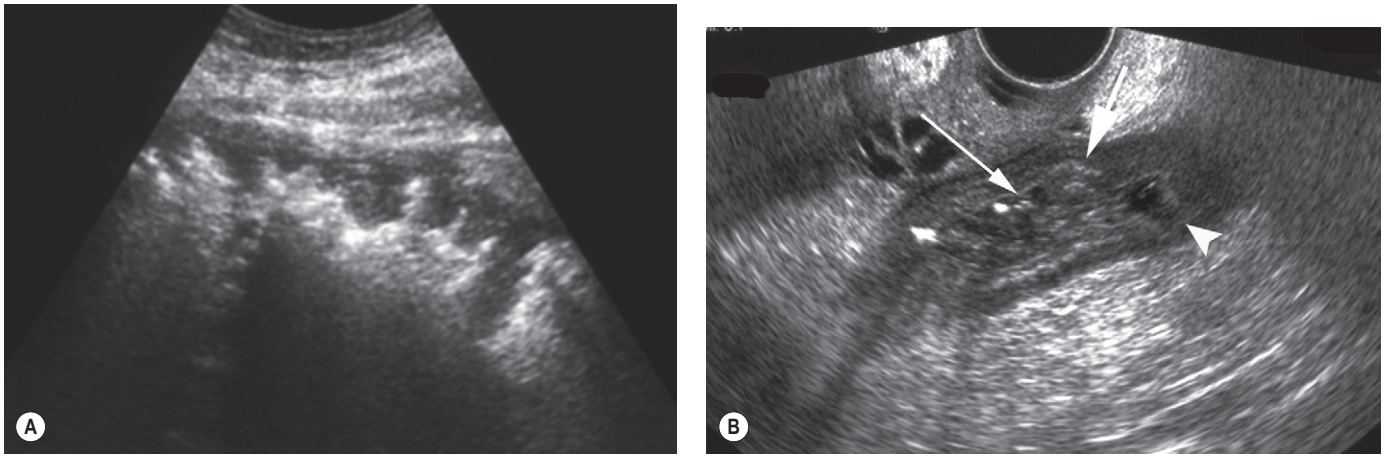


Figure 20.21 Pseudomembranous colitis. A: Longitudinal scan of the descending colon shows marked polypoid thickening of the colonic wall and narrowing of the lumen. **B:** Transvaginal scan shows diffusely thickened colon (arrow) with preserved stratification. Note deep ulcer (arrowhead) causing mucosal disruption and small linear pseudomembranes (thin arrow).

bowel obstruction. An echogenic peritoneum has also been reported in tuberculous infections of the gastrointestinal tract.

Amoebic colitis

Amoebic intestinal infection is caused by the protozoal organism *Entamoeba histolytica*. The trophozoite invades the intestinal mucosa causing colitis and disseminates through the portal bloodstream to cause abscesses, typically in the liver. Patients with intestinal infection may present with diarrhoea, abscesses and systemic symptoms. Pathological findings include discrete colonic ulcers, segmental colonic involvement or diffuse colitis. The ascending colon is frequently involved and the terminal ileum is invariably spared.

Ultrasonographically amoebic colitis manifests as diffuse, poorly reflective thickening of the colon (Fig. 20.20). Short segmental involvement may present as a mass lesion (termed 'amoeboma'), which is difficult to differentiate from a tumour. Amoebomas are typically seen in the caecum. The presence of a liver abscess with right colonic abnormality should alert the ultrasonologist to the presence of amoebic colitis. The normal terminal ileum helps to distinguish amoebic colitis from Crohn's colitis. A dilated, non-tender appendix has been reported in cases of amoebic colitis.

Pseudomembranous colitis

There has been a significant rise in the incidence of pseudomembranous colitis, mainly due to the increased use of prophylactic and broad-spectrum antibiotics. Antibiotic treatment leads to alteration in the colonic bacterial flora leading to proliferation of *Clostridium difficile*. Toxins produced by *Clostridium difficile* lead to pseudomembranous colitis that commonly presents with diarrhoea, abdominal pain, distension and systemic symptoms. Patients may occasionally present with an acute abdomen.

The most common ultrasonographic feature of pseudomembranous colitis is diffuse thickening of the colonic wall (Fig. 20.21).[43] The thickening varies with the severity of the disease but is generally much more marked than in other colitides. Typically the haustral pattern is preserved although the haustral thickening may have a polypoid appearance with marked narrowing of the lumen. Stratification of bowel layers may be preserved in mild cases. Scanning with high-frequency transducers may reveal mucosal defects caused by ulcers (Fig. 20.21). Pseudomembranes, which are the hallmark of this disease, are seen as linear, bright structures and they are best visualised on a real-time examination. Ascites may be detected in the majority of patients. In severe cases there is almost complete effacement of the lumen due to the mural oedema. The rectosigmoid region is most commonly affected, with contiguous

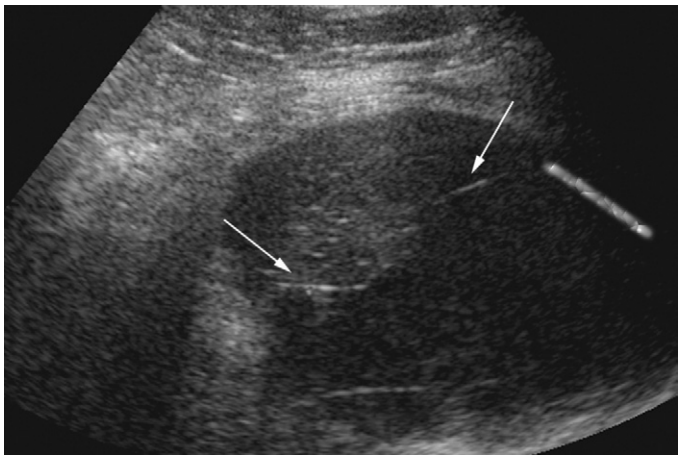


Figure 20.22 Typhlitis in a neutropenic patient. Diffuse, poorly reflective, mass-like appearance of the caecum with loss of normal mural pattern. Pneumatosis is seen as bright, linear areas (arrows) within the bowel wall.

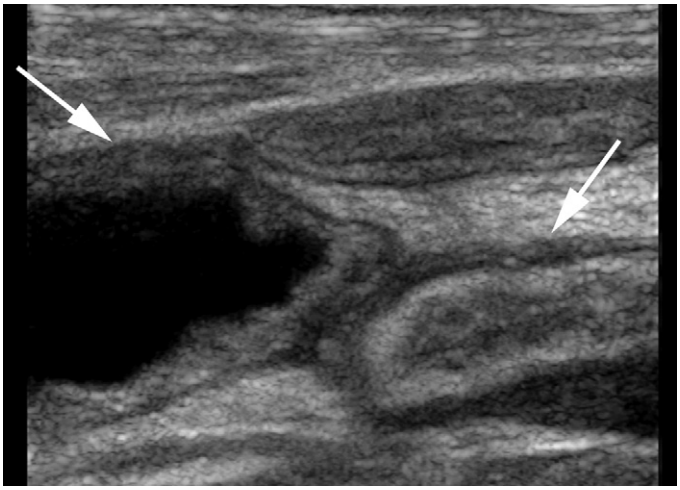


Figure 20.23 Infectious enterocolitis. Submucosal and mucosal thickening of the terminal ileum and caecum (arrows) with preserved stratification in a patient with *Yersinia* enterocolitis. Note lack of mesenteric inflammation or fibrofatty proliferation.

proximal involvement. Isolated involvement of the right colon is rare (<5%).

Typhlitis

Typhlitis or neutropenic enterocolitis is encountered in patients with immunosuppressive disorders (e.g. acquired immune deficiency syndrome or leukaemia), transplant recipients or after chemotherapy. The underlying pathological mechanism is considered to be secondary to mucosal damage of the bowel with subsequent bacterial or fungal invasion. The most commonly involved site is the caecum and ascending colon, although any bowel segment including the small intestine may be involved. The characteristic pathological findings of neutropenic enterocolitis are oedema, ulceration and inflammation of the bowel wall. Advanced cases may also have haemorrhagic necrosis of the bowel wall.[44]

The ultrasound features of neutropenic enterocolitis include diffuse bowel wall thickening and oedema of the right colon and distal ileum (Fig. 20.22). The affected segment may appear mass-like as there is loss of the typical layered and haustral pattern. Pericaecal stranding, ascites and pneumatosis may also be present.[45]

The differential diagnosis in the appropriate clinical setting of known neutropenia includes infective colitis (e.g. pseudomembranous colitis) and graft-versus-host reaction. The combined involvement of small and large bowel favours neutropenic enterocolitis over pseudomembranous colitis. Isolated right-sided pseudomembranous colitis is uncommon and patients typically have greater bowel wall thickening. Patients with graft-versus-host reaction have generalised involvement of the small and large bowel. Identification of neutropenic enterocolitis is important in order to initiate appropriate medical treatment.

Other infections

Other less common organisms that cause colitis include *Yersinia*, *Campylobacter* and *Salmonella* infections. In all these infections the terminal ileum and/or the caecum are involved. Ultrasonographically the bowel thickening is moderate and limited to mucosa and submucosa.[5] Usually there is no mesenteric fat involvement, fistulation or abscesses formation. Prominent haustrations of the right colon have been reported in these infections. *Yersinia* enterocolitis is usually associated with enlarged mesenteric lymph nodes and there is ileal and colonic thickening (Fig. 20.23). *Campylobacter* and *Salmonella* infections mainly cause colonic thickening and minimal small bowel involvement. *Yersinia* enterocolitis in particular can clinically mimic acute appendicitis and it is important to visualise the normal appendix, to exclude acute appendicitis.

Infective colitides

- Tuberculous colitis involves the ileocaecal region and there may be associated cavitating lymphadenopathy, ascites and omental thickening.
- Amoebic colitis may present as a caecal mass (amoeboma).
- *Campylobactor* and *Salmonella* cause modest thickening of the colonic mucosa.
- *Yersinia* enterocolitis causes modest thickening of the colonic and ileal mucosa with associated lymphadenopathy.
- Typhlitis commonly involves the caecum and ascending colon.
- Pseudomembranous colitis caused marked mural thickening, prominent haustral folds and ascites.

Ischaemia

The majority of cases of ischaemic colitis are due to non-occlusive vascular disease. The most common cause is vascular hypoperfusion due to arteriosclerosis, vasogenic shock and cardiac conditions. Ischaemia due to vascular occlusion by thrombus, emboli or other causes is less frequent. The most commonly affected site is the splenic flexure, followed by descending and sigmoid colon. Ischaemic colitis is the commonest vascular disorder of the gastrointestinal tract in patients over 65 years of age.

Ultrasonography has a high degree of sensitivity for detecting colonic abnormalities in ischaemic colitis. Ultrasonographic findings in ischaemic colitis include segmental or circumferential colonic wall thickening, pericolic changes, reduced or absent peristalsis and diminished blood flow on Doppler studies (Fig. 20.24). Typically the wall stratification is preserved and loss of stratification is indicative of advanced transmural ischaemia and a worse prognosis.[46] Absence of Doppler flow in the abnormal segment is also considered to be a sign of worse clinical outcome. High resistive index blood flow (>0.60) on Doppler studies has also been reported. Ascites may also be present in cases with established ischaemic changes and infarcted bowel segments demonstrate mural pneumatosis.

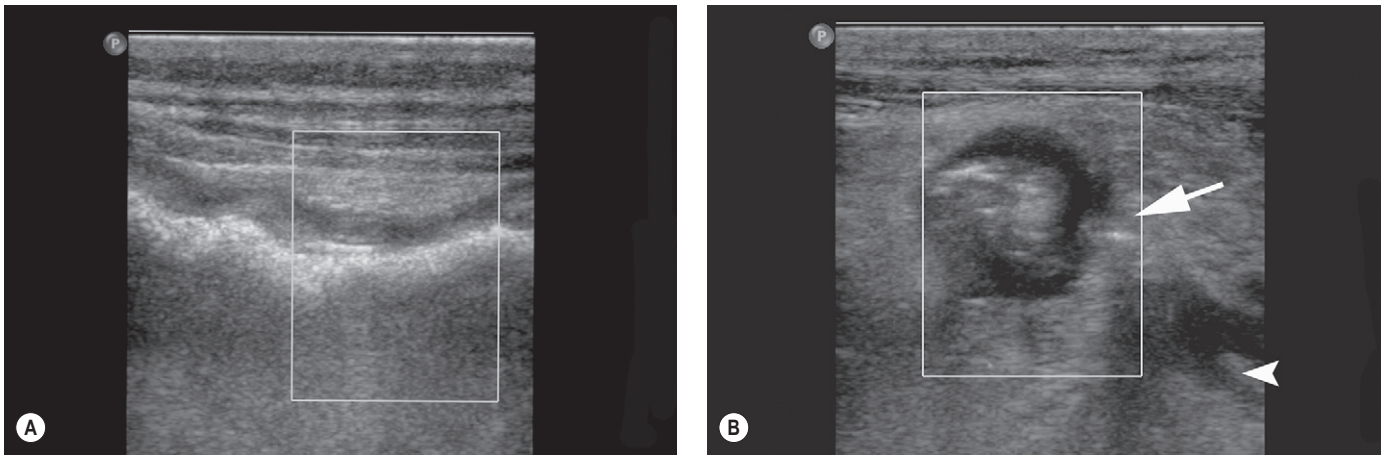


Figure 20.24 Ischaemic colitis. A: Longitudinal view shows thickened descending colon with absence of blood flow. The mural stratification is maintained. **B:** Transverse view shows diffuse, poorly reflective thickening (arrow), loss of the mural stratification and absence of blood flow. Focal area of pneumatosis is seen (arrow) with oedema of the paracolic fat and ascites (arrowhead).

Tumours

Although ultrasound is not the primary modality for diagnosis of colonic cancer, the widespread use of ultrasonography in abdominal conditions may result in the incidental detection of these tumours. Tumours of the colon typically manifest as localised, poorly reflective masses related to the bowel. Thickening of the bowel can produce the 'pseudo-kidney' appearance (Fig. 20.25).[47] Ultrasonographic features commonly associated with colonic cancer include localised, eccentric mural thickening, an irregular contour, abnormal or lack of peristalsis and loss of the layered appearance of the bowel wall.[48] Colonic tumours can also manifest as circumferential thickening of the bowel or as a polypoid mass, and the thickening is usually more marked than that seen in infective or inflammatory colitides (Fig. 20.25). Mucinous adenocarcinomas may contain calcifications that are seen as echogenic foci with shadowing on ultrasonography. Abrupt loss of mural stratification is also typical of colon cancer. Locally advanced tumours show infiltration of the adjacent fat planes, other abdominal viscera and liver metastases (Fig. 20.25). Serosal or omental metastases that involve the colon typically appear as poorly reflective infiltrative or mass lesions.

Small polypoid lesions may not be reliably detected on transabdominal ultrasonography; however, hydrocolonic ultrasonography has been reported to have a high degree of accuracy in the detection of such lesions.[24] Transabdominal scanning has been shown to have a high detection rate of right-sided and rectal cancers.[49]

Colonic lymphomas are rare and typically seen in immunocompromised patients, or those who have undergone organ transplantation. The commonest type of large bowel lymphoma is the B-cell type and they manifest with marked bowel wall thickening. The mural thickening may be circumferential, eccentric or nodular. Aneurysmal dilatation of the lumen may be seen, which is thought to be secondary to autonomic neural plexus destruction by tumour infiltration (Fig. 20.26).

The colon is the commonest site involved by gastrointestinal lipomas. Colonic lipomas are generally asymptomatic unless they cause bleeding or intussusception. They are typically seen as polypoid intraluminal lesions with high reflectivity (Fig. 20.27).

Miscellaneous conditions

Endometriosis

Endometriosis affects women of childbearing age and typically manifests with pain or infertility. Endometriosis is defined as the presence of endometrial tissue outside the uterine cavity and the myometrium. The most frequent locations are in the pouch of Douglas, with other sites having a lesser frequency. The rectovaginal septum may also be frequently involved. When there is bowel involvement, patients may complain of symptoms similar to irritable bowel syndrome. Deeper invasion of the bowel wall may cause scarring and stricture formation that can lead to obstruction.[50] The reported incidence of intestinal involvement ranges from 3% to 34% and in up to 70% of cases the rectum or sigmoid is involved.[51] Other less common sites include the appendix, caecum and ileum.

Transabdominal ultrasonography should be combined with endo-cavitary scanning (endorectal or transvaginal) for a comprehensive assessment of colonic endometriosis. Endometriomas can present as nodular, plaque-like, cystic or complex lesions. Small nodules or plaque-like lesions are the most difficult to demonstrate ultrasonographically. These lesions are typically of reduced reflectivity on ultrasonography (Fig. 20.28) and may be only seen on transrectal examinations. Larger nodules are more easily demonstrated on transabdominal scanning and appear as low-reflectivity lesions and can cause puckering and kinking of the bowel wall. Attachment of these lesions to the colon is confirmed on dynamic scans during respiration. Larger nodules can demonstrate blood flow on Doppler studies. Accurate assessment of the depth of rectal wall involvement can be made on transrectal ultrasonography, which is useful in surgical planning.

Intussusception

Colonic intussusception is rare in adults and is most commonly associated with a malignant tumour.[52] The commonest reported type is an ileocolic intussusception. Lipomas are the most common benign cause of colonic intussusception. Ultrasonographically the findings are that of a bowel mass with concentric layers of hyper- and hypoechogenicity. On longitudinal views the alternating layers produce a trident or pitchfork appearance.[53] The intussusception may contain mesenteric fat and the bowel may appear thickened due to oedema (Fig. 20.29). Contained mesenteric vessels may show normal Doppler signal. The finding of an intussusception in an adult should raise the suspicion of an underlying tumour.

Epiploic appendagitis

Appendices epiploicae are fatty tags attached to the serosal surface of the colon. They usually measure 1–2 cm in thickness and 2–5 cm in length. Venous infarction or torsion of these appendages may result in localised inflammation, which is termed epiploic

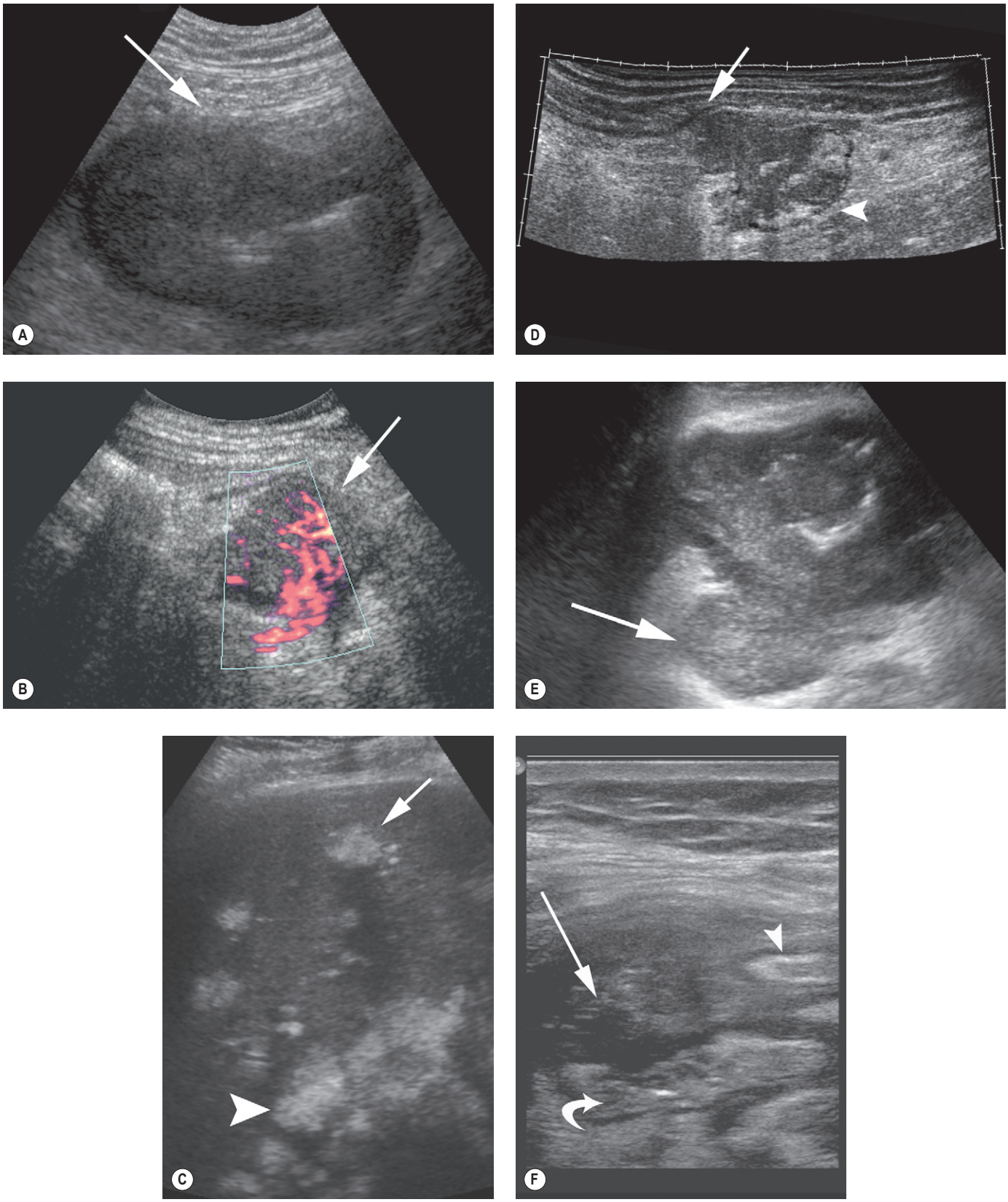


Figure 20.25 **Colonic tumours. A:** Diffuse, eccentric thickening of the colon (arrow) producing the pseudo-kidney sign. **B:** Polypoid intraluminal mass with a dilated feeding vessel (arrow). **C:** Mucinous colonic tumour shows extensive calcification in the hepatic flexure tumour (arrowhead) and calcified liver metastases (arrow). **D:** Locally advanced colonic tumour shows extensive infiltration of the paracolic fat and peritoneum (arrow). Arrowhead = colon. **E:** Polypoid colonic mass with loss of stratification, marked mural thickening and extension into pericolonic fat (arrow). **F:** Recurrent tumour (arrow) seen as diffuse, low-reflectivity lesion involving the colon (curved arrow) and ileum (arrowhead).

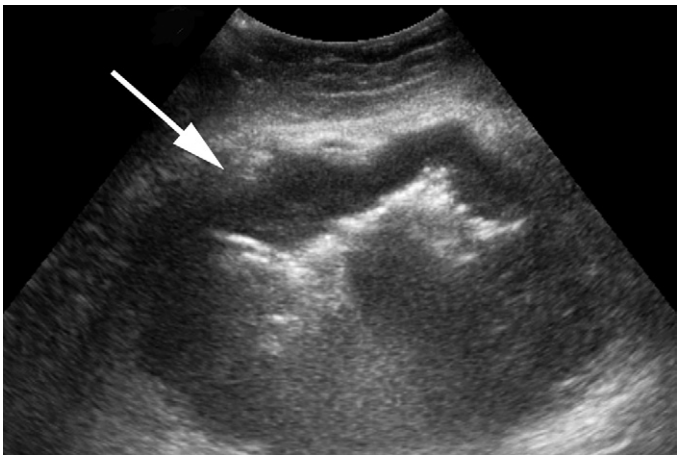


Figure 20.26 Colonic lymphoma. Circumferential thickening of a long segment of the sigmoid colon (arrow) is seen with distended, air-filled lumen (aneurysmal dilatation).

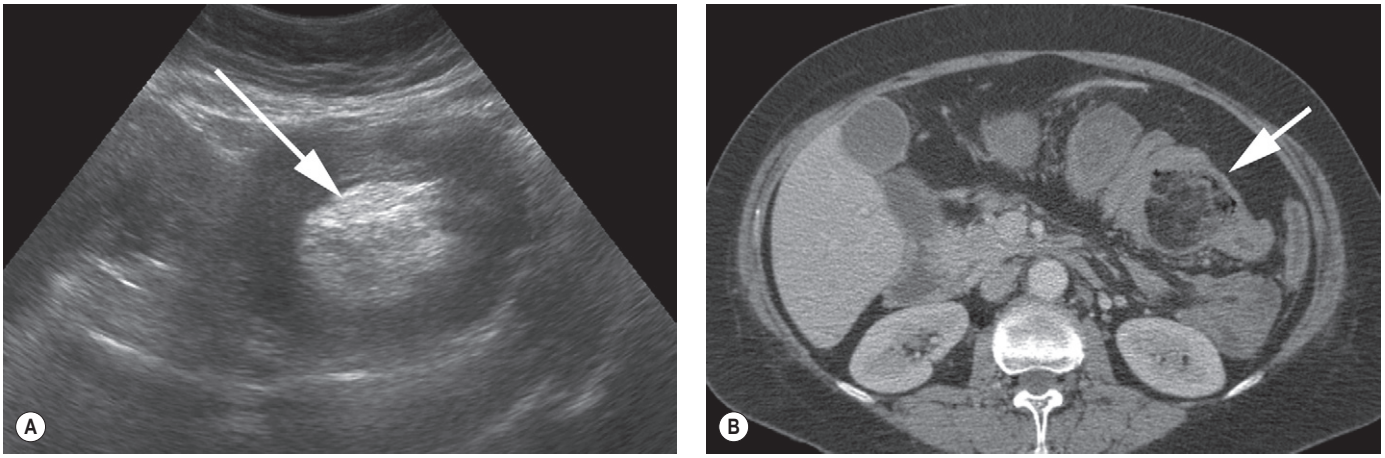


Figure 20.27 Lipoma. A: Transverse image of the transverse colon shows a bright, reflective mass (arrow) filling the colonic lumen. **B:** Axial CT image confirms the colonic lipoma as a fatty intraluminal lesion (arrow).

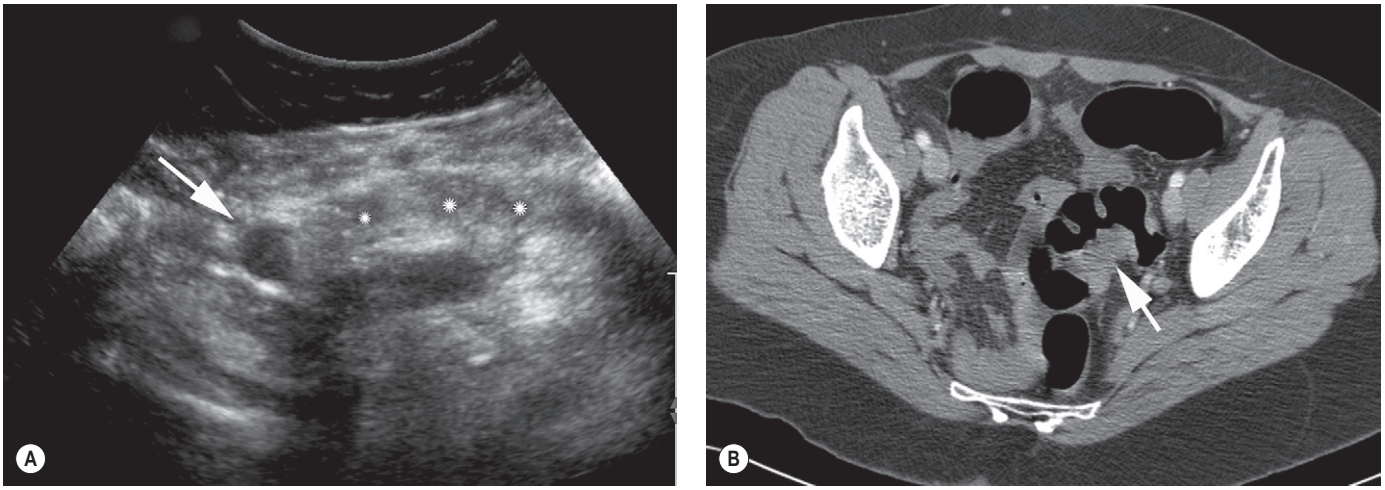


Figure 20.28 Endometriosis. A: Nodular, poorly reflective lesion (arrow) seen attached to the sigmoid colon (asterisks). **B:** Axial CT image shows enhancing lesion (arrow) attached to the sigmoid.

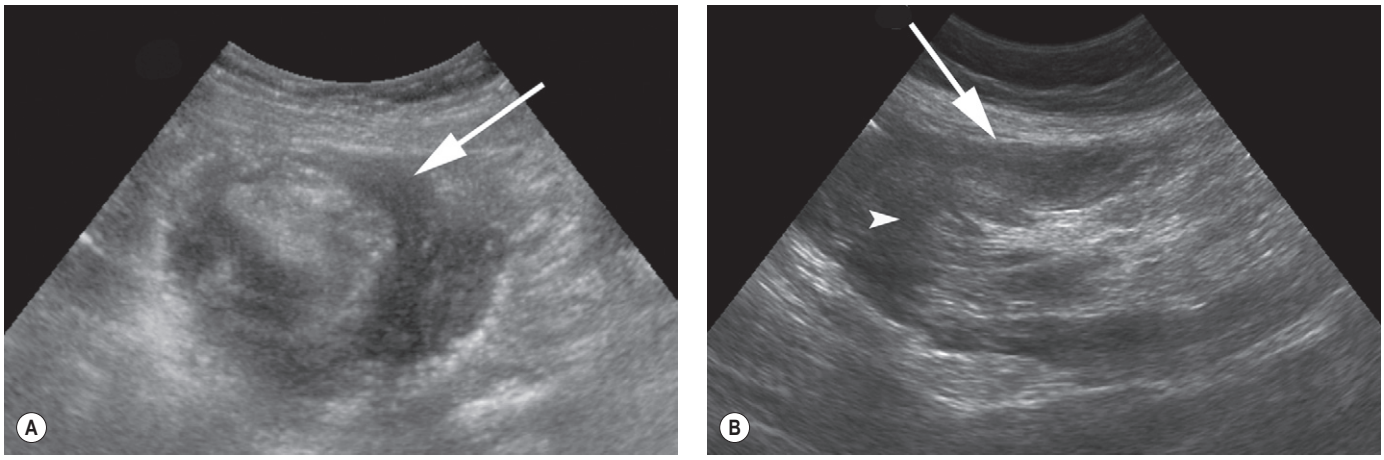


Figure 20.29 Intussusception. A: Ileocolic intussusception seen as a target lesion with an alternating high and low reflective pattern (arrow). **B:** Longitudinal view shows ileal segment and mesenteric fat (arrowhead) inside the colonic lumen (arrow). A trilaminar or trident appearance is evident.

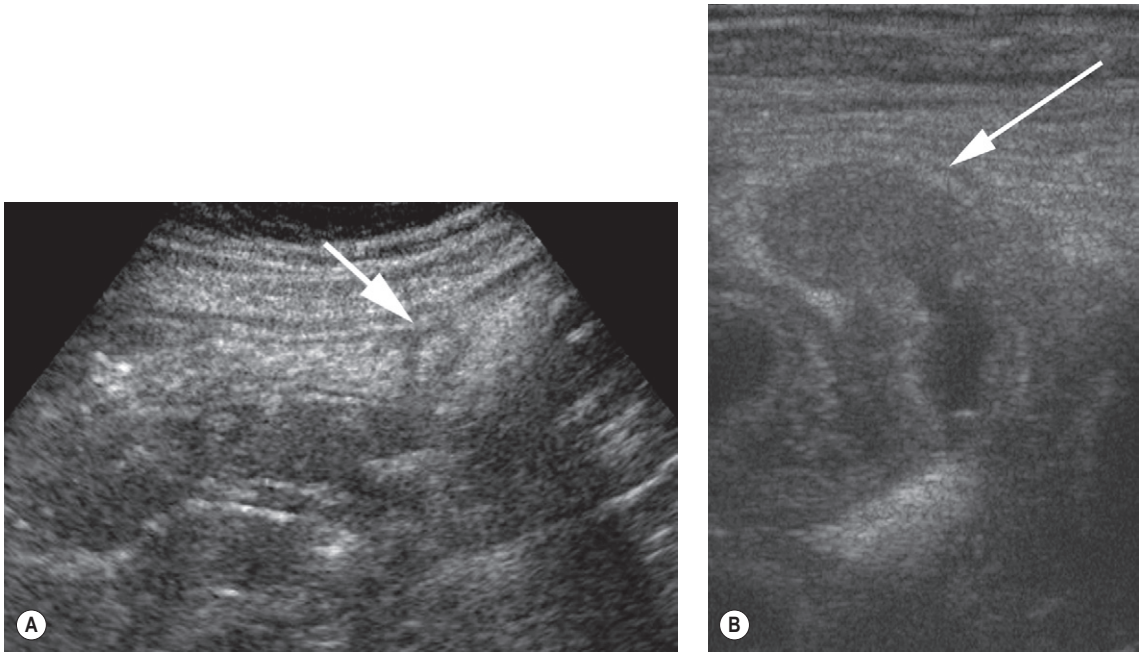


Figure 20.30 Epiploic appendagitis. A: Lenticular lesion with a dark rim (arrow) adjacent to the colon. **B:** Epiploic appendagitis seen as a lenticular echogenic lesion (arrow) arising from the colon.

appendagitis. Patients may present with acute abdominal pain and epiploic appendagitis may mimic diverticulitis or appendicitis. It has been reported that 2.3–7.1% of patients with suspected diverticulitis actually have epiploic appendagitis.[54] It is important to diagnose this entity correctly as the treatment is conservative management.

On ultrasonography the inflamed appendage is seen as a lenticular, echogenic lesion at the site of maximum tenderness (Fig. 20.30).[55] Real-time scanning during deep inspiration and expiration shows the attachment of the mass to the colon. There may be a well-defined low-reflectivity rim around the lesion that corresponds to the inflamed visceral peritoneum. Inflammation of the adjacent pericolic fat is often associated with epiploic appendagitis. Occasionally internal poorly reflective areas may be seen secondary to haemorrhagic foci within the mass.

RECTUM AND ANAL CANAL

The rectum can be visualised on transabdominal ultrasonography, particularly through a well-distended bladder. However, detailed assessment of the rectum and anal canal can only be performed via transrectal or endoanal ultrasonography using high-frequency transducers.[56]

Ultrasound technique

High-frequency probes (≥10 MHz), axial 360° view to assess sphincters and good near field resolution are required for optimal assessment of the anal canal. These prerequisites can be met by a

mechanical rotating single-crystal transducer. More recently fixed crystals with 360° field of view have been developed for endoanal ultrasonography. Biplane capabilities on a single transducer that allows axial and perpendicular views and Doppler capability have also been developed.[57,58] Alternative techniques such as transvaginal and transperineal scanning have also been advocated for evaluation of the anal sphincters. However, there are limitations to these approaches; firstly transvaginal scanning can only be used in women, and secondly, the anatomical configuration of the vagina and anal canal with the perineal body in between does not allow true axial imaging of the sphincters. Therefore only an oblique view of the anal canal can be obtained via the transvaginal approach, which is suboptimal for assessing the circular sphincter complex. Use of transvaginal and transperineal scanning should be reserved as an adjunct to standard endosonography and may be particularly useful in stenotic anal lesions or tumours where the standard endoanal approach may not be possible.

For an endosonographic examination, the probe is inserted into the rectum and withdrawn gently through the anal canal to obtain a view of the sphincter complex. Endoanal ultrasonography should be performed with the patient in the prone position as this provides a symmetrical view of the sphincter complex and also allows accurate views of the anterior aspect of the external sphincter.[59] Although scanning in the lateral decubitus position may be easier and more comfortable for the patient, it produces distortion of the sphincter complex.

Degassed water can be instilled to provide a good ultrasonographic window for examination of the rectum. This method is useful in assessing the rectal tumours as it reduces overstaging by decreasing artefacts produced by faecal matter, rectal air or the tumour itself.

The scan should be oriented as a clock-face in such a way that 3 o'clock corresponds to the left side of the patient. Images are obtained at high, mid and low anal canal levels. Measurements of the sphincter thickness should be obtained at the 3 and 9 o'clock positions. The internal sphincter measures approximately 2 mm in the normal adult and it gradually thickens with advancing age. A thickness of greater than 3.5 mm is abnormal in any age. The length of the sphincters may be determined on volume or three-dimensional scans. Ascertaining the length of the sphincter is important in order to assess the level of disruption.

Indications for endoanal sonography

- Assessment of sphincter abnormalities.
- Diagnostic work-up of faecal incontinence and evaluation of anal pain.
- Assessment of anal sepsis.
- Staging of anorectal tumours, particularly prior to local treatment.

Normal anatomy

Anal canal

On endoanal ultrasonography four distinct layers in the anal canal can be determined (Fig. 20.31).[60] These are:

1. The subepithelium, which is seen as a moderately echogenic layer that is adjacent to the probe surface. The subepithelium is of uniform echogenicity and may contain venous channels.
2. The internal sphincter is seen as a clearly defined layer with low reflectivity. It is circular in shape and measures 2–3 mm in the normal adult. There is some asymmetry of the internal sphincter high in the anal canal. This asymmetry is more prominent in females where the anterior aspect is ill-defined as the sphincter merges with the perineal body. The internal sphincter terminates at the dentate line.
3. The longitudinal muscle is seen as a moderately reflective layer in between the internal and external sphincters and is a continuation of the longitudinal muscles of the rectum.

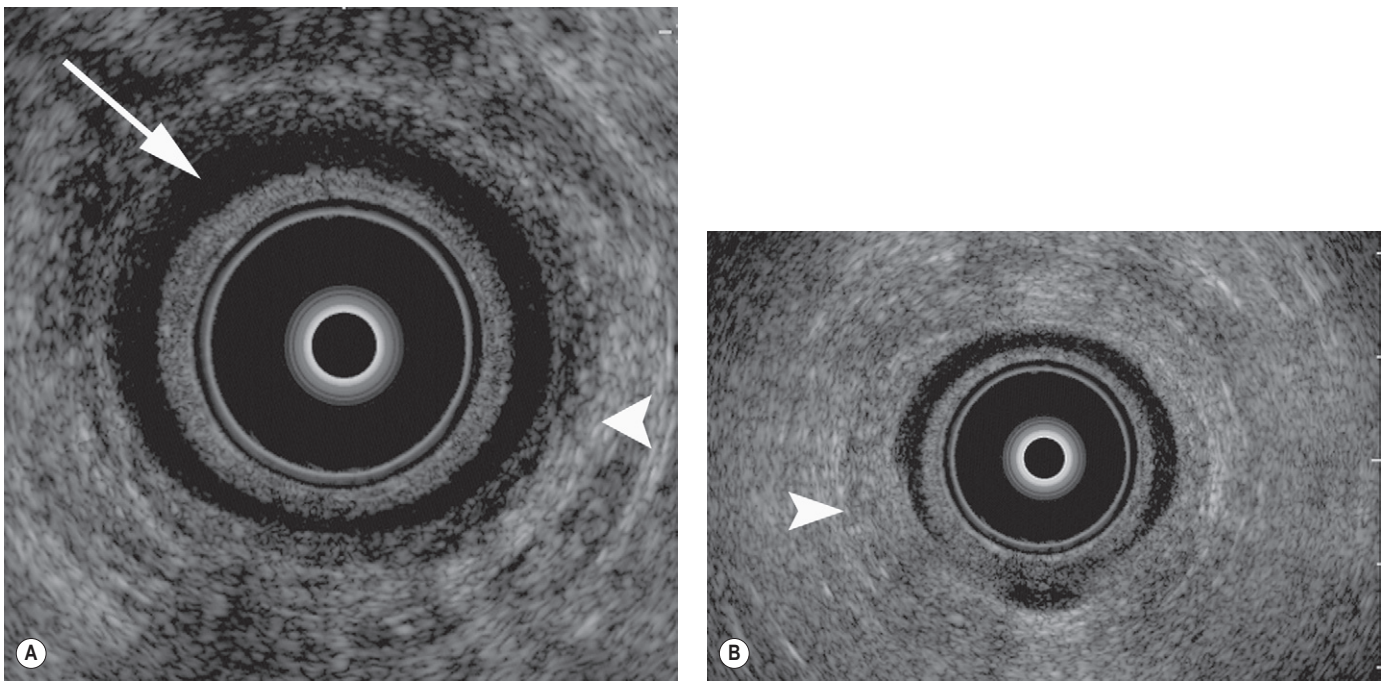


Figure 20.31 Normal anal anatomy. A: Image at high level shows the four layers. Arrow = internal sphincter; Arrowhead = external sphincter. Bright subepithelial layer is seen adjacent to the endoanal probe. Moderately reflective longitudinal muscle layer is between the external and internal sphincters. Amorphous appearing perineal body is seen anteriorly. **B:** Image at low level shows brightly reflective fibres of the subcutaneous external sphincter (arrowhead). The poorly reflective internal sphincter is seen ending at this level.

4. The external sphincter is composed of striated muscle and is of moderate and varied reflectivity. With ageing there is increased thickening of the internal sphincter and increased reflectivity.

Endoanal images should be obtained at high, mid and low levels in the anal canal. The high level corresponds to the level of the puborectalis and deep external sphincter. In males the external sphincter is roughly symmetrical whereas in females the anterior portion of the external sphincter is deficient and replaced by the perineal body. The internal sphincter and longitudinal muscle is clearly visualised at this level.

The mid level corresponds to the superficial part of the external sphincter. The internal sphincter terminates at the lower end of this level. At this level the sphincters are symmetrical and the pubococcygeal ligaments are seen posteriorly.

The low level starts caudal to the termination of the internal sphincter. The longitudinal muscle may appear slightly wider at this level. The predominant structure at this level is the subcutaneous part of the external sphincter.

Rectum

Typically the rectum demonstrates a five-layer pattern on transrectal ultrasonography. These layers are seen as alternating bands of increased and reduced reflectivity. The balloon–mucosa interface, submucosal and serosal layers appear bright; whereas the muscularis mucosae and muscularis propria are of reduced reflectivity.

Anorectal tumours

Endoanal and transrectal ultrasonography can be used to stage anal tumours based on depth of invasion. Typically anal cancers are poorly reflective and clearly demarcated from adjacent structures. Tumour confined to the subepithelium is classed as T1; limited to sphincter muscles is classed as T2; extending through the external sphincter is classed as T3; involving adjacent pelvic structures is classed as T4.

Transrectal ultrasonography has high accuracy in the staging of rectal cancer.[61] A meta-analysis has indicated that ultrasonography has significantly higher specificity for predicting muscularis propria and perirectal tumour extension compared to MRI or CT.[62] Perirectal invasions are seen as poorly reflective extensions traversing the rectal wall and extending into the adjacent serosa and mesorectum (Fig. 20.32). In routine practice, overstaging is more of a problem than understaging. This is because most tumours are surrounded by inflammatory and desmoplastic reaction around their margins.[63] It is difficult to distinguish between desmoplastic and inflammatory reaction from tumour infiltration on ultrasonography, which leads to overstaging. Another disadvantage of endoanal ultrasonography is the inability to evaluate stenotic tumours.

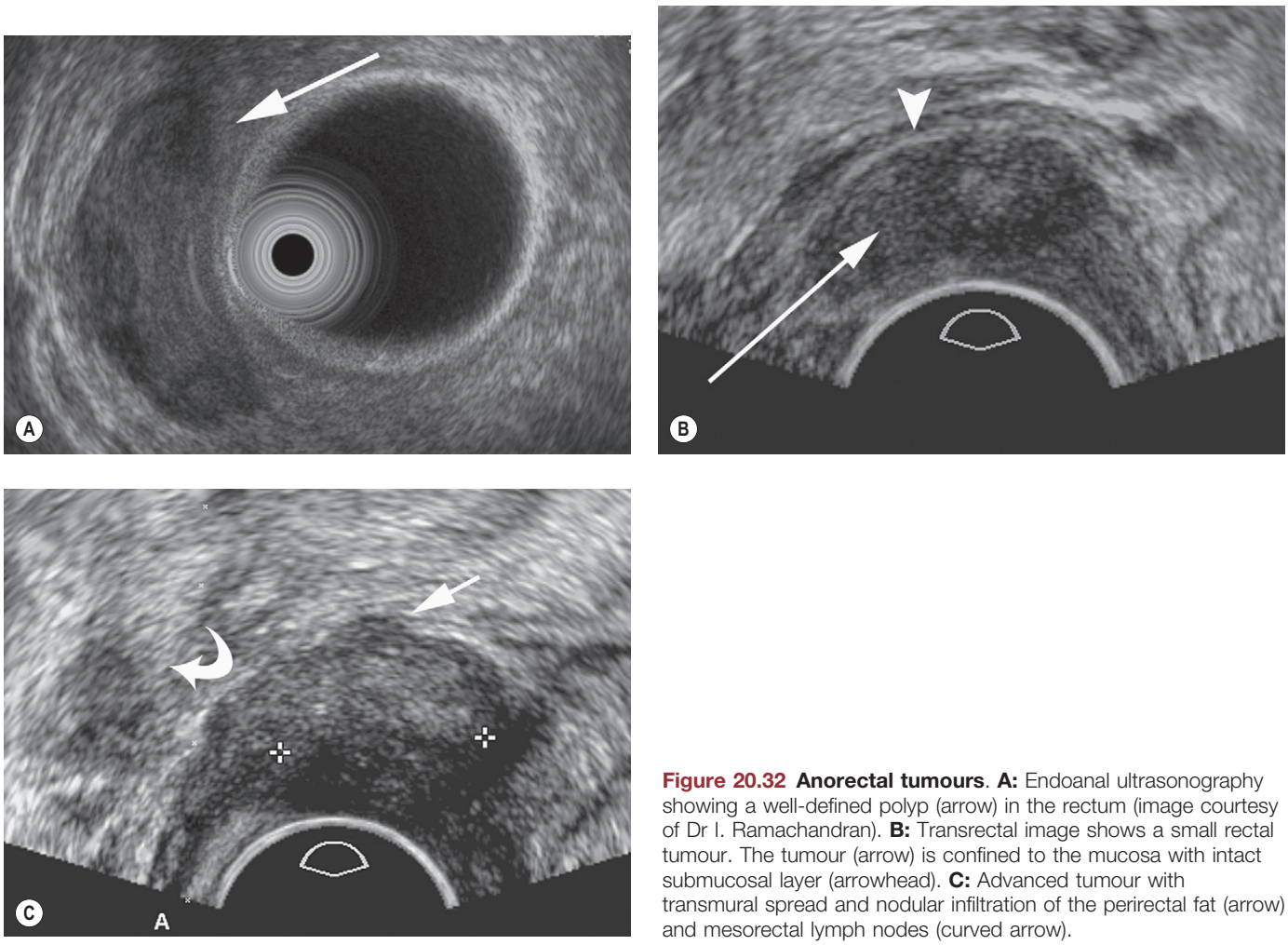


Figure 20.32 Anorectal tumours. **A:** Endoanal ultrasonography showing a well-defined polyp (arrow) in the rectum (image courtesy of Dr I. Ramachandran). **B:** Transrectal image shows a small rectal tumour. The tumour (arrow) is confined to the mucosa with intact submucosal layer (arrowhead). **C:** Advanced tumour with transmural spread and nodular infiltration of the perirectal fat (arrow) and mesorectal lymph nodes (curved arrow).

Endoanal ultrasonography can also be used in the follow-up of rectal cancers. Tumour recurrence typically manifests as an amorphous, poorly reflective mass. Endoanal ultrasound can be used to perform targeted biopsies of the bowel or extramural lesions.

Anal sepsis

Endoanal ultrasonography is useful in the detection of anal sepsis and in particular the identification of internal opening of fistula-in-ano.[64] It must be borne in mind that the track leading up to the mucosal surface is rarely seen; rather the site is identified as a poorly reflective area in the intersphincteric space adjacent to the internal sphincter (Fig. 20.33). Trans-sphincteric fistulae are seen as tracts that extend across the external sphincter into the ischioanal fossa. An inherent disadvantage of using high-resolution probes in endoanal ultrasonography is the inability to resolve ischioanal and supralevator infections. Trans-sphincteric tracks and ischioanal or ischiorectal extensions are better seen on cross-sectional examinations such as MR imaging. Endoanal ultrasonography cannot reliably distinguish between infection and fibrosis as both appear as linear tracks of low reflectivity. Hydrogen peroxide injection and 3D imaging can be used to demonstrate opening and anatomy of the track.[65]

Anal trauma

Loss of continuity of any sphincter is abnormal. Marked thinning or breaks in the internal or external sphincters are a sign of trauma. These defects may be acquired as a result of injury sustained during labour or after anal stretch procedures. Obstetric tears are typically situated anteriorly and if the internal sphincter is involved, the defect is seen is the same segment.[66] Isolated tears of the internal sphincter are not seen in obstetric injuries (Fig. 20.34). Well-defined defects may be seen in the internal sphincters after lateral sphincterotomy procedures.

External sphincter injuries most commonly relate to obstetric injuries. Episiotomies are typically seen as well-defined scars in the right lateral quadrant. Penetrating and traumatic anal sphincter injuries are seen as well-defined tracks and may be seen in any quadrant.

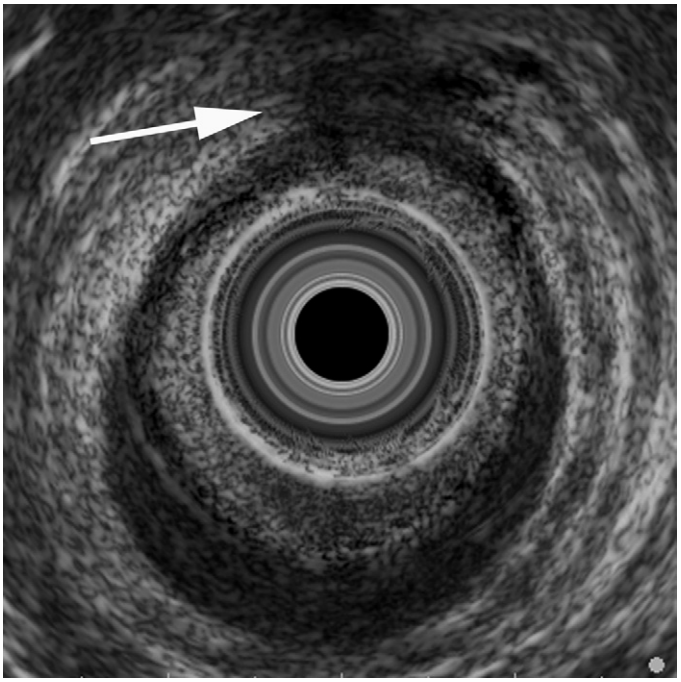
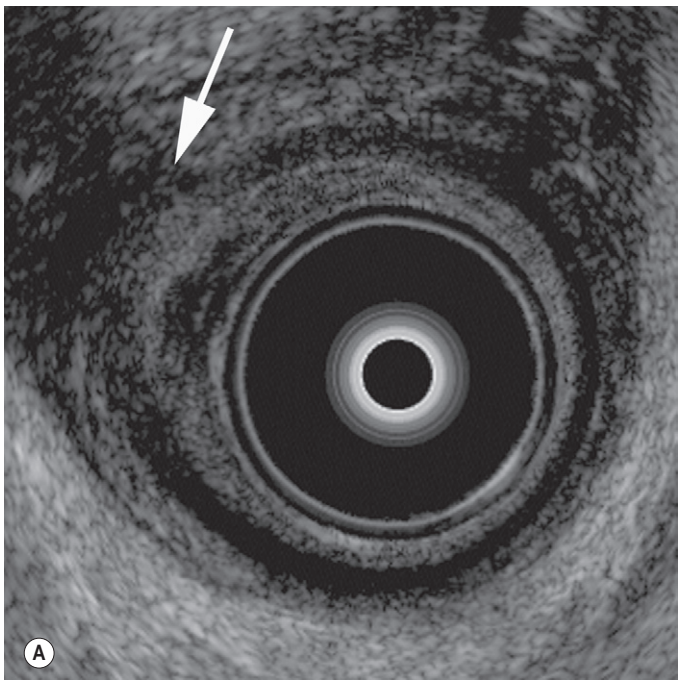


Figure 20.33 Anal sepsis. Fistula-in-ano at 12 o'clock position seen as a poorly reflective area (arrow) associated with a posterior horse-shoe abscess in the intersphincteric plane.



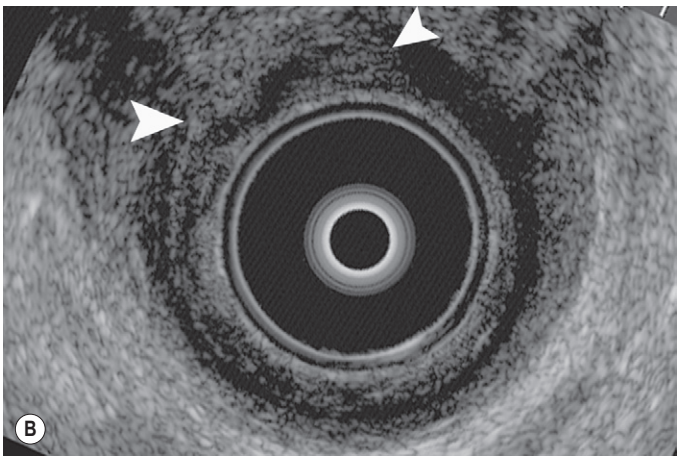


Figure 20.34 Anal trauma. **A:** Obstetric injury during labour. There is break of the internal and external sphincters at the 10 o'clock position (arrow). **B:** Multiple disruptions of the sphincters (arrowheads) after penetrating anal injury (image courtesy Dr I Ramachandran).

Anal sphincter abnormalities

- Obstetric injuries are commonly situated anteriorly and involve internal and external sphincters.
- Isolated internal sphincter injuries are not seen in obstetric injuries.
- Traumatic injuries may occur in any quadrant.
- Solitary rectal ulcer syndrome is the most common cause of internal sphincter thickening.

Miscellaneous conditions

Solitary rectal ulcer syndrome

Solitary rectal ulcer syndrome is the commonest cause of internal sphincter thickening.[67] The thickening is most commonly in the range of 3.5–4.5 mm. There is also associated thickening of the subepithelium which is thought to be secondary to intra-anal intussusception.[68]

Other sphincter abnormalities

Marked thickening of the internal sphincter over 5 mm suggests internal sphincter myopathy, a genetic disorder affecting women. Internal sphincter less than 2 mm in thickness suggests age-related degeneration. Manual dilatation or anal stretch procedures can cause multiple tears or fragmentation of the external sphincter (Fig. 20.34). Fibrosis and granulation in the sphincters are seen as areas of heterogeneous signal.

REFERENCES

1. Puylaert JB. Acute appendicitis: US evaluation using graded compression. Radiology 1986;158(2):355–360.
2. Yabunaka K, Katsuda T, Sanada S, Fukutomi T. Sonographic appearance of the normal appendix in adults. J Ultrasound Med 2007;26(1):37–43.
3. Lee J, Jeong YK, Hwang JC, et al. Graded compression sonography with adjuvant use of a posterior manual compression technique in the sonographic diagnosis of acute appendicitis. AJR Am J Roentgenol 2002;178(4):863–868.
4. Puylaert JB, Rutgers PH, Lalisang RI, et al. A prospective study of ultrasonography in the diagnosis of appendicitis. N Engl J Med 1987;317(11):666–669.
5. Puylaert JB. Ultrasound of acute GI tract conditions. Eur Radiol 2001;11(10):1867–1877.
6. Kessler N, Cyteval C, Gallix B, et al. Appendicitis: evaluation of sensitivity, specificity, and predictive values of US, Doppler US, and laboratory findings. Radiology 2004;230(2):472–478.
7. Chan I, Bicknell SG, Graham M. Utility and diagnostic accuracy of sonography in detecting appendicitis in a community hospital. AJR Am J Roentgenol 2005;184(6):1809–1812.
8. Keyzer C, Zalcman M, De Maertelaer V, et al. Comparison of US and unenhanced multi-detector row CT in patients suspected of having acute appendicitis. Radiology 2005;236(2):527–534.
9. Quillin SP, Siegel MJ, Coffin CM. Acute appendicitis in children: value of sonography in detecting perforation. AJR Am J Roentgenol 1992;159(6):1265–1268.
10. van Breda Vriesman AC, Puylaert JBCM. Mimics of appendicitis: alternative nonsurgical diagnoses with sonography and CT. AJR Am J Roentgenol 2006;186(4):1103–1112.
11. Puylaert JB, van der Zant FM. Mesenteric lymphadenitis or appendicitis? AJR Am J Roentgenol 1995;165(2):490.
12. Puylaert JB, Oudenhoven LF, Koumans RK. Right-sided diverticulitis masquerading as acute appendicitis. Ned Tijdschr Geneeskd 1998;142(23):1350.
13. Menten R, Lebecque P, Saint-Martin C, Clapuyt P. Outer diameter of the vermiform appendix: not a valid sonographic criterion for acute appendicitis in patients with cystic fibrosis. AJR Am J Roentgenol 2005;184(6):1901–1903.
14. Pickhardt PJ, Levy AD, Rohrmann CA, Kende AI. Primary neoplasms of the appendix manifesting as acute appendicitis: CT findings with pathologic comparison. Radiology 2002;224(3):775–781.
15. Connor SJ, Hanna GB, Frizelle FA. Appendiceal tumors: retrospective clinicopathologic analysis of appendiceal tumors from 7,970 appendectomies. Dis Colon Rectum 1998;41(1):75–80.
16. Pickhardt PJ, Levy AD, Rohrmann CA, Kende AI. Primary neoplasms of the appendix: radiologic spectrum of disease with pathologic correlation. Radiographics 2003;23(3):645–662.
17. Moertel C, Weiland L, Nagorney D, Dockerty M. Carcinoid tumor of the appendix: treatment and prognosis. N Engl J Med 1987;317(27): 1699–1701.
18. Pickhardt PJ, Levy AD, Rohrmann CA, et al. Non-Hodgkin's lymphoma of the appendix: clinical and CT findings with pathologic correlation. AJR Am J Roentgenol 2002;178(5):1123–1127.
19. Ripollés T, Martínez MJ, Morote V, Errando J. Appendiceal involvement in Crohn's disease: gray-scale sonography and color Doppler flow features. AJR Am J Roentgenol 2006;186(4): 1071–1078.
20. Baldisserotto M, Cavazzola S, Cavazzola LT, et al. Acute edematous stump appendicitis diagnosed preoperatively on sonography. AJR Am J Roentgenol 2000;175(2):503–504.
21. Shin L, Halpern D, Weston S, et al. Prospective CT diagnosis of stump appendicitis. AJR Am J Roentgenol 2005;184:S62–64.
22. Bru C, Sans M, Defelitto MM, et al. Hydrocolonic sonography for evaluating inflammatory bowel disease. AJR Am J Roentgenol 2001;177(1):99–105.
23. Limberg B. Diagnosis of acute ulcerative colitis and colonic Crohn's disease by colonic sonography. J Clin Ultrasound 1989;17(1):25–31.
24. Limberg B. Diagnosis and staging of colonic tumors by conventional abdominal sonography as compared with hydrocolonic sonography. N Engl J Med 1992;327(2):65–69.
25. Chui DW, Gooding G, McQuaid KR, et al. Hydrocolonic Ultrasonography in the detection of colonic polyps and tumors. N Engl J Med 1994;331(25):1685–1688.
26. Tong SC, Pitman M, Anupindi SA. Best cases from the AFIP: ileocecal enteric duplication cyst: radiologic-pathologic correlation. Radiographics 2002;22(5):1217–1222.
27. Barr LL, Hayden CK, Stansberry SD, Swischuk LE. Enteric duplication cysts in children: are their ultrasonographic wall characteristics diagnostic? Pediatr Radiol 1990;20(5):326–328.
28. Sinha R. Jejunal diverticulosis: sonographic diagnosis. J Clin Ultrasound 2006;34(2):84–87.
29. Pradel J, Adell J, Taourel P, et al. Acute colonic diverticulitis: prospective comparative evaluation with US and CT. Radiology 1997;205(2):503–512.
30. O'Malley ME, Wilson SR. US of gastrointestinal tract abnormalities with CT correlation. Radiographics 2003;23(1):59–72.
31. Vijayaraghavan SB. High-resolution sonographic spectrum of diverticulosis, diverticulitis, and their complications. J Ultrasound Med 2006;25(1):75–85.
32. Wilson S, Toi A. The value of sonography in the diagnosis of acute diverticulitis of the colon. AJR Am J Roentgenol 1990;154(6):1199–1202.
33. Ledermann HP, Borner N, Strunk H, et al. Bowel wall thickening on transabdominal sonography. AJR Am J Roentgenol 2000;174(1):107–115.
34. Oudenhoven LF, Koumans RK, Puylaert JB. Right colonic diverticulitis: US and CT findings – new insights about frequency and natural history. Radiology 1998;208(3):611–618.
35. Fraquelli M, Colli A, Casazza G, et al. Role of US in detection of Crohn disease: meta-analysis. Radiology 2005;236(1):95–101.
36. Horsthuis K, Bipat S, Bennink RJ, Stoker J. Inflammatory bowel disease diagnosed with US, MR, scintigraphy, and CT: meta-analysis of prospective studies. Radiology 2008;247(1):64–79.
37. Sarrazin J, Wilson S. Manifestations of Crohn disease at US. Radiographics 1996;16(3):499–520.
38. Maconi G, Sampietro GM, Russo A, et al. The vascularity of internal fistulae in Crohn's disease: an in vivo power Doppler ultrasonography assessment. Gut 2002;50(4):496–500.
39. Gritzmann N, Hollerweger A, Macheiner P, Rettenbacher T. Transabdominal sonography of the gastrointestinal tract. Eur Radiol 2002;12(7):1748–1761.
40. Chaubal N, Dighe M, Shah M, Chaubal J. Sonography of the gastrointestinal tract. J Ultrasound Med 2006;25(1):87–97.
41. Lee DH, Ko YT, Yoon Y, Lim JH. Sonographic findings of intestinal tuberculosis. J Ultrasound Med 1993;12(9):537–540.

42. Lee DH, Lim JH, Ko YT, Yoon Y. Sonographic findings in tuberculous peritonitis of wet-ascitic type. Clin Radiol 1991;44(5):306–310.
43. Ramachandran I, Sinha R, Rodgers P. Pseudomembranous colitis revisited: spectrum of imaging findings. Clin Radiol 2006;61(7): 535–544.
44. Kirkpatrick IDC, Greenberg HM. Gastrointestinal complications in the neutropenic patient: characterization and differentiation with abdominal CT. Radiology 2003;226(3):668–674.
45. Teefey S, Montana M, Goldfogel G, Shuman W. Sonographic diagnosis of neutropenic typhlitis. AJR Am J Roentgenol 1987;149(4):731–733.
46. Ripollés T, Simó L, Martínez-Pérez MJ, et al. Sonographic findings in ischemic colitis in 58 patients. AJR Am J Roentgenol 2005;184(3): 777–785.
47. Anderson DR. The pseudokidney sign. Radiology 1999;211(2):395–397.
48. Shirahama M, Koga T, Ishibashi H, et al. Sonographic features of colon carcinoma seen with high-frequency transabdominal ultrasound. J Clin Ultrasound 1994;22(6):359–365.
49. Lee DH, Ko YT, Shin GH, et al. Sonographic detection of rectal carcinoma. Clin Imaging 2002;26(1):30–34.
50. Doniec JM, Kahlke V, Peetz F, et al. Rectal endometriosis: high sensitivity and specificity of endorectal ultrasound with an impact for the operative management. Dis Colon Rectum 2003;46(12):1667–1673.
51. Carbognin G, Guarise A, Minelli L, et al. Pelvic endometriosis: US and MRI features. Abdom Imaging 2004;29(5):609–618.
52. Kim YH, Blake MA, Harisinghani MG, et al. Adult intestinal intussusception: CT appearances and identification of a causative lead point. Radiographics 2006;26(3):733–744.
53. Huang BY, Warshauer DM. Adult intussusception: diagnosis and clinical relevance. Radiol Clin North Am 2003;41(6):1137–1151.
54. van Breda Vriesman AC, Lohle PN, Coerkamp EG, Puylaert JB. Infarction of omentum and epiploic appendage: diagnosis, epidemiology and natural history. Eur Radiol 1999;9(9):1886–1892.
55. Rioux M, Langis P. Primary epiploic appendagitis: clinical, US, and CT findings in 14 cases. Radiology 1994;191(2):523–526.
56. Bartram CI, Frudinger A. Handbook of anal endosonography. Petersfield: Wrightson Biomedical; 1997.
57. Berton F, Gola G, Wilson SR. Perspective on the role of transrectal and transvaginal sonography of tumors of the rectum and anal canal. AJR Am J Roentgenol 2008;190(6):1495–1504.
58. Sudakoff GS, Quiroz F, Foley WD. Sonography of anorectal, rectal, and perirectal abnormalities. AJR Am J Roentgenol 2002;179(1): 131–136.
59. Law PJ, Bartram CI. Anal endosonography: technique and normal anatomy. Gastrointest Radiol 1989;14(4):349–353.
60. Frudinger A, Bartram CI, Halligan S, Kamm M. Examination techniques for endosonography of the anal canal. Abdom Imaging 1998;23(3):301–303.
61. Heneghan JP, Salem RR, Lange RC, et al. Transrectal sonography in staging rectal carcinoma: the role of gray-scale, color-flow, and Doppler imaging analysis. AJR Am J Roentgenol 1997;169(5): 1247–1252.
62. Bipat S, Glas AS, Slors FJM, et al. Rectal cancer: local staging and assessment of lymph node involvement with endoluminal US, CT, and MR imaging – a meta-analysis. Radiology 2004;232(3): 773–783.
63. Maier AG, Barton PP, Neuhold NR, et al. Peritumoral tissue reaction at transrectal US as a possible cause of overstaging in rectal cancer: histopathologic correlation. Radiology 1997;203(3):785–789.
64. Halligan S, Stoker J. Imaging of fistula in ano. Radiology 2006;239(1):18–33.
65. Buchanan GN, Bartram CI, Williams AB, et al. Value of hydrogen peroxide enhancement of three-dimensional endoanal ultrasound in fistula-in-ano. Dis Colon Rectum 2005;48(1):141–147.
66. Frudinger A, Ballon M, Taylor SA, Halligan S. The natural history of clinically unrecognized anal sphincter tears over 10 years after first vaginal delivery. Obstet Gynecol 2008;111(5):1058–1064.
67. Halligan S, Sultan A, Rottenberg G, Bartram CI. Endosonography of the anal sphincters in solitary rectal ulcer syndrome. Int J Colorectal Dis 1995;10(2):79–82.
68. Marshall M, Halligan S, Fotheringham T, et al. Predictive value of internal anal sphincter thickness for diagnosis of rectal intussusception in patients with solitary rectal ulcer syndrome. Br J Surg 2002;89(10):1281–1285.

CHAPTER

21 Kidneys: anatomy and technique

Paul L. Allan

NORMAL ANATOMY AND ANATOMICAL RELATIONS 413

RENAL ANATOMY 413

TECHNIQUES OF EXAMINATION 415
Positioning and access 415
Renal size 415
Cortical and parenchymal thickness 415
Perirenal structures 417
Renal vessels 417
Ectopic kidneys, technique 418
Nephroptosis 418

NORMAL APPEARANCES ON ULTRASOUND 418
Renal parenchyma 418
Cortex and medulla 418
Fetal lobation 420
Splenic humps 420
Septa of Bertin 420
The renal sinus, collecting system and vessels 421

CONGENITAL VARIANTS OF RENAL STRUCTURE AND POSITION 423
Duplex collecting system and ureters 423
Ectopic kidneys 423
Horseshoe kidneys 424
Hypoplasia and atrophy 425
Congenital solitary kidney 425

NORMAL ANATOMY AND ANATOMICAL RELATIONS

The kidneys lie in the retroperitoneal fat on either side of the vertebral column with the left kidney usually lying at a slightly higher level than the right.[1] They are a little flattened in transverse section and oval in the longitudinal plane resulting in an ellipsoidal shape. They are positioned with their long axes diverging inferiorly so that the lower poles are more lateral and anterior than the upper poles. The longer axis of the transverse plane is also angled at about 45° so that the hilum of each kidney lies more anteriorly than the lateral border.

The psoas muscles are related to the medial aspects of both kidneys. On the right side the right lobe of the liver covers the lateral aspect and much of the anterior surface of the kidney; the hepatic flexure of the colon and the duodenum are also related to the anterior surface. Medially the hilum of the right kidney lies adjacent to the inferior vena cava (IVC) with the right adrenal gland above its upper pole. On the left side the spleen lies adjacent to the lateral aspect of the upper pole and the left adrenal gland lies superiorly and anteromedially. Inferiorly the splenic flexure of the colon lies anterolaterally and the tail of the pancreas extends over the middle portion of the anterior surface. Medially the hilum of the left kidney is related to the abdominal aorta (Fig. 21.1).

The kidneys are surrounded by the perirenal fat, which is confined by the anterior and posterior renal fascia; these are sometimes referred to as Gerota's fascia and they separate the perirenal space from the anterior and posterior pararenal spaces. These fascial planes are not usually seen on ultrasound, but their presence may influence the development or appearances of retroperitoneal collections of fluid and inflammatory changes (Fig. 21.2).[2]

On the right side a reflection of the parietal peritoneum passes up between the inferior surface of the liver and the anterior surface of the kidney; this is the posterior subhepatic space (hepatorenal fossa or Morison's pouch). On the left side the lesser sac lies in front of the kidney. Fluid may accumulate in these spaces when ascites is present.

RENAL ANATOMY

The length of the normal adult kidney is usually given as 10–12 cm but there is a wider range of 7–14 cm in patients with normal renal function.[3,4] Renal size is related to sex, age and build of the individual.[5] The length can even vary in the same individual between scans depending on the state of hydration at the time of examination.[6] Pregnancy also causes an increase in overall renal size.[7] Ultrasound measurements of renal length tend to be shorter than those obtained on intravenous urography as there is no magnification factor and no osmotic diuresis induced by intravenous contrast agents.[3] Conversely, on urography some foreshortening of the kidney occurs due to the slight tilt of the kidneys in an anteroposterior plane and this can lead to an underestimation of true renal length.[8] Studies comparing ultrasound and CT have shown that they measure similar renal lengths.[9]

The kidney is surrounded by a fibrous capsule which demarcates it from the surrounding perirenal fat. The cortex forms the outer part of the renal parenchyma surrounding the medulla, which is made up of the renal pyramids arranged around the renal sinus. Projections of the cortex extend down to the renal sinus between the pyramids; these are called septa (or columns) of Bertin.[10]

The renal sinus contains the collecting system together with the major arteries and veins; these structures are surrounded by fat which fills the renal sinus. The tips of the pyramids project into the calyces of the collecting system, and the calyces join up to form the renal pelvis. The renal sinus opens on the medial aspect of the kidney; most of the renal pelvis is usually within the renal sinus but it can project outside the kidney to some extent, producing an extrarenal pelvis which may be confused with a parapelvic cyst or pathological fluid collection on ultrasound.

In the extrarenal part of their courses the renal arteries lie behind the renal veins, but as they approach the hilum they divide into segmental branches which pass in front and behind the renal pelvis. Similarly, branches of the renal veins pass in front and behind the renal pelvis, although the main renal veins lie in front of the arteries outside the kidney. About 40% of people have a single main artery and vein on each side; accessory renal arteries are found in 40%, more commonly on the left side.[11] Within the hilum the segmental

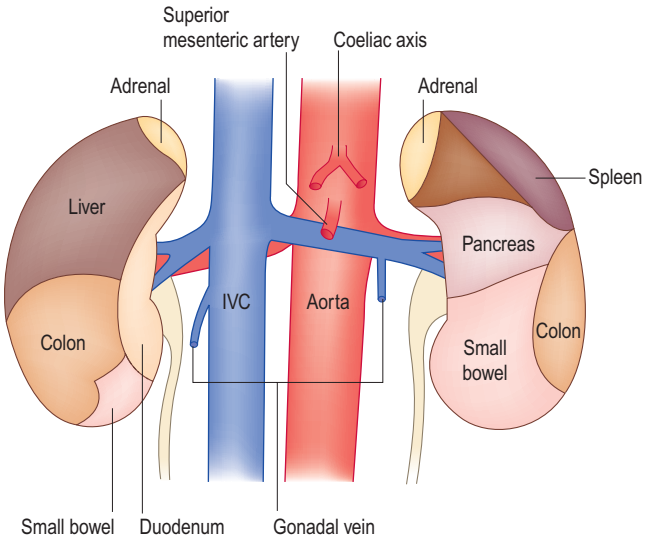


Figure 21.1 Anatomical relations of the kidneys. Diagrammatic representation indicating the major anatomical structures that are related to the kidneys.

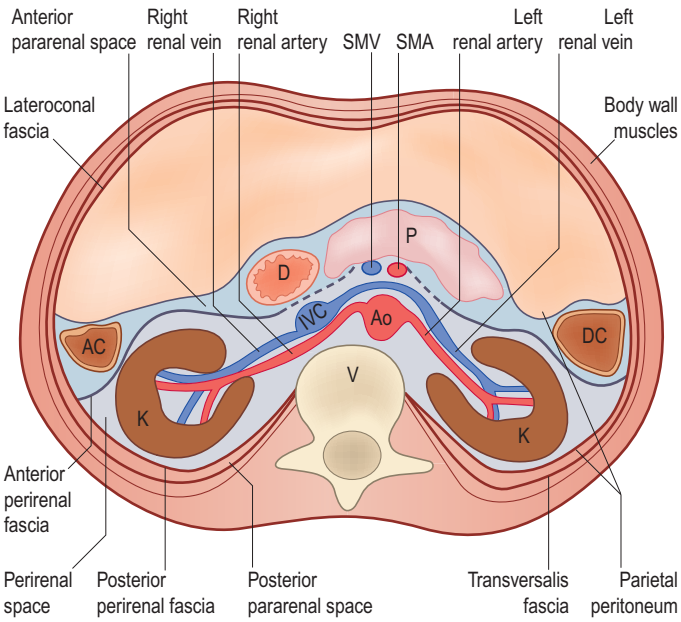


Figure 21.2 Fascial planes of the abdomen. The transversalis, lateroconal and perirenal fascia determine the localisation of fluid collections and infections in the renal areas. AC, ascending colon; Ao, aorta; DC, descending colon; D, duodenum; IVC, inferior vena cava; K, kidney; SMA, superior mesenteric artery; SMV, superior mesenteric vein; P, pancreas; V, vertebral body.

branches of the renal artery divide into interlobar branches which penetrate the parenchyma. As they approach the bases of the pyramids they give off small branches which run around the corticomedullary junctions; these are called the arcuate arteries (Fig. 21.3).[10]

The developing kidney is formed from a number of lobes in the fetus, typically about 14.[12] These combine together and merge but traces of fetal lobes may persist on the surface of adult kidneys. The lobes can be grouped into anterior and posterior components. In the past these have been called renunculi[13] and the highly reflective line sometimes seen running obliquely through the kidney from anteriorly near the upper pole to posteriorly near the lower pole

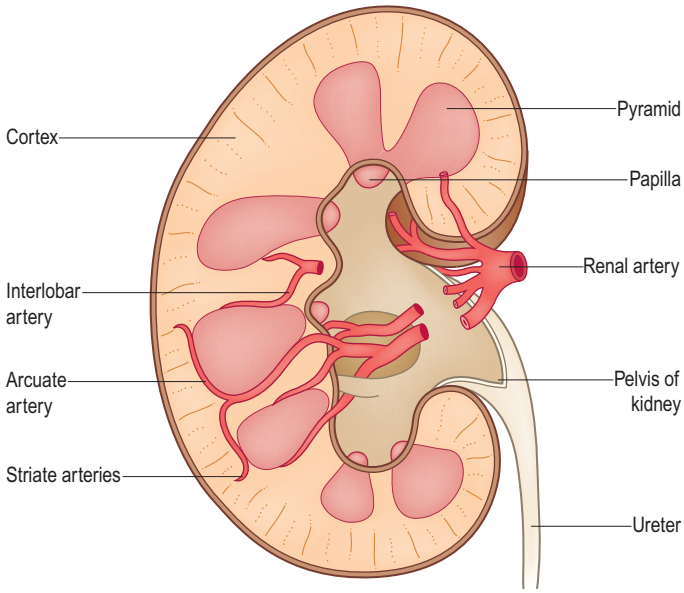


Figure 21.3 Divisions of the renal artery. The major branchings of the renal artery follow a predictable pattern. The major branches indicated here may be detectable on ultrasound, especially with colour flow imaging (reproduced from Allan, McDicken, Pozniak & Dubbins, Clinical Doppler Ultrasound 2nd edition, 2006, Churchill Livingstone).

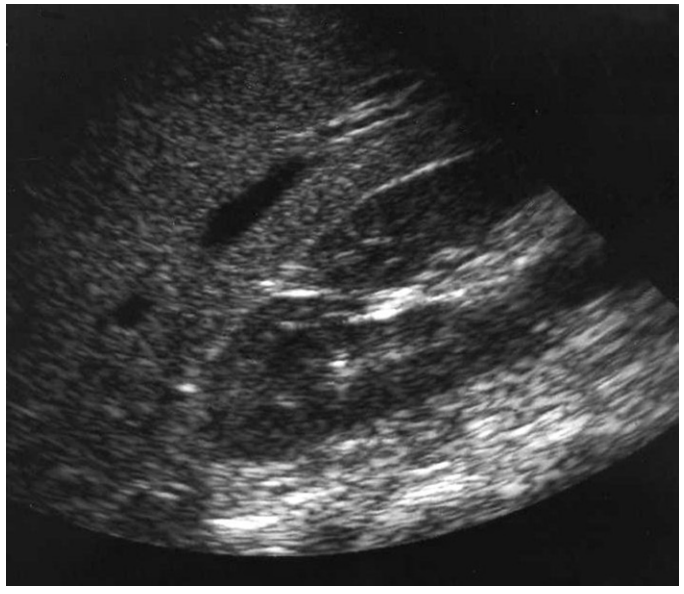


Figure 21.4 A junctional parenchymal defect or highly reflective line is seen on the anterior aspect of the cortex; this probably represents an extension of sinus/hilar fat near the medial aspect of the kidney rather than a septum between two 'renunculi'.

was considered to represent connective tissue at the junction of the two components: the parenchymal junctional defect.[14,15] This line is seen more frequently in children but may also be seen in adults (Fig. 21.4). However, subsequent reassessment of this aspect of renal anatomy suggests that this line represents an extension into the parenchyma of hilar or sinus fat in patients with a deep renal sinus, rather than a true plane of fusion between embryological components.[16]

TECHNIQUES OF EXAMINATION

Positioning and access

Despite their size it can sometimes be difficult to image normal kidneys adequately and various manoeuvres, together with various positions of the patient and the transducer, may be required for a satisfactory examination.

The examination usually commences with the patient supine. The right kidney is assessed first as it is usually easier to examine than the left kidney. The liver is used as an acoustic window to the kidney and the transducer is placed in subcostal and/or intercostal positions (Fig. 21.5). Varying the degree of respiration by asking the patient to take deep breaths, or to distend his/her abdomen may be of value. If there are gas-filled loops of bowel in the hepatorenal fossa or interposed between the liver and abdominal wall, it may be helpful to raise the patient's right side and scan from a lateral or posterolateral approach.

The left kidney is more difficult to visualise because gas in the small bowel and splenic flexure may interfere with an anterior or anterolateral approach. It is therefore better to start searching for the kidney from a posterolateral approach with the left side of the patient raised by approximately 45°. If this is still unsuccessful then examination of the patient in the full right lateral decubitus position with a pillow under the right flank and the left arm extended over the head may allow access to the left kidney. The spleen can provide an acoustic window to the upper pole of the kidney and if there is splenomegaly, this window is extended to include more of the kidney.

The posterior approach is rarely required in adults (except for renal biopsy localisation) as modern real-time equipment is usually able to provide adequate images from more anterior approaches. The thick paraspinal muscles distort both the transmitted and reflected sound waves, impairing the quality of the image, and the ribs may obscure parts of the upper poles, particularly on the left. In young children prone scanning remains a useful approach (see Chapter 71).

Once a kidney has been located, it should be examined in a systematic fashion. An overall impression of renal size and cortical thickness can be obtained quite rapidly and, with experience, a feeling for the normal range of appearances at various ages is developed.

Points of technique

Access to the right kidney: usually through the liver which acts as an acoustic window.
Access to the left kidney: usually best from a lateral, or posterolateral approach.
Doppler of renal vessels: initial location and targeting performed during quiet respiration, final assessment with suspended respiration.
Renal artery origins: may be seen from a transhepatic scan in the coronal plane.
Renal length measurement: ensure longest axial length is obtained by rotating transducer around its longitudinal axis.

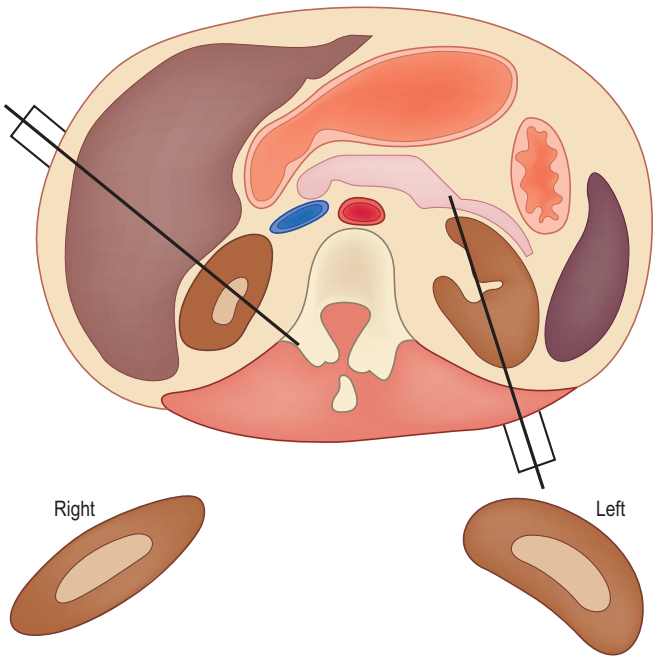


Figure 21.5 Access sites for the kidneys. Line diagram showing the usual access sites for the right and left kidneys and diagrams showing the normal renal shapes as seen from these approaches.

Renal size

To measure the overall length the longest craniocaudal length is found by rotating the probe around its vertical axis. Care must be taken to measure the longest length as it is easy to obtain a false, low measurement due to the ellipsoidal shape of the kidney (Fig. 21.6). If a measurement is to be recorded it is important that this is the longest length, especially if serial measurements are likely to be made. With careful technique serial measurements accurate to within 1 cm (approximately 10%) can be obtained in 95% of cases in children,[17] although larger limits of agreement up to 1.85 cm between pairs of sonographers have been reported in adults.[18] Renal length can be measured easily and quickly in most patients and provides a reasonable estimate of overall renal size, but care should be taken in attributing significance to differences between measurements of less than 10–12 mm. A more accurate estimate of the size of the kidneys is sometimes necessary and in these cases an assessment of the renal volume can be made. This is best performed by measuring the area of the kidney in serial slices and subsequently calculating the volume.[19] However, this is very time-consuming and an alternative is to use a modified three-dimensional ellipsoidal formula where the length, anteroposterior and transverse diameters are multiplied by a constant,[20] whose value is still the subject of some debate but is around 0.5.[7,20] In practice the errors in the ultrasound measurements are of the order of 5% and there is thus no logic in using a correction factor with more than two significant figures. A factor of 0.5 is therefore an entirely acceptable compromise. The precise value is probably not as important as consistency in measurement technique, so that changes in volume over a period of time can be measured. Normal values for renal length in adults are given in Table 21.1.

Volume measurements are of particular value in the assessment of transplants, or post-nephrectomy patients to assess compensatory hypertrophy; slight increases in volume have been reported in insulin-dependent diabetics, particularly those with albuminuria.[21,22]

Cortical and parenchymal thickness

Cortical thickness can also be measured if desired but this is more variable, even in kidneys with normal function. It can vary depending on the age and size of the patient and depends also on the angle of viewing, as the cortex tends to be thicker laterally than medially. This, and the slight flattening of the kidney in the anteroposterior plane, account for the different shapes when the two kidneys are viewed from the usual anterolateral and posterolateral directions for right and left respectively (Fig. 21.5). The cortical thickness is the distance between the capsule and the outer margin of the

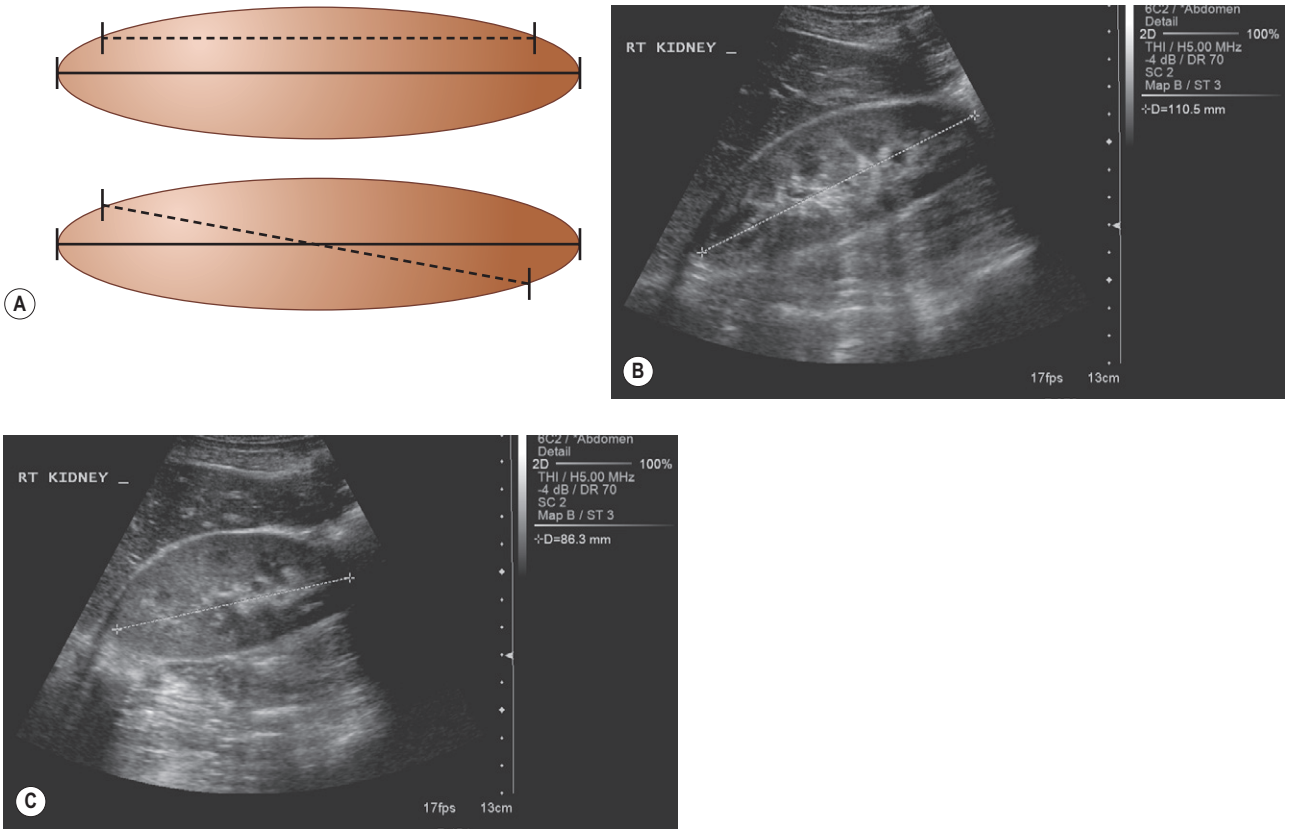


Figure 21.6 Renal length measurement. A: Line diagram to show the renal length measurement and possible sources of error in obtaining maximum lengths by failing to get the best scanning plane. **B** and **C:** A normal kidney with true maximum length of 11 cm shown to have an apparent length of 8.6 cm due to inaccurate orientation.

Table 21.1 Normal (median) renal length in adults (adapted from Emamian et al.[5])

	Women (cm)	Men (cm)
Left kidney	11.0 (9.9–12.1)	11.5 (10.4–12.6)
Right kidney	10.7 (9.5–12.0)	11.2 (10.1–12.4)

Figures in brackets are 10th and 90th centiles.

medullary pyramid; it must be distinguished from parenchymal thickness, which is the distance between the capsule and the margin of the sinus echoes (Fig. 21.7). This latter measurement is easier to perform and corresponds better with the assessment used on urography examinations when a line is drawn through the outer margins of the calyces. It is important, if serial measurements are being taken, to specify whether a measurement refers to cortical or parenchymal thickness as consistency is necessary for reliable comparison. Due to the variations in overall size and cortical thickness in normal kidneys and the degree of overlap with diseased kidneys, it is difficult to define upper and lower limits for these measurements in normal patients. Both renal length and parenchymal thickness tend to be smaller in patients with impaired renal function, although significant overlap occurs between different diagnostic groups.[23] In practice, an overall impression of length, volume and cortical thickness often allows an experienced sonographer to assess general renal size in relation to the clinical condition of the patient.

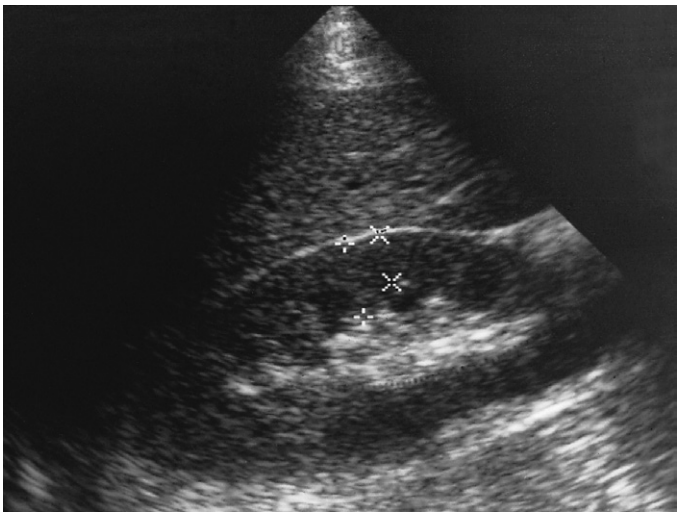


Figure 21.7 Measurement of cortical thickness. Scan showing the difference in values between measurement of cortical thickness from the capsule to the outer border of the pyramid (x), and parenchymal thickness from the capsule to the outer margin of the sinus echoes (+).

Care must be taken to include the whole kidney in longitudinal section, otherwise peripheral abnormalities may be missed. This can be avoided by rocking the transducer so that the beam passes from one side to the other. When the longitudinal examination is completed the probe is turned through 90° and the kidney is examined in the transverse plane, again ensuring that it is examined completely from top to bottom.

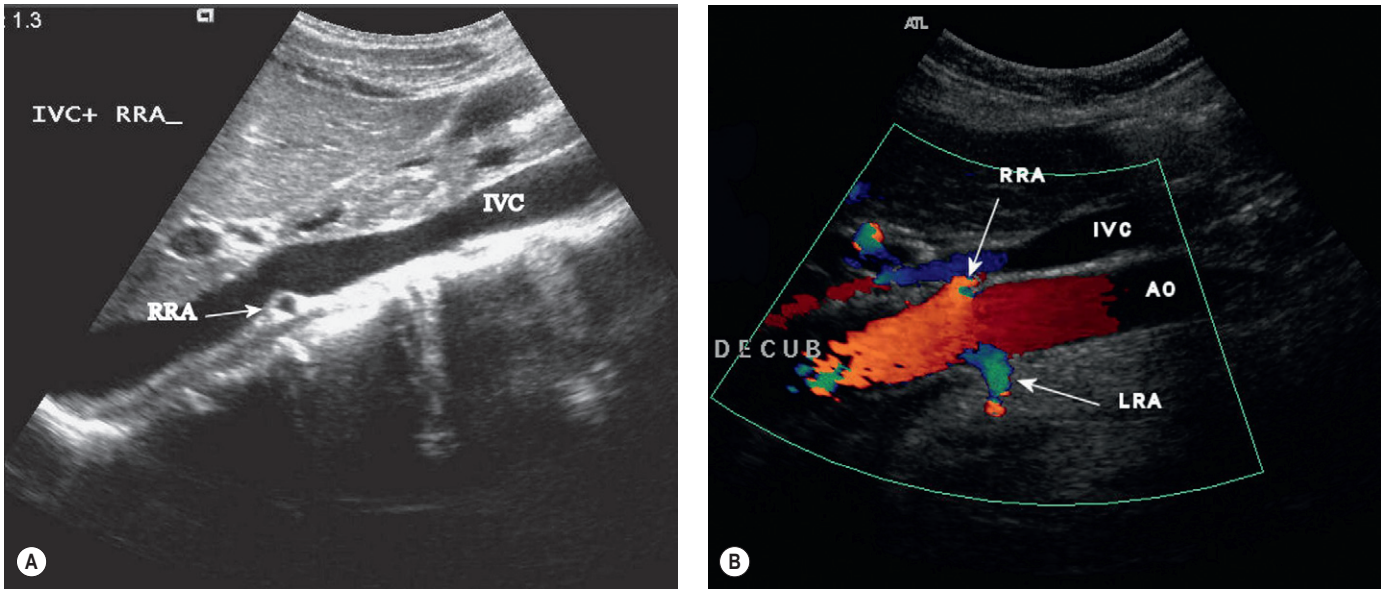


Figure 21.8 **Renal arteries. A:** The right renal artery (RRA, arrow) is seen passing behind the inferior vena cava (IVC). **B:** Decubitus/Coronal view from the right flank showing the origins of the renal arteries. Ao, aorta; LRA, left renal artery.

In addition to assessing the overall size and structure of the kidney, note should be made of the cortical reflectivity compared with the adjacent liver or spleen, the degree of corticomedullary differentiation, and the size and appearance of the medullary pyramids.

Perirenal structures

The movement of the kidney during respiration may be impeded by a variety of intra- and extrarenal abnormalities, thus providing useful diagnostic clues. In addition, in patients with small fibrotic kidneys, the movement of the kidney in the perirenal tissues may allow their identification and definition in difficult cases.

The perirenal fat, pararenal areas and adrenal areas should all be assessed briefly. If renal abnormalities are present, other more remote sites such as the liver, para-aortic areas, IVC, line of the ureters, pelvis and the bladder may need to be examined.

Renal vessels

Assessment of the renal vessels by imaging and Doppler may be required. In slim patients the renal arteries can often be identified on colour Doppler from an anterior approach as they leave the aorta, the right renal artery being located as it passes behind the IVC (Fig. 21.8A); the left renal artery is more difficult to demonstrate[24] and accessory arteries are usually not visualised.[25] In some patients use of both decubitus positions with the upper arm raised may allow visualisation of the renal arteries (Fig. 21.8B). Using a flexible approach, the origins and proximal segments of one or both arteries can be detected in a significant number of patients, although this may take some time. The intrarenal arteries are easier to demonstrate within the renal sinus, or the interlobar segments. They are identified using colour Doppler with the patient breathing quietly, rather than holding their breath, as this induces dyspnoea and increases respiratory movement of the kidney when the patient breathes. Spectral Doppler waveforms can be recorded as necessary during short periods of suspended respiration; it is good practice to obtain spectral traces from the upper, middle and lower segments of the kidney so that any significant differences due to accessory arteries are detected and resistive indices for each side can be averaged.[26] The use of echo-enhancing agents can improve visualisation of both the main renal arteries and their intrarenal branches, together with a reduction in the time necessary to perform the examination.[27]

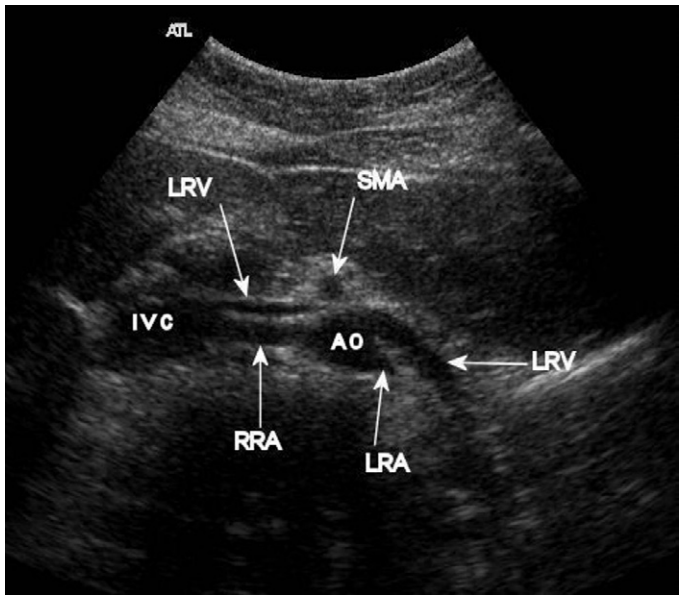


Figure 21.9 **Transverse view showing the left renal vein** passing between the superior mesenteric artery (SMA) and the aorta and the origins of the renal arteries. Ao, aorta; IVC, inferior vena cava; LRA, left renal artery; LRV, left renal vein; RRA, right venal vein.

Similarly the renal veins can be visualised both from an anterior or anterolateral approach; the left renal vein may be seen as it passes behind the superior mesenteric artery and in front of the aorta (Fig. 21.9). It often appears to be narrowed at this point with some peripheral dilatation but this is a normal appearance and not a sign of obstruction.[28] The right renal vein is shorter and is seen passing medially from the hilum of the kidney to the IVC. In fatter or more difficult patients it may be necessary to try to locate the vessel at or near the hilum of the kidney from a lateral approach and trace it

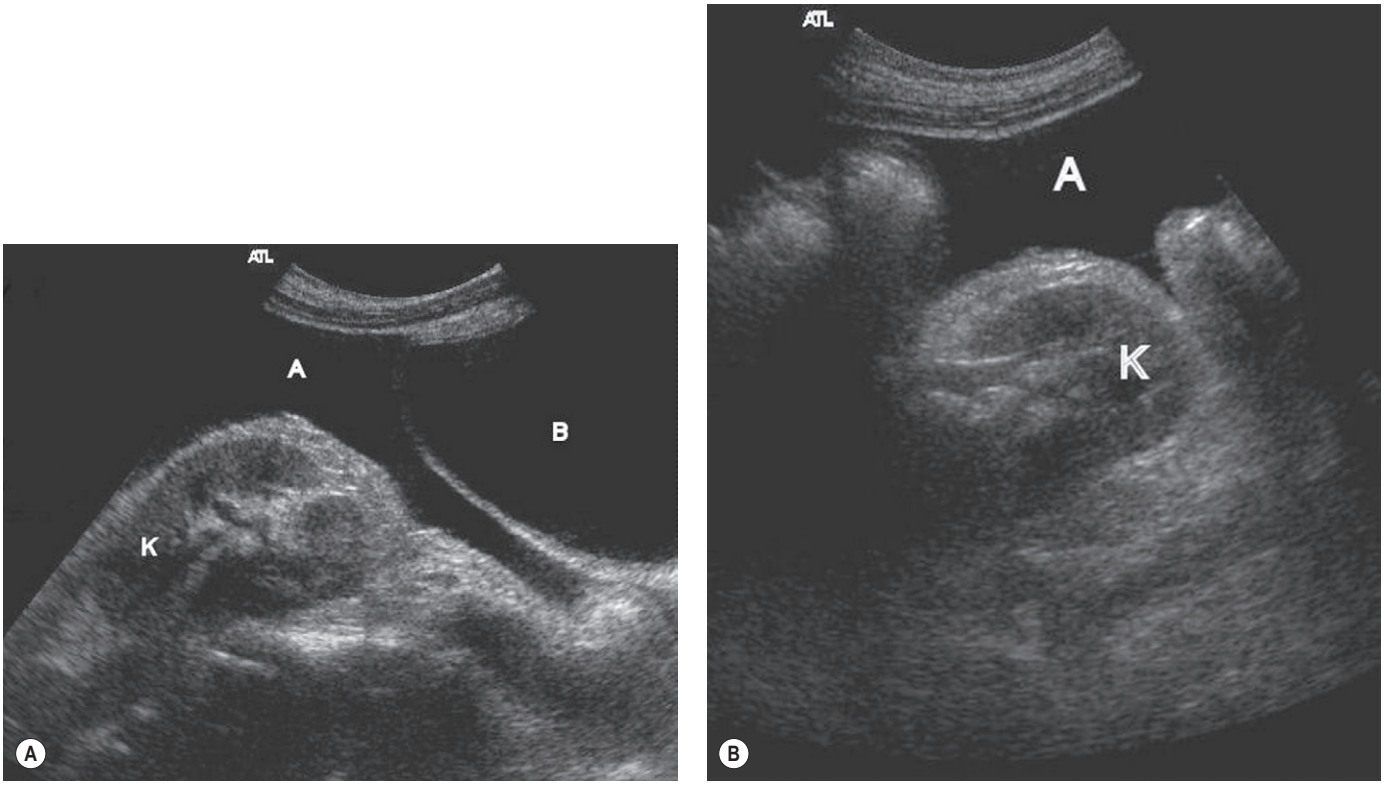


Figure 21.10 A and B: Two views of an ectopic left kidney (K) lying adjacent to the iliac vessels and bladder (B) in a patient with ascites (A).

proximally as far as possible towards the IVC or aorta, but it may be impossible to demonstrate the entire length in many obese patients.

Ectopic kidneys, technique

If a normal kidney is not seen in the renal fossa, the possibility that the kidney is atrophic or hypoplastic must be considered. The contralateral kidney should be reassessed for evidence of compensatory hypertrophy. If it is unusually large, this implies that the other kidney is non-functional or absent, while a normal-sized contralateral kidney implies that there may well be another kidney present somewhere with a reasonable amount of functioning tissue.

The patient should then be carefully examined beginning with the renal fossa on the side of the missing kidney, passing down the flank and psoas muscle into the pelvis (Fig. 21.10). If this does not reveal the missing kidney, the pelvis should be searched carefully and also the opposite flank to detect crossed renal ectopia. The ectopic kidney may look like a kidney but it may also be somewhat indeterminate in nature. In these cases, colour Doppler may show a regular, renal pattern of vascularity.

Nephroptosis

Examination for ptosis of a kidney is not usually very rewarding on ultrasound as it is difficult to find stable landmarks to compare the renal position when the patient moves from horizontal to vertical, or supine to decubitus positions. Assessing the position of the kidney in relation to the twelfth rib in the prone and erect position may give some assessment of vertical movement. Alternatively, lumbar transverse processes can be identified in slim patients and used as fixed reference points. Examination in the lateral decubitus positions may reveal significant medial mobility of the kidney, particularly on the right (Fig. 21.11). The significance of moderate or even marked degrees of vertical movement is controversial; medial movement may be of greater clinical importance. Patients should therefore be examined in both decubitus positions as well as supine and upright if symptoms are attributed to nephroptosis.[29,30]

NORMAL APPEARANCES ON ULTRASOUND

Renal parenchyma

Cortex and medulla

The normal kidneys can usually be identified without difficulty because of the difference in reflectivity between the parenchyma and surrounding fat. The outer margin of the cortex is well defined due to the renal capsule, but the inner margin of the parenchyma, adjacent to the echoes from the sinus fat, is less well defined (Fig. 21.12). The renal cortical reflectivity can be assessed subjectively by comparison with that of the adjacent liver or spleen, assuming that these organs are normal.[31]

Normal cortex has a reflectivity less than that of the adjacent liver and spleen but the degree of difference is, to some extent, equipment dependent and this distinction may be less obvious with some makes of scanner, or with particular settings for pre- and post-processing (see Chapter 1).[32] However, if the renal cortex is brighter than the normal liver, this strongly suggests the presence of parenchymal disease.

The medullary pyramids are less reflective than the cortex and can be identified with modern equipment as echo-poor oval structures, evenly distributed around the inner margin of the cortical

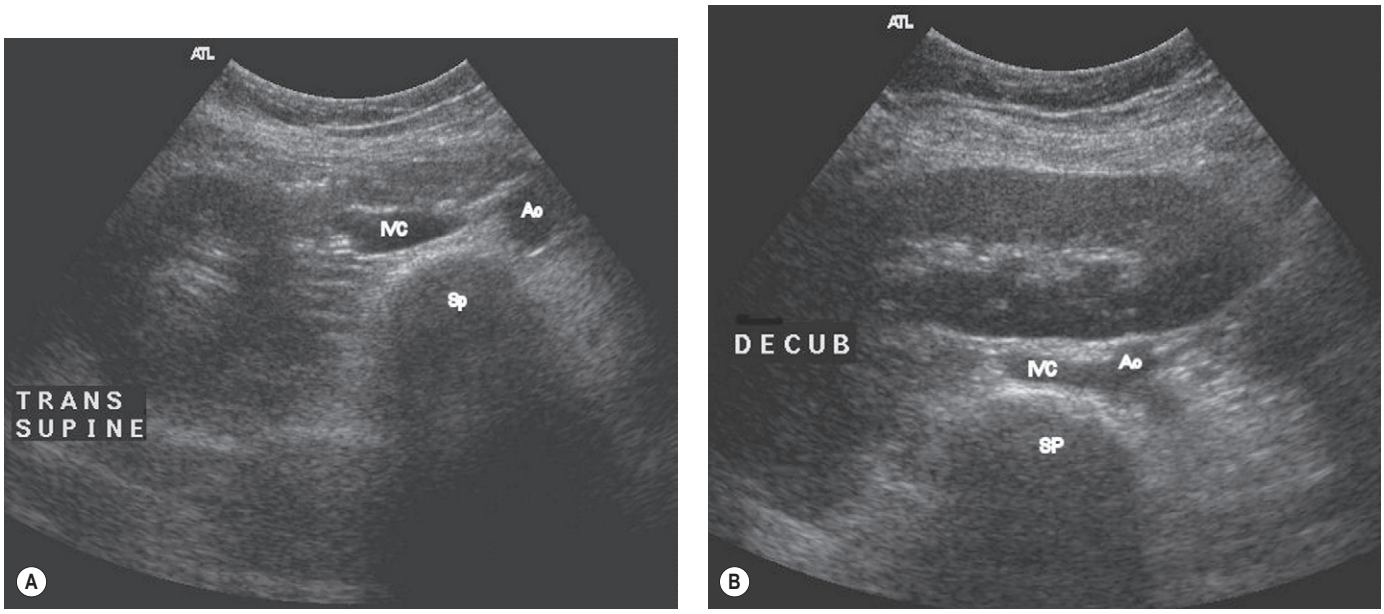


Figure 21.11 **Nephroptosis. A:** The right kidney is seen in a normal position on a transverse scan. **B:** With the patient lying on the left side, the kidney is seen to have crossed the midline and now lies across the spine (Sp) with much of it lying to the left of the aorta (Ao). This was asymptomatic and an incidental finding. IVC, inferior vena cava.

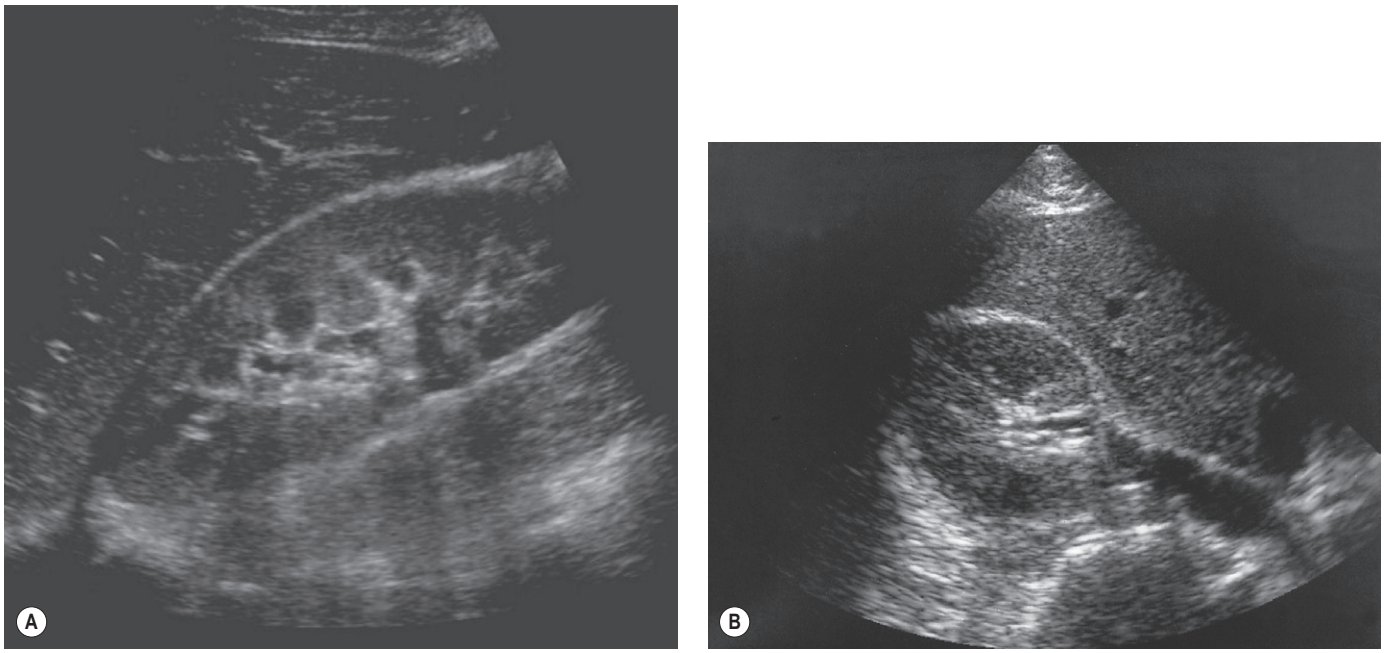


Figure 21.12 **Normal kidney. A:** Normal kidney showing cortex and pyramids with bright central sinus echoes. **B:** Transverse view of a normal kidney at the level of the renal hilum. The renal vein can be seen passing out of the plane of image towards the IVC.

parenchyma adjacent to the sinus echoes.[33,34] Small, highly reflective foci may be seen at the margins between the medullary pyramids and the adjacent cortex representing the interlobar and arcuate arteries (Fig. 21.13); their nature can be confirmed by Doppler. The margin between the pyramids and the adjacent cortex is usually well defined but in the presence of generalised parenchymal inflammation or oedema, this corticomedullary differentiation may be lost or, in some circumstances, enhanced.[31] This feature is more readily detected in transplants where visualisation is better because their superficial position allows high-frequency transducers, e.g. 5–7.5 MHz, to be used (see Chapter 28).

Assessment of parenchymal thickness around the margin of a kidney helps to detect and assess scarring secondary to childhood pyelonephritis, reflux or infarction. The parenchyma normally thins with age[5,35] but part of this impression of thinning is due to the development of sinus lipomatosis where the amount of fat in the renal sinus is increased.[29] This results in thinning of the parenchyma but there is a less marked decrease in renal length because the parenchymal atrophy is compensated, to some extent, by the increase in fat.[4] Normal values for parenchymal thickness have not been published but some authors suggest that a thickness less than 1.5 cm is indicative of thinned parenchyma.[22]

Fetal lobation

The adult kidney is formed in the fetus from several lobes.[9] Lobations may often be seen in neonates but usually disappear as the kidney matures, although they may still be seen in some adults.[11] Normally these coalesce to such an extent that differentiation is not possible on ultrasound. Occasionally one or more may remain apparent and produce a bulge in the renal outline which may be difficult to distinguish from a tumour or from focal hypertrophy adjacent to a cortical scar. In these cases of 'persistent fetal lobation', careful examination often shows that the cortical indentation overlies the interval between pyramids rather than a pyramid itself, which is the case with cortical scarring.[34]

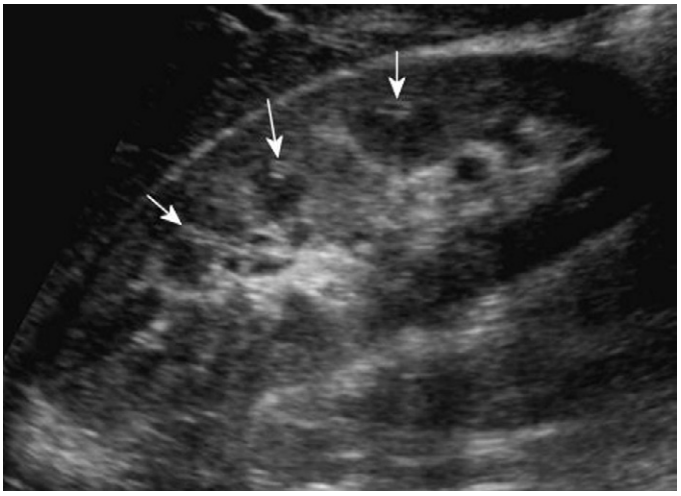


Figure 21.13 Intrarenal arterial branches. A normal kidney showing the cortex and medullary pyramids with the arcuate arteries (arrows) visible as small reflective foci in the junctional region between cortex and medulla.

Splenic humps

Splenic humps and other developmental cortical bulges are due to minor adaptations of the renal contour to adjacent organs. Their appearance may suggest a mass but careful examination usually confirms a uniform parenchymal thickness between the capsule and the renal sinus echoes and normal renal architecture (Fig. 21.14). Colour Doppler will show a normal distribution of vessels in this region.

Septa of Bertin

As the fetal lobes coalesce, the cortex of the deeper parts of a lobe becomes included within the kidney.[9] These portions of cortex from adjacent lobes project down to the renal sinus as the septa of Bertin between the papillae and normally do not produce any distortion of parenchymal anatomy (Fig. 21.15). Occasionally they are unusually prominent and distort the normal renal structure, simulating a tumour.[36] They can usually be differentiated from tumour on ultrasound as the renal cortical outline is not usually distorted even by a large septum of Bertin, and the septa are usually of similar reflectivity to the remainder of the cortex. However, reports of slightly increased reflectivity in a few childhood cases have been made.[36] The normal vascular pattern on colour Doppler also helps in distinguishing these prominent septa from tumours. The renal sinus echoes may show a characteristic pincer-like splaying around the enlarged septum as the sinus fat extends along the margin of the cortical tissue around the calyces of the adjacent lobes.[37]

Normal renal mass-like lesions

Prominent septum of Bertin: coalescence of cortex from adjacent fetal lobes.
Splenic hump: indentation from the spleen on the lateral aspect of the left kidney.
Fetal lobation: persistence of the outline of a fetal lobe.
Renal sinus lipomatosis: increase in the amount and prominence of the fat in the renal sinus around the collecting system, usually related to age and obesity.

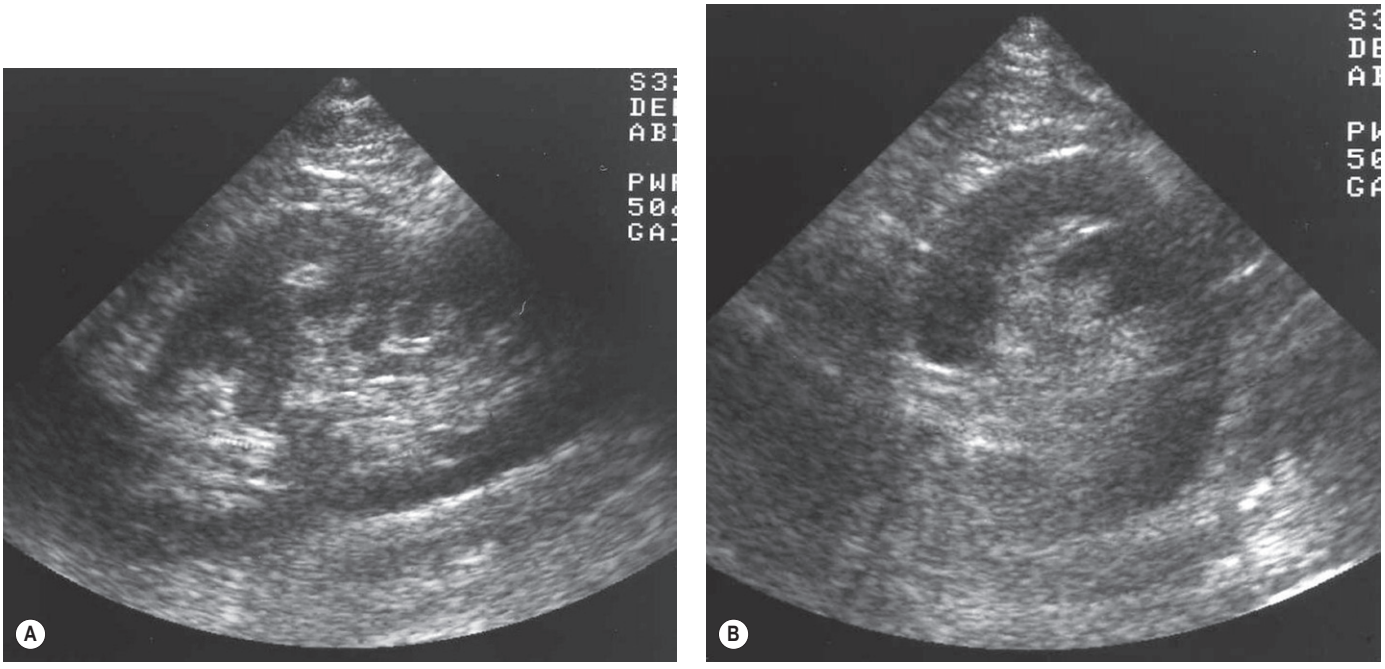


Figure 21.14 Renal splenic hump. A: Longitudinal view of a left kidney with a splenic hump. **B:** The bright echoes in the hump represent sinus fat, confirmed on this transverse view.

These normal cortical variants can often be distinguished on ultrasound, but if doubts persist echo-enhancing agents are of value in confirming normal parenchyma, as their use shows enhancement identical to normal parenchyma and a normal pattern of vessels. CT and MR scanning may also be helpful and if doubt persists, an isotope scan will show normal parenchymal uptake.



Figure 21.15 Septum of Bertin (arrows) at the upper pole extending into the renal sinus echoes.

The renal sinus, collecting system and vessels

The renal sinus is normally seen as an area of high reflectivity (the 'central echo complex') due to the fat that surrounds the blood vessels and collecting system. The outline of the renal sinus can vary from smooth to moderately irregular with small components extending around the papillae and septa of Bertin. In some patients – the elderly, patients on steroid treatment and the obese – the fat of the renal sinus can increase in amount, a change known as sinus lipomatosis.[4,38] This may be apparent on ultrasound but if any doubt persists, a CT scan can be of help in assessment. Conversely, the amount of fat in the renal sinus is reduced in cachectic patients and neonates and the renal sinus is then less well visualised. Tumour infiltration or oedema should be considered if the sinus echoes are indistinct or absent in patients who are not cachectic.

The components of the collecting system and major branches of the arteries and veins may be distinguished within the renal sinus in some patients (Fig. 21.16). In patients who are dehydrated to any extent (including an overnight fast) the peripheral collecting system is not usually visible, but in those undergoing a diuresis, or in patients with a full bladder, the renal pelvis and its major tributaries can be distinguished as 'splitting' of the renal sinus echoes.[39] If this is suspected, or if there is a question of possible obstruction, a repeat scan when the diuresis is completed and the bladder has been emptied should demonstrate emptying of the upper collecting system (Fig. 21.17).

Some prominence of the collecting system is often seen in pregnancy.[40] Slight distension of the pelvis and its main branches is apparent as early as 12 weeks gestation and by 20 weeks this is detected in up to three-quarters of patients on the right side; slightly fewer show similar changes on the left. By 36 weeks gestation more obvious dilatation may be shown in about two-thirds of patients (Fig. 21.18). These changes usually disappear quickly after delivery (within 48 hours) although minor distension of the collecting system may persist.[40,41] The cause of this dilatation is a matter of some debate but mechanical factors from the enlarging uterus, hormonal factors, increased blood flow and parenchymal hypertrophy have all been implicated.[41]

The renal pelvis usually lies predominantly within the renal sinus but it may lie partly or completely outside the kidney. In this situation the extrarenal component may act as a sump for urine,

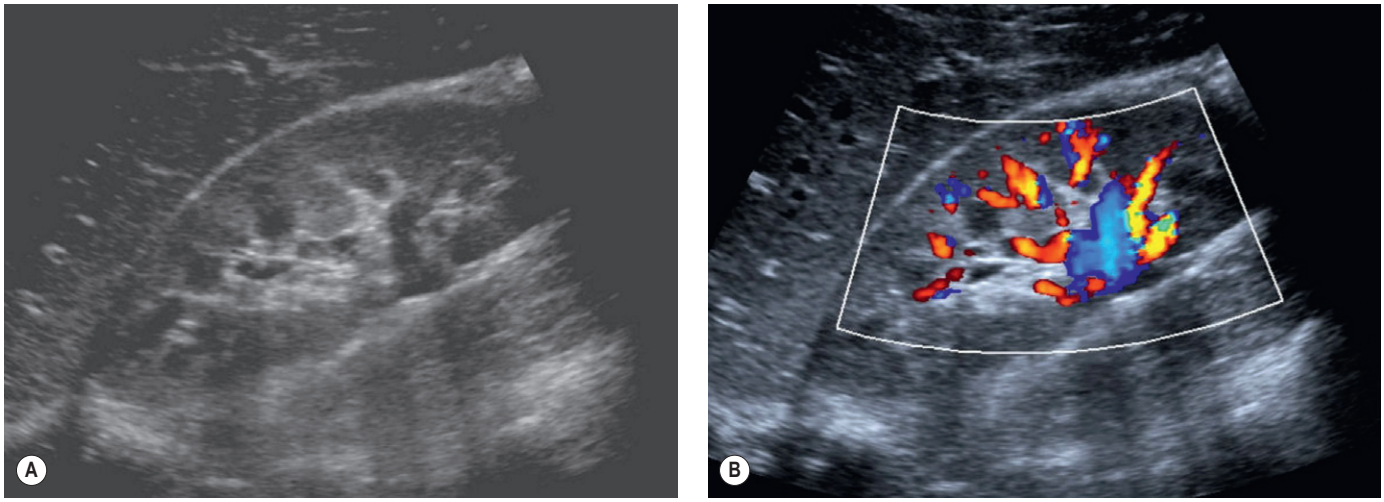


Figure 21.16 Intrarenal vessels. A: The normal renal sinus showing several small echo-free spaces which correspond to the main branches of the arteries and veins together with central components of the collecting system. **B:** Colour Doppler confirms the vascular nature of these spaces. These do not extend to the peripheral parts of the sinus, unlike dilated calyces which can be followed outwards.

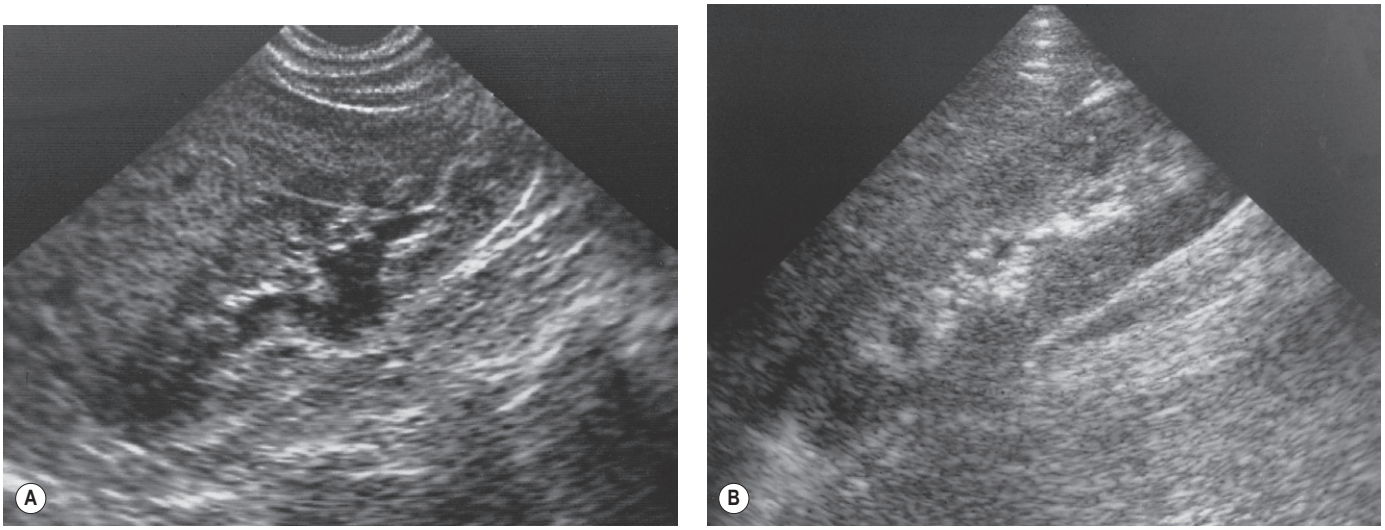


Figure 21.17 Physiological hydronephrosis. A: Pre- and **B:** post-micturition images (on different machines) of the right kidney showing resolution of dilatation of the collecting system following emptying of the bladder.

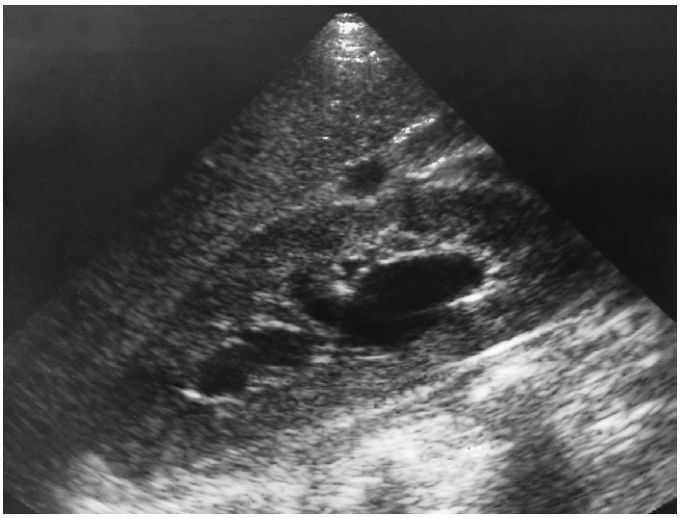


Figure 21.18 Physiological hydronephrosis of pregnancy. Moderate distension of the collecting system in a non-obstructed kidney during the third trimester of pregnancy.

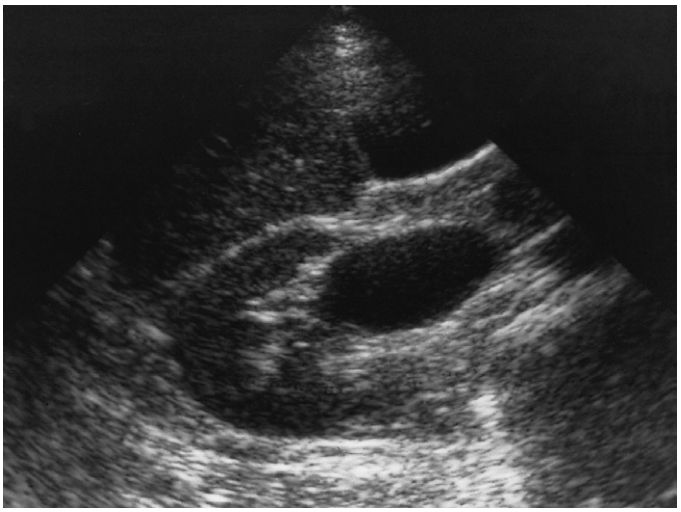


Figure 21.19 Prominent extrarenal pelvis. Transverse view of a kidney with a prominent extrarenal pelvis which might be mistaken for a parapelvic cyst or collection.

showing as a collection of fluid close to the medial aspect of the kidney on ultrasound (Fig. 21.19). The distinction from obstruction, parapelvic cyst or other collections may be difficult but careful examination, particularly in the transverse plane, usually defines the true nature of the appearances, especially if calyces are seen connecting to the 'collection'. Duplex systems may also be identified as the sinus echoes of the two moieties are separated by parenchymal tissue.

The renal vessels can often be visualised and examined with Doppler. In some patients the normal veins may be sufficiently prominent to simulate early obstruction, although their true nature is apparent on colour Doppler. The normal renal vascular bed has a low resistance so the arterial signals show high diastolic flow (Fig. 21.20). This feature is seen in the main renal arteries, the interlobar arteries and the arcuate arteries.[42] The resistance index (RI) in the renal arteries is consequently relatively low with typical normal values of 0.58–0.64 being reported.[43] It should be noted that the RI shows greater variability in children: one study reported a range from 0.34 to 0.94 in a group of children aged 1–15 years, with no significant relationship between age, renal size or gender.[43] The RI also tends to be higher in older patients (over the age of 60 years).[44] Care must therefore be taken when interpreting Doppler findings in these patients as a high RI may be due to physiological factors, rather than pathology. In the majority of the adult population, however, an RI of 0.7 is considered to be the upper limit of normal.[45] The shape of the renal artery waveform is discussed in the section on renal artery stenosis in Chapter 23.

The veins are fairly wide and the blood within them is normally echo-free except for the inconstant demonstration of moving echoes from red cell rouleaux. The left renal vein may show some dilatation distal to the point where it passes between the aorta and the superior mesenteric artery; this is a normal variant and does not represent significant obstruction.[28]

The kidneys normally move down with inspiration. The degree of travel is similar to that of adjacent liver on the right and of the spleen on the left. Real-time ultrasound allows for slight differences in the movement of the kidneys in relation to adjacent structures to be detected. Loss of respiratory movement may be due to diaphragmatic paralysis but if this is not the case then it may be a sign of intra- or perirenal pathology producing some fixation of the kidney.

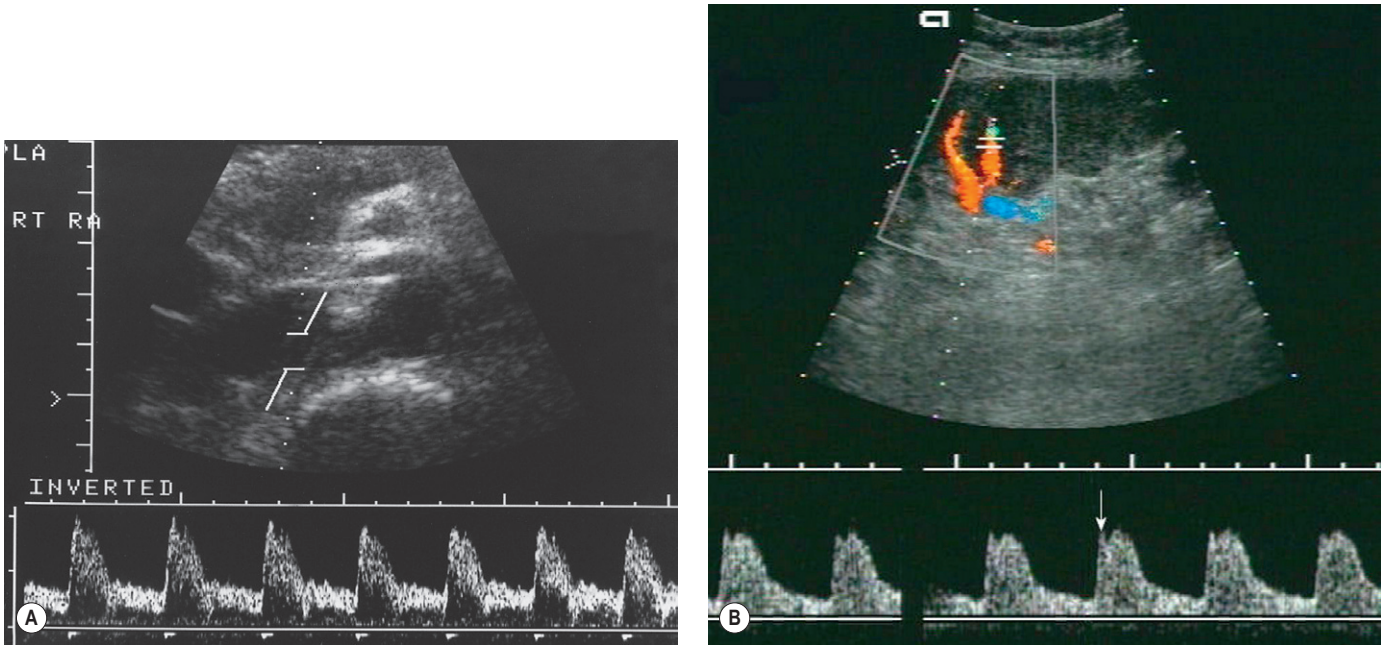


Figure 21.20 **A:** Doppler signal from the right renal artery, as it passes behind the IVC showing the normal high diastolic flow. **B:** The normal intrarenal waveform showing the characteristic early systolic peak (ESP) (arrow).

CONGENITAL VARIANTS OF RENAL STRUCTURE AND POSITION

Duplex collecting system and ureters

Minor degrees of separation of the upper and lower parts of the collecting systems may not be apparent on ultrasound. More marked degrees show as two separate renal sinus complexes separated by tissue with the reflectivity and texture of normal cortex (a septum of Bertin; Fig. 21.21). The point of junction of the ureters from the two separate moieties may be identified if it is high (in the region of the renal pelvis) but separate ureters can be difficult to trace down towards the bladder unless they are dilated. The ureter from the lower moiety usually enters the bladder in the region of the trigone, whereas the upper moiety ureter may be normally located or situated ectopically into the inferior bladder, upper urethra, or any other derivative of the embryonic mesonephric duct.[12] Examination of the bladder may show a ureterocele, usually associated with the ureter from the upper moiety.

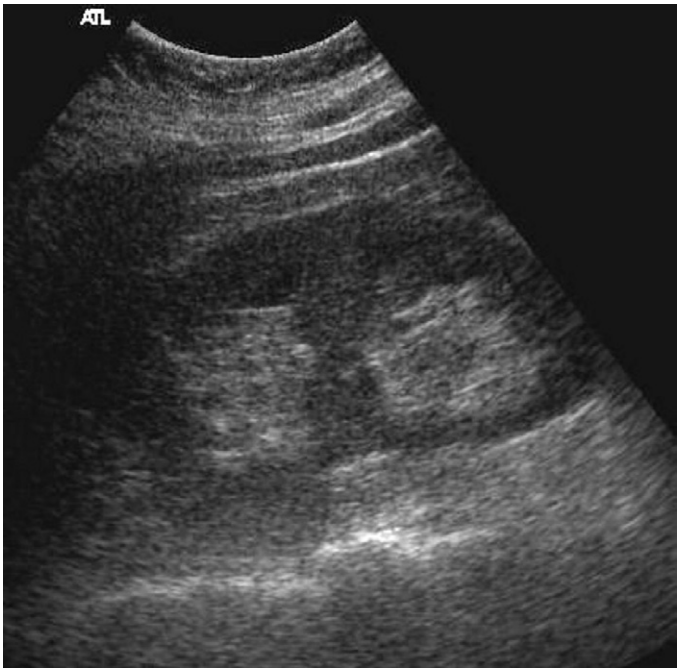


Figure 21.21 **Duplex collecting system.** Image of the left kidney showing a column or bar of cortex separating the renal sinus echoes into two parts in a patient with duplication of the collecting system and upper ureters.

Ectopic kidneys

The kidneys may develop anywhere along the urogenital ridge of the fetus and so, if they are not in a normal position, they should be searched for along the psoas muscles and down into the pelvis (see Fig. 21.10). Ectopic kidneys are more common on the left side, some 80% of them being found at, or below, the level of the iliac crest on the ipsilateral side.[46] An ectopic kidney can be recognised by its overall similarity in shape, size and structure to normal kidneys, although like horseshoe kidneys (see below) ectopic kidneys are associated with malrotation and a predisposition to dilatation of the collecting system.[47] However, pelvic kidneys may develop with unusual shapes and degrees of rotation and also may show some dilatation of the collecting system.[48] These unusual features may make an ectopic kidney difficult to recognise as a kidney, especially if it is an unexpected finding and presents as a mass during an examination (Fig. 21.22A). The overall appearance may lead to confusion with a bowel tumour or lymph node mass, by the unwary; colour Doppler is of value as it usually shows the vascular architecture compatible with renal vessels (Fig. 21.22B). Conversely the colon may lie in the vacant renal fossa and this may give a false impression of a normally situated kidney.[49]

The ectopic kidney usually lies on the correct side of the abdomen or pelvis; much more rarely, approximately 1 in 1000 births, it lies on the opposite side under a normally positioned kidney (crossed renal ectopia). The crossed, ectopic kidney is almost always fused

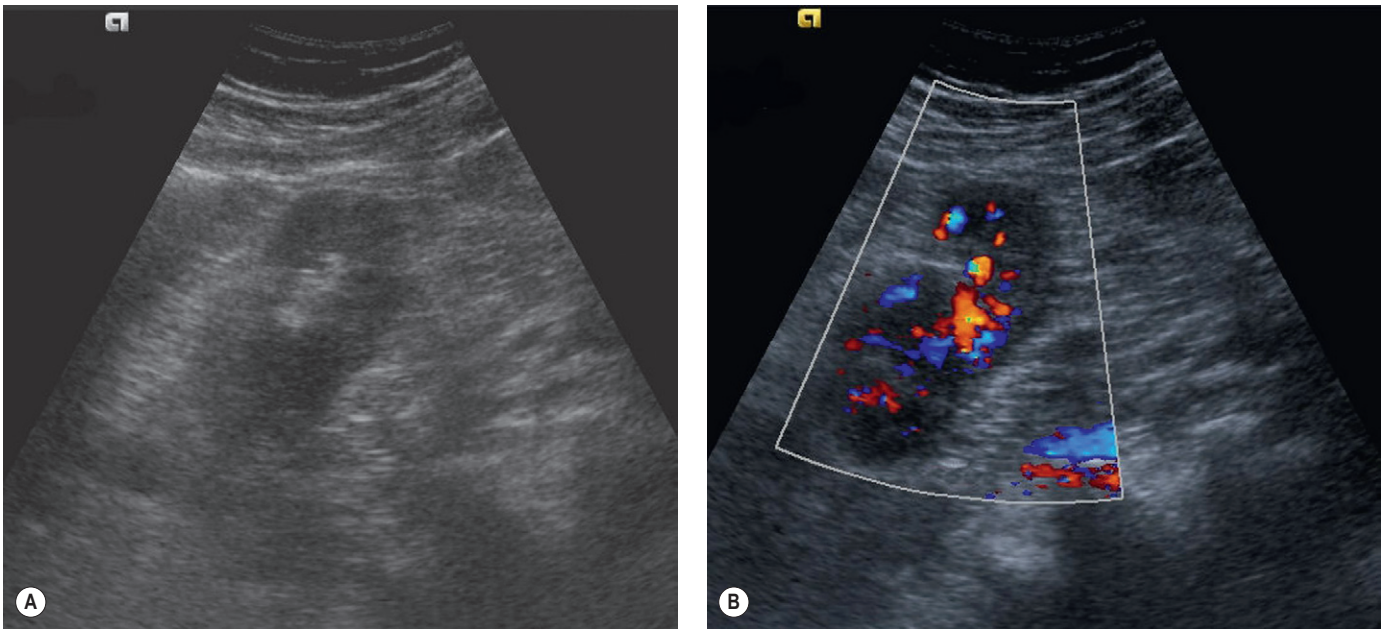


Figure 21.22 **Ectopic kidney. A:** Ectopic kidney in the right iliac fossa. **B:** Colour Doppler shows regular renal arrangement of vessels.

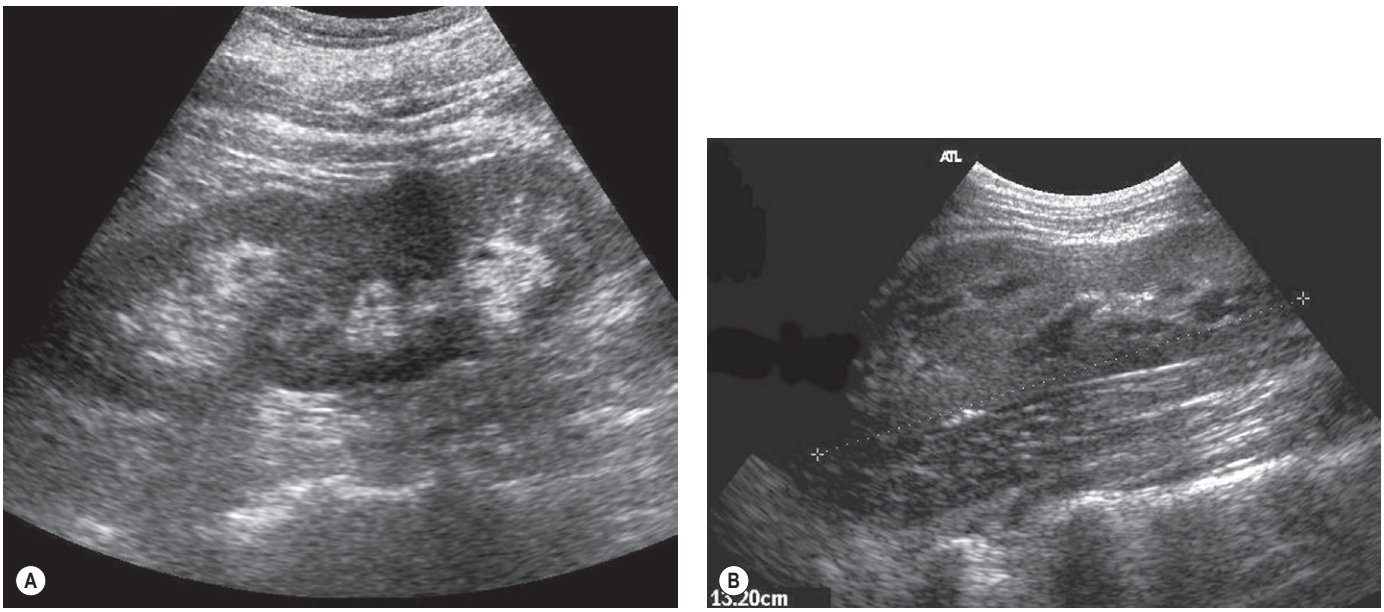


Figure 21.23 **Crossed fused renal ectopia. A:** A large (13.2 cm) reniform mass lies on the right psoas muscle. No kidney could be seen in the left abdomen. **B:** Another crossed fused ectopia in which the two components are easily distinguished.

with the other kidney (crossed fused renal ectopia) to produce a long, kidney-shaped flank mass, usually with two sinus echo complexes (Fig. 21.23).[48] In crossed renal ectopia the ureter from the ectopic kidney crosses the midline to enter the bladder on the normal side.[12]

Pancake kidneys are fused ectopic kidneys, usually lying centrally in a low abdominal or pelvic position. The normal renal outlines are not clearly seen and distortions of the renal sinus may add to the difficulties in recognition, although the absence of normal kidneys in the renal fossae should alert the examiner to the possibility (Fig. 21.24).[48] Again, colour Doppler is of value in demonstrating a renal pattern of vessels. If there is doubt over the nature of a possible ectopic kidney a DMSA isotope scan will confirm the presence of renal tissue but CT or arteriography may be required in a few cases for full assessment.

Horseshoe kidneys

Horseshoe kidneys are a congenital variant, occurring in about 1 in 400 of the population, where the kidneys are linked by tissue between their lower poles.[47,50] The size of this bridge or 'isthmus' varies from a thin connective tissue band to a full thickness of renal parenchyma (Fig. 21.25): usually there is some functioning parenchyma across the midline. Visualisation of the isthmus depends on its size and the build of the patient; it lies in front of the aorta and IVC and it may be confused with a lymph node mass, pancreatic tumour, aortic aneurysm, retroperitoneal fibrosis or dilated bowel.[51] Even if the isthmus cannot be identified, the presence of a horseshoe kidney may be suspected from the abnormal shape and orientation of the renal components.[52] The long axis of a kidney making up part

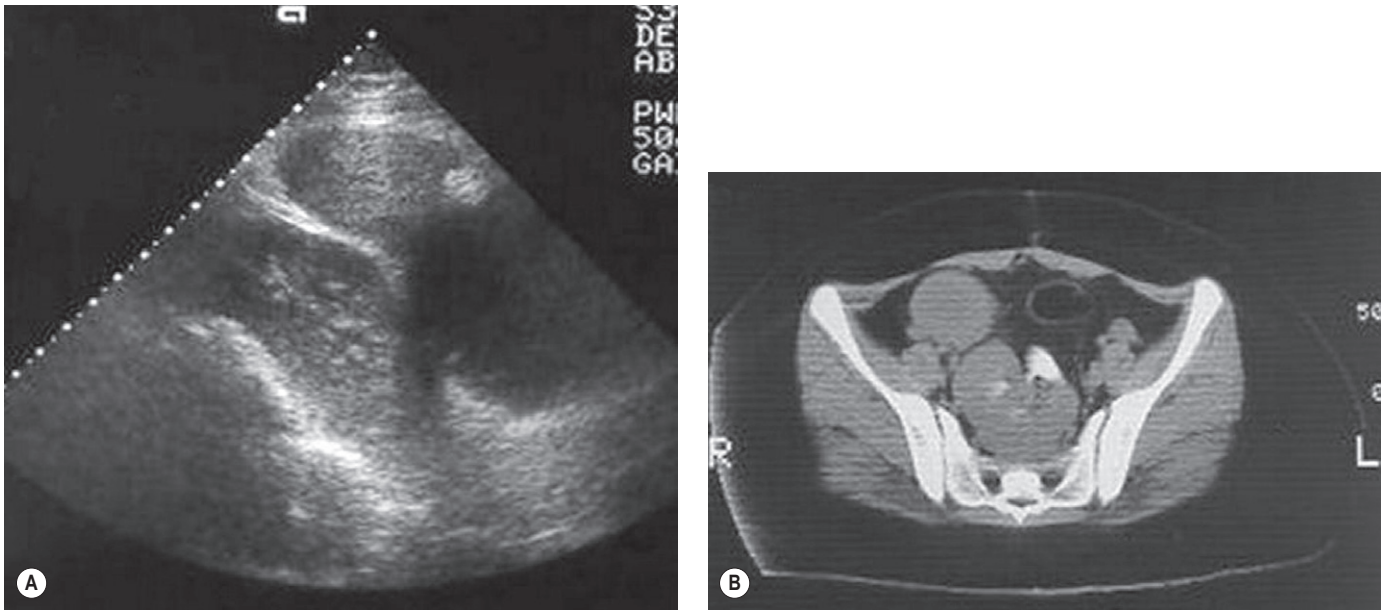


Figure 21.24 **Pancake kidney. A:** Part of a pancake kidney lying centrally in the pelvis above the bladder. A second component is seen lying anteriorly. **B:** CT scan confirms the ectopic kidney.

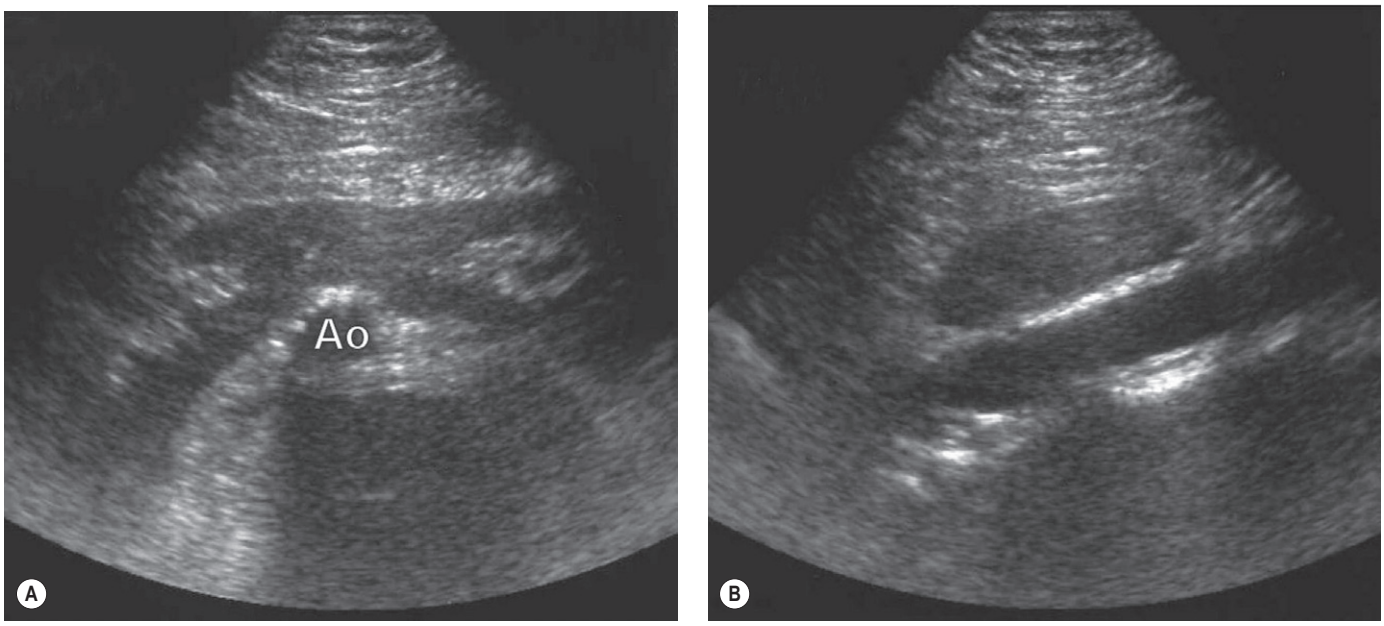


Figure 21.25 **Horseshoe kidney. A:** Transverse scan showing a horseshoe kidney with the isthmus crossing in front of the aorta (Ao); the renal sinus echoes can be seen in the right and left renal components. **B:** Longitudinal scan showing the isthmus of the horseshoe kidney anterior to the aorta.

of a horseshoe anomaly is more vertical than normal and is positioned with the lower pole more medial than the upper pole. In addition, there is a degree of malrotation so that the collecting systems are directed more anteriorly than normal.

Hypoplasia and atrophy

The distinction between these two abnormalities can be difficult on ultrasound alone unless there are signs of pre-existing renal disease such as cortical scarring or a dilated collecting system. A relatively large renal artery or vein is an indication of atrophy since hypoplastic kidneys have small vessels that are difficult to visualise (Figs 21.26 and 21.27). However, many cases of 'congenital hypoplasia' are thought to result from intra-uterine insults which have affected renal development and it may not be possible to make an accurate distinction between true congenital hypoplasia and acquired change.[53] Ultrasound provides information on the size of the contralateral kidney but estimates of relative function are best carried out with isotope renography.

Congenital solitary kidney

A congenital solitary kidney is more common than ectopia with an incidence of approximately 1 in 1300 neonates,[54] it is more common on the left side.[46] The unilateral absence of a kidney may be due to aplasia or agenesis, with aplasia being more common; the

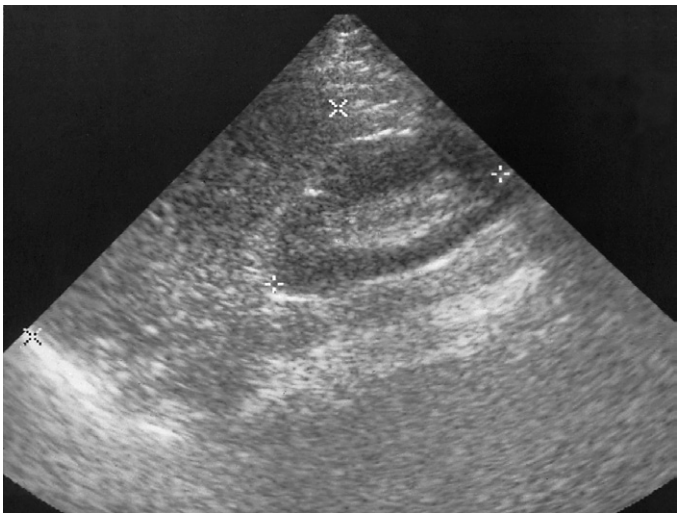


Figure 21.26 Hypoplastic kidney. A small but otherwise normal-appearing kidney suggestive of hypoplasia. Renal length 6.08 cm.

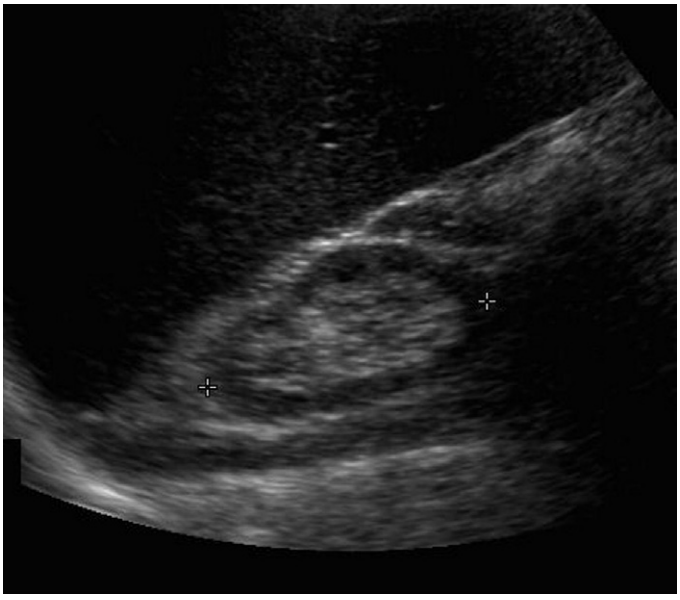


Figure 21.27 Atrophic kidney. A small atrophic kidney measuring 5.8 cm. There are no specific features to suggest the aetiology.

Congenital variants

Ectopic kidney: a kidney which is sited in an abnormal location.
Crossed renal ectopia: an ectopic kidney which is sited on the contralateral side of the abdomen.
Crossed, fused renal ectopia: the ectopic kidney is on the contralateral side of the abdomen and fused to the normotopic kidney on this side.
Congenital solitary kidney: One of the kidneys fails to develop (agenesis), or starts to develop but subsequently fails and atrophies (aplasia).
Horseshoe kidney: the two kidneys are linked by a bridge of tissue between their lower poles, this may be a simple fibrous band, or functioning renal tissue.
Duplex kidney: the renal collecting system is divided into two moieties and the ureters from these may join between the kidney and the bladder, or have separate insertions into the bladder.

development of the fetal kidney starts but then fails and the renal tissue subsequently atrophies.[55] Neonatal scanning shows the failed kidney, which subsequently shrinks and involutes. Agenesis is rarer; here, the renal tissue fails to develop and so there is no visible renal tissue.[54] In distinction from renal ectopia, the contralateral kidney shows compensatory hypertrophy. A loop of bowel, usually colon, may lie in the vacant renal fossa and this can be mistaken for a kidney.[49] The diagnosis may be suggested by ultrasound but it may require confirmation by isotope studies, CT or angiography in order to exclude an atrophic or ectopic kidney.

REFERENCES

1. Harrison RG. The urogenital system. In: Romanes GJ, editor. Cunningham's textbook of anatomy. 12th edn. Oxford: Oxford University Press; 1981. p. 531.
2. Myers MA. The extraperitoneal spaces: normal and pathologic anatomy. In: Myers MA, Dynamic radiology of the abdomen. New York: Springer-Verlag; 1976. p. 116.
3. Brandt TD, Neimann HL, Dragowski MJ, et al. Ultrasound determination of normal renal dimensions. J Ultrasound Med 1982;1:49–52.
4. Cronan JJ, Rosenfield AT. Normal size of the adult kidney by real-time ultrasound (abstract). AJR Am J Roentgenol 1990;154:195.
5. Emamian SA, Nielsen MB, Pedersen JF, Ytte L. Kidney dimensions at sonography: correlation with age, sex and habitus in 665 adult volunteers. AJR Am J Roentgenol 1993;160:83–86.
6. Wolpert SM. Variation in kidney length during the intravenous pyelogram. Br J Radiol 1965;38:100–103.
7. Cietak KA, Newton JR. Serial quantitative maternal nephro-sonography in pregnancy. Br J Radiol 1985;58:405–413.
8. Farrant P, Meire HB. Ultrasonic measurement of renal inclination; its importance in measurement of renal length. Br J Radiol 1978;51:628–630.
9. Kang KY, Lee YJ, Park SC, et al. A comparative study of methods of estimating kidney length in kidney transplantation donors. Nephrol Dial Transplant 2007;22(8):2322–2327.
10. Hodson J. The lobar structure of the kidney. Br J Urol 1972;44:246–261.
11. Pick JW, Anson BJ. The renal vascular pedicle. Analysis of 430 body-halves. J Urol 1940;44:411–434.
12. Williams H. Renal revision: from lobulation to duplication – what is normal? Arch Dis Child Online 2007;92:ep152–ep158.
13. Dalla Palma L, Rossi M. Advances in radiological anatomy of the kidney. Br J Radiol 1982;55:404–412.
14. Carter AR, Horgam JG, Jennings TA, Rosenfield AT. The junctional parenchymal defect. A sonographic variant of renal anatomy. Radiology 1985;154:499–502.
15. Kenney IJ, Wild SR. The renal parenchymal junctional line in children: ultrasonic frequency and appearances. Br J Radiol 1987;60:865–868.
16. Dalla Palma L, Bazzichi M, Cressa C, Tommasini G. Radiological anatomy of the kidney revisited. Br J Radiol 1990;63:680–690.
17. Hederstrom E, Forsberg L. Accuracy of repeated kidney size estimation by ultrasonography and urography in children. Acta Radiol 1985;26:603–607.
18. Ablett MJ, Coulthard A, Lee REJ, et al. How reliable are ultrasound measurements of renal length in adults? Br J Radiol 1995;68:1087–1089.
19. Rasmussen SN, Haase L, Kjeldsen H, Hancke S. Determination of renal volume by ultrasound scanning. J Clin Ultrasound 1978;6:160–164.
20. Hricak H, Lieto R P. Sonographic determination of renal volume. Radiology 1983;148:311–312.
21. Christiansen JS, Gamelgaard J, Frandsen M, Parving HH. Increased kidney size, glomerular filtration rate and renal plasma flow in short-term insulin dependent diabetics. Diabetologia 1981;20:451–456.
22. Feldt-Rasmussen B, Hegedus L, Mathiesen ER, Deckert T. Kidney volume in type 1 (insulin dependent) diabetic patients with normal or increased urinary albumen excretion: effect of long-term improved metabolic control. Scand J Clin Lab Invest 1991;51:31–36.
23. Roger SD, Beale AM, Cattell WR, Webb JAW. What is the value of measuring renal parenchymal thickness before renal biopsy? Clin Radiol 1994;49:45–49.
24. Robertson R, Murphy A, Dubbins PA. Renal artery stenosis: the use of duplex ultrasound as screening technique. Br J Radiol 1988;61:196–201.
25. Desberg AL, Paushter DM, Lammert GK, et al. Renal artery stenosis: evaluation with color flow imaging. Radiology 1990;177:749–753.

26. Keoghan MT, Kliewer MA, Hertzberg BS, et al. Renal resistive indices: variability in Doppler US measurement in a healthy population. Radiology 1996;199:165–169.
27. Karasch T, Rubin J. Diagnosis of renal artery stenosis and renovascular hypertension. Eur J Ultrasound 1998;7(Suppl. 3):S27–S39.
28. Buschi AJ, Harrison RB, Brenbridge AN, et al. Distended left renal vein: CT/sonographic normal variant. AJR Am J Roentgenol 1980;135:339–342.
29. Atlas SW, Rochester D, Panella JJ, Larson R. The utility of ultrasound in the diagnosis of wandering abdominal viscera. J Clin Ultrasound 1985;13:275–277.
30. Patel AS, Barber-Riley WP. Symptomatic medial nephroptosis. Br J Radiol 1982;55:244–246.
31. Rosenfield AT, Siegel NJ. Renal parenchymal disease. Histopathologic–sonographic correlation. AJR Am J Roentgenol 1981;137:793–798.
32. Platt JF, Rubin JM, Bowerman RA, Maru CS. The inability to detect kidney disease on the basis of echogenicity. AJR Am J Roentgenol 1988;151:317–319.
33. Rosenfield AT, Taylor KJW, Grade M, DeGraaf CS. Anatomy and pathology of the kidney by grey-scale ultrasound. Radiology 1978;128:737–744.
34. Marchal G, Verbeken E, Ogen R, et al. Ultrasound of the normal kidney: a sonographic, anatomic and histologic correlation. Ultrasound Med Biol 1986;12:999–1009.
35. MacLachlan M, Wasserman P. Changes in size and distensibility of the ageing kidney. Br J Radiol 1981;54:488–491.
36. Hardwick D, Hendry GMA. The ultrasonic appearances of the septa of Bertin in children. Clin Radiol 1984;35:107–112.
37. Mahoney BS, Brooke-Jeffrey R, Laing FC. Septa of Bertin: a sonographic pseudotumour. J Clin Ultrasound 1983;11:317–319.
38. Yeh H, Milty HA, Wolf BS. Ultrasound of renal sinus lipomatosis. Radiology 1977;124:799–801.
39. Morin ME, Baker DA. The influence of hydration and bladder distension on the sonographic diagnosis of hydronephrosis. J Clin Ultrasound 1979;7:192–194.
40. Cietak KA, Newton JR. Serial qualitative maternal nephrosonography in pregnancy. Br J Radiol 1985;58:399–404.
41. Peake SC, Roxburgh HB, Langlois SL. Ultrasonic assessment of the hydronephrosis of pregnancy. Radiology 1983;146:167–170.
42. Taylor KJW, Burns PN, Woodcock JP, Wells PNT. Blood flow in deep abdominal vessels: ultrasonic pulsed Doppler analysis. Radiology 1985;154:487–493.
43. Platt JF, Ellis JH, Rubin JM. Examination of the native kidneys with duplex Doppler ultrasound. Semin Ultrasound CT MR 1991;12:308–318.
44. Gill B, Palmer LS, Koenigsberg M, Laor E. Distribution and variability of resistive index values in undilated kidneys in children. Urology 1994;44:897–901.
45. Terry JD, Rysavy JA, Frick MP. Intrarenal Doppler: characteristics of ageing kidneys. J Ultrasound Med 1992;11:647–651.
46. Meyers MA, Whalen JP, Evans JA, Viamonte M. Malposition and displacement of bowel in renal agenesis and ectopia: new observations. AJR Am J Roentgenol 1973;117:323–333.
47. Singer A, Simmons MZ, Maldjian PD. Spectrum of congenital renal anomalies presenting in adulthood. Clin Imaging 2008;32: 183–191.
48. Sanders RC. Normal ultrasonic anatomy of the genitourinary system. In: Resnick MI, Sanders RC, editors. Ultrasound in urology. 2nd edn. Baltimore: Williams & Wilkins; 1984. p. 76.
49. Mascatello V, Lebowitz RL. Malposition of the colon in left renal agenesis and ectopia. Radiology 1976;120:371–376.
50. Whitehouse GH. Some urographic aspects of the horseshoe kidney anomaly – a review of 59 cases. Clin Radiol 1975;25:107–114.
51. Mindell HJ, Kupic EA. Horseshoe kidney: ultrasonic demonstration. AJR Am J Roentgenol 1977;129:526–527.
52. Bannerjee B, Brett I. Ultrasound diagnosis of horseshoe kidney. Br J Radiol 1991;64:898–900.
53. Friedland GW. Congenital anomalies of the urinary tract. In: Friedland GW, Filly R, Goris ML, et al, editors. Uroradiology: an integrated approach. New York: Churchill Livingstone; 1983. p. 1483.
54. Hiraoka M, Tsukahara H, Ohshima Y, et al. Renal aplasia is the predominant cause of congenital solitary kidneys. Kidney Int 2002;61:1840–1844.
55. Hitchcock R, Burge DM. Renal agenesis: an acquired condition? J Paediatr Surg 1994;29:454–455.

CHAPTER 22

Pelvi-ureteric dilatation

Tze M. Wah

INTRODUCTION 428

CAUSES OF PELVI-URETERIC DILATATION 428
Physiological 428
Normal circumstances 428
Pregnancy 428
Pathological 429
Stones 430
Tumour 431
Blood clot 434
Papillary necrosis 434
Infections 434
Congenital 435
Bladder outflow obstruction 436
Compression by intrapelvic mass 438
Iatrogenic 438
Trauma 438

DIAGNOSIS 438

ULTRASOUND APPEARANCES – ANATOMICAL EVIDENCE 439

FUNCTIONAL EVIDENCE USING DOPPLER TECHNIQUE 440
Renal blood flow changes 440

DOPPLER TECHNIQUE 441
Normal RI 441
Abnormal RI 441
Ureteric jets 441

MANAGEMENT OF OBSTRUCTIVE UROPATHY 441
Pyonephrosis 442
Percutaneous nephrostomy 443

INTRODUCTION

Pelvi-ureteric dilatation does not always equate to obstruction or indicate pathology. This appearance can be physiological, secondary to urinary tract reflux disease and is sometimes seen in a non-obstructed system when the bladder is too full.[1,2] In fact, occasionally severe functional obstructive uropathy can present without any evidence of or with minimal pelvi-ureteric dilatation. If there is no significant clinical suspicion for urinary tract system obstruction, this is likely to cause delayed diagnosis and management.[3]

When there is evidence of pelvi-ureteric dilatation on imaging, this finding suggests that there may be urinary tract obstruction distal to the dilatation in patients presenting with clinical symptoms. Ultrasound has been routinely used to assess patients and is very sensitive in detecting pelvi-ureteric dilatation in patients with normal or abnormal renal function.[4–6] Other adjuvant methods during ultrasound scanning such as renal artery resistance index measurement and colour Doppler examination of the ureteric jets may be useful in providing more evidence for urinary tract obstruction in difficult cases.[7]

Over the last few years, however, there has been increasing usage of unenhanced computed tomographic examination of the kidneys, ureter and bladder (CT KUB) as a first-line examination from acute admission or accident and emergency referral to assess patients with loin pain.[8–10] This is because obstructing stones within the ureter may or may not cause pelvi-ureteric dilatation in the early stage and CT KUB is definitely the most sensitive modality in assessing these patients.[9–11] Ultrasound may then be used as a second-line follow-up scan in patients with hydronephrosis caused by an obstructing ureteric stone if treated conservatively.[12]

CAUSES OF PELVI-URETERIC DILATATION

Physiological

Normal circumstances

Mild pelvi-ureteric dilatation is a relatively common finding in our clinical practice. The commonest cause is as a result of an over-full bladder for the ultrasound examination. These usually resolve when the bladder is completely emptied. Another frequent presentation is an extrarenal pelvis; this is usually accompanied by a non-dilated intrarenal pelvicalyceal system.

Pregnancy

It is common in normal pregnancy, from around 6–10 weeks onwards, to present with non-obstructing mild pelvi-ureteric dilatation. This is partly due to extrinsic compression from the gravid uterus on the ureters and partly from hormonal factors. This can involve both ureters, but is commoner and more marked on the right than the left, with increasing severity throughout the pregnancy.[13] Following delivery, the appearances resolve rapidly but may persist for up to 3 months postpartum. The resistive index for the pregnant female is similar to that of her non-pregnant counterpart. Therefore in a pregnant female with pelvi-ureteric dilatation, a normal RI would confirm the findings are dilated but non-obstructive.[14]

However, suspicion for obstruction or ureteric colic in pregnancy does present an imaging dilemma. This should be raised when the patient is symptomatic, and ultrasound following hydration is usually the first-line investigation to assess the pregnant woman. The ureter is usually dilated and can be followed to the region of the common iliac artery where it then tapers off. Findings on ultrasound that should prompt further investigation are: a dilated ureter beyond the common iliac artery suggestive of pathological obstruction, and internal echoes within the dilated pelvicalyceal system suggestive of infection caused by distal obstruction. In this situation, complementary techniques using Doppler, particularly the intrarenal RI difference, and evaluation of ureteric jets, should be used. Most pregnant women with suspected obstructive uropathy would benefit from MR urography in a centre with this

expertise.[15,16] In late pregnancy when the pregnant woman presents with physiological painful hydronephrosis, the ureter is dilated to the middle third, which usually tapers off and has a smooth outline on the MR urogram (Fig. 22.1). In contrast, those with pathological painful hydronephrosis in pregnancy, renal oedema and a dilated ureter can be traced to the source of obstruction on the T2-weighted sequences on MR urogram (Fig. 22.2A and B). The role of intravenous urography is now obsolete in the assessment of pregnant women with symptoms of acute renal colic.[17]

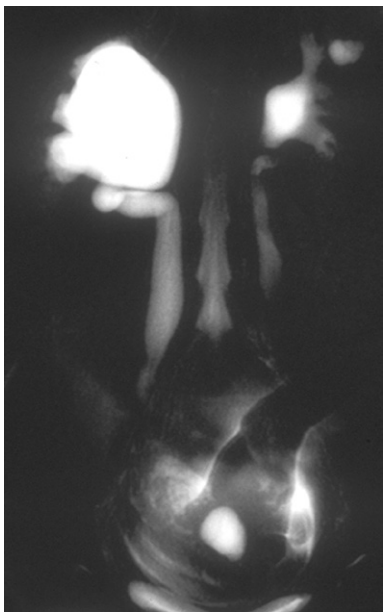


Figure 22.1 Coronal MR urography shows normal physiological dilatation of the right pelvicalyceal system with a dilated and smooth ureter that tapers off at the middle third. (Courtesy of Dr John Spencer.)

Pathological

It is important to diagnose obstructive uropathy promptly in order to salvage the renal tissues and prevent irreversible renal failure as a result of late diagnosis. Ultrasound plays an important role in the early assessment of patients with suspected voiding difficulty and renal colic or loin pain when unenhanced CT is not available or contraindicated.

Causes of obstructive uropathy

1. Stones
2. Tumour – renal cell carcinoma and transitional cell carcinoma
3. Blood clot
4. Papillary necrosis
5. Infections – tuberculosis, fungal infection, infective stricture
6. Congenital
   a. Idiopathic PUJ obstruction
   b. Posterior urethral valves
   c. Ureterocele
7. Bladder outflow obstruction
   a. Prostate problems – prostatic hyperplasia and prostate cancer
   b. Urethral stricture
8. Compression by intrapelvic mass
   a. Gynaecological causes: cervical carcinoma, endometriosis
   b. Lymph node enlargement
   c. Inflammatory disease
9. Iatrogenic
10. Trauma

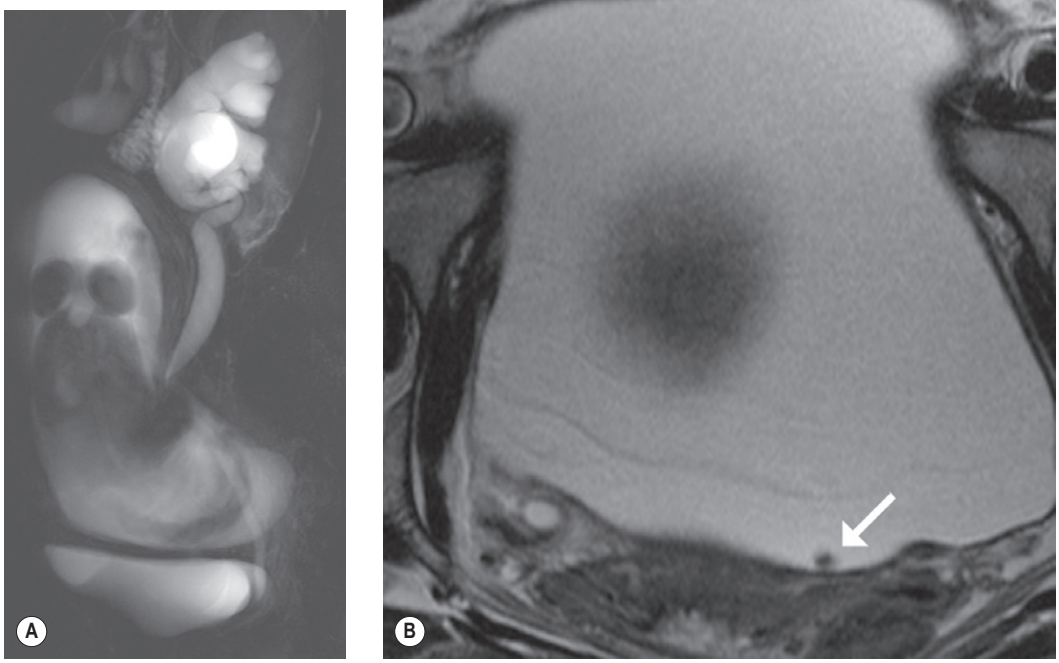


Figure 22.2 A: Coronal oblique thin slice MR urography shows an oedematous right kidney with high signal fluid around the kidney and a dilated ureter that can be traced past the gravid uterus to the right ureteric orifice. **B:** Axial thin slice T2-weighted MR urography of the bladder shows the swollen right ureteric orifice and a small passed stone in the bladder that is seen as a round signal void area in the dependent part (arrow). (A and B courtesy of Dr John Spencer).

Stones

Stones are one of the commoner causes of obstructive uropathy. In the context of pelvi-ureteric dilatation, stones may lie anywhere along the urinary tract system causing proximal obstruction. Patients usually present with acute loin pain and have complete or partial obstructive uropathy on the symptomatic side. They may also present in association with urinary tract infections or haematuria. Occasionally, presentation may be with a staghorn calculus which occupies and obstructs the whole of the renal pelvicalyceal system.

Renal stones

On ultrasound, a renal stone is usually seen as a highly reflective focus with well-defined posterior acoustic shadowing (Fig. 22.3). This is because the stone tends to absorb all the transmitted incident sound waves with greater definition when the stone has a rougher surface or is smaller, but not smaller than the beam width of the sound waves, which will make it invisible.[18,19] Most of the stones (in 90% of cases) are detected by meticulous ultrasound scanning. These stones are usually located within the collecting system. However, these stones occasionally may be seen within the reflective renal sinus, dilated pelvicalyceal collecting system or apparently within the parenchyma in the non-dilated calyx.[20]

To optimise stone detection, all operators must use the highest possible transducer frequency and ensure that the stone lies within the focal zone of the beam.[21] Gain reduction may also enhance the detection of the posterior acoustic shadowing.

The composition of the stone does not usually influence the ability of ultrasound to detect it, and both radiolucent urate stones and calcified stones are equally easily visualised.[21,22] The larger stones are usually easier to identify but some very large stones, e.g. staghorn calculi or large matrix calculi, may not have associated acoustic shadowing due to their proteinaceous content and these tend to render them difficult to demonstrate on ultrasound (Fig. 22.4A and B).[23,24] They can often be less obvious on ultrasound than on the plain radiograph, because dense shadows within the pelvicalyceal system may obscure any collecting system dilatation and may also be misinterpreted as bowel gas shadowing. Frequently as a result of the lobulated shape of the stone within the collecting system, this can be mistaken for numerous separate calculi within the collecting system instead (Fig. 22.5A and B). In fact coronal scanning is more helpful than sagittal scanning when checking for the presence of staghorn calculi. It is important to be aware that when there is a suspicion of staghorn calculi, the plain radiograph for confirmation or unenhanced CT for treatment planning is better than ultrasound at assessing the stone bulk in these patients.

In general most (90%) of stones greater than 5 mm are seen on ultrasound and very few stones less than 5 mm are seen despite the fact they lie within the focal zone of the transducer.[25] Occasionally, the tiny stones may produce 'comet-tail' artefacts.[26] In addition, ultrasound tends to overestimate stone size,[27] and in the clinical scenario where information regarding the exact stone size is required, unenhanced CT should be considered.

The location of the stone may influence its visibility; for example, stones within the renal sinus can be difficult to detect due to the heterogeneous tissue surrounding the stone which tends to defocus the ultrasound beam.[25] This is compounded by the fact that the normal renal sinus structure can also produce posterior acoustic shadowing.[28] Although in general stones are more easily seen in the dilated pelvicalyceal system, these may not be seen if they are impacted within the pelvi-ureteric junction.[29] Occasionally, when the kidney has abnormal increased reflective parenchyma such as in chronic renal failure (Fig. 22.6) this makes the stone harder to demonstrate.

Ultrasound is usually very good for stone detection but sometimes it may not be able to distinguish the exact location or part of the collecting system in which the stone resides. In particular, it cannot normally differentiate parenchymal or papillary calcification from a calyceal stone, or vascular calcification from a small stone.[28,30] In fact there are a variety of causes of masses in the pelvicalyceal system that may mimic calculi.[31] Whenever there is doubt as to the nature of calcification on ultrasound, either a plain radiograph or CT (with or without contrast) could be used to assess further.

Types of renal calculi

1. *Calcium stones*. Commonest and are associated with abnormal calcium metabolism.
2. *Struvite (triple phosphate) stones*. Usually form staghorn calculus and are associated with urinary tract infections.
3. *Uric acid stones*. Usually associated with gout.
4. *Cystine stones*. Rarest and are associated with abnormal amino acid metabolism.



Figure 22.3 Axial US shows a small stone around the midpolar region which displays intense distal acoustic shadowing (arrow).

Ureteral stones

Ultrasound can be used to detect stones in the upper ureter, the distal ureter or around the vesico-ureteric junction portion of the ureter behind a filled bladder[29] (Fig. 22.7A and B). Many other approaches have been advocated to visualise the distal ureteral stone using the transvaginal, rectal or perineal route.[32–34] Obstructing calculi causing dilatation in the mid-ureter may also be seen adjacent to the common iliac vessels but these are often not visualised. The most difficult scenario is when the stone is not causing any ureteric dilatation and ultrasound is unhelpful in delineating the cause or the level of obstruction (Fig. 22.8A and B). However, currently this group of patients presenting acutely with loin pain are investigated primarily with unenhanced CT KUB[8–10] (Fig. 22.9).

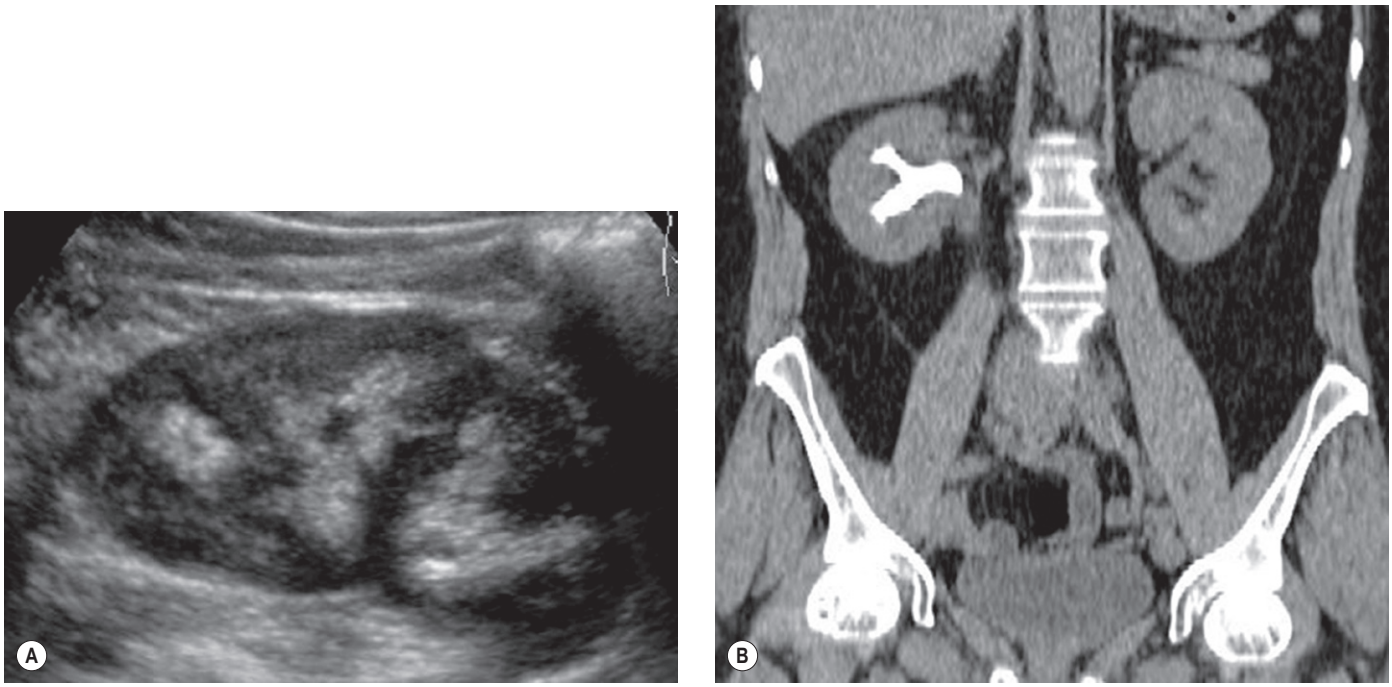


Figure 22.4 **Staghorn calculus. A:** Longitudinal US shows that there is echogenic material in the pelvicalyceal system but this does not cast posterior acoustic shadowing; this should raise suspicion of a staghorn calculus. **B:** Unenhanced CT (CT KUB) in the coronal plane shows the staghorn calculi in the right kidney.

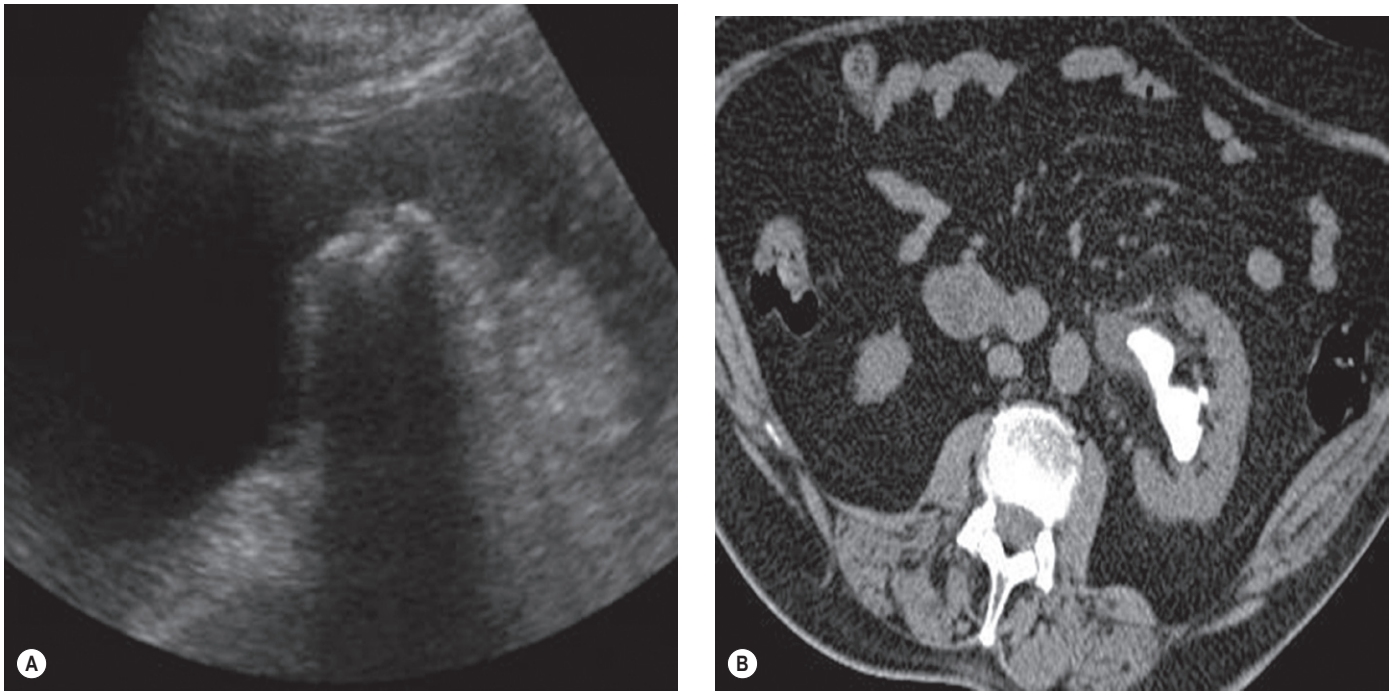


Figure 22.5 **Staghorn calculus. A:** Longitudinal US here can be misleading as the appearances suggest two fragments of stones within the calyces; ultrasound underestimates the extent of the staghorn calculi in the left kidney, which is better seen on the unenhanced axial CT KUB **(B)**.

Tumour

Ultrasound remains the first-line investigation in patients presenting with both microscopic and macroscopic haematuria, especially in the younger patient.[17] It is very sensitive at detecting larger renal masses (>2.5 cm) and renal cysts. CT urography is used increasingly to problem-solve cases of haematuria of unknown cause or in the assessment of a patient's upper tracts when there is known bladder transitional cell carcinoma. Depending on the CT urographic technique, it can usually be used to detect stones (on the unenhanced phase), as well as both renal cell carcinoma and transitional cell carcinoma during the combined nephrographic and excretory phase in the two-series technique.

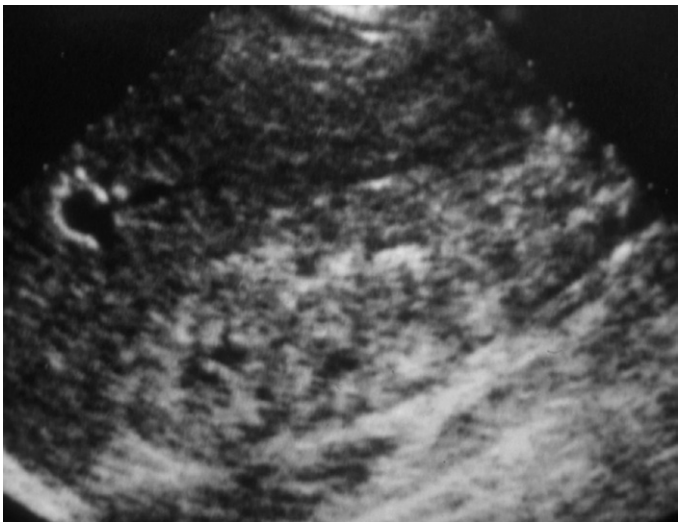


Figure 22.6 Longitudinal US shows a small right shrunken kidney with very echogenic parenchyma in end-stage renal disease.

Masses in the pelvicalyceal system visible with ultrasound[2]

- Soft tissue pattern
  - Tumour: transitional cell carcinoma, invasive renal cell carcinoma
  - Blood clot
  - Fungus ball
  - Papilla: normal or sloughed papilla
  - Pyonephrosis
  - Leukoplakia
  - Malacoplakia
- Stone pattern
  - Stone – radio-opaque or radiolucent
  - Gas
  - Foreign material: catheter, stent
  - Transitional cell carcinoma with calcification
  - Post-ESWL (extracorporeal shock-wave lithotripsy) fragments
  - Calcified necrotic papillae
  - Vascular calcification – pericalyceal
  - Papillary or parenchymal calcification

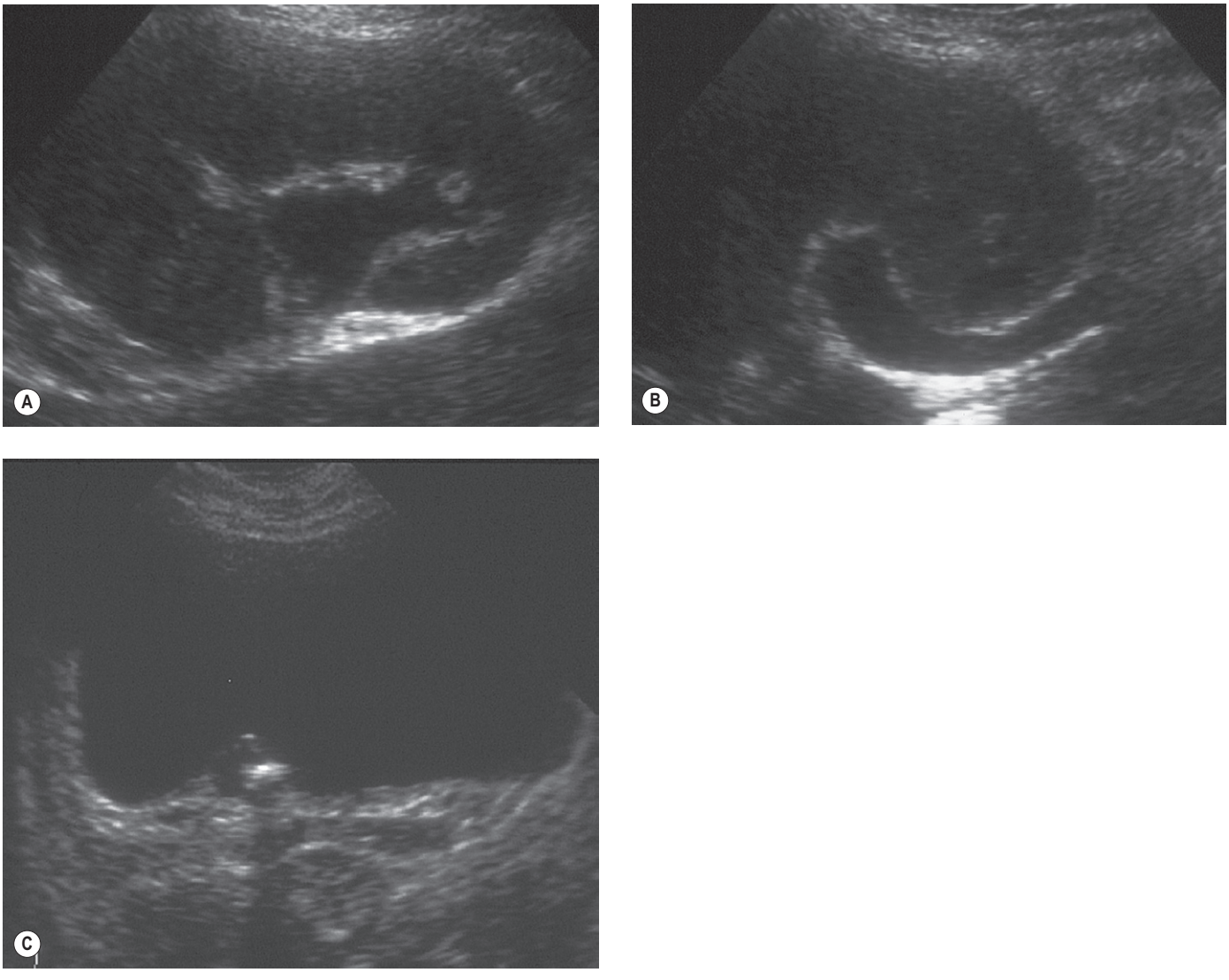


Figure 22.7 Longitudinal US shows a dilated right pelvicalyceal system (A) and hydroureter that can be traced to the vesico-ureteric junction **(B)**. The obstruction is caused by an echogenic obstructing stone seen on the axial bladder US examination **(C)**.

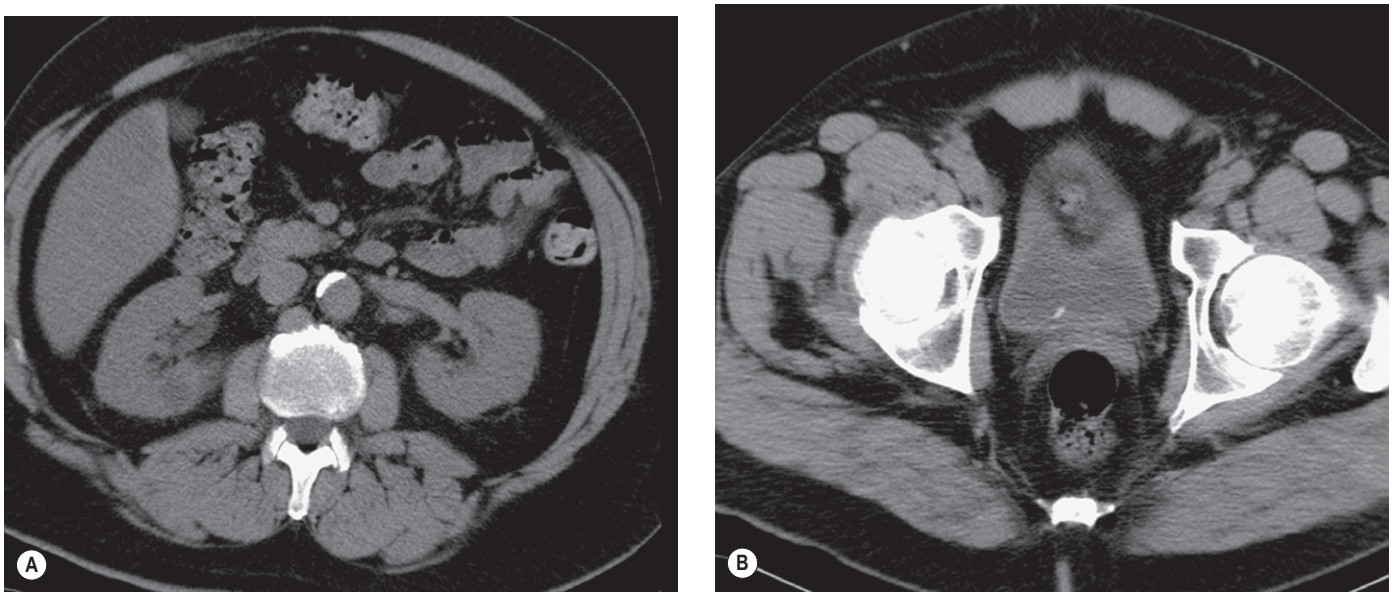


Figure 22.8 **Unenhanced axial CT KUB** shows **(A)** no hydronephrosis or secondary signs of obstructive uropathy in a patient presenting with acute right renal colic. A small stone is seen at the vesico-ureteric junction causing the obstruction **(B)**.



Figure 22.9 **Coronal oblique unenhanced CT KUB** shows a tiny 3 mm stone impacted in the left upper ureter causing minimal pelvicalyceal dilatation but demonstrates the secondary signs of obstruction on CT such as perinephric fluid stranding.

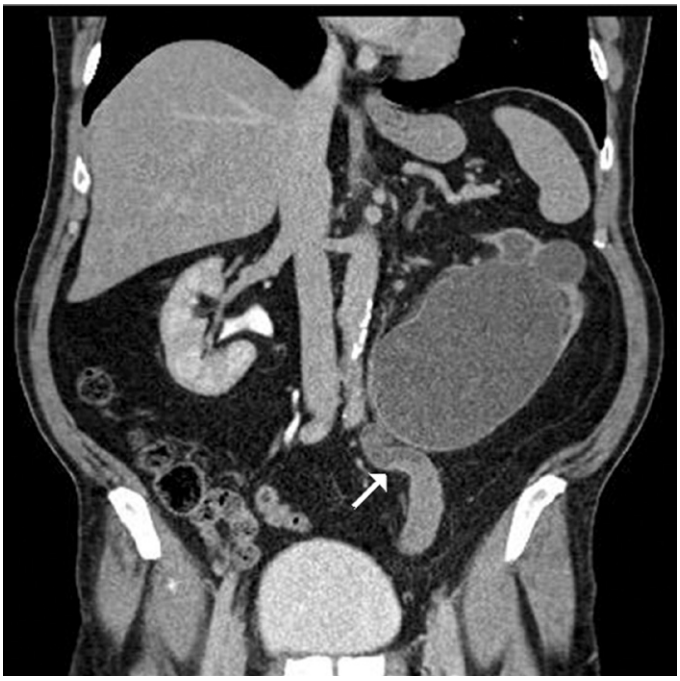


Figure 22.10 **Coronal CT urography shows a markedly dilated left pelvicalyceal system** and ureter that can be traced to the enhancing transitional cell carcinoma in the distal ureter (arrow).

Typically, the pelvi-ureteric dilatation is caused by an obstructing urothelial tumour and transitional cell carcinoma is the commonest cause. Renal cell carcinoma is a tumour sited within the renal parenchyma. It only causes pelvicalyceal dilatation when it is large enough to cause localised obstruction or when it infiltrates the collecting system by local invasion.

Transitional cell carcinoma (TCC)

Transitional cell carcinoma is the commonest uroepithelial tumour. The less common causes of uroepithelial tumours are: squamous cell carcinoma (10%) and adenocarcinoma (<1%).[35]

Usually transitional cell carcinoma presents early as mucosal irregularity within the pelvicalyceal system and this is more easily detected on the urographic examination than by ultrasound. CT urography is the most sensitive investigation for this purpose and should be used in preference to intravenous urography[17,36–39] (Fig. 22.10).

Ultrasound usually demonstrates the larger transitional cell carcinoma as masses within the renal sinus. They can be either isoechoic or hypoechoic masses within the renal parenchyma and are separated from the renal parenchyma by a band of echogenic renal sinus[40,41] (Fig. 22.11). Very rarely, it can mimic a renal stone due to encrustation of keratin or urinary salts on the surface of the tumour.[42] TCC is usually fairly poorly vascularised and therefore



Figure 22.11 Longitudinal US shows soft tissue filling the mid and lower pole calyces consistent with transitional cell carcinoma. This is causing obstructive dilatation of the upper pole calyces.

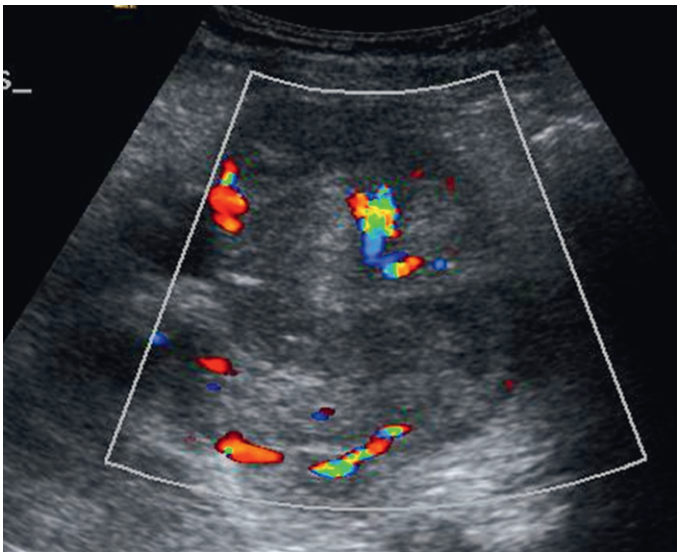


Figure 22.12 Longitudinal US shows absent vascular flow within the transitional cell carcinoma filling the mid and lower pole calyces.

does not display a Doppler signal (Fig. 22.12). Sometimes TCC obstructs the pelvicalyceal system and can be visualised as an intra-luminal mass within a dilated collecting system or within the bladder (Fig. 22.13A–C). In the advanced stages, TCC may invade the renal parenchyma and this is indistinguishable from renal cell carcinoma. In the late stage it can also invade the renal vein and inferior vena cava, very similar to renal cell carcinoma.[43]

It is important to be aware that there are many other causes of masses within the collecting system. Blood clot can typically be confused with TCC but normally resolves with time. Fungus balls can mimic TCC but this is usually seen as a very echogenic mass.[44,45] Other causes include prominent renal papillae that have projected into a dilated pelvicalyceal system[46] or a sloughed papilla can be seen as a mobile intra-luminal mass; lymphoma and extramedullary haemopoiesis that infiltrate the renal sinus may also simulate TCC on ultrasound.[47]

Renal cell carcinoma

Renal cell carcinoma can sometimes cause localised collecting system obstruction secondary to a mass effect, usually from a lower pole renal tumour causing pelvi-ureteric junction (PUJ) obstruction or from direct invasion into the collecting system in an advanced stage, making it difficult to differentiate from a transitional cell carcinoma.

Ultrasound usually detects the renal cell carcinoma when large and typically it is a heterogeneous mass with central necrosis and/or calcification. It is highly vascular and displays disorganised and increased Doppler signals within the mass, and occasionally high-velocity arteriovenous shunts can be detected within the tumour. In addition, it usually invades the renal vein and inferior vena cava. Contrast-enhanced CT is used for staging purposes.

Blood clot

Blood clot within the dilated pelvicalyceal system is also known as haemo-hydronephrosis. This can be due to trauma, an infective process or malignancy. Often it is impossible to delineate whether the blood clot is causing the obstruction or is the result of an obstructing lesion causing the bleeding. Any patient presenting with acute renal colic from a blood clot should be investigated fully in order to establish the diagnosis. Ultrasound usually shows low level echoes in the urine within a dilated collecting system, very similar to those of pyonephrosis, and clinical correlation is usually the only way to differentiate the two clinical settings (Fig. 22.14A and B). Occasionally an echogenic blood clot can be seen within the renal sinus[48] or impacted at the pelvi-ureteric junction.

Papillary necrosis

The renal papillae are situated in the renal medulla adjacent to the calyces. The renal medulla and papillae are vulnerable to ischaemic necrosis partly because of the special blood supply arrangement and partly due to the hypertonic environment. They are particularly susceptible to ischaemia as a result of hypoxia at the medullary junction in individuals with diabetes or on long-term anti-inflammatory medication or due to analgesia overuse/abuse. Other causes include sickle cell disease, pyelonephritis, renal vein thrombosis, tuberculosis and obstructive uropathy. Those renal papillae that necrose, slough off and blunt the calyces. The sloughed papillae may be impacted in the infundibulum of the calyces and cause calyceal obstruction.

It is difficult to detect papillary necrosis on ultrasound unless it is at an advanced stage.[49,50] Features may include a prominent pelvicalyceal system with increased cortico-medullary differentiation. The investigation of choice is with conventional intravenous urography (Fig. 22.15);[49,50] however, CT urography is used increasingly to assess some patients in selected indications. Contrast-enhanced CT urography is often better at depicting a full range of classical features including contrast material-filled clefts in the renal medulla, non-enhanced lesions surrounded by rings of excreted contrast material, and hyperattenuated medullary calcification.[51]

Infections

Infections within the pelvicalyceal system and ureter can present with localised infundibular, PUJ or ureteric strictures. The common causes are tuberculosis[52] and fungal infections.

An infundibular stricture usually results in a localised proximal calyceal dilatation and appears as a rounded fluid-filled space. This can be seen adjacent to the margin of the renal sinus, but sometimes within the sinus. The ultrasound appearances of the obstructive calyceal dilatation are indistinguishable from non-obstructive calyceal dilatation and frequently urographic techniques such as CT urogram are required for a more definitive diagnosis.

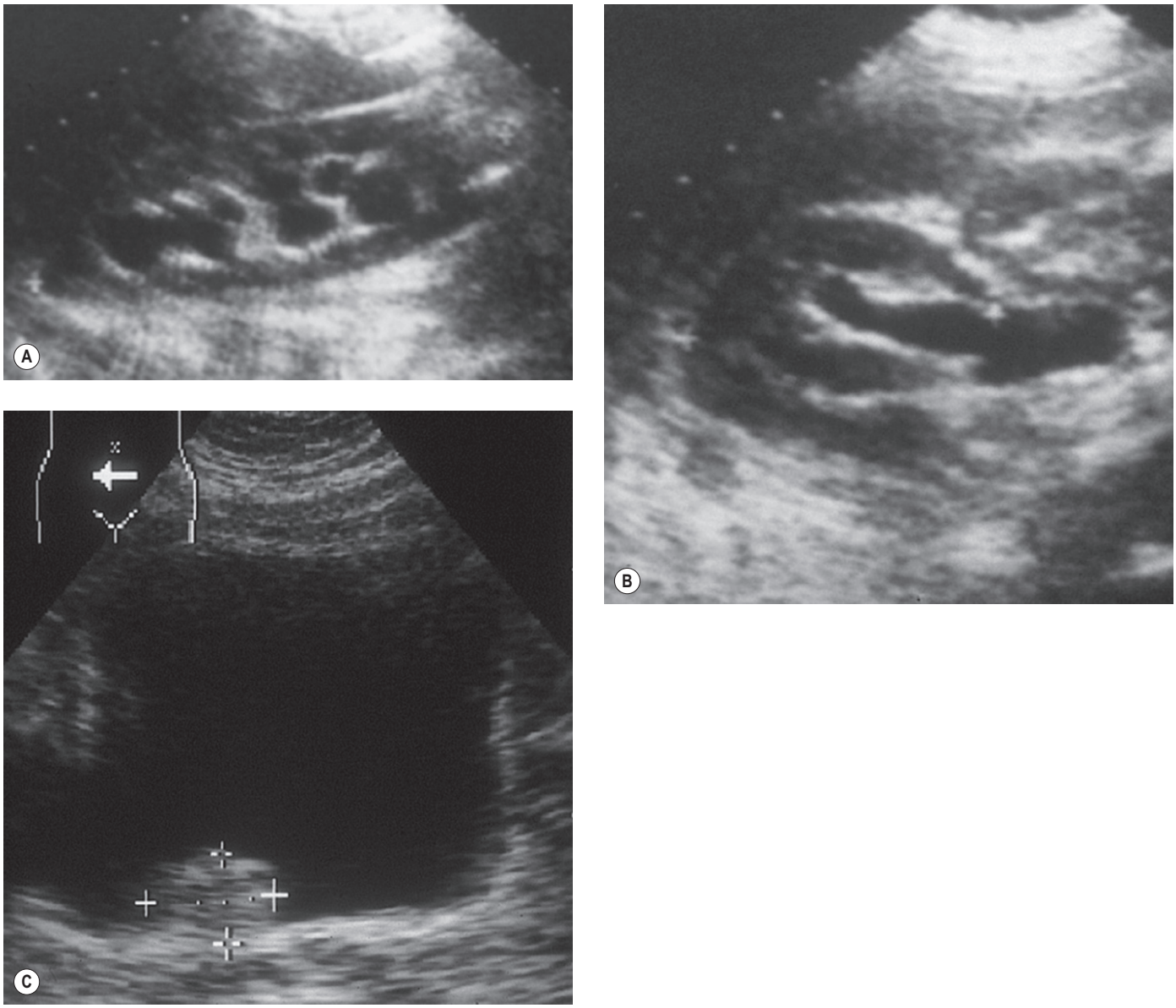


Figure 22.13 Longitudinal and axial US shows a dilated pelvicalyceal system (A and B) caused by a small transitional cell carcinoma at the right vesico-ureteric junction **(C)**.

Congenital

There are many congenital causes that give rise to pelvi-ureteric dilatation on imaging. It is important to recognise these, as with each cause, there are other accompanying abnormalities and early treatment and intervention could potentially salvage renal function.

Obstructed moiety in a duplex kidney

Duplex kidney is the commonest congenital abnormality of the urinary tract with a reported urographic incidence of around 2%.[53] Duplex kidney formation is a result of early divisions of the ureter to reach the metanephros during embryogenesis. The two parts of the duplex kidney are usually joined at a slight twist. Typically there is a smaller upper moiety with only two major calyces and a larger lower moiety with three major calyces.

Duplex kidney is a relatively common variant that may remain concealed in the absence of associated complications. However, it frequently occurs in association with other urinary tract anomalies such as a ureterocele and ectopic vesical insertion of the ureter draining the upper moiety causing ureteric obstruction, or a defective vesico-ureteric junction valve mechanism causing vesico-ureteral reflux to the lower moiety.[54] Both situations may present on imaging with a hydronephrotic moiety.[55]

Rare presentation of PUJ obstruction of either moiety may occur in the duplex kidney. PUJ obstruction of the lower moiety in the duplex kidney[56] has a 2% reported incidence in children with duplex kidneys.[57] Rarely, late presentation, in adult life, of lower moiety PUJ obstruction with pyonephrosis had also been described[58] (Fig. 22.16A–C). PUJ obstruction of the upper moiety is very rare. It is postulated that the incomplete ureteral duplication has predisposed the upper moiety to recurrent UTIs secondary to uretero-ureteral (or so-called 'yo-yo') reflux from retrograde peristalsis and incomplete urinary drainage.[59] The upper moiety PUJ obstruction may have developed subsequent to recurrent urinary reflux with subsequent inflammation and kinking of the PUJ.[60] This too may present late in adult life with pyonephrosis (Fig. 22.17A–C).

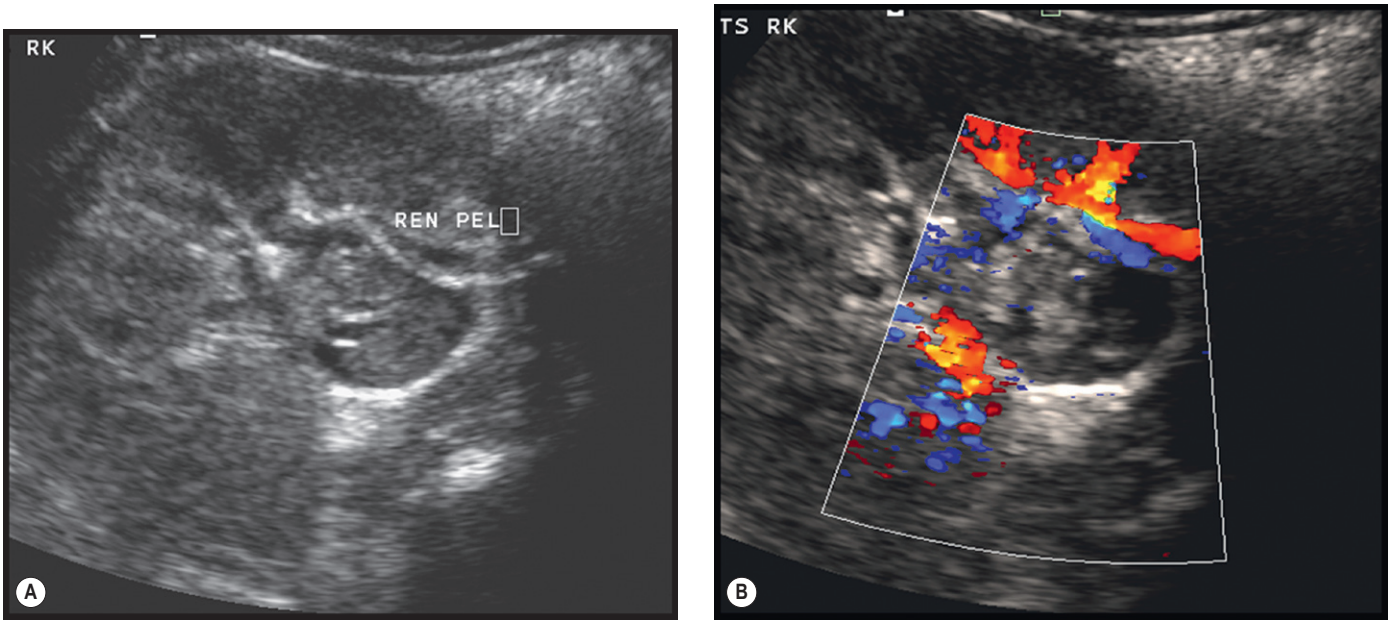


Figure 22.14 Axial US shows low level echoes within a mildly dilated pelvicalyceal system consistent with blood clot **(A)**. There is no colour Doppler signal within it **(B)**. The patient presented with haematuria.



Figure 22.15 Intravenous urography shows renal papillary necrosis in a patient using long-term non-steroidal therapy for chronic right loin pain due to a renal pelvic stone.

On ultrasound this may show as a localised dilated pelvicalyceal system simulating a PUJ obstruction in the upper or lower moiety; the overlying parenchyma is usually thinned and highly echogenic. When associated with a ureterocele, the superior fluid collection can usually be traced medially along an apparently normal kidney as it becomes continuous with the dilated ureter.[61] The ureter may be markedly dilated and tortuous, and whilst the mid-ureter is usually obscured by bowel gas, the distal ureter can be seen behind a full bladder.[62] A ureterocele may be seen as a localised more dilated area of the distal ureter at its insertion or, if big, may be seen within the bladder lumen. This usually dilates with the passage of the urine and may not be obvious unless the operator has observed this area carefully for a few minutes during scanning.[61] Sometimes there are also numerous cysts associated with it as part of a dysplastic process.[2] The ultrasound appearances can usually be confirmed with conventional intravenous urography (IVU) or increasingly with CT urography. In the presence of pyonephrosis, a fluid debris appearance may be seen on the dependent part during ultrasound examination (Figs 22.16B and 22.17B) and it is extremely important to recognise this urological emergency as prompt intervention could be life-saving.

Idiopathic PUJ obstruction

Idiopathic PUJ obstruction may occur at any age and is increasingly being detected early during antenatal ultrasound examination. It is usually caused by an abnormal ring of collagen replacing the smooth muscle of the renal pelvis at the PUJ.[63,64] The peristaltic waves that start off in the calyces fail to progress smoothly down the ureter beyond that abnormal ring of collagen and result in an obstructive uropathy.

Most cases are detected during antenatal ultrasound, occasionally as an incidental finding, and in adults it may present with pain during binge drinking, pyonephrosis, a palpable loin mass or gastrointestinal symptoms.

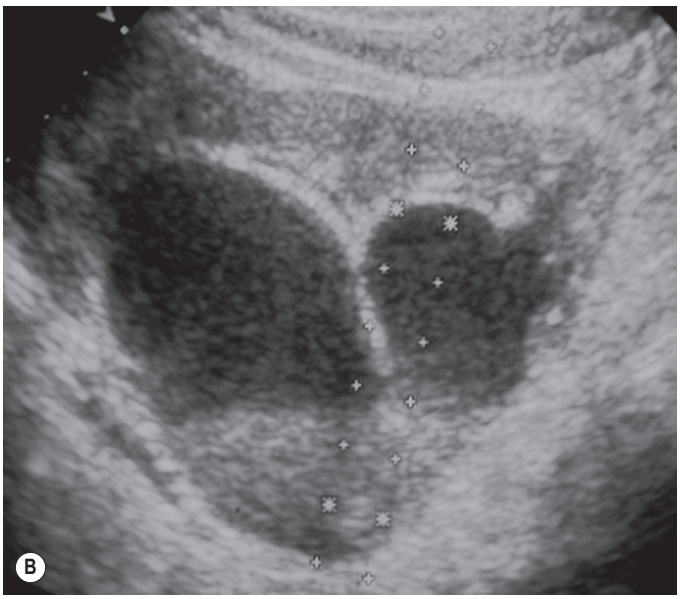
On imaging, the renal pelvis is disproportionately dilated when compared with the calyces and the intravenous urography shows characteristic appearances (Fig. 22.18). Diuresis renography with ^{99m}technetium-labelled MAG-3 is very useful to confirm the diagnosis of PUJ obstruction as well as to quantify the relative renal function in the kidneys before deciding on any potential surgical option.

Bladder outflow obstruction

Bladder outflow obstruction is a fairly common cause of urinary upper tract dilatation. Prostate-related problems are the commonest cause in males, which could be related to either benign prostatic hyperplasia or malignant prostate cancer. Occasionally, a urethral stricture resulting from infection, a congenital abnormality or an iatrogenic cause, could also cause upper tract obstruction.

During ultrasound examination, it is most important to differentiate upper tract dilatation as a result of reflux from a high pressure bladder from those situations where it is caused by intrinsic or extrinsic factors of ureteric obstruction. This is because the former





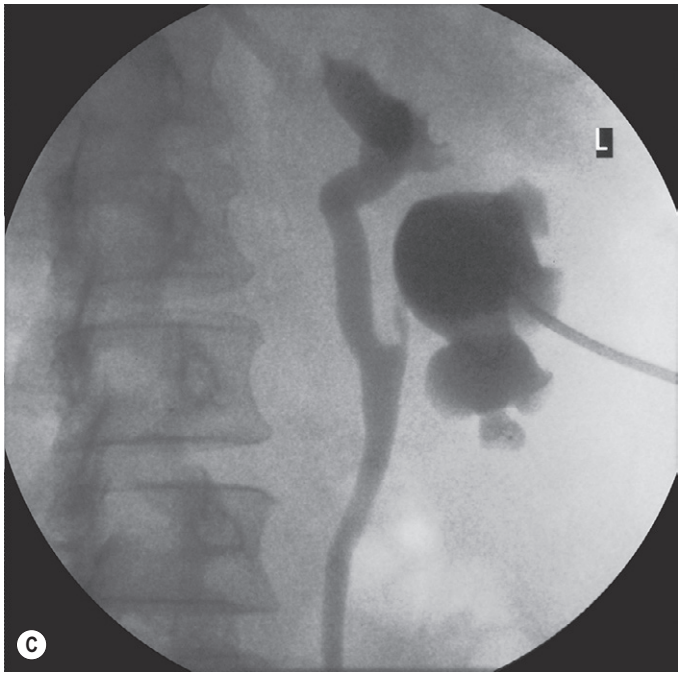


Figure 22.16 **PUJ obstruction in a duplex kidney. A:** IVU shows a duplex left kidney with PUJ obstruction of the lower moiety in a patient presenting with left loin pain and fever. **B:** Ultrasound shows a dilated pelvicalyceal system with low level echoes/debris seen in the dependent part consistent with pyonephrosis. Subsequent drainage of this infected system yielded pus. **C:** The nephrostogram confirms the left lower moiety PUJ obstruction.

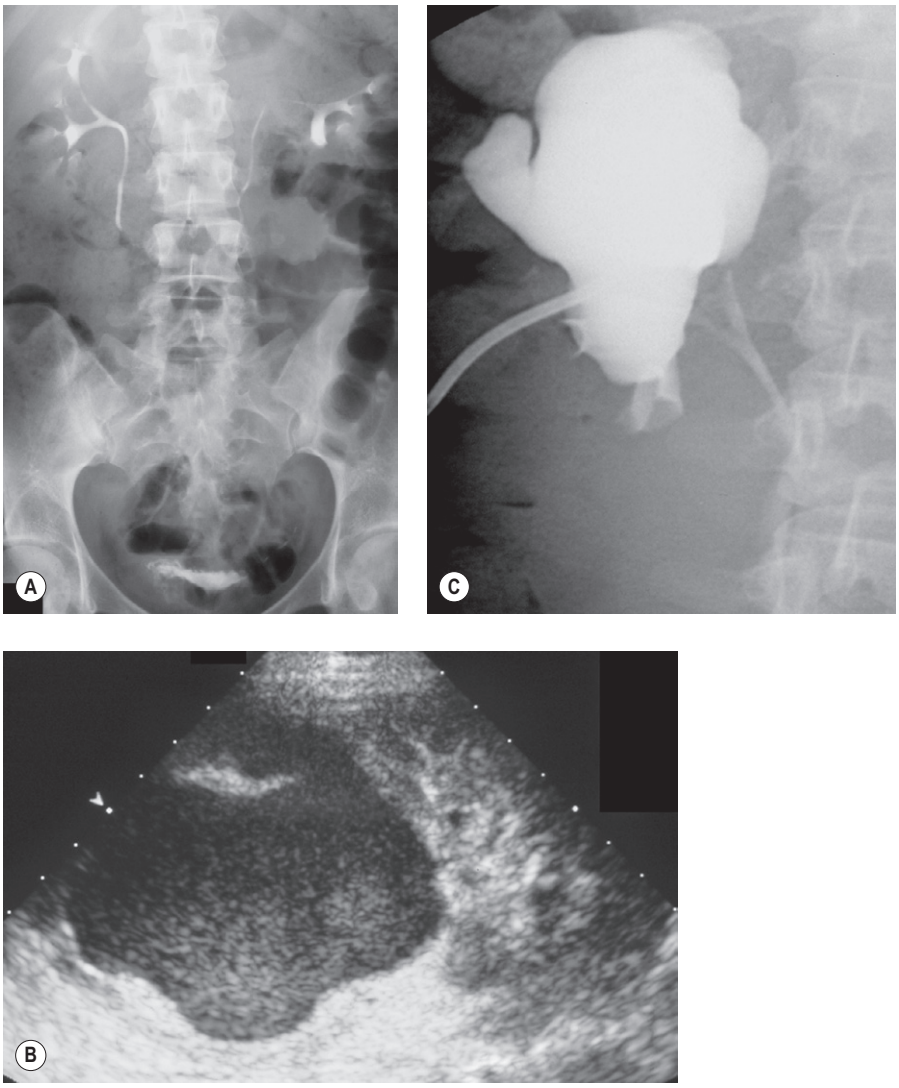


Figure 22.17 Pyonephrosis. A: IVU shows the classic drooping lily sign on the left suggesting an obstructed left upper pole moiety in a duplex system. **B:** A subsequent ultrasound shows an obstructed system which contains internal echoes at the dependent part consistent with pyonephrosis in a patient presenting with fever and loin pain. **C:** The nephrostogram following drainage of this infective obstructed system shows a marked dilated upper moiety pelvicalyceal system and a very tight PUJ.

will usually resolve when draining the bladder after an interval of either urethral or suprapubic catheterisation. Therefore a repeat scan following catheterisation, usually after 5–7 days, is important to ensure resolution of the upper tract dilatation.

Compression by intrapelvic mass

There are many causes within the pelvis that could lead to a dilated pelvi-ureteric system, including gynaecological causes such as cervical carcinoma, endometriosis, pelvic lymphadenopathy and inflammatory disease.

Iatrogenic

Iatrogenic injury to the ureter is quite common. There are many causes; the commoner causes include ligation of the ureter during gynaecological procedures, ureteral injury during ureteroscopic examination (Fig. 22.19) or, rarely, upper ureteral injury from percutaneous ablative therapy of renal cell carcinoma that lies in close apposition to the ureter.

Trauma

Both blunt and penetrating renal trauma can result in catastrophic renal injury where there is evidence of PUJ disruption. Frequently, on ultrasound, perirenal fluid may be detected but the PUJ disruption is not normally seen. Contrast-enhanced CT with excretory phase is the imaging technique to detect this high-grade renal injury.

DIAGNOSIS

Ultrasound is a very sensitive imaging modality for detecting a dilated pelvicalyceal system, even in mild pelvicalyceal dilatation. This is especially important because mild dilatation is a well-recognised finding and often difficult to detect in some patients with severe high-grade obstruction. This usually occurs in the presence of an obstructing calculus or in chronic obstruction caused by retroperitoneal fibrosis or malignancy. Occasionally, the obstructed system may not be dilated on all imaging modalities including CT or antegrade studies. The renal function usually improves after an interval of drainage either with percutaneous nephrostomy or ureteric stent insertion. This finding is thought to be related to a low urinary flow rate as a result of dehydration, underlying renal parenchymal disease, intermittent obstruction by stone or decompression of the pelvicalyceal system through rupture of a calyceal fornix. Fortunately, the clinical suspicion does assist the prompt diagnosis of obstruction in patients with mild pelvicalyceal system dilatation. This had been demonstrated by Kamholtz et al., where



Figure 22.18 IVU shows a classic left idiopathic PUJ obstruction that remains obstructed at 4 hours post contrast enhancement.

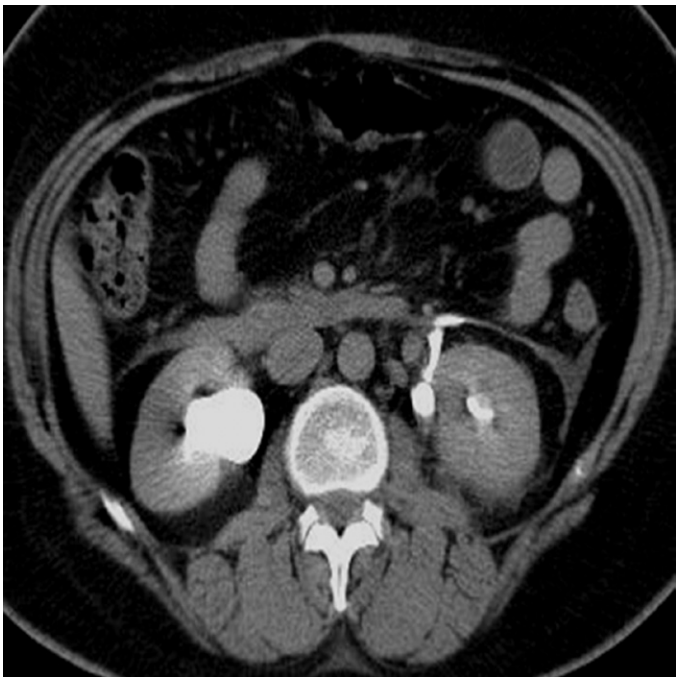


Figure 22.19 Axial CT urography shows contrast leaking around the left PUJ consistent with perforation of the ureter following ureteroscopy for endoscopic stone extraction.

obstruction was present in 56% of the clinically suspected group, versus 6% in the group in which it was not clinically suspected.[65]

However, ultrasound generally has a poor specificity with a reported high false positive rate of up to 26%[4–6] in assessing urinary tract obstruction. Ultrasound is less specific than other imaging modalities such as a urographic study because it provides less anatomical detail, poor visualisation of the ureter and provides no functional information about the drainage system. Largely, this is because ultrasound can visualise a normal fluid-filled collecting system and the causes can vary from osmotic diuresis to back pressure from a distended fluid-filled bladder. In addition, there are a variety of other causes that could contribute to the false positive ultrasound findings.

Causes of false positive ultrasound in obstruction[2]

- Normal
  - Anatomical variant, e.g. compound calyx, extrarenal pelvis
  - Diuresis
  - Distended bladder
- Dilated but non-obstructed
  - Vesico-ureteric reflux
  - Dilated system from previous obstruction
  - Abnormal calyx, e.g. reflux, papillary necrosis, calyceal diverticula
- Other renal fluid collections
  - Cystic disease
  - Normal intrarenal vessels
  - Renal artery aneurysm

ULTRASOUND APPEARANCES – ANATOMICAL EVIDENCE

It is important to ensure that the bladder is empty when the kidneys are examined for pelvicalyceal dilatation. This is because an excessively full bladder can cause mild dilatation of the pelvicalyceal system and ureter.[66]

The dilated pelvicalyceal system is usually seen as a central multiloculated fluid collection within the renal sinus. The medially located larger round renal pelvis can be traced to the dilated calyces via the infundibula. It is important to differentiate this from parapelvic cysts, where the cysts remain separate, whereas in hydronephrosis, the fluid collections communicate with each other and produce the 'Mickey Mouse sign' (Fig. 22.20A and B).

When the pelvicalyceal system dilates, the echogenic renal sinus fat is usually displaced around it. The renal sinus fat is very well seen in mild and moderate hydronephrosis but is usually invisible in marked hydronephrosis. When there is severe hydronephrosis, differentiation of dilated calyces and the renal pelvis can be difficult. The degree of hydronephrosis is graded to provide an indicator of the severity of the obstruction. The grades are: mild (grade 1), moderate (grade 2) and marked (grade 3)[4] (Fig. 22.21A–D).

During ultrasound examination, it is routine to assess the renal length and parenchymal thickness. Longstanding chronic obstruction will usually result in parenchymal thinning.

The renal cortex can return to normal if the cause of obstruction is resolved promptly.

Assessment of the dilated ureter in obstructive uropathy is possible depending on the operator's experience. The dilated proximal ureter adjacent to the renal pelvis may be seen if the transducer is angled anteriorly. The dilated mid-ureter may be delineated as it crosses the common iliac vessels anterior around the pelvic brim.

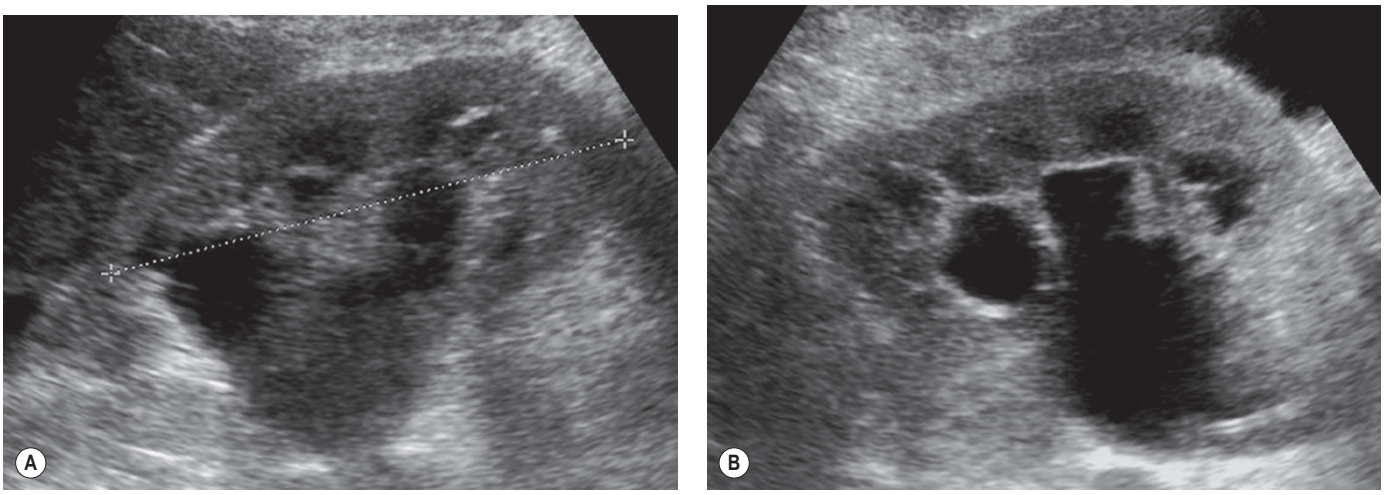
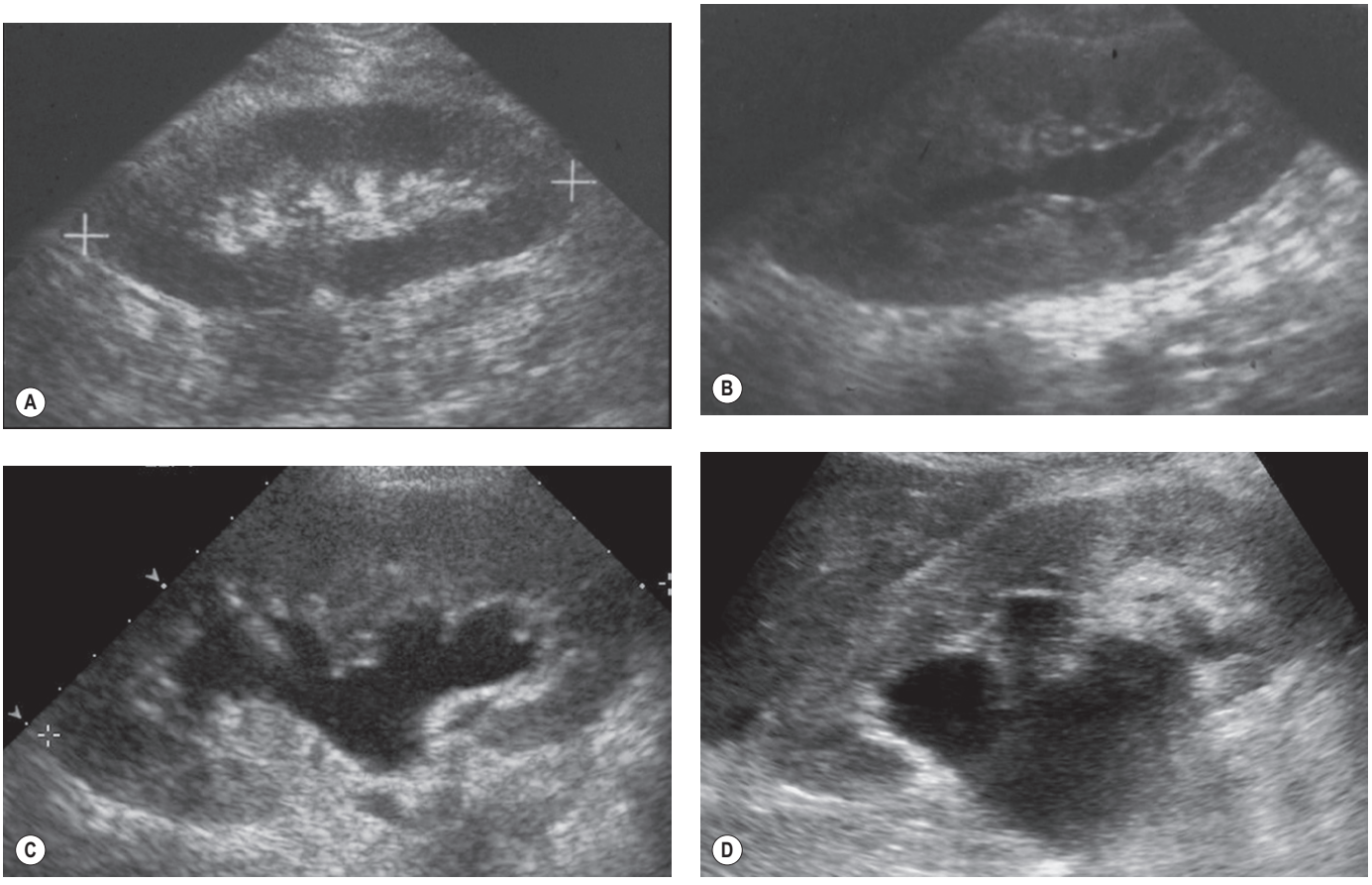


Figure 22.20 **Longitudinal (A) and axial (B) ultrasound shows the Mickey Mouse sign.**



Figures 22.21 **Longitudinal ultrasound shows the grading of hydronephrosis. A:** Non-dilated pelvicalyceal system. **B:** Mild hydronephrosis. **C:** Moderate hydronephrosis. **D:** Marked hydronephrosis.

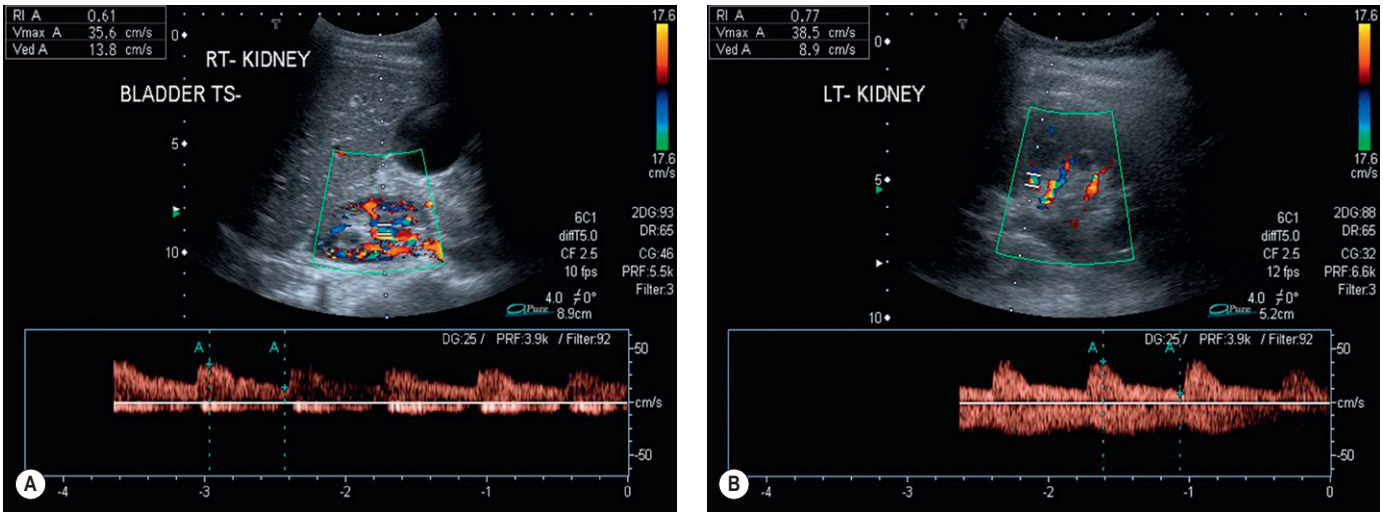
As for the dilated distal ureter, this may be shown behind the urine-filled bladder.

Whenever there is evidence of pelvi-ureteric dilatation, the cause of obstruction should be obtained if possible. Often complementary imaging such as CT (with or without contrast), retrograde studies and MR urography may be required to delineate the cause. The choice of the test will be dependent on patient factors such as the renal function and the clinical suspicion for the cause of obstruction.

FUNCTIONAL EVIDENCE USING DOPPLER TECHNIQUE

Renal blood flow changes

Complete acute obstructive uropathy is normally accompanied by altered renal blood flow and raised renal pelvic pressure. In the



Figures 22.22 Reflective index (RI). Doppler ultrasound shows a normal RI in the right kidney **(A)** and abnormal RI (= 0.77) in the obstructed left kidney **(B)** in a patient who presented acutely with left loin pain. (Courtesy of Jane Smith.)

early stage (within the first few hours post obstruction), there is increased renal blood flow which is likely to be related to the dilatation of the afferent arterioles in the acute setting.[67]

At the intermediate stage (3–5 hours post obstruction), the renal blood flow decreases, probably as a result of prostaglandins and other vasoactive substances due to induced vasoconstriction of the afferent arterioles.[68] This usually persists for 24 hours, and at the same time, the pressure within the collecting system normalises towards the baseline.

The renal blood flow can be evaluated with the ultrasound Doppler technique using the resistance index (RI).[69–71] The time lines for the RI changes are as expected from the pathophysiology of obstructive uropathy, increasing 6 hours post acute obstructive uropathy and remaining at a peak from 6 to 48 hours. Thereafter the RI remains elevated but less markedly so than in the earlier stage.[71]

DOPPLER TECHNIQUE

Normal RI

Measurement of the RI should be obtained from the interlobar or arcuate arteries. This is sampled using a sample volume of 2–5 mm and with a low frequency range (low pulse repetition frequency) and a low wall filter.[7] At least three measurements need to be sampled from three different sites and with three to five waveforms recorded from each site in order to allow calculation of an average RI.[72]

The normal RI is less than 0.7,[73] though it is higher in neonates and infants. In the first year, the RI is usually greater than 0.7 and it may persist at this level for up to 4 years.[74] In the adult, there is a wide variability in the RI even amongst normal individuals. In addition, this measurement also varies depending on the site of sampling; hence it is important to obtain an average measurement.

Abnormal RI

In adults, a dilated non-obstructed pelvicalyceal system and a dilated obstructed pelvicalyceal system have an RI of less than and greater than 0.7, respectively.[73] In addition, a difference in RI greater than 0.06–0.1 between the two kidneys is a significant indicator of obstruction on the side with the raised RI.[75]

However, an increase in RI is a non-specific indicator for obstruction. This is because RI tends to increase in a wide range of renal pathologies such as chronic renal disease, acute tubular necrosis, haemolytic uraemic syndrome, acute renal vein thrombosis, pyelonephritis, renal transplant rejection and subcapsular renal collection.[76–79]

In acute obstructive uropathy caused by a ureteric stone, the RI elevation occurs around 6–8 hours post obstruction.[71,75,80] The most useful indicator is the inter-renal RI difference for locating the site of obstruction[71,75] (Fig. 22.22A and B). This may be demonstrated in up to 20% of subjects without pelvicalyceal system dilatation.[75,80] However, many studies have a lower sensitivity (42–44%)[81,82] when compared with Platt's group (87%).[80] This could be due to the wide range of RIs in normal subjects, time-related response of the RI to the obstruction, possibility of partial or intermittent obstruction, hydration status and probably the use of analgesics that are vasodilators.[83]

In chronic obstructive uropathy, taking serial RI measurements 30 minutes after intravenous furosemide administration has been advocated, as this has been shown to be more sensitive than without furosemide.[84] Sensitivity was 95% in detecting renal obstruction when an RI threshold of greater than 0.75 was used to diagnose urinary tract obstruction.[84]

Ureteric jets

Ureteric jets may be visualised when scanning a full bladder as highly echogenic streams on greyscale ultrasound or as areas of colour on Doppler examination.[85,86] The ureteric jets are usually symmetrical on both sides.[86]

For optimal assessment, the patient should be hydrated with 600 mL to 1 L of fluid. About 15–30 minutes following hydration, the bladder should be examined for a period of at least 5 minutes to look for the jet of urine. In high-grade obstruction, most patients demonstrate no ureteric jet; conversely, in low-grade obstruction, very few patients have abnormal flow[86] (Fig. 22.23A and B).

MANAGEMENT OF OBSTRUCTIVE UROPATHY

The management of obstructive uropathy is very much dependent on the cause of obstruction. Ultrasound is very sensitive in detecting urinary tract obstruction but in most cases has difficulty in delineating the cause. Today, CT KUB and contrast-enhanced CT

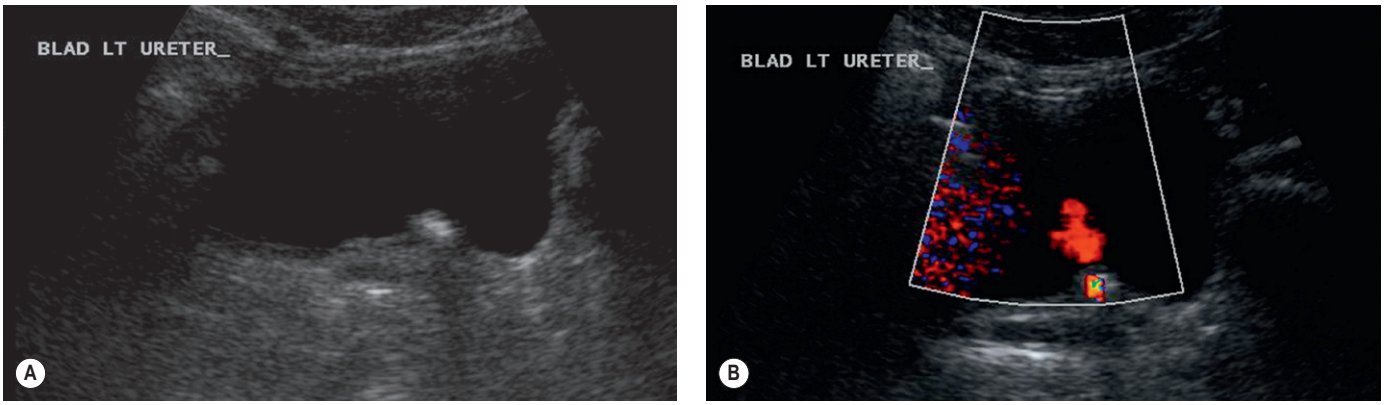


Figure 22.23 **A:** Axial ultrasoundshows a left vesico-ureteric junction stone. **B:** Doppler ultrasound shows that there is flow past the stone suggesting that the stone is causing only an incomplete obstruction.

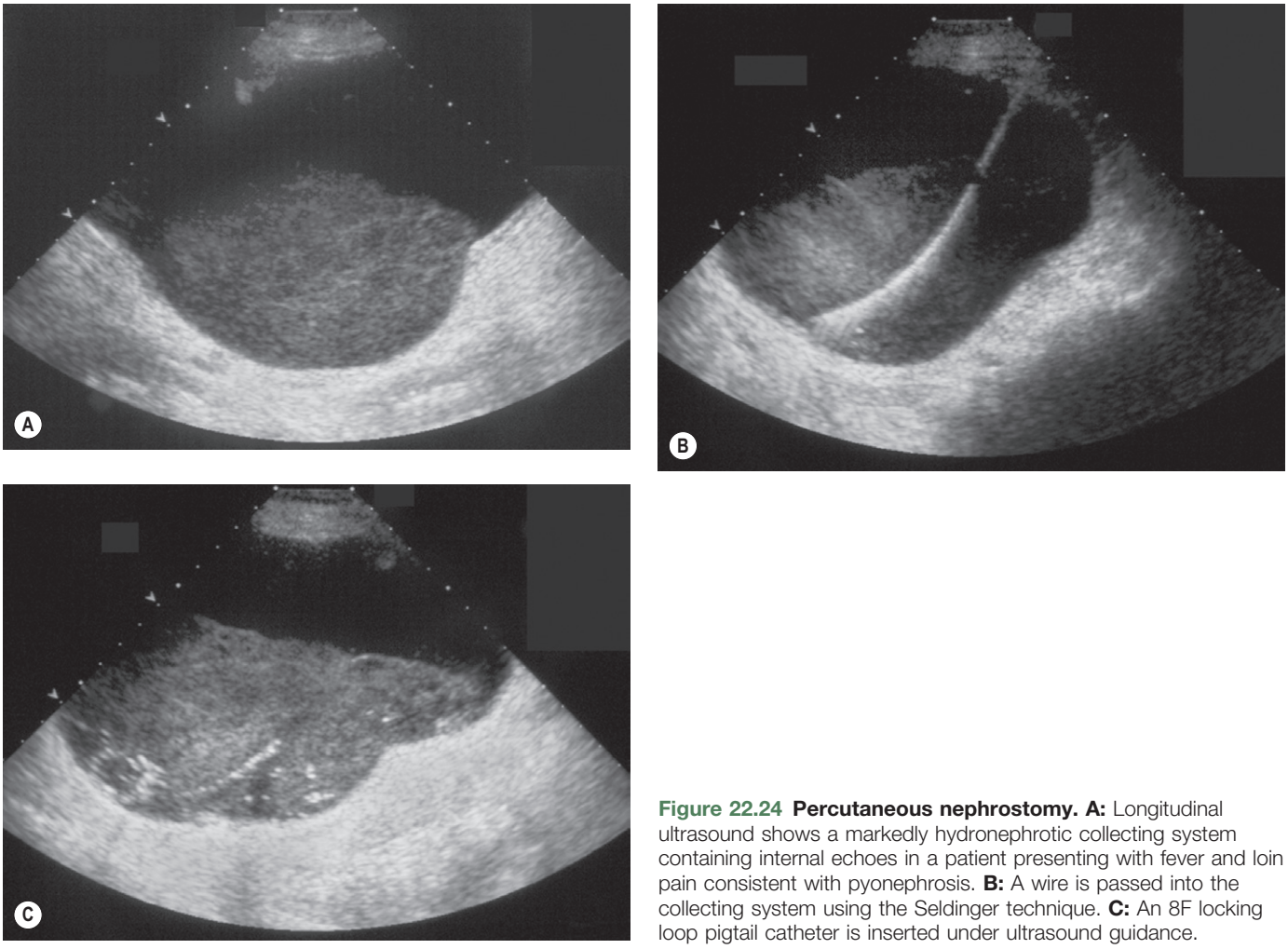


Figure 22.24 **Percutaneous nephrostomy. A:** Longitudinal ultrasound shows a markedly hydronephrotic collecting system containing internal echoes in a patient presenting with fever and loin pain consistent with pyonephrosis. **B:** A wire is passed into the collecting system using the Seldinger technique. **C:** An 8F locking loop pigtail catheter is inserted under ultrasound guidance.

(with excretory phase) are the investigations of choice depending on the clinical scenario.

MAG-3 renogram is very useful in assessing the relative function of the obstructed and non-obstructed kidneys. This information will allow the clinician to determine whether there is any mileage in saving the chronically obstructed kidney.

The treatment of obstructive uropathy is essentially dependent on the cause and radiologists are frequently involved in the acute setting when there is a need to relieve an obstructed system in the event of crushing renal failure or when there is evidence of pyonephrosis.

Pyonephrosis

Pyonephrosis is a urological emergency and performing percutaneous nephrostomy in this situation is very rewarding as it is a life-saving procedure.

The patient normally presents with loin pain and fever. Ultrasound will reveal an obstructed pelvicalyceal system which contains internal echoes consistent with an infected system (Figs 22.20B and 22.21B).

Percutaneous nephrostomy

Ultrasound is the modality of choice to guide the puncture of the dilated pelvicalyceal system. Both free hand and guide attachments fixed to the ultrasound transducer techniques are safe and widely practised.[87] Assessing the dilated system is usually achieved with a 19G or 20G sheathed needle through the perinephric tissue along the line of the ultrasound beam. Local anaesthetic is infiltrated under ultrasound guidance and the procedure is performed under breath holds during suspended inspiration in the cooperative patient or during gentle respiration in confused patients. When the dilated system is successfully accessed, a small amount of the infected urine should be sent for microbiology assessment. All patients with suspected pyonephrosis should be given prophylactic antibiotics before the collecting system is punctured because puncturing of the system can lead to septicaemia.

Depending of the configuration and degree of the dilatation, Seldinger and one-stab techniques may be used to site the nephrostomy. In moderate to marked hydronephrosis, both the Seldinger technique (Fig. 22.24A–C) and the one-stab technique using the trocar assembly can be easily performed using ultrasound guidance alone. When the system is minimally dilated, the Seldinger technique is usually performed using both ultrasound and fluoroscopic guidance in the interventional suite.

REFERENCES

1. Talner LB. Urinary obstruction. In: Grainger RG, Allison DJ, editors. Diagnostic radiology. Edinburgh: Churchill Livingstone; 1997. p. 1419.
2. Amis ES, Cronan JJ, Pfister RC, Yoder IC. Ultrasonic inaccuracies in diagnosing renal obstruction. Urology 1982;19:101–105.
3. Curry NS, Gobien RP, Schabel SI. Minimal dilatation obstructive nephropathy. Radiology 1982;143:531–534.
4. Ellenbogen PH, Scheible FW, Talner BL, Leopold GR. Sensitivity of grey scale ultrasound in detecting urinary tract obstruction. AJR Am J Roentgenol 1978;130:731–733.
5. Talner LB, Scheible W, Ellenbogen PH, et al. How accurate is ultrasonogaphy in detecting hydronephrosis in azotaemic patients? Urol Radiol 1981;3:1–6.
6. Webb JAW, Reznek RH, White FE, et al. Can ultrasound and computed tomography replace high dose urography in patients with impaired renal function? Q J Med 1984;53:411–425.
7. Platt JF. Duplex Doppler evaluation of native kidney dysfunction: obstructive and non-obstructive disease. AJR Am J Roentgenol 1992;158:1035–1042.
8. Chowdhury FU, Kotwal S, Raghunathan G, et al. Unenhanced multidetector CT (CT KUB) in the initial imaging of suspected acute renal colic: evaluating a new service. Clin Radiol 2007;62(10):970–977.
9. Pfister SA, Deckart A, Laschke S, et al. Unenhanced helical computed tomography vs intravenous urography in patients with acute flank pain: accuracy and economic impact in a randomized prospective trial. Eur Radiol 2003;13:2513–2520.
10. Sandhu C, Anson KM, Patel U. Urinary tract stones – Part 1: Role of radiological imaging in diagnosis and treatment planning. Clin Radiol 2003;58:415–421.
11. Heidenreich A, Desgrandchamps F, Terrier F. Modern approach of diagnosis and management of acute flank pain: review of all imaging modalities. Eur Urol 2002;41:351–362.
12. Dhar M, Denstedt JD. Imaging in diagnosis, treatment, and follow-up of stone patients. Adv Chronic Kidney Dis 2009;16(1):39–47.
13. Cietak KA, Newton JR. Serial qualitative maternal nephrosonography in pregnancy. Br J Radiol 1985;58:399–404.
14. Hertzberg BS, Carroll BA, Bowie JD, et al. Doppler US assessment of maternal kidneys: analysis of intrarenal resistivity indexes in normal pregnancy and physiologic pelvicaliectasis. Radiology 1993;186:689–692.
15. Spencer JA, Tomlinson AJ, Weston MJ, Lloyd SN. Early report: comparison of breath-hold MR excretory urography, Doppler ultrasound and isotope renography in evaluation of symptomatic hydronephrosis in pregnancy. Clin Radiol 2000;55(6):446–453.
16. Spencer JA, Chahal R, Kelly A, et al. Evaluation of painful hydronephrosis in pregnancy: magnetic resonance urographic patterns in physiological dilatation versus calculous obstruction. J Urol 2004;171(1):256–260.
17. Royal College of Radiologists. Making the best use of clinical radiology services (MBUR) 6th edn, Uroradiology Section 2007. Available at: http://mbur.nhs.uk.
18. Sommer FG, Taylor KJW. Differentiation of acoustic shadows due to calculi and gas collections. Radiology 1980;135:399–403.
19. Rubin JH, Adler RS, Bude RO, et al. Clean and dirty shadowing at US: a reappraisal. Radiology 1991;181:231–236.
20. Haddad MC, Sharif HS, Shahed MS, et al. Renal colic: diagnosis and outcome. Radiology 1992;184:83–88.
21. King W, Kimme-Smith C, Winter J. Renal stone shadowing: an investigation of contributing factors. Radiology 1985;154:191–196.
22. Pollack HM, Arger PH, Goldberg BB, Mulholland SG. Ultrasonic detection of non-opaque renal calculi. Radiology 1978;127:233–237.
23. Weill FS, Bihr E, Rohmer P, Zeltner F. Renal sonography. Berlin: Springer-Verlag; 1987. p. 54.
24. Zwirewich CV, Buckley AR, Kidney MR, et al. Renal matrix calculus: sonographic appearance. J Ultrsound Med 1990;9:61–64.
25. Kimme-Smith C, Perella RR, Kaveggia LP, et al. Detection of renal stones with real time sonography: effect of transducers and scanning parameters. AJR Am J Roentgenol 1991;157:975–980.
26. Scanlan KD. Sonographic artifacts and their origins. AJR Am J Roentgenol 1991;156:1267–1272.
27. Choyke PL, Pahira JH, Davros WJ, et al. Renal calculi after shock-wave lithotripsy: US evaluation with an in-vitro phantom. Radiology 1989;170:139–144.
28. Middleton WD, Dodds WJ, Lawson TL, Foley WD. Renal calculi: sensitivity for detection with ultrasound. Radiology 1988;167:239–244.
29. Baumgartner BR, Steinberg HV, Ambrose SS, et al. Sonographic evaluation of renal stones treated by extracorporeal shock-wave lithotripsy. AJR Am J Roentgenol 1987;149:131–135.
30. Kane RA, Manco LG. Renal arterial calcification simulating nephrolithiasis on sonography. AJR Am J Roentgenol 1983;140:101–104.
31. Amis ES, Hartman DS. Renal ultrasonography 1984: a practical overview. Radiol Clin North Am 1984;22:315–332.
32. Laing FC, Benson CB, DiSalvo DN, et al. Distal ureteral calculi: detection with vaginal US. Radiology 1994;192:545–548.
33. Lerner RM, Rubens D. Distal ureteral calculi: diagnosis by transrectal sonography. AJR Am J Roentgenol 1986;147:1189–1191.
34. Hertzberg BS, Kliewer MA, Paulson EK, Carroll BA. Distal ureteral calculi: detection with transperineal sonography. AJR Am J Roentgenol 1994;163:1151–1153.
35. Leder RA, Dunnick NR. Transitional cell carcinoma of the pelvicalices and ureter. AJR Am J Roentgenol 1990;155:713–722.
36. Korobkin M. CT urography. Eur Radiol 2005;15(Suppl 4):D82–D84.
37. Caoili EM, Cohan RH, Inampudi P, et al. MDCT urography of upper tract urothelial neoplasms. AJR Am J Roentgenol 2005;184(6): 1873–1881.
38. Noroozian M, Cohan RH, Caoili EM, et al. Multislice CT urography: state of the art. Br J Radiol 2004;77 Spec No 1:S74–S86.
39. Van Der Molen AJ, Cowan NC, Mueller-Lisse UG, et al. CT Urography Working Group of the European Society of Urogenital Radiology (ESUR). CT urography: definition, indications and techniques. A guideline for clinical practice. Eur Radiol 2008;18(1):4–17.
40. Subramanyam BR, Raghavendra BN, Madamba MR. Renal transitional cell carcinoma: sonographic and pathologic correlation. J Clin Ultrasound 1982;10:203–210.
41. Grant DC, Dee GJ, Yoder IC, Newhouse JH. Sonography in transitional cell carcinoma of the renal pelvis. Urol Radiol 1986;8:1–5.
42. Janetschek G, Putz A, Feichtinger H. Renal transitional cell carcinoma mimicking stone echoes. J Ultrasound Med 1988;7:83–86.
43. Hartman DS, Pyatt RS, Dailey E. Transitional cell carcinoma of the kidney with invasion into the renal vein. Urol Radiol 1983; 5:83–87.
44. Stuck K, Silver TM, Jaffe MH, Bowerman RA. Sonographic demonstration of renal fungus balls. Radiology 1981;142:473–474.
45. Kintanar C, Cramer BC, Reid WD, Andrews WL. Neonatal renal candidiasis: sonographic diagnosis. AJR Am J Roentgenol 1986; 147:801–805.
46. Dillard JP, Talner LB, Pinckney L. Normal renal papillae simulating calyceal defects on sonography. AJR Am J Roentgenol 1987; 148:895–896.

47. Tuite MJ, Weiss SL. Ultrasound and computed tomographic appearance of extramedullary haemopoiesis encasing the renal pelvis. J Clin Ultrasound 1991;19:238–240.
48. Rosenfield AT, Taylor KJ, Dembner AG, Jacobson P. Ultrasound of renal sinus: new observations. AJR Am J Roentgenol 1979; 133(3):441–448.
49. Ulreich S. Ultrasound in the evaluation of renal papillary necrosis. Radiology 1983;148(3):864.
50. Hoffman JC, Schnur MJ, Koenigsberg M. Demonstration of renal papillary necrosis by sonography. Radiology 1982;145:785–787.
51. Jung DC, Kim SH, Jung SI, et al. Renal papillary necrosis: review and comparison of findings at multi-detector row CT and intravenous urography. Radiographics 2006;26(6):1827–1836.
52. Premkumar A, Lattimer J, Newhouse JH. CT and sonography of advanced urinary tract tuberculosis. AJR Am J Roentgenol 1987; 148:65–69.
53. Privett JT, Jeans WD, Roylance J. The incidence and importance of renal duplication. Clin Radiol 1976;27:521–530.
54. Hartman GW, Hodson CJ. The duplex kidney and related abnormalities. Clin Radiol 1969;20:387–400.
55. Nusbacher N, Bryk D. Hydronephrosis of the lower pole of the duplex kidney: another renal pseudotumour. Am J Roentgenol 1978;130:967–969.
56. Fernbach SK, Zawin JK, Lebowitz RL. Complete duplication of the ureter with ureteropelvic junction obstruction of the lower pole of the kidney: imaging findings. Am J Roentgenol 1995;164:701–704.
57. Snyder HM 3rd, Lebowitz RL, Colodny AH, et al. Ureteropelvic junction obstruction in children. Urol Clin North Am 1980;7:273–290.
58. Wah TM, Weston MJ, Irving HC. Lower moiety pelvic-ureteric junction obstruction (PUJO) of the duplex kidney presenting with pyonephrosis in adults. Br J Radiol 2003;76(912):909–912. Erratum in: Br J Radiol 2004;77(915):269.
59. Campbell JE. Ureteral peristalsis in duplex renal collecting systems. AJR Am J Roentgenol 1967;99:557–584.
60. Whitaker RH, Flower CD. Ureters that show both reflux and obstruction. Br J Urol 1979;51:471–474.
61. Mascatello VJ, Smith EH, Carrera GF, et al. Ultrasonic evaluation of the obstructed duplex kidney. AJR Am J Roentgenol 1977;129:113–120.
62. Nussbaum AR, Dorst JP, Jeffs RD, et al. Ectopic ureter and ureterocele: their varied sonographic manifestations. Radiology 1986;159:227–235.
63. Gosling JA, Dixon JS. The structure of the normal and hydronephrotic upper urinary tract. In: O'Reilly PH, Gosling JA, editors. Idiopathic hydronephrosis. Berlin: Springer; 1982.
64. Notley RG. The structural basis for normal and abnormal ureteric motility. Ann R Coll Surg Engl 1971;49:248.
65. Kamholtz RG, Cronan JJ, Dorfman GS. Obstruction and the minimally dilated renal collecting system: US evaluation. Radiology 1989;170:51–53.
66. Morin ME, Baker DA. The influence of hydration and bladder distension on the sonographic diagnosis of hydronephrosis. J Clin Ultrasound 1979;7:192–194.
67. Vaughan ED, Shenasky JH, Gillenwater JY. Mechanism of acute haemodynamic response to ureteral occlusion. Invest Urol 1971;9:109–118.
68. Curhan GC, Zeidl ML. Urinary tract obstruction. In: Brenner BM, editor. The kidney. Philadelphia: WB Saunders; 1996. p. 1944.
69. Dodd GD, Kaufman PN, Bracken RB. Renal artery duplex Doppler ultrasound in dogs with urinary obstruction. J Urol 1991;145:644–646.
70. Ulrich JC, York JP, Koff SA. The renal vascular response to acutely elevated intrapelvic pressure: resistance index measurements in experimental obstruction. J Urol 1995;154:1202–1204.
71. Opdenakker L, Oyen R, Vervlossen I, et al. Acute obstruction of the renal collecting system: the intrarenal resistive index is a useful yet time dependent parameter for diagnosis. Eur Radiol 1998;8:1429–1432.
72. Keogan MT, Kliewer MA, Hertzberg BS, et al. Renal resistive indexes: variability in Doppler US measurement in a healthy population. Radiology 1996;199:165–169.
73. Platt JF, Rubin JM, Ellis JH. Distinction between obstructive and non-obstructive pyelocaliectasis with duplex Doppler sonography. AJR Am J Roentgenol 1989;153:997–1000.
74. Bude RO, DiPietro MA, Platt JF, et al. Age dependency of the renal resistive index in healthy children. Radiology 1992;184:469–473.
75. Rodgers PM, Bates JA, Irving HC. Intrarenal Doppler ultrasound studies in normal and acutely obstructed kidneys. Br J Radiol 1992;65:207–212.
76. Platt JF, Ellis JH, Rubin JM, et al. Intrarenal arterial Doppler sonography in patients with non-obstructive renal disease: correlation of resistive index with biopsy findings. AJR Am J Roentgenol 1990;154:1223–1227.
77. Mostbeck GH, Kain R, Mallek R, et al. Duplex Doppler sonography in renal parenchymal disease. Histopathologic correlation. J Ultrasound Med 1991;10:189–194.
78. Platt JF, Rubin JM, Ellis JH. Acute renal failure: possible role of duplex Doppler US in distinction between acute prerenal failure and acute tubular necrosis. Radiology 1991;179:419–423.
79. Patriquin HB, O'Regan S, Robitaille P, Paltiel H. Hemolytic-uremic syndrome: intrarenal arterial Doppler patterns as a useful guide to therapy. Radiology 1989;172:625–628.
80. Platt JF, Rubin JM, Ellis JH. Acute renal obstruction: evaluation with intrarenal duplex Doppler and conventional US. Radiology 1993; 186:685–688.
81. Tublin ME, Dodd GD, Verdile VP. Acute renal colic: diagnosis with duplex Doppler US. Radiology 1994;193:697–701.
82. Older RA, Stoll HL, Omary RA, Watson LR. Clinical value of renovascular resistive index measurement in the diagnosis of acute obstructive uropathy. J Urol 1997;157:2053–2055.
83. Cronan JJ, Tublin ME. Role of the resistive index in the evaluation of acute renal obstruction. AJR Am J Roentgenol 1995;164: 377–378.
84. Mallek R, Bankier AA, Etele-Hainz A, et al. Distinction between obstructive and nonobstructive hydronephrosis: value of diuresis duplex Doppler sonography. AJR Am J Roentgenol 1996;166:113–117.
85. Burge HJ, Middleton WD, McClennan BL, Hildebolt CF. Ureteral jets in healthy subjects and in patients with unilateral ureteral calculi: comparison with colour Doppler US. Radiology 1991;180:437–442.
86. Dubbins PA, Kurtz AB, Darby J, Goldberg BB. Ureteric jet effect: the echographic appearance of urine entering the bladder. Radiology 1981;140:513–515.
87. Wah TM, Weston MJ, Irving HC. Percutaneous nephrostomy insertion: outcome data from a prospective multi-operator study at a UK training centre. Clin Radiol 2004;59:255–261.

CHAPTER

23 Medical diseases of the kidney

Paul L. Allan

INTRODUCTION 445

ULTRASOUND FEATURES OF MEDICAL RENAL DISEASE 445
Renal size 445
Cortical changes 446
Medullary changes and corticomedullary differentiation 446
Renal vessels and Doppler studies 447

MEDICAL RENAL DISEASES 447
Vascular disorders 447
Renal vein thrombosis 447
Renal artery occlusion 448
Renal artery stenosis 448
Hypertensive renal disease 449
Acute tubular necrosis 449
Glomerulonephritis 449
Renal papillary necrosis 449
Medullary sponge kidney 450
Nephrocalcinosis 451

MISCELLANEOUS DISORDERS 451
Acute interstitial nephritis 451
Acute cortical necrosis 452
Amyloid and the kidneys 452
Diabetes mellitus 452
Connective tissue disorders 453
Sickle cell disease 453
Hepatorenal syndrome 453

END-STAGE RENAL DISEASE, DIALYSIS AND ACQUIRED CYSTIC DISEASE 453
Acquired cystic disease of the kidney 453
Dialysis patients 454

RENAL BIOPSY 455
Indications and contraindications 455
Technique 456
Complications 456
Renal transplant biopsy 457

INTRODUCTION

A wide range of disorders can affect the parenchyma of the kidney, producing varying degrees of acute or chronic impairment of function. Patients may be referred for ultrasound with one of several different clinical pictures. They may have suffered a sudden deterioration in function with no previous history of renal disease, or may have known renal impairment but have deteriorated suddenly or more quickly than was expected from their clinical history.

Ultrasound is a valuable investigation in the assessment of patients with impaired renal function from any cause as it does not rely on function or require the administration of intravascular contrast. Contrast medium may be deleterious to already impaired kidneys which may not have sufficient residual function for adequate concentration of contrast for satisfactory visualisation. Ultrasound demonstrates the presence, size and appearance of the kidneys but, most importantly, it will demonstrate whether there is obstruction of the outflow from the kidney. Although this is the cause of impaired function in only some 10% of patients with acute renal failure,[1] it is important that it should be recognised as quickly as possible so that relief of the obstruction can be obtained by the most suitable technique.

In the majority of cases obstruction will not be demonstrated but ultrasound is still of value as it can give information on the overall size of the kidneys, the thickness and reflectivity of the cortex, the prominence of the medullary pyramids and the degree of corticomedullary differentiation. Although changes in these features are non-specific they may, in conjunction with the clinical picture, provide further clues to the nature of the renal abnormality and the likelihood of recovery. Doppler ultrasound allows assessment of blood flow in the renal arteries and veins, which is of value, especially if a vascular aetiology is suspected. Ultrasound can also be used to guide biopsy procedures (see Chapter 11).

Unfortunately ultrasound does not distinguish reliably between the various causes of acute or chronic renal failure. Many attempts have been made to correlate the ultrasound appearances of the kidneys with the type of disease, its severity and its outcome but with little success.[2–6] Some clues can be obtained from the overall appearances of the kidney, analogous to the changes seen on urography. Focal cortical scarring with normal cortical reflectivity and no calyceal dilatation may be seen in segmental renal infarction, whereas focal scarring with dilated or prominent calyces raises the possibility of chronic pyelonephritis or reflux nephropathy. A dilated collecting system with diffuse cortical loss implies chronic obstruction or vesico-ureteric reflux, whereas prominent or dilated calyces without cortical loss suggests obstruction or perhaps renal papillary necrosis.

ULTRASOUND FEATURES OF MEDICAL RENAL DISEASE

Renal size

In acute disorders when there is oedema or inflammatory infiltrate, there is usually swelling of the parenchyma and an increase in overall size (Fig. 23.1). However, in the majority of cases of acute or subacute medical renal disease the size of the kidneys remain within normal limits. In chronic renal disease the kidneys tend to contract as fibrotic changes develop, but the degree to which this occurs is very variable and correlation with renal function as well as with the type of pathology is poor.[2–4] In some types of chronic renal disease, such as amyloid, the kidneys may enlarge in the initial stages but later contract. Enlargement may also occur if severe acquired cystic disease of renal failure develops. In addition, the kidneys are often large in diabetic patients until nephrosclerosis supervenes, when they may shrink to normal or below normal size (see below).



Figure 23.1 Acute glomerulonephritis. An enlarged kidney with increased cortical reflectivity and thickness in a patient with acute glomerulonephritis. There is also some loss of corticomedullary differentiation.

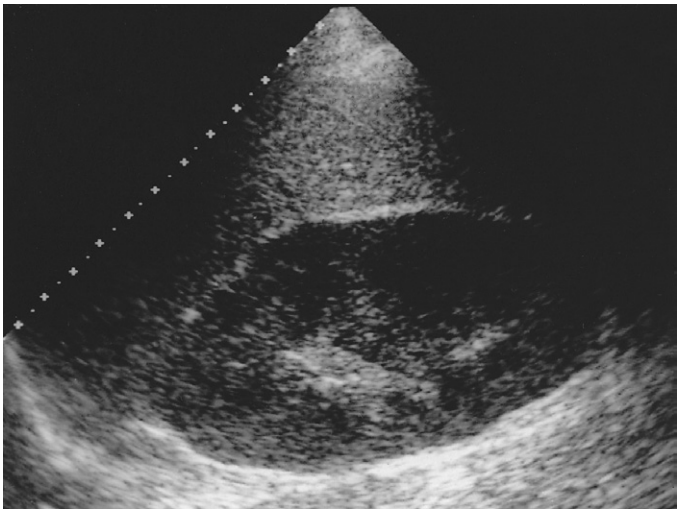


Figure 23.2 Acute renal failure. A swollen echo-poor kidney with loss of corticomedullary differentiation in a patient with acute renal failure.

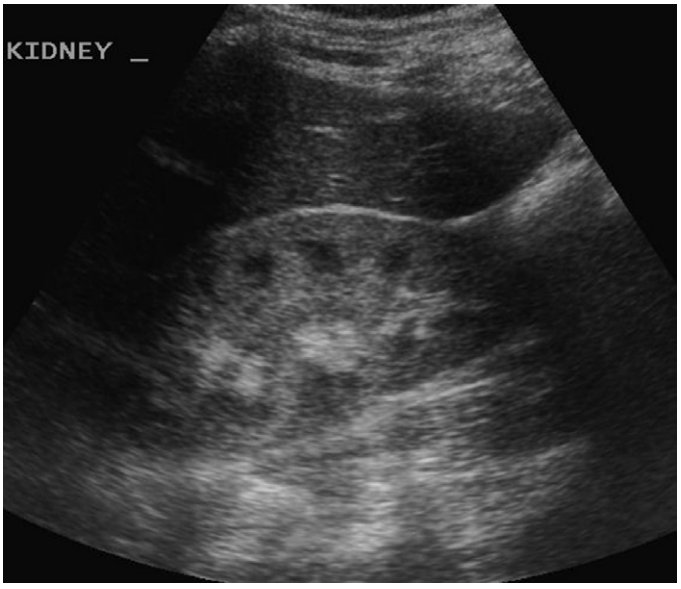


Figure 23.3 Glomerulonephritis and nephrotic syndrome. Increased prominence of the pyramids in a patient with glomerulonephritis and nephrotic syndrome.

Features of renal parenchymal disease

Change in size of kidneys: the kidneys may swell in acute disorders and tend to contract with chronic disease.
Increased or decreased reflectivity: increased parenchymal reflectivity is associated with inflammatory infiltration; decreased reflectivity with oedema or infiltration.
Loss of corticomedullary differentiation: seen with medullary inflammation or early calcinosis.
Scarring: occurs in the cortex of a renal lobule; fetal lobation indentations occur between lobules.
Changes in blood flow: most parenchymal diseases result in a non-specific elevation of the resistance index.

Cortical changes

In acute nephropathies the cortex may swell and increase in thickness. The cortical reflectivity may be either reduced (Fig. 23.2), as in acute renal vein thrombosis, or markedly increased, as in some cases of acute glomerulonephritis and acute interstitial nephritis (Fig. 23.3). Assessment of cortical reflectivity can be difficult. In the past it was compared to that of the adjacent liver or spleen – assuming that these were normal – and an estimate made of whether the reflectivity was less than, equal to or greater than the liver or spleen. In extreme cases of disease the reflectivity of the cortex can be similar to the renal sinus.[2] Normal cortex is generally less reflective than the liver or spleen. However, some modern ultrasound machines may not demonstrate much difference between the kidney and the adjacent liver in normal patients.[5,7] This is a feature of the equipment pre- and post-processing characteristics and these should be optimised to enhance display of subtle contrasts between low-amplitude echoes.

In chronic disease the reflectivity of the cortex is also variable. While the cortex may show no apparent change in appearance in some patients with severely impaired function, there is a tendency for cortical thinning to occur. This is usually proportional to the overall decrease in renal length but there is no consistent correlation with the underlying renal disease.[8] Some conditions, such as vesicoureteric reflux or segmental infarction, result in cortical scarring. Scarring can be distinguished from fetal lobation by assessing the relationship of the defect to the underlying pyramid and calyx. With fetal lobation the cortical indentation overlies the interval between pyramids rather than overlying a pyramid itself, which is the case with cortical scarring.

Calcification in the cortex may be apparent following acute cortical necrosis and rarely in some cases of chronic glomerulonephritis.

Medullary changes and corticomedullary differentiation

The medullary pyramids may be more prominent in many cases of parenchymal disease as the increased cortical reflectivity increases contrast with the echo-poor medullary tissue. In other cases there may be a decrease in the degree of corticomedullary differentiation so that the pyramids are poorly defined or even indistinguishable

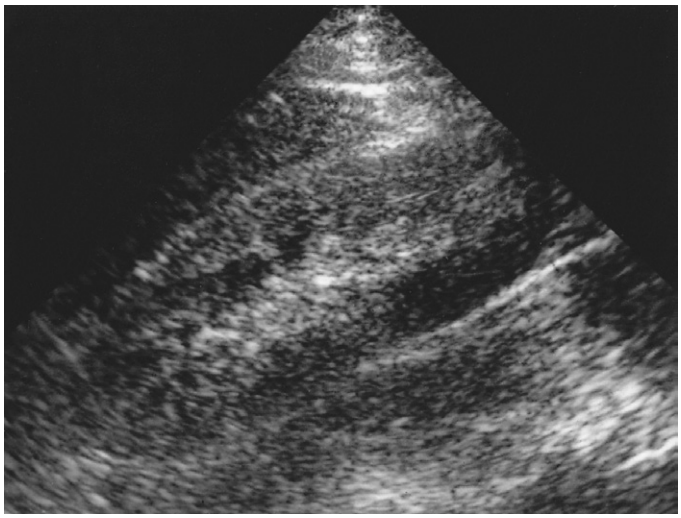


Figure 23.4 Acute glomerulonephritis. Loss of corticomedullary differentiation in a patient with acute glomerulonephritis.

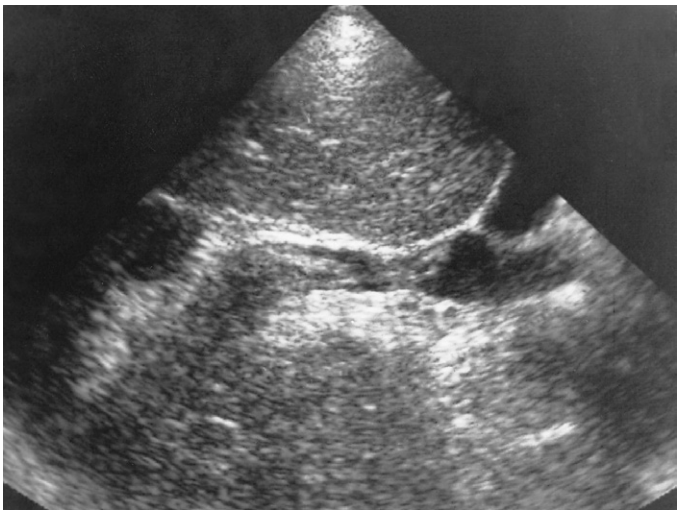


Figure 23.6 Tumour thrombus in the right renal vein extending into the IVC in a patient with renal cell carcinoma.

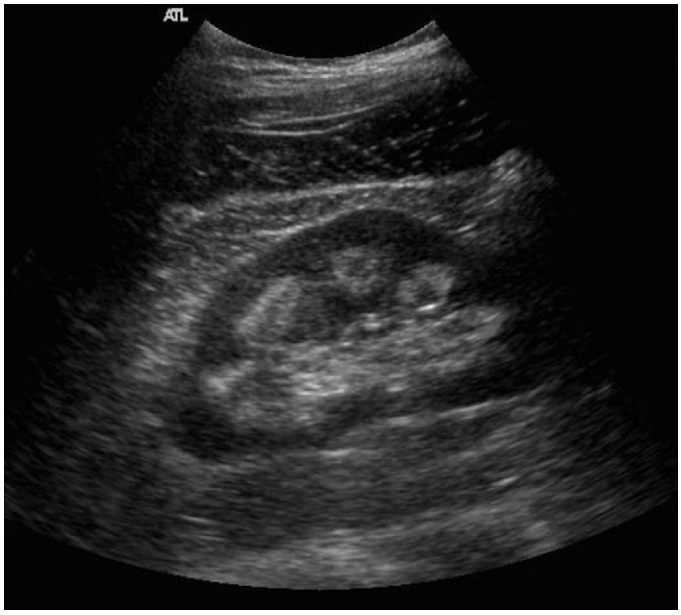


Figure 23.5 Nephrocalcinosis. Increased reflectivity of the medullary pyramids in a patient with early nephrocalcinosis.

as separate structures (Fig. 23.4). However, as with cortical reflectivity, there is no correlation with the aetiology of the renal disease.[3] In acute conditions involving primarily the medulla, such as acute tubular necrosis, the pyramids can be enlarged due to oedema. Increased medullary reflectivity can be detected in nephrocalcinosis of any aetiology (Fig. 23.5) and also in some other conditions such as gout.

Renal vessels and Doppler studies

Doppler signals can be obtained from the main renal arteries, their major branches and the interlobar vessels.[9–12] The renal circulation is normally of a low-resistance type with good diastolic flow, the normal resistance index (RI) in adults is less than 0.7,[13] and both kidneys should show similar values; a difference in RI of greater than 0.1 implies unilateral abnormality. The shape of the spectral waveform is important, particularly in the assessment of renal artery stenosis. Parenchymal disease can also alter the pattern of blood flow to a variable degree depending on the severity of involvement of the vessels with a resulting increase in the RI. There is a tendency for the RI to be higher in patients with acute tubulointerstitial disease[14] but these changes are not consistent or specific and are of little diagnostic value in distinguishing between different pathologies.[5,13]

Although, from the foregoing discussion, it would appear that ultrasound has little to offer in differentiating between the various causes of acute and chronic renal disease, useful information can be obtained from both imaging and Doppler, which in conjunction with the clinical history, biochemical findings and biopsy result (if performed) will allow a diagnosis to be reached, management decisions made and prognosis assessed.

MEDICAL RENAL DISEASES

Vascular disorders

Renal vein thrombosis

Renal vein thrombosis may be seen in up to 40% of septic or dehydrated infants.[15] Acute presentation with renal vein thrombosis is rare in adults. When it does occur it is generally unilateral or restricted to one segment and clinical renal failure does not occur, but it may occasionally be bilateral. It is most commonly associated with the nephrotic syndrome, which it is often considered to cause; however, it usually occurs on a background of pre-existing renal disease, most commonly membranous nephropathy producing the nephrotic syndrome, so that the venous thrombosis is a result of the underlying renal pathology rather than being the cause.[16] It is also associated with systemic lupus erythematosus, diabetes, glomerulonephritis, hypovolaemic shock and renal transplantation.[15] In some patients various abnormalities of coagulation, involving clotting factors, the fibrinolytic system and platelets, can be demonstrated. Other conditions which are associated with the development of renal vein thrombosis in the adult are trauma, oral contraceptives and steroid administration. Dehydration is more commonly associated with renal vein thrombosis in infants, although it may occur in adults, particularly in hot climates. Renal cell carcinoma may invade the renal vein and produce a tumour thrombus which can, like ordinary thrombus, extend into the inferior vena cava (IVC) and provide a source of emboli (Fig. 23.6).[17]

Left renal vein occlusion in males may present initially as an acute left varicocele, however, this is extremely rare.

On ultrasound the appearances depend on the degree of venous obstruction, the speed with which it has developed and the amount of collateral flow. Sudden complete occlusion of the main renal vein produces an enlarged, echo-poor kidney.[16,18,19] The changes develop over the initial 24 hours and are due to swelling of the parenchyma. Echo-free areas of haemorrhagic infarcts can be distinguished within the generally echo-poor tissue and the renal sinus echoes may be markedly compressed by the swollen parenchyma. After 10–14 days the kidney starts to shrink and over a period of 1–2 months this results in a small kidney with abnormally high reflectivity. Corticomedullary differentiation is initially preserved but is lost after 3–4 weeks as the kidney contracts. The renal veins can appear larger than normal and thrombus may be demonstrated within them with extension into the IVC in some patients. In patients with intrarenal segmental vein occlusion, focal areas of oedema and reduced reflectivity may be seen.

Colour Doppler examination is useful in confirming the lack of venous flow in the main renal veins and within the kidney parenchyma in severe cases.[10] In more severe cases the renal artery flow reduces to the baseline in diastole, or may even show reverse diastolic flow.[20] In patients with occlusion of segmental intrarenal veins venous Doppler signals may still be apparent within the renal parenchyma and the only clue to venous thrombosis may be a decrease in arterial diastolic flow, secondary to the increased intrarenal vascular resistance.[15] In cases of renal cell carcinoma extending into the renal vein it is not usually possible to demonstrate flow in the tumour thrombus to enable diagnosis but the clinical situation normally indicates the nature of the 'thrombus'.[13]

Renal artery occlusion

Sudden renal infarction can occur from various causes including atheromatous plaque haemorrhage, aortic dissection, emboli and traumatic avulsion. Unilateral renal artery occlusion does not produce renal failure and without Doppler may be difficult to detect with ultrasound. In the immediate acute stage following complete arterial occlusion the affected kidney may be normal in size and have normal reflectivity but a small increase in size compared with the perfused contralateral kidney may be demonstrated. In some patients a subcapsular 'halo' or rim of echo-poor tissue can be seen which is thought to correspond to oedematous perfused tissue fed by capsular collateral vessels.[21] In the longer term the affected kidney slowly shrinks with smooth margins and no dilatation of the collecting system. Colour or power Doppler ultrasound fails to show any arterial flow within the kidney; echo-enhancing agents will increase diagnostic certainty if there is any doubt over the diagnosis.

Acute segmental infarction results in a localised area of swelling with reduced reflectivity which appears some 8–24 hours after occlusion. After several weeks the infarcted area contracts and ultimately forms a highly reflective scar.[21] Focal renal infarction can result from local atheroma, or emboli. It may also be seen in sickle cell disease.

Renal artery stenosis

Narrowing of the renal arteries can cause hypertension and may be implicated in up to 5% of patients with hypertension. In one study with patients selected for ultrasound and Doppler assessment for possible renal artery stenosis, there was a prevalence of 22% for renal artery stenosis of >60% diameter reduction.[22] The commonest causes are atheroma and fibromuscular dysplasia of the vessel wall; other causes include aortic aneurysm, arteritis, emboli, neurofibromatosis and trauma. It is important to make the diagnosis since correction of the stenosis may allow cessation of drug therapy, or at least make therapeutic control easier.

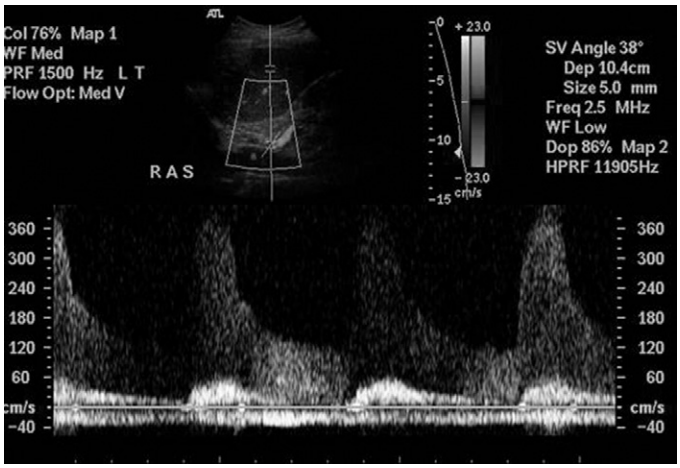


Figure 23.7 Renal artery stenosis. Colour Doppler of the origin of the left renal artery showing a markedly elevated PSV in excess of 3.6 m/s indicative of renal artery stenosis. (Courtesy Dr G. Baxter.)

In a patient with unilateral renal artery stenosis the affected kidney is usually of normal shape and size unless the stenosis is greater than 60%, when a small decrease in size may be found.[23]

Doppler can be used to examine the main renal arteries and also the intrarenal vessels. Initial reports suggested that the main renal arteries could be examined adequately in up to 80% of patients (Fig. 23.7).[12,24] However, it became apparent that in routine practice these examinations took a significant time to perform and problems existed with not only locating the main renal arteries and obtaining adequate waveforms but also locating accessory renal arteries, which are present in up to 40% of individuals.[25–27] Nevertheless, with appropriate training and sufficient time, more recent studies have demonstrated the main renal arteries in over 90% of cases, although visualisation of accessory arteries remains a problem.[22,28] Attention was then given to the Doppler waveform changes that might be seen in the intrarenal vessels as a result of a proximal stenosis in the main artery and again, initial reports suggested that measuring the systolic acceleration together with the RI and assessing changes in the waveform shape allowed diagnosis of significant proximal stenoses.[29–31] However, it again became apparent that the situation was less than straightforward. These criteria only detect reliably stenoses of greater than 70–80% but not lesser stenoses, and the shape of the waveform is not simply related to the pressure drop across the stenosis but also to the compliance of the renal arteries.[32] Coexisting renal parenchymal disease may also affect the waveform due to changes in peripheral resistance.

Other parameters, including the acceleration index and lowering of the resistance index or pulsatility index, have been assessed but have proved less popular in routine practice.

There is quite large variation in the literature around the best cut-off levels, particularly for the renal artery peak systolic velocity (PSV) and the renal artery/aorta velocity ratio (RAR). One review of the literature showed that the renal artery PSV had the highest performance characteristics with an expected sensitivity of 85% and specificity of 92%; additional measurements did not increase the accuracy achieved with the single PSV measurement.[33] The following criteria have proved useful in the assessment of renal artery stenosis:

- PSV greater than 180 cm/s correlates with stenoses >60%,[15] providing the vessel is adequately visualised.
- An RAR equal to or greater than 3.5: the velocity in the upper abdominal aorta and the renal artery at the site of the stenosis are measured; a ratio equal to or greater than 3.5 correlates with stenoses greater than 60%.[34] However, measurement of

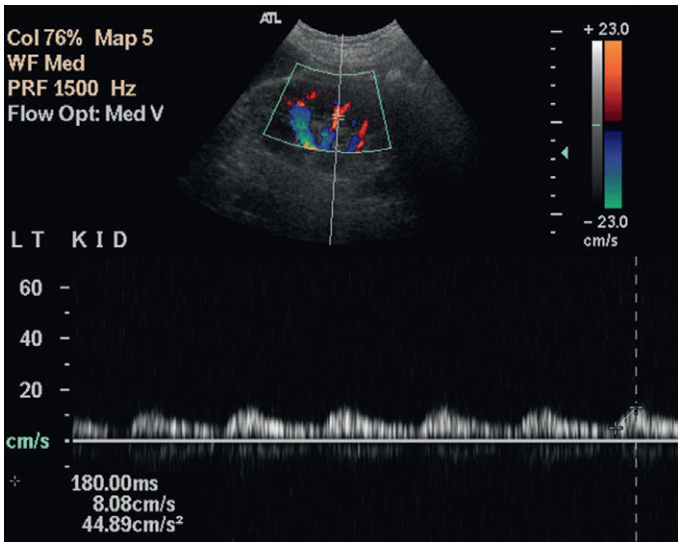


Figure 23.8 Renal artery stenosis. Parenchymal arterial waveform showing a tardus parvus pattern with a prolonged acceleration time of 0.18 s and a reduced peak systolic shift.

Features of significant renal artery stenosis

Elevated peak systolic velocity: velocities in the stenotic segment >1.8–2.0 m/s correlate well with stenoses of >60% diameter reduction.

Renal artery/Aorta ratio: an RAR >3.5 correlates with stenoses >60%.

Acceleration time: an AT >0.07 s correlates with a stenosis >60%.

Loss of the early systolic peak (ESP): proximal stenosis results in changes to the intrarenal waveform with loss of the ESP and a 'tardus parvus' appearance.

true velocities may be a problem as adequate visualisation of the renal artery for angle correction can be difficult.[12,23]

- Acceleration time greater than 0.07 s: this is measured in the intrarenal arteries and is the time taken from the start of the systolic acceleration to the systolic peak (Fig. 23.8).[27,29]
- Loss of the early systolic peak and tardus parvus waveform: the normal intrarenal renal artery waveform shows a small peak at peak systole; loss of this and progressive flattening of the waveform due to slower acceleration (tardus) and slower peak velocities (parvus) correlates with a proximal stenosis >60% (Fig. 23.8).[30]

The value of Doppler in the assessment of renal artery stenosis is that a positive diagnosis indicates a significant lesion but if the study is technically inadequate or has an indeterminate or negative result, it does not rule out a lesion and further imaging with isotopes or magnetic resonance angiography will be required. The use of echo-enhancing agents improves the visualisation of both the main and peripheral arteries, together with the diagnostic yield, but their role has yet to be fully defined.[35,36]

Hypertensive renal disease

The links between hypertension and the kidney involve complex haemodynamic, endocrine and metabolic interactions. Renal artery disease can cause hypertension (see 'Renal artery stenosis') but conversely hypertension can cause renal disease. In this case the changes primarily affect the interlobar arteries and afferent arterioles, producing few changes on ultrasound.[37] The renal size may be symmetrically and modestly reduced but this is difficult to assess on ultrasound as it is often not possible to show a significant difference between the two sides. If a patient presents in chronic renal failure with small kidneys and hypertension it is not possible to determine whether the hypertension produced nephrosclerosis and renal failure or if the hypertension is the result of chronic renal disease.[34]

Acute tubular necrosis

This is the commonest cause of acute renal failure in hospital patients; usually several factors combine to precipitate acute tubular necrosis (ATN) including hypotension, sepsis, drugs, contrast agents, dehydration and haemoglobinuria/myoglobinuria. Some two-thirds of patients will have more than one factor implicated.[38]

On ultrasound the kidneys may be unremarkable but some patients show an increase in renal size, particularly in the anteroposterior diameter, together with enlarged, well-defined pyramids.[39,40] Other patients may show an increase in cortical reflectivity with preservation of corticomedullary differentiation. There is some evidence that the aetiology of ATN in this latter group is more often a toxic insult, such as gentamicin or ethylene glycol poisoning. Those patients with prominent pyramids are more likely to have sustained ischaemic or hypotensive damage.[41]

Doppler ultrasound shows an elevated RI in the intrarenal arteries in the majority of patients with ATN.[42] Although there is some overlap with other causes of acute renal failure, kidneys with ATN tend to show significantly higher RI values (mean 0.85); there is also a tendency for patients who have persistent renal dysfunction to have higher RI values than those who recover adequate renal function.[42]

In renal transplant patients, acute tubular necrosis may be a cause of impaired renal function particularly in the postoperative period. Unfortunately ultrasound is unable to distinguish reliably between ATN and other causes of impaired renal function, such as acute rejection or drug toxicity, and biopsy is required for accurate diagnosis.[43]

Glomerulonephritis

This term covers a variety of conditions which primarily affect the glomerulus. Clinically they are defined by any precipitating factors, the clinical presentation and the findings on biopsy. The appearances on ultrasound are completely non-specific in terms of the pathological type, the degree of renal impairment and the prognosis.[2,3] There is some correlation between the degree of reflectivity and interstitial infiltrative changes or fibrosis but this is not of any value in determining the cause of renal impairment or predicting the outcome.[5,6,44,45]

In the acute stages the kidneys can be normal in appearance or they may show increased cortical reflectivity; they may be normal in size or enlarged. If chronic renal disease develops there is a tendency for the kidneys to shrink but the degree to which this occurs is variable, as is the amount of increased cortical reflectivity which develops or persists. Changes in corticomedullary differentiation also occur, with loss of definition being broadly related to the degree of inflammation and cellular infiltrate within the parenchyma (Fig. 23.4). In post-streptococcal glomerulonephritis there have been reports of multiple intrarenal echo-poor masses separated by highly reflective bands of tissue, although this is not an invariable feature.[46]

Renal papillary necrosis

This disorder is caused by one of many different processes affecting the medullary pyramids and leading to ischaemic necrosis of them. Analgesic abuse, diabetes, sickle cell trait/disease, infection, ureteric obstruction and vesico-ureteric reflux are the commonest

causes but a variety of vasculitic and other conditions have been described in association with this disorder.[47]

The renal pyramids are more vulnerable to ischaemic change because of the specific arrangement of their blood supply and their hypertonic environment so that conditions which further reduce blood flow or oxygenation produce ischaemic change.[48] The initial changes of central or peripheral papillary necrosis are not visualised on ultrasound but are well seen on intravenous urography and CT. If total papillary necrosis develops, these changes can be detected on ultrasound (Fig. 23.9). Calcification of affected papillae may occur, causing highly reflective regions in the papillae.[49] The affected papillae may slough off, producing small round or triangular cystic areas in the medullary region that can be demonstrated on ultrasound.[50] These sloughed papillae may cause ureteric obstruction and, if they are calcified, may be mistaken for calculi.[51] In the initial stages the renal size and outline are normal but some loss of renal volume does occur in chronic stages and the renal outline may become a little irregular due to areas of atrophy and compensatory hypertrophy, especially if analgesic intake has ceased.[47]

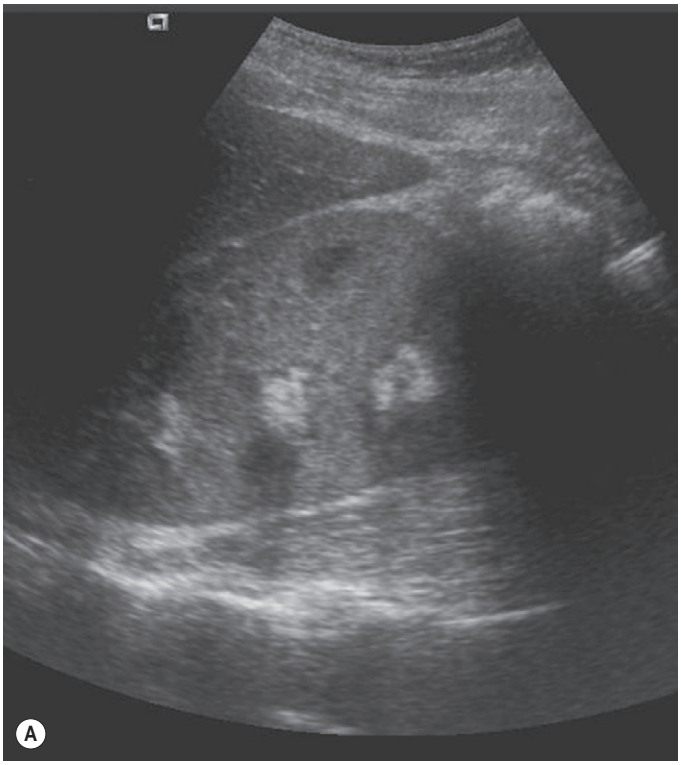
Medullary sponge kidney

In this condition there is dilatation of the distal collecting tubules in the medullary papillae. The aetiology is uncertain but it is probably a developmental anomaly and links with various other disorders such as hemi-hypertrophy, Ehlers–Danlos syndrome, Marfan's syndrome and Caroli's disease have been reported.[52] The true prevalence in the population is unknown as most patients remain asymptomatic unless calculi, haematuria or pain develop. Estimates of 0.5% of all intravenous urograms have been suggested[53] and approximately 17% of patients with renal calculi have been shown to have medullary sponge kidney.[54]

The diagnosis is usually made on urography, or CT, but ultrasound may show early nephrocalcinosis before this is seen radiographically, or even with CT.[55] Usually several pyramids are involved but occasionally the abnormalities may be limited to just two or three pyramids. If calculi form these may be detected in the region of the pyramids or calyces (Fig. 23.10) and if ureteric obstruction results then this too can be detected on ultrasound.



Figure 23.9 Papillary necrosis. Small cystic areas containing necrotic papilla fragments in the periphery of the sinus echoes in a patient with papillary necrosis.



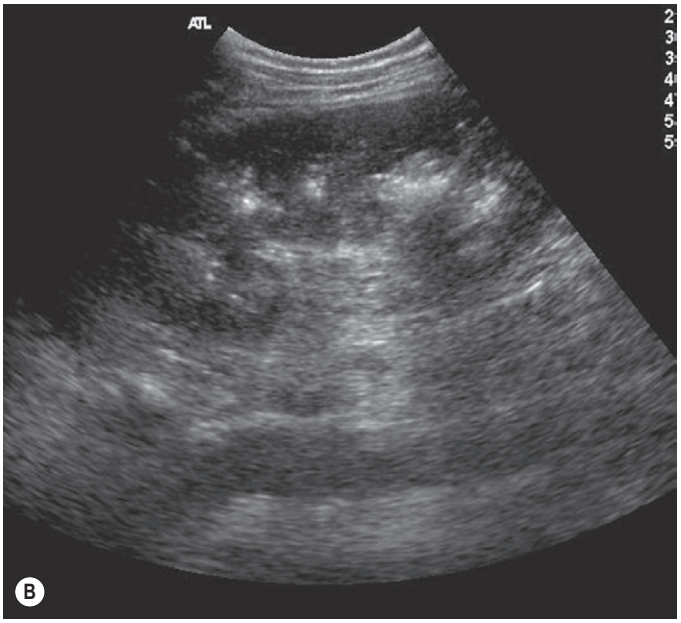


Figure 23.10 Medullary sponge kidney. A and B: Two examples of medullary sponge kidneys with calcifications in the medullary pyramids in two different patients.

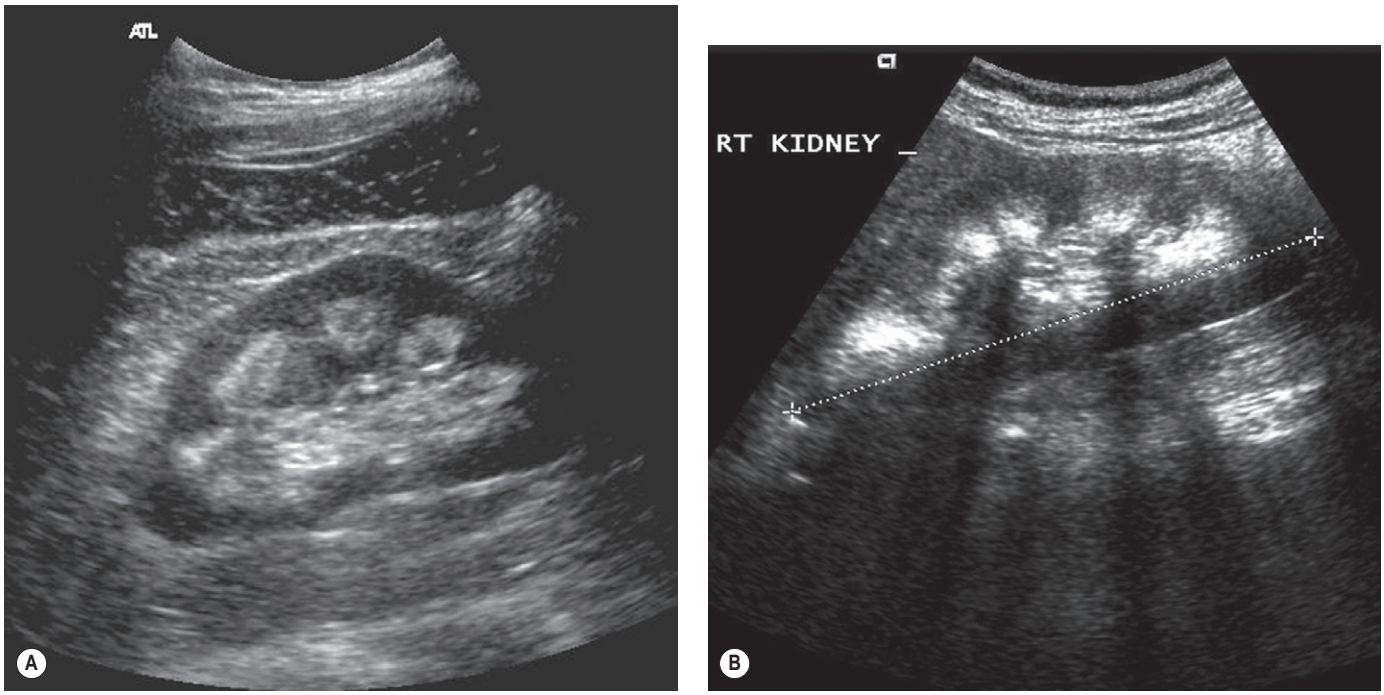


Figure 23.11 **Nephrocalcinosis. A:** Moderate changes of nephrocalcinosis in a patient with renal tubular acidosis. **B:** More marked changes in another patient with hypercalcaemia.

Nephrocalcinosis

This term embraces a varied group of disorders in which calcification is deposited within the renal parenchyma. The calcification is usually medullary in site but rarely may be cortical. Many disorders have been associated with medullary calcification including renal tubular acidosis, primary hyperoxaluria and papillary necrosis. Conditions resulting in hypercalcaemia or hypercalciuria can also produce nephrocalcinosis and these include primary hyperparathyroidism, sarcoid, vitamin D excess, hypercalcaemia of malignancy and Cushing's syndrome. Long-term ingestion of furosemide can also result in medullary nephrocalcinosis in children and adults.[56] An idiopathic form of nephrocalcinosis is occasionally seen. Cortical calcification has been reported in patients who have had acute cortical necrosis in the past and is also seen on rare occasions in patients with chronic glomerulonephritis.

On ultrasound the areas of calcium deposition are seen as highly reflective regions within the renal parenchyma, most commonly in the region of the pyramids (Fig. 23.11). This is usually diffusely distributed within the medullary pyramids but may be seen as a peripheral ring around the margin of the pyramids. Acoustic shadowing is frequently not present as the calcific foci are much smaller than the beam width (Fig. 23.5), particularly in early cases.[55,57] A similar appearance with highly reflective pyramids and variable acoustic shadowing is seen in patients with hyperuricaemia.[55]

In patients who have had acute cortical necrosis, calcification may develop at the interface between viable and necrotic areas[58] and this may be seen as early as 6 days after the onset.

Causes of renal calcification

- Medullary pyramids
  - Medullary sponge kidney
  - Hypercalcaemia/hypercalciuria (hyperparathyroidism, sarcoid, vitamin D excess, milk/alkali syndrome, malignancy, immobilisation
  - Long-term furosemide (frusemide) usage
  - Renal tubular acidosis
  - Renal papillary necrosis (RPN)
  - Hyperoxaluria
- Cortical
  - Acute cortical necrosis
  - Chronic glomerulonephritis
  - Alport syndrome
  - Sickle cell disease
- Collecting system and renal sinus
  - Renal calculi
  - Sloughed papilla in RPN
  - Arterial calcification

MISCELLANEOUS DISORDERS

Acute interstitial nephritis

This condition is a cause of acute renal failure and is characterised by inflammatory cell infiltration of the interstitial tissues in the kidney. It is most commonly precipitated by drugs or various infections but it may also be associated with connective tissue disorders and malignant infiltration. Clinically it may mimic acute tubular necrosis (ATN) as a degree of tubular dysfunction is often present and the disorder is more accurately described as acute tubulointerstitial nephritis. As with ATN the kidneys may be normal in size or enlarged, depending on the severity of the infiltrate. The reflectivity of the cortex may be normal or increased, and the finding of markedly increased cortical reflectivity in a patient with acute renal failure raises the possibility of acute interstitial nephritis.[59] However, the appearances are non-specific (Fig. 23.12) and renal biopsy is required to make the diagnosis in those patients who do not show an improvement following removal of the likely precipitating agent.[60]



Figure 23.12 Chronic interstitial nephritis. A small bright kidney in a dialysis patient with end-stage renal disease following acute interstitial nephritis.

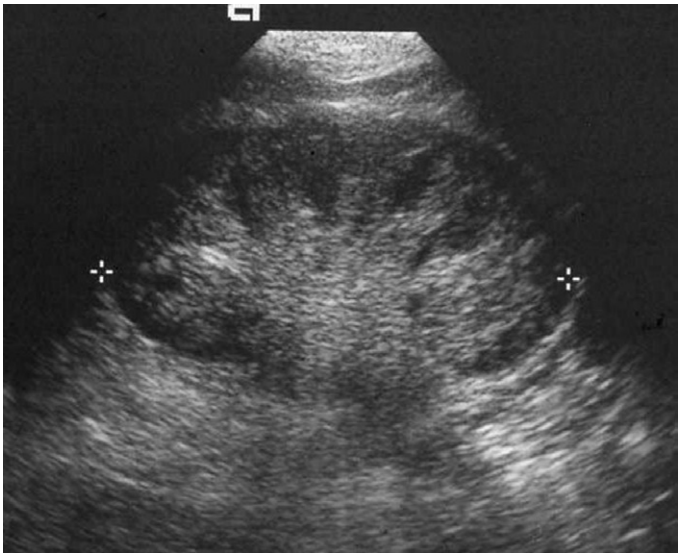


Figure 23.13 Acute cortical necrosis. There is a generalised increase in the parenchymal reflectivity but with a persistent rim of lower reflectivity in the subcapsular region.

Acute cortical necrosis

This is a rare cause of acute renal failure. It is often associated with postpartum haemorrhage and other obstetric emergencies, such as eclampsia and puerperal sepsis. Non-obstetric causes include snake bites, acute pancreatitis and other causes of severe shock and sepsis. The necrosis of the cortex seems to be the result of acute ischaemia as there are ischaemic changes within the cortex with sparing of a thin rim of peripheral tissue which is supplied by capsular vessels. On ultrasound there is loss of the normal corticomedullary differentiation within the parenchyma and patchy areas of increased reflectivity may be seen.[58] The outer margin of perfused cortex may be identified as a rim of echo-poor tissue adjacent to the capsule (Fig. 23.13). Calcification can develop at the junction between viable and necrotic tissue and this may appear within a few days.[58]

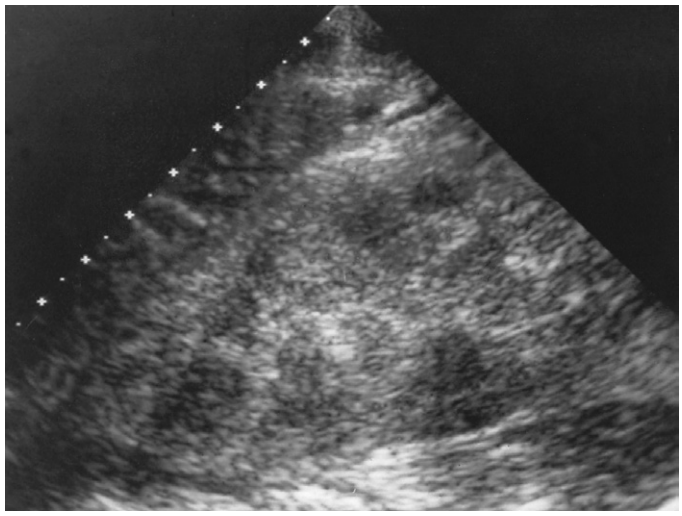


Figure 23.14 Renal amyloid. An enlarged kidney with patchy increase in cortical reflectivity in a patient with amyloid.

Amyloid and the kidneys

Amyloid is a disease complex that results in the extracellular deposition of insoluble fibrillar protein material with a β-pleated sheet configuration.[61] The term 'amyloidosis' covers a spectrum of disorders which result in a variety of abnormal proteins with this configuration being produced. These can be separated on the basis of the distribution of amyloid protein into systemic or localised forms, and further subgroups can be defined depending on the nature of the amyloid protein and the clinical associations or context of the condition. The most significant amyloid proteins are amyloid light chain (AL), amyloid A protein (AA) and β_2-microglobulin. Systemic amyloidosis accounts for some 85% of cases and includes the idiopathic (or primary) type, myeloma-related, reactive and familial forms of amyloid. AL amyloidosis is associated with primary amyloid and myeloma, whereas AA proteins are found mainly in secondary amyloid associated with chronic inflammation, chronic infections or neoplasms, particularly renal cell carcinoma. β_2-microglobulin amyloidosis is a type of secondary amyloid that is related to long-term haemodialysis.[62] Localised amyloid includes that confined to a single organ, the focal and senile forms of the disease.[61]

The kidneys are often involved in the systemic forms of amyloid with 90% of primary amyloid patients having proteinuria and 50% azotaemia at the time of presentation; 30% will develop the nephrotic syndrome. Similar clinical findings occur in myeloma-related and secondary amyloid.

In the acute or early stages of the disease the kidneys may be large and oedematous but, depending on the severity and duration of renal involvement, they decrease in size over a period of time and small, contracted kidneys are found in chronic cases.[63] On ultrasound enlarged amyloid kidneys are often seen to have increased cortical reflectivity which is usually uniform but may be patchy in its distribution (Fig. 23.14). The amyloid protein is deposited mainly in the cortex so that corticomedullary differentiation is preserved and the pyramids are normal in size.[64] As chronic changes develop, no distinguishing features can be seen on ultrasound to allow differentiation from other causes of chronic renal disease, although the presence of an amyloid-related disorder such as rheumatoid arthritis or systemic lupus erythematosus may suggest the nature of the renal changes.

Diabetes mellitus

Diabetes affects the kidneys primarily through vascular changes, although recurrent infections may also play a part in impairment

of renal function, and papillary necrosis may be seen. As with many other conditions, the appearances on ultrasound are inconstant, with variable changes in size and reflectivity as the disease progresses. One interesting feature of diabetic nephropathy is that the glomerular filtration rate increases during the initial stages and this is associated with a small but measurable increase in overall renal size.[65,66] This has been reported in both type 1 (insulin dependent) and type 2 (non-insulin dependent) diabetics. In the former, one study[67] reported that the increase in size was most marked in those patients with microalbuminuria with a mean standardised volume of 372 (±24) mL/1.73 m^2, compared with 299 (±49) mL in diabetics without albuminuria and 245 (±53) mL in normal controls. In type 2 diabetics another study[68] reported similar findings, with diabetic kidneys having a mean volume of 314 mL (±73) compared with 228 mL (±59) in normal controls. As chronic changes supervene in diabetic kidneys, however, they decrease in size, although their reflectivity is usually unchanged or only slightly increased.[69]

Doppler studies show an increased RI in those patients with established nephropathy compared with those patients with normal renal function, or only mild nephropathy. In one study[70] the mean RI in patients with established nephropathy was 0.83 (±0.11), compared with values of less than 0.65 in patients with normal or mildly impaired renal function.

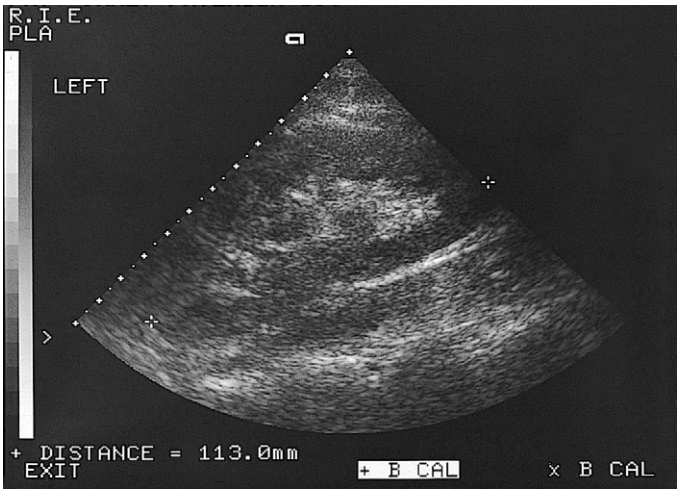


Figure 23.15 Systemic lupus erythematosus. A kidney in a patient with lupus nephritis showing a generalised increase in cortical reflectivity but with an ill-defined region of reduced reflectivity centrally.

Connective tissue disorders

Connective tissue disorders such as systemic lupus erythematosus (SLE), systemic sclerosis and rheumatoid arthritis may affect the kidneys in a variety of ways, either directly or as a result of drug therapy. Vasculitis and glomerulonephritis can occur but the ultrasound appearances are non-specific and no different from the spectrum seen in other progressive renal parenchymal disorders with a variable increase in reflectivity and normal or decreased renal length.[71] Some reports[72] have suggested that lupus nephritis can be recognised by the presence of focal echo-poor areas in generally highly reflective parenchyma (Fig. 23.15) but this has not been confirmed.[2,3,71] Amyloid may develop, especially in patients with rheumatoid arthritis, but no distinguishing features are apparent to differentiate this from other causes of amyloid.

Doppler studies in patients with SLE show an increase in the RI, which correlates with more chronic disease and a poorer outcome in terms of renal function.[73]

Sickle cell disease

Patients with sickle cell disease may develop papillary necrosis (see above) but in addition other changes have been reported on ultrasound in the kidneys of patients with both homozygous (SS) sickle cell disease, or sickle cell trait (SC). Increased reflectivity can be seen in up to a quarter of teenagers without symptoms of renal disease.[74] This may be distributed focally in the renal medulla or diffusely throughout the parenchyma. The explanation for these changes have not been clarified but it has been suggested[74] that the focal medullary changes may be due to mild nephrocalcinosis or possibly iron deposition and the diffuse changes to interstitial and glomerular changes that are found in sickle cell disease; however, further work is required. In another report from the same cohort of subjects,[75] the same group reported that the mean and height-adjusted renal length was greater in patients with the homozygous than with the heterozygous form of the disease, which in turn were greater than the measurements for normal controls. The changes in the renal microcirculation result in an increase in the vascular resistance, which is reflected in an increase in the resistance and pulsatility indices, especially in patients with severe disease.[76] An increase in the resistive index has been reported as an early predictor of renovascular changes in sickle cell disease and can alert clinicians to the early stages of these changes.[77] Sickle cell disease is a rare cause of renal cortical calcification.

Hepatorenal syndrome

Renal dysfunction can occur in patients with established liver disease. Hepatorenal syndrome is the development of renal failure in patients with advanced chronic liver disease, or occasionally fulminant hepatitis.[78] One of the main features of this disorder is intense vasoconstriction of the renal vascular bed, which usually precedes any increase in serum creatinine or other clinical signs of renal dysfunction. This raised vascular resistance can be detected as an increase in the RI,[79] patients with a raised RI being more likely to develop renal dysfunction and hepatorenal failure. A raised renal RI prior to liver transplantation has been associated with a more protracted and difficult postoperative recovery.[80] However, normal function and resistance index often resume following successful liver transplantation.[78]

END-STAGE RENAL DISEASE, DIALYSIS AND ACQUIRED CYSTIC DISEASE

Many diseases progress slowly to complete renal failure as nephrons are destroyed and the kidney becomes unable to maintain adequate function. The kidneys are usually contracted (Fig. 23.16) but the appearances do not correlate with the underlying pathology, except in cases of adult polycystic disease.

Small, contracted kidneys can be difficult to recognise on ultrasound, particularly on the left side, as their reflectivity may be very similar to that of adjacent perirenal fat. Larger kidneys are less difficult to locate. Sometimes the outline of a small kidney is only apparent from its pattern of movement during respiration.

Acquired cystic disease of the kidney

The native kidneys of patients with end-stage renal disease are not simply small, contracted, fibrotic lumps. In a significant proportion of patients (60%) proliferative changes lead to the development of small cysts and adenomas,[81,82] a condition called acquired cystic disease of the kidney (ACDK). These changes are usually seen in dialysis patients but they may be encountered occasionally in patients with severe renal impairment who have not yet reached dialysis.[82] Rarely malignant changes can occur and this should be suspected in any dialysis patient who develops loin pain or haematuria.[81]

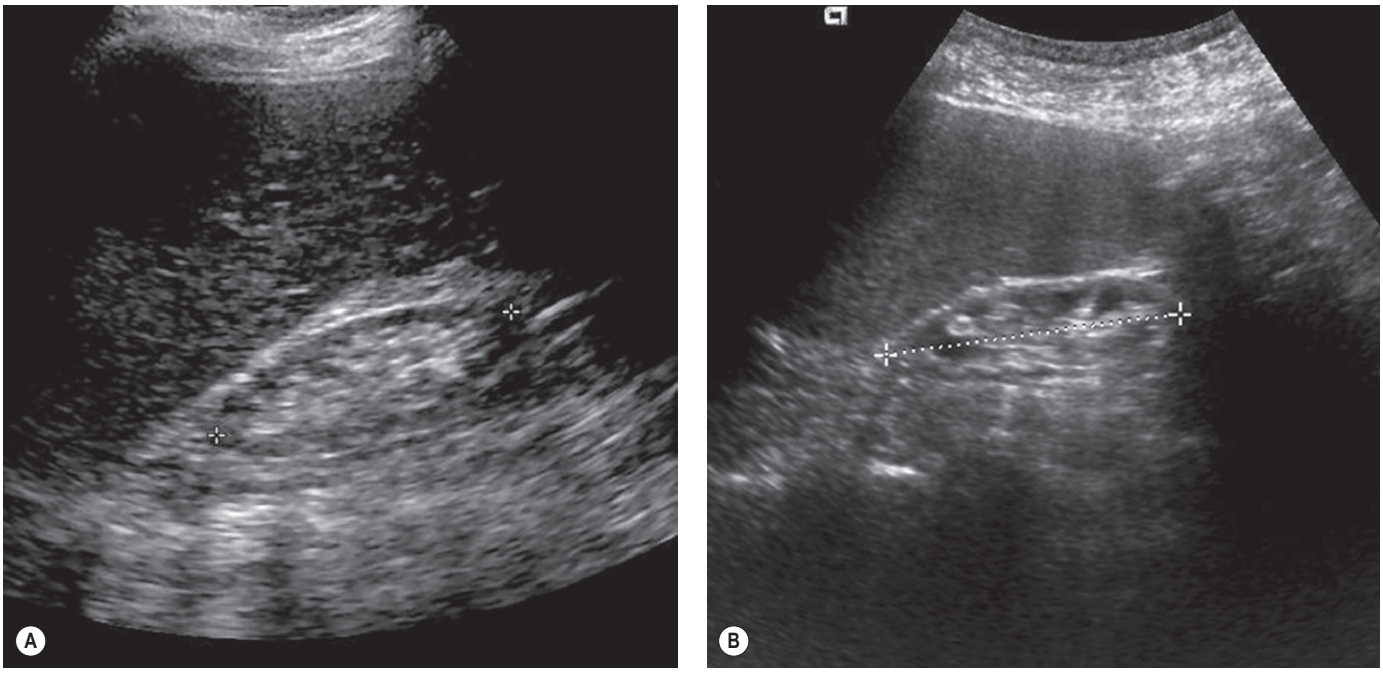


Figure 23.16 **End-stage renal disease. A and B:** Two examples of small contracted kidneys (6 cm) in patients with end-stage renal disease.

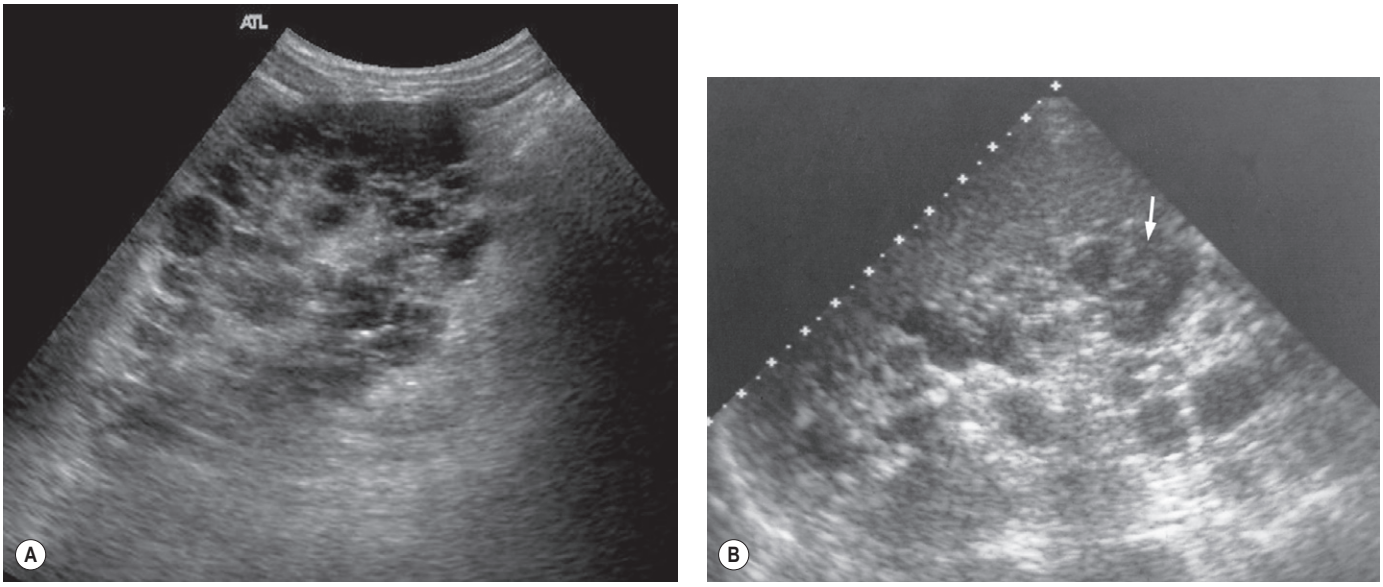


Figure 23.17 **Acquired cystic disease of the kidneys. A:** Marked changes of acquired cystic disease of the kidney showing multiple echo-poor areas throughout. **B:** A different case with a solid lesion towards the lower pole anteriorly (arrow).

The ultrasound appearances vary from a few echo-poor cyst-like areas to multiple, usually small, cysts. In severe cases the kidneys may be enlarged. Differentiation of small cysts from small adenomas may be difficult on ultrasound (Fig. 23.17) but this is probably not clinically significant in most cases as postmortem studies show a mixture of cystic and solid proliferative changes throughout the kidneys.[83] It is, however, important to identify larger or enlarging, solid lesions which may represent malignant neoplasms.

The severity of the changes of ACDK is related to the duration of time on dialysis, either haemodialysis or continuous ambulatory peritoneal dialysis (CAPD). Associations with age, sex, type of disease and haematocrit have also been suggested but the evidence for these is still inconclusive. Long-term follow-up shows that the changes progress slowly and are more pronounced in men.[84] The changes tend to persist after transplantation[85] but a functioning transplant appears to protect against the development of these changes in patients without ACDK before operation and there is some evidence to suggest that they may even reverse in some cases following a successful transplant.[86,87]

Dialysis patients

Patients in end-stage renal failure require dialysis to maintain metabolic stability. Two forms have been developed: haemodialysis (HD) and continuous ambulatory peritoneal dialysis (CAPD). Ultrasound can play a part in the assessment of complications arising in both groups of patients.

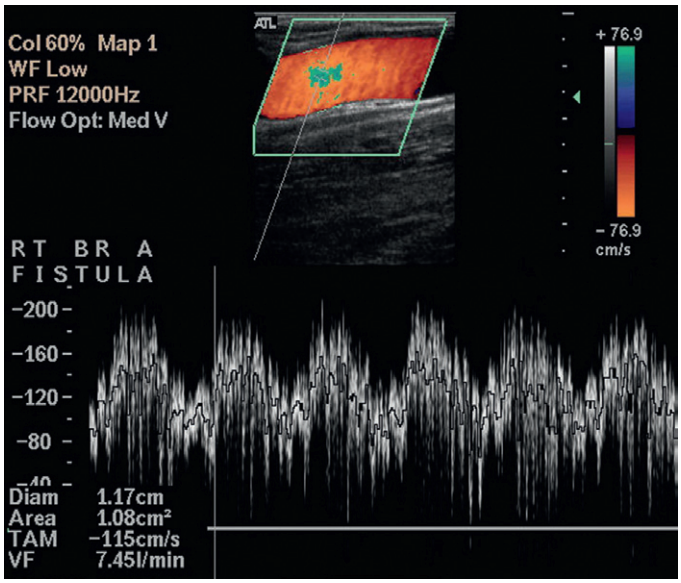


Figure 23.18 Excessive flow in a dialysis fistula. Calculating the area of the brachial artery and the time-averaged mean flow allows an estimate of the volume flow to be reached. In this case, flow is in excess of 7 L/min, which is well above normal values.

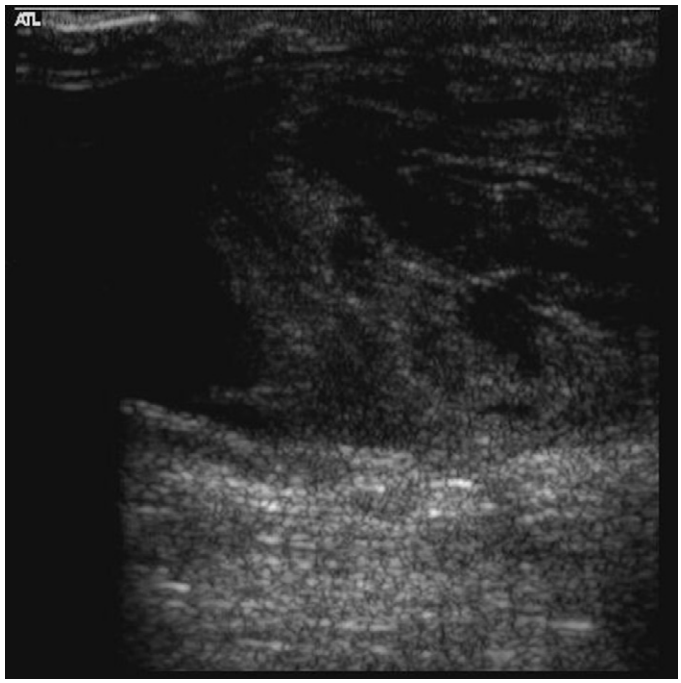


Figure 23.19 Thrombosed dialysis fistula. Echogenic thrombus is visible within the venous side of the fistula.

In haemodialysis patients, ultrasound can be used to assess the arteriovenous shunts used for dialysis and, using Doppler, an estimate of the flow rate can be made in the shunt itself, or in the artery above the shunt (Fig. 23.18).[88,89] Doppler can also be of value in the detection of stenoses or thromboses, especially if colour flow techniques are used (Fig. 23.19).[90]

The complications of continuous ambulatory peritoneal dialysis include localised collections in the anterior abdominal wall at the site of the catheter insertion. These can be assessed with ultrasound, as can intraperitoneal collections of localised fluid or abscesses. If necessary, ultrasound-guided aspiration can be performed for diagnosis or treatment. Sclerosing peritonitis is a condition in which there is generalised thickening of the mesentery and omentum leading to loss of peritoneal permeability and the development of loculated collections.[91] Various causes for this have been suggested including acetates, chlorhexidine cleansing solutions, plasticisers from bags and tubing, or subclinical infections with bacteria or fungi. Since procedures for handling dialysis fluid have been altered to reduce exposure to these factors, the incidence of this condition has fallen, although it is still encountered occasionally. Ultrasound shows thickening of the omentum which surrounds loops of bowel and these may show evidence of a degree of obstruction (see Chapter 19).[91,92] A thickened omental 'cake' may also be seen (Fig. 23.20).

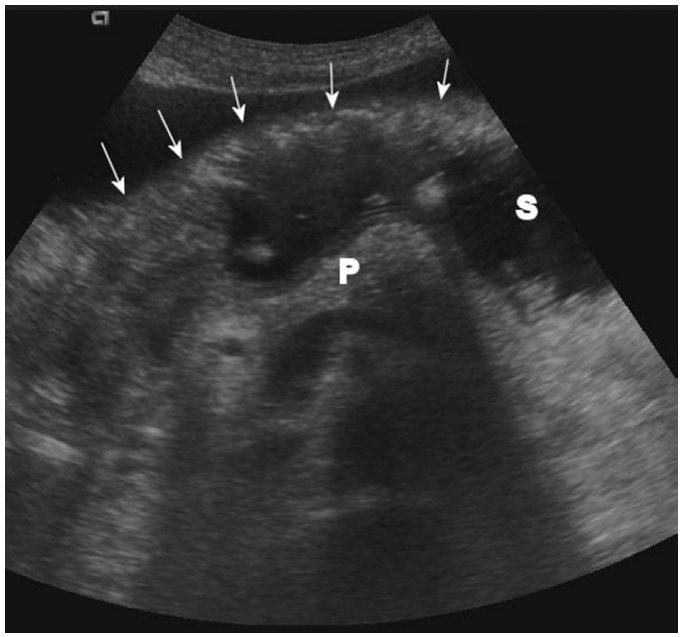


Figure 23.20 Sclerosing peritonitis. A band of thickened peritoneum (arrows) is seen lying anterior to the stomach (S) and pancreas (P) in a patient on peritoneal dialysis.

RENAL BIOPSY

In many patients with impaired renal function the diagnosis of the cause may not be apparent from the history, examination and investigations. In addition, the information that can be obtained from ultrasound examination, or indeed any other imaging technique, is limited and biopsy is often required to make the diagnosis and guide treatment options. This is the main indication for biopsy of native kidneys. The other main indication for renal biopsy is to carry out a targeted biopsy of a focal lesion to confirm or exclude a diagnosis of malignancy. Real-time ultrasound is the best guidance method for renal biopsy as it allows direct visualisation of the needle down to the kidney (Fig. 23.21).[93] A variety of sizes and types of cutting needle are available for renal biopsy.[94]

Indications and contraindications

The patient should be able to cooperate and obey instructions. Very nervous patients may require some sedation but this is not usually necessary. Blood pressure should be controlled and less than 140/90 mmHg as the risks of bleeding are increased above this level. Clotting parameters should be checked. Platelets should be >80000/mL but biopsy may be clinically justified in urgent cases

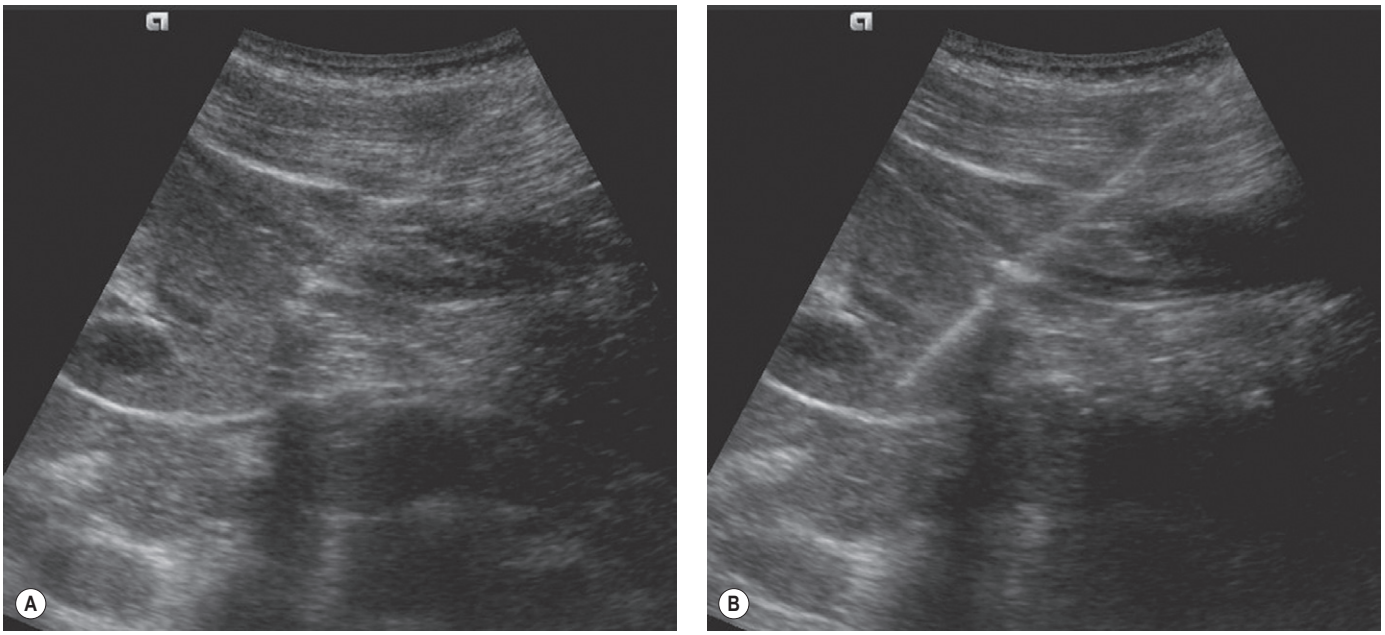


Figure 23.21 Visualisation of biopsy needle. A: The end of the needle is seen adjacent to the renal parenchyma at the lower pole. **B:** Following activation of the needle, this is now seen within the cortex of the lower pole.

with platelets between 40 000 and 80 000/mL. Below 40 000/mL a platelet transfusion should be instituted to cover the biopsy. The PTR should be <1.2 but urgent biopsy with a PTR <1.4 may be justified. A PTR >1.4 should be treated with appropriate blood products prior to or during biopsy.

After appropriate informed consent has been obtained, the kidneys are scanned with the patient supine to assess overall shape and size, as well as to exclude obstruction as a potential cause of the impaired renal function. If the kidneys are significantly reduced in length (<9 cm) with thinned parenchyma (<15 mm) it is generally considered that there is irreversible disease and the amount of useful tissue retrieved at biopsy may not be adequate for accurate diagnosis. However, this is not always the case and some patients with parenchymal thickness <15 mm may still have potential for improvement with appropriate treatment.[4] A further potential problem with thinned parenchyma is that the biopsy needle is more likely to impinge on the larger blood vessels in the renal sinus, which will increase the risk of post-biopsy haemorrhage.

Technique

For biopsy of the native kidneys, the patient is best positioned prone with a pillow under the stomach to compress the kidneys posteriorly. If the patient is unable to lie prone, then a semi-decubitus position can be used. In patients with haematuria loin pain syndrome it has been suggested that biopsy of the more symptomatic side may be of value; patients with a focal lesion will also have the side for biopsy predetermined. Otherwise, the kidney to be identified is chosen as the one that is easier to biopsy safely, as whatever process is present will affect both kidneys. Usually, the left kidney is preferred, as it is more easily seen below the twelfth rib and is normally the one nearer the operator. The aim of the exercise is to target the lower pole of the kidney, so that the larger vessels in the renal sinus are less likely to be punctured.

After appropriate skin cleansing, local anaesthetic is instilled into the skin and subcutaneous tissues. The amount required will vary from patient to patient; in sensitive patients use of a spinal needle under direct ultrasound control to infiltrate anaesthetic down to the renal capsule may be required; in other patients, anaesthetising the skin and subcutaneous tissues may be all that is required.

Biopsy is undertaken using a spring-loaded cutting needle. In our experience an 18-gauge needle retrieves adequate samples for diagnosis in the majority of cases[95] but a 16-gauge needle may also be used without increasing significantly the risk of post-procedural haemorrhage. The needle is inserted under direct ultrasound control to just above the lower pole of the kidney. The patient can be asked to vary the depth of respiration to place the kidney in the appropriate location and then asked to hold their breath. The needle is then advanced until the tip is seen to impinge on the capsule and the kidney to move slightly in response to gentle pressure from the needle (Fig. 23.21). The biopsy device is then activated and the needle withdrawn. Care must be taken when the needle tip is close to the capsule to ensure that it does not lacerate the kidney as the kidney moves with respiration.

In normal circumstances, two satisfactory cores of tissue are sufficient, although more may sometimes be required for specific histological techniques. Our practice is to put the first core into formaldehyde for standard fixing and staining procedures. For the second core, 2–3 mm of tissue from the cortical (outer) end of the sample are removed and put into glutaraldehyde for electron microscopy and the remainder is put onto filter paper in a container with a small amount of isotonic solution to be kept fresh for immunofluorescence studies, or frozen section.

Following the procedure the patient is returned to the ward and asked to lie quietly in bed for 4–6 hours with half-hourly pulse and blood pressure checks. If all is satisfactory, then the patient can resume normal activity, or go home, if the biopsy is being performed as a day case procedure.

Complications

Complications following renal biopsy are usually mild and self-limiting. Pain or discomfort at the site of biopsy may occur when the anaesthetic wears off but can usually be treated with oral analgesia. More severe pain may be associated with bleeding and haematoma formation.

Post-biopsy haemorrhage may result in mild haematuria, or a small perirenal haematoma; these bleeds are usually self-limiting but, rarely, more severe haemorrhage may require angiography and embolisation. Haemorrhage can also occur if an intercostal

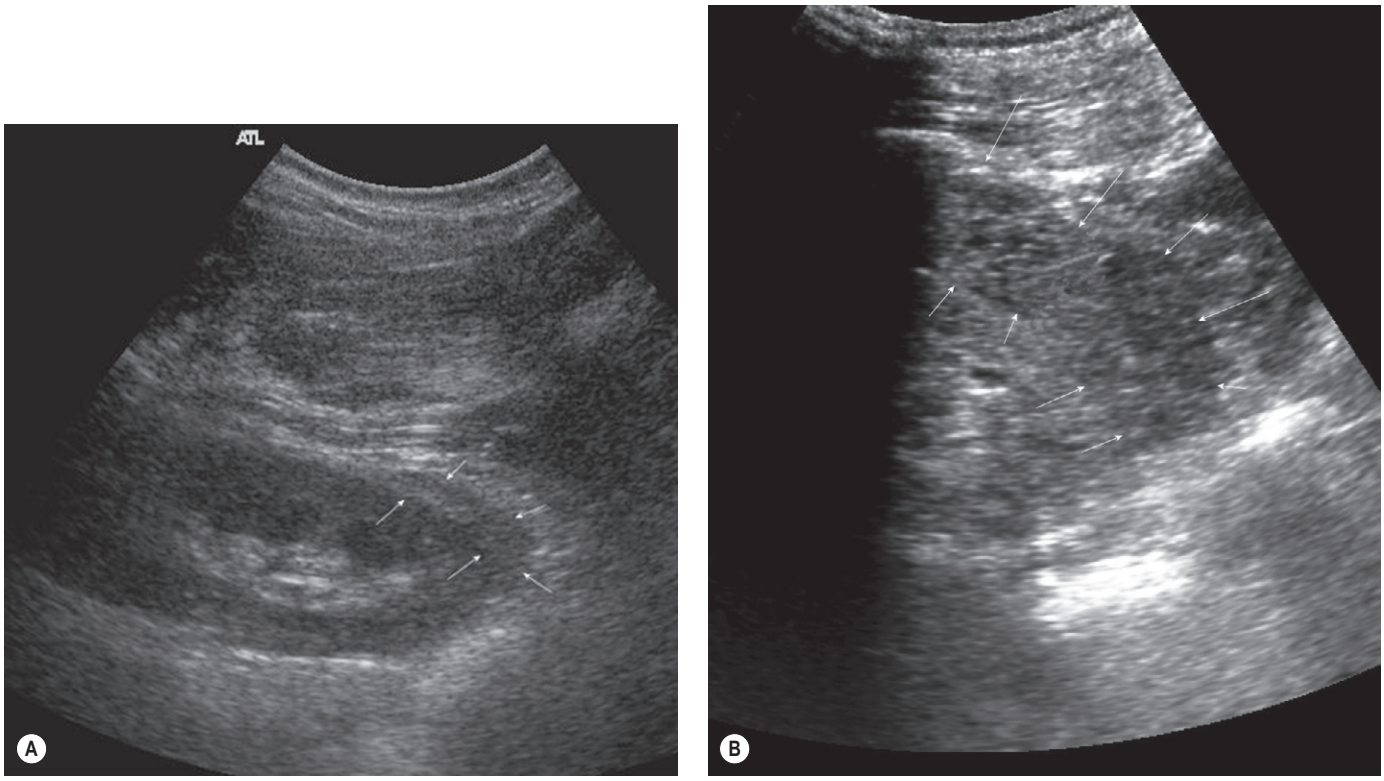


Figure 23.22 Post-biopsy haematomas. A: A small haematoma at the lower pole following renal biopsy (arrows). **B:** A larger haematoma, which was associated with significant haematuria and clot retention (arrows).

Complications from renal biopsy

Discomfort/pain: usually self-limiting and treated with oral analgesia.
Perirenal haematoma: can be seen in many patients if looked for with CT. Significant haematoma (>2 cm) seen in 2%.
Haematuria: macroscopic haematuria seen in 3–5%, usually self-limiting.
Clot retention/ureteric obstruction: rare.
Arteriovenous fistula formation: occurs in up to 10% of biopsies but most are clinically insignificant; approximately1% require intervention.
Puncture of adjacent organ: rare.

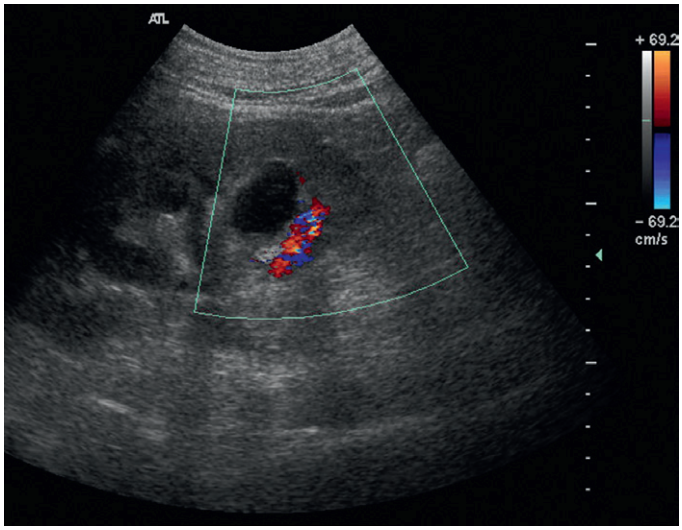


Figure 23.23 Post-biopsy arteriovenous fistula. Abnormal flow on colour Doppler at the lower pole of a native kidney following biopsy. Note the high colour scale of 69 cm/s and the dilated calyces as a result of clot retention.

vessel is damaged; this is more likely if an intercostal or subcostal approach is used with the patient in a non-supine position. Perirenal haematomas can be demonstrated in many patients following biopsy (Fig. 23.22), if these are looked for with ultrasound or CT scanning; one study reported evidence of post-biopsy haemorrhage on CT in 90% of renal biopsies.[96] However, the vast majority of these are not of clinical significance. Haematuria may result in ureteric obstruction from blood clot, or in severe cases, clot retention of the bladder.

Similarly, arteriovenous fistulae can be demonstrated in up to 10% of renal biopsies if they are looked for using colour Doppler ultrasound shortly after biopsy (Fig. 23.23),[96,97] but most of these will not be clinically relevant and will reduce or close off spontaneously. Should a fistula that is associated with significant haematuria persist, then arteriography and embolisation can be used to rectify the situation.

Puncture of adjacent structures and organs is more likely with the patient in a non-standard position for biopsy, when access and visualisation of the kidney, needle and adjacent structures may be suboptimal. The spleen, colon, pleura and lung are all potential sites of inadvertent puncture if due care is not taken during the procedure.

Renal transplant biopsy

The same general principles hold for biopsy of a renal transplant. Assuming that there are no contraindications to biopsy, the site

selected for biopsy is usually the more accessible pole of the kidney. This will depend to some extent on the location and orientation of the transplant. If possible, it is better not to traverse the peritoneal cavity, which may come down over part of the kidney. Suitable access may be achieved with an approach below the incision in a fairly horizontal plane, rather than a vertical approach through the lower abdominal wall. Depending on the position chosen it is worth using colour Doppler to identify the inferior epigastric artery, if there is a possibility that this may lie in the region of the needle track.

Either 18-gauge or 16-gauge needles can be used and two cores should be obtained. In cases of recent transplantation, where the main diagnostic dilemma is distinction between rejection and acute tubular necrosis, it is not necessary to provide a specimen for electron microscopy. However, in cases of renal transplant dysfunction occurring months or years after transplantation, it is useful to include a specimen for electron microscopy, as one of the causes for the deterioration of function in the transplant may be return of the original disease process that caused renal failure in the first place.

Transplants that have been in place for several years may develop a chronic graft versus host reaction around them. This is not usually of clinical significance but the dense fibrotic shell that may form around the kidney in these circumstances can be difficult to pierce with the biopsy needle unless firm pressure is applied to ensure that the needle goes forward into the kidney when activated and that it does not simply bounce back and recoil from the kidney.

REFERENCES

1. Ritchie WW, Whitely Vick C, et al. Evaluation of azotaemic patients: diagnostic yield of initial ultrasound examination. Radiology 1988;167:245–247.
2. Hricak H, Cruz C, Romanski R, et al. Renal parenchymal disease: sonographic–histologic correlation. Radiology 1982;144:141–147.
3. Quaia E, Bertolotto M. Renal parenchymal diseases: is characterization feasible with ultrasound? Eur Radiol 2002;12:2006–2020.
4. Burkhardt H, Hahn T, Gladisch R. Is kidney size a useful predictor of renal function in the elderly? Clin Nephrol 2003;59:415–422.
5. Webb JAW. The role of ultrasonography in the diagnosis of intrinsic renal disease. Clin Radiol 1994;49:589–591.
6. Moghazi S, Jones E, Schroepple J, et al. Correlation of renal histopathology with sonographic findings. Kidney Int 2005;67:1515–1520.
7. Platt JF, Rubin JM, Bowerman RA, Marn CS. The inability to detect kidney disease on the basis of echogenicity. AJR Am J Roentgenol 1988;151:317–319.
8. Roger SD, Beale AM, Catell WR, Webb JAW. What is the value of measuring renal parenchymal thickness before renal biopsy? Clin Radiol 1994;49:45–49.
9. Taylor KJW, Burns PN, Woodcock JP, Wells PNT. Blood flow in deep abdominal vessels: ultrasonic pulsed Doppler analysis. Radiology 1985;154:487–493.
10. Rifkin MD, Pasto ME, Goldberg BB. Duplex Doppler examination in renal disease: evaluation of vascular involvement. Ultrasound Med Biol 1985;11:341–346.
11. Avasthi PS, Greene ER, Scholler C, Fowler CR. Non-invasive diagnosis of renal vein thrombosis by ultrasonic echo-Doppler flowmetry. Kidney Int 1983;23:882–887.
12. Robertson R, Murphy A, Dubbins PA. Renal artery stenosis: the use of duplex ultrasound as a screening technique. Br J Radiol 1988;61:196–201.
13. Platt JF, Ellis JH, Rubin JM. Examination of the native kidneys with duplex Doppler ultrasound. Semin Ultrasound CT MR 1991;12:308–318.
14. Platt J F, Ellis J F, Rubin J M, et al. Intrarenal arterial Doppler sonography in patients with nonobstructive renal disease: correlation of resistive index with biopsy findings. AJR Am J Roentgenol 1990;154:1223–1227.
15. Zubarev AV. Ultrasound of renal vessels. Eur Radiol 2001;11:1902–1915.
16. Clark RA, Wyatt GM, Colley DP. Renal vein thrombosis: an underdiagnosed complication of multiple renal abnormalities. Radiology 1979; 132:43–50.
17. Schwerk WB, Schwerk WN, Rodeck G. Venous renal tumour extension: a prospective US evaluation. Radiology 1985; 156:491–495.
18. Hricak H. Sonographic manifestation of renal vein thrombosis: experimental study. Invest Radiol 1981; 16:30–35.
19. Rosenfield AT, Zeman RK, Cronan JJ, Taylor KWT. Ultrasound in experimental and clinical renal vein thrombosis. Radiology 1980;137:735–741.
20. Parvey HR, Eisenberg RL. Image directed Doppler sonography of the intrarenal arteries in acute renal vein thrombosis. J Clin Ultrasound 1990;18: 512–516.
21. Spies JB, Hricak H, Slemmer T. Sonographic evaluation of experimental acute renal arterial occlusion in dogs. AJR Am J Roentgenol 1984;142:341–346.
22. Labropoulos N, Ayuste B, Leon LR. Renovascular disease among patients referred for renal duplex ultrasonography. J Vasc Surg 2007;46:731–737.
23. Guzman RP, Zierler RE, Isaacson JA, et al. Renal atrophy and arterial stenosis: a prospective study with duplex ultrasound. Hypertension 1994;23:346–350.
24. Greene ER, Avasthi PS, Hedges JW. Non-invasive Doppler assessment of renal artery stenosis and haemodynamics. J Clin Ultrasound 1987;15:653–659.
25. Pick JW, Anson BJ. The renal vascular pedicle, anatomical study of 430 body halves. J Urol 1940;44:411–434.
26. Desberg AL, Paushter DM, Lammert GK, et al. Renal artery stenosis: evaluation with color Doppler flow imaging. Radiology 1990;177:749–775.
27. Berland LL, Koslin DB, Routh WD, Keller FS. Renal artery stenosis: prospective evaluation with color duplex US compared with angiography. Radiology 1990;174:421–442.
28. Li J, Jiang Y, Zhang S, et al. Evaluation of renal artery stenosis with hemodynamic parameters of Doppler sonography. J Vasc Surg 2008;48:323–328.
29. Handa N, Fukanaga R, Etani H, et al. Efficacy of echo-Doppler examination for the evaluation of renovascular disease. Ultrasound Med Biol 1988;14:1–5.
30. Stavros AT, Parker SH, Yakes WF, et al. Segmental stenosis of the renal artery: pattern recognition of tardus and parvus abnormalities with duplex sonography. Radiology 1992;184:487–492.
31. Schwerk WB, Restrepo IK, Stellwaag M, et al. Renal artery stenosis: grading with image-directed Doppler US evaluation of renal resistive index. Radiology 1994;190:785–790.
32. Bude RO, Rubin JM. Detection of renal artery stenosis: it is more complicated than originally thought. Radiology 1995;196:612–613.
33. Williams GJ, Macaskill P, Chan SF, et al. Comparative accuracy of renal duplex sonographic parameters in the diagnosis of renal artery stenosis: Paired and unpaired analysis. AJR Am J Roentgenol 2007;188:798–811.
34. Kohler TR, Zierler RE, Martin RL, et al. Noninvasive diagnosis of renal artery stenosis by ultrasonic duplex scanning. J Vasc Surg 1986; 4:450–456.
35. Karasch T, Rubin J. Diagnosis of renal artery stenosis and renovascular hypertension. Eur J Ultrasound 1998;7(suppl 3):S27–S39.
36. Correas JM, Claudon M, Tranquart F, Hélénon AO. The kidney: imaging with microbubble contrast agents. Ultrasound Q 2006;22:53–66.
37. Luke RG. Nephrosclerosis. In: Schreier RW, Gottschalk CW, eds. Diseases of the kidney. 4th edn. Boston: Little Brown; 1988. p. 1573–1595.
38. Rasmussen HH, Ibel LS. Acute renal failure. Multivariate analysis of causes and risk factors. Am J Med 1982;73:211–218.
39. Rosenfield A. Experimental acute tubular necrosis: ultrasound appearance. Radiology 1985;157:771–774.
40. Nomura G, Kinoshita E, Yamagata Y, Koga N. Usefulness of renal ultrasonography for assessment of severity and course of acute tubular necrosis. J Clin Ultrasound 1984;12:135–139.
41. Rosenfield AT, Zeman RK, Cicchetti DV, Siegel NJ. Experimental acute tubular necrosis: US appearance. Radiology 1985;157:771–774.
42. Platt JF, Rubin JM, Ellis JH. Acute renal failure: possible role of duplex Doppler US in distinction between acute prerenal failure and acute tubular necrosis. Radiology 1991;179:419–423.
43. Cosgrove DO, Chan KE. Renal transplants: what ultrasound can and cannot do. Ultrasound Q 2008;24:77–87.
44. Paivansalo M, Huttunen K, Suramo I. Ultrasonographic findings in renal parenchymal disease. Scand J Urol Nephrol 1985;19:119–123.
45. Page JE, Morgan SH, Eastwood JB, et al. Ultrasound findings in renal parenchymal disease: comparison with histological appearances. Clin Radiol 1994;49:867–870.
46. Rochester D, Aronsen AJ, Bowie JD, Kunzman A. Ultrasonic appearance of acute poststreptococcal glomerulonephritis. J Clin Ultrasound 1978;6:49–50.

47. Nanra RS. Analgesic induced renal disease. In: Schrier RW, Gottschalk CW, eds. Diseases of the kidney. 4th edn. Boston: Little Brown; 1988. p. 1202–1207.
48. Jung DC, Kim SH, Jung SI, et al. Renal papillary necrosis: review and comparison of findings at multi-detector row CT and intravenous urography. Radiographics 2006;26:1827–1836.
49. Weber M, Braun B, Kohler H. Ultrasonic findings in analgesic nephropathy. Nephron 1985;39:216–222.
50. Hoffman JC, Schnerr MJ, Koenigsberg M. Demonstration of renal papillary necrosis by sonography. Radiology 1982;45:785–787.
51. Cheung H, Chan PSF, Metreweli C. Case report: echogenic necrotic renal papillae simulating calculi. Clin Radiol 1992;46:61–62.
52. Yendt ER. Medullary sponge kidney. In: Schrier RW, Gottschalk CW, eds. Diseases of the kidney. 4th edn. Boston: Little Brown; 1988. p. 573–582.
53. Palubinskas AJ. Renal pyramidal structure opacification in excretory urography and its relation to medullary sponge kidney. Radiology 1963;81:963–970.
54. Sage MR, Lawson AD, Marshall VR, Ryall RL. Medullary sponge kidney and urolithiasis. Clin Radiol 1982;33:435–438.
55. Toyoda K, Miyamoto Y, Ida M, et al. Hyperechoic medulla of the kidneys. Radiology 1989;173:431–434.
56. Kim Y-G, Kim B, Kim M-K, et al. Medullary nephrocalcinosis associated with long-term furosemide abuse in adults. Nephrol Dial Transplant 2001;16:2303–2309.
57. Glazer GM, Callen PW, Filly RA. Medullary nephrocalcinosis: sonographic evaluation. AJR Am J Roentgenol 1982;138:55–57.
58. Sefczek RJ, Beckman I, Lupetin AR, Dash N. Sonography of acute cortical necrosis. AJR Am J Roentgenol 1984;142:553–554.
59. Gross HH, Hricak H, Filly RA. Ultrasonography in patients with acute renal failure. In: Resnick MI, Sanders RC, eds. Ultrasound in urology. 2nd edn. Baltimore: Williams & Wilkins; 1984. p. 147–168.
60. Kodner CM, Kudrimoti A. Diagnosis and management of acute interstitial nephritis. Am Fam Physician 2003;67:2527–2534.
61. Scott PP, Scott WW, Siegelman SS. Amyloidosis: an overview. Semin Roentgenol 1986;21:103–112.
62. Kim SH, Han JK, Lee KH, et al. Abdominal amyloidosis: spectrum of radiological findings. Clin Radiol 2003;58:610–620.
63. Ekelund L. Radiographic findings in renal amyloidosis. AJR Am J Roentgenol 1977;129:851–853.
64. Subramanyam BR. Renal amyloidosis in juvenile and rheumatoid arthritis: sonographic features. AJR Am J Roentgenol 1981;136:411–412.
65. Christiansen JS, Gamelgaard J, Frandsen M, Parving HH. Increased kidney size, glomerular filtration rate and renal plasma flow in short term insulin dependent diabetics. Diabetologia 1981;20:451–456.
66. Segel MC, Lecky JW, Slasky BS. Diabetes mellitus: the predominant cause of bilateral renal enlargement. Radiology 1984;153:341–342.
67. Feldt-Rasmussen B, Hegedus L, Mathiesen ER, Deckert T. Kidney volume in type 1 (insulin dependent) diabetic patients with normal or increased urinary albumen excretion: effect of long-term improved metabolic control. Scand J Clin Lab Invest 1991;51:31–36.
68. Derchi LE, Martinoli C, Saffioti S, et al. Ultrasonic imaging and Doppler analysis of renal changes in non-insulin dependent diabetes mellitus. Acad Radiol 1994;1:100–105.
69. Banholzer P, Haslbeck M, Edelman E, et al. Sonographic changes in the size of the kidneys in type I diabetes as a method of early detection of diabetic nephropathy. Ultraschall Med 1988;9:255–259.
70. Platt JF, Rubin JM, Ellis JH. Diabetic nephropathy: evaluation with renal duplex Doppler US. Radiology 1994;190:343–346.
71. Stanley JH, Cornella R, Loevinger E, et al. Sonography of systemic lupus nephritis. AJR Am J Roentgenol 1984;142:1165–1168.
72. Longmaid HE, Rider E, Tymkin J. Lupus nephritis. New sonographic findings. J Ultrasound Med 1987;6:75–79.
73. Platt JF, Rubin JM, Ellis JH. Lupus nephritis: predictive value of conventional and Doppler US and comparison with serologic and biopsy parameters. Radiology 1997;203:82–86.
74. Walker TM, Serjeant GR. Increased renal reflectivity in sickle cell disease: prevalence and characteristics. Clin Radiol 1995;50: 566–569.
75. Walker TM, Beardsall K, Thomas PW, Serjeant GR. Renal length in sickle cell disease: observations from a cohort study. Clin Nephrol 1996;46:384–388.
76. Aikimbaev KS, Oguz M, Guvenc B, et al. Spectral pulsed Doppler of renal vascular resistance in sickle cell disease: clinical implications. Br J Radiol 1996;69:1125–1129.
77. Taori KB, Chaudhary RS, Attarde V, et al. Renal Doppler indices in sickle cell disease: early radiological predictors of renovascular changes. AJR Am J Roentgenol 2008;191:239–242.
78. Mukerjee S. Hepatorenal syndrome. eMedicine, 2008: http://www.emedicine.com/med/topic1001.htm.
79. Platt JF, Ellis JH, Rubin JM, et al. Renal duplex Doppler ultrasonography: a noninvasive predictor of kidney dysfunction and hepatorenal failure in liver disease. Hepatology 1994;20:362–369.
80. Platt JF, Marn CS, Baliga PK, et al. Renal dysfunction in hepatic disease: early identification with renal duplex Doppler US in patients who undergo liver transplantation. Radiology 1992;183:801–806.
81. Thompson BJ, Jenkins DAS, Allan PL, et al. Acquired cystic disease of the kidney: an indication for renal transplantation? BMJ 1986;293:1209–1210.
82. Mickisch O, Bommer J, Bachman S, et al. Multicystic transformation of kidneys in chronic renal failure. Nephron 1984;38:93–99.
83. Hughson MD, Hennigar GR, McManus JFA. Atypical cysts, acquired renal cystic disease, and renal cell tumours in end stage dialysis kidneys. Lab Invest 1980;42:475–480.
84. Ishikawa I, Saito Y, Asaka M, et al. Twenty year follow-up of acquired renal cystic disease. Clin Nephrol 2003;59:153–159.
85. Heinz-Peer G, Schoder M, Rand T, et al. Prevalence of acquired cystic kidney disease and tumors in native kidneys of transplant recipients: a prospective US study. Radiology 1995;195:667–671.
86. Vaziri ND, Darwish R, Martin DC, Hosteller J. Acquired renal cystic disease in renal transplant recipients. Nephron 1984;37:203–205.
87. Ishikawa I, Yuri T, Kitada H, Shinoda A. Regression of acquired cystic disease of the kidney after successful renal transplantation. Am J Nephrol 1983;3:310–314.
88. Moran MR, Rodriguez JMR, Boyero MR, et al. Flow of dialysis fistulas. Non-invasive study performed with standard Doppler equipment. Nephron 1985;40:63–66.
89. Weber M, Kuhn FP, Quintes W, et al. Sonography of arterio-venous fistulae in dialysis patients. Clin Nephrol 1984;22:258–261.
90. Middleton WD, Picus DD, Marx MV, Melsen GL. Color Doppler sonography of haemodialysis vascular access: comparison with angiography. AJR Am J Roentgenol 1989;152:633–639.
91. Holland P. Sclerosing encapsulated peritonitis in chronic ambulatory peritoneal dialysis. Clin Radiol 1990;41:19–23.
92. Hollman A, McMillan M, Briggs JD, et al. Ultrasound changes in sclerosing peritonitis. following continuous ambulatory peritoneal dialysis. Clin Radiol 1991;43:176–179.
93. Cronan JJ. Percutaneous biopsy. Radiol Clin North Am 1996;34:1207–1223.
94. Murchison J, Cozens N, Allan PL, Winney RJ. Comparison of 18G renal biopsy with conventional 14G technique. Br J Radiol 1992;65:594–597.
95. Cozens NJ, Murchison JT, Allan PL, Winney RJ. Conventional 15G needle technique for renal biopsy compared with ultrasound-guided spring-loaded 18G needle biopsy. Br J Radiol 1992;65: 594–597.
96. Hergesell O, Felten H, Andrassy K, et al. Safety of ultrasound guided percutaneous renal biopsy: retrospective analysis of 1090 consecutive cases. Nephrol Dial Transplant 1998;13: 975–977.
97. Werner M, Oshadchy A, Plotkin E, et al. Increased detection of early vascular abnormalities after renal biopsies by color Doppler sonography. J Ultrasound Med, 2007;26:1221–1226.

CHAPTER

24

Infectious diseases of the kidney

Paul L. Allan

INTRODUCTION 460

ACUTE BACTERIAL PYELONEPHRITIS 460

LOBAR NEPHRONIA 460

RENAL AND PERIRENAL ABSCESSES 462

PYONEPHROSIS 462

CHRONIC PYELONEPHRITIS 462

XANTHOGRANULOMATOUS PYELONEPHRITIS 463

MALACOPLAKIA 463

OTHER INFECTIONS 463
Tuberculosis 463
Fungal infections 464
Parasites 464
Hydatid disease 464
Schistosomiasis 464
HIV-associated nephropathy 465

INTRODUCTION

The kidneys can be infected by a variety of organisms which enter from the bloodstream or, more commonly, ascend from the lower urinary tract. The most frequent form of infection is acute pyelonephritis, which most commonly affects women between the ages of 15 and 40 years. Most of these cases respond to antibiotics and do not require imaging or further investigation. Imaging is required for renal infections occurring in children, adult males, or females with recurrent infections. The aim of imaging is to identify any underlying structural abnormality which may predispose to infection, or to assess the state of the kidneys in cases of severe infection. Several factors other than anatomical abnormalities may predispose to renal infections. These include: obstruction, reflux, calculi, diabetes, immunosuppression, neuropathic bladder and urinary tract instrumentation or catheterisation. Organisms enter the renal parenchyma through the collecting tubules and initially affect the relevant lobe before spreading to the rest of the parenchyma. Haematogenous infection may occur from remote foci of infection such as skin or dental sepsis, osteomyelitis, pulmonary tuberculosis; intravenous drug abusers are more at risk from all forms of haematogenous spread. In haematogenous infection the infective foci develop within the renal parenchyma and often have a non-lobar distribution.[1,2]

Renal infection may predominantly affect the collecting system, the parenchyma, or both. Parenchymal involvement can be focal or diffuse. This has led to a multiplicity of terms that describe the abnormalities and significant confusion as to their meaning. One review article[1] lists 16 different terms that have been used to describe stages in the spectrum between acute pyelonephritis and renal abscess. The following sections describe the main stages in this spectrum and the findings that are seen on ultrasound.

ACUTE BACTERIAL PYELONEPHRITIS

The majority of bacterial infections of the renal parenchyma and collecting system respond rapidly to antibiotics and there are no significant sequelae. In more severe cases, the infection produces more marked inflammatory damage in the renal parenchyma which may be focal or diffuse; focal changes may also result from variable clearing of diffuse disease. When the renal parenchyma is severely affected, the condition is sometimes called acute bacterial nephritis; this is often associated with diabetics or immunosuppression.[3]

In some patients, often those with diabetes or with an obstructed collecting system, the bacterial flora are mixed and produce gas (emphysematous pyelonephritis). This type of infection produces a severe, diffuse necrotising inflammation, which has a mortality of up to 30%.[2,4] Pockets of gas are seen within the collecting system and parenchyma, often in a subcapsular distribution and sometimes in the perinephric tissues. If the gas is confined to the collecting system the condition is known as emphysematous pyelitis.

In patients with simple acute pyelonephritis, ultrasound is not normally indicated but, if it is performed, the kidneys usually appear normal or may be slightly swollen with reduced cortical reflectivity and loss of corticomedullary differentiation (Fig. 24.1).[5] In more severe cases the swelling and oedema are more marked with compression of the sinus echoes and there may be acoustic enhancement distal to the kidney. These changes can be diffuse or patchily distributed throughout the kidney. In some cases areas of increased reflectivity may be seen, which are thought to correspond to regions of haemorrhagic necrosis.[6] Thickening of the walls of the collecting system has been reported but this is a non-specific finding that has been described in other conditions, such as pyonephrosis and fungal infections.[7] Doppler ultrasound might be expected to show hyperaemia in acute pyelonephritis but flow is often segmentally reduced as a result of the oedema and raised intracapsular pressure; hyperaemia may be seen around areas of focal inflammation. In emphysematous pyelonephritis gas is seen as focal areas of increased reflectivity with 'dirty' distal acoustic shadowing, in contrast to calculi which tend to cast 'clean' shadows. Following resolution of the infection, there are normally no residual changes visible on ultrasound but following severe focal inflammation, cortical scarring may develop.[8]

LOBAR NEPHRONIA

In the spectrum between diffuse infection and the development of a frank abscess, there is a stage where there is acute focal pyelonephritis with progressive, severe, focal inflammation but in which necrosis and pus formation have not yet occurred. This is known as lobar nephronia, or a pre-abscess state.[1] These changes may resolve with treatment over a period of several weeks (Fig. 24.2A and B), or progress to frank abscess formation.

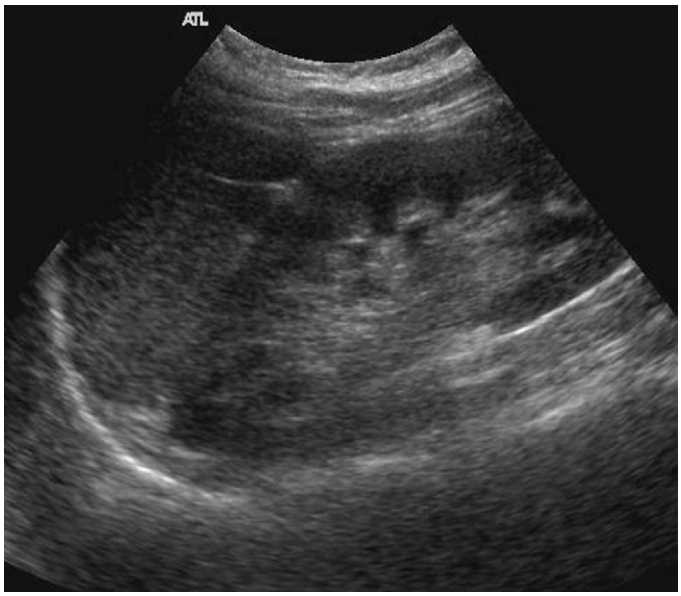
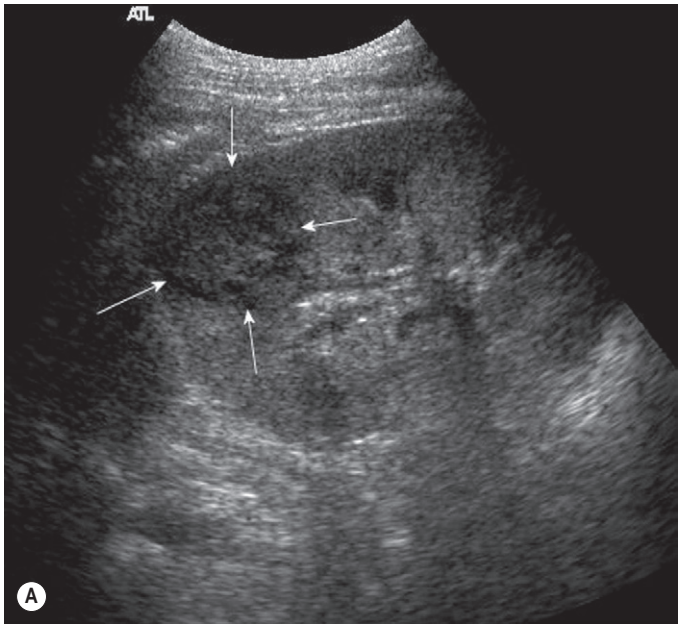
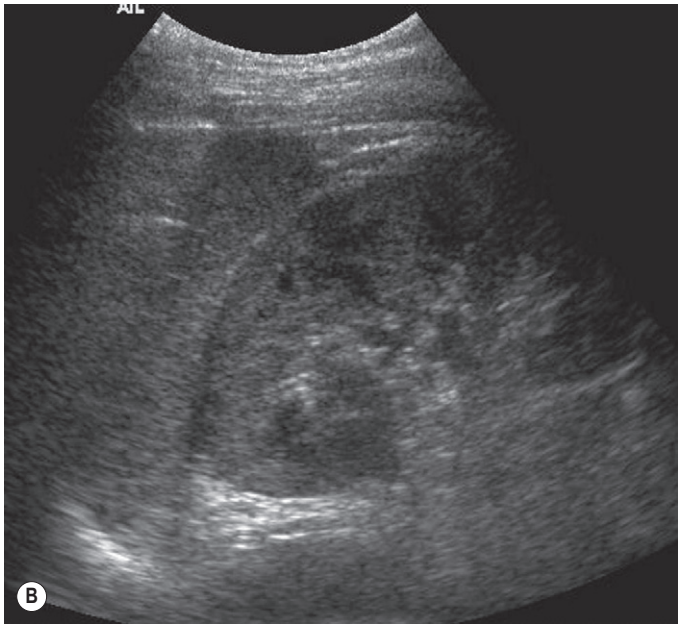


Figure 24.1 Acute pyelonephritis. Ultrasound of the kidney shows some reduction in parenchymal reflectivity but no other significant changes.





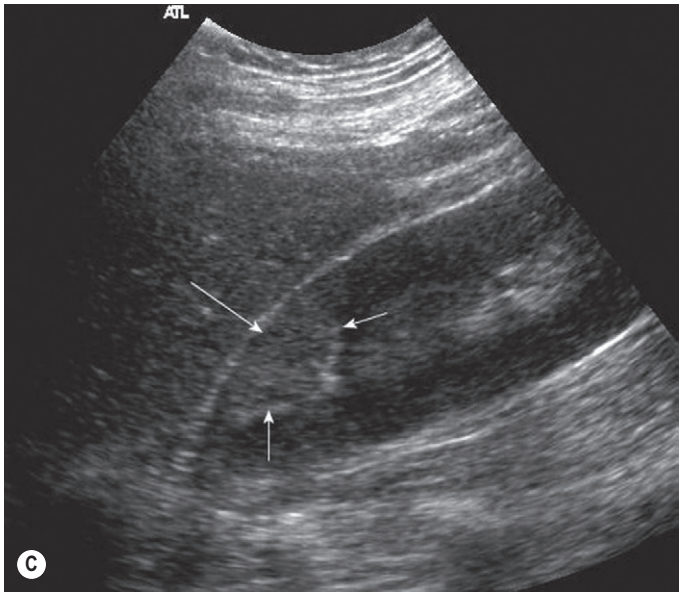


Figure 24.2 Lobar nephronia. A: A focal area of reduced echogenicity (arrows) at the upper pole of the right kidney in a patient with pyelonephritis. **B:** The same region 6 weeks later showing complete resolution. **C:** A second case showing focal increased echogenicity at the upper pole of the right kidney (arrows) in another patient with acute pyelonephritis.

Ultrasonic features of renal bacterial infections

In most cases ultrasound is not indicated.
In most cases ultrasound will not show any significant changes.
Ultrasound is indicated for renal infections in children, adult males, or females with recurrent infections.
Lobar nephronia: focal inflammation in the renal parenchyma.
Abscess: collection of pus and necrotic material within the renal parenchyma.
Pyonephrosis: infected, obstructed collecting system.

On ultrasound there is a focal area of reduced reflectivity, which may show some mass effect[9] but does not characteristically show increased sound transmission, in contradistinction to an abscess; it may, however, be difficult to distinguish a region of lobar nephronia from an abscess, or alternatively, an area of simple focal inflammation.[1] Other workers have suggested that focal areas of increased echogenicity (Fig. 24.2C) are more common[10] and this finding may also be seen if haemorrhage has occurred into the inflammatory mass, when patchy areas of increased reflectivity will be seen within it.[6]

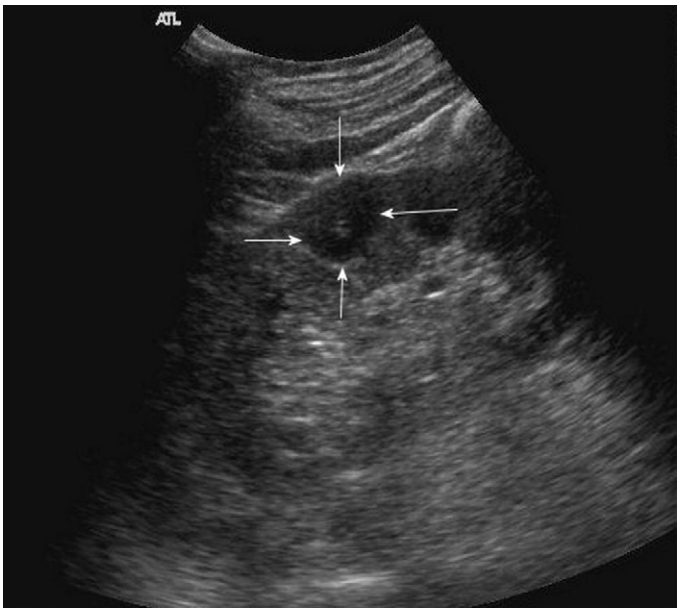


Figure 24.3 Renal abscess. A focal area of reduced attenuation in the parenchyma of the kidney (arrows); a slightly irregular posterior wall is apparent, together with low level echoes within the lesion.

RENAL AND PERIRENAL ABSCESSES

Intrarenal abscesses may develop in kidneys with severe infections that have not been treated with antibiotics, or which have been treated inadequately; they may also be the result of haematogenous spread from distant sites of sepsis.[5] They may be single or multiple; smaller abscesses may coalesce into a single cavity.[11] Small intrarenal abscesses resolve with appropriate antibiotic therapy but larger collections require percutaneous drainage (see Chapter 43). A pre-existing simple renal cyst may become infected in renal sepsis and may be indistinguishable from an abscess. Sometimes an intrarenal infection will extend through the capsule and spread to the perirenal space; perirenal abscesses may also result from extrarenal infection such as in Crohn's disease. Alternatively an intrarenal abscess may extend into the collecting system, producing a pyonephrosis.

Ultrasonically an abscess appears as a focal area of reduced or absent reflectivity (Fig. 24.3), or occasionally of increased reflectivity if there is gas within the collection. Increased sound transmission is usually apparent and layering or movement of debris within the cavity may be seen. The cavity itself may be unilocular or multilocular.[3] The wall can be difficult to discern but may be seen to be thickened and irregular, making distinction from a cystic neoplasm difficult. Small abscesses may be difficult to detect in a kidney showing changes of diffuse inflammation. Perinephric collections are seen as areas of fluid and debris in the retroperitoneum around the kidney.

Infected cysts tend to have smoother walls and tend to show greater sound transmission than an abscess[3] but distinction may be impossible. Conversely, haemorrhage into a cyst produces internal echoes suggestive of an abscess; if there is any doubt then diagnostic aspiration should be considered. MRI may also be of value in distinguishing haemorrhage from infection, particularly in patients with autosomal dominant polycystic kidney disease (ADPKD).

PYONEPHROSIS

Pyonephrosis develops in cases of hydronephrosis when the stagnant urine becomes infected from renal sepsis, associated calculi, instrumentation or haematogenous spread. In pyonephrosis the collecting system is usually markedly dilated but occasionally this may not be the case; thickening of the walls and contraction may be seen. Low-level echoes from the pus and debris within the infected collecting system can be seen but it may be necessary to turn up the gain to appreciate this feature (Fig. 24.4). An associated calculus or staghorn may be apparent but it should be remembered that a large staghorn may obscure a dilated collecting system, leading to a false negative examination. Gas may be present in the collecting system, and this confirms the diagnosis (in the absence of recent instrumentation) but it may be confused with calculi and not recognised. Layering or movement of debris within the collecting system is a characteristic feature[1] but up to 40% of pyonephroses may not show debris and may be mistaken for simple hydronephrosis.[12,13] Conversely, haemorrhage into a sterile hydronephrosis produces echoes within the collecting system leading to a false positive diagnosis.[13] It is therefore imperative that diagnostic aspiration is carried out in any case where there is doubt concerning the presence or absence of pyonephrosis because urgent nephrostomy is required to preserve any residual function and reduce the chance of fatal septicaemia.

CHRONIC PYELONEPHRITIS

Acute bacterial pyelonephritis does not usually result in long-term chronic infection and renal parenchymal damage in adults. Most cases of chronic pyelonephritis develop in childhood as a result of reflux and the associated recurrent infections.[1] These episodes damage the developing renal tissues in the young kidney, producing a typical appearance of a cortical scar overlying a dilated calyx (Fig. 24.5). Hypertrophy of normal adjacent renal tissue may emphasise the scar. In addition, focal areas of increased reflectivity may be seen scattered in the parenchyma, representing areas of fibrosis.[1] However, DMSA scintigraphy is more sensitive than ultrasound for these problems. Severe cases result in marked renal atrophy and scarring, with calyceal clubbing, thickening and dilatation of the collecting system.[2]

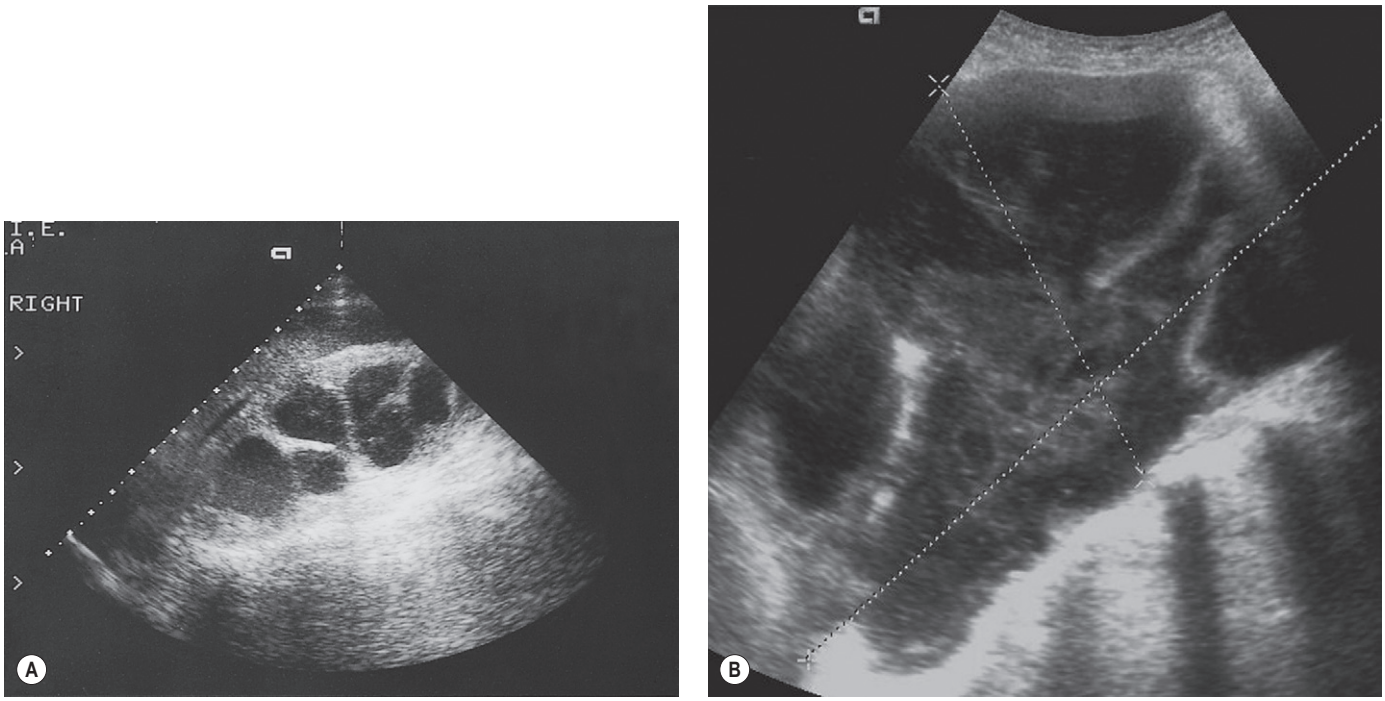


Figure 24.4 **Pyonephrosis. A:** An obstructed kidney with superimposed pyonephrosis. Low-level echoes from debris are visible in the dilated collecting system. **B:** A chronically obstructed pyonephrosis with marked parenchymal loss and significant debris within the collecting system.

XANTHOGRANULOMATOUS PYELONEPHRITIS

This is a rare chronic inflammatory condition which may develop in cases of chronic obstruction of a calyx, the renal pelvis or a ureter. It is believed to result from an atypical, incomplete immune response to acute bacterial infection.[2] Chronic inflammatory change extends through the transitional epithelium of the obstructed segment resulting in destruction, cavitation, chronic abscess formation and fibrosis.[1] The affected kidney, or renal segment, is destroyed and replaced by chronic granulomatous inflammatory tissue containing lipid-laden macrophages (xanthoma cells).

Ultrasound shows a mass in the renal fossa but the normal renal architecture cannot be distinguished, although the overall shape of a kidney is often preserved (Fig. 24.6).[14,15] Multiple areas of decreased reflectivity, representing dilated calyces and abscess cavities, may be visible but echogenic material within these spaces may be indistinguishable from the granulomatous tissues. Associated calculi, including staghorn calculi, may also be apparent but often they are difficult to see clearly; the renal pelvis is characteristically fibrotic and contracted rather than dilated. In cases of focal involvement the affected region is seen as an area of reduced reflectivity and may be difficult to distinguish from a tumour. The perirenal space may also be involved in the chronic inflammatory process.[16]

MALACOPLAKIA

Malacoplakia is another rare inflammatory response to chronic infection in which there is impaired histiocyte response to ingested bacteria.[2,5] It is more common in females and those who are immunocompromised in some way. It most frequently affects the bladder but any urothelial lining can be affected, including the ureter and renal pelvis.

Ultrasound typically shows a poorly defined hypoechoic mass, which can mimic a tumour, or diffuse enlargement of the affected kidney with distortion of the central echo complex. Bladder lesions may result in ureteric obstruction without direct renal involvement.

OTHER INFECTIONS

Tuberculosis

Tuberculosis of the renal tract is usually due to haematogenous spread of tubercle bacilli from the lungs, although often it does not manifest itself for 10–20 years after the primary infection[1] and less than 50% of patients in whom urinary tuberculosis is ultimately diagnosed have abnormal results on chest radiography.[2] The infection affects the kidney in two ways: parenchymal infection results in abscess cavities, granulation and calcification, and these changes may be focal or generalised throughout the kidney; secondly, the infection also affects the ureters and collecting system, producing strictures and dilatation of calyces or the collecting system and ureter.

The changes on ultrasound[17] reflect these patterns of involvement. The kidney may show focal or diffuse disorganisation of architecture, with areas of reduced reflectivity corresponding to abscesses and debris-filled cavities; focal areas of increased reflectivity from areas of calcification may also be apparent. Parenchymal masses, cavities and mucosal thickening can also be distinguished with modern equipment.[18] In addition, strictures in the ureter or parts of the collecting system result in a generalised or focal dilatation; however, the process results in fibrosis and contraction so that an affected renal pelvis may not be visible if it is contracted.[1] In advanced cases a small, calcified kidney is seen (autonephrectomy) (Fig. 24.7). Ultrasound-guided fine-needle

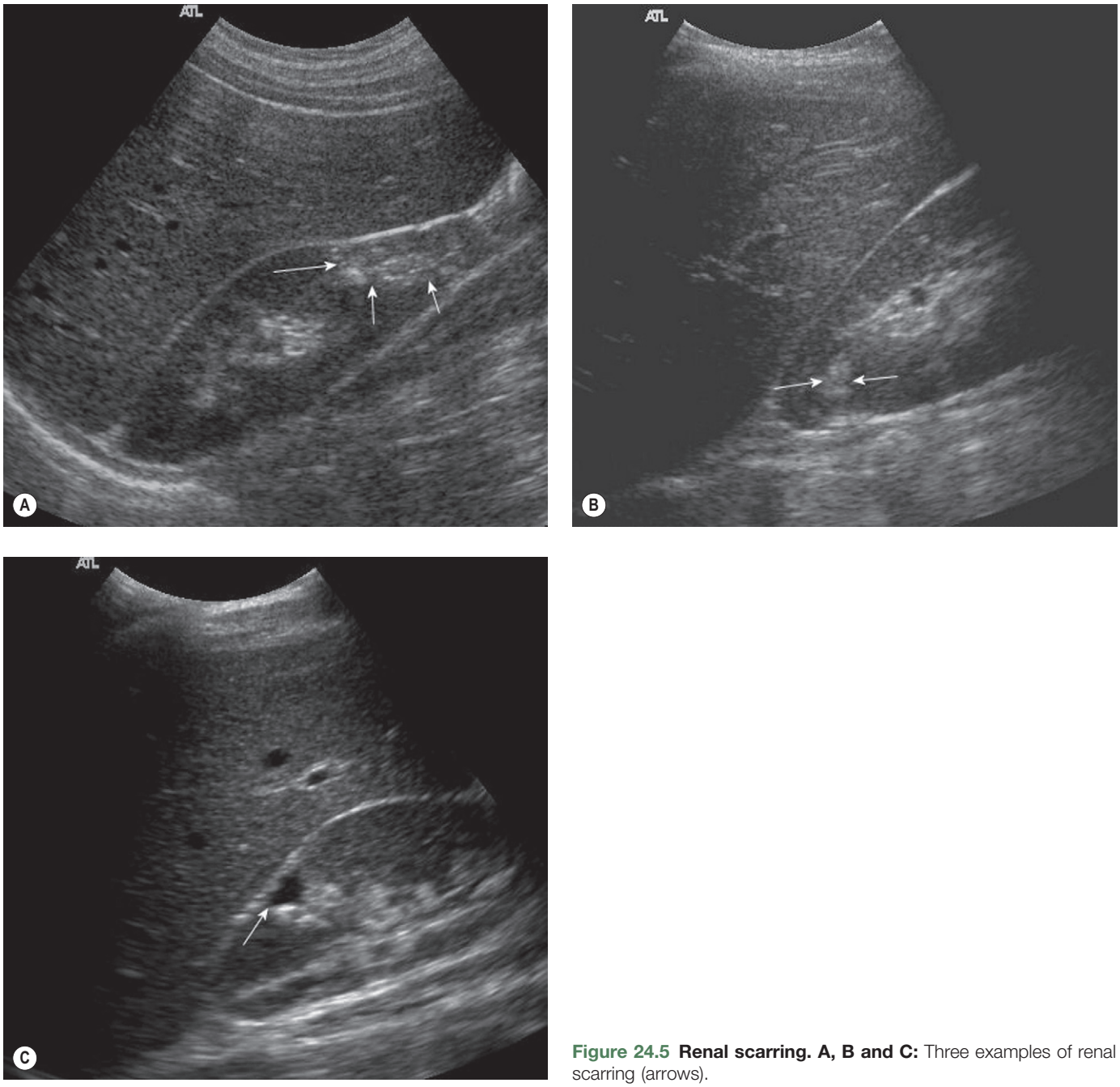


Figure 24.5 Renal scarring. A, B and C: Three examples of renal scarring (arrows).

aspiration for cytology and bacteriology is reported to be of value in the diagnosis of renal tuberculosis in cases with persistently negative urine culture.[19]

Fungal infections

A variety of fungi can affect the kidneys, usually in patients with predisposing factors such as immunosuppression, diabetes or cachexia, or in premature infants. The most common fungal agent is *Candida* and the infection may involve the whole kidney or affect mainly the papillae and medulla. A fungal mass (mycetoma) may be seen in a dilated calyx or collecting system and these may result in ureteric obstruction if they pass distally into the ureter.[20]

Parasites

Hydatid disease

Echinococcal involvement of the kidney is rare and is usually associated with hydatid disease elsewhere. The appearances on ultrasound[21,22] are similar to those seen in hepatic hydatid disease with a thick-walled cyst, which often contains daughter cysts; a detached internal membrane, hydatid 'sand' and wall calcification may also be seen (see Chapter 9).

Schistosomiasis

Schistosoma haematobium congregates in the venous plexi around the bladder and ureters. There is a significant inflammatory response

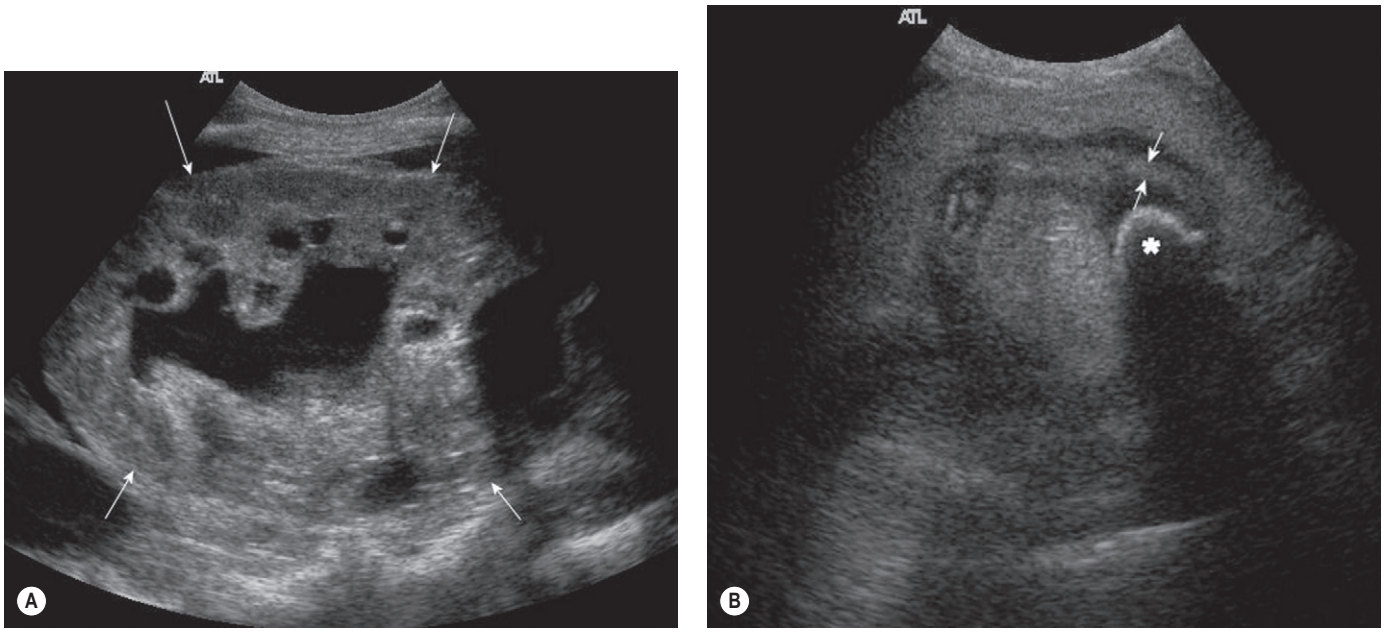


Figure 24.6 Xanthogranulomatous pyelonephritis. A: An enlarged kidney (thin arrows) with loss of normal architecture and multiple cystic areas around a dilated collecting system. **B:** A different patient with loss of architecture, thickening of the collecting system walls (arrows) with a calculus (*) and debris in the collecting system.

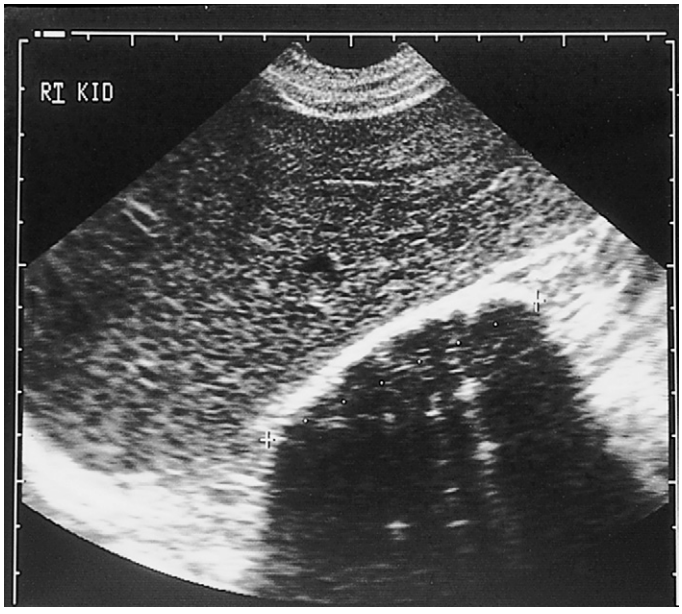


Figure 24.7 Tuberculous autonephrectomy. A small, densely calcified kidney in the right renal fossa.

secondarily from the effects of drugs used in antiviral therapy. In addition to proteinuria, these patients also have signs of impairment of renal function and may develop acute renal failure. Biopsy shows focal segmental glomerulosclerosis, focal glomerulonephritis and interstitial inflammatory change.[24,25] Tubular abnormalities have also been reported with irregular areas of dilatation and occasional small cystic spaces in both the cortex and medulla[26] on histology.

The ultrasound appearances reflect these changes: the kidneys may be of normal size, or enlarged; a non-specific increase in cortical reflectivity has been reported in up to 60% of AIDS patients with impaired renal function[27] and whilst increased echogenicity is associated with nephropathy, normal parenchymal echogenicity suggests a low likelihood of nephropathy.[28] An unusual pattern of focal calcification may be seen in the cortex and medulla, which may be dense and punctate or less dense and more diffuse; these lesions have been reported in patients with infection by *Mycobacterium avium intracellulare*, *Pneumocystis carinii* or histoplasmosis.[29,30]

AIDS patients are also more likely to suffer from renal infections, both bacterial and fungal. Treatment of toxoplasmosis involves the use of sulphadiazine, which may result in crystalluria and renal failure in which echogenic material may be seen in the renal parenchyma and collecting system; obstruction may also result from the urinary deposits.[31] They have an increased risk of developing non-Hodgkin's lymphoma, which has a predilection for extranodal sites such as the kidney, and Kaposi's sarcoma, which tends to affect the lower urinary tract rather than the kidney itself.[31]

to the eggs produced by the adult worms, which results in chronic inflammation and fibrosis. This results in ureteric and vesical fibrosis, which in turn, produce dilatation and obstructive changes in the kidneys.

HIV-associated nephropathy

The main renal complication in patients with human immunodeficiency virus infection is HIV-associated nephropathy,[23] which can result directly from infection of renal tissue by the HIV virus, or

Other renal infections

Tuberculosis: parenchymal and urothelial effects.
Fungal: more common in diabetes and other immunocompromised states.
Parasitic: Hydatid and *Schistosoma haematobium* are the most frequent parasites affecting the kidneys.
Viral: HIV nephritis as well as changes resulting from chemotherapy and secondary infections.

REFERENCES

1. Goldman SM, Fishman EK. Upper urinary tract infection: the current role of CT, ultrasound and MRI. Semin Ultrasound CT MR 1991;12:335–360.
2. Craig WD, Wagner BJ, Travis D. Pyelonephritis: radiologic-pathologic review. Radiographics 2008;28:255–276.
3. Papanicolaou N, Pfister RC. Acute renal infections. Radiol Clin North Am 1996;34:965–995.
4. Davidson AJ, Talner LB. Urographic and angiographic abnormalities in adult-onset acute bacterial nephritis. Radiology 1973;106:249–256.
5. Vourganti S, Agarawal PK, Bodner DR, Dogra VS. Ultrasonic evaluation of renal infections. Radiol Clin North Am 2006;44:763–775.
6. Rigsby CM, Rosenfield AT, Glickman MG, Hodson J. Haemorrhagic focal bacterial nephritis: findings on gray scale sonography and CT. Am J Roentgenol 1986;146:1173–1177.
7. Nicolet V, Carignan L, Dubuc G, et al. Thickening of the renal collecting system: a non-specific finding at ultrasound. Radiology 1988;168:411–413.
8. Soulen MC, Fishman EK, Goldman SM. Sequelae of acute renal infections. Radiology 1989;173:423–426.
9. McKinstry CS. Acute lobar nephronia. Br J Radiol 1985;58:1217–1219.
10. Farmer KD, Gellett LR, Dubbins PA. The sonographic appearance of acute focal pyelonephritis: 8 years experience. Clin Radiol 2002;57:483–487.
11. Dembry LM, Andriole VT. Renal and perirenal abscesses. Infect Dis Clin North Am 1997;11:663–680.
12. Coleman BG, Arger PH, Mulhearn Jr CB, et al. Pyonephrosis: sonography in the diagnosis and management. Am J Roentgenol 1981;137:939–943.
13. Jeffrey RB, Laing FC, Wing WV, Hoddick W. Sensitivity of sonography in pyonephrosis: a re-evaluation. Am J Roentgenol 1985;144:71–73.
14. VanKirk OC, Go RT, Wedel VJ. Sonographic features of xanthogranulomatous pyelonephritis. Am J Roentgenol 1980;134:1035–1039.
15. Hartman DS, Davies Jr CJ, Goldman SM, et al. Xanthogranulomatous pyelonephritis: sonographic–pathologic correlation of 16 cases. J Ultrasound Med 1984;3:481–488.
16. Loffroy R, Guiu B, Watfa J, et al. Xanthogranulomatous pyelonephritis in adults: clinical and radiological findings in diffuse and focal forms. Clin Radiol 2007;62:884–890.
17. Premkumar A, Lattimer J, Newhouse JH. CT and sonography of advanced urinary tract tuberculosis. Am J Roentgenol 1987;148:65–69.
18. Vijayaraghavan SB, Kandasamy SV, Arul M, et al. Spectrum of high resolution sonographic features of urinary tuberculosis. J Ultrasound Med 2004;23:585–594.
19. Das KM, Vaidyanathan S, Rajwanshi A, Indudhara R. Renal tuberculosis: diagnosis with sonographically guided aspiration cytology. Am J Roentgenol 1992;158:571–573.
20. Shimada S, Nakagawa H, Shintaku I, et al. Acute renal failure as a result of bilateral ureteral obstruction by *Candida albicans* fungus balls. Int J Urol 2006;13:1121–1122.
21. Zmerli S, Ayed M, Horchani A, et al. Hydatid disease of the kidney: diagnosis and treatment. World J Surg 2001;25:68–74.
22. Vargas-Serrano B, Ferrierro-Arguelles C, Rodriguez-Romero R, del Rio M. Imaging findings in renal hydatid disease. Eur Radiol 1997;7: 548–551.
23. Waytt CM, Klotman PE, D'Agati VD. HIV-associated nephropathy: clinical presentation, pathology and epidemiology in the era of antiretroviral therapy. Semin Nephrol 2008;28:513–522.
24. Schaffer RM, Schwartz GE, Becker JA, et al. Renal ultrasound in acquired immune deficiency syndrome. Radiology 1984;153:511–513.
25. Bourgoignie JJ, Meneses R, Ortiz C, et al. The clinical spectrum of renal disease associated with human immunodeficiency virus. Am J Kidney Dis 1988;12:131–137.
26. Hamper UM, Goldblum LE, Hutchinson GM, et al. Renal involvement in AIDS: sonographic–pathologic correlation. Am J Roentgenol 1988;150:1321–1325.
27. Miles BJ, Melser M, Farah R, et al. The urological manifestations of the acquired immunodeficiency syndrome. J Urol 1989;142:771–773.
28. Atta MG, Longenecker JC, Fine DM, et al. Sonography as a predictor of human immunodeficiency virus-associated nephropathy. J Ultrasound Med 2004;23:603–610.
29. Falkoff GE, Rigsby CM, Rosenfield AT. Partial combined cortical and medullary nephrocalcinosis: US and CT patterns in AIDS-associated MAI infection. Radiology 1987;162:343–344.
30. Kay CJ. Renal disease in patients with AIDS: sonographic findings. Am J Roentgenol 1992;159:551–554.
31. Kane D, Murphy JM, Keating S, et al. Renal ultrasonic findings in sulphadiazine-induced renal failure. Br J Radiol 1996;69:925–928.

CHAPTER

25 Vascular disorders of the kidney

Dennis L. Cochlin

INTRODUCTION 467

RELEVANT VASCULAR ANATOMY 468

RENAL DOPPLER STUDIES – THE NORMAL PATTERN 469
The colour flow map 469
The spectral (pulsed wave) arterial pattern 469

THE TECHNIQUE OF RENAL DOPPLER STUDIES 470
Study of the intrarenal vessels 470
Study of the main renal trunks 471

RENOVASCULAR HYPERTENSION – RENAL ARTERY STENOSIS 473
Clinical considerations 473
Screening hypertensive patients for renal artery stenosis 474
Simple greyscale ultrasound studies in hypertension 474
How should patients be screened for renal artery stenosis? 474
Catheter angiography 474
CT angiography 474
MR angiography 475
Captopril isotope renography 475
The captopril test 475
Doppler ultrasound 475
Abnormalities on greyscale ultrasound studies in hypertension 475
Abnormalities in renal Doppler studies in hypertension 475
Increased velocity 475
Flow disturbance (turbulence) 476
Damping – the parvus tardus waveform 476
The technique of Doppler studies for renal artery stenosis 476
Doppler study of the intrarenal vessels 477
Limitations of the damped (parvus tardus) waveform 477
Doppler study of the renal trunk 477
Children with hypertension 477
Hypertension in patients with renal transplants 477

RENAL ARTERY OCCLUSION AND RENAL INFARCTION 477
Greyscale ultrasound appearances 477
Doppler ultrasound appearances 478

RENAL VEIN THROMBOSIS 478
Symptoms 478
Greyscale ultrasound appearances 479
Doppler ultrasound appearances 479

RENAL CELL CANCER – PROPAGATION INTO THE RENAL VEIN AND INFERIOR VENA CAVA 480

ARTERIOVENOUS FISTULA 481
Symptoms and signs 481
Doppler ultrasound appearances 481

ARTERIOVENOUS MALFORMATIONS (CONGENITAL ARTERIOVENOUS FISTULAE) 481
Symptoms and signs 482
Greyscale ultrasound appearances 482
Doppler appearances 482

RENAL ARTERY ANEURYSM 482
Symptoms 483
Prognosis 483
Ultrasound appearances 483

VASCULAR ASPECTS OF RENAL PARENCHYMAL DISEASE AND DOPPLER STUDIES 483
Vascular response to renal disease 483
Acute tubular necrosis (ATN) 484
Doppler appearances 484
Contrast-enhanced ultrasound appearances 484
Renal diseases other than ATN 484
Small vessel disease 484
Acute glomerulonephritis (GN) 484
Tubulo-interstitial disease 484
Vasculitis 484
Hepatorenal syndrome 484
Chronic renal failure 484

ACUTE URETERIC OBSTRUCTION 484

INTRODUCTION

Diagnostic ultrasound with Doppler studies is a powerful tool in the investigation of vascular disorders of the kidney. It is non-invasive, involves no radiation and, in most cases, does not require a contrast agent.

The most common renovascular disorder that results in an ultrasound Doppler study is suspected renal artery stenosis in severely hypertensive patients. In these patients Doppler ultrasound is one of several diagnostic tests that may be used. It has strengths and weaknesses. These will be discussed.

Less common renal vascular disorders are arteriovenous fistulae, vascular malformations, aneurysms, renal artery occlusion resulting in total renal or segmental infarction and renal vein thrombosis. Doppler ultrasound studies are very useful in all of these conditions.

The small vessels of the kidney are affected in several diseases, the most common being diabetic nephropathy. The small vessels are affected in almost any chronic and most acute diseases that affect renal function. Doppler studies may be useful in some cases, an example being the distinction of acute tubular necrosis from pre-renal failure.

Ultrasound contrast agents are a method of studying perfusion dynamics in tissues. Their use in renal pathology has yet to be fully evaluated, but they do show promise in the study of both the native and the transplant kidney.

Doppler studies are commonly used in the transplant kidney. In this chapter the transplant kidney is discussed where the same pathology affects both the native and transplant kidney: renal artery stenosis, arteriovenous fistula, acute tubular necrosis. Although this causes some overlap with the chapter on the transplant kidney, this is necessary for a complete discussion. The use

of Doppler studies in transplant rejection is not discussed in this chapter.

RELEVANT VASCULAR ANATOMY

The renal arteries normally arise from the aorta about 1.5 cm below the origin of the superior mesenteric artery. The renal artery origins may leave the aorta at a near right angle, or may have a shallower angle. They usually run in a lateral direction although the right renal artery origin often leaves the aorta anterolaterally and then curves downwards and backwards.

The right renal artery passes behind the inferior vena cava, then roughly posterior to the renal vein to the renal hilum. The left renal artery runs more directly behind the left renal vein (though not always directly behind) to the left renal hilum (Fig. 25.1).

Accessory renal arteries are common. It has been estimated that 22% of patients have more than one artery on one or both sides, and 2% have three or more accessory arteries (most accessory arteries are missed on ultrasound Doppler studies). Accessory renal arteries usually arise from the aorta separately from the main trunk (Fig. 25.2). They occasionally arise from the common iliac artery, the superior mesenteric, inferior mesenteric, adrenal or right hepatic arteries. They enter the kidney towards the poles rather than at the hila. Most enter the lower pole.

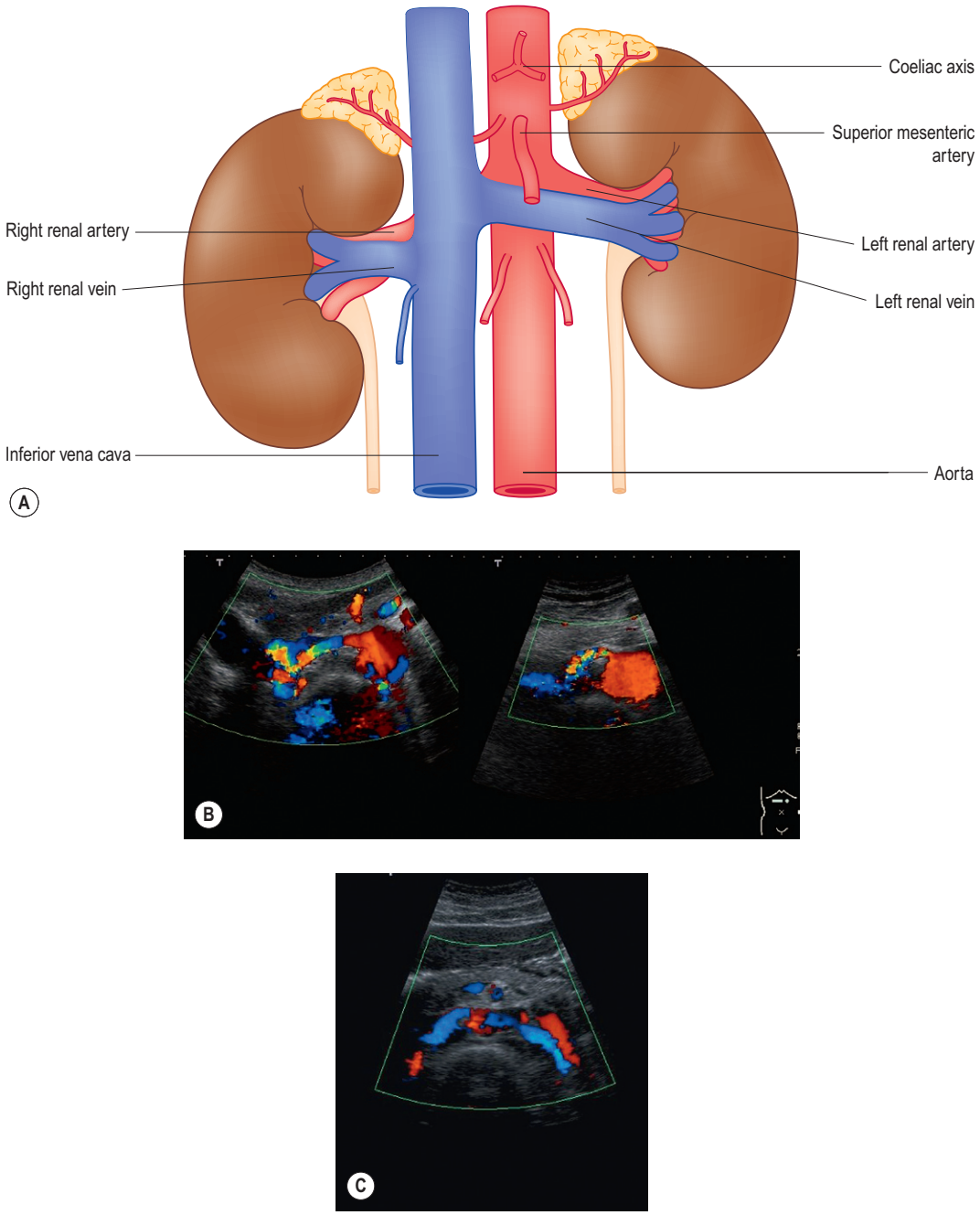


Figure 25.1 The main renal arteries. A: An anatomical diagram. **B, C**: axial plane scans. **B:** The right renal artery is seen passing posterior to the vena cava. The right-hand image shows a lateral origin and in the case shown on the left, the right renal artery leaves the aorta in an anterolateral direction. **C:** The left renal artery runs posterior to the renal vein.

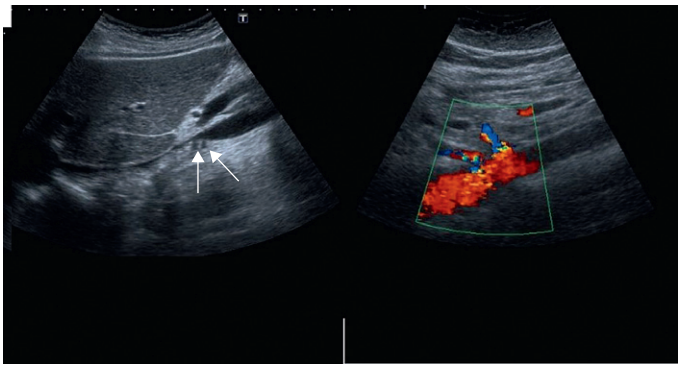
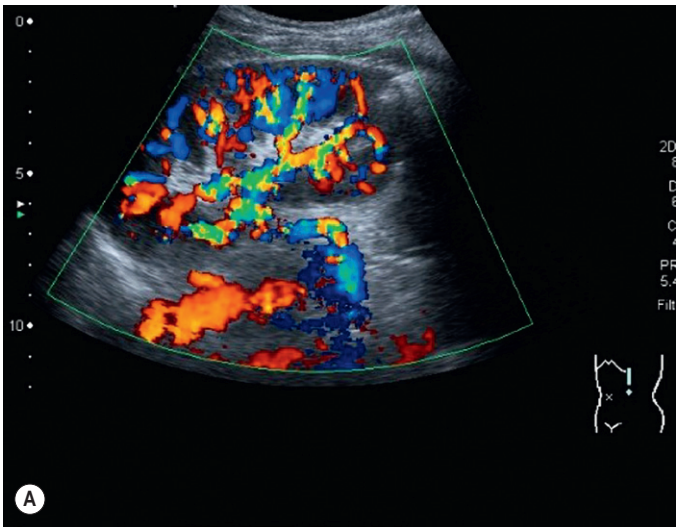


Figure 25.2 Accessory renal arteries. The right-hand image is a sagittal view through the inferior vena cava. It shows two right renal arteries (arrows). This is often a good view for detecting accessory right renal arteries but only works in slim patients. In the left-hand image, the two renal arteries are seen in an oblique longitudinal scan of the aorta.



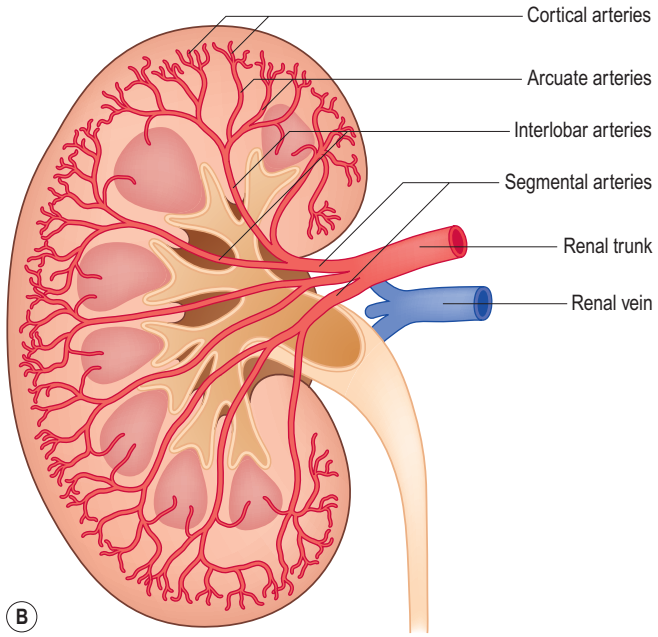


Figure 25.3 The renal arteries are seen dividing into the smaller intrarenal branches. **A:** Colour Doppler. **B:** Line diagram.

The renal arteries divide into a variable number of branches usually at or just before the renal hila, although 15% of renal arteries divide early. The branches form two groups that supply the anterior and posterior parts of the kidney respectively. These enter the kidney, where they are termed segmental arteries. The segmental arteries divide into the interlobar arteries which run between the pyramids into the cortex, where they branch into arcuate arteries which form arcades around the corticomedullary junction. The arcuate arteries then give off many cortical arteries that run radially into the cortex. These give off the afferent glomerular arteries (Fig. 25.3).

About 90% of the renal blood flow supplies the renal cortex; only 10% the medullary pyramids. This fact is relatively unimportant in Doppler studies, but is important in the understanding of contrast-enhanced studies (Fig. 25.4).

The right renal vein runs anterior to the artery to enter the vena cava. The left renal vein also runs anterior to the artery. It usually runs more truly parallel to the artery than the right (Fig. 25.1), although it often 'wanders' slightly. It usually runs between the aorta and the superior mesenteric artery. Occasionally it runs posterior to the aorta (retro-aortic), and occasionally it divides into two branches that run anterior and posterior to the aorta (circumaortic).

RENAL DOPPLER STUDIES – THE NORMAL PATTERN

In order to understand the changes that occur in renal pathology, it is necessary to first understand the pattern in the normal kidney. There follows a brief description.

The colour flow map

The colour flow Doppler map reveals the arterial and venous anatomy of the main renal arteries and veins and the intrarenal arteries and veins. In slim patients, children and transplanted kidneys, the intrarenal arteries may be seen down to the level of small cortical arteries. In larger patients only the more central vessels are seen (Fig. 25.3A).

The spectral (pulsed wave) arterial pattern

Arterial waveforms anywhere in the body may be divided into two broad types, high resistance (or triphasic) and low resistance (or biphasic). As the kidneys are normally always active, they have low arteriolar resistance. The normal renal artery waveform therefore has a low resistance or biphasic waveform (Fig. 25.5).

The important aspects of the waveform are:

1. The rapid rise from the beginning to the end of systole. The beginning of systole is found by extrapolating the systolic curve back to the baseline. The end of systole is marked by a brief reduction in velocity which causes a small spike followed by a notch. These are termed the first systolic peak and the systolic notch. The systolic notch is caused by closure of the aortic valve. It is sometimes clearly visible, sometimes difficult to see. The line of the maximum velocity envelope that joins the beginning of systole to the first peak is called the systolic rise curve (the normal 'curve' is usually nearly a straight line). The time from the beginning to the end of the systolic curve and the slope of the curve may be measured. The systolic curve is important in the diagnosis of arterial stenosis and this is discussed later.

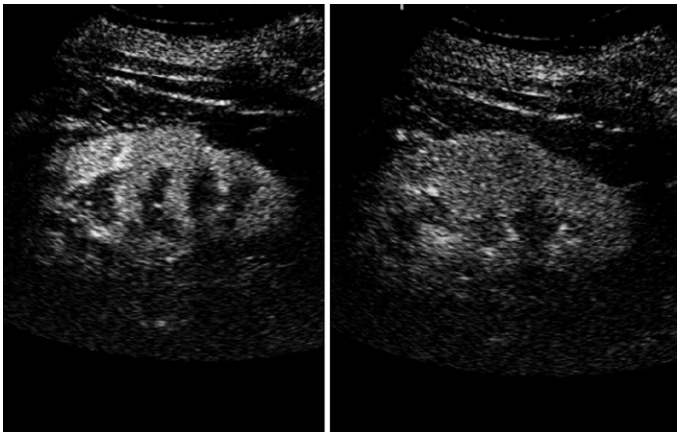


Figure 25.4 Contrast-enhanced ultrasound study (CEUS) of a normal kidney. Right: At 15 seconds following intravenous injection of contrast the cortex is well perfused (white). As the renal pyramids receive only 10% of the renal blood flow, at this stage there is less contrast in them and they appear relatively dark. Left: At 25 seconds sufficient contrast has accumulated in the renal pyramids to make them an equal contrast density to the cortex.

2. In the main renal trunk and its major branches, the systolic peak may be rounded or pointed. The peak velocity is about 1.5 metres per second, varying between 1.0 and 2.0 metres per second. As the intrarenal arteries branch into ever smaller arteries, the systolic peak becomes more rounded and the peak velocity becomes lower.
3. From the systolic peak there is a gentle curve to the end of diastole, and then the next systolic rise. The velocity at the end of diastole is between 0.4 and 0.3 of the peak systolic velocity. This may be quantified by several ratios, the most common being the resistance index (RI). The difference between the systolic and diastolic velocities decreases a little (the RI increases) in the smaller arteries towards the periphery of the kidney.

As the arteries branch towards the periphery of the kidney, their velocities decrease and the Doppler trace becomes lower. In perfectly healthy kidneys, the shape of the waveform is maintained. In many older patients and in patients with small vessel disease the waveform becomes progressively damped. This phenomenon is present in many older patients, including those with apparently normal renal function. It may well, however, be due to subclinical vascular disease.

The flow pattern in the renal veins is unremarkable. It varies from continuous to weakly pulsatile flow.

THE TECHNIQUE OF RENAL DOPPLER STUDIES

Study of the intrarenal vessels

Study of the intrarenal vessels is relatively straightforward. It is important, however, to achieve an appropriate scan angle. The best scan plane extends from the renal periphery towards the hilum. In this plane most of the vessels run more or less towards the transducer. This ensures that most of the vessels have a long length visible in the scan plane. Also the Doppler angle is good. In order to achieve this plane the patient needs to lie in a supine oblique position. The kidneys are scanned from an oblique posterior approach. The longitudinal plane is usually used, though a transverse plane is also suitable. In the longitudinal plane the blood vessels in the upper and lower poles of the kidney lie at a disadvantageous angle for Doppler study. This may give the false impression of hypovascularity at the poles. This may be partially rectified by changing the angle of the transducer.

A standard general abdominal transducer is used, generally a curved array transducer imaging at about 3–5 MHz. Such a transducer would normally use 2–3 MHz for the Doppler image. Doppler settings should be appropriate. Power Doppler is more sensitive and is not angle dependent. In practice, however, the colour Doppler on most machines is so good that power Doppler is not necessary. Which is used depends on individual preference based on which ultrasound system is used.

As more peripheral arteries are studied, their normal velocity measurements drop. Also as the angle between the ultrasound beam and the artery becomes greater, as would be predicted by the Doppler equation, the height of the spectral graph decreases. This often gives a false impression of damping. A poor Doppler angle in a peripheral vessel may therefore mimic a damped waveform. Also in many elderly patients and patients with small vessel disease, there may be true damping in the peripheral arteries. This may lead to a false diagnosis of renal artery stenosis. Care should be taken to study the larger segmental or interlobar arteries, and to achieve a good angle (less than 60°). The larger intrarenal veins often have weakly pulsatile waveforms that may mimic a damped arterial waveform. It is often not easy, given the number and

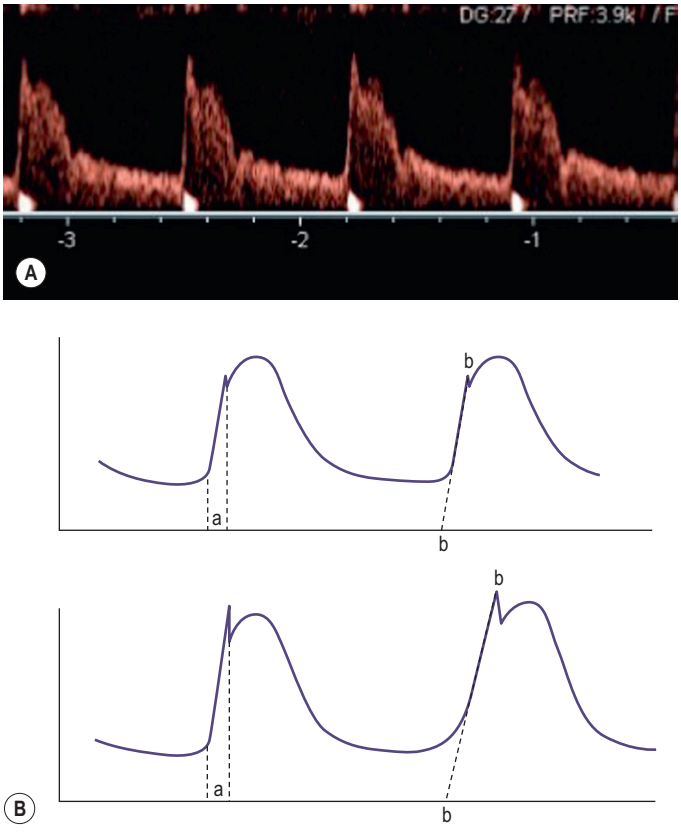


Figure 25.5 Normal renal artery waveform. The important features of the renal artery waveform are shown. **A:** Doppler ultrasound image. **B:** The systolic spike may be lower than the systolic peak as in the upper diagram, or higher as in the lower diagram. *a* is the systolic rise time (acceleration time); *b–b* is the systolic rise curve or upstroke (acceleration index).

complexity of intrarenal vessels, to be sure of these factors. It is necessary therefore to study at least three arteries to be sure of the waveform.

Study of the main renal trunks

The main renal artery trunks are seen on an oblique scan plane through the kidney with the beam angled towards the renal hilum (Fig. 25.6). Sometimes a plane transverse to the length of the kidney works best, sometimes a plane along the length of the kidney works better. Often in these planes the whole of the renal artery may be seen from the hilum to the aorta but sometimes only the distal portion is visualised. If this is the case, then the patient is asked to lie supine and the aorta is scanned. The position of the superior mesenteric artery origin is found on the sagittal scan. Axial views are then obtained and the scan plane is moved slowly caudad until the renal artery origins are seen (Fig. 25.1). In order to get a good angle of insonation the transducer may have to be tilted to the left for the right renal artery and vice versa. The renal arteries usually run in a transverse plane that is tilted in the postero-caudal direction, though sometimes in the postero-cranial direction, and sometimes the right renal artery origin points anterolaterally. Good angles of insonation are often not possible from this approach as the arteries tend to run parallel to the transducer. In large patients and in patients with overlying bowel gas, scans from the anterior approach often fail.

Having found the renal arteries on the colour map, it is necessary to study them by spectral (duplex) Doppler (Figs 25.7–25.14). An abnormal colour pattern, with turbulence and colour aliasing may suggest a stenosis, but it is the spectral pattern that is diagnostic. As stated earlier, a good angle between the ultrasound

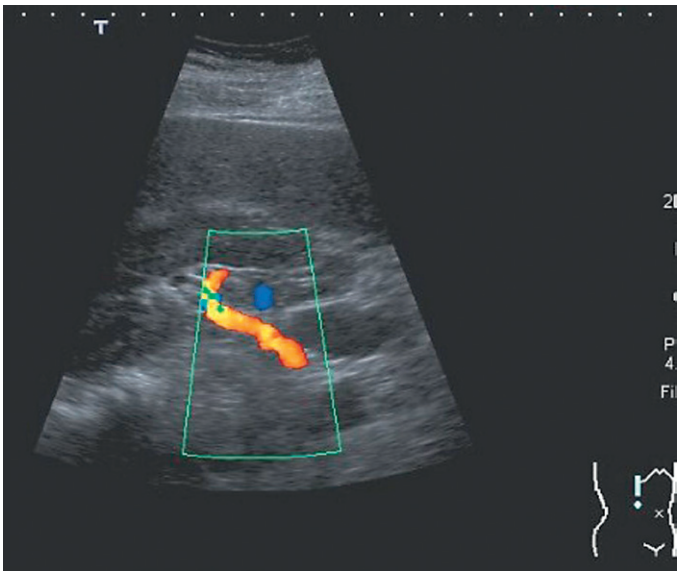


Figure 25.6 The renal artery viewed through the kidney. Sometimes the whole renal artery is readily seen as shown here, but sometimes the artery is tortuous and only portions of the artery are seen in any one scan plane. A diagnostic study is still possible.

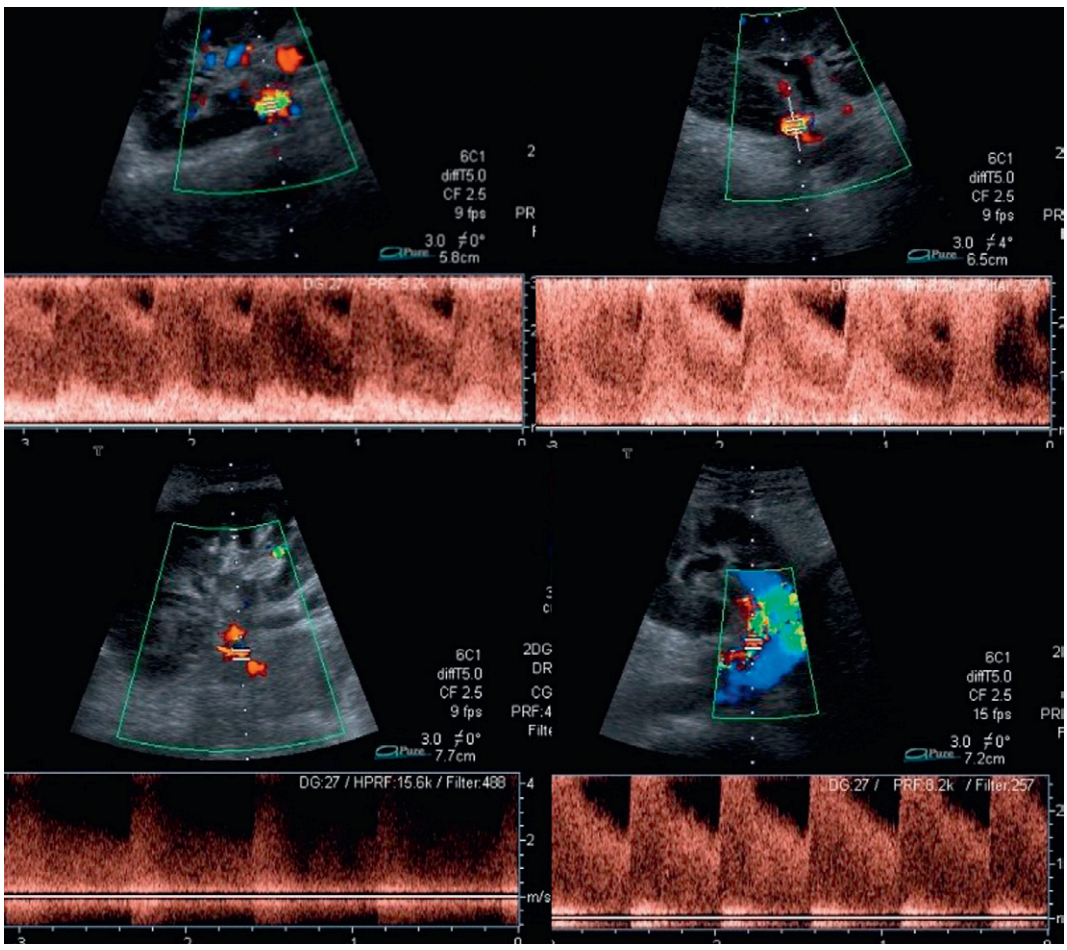


Figure 25.7 Renal artery stenosis. Four cases. All show the characteristic colour flow pattern and high velocity on the spectral graph.

Top right: The line of the artery is not clearly seen, so angle correction cannot be applied. Angle correction is not necessary in this case as the indicated peak systolic velocity is more than 3 metres per second. Any angle correction would increase this figure. Tissue vibration is visible on the colour Doppler image.

Top left: In this case the depth meant that the PRF could not be set lower. The peak velocity is, however, clearly more than 3 metres per second.

Bottom left: In this case velocity is not as high, but still well over the threshold of 2 metres per second.

Bottom right: In this young woman with fibromuscular dysplasia there is high velocity at a stenosis in the mid-renal artery.

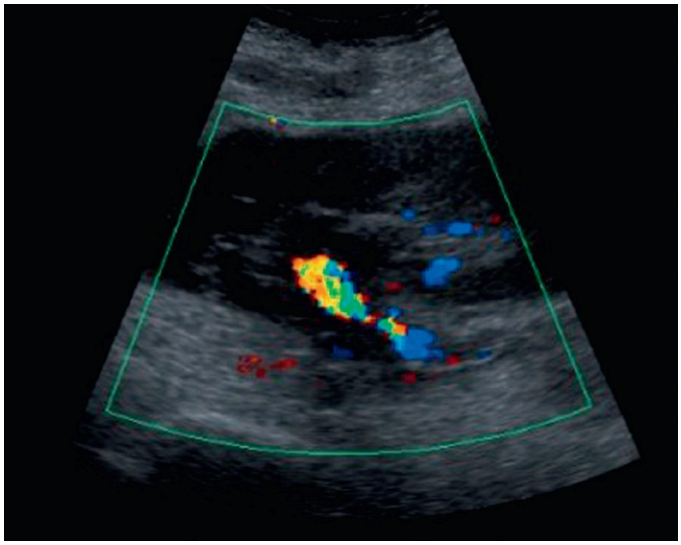


Figure 25.8 **Renal artery stenosis.** The stenosis is seen on the colour map image as a narrow segment of artery. Often the narrowing is not as clearly seen. Even when it is well seen, spectral Doppler is necessary to confirm the stenosis and to assess its severity.

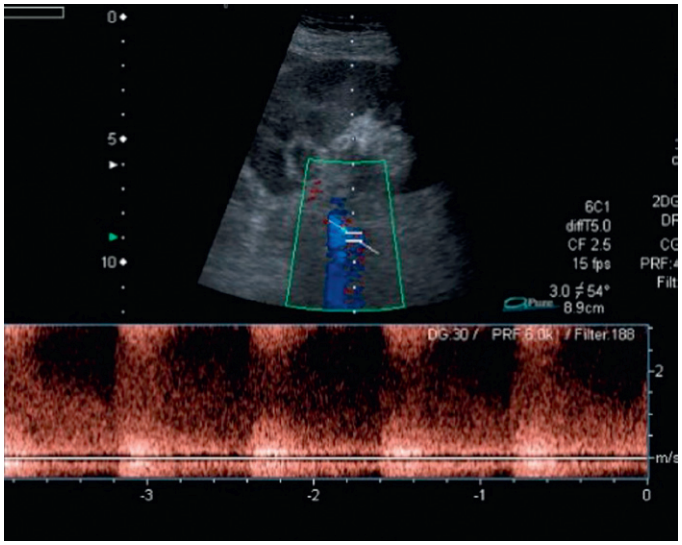


Figure 25.9 **Renal artery stenosis.** The spectral waveform is 'pale'. This is because the power is spread over a larger range of velocities. The waveform is nevertheless sufficiently clear to establish high velocity and diagnose renal artery stenosis.

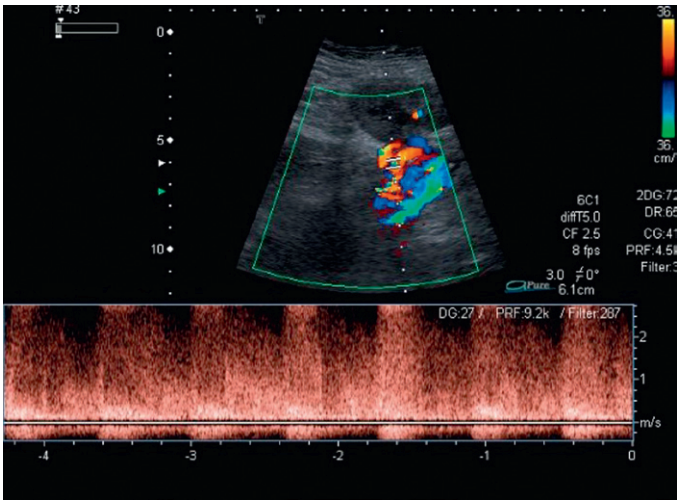


Figure 25.10 **Renal artery stenosis.** Just distal to the stenosis there is high velocity and flow disturbance.

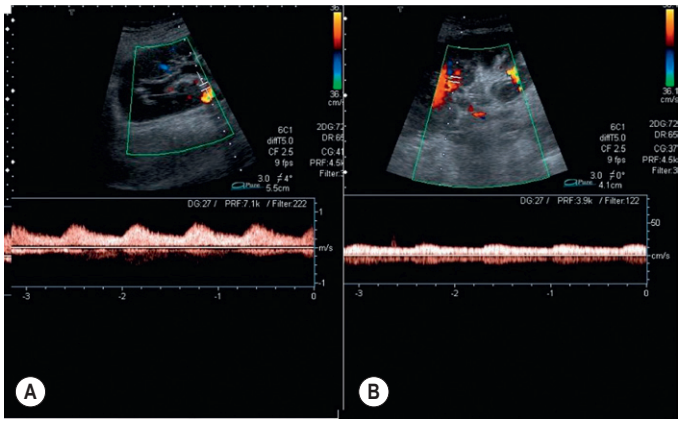


Figure 25.12 **Renal artery stenosis.** Damped (tardus parvus) waveform. **A:** Distal to the stenosis, but still in the main artery, the waveform is flattened, with a low rise to the systolic peak and a low flat systolic peak. No measurements have been made as the waveform is obviously abnormal. **B:** Damping in a peripheral artery.

beam and the line of the artery (the Doppler angle) is very important in order to avoid error. An angle of less than 60° is ideal, though it is not always possible, particularly from the anterior approach. Spectral studies are best obtained in a breath hold; however, this is not always possible. Diagnostic traces may be obtained with the patient breathing; usually at the end of expiration. A long series of traces, as may be produced in a breath hold, will not be obtained, but one full systolic/diastolic waveform is all that is needed for interpretation.

It must be understood that in the detection of renal artery stenosis, the changes in waveform that are being sought may only be present in a short length of the artery. The turbulence is only present for about 1 cm, the increased velocity for less. While the majority of stenoses due to atheroma occur at or near the renal artery origin, some occur along the artery, and occasionally even in segmental arteries. Stenoses due to fibromuscular hyperplasia typically occur distal to the origin and are often multiple. It is therefore necessary to study the renal artery at more than one site, the minimum being three points, origin, mid and hilar. It is sometimes possible to run the pulsed wave Doppler along the frozen colour image of the artery and to study, in real-time, the whole length. This is ideal.

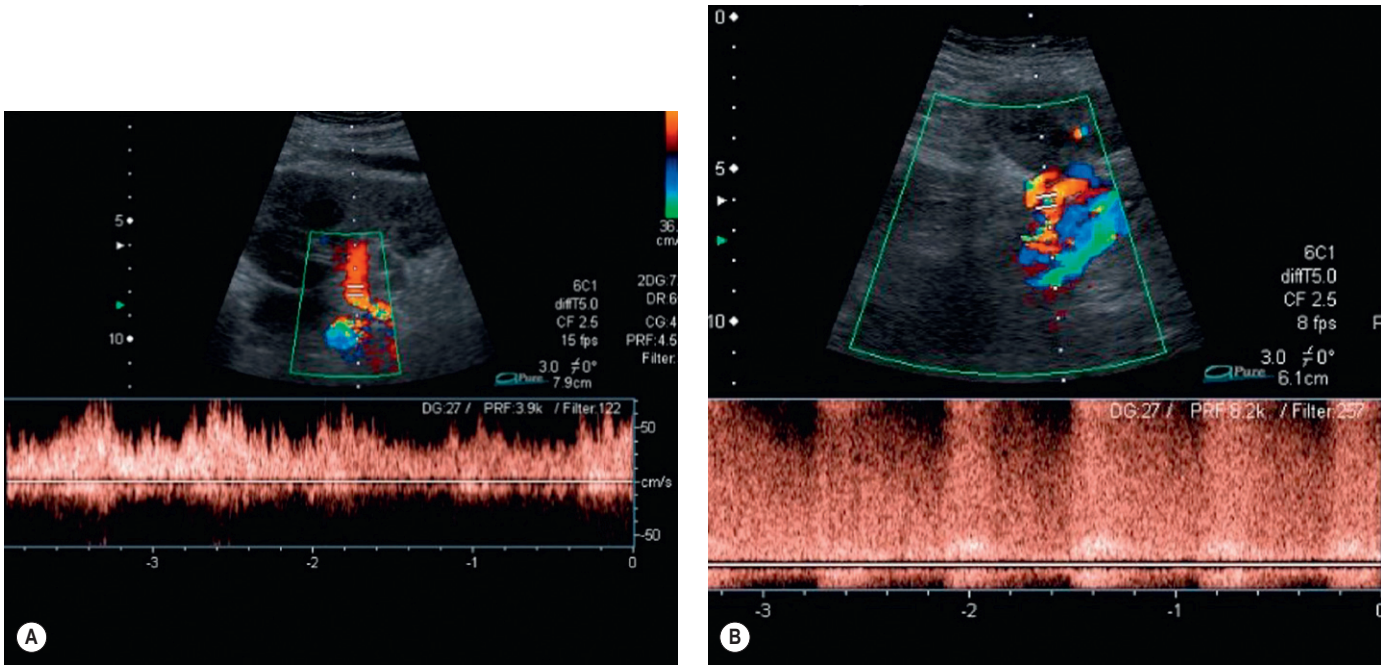


Figure 25.11 Renal artery stenosis. Flow disturbance. **A:** There is a very irregular 'spiky' maximal velocity envelope, with bright, high power signal at all velocities, including reversed velocities displayed below the baseline (turbulence). **B:** In this case the envelope is smoother, but there is bright, high power signal at all velocities (spectral broadening). Compare the normal renal artery waveform shown in Figure 25.5 where the high signal is concentrated near the maximum velocity envelope.

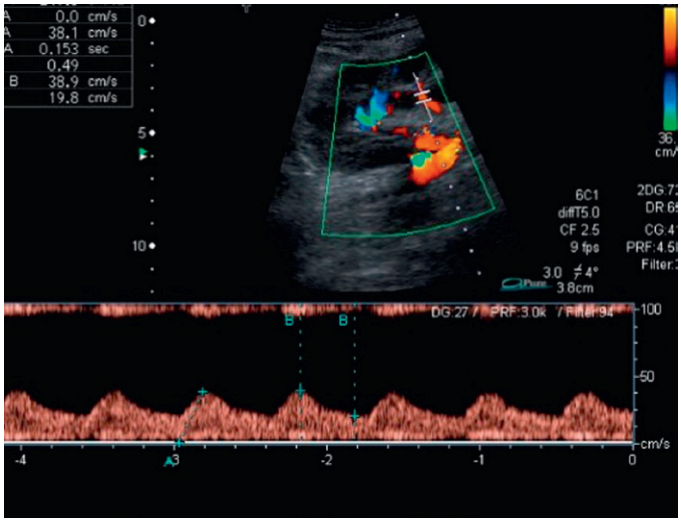


Figure 25.13 Renal artery stenosis. Damped waveform – measurements. The first measurement (A) is the systolic rise time, the second (B) is the resistance index.

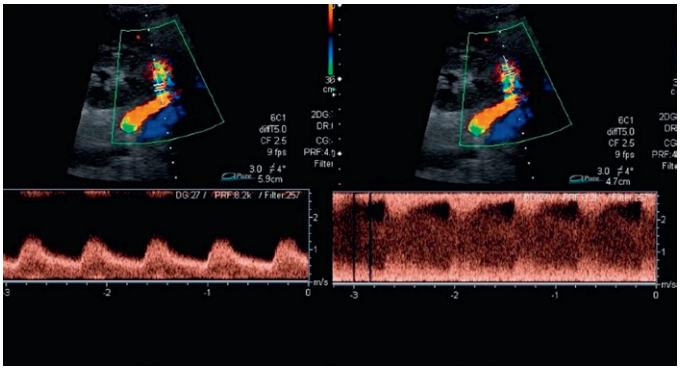


Figure 25.14 Renal transplant study. Renal artery stenosis. Left: Just proximal to the stenosis the waveform is normal. Right: At the stenosis there is high velocity. There is also flow disturbance. Note the dramatic change from left to right.

RENOVASCULAR HYPERTENSION – RENAL ARTERY STENOSIS

Clinical considerations

The kidneys control blood pressure through excretion of enzymes (renin and angiotensin). Several forms of renal disease or damage may upset this mechanism and cause hypertension. These include renal artery stenosis, renal trauma, polycystic kidney disease, scarring and almost any chronic renal disease (Table 25.1). Most important to this chapter is renal artery stenosis. This is important for several reasons. First, it is a potentially treatable cause. Second, the situation is complicated by the fact that hypertension itself can cause renal damage. Thus, renal artery stenosis in one kidney may cause hypertension, and the hypertension may damage the other kidney. Third, treatment of hypertension with acetylcholinesterase inhibitors (ACE inhibitors) in patients with renal artery stenosis will cause renal damage and may result in renal failure. Fourth, there is evidence that Doppler studies may be used to help select patients for angioplasty. A resistance index of more than 0.8 in the arteries distal to the stenosis indicates that angioplasty is likely to have a poor result.[1,2] Finally, Doppler studies are an appropriate method of follow-up after angioplasty.

Table 25.1 Renal causes of hypertension

Renovascular causes

1. Renal artery stenosis – due to atheroma or fibromuscular hyperplasia
2. Renal arteriovenous fistula or malformation
3. Renal artery aneurysm

Renal non-vascular causes

1. Polycystic kidneys
2. Scars
3. Almost any chronic renal disease
4. Renal trauma (Page kidney)

Table 25.2 Indications for renovascular screening in hypertension

1. Severe hypertension
2. Difficult to control 'brittle hypertension'
3. Severe rapid onset – flash pulmonary oedema
4. Onset at a young age (less than 30 years old) or in children
5. A renal bruit on clinical examination
6. A previous ultrasound study showing a significant discrepancy in renal size
7. Deterioration of renal function after onset of treatment with ACE inhibitors

Relative indications

8. Late age of onset (more than 60 years)
9. Severe coexisting atheromatous disease

Screening hypertensive patients for renal artery stenosis

Hypertension is very common. The vast majority of cases are classified as idiopathic, or essential hypertension, i.e. no cause may be identified. Renovascular or renal hypertension accounts for a small minority of cases. It is commonly felt that to screen all hypertensive patients for renal or renovascular disease is impractical. It is therefore common practice to screen selected cases only.

Current trials appear to show little long-term benefit from renal artery angioplasty in cases of atheromatous stenosis. There appears to be little improvement in hypertension or prevention of progression to renal failure as compared with patients treated by best medical treatment. This is despite good technical results. This could be interpreted as making the diagnosis of renal artery stenosis unnecessary in these patients, although a diagnosis would still be important in stenoses due to fibromuscular dysplasia and in the transplanted kidney. Others would take the view that a diagnosis is important even if it does not alter management. Whatever the arguments, current practice is to screen patients for certain indications.

For current indications for screening see Table 25.2. It is clear that some of these indications are imprecise. The level, for instance, of hypertension that constitutes sufficient severity to indicate screening will vary with different clinicians.

Simple greyscale ultrasound studies in hypertension

It is common practice in selected patients to perform a renal ultrasound study. As this is a non-invasive, simple and relatively inexpensive study, selection need not be as strict as for vascular (catheter, CT, MRI angiographic or Doppler) studies. Greyscale ultrasound will detect many of the renal causes of hypertension listed in Table 25.1. Enlargement of the adrenal glands may also be detected indicating possible phaeochromocytoma, although ultrasound is inferior to CT in imaging the adrenals. Although a number of renal pathologies are reported to cause hypertension, detection of many, such as scarring, may be coincidental. The only definite causes are polycystic kidneys and significant renal artery stenosis (or rarely renal arteriovenous fistula or renal artery aneurysm).

A significant discrepancy in renal size increases the probability of renal artery stenosis and is an indication for further screening.

How should patients be screened for renal artery stenosis?

This is a controversial question and there is no consensus.

There are several methods of screening for suspected renovascular hypertension (Table 25.3).

Table 25.3 Methods of screening for suspected renovascular hypertension

Method	Advantages	Disadvantages
Catheter angiogram	Most accurate* 'gold standard'	Invasive. Uses contrast. Expensive
CT angiogram	Less invasive	Uses contrast. High radiation. Expensive
MR angiogram	Non-invasive	Only marginally less accurate* than CTA. Expensive
Doppler ultrasound	Non-invasive	Very operator dependent. Poor in large patients
Captopril isotope renogram	Non-invasive	Low accuracy*
Captopril test		Least accurate*

**The term 'accurate' although scientifically imprecise is used here for brevity.*

Catheter angiography

Catheter angiography is undoubtedly the test that has the highest sensitivity and specificity, especially if combined with pressure measurements across a suspected stenosis. It is correctly regarded as the 'gold standard' against which other tests should be judged. The disadvantages are that it is invasive and expensive. It involves the administration of iodinated contrast. This is nephrotoxic and is contraindicated if there is significant coexisting renal dysfunction, which is often the case. The radiation dose is also high. In many centres catheter angiography is reserved for those cases where a definite diagnosis of renal artery stenosis has been made on other tests, in which case the angiogram is part of the therapeutic angioplasty.

CT angiography

Computed tomography (CT) angiography is a non-invasive alternative to diagnostic catheter angiography. Modern machines capable of fine slice image acquisition enable reconstructions of the image in any plane without loss of resolution. Nevertheless sensitivity and specificity are lower than those of catheter studies and pressure measurements cannot be performed. Iodinised contrast is used and the radiation dose is high.

Table 25.4 Tests for renal artery stenosis[3]

Test	Area under the curve
Contrast-enhanced CT	0.99
Contrast-enhanced MRI	0.99
Non-contrasted MRI	0.97
Doppler ultrasound	0.93
Captopril isotope study	0.89
Captopril test	0.72

MR angiography

Magnetic resonance angiograms may be obtained without the use of gadolinium contrast, using flow-specific sequences. The quality of these is, however, generally considered too low for use in the detection of renal artery stenosis. MR angiograms with gadolinium are of higher quality, comparable to multislice CT, with similar accuracy (Table 25.4). They were considered as an alternative to CT angiography in patients with renal impairment, but the possible link between gadolinium use in patients with renal impairment and nephrogenic sclerosing dermopathy is a contraindication to use of the technique in patients with poor renal function.

Captopril isotope renography

Captopril isotope renography relies on changes in the shape of the uptake curve of an isotope renogram after administration of captopril if a renal artery stenosis is present. The technique is non-invasive and radiation dose in low. Sensitivity and specificity are, however, also low.

The captopril test

This is the least accurate test and is not now used.

Doppler ultrasound

The main disadvantage of Doppler ultrasound is that it is extremely operator dependent with a long learning curve. It is more difficult to perform and sometimes technically not possible in large patients and in patients who cannot hold their breath. The percentage of cases that end as technical failures depends on the skill of the operator, the quality of the equipment and also on the criteria of a technically successful test. Some studies have reported technical failure rates of 40%, others less than 10%. These apparently daunting facts have led some to regard Doppler studies as inappropriate in the investigation of renal artery stenosis. In the view of the author this is not true.

In children, slim young women with suspected fibromuscular dysplasia and in transplant kidneys, Doppler ultrasound has a high technical success rate and high sensitivity and specificity. Overall 'accuracy' in all patients with suspected renovascular hypertension has been a subject of much debate. A comprehensive meta-analysis[3] quoted on the Cochrane database using catheter angiography as the gold standard has shown that Doppler ultrasound has a high sensitivity and specificity. This indicates that it is a highly appropriate test (Table 25.4).

While any analysis is open to debate, it is clear that, next to catheter angiography, contrast-enhanced CT or contrast-enhanced MRI are the most accurate tests. Doppler ultrasound is, however, not far behind. This would seem to support those who advocate Doppler ultrasound as the primary screening test for patients at high risk on clinical grounds of having renal artery stenosis. As opinions and practices vary so greatly, I will outline current practice in my department. That is not to say that it is necessarily best practice.

Table 25.5 Criteria for small kidneys

Right >2.5 cm smaller than left
Left >1.5 cm smaller than right

Patients with a high or moderately high suspicion of renal artery stenosis on clinical grounds (Table 25.2) have renal Doppler studies. Those that have a positive diagnosis or a high probability on the Doppler study proceed to catheter angiography and are consented for angioplasty at the same procedure provided the angiogram confirms the diagnosis.

Those that have equivocal renal Doppler studies, those in whom the Doppler study is a technical failure and those in whom the Doppler study is negative, but there is a very high or increasingly high clinical suspicion of renal artery stenosis, have contrast CT (or sometimes contrast MRI) studies.

Patients with hypertension but an intermediate or low suspicion of renal artery stenosis have ultrasound studies, without Doppler, and careful measurement of renal length.

Abnormalities on greyscale ultrasound studies in hypertension

Ultrasound is widely used in patients with hypertension. The conditions that may cause renal hypertension are listed in Table 25.1.

There are a number of pathologies other than renal artery stenosis that cause small kidneys, and these may all be found in patients with hypertension. However, whilst the combination of a small kidney and hypertension may be coincidental, the combination increases the probability of renal artery stenosis sufficiently to warrant a renal Doppler study.

Renal size may be measured in absolute terms, usually pole to pole length. Tables are available that relate renal size to patient size, and in children to age (see Chapter 21). It is more common, however, to make a more general judgement on renal size – less than 9 cm being regarded as small in adults, with subjective allowance being made for patient height and age. Comparison of the length on both sides is usually made. As the left kidney is commonly longer than the right, a different figure is used for each side (Table 25.5).

It is important to know, however, that measurement of renal length on an ultrasound study is imprecise. It is very important to ensure that a scan plane is obtained that includes the whole length of the kidney. Even with careful technique there is some lack of reproducibility. Nevertheless, the technique is sufficiently accurate for clinical use.

Abnormalities in renal Doppler studies in hypertension

An arterial stenosis causes changes in the blood flow pattern. These may be detected on a Doppler study. Proximal to the stenosis the flow pattern is usually normal. The exception to this is a very severe stenosis causing near or total occlusion. In this case there is absent or sometimes reversed diastolic flow. At the stenosis there is increased peak systolic velocity. Immediately distal to the stenosis there is flow disturbance (spectral broadening, turbulence) and in the distal arteries there is a damped waveform.[4] Each of these features will be discussed in turn.

Increased velocity

Increased velocity at a stenosis is due to the Venturi effect caused by the narrowing. This may be compared with squeezing the end of a garden hosepipe to increase the velocity and length of the water jet. The increase in velocity only occurs at a certain degree of

Table 25.6 Criteria for increased peak systolic velocity

High specificity

1. 2.2 metres per second
2. >3.5× velocity in the renal artery proximal to the stenosis or the opposite renal artery
3. >3.5× the velocity in the aorta or the iliac artery (renal-aortic ratio and reno-ileal ratio)

Good compromise of sensitivity and specificity

1. >2 metres per second
2. >2× velocity in the renal artery proximal to the stenosis or the opposite renal artery
3. >2× the velocity in the aorta or the iliac artery (renal aorto-renal and reno-ileal ratios)

High sensitivity

1. >1.8 metres per second
2. >1.5× the velocity in the renal artery proximal to the stenosis or the opposite renal artery
3. >1.5× the velocity in the aorta or the iliac artery (aorto-renal and ileo-renal ratios)

severity of stenosis, which is generally accepted to be about 60–70% stenosis. There are several ways of defining the level of peak systolic velocity that indicates a significant stenosis. Table 25.6 gives a set of typical values. The levels chosen depend on whether priority is given to high sensitivity or high specificity. In our department we use the 'compromise' criteria.

The elevated velocity is only present in a small length of artery at and immediately distal to the stenosis. It is important therefore to study the whole artery with a minimum of three points being studied. Careful angle correction is also necessary, with an angle of insonation of less than 60° being highly advantageous.

The colour map may show the high velocity as aliasing. This produces a confused area of mixed colour (Fig. 25.7). The appearances on colour are, however, highly dependent on settings and angles. They cannot be relied on in isolation, though they often indicate a part of the artery that warrants further investigation by spectral Doppler. The actual stenosis may sometimes be seen as a narrowed area of artery, but often this feature is not easily appreciated (Fig. 25.8).

The spectral Doppler waveform shows a high systolic peak indicating high velocity (Fig. 25.7). At the point of high velocity the spectral waveform often appears pale. This is because the power is spread over a larger velocity range (Fig. 25.9). Although the high-velocity jet occurs at the stenosis and flow disturbance occurs immediately distal to the stenosis, there is an area where there is both high velocity and flow disturbance (Fig. 25.10).

As well as these changes being shown on the spectral waveform, they also have a characteristic sound on audio Doppler. The pitch increases and the volume decreases. It is easy to recognise once heard.

Renal artery stenosis

- In atheromatous renal artery stenosis, the long-term results of angioplasty and stenting are poor. The need for diagnosis is therefore debatable.
- In cases of fibromuscular hyperplasia and in transplanted kidneys, the results of angioplasty and stenting are reasonably good, so a diagnostic test is required.
- Doppler ultrasound, in experienced hands, though inferior to CT angiography or MR angiography, is a good test.
- Combining two or more criteria, i.e. elevated peak systolic velocity, turbulence, damping of the distal waveforms, improves accuracy.

Table 25.7 Definition of common parameters

Systolic rise time	Time between the beginning and end of the systolic rise curve
Systolic upstroke	Systolic frequency/second
Acceleration index	Systolic upstroke/carrier frequency
Resistance index, RI	(S – D)/S where S = systolic velocity and D = diastolic velocity

Parameters of a damped waveform:

1. Systolic rise time >100 milliseconds
2. Systolic acceleration index <3.75 kHz/s
3. Resistance index >0.7 (>0.8 indicates a poor result if angioplasty is performed)

Flow disturbance (turbulence)

Flow disturbance (loosely termed turbulence) occurs distal to stenosis for a length of about 1 cm and may be detected in stenoses of over 40%. Flow disturbance is characterised by a chaotic pattern of colour on the colour flow map. This is, however, unreliable as other factors such as aliasing may occur if the pulse repetition frequency (PRF) is too high, and may mimic turbulence. The pattern on spectral Doppler is more reliable. The waveform has an irregular outline to the maximal velocity envelope. There is high power flow at all velocities, including reversed flow. This is termed spectral broadening. This causes a very white spectral pattern from the baseline to the irregular maximal velocity envelope and below the baseline (Fig. 25.11). Flow disturbance also has a characteristic sound on audio Doppler.

Damping – the parvus tardus waveform

A damped waveform is found in all the arteries distal to a severe stenosis. To cause this there must be a significant pressure drop across the stenosis. As with other parameters, the degree of stenosis that causes damping is debated, but it probably occurs somewhere between a 60% and an 80% or more stenosis. The waveform is flattened, hence the term damped. More accurately there is a slow rise to the systolic peak. There is decreased maximal systolic and diastolic velocity, but the systolic velocity is decreased to a greater extent than the diastolic. Hence the difference between systolic and diastolic velocities is reduced (Fig. 25.12). The waveform has been termed the parvus tardus (low and slow) waveform. Parvus refers to the decreased velocities, tardus to the slow rise to the systolic peak.

The two features of the waveform may be quantified. The slow rise to the systolic peak may be measured by placing a cursor on the baseline at the beginning of systole. This may be extrapolated from the spectral curve. Another cursor is placed at the first systolic peak. This is a small peak followed by a notch and is caused by closure of the aortic valve (Fig. 25.13). From the position of these two points the time between them (the systolic rise time) and the slope of the systolic rise (the systolic upstroke) or the systolic acceleration may be calculated. There is software on most ultrasound machines that will do this. The decreased difference between systolic and diastolic velocities may be measured by obtaining any ratio between them. The ratio most commonly used is the resistance index (RI) (Fig. 25.13). Normal values are also available for this. Normal values and those that indicate renal artery stenosis are available (Table 25.7).

The technique of Doppler studies for renal artery stenosis

The general technique of renal Doppler studies is described earlier in this chapter. A complete study should ideally include a colour

Doppler study of the whole volume of the kidney with pulsed wave Doppler (spectral analysis) of at least three segmental or interlobar arteries and a colour Doppler study of the main renal arteries. A search should be made for accessory renal arteries (though they are often missed). This is obviously a theoretical limitation of renal Doppler as it is recognised that stenoses in accessory renal arteries may cause hypertension. In practice, however, this is so uncommon that it does not invalidate the use of Doppler ultrasound in the investigation of hypertension.

Some centres study the intrarenal vessels only. This is undoubtedly a quicker and more practical method of screening, but has limitations.[5,6] These are discussed below.

Doppler study of the intrarenal vessels

Study of the intrarenal arteries is far easier than study of the main trunk (see the section on the technique of renal Doppler studies) and may be achieved in almost 100% of patients (some extremely large patients may be technical failures). The limitations of this are discussed below. It is common practice, however, to start the Doppler study with the intrarenal arteries.

Limitations of the damped (parvus tardus) waveform

Some care should be taken when interpreting the presence or absence of a damped waveform in isolation. Only severe stenoses cause distal damping. There must be a significant pressure drop across the stenosis.

Also it may be demonstrated that to produce a damped waveform, the arteries distal to a stenosis must be compliant (elastic). This may not be the case if there is extensive atheroma or, in a transplanted kidney on immunosuppressants, which may cause the renal artery to be encased in fibrous tissue.

There are conditions other than arterial stenosis that may produce a damped waveform. These include chronic renal failure from almost any cause, small vessel disease, old age (probably also due to subclinical small vessel disease), severe aortic valve stenosis and coarctation of the aorta. In the transplanted kidney, iliac artery stenosis and chronic rejection may cause damping. It follows that a damped waveform should not be relied on in isolation, particularly if renal function is poor. Peripheral renal arteries have low velocities. This may mimic damping, particularly if the Doppler angle is poor. This is discussed in the section on the technique of renal Doppler studies.

Doppler study of the renal trunk

Because of the limitations of a study of the intrarenal arteries alone, most centres will include a study of the main renal artery.[7] For more details see the section on the technique of renal Doppler studies. This is technically more difficult, particularly in large patients and those who cannot hold their breath. Technical failure rates of up to 40% have been reported. In most centres the figure is probably lower than this, but a technical failure rate of 10–20% is common. Accessory renal arteries, present in about 22% of people, are usually not detected.

Children with hypertension

Renal Doppler studies on children are often technically easier than in adults. While young children may find it difficult to stay still, the relative closeness of the renal arteries to the transducer and the ability to displace overlying bowel gas with light transducer pressure outweigh the disadvantages. Technical failures are less common than in adults. This makes Doppler ultrasound an appropriate diagnostic test in children with hypertension. The Doppler signs and velocity values are the same as in adults.

Hypertension in patients with renal transplants

The principles of Doppler detection of renal artery stenosis are similar in transplanted kidneys. There are, however, some differences, which are discussed here, though reference should also be made to Chapter 28. Hypertension is common in renal transplant recipients. Most cases have no identifiable cause. Renal artery stenosis is, however, relatively common in renal transplants.

As stated, many renal transplant patients are hypertensive. Factors that raise the possibility of a stenosis are severe hypertension, sudden onset or worsening of the hypertension and difficulty in controlling the hypertension. These factors are indications for a renal Doppler study.

The transplanted kidney is far easier to study by Doppler than the native kidney. It is near the body surface and moves little with respiration (Fig. 25.14). If there is more than one renal artery, then this will be known from the operation report. Technical failures in Doppler studies of the transplanted kidney are therefore unusual.

The Doppler features of renal artery stenosis, whatever the aetiology, are the same in the transplanted kidney as in the native kidney. There is usually mild to moderate turbulence at the transplant artery origin. This is due to the surgical anastomosis and should not be interpreted as a sign of stenosis unless severe or accompanied by high velocity or distal damping. The transplanted renal artery often has one or two bends. At a bend in an artery there is increased velocity. If the bend is tight, the peak systolic velocity may even exceed 2 metres per second. There will, however, be no turbulence or distal damping.

RENAL ARTERY OCCLUSION AND RENAL INFARCTION

Renal artery occlusion may be chronic (of gradual onset) or acute. The aetiology, presentation, symptoms, signs and imaging appearances are different in the two forms of the disease. Renal infarction is a result of real artery occlusion.

Chronic renal artery occlusion occurs when renal arteries that are stenosed, usually due to atheroma, slowly progress to complete occlusion. Symptoms and signs are similar to those of severe stenosis with hypertension and renal impairment, particularly if the disease is bilateral or superimposed on other chronic renal diseases such as hypertensive nephropathy. As there is slow progression there are no acute symptoms.

Acute renal artery occlusion occurs when thrombus or cholesterol plaque breaks off from a proximal source and occludes the vessel. Occlusion of the main trunk affects the whole kidney; occlusion of a branch artery causes a segmental infarct. The source of thrombus is usually aortic or proximal renal artery atheroma, mural thrombus in an aortic aneurysm or from the left heart in cases of ventricular infarct with mural thrombus, atrial fibrillation or subacute bacterial endocarditis. Aortic dissection or dissection of the renal artery, often caused by angiography catheter studies, are other causes. Symptoms of acute renal artery occlusion are sudden onset of flank or lower back pain, nausea and vomiting. There is usually haematuria, proteinuria and hypertension. Bilateral occlusion results in acute renal failure with anuria.

Segmental infarcts may also occur in renal transplants when there is a small polar accessory artery. These small arteries often thrombose in the immediate postoperative period.

Greyscale ultrasound appearances

There is little published material on this subject. In cases of chronic occlusion the kidney slowly shrinks to a small ‘end-stage’ kidney. Acute occlusion causes initial swelling of the kidney, which rapidly

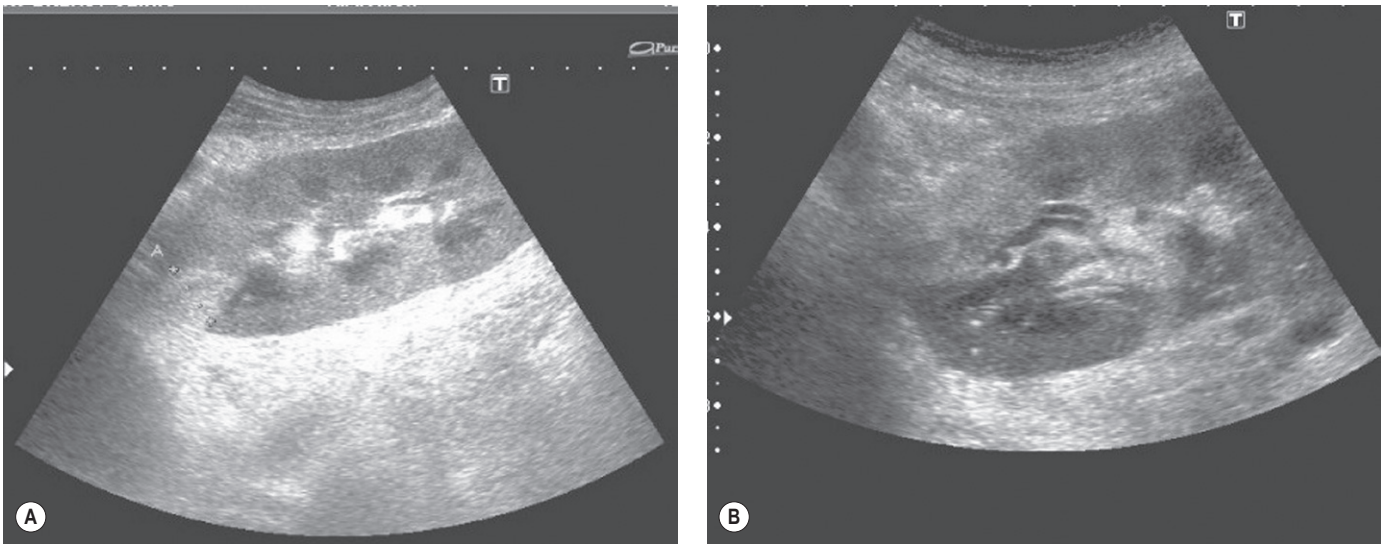


Figure 25.15 Renal infarct. A: Two days after the onset of pain there is a well-defined hyperechoic wedge shape area indicating the infarct. **B:** A larger infarct showing a hyperechoic area. Typically larger infarcts are less wedge shaped than smaller ones.

becomes inhomogeneous, with areas of increased and decreased echodensity and loss of the normal corticomedullary architecture (Fig. 25.16). Over the next few weeks the kidney shrinks. Acute infarcts cause wedge-shaped areas of increased echodensity that increase further in echodensity over several days (Fig. 25.15). Over the next few weeks the area shrinks and eventually becomes a focal scar.

Doppler ultrasound appearances

In both acute and chronic renal artery occlusion there is little Doppler flow within the kidney although some colour flow may still be visible at the periphery from capsular arteries, or at the poles from accessory vessels (Fig. 25.16). At the renal hilum spectral Doppler may show 'blips' of systolic flow with no flow during the rest of the cycle. This may represent true flow past the thrombus at peak systole only, or may represent transmitted pulsation.

Infarcts have no Doppler flow in the infarcted area (Fig. 25.17). This is often very difficult to demonstrate with smaller infarcts.[8] If doubt remains regarding renal perfusion then intravenous ultrasound contrast will clarify. Infarcts are shown as areas of non-perfusion (Fig. 25.18). In total renal artery occlusion there is no perfusion in most of the kidney, though there may be small patches of perfusion from capsular or accessory vessels.

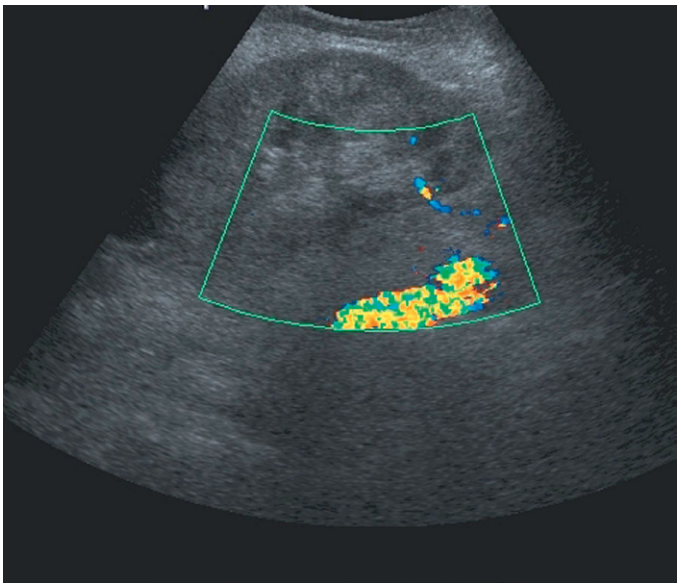


Figure 25.16 Acute renal artery occlusion. The swollen, inhomogeneous kidney is avascular, except for a small accessory upper pole artery.

RENAL VEIN THROMBOSIS

Renal vein thrombosis most commonly occurs in debilitated, dehydrated infants. Renal vein thrombosis may also affect adults. The most common cause is membranous glomerulonephritis and about 50% of patients with this condition develop renal vein thrombosis. There are other less common causes (Table 25.8). Transplanted kidneys may also develop renal vein thrombosis. Thrombosis usually occurs within the first 10 days after transplantation.

Renal tumours may propagate into the renal vein and inferior vena cava. This is referred to as tumour thrombus. It is, however, a separate entity from renal vein thrombosis and is considered separately (see Chapter 27).

Symptoms

Renal vein thrombosis may be of chronic or acute onset. Symptoms differ in the two forms.

Most cases are chronic. The thrombus begins in the peripheral veins and propagates centrally. Symptoms are often insignificant. Renal failure may result if thrombosis is bilateral or in a solitary or dominant kidney. In cases where there is background renal failure, there may be a rapid deterioration in renal function. Often, however, collateral venous channels dilate rapidly and renal failure does not occur. It is likely that many such cases escape detection.

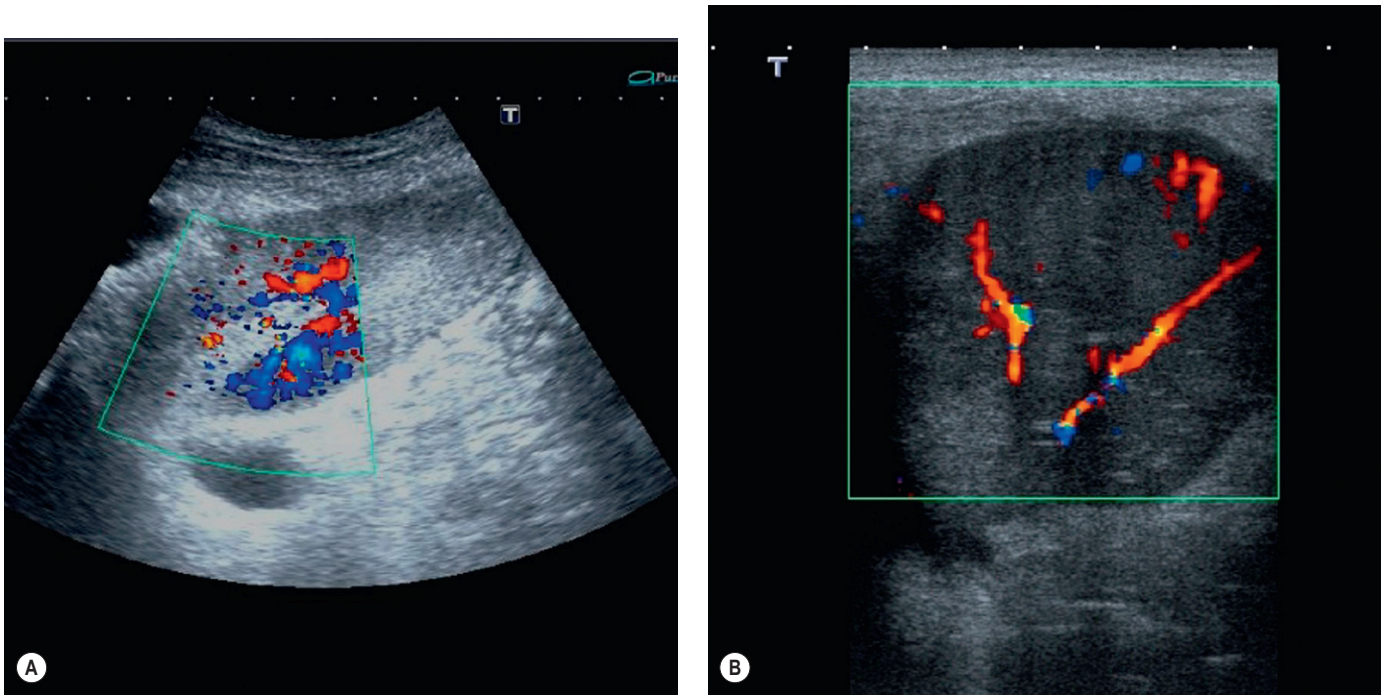


Figure 25.17 **Renal infarcts. A:** A colour flow image of the same case as shown in Figure 25.15A.There are vessels with Doppler flow either side of, but not in, the infarct. **B:** Another case with multiple infarcts. A few vessels are seen, but the vasculature is clearly abnormal.

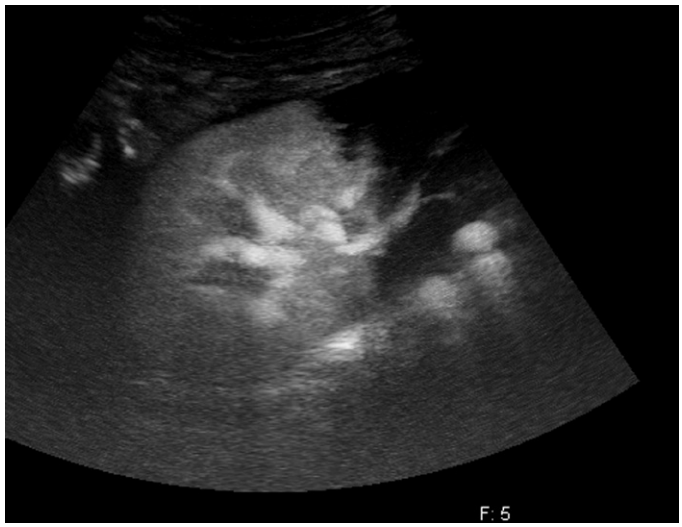


Figure 25.18 **A large renal infarct.** IV contrast (SonoView, Bracco), low MI technique. The non-infarcted part of the kidney shows normal enhancement in the arterial phase. The infarcted pole shows no enhancement.

Table 25.8 **Causes of renal vein thrombosis**

1. Membranous glomerulonephritis
2. Hypercoagulability states
3. Dehydration
4. Compression from retroperitoneal fibrosis, retroperitoneal tumour or pancreatic tumours

In acute renal vein thrombosis occlusion of the large veins occurs de novo. Patients have loin pain and haematuria. As with chronic cases, if bilateral or in a solitary or dominant kidney, renal failure occurs with its symptoms and signs. In acute cases, some of the thrombus may become detached and cause pulmonary embolus. Left renal vein thrombosis in males may present with an acute left varicocele.

In transplanted kidneys collateral veins are absent so chronic as well as acute renal vein thrombosis presents with pain over the kidney and haematuria. The swollen kidney may be palpable. As transplanted kidneys are the only well-functioning kidney, there is an acute increase in serum creatinine.

Greyscale ultrasound appearances

In acute cases the kidney is initially swollen and inhomogeneous. There may be hyperechoic and hypoechoic areas in the renal parenchyma. There is loss of the normal corticomedullary architecture.

Low echodensity thrombus may be seen distending the renal vein, though in the early stages the thrombus is often isoechoic with blood and is not visible.

In chronic cases the kidney initially appears normal or minimally swollen, but in the majority of cases, recovers and returns to a normal appearance. In some cases the kidney becomes inhomogeneous with a similar appearance to cases of acute thrombosis (Fig. 25.19). This appearance is perhaps due to intrarenal haemorrhage.

In severe cases of acute or chronic renal vein thrombosis the kidney may not recover, and shrinks to a small, usually homogeneous end-stage kidney.

Doppler ultrasound appearances[9]

The classic Doppler appearances only occur early in severe cases of acute renal vein thrombosis. They become less characteristic as collateral channels open. As collaterals are not present in the transplant kidney, the classic changes last longer.



Figure 25.19 Chronic renal vein thrombosis. The kidney is inhomogeneous with loss of the normal architecture.

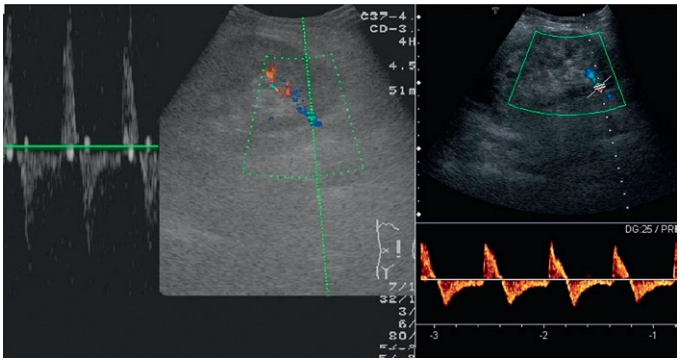


Figure 25.20 Renal vein thrombosis. Two different cases. In both cases, colour flow is seen at the hilum and in a few central vessels, but no further. The spectral waveforms are slightly different in both cases but both show a narrow systolic component with abrupt reversal of flow.

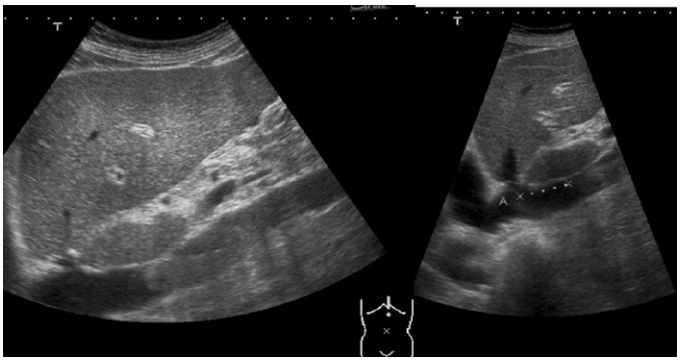


Figure 25.21 Renal cell cancer extending into the IVC. The moderately echodense tumour is seen with its upper border below the hepatic veins (right-hand image). The distance between the cranial extent of the tumour and the hepatic vein–IVC junction has been measured (left-hand image). This is very useful in planning the surgery.

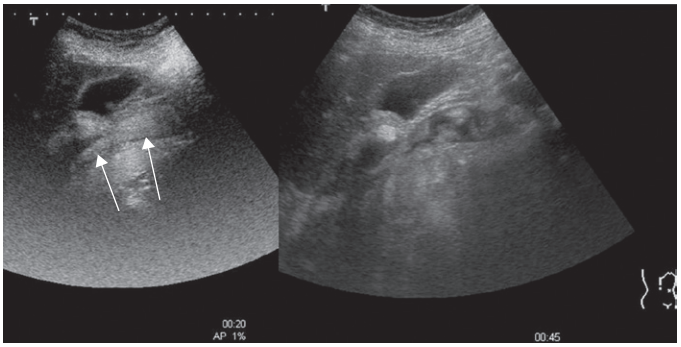


Figure 25.22 Renal cell cancer extending into the IVC: contrast-enhanced ultrasound scan. In this case the CT images suggested possible tumour in the IVC but were non-diagnostic. Greyscale ultrasound and Doppler were also equivocal. A contrast-enhanced study shows that there is no IVC tumour. Left: A low MI scan showing flowing blood filling the lumen (arrows). Right: A normal MI scan shows the contrast-enhanced blood swirling. This was clearly seen in real-time, and explained the equivocal on CT or non-enhanced scan.

The colour Doppler image shows severely reduced flow. The classical spectral Doppler pattern occurs in the arterial trace with reverse diastolic flow with a diastolic notch, which has led to the description of the waveform as a 'reversed M pattern'. In addition, there is severely reduced or absent venous flow (Fig. 25.20).

In the native kidney as collaterals open, the arterial flow changes from a less characteristic reverse diastolic pattern over time to a normal pattern. Often the ultrasound scan is performed some days after the onset of symptoms. In these cases there is usually a swollen inhomogeneous kidney with non-specific reverse diastolic flow, reduced diastolic flow or a normal Doppler pattern. In these cases it is not possible to make a definitive diagnosis.

Renal vein thrombosis

- There is a characteristic arterial waveform that may establish the diagnosis.
- In the native kidney the characteristic waveform is only seen for a short time before collateral veins open up.
- In the transplanted kidney, the characteristic waveform persists longer.

RENAL CELL CANCER – PROPAGATION INTO THE RENAL VEIN AND INFERIOR VENA CAVA

Advanced renal cell cancers may propagate into the lumen of the renal vein and up the inferior vena cava (IVC). They may extend as far as the right atrium. Propagation along the lumen, however, while it is a poor prognostic sign, does not render the tumour inoperable. The extent of tumour thrombus does though affect the planning of surgery. Basically extension close to the level of the hepatic veins means that the veins cannot be clamped, extension to the diaphragm means that the chest has to be opened and extension to the right atrium means that the heart may have to be opened. Imaging is usually done with CT or MRI. Ultrasound can also be useful. There is increasing use of ultrasound in cases where CT or MRI is equivocal, usually because of flow artefacts (Figs 25.21, 25.22).

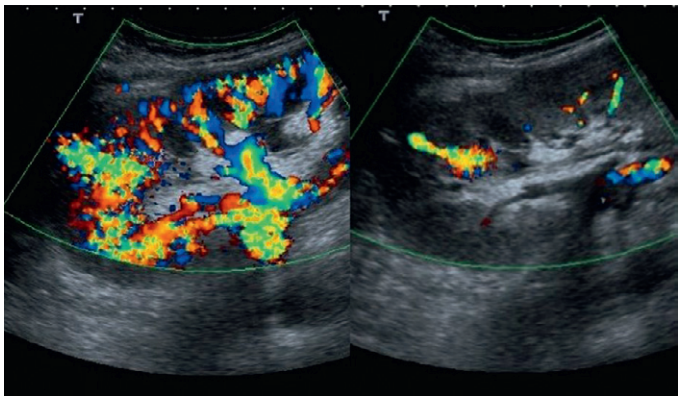


Figure 25.23 Post-traumatic arteriovenous fistula. Left: There is a mosaic of colour in the upper pole due to high turbulent flow but also tissue vibration. Right: Adjustment of gain, PRF and frequency reduce the confusing mass of colour until only the high flow in the fistula is seen.

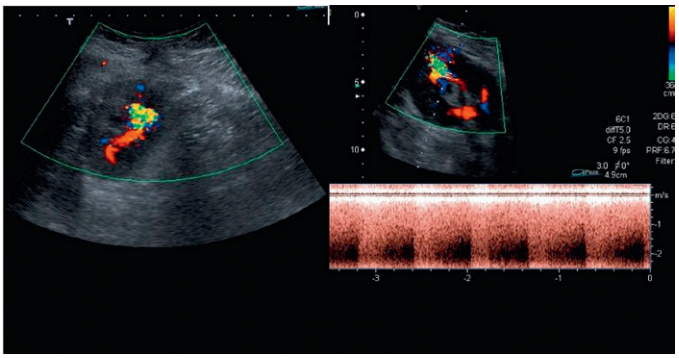


Figure 25.24 Arteriovenous fistula. Left: Changing the scan plane reveals the feeding artery. Right: There is high-velocity, low-resistance turbulent flow in the fistula on spectral Doppler.

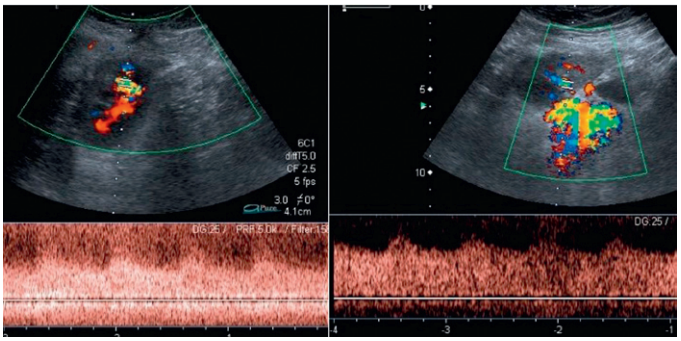


Figure 25.25 Arteriovenous fistula. Left: There are high systolic velocities through the fistula. The systolic peak is broadened. Right: The venous waveform. There is a weakly pulsatile (arterialised) waveform. There is turbulence.

ARTERIOVENOUS FISTULA

An arteriovenous fistula is a communication between an artery and vein, either direct or via a pseudoaneurysm. Most are caused by diagnostic renal biopsy. Other causes are radio-frequency (RF) ablation of renal tumours, stab wounds and blunt trauma.

Arteriovenous fistulae and pseudoaneurysms are common following renal biopsy. Some studies where all post-biopsy patients were imaged have shown that 15–50% develop a fistula. The vast majority are asymptomatic or have only transient symptoms (haematuria and flank pain). The majority presumably thrombose or remain small with low flow. A very small minority, less than 1%, are either sufficiently large de novo, or enlarge over time to present with symptoms or signs such as haematuria, loin pain, hypertension or deteriorating renal function.

Symptoms and signs

Post-biopsy fistulae may present acutely immediately after the biopsy with persistent haematuria. Others present weeks or months later with deteriorating renal function due to a 'steal' phenomenon. Renal dysfunction may be clinically evident, even though only one kidney is involved, because there is normally underlying renal dysfunction, this being the reason for the biopsy. Conversely the existence of renal dysfunction may mask the symptoms and signs of a fistula, as they may be misinterpreted as deterioration in the underlying condition. Hypertension or loin pain may occur. Haematuria does not often occur as a late presentation.

Arteriovenous fistulae in asymptomatic patients are sometimes detected incidentally on subsequent scans. This is particularly common in the transplant kidney.

Doppler ultrasound appearances[10]

The first indication on the Doppler scan that an arteriovenous fistula may be present is a focal increase in colour on the colour Doppler image. The pattern is often a mosaic of colour caused by high blood flow and by tissue vibration around the fistula. This is essentially a colour demonstration of the same vibration that causes a bruit (Fig. 25.23). Adjusting the Doppler settings to produce less colour (reducing gain, increasing PRF and lowering the frequency) results in the flow in normal vessels becoming less visible, whilst the high flow in the fistula remains bright (Fig. 25.23). The feeding artery and draining vein may sometimes be seen as relatively wide vessels travelling almost directly between the fistula and the hilum.

Arteriovenous fistula

- The fistula is usually clearly visible as a focus of increased colour on the colour flow image.
- The appearances of an arteriovenous fistula are confirmed by adjusting the colour flow parameters and by pulsed wave spectral analysis.

Spectral Doppler studies typically show a low resistance flow in the feeding artery with elevated diastolic velocity, resulting in a low resistance index (RI), typically less than 0.5. There is usually flow disturbance (turbulence) characterised by an irregular 'spiky' spectral waveform and small spikes below the baseline indicating elements of reversed flow (Fig. 25.24). There is often also an elevated systolic velocity through the actual fistula (Fig. 25.25). The draining vein has pulsatile flow similar to the arterial flow and it may be difficult to distinguish between the artery and vein (Fig. 25.25).

ARTERIOVENOUS MALFORMATIONS (CONGENITAL ARTERIOVENOUS FISTULAE)

A renal arteriovenous malformation (AVM) is a congenital vascular malformation, usually involving several vessels and containing one or more arteriovenous fistulae. They are sometimes referred to as congenital arteriovenous fistulae.

They are uncommon. Prevalence from autopsy series is about 1 per 100 000 and the incidence in patients being investigated for all urological conditions is about 1 per 3000–7500, although most practices see them only rarely.

There are two types of AVM. The most common is the circoid type, which lies deep to the uroepithelium in the lamina propria and often causes haematuria.

The less common type is the cavernous AVM, which consists of a single feeding artery and a single draining vein communicating via a cavernous chamber. These resemble a post-biopsy or traumatic fistula, but are histologically different. The cavernous chamber has vascular walls while the pseudoaneurysm that may be present in an acquired fistula has no true cellular wall.

Renal AVMs may be associated with renal artery aneurysms.

Symptoms and signs

Renal arteriovenous fistulae usually present in young adults with recurrent macroscopic haematuria. Bleeds are more common and often more severe in pregnancy. Hypertension is also common in patients with AVMs, thought to reflect relative ischaemia in the tissues distal to the AVM. Some patients with high flow AVMs present with left heart failure. Occasionally asymptomatic AVMs are found on renal Doppler studies or angiograms performed for other reasons.

Greyscale ultrasound appearances

AVMs are usually not detected on a greyscale ultrasound study.

Doppler appearances[11,12]

Descriptions of Doppler appearances are sparse; however, the appearances are similar to those of acquired AV fistulae. Circoid and cavernous AVMs may be distinguished by their vascular patterns (Figs 25.26–25.29).

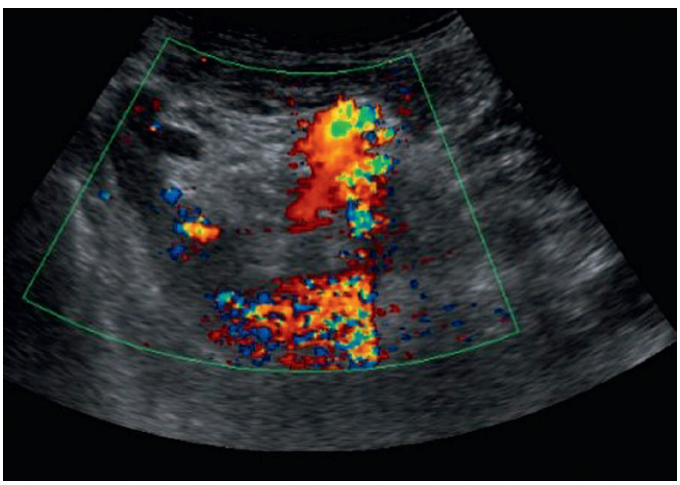


Figure 25.26 Arteriovenous malformation. Tissue vibration. There is a mass of colour due to vascular flow but also tissue vibration around the vessels.

RENAL ARTERY ANEURYSM

Renal artery aneurysms have the same characteristics as aneurysms elsewhere. They may occur in the main renal trunk (extraparenchymal), or in one or more of the intrarenal arteries (intraparenchymal). The aetiology of the two types differs (Table 25.9).

As with other aneurysms, they may be divided into three types according to their shape and two types according to their position (Table 25.10).

The incidence in postmortem studies is 1 in 1000. Their prevalence is equal in men and women, although they have a greater tendency to bleed during pregnancy.

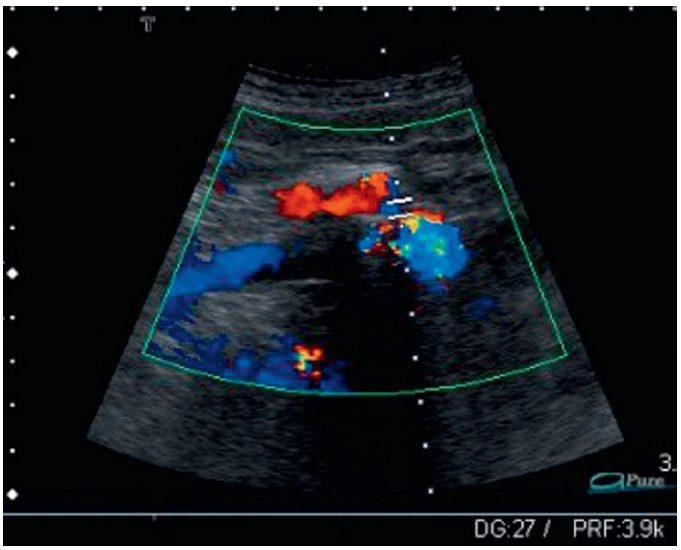


Figure 25.27 Cavernous arteriovenous malformation. The large single feeding artery and draining vein are shown.

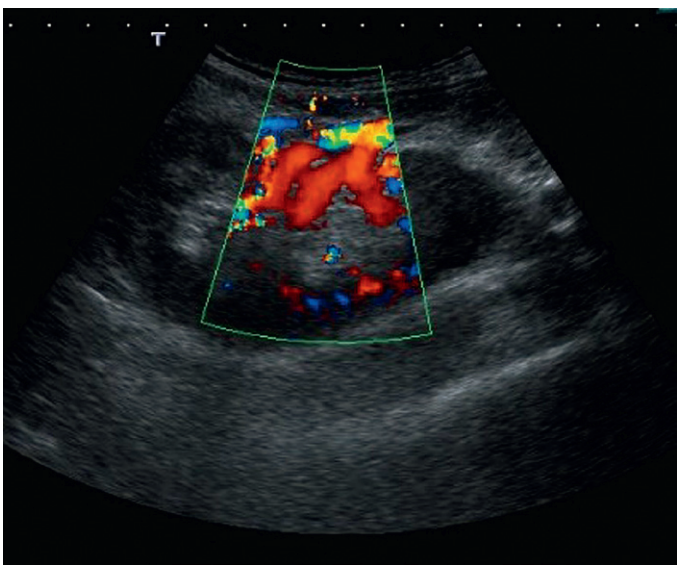


Figure 25.28 Circoid arteriovenous malformation. There is a knot of multiple vessels.

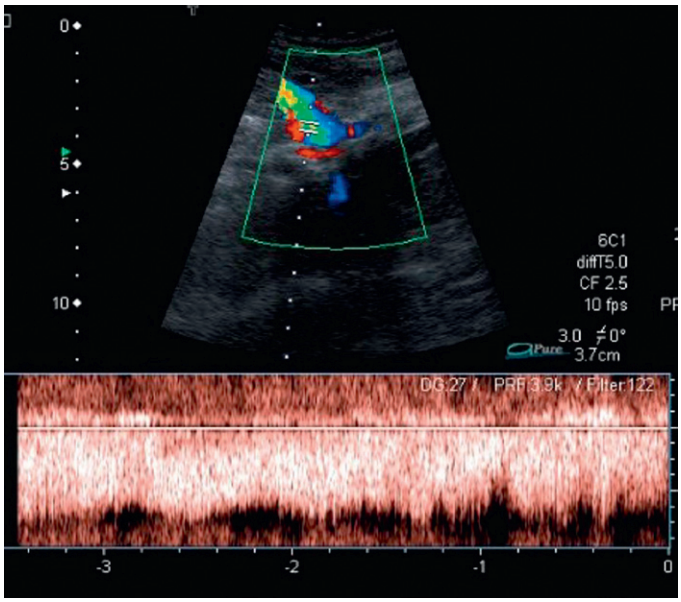


Figure 25.29 Arteriovenous malformation. There is high velocity, turbulent and slightly pulsatile 'arterialised' flow in the draining vein.

Table 25.9 Aetiology of renal artery aneurysms

Extraparenchymal (85%)	
Saccular or fusiform	Fibromuscular, dysplasia Kawasaki disease
False or dissecting	Blunt trauma, surgery, angiographic catheter injury
Intraparenchymal (15%)	
	Polyarteritis nodosa Neurofibromatosis Tuberculosis Mycotic Ehlers–Danlos syndrome

Table 25.10 Types of renal artery aneurysms

Extraparenchymal	Saccular (70%) Fusiform (20%) Dissecting (10%)
Intraparenchymal	Saccular

Symptoms

Most are asymptomatic and may never cause any problems. They may present when they rupture, which is usually a catastrophic event with severe shock and is often fatal. Less often they leak slowly, presenting with flank pain and/or haematuria. They may cause hypertension.

In some cases the hypertension is due to a narrowing of the artery associated with the aneurysm, the mechanism being the same as with renal artery stenosis. In other cases when there is no stenosis, thromboemboli in the distal vessels originating from the mural thrombus in the aneurysm have been suggested as an aetiological cause. Renal infarcts may be demonstrated by enhanced CT (and potentially by contrast-enhanced ultrasound) in many cases.

Renal aneurysms may obstruct the collecting system, causing hydronephrosis resulting in flank pain.

Finally patients with intraparenchymal aneurysms usually present with symptoms of the primary causative pathology.

Prognosis

A renal artery aneurysm is said to be at high risk of rupture if it is greater than 2 cm and at intermediate risk if it is between 1.5 cm and 2 cm. Intraparenchymal aneurysms are usually very small (microaneurysm) and not at risk of rupture.

Ultrasound appearances

There are few descriptions of the ultrasonic appearances of renal artery aneurysms. The ultrasound appearances of aneurysms per se are well described, and those originating from the renal artery have typical features. It is possible that renal artery aneurysms may be misinterpreted as cortical or parahilar cysts if Doppler is not used. This is particularly true of small intraparenchymal aneurysms. The main renal trunk is notoriously difficult to study and unless a dedicated Doppler study is performed, on a cursory look, with colour Doppler, renal artery aneurysms will often be missed.

Renal artery aneurysm

- These are rare.
- They are visible on the colour flow image.
- A tortuous artery may simulate the appearance.

VASCULAR ASPECTS OF RENAL PARENCHYMAL DISEASE AND DOPPLER STUDIES

Doppler studies are widely used, in conjunction with diagnostic biopsy, in the investigation of renal transplant dysfunction. This is not discussed further here but is covered in Chapter 28. Doppler studies are less widely used in the investigation of parenchymal disease, as opposed to primarily vascular disease, in the native kidney. Doppler studies do have a role, however, and contrast-enhanced ultrasound, while not in routine clinical use in the kidney, may play a part in the future.[13–15]

Vascular response to renal disease

In order to understand the Doppler changes that occur in renal disease it is important to understand how the disease may affect the blood vessels.

The disease may damage the medium-sized and small vessels of the kidney. This may cause increased vascular resistance resulting in an elevated RI on the Doppler study. The most common diseases to do this are diabetic nephropathy, atherosclerosis and vasculitis, though other chronic renal diseases may also do so.

Other diseases may affect the blood vessels by altering arteriolar muscle tone. There may also be parenchymal changes around the

blood vessels that cause vasoconstriction. Increased intrarenal pressure may have a similar effect. The combination of factors that may affect the blood flow pattern is therefore complex.[16]

Despite this complexity, however, there are only four ways in which renal parenchymal disease may affect renal Doppler studies: lowering the resistance index, increasing the resistance index and decreasing or increasing overall blood flow through the kidney. Vascular resistance may be objectively measured by the RI.

Parenchymal disease

- Doppler may distinguish ATN from pre-renal failure.
- The use of Doppler in obstruction is controversial.
- Doppler changes do occur in other renal parenchymal diseases, but it is not at present used clinically in these conditions.

Acute tubular necrosis (ATN)

Acute tubular necrosis (ATN) is one pathology where Doppler ultrasound is clinically useful, both in the transplant and the native kidney. It occurs in response to acute renal ischaemia, following an episode of hypotension secondary to various causes. Recovery is usually clinically complete, though there may often be some permanent subclinical damage. Some severe cases progress to cortical necrosis with permanent renal failure.

Doppler appearances

Acute tubular necrosis causes marked arteriolar vasoconstriction; the degree of vasoconstriction is related to the severity of the ATN. The Doppler hallmark of ATN is therefore reduced diastolic flow, reflected as an elevated resistance index (RI). The more severe the condition, the more marked is the reduction in diastolic flow; very severe cases have reverse diastolic flow. Prolonged reversal of diastolic flow carries a poor prognosis with a high proportion not recovering renal function.

The main differential diagnosis in cases of ATN is often pre-renal failure. In pre-renal failure the Doppler flow pattern is normal. Doppler studies may therefore distinguish between the two conditions.[17] Indeed there are few conditions (apart from renal vein thrombosis) other than ATN in the native kidney that cause reduced diastolic flow in acute renal failure.

When recovery from ATN occurs, it is rapid. During the first few hours after recovery there is a hyperaemic diuretic phase. Doppler studies during this phase show increased diastolic flow, higher than normal (RI less than 0.6). The Doppler changes may precede the diuresis by a few hours.

Contrast-enhanced ultrasound appearances

In cases of ATN contrast-enhanced ultrasound appears to show a variable reduction in cortical perfusion but a far more marked reduction in medullary perfusion. Flow to the medulla is delayed and reduced. The pyramids remain visible as hypoperfused areas throughout the scan. Although this pattern has been observed, its clinical utility, sensitivity and specificity have not at this time been validated by trials.

Renal diseases other than ATN

Neither Doppler nor contrast-enhanced ultrasound studies are in routine clinical use in these diseases. Some knowledge of the changes that occur is available, although, in most cases, such studies will not replace diagnostic renal biopsy. In some diseases a Doppler study may be an aid in assessing the prognosis of the disease.

Small vessel disease

Small vessel disease of the kidney may result from diabetes mellitus, nephrosclerosis or almost any cause of chronic renal failure. In early cases, Doppler studies show a variable pattern and are generally unhelpful. In advanced cases the arteriolar and arterial bed is damaged. The RI may be elevated in the larger arteries, although there is often damping in the peripheral arteries. The RI is elevated in a large proportion of older patients with normal creatinine levels. Although the cause is uncertain, the elevation is probably due to subclinical small vessel disease.

Acute glomerulonephritis (GN)

Published data, though sparse, suggest that the Doppler pattern varies with the type of GN.

Acute primary or secondary GN causes hypervascularity which is seen on colour Doppler. The RI is normal or slightly low.

Acute crescentic or proliferative GN causes reduced parenchymal perfusion and an elevated RI.

Tubulo-interstitial disease

Tubulo-interstitial disease causes reduced renal parenchymal perfusion and an elevated RI.

Vasculitis

In polyarteritis nodosa, thrombocytopenic purpura and haemolytic uraemic syndrome the resistance index is elevated and cortical perfusion is decreased. In severe cases the decreased cortical perfusion is sufficiently marked to be subjectively appreciated on a colour Doppler study. It has been shown that the level of the RI may predict the outcome of haemolytic uraemic syndrome in children.[18]

Hepatorenal syndrome

The resistance index tends to be very high in hepatorenal syndrome. An elevated RI in patients with severe hepatic failure, even with a normal creatinine level, indicates a high probability of renal dysfunction or failure following hepatic transplantation.[19]

Chronic renal failure

Failed kidneys, whatever the cause, show reduced parenchymal perfusion and a damped waveform in the peripheral arteries.

ACUTE URETERIC OBSTRUCTION

Acute ureteric obstruction causes a degree of renal shutdown as a physiological protective mechanism. The biochemical pathway by which this is achieved is well documented and results in arteriolar vasoconstriction, reduced diastolic flow and elevation of the RI. Shutdown occurs a few hours after onset of obstruction, but timing is variable, as is the degree of shutdown.

The reduction in diastolic flow, although small, has been used to aid in the diagnosis of acute obstruction.[20–23] The RI is usually compared in both kidneys. The difference should be less than 0.6 to 1 (published values vary). The use of non-contrast CT (CT KUB) in suspected ureteric calculus has resulted in Doppler studies being seldom used for this purpose. They are used in pregnant women, however, to help distinguish physiological dilatation of pregnancy from calculus obstruction. In physiological dilatation of pregnancy the RI is normal.

REFERENCES

1. Radermacher J, Chavan A, Bleck J, et al. Use of Doppler ultrasonography to predict the outcome of therapy for renal artery stenosis. N Engl J Med 2001;334:410–417.
2. Soulez G, Therasse E, Qanadi SD, et al. Prediction of clinical response after renal angioplasty. Respective value of renal Doppler sonography and scintigraphy. AJR Am J Roentgenol 2003;184(4):1029–1032.
3. Vasbinder GB, Nelemans PJ, Kessels AG, et al. Diagnostic tests for renal artery stenosis in patients suspected of having renovascular hypertension: a meta-analysis. Ann Intern Med 2001;135(6):401–411.
4. Williams GJ, Macaskill P, Chan SF, et al. Comparative accuracy of renal duplex sonography parameters in the diagnosis of renal artery stenosis; paired and unpaired analysis. AJR Am J Roentgenol 2007;188(3):798–811.
5. Dermipolat G, Ozbek SS, Parilder M. Reliability of intrarenal Doppler sonography paramaters of renal artery stenosis. J Clin Ultrasound 2003;31:346–351.
6. Motew SJ, Cherr GS, Craven TE, et al. Renal duplex sonography. Main renal artery versus hilar analysis. J Vasc Surg 2000;32(3):462–469.
7. Ripolles T, Aliaga R, Morote V. Utility of intrarenal Doppler ultrasound in the diagnosis of renal artery stenosis. Eur Radiol 2001;40(1):54–63.
8. Yucel C, Ozdemir H, Akpek S, et al. Renal infarct; contrast-enhanced power Doppler sonographic findings. J Clin Ultrasound 2001;29(4): 237–242.
9. Parvey HR, Isenberg RL. Image-directed Doppler sonography of the intrarenal arteries in acute renal vein thrombosis. J Clin Ultrasound 1990;18:512–516.
10. Renowden SA, Bleddyn J, Cochlin DL. Sonography in the diagnosis of post biopsy arteriovenous fistulae in the transplanted kidney. Clin Radiol 1992;45(4):233–237.
11. Cisterino SJ, Malave SR, Neilman HL. Congenital renal arteriovenous malformations: ultrasonic appearance. J Urol 1981;126(2):238–239.
12. Naganama H, Ashida H, Konno K, et al. Renal arterial malformation: sonographic findings. Abdom Imaging 2001;26:661–663.
13. Robbin M, Lockhart M, Barr R. Renal imaging with ultrasound contrast: current status. Radiol Clin North Am 2003;41:963–978.
14. Kim JH, Eun JW, Lee HK, et al. Perfusion abnormality. Coded harmonic angio-ultrasound with contrast agent. Acta Radiol 2003;44(2):166–171.
15. Puls R, Holsten N, Lemke M, et al. Perfusion abnormalities of kidney parenchyma: microvascular imaging with contrast-enhanced colour and power Doppler ultrasonography – preliminary results. J Ultrasound Med 2000;19(12):817–821.
16. Tublin ME, Bude RO, Platt JF. Review. The resistive index in renal Doppler sonography: where do we stand? AJR Am J Roentgenol 2003;180:885–892.
17. Platt JF, Rubin JM, Ellis JH. Acute renal failure: possible role of Duplex Doppler ultrasound in distinction between acute pre-renal failure and acute tubular necrosis. Radiology 1991;179:419–423.
18. Patriquin HB, O'Regan S, Robitaille P, et al. Hemolytic–uremic syndrome; intrarenal Doppler patterns as a useful guide to therapy. Radiology 1989;172:625–628.
19. Platt JF, Marn CS, Baliga PK, et al. Renal dysfunction in hepatic disease: early identification with renal duplex Doppler US in patients who undergo liver transplantation. Radiology 1992;186:801–806.
20. Platt JF, Rubin JM, Ellis JH, DiPietro MA. Duplex Doppler US of the kidney; differential diagnosis of obstructive from nonobstructive dilatation. Radiology 1989;171:515–517.
21. Platt JF. Advances in ultrasonography of urinary tract obstruction. Abdom Imaging 1998;23(1):3–9.
22. Webb JA. Ultrasonography and Doppler studies in the diagnosis of renal obstruction. BJU Int 2000;86(Suppl):25–32.
23. Renowden SA, Cochlin DL. The potential use of dieresis Doppler obstruction in PUJ obstruction. Clin Radiol 1992;46:94–96.

CHAPTER

26

Renal cystic disorders

Michael J. Weston

INTRODUCTION 486

SIMPLE RENAL CYSTS 486
Prevalence 486
Natural history 486
Symptoms 486
Ultrasound features 487
Differential diagnosis 487
Multiple simple cysts 488

COMPLICATED RENAL CYSTS 488
Septations 488
Haemorrhage 490
Infection 490
Calcification 491
Cystic malignancy 492

DIFFERENTIAL DIAGNOSIS OF A RENAL CYST 493
Pyramids 493
Renal papillary necrosis 493
Calyceal and renal pelvic diverticula 493
Dilated pelvicalyceal system 493
Lymphatic cysts 493
Haematoma 495
Arteriovenous malformations and aneurysms 495
Renal abscess 496
Multilocular cystic nephroma/mixed epithelial and stromal tumour (MEST) 497
Localised cystic disease 498

CYSTIC DISEASES OF THE KIDNEY 498
Acquired cystic kidney disease (ACKD) 498
Multicystic dysplastic kidney 498
Polycystic kidney disease 499
Von Hippel–Lindau disease 500
Tuberous sclerosis complex 502
Medullary cystic disease 502

INTRODUCTION

The kidneys are routinely examined as part of an abdominal or pelvic ultrasound scan, which is often being performed for diagnostic reasons other than renal symptoms. Likewise, the kidneys are necessarily seen during CT examination of the abdomen. Renal pathology is common, so it is not surprising that many focal renal lesions are detected incidentally during investigation for other symptoms. The commonest incidental renal lesion that may be found is a simple renal cyst. Ultrasound has a very high accuracy in cyst characterisation. Finding a solid renal tumour as an incidental finding confers a prognostic advantage over those whose tumours are found because of symptoms. It is important that the operator knows which incidental renal lesions can be safely categorised and ignored and those that need further investigation and treatment.

SIMPLE RENAL CYSTS

Simple renal cysts are the commonest renal mass lesion. They become more prevalent with increasing age and are a normal part of the process of ageing. Some believe cyst formation is related to nephron loss. Multiple cysts are common in patients with advanced renal disease so there is a hypothesis that even isolated cysts may be associated with early nephron loss. This is supported by the finding that renal length is less in those with cysts.[1] There is, however, dispute as to whether renal function is less in those with one or two cysts. Some authors have found a relationship,[2] whereas others have found no evidence of a decreased glomerular filtration rate.[3] It is certainly clear that multiple cysts are associated with a raised serum creatinine. There is also some evidence of an association with hypertension and multiple[3] or giant cysts. The mechanism may be mechanical compression of the renal arteries causing a functional stenosis; drainage of a giant cyst has been reported to cause normalisation of blood pressure.[4]

Prevalence

The prevalence of simple cysts increases with age: 4.3% in those aged 29 years or less, 15.3% in the fourth decade, 21.8% in the fifth decade, 23.3% in the sixth decade and 32.6% in those aged over 60.[5] Different ethnic populations report different incidences, with a Middle Eastern study giving an overall prevalence of 4.2%,[6] and a Chinese study 10.7%.[7] Obviously the age distribution studied will influence the overall prevalence. Cysts are generally twice as common in men as in women.

Natural history

The majority of simple renal cysts will increase in size with time. There is also an increase in the number of cysts with time. On average cysts increase by 1.6 mm or 3.9% per year,[8] with a tendency for size increase to be more rapid in younger patients. The rate and pattern of growth of benign cysts is no different to that of cysts that harbour neoplasia.

Symptoms

The vast majority of simple cysts are asymptomatic. Large cysts may be symptomatic due to pressure effects on adjacent structures, leading to discomfort, haematuria, hypertension and urinary obstruction. Simple cysts may become symptomatic when they undergo a complication such as haemorrhage, infection or rupture.[9]

Rupture is associated with severe abdominal pain and haematuria and may be spontaneous, iatrogenic or traumatic in origin. Treatment is conservative and following rupture a cyst may disappear for ever.

The great majority of cysts require no treatment. Intervention is only required for symptomatic cysts that affect renal function. This intervention can be surgical or radiological. Ultrasound-guided

aspiration with continuous negative-pressure drainage or aspiration and then instillation of a sclerosing agent such as alcohol, tetracycline or acetic acid can give success rates in relieving symptoms of 75–95%. Different authors advocate different techniques; for example, one paper showed that giant cysts are best treated with continuous negative-pressure drainage[10] and another showed acetic acid is better than alcohol.[11] Surgery is usually laparoscopic and may involve excision or marsupialisation of the cyst.

Ultrasound features

The typical ultrasound features are of a hypoechoic fluid collection arising from the kidney with the following features (Fig. 26.1):

- no internal echoes
- a rounded or oval shape
- increased through transmission of sound
- an imperceptible, smooth wall with a sharply defined margin
- no signal on colour Doppler.

Vessels seen on colour Doppler are deviated around a cyst. Cysts usually arise in the cortex and may be exophytic. Cyst sizes range from a few millimetres to many centimetres. The smaller cysts less than 2 cm in size may show internal echoes due to partial volume effects from the adjacent tissue because the ultrasound beam has width. Cysts of a few millimetres may also not show distal acoustic enhancement for the same reason. Reverberation echoes from strong proximal reflectors such as the skin surface may occur within a cyst (Fig. 26.2). These should fade out the deeper into the cyst they go and harmonic imaging will help reduce their appearance.

A renal cyst should show contact with the kidney it arises from and the 'beak' sign of a small amount of renal tissue extending around its margin should be present (Fig. 26.3). Occasionally other adjacent organs may produce cysts, such as in the adrenal gland, the pancreatic tail or in the retroperitoneum. If these lesions are large it may be difficult to separate them from the kidney and identify their organ of origin. Differential movement of the kidney and the cyst during respiration indicates that the kidney is not the source of the cyst.

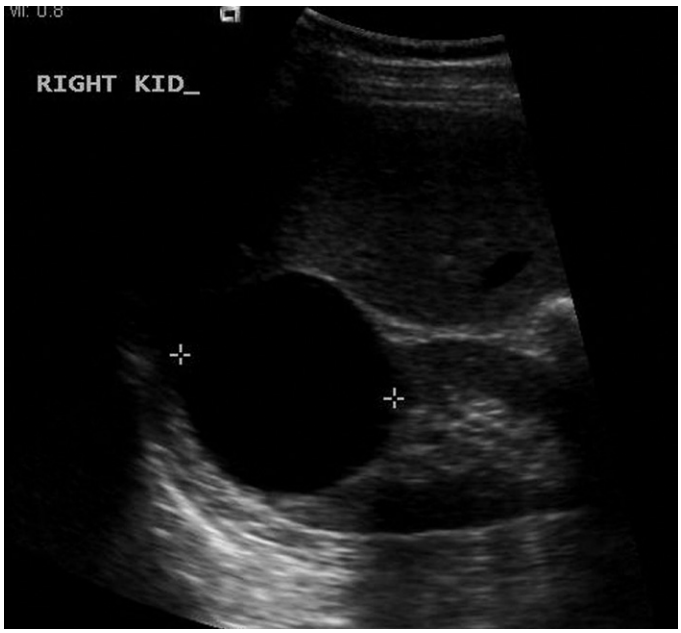


Figure 26.1 Simple renal cyst (between cursors) on the upper pole of the kidney. Note the increased through transmission of sound and the clearly defined margins.

Differential diagnosis

Any other fluid-containing structure can potentially mimic the appearance of a simple cyst; for example, dilated calyces in hydronephrosis, a calyceal diverticulum, a large extrarenal pelvis, aneurysm, abscess, perinephric collection, and haematoma can all cause confusion. Some solid lesions might do the same, most commonly a prominent pyramid in an echogenic cortex. Good examination technique and assessing adjacent structures, as well as checking the clinical history and signs, will help avoid these mistakes.

Malignant transformation of an established simple cyst is exceptionally rare and may never happen but it is possible for a renal cell carcinoma to present as an apparently simple cyst initially.[12] Reports of these rare malignant, simple cysts usually show that the cyst is large and symptomatic in its own right at presentation. Likewise, in endemic areas of the world, hydatid disease may very rarely present as a simple renal cyst.[13] Consequently, some caution needs to be exercised before dismissing a lesion as a simple cyst; but once the diagnosis of a simple cyst is established, then no further imaging follow-up is necessary.



Figure 26.2 Reverberation artefact. The near wall of the renal cyst closest to the transducer is obscured by reverberation echoes arising from the strongly reflective subcutaneous fat.

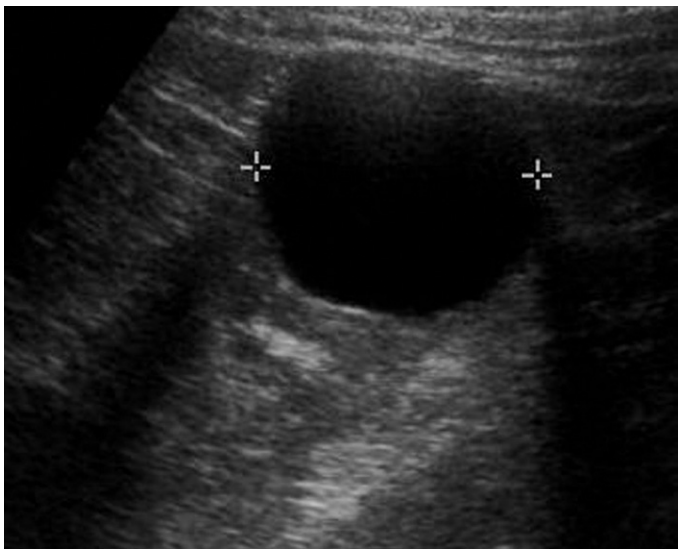


Figure 26.3 'Beak' sign. The margins of the kidney extend around the cyst to form a small beak of renal tissue – this confirms the cyst is renal in origin.

Multiple simple cysts

The likelihood of finding more than one cyst in a kidney increases with age. Each cyst should retain the characteristics of a simple cyst.

Simple renal cysts

- Commonest renal mass lesion.
- Increase in prevalence with age.
- Increase in size with age.
- Usually asymptomatic.
- Symptoms due to local pressure effects, infection and haemorrhage.
- Malignant transformation virtually never occurs.



Figure 26.4 Multiple simple renal cysts. The kidney is normal size and has several large simple cysts distorting its outline. The fine septations seen in one of the cysts do not stop it being regarded as simple.

Some syndromes produce multiple renal cysts, but once established these syndromes usually have innumerable cysts affecting both kidneys equally. Multiple simple cysts associated with the normal ageing process may affect the two kidneys in an asymmetric way and they will always remain countable. The cysts are often of disparate size (Fig. 26.4).

COMPLICATED RENAL CYSTS

Complicated renal cyst refers to any cyst that does not display entirely simple features. The aim is to identify those features that raise the likelihood of underlying haemorrhage, infection, ischaemia or malignancy and also to identify those cysts that even though complicated need no further action.

Septations

A few fine septations of less than 1 mm thickness do not stop a cyst from being regarded as simple. An arbitrary distinction exists that when a cyst contains more than three or four septations, it is termed multiloculated. The concern arises when septations are thicker than a millimetre or show nodularity. It has been suggested that finding cysts within septa is a marker of malignancy in paediatric cysts.[14] Alternatively, finding blood flow in a septum with colour Doppler, particularly high-velocity pulsatile flow, is a marker of malignancy.[15] More recently, work has concentrated on the role of contrast-enhanced ultrasound in detecting malignancy. There is a tendency for the contrast-enhanced ultrasound to upgrade the level of concern over a cyst compared with multislice CT scans[16] and there is some evidence that the diagnosis of cystic malignancy is more accurate with contrast-enhanced ultrasound.[17] All of this work is based on the Bosniak grading system derived from his seminal paper on CT grading published in 1986.[18] There have been numerous papers proving the worth of the system and updating its relevance to modern scanners and contrast-enhanced ultrasound (Table 26.1).

Table 26.1 Bosniak renal cyst classification system

Category I	Benign simple cyst with imperceptible wall that does not contain septa, calcifications or solid components. Water attenuation is seen at CT and the contents are anechoic at US. No enhancement is seen with contrast agents	No intervention needed
Category II	Benign cystic lesion that may contain a few thin (<1 mm) septa (Fig. 26.5A) in which perceived but not measurable contrast enhancement may be found at CT. Likewise, a few microbubbles of contrast agent may be seen in the septa at US. Fine calcification or a short segment of slightly thickened calcification may be seen in the septa. Hyperdense cysts on CT of less than 3 cm size and with no complexity or enhancement are in this group too	No intervention needed
Category IIF	Cysts may contain multiple thin (<1 mm) septa. There may be minimal thickening of wall or septa (Fig. 26.5B), which may contain calcification that may be thick and nodular (Fig. 26.5C). Perceived but not measurable enhancement of thin septa at CT or a few microbubbles seen at US are allowed but there are no enhancing soft tissue components. Totally intrarenal, non-enhancing, hyperdense cysts of less than 3 cm at CT are included in this group	Lesions are thought to be benign but follow-up is needed to prove the stability of the lesion. Risk of malignancy 5%
Category III	Cystic masses with thickened irregular or smooth walls or septa and in which there is measurable enhancement present. This category includes complicated haemorrhagic or infected cysts, multilocular cystic nephroma and cystic neoplasms (Fig. 26.5D)	Surgical intervention is needed as neoplasm cannot be excluded. Histology is needed for diagnosis. Risk of malignancy 25–100%
Category IV	Clearly malignant cystic masses which as well as enhancing walls and septa also have distinct enhancing soft tissue components independent of a wall or septa (Fig. 26.5E, F)	Clearly malignant and need to be removed

From Ascenti et al.[19] and based on Israel and Bosniak.[20]

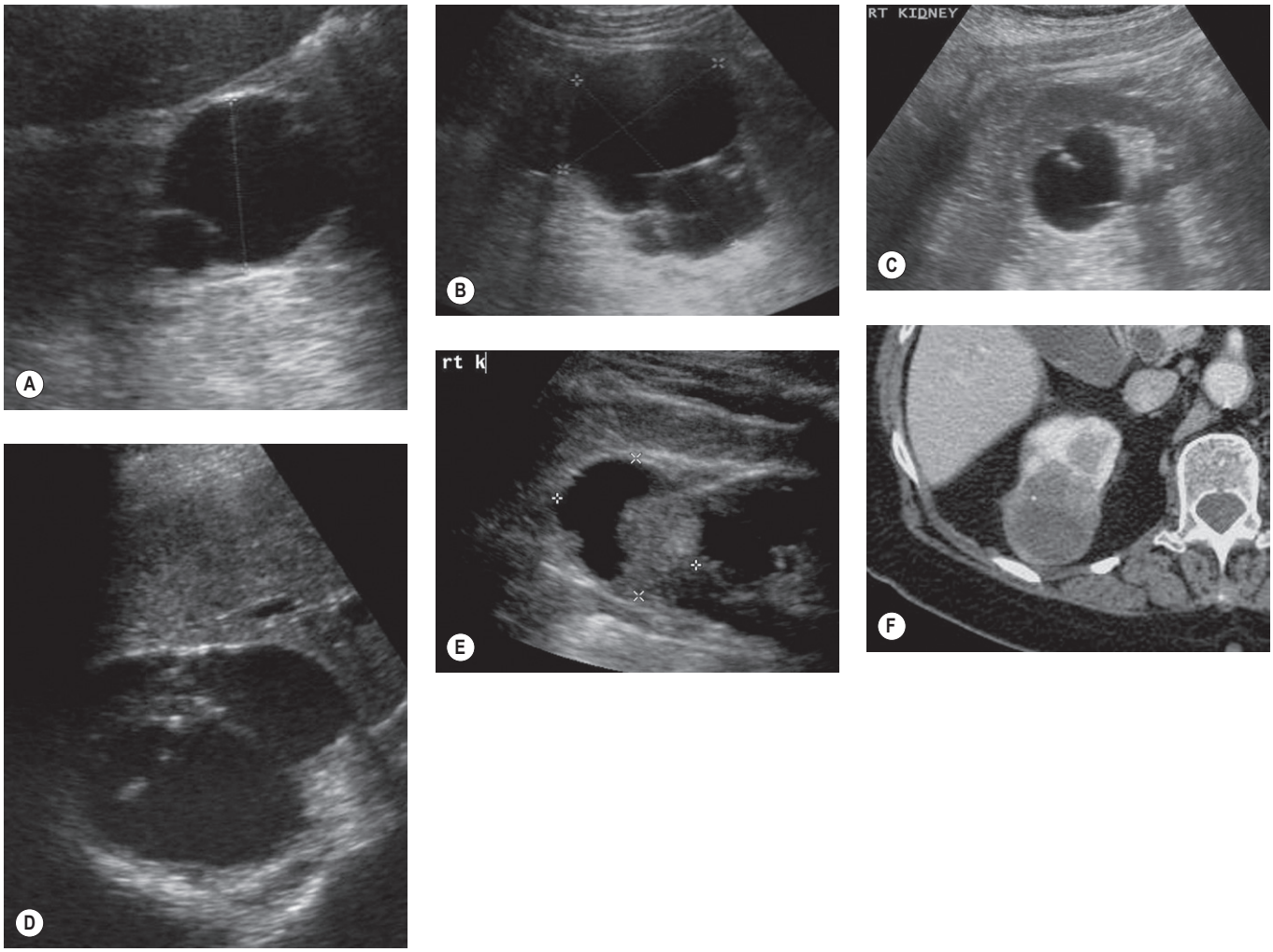


Figure 26.5 **A sequence of cysts to illustrate the Bosniak categories. A:** A single fine septum is seen, placing this cyst in category II. **B:** The septa show minimal thickening, category IIF. **C:** There is nodular calcification on the septa, category IIF. **D:** There is a more complex area adjacent to the septa that showed enhancement on CT, category III. **E and F:** Frankly malignant lesion with an obvious solid component, category IV, shown on US **(E)** and CT **(F)**.

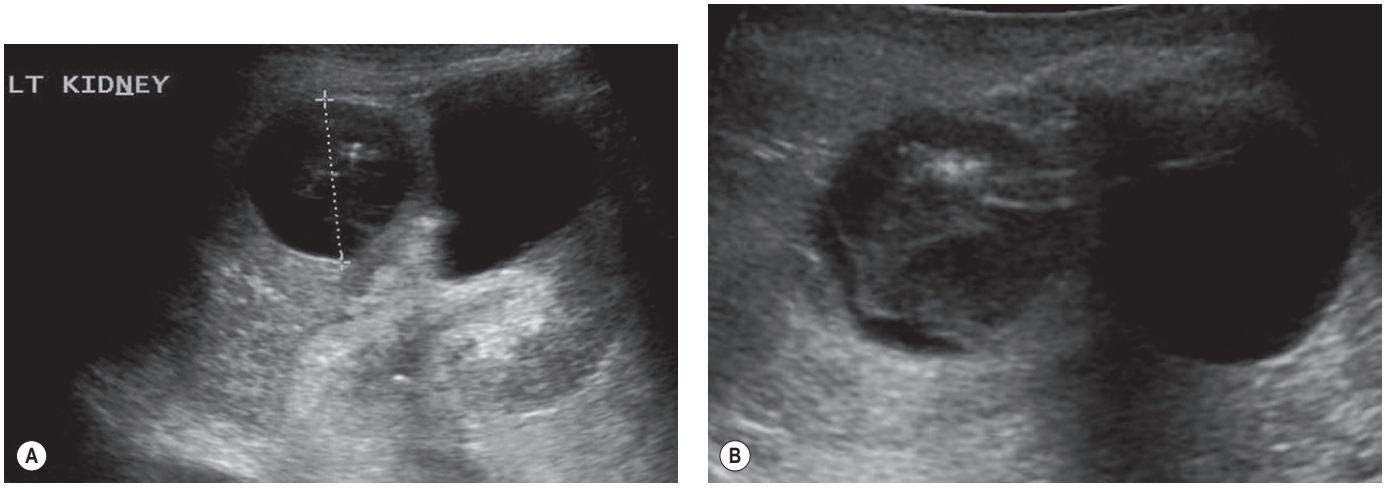


Figure 26.6 **Clot retraction in a haemorrhagic renal cyst.** The overview **(A)** and a more magnified view **(B)** of the organised echoes in one of the cysts. These represent clot within the cyst.

Haemorrhage

Cysts should have anechoic contents; when this is not the case, the echoes may be due to haemorrhage, infection, proteinaceous material or colloid. The rate of haemorrhage into simple cysts is based on studies predating the advent of sophisticated ultrasound, but is usually quoted as about 6%. There is a greater rate of haemorrhage in patients with polycystic kidney disease, which is, in part, due to the great number of cysts present and their greater vulnerability to trauma because of the large size of the kidneys. A fresh haemorrhage is anechoic, gaining echoes over time. These echoes may settle out to form layers. Eventually, clot retraction (Fig. 26.6), calcification and thickening of the cyst wall or formation of septa may occur. Haemorrhagic cysts are associated with malignancy. Haemorrhage is hyperdense on CT and is included in Bosniak's classification. Follow-up of haemorrhagic cysts is prudent either with US or CT to ensure they are benign. Conversely, benign haemorrhagic cysts may mimic malignancy and lead to unnecessary surgery.[21] Careful evaluation with contrast-enhanced US or CT should avoid this mishap.

Perirenal haemorrhage (Fig. 26.7) is also associated with renal cystic disease, with large retroperitoneal bleeds[22] or haemoperitoneum[23] being reported in association with acquired cystic kidney disease in those on dialysis. Other renal mass lesions, such as angiomyolipomas or renal cell carcinomas, may also produce perirenal haemorrhage.[24] The bleed may be large enough to obliterate the underlying lesion and mimic the features of a complex cystic mass. If initial imaging does not reveal the underlying cause it is imperative that follow-up imaging is performed once the haematoma has resolved to look for the underlying cause. It may take up to a year for a tumour to manifest itself.[25]

Infection

A pre-existing cyst may become infected or an infection may manifest as an abscess or other complex cystic lesion. Infection of a pre-existing cyst is either via haematogenous spread or by direct inoculation during trauma or iatrogenic cyst puncture.

A pre-existing cyst that has become infected may remain indistinguishable from a simple cyst or it may attain quite complex appearances. It is the clinical picture of fever, flank pain and a raised white cell count that points towards infection. Infected cysts may contain echogenic fluid, which may layer out with dependent debris (Fig. 26.8) and the walls may thicken up due to inflammatory change. Contained gas may be present. At this point, an infected cyst is to all intents and purposes no different to an abscess. Such an abscess may spontaneously rupture.[26] It is best to aspirate and drain infected cysts or abscesses as they are relatively resistant to antibiotic treatment.

Patients with polycystic kidney disease may present with symptoms of an infected cyst. It may be impossible to tell with ultrasound alone which of the many cysts is the infected one. Positron emission tomography combined with CT can allow accurate identification of the culprit.[27]

Hydatid (echinococcosis) cysts of the kidney represent a rare form of renal infection. Even though hydatid disease is endemic in

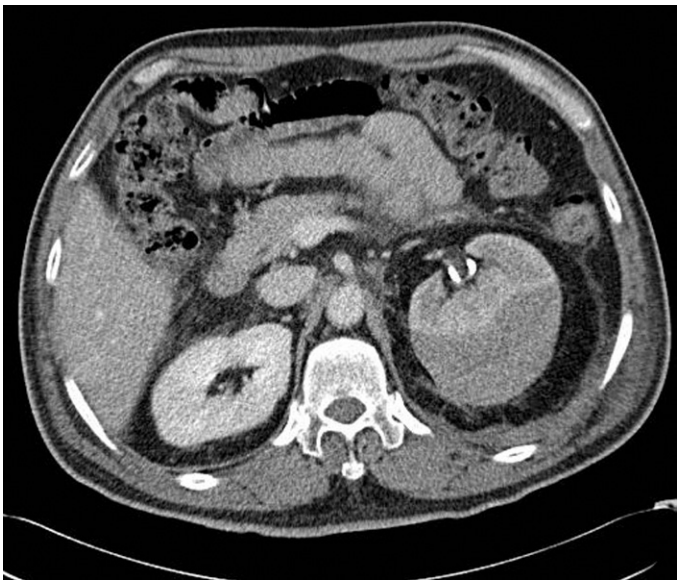


Figure 26.7 CT scan showing a subcapsular haematoma compressing the renal substance.

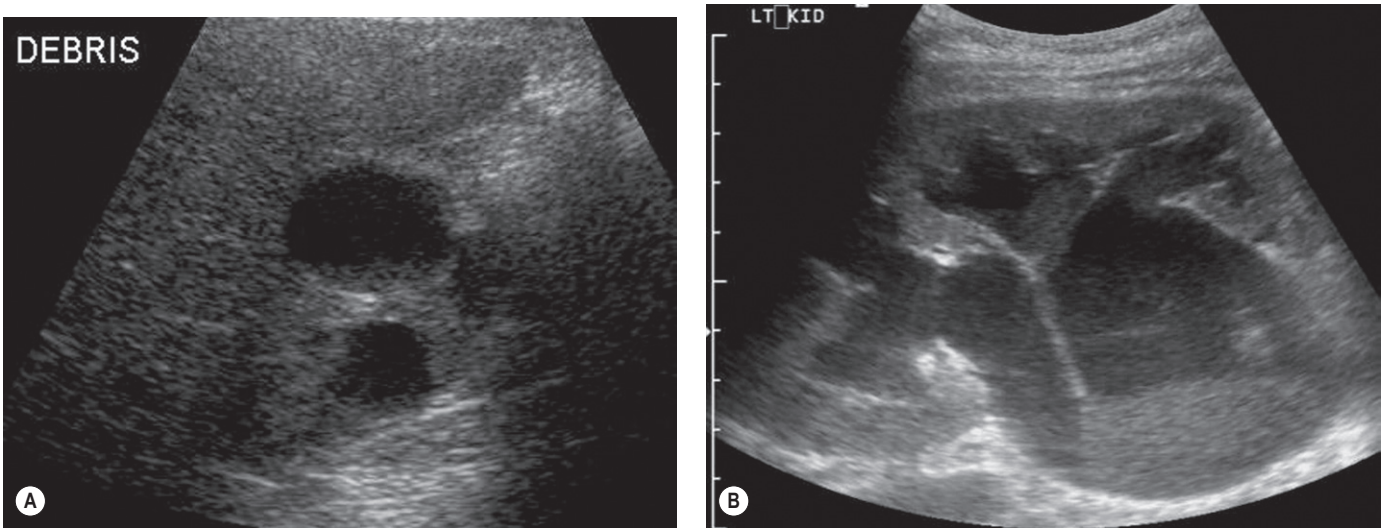


Figure 26.8 Debris. A: Layering of debris in the dependent portion of the cyst is seen secondary to infection. **B:** Similar layering out of debris is seen in this kidney with pyonephrosis.

Cysts with echogenic contents

- First, ensure echoes are not due to artefact, such as reverberation.
- Blood, pus, colloid and proteinaceous material may all look similar.
- Clinical symptoms, such as fever, help to distinguish the lesions.
- Blood will mature over time, becoming more echogenic and showing clot retraction.
- Debris of any sort may form layers of echogenicity within the cyst.
- An infected cyst will clinically behave much the same as a primary abscess.
- Aspiration of infected cysts or abscesses is advised as they are relatively resistant to antibiotics.

many parts of the world, renal involvement occurs in only 4% of confirmed hydatid disease. The commonest sites of involvement are hepatic (75%) or pulmonary (15%). Hydatiduria is the only specific sign of renal involvement and is rarely seen. Eosinophilia only occurs in about 50% of cases. Consequently, in endemic areas an open mind needs to be kept when evaluating cystic lesions. The characteristic features of daughter cysts within the main cyst, floating membranes and fine calcification are not reliably seen. Occasionally, hydatid may even present as a simple cyst.[13] Calcification of a hydatid cyst does not imply inactivity but can occur in all stages;[28] it is stability of the cyst over time that more reliably predicts inactivity.

Calcification

Calcification is reported in 1–3% of renal cysts.[29] CT is usually better at detecting calcification than ultrasound. Bright foci in cyst walls or septa that show ring-down artefact are often seen on ultrasound but do not correlate with calcification on CT images. Most calcifications have occurred as a result of a previous cyst complication, such as bleeding or inflammation. There is also an association of cyst calcification with malignancy so the art is to distinguish calcification that can be ignored from that which requires further investigation. Israel and Bosniak have shown that the coexistence of enhancing soft tissue elements is far more important than the presence of calcification in diagnosing malignancy.[30] Magnetic resonance (MR) scans are probably best at showing enhancement in calcified masses as calcification is less apparent on MR and does not detract from the appreciation of the enhancement.

A smooth amount of calcification deposited around a wall or septum can be considered benign (Fig. 26.9). If the calcification is thick and nodular but without obvious enhancement then it can be followed up. Only if there is enhancement associated with the calcification should the lesion be considered surgical.

Renal cyst calcifications are much commoner in patients with polycystic kidney disease (Fig. 26.10) with up to 50% of patients having calcifications.[31] Calcifications are commoner in those with larger kidneys and poor renal function. The greater number of

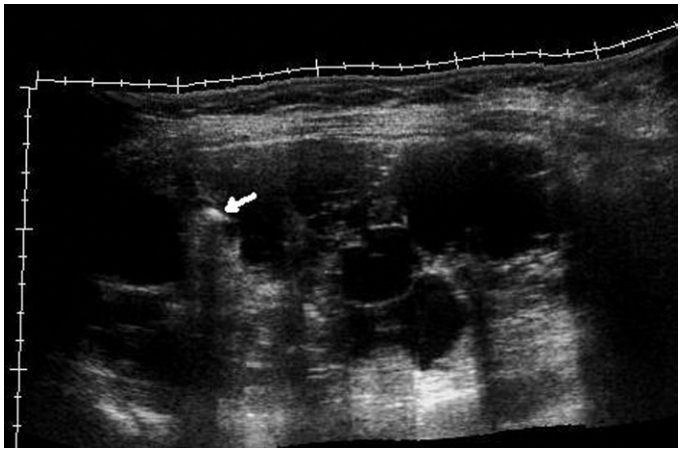
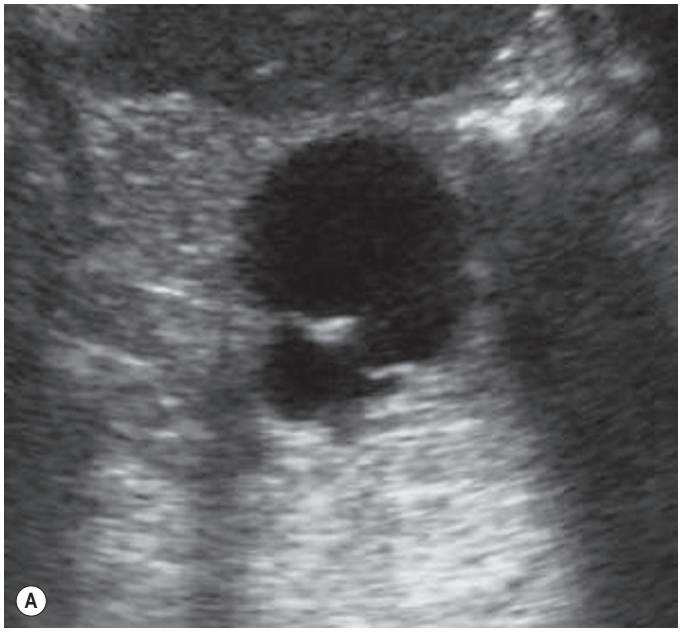


Figure 26.10 A polycystic kidney showing a dense focus of calcification (arrow) with acoustic shadowing.



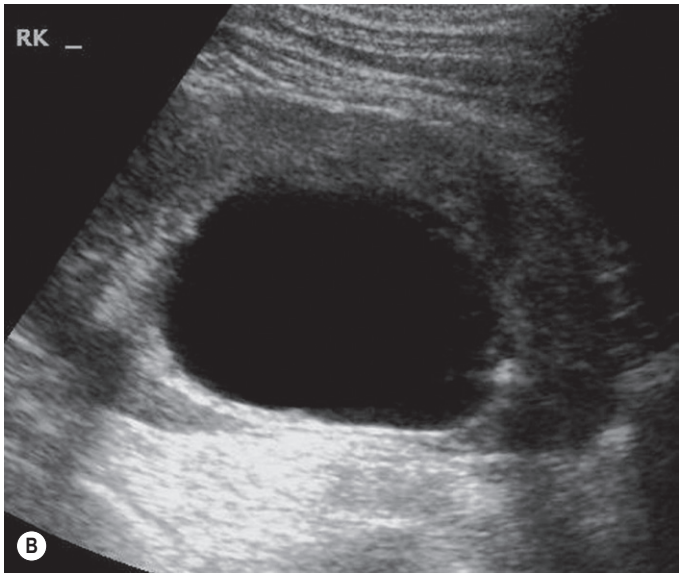


Figure 26.9 Calcification. A: A small bright focus is seen on an otherwise thin septum in the cyst. This is a small benign calcification. **B:** Shows another example in a larger cyst. The calcification shows acoustic shadowing. Care needs to be taken to distinguish this from an erroneous diagnosis of a dilated renal pelvis containing a stone.

calcifications is merely a reflection of the greater propensity to cyst haemorrhage or infection seen in polycystic kidney disease.

Milk of calcium cysts contain a colloidal suspension of calcium crystals (viscous collection of calcium carbonate, calcium phosphate or calcium oxalate); these gravitate to form a layer of dependent high-reflectivity, which is enough to form shadowing. These cysts are usually asymptomatic. They represent a calyceal diverticulum that has lost its communication with the collecting system. A pitfall is to mistake a milk of calcium cyst for a calculus,[32] though in some cases of stasis, milk of calcium may form in calyces. Demonstrating the characteristic layering is diagnostic, but often better seen on CT.

Cystic malignancy

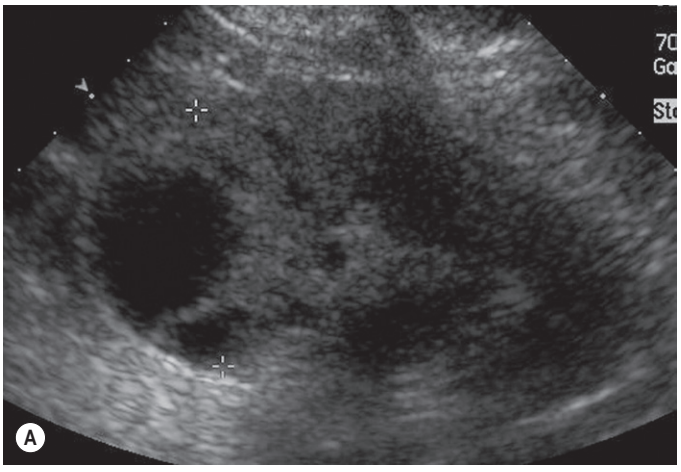
The initial premise of the Bosniak classification was to identify cysts that did not require surgery. Grades I and II do not need surgery, whereas grades III and IV should be offered surgery, with an increased likelihood of malignancy being found in the higher grade. An absence of change in grade IIF lesions helps support the contention that they are benign. Some authors advocate biopsy of grade III lesions in an attempt to avoid unnecessary surgery,[33] though there is always the problem of sampling error leading to a false negative diagnosis, as well as the risk of tumour seeding down the needle track. The best chance of cure for renal cell carcinoma is excision of the primary mass before it has metastasised, hence a high index of suspicion needs to be maintained for cystic masses. Approximately 1 in 10 renal cell carcinomas will manifest primarily as a cystic mass. The presence of enhancement with intravenous contrast agents (on ultrasound, CT or MR) dramatically increases the likelihood that a lesion is malignant.

Extensively cystic renal neoplasms such as might be classified as Bosniak II or III lesions fall into one of three diagnoses: multilocular cystic renal cell carcinoma, cystic nephroma and mixed epithelial and stromal tumour (MEST) of the kidney.[34] These conditions are indistinguishable preoperatively and biopsy is often misleading. Multilocular cystic renal cell carcinoma probably only forms 4% of all renal cell carcinomas (Fig. 26.11).[35] Whatever the diagnosis, prognosis is generally good and nephron-sparing surgery should be considered.

Most renal cell carcinomas showing central cystic change are unilocular with thick irregular walls because they have undergone central necrosis (50%). The cystic component usually shows low-level echoes. Next most commonly (30%), a cystic mass might have several cystic spaces with thick nodular intervening masses containing adenocarcinoma. Asymmetric necrosis of a carcinoma produces a cystic mass with a solid mass eccentrically placed in its wall (Fig. 26.12).[36] These three patterns with their substantial solid components are quite different to the lesions described in the previous paragraph and will all fall into the Bosniak IV category requiring surgery.



Figure 26.11 Renal cell carcinoma. A coronal reformatted image from a CT scan showing a multilocular cystic renal cell carcinoma at the upper pole of the right kidney.



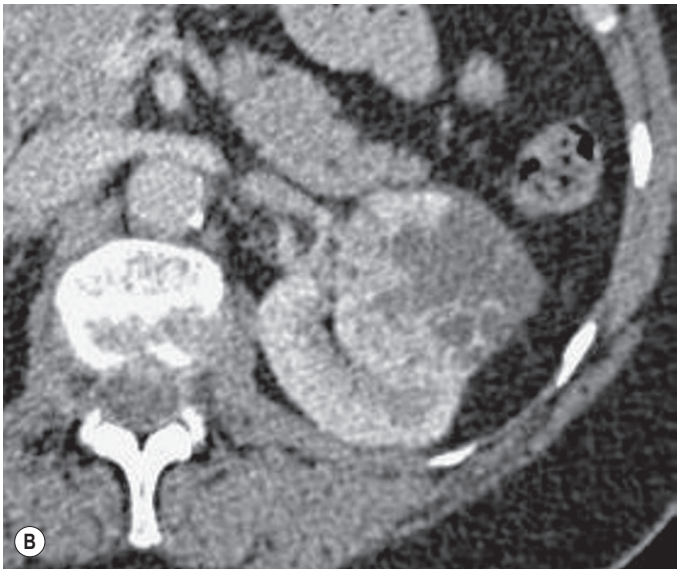


Figure 26.12 Asymmetric necrosis. Ultrasound **(A)** and CT **(B)** of a renal cell cancer that has shown asymmetric necrosis to produce a cystic mass with an eccentrically placed solid mass in its wall.



Figure 26.13 A kidney with an abnormally echo-bright cortex. This is causing one of the inferior pole pyramids to stand out as an echo-poor structure (arrowhead) – it is not a cyst.

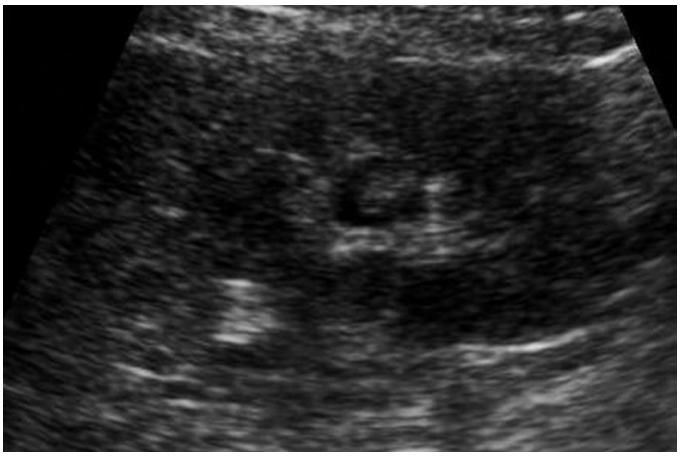


Figure 26.14 This small cystic structure with a central echogenic focus represents papillary necrosis with a central sloughed papilla.

Cystic malignancy

- The Bosniak classification helps to identify those cysts that do not need intervention or follow-up.
- Enhancing soft tissue elements in a cystic mass are most important in the diagnosis of malignancy.
- Most cystic tumours are those solid lesions that have undergone necrosis and liquefaction.
- Calcification alone is not a good marker of malignancy.
- Primary cystic renal cell carcinomas are usually multilocular and may be indistinguishable on imaging from benign diagnoses such as cystic nephroma.
- Renal cell carcinoma can very rarely present as an apparently simple cyst, but they are usually large and symptomatic in their own right.

DIFFERENTIAL DIAGNOSIS OF A RENAL CYST

Pyramids

Sonographically the pyramids show as evenly spaced, echo-poor, inverted triangles pointing toward the renal pelvis. When the renal cortex is echo-bright then the pyramids can stand out very clearly and mimic the presence of small cysts (Fig. 26.13). Normal paediatric kidneys have a bright cortex. Adults show a bright cortex as a non-specific response to intrinsic renal disease such as glomerulonephritis, acute tubular necrosis or acute transplant rejection.

Renal papillary necrosis

This may manifest as single or multiple small cystic cavities within the medullary pyramids. They may be continuous with the calyces and be associated with hydronephrosis. One characteristic feature is that the cystic cavity may contain an echogenic focus which may even be calcified; these represent the sloughed papilla (Fig. 26.14).

Calyceal and renal pelvic diverticula

Fluid-containing lesions that communicate with the renal collecting system can be impossible to distinguish from renal cysts on ultrasound alone. The presence of milk of calcium can help (Fig. 26.15). CT urography or conventional urography is required to demonstrate the connection, with excreted contrast medium entering the diverticulum.

Dilated pelvicalyceal system

Errors of diagnosis can occur both ways; peripelvic cysts can mimic hydronephrosis and obstructed calyces (Fig. 26.16) may mimic a cyst. Ideally the communication between the different parts of the dilated pelvicalyceal system should provide the diagnosis but sometimes these communications may be hard to see on ultrasound or they may be pathologically absent. An example would be an obstructed calyx due to tumour, appearing like an isolated cyst. Alternatively, multiple peripelvic cysts can falsely seem to communicate with each other because of artefactual signal drop-out from the walls.

Classically, the obstructed upper moiety of a duplex kidney may simulate an upper pole renal cyst. This mistake is most easily made if the obstruction occurred in utero so that the surrounding cortex has had time to become atrophic and non-functioning (Fig. 26.17). Similar appearances do also occur following obstruction to an upper moiety in adulthood but it is more likely that the structure of the branching calyceal system will be maintained. Finding a ureterocele in the bladder may aid diagnosis.

Chronic obstruction at the pelvi-ureteric junction can lead to complete atrophy of the renal cortex, leaving the residual appearance of a large cyst. The later in life this occurs, the more likely there will still be structural features of a branching calyceal system remaining. A dilated extrarenal pelvis should not be confused with a parapelvic cyst once the communication with the rest of the calyceal system is identified.

CT urography is the best way to establish whether there is communication or not between the lesion and the pelvicalyceal system. Alternatively, it has been shown that measuring the size of the 'cyst' before and after a 1.5 litre fluid load will distinguish between a cyst and renal obstruction; an increase in size of the lesion indicates renal obstruction.[37] This technique does require the kidney to have some function, otherwise it does not work.

Lymphatic cysts

Cysts in the renal sinus are found in two forms: parapelvic and peripelvic.[38] Parapelvic cysts are parenchymal in origin and are similar to any other simple cortical cyst (Fig. 26.18). They are usually solitary and seen in 1.5% of autopsies. Peripelvic cysts arise by lymphatic ectasia and are usually multiple and septated. They often

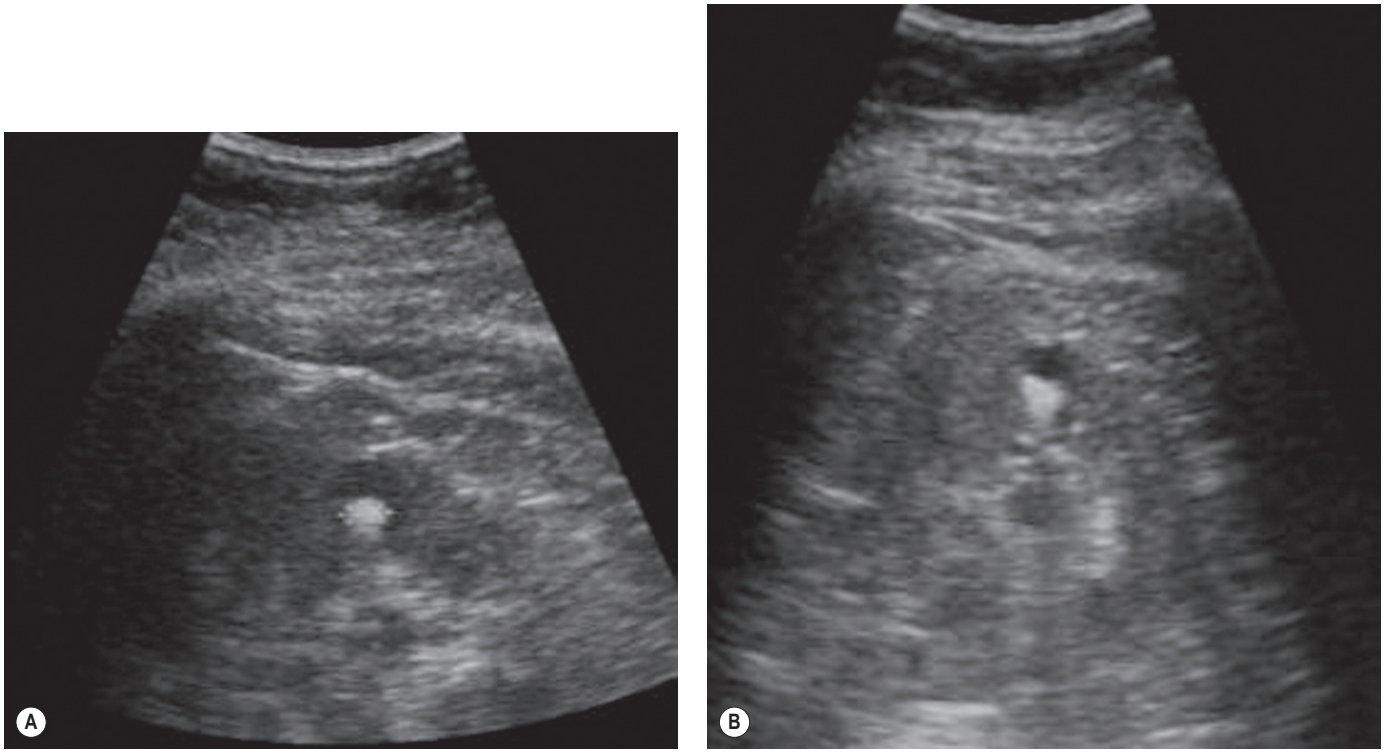


Figure 26.15 Two views of a paracalyceal cyst containing milk of calcium. This casts an acoustic shadow.



Figure 26.16 A hydronephrotic kidney, imaged so that only the evenly spaced dilated calyces are seen. These might be mistaken for cysts were it not for other imaging planes showing they are part of the pelvicalyceal system.

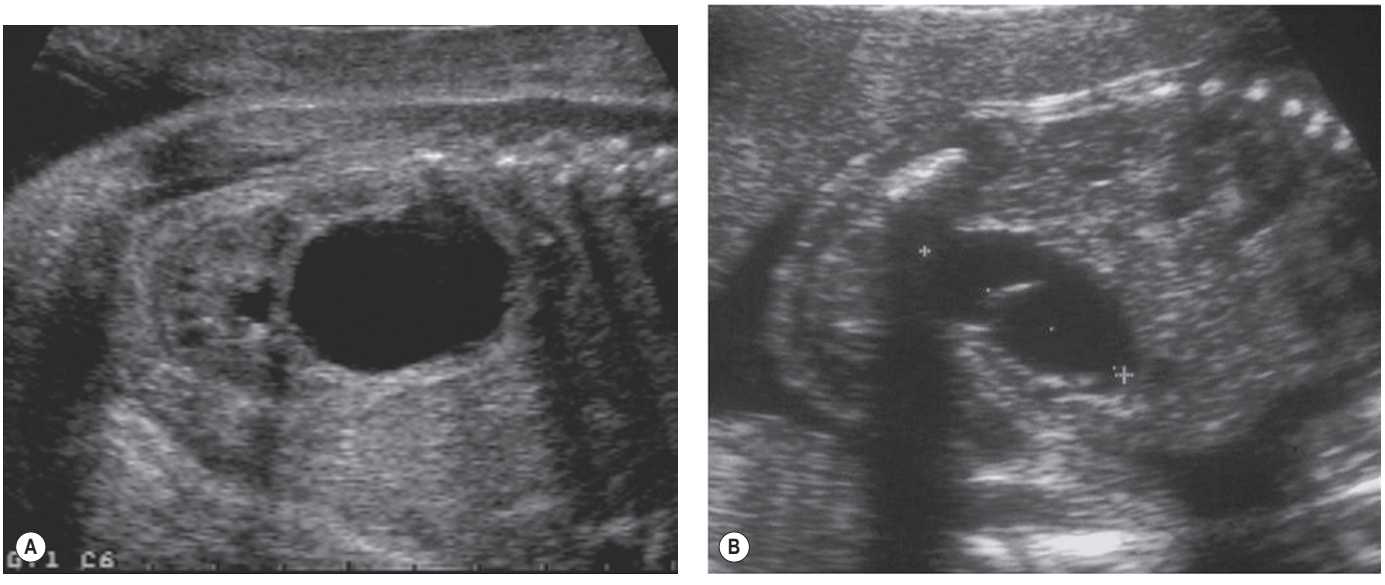


Figure 26.17 A fetal example of an obstructed upper moiety in a duplex kidney resembling a cyst **(A)** and associated with a ureterocele **(B)**.

are elongated and run alongside the adjacent pelvicalyceal system (Fig. 26.19).

Renal lymphangiectasia and lymphangiomas are part of the same spectrum of lymphatic ectasia and may occur in the peripelvic space or perirenal space.[39] The usual diagnostic error is to confuse them with hydronephrosis rather than cysts.[40] Very rarely, the lymphangioma is shown to communicate with the excretory system.[41] Peripelvic lymphangiectasia is associated with perivascular cysts (probably dilated lymph vessels), most easily seen in the peri-aortic space. Perirenal cysts seen in lymphangiectasia appear to arise in a capsular location rather than from the renal cortex.[42]

Lymphangiectasia and lymphangiomas are benign lesions. Intervention is only needed if they are causing pain by local space-occupying effects. Occasionally, resection of a lesion thought to be a cystic neoplasm preoperatively turns out to be a lymphangioma on postoperative histology.

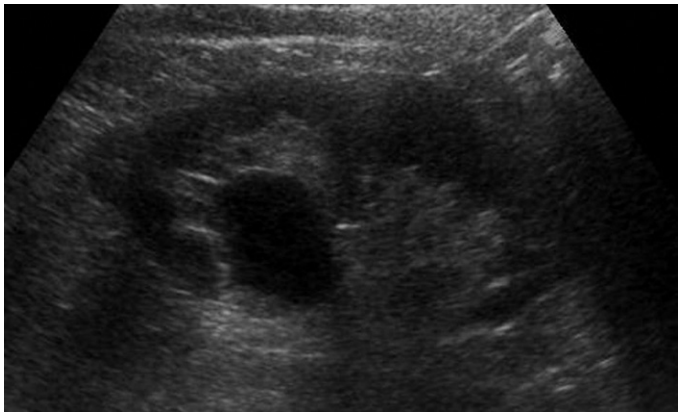


Figure 26.18 A parapelvic cyst. These are usually single as seen here; they arise from the cortex and are identical to any other cortical cyst.

Haematoma

A recent haematoma may be indistinguishable from a cyst. The diagnosis should be suspected if there is a history of trauma. Sequential ultrasound scans will show development of echoes within the lesion as it matures and eventually clot retraction (a pattern analogous to the maturation of a haemorrhagic ovarian cyst). Doppler ultrasound is useful to show that the kidney is still perfused after renal trauma. Iatrogenic trauma, usually following biopsy, may show a focal haematoma and be associated with aneurysm or arteriovenous fistula formation. Despite this, most iatrogenic haematomas or arteriovenous fistulae are not associated with long-term sequelae and usually resolve spontaneously.[43] Contrast-enhanced CT is the preferred imaging modality in the assessment of blunt renal trauma. It not only shows the renal trauma but is sensitive for associated trauma to other abdominal viscera.

Some haematomas occur spontaneously as a result of an unsuspected underlying lesion such as an angiomyolipoma.[44] Other tumours are also implicated, e.g. metastatic trophoblastic tumour.[45] These spontaneous bleeds usually adopt a subcapsular location and compress the underlying parenchyma (Fig. 26.20). Rarely, over the long term, osmotic forces may cause the subcapsular haematoma to swell and compress the kidney enough to compromise its function – the so-called 'page' kidney. The compressed kidney may be hard to discern around the margin of the 'cyst' on ultrasound.

Arteriovenous malformations and aneurysms

Arteriovenous malformations and aneurysms (Fig. 26.21) may appear identical to a simple cyst on greyscale ultrasound. Big dilated veins may mimic a dilated pelvicalyceal system. These

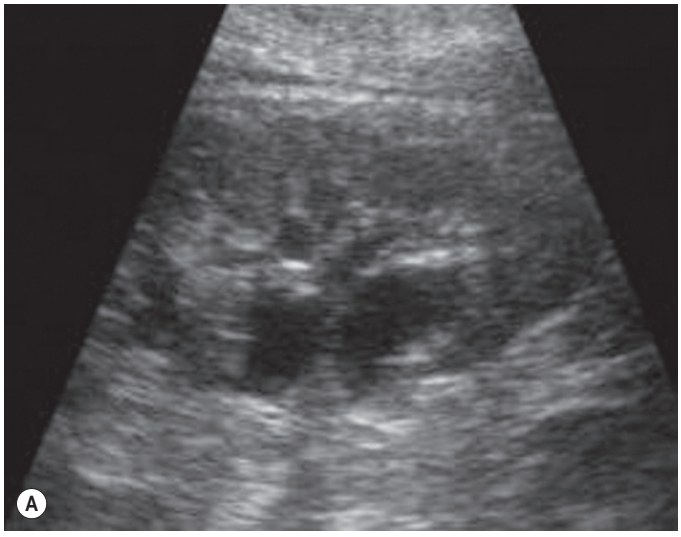




Figure 26.19 Peripelvic cysts. Ultrasound **(A)** shows elongated cysts paralleling the course of the pelvicalyceal system. They are easy to mistake for hydronephrosis but CT urography **(B)** shows the contrast-filled pelvicalyceal system running between the cysts.

entities, however, show no diagnostic difficulty once they are interrogated with colour Doppler ultrasound, although some care needs to be taken with lesions showing very low, slow flow with compensatory adjustment of the Doppler parameters to allow detection. Occasionally CT will misinterpret a venous varix as an enhancing mass.[46] These vascular anomalies may have no symptoms and can be picked up incidentally on investigations done for other purposes.[47]

Renal abscess

Before antibiotics, haematogenous spread of *Staphylococcus aureus* was the common cause of renal and perirenal abscess formation. In recent times, it is more common for infection to be caused by *Escherichia coli* and *Klebsiella pneumoniae* from ascending infections of the lower urinary tract.[48] Renal abscesses from haematogenous spread usually arise in the renal cortex and those from ascending infection in the medulla. Perirenal abscesses arise from rupture of a renal abscess or direct haematogenous spread. Common underlying conditions include diabetes mellitus, cirrhosis, urinary obstruction and stones.

Ultrasound signs may be non-specific initially, showing global enlargement of the kidney and a focal mass (Fig. 26.22). If progression to true abscess occurs then typical appearances are of a thick-walled mass with a liquefied centre containing turbid echoes (Fig. 26.23). CT outperforms ultrasound in identifying abscess formation[49] and is indicated if ultrasound is inconclusive. Ultrasound alone has a risk of incorrect diagnosis about 14 times higher than when combined with CT scan. Ultrasound tends to miss perinephric abscesses associated with pyonephrosis, and gas-forming abscesses. Emphysematous infections carry a risk of misdiagnosis 19 times greater with ultrasound alone than with CT. CT is also better at identifying underlying stones than ultrasound. Ultrasound is particularly insensitive to mid-ureteric calculi.

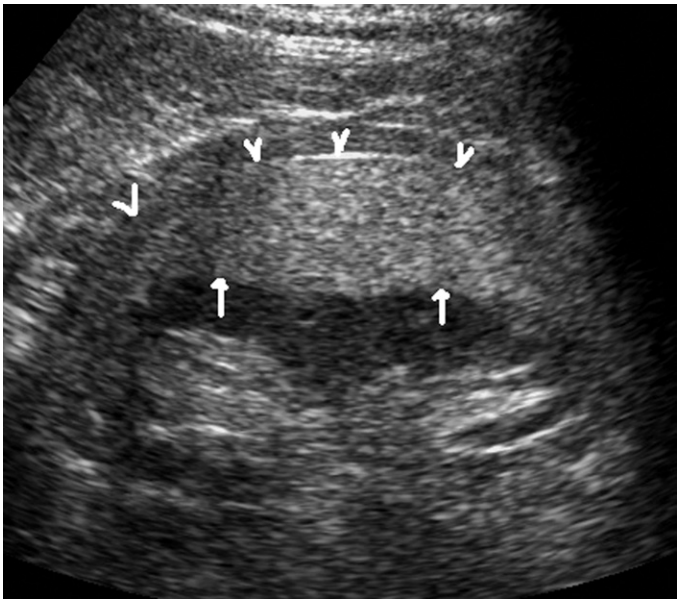
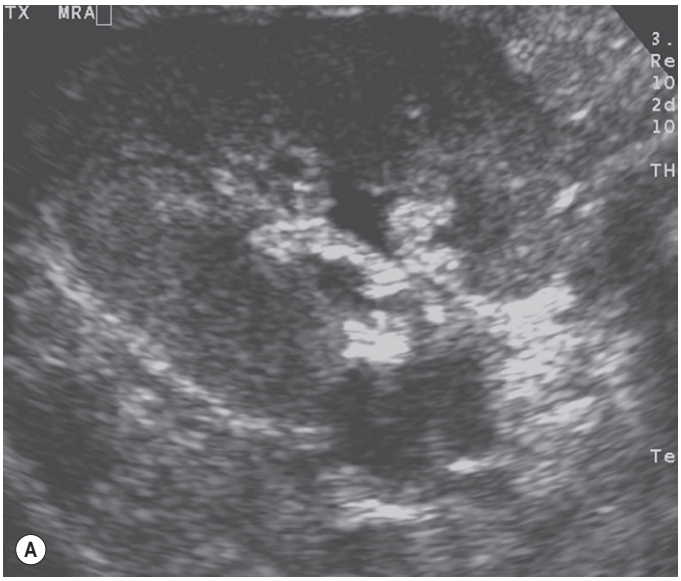


Figure 26.20 The subcapsular haematoma shows as an echogenic collection (arrowheads) compressing the kidney (arrows) beneath it.



Figure 26.22 The upper half of this kidney can be seen to be swollen and of increased echogenicity compared to the lower half. This patient had typical symptoms of flank pain and fever. These are the appearances of a focal pyelonephritis.



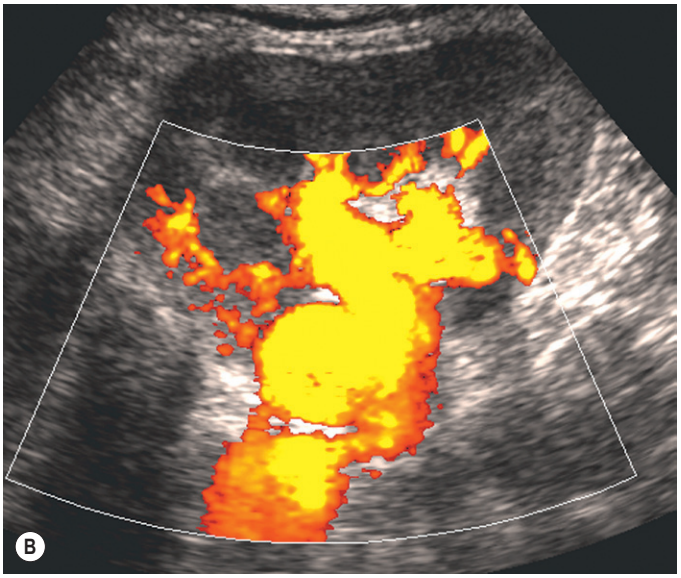


Figure 26.21 Aneurysm. The sonolucent structure by the hilum of this transplant kidney could be mistaken for a cyst on greyscale ultrasound **(A)** but power Doppler **(B)** clearly shows it is an aneurysm containing blood flow.

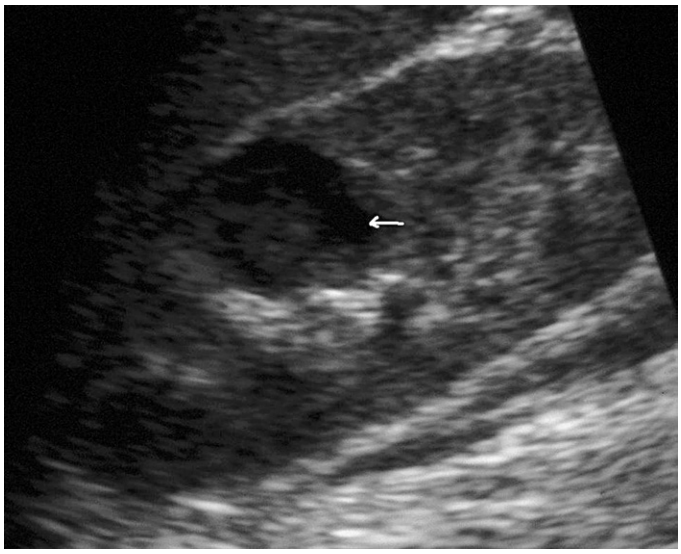


Figure 26.23 A small focal cystic collection (arrow) in the interpolar cortex of the kidney. Given the patient's symptoms of fever and flank pain, this is a small abscess.

The appearances of infected cysts have been discussed above (Fig. 26.24). If they progress to abscess formation they may be indistinguishable from a primary abscess. Depending on the size of the abscess and the patient's symptoms, ultrasound can be used to guide drainage of an abscess or to monitor its resolution with antibiotic therapy.

Multilocular cystic nephroma/mixed epithelial and stromal tumour (MEST)

A multilocular cystic nephroma is a rare lesion that is classically characterised as a discrete, unilateral collection of anechoic, non-communicating cysts, all grouped within a thick fibrous capsule (Fig. 26.25). If the individual cysts are small the overall lesion may appear as a more solid mass. No mural nodules are seen but there may be fine calcification. Typically, these lesions are seen in boys less than 2 years of age or in women in their fifth and sixth decades. Pathological disagreement in the past has led to an array of synonyms: benign cystic nephroma, cystic hamartoma, multilocular cystadenoma, cystic Wilms' tumour, benign cystic differentiated nephroblastoma, and segmental polycystic kidney, to name a few.

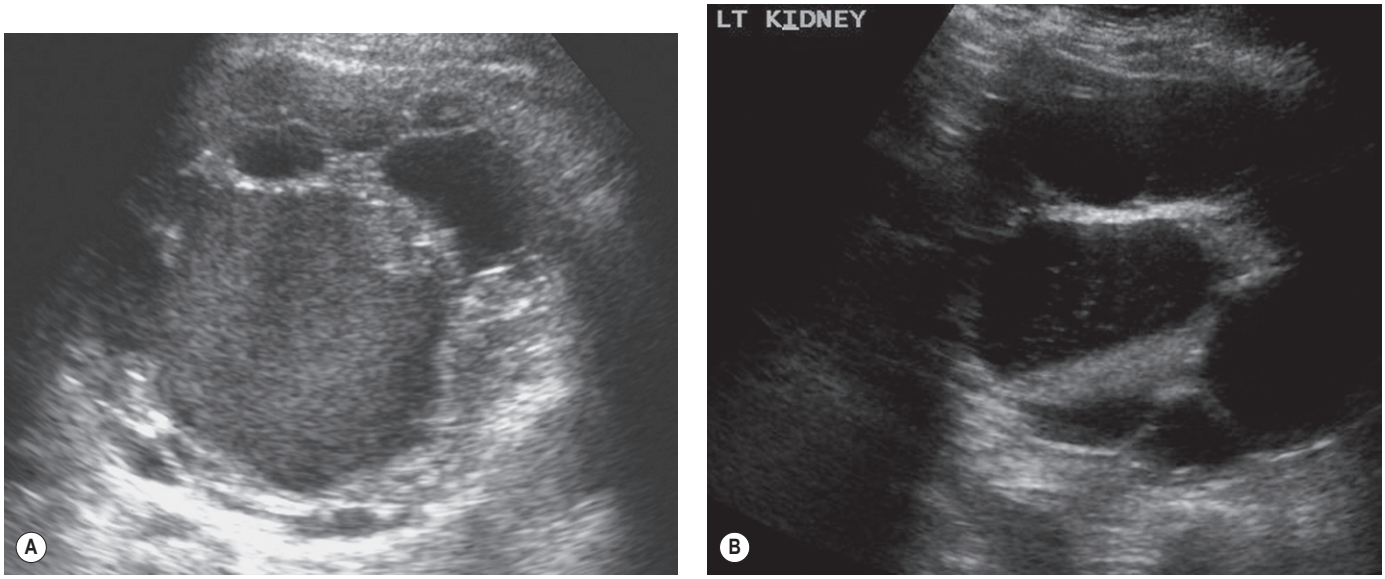


Figure 26.24 Infected cysts may look identical to a thick-walled abscess and have uniform internal echoes **(A)**. Layering of debris may also occur **(B)**.

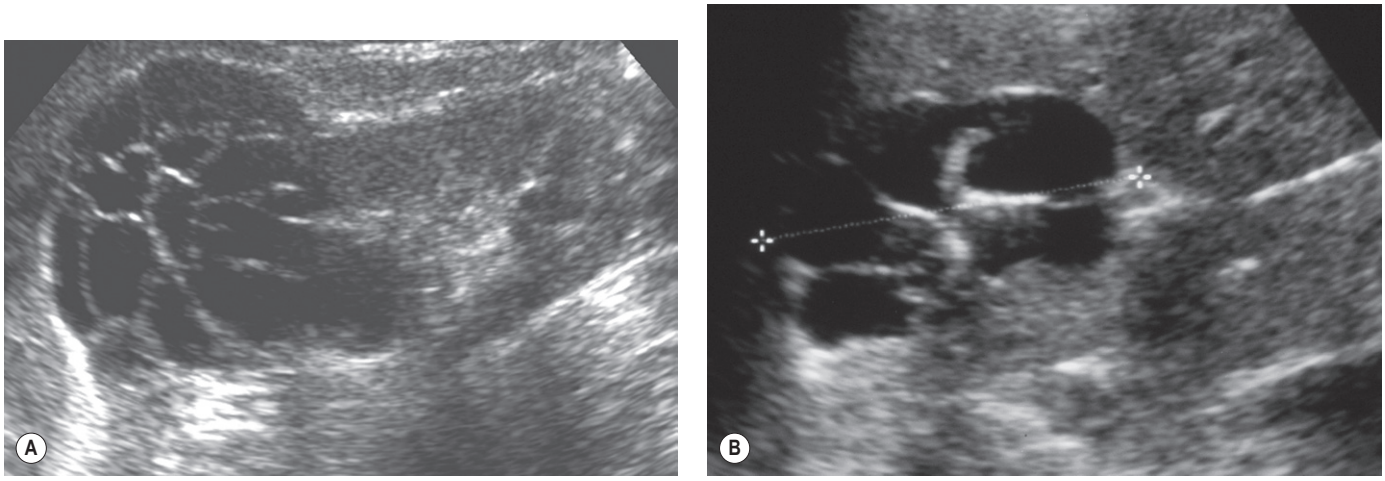


Figure 26.25 Cystic nephroma. A and B: Two examples of a focal collection of cysts surrounded by a capsule as seen in cystic nephromas. Differentiation from a multilocular cystic carcinoma can be impossible preoperatively.

Recently described is a new entity, the mixed epithelial and stromal tumour. It is likely that this forms part of the same spectrum as a multilocular cystic nephroma.[50] Morphologically they are the same, with multiple non-communicating cysts, though there are histological differences.

The difficulty with these lesions, be they cystic nephroma (CN) or MEST, is to distinguish them from multilocular cystic malignancy. Other potential diagnostic confusions can exist with multicystic dysplastic kidney or abscesses. Both CN and MEST are likely to be graded as Bosniak III lesions on imaging, with MEST more likely to show enhancing nodules. Both CN and MEST are benign entities that are usually treated with excision, the true diagnosis being made following resection. One series, however, reports two patients with CN having concomitant renal cell carcinomas and one patient with MEST having a sarcomatous component.[51]

Localised cystic disease

Simple renal cysts may occur in an asymmetric fashion and occasionally the only cysts present will be clustered together in one part of one kidney. It should be possible to identify each cyst as a separate entity, although if cysts are abutting each other their walls may be mistaken for a dividing septum in a single cyst. Other differential possibilities to be kept in mind are multicystic dysplastic change in one moiety of a duplex kidney or focal dilation of one part of the collecting system.

Differential diagnosis of a renal cyst

- Medullary pyramids – evenly spaced, triangular shape.
- Papillary necrosis – typical position of a pyramid and may contain an echogenic focus.
- Hydronephrosis – dilated calyces show communication with each other.
- Lymphatic cysts – may be impossible to distinguish from the pelvicalyceal system without using CT urography.
- Haematoma – recent history of trauma is helpful. Look for an underlying lesion.
- Aneurysms – colour Doppler helps avoid misdiagnosis.
- Abscesses – clinical features of fever and raised white cell count.
- Hydatid – be aware of this in people from endemic areas.
- Cystic nephroma – multiloculated benign tumours; diagnosis may not be possible without histology.

CYSTIC DISEASES OF THE KIDNEY

This group of cystic diseases includes inherited, developmental and acquired cystic diseases. Pathologically there are many diagnoses: polycystic kidney disease, dominant or recessive; multicystic dysplastic kidney; pluricystic kidney of the multiple malformation syndromes; juvenile nephronophthisis and medullary cystic disease, medullary sponge kidney, primary glomerulocystic disease; glomerulocystic kidneys associated with systemic disorders; cystic kidney in tuberous sclerosis and in von Hippel–Lindau disease; and acquired cystic renal disease of long-term dialysis, to name a few.[52] Sometimes clinical and gross appearances are enough to characterise the disease and in others histological and molecular studies will be needed.

Acquired cystic kidney disease (ACKD)

This describes the process of cyst formation in a non-cystic failing kidney. Cysts form from dilated renal tubules and increase in size and number with the length of renal insufficiency.[53] The tubules may be obstructed by oxalate crystals, interstitial fibrosis or hyperplasia. Cysts continue to form in end-stage failure and development of ACKD is associated with being on dialysis, whether haemodialysis or peritoneal. Men are much more commonly affected. The rate of increase in size is greatest in young men and this may mimic the onset of polycystic disease. The longer someone has been on dialysis the more likely they are to have ACKD. Transplantation of a functioning kidney gives protection against the development of ACKD and may even cause some changes to regress. There is a well-known association with cystic renal cell carcinoma, occurring in 19% of those with ACKD.[53] Failure of a cyst to regress following transplantation when all the other cysts are regressing is suspicious for the development of renal cell carcinoma. The Bosniak classification is useful to assess the risk of malignancy in each cyst, but since the likelihood of renal carcinoma in complicated cysts of ACKD is high (about 50%), it is prudent to offer resection even in Bosniak IIF lesions.

Most patients with ACKD are asymptomatic but flank pain, haematuria and colic may develop if the cysts rupture or bleed.

Typical ultrasound features are of a small, bright kidney containing a number of small (0.5–3.0 cm) cysts, either cortical or medullary (Fig. 26.26). Cysts are commoner at areas of scarring. If enough cysts develop the kidney may become enlarged. Small cysts may be indistinguishable from solid lesions. Haemorrhagic complications have the same imaging appearances as in other cysts. One series showed that over a 7-year period, 17% of ACKD patients suffered large haemorrhagic cysts and 13% large perinephric haematomas.[54] If patients are also being treated with anticoagulants, then episodes of haemorrhage are more likely to occur and they may be large enough to be life-threatening.

Interestingly, the transplant kidney, even if left in place after it has failed, almost never develops ACKD.

Acquired cystic kidney disease

- Associated with dialysis, prevalence increasing with increasing length of dialysis.
- Cysts of 0.5–3.0 cm form in failing kidneys that are not otherwise cystic.
- Usually asymptomatic.
- Commoner in men.
- Renal transplantation provides protection against developing cysts.
- Increases the likelihood of spontaneous renal haemorrhage.
- Strong association with cystic renal cell carcinoma.

Multicystic dysplastic kidney

The aetiology of multicystic dysplastic kidney is thought to be ureteric atresia during early fetal life. It can affect one or both kidneys and can involve one moiety of a duplex kidney alone. The kidney or part of the kidney affected is necessarily non-functioning because of the ureteric atresia. Consequently, bilateral multicystic dysplastic kidney is incompatible with life – babies die at birth due to the pulmonary hypoplasia caused by the lack of liquor (liquor being essentially fetal urine). A single multicystic dysplastic kidney is, however, compatible with a normal life as the other kidney provides all the function. A multicystic dysplastic kidney often atrophies during childhood such that in later life the affected person only appears to have one kidney. Earlier concerns that the multicystic dysplastic kidney may be associated with development of tumour or hypertension appear to be unfounded, though surgeons may remove a persistent multicystic dysplastic kidney. The main clinical concern is the association with a contralateral uropathy in up to 40% of cases. This usually takes the form of either pelviureteric obstruction or vesico-ureteric reflux. Reflux may cause the

normal contralateral kidney to have reduced growth.[55] Most cases of multicystic dysplastic kidney are sporadic but there has been the occasional reported instance of familial recurrence.[56]

Ultrasound features are of numerous discrete cysts of varying sizes replacing all or nearly all of the renal substance (Fig. 26.27). The cysts show no inter-communication, distinguishing them from a hydronephrosis. The outline of the kidney is uneven due to the presence of the cysts.

A similar process of post-obstructive cystic dysplasia (Fig. 26.28) of the kidney may occur as a response to urinary tract obstruction at other times in utero. In these instances, the kidney may show a hydronephrotic renal pelvis surrounded by a cortex replaced by innumerable cysts of different sizes. Otherwise, distinction from a true multicystic dysplastic kidney may be impossible on imaging. Ureteroceles are occasionally seen on the ipsilateral side to a multicystic dysplastic kidney.

Polycystic kidney disease

Autosomal recessive polycystic kidney disease (ARPKD) may present in utero or in childhood and has been categorised into perinatal, neonatal, infantile and juvenile forms. All forms are caused by the same genetic defect related to chromosome 6p21.[57] Pathologically the features are of bilateral kidney involvement with multiple microcysts and liver involvement with portal and interlobular fibrosis. The ultrasound features are of bilateral, symmetrically enlarged, smooth-outlined kidneys (Fig. 26.29). They are of generally increased reflectivity due to the numerous interfaces provided by the microcysts (each being too small to individually resolve). Occasionally a discrete cyst may develop and the brightness of the kidney may reduce around its periphery as the size of the microcyst expands. The kidneys may appear normal initially. A not uncommon scenario is for the kidneys to look normal at the

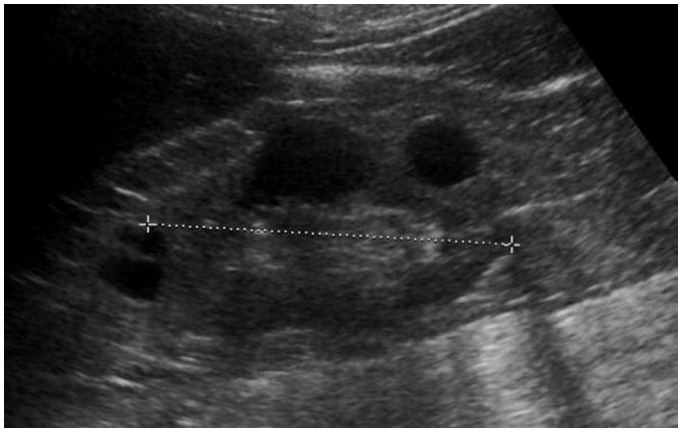


Figure 26.26 Acquired cystic kidney disease. Typically as a kidney fails it becomes small, bright and develops small cortical cysts.

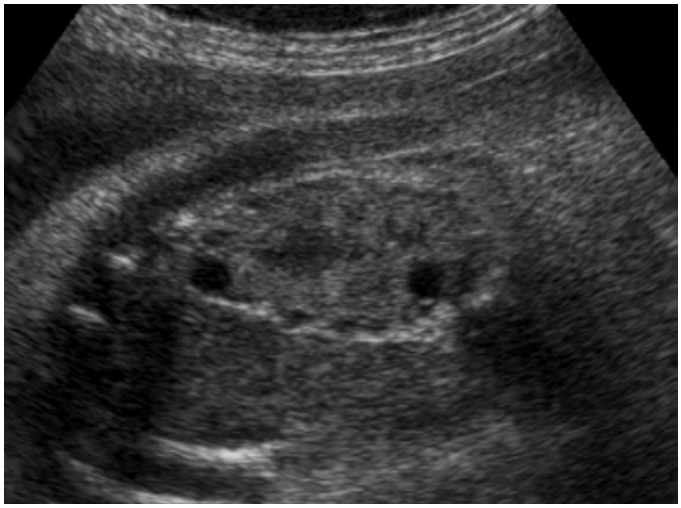


Figure 26.28 Longitudinal view of a fetal kidney with post-obstructive cystic dysplasia.



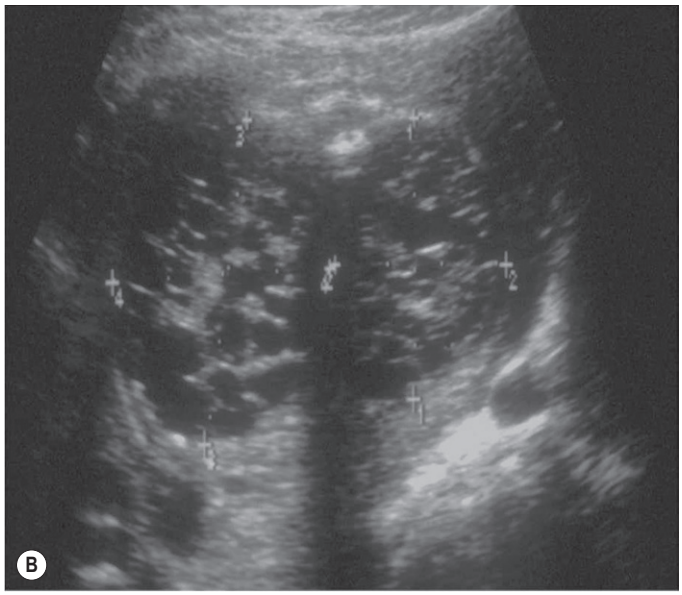


Figure 26.27 Multicystic dysplastic kidney. A: Transverse view of the fetal abdomen shows a unilateral right multicystic dysplastic kidney between the cursors and a normal left kidney; prognosis is good. **B:** Bilateral multicystic dysplastic kidneys in a fetus; prognosis is poor as there is no urine production and hence no liquor.

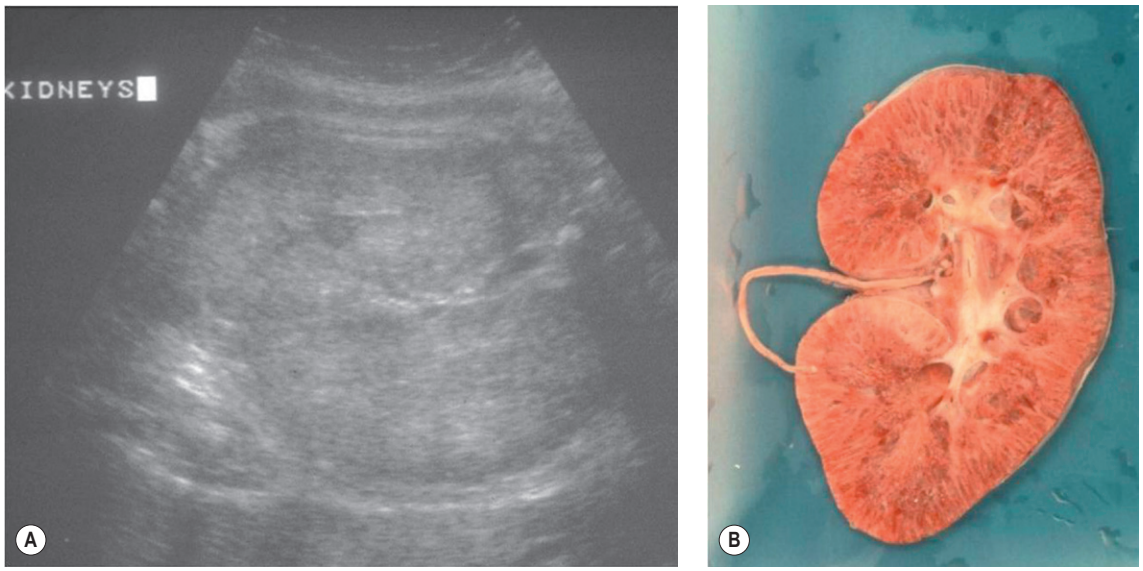


Figure 26.29 Autosomal recessive polycystic kidney disease. A: Longitudinal view of a fetus with ARPKD. The kidneys are symmetrically smooth, bright and large. There is no liquor, indicating these kidneys have ceased to function. **B:** Pathological specimen of an autosomal recessive polycystic kidney showing numerous tiny elongated cysts peripherally.

time of the 20-week in-utero anatomy scan but to have become enlarged and non-functioning by term pregnancy. If the condition is diagnosed in utero, then the prognosis is generally poor and the baby may succumb at birth due to underdeveloped lungs caused by a lack of liquor. Those that have a lesser degree of renal involvement are usually diagnosed at a later age; they may have better renal function but will suffer from portal hypertension secondary to the hepatic cysts and periportal fibrosis. Children who survive the perinatal period have a better prognosis than is generally perceived.[58] The parents have a 1 in 4 chance of having another affected child.

Autosomal dominant polycystic kidney disease (ADPKD) usually presents in the fourth or fifth decade of life with renal impairment, hypertension, haematuria and abdominal pain. The commonest mode of presentation is with hypertension.[59] The condition may also be detected serendipitously during ultrasound imaging for other reasons. ADPKD is caused by a mutation in PKD1 (chromosome 16p13.3) or PKD2 (chromosome 4q21–23).[60] Those with the PKD2 mutation show a lesser severity of disease. Screening of offspring of affected adults is normally by ultrasound. The essence of the test is that renal cysts in normal people are rare below the age of 30 so detection of cysts forms the basis of diagnosis. The criteria have been modified recently so that if the genotype of the family is unknown, those with the less severe PKD2 form will not be missed.[61] The presence of three or more renal cysts (unilateral or bilateral) in those aged 15 to 39 years, two or more cysts in each kidney at ages 40 to 59 years, and four or more cysts in each kidney for those over 60 years of age is enough in the presence of an established family history to confirm the diagnosis. Conversely, an at-risk individual older than 40 years who has fewer than two renal cysts does not have the disease.

Once the condition of ADPKD becomes established, innumerable renal cysts of varying sizes disrupt the normal architecture of the kidney and the kidneys become considerably enlarged (Fig. 26.30). The size of the kidneys is related to renal function and hypertension; an increase in cyst volume correlates with decline in renal function. Magnetic resonance can be used to obtain volumes of the entire kidney in a reproducible fashion and show changes over as short a period as 6 months.[62] Liver cysts occur in up to 67% of those with ADPKD and increase in size and number with age. Women suffer more severe liver disease than men. Cysts may occur in other organs too, being reported in seminal vesicles, pancreas, spleen and ovary.

Patients with ADPKD suffer from infective or haemorrhagic complications of their renal cysts. The symptoms and signs are the same as the same complication in someone with an isolated cyst but because there are so many cysts the frequency with which an ADPKD individual is affected is greater. It can be difficult to tell which cyst of the many present is responsible for the patient's symptoms. Positron emission tomography helps to identify the culprit.[27] Polycystic kidneys are more likely to suffer from trauma because they are enlarged. Calculi are seen in up to 20% of ADPKD patients. Smaller calculi usually pass spontaneously even if renal function is impaired. The management of larger calculi is complicated by the presence of the cysts, percutaneous techniques and lithotripsy being relatively contraindicated.

Von Hippel–Lindau disease

Von Hippel–Lindau disease is inherited in an autosomal dominant fashion with variable expression and penetrance of the gene and is characterised by the development of a variety of benign and malignant tumours.[63] The spectrum of clinical manifestation is wide. It usually presents after the second decade of life and will feature one or more of the following: renal cysts 75%; cerebellar haemangioblastoma 35–60%; retinal angiomatosis 50%; renal adenocarcinoma 25–45% (Fig. 26.31); phaeochromocytoma 10%; endolymphatic sac tumours; epididymal cystadenomas; and pancreatic cysts and tumours. The commonest causes of death are renal cell carcinomas and complications from cerebellar haemangioblastomas.

Genetic testing is available, but, because the syndrome may manifest in many different ways, imaging is essential in identifying tumours. Screening is advocated as the tumours in von Hippel–Lindau disease are treatable and early detection allows more conservative procedures, in turn improving the patient's length and quality of life.

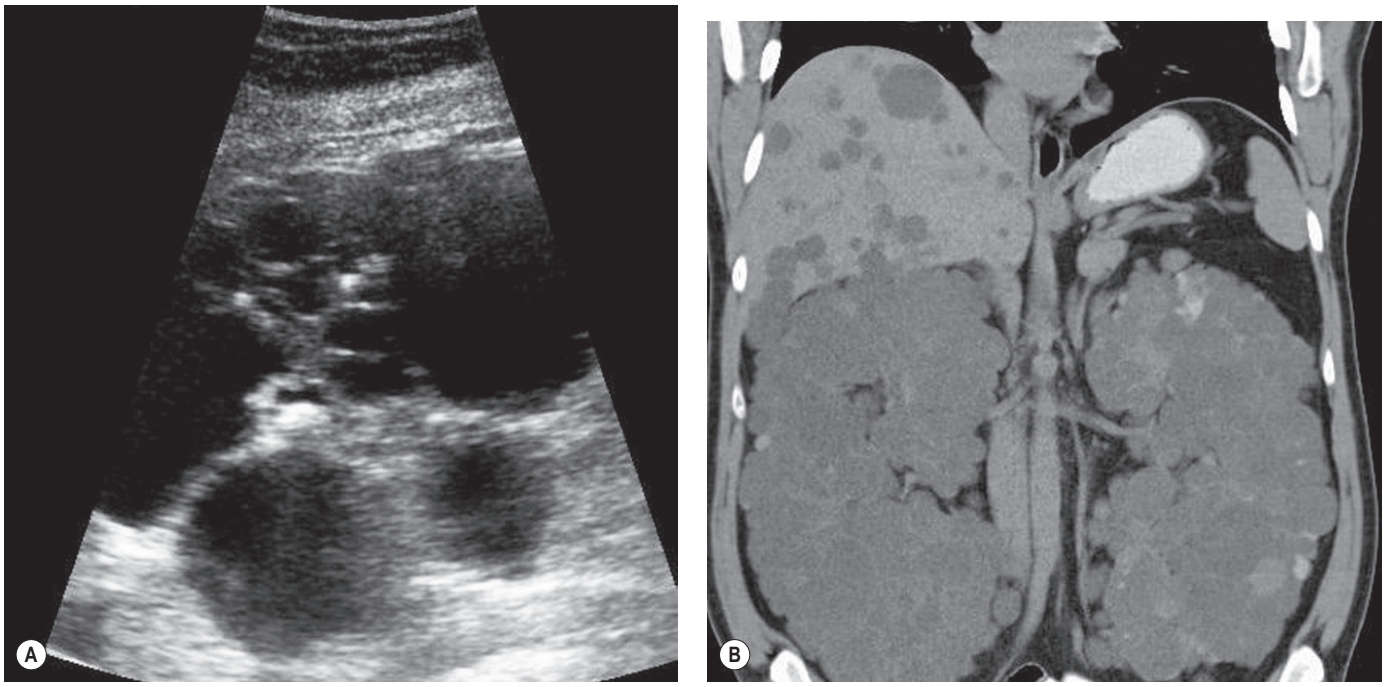


Figure 26.30 **Autosomal dominant polycystic kidney disease** on ultrasound **(A)** and coronal reformatted CT **(B)**. Note the differing sizes of the cysts and that there are cysts in the liver. This is an advanced example with the kidneys greatly enlarged by innumerable cysts. Earlier in the onset of the disease the cysts may be much less numerous.

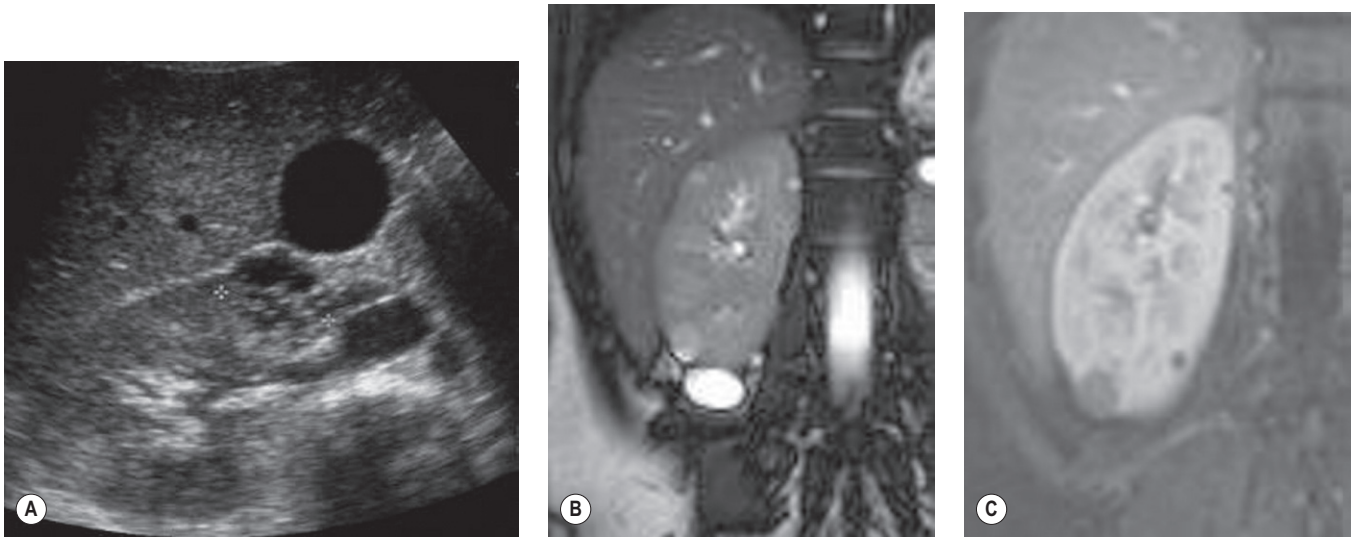


Figure 26.31 **Von Hippel–Lindau disease.** Screening is used to detect the onset of renal disease with either cysts or solid tumours. **A:** A complex cyst developing next to a more simple cyst. Magnetic resonance **(B, C)** is a better tool to assess the kidneys once the initial lesions are detected by ultrasound screening.

Renal cysts may be the first manifestation of the disease. Ultrasound of the abdomen is used as a screening test in asymptomatic carriers of the gene. Renal cysts are usually cortical and measure 0.5–3.0 cm in size. Once ultrasound screening detects a patient is affected by renal cysts, it is reasonable to proceed to MR for follow-up. This is because the renal adenocarcinomas that occur in conjunction with the cysts are multifocal and small within one kidney (87%) or bilateral (75%) and ultrasound is relatively insensitive in their detection. Nephron-sparing treatments are usually offered, either partial nephrectomy or radio-frequency ablation. Ultrasound may also identify cysts in the pancreas, liver and adrenals.

Tuberous sclerosis complex

Tuberous sclerosis is characterised by mental disability, seizures and cutaneous adenoma sebaceum. It is an autosomal dominant hereditary neurocutaneous disorder with hamartomatous lesions involving the brain, skin, kidney, heart and other organs. Renal manifestations are mainly angiomyolipomas, cysts and cancer.[64] Renal lesions occur in 57% of patients and of these angiomyolipomas occurred in 85%, cysts in 45% and renal carcinoma in 4%.[65] Renal cysts and angiomyolipomas may be the only manifestation of the disease in childhood, with an average age of onset of 11 years but some appearing as early as 3 years. Both cysts and angiomyolipomas increase in size and number with increasing age. Angiomyolipomas are commoner in female patients but renal cysts are equally distributed between the sexes.

The renal cysts have typical ultrasound features. Angiomyolipomas are seen as focal masses of increased echogenicity in the cortex, some of which are exophytic (Fig. 26.32). They are usually small in tuberous sclerosis but may be very numerous, replacing the entire renal substance (Fig. 26.33). Occasionally tuberous sclerosis patients may show larger angiomyolipomas. If they are larger than 4 cm, they have an increased chance of spontaneous bleeding.

Medullary cystic disease

This is a complex group of disorders comprising juvenile nephronophthisis, medullary cystic renal degeneration and renal retinal dysplasia. Extensive molecular work has enabled the identification of genes on chromosomes 1 and 16.[66] Presentation of these disorders is with renal failure in childhood or early adulthood. Since molecular diagnostics are not yet a feasible clinical tool, ultrasound can be used for screening, though clinical acumen remains important.[67]

Ultrasound identifies four main findings: renal hyperechogenicity, poor corticomedullary differentiation, small kidney size and corticomedullary cysts.[68] These cysts may be multiple and usually 1–2 cm in size. They lie in the medulla or at the corticomedullary junction and are thought to be dilated distal convoluted tubules. The cysts usually appear later in the course of the disease than the cortical hyperechogenicity. The outline of the kidneys remains smooth.

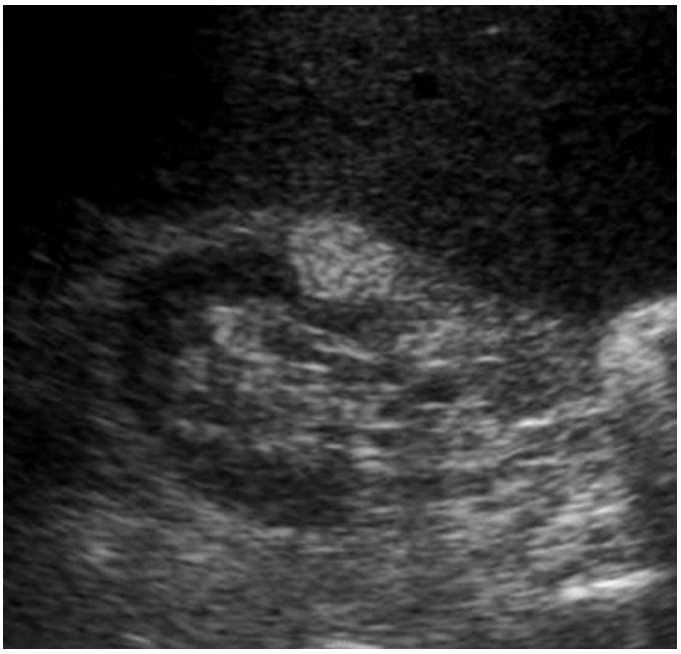


Figure 26.32 Tuberous sclerosis may manifest very variably. This patient has a solitary, exophytic angiomyolipoma seen as a focal echogenic mass on ultrasound; 45% will have a simple renal cyst too.

Syndromes with renal cysts

- Multicystic dysplastic kidney – occurs in utero. Kidney is non-functioning. The bilateral form is fatal. Kidney has numerous cysts of varying size distorting its outline.
- Autosomal recessive polycystic kidney disease – may present in utero. Both kidneys are symmetrically affected. Cysts are too small to resolve on ultrasound so kidneys look big, bright and smooth.
- Autosomal dominant polycystic kidney disease – presents in fourth or fifth decade of life. Cysts are seen in both kidneys and the liver. Kidneys may become massively enlarged by cysts. Complications of infection, haemorrhage and renal failure occur.
- Von Hippel–Lindau disease – autosomal dominant, usually presents in the second decade of life. Ultrasound screening used to look for renal cysts. Concern is the development of multifocal renal cell carcinomas.
- Tuberous sclerosis – autosomal dominant but very variable in presentation. Renal cysts occur but the renal lesions of greatest concern are angiomyolipomas; these may bleed.

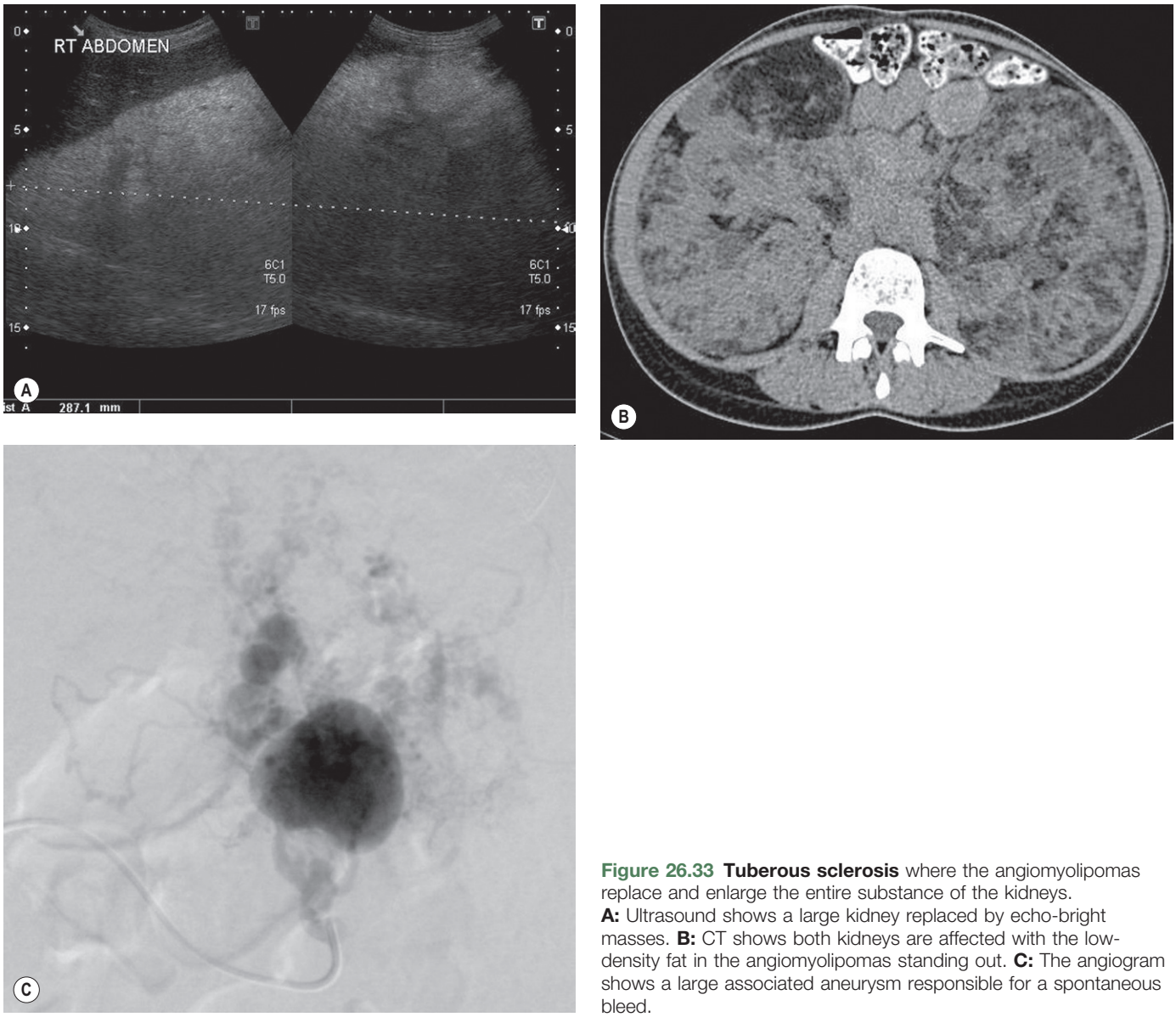


Figure 26.33 **Tuberous sclerosis** where the angiomyolipomas replace and enlarge the entire substance of the kidneys. **A:** Ultrasound shows a large kidney replaced by echo-bright masses. **B:** CT shows both kidneys are affected with the low-density fat in the angiomyolipomas standing out. **C:** The angiogram shows a large associated aneurysm responsible for a spontaneous bleed.

REFERENCES

1. Al-Said J, O'Neill WC. Reduced kidney size in patients with simple renal cysts. Kidney Int 2003;64:1059–1064.
2. Al-Said J, Brumback MA, Moghazi S, et al. Reduced renal function in patients with simple renal cysts. Kidney Int 2004;65:2303–2308.
3. Chin HJ, Ro H, Lee HJ, et al. The clinical significances of simple renal cyst: is it related to hypertension or renal dysfunction? Kidney Int 2006;70:1468–1473.
4. Giannakopoulos X, Charalabopoulos K, Charalabopoulos A, et al. Giant simple renal cyst complicated with hypertension. Int J Clin Pract Suppl 2005;147:69–71.
5. Marumo K, Horiguchi Y, Nakagawa K, et al. Incidence and growth pattern of simple cysts of the kidney in patients with asymptomatic microscopic haematuria. Int J Urol 2003;10:63–67.
6. Mosharafa AA. Prevalence of renal cysts in a Middle-Eastern population: an evaluation of characteristics and risk factors. BJU Int 2008;101:736–738.
7. Chang CC, Kuo JK, Chan WL, et al. Prevalence and clinical characteristics of simple renal cyst. J Chin Med Assoc 2007;70:486–491.
8. Terada N, Arai Y, Kinukawa N, Terai A. The 10-year natural history of simple renal cysts. Urology 2008;71:7–11.
9. Eknoyan G. A clinical view of simple and complex renal cysts. J Am Soc Nephrol 2008 Sep 5 (epub ahead of print).
10. Zerem E, Imamovic G, Omerovic S. Symptomatic simple renal cyst: comparison of continuous negative-pressure catheter drainage and single-session alcohol sclerotherapy. AJR Am J Roentgenol 2008;190:1193–1197.
11. Cho DS, Ahn HS, Kim SI, et al. Sclerotherapy of renal cysts using acetic acid: a comparison with ethanol sclerotherapy. Br J Radiol 2008 Sep 1 (epub ahead of print).
12. Lin CJ, Chen YC, Chen HH, et al. Renal cell carcinoma presenting as a huge simple renal cyst. Med Oncol 2008;25:104–106.
13. Kilciler M, Bedir S, Erdemir F, et al. Isolated unilocular renal hydatid cyst: a rare diagnostic difficulty with simple cyst. Urol Int 2006;77:371–374.
14. Duncan AW, Charles AK, Berry PJ. Cysts within septa: an ultrasound feature distinguishing neoplastic from non-neoplastic renal lesions in children? Pediatr Radiol 1996;26:315–317.
15. Hirai T, Ohishi H, Yamad R, et al. Usefulness of color Doppler flow imaging in differential diagnosis of multilocular cystic lesions of the kidney. J Ultrasound Med 1995;14:771–776.
16. Clevert DA, Minaifar N, Weckbach S, et al. Multislice computed tomography versus contrast enhanced ultrasound in evaluation of

complex cystic renal masses using the Bosniak classification system. Clin Hemorrheol Microcirc 2008;39:171–178.
17. Quaia E, Bertolotto M, Cioffi V, et al. Comparison of contrast-enhanced sonography with unenhanced sonography and contrast-enhanced CT in the diagnosis of malignancy in complex cystic renal masses. AJR Am J Roentgenol 2008;191:1239–1249.
18. Bosniak MA. The current approach to renal cysts. Radiology 1986;158:1–10.
19. Ascenti G, Mazziotti S, Zimbaro G, et al. Complex cystic renal masses: characterization with contrast-enhanced US. Radiology 2007;243: 158–165.
20. Israel GM, Bosniak MA. How I do it: evaluating renal masses. Radiology 2005;236:441–450.
21. Fujii Y, Higashi Y, Owada F, et al. Benign haemorrhagic renal cysts mimicking cystic renal cell carcinoma. Hinyokika Kiyo 1993;39:1113–1117.
22. Moore AE, Kujubu DA. Spontaneous retroperitoneal hemorrhage due to acquired cystic kidney disease. Hemodial Int 2007;11(Suppl 3): S38–S40.
23. Borras M, Valdivielso JM, Egido R, et al. Haemoperitoneum caused by bilateral renal cyst rupture in an ACKD peritoneal dialysis patient. Nephrol Dial Transplant 2006;21:789–791.
24. Zhang JQ, Fielding JR, Zou KH. Etiology of spontaneous perirenal hemorrhage: a meta-analysis. J Urol 2002;167:1593–1596.
25. Prando A, Prando D, Prando P. Renal cell carcinoma: unusual imaging manifestations. Radiographics 2006;26:233–244.
26. Vaidyanathan S, Hughes PL, Oo T, Soni BM. Spontaneous rupture of an infected renal cyst and external drainage through a lumbar surgical scar in a male patient with cervical cord injury: a case report. J Med Case Reports 2008;2:154.
27. Soussan M, Sberro R, Wartski M, et al. Diagnosis and localisation of renal cyst infection by 18F-fluorodeoxyglucose PET/CT in polycystic kidney disease. Ann Nucl Med 2008;22:529–531.
28. Hosch W, Stojkovic M, Janisch T, et al. The role of calcification for staging cystic echinococcosis. Eur Radiol 2007;17:2538–2545.
29. Hartman DS, Choyke PL, Hartmann MS. A practical approach to the cystic renal mass. Radiographics 2004;24:S101–S115.
30. Israel GM, Bosniak MA. Calcification in cystic renal masses: is it important in diagnosis? Radiology 2003;226:47–52.
31. Levine E, Grantham JJ. Calcified renal stones and cyst calcifications in autosomal dominant polycystic kidney disease: clinical and CT study in 84 patients. AJR Am J Roentgenol 1992;159:77–81.
32. Vaidyanathan S, Hughes PL, Soni BM. Bilateral renal milk of calcium masquerading as nephrolithiasis in patients with spinal cord injury. Adv Ther 2007;24:533–544.
33. Harisinghani MG, Maher MM, Gervais DA, et al. Incidence of malignancy in complex renal masses (Bosniak category III): should imaging-guided biopsy precede surgery? AJR Am J Roentgenol 2003;181:755–758.
34. Hora M, Hes O, Michal M, et al. Extensively cystic neoplasms in adults (Bosniak classification II or III) – possible 'common' histological diagnoses: multilocular cystic renal cell carcinoma, cystic nephroma, and mixed epithelial and stromal tumour of the kidney. Int Urol Nephrol 2005;37:743–750.
35. Gong K, Zhang N, He Z, et al. Multilocular cystic renal cell carcinoma: an experience of clinical management for 31 cases. J Cancer Res Clin Oncol 2008;134:433–437.
36. Cai S, Li J, Jiang Y, et al. Sonographic patterns and differential diagnoses of cystic renal carcinomas. Chin Med Sci J 2002;17: 164–167.
37. Nicolau C, Vilana R, Del Amo M, et al. Accuracy of sonography with a hydration test in differentiating between excretory renal obstruction and renal sinus cysts. J Clin Ultrasound 2002;30:532–536.
38. Amis ES, Cronan JJ. The renal sinus: an imaging review and proposed nomenclature for sinus cysts. J Urol 1988;139:1151–1159.
39. Wadhwa P, Kumar A, Sharma S, et al. Renal lymphangiomatosis: imaging and management of a rare renal anomaly. Int Urol Nephrol 2007;39:365–368.
40. Sarikaya B, Akturk Y, Bekar U, Topaloglu S. Bilateral renal lymphangiomatosis mimicking hydronephrosis: multidetector CT urographic findings. Abdom Imaging 2006;31:732–734.
41. Pancione L, Giacomelli G, Moroni M, et al. Lymphangioma communicating with the excretory system. Minerva Urol Nefrol 2008;60:65–67.
42. Surabhi VR, Menias C, Prasad SR, et al. Neoplastic and non-neoplastic disorders of the perirenal space: cross-sectional imaging findings. Radiographics 2008;28:1005–1017.
43. Chichakli R, Krause R, Voelzke B, Turk T. Incidence of perinephric hematoma after percutaneous nephrolithotomy. J Endourol 2008;22:1227–1232.
44. Lenton J, Kessel D, Watkinson AF. Embolisation of renal angiomyolipomas: immediate complications and long-term outcomes. Clin Radiol 2008;63:864–870.
45. Vijay RK, Kaduthodil MJ, Bottomley JR, Abdi S. Metastatic gestational trophoblastic tumour presenting as spontaneous subcapsular renal haematoma. Br J Radiol 2008;81:e234–e237.
46. Deibler AR, Nadig SN, Curry N, et al. Intrarenal varix presenting as an enhancing renal mass with calcifications. J Urol 2001;166:997–998.
47. Asakuma J, Miyajima A, Sawazaki H, et al. Incidentally discovered giant renal arteriovenous malformation. Int J Urol 2001;8:322–325.
48. Lee BE, Seol HY, Kim TK, et al. Recent clinical overview of renal and perirenal abscesses in 56 consecutive cases. Korean J Intern Med 2008;23:140–148.
49. Stojadinovic M, Micic S, Milovanovic D. Ultrasonographic and computed tomography findings in renal suppurations: performance indicators and risks for diagnostic failure. Urol Int 2008;80:389–397.
50. Jevremovic D, Lager DJ, Lewin M. Cystic nephroma (multilocular cyst) and mixed epithelial and stromal tumour of the kidney: a spectrum of the same entity? Ann Diagn Pathol 2006;10:77–82.
51. Lane BR, Campbell SC, Remer EM, et al. Adult cystic nephroma and mixed epithelial and stromal tumor of the kidney: clinical, radiographic, and pathologic characteristics. Urology 2008;71: 1142–1148.
52. Bisceglia M, Galliani CA, Senger C, et al. Renal cystic diseases: a review. Adv Anat Pathol 2006;13:26–56.
53. Schwarz A, Vatandaslar S, Merkel S, Haller H. Renal cell carcinoma in transplant recipients with acquired cystic kidney disease. Clin J Am Soc Nephrol 2007;2:750–756.
54. Levine E, Slusher SL, Grantham JJ, Wetzel LH. Natural history of acquired renal cystic disease in dialysis patients: a prospective longitudinal CT study. AJR Am J Roentgenol 1991;156:501–506.
55. Fanos V, Sinaguglia G, Vino L, et al. Multicystic dysplastic kidney and contralateral vesicoureteral reflux. Renal growth. Minerva Pediatr 2001;53:95–98.
56. Belk RA, Thomas DF, Mueller RF, et al. A family study and the natural history of prenatally detected unilateral multicystic dysplastic kidney. J Urol 2002;167:666–669.
57. Sessa A, Righetti M, Battini G. Autosomal recessive and dominant polycystic kidney diseases. Minerva Urol Nefrol 2004;56:329–338.
58. Guay-Woodford LM, Desmond RA. Autosomal recessive polycystic kidney disease: the clinical experience in North America. Pediatrics 2003;111:1072–1080.
59. Rabbani MA, Ali SS, Murtaza G, et al. Clinical presentation and outcome of autosomal dominant polycystic kidney disease in Pakistan: a single centre experience. J Pak Med Assoc 2008;58:305–309.
60. Harris PC, Torres VE. Polycystic kidney disease. Annu Rev Med 2008 Oct 23: epub ahead of print.
61. Pei Y, Obaji J, Dupuis A, et al. Unified criteria for ultrasonographic diagnosis of ADPKD. J Am Soc Nephrol 2008 Oct 22: epub ahead of print.
62. Kistler AD, Poster D, Krauer F, et al. Increases in kidney volume in autosomal dominant polycystic kidney disease can be detected within 6 months. Kidney Int 2008 Oct 29: epub ahead of print.
63. Leung RS, Biswas SV, Duncan M, Rankin S. Imaging features of von Hippel–Lindau disease. Radiographics 2008;28:65–79.
64. Fatihi el M, Khanfri N, Niang A, et al. Renal manifestations of tuberous sclerosis complex. Ann Med Interne (Paris) 2003;154:255–258.
65. Rakowski SK, Winterkorn EB, Paul E, et al. Renal manifestations of tuberous sclerosis complex: incidence, prognosis, and predictive factors. Kidney Int 2006;70:1777–1782.
66. Scolari F, Ghiggeri GM. Nephronophthisis-medullary cystic kidney disease: from bedside to bench and back again. Saudi J Kidney Dis Transpl 2003;14:316–327.
67. Rohatgi R. Clinical manifestations of hereditary cystic kidney disease. Front Biosci 2008;13:4175–4197.
68. Chuang YF, Tsai TC. Sonographic findings in familial juvenile nephronophthisis-medullary cystic disease complex. J Clin Ultrasound 1998;26:203–206.

CHAPTER

27 Solid renal masses

Michael J. Weston and Tze M. Wah

INTRODUCTION 505

PSEUDO-TUMOURS 505
Column of Bertin 505
Dromedary hump 505
Persistent fetal lobulation versus renal scarring 505
Splenorenal fusion 505
Focal pyelonephritis 507
Xanthogranulomatous pyelonephritis 507
Granulomatous renal pseudo-tumours 507
Extramedullary haematopoiesis 507
Arteriovenous malformations 507

BENIGN SOLID MASSES 508
Adenoma 508
Papillary adenoma 508
Metanephric adenoma 508
Management 508
Oncocytoma 508
Appearances 508
Angiomyolipoma 509
Appearances 510
Differential diagnosis 511
Treatment 512
Other benign solid renal masses 512

MALIGNANT RENAL MASSES 512
Renal cell carcinoma 512
Presentation 513
Screening 513
Appearances 513
Rare presentations 513
Staging 513
Treatment 517
Collecting duct and medullary carcinoma 517
Transitional cell carcinoma 517
Aetiology 517
Symptoms 518
Ultrasound findings 518
Other tests 519
Patterns of spread 520
Treatment 520
Lymphoma 521
Leukaemia 521
Metastases 521
Sarcoma and other rare renal tumours 521
Hereditary tumours and syndromes 522

MINIMALLY INVASIVE TREATMENT OF RENAL CELL CARCINOMA 522
Radio-frequency ablation of renal cell carcinoma 523

INTRODUCTION

Cystic renal masses are the commonest renal mass lesions. They are discussed in Chapter 26. Solid renal masses, although less common than cysts, are still often detected serendipitously during cross-sectional imaging performed for other reasons. It has been the practice in the past to assume all solid renal masses are renal cell carcinoma, especially if they showed enhancement with contrast medium, proof being obtained only after radical nephrectomy. Nowadays, it is possible to recognise benign solid renal masses with imaging, so that surgery can be avoided. There are also a variety of pseudo-tumours that can mimic the presence of a true mass and provide a pitfall for the unwary.

PSEUDO-TUMOURS

Renal pseudo-tumours can be categorised as developmental, infectious, granulomatous or vascular in nature.[1] Ultrasound can identify most of these lesions if care is taken, but on occasion recourse to CT or MRI will be needed to confirm their nature.

Column of Bertin

This is a normal part of the kidney, comprising normal cortical tissue extending between the renal pyramids and projecting into the renal sinus fat. This cortex can be hypertrophied and can resemble a mass (Fig. 27.1), often of slightly greater echogenicity than the cortex because of anisotrophy. It is most commonly seen in the middle third of the kidney and more frequently on the left than the right. If contrast medium is given, either ultrasonic microbubbles or CT, the column of Bertin will show the same enhancement as normal cortex.

Dromedary hump

This is a focal bulge on the lateral margin of the left kidney, formed as an adaptation to the available space next to the spleen (Fig. 27.2). Enhancement with contrast agents is the same as normal cortex.

Persistent fetal lobulation versus renal scarring

The fetal kidneys have prominent lobes that may be separated by indentations on the cortical surface. These contours have usually diminished by birth but occasionally persist into adulthood. The indentations are positioned in between the renal pyramids, which is in contrast to true renal scarring from reflux nephropathy where the scar overlies the pyramid (Fig. 27.3). Cortical infarcts do produce scars between the pyramids, but they are usually isolated. The abnormality of the cortical contour produced by any of these mechanisms may mimic the presence of a focal renal lesion. Likewise, preserved normal cortex within a very scarred kidney may mimic the appearance of a mass.

Splenorenal fusion

Heterotopic splenic tissue very rarely occurs within the kidney, either congenitally or secondarily due to splenosis following

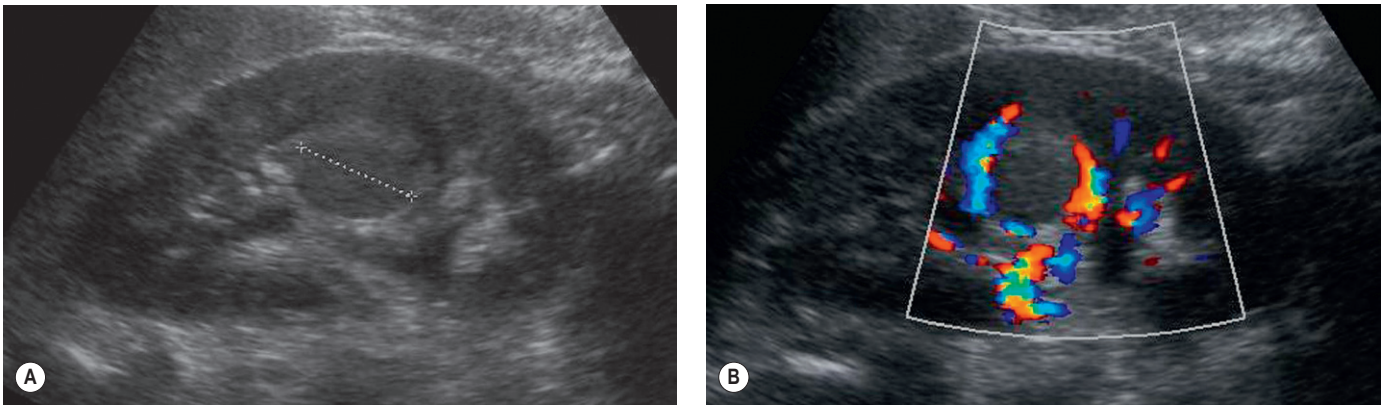


Figure 27.1 Column of Bertin. This is a normal projection of cortical tissue into the renal sinus fat. It can appear slightly more echogenic than normal cortex and can appear mass-like due to hypertrophy as in **A**. Colour Doppler **(B)** shows the normal vascularity around the column.

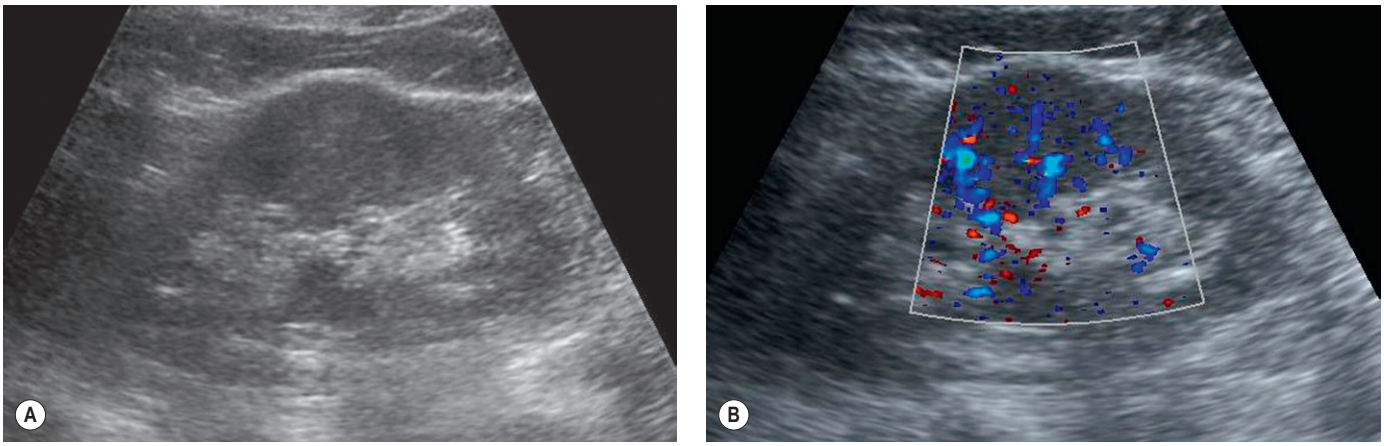


Figure 27.2 Dromedary hump. This is a normal variant seen on the left kidney only; a focal bulge on the lateral margin of the kidney that can simulate a mass, as in **A**. Colour Doppler **(B)** shows it to have normal vascularity.

Categorisation of renal pseudo-tumours[1]

Developmental:
- Columns of Bertin
- Fetal lobulation
- Dromedary hump
- Splenorenal fusion
- Cross-fused renal ectopia

Infectious:
- Abscess
- Focal pyelonephritis
- Scarring

Granulomatous:
- Xanthogranulomatous pyelonephritis
- Sarcoidosis
- Malacoplakia
- Tuberculosis

Vascular:
- Extramedullary haematopoiesis
- Arteriovenous malformation
- Renal pelvic haematomas
- Subcapsular haemorrhage

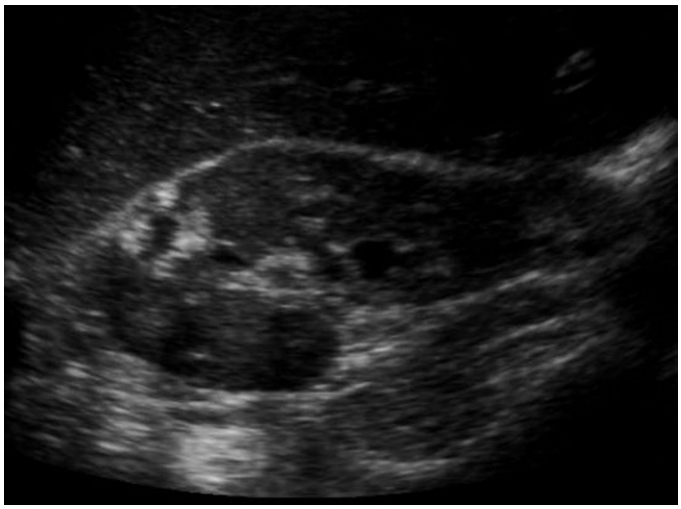


Figure 27.3 Dense calcification is seen in the renal cortex at the site of a scar – identified as such by its relationship to the underlying renal pyramid.

splenectomy or splenic trauma. The heterotopic splenic tissue forms a mass within the kidney, which is either asymptomatic or found as a result of a search for causes of anaemia (hypersplenism). The diagnosis should be considered in those who have had splenectomy or splenic trauma in the past. Cross-sectional imaging simply demonstrates an enhancing mass, but a radioisotope ^{99m}Tc sulphur colloid scan will show uptake, confirming the splenic nature of the lesion.

Focal pyelonephritis

Lobar nephronia, acute focal pyelonephritis and focal bacterial nephritis are synonyms for the same condition. In essence, the condition is a focal area of pyelonephritis within a lobar distribution. It is commoner in diabetics and immunocompromised people. It represents an inflammatory mass that does not contain any pus, although progression to an abscess will occur if treatment is inadequate. Ultrasound shows a mass or wedge-shaped area that extends from the medulla to the cortical margin (Fig. 27.4). It can be of increased, decreased or similar reflectivity to normal cortex.[2] The absence of a cortical bulge helps to distinguish the condition from a tumour, though, since the clinical presentation is one of infection with fever, flank pain and pyuria, the diagnosis is not normally in doubt. Harmonic imaging improves detection of focal pyelonephritis and it can be used to monitor resolution with treatment. Microbubble contrast agents can perform a similar role.

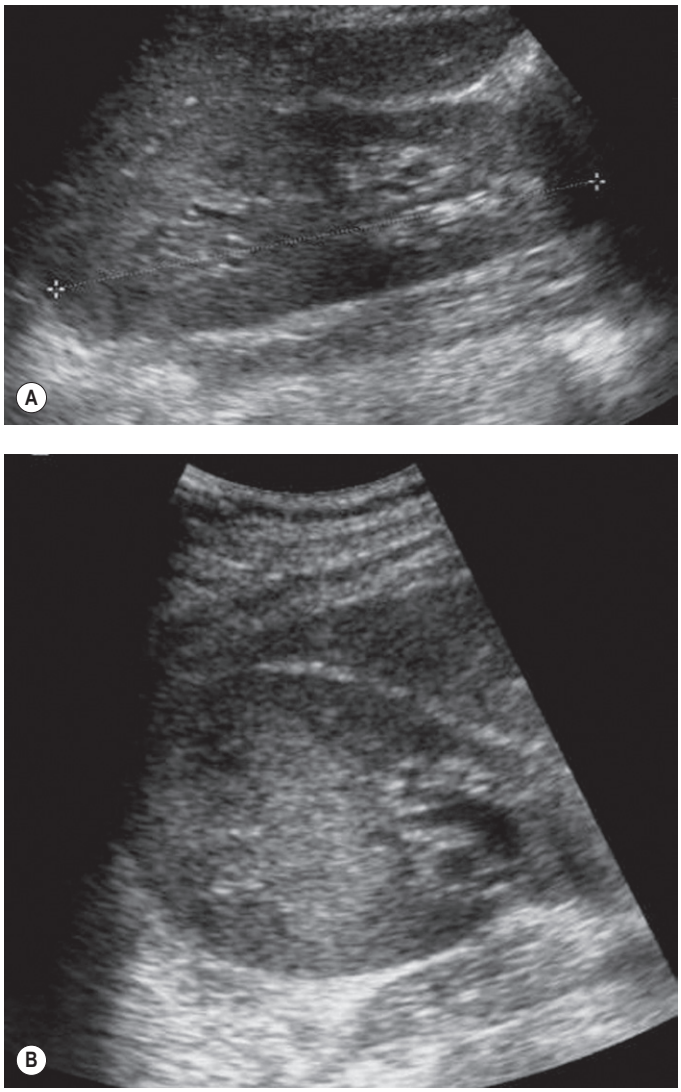


Figure 27.4 Focal pyelonephritis. Longitudinal **(A)** and transverse **(B)** views of the right kidney showing focal increased echogenicity in the upper pole of the kidney. The history of fever, flank pain and urinary tract infection made the diagnosis of focal pyelonephritis.

Xanthogranulomatous pyelonephritis

This is a rare inflammatory condition, usually secondary to chronic renal tract obstruction due to stones (70% will have a staghorn calculus). The infection results in destruction of the normal renal cortex. A characteristic feature pathologically is the presence of xanthoma cells, which are lipid-laden macrophages. These produce areas in the resulting mass that contain enough fat for it to be detectable at CT scan. Diabetic patients are particularly prone to developing xanthogranulomatous pyelonephritis. Presentation is with chronic ill-health rather than any features of acute infection.

Ultrasound will show single or multiple low-echo masses in the parenchyma of an enlarged kidney and a central echogenic focus due to the obstructing calculus. No recognisable kidney structure may remain. There is no sign on ultrasound that confirms the diagnosis, but CT may be helpful by showing the presence of fat and calculi. If the mass has arisen in the absence of calculi it is more likely that a misdiagnosis of renal cell carcinoma will be made.

Xanthogranulomatous pyelonephritis

- A mimic of malignancy.
- Associated with calculi and diabetes.
- A chronic infective complication of renal obstruction.
- No characteristic features on US.
- CT may identify the fat present in the lipid laden macrophages.

Granulomatous renal pseudo-tumours

Sarcoidosis, malacoplakia and tuberculosis can all produce focal or multifocal abnormalities in the kidneys that might mimic renal metastases or lymphoma. There are no specific imaging features; biopsy is generally required to make the diagnosis.

Extramedullary haematopoiesis

Failure of haematopoiesis in the bone marrow prompts other sites to transform to undergo haematopoiesis. The common sites are spleen, liver and lymph nodes but many other areas may uncommonly transform too, including the kidney. Myelofibrosis, chronic myeloproliferative disorder and polycythaemia vera are common causes. A renal mass in association with these diseases should give pause for thought. There are no specific imaging features and biopsy will be needed to make the distinction from lymphoma or other tumours.

Arteriovenous malformations

Colour-flow Doppler should make this diagnosis straightforward at ultrasound. Care needs to be taken though, as although most arteriovenous malformations will be secondary to trauma or congenital, they are occasionally associated with underlying renal cell carcinomas. In this instance the shunt may be so large and the cancer so small that the tumour is relatively hard to discern. Magnetic resonance can be useful in this context.

BENIGN SOLID MASSES

Adenoma

There used to be an arbitrary distinction made in the past that solid lesions less than 3 cm in size were benign and they were often called adenomas. It is now apparent that the diagnosis of a renal adenoma is no longer tenable on imaging.

It is considered that all clear cell containing tumours are carcinomas and that there is no such thing as a clear cell adenoma.[3] Even very small clear cell tumours may show metastasis so it is better to consider these lesions as having greater or lesser aggressiveness depending on their presentation.

Papillary adenoma

Papillary adenomas do exist and may be found in about 40% of autopsies of those aged over 70 years.[4] They are also found in sclerosed end-stage kidneys and in acquired cystic disease kidneys. There is a continuum of development to transformation to carcinoma. It is important to realise that by definition (WHO 2004 classification) papillary adenomas are all less than 5 mm in size. Histological features are identical to papillary carcinomas, although the carcinomas may exhibit greater amounts of chromosomal aberration. There is no imaging test or feature to allow distinction from any other small tumour.

Metanephric adenoma

Metanephric adenoma is considered a rare benign renal neoplasm with a peak incidence in the fifth decade of life (range from 5 to 83 years) and is commoner in women.[4] They represent 1% of renal tumours less than 7 cm in size.[3] Half are found incidentally and 10% are associated with polycythaemia. The polycythaemia promptly resolves once the tumour is removed or ablated. Histogenetically they are considered to be at the most hyper-differentiated, benign end of the nephroblastoma spectrum. This may account for the report of metastasis in two recent cases.[5] Metanephric adenoma typically appears as a well-defined, unencapsulated, solid mass. Ultrasound shows a hyper-echogenic lesion that also has increased through transmission of sound.[6] CT shows them to be of increased attenuation compared to normal kidney on unenhanced scans. Larger lesions may be expansile and may show cystic degeneration and calcification. There are no distinguishing features on imaging that allow these tumours to be separated prospectively from a renal cell carcinoma.

Management

Small solid renal lesions present a management problem as there is no way with imaging to tell if they are benign or not (Fig. 27.5). However, it is known that small tumours usually grow slowly, usually less than 0.5 cm per year, and that these tumours are most unlikely to metastasise whilst they are smaller than 3 cm. It is also known that the majority of benign tumours are less than 4 cm in size.[7] Options for management include 'watchful waiting' or surveillance, particularly in elderly patients or those too unfit to survive intervention. New techniques are being tried: laparoscopic partial nephrectomy, enucleation, ablation and high-intensity focused ultrasound.[8] These have to be weighed against traditional open surgical techniques. Clearly, there is a need for histological proof in these non-traditional approaches such as ablation to ensure that like is being compared with like in terms of outcome. Ultrasound-guided biopsy is advocated in the diagnosis of small renal masses, particularly those that are homogeneous and non-cystic,[9] as it is these that are most likely to be benign. Another series[10] showed that renal biopsy of focal masses altered the clinical decision-making in 60% of cases. There was no evidence of any tumour seeding in their series of 152 biopsies.

Oncocytoma

Oncocytomas are commoner in men, usually asymptomatic and most often found by chance in the sixth or seventh decade. The tumour contains oncocytes, large cells with mitochondria-rich, eosinophilic cytoplasm. They represent up to 6% of all renal epithelial neoplasms and generally follow a benign course without metastasis. Most are not correctly diagnosed before operation, only 20% in one series,[11] being usually mistaken for renal cell carcinoma. There is also the problem that oncocytomas may be associated with renal cell carcinoma either as hybrid tumours or as two adjacent lesions that have grown into each other (collision tumours).

Appearances

Ultrasound appearances may vary, with oncocytomas displaying all types of echogenicity from reduced to increased reflectivity. The characteristic feature associated with oncocytomas is the presence of a central scar and a spoke-wheel pattern of enhancement. This is

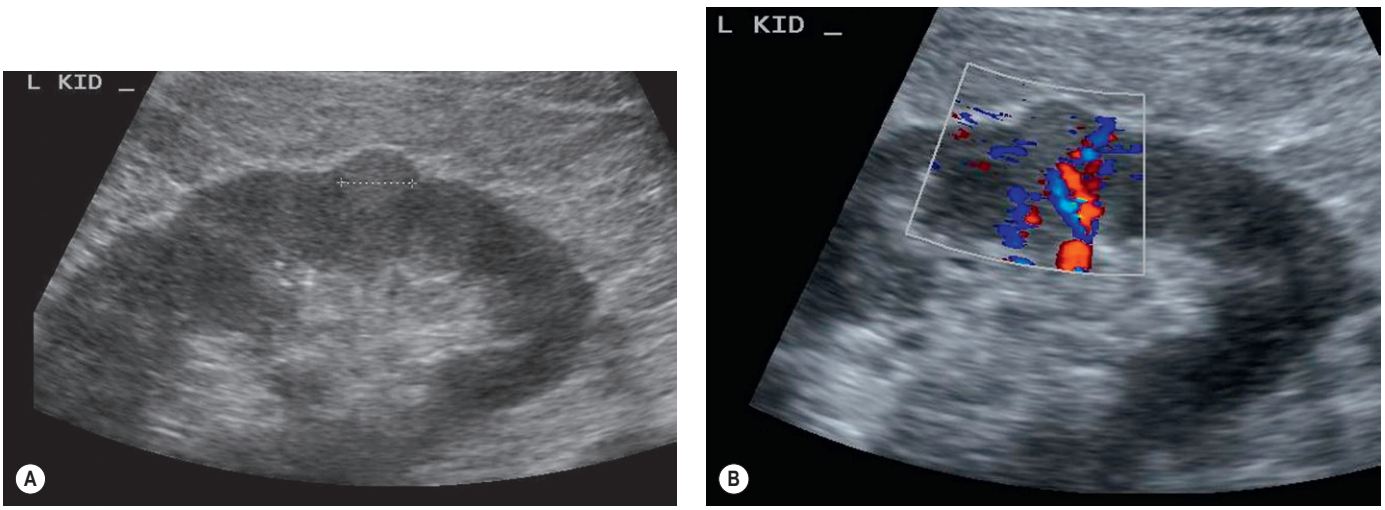


Figure 27.5 Small renal tumours may be uncharacterised on imaging. This is an 11 mm echogenic lesion that looked like normal cortex on CT but is clearly different on US **(A)** and shows deviation of adjacent vessels **(B)**.

quoted, depending on the series, as occurring in between 30% and 90% of oncocytomas,[12] although it is not a specific feature, being also seen in chromophobe cell renal carcinoma.[13] Oncocytomas may be up to 15 cm in size, though on average they are about 5 cm at diagnosis. They commonly have a lobulated margin. Not all oncocytomas grow but just over 50% do and their growth rate is similar to that of renal cell carcinoma at 0.5 cm per year.[14] It is even possible for oncocytomas to display renal vein extension,[15] although particular care is then needed to distinguish them histologically from a chromophobe renal cell carcinoma (RCC), an oncocytic variant of papillary RCC and the granular variant of clear cell RCC. Finally, oncocytomas may be multifocal and bilateral[16] and central cystic degeneration is reported to occur rarely.

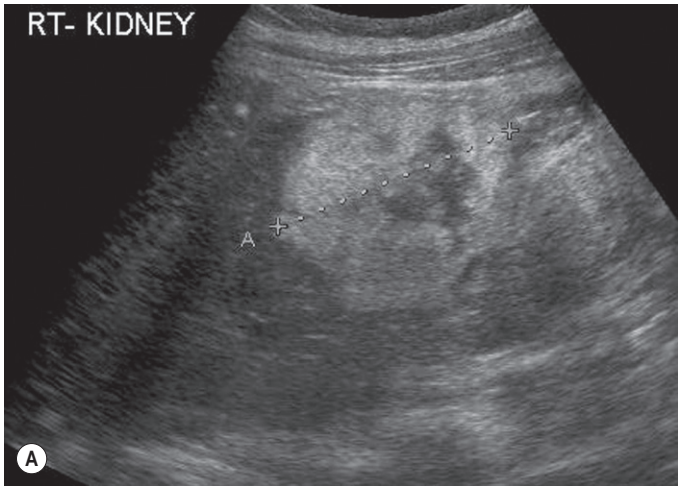
Consequently, there are no imaging features that allow a confident diagnosis of oncocytoma or its distinction from renal cell carcinoma. Biopsy is unhelpful as oncocytoma rests are occasionally found in adenocarcinomas or in collision tumours as described above. A final diagnosis can only be made after the entire lesion has been examined histologically. If the diagnosis is suspected preoperatively then nephron-sparing techniques are appropriate. It does raise a problem with appropriate categorisation of the tumour if ablation treatments are used that rely on a biopsy for diagnosis.

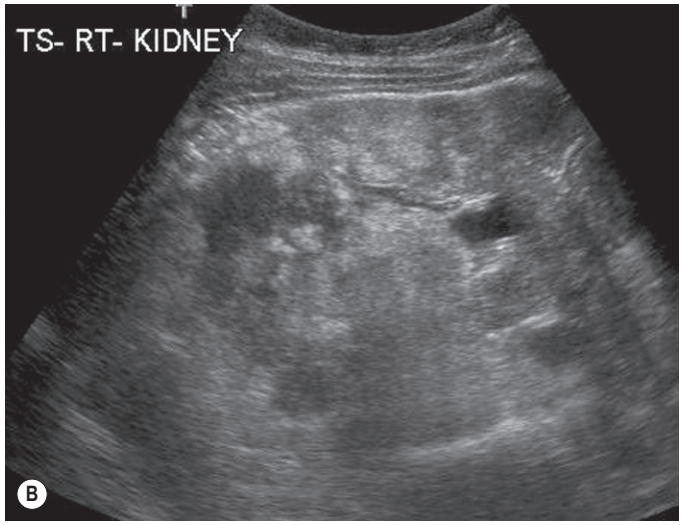
Oncocytoma

- Benign renal tumour.
- Usually asymptomatic.
- Most are only diagnosed after operation to remove a mass thought to be malignant.
- Characteristic central scar and spoke-wheel enhancement not seen in all oncocytomas and may be seen in some RCCs.
- Oncocytoma can be associated with RCC and can form collision tumours.
- Biopsy is unhelpful.
- Nephron-sparing techniques are appropriate.

Angiomyolipoma

Angiomyolipomas (AMLs) are benign mesenchymal neoplasms (hamartomas) that, as their name suggests, contain blood vessels, smooth muscle and fat in varied proportions. They are relatively common, the exact prevalence quoted depending on whether operative or postmortem studies are cited. For instance, the incidence in a surgical series[17] looking at resection of masses smaller than 4 cm was 9%, whereas in a postmortem study[18] they formed 4% of all renal tumours. AMLs are usually diagnosed as incidental





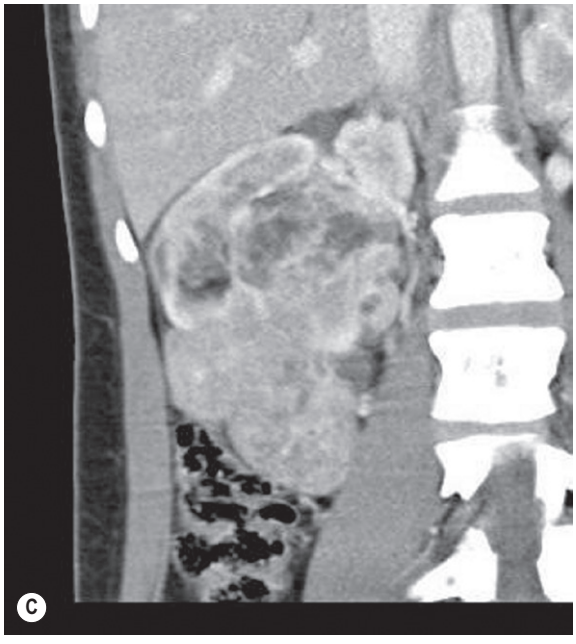


Figure 27.6 Tuberous sclerosis. Eighty per cent of tuberous sclerosis patients will have angiomyolipomas, and they may be numerous and distort and enlarge the kidney. Longitudinal **(A)** and transverse **(B)** ultrasound images show the kidney is disorganised by several echogenic masses. CT scan **(C)** shows how an AML can enhance, and finding the fat within them can be difficult.

findings at imaging but they can present with flank pain and bleeding. They are commoner in women by a factor of four and usually found after the age of 40 years.

AML may exist as an isolated entity (about 80% of the total) or in about 20% be associated with tuberous sclerosis or pulmonary lymphangiomyomatosis. Tuberous sclerosis is an autosomal dominant neurocutaneous syndrome that has benign congenital tumours in multiple organs.[19] The classic triad of epilepsy, mental disability and adenoma sebaceum is relatively uncommon, so radiology plays a part in finding the tumours: cardiac rhabdomyomas, renal AMLs and subependymal tubers, though many different organs may be affected. Eighty per cent of tuberous sclerosis patients will have renal AMLs (Fig. 27.6).

Appearances

AML may occur as single or multiple lesions in one or both kidneys. The sporadic lesions are usually in middle-aged women and unilateral whereas in tuberous sclerosis, lesions are more likely to be small and multiple. The appearance of an AML depends on the proportion of each of the different tissues. Typically, on ultrasound, the fat in the AML produces a highly reflective mass, with brightness similar to renal sinus fat (Fig. 27.7). Up to a third of AMLs may show acoustic shadowing. Larger lesions may show intralesional aneurysms as well as hypervascular components. It is these that predispose to spontaneous haemorrhage (Fig. 27.8). The likelihood of spontaneous bleeding increases once an AML is larger than 4 cm

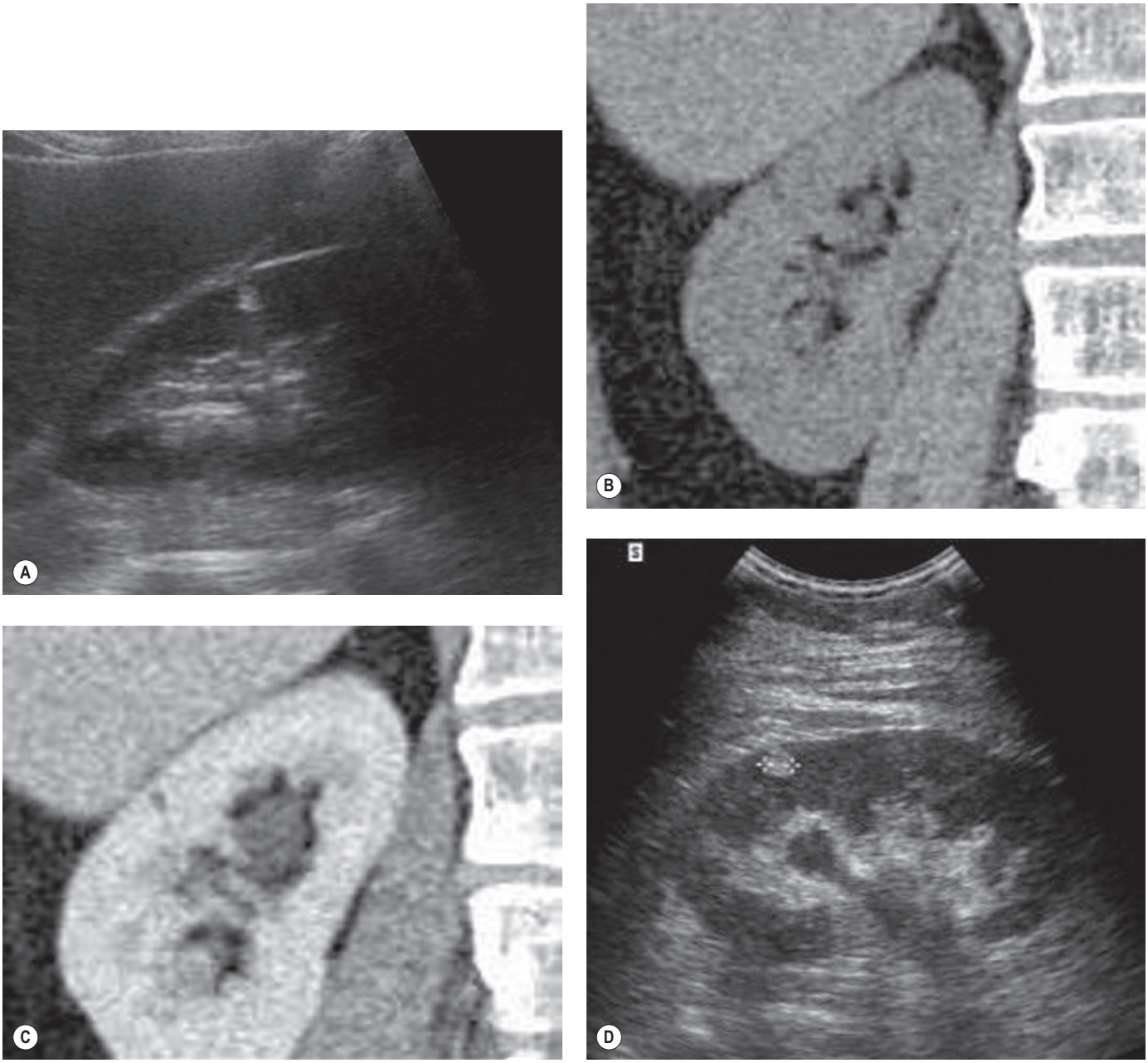


Figure 27.7 A small angiomyolipoma seen on US **(A)** and CT **(B, C)**. Ultrasound shows a small brightly echogenic focus in the renal cortex. The CT scans, both unenhanced and enhanced, show a small focus of cortical fat to correspond to the AML. **D:** A slightly larger AML in the renal cortex in another patient.

in size or there is an aneurysm of over 5 mm diameter. Spontaneous renal bleeding into the subcapsular and perirenal space is associated with AML (Wunderlich syndrome). If bleeding occurs into the AML it alters its appearance and may make diagnosis difficult.

Most AMLs are smaller than 3 cm, are intracortical and appear as a discrete round mass. Larger lesions may have a lobulated outline and may be exophytic from the kidney. Colour Doppler may show the arteriovenous fistulae or aneurysms that AML may contain.

Differential diagnosis

Milk of calcium cysts may mimic the ultrasound appearances of a small intracortical, bright AML (Fig. 27.9). CT scan will readily distinguish them. A third of small renal cell carcinomas are echogenic, some as bright as an AML. There are sonographic distinguishing features: a hypoechoic rim, intra-lesional cysts and calcification are common in carcinoma but not in AML; shadowing may be seen in AML but not in carcinomas. CT and MR can be used

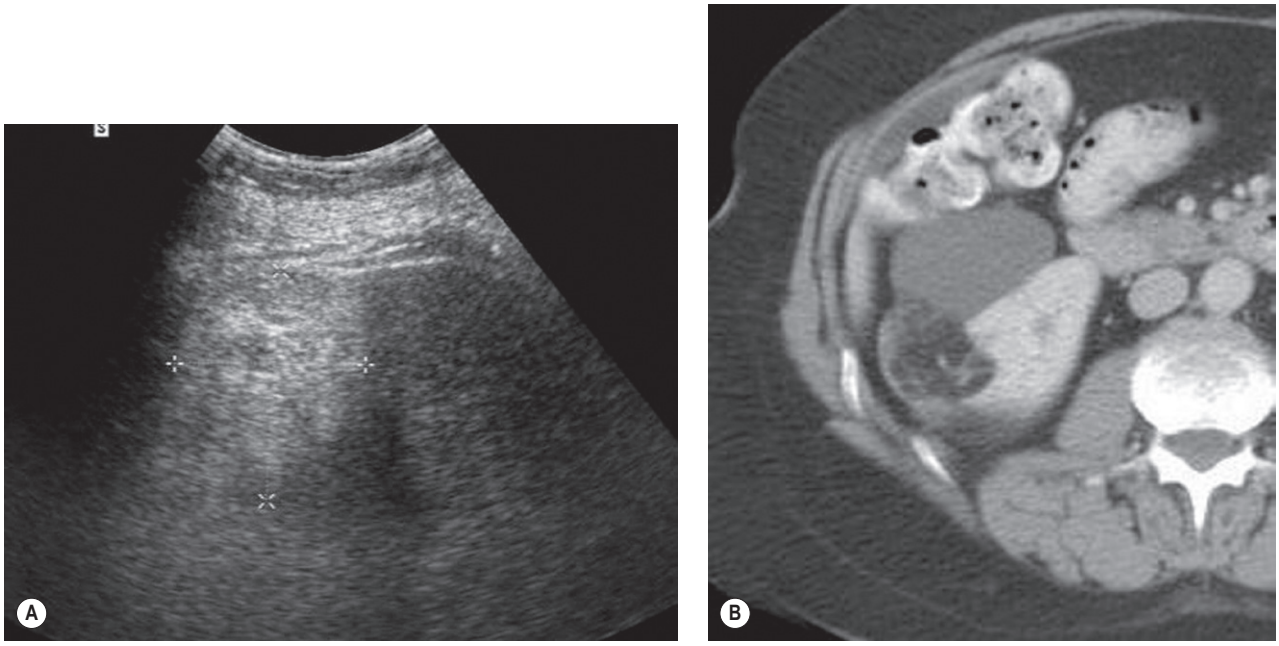


Figure 27.8 A large AML on ultrasound **(A)** associated with a perinephric haematoma on CT **(B)**. The CT shows the AML contains predominantly fat.

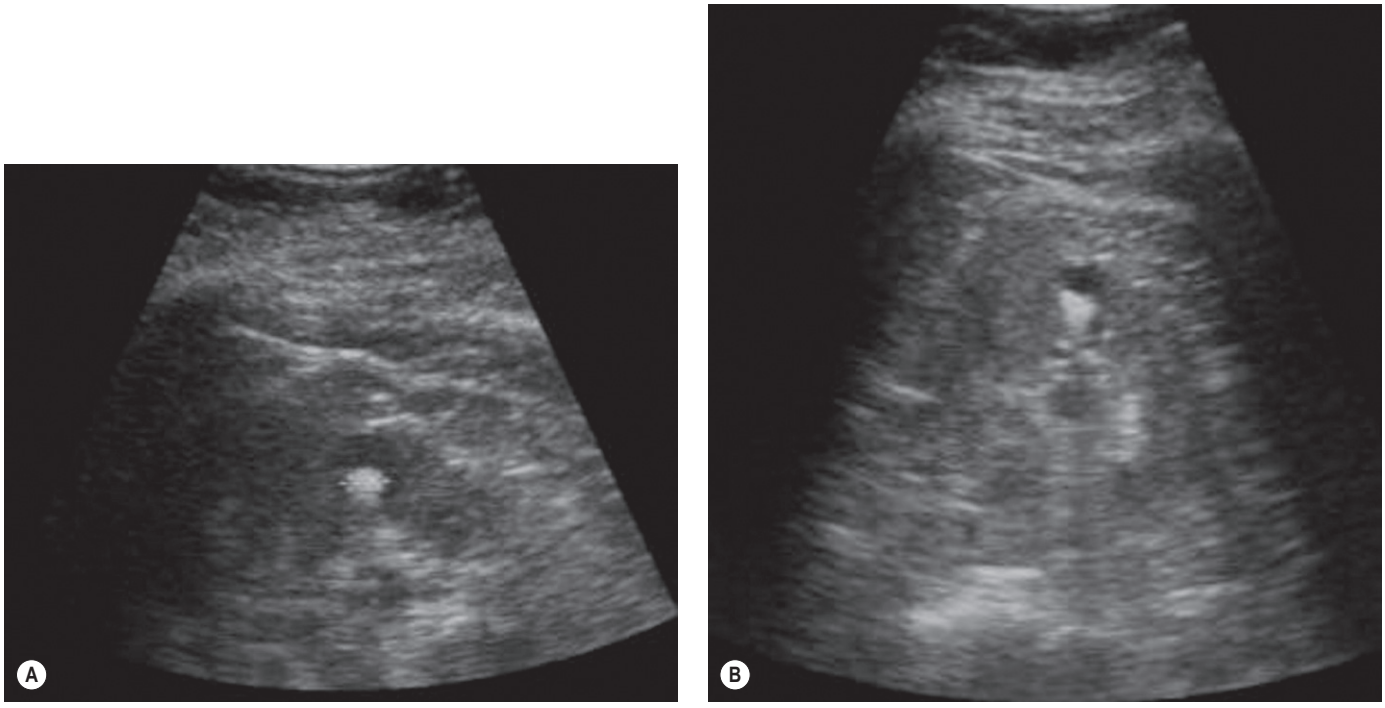


Figure 27.9 Milk of calcium cyst. Transverse **(A)** and longitudinal **(B)** views showing how these cysts can mimic the appearance of a small cortical AML.

to confirm the presence of fat and make the diagnosis of AML though even this has pitfalls. Fat may be present in a few renal cell carcinomas[20] and is commoner in the papillary cell variant,[21] although these tumours often have calcification too which is not seen in AML. Up to 5% of AMLs will contain minimal or no fat[4] and be potentially indistinguishable from carcinoma, although ultrasound shows a very uniform isoechoic appearance and CT will show increased attenuation on unenhanced images.[22] A perirenal liposarcoma can mimic the appearances of a large exophytic AML. In this instance, an AML is likely to show a marginal defect in the kidney and enlarged tumoral vessels, whereas a liposarcoma is more likely to show smooth compression of the kidney and extension outside of the perirenal space. Biopsy is not often needed in the diagnosis of typical fat-rich AML but it may be helpful in fat-poor lesions or in suspected liposarcoma.[23] A meta-analysis of the published literature has concluded that all non-calcified, echogenic lesions found on ultrasound in the kidney require a CT scan to rule out a renal cell carcinoma.[24]

Treatment

Small AMLs (less than 4 cm) do not need to be treated. Asymptomatic lesions need no more than conservative treatment and follow-up. Lesions larger than 4 cm should be removed using nephron-sparing techniques in order to prevent the occurrence of complications, primarily those of spontaneous haemorrhage. Those patients that present with spontaneous bleeding should be considered for coil embolisation at catheter angiography if the bleeding is active and ongoing. Surgery is reserved for when the patient has recovered from the acute episode of bleeding.

Angiomyolipoma

- Benign mesenchymal neoplasm.
- Commoner in women.
- 20% of AML are associated with tuberous sclerosis.
- May be single or multiple.
- Typically appear as a bright cortical mass.
- AMLs bigger than 4 cm have an increased chance of bleeding.
- Potential problem distinguishing AML from small bright RCC.
- CT or MR can be used to confirm fat in an AML.

Other benign solid renal masses

Other benign solid tumours do occur but they are generally very rare or not often detected on imaging.[4]

- *Haemangioma*. These are rare lesions that are typically solitary and arise from the renal pyramids. They characteristically show early intense enhancement with ultrasonic contrast agents that persist on delayed imaging. They are associated with syndromes such as Sturge–Weber and Klippel–Trénaunay and may cause haematuria and renal colic.
- *Leiomyoma*. These are rare lesions that typically arise from the renal capsule. They may be quite large and show cystic degeneration or haemorrhage.
- *Reninoma*. An extremely rare tumour that produces a triad of findings: poorly controlled hypertension; hypokalaemia; and high plasma rennin levels. Usually found in young adults and smaller than 3 cm in size, there are no specific imaging findings.
- *Medullary fibromas*. Autopsy series describe these lesions commonly but as they are usually less than 5 mm in size they are not often found on imaging. Their typical location is in the renal pyramid.

MALIGNANT RENAL MASSES

Renal cell carcinoma

Renal cell carcinoma (RCC) accounts for about 2% of adult malignancies and represents about 90% of adult primary renal tumours. Most of these tumours occur sporadically, but there is an association with von Hippel–Lindau disease (Fig. 27.10) and tuberous sclerosis. There is a male to female preponderance of two to one. The peak age of incidence is 50 to 70 years. Predisposing risk factors include smoking, long-term dialysis and exposure to lead, cadmium or diethylstilbestrol.

Renal cell carcinoma is thought to arise from the convoluted tubules of the renal cortex; 70–80% are of the clear cell type, 10–15% are papillary cell and about 5% are chromophobe-type. The features seen on ultrasound do not bear any useful relationship to the cell type of the renal cell carcinoma, although papillary tumours are

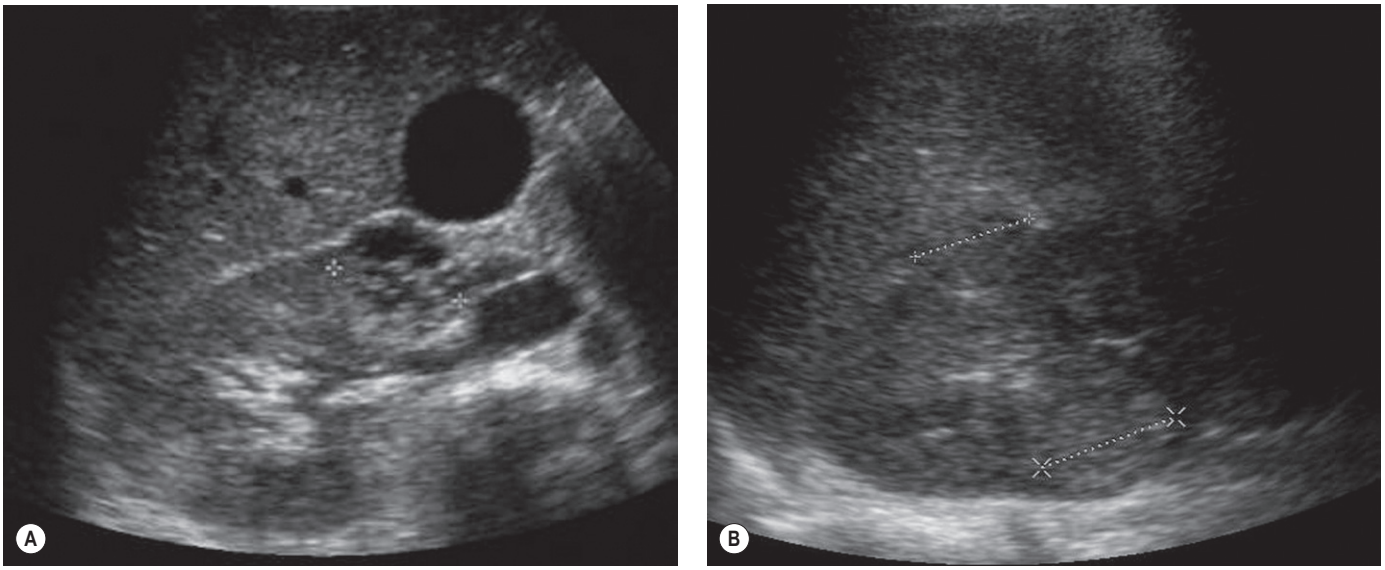


Figure 27.10 Von Hippel–Lindau disease. A and B: There are at least three renal lesions seen in this patient with von Hippel–Lindau disease. They have subsequently grown and proved themselves to be renal cell carcinomas.

more likely to show poor enhancement with contrast agents on CT scan and chromophobe tumours may have a homogeneous bright ultrasound texture without necrosis.

Presentation

Common symptoms at presentation are painless haematuria, flank pain and a palpable mass together with anorexia and weight loss. However, with the increasing use of cross-sectional imaging for other reasons, the proportion of tumours that are detected at less than 3 cm in size is increasing; these are chance findings prior to any symptoms.

There is a belief that finding a varicocele in a man should prompt a search of the kidneys for an underlying cancer, but this is an association based on very old papers from before the days of cross-sectional imaging. The cancers described in those papers were huge and clinically palpable. Current evidence suggests that both conditions are relatively common and can be expected to coexist in a few people. Young men presenting with a varicocele do not have an increased rate of renal cancer. In older men, late presentation of varicocele may, rarely, be due to tumour thrombus spread along the left renal vein obstructing the gonadal vein but there is no true association between a varicocele and renal cancer. In contrast, there is an association between non-Hodgkin's lymphoma and renal cell carcinoma, particularly in those patients with bulky abdominal disease.[25] Imaging does not allow differentiation between the two diagnoses so biopsy is required.

Some patients present with spontaneous renal or perirenal haemorrhage. This blood may be enough to obliterate the underlying tumour on initial imaging. Consequently, follow-up imaging will be needed once the acute bleed has resolved to look for an underlying tumour.

Screening

Since between 25% and 40% of tumours are found incidentally, interest has been raised in providing a screening service. An initial ultrasound study of 9959 volunteers yielded only 9 cancers (0.1%); sensitivity at 1-year follow-up was 82% but the positive predictive value was only 50%.[26] A further ultrasound study looking at a more focused elderly population of 6678 volunteers found an incidence of solid renal tumours of 0.32%.[27] Screening with ultrasound is well tolerated and those treated show good survival rates. One group in whom screening is worthwhile is those with acquired cystic disease of the kidney secondary to renal failure.[28] They have a prevalence of cancer of 19%, 50% due to clear cell and 50% due to papillary carcinoma.

Appearances

Ultrasound features are of a solid tumour mass, distorting the normal renal architecture often with a 'ball' pattern of growth rather than an infiltrative pattern (Fig. 27.11).[29] Reflectivity may be increased, decreased or similar when compared to the normal renal cortex. The larger tumours are more likely to be of similar reflectivity but may also have central necrosis or haemorrhage (Fig. 27.12). Tumours less than 3 cm in size are more likely to be of increased echogenicity: hence the need for care when differentiating them from angiomyolipoma, which will also appear bright (Fig. 27.13). Calcification is found in 30% of RCCs but not in angiomyolipoma. This calcification may be rim-like but is more commonly central. CT and MR can be used to look for fat, which indicates an angiomyolipoma rather than an RCC.

The differential diagnosis of a solid or partly solid renal mass on ultrasound includes tumours, haematomas, infections and the pseudo-tumours described earlier in this chapter. Ultrasound contrast agents can enable distinction of these lesions. Hyperenhancement in the late phase (30–90 seconds after agent injection) is the most useful feature indicating a renal cell carcinoma (Fig. 27.14).[30] Heterogeneity of enhancement is also an indicator of malignancy, as most angiomyolipomas show a smooth enhancement pattern which washes out in the late phase. One pitfall is that some papillary cancers may not show much enhancement.

Colour and spectral Doppler features of high velocity and turbulence are non-specific and do not help in the diagnosis of tumour but will help distinguish cystic from solid lesions (Fig. 27.15). The pattern of vessels on colour Doppler may help indicate a pseudotumour such as a prominent column of Bertin.

Multiple tumours may develop in an asynchronous or synchronous fashion. A patient who has one kidney removed for a sporadically occurring tumour has a 2% chance of another tumour developing in the remaining kidney. There is also a 2% chance that a tumour in the contralateral kidney may exist at the time of initial diagnosis. Synchronous occurrence of more than one tumour in the same kidney is quoted as 5% but some histological studies of nephrectomy specimens quote a higher rate, up to 25%, but the tumours are usually less than 5 mm in size. Finding more than one tumour should prompt a search for associated syndromes such as von Hippel–Lindau disease.

Rare presentations

Occasionally, the metastases from renal cell cancer may become apparent before the primary tumour in the kidney can be detected.[25] An example is the development of para-aortic adenopathy with no detectable primary tumour. Arteriovenous malformations (AVMs) are associated with renal cell cancer. These AVMs can be large enough to obscure visualisation of the tumour. We know of two patients in whom the initial diagnosis was thought to be pancreatic neuroendocrine tumours with an incidental renal AVM but which turned out to be renal cell cancer metastases to the pancreas from a tumour hidden by the AVM. Occasionally, RCC can present as a single large cyst (Fig. 27.16). This is not a cyst that has turned malignant but an RCC that has always been cystic.

Staging

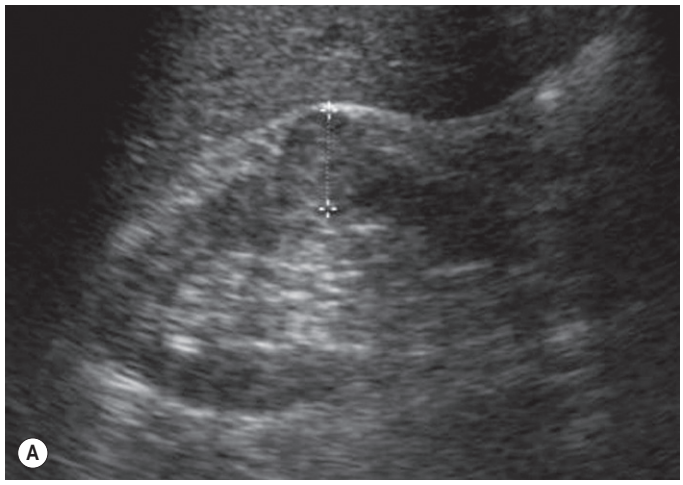
Renal cell carcinoma spreads either locally into adjacent structures or by haematogenous spread. Survival worsens as the stage of the

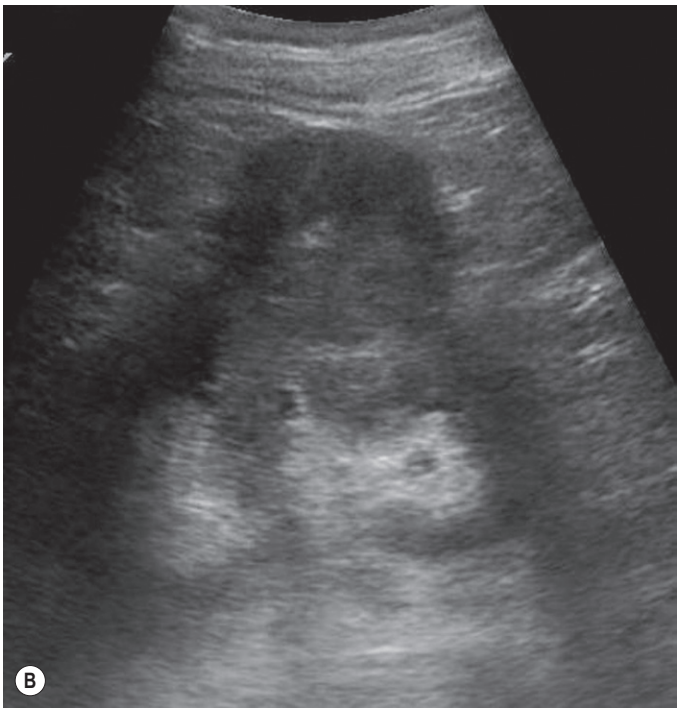
Renal cell carcinoma: aetiology and presentation

- 2% of adult malignancies.
- Most are sporadic.
- Commoner in men.
- Increased risk in smokers, dialysis patients and those with von Hippel–Lindau disease.
- Up to 80% are clear cell type.
- Painless haematuria is the classic presentation.
- Often an incidental finding on cross-sectional imaging.
- Screening the general population is not proven.

Renal cell carcinoma: appearances

- Deforms the kidney with a 'ball' pattern of growth.
- Small tumours more likely to be bright on US – a hypoechoic rim is sometimes seen in RCC but not in AML.
- Larger tumours more likely to have central necrosis and bleeding.
- Calcification is seen in RCC but not AML.
- Ultrasound contrast agents have a role.
- Synchronous occurrence of another RCC between 2% and 5%.





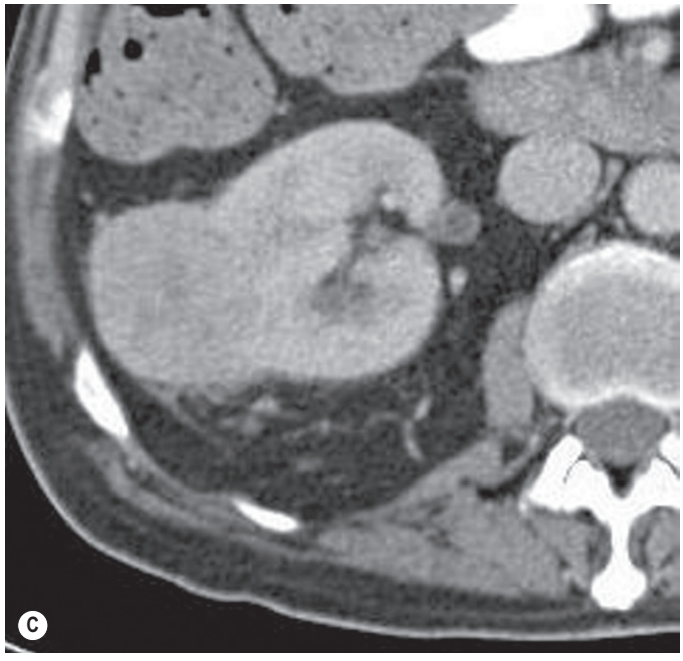
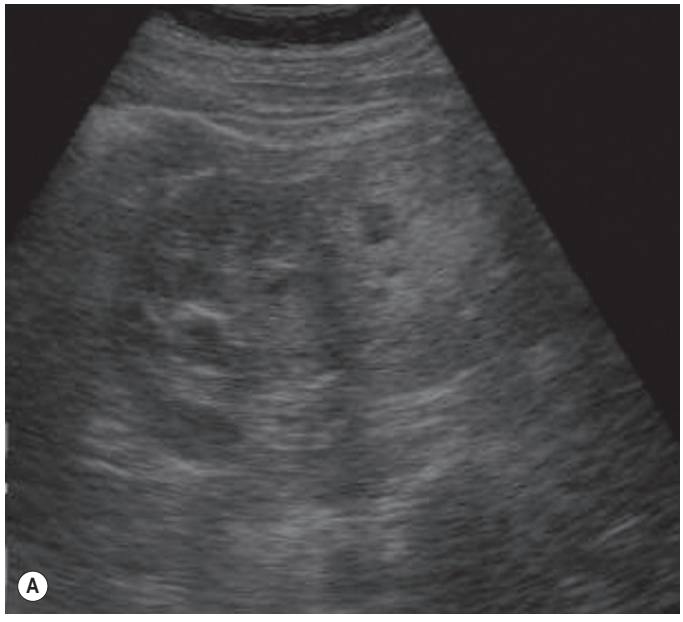


Figure 27.11 **Renal cell carcinoma. A:** A small exophytic RCC. **B:** Larger RCC may show some heterogeneity of echo. **C:** CT scan of the lesion seen in **B**.



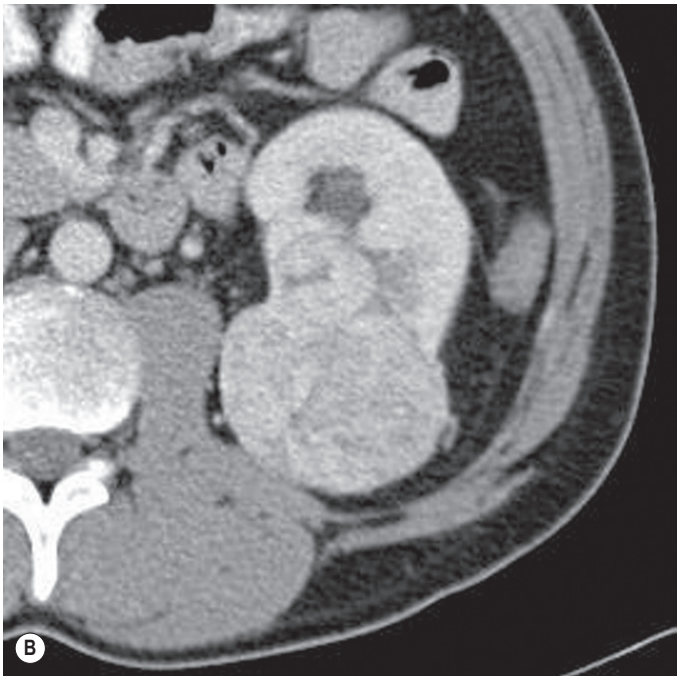


 Figure 27.12 **Renal cell carcinoma. A:** Ultrasound shows an exophytic tumour with some central low-echo areas that could be necrosis. **B:** CT of the same lesion.

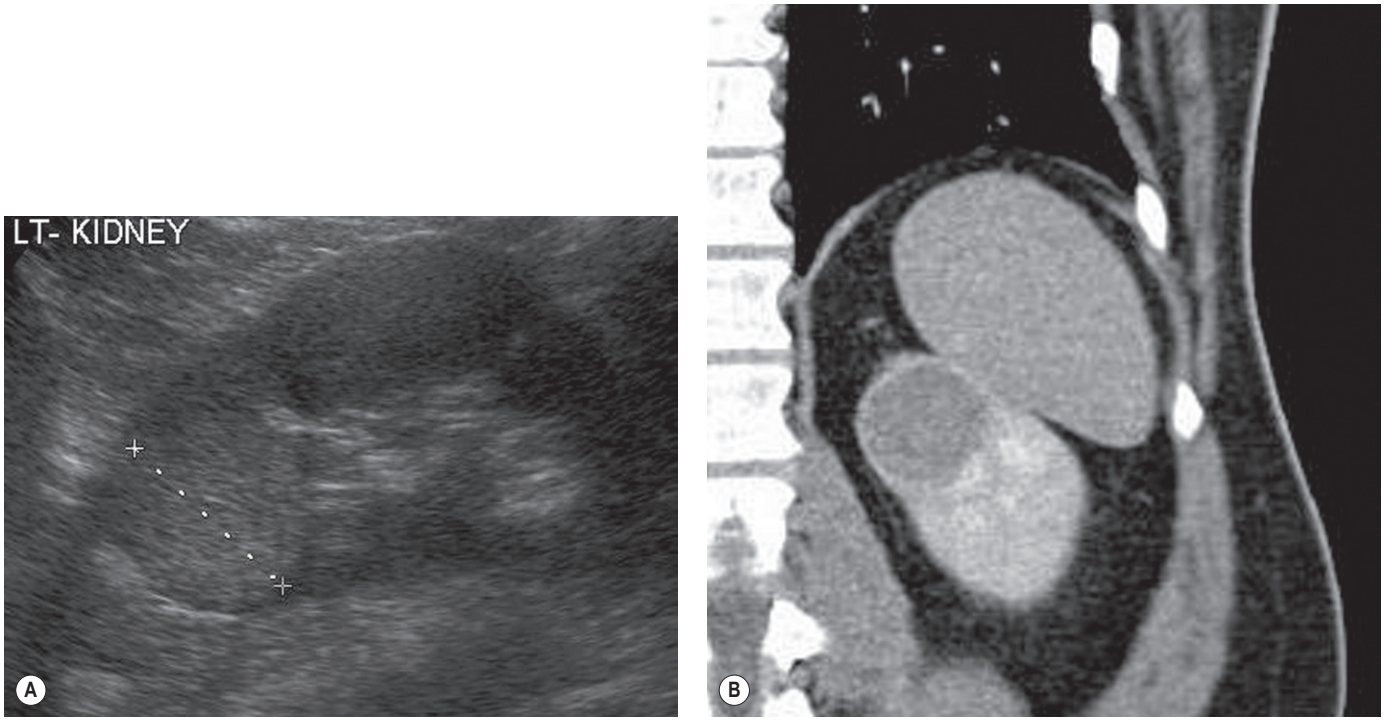


Figure 27.13 **Renal cell carcinoma. A:** Ultrasound shows a uniformly echogenic mass that could be mistaken for an AML. **B:** CT scan shows there is no fat in the lesion, confirming it is an RCC and not an AML.

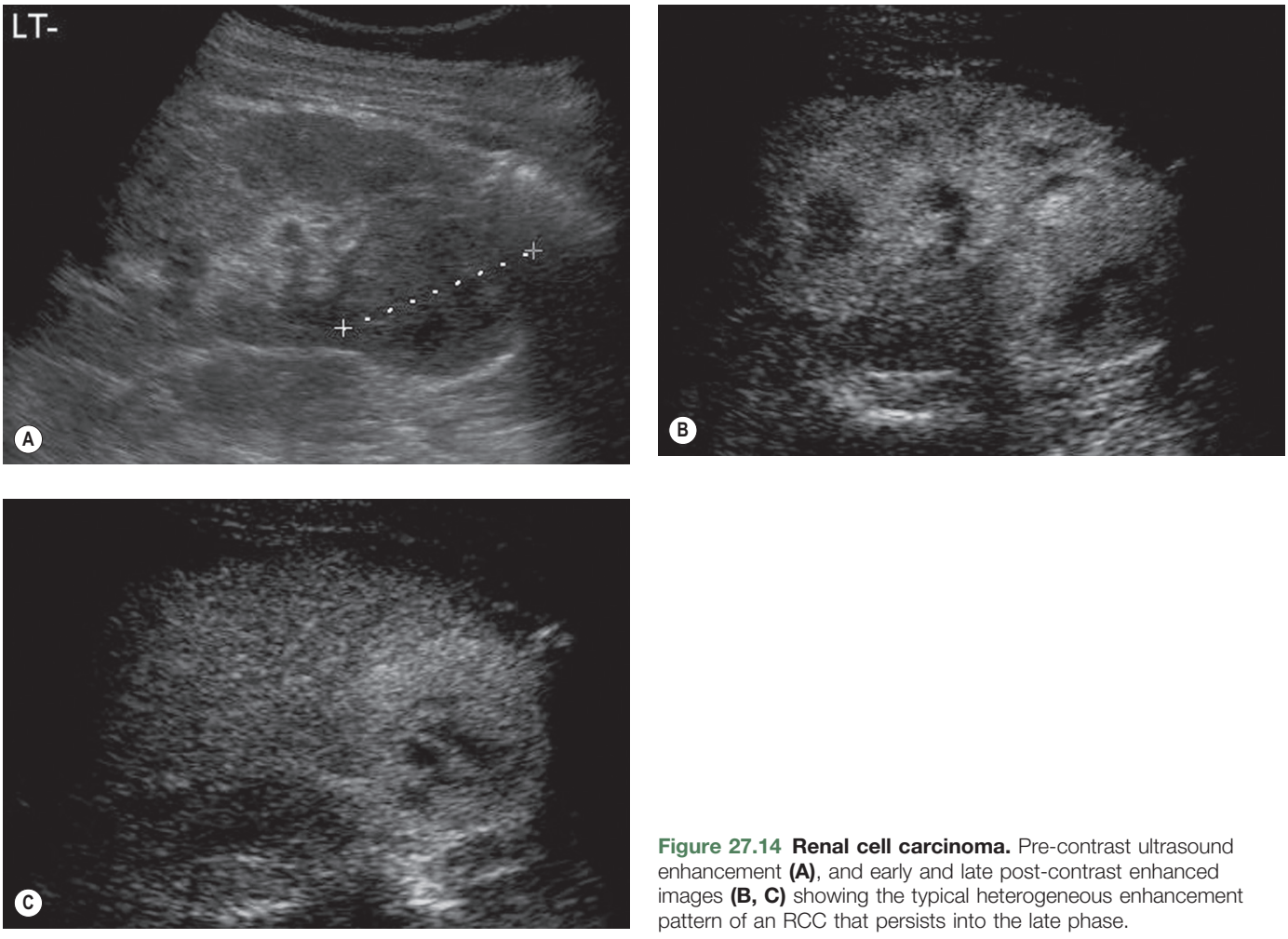


Figure 27.14 **Renal cell carcinoma.** Pre-contrast ultrasound enhancement **(A)**, and early and late post-contrast enhanced images **(B, C)** showing the typical heterogeneous enhancement pattern of an RCC that persists into the late phase.

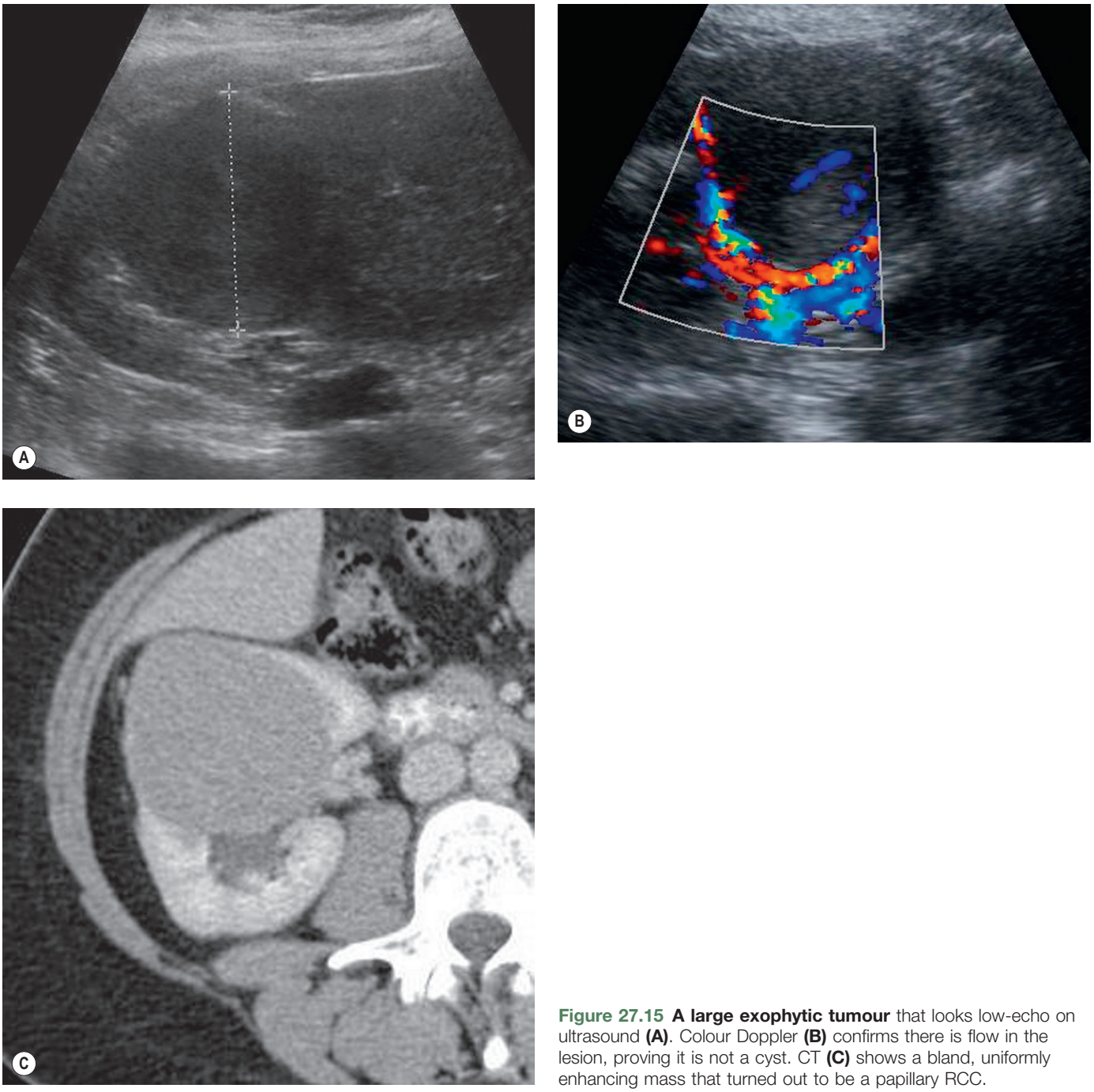


Figure 27.15 A large exophytic tumour that looks low-echo on ultrasound **(A)**. Colour Doppler **(B)** confirms there is flow in the lesion, proving it is not a cyst. CT **(C)** shows a bland, uniformly enhancing mass that turned out to be a papillary RCC.

tumour worsens (Table 27.1). Characteristically, the tumour invades into the renal vein (30%) and tumour thrombus can propagate along this vein into the IVC (5–10%) and right atrium. Ultrasound can show thrombus in the vein provided it is possible to identify the vein. Thrombus may cause the vein to be enlarged. Colour Doppler can help in identifying tumour thrombus. CT and MR are better than US at demonstrating venous involvement. Distant metastases can be to any site but there is a predilection for pulmonary metastases. Bone metastases are usually lytic and expansile. Local spread can occur through Gerota's fascia to cause fixity to adjacent organs. Ultrasound palpation during respiration may show the liver and kidney to move as one rather than relative to each other. Local spread is also to retroperitoneal nodes. CT scan of the chest and abdomen is the optimum test to stage the tumour. MR can provide

Table 27.1 Staging and survival of renal cell carcinoma[31]

Stage	Description	Survival
Stage I	Tumour confined to kidney	5 years: 67%; 10 years: 56%
Stage II	Invasion of perinephric fat	5 years: 51%; 10 years: 28%
Stage III	Venous or nodal involvement	5 years: 33%; 10 years: 20%
Stage IV	Invasion of adjacent organs or distant metastases	5 years: 13%; 10 years: 3%

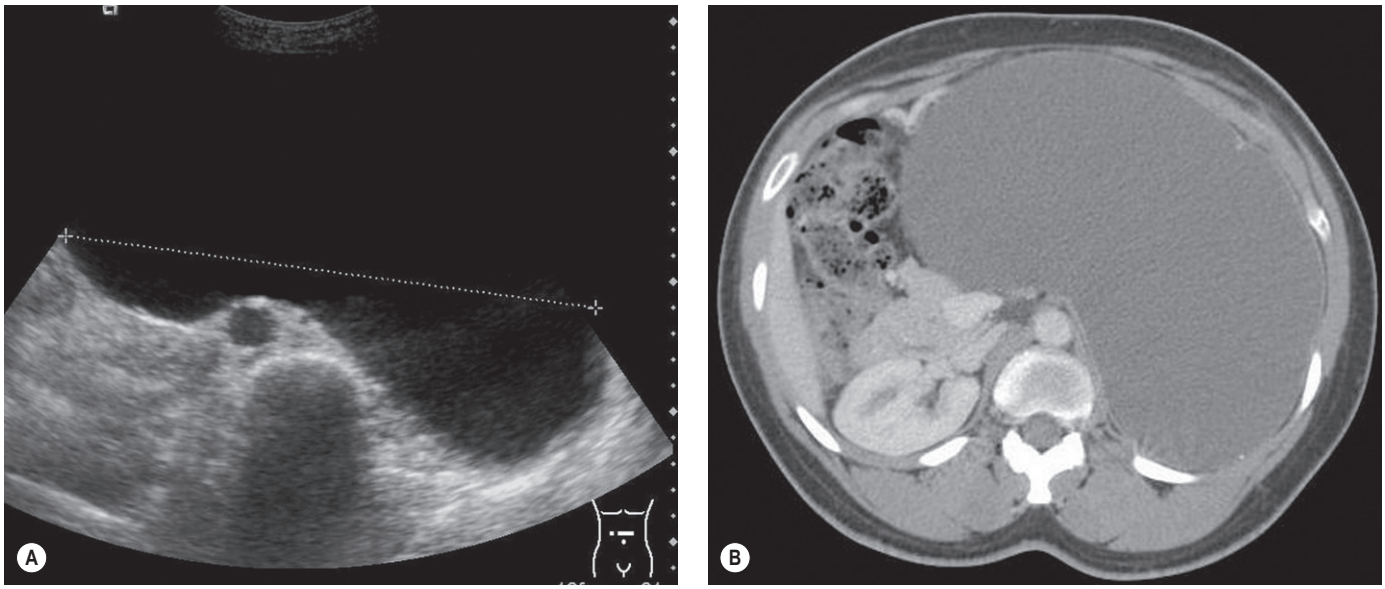


Figure 27.16 A rare example of a large, purely cystic RCC on US **(A)** and CT **(B)**. Other than size, there are no features to suggest malignancy.

good local staging and may demonstrate the extent of tumour thrombus better than other tests but it is insensitive for lung metastases.

Treatment

Surgery with radical nephrectomy is the standard treatment. It may be useful in large tumours to angiographically embolise the tumour preoperatively to ease dissection and reduce blood loss. Surgery can still be useful, even in people with known metastases. It has a cytoreductive effect that can improve the effect of adjuvant treatments.

Partial nephrectomy can be offered as a nephron-sparing technique in those whose tumours do not transgress the renal hilum. Surgery may be done as a traditional open procedure or laparoscopically.

Ablative techniques such as radio-frequency ablation are a good alternative in smaller tumours and are discussed separately at the end of this chapter.

Chemotherapy, immunotherapy and radiotherapy all have appropriate uses for the management of disseminated disease.

Collecting duct and medullary carcinoma

Collecting duct carcinoma differs from renal cell carcinoma in two main ways. Firstly, instead of arising from the convoluted tubules of the renal cortex as RCC cell types do, it arises from the renal medulla, possibly the distal collecting ducts of Bellini.[32] Secondly, it has an infiltrative pattern of growth rather than a 'ball-like' mass lesion. There is a 2:1 preponderance of men affected and the mean age at presentation is 55 years. It has a central and medullary pattern of infiltration, although these tumours tend to be large at presentation (around 8 cm), which can hide their central origin. It is an aggressive tumour with a relatively poor prognosis.[33] It tends to be isoechoic to normal parenchyma but some of the tumours are bright and since they are large lesions, this is another potential distinguishing feature from RCC as most bright RCCs are smaller than 3 cm. Overall, though the diagnosis may be suspected because of a central infiltrative pattern, the imaging features are not sufficient to make the diagnosis (Fig. 27.17). Furthermore, transitional cell carcinoma (TCC) arising in the pelvicalyceal system may also show a central infiltrative pattern. This is an important distinction to make as TCC is treated by nephroureterectomy rather than just nephrectomy alone. Histology is required.

Renal medullary carcinoma is sometimes confused with collecting duct tumours but the lesions are distinct clinical entities. Renal medullary carcinoma occurs almost exclusively in people with sickle cell trait and affects a young age group, 15 to 27 years old. The commonest presentation is with gross painless haematuria. The tumours have a predilection for the right kidney. They are centrally located and infiltrative. Most have central necrosis. Metastases are usually present at initial diagnosis. The literature suggests that these tumours are not readily visible at sonography[34] and hence people with sickle cell trait and gross haematuria should be investigated with CT.

Transitional cell carcinoma

Tumours of the renal pelvis represent 10% of solid renal tumours, with the majority of these being transitional cell carcinomas (TCCs). The great majority of TCCs arise in the bladder, with only 5% of TCCs arising in the upper tracts. This is because the bladder has a much greater surface area of urothelium and because urine remains in contact with it for greater periods of time. The majority of upper tract TCCs occur in the extrarenal pelvis, some in the infundibular regions and only a quarter in the ureter.[35] The left and right kidneys are affected equally and 2 – 4% of renal TCCs will occur bilaterally. Any patient with TCC of the bladder has a 4% risk of developing upper tract TCC. This same risk persists even after cystectomy.[36] If the upper tract tumour is the presenting lesion, there is a 30% risk of developing a bladder tumour. Because multicentric TCC and synchronous or metachronous presentations are common, urological follow-up needs to be systematic and accurate.

Aetiology

Men are affected three times more often than women. The peak age at presentation is between 50 and 70. Smoking is an important risk factor, increasing the relative risk two to three times. Carcinogenic substances excreted in the urine act locally on the urothelium: these

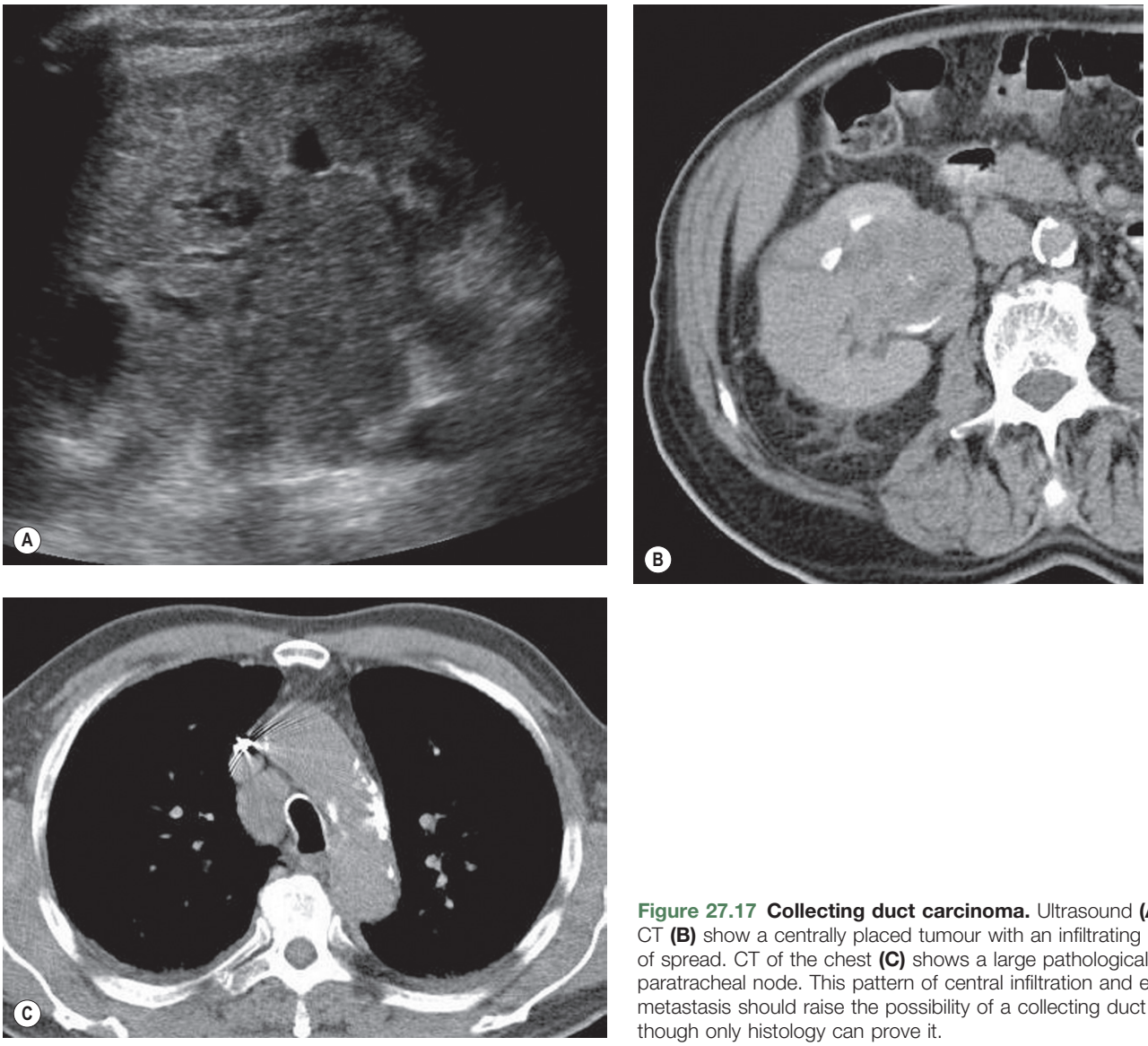


Figure 27.17 Collecting duct carcinoma. Ultrasound **(A)** and CT **(B)** show a centrally placed tumour with an infiltrating pattern of spread. CT of the chest **(C)** shows a large pathological paratracheal node. This pattern of central infiltration and early metastasis should raise the possibility of a collecting duct tumour, though only histology can prove it.

include; aniline, benzidine, aromatic amine, azo dyes, cyclophosphamide and heavy caffeine consumption.[37] Analgesic abuse particularly of phenacetin predisposes to a highly invasive type of TCC. Structural anomalies, such as horseshoe kidney, that lead to stasis of urine and prolong the contact time of any carcinogen are also associated with an increased prevalence of this disease.

Symptoms

The most common presenting symptom is haematuria. The standard work-up for haematuria has been urine cytology, cystoscopy and intravenous urography (IVU) in the past. IVU was superseded by ultrasound as the initial screening tool because of its better ability to pick up solid parenchymal renal masses and because most upper tract urothelial tumours cause some degree of pelvicalyceal dilation.[38] However, the advent of multidetector CT scans has meant that CT urography has become the most sensitive screening tool and is rapidly replacing ultrasound in the initial work-up.[39]

Ultrasound findings

The ultrasound appearances of TCC are variable depending on whether the tumour is sessile or papillary and whether it produces a hydronephrosis or not. Generally, tumours by the time they become visible on ultrasound look like a central soft tissue mass surrounded by the echogenic fat of the renal sinus (Fig. 27.18). Squamous metaplasia leads to formation of keratin pearls that look like highly echogenic foci within the mass or on its surface. There may be dilated calyces around the mass. TCC has an infiltrative pattern of growth so the reniform shape of the kidney is not lost until late in the disease. Sometimes the dilation of the surrounding calyces is the only ultrasonic sign of the disease (Fig. 27.19).

Fat within the normal renal sinus can appear as relatively low-echo and mimic a tumour. This pitfall in diagnosis can be avoided by assessing if there is posterior acoustic shadowing, an ill-defined posterior margin and traversing hilar vessels. These three signs indicate it is just low-echo fat. Tumour will displace vessels and have a defined posterior margin.

Dilation of the pelvicalyceal system with urine can provide a negative contrast that allows the presence of small filling defects or sessile thickening of the urothelium to be appreciated (Fig. 27.20). Blood clots or infective debris can mimic soft tissue masses. Finding blood flow within a mass confirms it is tumour, although conversely the absence of blood flow does not mean it is not tumour (Fig. 27.21). Doppler studies are otherwise unhelpful as tumour grade, stage and size are not related to vascularity.[40]

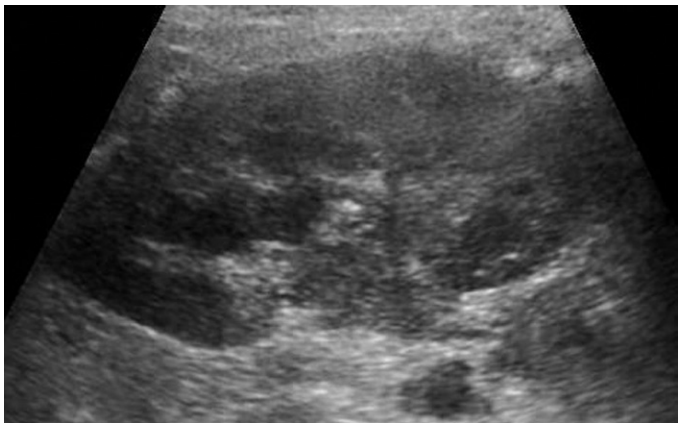


Figure 27.18 Transitional cell carcinoma. Ultrasound shows the renal pelvis is filled with lower-echo tissue surrounded by the echogenic sinus fat. This was proven to be TCC. Note the posterior margin is well defined – unlike a normal low-echo renal sinus that will have a poorly defined posterior margin and shadowing.

Finding unexplained dilation of the pelvicalyceal system on ultrasound should prompt further investigation.

Other tests

The best radiological investigation is a CT urogram (Fig. 27.22). This will accurately depict stones and has a high sensitivity for TCC in

Upper tract transitional cell carcinoma

- 8–10% of solid renal tumours.
- 4% of people with bladder TCC will develop an upper tract lesion.
- Commoner in men.
- Usually presents with haematuria.
- Typically has an infiltrative pattern of growth, retaining the renal shape.
- Focal dilatation of calyces may be the only sign on US.
- Multidetector CT urography is the best imaging test.
- Standard treatment is nephroureterectomy.

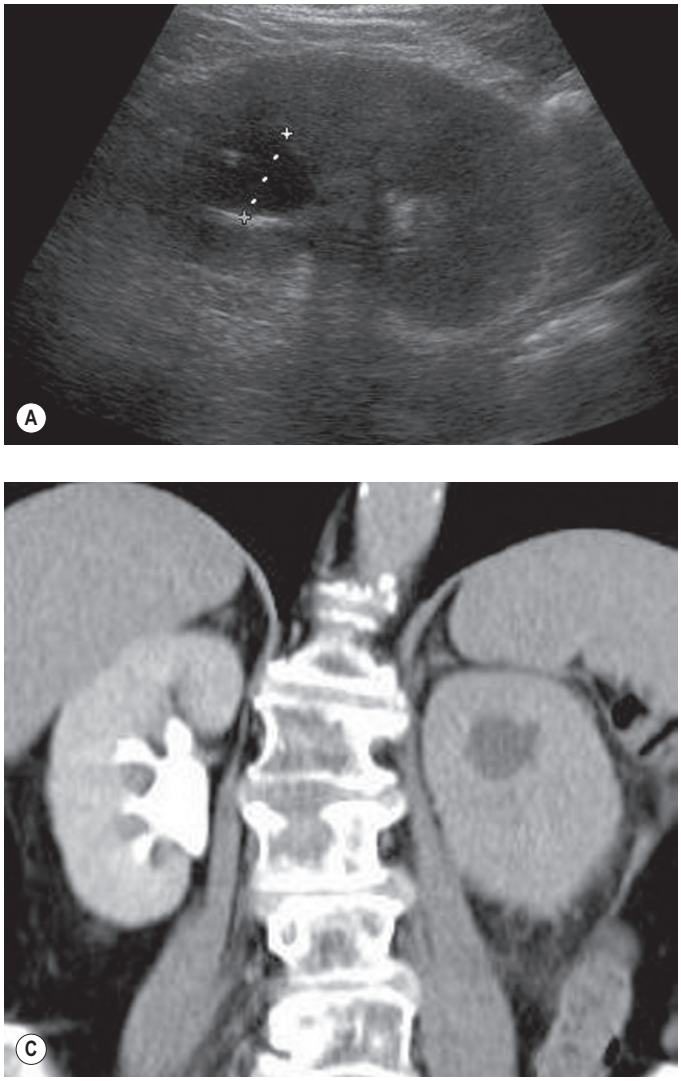


Figure 27.19 Transitional cell carcinoma. Ultrasound **(A)** shows the upper pole calyx is dilated but it is hard to identify anything else in the kidney. Axial CT **(B)** shows the left kidney is diffusely replaced by tumour (TCC) – compare it to the normal right kidney. CT in the coronal urographic phase **(C)** shows the right kidney excretes normally but the left does not. The dilated upper pole calyx is shown as well.

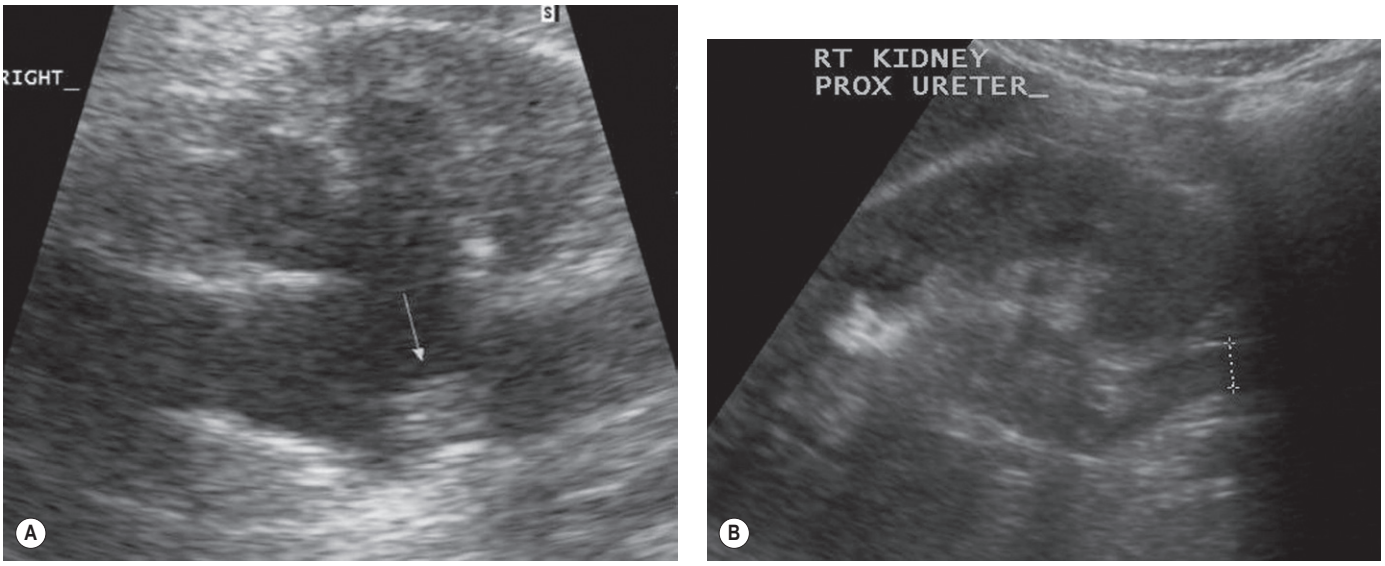


Figure 27.20 **A:** The urine in the dilated renal pelvis acts to outline a small mural nodule of tissue (arrow). **B:** The renal pelvis and proximal ureter are filled with material. Ultrasound cannot tell if this is tumour or blood clot.

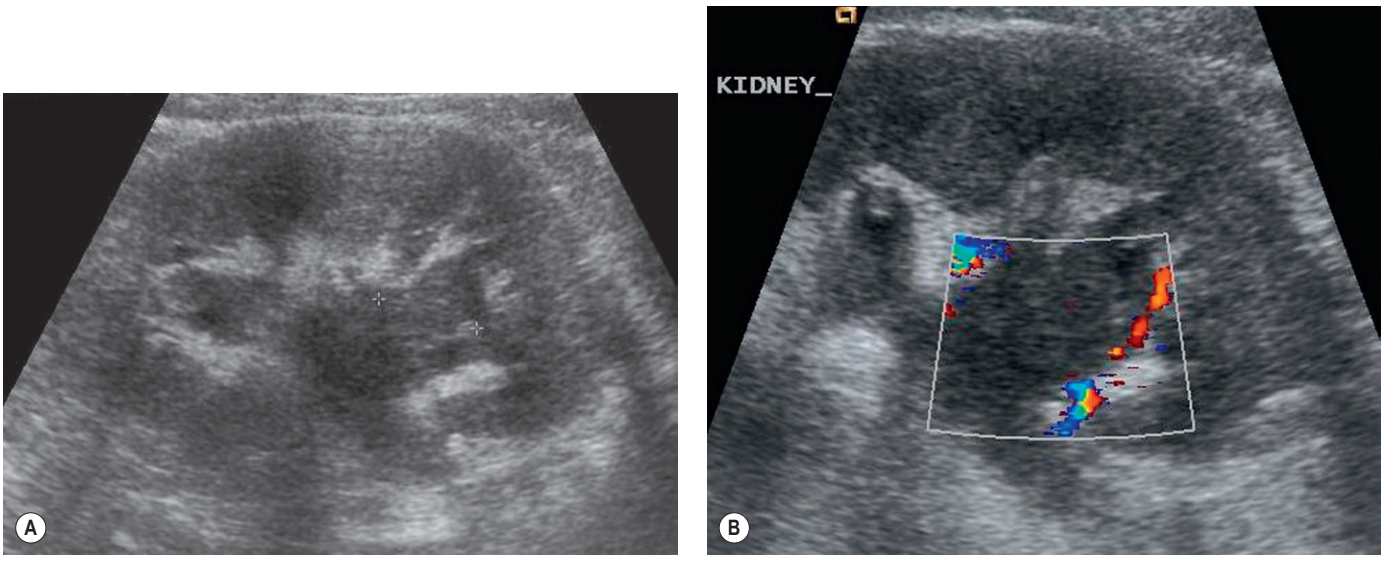


Figure 27.21 **Transitional cell carcinoma. A:** A soft tissue mass fills the lower pole calyces. **B:** Colour Doppler does not show any blood flow in the lesion but this does not mean that it is not tumour. It was subsequently proven to be TCC.

the upper tract. If there is a contraindication to intravenous contrast agents, then MR urography is an acceptable alternative although it is less sensitive for small lesions. If doubt remains about the diagnosis, ureteroscopy is needed. This can be combined with biopsy or retrograde pyelography as needed.

Patterns of spread

The tumour stage (Table 27.2) at diagnosis influences the likelihood of local recurrence and metastases and is consequently the most useful determinant in predicting survival.[41] Metastases are primarily to lymph nodes, bone and lung. Histological grading of the TCC into different degrees of differentiation also affects survival.

Treatment

Standard treatment of upper tract TCC requires total nephroureterectomy and excision of a bladder cuff at the site of ureteric insertion.

Table 27.2 Staging and survival of renal TCC[41]

Stage	Description	5-year survival
Tis	Carcinoma in situ	
T1	Invades subepithelial connective tissue	77–80%
T2	Invades the muscle layer	44%
T3	Invades beyond the muscle layer into peri-ureteric fat or renal parenchyma	0–20%
T4	Invades adjacent organs, the abdominal wall or through the kidney into perinephric fat	

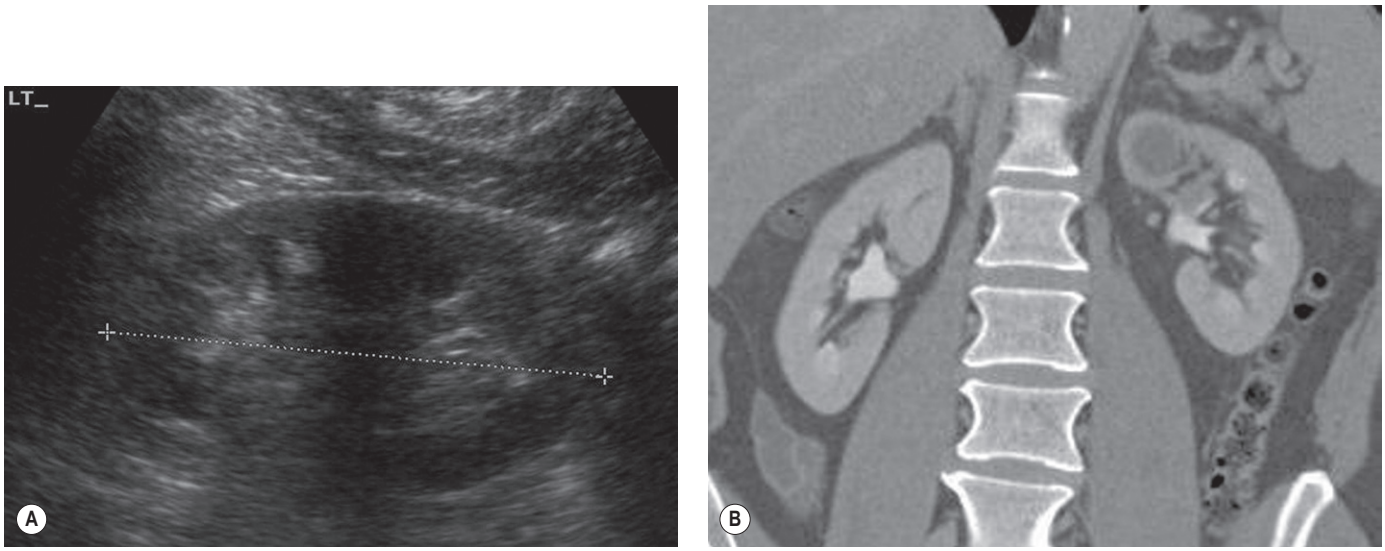


Figure 27.22 Transitional cell carcinoma. A: Ultrasound of the kidney failed to identify a tumour. **B:** CT urogram shown in the coronal plane revealed a TCC filling the upper pole calyces on the left. It is for this reason that CT urography is replacing ultrasound in many centres in the investigation of unexplained haematuria.

Laparoscopic techniques and partial resection may be appropriate in selected patients with bilateral tumours, poor renal function or poor operative risk. Metastases may be treated with chemotherapy or radiotherapy.

Lymphoma

Primary renal lymphoma is a contested diagnosis and is certainly very rare, comprising less than 3% of all renal lymphomas. The kidneys do not contain intrinsic lymphoid tissue. Secondary involvement of the kidney by lymphoma as part of a systemic process by either direct extension or haematogenous spread is the normal manifestation. Six per cent of lymphomas at presentation will have renal involvement and this rises to 60% by the time of death from lymphoma. Non-Hodgkin's lymphoma affects the kidney ten times more commonly than Hodgkin's lymphoma.

Ultrasound is less sensitive than CT or MR at detecting renal involvement.[42] The ultrasonic features are usually of several hypoechoic masses distorting the renal outline or a diffuse involvement producing renal enlargement. It is less common to find a single mass (Fig. 27.23). Rarely, lymphoma may manifest as a rind of low-echo tissue surrounding the kidney (a so-called 'collar' of disease) (Fig. 27.24). The tumour is typically hypovascular on colour Doppler. Lymphoma does not usually show cystic degeneration nor does it centre in the sinus or collecting system. There are overlapping signs on ultrasound between lymphoma, metastases and primary renal carcinoma, so the clinical history and presentation is important.

Most cases of renal lymphoma are diagnosed during CT staging of the known disease. If this is not the case and the renal lesion is the initial manifestation, then biopsy is needed to distinguish lymphoma from metastases. The correct diagnosis of lymphoma will avoid unnecessary nephrectomy, as lymphoma is correctly treated with chemotherapy. Complete remission can be achieved in almost 60% of cases.

Leukaemia

There is a very rare initial manifestation of leukaemia in the paediatric population whereby the kidneys are diffusely infiltrated and enlarged by immature blast cells.[43]

Lymphoma and metastases

- 6% of lymphoma patients have renal involvement at presentation.
- Renal involvement is commoner in non-Hodgkin's lymphoma.
- Metastases to the kidney are very common on autopsy studies.
- Lung, breast and melanoma are common primary sites.
- Multiple small renal masses without a known primary need biopsy to distinguish RCC, lymphoma and metastasis.

Metastases

Renal cell carcinoma may be the most common primary renal malignancy, but overall, metastases to the kidney are the commoner lesions. Autopsy studies show that kidneys are the fifth most common site for metastases.[29] However, metastases to the kidneys are diagnosed much less commonly during life. This is because renal metastatic disease is usually a late event in the course of a malignancy, often as part of widespread dissemination. The commonest primary sites are lung, breast, melanoma and the contralateral kidney. Ultrasound usually shows multiple masses which are low-reflective. These are usually small and intraparenchymal. It is less common for renal metastasis to present as a solitary mass but if they do they can mimic a renal primary. If a patient is known to have another primary tumour, even one in remission, then a renal mass biopsy is needed to distinguish a metastasis from a renal adenocarcinoma. Melanoma metastases are particularly prone to causing perinephric haemorrhage.

Sarcoma and other rare renal tumours

Sarcomas represent only 1% of renal malignancies. The ultrasound appearances are often indistinguishable from other tumours and the diagnosis is usually only made after resection. The commonest form of sarcoma in the kidney is a leiomyosarcoma, which is very similar in appearance to a retroperitoneal sarcoma (Fig. 27.25), and may be solid or occasionally cystic. The prognosis is poor, with 5-year survival rates of about 30%.

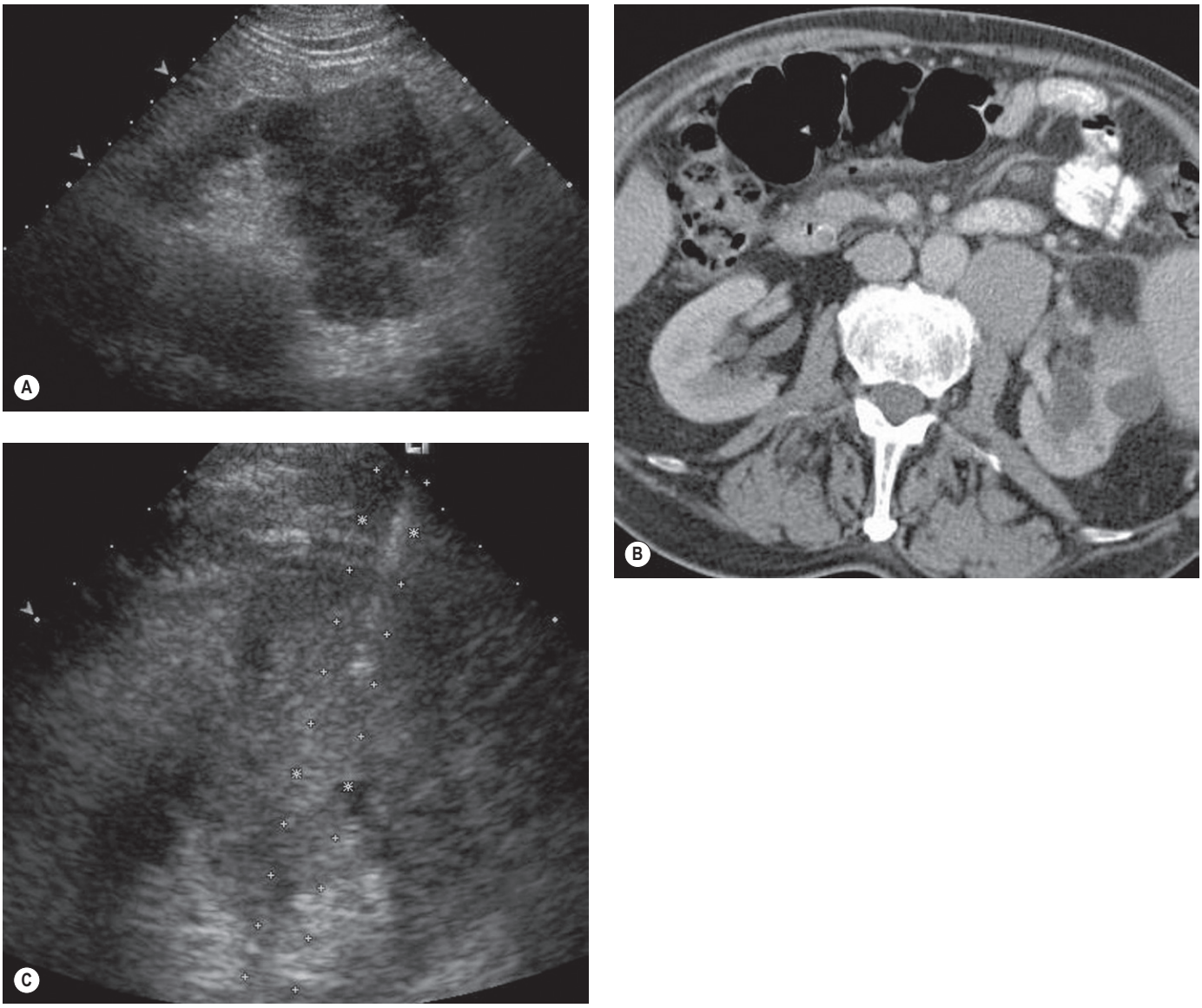


Figure 27.23 **Lymphoma.** Ultrasound **(A)** shows a mass in the lower pole of the left kidney. CT **(B)** confirms the renal abnormality but also shows a huge left para-aortic node. Ultrasound guided biopsy **(C)** of the renal mass confirmed it was a lymphoma.



Figure 27.24 **An echogenic rind of tissue** surrounding the whole kidney. Differential includes a recent bleed but this kidney turned out to be involved by lymphoma.

Hereditary tumours and syndromes

Von Hippel–Lindau disease, tuberous sclerosis and other hereditary causes of renal tumours are discussed in Chapter 26 on cystic diseases.

MINIMALLY INVASIVE TREATMENT OF RENAL CELL CARCINOMA

The incidence of renal cell carcinoma is increasing, with over 6000 new cases per year in the UK and 30 000 new cases per year in the United States.[44,45] It has a male to female ratio of 2:1.[44] Traditionally, renal cell carcinoma has been treated with open nephrectomy as the gold standard procedure.[46] However, it is now widely accepted that small renal cell carcinomas can be treated with minimally invasive and nephron-sparing techniques. The evolving techniques

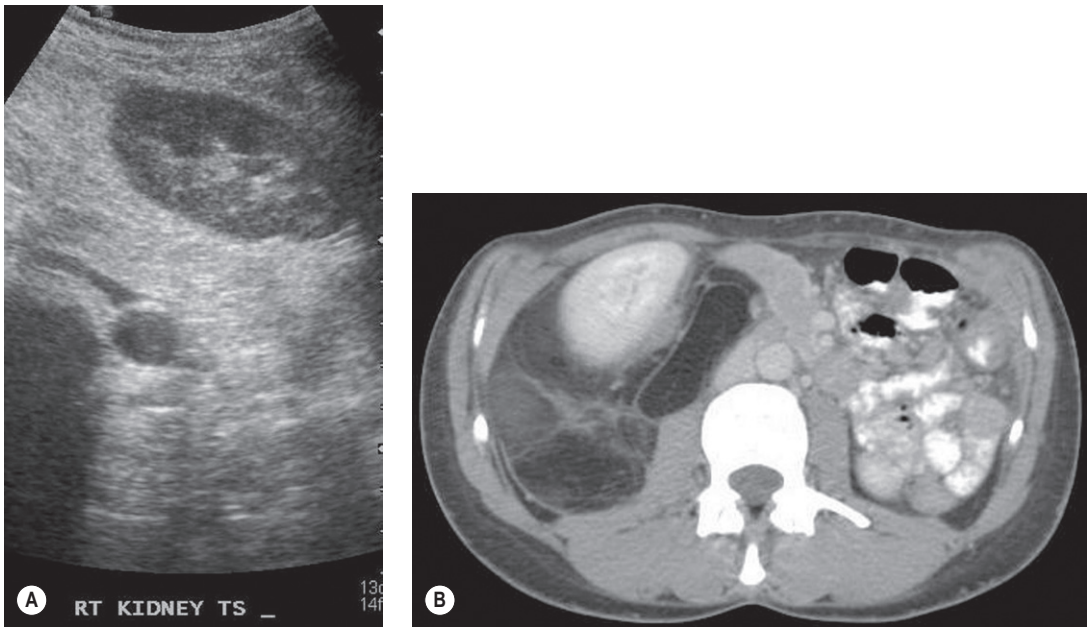


Figure 27.25 Retroperitoneal liposarcoma. A: Ultrasound shows the right kidney is displaced and surrounded by increased fat. **B:** CT confirms the extensive retroperitoneal fat which on resection was confirmed to be due to a liposarcoma.

currently available are image-guided energy ablative therapy and laparoscopic partial nephrectomy.

Nowadays, there are many new developments in energy ablative technologies to treat renal cell carcinoma. These are either with heat-based ablative energy, such as radio-frequency ablation (RFA) or microwaves, or with cold-based ablative energy such as cryoablation.[47–53] Preliminary results show that treatment is safe and effective, with good medium-term outcome data, for both RFA and cryoablation therapy of small renal cell carcinomas.[47–52]

RFA had initially enjoyed greater popularity in interventional radiology because of the smaller RFA needle electrode size, which allowed radiologists to perform image-guided treatment with ease. Recently, cryoablation is also gaining momentum as there is a new comparable-sized needle electrode (around 17G) available for the radiologist to use with image guidance. Microwave therapy is a new technology and many operators believe that there is great potential for this technology in the future. Currently this treatment is only available in selected research institutions around the world.

Minimally invasive therapy of renal cell carcinomas is evolving rapidly. Only time will tell which type of energy-based ablative therapy will be the optimum treatment option. However, regardless of the type of energy we might use for treatment in the future, most published series agree that image-guided treatment of small RCCs has great promise and long-term outcome data are currently awaited to validate the treatment.

The energy ablative therapy may be delivered via open surgery, a laparoscopic approach or via image guidance under ultrasound (US), computed tomography (CT) or magnetic resonance imaging (MRI).

The majority of interventional radiologists involved in this therapy utilise CT as the main imaging guidance technique to treat renal cell carcinomas. This is because CT is more widely available and cost effective than open MRI for guidance. CT allows good visualisation of all the electrode tips, especially with multi-tined expandable electrodes; this is important for accurate needle electrode positioning. Precise visualisation of the tips of the tines is crucial in order to avoid thermal injury to surrounding intra-abdominal viscera such as colon or retroperitoneal structures during the ablative treatment. It also allows operators to perform the hydro-dissection technique. In addition, CT is particularly useful when treating posteriorly located renal cell carcinomas or if the tumour predominantly has a parenchymal or central location, as this allows easier targeting of the tumour. Monitoring of the treatment response during and after the energy ablation can be performed with a contrast-enhanced examination using CT in patients without contrast allergy or impaired renal function. There are a small number of operators who prefer to use ultrasound guidance to insert the initial needle electrode and then use CT to assess the needle electrode's position in relation to the adjacent intra-abdominal structures.

Radio-frequency ablation of renal cell carcinoma

Radio-frequency ablation destroys tumour by using the frictional heat generated by radio-frequency waves. When the temperature rises above 60°C, this leads to cell death by destruction of the cellular membrane and denaturing of proteins. The technologies that are available in commercial markets currently are either impedance or temperature controlled systems.

All treatments should ideally be performed in the CT interventional suite with both CT and US available to guide the therapy. All established centres worldwide primarily use CT to guide treatment and peri-procedural monitoring of treatment. Many operators who started with US guidance alone have since realised that it is inadequate for needle placement and it limits targeting for more awkwardly positioned tumours such as those located close to the bowel or ureter.

For US-guided treatment, the RFA needle electrode can be inserted directly under US guidance (Fig. 27.26). During the thermal ablation, an echogenic cloud becomes visible (Fig. 27.27), and this tends to obscure the needle electrode. This makes subsequent needle readjustment difficult if only US guidance is used for treatment. Therefore, all established centres treating complex renal tumours use CT to check the needle electrode's position during treatment and subsequent repositioning of the needle electrode.

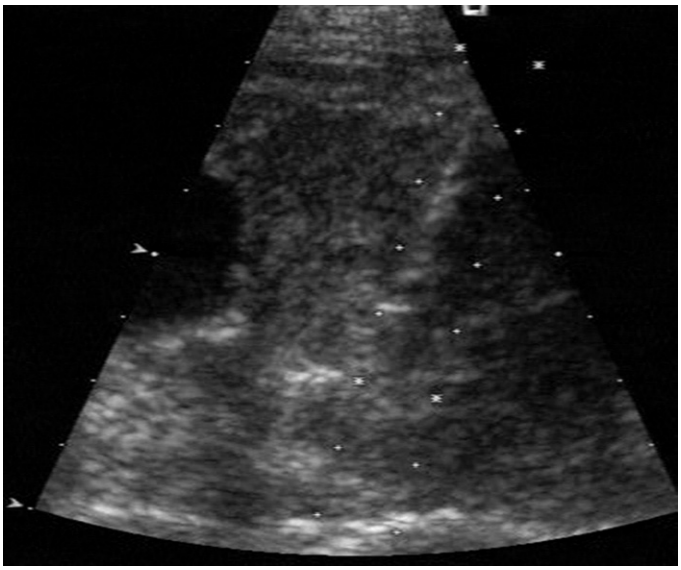


Figure 27.26 The RFA needle electrode can be inserted directly under US guidance.

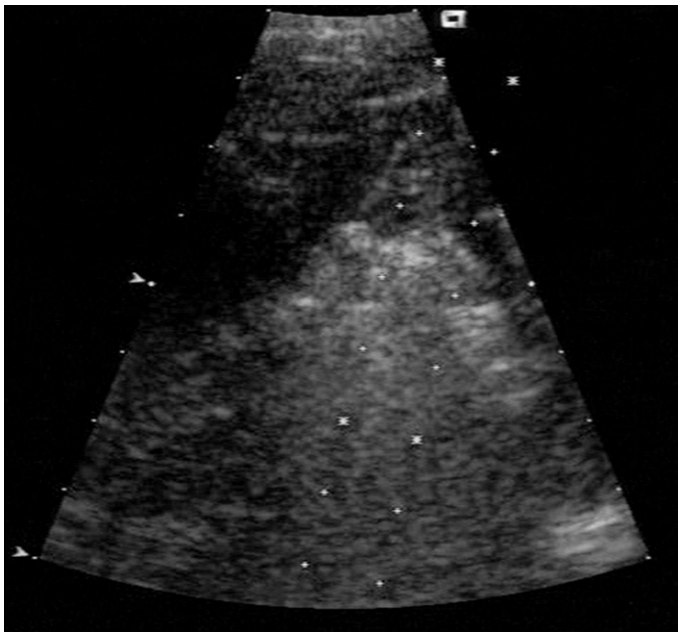


Figure 27.27 An echogenic cloud is visible during thermal ablation and this tends to obscure the needle electrode for subsequent placement.

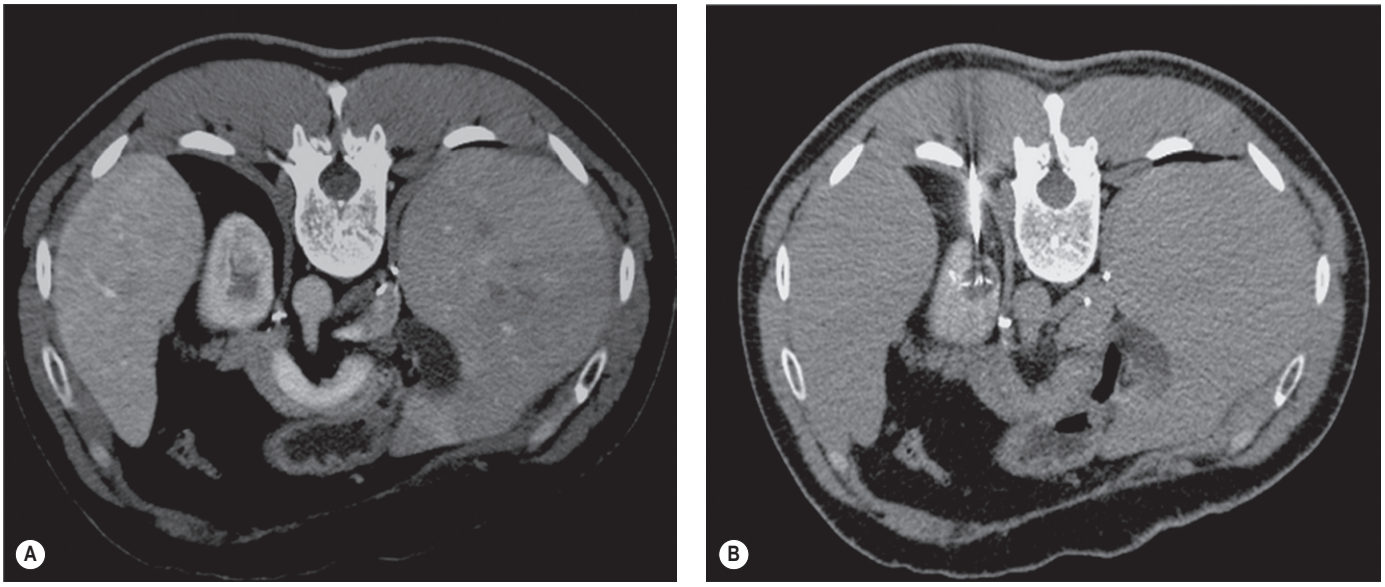


Figure 27.28 A: The contrast-enhanced CT shows a small renal cell carcinoma at the upper pole of the left kidney **B:** The RFA needle is inserted into the tumour under CT guidance.

For CT-guided treatment, this may involve using US or CT for the initial needle electrode placement (Fig. 27.28). CT is then used to check the position of the needle electrode, especially with the multi-tined probe where some of the tines could be in close relation to colon or ureter. If the tumour is too close to any intra-abdominal structure such as the colon, a hydrodissection technique may be required to move the colon away from the tumour in order to avoid thermal injury.[54]

For centrally located renal tumours or a tumour closely related to the ureter, a cold pyeloperfusion technique can be used to minimise the risk of thermal injury to the collecting system. If such an injury occurs, it causes a subsequent ureteric stricture.[55,56]

Patient selection is crucial. The referral should come from the cancer network, according to the NICE recommendations. As the treatment evolves, indications have expanded from curative to palliative intent. The indications include non-surgical candidates, patients with a solitary kidney, and von Hippel–Lindau disease patients with RCC. Patients with metastatic disease undergoing immunotherapy may also be considered for this therapy to debulk the primary tumour.

Evaluation prior to treatment includes attending the tumour ablation clinic for staging and counselling, laboratory investigations such as clotting and baseline renal function, and biopsy of the tumour either before/just prior to therapy.

Factors that influence the outcome of the therapy are size and location. For tumours smaller than 3 cm in diameter, complete ablation can be achieved in 90% of the cases treated with a single treatment session. For tumours between 3 and 5.5 cm, 100% successful ablation is achievable with exophytic tumours and 70% of the cases are treated in a single session.[57] The tumour locations can be divided into: exophytic, parenchymal, central/mixed location. The exophytic tumours have the best treatment outcome from the oven heat effect. This is due to the surrounding pararenal fat acting as a heat insulator to maximise the ablation effect.

Pre RFA imaging often consists of a combination of US, CT and MRI. They are used for staging, planning of therapy and as a baseline for post RFA changes. After RFA, imaging follow-up is variable depending on the operator's experience. Most institutions have patient follow-up at 1, 3, 6 and 12 months post treatment and annually thereafter. Contrast-enhanced US may be useful for those who still use US guidance alone to guide re-treatment (Fig. 27.29). It is well recognised that cross-sectional imaging with CT (Fig. 27.30) and/or MRI (Fig. 27.31), depending on the availability of resources, are the best imaging techniques for follow-up.

After the procedure, the patient is monitored for gross haematuria. They must be able to pass urine before discharge. If there is concern regarding complications then early imaging is advised. Minor complications are more common. These are microscopic

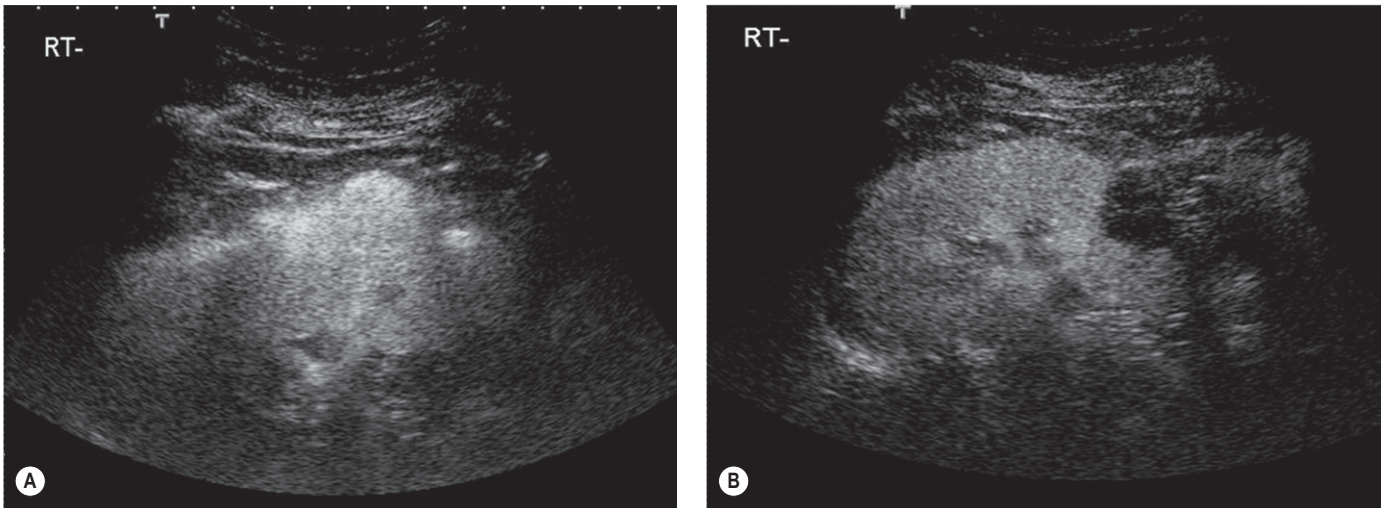


Figure 27.29 **A:** The contrast-enhanced US shows a small renal cell carcinoma at the lower pole of the right kidney **B:** Post RFA, the zone of ablation is seen as an echo-poor area, following US contrast administration.

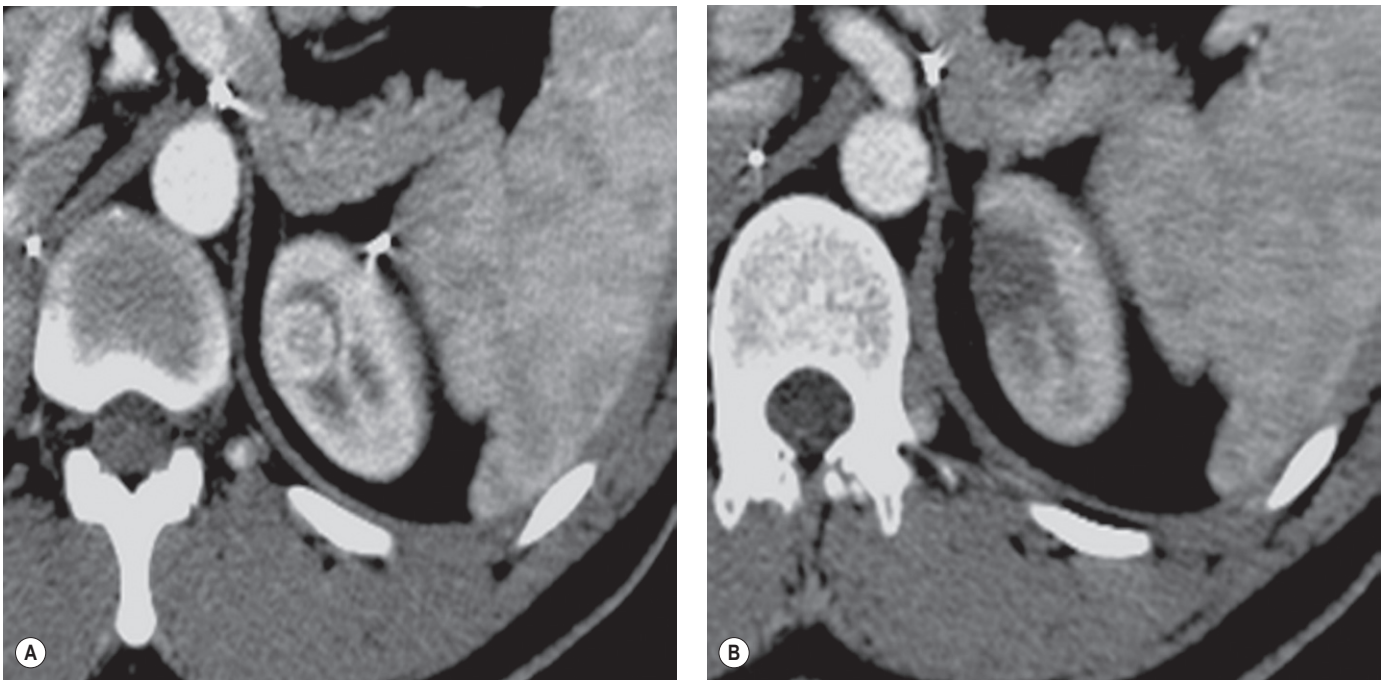


Figure 27.30 **A:** The contrast-enhanced CT shows a small renal cell carcinoma at the upper pole of the left kidney, **B:** Post RFA, the CT shows lack of enhancement within the zone of ablation.

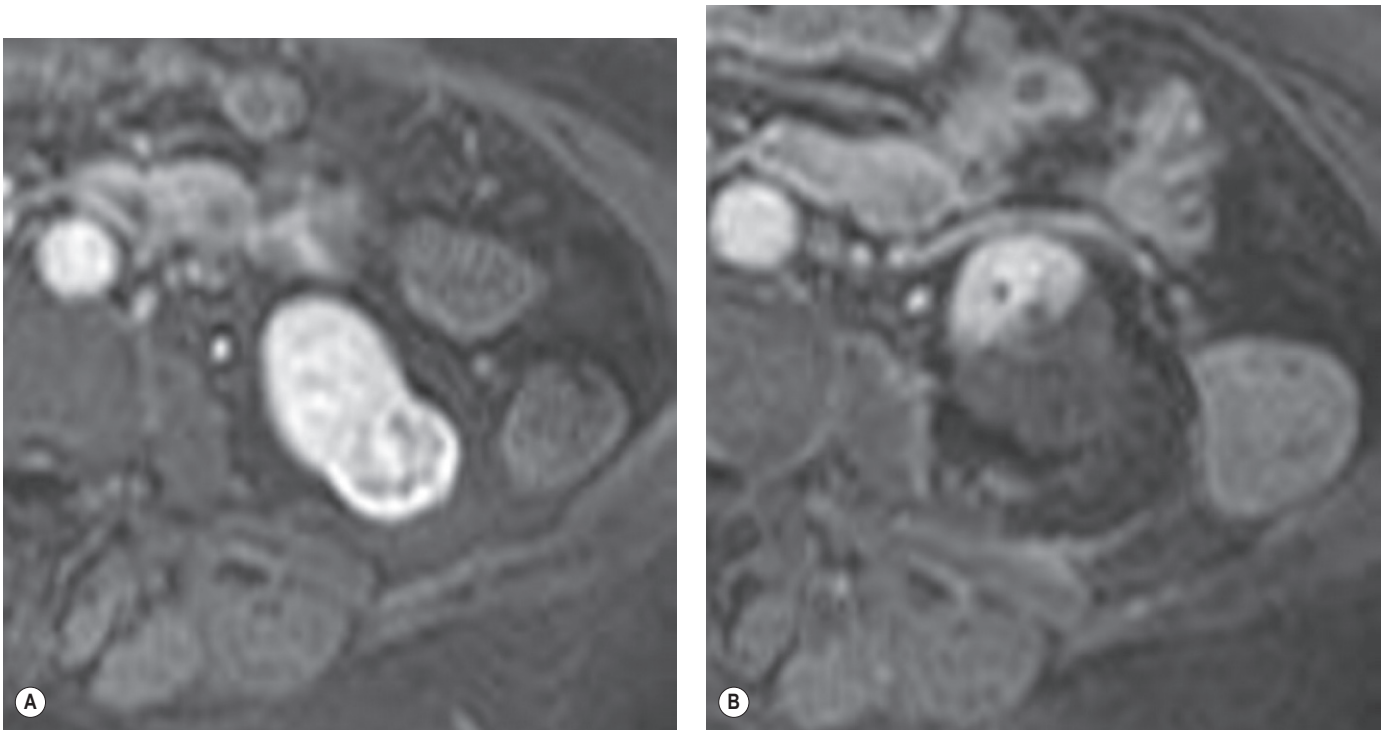


Figure 27.31 **A:** The contrast-enhanced MRI shows a small renal cell carcinoma at the lower pole of the left kidney **B:** Post RFA, the MRI shows a clear margin of the ablated zone that displays a lack of enhancement.

Ablation treatment of renal cell carcinoma

- Radio-frequency ablation, microwave ablation and cryoablation are all possible.
- Image-guided approaches favour CT over US.
- Tumours less than 5.5 cm are suitable for treatment.
- Exophytic tumours give the best results.
- Risk of damage to adjacent structures can be minimised with hydrodissection or pyeloperfusion.
- Best performed within a multidisciplinary cancer network environment.

haematuria in up to two-thirds of cases, perirenal haematoma and post RFA syndrome.[58] Major complications are rare and include haemorrhage that requires blood transfusion, renal failure from acute tubular necrosis, urinoma/calyceal-cutaneous fistula and ureteric injury.[49,59,60]

In order to set up a programme, good core interventional radiology skills are required for those performing the procedure, as the technical success and complication rate is directly related to the operator's experience.[61] Service development also requires cooperative work within a cancer network, adequate resources and a multidisciplinary team approach. To date, renal RFA is a safe and minimally invasive technique with good medium-term outcome data (within 5 years). Currently, long-term outcome data are awaited, though it is hoped and expected that these will be comparable to surgery.

REFERENCES

1. Bhatt S, MacLennan G, Dogra V. Renal pseudotumors. AJR Am J Roentgenol 2007;188:1380–1387.
2. Dubbins P. Ultrasound in acute urinary tract infection. BMUS Bull 2003;11:25–29.
3. Algaba F. Renal adenomas: Pathological differential diagnosis with malignant tumors. Adv Urol 2008; epub.
4. Prasad SR, Surabhi VR, Menias CO, et al. Benign renal neoplasms in adults: Cross-sectional imaging findings. AJR Am J Roentgenol 2008;190:158–164.
5. Bastos Netto JM, Esteves TC, Mattos RD, et al. Metanephric adenoma: a rare differential diagnosis of tumor in children. J Pediatr Urol 2007;3:340–341.
6. Fielding JR, Visweswaran A, Silverman SG, et al. CT and ultrasound features of metanephric adenoma in adults with pathologic correlation. J Comput Assist Tomogr 1999;23:441–444.
7. Li G, Cuilleron M, Gentil-Perret A, Tostain J. Characteristics of image-detected solid renal masses: implication for optimal treatment. Int J Urol 2004;11:63–67.
8. Ramirez ML, Evans CP. Current management of small renal masses. Can J Urol 2007;14(Suppl 1):39–47.
9. Reichelt O, Gajda M, Chyhrai A, et al. Ultrasound-guided biopsy of homogenous solid renal masses. Eur Radiol 2007;52:1421–1426.
10. Maturen KE, Nghiem HV, Caoili EM, et al. Renal mass core biopsy: accuracy and impact on clinical management. AJR Am J Roentgenol 2007;188:563–570.
11. Fan YH, Chang YH, Huang WJ, et al. Renal oncocytoma: clinical experience of Taipei Veterans General Hospital. J Chin Med Assoc 2008;71:254–258.
12. de la Cruz Burgos R, Martel Villagran J. Renal oncocytoma. Fundamental radiologic manifestations and enhancement patterns in tri-phase helical CT. Radiologica 2007;49:109–114.
13. Kondo T, Nakazawa H, Sakai F, et al. Spoke-wheel-like enhancement as an important imaging finding of chromophobe cell renal carcinoma: a retrospective analysis on computed tomography and magnetic resonance imaging studies. Int J Urol 2004;11:817–824.
14. Siu W, Hafez KS, Johnston WK 3rd, Wolf JS Jr. Growth rates of renal cell carcinoma and oncocytoma under surveillance are similar. Urol Oncol 2007;25:115–119.
15. Hes O, Michal M, Sima R, et al. Renal oncocytoma with and without intravascular extension into branches of renal vein have the same morphological, immunohistochemical, and genetic features. Virchows Arch 2008;452:193–200.
16. Mogorovich A, Giannarini G, De Maria M, et al. Multifocal and bilateral renal oncocytoma: a case report and review of the literature. Arch Ital Urol Androl 2007;79:130–134.
17. Ameri C, Contreras P, Villasante N, et al. Solid renal masses up to 4 cm. Analysis of the diagnostic procedures, TNM staging and surgical treatment. Actas Urol Esp 2006;30:772–783.

18. Kozlowska J, Okon K. Renal tumours in post-mortem material. Pol J Pathol 2008;59:21–25.
19. Umeoka S, Koyama T, Miki Y, et al. Pictorial review of tuberous sclerosis in various organs. Radiographics 2008;28:e32.
20. Strotzer M, Lehner KB, Becker K. Detection of fat in a renal cell carcinoma mimicking angiomyolipoma. Radiology 1993;188:427–428.
21. Garin JM, Marco I, Salva A, et al. CT and MRI in fat-containing papillary renal cell carcinoma. Br J Radiol 2007;80:e193–e195.
22. Jinzaki M, Tanimoto A, Narimatsu Y, et al. Angiomyolipoma: imaging findings in lesions with minimal fat. Radiology 1997;205:497–502.
23. Nelson CP, Sanda MG. Contemporary diagnosis and management of renal angiomyolipoma. J Urol 2002;168:1315–1325.
24. Farrelly C, Delaney H, McDermott R, Malone D. Do all non-calcified echogenic renal lesions found on ultrasound need further evaluation with CT? Abdom Imaging 2008;33:44–47.
25. Prando A, Prando D, Prando P. Renal cell carcinoma: unusual imaging manifestations. Radiographics 2006;26:233–244.
26. Filipas D, Spix C, Schulz-Lampel D, et al. Screening for renal cell carcinoma using ultrasonography: a feasibility study. BJU Int 2003;91:595–599.
27. Malaeb BS, Martin DJ, Littooy FN, et al. The utility of screening renal ultrasonography: identifying renal cell carcinoma in an elderly asymptomatic population. BJU Int 2005;95:977–981.
28. Schwarz A, Vatandaslar S, Merkel S, Haller H. Renal carcinoma in transplant recipients with acquired cystic kidney disease. Clin J Am Soc Nephrol 2007;2:750–756.
29. Dyer R, DiSantis DJ, McClennan BL. Simplified imaging approach for evaluation of the solid renal mass in adults. Radiology 2008;247: 331–343.
30. Fan L, Lianfang D, Jinfang X, et al. Diagnostic efficiency of contrast-enhanced ultrasonography in solid renal parenchymal lesions with maximum diameters of 5 cm. J Ultrasound Med 2008;27:875–885.
31. Ho SSY. Renal cell carcinoma. In: Ahuja AT, editor. Diagnostic imaging, ultrasound. Salt Lake City: Amirsys; 2007.
32. Pickhardt PJ, Siegel CL, McLarney JK. Collecting duct carcinoma of the kidney: are imaging findings suggestive of the diagnosis? AJR Am J Roentgenol 2001;176:627–633.
33. Prasad SR, Humphrey PA, Catena JR, et al. Common and uncommon histologic subtypes of renal cell carcinoma: imaging spectrum with pathologic correlation. Radiographics 2006;26:1795–1806.
34. Blitman NM, Berkenblit RG, Rozenblit AM, Levin TL. Renal medullary carcinoma: CT and MRI features. AJR Am J Roentgenol 2005;185: 268–272.
35. Browne RFJ, Meehan CP, Colville J, et al. Transitional cell carcinoma of the upper urinary tract: spectrum of imaging findings. Radiographics 2005;25:1609–1627.
36. Tran W, Serio AM, Raj GV, et al. Longitudinal risk of upper tract recurrence following radical cystectomy for urothelial cancer and the potential implications for long-term surveillance. J Urol 2008;179: 96–100.
37. Gupta R, Paner GP, Amin MB. Neoplasms of the upper urinary tract: a review with focus on urothelial carcinoma of the pelvi-calyceal system and aspects related to its diagnosis and reporting. Adv Anal Pathol 2008;15:127–139.
38. Datta SN, Allen GM, Evans R, et al. Urinary tract ultrasonography in the evaluation of haematuria – a report of over 1,000 cases. Ann R Coll Surg Engl 2002;84:203–205.
39. Anderson EM, Murphy R, Rennie AT, Cowan NC. Multidetector computed tomography urography (MDCTU) for diagnosing urothelial malignancy. Clin Radiol 2007;62:324–332.
40. Horstman WG, McFarland RM, Gorman JD. Color Doppler sonographic findings in patients with transitional cell carcinoma of the bladder and renal pelvis. J Ultrasound Med 1995;14:129–133.
41. Papatsoris AG, Chrisofos M, Skolarikos A, et al. Upper urinary tract transitional cell carcinoma: a 10-year experience. Tumori 2008;94: 75–78.
42. Sheth S, Ali S, Fishman E. Imaging of renal lymphoma: patterns of disease with pathologic correlation. Radiographics 2006;26:1151–1168.
43. Pradeep R, Madhumathi DS, Lakshmidevi V, et al. Bilateral nephromegaly simulating Wilms tumour: a rare initial manifestation of acute lymphoblastic leukaemia. J Pediatr Hematol Oncol 2008;30:471–473.
44. Office for National Statistics. Registrations of cancer diagnosed in 2003, England. ONS; 2006.
45. Landis SH, Murray T, Bolden S, Wingo PA. Cancer statistics, 1999. CA Cancer J Clin 1999;49(1):8–31.
46. Lee CT, Katz J, Shi W, et al. Surgical management of renal tumors 4 cm or less in a contemporary cohort. J Urol 2000;163(3):730–736.
47. McDougal WS, Gervais DA, McGovern FJ, Mueller PR. Long-term follow up of patients with renal cell carcinoma treated with radio frequency ablation with curative intent. J Urol 2005;174(1):61–63.
48. Gervais DA, McGovern FJ, Arellano RS, et al. Radiofrequency ablation of renal cell carcinoma: part 1, Indications, results, and role in patient management over a 6-year period and ablation of 100 tumors. AJR Am J Roentgenol 2005;185(1):64–71.
49. Gervais DA, Arellano RS, McGovern FJ, et al. Radiofrequency ablation of renal cell carcinoma: part 2, Lessons learned with ablation of 100 tumors. AJR Am J Roentgenol 2005;185(1):72–80.
50. Levinson AW, Su LM, Agarwal D, et al. Long-term oncological and overall outcomes of percutaneous radio frequency ablation in high risk surgical patients with a solitary small renal mass. J Urol 2008;180(2):499–504; discussion 504. Epub 2008 Jun 11.
51. Permpongkosol S, Link RE, Kavoussi LR, Solomon SB. Percutaneous computerized tomography guided cryoablation for localized renal cell carcinoma: factors influencing success. J Urol 2006;176(5):1963–1968; discussion 1968.
52. Hinshaw JL, Shadid AM, Nakada SY, et al. Comparison of percutaneous and laparoscopic cryoablation for the treatment of solid renal masses. AJR Am J Roentgenol 2008;191(4):1159–1168.
53. Trembley BS, Ryan TP, Strohbehn JW. Interstitial hyperthermia: physics, biology and clinical aspects. In: Urano M, Douple E, editors. Physics of microwave hyperthermia in hyperthermia and oncology, vol 3. Utrecht, the Netherlands: Verlag Springer; 1992. p. 11–98.
54. Farrell MA, Charboneau JW, Callstrom MR, et al. Paranephric water instillation: a technique to prevent bowel injury during percutaneous renal radiofrequency ablation. AJR Am J Roentgenol 2003;181(5): 1315–1317.
55. Wah TM, Koenig P, Irving HC, et al. Radiofrequency ablation of a central renal tumor: protection of the collecting system with a retrograde cold dextrose pyeloperfusion technique. J Vasc Interv Radiol 2005;16(11):1551–1555.
56. Cantwell CP, Wah TM, Gervais DA, et al. Protecting the ureter during radiofrequency ablation of renal cell cancer: a pilot study of retrograde pyeloperfusion with cooled dextrose 5% in water. J Vasc Interv Radiol 2008;19(7):1034–1040.
57. Gervais DA, McGovern FJ, Wood BJ, et al. Radio-frequency ablation of renal cell carcinoma: early clinical experience. Radiology 2000;217(3):665–672.
58. Wah TM, Arellano RS, Gervais DA, et al. Image-guided percutaneous radiofrequency ablation and incidence of post-radiofrequency ablation syndrome: prospective survey. Radiology 2005;237(3):1097–1102.
59. Wah TM, Irving HC. Acute tubular necrosis following radiofrequency ablation of a renal cell carcinoma. Cardiovasc Intervent Radiol 2007 Nov 6 (epub ahead of print).
60. Wah TM, Irving HC. Infectious complications after percutaneous radiofrequency ablation of renal cell carcinoma in patients with ileal conduit. J Vasc Interv Radiol 2008;19(9):1382–1385.
61. Poon RT, Ng KK, Lam CM, et al. Learning curve for radiofrequency ablation of liver tumors: prospective analysis of initial 100 patients in a tertiary institution. Ann Surg 2004;239(4):441–449.

CHAPTER

28

Renal transplantation

Grant M. Baxter

DEVELOPMENT OF RENAL TRANSPLANTATION 528

BACKGROUND 528

INDICATIONS AND CONTRAINDICATIONS TO TRANSPLANTATION 529

DONOR SUPPLY 529

HISTOCOMPATIBILITY TESTING 529

PREOPERATIVE MANAGEMENT 529

SURGERY 529

IMMUNOSUPPRESSION 529

IMAGING THE TRANSPLANTED KIDNEY 530

EARLY COMPLICATIONS 532
- Acute tubular necrosis 532
- Acute rejection 532
- Ultrasound in delayed function 532
- Arterial thrombosis 533
- Venous thrombosis 534
- Obstruction 535
- Haemorrhage 535
- Urinary leak 535
- Post-transplant collections 535
- Ciclosporin and tacrolimus toxicity 536
- Infection 536

LATE COMPLICATIONS 537
- Ureteric stenosis 537
- Transplant artery stenosis 537
- Arteriovenous fistulae 538
- Ciclosporin and tacrolimus toxicity 539
- Acute rejection 539
- Chronic rejection 539
- Urinary tract infection 540
- Recurrent disease 540
- Other complications 540

COMBINED RENAL AND PANCREATIC TRANSPLANTATION 541

USE OF MICROBUBBLE CONTRAST AGENTS 542
- Hydronephrosis 542
- Monitoring in the early postoperative transplant period 542
- Vascular applications 546
  - Vascular occlusion 546
  - Renal artery stenosis 546
- Renal masses 546
- Potential applications 546

DEVELOPMENT OF RENAL TRANSPLANTATION

Renal transplantation is now regarded as a successful and routine procedure. However, the road to success has been paved with many setbacks along the way and indeed this journey dates back to the first experimental attempts of Carrel at transplantation at the beginning of the twentieth century, this seminal work resulting in the Nobel prize of 1912.[1] Non-immunosuppressed attempts at transplantation followed in the 1950s and were superseded by the more successful outcome of twin to twin transplants later that decade.[2] However, this work was interrupted by many severe setbacks and pitfalls, leading many groups at the time to question whether further work in this area was both justified and likely to be successful.

Despite these issues, with a better understanding of tissue rejection, the introduction of steroids and azathioprine in 1963,[3] and more specifically the use of cyclosporin A by Calne et al. in the 1970s,[4] the door to progress was opened and many groups were encouraged to persevere.

Further development and progress of surgical techniques, combined with new more effective anti-rejection therapy with reduced toxicity, led to renewed enthusiasm. The addition of ultrasound as a diagnostic aid in the 1970s followed by Doppler a decade later and a rapid development of interventional radiological techniques all combined to give renewed impetus and these now represent routine, primary imaging examinations in this patient group.[5–7] These advances resulted in more successful clinical outcomes and the routine operation we now all take for granted. It is safe to say, however, that without the dedication and fortitude of these early pioneers, it is unlikely that such progress would have been achieved and indeed a debt of gratitude is owed to those in the early pioneering and informative years.

BACKGROUND

The number of patients with end-stage renal disease is rising and will continue to do so; it is not expected to plateau before the middle of the twenty-first century. This reflects a combination of an ageing population and a significant improvement in the long-term prognosis of patients with this condition, particularly those with co-morbid diseases such as diabetes mellitus.[8,9] Clearly this has public health resource implications and is unremitting in terms of diagnosis, treatment and long-term surveillance. It is therefore easy to appreciate that this constitutes a serious and chronic health resource issue.[10]

There are a number of treatment options for end-stage renal disease and these include haemodialysis, peritoneal dialysis and renal transplantation. Of these, there is no doubt that transplantation is the treatment of choice; however, there are limitations to the number of operations that can be performed. These are well recognised, not just by the medical staff involved, but also by the general public and the many and diverse public health campaigns which highlight the continuing shortage of suitable donor kidneys.[11] Thankfully, improvements including better donor recipient matching,[12,13] the use of more potent immunosuppressive regimens, together with improved surgical techniques, have all resulted in improved outcomes. The 1- and 5-year graft survival in Europe has been improving since the mid-1990s and current figures show a 1-year graft survival of 90% with a 5-year survival of 80%; there are slightly higher values for living donor kidneys and slightly lower values for second and subsequent transplants (www.uktransplant.org).

There is universal agreement that renal transplantation is the treatment of choice for end-stage renal failure. A successful renal transplant will provide a glomerular infiltration rate (GFR) of up to 50–60 mL per minute, which although only half of the normal adult value, is nevertheless sufficient to return the vast majority of patients to a normal, independent lifestyle. Such an improvement in the quality of life is difficult and some would say impossible to measure; however, in the harsh world of health economics, it is clear that the cost benefits of successful transplantation far outweigh those of failure. This is one reason why resources are targeted on the pre-, peri- and immediate post-transplantation period in order to help ensure as positive an outcome as possible. The average life expectancy of a transplant kidney is approximately 7–10 years, increasing to 15–20 years with a live donor organ. Although there are many and varied imaging techniques used when dealing with the transplant patient, there is no doubt that ultrasound remains central and crucial to the management of these patients and is very useful both in the early postoperative period as a non-invasive indicator of renal transplant dysfunction and in the long-term follow-up of many of these patients, particularly those with suspected renal artery stenosis.

INDICATIONS AND CONTRAINDICATIONS TO TRANSPLANTATION

There are few contraindications to renal transplantation and this treatment option should be considered for all patients with end-stage renal failure that is of a severity to require dialysis. Those unfit for transplantation are generally those who are unfit for general anaesthesia or surgery, such as those with severe cardiac disease, severe arteriopathy and severe respiratory disease. In addition, the known potential issues of immunosuppression in the context of a pre-existing infection and malignancy should be considered, as should the risk of recurrence of the renal disease, which is particularly evident in those patients with oxalosis or active vasculitis.

DONOR SUPPLY

Initially the main sources of organ transplantation were either brain-dead, ventilated organ donors or live related donors. The majority of transplants in the developed world are cadaveric in origin, whereas live related operations predominate in the developing countries. The number of transplant operations is more or less constant annually, with perhaps a slight fall in the past few years reflecting the known shortage of transplant donors. Although cadaveric transplants have clearly reduced in number, this has been partially compensated for by an increase, particularly in the developed world, in the number of live donor transplants. This latter group includes both live related and live unrelated transplantations which are now feasible and routine with a very similar outcome and prognosis. A number of small technical differences exist in terms of the surgical technique and recipient outcome between cadaveric and live donor transplants; however, the overall management of the recipient can be regarded as similar in both types.

HISTOCOMPATIBILITY TESTING

In order to reduce to a minimum the risk of rejection, the detection of donor-specific antibodies in the lymphocyte cross-match test is a contraindication to transplantation.

The risk of subsequent episodes of acute rejection is partially dependent upon the degree of HLA matching between donor and recipient. The genes that determine the HLA antigens are located on chromosome 6.[14,15] The importance of such HLA matching is reflected in the improved graft survival of a fully HLA matched graft (T-half 17.3 years), compared with an incomplete HLA miss matched graft (T-half 7.8 years),[16,17] where T-half is the time taken for 50% of transplants that are functioning at one year to fail.

PREOPERATIVE MANAGEMENT

The transplant procedure should ideally be performed within 24 hours of organ retrieval and at worst, 48 hours. During this period the recipient will have been chosen, appropriately prepared for the operation with screening for infection and cardiorespiratory reserve assessment, and initial dialysis undertaken, if any fluid or metabolite imbalance requires recorrection.

A live related donor, who can be either a family member or close friend, is screened with a combination of clinical history, examination and HLA status assessment. Other assessment tests for live donors will vary from centre to centre but will include a 24-hour creatinine clearance, serology, liver function tests, DMSA scan and either MRI or CT to assess anatomy; renal arteriography is largely reserved for difficult cases.

SURGERY

Traditionally the transplant vessels are anastomosed to the external iliac artery and vein in the case of the cadaveric transplant, and to the internal iliac vessels in a live related procedure. More than one artery may be present in 18–30% of the population; this can create technical difficulties for the surgeon. In the case of a cadaveric transplant this is addressed by suturing these vessels to a common Carrel patch.[18] Those receiving a third transplant kidney may require an intraperitoneal approach to the iliac vasculature. The vesico-ureteric anastomosis is performed by implanting the shortened ureter into the dome of the bladder. A point worthy of consideration is that this procedure may result in ischaemia of the lower end of the ureter, particularly if the lower ureter is too long and affected by devascularisation at the time of retrieval. This can on occasion become functionally significant. In many centres, a ureteric stent is placed across the uretero-vesical anastomosis, which is normally removed at 3 months (Fig. 28.1).

Postoperative complications vary from centre to centre but include bleeding (less than 1%), major vascular occlusion of the transplant artery or vein (1–2%), wound infection (1.6–6.3%) and a number of urological complications including obstruction, haematuria and anastomotic leak (1.3–7%).[19–22]

IMMUNOSUPPRESSION

The aim of immunosuppression is to prevent rejection but not at the expense of inducing infective complications or serious drug

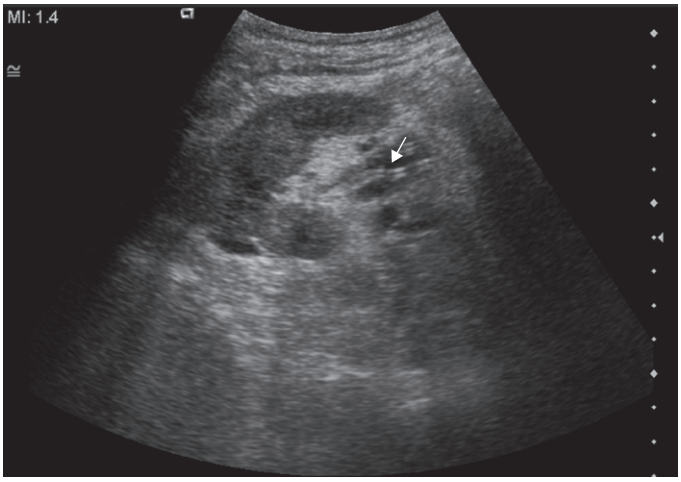


Figure 28.1 **Normal functioning transplant kidney** in the early postoperative period. A ureteric stent (arrow) can be seen within the renal pelvis.

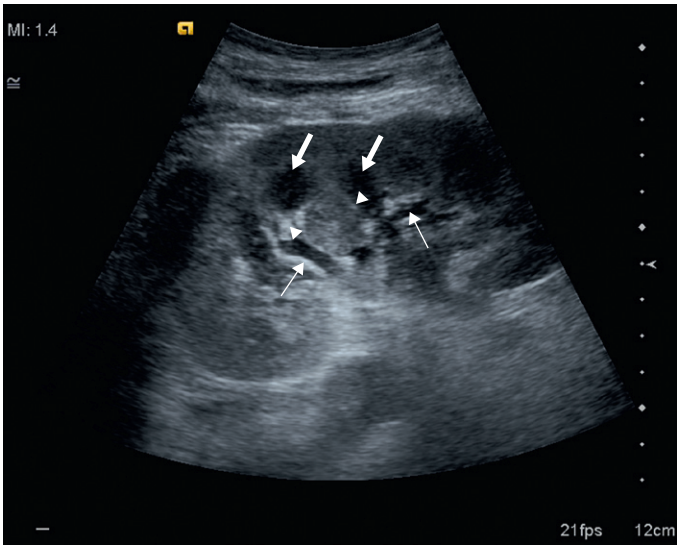


Figure 28.2 **Normal transplant kidney.** The renal pyramids (thick arrows) are regularly spaced and hypoechoic relative to the cortex. They do not communicate and are readily differentiated from calyceal dilatation. A column of Bertin is easily visualised (arrowheads). The segmental vessels (thin arrows) can also be seen within the renal sinus.

Ultrasound and renal transplantation

- 1- and 5-year graft survivals are currently 90% and 80% respectively.
- A combination of an ageing population and increased requirements for renal transplantation constitutes a major public health and ethical issue.
- Contraindications to transplantation are few.
- Early disease recurrence after transplantation is high in patients with oxalosis or active vasculitis.
- Immunologically well-matched kidneys have a favourable outcome.

toxicity. A number of options now exist with the various drug regimen combinations. The conventional regimen is likely to include a combination of ciclosporin (cyclosporin A), azathioprine and steroids (prednisolone). However, a number of newer agents exist including tacrolimus,[23] mycophenolate[24] and sirolimus (rapamycin); these are often used in the therapeutic cocktail. Other alternatives include antibody therapies such as anti-interleukin-2; these are effective and less toxic than the more traditional humoral agents which include OKT3 and antithymic globulin. These are often reserved for high-risk patients. Clearly the range and increased number of such options means that the immunosuppressive regimens will vary from centre to centre.

The treatment of established acute rejection is normally with high-dose oral or intravenous steroids and, in resistant cases, with immuno-depletion using antibody therapy or tacrolimus. Unfortunately no effective treatment exists for either hyperacute or chronic rejection.

IMAGING THE TRANSPLANTED KIDNEY

Normally the renal transplant can be visualised easily in either iliac fossa as it lies a few centimetres beneath the skin surface and is therefore very easily accessible using ultrasound. Orientation of the kidney can be variable depending on the surgical technique employed and it is important for the sonographer to develop a clear idea of the alignment of the kidney. As for any ultrasonic technique, resolution clearly depends on a number of well-established factors including the depth of the transplant beneath the skin surface, the presence or absence of postoperative oedema, the amount of subcutaneous fat and patient build. In general a 4 MHz probe will give a very good overall assessment of the kidney, perirenal structures and potential peri-transplant collections; it also allows interrogation not only of the intrarenal transplant vasculature but also of the more deeply situated iliac vessels and the anastomoses of the main transplant vessels. A higher-frequency probe, such as 7 MHz, gives excellent near-field resolution and beautiful anatomical detail of the renal transplant and high quality colour Doppler from within the kidney; however, in all but the thinnest of patients, use of such a probe will probably at best be suboptimal, and in some will not allow visualisation of the more deeply situated vascular structures.

There is no difference morphologically between the renal transplant and the native kidney. The renal parenchyma peripherally is well defined with a bright echogenic pattern centrally representing the renal sinus fat. For the reasons defined above, the improved resolution of the renal transplant makes identification of the renal pyramids much more common; these are hypoechoic relative to the adjacent renal cortex. In addition, they are regularly spaced with no communication between them; this is a useful differentiating feature from calyceal dilatation (Fig. 28.2).

In the early postoperative period it is not unusual to observe a mild degree of hydronephrosis in the transplant kidney. This is largely the result of some postoperative oedema producing lower ureteric compression in and around the vesicoureteric anastomosis. Although this may resolve with time, it can be variable. However, assuming renal function to be normal, a minor degree of dilatation is often documented as a baseline feature to which subsequent examinations can be compared.

On occasion it can be confusing and difficult to differentiate the renal transplant artery and vein at the renal hilum from a dilated or prominent renal pelvis using real-time imaging alone. The situation can easily be clarified with the use of colour Doppler ultrasound.

The bladder should be imaged routinely during all examinations when visible and should be echo-free. The presence of intravesical turbid echoes may indicate either haemorrhage or infection, depending on the clinical situation.

Colour Doppler ultrasound is an extremely valuable tool in the assessment of the renal transplant for a number of different reasons.

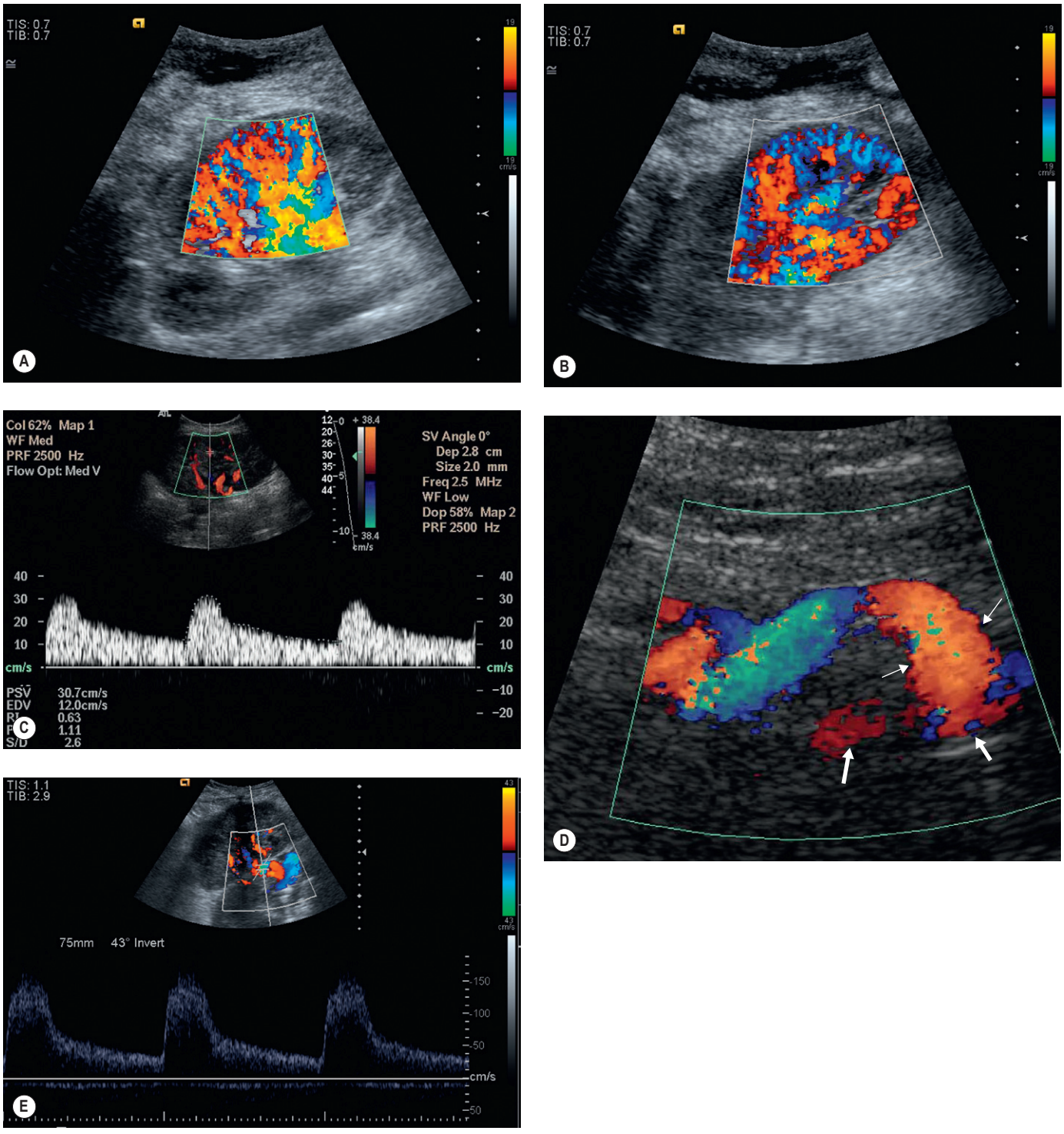


Figure 28.3 A and B: Normal colour Doppler scan of the transplant kidney. The intrarenal vessels are well visualised and extend to the periphery of the cortex. The arterial (red) and venous (blue) branches can be easily distinguished. **C:** Normal spectral Doppler waveform from an interlobar artery. Having selected and drawn around an appropriate arterial waveform the machine has automatically calculated both the PI and RI (1.11 and 0.63 respectively). **D:** Normal colour Doppler scan of the origin of the transplant renal artery (thin arrows) as it arises from the external iliac artery (thick arrows). **E:** Spectral Doppler waveform of the transplant renal artery just distal to its origin. The normal renal artery waveform is well demonstrated and has a peak systolic velocity of 1.50 m/s.

Primarily it provides an instantaneous appreciation of the intrarenal vasculature and therefore gives a global impression of overall transplant perfusion. In addition, it can easily identify the transplant artery and vein and track these back to their anastomoses with the iliac vessels. Although such information is purely visual and qualitative in many circumstances, it is both helpful and reassuring (Fig. 28.3A, B). As with all Doppler techniques, in order to acquire quantitative information spectral Doppler analysis is required (Fig. 28.3C). The technique of using colour Doppler and spectral Doppler analysis in the transplanted kidney has much in common with techniques used elsewhere in the vascular tree: the vessel is first identified using colour Doppler, the spectral gate is placed over the

lumen of the vessel and a spectral Doppler tracing obtained. With regard to the transplant kidney, the spectral Doppler waveform is characteristically of low resistance and has been described as having a 'ski slope' appearance with diastolic flow normally being at least a third of the peak systolic value. Any reduction in diastolic flow may reflect a pathological process and increased peripheral resistance in the kidney. Colour Doppler ultrasound is used most effectively in the early transplant period when serial studies are performed regularly until renal function is satisfactory.

There are a number of Doppler indices that can be measured, including the pulsatility index (PI), resistive index (RI), the systolic to diastolic and diastolic to systolic ratios. Although all of these parameters may be used, the most commonly utilised ones are the pulsatility index (PI) and the resistive index (RI); there is no perceived advantage for one over the other.

$$\text{PI} = \frac{\text{peak systolic velocity} - \text{end-diastolic velocity}}{\text{time-averaged mean velocity}}$$

$$\text{RI} = \frac{\text{peak systolic velocity} - \text{end-diastolic velocity}}{\text{peak systolic velocity}}$$

The main transplant artery can often be difficult to visualise due to its course, which can range from mildly curved to severely tortuous (Fig. 28.3D). A wide range of normal peak systolic velocities have been quoted for the artery, possibly as a result of this tortuosity. At our centre a cut-off value of 2.5 m/s is used.[25,26] Any value below this level is regarded as normal, whereas values above this level are taken to represent a significant transplant artery stenosis. Other centres have looked at this issue and some of these have chosen as their cut-off level a slightly higher value at 3 m/s.[27] Such differences could be explained by the use of different ultrasound systems, or differences in technique. Differences in the group of patients being evaluated may also be pertinent; our original study[28] was performed on high-risk patients; whereas those in the 3 m/s study were patients at low risk for renal artery stenosis.[27] The examination of the renal vessels can be time-consuming and quite an exacting procedure depending on the nature of the anatomy. Precise Doppler angle correction to ensure an accurate velocity reading is of paramount importance (Fig. 28.3E).

There are no specific Doppler values for normal velocity in the transplant renal vein; however, most often the prime consideration with regard to this vessel, at least in the early transplant period, is simply to identify whether flow is present or absent. It is also vital that the iliac artery and vein are identified, primarily to distinguish them from the renal vessels and, secondarily, to exclude a more proximal lesion in the iliac vessel such as a stenosis in the iliac artery which may contribute to, or be the sole cause of, impaired renal function.

Ultrasound technique

- A 4 MHz ultrasound probe gives the best overall assessment of the transplant kidney.
- Mild hydronephrosis is 'normal' in the early postoperative transplant period.
- Serial colour and spectral Doppler ultrasound measurements can be used to monitor transplant dysfunction and response to therapy.
- The PI and RI are the most commonly used Doppler indices; there is no advantage of one over the other.
- The transplant and iliac vessels should always be identified separately to avoid confusion.
- The peak systolic velocity in the transplant artery is normally <2.5 m/s.

EARLY COMPLICATIONS

Complications of renal transplantation are both varied and numerous. They include parenchymal insults such as acute tubular necrosis (ATN), acute rejection or both, vascular occlusion, obstruction, urinary leak, collections, infections and drug toxicity related to antirejection therapy. Some of these complications can be differentiated through a combination of clinical history, bacteriology and ultrasound. In practice the main differential diagnosis often lies between acute rejection and acute tubular necrosis, which can be a difficult diagnosis clinically as symptoms are generally absent. As both entities require different approaches to treatment, early and accurate diagnosis is essential. Although many groups have tried, it has not been possible to differentiate these entities using colour Doppler imaging and, for definitive diagnosis, a histological sample is still required.[29,30] Despite this limitation ultrasound remains useful in its dual rule of not only helping to assess transplant dysfunction but also monitoring response to therapy.[31]

Acute tubular necrosis

Acute tubular necrosis is common in the early transplant period, with up to 30% of patients requiring dialysis in the early postoperative period. Delayed graft function is rare in the live related donor situation. Acute tubular necrosis is primarily related to both the donor and the donor kidney and, in particular, the warm ischaemic time. In patients with established acute tubular necrosis requiring dialysis, recovery generally occurs within 1–2 weeks of transplantation, although it may be delayed for significant longer periods of time of up to 3 months.

Acute rejection

The diagnosis of acute rejection is by biopsy. In experienced hands this is generally safe, with a complication rate of less than 5% for haemorrhage requiring blood transfusion and significant pain requiring analgesia.[32] The recommended technique for transplant biopsy is to use an automated core biopsy/cutting needle system under direct ultrasonic guidance.[33–35] Needle sizes can vary from 14- to 18-gauge. In our institution we normally employ a 16-gauge needle, with at least two cores of tissue being obtained and, on occasion, three. Acute rejection can affect up to 40% of patients and peaks at 1–3 weeks post transplantation. Assuming the condition is recognised early, it is normally treated with high-dose steroids or antibody therapy. In general, patients are normally asymptomatic, although severe rejection can be accompanied by a flu like illness consisting of pyrexia and graft tenderness. Acute rejection must always be considered in patients with deteriorating renal function, and, as with acute tubular necrosis, it is often difficult to diagnose, particularly in those patients with non-functioning grafts. Unfortunately the occurrence of acute rejection, even if treated successfully, is an adverse long-term prognostic indication.[36]

Ultrasound in delayed function

Whilst the appearances of acute rejection have been well documented on real-time imaging,[37] these would now be regarded largely in an historical context and should essentially no longer be seen, particularly in the early postoperative transplant period; these classic features occur late, well after the onset of the rejection process. In addition, the findings are so arbitrary, varied and inconsistent that they are of limited value. Features that have been described include a reduction in cortical medullary differentiation, reduction in renal sinus echoes, both increased and reduced renal parenchymal echoes, increased cortical reflectivity and so forth. It is noteworthy, however, that observations of increased renal length[38] and cross-sectional area[39] have been reported in patients

with acute rejection and, although acute tubular necrosis has been described as causing a minimal increase in renal length, these features are much less marked when compared with those of acute rejection. Irrespective of these observations, none of these measurements have been adopted in routine clinical practice.

With regard to Doppler ultrasound, there have been a significant number of studies performed testing the potential value of this technique in differentiating acute rejection from acute tubular necrosis, as a non-invasive alternative to renal transplant biopsy. Some of these initial results were both confusing and contradictory; the reasons for this have been well recognised and include inhomogeneous study populations, inadequately defined end points and differing diagnostic criteria. In retrospect, the expectation of being able to ascribe some form of histological value to a non-invasive ultrasound test was probably, at best, optimistic. However, this technique continues to perform a useful clinical role in monitoring such patients with delayed function.[40]

The role of colour Doppler in the early postoperative period is therefore to help provide an overall qualitative impression of renal perfusion and on specific spectral Doppler analysis, quantify this with serial measurements. At our institution scanning is performed three times per week until renal function is established. Although differentiation of pathological entities, such as acute tubular necrosis from acute rejection is not possible, serial measurement of the pulsatility and resistive indices, in conjunction with the many clinical and biochemical findings, help the renal physician decide whether to proceed or refrain from renal biopsy (Table 28.1). A PI less than 1.5 or RI less than 0.7 is normal; a PI greater than 1.8 or an RI greater than 0.7 should be regarded as abnormal. It is well recognised that both acute tubular necrosis and acute rejection can elevate both these values.[41,42] However, the higher the ratio, the greater is the likelihood of acute rejection.[43] Complete absence, or reversal of diastolic flow is likely to be due to acute rejection in the majority of cases. A normal resistive index or pulsatility index, however, does not exclude graft dysfunction and has been noted in up to 50% of patients with biopsy-proven rejection. Once a histological diagnosis has been established, monitoring of treatment regimens can be documented using serial spectral Doppler measurements[31] (Fig. 28.4).

With regard to the colour flow technique itself, power Doppler ultrasound has been promoted as a synergistic tool to colour Doppler, or even a replacement. However, there is no evidence to date that has shown any improvement of the power Doppler technique over conventional colour Doppler,[44] and in the opinion of many, the loss of directional flow information in many circumstances is disadvantageous for vessel identification, or in the detection of renal artery stenosis.

Other indices, including the acceleration time, have shown interesting results in the early transplant period with a short acceleration time on day 1 being associated with a longer duration of delayed function and an acceleration time of less than 90 ms on day 5 being associated with a high risk of rejection.[45] However, these results were published a number of years ago and they remain to be substantiated. Conventional resistive and pulsatility index measurements remain the mainstay for monitoring transplanted kidneys using Doppler ultrasound. With regard to renal graft outcomes, it has also been shown that a resistive index of greater than 80, measured at least 3 months following transplantation, is associated with subsequent poor graft performance and failure.[46] This work, again, has still to be substantiated and indeed an earlier prognostic value within 1 or 2 weeks of transplantation would be clinically more useful than a post 3-month assessment.

Table 28.1 Causes of elevation of PI/RI in the early transplant period

Acute rejection
Acute tubular necrosis
Hydronephrosis
Pyelonephritis
Extrarenal collection; in up to 50%; lymphocele commonest
Ciclosporin toxicity; normally no effect on RI/PI
Renal vein thrombosis; reverse diastolic flow

Arterial thrombosis

Arterial thrombosis is rare and affects less than 1% of transplants.[47] It is often clinically silent and occurs in the early transplant period. It may be discovered either incidentally at a routine isotope renogram or on colour Doppler imaging scan in a patient with

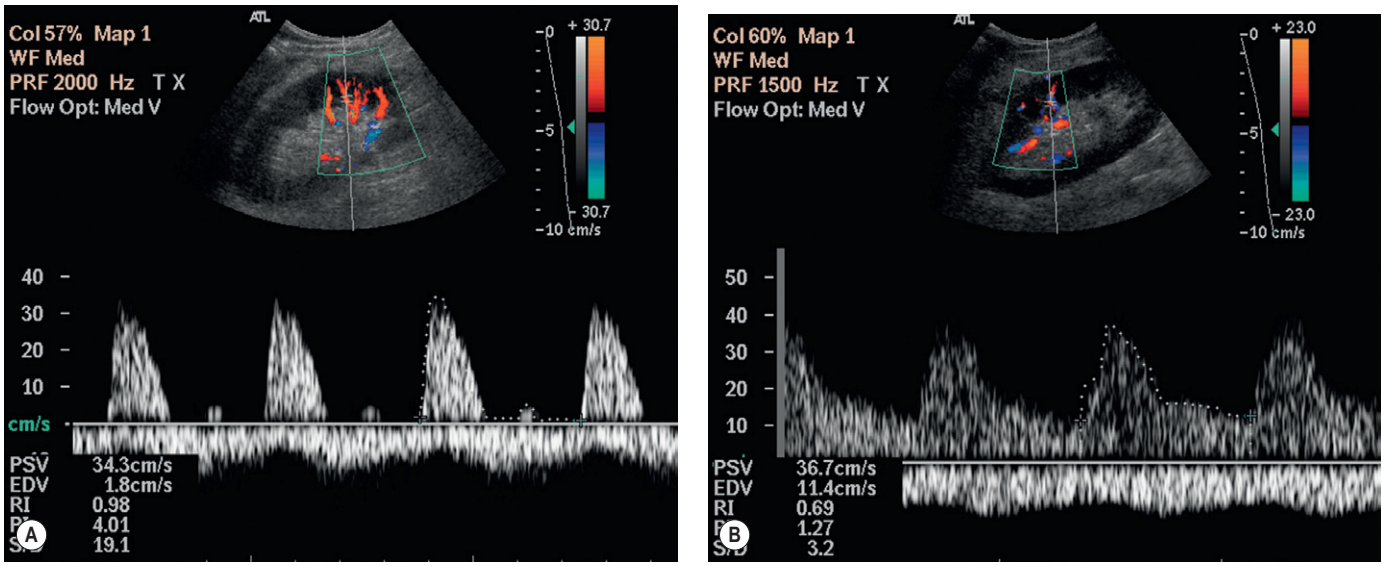


Figure 28.4 Delayed function. A: Spectral Doppler waveform from a kidney with delayed function in the first week of transplantation. This shows complete absence of flow in diastole with a only a small segment remaining. The PI was markedly elevated at 4.01. This prompted renal biopsy, which showed acute rejection. Appropriate anti-rejection treatment was started; the scan a few days later **(B)** showed restoration of normal diastolic flow and a PI of 1.27 consistent with a favourable response to treatment.

presumed delayed function. Predisposing factors include multiple renal vessels, paediatric donor kidneys and atherosclerosis in either the donor or recipient. The process is generally irreversible, resulting in graft infarction and subsequent nephrectomy. If the graft has multiple arteries, it is possible for one vessel to thrombose resulting in focal segmental infarction but renal function may remain stable and satisfactory in the long term, depending upon the volume of kidney spared.

The ultrasonic features of main artery thrombosis are striking, with complete absence of flow in both the kidney and the renal artery both on colour Doppler and spectral Doppler analysis. In this situation it is important to confirm that the ultrasound machine settings are optimised and adjusted for maximum sensitivity for the detection of low velocity flow. A good way of confirming thrombosis is to search for flow in alternative vessels either at similar depth to the transplant kidney or deeper to it, such as demonstrating flow within the deeper iliac artery and vein (Fig. 28.5). On occasion, a Doppler waveform may still be obtained from the main transplant artery; if this is the case, it is usually very abnormal with absent diastolic flow and significantly reduced amplitude. Assuming the colour features are as described above, this should not alter the suspected diagnosis.

It is important to remember that absent intrarenal flow may also be seen in a number of other conditions, including hyperacute rejection or renal vein thrombosis. In both of these scenarios, however, colour Doppler will show flow in the main transplant artery, which on spectral Doppler analysis will show reversed diastolic flow.[48] On occasion, trauma may be the cause of acute arterial occlusion secondary to intimal dissection. This is, however, generally outside the early transplant period and the clinical history is normally highly suggestive.

Venous thrombosis

Venous thrombosis normally causes acute pain and swelling of the graft, often in association with an abrupt cessation of renal function and urine output. It is more common than arterial occlusion. A typical patient may be between the third and eighth postoperative day; if the patient has delayed graft function then pain and tenderness will predominate, if the kidney is functioning then the sudden onset of anuria with or without pain will cause clinical concern.[49] Although withholding ciclosporin and tacrolimus in the early postoperative period and the use of subcutaneous heparin or aspirin are thought to help avoid this complication, none of these options have been proven in clinical trials. Ideally a high index of suspicion is required in order that early diagnosis and intervention may salvage the transplant kidney. However, nephrectomy is still required in the vast majority of these cases.

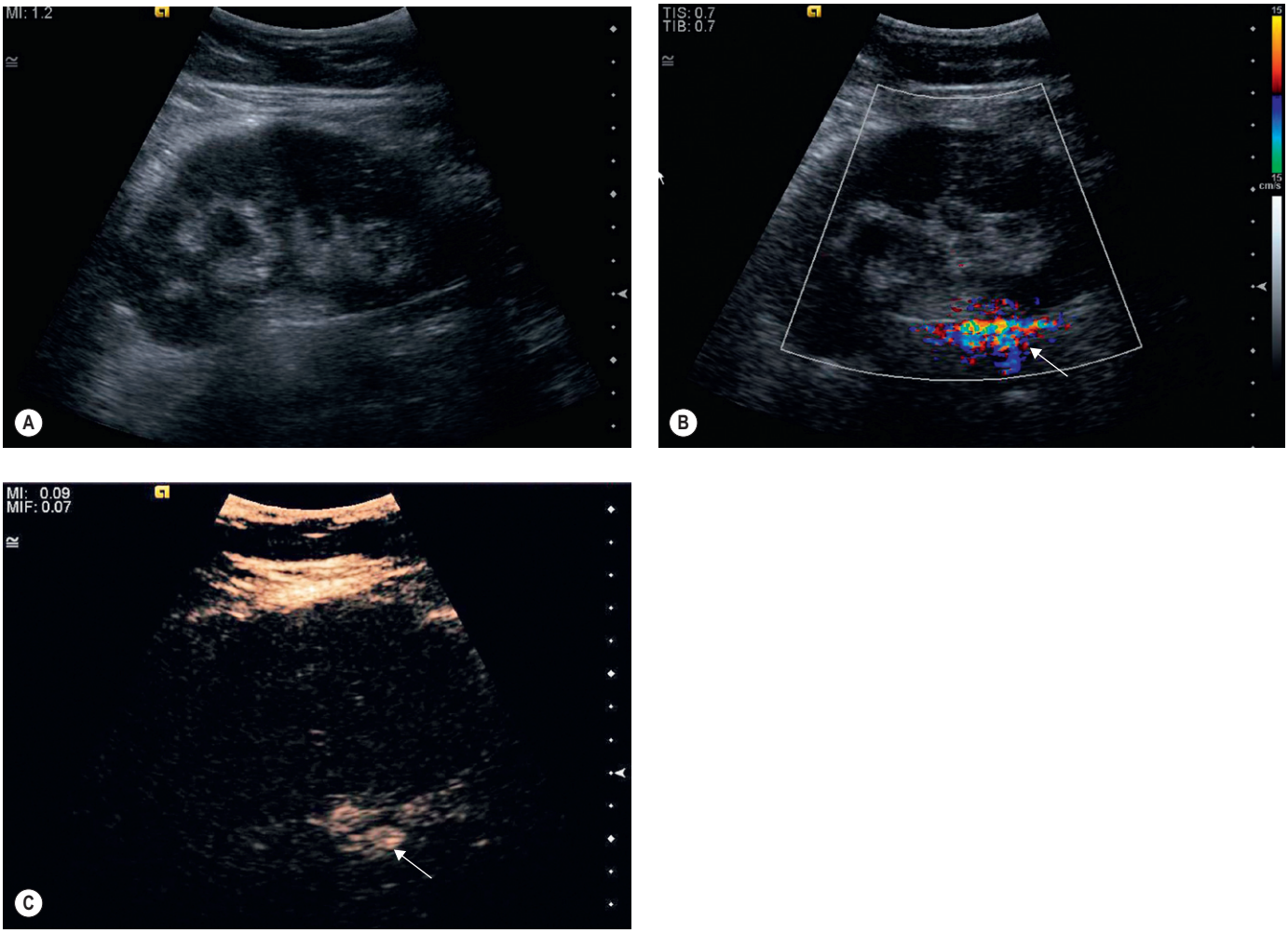


Figure 28.5 **Absent intrarenal flow. A:** B-mode image showing a normal looking transplant kidney. **B:** Colour Doppler scan of the same kidney. The PRF or colour velocity scale is set low for increased sensitivity. Despite this there is complete absence of intrarenal flow. Flow, however, can be visualised in the iliac artery (arrow) with some flash artefact in the surrounding tissues. The appearances are those of renal artery occlusion. **C:** The same kidney following the injection of intravenous microbubble contrast agent. This confirms patency of the iliac artery (arrow) but complete absence of intrarenal flow.

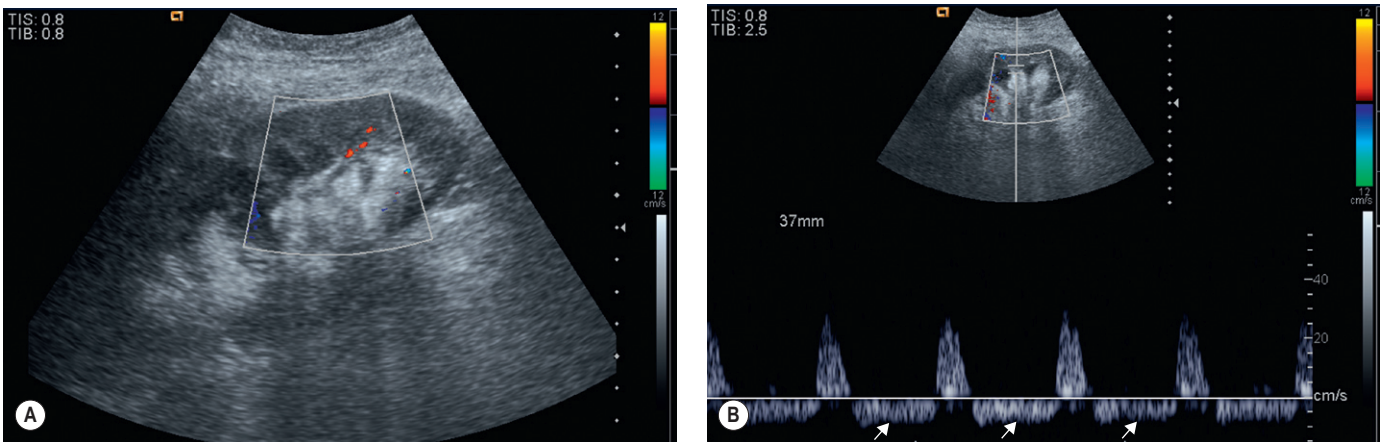


Figure 28.6 Colour Doppler ultrasound from a patient who had graft tenderness and absent urine output in the early postoperative period. Significantly reduced flow is noted within the kidney **(A)** with only one definite arterial vessel seen in the upper pole. Venous flow was absent throughout the kidney and the main transplant vein. Spectral Doppler sampled from an intrarenal artery **(B)** showed reverse diastolic flow (arrows). The features are those of renal vein thrombosis. A graft nephrectomy was performed.

Table 28.2 Reverse diastolic flow in the transplant artery

Indicative of severe change
Poor prognosis: 30% with reversed diastolic flow in the artery come to nephrectomy cf. 1–2% without
Non-specific sign
Can be seen in: severe rejection
severe ATN
renal vein thrombosis
Reverse diastolic flow suggests renal vein thrombosis

The ultrasonic diagnostic criteria for venous thrombosis include a dilated renal vein with visible echogenic thrombus, intrarenal venous thrombus, absent flow in the transplant vein on colour Doppler imaging and reverse diastolic flow in the renal artery (Table 28.2), or indeed in the main intrarenal arterial vessels on spectral Doppler analysis[50,51] (Fig. 28.6). A low-amplitude parvus tardus venous waveform has been described in the intrarenal arterial tree in patients with this condition in whom it is thought that the renal vein occlusion is incomplete with a small amount of residual intravenous flow remaining. Only a limited number of cases have been described and it is not clear in such cases if this alters outcome, or if the prognosis remains as universally poor as for complete venous occlusion.[52]

Obstruction

Ureteric obstruction occurs in 1.3–10.2% of all transplants.[53] Early obstruction within 3 days of transplantation normally reflects either ureteric or bladder thrombus and can be relieved by simple measures such as bladder irrigation. Obstruction thereafter may be due to a distal ureteric stenosis or to external compression of the ureter by a large lymphocele, haematoma or abscess. If warranted, such collections can be drained percutaneously, which will offer either temporary or permanent relief. In patients with suspected ureteric stenosis, nephrostomy followed by a contrast nephrostogram is normally performed. Depending on a number of differing circumstances, the treatment options involve either reoperation or percutaneous stenting and monitoring of renal function.

Although a dilated collecting system can be clearly visualised with ultrasound it is important that this feature is not interpreted in isolation and is reviewed in conjunction with the biochemical data, as a degree of prominence of the collecting system can exist secondary to denervation of the renal pelvis and this does not equate to obstruction. It is also important to remember that hydronephrosis should always be considered as a cause of an elevated pulsatility or resistive index, particularly in the early transplant period.

Haemorrhage

This can occur from two sites: the transplant kidney or the wound. It is normally easily detected with ultrasound and is self-limiting. Intervention may occasionally be required to identify any bleeding point and subsequent haematoma. Catastrophic haemorrhage is rare and generally occurs secondary to either vascular rupture or an anastomotic breakdown. These latter two conditions are more likely when there is an associated deep wound infection, or post-biopsy haemorrhage.

Urinary leak

Urinary leaks may occur in up to 6% of renal transplant patients and are due to disruption and breakdown of the vesico-ureteric anastomosis, or necrosis of the distal ureter itself.[54] Symptoms include increasing abdominal pain, reduction in urine output and, on occasion, leakage of urine from the wound site. Ultrasound may demonstrate a new collection (Fig. 28.7), whereas a cystogram may show a bladder leak. On occasion, an isotope study can be helpful to demonstrate small leaks. Treatment is traditionally surgical repair although a temporising nephrostomy may be helpful in certain clinical situations.

Post-transplant collections

Various types of collection may occur in the post-transplant period and include abscess, haematoma (Fig. 28.8), lymphocele and urinoma (Fig. 28.7). Ultrasound can clearly identify the collection but cannot differentiate between the four different entities. The presence of internal echoes may be seen more frequently in abscesses and haematomas but normally the clinical findings in conjunction with the ultrasonic appearances are likely to indicate the nature of the collection. If doubt persists and definitive diagnosis is required, then percutaneous aspiration with or without formal drainage can be performed.

The most common collection is a lymphocele, occurring in 0.6–18% (Fig. 28.9). Although these can be treated with various sclerosants in an attempt to cure, the success of this approach has been mixed. Recognised treatment options are now based on laparoscopic marsupialisation, which is both safe and effective.[55,56]

Ciclosporin and tacrolimus toxicity

Both of the above agents are calcineurin inhibitors and represent a major advance in organ transplantation. Unfortunately there are side effects with both these agents as they are nephrotoxic, producing a reversible renovascular constriction acutely and an interstitial fibrosis chronically.[57] As a result of this, recovery from acute tubular necrosis may be delayed and, indeed, these drugs may induce irreversible chronic damage to the transplant kidney. Furthermore, a diagnosis of nephrotoxicity in the acute setting of a non-functioning graft is notoriously difficult and therefore many clinicians avoid the use of these drugs if possible. Serum drug levels and renal biopsy are traditional but imperfect methods of diagnosis of toxicity. Ultrasound is generally unremarkable, as these drugs do not produce any significant change in diastolic flow.[58] Occasionally a reduction in diastolic flow has been noted, but this is non-specific.

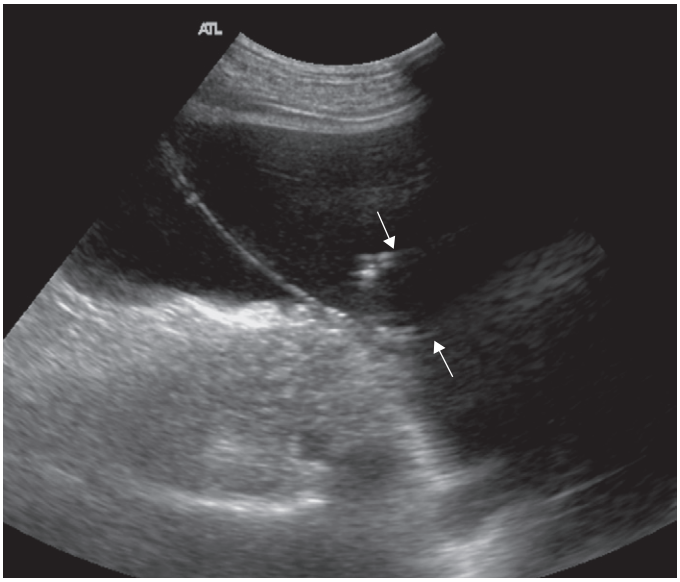


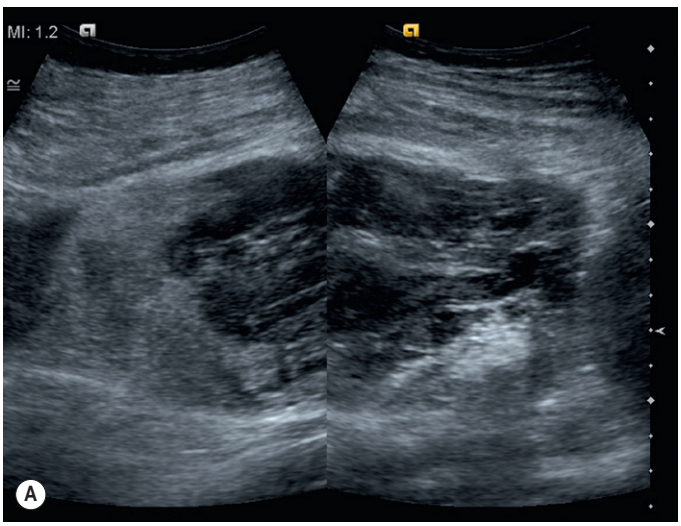
Figure 28.7. Longitudinal scan of a large cystic collection just superior to the bladder. An 8F pigtail catheter was inserted and can be easily identified (arrows). Analysis of the drainage fluid showed this to be urine, i.e. the collection was a urinoma.

Infection

The transplant patient is prone to a number of infections, particularly those of the chest, wound and urinary tract, in the early postoperative period. Wound infections are likely to be due to *Staphylococcus*, whereas urinary catheters and reflux predispose to urinary tract infections. The latter can cause a deterioration in renal function which may be indistinguishable from acute rejection and, although rare, it is not unknown for pyelonephritis to be diagnosed on transplant biopsy in patients with suspected acute rejection. Ultrasound has little or no role in the diagnosis of infection, although it is important to remember that infection may adversely affect the pulsatility and resistive ratios.

Acute complications

- 10–30% of patients require dialysis for ATN following transplantation.
- Acute rejection can develop in up to 40% of patients following transplantation.
- Colour and spectral Doppler are necessary for graft monitoring; a PI <1.5 or RI <0.7 is normal.
- Vascular occlusions, ureteric obstruction, collections and infection can all elevate the PI and RI indices.
- Arterial and venous occlusions carry a poor prognosis and often result in transplant nephrectomy.
- Most transplant collections are benign; drainage is only performed when appropriate.
- Ciclosporin toxicity has no effect on Doppler indices; diagnosis is suspected on blood levels or at biopsy.



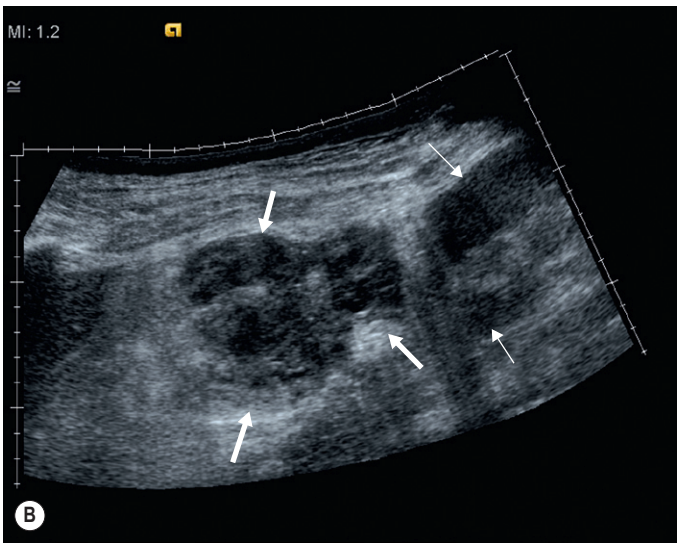


Figure 28.8 A: A large postoperative psoas collection is noted. This is of mixed echogenicity. The patient's haemoglobin had fallen significantly. The appearances are consistent with haematoma. **B:** The transplant kidney (arrows) lies inferior to the psoas haematoma (thick arrows).

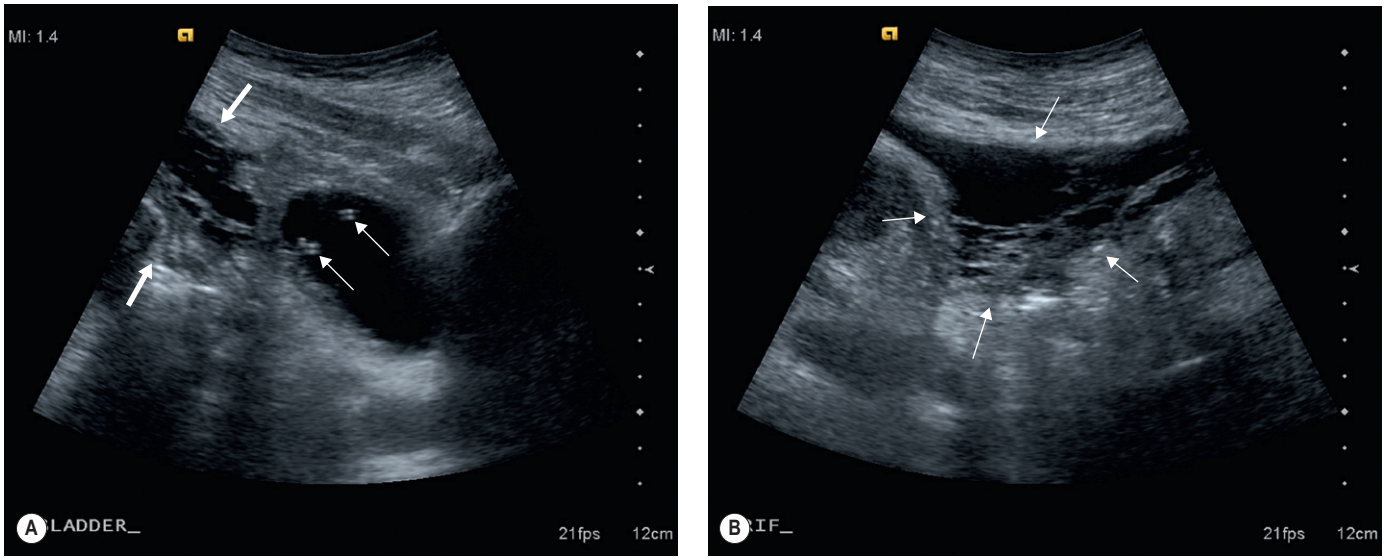


Figure 28.9 **A:** A peri-transplant collection (thick arrows) superior to the bladder had been unchanged over a number of years. A ureteric stent is also noted within the bladder (thin arrows). **B:** This collection (arrows) was partially septated and presumed to be a lymphocele. The patient was asymptomatic and therefore no treatment was indicated.

LATE COMPLICATIONS

Ureteric stenosis

As mentioned previously, the lower end of the transplant ureter is prone to ischaemia, which can result in secondary stricture formation, hydronephrosis and deterioration in renal function. This is largely related to the surgical technique as the vascular supply to the lower two-thirds of the donor ureter is lost when the kidney is excised; the main supply to the remaining upper third of the ureter in the transplant kidney is supplied by vessels from the transplant kidney. An over-long ureter therefore is at risk of an ischaemic related stenosis at its lower end. This complication can progress insidiously with a deterioration in overall renal function as a late event. In view of this, routine ultrasound screening is therefore performed to detect any signs of developing ureteric stenosis as early as possible, so as to prevent permanent severe renal damage. Annual review scans are strongly encouraged.

Transplant artery stenosis

Transplant artery stenosis occurs in up to 10% of patients,[59] the clinical suspicion being elevated in patients who have hypertension resistant to traditional therapy, a deterioration in renal function of unknown cause, a combination of the two, or a reduction in renal function following ACE (angiotensin-converting enzyme) inhibitor therapy. A number of predisposing factors are recognised, including renal donor arterial sclerosis and when small paediatric renal donor arteries are anastomosed to adult patients' vessels (Table 28.3). Opinions vary as to the best diagnostic test, with advocates for isotope renography, angiography, magnetic resonance angiography and ultrasonography.[28,60,61] The eventual choice, as in a number of situations, will depend upon local expertise and availability of technology. In common with a number of other centres, we currently use colour Doppler ultrasound as a first-line imaging test and if this confirms a stenotic lesion, proceed to arteriography with a view to percutaneous angioplasty and stenting after appropriate clinical discussion.

The transplant kidney artery is known to course in a very variable fashion with numerous twists and turns from its anastomosis on the iliac artery to the renal hilum. Because of this, colour Doppler ultrasound can be difficult to perform and requires accurate angle correction for precise spectral Doppler quantification and velocity measurement. In addition, it can be difficult to distinguish a focal stenosis from renal artery tortuosity. As the latter may also alter haemodynamics and thus peak systolic velocity readings, this clearly represents a significant potential pitfall of the technique. Although some of these twists and turns can be better delineated with power Doppler, the disadvantage of this technique is that a stenosis can be masked; therefore colour Doppler still remains the preferred option (Fig. 28.10).

The examination of the transplant renal artery must begin with an interrogation of the proximal iliac artery, as a stenosis in this vessel may adversely affect and reduce renal function[62] (Fig. 28.11). With regard to transplant artery stenosis, the majority of these lesions occur at, or close to, the anastomosis with the iliac artery and produce an area of aliasing on colour Doppler indicative of a focus of elevated velocity (Fig. 28.12A). In our centre a peak systolic velocity of 2.5 m/s or greater within the transplant renal artery is considered to be diagnostic of transplant artery stenosis[28] (Fig. 28.12B). We have found this to be accurate, but a range of values does exist and other workers have found a velocity of 3 m/s to be a better discriminator,[25,27] although this level is based upon a study

Table 28.3 Transplant artery stenosis

Occurs within 3 years of transplantation
Incidence 3 – 12%
More common in cadaveric and young kidney donors than in living related donors
Clinical presentation includes renal dysfunction, hypertension, graft bruit, deterioration in function with ACE inhibitor
Most stenoses (>50%) occur at the anastomosis or just distal to it
Anastomotic: Aetiology: focal intimal fibrosis
End to end three times as common as end to side
Proximal: Aetiology: atheroma donor vessel or clamp injury
Distal: Aetiology: intimal hyperplasia
More common in end to side anastomoses

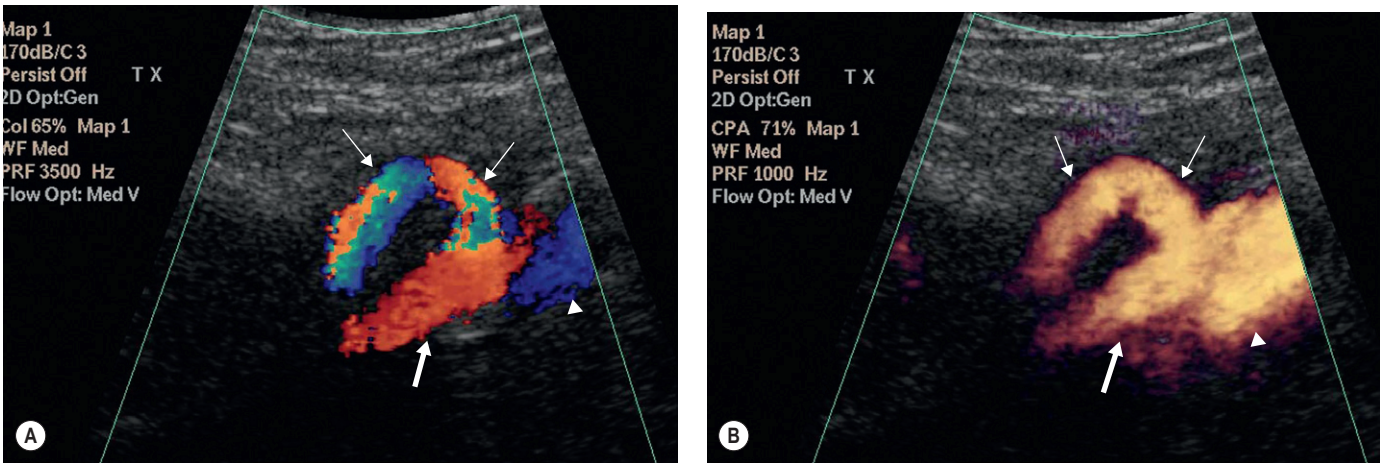


Figure 28.10 **A:** Colour Doppler scan of the transplant artery (arrows) at its origin from the external iliac artery (thick arrow). The change in direction of flow within the transplant artery is easily appreciated. The external iliac vein (arrowhead) is also clearly visualised and differentiated due to the colour coding. **B:** Power Doppler scan of the same area as in **A** with exactly the same labelling for comparison. There is no sense of flow direction and vessel identification is harder as a consequence.

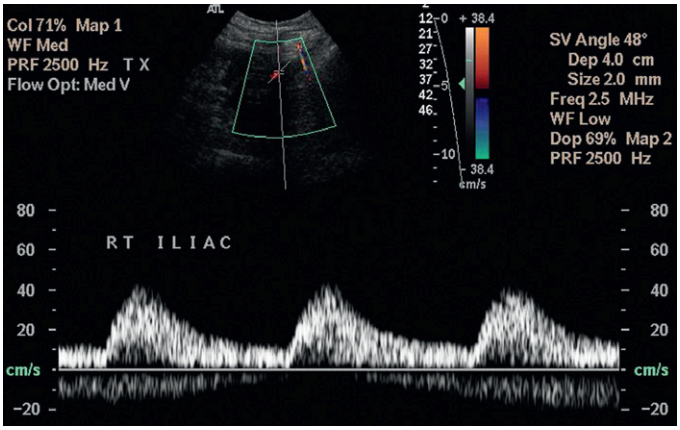


Figure 28.11 **A low-amplitude monophasic waveform throughout the iliac artery.** This was secondary to proximal iliac disease. Iliac disease (stenosis or occlusion) can not only affect the transplant artery waveforms but may cause a reduction in renal function.

group of lower risk patients. Clearly, exact cut-off levels will depend upon many factors and departments should review and audit the level that is appropriate for their practice.

Secondary Doppler findings of renal artery stenosis include marked downstream turbulence (Fig. 28.12C), spectral broadening and flow reversal, all of which may be seen distal to the primary stenotic site and help add weight and confidence to the primary diagnostic findings. The transplant kidney, being superficial in position, contributes to the relative ease of examination of the main transplant vessels, which can almost invariably be identified in all patients. Reliance on the secondary signs of stenosis, such as the parvus tardus effect within the intrarenal arterial vessels (Fig. 28.12D), as an aid to primary diagnosis is therefore less important than it would be in the native kidney.[28] Kidneys with dual arteries may have a stenosis affecting only one of the vessels and care must be taken to examine both components (Fig. 28.13). As well as main transplant vessel lesions, intrarenal branch stenoses have been described although these are difficult to diagnose with all modalities, even angiography.

Clinically it can be difficult to know which patients to refer for therapeutic angioplasty/stent and which simply to observe and treat conservatively. Any intervention must be clinically justified as many of these patients remain clinically stable, or even improve over time; it has also been shown that the majority of these lesions are stable and non-progressive.[63]

A recently published study, although not randomised, demonstrated that for two largely equivalent groups a conservative approach to transplant artery stenosis was as optimal in terms of renal function and blood pressure control as intervention over a course of 3 years.[64] Any therapeutic interventional procedure, together with their potential risks, must be clinically justified, particularly as the benefits of a more conservative approach become appreciated. Nevertheless, transplant artery stenting remains a useful therapeutic option for a number of patients, such as those with episodes of flash pulmonary oedema.

Colour Doppler ultrasound is helpful not only in diagnosis, but also in monitoring these patients to detect signs of disease recurrence[65] in those previously treated with angioplasty and/or stenting. Both the intrarenal pulsatility and resistive indices together with the peak systolic velocity in the transplant artery have been shown to be effective detectors of recurrence. In our centre, the preferred measurement is the peak systolic velocity.

Arteriovenous fistulae

Arteriovenous fistulae (AVF) can result from previous renal transplant biopsy and have an incidence of approximately 1–2%. In general most are of little clinical significance and resolve spontaneously as reflected in one study where, with an incidence of up to 10% following biopsy, all but one of the ten fistulae had resolved on follow-up scans.[66] In another study the incidence was 16.7%, with 75% closing within a month and 25% persisting longer than one year (three patients).[67] Those AVFs that persist normally give rise to very pathognomonic and spectacular colour Doppler appearances. Clinically they have been considered to be a potential cause of both hypertension and impaired renal function but neither of these scenarios is a common problem. In practice, these lesions are often simply observed and radiological intervention is only considered if a fistula is actively bleeding or significantly increasing in size and causing a 'steal syndrome' from the kidney, when the benefits of embolisation may be considered to outweigh those of conservative management.

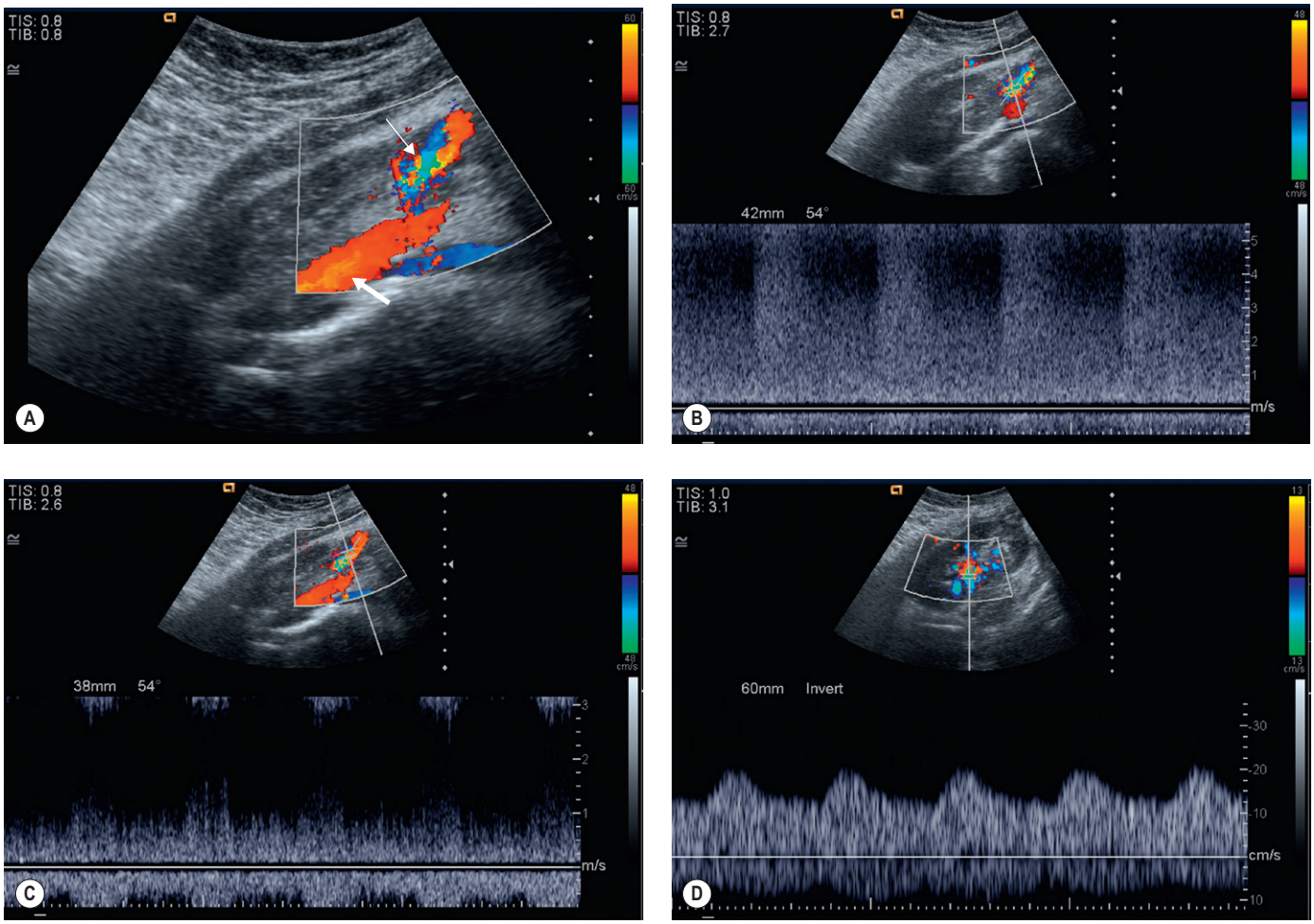


Figure 28.12 Transplant artery stenosis. A: Colour Doppler image at the origin of the transplant renal artery demonstrating an area of aliasing (arrow) within the proximal transplant artery with normal laminar flow within the iliac artery (thick arrow). The aliasing was focal and the colour velocity scale was set high. The appearances are those of a transplant artery stenosis. **B:** Spectral Doppler waveform through the area of aliasing in the transplant artery showed a markedly elevated peak systolic velocity of 5 m/s and spectral broadening, all features of a renal artery stenosis. **C:** Spectral Doppler downstream from the main stenosis showing marked turbulence as demonstrated by the marked and varied irregularity of the waveform itself. **D:** Spectral Doppler waveform from a segmental renal artery in the same patient showing the parvus tardus effect indicative of a more proximal stenosis.

The ultrasonic appearances of an AVF include a focus of high flow on colour Doppler with spectral Doppler showing both arterial and venous components. This is easily differentiated from 'high flow' that may be present in other parts of the transplant kidney by the simple manoeuvre of increasing the pulse repetition frequency (PRF) to a level that results in non-visualisation of the normal intrarenal vasculature on colour Doppler, with only the pathological high flow in the fistula being observed. This simple manoeuvre is in itself diagnostic (Fig. 28.14). On further analysis the spectral Doppler arterial waveform shows an increase in both systolic and diastolic flow within the affected area of the fistula and as a result the pulsatility index or resistive index will either remain normal or will be slightly reduced when compared with that of the normal surrounding vessels.[68] Venous flow can be either normal or turbulent and a large draining vein with arterialised flow may also be visualised.

Ciclosporin and tacrolimus toxicity

Both these drugs have been discussed previously and their toxic effects on renal function are well recognised. Continued administration may lead to a progressive deterioration in function, which can be difficult to differentiate from chronic rejection and therefore often a therapeutic trial of dose reduction or conversion to an alternative immunosuppressive agent may be required. Following this, a small but significant number of patients may respond positively.

Acute rejection

Acute rejection is an unusual late complication. If present, non-compliance with drug therapy should be strongly considered. Diagnosis and treatment are as previously discussed for acute rejection in the postoperative period.

Chronic rejection

Chronic rejection leads to a gradual deterioration of renal function beginning at least 3 months following transplantation with biopsy appearances of fibrous intimal thickening, interstitial fibrosis and tubular atrophy. The most consistent predisposing factor is that of previous episodes of acute rejection. There is no effective treatment and all efforts are concentrated towards preventing episodes of acute rejection as a method to retard the progress of chronic

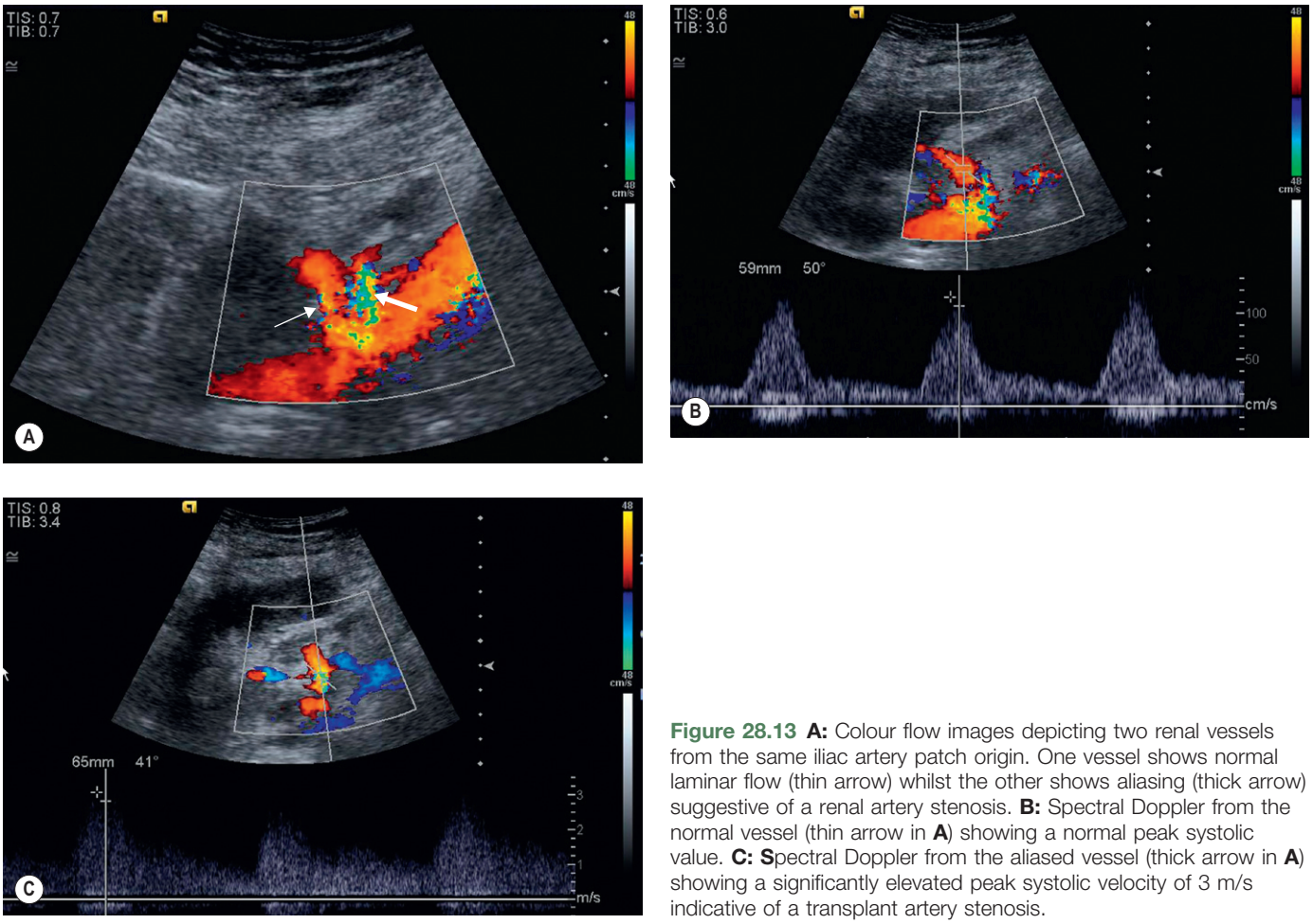


Figure 28.13 **A:** Colour flow images depicting two renal vessels from the same iliac artery patch origin. One vessel shows normal laminar flow (thin arrow) whilst the other shows aliasing (thick arrow) suggestive of a renal artery stenosis. **B:** Spectral Doppler from the normal vessel (thin arrow in **A**) showing a normal peak systolic value. **C: S**pectral Doppler from the aliased vessel (thick arrow in **A**) showing a significantly elevated peak systolic velocity of 3 m/s indicative of a transplant artery stenosis.

rejection. Ultrasonic features of chronic rejection include increased transplant echogenicity and a reduction in the normal number of intrarenal vessels. These signs, however, are of minimal prognostic significance as renal function does not correspond with the appearances and the role of ultrasound is limited in diagnosis (Fig. 28.15).

Urinary tract infection

Asymptomatic bacteriuria is common and has a good prognosis. Symptomatic infections are also common and can cause pyuria, pyelonephritis (Fig. 28.16) and a temporary reduction in overall graft function. Repeated infections can lead to underlying structural abnormalities such as calculi (Fig. 28.17), obstruction and reflux (Fig. 28.18). Chronic repeated infections occasionally lead to malacoplakia.

Recurrent disease (Table 28.4)

A number of forms of glomerulonephritis may cause recurrent disease in the transplant kidney, although early recurrence and graft failure is rare. Recurrent disease is more commonly seen in long-term recipients with diabetes mellitus, amyloidosis and cystinosis. In patients with oxalosis or active vasculitis, disease recurrence and renal damage are more common in the earlier stages following transplantation.[69] Ultrasound again has no specific role apart from excluding the known treatable causes of reduced renal function which have been described.

Chronic complications

- The lower end of the transplant ureter is at risk of an ischaemic related stricture.
- Transplant artery stenosis occurs in up to 10% of patients.
- The peak systolic velocity in the transplant renal artery is the best measurement for the detection of RAS. Cut-off values vary between 2.0 and 3.0 m/s.
- In our institution the cut-off value is 2.5 m/s.
- AVFs have an incidence of 1–2%. The vast majority are benign but ultrasonically interesting.
- Vascular steal is uncommon.
- Chronic rejection is a diagnosis of exclusion for which there is no effective treatment.
- Long-term risk factors are related to cardiovascular disease, infection and the risk of malignancy.

Other complications

Increased morbidity and mortality following renal transplantation is normally due to either cardiovascular disease, malignancy, or infection secondary to immunosuppression. Cardiovascular risk factors include hypertension, left ventricular hypertrophy and altered liver profile. To date no specific targeting of these areas has shown any survival improvement.

In contrast, however, the incidence of infection has been significantly reduced. Improvements in immunosuppression regimens

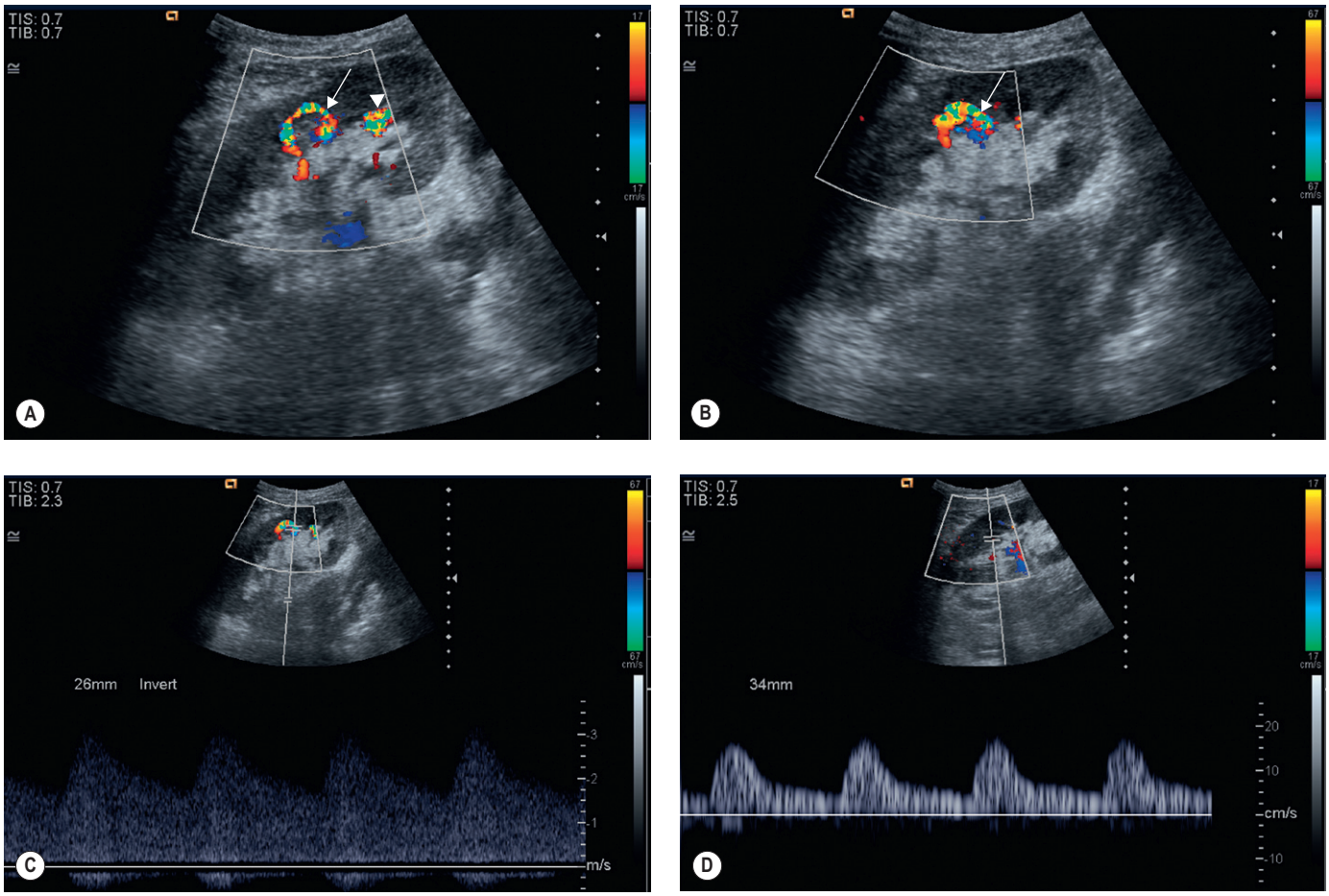


Figure 28.14 **A:** Colour flow image of a transplant kidney demonstrates a focus of high flow (arrow); the velocity scale is set at a low level. Another area of apparent focal flow is also noted (arrowhead). **B:** The same patient as in **A**; however, this time the velocity scale has been significantly increased. Now, only the pathological high flow of the AVF persists (arrow). These appearances are pathognomonic of an AVF. **C:** Spectral Doppler of the feeding artery to the AVF shows markedly elevated peak systolic (3 m/s) and diastolic values (1.5 m/s). **D:** A normal intrarenal Doppler waveform from a different area of the kidney for comparison.

Table 28.4 Late complications of renal transplantation

Renal artery stenosis
Arteriovenous fistula
Hydronephrosis
Recurrence of disease
Chronic rejection
Malignancy
Infection

and improved targeting of these agents in combination with an increased awareness of the different types of infection that may occur have all contributed to improved outcomes.

Malignancy remains an issue and with the increased longevity of transplanted kidneys, the number of malignancies developing is slowly increasing (Fig. 28.19). The most likely lesions following transplantation are skin-related malignancy, cervical cancer and non-Hodgkin's lymphoma. It is therefore obvious that careful supervision of the transplant population is required so that earlier diagnosis may result in improved prognosis for each of these disorders.[70]

COMBINED RENAL AND PANCREATIC TRANSPLANTATION

A detailed description of combined organ transplantation is beyond the scope of this chapter. As for the renal transplantation, patient selection is crucial and depends upon a multidisciplinary pre-transplantation evaluation team. A successful outcome will restore blood glucose levels to normal, improve neuropathy in most patients and prevent recurrence of diabetic nephropathy in the new kidney. It may also prevent the secondary complications of diabetes but the effect on established lesions is not clear.

The standard surgical technique results in anastomosis of the pancreatic veins, and thus pancreatic endocrine production, to the iliac vein with exocrine drainage via the pancreatic duct drained to the bladder.[71] However, this is gradually being replaced in many centres by endocrine drainage to the portal system and drainage of the exocrine secretions to the bowel. The transplant kidney is dealt with in the standard surgical manner.

Vascular complications are the most common and occur in 12% of patients; 5% of vascular complications are arterial and 7% venous. Other complications include rejection, infection and allograft pancreatitis. The overall survival of a combined pancreatic renal transplant is 83%, 72.9% and 65.5% at 1, 3 and 5 years respectively.

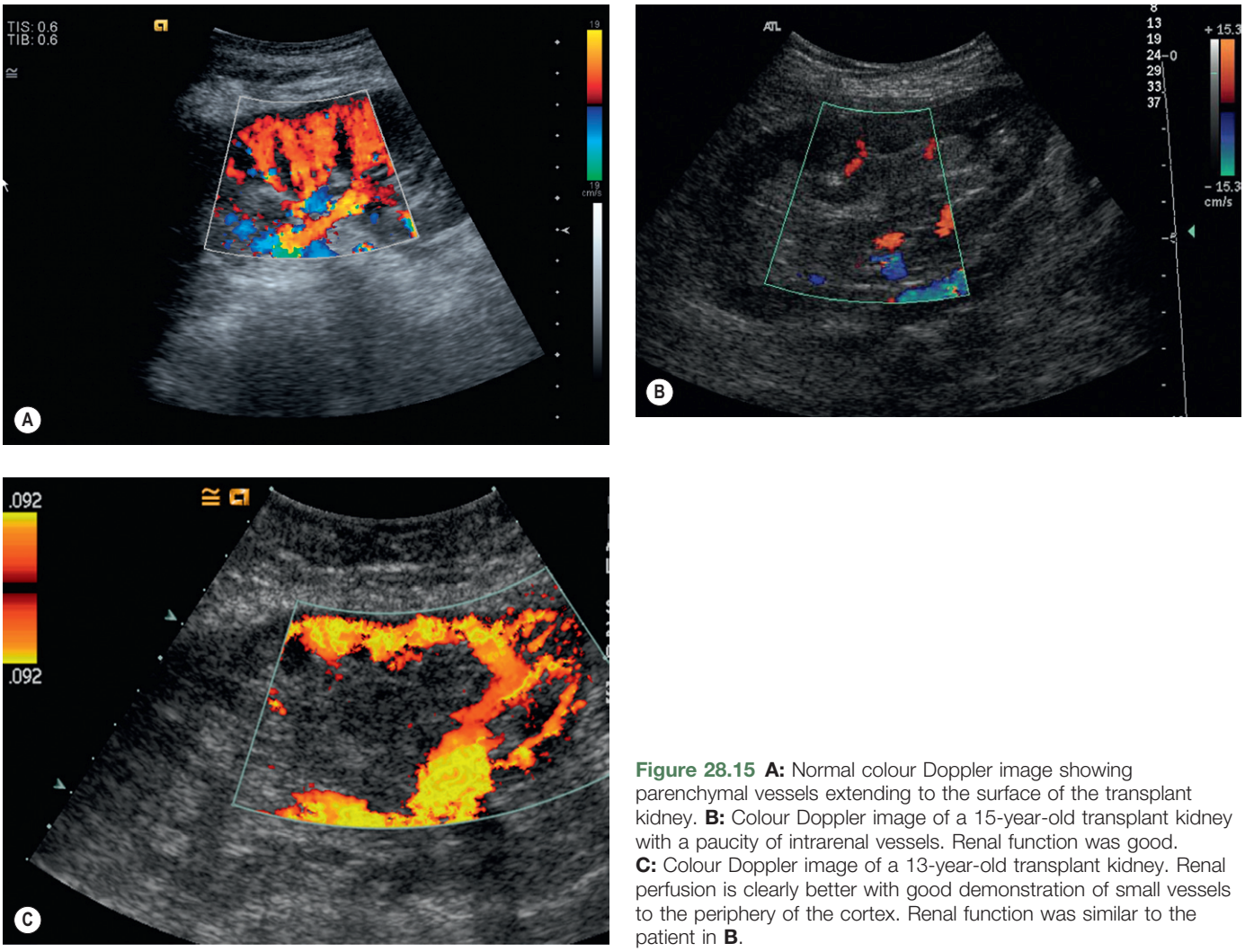


Figure 28.15 **A:** Normal colour Doppler image showing parenchymal vessels extending to the surface of the transplant kidney. **B:** Colour Doppler image of a 15-year-old transplant kidney with a paucity of intrarenal vessels. Renal function was good. **C:** Colour Doppler image of a 13-year-old transplant kidney. Renal perfusion is clearly better with good demonstration of small vessels to the periphery of the cortex. Renal function was similar to the patient in **B**.

USE OF MICROBUBBLE CONTRAST AGENTS

Imaging of the transplant kidney has been described earlier in the chapter. Given the relatively superficial position of the transplanted kidney and the improvements in resolution of ultrasound over time, imaging of the transplant is, for most patients, relatively straightforward. It is therefore difficult to imagine a situation when the use of a microbubble contrast agent may be helpful in the transplant kidney. However, many questions remain unanswered with conventional imaging and whilst no definitive and proven renal transplant application currently exists, a large amount of preliminary work is being undertaken to see if functional imaging using microbubbles may be of help in the assessment of renal transplants.[72,73]

Functional contrast studies remain very much in development and therefore the applications discussed below are to some extent under assessment, rather than being routinely employed clinically.

Hydronephrosis

Many 'normal' transplant kidneys have some element of pelvicalyceal dilatation. In the early postoperative period, approximately 35–40% of kidneys will suffer from delayed function and it is difficult to know the significance of these mild hydronephrotic changes. It has been shown in animal studies that after creating an obstructive hydronephrosis and thereby increasing the intrarenal pressure, the time intensity curve measured after microbubble injection is altered in those kidneys with severe acute obstruction.[74] The clinical situation, however, is different from the idealised setting of the laboratory, although this may remain one potential application of microbubbles in the assessment of transplant kidneys.

Monitoring in the early postoperative transplant period

Delayed function is normally due to either acute tubular necrosis (ATN) or acute rejection. This can be difficult to assess as symptoms are generally absent. A number of centres use serial spectral Doppler to judge if there is any deterioration or improvement over time; however, if a definitive diagnosis is required, then transplant biopsy is performed. Although few centres still perform nuclear medicine routinely, it is interesting to note that an intravenous injection of a microbubble contrast agent produces a very similar time intensity arterial curve to that obtained at renography in native kidneys; it therefore provides both functional information and excellent greyscale anatomy.[75] It is difficult to say what impact this technique may have for the management of transplant kidneys (Figs 28.20 and 28.21).

It is too early to determine whether there is hidden information in these microbubble time intensity curves that may help

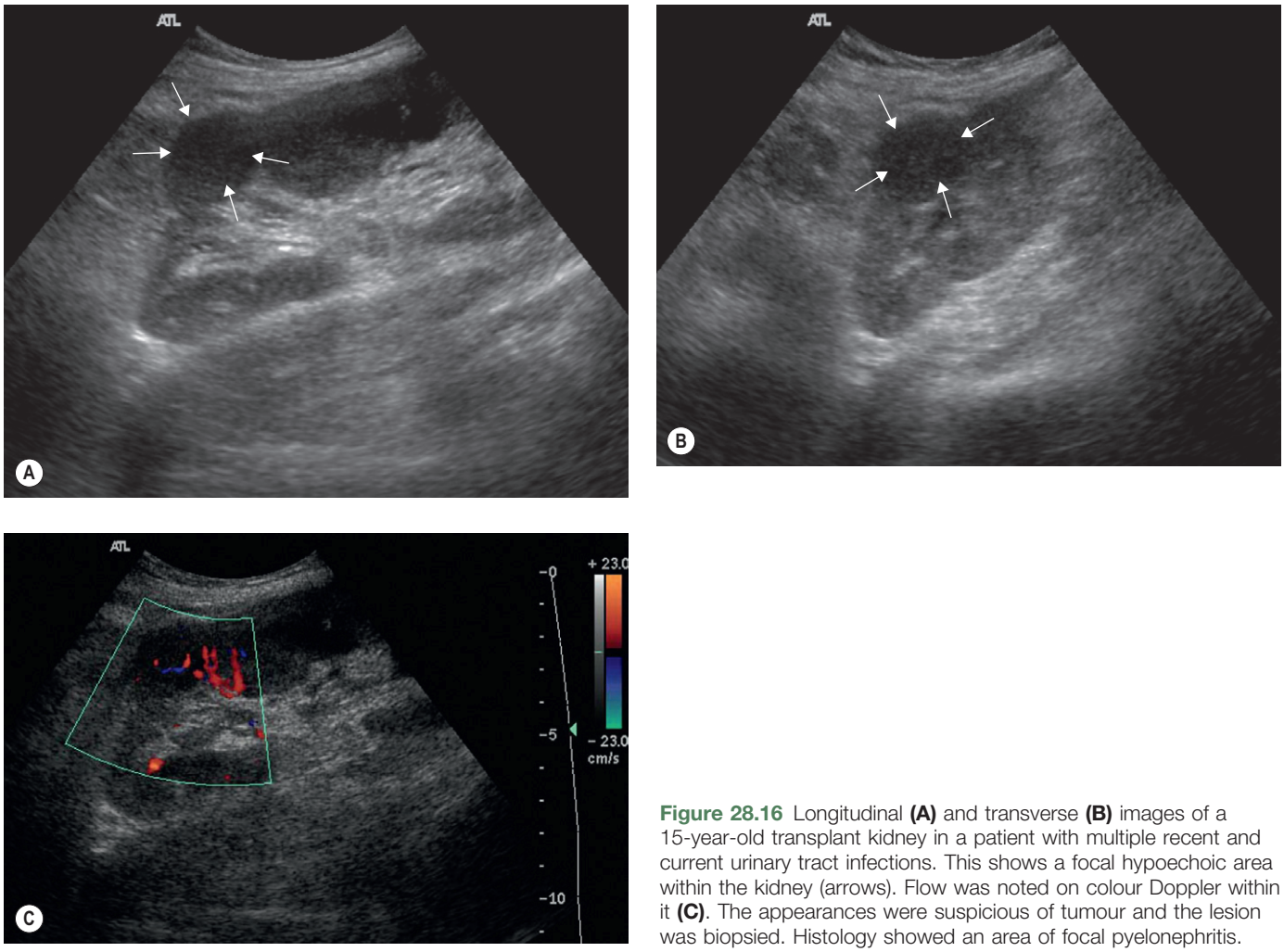


Figure 28.16 Longitudinal **(A)** and transverse **(B)** images of a 15-year-old transplant kidney in a patient with multiple recent and current urinary tract infections. This shows a focal hypoechoic area within the kidney (arrows). Flow was noted on colour Doppler within it **(C)**. The appearances were suspicious of tumour and the lesion was biopsied. Histology showed an area of focal pyelonephritis.

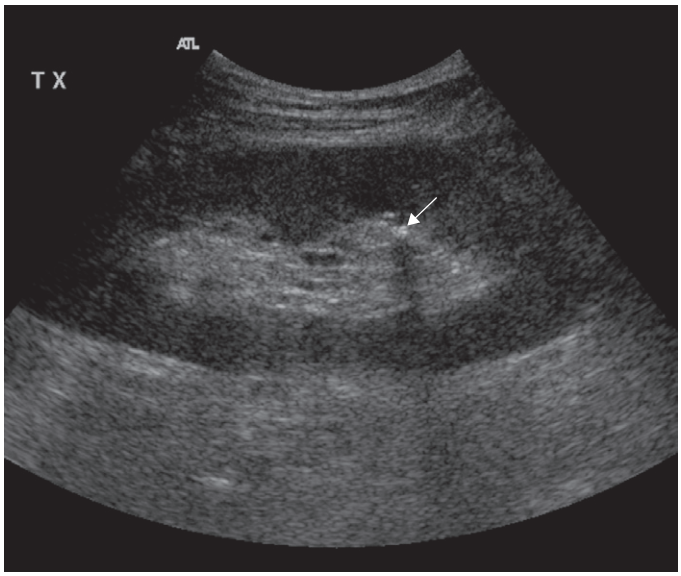


Figure 28.17 **A group of three small calculi.** One with distal acoustic shadowing (arrow) is seen at the lower pole of the transplant kidney.

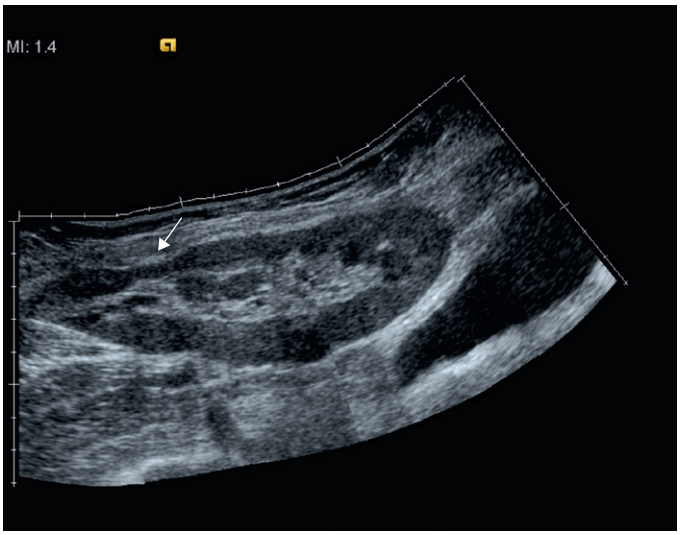


Figure 28.18 **Extended field-of-view scan of a transplant kidney** showing focal cortical loss at the upper pole (arrow) secondary to reflux.

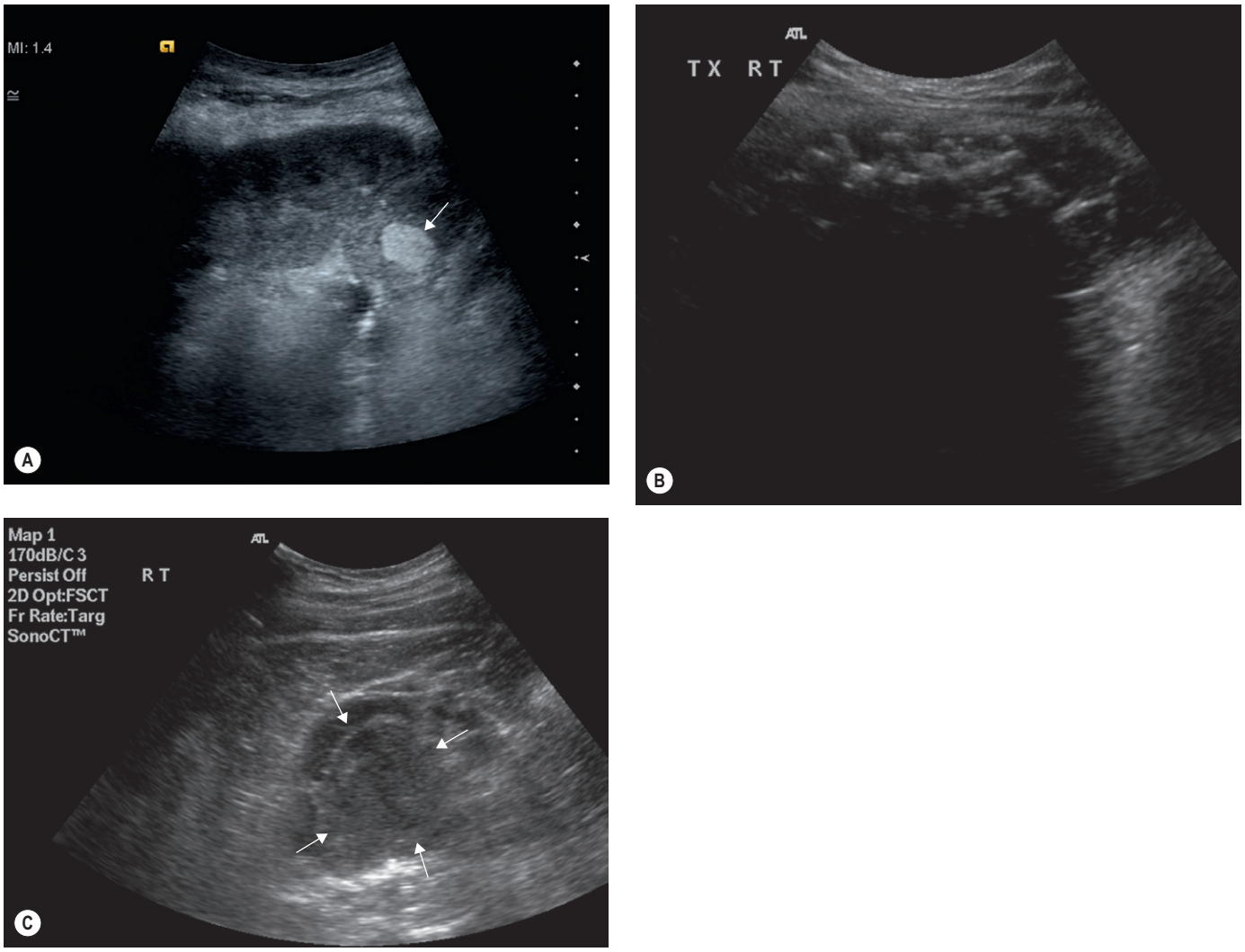


Figure 28.19 **A:** Real-time image of a normal transplant kidney with a sharply defined echogenic lesion (arrow) at its pole. The appearances are those of a benign angiomyolipoma. **B:** A chronic non-functioning transplant kidney with extensive internal calcification and distal acoustic shadowing akin to autonephrectomy. **C:** The same patient as in **B**. The patient presented with haematuria. It is important to check not only the transplant kidney(s) in this situation but also the native kidneys. A scan of the right kidney showed a renal tumour (arrows) accounting for his symptomatology.

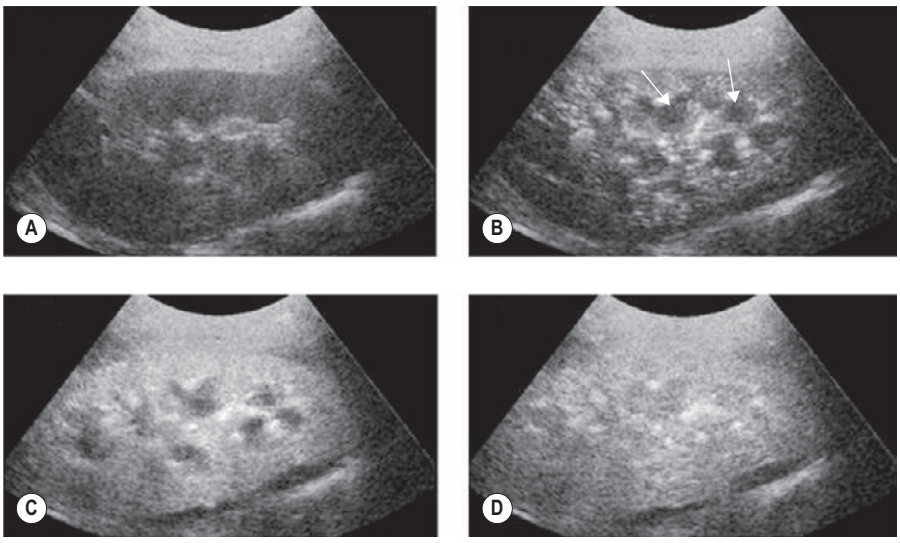


Figure 28.20 **A series of images taken from a dynamic study of a transplant kidney** following the intravenous injection of a microbubble agent. This study was conducted in the early postoperative phase as the kidney had delayed function. **A:** The baseline scan prior to contrast injection. **B:** Shortly after injection; this shows good cortical enhancement highlighted against the darker pyramids (arrows). **C and D:** Later images which show an even distribution of contrast in both the cortex and pyramids.

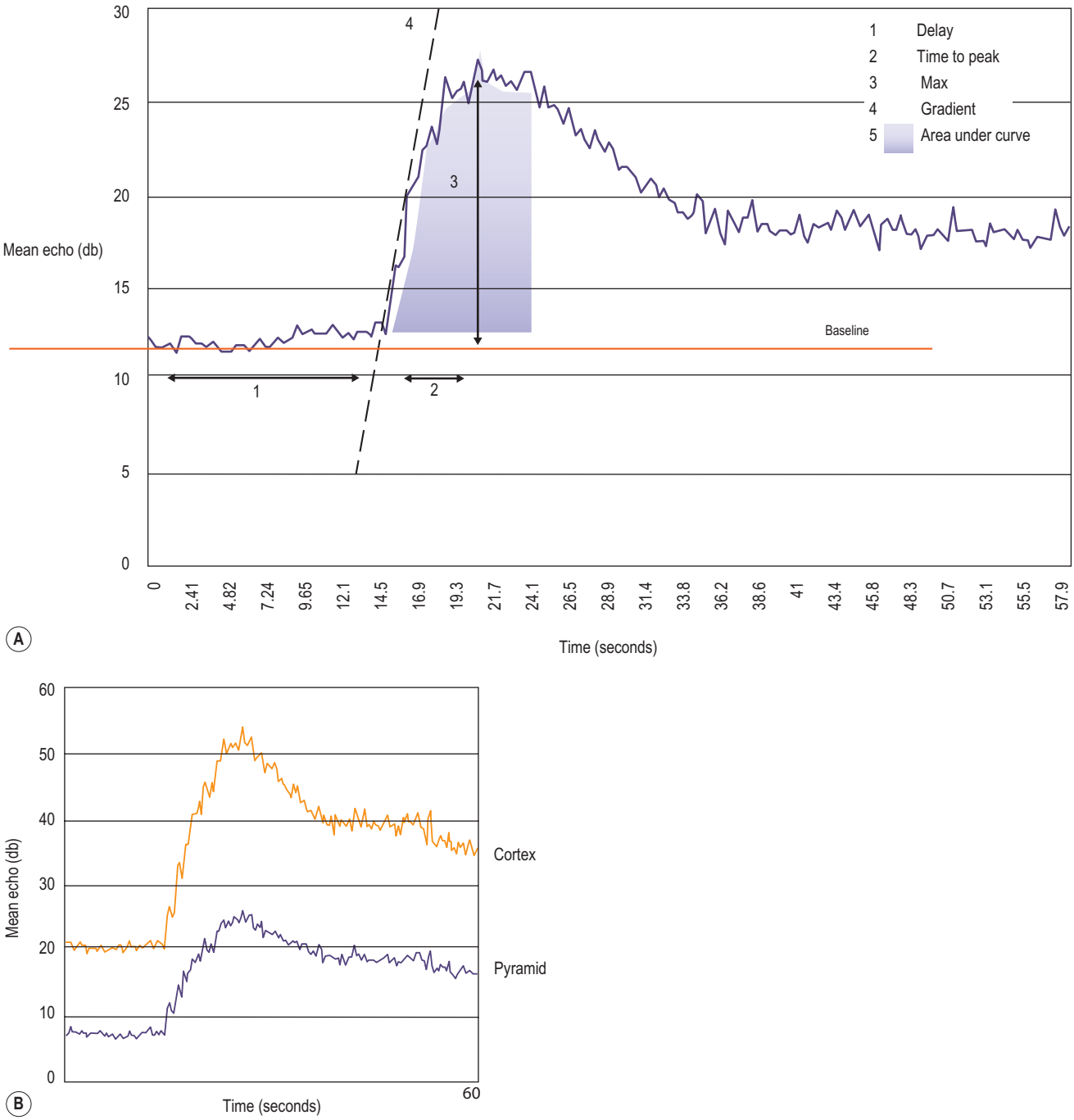


Figure 28.21 **A:** A time intensity curve from the renal cortex during dynamic microbubble injection. Various parameters can be measured including the arrival time from injection, the gradient of the curve, time to peak and peak value, and the area under the curve. **B:** Graph of uptake following microbubble injection showing cortical and pyramidal time intensity curves.

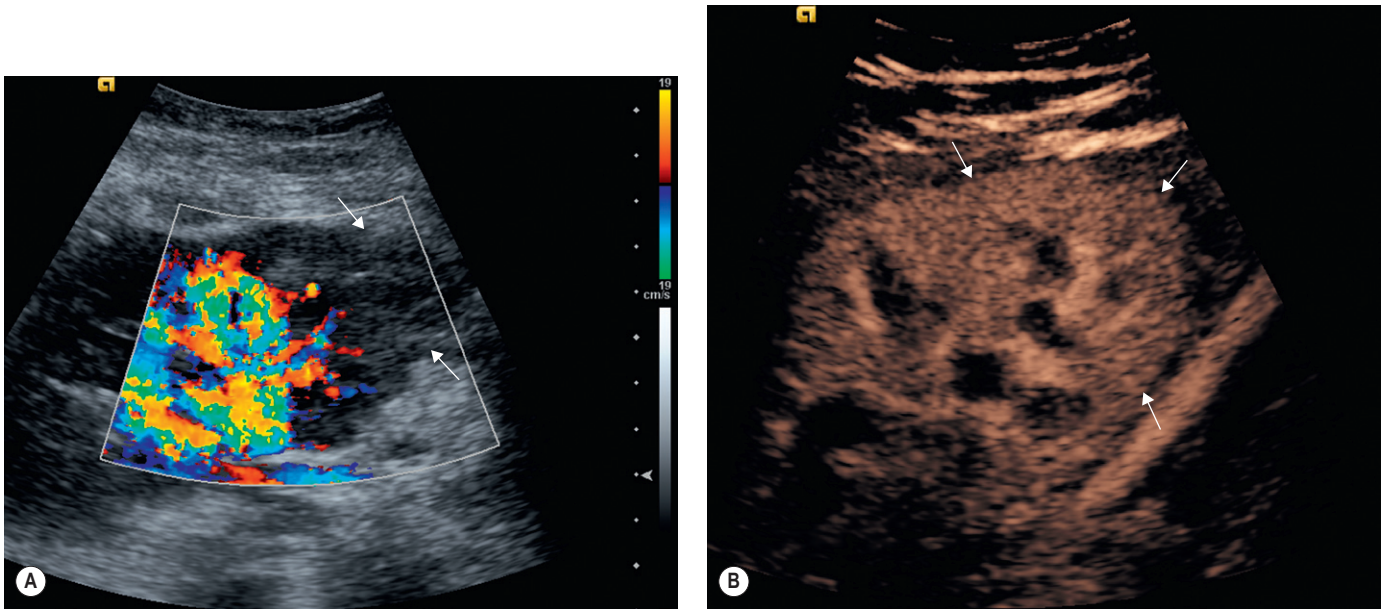


Figure 28.22 **A:** Baseline colour Doppler scan shows minimal flow to the pole of the transplant kidney (arrows). It was not clear if this was a technical problem, or an area of infarction. **B:** Following injection of microbubbles it is clear that the agent has been evenly distributed to all areas of the transplant kidney (arrows). There is no evidence of focal infarction and the appearances on colour Doppler were presumably therefore technical in origin.

differentiate the various pathological entities, or even if there is some hidden prognostic information on the longevity of the renal transplant. Differences have been noted in the time to peak enhancement values and the wash in and wash out curves between normal transplant kidneys and those with a parenchymal insult such as acute tubular necrosis or acute rejection. In addition, heterogeneous enhancement of the cortex with microbubbles was noted in the kidneys with acute parenchymal disease.[76] Furthermore it has also been shown that with this dynamic method the arterial venous transit time can be calculated – again clinical applications of such a technique are unknown.

Microbbubles

- Functional studies with microbubbles have demonstrated similar curves to isotope studies.
- Transit studies with microbubbles may prove helpful in the future.
- Contrast-enhanced ultrasound is generally not required in the diagnosis of transplant artery stenosis, or major vessel occlusion.
- Segmental infarction of the transplant kidney is easily visualised with microbubble-enhanced ultrasound.
- Microbubbles can help in the differentiation of 'complicated cysts'.
- Early results from microbubble studies are encouraging; however, standardisation of the functional technique is required.

Vascular applications

Vascular occlusion

The diagnosis of renal artery occlusion is a catastrophic event for any transplant patient. It is rare that a contrast-enhanced study would be required to confirm this diagnosis. Sometimes, however, multiple renal arteries are transplanted with the kidney and one may suffer damage in the early postoperative period. It is useful to know if there has been segmental infarction and the extent of such involvement. This can be a difficult diagnosis to make confidently in some patients on conventional colour Doppler scanning and a more dynamic analysis of the renal circulation following the injection of a microbubble contrast agent is much more revealing in this clinical situation (Fig. 28.22). It has been shown that use of such an agent can quantify both total and regional blood flow in dogs;[77] this may be one of the more clinically useful applications of these agents in relation to renal transplantation. In some circumstances such as with patients with reduced renal function in the early transplant period for unknown reasons, it has occasionally been enlightening to see focal areas of unsuspected renal infarction (Fig. 28.23).

Renal artery stenosis

The vast majority of transplant artery stenoses can be diagnosed with conventional colour Doppler. The routine use of a microbubble agent is not normally required but in the relatively rare circumstances when the vessel is difficult to visualise due to patient build, deeply situated vessels, bowel gas etc., microbubbles may have a limited role.

Renal masses

Transplant kidneys, like the native kidney, may develop cysts or tumours. With increased longevity of the transplant kidney, a definite but small increase in the incidence of tumours has been noted in the transplant population. These can occur at multiple sites; however, the differentiation of a cyst from a tumour, or clarification of the nature of a 'complicated cyst' can be helped with the use of microbubble agents[78] (Fig. 28.24). It is important to remember, however, that complementary imaging also includes CT and on occasion MRI.

Potential applications

A number of other potential applications of microbubble time intensity curves can be considered for the future. These may address issues including their relationship with eGFR and creatinine and any potential predictive value for the overall prognosis for the

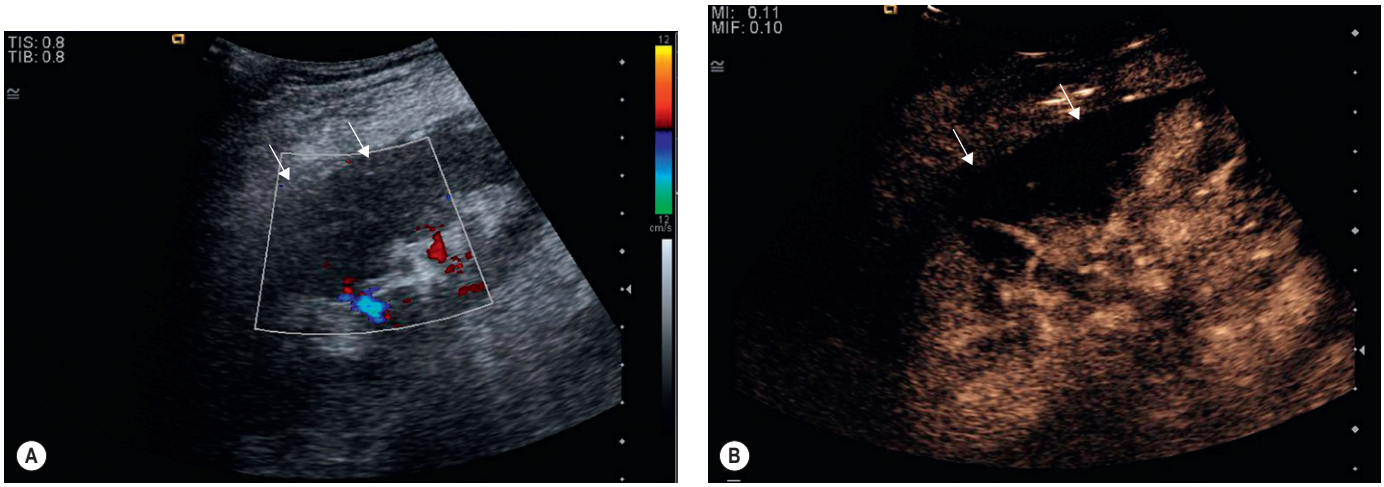


Figure 28.23 **A:** Colour Doppler ultrasound of a transplant kidney in the early postoperative period showing a lack of colour flow from the cortex anteriorly (arrows). It was not clear if this was technical, or if the vascular supply to this area was compromised. **B:** Following the injection of microbubbles, it can be seen that the anterior cortex is devoid of perfusion (arrows). This wedge-shaped defect is in keeping with an area of infarction.

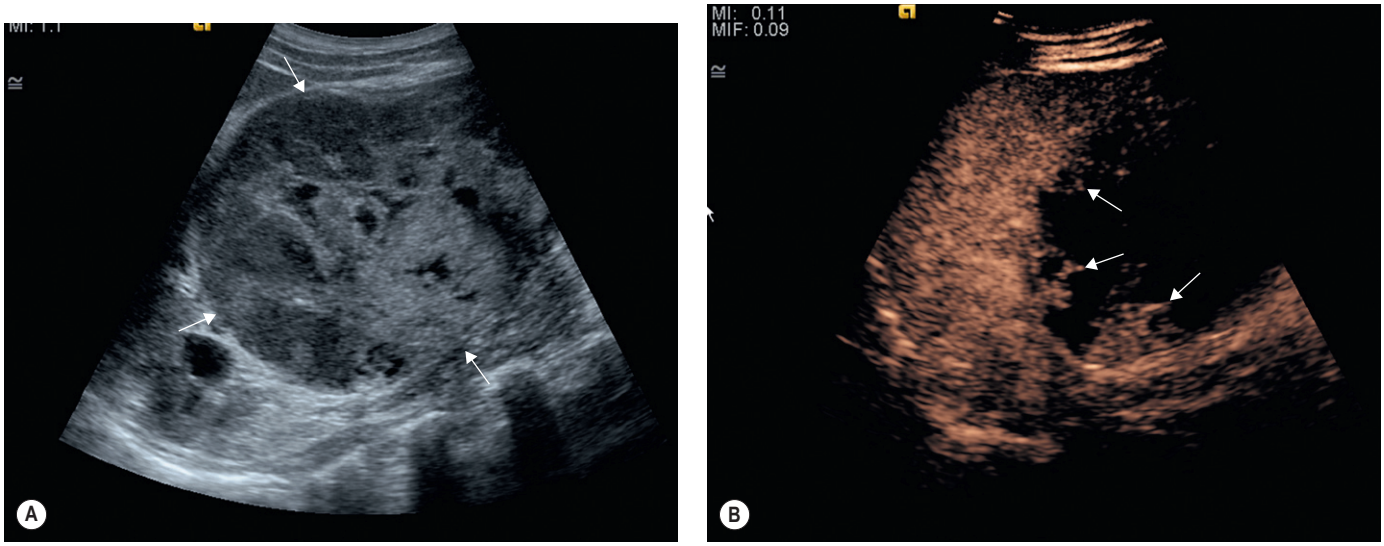


Figure 28.24 **A:** Real-time scan of a native kidney in a patient with loin pain, hypotension and falling haemoglobin. A large inhomogeneous mass was visualised (arrows). The diagnosis was either one of a bleed into a cyst or tumour. **B:** Following the injection of a microbubble agent it was obvious that the lesion was not simple. Focal areas of contrast enhancement (arrows) were seen around the wall of the lesion. The appearances were therefore those of a cystic tumour with internal haemorrhage.

transplant kidney, prediction of chronic rejection, or indeed any potential applications in the monitoring of drug-related studies. All of these areas remain potential fruitful areas of clinical research.

REFERENCES

1. Hamilton D. Alexis Carrel and the early days of tissue transplantation. Transplant Rev 1987;2:1–15.
2. Murray JE, Merrill JP, Harrison JH. Kidney transplantation between seven pairs of identical twins. Ann Surg 1958;148:343–359.
3. Starzl TE. Experience in renal transplantation. Philadelphia: Saunders; 1964.
4. Calne RY, White DJG, Thiru S, et al. Cyclosporin A in patients receiving renal allografts from cadaveric donors. Lancet 1978;ii:1323–1327.
5. Akbar SA, Jafri SZ, Amendola MA, et al. Complications of renal transplantation. Radiographics 2005;25:1335–1356.
6. Baxter GM. Ultrasound of renal transplantation. Clin Radiol 2001;56:802–818.
7. Sandhu C, Patel U. Renal transplantation dysfunction: the role of interventional radiology. Clin Radiol 2002;57: 772–783.
8. Charra B, Calemerd E, Ruffet M, et al. Survival as an index of the adequacy of dialysis. Kidney Int 1992;41:1286–1291.
9. Vincenti F. A decade of progress in kidney transplantation. Transplantation 2004;77:S52–S61.
10. Valderrabano F, Jones EHP, Mallick NP. Report on the management of renal failure in Europe XXIV, 1993. Nephrol Dial Transplant 1995;10(suppl 51):1–25.
11. Gore SM, Cable DJ, Holland AJ. Organ donation from intensive care units in England and Wales – two year confidential audit of deaths in intensive care. Br Med J 1992;304:349–355.
12. Takemoto S, Terasaki PI, Cecka JM, et al. Survival of nationally shared HLA-matched kidney transplants from cadaveric donors. N Engl J Med 1992;327:834–839.

13. The Canadian Multicentre Transplant Study Group. A randomised clinical trial of cyclosporin in cadaveric renal transplantation: analysis at three years. N Engl J Med 1986;314:1219–1220.
14. Robinson MT, Kindt TJ. Major histocompatibility complex antigens and genes. In: Paul W, ed. Fundamental immunology. New York: Raven Press; 1989. p. 489–539.
15. Krensky AM. Transplant immunobiology in paediatric nephrology. 3rd edn. Baltimore: Williams & Wilkins; 1993. p. 1373–1389.
16. Jamison RL, Wilkinson R. The pretransplant selection and evaluation of donor and recipient. In: Nephrology. New York: Chapman & Hall; 1997. p. 1072–1082.
17. Opelz G. Correlation of HLA matching with kidney graft survival in patients with or without cyclosporine treatment. Transplant 1985;40:240–243.
18. Basaran O, Moray G, Emiroglu R, et al. Graft and patient outcomes among recipients of renal grafts with multiple arteries. Transplant Proc 2004;36:102–104.
19. Robles J, Errasti P, Abad J, et al. Surgical complications in renal transplantation: determinant factors. Transplant Proc 1995;27:2258–2259.
20. Lai M, Huang C, Chu S, et al. Surgical complications in renal transplantation. Transplant Proc 1994;26:2165–2166.
21. Gruber S, Chavers B, Payne W, et al. Allograft renal vascular thrombosis – lack of increase with cyclosporin immunnosuppression. Transplantation 1989;47:475–478.
22. Hakim N, Benedetti E, Pirenne J, et al. Complications of ureterovesical anastomosis in kidney transplant patients: the Minnesota experience. Clin Transplant 1994;8:504–507.
23. Vincenti F, Laskow DA, Neylan JF, et al. One year follow up of an open label trial of FK506 for primary kidney transplantation. Transplantation 1996;61:1576–1581.
24. European Mycophenolate Mofetil Cooperative Study Group. Placebo controlled study of mycophenolate mofetil combined with cyclosporin and corticosteroids for prevention of acute rejection. Lancet 1995;345:1321–1325.
25. de Morais RH, Muglia VF, Mamere AE, et al. Duplex Doppler sonography of transplant renal artery stenosis. J Clin Ultrasound 2003;31:135–141.
26. Li J, Ji Z, Cai S, et al. Evaluation of severe transplant renal artery stenosis with Doppler sonography. J Clin Ultrasound 2005;33: 261–269.
27. Patel U, Khaw KK, Highes NC. Doppler ultrasound for the detection of renal transplant artery stenosis – threshold peak systolic velocity needs to be higher in low-risk or surveillance population. Clin Radiol 2003;58:772–777.
28. Baxter GM, Ireland H, Moss JG, et al. Colour Doppler ultrasound in renal transplant artery stenosis: which Doppler index? Clin Radiol 1995;50:618–622.
29. Genkins SM, Sanfilippo FP, Carroll BA. Duplex Doppler sonography of renal transplants: lack of sensitivity and specificity in establishing pathologic diagnosis. AJR Am J Roentgenol 1989;152: 535–539.
30. Rigsby CM, Taylor KJW, Weltin G, et al. Renal allografts in acute rejection: evaluation using duplex sonography. Radiology 1986;158:375–378.
31. Hollenbeck M, Hilbet N, Meusel F, et al. Increasing sensitivity and specificity of Doppler sonographic detection of renal transplant rejection with serial investigative technique. Clin Invest 1994;72:609–615.
32. Wilczek HE. Percutaneous needle biopsy of the renal allograft. Transplantation 1990;50:790–797.
33. Tang S, Li JH, Lui SL, et al. Free hand, ultrasound guided percutaneous renal biopsy: experience from a single operator. Eur J Radiol 2002;41(1):65–69.
34. Freda A, Van Dijk LC, Van Oostaijen JA, Pattynama PM. Complication rate and diagnostic yield of 515 consecutive ultrasound guided biopsies of renal allografts and native kidneys using a 14-gauge Biopsy gun. Eur Radiol 2003;13(3):527–530.
35. Chan R, Common AA, Marcuzzi D. Ultrasound guided renal biopsy: experience using an automated core biopsy. Can Assoc Radiol J 2000;51(2):107–113.
36. Pirsch JD, Ploeg RJ, Gange S, et al. Determinants of graft survival after renal transplantation. Transplantation 1996;61:1581–1585.
37. Cochlin DLL, Wake A, Salaman JR, Griffin PJA. Ultrasound changes in the transplant kidney. Clin Radiol 1988;39:373–376.
38. Pozniak MA, Kelcz F, D'Alessandro A, et al. Sonography of renal transplants in dogs: the effect of acute tubular necrosis, cyclosporin nephrotoxicity and acute rejection on resistive index and renal length. AJR Am J Roentgenol 1992;158:791–797.
39. Parvin SD, Rees Y, Veitch PS, et al. Objective measurement by ultrasound to distinguish Cyclosporin A toxicity from rejection. Br J Surg 1986;73:1009–1011.
40. Jakobsen JA, Brabrand K, Egge TS, Hartmann A. Doppler examination of the allografted kidney. Acta Radiol 2003;44(1): 3–12.
41. Chudek J, Kolonko A, Krol R, et al. The intrarenal resistance parameters measured by duplex Doppler ultrasound shortly after kidney transplantation in patients with immediate, slow and delayed graft function. Transplant Proc 2006;38:42–45.
42. Datta R, Sandhu M, Saxena AK, et al. Role of duplex Doppler and power Doppler sonography in transplanted kidneys with acute renal parenchymal dysfunction. Australas Radiol 2005;49:15–20.
43. Hillburn MD, Bude RO, Murphy KJ, et al. Renal transplant evaluation with power Doppler ultrasound. Br J Radiol 1997;70:39–42.
44. Chow L, Sommer FG, Huang J, Li KC. Power Doppler imaging and resistance index measurement in the evaluation of acute renal transplant rejection. J Clin Ultrasound 2001;29(9):483–490.
45. Merkus JWS, Hoitsma AJ, van Asten WNJC, et al. Doppler spectrum analysis to diagnose rejection during post transplant acute renal failure. Transplantation 1994;58:570–576.
46. Radermacher J, Mengel M, Ellis S, et al. The renal arterial resistive index and renal allograft survival. N Engl J Med 2003;349(2): 115–124.
47. Orlic P, Vukas D, Drescik I, et al. Vascular complications after 725 kidney transplantations during 3 decades. Transplant Proc 2003;35:1381–1384.
48. Kaveggia LP, Perella RR, Grant EG, et al. Duplex Doppler sonography in renal allografts: the significance of reversed flow in diastole. AJR Am J Roentgenol 1990;155:295–298.
49. Penny MJ, Nankivell BJ, Disney APS, et al. Renal graft thrombosis: A survey of 134 consecutive cases. Transplantation 1994;58:565–569.
50. Baxter GM, Morley P, Dall B. Acute renal vein thrombosis in renal allografts: new doppler ultrasonic findings. Clin Radiol 1991;43:125–127.
51. Reuther G, Wanjura D, Bauer H. Acute renal vein thrombosis in renal allografts: detection with duplex Doppler ultrasound. Radiology 1989;170:557–558.
52. MacLennan AC, Baxter GM, Harden P, Rowe PA. Renal transplant vein occlusion; an early diagnostic sign? Clin Radiol 1995;50:251–253.
53. Kocak T, Nane I, Ander H, et al. Urologic and surgical complications in 362 consecutive living related donor renal transplantations. Urol Int 2004;72:252–256.
54. Karam G, Maillet F, Parant S, et al. Ureteral necrosis after kidney transplantation: risk factors and impact on graft and patient survival. Transplantation 2004;78:725–729.
55. Duepree HJ, Fornara P, Lewejohann JC, et al. Laparoscopic treatment of lymphoceles in patients after renal transplantation. Clin Transplant 2001;15(6):375–379.
56. Risaliti A, Corno V, Donini A, et al. Laparoscopic treatment of symptomatic lymphoceles after kidney transplantation. Surg Endosc 2000;14(3):293–295.
57. Myers BD, Sibley R, Newton L, et al. The long term course of cyclosporin associated chronic nephropathy. Kidney Int 1988;33:590–600.
58. Heine GH, Girndt M, Sester U, Kohler H. No rise in renal Doppler resistance indices at peak serum levels of cyclosporin A in stable kidney transplant patients. Nephrol Dial Transplant 2003;18(8):1639–1643.
59. Gray DWR. Graft renal artery stenosis in the transplanted kidney. Transplant Rev 1994;8:15–21.
60. Erley CM, Duda SH, Wakat JP, et al. Non invasive procedures for diagnosis of renovascular hypertension in renal transplant recipients and prospective analysis. Transplantation 1992;54:863–867.
61. Gedroyc WM, Negus R, al Kautoubi A, et al. Magnetic resonance angiography of renal transplants. Lancet 1992;339:789–791.
62. Voiculescu A, Hollenbeck M, Plum J, et al. Iliac artery stenosis proximal to a kidney transplant: clinical findings, duplex sonographic criteria, treatment and outcome. Transplantation 2003;76(2):332–339.
63. Butorovic-Ponikvar J. Renal transplant artery stenosis. Nephrol Dial Transplant 2003;18(Suppl. 5):74–77.
64. Geddes CC, McManus SK, Koteeswaran S, Baxter GM. Long term outcome of transplant renal artery stenosis managed conservatively or by radiological intervention. Clin Transplant 2008;22:572–578.

65. Ruggenenti P, Mosconi L, Bruno S, et al. Post transplant renal artery stenosis: the hemodynamic response to revascularisation. Kidney Int 2001;60(1):309–318.
66. Merkus JWS, Zeebregts CJAM, Hoitsma AJ, et al. High incidence of arteriovenous fistula after biopsy of kidney allografts. Br J Surg 1993;80:310–312.
67. Brandenburg VM, Frank RD, Riehl J. Color coded duplex sonography of arteriovenous fisulae and pseudoaneurysms complicating percutaneous renal allograft biopsy. Clin Nephrol 2002;58(6):398–404.
68. Renowden SA, Blethyn J, Cochlin DLL. Duplex and color flow sonography in the diagnosis of post biopsy arteriovenous fistulae in the transplant kidney. Clin Radiol 1992;45:233–237.
69. Matthew TH. Recurrent disease after transplantation. Transplant Rev 1991;5:31–45.
70. Penn I. Cancer is a complication of severe immunosuppression. Surg Gynaecol Obstet 1986;162:603–610.
71. Sidhu PS, Baxter GM. Pancreas transplantation. In: Ultrasound of abdominal transplantation. Stuttgart: Thieme International; 2002:125–130.
72. Schlosser T, Pohl C, Veltmann C, et al. Feasibility of the flash-replenishment concept in renal tissue: which parameters affect the assessment of the contrast replenishment? Ultrasound Med Biol 2001;27(7):937–944.
73. Cosgrove D, Eckersley R, Blomley M, Harvey C. Quantification of blood flow. Eur Radiol 2001;11(8):1338–1344.
74. Claudon M, Barnevolt CE, Taylor GA, et al. Renal blood flow in pigs: changes depicted with contrast enhanced harmonic US imaging during acute urinary obstruction. Radiology 1999;212:725–731.
75. Hosotani Y, Takahashi N, Kiyomoto H, et al. A new method for evaluation of split renal cortical blood flow with contrast echography. Hypertension Res 2002;25(1):77–83.
76. Lefevre F, Correas JM, Briancon S, et al. Contrast enhanced sonography of the renal transplant using triggered pulse inversion imaging: preliminary results. Ultrasound Med Biol 2002;28(3): 303–314.
77. Wei K, Le E, Bin JP, Coggins M, et al. Quantification of renal blood flow with contrast enhanced ultrasound. J Am Coll Cardiol 2001;37(4):1135–1140.
78. Correas J, Claudon M, Tranquart F, Helenon O. Contrast enhanced ultrasonography: renal applications. J Radiol 2003;84(12 pt 2): 2041–2054.

CHAPTER

29

Ultrasound of the bladder

Jonathan L. Richenberg

INTRODUCTION 550

ANATOMY 550
Gross anatomy 550
Microscopic anatomy 550

TECHNIQUES 551
Transabdominal imaging 551
Colour duplex imaging: ureteric jets 551
Endocavity ultrasound 551
Harmonic imaging 551
Contrast media: caution and new horizons 552

FUNCTIONAL ASPECTS OF BLADDER ULTRASOUND 553
Lower urinary tract symptoms 553
Bladder volume and bladder emptying (residue) 553
Accuracy of volume estimation at different volumes and in bladder shapes 554
Comparison of differing technologies in bladder volume estimation 554
Ultrasound and flowmetry 554
Flow patterns 555

STRUCTURAL ASPECTS OF BLADDER ULTRASOUND 556
Overview 556
Lumen 556
Stones 556
Foreign bodies 556
Ureteroceles 558
Urachus 559
Bladder wall 560
Wall thickness 560
Diffuse increase in bladder wall thickness 560
Tumours and bladder masses 561
Tumour detection 562
Staging bladder cancer 563
Tumour follow-up 564
Invasion of the bladder from adjacent tumours 565
Diverticula of the bladder 566
Fistula to the bladder 566

PATHOLOGY OUTSIDE THE BLADDER 566
Extrinsic masses 567

SPECIFIC CONDITIONS 568
Inflammatory/infective 568
Pregnancy-related pathology of the bladder 568
Placenta percreta 568
Endometriosis of the bladder 568
Postoperative 568
Conduits and partial resections 568
Trauma 569

PROCEDURES 569
Suprapubic catheterisation 569
Urinary bladder catheter balloon puncture 569

INTRODUCTION

Ultrasound is a dynamic examination, with the huge benefit over other cross-sectional imaging of direct patient contact. The examination can be tailored to the patient's physical state and to their clinical problem. Supplementary ultrasound views can be acquired immediately, as dictated by any clinical history elicited. Ultrasound of the bladder is usually performed as part of a more comprehensive examination of the urinary tract, or in the assessment of the pelvis as a whole. As such, the 'ideal' scanning sequence will be determined by the appearances of the kidneys or other organs. This chapter sets out to embody all aspects of bladder ultrasound, in the expectation that in daily practice, the examination of the lower urinary tract will be adapted to each patient.

ANATOMY

Gross anatomy

The bladder is a midline structure, supported by the pelvic floor (levator ani and obturator internus muscles), and protected by the pubic bones anteriorly. From puberty, the bladder, when empty, is confined to the pelvic cavity. Its macroscopic anatomy varies according to its degree of distension. When empty, the anterior wall points toward the symphysis pubis; the middle umbilical ligament, contiguous superiorly with the umbilicus, arises from the anterior wall. The posterior wall (when empty) is triangular, pointing inferiorly toward the rectum. The immediate posterior relations are, in the male, the distal ends of the vas deferens, the seminal vesicles or, in the female, the inferior uterus and cervix and vagina. The dome or superior surface is bounded by peritoneum, the sigmoid colon and loops of small bowel. As the bladder begins to fill, it rises out of the pelvis, and the superior margin enters the abdominal cavity, causing the peritoneal reflection to ascend. By the time the bladder contains 500 mL of urine, it has adopted an oval shape approximately 12 cm in long axis. The lateral walls bow outwards separated from the pelvic side walls by the iliac vessels and lymph nodes. The inferior margin of the bladder is relatively fixed, altering little in position regardless of the degree of bladder distension.

In the male, the base of the bladder sits on the prostate, to which it is bound by the puboprostatic ligaments. In the female, the posterior inferior bladder melds through alveolar tissue to the anterior surface of the cervix and upper vagina. More superiorly, the posterior female bladder is separated from the uterus by the vesicouterine peritoneal reflection.

Microscopic anatomy

The bladder wall is formed of four layers: the serosa (outermost, formed from the peritoneum), the muscular layer, the submucosa and the mucosa. The muscular layer (detrusor muscle) comprises

three bands of smooth muscle fibres arranged variously in longitudinal and circular array. The layers cannot be distinguished on ultrasound. The muscle fibres form the involuntary internal sphincter at the bladder neck.

The deep muscle fibres are bound by the submucosa to the mucosa, in the most part a loose affiliation so that the mucosa can 'ruck up' when the bladder is empty, becoming stretched and smooth as the bladder distends. The mucosa is continuous with that of the ureters (and therefore with the mucosa of the collecting systems of the kidneys) and with that of the urethra. Transitional cell epithelium lines the mucosa.

The base is the most complex part of the bladder, the sensitive trigone being triangular in shape and receiving the left and right ureter posteriorly, and opening to the urethra anteriorly. The mucosa over the trigone is always smooth, even when the bladder is empty because uniquely it is firmly attached to the muscular layer. The distal ureters pass obliquely through the bladder wall, the ureteric openings marking the posterior border of the trigone. Their course is visible on ultrasound.

The urothelium is not just a barrier, but is active in bladder function, having an afferent innervation with an important role in the reflex responses to bladder filling and distension. Within the urothelium, there is a dense muscarinic receptor population, which mediates the release of a diffusible inhibitory factor that inhibits smooth muscle contraction.[1]

The bladder derives its blood supply from the internal iliac arteries, predominantly via the superior, middle and inferior vesical arteries, supplemented by the obturator and inferior gluteal branches of the internal iliac arteries. The venous drainage forms a rich plexus of vessels around the inferior and fundal surfaces.

TECHNIQUES

Transabdominal imaging

The default examination of the bladder is via a suprapubic or lower abdominal window (Fig. 29.1). Modern ultrasound platforms will give excellent views of the whole viscus and information about the posterior vesical space at frequencies of 5 MHz, using a curvilinear array. Adjusting the time gain curve (TGC) so that it is 'flat' or even 'j' shaped reduces reverberation artefact. Use of compound harmonic imaging is advocated for a similar reason.

The bladder must be moderately full, typically 300–400 mL volume, for a meaningful examination. Scans are conducted from the dome down to the base of the bladder and by angling the transducer posteriorly and inferiorly, reasonable views of the prostate should be obtained in male patients. This provides an approximate estimation of prostate volume.

In patients with retention, notably chronic retention, the bladder may hold up to 1000 mL and scanning necessarily is periumbilical or even more cranially. In these cases, reporting the anatomical level for the dome of the bladder (e.g. centimetres above the umbilicus) is very helpful.

The ultrasound examination should include views of the trigone to show the vesico-ureteric junctions and the bladder neck (Fig. 29.1C and D).

Colour duplex imaging: ureteric jets

With the peristalsis of the ureter, the urine is propelled from the kidney to the bladder, emptying sporadically through the vesicoureteric junction into the bladder lumen. This may be seen during real-time ultrasound as a 'shimmer' on greyscale imaging, much more easily appreciated as a 'jet' or 'flame' using colour duplex imaging (Fig. 29.2). The duplex imaging detects the turbulence of the intravesical urine caused by the urine being 'squirted' from the ureter. Turbulence will only be detected if the specific gravity of the urine in the bladder and the urine from the ureter are different. Fortunately, most patients for bladder ultrasound have been asked to drink sufficient amount of fluid to fill their bladder, and the urine excreted by the kidneys is likely to be more dilute than that in the bladder.

With regard to the jets on colour duplex imaging:[2,3]

- They assist in identifying the ureteric orifice.
- Their duration varies 0.4 s to 7.5 s and depends largely on fluid intake.[2,3] Duration can vary in an individual by up to 2 s from one jet to another.[2] The interval between jets can be as low as 2 s or up to 2.5 min.[3]
- The direction of a normal jet is anteromedial and upward.
- Several flow patterns may be observed, including discrete jets, ureteric streaming, and rest periods.[3]
- Absence of jets in patients with acute obstruction from ureteric calculus suggests high-grade obstruction.[4] Indeed, in children, unilateral absence of a jet from the dilated side or significant asymmetry in jet frequency indicates upper tract obstruction.[4] A recent study has shown that when there is less than one jet detected from the dilated side in comparison to four (combined jets from both ureters), there is an 87% sensitivity and 96% specificity for obstruction in children with unilateral hydronephrosis.[5]
- In the stented ureter, looking for ureteric jets is not helpful.[6]

The detection of ureteric jets, especially when the jet frequency is comparable between the left and right side when scanning for several minutes, helps to exclude significant obstruction to the ureter. However, analysing ureteric jets is only an adjunct to urinary tract ultrasound and must be interpreted alongside evidence of renal obstruction.[7] In particular, failure to detect jets bilaterally does not usually imply obstruction to both kidneys, but rather that the difference in specific gravity of the urine from the kidneys compared with that in the bladder is too insignificant for turbulence to be detected.

Endocavity ultrasound

In rare circumstances, the base of the bladder is best assessed by transrectal ultrasound (TRUS). This can be helpful if there is concern about pathology at the trigone or when a mass may be invading the urethra from the bladder. Likewise, TRUS is invaluable when there is invasion between the prostate and the bladder, irrespective of the origin of the tumour.

Transvaginal ultrasound has a role in evaluating the mobility of the bladder neck. Techniques have been developed that ensure the endocavity probe does not affect the pelvic floor motion.[8,9] The bladder neck tends to lie more inferiorly and more posteriorly at rest in incontinent women when compared to continent women, with more descent on straining and less elevation on squeezing.[8] In a large study of women with primary stress incontinence, ultrasound revealed bladder neck funnelling in just over one-third of subjects, and this correlated with low pressure incontinence; the worth of the study is in the high negative predictive value (93%), so that absence of bladder neck funnelling more or less excludes the detection of low pressure leak on formal urodynamics.[10]

Endovaginal US is performed routinely in women presenting with postmenopausal bleeding, and in this population, it can detect unsuspected bladder tumours[11] – indeed, a small proportion of those scanned for 'postmenopausal bleeding' may have macroscopic haematuria rather than blood loss per vaginam, emphasising the worth of transabdominal and transvaginal ultrasound of the bladder in this patient group.

Harmonic imaging

Harmonic imaging is increasingly being used as the 'default setting' in renal tract imaging, many platforms performing the

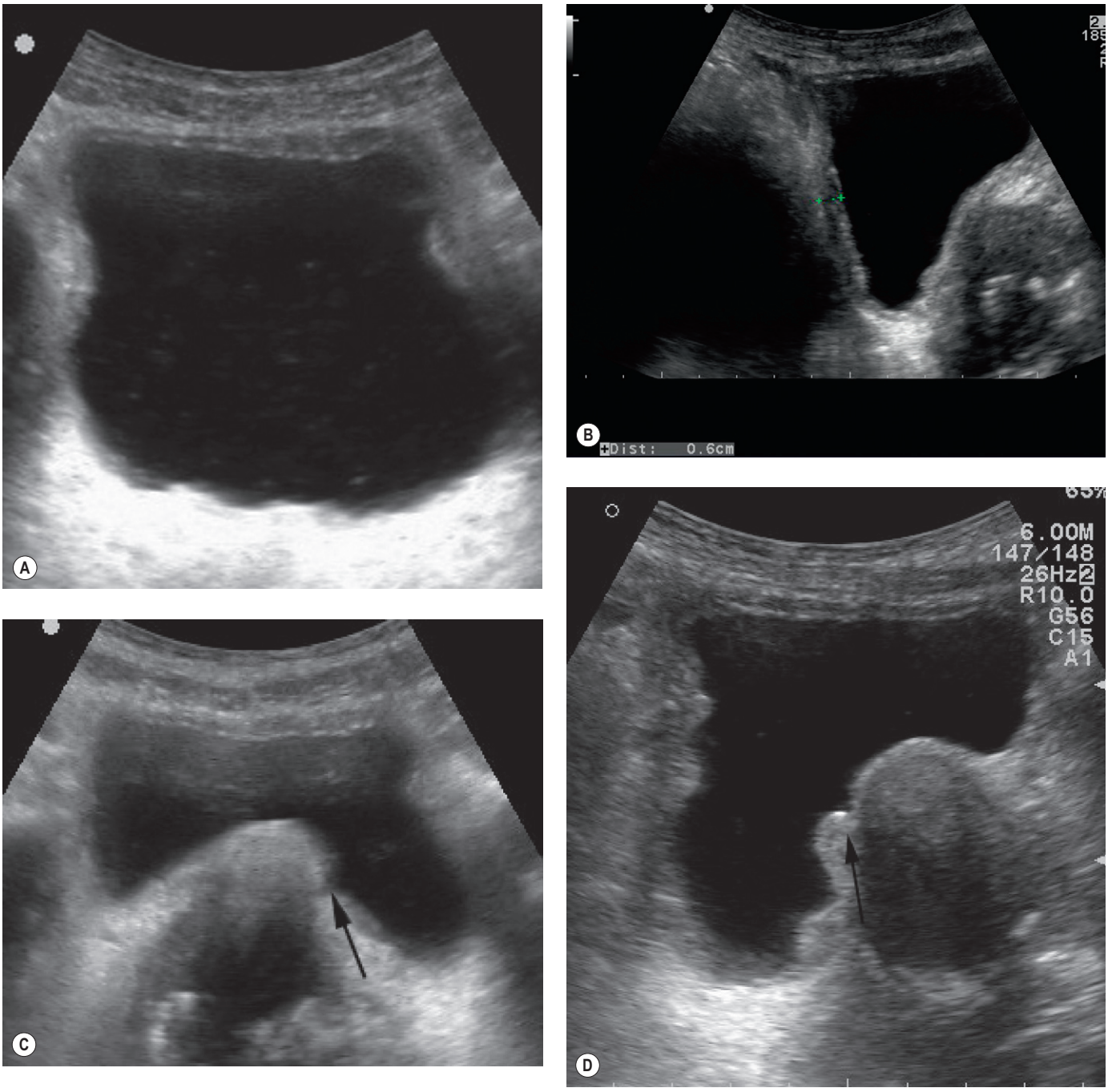


Figure 29.1 **Transabdominal scan of bladder** in axial **(A)** and sagittal **(B)** section. The wall thickness is best estimated on the sagittal section. The bladder base is the point of entry of both ureters and the point of exit for the urethra; in men, the bladder base may be elevated because of prostatic hypertrophy. In the axial **(C)** and sagittal **(D)** images of the bladder base, the displaced left ureteric orifice is shown by the black arrow.

post-processing of the fundamental image unless the harmonic mode is actively turned off. This is because in children[12] and adults harmonic imaging has been proven superior in visualising the renal tract.[13]

Contrast media: caution and new horizons

Ultrasound has one incontrovertible and significant advantage over computed tomography (CT): the absence of ionising radiation. It cannot 'trump' magnetic resonance imaging (MRI) in the same way, and MRI has had the ascendancy over ultrasound in bladder mass imaging for a decade or so. One of the benefits of MRI over ultrasound has been the use of gadolinium-based contrast agents in MRI to evaluate enhancement of lesions and thereby provide functional as well as structural information.

For two reasons, the 'contrast argument' looks set to swing back in favour of ultrasound, at least in a select group of patients. The first reason is the recognition of a new condition by Cowper et al. in 2000, called nephrogenic systemic fibrosis (NSF).[14] This is a rare but disabling condition in which the skin becomes indurated and painful, resulting in contractures. It is also associated with visceral sclerosis. The development of NSF is strongly linked to the usage of gadolinium contrast agents in patients with advanced renal impairment.[15] Thus, recognising that iodinated contrast media are

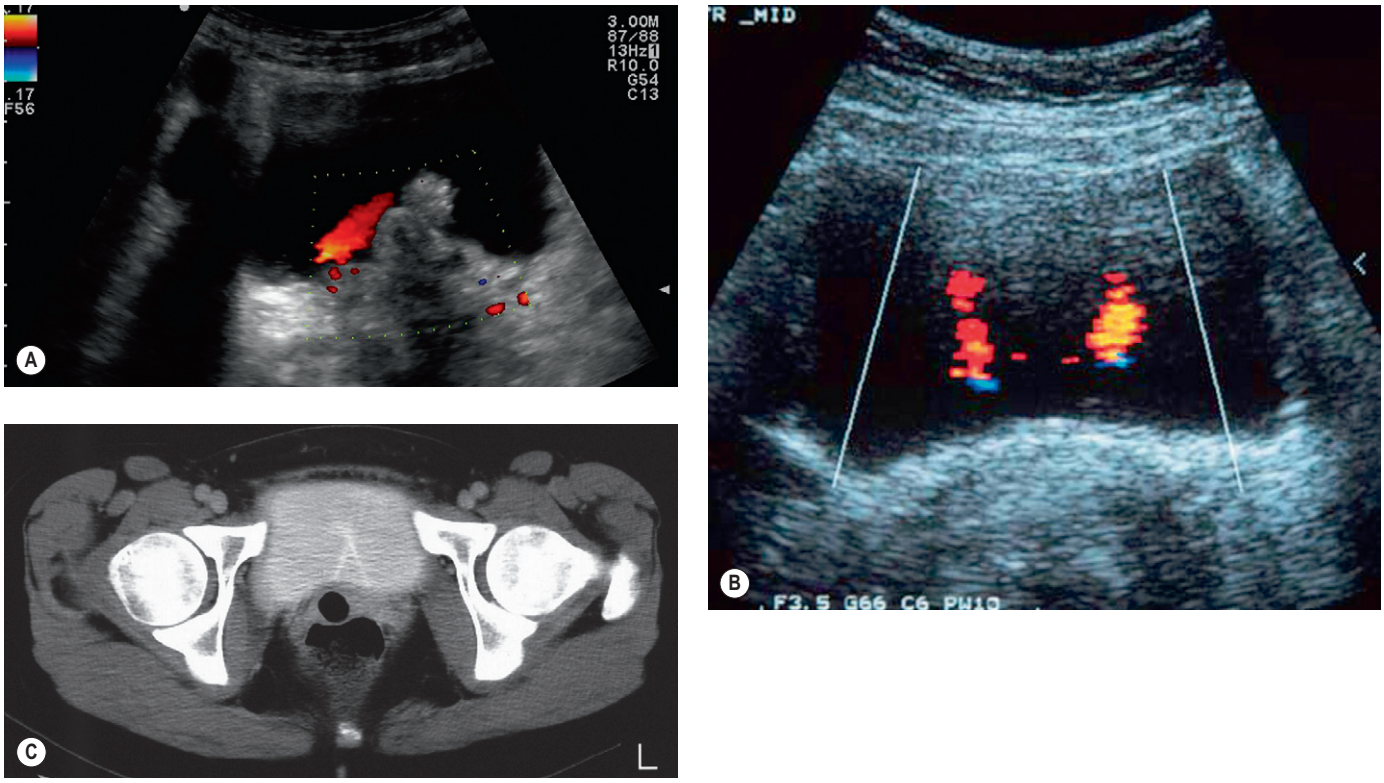


Figure 29.2 Ureteric jets on colour duplex imaging: from the right ureter **(A)**, both ureters **(B)** and on **(C)** CT from both ureters. Note the displacement of the right ureteric orifice in **A** by prostatic hyperplasia.

contraindicated in patients with renal impairment,[16] and acknowledging that gadolinium-based agents should be eschewed in advanced renal disease, ultrasound becomes more attractive in evaluating the bladder (and renal tract as a whole) in a very relevant group of patients that are needful of such imaging.

The second reason that ultrasound may in the future challenge MRI in bladder imaging is the development of microbubble ultrasound contrast agents. These agents have been used increasingly in hepatic imaging, and are being used with some benefit when scanning renal masses. Contrast-enhanced ultrasound, improving the signal-to-noise ratio in regions of low volume blood flow, has shown promise in the detection of otherwise occult prostate cancer, and it is hoped that it might be used to good effect when trying to resolve the aetiology of focal bladder wall thickening.

Work on children with suspected vesico-ureteric reflux has looked at harmonic imaging using phase or pulse inversion technology and contrast harmonic imaging after intravesical administration of ultrasound-based contrast medium (microbubbles).[17] The refluxing microbubbles are much more conspicuous in the harmonic imaging, such that in 8 out of 27 kidney-ureter units, the reflux was detected using only the harmonic imaging modalities. Harmonic imaging with ultrasound contrast has been shown to be equivalent to conventional micturating cystourethrography in the detection of reflux in the paediatric population.[18]

FUNCTIONAL ASPECTS OF BLADDER ULTRASOUND

Lower urinary tract symptoms

Lower urinary tract symptoms, or LUTS, are a non-sex-specific, non-organ-specific group of symptoms, which are sometimes age-related and progressive.[19]

Summary of lower urinary tract symptoms (LUTS) (based on personal communication, Professor Christopher Chapple, Sheffield Teaching Hospitals)

Storage	Voiding	Post-micturition
• Frequency • Urgency • Nocturia • Incontinence	• Slow stream • Spraying • Intermittency • Hesitancy • Straining • Terminal dribble	• Post-micturition dribble • Feeling of incomplete emptying

Bladder volume and bladder emptying (residue)

Much has been written about the role and accuracy of ultrasound in estimating bladder volume. The emphatic conclusion is that transabdominal ultrasound is a safe, reasonably accurate and cheap method to determine the volume of urine in the bladder. This holds for pre- and post-micturition estimation, and is true in adult[20,21] and paediatric[22–24] patient groups. A formal review of the literature from 1966 to 1999 identified 504 subjects in 16 validity studies (in which ultrasound estimation is compared with actual bladder volume). Where reported, the index of concordance for estimating bladder volume varied from 0.914 to 0.983.[25] This level of accuracy is usually sufficient for clinical purposes where the degree of tolerance is relatively wide.[26]

From a clinical point of view, the thresholds for bladder volume are:

- 0–50 mL: insignificant
- 51–100 mL: borderline – to be interpreted together with anatomical appearances, flow rate chart and the patient's

Calculating bladder volume

$$V = (L \times A \times T) \times C \text{ mL}$$

where V = volume, L = longitudinal length, A = maximum anteroposterior diameter, T = maximum transverse diameter and C is a coefficient.

C ranges from 0.5 to 0.625 based on differing algorithms and essentially assuming that the bladder is spherical.

Sphere volume = $4/3 \times \pi \times r^3$ where r is the radius equivalent to half the diameter. The measurements L, A and T are all diameters so the formula can be rewritten:

$$\begin{aligned}\text{Sphere volume} &= 4/3 \times \pi \times (d/2)^3 \\ &= 4/3 \times \pi \times d^3/8 \\ &= 1/6 \times \pi \times d^3 \\ &= 0.52 \times d^3\end{aligned}$$

C can be up to 0.625; more usually in practice the formula would be:

$$V = (L \times A \times T) \times 0.6 \text{ mL}$$

See Dicuio et al.[28] and Yip et al.[29] for a more complete mathematical treatment of the formulae for bladder volume calculation. The conclusion from these papers is that the more simplistic formulae (as above) are as precise as more complex methods such as the double area method and the double ellipsoid method.

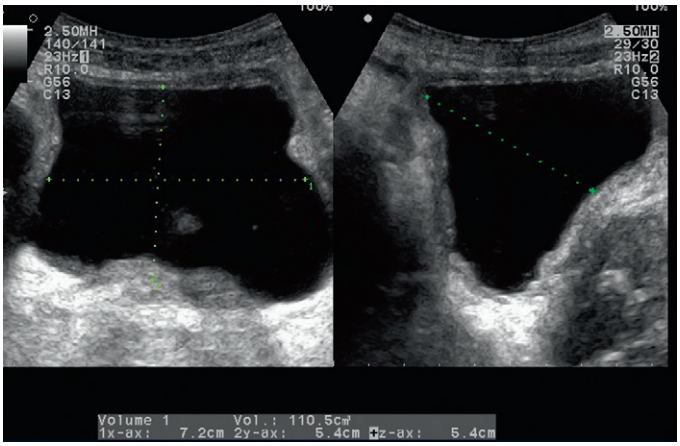


Figure 29.3 Bladder volume estimation: orthogonal diameters of the bladder shown on split screen; the maximum diameters are used, the image being frozen first in the axial and then in the sagittal plane. Most ultrasound platforms automatically calculate the bladder volume (in this case >100 mL).

symptoms. Often patients have drunk exuberantly prior to the scan, so that the bladder fills up rapidly after first void

- >150 mL: indicates retention.

Clearly the latitude in most cases is wide enough for the ultrasound-predicted bladder volume to be clinically relevant. In 80 postoperative patients, ultrasound (against catheter volume) was 97.7% specific, with a negative predictive outcome of 89.5%, obviating the use of catheterisation in those with a bladder residual volume of <150 mL.[27]

Accuracy of volume estimation at different volumes and in bladder shapes

Once ultrasound has been performed, the bladder volume can be estimated by a number of formulae.[28] The most common method is to measure the longitudinal, the transverse and the anteroposterior diameter. These are best 'captured' by splitting the screen into two halves, the left screen revealing the transverse image of the bladder at its widest point, the right screen the sagittal image (Fig. 29.3).

The straightforward method of measuring the three linear, orthogonal diameters, and multiplying the values together, is as precise in estimating bladder volume as more mathematically complex techniques, notably the ellipsoid and area methods, although the tendency is to underestimate the true volume.[30] The limitations of ultrasound-based bladder volume remain even when the bladder contains more than 150 mL of fluid, so the predicted bladder volume must be interpreted with a degree of caution and only ever offered as an estimate, not a true value. Because of this tendency to underestimation, of up to 20% in calculated bladder volume, some institutions advocate the use of individually determined proportionality constants to improve the accuracy of residual bladder volume determinations.[31] However, each institution needs to define a specific algorithm, and this may be dependent not simply on the hospital setting but on the specific ultrasound platform used; moreover, a personal computer has to be connected to the ultrasound imaging unit. The increased complexity albeit with a more accurate volume estimation is not warranted in the majority of clinical settings.

In augmented bladders, ultrasound is not accurate in estimating urinary volume, because there is no reliable geometry to the neobladder. Ultrasound can provide an idea of the degree of filling, and more relevant, retention in the augmented bladder, but in this specialist postoperative group, catheterisation through the ileal conduit, with confirmation of complete drainage by ultrasound, is the recommended method by which residual volume is measured.[32]

Comparison of differing technologies in bladder volume estimation

Voided volume measurements or catheter volume measurements are taken as the 'gold standard' in studies that set out to determine the accuracy of various ultrasound methods for calculating the volume of the bladder.

A recent comparison of a dedicated bladder, non-real-time volume calculator (BladderScan BVI 3000) with a real-time three-dimensional (3D) ultrasound system and with a real-time portable 2D ultrasound platform with iterative bladder volume calculation (Bardscan II) has been undertaken on 34 patients. Significant correlation between the voided and calculated bladder volumes were achieved with each method, but the 'accuracy and level of clinical agreement was greatest when using the 3D ultrasound system to calculate the bladder volume'; the portable 2D ultrasound system tended to underestimate the bladder volume by 5–10%.[33] In postoperative patients in the urodynamics clinic, Bardscan II performed well against catheter volume measurements with a correlation coefficient >0.98.[34] In the paediatric setting, however, where the volumes are much lower, conventional ultrasound measurements should be used in preference to the BladderScan automated system.[35]

The use of 3D ultrasound over bladder volumes 100–400 mL appears accurate with only a minor underestimation of volume (~3%).[36]

Ultrasound and flowmetry

The quantification of bladder volume alone is limited. Ultrasound of the urinary tract (that is, the kidneys as well as the bladder) should be augmented by data from a flowmeter.[37] The majority of flowmeters in hospital practice are spinning disc types (rather than weight transducer flowmeters). The urine flow rate is charted by

attaching the flowmeter to a chart recorder. A graph is produced for each micturition episode, from which peak flow rate (mL per second), mean flow rate (mL per second), time to peak flow (seconds), voiding time (seconds), and time of micturition (seconds) can all be derived. These data can then be interpreted with the residual volume, derived from ultrasound of the bladder immediately post void, along with visual analysis of the shape of the flowmeter tracing.

Overall, the ultrasound and uroflowmeter examination is non-invasive and provides information about bladder function, bladder anatomy, bladder anomalies and bladder capacity. There are a couple of caveats:

- Flow charts where the total voided is less than 125–150 mL are limited; it is better to ultrasound the patient as a matter of routine before sending for flow rate measurement, ensuring that the pre-micturition volume (by ultrasound measurement) is larger than 200 mL. In an Italian study, on 67 men in their 60s and 70s, a voided volume of greater than 125 mL (>150 mL) necessitated a pre-voiding bladder scan volume greater than 200 mL (>250 mL), which in the study decreased the number of non-eligible flow rate recordings from 23.9% to 4.5% (31.3% to 4.5%).[38]
- Similarly, sending patients with abnormally distended bladders for 'physiological' flow measurements is ill advised, as the normal innervation that triggers micturition can be upset with abnormally full bladders, especially in the clinic setting.
- If residual volume exceeds 100 mL, the patient should be sent to urinate again, and a repeat post (second) micturition bladder volume calculated.

Of the various parameters, post-micturition residue and maximum flow rate (as well as prostate volume that can be easily estimated by transabdominal ultrasound) are the most useful in the prediction of urodynamically proven bladder outflow obstruction.[39]

Flow patterns

In normal subjects the flow tracing is bell-jar shaped.[44,45] The delay to peak flow is between 3 and 8 seconds, and the peak rate 35–40 mL/s (men), and approximately 50 mL/s in women (Fig. 29.4). The abnormal traces – low, high or intermittent flow patterns – signify defined pathologies, but the classification also relies on the volume of post-micturition residue.

Complete bladder emptying and high flow

When the flow rate is supra-normal, the inference is that voiding occurs at high pressure, either because of abdominal muscle augmentation ('straining') or because the detrusor muscle is overly active (a primary or neurological problem, rather than compensatory hyperactivity to overcome outflow resistance).

Complete bladder emptying and low flow

When the flow rate is reduced, the inference is that either there is outflow obstruction or there is a weakened, poorly functioning detrusor muscle.

Outflow obstruction may be mechanical or neurological. The former is most commonly due to prostatic hyperplasia, and the bladder wall will be thickened and the bladder base elevated. Urethral strictures may also result in thickening of the bladder wall with low flow. The mean flow rate is more than 50% of the value

Urine flow rates

Post-void residual[40]
Population: 477 randomly selected community-dwelling white men.
Median post-void residual 9.5 mL (2.5–35.4 mL 25–75%).
Post-void residual ≥50 mL much more likely as prostate >30 mL.
Post-void residual urine volume poorly correlates with peak urinary flow rate.

Urine flow rate[41]
Population 514 men (17–84 years) who subjectively felt that their urination was normal and were objectively demonstrated to be without prostatic hyperplasia.
Maximum flow rate: 20.7 ± 7.3 mL/s in a mean voided volume of 290.7 ± 123.2 mL.
Voided volume decreases with age; with declining maximum flow rate bladder capacity diminishes with age.

Functional bladder capacity (FBC)[42]
Functional bladder capacity defined as largest voided volume in 24-hour period.
Population: 1688 men 50 to 78 years old.
Strongly related to LUTS.
Lower in men with a reduced maximum flow rate (less than 15 mL/s) independent of the post-void residual volume.

LUTS[42]
Dependent on age.
Correlates with a reduced flow rate.
Associated with large post-void residual volume.
More frequent as FBC falls.

Bladder compliance (BC)[43]
Population: 170 men aged 50+ years with an International Prostate Symptoms Score (IPSS) of ≥7 and a peak flow rate (Qmax) of ≤15 mL/s.
The mean BC = 32 ± 2 mL/cm water, decreasing significantly with age and falling peak flow rate.

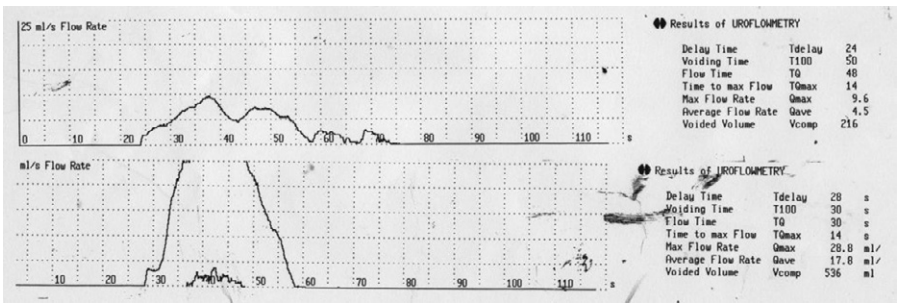


Figure 29.4 Uroflowmetry in a normal 36-year-old man (lower trace) and in a 69-year-old man with detrusor failure (upper trace). Compare the normal bell-shaped curve with the flat and persistent slower flow in the patient whose bladder is failing. As expected, a significant residue (>150 mL) was recorded post void in the 69-year-old.

of the maximum flow rate, with a slow and protracted decline in flow rate from the peak (the peak itself is, of course, reduced). In obstruction due to urethral strictures, the trace tends to be very level with barely a discernible peak; the maximum rate being not only suppressed but very close in value to the mean rate.

Neurological outflow obstruction is seen when there is incoordination between detrusor contraction and bladder sphincter relaxation. This is referred to as bladder neck dyssynergia. The incoordination may be part of a wider neurological deficit – spinal tumour, Parkinson's disease or multiple sclerosis – but it is also seen in otherwise healthy young men, in whom it is ascribed to a primary failure of the sympathetic nervous system to relax the sphincter mechanism at the time of voiding.

Failure of the detrusor may be idiopathic (anecdotally suggested that the patient, normally female, has held on to their urine for long periods throughout their life), or it may be due to failure of the detrusor following longstanding outflow obstruction. The idiopathic group manages to empty the bladder completely, albeit with a slow and sustained flow pattern.

Incomplete bladder emptying and low flow

This combination is the end result of long-term outflow obstruction. Characteristically, ultrasound will reveal abnormalities of the bladder wall, such as thickening, trabeculation and diverticula, all indicative of long-term resistance. The ability of the detrusor to overcome the outflow resistance has been surpassed, and the bladder can no longer completely empty. Frequently, the patients will volunteer that they have the urge to urinate only a short while after they have just been, as the stretched detrusor recovers following the initial micturition (Fig. 29.4).

Intermittent flow pattern

This signifies near complete detrusor failure, voiding occurring by abdominal straining. The amount of residual urine is variable, reducing as the abdominal muscles become more accustomed to emptying the bladder.

Limitations of flowmetry

Complete evaluation of bladder function – more specifically, detrusor compliance and detrusor stability – requires formal, invasive urodynamics. This is because lower urinary tract symptoms are non-specific and common to bladder outflow obstruction, detrusor failure, detrusor instability, detrusor-sphincter dyssynergia and even to bladder infection. Uroflowmeter assists in classifying by flow rate and degree of emptying, but does not give reliable information on intravesical pressure or on bladder shape and pelvic floor movements during micturition. These parameters are within the realm of invasive urodynamics.

STRUCTURAL ASPECTS OF BLADDER ULTRASOUND

Overview

Ultrasound images can give a wealth of accurate data about the bladder, its contents and its relationship to the adjacent organs.

The following discussion is based on classical radiological classification: pathology within the lumen, pathology within the wall of the bladder and lesions extrinsic to, but nevertheless, affecting the bladder or its function. This is very apposite, mirroring the systematic evaluation of the pelvis during an ultrasound examination.

Overview

The bladder lumen
- Capacity, especially post-micturition residue
- The presence of blood or debris within the urine (echogenicity of the urine)
- The presence of gas within the bladder
- Foreign bodies or calculi within the bladder
- The position of bladder catheters and the state of any retaining balloons
- Ureteric function (ureteric jets)

The bladder wall
- Thickness
- Smoothness or trabeculation or diverticula
- Focal masses

External to the bladder
- The distal ureters
- The prostate
- Extrinsic masses including urachal element
- Pelvic organs

Lumen

Normal urine is anechoic. Indeed, when scanning transabdominally, the TGC (time gain curve) may usefully be altered to a 'j-shape' to minimise artefact in the far field and optimise visualisation of the posterior bladder wall. When echoes are returned from the urine (spectral reflectors), it means that the urine contains debris, or crystals, or blood or pus (Fig. 29.5). Obviously, inspection of the urine, voided or catheter specimen, will suggest the likely source of the spectral effect. If the urine appears clear to the naked eye, it should be sent for microscopy and culture, looking for inflammatory cells, pathogens and crystals.

Stones

Stones in the urinary tract are common; the majority develop in the upper tracts, with only 5% in the bladder. Calculi within the bladder may have come from the upper tracts, or they may develop primarily within the bladder itself due either to diet (limited to all intents and purposes to children in developing nations) or to urinary stasis. Stasis, in turn, occurs because of neuropathic problems or because of outflow obstruction. In the developed world, bladder calculi are associated in 25–35% of cases with urinary tract infection.[46] Foreign bodies also predispose the patient to bladder stones.

Unlike radiography all bladder calculi are detectable by ultrasound – there is no equivalent of a radiolucent stone. They are characteristically well-defined ellipsoid echogenic structures, mobile and casting an intense acoustic shadow (Figs 29.6 and 29.7).

Foreign bodies

Occasionally foreign bodies may be introduced into the bladder. The most literal foreign body is the Foley balloon catheter, placed either perurethrally or transcutaneously (suprapubic). The catheter itself and retaining balloon when inflated are easily visualised on ultrasound (Fig. 29.8). Another iatrogenic foreign body is the ureteric JJ stent, which may be placed between the renal pelvis and the bladder lumen either antegradely or retrogradely. This has a distinctive appearance on ultrasound: thin echogenic parallel lines (tram lines), which curve away from the ureteric orifice of the stented ureter (Fig. 29.9).

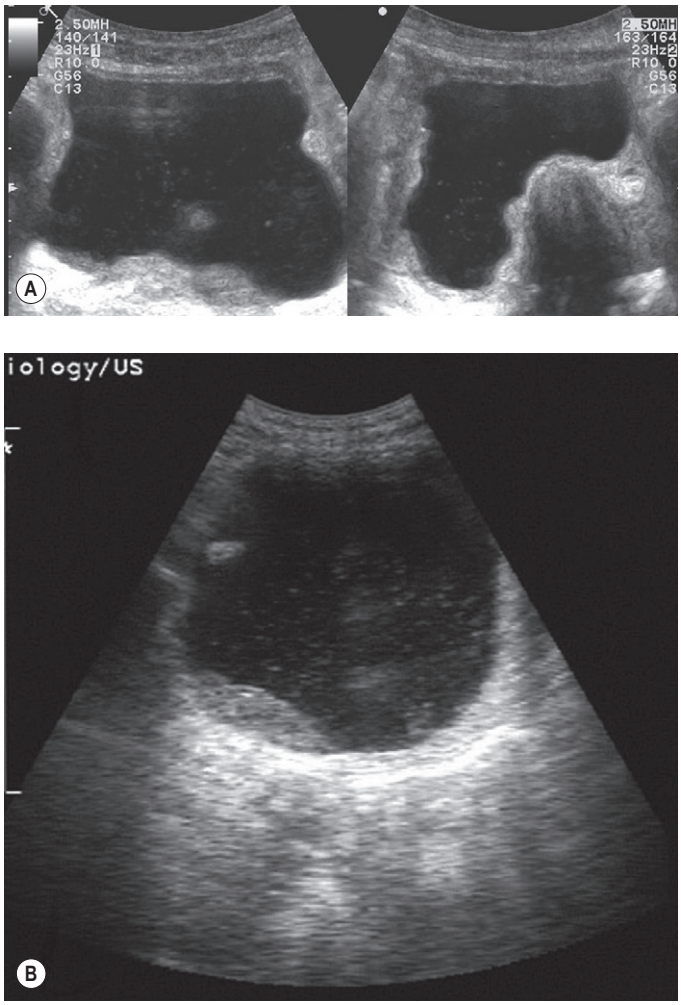


Figure 29.5 **Echogenic urine.** Axial **(A)** and sagittal **(B)** transabdominal ultrasound views of the urinary bladder, showing echogenic urine in a patient with urosepsis.

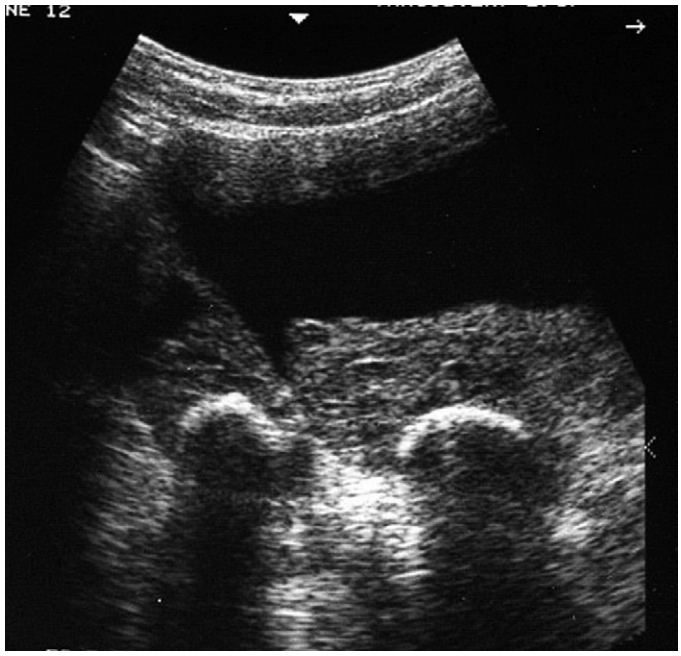
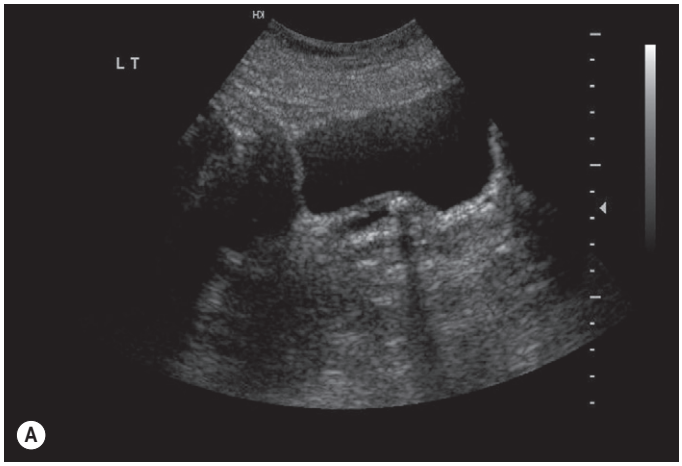


Figure 29.6 **Bladder stones.** Two large (>1 cm) stones and debris settling out in a dependent fashion in the bladder of a patient with spina bifida, resulting from a neuropathic bladder. The stones are echogenic and cast acoustic shadows. On real-time imaging, the stones were mobile.



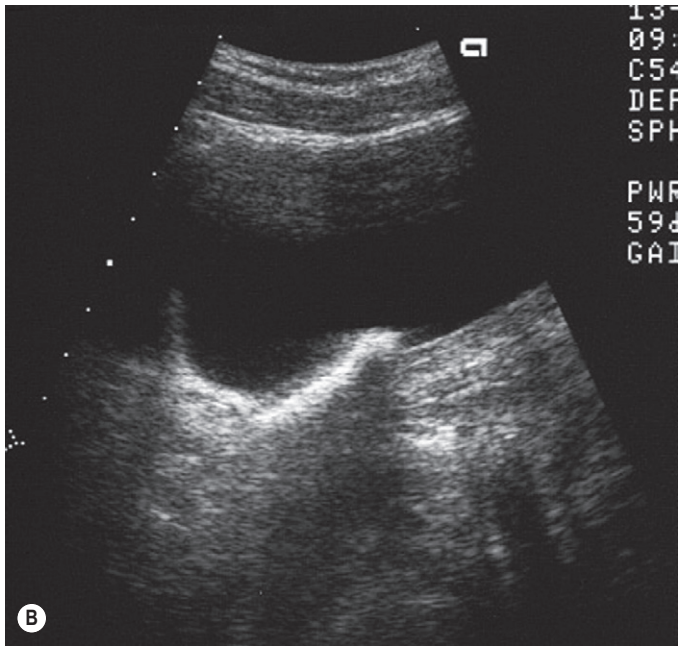


Figure 29.7 **Bladder stones. A:** Stone (4–5 mm) in the distal ureter with proximal dilation of the ureter. At this size and site, the patient can be managed expectantly. The stone is likely to pass spontaneously. Serial ultrasound can be employed to document passage of the stone into the bladder. Intervention would be indicated only if the stone failed to pass over 48 hours, the patient suffered intractable pain, or urosepsis. Contrast advocacy of conservative management with **(B)** a 'steinstrasse' – multiple stone fragments in the distal ureter following extracorporeal shock-wave lithotripsy treatment to a renal calculus. In the steinstrasse, urgent retrograde JJ ureteric stent placement is advised.

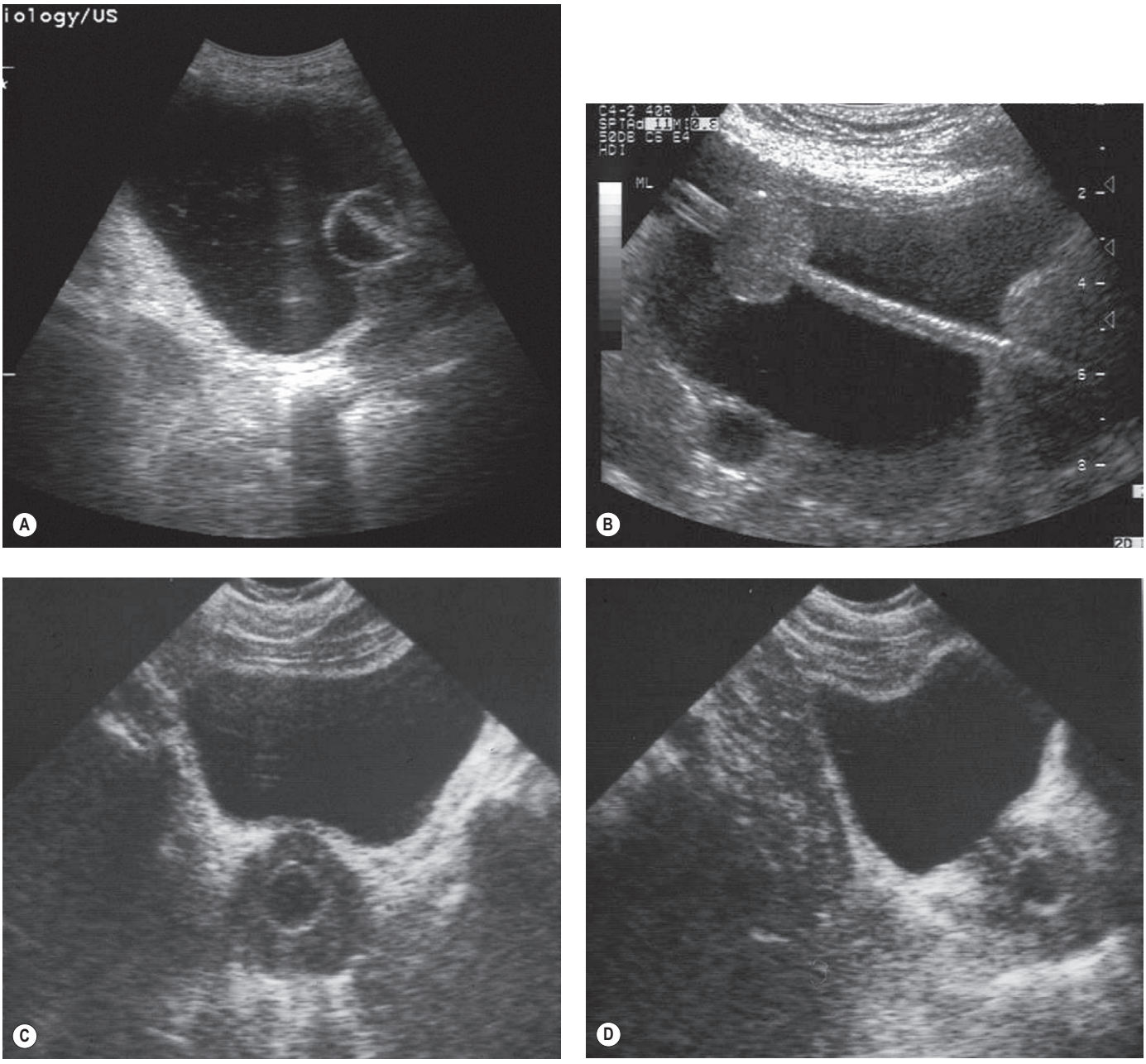


Figure 29.8 Typical appearances of Foley balloon catheters (per-urethral), with saline-filled balloon lying on the trigone **(A)** and the catheter lying more proximally the balloon filled with unknown fluid of moderately high echogenicity **(B)**. Occasionally, the Foley catheter may be inserted short, the balloon inflated in the urethra. In this case, axial **(C)** and sagittal **(D)** images confirm that the catheter has not entered the bladder lumen, the retaining balloon visible in the prostatic urethra.

Less commonly, patients may insert foreign bodies perurethrally into the bladder. These are usually detected by plain radiography, but ultrasound may be useful, especially if the object is not radiodense (e.g. a plastic drinking straw) (Fig. 29.10). Naturally, the sonographic findings will depend on the particular foreign body inserted.

Ureteroceles

The term 'ureterocele' refers to the ballooning of the distal ureter. When the ureterocele is mostly within the submucosa, and only a part projects into the bladder neck or urethra, it is defined as ectopic; when the ureterocele and its orifice are contained by the bladder, it is defined as intravesical. The latter, due to herniation of the lower ureter and opening through the bladder wall, are seen on ultrasound as a cystic mass within the bladder, defined by a smooth and thin wall (Fig. 29.11). The ureterocele can be seen on real-time imaging to 'peristalse', intermittently discharging and then refilling. The intravesical ureterocele is usually an incidental finding, but it can be complicated by stone formation or it can, occasionally, cause obstruction to the upper tract (Fig. 29.12). Most are discovered on ultrasound or other imaging by chance, being bilateral in 30–40% of cases.

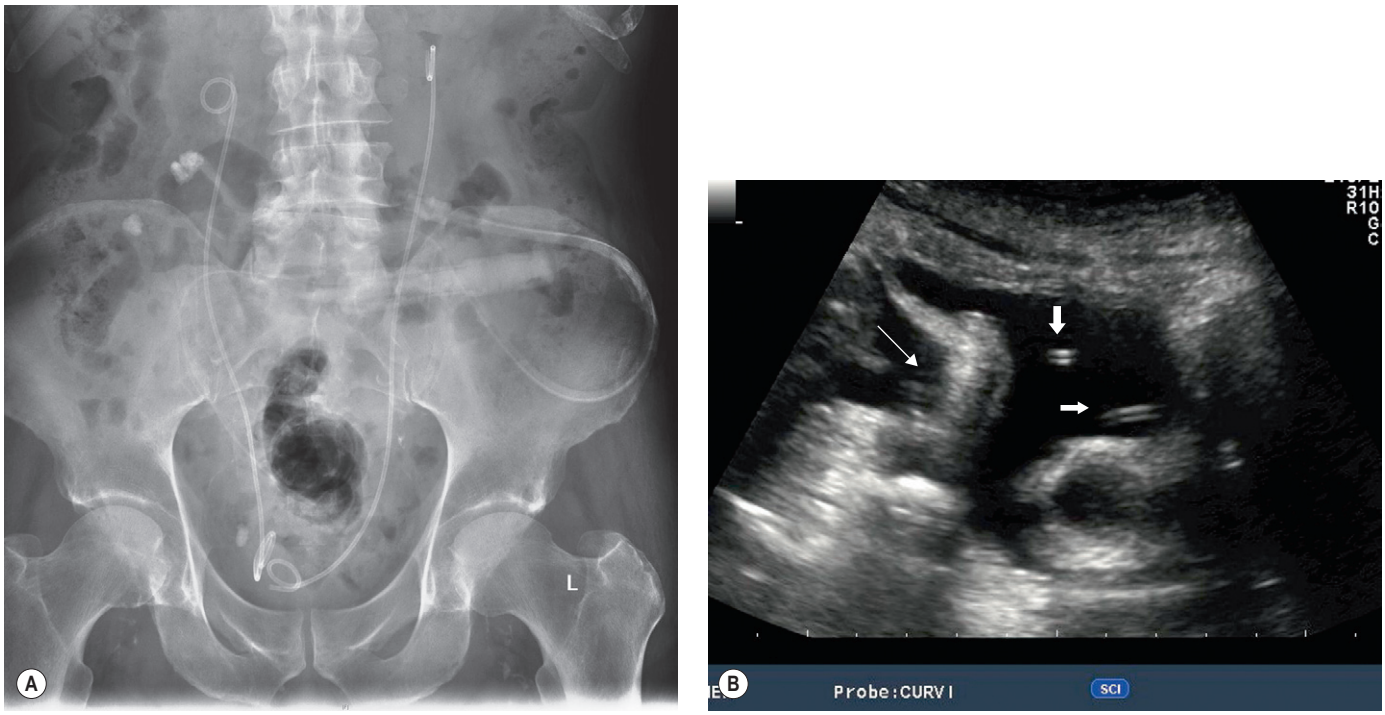


Figure 29.9 **Bilateral ureteric JJ stents** shown on KUB X-ray **(A)**. The stent in the bladder on ultrasound **(B)** appears as a pair of parallel lines which are echogenic (white arrowheads). In this image, the stent is forming a 'J' and therefore is seen in the anterior and posterior half of the bladder. Note also the Foley balloon catheter lying posteriorly. Unfortunately, despite insertion of bilateral JJ stents and long-term bladder catheterisation, the patient went into end-stage renal failure from chronic bladder outflow obstruction (uropathy). The peritoneal dialysate is manifest as anechoic fluid within the abdominal cavity (thin white arrow).



Figure 29.10 **Radiograph to show a glass bracelet** within the bladder lumen. When radio lucent foreign bodies are suspected, such as drinking straws, ultrasound of the bladder is advised as the first line of investigation.

An ectopic ureterocele arises because the ureteral bud commences more inferiorly than normal from the mesonephric duct, so that the ureteric orifice is distal to the bladder neck. If this occurs in the sole ureter draining the kidney (20% of ectopic ureteroceles), the kidney is usually atrophic. Fortunately, 80% of ectopic ureteroceles are seen in duplex systems, and therefore, identifying an ectopic ureterocele must alert the radiologist to the possibility of a duplex ureter, the ureterocele always being associated with the upper moiety ureter (as it descends and crosses the lower moiety ureter to insert in an ectopic position in the low bladder or inferior to the bladder). Careful ultrasound of the ipsilateral kidney may suggest a duplex system, in which the upper moiety is hydronephrotic. A comprehensive discussion on the embryology of ureteroceles can be found in Barth et al.[47]

Urachus

The urachus is an embryonic remnant resulting from involution of the allantoic duct and the ventral cloaca.[48] Attaching the bladder dome to the umbilicus, the urachus should close during gestation. Failure of closure is not uncommon, the urachus being reported as present in up to 30% of adults.[48] In children under 16, the urachus may be present in up to two-thirds of studies.[49] On ultrasound, the urachus presents as a cystic tubular structure in the midline, inferior to the rectus muscle (Fig. 29.13). When patent it can have a length up to 15 cm, and occasionally may exhibit pathology including a diverticulum, cyst (a small part of the duct is pinched off, with closure superiorly and inferiorly),[50] and very occasionally, a tumour can develop within a patent urachus. These are invariably adenocarcinomas with a poor prognosis. Their diagnosis is vexatious, presenting as a mass superior to the bladder dome in the anterior abdomen. They are best assessed by CT.[51]

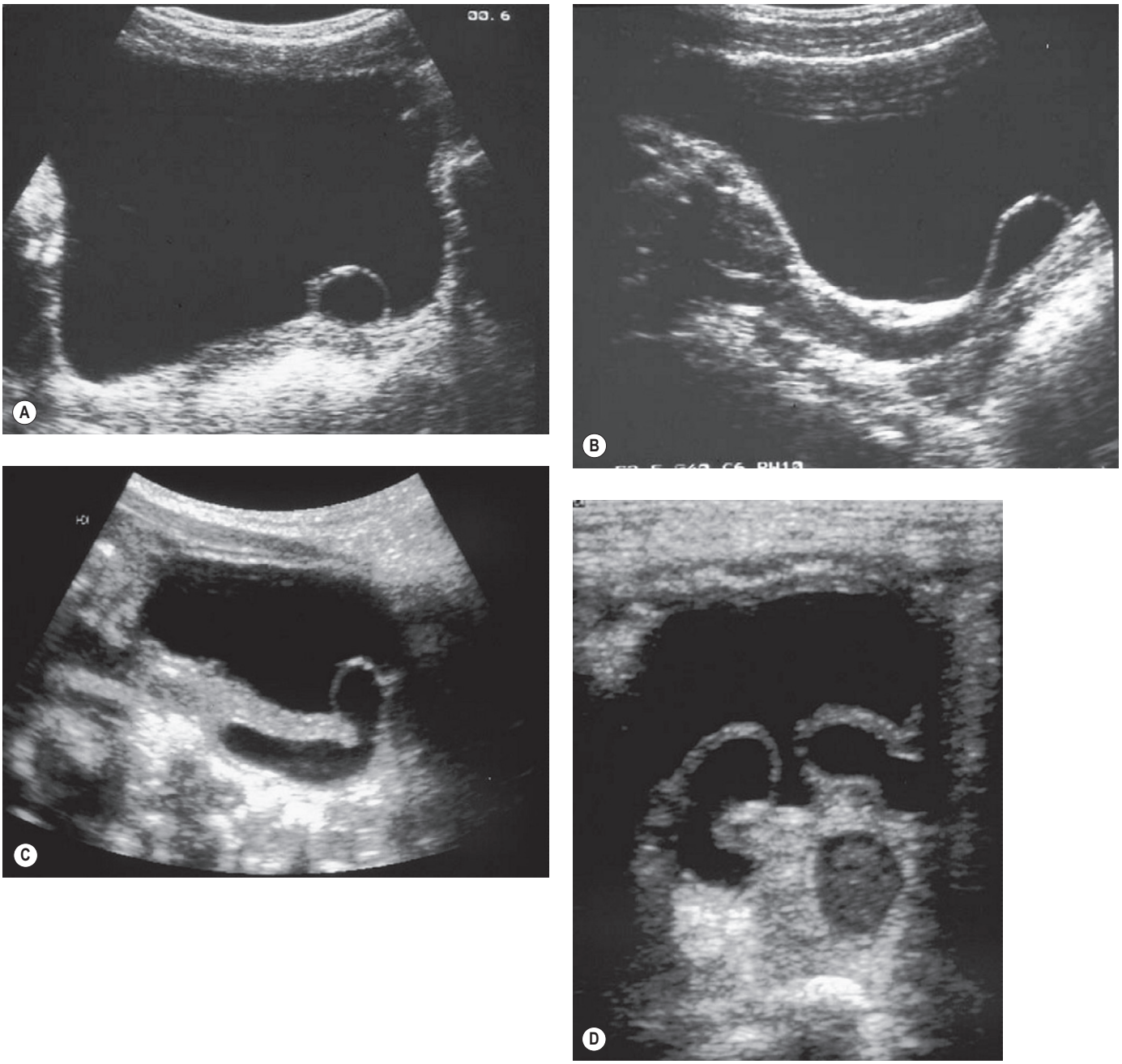


Figure 29.11 Transabdominal ultrasound views (A, B, C, D) showing simple ureteroceles in different patients. Note the mild dilatation of the ureter in images **(B)** and **(C)**. There are bilateral ureteroceles in image **(D)**. In all cases, the uretrocele has a smooth and thin wall.

Bladder wall

Wall thickness

Transabdominal ultrasound of a bladder containing 300 mL or greater of urine gives a very accurate measurement of bladder wall thickness. In a normal bladder, this will be 3 mm or less. The corresponding figure when the bladder is empty is 5 mm.

Diffuse increase in bladder wall thickness

If there is outflow obstruction, the bladder wall may hypertrophy. In men this is almost a normal finding with increasing age as the prostate begins to cause mechanical outflow obstruction. Neurological incoordination can also lead to hypertrophy of the muscle (Fig. 29.14).

The bladder wall can become thickened if there is inflammation or infection, although this is not inevitably global, as in the case of outflow obstruction. The thickening is due to oedema rather than muscle hypertrophy. It may be associated with increased vascularity, demonstrated on colour flow imaging. The patient is likely to have symptoms of dysuria, frequency and urgency. For a fuller discussion about cystitis, see 'Specific conditions' below.

Focal thickening of the bladder wall due to tumour is dealt with in the subsequent section.

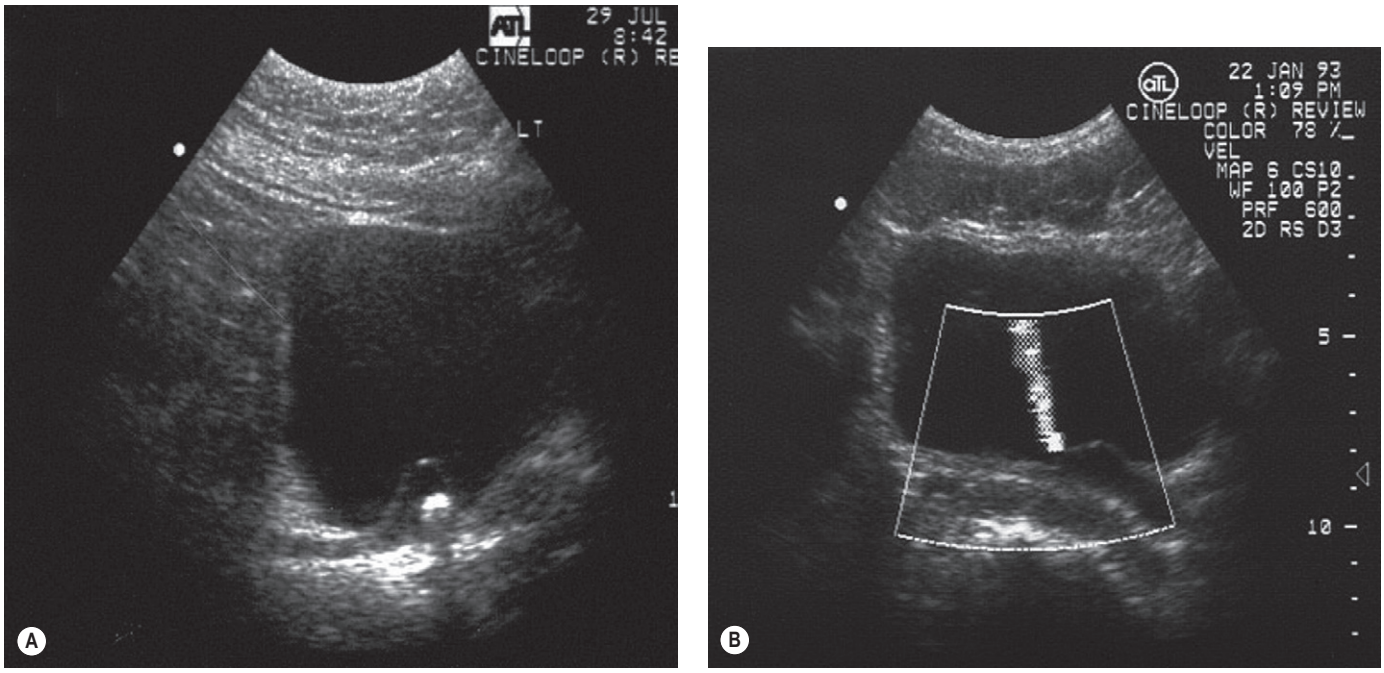


Figure 29.12 **Ureterocele. A:** A small stone complicates an otherwise simple ureterocele. **B:** Concern that mild ureteric dilatation signifies obstruction associated with a ureterocele is allayed by the prominent and episodic ureteric jet well shown on colour duplex imaging.

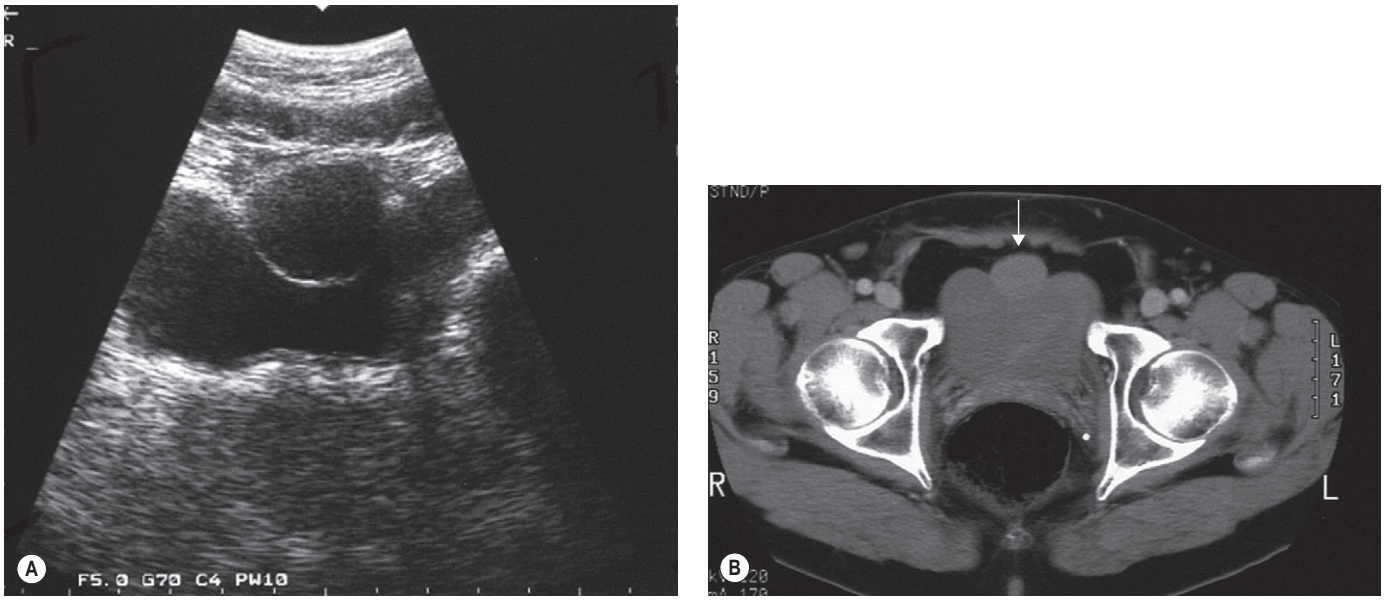


Figure 29.13 **Urachal cyst. A:** Transabdominal ultrasound reveals a cystic structure anterior to the bladder and deep to the abdominal wall. The differential diagnosis includes a urachal element, a bladder wall tumour such as a leiomyoma or, in women, an endometrial deposit. Note the mass effect, suggesting the lesion is extrinsic to the bladder. A non-enhanced CT **(B)** indicates that the lesion (white arrow) has increased density, suggesting the contents might be haemorrhagic or contain (as in this case) slightly calcific fluid, within a closed off urachal cyst.

Tumours and bladder masses

Cancer involving the bladder may be primary, secondary or a manifestation of local invasion from adjacent organs. Primary carcinoma is a relatively common condition, with, according to the National Cancer Institute, 68 810 estimated new cases and 14 100 deaths from bladder cancer in the United States in 2008 (http://www.cancer.gov/cancertopics/types/bladder). In 2004, an estimated 60 200 new patients were diagnosed with bladder cancer in the United States, and 12 700 of those patients died from the disease (http://www.emedicine.com/med/topic2344.htm.), indicating that the frequency of the disease is increasing. Men are affected three to four times more commonly than women, but women tend to fare worse from the disease. The median age for diagnosis is 60–70 years. For data relevant to the United Kingdom, see Table 29.1.

In the developed world, urothelial cancer, more commonly referred to as transitional cell cancer, comprises 90% of these cases,



Figure 29.14 This patient has bladder outflow obstruction secondary to prostatic hyperplasia. The bladder wall is globally hypertrophied, with trabeculation, as a consequence, ensuring that the intravesical pressure is sufficient for the bladder to empty through the compromised urethra.

Table 29.1 Number of deaths from bladder cancer in the United Kingdom, 2006

	England	Wales	Scotland	N. Ireland	UK
Males	2675	165	281	56	3,177
Females	1371	84	144	37	1,636
Persons	4046	249	425	93	4,813

Source: http://info.cancerresearchuk.org/cancerstats/types/bladder/mortality/.

Causes of outflow obstruction

Mechanical
- Prostate – mostly benign hyperplasia, occasionally prostate cancer
- Urethral strictures
- Bladder neck stenosis

Functional
- Bladder neck dyssynergia
- Anticholinergics and other drugs
- Peripheral neuropathy – diabetes mellitus, spinal cord/cauda equine disease
- Central nervous system – multiple sclerosis, trauma, tumours

with squamous (5%) and adenocarcinoma (2%) forms less common. Worldwide, squamous cell cancer (SCC) of the bladder predominates (75%), being associated with chronic infection and inflammation – and associated with bladder infection by *Schistosoma haematobium* in the tropics. In Europe, SCC is again a consequence of long-term inflammation associated with bladder catheters and/or stones. Urothelial cancer – the subtype most commonly encountered in Europe – has a strong link with cigarette smoking, although occupational exposure to arylamines has been implicated in the past.[52]

The remaining primary malignancies of the bladder are non-urothelial: non-small cell cancer or muscle tumours (the majority leiomyosarcoma or in children rhabdomyosarcoma). Primary lymphoma (submucosal origin) and metastases to the bladder from alternative primary tumours are rare. Local invasion from prostate cancer or from gynaecological or bowel cancer is well recognised.

Tumours may be sessile, papillary or nodular. Not uncommonly, there is involvement of more than one site. The detection of the sessile tumours remains in the domain of the urologist, at cystoscopy. Malignancies that stand proud of the lumen can be detected with imaging, and here ultrasound plays a pivotal role. Approximately 40–45% of bladder tumours show muscle invasion at presentation and this can also be inferred by imaging.

Tumour detection

The accuracy of transabdominal ultrasound in detecting superficial bladder tumours was assessed more than 20 years ago,[53,54] with a reported detection rate of 50–94% and false positive rate of 11% at that time. The detection rate for tumours greater than 5 mm (82%) was unsurprisingly far better than for tumours less than 5 mm (38%). In fact, the place of ultrasound of the bladder in cancer detection became firmly established more from clinical and cost drivers than from somewhat artificial audits of ultrasound detection rates. The majority of patients with bladder cancer present with haematuria,[52] and the first-line investigations for haematuria are widely accepted nowadays as ultrasound of the urinary tract and cystoscopy, with computed tomography (CT), notably CT urography (having replaced intravenous urography), a second-line investigation. Strategies using cystoscopy or ultrasound as the initial diagnostic test have repeatedly been shown to minimise cost and morbidity while maintaining diagnostic accuracy.[55–57]

By the beginning of this millennium, detection of bladder cancer by transvesical ultrasound in patients with haematuria, has reported sensitivity of 63%, and specificity of 99%. These figures come from a series of just over 1000 patients in whom 83% had macroscopic haematuria, 15% had microscopic haematuria and 2% had unspecified haematuria.[58]

Patients with bladder cancer may also present, in the absence of haematuria, with lower urinary tract symptoms. This group, too, is routinely sent for ultrasound and therefore by default, ultrasound is frequently the first investigation offered to a patient with bladder cancer: the symptoms appropriately dictate the best investigation and ultrasound provides the opportunity to detect the tumour.

The detection rate of bladder cancer by ultrasound depends on size of tumour, and on location. Detection by ultrasound may fall to less than 50% for tumours on the anterior and inferior bladder wall,[59] and generally anterior wall tumours are poorly detected: the near-field images are less conspicuous being usually adjacent to more echogenic material in the pre-vesical space, as opposed to the stark contrast of a soft tissue echogenic lesion on the side or posterior wall, outlined by poorly echogenic urine (Figs 29.15 and 29.16).

Needless to say, with variable detection rates and a weakness of ultrasound to note anterior wall lesions, the ultrasound examination should always be complemented by cystoscopy. In addition to improving evaluation of the entire bladder lumen, cystoscopy can confirm the findings, allow histological sampling, and permit examination of the urothelium for sessile lesions or carcinoma in situ which ultrasound cannot detect.[59,60] Most bladder transitional cell tumours are superficial, i.e. there is no muscle invasion (Ta, T1 or carcinoma in situ). A recently published small prospective study suggests that virtual cystoscopy (reformatted thin slice CT images) is nearly as accurate as conventional cystoscopy, being notably better than transabdominal ultrasound in the detection of polypoid tumours, or tumours less than 1 cm in diameter.[61] This resonates with a study of 69 patients with urinary bladder

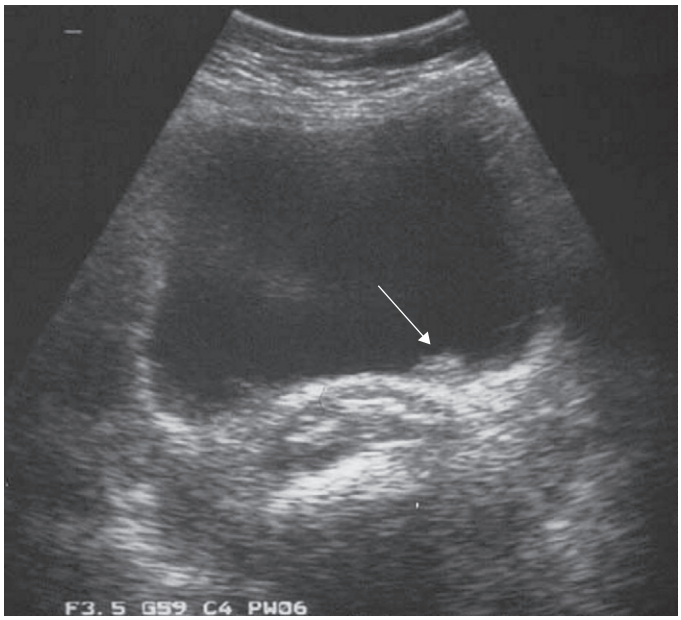


Figure 29.15 **Sessile tumour** lies on the posterior bladder wall to the left of the midline (white arrow).

TNM staging

- CIS – carcinoma in situ, high-grade dysplasia, confined to the epithelium
- Tx – primary tumor cannot be evaluated
- T0 – no primary tumour
- Ta – papillary tumour confined to the epithelium
- T1 – tumour invasion into the lamina propria
  - T1a – superficial submucosal invasion
  - T1b – deep submucosal invasion
- T2 – tumour invasion into the muscularis propria
  - T2a – superficial muscle affected
  - T2b – deep muscle affected
- T3 – tumour involvement of the perivesical fat
  - T3a – microscopic perivesical invasion
  - T3b – macroscopic invasion
- T4 – tumour involvement of adjacent organs such as prostate, rectum or pelvic side wall
  - T4a – prostate, uterus or vagina invaded
  - T4b – pelvic side wall or abdominal wall invaded
- N+ – lymph node metastasis
- M+ – metastasis

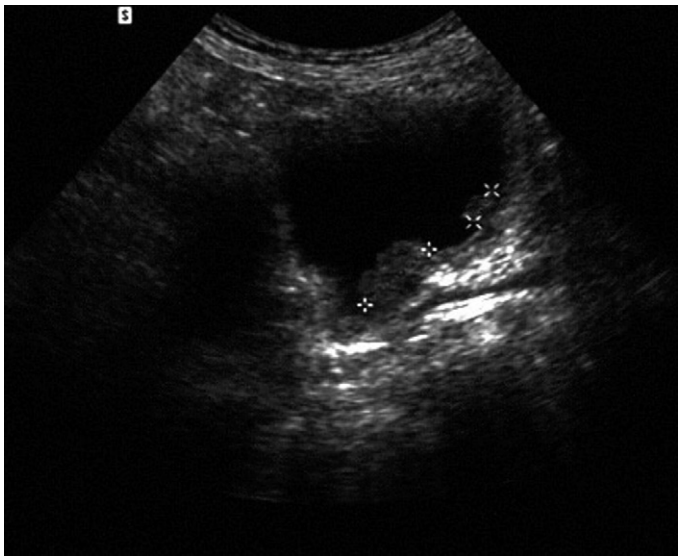


Figure 29.16 **Urothelial tumour.** Ultrasound is not limited, and may, as in this case, detect multiple sites of urothelial tumour within the bladder. Tumour deposits on the posterior wall are more conspicuous than those on the anterior wall.

cancer using 3D ultrasound and ultrasound angiography assessed resistance index and tumour vascularisation.[62] The paper quotes an impressive 100% detection of T1 tumours on 3D ultrasound, 87% for T2 disease, with an overall detection rate of 96%.

The promise of 3D ultrasound, volumetric scans and virtual cystoscopy using ultrasound volumes offered by the technological advances in transducer design and by the breath-taking blossoming of computer-aided reconstruction, however, is beguiling. For all the attraction of avoiding the intrusiveness of cystoscopy, it is difficult to foresee the day when direct visualisation of the bladder mucosa will ever be rivalled by ultrasound. There have also been technological advances in cystoscope design to rival those in ultrasound, making cystoscopy a much less uncomfortable experience for patients than previously. A more sanguine advocate might champion 3D ultrasound as a tool in the differential diagnosis of bladder lesions in patients with haematuria.[63] Three-dimensional technologies seem superior to conventional 2D imaging when a wider gamut of pathologies in addition to tumours, e.g. diverticula, mucosal folds simulating disease, and prostatic in-growth, are considered. In the 42 patients presented, 3D ultrasound detected all bladder cancers seen at cystoscopy, as well correctly 'labelling' 70% of the non-malignant abnormalities also seen on cystoscopy.[63] With the imminent advent of volumetric scanning by most manufacturers, the number of cystoscopies in haematuria of benign cause may diminish.

Staging bladder cancer

The TNM classification is used for bladder cancer. Five-year survival for T1 disease is between 80% and 100% and for T2, approximately 65–80%. The crucial distinction is between T3a and T3b disease: surgical cure is effectively impossible in the latter group with 5-year survival typically 30–40%. Imaging is vital in assisting in establishing the T stage, and cross-sectional imaging, usually CT, in gauging the N and M stage.

Transabdominal ultrasound has a reported accuracy of 79–84%.[54,64] The loss of accuracy is not due to lack of sensitivity, but rather because specificity is limited because ultrasound cannot distinguish tumour from focal cystitis, asymmetric muscle hypertrophy or from haematoma (Figs 29.17 and 29.18).

Preoperative staging of bladder masses by 3D ultrasound has been compared with histopathology staging of the transurethral resection material or the cystectomy specimens.[65] In 63 patients, concordance was: pTa 66%, pT1 83%, T2 or worse, 100%. The hope is that 3D ultrasound may benefit in identifying patients whose stage is worse than T1, notably in patients where cystoscopic biopsies do not contain muscle, and the T stage cannot be determined.

In the early 1980s, a rush of papers proposed that transurethral ultrasound was the method of choice for (T) staging bladder cancer,[63,66–68] with acknowledgement that Ta and T1 disease tended to be over-staged. Some authors went as far as concluding that transurethral ultrasound is 'particularly helpful in the evaluation of

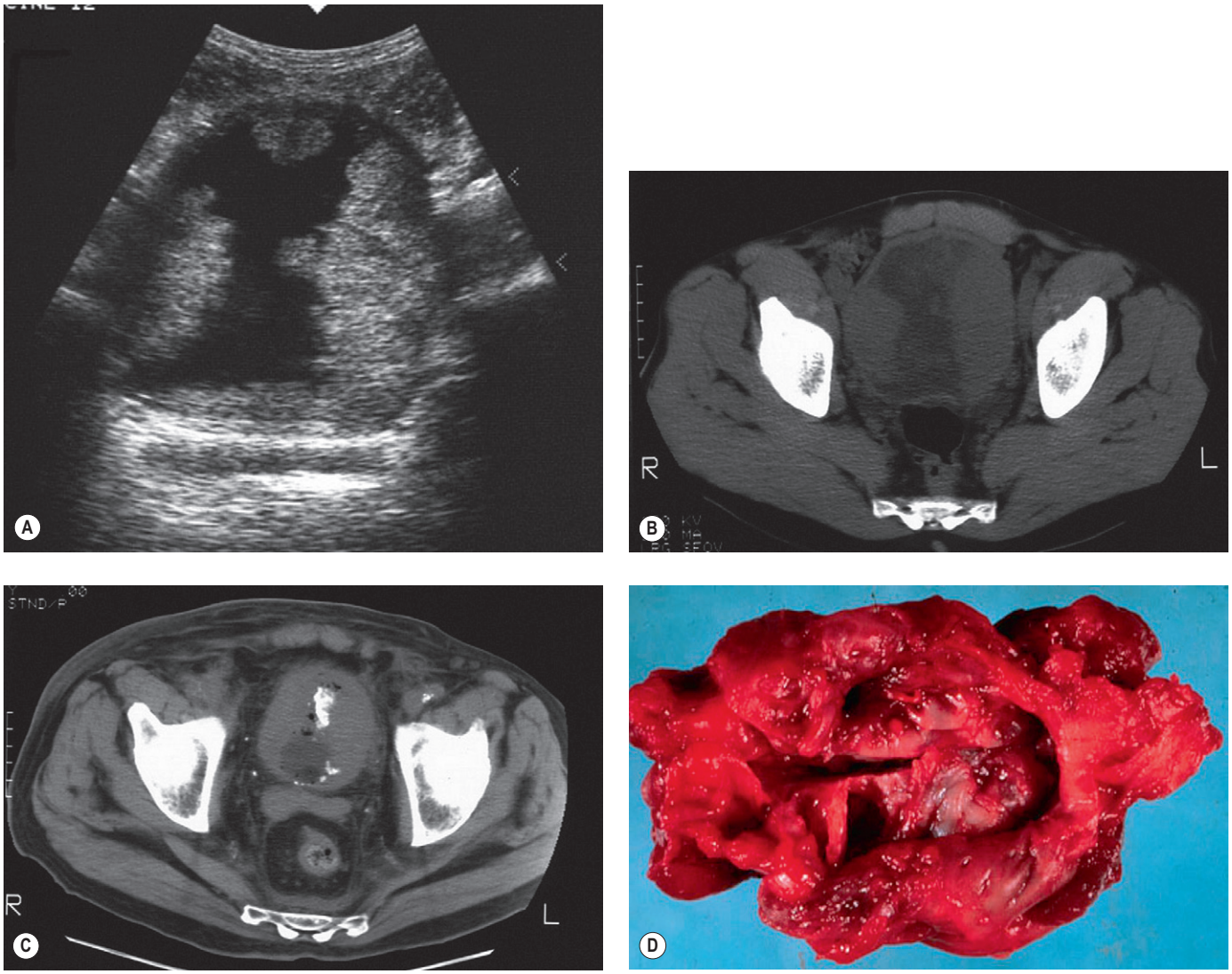


Figure 29.17 **Tumour staging. A:** Extensive bladder cancer on the lateral and anterior walls. On the left lateral wall, ultrasound suggests muscle invasion (T2 at least), but it is unlikely that there is macroscopic extension into the perivesical fat (T3). **B:** Non-enhanced CT in the same patient confirms T2 rather than T3 disease. **C:** Compare with the CT in another patient (urographic phase, contrast in bladder, with Foley balloon catheter); here there is stranding of the perivesical fat at 4 o'clock indicating T3 disease. **D:** Post-cystectomy specimen, bladder opened, showing the large malignancy on the lateral wall.

more deeply infiltrating tumours [and] intravesical sonography constitutes a major extension of the diagnostic spectrum for T classification of bladder carcinoma'.[69] By 1991, the vogue for transurethral scanning had waned.[70]

With further advances in technology, endoluminal ultrasonography is being evaluated with comparison of differing radiological staging to pathological staging. The endoluminal diagnostic accuracy of 84% compared favourably with that of CT (44%) and even MRI (82%).[71] An earlier paper in which intravesical ultrasonic scanning was performed in 74 patients with 84 bladder tumours quotes an accuracy of T staging by intravesical ultrasound as 94% of the 82 visible tumours.[72] A second paper from Japan is more guarded about high-frequency endoluminal ultrasound (using 20 MHz miniature transducers) because of their limited penetration.[73] Moreover, there has been little subsequently published about endoluminal ultrasonography, with a reference in 2005 to a new cystofibrescope incorporating ultrasound.[74]

Tumour follow-up

A central tenet in managing patients with bladder transitional cell cancer (and indeed in patients with TCC of the upper tracts) is that (1) there is a risk of TCC developing elsewhere in the urogenital tract and (2) superficial tumours treated locally are likely to recur. There is, therefore, an absolute need to enrol the patients into a surveillance programme.

As stated above, most bladder cancer is superficial at presentation, and is treated by resection and local chemotherapy (mitomycin or BCG instillation). In other words, most patients with TCC do not need cystectomy but conversely do need regular check cystoscopy. The follow-up regimen must take into account the patient's general state of health, as well as the tumour stage and grade and number. These latter parameters are used to stratify patients into high risk of local muscle invasion (15–25% of patients) and low risk of invasion.[52]

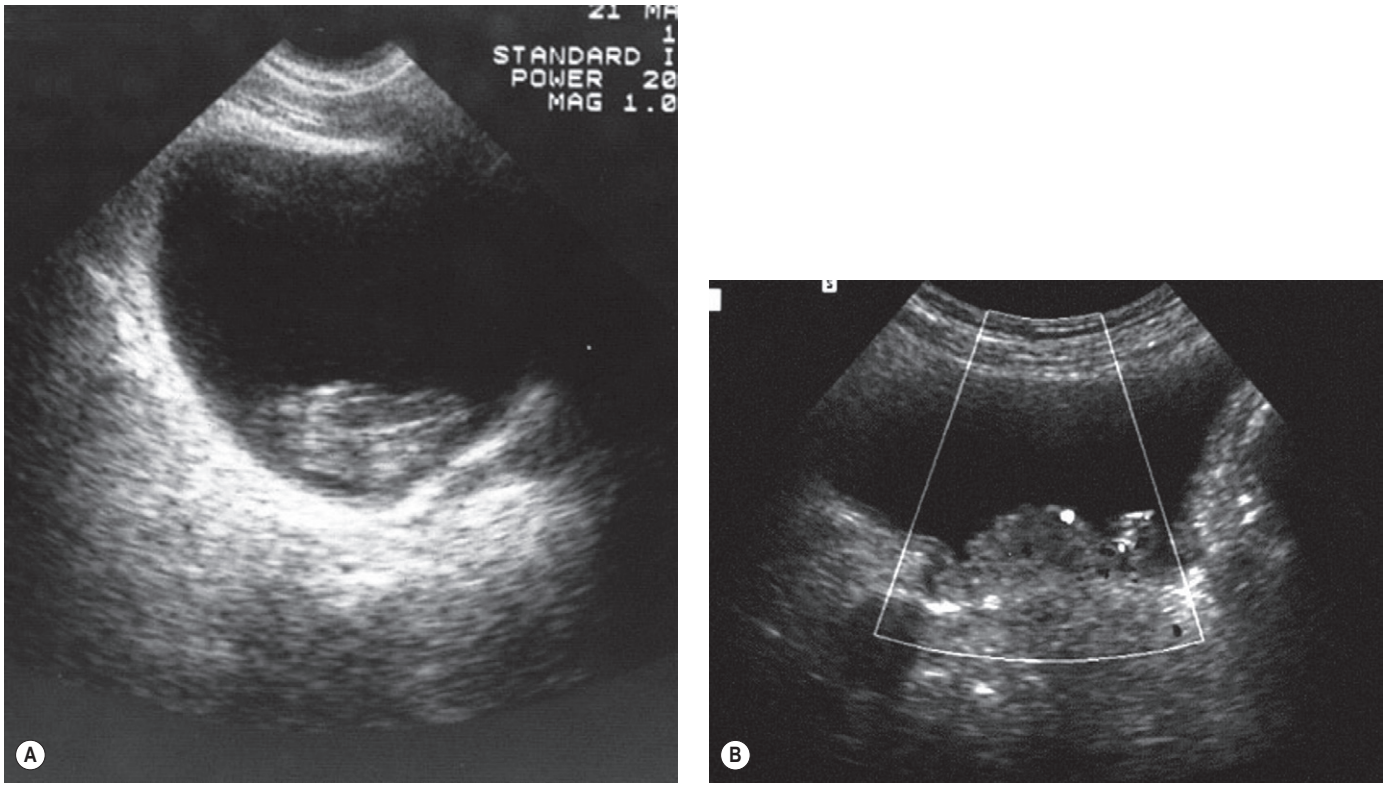


Figure 29.18 **Tumour staging: low specificity. A:** Mass in bladder in patient with macroscopic haematuria. Cystoscopy found bladder clot, but no tumour. **B:** Use of colour duplex imaging shows flow in the periphery of a mass in another patient: the flow would not be seen in blood clot, and cystoscopy confirmed a mass adjacent to the trigone.

Once a patient has been classified as being at low risk of invasion – G1 disease, stage T1 or less – or has been shown on repeat cystoscopy to have minimal episodes of recurrence, ultrasound can be utilised to reduce the frequency of cystoscopic surveillance.[53,75,76] Dershaw and Scher reported a small cohort of 23 patients with known TCC of the bladder.[77] On 58 serial transabdominal scans, ultrasound correctly identified change (growth and regression) in 83% of cases, being unreliable when interval surgery had occurred. Ultrasound was likewise shown to be limited in distinguishing oedema from sessile recurrence. The key observation from the study is that in no case in which the bladder wall was normal on sonography was tumour found (Fig. 29.19). Others have proposed combined transrectal and transabdominal ultrasound with or without cytology as an alternative to repeated cystoscopy.[78,79] Ultrasound was generally preferred over rigid cystoscopy, although the transrectal probe was less popular![78] When combined with cytology in a study of 125 patients, detection rate of recurrent tumours was 93%, and 97% of the patients with recurrent tumour would have been referred for cystoscopy, and 3 patients would have mistakenly been sent for cystoscopy (false positive rate 2–3%).[79] The authors concluded that 'combination ultrasound and cytology may be a satisfactory alternative to check cystoscopy in certain categories of bladder tumours'. A Scandinavian paper[80] is more explicit, advocating transabdominal ultrasonic scanning in place of routine cystoscopy (after the first check cystoscopy) in patients with low-grade Ta disease which shows no progression after the primary transurethral treatment with cystoscopy reserved for patients with frequently recurring urinary bladder tumours, tumours of high grade regardless of T stage, patients with T1 disease regardless of grade and those with carcinoma in situ.

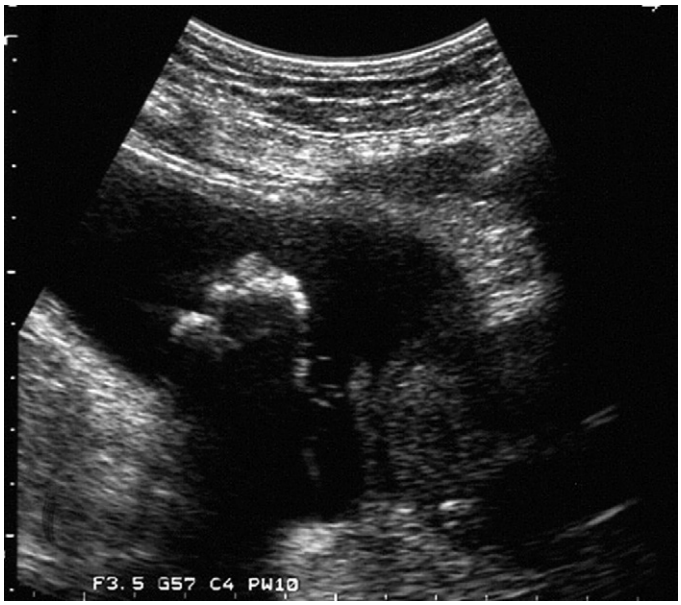


Figure 29.19 **During ultrasound surveillance in a patient with G1pTa bladder cancer** (transitional cell), following a course of intravesical chemotherapy (BCG), recurrent polypoid disease may be noted. In this case, there is calcification within the fronds of the recurrent tumour, ascribed to inflammatory reaction to the BCG. This manifests as an echogenic rim where the tumour projects into the bladder lumen. Recurrence was confirmed at follow-up cystoscopy.

Invasion of the bladder from adjacent tumours

Local invasion of the bladder may be from the prostate in men, cervix or uterus in women, or the rectum. Urothelial cancer

developing in the urethra is relatively rare, and when there is contiguous TCC between the bladder base and proximal urethra, usually the primary will have developed in the bladder; the distinction, in any case, is academic.

Transrectal ultrasound (TRUS) is the primary imaging modality of choice for assessing prostate tumours that may have invaded the bladder base. Magnetic resonance imaging (MRI) has an important role in secondary investigation of these low pelvic masses. The provenance of the primary (urothelial tumour or prostatic adenocarcinoma) is established by transurethral resection or transrectal ultrasound-guided biopsy, with staining for urothelial tumour markers and for prostate-specific antigen (PSA). In a similar vein, transvaginal ultrasound (TVUS), supplemented if necessary by MRI, is the best way to evaluate local invasion of the bladder by cancer of the cervix.[81] The parameters to be noted include morphology and bulk of the cervical tumour, thickening and echogenicity of the bladder wall, and mobility of the cervix over the lower bladder wall. This last feature is feasible because ultrasound is a real-time examination, unlike MRI. MRI, on the other hand, is superior in elucidating tumour morphology and size. On both TVUS and MRI, progressive involvement of the bladder is apparent as: disruption of the endopelvic fascia, focal mural thickening, changes in the bladder mucosa and interruption of the entire bladder wall.[81]

Transvesical ultrasound is accurate in detecting posterior bladder wall invasion by rectal cancer, but contrast-enhanced CT and contrast-enhanced MRI are universally acknowledged as the gold standard in imaging rectal cancer, and in assessing changes in the posterior pelvis (Fig. 29.20).

Diverticula of the bladder

A diverticulum (plural: diverticula) is an out-pouching of the mucous and submucous membranes through the muscle wall. They result from prolonged elevation of the intravesical pressure. Their most common associations are:

- benign prostatic hypertrophy
- urethral stricture
- neuropathic (high pressure) bladder.

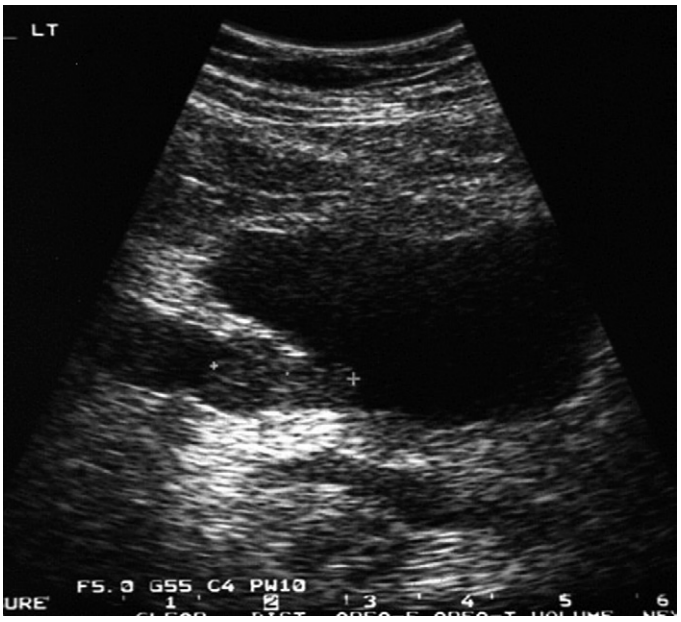


Figure 29.20 Tumour (urothelial cancer) in the distal left ureter detected on transabdominal ultrasound through a full bladder. Unsurprisingly, there is dilatation of the ureter above the tumour. The 53-year-old patient presented with microscopic haematuria, and underwent standard first-line investigations, including renal tract ultrasound.

Having no muscle coat, diverticula do not empty reliably during micturition. They therefore predispose to infection, secondary to the urinary stasis. Stones are also liable to become trapped in a diverticulum. Bladder cancer can, of course, develop with the mucosa of a diverticulum, and because of the potential for local chronic inflammation from infection or stone entrapment, it is not unreasonable to proffer that squamous cell cancer may have a higher incidence in bladder diverticula than in normal bladder mucosa.

Ultrasound is an ideal modality to detect bladder diverticula. Real-time scanning in limitless planes means that the communication between the bladder and the 'para-vesical cystic collection' can be located, the so-called neck of the diverticulum (Fig. 29.21A). Moreover, scanning post void, the degree of urinary retention within the diverticulum can be readily assessed. Endovaginal views, and colour Doppler interrogation can also assist in diagnosing bladder diverticula, specifically in distinguishing it from other pelvic cystic masses.[82] Once identified, ultrasound will determine whether there is debris or stones within the diverticulum, and will prompt the clinician to perform directed cystoscopy if focal wall thickening is suggested by ultrasound (Fig. 29.21B). Ultrasound is also useful in suggesting that a diverticulum may contain tumour.[83]

Fistula to the bladder

A fistula is defined as an abnormal communication between two epithelialised surfaces. Fistulae to the bladder can therefore be to the vagina or uterine cavity in women, or to the bowel or abdominal wall in men or women. A fistula is not, in itself, pathology: it may be as a consequence of malignancy, infection, trauma, including iatrogenic trauma, or inflammatory conditions (Table 29.2).

The clinical pointers that a patient may have a bladder fistula are offensive urine/faeculent urine, pneumaturia, or, in fistulation to the female genital tract, constant wetness/passing fluid per vagina. Pneumaturia or gas in the urine is a very specific finding, strongly suggestive of a fistula between the bowel and bladder. It is a symptom that needs to be specifically enquired of when a fistula is suspected clinically. In the case of fistula to the skin, the symptoms and signs will be self-evident. The ultrasound findings in fistulation to the bladder include (when the fistula is to bowel) echogenic gas in the anterior part of the lumen, casting a dirty shadow and severely attenuating the beam, limiting evaluation of the deeper part of the bladder.[84] When the posterior bladder is visualised, the urine will be echogenic. The responsible pathology may be visible – a tumour mass or a diverticular abscess, for example.

The ultrasound findings of fistula between bladder and the female genital tract are less dramatic.[85]TVUS may locate the tract to the vagina, and the presence of fluid within the upper vagina may also be a clue.[86,87] A report from Munich assessing the efficacy of ultrasound contrast media in the diagnosis of vesico-vaginal fistulae concluded that observation of a jet through the bladder wall reliably pinpointed the fistula in over 90% of cases,[88] stressing that the examination is less invasive than cystoscopy and the lack of radiation exposure.

Vesico-uterine fistulae are rare, usually secondary to gynaecological or obstetric procedures. MRI is the method of choice in the diagnosis and preoperative assessment of these fistulae, but ultrasound may detect echogenic bubbles in the tract between the bladder and uterus.[89] Sonography is also useful by scanning with a full and empty bladder, demonstrating a focal area of proximity between bladder and uterus regardless of the degree of bladder filling.

PATHOLOGY OUTSIDE THE BLADDER

Symmetrical compression of the bladder, associated with elevation of the bladder floor, has a striking appearance on ultrasound, with

Table 29.2 Fistulae to bladder by site and aetiology

Fistula to	Malignancy	Inflammation	Trauma	Other
Large bowel	Cancer rectum or sigmoid colon; cancer bladder	Diverticulitis Crohn's disease	Gun shot (endoscopy)	Post radiotherapy Post surgery
Small bowel	Cancer small bowel; bladder cancer	Crohn's disease	Penetrating injury	(Post radiotherapy)
Vagina	Cancer cervix, cancer vagina, cancer bladder			Post radiotherapy
Uterus	Endometrial cancer, bladder cancer		Post caesarean section Penetrating injury	Post radiotherapy
Skin	(Bladder cancer)	Subcutaneous infection	Penetrating injury	Post radiotherapy

Brackets () denote theoretical aetiology rarely if ever encountered in clinical practice.

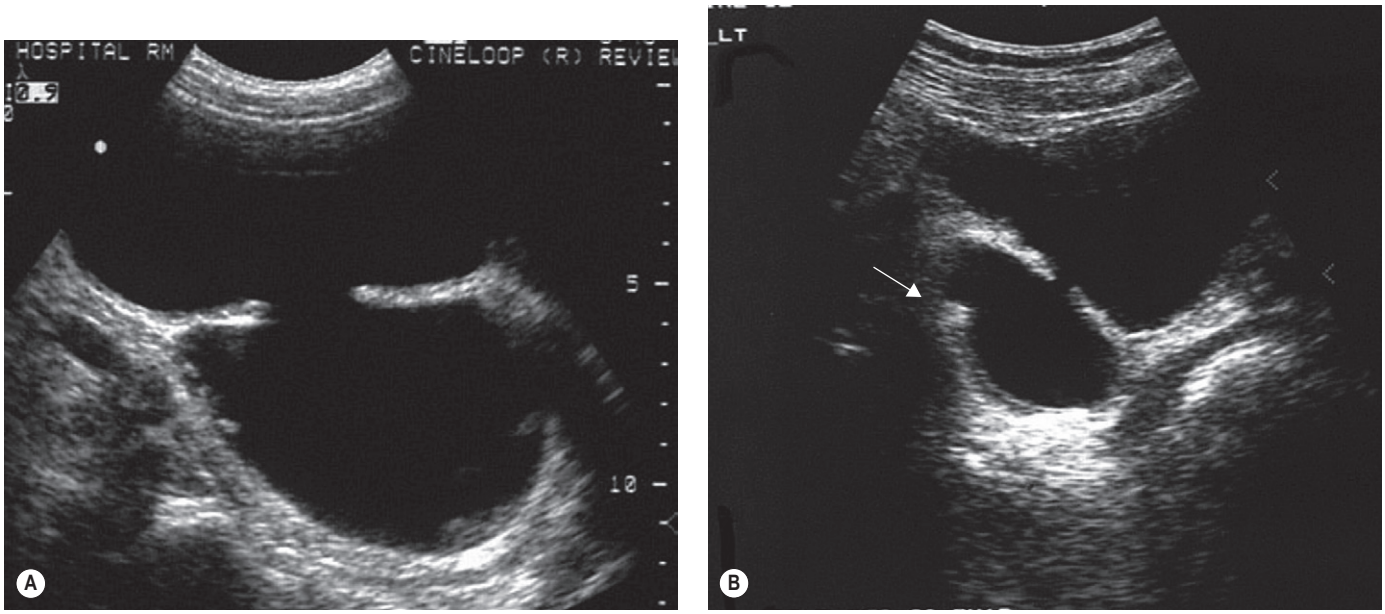


Figure 29.21 Bladder diverticula. A: Wide-necked posterior wall bladder diverticulum containing sludge and debris. **B:** Bladder diverticulum complicated by small echogenic stone.

the bladder taking on the shape of an inverted fir cone. The differential for this appearance is easy to resolve with clinical history: in the well patient, almost always male, *pelvic lipomatosis* is suspected; following trauma, the diagnosis is *pelvic haematoma;* when there is a longstanding history of LUTS, consider *chronic cystitis.*

Extrinsic masses

Ultrasound is very sensitive in detecting physiological and pathological enlargement of the solid pelvic organs (Fig. 29.22). Thus, the gravid uterus or a subserosal leiomyoma can be detected readily, and the extrinsic mass effect on the bladder assessed. The commonest cause of pressure on the bladder from an adjacent organ is benign prostatic hypertrophy. In addition to possible bladder outflow obstruction, with wall thickening, the median lobe of the prostate may enlarge and indent the base of the bladder.

Malignant involvement of the bladder can be seen in cancers of the rectosigmoid, when the invasion may be complicated by a fistula. Loss of the normal separation between the rectum and posterior bladder wall, coupled with a soft tissue mass and air in the bladder (manifest by an echogenic layer in the non-dependent part of the lumen which casts a 'dirty' shadow), are highly suggestive



Figure 29.22 Extrinsic compression of the posterolateral bladder wall by an enlarged ovary in a patient with confirmed polycystic ovarian syndrome.

of a gastrointestinal malignancy invading the bladder. The same findings can be seen in local invasion of the bowel by a bladder mass, but this is much less commonly encountered than bowel invading bladder.

Prostate cancer can invade the bladder base, frequently progressively occluding the ureteric orifices. In these cases, the patient may present in acute renal failure with bilateral asymmetric hydronephrosis. In women, cervical cancer can behave in the same way. When the bladder base is involved, the ultrasound findings include ureteric and pelvicaliceal dilation, inferior bladder wall focal thickening and a soft tissue mass in the lower pelvis. Transrectal ultrasound for prostate cancer and transvaginal ultrasound for cervical cancer are more sensitive in demonstrating the primary origin of disease and the invasive soft tissue mass than transvesical imaging.

SPECIFIC CONDITIONS

Inflammatory/infective

Cystitis has several causes. Ultrasound cannot distinguish between the different aetiologies. Indeed, the bladder usually appears normal in acute cystitis; and when there is abnormality, the appearances are non-specific, being seen also in patients with tumour. In short, the clinical diagnosis of cystitis is confirmed by urine analysis and cystoscopy.[90]

There are a number of features that can be seen in cystitis that can suggest the diagnosis:

- Calcification in the bladder wall – this is most commonly an indicator of schistosomiasis infection, and can also be seen in tuberculosis or following radiation.
- Gas in the bladder wall, often associated with gas in the lumen: this is a significant finding with a relatively grave prognosis, signifying emphysematous cystitis. The condition is almost exclusive to those with a long history of diabetes mellitus.
- Multiple echoes within the urine, especially in the clinical setting of a patient with signs of infection, suggest infective cystitis or even pyocystitis.
- In chronic cystitis, the bladder wall becomes thickened, bladder capacity is reduced and the detrusor irritable.
- Infection in adjacent organs can result in sympathetic cystitis in the bladder: ultrasound may reveal an inflamed appendix or myotubular disease. If there is sigmoid diverticulitis, a fistula may develop in which case the ultrasound examination may reveal gas in the bladder, and debris/faeces lying in the dependent portion of the bladder.
- It is important to stress that the findings are non-specific, and ultrasound must be interpreted in the wider clinical picture, as malignancy and cystitis have a broad overlap on imaging.[91]

Causes of cystitis

Infective
- Viral
- Fungal
- Protozoal – schistosomiasis
- Tuberculosis
- Malacoplakia

Iatrogenic
- Post radiotherapy or chemotherapy
- Medications
- Catheters

Other
- Vasculitis
- Eosinophilic
- Interstitial
- Granulomatous

Emphysematous
- Gangrenous
- Empyema

Pregnancy-related pathology of the bladder

The most important pregnancy-related problem in the urinary tract, by an order of magnitude, is infection (UTI). This is mostly managed without the need for imaging. In some cases, renal tract ultrasound is indicated, mostly concentrating on the upper tracts, seeking out stones, undue hydronephrosis or complications of the UTI. Bladder ultrasound is generally not critical in this setting.

There are two pathologies related to pregnancy and birth that can affect the bladder. These are:

1. Fistula between the bladder and the uterus post caesarean section. Ultrasound in this case may hint at the problem, with the posterior wall of the uterus adherent to the bladder regardless of the time of filling of the bladder. A small convexity of the bladder wall where it is closely apposed to the uterus can sometimes be detected. Nevertheless, the diagnosis is reliant on cystoscopy, cystography or sagittal T2 MRI.
2. Placenta percreta.

Placenta percreta

Rarely, the placenta invades through the decidual lining of the uterine cavity, into the uterine muscle (placenta accreta). More rarely still, trophoblastic tissues penetrate the serosa of the uterus and may extend directly into the bladder.[92–94] With the ubiquitous use of prenatal ultrasound, this uncommon but potentially fatal condition may be detected by ultrasound, especially as 3D ultrasound becomes more commonplace.[92,95,96]

Endometriosis of the bladder

Occasionally the endometrial glands and stroma can implant in the urinary bladder wall. The patient will then present with cyclical haematuria, coinciding with menstruation. Bladder wall endometriomas are usually hyperechoic, with internal septations.[97–99] While clinical presentation and ultrasound findings may suggest the diagnosis, the diagnosis is made by cystoscopy and biopsy.[100]

Postoperative

Conduits and partial resections

There are several operations to augment the urinary bladder, either in patients with low capacity bladders, or as part of neo-bladder formation following cystectomy. In the cystectomised patient, the neo-bladder may be formed by attaching a pouch fashioned from bowel onto the trigone, resulting in a functional unit with preserved micturition. Alternatively, a pouch may be drained via a conduit to the abdominal wall, the stoma being 'continent' (drained by intermittent catheterisation) or 'incontinent' (urostomy and stoma bag). Regardless of the surgical variance, the augmented bladder tends to have an irregular shape, with irregular, fronded mucosal membrane forming the wall.[101] Because of the irregularity, ultrasound is mostly limited to estimating post-micturition volumes, gauging roughly the capacity of the neo-bladder, and looking for stones within the lumen.[102]

Types of bladder trauma

Nature
- Penetrating injury: bullet or knife
- Iatrogenic
- Obstetric
  - Pressure necrosis: bladder neck – fistula
  - Caesarean section
- Puncture by bone spicule in pelvic fracture (road traffic accident, fall, riding or sporting injury, etc.)
- Radiation
- Spontaneous

Type
- Simple:
  - Intraperitoneal
  - Extraperitoneal
  - Combined
- With urethral involvement
- With rectal involvement

Key points in the management of bladder trauma

- Injury to the lower urinary tract often as part of more widespread abdominal/pelvic trauma.
- The most important message is: avoid compounding the initial trauma with iatrogenic injury (injudicious passage of a urethral catheter).
- If the patient develops retention and a urethral injury cannot be excluded: insert suprapubic catheter.
- If the urethra is damaged, suprapubic catheterisation is indicated and definitive treatment of the urethra deferred for 6 or more weeks.
- Ultrasonography is not a routine investigation in the initial assessment of urethral injuries but can be useful in determining the position of pelvic haematoma and the high riding bladder, when a suprapubic catheter is indicated.
- In polytrauma, CT of the pelvis is usually available, and this can suggest with surprising accuracy the extent and type of urethral injury and bladder injury.
- The MRI suite is no place for the acute trauma patient.

Trauma

FAST (focused assessment with sonography in trauma) is widely practised in the Accident and Emergency Departments in Europe and Australasia. In the acute setting, the scan sets out to detect free fluid in the abdomen. The fluid may be due to internal bleeding or it may indicate rupture of a viscus, including, of course, the bladder.

Isolated bladder trauma is rare, and usually iatrogenic in aetiology. As such, it is commonly recognised at the time of injury, and imaging is not required. When the bladder is injured, it is more commonly in conjunction with more widespread trauma, frequently associated with bony and soft tissue pelvic damage. In these circumstances, current practice would be to resuscitate the patient and undertake emergency contrast-enhanced CT. The role of ultrasound is limited in this setting.

Ultrasound, nevertheless, does, indirectly have a bearing on bladder trauma management. For example, when there is intraperitoneal rupture of the bladder, as may occur when the distended bladder is compressed, typically in a road traffic accident, the urine will escape from a rent in the bladder dome, and manifest as free fluid on the FAST scan.

Ultrasound may also be invaluable in the acute setting when there is suspected urethral injury, specifically when urethral disruption is suspected. The examination may confirm a bladder containing urine in spite of the patient's inability to void, and the bladder may be unusually high in the pelvis, having lost its anchor to the urogenital diaphragm. The urine may be echogenic, indicating blood within the lumen, but in an isolated urethral injury, the urine will be anechoic. Naturally, the presence of echogenic urine in the setting of trauma suggests possible injury to the kidneys or ureters, alerting the clinical team without the need to examine the urine for haematuria. When urethral or bladder injury is suspected, the acute management is insertion of a Foley balloon catheter, and if there is urethral tear, this should be via a suprapubic approach, best performed under ultrasound guidance. See 'Procedures' below.

Key points in bladder trauma are presented in the following boxes.

Patterns of bladder rupture following trauma

- Peritoneum covers superior surface.
- Anterosuperior perforation: urine into peritoneal cavity, or Retzius space or both.
- Posterosuperior perforation: peritoneal cavity or retroperitoneum or both.
- Base supported by fascia and urogenital diaphragm and pelvic floor muscles.
- Superior fascia prevents leak into pelvis.
- Inferior fascia (melding to Colles' and Scarpa's fascia and dartos muscle) prevents leak into perineum.
- In intraperitoneal rupture, pelvic fracture seen in 75%.
- In extraperitoneal rupture, pelvic fracture seen in 99%.
- Intraperitoneal combined with extraperitoneal rupture in 5%.

PROCEDURES

Suprapubic catheterisation

Suprapubic catheterisation has been alluded to in the previous section. In addition to its use in the management of pelvic/urethral trauma, it may be necessary in acute urinary retention when per-urethral catheter passage is impossible – for example when there is a tight urethral stricture or a false passage. Traditionally, suprapubic catheterisation is performed by the urology middle grade, without the assistance of real-time imaging. As with all modern medical practice, there has been a drift in the past few years to requesting radiological input with real-time ultrasound in placing the catheter.

The ultrasound readily identifies the bladder, confirms it is sufficiently full, can predict the depth of the tract, can identify any vessels in the skin or subcutaneous tissues (with colour flow imaging), and can confirm when the trocar has penetrated the anterior bladder wall.

Urinary bladder catheter balloon puncture

Occasionally, removal of a Foley bladder catheter is impossible because the retaining balloon will not deflate. Almost invariably the balloon has inadvertently been inflated with saline rather than water, and the solution has reacted with the rubber to crystallise. In these cases, ultrasound is invaluable, being used in real-time to guide a 22-gauge spinal needle transcutaneously through the bladder wall and into the balloon. The balloon usually has to be punctured several times, because the problem is not so much with the rubber membrane but with the 'congealed' saline contents. The operator can see when the retaining balloon has burst, and only then withdraw the catheter, avoiding undue trauma to the bladder base and urethra (or to the bladder wall and perivesical tissues in the case of a suprapubic catheter).

REFERENCES

1. Chess-Williams R. Muscarinic receptors of the urinary bladder: detrusor, urothelial and prejunctional. Auton Autacoid Pharmacol 2002;22:133–145.
2. Jequier S, Paltiel H, Lafortune M. Ureterovesical jets in infants and children: duplex and color Doppler US studies. Radiology 1990;175:349–353.
3. Cox IH, Erickson SJ, Foley WD, Dewire DM. Ureteric jets: evaluation of normal flow dynamics with color Doppler sonography. AJR Am J Roentgenol 1992;158:1051–1055.
4. Cvitkovic KA, Brkljacic B, Rados M, Galesic K. Doppler visualization of ureteric jets in unilateral hydronephrosis in children and adolescents. Eur J Radiol 2001;39:209–214.
5. de Bessa Júnior J, Dénes F, Chammas M, et al. Diagnostic accuracy of color Doppler sonographic study of the ureteric jets in evaluation of hydronephrosis. J Pediatr Urol 2008;4:113–117.
6. Patel U, Kellett MJ. Ureteric drainage and peristalsis after stenting studied using colour Doppler ultrasound. Br J Urol 1996;77: 530–535.
7. Blomley MJ, Ramsey CM, Cosgrove DO, et al. The ureteric jet index: a novel measure of divided renal function. Clin Radiol 1997;52:771–774.
8. Hol M, van Bolhuis C, Vierhout ME. Vaginal ultrasound studies of bladder neck mobility. Br J Obstet Gynaecol 1995;102:47–53.
9. Mouritsen L, Strandberg C, Frimodt-Moller C. Bladder neck anatomy and mobility: effect of vaginal ultrasound probe. Br J Urol 1994;74:749–752.
10. Huang WC, Yang JM. Bladder neck funneling on ultrasound cystourethrography in primary stress urinary incontinence: a sign associated with urethral hypermobility and intrinsic sphincter deficiency. Urology 2003;61:936–941.
11. Granberg S, Wikland M, Norstrom A. Endovaginal ultrasound scanning to identify bladder tumors as the source of vaginal bleeding in postmenopausal women. Ultrasound Obstet Gynecol 1991;1:63–65.
12. Bartram U, Darge K. Harmonic versus conventional ultrasound imaging of the urinary tract in children. Pediatr Radiol 2005;35: 655–660.
13. Dana A, Hélénon O. [Urinary tract imaging: conventional radiology and ultrasound]. J Radiol 2004;85:159–168.
14. Cowper SE, Robin HS, Steinberg SM. Scleromyxoedema-like cutaneous diseases in renal dialysis patients. Lancet 2000;356:1000–1001.
15. Swaminathan S, Shah SV. New insights into nephrogenic systemic fibrosis. J Am Soc Nephrol 2007;18:2636–2643.
16. Aspelin P, Aubry P, Fransson SG. Nephrotoxic effects in high-risk patients undergoing angiography. N Engl J Med 2003;348:491–499.
17. Darge K, Zieger B, Rohrschneider W, et al. Contrast-enhanced harmonic imaging for the diagnosis of vesicoureteral reflux in pediatric patients. AJR Am J Roentgenol 2001;177:1411–1415.
18. Darge K, Moeller R-T, Trusen A, et al. Diagnosis of vesicoureteric reflux with low-dose contrast-enhanced harmonic ultrasound imaging. Pediatr Radiol 2005;35:73–78.
19. Chapple CR, Wein AJ, Abrams P, et al. Lower urinary tract symptoms revisited: a broader clinical perspective. Eur Urol 2008;54:563–569.
20. Poston GJ, Joseph AE, Riddle PR. The accuracy of ultrasound in the measurement of changes in bladder volume. Br J Urol 1983;55:361–363.
21. Marks LS, Dorey FJ, Macairan ML, et al. Three-dimensional ultrasound device for rapid determination of bladder volume. Urology 1997;50:341–348.
22. Rosseland LA, Bentsen G, Hopp E, et al. Monitoring urinary bladder volume and detecting post-operative urinary retention in children with an ultrasound scanner. Acta Anaesthesiol Scand 2005;49:1456–1459.
23. Hiraoka M, Tsukahara H, Tsuchida S, et al. Ultrasonographic evaluation of bladder volume in children. Pediatr Nephrol 1993;7:533–535.
24. Chan H. Noninvasive bladder volume measurement. J Neurosci Nurs 1993;25:309–312.
25. Nwosu CR, Khan KS, Chien PF, Honest MR. Is real-time ultrasonic bladder volume estimation reliable and valid? A systematic overview. Scand J Urol Nephrol 1998;32:325–330.
26. Ravichandran G, Fellows GJ. The accuracy of a hand-held real time ultrasound scanner for estimating bladder volume. Br J Urol 1983;55:25–27.
27. Maymon R, Gilboa S, Abramowicz JS, et al. Ultrasonic validation of residual bladder volume in postvaginal hysterectomy patients. Gynecol Obstet Invest 1991;31:226–230.
28. Dicuio M, Pomara G, Menchini Fabris F, et al. Measurements of urinary bladder volume: comparison of five ultrasound calculation methods in volunteers. Arch Ital Urol Androl 2005;77:60–62.
29. Yip SK, Sahota D, Chang AM. Determining the reliability of ultrasound measurements and the validity of the formulae for ultrasound estimation of postvoid residual bladder volume in postpartum women. Neurourol Urodyn 2003;22:255–260.
30. Hvarness H, Skjoldbye B, Jakobsen H. Urinary bladder volume measurements: comparison of three ultrasound calculation methods. Scand J Urol Nephrol 2002;36:177–181.
31. Hwang JY, Byun SS, Oh SJ, Kim HC. Novel algorithm for improving accuracy of ultrasound measurement of residual urine volume according to bladder shape. Urology 2004;64:887–891.
32. Barrington JW, Jones A, Robinson J, Stephenson TP. Estimation of bladder volume using portable ultrasound in clam enterocystoplasty patients. J Urol 1996;155:82–83.
33. Ghani KR, Pilcher J, Rowland D, et al. Portable ultrasonography and bladder volume accuracy – a comparative study using three-dimensional ultrasonography. Urology 2008;72:24–28.
34. Abdel-Fattah M, Barrington JW. The accuracy of Bardscan: a new tool for the measurement of the bladder volume. J Obstet Gynaecol 2005;25:186–188.
35. Dudley NJ, Kirkland M, Lovett J, Watson AR. Clinical agreement between automated and calculated ultrasound measurements of bladder volume. Br J Radiol 2003;76:832–834.
36. Byun SS, Kim HH, Lee E, et al. Accuracy of bladder volume determinations by ultrasonography: are they accurate over entire bladder volume range? Urology 2003;62:656–660.
37. Boothroyd AE, Dixon PJ, Christmas TJ, et al. The ultrasound cystodynamogram – a new radiological technique. Br J Radiol 1990;63:331–332.
38. Dicuio M, Creti S, Di Campli A, et al. Usefulness of a prevoiding transabdominal sonographic bladder scan for uroflowmetry in patients involved in clinical studies of benign prostatic hyperplasia. J Ultrasound Med 2003;22:773–776.
39. Vesely S, Knutson T, Fall M, et al. Clinical diagnosis of bladder outlet obstruction in men with lower urinary tract symptoms: reliability of commonly measured parameters and the role of idiopathic detrusor overactivity. Neurourol Urodyn 2003;22:301–305.
40. Kolman C, Girman CJ, Jacobsen SJ, Lieber MM. Distribution of post-void residual urine volume in randomly selected men. J Urol 1999;161:122–127.
41. Kuo HC. The uroflowmetry in normal men and after prostatectomy. Eur Urol 1997;31:447–452.
42. Blanker MH. Voided volumes: normal values and relation to lower urinary tract symptoms in elderly men, a community-based study. Urology 2001;57:1093–1098.
43. Madersbacher S, Pycha A, Klingler C, et al. Interrelationships of bladder compliance with age, detrusor instability, and obstruction in elderly men with lower urinary tract symptoms. Neurourol Urodyn 1999;18:3–15.
44. Abrams P. Urodynamics. Basel: Birkhäuser; 2005.
45. Patel U, Rickards D. Imaging and urodynamics of the lower urinary tract. New York: Taylor & Francis; 2005.
46. Papatsoris AG, Varkarakis I, Dellis A, Deliveliotis C. Bladder lithiasis: from open surgery to lithotripsy. Urol Res 2006;34: 163–167.
47. Barth R, Nino-Murcia M, DeVries PA, Friedland GW. Congenital anomalies of the urinary tract. In: Pollack HM, McClennan BL, editors. Clinical urography (vol. 1, part III). Philadelphia: Saunders; 2000. p. 661–911.
48. Cappele O, Sibert L, Descargues J, et al. A study of the anatomic features of the duct of the urachus. Surg Radiol Anat 2001;23:229–235.
49. Robert Y, Hennequin-Delerue C, Chaillet D, et al. Urachal remnants: sonographic assessment. J Clin Ultrasound 1996;24: 339–344.
50. Contin F, Cappellari F, Campobasso P, Canale M. [Echographic features of urachal cysts]. Radiol Med (Torino) 1992;83:783–786.
51. Descazeaud A. [Urachal diseases]. Ann Urol (Paris) 2007;41:209–215.
52. Amling CL. Diagnosis and management of superficial bladder cancer. Curr Probl Cancer 2001;25:219–278.
53. Malone PR, Weston-Underwood J, Aron PM, et al. The use of transabdominal ultrasound in the detection of early bladder tumours. Br J Urol 1986;58:520–522.
54. Denkhaus H, Crone-Munzebrock W, Huland H. Noninvasive

ultrasound in detecting and staging bladder carcinoma. Urol Radiol 1985;7:121–131.
55. Corwin HL, Silverstein MD. The diagnosis of neoplasia in patients with asymptomatic microscopic hematuria: a decision analysis. J Urol 1988;139:1002–1006.
56. Jaffe JS, Ginsberg PC, Gill R, Harkaway RC. A new diagnostic algorithm for the evaluation of microscopic hematuria. Urology 2001;57:889–894.
57. Brehmer M. Imaging for microscopic haematuria. Curr Opin Urol 2002;12:155–159.
58. Datta SN, Allen GM, Evans R, et al. Urinary tract ultrasonography in the evaluation of haematuria – a report of over 1,000 cases. Ann R Coll Surg Engl 2002;84:203–205.
59. Ozden E, Turgut AT, Turkolmez K, et al. Effect of bladder carcinoma location on detection rates by ultrasonography and computed tomography. Urology 2007;69:889–892.
60. Khadra MH, Pickard RS, Charlton M, et al. A prospective analysis of 1,930 patients with hematuria to evaluate current diagnostic practice. J Urol 2000;163:524–527.
61. Lopes RI, Nogueira L, Albertotti CJ, et al. Comparison of virtual cystoscopy and transabdominal ultrasonography with conventional cystoscopy for bladder tumor detection. J Endourol 2008;22: 1725–1729.
62. Mazo EB, Gazhonova VE, Chepurov DA. [Three-dimentional echography in diagnosis and staging of urinary bladder cancer]. Urologiia 2005;6–12.
63. Nakamura S, Niijima T. Staging of bladder cancer by ultrasonography: a new technique by transurethral intravesical scanning. J Urol 1980;124:341–344.
64. Abu-Yousef MM, Narayana AS, Franken EA Jr, Brown RC. Urinary bladder tumours studied by cystosonography. Radiology 1984;153:223–226.
65. Wagner B, Nesslauer T, Bartsch G Jr, et al. Staging bladder carcinoma by three-dimensional ultrasound rendering. Ultrasound Med Biol 2005;31:301–305.
66. Braeckman J, Denis L. The practice and pitfalls of ultrasonography in the lower urinary tract. Eur Urol 1983;9:193–201.
67. Holm HH, Juul N, Torp-Pedersen S, et al. Bladder tumor staging by transurethral ultrasonic scanning. Eur Urol 1988;15:31–33.
68. Devonec M, Chapelon JY, Codas H, et al. Evaluation of bladder cancer with a miniature high frequency transurethral ultrasonography probe. Br J Urol 1987;59:550–553.
69. Jaeger N, Radeke HW, Adolphs HD, et al. Value of intravesical sonography in tumor classification of bladder carcinoma. Eur Urol 1986;12:76–84.
70. Schulze S, Holm-Nielsen A, Mogensen P. Transurethral ultrasound scanning in the evaluation of invasive bladder cancer. Scand J Urol Nephrol 1991;25:215–217.
71. Saga Y, Numata A, Tokumitsu M, et al. Comparative study of novel endoluminal ultrasonography and conventional transurethral ultrasonography in staging of bladder cancer. Int J Urol 2004;11:597–601.
72. Salo JO. Intravesical ultrasound for staging bladder tumours. Scand J Urol Nephrol 1987;21:203–207.
73. Horiuchi K, Tsuboi N, Shimizu H, et al. High-frequency endoluminal ultrasonography for staging transitional cell carcinoma of the bladder. Urology 2000;56:404–407.
74. Horiuchi K, Shimizu H, Yoshida K, Nishimura T. New ultrasonic cystofiberscope for staging bladder tumors. J Endourol 2005;19:130–132.
75. Malone PR. Transabdominal ultrasound surveillance for bladder cancer. Urol Clin North Am 1989;16:823–827.
76. Vera-Donoso CD, Llopis B, Oliveet F, et al. Follow-up of superficial bladder cancer: how to spare cystoscopies? Eur Urol 1990;17:17–19.
77. Dershaw DD, Scher HI. Serial transabdominal sonography of bladder cancer. AJR Am J Roentgenol 1988;150:1055–1059.
78. Davies AH, et al. Flexible cystoscopy compared with ultrasound in the detection of recurrent bladder tumours. Br J Urol 1991;67:491–492.
79. Davies AH, Cranston D, Turner WH, et al. The role of abdominal and transrectal ultrasound and cytology in the detection of recurrent bladder tumours. Eur Urol 1990;18:124–126.
80. Rosenkilde OP, Jørgensen PM, Roed-Petersen K, et al. Control for recurrences of urinary bladder tumours by transabdominal ultrasonic scanning. Scand J Urol Nephrol 1985;19:105–107.
81. Huang WC, Yang JM, Yang YC, Yang SH. Ultrasonographic characteristics and cystoscopic correlates of bladder wall invasion by endophytic cervical cancer. Ultrasound Obstet Gynecol 2006;27:680–686.
82. Maynor CH, Kliewer MA, Hertzberg BS, et al. Urinary bladder diverticula: sonographic diagnosis and interpretive pitfalls. J Ultrasound Med 1996;15:189–194.
83. Saez F, Peña JM, Martinez A, et al. Carcinomas in vesical diverticula: the role of ultrasound. J Clin Ultrasound 1985;13:45–48.
84. Long MA, Boultbee JE. Case report: the transabdominal ultrasound appearances of a colovesical fistula. Br J Radiol 1993;66:465–467.
85. Ramamurthy S, Vijayan P, Rajendran S. Sonographic diagnosis of a uterovesical fistula. J Ultrasound Med 2002;21:817–819.
86. Carrington BM, Johnson RJ. Vesicovaginal fistula: ultrasound delineation and pathological correlation. J Clin Ultrasound 1990;18:674–677.
87. Yang JM, Su TH, Wang KG. Transvaginal sonographic findings in vesicovaginal fistula. J Clin Ultrasound 1994;22:201–203.
88. Volkmer BG, Kuefer R, Nesslauer T, et al. Colour Doppler ultrasound in vesicovaginal fistulas. Ultrasound Med Biol 2000;26:771–775.
89. Huang SC, Yao BL, Chou CY. Transvaginal ultrasonographic findings in vesico-uterine fistula. J Clin Ultrasound 1996;24:209–212.
90. Browne RF, Zwirewich C, Torreggiani WC. Imaging of urinary tract infection in the adult. Eur Radiol 2004;4(Suppl 3):E168–E183.
91. Afroz S, Taher MA. Cystitis mimicking bladder cancer on sonography. AJR Am J Roentgenol 1988;151:1252–1253.
92. Litwin MS, Loughlin KR, Benson CB, et al. Placenta percreta invading the urinary bladder. Br J Urol 1989;64:283–286.
93. Silber SJ, Breakey B, Campbell D, et al. Placenta percreta invading bladder. J Urol 1973;109:615–618.
94. Teo RE, Ahmed M, Chilton CP. Placenta percreta involving urinary bladder. Br J Urol 1996;78:140.
95. Campani R, Bottinelli O, Calliada F, Coscia D. The latest in ultrasound: three-dimensional imaging. Part II. Eur J Radiol 1998;27(Suppl 2):S183–S187.
96. Hull AD, Salerno CC, Saenz CC, Pretorius DH. Three-dimensional ultrasonography and diagnosis of placenta percreta with bladder involvement. J Ultrasound Med 1999;18:853–856.
97. Kinkel K, Frei KA, Balleyguier C, Chapron C. Diagnosis of endometriosis with imaging: a review. Eur Radiol 2006;16n:285–298.
98. Goodman JD, Macchia RJ, Macasaet MA, Schneider M. Endometriosis of the urinary bladder: sonographic findings. AJR Am J Roentgenol 1980;135:625–626.
99. Park SB, Kim JK, Cho KS. Sonography of endometriosis in infrequent sites. J Clin Ultrasound 2008;36:91–97.
100. Pastor NH, Donate MMJ, Giménez BJM, et al. [Bladder endometriosis. Report of two cases and bibliographic review, with special focus on Spanish articles.] Arch Esp Urol 2006;59:111–122.
101. Ralls PW, Barakos JA, Skinner DG, et al. Imaging of the Kock continent ileal urinary reservoir. Radiology 1986;161:477–483.
102. McInerney PD, DeSouza N, Thomas PJ, Mundy AR. The role of urodynamic studies in the evaluation of patients with augmentation cystoplasties. Br J Urol 1995;76:475–478.

CHAPTER

30

The prostate and seminal vesicles

Uday Patel

INTRODUCTION 572

EMBRYOLOGY 572

GROSS ANATOMY OF THE PROSTATE 572

SURFACE RELATIONS OF THE PROSTATE 572

PERIPROSTATIC FASCIA 573

THE PROSTATIC CAPSULE 573

ZONAL ANATOMY OF THE GLAND 573

BLOOD SUPPLY OF THE PROSTATE AND SEMINAL VESICLES 574

PROSTATIC NERVE SUPPLY 574

PROSTATIC LYMPHATIC DRAINAGE 574

THE SEMINAL VESICLES, EJACULATORY DUCTS AND SPHINCTERS 574

TRANSRECTAL ULTRASOUND OF THE PROSTATE AND ACCESSORY STRUCTURES 574

SONOGRAPHIC APPEARANCES OF THE NORMAL PROSTATE GLAND 576
Normal prostate vascularity 576

SONOGRAPHIC APPEARANCES OF THE NORMAL SEMINAL VESICLES AND EJACULATORY DUCTS 576

CONGENITAL OR DEVELOPMENTAL ANOMALIES 579

ACQUIRED ABNORMALITIES 579
Benign prostate hyperplasia or hypertrophy (BPH) 579
Prostatitis 582
Cysts of the prostate gland and associated structures 583
TRUS and evaluation of male infertility 584
TRUS and haematospermia 584

ACQUIRED ABNORMALITIES: MALIGNANT 585
Carcinoma of prostate 585
TRUS diagnosis of prostate cancer 585
Staging of prostate cancer 585
Follow-up of prostate cancer or assessment of suspected recurrent tumour 587

UNUSUAL TRUS ABNORMALITIES 587

TRUS-GUIDED INTERVENTION 587
Prostate biopsy 587
Principles of prostate biopsy 587
Biopsy of the post-prostatectomy bed 590
Drainage of prostate abscess, cyst or seminal vesicles 591

INTRODUCTION

Not all animals have a fully developed, anatomically recognisable prostate gland. The human is one, also interestingly the dog, and both species are prey to the common prostatic diseases of enlargement, prostatitis and prostate cancer, though curiously, in dogs an enlarged prostate is more likely to obstruct the colon, rather than the bladder. The word 'prostate' is of Greek origin – *protector or guardian* – reflecting the gland's role as a 'doorkeeper' to the bladder, a role it serves well, protecting the male from the minor stress leakage not uncommon among females of any age. Its anatomy is complicated only because it has undergone revision. Classical texts describe a lobar anatomy, now discarded as inaccurate and replaced with a zonal subdivision. Conveniently, these zones can be clearly identified on ultrasound (US), hence its central role in imaging of the prostate gland.

EMBRYOLOGY

The prostate originates from the urogenital sinus, as outpouchings from the prostatic part of the urethra between the 9th and 12th weeks of fetal life. This develops into the glandular, stroma and smooth muscles of the gland; but the seminal vesicles and ejaculatory ducts (and possibly the central zone, see below) are of Wolffian duct origin. Skene's glands found in the female urethra are the female homologue of the prostate.

GROSS ANATOMY OF THE PROSTATE

Of no vital physiological function, the gland is situated between the bladder and the muscles of the pelvic floor. In shape it approximates to an inverted cone. Thus the base of the gland is situated superiorly and the prostate apex is paradoxically its most inferior portion, adjacent to the external urethral sphincter. Dimensions of the non-enlarged gland are up to 3 cm in height, 2.5 cm in depth and 4 cm in width and its volume is less than 25 mL, or the size of an apricot. Like the apricot, the gland also has a midline groove, which is palpable but strangely not identifiable on imaging. Beyond the age of 40 years, with the onset of benign prostatic hyperplasia, the gland commonly enlarges.

SURFACE RELATIONS OF THE PROSTATE

The gland lies within the lower pelvis, where it funnels down towards the perineum. The symphysis pubis lies in front, particularly over the lower gland. The posterior relations are the rectum, with the seminal vesicles lying in between, behind the bladder neck. The lateral surfaces abut the pelvic side walls and the levator ani muscles. The neurovascular bundles, which contain the arteries and neural supply of the gland, are located posterolaterally and are vulnerable during surgical dissection, which can lead to erectile dysfunction, as some of the neural fibres also supply the corpora cavernosa of the penis.

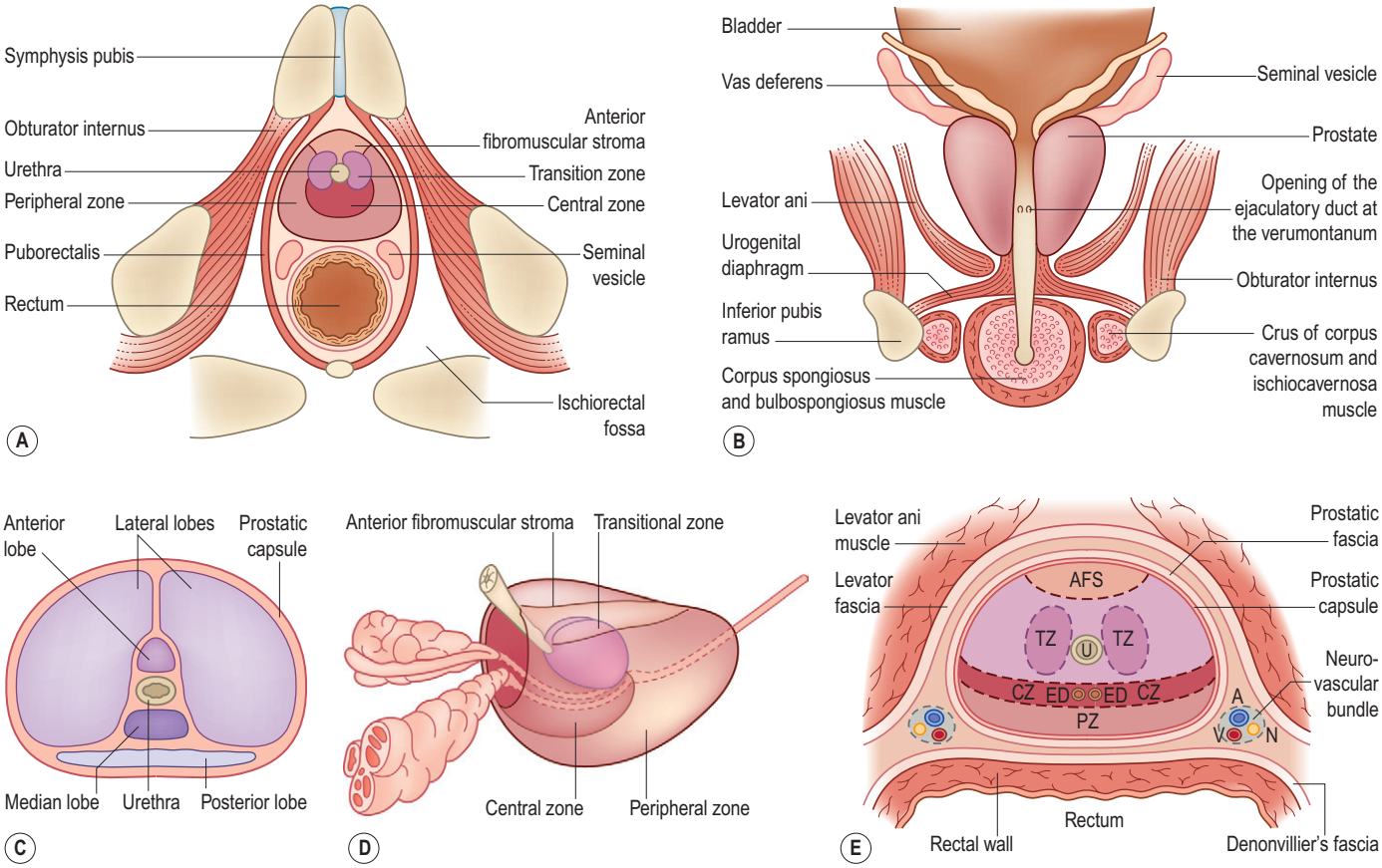


Figure 30.1 **The anatomy of the prostate gland and surrounding structures. A and B:** Axial and coronal line illustrations of the prostate gland and its immediate anatomical relationships (modified from Patel U, Rickards D, Handbook of Transrectal Ultrasound and Biopsy of the Prostate, Martin Dunitz 2002). **C:** Line illustration of the classical lobar anatomical model, which is now known to be inaccurate, although certain terminological derivations are still sometimes used, e.g. median lobe enlargement. **D:** The zonal model of the gland (modified from Patel U, Diseases of the bladder and prostate, in Ultrasound of the Urogenital System, Baxter G, Sidhu P, Eds, Thieme, 2006). As well as being more accurate, this has clinical correlates (see text) and the zones can be differentiated on imaging. **E:** The fascial planes around the gland. These planes are not generally identifiable on ultrasound, except for the capsule (AFS, anterior fibromuscular stroma; TZ, transition zone; CZ, central zone; PZ, peripheral zone; ED, ejaculatory duct; A, artery; V, vein; N, nerve).

Further surgical, and radiological, landmarks are the bladder neck (cephalad), the external sphincter (caudal) and the dorsal vein complex (anterior), which overlies the apex of the gland. The urinary sphincters (i.e. the bladder neck and the external sphincter, the latter being more important for continence) fuse with the prostate gland. All these structures are usually identifiable on sonography.

PERIPROSTATIC FASCIA

The prostate is surrounded by three fascial layers (Fig. 30.1). Denonvillier's fascia is a fused layer of connective tissue behind the gland, separating it from the rectum. Over the anterior surface lies the prostatic fascia, which is superficial to the prostatic venous plexus, but beneath the dorsal vein of the penis. As it passes posterolaterally, the prostatic fascia fuses with the third fascia – the levator fascia – to form the lateral pelvic fascia. None of these fascial plains are identifiable on ultrasound.

THE PROSTATIC CAPSULE

The prostate does not have a true fibro-elastic capsule (Fig. 30.1), but the surrounding 2–3 mm of stromal tissue is seen as a distinct boundary on imaging, including transrectal ultrasound (TRUS). It can also be identified pathologically and is loosely termed the 'prostate capsule'. This capsule thins towards the apex, making local cancerous spread more likely at the apex. Further areas of capsular weakness are around the base of the gland, where the ejaculatory ducts pierce through, and those points along the posterolateral margins perforated by the neural and vascular supplies. All these also represent points of early local cancer spread and should be especially inspected on TRUS.

ZONAL ANATOMY OF THE GLAND

Classical anatomists believed in a lobar prostate anatomy, based on dissections along natural planes of the embryological prostate (Fig.

30.1). Five lobes were described – the anterior, middle, posterior and two lateral lobes. The anterior lobe was that small area of the gland anterior to the urethra; the median lobe the region between the ejaculatory ducts and the proximal urethra. The remaining gland at the back and to the sides represented the posterior and lateral lobes. In reality, clear lobar anatomical distinction is not demonstrable in the adult gland, and the model has now fallen into disuse, to be replaced by a zonal model[1] based on glandular differentiation (Fig. 30.1). These zones also closely correlate with radiological and histological anatomy. Three zones are described – the peripheral, central and transition zones – though some texts, inaccurately, consider the peri-urethral glands as a further zone.

The peripheral zone (PZ) accounts for most of the gland in the young adult (>70%). It lies behind the urethra and is bulkier around the base. Its lateral margins project substantially anterior, such that this zone is seen to 'cup' the gland on axial TRUS. These 'cups' are termed the posterolateral margins or the anterior horns, adjacent to the neurovascular bundles. The second largest glandular portion is the central zone (CZ, about 25% of the non-enlarged gland), which lies anterior to the PZ and behind the proximal urethra (similar to the median lobe of the old lobar model). The ejaculatory ducts traverse the CZ. The transition zones (TZ) are two glandular areas adjacent to the urethra, and account for less than 5% of the gland in the absence of benign prostatic hyperplasia (BPH). Histologically, the zones demonstrate subtle microscopic differences and it is believed that the CZ may be of Wolffian duct origin as it partly resembles the seminal vesicle epithelium. Further histological components of the gland are the fibromuscular stroma, which lie most anterior to the urethra. Unlike the zones, neither the anterior fibromuscular stroma nor the peri-urethral glands are clearly identifiable on US or of much clinical importance. Terminologically, the gland is sometimes also divided into an outer and inner gland,[2] with the outer gland comprising the PZ and CZ and the inner gland the TZ and peri-urethral glands. This nomenclature is often used loosely in clinical practice to differentiate that part of the gland more likely to harbour cancer (i.e. the PZ) from the rest of the gland.

For the radiologist, the value of the zonal model is that it correlates with the common prostate pathologies.[3] For unknown reasons, cancer most commonly originates in the PZ, whilst benign prostatic hyperplasia (BPH) is principally a disease of the TZ and the peri-urethral glands. Prostatitis, the third commonest prostate disease, can affect any zone.[2]

BLOOD SUPPLY OF THE PROSTATE AND SEMINAL VESICLES

The main arterial supply to the prostate and seminal vesicles arises from the inferior vesical artery, which is a branch of the anterior division of the internal iliac artery. The distal arterial branches can be grouped into capsular and urethral branches. The capsular branches are located in the lateral pelvic fascia, posterolateral to the bladder, and supply the outer prostate. The urethral branches of the inferior vesical artery enter the prostate at the junction of the bladder and prostate, and supply the central portion. This arterial distribution is recognisable on TRUS, with 'normal' flow being greatest around the periphery and the urethra.

Venous drainage is more complex, and their surgical control is an important step during prostatectomy. The dorsal vein of the penis divides into three branches that also drain the prostate. A single superficial branch lies anterior to the prostatic fascia. The right and left lateral deep branches pass posterolaterally, beneath the prostatic fascia. These veins are not clearly separable during TRUS. All of the major branches interconnect with adjacent venous complexes, particularly the lateral pelvic plexi (e.g. the internal pudendal vein, obturator and pelvic plexi), and this ramifying venous system finally drains into the iliac veins; in addition some veins also communicate with the lumbar venous complex of Batson. This posterior venous outlet, coupled with the propensity of early periprostatic tumour spread because of the deficient prostate capsule (as described above), accounts for the early spread of prostate cancer to the pelvic and lumbar bones.

PROSTATIC NERVE SUPPLY

From an imaging perspective, the vascular bundles act as a landmark for the neural plexus as the nerves are not otherwise identifiable. They contain fibres from the inferior hypogastric plexus, parasympathetic fibres from the pelvic splanchnic nerves (S2, 3 and 4) and sympathetic fibres from the sacral sympathetic trunks. The resulting plexus runs along the pelvic side wall, and at the level of the prostate is situated within the lateral pelvic fascia, superficial to the prostatic fascia, intimately related to and inseparable from the vascular bundles.

The major relevance of the prostatic nerves to the imager is merely to appreciate that the gland is to a degree sensate, and that local anaesthetic is of benefit during prostate biopsy.

PROSTATIC LYMPHATIC DRAINAGE

Prostatic lymphatics drain into the periprostatic subcapsular network, and then to the internal iliac, external iliac and obturator chains. There is no constant sentinel node described for prostate cancer spread, but the commonest affected is the obturator node. Although theoretically within reach of TRUS, the periprostatic nodes are in practice rarely visualised on US.

THE SEMINAL VESICLES, EJACULATORY DUCTS AND SPHINCTERS

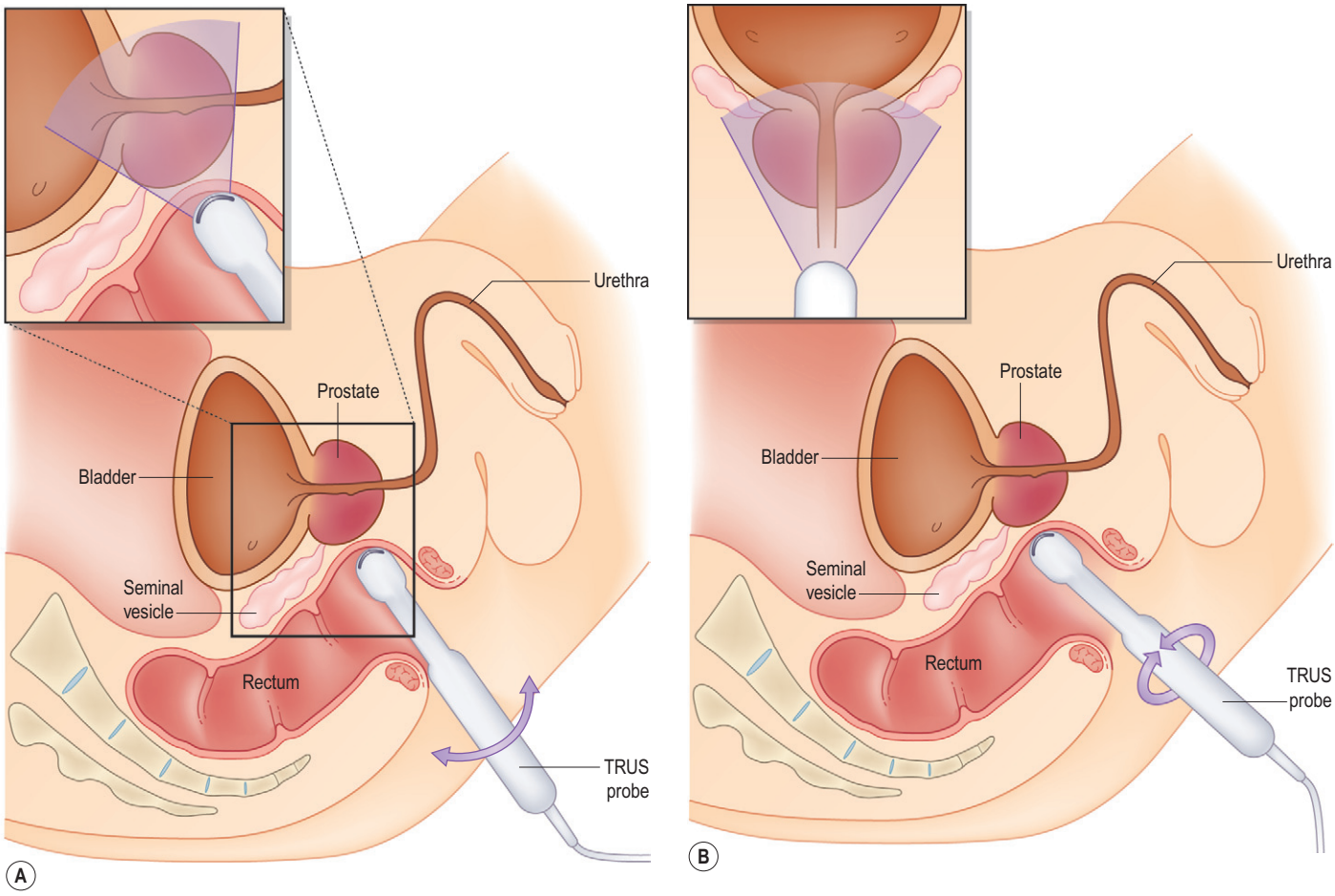
The seminal vesicles, ejaculatory ducts and urethral sphincters (Fig. 30.1) are important para-prostatic structures as they may be either individually diseased or involved as a part of prostate disease. The seminal vesicles (SVs) are positioned above the prostate, against the posterior wall of the bladder. The ureter passes superomedial to the seminal vesicles and the neurovascular bundles lie in the groove between the prostate and vesicle. Blood supply to the vesicles is from branches of the middle rectal and inferior vesical arteries.

Anterior to, and eventually medial to, each vesicle lies the ductus (or vas) deferens. The ampulla (or duct) of the seminal vesicle fuses with the ampulla of the vas to form the ejaculatory duct (ED), which punctures the base of the gland, traverses anteroinferioly through the central zone and empties into the prostatic urethra at the verumontanum. The duct is a potential pathway for local tumour extension into the seminal vesicles.

Urinary continence is dependent on the bladder neck and the external urethral sphincter. The bladder neck has smooth muscle fibres contiguous with those of the prostate and seminal vesicles (the bladder neck is sometimes termed the internal sphincter). The external sphincter is composed of striated muscle, responsible for voluntary control of continence. Its preservation is of prime concern during prostatic surgery. On US, the position of both sphincters is identifiable, as they are more hypoechoic than prostate, or of mixed echogenicity.

TRANSRECTAL ULTRASOUND OF THE PROSTATE AND ACCESSORY STRUCTURES

Although the gland may be visualised on transabdominal scanning, the views are too poor for diagnosis but the dimensions may be



TRUS examination of the prostate

Preparation: None specific

Position: Left lateral position

Probe: 5–10 MHz. An end-firing probe is best, but combined axial/longitudinal probes are also available

Method: Adjust scan parameters. Adjust focal zones to encompass the whole gland and gain until entire gland is well seen. Decrease frequency and adjust the time gain compensation for large glands. Next, scan gland in both planes from base to apex and from side to side

Images: recorded in

a. Axial plane – base, mid- and apex

b. Longitudinal plane – midline, left and right para-sagittal

Assess:

1. Measure gland volume (formula: height × width × length × 0.52)
2. Note echotexture, nodules and gland symmetry
3. Evaluate the capsule
4. Scrutinise blind areas in both planes – posterolateral margins (also sometimes called anterior horns), base, apex and far anterior gland (decrease frequency to 5–7.5 MHz)
5. Assess neurovascular bundle symmetry
6. Seminal vesicle/Ejaculatory duct assessment – scan in both axial and longitudinal planes, although axial plane is better for SVs and longitudinal for EDs
7. Colour Doppler imaging

Notes: Gland volume is more accurately measured by planimetry. The formula above becomes increasingly inaccurate with glands >80 mL.

Figure 30.2 The technical details of transrectal ultrasound scanning of the prostate gland and its surrounding structures. A and **B** illustrate how to scan in the axial and longitudinal planes using the most commonly used end-firing TRUS probe. Note the rocking **(A)** and rotating **(B)** movements necessary for scanning in the axial and longitudinal planes respectively. A systematic approach to scanning is important and these are listed in the table. The last image **(C)** shows how the gland volume is measured.

measured, albeit imprecisely. In contrast, the prostate can be seen with sub-millimetre precision using a transrectal probe.[4] Varieties of probe designs are available. Radiology departments favour the more versatile end-firing probe which requires a fanning or rocking motion (Fig. 30.2), unlike the simple advancement or rotation movements necessary for true axial/longitudinal probes. Modern probes scan at a frequency of 5–10 MHz, but are also capable of multifrequency scanning and prostate biopsy as well. For most glands 7.5–10 MHz is adequate, but large glands require 5–MHz to inspect the anterior structures or the bladder neck.

The left lateral position is best for scanning, and the higher the knees are flexed the easier the examination for both patient and

Tips and tricks

- The higher the knees are flexed, the easier the examination for the patient as probe introduction is easier.
- For easier probe introduction, ask the patient to take deep breaths in and out, and advance the probe during each expiration and follow the normal contours of the rectum. Deep breathing reduces the anal sphincter contraction that occurs during breath hold, and especially during Valsalva manoeuvre.
- If views are poor, it may be due to poor rectal wall contact – point the probe tip anteriorly.
- If the anterior part of the gland is poorly seen, reduce the frequency to 5–7.5 MHz, increase the gain and focal depth.
- Evaluate all suspected abnormalities in at least two different planes, especially the 'blind areas' of the gland – the posterolateral margins, apex and the base.

Indications for TRUS

Established indications

- Measurement of prostate size
- Targeting for prostate biopsy
- Evaluation of haematospermia
- Evaluation of azoospermia or ejaculatory dysfunction
- Evaluation of acute prostatitis and suspected prostatic abscess
- Staging of prostate cancer (although this is not as accurate as MRI, it is useful when MRI findings are equivocal)

Indicated in selected cases

- Assessment of benign prostate hyperplasia
- Assessment of patients with negative biopsy but rising prostate-specific antigen (using colour Doppler imaging)
- Recurrent bladder outflow obstruction
- Evaluation of the prostate bed after radical prostatectomy

operator. No special preparation is necessary. Some urine in the bladder is helpful, but over-distension will lead to urinary urge as the probe is moved around. The lubricated, condom-covered probe is inserted into the anus and directed slightly posterior, to follow the natural contour of the lower rectum. Deep breathing through an open mouth helps to relax the anal sphincter and the probe is incrementally advanced, during each expiration. This manoeuvre is especially useful in those with a narrow anus or tight sphincter.

The probe should be advanced till the gland is seen anteriorly – about 10 cm beyond the anal margin – and the gland scanned in a systematic manner (summarised in Fig. 30.2). Magnification should be adjusted until the entire gland is visualised on the screen.[2] Multiple focal zones are more useful with modern probes, and the focal depth adjusted to encompass the whole gland.

First the gland size should be measured (Fig. 30.3). Studies have shown that the correlation between the volume and true prostate weight is between 0.82 and 0.99.[5] The correlation is poorer for large glands (>80 mL) as they deviate from the semi-ellipsoid shape, assumed by the formula used for volume calculation. Next the gland should be examined in the axial plane from the base to the apex.

The echogenicity of the glandular zones should be compared between the two sides and note made of any asymmetry. The gland should then be scanned in the longitudinal plane and asymmetry again noted. Any suspected abnormality should be examined in two planes, as only those seen on both will be true abnormalities. This is especially useful near the gland base and apex, as otherwise partial voluming of adjacent seminal vesicles or urethra can be misinterpreted as hypoechoic abnormalities. The far lateral edge of the gland is another blind spot that should also be scrutinised in both planes. Finally, the seminal vesicles, ejaculatory ducts, vasa and the external urethral sphincter should be examined.

Colour flow imaging can be of some diagnostic value[6] and should be used routinely. The colour window should be enlarged to encompass the entire gland in the axial view. The gain should be reduced till there is no 'flow', and then slowly increased till flow commences around the capsule and the urethra. A low flow setting is useful. This is 'normal' prostate vascularity (see under 'Blood supply of the prostate and seminal vesicles' – above – for explanation). Flow characteristics should be slowly evaluated in the axial plane, from the base to the apex of the gland, and any focal intraparenchymal flow asymmetry noted. Intravenous contrast will augment flow,[7] normal or abnormal, but is not yet used routinely. Duplex Doppler US has no diagnostic role in the prostate and sonoelastic imaging, or elastography, is still being explored. The accepted indications for TRUS are well described.

SONOGRAPHIC APPEARANCES OF THE NORMAL PROSTATE GLAND

In the young man, the gland is homogeneous[2,4] and the zones difficult to differentiate, but generally the peripheral zone is hyperechoic relative to the central and transition zones (Figs 30.3 and 30.4). This echo-differentiation is further boosted by glandular enlargement, because of compression of the peripheral zone, but normally the central and transition zones cannot be separated from each other (the position of the CZ can usually only be inferred from the location of the ejaculatory ducts).

The anterior fibromuscular stroma is not easily defined either. Although there is no histological prostate capsule, the distinction between the gland and surrounding fat is so distinct that a 'sonographic' capsule can be seen. The levator ani muscles are seen as linear mixed echogenic lateral boundaries of the prostatic bed. The urethra is seen as a line, also of mixed echogenicity, but has no lumen at rest. With muscular hypertrophy the urethra, and bladder neck, become increasingly hypoechoic and sound attenuating, a common finding with prostate gland enlargement. Just beyond the apex can be seen the hypoechoic external urethral sphincter. In the longitudinal plane, the non-enlarged gland should not elevate the bladder base. Elevation is seen with glandular enlargement, especially if the CZ is enlarged, and the term 'median' lobe enlargement still has some loose clinical value.

Highly reflectile, non-shadowing foci may be seen within the ducts of the inner gland, so-called corpora amylacea (Fig. 30.5) representing mucoproteins. They have no clinical significance. Scattered calcification is also sufficiently common to be considered a 'normal' finding. Heavier focal calcification may represent prostatitis (see below) or calculi within the ejaculatory ducts or urethra; and only very rarely is prostate cancer calcified.

Normal prostate vascularity

On colour Doppler US,[6,7] the normal gland has strong vascular signals from the neurovascular bundles, the pericapsular arteries and the peri-urethral branches (Fig. 30.6) but there is little internal or parenchymal flow. Importantly, like the overall gland echogenicity, normal parenchymal vascularity is broadly symmetrical.

SONOGRAPHIC APPEARANCES OF THE NORMAL SEMINAL VESICLES AND EJACULATORY DUCTS

For seminal vesicles, both transverse and longitudinal scans are helpful (Fig. 30.7). Ejaculatory ducts are best seen in the

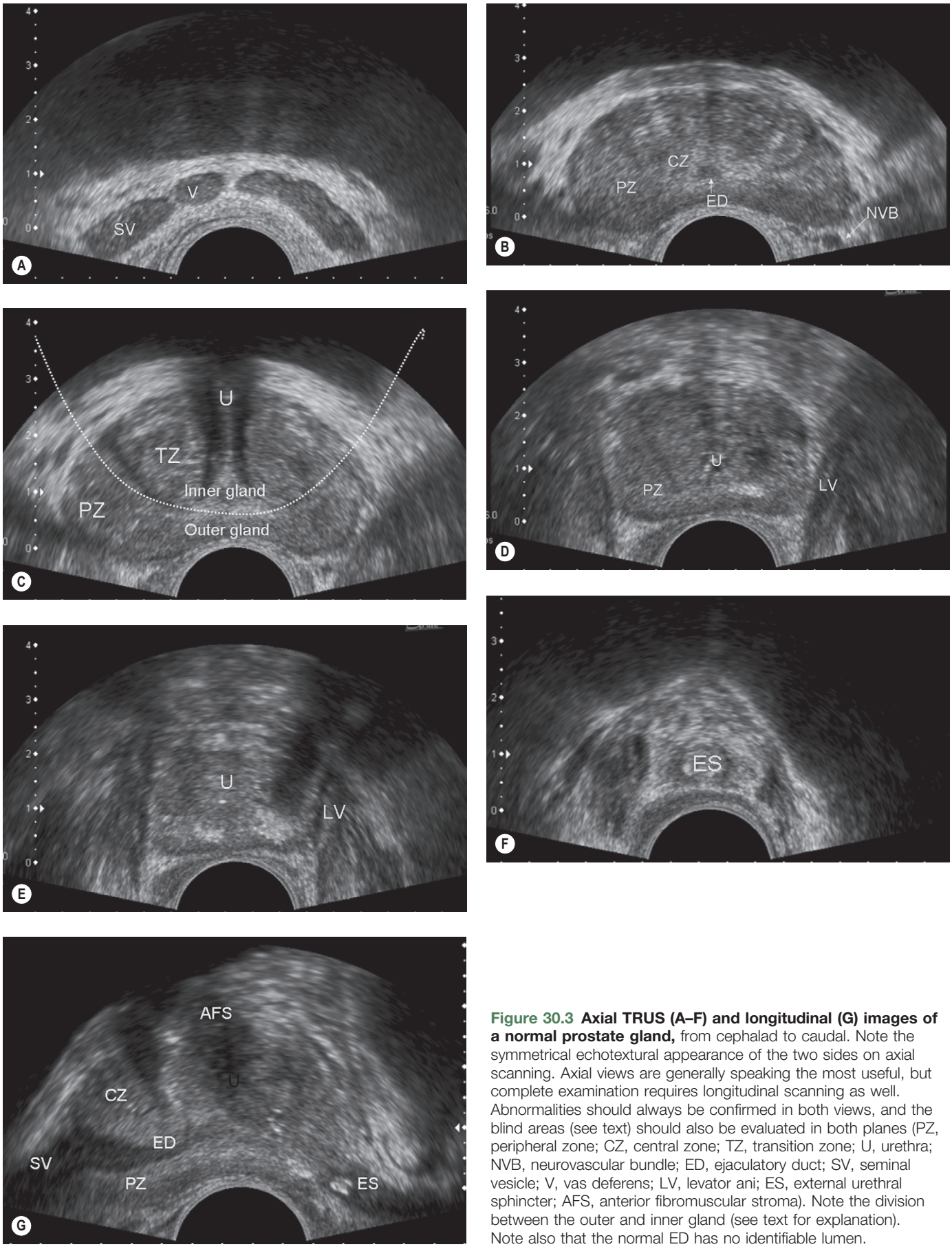


Figure 30.3 Axial TRUS (A–F) and longitudinal (G) images of a normal prostate gland, from cephalad to caudal. Note the symmetrical echotextural appearance of the two sides on axial scanning. Axial views are generally speaking the most useful, but complete examination requires longitudinal scanning as well. Abnormalities should always be confirmed in both views, and the blind areas (see text) should also be evaluated in both planes (PZ, peripheral zone; CZ, central zone; TZ, transition zone; U, urethra; NVB, neurovascular bundle; ED, ejaculatory duct; SV, seminal vesicle; V, vas deferens; LV, levator ani; ES, external urethral sphincter; AFS, anterior fibromuscular stroma). Note the division between the outer and inner gland (see text for explanation). Note also that the normal ED has no identifiable lumen.

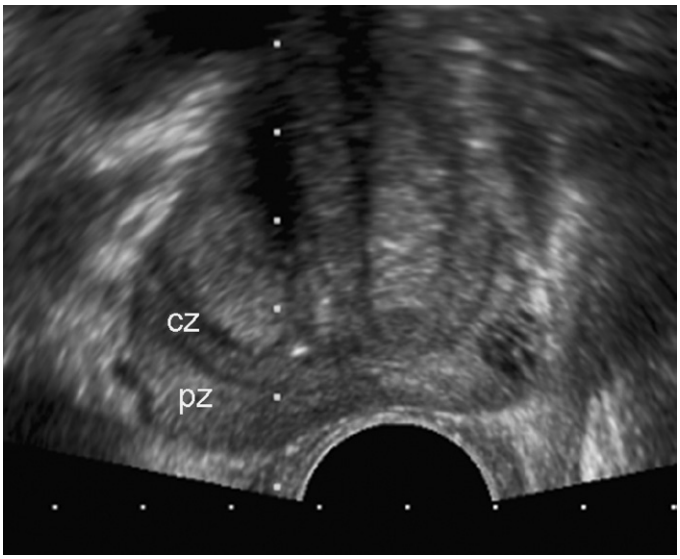


Figure 30.4 Normally the peripheral and central zones cannot be easily differentiated, but they are clearly seen in this case. There is no especial disease of the central zone, except that it is felt to be of the same embryological origin as the Wolffian duct structures and may be absent when there are anomalies of this duct. pz, peripheral zone; cz, central zone.

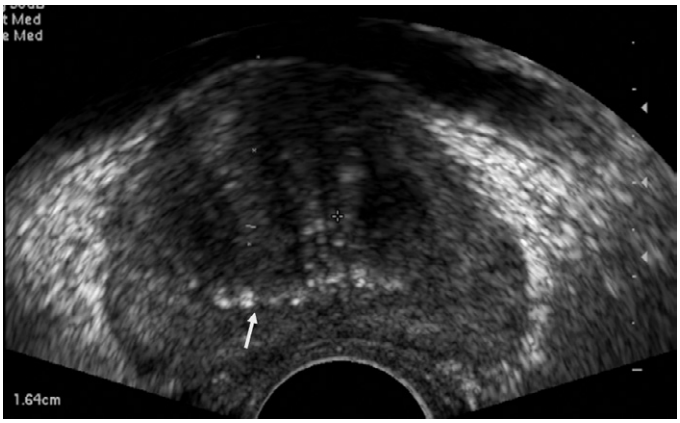


Figure 30.5 Non-shadowing reflectile hyperechoic opacities (arrow) are commonly seen on TRUS. These are felt to represent mucoproteins in the duct, so called corpora amylacea.

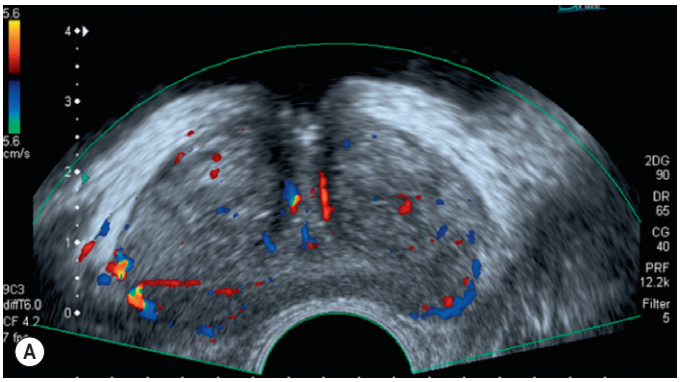
longitudinal view. The normal vesicle has a width of about 1.5 cm, is usually about 4 cm long and is symmetrical with its counterpart vesicle. Although normal size ranges have been described, in practice size estimation is of no clinical value.

On good quality ultrasound the seminal vesicle epithelium may be identified with its separate mucosal layers (Fig. 30.4), but the value of SV epithelium analysis on US has not been explored. Often the lumen, and its swirling contents, may also be visualised. This is normal physiological distension, is symmetrical (Fig. 30.7A) and can be differentiated from true seminal vesicle dilatation by repeating the scan after ejaculation. True dilatation is usually, but not always, asymmetric and associated with vasal/ejaculatory duct dilatation. With agenesis of the SV, the ipsilateral vas is usually also absent. In the longitudinal view, an important assessment, especially in those with suspected prostate cancer, is the angle at which the vesicle enters the gland. At this point, the periprostatic fat creates an acute hyperechoic angle (Fig. 30.7C), which is lost in the presence of extracapsular extension of cancer into the SVs.

On modern machines, the normal ejaculatory ducts are readily seen as hyperechoic tramlines on longitudinal scans and as composite midline ovoid structures in the axial view. The normal duct has no identifiable lumen, and its lumen diameter is described as <0.1 mm. In practice, if a lumen is seen then this means a dilated duct. One route for cancer spread into the seminal vesicles is along the ejaculatory ducts; however, duct infiltration per se is rarely identified on US.

Normal TRUS appearances

- In the young man, with a non-enlarged gland, zonal differentiation may be difficult.
- The peripheral zone is the most hyperechoic.
- Normal gland volume is <25 mL.
- Appearances change with enlargement – the peripheral zone may become even more hyperechoic and thin.
- Usually the central zone is not identifiable as separate, but its position can be determined by the presence of the ejaculatory ducts.
- The prostate capsule, though identifiable on US, is not a true capsule.
- Vascularity on colour Doppler imaging is symmetrical, with peripheral and peri-urethral flow, and no/low parenchymal flow.
- The non-dilated ejaculatory duct has no identifiable lumen.
- The seminal vesicles may appear distended due to normal physiological storage.



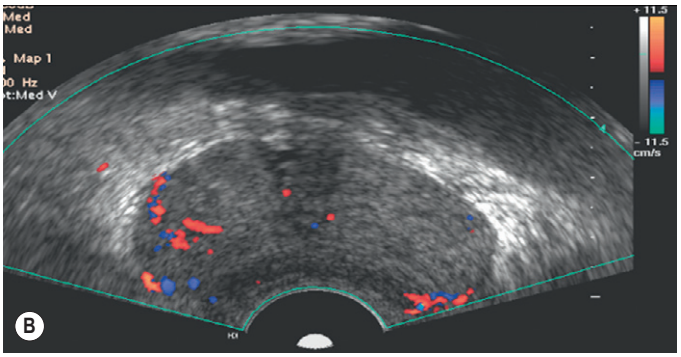


Figure 30.6 A: Normal prostate vascularity on colour Doppler ultrasound, with strong signals in the capsular and peri-urethral vessels but no substantial focal parenchymal or intra-prostatic flow. In comparison, **B** shows increased focal flow from the right inner gland. There is no focal nodule in this area on the greyscale image, but this area should be targeted during biopsy, especially in those with previous negative biopsies.

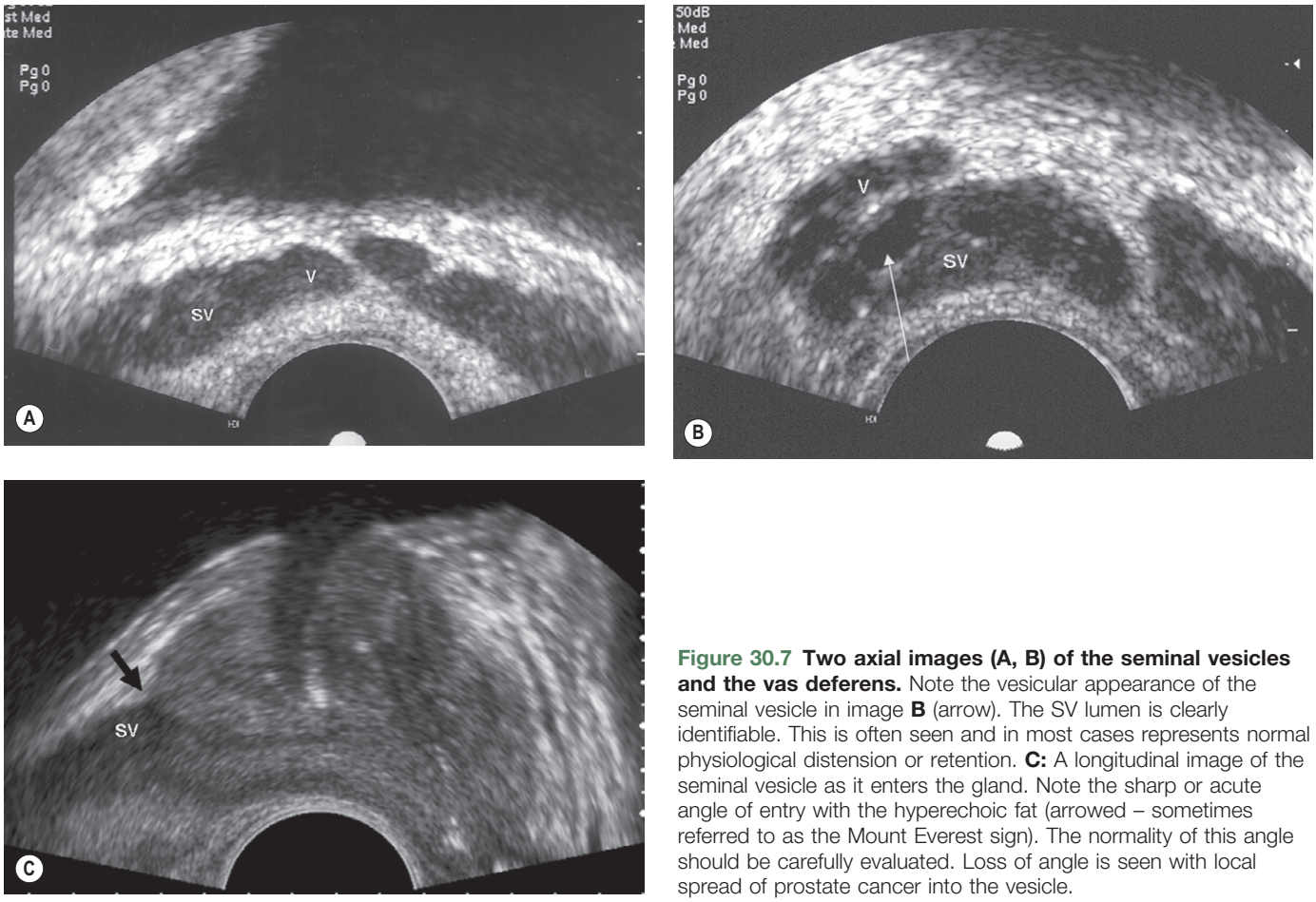


Figure 30.7 Two axial images (A, B) of the seminal vesicles and the vas deferens. Note the vesicular appearance of the seminal vesicle in image **B** (arrow). The SV lumen is clearly identifiable. This is often seen and in most cases represents normal physiological distension or retention. **C:** A longitudinal image of the seminal vesicle as it enters the gland. Note the sharp or acute angle of entry with the hyperechoic fat (arrowed – sometimes referred to as the Mount Everest sign). The normality of this angle should be carefully evaluated. Loss of angle is seen with local spread of prostate cancer into the vesicle.

On vascular imaging, normal flow is barely seen in the epithelium, even on high sensitivity settings. Abnormal flows are asymmetric and involve the lumen and surrounding fat planes and infiltrated tissue. However, the diagnostic value of seminal vesicle colour Doppler has also not been extensively studied or reported.

CONGENITAL OR DEVELOPMENTAL ANOMALIES

The prostate gland is absent in hermaphrodites. There are no other described congenital or developmental anomalies of the prostate gland, but very rarely, the prostate may be hypoplastic, e.g. with prune belly syndrome or in those with low testosterone levels or retarded sexual development. The seminal vesicles, vasa and/or ejaculatory duct may be absent as a combined maldevelopment of the Wolffian duct (additionally the bladder trigone and the CZ may be deficient with a wide bladder neck).

These abnormalities are rare but those of the Müllerian duct or, more commonly, utricle development are often seen on TRUS (5–8.6%), as midline cystic structures.[8] They are round in the axial plane and teardrop shaped on longitudinal scanning, and may extend above the prostate gland. The majority are incidental findings and may be slightly thick-walled but are always transonic, unless after internal bleeding or infection. Small amounts of internal debris may be mistaken for wall thickening. If there is doubt, then a re-scan in the other lateral position will often clarify. Occasionally they may be calcified and clinical presentations include haematospermia and obstructive infertility. Giant cysts may obstruct urinary flow (usually seen in teenagers) and bilateral Müllerian cysts may be associated with unilateral renal agenesis.[9] Tumours of these structures are rarely seen.

Müllerian cysts (Fig. 30.8) do not communicate with the urethra, unlike a persistent prostatic utricle (or 'utricle cyst') which may communicate. Persistent utricles, sometimes mega-utricles, are often associated with hypospadias or genital anomalies. Seminal vesicle cysts are rare. In isolation they are inconsequential, but multiple SV cysts are associated with adult polycystic kidney disease.[10]

In practice it may be difficult to differentiate Müllerian from utricle cysts, but the latter are smaller and do not extend beyond the gland. Cyst content, which can be sampled via the transrectal route (see below), may be helpful. Müllerian duct cysts should have no prostate-specific antigen (PSA) expression. Utricle cyst fluid may or may not contain sperm, depending on whether they communicate with the urethra and ejaculatory ducts.

ACQUIRED ABNORMALITIES

Benign prostate hyperplasia or hypertrophy (BPH)

After the 40th year, the prostate hypertrophies and above the age of 50 years, over 50% will have some degree of BPH. The glandular

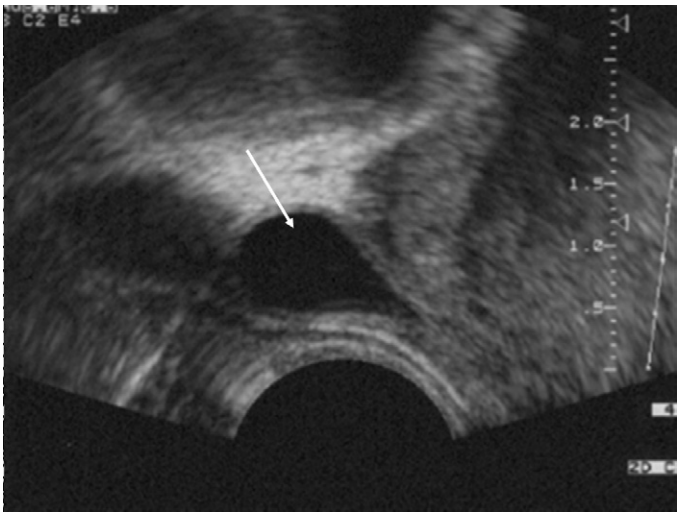


Figure 30.8 Longitudinal view of a midline cyst (arrow). This could represent either a Müllerian remnant cyst or a Utricle cyst. There is no reliable way on imaging of distinguishing them apart. It is said that Müllerian remnant cysts are more likely to extend outside the gland (as in this case).

and stromal elements both enlarge, particularly in the transition zone and the peri-urethral glands. BPH of the PZ or the CZ is less common. Hypertrophy may be diffuse or as distinct adenomas, and there is also hypertrophy of the peri-urethral muscles. But there is no direct relation between size, degree of BPH or adenomas and reduced urinary flow or other lower urinary tract symptoms. Men with symptomatic BPH can also present with a variety of symptoms. Some present with irritative symptoms (frequency, nocturia) rather than significantly reduced flow rates. Others may present with urgency and stress incontinence, due to secondary detrusor overactivity. Thus, the entire symptom complex secondary to prostate gland enlargement is conveniently referred to as lower urinary tract symptoms (or LUTS).

A variety of sonographic abnormalities are seen (Figs 30.9–30.11; Table 30.1). The commonest anatomical findings are asymmetric enlargement with a deviated urethra and elevated bladder base. The earliest sonographic change is heterogeneity of the inner gland (Fig. 30.9). Other findings are compression of the PZ (Fig. 30.9), which consequently may appear even more hyperechoic, and numerous nodules of various sizes and appearances. These nodules, or adenomas, will be well defined and if close to the edge, will elevate but not infiltrate the capsule. On vascular imaging, there is generally no internal flow within the nodules. Some of these appearances unfortunately overlap with those of central gland tumours, but the latter are more uniformly hypoechoic, with poorly defined edges, and may demonstrate internal vascularity. Occasionally,

Table 30.1 Common benign prostate pathology – TRUS features

Pathology	Site	TRUS features
Benign prostatic hyperplasia (BPH) (Note: Correlation between TRUS findings of BPH, prostate volume and outflow obstruction is poor)	TZ or central gland	• Gland enlargement – >25 mL • Heterogeneous changes in 2/3, homogenous in rest • Thinning of the PZ • Lobar asymmetry • Narrowed, deviated urethra • Nodules in the TZ – usually mixed reflectivity with well-defined boundaries (unlike malignancy). Peripheral flow on colour Doppler • Capsule may bulge, but is always intact • Cystic degeneration of nodules • Bladder base is elevated ('median lobe' may be enlarged)
Acute or chronic prostatitis (Note: Data on many of these features is anecdotal or not thoroughly established. Clinical correlation is necessary)	PZ or TZ/CZ	Acute: • Diffuse or focal hypoechogenicity • Focal or generalised increased vascularity • Abscess (thick-walled focal hypoechoic/cystic areas of increased vascularity) Chronic: • Echogenic foci • Prominence of the periprostatic venous plexus • Thickening of the 'capsule' of the gland • Calcification, often heavy, of inner gland • Mild/Moderate increased flow on colour Doppler (focal or global)
Obstructive infertility	Ejaculatory ducts, seminal vesicles	• Dilated EDs and/or SVs • ED stricture • ED calculi • Masses (usually developmental cysts, e.g. Müllerian) obstructing EDs • Absent Vasa/EDs
Retrograde ejaculation	Ejaculatory ducts, bladder neck	• Open bladder neck or TURP cavity • Normal EDs and SVs
Haematospermia	EDs, SVs, prostate	• ED calculi • Developmental cysts • Prostatitis • Prostate cancer

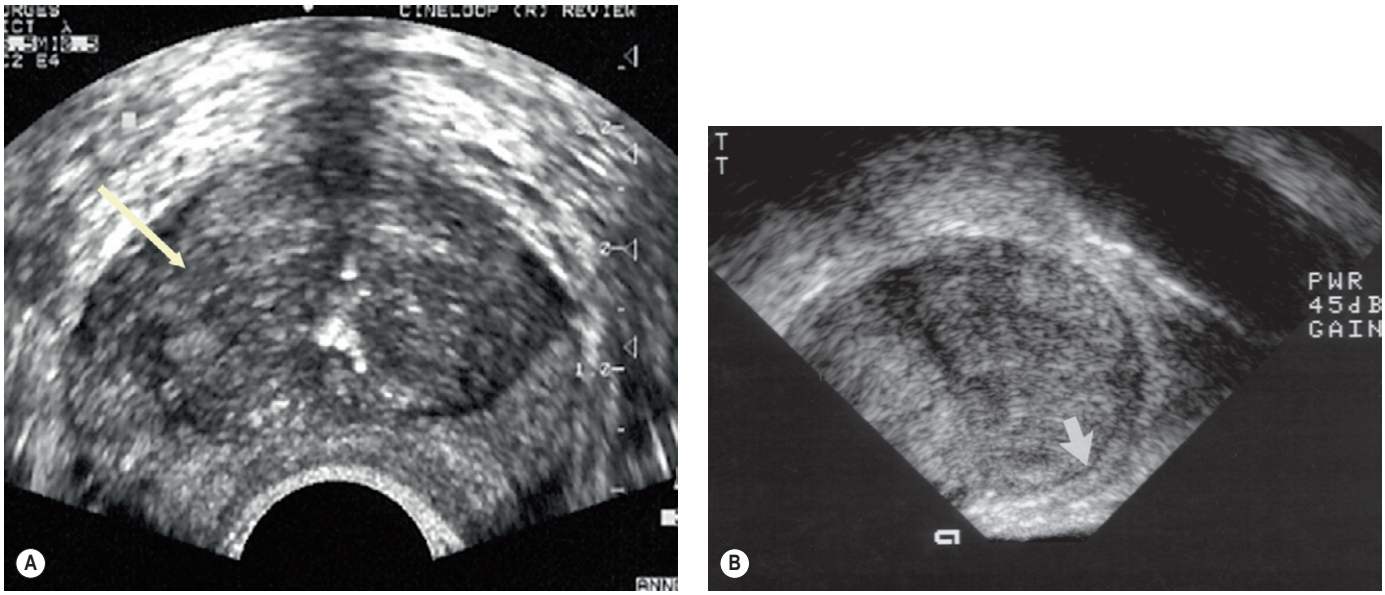


Figure 30.9 **Benign prostate hyperplasia. A and B:** Axial scans of patients with BPH. Note the heterogeneous echotexture of the inner gland (arrow) representing BPH affecting the transition zone. Note also how the naturally hyperechoic quality of the peripheral zone is further accentuated by compression due to inner gland enlargement. An extreme example of this is seen in **B** (arrow points to the compressed PZ).

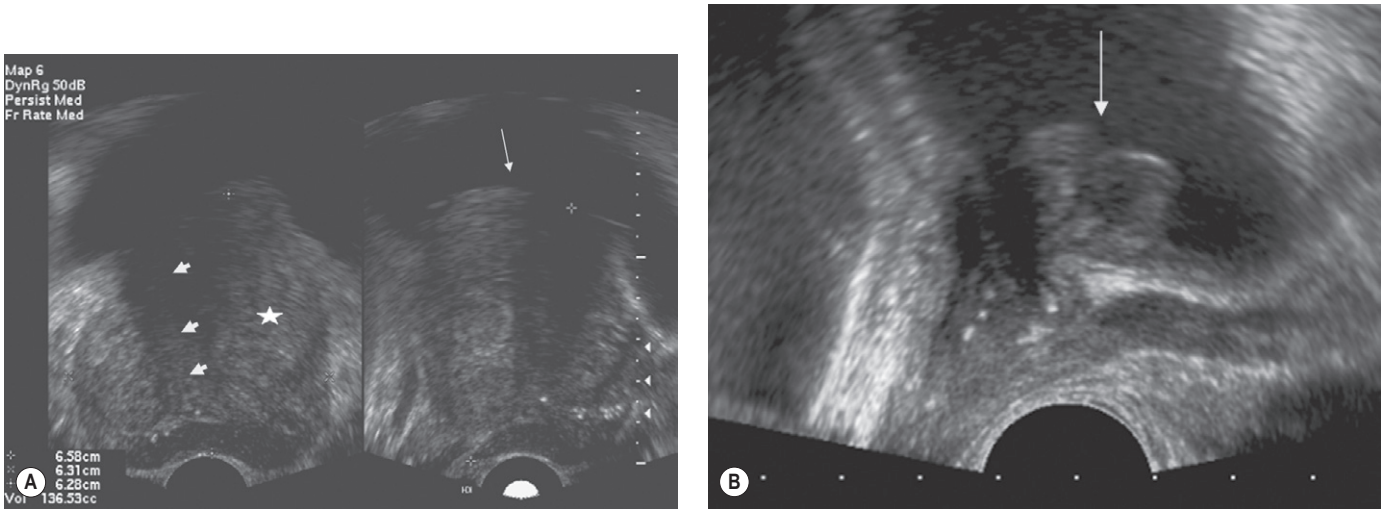


Figure 30.10 **Benign prostate hyperplasia. A:** This image demonstrates many of the typical anatomical findings of a gland with BPH. The star indicates asymmetrical enlargement, with a disproportionately larger left lobe. The arrowheads point to a deviated prostatic urethra and the thin arrow to the elevated bladder base. The size has been measured (bottom left of image). Note also that the entire peripheral zone is hypoechoic, which proved to be malignant on biopsy. **B:** This gland is nominally of normal size (25 mL) but BPH has resulted in disproportionate enlargement of the 'median lobe' (arrow), which is protruding into the bladder

adenomas can be seen in the PZ, again distinguished by a well-defined edge, mixed echogenicity and peripheral flow.

TRUS has not been proven to add much useful information in the evaluation of the patient presenting with suspected BPH, reduced flow rates or LUTS, apart from prostate sizing. Recent data suggest that there is a link between size and eventual bladder retention, and need for surgery. Another use for size estimation is that glands >100 mL may be better treated by retropubic prostatectomy, rather than transurethral resection. TRUS is also not of proven value in the follow-up of the patient on conservative or pharmacological management of known BPH. 5-Alpha reductase agents can decrease the gland size by up to 25%, but repeated TRUS for size estimation does not directly influence management. Rarely, TRUS may provide useful diagnostic information. Occasionally, an obstructing cyst at the bladder neck may be seen. Such cysts can be aspirated under TRUS guidance to relieve obstructive symptoms but the benefit is temporary.

The value of TRUS for evaluating recurrent outflow obstruction has also not been proven. On scanning, regrowth and restriction of the bladder neck may be seen, but does not influence management as much as urinary flowmetry and post-void residues. TRUS also tends to underestimate the size of the cavity after transurethral resection of the prostate (TURP), unless examined with a moderately full bladder. A good cavity is 1–2 cm in diameter and extends towards the apex of the gland (Fig. 30.12). Compromised cavities occur because of inadequate resection, when TRUS will show a tiny cavity or none at all, and bladder neck stricture will show a mid-prostatic cavity with a closed echogenic bladder neck. In recurrent hyperplasia, an adenoma may be seen reducing the TURP cavity (Fig. 30.13).

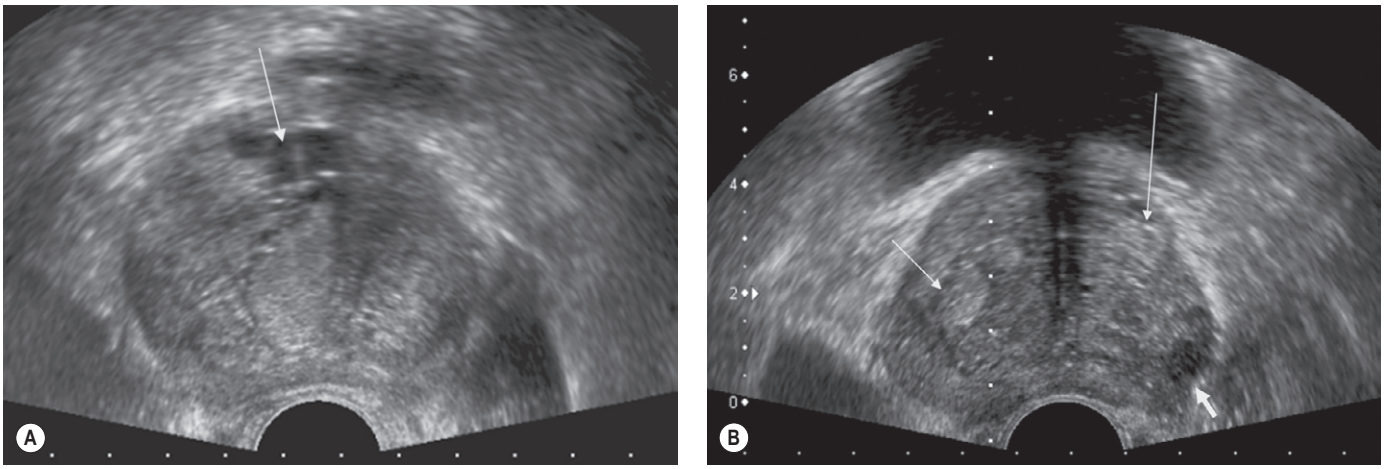


Figure 30.11 Prostate gland with background BPH. A: Cystic changes are present anteriorly (arrow). These are believed to represent degenerative adenomas rather than obstructed ducts or gland structures. **B:** Bilateral hyperechoic nodules in the inner gland, consistent with adenomas (arrows), and a solitary hypoechoic adenoma in the left lobe (short arrow).

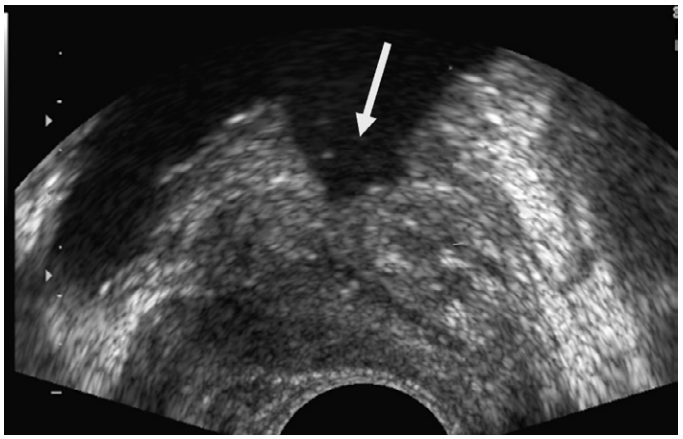


Figure 30.12 An example of a good transurethral resection cavity. However, there is no clear correlation between the size of the cavity and the recurrence of poor urinary flow.

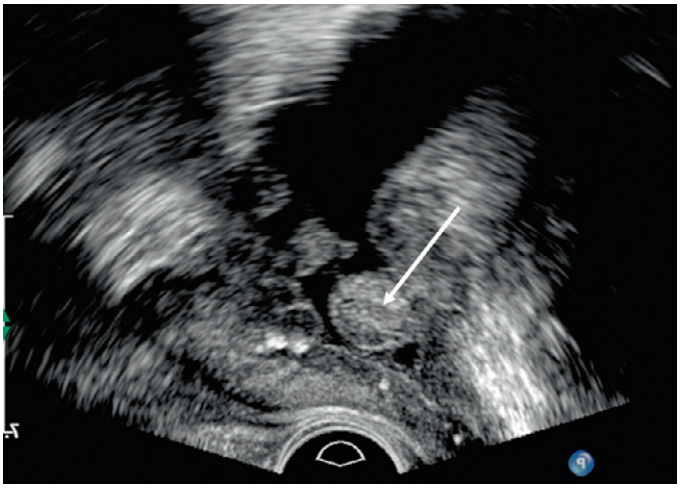


Figure 30.13 Longitudinal TRUS view showing regrowth of benign prostate hyperplasia, with a prominent adenoma (arrow) protruding into the TURP cavity.

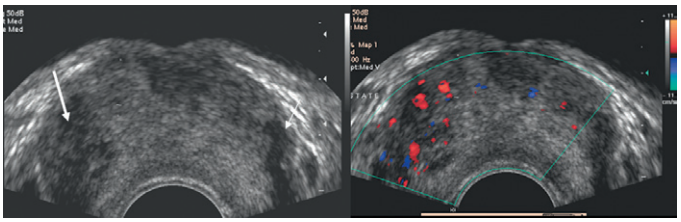


Figure 30.14 Axial images showing focal prostatitis. On the left-hand image, there is a large echo-poor area affecting the right inner gland (arrow), and to a lesser extent the left inner gland (thin arrow). The larger area is shown to be of increased vascularity on colour Doppler ultrasound in the second image. The appearances are consistent with acute prostatitis, with early abscess formation.

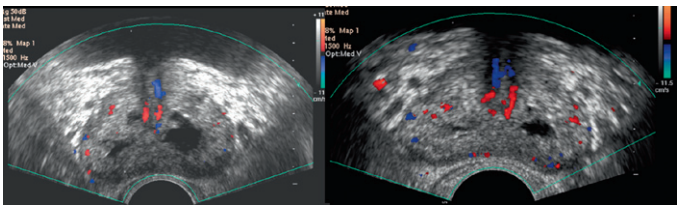


Figure 30.15 Axial images showing bilateral inner gland cavities, representing abscesses. The second image (right hand) was taken after TRUS-guided aspiration of the abscess in the left lobe.

Prostatitis

The clinical, pathological and sonographic features of prostatitis vary widely (Table 30.1). Acute prostatitis is uncommon but can occur in the young man, and is due to infection by the usual urinary tract organisms. Systemic signs of infection are present, and the prostate gland is tender on rectal examination. On TRUS, the gland may show increased generalised or focal vascularity (Fig. 30.14). The gland is of focal or generalised decreased echogenicity and the capsule is thick or ill defined.[11] An abscess may be seen as focal cystic degeneration (Fig. 30.15), with a thick capsule and/or air,[12] and may be drained by TRUS-guided aspiration (see below). However, the gland may also be entirely unremarkable.

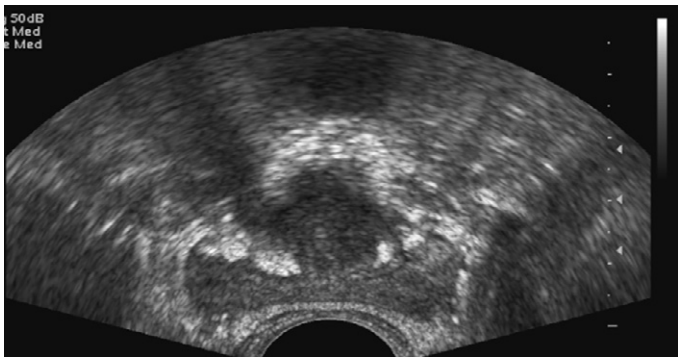


Figure 30.16 Axial image of one of the described appearances of chronic prostatitis, with heavy inner gland calcification.

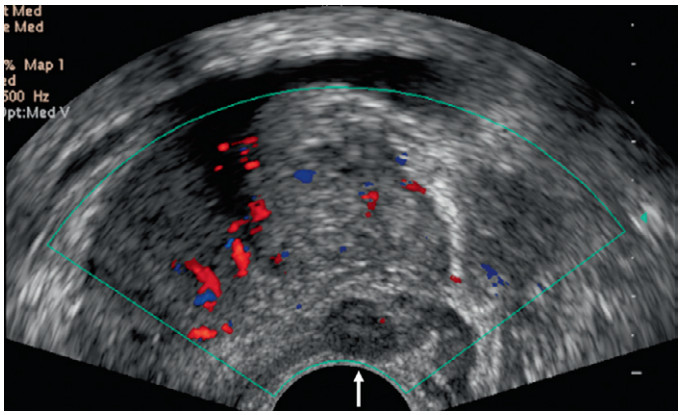


Figure 30.17 An axial TRUS image showing the typical sonographic appearances of granulomatous prostatitis, with a discrete hypoechoic (or mixed echoic) nodule located in the peripheral zone (arrow). This elevates, but does not penetrate through the capsule. The vascularity is either normal or mildly elevated. Similar appearances may be seen with malignancy or a BPH nodule.

Chronic prostatitis is more common. The cause is still unknown, but thought to be non-bacterial. Symptoms are vague and persistent perineal discomfort is commonest. Reduced urinary flow and incomplete emptying may also feature. On TRUS, the signs are as non-specific as the symptoms – distension of the periprostatic veins, dystrophic inner gland (Fig. 30.16) and peri-urethral calcification or hyperechoic thickening of the capsule have all been described.[2] But their specificity is limited and findings need to be correlated with the clinical picture and biochemistry of prostate secretions after massage. Although midline cysts are often seen, presumed to be utricle cysts, their relationship with recurrent prostatitis is not established. This merits study as utricle cysts can communicate with the urethra.

Less common causes of prostatitis are eosinophilic prostatitis or granulomatous infections. Most granulomatous infections are idiopathic but tuberculosis (TB), either infective or the result of BCG instillation to treat bladder transitional cell carcinoma, may be a cause. On TRUS, a TB gland may be of diffusely decreased echogenicity or characteristically a mixed echotexture nodule may be seen in the peripheral zone. Caseating nodules are rarely seen. Other non-infective causes of prostatitis are sarcoidosis and Wegener's granulomatosis. Their appearances are non-specific.

A separate entity, granulomatous prostatitis,[13] has more distinct clinical and ultrasound features. Typically, a nodule can be palpated in the posterior gland, and on ultrasound a bulging nodule of mixed echotexture is seen (Fig. 30.17). Crucially, the capsule and the periprostatic fat planes are intact and the nodule is well defined – thus similar to a BPH nodule occurring in the PZ, except it can exhibit increased internal vascularity, like cancerous nodules. Occasionally the nodule is hypoechoic and entirely indistinguishable from prostate cancer. Its close clinical and sonographic resemblance to prostate cancer is the major importance of this enigmatic form of prostatitis. They can also be persistent.

Table 30.2 Cysts of the prostate gland and associated structures

Developmental

1. **Müllerian remnant cysts** – midline, usually extend above the gland. Can be large. No sperm. No communication with urethra
2. **Utricle 'cysts'** – midline, at the level of the verumontanum, intra-glandular. Usually less than 1 cm. Rarely may contain sperm. May communicate with urethra

Acquired

1. **Duct ectasia** – mild distension of normal ducts. Very common
2. **Ejaculatory duct cysts** – just lateral to midline. Post inflammation or TURP. Contain sperm or calculi with seminal vesicle dilatation
3. **Cystic degeneration of BPH nodules** – commonest cysts. In transition zone
4. **Retention cysts** – due to dilatation of gland acini. May cause obstruction if located close to the bladder neck ('ball valve' obstruction)
5. **'Cavitary prostatitis'** – rare, due to prolonged inflammation. Multiple cysts
6. **Abscess** – post prostatitis, commoner in diabetics and after bladder catheterisation. Thick-walled and septated
7. **Cystic prostate cancer** (very rare)

Benign prostate diseases

- The sonographic features of prostatitis are non-specific (distension of periprostatic veins, dystrophic inner gland, focal calcification).
- Focal or diffusely low echogenicity, increased vascularity and/or an abscess may be seen with acute prostatitis.
- Granulomatous prostatitis is a very close sonographic mimic of prostate cancer.
- Benign prostate hyperplasia commences in the transition zone and the peri-urethral glands.
- Adenomas due to BPH are generally of mixed echogenicity, but with a well-defined edge and peripheral vascularity.
- Cystic lesions are rarely malignant.

Cysts of the prostate gland and associated structures

The vast majority are benign[8] and have characteristic locations (Table 30.2). The commonest is a utricle cyst (Fig. 30.18A). These have been dealt with above (under congenital or developmental anomalies), as have Müllerian remnant and seminal vesicle cysts. In the older man, cystic areas usually represent areas of degeneration within BPH nodules. More diffuse, smaller cysts can be seen with ductal ectasia (Fig. 30.18B) and abscesses can be cystic masses. Cystic prostate cancers (Fig. 30.18C) are very rare. Histologically they are indistinguishable from common prostate cancers. Although

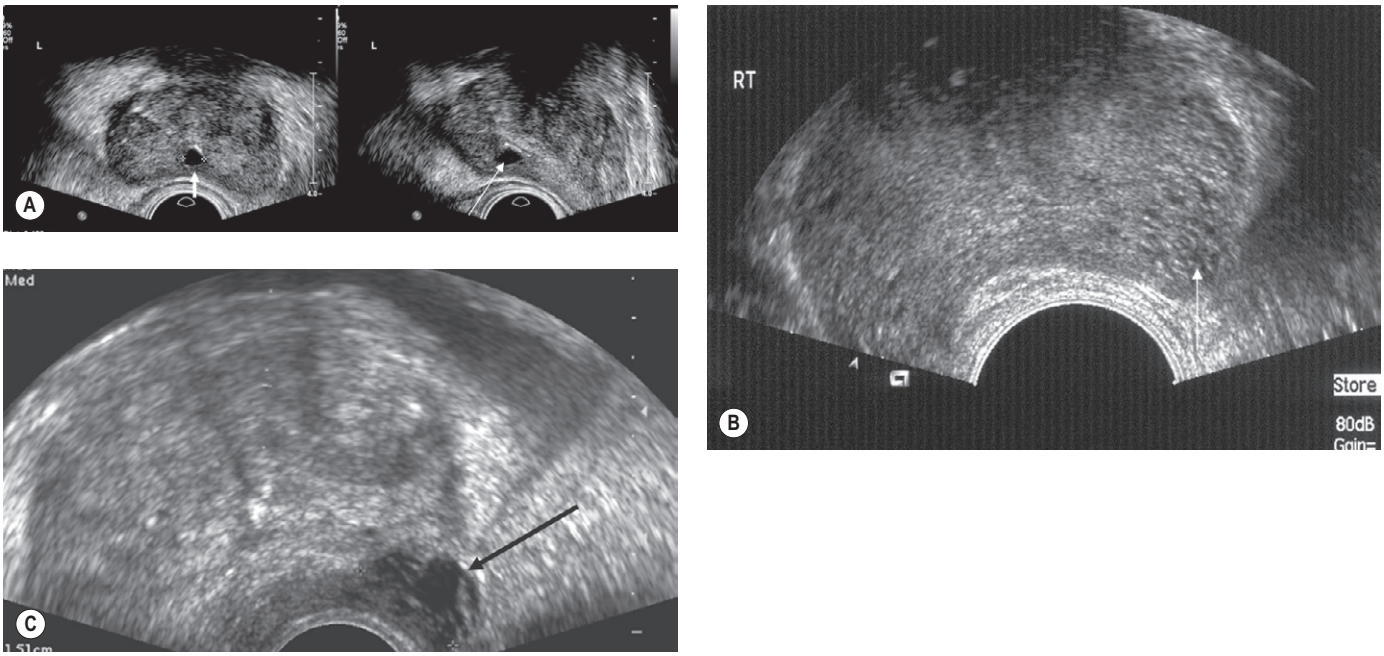


Figure 30.18 **Cysts. A:** Axial and longitudinal images of a typical utricle cyst (arrow). Note its midline position, good definition, and transonic nature. It is entirely intra-prostatic and of teardrop shape on the longitudinal image. **B:** Axial image showing normal ductal ectasia of the peripheral zone (arrow). This has no clinical significance. **C:** An example of a cystic prostate carcinoma. These are rare.

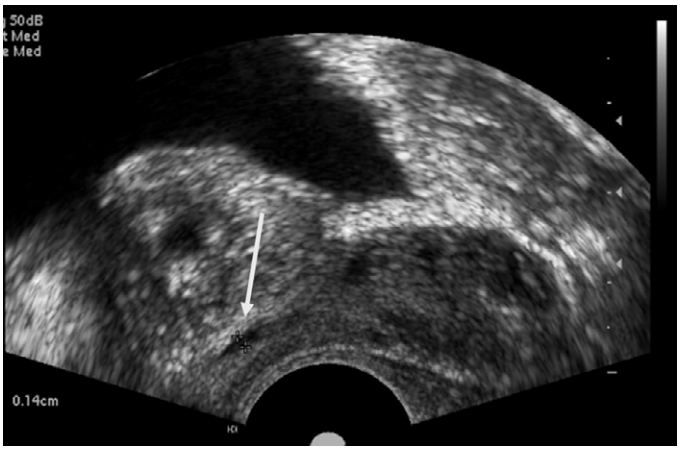


Figure 30.19 **A minimally dilated ejaculatory duct** (arrow). Normal ducts have no identifiable lumen (note that this sagittal image is inverted, with the seminal vesicles on the right side of the image).

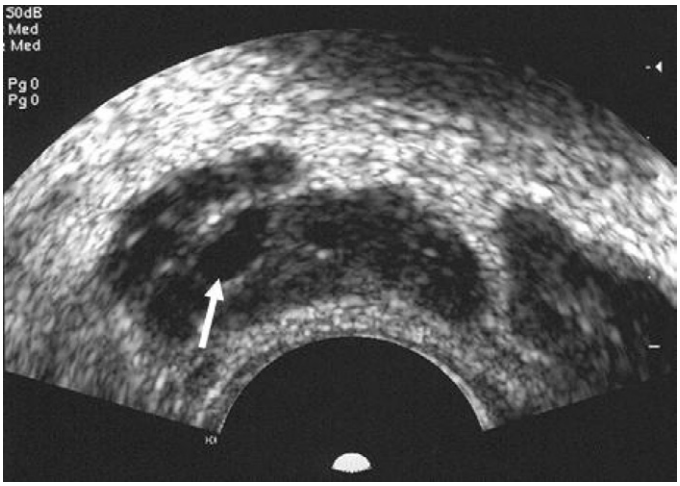


Figure 30.20 **Mild seminal vesicle distension** (arrow) (note how the lumen of the right seminal vesicle is clearly visualised) can be a normal finding (unlike the ejaculatory duct – see Fig. 30.19). This can be confirmed as normal physiological storage by repeat scanning following ejaculation.

mucinous prostate cancers can occur, their TRUS appearances are said to be non-specific. Nevertheless, it is best to assume that semi-solid cysts in the PZ are possible neoplasms, unless proven otherwise, although other nodules of the PZ, e.g. BPH or granulomatous prostatitis, can also be cystic.

TRUS and evaluation of male infertility

Routine imaging is not useful, but TRUS may provide valuable information in men (Table 30.1) with reduced or an unrecordable sperm count.[14,15] Ejaculatory duct obstruction is suggested by dilatation of the ducts (normal ducts have no identifiable lumen – Fig. 30.19) and/or seminal vesicles. Mild vesicular distension can be seen with normal physiological storage (Fig. 30.20) and can be identified by repeat scanning after ejaculation. True obstruction may be due to calculi in the ducts (Fig. 30.21), with or without duct stricturing. Occasionally a large Müllerian remnant or utricle cyst may obstruct the ducts (Fig. 30.22); or the seminal vesicles, vasa and ejaculatory ducts may all be absent as part of a generalised maldevelopment of the embryological Wolffian duct. The commonest cause of retrograde ejaculation is post TURP, but a rarer cause is dyssynergia of the external sphincter.

TRUS and haematospermia

An isolated episode of haematospermia is very common, and a cause is seldom identified, even after extensive investigation. Such

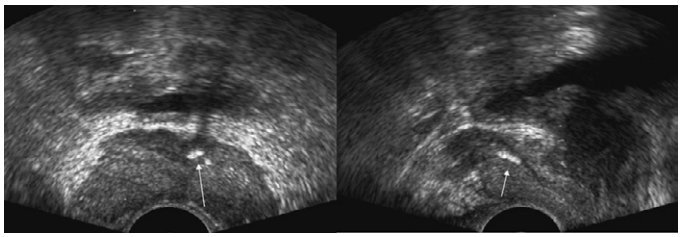


Figure 30.21 Midline axial and longitudinal images showing a calculus in the left ejaculatory duct (arrow).

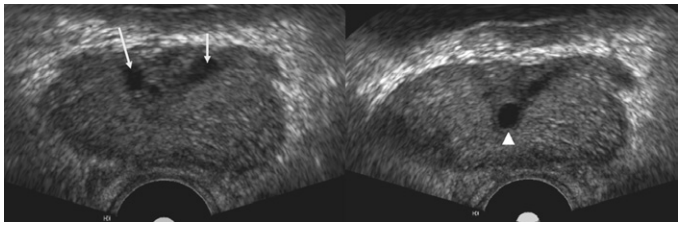


Figure 30.22 Two midline axial images through the base of the prostate gland, showing that both ejaculatory ducts are dilated (arrows) secondary to a midline cyst (arrowhead) which could be either a Müllerian remnant cyst or a utricle cyst.

cases do not merit TRUS evaluation. However, repeated episodes should be examined; causes include ejaculatory duct calculi (Fig. 30.23) or bleeding into a Müllerian remnant or utricle cyst (Fig. 30.24).[16] Other causes that may be identified are prostatitis or other inflammatory causes, but cancer, of the gland, SVs or EDs, is an extremely uncommon cause; in which case, the tumour is obvious and hypoechoic.

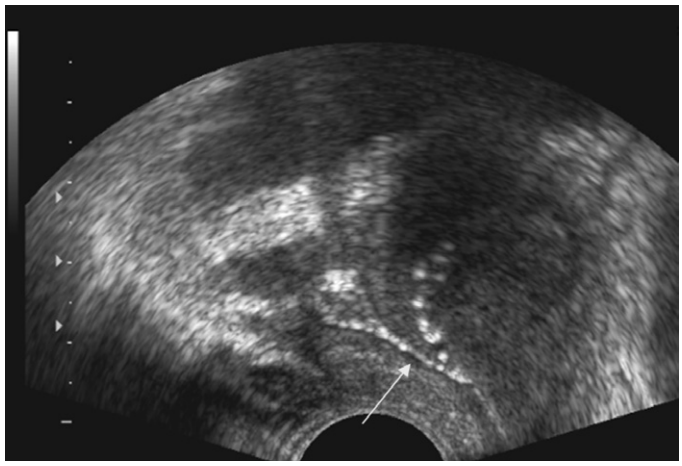


Figure 30.23 Diffuse calcification (arrow) involving the ejaculatory duct in a man with haematospermia (note that the seminal vesicles are on the right-hand side of the image).

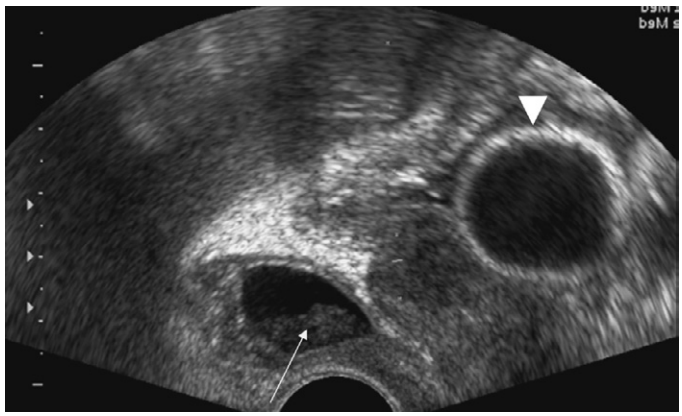


Figure 30.24 Haematospermia. A longitudinal image showing a Müllerian remnant cyst that has bled internally (arrow). The patient has a urethral catheter in place (balloon of catheter – arrowhead).

ACQUIRED ABNORMALITIES: MALIGNANT

Carcinoma of prostate

TRUS diagnosis of prostate cancer

Now the commonest non-cutaneous male cancer over 80% originate in the peripheral zone.[3] The remainder arise in the central/transition zone or are anteriorly infiltrating peripheral zone cancers. As the peripheral zone is the most homogeneous of the zones, even in the presence of marked hyperplasia, most cancers should be easily visible. Yet this is not so. Although highly variable appearances have been described (illustrated in Fig. 30.25, and also see Figs 30.26 and 30.27),[4] ranging from hypoechoic to hyperechoic, in modern practice most cancers are isoechoic or barely visible; a reflection of the downward stage migration of prostate cancer at presentation. Table 30.3 illustrates the various types and locations of abnormality that may be seen with prostate cancer, and their diagnostic reliability.

Often the abnormality is subtle, and careful examination is important. The posterolateral 'horns', apices and the base of the gland close to the seminal vesicles are areas of higher cancer incidence and also relative 'blind' areas; they should be scrutinised in multiple orientations and the two sides compared. Even then, described abnormalities are not specific enough as inflammation, hyperplasia, prostatic intra-epithelial neoplasia and necrosis can all look similar.[2,4]

Study of gland vascularity improves the specificity – by about 5–10%,[17] and this performance is only slightly further improved by the use of power (or colour energy) Doppler or the use of ultrasound contrast media.[7] Three general flow patterns have been described (Fig. 30.25) – focal flow, increased flow around a nodule or asymmetric flow with increased number and size of vessels on the side harbouring tumour. When seen in association with a hypoechoic nodule, all three are highly suggestive of cancer; but in the more difficult area of isoechoic tumour, flow is disappointingly often normal or unhelpful. Simple 3D TRUS systems and elastography are now becoming available, but their value is unproven. In current practice, TRUS is accurate if the described changes are seen in the presence of a significantly elevated prostate-specific antigen (PSA) level, but not accurate for confident exclusion of prostate cancer in those with mildly elevated PSA (especially if <10 ng/mL). Prostate biopsy (covered below) is necessary to confirm suspected malignancy or to confidently exclude low-volume or isoechoic cancer in all patients with clinical suspicion of tumour.

Staging of prostate cancer

As most tumours in contemporary practice are isoechoic, staging by TRUS is only applicable in the minority with visible cancers (Table 30.3). Tumour volume – T2 staging – is inaccurately assessed

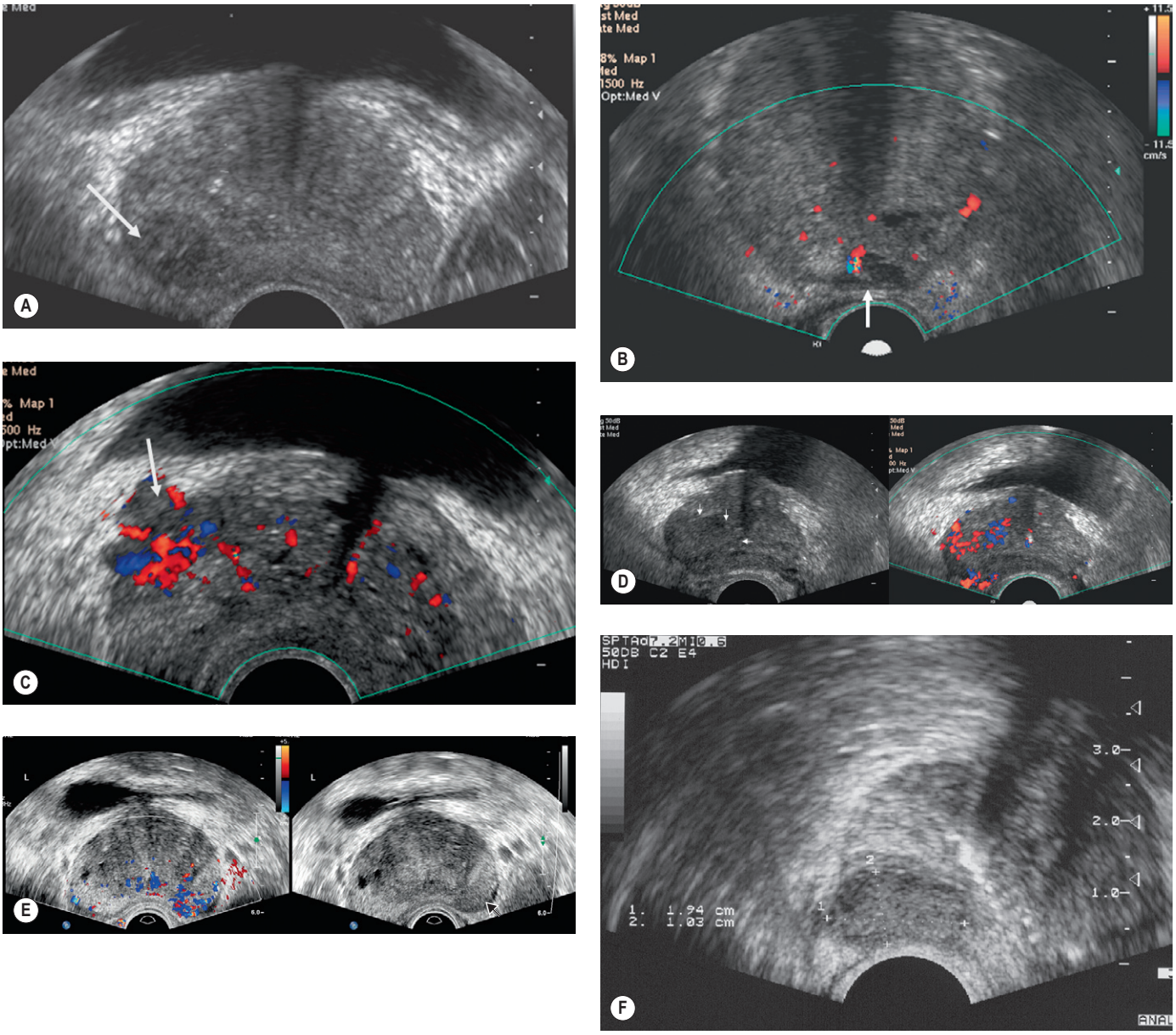


Figure 30.25 **Prostate cancer. A:** A diffuse mixed echotexture abnormality (arrow) affecting the right peripheral zone that proved to be a Gleason 3+3 cancer on biopsy. **B:** A well-defined hypoechoic abnormality in the midline peripheral zone of mildly increased vascularity (arrow), extending into the left inner gland. This proved to be a Gleason 3+3 cancer on biopsy. **C:** The arrow points to a mixed echotexture nodule in the right inner gland, extending into the periprostatic fat, and of increased vascularity. This proved to be Gleason 4+4 tumour on biopsy. **D:** Note the asymmetry and enlargement of the right lobes. The differentiation between the right peripheral zone and inner gland is lost (outlined by arrows). This area is also of increased vascularity. This proved to be a Gleason 5+5 tumour on biopsy. **E:** A subtle cancer located in the left peripheral zone (arrow), but of increased vascularity. This proved to be a Gleason 3+3 tumour on biopsy. **F:** A large tumour of mixed echogenicity located in the right peripheral zone.

on TRUS, but bilateral nodules imply stage T2C disease. Regarding T3/4 staging,[2,4,18] the areas of the prostate gland where local invasion is more likely are the neurovascular bundles, the seminal vesicles (Figs 30.26, 30.27), the ejaculatory ducts, the apex of the gland and the prostate capsule, immediately adjacent to the tumour. All are areas of relative weakness of the prostate capsule, where structures pierce through the capsule, which is consequently thin or deficient.

Extracapsular extension (ECE) – T3A disease – is best seen on axial scans. Early ECE is seen as an irregular hypoechoic bulge of the capsule, but a long line of contact is a surrogate indicator of a high likelihood of local invasion. If tumour is seen to extend into the periprostatic fat, then advanced ECE is diagnosed. Neurovascular bundle involvement will create an asymmetry of these structures, best appreciated on axial views. The sign of seminal vesicle involvement – T3B disease – is loss of the acute angle between the

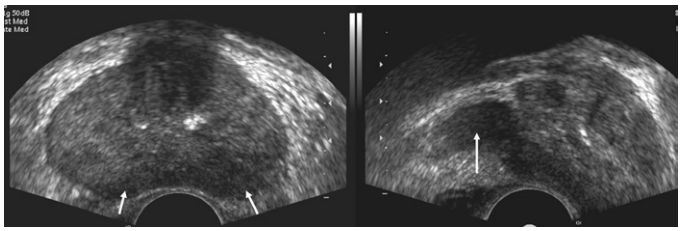


Figure 30.26 A locally advanced prostate cancer. On the left-hand image the hypoechoic tumour (arrows) is seen to involve both peripheral zones and on the right-hand (longitudinal) image the hypoechoic change extends into the seminal vesicle (arrow). This is therefore a T3b tumour.

Prostate cancer

- The commonest non-cutaneous cancer in males.
- Over 80% originate in the peripheral zone.
- In modern practice the majority of cancers are isoechoic.
- The commonest sonographic sign is a hypoechoic nodule or region in the peripheral zone with internal vascularity.
- Colour Doppler imaging further improves specificity by about 10% when compared to greyscale TRUS.
- Staging by TRUS is only 56–86% accurate.
- Current practice favours 10- or 12-core biopsy pattern.

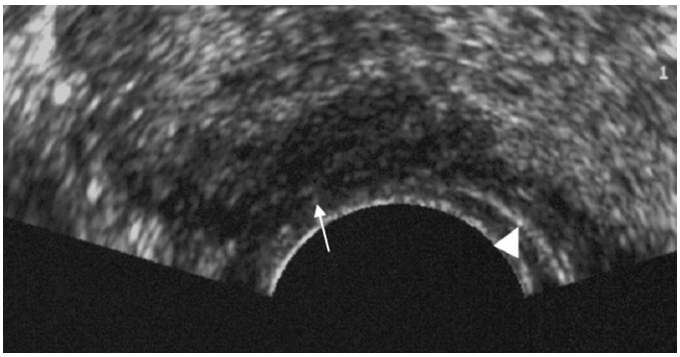


Figure 30.27 Prostate cancer. Note that the fat plane between the prostate gland and the rectal wall (arrowhead) is lost adjacent to the tumour in the right peripheral zone (arrow). This is therefore a T3a tumour.

vesicle and the prostate base in the longitudinal plane. Extension inferiorly from the gland apex into the membranous urethra –T4 disease – is very difficult to recognise; but tumour reaching up to the levator muscles – also T4 disease – can be recognised. Enlarged nodes are seldom seen as the focal length of TRUS is restricted. For this pelvic US is better, and MRI or CT best.

The accuracy of TRUS in local staging is only modest. Reported sensitivity, specificity and accuracy ranges are 50–92%, 46–91% and 58–86% respectively for ECE. For seminal vesicle involvement the sensitivity is 22–60%, specificity about 88% and accuracy 78%; but it should be understood that these are historical figures and modern TRUS staging may perform more poorly still, as contemporary cancers are isoechoic. Colour Doppler is not of proven value and for non-invasive staging magnetic resonance imaging is most accurate, and a sensitivity of 91% and specificity of 96% for MRI with spectroscopy have been reported,[19] although modern studies report lower figures of 78% and 88% respectively.[20]

Clinical outcome of prostate cancer is also dependent on the histological score (the Gleason score) and this is determined from the prostate biopsies; and further, less specific, measures of clinical outcome include the number of prostate biopsies that reveal cancer, the percentage of the core length involved by cancer and whether biopsies from both lobes were positive.

Follow-up of prostate cancer or assessment of suspected recurrent tumour

TRUS is of limited value[2] and cannot replace PSA estimation for disease monitoring. After radiotherapy, the gland can vary from diffusely hypoechoic to a mixed echo pattern, with or without a prominent 'capsule'. The value of colour Doppler has not been established (Fig. 30.28). After prostatectomy, findings depend on the level of the PSA or the rate of rise of the PSA (the PSA velocity). High levels and velocity are more indicative of metastatic disease, but a slow rise is seen in those with local prostate bed recurrence. In the latter case, hypoechoic nodular areas (Fig. 30.29) in the prostate bed, of increased flow, may be seen; however, fibrosis can look similar and biopsy confirmation is necessary.

Prostate ablation, by high-frequency ultrasound or cryotherapy, leaves a large cavity, which is markedly stiff and fibrotic but avascular on colour Doppler US. Residual tumour can be difficult to identify, and biopsy is required.

UNUSUAL TRUS ABNORMALITIES

Other rare prostate abnormalities may be seen (Fig. 30.30) and their sonographic findings are described in Table 30.4.

TRUS-GUIDED INTERVENTION

Prostate biopsy

Principles of prostate biopsy

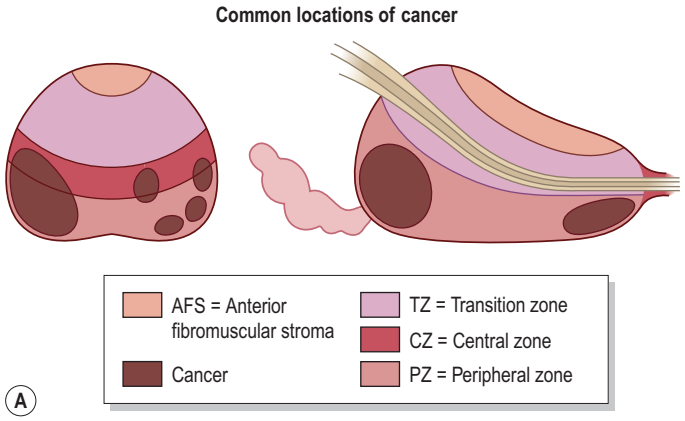
Uniquely among image-guided biopsies, prostate biopsy is not (generally) lesion directed. As discussed, most prostate cancers in contemporary practice are isoechoic or diagnostically non-specific. Being invisible, targeted biopsies are naturally not feasible. So prostate biopsy is a sampling technique,[21] but sampling is systematic, not random, and biopsies are targeted onto the portion of the prostate most likely to harbour cancer – i.e. the peripheral zone.

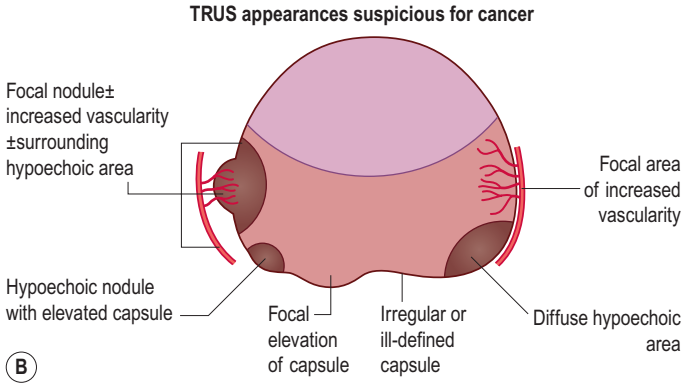
Modern probe biopsy is via the transrectal route and the transperineal route is reserved for brachytherapy implantation or template-based biopsy techniques. The advantage of the transrectal route is its convenience, but there is a higher risk of infection and per-rectal bleeding – range of 0–4% and 1.3–58% respectively in pooled data.[22] Thus antibiotic prophylaxis is necessary; the agent of choice varies but a 5-quinolone is most often used, e.g. ciprofloxacin. The comfort level of the procedure has also been improved by the use of local anaesthesia.[23]

The number of biopsies necessary to confidently exclude clinically significant prostate cancer undergoes constant change.[21] This reflects the changing demographics of tumours at presentation. Early stage tumours are smaller in volume and naturally only identifiable by wider sampling. Six cores, targeted onto the peripheral zone, was the historical practice standard, but as this missed many cancers (19–31%) 10 or 12 cores are now recommended in the UK[24]

Table 30.3 Prostate cancer – illustration of the various features described on transrectal ultrasound (figure modified from Patel U, Rickards D, Handbook of Transrectal Ultrasound and Biopsy of the Prostate, Martin Dunitz, 2002)

Prostate cancer	Site	TRUS features
Diagnosis		
There is a correlation between PSA level and sono-visibility. Below 10 ng/mL less than 30% are seen, but this rises to >75% if PSA level is >20 ng/mL. In modern practice most tumours are not visualised as the median PSA is <10 ng/mL	PZ – 75% TZ/CZ – 25%	Strongly suggestive: • Hypoechoic nodules with indistinct edge in PZ • Diffuse hypoechogenicity in PZ • Nodule with surrounding altered echogenicity • Hypoechoic area in PZ with increased vascularity Moderately suggestive: • Hyperechoic or isoechoic focal bulge of the PZ • Irregular or ill-defined capsule Weakly suggestive: • Hypoechoic nodule in the inner gland • Focal increase in vascularity of an isoechoic area in the PZ • Focal increase in vascularity in the inner gland
Staging		
Accuracy – 50–92% for extracapsular extension, 78% for seminal vesicle extension; but these are historical figures. There are no modern data available, but modern accuracy is likely to be poorer still, as most cancers diagnosed now are early stage, with PSA <10 ng/mL		Extracapsular extension: • Irregular hypoechoic bulge of capsule • Infiltration into periprostatic fat Neurovascular bundle: • Asymmetry • Enlargement Seminal vesicle (SV) involvement: • Loss of angle between SV and base of gland • Enlargement of SV High Gleason grade: • High flow on Doppler US may signify higher Gleason grades





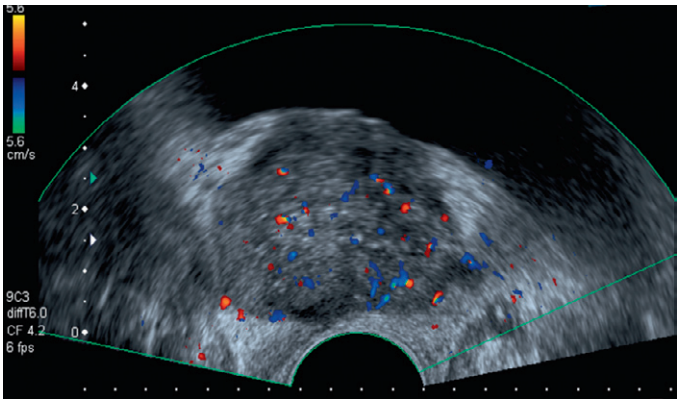


Figure 30.28 An example of recurrent tumour post radiotherapy. The appearances of the gland after radiotherapy (or brachytherapy) are highly variable but normally uniform be it hypoechoic or isoechoic and symmetrical. Residual tumour can only be identified on biopsy. This example shows clear asymmetry of appearances, with hypoechoic change in the left lobe with mildly increased vascularity. Recurrent tumour was confirmed on biopsy.



Figure 30.29 Longitudinal view of a recurrent tumour, seen as a hypoechoic nodule (arrow), after radical prostatectomy. These appearances are non-specific and postoperative fibrosis can look the same. If increased vascularity is seen then tumour is more likely.

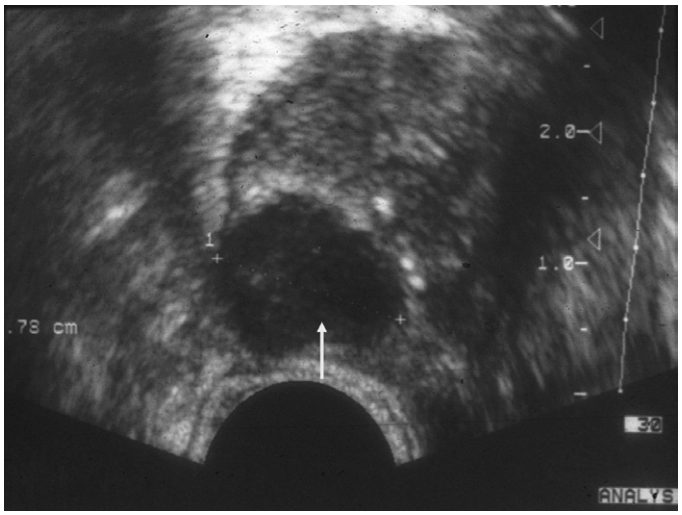


Figure 30.30 A large hypoechoic nodule (arrow) located in the right peripheral zone. This was due to tuberculosis.

Table 30.4 Unusual abnormalities of the prostate gland

		TRUS findings
Tuberculosis	May be secondary to intravesical BCG for treatment of bladder cancer	Like prostatitis
Sarcoidosis		Non-specific
Infarction	Particularly after catheterisation	Hypoechoic nodules
Lymphoma	Usually non-Hodgkin's	Large hypoechoic masses throughout the gland with periprostatic infiltration
Leukaemia		Non-specific
Metastasis	Lung, melanoma	Non-specific
Comedocarcinoma		Hypoechoic nodules with multiple small hyperechoic foci
Primitive neuroectodermal tumour		Multilobulated, multinodular
Cystic adenoid carcinoma		Normal or hypoechoic nodule
Sarcoma		Huge heterogeneous mass between bladder and rectum
Solitary fibrous tumour		Hypoechoic nodule
Rhabdomyosarcoma		Isoechoic
Other rare cancers		Non-specific

Note: the data on many of these are sparse. Usually merely a few case reports.

Preparation and equipment necessary for transrectal ultrasound-guided prostate biopsy

- Stop warfarin till INR <1.3. Stop clopidogrel for 10 days. Data show that aspirin may be continued safely, but many practitioners stop for 7 days prior the biopsy. Commence antibiotics at least one hour before biopsy.
- Biopsy attachment. Either a disposable unit or a reusable metal guide.
- 15–20 cm long, 22G spinal needle, 10 mL syringe and 1% plain lidocaine for local anaesthesia.
- Fresh 18G biopsy needle, with biopsy 'gun' or device. Needle length longer than the length of the biopsy guide. Seminal vesicle biopsies are easier with a 20 cm long needle. Core length of the needle 'notch' should be 1.5–2.0 cm, but seminal vesicle biopsy requires a shorter core length of 1 cm.
- Separate pots with formalin-saline solution for each core so the anatomical position of the tumour is known.
- A small pot of sterile saline to swizzle and clean the needle tip of formalin between biopsies.

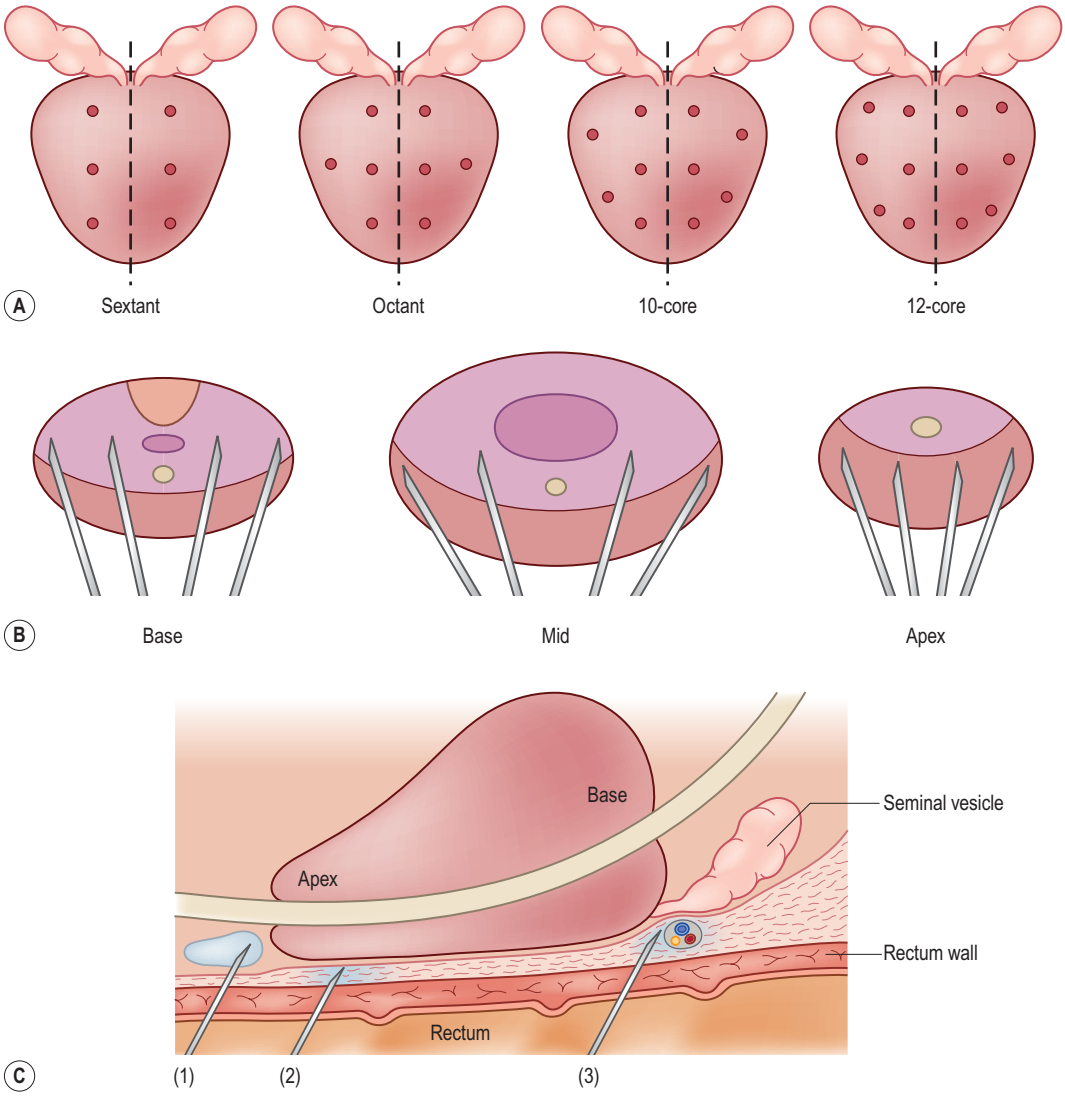


Figure 30.31 **The principles behind prostate biopsy** (or more accurately prostate gland sampling) and the method of prostate anaesthesia. The first row **(A)** illustrates the various biopsy schemes used, in the coronal plane. The first is the classical sextant pattern. This misses about 25% of cancers. The next three schemes illustrate the octant, 10-core and 12-core regimes respectively. In current practice the 10- or 12-core regime is favoured, but this may change in the future with further down-migration of prostate cancer at presentation.

Prostate biopsy is a systematic sampling technique, and this is further emphasised in the second row **(B)** showing that cores are preferentially targeted onto the peripheral zone as most cancers arise here. Note how the needle trajectories have been aimed anterolaterally to maximise peripheral zone sampling.

The last row **(C)** illustrates the various methods for anaesthetising the gland. In (1) the needle is advanced to just outside the apex and the local anaesthetic injected to create a pool around it. In (2) the injection has been made into Denonvillier's fascia, just beyond the rectal wall. In the last example (3), the local anaesthetic has been introduced around the neurovascular bundle, between the base of the gland and the seminal vesicle. Any of these three sites can be used, as none is of proven superiority, but both sides should be injected for maximum effect. Injection directly into the gland is of no benefit. (Note that image **C** is inverted, with the apex of the gland on the left-hand side, as this is the orientation used during TRUS-guided interventions on most machines.)

– but there are no firm recommendations by other national bodies – though some have made a case for 14–18, or more.[21] Figure 30.31 illustrates the principles of targeting and summarises the technique.

In a minority, in spite of repeated negative 12-core biopsies, there continues to be a suspicion of an undisclosed cancer, e.g. rising PSA levels. In this case saturation biopsy can be carried out.[25] The definition of saturation is subjective, but most agree that at least 24 (and up to 40) cores should be taken and that the entire gland, both inner and outer portions, should be sampled. This can be carried out via the transrectal route, or more precisely by transperineal needle puncture using a template,[26] under sedation or general anaesthesia. The relative safety of both methods has been described, but either method is associated with a significant risk of temporary outflow obstruction (5–10%), which may require bladder catheterisation for a few days.

Biopsy of the post-prostatectomy bed

After total prostatectomy the PSA level should be near undetectable. If not, or if the PSA later starts rising, there is the possibility of residual prostate cancer. This is more likely if there were positive

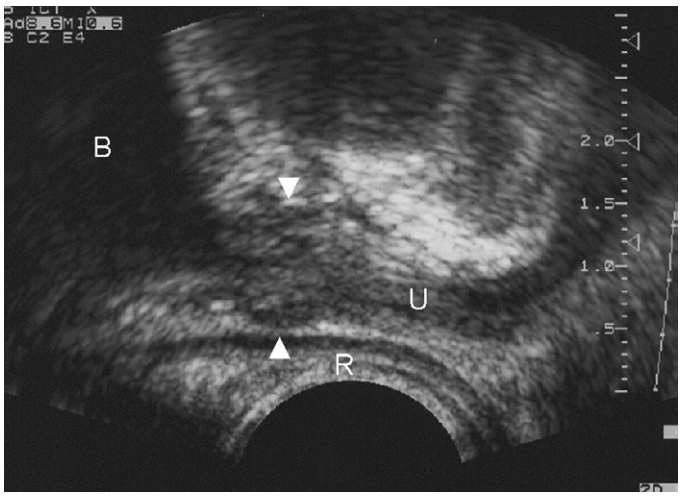


Figure 30.32 Normal appearance of the prostate bed post radical prostatectomy. The anastomosis is shown between the arrowheads. Note the overall symmetrical appearance, of a mixed echotexture. Hypoechoic areas could represent either recurrent tumour or fibrosis. Only biopsy can confidently differentiate. (B, bladder; U, urethra; R, rectal wall.)

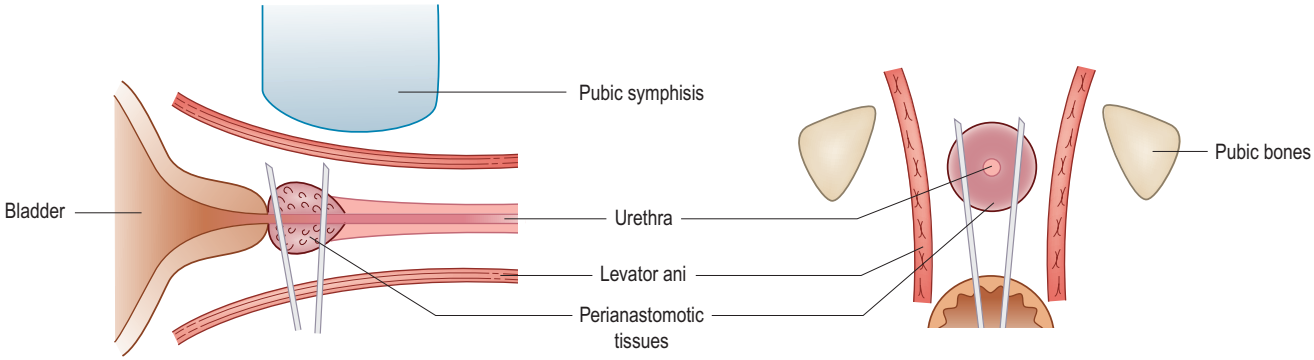


Figure 30.33 Needle targeting when the prostate bed is biopsied following radical prostatectomy.

surgical margins post-prostatectomy – which occurs in 10–40% of cases, depending on surgical expertise and patient selection. If appropriate investigations (bone scan and CT/MRI) are negative for occult metastatic disease, residual/recurrent disease at the anastomosis needs to be excluded.

On TRUS, the anastomosis and its surrounding tissues are normally symmetric and of mixed echotexture (Fig. 30.32), representing postoperative fibrosis and normal tissues. Recurrent tumour is more likely to be hypoechoic and of (mildly) increased vascularity.[2,25] The seminal vesicle beds should also be examined, as this may be the site of residual cancer in some cases, especially in those with basal positive margins. In either case biopsy confirmation may be necessary. This is easily carried out under TRUS guidance (Fig. 30.33).[27] Local anaesthetic can be used and is effective, but injection may be difficult because of the fibrosis. Also, this may lead to temporary loss of bladder control as the external sphincter may become anaesthetised. The bladder should be emptied before biopsy. There are few data regarding complications, but these are believed to be no greater than after conventional prostate biopsy and antibiotics should be given. At least two cores, but ideally four, should be taken, one from either side and just above the anastomosis.

Drainage of prostate abscess, cyst or seminal vesicles

Prostate abscesses are generally treated with antibiotics, but drainage should be considered if clinical response is poor. In such a case simple TRUS-guided needle aspiration can be performed. Occasionally, cyst drainage of utricle or Müllerian remnants may be performed to sample contents. Although the transrectal route is simplest and can be carried out safely, the transperineal route will reduce the risk of introduced infection or contamination.

Injection of seminal vesicles or ejaculatory ducts with iodinated contrast under combined TRUS/fluoroscopic guidance is an elegant method for confirming obstructive infertility, or to show communication between a utricle cyst and the urethra.[28]

REFERENCES

1. McNeal JE. The zonal anatomy of the prostate. Prostate 1981;2:35–49.
2. Patel U, Rickards D. Handbook of transrectal ultrasound and biopsy of the prostate. London: Martin Dunitz; 2002.
3. McNeal JE, Redwine EA, Freiha FS, et al. Zonal distribution of prostatic adenocarcinoma. Correlation with histologic pattern and direction of spread. Am J Surg Pathol 1988;12(12):897–906.
4. Coakley FV, Hricak H. Radiologic anatomy of the prostate gland: a clinical approach. Radiol Clin North Am 2000;38:15–30.
5. Terris MK, Stamey TA. Determination of prostate volume by transrectal ultrasound. J Urol 1991;145(5):984–987.
6. Kelly IM, Lees WR, Rickards D. Prostate cancer and the role of color Doppler US. Radiology 1993;189:153.
7. Halpern EJ, Rosenberg M, Gomella LG. Prostate cancer: contrast-enhanced US for detection. Radiology 2001;219(1):219–225.
8. Nghiem HT, Kellman GM, Sandberg SA, et al. Cystic lesions of the prostate. Radiographics 1990;10:635–650.
9. Gilsanz V. Duplicated Mullerian duct remnants: unilateral occlusion and ipsilateral renal agenesis in a male. AJR Am J Roentgenol 1981;137:174–175.
10. Danaci M, Alpolat T, Bastemir M, et al. The prevalence of seminal vesicle cysts in autosomal dominant polycystic kidney disease. Nephrol Dial Transplant 1998;13:2825–2828.
11. Langer JE, Cornud F. Inflammatory disorders of the prostate and the distal genital tract. Radiol Clin North Am 2006;44(5):665–677.

12. Papanicolaou N, Pfister R, Stafford S, et al. Prostate abscess: imaging with transrectal sonography and MRI. AJR Am J Roentgenol 1987;149:981–982.
13. Clements R, Thomas KG, Griffiths GJ, Peeling WB. Transrectal ultrasound appearances of granulomatous prostatitis. Clin Radiol 1993;47(3):174–176.
14. Kuligowska E, Fenlon HM. Transrectal US in male infertility: spectrum of findings and role in patient care. Radiology 1998;207(1): 173–181.
15. Meacham RB, Townsend RR, Drose JA. Ejaculatory duct obstruction: diagnosis and treatment with transrectal sonography. AJR Am J Roentgenol 1995;165:1463–1466.
16. Torigian DA, Ramchandani P. Hematospermia: imaging findings. Abdom Imaging 2007;32(1):29–49.
17. Pallwein L, Mitterberger M, Pelzer A, et al. Ultrasound of prostate cancer: recent advances. Eur Radiol 2008;18(4):707–715.
18. Presti JC Jr, Hricak H, Narayan PA, et al. Local staging of prostatic carcinoma: comparison of transrectal sonography and endorectal MR imaging. AJR Am J Roentgenol 1996;166(1):103–108.
19. Choi YJ, Kim KJ, Kim N, et al. Functional MR imaging of prostate cancer. Radiographics 2007;27:63–77.
20. Ocak I, Bernardo M, Metzger G, et al. Dynamic contrast enhanced MRI of prostate cancer at 3T: a study of pharmacokinetic parameters. AJR Am J Roentgenol 2007;189:W192–W201.
21. Raja J, Ramachandran N, Munneke G, Patel U. Current status of transrectal ultrasound-guided prostate biopsy in the diagnosis of prostate cancer. Clin Radiol 2006;61(2):142–153.
22. Ghani KR, Dundas D, Patel U. Bleeding after transrectal ultrasonography-guided prostate biopsy: a study of 7-day morbidity after a 6, 8 and 12 core protocol. BJU Int 2004;94:1014–1020.
23. Lee-Elliott CE, Dundas D, Patel U. Randomized trial of lidocaine vs lidocaine/bupivacaine periprostatic injection on longitudinal pain scores after prostate biopsy. J Urol 2004;171(1):247–250.
24. http://www.cancerscreening.nhs.uk/prostate/pcrmp01.pdf (accessed 20 September 2008).
25. Stewart CS, Leibovich BC, Weaver AL, Lieber MM. Prostate cancer diagnosis using a saturation needle biopsy technique after previous negative sextant biopsies. J Urol 2001;166:86–92.
26. Bott SR, Henderson A, Halls JE, et al. Extensive transperineal template biopsies of prostate: modified technique and results. Urology 2006;68(5):1037–1041.
27. Wasserman NF, Kapoor DA, Hildebrandt WC, et al. Transrectal ultrasound in evaluation of patients after radical prostatectomy. Part 1: Normal post-operative anatomy. Part 2: TRUS and biopsy findings in the presence of residual and early recurrent prostatic cancer. Radiology 1992;185:361–377.
28. Lawler LP, Cosin O, Jarow JP, Kim HS. Transrectal US-guided seminal vesiculography and ejaculatory duct recanalization and balloon dilation for treatment of chronic pelvic pain. J Vasc Interv Radiol 2006;17(1):169–173.

CHAPTER

31 Diseases of the testis and epididymis

Paul S. Sidhu

INTRODUCTION 593

ULTRASOUND EXAMINATION TECHNIQUE 593

ANATOMY 593
Embryology 593
Scrotal sac and testicular anatomy 594
Vascular anatomy 594

NORMAL ULTRASOUND APPEARANCES OF THE SCROTAL SAC, TESTIS AND EPIDIDYMIS 595
Normal variants and artefacts 595
Trans-mediastinal artery 595
Two-tone testis 597
Rete testis 597
Appendix testis 598
Polyorchidism 598

INTRA-TESTICULAR ABNORMALITIES 598
Focal lesions: neoplastic lesions 598
Germ cell tumours 599
Non-germ cell tumours 600
Lymphoma 601
Leukaemia 602
Metastasis 602
Focal lesions: non-neoplastic lesions 602
Epidermoid cyst 602
Splenogonadal fusion 603
Adrenal rest cells 603
Segmental infarction 603
Other tumour-like testicular lesions 604
Testicular microlithiasis and macrocalcification 607

EXTRA-TESTICULAR ABNORMALITIES 608
Extra-testicular focal lesions 608
Epididymal cysts and spermatoceles 608
Tubular ectasia and vasectomy 608
Sperm granuloma 608
Benign neoplasms 609
Malignant neoplasms 610
Extra-testicular calcification 611
Extra-testicular non-focal lesions 612
Inguinal hernia 612
Fluid collections 612
Varicocele 612

ACUTE SCROTUM 612
Inflammatory disease 614
Epididymo-orchitis and epididymitis 614
Chronic epididymitis 615
Orchitis 615
Trauma 615
Spermatic cord torsion 616
Spontaneous de-torsion 617
Torsion of an appendage 617
Fournier's gangrene 618

SCROTAL WALL ABNORMALITIES 618

INTRODUCTION

Despite the widespread use of more sophisticated imaging techniques, delineation of the contents of the scrotum remains firmly within the domain of ultrasound. As a consequence, ultrasound is recognised as the first-line and often only imaging modality employed in the assessment of scrotal abnormalities. The superficial nature of the scrotal sac and contents lends itself to thorough and accurate imaging with ultrasound. Technical advances in transducer design and image processing have further improved ultrasound diagnosis of diseases of the scrotal contents, with colour Doppler adding important information. This chapter will deal with aspects related to the testis and epididymis, detailing both normal ultrasound features and those features related to disease processes.

ULTRASOUND EXAMINATION TECHNIQUE

Examination should take place in a private setting in the presence of a chaperone, with the assessor using a gloved hand for the examination. The ultrasound gel should be warm with ample amounts applied (artefact from scrotal hair is a common problem). The scrotal sac may be held in a steady position by placing a towel beneath the sac and stabilised by the patient crossing his ankles. The penis is held against the anterior abdominal wall by the patient and covered with a towel. A high-frequency linear array probe (7–12 MHz) should be used, with sensitive colour and spectral Doppler capabilities. Usually the probe length (>5 cm) should allow accurate longitudinal length measurements of the testis. Initially both testes are examined in the transverse plane, in order to produce the 'spectacle' view to allow comparison of testicular parenchyma features; important if a unilateral global testicular problem is suspected (Fig. 31.1). The examination of the entire scrotal sac should include both the transverse and longitudinal planes, documenting any abnormalities present. Testicular volume may be calculated and colour Doppler ultrasound will confirm vascular supply. If the ultrasound examination fails to detect a 'lump' as felt by the patient, the patient should palpate the lesion and hold this between two fingers to be re-examined with ultrasound.

ANATOMY

Embryology

Over the seventh month of fetal development the testes descend into the scrotal sac. A dense layer of fibrous connective tissue, the

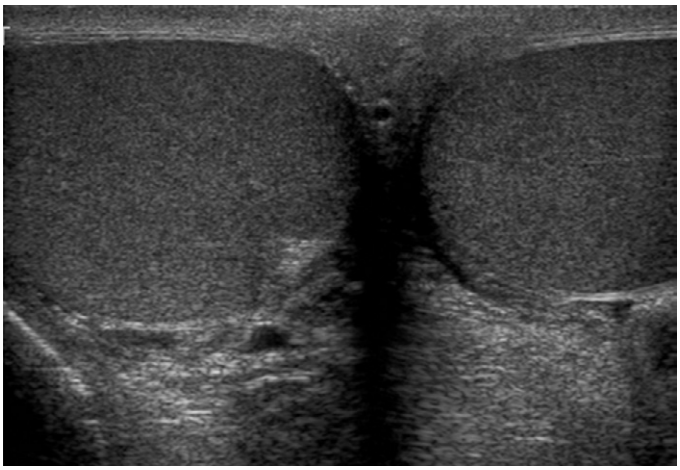


Figure 31.1 Normal testis. A transverse view through both the testes, the 'spectacle view' allows comparison of the reflectivity of the two testes, normal in this patient. A spectacle view is of particular importance in infiltrative lymphoma and leukaemia.

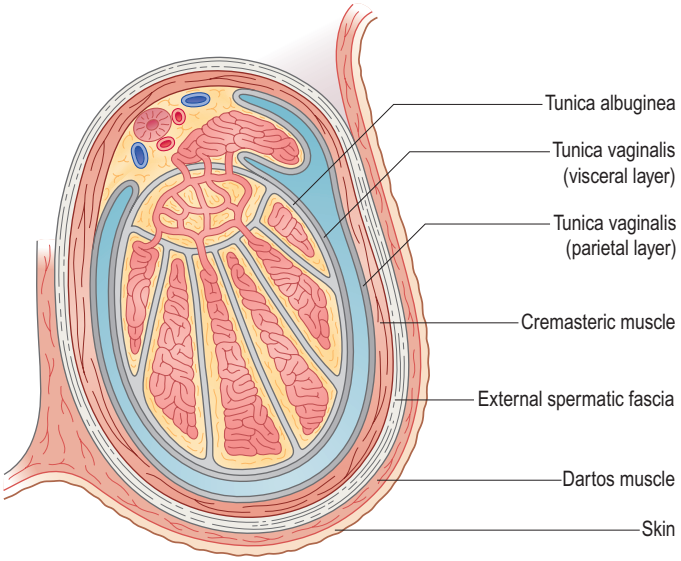


Figure 31.2 The anatomical layers surrounding the normal testis. The blue shaded area between the two layers of the tunica vaginalis is the area of fluid accumulation which gives rise to a hydrocele (from Sidhu PS, Clinical Radiology 1999; 54:343–352).

tunica albuginea, forms a capsule that covers the testis. The testis is then further covered by a reflected fold of the processus vaginalis that becomes the visceral layer of the tunica vaginalis, with the remainder of the peritoneal sac forming the parietal layer of the tunica vaginalis. The visceral layer of the tunica vaginalis covers the testes and the epididymis, whereas the parietal reflection covers the anterior and lateral parts of the testes and the epididymis leaving a 'bare area' to which the mesentery of the testis is attached; this is important in understanding the 'bell-clapper' deformity and spermatic cord torsion. A reflection of the tunica albuginea forms the mediastinum testis, within which the rete testis forms.[1]

Scrotal sac and testicular anatomy

The scrotum is divided into two separate chambers by the median raphe, which is continuous with the dartos muscle. The layers of the scrotal sac consist of skin, dartos muscle, external spermatic fascia, the cremasteric fascia and the internal spermatic fascia (Fig. 31.2). Beneath this is the parietal layer of the tunica vaginalis. A potential space exists between the two layers of the tunica vaginalis allowing fluid accumulation. The visceral layer of the tunica vaginalis covers the inelastic tunica albuginea, which gives rise to multiple thin septations that extend to the mediastinum testis dividing the testis into 200–250 lobules containing the seminiferous tubules. The seminiferous tubules form the tubuli recti that enter the mediastinum as the rete testis, eventually draining into the epididymis and then into the vas deferens. The epididymis consists of three segments: the head (globus major), the body and the tail (globus minor). The head is formed of efferent ductules from the rete testis, forming a single convoluted duct, the ductus epididymis, up to 6 metres in length. The ductus epididymis has a very tortuous route from the head to the tail of the epididymis, where it turns around to exit into the spermatic cord from the epididymal head.

Vascular anatomy

The arterial supply to the scrotal sac and contents arises from three sources: the *testicular artery* (arising from the aorta and supplying the testis), the *cremasteric artery* (a branch of the inferior epigastric artery, supplying the scrotal sac and the coverings of the spermatic cord), and the *artery to the ductus deferens* (arising from the superior vesicle artery) (Fig. 31.3). The testicular artery branches into the testis, piercing the tunica albuginea in a layer termed the tunica vasculosa. These branches course along the

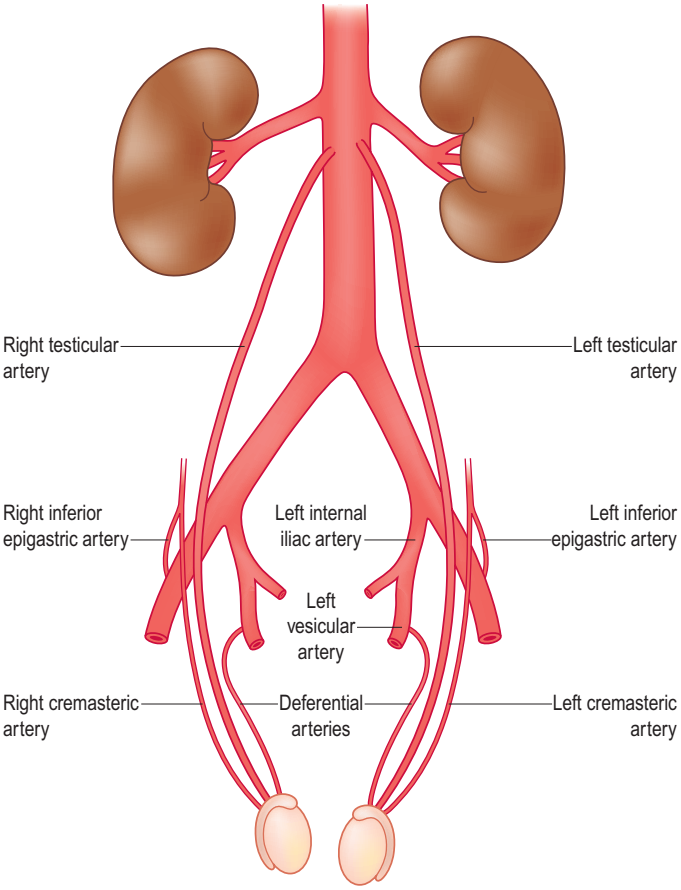


Figure 31.3 Normal arterial anatomy of the testis (from Sidhu PS, Clinical Radiology 1999; 54:343–352).

septum to converge on the mediastinum and then form recurrent rami through the parenchyma. Veins exit the testes at the mediastinum and join the veins draining the epididymis to form the pampiniform plexus at the superior aspect of the testes. The cremasteric plexus (mainly draining extra-testicular blood) lies posterior to the pampiniform plexus. The right testicular vein drains directly into the inferior vena cava below the level of the right renal vein, whereas the left testicular vein drains into the left renal vein (Fig. 31.4). These three arteries and the veins are loosely held together by connective tissue along with nerves, lymph vessels and the vas deferens in the spermatic cord.[2] The spermatic cord runs from the deep inguinal ring into the scrotum. There are anastomoses between these arteries; these are not sufficient to prevent testicular ischaemia when the testicular artery is compromised.[3] Although it is not possible to identify a named artery within the spermatic cord, colour Doppler is able to demonstrate the three individual arteries within it (Fig. 31.5). Despite anastomoses existing between the testicular, deferential and cremasteric arteries, one of the arteries will consistently show a significantly lower resistance index than the other two.

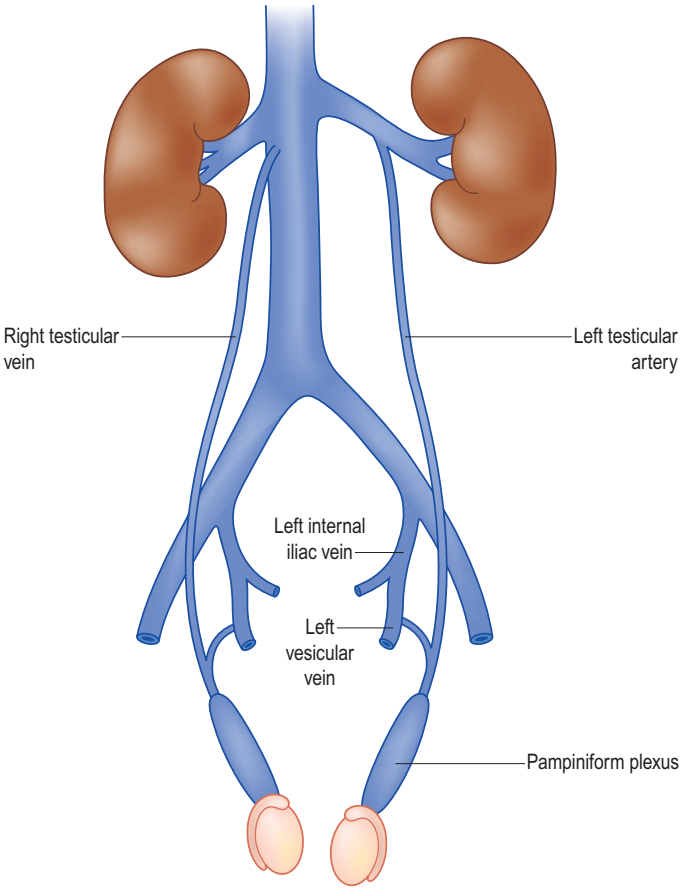


Figure 31.4 Normal venous drainage of the testis (from Sidhu PS, Clinical Radiology 1999; 54:343–352).

NORMAL ULTRASOUND APPEARANCES OF THE SCROTAL SAC, TESTIS AND EPIDIDYMIS

The scrotal wall appears as three layers: an outer hyper-reflective layer, a hypo-reflective intermediate and a hyper-reflective inner layer corresponding to the tunica albuginea. The scrotal wall normally measures 3–7 mm. The testes are homogeneous and of medium level reflectivity. At birth the testis measures approximately 1.5 cm in length and 1.0 cm in width, and before 12 years of age the testicular volume is 1–2 mL. In the adult, testicular length may be up to 5 cm. Volume measurement is calculated using the formula; length × width × height × 0.51 (Fig. 31.6). A total volume (both testes) of >30 mL is indicative of normal function.[4] A testicular volume >2 mL allows reliable appreciation of intra-testicular colour Doppler flow.[5] The mediastinum testis is seen as a highly reflective linear structure at the posterior-superior aspect of the testicle, draining the seminiferous tubules of the testes into the rete testis (Fig. 31.7). The rete testis is a low reflective area at the hilum of the testis with finger-like projections into the parenchyma (Fig. 31.8).[6] Apart from these projections, the parenchyma of the testis should remain of homogeneous reflectivity. The appendix testis (a vestigial remnant of the Müllerian duct) is present in the majority of patients, most commonly at the superior testicular pole or in the groove between the testis and the head of the epididymis medially.[7] There is marked variation in the size and appearance of an appendix testis; it is usually oval, although a stalk-like cystic structure (cyst of Morgagni) is occasionally seen (Fig. 31.9).

The epididymis is 6–7 cm in length. The head (globus major) is a pyramid-shaped structure lying superior to the upper pole of the testis. The body courses along the posterolateral aspect of the testicle. The tail (globus minor) is slightly thicker than the body and can be seen as a curved structure at the inferior aspect of the testicle where it becomes the proximal portion of the ductus deferens. The body and tail are of similar or slightly lower reflectivity when compared with the testis, whilst the head is of slightly higher reflectivity (Fig. 31.10). Colour Doppler signal may be identified in the normal epididymis. The appendix epididymis is not as frequently seen as the appendix testis. It is part of the mesonephric (Wolffian duct), and projects from the epididymis from different sites, most commonly the head. It usually has a stalk-like appearance. The globus major measures 10–12 mm in diameter, the body less than 4 mm (average 1–2 mm) in diameter.

Normal variants and artefacts

Trans-mediastinal artery

A large branch of the testicular artery may split off and traverse the testis to form capsular branches at the opposite aspect: the trans-mediastinal artery. An intra-testicular artery traverses the testis in a centrifugal direction in a reported 52% of patients, unilateral in half.[8] The artery is readily identified with colour Doppler ultrasound, returns a low resistance spectral Doppler waveform and is accompanied by the trans-mediastinal vein (Fig. 31.11).

Anatomy

- Tunica albuginea covers the testis; a reflection forms the mediastinum testis.
- Two layers of tunica vaginalis (visceral and parietal) leave a small bare area.
- Three arteries supply the scrotum: testicular artery, cremasteric artery and the artery to the ductus deferens.
- The pampiniform plexus drains into the testicular vein.

Ultrasound appearances

- The normal testis is of medium level, homogeneous reflectivity.
- The mediastinum testis is a linear, high reflective structure.
- The 'spectacle' transverse view through both testes is essential.
- The epididymal head is a pyramidal structure; the epididymal body is of lower reflectivity.
- The testicular and epididymal appendices are present at the superior aspect.

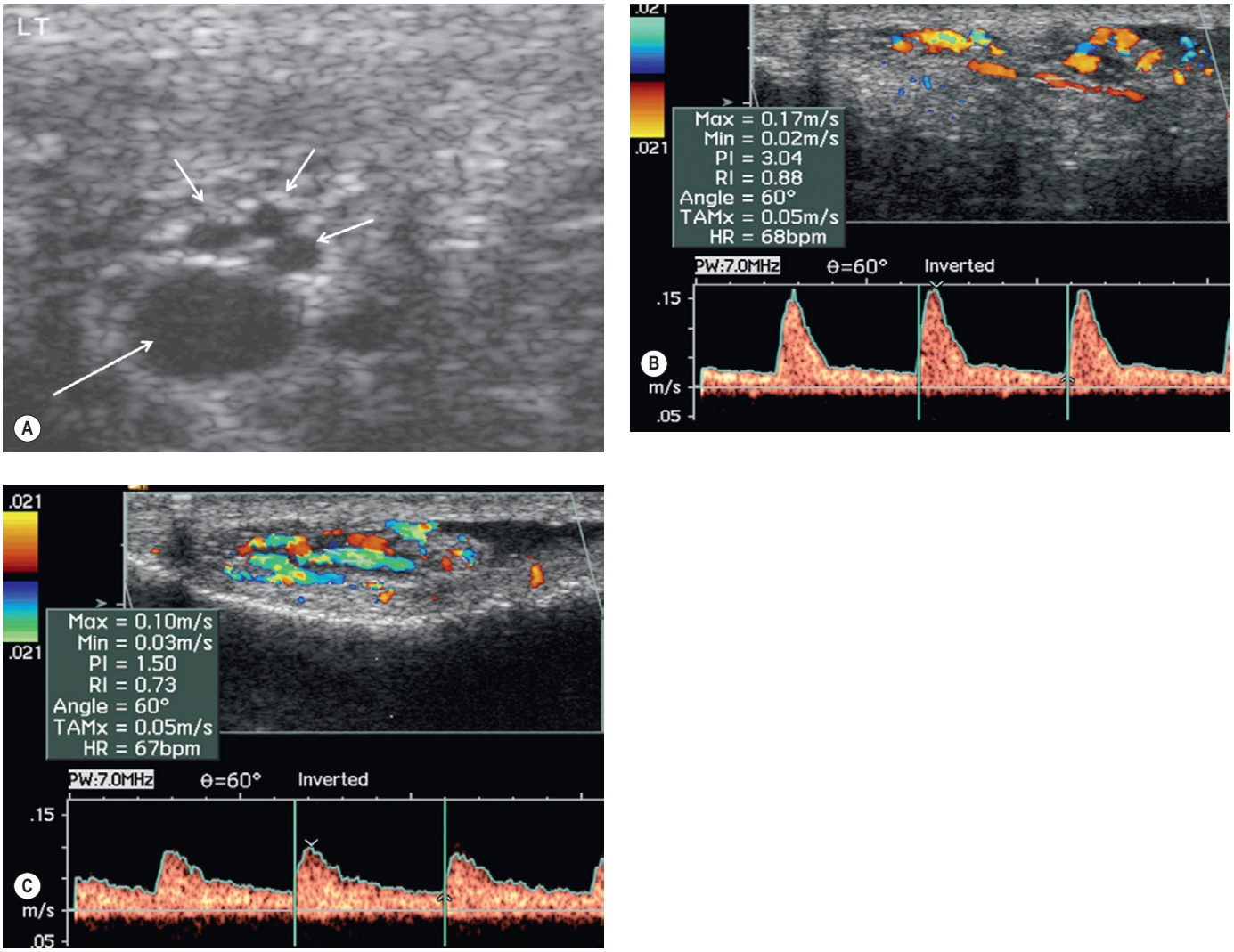


Figure 31.5 Spermatic cord Doppler ultrasound. A: A transverse image through the spermatic cord, demonstrating the testicular vein (long arrow) and the three arteries (short arrows) that are present in the spermatic cord: the *testicular artery*, the *cremasteric artery* and the *artery to the ductus deferens*. **B:** Spectral Doppler analysis of one of the arteries in the spermatic cord demonstrates a high resistance pattern (resistance index 0.88), implying that this is either the cremasteric artery or the artery to the ductus deferens. **C:** Spectral Doppler analysis of one of the arteries in the spermatic cord demonstrates a low resistance pattern (resistance index 0.73), implying that this is the testicular artery.

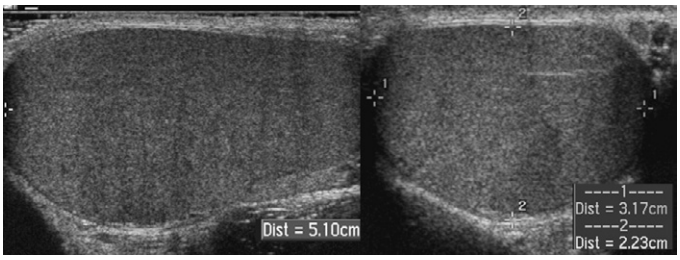


Figure 31.6 Testicular volume. Method for measuring testicular volume in a normal patient. The right testis measures 5.1 × 3.2 × 2.2 cm, giving a volume of 18.3 mL.

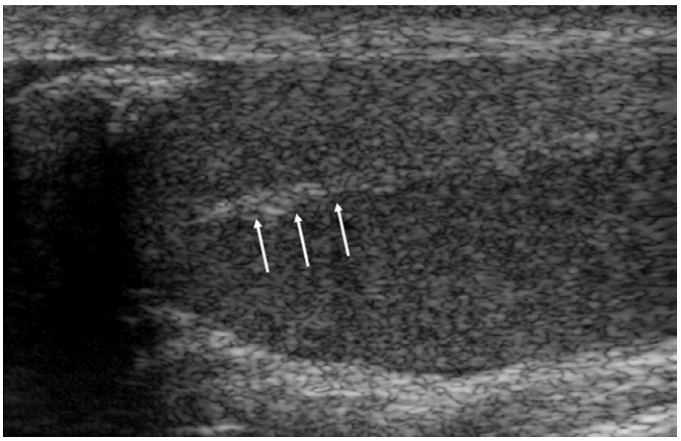


Figure 31.7 Mediastinum testis. The mediastinum testis is seen as a highly reflective linear structure at the posterior-superior aspect of the testicle (arrows) draining the seminiferous tubules of the testes into the rete testis.

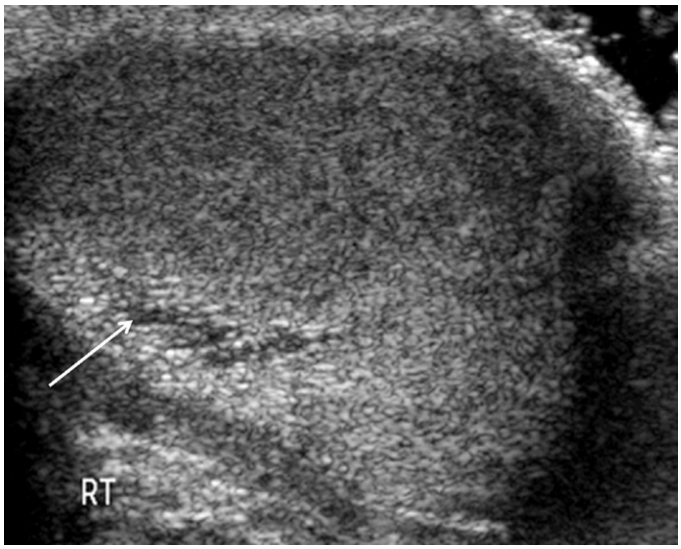


Figure 31.8 Normal rete testis. The rete testis (RT) is a low reflective area at the hilum of the testis with finger-like projections into the parenchyma (arrow).

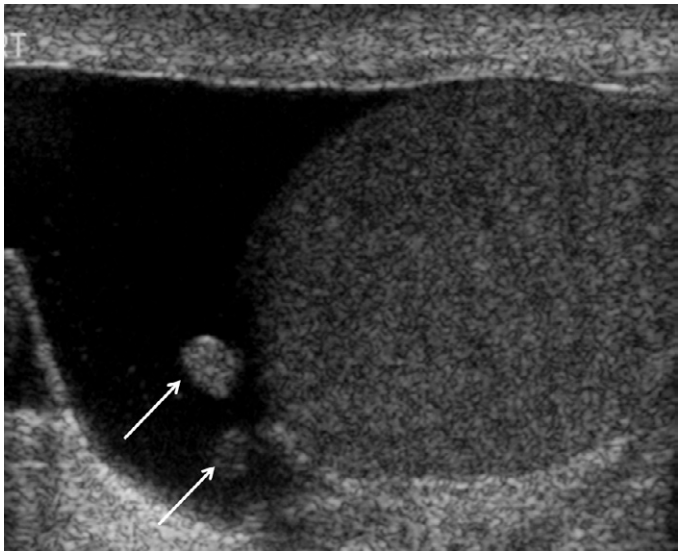


Figure 31.9 Appendix testis and epididymis. There is marked variation in the size and appearance of an appendix testis and epididymis (arrows); usually oval, although a stalk-like cystic structure is occasionally seen.

Two-tone testis

The term 'two-tone' describes the appearances of an artefact within the testis where an intra-testicular artery produces acoustic shadowing resulting in a discrete uniform area of decreased reflectivity posterior to the artery (Fig. 31.12). This artefact is caused by refractive shadowing at both edges of the intra-testicular artery. The reflectivity of the remainder of the testis is normal. The use of colour Doppler ultrasound readily confirms the presence of the intra-testicular artery as being the source of the artefact.[9]

Rete testis

The rete testis is located in the mediastinum testis. Microscopically the rete testis is composed of three parts: the septal (interlobular) portion containing the tubuli recti, the tunical (mediastinal) portion consisting of a network of channels, and the extra-testicular rete,

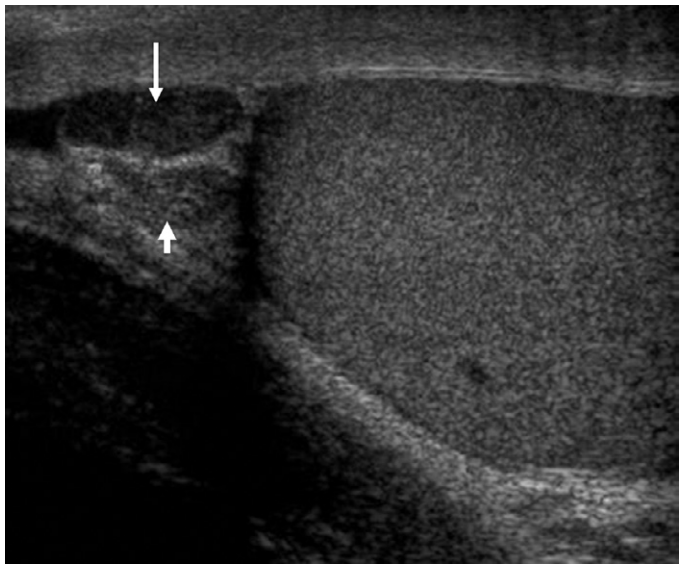


Figure 31.10 Normal epididymal head. The normal triangular shaped epididymal head. The changes in reflectivity of the epididymis are demonstrated; the low reflectivity of the body (long arrow) alters in the head of the epididymis (short arrow) to a higher reflectivity.

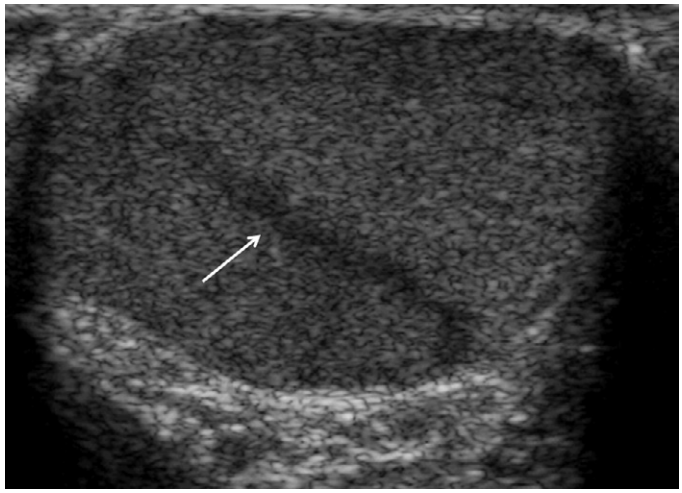


Figure 31.11 Trans-mediastinal artery and vein. Linear low reflective structure traverses the testis (arrow).

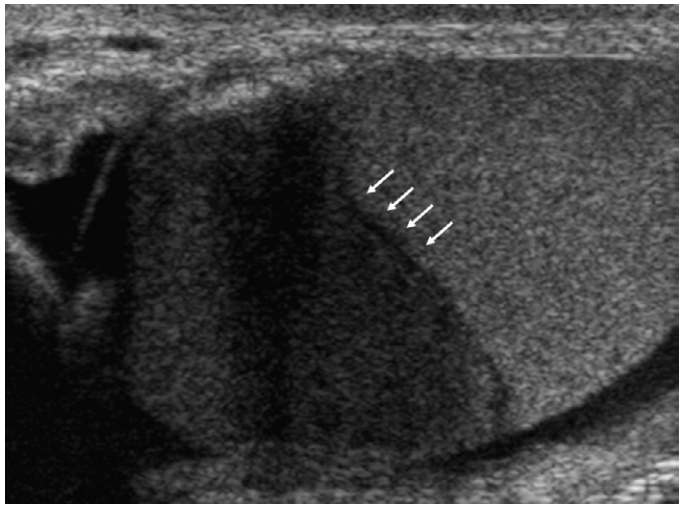


Figure 31.12 'Two-tone' testis. There is a well-demarcated low reflective appearance generated through the testis (arrows) which does not appear to be related to a pathological cause.

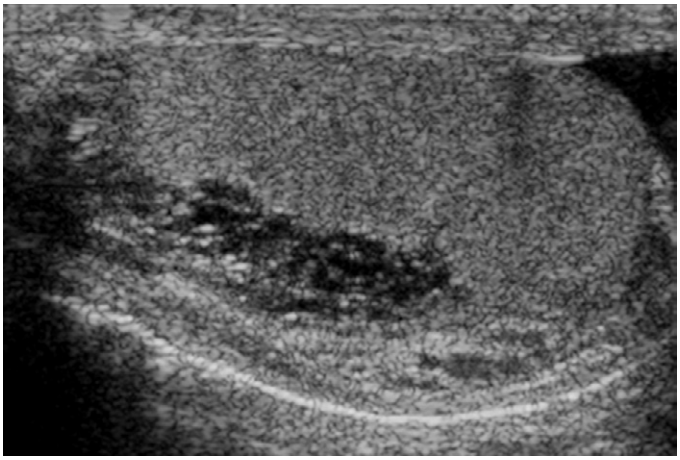


Figure 31.13 Rete testis. A florid example of a rete testis, with a number of cysts of varying size present adjacent to the mediastinum of the testis.

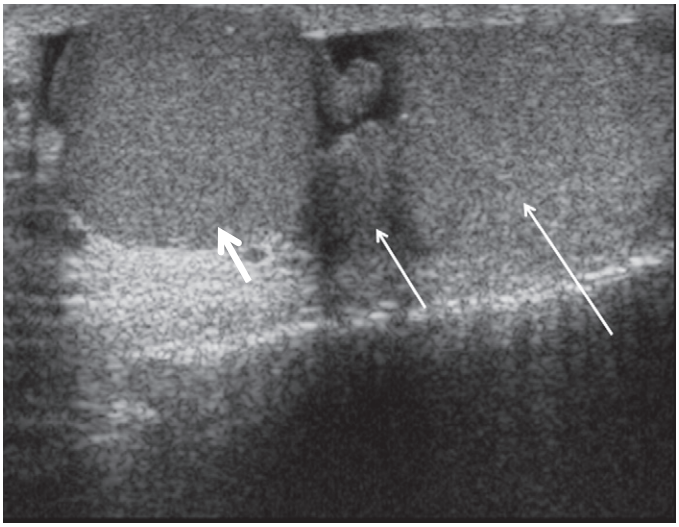


Figure 31.14 Polyorchidism. A normal testis (long arrow) with a normal epididymal head (short arrow) and a further mass, isoreflective to the normal testis (thick short arrow) lying in a superior position, representing an extra testicle: polyorchidism.

comprising the irregularly shaped lacunar spaces which connect to the efferent ducts. Seminiferous tubules contained within 250 lobules join the tubuli recti and the efferent ducts drain out into the epididymis. On ultrasound, the rete testis has a spectrum of appearances ranging from a faintly visible ill-defined area of decreased reflectivity (18% of patients) at the testicular hilum to a coarse tubular appearance with finger like projections into the parenchyma (Fig. 31.13).[6]

Appendix testis

A remnant of the paramesonephric and mesonephric ducts may remain to form the appendix testis (hydatid of Morgagni) and appendix epididymis respectively. Three further appendages, not seen on ultrasound, have been identified microscopically: the paradidymis (appendix of the cord or organ of Giraldés) arising from the spermatic cord and the superior and inferior vas aberrans of Haler. The appendix testis can measure between 1 and 7 mm in length, and may be present in up to 92% of patients, bilateral in 69%. The appendix testis is usually of similar reflectivity to the head of the epididymis, best seen in the presence of a hydrocele, with a variable morphology. It is most commonly oval shaped and sessile but it may appear 'stalk-like' and pedunculated, cystic or even calcified.[7] The 'stalk-like' and cystic appendices are associated with an increased likelihood of appendiceal torsion recognised as a cause of acute scrotal pain. The epididymal appendix is less frequently seen on ultrasound (6%), has a length of between 3 and 8 mm, is more frequently stalked and like the testicular appendix may undergo torsion, although less commonly. On occasion both an epididymal and testicular appendage may be seen in the same patient (Fig. 31.9).

Polyorchidism

Polyorchidism (more than two testes) is a rare condition and most commonly involves a bifid or duplicated testis with a single epididymis, with a uniform surrounding tunica albuginea (Fig. 31.14).[10] It usually presents as a painless mass and occurs more often on the left. The supernumerary testes may or may not have reproductive potential depending on the attachment to a draining vas deferens and epididymis. Type 1 abnormality has reproductive potential and type 2 does not. Based on the embryological development polyorchidism may be classified into four types:[11] *type A*: the supernumerary testis lacks either an epididymis or vas deferens; *type B*: the supernumerary testis has an epididymis but no vas deferens and the epididymis may be connected to the normal ipsilateral testis (type B2) or have no connection (type B1); *type C*: the supernumerary testis has a separate epididymis but shares the vas deferens with the ipsilateral testes in either a parallel or longitudinal fashion; *type D*: the supernumerary testis may have a completely separate epididymis and vas deferens and is the least common.

The ultrasound features are those of a well-defined rounded lesion occurring either superior or inferior to the ipsilateral testicle with identical reflectivity and colour Doppler signal as the ipsilateral testis. The length of the two ipsilateral testes added together equates to the length of the contralateral testicle. Polyorchidism has been reported in association with rete testis and microlithiasis.[12] Various malignancies have been reported in the supernumerary testes. Management is conservative unless there are associated complicating features.

INTRA-TESTICULAR ABNORMALITIES

Focal lesions: neoplastic lesions

Testicular carcinoma represents 1% of all neoplasms in men and is the most common malignancy in the 15–34-year-old age group.[13] A second peak of prevalence occurs in the 71–90-year-old age group, with metastasis and lymphoma most common. A third smaller peak occurs in children where yolk sac tumours and teratoma occur. There has been an unexplained increase in the prevalence of testicular carcinoma over the past 70 years, and testicular carcinoma is predominantly a cancer of white males. The most common presenting symptom is a painless scrotal mass; only 10% of patients present with pain. A smaller number of patients present with metastases or rarely with endocrine abnormalities such as gynaecomastia. Survival rates for testicular carcinoma approach 95%.[13]

There are well-documented risk factors for the development of testicular carcinoma: previous testicular tumour, family history, cryptorchidism, infertility and intersex syndromes. There remains an increase in risk in the contralateral testis even following removal of the undescended testis. Testicular tumours may be divided into germ cell and non-germ cell tumours; 95% of testicular tumours are germ cell tumours which arise from spermatogenic cells. Non-germ

Table 31.1 Classification of testicular tumours

Germ cell tumours
Precursor lesions:
Intra-tubular germ cell neoplasia
Tumours of one histological type:
Seminoma
Classic
Spermatocytic
Embryonal carcinoma
Yolk sac tumour
Choriocarcinoma
Teratoma
Mature
Immature
With malignant transformation
Tumours of more than one histological type
Non-germ cell tumours (sex cord and stromal tumours)
Leydig cell tumour
Sertoli cell tumour
Granulosa cell tumour
Fibroma-thecoma
Tumours with both sex cord and stromal cells and germ cells
Gonadoblastoma
Lymphoid and haematopoietic tumours
Lymphoma
Leukaemia
Metastasis

cell tumours derive from sex cords (Sertoli cells) and stroma (Leydig cells); these tumours are malignant in 10% of cases. Lymphoma, leukaemia and metastases may manifest as testicular tumours (Table 31.1).

Most testicular tumours are of homogeneous, low reflectivity in comparison to the surrounding testicular parenchyma, although a wide range of appearances occur including high reflective, heterogeneous lesions with areas of calcification and cystic change.[14] Larger tumours demonstrate increased vascularity,[15] although with the newer high-frequency transducers, malignant vascularity may also be identified in small volume tumours.[16]

Germ cell tumours

The precursor of germ cell tumours is thought to be intra-tubular germ cell neoplasia; if development is along a 'uni-potential' gonadal line a seminoma will form but if development occurs along a 'toti-potential' gonadal line, a non-seminomatous tumour will develop. The 'toti-potential' cells may remain undifferentiated (embryonal carcinoma) or develop toward embryonic differentiation (teratoma) or extraembryonic differentiation (yolk sac tumours, choriocarcinoma). Multiple histological types occur together (mixed germ cell tumour) as these 'toti-potential' cells develop along multiple pathways.

Most germ cell tumours spread via the lymphatic system rather than haematogenous, except for choriocarcinoma. Normally testicular lymphatic drainage follows the testicular vein, occurring in a predictable pattern. Orchidectomy for all testicular tumours is performed through an inguinal approach to avoid skin involvement and spread to the external iliac nodes. Staging of testicular carcinoma follows the TNM (tumour, node, metastasis) classification.[17] Tumour markers play an important role in diagnosis, staging, prognosis and follow-up of germ cell tumours. The most important tumour markers are alpha-fetoprotein, human chorionic gonadotrophin and lactate dehydrogenase. Although not always raised, specific patterns are seen: alpha-fetoprotein is raised in yolk sac tumours and teratomas, human chorionic gonadotrophin is raised in choriocarcinoma. Documentation of the tumour markers is essential to calculate clearance rate or marker persistence following treatment.

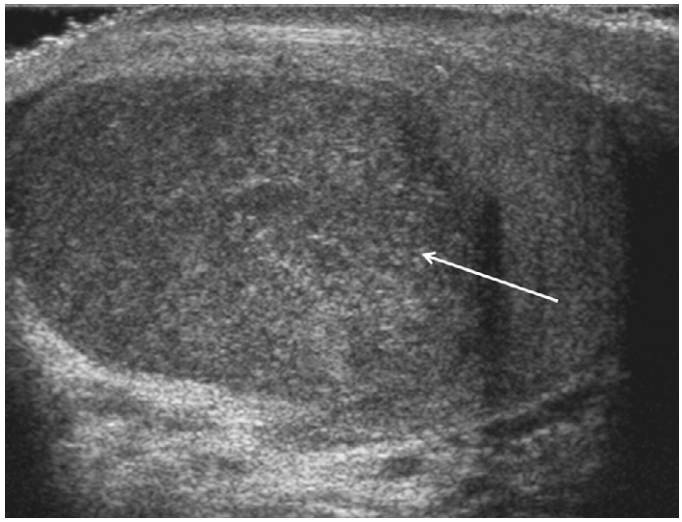


Figure 31.15 Seminoma. A low reflective mass lying within testicular parenchyma, with a well-delineated border (arrow) demonstrating features of a seminoma.

Seminomatous germ cell tumours

Seminoma is the most common pure germ cell tumour, accounting for up to 35–50% of cases, occurring in a slightly older patient group of 40 years. Seminoma represents the most common solid tumour in young men with the highest rates reported in Europe, Scandinavia and North America. There is a white:black ratio of 5:1. Seminomas may be bilateral in 2–5% of cases, and are most often associated with cryptorchidism. The ultrasound appearances reflect the uniform cellular nature of the tumour; uniformly of low reflectivity although larger tumours may be heterogeneous, lobulated or present as multinodular areas in continuity (Fig. 31.15). These tumours are extremely radiosensitive.

Non-seminomatous germ cell tumours

The non-seminomatous germ cell tumours, a collective group of various cell types, affect younger patients (20–30 years) than seminomatous germ cell tumours and are more aggressive with frequent visceral metastases.

Mixed germ cell tumours

Mixed germ cell tumour contains more than one germ cell component; any combination of cell type can occur. The most common combination is a teratoma and embryonal cell carcinoma (previously called teratocarcinoma). The average age of presentation is 30 years. These tumours constitute up to 20–40% of all germ cell tumours and are more common than the pure histological forms of testicular tumours. On ultrasound the appearances reflect the diverse nature of the histology with areas of calcification, cystic change, haemorrhage and necrosis (Fig. 31.16).

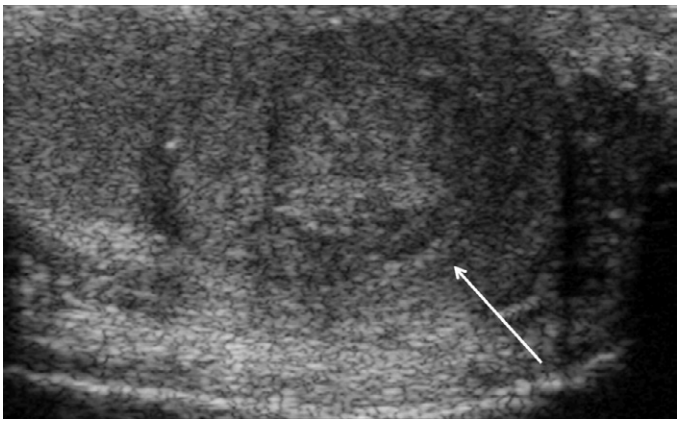


Figure 31.16 Mixed germ cell tumour. A focal mass (arrow), a mixed germ cell tumour, is present at the lower aspect of the testis, heterogeneous but mainly high reflectivity and is not as clearly defined as the examples of seminoma.

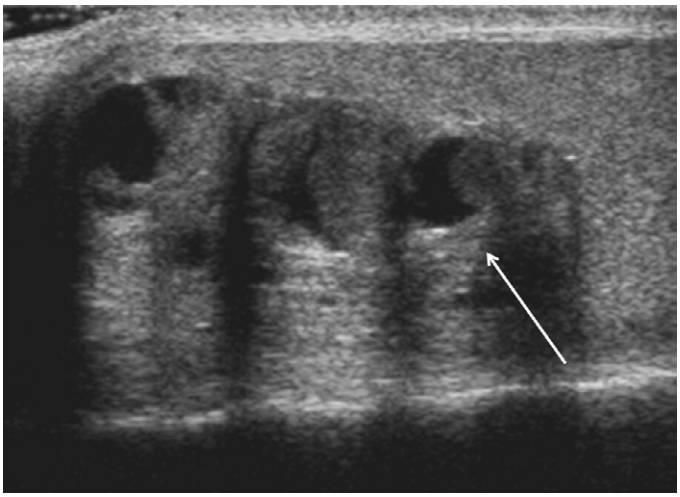


Figure 31.17 Embryonal cell tumour. Often a component of mixed germ cell tumours, this is an example of a pure embryonal cell tumour that is ill defined, lobulated and partly cystic (arrow).

Embryonal cell carcinoma

This is the second most common tumour after seminoma; embryonal carcinoma is present in 87% of mixed germ cell tumours, but in the pure form accounts for 2% of all testicular tumours. Embryonal carcinoma affects younger men (25–35 years) and tends to be more aggressive; a significant number will present with metastases. These tumours are often heterogeneous, ill defined and blend imperceptibly into adjacent testicular parenchyma (Fig. 31.17).

Choriocarcinoma

Choriocarcinoma is a rare tumour, occurring in a pure form in <1% of patients but in a mixed germ cell tumour in 8% of patients, where it is highly malignant. Choriocarcinoma carries the worst prognosis of any germ cell tumour; a high level of human chorionic gonadotrophin confers a poor prognosis and often results in gynaecomastia. Ultrasound will demonstrate a heterogeneous solid mass with areas of haemorrhage, necrosis and calcification. These tumours show a tendency to haematogenous spread.

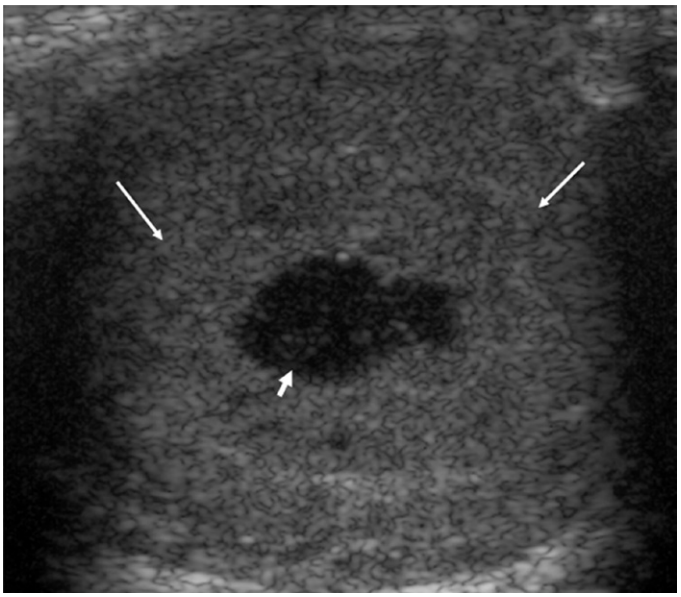


Figure 31.18 Yolk sac tumour. The imaging features are non-specific and are similar to a mixed germ cell tumour (arrows) with cystic change (short arrow) and areas of calcification.

Yolk sac tumour

Yolk sac tumours (endodermal sinus tumour) are the infantile form of embryonal cell carcinoma and account for 80% of childhood (<2 years) tumours but are rare in adults except as a component of mixed germ cell tumours. Elevation of alpha-fetoprotein levels is present. The imaging features are non-specific and are similar to a mixed germ cell tumour with cystic change and areas of calcification (Fig. 31.18).

Teratoma

Teratoma constitutes 5–10% of primary testicular tumours, divided into mature, immature and teratoma with malignant transformation according to the presence of derivatives of the different germinal layers (endoderm, mesoderm and ectoderm). Teratoma is the second most common testicular tumour in children (<4 years), and teratoma cells occur in over 50% of adult cases of mixed germ cell tumours. A teratoma tends to be a complex tumour, and the ultrasound features are those of a well-defined complex mass with cystic change (Fig. 31.19). Calcification may be present. Malignant transformation into a teratocarcinoma occurs (Fig. 31.20). In the prepubertal testes a pure teratoma runs a benign course and testis-sparing surgery may be undertaken. This is not true for the postpubertal teratoma, which will metastasise irrespective of the histological features. Spread is via the lymphatic route and the 5-year survival rate is 70%.

'Regressed' or 'burnt-out' germ cell tumours

Patients may present with widespread metastases but no primary tumour except for an area of calcification or fibrosis within an often atrophic testis.[18] The pathogenesis of this phenomenon may be the result of a high metabolic rate of the tumour, which outgrows its blood supply and involutes (Fig. 31.21).

Non-germ cell tumours

Non-germ cell tumours (gonadal stromal tumours) account for 3–6% of all testicular tumours. The prevalence of non-germ cell tumours is higher in the paediatric age group, constituting 30% of

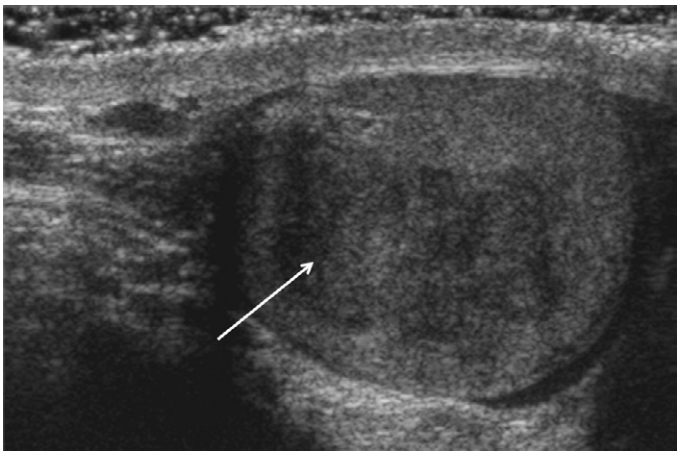


Figure 31.19 Teratoma. There is a lobulated defined teratoma at the upper aspect of the testis (arrow).

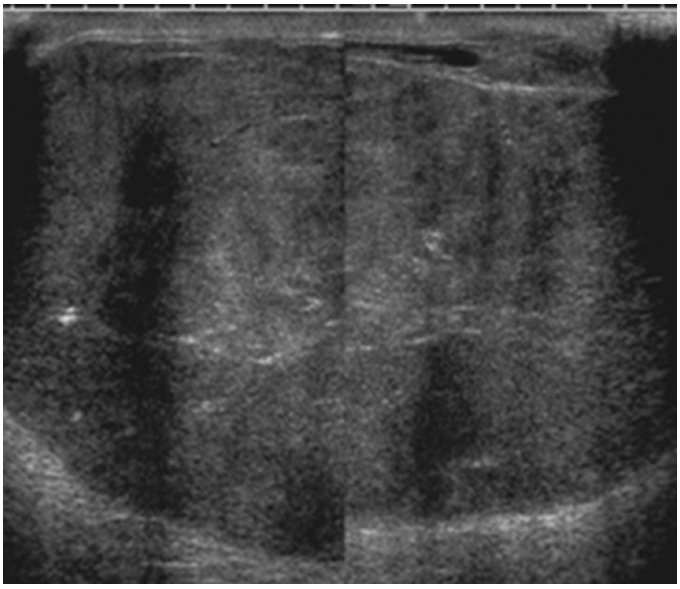


Figure 31.20 Teratocarcinoma. A mixed reflective tumour replacing normal tissue in the testis with areas of calcification; histology demonstrates this to be a teratocarcinoma.

all testicular tumours. Nearly all non-germ cell tumours are benign (90%), but there is no clear ultrasound criterion that allows differentiation from malignant testicular tumours. These non-germ cell tumours contain Leydig, Sertoli, thecal, granulosa or lutein cells and fibroblasts. When combined with germ cell tumours they are called gonadoblastomas.

Leydig cell tumours

The majority are Leydig cell tumours, which occur across all age groups predominantly between 20–50 years, and account for 3% of all testicular tumours. Patients demonstrate symptoms related to androgen or oestrogen secretion by the tumour, which includes precocious virilisation, gynaecomastia or decreased libido (30%). This is the most common tumour seen as an incidental ultrasound finding in infertile men.[19] On ultrasound Leydig cell tumours are small, commonly of low reflectivity with cystic change. Use of colour Doppler ultrasound may demonstrate poor internal colour Doppler flow with increased peripheral vascularity when small. Internal vascularity increases with tumour size (Fig. 31.22).

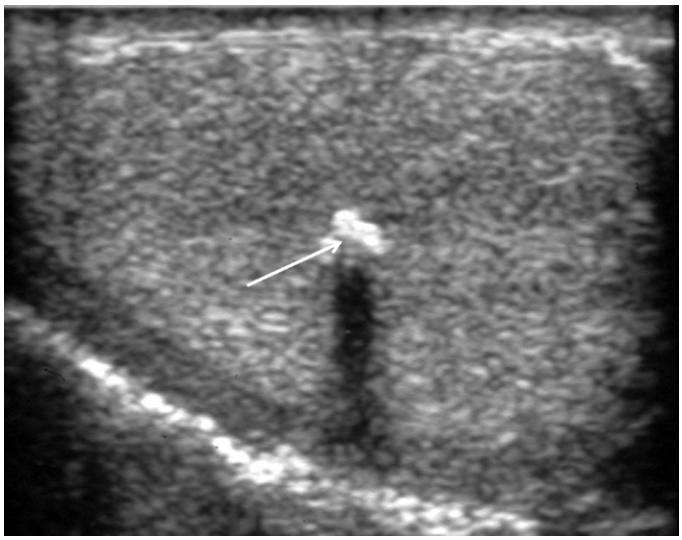


Figure 31.21 'Burnt-out' tumour. A focal clump of calcification (arrow) is present in the central aspect of the testis on ultrasound in a patient with a retroperitoneal germ cell tumour: a 'burnt-out' testicular tumour.

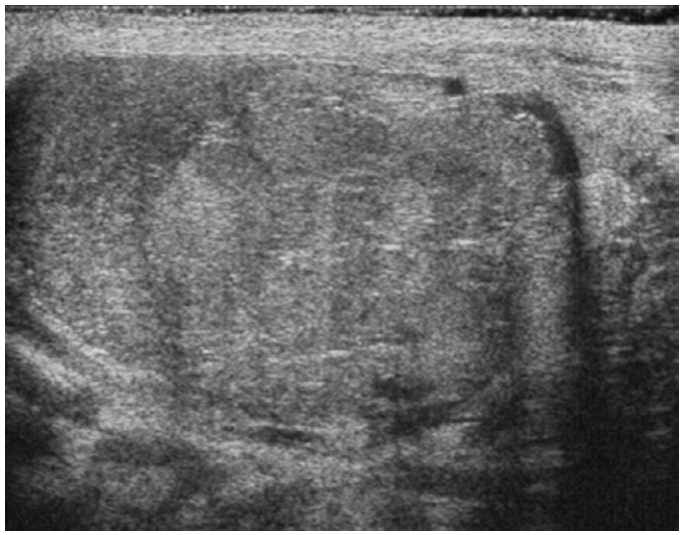


Figure 31.22 Leydig cell tumour. A large mixed reflective, heterogeneous tumour at the lower aspect of the testis which on histological examination was found to be a Leydig cell tumour.

Sertoli cell tumours

Sertoli cell tumours constitute 1% of all testicular tumours, and are less likely than Leydig cell tumours to secrete hormones. On ultrasound the Sertoli cell tumours are well circumscribed, round and lobulated.

Lymphoma

Testicular lymphoma may be the primary site of involvement, the initial manifestation of widespread disease or the site of recurrence. Testicular lymphoma, which accounts for 5% of testicular tumours, is the most common testicular tumour in the over 60-year-old age group, the most common secondary tumour of the testis, and the most common bilateral tumour. It is unusual to develop testicular disease in lymphoma; only 0.3% of patients with lymphoma have testicular involvement. The most common type of lymphoma to

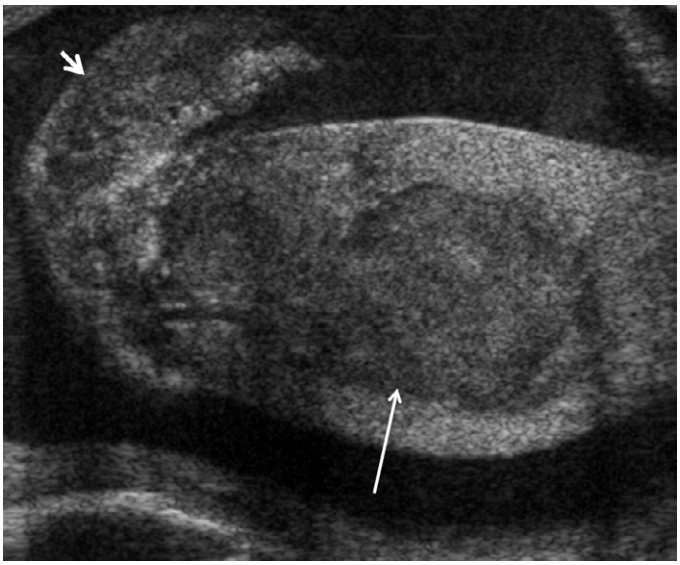


Figure 31.23 Lymphoma. There is enlargement of the testis, with a central mass of uniform low reflective appearance (arrow) extending into the epididymis (arrowhead). A surrounding hydrocele is present in a patient with testicular lymphoma.

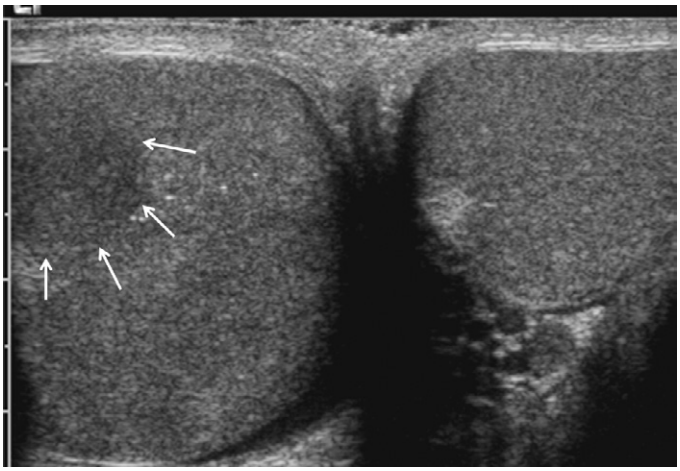


Figure 31.24 Leukaemia. A larger right testis with the suggestion of areas of lower reflectivity (arrows) in a patient with acute myeloid leukaemia.

affect the testis is non-Hodgkin's lymphoma, usually of the diffuse histiocytic type. The ultrasound appearances of testicular lymphoma are similar to germ cell tumours, particularly a seminoma: discrete low reflective lesions with increased colour Doppler flow. However, complete testicular involvement may be seen, emphasising the need to compare the reflectivity of both testes (Fig. 31.23).

Leukaemia

Testicular involvement in acute leukaemia is estimated at 64% and in chronic leukaemia at 25%. Primary leukaemia of the testis is rare, although it is a common site of recurrence in children. The blood–testis barrier prevents chemotherapy agents from dealing with intra-testicular leukaemia cells. The ultrasound appearances are very variable, being unilateral or bilateral, diffuse or focal, low or high reflectivity with increased colour Doppler flow (Fig. 31.24).[20] Differentiation from inflammatory disease is difficult without a full clinical history.

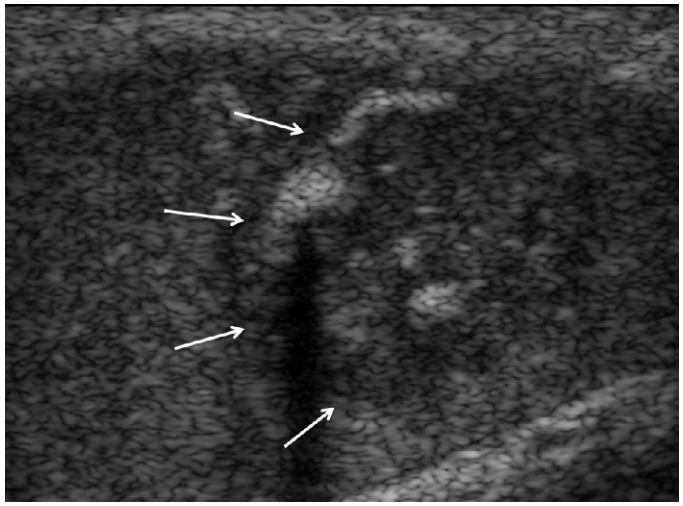


Figure 31.25 Metastasis. A secondary lesion (arrows) with calcification which on histology was an adenocarcinoma.

Testicular tumour

- Represents 1% of all male neoplasms; higher incidence in 15–34-year age group.
- Commonly presents as a painless scrotal mass.
- Multiple histological cell types occur together; seminoma and mixed germ cell tumours are the most common.
- Tumour spread is via the lymphatic system.
- Ultrasound is unable to differentiate germ cell from non-germ cell tumours.
- Nearly all non-germ cell tumours are benign.
- Lymphoma occurs in the over-60 age group.

Metastasis

Metastasis to the testis is unusual, with the most frequent primary sites being the prostate, lung, melanoma, colon and kidney.[21] Metastases occur most commonly in patients over 50 years of age. Metastasis usually occurs in advanced disease and is indistinguishable on ultrasound from a primary tumour (Fig. 31.25).

Focal lesions: non-neoplastic lesions

Epidermoid cyst

The pathogenesis of an epidermoid cyst is uncertain. It is likely it either arises from monodermal development of a teratoma or as a result of squamous metaplasia of surface mesothelium. These are benign lesions with no malignant potential. Epidermoid cysts comprise 1% of all testicular tumours and are true cysts, containing a cheesy laminated material. Patients are usually between 20 and 40 years at presentation. Classically on ultrasound, epidermoid cysts are well circumscribed with a high reflective border and internal laminations giving an 'onion-ring' appearance (Fig. 31.26). These lesions are avascular on colour Doppler ultrasound. There are four types of appearance documented on ultrasound: (i) classic onion ring configuration; (ii) densely calcified mass; (iii) peripheral rim or central calcification; and (iv) mixed pattern.[22] The treatment for epidermoid cyst is either enucleation or orchidectomy and as the ultrasound findings are frequently non-specific, orchidectomy is often performed.

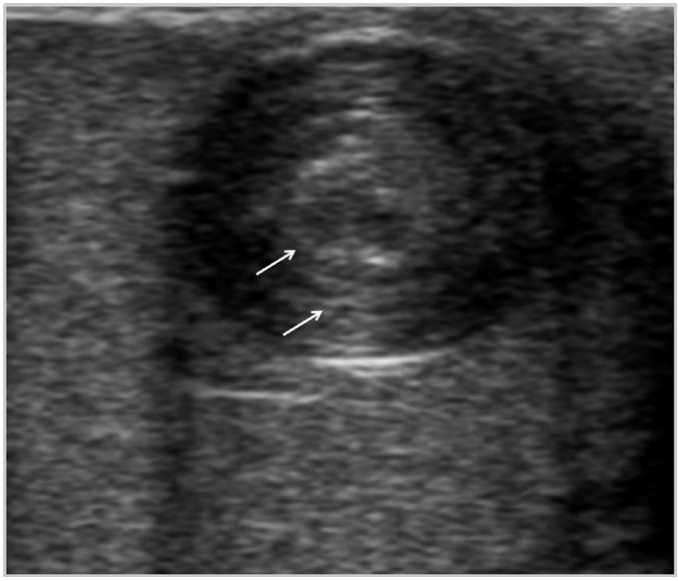


Figure 31.26 Epidermoid cyst. An epidermoid cyst demonstrating a well-circumscribed low reflective appearance with a high reflective border and internal laminations (small arrows) giving an 'onion-ring' appearance.

Splenogonadal fusion

Splenogonadal fusion is a rare condition where an accessory spleen exists within the scrotum or pelvis fused to the gonadal organs; the majority of cases occur on the left side. Splenogonadal fusion is far more common in males, where presentation is usually with a scrotal mass.[23] There are two types described, continuous and discontinuous. In the more common continuous type, a cord connects the normal and ectopic spleen; this cord may be beaded with small splenunculi. In the discontinuous type there is no cord present. There are several recognised associations with splenogonadal fusion; inguinal hernia and cryptorchidism are the most common, with micrognathia, peromelia, cleft palate, cardiac defects and several other rarer congenital anomalies also reported. The appearance of splenogonadal fusion on ultrasound resembles a mass within the scrotal sac of low reflectivity in comparison to the normal testicular parenchyma. The mass may not be seen separate to the testis and as such will be readily confused with a primary testicular tumour (Fig. 31.27). Colour Doppler ultrasound flow in the abnormal tissue assumes a pattern similar to that seen in the central aspect of the normal testis or that seen in splenic tissue.[24] Should the diagnosis be considered, a 99mTc-sulphur colloid scan will demonstrate uptake within the ectopic splenic tissue.

Adrenal rest cells

Testicular adrenal rest tumours are benign adenocorticotrophic hormone (ACTH)-dependent lesions that are asymptomatic and occur in patients with congenital adrenal hyperplasia. Increased ACTH levels prevent involution of aberrant adrenal cortical cells that migrate with gonadal tissues in fetal life. The testicular adrenal rests are usually less than 5 mm and can normally be found in the testis and surrounding tissues in 7.5–15% of neonates and 1.6% of adults. Ectopic adrenal rest cells within the testis develop as a tumour-like abnormality in response to elevated circulating ACTH. The intra-testicular nodules of adrenal rests can gradually expand and destroy the testicular parenchyma, resulting in low testosterone production and infertility. Treatment with steroid therapy can stabilise or regress these lesions, and aids the diagnosis. These tumours usually appear as focal low reflective abnormalities with abnormal colour flow and are often bilateral (Fig. 31.28).[25]

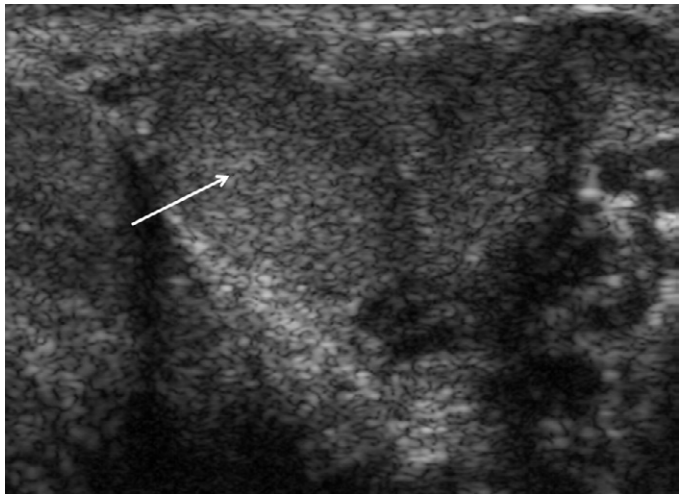


Figure 31.27 Spleno-gonadal fusion. A subtle, defined lesion at the upper aspect of the testis (arrow) which has the appearances of a primary testicular tumour.

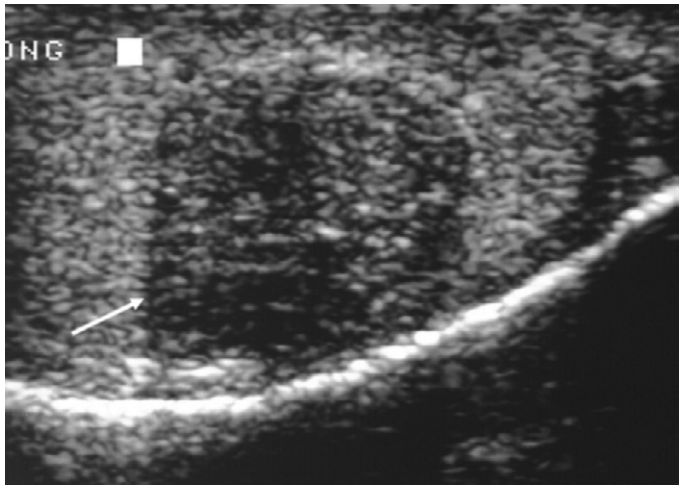


Figure 31.28 Adrenal rest cells. A focal low reflective area in the central aspect of the testis (arrow); adrenal rest cells (reproduced with permission from Giles Rottenberg, London and the Editor. Houghton R, Rottenberg G. Testicular lumps. Imaging 2005; 17:101–112).

Segmental infarction

Global testicular infarction is well recognised, usually as a result of torsion of the spermatic cord, severe epididymo-orchitis or trauma.[26] Segmental testicular infarction is, however, rare and is usually diagnosed following orchidectomy. The predisposing factors to segmental infarction include polycythaemia, intimal fibroplasia of the spermatic artery, sickle cell disease, hypersensitivity angiitis and trauma, although the majority are idiopathic in origin.[27] Patients with segmental infarction tend to be older than those with global testicular infarction arising from spermatic cord torsion, usually between 20 and 40 years. Segmental testicular infarction is characterised by poor or absent flow on colour Doppler ultrasound in a focal low reflective area with no posterior acoustic enhancement. The low reflective area may be wedge-shaped or assume a more rounded appearance.[27] Focal expansion of a pole of the testis may mimic a primary testicular tumour and colour Doppler ultrasound provides a useful discriminatory tool (Fig. 31.29).[28] Serial ultrasound examinations of an area of infarction will demonstrate reduction in size of the lesion.

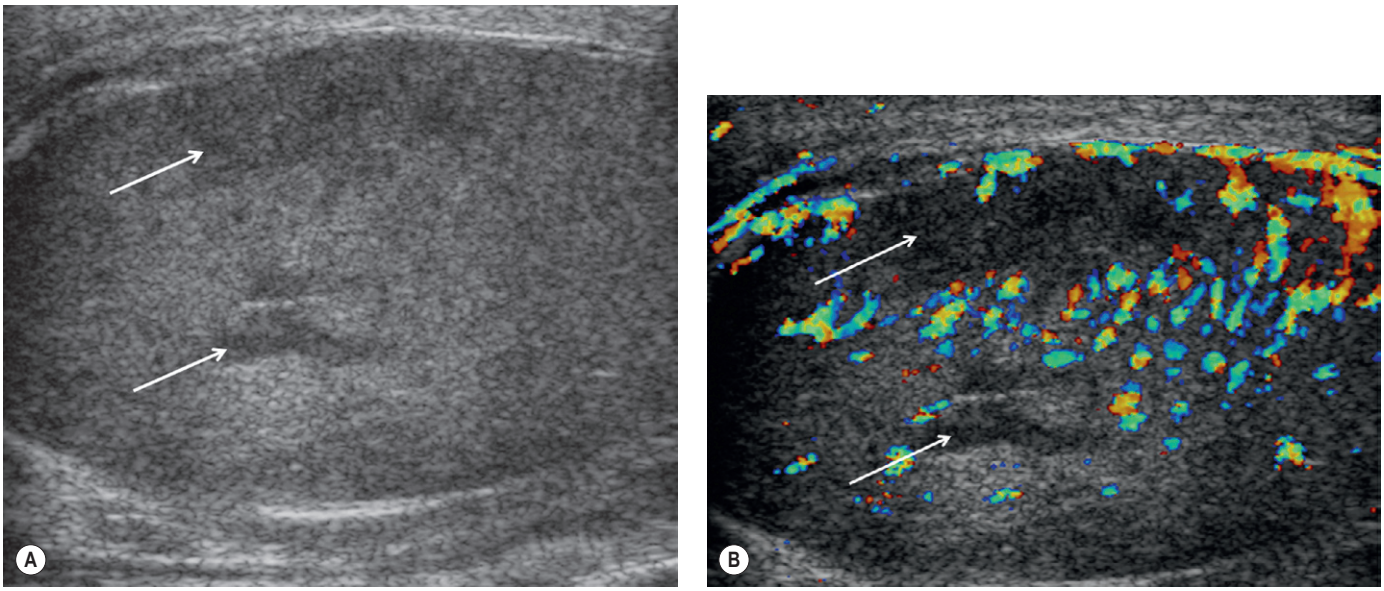


Figure 31.29 Segmental infarction. A: Two focal areas of low reflectivity (arrows) in a testis of a patient complaining of acute testicular pain with no evidence of inflammatory disease. **B:** The colour Doppler appearances (arrows) demonstrate absence of flow to the area, suggesting a segmental infarction as the cause of the appearances.

Other tumour-like testicular lesions

A number of other focal testicular lesions may cause clinical and ultrasound confusion: granulomatous epididymo-orchitis, sarcoidosis, tubular ectasia and cysts either intraparenchymal or adjacent to the tunica albuginea.

Sarcoidosis

Sarcoidosis is a multisystem disorder characterised by non-caseating epithelioid granulomas. Sarcoid most commonly involves the epididymis; solitary testicular involvement is uncommon. Differentiation from a primary testicular malignancy is challenging. However, if there is clinical evidence of sarcoid elsewhere, if the intra-testicular lesions are multifocal or if there is associated epididymal involvement, a more confident ultrasound diagnosis may be offered (Fig. 31.30). The reported incidence of genital involvement at postmortem is 4–4.5% but only 0.5% of these patients had clinical symptoms. Testicular sarcoid presents with a mass which may be painful. On ultrasound sarcoid appears as a low reflective focal lesion.[29,30] Without these associated symptoms or features, tissue biopsy for pathological evaluation may be required.

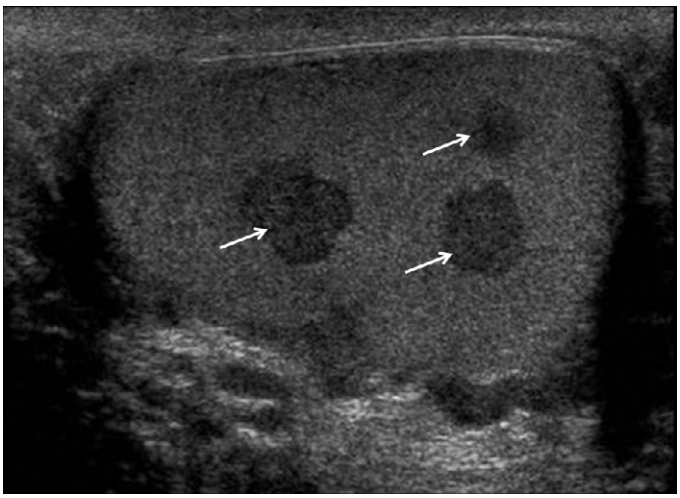


Figure 31.30 Testicular sarcoid. Three focal lesions within the testis in a patient with sarcoidosis (reproduced with permission from Stewart VR, Sidhu PS. The testis: the unusual, the rare and the bizarre. Clinical Radiology 2007; 62:289–302).

Focal orchitis and abscess formation

Pure orchitis is uncommon; the testis is frequently involved when epididymitis occurs resulting in epididymo-orchitis. Pure orchitis most often arises as a result of the paramyxovirus causing mumps. On ultrasound, the testis is enlarged with either diffuse low reflectivity with pure orchitis or more commonly focal areas of low reflectivity when associated with epididymitis. On occasion a focal abnormality may be produced that mimics a tumour, which should regress with serial ultrasound examinations (Fig. 31.31). Abscess formation may occur, particularly with severe epididymo-orchitis, where the abscess demonstrates low reflectivity with peripheral but no internal colour Doppler signals (Fig. 31.32).[31] The internal echoes of the abscess may vary depending on the age, but should be predominantly fluid-filled with septations (Fig. 31.33). If an abscess ruptures through the tunica albuginea, a pyocele may develop and this may further form a fistula to the skin surface. Idiopathic granulomatous orchitis can also present as a focal mass or diffuse enlargement of a testis and is indistinguishable from a tumour at ultrasound.

Intra-testicular haematoma

Testicular rupture, extra-testicular haematoma and a haematocele are the most common sequelae of testicular trauma. An uncommon finding is an isolated intra-testicular haematoma, which has a variable appearance on ultrasound with a temporal change in characteristics on repeat ultrasound.[32] A history of trauma to the scrotum should prompt the diagnosis. Acutely the haematoma appears as patchy increased reflectivity that becomes darker and decreases in size as the haematoma retracts, to eventually resolve completely. The haematoma demonstrates no colour Doppler flow, a low reflective rim thought to represent surrounding oedema, and internal

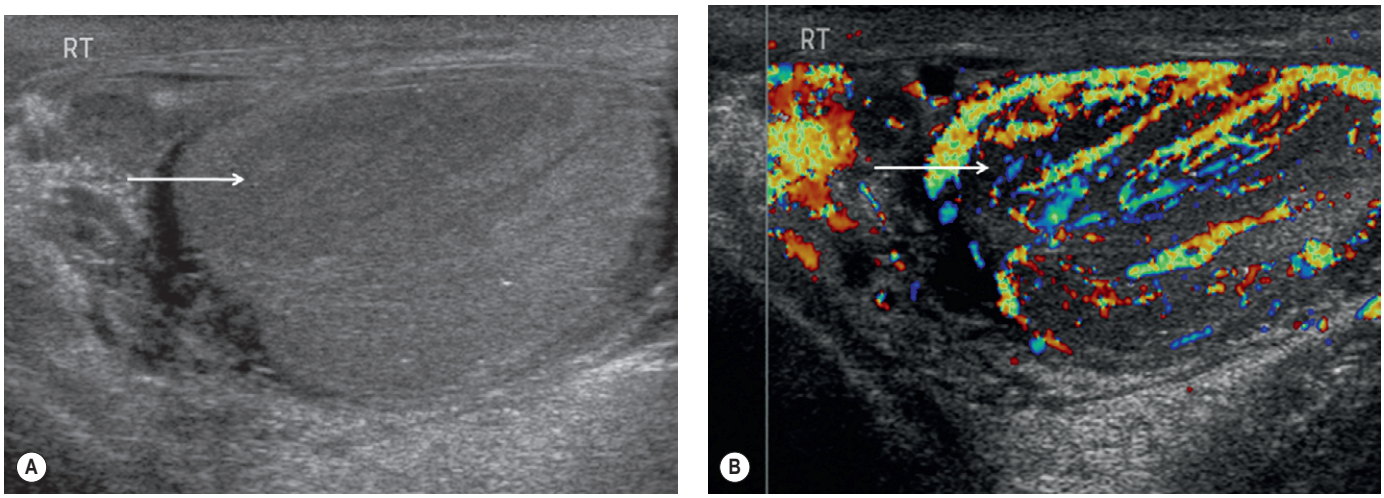


Figure 31.31 Focal orchitis. A: An area of low reflectivity at the upper aspect of the testis (arrow) in a patient with focal orchitis. **B:** The colour Doppler image demonstrates increased colour flow (arrow) to the area with vessels arranged in a uniform pattern conforming to the normal anatomical distribution of vessels.



Figure 31.32 Intra-testicular abscess. A poorly defined focal area of mixed reflectivity (between cursors) in a patient with epididymitis (arrow) representing a focal abscess.

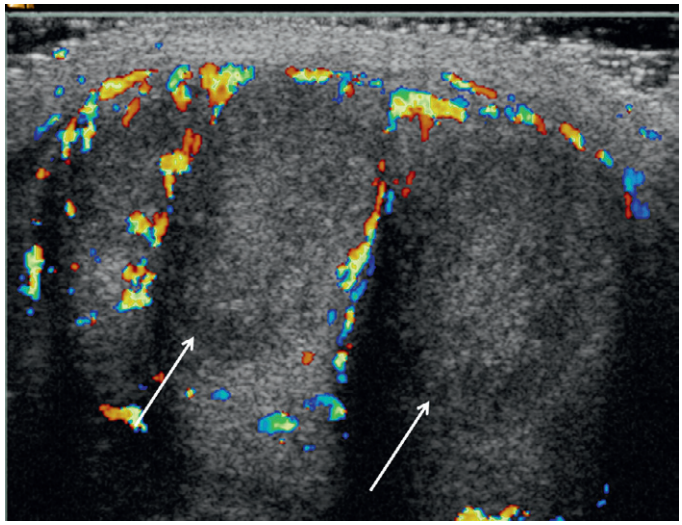


Figure 31.33 Intra-testicular abscesses. Colour Doppler ultrasound demonstrates absence of colour signal within these mass lesions (arrows), with increased flow around the periphery. The patient responded to antibiotic therapy.

echoes (Fig. 31.34). The most important differential is that of an intra-testicular tumour but a lack of lesion vascularity and the clinical history should lead to the correct diagnosis. The addition of normal tumour markers and a decrease in lesion size on sequential scans are useful.

Postoperative and post-biopsy testis

Following surgery to the pelvis, prostate and scrotum, oedema of the scrotal wall is a frequent finding, causing thickening visible on ultrasound. Often there is oedema of the testicular parenchyma causing a characteristic 'crazy-paving' appearance as the oedema follows anatomical boundaries. Following biopsy, a surgical scar may be seen as a localised alteration in parenchymal reflectivity extending to the surface of the testis.

Intra-testicular cysts

Intra-testicular cysts were thought to be rare but are now seen as incidental findings in 8–10% of ultrasound examinations.[33] These

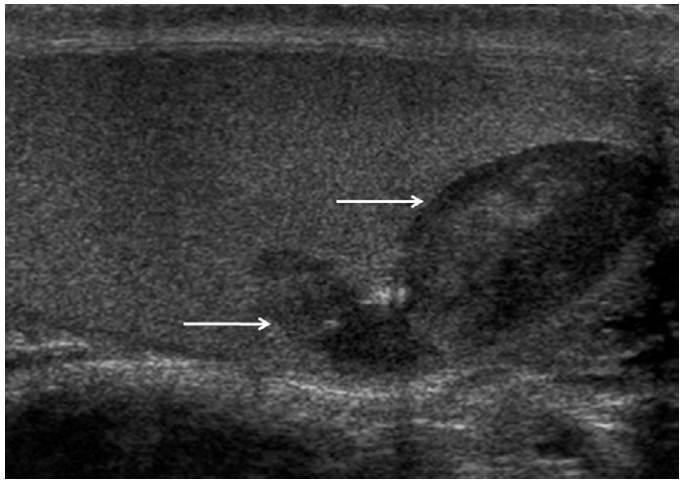


Figure 31.34 Intra-testicular haematomas. Two areas of predominantly low reflectivity (arrows) but with central high reflectivity in a patient following a motorcycle accident.

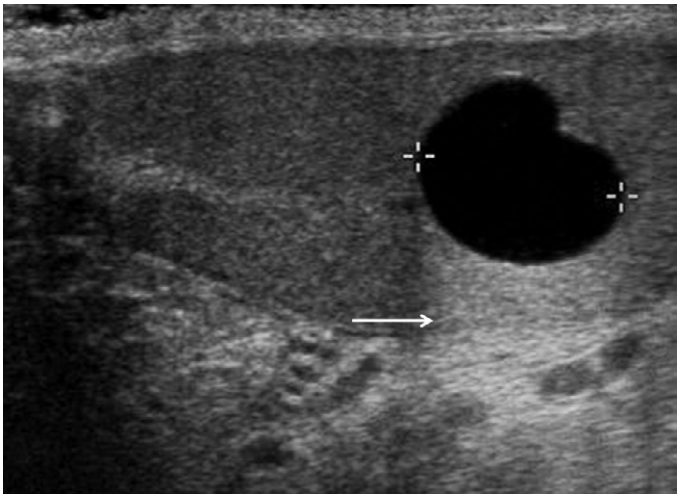


Figure 31.35 Intra-testicular cyst. A large low reflective lesion (between cursors) within the testis demonstrating posterior acoustic enhancement (arrow): a testicular cyst.



Figure 31.37 Tunica vaginalis cyst. In the presence of a large hydrocele, this tunica vaginalis cyst (arrow) is readily visible.

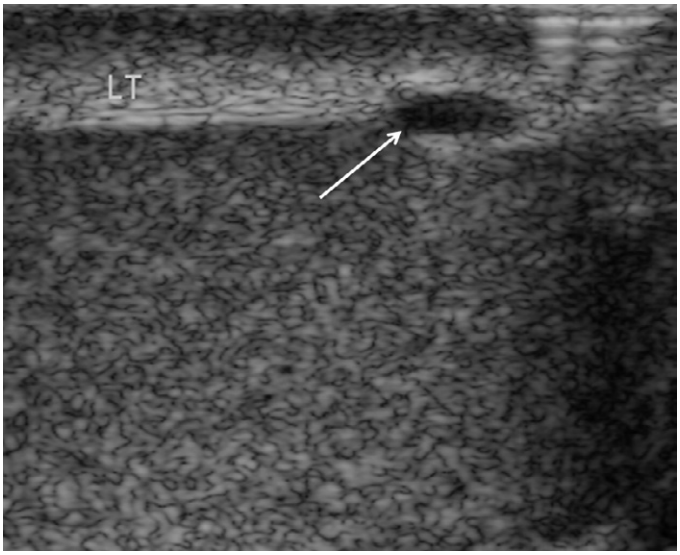


Figure 31.36 Tunica albuginea cyst. A small cyst (arrow) is situated in the line of the echogenic tunica albuginea. These tunica albuginea cysts are frequently palpated by the patient and give rise to concern.

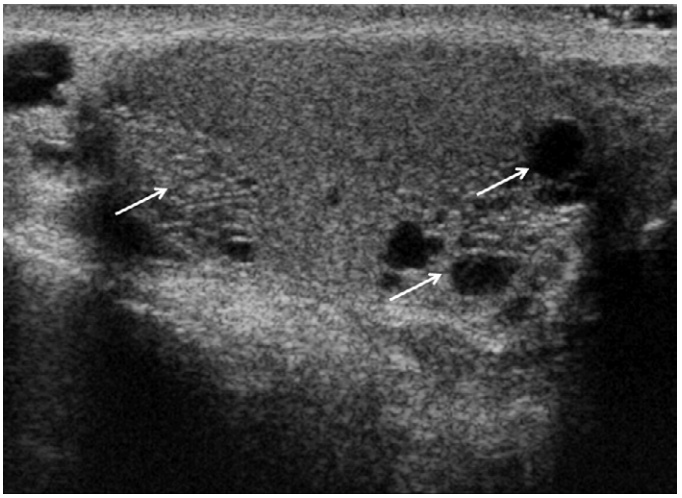


Figure 31.38 Dilated cystic rete testis. The central aspect of the testis; along the line of the mediastinum testis are multiple areas of cystic dilatation (arrows) of varying size in keeping with dilatation of the rete testis.

cysts are rarely palpated and even if large are not firm. Simple cysts are well-delineated anechoic round structures, with a thin smooth wall and posterior acoustic enhancement (Fig. 31.35). The origin of the intra-testicular cyst is uncertain: congenital, traumatic or post-inflammatory. These cysts are often near the mediastinum testis and may arise from an anomalous efferent duct. The cysts may be as large as 30 mm and careful examination is required to exclude any wall irregularity which may suggest a cystic tumour.

Tunica albuginea cyst

Tunica albuginea cysts are located within the dense tissue of the closely adherent tunica albuginea (Fig. 31.36). The origin is unknown but may be mesothelial. These cysts are usually solitary, unilocular and readily palpated by the patient as a firm nodule on the surface of the testis giving concern. These lesions are often difficult to see with ultrasound and the patient's cooperation is invaluable in locating the lesion.

Tunica vaginalis cyst

A tunica vaginalis cyst arises from either the visceral or parietal layer of the tunica vaginalis (Fig. 31.37).

Dilatation of the rete testis

Cystic ectasia of the rete testis results from the partial or complete obstruction of the efferent ducts often by inflammation or trauma, and causes dilatation of the rete testis in an asymmetrical unilateral distribution (Fig. 31.38). However, cystic ectasia of the rete testis often occurs in a bilateral and symmetrical distribution in the older patient. The differential diagnosis is of a malignant cystic testicular tumour although the bilateral nature of ectasia usually suggests the diagnosis. The ultrasound appearances of a dilated rete testis are multiple low reflective oval or rounded structures, which do not demonstrate vascular flow within the mediastinum testes.[6] The cysts usually measure a few millimetres in diameter but may be as

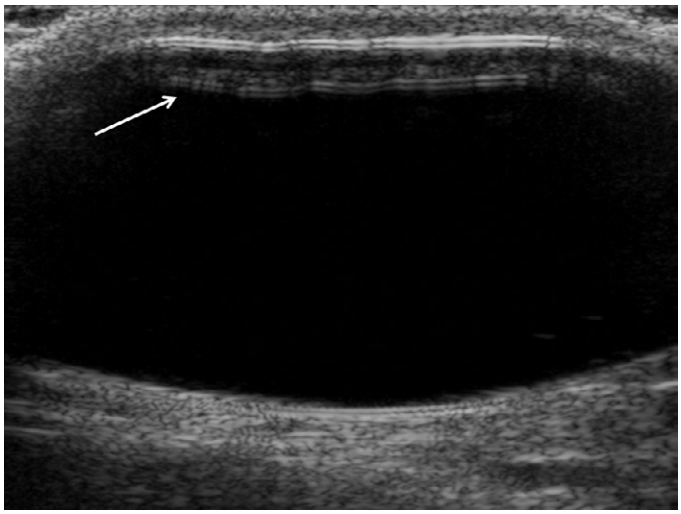


Figure 31.39 Testicular prosthesis. A silicone testicular prosthesis of uniform low reflectivity demonstrating some reverberation artefact (arrow).

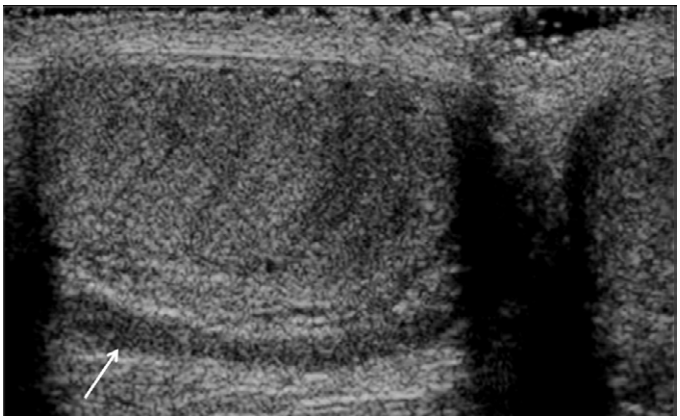


Figure 31.40 Testicular atrophy in an 80-year-old man, demonstrating a heterogeneous appearance of the testis and a normal appearing epididymis (arrow).

large as 7 cm.[34] Whilst this is a benign entity it may be of significance in a patient suffering from azoospermia as this implies there is obstruction of the ipsilateral spermatic ducts. Distension of the rete testes has been described in association with a seminoma, teratoma and an epididymal cystadenoma, where the obstruction of the tubules by tumour is thought to be responsible.[33] Therefore careful examination to exclude an associated tumour should be performed.

Cystic dysplasia of the testis

Although cystic dysplasia is similar in appearance to a dilated rete testis, this is thought to represent a rare congenital anomaly and is usually diagnosed in childhood.[6]

Testicular prosthesis

Following orchidectomy, patients may elect to have a testicular prosthesis inserted, normally made of silicone. A testicular prosthesis has a characteristic appearance on ultrasound (Fig. 31.39).

Atrophy

Testicular atrophy may occur following cryptorchidism, inflammation, torsion of trauma, hypothyroidism, oestrogen treatment, liver cirrhosis, hypopituitary disease and ageing. The testis is globally reduced in size, usually unilateral with changes in testicular reflectivity related to the underlying cause, but usually of lower reflectivity. While volume and vascularity of the testis are reduced, the epididymis remains normal. Atrophy is a natural phenomenon of ageing where changes in the normal testis reflectivity, usually of a heterogeneous nature, may occur (Fig. 31.40).[35]

Testicular microlithiasis and macrocalcification

Testicular microlithiasis describes the appearance of multiple tiny bright foci, measuring 1–2 mm in diameter, which may be unilateral or bilateral (Fig. 31.41). The number of calcified foci and the pattern of distribution can vary, being either very diffuse or more peripherally clustered.[36] Testicular microlithiasis has been

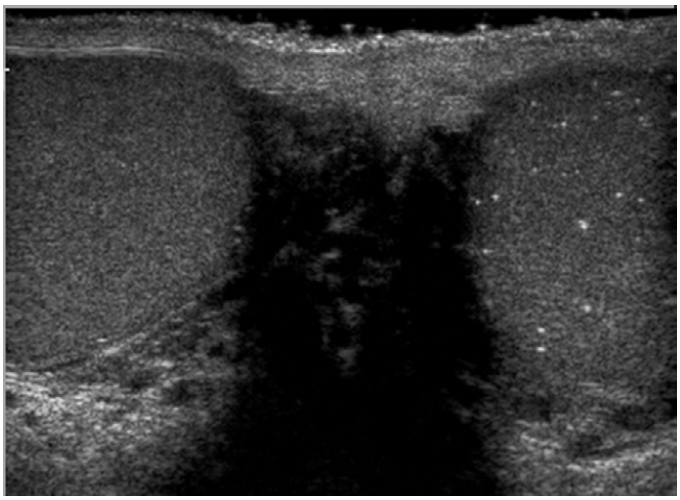


Figure 31.41 Testicular microlithiasis. Spectacle view with unilateral left-sided classical testicular microlithiasis.

arbitrarily classified into 'limited', defined as fewer than five microliths per ultrasound field, or 'classical', defined as more than five microliths per field.[36] A further definition, 'florid', where there are innumerable microliths per ultrasound field, has also been suggested.[37] The prevalence of all forms of testicular microlithiasis is reported at 0.6%–9.0%.[38,39] Testicular microlithiasis is characterised by the formation of microliths from degenerating cells in the seminiferous tubules. Acoustic shadowing is not seen, probably due to the small size of the calcifications. Although usually an incidental finding during the investigation of testicular symptoms, testicular microlithiasis has been associated with various medical conditions, including infertility, cryptorchidism, Klinefelter's syndrome, Down's syndrome and pulmonary alveolar microlithiasis.

Testicular microlithiasis has also been found in association with benign and malignant tumours in the testis, with reports indicating seminoma as the commonest tumour to occur in association with testicular microlithiasis (Fig. 31.42).[40] Furthermore a high number of patients with intra-tubular germ cell neoplasia have testicular

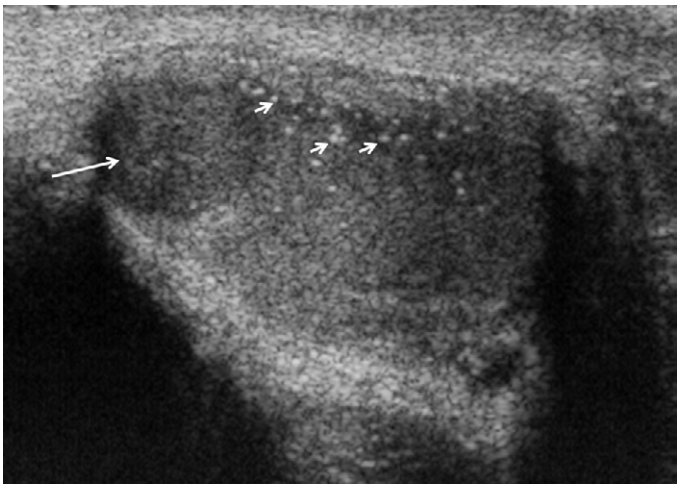


Figure 31.42 Seminoma with testicular microlithiasis. Testicular microlithiasis (short arrows) in association with a seminoma (arrow) in an atrophic testis. There is an increased prevalence of primary testicular tumours in the presence of testicular microlithiasis.

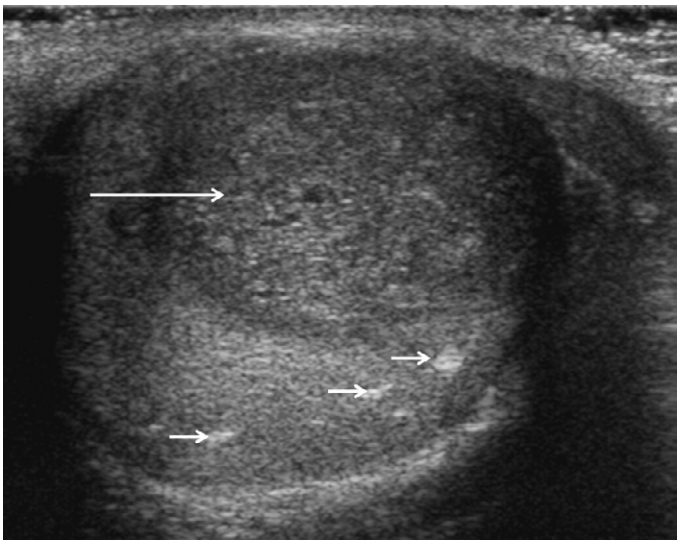


Figure 31.43 Seminoma with testicular macrocalcification. A seminoma is present in the upper aspect of the testis (long arrow), with focal areas of macrocalcification lying outside the tumour margins (small arrows).

microlithiasis; approximately 50% of patients with intra-tubular germ cell neoplasia develop testicular cancer within 5 years.[41] As a consequence, the significance of finding isolated testicular microlithiasis is as yet uncertain; surveillance with ultrasound on an annual basis is advocated.[38] A number of case reports have detailed the development of a primary testicular tumour whilst on an ultrasound surveillance programme.[39,42]

The association of testicular macrocalcification within benign testicular lesions is well documented and can be found in association with intra-testicular cysts and epidermoid tumours. Benign intratesticular tumours, commonly derived from the Sertoli and Leydig cells of the seminiferous tubules, are difficult to distinguish from malignant tumours and these too demonstrate calcification. Large smooth curvilinear calcification at the periphery of a tissue mass has been shown in Sertoli cell tumours. Granulomatous disease within the testes can also present with a low reflective mass and areas of calcification within.[43] The presence of macrocalcification in association with malignant tumours has also been noted, particularly with the entity of 'burnt-out' tumours, and recently macrocalcification has been associated with a higher prevalence of primary testicular tumours (Fig. 31.43).[44]

Testicular microlithiasis

- Small 1–2 mm highly reflective areas with no posterior acoustic shadowing.
- May be bilateral or unilateral.
- Associated with an increased prevalence of testicular malignancy.
- High numbers of patients with testicular microlithiasis have intra-germ cell neoplasia.
- Annual ultrasound surveillance is suggested.

EXTRA-TESTICULAR ABNORMALITIES

Extra-testicular focal lesions

Extra-testicular solid tumours are rare; the majority of extra-testicular lesions are cystic abnormalities of the epididymis. Primary solid tumours of the extra-testicular tissues are normally benign although malignant lesions are seen. The reported prevalence of extra-testicular solid tumours varies between 3% and 16% of all patients referred for scrotal ultrasound.[45] Metastases may also occur in the extra-testicular space.

Epididymal cysts and spermatoceles

Extra-testicular cysts are commonly found in the spermatic cord, epididymis (Fig. 31.44), tunica albuginea or tunica vaginalis. Epididymal cysts are most commonly found in the epididymal head, contain clear serous fluid and on ultrasound demonstrate typical features of a cyst with posterior acoustic enhancement and may be seen in up to 40% of patients. A spermatocele consists of cystic dilatation of tubules of the efferent ductules and occurs in the epididymal head (Fig. 31.45), often containing low reflective debris representing spermatozoa, lymphocytes, cellular debris, fat and proteinaceous fluid.[46] The differentiation between a spermatocele and a simple cyst is unimportant and they may be indistinguishable on ultrasound. Spermatocele is though to be more common than an epididymal cyst and more frequent in the epididymal head. These cystic structures are normally painless unless inflamed, a rare occurrence (Fig. 31.46). Spermatocele may be large (>4 cm) and mimic a hydrocele; differentiation is usually attained by demonstrating fluid anterior to the testis in a hydrocele.

Tubular ectasia and vasectomy

Following vasectomy, the epididymis has a characteristic appearance of dilatation, with an inhomogeneous appearance on ultrasound described as ectasia of the epididymis. These appearances are unrelated to symptoms and are seen in 45% of patients (Fig. 31.47). There may be an associated spermatocele and sperm granuloma.

Sperm granuloma

A sperm granuloma occurs secondary to inflammation, trauma and vasectomy, and is thought to be a granulomatous reaction to extravasated sperm cells. Causative factors include infection, trauma or a vasectomy; 3–5% of vasectomy patients develop a sperm granuloma. On ultrasound a sperm granuloma is well

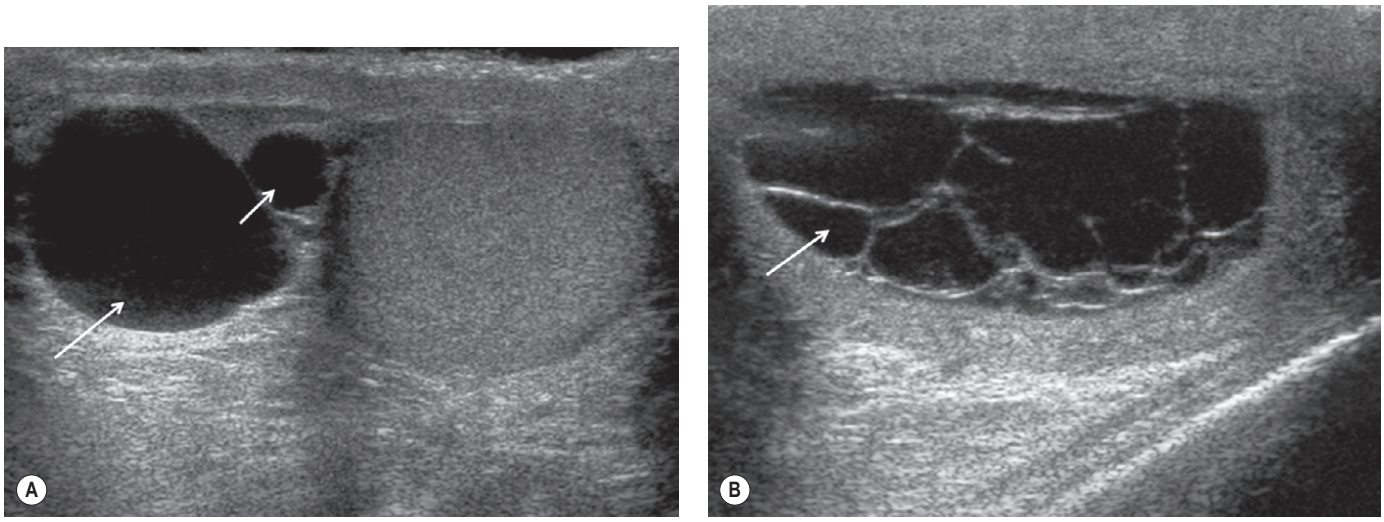


Figure 31.44 Epididymal head cysts. A: Two cysts are present in the epididymal head (short and long arrows). **B:** A septated epididymal head cyst (arrow).

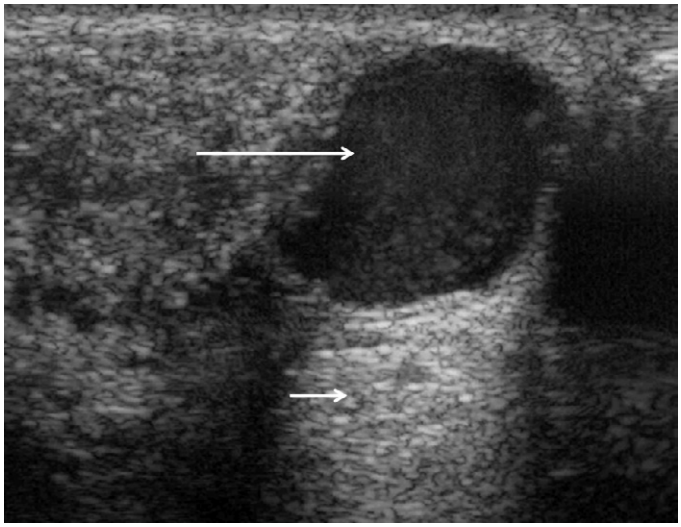


Figure 31.45 Spermatocele. A cyst in the epididymal tail demonstrates debris (long arrow) that is 'layering' and produces posterior acoustic enhancement (short arrow): a spermatocele.

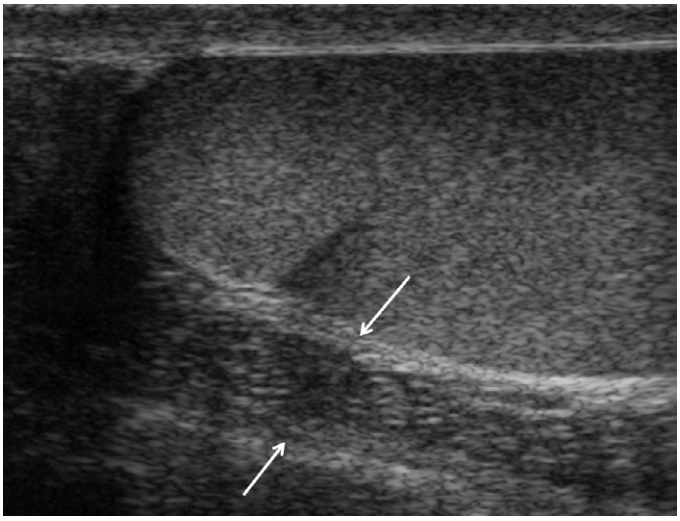


Figure 31.47 Post-vasectomy. The epididymis is dilated (between arrows, >4 mm) in a patient who has undergone a vasectomy, with a characteristic reflective pattern demonstrated.

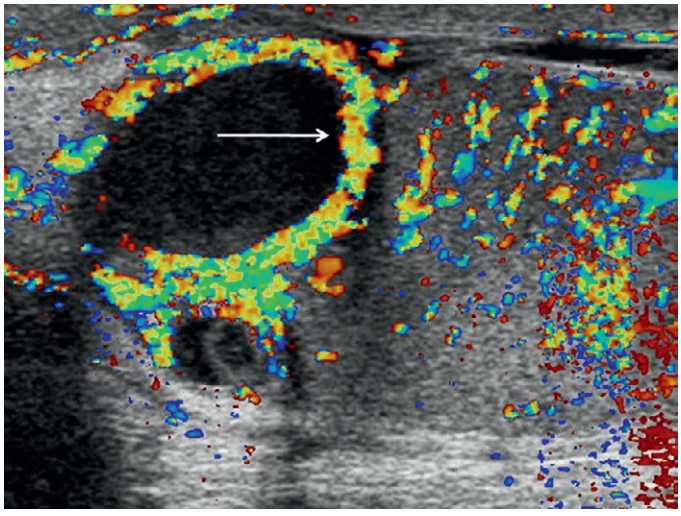


Figure 31.46 Inflamed spermatocele. On colour Doppler ultrasound there is increased colour Doppler flow to the periphery of the spermatocele (arrow) in keeping with inflammatory change.

demarcated, of low or high reflectivity, is avascular on colour Doppler flow, found in the epididymis, and often painful in the early stages (Fig. 31.48).[47]

Benign neoplasms (Table 31.2)

Tumours of the epididymis, spermatic cord and extra-testicular tissues are rare, seen in the older patient and are often benign (but not in children).

Lipoma

This is the most common benign tumour of the extra-testicular space and it is commonly found in the spermatic cord.[48] Patients of all ages are affected, with the tumour manifesting as a non-tender scrotal lump. At ultrasound a lipoma has a homogenous high to iso-reflective appearance, and varies in size (Fig. 31.49). Magnetic resonance (MR) imaging will confirm the fat content of the lesion, prior to excision if necessary.

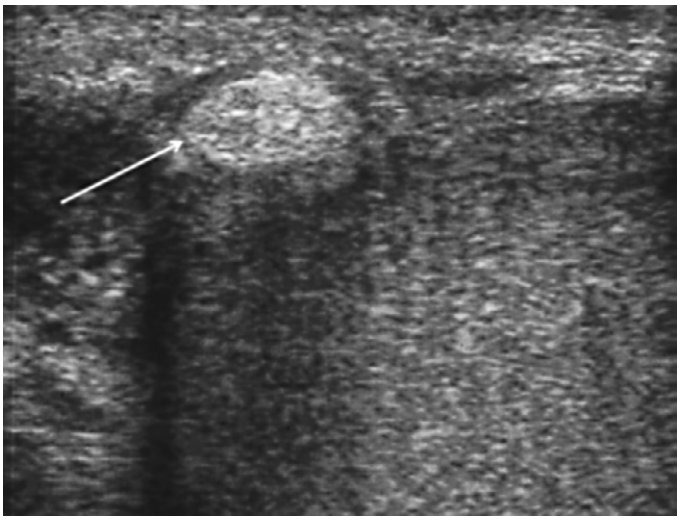


Figure 31.48 Sperm granuloma. A focal high reflective lesion in the epididymis (arrow) which is painful: a sperm granuloma.

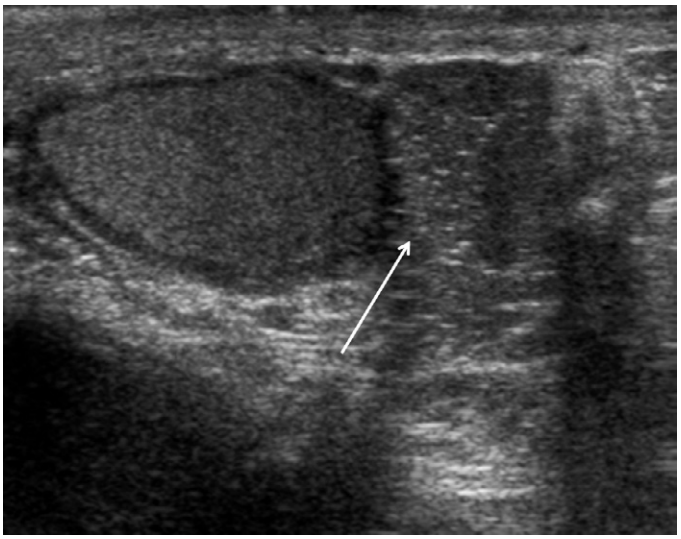


Figure 31.49 Lipoma. A focal extra-testicular lesion (arrow) in keeping with a lipoma.

Table 31.2 Extra-testicular neoplasms

Benign
Adenomatoid tumour
Leiomyoma
Lipoma
Haemangioma
Cystadenoma
Fibrous pseudo-tumour
Sclerosing lipogranuloma
Malignant
Rhabdomyosarcoma
Liposarcoma
Leiomyosarcoma
Malignant schwannoma
Malignant fibrous histiocytoma
Pleomorphic hyalinising angiectatic tumour
Metastases (in order of frequency)
Prostate
Kidney
Stomach
Colon
Ileum (carcinoid tumour)
Pancreas

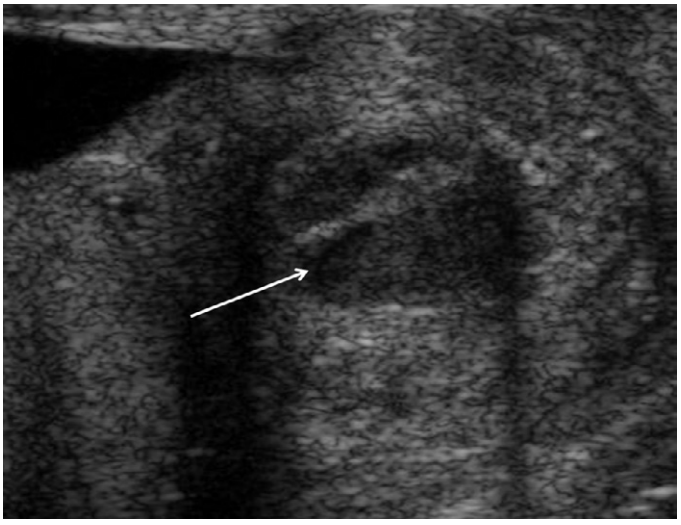


Figure 31.50 Adenomatoid tumour. A focal low reflective mass (arrow) present in the tail of the epididymis with a linear highly reflective septum.

Adenomatoid tumour

This is the most common tumour of the epididymis, accounting for 30% of all tumours of the extra-testicular space; probably of a mesothelial origin. Adenomatoid tumours usually occur in the patient of 20 years or older, present as a painless mass, are slow growing and arise in the tail of the epididymis (four times as common as in the head) and are predominantly left-sided. The ultrasound appearance is non-specific; the majority are iso-reflective to the epididymis, well defined, oval in shape and can be cystic (Fig. 31.50).[49] Resection is normally curative, but will interfere with sperm ejaculation on the side of the resection.

Leiomyoma

This is the second commonest tumour of the epididymis, with a prevalence of 6%. It commonly manifests in the fifth decade, frequently involving the epididymal head, and is often associated with a hydrocele. The patient presents with a slow-growing non-tender mass. On ultrasound there are no specific features; it may be cystic or solid and contain areas of calcification.[50]

Other benign tumours

Other rare benign tumours of the extra-testicular space include haemangiomas (Fig. 31.51),[51] which may be indistinguishable from a varicocele, and a papillary cystadenoma associated with von Hippel–Lindau disease, appearing as a solid lesion with small cystic spaces in the head of the epididymis. A fibrous pseudo-tumour (Fig. 31.52) may result from a prior history of trauma, haematocele or from epididymo-orchitis.

Malignant neoplasms

Malignant lesions of the extra-testicular space are rare, usually present as a mildly painful enlarging mass, and the vast majority are sarcomas.

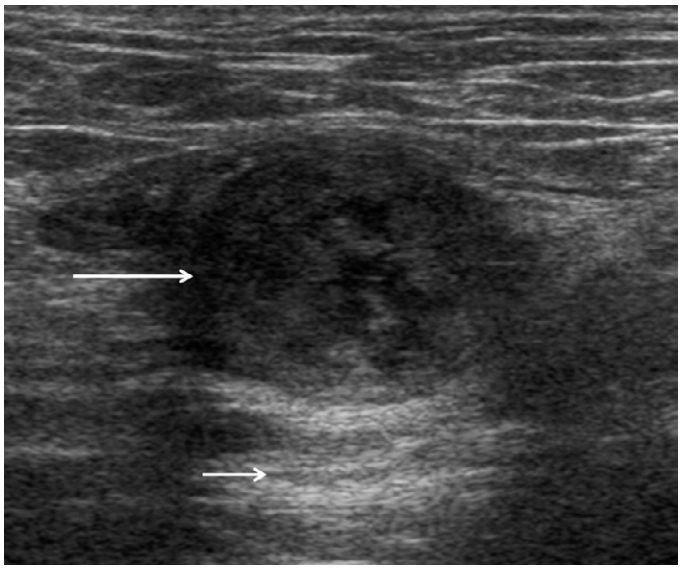


Figure 31.51 Cavernous haemangioma of the spermatic cord. A well-circumscribed lesion of the spermatic cord containing pockets of low reflectivity (long arrow) that demonstrate colour Doppler flow, with posterior acoustic enhancement (short arrow) along the line of the spermatic cord: a cavernous haemangioma.

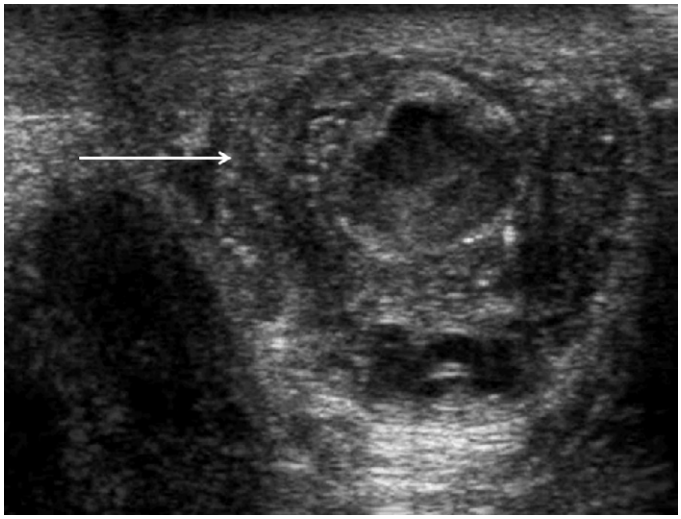


Figure 31.52 Fibrous pseudo-tumour. A fibrous pseudo-tumour of the epididymal tail (arrow) demonstrating a spectrum of different reflectivity.

Rhabdomyosarcoma

This is the most common sarcoma of the spermatic cord (40% of extra-testicular malignant lesions), peaking at ages 5 and 16 years. The most common presentation is of an enlarging painless mass, but as an aggressive tumour it may present with metastases. On ultrasound features are non-specific: variable reflectivity with areas of necrosis and haemorrhage and increased colour Doppler flow of low resistance.[52]

Liposarcoma

This is very rare, usually arises from the spermatic cord, is of low-grade malignancy, and spreads locally. Patients present with a slow-growing fluctuant mass. Ultrasound demonstrates a highly reflective mass of varying size.

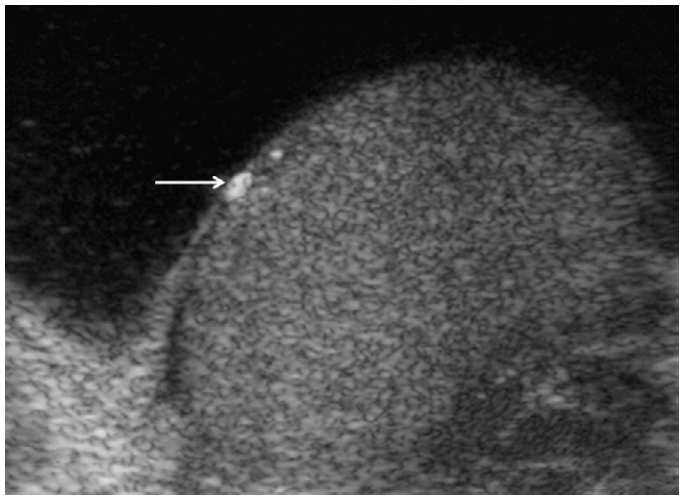


Figure 31.53 Tunica vaginalis calcification. A focus of high reflectivity adjacent to the outer border of the testis casting an acoustic shadow (arrow): calcification within the tunica vaginalis.

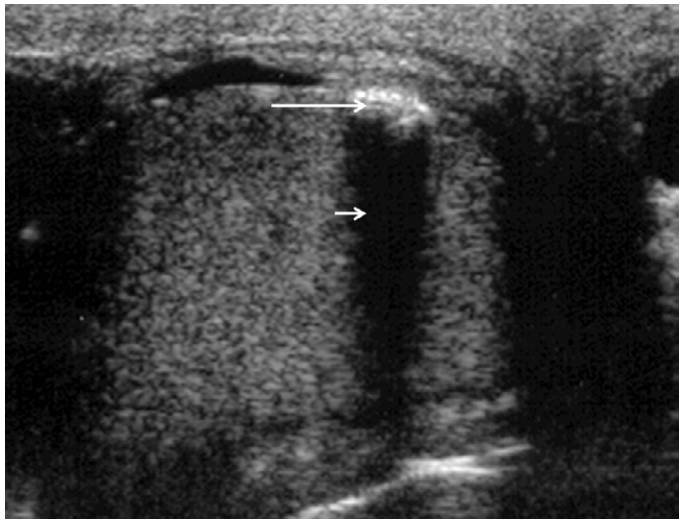


Figure 31.54 Tunica albuginea calcification. A focus of high reflectivity in the tunica albuginea (long arrow) causing extensive posterior acoustic shadowing (short arrow).

Other malignant neoplasms

Other rare malignant lesions of the extra-testicular space include leiomyosarcoma, which is seen as a predominantly low reflective mass,[53] malignant schwannoma and malignant fibrous histiocytoma. A mesothelioma may develop from the tunica vaginalis in patients exposed to asbestos.[54] Lastly, metastases to the extra-testicular space occur from a testicular primary tumour and from renal, prostate and gastrointestinal tumours.

Extra-testicular calcification

Calcification within the epididymis is frequent and usually represents benign disease. The tunica vaginalis may occasionally calcify, producing a plaque with acoustic shadowing (Fig. 31.53), as will calcification in the tunica albuginea (Fig. 31.54). Calcification in or adjacent to the epididymis is a common finding and is usually due to chronic epididymitis. Haematoma and sperm granulomas (sperm extravasation with granuloma formation) may occur and produce a solitary, highly reflective area within the epididymis. The appendix epididymis and appendix testis may calcify and are recognised

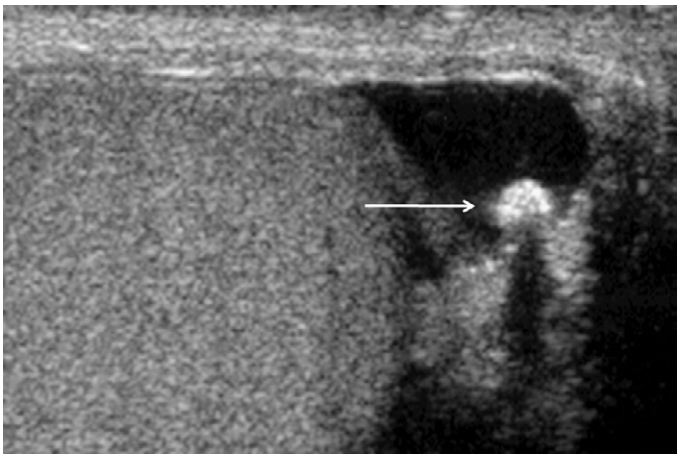


Figure 31.55 Scrotal pearl. The high reflective area (arrow) lying free within a small hydrocele within the scrotal sac represents a 'scrotal pearl', and causes posterior acoustic shadowing.

Extra-testicular lesions

- Nearly all are benign abnormalities.
- The majority are epididymal head cysts.
- Lipomas occur commonly.
- Adenomatoid lesions are commonest in the epididymis.
- Rhabdomyosarcoma occurs between the ages of 5 and 16 years.

by their characteristic position and shape.[43] Calcifications present in between the two layers of the tunica vaginalis have a characteristic appearance and are termed 'scrotal pearls', often best seen in the presence of a hydrocele (Fig. 31.55). A scrotal pearl, often palpated by the patient, is usually freely mobile within a hydrocele. They may arise from inflammation of the tunica vaginalis or from remnants of an appendix testis or epididymis.

Extra-testicular non-focal lesions

Inguinal hernia

Inguinal hernias are a common cause of a scrotal swelling. Physical examination is normally sufficient to arrive at the diagnosis of an intra-scrotal inguinal hernia; ultrasound may be useful in the difficult cases. On ultrasound the hernia contains bowel or omentum giving rise to peristalsis of fluid-filled loops of bowel, air within bowel or high reflective omental fat.

Fluid collections

Hydrocele, pyocele and haematocele

Between the two layers of the tunica vaginalis, there is normally a little serous fluid present, and this may be visualised in up to 85% of asymptomatic men. When the collection of fluid becomes large, a hydrocele develops, the commonest cause of a painless scrotal swelling. The fluid accumulation is confined to the anterior and lateral aspects of the scrotum, sparing the bare area of the testis; the testis appears to lie in a posterior location within the scrotal sac. A hydrocele is normally of low reflectivity, with posterior acoustic enhancement, but may contain multiple echoes in the presence of cholesterol crystals (Fig. 31.56).[55] Hydroceles may be idiopathic or develop secondary to trauma (haematocele), infection (pyocele), torsion or tumour, or be congenital (secondary to a patent processus vaginalis). The testis is normally displaced to the posterior aspect of the scrotal sac in the presence of a hydrocele, in contrast to the inferior position when a large epididymal cyst causes displacement of the testis.

Varicocele

A varicocele is present in up to 15% of adult male patients. Varicoceles are caused by incompetent valves in the internal spermatic vein. Impaired drainage is more evident when standing upright or during a Valsalva manoeuvre, which renders the varicocele more prominent. Varicoceles are left-sided in 78%, right-sided in 6% and bilateral in 15%. This abnormal dilatation of veins arises more often on the left as a consequence of the angle at which the left testicular vein enters the left renal vein. The normal veins of the pampiniform plexus measure 0.5–1.5 mm and a vein diameter of greater than 2 mm should be considered abnormal.[56] On ultrasound, a varicocele consists of multiple low reflective serpiginous tubular structures of varying size, best seen superior and lateral to the testis. If large the varicocele may extend to the inferior aspect of the testis (Fig. 31.57). Tumbling low-level echoes may be identified on real-time imaging, secondary to low flow. Ultrasound in the supine and erect positions as well as following the Valsalva manoeuvre will help identify the varicocele and document retrograde filling. Examination of the left kidney is advocated in the presence of a varicocele to exclude a renal tumour in all patients by many clinicians, without much supporting evidence as to the prevalence of this association.[57] This is probably only really indicated in the presence of a varicocele that has recently arisen in patients over the age of 40 years. Occasionally an intra-testicular varicocele may occur (Fig. 31.58) with an incidence quoted at <2% in a symptomatic population.[58] The ultrasound appearances of an intra-testicular varicocele are anechoic serpiginous or cystic structures radiating from the mediastinum testis. The appearance on colour and spectral Doppler examination is characteristic, as an intra-testicular varicocele demonstrates vascular flow, differentiating this from other cystic structures such as a prominent rete testis or an intra-testicular cyst. An intra-testicular varicocele will behave in a similar fashion to an extra-testicular varicocele, increasing in size and demonstrating retrograde flow on Valsalva manoeuvre. A common clinical presentation is with testicular pain attributed to stretching of the tunica albuginea secondary to venous congestion.

A classification of varicoceles based on clinical features is as follows: grade 1, varicocele is palpable only during the Valsalva manoeuvre; grade 2, readily palpable without the need for the Valsalva manoeuvre; and grade 3, visible on inspection.[59] Identification of a varicocele in patients being investigated for infertility may be of relevance, although testicular volume, ultrasound appearances and Doppler studies may also be of importance.

ACUTE SCROTUM

Acute scrotal pain is a common urological emergency for which epididymo-orchitis is the commonest cause. The most important diagnostic distinction to be made in patients presenting with acute scrotal pain is between acute spermatic cord torsion and the other causes of acute scrotal pain (Table 31.3). The treatment for acute spermatic cord torsion is urgent surgical exploration to maintain viability of the testis and avoid testicular infarction. Diagnostic accuracy is therefore imperative in order to identify those patients that require immediate surgical intervention as well as avoiding unnecessary surgery in patients with a non-surgical cause for acute testicular pain. In the emergency setting, the ready availability of greyscale ultrasound, with the ability to assess testicular vasculature on colour Doppler, allows ultrasound to remain the imaging modality of choice. Clinical examination can be notoriously

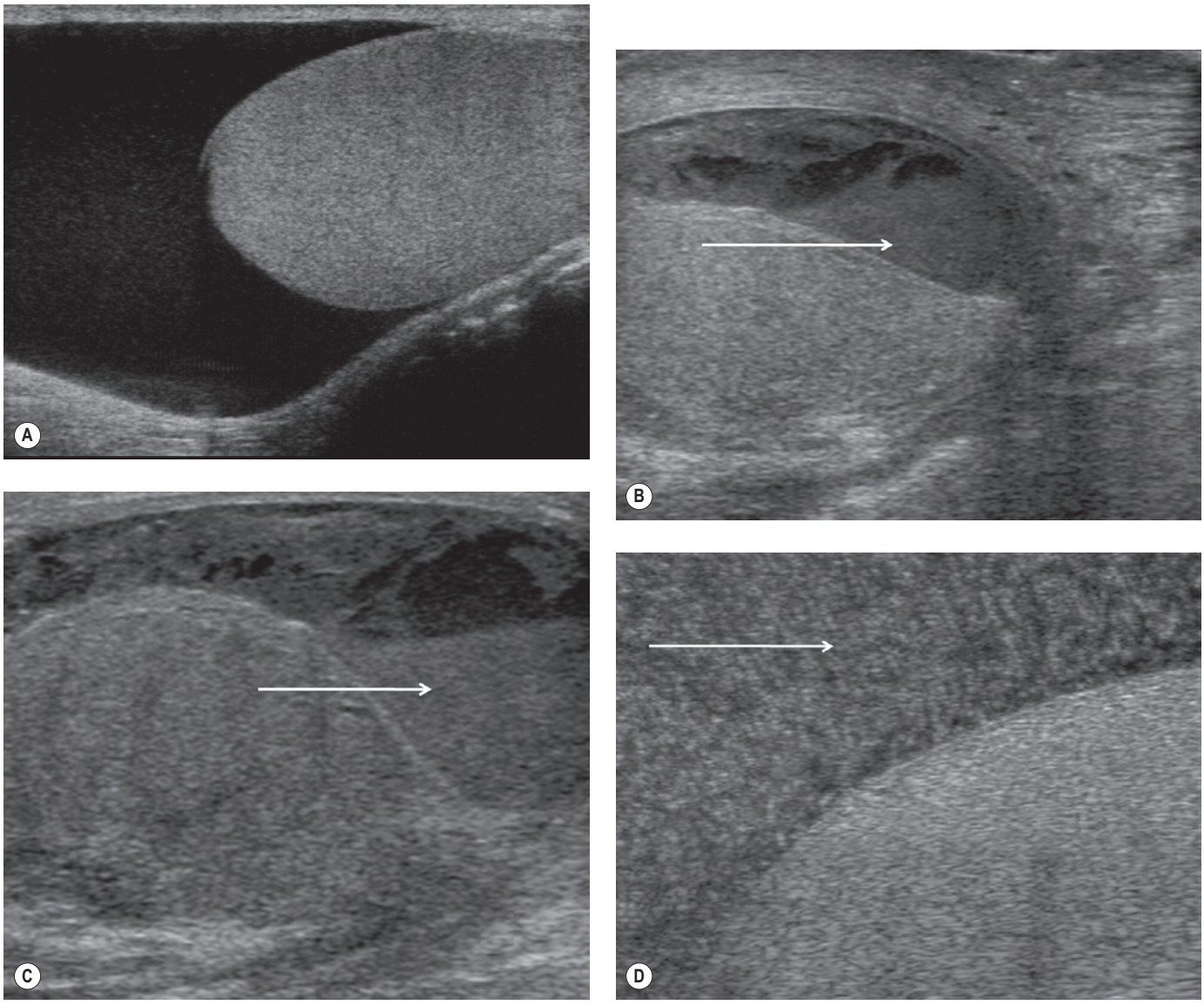


Figure 31.56 Extra-testicular fluid collections. A: The testis is displaced inferiorly by a large hydrocele without any echogenic debris visible: a simple hydrocele. **B:** A pyocele in a patient with severe epididymo-orchitis with echogenic debris (arrow) representing pus. **C:** A haematocele in a patient following blunt testicular trauma, with 'layering' of echogenic debris seen (arrow). **D:** Extensive highly reflective material within a chronic hydrocele representing cholesterol crystals (arrow).

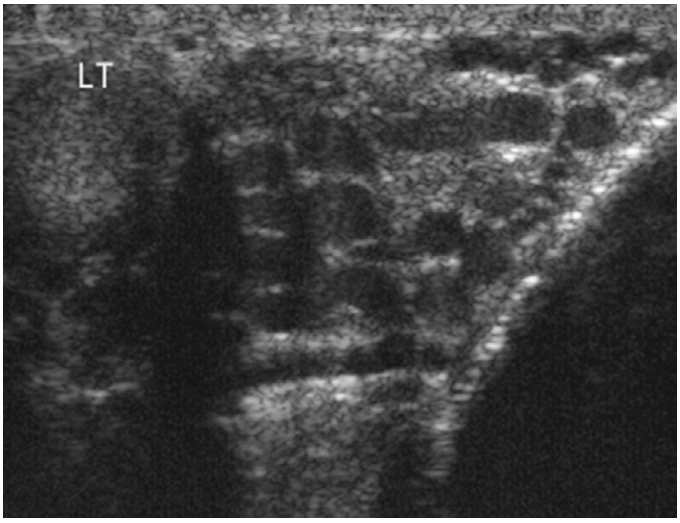


Figure 31.57 Extra-testicular varicocele. Serpiginous dilated (>2 mm) veins at the lower aspect of the testis; a testicular varicocele. LT, left testis.

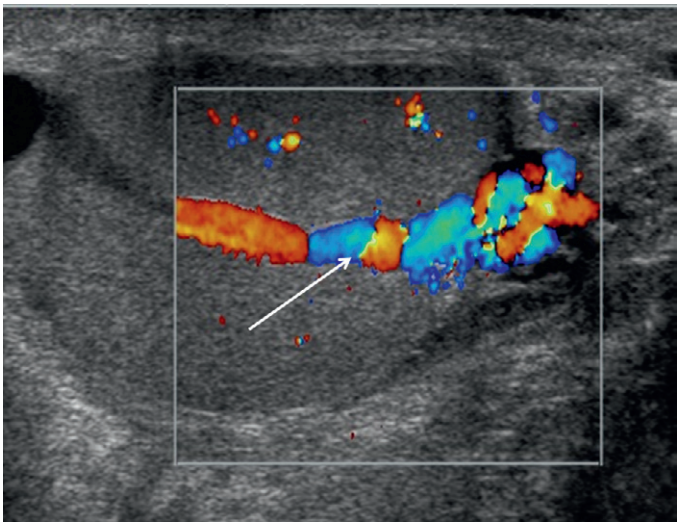


Figure 31.58 Intra-testicular varicocele. With the Valsalva manoeuvre there is filling of the tubular structure with colour: an intra-testicular varicocele (arrow).

inaccurate in distinguishing the causes of acute scrotal pain. In particular, the clinical discrimination between acute epididymo-orchitis and spermatic cord torsion can be virtually unachievable; imaging may play an important role. Familiarity with the ultrasound features of common causes of acute scrotal pain is therefore a necessity for the emergency on-call radiologist in order to provide complementary information for the clinical team to aid accurate diagnosis in these patients.

Inflammatory disease

Epididymo-orchitis and epididymitis

Epididymo-orchitis and epididymitis predominantly affects the sexually active male of less than 40 years, the older patient with urological disease and the prepubertal boy with an associated urogenital anomaly.[60] The main causative organisms in sexually transmitted diseases are *Chlamydia trachomatis* and *Neisseria gonorrhoeae*, whereas in prepubertal boys and in men over the age of 40 years, the organisms responsible are *Escherichia coli* and *Proteus mirabilis*. Epididymitis causes acute scrotal pain of varying intensity and pyuria with fever; at clinical examination the epididymis may be palpated as a thickened tender structure separate from the testis.

On ultrasound, the epididymis may be involved in focal areas (often the lower is affected first) or in a global pattern, with enlargement, decreased reflectivity and increased colour Doppler flow (Fig. 31.59).[61,62] The presence of increased colour Doppler flow to the inflamed epididymis is the hallmark of hyperaemia and usefully aids the diagnosis of epididymitis and epididymo-orchitis. On spectral Doppler ultrasound, there is a high-flow, low resistance waveform.[63] There is often a reactive hydrocele, with septations if a pyocele develops and scrotal wall thickening. The infection often spreads to the adjacent testis (epididymo-orchitis), seen as patchy areas of low reflectivity and increased colour Doppler signal, an appearance that may persist for several months following treatment.[64] In addition, with focal ultrasound changes of the testes it is difficult to exclude a malignant lesion. It is therefore important that diffuse heterogeneous hyper-reflectivity and focal changes of the testes in suspected orchitis be followed up to ensure complete resolution and rule out neoplasm.[65]

Venous infarction of the testis may occur in patients with severe epididymo-orchitis where localised oedema occludes the venous drainage of portions of the testis or the entire testis (Fig. 31.60). The

Table 31.3 Causes of acute scrotal pain

Acute epididymo-orchitis
Acute spermatic cord torsion
Intermittent torsion of the spermatic cord
Acute testicular trauma
Chronic epididymo-orchitis
Acute segmental testicular infarction
Henoch–Schönlein purpura
Patent processus vaginalis with acute appendicitis
Intra-testicular tumours

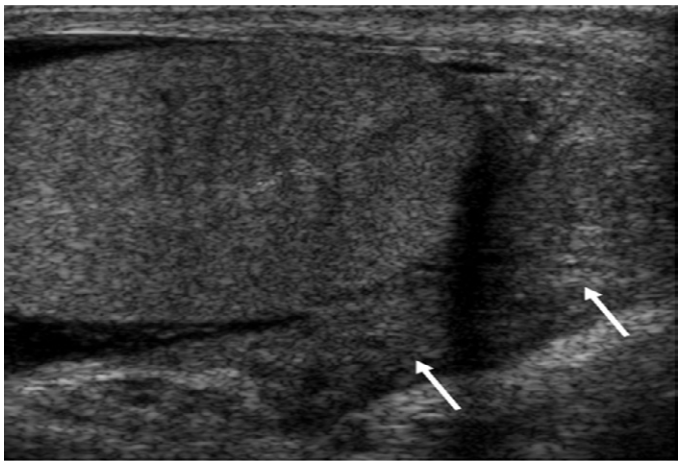


Figure 31.59 Epididymitis. The epididymis is enlarged, of mixed reflectivity (arrows) with an accompanying hydrocele: acute epididymitis.

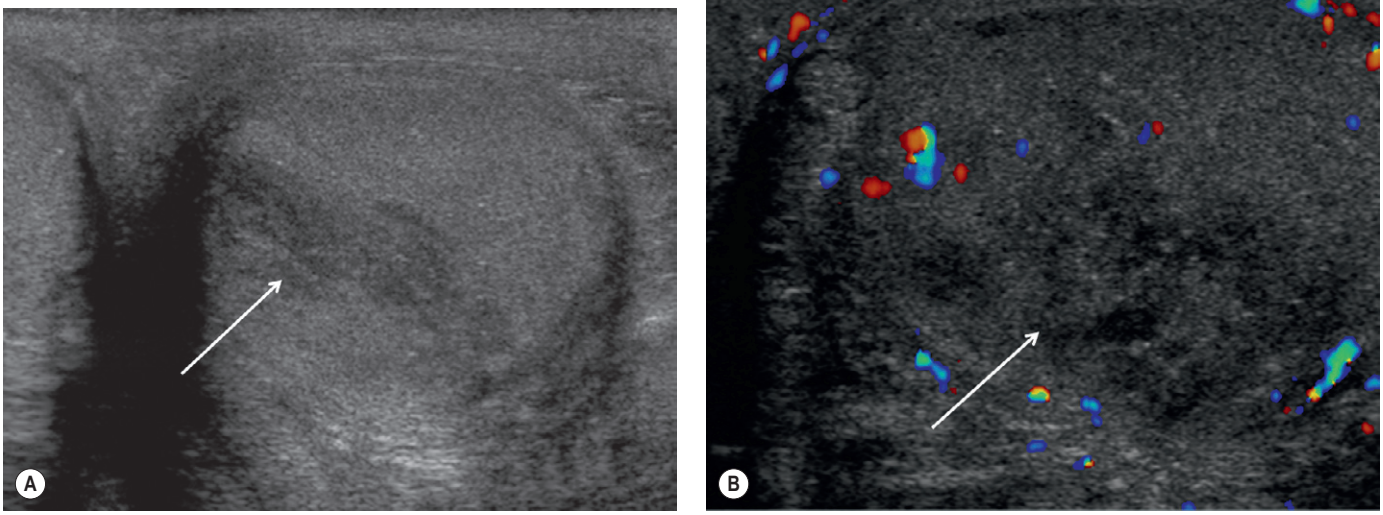


Figure 31.60 Venous infarction. A: There is an area of irregularity and mixed reflectivity present in the posterior aspect of the testis (arrow) in a patient with severe epididymitis. **B:** Colour Doppler ultrasound demonstrates absence of flow signal in the mixed reflective region of the testis (arrow): testicular venous infarction following severe acute epididymitis. There is usually increased colour Doppler flow in orchitis.

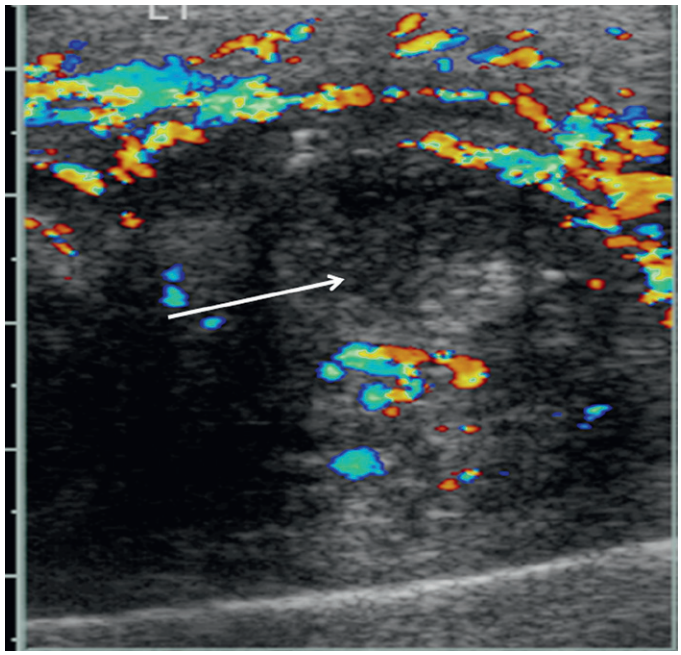


Figure 31.61 Epididymal abscess. There is a focal area of mixed reflectivity (arrow), containing debris, in the tail of the epididymis in a patient with acute epididymitis not responding to antibacterial therapy. Colour Doppler demonstrates increased colour signal from around the low reflective area, and absence of colour Doppler signal within the lesion: an epididymal abscess.

Epididymo-orchitis

- Acute onset of pain.
- Focal or diffuse enlargement of the epididymis.
- Increased colour Doppler flow to the affected areas.
- Orchitis is a common occurrence.
- Abscess is a potential complication.

testis appears of low reflectivity, is swollen and there is absent colour Doppler flow.[66] Indirect evidence of venous infarction is suggested by reversal of arterial flow in diastole when the testicular artery in the spermatic cord is interrogated with spectral Doppler ultrasound.[67]

Other complications include abscess formation (low reflective area surrounded by increased colour Doppler signal) (Fig. 31.61), pyocele, testicular atrophy and chronic pain.

Chronic epididymitis

Chronic epididymitis results in persistent pain and on ultrasound an enlarged epididymis with increased reflectivity is seen with areas of calcification. Tuberculous epididymitis may present in a similar fashion to bacterial epididymitis but will not respond to standard antibiotic treatment. Ultrasound features are not specific, although chronic disease with calcification and indolent abscess formation discharging onto the skin may be present (Fig. 31.62).[68]

Orchitis

Usually the testis is affected in patients with epididymitis giving rise to epididymo-orchitis. Primary orchitis without associated epididymitis is relatively rare but may be caused by HIV or mumps

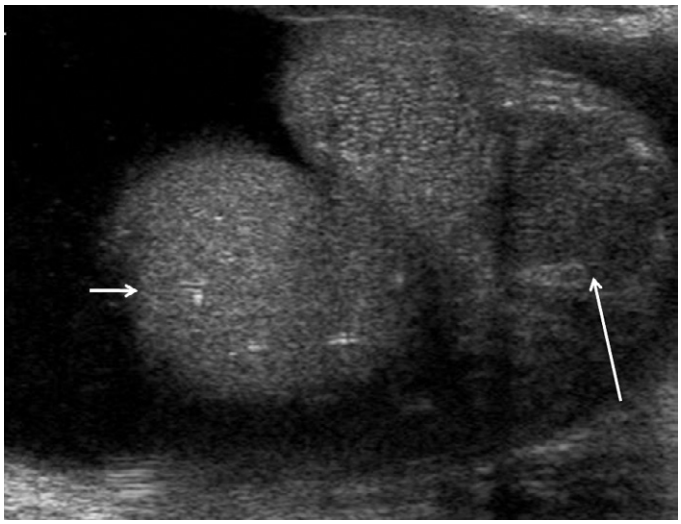


Figure 31.62 Tuberculous epididymitis. A focal area of reduced reflectivity within an enlarged epididymis (long arrow) in a patient with urogenital tuberculosis. A hydrocele is present; the testis is marked with a short arrow.

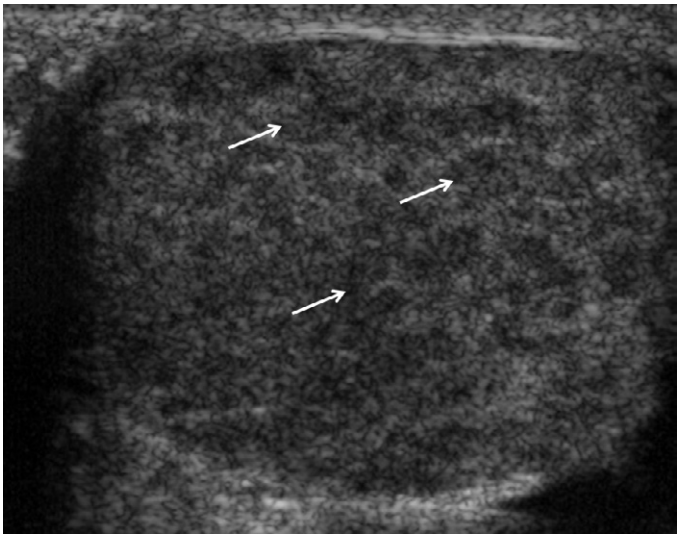


Figure 31.63 Complicated orchitis. There are multiple areas of low reflectivity (arrows) in this testis in a patient with severe orchitis.

virus.[69] The great range of appearances seen on ultrasound in acute orchitis may give rise to confusion. Initially oedema of the testis occurs with associated pain; the ultrasound appearances are those of a diffuse low reflective pattern.[64] The appearances then evolve to areas of patchy low reflectivity with an increase in colour Doppler flow, with the presence of intra-testicular venous flow thought to be characteristic of orchitis.[61] As the condition progresses, areas of venous infarction occur with associated haemorrhage, giving rise to areas of mixed or increased reflectivity. Complications include abscess formation, infarction and necrosis (Fig. 31.63). Following treatment and healing, changes may resolve completely or often there is loss of volume of the testis with fibrosis giving a heterogeneous pattern on ultrasound.[64]

Trauma

Testicular trauma is commonly seen following motor vehicle accidents, athletic injury or a straddle injury. The mobility and elasticity of the scrotal tissues provides protection for the testis in the event

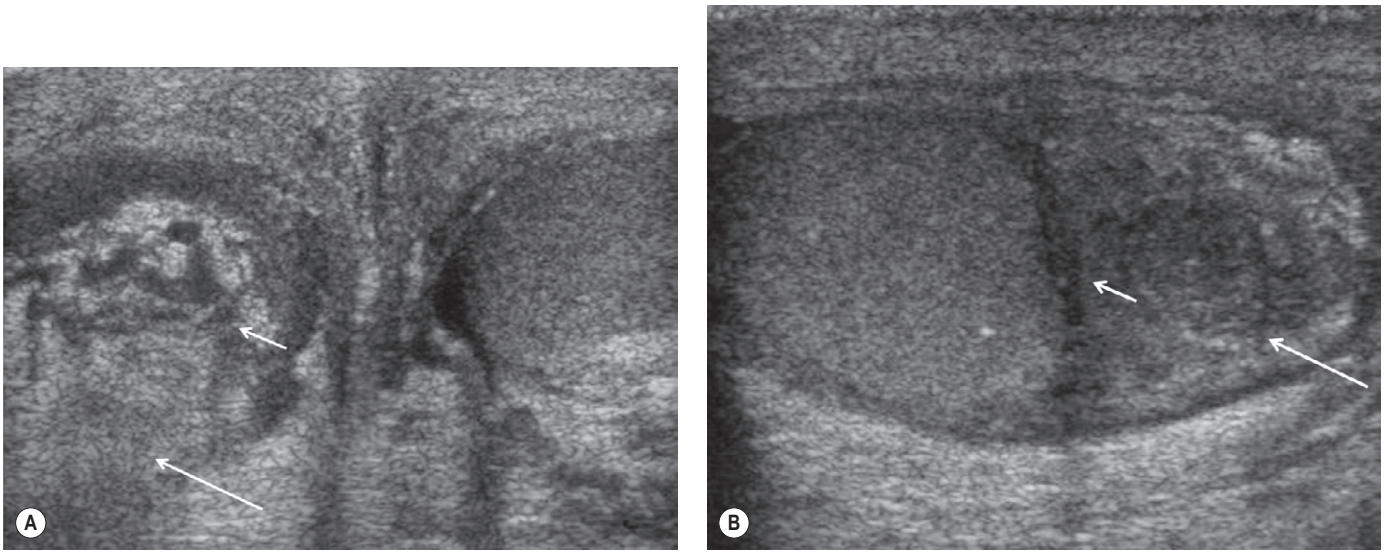


Figure 31.64 Testicular trauma. A: Spectacle view of trauma to the right testis (short arrow) with a heterogeneous appearance and loss of clarity of the tunica albuginea (long arrow) suggesting a testicular rupture. **B:** Ultrasound of the testis following trauma demonstrating a fracture line (short arrow) through the mid-aspect of the testis and disruption of the lower testicular pole with a heterogeneous appearance of haemorrhage (long arrow).

of trauma. However, forceful compression of the scrotal contents against the pubic ramus or impact with objects moving at high velocity can result in serious injury.

Blunt trauma accounts for 85% of testicular injuries and penetrating injuries for 15%. Blunt scrotal trauma may result in a variety of injuries including testicular rupture, torsion, dislocation, haematoma or contusion. Epididymal, scrotal wall and urethral injury may also be seen. Pain and swelling of the scrotum following trauma makes clinical examination extremely difficult. Ultrasound is useful in the context of trauma and can help to exclude or confirm testicular rupture and differentiate testicular haematoma from haematocele (Fig. 31.64). Testicular rupture is a surgical emergency. On ultrasound, in testicular rupture, there is discontinuity of the tunica albuginea, irregular heterogeneous testicular margins, a haematocele and diminished colour Doppler flow to the affected area.[70] Direct visualisation of a fracture site is unusual; more often parenchymal heterogeneous areas are seen. A haematoma will initially be seen as a high reflective area but with evolution over time, will subsequently manifest as a low reflective complex cystic structure.

Spermatic cord torsion

Testicular torsion occurs when the spermatic cord is twisted and the correct term is spermatic cord torsion. A narrow mesenteric attachment from the spermatic cord to the testes and epididymis is regarded as the dominant cause, a slender attachment occurring as a result of a small testicular bare area. This allows the testes to fall forward within the cavity of the tunica vaginalis and then to rotate like a 'bell-clapper': the 'intravaginal' type of torsion, as the gubernaculum is fixed to the scrotal wall preventing the rotation of the tunica vaginalis.[71] In neonates, the gubernaculum is not attached to the scrotal wall and the entire testes, epididymis and the tunica vaginalis twist in a vertical axis on the spermatic cord, termed 'extravaginal' torsion.[72] Neonatal torsion is rare, occurring in the prenatal period and associated with an inguinal hernia. Factors other than an anatomical anomaly may predispose to spermatic cord torsion since the incidence of torsion (0.025%) is far less than the incidence of 'bell-clapper' deformities.

Two factors are of importance in spermatic cord torsion: the extent of the spermatic cord twist (90° to three complete twists) and the duration of the torsion. The initial disruption will be to the venous and lymphatic drainage, rather than to the arterial input of the testes, and venous infarction occurs earlier. Scrotal oedema is an early feature as the lower pressure cremasteric plexus is the first vascular channel to be affected. Areas of testicular infarction begin to appear within 2 hours of complete occlusion of the testicular artery, irreversible ischemia occurs after 6 hours and complete infarction is established by 24 hours.[73] Intra-vaginal torsion most commonly occurs between the ages of 12 and 18 years, with a reported incidence of 1 in 4000 males younger than 25 years.[74] Torsion commonly arises as puberty approaches, when testicular volume may increase by a factor of five, thereby increasing the propensity of the testis to fall forward and rotate.

Clinically intra-vaginal torsion presents with pain of sudden or insidious onset and is followed by swelling of the ipsilateral scrotum. The main clinical dilemma remains the distinction between spermatic cord torsion and acute epididymo-orchitis. Establishing the diagnosis is important since in acute epididymo-orchitis, resolution with minimal intervention is the rule unless complications, such as an abscess, supervene; by contrast surgery is mandatory for torsion. The diagnostic dilemma is compounded by the occasional similarity in clinical presentation: fever and pyuria may occur in both conditions.

In spermatic cord torsion, the ultrasound appearances are variable depending on the time elapsed from the onset of symptoms. With the development of congestion and infarction, the testes appear abnormally enlarged with decreased reflectivity[75] (Fig. 31.65). The tunica albuginea and the mediastinum testis appear of relatively high reflectivity, and a small amount of fluid may pool in the lower pole of the sac of the tunica vaginalis. Later, as infarction is established, haemorrhage may cause increased reflectivity and heterogeneity; this is particularly true in missed torsion and 'chronic' torsion (symptoms present for more than 10 days). Enlarged, thrombosed pampiniform plexus veins, within the spermatic cord, may be visible and there may be an abrupt change in calibre of the spermatic cord below the point of torsion. This results in an enlarged, twisted spermatic cord superior and posterior to the epididymal head, containing round anechoic structures representing veins.[76] This may resemble the whirlpool pattern encountered with MR imaging[77] (Fig. 31.66). Skin thickening of the scrotum may be present as a manifestation of venous congestion.

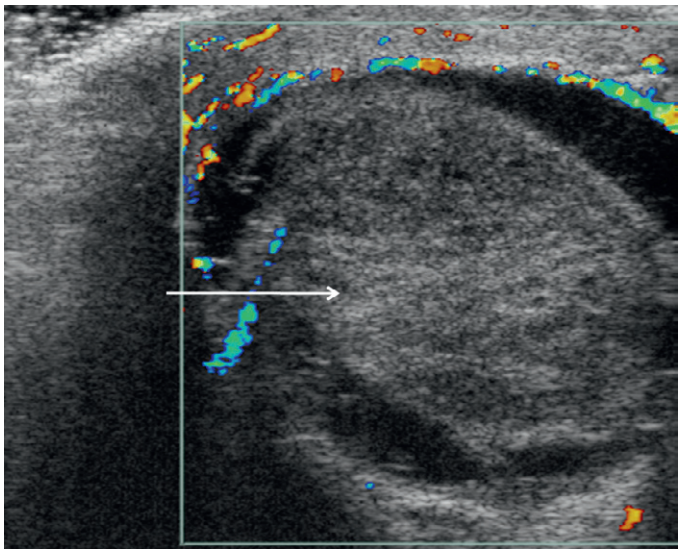


Figure 31.65 Missed spermatic cord torsion. The testis is enlarged and heterogeneous (arrow) with a surrounding hydrocele. No colour Doppler flow is identified within the testis but there is colour Doppler signal within the para-testicular tissues. The ultrasound was performed 24 hours after the onset of symptoms.

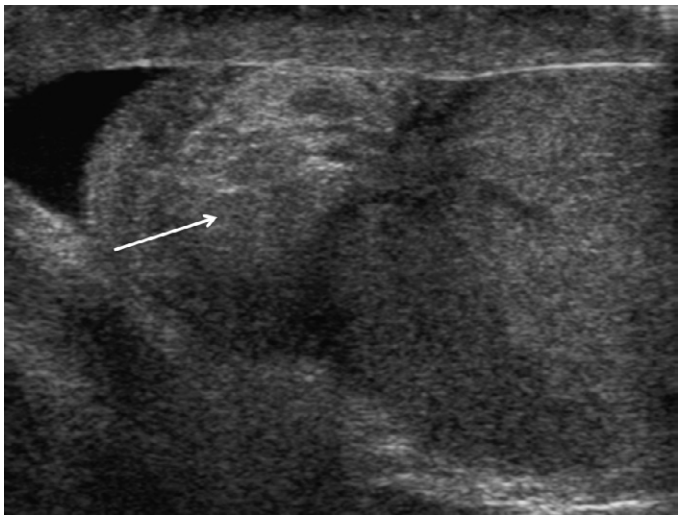


Figure 31.66 Whirlpool sign of spermatic cord torsion. The appearance of a 'whirlpool' above the testis (arrow), and separate from the epididymis, which represents the torted spermatic cord.

The basis for the ultrasound diagnosis of spermatic cord torsion is the absence or decreased flow in the symptomatic testis compared to the asymptomatic testis. Colour Doppler ultrasound allows visualisation of intra-testicular blood flow; in torsion blood flow is either reduced or absent, whereas it may be increased in epididymo-orchitis.[61] Therefore colour Doppler ultrasound is most useful in rapidly differentiating acute spermatic cord torsion from epididymo-orchitis. Although colour Doppler ultrasound is of value in the adult testes it is less sensitive for the detection of blood flow in children, since symmetry of blood flow is less well established and is dependent on testicular size.[5] A further limitation with colour Doppler ultrasound is the entity of epididymo-orchitis complicated by testicular infarction.[66] In these cases, a reversal of diastolic flow in the testicular artery is thought to be characteristic of venous thrombosis, and when combined with the greyscale and colour Doppler ultrasound appearances of the inflamed epididymis, should allow a correct diagnosis to be reached.[78] Currently, there is no single clinical feature or imaging examination that can reliably distinguish torsion from other causes of testicular pain.[26]

Spermatic cord torsion

- Occurs commonly between the ages of 12 and 18 years.
- A 'bell-clapper' deformity predisposes to torsion.
- Testicular ischaemia depends on the degree and duration of the torsion.
- Diagnosis of torsion is a clinical skill.
- Ultrasound is able to differentiate acute epididymitis/epididymo-orchitis as a cause of pain.

Spontaneous de-torsion

A pitfall of the use of colour Doppler ultrasound in the assessment of the acute scrotum, and in the desire to exclude the presence of spermatic cord torsion, is the entity of a spontaneous de-torsion. The susceptible testis undergoes torsion, and then spontaneously untwists, resulting in hyperaemia of the previously ischaemic testis. On ultrasound, the B-mode appearances may be unremarkable, but an increase in colour Doppler flow may resemble acute epididymo-orchitis, resulting in a misinterpretation and possibly severe consequences for the patient.

Torsion of an appendage

Torsion of the testicular (or epididymal) appendage is considered to be more common than spermatic cord torsion and an important differential diagnosis among boys under the age of 13 years who present acutely with a painful scrotum. Although most frequently presenting in patients between 7 and 13 years of age, torsion of a testicular appendage can occur at any age. The onset may be associated with trauma or exercise, with pain, erythema, tenderness and scrotal swelling common presenting symptoms.[26] In light-skinned individuals the palpable, infarcted, tender appendage may be visible at the upper pole of the testis; this 'blue-dot' sign is reported to occur in up to 21% of patients presenting with torsion of an appendage.[79]

With torsion of a testicular appendage, the testis itself usually appears normal on ultrasound with a normal low resistance arterial supply. There is often an associated localised upper pole hydrocele and an inflammatory reaction in the epididymis, which is often enlarged. The torted appendage may have a variable appearance most commonly of increased homogeneous reflectivity, although up to 30% are reported as being of low reflectivity surrounded by an area of increased perfusion (Fig. 31.67).[80] Colour Doppler studies may demonstrate an avascular mass separate from the testis and epididymis and an inflammatory reaction with increased blood flow in adjacent structures. With time the appendix becomes increasingly of higher reflectivity, indicating the onset of calcification, eventually completely detaching itself.

Torsion of an appendage

- More common in 7–13-year-old age group.
- The testis is normal on ultrasound.
- Ultrasound demonstrates a highly reflective appendage with a surrounding hydrocele.
- Surgical exploration is not indicated; treatment is conservative.

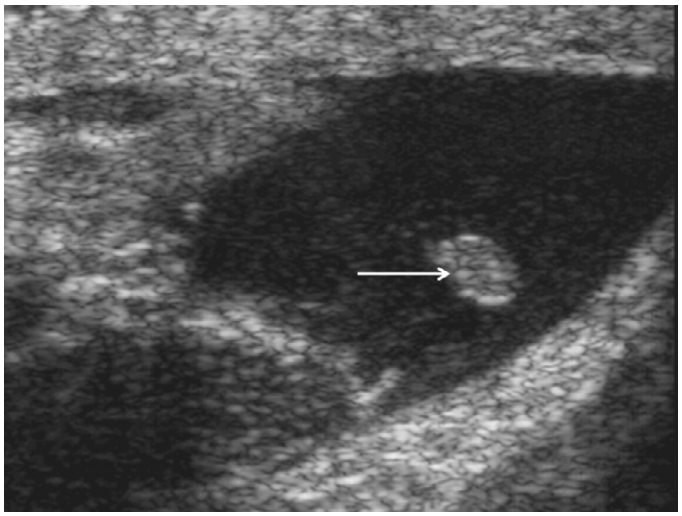


Figure 31.67 Torsion of the appendix test. A hydrocele surrounds the upper aspect of the testis, with a prominent appendix testis (arrow) seen; appearances are those of torsion of an appendix in a patient with the appropriate symptoms of sudden onset of testicular pain.

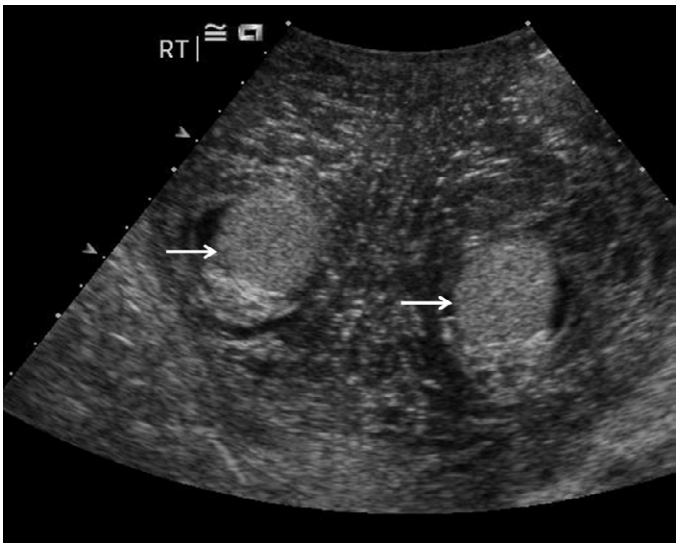


Figure 31.69 Scrotal wall oedema. There is gross oedema of the scrotal sac surrounding the normal testes (arrows) in a patient with post-surgical scrotal oedema.

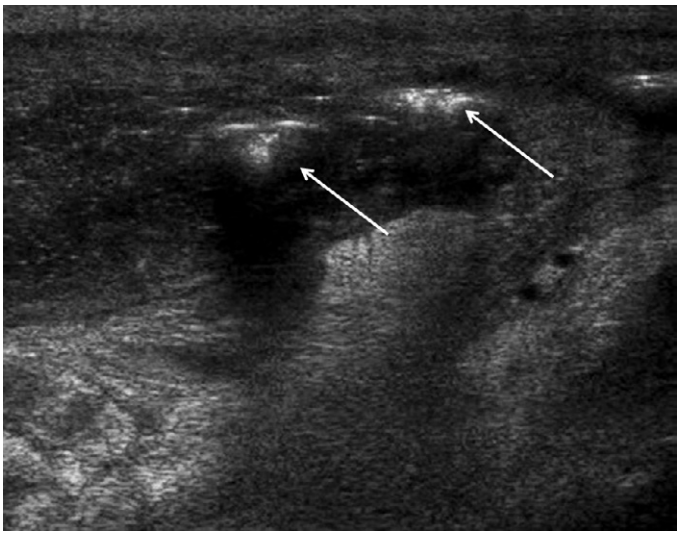


Figure 31.68 Fournier's gangrene. Ultrasound features seen are of scrotal wall thickening and normal underlying testes. Ultrasound of the scrotal wall demonstrates multiple pockets of gas (arrows), which appear as high reflective foci causing 'dirty shadowing'.

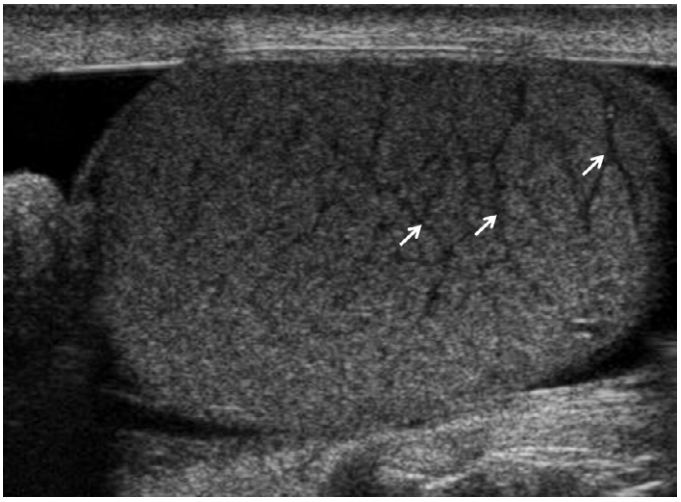


Figure 31.70 Intra-testicular oedema. Intra-testicular serpiginous low reflectivity (short arrows) following anatomical boundaries.

Fournier's gangrene

Fournier's gangrene is an aggressive necrotising fasciitis of the perineum which occurs most frequently in males aged 50–70 years. Associated co-morbidities are common, with diabetes mellitus found in 40–60% of patients.[81] Fournier's gangrene usually arises secondary to local infection, with multiple organisms involved: *Klebsiella*, *Streptococcus*, *Proteus* and *Staphylococcus* are commonly reported. Treatment is immediate surgical resection of the devitalised tissues as the condition carries a high morbidity and mortality rate. The rate of progression of fascial necrosis is reported as up to 2–3 cm/hour.[82] Prompt diagnosis is vital; mortality increases to 11.5% at 24 hours diagnostic delay and a diagnostic delay of 6 days results in a mortality rate of 75%.[82] The average delay from the onset of symptoms to diagnosis is 5 days. Anaerobic bacterial metabolism produces soft tissue gas that can be detected clinically as crepitus. Ultrasound has been reported to detect gas before it becomes clinically palpable, therefore expediting the diagnosis.[83] The ultrasound features of Fournier's gangrene are scrotal wall thickening containing multiple pockets of gas, which appear as high reflective foci causing 'dirty shadowing', and are said to be pathognomonic.[84] The underlying testes appear normal, protected by their separate blood supply (Fig. 31.68).

SCROTAL WALL ABNORMALITIES

Scrotal wall oedema may occur in many conditions: heart failure, liver failure, lymphatic obstruction and venous obstruction. Lymphoedema of the scrotal wall is classically described in filarial worm infestations[85] (Fig. 31.69). Testicular oedema results in fluid tracking into the interstitial tissues of the testis as a consequence of marked subcutaneous oedema of the scrotal sac. This gives rise to low reflective linear branching throughout the testes, giving a 'crazy paving' appearance.[86] The linear branching low reflective areas demonstrate no colour Doppler signal (Fig. 31.70).

REFERENCES

1. Langman J. Genital system. Medical embryology. 3rd edn. Baltimore: Williams and Wilkins; 1975. p. 175–200.
2. The reproductive organs of the male. In: Williams PL, Warwick R, Dyson M, Bannister LH, editors. Gray's anatomy. 37th edn. London: Churchill Livingstone; 1989. p. 1424–1434.
3. Aziz ZA, Satchithananda K, Khan M, Sidhu PS. High-frequency color Doppler ultrasonography of the spermatic cord arteries: resistive index variation in a cohort of 51 healthy men. J Ultrasound Med 2005;24:905–909.
4. Paltiel HJ, Diamond DA, Di Canzio J, et al. Testicular volume: comparison of orchidometer and US measurements in dogs. Radiology 2002;222:114–119.
5. Ingram S, Hollman AS. Colour Doppler sonography of the normal paediatric testis. Clin Radiol 1994;49:266–267.
6. Sellars MEK, Sidhu PS. Pictorial review: ultrasound appearances of the rete testis. Eur J Ultrasound 2001;14:115–120.
7. Sellars MEK, Sidhu PS. Ultrasound appearances of the testicular appendages: pictorial review. Eur Radiol 2003;13:127–135.
8. Middleton WD, Meredith MW. Analysis of intratesticular arterial anatomy with emphasis on transmediastinal arteries. Radiology 1993;189:157–160.
9. Bushby LH, Sellars ME, Sidhu PS. The "two-tone" testis: spectrum of ultrasound appearances. Clin Radiol 2007;62:1119–1123.
10. Rifkin MD, Kurtz AB, Pasto ME, Goldberg BB. Polyorchidism diagnosed preoperatively by ultrasonography. J Ultrasound Med 1983;2:93–94.
11. Leung AK. Polyorchidism. Am Fam Physician 1988;38:153–156.
12. Rajbabu K, Morel JC, Thompson PM, Sidhu PS. Multi-cystic (rete testis) supernumerary testis in polyorchidism with underlying microlithiasis: ultrasound appearances. Aust Radiol 2007;51: B56–B58.
13. Greenlee RT, Hill-Harmon MB, Murray T, Thun M. Cancer Statistics, 2001. CA Cancer J Clin 2001;51:15–36.
14. Grantham JG, Charboneau JW, James EM, et al. Testicular neoplasms: 29 tumors studied by high-resolution US. Radiology 1985;157: 775–780.
15. Horstman WG, Melson GL, Middleton WD, Andriole GL. Testicular tumours: Findings with color Doppler US. Radiology 1992;185: 733–737.
16. Sidhu PS, Sriprasad S, Bushby LH, et al. Impalpable testis cancer. BJU Int 2004;93:888.
17. Woodward PJ, Schwab CM, Sesterhenn IA. Extratesticular scrotal masses: radiologic-pathologic correlation. Radiographics 2003;23: 215–240.
18. Comiter CV, Renshaw AA, Benson CB, Loughlin KR. Burned-out primary testicular cancer: sonographic and pathological characteristics. J Urol 1996;156:85–88.
19. Carmignani L, Gadda F, Gazzano G, et al. High incidence of benign testicular neoplasms diagnosed by ultrasound. J Urol 2003;170: 1783–1786.
20. Rayor RA, Scheible W, Brock WA, Leopold GR. High resolution ultrasonography in the diagnosis of testicular relapse in patients with acute lymphoblastic leukaemia. J Urol 1982;128:602–603.
21. Garcia-Gonzalez R, Pinto J, Val-Bernal JF. Testicular metastases from solid tumours: an autopsy study. Ann Diagn Pathol 2000;4:397–400.
22. Atchley JTM, Dewbury KC. Ultrasound appearances of testicular epidermoid cysts. Clin Radiol 2000;55:493–502.
23. Carragher AM. One hundred years of splenogonadal fusion. Urology 1990;35:471–475.
24. Stewart VR, Sellars ME, Somers S, et al. Splenogonadal fusion: B-mode and color Doppler sonographic appearances. J Ultrasound Med 2004;23:1087–1090.
25. Avila NA, Premkumar A, Shawker TH, et al. Testicular adrenal rest tissue in congenital adrenal hyperplasia: findings at gray-scale and color Doppler US. Radiology 1996;198:99–104.
26. Sidhu PS. Clinical and imaging features of testicular torsion: role of ultrasound. Clin Radiol 1999;54:343–352.
27. Bilagi P, Sriprasad S, Clarke J, et al. Clinical and ultrasound features of segmental testicular infarction: six-year experience from a single centre. Eur Radiol 2007;17:2810–2818.
28. Sriprasad SI, Kooiman GG, Muir GH, Sidhu PS. Acute segmental testicular infarction: differentiation from tumour using high frequency colour Doppler ultrasound. Br J Radiol 2001;74:965–967.
29. Rehman J, Rizkala ER, Chughtai B, Khan SA. Hypoechoic testicular mass: a case of testicular and epididymal sarcoidosis. Urology 2005;66:e9–e10.
30. Eraso CE, Vrachliotis TG, Cunningham JJ. Sonographic findings in testicular sarcoidosis simulating malignant nodule. J Clin Ultrasound 1999;27:81–83.
31. Mevorach RA, Lerner RM, Dvoretsky PM, Rabinowitz R. Testicular abscess: diagnosis by ultrasonography. J Urol 1986;136:1213–1216.
32. Purushothaman H, Sellars ME, Clarke JL, Sidhu PS. Intra-testicular haematoma: differentiation from tumour on clinical history and ultrasound appearances in two cases. Br J Radiol 2007;80:e184–e187.
33. Hamm B, Fobbe F, Loy V. Testicular cysts: differentiation with US and clinical findings. Radiology 1988;168:19–23.
34. Rouviere O, Bouvier R, Pangaud C, et al. Tubular ectasia of the rete testis: a potential pitfall in scrotal imaging. Eur Radiol 1999;9: 1862–1868.
35. Harris RD, Chouteau C, Patrick M, Schned A. Prevalence and significance of heterogeneous testes revealed on sonography: ex vivo sonographic-pathologic correlation. AJR Am J Roentgenol 2000;175: 347–352.
36. Backus ML, Mack LA, Middleton WD, et al. Testicular microlithiasis: imaging appearances and pathologic correlation. Radiology 1994;192: 781–785.
37. Amaechi I, Sidhu PS. Testicular microlithiasis and macrocalcification: prevalence of tumors and follow-up in a single center over 10 years. Eur Radiol Suppl 2008;18:175.
38. Miller FNAC, Sidhu PS. Does testicular microlithiasis matter? A review. Clin Radiol 2002;57:883–890.
39. Poulsen J, Sidhu PS, Holm M. Testicular microlithiasis – a sinister condition? In: Dawson C, Muir GH, editors. The evidence for urology. Shrewsbury, UK: TFM Publishing; 2005. p. 31–38.
40. Ganem JP, Workman KR, Shaban SF. Testicular microlithiasis is associated with testicular pathology. Urology 1999;53:209–213.
41. Skakkebaek NE, Berthelsen JG, Giwercman A, Muller J. Carcinoma-in-situ of the testis: possible origin from gonocytes and precursor of all types of germ cell tumours except spermatocytoma. Int J Androl 1987;10:19–28.
42. Gilbert S, Nuttall MC, Sidhu PS, Ravi R. Metachronous testicular tumors developing 5 and 9 years after the diagnosis of testicular microlithiasis. J Ultrasound Med 2007;26:981–984.
43. Bushby LH, Miller FNAC, Rosairo S, et al. Scrotal calcification: ultrasound appearances, distribution and aetiology. Br J Radiol 2002;75:283–288.
44. Miller FNAC, Rosairo S, Clarke JL, et al. Testicular calcification and microlithiasis: association with primary intra-testicular malignancy in 3,477 patients. Eur Radiol 2006;17:363–369.
45. Frates MC, Benson CB, DiSalvo DN, et al. Solid extratesticular masses evaluated with sonography: pathologic correlation. Radiology 1997;204:43–46.
46. Rifkin MD, Kurtz AB, Goldberg BB. Epididymis examined by ultrasound: correlation with pathology. Radiology 1984;151:187–190.
47. Ramanathan K, Yaghoobian J, Pinck RL. Sperm granuloma. J Clin Ultrasound 1986;14:155–156.
48. Lioe TF, Biggart JD. Tumours of the spermatic cord and paratesticular tissue. A clinicopathological study. Br J Urol 1993;71:600–606.
49. Makarainen HP, Tammela TL, Karttunen TJ, et al. Intrascrotal adenomatoid tumors and their ultrasound findings. J Clin Ultrasound 1993;21:33–37.
50. Hertzberg BS, Kliewer MA, Hertzberg MA, Distell BM. Epididymal leiomyoma: sonographic features. J Ultrasound Med 1996;15:797–799.
51. Stewart VR, Sriprasad S, Pomplun S, et al. Sonographic features of a spermatic cord capillary hemangioma. J Ultrasound Med 2007;26: 139–142.
52. Wood A, Dewbury KC. Case report: paratesticular rhabdomyosarcoma – colour Doppler appearances. Clin Radiol 1995;50:130–131.
53. Stein A, Kaplun A, Sova Y, et al. Leiomyosarcoma of the spermatic cord: report of two cases and review of the literature. World J Urol 1996;14:59–61.
54. Kuwabara H, Uda H, Sakamoto H, Sato A. Malignant mesothelioma of the tunica vaginalis testis. Report of a case and review of the literature. Acta Pathol Jpn 1991;41:857–863.
55. Gooding GA, Leonhardt WC, Marshall G, et al. Cholesterol crystals in hydrocoeles; sonographic detection and possible significance. AJR Am J Roentgenol 1997;169:527–529.
56. Dogra VS, Gottlieb RH, Oka M, Rubens DJ. Sonography of the scrotum. Radiology 2003;227:18–36.
57. El-Saeity NS, Sidhu PS. 'Scrotal varicocele, exclude a renal tumour'. Is this evidence based? Clin Radiol 2006;61:593–599.
58. Das KM, Prasad K, Szmigielski W, Noorani N. Intratesticular varicocele: evaluation using conventional and Doppler sonography. AJR Am J Roentgenol 1999;173:1079–1083.

59. Dublin L, Amelar RD. Varicocele size and results of varicocelectomy in selected subfertile men with varicocele. Fertil Steril 1970;21:606–609.
60. Siegal A, Snyder H, Duckett JW. Epididymitis in infants and boys: underlying anomalies and efficacy of imaging modalities. J Urol 1987;138:1100–1103.
61. Horstman WG, Middleton WD, Melson GL. Scrotal inflammatory disease: Color Doppler US findings. Radiology 1991;179:55–59.
62. Fitzgerald SW, Erickson SJ, Dewire DM, et al. Color sonography in the evaluation of the adult acute scrotum. J Ultrasound Med 1992;11: 543–548.
63. Brown JM, Hammers LW, Barton JW, et al. Quantitative Doppler assessment of acute scrotal inflammation. Radiology 1995;197:427–431.
64. Cook JL, Dewbury K. The changes seen on high-resolution ultrasound in orchitis. Clin Radiol 2000;55:13–18.
65. Amaechi I, Sidhu PS. Ultrasound in the assessment of the "on-call" acute scrotum. Imaging 2008;20:131–138.
66. Eisner DJ, Goldman SM, Petronis J, Millmond SH. Bilateral testicular infarction caused by epididymitis. AJR Am J Roentgenol 1991;157: 517–519.
67. Sanders LM, Haber S, Dembner A, Aquino A. Significance of reversal of diastolic flow in the acute scrotum. J Ultrasound Med 1994;13: 137–139.
68. Drudi FM, Laghi A, Iannicelli E, et al. Tubercular epididymitis and orchitis: US patterns. Eur J Radiol 1997;7:1076–1078.
69. Dogra VS, Bhatt S. Acute painful scrotum. Radiol Clin North Am 2004;42:349–363.
70. Herbener TE. Ultrasound in the assessment of the acute scrotum. J Clin Ultrasound 1996;24:405–421.
71. Corriere JN. Horizontal lie of the testicle: a diagnostic sign and torsion of the testis. J Urol 1972;107:616–617.
72. Blackhouse KM. Embryology of testicular descent and maldescent. Urol Clin North Am 1982;9:315.
73. Luker GD, Siegel MJ. Color Doppler sonography of the scrotum in children. AJR Am J Roentgenol 1994;163:649–655.
74. Williamson RCN. Torsion of the testis and allied conditions. Br J Surg 1976;63:465–476.
75. Hricak H, Lue TF, Filly RA, et al. Experimental study of the sonographic diagnosis of testicular torsion. J Ultrasound Med 1983;2:349–356.
76. van Dijk R, Karthaus HFM. Ultrasonography of the spermatic cord in testicular torsion. Eur J Radiol 1994;18:220–223.
77. Vijayaraghavan SB. Sonographic differential diagnosis of acute scrotum: real-time whirlpool sign, a key sign of torsion. J Ultrasound Med 2006;25:563–574.
78. Dogra VS, Rubens DJ, Gottlieb RH, Bhatt S. Torsion and beyond: new twists in spectral doppler evaluation of the scrotum. J Ultrasound Med 2004;23:1077–1085.
79. McCombe AW, Scobie WG. Torsion of scrotal contents in children. Br J Urol 1988;61:148–150.
80. Lerner RG, Mevorach RA, Hulbert WC, Rabinowitz R. Color Doppler US in the evaluation of acute scrotal disease. Radiology 1990;176: 355–358.
81. Stamenkovic I, Lew PD. Early recognition of potentially fatal necrotizing fasciitis. The use of frozen-section biopsy. N Engl J Med 1984;28:1689–1693.
82. Paty R, Smith AD. Gangrene and Fournier's gangrene. Urol Clin North Am 1992;19:149–162.
83. Kane CJ, Nash P, McAninch JW. Ultrasonographic appearance of necrotizing gangrene: aid in early diagnosis. Urology 1996;48:142–144.
84. Rajan DK, Scharer A. Radiology of Fournier's gangrene. AJR Am J Roentgenol 1998;170:163–168.
85. Grainger AJ, Hide IG, Elliot ST. The ultrasound appearances of scrotal oedema. Eur J Ultrasound 1998;8:33–37.
86. Stewart VR, Sidhu PS. The testis: the unusual, the rare and the bizarre. Clin Radiol 2007;62:289–302.

CHAPTER

32 Ultrasound of the penis

Anthony J. Edey, C. Jason Wilkins and Paul S. Sidhu

INTRODUCTION 621

NORMAL ANATOMY AND ULTRASOUND APPEARANCES 621

ERECTILE DYSFUNCTION 621
Background 621
Physiology of the erectile process 623

STIMULATED COLOUR DOPPLER ULTRASOUND 623
Pharmacological agents 623
Technique 623
Baseline imaging 623
Normal response 624
Arteriogenic erectile dysfunction 624
Veno-occlusive erectile dysfunction 624
Further imaging 625
False venous leak 626

PRIAPISM 627
Non-ischaemic priapism 627
Ischaemic priapism 627

PEYRONIE'S DISEASE 627

PENILE FIBROSIS 628

PENILE MASSES 628

PENILE TRAUMA 629

URETHRAL ULTRASOUND 629

INTRODUCTION

Ultrasound plays an important role in the evaluation of penile pathology. High-frequency 'small parts' linear transducers allow interrogation of the greyscale anatomy and dynamic vascular imaging of the normal and diseased penis. Diagnostic images can be obtained with few artefacts in a non-invasive manner and without exposure to ionising radiation. Ultrasound of the penis has been useful in the assessment of erectile dysfunction, but is also valuable in the assessment of Peyronie's disease, penile masses, priapism and following trauma.

NORMAL ANATOMY AND ULTRASOUND APPEARANCES

The penis is composed of three cylindrical structures of erectile tissue: two dorsal corpora cavernosa and a ventral corpus spongiosum containing the penile urethra. The spongiosum is smaller proximally but expands distally to form the glans penis (Fig. 32.1). The corpora cavernosa contain sinusoidal tissue which is markedly distensible and is essential to the erectile process. A tough, non-distensible fibrous capsule, the tunica albuginea, invests the corpora cavernosa, with a much thinner layer covering the corpus spongiosum.[1] There are two layers of fascia enveloping the shaft of the penis beneath the skin. The dartos fascia is superficial and is in continuity with Scarpa's fascia of the abdomen and the dartos fascia of the scrotum. Deep to the dartos fascia lies Buck's fascia, which covers the corpora cavernosa and corpus spongiosum and attaches posteriorly to the suspensory ligaments of the penis, allowing the erect penis to achieve a horizontal or greater angle.[2] The normal arterial supply to the penis is via the internal pudendal artery (a branch of the anterior division of the internal iliac artery), which divides into terminal branches, the dorsal penile artery (supplying the glans penis), the cavernosal artery (supplying the corpora cavernosa) and the bulbar artery (supplying the bulb and the corpus spongiosum) (Fig. 32.2). The cavernosal arteries give the main contribution to erectile function and anatomical variations are common. Emissary veins pierce the tunica albuginea, and drain into the deep dorsal vein via the spongiosal, circumflex and cavernosal veins.[3]

Ultrasound identifies the paired corpora cavernosa, the cavernosal arteries, the tunica albuginea and the corpus spongiosum (Fig. 32.3). The corpora cavernosa are of intermediate reflectivity. Buck's fascia and the tunica albuginea are indistinguishable as they surround the corpora and appear as a thin low reflective envelope (<2 mm thick). Overlying the corpus spongiosum, Buck's fascia is visible as a separate high reflectivity line. The corpus spongiosum is of slightly higher reflectivity than the corpora cavernosa. The highly reflective walls of the cavernosal arteries are usually clearly identified at the base of the penis and can often be identified as two parallel, highly reflective lines on longitudinal imaging (Fig. 32.4). The normal urethra is not identified.

Anatomy

- Ventral highly reflective corpus spongiosum expands to form the glans penis.
- Dorsal paired low reflective corpora cavernosa
  - enveloped by the thin highly reflective tunica albuginea
  - distensible sinusoidal tissue essential for erectile function.
- Internal pudendal artery divides into
  - dorsal penile artery, bulbar artery and the cavernosal arteries.
- Venous drainage via the superficial and deep dorsal veins
  - emissary veins pierce the tunica albuginea, draining into dorsal veins via cavernosal, spongiosal and circumflex veins
  - the emissary vein/tunica region is the site of the veno-occlusive mechanism.

ERECTILE DYSFUNCTION

Background

Erectile dysfunction is defined as the inability to achieve or maintain an erection adequate for sexual satisfaction. The Massachusetts Male Aging Study found that 35% of men aged 40–70 years reported moderate or complete erectile dysfunction.[4] Severity and

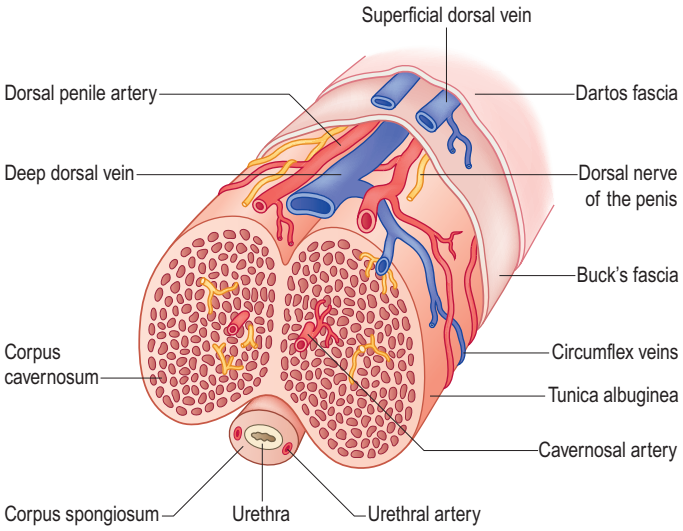


Figure 32.1 Anatomy of the penis. (Modified from Baxter GM and Sidhu PS. Ultrasound of the Urogenital System. Thieme, Stuttgart, 2006, Ch. 12, Diseases of the penis with functional evaluation by Wilkins CJ, Sidhu PS.)

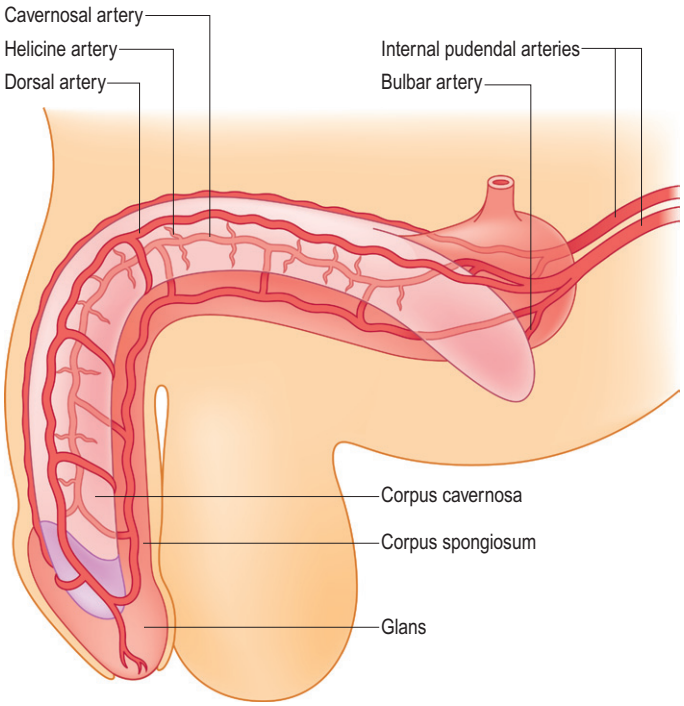


Figure 32.2 Arterial supply of the penis.

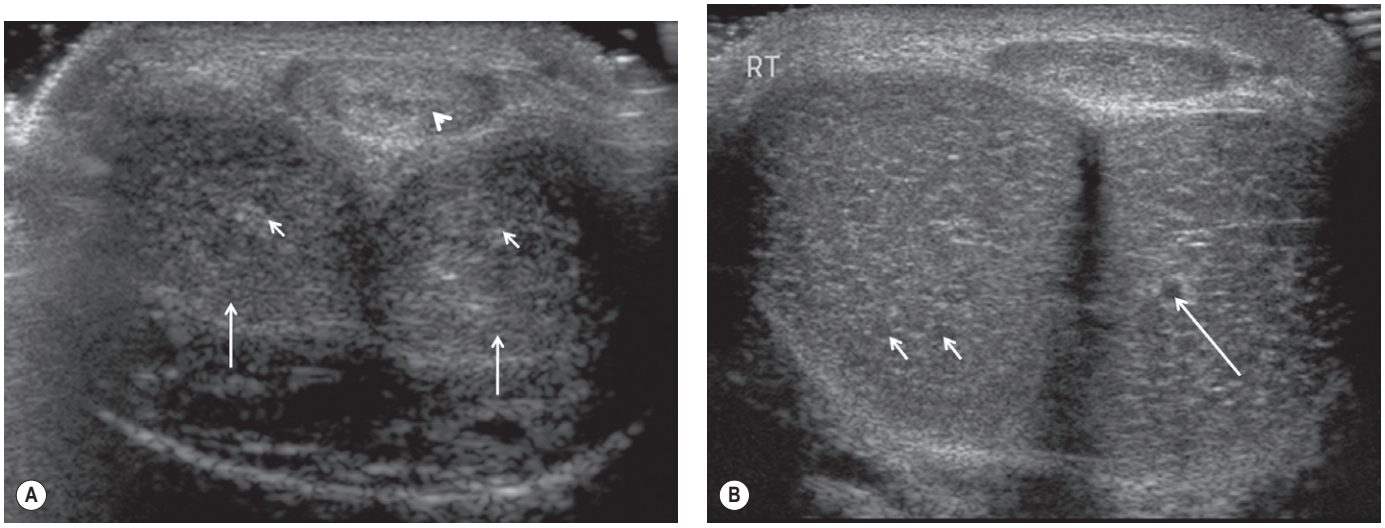


Figure 32.3 Ultrasound appearances of the penis. A: In the flaccid state, the paired corpora cavernosa (long arrows) are of low reflectivity and contain the cavernosal arteries (short arrows). The higher reflective corpora spongiosum (arrowhead) contains the urethra. **B:** During tumescence, the corpora cavernosa expand with blood resulting in pockets of low reflectivity forming (short arrows). The cavernosal arteries are more prominent (long arrow).

prevalence increase with age and it is estimated that between 20 and 30 million men in the USA are affected by erectile dysfunction.[5]

Following the discovery that intra-cavernosal injection of vasoactive agents can produce an erection in the absence of sexual arousal, our understanding of the physiology of the erectile process has improved.[6] Recently, the introduction of effective oral therapies such as sildenafil, a phosphodiesterase type 5 (PDE-5) inhibitor, has revolutionised the management of erectile dysfunction. There has been a decline in the role of stimulated colour Doppler ultrasound (CDUS) and other radiological tests in the evaluation of erectile dysfunction. Often a 'trial' of a PDE-5 inhibitor serves as an initial diagnostic test: efficacy confirms the adequacy of penile arterial inflow and veno-occlusive erectile mechanisms and eliminates the need for further testing. Furthermore, surgical procedures for the

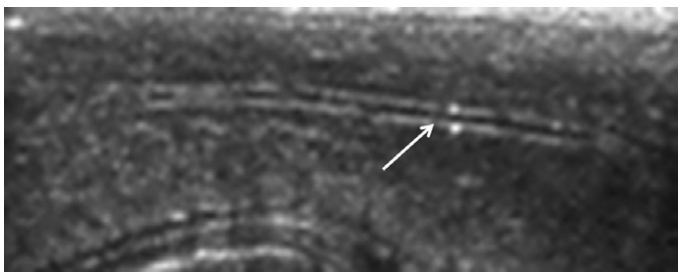


Figure 32.4 Longitudinal image of the prominent cavernosal artery (arrow).

treatment of venous leaks have poor long-term clinical outcomes. Despite this, patient pressure means that surgical correction for venous leak, whilst controversial, is still carried out in some centres. The use of arterial reconstructive surgery is indicated only in a small group of patients with new onset focal arterial occlusion with few or no features of systemic vascular disease.[7,8]

However, a CDUS examination remains useful; experience shows that many patients benefit psychologically from a normal test result. Additionally, CDUS imaging of the penis is important in the pre-assessment of patients due to undergo revascularisation surgery following penile trauma, and to document vascularity prior to surgery for Peyronie's disease.[9] There is also evidence that erectile dysfunction may be an early marker of peripheral and coronary atherosclerotic disease.[10] Pooled data suggests that a normal arterial response to prostaglandin E1 has a negative predictive value for the presence of coronary artery disease of 84%, whilst a diminished response has a positive predictive value of 32%.

Physiology of the erectile process

Penile erection is the consequence of neurovascular events triggered by a combination of psychological and hormonal factors. Increased cavernosal artery blood flow results in filling of the sinusoids of the corpora cavernosa. This leads to an elevation of pressure in the corpora as the sinusoids distend within the non-compliant tunica albuginea. The rise in intra-tunica pressure compresses the sub-tunica venous plexuses between the trabecula and tunica albuginea. In turn, this partially occludes venous drainage from the penis and results in tumescence. Complete occlusion of venous outflow is achieved during sexual activity by compression of the engorged corpora cavernosa at their base by contraction of the ischio-cavernosal muscles. This final stage results in rigidity. During tumescence intra-cavernous pressures reach approximately 100 mmHg and when rigid the pressure may rise to several hundred mmHg.

Erectile dysfunction is the result of a failure of this process and may be due to neurogenic, psychogenic, vascular (arterial or venous) causes, or as the result of disruption of the tunica albuginea, post-traumatic or more commonly due to Peyronie's disease. Alternatively it may be due to patient medication or systemic disorders such as diabetes mellitus with multifactorial causes not uncommon.

STIMULATED COLOUR DOPPLER ULTRASOUND

Pharmacological agents

Prostaglandin E-1 (PGE-1) is the most widely used agent for pharmacological stimulation of the penis. The normal dosage of PGE-1 is between 10 and 20 μg. Practice varies, but most commonly 20 μg is administered at the outset of the test. An alternative is to assess the erectile response after an initial dose of 10 μg and if inadequate a second 10 μg injection is administered. However, the examination is significantly shortened with the single dose method and use of a single dose minimises patient discomfort and anxiety. PGE-1 is widely reported as a safe treatment but there is a small risk of priapism (less than 1%).[11] Papaverine, the second most commonly used stimulant, has a reported incidence of iatrogenic priapism of up to 18%.[12] Regardless, patients should be fully informed of the risks and given appropriate advice. One possible strategy is that patients with an erection lasting longer than 4 hours be given direct access to an on-site urology opinion to ensure prompt treatment. During stimulated CDUS, absence of cavernosal artery flow or a resistance index greater than 1.00 (absent diastolic flow) was thought to be highly specific in predicting priapism. However, experience suggests that absence of diastolic flow is a frequent occurrence in the 'normal' responder, and is not a sinister finding.[13] More recent work has found that the absence of systolic flow at 1 hour following intracavernosal injection of a stimulant is a more useful predictor and warrants immediate treatment and admission.[14] Imaging all patients at 1 hour post procedure would be impractical and a 4-hour return to receive prompt treatment based on patient self-assessment has been shown to work well.[3]

Technique

The stimulated CDUS examination should be performed with a chaperone, in a setting that offers patient privacy with little possibility of interruption. A high-frequency linear 'small parts' transducer with a small footprint is required. Intra-cavernosal injection of PGE-1 is performed with a small-bore needle (typically 30G). The ideal injection site is between the proximal and mid thirds of the shaft at the dorsolateral aspect. Following injection of the vasoactive substance the angle-corrected velocity of either the left or the right cavernosal artery is recorded at 5-minute intervals from baseline up to 30 minutes.[15] Tumescence and rigidity are documented.

Colour flow Doppler ultrasound of the cavernosal arteries should be performed with the probe positioned at the base of the penis on the ventral surface. The angle for Doppler analysis needs to be optimised (<60°) with box-steering, angle correction and orientation of the probe to ensure reproducible, valid measurements. The peak systolic velocity (PSV) of the cavernosal artery varies according to the location of sampling, with higher velocities more proximally.[16] Measurement of the spectral Doppler trace is most reproducible at the base of penis where the angle of the cavernosal vessel is not parallel with the probe.[9] Self-stimulation has been advocated as an adjunct to pharmacological stimulation in order to obtain a maximal response, although the risk of ejaculation (which would necessitate a repeat of the test on a separate occasion) needs to be considered and patients should be advised to stop prior to this.[17]

Baseline imaging

Baseline B-mode US imaging is performed in longitudinal and transverse planes with the penis held by the patient in the anatomical position. Before injection of the stimulant detailed ultrasound examination of the penis is required. This allows selection of an appropriate site for injection. Significant abnormalities such as fibrotic plaque disease, focal cavernosal fibrosis, arterial calcification or tunica disruption may be detected. Ultrasound imaging prior to injection allows the observer to distinguish between true calcification/fibrosis abnormalities and the spurious appearance of calcification/fibrosis of the corpora which may occur following inadvertent intra-cavernosal injection of air bubbles[18] (Fig. 32.5). The cavernosal arteries range in diameter from 0.3 mm in the flaccid

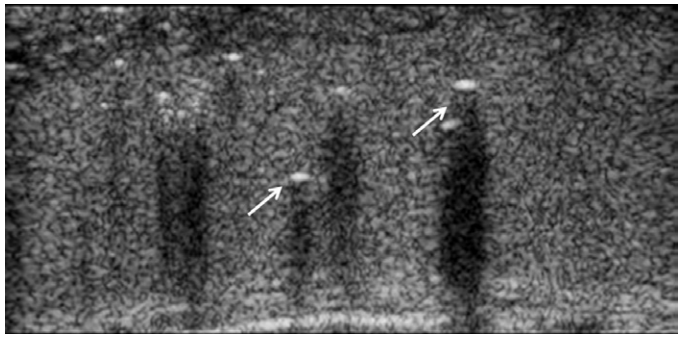


Figure 32.5 Air in the corpora cavernosa. Following the intra-cavernosal injection of a vasoactive substance, air (arrows) causing acoustic shadowing is present at the injection site in the corpora cavernosa.

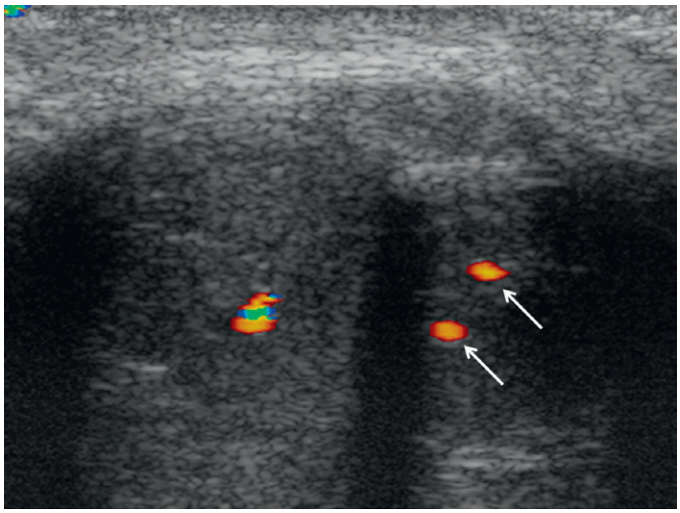


Figure 32.6 Cavernosal artery duplication. In this transverse image of the penis, there are two (arrows) cavernosal arteries present in the left corpora cavernosa.

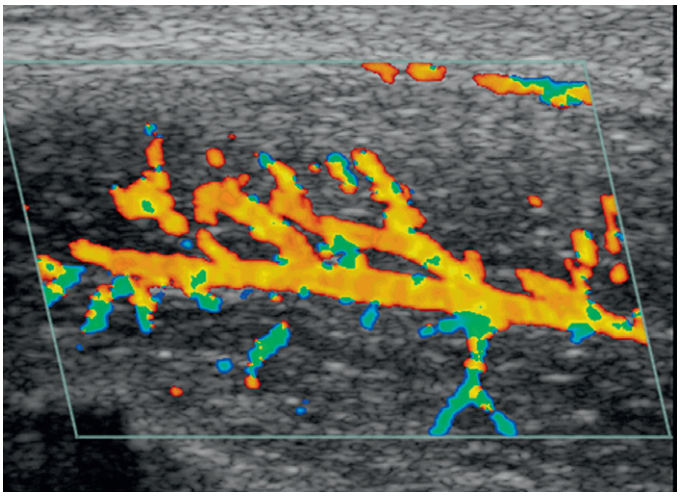


Figure 32.7 Helicine branches of the cavernosal artery following pharmaco-stimulation.

state to 1.0 mm during erection.[6,7,19] The PSV of the cavernosal artery in the flaccid penis in normal patients is 10–15 cm/s. This value should be documented and further sampling during the study should be performed in the same location.

Normal response

During the pharmacologically induced erection, dynamic assessment of the spectral Doppler waveform is performed. Maximal arterial engorgement occurs early in tumescence and allows colour mapping of the vessels. Variations such as bifurcation, duplication and a common origin of the cavernosal arteries are often seen[20] (Fig. 32.6). Cross communications between left and right cavernosal arteries are present in virtually all patients.[19] Anomalies may lead to a reduction in the PSV in the absence of significant arterial insufficiency and therefore measurements obtained may result in false positive results.[21] If there is definite asymmetry of the cavernosal arteries, this should be documented and both arteries sampled during the course of the assessment. A focal stenosis may result in high-velocity 'jets' at the site of narrowing on colour Doppler US and, more distally, in damped pulsatility. The helicine arteries are not visible in the flaccid penis but become apparent during the onset of erection and branch in a radial direction from the cavernosal arteries (Fig. 32.7). During the course of tumescence, erection and full rigidity the helicine arteries become less visible as progressive venous occlusion leads to a reduction and finally cessation of penile inflow.[19]

Pharmacologically induced erection follows a predictable sequence of changes on CDUS in patients without erectile dysfunction. Schwartz et al.[22] divided this sequence into stages.

- **Phase 0**: Prior to injection the dorsal arteries of the penis are more clearly identified than the cavernosal arteries. In about one-third of patients colour and spectral Doppler analysis of the cavernosal artery prior to stimulation is not possible. The normal spectral waveform at this stage is monophasic with a high resistance pattern showing minimal or no diastolic flow.
- **Phase 1**: Follows pharmaco-stimulation and marks the onset of erection. During phase 1 the systolic and diastolic flow increase results in continuous flow throughout the cardiac cycle. In normal volunteers PSV is usually greater than 35 cm/s and the peak end-diastolic velocity (EDV) is greater then 8 cm/s.
- **Phase 2:** As pressure increases within the corpora cavernosa there is a progressive decrease in the diastolic flow. The development of tumescence and subsequent veno-occlusion results in a reduction in diastolic flow.
- **Phase 3:** Corresponds to no diastolic flow.
- **Phase 4**: Characterised by reversal of diastolic flow and represents full erection (Fig. 32.8).
- **Phase 5:** The final stage of rigidity, usually not seen in clinical practice, shows a decrease in systolic velocities, which may approach zero.[22]

This sequence of events has a variable time course. Assessment over 30 minutes is occasionally required to ensure that the maximal effect has been attained, although 20 minutes is normally sufficient.[23]

Arteriogenic erectile dysfunction

Maximal PSV of the cavernosal artery following injection of vasoactive agents is the most accurate indicator of arterial disease. The average PSV in normal volunteers is between 30 and 40 cm/s.[24] A PSV of ≥35 cm/s is unequivocally normal, whilst a PSV of <25 cm/s following adequate stimulation indicates definite arterial insufficiency.[18] Intermediate values are not specific and in this group sildenafil is often used as some will have mild to moderate arterial insufficiency and may benefit[25] (Fig. 32.9).

Some authors suggest that arteriogenic erectile dysfunction can be diagnosed on the basis of the PSV in the flaccid penis. One study showed that a cut-off value of 10 cm/s for the PSV in the non-erect penis was 96% sensitive and 92% specific in the diagnosis of arteriogenic erectile dysfunction.[26] The degree of change in the diameter of the cavernosal artery during the erectile process provides some insight into the degree of arterial insufficiency. In normal patients the vessel increases in size by 75–100%, whereas in patients with arteriogenic erectile dysfunction this figure is usually less than 75%.[23] However, the increase in the baseline diameter following pharmacological stimulation does not correlate with either the measured PSV or clinical grading of erection and it is not routine to measure arterial diameters.[27]

Veno-occlusive erectile dysfunction

Ultrasound may be used to diagnose veno-occlusive dysfunction in patients with normal arterial inflow. Having established a normal arterial response with a PSV >35 cm/s, an EDV of >5 cm/s is usually accepted as the level above which a venous leak is

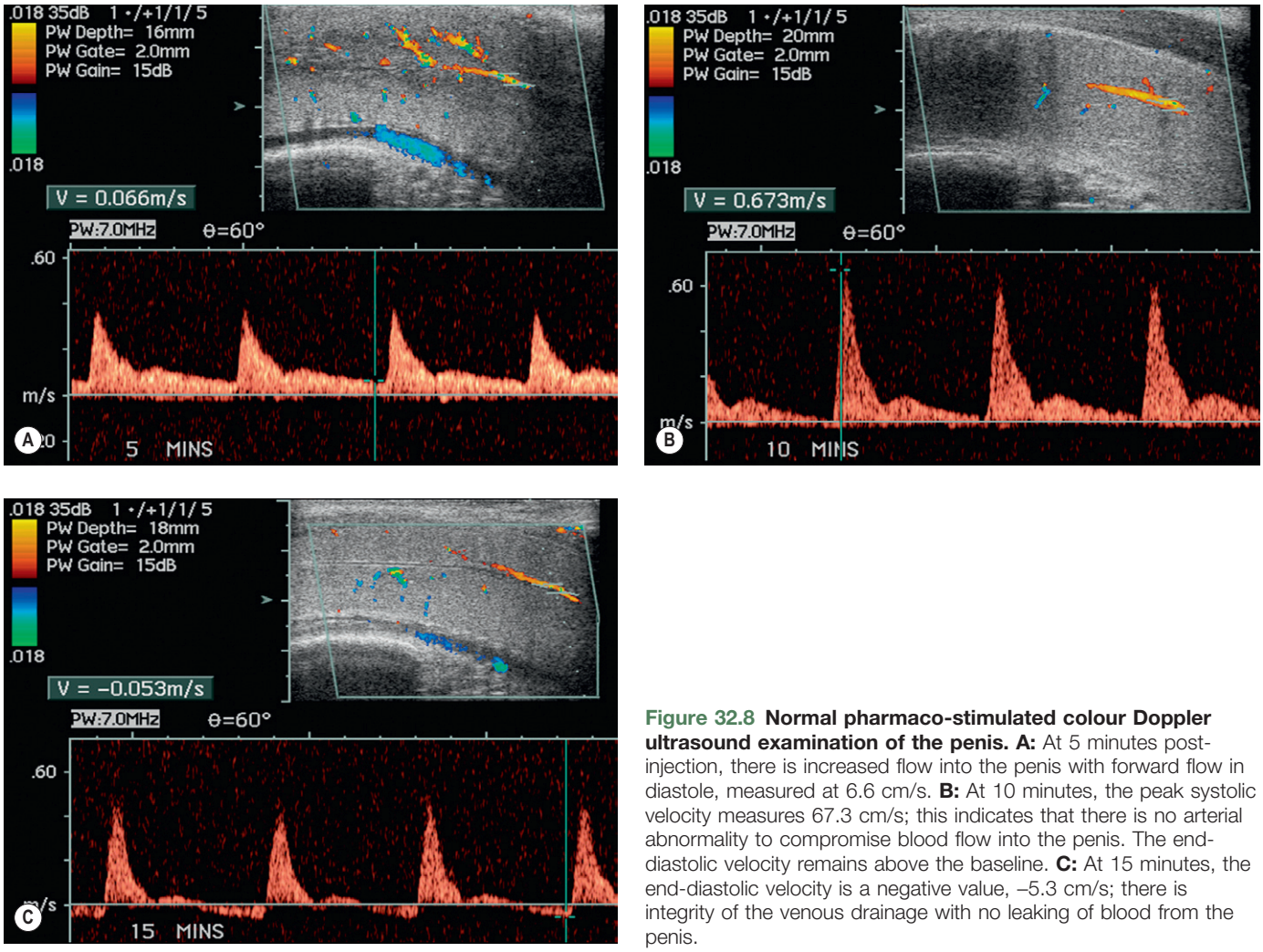


Figure 32.8 Normal pharmaco-stimulated colour Doppler ultrasound examination of the penis. A: At 5 minutes post-injection, there is increased flow into the penis with forward flow in diastole, measured at 6.6 cm/s. **B:** At 10 minutes, the peak systolic velocity measures 67.3 cm/s; this indicates that there is no arterial abnormality to compromise blood flow into the penis. The end-diastolic velocity remains above the baseline. **C:** At 15 minutes, the end-diastolic velocity is a negative value, –5.3 cm/s; there is integrity of the venous drainage with no leaking of blood from the penis.

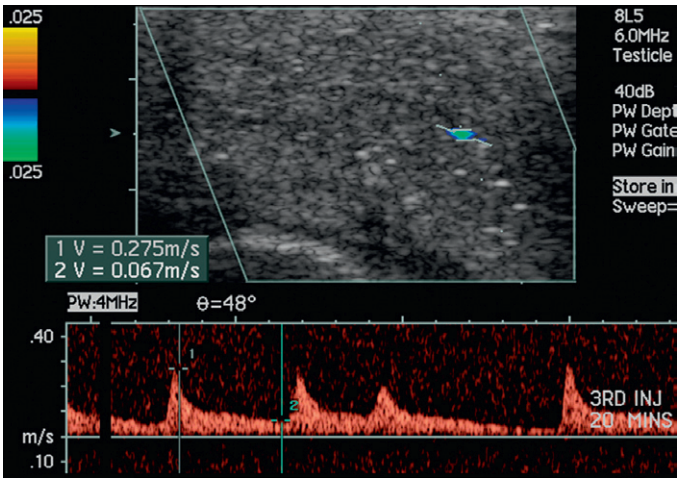


Figure 32.9 Arterial erectile dysfunction. The peak systolic velocity remains at 27.5 cm/s despite three doses of PGE-1. The end-diastolic velocity remains elevated at 6.7 cm/s; venous integrity cannot be assessed in the presence of arterial erectile dysfunction.

present.[28,29] The resistive index (RI) may be used as an alternative measure for the diagnosis. An RI of less than 0.8 with a normal PSV is also regarded as diagnostic of a venous leak.[30] An RI of 1.0 is normal. In young patients with good arterial input, reversal of EDV should normally be seen and it may be appropriate to lower the EDV threshold in this group. As well as forward diastolic flow in the cavernosal artery, continuous flow in the dorsal vein or other abnormal draining veins may also be seen, but is not a requisite for diagnosis[3] (Fig. 32.10).

Further imaging

The diagnosis of venous incompetence on ultrasound requires normal arterial inflow. In cases with mixed aetiology of erectile dysfunction an indeterminate result may be obtained and reflects both arterial inflow insufficiency and venous leak. In this group of patients, cavernosography and arteriography may be required. Cavernosography with cavernosometry remains the diagnostic reference standard for the diagnosis of venous leak, as this technique measures outflow resistance without the need for adequate arterial inflow as well as mapping the sites of incompetence.[31] Therefore, following a positive CDUS for venous leak, cavernosography is

usually required if surgical venous ligation is planned. As previously discussed, surgical intervention for venous leak has a limited success rate and its effects may be short-lived. However, it is a relatively minor surgical procedure and may be the treatment option of choice for young patients, providing a temporary improvement in symptoms. An alternative treatment is coil embolisation via a direct approach using a draining vein.[32]

False venous leak

Anxiety following injection of PGE-1 may lead to a false positive result for venous leak due to elevated adrenergic tone.[11] Increased levels of adrenaline prevent complete relaxation of the sinusoidal smooth muscle in the corpora cavernosa and result in a failure of the normal veno-occlusive mechanism required for an erection. On CDUS this is characterised by forward flow in the cavernosal artery throughout the cardiac cycle and is indistinguishable from a positive finding of venous incompetence. In patients with a suboptimal response to PGE-1 injection and features of venous incompetence the study may be supplemented by an intra-cavernosal injection of phentolamine. Phentolamine is an alpha-adrenoreceptor antagonist and has been found to be safe at an intra-cavernosal dose of 2 mg with no significant impact on systemic blood pressure. In a study by Aversa et al.[33] phentolamine normalised erectile response in 20/26 patients initially diagnosed with venous leak following injection with PGE-1 (Fig. 32.11). Phentolamine led to a statistically significant increase in the grade of erection, PSV and a decrease in EDV in this study.[33] Similar results have been reported in other studies.[11] The concern that intra-cavernosal injection of multiple vasoactive agents may lead to an increased risk of priapism is unfounded.[11,33]

The marked reduction in false positive results has led many authors to recommend that intra-cavernosal phentolamine is necessary before a venous leak can be diagnosed by CDUS assessment in the younger patient. Furthermore, phentolamine, as an oral preparation, may offer a therapeutic approach in this very specific group of patients.[34,35] Venous leak not reversed by phentolamine is highly predictive of a structurally based abnormality.

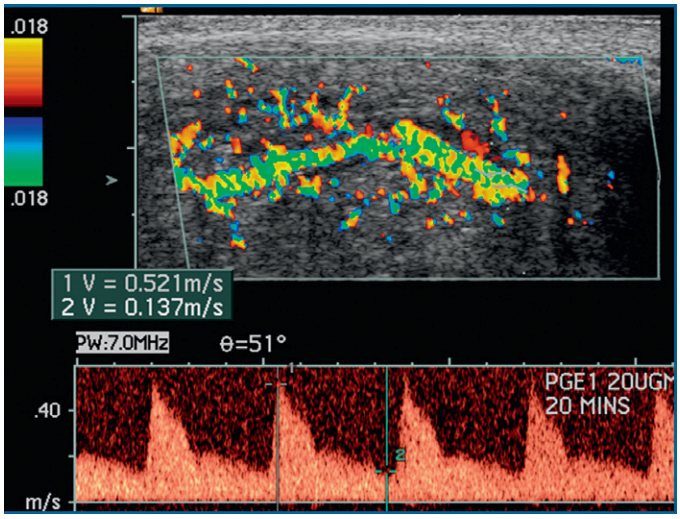
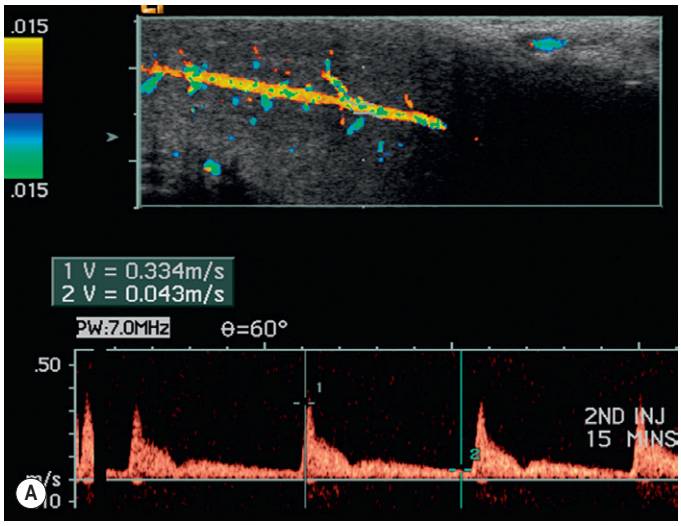


Figure 32.10 Venous erectile dysfunction. At 20 minutes following pharmaco-stimulation, the peak systolic velocity measures 52.1 cm/s; there is no arterial erectile dysfunction. However, the end-diastolic velocity measures 13.7 cm/s; this is a clear example of a venous cause for erectile dysfunction.

Haemodynamic parameters for stimulated colour Doppler ultrasound

- Adequate arterial inflow if PSV >35 cm/s.
- Borderline arterial inflow if PSV between 35 cm/s and 25 cm/s.
- Arterial insufficiency if PSV <25 cm/s.
- If PSV >35 cm/s a venous leak is diagnosed if EDV >5 cm/s.
- Reversal of end-diastolic flow is expected in younger patients with an adequate arterial inflow.
- Phentolamine may be required in young patients to avoid a spurious diagnosis secondary to anxiety-induced adrenergic drive.



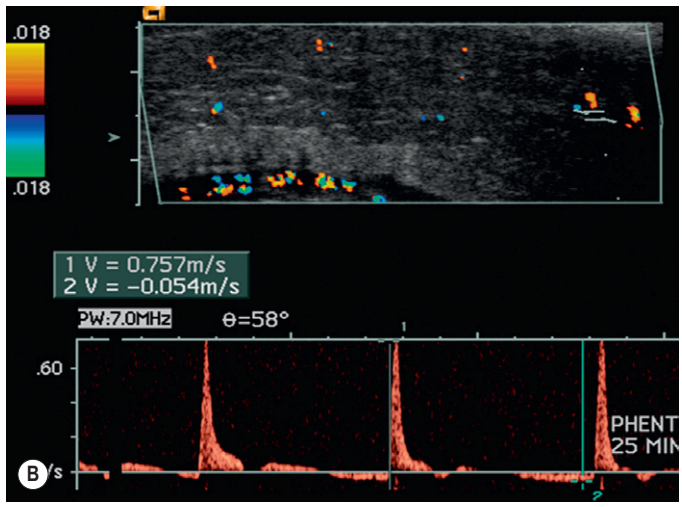


Figure 32.11 Colour Doppler ultrasound response to intra-cavernosal phentolamine. A: Following pharmaco-stimulation with PGE-1 in this young patient, the peak systolic velocity and the end-diastolic velocity are difficult to interpret; arterial input may be insufficient to prevent a venous leak. **B:** At 25 minutes, 5 minutes after a 2 mg dose of phentolamine, the peak systolic velocity increases to 75.7 cm/s and the end-diastolic velocity is negative at –5.4 cm/s; the arterial and venous mechanisms are intact.

PRIAPISM

Priapism is defined as an erection that is maintained in the absence of sexual stimulation.[17] There are two principal categories: non-ischaemic and ischaemic priapism. A further subgroup of 'stuttering' or recurrent priapism has been proposed.[36] Rarely, priapism may be a manifestation of an aorto-caval fistula.[37] Diagnosis of priapism is clinical and relies on the history, examination and analysis of blood aspirated from the cavernosa. However, ultrasound provides clinically useful information that may help management.[38]

Non-ischaemic priapism

Non-ischaemic, high-flow or post-traumatic priapism is a manifestation of damage to the cavernosal arteries resulting in fistula formation between the high-pressure arterial system and the low-pressure cavernosal sinusoids.[17] Clinically patients present with prolonged tumescence from the time of injury. On aspiration the cavernosal blood is oxygenated. Presentation may not be immediate as it is usually painless. Patients with non-ischaemic priapism may still be able to achieve an erection following sexual stimulation.

B-mode imaging reveals a hypoechoic intra-cavernosal region around the damaged cavernosal artery. This abnormality is localised to the site of cavernosal disruption and haematoma formation resulting from arterial extravasation.[38] There is elevation of the cavernosal artery PSV and high forward diastolic flow at spectral Doppler US examination. The draining veins are often prominent and may exhibit arterialised waveforms.[18] Colour Doppler ultrasound allows direct imaging of the arterio-sinusoidal fistula. This is identified as a focus of high-velocity, turbulent flow superimposed on the hypoechoic region demonstrated on greyscale imaging.[39] Elective arterial embolisation of the internal pudendal or cavernosal artery is often the first-line management of non-ischaemic arterial priapism.[40,41]

Ischaemic priapism

Ischaemic or low-flow priapism is a compartment syndrome caused by veno-occlusive problems such as sickle cell disease, or by intracavernosal injection of vasoactive agents (Fig. 32.12). Ischaemic priapism presents with a painful persistent tumescence of the corpora cavernosa but a soft glans and is a urological emergency that requires prompt treatment. The diagnosis is usually clinical. Aspiration of the cavernosal blood is both therapeutic and diagnostic. Ischaemic priapism is confirmed by the presence of deoxygenated blood and a low pH. A low pH indicates a severe degree of ischaemia and compounds the risk of corporal fibrosis with concomitant loss of erectile function. Imaging is not usually required before therapeutic intervention but may have a role if first-line measures including aspiration of cavernosal blood and phenylephrine injection fail to significantly improve blood flow.[7]

On B-mode imaging there is engorgement of the cavernosal sinusoids as seen in a physiological erection. Due to sedimentation of the corpuscular component of blood a fluid–fluid level within the corpora cavernosa is visible on ultrasound of the penis if the patient is left supine for a few minutes with no penile manipulation.[38] Colour Doppler ultrasound findings are of low or absent diastolic flow with variable, but usually not high, arterial inflow consistent with a high resistance vascular bed.[18]

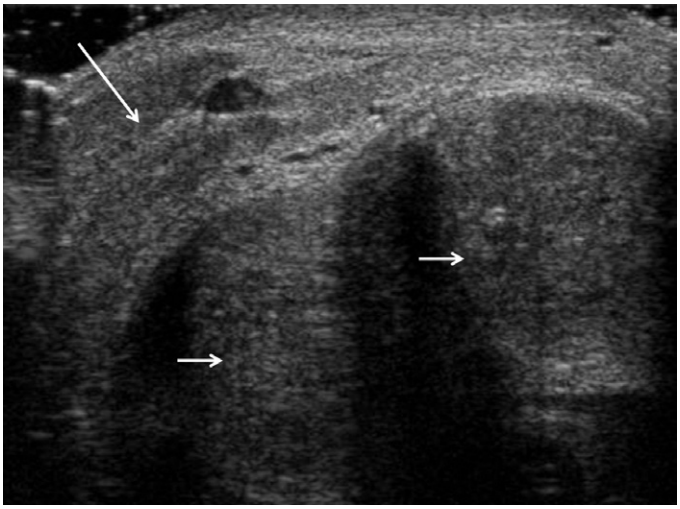


Figure 32.12 Ischaemic priapism. In this patient with sickle cell disease, there is engorgement of the corpora cavernosa (short arrows) and oedema of the overlying tissue (long arrow).

Priapism

Non-ischaemic:
- High PO_2; oxygenated corporal blood on aspiration.
- Spectral Doppler waveforms show continuous increased systolic and diastolic flow with a low resistance pattern.
- In the post-traumatic patient AV fistula may be identified and can guide therapy.

Ischaemic:
- Low PO_2; deoxygenated corporal blood on aspiration.
- Spectral Doppler waveforms show low or absent diastolic flow with a high resistance pattern.
- Oedema.

Differentiation is necessary as ischaemic priapism requires urgent treatment.

PEYRONIE'S DISEASE

Peyronie's disease is defined as a combination of penile pain and deformity with or without palpable penile plaques. The lack of a consensus definition is reflected in the range of reported incidence (1–10% of the adult male population).[42] The incidence is highest in the 40–60-year-old group. Peyronie's disease is characterised by formation of plaques in the tunica albuginea of the penis. Peyronie's disease most commonly presents with a dorsal curvature of the penis. However, other malformations including penile shortening, bottle-neck deformities (due to annular plaques) and indentations, may all occur. Erectile dysfunction is a common association found in 20–40% of such patients. Fibrotic plaque formation results from vascular inflammation but the aetiology is controversial. Evidence does not corroborate the long-held belief that trauma is a primary cause.[43] Peyronie's disease may be associated with Dupuytren's contracture.

On ultrasound plaques are most commonly identified peripherally over the dorsum of the penis (Fig. 32.13). Imaging in the region of maximal deformity or at the site of a palpable lesion will invariably demonstrate an abnormality. Recent work suggests that the fibrotic lesions may be classified into three groups: firstly, hyperechoic foci with no acoustic shadow (Fig. 32.14); secondly, those lesions with an acoustic shadow; and thirdly, calcified lesions. Abnormalities are rarely hypoechoic.[44] It has been suggested that the first group represents active fibrotic foci which frequently resolve spontaneously. The presence of calcified plaques is consistent with established, non-reversible disease.[45] Abnormal plaques

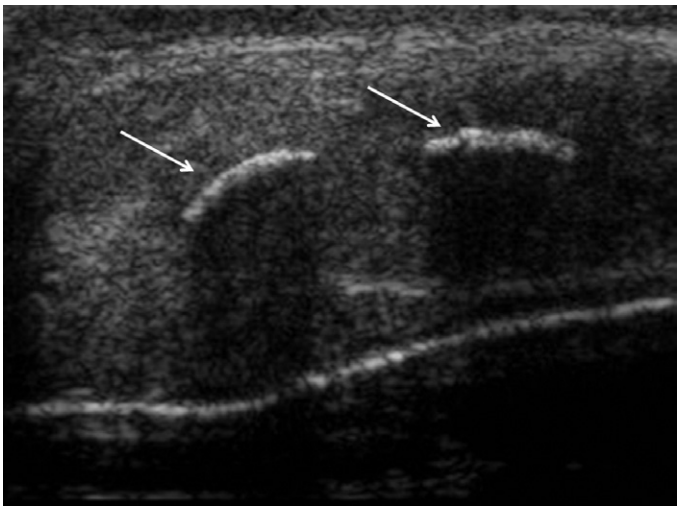


Figure 32.13 Peyronie's disease. Linear calcification (arrows) in the corpora cavernosa, causing acoustic shadowing; likely Peyronie's disease.

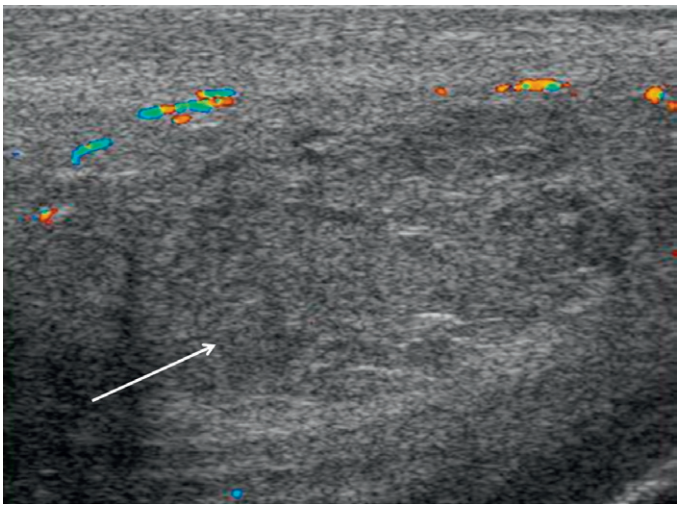


Figure 32.15 Malignant tumour of the penis. A poorly vascularised mass (arrow) in the distal shaft of the penis; a squamous cell carcinoma.

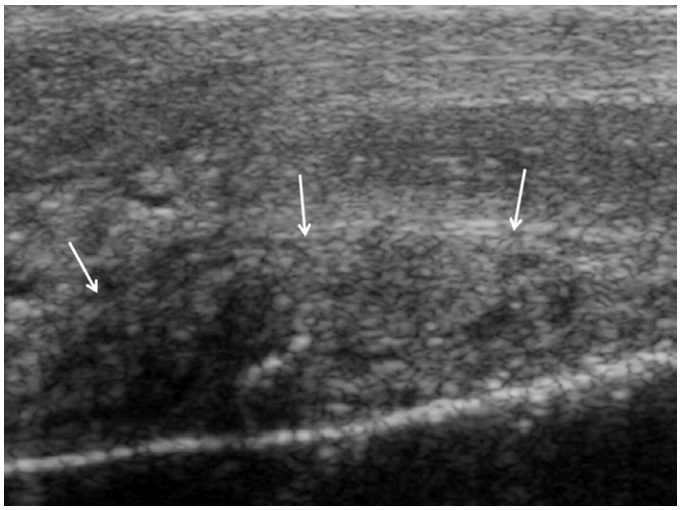


Figure 32.14 Peyronie's disease. Focal area of altered reflectivity (arrows) in the corpora cavernosa; likely Peyronie's disease.

Peyronie's disease

- Plaques may or may not be calcified.
- In the flaccid state plaques can be difficult to visualise, but may become apparent during tumescence; image at the site of maximal curvature.
- Both arterial and venous diseases are more common in Peyronie's disease – mixed aetiology is often present requiring careful assessment to guide therapy.
- Plaques and/or fibrosis may occur following treatment with PGE-1 and can necessitate cessation of treatment.

may extend beyond those that are palpable to involve the corporal tissue or the inter-cavernosal septum and these may be visible on ultrasound.[46] Focal or diffuse thickening of the tunica (which becomes more apparent following pharmacological stimulation) may be the only ultrasound feature.[47]

Distortion of the tunica albuginea results in a higher incidence of venous erectile dysfunction than in the general population. Rarely, plaque may encase the cavernosal arteries and cause arterial erectile dysfunction.[48] Furthermore, there is also an increased incidence of arterial and mixed vascular abnormalities.[49] B-mode assessment of calcification allows patient selection for lithotripsy therapy, and CDUS examination is important prior to possible corrective surgery, to ascertain the course of the cavernosal arteries in relation to plaques.[50]

PENILE FIBROSIS

Penile fibrosis may result from a number of causes. Without prompt treatment ischaemic priapism will cause fibrosis of the cavernosal tissue, producing diffuse cavernosal fibrosis. On ultrasound this is recognisable as replacement of normal sinusoidal tissue in the corpora cavernosa by ill-defined hyperechoic regions. Regular self-injection with intra-cavernosal stimulation therapy for erectile dysfunction, in particular papaverine, may cause focal areas of penile fibrosis to develop.[51] Ultrasound examination can delineate areas of fibrosis allowing follow-up and guiding decisions on therapy.[52] In some patients there may be intra-corporal calcification without any associated plaque and this is thought to result from regions of focal fibrosis or possibly previous trauma.[53]

PENILE MASSES

Primary penile malignancies are rare. Squamous cell carcinoma accounts for up to 95% of malignancies of the penis and is most commonly located at the glans (Fig. 32.15). Squamous cell carcinoma is associated with human papilloma virus (types 16 and 18) and is more common in the developing world. Other primary malignancies include melanomas, basal cell carcinoma and lymphoma.[54] Metastatic spread of malignancy to the penis may be either haematogenous or lymphatic. Metastases should be suspected in patients with a known primary malignancy and new onset priapism. Ultrasound is the preferred imaging modality for penile malignancy.[21,55] Ideally, it should be performed following injection of PGE-1. Ultrasound can assist in identifying the depth of tumour invasion and, specifically, allows evaluation of corpora cavernosal infiltration. It has been shown to be more accurate than clinical examination in determining the extent and size of the

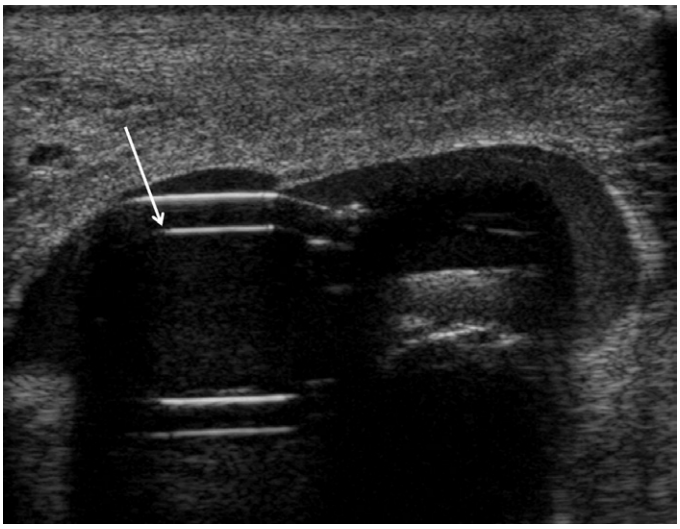


Figure 32.16 Penile prosthesis. The low reflective area (arrow) within the shaft of the penis is clearly of an artificial nature.

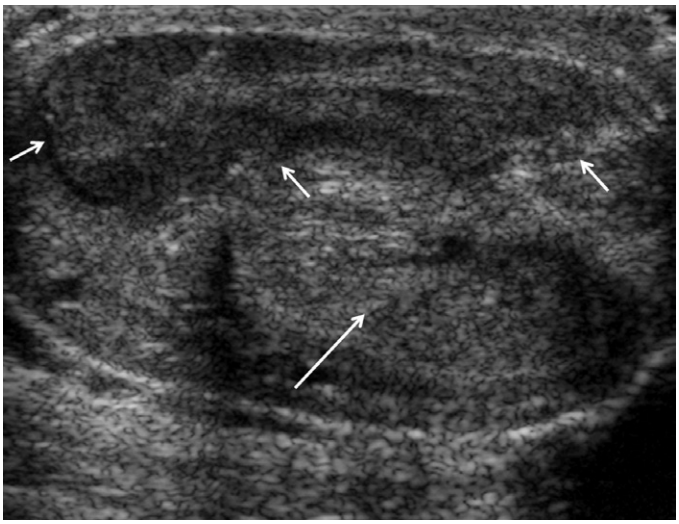


Figure 32.17 Penile fracture. A transverse image through the penis demonstrating a haematoma (short arrows) displacing the normal structures of the penis (long arrow) as a consequence of a fracture.

tumour.[56] Detection of local lymph nodes is readily performed using ultrasound; however, assessment of microscopic infiltration is not possible.[21,55]

On ultrasound squamous cell carcinoma tends to be hypoechoic, relatively heterogeneous and typically poorly vascularised on CDUS. Interruption of the echogenic tunica albuginea indicates malignant infiltration.[57] Ultrasound is of limited value in large tumours and MR imaging is generally indicated in this context. The appearances of secondary disease are similar to those of primary penile cancer involving the corpora.[58]

Other masses occurring in the penis include those found in the skin and subcutaneous tissues elsewhere including cysts, lipomas and neurofibromas. A further unusual 'mass' which may be encountered is a penile prosthesis, easily identifiable by parallel highly reflective walls and the 'man-made' symmetrical structure (Fig. 32.16).

PENILE TRAUMA

Blunt trauma to the flaccid penis rarely causes a fracture, but may result in extra-tunica or cavernosal haematoma formation. Penile fractures most commonly occur as a result of compression of the erect penile shaft against the pubic symphysis during sexual intercourse. Presentation is usually acute with a history of pain, swelling and sudden loss of tumescence during intercourse.[43] The principal role of ultrasound in the acute setting is to identify defects in the tunica albuginea and to allow assessment of the extent of acute haematoma formation (Fig. 32.17). Ultrasound aids diagnosis in cases where the history or clinical findings are atypical. Identification of a tunica defect should prompt immediate surgical repair as delay in treatment of over 24 hours following the initial injury significantly increases the risk of long-term sequelae.[59]

Complications of penile fracture include corporal fibrosis with or without plaque formation, disruption of the tunica albuginea and urethral disruption.[59,60] Urethral injury may be present in up to 20% of cases.[61] If there is clinical concern about a urethral injury then formal urethrography is required. Erectile dysfunction due to impairment of the veno-occlusive mechanism may also occur.[62]

URETHRAL ULTRASOUND

Formal urethrography supplemented by urethroscopy remains the imaging modality of choice for the assessment of the male urethra. Urethrography involves ionising radiation, whilst urethroscopy is invasive and may introduce infection. Ultrasound allows visualisation of the structures around the urethra whilst these other techniques essentially provide luminal views. Some practitioners have advocated the use of ultrasound for evaluating the urethra. Using high-frequency linear probes the normal anterior (bulbar and penile) urethra is visualised when distended with fluid. Lidocaine gel or normal saline may be used to obtain urethral distension in a retrograde direction via the urethral meatus in a manner analogous to conventional urethrography. Alternatively, antegrade passage of urine with constriction of outflow at the glans by means of a clamp or the patient's fingers during the ultrasound examination may be utilised. Images are acquired in longitudinal and transverse planes. Imaging of the posterior urethra is more problematic but may be performed with a transrectal probe. Micturating images of the posterior urethra with the probe in situ allow high-resolution images of the posterior urethra. However, the self-evident problems of micturition with the probe in place limit the value of this technique.

The anterior (bulbar and penile) urethra is of relatively uniform diameter and measures up to 1.0 cm across. The walls are smooth and highly reflective. Strictures, intra-luminal masses and calculi are well visualised.

Ultrasound of the urethra serves as an important adjunct to other imaging modalities in the evaluation of stricturing disease. In particular, bulbar urethral strictures, which tend to be focal, benefit from ultrasound evaluation in order to determine the best treatment. The presence of abnormal peri-urethral tissue, which measures more than 3 mm, is predictive of poor outcome unless surgical resection is performed.[63] Ultrasound has been shown to be more accurate in the measurement of the length of strictures in the bulbar urethra than conventional urethrography.[64] Accurate evaluation of stricture length is important as it in part determines the decision to graft or excise a stricture.[63]

REFERENCES

1. Williams PL, Warwick R, Dyson M, Bannister LH. Splanchnology. In: Williams PL, Warwick R, Dyson M, Bannister LH, editors. Gray's anatomy. 37th edn. London: Churchill Livingstone; 1989. p. 1432–1433.
2. Bella AJ, Brant WO, Lue TF. Penile anatomy. In: Bertolotto M, editor. Color Doppler US of the penis. Berlin: Springer; 2008. p. 11–14.

3. Wilkins CJ, Sidhu PS. Diseases of the penis with functional evaluation. In: Baxter GM, Sidhu PS, editors. Ultrasound of the urogenital system. Stuttgart: Thieme; 2006. p. 181–192.
4. Feldman HA, Goldstein I, Hatzichristou DG, et al. Impotence and its medical and psychosocial correlates: results of the Massachusetts Male Aging Study. J Urol 1994;151:54–61.
5. Benet AE, Melman A. The epidemiology of erectile dysfunction. Urol Clin North Am 1995;22:699–709.
6. Virag R. Intracavernous injection of papaverine for erectile failure. Lancet 1982;2(8304):938.
7. Montague DK, Jarow J, Broderick GA, et al. American Urological Association guideline on the management of priapism. J Urol 2003;170:1318–1324.
8. Montague DK, Jarow JP, Broderick GA, et al. Chapter 1: The management of erectile dysfunction: an AUA update. J Urol 2005;174:230–239.
9. Golijanin D, Singer E, Davis R, et al. Doppler evaluation of erectile dysfunction – part 1. Int J Impot Res 2007;19:37–42.
10. Montorsi P, Ravagnani PM, Galli S, et al. Association between erectile dysfunction and coronary artery disease: matching the right target with the right test in the right patient. Eur Urol 2006;50:721–731.
11. Gontero P, Sriprasad S, Wilkins CJ, et al. Phentolamine re-dosing during penile dynamic colour Doppler ultrasound: a practical method to abolish a false diagnosis of venous leakage in patients with erectile dysfunction. Br J Radiol 2004;77:922–926.
12. Lomas GM, Jarow JP. Risk factors for papaverine-induced priapism. J Urol 1992;147:1280–1281.
13. Cormio L, Bettocchi C, Ricapito V, et al. Resistance index as a prognostic factor for prolonged erection after penile dynamic colour Doppler ultrasonography. Eur Urol 1998;33:94–97.
14. Shamloul R, Ghanem HM, Salem A, et al. The value of penile duplex in the prediction of intracavernous drug-induced priapism. Int J Impot Res 2004;16:78–79.
15. Govier FE, Asase D, Hefty TR, et al. Timing of penile color flow duplex ultrasonography using a triple drug mixture. J Urol 1995;153:1472–1475.
16. Kim SH, Paick JS, Lee SE, et al. Doppler sonography of deep cavernosal artery of the penis: variation of peak systolic velocity according to sampling location. J Ultrasound Med 1994;13:591–594.
17. Mihmanli I, Kantarci M. Erectile dysfunction. Semin Ultrasound CT MRI 2007;28:274–286.
18. Wilkins CJ, Sriprasad S, Sidhu PS. Colour Doppler ultrasound of the penis. Clin Radiol 2003;58:514–523.
19. Bertolotto M, Lissiani A, Pizzolato R, Fute MD. US anatomy of the penis: common findings and anatomical variations. In: Bertolotto M, editor. Color Doppler US of the penis. Berlin: Springer; 2008. p. 25–38.
20. Jarrow JP, Pugh VW, Routh WD, Dyer RB. Comparison of penile duplex ultrasonography to pudendal arteriography. Variant penile arterial anatomy affects interpretation of duplex ultrasonography. Invest Radiol 1993;28:806–810.
21. Mancini M, Bartolini M, Maggi M, et al. The presence of arterial anatomical variations can affect the results of duplex sonographic evaluation of penile vessels in impotent patients. J Urol 1996;155: 1919–1923.
22. Schwartz AN, Wang KY, Mack LA, et al. Evaluation of normal erectile function with color flow Doppler sonography. AJR Am J Roentgenol 1989;153:1155–1160.
23. Chiou RK, Alberts GL, Pomeroy BD, et al. Study of cavernosal arterial anatomy using color and power Doppler sonography: impact on hemodynamic parameter measurement. J Urol 1999;162:358–360.
24. Golijanin D, Singer E, Davis R, et al. Doppler evaluation of erectile dysfunction – part 2. Int J Impot Res 2007;19:43–48.
25. Benson CB, Aruny JE, Vickers MA. Correlation of duplex sonography with arteriography in patients with erectile dysfunction. AJR Am J Roentgenol 1993;160:71–73.
26. Roy C, Saussine C, Tuchmann C, et al. Duplex Doppler sonography of the flaccid penis: potential role in the evaluation of impotence. J Clin Ultrasound 2000;28:290–294.
27. Patel U, Lees WR. Penile sonography. In: Solibiati L, Rizzatto G, editors. Ultrasound of superficial structures. London: Churchill Livingstone; 1995. p. 229–242.
28. Quam JP, King BF, James EM, et al. Duplex and color Doppler sonographic evaluation of vasculogenic impotence. AJR Am J Roentgenol 1989;153:1141–1147.
29. Bassiouny HS, Levine LA. Penile duplex sonography in the diagnosis of venogenic impotence. J Vasc Surg 1991;13:75–82.
30. Kassouf W, Carrier S. A comparison of the International Index of Erectile Function and erectile dysfunction studies. BJU Int 2003;91:667–669.
31. Lue TF, Hricak H, Schmidt RA, Tanagho EA. Functional evaluation of penile veins by cavernosgraphy in papaverine-induced erection. J Urol 1986;135:479–482.
32. Fowlis GA, Sidhu PS, Jager HR, et al. Preliminary report: combined surgical and radiological penile vein occlusion for the management of impotence caused by venous-sinusoidal incompetence. Br J Urol 1994;74:492–496.
33. Aversa A, Rocchietti-March M, Caprio M, et al. Anxiety-induced failure in erectile response to intracorporeal prostaglandin-E1 in non-organic male impotence: a new diagnostic approach. Int J Androl 1996;19:307–313.
34. Goldstein I. Oral phentolamine: an alpha-1, alpha-2 adrenergic antagonist for the treatment of erectile dysfunction. Int J Impot Res 2000;12(Suppl. 1):S75–S80.
35. Wespes E, Rondeux C, Schulmann CC. Effect of phentolamine on venous return in human erection. Br J Urol 1989;63:95–97.
36. Muneer A, Minhas S, Arya M, Ralph DJ. Stuttering priapism – a review of the therapeutic options. Int J Clin Pract 2008;62:1265–1270.
37. Gordon S, Marsh P, Day A, Chappell B. Priapism as the presenting symptom of an aortocaval fistula. Emerg Med J 2004;21:265.
38. Bertolotto M, Mucelli FP, Liguori G, Sanabor D. Imaging priapism: the diagnostic role of color Doppler US. Color Doppler US of the penis. Berlin: Springer; 2008. p. 79–88.
39. Bertolotto M, Mucelli RP. Nonpenetrating penile traumas: sonographic and Doppler features. AJR Am J Roentgenol 2004;183:1085–1089.
40. Walker TG, Grant PW, Goldstein I, et al. 'High-flow' priapism: treatment with superselective transcatheter embolization. Radiology 1990;174:1053–1054.
41. Kang BC, Lee DY, Byun JY, et al. Post-traumatic arterial priapism: colour Doppler examination and superselective arterial embolization. Clin Radiol 1998;53:830–834.
42. Brant WO, Bella AJ, Lue TF. Peyronie's disease: etiology and treatment. In: Bertolotto M, editor. Color Doppler US of the penis. Berlin: Springer; 2008. p. 55–60.
43. Zargooshi J. Penile fracture in Kermanshah, Iran: report of 172 cases. J Urol 2000;164:364–366.
44. Bertolotto M, Coss M, Neumaier CE. US evaluation of patients with Peyronie's disease. In: Bertolotto M, editor. Color Doppler US of the penis. Berlin: Springer; 2008. p. 61–70.
45. Bekos A, Arvaniti M, Hatzimouratidis K, et al. The natural history of Peyronie's disease: an ultrasonography-based study. Eur Urol 2008;53:644–650.
46. Brant WO, Bella AJ, Garcia MM, et al. Isolated septal fibrosis or hematoma – atypical Peyronie's disease? Eur Urol 2007;177:179–182.
47. Brock G, Hsu GL, Nunes L, et al. The anatomy of the tunica albuginea in the normal penis and Peyronie's disease. J Urol 1997;157:276–281.
48. Bertolotto M, de Stefani S, Martinoli C, et al. Color Doppler appearance of penile cavernosal-spongiosal communications in patients with severe Peyronie's disease. Eur Radiol 2002;12: 2525–2531.
49. Kadioglu A, Tefekli A, Erol H, et al. Color Doppler ultrasound assessment of penile vascular system in men with Peyronie's disease. Int J Impot Res 2000;12:263–267.
50. Levine LA, Coogan CL. Penile vascular assessment using color duplex sonography in men with Peyronie's disease. J Urol 1996;155: 1270–1273.
51. Pery M, Rosenberger A, Kaftori JK, Vardi Y. Intracorporeal calcifications after self-injection of papaverine. Radiology 1990;176: 81–83.
52. Chew KK, Stuckey BG, Earle CM, et al. Penile fibrosis in intracavernosal prostaglandin E1 injection therapy for erectile dysfunction. Int J Impot Res 1997;9:225–229.
53. Doubilet PM, Benson CB, Silverman SG, Gluck CD. The penis. Semin Ultrasound, CT, MRI 1991;12:157–175.
54. Kayes O, Ahmed HU, Arya M, Minhas S. Molecular and genetic pathways in penile cancer. Lancet Oncol 2007;8:420–429.
55. Algaba A, Horenblas S, Pizzocaro-Luigi PG, et al. EAU guidelines on penile cancer. Eur Urol 2002;42:199–293.
56. Agrawal A, Pai D, Ananthakrishnan N, et al. Clinical and sonographic findings in carcinoma of the penis. J Clin Ultrasound 2000;28: 399–406.
57. Bertolotto M, Serafini G, Dogliotti L, et al. Primary and secondary malignancies of the penis: ultrasound features. Abdom Imaging 2005;30:108–112.

58. Vapnek JM, Hricak H, Carroll PR. Recent advances in imaging studies for staging of penile and urethral carcinoma. Urol Clin North Am 1992;19:257–266.
59. El Bahnasawy MS, Gomha MA. Penile fractures: the successful outcome of immediate surgical intervention. Int J Impot Res 2000;12:273–277.
60. Asgari MA, Hosseini SY, Safarinejad MR, et al. Penile fractures: evaluation, therapeutic approaches and long-term results. J Urol 1996;155:148–149.
61. Fergany AF, Angermeier KW, Montague DK. Review of Cleveland Clinic experience with penile fracture. Urology 1999;54:352–355.
62. Gontero P, Sidhu PS, Muir GH. Penile fracture repair: assessment of early results and complications using color Doppler ultrasound. Int J Impot Res 2000;12:125–129.
63. Morey AF, McAninch JW. Sonographic staging of anterior urethral strictures. J Urol 2000;163:1070–1075.
64. Nash PA, McAnich JW, Bruce JE, Hanks DK. Sono-urethrography in the evaluation of anterior urethral strictures. J Urol 1995;154:72–76.

CHAPTER

33

Adrenals

Keith Dewbury and Elizabeth E. Rutherford

INTRODUCTION 632

ANATOMY AND SCANNING TECHNIQUES 632

NORMAL APPEARANCES 633

CONGENITAL ANOMALIES 634
Agenesis 634
Hyperplasia (adrenogenital syndromes) 634
Discoid adrenal 634

ADRENAL CYSTS 634

ADRENAL HAEMORRHAGE 635

HYPERPLASIA 635

ADRENAL CALCIFICATION 635

TUMOURS 635
Benign 636
Adenomas 636
Myelolipomas 636
Phaeochromocytoma 637
Malignant 637
Adrenal cortical carcinoma 637
Neuroblastoma 637
Metastases 640

ROLE OF CT AND MRI IN CHARACTERISATION OF ADRENAL LESIONS 642

INTRODUCTION

The adrenal glands are small, paired organs which lie anteromedial to the upper pole of the kidneys and may therefore be challenging to visualise with ultrasound. Initial descriptions of adrenal ultrasound reported that the right adrenal was easier to visualise than the left.[1,2] Recent improvements in ultrasound technology have increased the sensitivity of abdominal ultrasound in the detection of adrenal lesions such that lesions less than 1 cm may be identified. Lesion detection, however, depends on a number of factors, in particular patient habitus, and whilst lesions as small as 5 mm can be detected if visualisation is good, when imaging is suboptimal, lesions under 2 cm in diameter may not be identified. In cases where there is doubt as to the presence of a lesion or in obese patients where an adrenal lesion is suspected, computed tomography (CT) is the initial imaging modality of choice. Whilst magnetic resonance (MR) and CT imaging are undoubtedly better imaging modalities for characterisation of adrenal masses, there are certain lesions that have characteristic ultrasound appearances. Adrenal lesions detected at ultrasound may be the first manifestation of malignancy or may be benign and incidental. Ultrasound of the adrenal glands is also particularly useful in children, when radiation dose reduction is paramount and the glands are more readily visualised than in adults.

ANATOMY AND SCANNING TECHNIQUES

Embryologically, the adrenal cortex is of mesodermal origin and the medulla develops from neuroectodermal tissue. The cortex produces hormones including cortisol, aldosterone and androgens and consists of three layers: the zona glomerulosa (outermost layer), zona fasciculata (largest, middle layer) and the zona reticularis (innermost layer). The more central adrenal medulla is smaller and secretes adrenaline, noradrenaline and dopamine. The adrenal glands are yellowish in colour, weigh approximately 4 g each and measure 3–6 cm in length, 2–3 cm in width and 2–6 mm in thickness. Each consists of an anteromedial ridge from which two thin limbs extend posteriorly.

The right adrenal is pyramidal in shape, lying between the inferior vena cava (IVC) and right crus of diaphragm. The inferior aspect of the gland never extends caudally to the level of the renal vessels.[3] The left adrenal is crescentic in shape and lies more cranially than its counterpart. The medial and lateral limbs are also shorter than those on the right. It lies lateral or slightly posterior to the aorta and lateral to the left crus of diaphragm. Superiorly, it lies posterior to the lesser sac, and more inferiorly, it is posterior to the pancreas. The glands receive their blood supply from the inferior phrenic arteries, renal arteries and directly from the aorta. There is usually a single adrenal vein that drains into the vena cava on the right and into the left renal vein on the left.[4]

The position of the adrenals as described requires an intercostal scanning approach using the acoustic window of the liver on the right and the spleen on the left. To visualise the right adrenal, the transducer is placed in the ninth or tenth intercostal space in the mid or anterior axillary line. Scanning transversely, the transducer is gently rotated to move the field of view from the renal hilum upwards to a few centimetres above the kidney, concentrating on the region behind the IVC and directly adjacent to the right diaphragmatic crus. In the upper transverse section on the right a vertical linear or curvilinear structure corresponding to the anteromedial ridge and medial limb is seen. In the middle section both limbs are seen as an inverted 'V' or 'Y'. Through the inferior portion of the gland only the lateral limb may be seen as a horizontal band. Coronal or longitudinal sections are obtained by rotating the transducer through 90°. The upper pole of the right kidney is located and the transducer angled medially. Both limbs of the gland may be simultaneously displayed as a thin, long inverted 'V'- or 'Y'-shaped structure up to 6 cm in length. A further small medial angulation is necessary to visualise the anteromedial ridge of the gland in this plane where it lies posterior to the IVC.

The left adrenal gland is more difficult to image because of the smaller acoustic window available through the spleen. The transducer is placed on the eighth or ninth intercostal space in the posterior axillary line, avoiding stomach or bowel gas, to give a coronal scan. The upper pole of the kidney should first be located through the spleen. A small angulation of the transducer towards the anterior aspect of the kidney will demonstrate the left adrenal gland in the perirenal space between spleen, kidney and left diaphragmatic crus. This is best recognised when both limbs are shown, displaying

the characteristic 'V' shape. A transverse section is obtained by rotating the transducer through 90°. Due to the relative difficulty in demonstrating the left adrenal gland, additional views in right lateral decubitus and erect positions may be helpful. With high-resolution real-time scanning, the normal right adrenal gland is demonstrated in 92% of patients and the left gland in 71%.[5]

Normal adrenal gland

- Measures up to 0.6 × 3 × 6 cm.
- Blood supply: inferior phrenic arteries, renal arteries, aorta.
- Right: pyramidal in shape; left: crescentic shape.
- Right adrenal visualised in 92%; left in 71%.
- Medulla: linear reflective structure, seen in neonates and 13% of adults.
- Flat or concave contour.

NORMAL APPEARANCES

The adrenal cortex appears of low reflectivity on ultrasound. The medulla is seen as a thin linear reflective structure in the centre of the cortex in up to 13% of adults[5] (Fig. 33.1). This is a particularly prominent feature in the neonatal or fetal adrenal gland (Fig. 33.2). At birth the neonatal adrenal cortex is relatively thick and is composed of two layers: the thick fetal zone (primitive cortex) occupying 80% of the gland and the thin peripheral zone that becomes the adult cortex.[6] The fetal cortex synthesises most of the precursors for maternal oestrogens and is one of the main consumers of placental progesterone. It involutes after birth and disappears by the age of one year.

The neonatal adrenal gland is readily visualised for several reasons:

1. The infant gland is proportionally larger. At birth it is one-third of the size of the kidney, for which it can be mistaken if the kidney does not lie in its normal position. During the first week of life, the adrenal reduces in size.[6]
2. The small amount of perirenal fat in neonates allows for better resolution.
3. The small size of the subject means that higher frequency transducers are routinely used, further optimising overall resolution.

The contour of the normal adrenal gland is flat or concave and convexity should be regarded with suspicion. It is important to examine the whole of each gland since small masses may affect only part of the gland, leaving the remainder with a normal appearance. Upper pole renal cysts and masses may be mistaken for adrenal lesions and similarly a prominent diaphragmatic crus or splenunculus may also mimic adrenal pathology.



Figure 33.1 Longitudinal ultrasound image of a normal right adult adrenal gland. The body of the gland (arrow) and both limbs (arrowheads) can be clearly delineated.

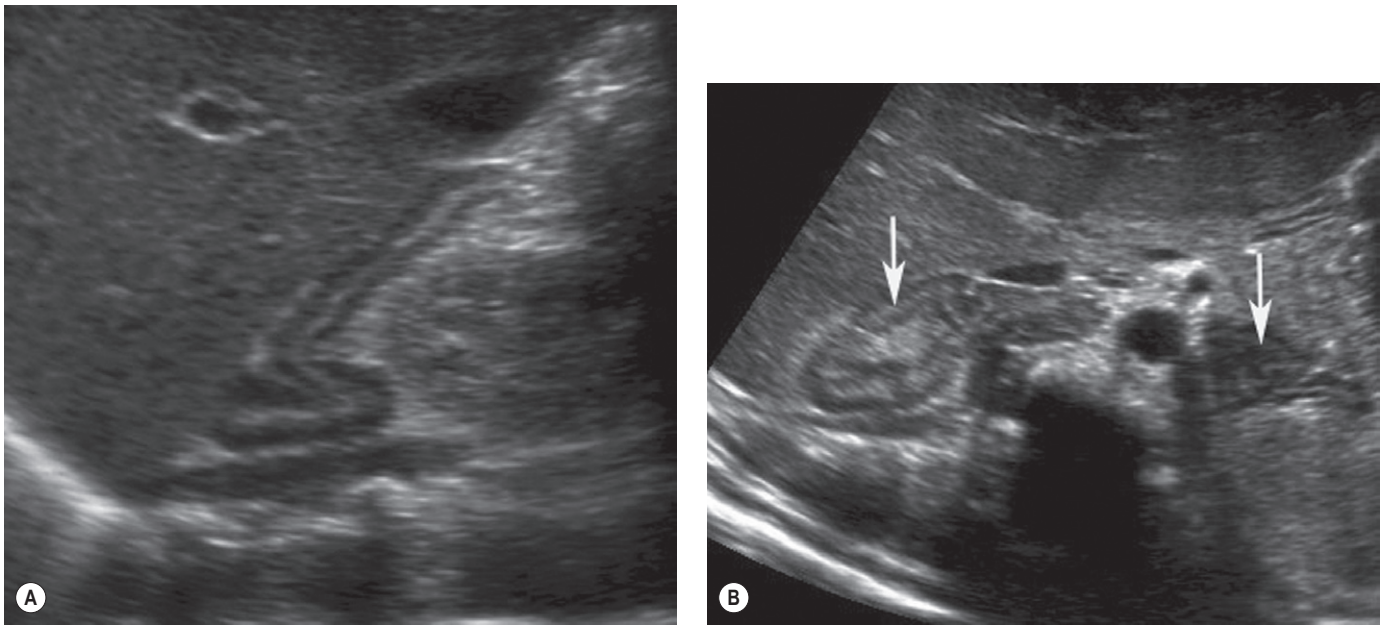


Figure 33.2 Normal neonatal adrenal glands. A: Longitudinal view of the right adrenal gland in a neonate. Note the clear distinction between the low reflectivity cortex and higher reflectivity medulla. **B:** Transverse image showing both adrenal glands (arrows) in a neonate.

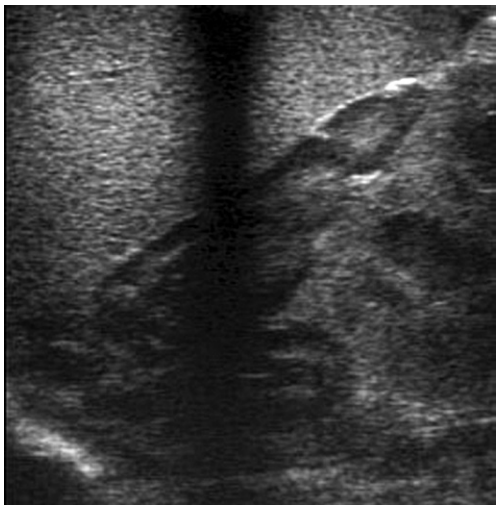
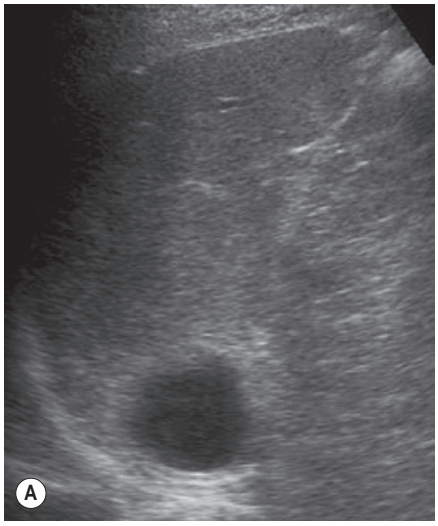


Figure 33.3 Congenital adrenal hyperplasia. Note the large size of the gland (compared with the normal neonatal adrenal – Fig. 33.2A) and pronounced corticomedullary differentiation.



Figure 33.4 Discoid adrenal. Longitudinal image in a neonate. There is left renal agenesis. The flattened elongated left adrenal gland is well visualised through the spleen. Note the marked corticomedullary differentiation.



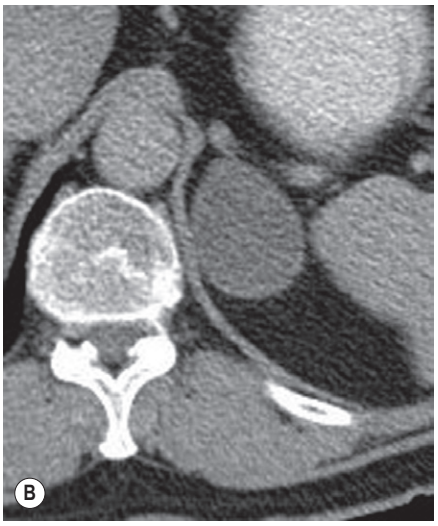


Figure 33.5 Adrenal cyst. A: Well-defined anechoic left adrenal lesion, typical of a simple cyst. **B:** Corresponding axial CT image showing a homogeneous cystic left adrenal lesion with a thin wall.

CONGENITAL ANOMALIES

Agenesis

Unilateral adrenal agenesis is described[7] but is rare. The contralateral gland will characteristically show compensatory hypertrophy. Bilateral adrenal agenesis is not compatible with life.

Hyperplasia (adrenogenital syndromes)

Congenital adrenal hyperplasia is an autosomal recessive disorder due to an inborn error of metabolism. A number of syndromes are described;[8] the most common are termed 'adrenogenital syndromes' and demonstrate clinical manifestations of virilisation. Ultrasound is useful in assessing adrenal size in this situation (Fig. 33.3).

Discoid adrenal

The adrenal gland is normally present in patients with renal agenesis. Renal agenesis may be associated with the loss of the normal folding of the adrenal gland into a medial and lateral wing. The gland becomes flattened and elongated, producing a typical discoid shape. This may be particularly well seen in neonates when the gland is proportionally larger and the zonal architecture is still seen (Fig. 33.4).

ADRENAL CYSTS

Adrenal cysts are benign and rarely symptomatic, most being encountered as incidental findings, which do not require any intervention.[9] If they become large, however, adrenal cysts may cause discomfort or pain due to displacement of adjacent structures. They are usually unilateral but occur with equal frequency on both sides and are three times more common in women than men. Cysts are well-defined anechoic structures and usually have a thin wall (Fig. 33.5). Occasionally, the cyst wall may calcify.

Adrenal cysts can be divided into the following subtypes:

- **Endothelial.** This is the most common adrenal cyst, accounting for nearly half of all reported cases.[10] These are mostly lymphangiomatous in origin but some are angiomatous.

- **Pseudocysts.** These may occur as the result of haemorrhage or tumour and account for approximately 40% of adrenal cysts.
- **Epithelial.** Epithelial glandular cysts account for 9% of adrenal cysts.
- **Parasitic.** Echinococcal infection is the most common cause.

ADRENAL HAEMORRHAGE

Adrenal haemorrhage is most commonly related to trauma and can occur in up to 25% of severely injured patients.[11] In most cases this will be associated with ipsilateral thoracic, abdominal or retroperitoneal injury.[12] The majority of such patients will be imaged with a 'multitrauma' CT scan which will detect adrenal haemorrhage and so ultrasound has a limited role in this regard.

The neonatal adrenal gland undergoes a marked reduction in size following birth. The vessels in the primitive adrenal cortex become distended and are prone to haemorrhage. The exact cause of haemorrhage in neonates is unknown, but stress and birth trauma, anoxia and systemic disease are all implicated. Infants usually present within 2–7 days of birth. Haemorrhage is more commonly seen on the right side although up to 10% are bilateral.[13–15]

In adults the hypertrophic adrenal gland caused by adrenocorticotrophic hormone (ACTH) therapy or severe stress may also be more prone to haemorrhage. Sepsis secondary to meningococcal infection and anticoagulant therapy can also predispose to haemorrhage. Division of the right adrenal vein during orthotopic liver transplantation has also been reported to cause venous congestion and haemorrhagic infarction of the right adrenal gland.[16]

At ultrasound, adrenal haemorrhage has a variable appearance depending on the timing of imaging. Acutely, adrenal haematomas are often anechoic but may be more reflective due to fibrin strand formation as resolution occurs (Fig. 33.6). They become smaller and reduce in reflectivity over time. Haematomas may completely resolve, calcify or remain as a residual adrenal cyst[13] and they rarely require any intervention. Serial ultrasounds are, however, useful in excluding an underlying tumour as a cause for adrenal haemorrhage. Where there is any doubt as to the diagnosis or concern regarding underlying adrenal pathology, CT and/or MRI can be useful to confirm the presence of haemorrhage and also have a role in follow-up. In neonates, however, ultrasound remains the imaging modality of choice.

HYPERPLASIA

Diffuse adrenal enlargement may occur in diffuse bilateral hyperplasia in conditions such as Cushing's syndrome. In most patients the enlargement will be slight and this is extremely difficult to detect with confidence using ultrasound. When the glands are significantly enlarged (approximately double their normal size), demonstration of the medulla allows differentiation of hyperplasia from a diffuse infiltrative process such as lymphoma, when the medulla cannot be identified.[17,18]

ADRENAL CALCIFICATION

Adrenal calcification may rarely be noted as an incidental finding on plain abdominal X-rays or at routine ultrasound examination of the upper abdomen. It can result from previous adrenal haemorrhage or be related to adrenal tuberculous infection. A less commonly seen pattern of curvilinear calcification may be seen in the wall of an adrenal cyst.

TUMOURS

It is most common for adrenal tumours to enlarge the adrenal gland focally, although diffuse enlargement may occur. A focal mass is normally oval or round and may vary enormously in size. A small adrenal mass is easier to delineate than the normal adrenal gland because its diameter usually exceeds that of the adrenal. Its overall reflectivity is low, in contrast to the high reflectivity of the surrounding fat. Ultrasound has been reported to have an overall accuracy of 95% in the evaluation of adrenal masses over 1 cm in size.[19] Even when a normal adrenal gland is not visualised, if the adrenal area is thoroughly scanned and no mass can be identified, tumour can be fairly confidently excluded.[20] To differentiate an adrenal from a renal mass, a separating interface must be demonstrated. A right adrenal tumour typically compresses or displaces the IVC forwards.[21] A large adrenal tumour usually displaces the upper pole of the kidney laterally or the whole kidney inferiorly. Occasionally, the tumour may extend downwards anterior to the kidney without much displacement. Larger masses may indent the liver or kidney. Whilst smaller tumours are usually fairly

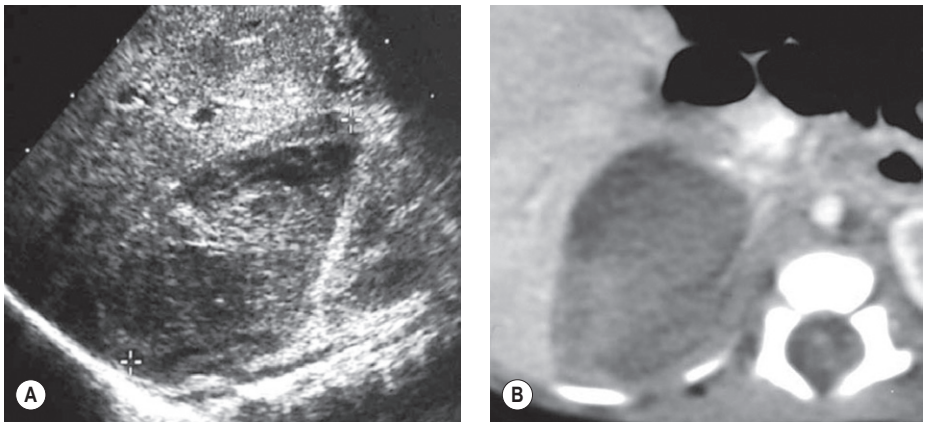


Figure 33.6 Subacute right adrenal haemorrhage in a neonate. A: The ultrasound appearances are of a solid mixed reflectivity mass. **B:** CT image in the same child confirms the presence of mixed attenuation within the right adrenal, with higher attenuation areas signifying recent haemorrhage.

homogeneous, focal areas of necrosis or haemorrhage are more likely to occur in larger masses, resulting in a more heterogeneous appearance.[21]

Benign

Adenomas

These tumours are common incidental findings, being reported in up to 3% of adult autopsies.[22] Approximately 10% of adrenal adenomas are bilateral and their incidence increases with age. They are usually small and measure 1–2 cm in diameter. Whilst most adenomas are non-functioning and detected incidentally, they may be hyperfunctioning and present with symptoms related to excessive hormone (cortisol or aldosterone) secretion.

Adenomas that secrete excessive amounts of cortisol result in Cushing's syndrome, which is characterised by truncal obesity, hirsutism, amenorrhoea, hypertension and weakness and can also be caused by adrenal hyperplasia, adrenal carcinoma or exogenous corticosteroid administration. Conn's syndrome results from the excessive secretion of aldosterone, which is due to an adrenal adenoma in 70% of cases. Women are more likely to have hyperaldosteronism due to an adenoma, whereas men with hyperaldosteronism are more likely to have underlying adrenal hyperplasia.[23,24] Symptoms include hypertension, weakness, tetany and ECG abnormalities and biochemical tests reveal hypokalaemia, hypernatraemia and raised urine and serum aldosterone levels.

The majority of adrenal adenomas are found incidentally at CT examination, although routine abdominal ultrasound may also detect them. The intracytoplasmic lipid content of adrenal adenomas allows their diagnosis by unenhanced CT imaging[25] or opposed phase chemical shift MRI.[26] At unenhanced CT imaging, 98% of homogeneous adrenal masses with a CT attenuation value of 10 Hounsfield units or less will be benign, with the majority of these being adenomas, although 29% of adenomas will have a greater attenuation value and are hence indistinguishable from non-adenomas, including metastases.[27] At ultrasound, adrenal adenomas appear solid, rounded (Fig. 33.7) or slightly flattened (Fig. 33.8) and well defined. They are homogeneous and of low reflectivity.

Myelolipomas

Adrenal myelolipoma is a rare cortical tumour composed of varying proportions of fat and bone marrow elements.[28,29] There is no malignant potential and the lesions are endocrinologically non-functioning. They arise in the zona fasciculata of the gland. Myelolipomas are usually asymptomatic and discovered incidentally although they may cause symptoms if they undergo haemorrhage or become large and exert a local pressure effect on adjacent structures. They have a prevalence at postmortem of 0.08% to 0.2%.[30] On ultrasound these rare tumours are characteristically highly reflective,

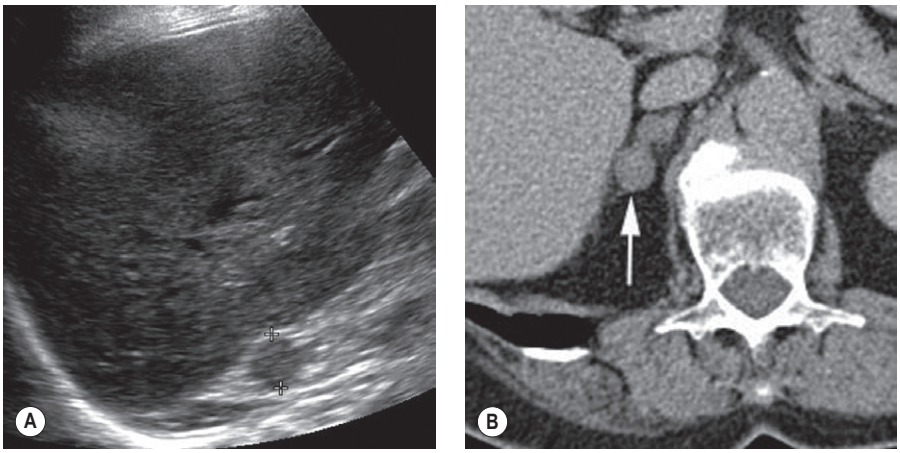


Figure 33.7 Rounded adrenal adenoma. **A:** Well-defined, small rounded right adrenal lesion (callipers). **B:** CT in the same patient confirmed this to represent an adrenal adenoma (arrow).

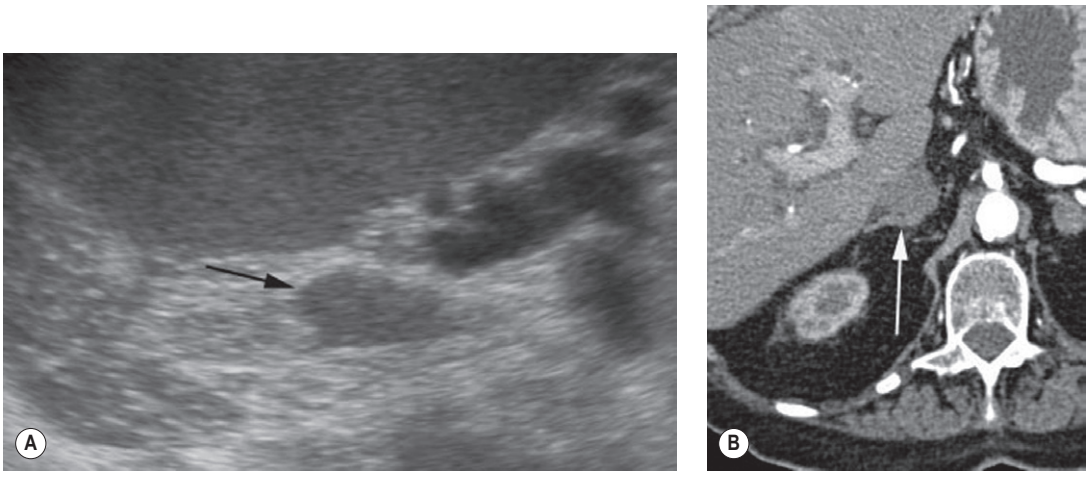


Figure 33.8 Flattened adrenal adenoma. A: Well-defined, low reflectivity right adrenal lesion with a more linear morphology (arrow). **B:** CT in the same patient confirmed a right adrenal adenoma (arrow).

due to their fat content (Fig. 33.9A). They may also contain calcification. If discovered incidentally at ultrasound, CT should be performed to confirm the presence of fat in these lesions (Fig. 33.9B).

Phaeochromocytoma

Phaeochromocytomas are endocrinologically active tumours that secrete adrenaline and noradrenaline, causing paroxysmal headache, palpitations, excessive perspiration and hypertension. They are found in up to 1% of patients with hypertension. The majority arise within the chromaffin cells of the adrenal medulla but up to 10% arise in the autonomic nervous tissue, particularly in the organs of Zuckerkandl.[31] The majority of adrenal phaeochromocytomas are benign but 5–10% are malignant and up to 5% are multiple. Multiple lesions are frequently associated with various hereditary syndromes, e.g. multiple endocrine neoplasia (MEN) type IIa and IIb, von Hippel–Lindau syndrome, neurofibromatosis and tuberous sclerosis. The diagnosis may be confirmed by biochemical assay for urinary catecholamines and metabolites, e.g. vanillylmandelic acid (VMA).

Phaeochromocytomas may be large or small at presentation. The right adrenal is more commonly affected than the left. Typically, when small they are well-defined, round or oval masses with a uniform reflectivity. Larger tumours frequently undergo necrosis or haemorrhage with loss of homogeneity, and calcification may be seen (Figs 33.10 and 33.11).

Benign adrenal lesions

- Adenomas (solid, low reflectivity, rounded or flattened).
- Myelolipomas (highly reflective due to fat content).
- Phaeochromocytoma (90% benign, variable appearance ± calcification).
- Lipomas.
- Cysts.
- Ganglioneuromas.
- Haemangiomas.

Other rare benign adrenal lesions include ganglioneuromas, haemangiomas[32] and lipomas. The ultrasound features of these tumours are non-specific and hence the diagnosis is usually made histologically.

Malignant

Adrenal cortical carcinoma

Primary adrenal cortical carcinoma is rare, accounting for 0.2% of all cancer deaths. It can arise from any of the layers of the adrenal cortex. Approximately half of tumours are endocrinologically active[33] and therefore present earlier with features of excess hormone production such as Cushing's syndrome. Non-functioning tumours are often therefore large and have invaded the adrenal vein and IVC by presentation. Colour Doppler examination may therefore be useful to assess for venous invasion. Nodal and blood-borne metastases are common and tumour recurrence following surgery is common. Adrenal carcinoma has a variable appearance at ultrasound with larger lesions often exhibiting central necrosis or haemorrhage. Tumours are usually well defined and some lesions may contain calcification (Fig. 33.12).

Neuroblastoma

Neuroblastoma is the second most common abdominal tumour of childhood (after Wilms' tumour), with 80% occurring in children under 5 years of age and one-third under 2 years of age. It accounts for approximately 15% of childhood cancer deaths.[34] Under 1 year of age the tumour may spontaneously regress or differentiate into a ganglioneuroma. Approximately 35% of neuroblastomas arise in the adrenal medulla, with the extra-adrenal paraspinal ganglia and posterior mediastinum being other common sites.[35] Neuroblastoma may present as an asymptomatic abdominal mass or present with symptoms related to metastases or the secretion of catecholamines. There may be generalised debility with weight loss and fever. Up to three-quarters of patients have metastases at the time of presentation, with the most commonly affected sites being the bone marrow, lymph nodes, liver and skin.[36]

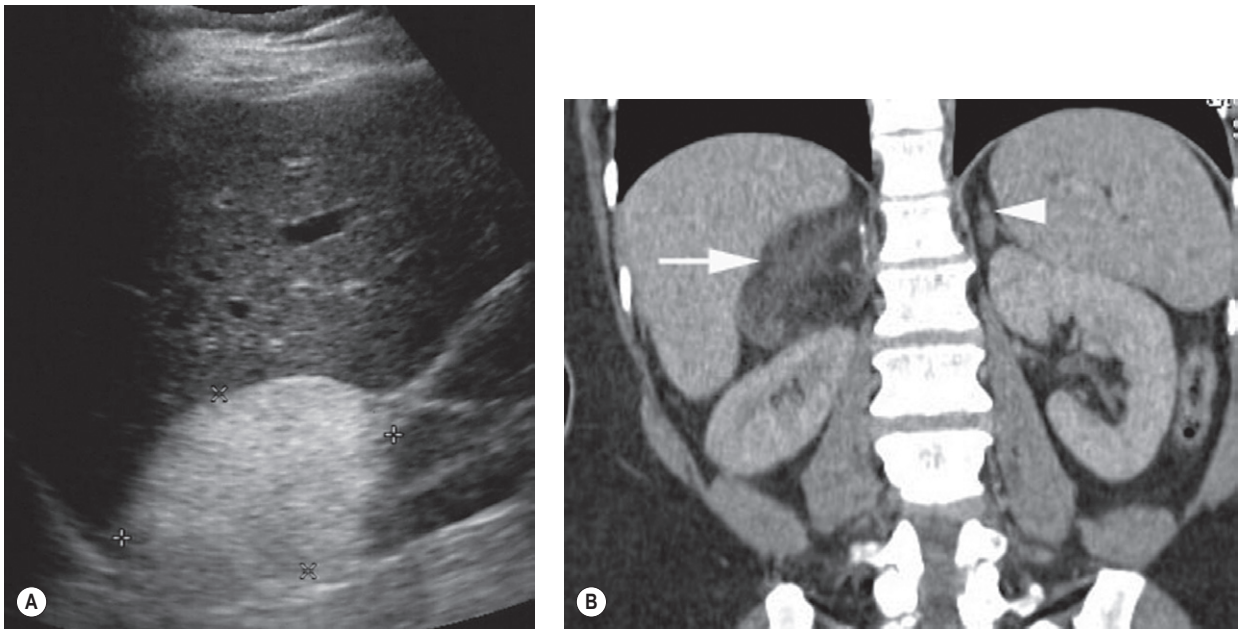


Figure 33.9 Myelolipoma. A: Longitudinal ultrasound image showing homogeneously highly reflective right adrenal mass, typical of a myelolipoma. **B:** Coronal CT reformat in the same patient confirms the presence of fat in the right adrenal lesion (arrow), which also contains some linear calcification medially. The left adrenal gland (arrowhead) is normal.

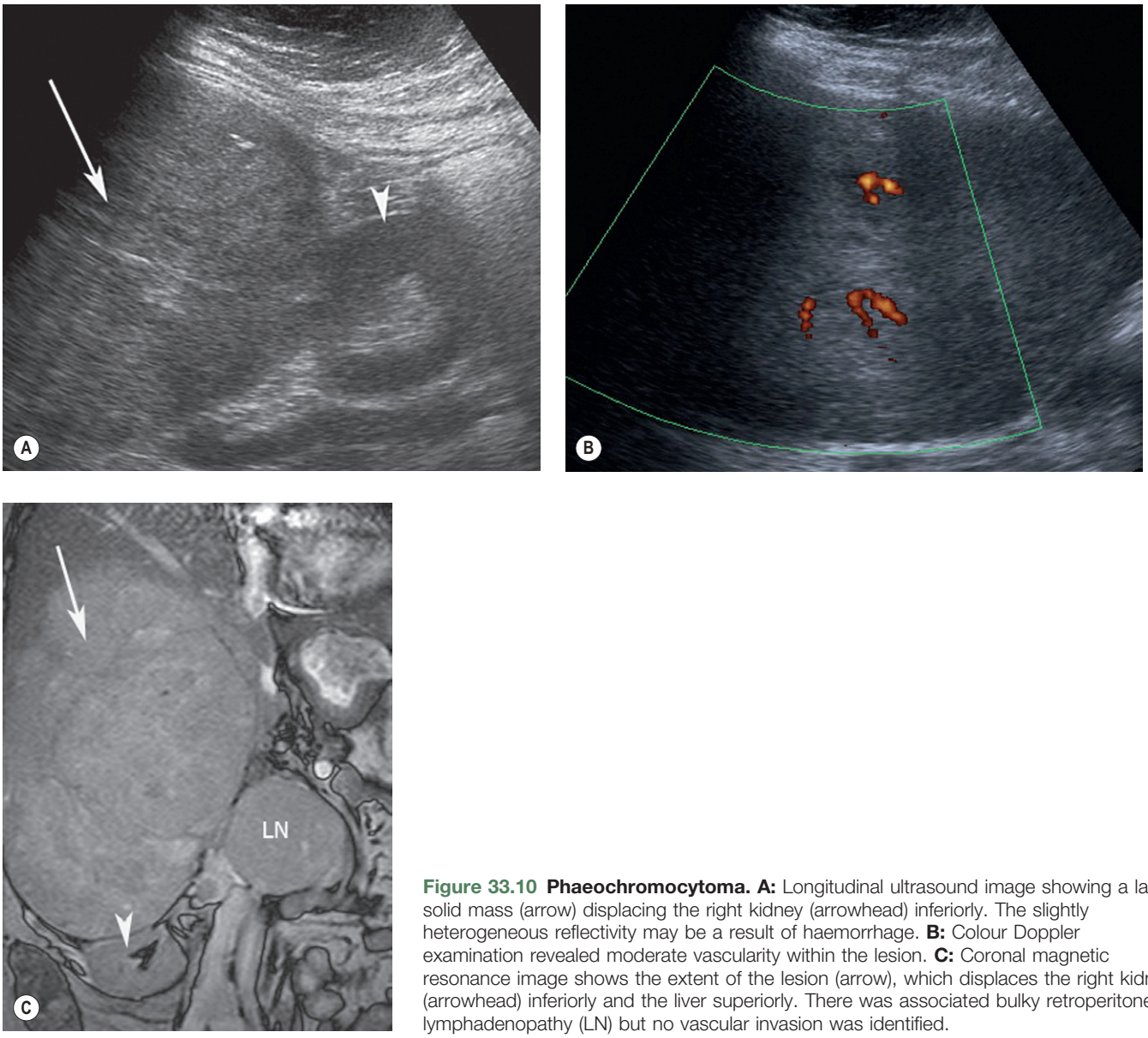


Figure 33.10 **Phaeochromocytoma. A:** Longitudinal ultrasound image showing a large solid mass (arrow) displacing the right kidney (arrowhead) inferiorly. The slightly heterogeneous reflectivity may be a result of haemorrhage. **B:** Colour Doppler examination revealed moderate vascularity within the lesion. **C:** Coronal magnetic resonance image shows the extent of the lesion (arrow), which displaces the right kidney (arrowhead) inferiorly and the liver superiorly. There was associated bulky retroperitoneal lymphadenopathy (LN) but no vascular invasion was identified.

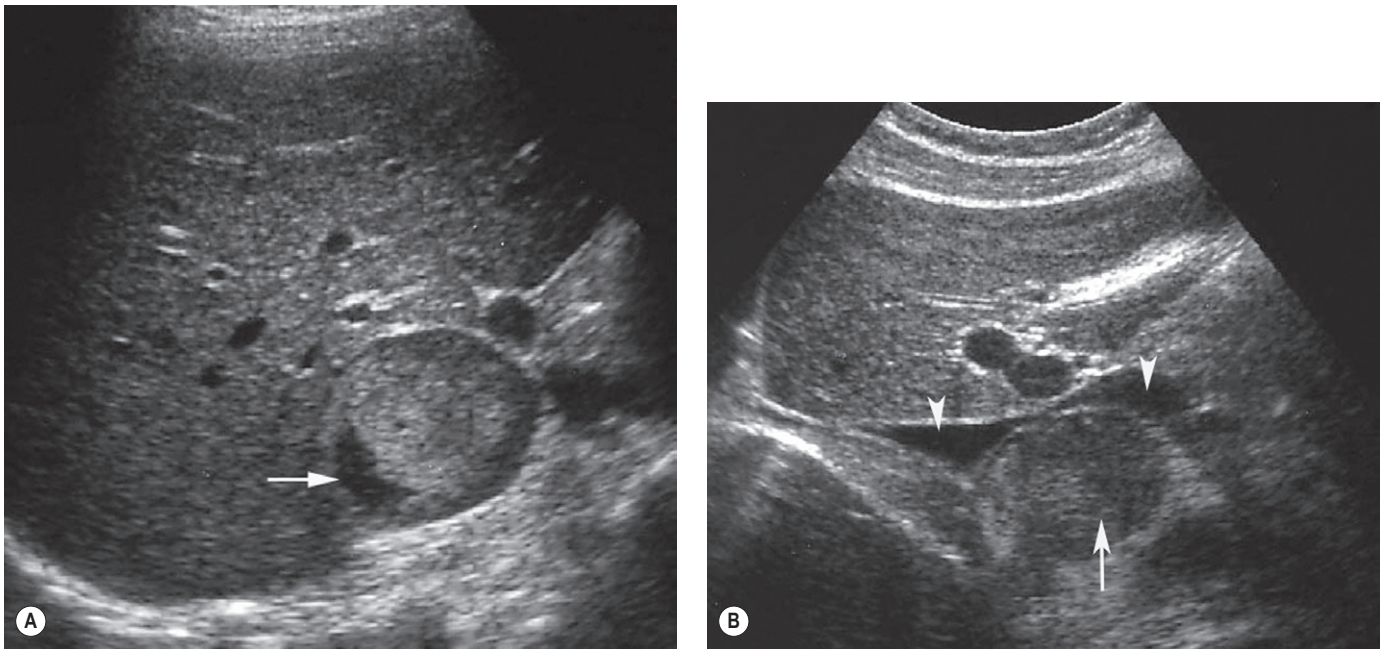


Figure 33.11 **Phaeochromocytoma. A:** Well-defined rounded right adrenal lesion. Note the slightly increased reflectivity of the lesion compared to the adjacent liver. There is also a small necrotic area (arrow), which is a typical finding in phaeochromocytomas. **B:** Note how the lesion (arrow) indents the posterior aspect of the IVC (arrowheads) – this is a typical finding with adrenal lesions.

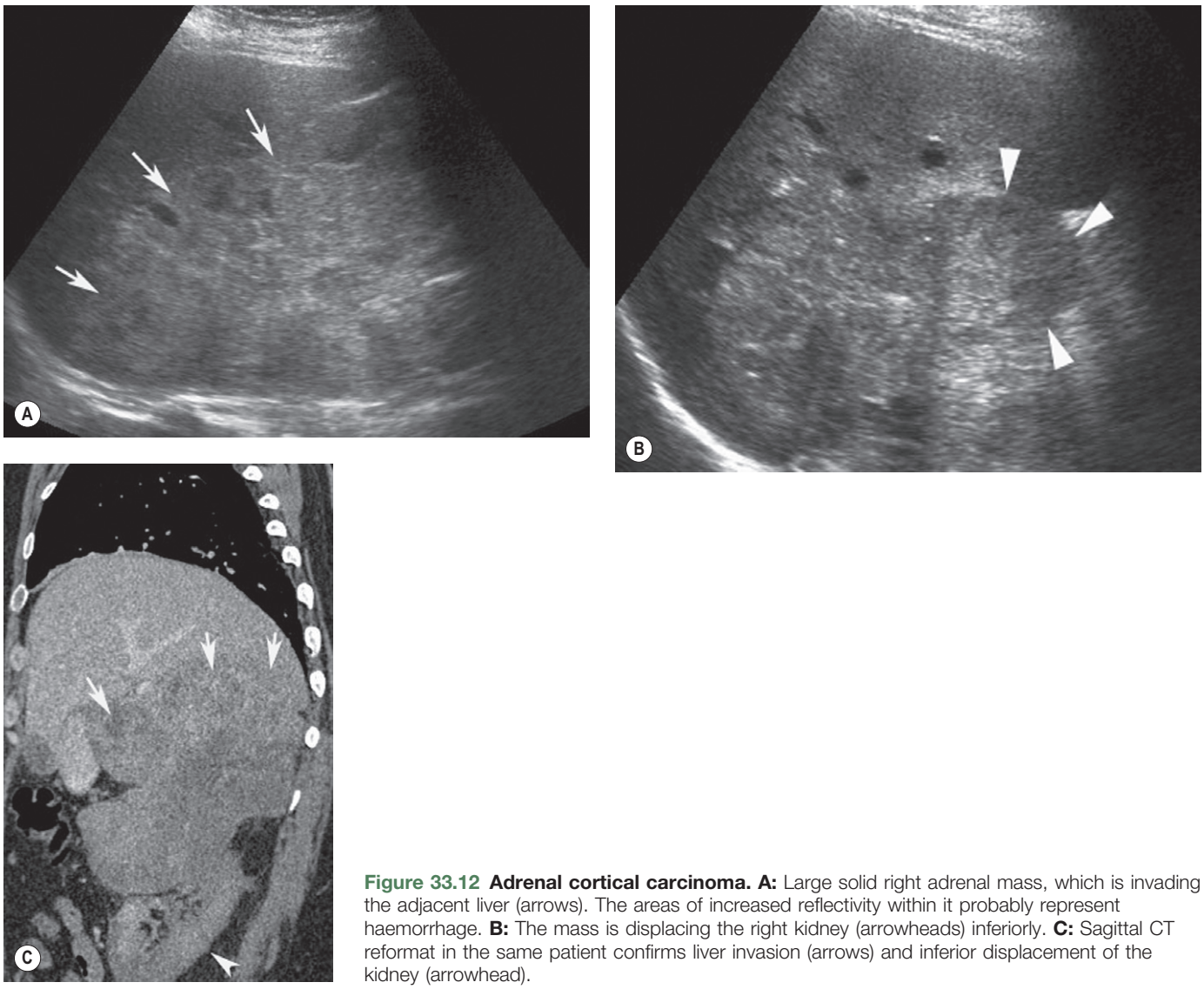


Figure 33.12 **Adrenal cortical carcinoma. A:** Large solid right adrenal mass, which is invading the adjacent liver (arrows). The areas of increased reflectivity within it probably represent haemorrhage. **B:** The mass is displacing the right kidney (arrowheads) inferiorly. **C:** Sagittal CT reformat in the same patient confirms liver invasion (arrows) and inferior displacement of the kidney (arrowhead).

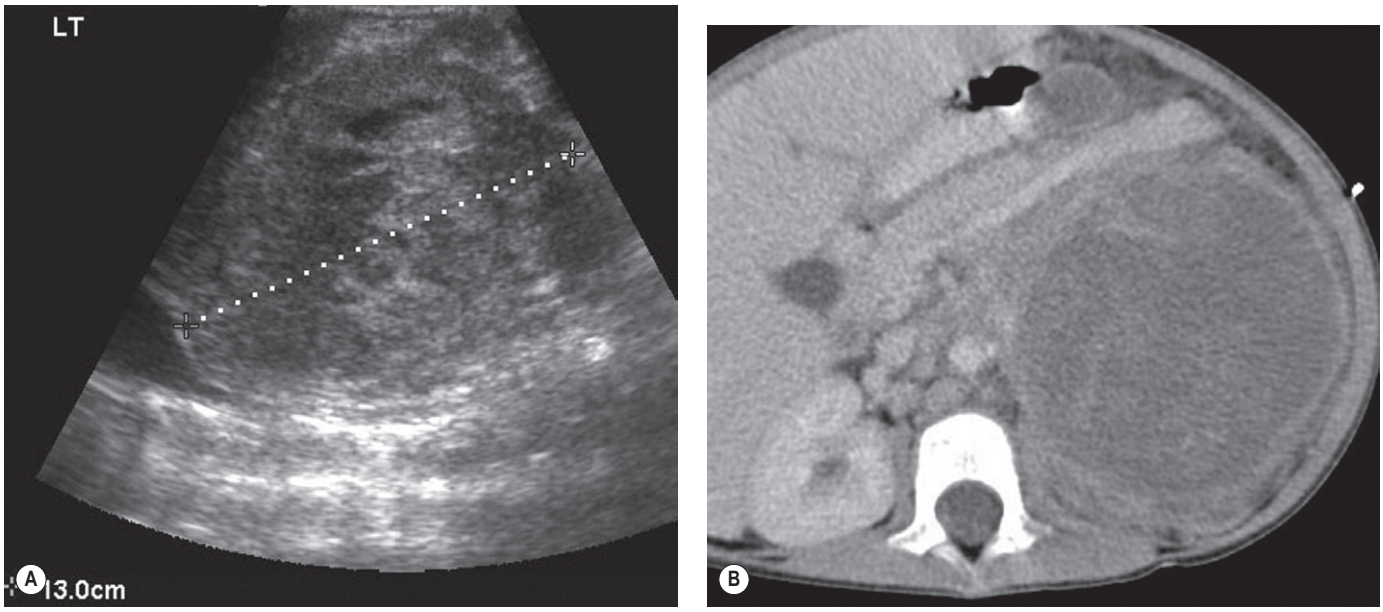


Figure 33.13 **Neuroblastoma in a child. A:** Ultrasound image showing a mixed reflectivity rounded 13 cm left adrenal lesion that is slightly ill defined. A small left pleural effusion is present. **B:** CT scan in the same patient confirms the mixed attenuation nature of the lesion and helps in planning subsequent management.

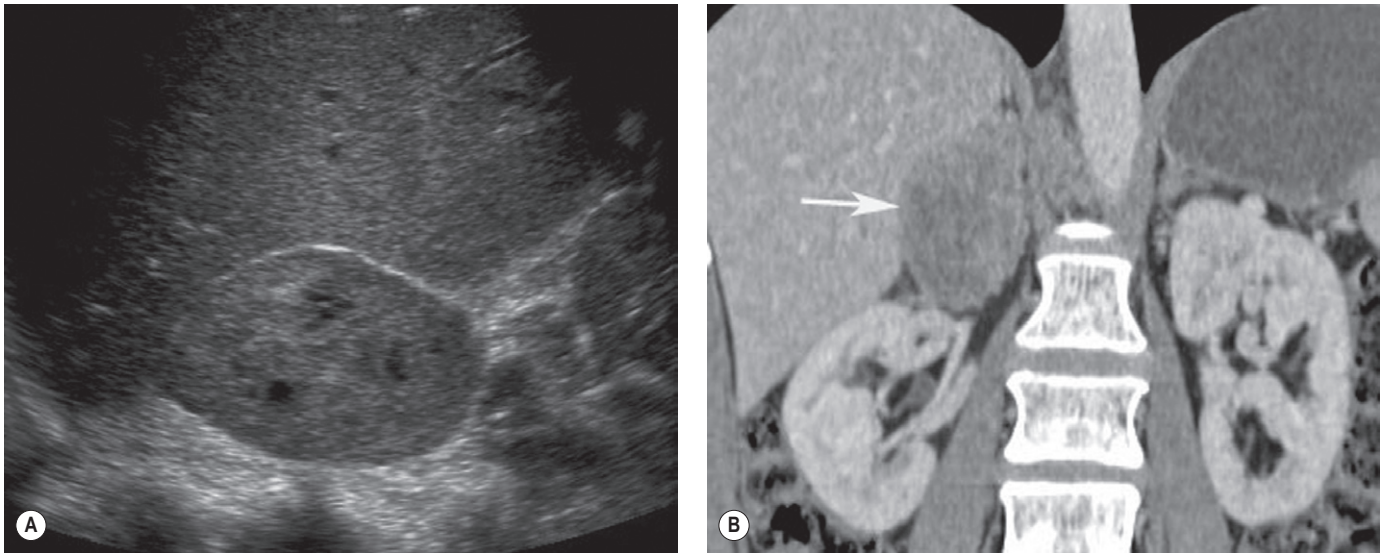


Figure 33.14 **Adrenal metastasis. A:** Ultrasound imaging revealed a well-defined low reflectivity with central necrotic areas. **B:** Coronal CT reformat showing the right adrenal lesion (arrow) with a normal contralateral gland. The primary tumour in this case was unknown.

Ultrasound is useful for assessing the local extent of the primary tumour and for the detection of liver metastases, although further imaging with CT or MR is performed for initial tumour staging. Neuroblastomas are typically heterogeneous and predominantly of high reflectivity although sometimes cystic areas are seen within the lesion, corresponding to areas of haemorrhage or necrosis (Fig. 33.13). Calcification is present in at least 30%.[34] The margins of the tumour are usually ill defined. Neuroblastoma will often cross the midline and displace the ipsilateral kidney.[37] It is important to delineate the relationship of the mass to the IVC and aorta before surgery is planned as they may be encased by tumour, and colour Doppler examination is useful to evaluate their patency. Ultrasound is particularly valuable in the follow-up of those children who undergo chemotherapy to monitor the response of the tumour whilst minimising radiation dose.

Metastases

The adrenal glands are the fourth most common site in the body for metastases after the lungs, liver and bones. Common primaries to metastasise to the adrenals include bronchial, renal, colonic and breast carcinomas in addition to melanoma. The adrenals may also be involved with non-Hodgkin's lymphoma. Metastases are usually rounded or oval and poorly reflective[38,39] (Figs 33.14 and 33.15).

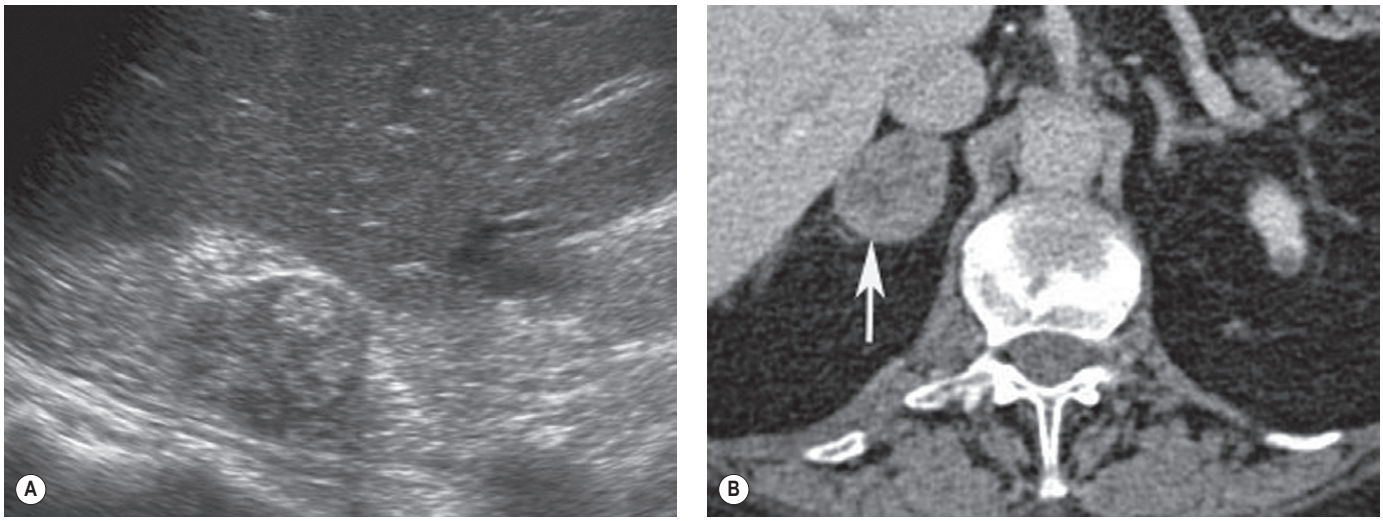


Figure 33.15 **Adrenal metastasis. A:** Right adrenal metastasis with central areas of increased reflectivity, likely to reflect haemorrhage. **B:** Axial CT image in the same patient confirms the heterogeneous nature of the adrenal metastasis (arrow). The left adrenal is normal in appearance.

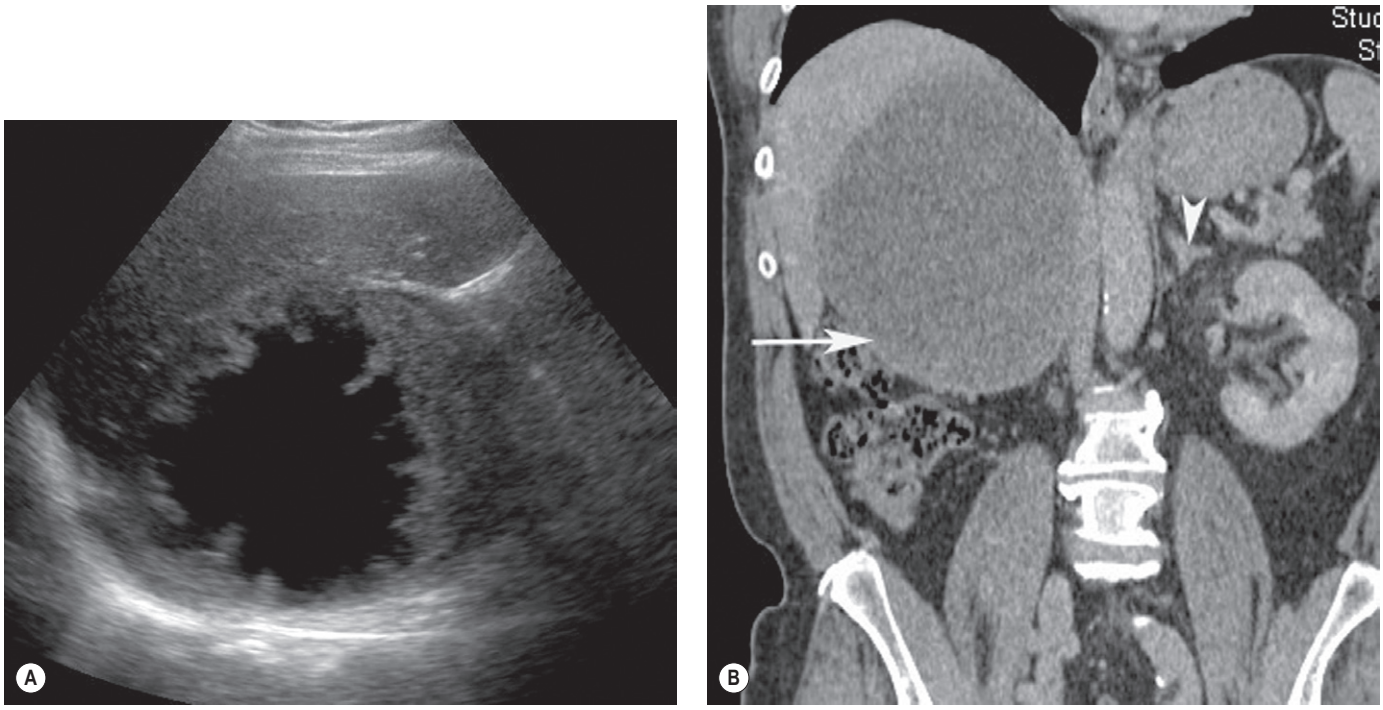


Figure 33.16 **Adrenal metastasis. A:** Ultrasound image of a huge right adrenal lesion in a patient who had undergone a previous right nephrectomy for renal cell carcinoma. Note the irregular soft tissue around the periphery and central anechoic necrotic component. **B:** Coronal CT reformat in the same patient confirms the presence of a large, predominantly cystic right adrenal lesion (arrow). The left adrenal is normal (arrowhead). Note the previous right nephrectomy.

Malignant adrenal lesions

- Metastases (primaries include lung, kidney, colon, breast, melanoma).
- Adrenal cortical carcinoma:
  - 50% hormonally active – well-defined, small ± calcification
  - 50% non-functioning – larger, central necrosis ± venous invasion.
- Neuroblastoma (children), 75% metastases at diagnosis, 30% have calcification.
- Phaeochromocytoma (10% malignant).

They may be unilateral or bilateral and can be heterogeneous due to the presence of central necrosis or haemorrhage (Fig. 33.16). They rarely contain calcification.[40] Visualisation of both adrenal areas should be part of the routine assessment of any patient with primary malignancy. Ultrasound alone will not differentiate between a metastasis and a benign adenoma (adrenal lesions found in patients with a known primary tumour are equally likely to be benign adenomas as metastases) and colour Doppler ultrasound is not helpful in this differentiation.[40,41]

ROLE OF CT AND MRI IN CHARACTERISATION OF ADRENAL LESIONS

Whilst ultrasound has the ability to distinguish between lesions such as cysts, myelolipomas and hyperplasia, its role is limited in characterising other adrenal lesions which have an overlapping spectrum of appearances, and further imaging with either CT or MRI is necessary for diagnosis. Increased use of cross-sectional imaging has also led to large numbers of adrenal lesions being incidentally detected at imaging performed for an unrelated indication (up to 5% of CT scans performed for indications other than suspected adrenal pathology).[42] These 'incidentalomas' can be further evaluated with unenhanced CT where an attenuation value less than 10 Hounsfield units is useful in predicting benignity.[27] However, a proportion of lesions with higher attenuation values will also be benign, including some adrenal adenomas which are lipid-poor. CT differentiation between benign and malignant adrenal lesions may be improved by calculation of the percentage enhancement washout following administration of intravenous contrast.[43] Benign lesions exhibit greater than 50% washout of enhancement on a 10-minute delayed CT scan whereas malignant lesions demonstrate less than 50% washout. Chemical shift MRI has been shown to have similar sensitivity and specificity to CT in the characterisation of adrenal lesions.[44] Comparison of in phase and out of phase MR sequences allows identification of benign adenomas by virtue of their lipid content, which results in loss of signal intensity on opposed phase imaging.[26] Despite these techniques, some adrenal lesions cannot be identified with certainty and particularly where diagnosis could potentially alter treatment (e.g. patients with known malignancy), confirmation may be sought by percutaneous biopsy, which can be performed under ultrasound or CT guidance, depending on the size of the lesion and ease of access to it. In children, however, ultrasound remains the primary imaging modality for the adrenal glands as visualisation is generally good without the associated problems of keeping a baby or child still for CT/MR imaging. Keeping radiation dose to a minimum is also of paramount importance in paediatrics and ultrasound has the advantage of allowing follow-up examinations without concerns regarding radiation dose.

REFERENCES

1. Sample WF. A new technique for the evaluation of the adrenal gland with grey scale ultrasonography. Radiology 1977;124:463–469.
2. Yeh HCH. Sonography of the adrenal glands: normal glands and small masses. AJR Am J Roentgenol 1980;135:1167–1177.
3. Brownlie K, Kreel L. Computer assisted tomography of normal suprarenal glands. J Comput Assist Tomogr 1978;2:1–20.
4. McMinn RMH, editor. Last's anatomy. Regional and applied. 9th edn. London: Churchill Livingstone; 1994.
5. Marchal G, Gelin J, Verbeken E, et al. High resolution real time sonography of the adrenal glands: a routine examination? J Ultrasound Med 1986;5:65–68.
6. Scott EM, Thomas A, McGarrigle HH, Lachelin GC. Serial adrenal ultrasonography in normal neonates. J Ultrasound Med 1990;9:279–283.
7. Mitty HA. Adrenal embryology, anatomy and imaging techniques. In: Pollack HM, editor. Clinical urography: an atlas and textbook of urologic imaging. Philadelphia: Saunders; 1990. p. 2291–2305.
8. White PC, New MI, Dupont B. Congenital adrenal hyperplasia. N Engl J Med 1987;316:1519–1524.
9. Scheible W, Coel M, Siemers PT, Siegel H. Percutaneous aspiration of adrenal cysts. AJR Am J Roentgenol 1977;128:1013–1016.
10. Foster DG. Adrenal cysts: review of literature and report of case. Arch Surg 1986;92:131–143.
11. Murphy BJ, Casillas J, Yrizarry JM. Traumatic adrenal hemorrhage: radiologic findings. Radiology 1988;169:701–703.
12. Burks DW, Mirvis SE, Shanmuganathan K. Acute adrenal injury after blunt abdominal trauma: CT findings. AJR Am J Roentgenol 1992;158:503–507.
13. Pery M, Kaftori J K, Bar-Maor J A. Sonography for diagnosis and follow up of adrenal haemorrhage. J Clin Ultrasound 1981;9:397–401.
14. Mittelstaedt CA, Volberg FM, Merten DF, Brill PW. The sonographic diagnosis of neonatal haemorrhage. Radiology 1979;131:453–457.
15. Mineau DE, Koehler PR. Ultrasound diagnosis of neonatal adrenal haemorrhage. AJR Am J Roentgenol 1979;132:443–444.
16. Bowen AD, Keslar PJ, Newman B, Hashida Y. Adrenal haemorrhage after liver transplantation. Radiology 1990;176:85–88.
17. Paling MR, Williamson BRJ. Adrenal involvement in non-Hodgkins lymphoma. AJR Am J Roentgenol 1983;141:303–305.
18. Yeh HC. Ultrasonography of the adrenals. Semin Roentgenol 1988;23:250–258.
19. Sample WF. Adrenal ultrasonography. Radiology 1978;127:461–466.
20. Yeh HC. Ultrasonography of normal adrenal gland and small adrenal masses. AJR Am J Roentgenol 1980;135:1167–1177.
21. Yeh HC, Mitty HA, Rose J, et al. Ultrasonography of adrenal masses: unusual manifestations. Radiology 1978;127:475–483.
22. Dunnick NR. Adrenal imaging: current status. AJR Am J Roentgenol 1990;154:927–936.
23. Conn JW, Knopf RF, Nesbit RM. Clinical characteristics of primary aldosteronism from an analysis of 145 cases. Am J Surg 1964;107: 159–172.
24. Grant CS, Carpenter P, Van Heerden JA, et al. Primary aldosteronism. Arch Surg 1984;119:585–589.
25. Lee MJ, Hahn PF, Papanicolau N, et al. Benign and malignant adrenal masses: CT distinction with attenuation coefficients, size, and observer analysis. Radiology 1991;179:415–418.
26. Mitchell DG, Crovello M, Matteucci T, et al. Benign adrenocortical masses: diagnosis with chemical shift MR imaging. Radiology 1992;185:345–351.
27. Boland GW, Lee MJ, Gazelle GS, et al. Characterization of adrenal masses using unenhanced CT: an analysis of the CT literature. AJR Am J Roentgenol 1998;171:201–204.
28. Behan M, Martin EC, Meucke EC, Kazam E. Myelolipoma of the adrenal: two cases with ultrasound and CT findings. AJR Am J Roentgenol 1977;129:993–996.
29. Rao P, Kenney PJ, Wagner BJ, et al. Imaging and pathological features of myelolipoma. RadioGraphics 1997;17:1375–1385.
30. Musante F, Derchi LE, Zappasodi F, et al. Myelolipoma of the adrenal gland: sonographic and CT features. AJR Am J Roentgenol 1988;151: 961–964.
31. Bowerman RA, Silver TM, Jaffee MH. Sonography of adrenal phaeochromocytoma. AJR Am J Roentgenol 1981;137:1227–1237.
32. Vergas AD. Adrenal haemangioma. Urology 1980;16:389–390.
33. Hamper UM, Fishman EK, Harman DS, et al. Primary adrenocortical carcinoma: sonographic evaluation with clinical and pathologic correlation in 26 patients. AJR Am J Roentgenol 1987;148:915–919.
34. Lonergan GJ, Schwab CM, Suarez ES, Carlson CL. Neuroblastoma, ganglioneuroblastoma, and ganglioneuroma: radiologic–pathologic correlation. Radiographics 2002;22:911–934.
35. Rha SE, Byun JY, Jung SE, et al. Neurogenic tumors in the abdomen: tumor types and imaging characteristics. Radiographics 2003;23:29–43.
36. Hiorns MP, Owens CM. Radiology of neuroblastoma in children. Eur Radiol 2001;11:2071–2081.
37. White SJ, Stuck KJ, Blane CE, Silver TM. Sonography of neuroblastoma. AJR Am J Roentgenol 1983;141:465–468.
38. Cunningham JJ. Ultrasonic findings in 'primary' lymphoma of the adrenal area. J Ultrasound Med 1983;2:467–469.
39. Forsythe JR, Gosink BB, Leopold GR. Ultrasound in the evaluation of adrenal metastases. J Clin Ultrasound 1977;5:31–34.
40. Dunnick NR, Korobkin M, Francis I. Adrenal radiology: distinguishing benign from malignant adrenal masses. AJR Am J Roentgenol 1996;167:861–867.
41. Ghiatas AA, Chopra S, Schnitker JB. Is sonographic flow imaging useful in the differential diagnosis of adrenal masses? Br J Radiol 1996;69:1005–1008.
42. Kloos RT, Gross MD, Francis IR, et al. Incidentally discovered adrenal masses. Endocr Rev 1995;16:460–484.
43. Peña CS, Boland GW, Hahn PF, et al. Characterization of indeterminate lipid-poor adrenal masses: use of washout characteristics at contrast-enhanced CT. Radiology 2000;217:798–802.
44. Outwater EK, Siegelman ES, Huang AB, Birnbaum BA. Adrenal masses: correlation between CT attenuation value and chemical shift ratio at MR imaging with in-phase and opposed-phase sequences. Radiology 1996;200:749–752.

CHAPTER

34 Pelvic anatomy and scanning techniques

Tracey Hughes

INTRODUCTION 645

TECHNIQUE: AN OVERVIEW 645

PELVIC ANATOMY 646
Skeleton 646
Muscles 647
Pelvic viscera 647
The ovaries 647
The uterus 648
Uterine tubes 649
The vagina 649

PHYSIOLOGY OF THE FEMALE SEXUAL CYCLE 649

TECHNIQUE AND ULTRASOUND ANATOMY 649
Transabdominal scanning 649
Transvaginal scanning 651
Ultrasound anatomy 652
Uterus 652
Cervix 653
Uterine tubes 653
Ovaries 654
Technique 654
Anatomy 654

HAEMODYNAMICS OF THE UTERUS AND OVARIES AS REPRESENTED BY DOPPLER ULTRASOUND 655

CONGENITAL ANOMALIES OF THE FEMALE GENITAL TRACT 655

Factors influencing the ultrasound appearance of the female reproductive organs

- Age
- Parity
- Phase of reproductive cycle
- Hormonal contraception
- Hormone replacement therapy
- Tamoxifen
- Congenital anomalies

This chapter aims to familiarise the reader with the anatomy and scanning techniques of the female pelvis. It sets out an overview of the techniques. This is followed by a description of pelvic anatomy and reproductive physiology. A more detailed account of the scanning techniques is then given and this is closely aligned with a description of the ultrasound anatomy. Next the haemodynamics of the uterus and ovaries are described. Finally there is an account of congenital anomalies of the female reproductive system with a description of the ultrasound findings.

Ultrasound of the female reproductive organs is undertaken by range of health care professionals including radiographers, radiologists, midwives and gynaecologists. Throughout this chapter the term ultrasonographer is used in its broadest sense.

INTRODUCTION

All diagnostic imaging requires a thorough knowledge of normal anatomy and its variants before abnormality may be recognised. In this respect the female pelvis is particularly complex as the anatomy of the reproductive organs changes with age, phase of menstrual cycle, parity and extrinsic hormonal influences such as hormonal contraception, hormone replacement therapy and anti-oestrogens such as tamoxifen. Moreover, if a transabdominal ultrasound examination of the pelvis is performed when the urinary bladder is underfilled, the images may be suboptimal. Thus, ultrasound findings should be correlated appropriately, requiring that the ultrasonographer has knowledge not just of pelvic anatomy but of reproductive physiology. In addition they should ideally be aware of any relevant patient medication and attention should be paid to the adequacy of patient preparation. Frequently the information the ultrasonographer requires to make a meaningful interpretation of the scan findings is not given by the referring clinician. This may not necessarily present a problem as the sonographer can always ask the patient directly. In so doing this may go some way to putting the patient at her ease, particularly if a transvaginal scan is to be carried out.

The overall complexity of the female reproductive system is compounded by the numerous, though relatively infrequent, congenital anomalies that may arise from it.

TECHNIQUE: AN OVERVIEW

There are two ultrasound scanning techniques for imaging the female pelvis: transabdominal/transcutaneous (TA) and transvaginal (TV) scanning.

TA scanning provides a panoramic view of the pelvis but not fine detail. It allows assessment of the reproductive organs and their relationship to the neighbouring anatomy. The wide field of view will often accommodate a large pelvic mass. Abdominal extension of such a mass can be scanned with the same transducer as well as enabling a search for any evidence of relevant associated pathology such as peritoneal/omental or serosal liver deposits.

For a TA scan to be effective the patient's bladder should be full. This said, in slim individuals it is possible to obtain remarkably good pelvic images when the bladder is empty. The full bladder, however, serves as an acoustic window, lifts the bowel away from the reproductive organs and introduces a degree of retroflexion to the frequently anteverted uterus, maintaining a favourable angle of insonance relative to the long axis of the endometrium. Thus the patient should drink 500–750 mL of still fluid 1 hour prior to the examination. Most women are able to tolerate a full bladder but it can become problematic if an ultrasound list is not running to time. TA scanning is generally performed using a curved array 2–5 megahertz (MHz) transducer. In slim individuals scanning at these frequencies is often adequate but image quality may be

compromised in women with a raised body mass index. Tissue harmonics often optimises the images by reducing noise and reverberation artefact.

TV scanning is performed using a 4–8 MHz curved array transducer. As such the images are of high resolution with a small field of view. The detail of the endometrium and internal architecture of the ovaries is often exquisite. Thus a TV scan should never be omitted if the clinical indication suggests gynaecological pathology and the pelvic anatomy has not been well seen on TA scanning, or if endometrial pathology is suspected. The bladder should be emptied prior to a TV scan. It is imperative to explain clearly to the woman what the examination entails and to obtain verbal consent. Complete privacy must be guaranteed and a female chaperone should be present. In general women are quite accepting of this examination technique and are relieved to empty their bladder, particularly if they have initially undergone a TA scan. When the examination is complete it is mandatory to clean the transducer with an antimicrobial agent. This is also true of the transabdominal probe following a TA scan.

Both a TA and a TV scan may be necessary to obtain the maximum amount of information from a single examination. Both techniques lend themselves to guided biopsies, aspirations and drainages.

Transabdominal and transvaginal scanning

Transabdominal scanning
- Full bladder
- 2–5 MHz curved array transducer
- Large field of view
- Upper abdomen may be assessed

Transvaginal scanning
- Empty bladder
- 4–8 MHz curved array endovaginal transducer
- High resolution, small field of view
- Verbal consent

It is a medicolegal requirement that all ultrasound examinations be reported. Ideally this should be within a radiology information system (RIS) but failing this a report should be written in the patient's medical records. Similarly all images captured during the course of a scan should be archived within a picture archiving and communication system (PACS). Both these measures serve as a permanent record that an examination has taken place and allow the ultrasonographer to compare old with new studies. Reporting and archiving also facilitates audit.

PELVIC ANATOMY

Skeleton

The skeleton and attached muscles provide the framework upon which the pelvic viscera are supported. Knowledge of them provides a fuller understanding of pelvic anatomy as a whole. The articulated hip bone, sacrum and coccyx enclose the pelvic cavity. The brim of this cavity, the pelvic brim, is formed by the pubic crest, the pectineal line of the pubis, the arcuate line of the ilium and the ala and promontory of the sacrum. The plane of the pelvic brim is oblique, being 35–50° up from the horizontal. It is also known as the pelvic inlet and is orientated anteriorly. Below the level of the pelvic brim is called the true pelvis. The long posterior wall of the true pelvis is formed by the concavity of the sacrum and coccyx. The short anterior wall consists of the pubic symphysis and the bodies of the paired pubic bones and their rami. It is bound laterally by the inner aspects of the quadrangular area of the fused ilium and ischium (Fig. 34.1). The outlet to the true pelvis faces posteriorly.

The greater pelvis or false pelvis lies above the pelvic brim. It consists of the paired iliac wings, the inner surfaces of which form the iliac fossae and the posterior abdominal wall. Anteriorly there is no bony wall to the greater pelvis. Instead it is formed by the aponeuroses of the anterolateral abdominal wall muscles and the rectus abdominis. The cavity of the greater pelvis is effectively the lower abdominal cavity.[1]

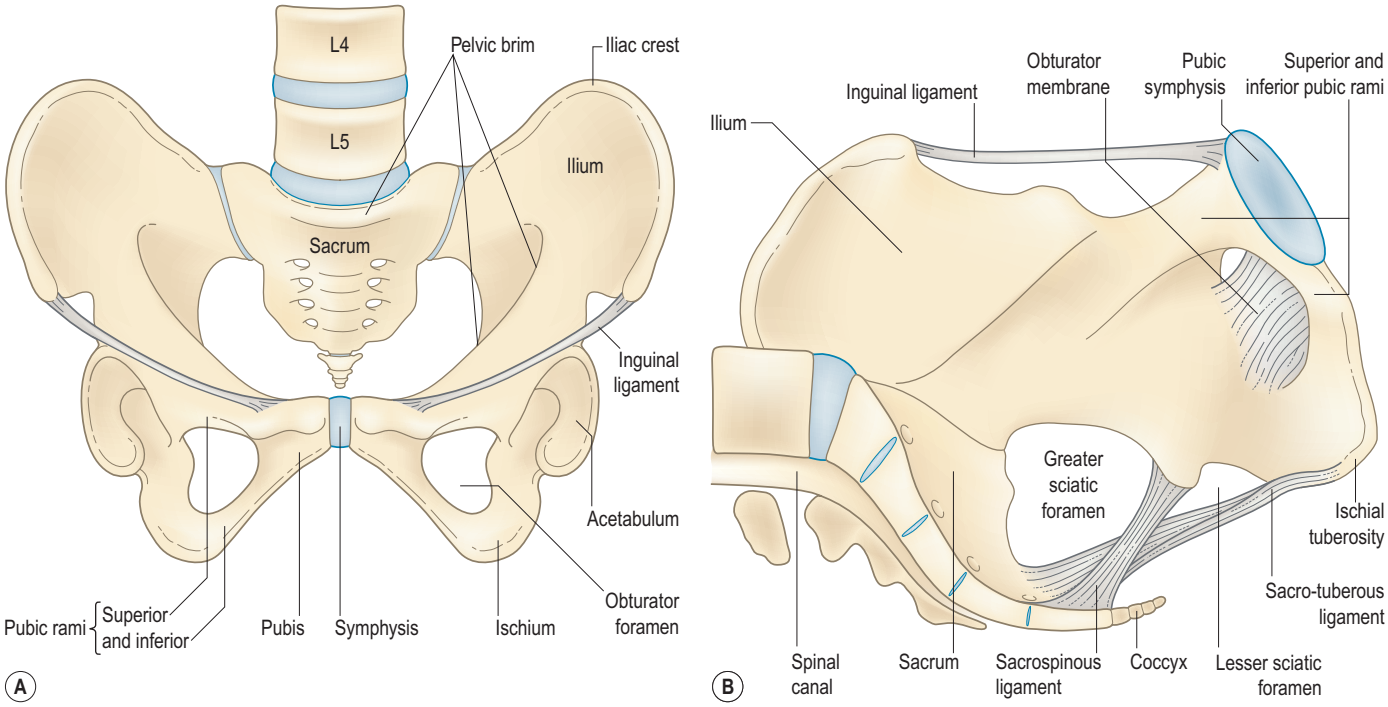


Figure 34.1 The bony pelvis. A: A frontal view showing the pelvic brim. **B:** A view from the right of the medial aspect of the left pelvic bones.

Muscles

There are four paired muscles of the true pelvis. The lateral group are obturator internus and piriformis. These are also lower limb muscles. The medial group are levator ani and coccygeus. These latter two muscles constitute the pelvic floor and in the midline are slung around the urethra, vagina and anal canal. These three effluent channels pierce the pelvic floor to enter the perineum.

Obturator internus has a broad origin from the body of the ischium and the obturator membrane which covers most of the obturator foramen of the ischium. It extends upwards to the pelvic brim. The fibres of obturator internus converge towards the lesser sciatic notch where they leave the pelvis to attach to the greater trochanter of the femur. This muscle is covered by the obturator fascia. Posterior and superior to obturator internus is piriformis, which arises from the middle three sacral segments. It runs transversely to the greater sciatic foramen, exiting the pelvis to attach to the greater trochanter (Fig. 34.2).

The levator ani consists of three main parts: puborectalis, pubococcygeus and iliococcygeus. Their fibres are continuous and arise from the body of the pubis, the obturator fascia and the ischial spine. The muscle fibres run posteroinferiorly to the midline to insert in the coccyx, the levator raphe and the anococcygeal ligament.

Coccygeus arises from the ischial spine. From here its fibres fan out to be inserted into the coccyx and the lowest sacral segment (Fig. 34.3).

The muscles of the greater pelvis are those of the posterior abdominal wall, psoas major and iliacus. The psoas muscle arises from the five lumbar vertebrae. It passes downwards along the pelvic brim, beneath the inguinal ligament in the groin to attach to the lesser trochanter. Iliacus arises from the iliac bone and passes under the inguinal ligament. Its tendon fuses with that of the psoas muscle to insert into the lesser trochanter[2] (Fig. 34.4).

Pelvic viscera

The ovaries

The ovaries are the paired female sex organs. They are composed of fibrous tissue in which ova are embedded. In the embryo and fetus the ovaries are sited in the lumbar region near kidneys and gradually descend into the true pelvis. In the adult the ovaries are mobile and their position varies with parity and degree of bladder and intestinal filling. During pregnancy they are lifted high in the pelvis, becoming entirely abdominal by the third trimester.

In the nulliparous woman the ovaries occupy the ovarian fossae on the pelvic side walls. The upper pole is tilted laterally and is overlapped by the infundibulum of the uterine tube. The lower pole is tilted medially towards the uterus to which it is attached by the suspensory ligament of the ovary. The ovaries are suspended from the anterior border by a fold of peritoneum, the mesovarium, which attaches it to the broad ligament. The lateral ovarian surface contacts parietal peritoneum behind which lies the angle between the internal and external iliac vessels, the ureter, obturator vessels and nerves and the origin of the uterine artery. Thus the iliac vessels

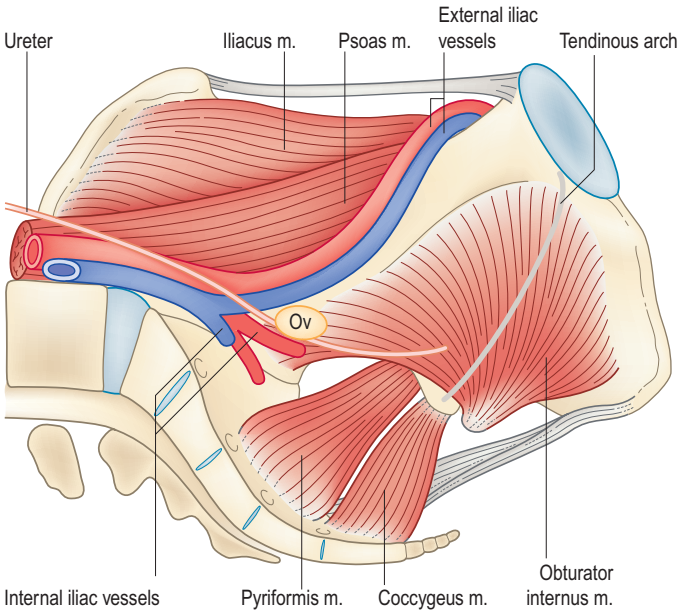


Figure 34.2 Left pelvic side wall viewed from the right showing the lateral group of muscles of the true pelvis. Coccygeus and the muscles of the false pelvis are also shown. The iliac vessels are superimposed along with the left ovary in the left ovarian fossa. Note the location of the ureter.

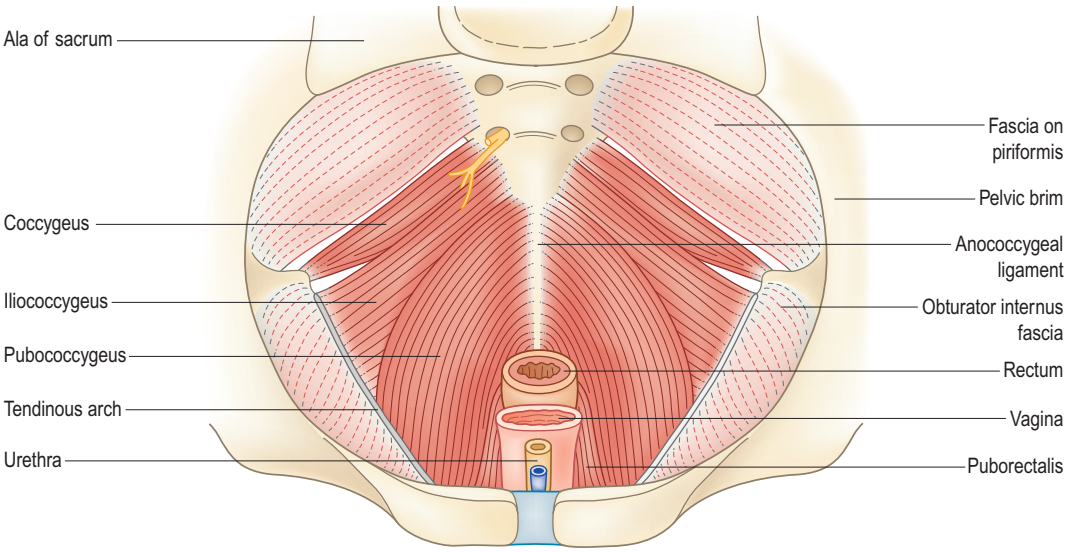


Figure 34.3 The female pelvic floor viewed from above (modified from Sinnatamby CS, Last's Anatomy, Regional and Applied, 11th edn, 2006, Churchill Livingstone).

serve as a useful landmark when trying to locate the ovaries during an ultrasound examination. The medial ovarian surface faces the uterus and the uterine vessels within the broad ligament (Figs 34.2 and 34.5).

On the right side superolateral to the ovary are the ileocaecal junction, the caecum and the appendix. On the left is the sigmoid colon and rectosigmoid junction. This is important to bear in mind when scanning a woman presenting with iliac fossa pain in terms of a differential diagnosis.[3]

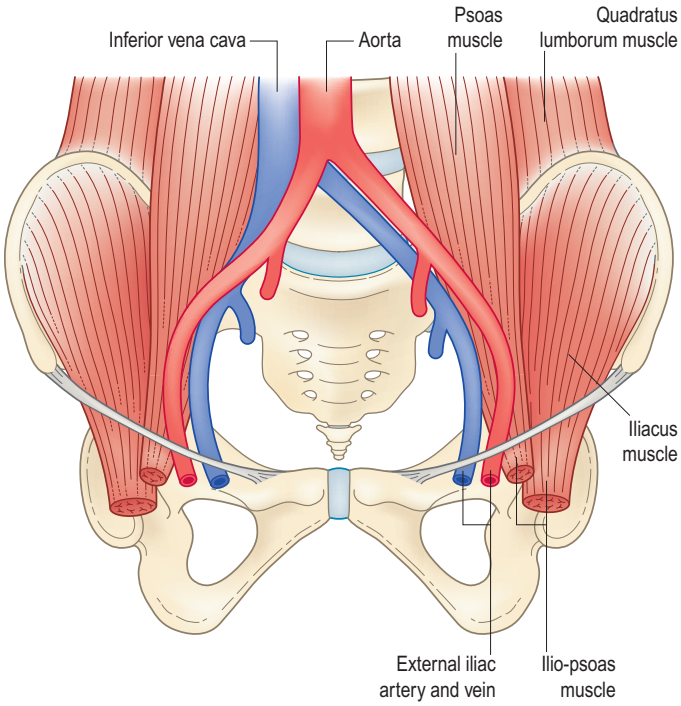


Figure 34.4 Frontal view of the pelvis showing the muscles of the false pelvis. The major blood vessels are shown.

Blood supply

The ovarian artery is a branch of the abdominal aorta arising just below the origin of the renal arteries. It runs down behind peritoneum in the paracolic gutter and crosses the ureter and psoas muscle. Crossing the pelvic brim the vessel enters the suspensory ligament of the ovary to enter the lateral end of the broad ligament below the uterine tube. It divides into branches that supply the ovary, the uterine tube and the skin of the labium majus.

Ovarian veins form a plexus in the mesovarium and suspensory ligament, draining into paired ovarian veins that accompany the ovarian artery and drain into the inferior vena cava on the right and the renal vein on the left.[3]

The uterus

Whilst described as midline, the uterus is rarely exactly in the midline, particularly in parous women. The non-pregnant uterus has a slit-like cavity and lies within the true pelvis. Superolaterally the cavity is continuous with the uterine tubes. Inferiorly it leads into the endocervical canal and on into the vagina. The overall tubular anatomy may be referred to as the uterovaginal canal.

The uterus is likened to a flattened pear. It is made up of the fundus, body, isthmus and cervix. The fundus is the broadest component and projects above the entry points of the paired uterine tubes. The bilateral upper angles into which the tubes feed are the cornua. The uterine body tapers below this to the cervix, the junction between the body and cervix being the isthmus. The cervix projects into the vaginal vault, forming the vaginal fornix; this is deepest posteriorly.

The uterine body and the posterior surface of the cervix are enclosed in peritoneum. Laterally this fold of peritoneum becomes the broad ligament. When anteverted the anterior uterine surface rests on the bladder and the peritoneal covering reflects off it at the level of the internal cervical os onto the bladder, forming the vesico-uterine pouch. The posterior uterine and cervical surface faces upwards, having loops of bowel lying upon it. The peritoneum reflects off this at the level of the posterior vaginal fornix onto the rectum, forming the recto-uterine pouch or the pouch of Douglas (Fig. 34.5).

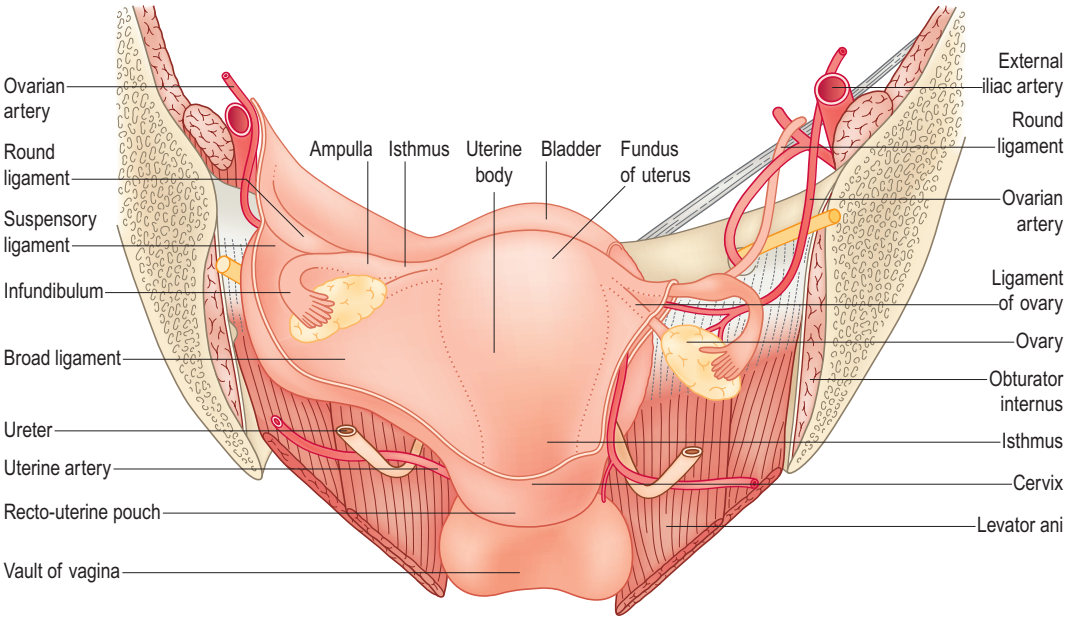


Figure 34.5 Coronal view of the female pelvis viewed from behind showing the uterus, tubes, ovaries and related structures. The broad ligament has been removed on the right side (modified from Sinnatamby CS, Last's Anatomy, Regional and Applied, 11th edn, 2006, Churchill Livingstone).

Table 34.1 Variation in uterine size and cervical:fundal ratio with age

	Length (cm)	Width (cm)	Depth (cm)	Cervix:fundus
Infantile	3.4		1.26	1:1
Prepubertal	3.0	1.5	1.0	2:1
Nulliparous	7.1	4.6	3.3	1:2
Multiparous	8.9	5.8	4.3	1:3
Postmenopausal	7.9	4.9	3.2	1:1

The long axis of the uterus relative to the vagina describes uterine version while the long axis of the uterine body relative to the cervix describes uterine flexion. The normal position of the long axis of the uterus relative to the vagina is anteversion but up to 20% of nulliparous females may have a retroverted uterus.

The outer uterine layer is the myometrium. It is a fibromuscular layer composed of smooth muscle and connective tissue. There is an inner layer of longitudinal smooth muscle and a circular outer layer.

The innermost uterine layer is a mucous membrane, the endometrium. This is subject to hormonal influences and cyclical changes.[4]

The variation in uterine size with age, parity and menopausal status is shown in Table 34.1.[5–7] The size of the uterine body relative to the cervix is subject to change throughout a female's lifetime. In the neonate the uterus is only slightly smaller than that of a prepubertal child. The cervix and fundus are approximately equal in size. The endometrium is hypertrophied in response to maternal hormones and is seen as an echogenic bilayer on ultrasound.[5] A prepubertal cervix is larger than the uterine body and fundus by a ratio of 2:1. Endometrial echoes are absent and only the echogenic midline interface is visible.[6] After puberty the fundus enlarges such that in the reproductive years the cervix to body ratio is 1:2 in nulliparous women and 1:3 in parous women. After the menopause the uterus atrophies and the ratio becomes 1:1.

Uterine tubes

The uterine tubes are approximately 10 cm in length and divided into four segments. The medial extremity is the short intramural component. It is surrounded by myometrium. Next is a narrow, straight segment, the isthmus. This lies in the upper edge of the broad ligament. Beyond this is the wider ampulla. The lateral extremity is the expanded open end, the infundibulum, which lies behind the broad ligament adjacent to the pelvic side wall (Fig. 34.5).

Blood supply

The uterus and tubes receive their blood supply from the uterine artery and ovarian artery, branches of the internal iliac artery and the aorta, respectively. The uterine artery runs in the base of the broad ligament medially to the cervix. Here it gives branches to the upper vagina and cervix. It ascends in the broad ligament giving off branches to the myometrium and reaches the cornua, where it turns laterally. It then anastomoses with branches of the ovarian artery supplying the uterine tube.

The uterine vein follows a similar course to the artery, ultimately draining into the internal iliac veins.[4]

The vagina

The vagina is midline. It is a distensible, approximately 10 cm long, fibromuscular tube that passes posterosuperiorly from the introitus to the cervix. The vagina lies along the same plane as the pelvic brim at 60° to the horizontal. It is an H-shaped slit in the transverse plane, its anterior and posterior walls being in apposition. The vagina serves as a useful landmark when performing a TA scan. The upper vagina expands to receive the cervix, which projects into it. Surrounding the cervix is the vaginal fornix, which is deepest posteriorly, and this generally is where the tip of the transducer would be positioned when examining the uterus during a TV scan.

PHYSIOLOGY OF THE FEMALE SEXUAL CYCLE

The female sexual cycle is often a 28-day cycle but this is variable, with some women having shorter and others longer cycles. Day one of the cycle is the first day of menstruation. In a postpubertal female the ovarian changes are dependent upon two hormones secreted by the anterior pituitary gland, follicle-stimulating hormone (FSH) and luteinising hormone (LH). In the first few days of the cycle there is a modest increase in FSH and LH levels. This stimulates growth of 6–12 primary follicles within the ovary and is called the follicular phase. The follicles grow and secrete oestrogen. After a week or so of growth one follicle becomes dominant while the others involute. During this time the levels of LH and, to a lesser extent FSH, rise sharply, stimulating rapid follicular growth, decreasing oestrogen production and increasing progesterone secretion. A mid-cycle LH surge promotes ovulation and the follicle ruptures. This would occur at day 14 in a regular 28-day cycle. Following ovulation LH causes luteinisation of the ruptured follicle, converting it into the corpus luteum. This is the luteal phase. The corpus luteum secretes progesterone and oestrogen, which prepare the endometrium to receive a fertilised ovum. If fertilisation does not occur the corpus luteum, which has a lifespan of around 12 days, involutes. Consequently progesterone and oestrogen levels fall and menstruation takes place.

Following menstruation there is a thin residual layer of endometrium. Rising oestrogen levels cause endometrial regeneration and proliferation, hence this is known as the proliferative phase. The endometrial proliferative phase coincides with the follicular phase of the ovary. After ovulation and the development of the corpus luteum, oestrogen and progesterone levels rise, causing further endometrial proliferation and secretory development. This is called the secretory phase and it coincides with the ovarian luteal phase[8] (Fig. 34.6).

TECHNIQUE AND ULTRASOUND ANATOMY

Transabdominal scanning

The technique of transabdominal scanning uses the bladder as an acoustic window. In the longitudinal or sagittal plane by angling the transducer inferiorly the vagina is visualised as a linear, midline

structure. The walls are hypoechoic and the apposed anterior and posterior walls produce a hyperechoic midline stripe. In the transverse plane the vagina appears as a flattened rectangle with a hyperechoic midline stripe. The upper vagina is seen to expand to accommodate the cervix (Fig. 34.7).

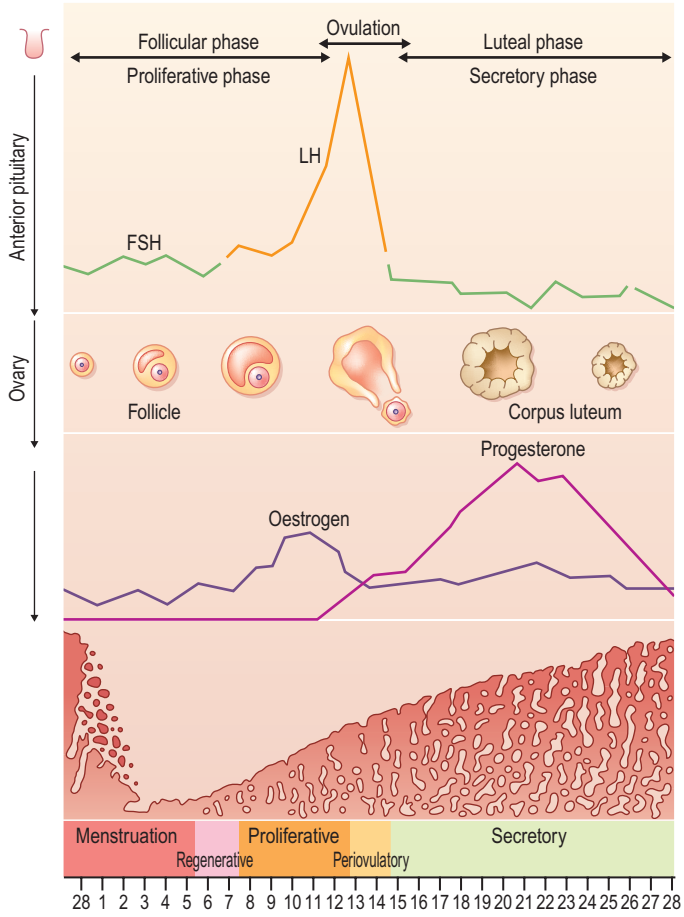


Figure 34.6 The physiology of the female sexual cycle (modified with permission from Bates JA, Practical Gynaecological Ultrasound, 2nd edn, 2006, Cambridge University Press).

With less caudal angulation the uterus occupies the field of view. In the longitudinal plane the hypoechoic myometrium surrounds the endometrium. The endometrium coats the uterine cavity and is generally hyperechoic relative to the myometrium. In the non-pregnant uterus the cavity is a potential space that is represented by the echogenic line of the apposed anterior and posterior endometrial surfaces.

By turning the transducer 90° the uterus becomes ovoid. The myometrium surrounds the inner oval of the endometrium in the body. Angling cephalad towards fundus the endometrium elongates as it extends to the cornua. The serosal surface of the uterus should be smooth (Fig. 34.8).

The position of the ovaries is variable. With the transducer orientated in the transverse plane and the uterine fundus in the centre of the field of view, if the ovaries are in their usual anatomical location, each may be visualised next to the iliac vessels and the pelvic side wall. A degree of angulation to each side may be necessary. Imaging

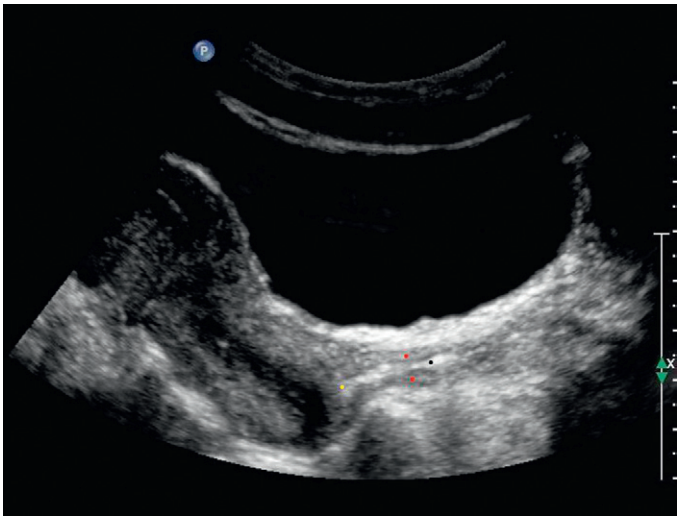
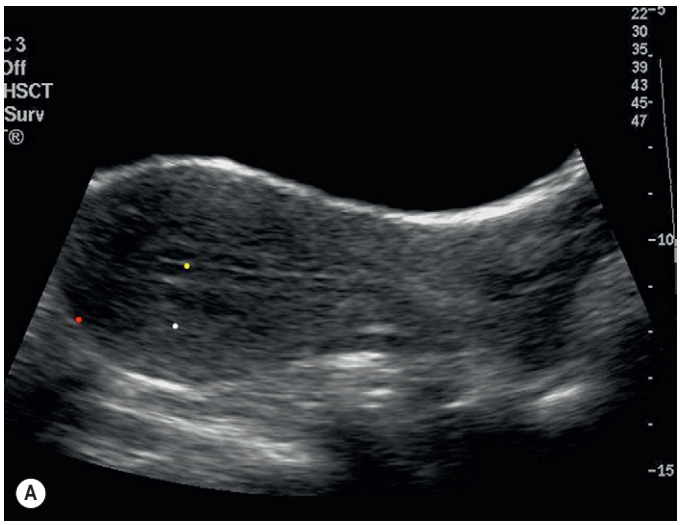


Figure 34.7 TA scan longitudinal plane showing the hyperechoic midline echo of the apposed anterior and posterior vaginal walls (black dot). Note the hypoechoic vaginal walls (red dots). The upper vagina expands to accommodate the cervix (yellow dot).



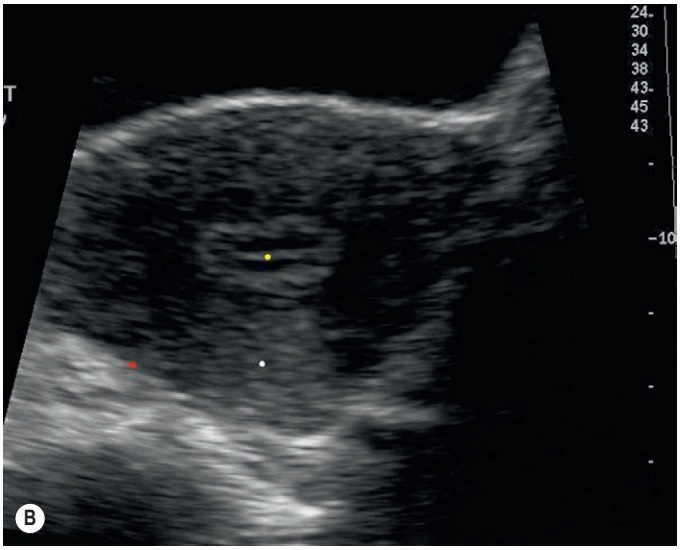


Figure 34.8 TA scan (A) longitudinal/sagittal and **(B)** transverse images of the uterus. The serosal surface is smooth (red dot). The myometrium is homogeneous and hypoechoic relative to the endometrium (white dot). The midline stripe is hyperechoic (yellow dot).

the ovaries in the longitudinal plane often requires insonating from the contralateral side of the bladder. Thus to image the right ovary the transducer is placed on the skin to the left of the midline on the lower anterior abdominal wall. It is angled obliquely such that the ultrasound beam passes through the bladder towards the right iliac vessels and pelvic side wall, where the ovary should come into view. The opposite is true for the left ovary (Fig. 34.9).

TA scanning provides an overview of the ovarian position. It is complementary to TV scanning when the ovaries are not in their normal anatomical position such as in the pouch of Douglas or when they are lifted out of the true pelvis in the presence of an enlarged, fibroid uterus.

The pelvic musculature is best appreciated on TA scanning. The muscles lie posterior and lateral to the uterus and are depicted as well-defined, linear structures of homogeneous, low-level echogenicity.

Transvaginal scanning

To master the technique of transvaginal scanning requires practice and patience. Prior to scanning a patient, the transducer must be covered with a clean probe cover containing coupling gel. This is also used on the outside surface of the probe cover at its tip. The positioning of the woman must allow the operator to have adequate leverage of the probe handle. This can be achieved in a number of ways. A useful manoeuvre is to ask the patient to lie supine on the examination couch so that her bottom is right at the foot end of the couch and her head is at its centre. A chair is placed at a lower level than the couch at the foot end. The woman bends her legs at the knees in order that her feet can rest on the chair.

The transducer is gently introduced into the vagina and advanced until it meets resistance. At this point the tip is in the posterior fornix. In the presence of an anteverted uterus the handle of the probe often requires lowering towards the floor so that the ultrasound beam passes through the entire organ. When the uterus is retroverted the handle may require elevation. Once the uterus has been located and the operator has centred it on the monitor, a frequent mistake of novices to the technique is that of moving the transducer too quickly and too far. Movements of the transducer should be small, otherwise the uterus will no longer be in the centre of the field of view, and slow so that the region of interest is systematically interrogated. Individuals with a radiology background usually view the image with the apex of the scan sector positioned at the top of the screen. As such, in anteversion in the sagittal plane the fundus will be on the left-hand side of the monitor and in retroversion it will be on the right (Fig. 34.10). A perfect, though not always achievable, sagittal midline image should have an uninterrupted echogenic midline stripe. Ideally this should extend from the fundus to the external cervical os, and represents the apposed anterior and posterior endometrial and endocervical mucosal surfaces. It is from this midline image that endometrial thickness is measured. It ensures an accurate measurement with no obliquity. Effectively the two endometrial layers are measured from the anterior interface between the myometrium and endometrium to the posterior interface (Fig. 34.10). It is entirely normal to have a tiny volume of fluid in the uterine cavity in pre- and postmenopausal women. In premenopausal women this may be around the time of ovulation and during menstruation. If fluid is present, the endometrial thickness measurement should not include the fluid. The single endometrial layers are measured and added together. If it is not possible to define the echogenic midline stripe within the endometrium or if the stripe is interrupted, it may be a sign of pathology within the uterine cavity. Such pathology might include an endometrial polyp or a polypoid fibroid.

In the sagittal plane it is important to pan from side to side (parasagittal to parasagittal) so that the entire uterus is assessed.

Turning the transducer 90° with the leading edge towards the operator produces a transverse image of the uterus. When the

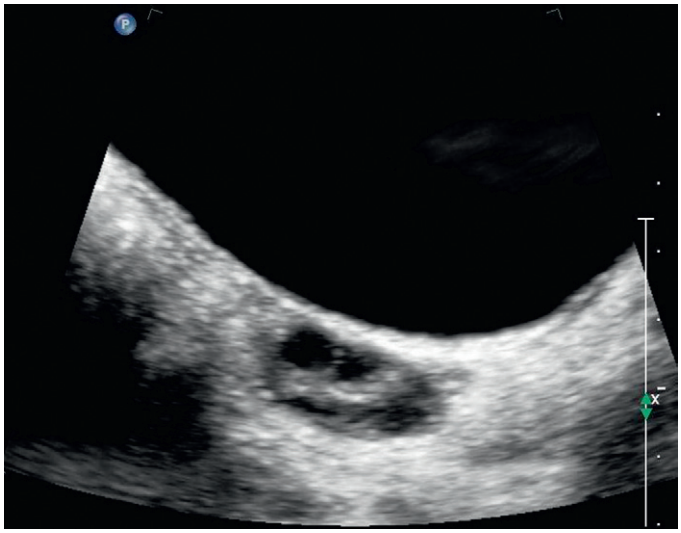


Figure 34.9 TA scan of right ovary. The image is achieved by insonating obliquely from the left through the bladder to the right pelvic side wall.

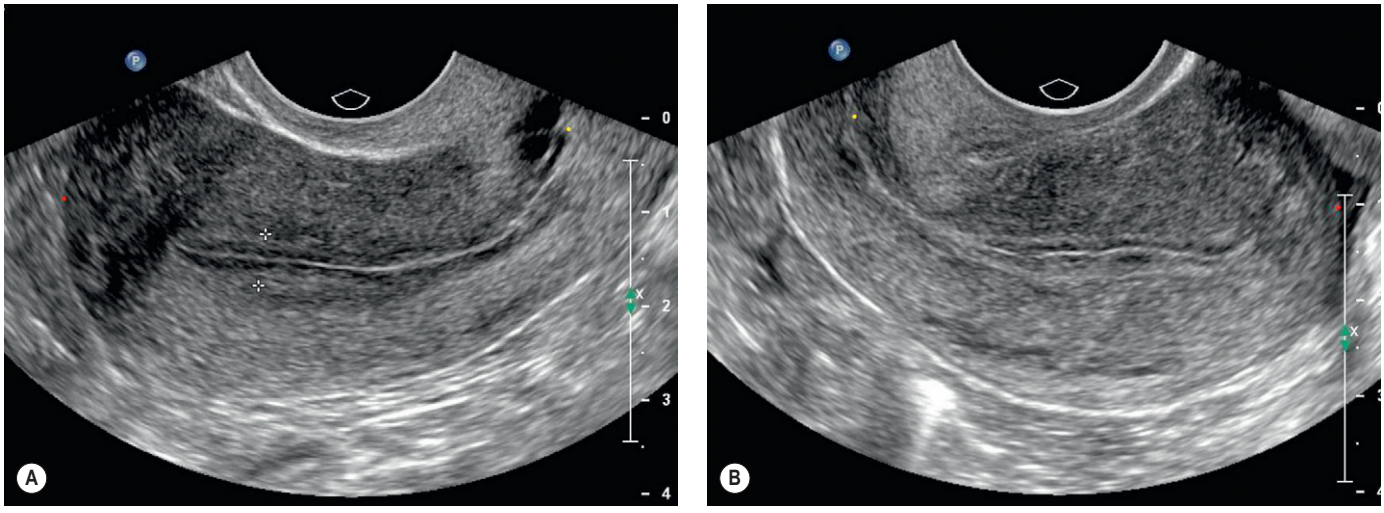


Figure 34.10 TV scan sagittal midline image of **(A)** an anteverted uterus with the fundus (red dot) to left and the cervix (yellow dot) to the right. The callipers are measuring the endometrial thickness. **B:** The fundus to right in retroversion.

uterus is anteverted, panning through it from fundus to cervix requires the probe handle to be gradually elevated from a position of relative depression. The opposite is true in retroversion. The transverse plane allows full assessment of the myometrium from serosa to endometrial interface. It also allows visualisation of the endometrium as it extends out to the cornua (Fig. 34.11). Careful attention should be paid here as the cornua are a hysteroscopic blind spot.

Ultrasound anatomy

Uterus

The serosal surface of the uterus is smooth. The myometrium returns intermediate level homogeneous echoes. Vessels are seen penetrating the outer myometrium and these correspond to the arcuate branches of the uterine circulation[9] (Fig. 34.12). There is an echo-poor inner layer of inner myometrium. It has been described as the subendometrial halo and is composed of tightly packed muscle cells with an increased vascularity. This myometrial layer may play a role in stripping the endometrium during menstruation and promoting sperm transport.[10] It corresponds to the junctional zone of subendometrial myometrium demonstrated on magnetic resonance imaging[11] (Fig. 34.13).

The endometrium should be well defined with a smooth, clear interface between it and the underlying myometrium. In addition, its echogenicity should be uniform throughout.

During the early proliferative phase of the reproductive cycle the endometrium is isoechoic or slightly hyperechoic to the outer myometrium. As this phase progresses, the endometrium develops a multilayered configuration. Viewing from anterior to posterior, adjacent to the inner myometrium, the anterior endometrium has an outer hyperechoic basal layer. Next is an inner hypoechoic functional layer. This appearance is repeated in the posterior endometrium, the two being separated by the midline echo representing the apposed anterior and posterior surfaces. This has been

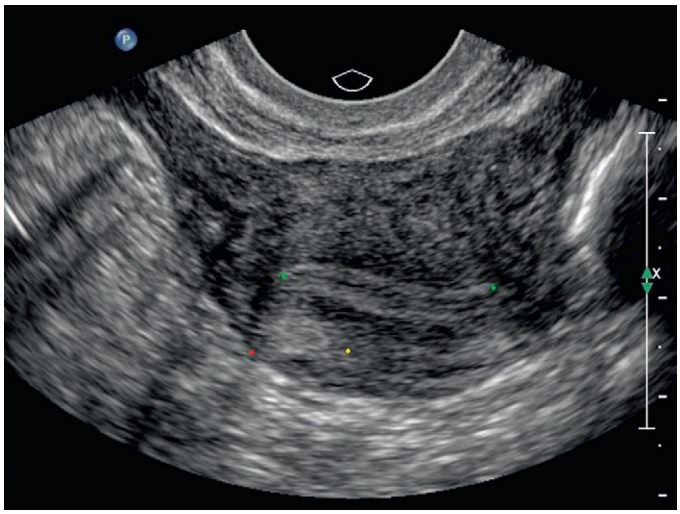


Figure 34.11 TV scan transverse image of the uterus showing a smooth serosal surface (red dot), homogeneous myometrium (yellow dot) and the endometrium elongating out towards the cornua (green dots).

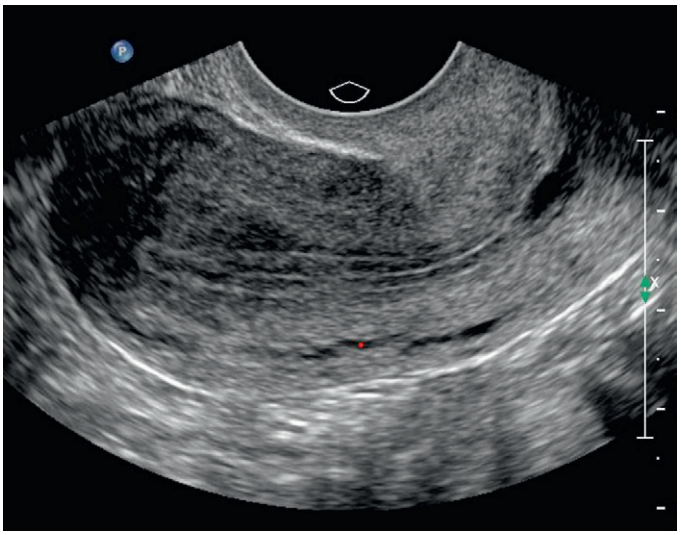


Figure 34.12 Uterus. TV scan sagittal image showing linear anechoic structures (red dot) in the periphery of the posterior myometrium. These represent the arcuate branches of the uterine circulation.

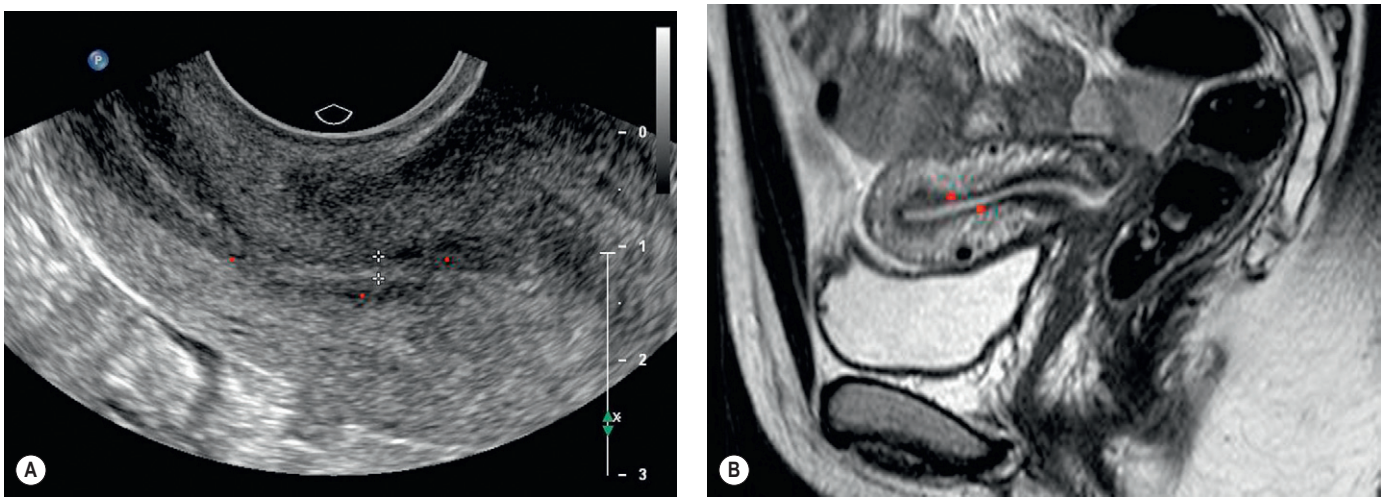


Figure 34.13 Uterus. A: TV scan sagittal plane. Retroverted uterus with a hypoechoic subendometrial halo (red dots) representing the inner myometrium. The callipers are measuring the endometrial thickness. **B:** T2-weighted midline sagittal magnetic resonance image of the uterus showing the hypointense subendometrial junctional zone (red dots) of the myometrium.

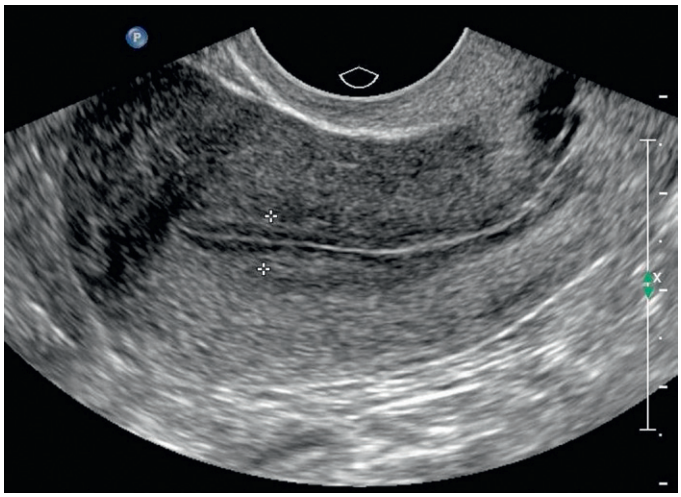


Figure 34.14 TV scan sagittal image of an anteverted uterus. The endometrium exhibits the multilayered appearance of a proliferative phase endometrium. There is an outer, basal hyperechoic layer (red dots) and an inner hypoechoic functional layer (yellow dots). The midline stripe is hyperechoic. This is the triple line sign.

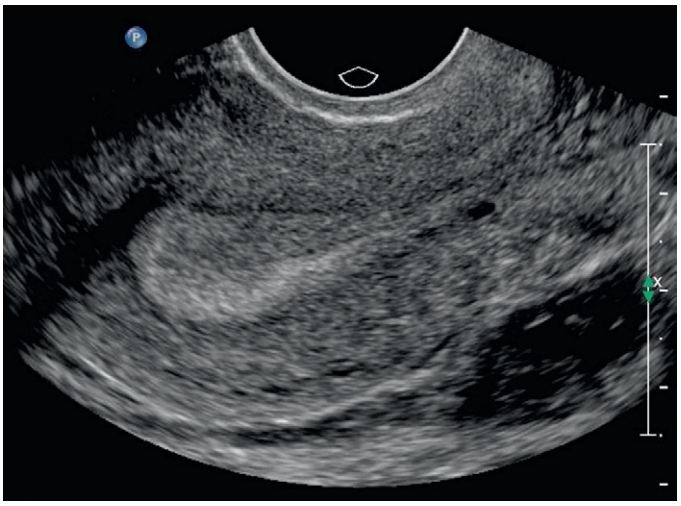


Figure 34.15 TV scan midline sagittal image of an anteverted uterus. The endometrium is secretory and is uniformly hyperechoic.

Cyclical changes in the appearance of the endometrium

Proliferative phase: thickness 4–8 mm
Early – isoechoic or slightly hyperechoic to outer myometrium
Late – multilayered/triple line sign

Secretory phase: thickness 8–16 mm
Layers disappear
Uniformly hyperechoic to outer myometrium

Menstrual phase: thickness 1–4 mm
Thin
Irregular
May be fluid in cavity

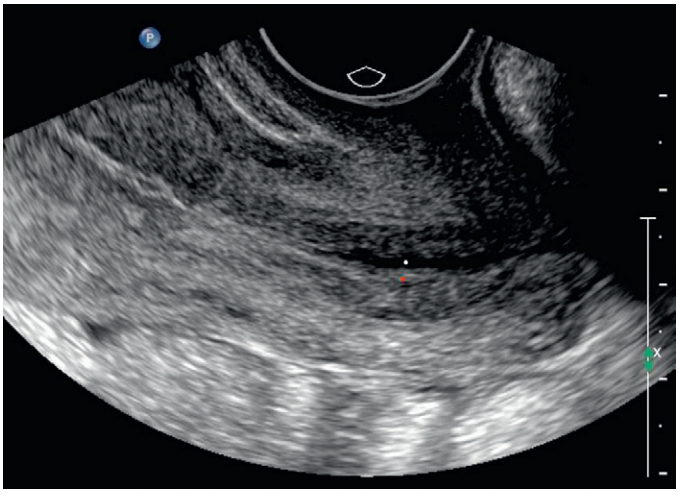


Figure 34.16 TV scan of the cervix of an anteverted uterus in the sagittal plane. There is a trace of fluid in the endocervical canal (white dot). The cervical mucosa is hyperechoic (red dot).

described as the triple line sign. The bilayer may measure up to 8 mm[9–12] (Fig. 34.14).

The layers gradually disappear during the secretory phase. The endometrium becomes uniformly hyperechoic relative to the outer myometrium and achieves its maximum thickness with the bilayer measuring up to 16 mm (Fig. 34.15). This is due to the presence of oedema and the endometrial glands being distended with mucus and glycogen.[9,12]

Menstruation is not a contraindication to a TV scan but if endometrial pathology is suspected the proliferative phase is optimum for endometrial evaluation. During menses the endometrium is thinned and irregular, measuring between 1 mm and 4 mm. There may be fluid within the uterine cavity.

After the menopause the endometrium atrophies and an endometrial thickness greater than 4 mm is considered to be abnormal.[13–15]

Cervix

By withdrawing the transducer by 2–3 cm the cervix is visualised. Unlike the uterine body, the ectocervix is amenable to direct visualisation during the course of an internal gynaecological examination and to even closer inspection at colposcopy. Thus gynaecologists are not fully reliant upon ultrasound to evaluate the cervix. It does, however, enable inspection of the endocervical canal, the surrounding layers of cervical stroma and muscle, and the serosal surface. Pathology such as a cervical fibroid that may not be seen clinically may be assessed ultrasonically. The endocervical canal appears as a central echogenic stripe and represents the cervical mucosa. The cervical stroma and muscle layer has a similar echogenicity to the outer myometrium.[9] The serosal surface is smooth (Fig. 34.16).

Uterine tubes

The diameter of the uterine tubes is so small that normal tubes are beyond the resolution capabilities of even a high-frequency vaginal transducer. In the presence of ascites the broad ligament and its contents, including the tubes, are more easily seen. Tubal patency may be determined using hystero-contrast sonography (HyCoSy). This is a procedure whereby the endocervical canal or uterine cavity is cannulated with a catheter. This is held in place by inflating a small balloon with air or water. Then contrast is instilled.

The ultrasound contrast agent is a positive contrast agent consisting of microbubbles. The contrast is instilled whilst performing a TV scan and tubal patency is assessed. The National Institute for Health and Clinical Excellence (NICE) recommend HyCoSy as an initial investigation of tubal patency in the assessment of women with fertility problems.[16]

Ovaries

Technique

A useful technique to localise the ovaries with TV ultrasound is to position the transducer in the transverse plane at the level of the uterine fundus. From here follow the endometrium laterally as it extends out towards the cornua. Beyond the cornua it is often possible to visualise a hypoechoic, linear structure. This represents the broad ligament and its contents (Fig. 34.17). This should be followed laterally to its outer limit where the ovary should be located adjacent to the iliac vessels. By applying gentle pressure on the skin in the relevant iliac fossa the image of the ovary may become clearer as bowel loops are displaced. In addition, the ovary is pushed downwards towards the transducer tip. This technique is akin to a gynaecological bimanual examination. Ovaries in women of reproductive age are generally straightforward to locate because of the presence of anechoic follicles. If an ovary is not in the expected anatomical location, it may be found in the pouch of Douglas or around the peripheries of the uterus. When the uterus is enlarged the ovaries may have been lifted out of the true pelvis and therefore beyond the range of a TV probe.

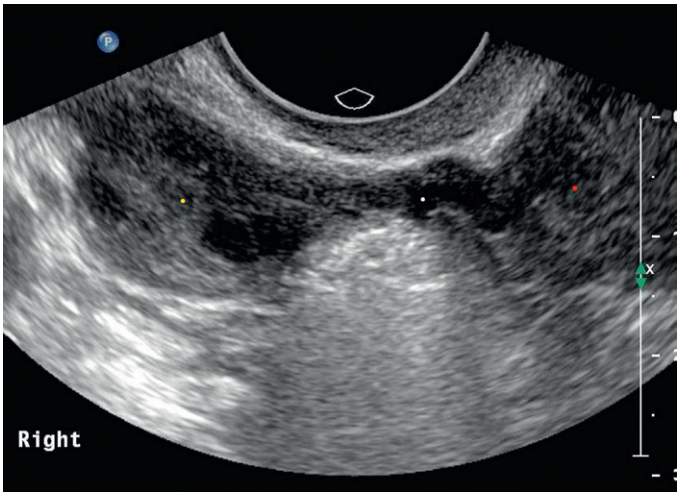


Figure 34.17 Ovaries. TV scan transverse image of right cornual region (red dot) and right ovary (yellow dot). The hypoechoic linear structure (white dot) to the right of the ovary represents the broad ligament and its contents.

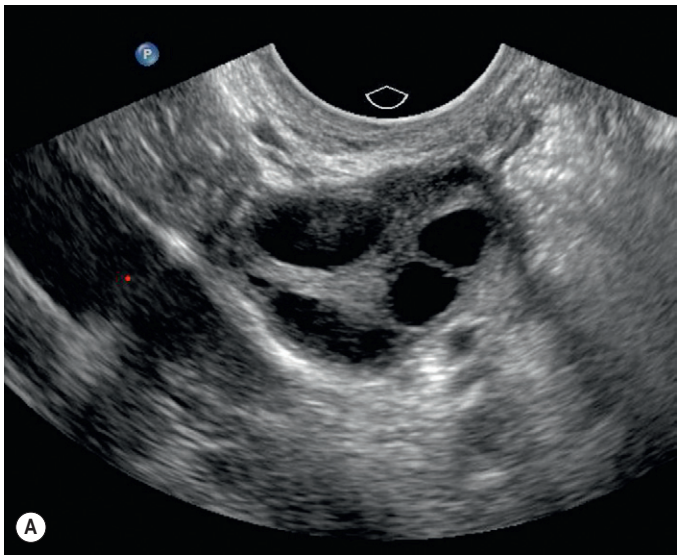
Anatomy

Ovarian shape is variable, ranging from almond shaped to spherical. An outer cortex of the ovary contains immature follicles and it is here that cyclical changes are observed. During the follicular phase the follicles grow, appearing as peripheral anechoic structures. Usually only one will reach 10 mm becoming the dominant follicle (Fig. 34.18). As it matures the dominant follicle may reach 25 mm in diameter. Within it, it is possible to depict the cumulus oophorus, which represents the oocyte surrounded by a cluster of granulosa cells. It gives rise to a cyst within a cyst appearance and is a sign of impending ovulation.[9] Following ovulation the ovary enters the luteal phase. The follicle deflates and the wall becomes irregular.[17] This is the corpus luteum, the appearance of which ranges from a cystic structure with an irregular, echogenic wall to a cystic structure containing a fine latticework of septations (Fig. 34.19). The variability represents haemorrhage in its different manifestations.[18] It is normal to see a small volume of free fluid in the pouch of Douglas following ovulation.

Ovarian volume changes with age, menopausal status, phase of menstrual cycle and external hormonal influences. It is calculated using the formula for an ellipse:

$$\text{Volume}\ (\text{cm}^3) = \text{length} \times \text{width} \times \text{depth}\ (\text{anteroposterior diameter}) \times 0.53$$

Table 34.2 shows age-related differences in ovarian volume[19] and Table 34.3 shows age-related differences in ovarian dimensions.[3,11]



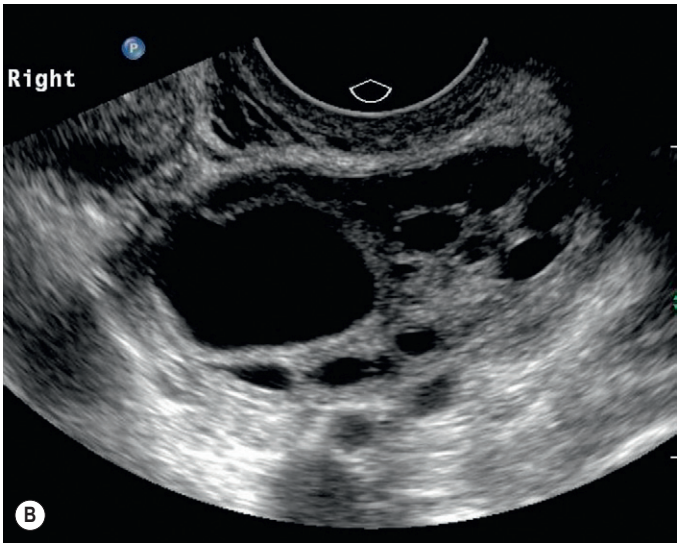


Figure 34.18 Ovarian follicle. A: TV scan longitudinal image through the right ovary during the follicular phase. Note the iliac vessels posterior to the ovary (red dot). **B:** The dominant follicle.

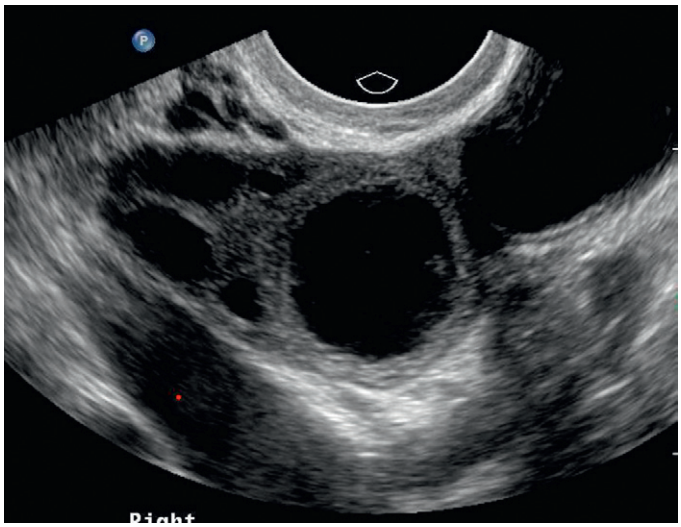


Figure 34.19 TV scan longitudinal image of the right ovary during the luteal phase. The predominantly anechoic structure with the thick echogenic wall and containing internal echoes represents the corpus luteum. Note the iliac vessels posterior to the ovary (red dot).

Cyclical changes in the ovaries

Follicular phase
Early – several peripheral anechoic follicles appear.
Mid – one follicle grows to >10 mm to become the dominant follicle.
Periovulatory – cumulus oophorus may be visible.

Ovulation
Dominant follicle deflates. May be fluid in pouch of Douglas.

Luteal phase
Corpus luteum – thick, echogenic, irregular wall. Internal echoes/septations representing haemorrhage. Hypervascular wall with low resistance waveform on pulsed wave Doppler.

Table 34.2 Age-related differences in ovarian volume

	Mean ovarian volume (cm^3)	Range (cm^3)
Prepubertal	3.0	0.75–2.32
Reproductive	9.8	1.2–11.8
Postmenopausal	5.8	3.5–7.5

HAEMODYNAMICS OF THE UTERUS AND OVARIES AS REPRESENTED BY DOPPLER ULTRASOUND

In women of reproductive age the haemodynamics of the ovarian and uterine arteries undergo cyclical changes. These changes can be assessed using Doppler ultrasound.

The uterine arteries are located just lateral to the cervix. The blood flow within them in the non-gravid state is typically of high velocity and high resistance. A diastolic notch is seen on the pulsed wave Doppler trace[9,20] (Fig. 34.20). The arcuate and subendometrial arteries are best depicted by placing the colour box on the myometrium. These vessels have similar haemodynamics to the uterine arteries. The pulsatility index, which represents resistance to blood flow, within the uterine, arcuate and subendometrial arteries vessels is highest just after ovulation, whereas it is lowest 7–12 days following ovulation.[21]

The ovarian arteries and intraovarian arterioles exhibit even greater cyclical changes than the uterine arteries. These changes occur in the ovary containing the dominant follicle and subsequently the corpus luteum. Maximum resistance is observed during the early proliferative phase. With the development of the dominant follicle the resistance gradually decreases. The pulsatility index is at its lowest in the presence of the corpus luteum. This reflects neovascularisation within the wall of the corpus luteum[9,16,21,22] (Fig. 34.21). The flow velocity and pulsatility index remain relatively constant throughout the reproductive cycle in the non-dominant ovary.

CONGENITAL ANOMALIES OF THE FEMALE GENITAL TRACT

Müllerian duct anomalies (MDAs) are congenital anomalies of the female genital tract. They arise as a result of non-development or non-fusion of the Müllerian ducts or failed resorption of the uterine or vaginal septa. Their reported prevalence in the general population is 1%. The importance of MDAs lies in the association of some types with recurrent spontaneous abortions, premature delivery, abnormal fetal lie and dystocia at delivery. In addition, some anomalies are associated with obstruction of the genital tract.

Embryologically the uterine tubes, uterus, cervix and upper two-thirds of the vagina originate from paired Müllerian or paramesonephric ducts. The lower third of the vagina originates from the urogenital sinus. At 6 weeks gestation the paired ducts grow caudally crossing over the Wolffian or mesonephric ducts to meet in the midline. Cranially the uterine tubes remain unfused whilst caudally the urogenital sinus invaginates to form the lower third of the vagina. Fusion and reabsorption of the midline uterine and vaginal septum along with the transverse vaginal septum takes place by 10.5 weeks.

The urinary and genital tracts arise from a common ridge of mesoderm, with both relying upon normal development of the

Table 34.3 Age-related differences in ovarian dimensions

	Length (cm) [range]	Width (cm)	Depth (cm)
Neonate	1.3	0.6	0.4
Reproductive	3.0 [2.5–5.0]	2.0 [1.5–3.0]	1.0 [0.1–1.5]
Postmenopausal (early)	2.0	1.5	0.5
Postmenopausal (late)	1.5	1.5	0.5

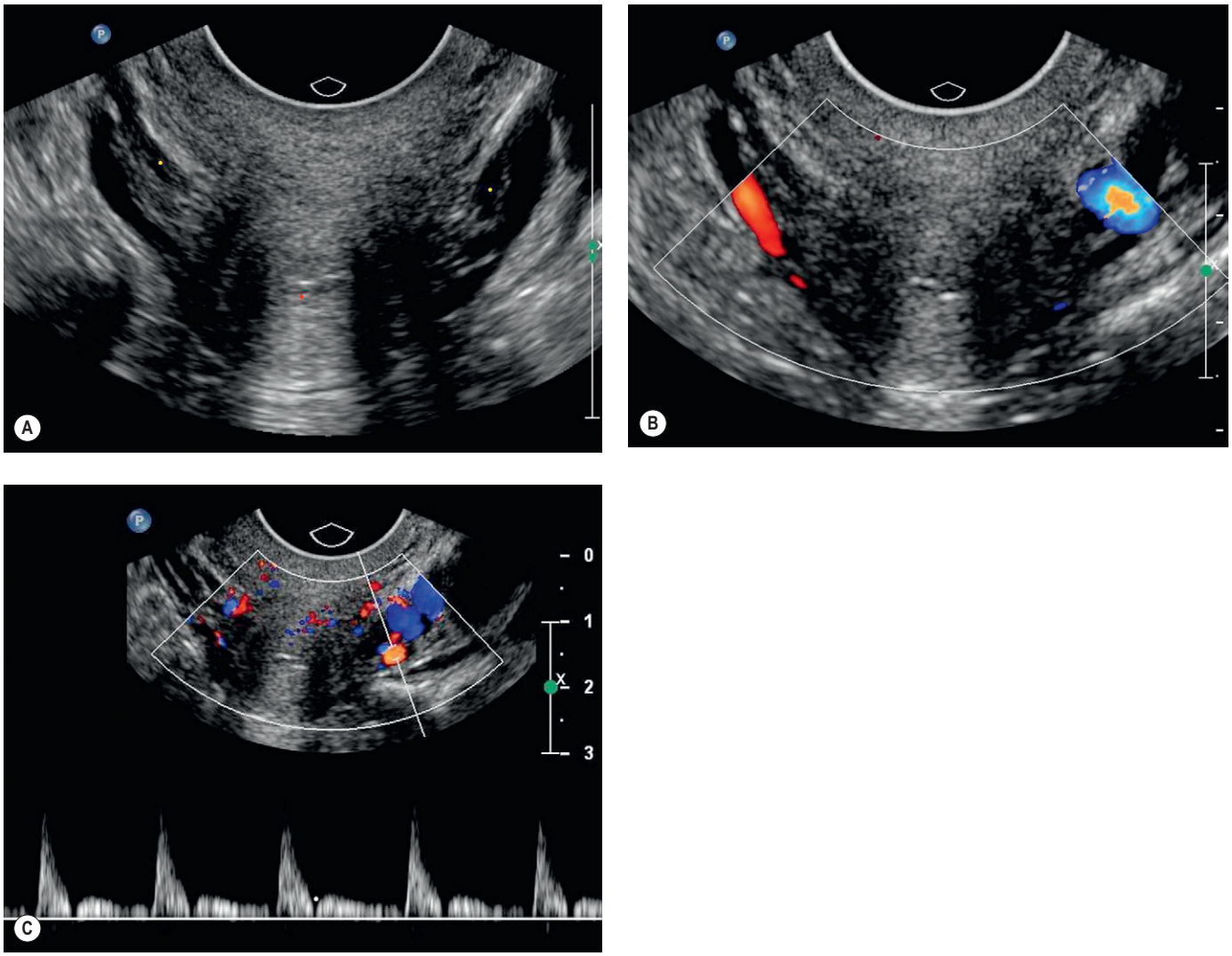


Figure 34.20 Uterine arteries. TV scan transverse image through the cervix (red dot) demonstrating **(A)** the uterine arteries laterally (yellow dots). **B:** Uterine arteries with colour flow Doppler. **C:** Uterine arteries with both colour flow and pulsed wave Doppler. There is a diastolic notch (white dot) in the pulsed wave Doppler trace.

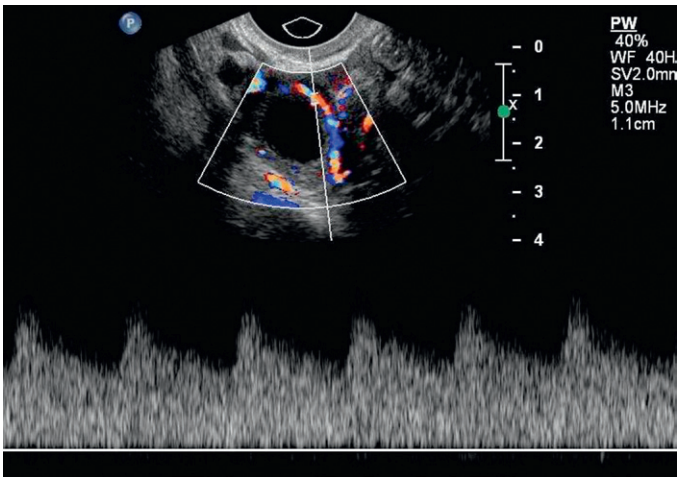


Figure 34.21 TV scan. Image of a right ovary during the luteal phase. It demonstrates neovascularisation within the wall of the corpus luteum with a low resistance waveform on pulsed-wave Doppler.

mesonephric system. The mesonephric ducts give rise to the ureters, renal calyces and collecting tubules. Abnormal development of the mesonephric and paramesonephric ducts may be associated with renal anomalies. Renal agenesis is the most common association but others include crossed ectopy, cystic renal dysplasia and duplicated collecting systems. In this respect when a uterine congenital anomaly is suspected at ultrasound, the kidneys should be scanned as well.

Ovarian development is entirely separate from the development of the uterovaginal canal and is not associated with MDAs.[23] Figure 34.22 illustrates the American Fertility Society's classification of MDAs.[24]

It is acknowledged that magnetic resonance imaging is the optimum imaging modality for characterising MDAs, having a reported accuracy of up to 100%.[23] Anomalies, however, are frequently detected incidentally during a pelvic ultrasound examination in women being scanned for gynaecological problems other than subfertility. They may also be detected at hysterosalpingography in the investigation of subfertility. Ultrasound characterisation is optimised by scanning during the secretory phase. This is because the uterine cavity or cavities are most obvious during this phase of the reproductive cycle as the endometrium is at its thickest and most echogenic. Ultrasound has an accuracy of up to 92%. Its

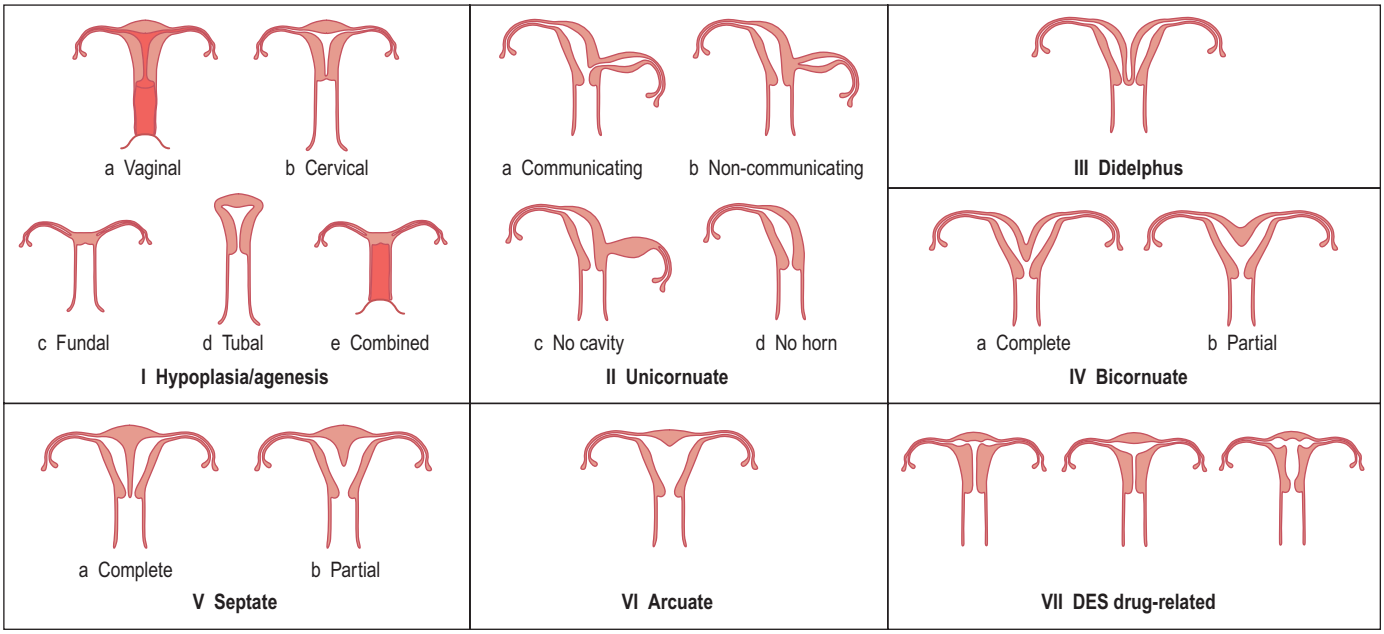


Figure 34.22 Müllerian anomalies: the American Fertility Society classification (reproduced with permission from *Fertility and Sterility* 1988; 47(6):952).

limitations are in part due to the overlap in the findings of some anomalies. It should be noted that three-dimensional ultrasound has been shown to be superior to conventional two-dimensional ultrasound in the assessment of uterine anomalies. Its superiority lies in its ability to better delineate the fundal contour and to calculate uterine volume.[23,25]

Class I anomalies constitute agenesis or hypoplasia and comprise 5–10% of MDAs. The hypoplasia may be vaginal, cervical, fundal, tubal or combined. The ovaries, however, are normal as they are not Müllerian in origin. Mayer–Rokitansky–Kuster–Hauser syndrome is the most common variant, comprising complete vaginal agenesis and a 90% association with uterine agenesis. On ultrasound the uterus is absent whilst the ovaries are in their usual anatomical location.[23]

Class II anomalies comprise the unicornuate uterus and its variants. These account for 20% of MDAs and result from complete or incomplete development of one of the Müllerian ducts. There may be: (a) a communicating rudimentary horn, (b) a non-communicating rudimentary horn, (c) a rudimentary horn with no endometrial cavity or (d) no rudimentary horn. A solitary uterine horn accounts for 35% of unicornuate uteri while the remainder have a rudimentary horn. In the presence of a cavitary, non-communicating rudimentary horn, there is an association with dysmenorrhoea and haematometra at menarche, and also endometriosis. Women with a class II anomaly can sustain a normal pregnancy but there is an increased risk of spontaneous abortion (41–62%) and premature delivery (10–20%). These anomalies are not easily recognised ultrasonically. The uterine body in subtype d is usually smaller than a normal, nulliparous corpus but this size discrepancy may not be noticeable on ultrasound. The corpus may appear asymmetric, ellipsoidal and laterally deviated. In the other subtypes the rudimentary horn may be mistaken for an adnexal mass.[23,26–28]

Class III anomalies are characterised by complete duplication of the uterus and cervix. Uterus didelphys accounts for 5% of MDAs and is due to non-fusion of the Müllerian ducts. There is often both a vertical and a transverse vaginal septum. The latter may cause obstruction of the ipsilateral vagina and uterus that can give rise to a haematometrocolpos. A further complication of this is retrograde menstruation from the blood-filled uterine cavity down the uterine tube. As a consequence haematosalpinx, endometriosis and pelvic adhesions have been described. On ultrasound two separate, divergent uterine horns are identifiable with a deep cleft between them. Within these are two separate, non-communicating endometrial cavities and two cervices are present[23,27] (Fig. 34.23).

The class IV anomaly is the bicornuate uterus, which constitutes 10% of MDAs. It results from incomplete fusion of the superior segments of the uterovaginal canal. There are two symmetrical uterine horns with an intervening cleft. The horns are most often fused at the isthmus, giving rise to the bicornuate unicollis uterus. In a bicornuate bicollis uterus there is cervical duplication. In both types the two endometrial cavities communicate (Fig. 34.24). There is an increased risk of spontaneous abortion (28–35%) and preterm labour (14–23%). In addition, this anomaly is associated with the highest incidence of cervical incompetence in comparison to other MDAs. Ultrasonically a large fundal cleft is present and the uterine horns are widely divergent[23,27,28] (Fig. 34.25).

Class V anomalies are most common, comprising 55% of MDAs. The septate uterus results from complete or partial failure of resorption of the midline septum. This anomaly has the highest association with recurrent abortions and premature delivery. The septum is midline, arising from the fundus. A complete septum extends to the external cervical os and a partial septum is of variable length. All partial septa contain myometrium, whereas complete septa contain myometrium in the upper segment and fibrous tissue in the lower segment. Ultrasonically the fundal contour is flat, convex or mildly concave. In the fundal region the septum has a similar echogenicity to myometrium and in the presence of a complete septum the caudal portion is hypoechoic[23,27,28] (Fig. 34.26).

The class VI anomaly is the arcuate uterus. It differs only slightly from the normal uterine morphology and has no clinically significant implications. It is characterised by a mild indentation of the endometrium at the fundus due to near complete resorption of the uterovaginal septum. Ultrasonically there is a normal fundal contour and smooth indentation of the fundal myometrium.[23,27]

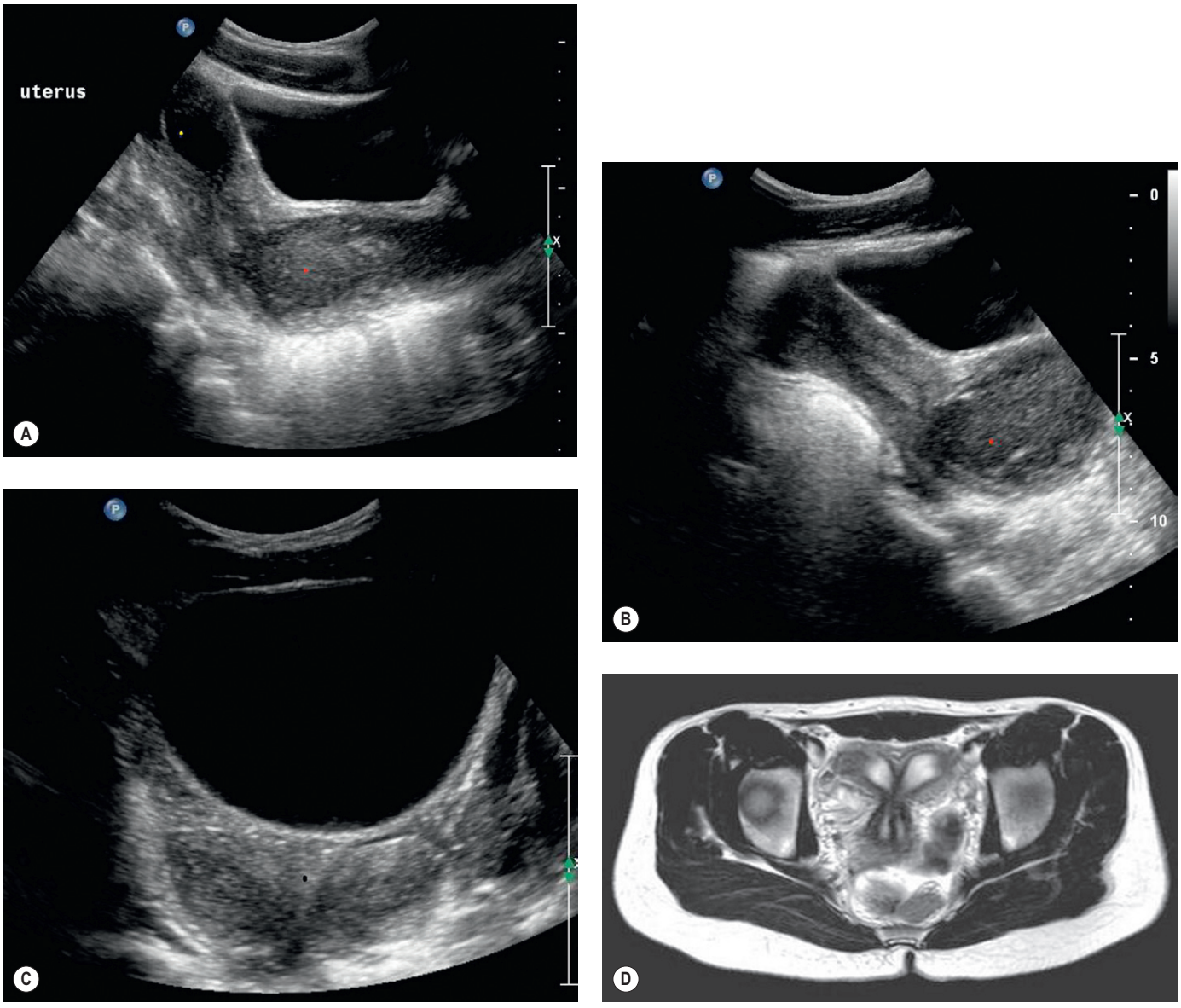


Figure 34.23 **Uterus didelphys. A:** TA scan sagittal image of a right haematometrocolpos in a uterus didelphys. The red dot indicates the haematocolpos and the yellow dot indicates the haematometra. **B:** Non-distended left uterus with haematocolpos (red dot) still visible. **C:** Transverse image of both non-distended, widely divergent, uteri. The black dot indicates the deep cleft between them. This image has been acquired following excision of a transverse vaginal septum. **D:** Axial T2-weighted magnetic resonance image showing divergent, non-distended uteri.

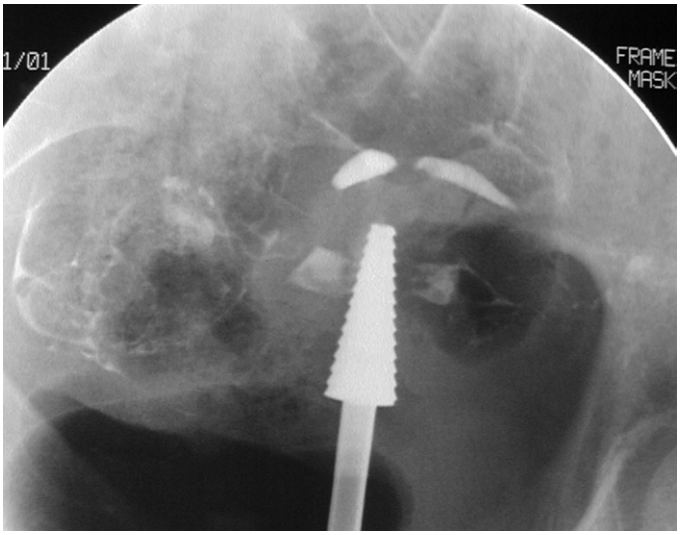


Figure 34.24 **Hysterosalpingogram** demonstrating a bicornuate, unicollis uterus.

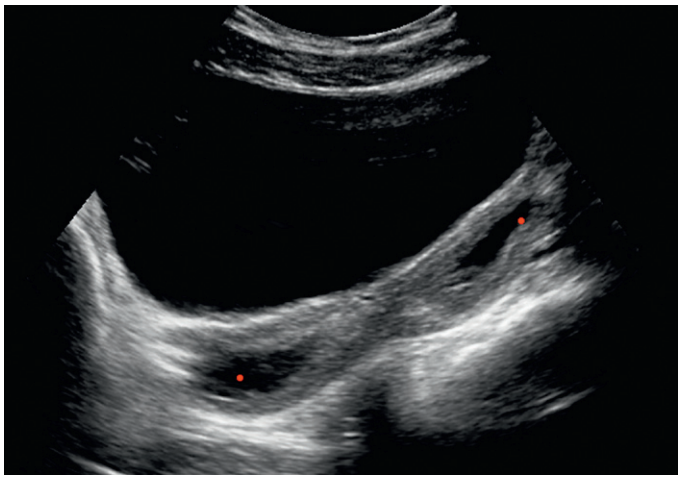


Figure 34.25 TA scan transverse image demonstrating diverging uterine horns (red dots) in a bicornuate uterus.

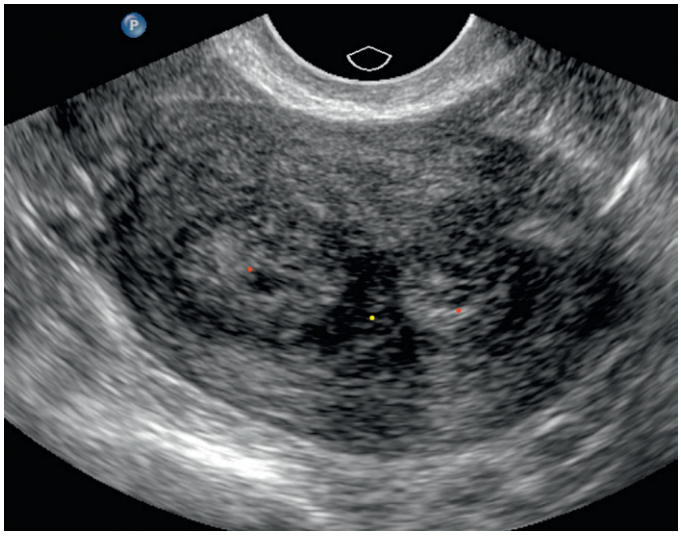


Figure 34.26 TV scan transverse image through uterine body demonstrating a septate uterus with two discrete, echogenic endometria (red dots) separated by a hypoechoic structure (yellow dot). This is either a muscular or fibrous septum.

Class VII anomalies represent the consequences of in-utero exposure of the female fetus to diethylstilbesterol (DES). DES is a synthetic oestrogen introduced in 1948 and given to women experiencing recurrent spontaneous abortions and premature deliveries up until 1971. The structural anomalies described in women who were exposed in utero to DES include a hypoplastic uterine cavity, shortened upper uterine segment, T-shaped uterus, hypoplastic cervix, transverse septa, circumferential vaginal or cervical ridges, and cervical hood or collar. Tubal anomalies have also been described including tubal shortening and fimbrial abnormalities. Women exposed to DES in utero also have an increased risk of developing vaginal clear cell carcinoma.[23]

REFERENCES

1. Newell RLM, Williams A, editors. Pelvic girdle, gluteal region and hip joint. In: Gray's anatomy: the anatomical basis of clinical practice. 39th edn. Edinburgh: Elsevier Churchill Livingstone; 2005.
2. Mundy RA, Healy JC, editors. True pelvis, pelvic floor and perineum. In: Gray's anatomy: the anatomical basis of clinical practice. 39th edn. Edinburgh: Elsevier Churchill Livingstone; 2005.
3. Ind T, Healy JC, editors. Ovaries. In: Gray's anatomy: the anatomical basis of clinical practice. 39th edn. Edinburgh: Elsevier Churchill Livingstone; 2005.
4. Ind T, Healy JC, editors. Uterus. In: Gray's anatomy: the anatomical basis of clinical practice. 39th edn. Edinburgh: Elsevier Churchill Livingstone; 2005.
5. Nussbaum AR, Sanders RC, Douglas Jones M. Neonatal uterine morphology as seen on real-time US. Radiology 1986;160:641–643.
6. Hernanz-Schulman M. Pediatric gynecologic imaging. In: Clinical gynecologic imaging. Philadelphia: Lippincott-Raven; 1997.
7. Platt JF, Bree RL, Davidson D. Ultrasound of the normal nongravid uterus: correlation with gross and histopathology. J Clin Ultrasound 1990;18:15–19.
8. Guyton AC. Female physiology before pregnancy and the female hormones. In: Textbook of medical physiology. 8th edn. Philadelphia: WB Saunders; 1991.
9. Gratton D, Harrington C, Holt SC, Lyons EA. Normal pelvic anatomy using transvaginal scanning. Obstet Gynecol Clin North Am 1991;18:4.
10. NICE Clinical Guidelines. Fertility: assessment and treatment for people with fertility problems. 2004.
11. Fleischer AC, Kepple DM. Normal pelvic anatomy as depicted by various sonographic techniques. In: Clinical gynaecologic imaging. Philadelphia: Lippincott-Raven; 1997.
12. Tetlow RL, Richmond I, Manton DJ, et al. Histological analysis of the uterine junctional zone as seen by transvaginal ultrasound. Ultrasound Obstet Gynecol 1999;14:188–193.
13. Nalaboff KM, Pellerito JS, Ben-Levi E. Imaging the endometrium: disease and normal variants. Radiographics 2001;21:1409–1424.
14. Epstein E, Valentin L. Managing women with post-menopausal bleeding. Best Practice and Research: Clinical Obstetrics and Gynaecology 2004;18(1):125–143.
15. Gupta JK, Chien FW, Voit D, et al. Ultrasonographic endometrial thickness for diagnosing endometrial pathology in women with postmenopausal bleeding: a meta-analysis. Acta Obstet Gynaecol Scand 2002;81:799–816.
16. Gull B, Karlsson B, Milsom I, et al. Transvaginal sonography of the endometrium in a representative sample of postmenopausal women. Ultrasound Obstet Gynecol 1996;7:322–327.
17. Fleischer AC, Vasquez JM, Kepple DM. Transvaginal sonography in gynaecologic fertility disorders. In: Clinical gynaecologic imaging. Philadelphia: Lippincott-Raven; 1997.
18. Timor-Tritsch IE. Relevant pelvic anatomy. In: Ultrasound in gynecology. 2nd edn. Philadelphia: Churchill Livingstone Elsevier; 2007.
19. Cohen HL, Tice HM, Mandel FS. Ovarian volumes measured by US: Bigger than we think. Radiology 1990;160:641–643.
20. Timor-Tritsch IE. Color Doppler mapping in gynecology. In: Ultrasound in gynecology. 2nd edn. Philadelphia: Churchill Livingstone Elsevier; 2007.
21. Sladkevicius P, Valentin L, Marsal K. Blood flow velocity in the ovarian and uterine arteries during the normal menstrual cycle. Ultrasound Obstet Gynecol 1993;3:199–208.
22. Scholtes MCW, Wladimiroff JW, van Rijen HJM. Uterine and ovarian flow velocity waveforms in the normal menstrual cycle: a transvaginal Doppler study. Fertil Steril 1989;52(6):981–985.
23. Triano RN, McCarthy SM. State of the art: Mullerian duct anomalies: imaging and clinical issues. Radiology 2004;233:19–34.
24. The American Fertility Society. The American Fertility Society classification of adnexal adhesions, distal tubal occlusion secondary to tubal ligation, tubal pregnancies. Mullerian anomalies and intrauterine adhesions. Fertil Steril 1988;49:944–955.
25. Wu HM, Hsu CC, Huang KE. Detection of congenital Mullerian duct anomalies using three dimensional ultrasound. J Clin Ultrasound 1997;25:487–492.
26. Brody JM, Koelliker SL, Frishman GN. Unicornuate uterus: imaging appearance, associated anomalies and clinical implications. AJR Am J Roentgenol 1998;171:1341–1347.
27. Pellerito JS, McCaarthy SM, Doyle MB, et al. Diagnosis of uterine anomalies: relative accuracy of MR imaging, endovaginal sonography, and hysterosalpingography. Radiology 1992;183:795–800.
28. Dykes TM, Siegel C, Dodson W. Imaging of congenital uterine anomalies: review and self-assessment module. AJR Am J Roentgenol 2007;189(3):S1–S10.

CHAPTER

35

Ovaries

Diane DeFriend

NORMAL SIZE AND APPEARANCES 660
Position 660
Size 660
Appearances 661
Cyclical variations 661

FUNCTIONAL CYSTS 663
Follicular cysts 663
Corpus luteal cysts 663
Haemorrhagic cysts 663
Paraovarian cysts 664
Peritoneal inclusion cysts 664
Ovarian remnant syndrome 666
Postmenopausal cysts 666
Polycystic ovary syndrome (PCOS) 666
Hyperreactio luteinalis and ovarian hyperstimulation syndrome 667
Theca lutein cysts 667
Ovarian hyperstimulation syndrome 667

OVARIAN TORSION 668

CHARACTERISATION OF AN ADNEXAL MASS 668

BENIGN VERSUS MALIGNANT OVARIAN LESIONS 670

OVARIAN TUMOURS 670
Symptoms 671
Classification 671
Epithelial neoplasms 671
Serous tumours – serous cystadenoma and cystadenocarcinoma 671
Mucinous tumours – mucinous cystadenoma and cystadenocarcinoma 672
Pseudomyxoma peritonei 672
Endometrioid tumours 673
Clear cell tumours 674
Brenner (transitional cell) tumours 674
Germ cell tumours 674
Mature teratoma (dermoid) 674
Immature teratomas 676
Dysgerminomas 676
Yolk sac tumours (endodermal sinus tumours) 676
Sex cord stromal tumours 677
Granulosa cell tumours 677
Fibromas/thecomas 678
Sertoli–Leydig cell tumours (androblastoma) 678
Metastatic tumours 678
Lymphoma 680
Screening 680

ENDOMETRIOSIS 680

PELVIC INFLAMMATORY DISEASE 682

NORMAL SIZE AND APPEARANCES

Despite technological advances in other imaging techniques, ultrasound remains the initial investigation of choice for evaluation of the ovaries. The ovaries vary in appearance in relation to age and the menstrual cycle and it is essential to appreciate the range of normal appearances in order to correctly identify and characterise pathology.

Position

The ovaries are paired, oval structures which usually lie posterolateral to the uterus, attached to the posterior leaf of the broad ligament by a double fold of peritoneum, the mesovarium, which conveys the ovarian vessels. The ovary usually has a craniocaudal axis, with its tubal extremity uppermost, and its uterine extremity attached to the upper angle of the uterus by the ovarian ligament, also known as the round ligament of the ovary. This is continuous with the round ligament (of the uterus), which extends from the uterine cornua to the pelvic wall and crosses forwards to traverse the inguinal canal and terminate in the labium majus (Fig. 35.1). These ligaments are remnants of the fetal gubernaculum and are not generally visualised by ultrasound unless outlined by ascites (Fig. 35.2). The part of the broad ligament extending between the attachment of the mesovarium and the lateral wall of the pelvis is sometimes called the suspensory ligament of the ovary.

The ovary usually lies on the peritoneum of the pelvic side wall, in the angle between the internal and external iliac vessels, and its position anterior to the internal iliac vessels serves as a useful reference for its identification (Fig. 35.3). The position of the ovaries may be variable, however, due to factors such as laxity of the ligaments and in practice, a search for the ovaries should be made from the pouch of Douglas (Fig. 35.4) to the superolateral aspect of the uterus. Previous surgery can also alter the position, and after hysterectomy the ovaries may lie medially, directly superior to the vaginal vault.[1]

Size

The ovaries vary in size according to age and also in relation to the stage of the menstrual cycle.

Ovarian volume is considered to be the best method for determining ovarian size. The volume of the ovary can be calculated using the formula, length × width × anteroposterior diameter × 0.523 (i.e. the formula for a prolate ellipse).

The reported normal range of ovarian volumes for adult menstruating females has varied between series. This may reflect a number of factors, such as the scan technique used (transabdominal versus transvaginal) and the different populations studied (asymptomatic versus symptomatic). Furthermore, fluctuation in ovarian size throughout the menstrual cycle makes defining normal ovarian volumes difficult. Merz et al. recorded a mean ovarian volume of 7–8 cm^3 with a standard deviation of approximately 2.5 in premenopausal women using transvaginal ultrasound.[2]

In postmenopausal women, ovarian size depends on the time since the menopause, with a number of studies showing that ovarian volume decreases with increasing time elapsed.[2,3] Tepper et al. have established normal values for ovarian volume, according to menopausal age, in healthy postmenopausal women and found that mean ovarian volume decreased from 8.6 cm^3, in the first year

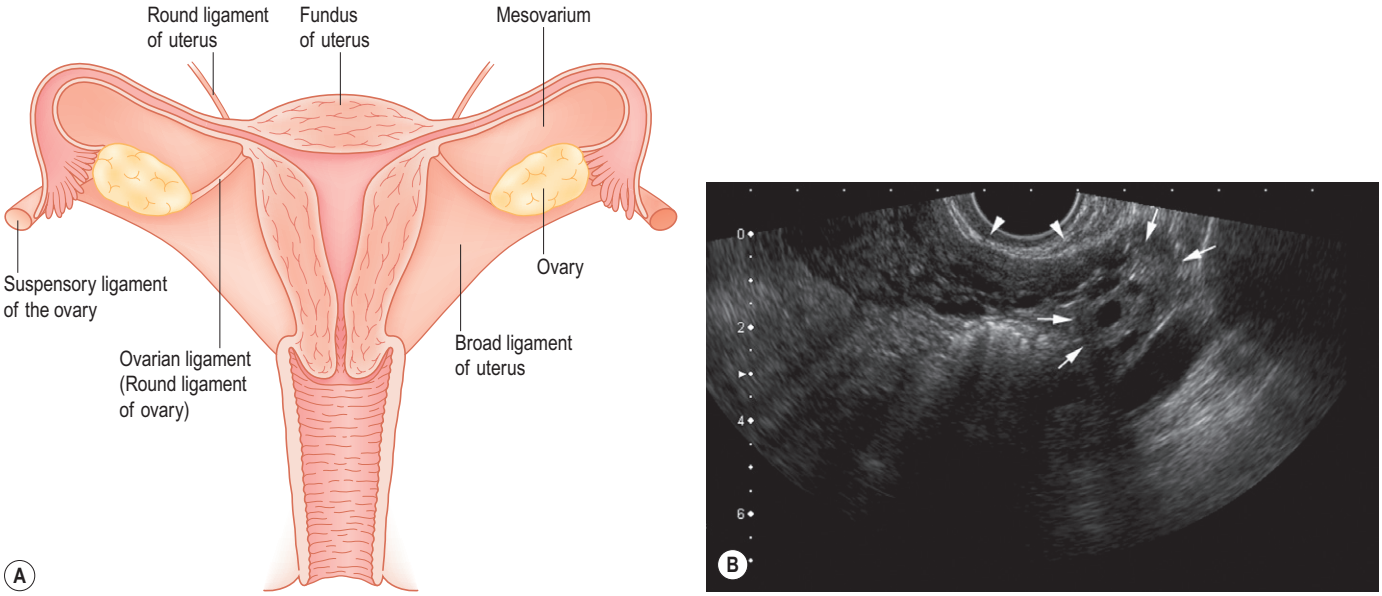


Figure 35.1 **A:** Diagram showing the uterus and ovaries and their related ligaments. **B:** Left adnexa. Transverse, transvaginal ultrasound image, demonstrating the superior aspect of the broad ligament (arrowheads), and the left ovary (arrows).

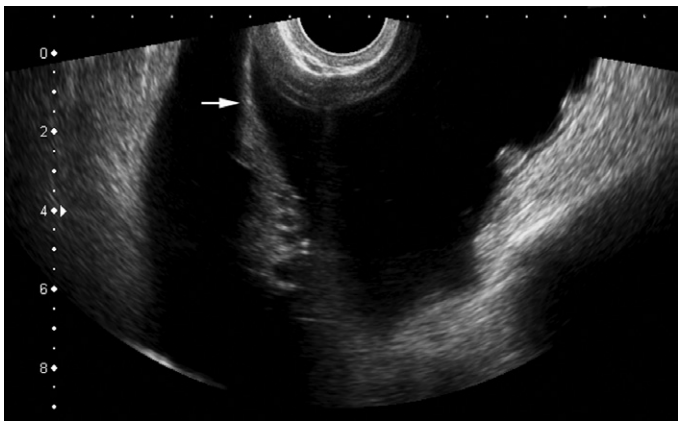


Figure 35.2 **Transvaginal ultrasound image demonstrating the ovarian ligament** (arrow). This ligament is not usually seen but can be visualised when outlined by ascites.

Table 35.1 Ovarian volume in relation to the number of years since the menopause

Years since menopause	Ovarian volume (cm^3), mean ± SD
1–2	6.2 ± 2.7
3–4	5.2 ± 1.6
5–6	4.0 ± 1.8
7–8	3.1 ± 1.3
9–10	2.8 ± 2.1
11–12	2.4 ± 1.3
13–14	2.2 ± 1.3
15+	2.2 ± 1.4

Data adapted from Tepper et al.[3]

post menopause, to 2.2 cm^3, after 15 years (Table 35.1).[3] Tepper, in association with others, has also tried to determine whether different ovarian volume cut-off values can distinguish between normal, benign and malignant lesions in postmenopausal women. In a study of 362 postmenopausal women prior to gynaecological surgery, an ovarian volume of less than 8 cm^3 had a 100% negative predictive value for ovarian cancer. They concluded, however, that it was not possible to define a cutoff value to distinguish between benign and malignant lesions and that any enlarged ovary, >8 cm^3, in a postmenopausal woman may contain a malignancy.[4]

Appearances

The ovary consists of a fibrous stroma covered by a single layer of cuboidal epithelium. The tunica albuginea is a layer of fibrous tissue immediately deep to the epithelium. The stroma is made up of a peripheral cortex and central medulla. The cortex contains numerous follicles, which contain female gametes in various stages of development, while the central medulla is highly vascular and contains few follicles. Ultrasonically the normal ovary is of relatively homogeneous echotexture. The follicles, which help in the identification of the ovary, are seen as echo-free areas, predominantly in the cortex, while the central medulla is more echogenic. The size of the follicles varies with the stage of the menstrual cycle and with age, and in practice, the postmenopausal ovary is harder to find because of its small size and the fact that it contains fewer or no follicles (Fig. 35.5). Ability to visualise both ovaries in postmenopausal women with transvaginal scanning has been reported to be possible in between 60% and 97% cases.[2,3] However, if a thorough examination with a transvaginal probe fails to identify a postmenopausal ovary it is unlikely that a significant pathology will remain undetected.

Cyclical variations

The appearance of the premenopausal ovary varies in response to the gonadotrophic hormones, follicule-stimulating hormone (FSH) and luteinising hormone (LH) secreted by the anterior pituitary. Three phases of the ovarian cycle are recognised ultrasonically, the follicular phase, ovulation and the luteal phase.

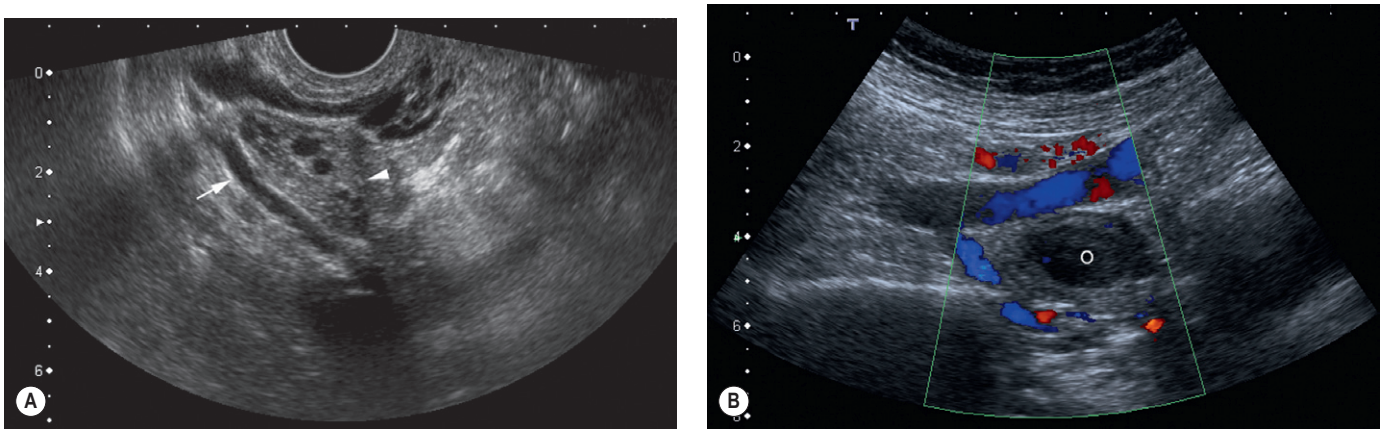


Figure 35.3 Position of the ovary in relation to the iliac vessels. A: Transvaginal scan showing the position of a normal ovary (arrowhead) anterior to the iliac vessels (arrow). **B:** Transabdominal scan showing a normal ovary (O) visualised between the internal and external iliac vessels.

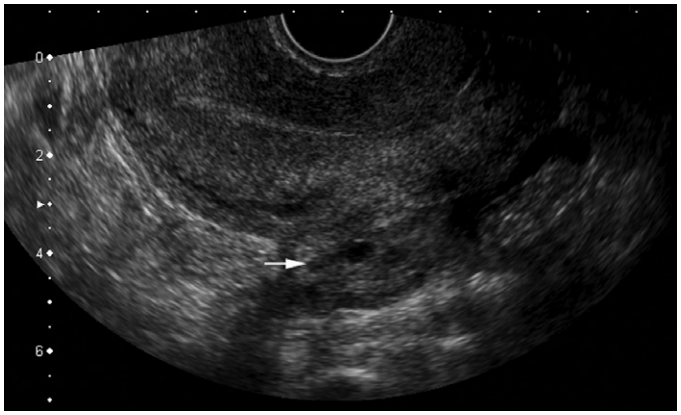


Figure 35.4 Transvaginal image showing a normal ovary (arrow), lying within the pouch of Douglas.

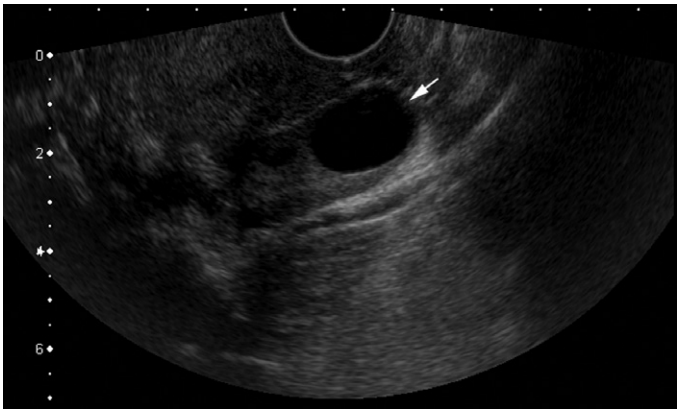


Figure 35.6 Transvaginal image of an ovary, containing a dominant follicle (arrow), in the follicular phase of the ovarian cycle.

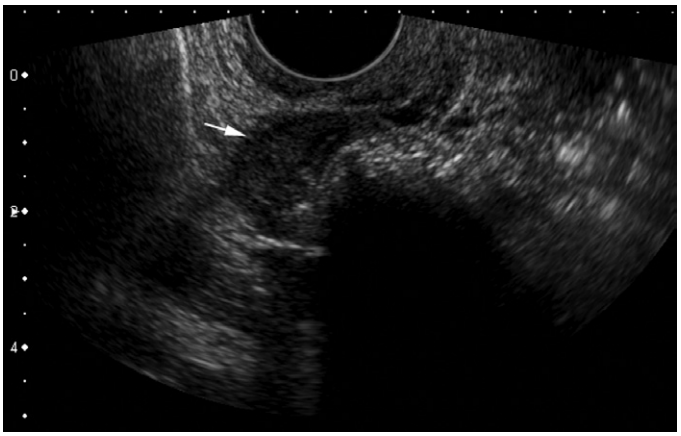


Figure 35.5 Transvaginal image showing a normal postmenopausal ovary (arrow). The ovary lies adjacent to bowel, which is causing acoustic shadowing.

The follicular phase begins on the first day of menses and continues to ovulation, 10–14 days later. During the follicular phase, the ovaries contain several immature follicles, typically less than 1 cm, with a dominant follicle becoming evident by day 8–12 (Fig. 35.6). The dominant follicle reaches a pre-ovulation, mean diameter of between 20–23 mm.

There are no reproducible sonographic signs which reliably predict ovulation, but a cumulus oophorus may be seen, as an eccentric, echogenic or cyst-like mural protrusion, 12–24 hours prior to ovulation. Some fluid may be present in the pouch of Douglas, particularly after ovulation, with the fluid formed predominantly from the active ovary.

In the luteal phase, a corpus luteum, which forms from the ruptured follicle, can be seen in most cases. The function of the corpus luteum is to produce hormones to support the early pregnancy prior to the placenta taking over. The corpus luteum may have a varied appearance on ultrasound, reflecting its maturation and involution. It may appear hypoechoic with thick walls. Haemorrhage is common and it often appears as an irregular or crenated cyst with low-level echoes and circumferential flow (Fig. 35.7A, B). In the absence of fertilisation, the corpus luteum begins to undergo involution and is eventually replaced by scar tissue to form a corpus

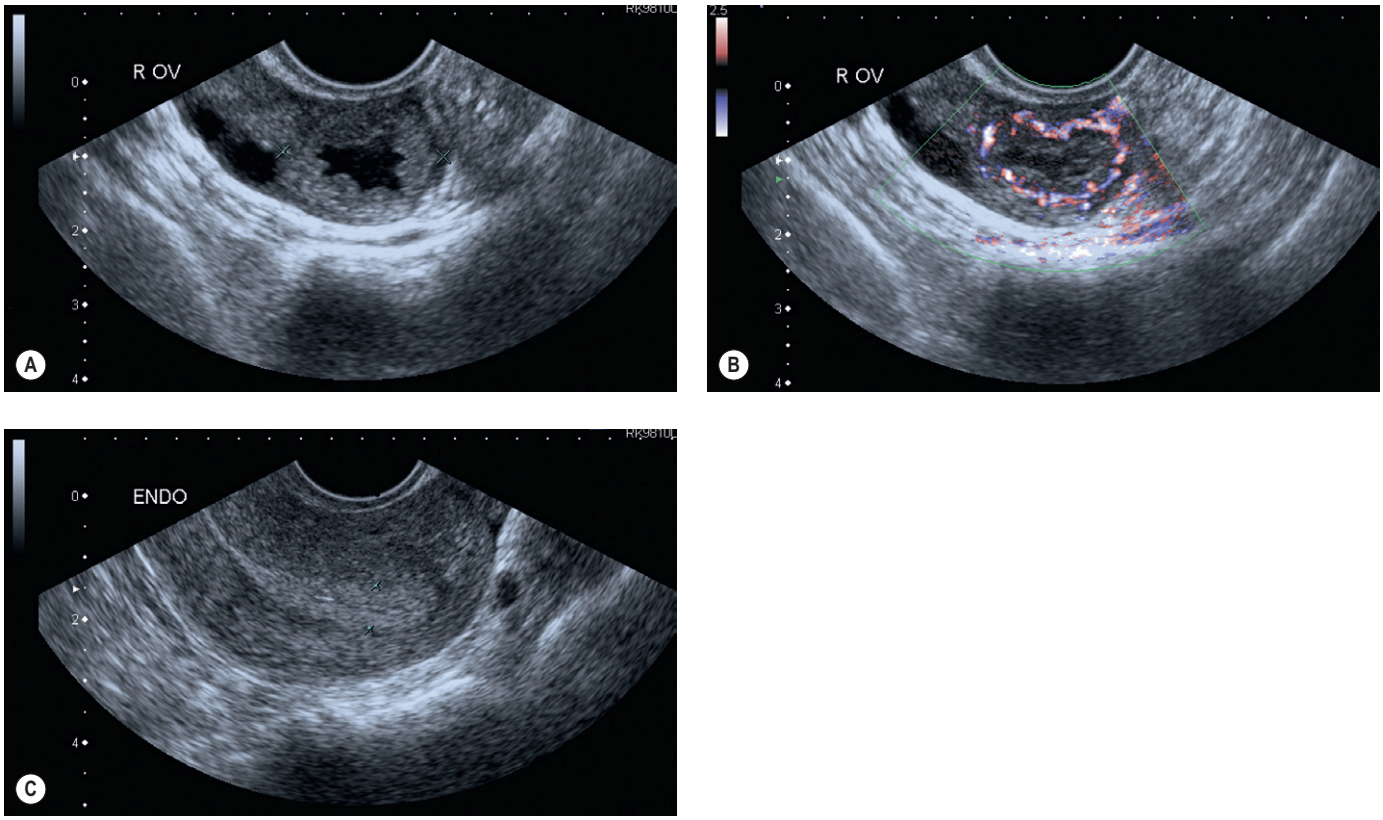


Figure 35.7 Corpus luteum. Transvaginal images showing **(A)** characteristic appearance of a crenated cyst (callipers) with internal echoes, **(B)** characteristic circumferential flow, and **(C)** the endometrium in the secretory phase of the cycle (callipers) of the same patient. The presence of a corpus luteum should correlate with an endometrium in the secretory phase.

albicans. The corpus luteum disappears shortly before, or with the onset of, menstruation and should not be visible more than 72 hours into the subsequent cycle.

It is important to relate the stage of the cycle of the ovary with that of the endometrium; thus the presence of a corpus luteum should correlate with the presence of a secretory endometrium (Fig. 35.7C). Recognition of these physiological changes of the ovary in relation to the menstrual cycle can help avoid unnecessary follow-up of functional cysts.

FUNCTIONAL CYSTS

Follicular cysts

The development of physiological follicles is a normal function of the ovary. Follicular cysts occur as a result of failure of ovulation, or failure of involution of a mature follicle. They are commonly seen at ultrasound, although their true incidence is unknown, as they are often asymptomatic. Most follicles are small, but as they mature can reach sizes of 2.5–3.0 cm. The term follicular cyst should therefore be reserved for cystic structures greater than this size, which can become as large as 20 cm. The typical appearance is of a unilocular cyst with no internal echoes, a thin smooth wall, and posterior acoustic enhancement. Follicular cysts are often detected incidentally and usually regress spontaneously (Fig. 35.8).

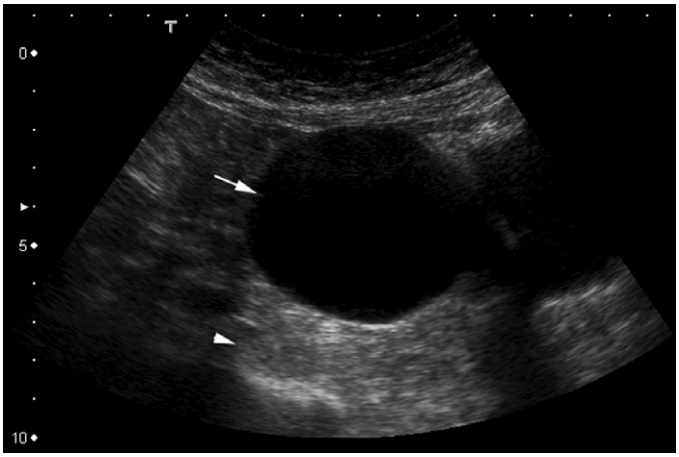


Figure 35.8 Transabdominal ultrasound image of a simple ovarian cyst (arrow), which contains anechoic fluid, has an imperceptible wall and shows posterior acoustic enhancement (arrowhead).

Corpus luteal cysts

Following ovulation, the corpus luteum forms from the ovulatory follicle. Corpus luteal cysts result from failure of involution of the corpus luteum. They are prone to haemorrhage and rupture, tending to be more symptomatic than follicular cysts, and patients often present with pain. Complex luteal cysts can mimic malignant lesions and follow-up may be required to ensure resolution.

Haemorrhagic cysts

Haemorrhage may occur in both types of functional cyst, although it is more common with corpus luteal cysts. Haemorrhagic cysts

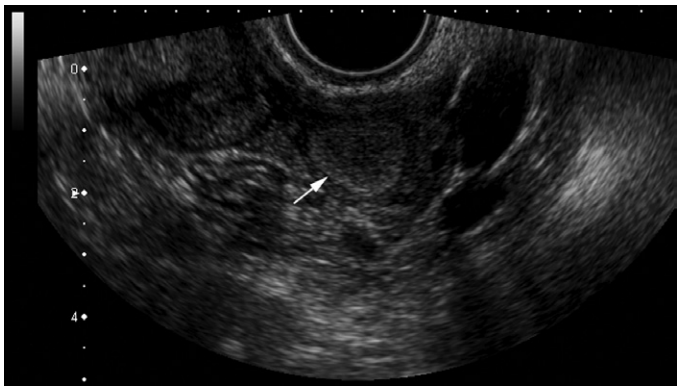


Figure 35.9 Haemorrhage. Transvaginal ultrasound image of an ovary containing an area of increased echogenicity (arrow), consistent with haemorrhage, which resolved on follow-up imaging.

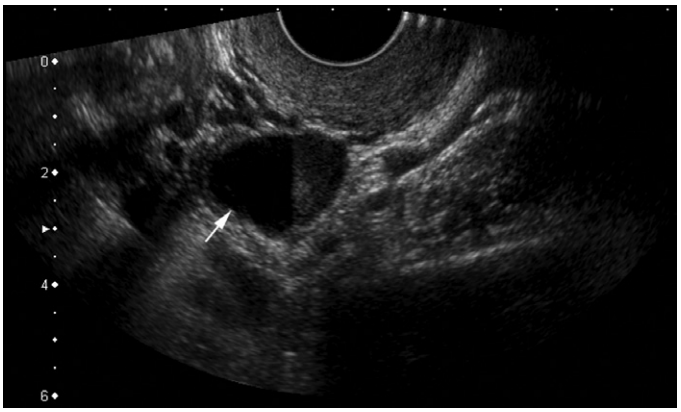


Figure 35.11 Haemorrhagic cyst (arrow) with a fluid level. The hyperechoic component layers inferiorly as opposed to a dermoid where the hyperechoic component tends to be located superiorly.

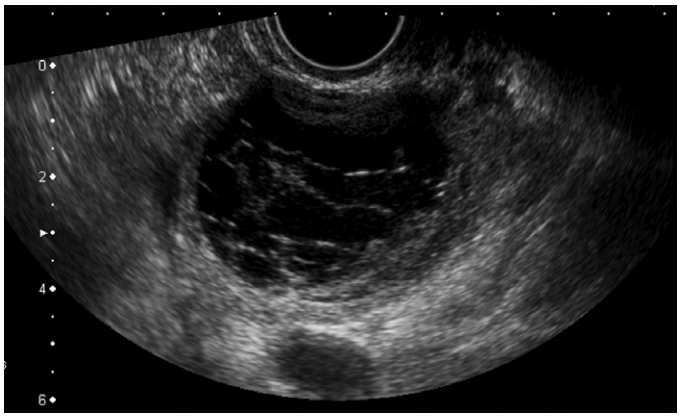


Figure 35.10 Reticular appearance of a haemorrhagic cyst. Transvaginal image showing a cyst containing a fine network of interfaces which are thought to correspond to fibrin strands.

have a variety of appearances at ultrasound, related to the changes in blood products with time. These include clot formation, retraction and lysis. Acute haemorrhage may be purely echogenic (Fig. 35.9) and can sometimes appear as a solid mass, although the presence of posterior acoustic enhancement helps to confirm the cystic nature of the lesion.

As the haemorrhage evolves it tends to develop a reticular appearance or a fine network of interfaces, which are thought to correspond to fibrin strands (Fig. 35.10). Fluid levels may be seen due to layering of the blood products (Fig. 35.11). With further organisation, solid areas of clot may be seen which later show retraction (Fig. 35.12).

The appearances of haemorrhagic cysts are clearly variable depending on their stage of evolution and thus they may simulate malignancies and other complex lesions. Patel et al. have identified fibrin strands and clot retraction in a smooth-walled cyst as the key features in the diagnosis of a haemorrhagic cyst.[5] It is important to try and distinguish these features from septa and solid mural nodules, which are more characteristic of neoplastic lesions. Septa are usually thicker and more reflective than fibrin strands.[5] Although septa may be multiple they usually appear discrete, as opposed to fibrin strands, which are typically mesh-like. Blood flow may be detected within septa but will not be observed within fibrin strands.

Retracting thrombus, which often has a concave margin, may be distinguished from mural nodules which are more typically convex[5] (Fig. 35.12). In addition, mural nodules tend to have a similar echogenicity to the cyst wall whereas thrombus is usually less echogenic.[5] While not all mural nodules will demonstrate blood flow, the presence of flow within a lesion effectively excludes thrombus. It is not always possible to make a definitive diagnosis, however, and resolving haemorrhage may sometimes contain apparent septa or mural nodules (Figs 35.13 and 35.14).

Management depends on clinical factors, including age and symptoms. Haemorrhagic cysts occur almost exclusively in relation to ovulation, and therefore should not occur in postmenopausal women. An asymptomatic lesion, which is characteristic for a haemorrhagic cyst, may not require follow-up. If a haemorrhagic lesion is suspected but appearances are atypical, a follow-up scan at 6–12 weeks is recommended, as most physiological lesions will show regression. Lesions that do not resolve may still be benign, such as an endometrioma, but persistent lesions will require gynaecological assessment regarding further treatment. A haemorrhagic cyst may be seen in association with an excess of fluid within the pouch of Douglas, which, in the correct clinical context, may indicate cyst rupture.

Paraovarian cysts

Paraovarian cysts account for 10% of adnexal masses.[6] They have been considered difficult to diagnose preoperatively,[7] although a recent retrospective study of 50 paraovarian cysts found that they were all correctly identified, by transvaginal scanning, prior to surgery.[8] They arise from the broad ligament and are usually of mesothelial or paramesonephric origin, and are less commonly derived from mesonephric remnants.[9,10] The cysts are most common in the third and fourth decades[6] and are often asymptomatic. They usually have the appearance of simple cysts although they may contain echoes and can be complicated by haemorrhage, infection or torsion. Paraovarian cysts containing neoplasm have also been described.[10] It is claimed that they are frequently located superior to the uterine fundus, particularly as they enlarge in size,[6] possibly explained by the mobility afforded by the broad ligament. Paraovarian cysts do not show cyclical changes and a specific diagnosis is only possible if the ipsilateral ovary can be demonstrated separate to the cyst[11] (Fig. 35.15).

Peritoneal inclusion cysts

Peritoneal inclusion cysts represent non-neoplastic, reactive mesothelial proliferation.[12] They are not true ovarian cysts, but

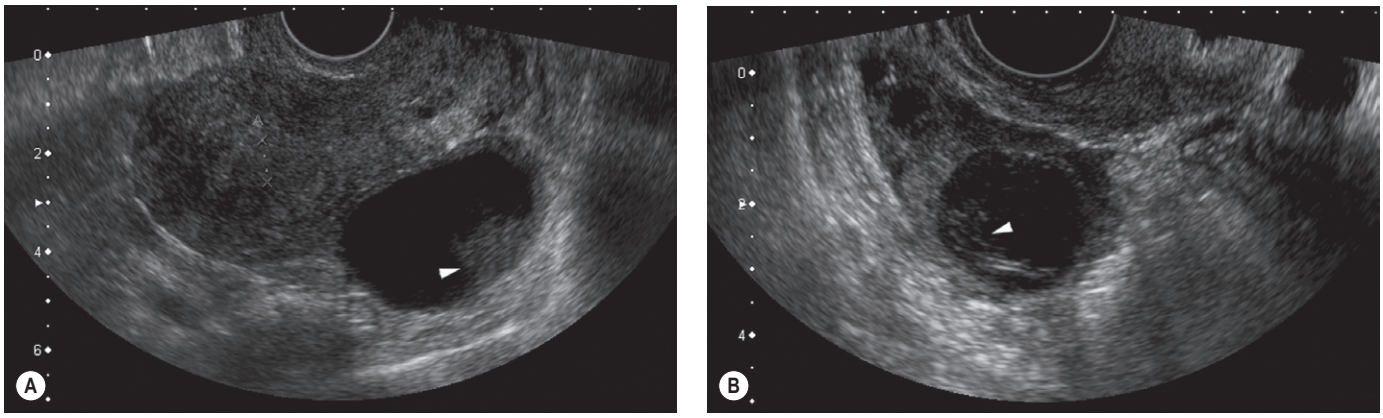


Figure 35.12 A and B: Clot retraction in haemorrhagic cysts. The clot in each of these haemorrhagic cysts has a concave margin (arrowhead), helping to distinguish it from a mural nodule.



Figure 35.13 Transvaginal ultrasound image of a haemorrhagic cyst (arrow). This contains apparent septa due to clot retraction but these resolved on follow-up imaging.

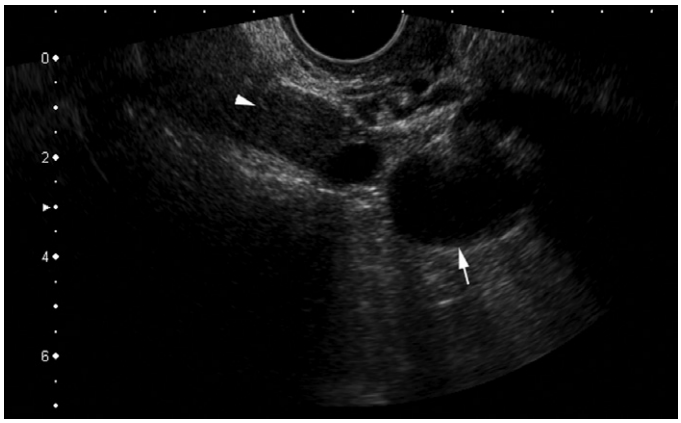


Figure 35.15 Transvaginal ultrasound image shows a cystic lesion (arrow) separate from the right ovary (arrowhead), which was proven at histology to be a paraovarian cyst.

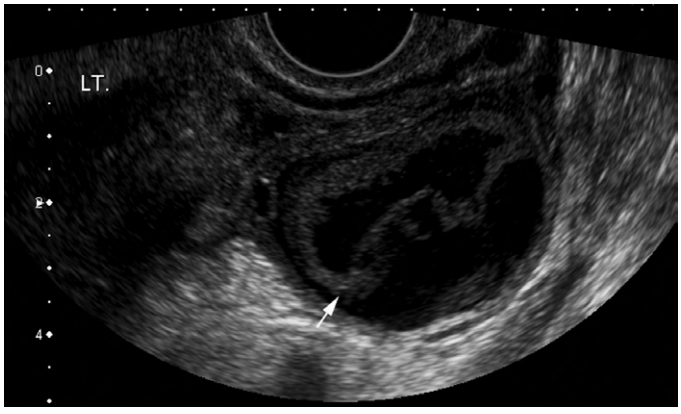


Figure 35.14 Haemorrhagic cyst with clot retraction. The internal echoes give the appearance of a thick wall and a septum (arrow), but these echoes showed movement on real-time scanning, did not show colour flow and resolved on follow-up imaging.

represent an accumulation of fluid, produced by the ovary, which fails to be resorbed by abnormal peritoneum and becomes contained by peritoneal adhesions. Their formation requires a functioning ovary and the presence of adhesions, and they therefore occur predominantly in premenopausal women with a history of previous surgery, pelvic inflammatory disease, trauma or endometriosis. Peritoneal inclusion cysts are lined by mesothelial cells and are also known as peritoneal pseudocysts or benign cystic mesothelioma, reflecting their origin. They have no malignant potential.[13] Clinically they often manifest as pain or a pelvic mass.

Ultrasonic appearances

Peritoneal inclusion cysts typically appear as multicystic, adnexal masses (Fig. 35.16). They are extra-ovarian, with fluid surrounding the ovary, without involvement of the parenchyma, and a key feature for their diagnosis is the presence of a normal, albeit sometimes distorted, ovary surrounded by septa and fluid. The ovary is not always identified, however, and may lie within the periphery of the cyst.[13,14] The walls of the cyst are formed by adjacent pelvic structures and acute angular margins are a characteristic feature. The differential diagnosis includes a paraovarian cyst or a hydrosalpinx.[13] Occasionally the entrapped ovary can be mistaken for a solid nodule, and dense adhesions may form thick septa, which may show vascularity, making distinction from an ovarian tumour difficult. A recent prospective study reports the sensitivity of transvaginal sonography in the diagnosis of peritoneal inclusion cysts as 62%, with a specificity of 96%.[12] A stable appearance on follow-up imaging, and the use of other imaging techniques, such as magnetic resonance imaging (MRI), may be helpful.

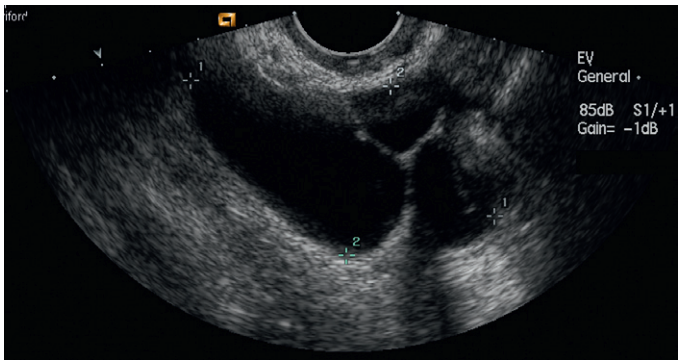


Figure 35.16 Transvaginal ultrasound image of a peritoneal inclusion cyst (between callipers), with fluid contained within septations which represent adhesions. The ovary itself is not clearly identified.

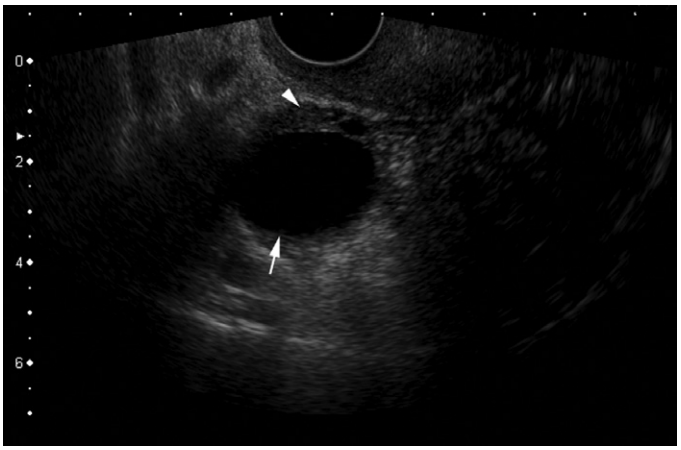


Figure 35.17 Transvaginal image of a cystic ovarian remnant (arrow), which was proven histologically. Ovarian tissue is identified within the wall of the cyst (arrowhead).

Peritoneal inclusion cysts often recur after surgery and their recognition at ultrasound may allow for a more conservative approach to treatment, such as hormonal therapies to suppress ovulation. Transvaginal aspiration has also been used for treatment, although cysts may recur.

Ovarian remnant syndrome

Ovarian remnant syndrome is an unusual condition, which occurs following a salpingo-oophorectomy where residual ovarian tissue is left, which can then result in pain or a pelvic mass. Incomplete excision of the ovaries is more common after difficult or repeated surgery, often for endometriosis or pelvic inflammatory disease, although it has occurred following surgery for removal of pelvic tumour.[15] The syndrome can occur from weeks to years following oophorectomy, and patients usually present with chronic pelvic pain, pain associated with a pelvic mass or an asymptomatic pelvic mass. Presentation with urinary symptoms, including obstructive uropathy, has also been reported.[15] Ovarian remnants may become incorporated within a peritoneal inclusion cyst.[16]

The sonographic appearance of ovarian remnants varies from small to large cystic masses, which may be simple or multiseptated cysts.[16] Distinction from peritoneal inclusion cysts, which often have a similar history, may be possible by finding the presence of ovarian tissue within the wall of a mass. Peritoneal inclusion cysts may contain a normal ovary within a cyst, whereas only a thin rim of tissue can usually be seen within an ovarian remnant[16] (Fig. 35.17).

Treatment is usually surgical excision by laparotomy or, more recently, laparoscopy, although hormonal treatments and percutaneous aspiration have been described.[16] Carcinoma developing in an ovarian remnant is rare, but has been reported.[17]

Postmenopausal cysts

With the increase in radiological imaging in general, and transvaginal ultrasound in particular, it has become apparent that ovarian cysts are common in postmenopausal women, with a reported prevalence of up to 20%.[18,19] Previously, surgery would have been considered the appropriate management for such cysts, but more recent studies have shown that the risk of malignancy in simple cysts under 5 cm in size is low (less than 1%) and furthermore that 50% of such cysts will resolve within 3 months[18,20,21] (Fig. 35.18). The Royal College of Obstetricians and Gynaecologists' guidelines recommend that postmenopausal cysts are assessed by transvaginal ultrasound and serum CA125 levels. Where CA125 levels are normal and simple cysts are less than 5 cm, conservative management may be appropriate with repeat US examinations every 4 months up to one year. Surgery should be considered for cysts greater than 5 cm or cysts that increase in complexity or size on follow-up.[18]

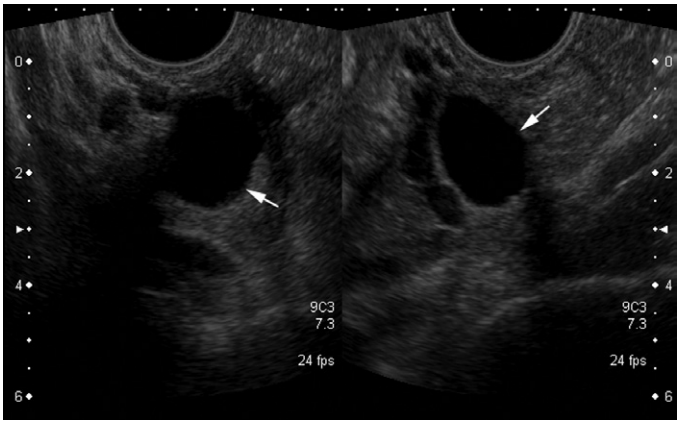


Figure 35.18 Postmenopausal cyst. Transvaginal, transverse and longitudinal, views of a simple postmenopausal cyst (arrow).

Polycystic ovary syndrome (PCOS)

PCOS is a syndrome of ovarian dysfunction associated with complex endocrine and metabolic disturbances. The key features of this syndrome include menstrual cycle changes and hyperandrogenism. Other manifestations include obesity, infertility, hirsutism and type 2 diabetes. The LH/FSH ratio is often, although not always, elevated and this is no longer a requisite for diagnosis. The definition of PCOS has recently been refined,[22] with two out of the following three criteria now required for a diagnosis (once appropriate tests have been performed to exclude other causes of androgen excess and menstrual disturbance such as congenital adrenal hyperplasia and Cushing's disease):

1. oligo- and/ or anovulation
2. clinical and/or biochemical signs of hyperandrogenism
3. finding of a polycystic ovary on ultrasound.

The new definition now includes a description of the morphology of the polycystic ovary (Fig. 35.19), which should have at least one of the following:

1. twelve or more follicles measuring 2–9 mm in diameter or
2. increased ovarian volume >10 cm^3.

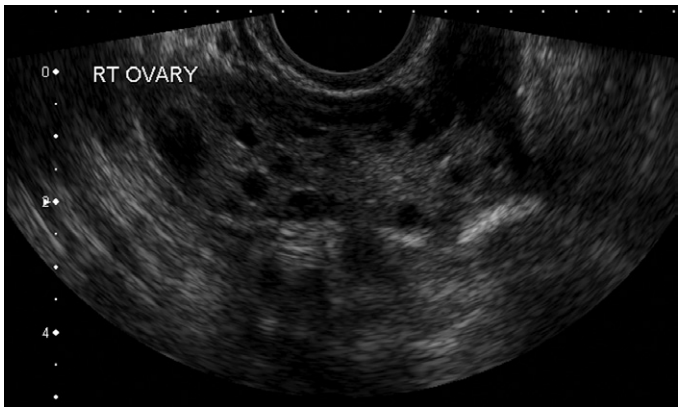


Figure 35.19 Transvaginal image of an enlarged ovary with multiple small follicles, consistent with a polycystic ovary.

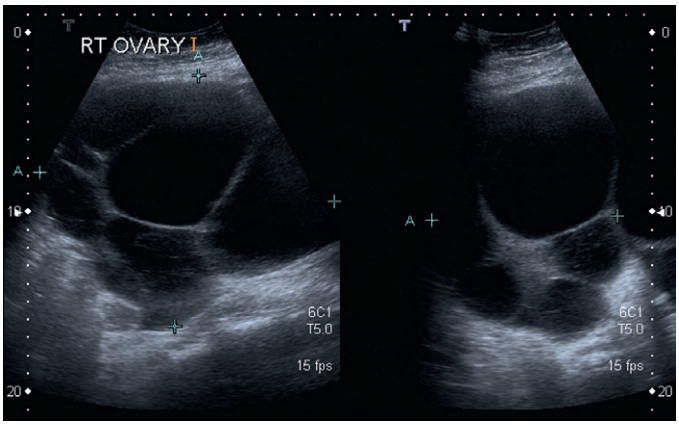


Figure 35.20 Ovarian hyperstimulation syndrome. Transabdominal images of a markedly enlarged ovary, with multiple cysts (between callipers). Mild ascites was present.

A single polycystic ovary is sufficient for the diagnosis, but if there is a follicle more than 10 mm in diameter, the scan should be repeated at a time of ovarian inactivity. A peripheral distribution of follicles and bright ovarian stroma are no longer required for the diagnosis. Other factors regarding optimal technique for scanning are outlined in the guidelines and include that:

- the transvaginal route should be used wherever possible, particularly with obese women
- the scan should ideally be performed in the first 3 days of the menstrual cycle, if practical, or at random if there is oligo- or amenorrhoea
- the number of follicles should be estimated in both the longitudinal and anteroposterior cross-sections of the ovary
- the size of follicles less than 10 mm should be expressed as the mean of the diameters measured on two sections.

It should be stressed that an ultrasound finding of a polycystic ovary is not by itself diagnostic of PCOS, which is a syndrome and requires the additional features described.[23] Likewise, if the clinical and biochemical features are present, an ultrasound is not required for the diagnosis. It is believed that 20% of women with polycystic ovaries have no symptoms.[22] While the previous criteria did not include ovarian appearance, some are concerned that the ultrasound criteria in the new definition are too broad. This could result in a low specificity with multifollicular ovaries being considered polycystic ovaries.[23]

The incidental discovery of a polycystic ovary can be an important finding to report. For example, in women with ovulatory infertility, where PCOS is not the cause, the presence of a polycystic ovary increases the risk of hyperstimulation syndrome if drugs are administered to stimulate the ovaries for assisted conception.[22]

Hyperreactio luteinalis and ovarian hyperstimulation syndrome

Theca lutein cysts

These are the largest of the functional cysts, and they result from excessive stimulation by gonadotrophins. They are seen primarily in patients with trophoblastic disease or as a result of iatrogenic administration of human chorionic gonadotrophin (hCG) for the treatment of infertility.

Hyperreactio luteinalis (HL) and ovarian hyperstimulation syndrome (OHSS) are both rare conditions during pregnancy. HL occurs during a spontaneous pregnancy and is characterised by the presence of multiple luteinised cysts secondary to hyperstimulation by hCG or increased sensitivity to hCG. HL occurs most commonly with hydatidiform mole or choriocarcinoma as well as other conditions resulting in high levels of hCG, such as multiple pregnancy. It has also been recorded with otherwise normal pregnancies.

This condition is usually asymptomatic or presents with mild abdominal symptoms. Ultrasound features are of bilaterally, or rarely unilaterally, enlarged ovaries which range in size from 3 to 20 cm. Multiple cysts and minimal stroma are said to give a 'spoke wheel' appearance.[24] Rarely, haemorrhage may occur into the cysts. Torsion or rupture can also occur and presentation in such cases is with acute pain. Ascites and pleural effusions are rare, although they may be seen in severe cases. Maternal virilisation is an associated finding in approximately 25% patients.[24]

Ovarian hyperstimulation syndrome

Ovarian hyperstimulation syndrome (OHSS) is an iatrogenic form of HL, following ovulation induction for the treatment of infertility. In addition to the enlarged ovaries (Fig. 35.20), this syndrome is characterised by ascites and pleural effusions. Systemic effects are thought to be due to vasoactive products released from hyperstimulated ovaries. In severe cases there may be marked fluid shifts with development of renal or liver dysfunction, acute respiratory distress syndrome (ARDS) and thrombotic complications.[25]

Most cases of severe ovarian hyperstimulation syndrome are seen following IVF treatment, but the condition can occur following any supraphysiological ovarian stimulation, including gonadotrophin ovulation induction and also, albeit rarely, with clomiphene alone.[25] Mild forms of the syndrome are common, affecting up to 33% of IVF cycles, but only 3–8% of IVF cycles are complicated by moderate or severe OHSS. Young lean women and those with polycystic ovaries are supposedly at increased risk and the severity is increased in cycles where conception occurs.

OHSS has rarely been reported to occur in spontaneously conceived pregnancies.[24] In these cases it may be difficult to distinguish severe HL from spontaneous OHSS. Whilst some authors distinguish the two on the basis of aetiology and clinical course, others view the conditions as a continuum.[24] In practice, the distinction is not important clinically as the treatment is the same.

OHSS has been classified according to severity, into mild, moderate, severe and critical grades.[26] In mild cases the ovaries usually measure less than 8 cm in association with mild abdominal symptoms, while in moderate cases the ovaries are larger, between 8 and 12 cm, with ultrasonic evidence of ascites. Severe disease is characterised by clinical ascites, with the ovaries often over 12 cm in size. With critical OHSS there may be tense ascites or a large hydrothorax, thromboembolic episodes and ARDS. Paracentesis may be helpful for the relief of symptoms and should be performed under

ultrasound guidance to avoid inadvertent puncture of the enlarged ovaries.

OVARIAN TORSION

Adnexal torsion is the partial or complete rotation of the ovarian pedicle on its long axis. It usually involves both the ovary and tube[27,28] and, if persistent, can result in infarction of the adnexal structures. Early intervention is important to attempt to preserve the ovary, but diagnosis is often difficult with both the clinical symptoms and signs and imaging features being non-specific.

Adnexal torsion has a prevalence of 2.7%.[29] It occurs predominantly in women of reproductive age or younger, and a pre-existing ovarian lesion is common.[30] Underlying lesions are usually benign, with teratoma being the most commonly reported, although underlying malignancy has been described. Torsion in the absence of an underlying condition is thought to be more common in children, where the adnexal structures are more mobile. When torsion occurs in postmenopausal women there is a higher incidence of an underlying lesion.[27] Other predisposing factors for torsion include pregnancy and ovulation induction. The right ovary is reported to be affected more frequently than the left in some series,[29,30] possibly related to the position of the colon on the left side.

The most common clinical presentation of torsion is acute onset of severe abdominal or pelvic pain often localised to a lower quadrant. Associated symptoms and signs include nausea and vomiting, leucocytosis and fever. A palpable abdominal mass may be present.[27] The absence of additional symptoms and signs does not, however, exclude the diagnosis.

The appearances of ovarian torsion are variable depending on whether it is partial or complete and on the presence or absence of a pre-existing mass. The most common sonographic finding is enlargement of the ovary or the presence of an adnexal mass, which may be cystic, solid or complex and which often reflects the underlying lesion (Fig. 35.21). Pelvic fluid is frequently an associated finding.[31] Previous reports suggest that the presence of multiple, small, peripheral follicles in a unilaterally enlarged ovary is a specific finding for torsion,[32,33] although other authors have failed to confirm this.[34] A recent review suggests that the only consistent greyscale finding in torsion is enlargement of the ovary or ovary mass complex and that other previously described findings, such as ground glass and cystic changes, are nonspecific.[35]

Various colour Doppler findings in torsion have been described but these are often conflicting. A number of studies have reported absence or abnormality of venous and/or arterial flow in association with torsion,[34] with some authors reporting the positive predictive value for torsion in the absence of venous flow as 94%.[36] However, others have shown normal arterial or arterial and venous flow in proven cases of torsion,[27] thought to be explained by either incomplete or intermittent torsion, or the presence of a dual arterial blood supply to the ovary (Fig. 35.22). Some have described a twisted vascular pedicle as a feature suggestive of ovarian torsion,[37] although this is not a specific finding. A more recent study has documented the sonographic whirlpool sign, i.e. the presence of hypoechoic vessels around the central axis of the twisted pedicle seen on greyscale imaging, as a more specific sign of ovarian torsion, with evidence of colour flow within this whirlpool of vessels an indicator of viability of the ovary.[31] Whilst the presence of this sign may be a good predictor of torsion, there is no indication, in this study, as to how often cases of torsion are likely to demonstrate this feature.

A recent retrospective review of 39 patients with proven torsion found that abdominal pain, vomiting, ovarian enlargement and absence of venous flow were the most common associations with torsion. However, ovarian enlargement, even in the presence of arterial and venous flow, is the most commonly associated ultrasound finding. The authors conclude that suspicion for torsion should be high if a patient presents with the appropriate clinical symptoms and ovarian enlargement, regardless of the presence or absence of flow. In these cases surgical exploration should not be delayed.[35]

CHARACTERISATION OF AN ADNEXAL MASS

Adnexal masses are a common clinical problem, with many women undergoing surgery for suspicious masses, the majority of which turn out to be benign. Ultrasound is usually the first-line investigation for evaluation of a suspected adnexal mass. It has high sensitivity for the detection of pelvic masses and for confirming that a mass is of ovarian as opposed to uterine origin, as well as excluding other pathologies such as bowel-related lesions.

The distinction from fibroids can be a particular problem, and not uncommonly a pedunculated or broad ligament fibroid may mimic an ovarian lesion or vice versa, especially where degeneration of a fibroid alters the characteristic ultrasonic appearances. In these instances, full assessment, often including further imaging with MRI, is appropriate.

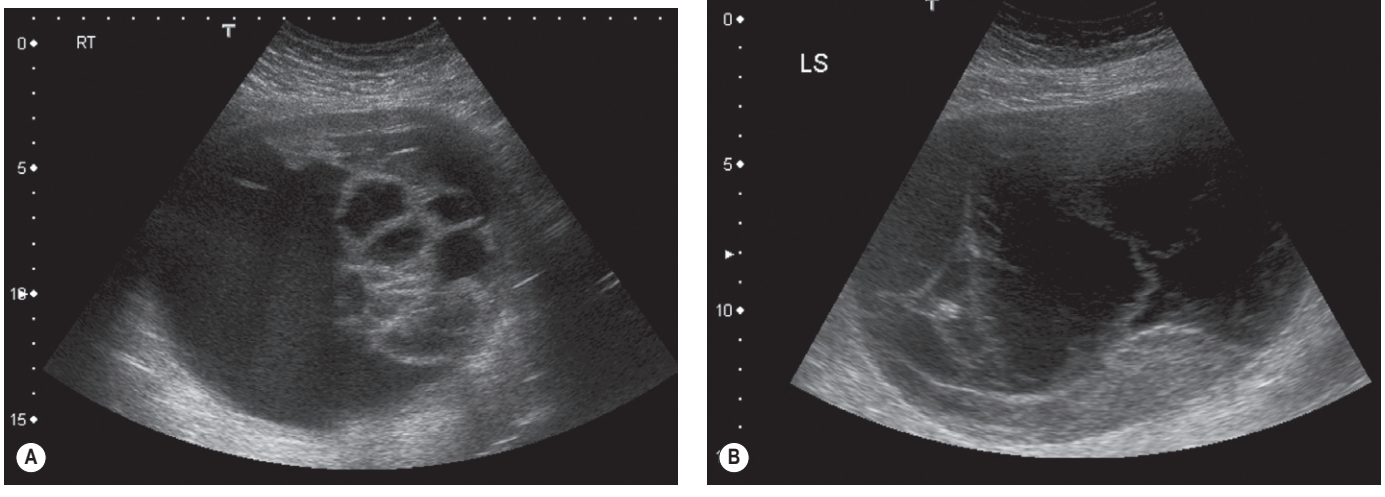


Figure 35.21 Two examples of pathologically proven torsion. A: No underlying cause could be identified. **B:** Torsion of a cystic epithelial tumour resulting in infarction. Both cases were associated with free fluid.

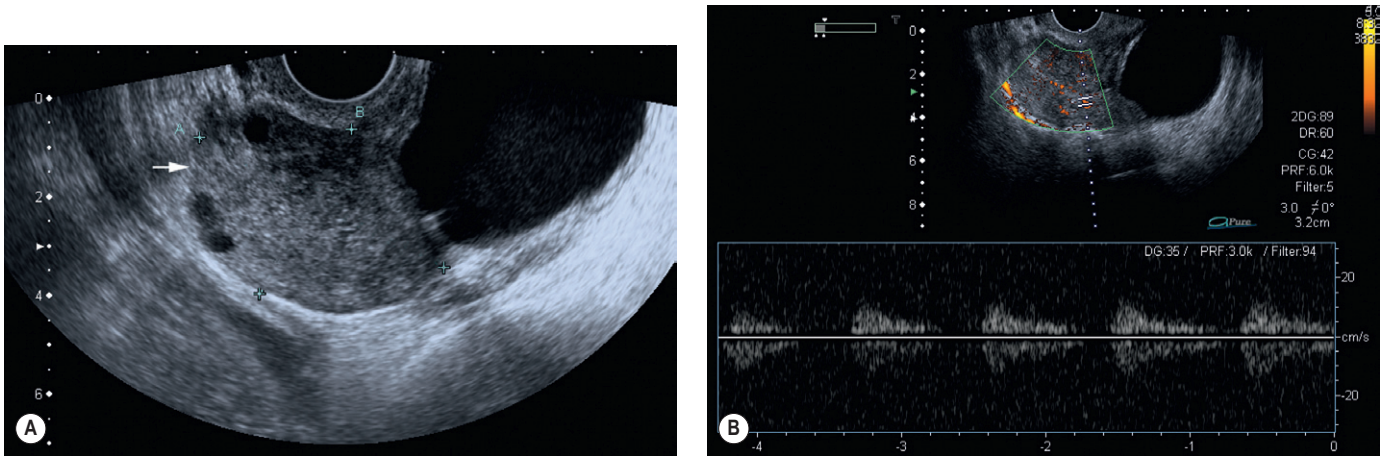


Figure 35.22 Surgically proven torsion of the ovary and tube. A: The enlarged ovary (arrow) shows peripheral follicles. **B:** Colour Doppler images show flow within the ovary and arterial flow is demonstrated with spectral Doppler.

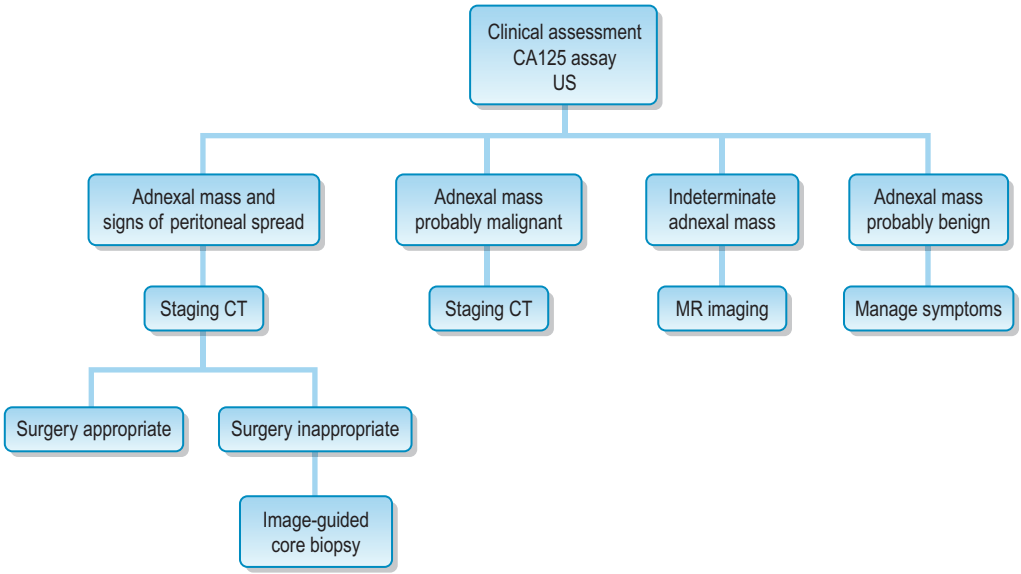


Figure 35.23 Pathway of imaging and intervention for suspected ovarian cancer. (Redrawn with permission from Investigating women with suspected ovarian cancer. Spencer JA et al. *Gynecologic Oncology* 108 (2008) 263. Elsevier.)

Ultrasound also has an important role in characterisation of an ovarian lesion, in order to inform decisions regarding treatment. The most important distinction is between a non-neoplastic or benign lesion as opposed to an ovarian cancer. Optimal surgical resection for ovarian cancer includes radical hysterectomy, bilateral oophorectomy and omentectomy with lymph node sampling, and best results are obtained when such extensive surgery is performed by specialist gynaecologists in cancer centres.[38] In benign or borderline malignant lesions more limited surgery, such as cystectomy or oophorectomy, may be appropriate and laparoscopic techniques may be an option. Optimal characterisation of lesions is therefore important in order to allow appropriate subspecialty referral, avoid inadequate surgery in malignant disease and likewise avoid inappropriate radical surgery for benign lesions.

Whilst ultrasound is useful in the characterisation of an ovarian mass, its limited specificity means that a number of lesions will remain indeterminate. A combination of clinical information (especially age and menopausal status), ultrasound features and tumour markers can be used to make decisions regarding further imaging or treatment strategies, with these decisions now generally made in the setting of the multidisciplinary team meeting (MDT).

Where clinical findings, ultrasound and CA125 levels suggest a benign lesion, follow-up imaging with ultrasound is recommended if symptoms do not require immediate surgery.

If they suggest a malignant lesion, either surgical staging or computed tomography (CT) is generally performed. CT is increasingly used to assess the extent of disease and suitability for surgery. In addition, CT can help to exclude other primary sites of tumour such as gastric or colonic carcinoma, which can mimic the appearance of ovarian cancer with peritoneal disease and ovarian masses. While MRI is superior to CT in assessing local spread of disease and is probably at least equivalent in terms of staging ovarian cancer, the limited availability of this technique means that CT remains the primary imaging modality for staging.

Where patients are considered for neoadjuvant chemotherapy, both ultrasound and CT may be helpful in guiding biopsy to obtain histology prior to treatment. While it may be appropriate to obtain histology for advanced tumours, biopsy is contraindicated for localised ovarian cancer, because of the potential to seed tumour and upstage the disease.

Indeterminate lesions with equivocal or contradictory findings on US, clinical examination and CA125 are best evaluated with

MRI, which serves as a problem-solving technique. MRI can provide tissue characterisation based on signal properties and has increased specificity for diagnosing benign lesions, such as endometriomas and teratomas, which can mimic malignancy on ultrasound examination.

BENIGN VERSUS MALIGNANT OVARIAN LESIONS (See Fig. 35.23)

While no single feature allows reliable distinction between benign and malignant lesions, a number of morphological features have been reported to be useful for characterisation. Well-defined, anechoic lesions are likely to be benign. With complex lesions, features reported to be more likely to indicate malignancy include large size, thick (>3 cm) irregular walls, thick (>3 cm) irregular septa, papillary nodules and solid elements. Not all authors consider size to be important.[39] The most significant feature is thought to be the presence of solid areas within an ovarian mass although a hyperechoic solid area is more likely to indicate a benign lesion on account of this being a particular feature of dermoids.[39] The presence of ascites is also suggestive of malignant disease.[39]

Greyscale ultrasound has a high sensitivity and negative predictive value for the characterisation of malignant masses, but has a low specificity and positive predictive value. Thus, as Stein has shown, whilst greyscale ultrasound can reliably predict benign lesions and is sensitive in the detection of malignancy, the low specificity means that many benign lesions are categorised as malignant on the basis of their morphology.[40]

The difficulties in distinguishing lesions purely on the basis of morphology led to a search for additional methods of discrimination, with colour and spectral Doppler initially appearing promising. The presence and distribution of colour flow have been considered important, with benign lesions tending to show peripheral flow and malignant lesions demonstrating internal flow.[41] However, others have demonstrated considerable overlap in flow patterns and again the low positive predictive value makes the use of colour Doppler alone unhelpful.[40]

The use of spectral Doppler is based on the presence of angiogenesis in malignant tumours. New vessels lack smooth muscle within their walls and this combined with arteriovenous shunting results in low resistance (increased diastolic) flow. Initial studies reported high sensitivities and specificities for spectral Doppler in distinguishing benign and malignant lesions.[42,43] Various thresholds for these parameters have been described, the most common using a pulsatility index (PI) of <1 or a resistive index (RI) of <0.4 as evidence of malignancy. Many studies have failed to confirm these findings, however, and there is too much overlap with benign lesions to make this a reliable technique.[40,44,45]

Despite the limitations, the use of Doppler imaging may still, however, be an important adjunct to morphological evaluation. A study using combined morphological and colour Doppler findings has emphasised the importance of interpreting the significance of flow in relation to its precise location, taking into account the morphological features. In this way, the addition of colour Doppler increased the specificity and positive predictive value for diagnosing malignancy, but the use of spectral Doppler did not improve diagnostic accuracy.[46] A recent meta-analysis has also suggested that a combination of morphology and colour Doppler is best for characterisation of adnexal masses.[47] Whilst spectral Doppler currently has little role in the characterisation of adnexal masses, colour flow continues to be used clinically and these findings help to define its role.

The possible contribution from combined colour Doppler sonography with three-dimensional imaging and the potential use of ultrasound contrast have been considered but await further investigation.[48]

Scoring systems using morphological features and Doppler criteria have been used to try and standardise the diagnosis of ovarian cancer by assigning numerical scores to ultrasound features. However, similar results are obtained when experienced sonographers use subjective criteria in conjunction with clinical information,[49] and pattern recognition is thought to be superior to scoring systems for discrimination between benign and malignant lesions.[50]

Ovarian masses – morphological ultrasound features suggestive of benign or malignant disease

Benign disease	Malignant disease
Small size	Large size
Thin walls <3 mm	Thick walls >3 mm
Smooth walls	Irregular walls
Purely cystic	Solid/Complex
Thin septa <3 mm	Thick septa >3 mm
	Papillary nodules (especially if large/multiple)
Highly echogenic solid component	Solid component
	Ascites
	Peritoneal implants
	Lymphadenopathy

Size: not all authors agree that size is important and whilst malignant tumours tend to be larger than benign tumours this is not a good discriminating feature.

Solid component: a solid component is the most significant predictor of a malignant ovarian mass. However, a highly echogenic solid component is more likely to indicate a benign mass, as this feature is strongly associated with teratomas.

OVARIAN TUMOURS

Ovarian cancer is the leading cause of mortality from gynaecological malignancy[51] and the fourth most common cause of cancer death in women.[52] The lifetime risk of developing ovarian cancer is approximately 1 in 48 for women in England and Wales.[53] There is, to date, no effective screening programme, and there are few specific symptoms and signs of ovarian cancer. Consequently the majority of women present with advanced stage disease with poor survival rates. Approximately 60–65% women present with stage III disease at the time of diagnosis. Whilst the 5-year survival approaches 80–90% for patients with stage I disease, it ranges from only 5% to 50% in women with stage III–IV disease.[54]

Increasing age is a risk factor for ovarian carcinoma but the age distribution varies with tumour type. Epithelial ovarian cancer is a disease of postmenopausal women, with a median age at diagnosis of 62 years, whereas germ cell and sex cord stromal tumours occur most often in the second and third decades of life.

The most consistently reported risk factor for ovarian cancer is uninterrupted ovulation, so that nulliparous women are at increased risk, as are those with an early menarche and a late menopause. Conversely, the risk is decreased with increasing parity, breastfeeding and the use of oral contraceptives.

A hereditary link is recognised in less than 5% of cases, with three recognised inherited syndromes of ovarian cancer:

1. breast and ovarian familial cancer syndrome, linked to the tumour suppressor gene BRCA1.
2. Lynch II syndrome, characterised by colon, breast, endometrial and ovarian cancers in family members.
3. site-specific ovarian cancer, the least common of the genetic syndromes, in which ovarian cancer is present in two or more first or second degree relatives.[55]

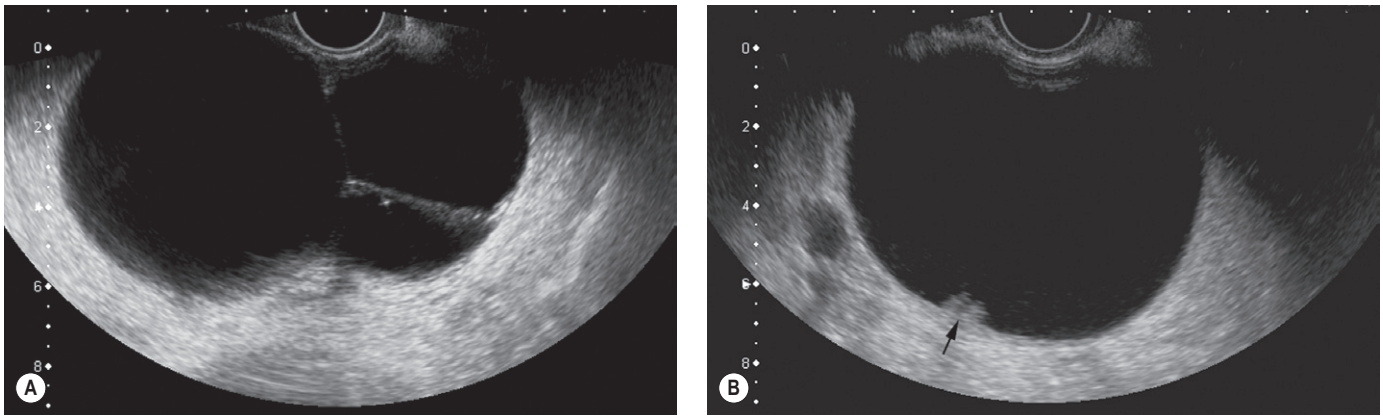


Figure 35.24 Benign serous cystadenoma. Transvaginal images showing **(A)** a thin-walled loculated lesion with hypoechic fluid. The septa are thin. **B:** A unilocular cyst with echo-free fluid and a small papillary nodule (arrow).

Table 35.2 Classification of ovarian neoplasms

Tumour type	As proportion of all ovarian tumours	Classification
Epithelial	65–70%	Serous cystadenoma/carcinoma Mucinous cystadenoma/carcinoma Endometrioid carcinoma Clear cell carcinoma Brenner tumour
Germ cell	15–20%	Mature teratoma/dermoid Immature teratoma Dysgerminoma Yolk sac tumour
Sex cord stromal	5–10%	Granulosa cell tumour Sertoli–Leydig cell tumour Fibroma Thecoma
Metastatic tumours	5–10%	

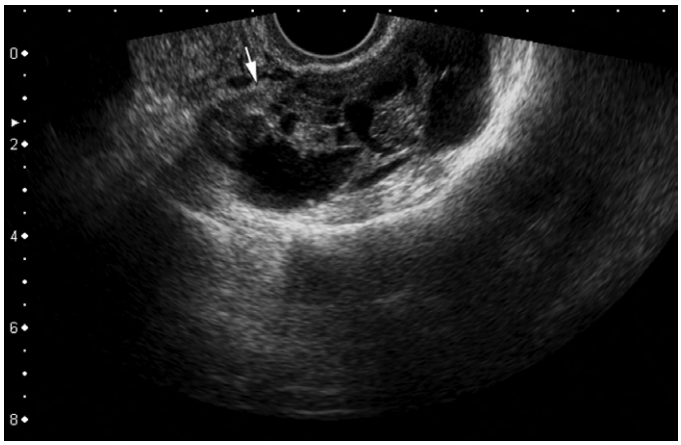


Figure 35.25 Serous cystadenocarcinoma. Transvaginal image shows a cystic lesion with prominent soft tissue elements (arrow). Colour flow was seen centrally within the soft tissue on Doppler imaging.

Symptoms

Symptoms of ovarian cancer are usually non-specific and patients may present with a palpable mass, abdominal pain or distension, weight loss or vague gastrointestinal symptoms. Hormonal activity may be associated with the sex cord stromal tumours but is rarely associated with epithelial tumours, with the exception of some endometrioid tumours.

Classification

Ovarian tumours may be primary or metastatic. They are classified on the basis of cell origin as epithelial, germ cell and sex cord stromal tumours (Table 35.2). While it is not the role of ultrasound to characterise tumours on a histological basis, imaging features may sometimes suggest a tumour subtype.

Epithelial neoplasms

Epithelial tumours are the most common type of ovarian neoplasm (Table 35.2). The majority of them are benign although most malignant ovarian neoplasms (85%) are of the epithelial type.[51] There is also a borderline category, otherwise known as 'tumours of low malignant potential'. These tumours have cytological features of malignancy but show no evidence of stromal invasion.[51] They are found in younger patients and have a better prognosis than their malignant counterparts.

Serous tumours – serous cystadenoma and cystadenocarcinoma

Serous tumours are the commonest type of epithelial neoplasms, comprising 30% of all ovarian neoplasms. Approximately 60% are benign, 25% malignant and 15% are classified as borderline or of low malignant potential.[51] Serous cystadenocarcinomas represent about 40% of malignant ovarian tumours. Cystadenomas have a peak incidence in women aged between 30 and 40 years, whereas cystadenocarcinomas are more common in perimenopausal and postmenopausal women. Approximately 20% of benign, but 50% of malignant serous tumours are bilateral.[51]

Ultrasonically, these tumours reflect their macroscopic appearance. They are predominantly cystic and may be either unilocular or multilocular with thin septa in the benign types (Fig. 35.24A). They contain largely echo-free, serous fluid. These tumours are characterised by papillary projections and their presence is the

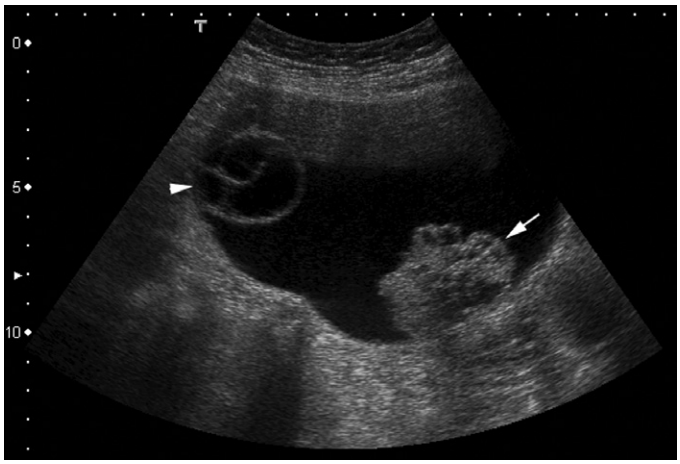


Figure 35.26 Borderline serous tumour. Transabdominal ultrasound image of a predominantly cystic mass with an irregular nodule (arrow), and septa (arrowhead). There are no specific features to distinguish this from other serous tumours.

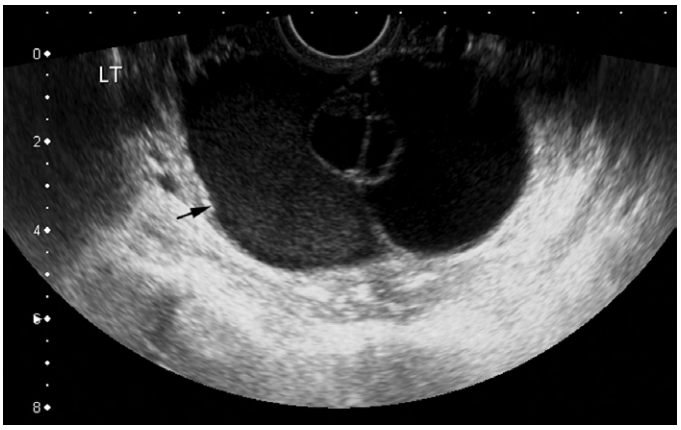


Figure 35.28 Mucinous cystadenoma. Transvaginal ultrasound image shows a multilocular tumour with low-level echoes (black arrow). Individual locules may vary in echogenicity due to difference in mucin content.

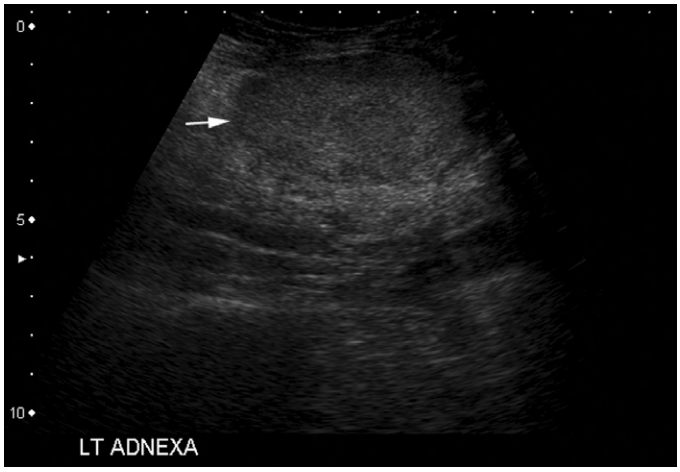


Figure 35.27 Peritoneal disease. Transabdominal image showing omental disease (arrow), on the left side in a woman with a serous ovarian carcinoma. When a complex mass is discovered at pelvic ultrasound, the scan should be extended to look for hydronephrosis and evidence of tumour spread, e.g. omental disease and ascites Ultrasound is less sensitive than other imaging techniques for the detection of peritoneal disease, but if it is identified it confirms the presence of advanced malignant disease.

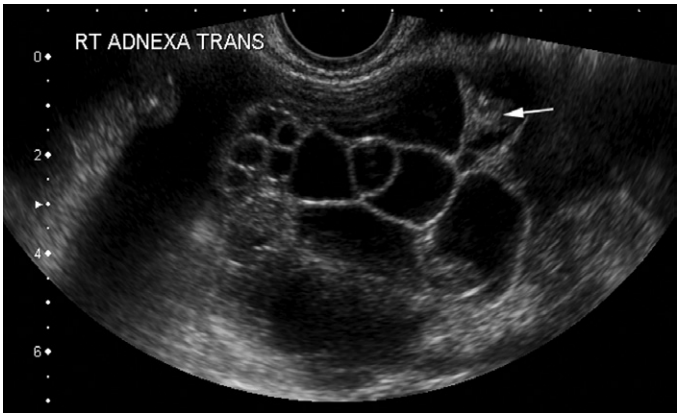


Figure 35.29 Borderline mucinous cystadenoma. Transvaginal image of a multilocular cystic lesion with some solid areas (arrow).

single best predictor of an epithelial neoplasm.[56] These projections are often absent, or small if present, in the benign forms (Fig. 35.24B). Profuse papillary projections are highly suggestive of borderline or malignant subtypes.[56] Malignant lesions tend to have more solid tissue overall (Fig. 35.25), with haemorrhage and necrosis seen more commonly than with benign lesions. Imaging features of borderline tumours may resemble benign or malignant neoplasms and there are no specific features that allow reliable differentiation[54,57] (Fig. 35.26).

Peritoneal carcinomatosis is seen more frequently in serous than mucinous cystadenocarcinomas.[56] Ultrasound is less sensitive than other imaging modalities in the detection of peritoneal spread,[58] but omental deposits may be identified (Fig. 35.27) and the use of a linear high-frequency probe may be helpful to improve visualisation of disease within the near field.

Mucinous tumours – mucinous cystadenoma and cystadenocarcinoma

Mucinous tumours are less common than serous tumours and account for 20–25% of ovarian tumours. Approximately 80% of them are benign, 10% borderline and 10% malignant. Mucinous tumours are less commonly bilateral than serous tumours, with 5% of the benign and 15–20% of the malignant lesions occurring bilaterally.[51]

These lesions are usually multilocular, with multiple thin-walled cysts, although they may be unilocular. They tend to be larger than serous tumours and they often contain echogenic fluid, reflecting their high mucin content (Fig. 35.28). Malignant lesions tend to have thicker walls and septa and contain more solid elements (Figs 35.29 and 35.30).

Pseudomyxoma peritonei

Pseudomyxoma peritonei is a rare condition in which there are peritoneal implants associated with massive mucinous ascites. The ascites surrounds the mesentery, bowel and organs and has mass effect, which can give rise to a characteristic scalloping of the surface of the liver and spleen.

Ovarian cancer – epithelial neoplasms

- Most malignant ovarian neoplasms are of the epithelial type.
- Malignant epithelial tumours are:
  - most common in postmenopausal women
  - uncommon before 40 years of age.
- Epithelial tumours are primarily cystic and when malignant are associated with varying proportions of solid tissue.
- Papillary projections are a characteristic feature of epithelial neoplasms.
- Serous cystadenocarcinomas are more often bilateral than mucinous (approximately 50% of serous and 15–20% of mucinous cystadenocarcinomas are bilateral).
- Peritoneal carcinomatosis is seen more often with serous than mucinous cystadenocarcinomas.
- Mucinous tumours may be associated with pseudomyxoma peritonei.



Figure 35.30 Mucinous cystadenocarcinoma. Transabdominal image of a large complex cystic and solid lesion (arrow). The prominent soft tissue elements increase the likelihood of malignancy.

It is most commonly associated with benign, borderline or malignant mucinous tumours of the appendix and ovary. It is now recognised that in the majority of cases the primary tumour is appendiceal with metastases to the ovaries[59] (Fig. 35.31).

Endometrioid tumours

Endometrioid tumours represent 10–15% of all ovarian carcinomas.

They are less common than mucinous tumours but are nearly always malignant, making them the second most common ovarian malignancy. Approximately 25% of endometrioid tumours are bilateral.[51] They are associated with endometrial hyperplasia or carcinoma in 20–30% of cases but most are thought to represent independent primary tumours.[51] Rarely, they are thought to arise from endometriosis.[60] Endometrioid tumours have a better prognosis than serous or mucinous tumours, which may be partly related to diagnosis at an earlier stage.

Endometrioid tumours have a non-specific ultrasound appearance and are usually part cystic and part solid (Fig. 35.32), although they can occasionally present as solid lesions particularly in postmenopausal patients. Endometrial thickening may be identified (Fig. 35.32).

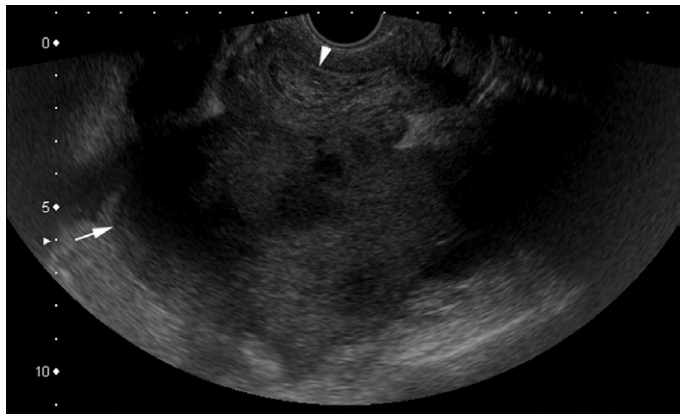
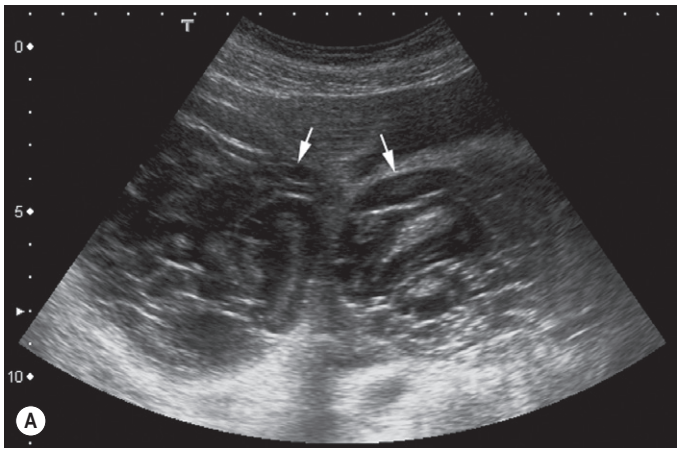


Figure 35.32 Endometrioid tumour. Transvaginal image showing a cystic and solid endometrioid tumour of the ovary (arrow), with associated thickening of the endometrium (arrowhead).



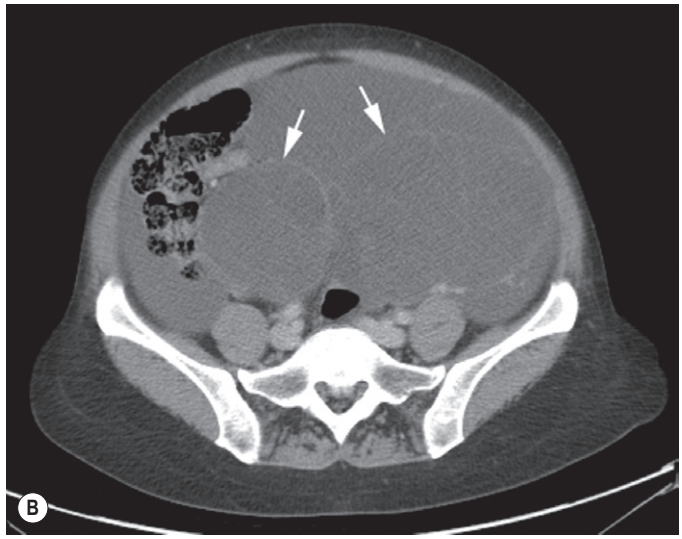


Figure 35.31 Pseudomyxoma peritonei. Transverse transabdominal ultrasound image **(A)** and axial contrast-enhanced CT scan **(B)** showing bilateral mucinous ovarian tumours (arrows). Mucinous ascites was present. A low-grade primary mucinous tumour of the appendix was identified at surgery and histology.

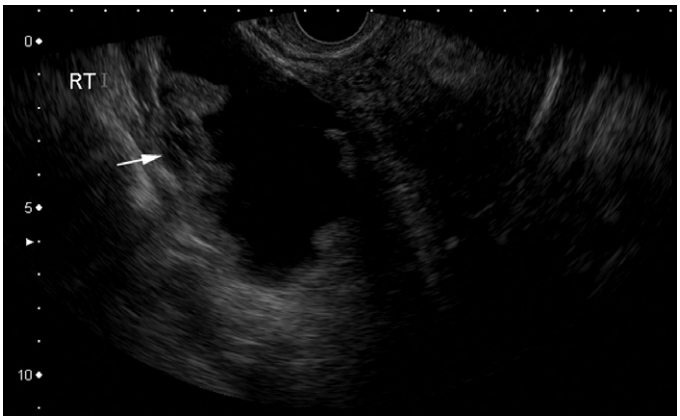


Figure 35.33 Clear cell tumour. Transvaginal image showing a cystic lesion with peripheral, solid areas (arrow). These appearances are non-specific.

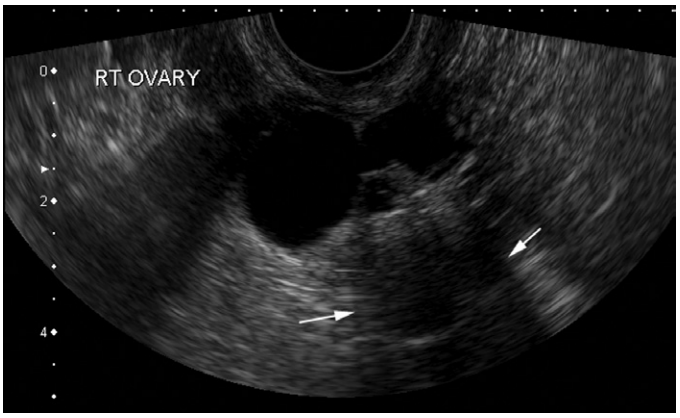


Figure 35.34 Brenner tumour in association with a mucinous cystadenoma. There is a complex cystic lesion with a solid area (arrows), which represents the Brenner tumour. These appearances are non-specific and the Brenner tumour was only identified histologically.

Clear cell tumours

Clear cell tumours make up approximately 10% of ovarian cancers and are nearly always malignant. They are bilateral in approximately 20% of cases and they also may arise in endometriosis.[56] They tend to have a better prognosis than other ovarian tumours as the majority of them present as stage 1 disease.

Sonographically, they appear as non-specific, predominantly cystic masses with some solid elements (Fig. 35.33).

Brenner (transitional cell) tumours

Brenner tumours, also known as transitional cell tumours because of their histological similarity to urothelium, are relatively rare[61] and are usually benign. They represent approximately 3% of ovarian tumours. They are often small and are usually discovered incidentally in women between their fifth and seventh decades.[61] They are usually unilateral.[61] Approximately 20% of Brenner tumours are associated with other epithelial tumours. They are typically solid homogeneous lesions and although extensive calcification may be seen, cystic areas are unusual except when due to coexistent cystic tumours.

On ultrasound examination, they tend to be small, typically 1–2 cm, hypoechoic lesions with associated shadowing and may contain calcification.[62] Their appearance is similar to other solid lesions and the differential diagnosis includes fibromas, fibrothecomas and pedunculated fibroids.[61] MRI may be helpful in characterising these lesions. When associated with other tumours they appear similar to complex cystic lesions (Fig. 35.34).

Germ cell tumours

Germ cell tumours represent approximately 15–20% of all ovarian tumours, with 95% of these being benign, cystic teratomas. Germ cell tumours also include immature teratoma, dysgerminoma and yolk sac tumours (embryonal carcinoma and choriocarcinoma).

Mature teratoma (dermoid)

Mature teratomas are the commonest benign neoplasms.[63] They are usually found in young women of reproductive age but can occur in all age groups including postmenopausal women. They are bilateral in up to 20% of cases.

They are composed of mature tissue elements from two or more embryonic germ cell layers (ectoderm/mesoderm/endoderm). Ectodermal elements predominate and they are alternatively known as dermoid cysts. They are almost always benign and usually

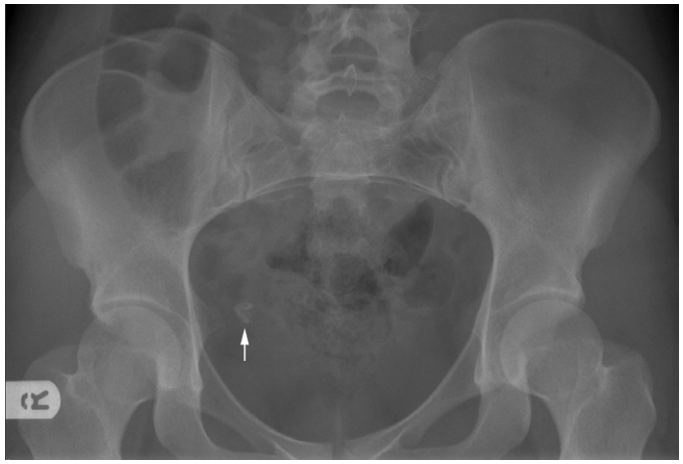


Figure 35.35 Pelvic radiograph showing teeth (arrow), within a dermoid on the right side of the pelvis.

contain sebaceous material as well as variable amounts of hair, teeth, bone and muscle (Fig. 35.35). Pathologically they often have a projection into the cyst cavity, the Rokitansky nodule, which usually contains hair or teeth.

Sonographically, mature teratomas have a broad spectrum of appearances on account of their variable internal composition. They are predominantly cystic but the presence of teeth and hair gives them complex features. Although their wide range of appearances can cause diagnostic difficulty they often show specific features.

Characteristic appearances include a cystic lesion with a dense echogenic nodule – the dermoid plug, or Rokitansky nodule. This plug represents an ingrowth of solid tissue from the tumour wall and usually shows shadowing due to the presence of calcification or hair within it[64] (Fig. 35.36). Teeth, bone and calcification usually produce an intensely echogenic nodule with well-defined shadowing, whereas the shadowing distal to sebum and hair, which occurs due to the multiple interfaces, is more ill defined and heterogeneous. A characteristic sign of a dermoid is an echogenic mass, containing sebaceous material and hair, with acoustic shadowing distally which obscures the posterior border of the lesion, resulting in the 'tip of the iceberg' sign[65] (Fig. 35.37). Fluid levels are a less common[66] but fairly specific finding, representing the interface between hair and sebum. Another characteristic appearance is

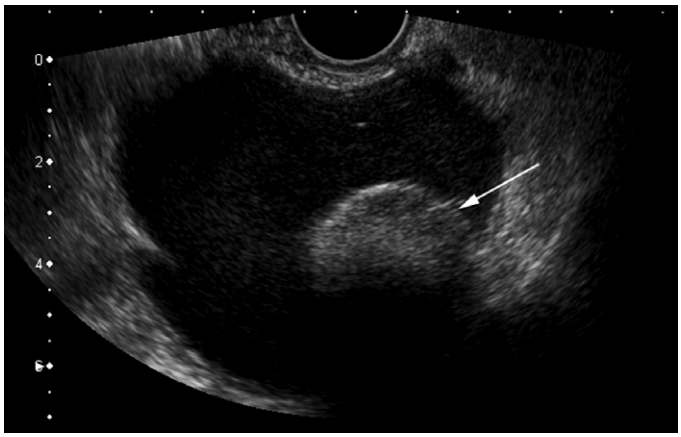


Figure 35.36 Dermoid cyst. Transvaginal image shows a cystic lesion containing echoes and a hyperechoic nodule (arrow) – the dermoid plug. The nodule shows posterior acoustic shadowing due to adipose tissue or calcification within the plug, or to hair arising from it.

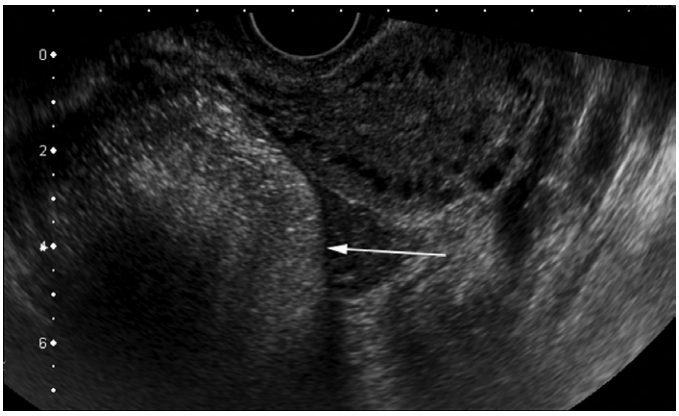
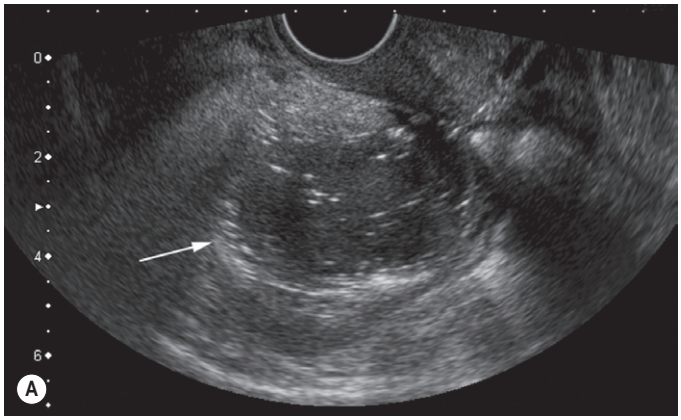


Figure 35.37 Dermoid cyst. Transvaginal ultrasound image of a dermoid (arrow), which demonstrates the 'tip of the iceberg sign'. Anterior bright echoes cause attenuation that obscures the posterior border of the lesion.



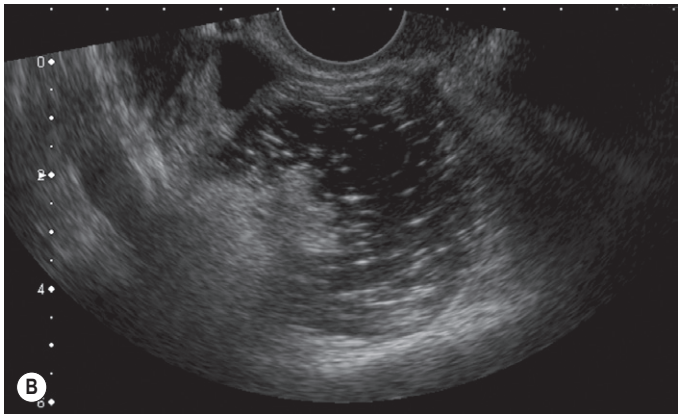


Figure 35.38 Transvaginal images showing examples of 'dermoid mesh'. A: A dermoid cyst (arrow), with multiple linear hyperechogenic interfaces or 'dermoid mesh' which is thought to be due to hair fibres. **B:** A dermoid cyst with echogenic lines and dots ('dermoid mesh') in association with an echogenic nodule, which shows the 'tip of the iceberg' sign.

multiple linear echogenic interfaces and echogenic dots in a cystic lesion, known as 'dermoid mesh', which is thought to be due to hair fibres (Fig. 35.38). The presence of multiple floating fat balls in a cystic tumour has also been reported as a rare, but possibly pathognomonic, sign for a cystic teratoma.[67] Caspi et al. have devised a simple classification system with a high diagnostic accuracy rate for the diagnosis of dermoids, based on the main pathognomonic patterns.[66]

Some studies have assessed the vascularity of dermoids, with most found to be avascular. Where vascularity was demonstrated it was shown to be peripheral only.[68,69]

Whilst a lesion may show the typical features of a dermoid, other tumours can on occasion show similar features, e.g. an echogenic plug,[70] echogenic lines or fluid levels. Patel et al. have reported that the positive predictive values for individual sonographic features associated with a dermoid are 80% for a shadowing echodensity, 75% for bright echoes, 50% for hyperechoic lines and dots and 20% for a fluid level. In their study,[71] while 74% of dermoids demonstrated more than one feature, none of the other masses did, giving a positive predictive value for more than one feature of 100% (Fig. 35.39).

In addition, atypical dermoids can occur, which may appear as purely cystic or occasionally solid lesions. Because of their echogenicity, dermoids can also be difficult to distinguish from bowel

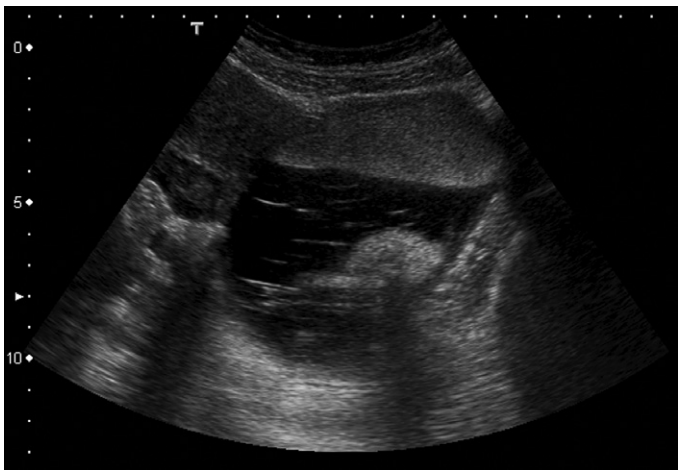


Figure 35.39 Dermoid cyst. Transabdominal image showing a dermoid cyst with a fluid level, in addition to a dermoid plug and 'dermoid mesh'. The presence of multiple characteristic features is highly predictive for a dermoid. In dermoid cysts the echogenic layer tends to lie superiorly, while in haemorrhagic cysts and endometriomas the echogenic blood tends to layer dependently.

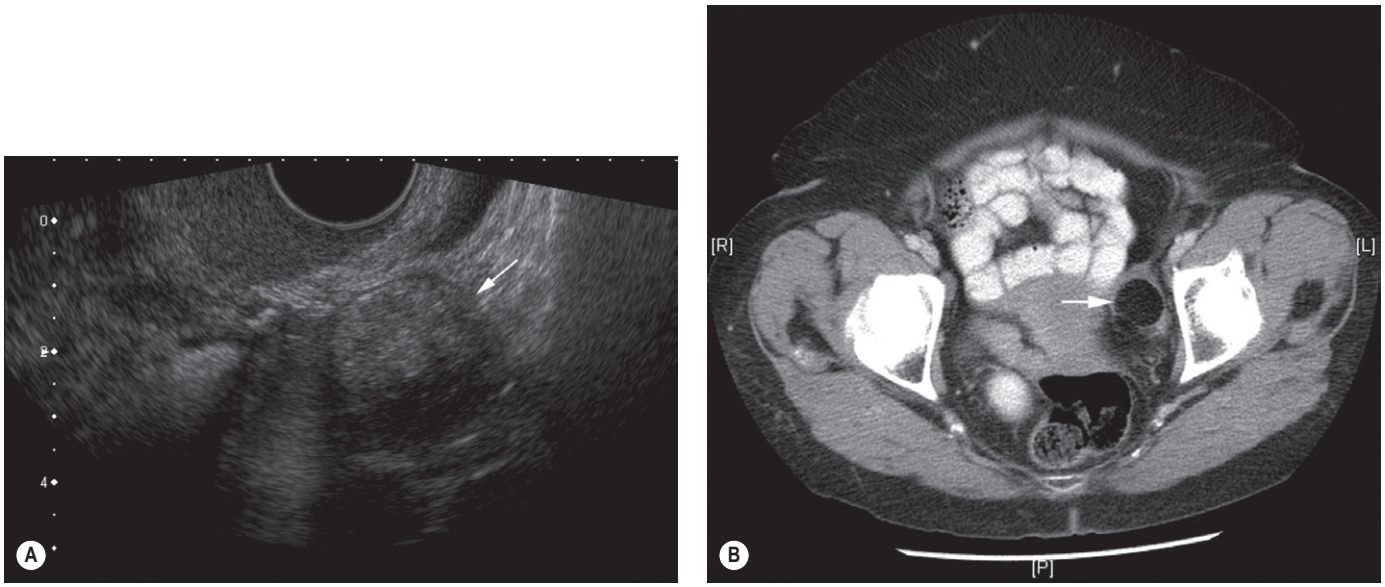


Figure 35.40 Dermoid cyst. Transvaginal scan **(A)** shows an echogenic dermoid (arrow) on the left side, which was difficult to distinguish from bowel. CT scan **(B)** in the same patient confirms the presence of a fat containing lesion (arrow), which is diagnostic of a dermoid. MRI, which does not involve ionising radiation, is now the most commonly used imaging modality to further evaluate a suspected dermoid.

Tumour markers

- CA125 is the most commonly used serum marker for ovarian cancer.
- Germ cell tumours may produce alpha-fetoprotein and hCG.

Ovarian tumours associated with endometrial hyperplasia/carcinoma

- Endometrioid carcinoma
- Granulosa cell tumours
- Thecoma/fibrothecoma (occasionally)

(Fig. 35.40) and small, echogenic dermoids may be mistaken for haemorrhagic lesions. Finally, a large dermoid may be identified but not recognised if some of its borders are obscured, on account of the limited field of view afforded by transvaginal sonography. This emphasises the importance of including a transabdominal scan for pelvic imaging, which is particularly important when a pelvic mass can be palpated but not visualised on transvaginal views.

Further imaging relies on identification of fat, for which MRI is now the most widely used imaging modality. Fat appears as high signal on T1-weighted MRI sequences and shows suppression on fat saturation sequences. This allows distinction from haemorrhage and confirmation of the diagnosis of a dermoid (Fig. 35.41). Although CT imaging also allows identification of fat (Fig. 35.40), it has the disadvantage of using ionising radiation.

Complications of dermoids include torsion, rupture and rarely malignant change. Torsion is the most frequent complication and is reportedly more common in pregnancy. Large dermoids are usually removed to prevent torsion. Rupture occurs rarely in approximately 1%. Malignant change is also rare, occurring in 1–2% of cases, with squamous carcinoma being the most common malignancy to develop.[57] Malignant transformation usually occurs in older women and may be recognised by the presence of enhancing nodules on MRI.

Immature teratomas

Immature teratomas represent less than 1% of all teratomas. They are rapidly growing malignant tumours, and are most common in the first two decades of life.

They tend to be unilateral and are predominantly solid or have prominent solid elements within a cyst at ultrasound examination.[54,57]

Dysgerminomas

Dysgerminomas represent 1–2% of ovarian neoplasms. They are malignant germ cell tumours, which resemble seminomas and are most common under 30 years of age. They are usually solid tumours and are predominantly unilateral.[57] They may be associated with elevated serum hCG levels.

Yolk sac tumours (endodermal sinus tumours)

These are rare malignant tumours, which occur mainly in children or young women. At ultrasound they are predominantly echogenic, solid masses[57] but can contain cystic and solid elements.[56] These tumours are associated with an elevated alpha-fetoprotein level.

Sonographic features of a dermoid cyst (teratoma)

The sonographic appearance of dermoids is highly variable. Characteristic appearances include:

- focal or diffuse high-amplitude echoes that attenuate the acoustic beam
- echogenic mural nodule, often with acoustic shadowing – dermoid plug
- 'tip of the iceberg' sign – acoustic shadowing posterior to an echogenic focus that obscures the posterior border of the lesion
- hyperechoic lines and dots – dermoid mesh
- fat–fluid levels.

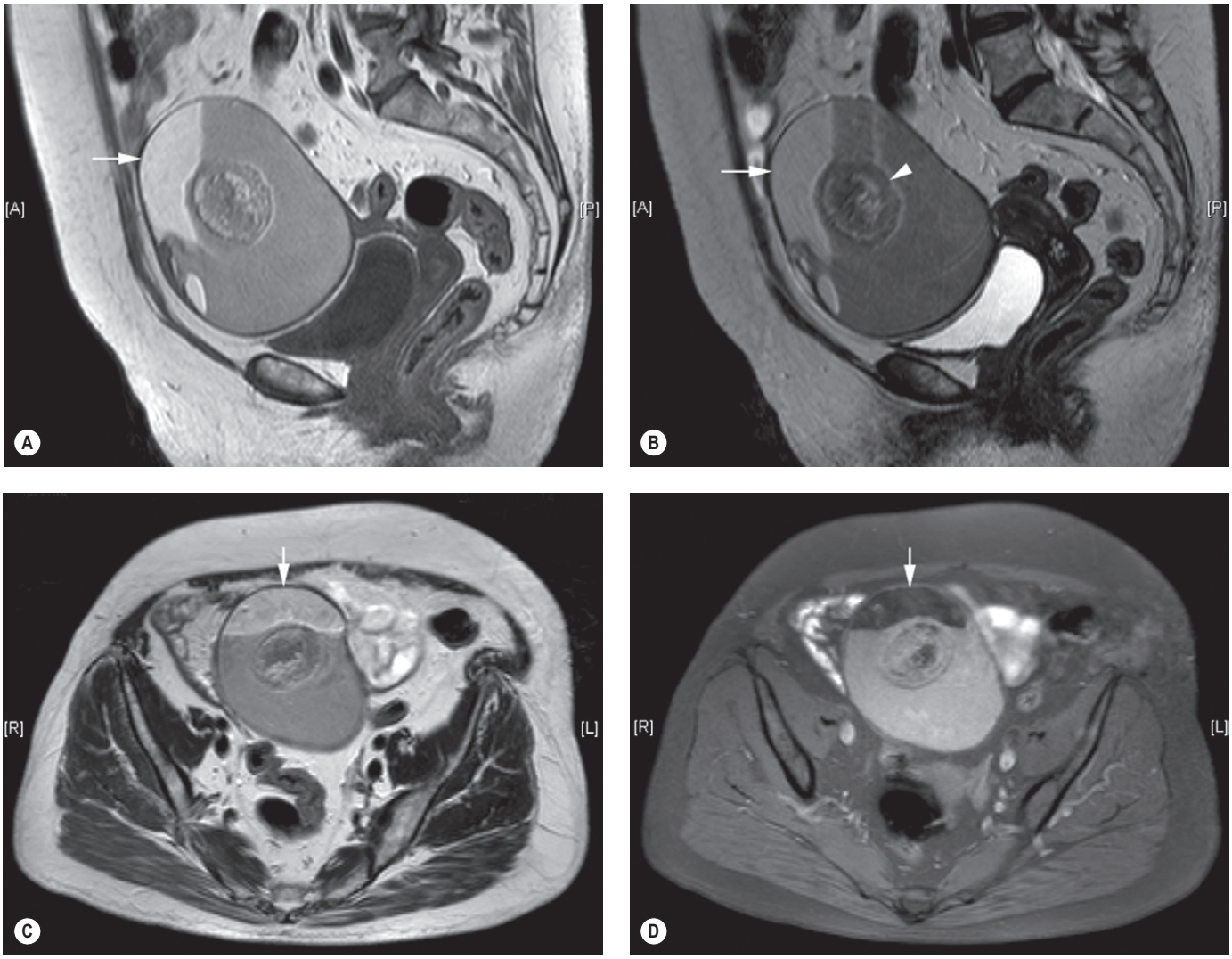


Figure 35.41 Dermoid. Sagittal T1-weighted **(A)** and T2-weighted **(B)** MR images and axial T1-weighted **(C)** and fat suppression sequences **(D)**. These show a cystic lesion with a fluid level and a central nodule (**B**, arrowhead). On the sagittal images (**A** and **B**) the fat is high signal on the T1-weighted image (**A**, white arrow) and intermediate signal on the T2-weighted image (**B**, white arrow). The signal intensity is equivalent to subcutaneous fat on both sequences. On the axial images (**C** and **D**) the high signal intensity fat (**C**, white arrow) on the T1-weighted images shows fat suppression (**D**, white arrow), confirming the presence of a dermoid. (Williams P & DeFriend D. Techniques in Gynaecological Imaging: Non Ultrasound Techniques. Radiology Integrated Training Initiative 2010: e-learning session 46_00036. Royal College of Radiologists, London).

Sex cord stromal tumours

Sex cord stromal tumours are derived from the sex cords and specialised stroma of the developing gonad. They represent 5–10% of ovarian neoplasms and approximately 2% of malignant ovarian neoplasms. They include granulosa cell tumours, fibromas, thecomas/fibrothecomas and Sertoli–Leydig cell tumours.

Granulosa cell tumours

Granulosa cell tumours are rare, accounting for 3% of all ovarian malignancies, but are the most common malignant sex cord stromal tumour. They include adult granulosa cell and juvenile granulosa cell tumours, with only the former discussed here. Adult granulosa cell tumours occur predominantly in perimenopausal or postmenopausal women, are unilateral in 95% cases and are generally of low-grade malignancy. They are the most common oestrogen-producing tumour, and manifest clinically as irregular bleeding in premenopausal women or as postmenopausal bleeding.[72] Approximately one-third of women with granulosa cell tumours will have endometrial hyperplasia[73] and up to 25% of patients will have endometrial carcinoma.[72] Granulosa cell tumours can occasionally be androgenic and present with virilisation.[54] They vary in size at presentation, with hormonally active tumours tending to present with a smaller size.[72] In contrast to epithelial tumours, more than 90% of granulosa cell tumours are confined to the ovary at presentation and hence have a better prognosis.[72]

Ultrasonically the appearances are non-specific and granulosa cell tumours may present as large multilocular cystic masses with solid components or as solid tumours[72,73] (Fig. 35.42). A more recent study suggests two typical patterns: (i) a solid mass with heterogeneous echogenicity of the solid tissue or (ii) a multilocular-solid mass with large solid areas but only rarely papillary projections.[74] It is reported that the virilising type are more commonly cystic.[72] Granulosa cell tumours have a propensity to rupture and up to 15% may present with haemoperitoneum.[54]

MRI may show more specific features, with high signal on T1-weighted imaging reflecting their propensity for haemorrhage and T2-weighted imaging showing a characteristic sponge-like appearance.[54,72]

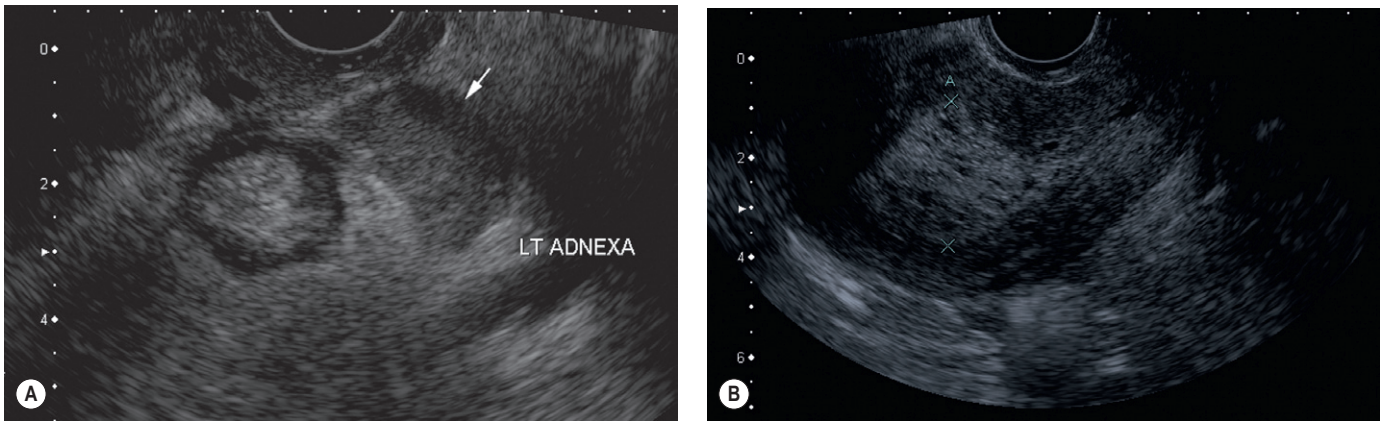


Figure 35.42 Granulosa cell tumour. Transvaginal scan of the left adnexa **(A)** and uterus **(B)** in a 62-year-old woman with postmenopausal bleeding. **A:** The left ovary (arrow) was enlarged as compared to the right and appeared to contain a solid mass. **B:** There is marked endometrial thickening (between callipers). Histology showed a granulosa cell tumour of the ovary and the endometrial thickening was shown to be endometrial hyperplasia. Granulosa cell tumours vary in size at presentation, with hormonally active tumours tending to present with a smaller size.

Fibromas/thecomas

Fibromas and thecomas represent a spectrum of benign tumours with predominantly oestrogen secreting thecal cells at one end and mainly non-hormone-secreting fibroblasts at the other. Many contain both theca cells and fibroblasts and are known as fibrothecomas.

Fibromas

Fibromas are the most common sex cord stromal tumour and constitute 3–4% of ovarian neoplasms. They are unilateral in 90% of cases. They are most common in perimenopausal or postmenopausal women.[75] Pure fibromas do not demonstrate significant hormonal effects, are often discovered incidentally and may reach relatively large sizes, 5–10 cm being the average diameter.[75]

Meigs' syndrome, the association of a benign ovarian tumour, usually a fibroma, with pleural effusions and ascites, occurs in 1–3% of patients with a fibroma. The ascites and pleural fluid resolve after removal of the tumour.[75] Ascites alone occurs in 10–15% of patients with a fibroma greater than 10 cm. Fibromas also occur in some patients with the basal cell naevus (Gorlin) syndrome, when they occur at a younger age, and are often bilateral and calcified.[72]

At ultrasound examination fibromas usually appear as homogeneous, hypoechoic masses, often with marked attenuation of sound (acoustic shadowing). These tumours have a similar composition to leiomyomas and, because sound transmission is poor through fibrous tissue, the sonographic beam is strongly attenuated (Fig. 35.43). They can, however, have a variable appearance and hyperechoic masses, acoustic enhancement[75,76] and calcification have been reported.[77] This variation in appearance may be related to a tendency for oedema and cystic degeneration in these tumours.[1] Although in most cases their appearance is non-specific, the pattern of a hypoechoic mass with acoustic shadowing should raise the possibility of a fibroma/thecoma.[76]

Fibromas have a relatively diagnostic appearance at MRI examination, where they appear as low signal lesions on both T1-weighted and T2-weighted sequences (Fig. 35.43).

The differential for fibromas includes pedunculated or parasitic leiomyomas and Brenner tumours, which although classified histologically as epithelial lesions, have an ultrasonic appearance similar to fibromas.

Thecomas

Thecomas are benign, solid, oestrogen-producing tumours, which like fibromas occur in perimenopausal and postmenopausal women. Like granulosa cell tumours they may present with menorrhagia or postmenopausal bleeding and are associated with endometrial carcinoma.

Thecomas appear similar to other solid tumours of the ovary with non-specific features at ultrasound[72] (Fig. 35.44).

Sertoli–Leydig cell tumours (androblastoma)

These tumours produce androgens and oestrogens and are the most common virilising tumours. They tend to occur in young women, less than 30 years, and are almost all unilateral. Whilst they are rare tumours (<0.5% of ovarian tumours), virilisation syndromes such as hirsutism and oligomenorrhoea are common clinical problems and these tumours may be discovered during a search for polycystic ovaries. They are considered low-grade malignancies.

Sertoli–Leydig cell tumours may go undetected at imaging because of their small size or there may be non-specific ovarian enlargement.[77] When they are identified at ultrasound they are usually isoechoic or hypoechoic solid masses,[72] although they may appear indistinguishable from granulosa cell tumours.[72,74] Calcification is unusual.[72]

Metastatic tumours

These account for 5–15% of malignant ovarian tumours.[78,79] Tumours that metastasise to the ovary include colon, breast, stomach, pancreas, melanoma and carcinoid.[54,80] The majority are from the gastrointestinal tract. The so-called Krukenberg tumour, strictly speaking, describes a secondary tumour from a gastrointestinal primary with signet-ring cells due to intracellular mucin secretion (Fig. 35.45).

Distinguishing between a primary ovarian and a metastatic tumour is important in terms of treatment options. Ovarian metastases may be solid or complex cystic masses of various sizes, but have been described as typically bilateral and predominantly solid, both at pathology and on imaging studies.[81–83] Shimizu et al. describe metastases as having clear tumour margins, an irregular hyperechoic solid pattern and moth-eaten cyst formation in contrast to primary ovarian cancers, which had unclear margins, an irregular hypoechoic solid pattern and papillary projections. They suggest that this distinction may be more obvious earlier in the development of metastases when they are predominantly solid, but becomes more difficult later as metastases become increasingly cystic and necrotic, resembling primary ovarian tumours.[84] Two more recent studies have looked particularly at imaging features of primary and secondary ovarian neoplasms to determine if there is a significant difference in their appearance. Brown et al. found no difference

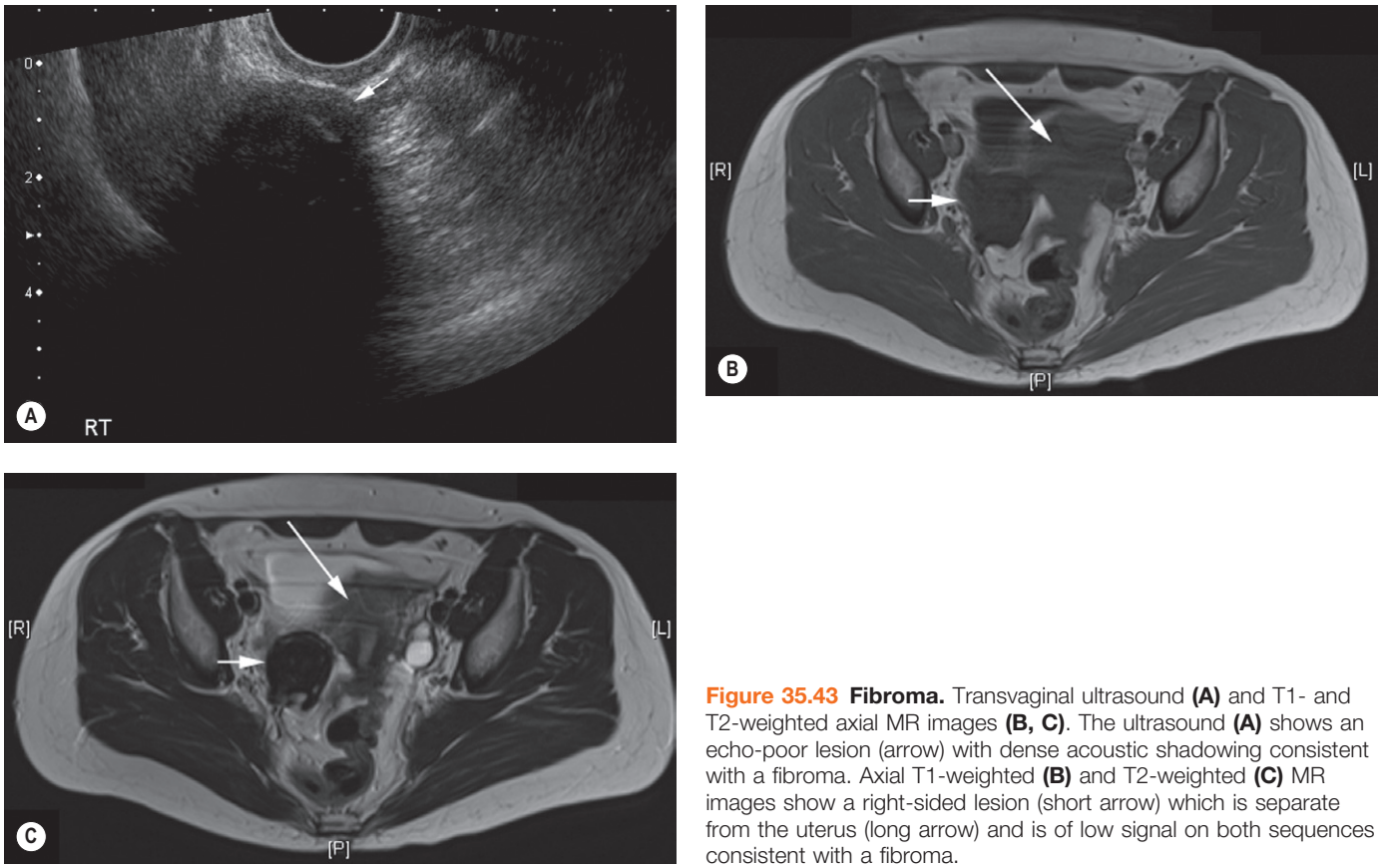


Figure 35.43 Fibroma. Transvaginal ultrasound **(A)** and T1- and T2-weighted axial MR images **(B, C)**. The ultrasound **(A)** shows an echo-poor lesion (arrow) with dense acoustic shadowing consistent with a fibroma. Axial T1-weighted **(B)** and T2-weighted **(C)** MR images show a right-sided lesion (short arrow) which is separate from the uterus (long arrow) and is of low signal on both sequences consistent with a fibroma.

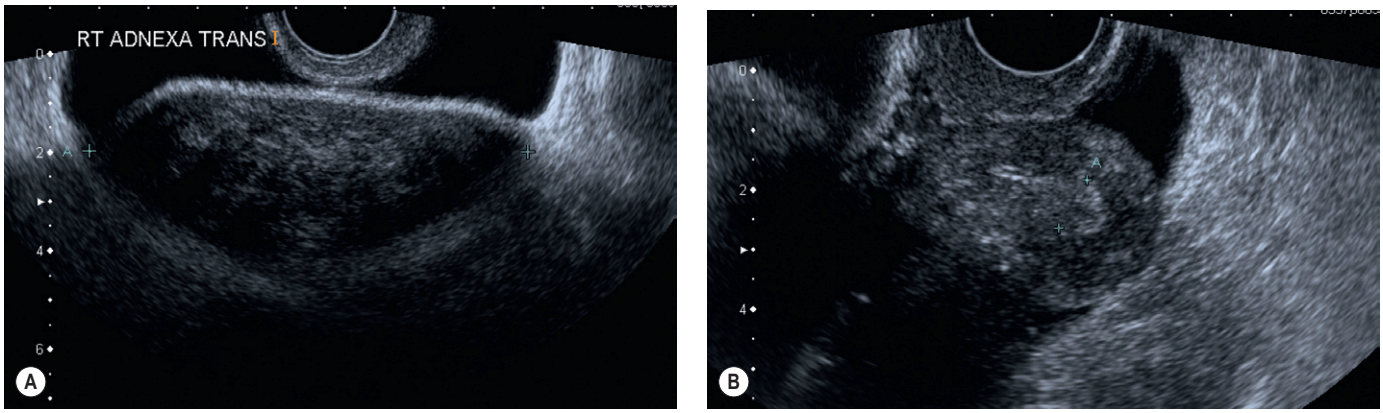


Figure 35.44 Fibrothecoma. Transvaginal ultrasound images **(A, B)** show an 8 cm solid lesion in a postmenopausal woman **(A)**. This was proven to be a fibrothecoma at histology. There was associated endometrial thickening (**B**, between callipers).

between them in terms of solidity, and although secondary neoplasms were more often bilateral than primary neoplasms, this was not a significant finding. The only statistically significant feature on ultrasound was multilocularity, which was more common in primary malignancy.[78] Alcazar also found no difference in terms of bilaterality, but metastatic tumours were significantly more often, purely or predominantly solid.[79] Overall they conclude that no imaging feature is highly accurate in distinguishing primary from secondary tumours.

These conflicting results may be partly explained by the different primary tumours studied. Pathological studies have shown that gastric, breast, lymphoma and carcinoid tumours often produce solid metastases in the ovaries. Colonic tumours, which are the most common primary site, may also produce solid tumours, but often produce cystic metastases similar to primary ovarian tumours. In support of this concept, Testa et al. have recently shown that ultrasound features of metastases differ depending on the origin of the primary. They found that metastases from stomach, breast, lymphoma or uterus were mostly solid while those from the colon, rectum, appendix or biliary tract were more heterogeneous with a multilocular appearance, with or without solid elements[85] (Fig. 35.46). A number of authors have acknowledged the difficulties in distinguishing between primary and secondary tumours. In practice the presence of bilateral or solid tumours may raise the possibility of a metastatic tumour and further imaging with CT and biopsy may be helpful.



Figure 35.45 Krukenberg tumour. Transabdominal ultrasound scan, showing bilateral, largely solid, Krukenberg tumours with ascites.

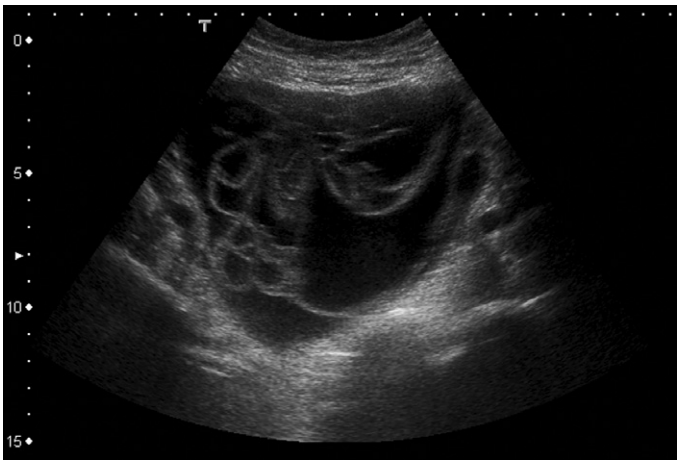


Figure 35.46 Transabdominal image, showing metastatic involvement of an ovary, secondary to a primary colonic carcinoma. The lesion is largely cystic with septa and solid elements. Flow was demonstrated within the septa on colour Doppler.

Lymphoma

Lymphoma of the ovary in the absence of lymph node or bone marrow involvement is rare. It is often bilateral and usually appears as a solid mass at ultrasound.

Screening

The poor outcome of ovarian cancer is largely related to late presentation and screening has been seen as a means to improve prognosis. Currently screening is not practical due to the relatively low prevalence of the disease and the limited specificity of the available techniques.

Measurement of CA125 and transvaginal ultrasound are the main techniques that have been evaluated for use in screening.

Serum CA125 is the most commonly used tumour marker for ovarian cancer. It is raised in 85% women with epithelial ovarian cancer as opposed to 1% of normal individuals, but its sensitivity is limited in early stage disease, and it detects less than 50% of stage I tumours. It is insensitive for mucinous and germ cell tumours. It also lacks specificity and can be raised in other gynaecological diseases such as benign tumours and endometriosis. CA125 therefore lacks both the sensitivity and specificity to be used alone as a screening technique.

Transvaginal ultrasound also lacks specificity, with too many unnecessary operations performed for each cancer detected. A combination of these techniques improves specificity.

Improved survival has been reported in some single arm and randomised control trials, but the impact on mortality and cost-benefits remain to be proven.

There are two main trials involving the general population currently underway. The first is the UK Collaborative Trial of Ovarian Cancer Screening (UKCTOCS) in England, Wales and Northern Ireland. This involves approximately 200 000 women aged 50–74 randomised to screening with transvaginal ultrasonography (TVS), or with CA125 which, if elevated, is followed by TVS, or to a control group. Screening is for 6 years and initial results will be available in 2012–2014.

The second trial is the ovarian arm of the Prostate, Colorectal, Lung and Ovarian Cancer screening trial, based in the USA, involving nearly 80 000 women aged 55–74 and using combined CA125 and TVS techniques and CA125 alone.

Other studies are looking at the value of screening in high-risk populations. The benefits of screening in this group are not proven and there is concern that screening may not be effective. There is one main UK trial, the UK Familial Ovarian Cancer Screening Study (UK FOCSS), which aims to include 5000 women and will report in 2011.

ENDOMETRIOSIS

Endometriosis is defined as the presence of functional endometrial glands and stroma outside of the uterus. The pathogenesis is unknown, with theories regarding its aetiology including implantation from retrograde menstruation and metaplastic differentiation of serosal surfaces. Endometriosis most commonly affects the ovaries. Other sites of involvement include the uterine ligaments, pouch of Douglas, fallopian tubes, rectosigmoid and bladder, in decreasing order of frequency.[86] Endometriosis may be present as peritoneal implants, adhesions and ovarian lesions with symptoms occurring due to cyclical bleeding into the implants. Repeated haemorrhage into ovarian implants results in blood-filled ovarian cysts known as endometriomas, or 'chocolate cysts'.

Endometriosis is a common condition, which is thought to affect 5–10% of all women. It is found predominantly in women of reproductive age and approximately 20% of women presenting with infertility are thought to have endometriosis.[87]

Patients usually present with infertility or chronic pelvic pain, typically dysmenorrhoea or dyspareunia. Some women are asymptomatic and the extent of the disease does not necessarily correlate with the severity of symptoms.

Small peritoneal implants are difficult to diagnose radiologically and ultrasound is of particular use for the identification of endometriotic ovarian cysts. Transrectal ultrasound has been used to assess endometriotic involvement of the rectovaginal septum and uterosacral ligaments[88] and other imaging modalities such as MRI have more recently been evaluated for detection of peritoneal implants.[86] Laparoscopy remains the gold standard for detection of disease.

Endometriomas have a variety of appearances at ultrasound, ranging from anechoic to echogenic cysts.[87] Septa and solid areas may be present.[89] They are often multiple and are bilateral in up to half of cases.[86] They are of variable size[87,90] and are often thick walled, although this is not a distinguishing feature.[89]

The classic description is a cystic lesion with homogeneous low-level echoes, which are more likely to be detected with transvaginal than transabdominal scanning[91,92] (Fig. 35.47). This characteristic appearance was found to occur in 95% of cases in a retrospective review.[89] This review also tried to establish which criteria are most important in distinguishing endometriomas from other adnexal

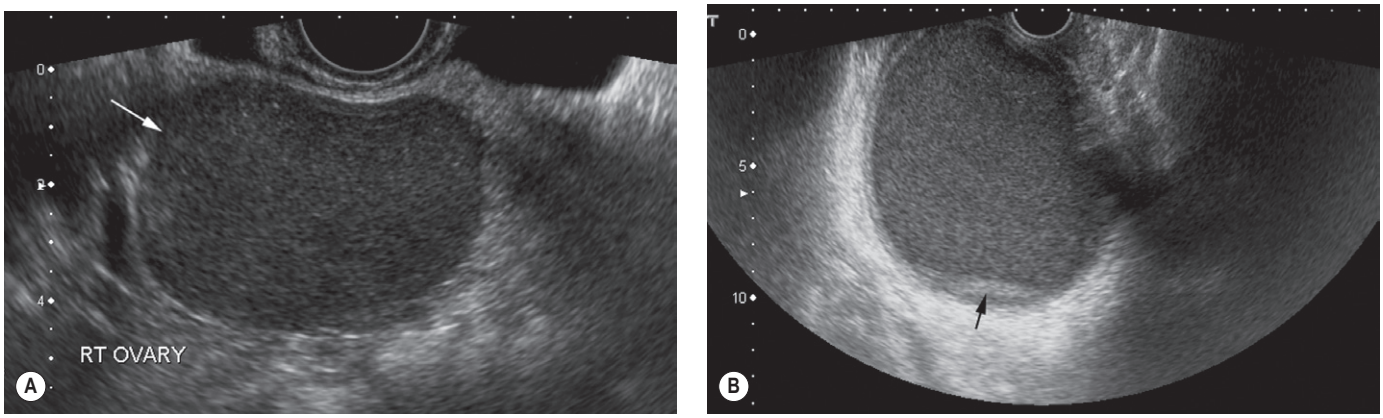


Figure 35.47 Transvaginal images showing typical appearances of an endometrioma. A: Unilocular cystic lesion with homogeneous low-level echoes (white arrow). **B:** There is the typical echo pattern with some echogenic layering (black arrow).

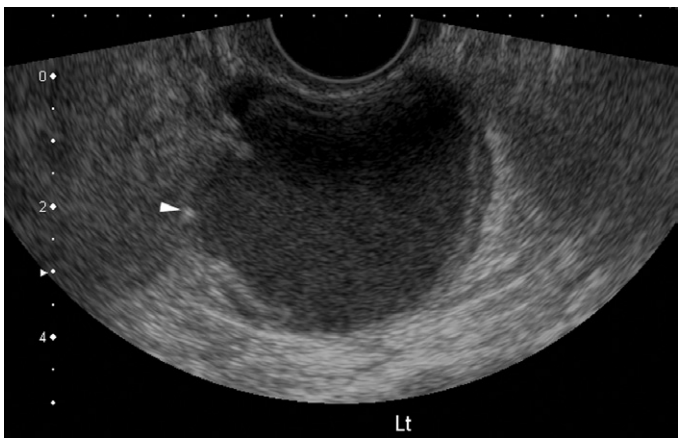


Figure 35.48 Transvaginal image of a typical endometrioma, with low-level echoes. Hyperechoic foci are demonstrated within the wall (arrowhead).



Figure 35.49 Transvaginal image showing a multiloculated endometrioma (arrow) with varying echo levels in the different locules.

lesions. They identified hyperechoic wall foci in 35% of endometriomas compared with only 6% of other lesions (Fig. 35.48). They suggest that the presence of hyperechoic wall foci in addition to the typical echo pattern, provided there are no neoplastic features, is highly predictive of an endometrioma. Endometriomas have classically been described as unilocular but they may be multilocular with varying echogenicity in the different locules. The presence of multilocularity, together with low-level echoes, in the absence of neoplastic features, increases the likelihood that a lesion is an endometrioma[89] (Fig. 35.49).

Endometriomas may mimic other adnexal lesions. They may have a similar appearance to haemorrhagic cysts, and clinical features such as an acute onset in the latter may be helpful in distinguishing them. Follow-up of lesions is a useful strategy, since haemorrhagic cysts will usually resolve whereas endometriomas will not. Atypical endometriomas may contain central calcification, which can make them difficult to distinguish from dermoid cysts.[93] They may also show clot retraction or wall nodularity, making distinction from neoplastic lesions difficult. This subgroup may benefit from further investigation with Doppler or MRI to assess vascularity of nodules. However, the routine use of colour Doppler does not appear to improve the diagnostic accuracy of transvaginal ultrasound alone in the diagnosis of endometriomas.[94]

MRI is more specific than ultrasound for the diagnosis of endometriomas, with lesions usually showing high signal on T1-weighted imaging and low signal or 'shading' on T2-weighted sequences. They do not show fat suppression and become more conspicuous on fat saturation sequences.

Complications of endometriosis include adhesions and some authors have emphasised the role of a bimanual ultrasound examination or use of gentle pressure with the transvaginal probe to demonstrate mobility or fixity of pelvic organs.[90,95] Malignant change is a rare (<1%) complication, with endometrioid tumours followed by clear cell tumours being the most common malignancies.[90]

Endometriosis

Occurs predominantly in women of reproductive age.
Most commonly affects the ovaries resulting in endometriomas or 'chocolate cysts'.

Endometriomas:
- Appearances at ultrasound may be diverse.
- Characteristic appearance is a cystic lesion with low-level echoes.
- Are often multiple and bilateral.
- May be multiloculated.
- May contain hyperechoic wall foci.

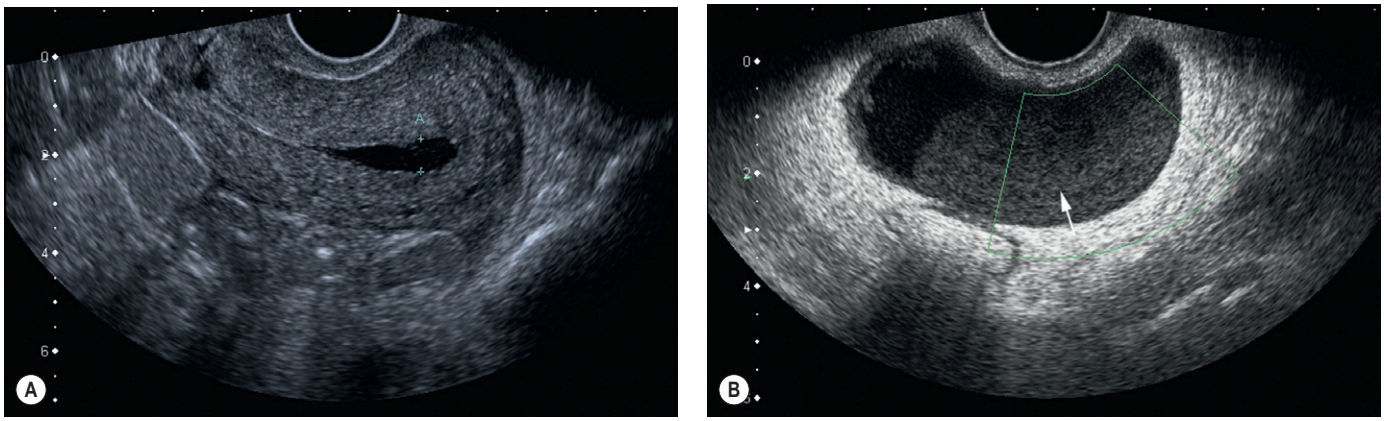


Figure 35.50 Pelvic inflammatory disease. Transvaginal images in a 38-year-old woman with clinical signs of PID. **A:** There is fluid within the endometrial canal (between callipers) consistent with endometritis. **B:** The fallopian tube is dilated and contains echoes (arrow), with no flow seen on colour Doppler, consistent with a pyosalpinx.

PELVIC INFLAMMATORY DISEASE

Pelvic inflammatory disease (PID) is a common condition, affecting predominantly women of reproductive age, which may present as acute or chronic pain. Complications include infertility and ectopic pregnancy. It is most often due to ascending genital tract infection, usually due to *Chlamydia trachomatis* or *Neisseria gonorrhoeae*. Rarer causes include actinomycosis and tuberculosis. It may be associated with the use of an intrauterine contraceptive device or instrumentation. Rarely, spread from adjacent pelvic infections such as appendicitis or diverticulitis may occur. While PID is usually bilateral, it may be unilateral in cases of direct spread. It may result in endometritis, pyosalpinx, tubo-ovarian complex or abscess or peritonitis. Peritonitis may involve the bowel serosa and can cause adhesions, small bowel obstruction or perihepatitis (Fitz-Hugh–Curtis syndrome).

Acute PID may present with pelvic pain, fever and vaginal discharge, and inflammatory markers are often raised.

PID may present a range of appearances at ultrasound depending on the spread and extent of the infection. In early or uncomplicated cases imaging may be unremarkable and the presence of a normal ultrasound scan does not exclude PID. Endometritis is essentially a clinical diagnosis and although ultrasound may show thickening of the endometrium and fluid within the endometrial cavity, these appearances are non-specific and may occur as a normal finding in the second half of the menstrual cycle (Fig. 35.50A). There may be free fluid within the pelvis, which can also be a normal finding, although excessive fluid or fluid-containing echoes is more suggestive of PID.

Involvement of the fallopian tube may present as a pyosalpinx, with a dilated, thick-walled, retort-shaped tube, which contains fluid, sometimes with low-level echoes (Fig. 35.50B). Features thought to assist in identification of dilated tubes at ultrasound include incomplete septa[96] and the 'waist sign', which refers to diametrically opposed indentations within the wall of a cystic, tubular, collection[97] (Fig. 35.51). The 'cogwheel sign' has been used to describe the cross-sectional appearance of a tube with thickened endosalpingeal walls, thought to be most typical of acute disease.[96] A dilated, thin-walled, fluid-filled structure with hyperechoic mural nodules, known as the 'string of beads sign', is believed to be more characteristic of a chronic hydrosalpinx[96] with the hyperechoic nodules thought to represent remnants of the salpingeal folds.

Involvement of the ovary results in a tubo-ovarian complex or tubo-ovarian abscess. Where there is inflammation of the tube and ovary but the anatomy of the structures is preserved, this is described as a tubo-ovarian complex (Fig. 35.52). In the more advanced stage of tubo-ovarian abscess there is complete breakdown of the normal architecture so that separate structures are no longer identified.[96] The typical appearance is of a complex, often multiloculated mass with variable septations and internal echogenicity (Fig. 35.53). It may be difficult to distinguish a tubo-ovarian abscess from a tumour or endometrioma, but with an abscess the patient is usually acutely ill with marked tenderness on examination with the transvaginal probe. Involvement of the ovary alone is rare but can occur with spread of infection from adjacent organs (Fig. 35.54).

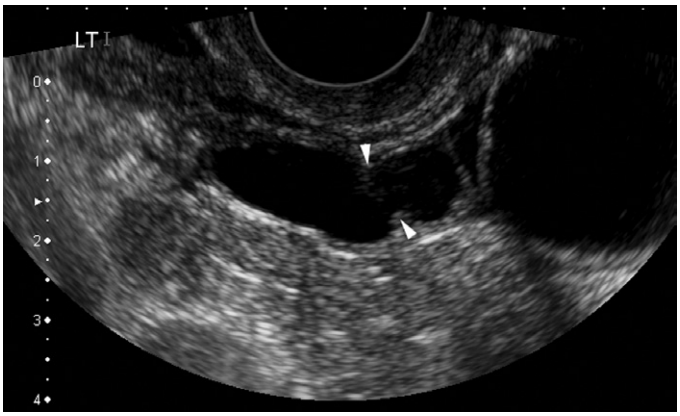


Figure 35.51 Transvaginal image of a hydrosalpinx, which demonstrates the waist sign (arrowheads).

Pelvic inflammatory disease

Affects mainly women of reproductive age.
Is usually due to an ascending infection.
May present as endometritis, hydro or pyosalpinx, tubo-ovarian complex or tubo-ovarian abscess.

Ovarian involvement:

- Tubo-ovarian complex – inflammation involves the tubes and ovaries but the anatomy is preserved.
- Tubo-ovarian abscess – there is a complete breakdown of the normal architecture so that separate structures are not identified.

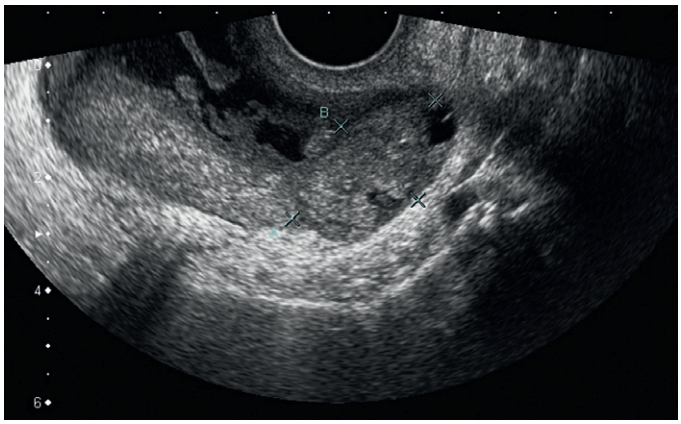


Figure 35.52 Transvaginal image which shows a tubo-ovarian complex. The ovary (between callipers) remains recognisable.

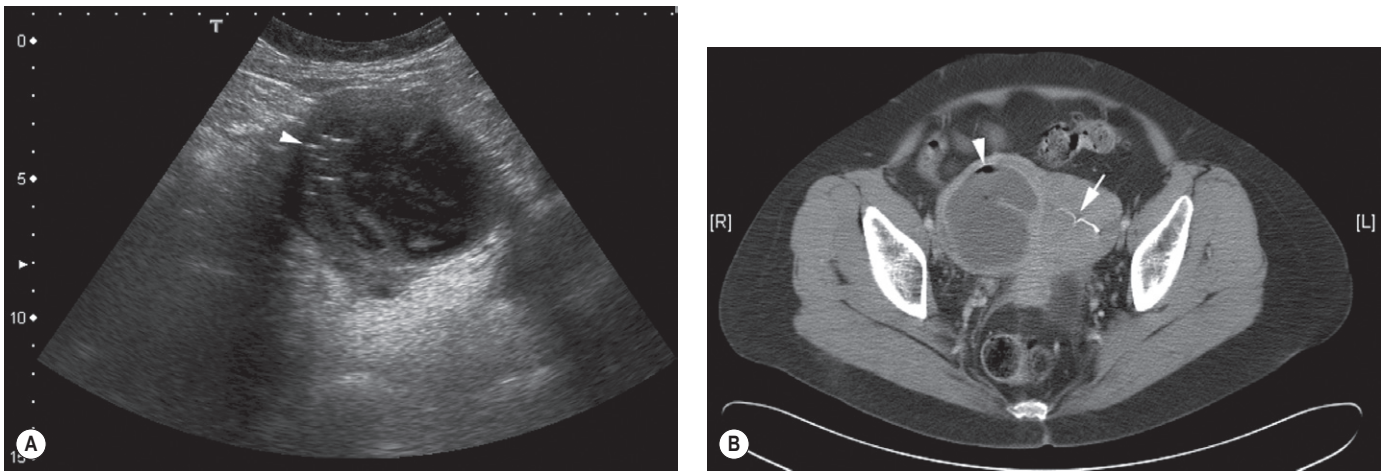


Figure 35.53 Tubo-ovarian abscess. Transabdominal ultrasound image **(A)** and axial contrast-enhanced CT scan **(B)** in a patient with clinical signs of infection. Ultrasound **(A)** shows a tubo-ovarian abscess, containing linear echoes (arrowhead) typical of gas. The tube and ovary could not be identified separately. CT scan **(B)** confirms the presence of an abscess with a locule of gas identified (arrowhead). Note the intrauterine contraceptive device (arrow), which increases the risk of PID.

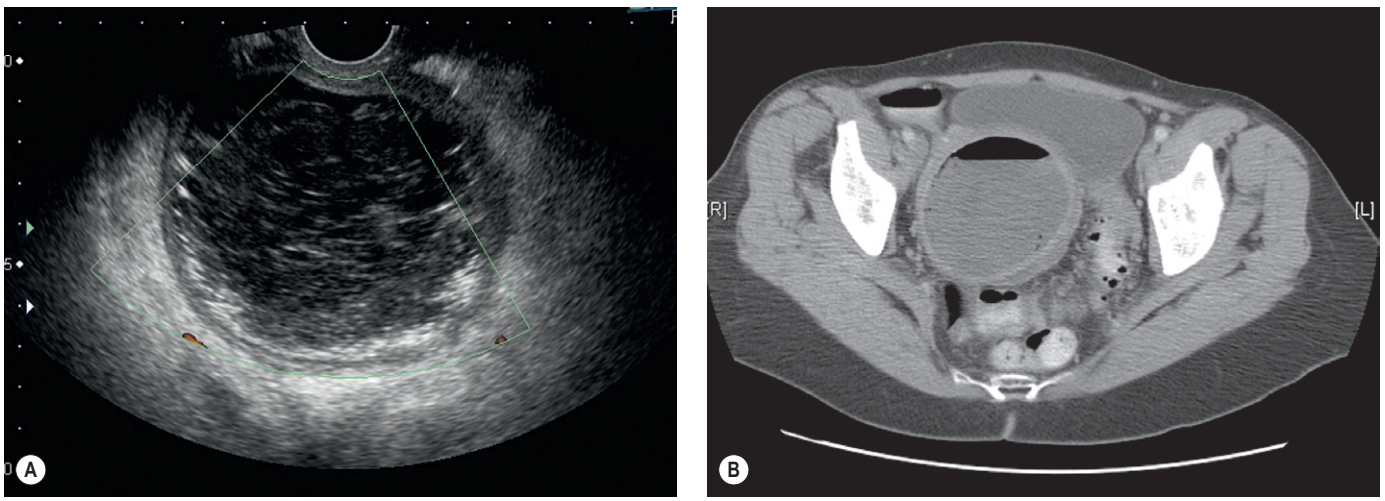


Figure 35.54 Ovarian abscess. Transvaginal ultrasound and axial CT scan in a patient with signs of infection. The patient had undergone a hysterectomy several years previously. **A:** Transvaginal ultrasound image showing a right ovarian lesion with multiple echoes within it. **B:** CT scan confirmed the presence of gas. The previous hysterectomy made an ascending infection an unlikely diagnosis. Surgery showed an ovarian abscess secondary to an inflamed appendix.

REFERENCES

1. Salem S. The uterus and adnexa. In: Rumack C, Wilson S, Charboneau J, editors. Diagnostic ultrasound. 2 edn. St Louis: Mosby; 1998. p. 519–573.
2. Merz E, Miric-Tesanic D, Bahlmann F, et al. Sonographic size of uterus and ovaries in pre- and postmenopausal women. Ultrasound Obstet Gynecol 1996;7(1):38–42.
3. Tepper R, Zalel Y, Markov S, et al. Ovarian volume in postmenopausal women – suggestions to an ovarian size nomogram for menopausal age. Acta Obstet Gynecol Scand 1995;(74):208–211.
4. Aviram R, Gassner G, Markovitch O, et al. Volumes of normal ovaries, ovaries with benign lesions, and ovaries with cancer in menopausal women: is there an optimal cut-off value to predict malignancy? J Clin Ultrasound 2008;36(1):1–5.
5. Patel MD, Feldstein VA, Filly RA. The likelihood ratio of sonographic findings for the diagnosis of hemorrhagic ovarian cysts. J Ultrasound Med 2005;24(5):607–614.
6. Athey PA, Cooper NB. Sonographic features of parovarian cysts. AJR Am J Roentgenol 1985;144:83–86.
7. Barloon TJ, Brown BP, Abu-Yousef MM, Warnock NG. Paraovarian and paratubal cysts: preoperative diagnosis using transabdominal and transvaginal sonography. J Clin Ultrasound 1996;24(3):117–122.
8. Savelli L, Ghi T, De Iaco P, Ceccaroni M, et al. Paraovarian/paratubal cysts: comparison of transvaginal sonographic and pathological findings to establish diagnostic criteria. Ultrasound Obstet Gynecol 2006;28(3):330–334.
9. Alpern MB, Sandler MA, Madrazo BL. Sonographic features of parovarian cysts and their complications. AJR Am J Roentgenol 1984;143(1):157–160.
10. Genadry R, Parmley T, Woodruff JD. The origin and clinical behaviour of the paraovarian tumour. Am J Obstet Gynecol 1977;129:873–880.
11. Kim JS, Woo SK, Suh SJ, Morettin LB. Sonographic diagnosis of paraovarian cysts: value of detecting a separate ipsilateral ovary. AJR Am J Roentgenol 1995;164(6):1441–1444.
12. Guerriero S, Ajossa S, Mais V, et al. Role of transvaginal sonography in the diagnosis of peritoneal inclusion cysts. J Ultrasound Med 2004;23(9):1193–1200.
13. Jain KA. Imaging of peritoneal inclusion cysts. AJR Am J Roentgenol 2000;174(6):1559–1563.
14. Savelli L, De Iaco P, Ghi T, et al. Transvaginal sonographic appearance of peritoneal pseudocysts. Ultrasound Obstet Gynecol 2004;23:284–288.
15. Phillips HE, McGahan JP. Ovarian remnant syndrome. Radiology 1982;142(2):487–488.
16. Fleischer AC, Tait D, Mayo J, et al. Sonographic features of ovarian remnants. J Ultrasound Med 1998;17(9):551–555.
17. Dereska NH, Cornella J, Hibner M, Magrina JF. Mucinous adenocarcinoma in an ovarian remnant. Int J Gynecol Cancer 2004;14(4):683–686.
18. RCOG. Guideline no 34. Ovarian cysts in postmenopausal women. London: Royal College of Obstetricians and Gynaecologists; 2003.
19. Patel MD. Practical approach to the adnexal mass. Radiol Clin North Am 2006;44:879–899.
20. Levine D. What is the significance of the incidental discovery of a unilocular ovarian cyst in a postmenopausal woman (either with or without a family history of ovarian cancer) during a pelvic sonographic examination to exclude ovarian carcinoma? AJR Am J Roentgenol 1994;163(1):215–216.
21. Goldstein SR, Subramanyam B, Snyder JR, et al. The postmenopausal cystic adnexal mass: the potential role of ultrasound in conservative management. Obstet Gynecol 1989;73(1):8–10.
22. Balen AH, Laven JSE, Tan S-L, Dewailly D. Ultrasound assessment of the polycystic ovary: international consensus definitions. Hum Reprod Update 2003;9(6):505–514.
23. Belosi C, Selvaggi L, Apa R, et al. Is the PCOS diagnosis solved by ESHRE/ASRM 2003 consensus or could it include ultrasound examination of the ovarian stroma? Hum Reprod 2006;21(12): 3108–3115.
24. Haimov-Kochman R, Yanai N, Yagel S, et al. Spontaneous ovarian hyperstimulation syndrome and hyperreactio luteinalis are entities in continuum. Ultrasound Obstet Gynecol 2004;24(6):675–678.
25. RCOG. The management of ovarian hyperstimulation syndrome – Green-top guideline No. 5. Royal College Obstetricians and Gynaecologists; 2006.
26. Mathur R, Evbuomwan I, Jenkins J. Prevention and management of ovarian hyperstimulation syndrome. Curr Obstet Gynaecol 2005;15(2):132–138.
27. Chiou S-Y, Lev-Toaff AS, Masuda E, et al. Adnexal torsion: new clinical and imaging observations by sonography, computed tomography, and magnetic resonance imaging. J Ultrasound Med 2007;26(10):1289–1301.
28. Kaakaji Y, Nghiem HV, Nodell C, Winter TC. Sonography of obstetric and gynecologic emergencies: Part II, gynecologic emergencies. AJR Am J Roentgenol 2000;174(3):651–656.
29. Hibbard L. Adnexal torsion. Am J Obstet Gynecol 1985;152:456–461.
30. Warner MA, Fleischer AC, Edell SL, et al. Uterine adnexal torsion: sonographic findings. Radiology 1985;154(3):773–775.
31. Vijayaraghavan SB. Sonographic whirlpool sign in ovarian torsion. J Ultrasound Med 2004;23(12):1643–1649.
32. Graif M, Itzchak Y. Sonographic evaluation of ovarian torsion in childhood and adolescence. AJR Am J Roentgenol 1988;150(3):647–649.
33. Graif M, Shalev J, Strauss S, et al. Torsion of the ovary: sonographic features. AJR Am J Roentgenol 1984;143(6):1331–1334.
34. Albayram F, Hamper UM. Ovarian and adnexal torsion: spectrum of sonographic findings with pathologic correlation. J Ultrasound Med 2001;20(10):1083–1089.
35. Shadinger LL, Andreotti RF, Kurian RL. Preoperative sonographic and clinical characteristics as predictors of ovarian torsion. J Ultrasound Med 2008;27(1):7–13.
36. Moshe B-A, Yuri P, Sami H. The effectiveness of spectral and color Doppler in predicting ovarian torsion. A prospective study. Eur J Obstet Gynecol Reprod Biol 2002;104(1):64–66.
37. Lee EJ, Kwon HC, Joo HJ, et al. Diagnosis of ovarian torsion with color Doppler sonography: depiction of twisted vascular pedicle. J Ultrasound Med 1998;17(2):83–89.
38. Spencer JA, Forstner R, Hricak H. Investigating women with suspected ovarian cancer. Gynecol Oncol 2008;108(2):262–264.
39. Brown DL, Doubilet PM, Miller FH, et al. Benign and malignant ovarian masses: selection of the most discriminating gray-scale and Doppler sonographic features. Radiology 1998;208(1):103–110.
40. Stein SM, Laifer-Narin S, Johnson MB, et al. Differentiation of benign and malignant adnexal masses: relative value of gray-scale, color Doppler, and spectral Doppler sonography. AJR Am J Roentgenol 1995;164(2):381–386.
41. Fleischer AC, Rodgers WH, Kepple DM, et al. Color Doppler sonography of ovarian masses: a multiparameter analysis. J Ultrasound Med 1993;12(1):41–48.
42. Kurjak A, Zalud I, Alfirevic Z. Evaluation of adnexal masses with transvaginal color ultrasound. J Ultrasound Med 1991;10(6):295–297.
43. Fleischer AC, Rodgers WH, Rao BK, et al. Assessment of ovarian tumor vascularity with transvaginal color Doppler sonography. J Ultrasound Med 1991;10(10):563–568.
44. Jain KA. Prospective evaluation of adnexal masses with endovaginal gray-scale and duplex and color Doppler US: correlation with pathologic findings. Radiology 1994;191(1):63–67.
45. Salem S, White LM, Lai J. Doppler sonography of adnexal masses: the predictive value of the pulsatility index in benign and malignant disease. AJR Am J Roentgenol 1994;163(5):1147–1150.
46. Buy JN, Ghossain MA, Hugol D, et al. Characterization of adnexal masses: combination of color Doppler and conventional sonography compared with spectral Doppler analysis alone and conventional sonography alone. AJR Am J Roentgenol 1996;166(2):385–393.
47. Kinkel K, Hricak H, Lu Y, et al. US characterization of ovarian masses: a meta-analysis. Radiology 2000;217(3):803–811.
48. Fleischer AC. Recent advances in the sonographic assessment of vascularity and blood flow in gynecologic conditions. Am J Obstet Gynecol 2005;193:294–301.
49. Timmerman D, Schwärzler P, Collins WP, et al. Subjective assessment of adnexal masses with the use of ultrasonography: an analysis of interobserver variability and experience. Ultrasound Obstet Gynecol 1999;13(1):11–16.
50. Valentin L. Use of morphology to characterize and manage common adnexal masses. Best Pract Res Clin Obstet Gynaecol 2004;18(1): 71–89.
51. Wagner BJ, Buck JL, Seidman JD, McCabe KM. From the archives of the AFIP. Ovarian epithelial neoplasms: radiologic-pathologic correlation. Radiographics 1994;14(6):1351–1374.
52. Jacobs I, Menon U. Screening for ovarian cancer. Best Pract Res Clin Obstet Gynaecol 2002;16(4):469–482.
53. Cancer Research UK. UK ovarian cancer incidence statistics. 2008.
54. Mironov S, Akin O, Pandit-Taskar N, Hann LE. Ovarian cancer. Radiol Clin North Am 2007;45(1):149–166.
55. Sohaib SA, Husband JE, Reznek R. Ovarian cancer. In: Husband JE, Reznek R, editors. Imaging in oncology. London: Taylor and Francis; 2004. p. 429–466.

56. Jung SE, Lee JM, Rha SE, et al. CT and MR imaging of ovarian tumors with emphasis on differential diagnosis. Radiographics 2002;22(6): 1305–1325.
57. Sutton CL, McKinney CD, Jones JE, Gay SB. Ovarian masses revisited: radiologic and pathologic correlation. Radiographics 1992;12(5): 853–877.
58. Tempany CMC, Zou KH, Silverman SG, et al. Staging of advanced ovarian cancer: comparison of imaging modalities – Report from the Radiological Diagnostic Oncology Group. Radiology 2000;215(3): 761–767.
59. Ronnett BM, Shmookler BM, Diener-West M, et al. Immunohistochemical evidence supporting the appendiceal origin of pseudomyxoma peritonei in women. Int J Gynecol Pathol 1997;16(1):1–9.
60. Tanaka YO, Yoshizako T, Nishida M, et al. Ovarian carcinoma in patients with endometriosis: MR imaging findings. AJR Am J Roentgenol 2000;175(5):1423–1430.
61. Green GE, Mortele KJ, Glickman JN, Benson CB. Brenner tumors of the ovary: sonographic and computed tomographic imaging features. J Ultrasound Med 2006;25(10):1245–1251.
62. Athey PA, Siegel MF. Sonographic features of Brenner tumor of the ovary. J Ultrasound Med 1987;6(7):367–372.
63. Koonings PP, Campbell K, Mishell Jr DR, Grimes DA. Relative frequency of primary ovarian neoplasms: a 10-year review. Obstet Gynecol 1989;74(6):921–926.
64. Quinn SF, Erickson S, Black WC. Cystic ovarian teratomas: the sonographic appearance of the dermoid plug. Radiology 1985;155(2):477–478.
65. Beller MJ. The "tip of the iceberg" sign. Radiology 1998;209(2): 395–396.
66. Caspi B, Appelman Z, Rabinerson D, et al. Pathognomonic echo patterns of benign cystic teratomas of the ovary: classification, incidence and accuracy rate of sonographic diagnosis. Ultrasound Obstet Gynecol 1996;7(4):275–279.
67. Tongsong T, Wanapirak C, Khunamornpong S, Sukpan K. Numerous intracystic floating balls as a sonographic feature of benign cystic teratoma: report of 5 cases. J Ultrasound Med 2006;25(12):1587–1591.
68. Kurjak A, Kupesic S, Babic MM, et al. Preoperative evaluation of cystic teratoma: what does color Doppler add? J Clin Ultrasound 1997;25(6):309–316.
69. Zalel Y, Caspi B, Tepper R. Doppler flow characteristics of dermoid cysts: unique appearance of struma ovarii. J Ultrasound Med 1997;16(5):355–358.
70. Hertzberg BS, Kliewer MA. Sonography of benign cystic teratoma of the ovary: pitfalls in diagnosis. AJR Am J Roentgenol 1996;167(5): 1127–1133.
71. Patel MD, Feldstein VA, Lipson SD, et al. Cystic teratomas of the ovary: diagnostic value of sonography. AJR Am J Roentgenol 1998;171(4):1061–1065.
72. Outwater EK, Wagner BJ, Mannion C, et al. Sex cord-stromal and steroid cell tumors of the ovary. Radiographics 1998;18(6):1523–1546.
73. Ko SF, Wan YL, Ng SH, et al. Adult ovarian granulosa cell tumors: spectrum of sonographic and CT findings with pathologic correlation. AJR Am J Roentgenol 1999;172(5):1227–1233.
74. Demidov VN, Lipatenkova J, Vikhareva O, et al. Imaging of gynecological disease (2): clinical and ultrasound characteristics of Sertoli cell tumors, Sertoli-Leydig cell tumors and Leydig cell tumors. Ultrasound Obstet Gynecol 2008;31(1):85–91.
75. Stephenson WM, Laing FC. Sonography of ovarian fibromas. AJR Am J Roentgenol 1985;144(6):1239–1240.
76. Athey PA, Malone RS. Sonography of ovarian fibromas/thecomas. J Ultrasound Med 1987;6(8):431–436.
77. Outwater EK, Marchetto B, Wagner BJ. Virilizing tumors of the ovary: imaging features. Ultrasound Obstet Gynecol 2000;15(5):365–371.
78. Brown DL, Zou KH, Tempany CMC, et al. Primary versus secondary ovarian malignancy: imaging findings of adnexal masses in the Radiology Diagnostic Oncology Group Study. Radiology 2001;219(1):213–218.
79. Alcazar JL, Galan MJ, Ceamanos C, Garcia-Manero M. Transvaginal gray scale and color doppler sonography in primary ovarian cancer and metastatic tumors to the ovary. J Ultrasound Med 2003;22(3): 243–247.
80. Cho KC, Gold BM. Computed tomography of Krukenberg tumors. AJR Am J Roentgenol 1985;145(2):285–288.
81. Athey PA, Butters HE. Sonographic and CT appearance of Krukenberg tumors. J Clin Ultrasound 1984;12(4):205–210.
82. Ulbright TM, Roth LM, Stehman FB. Secondary ovarian neoplasia. A clinicopathologic study of 35 cases. Cancer 1984;53:1164.
83. Hann LE, Lui DM, Shi W, et al. Adnexal masses in women with breast cancer: US findings with clinical and histopathologic correlation. Radiology 2000;216(1):242–247.
84. Shimizu H, Yamasaki M, Ohama K, et al. Characteristic ultrasonographic appearance of the Krukenberg tumor. J Clin Ultrasound 1990;18(9):697.
85. Testa A, Ferrandina G, Timmerman D, et al. Imaging in gynecological disease (1): ultrasound features of metastases in the ovaries differ depending on the origin of the primary tumor. Ultrasound Obstet Gynecol 2007;29(5):505–511.
86. Gougoutas CA, Siegelman ES, Hunt J, Outwater EK. Pelvic endometriosis: various manifestations and MR imaging findings. AJR Am J Roentgenol 2000;175(2):353–358.
87. Suren A, Osmers R, Dietrich M, et al. Sonomorphology of endometriotic cysts. Int J Gynecol Obstet 1998;62:155–165.
88. Fedele L, Bianchi S, Portuese A, et al. Transrectal ultrasonography in the assessment of rectovaginal endometriosis. Obstet Gynaecol 1998;91(3):444–448.
89. Patel MD, Feldstein VA, Chen DC, et al. Endometriomas: diagnostic performance of US. Radiology 1999;210(3):739–745.
90. Woodward PJ, Sohaey R, Mezzetti Jr TP. Endometriosis: Radiologic-Pathologic Correlation. Radiographics 2001;21(1):193–216.
91. Volpi E, De Grandis T, Zuccaro G, et al. Role of transvaginal sonography in the detection of endometriomata. J Clin Ultrasound 1995;23:163–167.
92. Spencer JA, Weston MJ. Imaging in endometriosis. Imaging 2003;15(2):63–71.
93. Asch E, Levine D. Variations in appearance of endometriomas. J Ultrasound Med 2007;26(8):993–1002.
94. Alcázar JL, Laparte C, Jurado M, López-García G. The role of transvaginal ultrasonography combined with color velocity imaging and pulsed Doppler in the diagnosis of endometrioma. Fertil Steril 1997;67(3):487–491.
95. Okaro E, Condous G, Khalid A, et al. The use of ultrasound-based 'soft markers' for the prediction of pelvic pathology in women with chronic pelvic pain – can we reduce the need for laparoscopy? BJOG 2006;113(3):251–256.
96. Timor-Tritsch IE, Lerner JP, Monteagudo A, et al. Transvaginal sonographic markers of tubal inflammatory disease. Ultrasound Obstet Gynecol 1998;12(1):56–66.
97. Patel MD, Acord DL, Young SW. Likelihood ratio of sonographic findings in discriminating hydrosalpinx from other adnexal masses. AJR Am J Roentgenol 2006;186(4):1033–1038.

CHAPTER

36

Uterus and vagina

Michael J. Weston

INTRODUCTION 686
Other tests 687

SYMPTOMS 688
Management of abnormal uterine bleeding 688

MYOMETRIUM 689
Uterine fibroids 689
Pregnancy and fibroids 690
Fertility and fibroids 691
Nomenclature of site of fibroids 691
Symptoms and fibroids 691
Ultrasound appearances of fibroids 691
Vascularity and malignant change 693
Treatment of fibroids 693
Adenomyosis 694
Symptoms of adenomyosis 694
Diagnosis of adenomyosis 694
Treatment of adenomyosis 695
Other myometrial lesions 695
Malignant mixed Müllerian tumours 695
Uterine sarcoma 695
Lymphoma and metastases 695
Lipoma 695
Arteriovenous malformation (AVM) 695
Gestational trophoblastic disease (GTD) 696
The postoperative uterus 697
Dilatation and curettage 697
Endometrial ablation 697
Caesarean section scars 697
Hysterectomy; subtotal hysterectomy; trachelectomy 697

ENDOMETRIUM 700
Endometrial hyperplasia 700
Endometrial polyps 700
Endometrial cancer 702
Aetiology 702
Symptoms 702
Diagnosis 702
Other investigations 705
Screening 705
Management 705
Medications and the endometrium 705
Oral contraceptive pill 705
Hormone replacement therapy (HRT) 705
Tamoxifen and anastrozole 706
Intrauterine devices 706
Endometritis 709
Asherman's syndrome/intrauterine synechiae 709
Haematometrium and other related conditions 709
The postpartum uterus 711
Retained products of conception (RPOC) 711

THE CERVIX 712
Benign conditions 713
Nabothian cysts 713
Cervical polyp 713
Cervical fibroid 713
Cervical incompetence 714
Cervical cancer 714
Aetiology 714
Symptoms 714
Ultrasound appearances 714
Other investigations 714
Management 715

THE VAGINA 715
Foreign bodies 715
Fluid-filled vaginal lesions 716
Solid vaginal lesions 716

INTRODUCTION

Ultrasound is well established as the initial imaging investigation of choice for the majority of pelvic symptoms in women. Professor Ian Donald first described its use in obstetrics and gynaecology in the 1960s[1] and Kratochwil first described transvaginal sonography in 1969.[2] Nowadays, although ultrasound should be used to build up the clinical picture in combination with history, examination and laboratory tests, it forms an indispensable part of patient evaluation, often more so in those whose condition precludes effective bimanual examination, such as the obese, those who are virgo intacta or those with postmenopausal atrophy. Ultrasound can also help to reduce the number of women who have to undergo invasive procedures like hysteroscopy.

Transabdominal and transvaginal scans are both required in order to fully assess the uterus. Transvaginal scan, done with an empty bladder, enables a high-frequency probe to be placed next to the uterus and good resolution images obtained of the uterine contents. This can be achieved whether the uterus lies in an anteverted or retroverted position. The head of the probe is able to be positioned against the side of the uterus so that the endometrial cavity lies perpendicular to the ultrasound beam (Fig. 36.1). The uterus does not always lie favourably for transvaginal examination. On occasion, more often so in the obese, the uterus will remain in an axial orientation so that the endometrial cavity runs directly away from the probe and parallel to the ultrasound beam. This produces relatively poor quality images. Sometimes bimanual manipulation using the free hand on the abdomen will allow the uterus to be moved to a more favourable position for imaging. Continuing to image whilst withdrawing the transvaginal probe will allow the vaginal walls to be seen as well as adjacent structures, like the urethra. Women who are unsuitable for transvaginal scan either due to age, preference or disability may tolerate a transperineal or translabial scan instead.

The transabdominal scan is usually performed with a full bladder (Fig. 36.2). The bladder displaces gas-filled bowel out of the pelvis and allows the gynaecological organs to be seen. It facilitates visualisation of large pelvic masses that otherwise would not be accessible to the transvaginal scan and also helps to provide an overview

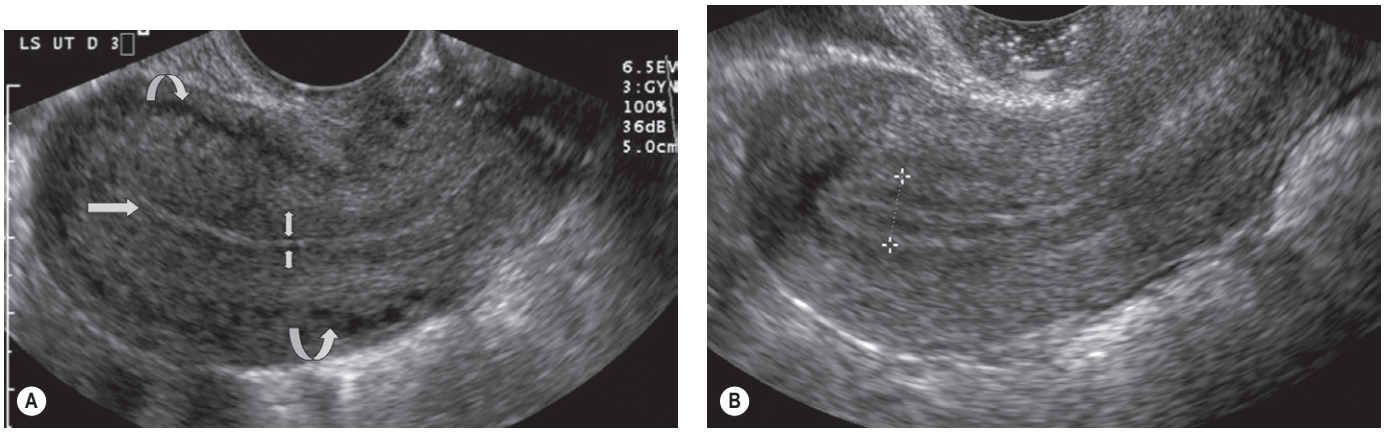


Figure 36.1 Uterus. A: Normal transvaginal longitudinal image of the uterus. Note the defined thin endometrial echo (arrow) and its dark myometrial halo (double-headed arrows). The halo should not be confused as being part of a trilaminar proliferative endometrium. Also note the prominent subserosal myometrial vessels (curved arrows). **B:** Normal transvaginal longitudinal image of the uterus. The endometrium is in the proliferative phase and shows a typical trilaminar pattern, between the callipers. The dark myometrial halo is present around the endometrium. Compare this to **A** where the endometrium is atrophic.



Figure 36.2 Normal transabdominal longitudinal image of the uterus, using the full bladder technique. The uterus is further away from the probe than in the transvaginal images but detail of the endometrium and myometrial halo is still visible.

of the pelvic relations. In slim women, it may not be necessary to have a full bladder in order to obtain good views of the uterus. Gentle pressure with the probe on the abdominal wall will bring the uterus into view within the near field of the probe and allow good resolution imaging. This can be especially useful in early pregnancy scans. The transabdominal approach also allows the kidneys to be checked for hydronephrosis, which might be secondary to gynaecological pathology.

Some authors advocate using just transvaginal ultrasound for dedicated clinics. An example might be a postmenopausal bleeding clinic where the evaluation of the endometrium is paramount. It is argued that it is more comfortable for the women to attend with an empty bladder than to struggle to fill their bladder. A transvaginal scan answers all the necessary questions and allows a decision to be made on the need for hysteroscopy. Opponents argue that, for a small expense of time, denying a transabdominal scan loses the opportunity to examine other pelvic organs and the kidneys. Women in the postmenopausal age group are likely to have other pathologies that might be missed without a transabdominal scan.

The ultrasound examination can be extended to include Doppler studies, contrast enhancement or the use of saline infusion to show the endometrial cavity. If large pelvic masses or malignancy are found then the examination should be extended to assess the upper abdomen for ascites, omental cake, lymphadenopathy and liver lesions. Ultrasound is not as sensitive as computed tomography for these findings, but it is specific. If disease spread is found on the initial ultrasound, it enables management to be appropriately focussed.

Other tests

Computed tomography (CT) offers very little in the evaluation of the uterus. It may coincidentally show a distended uterine cavity in scans performed for other reasons, but other tests will be required to determine if there is pathology present. Some authors believe that modern multidetector CT scanners with their ability to produce isometric voxels in multiplanar reconstructions may rival MR scans in their staging of the cervix but this is yet to be reliably proven. CT does provide useful assessment of lymphadenopathy and distant metastases in women with uterine or cervical cancers and it can show complications of treatment such as colo-vaginal fistulae or abscesses.

Magnetic resonance (MR) provides exquisite images of the uterus and cervix, demonstrating zonal anatomy on T2-weighted images (Fig. 36.3). It has a strong role in the local staging of endometrial and cervical cancers. Its use is best reserved for imaging once the diagnosis of cancer has already been made. Like ultrasound, MR cannot distinguish benign endometrial hyperplasia from cancer even with diffusion-weighted imaging, so biopsy remains necessary. Ultrasound is a cheaper and more readily available test to assess the endometrium prior to biopsy. MR has a role in the follow-up of cancers treated with chemo/radiotherapy and is also the best objective test to assess fibroids before and after uterine artery embolisation.

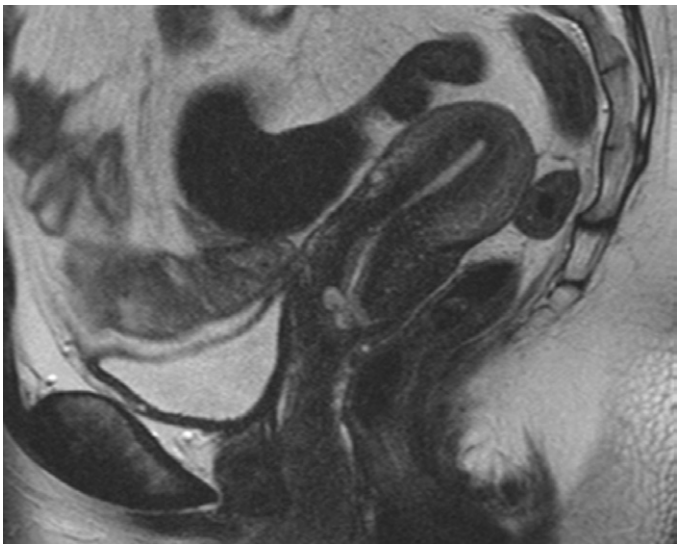


Figure 36.3 T2-weighted MR scan of a retroverted uterus. The zonal anatomy of the uterus is well shown, with a white endometrium, a dark junctional zone and a grey outer myometrium

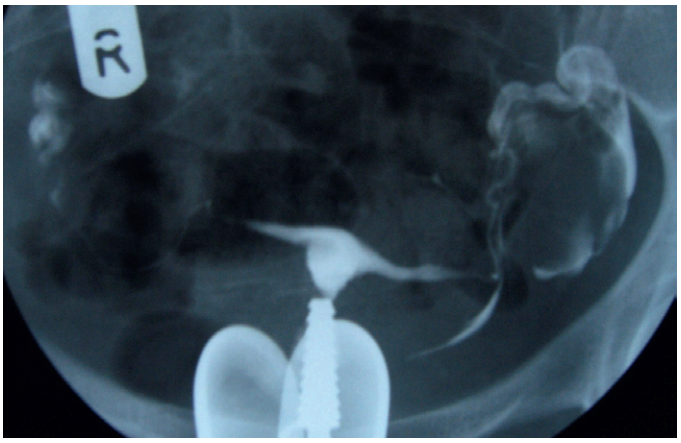


Figure 36.4 Hysterosalpingogram. Contrast medium outlines the endometrial cavity and traces out the fallopian tubes. Free spill is shown from the tube on the left.

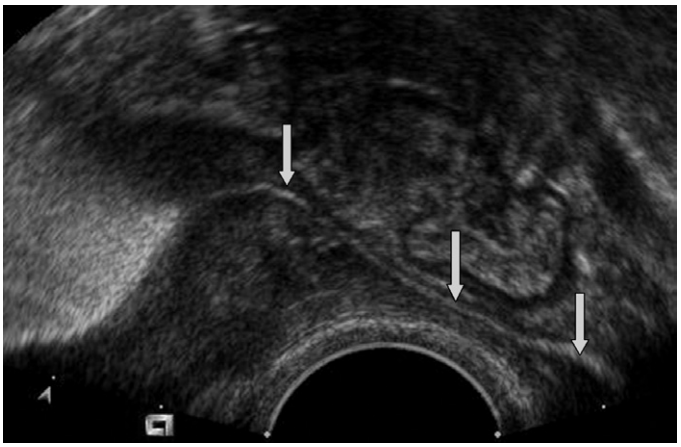


Figure 36.5 HyCoSy. Transvaginal image showing echogenic contrast agent filling the endometrial cavity and outlining the left fallopian tube (arrows).

Positron emission tomography (PET) has a role in looking for distant metastases when pelvic exenteration is being considered. PET looks for metabolically active tumour and can direct attention to nodes or nodules that might otherwise have been overlooked on other imaging. The combination of the PET image overlaid on a low-dose CT scan done at the same examination allows the site of activity to be localised.

Hysterosalpingogram (HSG) allows the uterine cavity and the patency of the fallopian tubes to be assessed (Fig. 36.4). It is most used in assisted conception units. The ultrasound equivalent hystero-contrast-sonography (HyCoSy) can be used in order to avoid radiation (Fig. 36.5). HyCoSy has a high degree of accuracy (over 90%) when demonstrating the fallopian tubes to be patent but suffers with a low accuracy of 50% when diagnosing tubal occlusion. HSG or laparoscopy and dye tests are required to confirm occlusion.

Hysteroscopy is the gynaecologists' main tool when assessing the endometrium. It can be done as an outpatient procedure with a small flexible scope or as a day-case procedure under anaesthesia with a rigid larger-calibre scope. The rigid scope allows directed biopsy or resection to be done. Otherwise, the flexible scope, outpatient procedure uses a pipelle biopsy catheter to obtain non-directed sampling of the endometrium. Saline infusion hysterography (SIH) is an ultrasound technique that may be used as an alternative to flexible hysteroscopy in the diagnosis of focal endometrial abnormalities. Patients report much lower pain scores with SIH.

SYMPTOMS

Symptoms arising from the uterus, cervix and vagina are mostly related to abnormal bleeding and this is the commonest presenting feature. Painful periods (dysmenorrhoea) or pain during sexual intercourse (dyspareunia) may occur. Some masses will cause local pressure symptoms and may result in urinary retention or hydronephrosis. Fever and discharge may point the way to pelvic inflammatory disease with uterine lesions varying from endometritis to a pyometrium. Loss of the threads from an intrauterine device will necessitate a scan to determine if the device is still present. Infertility is covered in Chapter 38.

Menorrhagia is defined as a measured menstrual loss of more than 80 mL per cycle. Other commonly used terms that might be seen on scan request cards are:

- *Dysfunctional uterine bleeding* (DUB): irregular or non-cyclical bleeding that results from endogenous or exogenous hormonal fluctuations, such as anovulation or hormone replacement therapy.
- *Intermenstrual bleeding* (IMB): bleeding between periods. This is often caused by uterine pathology such as an endometrial polyp.
- *Postcoital bleeding* (PCB): bleeding after sexual intercourse, usually as a result of cervicitis or vaginal wall pathology.
- *Postmenopausal bleeding* (PMB): bleeding that recommences more than a year after the last period. About 10–12% of cases will be due to a malignant cause.

Management of abnormal uterine bleeding

There are many causes of abnormal uterine bleeding as listed in Table 36.1. The uterus needs to be investigated in premenopausal women because of the probability of finding structural causes of the bleeding such as fibroids and polyps. Treating these causes will hopefully resolve the symptoms. Those women who do not have a structural cause for their bleeding are classified as having dysfunctional uterine bleeding (DUB). Approximately 55% of women investigated by hysteroscopy will have an apparently normal uterus and fall into this category of DUB. Ultrasound can be used

Table 36.1 Causes of abnormal vaginal bleeding

Uterus
Fibroids
Adenomyosis
Endometrial pathology
Hyperplasia
Polyp
Carcinoma
Pelvic inflammatory disease
Endometritis
Chronic
Postmenopausal atrophic
Coagulopathies
Congenital deficiencies
Thrombocytopenia
Leukaemia
Systemic disorders
Hypothyroidism
Systemic lupus erythematosus
Chronic liver failure
Obesity
Iatrogenic
Intrauterine devices
Anticoagulants
Progesterones
Cervix
Chronic cervicitis
Polyp
Carcinoma
Vagina
Atrophic vaginitis
Infection
Foreign body
Trauma
Carcinoma
Vulva
Squamous carcinoma
Melanoma
Non-gynaecological sources mistaken for vaginal bleeding
Haematuria
Rectal bleeding

to identify those women who do not need hysteroscopy by defining normality. It is less useful as a positive predictor as hysteroscopy will still be needed.

Medical treatment can be hormonal or non-hormonal. Progesterone is often used to stabilise menstrual loss. The oral contraceptive pill can also be used in those without contraindications and is particularly useful in younger women who also require contraception. Non-hormonal treatments such as tranexamic acid (improved haemostasis) or mefenamic acid (control of prostaglandin production in the uterus) can be tried.

The Mirena intrauterine system, although initially marketed as a contraceptive device, has become used for much wider indications including control of heavy bleeding. It comprises a slow-release cylinder of levonorgestrel around a conventional T-shaped frame. Levonorgestrel is a progesterone that has local effects on the endometrium and prevents proliferation. The system can be left in place for 5 years.

Surgical management varies from hysterectomy, through submucous fibroid resection and endometrial resection, to newer techniques of endometrial ablation and radiological techniques of uterine artery embolisation (UAE), transvaginal radio-frequency ablation (RFA) and high-intensity focused ultrasound (HIFU).

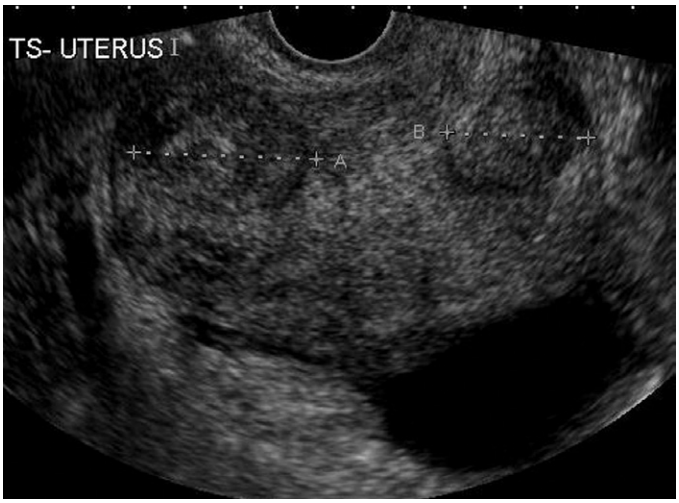


Figure 36.6 Transverse transvaginal view of the uterus showing two intramural fibroids (marked by callipers).

MYOMETRIUM

Uterine fibroids

Fibroids (also known as myomas, leiomyomas or fibroleiomyomas) are a benign uterine smooth muscle proliferation. The smooth muscle fibres are disposed in smooth concentric rings with a variable amount of fibrous tissue forming whorls of tissue. They are usually clearly demarcated and most commonly found in the body of the uterus (Fig. 36.6) though they may arise in the cervix or broad ligament and very rarely in the vagina.[3]

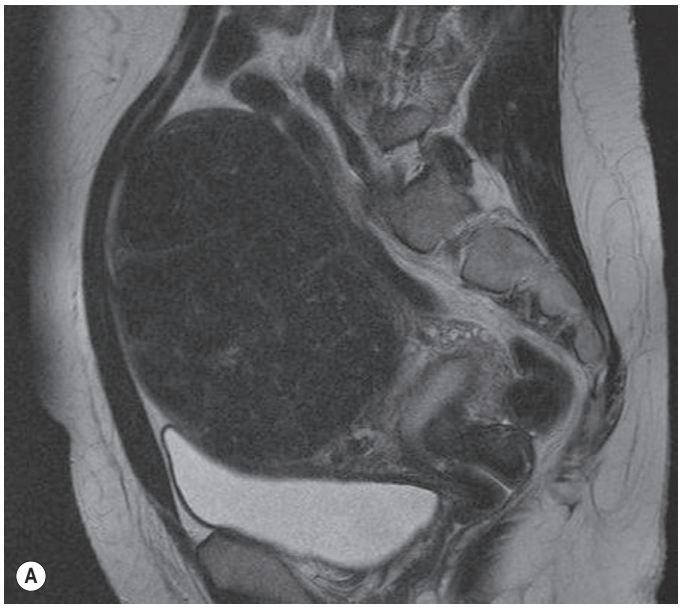
Fibroids are common, being present in more than 30% of women aged 40–60 years of age.[4] Risk factors for fibroids include nulliparity, obesity, family history, black race and hypertension. Interestingly, physical activity is thought to be protective against the development of fibroids, and not just because women with fibroids avoid exercise.[5] There is an association of polycystic ovary syndrome and the development of fibroids in African-American women.[6] There is clearly a relationship with oestrogen stimulation: nulliparity indicates continuous oestrogen stimulation without the interruption of pregnancy or lactation; obesity is associated with increased amounts of endogenous oestrogen being stored in body fat; tamoxifen and hormone replacement therapy treatment may result in enlargement of fibroids. Many medical treatments of fibroids are aimed at interrupting this oestrogen stimulation. Depo-Provera (medroxyprogesterone acetate),[7] mifepristone,[8] and gonadotrophin-releasing hormone[9] have all been shown to decrease fibroid size and improve quality of life. Likewise, the use of a Mirena intrauterine system in women with fibroids and menorrhagia has been shown to reduce menstrual blood loss and pain,[10] though the rate of expulsion of the device is higher in women with fibroids than in those without.

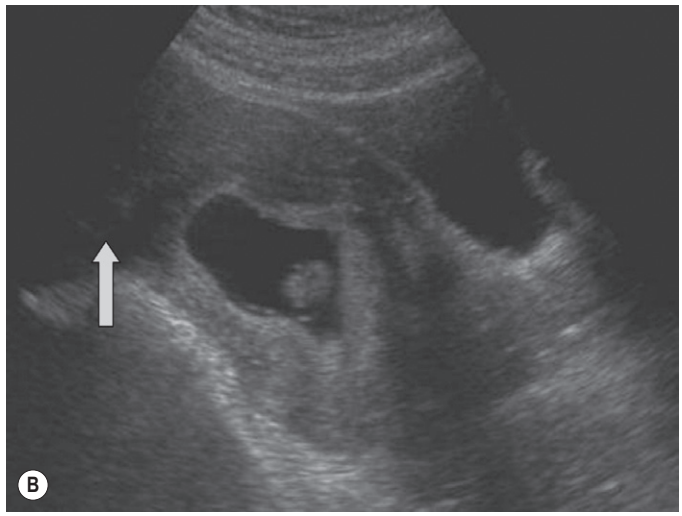
Fibroids change in size with age. They are unknown prior to puberty, they enlarge with time during the reproductive years and they reduce in size after the menopause.[11] Their size can vary from the imperceptible on ultrasound to lesions that fill the abdominal cavity. Size does not necessarily correlate with symptoms, the largest often being silent. Small fibroids affecting the endometrium can produce disproportionately severe symptoms, possibly by increasing the surface area of the endometrial cavity.

Pregnancy and fibroids

Pregnancy is often quoted as a cause of fibroid enlargement: whilst it is true that enlargement and central degeneration of fibroids may occur, this phenomenon is actually quite rare,[12] with the great majority of pregnant women showing no change in size of their fibroids (Fig. 36.7). Those that do change in size most commonly do so in the first trimester. Fibroids do impact on the management of some pregnancies[13] though most pregnancies are unaffected. Large (greater than 5 cm) submucosal and retroplacental fibroids seem to impart a greater risk for pain, vaginal bleeding, placental abruption, abnormally adherent placenta (accreta), growth restriction and preterm delivery. Very rarely fibroids in the lower segment or cervix may prevent a normal vaginal delivery. Uterine fibroids of 5 cm in size or larger are independently associated with caesarean section performed prior to the onset of labour and the risk increases with the size of the fibroid.[14] Myomectomy at the time of caesarean delivery carries a high risk of significant haemorrhage and is best avoided. Pyomyoma is the rare development of an infected fibroid in the postpartum period. It is uncommon since the advent of antibiotics but is potentially lethal. The formation of gas in the fibroid gives a distinctive pattern of increased echogenicity.[15]

Uterine contractions in pregnancy (Braxton Hicks) may mimic the presence of a fibroid by distorting the uterine contour, usually the inner contour rather than the outer. They can be distinguished by their normal echogenicity and because they are transient. Patience is required as it may take up to 20 minutes for them to relax and show that the apparent mass was only a contraction. Rim calcified fibroids may also confuse the sonographer by simulating the fetal head or if the rim is incompletely calcified, other fetal parts.





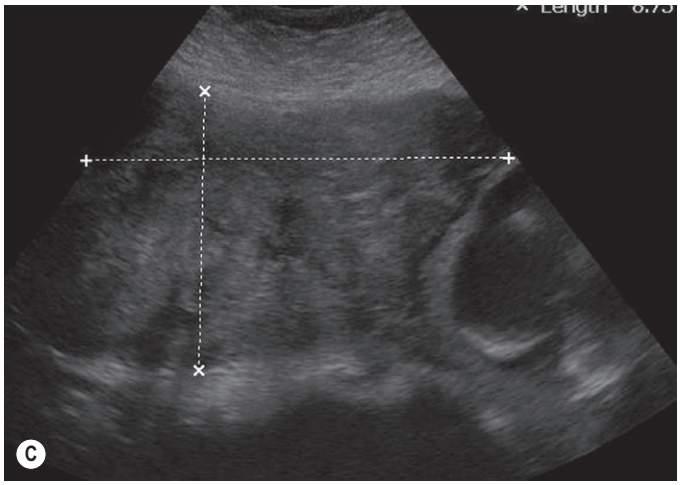


Figure 36.7 Pregnancy and fibroids. MR scan of the non-gravid uterus **(A)** shows a large subserosal fibroid arising from the anterior wall of the uterus and bending the uterus posteriorly. Ultrasound when the woman is pregnant shows the fibroid arising off the fundus of the uterus on the edge of image (arrow) **(B)** and it is shown fully in image **(C)** between the callipers. It has not enlarged or shown central degeneration.

Fertility and fibroids

Fibroids are implicated in subfertility. They may block the tubal ostia or prevent implantation of the embryo by distorting the uterine cavity. Endometrial thickness is no different between those with fibroids and those without, but in a study of those undergoing first assisted reproduction cycles, the rate of non-proliferative endometrial pattern and live birth rates (34% for those with fibroids versus 43% for those without) were significantly different.[16] Women with fibroids larger than 4 cm require an increased number of IVF cycles to achieve an ongoing pregnancy.[17]

Nomenclature of site of fibroids

The clinical symptoms that may arise, outside of pregnancy, depend on the site and size of the fibroid. Fibroids that lie entirely within the myometrium are termed intramural; those that distort the outer margin of the uterus are subserosal; and those that distort the endometrial cavity are submucosal. The degree of distortion caused by submucosal and subserosal fibroids may vary from a minor bump to a fully pedunculated fibroid.

The European Society of Hysteroscopy has classified submucosal fibroids into three groups: those that are pedunculated and entirely within the endometrial cavity are type 0; those that lie mostly within the cavity such that there is an acute angle between the wall of the cavity and the wall of the fibroid are type 1; and those that are mostly within the myometrium such that the angle between the cavity wall and the wall of the fibroid is obtuse are type 2. The purpose of the classification is to reflect the suitability for hysteroscopic resection of the fibroid. Submucosal fibroids may be expelled vaginally following treatments such as uterine artery embolisation or gonadotrophin-releasing hormone agonists.[18]

Subserosal fibroids have the same variety of extension through the uterine serosa. Fully pedunculated fibroids may provide diagnostic difficulty in distinguishing them from other adnexal masses. Degenerative cystic change in the fibroid may give it an appearance similar to an ovarian cyst.[19] A valuable sign is the 'bridging vascular' sign whereby the blood supply to the pedunculated mass is seen to arise from uterine vessels helping to confirm its pedunculated nature.[20] A fibroid that has its blood supply through a narrow pedicle runs the risk of twisting and cutting off the blood supply, the so-called torted pedunculated fibroid. This produces acute symptoms of pain and tenderness, not unlike any other cause of an acute abdomen. Torsion of other adnexal masses or ovaries will give similar symptoms. CT is usually better than ultrasound in establishing the diagnosis in the acute setting.[21] Those subserosal fibroids that extend laterally may lie within the layers of the broad ligament; indeed fibroids may develop entirely within the broad ligament, as can other rare variants of fibroids such as an angioleiomyoma.[22]

Symptoms and fibroids

A causal relationship is often difficult to establish, but fibroids are associated with menorrhagia, pelvic pain and pelvic or urinary obstructive symptoms[3] in addition to the fertility- and pregnancy-related conditions described above. Disorders of menstruation are the commonest presenting feature.

Urinary retention rarely affects women of reproductive years. The commonest causes are gynaecological surgery or pelvic masses. Large fibroids or fibroid uteri can act to distort the position of the cervix and bladder neck.[23] Hysterectomy in such cases has been shown to alleviate the urinary symptoms.

Torsion of a pedunculated fibroid is a well-recognised cause of acute pelvic pain. Much rarer is torsion of the whole uterus due to the presence of fibroids. It has been reported in association with uterine prolapse.[24] Another rare occurrence is inversion of the uterus. This can occur when a submucous fibroid is expelled through the cervix and pulls the uterus inside-out.

Deep dyspareunia (pelvic pain associated with sexual intercourse) has been shown to be unrelated to the presence of fibroids. Women with fibroids do not have any increased prevalence or severity of deep dyspareunia and their sexual function is unimpaired.[25]

Ultrasound appearances of fibroids

Fibroids produce a variety of ultrasound appearances depending on their size, number, position and the relative amount of fibrous tissue, smooth muscle and calcification within them. The typical appearance of an intramural fibroid is of a well-demarcated, round or oval lesion within the normal homogeneous myometrial echo (Fig. 36.8). Fibroids may be echo-poor, isoechoic to myometrium, or echo-bright. Increased reflectivity may be due to calcification, which can be punctuate, amorphous or rim in nature, or due to the presence of fat within the lesion; a so-called lipoleiomyoma (Fig. 36.9). The uterus can be enlarged by the presence of one or many

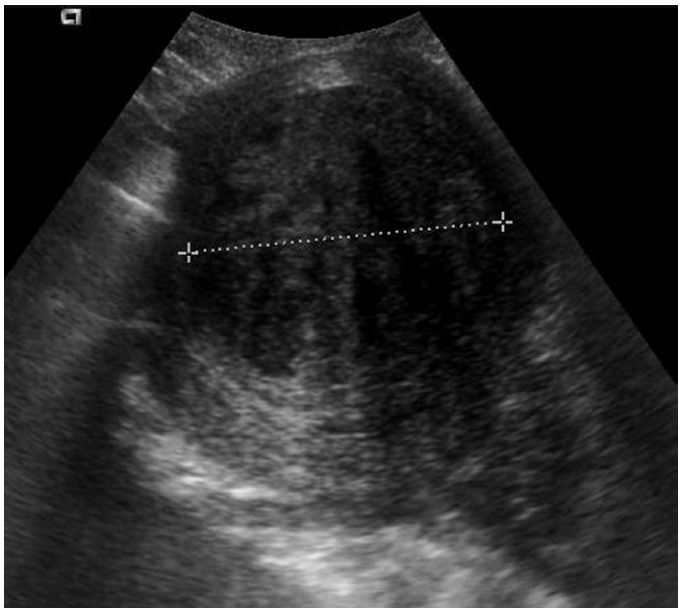


Figure 36.8 Transverse view of a fibroid in the uterine fundus. The fibroid is between the callipers. Note the streaky shadowing arising from the fibroid. A characteristic feature.



Figure 36.9 A small, round, bright fibroid is seen near to the cervix. A high fat content gives it the bright echogenicity and is typical of a lipoleiomyoma.

fibroids and the outline of the uterus may become lobulated (Fig. 36.10), often most easily seen where it pushes against the full bladder. Fibroids have a dense nature which impairs the passage of ultrasound so that most show posterior acoustic shadowing even without calcification. The whorled nature of a fibroid or internal calcification can lead to the typical 'venetian blind' pattern of acoustic shadowing with bands of diverging linear shadows (Fig. 36.11). Fibroids may be so dense or calcified that they prevent visualisation of other structures. Dense calcification of a fibroid is commoner in the postmenopausal age group and may be picked up as an incidental finding on an abdominal radiograph for other reasons. Calcification of the margins alone of a fibroid also occurs (Fig. 36.12). The presence of fibroids may prevent adequate examination of the rest of the pelvic organs; the endometrium and the ovaries may be obscured.

Fibroids can outgrow their blood supply and undergo central necrosis or cystic change (Fig. 36.13). This cystic change can vary from a simple cavity to a complex array of echogenicities with a surrounding irregular wall and septations. It is a not-uncommon diagnostic dilemma to distinguish a cystic fibroid from another potentially serious adnexal mass such as an ovarian tumour. When a mass is large enough it may be impossible to tell on ultrasound whether it is uterine or ovarian in origin. Magnetic resonance plays a very useful role here as it gives a better overall anatomical depiction of the pelvis[26] and may help identify the normal ovaries elsewhere. Indeed MR is ultrasound's complement as it can give precise fibroid mapping and characterisation:[27] because of this MR is the favoured imaging tool in the work-up for uterine artery embolisation and post-embolisation quantification of fibroid shrinkage.

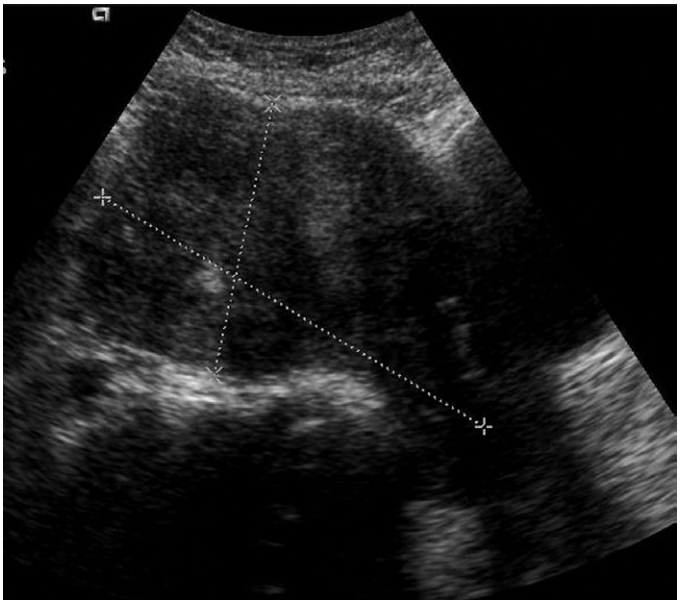


Figure 36.10 Transabdominal image of an enlarged fibroid uterus extending above the level of the bladder. Note its lobulated outline.

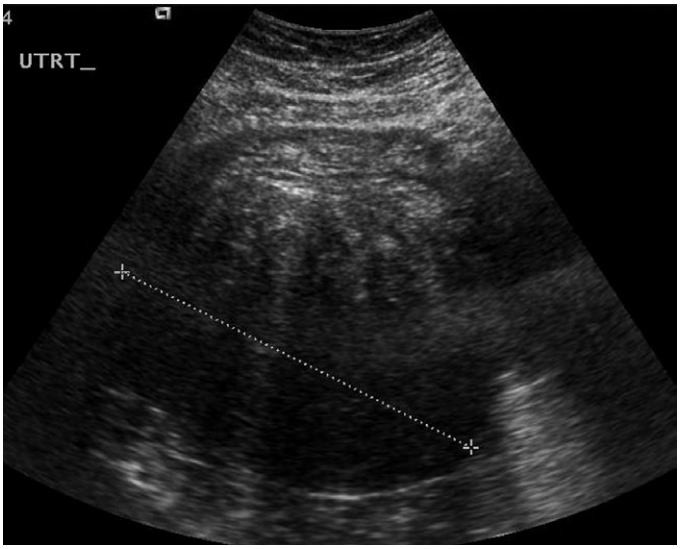
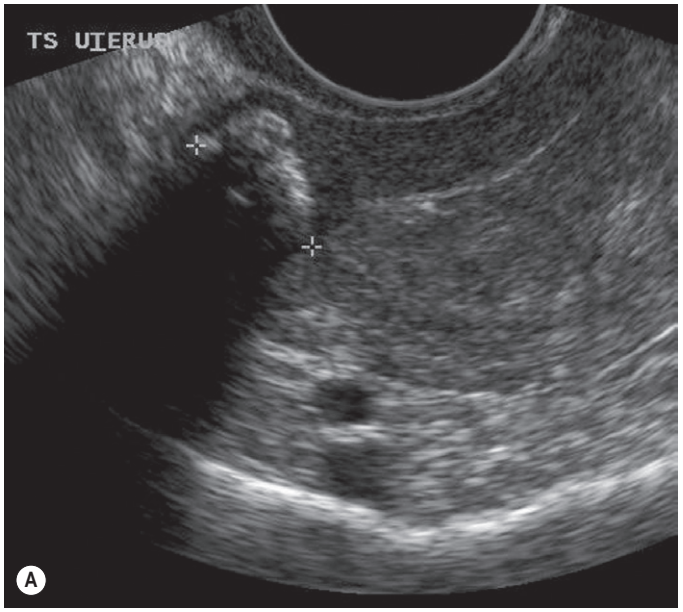


Figure 36.11 A large fibroid marked by the callipers is seen on transabdominal scan. It shows the streaky shadowing that is typical of a fibroid (and is also shown in Fig. 36.8).



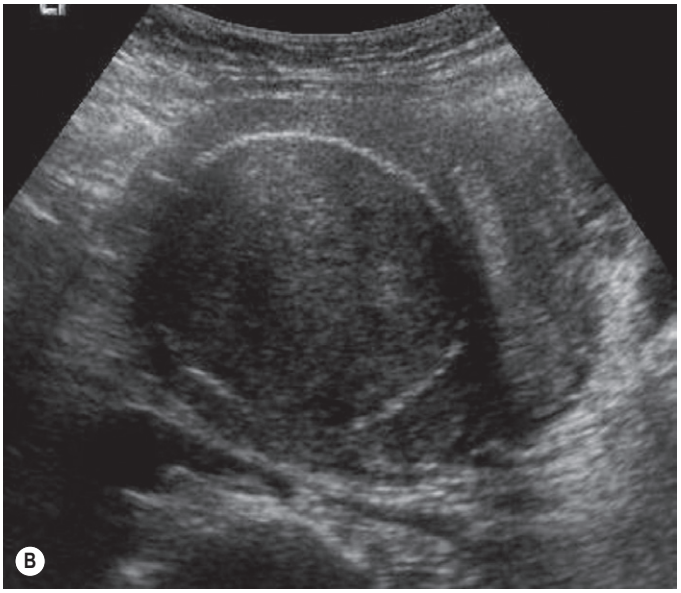


Figure 36.12 Calcified fibroids. A dense calcified fibroid with a strong acoustic shadow **(A)** and a rim calcified fibroid **(B)** are shown.

Submucosal fibroids need to be distinguished from endometrial polyps. Polyps typically show as homogeneously hyperechoic masses. Submucous fibroids are more likely to be hypoechoic. Lesions greater than 20 mm in size are much more commonly fibroids. Fibroids may have more than one feeding vessel whereas polyps never do.[28]

A retroverted uterus on transabdominal ultrasound can produce the misleading impression of a fundal fibroid; this is in part due to the axial lie of the uterus relative to the ultrasound beam and the consequent increase in sound attenuation. Transvaginal ultrasound easily resolves this issue. Duplication anomalies of the uterus, typically a bicornuate uterus, can also confuse as one fundus may mimic a fibroid. Identification of the endometrium in each horn resolves this issue. This can be more of an issue if there is a pregnancy in one horn and not the other.

Ultrasound has a high sensitivity for fibroids but only a relatively poor specificity (about 40% in one study) and a low negative predictive value. Adenomyosis is the most common final diagnosis in women with inaccurate ultrasound reports for uterine fibroids,[29] being found in both false positive and false negative reports. The diffusely enlarged uterus without a focal lesion that might in the past have been thought to represent numerous small intramural fibroid changes is more likely to be a manifestation of adenomyosis. Magnetic resonance is better able to differentiate the two conditions, though of course they often coexist.

Vascularity and malignant change

The blood flow through a fibroid can be very varied. The finding of central or peripherally placed vessels, their velocities and the impedance to flow show a very wide range of variation across benign fibroids. Some authorities believe that fibroids containing sarcoma are more likely to show increased vascularity and high-velocity flows; others believe that malignant mixed mesodermal tumours are more likely to have low-impedance flow;[30] however, these features are non-specific. Leiomyosarcomas are more likely to be larger than 8 cm in diameter (Fig. 36.14) and show central degeneration when diagnosed.[31] Magnetic resonance is also unable to distinguish leiomyosarcomas from cellular fibroids. The most useful indicator is a rapid increase in size of the lesion over time. It should be borne in mind that sarcomas do not generally arise in pre-existing fibroids but develop de novo. Furthermore, most leiomyosarcomas are diagnosed at postoperative histology rather than before resection.

Treatment of fibroids

Hysterectomy used to be the only effective surgical treatment. Women who wish to preserve or improve their fertility may opt for myomectomy. Hysteroscopic resection of submucous fibroids is well recognised. Uterine artery embolisation is well established as an alternative treatment with many papers reporting a 50–60% reduction in fibroid size[32] with up to a 95% rate of symptom relief.



Figure 36.13 Central necrosis of a large fibroid. Note the complex cystic centre with an irregular surrounding wall.

Fibroids

- 30% of women aged 40–60.
- Oestrogen stimulation a common causal factor; regression after menopause.
- Position: submucosal, intramural, subserosal and pedunculated.
- Symptoms: disorders of menstruation, pelvic pain and urinary symptoms.
- Ultrasound appearance variable but commonly attenuating with a streaky shadowing.
- Rapid growth suggests sarcoma.
- Treatments: medical, surgical, embolisation and ablation.

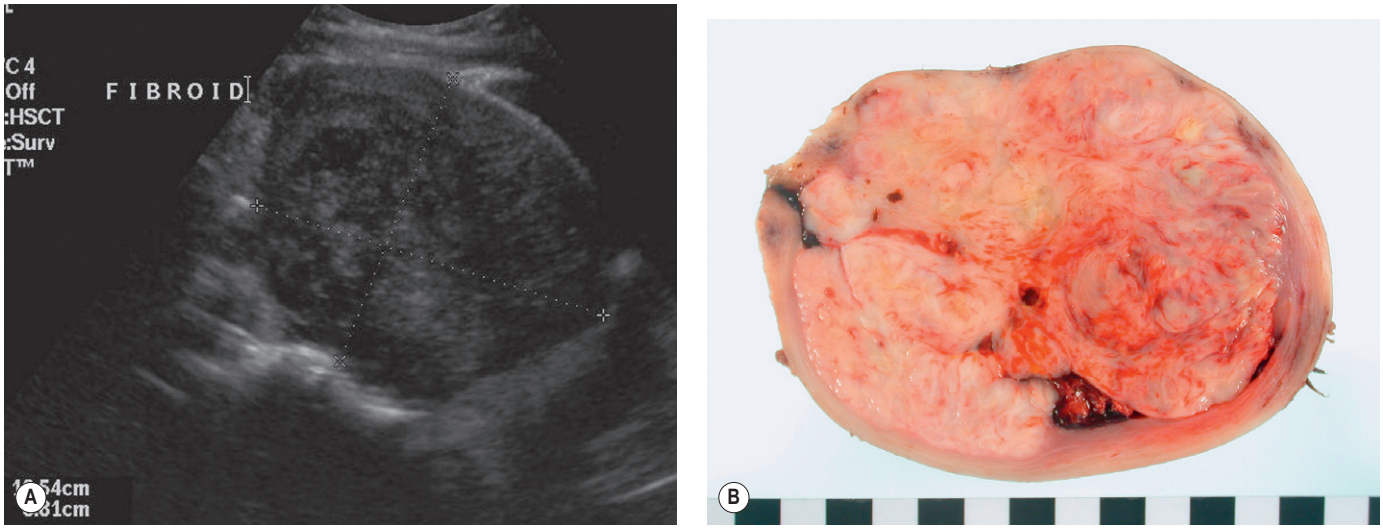


Figure 36.14 Leiomyosarcoma. Ultrasound **(A)** and pathological specimen **(B)** of a proven leiomyosarcoma. The only feature of note was the large size of the 'fibroid'. The diagnosis of sarcoma had not been suspected preoperatively.

Other new treatments include: radio-frequency thermal ablation done either transvaginally[33] or percutaneously;[34] and focused ultrasound ablation.[35]

Medical treatments (Depo-Provera (medroxyprogesterone acetate),[7] mifepristone,[8] and gonadotrophin-releasing hormone[9]) have all been shown to decrease fibroid size and improve quality of life. The use of the Mirena intrauterine system has been discussed earlier. The advent of the menopause relieves many women of their fibroid related symptoms.

Adenomyosis

This is a condition of migration of endometrial glands into the myometrium, which provokes an associated smooth muscle hyperplasia. It is most commonly encountered in the fourth and fifth decades of life and is strongly associated with endometriosis. Up to 80% of women with endometriosis will also have adenomyosis (though women with endometriosis as their main complaint usually present earlier in life, in the third and fourth decades). Adenomyosis is more common in multiparous women.

Symptoms of adenomyosis

Adenomyosis has been a difficult condition to diagnose before the advent of high quality transvaginal ultrasound or magnetic resonance. Consequently, its symptomatology is poorly understood. Certainly, some women will experience heavy or painful bleeding and a tender uterus which waxes and wanes through the cycle.[36] Many though will remain asymptomatic and the condition is only found as an incidental finding on imaging. Adenomyosis often coexists with other conditions and these produce confusion over related symptoms.

Diagnosis of adenomyosis

There is some overlap with the features in fibroid change, and fibroids and adenomyosis may coexist. The most specific signs of adenomyosis on ultrasound[37] are: subendometrial echogenic linear striations; a globular configuration to the uterus; and myometrial cysts (Fig. 36.15). The subendometrial striations have a high positive predictive value of 80%. The myometrial cysts are due to the endometrial glands still showing cyclic function. They are usually 1–5 mm in size and subendometrial, and not to be confused with the normal venous spaces seen in the subserosal layer. Other features (Fig. 36.16) which are less specific are: asymmetric thickening of the uterine walls; loss of definition of the endometrial/myometrial interface; and the formation of adenomyomas. Adenomyomas are usually poorly defined, echogenic masses that may contain cystic spaces, sited near the junctional zone.[38] They have features that overlap with fibroids but one useful feature is that they do not show the rim vascularisation that fibroids may do on colour Doppler. Bright echogenic subendometrial foci may be artefactually

Adenomyosis

- 80% of women with endometriosis also have adenomyosis.
- Many remain asymptomatic.
- Fibroids and adenomyosis may coexist.
- Diagnosis: subendometrial echogenic striations, globular shape to uterus and myometrial cysts.
- MR is a better diagnostic tool for adenomyosis.

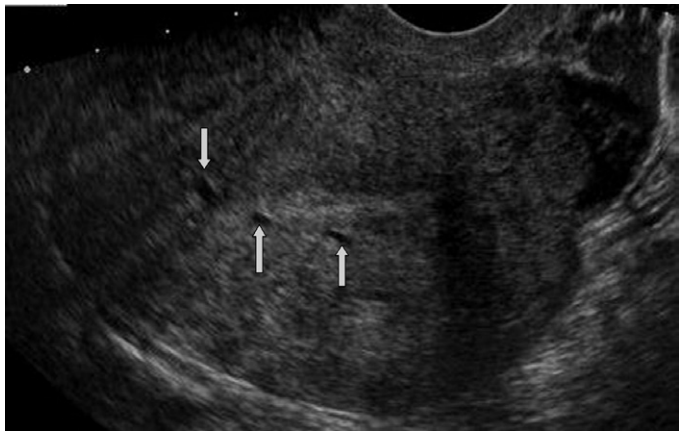


Figure 36.15 Adenomyosis. Three small cysts are seen in the myometrium adjacent to the endometrium (arrows). These are strong indicators of adenomyosis.

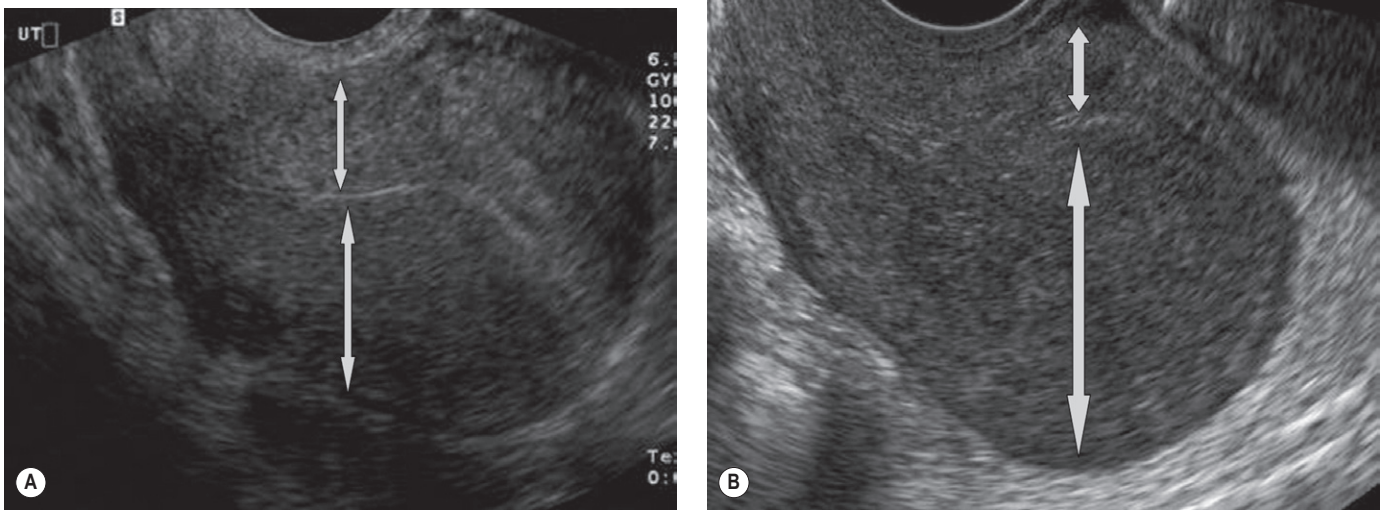


Figure 36.16 Adenomyosis. A and B: Both images show asymmetrical thickening of the uterine walls (double-headed arrows). There is also loss of definition of the endometrium in **(B)**.

produced by intravasation of air during saline infusion hysterography[39] so, ideally, ordinary transvaginal ultrasound should be done prior to any infusion. Overall, the diagnostic sensitivity of ultrasound is suboptimal, even in the best hands only ranging from 50% to 87%.[40] Magnetic resonance is the better imaging tool,[41] showing thickening of the low-signal junctional zone on T2-weighted imaging and the presence of foci of high signal in the myometrium due to haemorrhage (T1) or cystic endometrial glands (T2) (Fig. 36.17). It suffers much less from observer variation.

Adenomyosis can rarely be the origin of adenocarcinoma arising outside the normal endometrium. They may display a more aggressive histological subtype than conventional endometrial adenocarcinoma.

Treatment of adenomyosis

Generally, treatment is aimed at suppressing menstruation. Antiprostaglandins, sex hormones, danazol and gonadotrophin-releasing hormone analogues have all been tried.[42] Surgical procedures include endometrial ablation, laparoscopic electrocoagulation, radio-frequency ablation and adenomyoma resection. Uterine artery embolisation has also been used with promising results. Ultimately, if fertility is not desired, hysterectomy can be offered.

Other myometrial lesions

Malignant mixed Müllerian tumours

These rare tumours are usually aggressive and rapidly invasive. They most commonly present as an intracavitary mass with dilation of the endometrial canal. They tend to look hyperechoic on ultrasound; myometrial invasion is common and has a predilection for the uterine fundus.[43] They arise in pluripotential cells in the Müllerian duct system and are at least in part sarcomatous.

Uterine sarcoma

These are rare tumours with a peak incidence at 50–60 years of age. They mostly develop de novo rather than in pre-existing fibroids. They present with postmenopausal bleeding and are commonly quite bulky at presentation (Fig. 36.18). There are no distinguishing features on ultrasound to separate them from benign fibroids. The most useful sign is that of rapid enlargement. They are often highly vascular with central flow visible on colour Doppler. Histology is required for diagnosis.[31]

Lymphoma and metastases

Lymphomatous involvement of the uterus may occur as part of a generalised systemic disorder (usually non-Hodgkin's type with involvement of liver, spleen or lymph nodes) or as a primary manifestation. In the latter case, it invariably arises in the cervix rather than the uterine body and is usually B-cell in type. Ultrasound shows a uniformly hypoechoic mass which is rarely calcified, centred on the cervix. Magnetic resonance appearances may suggest the diagnosis but biopsy is needed.

Metastases to the uterus are usually to the endometrium, though they can be to the body or cervix as well. They are rare. Primary sites are often in the breast or stomach. There are no specific features on ultrasound.

Lipoma

Lipoleiomyomas are fat-rich fibroids, in distinction to pure lipomas. Both will look bright on ultrasound. Magnetic resonance is useful to prove the presence of fat. They are benign lesions.

Arteriovenous malformation (AVM)

These abnormal arterio-vascular communications may arise as a manifestation of abnormal placentation and retained products of conception or as a consequence of surgical curettage or trauma. They characteristically show as areas of intense signal on colour Doppler within the endometrium or myometrium (Fig. 36.19).[44] Tortuous feeding vessels may be visible on greyscale ultrasound. There is overlap with the appearances of trophoblastic disease, so serum beta human chorionic gonadotrophin (beta-hCG) levels should be checked. They usually present with persistent bleeding after miscarriage. Curettage can provoke massive haemorrhage and is best avoided.[45] Transcatheter arterial embolisation has been the standard treatment; however, the greater use of ultrasound after

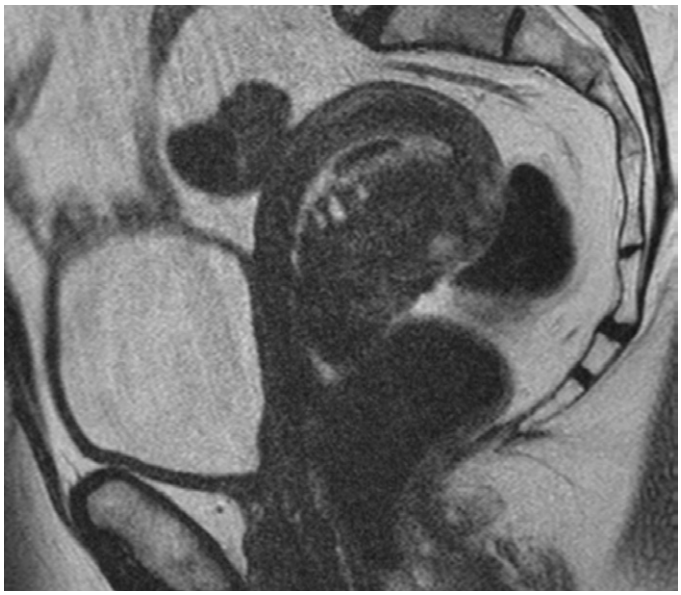


Figure 36.17 MR T2-weighted scan of a retroverted uterus. Small high-signal foci are seen extending into the myometrium from the endometrium. These are cystic endometrial glands diagnostic of adenomyosis.

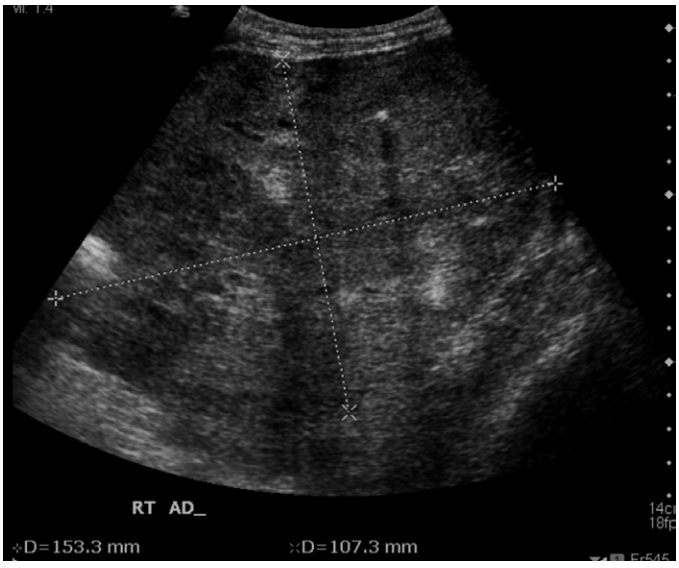


Figure 36.18 A 15 cm fibroid that proved to be a sarcoma at histology.

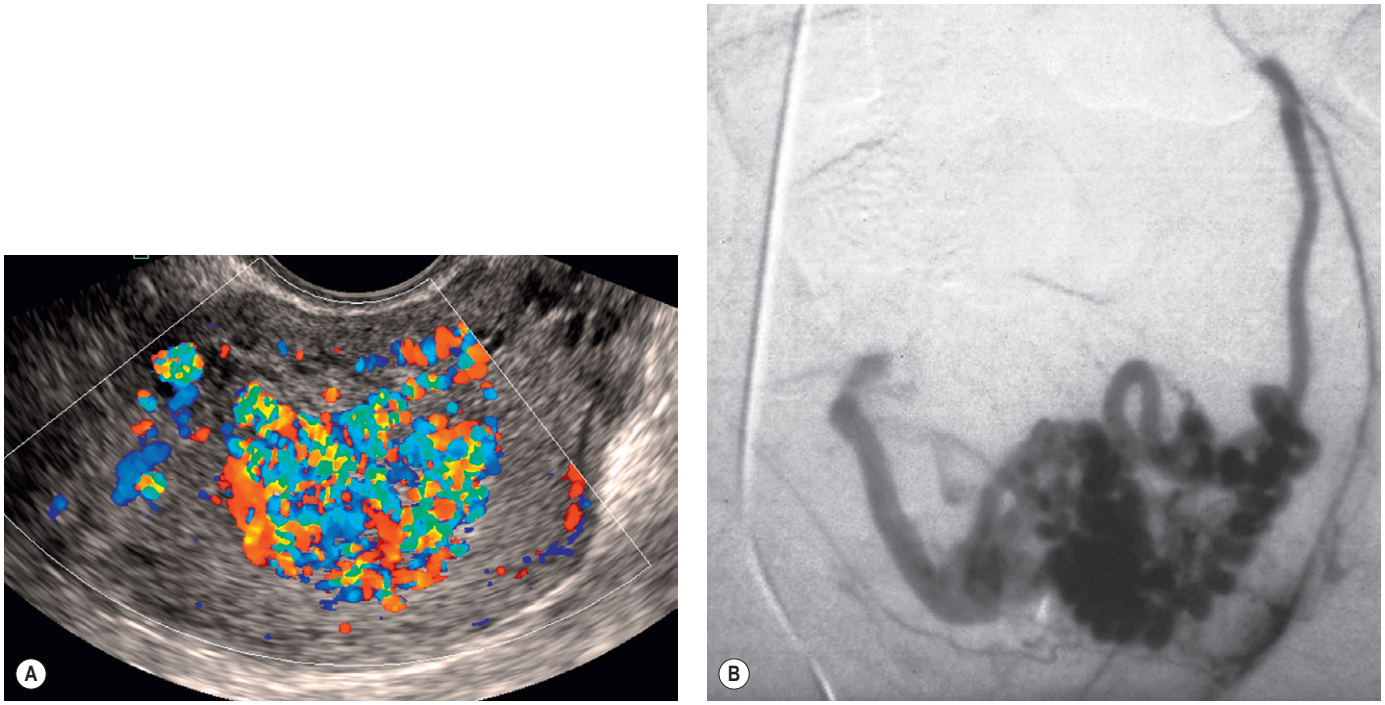


Figure 36.19 Arteriovenous malformation. Transverse view **(A)** of a bright, turbulent blush of colour Doppler signal due to an AVM following miscarriage, together with an arteriogram **(B)** demonstrating the tangle of vessels associated with a true AV fistula.

miscarriage has led to many more arteriovenous fistulae being recognised. Embolisation is still often needed for traumatic fistulae but those related to retained products of conception can be treated conservatively.[46] The malformation resolves once the products pass or resorb. Medical treatment to suppress menstruation is needed until this occurs.

Gestational trophoblastic disease (GTD)

GTD is always associated with products of conception be it following miscarriage, stillbirth, livebirth or termination. Three main categories are recognised: molar pregnancy, which can be partial or complete, invasive mole, and choriocarcinoma, listed in increasing order of invasiveness. Choriocarcinomas are fast growing and often metastasise early to the lungs. The incidence of GTD is about 1 in 2000 pregnancies, but it is far higher in the Far East. The classic presentation is with an enlarged uterus for menstrual age, elevated serum beta-hCG levels and vaginal bleeding. The typical second trimester appearance of a complete molar pregnancy is of a large soft tissue mass with numerous small cystic spaces filling the uterine cavity (Fig. 36.20). The lesions are highly vascular and show copious low-impedance flow on colour Doppler. There may be associated theca lutein cysts of the ovary because of the high beta-hCG levels.

A complete mole is characterised by diffuse trophoblastic proliferation in the absence of any embryonic parts. Partial moles are characterised by focal trophoblastic proliferation and the presence of embryonic or fetal tissue. They exhibit lower beta-hCG levels than complete moles. Complete moles can coexist with a normal pregnancy and must have formed in a dizygotic twin pregnancy.

Retained products of conception are common, occurring in about 17% of first trimester miscarriages and 40% of second trimester miscarriages but only about 6% of normal deliveries.[47] This raises the problem of distinguishing ordinary retained products (Fig. 36.21) from molar change. Features that favour molar change are findings that a mass has its epicentre in the myometrium, a depth of myometrial invasion greater than a third, venous lakes, mass dimension greater than 3.4 cm and endometrial thickness less than

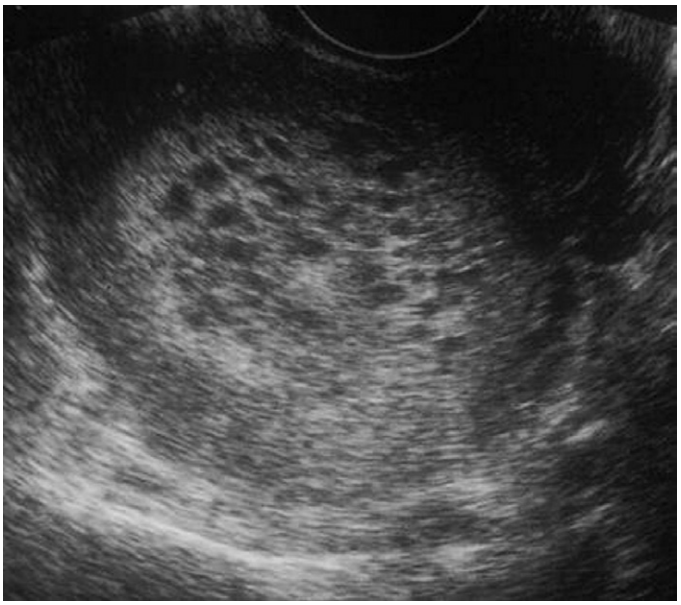


Figure 36.20 Molar pregnancy. The uterine cavity is distended by a soft tissue mass containing numerous small cystic spaces.

12 mm.[48] Looking for small cystic spaces, increased vascularity, ascites and ovarian cysts does not help distinguish the two. A significant proportion of first trimester moles only show minimal hydropic change and so will not show the small cystic spaces classically associated with moles.[49] Serial beta-hCG levels will help.

Ultrasound is valuable in the monitoring of treatment and in follow-up to assess recurrence. A combination of colour Doppler ultrasound and beta-hCG testing is effective, persistent tumour being shown by areas of increased vascularity and an abnormal uterine morphology. Magnetic resonance imaging is invaluable in

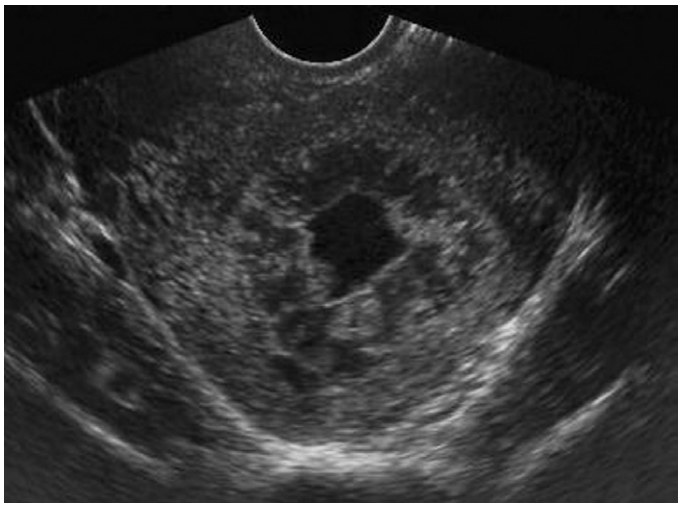


Figure 36.21 Hydropic decidua following miscarriage. Compare and contrast this with the molar change shown in Figure 36.20.

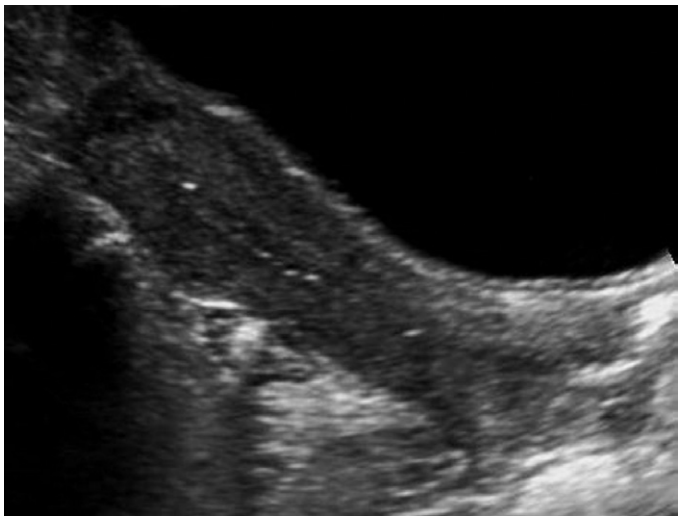


Figure 36.22 Transabdominal scan: small bright foci are seen along the basal layer of the endometrium. These indicate sites of old trauma and can indicate the presence of Asherman's syndrome.

assessing extrauterine spread, vascularity and staging.[50] Methotrexate chemotherapy has a 95% cure rate for gestational trophoblastic tumours.

The postoperative uterus

Dilatation and curettage

The use of newer techniques, involving hysteroscopy or thermal ablation, has rendered this procedure almost obsolete. It involves removing the superficial layer of the endometrium and if confined to this, complications are rare. If done after pregnancy, to remove retained products of conception, there is a greater chance of removing deeper layers of endometrium because the pregnant endometrium is very friable. This deeper resection may cause areas of fibrosis or adhesions to develop. This eventually produces a characteristic picture of small bright foci of echoes on the basal layer of the endometrium, some of which are calcified (Fig. 36.22). These adhesions, which form the basis of Asherman's syndrome,



Figure 36.23 Regrowth of endometrium following endometrial ablation; this example shows fundal reformation together with a small amount of retained intracavitary fluid.

are associated with subfertility and may need to be divided at hysteroscopy although this treatment is not always straightforward and subsequent pregnancies have a higher rate of complications, even including uterine rupture.[51]

Endometrial ablation

Coagulation of the endometrium using thermal energy is an alternative treatment to hysterectomy or medical treatment for dysfunctional uterine bleeding. The aim is to destroy the endometrium and reduce the cavity to a narrow fibrotic tube. The procedure works best if done when the endometrium is at its thinnest in the early part of the cycle. Follow-up ultrasound may show fluid in the cavity, adhesions and residual or regenerated endometrium (Fig. 36.23). Haematometrium is a potential complication and may be focal.

Caesarean section scars

Up to a third of pregnancies may be delivered by caesarean section. A lower segment horizontal incision just above the cervix is preferred, though many may be done through the cervix, especially if done during uterine contractions when the cervix is effaced.[52] In the first few days after operation the incision is visible on ultrasound as a well-defined oval area in the lower uterine segment, which may deform the posterior wall of the bladder. Suture material is shown as small punctate echogenic foci. These signs can take over 6 weeks to disappear and the rate of change is not affected by whether a one- or two-layer closure has been used.[53] Long term, a small echogenic line extending perpendicularly from the endometrium into the anterior myometrium just above the cervix is detectable in nearly all women who have had a caesarean section (Fig. 36.24).[54] This scar may be filled with fluid (Fig. 36.25). Its appearance does not predict whether or not it is at risk of rupture in future pregnancies. A caesarean section scar can also lead to abnormal implantation and adherence of an anterior placenta in future pregnancies or even be a site of ectopic pregnancy (Fig. 36.26).[55]

Hysterectomy; subtotal hysterectomy; trachelectomy

Hysterectomy is the most common major surgical procedure in women. If done for benign disease, then just the uterus and not the ovaries may be removed. If done for malignant disease, then surgery is more extensive and also requires removal of the ovaries and tubes, as well as lymph node dissection or further procedures



Figure 36.24 Caesarean section scar. This is the typical appearance of an old scar, seen as a thin white line (arrow) extending anteriorly from the endometrium just above the cervix.

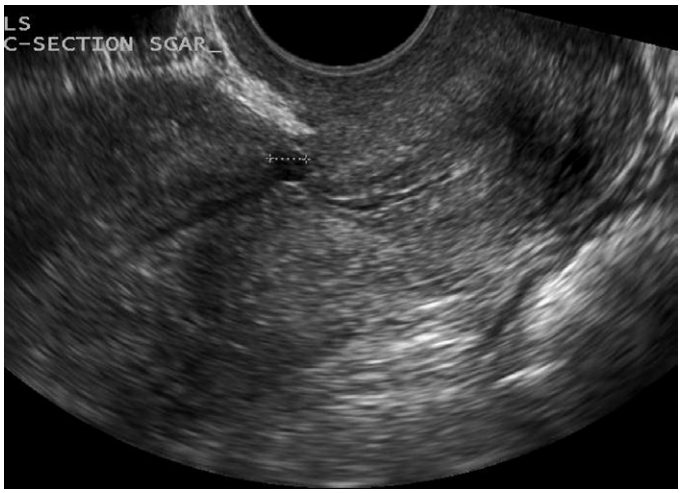


Figure 36.25 Caesarean section scar. This old scar has a little fluid within it (callipers). Note the line of the endometrium is deviated up toward it.



Figure 36.26 Caesarean section scar. An ectopic pregnancy is developing within an old scar.

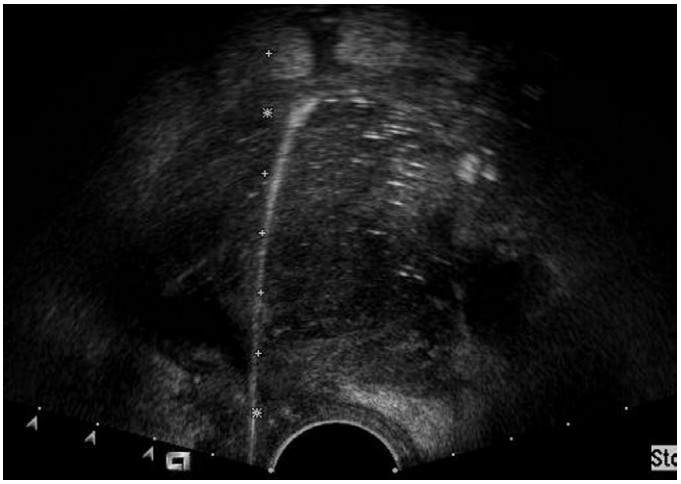


Figure 36.27 Drainage of a post-hysterectomy, pelvic collection. A transvaginal scan showing a guide-wire that has been placed through the vagina into the collection using a sheathed needle.

Postoperative changes

- Type of surgery affects postoperative appearances.
- Dilatation and curettage done after delivery is more likely to damage the myometrium.
- Endometrial ablation: adhesions, residual endometrium and haematometra may result.
- Caesarean section scars are readily visible in nearly all those who have had one. Its appearance does not predict future rupture.
- Haematoma, abscesses, urinomas and lymphoceles may all occur after hysterectomy.

where necessary for staging. Immediately postoperatively a small amount of free fluid in the pelvis is normal. Up to a third will develop a more significant sized collection and pyrexia may develop. The vault of the vagina is often left unsutured to facilitate postoperative drainage of these collections clinically. Haematomas may develop. These often show complex internal architecture with fluid levels and clot retraction. Ultrasound-guided drainage can be tried if clinical reopening of the vault and medical treatment with antibiotics is unsuccessful (Fig. 36.27). It is important to remember to treat the patient rather than the scan as many of these haematomas will resolve spontaneously. The anterior abdominal wall also needs to be checked for collections, either in the wound or in the rectus sheath. Other potential accumulations are: urinomas, lymphoceles and peritoneal inclusion cysts. Urinomas, following damage to the ureters or bladder, occur early. CT urography is the best way to make the diagnosis as the kidneys may not be dilated on ultrasound. Lymphoceles usually develop a week or two after surgery. They arise from the pelvic side wall and have a very variable appearance from a simple thin-walled cyst to a cyst with innumerable fine septations. Peritoneal inclusion cysts are usually a late occurrence (Fig. 36.28). The typical feature is that the cyst interleaves between bowel loops and shows walls with acute angles. Developing countries report a higher incidence of pelvic haematoma and more pelvic inflammatory disease.[56]

Long term just the residual vagina with a uniform thickness should be seen. A subtotal hysterectomy leaves the cervix in place. This appears as a smooth mass at the vault of the vagina and may show development of nabothian cysts. A trachelectomy is an

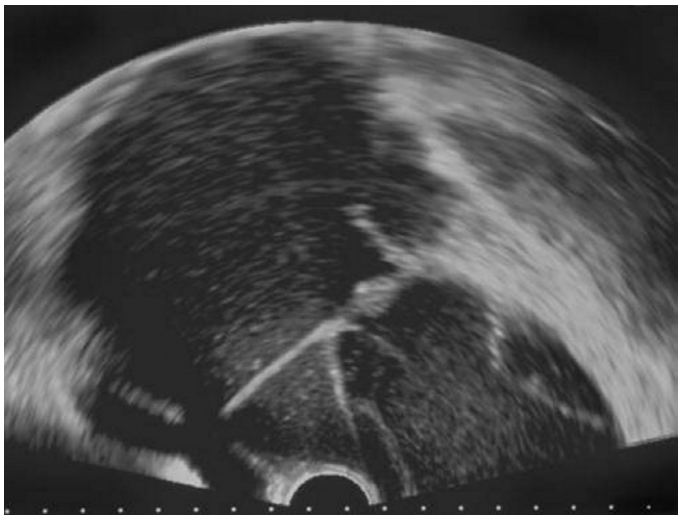


Figure 36.28 **Transvaginal view of a peritoneal inclusion cyst** as a long-term consequence of previous hysterectomy.



Figure 36.29 **Haematometrium** developed in the potential space left following removal of the cervix as part of a Manchester repair for prolapse. The opening left by the surgeon to allow drainage of blood into the vagina had stenosed up over time.

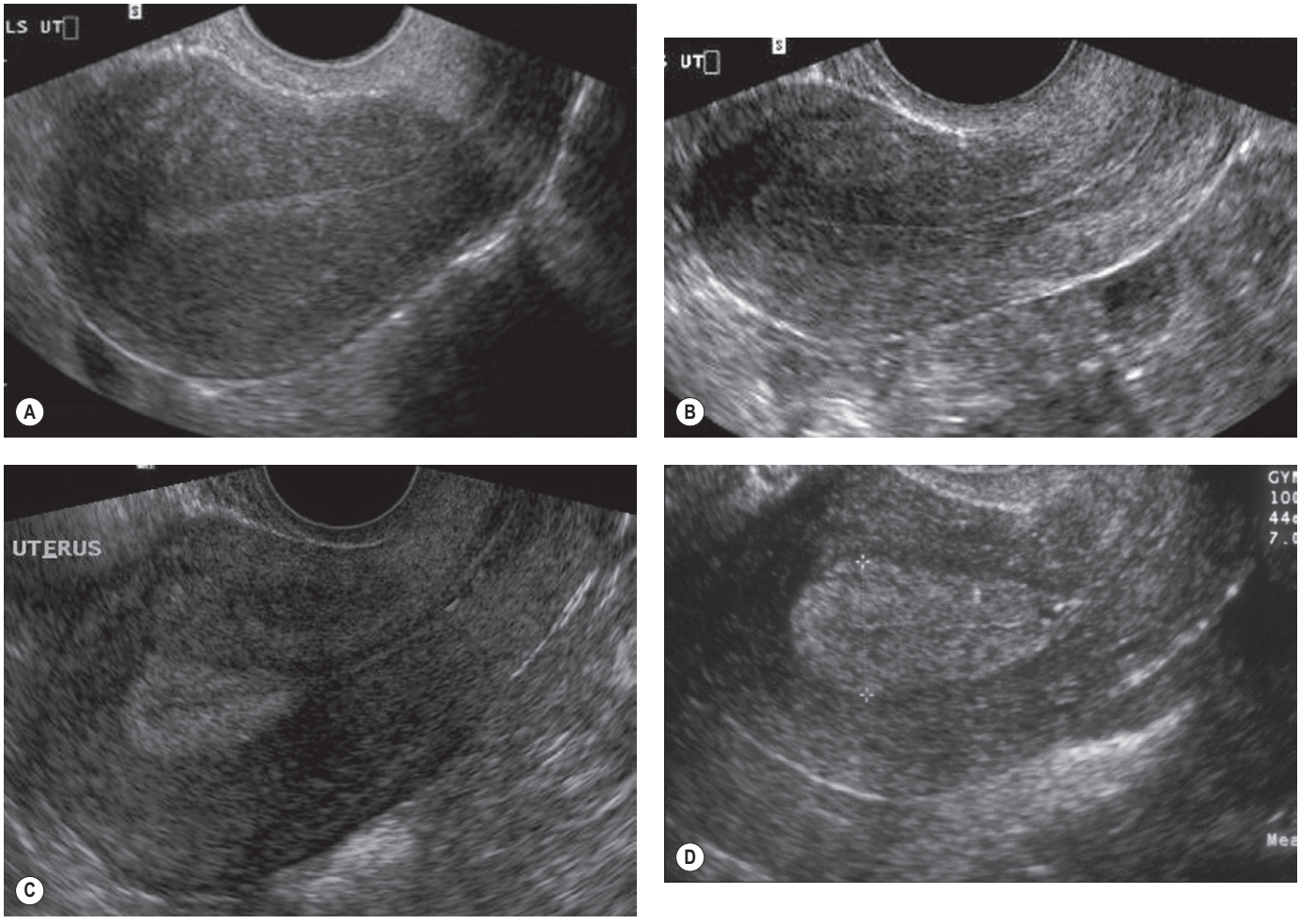


Figure 36.30 **The normal endometrium** in different phases of the menstrual cycle: menstrual **(A)**, proliferative **(B)**, peri-ovulatory **(C)** and secretory **(D)**.

uncommon operation done for early stage cervical cancer when the woman wishes to retain the ability to carry a pregnancy. The cervix is removed but the uterine body is left behind. Assisted conception will be needed if pregnancy is desired. A Manchester repair done for prolapse also removes the cervix and although a passage is left to allow uterine contents to escape, a haematometrium can result (Fig. 36.29).

Knowledge of the type and extent of surgery clearly affects the postoperative features and the likelihood of complications.

ENDOMETRIUM

The endometrium is a specialised form of mucous membrane whose appearance reliably reflects the hormonal status of the patient. The normal appearances (Fig. 36.30) and variation with age and menstrual cycle are described in Chapter 34. The active endometrium in premenopausal women measures up to 12 mm in double layer thickness; prior to menarche it is very thin and after the menopause it again atrophies and measures less than 5 mm thick. The thicker the endometrium becomes the more likely there will be pathology present. Oestrogen deficiency produces endometrial atrophy (Table 36.2). An inappropriate endometrial pattern for the stage of the menstrual cycle can suggest hormonal imbalance or ovarian dysfunction.

Endometrial hyperplasia

Endometrial hyperplasia can be divided into two categories based on the presence or absence of cytological atypia and further divided into simple or complex depending on the extent of architectural abnormalities.[57] Clinical presentation is with abnormal bleeding, most commonly in the perimenopasusal age group. Endometrial hyperplasia without atypia responds well to treatment with progestins but will need follow-up to ensure atypia does not develop. Women with atypical hyperplasia are offered hysterectomy, as atypia is a precursor to endometrioid endometrial cancer.[58] Ultrasound is unable to distinguish one form of hyperplasia from another. The presence of cystic spaces is unhelpful and a diagnosis of so-called cystic hyperplasia does not really exist or help in management.

Table 36.2 Causes of abnormal endometrial thickness

Causes of atrophy	Causes of increased thickness
Endogenous causes: premature ovarian failure perimenopausal period menopause excessive androgens	Secretory phase of normal cycle Decidual reaction in early pregnancy Infections, i.e. endometritis Endometrial hyperplasia/ polyp Endometrial carcinoma
Exogenous medications: oral contraceptive pill progesterone compounds Depo-Provera danazol	Increased endogenous oestrogen: ovarian tumours adrenal tumours Oestrogen-type medications: hormone replacement therapy tamoxifen/anastrozole
Pelvic irradiation	

Endometrial hyperplasia

- Presents with abnormal bleeding in the perimenopausal age group.
- Persistent thickening over 10 mm is predictive.
- Histology is needed to diagnose the presence of atypia.
- Atypia is a precursor to endometrial cancer.

Predictive features of an abnormal endometrium on ultrasound are a persistent thickening over 10 mm and an increased echogenicity that does not vary through the cycle in women who are premenopausal (Fig. 36.31). Hysteroscopy and biopsy are required for the diagnosis. Even biopsy runs a risk of under-calling the presence of atypia and coexistent cancer. Tamoxifen, used in the treatment of breast cancer, increases the risk of developing endometrial hyperplasia.

Endometrial polyps

These are a circumscribed overgrowth of endometrial tissue with or without some stroma. They are most commonly seen in the perimenopausal age group but occur at most ages. The number, size or site of polyps does not correlate with symptoms, which are typically related to intermenstrual bleeding or other menstrual symptoms. Many are asymptomatic. They vary in size from a few millimetres up to 5 cm but most are in the range of 5 to 10 mm. They may show a stalk and occasionally may be pedunculated and even protrude through the cervical canal.

Younger women presenting with infertility may be found to have polyps but it remains uncertain if polyps are a cause of infertility, or whether removing them improves outcome. The exception is those that block the tubal ostia.

Ultrasound features are typically of a focal area of echogenic endometrial thickening. Colour or power Doppler may show a feeding vessel (Fig. 36.32) but this is not essential for the diagnosis. An oval or fusiform shape is normal. Round lesions are more likely

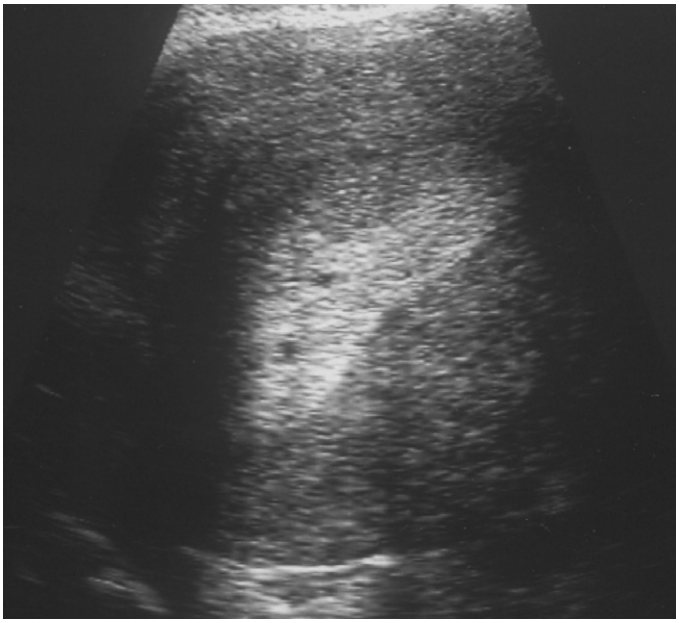


Figure 36.31 Endometrial hyperplasia. The endometrium shows a persistent thickening over 10 mm. It contains a couple of tiny cystic spaces but this is unhelpful in the diagnosis of cystic hyperplasia. Biopsy is needed to look for the presence of atypia.

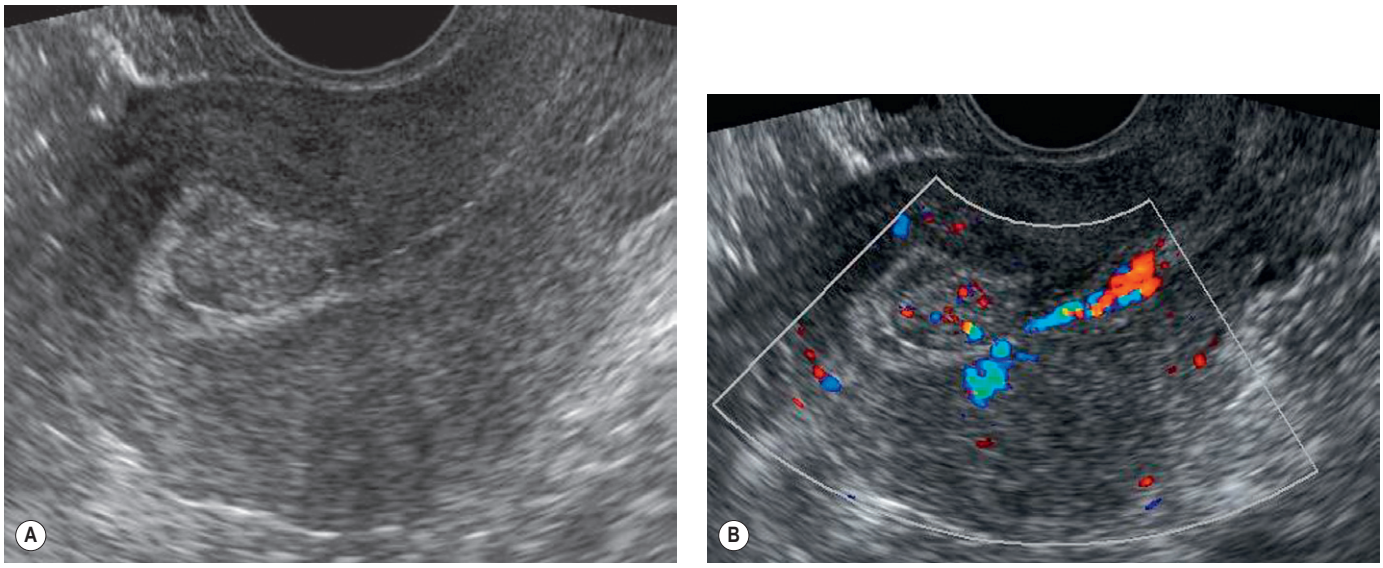


Figure 36.32 **Endometrial polyp (A)** with a single feeding vessel shown on colour Doppler **(B)**, though there are branching vessels within the polyp itself. Note that the polyp has an ovoid shape.

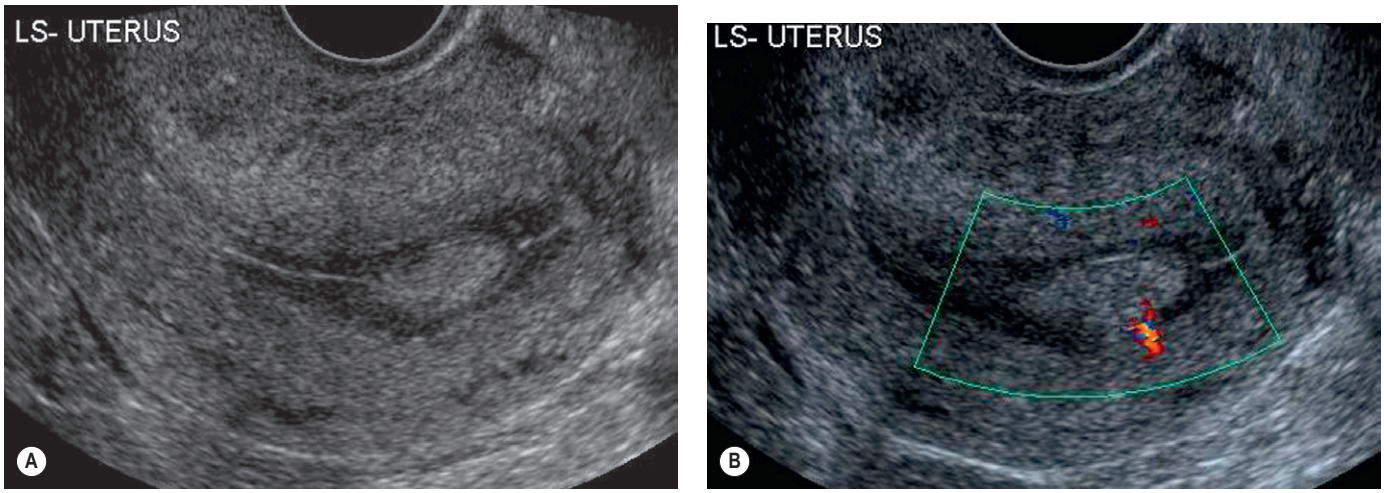


Figure 36.33 **Endometrial polyps** are easier to see in the proliferative phase of the cycle. The echogenicity of the ovoid polyp is outlined against the darker endometrium **(A)**. A single feeding vessel is also shown on colour Doppler **(B)**.

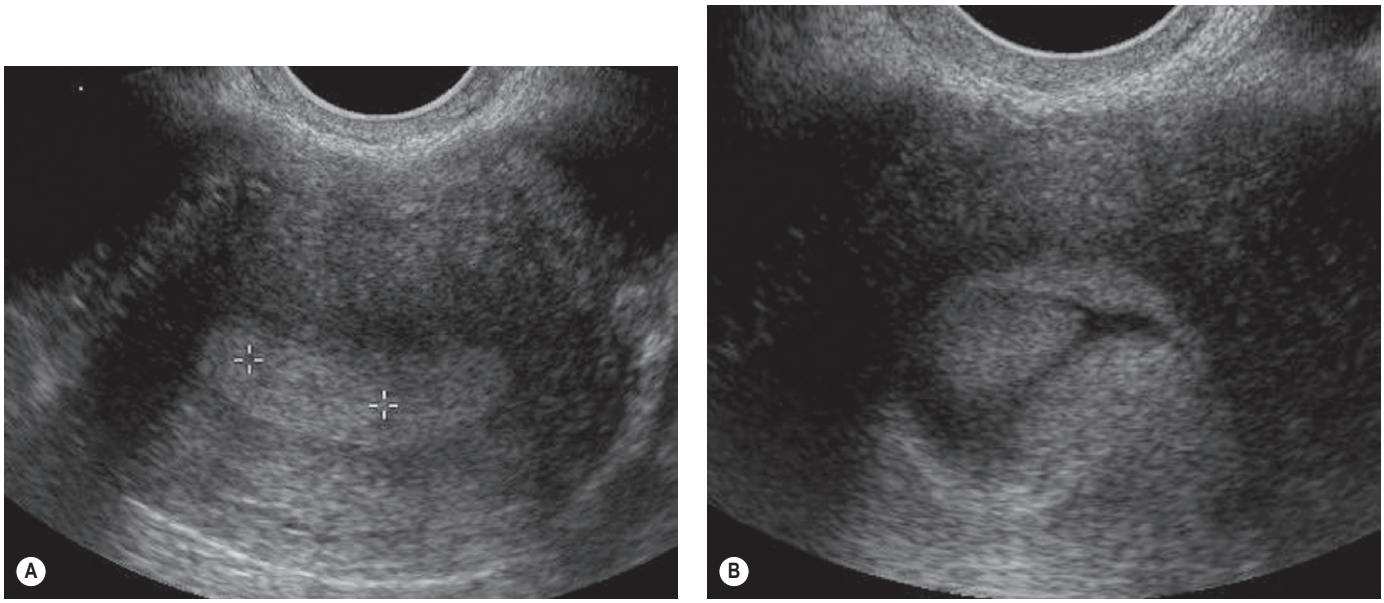


Figure 36.34 **Saline infusion hysterography.** The polyp is hard to see against the secretory phase endometrium **(A)** but is clearly outlined by saline in **(B)**.

to be submucosal fibroids. Small cystic areas may develop due to dilated glands within the polyp. Polyps are most easily seen in the proliferative phase when their echogenicity stands out against the relatively hypoechoic endometrium (Fig. 36.33). Later, in the secretory phase, the echogenicity of the endometrium may match that of the polyp and make it difficult to see. Occasionally a thin echogenic rim may be seen around a polyp due either to a band of compressed endometrium or to the interface with the cavity. Saline infusion hysterography can be used to reveal the polyp (Fig. 36.34). This is best done in the early proliferative phase when the endometrium is thin. Later in the cycle when the endometrium is thick, wrinkles from contractions may simulate sessile polyps. Polyps can be single or multiple. 3D ultrasound is better at giving a global depiction of multiple polyps than 2D.

Blood clots may mimic a polyp but will not be vascularised and will not be constant on repeat examinations. Submucosal fibroids are more likely to be round, be hypoechoic and to show shadowing (Fig. 36.35). Fibroids are more likely to have multiple feeding vessels which branch over the surface and may also have a layer of overlying endometrium. A history of pregnancy raises the possibility of other intracavitary masses, namely retained products of conception and gestational trophoblastic disease.

Most polyps are benign, particularly in the premenopausal age group. Polyps are associated with endometrial cancer, with 10% of cancer patients showing coexistent or malignant polyps. Ultrasound cannot distinguish a benign polyp from one with atypia, nor can ultrasound distinguish a benign polyp from coexistent endometrial cancer. Consequently, polyps should be removed and the endometrium sampled. Tamoxifen use is associated with an increased incidence of polyps and cancer.

Endometrial polyps

- Circumscribed overgrowth of endometrium.
- Any age but usually perimenopausal.
- Typically oval in shape on ultrasound.
- Best seen against the proliferative phase endometrium.
- Saline infusion hysterography helps to reveal them.
- Most are benign, but no imaging features to distinguish them from malignancy.
- Tamoxifen use is associated with polyp formation.

Endometrial cancer

Aetiology

There are various factors that increase the risk of developing endometrial cancer, namely: nulliparity, obesity, hypertension, diabetes, polycystic ovary syndrome, hereditary non-polyposis colorectal cancer and pelvic irradiation. A common causative factor is exposure to unopposed oestrogen, either from endogenous production from hormone-secreting tumours, or exogenous medication such as tamoxifen or hormone replacement therapy with oestrogen and no progestogen. Endometrial hyperplasia with atypia has a 25% risk of developing carcinoma. Most are adenocarcinomas. It is the commonest gynaecological malignancy and the fourth commonest cancer in women. The majority of women are postmenopausal, with the commonest ages being 50 to 65 years.

Symptoms

The most common presentation is with abnormal bleeding, typically postmenopausal bleeding. About 10% of women with postmenopausal bleeding will have endometrial cancer and the longer the interval between menopause and the onset of bleeding the greater the likelihood of cancer. Some present with a vaginal discharge rather than bleeding. An obstructed uterine cavity causing a haematometrium may present with pain.[59]

Diagnosis

The role of ultrasound falls into two main groups. Firstly, women who present with postmenopausal bleeding will be investigated with hysterography. Ultrasound can be used as a negative predictive tool to triage those women who do not need hysteroscopy. Secondly, asymptomatic women may have ultrasound scans for other reasons and ultrasound can be used to predict which of those need further investigation of their endometrium.

The typical feature is that endometrial cancer produces thickening of the endometrium (Fig. 36.36). Focal thickening is more concerning than diffuse and likewise an uneven echogenicity is more concerning than an even echo. Irregular branching of endometrial vessels on power Doppler is also a concerning sign[60] though addition of Doppler to the predictive score obtained from greyscale features barely increases performance (Fig. 36.37). Texture analysis

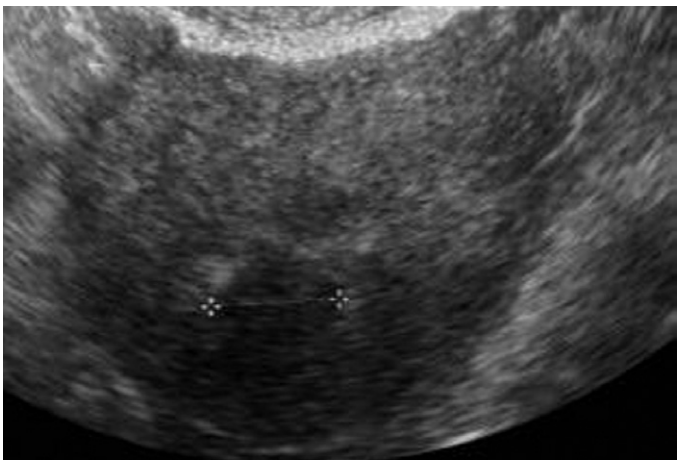


Figure 36.35 Submucous fibroid. In comparison with endometrial polyps, a submucous fibroid (between callipers) is more likely to be round, dark and shadowing.

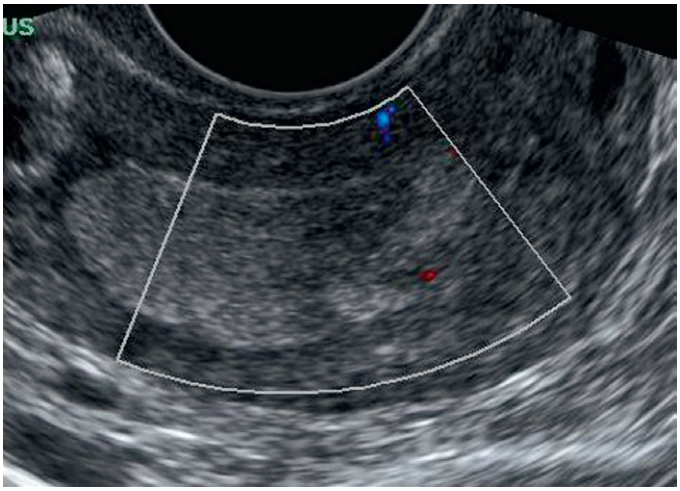


Figure 36.36 Grossly thickened endometrium in a postmenopausal woman. She was found to have endometrial cancer.

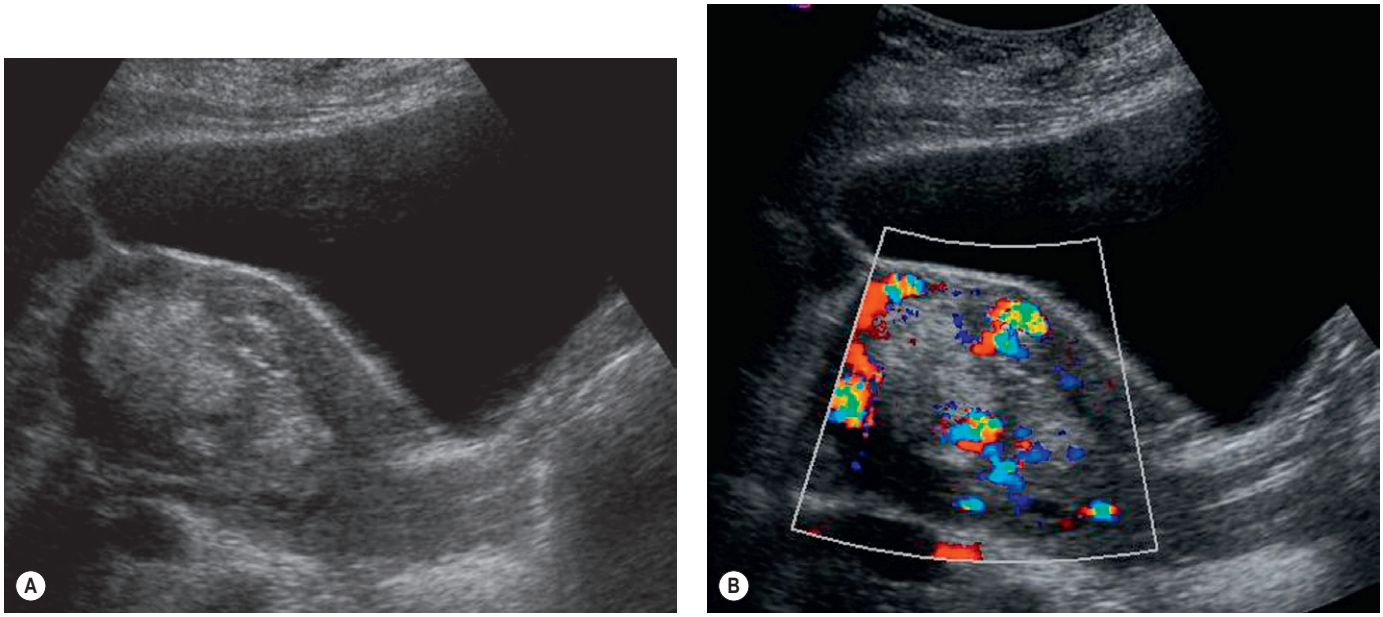


Figure 36.37 Endometrial cancer. Longitudinal transabdominal image **(A)** shows a bright irregular endometrium that disrupts the normal hypoechoic subendometrial layer. These features are strongly indicative of invasive endometrial cancer. The addition of colour Doppler **(B)** whilst showing irregular hypervascularity does not increase the predictive power of the scan.

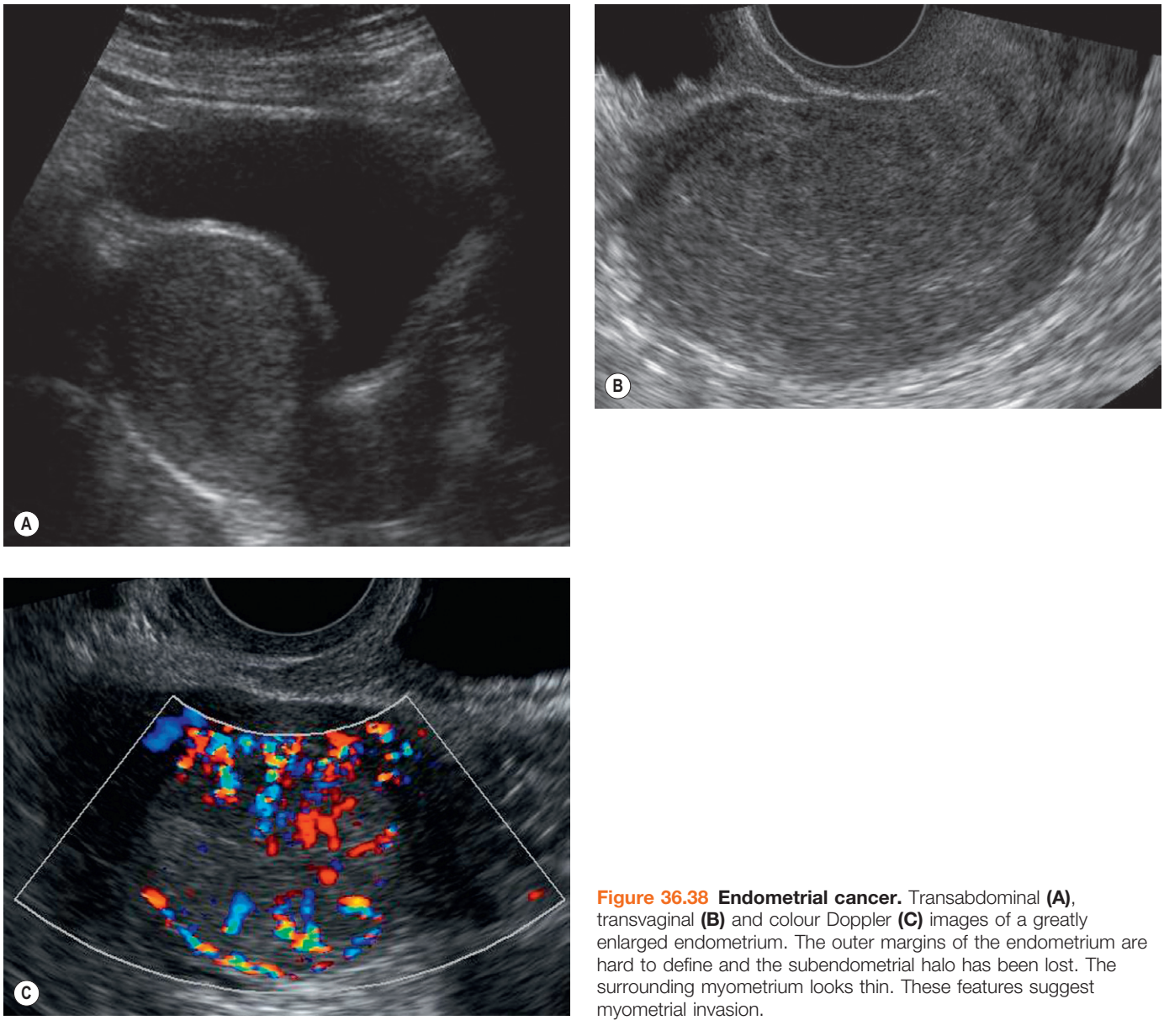


Figure 36.38 Endometrial cancer. Transabdominal **(A)**, transvaginal **(B)** and colour Doppler **(C)** images of a greatly enlarged endometrium. The outer margins of the endometrium are hard to define and the subendometrial halo has been lost. The surrounding myometrium looks thin. These features suggest myometrial invasion.

of the endometrium using a computer model has been proposed but has not found widespread acceptance.[61]

Staging and prognosis of endometrial cancer depends on the degree of myometrial invasion (Fig. 36.38). Stage 1a is confined to the endometrium, or invades the inner half of the myometrium and 1b the outer half. Ultrasound typically shows a low-echo, subendometrial, myometrial halo around the endometrium. Disruption of this layer suggests myometrial invasion (Fig. 36.39). However, prospective studies have shown that ultrasound is very unreliable at assessing invasion, with one study showing up to 30% incorrectly staged.[62]

Postmenopausal women should have an atrophic endometrium. It has been found that ultrasound has a high negative predictive value for endometrial cancer if the double-layer thickness is 4 mm or less (Fig. 36.40). Many centres use this as a triage tool to exclude women from unnecessary hysteroscopy. There are dissenting voices as a small proportion of women with cancer will have a thin endometrium, one study even claiming that up to 10% of women with cancer have a thickness less than 4 mm.[63] However, most studies are in accord with the Birmingham experience[64] that using a cut-off of 4 mm saves hysteroscopy without missing any cancers. An important caveat is that an unmeasurable endometrial thickness is an indication for hysteroscopy. Loss of the endometrial/myometrial distinction is potentially a sign of invasion and carries as high a risk of carcinoma as finding a markedly thickened endometrium.

The transvaginal ultrasound technique must show the entire length of the endometrium. Measurement of thickness is made in the longitudinal plane at the widest point. The hypoechoic inner myometrium (or subendometrial halo) should not be included. Likewise, any intracavitary fluid should not be included in the measurement (Fig. 36.41). The significance of any intracavitary fluid depends on the coexistent endometrial thickness but also on its echogenicity. Echo-free fluid and a thin endometrium is usually a benign condition,[65] but the presence of echoes in the fluid confers a greater risk of endometrial cancer[66] and both endocervical and endometrial sampling is advised.

Other ultrasound techniques that are used are saline infusion hysterography (SIH) and 3D ultrasound. SIH is advocated as a better way of visualising endometrial abnormalities and it certainly helps in the delineation of polyps and fibroids. However, it confers very little advantage over transvaginal ultrasound in the diagnosis of malignancy.[67] If SIH is used in the presence of endometrial cancer it does not cause any increased risk of extrauterine dissemination of the disease.[68]

3D ultrasound by enabling calculation of the endometrial volume can give higher specificities and better negative predictive values for endometrial cancer than using the endometrial thickness. However, there is no agreement between the various studies about the optimal volume to use as a cut-off. A range of values from 1.35 mL,[69] to 2.7 mL[70] to 3.56 mL[71] have been reported as optimal values by different authors. It seems that any centre would have to validate its own volume measurement before applying it. The use of endometrial thickness is a much more readily reproducible measurement across different centres.

Patient preference for ultrasound or hysteroscopy as the initial investigation for endometrial cancer differs depending on how the question is asked. Women asked which procedure they found more tolerable using a visual analogue pain score opted for ultrasound.[72] In contrast, when women were taught about the probability of finding endometrial cancer and the advantages and disadvantages of different diagnostic strategies they showed a clear preference for hysteroscopy and its greater diagnostic certainty.[73]

Advanced tumours at presentation are relatively rare because bleeding is generally an early symptom. However, some women will present with large uterine masses that can be mistaken for fibroids or an ovarian mass. Endometrial cancer can metastasise to

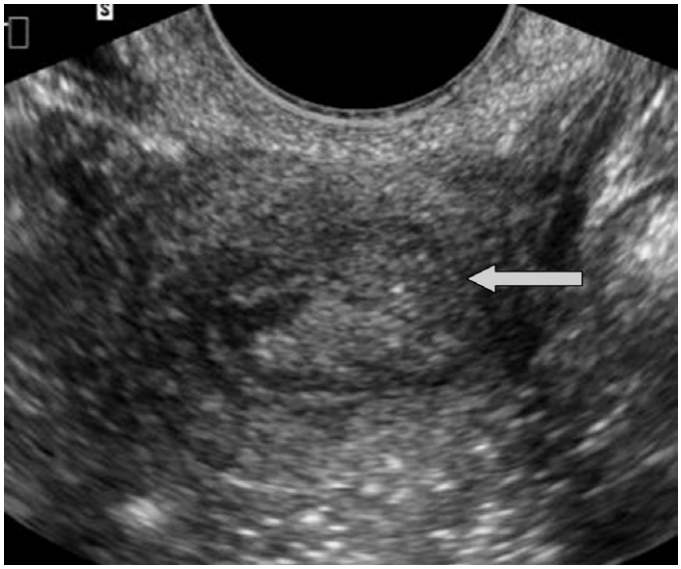


Figure 36.39 Endometrial cancer. Normal endometrium and a subendometrial layer are seen on the right, whereas there is a tumour on the left invading into the myometrium (arrow).

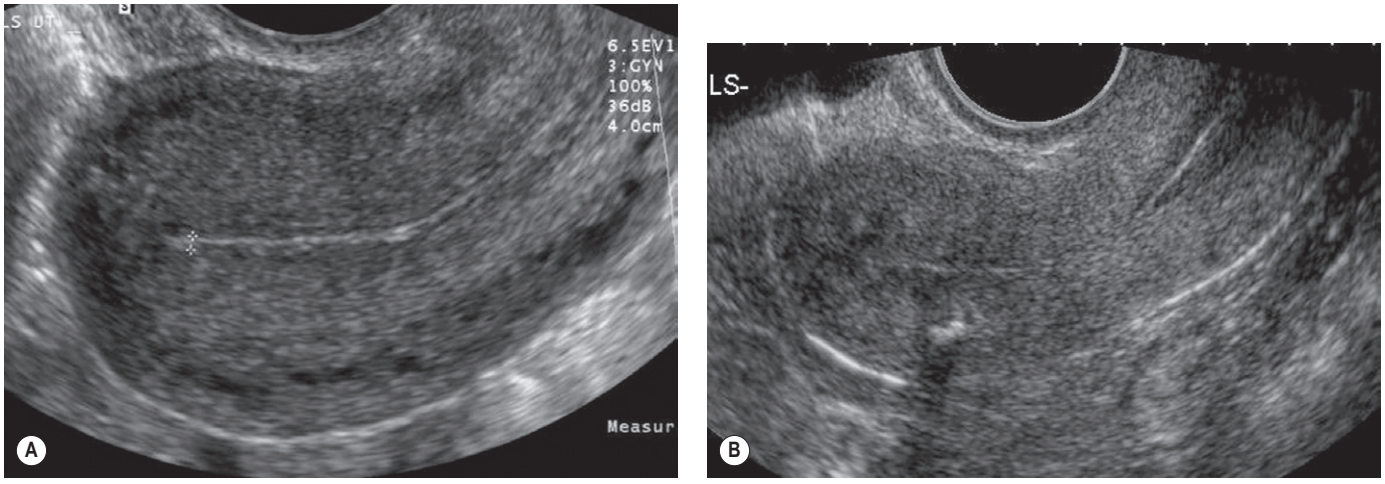


Figure 36.40 Atrophic endometrium: perimenopausal **(A)** and postmenopausal **(B)**. There are obvious subserosal venous spaces seen in **A** and a dense focus of myometrial calcification in **B** as well. The calcification is probably in an old fibroid.

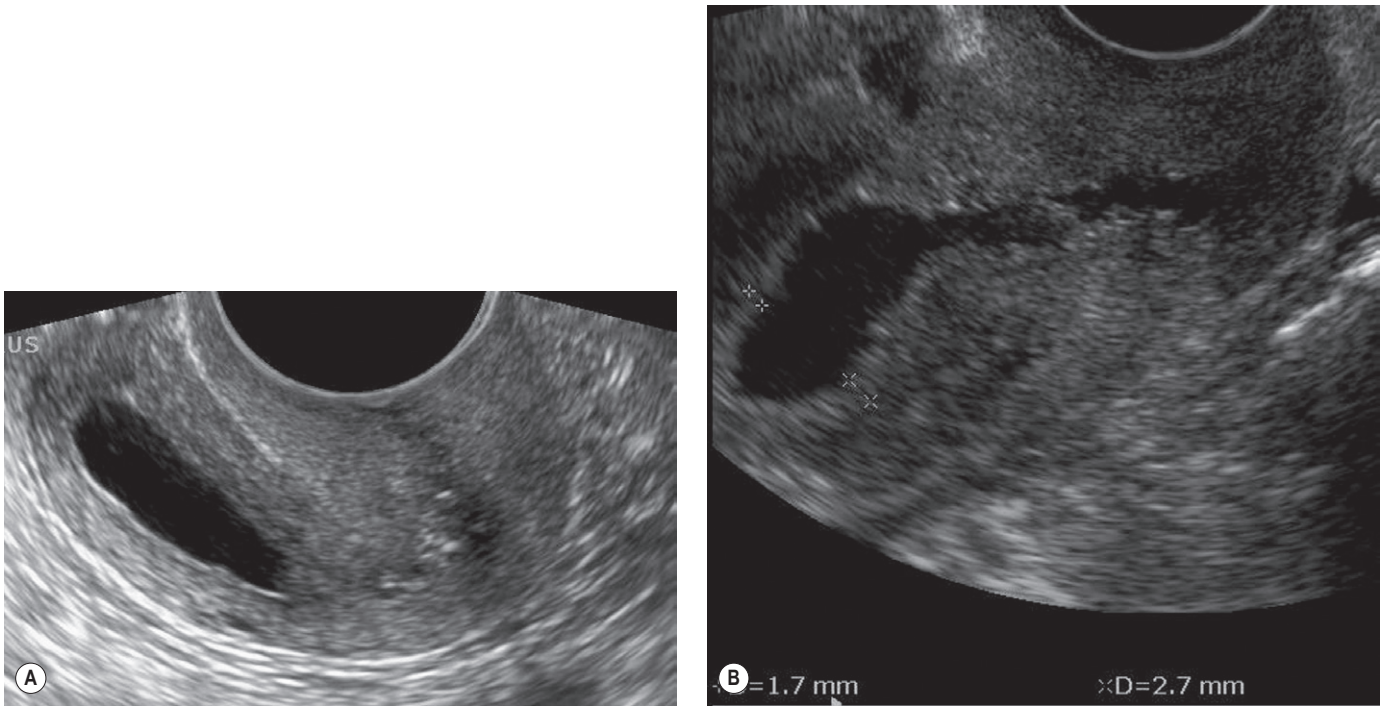


Figure 36.41 **If there is fluid in the endometrial cavity (A),** this should not be included in the endometrial thickness measurement. The double layer endometrial thickness in **(B)** is correctly measured, total 4.4 mm.

Endometrial cancer

- Commonest gynaecological malignancy.
- Exposure to unopposed oestrogen and to tamoxifen.
- Present with abnormal bleeding.
- Mainstay of diagnosis is hysteroscopy and biopsy.
- Ultrasound can be used for its negative predictive value in those with an endometrium less than 4 mm thick.
- Loss of the subendometrial dark halo suspicious for myometrial invasion.
- MR is the best imaging tool for staging.
- Screening of asymptomatic women is not effective.

the ovary to produce a large adnexal mass. Other signs of local spread with invasion into bowel and bladder, ascites, lymphadenopathy and evidence of distant metastases to the liver or lungs may also be present.

Other investigations

Once the diagnosis of endometrial cancer is established by biopsy, then an MR scan is the best imaging test for local staging (Fig. 36.42).[74] Some surgeons do not believe that preoperative staging by MR influences their choice of surgery or need to do lymphadenectomy. Surgery is needed to detect micrometastases that MR cannot see.

A CT scan is used for staging more advanced disease and provides a baseline for any chemoradiotherapy. PET is occasionally used when major pelvic exenterative surgery is being considered in order to improve detection of distant metastases that would be a contraindication to the planned surgery.

Screening

Screening the asymptomatic postmenopausal population has been advocated for the detection of endometrial cancer. Not every woman presents with postmenopausal bleeding. Asymptomatic endometrial cancer is thought to occur with an incidence of around 1.5 per 1000 screened women. The problem is that ultrasound has a relatively poor positive predictive value for cancer and using endometrial thicknesses over 8 mm generates a high number of false positives. Currently, there is no evidence to support screening asymptomatic women.

Management

Surgery is the mainstay of treatment for early stage disease, with hysterectomy, bilateral salpingo-oophorectomy and lymphadenectomy. Stage I and II disease (confined to the uterine body and cervix) carries a 96% 5-year survival. More advanced stage disease (Table 36.3) is treated with chemotherapy and radiotherapy tailored to the individual presentation.

Medications and the endometrium

Oral contraceptive pill

This is usually a combined oestrogen and progesterone preparation taken cyclically. There is also a progesterone only mini-pill. Characteristically, the endometrium appears as a 'single-line' which is a little thicker than that seen in postmenopausal woman.

Hormone replacement therapy (HRT)

This is a treatment aimed at alleviating postmenopausal symptoms produced by oestrogen deficiency. There is good evidence that HRT can improve health-related quality of life.[75] Hot flushes, night sweats, aching joints and muscles, insomnia and vaginal dryness are all improved but at a risk of increased breast tenderness, bleeding and vaginal discharge.[76] There are co-morbidities of an increased cardiovascular and thromboembolic risk.[77]

Unopposed oestrogen leads to endometrial hyperplasia, irregular bleeding and poor compliance. The hyperplasia carries a risk of

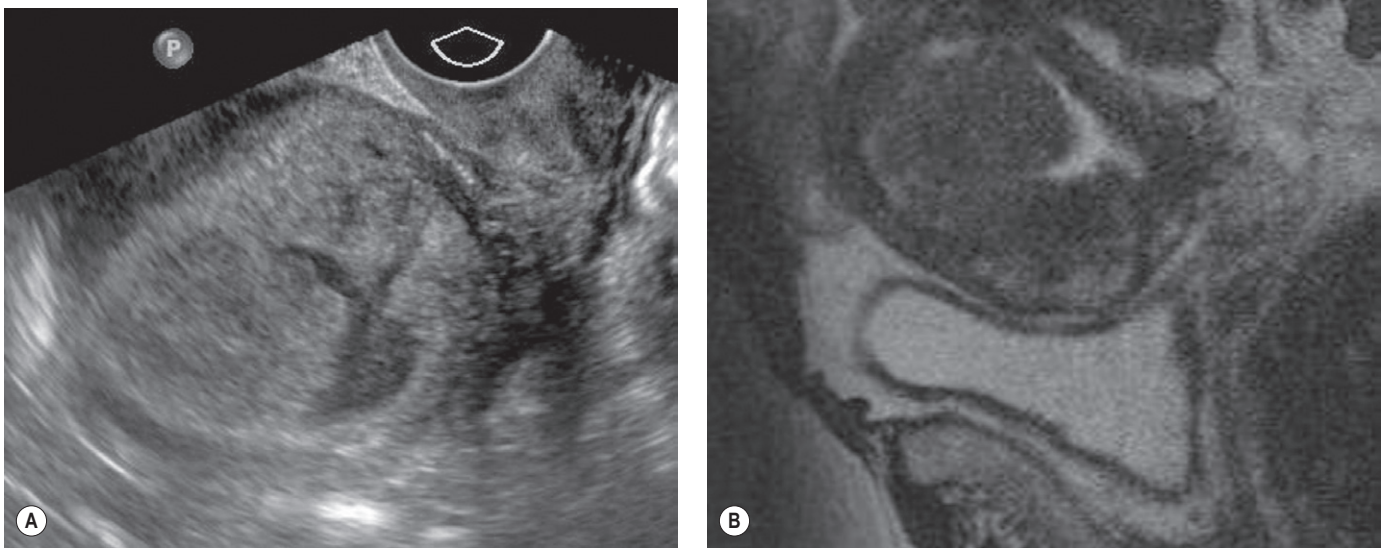


Figure 36.42 Local staging of endometrial cancer is best done with MR. A large endometrial tumour is seen on ultrasound **(A)**, which is shown by MR **(B)** to extend into the outer half of the myometrium – stage Ib.

Table 36.3 FIGO staging of endometrial carcinoma

Stage	Description
Ia	Confined to the endometrium or invasion into inner half of myometrium
Ib	Invasion into outer half of myometrium
II	Involvement of cervical stroma
III	Spread beyond the uterus confined to true pelvis
IV	Spread outside the true pelvis or involvement of bladder or bowel

developing endometrial carcinoma. Consequently, the main HRT regimens include a progestogen. This decreases hyperplasia and improves the woman's compliance with the treatment. The progestogen is added in two main ways:

1. continuous combined oestrogen and progesterone to produce permanent amenorrhoea and endometrial atrophy
2. cyclical/sequential; e.g. with oestrogen for days 1–25 and progesterone for days 15–25, giving a regular bleed.

The problem of irregular bleeding is less likely under the sequential regime but the continuous regime over the long term offers the better protection against hyperplasia.[78]

Ultrasound appearances are different between the two regimes. Continuous HRT should produce an atrophic endometrium less than 5 mm thick that does not vary through the month. The cyclical treatment may produce a variation in thickness of up to 3 mm through the cycle with some measuring over 8 mm at their thickest. Hence, endometrial thickness measurement in these women is best taken immediately post-bleed.

Tamoxifen and anastrozole

Tamoxifen is a selective oestrogen receptor modulator (SERM) that is widely used in the treatment of patients with breast cancer and for chemoprophylaxis in high-risk women.[79] It confers a significant survival advantage in oestrogen receptor positive breast cancer. It has paradoxical effects, with an antagonistic action against oestrogen receptors in the breast and an agonistic oestrogen action in the genital tract. This means tamoxifen produces endometrial pathology both benign and malignant, with an increased incidence of polyps, hyperplasia and carcinoma. About 40% of postmenopausal women on tamoxifen will have an endometrial thickness greater than 5 mm. Typically tamoxifen produces visible cystic spaces in the endometrial hyperplasia (Fig. 36.43). Saline infusion hysterography is helpful in looking for focal abnormalities in these women. A confounding factor in ultrasound assessment is that tamoxifen can also cause a form of reactivation of adenomyosis, producing an appearance in the subendometrial myometrium of multiple small cysts in an echogenic stroma. This can be indistinguishable from the endometrium and be mistaken for endometrial hyperplasia on ultrasound. Hysteroscopy or MR will enable the distinction.

Anastrozole (Arimidex) is an alternative therapy to tamoxifen in women with endocrine responsive breast cancer. Its advantage in the genital tract is that it reverses the endometrial changes produced by tamoxifen and reduces the need for hysteroscopy.[80] The mean reduction in endometrial thickness after changing from tamoxifen to anastrozole is 4.5 mm.[81] It also reduces the cystic appearance of the endometrium wrought by tamoxifen. Anastrozole is generally more expensive than tamoxifen. Anastrozole also acts to reduce fibroid size in premenopausal women.

Intrauterine devices

Intrauterine devices (IUDs) are deployed for two main reasons; either to act as a contraceptive device or to provide symptom relief from abnormal bleeding. The Mirena coil is a progestin (levonorgestrel) delivery system that leads to endometrial atrophy and can be used both for control of menorrhagia and as a contraceptive. Other IUDs used for contraception alone come in a variety of shapes (usually a 'T' or a '7') and may also be coated in copper. The major effect of all IUDs is to induce a local inflammatory reaction in the endometrium.[82] Copper ions released from copper IUD enhance the

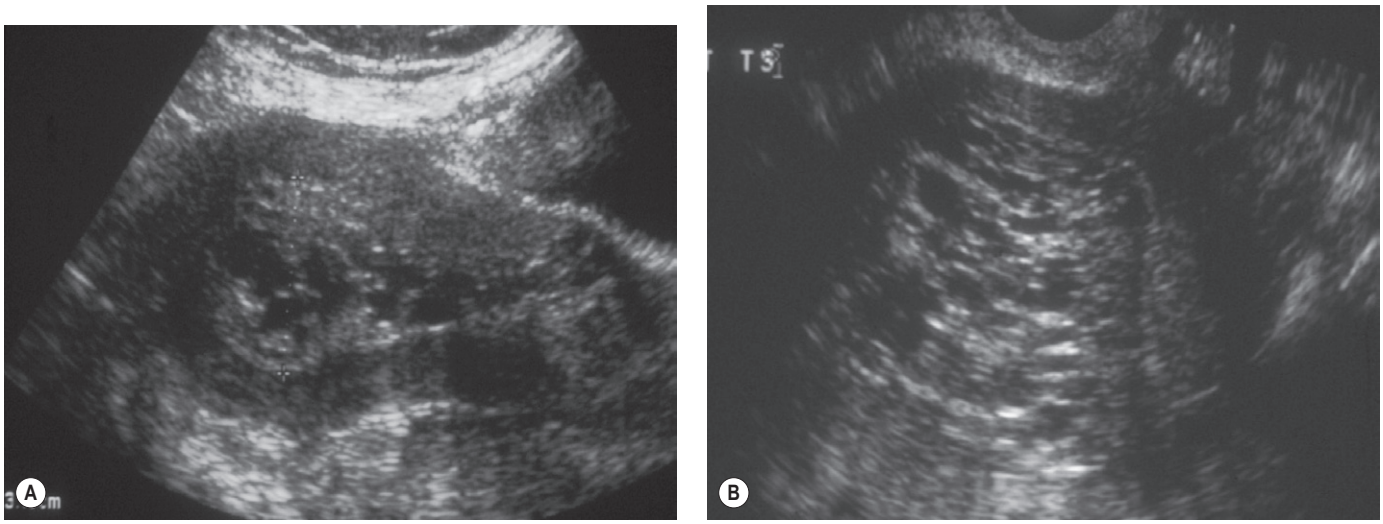


Figure 36.43 Cystic changes associated with tamoxifen usage, with apparently greatly enlarged endometrial width on transabdominal **(A)** and transvaginal **(B)** views. This can be misleading as some of these changes can be in old adenomyosis in the subendometrial layer.

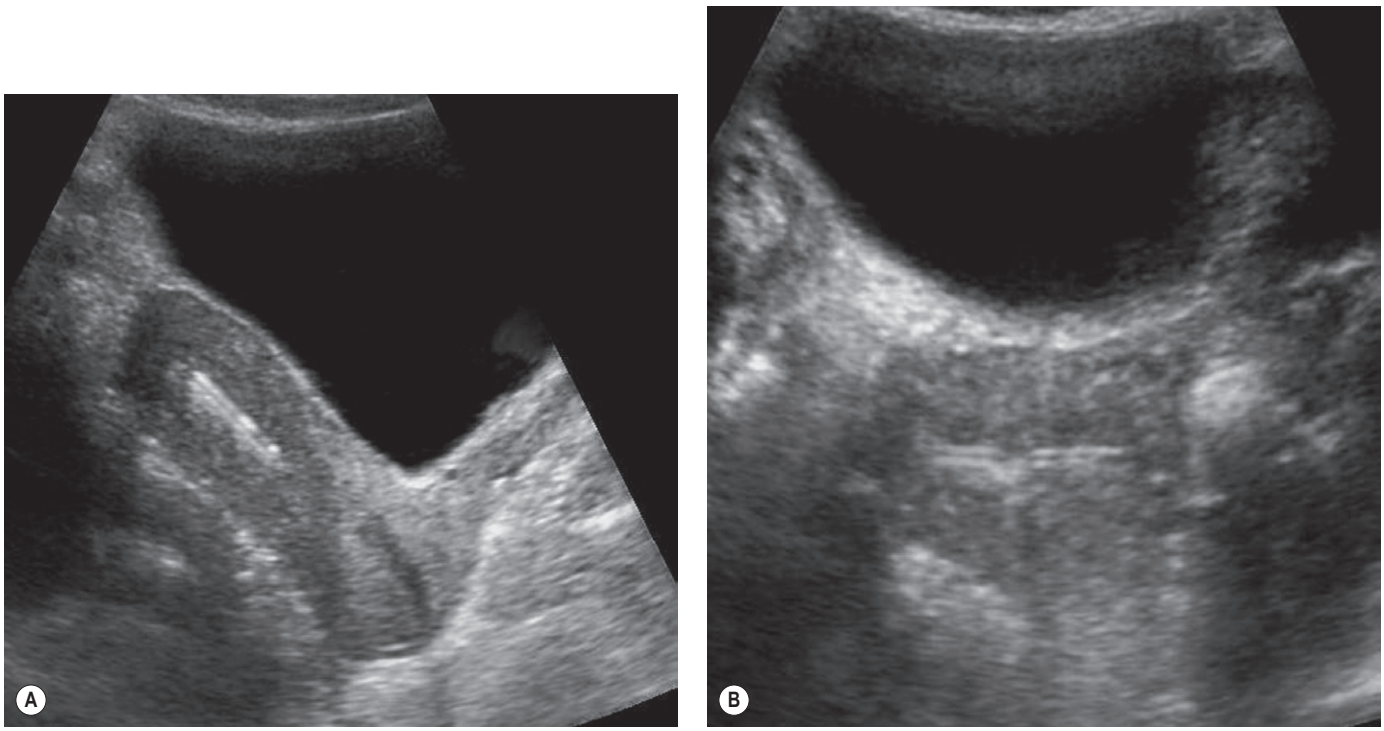


Figure 36.44 Normal 'T' shaped intrauterine device. Longitudinal image **(A)** shows the body of the device in the endometrial cavity and transverse image **(B)** shows the less echogenic T bar in the fundus.

local inflammatory reaction. This releases fluid into the lumen of the genital tract that is toxic to eggs and sperm. Far fewer sperm reach the egg, and any resultant fertilised egg is much less likely to survive the altered milieu of the uterus. The common belief that IUDs act to abort embryos in the uterus is not supported by the evidence.

The role of ultrasound is to confirm the site of an IUD and to look for potential complications. The IUD should be visualised as centrally located within the endometrial cavity (Fig. 36.44), with the crossbar (if present) in the fundal part of the cavity.[83] Typically, the IUD shows as a strong reflector casting an acoustic shadow. This is more so when viewed in cross-section than longitudinally because of the limitations of the ultrasound beam width. Early versions of the Mirena coil were poorly reflective and harder to see (Fig. 36.45). The cross bar is often less reflective than the body of the IUD. The strings may be seen in the cervical canal. Some IUDs produce very characteristic appearances, the Gynaefix appears as a row of six spots, the old-fashioned Lippes loop (Fig. 36.46) has a serpentine appearance but may also appear as a row of spots if seen in cross-section. Patients from China may show a ring-shaped IUD.

Complications of an IUD include low position, associated infection, migration into the myometrium, uterine perforation, associated intra- or extrauterine pregnancy and fragmentation of the IUD. If an IUD is known to be present but cannot be seen with

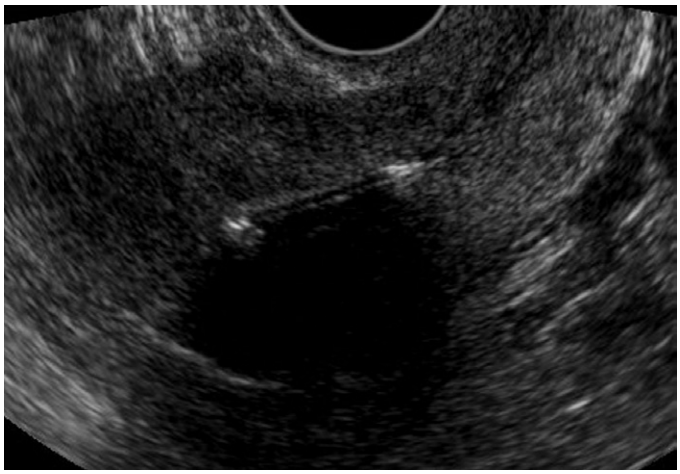


Figure 36.45 Mirena coil. Early versions were hard to visualise on ultrasound in the longitudinal plane but have become easier to see with more recent versions. The acoustic shadow helps.

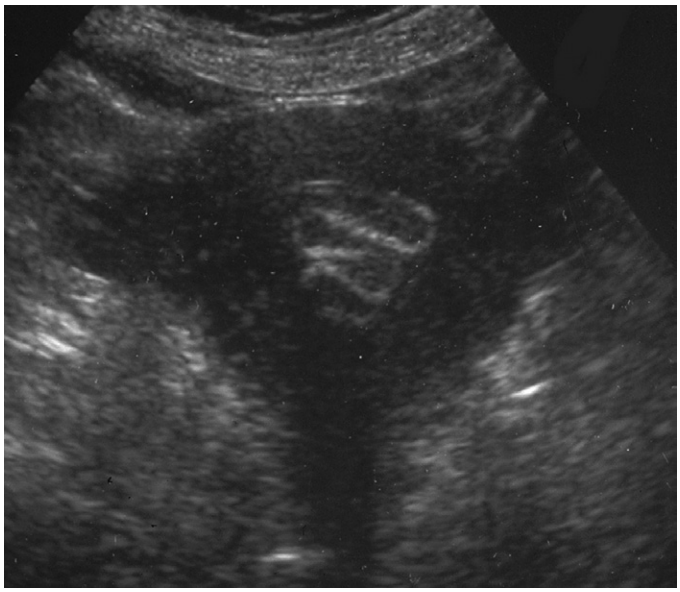


Figure 36.46 The serpentine appearance of a Lippes loop.

Intrauterine devices

- IUD used for contraception or as a local hormone delivery system.
- Ultrasound is used to confirm IUD location.
- Different IUDs have characteristic appearances.
- Complications: wrong position, infections, migration and perforation, pregnancy and secondary infertility.
- A plain radiograph will always show an IUD if one is present.
- Long-term IUD use is associated with actinomycosis.

ultrasound, a plain abdominal radiograph (Fig. 36.47) is helpful to show if an IUD is really present or has been expelled (usually with the menses). Expulsion of a modern IUD is rare (0.2%).

Nearly 80% of pregnancies associated with IUD use are related to the IUD having been expelled. Those pregnancies that do develop with an IUD present (Fig. 36.48) carry a greater risk of abortion and infection so there is general agreement regarding the desirability of removing the IUD as soon as pregnancy is diagnosed.[84]

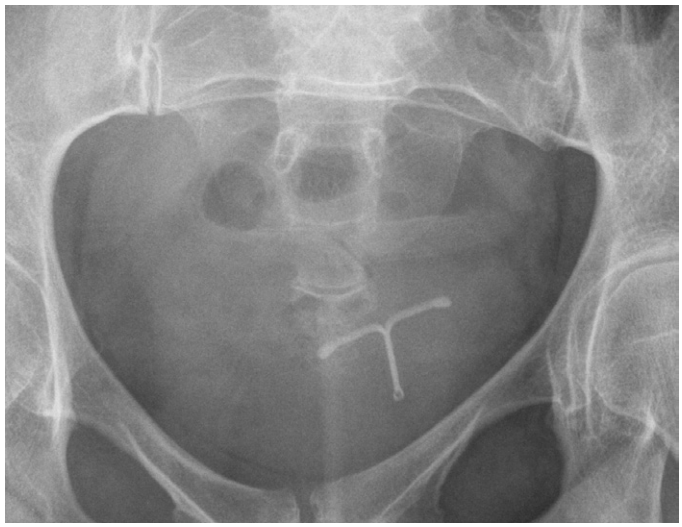


Figure 36.47 Plain film of the pelvis, confirming that an intrauterine device is present, even though it is not seen in the uterus on ultrasound.

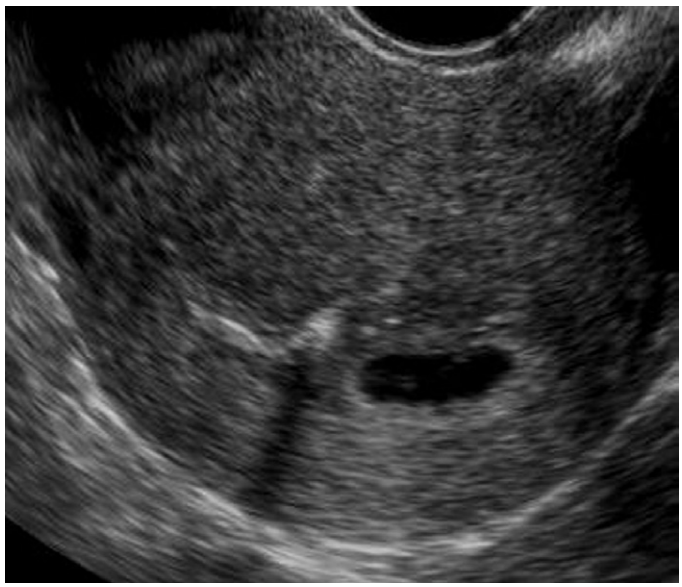


Figure 36.48 Early pregnancy in association with an intrauterine device.

Myometrial penetration or uterine perforation usually occurs at the time of IUD insertion, in up to 5%. It is associated with pain and bleeding. Ultrasound shows the IUD or part of it to lie in the myometrium (Fig. 36.49). Ultrasound is less good once the IUD is completely outside the uterus. CT can have a role to play here. IUDs are visible on both CT and MR (Fig. 36.50) although these are not primary tools of investigation.

Long-term use of an IUD is associated with infection with actinomycosis. Plastic IUDs have a higher infection rate than copper IUDs.[85] Actinomycosis can produce an indolent infection that causes a diffuse pelvic mass that may invade and displace other structures in the pelvis. It is a mimic for gynaecological malignancy and should be borne in mind whenever an IUD is present. Other infections and pelvic inflammatory disease are associated with IUD use and may lead to secondary infertility.

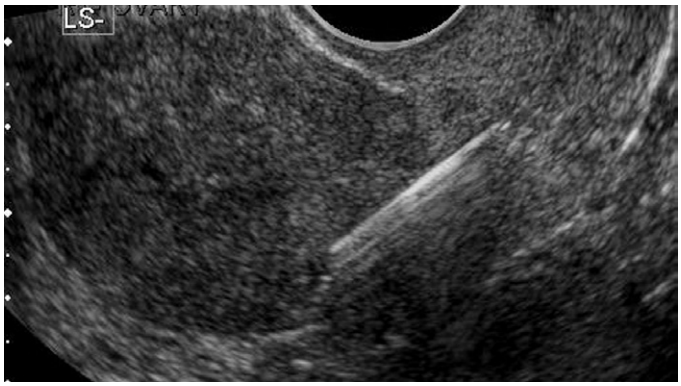


Figure 36.49 **The intrauterine device** penetrates the posterior myometrium. Most of these malpositions occur at the time of IUD insertion.

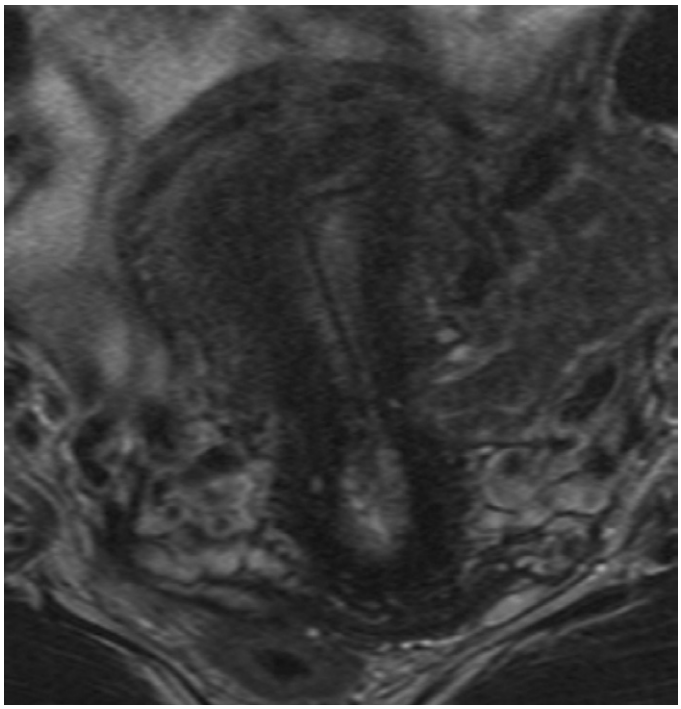


Figure 36.50 **MR scan showing an IUD** as a dark linear structure within the bright endometrium on T2-weighted images.

Endometritis

Infection of the endometrium is generally caused by ascending infection through the cervix. It may form part of a more generalised pelvic inflammatory disease or be localised. Iatrogenic causes include any invasive procedure, such as cervical biopsy, hysterosalpingogram, IUD insertion or endometrial instrumentation. Endometritis may also occur as a result of pregnancy, due to premature rupture of membranes, abortion, postpartum, or prolonged labour. The commonest clinical manifestation is pain and fever in the postpartum period.

Microbiologically, postpartum endometritis may be due to group B streptococcus alone or it may be polymicrobial with both anaerobic and aerobic organisms. In the setting of non-pregnancy-related pelvic inflammatory disease, the two commonest organisms are *Chlamydia trachomatis* and *Neisseria gonorrhoeae*.

Ultrasound examination may be limited by pain and often shows either normal or non-specific findings.[86] Endometritis is predominantly a clinical diagnosis as uncomplicated endometritis commonly looks normal. Ultrasound has merit in looking for complications such as a pyometrium, pelvic abscess or retained products of conception (RPOC). A large amount of echogenic fluid in the endometrial cavity raises the possibility of a pyometrium.

Non-specific ultrasound findings that may be seen (Fig. 36.51) are a thickened, heterogeneous endometrium, fluid in the endometrial cavity, free pelvic fluid, diffuse enlargement of the uterus and loss of the junction between endometrium and myometrium. Air in the uterine cavity postpartum may be a normal finding, seen in 21% of healthy women. Colour Doppler can help identify RPOC, which predisposes to endometritis. Hyperaemia occurs in endometritis but normal colour Doppler flow does not exclude the diagnosis. Endometritis and RPOC can coexist.

Endometritis

- Secondary to ascending infection through the cervix.
- Causes: iatrogenic (any invasive procedure), pregnancy related or part of generalised pelvic inflammatory disease (PID).
- C. trachomatis and N. gonorrhoeae; common in PID.
- Primarily a clinical diagnosis.
- There are no specific ultrasound features.
- Non-specific signs: thickened endometrium, fluid in cavity, free pelvic fluid, diffuse enlargement of uterus and loss of definition of the endometrial border.

Asherman's syndrome/intrauterine synechiae

Synechiae are intrauterine adhesions that cause the walls of the endometrial cavity to stick together at various sites. Asherman's syndrome is usually reserved for the more severe forms, with partial or complete obliteration of the endometrial cavity. The commonest cause is dilatation and curettage, particularly in the postpartum period when the uterus has a softened myometrium, which is more prone to damage. Retained placenta also increases the risk of adhesions.

Clinically, women present with hypo- or amenorrhoea, infertility, or if the woman does become pregnant, an increased risk of miscarriage and postpartum haemorrhage.

Small bright foci on the basal layer of the endometrium are the clue to the site of adhesions. These may commonly be seen in asymptomatic postmenopausal women, when they are of no consequence. However, in the symptomatic infertile woman, adhesions may be commonly missed on ordinary transvaginal sonography. Sonohysterography is the best way to demonstrate the adhesions. These vary from fine strands (Fig. 36.52) to thick septa. Dilation of the cavity with saline can cause pain in those with adhesions. Division of the adhesions can be achieved at hysteroscopy.

Haematometrium and other related conditions

Retention of blood or mucus within the genital tract leads to distension. The obstruction can be congenital or acquired. In children and adolescents the obstruction is usually congenital, which might be due to an intact hymen (1 in 1000) or an atresia or stenosis of the vagina (1 in 5000). These congenital lesions are associated with renal tract anomalies, so the ultrasound examination needs to be extended to include the kidneys. In the adult, the obstruction is usually at the cervix or high vaginal level.

The genital tract becomes dilated above the obstruction. If the dilation contains blood the terms used are:

- haematocolpos: vaginal distension – obstruction at vaginal level

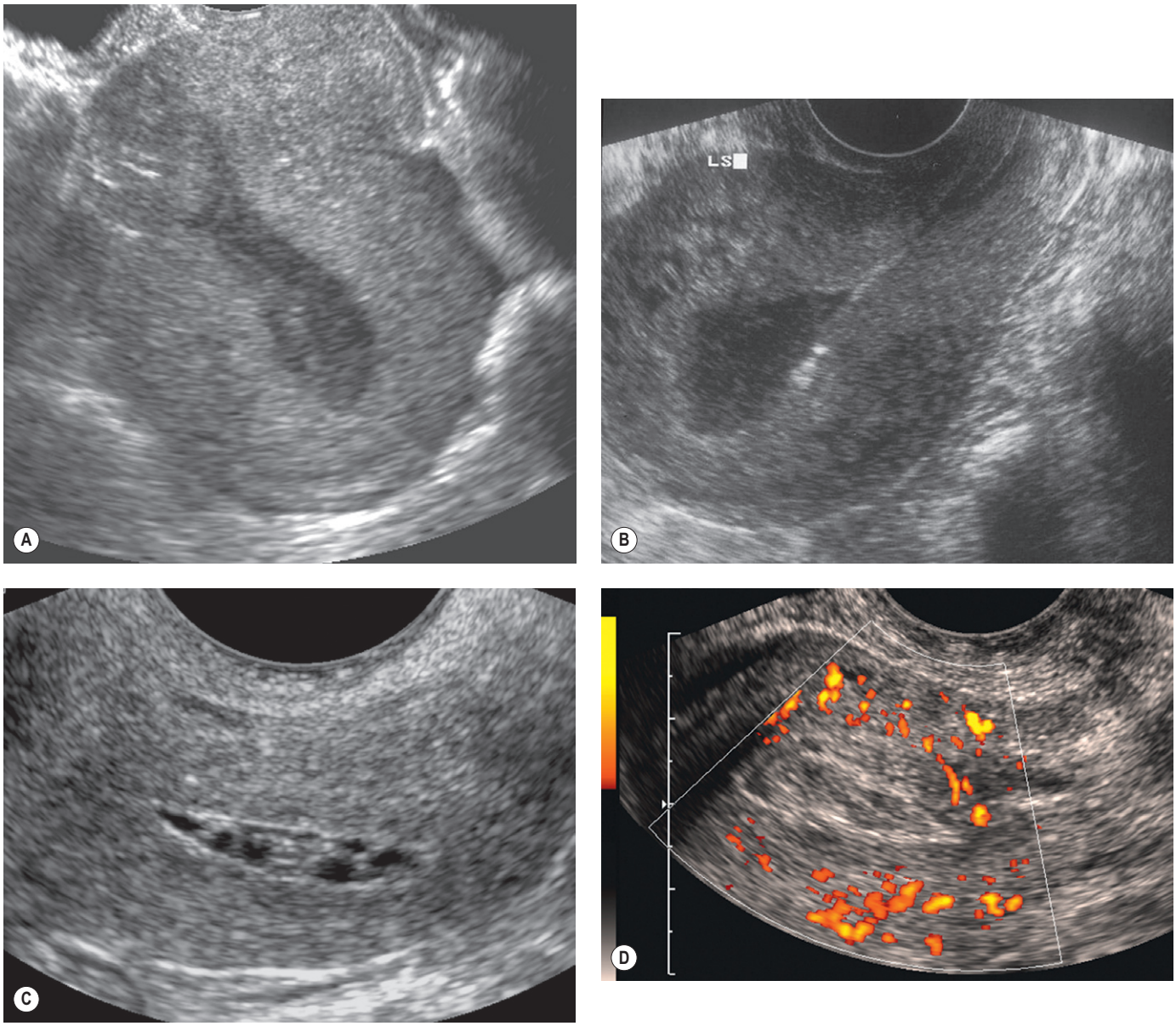


Figure 36.51 Endometritis. There are no specific signs on ultrasound for endometritis. Features that may be seen in association are: **(A)** retained fluid in the cavity after caesarean section (note the suture material in the fresh scar); **(B)** retained fluid and echogenic basal foci of tiny amounts of RPOC; **(C)** fluid and debris in the endometrial cavity; and **(D)** hypervascularity of the myometrium.

- haematometrocolpos: vaginal and uterine distension – obstruction at vaginal level
- haematometra: uterine distension – obstruction at cervical level
- haematosalpinx: dilation of fallopian tubes – obstruction at cornua.

If the lesion contains pus, substitute 'pyo' for 'haemato' and if it contains only secretions use 'hydro' instead.

The most common presentation of congenital lesions is with primary amenorrhoea. Cyclical pelvic pain, low back pain and urinary retention are all reported. Acute urinary retention can be the presenting complaint in an imperforate hymen.[87] Some may present as a huge paravaginal mass[88] – this is due to a vaginal septum dividing the vagina lengthways. The syndrome of Herlyn–Werner–Wunderlich comprises uterus didelphys (Fig. 36.53), an obstructed hemivagina and ipsilateral renal agenesis.[89] Problems with diagnosis can occur when one moiety of a uterus didelphys is obstructed. The unobstructed moiety is assumed to be a normal uterus and the adjacent obstructed moiety is misinterpreted as an adnexal cyst.

Treatment of these congenital variants can range from simple division of an obstructing membrane through to more extensive surgery required for more complicated Müllerian duct anomalies or cloacal malformations. MR provides the best anatomical information, although transrectal sonography has been used as well.[90]

Adults who develop secondary genital tract obstruction do so for a variety of reasons (Table 36.4). Cervical stenosis as a result of endometrial ablation may cause retrograde menstruation, endometriosis and delay in diagnosing endometrial cancer.[91] Unexplained postmenopausal haematometra needs to be investigated thoroughly to exclude an underlying malignant cause.[92] Post-radiotherapy stenosis usually occurs within a year of treatment. Occasionally, the uterus will be so distended that it mimics an adnexal cyst. Failure to find a normal uterus should always raise the possibility that the abnormal mass is the uterus.



Figure 36.52 Fluid in the endometrial cavity outlines fine strands or synechiae crossing the cavity.

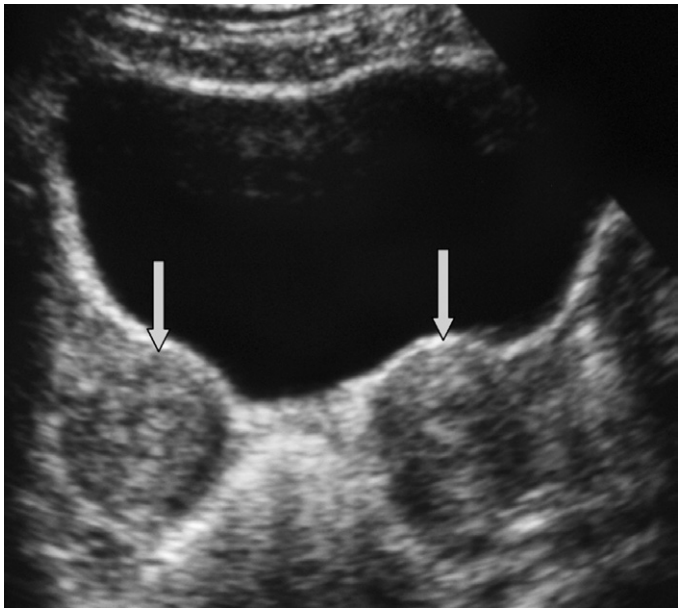


Figure 36.53 Uterus didelphys. Two separate uterine bodies are seen on this transverse view (arrows).

Table 36.4 Causes of adult cervical obstruction

Fibrotic cervical atrophy in the elderly
Tumour
Cervical, endometrial and vaginal tumour
Radiation therapy
External or intracavity
Trauma
Post cone biopsy or instrumentation

The ultrasound features are generally of a fluid-filled mass in the central pelvis (Fig. 36.54). Haematocolpos usually has a thin almost imperceptible wall, looks low-lying and tubular in shape and the uterus may be small and difficult to recognise at its top. Haematometrium usually presents with a thicker-walled mass and may, if severely distended, assume a rounded shape. The cervix is relatively indistensible so a haematometrocolpos often has an hourglass shape with the cervix forming the waist. The contents may be anechoic or exhibit a uniform echogenicity. No Doppler flow will be visible in the fluid. It is not possible to distinguish blood from mucus or pus on ultrasound. MR can distinguish blood but clinical features are needed to diagnose pus (pyometrium).

Congenital anomalies

- Covered in Chapter 34 also.
- The genital tract dilates above any congenital obstruction.
- An intact hymen is commonest cause.
- An MR scan is almost 100% accurate in diagnosing congenital gynaecological anomalies.
- There is an association with renal anomalies.
- Primary amenorrhoea commonest presentation of an obstructed tract.
- Ultrasound will show the dilated tract as a central fluid-filled mass.
- Failure to identify the uterus should always raise the possibility that an abnormal mass is in the uterus.

The postpartum uterus

The puerperium lasts about 6 weeks and is the postpartum period in which the uterus returns to its pre-pregnant state. Immediately after delivery the fundus of the uterus is palpable around 12 cm above the symphysis pubis. Ultrasound shows the enlarged uterus to have a smooth globular outline with a length of 20 cm. Up to a fifth of normal postpartum uteri will show air in the cavity. A small amount of fluid is also common. Uterine size diminishes rapidly, taking only a week to halve in weight (Fig. 36.55) and 6 weeks to involute to a size a little greater than its nulliparous state. Restoration of the endometrium takes about 3 weeks after the superficial layer of decidua is shed as lochia in the first few days after delivery.

Retained products of conception (RPOC)

This may occur following delivery or termination of pregnancy and is defined as incomplete uterine evacuation with retention of placental tissue within the uterus. Presentation is usually with postpartum haemorrhage, often within a few days, although sometimes delayed for a few weeks. Involution of the uterus becomes delayed and there is a risk of developing endometritis. RPOC is commoner after termination than after delivery, and it is least common after caesarean section (because the uterine cavity should have been inspected at the time of caesarean section). Abnormal implantation, placenta accreta, has a higher incidence of RPOC.

Ultrasound features show an overlap between a normal postpartum uterus and RPOC. The uterus may be inappropriately large and the endometrial cavity distended with fluid, blood clot, membranes and placenta. Blood clot and placenta can appear similarly reflective so it may not be possible to distinguish them (Fig. 36.56). Finding colour Doppler blood flow in the tissue, particularly low-impedance flow, indicates RPOC but its absence does not exclude it. Ultrasound overcalls the presence of RPOC in 34% of patients.[93]

Management includes surgical curettage. This should not be undertaken lightly because the postpartum uterus is more liable to damage. Hence, some authorities advocate the use of an endometrial thickness measurement to determine if surgical treatment is needed. The evidence is conflicting, with some papers finding a thickness of 13 mm, or more, useful with a sensitivity of 85% and specificity of 64% for RPOC,[94] whilst others find that there is no endometrial thickness measurement that allows distinction between chorionic villi or just decidua being present.[95] Another potential cause for confusion is the distinction of the normal low-impedance

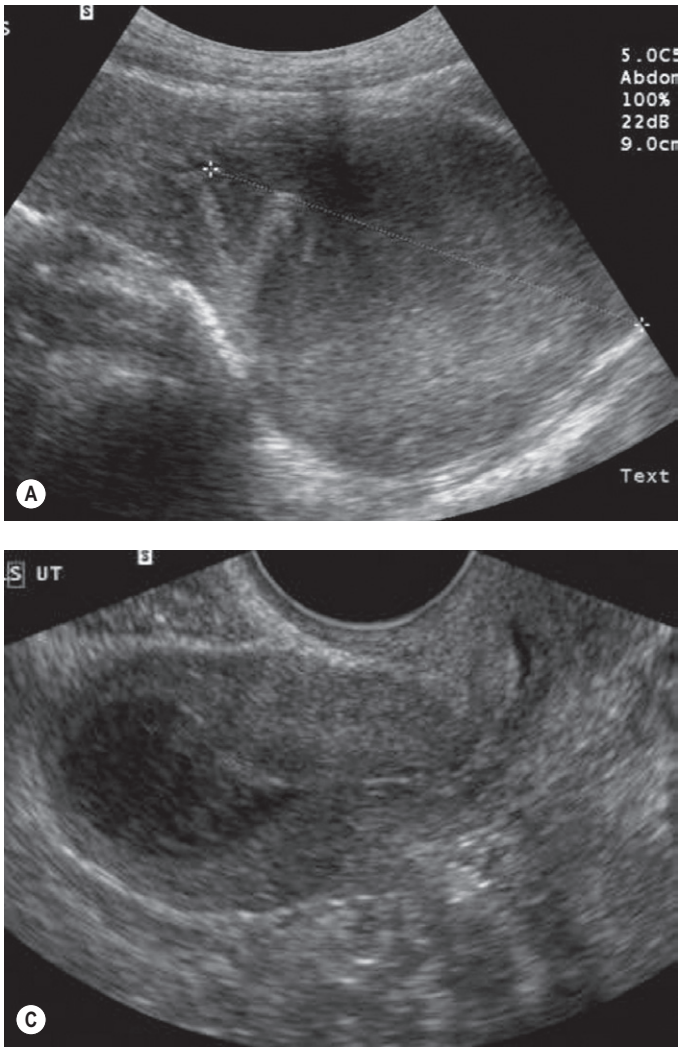


Figure 36.54 Obstructed genital tract. Longitudinal **(A)** and transverse **(B)** views of a vagina distended with blood and a normal uterus above it. This is a congenital haematocolpos in a 13-year-old. **C:** An acquired haematometrium in a postmenopausal woman.

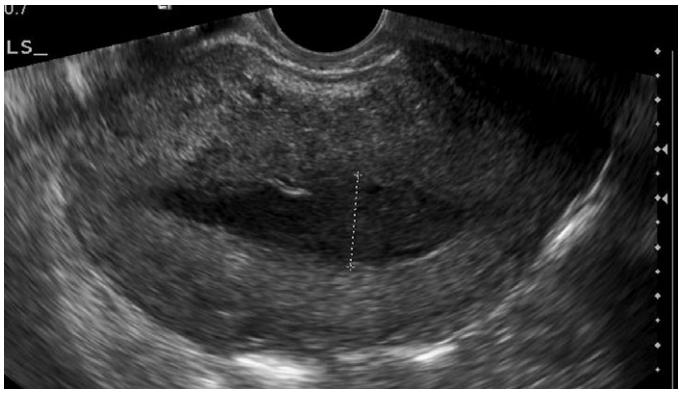


Figure 36.55 Transvaginal view of a postpartum uterus on day 8.

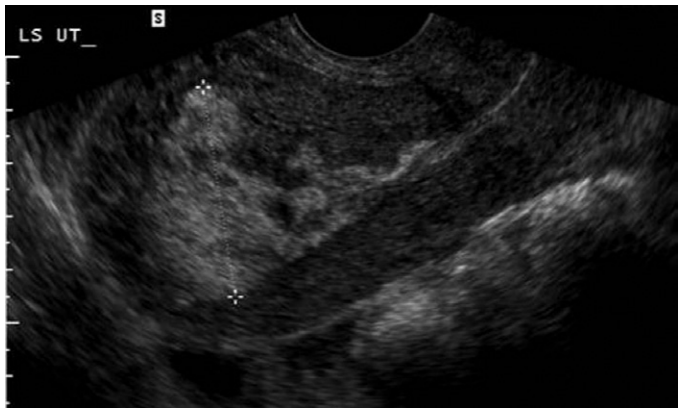


Figure 36.56 A substantial amount of retained products of conception is seen, with an endometrial cavity diameter of 40 mm. The bright echo tissue is a combination of placenta and blood clot. Ultrasound cannot tell them apart.

flow found in RPOC from the development of an associated AV malformation. Both can show substantial areas of colour flow with apparent feeding vessels. Recent work demonstrates that the diagnosis of AV malformation is overcalled considerably on ultrasound.[96] This has important implications for management as someone with an AV malformation would not generally be offered curettage.

THE CERVIX

The cervix is potentially overlooked on the ultrasound exam because it is relatively difficult to visualise and practitioners are drawn to examining the uterine body and endometrium and

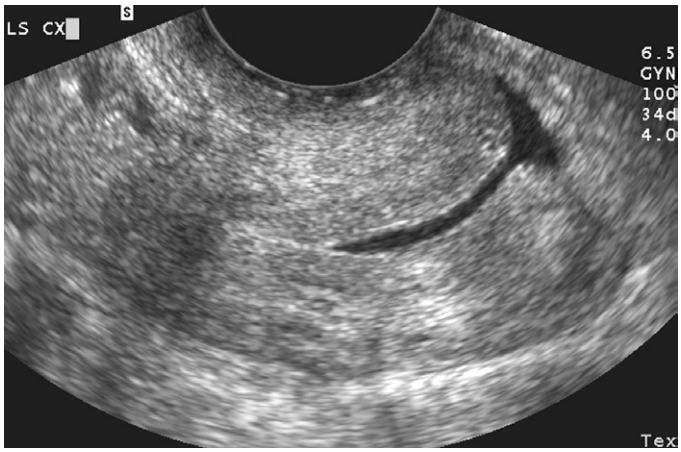


Figure 36.57 Transvaginal view of the cervix. A small amount of fluid outlines the endocervical canal.



Figure 36.58 Transvaginal view of a cervix containing several Nabothian cysts. They do not arise in the cervical canal.

looking for the ovaries. However, attention to detail allows the internal os, the endocervical canal and the external os to be identified (Fig. 36.57). Very specialised techniques with high frequency (20 MHz) intracervical transducers have shown promise in identifying carcinomas.[97] Transrectal ultrasound can also provide further information about the cervix and its adjacent tissue planes as the probe is a little further removed from the cervix than is usual on transvaginal scan.

Benign conditions

Nabothian cysts

These are retention cysts of the cervix and are a common benign finding, more so in those who have had children. Originally described as cysts visible on the ectocervix, the definition has come to include any retention cyst in the muscle of the cervix. Ultrasonically, they appear as echo-free cysts of 6–20 mm in size.[98] They are usually multiple and may distort the endocervical canal but they do not occur in the canal itself (Fig. 36.58). Debris can be occasionally seen in the cyst. It is of no consequence. Nabothian cysts do not resolve.

Cystic spaces centrally within the canal are due to dilated endocervical glands (Fig. 36.59). These usually give a tubular, multicystic appearance and are termed 'cystic endocervical mucus'. This may coexist with nabothian cysts. Both conditions are entirely innocent and have no predisposition to cancer.

A pitfall to avoid is mistaking a cervix filled with nabothian cysts for an enlarged ovary. Finding the endocervical canal and showing the relationship to the uterine body should prevent this error.

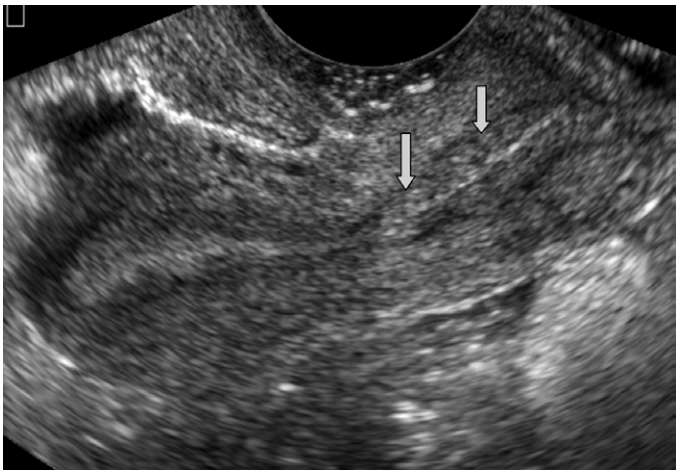


Figure 36.59 Prominent endocervical glands are visible (arrows) in this transvaginal view of the uterus. Note that they look different to the endometrium.

Cervical polyp

Cervical polyps are relatively common, being found in 5% of women referred for hysteroscopy,[99] although they may be difficult to see on ultrasound without saline contrast. Occasionally they become large but usually are only a few millimetres in size. Most are echogenic. They may be mistaken for pedunculated endometrial polyps or fibroids. Most cervical polyps are asymptomatic though some present with bleeding. There is no known malignant potential.

Cervical fibroid

Less than 10% of fibroids occur in the cervix (Fig. 36.60). They have the same ultrasound features as fibroids elsewhere in the uterus and most are small. Urinary frequency may be caused by large cervical fibroids pressing on the bladder. Cervical fibroids may also cause obstructed labour. MR imaging is often better in late pregnancy than ultrasound in defining the relationship and size of a cervical fibroid.

The benign cervix

- Nabothian cysts are often multiple.
- Nabothian cysts may mimic the appearances of an ovary – look for the relationship with the uterine body.
- Dilation of the endocervical canal with endocervical glands is an innocent phenomenon.
- Cervical polyps are common, but often not seen at ultrasound.
- Less than 10% of fibroids occur in the cervix.
- Cervical length monitoring in pregnancy can help predict those that will become incompetent.

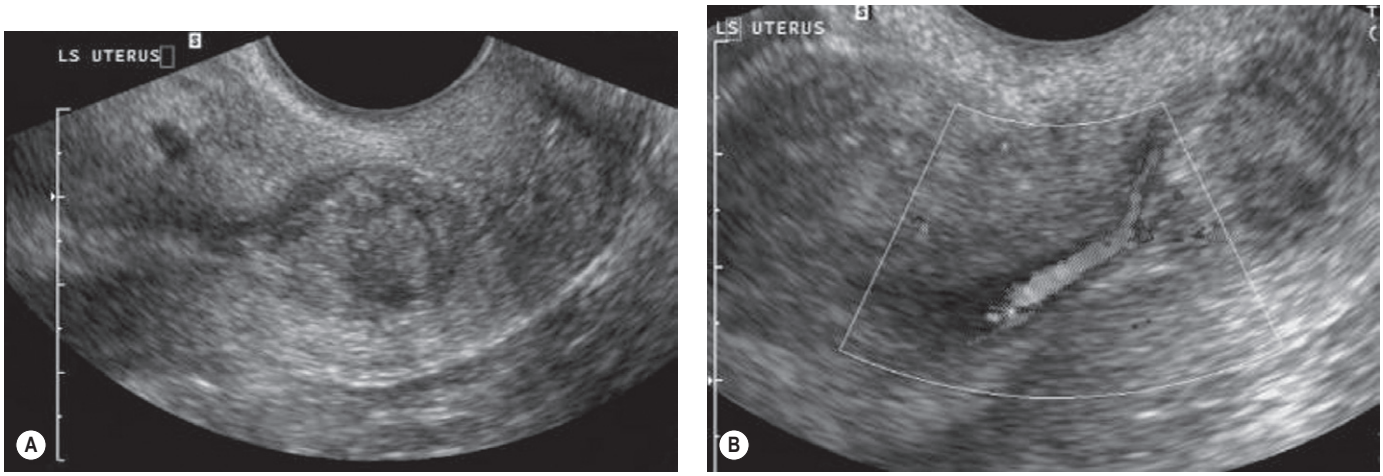


Figure 36.60 **A pedunculated fibroid** is seen to be prolapsed into the cervix **(A);** the pedicle is highlighted by colour Doppler, seen here in monochrome **(B)**.

Cervical incompetence

A history of second or early third trimester fetal loss, after painless dilation of the cervix, prolapse or rupture of membranes and expulsion of a live fetus despite minimal uterine activity, is characteristic for cervical incompetence.[100] The diagnosis of cervical incompetence is mostly based on the measurement of a shortened cervical length on transvaginal ultrasound.[101] Measurements of less than 25 mm in cervical length might predispose to preterm loss. Studies have been devoted to seeing if placing a cervical suture (cerclage) on the basis of ultrasound findings improves outcome. Whilst there is benefit in high-risk women (previous cone biopsy or dilatation and curettage in particular), those in low-risk groups[102] and those with multiple gestations[103] show no benefit of ultrasound-directed cerclage over conservative management. Another variable, other than length, is dilation of the internal os, or funnelling. This of itself predisposes to an adverse perinatal outcome.[104]

Ultrasound measurement is with transvaginal ultrasound, imaging the cervix in long axis. Normally the cervix is 40–42 mm in length with a 'T' shaped appearance at the internal os. When funnelling occurs the internal os develops a 'Y' shaped appearance. Finding bulging membranes through the cervix and into the upper vagina is likely to represent inevitable delivery.

Cervical cancer

Aetiology

Cervical cancer is the second most common gynaecological cancer. It is associated with the early onset of sexual activity, multiple partners and venereal disease. Smoking, low-socio-economic class and high parity are also associated. Human papilloma virus (HPV) is strongly implicated. A national vaccination programme for schoolgirls has been instituted in the UK with the intent of reducing the incidence of cervical cancer.

The peak incidence is at age 40 but with a change in society's attitude to sex there has been an increase in the number of younger women affected. Tumours arise at the adeno-squamous junction of the cervix, with 80–90% of tumours being squamous (and on the ectocervix) and 10–20% being adenocarcinoma (and in the endocervix). The position of the adeno-squamous junction in the cervical canal changes with age, so that older women are more likely to suffer endocervical tumours and growth, whereas younger women suffer an exophytic growth that extends inferiorly to the vagina. Other rare tumours may occur, including lymphoma, sarcoma, melanoma and metastases.

Symptoms

Cervical cancer is most often asymptomatic and is detected at routine screening with a cervical smear and cytology. A few present with abnormal bleeding. The diagnosis is confirmed clinically by a combination of colposcopy, local or cone biopsy. The cone biopsy obtains tissue from the endocervical canal so is less likely to miss the 20% or so of cancers that arise there. A cone biopsy may also be sufficient therapy in the precursor to cancer, cervical intra-epithelial neoplasia.

Ultrasound appearances

Ultrasound has little or no role to play in the early stages of cervical cancer, as the tumour is often indistinguishable from the normal cervix. Some authors dispute this,[105] and say that by use of transrectal ultrasound (TRUS), equivalent detection rates and staging as that by MRI can be achieved. TRUS has a particular advantage over MRI in detecting residual tumour after cone biopsy. The use of TRUS in cervical cancer has yet to gain any wide acceptance.

Three-dimensional ultrasound has been suggested as another tool that could be used to identify local infiltration of tumour,[106] although, again like TRUS, the technique is yet to find any widespread use.

Later stage disease may present on ultrasound as a mass distending the cervix (Fig. 36.61). Irregularity of the outer margin of the mass implies local tumour spread into the parametrium. Ultrasound may identify complications, namely invasion into the posterior bladder wall, obstruction to the ureters causing hydronephrosis and development of hydro/haematometra. Development of hydronephrosis indicates advanced stage disease and it may also be possible to see pelvic and retroperitoneal lymphadenopathy.

Other investigations

The mainstay of cervical cancer imaging is MRI. Direct multiplanar imaging and good contrast resolution between different tissues has allowed accurate local staging (Table 36.5). Finding an intact dark band around the cervix on axial T2-weighted images (the intact stromal ring) (Fig. 36.62) reliably stages the patient to stages I and IIa and hence eligible for surgical therapy.

CT has a role in more advanced disease as it reproducibly demonstrates lymph node, liver and lung involvement. PET-CT is used in women considering pelvic exenterative surgery, to ensure there is no disease outside the pelvis.

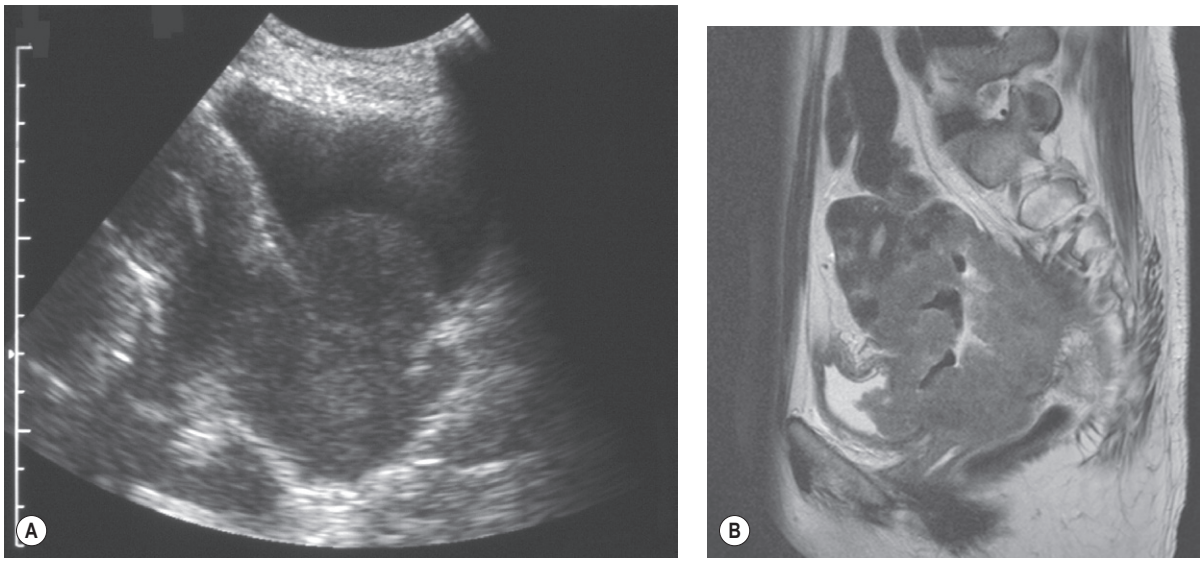


Figure 36.61 Cervical cancer. Ultrasound **(A)** of stage IV disease, with invasion of the bladder. MR scan **(B)** also shows a large cavitating mass replacing the cervix and invading the bladder.

Cervical cancer

- Second most common gynaecological cancer.
- New HPV vaccination programme recently instigated.
- Usually asymptomatic and found on screening.
- Ultrasound has little or no role in early stage disease.
- MR scan is the best imaging tool for staging.
- Ultrasound may detect complications such as hydronephrosis and bladder invasion.
- Surgery reserved for stage I and IIa disease.

Table 36.5 FIGO staging of cervical carcinoma

Stage	Description
I	Invasive carcinoma confined to cervix
II	Extends beyond the cervix, but not to either the pelvic side wall or the lower third of the vagina
IIa	No obvious parametrial involvement
IIb	Obvious parametrial involvement
III	The pelvic side wall or the lower third of the vagina are involved
IV	Spread beyond the pelvis or involvement of the bladder or rectum

Transrectal or transvaginal ultrasound-guided biopsies can be invaluable in confirming recurrent cervical cancer when clinically directed biopsies have failed to secure the diagnosis.[107]

Management

Surgery with or without adjuvant radiotherapy is reserved for stage I and stage IIa disease. Stage IIb and worse are generally treated with radiotherapy. Compromise to the renal tract will require ureteric stenting in order to preserve function.

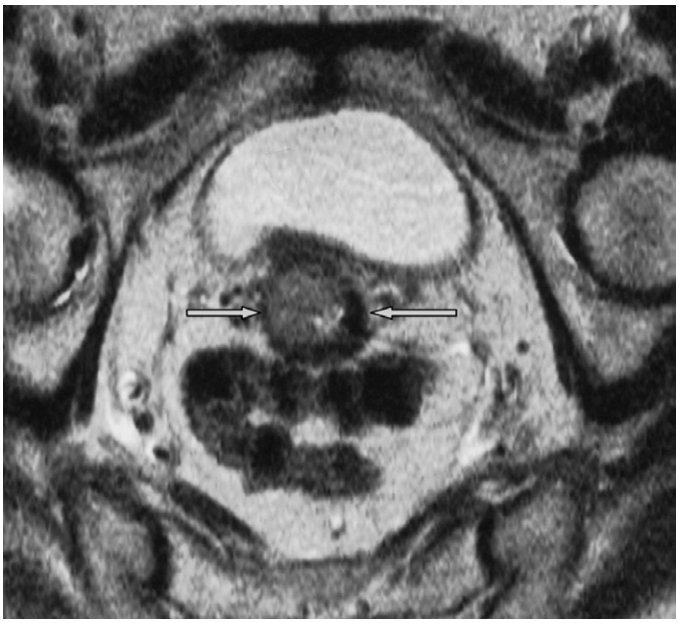


Figure 36.62 Cervical cancer. Transverse T2-weighted MR scan through the cervix: there is an intact stromal ring, shown by the dark band (arrows) surrounding the greyer central tumour.

THE VAGINA

Most vaginal pathology is assessed clinically but some anomalies will be found incidentally at pelvic ultrasound. Counter-intuitively, the transvaginal scan is least effective at identifying pathology as it is too close to the lesion or the probe may have gone past it before the operator starts looking. Transabdominal scans with a full bladder or transperineal scans show the vagina best.

Foreign bodies

A tampon is clearly seen because of the air it contains. It produces a well-defined, reflective linear shape with posterior acoustic

shadowing that lies centrally within the vagina. The innermost end of the tampon may abut and deform the posterior bladder wall.[108] Retained tampons or other foreign matter may provoke a vaginitis, and present with a bloody discharge. If they become infected a foul discharge will result and the toxic shock syndrome may develop.

A vaginal ring pessary is used in the treatment of prolapse. These produce a characteristic appearance on ultrasound. Any cross-section of the pessary produces two rounded lesions, each with a dense acoustic shadow. Typically, the transverse view of the pelvis will show these dense echogenicities laterally in the fornices. Tracing these 'masses' around confirms the ring shape of the pessary.

Gas may be present in the vagina, either as a result of instrumentation or recent sexual intercourse. Vaginal calculi are rare and may just be calcification of a retained foreign body. Vaginal septa or urinary reflux into the vagina can predispose to calculus formation.

Teflon injection used around the urethral sphincter in the treatment of urinary incontinence shows up as an echogenic amorphous mass adjacent to the vagina.

Fluid-filled vaginal lesions

Cystic lesions of the vagina are relatively common and usually represent benign lesions. A vaginal cyst may be an embryological derivative, ectopic tissue or urological abnormality.[109] Hydrocolpos arising as a result of an intact hymen or a congenital vaginal septum has been discussed earlier in the 'Haematometrium and other related conditions' section. There can be associated renal malformations so the kidneys should always be examined as part of the ultrasound scan. Hydrocolpos should not be confused with a small amount of free fluid, such as blood during menstruation or urine from a fistula or ectopic ureter. A history of persistent wetting should lead to the latter diagnosis. Standing the patient up and rescanning can also help.

Gartner's duct cysts are remnants of the embryological mesonephric duct[110] and are usually small, often multiple cysts that lie within or adjacent to the anterior vaginal wall (Fig. 36.63). Müllerian duct cysts are similarly remnants of the embryological paramesonephric duct system and are usually small and located anterolaterally. Both types of cyst can appear identical on ultrasound and only histological examination can tell them apart. Occasionally both types of cyst can be sufficiently large to prolapse through the introitus.[111] An MR scan is useful to give an overview of the anatomy. Both types of cyst are associated with renal anomalies. There are usually no symptoms and the cysts are soft to palpate.

Dilation of paraurethral glands can produce cysts adjacent to the vagina that sometimes compress the vagina. Similarly, paravaginal haematomas (most often seen after vaginal delivery) may compress the vagina and be mistakenly thought to be intravaginal. Endometriotic implants also occur.

Solid vaginal lesions

Fibroids very rarely occur within the vagina and may mimic prolapse.[112] Sometimes pedunculated submucosal fibroids can prolapse through the cervix into the vagina.[113] The fibroids display the same sonographic features as fibroids anywhere else. Neurofibromas occur in the vagina in people with neurofibromatosis.

Primary vaginal tumours account for only 1–2% of gynaecological malignancies, and most are squamous cell carcinomas and occur in the elderly. Adenocarcinomas and melanomas are much rarer. Tumours present with a vaginal discharge or blood loss. The diagnosis is invariably made clinically and confirmed by biopsy. Ultrasound shows the tumour as a low-echo mass lying within the upper third of the vagina, if it is visible at all. Spread of tumour is similar to cervical cancer and may cause hydronephrosis. The main imaging modality is MRI, with ultrasound having little if any role to play.

Rhabdomyosarcoma is the commonest soft tissue sarcoma of childhood and 20% will involve the genitourinary tract. In girls, most are vaginal in origin, although spread to or from the uterus also occurs. A rapidly enlarging mass which may protrude through the introitus is associated with vaginal bleeding. Staging with MR is the preferred imaging method, although ultrasound initially may find the mass incidentally (Fig. 36.64).

The vagina

- Transabdominal ultrasound often sees the vagina better than a TV scan.
- Tampons and pessaries have characteristic appearances.
- Cystic lesions may be due to an obstructed genital tract or due to embryological remnants.
- Reflux of urine into the vagina during voiding may mimic a cystic lesion.
- Solid lesions are uncommon and are usually fibroids or neurofibromas.
- Malignant lesions usually occur in the elderly and account for only 1–2% of gynaecological malignancies.
- Most malignancies are usually squamous cell carcinomas, although adenocarcinomas and melanomas do occur. The young may get rhabdomyosarcoma.

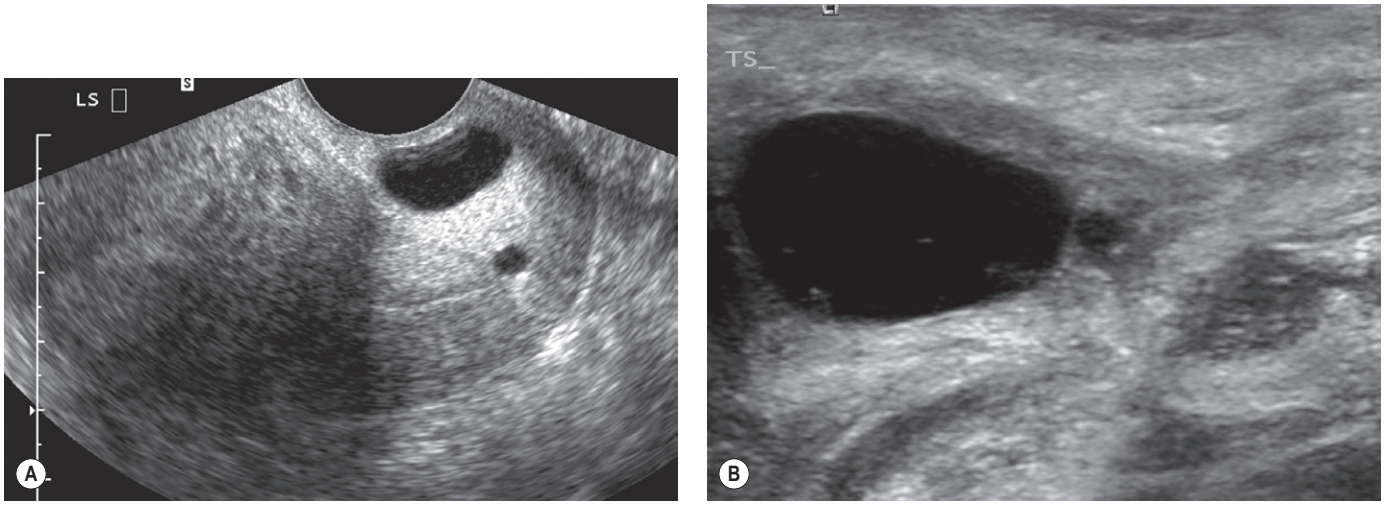


Figure 36.63 Gartner's duct cyst. An ovoid cyst is seen arising in the anterior vaginal wall adjacent to the cervix **(A)** and in close-up **(B)**.

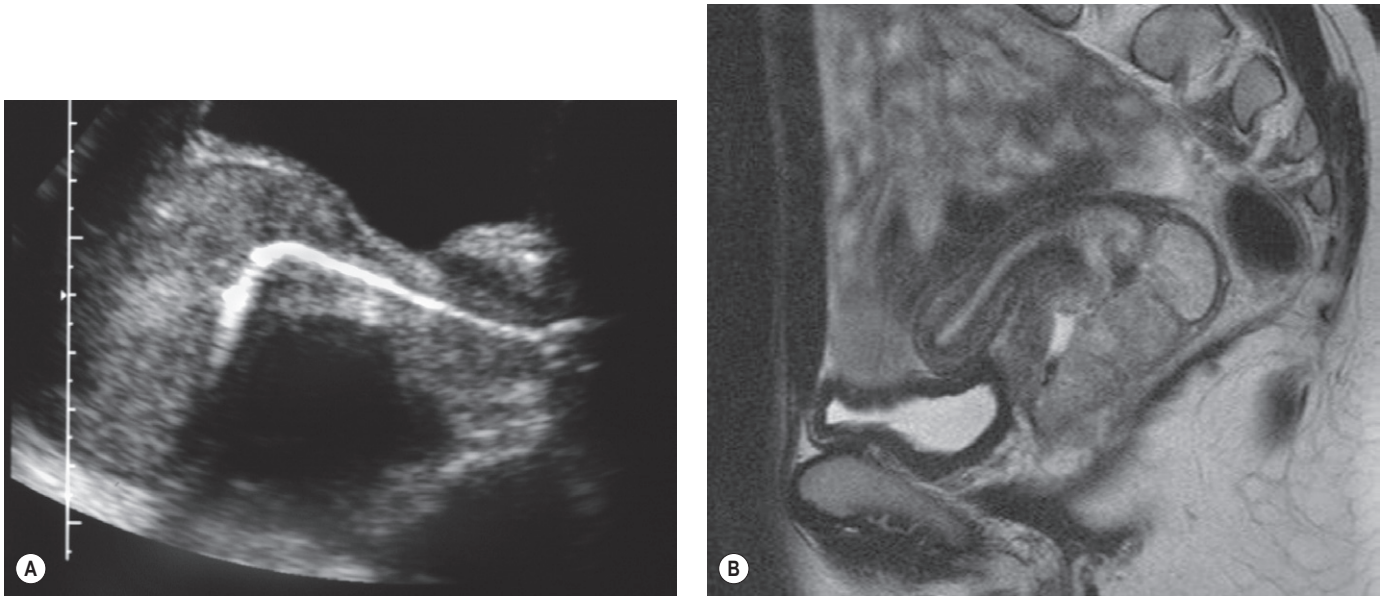


Figure 36.64 **Rhabdomyosarcoma.** The initial ultrasound **(A)** was thought to show a linear echogenic foreign body, but the MR **(B)** shows that in reality there is a large vaginal tumour with some central necrosis correlating with the echogenic region seen on ultrasound. The tumour was proven to be a rhabdomyosarcoma.

REFERENCES

1. Donald I. Use of ultrasonics in the diagnosis of abdominal swelling. BMJ 1963;2:1154–1155.
2. Kratochwil A. Ein neues vaginales Schnittbildverfahren. Geburtshilfe Frauenheilkd 1969;29:379–385.
3. Sherer DM, Cheung W, Gorelick C, et al. Sonographic and magnetic resonance imaging findings of an isolated vaginal leiomyoma. J Ultrasound Med 2007;26:1453–1456.
4. Evans P, Brunsell S. Uterine fibroid tumours: diagnosis and treatment. Am Fam Physician 2007;75:1503–1508.
5. Baird DD, Dunson DB, Hill MC, et al. Association of physical activity with development of uterine leiomyoma. Am J Epidemiol 2007;165:157–163.
6. Wise LA, Palmer JR, Stewart EA, Rosenberg L. Polycystic ovary syndrome and risk of uterine leiomyomata. Fertil Steril 2007;87:1108–1115.
7. Venkatachalam S, Bagratee JS, Moodley J. Medical management of uterine fibroids with medroxyprogesterone acetate (DepoProvera):a pilot study. J Obstet Gynaecol 2004;24:798–800.
8. Fiscella K, Eisinger SH, Meldrum S, et al. Effect of mifepristone for symptomatic leiomyomata on quality of life and uterine size: a randomised controlled trial. Obstet Gynecol 2006;108:1381–1387.
9. Chia CC, Huang SC, Chen SS, et al. Ultrasonographic evaluation of the change in uterine fibroids induced by treatment with a GnRH analog. Taiwan J Obstet Gynecol 2006;45:124–128.
10. Kaunitz AM. Progestin-releasing intrauterine systems and leiomyoma. Contraception 2007;75(6 Suppl):S130–S133.
11. Lurie S, Piper I, Woliovitch I, Glezerman M. Age-related prevalence of sonographically confirmed uterine myomas. J Obstet Gynaecol 2005;25:42–44.
12. Neiger R, Sonek JD, Croom CS, Ventolini G. Pregnancy-related changes in the size of uterine leiomyomas. J Reprod Med 2006;51:671–674.
13. Ouyang DW, Economy KE, Norwitz ER. Obstetric complications of fibroids. Obstet Gynecol Clin North Am 2006;33:153–169.
14. Vergani P, Locatelli A, Ghidini A, et al. Large uterine leiomyomata and risk of caesarean delivery. Obstet Gynecol 2007;109:410–414.
15. Nguyen QH, Gruenewald SM. Sonographic appearance of a postpartum pyomyoma with gas production. J Clin Ultrasound 2008;36:186–188.
16. Levens ED, Stegmann BJ, Feinberg EC, Larsen FW. Ultrasonographic characteristics of the endometrium among patients with fibroids undergoing ART. Fertil Steril 2008;89:1005–1007.
17. Vimercati A, Scioscia M, Lorusso F, et al. Do uterine fibroids affect IVF outcomes? Reprod Biomed Online 2007;15:686–691.
18. Wen L, Tseng JY, Wang PH. Vaginal expulsion of a submucosal myoma during treatment with long-acting gonadotrophin-releasing hormone agonist. Taiwan J Obstet Gynecol 2006;45:173–175.
19. Fogata ML, Jain KA. Degenerating cystic uterine fibroid mimics an ovarian cyst in a pregnant patient. J Ultrasound Med 2006;25:671–674.
20. Madan R. The bridging vascular sign. Radiology 2006;238:371–372.
21. Roy C, Bierry G, El Ghali S, et al. Acute torsion of uterine leiomyoma: CT features. Abdom Imaging 2005;30:120–123.
22. Cobellis L, Pecori E, Rigatti F, et al. A rare case of female pelvic mass: angioleiomyoma of the broad ligament. Eur J Gynaecol Oncol 2007;28:418–420.
23. Barnacle S, Muir T. Intermittent urinary retention secondary to a uterine leiomyoma. Int Urogynecol J Pelvic Floor Dysfunct 2007;18:1247–1248.
24. Nikolov A, Tiufekchieva E, Raicheva R. [Torsion of a non-gravid leiomyomatous uterus] Akush Ginekol (Sofiia) 2006;45:49–51.
25. Ferrero S, Abbamonte LH, Giordano M, et al. Uterine myomas, dyspareunia, and sexual function. Fertil Steril 2006;86:1504–1510.
26. Maizlin ZV, Vos PM, Cooperberg PL. Is it a fibroid? Are you sure? Sonography with MRI assistance. Ultrasound Q 2007;23:55–62.
27. Vitiello D, McCarthy S. Diagnostic imaging of myomas. Obstet Gynecol Clin North Am 2006;33:85–95.
28. Tamura-Sadamori R, Emoto M, Naganuma Y, et al. The sonohysterographic difference in submucosal uterine fibroids and endometrial polyps treated by hysteroscopic surgery. J Ultrasound Med 2007;26:941–946.
29. Harmanli OH, Bevilacqua SA, Dandolu V, et al. Adenomyosis interferes with accurate ultrasonographic detection of uterine leiomyomas. Arch Gynecol Obstet 2005;273:146–149.
30. Aviram R, Ochshorn Y, Markovitch O, et al. Uterine sarcomas versus leiomyomas: gray-scale and Doppler sonographic findings. J Clin Ultrasound 2005;33:10–13.
31. Exacoustos C, Romanini ME, Amadio A, et al. Can gray-scale and color Doppler sonography differentiate between uterine leiomyosarcoma and leiomyoma? J Clin Ultrasound 2007;35:449–457.
32. Tropeano G, Amoroso S, Scambia G. Non-surgical management of uterine fibroids. Hum Repro Update 2008;14:259–274.
33. Cho HH, Kim JH, Kim MR. Transvaginal radiofrequency thermal ablation: a day-care approach to symptomatic uterine myomas. Aust N Z J Obstet Gynaecol 2008;48:296–301.
34. Recaldini C, Carrafiello G, Lagana D, et al. Percutaneous sonographically guided radiofrequency ablation of medium-sized fibroids: feasibility study. AJR Am J Roentgenol 2007;189:1303–1306.

35. Hesley GK, Gorny KR, Henrichsen TL, et al. A clinical review of focused ultrasound ablation with magnetic resonance guidance: an option for treating fibroids. Ultrasound Q 2008;24:131–139.
36. Peric H, Fraser IS. The symptomatology of adenomyosis. Best Pract Res Clin Obstet Gynaecol 2006;20:547–555.
37. Kepkep K, Tuncay YA, Goynumer G, Tutal E. Transvaginal sonography in the diagnosis of adenomyosis: which findings are most accurate? Ultrasound Obstet Gynecol 2007;30:341–345.
38. Lee EJ, Joo HJ, Ryu HS. Sonographic findings of uterine polypoid adenomyomas. Ultrasound Q 2004;20:2–11.
39. Ors F, Lev-Toaff AS, Bergin D. Echogenic foci mimicking adenomyosis presumably due to air intravasation into the myometrium during sonohysterography. Diagn Interv Radiol 2007;13:26–29.
40. Levgur M. Diagnosis of adenomyosis: a review. J Reprod Med 2007;52:177–193.
41. Dueholm M, Lundorf E. Transvaginal ultrasound or MRI for diagnosis of adenomyosis. Curr Opin Obstet Gynecol 2007;19:505–512.
42. Levgur M. Therapeutic options for adenomyosis: a review. Arch Gynecol Obstet 2007;276:1–15.
43. Teo SY, Babagbemi KT, Peters HE, Mortele KJ. Primary malignant mixed Mullerian tumor of the uterus: findings on sonography, CT and gadolinium-enhanced MRI. AJR Am J Roentgenol 2008;191:278–283.
44. Huang MW, Muradali D, Thurston WA, et al. Uterine arteriovenous malformations: gray-scale and Doppler US features with MR imaging correlation. Radiology 1998;206:115–123.
45. Kwon JH, Kim GS. Obstetric iatrogenic arterial injuries of the uterus: diagnosis with US and treatment with transcatheter arterial embolisation. Radiographics 2002;22:35–46.
46. Jain K, Fogata M. Retained products of conception mimicking a large endometrial AVM: complete resolution following spontaneous abortion. J Clin Ultrasound 2007;35:42–47.
47. van den Bosch T, Daemen A, Van Schoubroeck D, et al. Occurrence and outcome of residual trophoblastic tissue: a prospective study. J Ultrasound Med 2008;27:357–361.
48. Betel C, Atri M, Arenson AM, et al. Sonographic diagnosis of gestational trophoblastic disease and comparison with retained products of conception. J Ultrasound Med 2006;25:985–993.
49. Fowler DJ, Lindsay I, Secki MJ, Sebire NJ. Histomorphometric features of hydatidiform moles in early pregnancy: relationship to detectability by ultrasound examination. Ultrasound Obstet Gynecol 2007;29:76–80.
50. Allen SD, Lim AK, Secki MJ, et al. Radiology of gestational trophoblastic neoplasia. Clin Radiol 2006;61:301–313.
51. Yu D, Wong YM, Cheong Y, et al. Asherman syndrome – one century later. Fertil Steril 2008;89:759–779.
52. Zimmer EZ, Bardin R, Tamir A, Bronshtein M. Sonographic imaging or cervical scars after Cesarean section. Ultrasound Obstet Gynecol 2004;23:594–598.
53. Hamar BD, Saber SB, Cackovic M, et al. Ultrasound evaluation of the uterine scar after caesarean delivery: a randomized controlled trial of one- and two-layer closure. Obstet Gynecol 2007;110:808–813.
54. Ofili-Yebovi D, Ben-Nagi J, Sawyer E, et al. Deficient lower-segment Cesarean section scars: prevalence and risk factors. Ultrasound Obstet Gynecol 2008;31:72–77.
55. Holland MG, Bienstock JL. Recurrent ectopic pregnancy in a caesarean scar. Obstet Gynecol 2008;111:541–545.
56. Seffah JD, Adanu RM. Sonographic findings in women with complications after hysterectomy. Int J Gynaecol Obstet 2008;100:160–162.
57. Brun JL, Descat E, Boubli B, Dallay D. Endometrial hyperplasia: a review [in French]. J Gynecol Obstet Biol Reprod (Paris) 2006;35:542–550.
58. Montgomery BE, Daum GS, Dunton CJ. Endometrial hyperplasia: a review. Obstet Gynecol Surv 2004;59:368–378.
59. Marchetti M, Vasile C, Chiarelli S. Endometrial cancer: asymptomatic endometrial findings. Characteristics of postmenopausal endometrial cancer. Eur J Gynaecol Oncol 2005;26:479–484.
60. Opolskiene G, Sladkevicius P, Valentin L. Ultrasound assessment of endometrial morphology and vascularity to predict endometrial malignancy in women with postmenopausal bleeding and sonographic endometrial thickness >or= 4.5mm. Ultrasound Obstet Gynecol 2007;30:332–340.
61. Michail G, Karahaliou A, Skiadopoulos S, et al. Texture analysis of perimenopausal and post-menopausal endometrial tissue in grayscale transvaginal ultrasonography. Br J Radiol 2007;80:609–616.
62. Kanat-Pektas M, Gungor T, Mollamahmutoglu L. The evaluation of endometrial tumors by transvaginal and Doppler ultrasonography. Arch Gynecol Obstet 2007; Nov29 Epub.
63. Tsikouras P, Liberis V, Galazios G, et al. TV sonographic assessment in postmenopausal women with bleeding. Eur J Gynaecol Oncol 2008;29:67–71.
64. Williams SC, Lopez C, Yoong A, McHugo JM. Developing a robust and efficient pathway for the referral and investigation of women with post-menopausal bleeding using a cut-off of <or= 4mm for normal thickness. Br J Radiol 2007;80:719–723.
65. Debby A, Malinger G, Glezeman M, Golan A. Intra-uterine fluid collection in postmenopausal women with cervical stenosis. Maturitas 2006;55:334–337.
66. Takacs P, De Santis T, Nicholas MC, et al. Echogenic fluid collection in postmenopausal women is a significant risk factor for disease. J Ultrasound Med 2005;24:1477–1481.
67. Takac I. Transvaginal ultrasonography with and without saline infusion in assessment of myometrial invasion of endometrial cancer. J Ultrasound Med 2007;26:949–955.
68. Takac I. Saline infusion sonohysterography and the risk of malignant extrauterine spread in endometrial cancer. Ultrasound Med Biol 2008;34:7–11.
69. Mansour GM, El-Lamie IK, El-Kady MA, et al. Endometrial volume as predictor of malignancy in women with postmenopausal bleeding. Int J Gynaecol Obstet 2007;99:206–210.
70. Yaman C, Habelsberger A, Tews G, et al. The role of three-dimensional volume in diagnosing endometrial cancer in patients with postmenopausal bleeding. Gynecol Oncol 2008 Jun 23 Epub.
71. Odeh M, Vainerovsky I, Grinin V, et al. Three-dimensional endometrial volume and 3-dimensional power Doppler analysis in predicting endometrial carcinoma and hyperplasia. Gynecol Oncol 2007;106:348–353.
72. Van den Bosch T, Verguts J, Daemen A, et al. Pain experienced during transvaginal ultrasound, saline contrast sonohysterography, hysteroscopy and office sampling: a comparative study. Ultrasound Obstet Gynecol 2008;31:346–351.
73. Timmermans A, Opmeer BC, Veersema S, Mol BW. Patients' preferences in the evaluation of postmenopausal bleeding. Br J Obstet Gynaecol 2007;115:1146–1149.
74. Spencer JA, Messiou C, Swift SE. MR staging of endometrial cancer: needed or wanted? Cancer Imaging 2008;8:1–5.
75. Welton AJ, Vickers MR, Kim J, et al. Health related quality of life after combined hormone replacement therapy: randomised controlled trial. BMJ 2008;337:a1190.
76. Barnabei VM, Cochrane BB, Aragaki AK, et al. Menopausal symptoms and treatment-related effects of estrogen and progestin in the Women's Health Initiative. Obstet Gynecol 2005;105: 1063–1073.
77. Vickers MR, MacLennan AH, Lawton B, et al. Main morbidities recorded in the women's international study of long duration oestrogen after menopause (WISDOM): a randomised controlled trial of hormone replacement therapy in postmenopausal women. BMJ 2007;335:239.
78. Lethaby A, Suckling J, Barlow D, et al. Hormone replacement therapy in post-menopausal women: endometrial hyperplasia and irregular bleeding. Cochrane Database Syst Rev 2004;3: CD000402.
79. Polin SA, Ascher SM. The effect of tamoxifen on the genital tract. Cancer Imaging 2008;8:135–145.
80. Garuti G, Cellani F, Centinaio G, et al. Prospective endometrial assessment of breast cancer patients treated with third generation aromatase inhibitors. Gynecol Oncol 2006;103:599–603.
81. Valenzano Menada M, Costantini S, Moioli M, et al. Evaluation of endometrial thickness in hormone receptor positive early stage breast cancer postmenopausal women switching from adjuvant tamoxifen treatment to anastrozole. Breast 2008 Jul 5. Epub ahead of print.
82. Ortiz ME, Croxatto HB, Bardin CW. Mechanisms of action of intrauterine devices. Obstet Gynecol Surv 1996;51(12 Suppl):S42–51.
83. Peri N, Graham D, Levine D. Imaging of intrauterine contraceptive devices. J Ultrasound Med 2007;26:1389–1401.
84. Sviggum O, Skjeldestad FE, Tuveng JM. Ultrasonically guided retrieval of occult IUD in early pregnancy. Acta Obstet Gynecol Scand 1991;70:355–357.
85. Keebler C, Chatwani A, Schwartz R. Actinomycosis infection associated with intrauterine contraceptive devices. Am J Obstet Gynecol 1983;145:596–599.
86. Boardman LA, Peipert JF, Brody JM, et al. Endovaginal sonography for the diagnosis of upper genital tract infection. Obstet Gynecol 1997;90:54–57.

87. Chang JW, Yang LY, Wang HH, et al. Acute urinary retention as the presentation of an imperforate hymen. J Chin Med Assoc 2007;70:559–561.
88. Asha B, Manila K. An unusual presentation of uterus didelphys with obstructed hemivagina with ipsilateral renal agenesis. Fertil Steril 2008 Jul 12 (epub ahead of print).
89. Ghirardo V, Cecchetto G, Minucci D, et al. Haematometra in uterus didelphys: a pitfall in teenagers with lower abdominal mass. Report of two cases. Paediatr Med Chir 2008;30:41–44.
90. Anguenot JL, Ibecheole V, Salvat J, Campana A. Hematocolpos secondary to imperforate hymen, contribution of transrectal echography. Acta Obstet Gynecol Scand 2000;79:614–615.
91. McCausland AM, McCausland VM. Long-term complications of endometrial ablation: cause, diagnosis, treatment and prevention. J Minim Invasive Gynecol 2007;14:399–406.
92. Bollapragada SS, Sircar S, Rae DW, Walker E. Unexplained postmenopausal hematometra. Acta Obstet Gynecol Scand 2006;85:121–123.
93. Sadan O, Golan A, Girtler O, et al. Role of sonography in the diagnosis of retained products of conception. J Ultrasound Med 2004;23:371–374.
94. Ustunyurt E, Kaymak O, Iskender C, et al. Role of transvaginal sonography in the diagnosis of retained products of conception. Arch Gynecol Obstet 2008;277:151–154.
95. Sawyer E, Ofuasia E, Ofili-Yebovi D, et al. Ultrasound Obstet Gynecol 2007;29:205–209.
96. Rufener SL, Adusumilli S, Weadock WJ, Caoili E. Sonography of uterine abnormalities in post partum and postabortion patients: a potential pitfall of interpretation. J Ultrasound Med 2008;27:343–348.
97. Dubinsky TJ, Reed SD, Grieco V, Richardson ML. Intracervical sonographic-pathologic correlation: preliminary results. J Ultrasound Med 2003;22:61–67.
98. Fogel SR, Slasky BS. Sonography of nabothian cysts. AJR Am J Roentgenol 1982;138:927–930.
99. Bajo J, Moreno-Calvo FJ, Uguet-de-Resayre C, et al. Contribution of sonography to the evaluation of benign cervical conditions. J Clin Ultrasound 1999;27:61–64.
100. Lotgering FK. Clinical aspects of cervical insufficiency. BMC Pregnancy Childbirth 2007;7(Suppl 1):S17.
101. Pugatsch R, Elad D, Jaffa AJ, Eytan O. Analysis of cervical dynamics by ultrasound imaging. Ann N Y Acad Sci 2007;1101:203–214.
102. Incerti M, Ghidini A, Locatelli A, et al. Cervical length < or = 25 mm in low-risk women: a case control study of cerclage with rest vs rest alone. Am J Obstet Gynecol 2007;197:315.e1–4.
103. Roman AS, Rebarber A, Pereira L, et al. The efficacy of sonographically indicated cerclage in multiple gestations. J Ultrasound Med 2005;24:763–768.
104. Rust OA, Atlas RO, Kimmel S, et al. Does the presence of a funnel increase the risk of adverse perinatal outcome in a patient with a short cervix? Am J Obstet Gynecol 2005;192:1060–1066.
105. Fischerova D, Cibula D, Stenhova H, et al. Transrectal ultrasound and magnetic resonance imaging in staging early cervical cancer. Int J Gynecol Cancer 2008;18:766–772.
106. Ghi T, Giunchi S, Kuleva M, et al. Three-dimensional transvaginal sonography in local staging of cervical carcinoma: description of a novel technique and preliminary results. Ultrasound Obstet Gynecol 2007;30:778–782.
107. Roy D, Kulkarni A, Kulkarni S, Thakur MH, et al. Transrectal ultrasound-guided biopsy of recurrent cervical carcinoma. Br J Radiol 2008 Jul 28 epub ahead of print.
108. Caspi B, Zalel Y, Katz Z, et al. The role of sonography in the detection of vaginal foreign bodies in young girls: the bladder indentation sign. Pediatr Radiol 1995;25(Suppl 1):S60–61.
109. Eilber KS, Raz S. Benign cystic lesions of the vagina: a literature review. J Urol 2003;170:717–722.
110. Deppisch LM. Cysts of the vagina: classification and clinical correlations. Obstet Gynecol 1975;45:632–637.
111. Kresowik J, Kennedy CM, Wing S, Galask RP. Prolapsing vaginal cyst: a case report. J Reprod Med 2007;52:852–854.
112. Leron E, Stanton SL. Vaginal leiomyoma – an imitator of prolapse. Int Urogynecol J Pelvic Floor Dysfunct 2000;11:196–198.
113. McCarthy S, Taylor KJW. Sonography of vaginal masses. AJR Am J Roentgenol 1983;140:1005–1006.

CHAPTER

37

Gynaecological intervention techniques

Michael J. Weston

INTRODUCTION 720

OMENTAL BIOPSY 720
Rationale 720
Method 720
Complications 722

TRANSVAGINAL BIOPSY OR CYST ASPIRATION 722
Rationale 722
Method 722
Complications 723

PELVIC ABSCESS DRAINAGE 724
Rationale 724
Method 724
Complications 727

SALINE INFUSION HYSTEROGRAPHY 727
Rationale 727
Method 727
Complications 728

INTRODUCTION

Ultrasound-guided interventional techniques all have a common theme and the basic principles of biopsy or drainage are universal. Chapters 11 and 43 discuss liver and general abdominal interventional procedures. The aim of this chapter is to cover interventions specific to female pelvic disease.

OMENTAL BIOPSY

Rationale

Ovarian cancer is best treated by primary cytoreductive surgery followed by chemotherapy. Women who present with typical imaging findings and an appropriate tumour marker profile of a raised CA125 can go straight to surgery without the need for biopsy, provided they are fit enough. If the woman is too debilitated to undergo primary surgery, then the next best option is for chemotherapy and when fit, interval debulking surgery. In this scenario, oncologists need to know that the tumour is ovarian before prescribing the chemotherapy regime. A biopsy therefore becomes necessary.[1]

Clinical trials are currently in progress to assess if primary chemotherapy and interval debulking surgery should become the standard management of ovarian cancer rather than the traditional primary cytoreductive surgery.

Women may present with peritoneal carcinomatosis, without either an obvious pelvic mass or an appropriate tumour marker profile. They may have a history of another tumour, such as breast cancer. A biopsy becomes necessary to distinguish between primary peritoneal carcinoma, and metastases from sites such as breast, colon, appendix, pancreas and stomach.[2–4] The treatment of these different tumours varies and debulking surgery is contraindicated in some. Modern histology techniques, including immunohistochemistry, allow a site-specific diagnosis to be made in over 90% of biopsies taken.

Seeding of tumour along a biopsy track or into the peritoneal cavity is a potential risk, though not one that has been quantified. Most reports are anecdotal. However, this perceived risk influences practice and routes of access. Consequently, percutaneous biopsies are not done in suspected malignancy unless there is already evidence of spread from the primary tumour. Computed tomography or MRI should be performed to stage the tumour before considering any biopsy. These scans not only stage the tumour but also allow planning of the biopsy procedure.

Method

The technique of percutaneous ultrasound-guided omental biopsy is no different to any other ultrasound-guided technique. The main challenge is to identify the abnormal omentum with ultrasound. This is easier to do if the site of disease is already known from CT or MRI but can still be done even if no prior scans are available. The presence of ascites helps to outline omental cake but it is not essential. Large omental deposits are identifiable because they adopt a sheet-like appearance on both transverse and longitudinal imaging (Fig. 37.1). This is in contradistinction to bowel that might look sheet-like in one plane but tubular in the other. The omental deposits can look bright or dark on ultrasound. Any detectable blood flow will have a random distribution rather than the more organised pattern seen in the wall of bowel. The highest frequency probe that allows visualisation is advised. Many women can have their omental disease identified with a linear 8 MHz probe.

Care needs to be taken to identify adjacent structures to the intended omental target so that they can be avoided. Time spent in preparation is never wasted and usually ensures the procedure goes quickly and smoothly once started.

The patient needs no preparation. Omental biopsy can be done as an outpatient procedure with the patient spending only 30–40 minutes in the department after the biopsy. It helps if they attend with a companion who will take them home. Clotting needs to be corrected if the patient has been formally anticoagulated; otherwise the use of aspirin is not a contraindication.

Skin preparation, a sterile drape and local anaesthetic are used. A sterile ultrasound-probe cover and a needle guide device are advised. Freehand needle guide techniques are possible but in my experience take longer both to do and to teach. An 18-gauge automated cutting needle is best. Studies have shown needle core techniques outperform fine-needle aspiration cytology in diagnostic rates without changing the risk of complications.[5]

A small nick in the skin with a scalpel blade and blunt dissection with small forceps facilitates passage of the needle through the skin and subcutaneous tissues. The needle guide technique requires the target to be lined up with the guide lines on the screen (Fig. 37.2). The ultrasound probe is then held very still and the needle advanced through the guide in a fairly quick movement until it reaches the

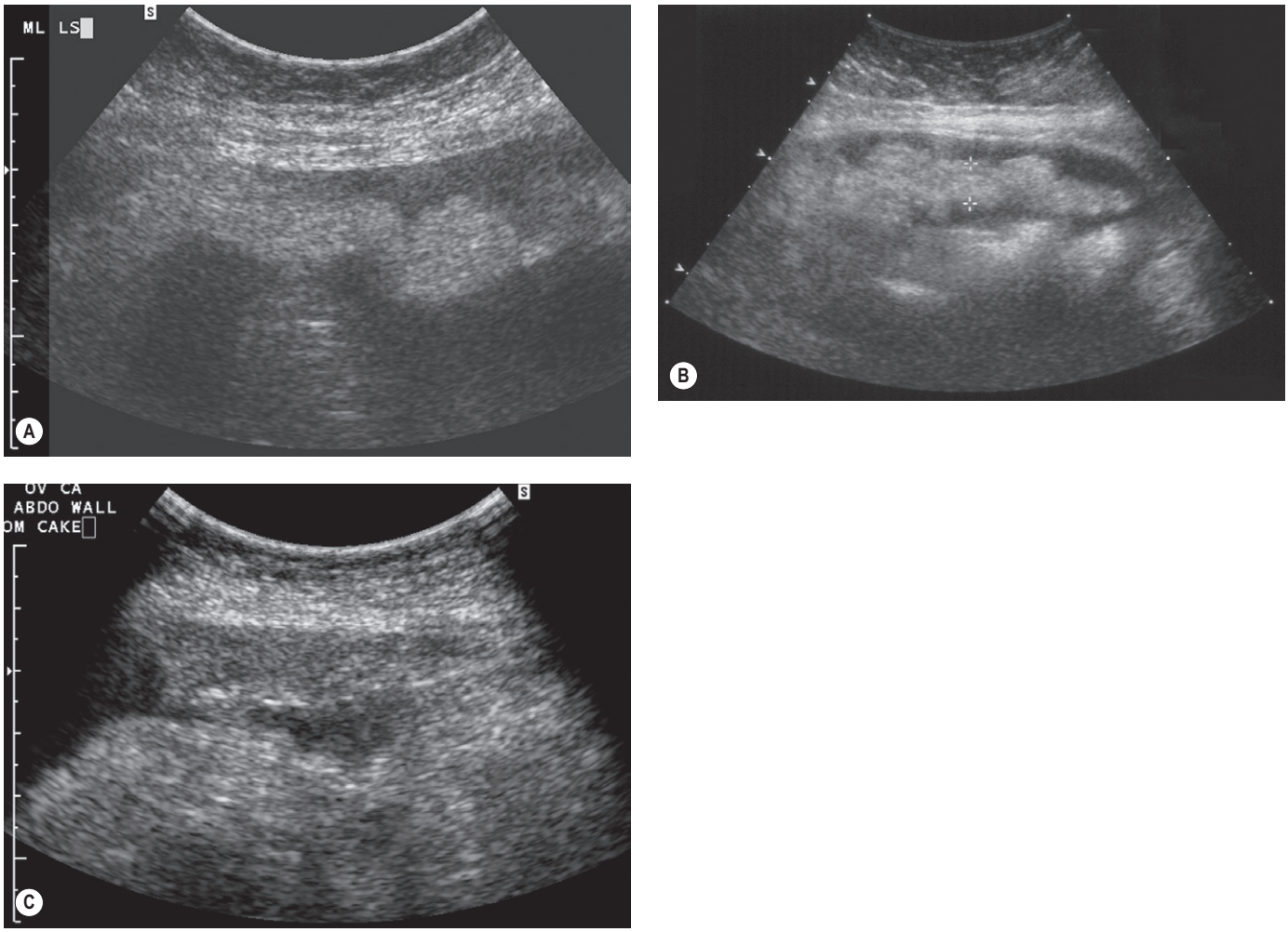


Figure 37.1 **Three examples of omental tumour. A:** The omental cake is seen as an irregular lumpy sheet within a large pool of ascites. The 'cake' is still seen as a sheet of tissue whether the probe is held in the transverse or longitudinal plane. **B:** Less ascites is present but it still outlines a sheet of omental tumour (between the callipers). Note that it has a lumpy outline similar to the disease seen in **A**. **C:** An example of a smaller amount of omental tumour, more adherent to the anterior abdominal wall.

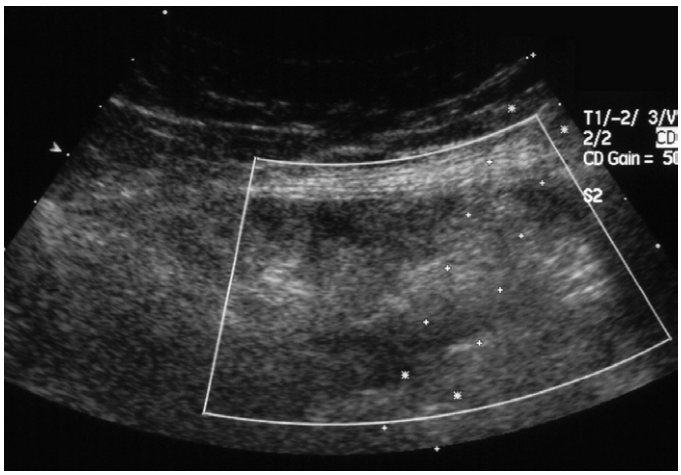


Figure 37.2 **Omental tumour** being scanned to plan the route of biopsy. A colour Doppler box is used to check there are no large vessels in the intended target. The needle guide lines are graduated with centimetre marks. This helps to judge where to place the biopsy needle and how far the needle will throw on firing.

Omental biopsy

- Percutaneous omental biopsy is safe.
- Imaging-guided biopsy avoids the need for laparoscopic or open biopsy.
- Technique is no different to any other biopsy.
- Time spent in preparation is never wasted.

target. The operator needs to ensure that they line up their needle with the guide so that when they push, the needle is not forced into a bend. The quick advancement of the needle through the guide improves visualisation of the tip of the needle. The position of the needle tip and the mechanism of firing the cutting mechanism will vary between manufacturers. The operator needs to be familiar with the needle they are using.

The core retrieved should be inspected to see if it contains the expected firm white tissue that most malignant deposits exhibit. The number of needle passes made depends on the quality of the specimen. Two good cores are usually enough to allow histology and various different immunohistochemistry stains.

Once the nick in the skin has stopped bleeding and a small dressing has been applied, the woman can sit up. They can leave straight away if they wish but most people prefer to sit for half an hour with a soft drink before leaving.

Complications

Percutaneous omental biopsy is a very well tolerated and extremely safe procedure. No significant complications have been recorded in several series. Bowel seems remarkably tolerant to the passage of an 18-gauge needle and no descriptions of bowel damage are reported. The occasional haematoma is seen (1 out of 90 patients in one series).

TRANSVAGINAL BIOPSY OR CYST ASPIRATION

Rationale

Masses in the pelvis may be inaccessible percutaneously because of intervening bowel, bladder or vascular structures. The transvaginal route of access can allow the probe to be positioned directly adjacent to the target lesion. The need for a biopsy is usually the same as described in the omental biopsy section above. One potential advantage of the transvaginal route is that if there is any seeding of tumour down the biopsy track it is not upstaging the tumour by spreading disease into a different compartment. However, it is still best avoided in lesions thought to be confined to the ovary (stage I).[6]

Aspiration of simple cysts is neither advised nor needed.[7] It has been shown that the rate of resolution of simple cysts is the same whether treated with watchful waiting or with aspiration. Cysts often recur after aspiration. Endometriomas in particular have a high rate of recurrence and are also quite painful to drain.

Women who are undergoing palliative treatment for peritoneal cancer may develop pelvic symptoms due to the local pressure effects of a malignant cyst. It is entirely reasonable to offer palliation of these symptoms by draining the cyst (Fig. 37.3).

Method

Transvaginal biopsy can be done as an outpatient procedure. No particular preparation is needed although clotting abnormalities require correction. The patient lies in the usual position for a transvaginal scan. Stirrups are not necessary. Some authorities advocate vaginal cleansing with povidone-iodine and a course of antibiotics as the vaginal route of access is only semi-sterile. However, in my own practice, I have found that the use of an antiseptic cream as the probe lubricant and no antibiotics has not resulted in any infective complications in almost one hundred biopsies.

Some authorities prefer to perform transvaginal biopsies under conscious sedation.[8] If this approach is used then fasting for 6 hours and adherence to your own institutional guidelines are required. Sedation is not essential, however, and in my practice I have found it is rarely needed. Careful discussion with the woman beforehand and an appropriate reassuring environment usually allow the biopsy to take place without undue discomfort.

A transvaginal transducer with a needle guide attachment is essential (Fig. 37.4). It should be possible in most cases to position the probe within a few millimetres of the lesion so that there is not much more than the vaginal wall for the needle to traverse before hitting the lesion (Figs 37.5 and 37.6). Once the target for biopsy is identified with due consideration to any intervening structures and blood vessels then the probe should be pushed gently but firmly. This is to stretch the vaginal wall and make it taut so that the needle will puncture it more readily. It is almost impossible to infiltrate

Transvaginal intervention

- Transvaginal biopsy is well tolerated.
- Sedation is not normally required.
- Draining simple cysts is no better than watchful waiting.
- Allows access to lesions that cannot be reached percutaneously.

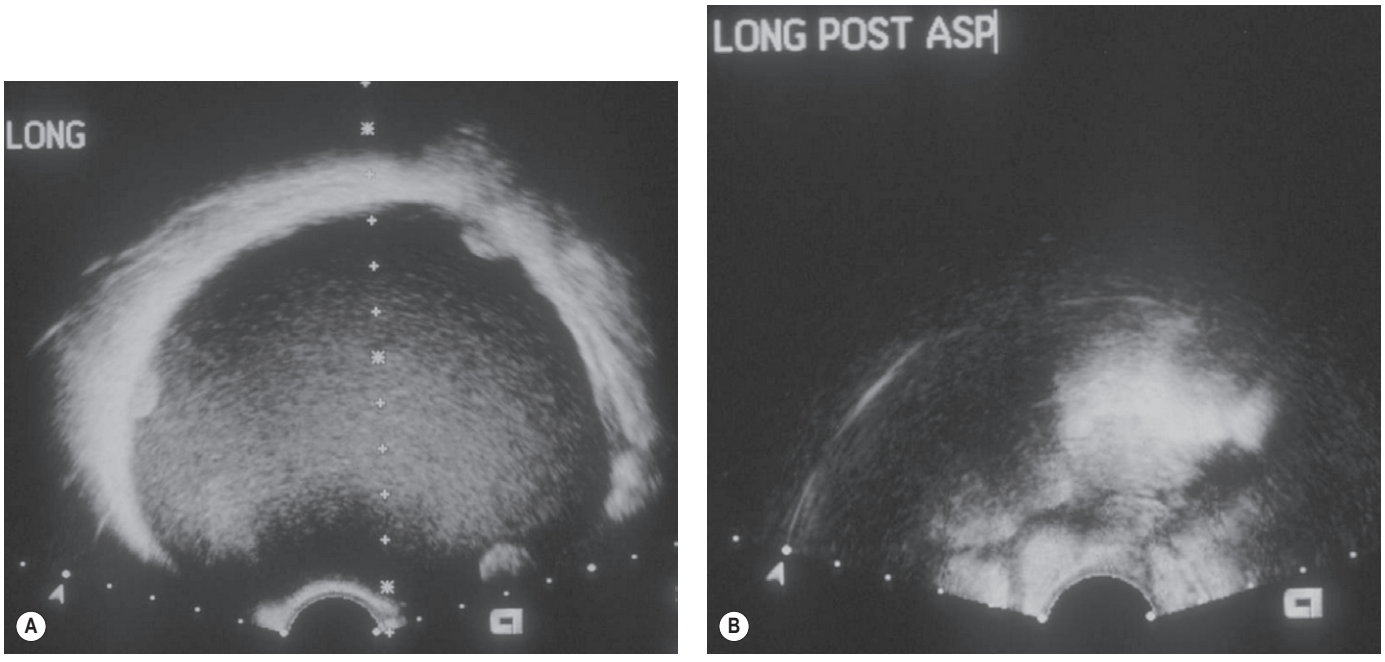


Figure 37.3 Transvaginal drainage of a malignant cyst to palliate pelvic symptoms. **A:** The large pelvic cyst clearly has tumour nodules around its margin. The transvaginal probe is pushed against the cyst to indent its margin and stretch the vaginal wall. Note that the amount of tissue the needle has to pass through to penetrate the cyst is minimal if it travels along the dotted guide line. **B:** The same cyst is shown collapsed and empty after successful transvaginal aspiration of its contents.

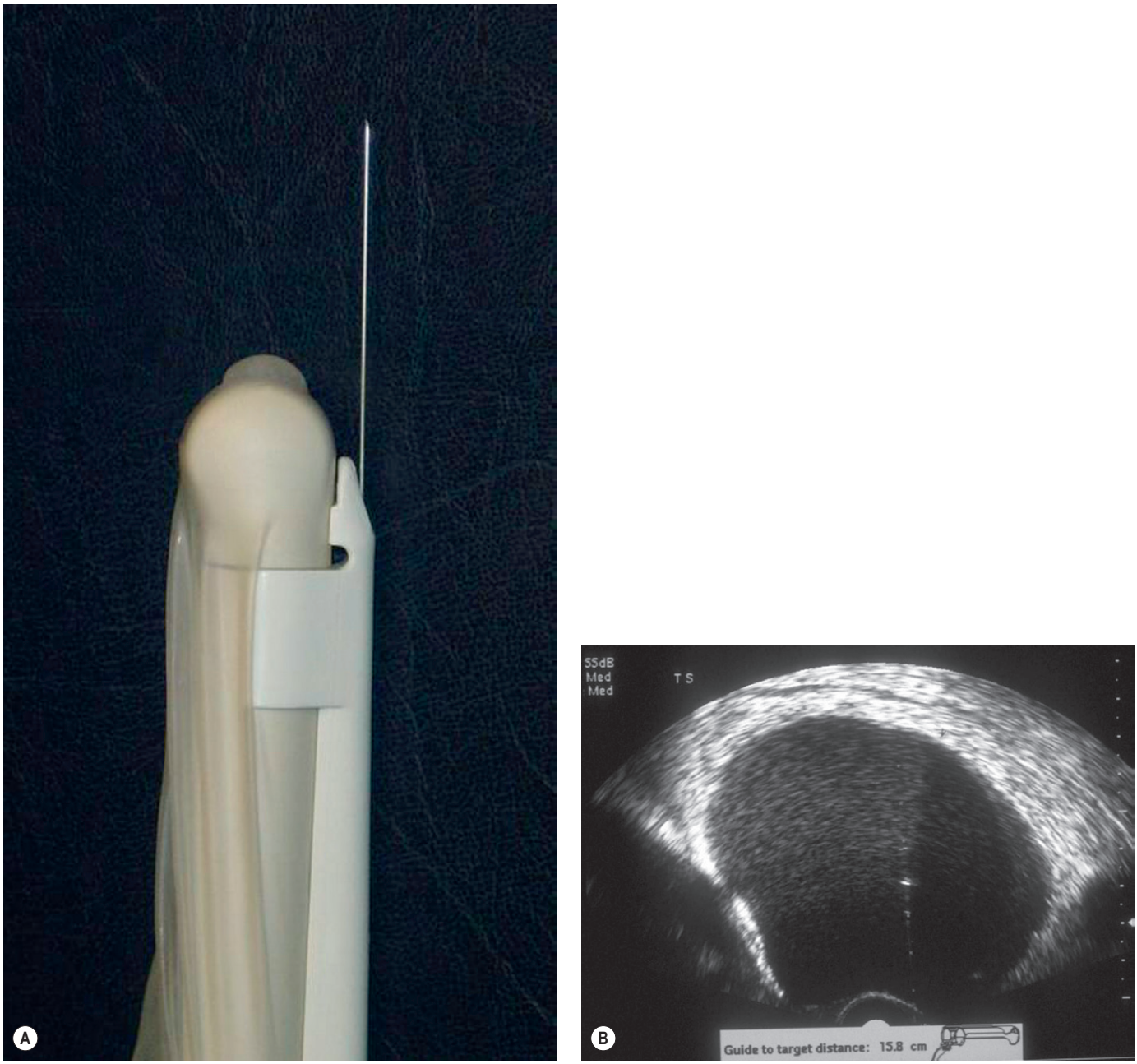


Figure 37.4 Transvaginal biopsy. **A:** An endoluminal ultrasound probe with a probe cover and needle guide attachment. A needle has been passed through the guide to show its route of passage relative to the probe. **B:** A transvaginal scan with the tip of the probe pushed into the margin of a cyst to stretch the vaginal wall. A needle has been passed into the cyst. The tip can be seen as a bright echo along the dotted needle guide line.

local anaesthetic adequately and doing so may cause more discomfort than just passing the biopsy needle. Generally, the least amount of needle manipulation is the most comfortable. A single pass with an 18-gauge core-biopsy needle is usually enough to sample a solid lesion though most women will allow a second pass if needed.

If a cystic lesion is being drained, this can usually be achieved through a 19-gauge sheathed needle. The needle is placed into the lesion using the same technique as described for a biopsy above. The metal inner part of the needle is removed and the outer plastic sheath left in the lesion. An assistant can then drain the lesion using a syringe and some connecting tubing to the back of the sheath.

Once the biopsy or drainage is done, the woman should be warned to expect a little vaginal bleeding not unlike menstrual loss. Most women are fit enough to leave the department after half an hour. It helps if they attend with a companion. Women who have been sedated will need somewhere to recover before they can be allowed home.

Complications

Complication rates are very low. Most of those described in the literature are related to draining endometriomas.[9]

PELVIC ABSCESS DRAINAGE

Rationale

Pelvic sepsis and abscess formation can be due to iatrogenic, gynaecological and non-gynaecological causes. Tubo-ovarian, diverticular, appendiceal and postoperative abscesses are most common. Many of these abscesses lie deep in the pelvis and are not accessible by percutaneous routes (Fig. 37.7). The transgluteal route may be available, but this is a painful and poorly tolerated path; especially if a drain is left in place. Endoluminal access either by transrectal or transvaginal route should be remembered.

The transrectal route is inherently non-sterile so should not be used to access collections that are not bowel related or which are not thought necessarily to be infected. Typically the transrectal route would be used to drain diverticular, appendiceal or post-bowel-surgery collections.

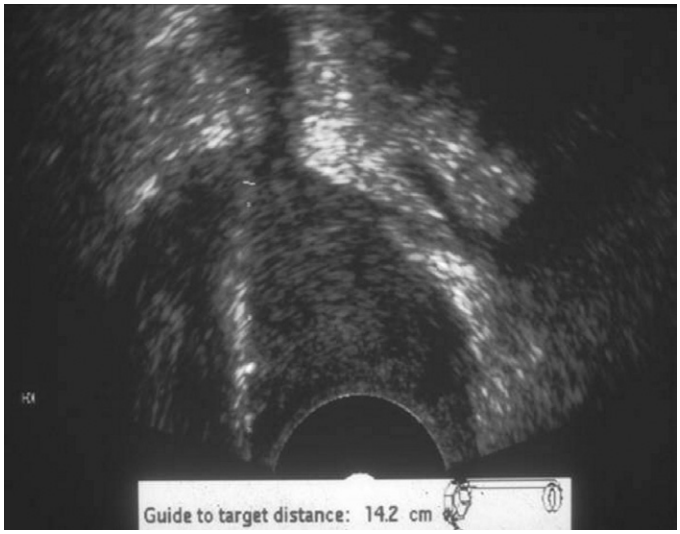


Figure 37.5 Transvaginal scan picture of a biopsy being taken of a solid nodule at the vaginal vault.

The transvaginal route is only semi-sterile but forms a better route of access to collections that may not be infected. It is typically used as a route of drainage for gynaecological tubo-ovarian abscesses. It is not used as a route to access bowel-related collections for fear of creating a colo-vaginal fistula.

Abscesses that contain a large amount of gas may be invisible to ultrasound or at least make differentiating them from bowel loops filled with gas difficult. CT scan is a better way of demonstrating gas-containing lesions (Fig. 37.8).

Method

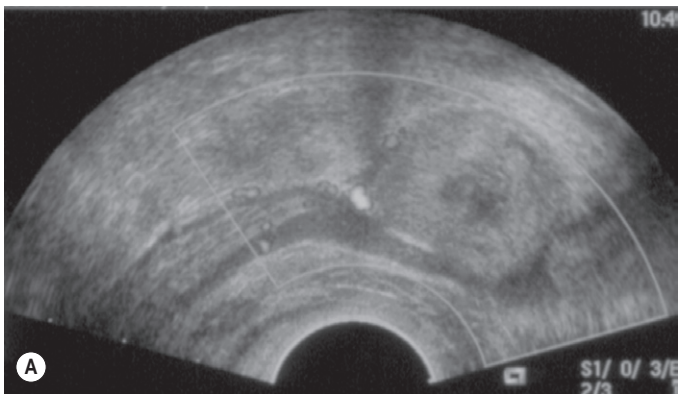
Review of CT or MR imaging is strongly advised as these scans form a reproducible overview of the extent of an abscess and its relationships. These scans help to plan the ultrasound intervention. All patients who have an abscess should be established on antibiotic therapy before any drainage procedure is attempted.

The preparation and technique of transvaginal needle puncture is described in the section above. The woman usually lies supine.

The transrectal route needs no preparation. Cleansing enemas in prostate biopsies have been shown to increase the rates of infection. The patient lies on their left-hand side with their knees curled up toward their stomach. It helps to have an assistant sit where they can be seen by the patient so that they can chat and provide reassurance. The transrectal probe should be covered with a condom and a needle guide affixed. Ultrasound gel provides lubrication of the passage of the probe through the anal canal. The feeling of the probe in the anus is often the part of the procedure that patients like least, particularly younger people. Remember that the rectum angles back toward the sacrum when advancing the probe beyond the anal canal.

Whether the transrectal or transvaginal route is used, the primary objective is to identify the abscess. Once found, the best position of the probe needs to be determined. It should be possible to position the probe so that there is only either rectal or vaginal wall between the probe and the lesion. Colour Doppler is used to locate and avoid any large blood vessels. Local anaesthetic is not usually required and, if given, is difficult to accurately position.

There are two ways to introduce a drainage catheter: over a guide-wire using the Seldinger technique or by direct puncture with the drainage catheter. An 8F catheter is usually large enough for most abscesses.



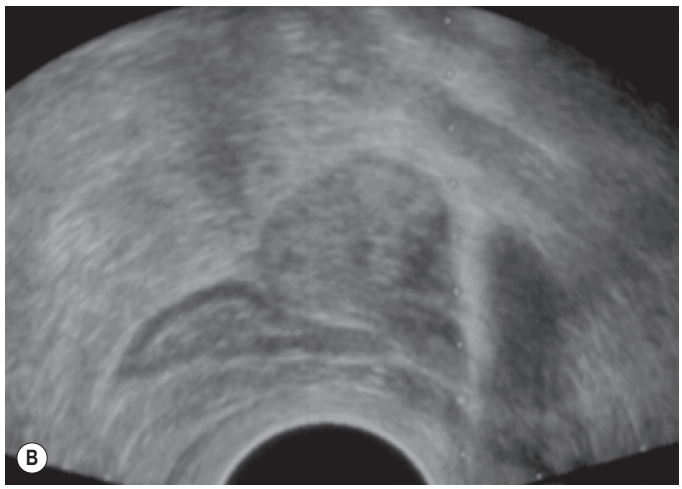
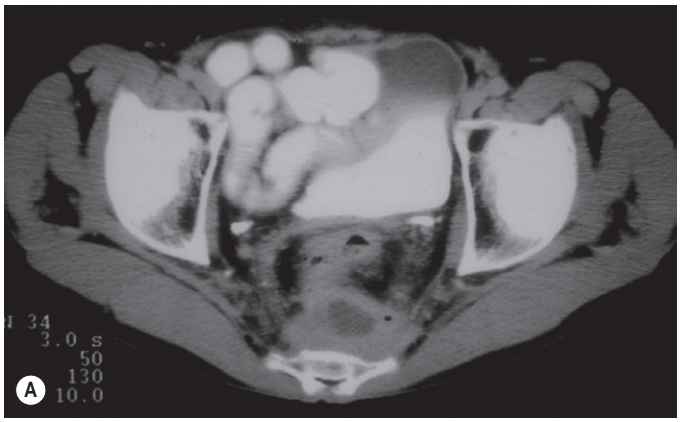
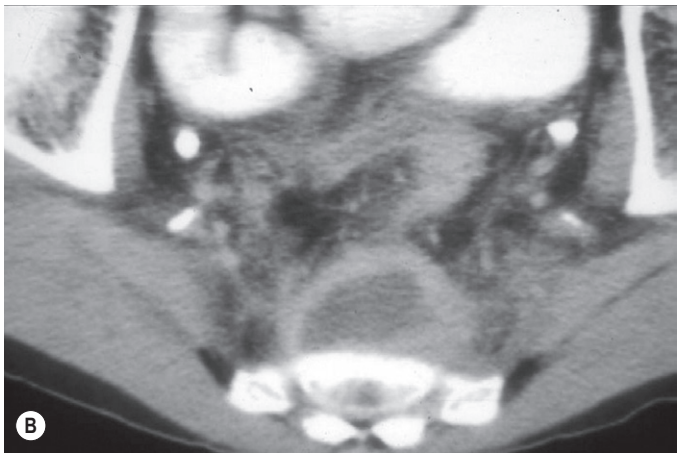


Figure 37.6 A: Rounded serosal tumour deposit on a loop of bowel. **B:** Transvaginal needle biopsy of the mass – note the bright white line from the cavitation artefact caused by firing the needle. A path has been chosen that avoids the bowel lumen.





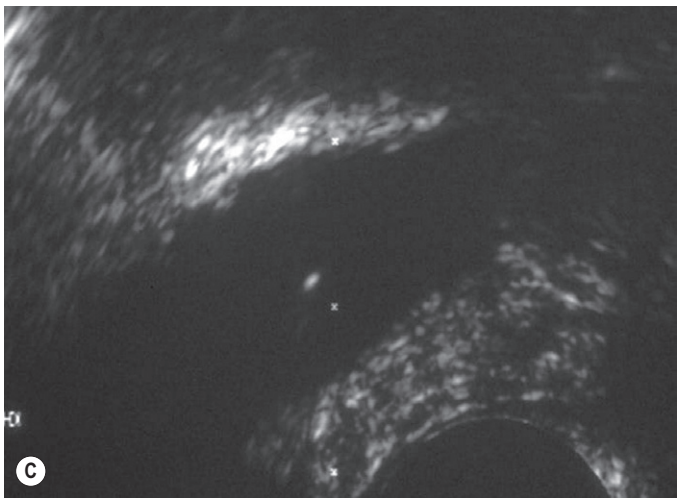
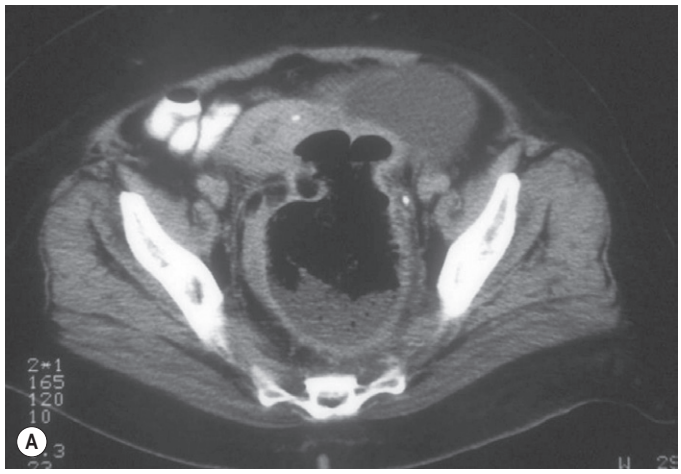


Figure 37.7 Transrectal aspiration of a small presacral abscess. A: Pelvic CT scan showing an abscess in front of the sacrum. Note that bowel and bladder prevent an anterior percutaneous approach to aspiration. A transgluteal approach would be possible but this route can be quite painful. **B:** Magnified view of the presacral abscess on CT. **C:** A transrectal ultrasound image showing the same presacral abscess with a needle tip in its centre. Only a short distance has had to be traversed for the needle to reach the lesion. The ultrasound probe has to be angled posteriorly for the lesion to be visualised.



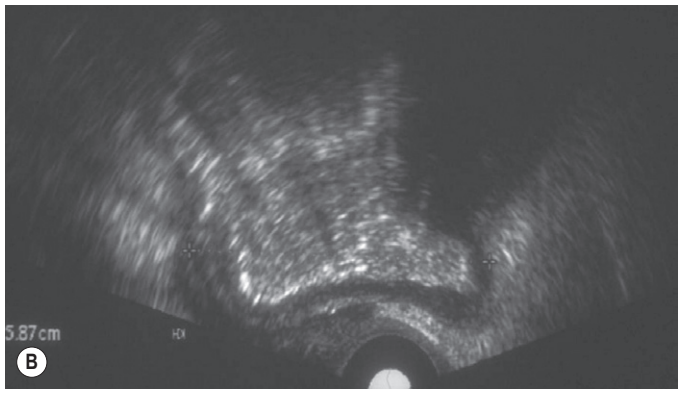




Figure 37.8 Gas makes abscesses hard to see with ultrasound. A: CT scan of a pelvic diverticular abscess containing mostly air. **B:** Transrectal ultrasound scan of the abscess. The gas renders the abscess invisible, leaving a only bright shadowing edge visible. **C:** CT scan of a postoperative pelvic abscess containing an air–fluid level. This abscess can be drained percutaneously using CT guidance. Alternatively, turning the patient so the gas is out of the way allows ultrasound to be used for guidance as well.

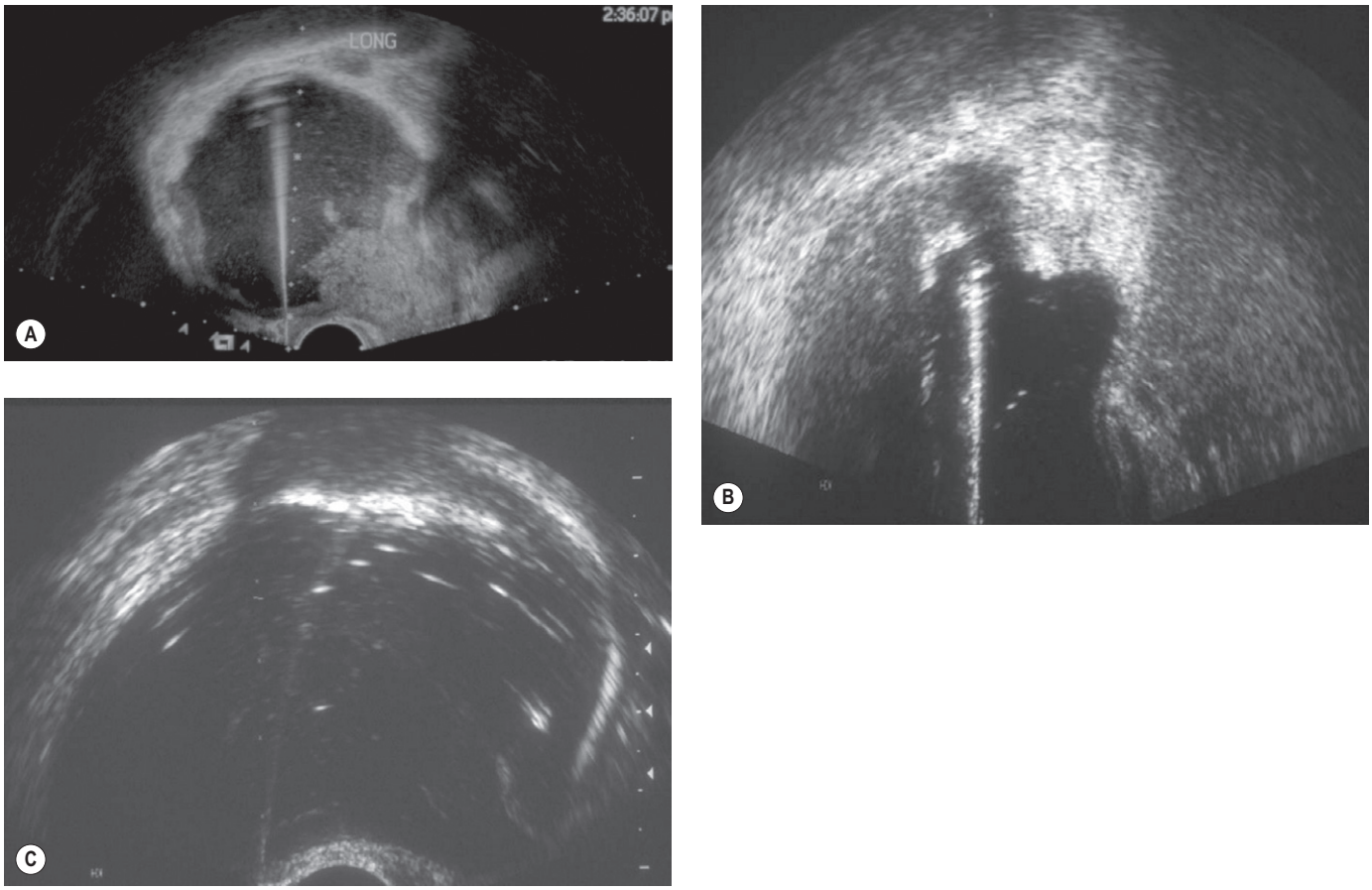


Figure 37.9 Three examples of a guide-wire placed transrectally into an abscess. A: Tumour related abscess. The wire is easily visible. **B:** Post-bowel-surgery abscess. The ultrasound probe is in the residual rectal stump. **C:** Diverticular abscess. The wire can be seen to be curled within the collection. Note that in all three cases the distance from rectum to the abscess is very small.

The direct puncture technique requires the needle guide to be of a large enough calibre to accommodate the catheter. This can be achieved by fixing a 'peel-away' sheath to the probe with rubber bands rather than using an ordinary needle guide. The path of the catheter through this sheath should be verified in a water-bath before the operator uses it for the first time on a patient. The catheter used should be chosen for its ability to pass through soft tissues without prior dilation and without undue force. The catheter needs to be longer than the sheath. Once the probe is in place and the abscess lined up with the proposed puncture route, the probe is pushed against the abscess to stretch the tissues and allow easier puncture. The catheter is advanced into the abscess. The probe and the peel-away sheath are then withdrawn, leaving the catheter behind. The peel-away sheath has to be peeled away, as its name suggests, in order to allow the catheter to pass through it and remain behind.

The guide-wire technique uses the usual proprietary needle guide to place a 19-gauge sheathed needle into the abscess. The metal needle is withdrawn leaving the outer plastic sheath. A 0.038 inch J guide-wire is passed into the abscess. This guide-wire is easily visible on ultrasound (Fig. 37.9). Once the wire is in place, the probe and guide are withdrawn, leaving the wire behind. Sequential dilators and then the final catheter can be passed over the wire into the lesion. Positioning of the catheter is done by tactile impression. It is important to push the dilators and catheter over the wire in the direction of the initial needle puncture. This ensures that the wire does not buckle out of the abscess and back into the rectum.

It is my experience that the Seldinger technique is the less painful method of introducing a catheter and that conscious sedation is not needed (whereas it may be with the one-step direct puncture method).

Once the catheter is in place, the abscess should be aspirated of pus until it is empty. This provides immediate relief. Spontaneous drainage of an abscess through an 8F catheter is relatively poor and, unless the abscess is aspirated to dryness, the catheter may become dislodged before the abscess has emptied. A transrectal catheter can be expected to become displaced the first time the patient opens their bowels. This does not matter provided the abscess was emptied. If it re-accumulates despite adequate antibiotic therapy, it can always be re-drained.

Pelvic abscess drainage

- CT or MR scans help in planning the intervention.
- Antibiotic therapy must be established before intervening.
- Transvaginal and transrectal routes are a safe, well-tolerated alternative to percutaneous drainage.
- Empty the abscess completely on first placing the catheter.

Complications

Theoretically, septicaemic shock, haematoma, haemorrhage and damage to adjacent organs are all possible. However, the literature does not report any of these events in the absence of blood dyscrasias and if antibiotics have been given.[10–13]

SALINE INFUSION HYSTEROGRAPHY

Rationale

This is the instillation of sterile saline into the endometrial cavity to act as a negative contrast agent in order to help demonstrate endometrial abnormalities. It is a minimally invasive, outpatient procedure designed to reduce the need for hysteroscopy. It is done as an adjunct to normal transvaginal ultrasound and in a department set up to offer the service, only adds 10 or 15 minutes to the appointment time for an ordinary scan. Studies on acceptability have shown that patients prefer saline infusion hysterography over outpatient flexible hysteroscopy.[14,15]

Saline infusion hysterography improves detection of focal endometrial abnormalities, polyps and submucous fibroids (Figs 37.10 and 37.11) and may improve the assessment of depth of invasion in endometrial cancer.

Some centres have advocated ultrasound-directed endometrial biopsy as a way of improving the detection of focal abnormalities over a blind pipelle biopsy.[16] Specific sampling devices have been designed for use during saline infusion hysterography.

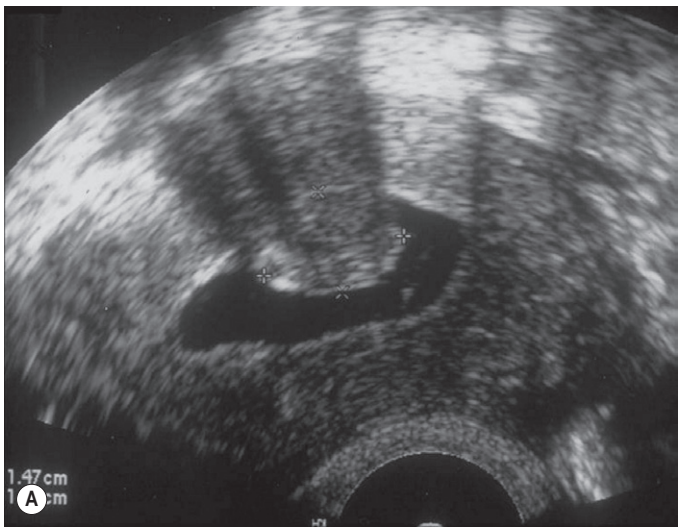
Method

Saline infusion hysterography is best done after menstruation and within the first 10 days of the cycle. If done during menstruation, blood clot may mimic the appearances of a polyp. Later in the cycle the cervix becomes less favourable for passage of a cannula. Most women will have a standard pelvic ultrasound scan done first, by both transabdominal and transvaginal routes. This is to ensure there is not some larger pathology or adnexal mass that might be missed by concentrating just on the endometrium.

A sterile catheter is prepared by attaching a syringe filled with saline to it and flushing it to expel any air. The saline should have been drawn up into the syringe in a slow steady fashion so as not to aerate the saline and render it opaque to ultrasound. Special hysterosonography catheters are made by several manufacturers; these come with a balloon that can be inflated to retain the catheter in the uterus and to prevent leakage of saline out through the cervical os (Fig. 37.12). They are relatively expensive. An alternative is to use a simple 6F infant feeding tube (which costs about 15 pence). The disadvantage of this is that without a balloon to hold it in place it may dislodge and saline might leak so fast through the os that the cavity is not distended. Women tolerate the simple tube better



Figure 37.10 Saline infusion hysterography picture of increased endometrial thickness.



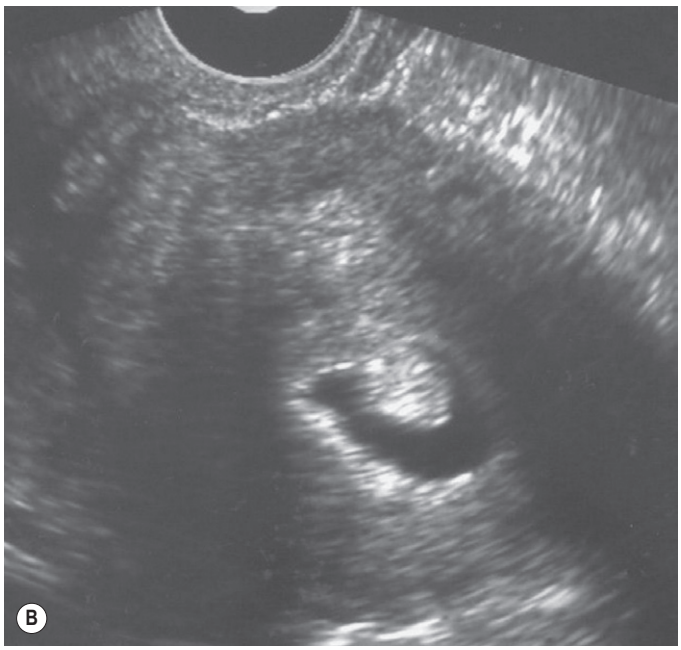


Figure 37.11 Pathology visible on saline infusion hysterography. A: Saline outlines a submucosal fibroid. Note that most but not all fibroids appear relatively echo-poor. **B:** Saline outlines an endometrial polyp. Note that most but not all polyps appear relatively echo-bright.

than the balloon catheter and it will be successful in 80% of examinations. If not, a balloon catheter can then be placed.

The woman lies supine, usually with her bottom raised on a wedge or pillow. A speculum is advanced into the vagina to allow visualisation of the cervix. The cervix is cleaned with povidone-iodine. If there are symptoms or signs of vulval or vaginal infection the procedure should not be done. The pre-prepared catheter is introduced through the cervix into the endometrial cavity. It may be necessary to grip the cervix and pull it down in order to straighten out the cervical canal and allow passage of the catheter. Occasionally a sound needs to be passed to dilate the cervix prior to catheter placement. The speculum is withdrawn, leaving the catheter in place. A standard transvaginal ultrasound probe is inserted in order to visualise the uterus. A few millilitres of saline are injected into the endometrial cavity whilst transvaginal ultrasound images are obtained.

If a balloon catheter is used, it may be necessary to deflate the balloon to allow visualisation of the full endometrial cavity. The balloon can otherwise obscure endometrial pathology.

The same technique can be used to instil a positive contrast agent to outline the fallopian tubes in women with delayed conception (Fig. 37.13).

Complications

Ascending infection, intravasation of saline and abdominal cramping pain are potential complications.

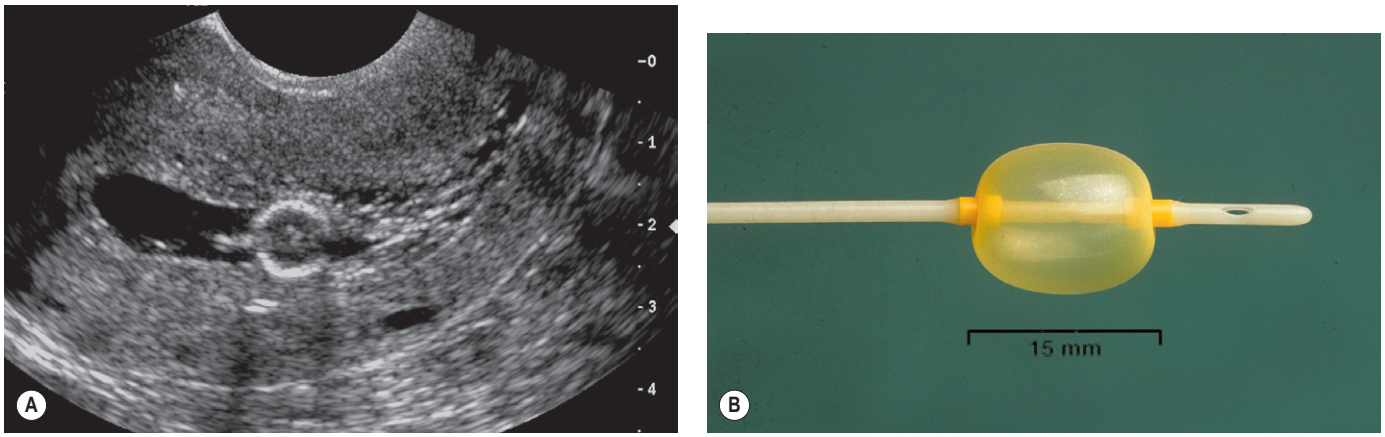


Figure 37.12 Saline infusion hysterography. A: Longitudinal transvaginal ultrasound view of the uterus. The endometrial cavity is distended with saline. The balloon of the catheter is visible in the cavity. **B:** View of the tip of a hysterography catheter with its balloon inflated.



Figure 37.13 A: Transvaginal ultrasound longitudinal view of a proliferative phase endometrium that appears to contain small cystic spaces. **B:** Transverse view of the same uterus with saline in the endometrial cavity. The small cyst is proven to be in the endometrium. Note the dense acoustic shadow cast by the infant feeding tube used as the hysterography catheter. **C:** Positive contrast agents can also be instilled in order to check fallopian tube patency. The contrast in the endometrial cavity casts a shadow that would obscure any endometrial detail. The contrast does, however, reveal the fallopian tube exquisitely.

REFERENCES

1. Spencer JA, Anderson K, Weston M, et al. Image guided biopsy in the management of cancer of the ovary. Cancer Imaging 2006;6:144–147.
2. Hewitt MJ, Anderson K, Hall GD, et al. Women with peritoneal carcinomatosis of unknown origin: efficacy of image-guided biopsy to determine site-specific diagnosis. Br J Obstet Gynaecol 2007;114:46–50.
3. Fischerova D, Cibula D, Dundr P, et al. Ultrasound guided tru-cut biopsy in the management of advanced abdomino-pelvic tumours. Int J Gynecol Cancer 2007 Aug 30, epub.
4. Que Y, Wang X, Liu Y, et al. Ultrasound-guided biopsy of greater omentum: an effective method to trace the origin of unclear ascites. Eur J Radiol 2008 Mar 5, epub.
5. O'Connell AM, Keeling F, Given M, et al. Fine-needle trucut biopsy versus fine-needle aspiration cytology with ultrasound guidance in the abdomen. J Med Imaging Radiat Oncol 2008;52:231–236.
6. Bret PM, Guibaud L, Atri M, Gillet P, et al. Transvaginal US-guided aspiration of ovarian cysts and solid pelvic masses. Radiology 1992;185:377–380.
7. Zanetta G, Lissoni A, Torri V, et al. Role of puncture and aspiration in expectant management of simple ovarian cysts: a randomised study. BMJ 1996;313:1110–1113.
8. O'Neill MJ, Rafferty EA, Lee SI, et al. Transvaginal interventional procedures: aspiration, biopsy and catheter drainage. Radiographics 2001;21:657–672.
9. Zanetta G, Trio D, Lissoni A, et al. Early and short-term complications after US-guided puncture of gynecologic lesions: evaluation after 1000 consecutive cases. Radiology 1993;189:161–164.
10. Alexander AA, Eschelman DJ, Nazarian LN, Bonn J. Transrectal sonographically guided drainage of deep pelvic abscesses. AJR Am J Roentgenol 1994;162:1227–1232.
11. Ryan RS, Mcgrath FP, Haslam PJ, et al. Ultrasound-guided endocavitary drainage of pelvic abscesses: technique, results and complications. Clin Radiol 2003;58:75–79.
12. Nielsen MB, Torp-Pedersen S. Sonographically guided transrectal or transvaginal one-step catheter placement in deep pelvic and perirectal abscesses. AJR Am J Roentgenol 2004;183:1035–1036.
13. Sudakoff GS, Lundeen SJ, Otterson MF. Transrectal and transvaginal sonographic intervention of infected pelvic fluid collections: a complete approach. Ultrasound Q 2005;21:175–185.
14. Rogerson L, Bates J, Weston M, Duffy S. A comparison of outpatient hysteroscopy with saline infusion hysterosonography. Br J Obstet Gynaecol 2002;109:800–804.
15. Van den Bosch T, Verguts J, Daemen A, et al. Pain experienced during transvaginal ultrasound, saline contrast sonohysterography, hysteroscopy and office sampling: a comparative study. Ultrasound Obstet Gynecol 2008;31:346–351.
16. Gorlero F, Nicoletti L, Lijoi D, et al. Endometrial directed biopsy during sonohysterography using the NiGo device: prospective study in women with abnormal uterine bleeding. Fertil Steril 2008;89:984–990.

CHAPTER

38

Ultrasound assessment of fertility

Stephen R. Killick

INTRODUCTION 730

CAUSES OF SUBFERTILITY 730
Endometriosis 730
Congenital uterine abnormalities 731
Uterine fibroids 731
Osseous metaplasia of the endometrium 732
Endometrial polyps 733
Hydrosalpinges 733
Polycystic ovaries and PCOS 733

HYSTEROSALPINGO-CONTRAST SONOGRAPHY FOR TUBAL PATENCY 734

SCANNING THROUGH AN IVF CYCLE 735
Downregulation 735
Follicular development 736
Oocyte capture 736
Embryo transfer 737
Ovarian hyperstimulation syndrome (OHSS) 738

INTRODUCTION

Specialists in reproductive medicine have come to rely heavily on ultrasound imaging, and IVF units incorporate their own dedicated ultrasound machines and ultrasonographers. Vaginal transducers are used almost exclusively in reproductive medicine because the close apposition of the reproductive organs to the vaginal fornices enables probes of high frequency and hence higher resolving power to be used. Serial observations of graafian follicle development within the ovary allow functional as well as structural assessments. Ovarian and uterine images are used as an aid to diagnosis, as a way of educating and counselling patients, and, characteristically, as a way of determining the functional response to treatment.

The management of subfertile couples begins with an assessment of the expected chances of natural conception given the ages, medical history, and lifestyle of both partners. Many couples retain an unrealistic expectation of their chances of conception.

The most informative way to display chances of conception is with the use of cumulative pregnancy rates (Fig. 38.1). No couple ever has a chance of conception greater than 1 in 3 per month and in population studies the chance of pregnancy is on average only 91% in the first year of trying.[1] Although there is some evidence that the incidence of infertility is decreasing in the developed world,[2] there is still a huge unmet need for medical services for subfertile couples.[1] The definition of infertility is usually taken to be lack of conception after one year of unguarded intercourse, although such a strict interpretation may not be clinically useful and in this chapter the term subfertility will be used to indicate a reduced chance of conception compared with what might be expected for a couple of given age and lifestyle.

CAUSES OF SUBFERTILITY

Subfertility may result from abnormalities in three general areas: the ejaculate, the ovulatory process, or pathology within the fallopian tubes and/or uterus. It is common to find a combination of these three factors in any one couple and there is also a significant proportion of couples for whom no obvious cause can be found for their inability to conceive (Fig. 38.2).

It is possible to use ultrasound as a way of diagnosing ovulation. Follicle rupture is said to have occurred if the diameter of the dominant ovarian follicle suddenly reduces to less than half its size within 24 hours.[3] However, in order to observe such an occurrence frequent scanning is obviously necessary, usually twice daily for several days, and hence the technique is limited to research applications. Moreover follicle rupture may occur without progesterone production and progesterone production may occur without follicle rupture (a luteinised unruptured follicle).[3,4]

The main diagnostic role of ultrasound is in determining the anatomy of the uterus and, in particular, the patency of the fallopian tubes.

Endometriosis

The classical ground glass appearance of endometriotic deposits is described in detail in Chapter 35 (Fig. 38.3) although it is worth mentioning that the majority of endometriosis will not be visible with ultrasound. However, small deposits may exhibit acute peritoneal tenderness or lead to quite dense fibrosis. Therefore note should be taken of areas within the pelvis that are tender to the vaginal probe or that do not exhibit the usual tissue compliance.

The significance of endometriosis from the reproductive point of view is far from simple. Endometriosis is common in women with normal fertility, but even more common in women with subfertility. Extensive deposits can, of course, cause considerable distortion to the pelvis or block the fallopian tubes completely. Ovarian endometriomas are thought to interfere with the process of ovulation and possibly affect the quality of the oocyte[5] but in the vast majority of cases the association between minimal endometriosis and subfertility remains unexplained. In the only randomised double-blind placebo-controlled study to address the problem,[6] laparoscopic destruction of minimal endometriosis was shown to improve fertility in subfertile women, but to nowhere near normal levels and to much less than could be achieved by IVF. The implication is that whatever results in pelvic endometriosis also results in subfertility and that treatment of the endometriosis does not eliminate what caused it to occur in the first place. It is pragmatic, in the light of current knowledge, to place cases of subfertility with minimal endometriosis in the 'unexplained' aetiological category.

The decision as to whether to surgically remove endometriotic deposits as part of a programme of fertility treatment is hence complex and should be taken on an individual patient basis. The ultrasonographer can help by determining the size and exact anatomical location of all deposits, and to determine whether these correspond to sites of any pelvic pain.

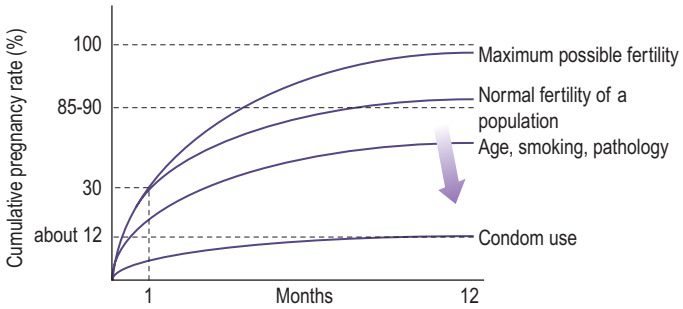


Figure 38.1 Cumulative pregnancy rates for a given population and factors which reduce the chances of conception.

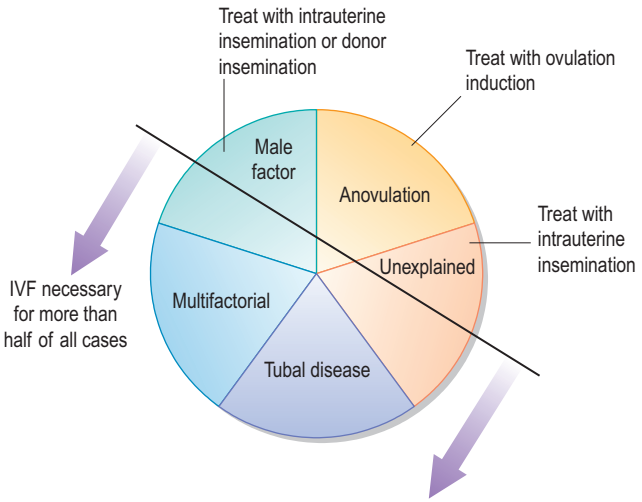


Figure 38.2 Pathology leading to reduced fertility and the treatments used in each case. Each category accounts for roughly a fifth of referrals to most clinics. IVF is the treatment of choice for more than half of all cases, giving a pregnancy rate in the region of 1 in 3 for women under 35 years. In order to decide on appropriate treatment, ultrasound (or an alternative technique) needs to be used to determine tubal patency in all cases except severe male factor, when IVF is the treatment of choice regardless of any coincident tubal disease.

Subfertility

- Some 10% of couples in any population fail to conceive during one year of trying.
- No couple ever has more than a 1 in 3 chance of conception per month.
- Age and lifestyle of both partners are major determinants of fertility.
- A significant proportion of couples have no detectable pathology to account for their subfertility.
- IVF is the most appropriate treatment for over half of the couples referred to a tertiary centre with infertility.
- Ultrasound imaging provides a good opportunity to educate and counsel couples about their problem.

Congenital uterine abnormalities

Abnormal Müllerian fusion and the multiple possible anatomical variants of the uterus that may result are described in Chapter 34. Although some congenital uterine anomalies undoubtedly have an effect on reproductive outcome by increasing the risk of miscarriage or preterm delivery,[7,8] any effect on the chances of conception is much more difficult to assess[9] because the anomalies are so variable, they are often associated with other pathology which might in itself affect fertility and their true prevalence in the general population is unknown. Even gross abnormalities such as complete uterine and vaginal septum may have little effect on fertility,[10] whereas minor anomalies such as arcuate uterus may be seen more frequently in subfertile women than in those presenting for other reasons.[11] Uterine anomalies are often associated with other relevant pathology which can be visualised during an ultrasound examination, including renal tract abnormalities and endometriosis.

The detection of uterine anomalies is one of the rare instances when the use of 3D ultrasound is a definite advantage. The coronal view of the uterus obtained by a 3D vaginal scan enables a clear comparison of the left and right sides, a transverse view of the fundus, and an appreciation of the shape of the uterine cavity. Such a view is particularly useful for the assessment of arcuate anomalies and septa (Fig. 38.4).

The vascularity and relative muscular and fibrous tissue components of uterine septa may influence their effect on reproductive function, and 3D ultrasound and Doppler assessments of these components may be helpful.[12]



Figure 38.3 A transverse view through the uterus and an adjacent ovarian endometrioma. A HyCoSy is being performed and contrast is seen in the distal end of the fallopian tube and spilling beneath the ovary. An endometrioma of this size is likely to reduce the chances of fertility despite patent fallopian tubes. B, balloon of catheter in uterine cavity; E, endometrioma; S, spill of contrast medium.

Uterine fibroids

Uterine fibroids are the commonest human tumour, with up to 70% of uteri eventually harbouring at least small examples.[13] Many women conceive and deliver normally without ever knowing they have fibroids, although as the tumours grow with age they are more likely to have an influence on the ability to conceive, particularly if they are submucous and encroach into the endometrial cavity.[14] The quantitative influence of fibroids on natural fertility is difficult to calculate but submucous fibroids may reduce pregnancy rates following IVF by up to 70%,[15] even when good quality embryos are obtained. The endometrium overlying fibroids is thought to be less able to support implantation and it is easy to imagine how a pedunculated fibroid could impair implantation by moving around within the uterine cavity.

The visualisation of submucous fibroids is enhanced by introducing a negative contrast agent such as saline into the uterine cavity[16]

(Figs 38.5A and B). The exact anatomical location of the fibroid, its size, the extent it protrudes into the cavity and the thickness of the overlying myometrium are all important when considering whether to undertake hysteroscopic myomectomy in order to enhance fertility.[17]

Osseous metaplasia of the endometrium

Osseous metaplasia of the endometrium is a rare condition, often occurring many years after a failed pregnancy, but the ultrasound appearances are characteristic. Small bony deposits within the uterine cavity create a hyper-reflective endometrium[18] with shadowing (Fig. 38.6). The cavity is indistensible when saline is injected

Fibroids

- Up to 70% of women will develop uterine fibroids.
- Submucous fibroids lower the chances of pregnancy from IVF by 70%.
- Hysteroscopic myomectomy can improve pregnancy rates.
- Fibroid size, position and overlying myometrium thickness determine whether hysteroscopic myomectomy can be performed.
- Saline infusion is essential for precise imaging of intrauterine pathology.

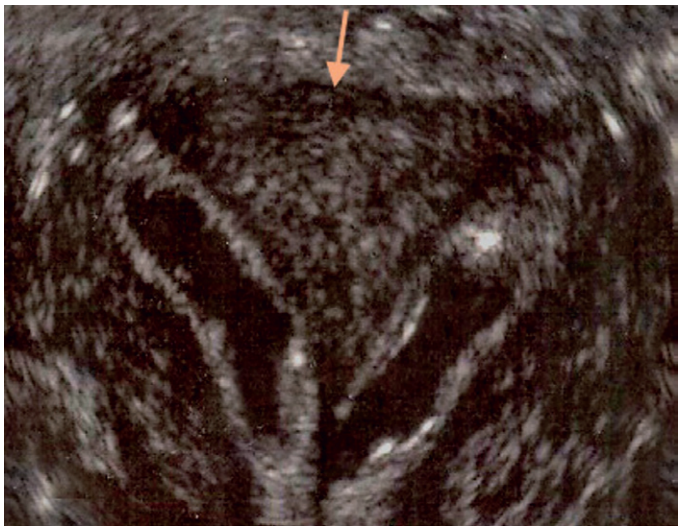


Figure 38.4 Coronal view of a septate uterus generated by 3D imaging. Saline has been instilled into the cervix and has filled both sides of the uterine cavity. There is no concave depression in the fundus (arrow), indicating that this is a septum and not two separate uteri. Hysteroscopic removal is therefore relatively simple but the advantage for fertility is unproven.



Figure 38.6 Osseous metaplasia of the endometrium. Note the extensive shadowing resulting from the bony deposits within the endometrium. An attempt at saline infusion did not distend the endometrium and resulted in pain for the patient. First published R-ITI copyright RCR.

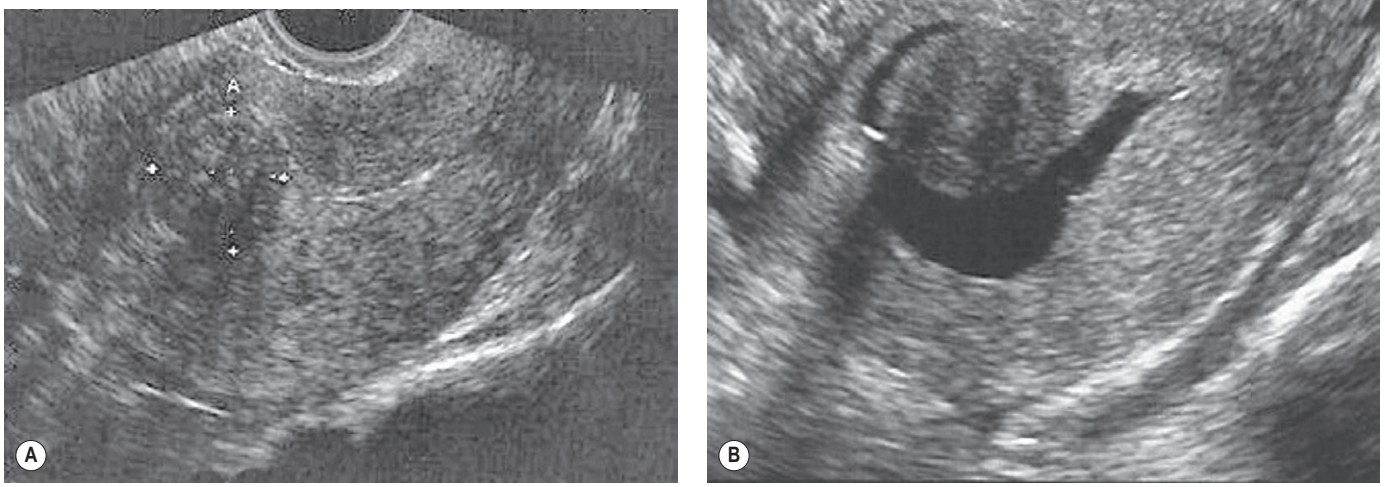


Figure 38.5 Submucous fibroid. Longitudinal views of the uterus showing a fundal fibroid **(A)** before and **(B)** after the instillation of saline into the uterine cavity. Saline infusion enables the fibroid to be seen as totally submucous and therefore comparatively easy to remove hysteroscopically. It is also possible to see the indentation created by the fibroid in the posterior endometrium. First published R-ITI copyright RCR.

and this may result in considerable pain for the patient. Pregnancy rarely occurs unless the deposits are removed hysteroscopically.

Endometrial polyps

Endometrial polyps are histologically similar to the endometrium and retain a little of their hormone sensitivity. Their relevance to implantation is hence far less than that of a submucous pedunculated fibroid. Nevertheless pregnancy rates in response to treatment with intrauterine insemination have been shown to increase after hysteroscopic polypectomy in a prospective randomised study.[19]

As for other intrauterine pathology, saline infusion is helpful for imaging endometrial polyps (Fig. 38.7) and should be utilised if the location and size need to be accurately determined. Polyps adjacent to the ostium of the fallopian tube may have a greater effect on fertility than those situated elsewhere.[20] Small polyps may only be apparent during a single ovarian cycle and therefore surgical removal should only be considered if the polyp persists after menstruation.



Figure 38.7 A small endometrial polyp on the posterior wall of the uterine cavity delineated by saline infusion. Such a polyp is of doubtful significance for fertility.

Hydrosalpinges

A hydrosalpinx results when the distal end of the fallopian tube becomes occluded by chronic infection. The walls of the fallopian tube initially thicken and the tube becomes swollen and oedematous, but with continued tissue destruction, probably over several years, the walls become devoid of muscle and the whole tube expands into a retort-shaped bag of fluid (Fig. 38.8B).

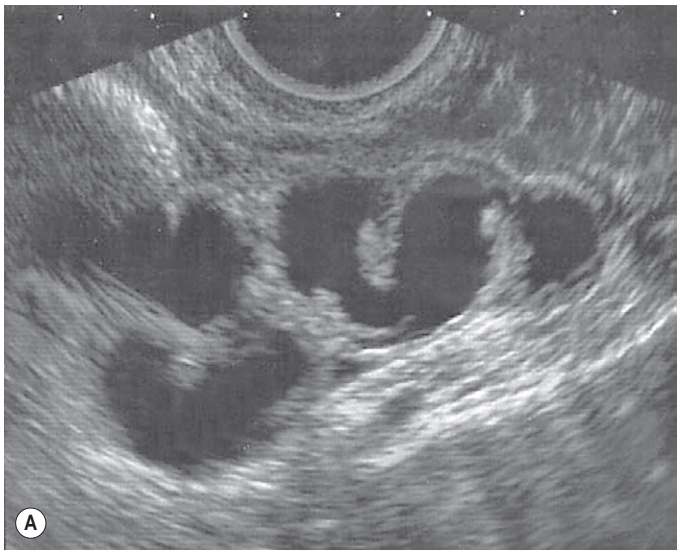
Quite apart from their obvious block to natural conception, hydrosalpinges lower implantation rates following IVF by 50%.[21] The presumed mechanism is the gradual leakage of small volumes of hydrosalpingeal fluid through the uterine end of the fallopian tube into the uterine cavity where it is embryotoxic and/or interferes with implantation. Either placing a clip on the fallopian tube adjacent to the uterus or removing the tubes completely at laparoscopy restores IVF pregnancy rates to those that would be expected in women without hydrosalpinges.[22] An alternative approach is to aspirate the hydrosalpinx under ultrasound control at the time of oocyte capture.[23]

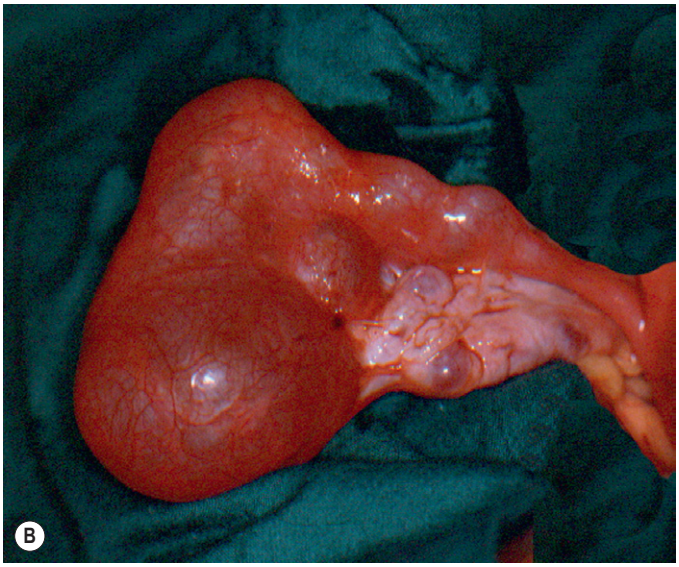
Hydrosalpinges are usually easy to identify with ultrasound (Fig. 38.8A). Their fluid content and hence their size may vary throughout the menstrual cycle and occasionally they may only become apparent during ovarian stimulation, when serum hormone levels are particularly high. If the fallopian tube expands into a hydrosalpinx when contrast is injected during HyCoSy (see below), there is a high risk of stimulating a recurrence of the pelvic infection and antibiotics should be prescribed.

Polycystic ovaries and PCOS

Polycystic ovarian syndrome (PCOS) is a poor term for women who have a particular ultrasonic appearance of their ovaries and disordered ovarian physiology, probably as a consequence of disordered carbohydrate metabolism, which can be recognised as insulin resistance. Such women may suffer with obesity, oligomenorrhoea, hirsutism and a number of long-term health risks such as cardiac ischaemia, type 2 diabetes and uterine carcinoma. Although the typical ovarian appearance of multiple small antral follicles arranged peripherally in an enlarged ovary with abundant stroma (Fig. 38.9) is one of the diagnostic criteria for the syndrome, other criteria must also be present for the diagnosis.[24]

There are many women whose ovaries appear polycystic but who do not have the syndrome.[25] However, such an ovarian appearance in an otherwise asymptomatic woman may not be without





Figures 38.8 Hydrosalpinges, how they typically appear **(A)** ultrasonographically and **(B)** at operation. First published R-ITI copyright RCR.

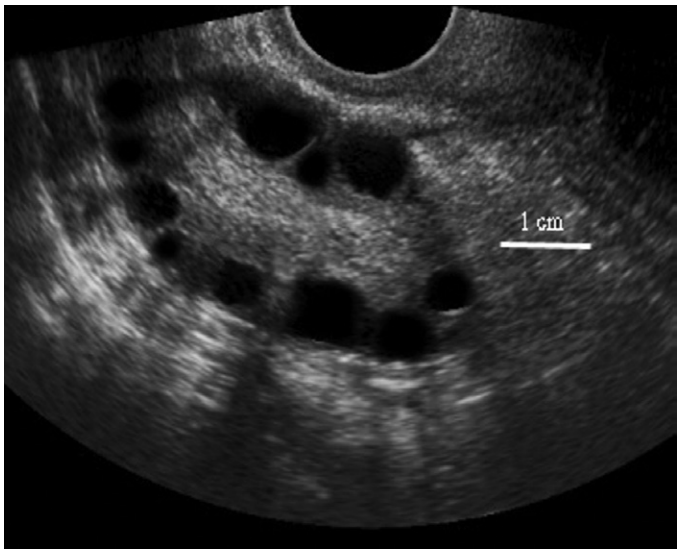


Figure 38.9 An ovary showing characteristic polycystic morphology: a volume greater than 10 cm^3, more than 12 follicles (11 seen in this plane) of less than 10 mm diameter situated peripherally (the so-called 'ring of pearls') around an increased body of stroma of increased echogenicity.

Polycystic ovaries

- Polycystic ovary morphology includes:
  - an ovarian volume of greater than 10 cm^3
  - at least 12 follicles of less than 10 mm diameter
  - a third of the volume is made up of stroma
  - the stroma appears hyper-reflective.
- Women with polycystic ovaries do not necessarily have the polycystic ovary syndrome.
- Not all polycystic ovaries are anovulatory.
- Women with polycystic ovaries are more likely to suffer ovarian hyperstimulation syndrome when stimulated to ovulate.

significance as the response to ovulation induction may be exaggerated and risk ovarian hyperstimulation (see below). The 'cysts' are functioning small antral follicles and can be stimulated to develop by fertility treatment.

The precise definition of what constitutes a polycystic ovarian appearance has changed over the years as ultrasound resolving power has increased. Current consensus[26] requires either ovary to have 12 or more follicles of less than 10 mm diameter or an increased ovarian volume of greater than 10 cm^3. Polycystic ovaries may ovulate, albeit intermittently, and a transient preovulatory follicle or a corpus luteum may temporarily enlarge the volume measurement and hence necessitate a second assessment in the early follicular phase if the diagnosis is in doubt.

Polycystic ovaries also have other distinguishing features. More than a third of their volume is stroma.[27] This increased stroma is the feature which primarily distinguishes polycystic ovaries from the multifollicular appearance seen during puberty and in hypothalamic amenorrhoea,[28] and appears to be functionally relevant as its volume correlates with serum androgen concentrations.[29] The stroma of a polycystic ovary may appear more echogenic than normal (normal is said to be less than that of the myometrium), probably as a result of increased vascularity and enhancement from the fluid in the surrounding small follicles.

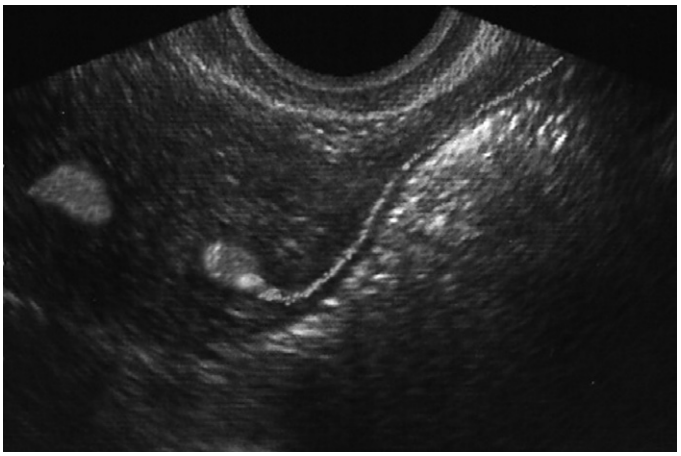


Figure 38.10 HyCoSy. This is a transverse view across the uppermost part of the endometrial cavity with the positive contrast medium Echovist in both cornual regions. Echovist can be seen to pass down the left fallopian tube, which is uncharacteristically straight, but no flow was seen on the right side for several minutes as the tube was in spasm.

HYSTEROSALPINGO-CONTRAST SONOGRAPHY FOR TUBAL PATENCY

The lumen of the fallopian tubes is extremely narrow, being only 1 mm diameter at its intramural part, where it passes from the endometrial cavity through the myometrium. In the non-pathological state there are no fluid interfaces to demarcate the tube and it is completely undetectable by unaided ultrasound.

Although a negative contrast medium is used to delineate the uterine cavity, a positive contrast medium is far superior for demonstrating the fallopian tube lumen. A supersaturated solution of galactose (Echovist, Bayer Schering Plough) was licensed for HyCoSy for many years and virtually all previously published work refers to its use, but it is no longer manufactured. The sulfur hexafluoride contrast agent SonoView (BRACCO) is now widely used although not currently licensed for HyCoSy. Positive contrast agents function because they contain microbubbles, hence they need to be freshly constituted immediately prior to use and become inactive within a short period of time. Their acoustic properties depend to a large extent on the size of the microbubbles.

The technique of hysterosalpingo-contrast sonography is usually abbreviated to HyCoSy. The technique consists of a baseline vaginal scan followed by the insertion of an intrauterine catheter and the gentle instillation of low volumes of contrast agent.[30] The fallopian tubes take up the agent by capillary action and it can be seen to pass along healthy tubes with the minimum of pressure (Fig. 38.10).

HyCoSy has good concordance with other tests of tubal patency although it is usually regarded as a screening test, with laparoscopy and dye as the gold standard. Screening is positive when contrast cannot be seen to pass through one or other of the tubes and in these circumstances a decision needs to be made as to whether to perform a laparoscopy to confirm the diagnosis of tubal obstruction. The sensitivity of HyCoSy screening is very high, approaching 100%, because the passage of contrast down the tube is distinctive and therefore if it is seen the tube is patent.[31] The specificity, however, is in the region of only 80% because the passage of contrast can be masked by bowel gas or just difficult to see in a tortuous tube. The predictive value of a screening test depends on the prevalence of the condition it is designed to screen for. Hence, if all subfertile referrals were to be screened, up to a third of tubes thought to be occluded by HyCoSy will in fact be patent. Nevertheless many unnecessary invasive laparoscopies can be avoided by HyCoSy screening and therefore the UK National Institute for Health and

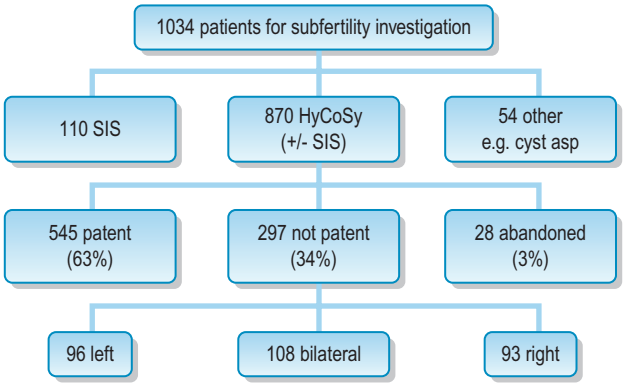


Figure 38.11 Results of HyCoSy and allied procedures in subfertile women over an 8-year period in the author's unit in Hull. All HyCoSy procedures were performed by unaided ultrasonographers. No analgesics other than non-steroidals were necessary and there were no cases of cervical shock. SIS, saline infusion sonogram.



Figure 38.12 3D coronal view of uterus with the positive contrast medium Echovist in the uterine cavity. Contrast could be seen to pass into both fallopian tubes but it is not possible to show the main part of the cavity and the origin of both fallopian tubes in the same plane. Hence only the left tube is shown. The balloon of the catheter is situated in the cervix.

HyCoSy

- There is grade A evidence that HyCoSy is the investigation of choice for all otherwise asymptomatic subfertile women.
- HyCoSy has the sensitivity to detect virtually all cases of fallopian tube occlusion.
- About two-thirds of the fallopian tubes that cannot be shown as patent using HyCoSy are truly occluded.
- A learning curve of up to 50 procedures may be necessary for those who do not have previous experience of vaginal scanning.
- If the semen analysis is abnormal tests of fallopian tube patency are unwarranted as IVF will probably be necessary even if both tubes are patent.
- Fallopian tubes may be diseased even if they are not occluded.

Clinical Excellence, NICE, recommends HyCoSy as the first-line investigation for tubal patency assessment in otherwise asymptomatic women.[32]

The procedure may be uncomfortable, particularly if larger volumes (>5 mL) or undue pressure is used, but in our unit more than 1000 procedures were performed over the first 8 years of our HyCoSy programme without the need for narcotic analgesia or any sort of resuscitation (Fig. 38.11). Pain may be reduced by warming the contrast medium[33] although this will reduce the time over which the medium is stable and effective. Salpingitis following the procedure is rare but the use of prophylactic antibiotics is recommended.

Fallopian tubes are muscular and can go into spasm for several minutes, effectively occluding the tube to the passage of contrast medium. A positive screen is defined as when a tube cannot be demonstrated as patent over a 5-minute period.[30] Some practitioners advocate the use of intravenous anti-spasmodics such as hyoscine but this is no more effective than merely waiting patiently for any spasm to recede.

Fallopian tubes are mobile and can twist and turn in their anatomical path from the uterus to the ovary so the vaginal probe may need to be angled and rotated in order to follow the contrast medium and it may not be possible to show more than a short length of tube at any one time. Doppler or 3D techniques can be employed but add little, if anything, to the diagnostic ability of the procedure, although 3D recordings have an advantage for retrospective reporting and demonstration purposes (Fig. 38.12). Several groups have criticised HyCoSy, either because of poor results or because of significant pain during the procedure. These instances may have been the result of inadequate training because the learning curve is shallow and an experience of up to 50 procedures[30] may be required before consistently reliable reports can be obtained from those who do not previously have experience of vaginal scanning.

Semen analysis should precede any assessment of fallopian tube patency because an abnormal ejaculate might necessitate IVF regardless of tubal status and hence tubal investigation becomes irrelevant. It should also be appreciated that just because a fallopian tube is shown to be patent it is not necessarily completely healthy. The delicate endosalpinx can be damaged by infection without the tube becoming blocked.

SCANNING THROUGH AN IVF CYCLE

During an IVF and embryo transfer (ET) cycle ultrasound is used to check for downregulation, to follow the response of the ovary to superovulation and then to facilitate both oocyte capture and embryo transfer.

Downregulation

During an IVF cycle the pituitary gland must be inhibited from delivering an luteinising hormone (LH) surge, which would result in premature luteinisation. This can be achieved by administering either superagonists or antagonists of gonadotrophin-releasing hormone (GnRH). If superagonists are used the gland is initially stimulated for several days in the luteal phase, and a check must be made that ovarian activity has ceased before superovulation can commence. The first scan in an IVF/ET cycle therefore checks that all the antral follicles within the ovary are small (<9 mm) and that the endometrium is thin (<5 mm).

A record of the antral follicle count at this time can be used to predict the probable number of oocytes which will be obtained during the cycle[34] and help to decide on the initial dose of follicle-stimulating hormone (FSH). Antral follicle counts reflect the number of oocytes remaining in the ovaries (the ovarian reserve) and hence the likely response to treatment and the likelihood of an early menopause.[35]

Follicular development

Ovarian follicular development during superovulated IVF treatment is stimulated by FSH injections. Once a cohort of follicles has emerged their growth is usually about 2 mm diameter every 24 hours. Ultrasound is used to determine the number and size of all follicles. In a superovulated ovary with as many as 10 follicles of different sizes crammed together, follicle shape is rarely spherical and a standard measure of size is necessary. Although linear measurements can be performed in all three planes or volume measurements determined by 3D imaging, this can be difficult and time-consuming and a reproducible standard is the mean follicle diameter as determined by the mean of the longest diameter and the diameter at right angles at the midpoint of the first measurement (Fig. 38.13). Serum oestradiol can be measured at intervals but is proportional to follicle growth (most precisely to the sum of the squared diameters because oestradiol must defuse out through the follicle basement membrane and diffusion is dependent on area) and hence adds little to the decisions which need to be made about FSH dose and the timing of the ovulatory trigger. A recent Cochrane review has not shown any improvement in pregnancy rates by adding routine serum oestradiol monitoring to ultrasound follicle monitoring.[36]

Patients progressing through IVF treatment often find the process stressful.[37] The ultrasonographer has an opportunity during the scanning sessions to provide support and counselling. This opportunity should not be missed. The male partner should be present during the scans. An explanation of the images and of the physiological processes taking place add to a couple's knowledge and understanding.

An ovulatory trigger in the form of human chorionic gonadotrophin (hCG) or LH is given when the majority of follicles are thought to be mature, usually when the lead follicle is about 20 mm diameter, so as to finalise the maturation of each oocyte ready for fertilisation.

The average number of oocytes harvested during a superovulated IVF cycle is about 10 or 11, but especially in younger women or in women with polycystic ovaries many more large antral follicles may develop and serum oestradiol levels may rise to 20 or 30 times the values seen during a spontaneous ovulatory cycle. It is important to recognise such an over stimulated ovary as early as possible because when the ovulatory trigger of hCG is given it can result in ovarian hyperstimulation syndrome (see below). There is, however, no precise definition of when an ovary is over-stimulated and risks of hyperstimulation syndrome must be carefully assessed in each case. The ovulatory trigger is withheld and the treatment cycle abandoned if more than a certain number of follicles develop and the risk of hyperstimulation syndrome becomes too high. An alternative approach is to 'coast' the ovary by continuing down-regulation whilst omitting FSH for several days.[38] The serum oestradiol may be a slightly better predictor of the risk of hyperstimulation syndrome and coasting is usually continued until oestradiol levels fall below an agreed threshold, usually about 10 000 pmol/L.

Ultrasound is also used to monitor ovulation induction in treatment cycles other than IVF, where the aim is to achieve conception by means of natural intercourse or intrauterine insemination. In these cases there is a risk of a multiple gestation if more than one pre-ovulatory sized follicle develops and so the assessment of follicle size and number is critical. Follicles greater than 14 mm in diameter are capable of ovulating viable oocytes leading to pregnancy[39] and if several such follicles develop it is necessary to withhold the ovulatory trigger and any further treatment, and for the couple to refrain from intercourse until the follicles regress.

Oocyte capture

Vaginal ultrasound with conscious sedation is by far the most common method of harvesting mature oocytes for IVF. Previous ultrasound approaches have been transvesical, perurethral and transcutaneous directly into the peritoneal cavity. These approaches may occasionally be necessary with ovaries congenitally or surgically displaced within the peritoneum. The procedure can also be performed under general anaesthesia if necessary.

A single or, more usually, double lumen needle is passed through a guide attached to the vaginal probe, through the lateral fornix of the vagina, through the peritoneum and into the ovary, its path indicated by a computer-generated line on the display (Fig. 38.14). The antral fluid of each follicle is aspirated and immediately

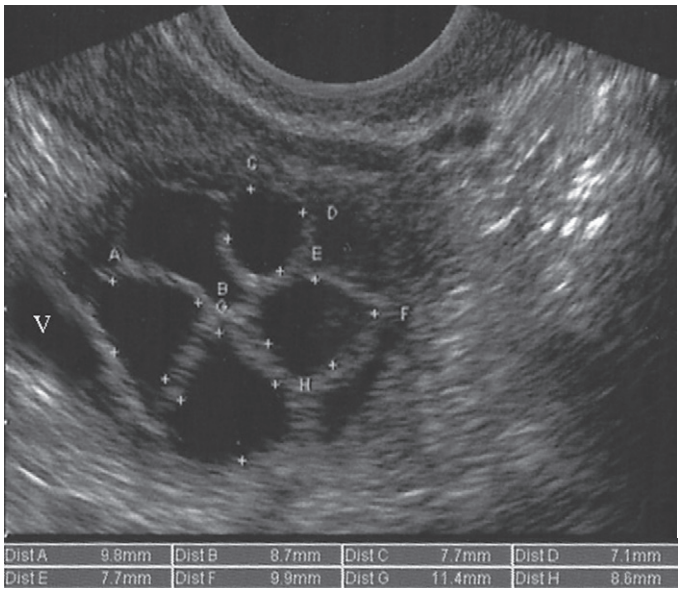


Figure 38.13 Image of a superovulated ovary showing the characteristic cartwheel appearance and multiple measured follicles. V, iliac vein.

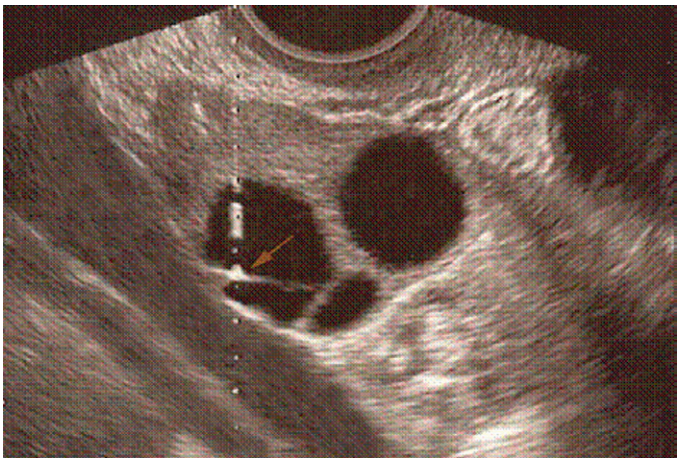


Figure 38.14 Oocyte capture. The superovulated ovary lies adjacent to the iliac vein and is seen actually indenting its wall. The iliac artery is seen beneath the vein. The oocyte capture needle has followed its projected path (the dots are 1 cm apart) and would now lie within the vein if it were not for the ovary. The tip of the needle is indicated with an arrow.

examined microscopically to identify the oocyte encased within its cumulus of granulosa cell. The antrum may need to be flushed with culture medium several times to obtain the oocyte.

There are several ways in which the quality of oocytes captured during IVF may be predicted. Oocytes from follicles less than 10 mm diameter are more likely to be immature and less likely to fertilise. Power Doppler can be used to visualise the neovascularisation around the follicle. Oocytes may be of a higher quality and more likely to lead to pregnancy if the vascularity extends around all four quadrants of the follicle.[40] In practice this is rarely performed because pregnancy can occur from oocytes from relatively poorly vascularised follicles so the measurement does not influence clinical decision.

Considering the adjacent bowel and blood vessels (Fig. 38.14) and the fact that the vagina is not disinfected prior to the procedure, it is reassuring that complications following vaginal oocyte capture are remarkably rare, being quoted as 0.42%.[41] Pelvic infection may occur, sometimes delayed for several days after the procedure, more commonly after an endometriotic cyst or hydrosalpinx has been drained at the same time and hence these procedures are best performed on a separate occasion.

Embryo transfer

Oocytes are fertilised in vitro and transferred through the cervix into the uterine cavity as a two- to eight-cell embryo 2 or 3 days later or as a blastocyst 5 days later. The technique of embryo transfer has a major influence on outcome and hence ultrasound has been utilised to try to minimise uterine stimulation and ensure correct embryo placement near the fundus.

There is ultrasound evidence to demonstrate why the technique of embryo transfer is so critical. Time lapse ultrasonic video imaging has shown that any uterine stimulation, such as touching the fundus with the embryo catheter or attaching a tenaculum to the cervix, at the time of ET is associated with an increase in uterine junctional zone contractions,[42] which can either expel embryos through the cervix or force them up into the fallopian tubes.[43] Such fallopian relocation probably occurs quite commonly after ET as some 4% of IVF pregnancies are tubal ectopics. An interesting historical note is that the first ever IVF pregnancy, before Louise Brown, was ectopic. Uterine junctional zone contractions have been shown to correlate inversely with the chances of successful implantation.[44]

Transvesical views can be used to watch the transcervical catheter deliver the embryos. The embryos are held within the catheter by two air bubbles which can be seen in the uterine cavity after the embryos have been expelled (Fig. 38.15). It is also possible to see a small vortex of fluid at the moment the embryos are expelled from the catheter. Whether it is helpful to perform ET under ultrasound control or not is controversial. Some publications have shown that such ultrasound guidance can increase implantation rates but a large prospective double-blind carefully controlled study has shown no effect,[45] at least not when ultrasound guidance is used routinely. It may be that if a careful assessment of uterine cavity length and direction is undertaken early in an IVF cycle (often referred to as a 'mock ET') then in straightforward cases no further advantage is obtained by ultrasound-guided ET.

Difficult cases, where the cervical canal is tortuous, may still require transabdominal ultrasound guidance, and, in a small number of cases, cervical pathology necessitates the transmyometrial transfer of embryos directly through the uterine wall. For transmyometrial transfer a needle guide similar to that used for oocyte capture is attached to the vaginal probe and a single lumen needle is introduced through either the anterior or posterior uterine wall depending on whether the uterus lies in an anteverted or retroverted position. The embryos are then transferred through the needle into the uterine lumen (Fig. 38.16). Not surprisingly this method of transfer is associated with increased junctional zone contractions.[46]

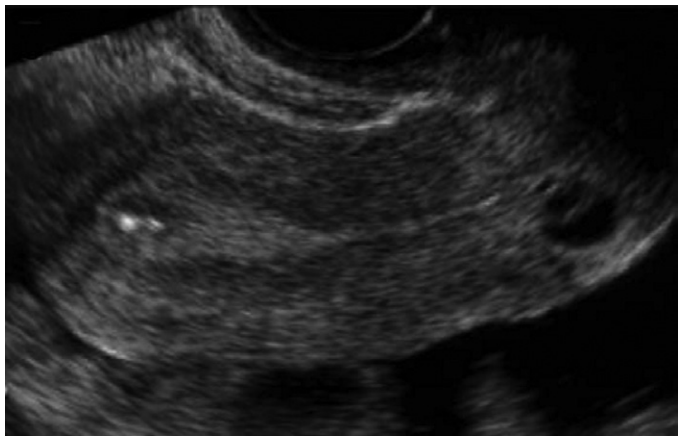


Figure 38.15 Longitudinal view of a uterus after embryo transfer. Note the thickened, homogeneously echogenic endometrium of the luteal phase and the two air bubbles, which have been introduced with the embryos, situated in the correct position 1 cm from the fundus. The superovulated ovary can be seen behind the uterus. A nabothian follicle is also seen within the cervix.

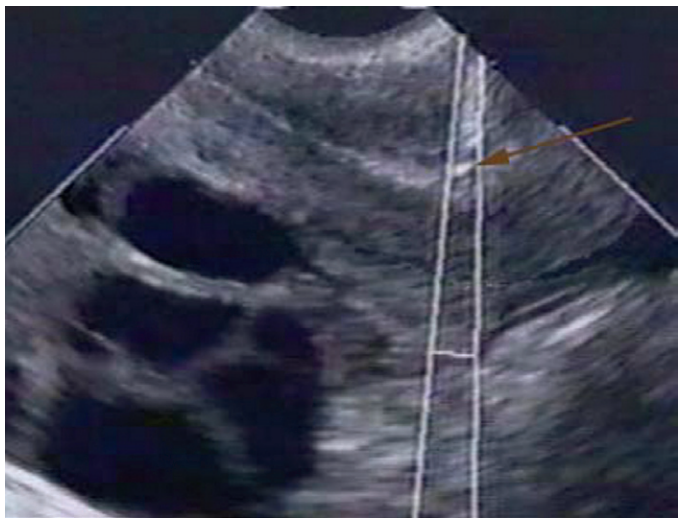


Figure 38.16 Transmyometrial embryo transfer. A needle has been passed through the wall of the uterus into the endometrial cavity. The tip is marked with an arrow. Note the large ovarian follicles behind the uterus which have refilled since their aspiration at the time of oocyte capture.

Power Doppler studies of the neovascularisation and blood flow within the endometrium have been used to try to predict the chances of implantation in much the same way as they have been utilised to predict oocyte quality by measuring perifollicular blood flow. Ng et al.[47] studied the endometrium at the time of oocyte capture and found the more usual endometrial measurements (thickness, volume, echogenic pattern) to be non-predictive of implantation but endometrial vascular indices – resistive index (RI), vascularisation index (VI) and vascularisation flow index (VFI) – to be predictive of a favourable outcome. Currently these measurements do not have a clinical usefulness as there are no ways to increase endometrial vascularity, or indeed endometrial receptivity in general.[48]

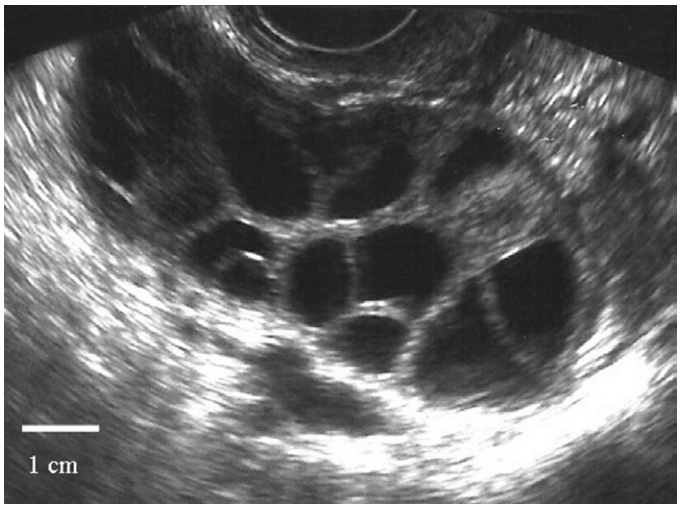


Figure 38.17 **Ovarian hyperstimulation syndrome.**

IVF

- Polycystic ovarian morphology predicts an increased risk of ovarian hyperstimulation.
- Antral follicle counts performed at downregulation correlate well with final number of oocytes obtained.
- Ultrasound monitoring of follicle growth is not aided by additional routine serum oestradiol measurements.
- Routine ultrasonically guided oocyte capture is safe and easily achievable under conscious sedation.
- Routine embryo transfer is not aided by ultrasound control if a mock embryo transfer has been performed.

Table 38.1 **Classification of severity of OHSS (modified to expand on the ultrasound features from Royal College of Obstetricians and Gynaecologists green-top guideline number 5. September 2006)**

Classification	Ultrasound features	Other features
Mild	Ovarian volume <8 cm^3 Free fluid in pelvis	Abdominal bloating Mild abdominal pain
Moderate	Ovarian volume 8–12 cm^3 Fluid in pelvis, elsewhere in abdomen and around kidneys	Moderate abdominal pain Nausea ± vomiting
Severe	Ovarian volume >12 cm^3 Fluid in pelvis, elsewhere in abdomen, around kidneys and in pleural cavity	Clinical ascites Pleural effusion Oliguria Haematocrit >45% Hypoproteinaemia
Critical	Ovarian volume >12 cm^3 Abundant fluid in pelvis, elsewhere in abdomen, around kidneys and in pleural cavity	Tense ascites Large pleural effusion Haematocrit >55% White cell count >25 000/mL Oliguria Thromboembolism Acute respiratory distress syndrome

Ovarian hyperstimulation syndrome (OHSS)

Ovarian hyperstimulation syndrome is very rarely seen except in superovulated treatment cycles, almost always IVF, and can only develop after an LH surge or hCG trigger. The quoted incidence of the clinical syndrome varies from 1% to 10%, although most women who undergo superovulation have some symptoms of a more minor degree. The syndrome is characterised by nausea and vomiting, abdominal distension, fluid retention, ascites and oliguria. There is a risk of breathlessness because of pleural effusions, venous thromboembolism because of haemoconcentration and renal failure because of reduced renal blood flow. Deaths have been reported but are rare.[49]

Hyperstimulation is more common in younger women and in women with polycystic ovaries. Recognising women at risk and taking action to prevent OHSS, such as coasting or abandoning the cycle of treatment, is preferable to managing the syndrome once it has developed.

The syndrome is classified into mild, moderate or severe[50] with the classification depending in part on the ultrasound appearances (Fig. 38.17), principally the degree of ovarian enlargement (Table 38.1). Intraperitoneal fluid can be seen in the pelvis and around the kidneys and in severe cases there is pleural effusion. Management is basically supportive but depends on the severity.

Since the syndrome is triggered by hCG and continued hCG injections, when administered to maintain the luteal phase, make the symptoms more severe, it seems appropriate to abandon embryo transfer if the diagnosis of OHSS has been made before this point so as to prevent any hCG secretion from a resulting pregnancy. The embryos can be cryopreserved and transferred at a later date. There is, however, no evidence that such a regimen modifies the clinical course of the condition.[51]

REFERENCES

1. Boivin J, Bunting L, Collins JA, Nygren K. International incidence of infertility prevalence and treatment seeking: potential need and demand for infertility medical care. Hum Reprod 2007;22(6):1506–1512.
2. Stephen EH, Chandra A. Declining estimates of infertility in the United States: 1982–2002. Fertil Steril 2006;86(3):516–523.
3. Qublan H, Amarin Z, Nawasreh M, et al. Luteinized unruptured follicle syndrome: Incidence and recurrence rate in infertile women with unexplained infertility undergoing intrauterine insemination. Hum Reprod 2006;21(8):2110–2113.
4. Killick SR, Elstein M. Pharmacologic production of luteinized unruptured follicles by prostaglandin synthetase inhibitors. Fertil Steril 1987;47(5):773–777.
5. Gupta S, Goldberg JM, Aziz N, et al. Pathogenic mechanisms in endometriosis-associated infertility. Fertil Steril 2008;90(2):247–257.
6. Marcoux S, Maheux R, Berube S. Laparoscopic surgery in infertile women with minimal or mild endometriosis. N Engl J Med 1997;337(4)217–222.
7. Woelfer B, Salim R, Banergee S, et al. Reproductive outcomes in women with congenital anomalies detected by three-dimensional ultrasound screening. Obstet Gynecol 2001;98:1099–1103.
8. Akar ME, Bayar D, Yildiz S, et al. Reproductive outcome of women with unicornuate uterus. Aust N Z J Obstet Gynaecol 2005;45(2):148–150.
9. Rackow BW, Arici A. Reproductive performance of women with Mullerian anomalies. Curr Opin Obstet Gynecol 2007;19(3):229–237.
10. Heinonen PK. Complete septate uterus with longitudinal vaginal septum. Fertil Steril 2006;85(3):700–705.
11. Tur-Kaspa I, Gal M, Hartman M, et al. A prospective evaluation of uterine abnormalities by saline infusion sonohysterography in 1,009 women with infertility or abnormal uterine bleeding. Fertil Steril 2006;86(6):1731–1735.

12. Kupesic S, Kurjak A. Role of three-dimensional ultrasound in diagnosis of uterine anomalies. Ultrasound Rev Obstet Gynecol 2005;5(3):194–200.
13. Baird DD, Dunson DB, Hill MC, et al. High cumulative incidence of uterine leiomyoma in black and white women: ultrasound evidence. Am J Obstet Gynecol 2003;188:100–107.
14. Somigliani E, Vercellini P, Daguati R, et al. Fibroids and female reproduction: a critical analysis of the evidence. Hum Reprod Update 2007;13(5):465–476.
15. Pritts EA. Fibroids and infertility: a systemic review of the evidence. Obstet Gynecol Surv 2001;56:483–491.
16. Botsis D, Papagianni V, Makrakis E, et al. Sonohysterography is superior to transvaginal sonography for the diagnostic approach to irregular uterine bleeding in women of reproductive age. J Clin Ultrasound 2006;34:434–439.
17. Sardo ADS, Mazzon I, Bramante S, et al. Hysteroscopic myomectomy: a comprehensive review of surgical techniques. Hum Reprod Update 2008;14(2):101–119.
18. Basu M, Mammen C, Owen E. Bony fragments in the uterus: an association with secondary subfertility. Ultrasound Obstet Gynecol 2003;22(4):402–406.
19. Perez-Medina T, Bajo-Arenas J, Salazar F, et al. Endometrial polyps and their implication in the pregnancy rates of patients undergoing intrauterine insemination: a prospective, randomized study. Hum Reprod 2005;20(6):1632–1635.
20. Yanaihara A, Yorimitsu T, Motoyame H, et al. Location of endometrial polyp and pregnancy rate in infertility patients. Fertil Steril 2008;90(1):180–182.
21. Zeyneloglu HB, Arici A, Olive DL. Adverse effects of hydrosalpinx on pregnancy rates after in vitro fertilization-embryo transfer. Fertil Steril 1998;7(3):492–499.
22. Kontoravdis A, Makrakis E, Pantos K, et al. Proximal tubal occlusion and salpingectomy result in similar improvement in in vitro fertilization outcome in patients with hydrosalpinx. Fertil Steril 2006;86(6):1642–1649.
23. Hammadieh N, Coomarasamy A, Ola B, et al. Ultrasound-guided hydrosalpinx aspiration during oocyte collection improves pregnancy outcome in IVF: a randomized controlled trial. Hum Reprod 2008;23(5):1113–1117.
24. Fauser BCJM, et al. (The Rotterdam ESHRE/ASRM-sponsored PCOS consensus workshop group). Revised 2003 consensus on diagnostic criteria and long-term health risks related to polycystic ovary syndrome. Hum Reprod 2004;19(1):41–47.
25. Hassan MA, Killick SR. Ultrasound diagnosis of polycystic ovaries in women who have no symptoms of polycystic ovary syndrome is not associated with subfecundity or subfertility. Fertil Steril 2003;80(4): 966–975.
26. Balen AH, Laven JSE, Tan SL, Dewailly D. Ultrasound assessment of the polycystic ovary: international consensus definitions. Hum Reprod Update 2003;9:505–514.
27. Fulghesu AM, Ciampelli M, Belosi C, et al. A new ultrasound criterion for the diagnosis of polycystic ovary syndrome: the ovarian stroma:total area ratio. Fertil Steril 2001;76:326–331.
28. Adams J, Polson DW, Abdulwahid N, et al. Multifollicular ovaries: clinical and endocrine features and response to pulsatile gonadotrophin releasing hormone. Lancet 1985;ii:1375–1379.
29. Kyei-Mensah A, Tan SL, Zaidi J, Jacobs HS. Relationship of ovarian stromal volume to serum androgen concentration in patients with polycystic ovary syndrome. Hum Reprod 1998;13:1437–1441.
30. Killick SR. Hysterosalpingo contrast sonography as a screening test for tubal patency in infertile women. J R Soc Med 1999;92: 628–631.
31. Schwarzler P, Concin H, Wohlgenannt K. Transvaginal sonographic assessment of the uterine cavity and the Fallopian tubes with echo-enhancing agents. Ultraschall Med 1997;18(1):8–13.
32. NICE clinical guideline number 11. Fertility: Assessment and treatment for people with fertility problems. Feb 2004.
33. Nirmal D, Griffiths AN, Jose G, Evans J. Warming Echovist contrast medium for hysterocontrastsonography and the effect on the incidence of pelvic pain. A randomized controlled study. Hum Reprod 2006;21(4):1052–1054.
34. Jayaprakasan K, Hilwah N, Kendall NR, et al. Does 3D ultrasound offer any advantage in the pretreatment assessment of ovarian reserve and prediction of outcome after assisted reproduction treatment? Hum Reprod 2007;22(7):1932–1941.
35. Lutchman Singh K, Davies M, Chatterjee R. Fertility in female cancer survivors: pathophysiology, preservation and the role of ovarian reserve testing. Hum Reprod Update 2005;11(1):69–89.
36. Kwan I, Bhattacharya S, McNeil A, Van Rumste MME. Monitoring of stimulated cycles in assisted reproduction (IVF and ICSI). Cochrane Database Syst Rev 2008;2:1469–1493X.
37. Verhaak CM, Smeenk JMJ, Evers AWM, et al. Women's emotional adjustment to IVF: a systematic review of 25 years of research. Hum Reprod Update 2007;13(1):27–36.
38. Aboulghar MA, Mansour RT. Ovarian hyperstimulation syndrome: classifications and critical analysis of preventive measures. Hum Reprod Update 2003;9(3):275–289.
39. Farhi J, West C, Patel A, Jacobs HS. Treatment of anovulatory infertility: The problem of multiple pregnancy. Hum Reprod 1996;11(2):429–434.
40. Bhal PS, Pugh ND, Chui DK, et al. The use of transvaginal power Doppler ultrasonography to evaluate the relationship between perifollicular vascularity and outcome in in-vitro fertilization treatment cycles. Hum Reprod 1999;14(4):939–945.
41. Bodri D, Guillen JJ, Polo A, et al. Complications related to ovarian stimulation and oocyte retrieval in 4052 oocyte donor cycles. Reprod BioMed Online 2008;17(2):237–243.
42. Lesny P, Killick SR. The uterine junctional zone and its contractions. Br J Obstet Gynaecol 2004;111(11):1182–1189.
43. Lesny P, Killick SR, Robinson J, Maguiness S. Transcervical embryo transfer as a risk factor for ectopic pregnancy. Fertil Steril 1999;72:305–309.
44. Fanchin R, Righini C, Olivennes F, et al. Uterine contractions as visualised by ultrasound alter pregnancy rates in IVF and embryo transfer. Hum Reprod 1998;13:1968–1974.
45. Drakeley AJ, Jorgensen A, Sklavounos J, et al. A randomised control trial of 2295 ultrasound-guided embryo transfers. Hum Reprod 2008;23(5):1101–1106.
46. Biervliet FP, Lesny P, Maguiness SD, et al. Transmyometrial embryo transfer and junctional zone contractions. Hum Reprod 2002;17(2): 347–350.
47. Ng EHY, Chan CCW, Tang OS, et al. The role of endometrial and subendometrial vascularity measured by three-dimensional power Doppler ultrasound in the prediction of pregnancy during frozen–thawed embryo transfer cycles. Hum Reprod 2006;21(6):1612–1617.
48. Killick SR. Ultrasound and the receptivity of the endometrium. Reprod BioMed Online 2007;15(1):63–67.
49. Cluroe AD, Synek BJ. A fatal case of ovarian hyperstimulation syndrome with cerebral infarction. Pathology 1995;27(4):344–346.
50. Royal College of Obstetricians and Gynaecologists. Green-top guideline number 5. September 2006.
51. D'Angelo A, Amso N. Embryo freezing for preventing ovarian hyperstimulation syndrome. Cochrane Database Syst Rev 2007;3:1469–1493.

CHAPTER

39

The first trimester, gynaecological aspects

Anne Marie Coady

TRANSVAGINAL SCANNING IN EARLY PREGNANCY 741

THE NORMAL FIRST TRIMESTER 741
Normal sonographic pregnancy development 741
- Thickening of the endometrium 741
- Appearance of the gestation sac 741
- The appearance of the yolk sac 743
- The appearance of the embryo 744
- The embryonic heartbeat 745
- Appearance of the membranes: the amnion and chorion 745
- Normal embryonic anatomy and fetal anomalies 746

Multiple pregnancy diagnosis 747
- Twinning 747

First trimester biometry 748
- Mean gestational sac diameter (MGSD) 748
- Crown–rump length (CRL) 749

EARLY PREGNANCY FAILURE 749
Failure of normal progression of the in-utero implantation 749
Sonographic diagnosis of early pregnancy failure 749
- Major criteria 750
- Minor criteria 750

EARLY PREGNANCY COMPLICATIONS 751
First trimester haemorrhage 751
- Subchorionic haemorrhage 752
- Crown–rump length 753

Early pregnancy failure due to ectopic implantation 753
Risk factors for ectopic pregnancy 753
The uterine findings in ectopic pregnancy 753
- Normal intrauterine pregnancy 753
- Endometrial appearances 754
- The pseudo-gestation sac 754

The adnexal findings in ectopic pregnancy 754
- Normal adnexal regions 754
- Tubal ring with yolk sac/tubal ring with embryo 754
- Complex mass 755
- Intraperitoneal fluid 756

The role of Doppler ultrasound in the diagnosis of ectopic pregnancy 756
Unusual ectopic gestations 757
- Interstitial ectopic gestation 757
- Cervical ectopic gestation 757
- Caesarean scar ectopic pregnancy 758
- Ovarian ectopic gestation 758

Negative ultrasound 760
The role of a discriminatory serum β-hCG level 760
Pregnancy of unknown location (PUL) 760

THE ROLE OF ULTRASOUND IN PREDICTING AN ABNORMAL PREGNANCY OUTCOME 761
Ultrasound bias and loss of reassurance: the ultrasound conundrum 761
Ultrasound in the prediction of early pregnancy loss 761
- The embryonic heart rate: embryonic bradycardia 761
- Mean gestational sac diameter in relation to the crown–rump length 761
- Yolk sac size and shape 761

FIRST TRIMESTER MASSES 762
Ovarian masses 762
Fibroids 763

GESTATIONAL TROPHOBLASTIC DISEASE 764
Complete hydatidiform mole 764
Partial hydatidiform mole (PHM) 764

THE ULTRASOUND DIAGNOSIS OF RETAINED PRODUCTS OF CONCEPTION 765

THE NON-SURGICAL MANAGEMENT OF ECTOPIC PREGNANCY 766
Methotrexate regimens 767

Ultrasound in the first trimester of pregnancy has come a long way from the first reports of Cacciatore et al.[1] to the present day. Not only does transvaginal ultrasound have the central role in diagnosis of first trimester problems but it is now involved in:

1. providing patients with choice in terms of therapy, frequently safely facilitating a wait and see policy
2. providing prognostic information on the likely outcome of a pregnancy
3. monitoring of methotrexate therapy in cervical, caesarean scar and interstitial ectopic pregnancies.

It is universally acknowledged that ultrasound has transformed the first trimester, providing knowledge and insight for physicians and parents alike into the embryology and physiology of a pregnancy. Some cautions must be sounded. The demands from doctors and parents have led to a rapidly expanding service; however, the quality of this service must not be compromised and must comprise the following:

1. Properly trained, accredited and dedicated staff, following a training programme that is recognised and regulated. Training must be continuous and must be audited.
2. High quality equipment that is properly maintained and replaced.
3. Properly constructed departmental guidelines and protocols, which should reassure and inspire confidence in both service providers and patients.

The use of transvaginal ultrasound has resulted in some unexpected side effects:

1. Loss of reassurance. A transvaginal scan can often detect a heartbeat in an embryo when it measures only 2 mm in size. However, the natural loss rate of very early embryos means that detecting a heartbeat so early is not as reassuring as expected.
2. An entirely new diagnostic concept: the pregnancy of unknown location (PUL). This is proving costly financially

and is increasing workload. As a consequence this is producing increased stress and anxiety for staff and parents alike.

The best scan is the scan performed to a high standard to answer a specific clinical question by properly trained ultrasound personnel. Whilst some uncertainty will always exist, this should not be uncertainty generated by poor technique, substandard knowledge or poor understanding of natural processes. With such a wonderful technique available to us, opening insights on a very remarkable process, we must first do no harm. The greatest concern relating to ultrasound safety comes not from the physical ultrasound process but from the use of the technique in unsafe hands.

TRANSVAGINAL SCANNING IN EARLY PREGNANCY

The first trimester of pregnancy is the time interval between the last menstrual period and the end of the twelfth completed week of gestation.

It was Sir Ian McDonald who described the first 12 weeks of pregnancy as the most 'crucial period of existence'.[2] It is not only a very dynamic phase of development but also an emotionally charged time with a high complication and loss rate.

The advent of high-resolution transvaginal ultrasound has enabled the anatomy and physiology of the human fetus and the adnexae to be visualised from as early as the third week post implantation.[3] As transvaginal scanning produces accurate images of the early gestational sac and its contents, it has provided clues to the epidemiology and pathophysiology of early pregnancy failure. Ultrasound has changed the medical approach to early pregnancy failure.

THE NORMAL FIRST TRIMESTER

Normal sonographic pregnancy development

The primary objective of transvaginal scanning in early pregnancy must be to be accurate. Characterisation of normality is of fundamental importance. Knowledge of the typical ultrasound appearances of normal early pregnancy and a good understanding of the pitfalls is essential for the diagnosis and management of early pregnancy failure.

It is fortunate that the development of a normal pregnancy occurs in a very predictable manner.[4] Every stage of development may be characterised by threshold and discriminatory levels.[5] These levels, in association with beta human chorionic gonadotrophin (β-hCG) levels, predict what should or should not be seen on ultrasound scan. The threshold level is the earliest age at which we would expect to see a pregnancy reach a certain sonographic milestone. The discriminatory level is that age at which failure to detect a certain biological landmark on ultrasound is not consistent with normal development and is therefore evidence of pregnancy failure. It is important to recognise and understand the sequence of sonographic embryology (Table 39.1). Without knowledge of the normal sequence of events and biological variation, the diagnosis of first trimester pathology is not possible.

Table 39.1 Normal stages of early pregnancy development as visualised sonographically

1. Thickening of the endometrium
2. Appearance of the gestation sac
3. Appearance of the yolk sac (to include development of the membranes)
4. Appearance of the embryo

Thickening of the endometrium

The first, quite non-specific, sign of early pregnancy is thickening of the endometrium to approximately 17 mm in true anteroposterior sagittal dimension (Fig. 39.1). The differential diagnosis for this finding includes:

1. late luteal phase of a normal cycle
2. very early ectopic gestation.

The intra-decidual sign has been reported within the homogeneously thickened endometrium. This is a highly reflective area within the thickened endometrium which is thought to represent the early implantation site.[6] This is very difficult to demonstrate and is therefore an unreliable finding.

Appearance of the gestation sac

The gestation sac is first seen as a tiny hypoechoic chorionic fluid collection within the thickened endometrium. The earliest a tiny gestation sac can be seen is approximately 4 weeks 4 days gestational age when it is only 2–3 mm in size (Fig. 39.2).[7]

The size of the gestation sac is quantified by the mean gestational sac diameter (MGSD). In the very early stages when the sac is round, a single chorionic margin to chorionic margin measurement will suffice. Once the sac is ovoid the measurement must be the mean of the three orthogonal measurements, each one taken from chorionic margin to chorionic margin of the gestational sac with the transverse measurement only taken from the transverse plane (Fig. 39.3).[8] The MGSD is an adequate estimation of gestational age in a normally developing pregnancy. The normal gestational sac grows at 1.1 mm per day.

At first, the gestation sac simply looks like a fluid collection within the endometrium. This is a non-specific sign of which there are other causes (Table 39.2; Figs. 39.4, 39.5). Recognition of the true gestation sac at this stage is dependent on subtle features of the sac itself (Table 39.3; Figs 39.6, 39.7). *The appearance of the yolk sac and then the embryo confirms the intrauterine collection as a true sac.*

The central endometrial cavity echo is formed by opposing margins of the endometrial lining. The true sac implants within the endometrium on one or other side of the central endometrial cavity

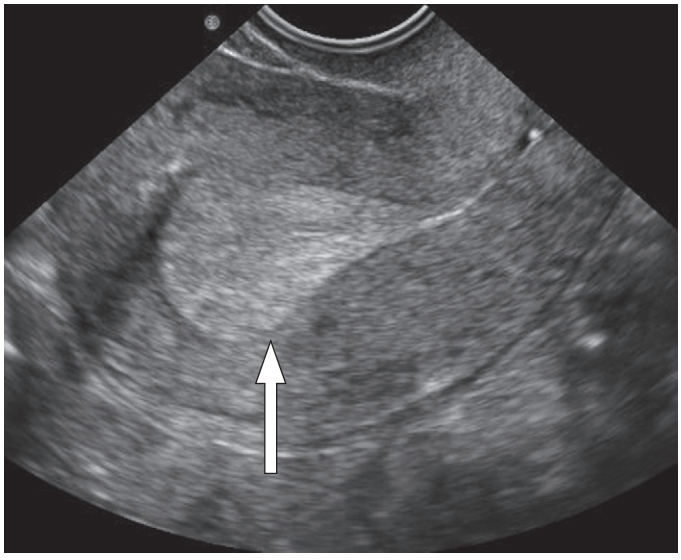


Figure 39.1 Homogenous thickening of the endometrium to 17 mm.

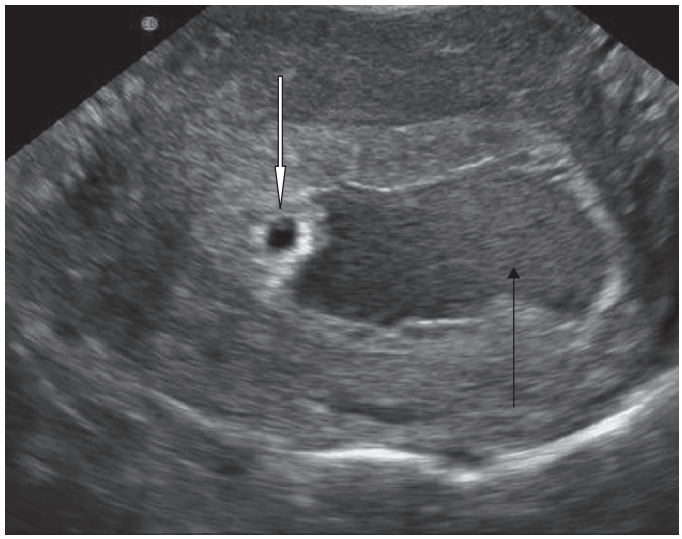


Figure 39.2 A tiny 4 week gestation sac (white arrow) only 2 to 3 mm in size accentuated by a large sub chorionic haematoma (black arrow).

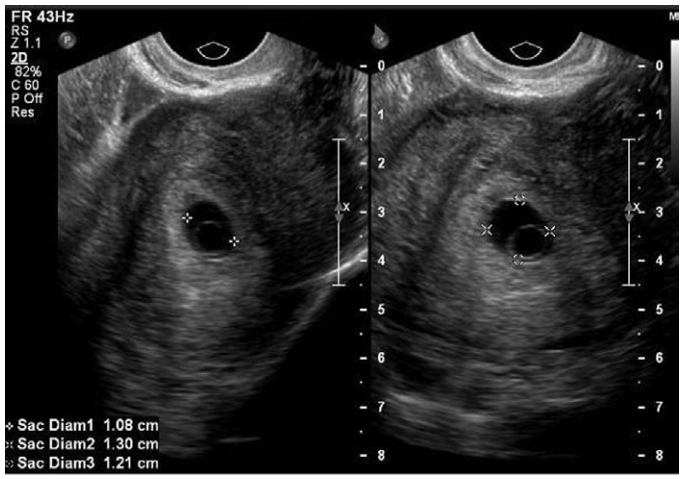


Figure 39.3 Measurement of the mean gestational sac diameter (MGSD).

Table 39.2 Causes of fluid within the endometrial cavity

1. Pseudo-sac of an ectopic gestation (Fig. 39.4)
2. Endometritis
3. Endometrial cyst (Fig. 39.5)
4. Haematoma

Table 39.3 Features of a normal intrauterine gestation sac when first seen at 2–3 mm in size at a gestational age of 4–4.5 weeks

1. Eccentric to the endometrial echo (Fig. 39.6)
2. Double decidual sac sign (Fig. 39.6)

These first 2 features are the most reliable

3. Round or oval in shape and is located in the fundal or midportion of the uterine cavity (Fig. 39.7)
4. It has a well-defined complete decidual reaction >2 mm (Fig. 39.7)

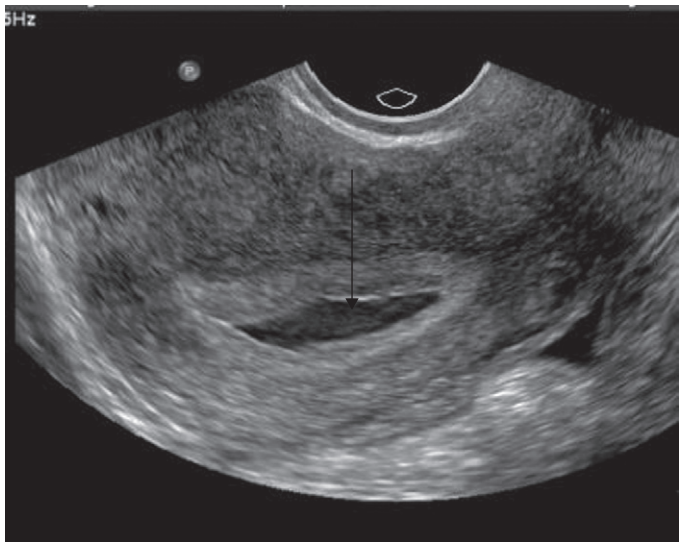


Figure 39.4 Pseudo sac of an ectopic pregnancy (arrow) which is simply fluid within the central endometrial cavity.

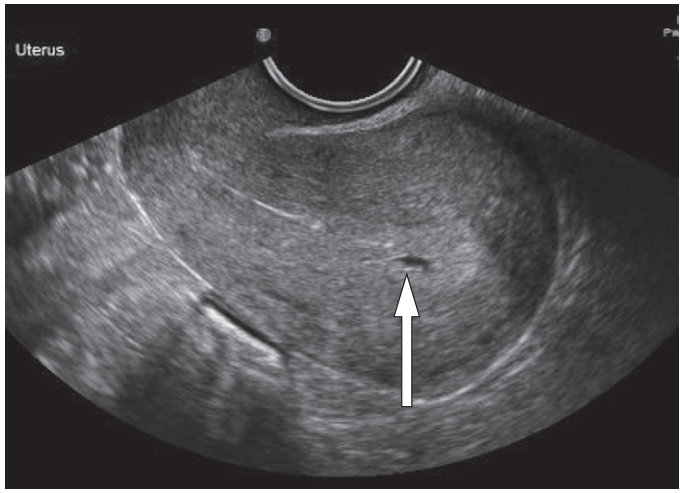


Figure 39.5 Endometrial cyst.

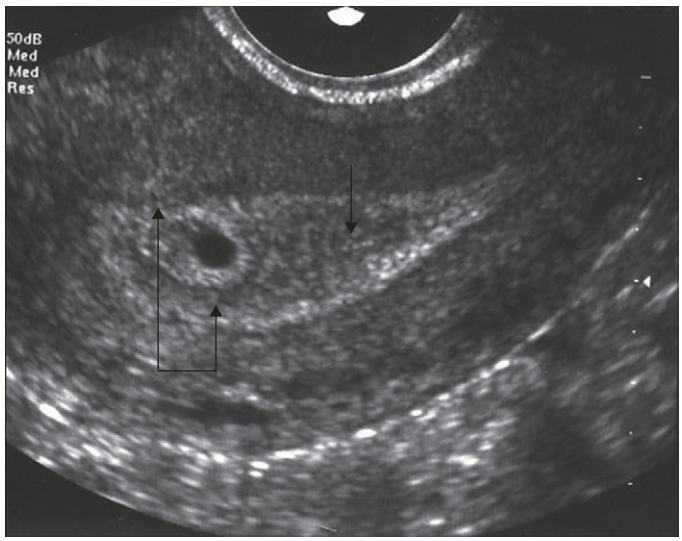


Figure 39.6 Demonstrating the position of the sac eccentric to the endometrial echo (single arrow) and the double decidual sac sign (double arrow).

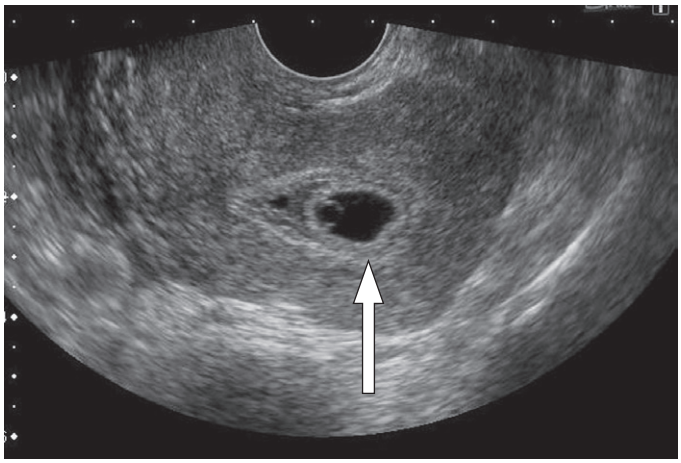


Figure 39.7 Well-defined complete decidual reaction >2 mm surrounding a normal round gestation sac.

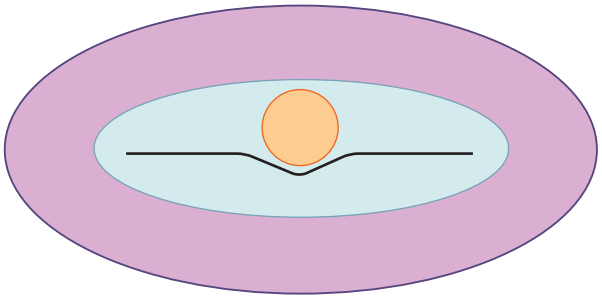


Figure 39.8 Diagrammatic illustration of what is visualised on ultrasound. The purple oval is the myometrium of the entire pregnant uterus. The pale blue oval is the thickened endometrium/the decidual layers of the pregnant uterus. The thin black line represents the central endometrial cavity echo. The orange circle is the gestation sac which is eccentric to the central endometrial echo and which has two decidual layers surrounding it.

echo.[9] A positive double decidual sac sign confirms a normal intrauterine pregnancy (Fig. 39.8).[10] The absence of this sign does not rule out an intrauterine gestation but suggests the existence of an abnormality.

There are important pitfalls and normal variations to the classic sonographic diagnostic criteria of the true gestation sac, not only in terms of shape but also in its location. An over-distended bladder will distort the sac when visualised on the transabdominal approach and fibroids can produce pronounced misshaping of the sac (Fig. 39.9). There is a normal lower uterine body implantation called a lower isthmus implantation, where the sac is low, unchanging and well established in the lower uterine cavity but not within a caesarean section scar (Fig. 39.10).

The appearance of the yolk sac

The yolk sac visualised sonographically is the secondary yolk sac located in the chorionic cavity (Fig. 39.11). The yolk sac is responsible for the initial biosynthetic, haematopoietic and absorptive functions of the embryo.[11] It is involved in the formation of the primitive gut and remains connected to the midgut by the vitelline duct, which can be demonstrated sonographically (Fig. 39.12).

The yolk sac is a thin-walled rounded structure whose walls gradually thicken. The yolk sac growth is linear to a maximum of 6 mm and it is never >6 mm in normal pregnancies at 10 weeks gestation (Fig. 39.13).[12] At 10 weeks it involutes or is incorporated

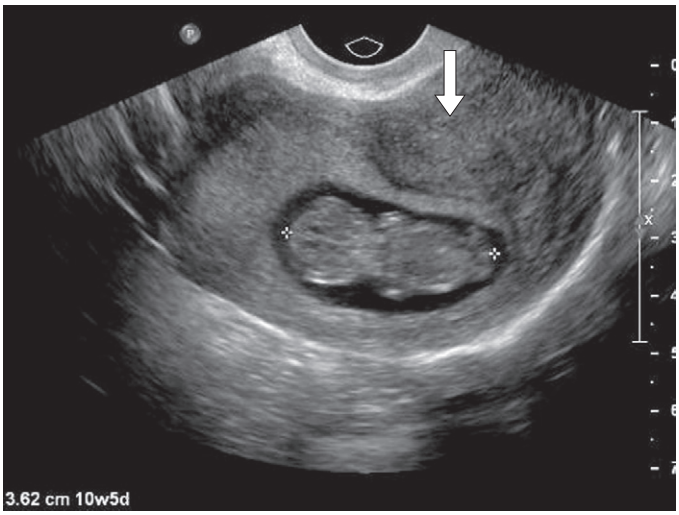


Figure 39.9 A fibroid (arrow) producing anterior compression of the gestation sac.

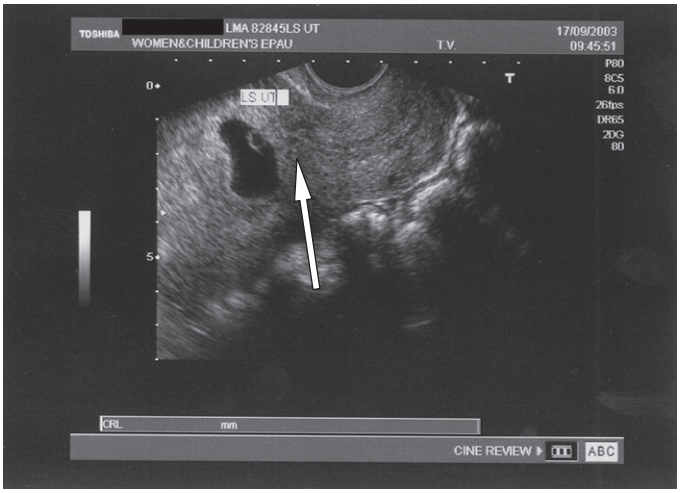


Figure 39.10 A low normal sac implantation within the uterine isthmus, the arrow at the level of the internal os.

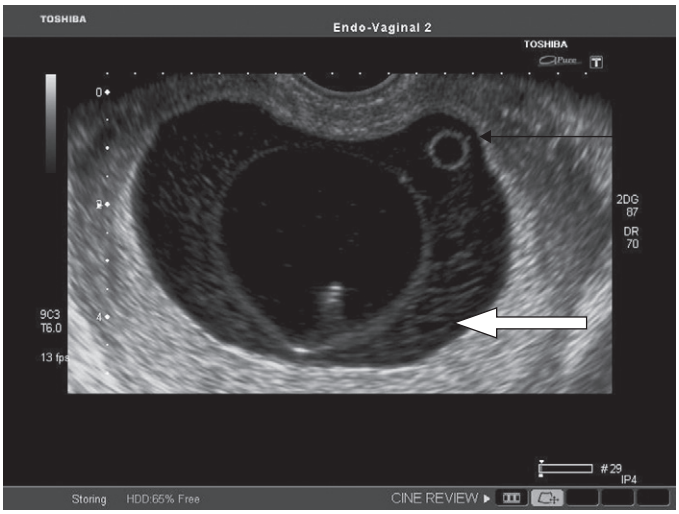


Figure 39.11 The yolk sac (black arrow) within the echogenic chorionic cavity (white arrow).



Figure 39.12 The normal yolk sac (black arrow) with the attached vitelline duct (white arrow).



Figure 39.13 The maximum size of the yolk sac is never more than 6 mm in transverse section at 10 weeks.

Table 39.4 Size of the gestation sac on transvaginal (TV) scanning with respect to yolk sac appearance and visualisation

1. When on TV the MGSD is 6 mm (5.5 weeks) the yolk sac is usually seen. This is the threshold level for yolk sac visualisation
2. When on TV the MGSD is 8 mm (5.7 weeks) the yolk sac is always seen
3. When on TV the MGSD is ≥13 mm (6.4 weeks) the yolk sac must be seen. This is the discriminatory level for yolk sac visualisation

into the primitive foregut. The main initial sonographic importance of the yolk sac is that it confirms that the fluid collection within the endometrium is indeed a true intrauterine sac. It is therefore important to be aware of the timing of the appearance of the yolk sac within the gestation sac, i.e. to be aware of the threshold and discriminatory levels of sac size and yolk sac visualisation (Table 39.4).[13]

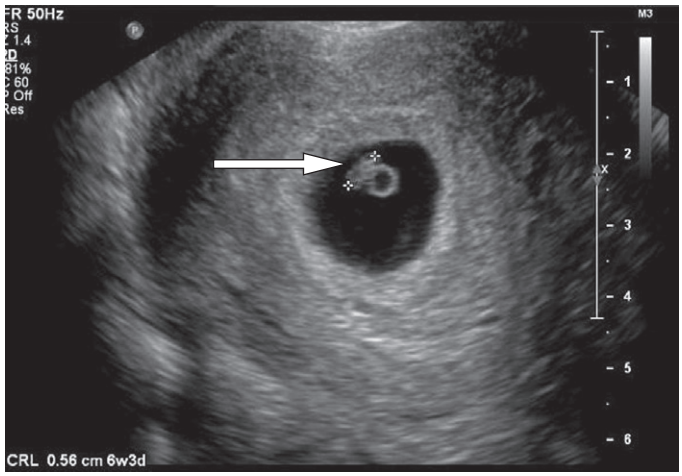


Figure 39.14 The embryo (arrow) first appears at the chorionic margin of the yolk sac.

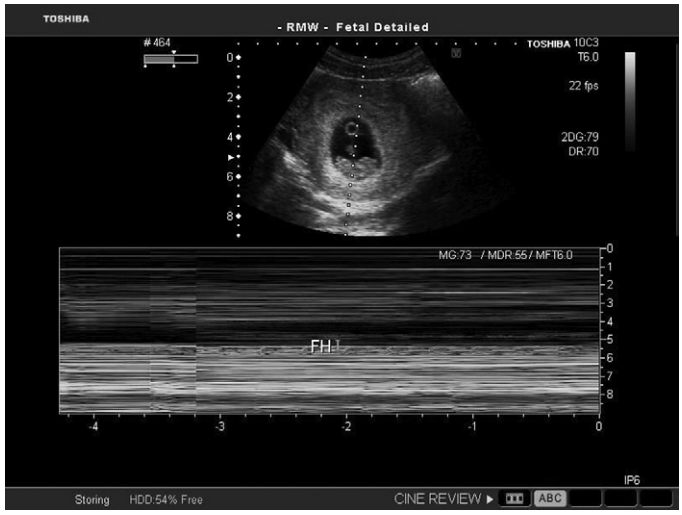


Figure 39.15 Cardiac activity in an embryo of >5 mm in size.

Defining features of the true gestation sac

- The early gestation sac is simply a tiny hypoechoic fluid collection.
- The eccentric location and the double decidual sac sign suggest a true intrauterine sac.
- The appearance of the yolk sac confirms the intrauterine collection as a true sac.
- A MGSD ≥13 mm (6.4 weeks) is the discriminatory level for yolk sac visualisation.
- A MGSD of 15–18 mm (6.4 weeks) is the discriminatory level for embryo visualisation.

The appearance of the embryo

The embryo is first seen as a disc adjacent to but distinct from the yolk sac, developing along the chorionic margin of the yolk sac (Fig. 39.14). It is approximately 2 mm in length at 5 weeks. Prior to this the beat of the developing embryonic heart can often be seen without the embryo itself.[14] Once it is larger than 2 mm it is discoid with a proportional width relative to its length. The normal embryonic growth rate is initially 1.2 mm/day. Once it measures 5 mm in a sac of 15–18 mm size (a gestational age of approximately 6.5 weeks), it will be seen consistently as a discrete structure and it will always have cardiac pulsations, if it is living (Fig. 39.15).[15]



Figure 39.16 Measurement of the crown–rump length (CRL).

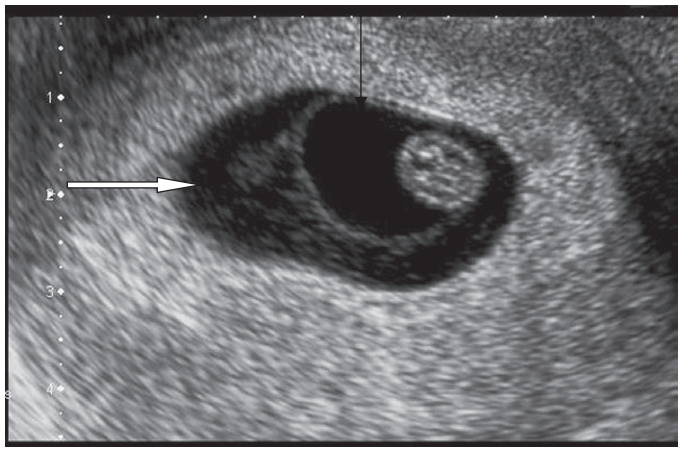


Figure 39.17 The echogenic chorion (white arrow) and the echo-poor amnion containing the embryo (black arrow).

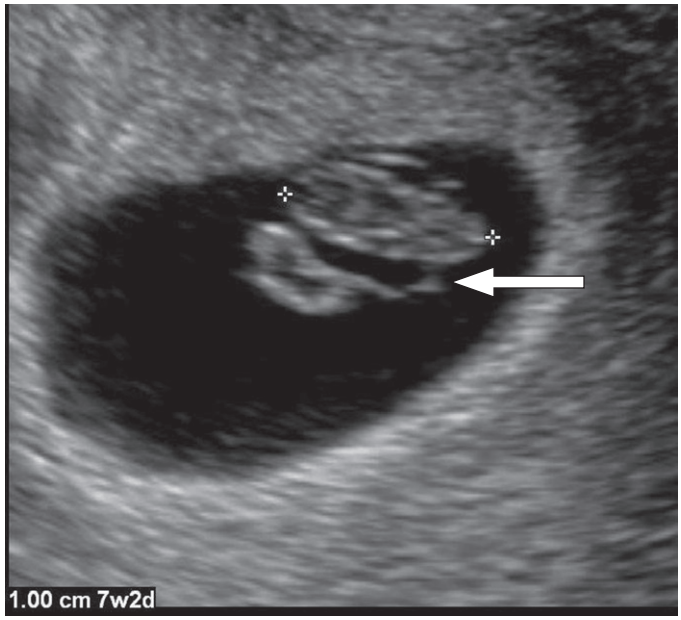


Figure 39.18 The amnion (arrow) slowly moving away from the developing embryo by accumulating amniotic fluid.

Table 39.5 Size of the gestation sac on transvaginal scanning (TV) with respect to embryonic appearance and visualisation

1. When on TV the MGSD is 10 mm (6 weeks) the embryo is usually seen. This is the threshold level for visualisation of the embryo
2. When on TV the MGSD is 15–18 mm (6.4 weeks) the embryo must be seen. This is the discriminatory level for visualisation of the embryo
3. By realising what the threshold and discriminatory levels for visualisation of the yolk sac and the embryo are, it will be seen that the diagnostic levels recommended for use by the Royal College of Obstetricians and Gynaecologists/ Royal College of Radiologists are very conservative but rightly so

The crown–rump length (CRL) is used to measure the embryo within the first trimester (Fig. 39.16). The term CRL is initially a misnomer as before 7 weeks there is no crown–rump differentiation to the embryo. The assumption is that the longest dimension of the embryo is the most accurate, which is true, provided other structures such as the yolk sac are not included in the measurement.

As with the yolk sac, it is extremely important to be aware of the timing of the appearance of the embryo within the gestation sac, i.e. to be aware of the threshold and discriminatory levels of sac size and embryo visualisation (Table 39.5).

The embryonic heartbeat

Embryonic heart pulsation is the earliest proof that the embryo is alive. Cardiac pulsation has been documented in utero by transvaginal scanning as early as 36 days menstrual age, the time when the heart tube starts to beat. Theoretically cardiac activity should always be evident when the embryo is over 2 mm in size. In around 5–10% of embryos between 2 and 4 mm it cannot be demonstrated, although the pregnancies will have a normal outcome.[14] From 5 to 9 weeks of gestation, there is a rapid increase in the mean heart rate from 110 to 175 bpm.[16]

Appearance of the membranes: the amnion and chorion

The chorionic cavity is the first cavity seen. The fluid is faintly echogenic (Fig. 39.17). The chorion contains the secondary yolk sac and the chorionic margin always leads to the placental margin. The chorion is gradually obliterated by expansion of the amnion and complete fusion is usually complete by 12 weeks.

The amnion appears at the same time as the yolk sac, i.e. when the MGSD is 6 mm (5–5.5 weeks). The amnion and the yolk sac produce an initial double bleb not seen sonographically. The amnion goes through a period of sonographic invisibility due to the fact that this is a very thin structure very close to the embryo. With newer ultrasound systems sonographic invisibility is less common. It is reliably seen once again at about week 7 when the accumulating amniotic fluid pushes it away from the embryo (Fig. 39.18). Visualisation of an amnion without an embryo is impossible in a normal gestation and the 'empty amnion sign' is universally predictive of pregnancy failure.[17]



Figure 39.19 **The normal fetal rhombencephalon (arrow).**

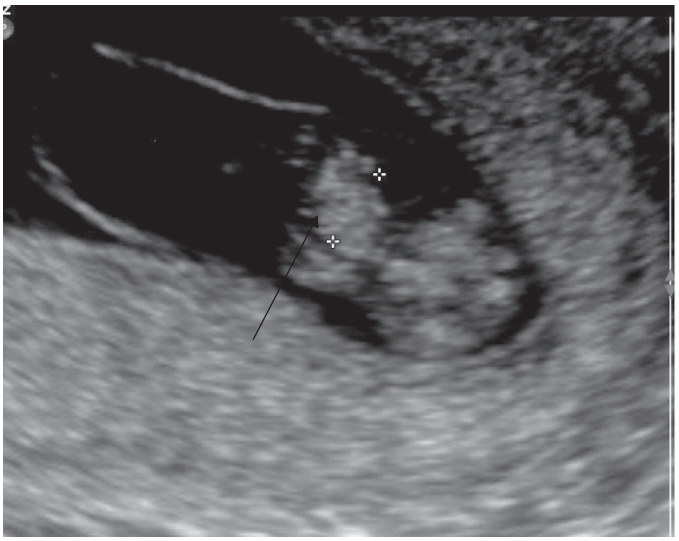


Figure 39.20 **The normal physiological echogenic omphalocele.**

Normal pregnancy development

- Normal pregnancy development occurs in a very predictable manner.
- When the embryo is over 2 mm in size cardiac activity should be evident.
- Chorionic cavity fluid is echogenic.
- The chorion is gradually obliterated by expansion of the amnion.
- The amnion appears at the same time as the secondary yolk sac.
- Visualisation of an amnion without an embryo is impossible in a normal gestation.

Normal embryonic anatomy and fetal anomalies

High-resolution transvaginal ultrasound allows visualisation of in-vivo embryology from as early as the third week post implantation. Knowledge of the early anatomical development of the fetus is essential as normal anatomy may mimic the sonographic appearances of fetal anomalies due simply to the early stage of development.[18]

The fetal rhombencephalon appears as a cystic structure in the posterior fossa beginning at 7 weeks menstrual age. It is well visualised by 8 weeks. It should not be mistaken for an intracranial cyst or hydrocephalus (Fig. 39.19). The telencephalic, mesencephalic vesicles and the bilateral echogenic choroid plexus can also be seen at 8 weeks.

The upper limb buds are seen at 8 weeks with the lower limb buds apparent by 9 weeks. At 8 weeks gestational age the first movements of the 15–20 mm embryo are detected. This movement is predominantly lateral flexion of the body. By 9 weeks gestation the 21–26 mm embryo is wriggling its body and actively moving its limbs.

Physiological herniation of the gut is present in embryos between 8 weeks 3 days and 10 weeks 4 days. This physiologic midgut hernia is a small (6–8 mm) echogenic mass protruding into the umbilical cord. It is never more than 8 mm in transverse measurement (Fig. 39.20).[19] The bowel should always have returned to the abdominal cavity by a CRL of 45 mm.

The kidneys do not reach their adult position until 11 weeks. The fetal bladder will be seen in 94% of normal fetuses by 13 weeks.[20] Amniotic fluid volume does not depend on fetal renal function until the second trimester and so an abnormal liquor volume cannot serve as an early indicator of severe renal disease and severe renal

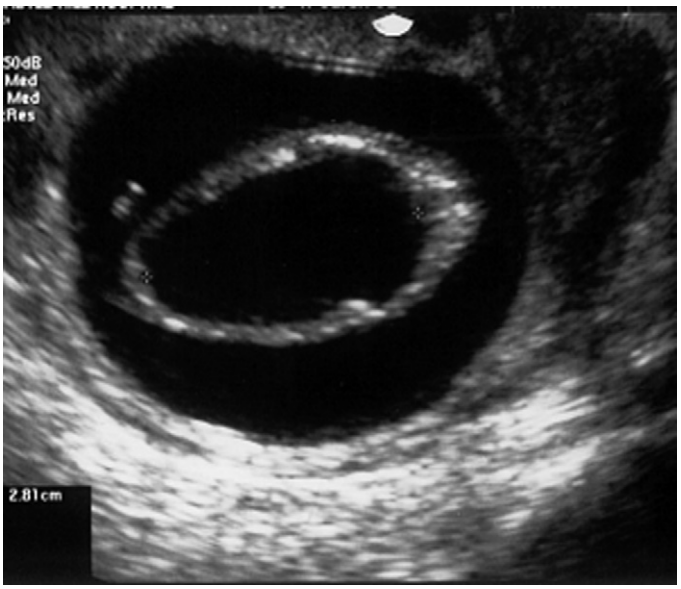


Figure 39.21 **LS of an abnormal fetal bladder** which measures 28 mm and is therefore abnormal i.e. first trimester megacystis.

anomalies cannot be diagnosed in the first trimester. However, anomalies of the lower renal tract such as megacystis, defined as a longitudinal measurement of the fetal bladder >8 mm, may be detected even at this early stage (Fig. 39.21). The normal fetal bladder measures less than 6 mm in longitudinal section at 10–14 weeks.[21]

Many severe anomalies may have a normal sonographic appearance in the first trimester. The most dramatic example is anencephaly, which may only become obvious after failure of ossification of the calvarium, which is normally complete by 12 weeks menstrual age. Anencephaly results from failure of closure of the rostral neuropore at 42 days menstrual age and is the end stage of a defect which begins with acrania and progresses through exencephaly to anencephaly. At approximately 8 weeks menstrual age, a fetal head may be identified in an anencephalic embryo. Whilst true acrania may not be diagnosed until the end of the twelfth completed week the diagnosis of exencephaly (extrusion of the brain tissue normal and abnormal) may be made at 11 weeks and indeed there are reports of even earlier diagnoses.[22] At 11 weeks, the brain in

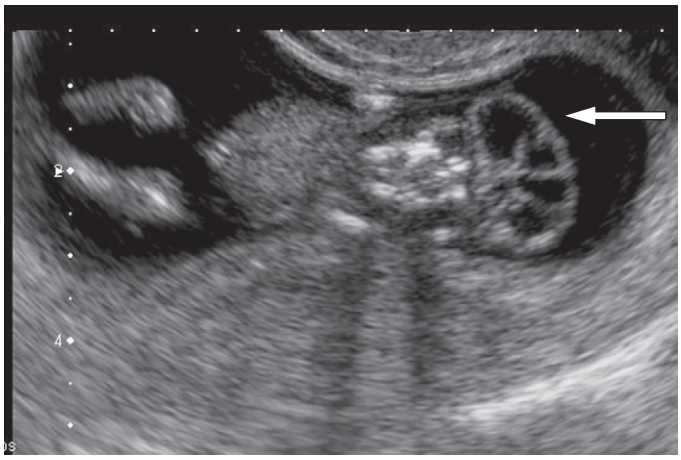


Figure 39.22 First trimester exencephaly with extrusion of the brain tissue (arrow).

Normal embryonic anatomy and fetal anomalies

- Normal embryologic anatomy may mimic the appearances of fetal anomalies.
- The rhombencephalon may be mistaken for an intracranial cyst or hydrocephalus.
- The upper limb buds and lower limb buds are seen on transvaginal scan at 8 and 9 weeks respectively.
- By 9 weeks gestation the 21–26 mm embryo is wriggling its body and moving its limbs.
- Physiological herniation of the gut occurs between 8 and 10 weeks.
- Physiological herniation must have resolved by a crown–rump length of 45 mm.
- Acrania may not be diagnosed until the end of the twelfth completed week of gestation.
- Exencephaly may be diagnosed at 11 weeks.

exencephaly appears as an abnormal mass of tissue extending above the head, which is sonographically referred to as the 'Mickey Mouse' sign (Fig. 39.22).[23]

Multiple pregnancy diagnosis

Twinning

Twinning occurs in 1% of all pregnancies. Two-thirds of all twins will be dizygotic, i.e. the embryos develop from two separate zygotes (two separately fertilised ova). One-third will be monozygotic twins, i.e. separation/splitting of one zygote.

The most important role of ultrasound in an early multiple pregnancy is to determine the chorionicity and amnionicity of the pregnancy. Ultrasound does not determine zygosity.[24]

Dizygotic twins will always have a dichorionic placentation. However, a monozygotic twin pair can have either a dichorionic placenta (40% of cases) or a monochorionic placenta (60%) depending on when splitting of the blastocyst occurs (Table 39.6).[25]

The presence of two gestation sacs, which can be seen as early as 4.5 to 5 weeks, is consistent with a dichorionic gestation. It is essential to ensure that two distinct gestation sacs are seen (Fig. 39.23). The most frequent early misdiagnosis of twinning is to misinterpret either a normal early structure such as the yolk sac as a second gestation sac or to diagnose a subchorionic haematoma or hydropic placental change as a gestation sac (Fig. 39.24). This should only present a problem prior to visualisation of the embryo. Such misinterpretations are in part responsible for the wide variability in reporting the 'vanishing twin'.[26] Disappearance of sacs or embryos is described throughout the first trimester, occurring more frequently earlier in gestation. A disappearance rate of 21% for dichorionic twins and 50% for monochorionic twins between 6 and 8 weeks has been reported, with no further spontaneous losses in either group from 8 to 13 weeks.[27]

The lambda sign or twin peak sign occurs in a dichorionic gestation when both placentas have formed adjacent to each other and is most reliable between 10 and 14 weeks. It represents placental tissue extending between the intertwin membranes. By 20 weeks it will no longer be seen in 7% of dichorionic gestations.[28] Absence of the lambda sign at this gestational age neither excludes a dichorionic gestation nor implies a monochorionic gestation. Different

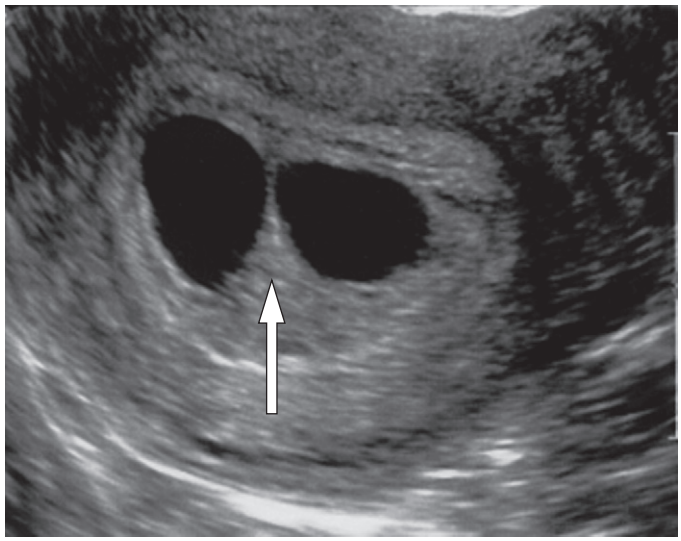


Figure 39.23 Two discrete gestation sacs with a positive lambda sign (arrow) at 8 weeks.

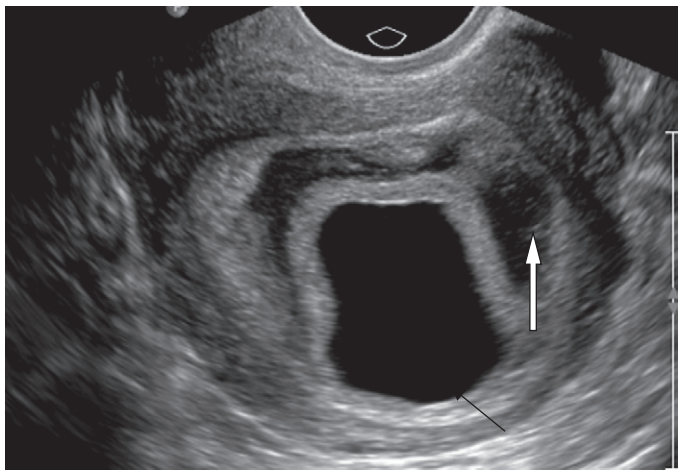


Figure 39.24 A retro membraneous haematoma (white arrow) adjacent to the true gestation sac (black arrow).

Table 39.6 Different monozygotic twin types

Time of division	Type of twinning
<4 days	Dichorionic diamniotic
4–8 days	Monochorionic diamniotic
8–13 days	Monochorionic monoamniotic
>13 days	Conjoined twins

Reproduced with permission from Elsevier.

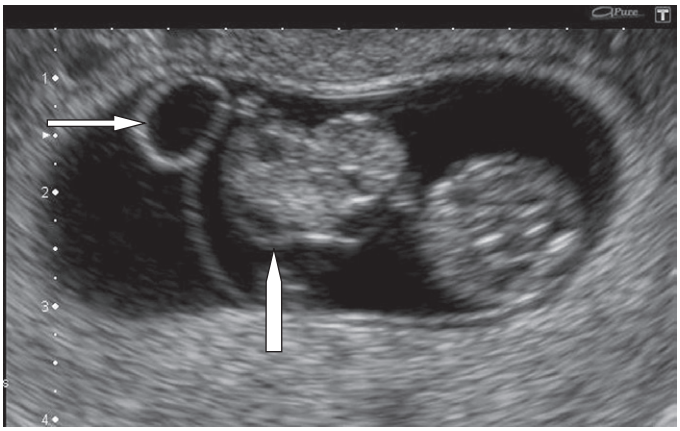


Figure 39.25 A single large yolk sac (thin arrow) in the chorionic cavity with 2 embryos, one showing abnormal development (block arrow) within a single amnion consistent with a MCMA pregnancy complicated by Twin Reversed Arterial Perfusion (TRAP) sequence.

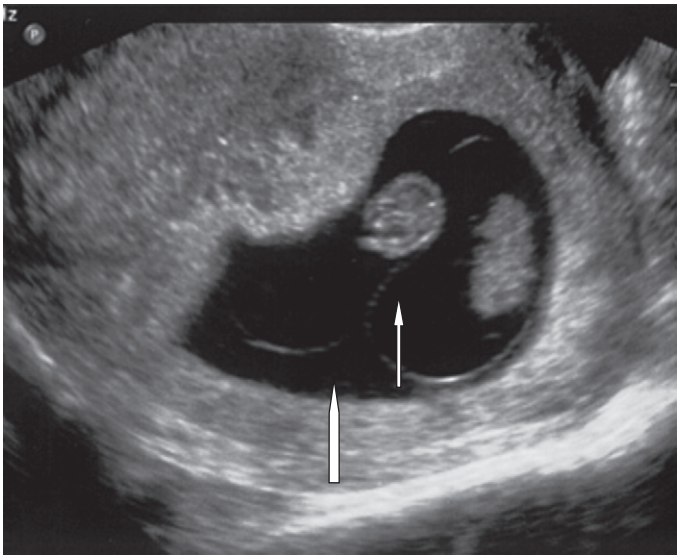


Figure 39.26 Two embryos each within their own amnion (thin arrow) within a single chorionic cavity (block arrow) consistent with a MCDA.

criteria then need to be used to establish chorionicity such as thickness of the intertwin membrane and fetal gender determination.[29]

Determining the amnionicity, in the presence of a single gestation sac and two embryos, depends upon visualisation of two discrete amnions. This is not easy early on because the amnion is thin and delicate. After 7 weeks, the differentiation between diamniotic and monoamniotic monochorionic gestation becomes easier as the developing amnion moves away from the embryo. Prior to that time determination of the amnionicity of a monochorionic pregnancy can be attempted by evaluating the number of yolk sacs. The very early embryonic disc lies within the forming amniotic cavity adjacent to the secondary yolk sac. One yolk sac implies a monochorionic monoamniotic (MCMA) pregnancy (Fig. 39.25). Two yolk sacs within a single chorionic cavity are consistent with a monochorionic diamniotic pregnancy (MCDA). It is often more prudent to wait until 10 weeks to confirm the amnionicity, at which stage the amnions of a diamniotic pregnancy will have enlarged sufficiently to contact each other and to form the thin intertwin membrane (Fig. 39.26).[30]



Figure 39.27 Conjoined twins; the type of union in this case is omphalophagus-xiphophagus.

Twinning

- Twinning occurs in 1% of all pregnancies.
- Two-thirds of twins will be dizygotic and one-third will be monozygotic.
- Dizygotic twins will always have a dichorionic placentation.
- The lambda (twin peak) sign occurs in a dichorionic gestation when both placentas have formed adjacent to each other.
- The lambda or twin peak sign is most reliable between 10 and 14 weeks.
- Absence of the lambda sign at 20 weeks gestation does not exclude a dichorionic gestation nor does it imply a monochorionic gestation.
- The perinatal mortality associated with twinning is six times that for singletons.
- The perinatal mortality of a monochorionic (MC) gestation is three to four times that of a dichorionic (DC) gestation.

Due to the increased perinatal mortality associated with twinning (six times that for singletons) with the mortality for a monochorionic (MC) gestation three to four times that of a dichorionic (DC) gestation, it is essential to determine chorionicity as soon as possible.[30]

Conjoined twins are extremely rare, occurring in 1 in 50 000 to 1 in 100 000 pregnancies. Conjoining can only occur in monozygotic pregnancies and is due to division of the zygote 13 days after fertilisation. The diagnosis may be missed prior to 10 weeks if a strict routine for scanning a pregnancy in the first trimester and careful separation with individual movement of the fetuses is not observed (Fig. 39.27).

First trimester biometry

Biological variability in embryonic development in the first trimester is minimal so it is possible to estimate the gestational age (GA) with a small margin of error. An accurate calculation of gestational age is essential for the correct evaluation of subsequent fetal growth during pregnancy.

Mean gestational sac diameter (MGSD)

The first structure that can be used to determine the gestational age is the gestational sac (GS). The measurement of the mean diameter of the sac can be obtained even if the yolk sac and embryo are not

Assessment of gestational age

- Measurement of the mean gestational sac diameter is the first parameter that can be used to determine gestational age.
- The rate of growth of the normal gestation sac is 1.1 mm/day.
- Measurement of the crown–rump length (CRL) between 6 and 12 weeks is the most accurate dating parameter.
- CRL measurements of gestational age are accurate to within 3–5 days.

visible provided the true nature of the gestation sac has been confirmed. The rate of growth of the gestation sac is 1.1 mm/day. The MGSD is an extremely useful way of placing the developing pregnancy along a developmental time line and monitoring progress. This measurement becomes less reliable with advancing gestation (Fig. 39.3).

Crown–rump length (CRL)

Between 6 and 12 weeks gestational age (GA), the measurement of the crown–rump length (CRL) of the embryo is most accurate for dating. The now classical study by Robinson and Fleming[31] on CRL is still the main reference for the assessment of gestational age in early pregnancy. There are no significant differences with measurements made by the transabdominal route or the transvaginal route. Because transvaginal scan provides superior resolution and more accurate identification of the embryonic structures than abdominal ultrasound, new charts have been developed for the period of gestation before 7 weeks. The original data of Robinson has been extrapolated from embryos of 7 mm in size down to embryos of 2 mm with preservation of accuracy and reliability.[31]

The accuracy of CRL measurements in determining gestational age is within 3–5 days. There is an optimum window for CRL measurement which is between 7 and 9 weeks using transvaginal scan. The confidence interval at 8 weeks is ±0.64 weeks and at 12 weeks is ±0.96 weeks.

EARLY PREGNANCY FAILURE

A pregnancy may fail either because the normal progression of the in-utero implantation ceases or because it does not implant within the uterus, i.e. it is an ectopic pregnancy.

Failure of normal progression of the in-utero implantation

Spotting or bleeding and cramping with a closed cervical os are common in early pregnancy, occurring in approximately 25% of patients.[32] About 50% of patients presenting with threatened miscarriage will have a normal outcome and 50% subsequently miscarry. The majority of pregnancy losses are sporadic and the commonest apparent cause of sporadic loss is a cytogenetic abnormality.

Two important features of early pregnancy loss need to be appreciated:

1. In patients presenting with threatened miscarriage who subsequently miscarry, the embryo is usually already dead at the time of presentation.
2. Spontaneous expulsion of the products of conception may be delayed.[33]

The highly charged emotional situation of an early pregnancy complication is not helped by inappropriate terminology. The use of appropriate ultrasound-based terminology is essential (Table 39.7).[34] Terms such as blighted ovum, anembryonic sac, trophoblastic bleeding, implantation bleeding and abortion are unacceptable and obsolete.

Table 39.7 Ultrasound-based terminology for early pregnancy problems

Diagnosis	Ultrasound appearance
Complete miscarriage in which there is usually cessation of pain and bleeding	Endometrial thickness <15 mm, no evidence of retained products
Incomplete miscarriage which clinically may still have pain and/or bleeding	Any thickening of the endometrium, heterogeneity of tissues or gestational sac
Delayed miscarriage in which clinically there is loss of pregnancy symptoms and usually minimal bleeding or pain	Gestational sac diameter >20 mm with no fetal pole or yolk sac. Fetal pole <6 mm with no fetal cardiac activity

Sonographic diagnosis of early pregnancy failure

Robinson's original statement relating to the fundamental importance of accurate ultrasound diagnosis of early pregnancy failure is still essential, i.e. the criteria that are formulated for the ultrasound diagnosis of early pregnancy failure must be capable of being applied retrospectively with complete reliability.[2,35]

The presence of embryonic cardiac activity is the single most important diagnostic finding indicating that the embryo is alive. Conversely sonographic demonstration that an embryo lacks cardiac motion is the most specific evidence of embryonic demise. This is only a reliable observation when the embryo has reached the discriminatory size of a CRL of 5 mm (6.2 weeks). For diagnostic purposes it is not how early cardiac activity can be visualised (2–3 mm embryos may demonstrate cardiac activity) but at what stage its absence is considered a definite sign of early pregnancy failure.[36]

The reliability of demonstration of lack of embryonic cardiac activity depends on a scrupulous scan technique and evaluation. The structure being measured must be an embryo and time should be spent trying to locate cardiac activity (Fig. 39.28). An inadequate, technically poor, transvaginal scan must be abandoned and repeated either by a more experienced observer or on a different occasion. If the embryonic size does not meet the diagnostic criteria for failure then the scan must be repeated after a week (allowing for an embryonic growth rate of 1.2 mm/day).[37]

In many patients, the embryo cannot be visualised at the time of initial sonographic examination and so the sonographic diagnosis of pregnancy failure cannot be made on the basis of embryonic cardiac activity. The diagnosis of pregnancy failure is possible based on gestational sac characteristics.[5,38]

The diagnostic ultrasound features of pregnancy failure prior to the visualisation of the embryo can be divided into major and minor criteria.

Major criteria:

1. gestation sac size characteristics
2. empty amnion sign
3. absence of growth of the gestation sac after a 7–10-day interval
4. gestation sac shape.

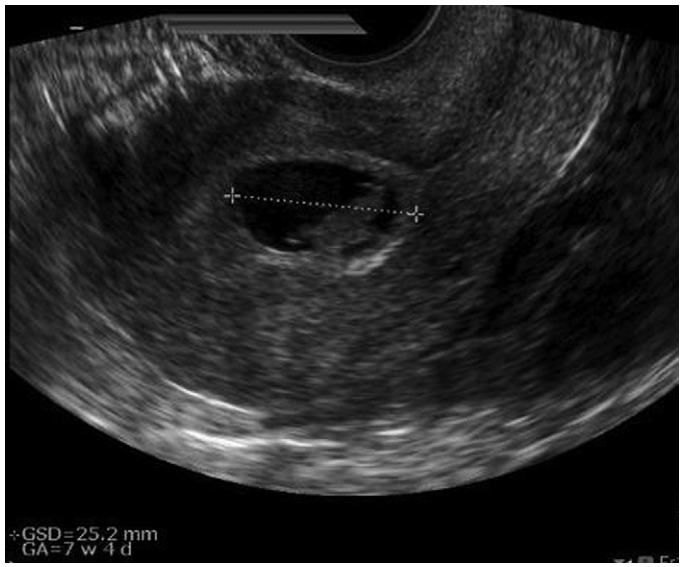


Figure 39.28 The structure being measured is not a sac and the mass within is definitely not an embryo.



Figure 39.30 The pathological double bleb sign due to an empty amnion (white arrow) adjacent to the yolk sac (black arrow).



Figure 39.29 A very large gestation sac lacking any discerning features such as yolk sac or embryo thereby fulfilling the RCR/RCOG criteria for failed pregnancy.

Minor criteria:

1. thin decidual reaction
2. irregular contour
3. absent double decidual sac sign
4. abnormally low position of the sac.

Major criteria

Gestation sac size

The most reliable indicator of abnormal outcome based on gestational sac characteristics is abnormal gestational sac size.

An abnormally large gestational sac is a sac of at least 25 mm MGSD on transabdominal scanning lacking an embryo, or a gestational sac of at least 20 mm MGSD on transvaginal scanning lacking a yolk sac or embryo (Fig. 39.29; Table 39.8). An abnormally large sac lacking an embryo is always abnormal and is usually due to an anembryonic gestation. This feature occurs in 45% of all failed first trimester pregnancies. These pregnancies contain a large number of chromosomal anomalies.[36,38]

Table 39.8 The discriminatory levels for gestational sac size

This is the gestational sac size correlated with absence of defining features:

Transabdominal MGSD >25 mm >8 weeks lacking an embryo
Transabdominal MGSD >20 mm >7.3 weeks lacking a yolk sac
Transvaginal MGSD >20 mm >7.3 weeks lacking an embryo or a yolk sac

These are the levels chosen by the Royal College of Radiologists/Royal College of Obstetricians and Gynaecologists, which are conservative levels.[37]

The empty amnion sign

As described earlier, at approximately 5.5 weeks menstrual age the amnion may be visualised as a 2 mm bleb adjacent to the yolk sac. The amnion becomes visible again when the CRL is about 8–12 mm as a thin, filamentous, rounded membrane surrounding the embryo. Visualisation of an amnion without an embryo is impossible in a normal gestation. The empty amnion sign is universally predictive of an anembryonic gestation. The double-bleb sign is a descriptive term applied to a pathologically empty amnion adjacent to the yolk sac (Fig. 39.30).[3,39]

Gestational sac shape

Grossly irregular contours/grossly aberrant shapes are readily recognised and reliably predict an abnormal outcome provided there is no distortion of the gestation sac by fibroids or an over-distended bladder. Only 10% of failed pregnancies demonstrate this feature (Fig. 39.31A and B).[5]

Minor criteria

Abnormally low position of the sac

An abnormally low position of the gestational sac within the endometrial cavity has been used as a prognostic feature of early pregnancy failure. Once an implantation in the isthmus has been

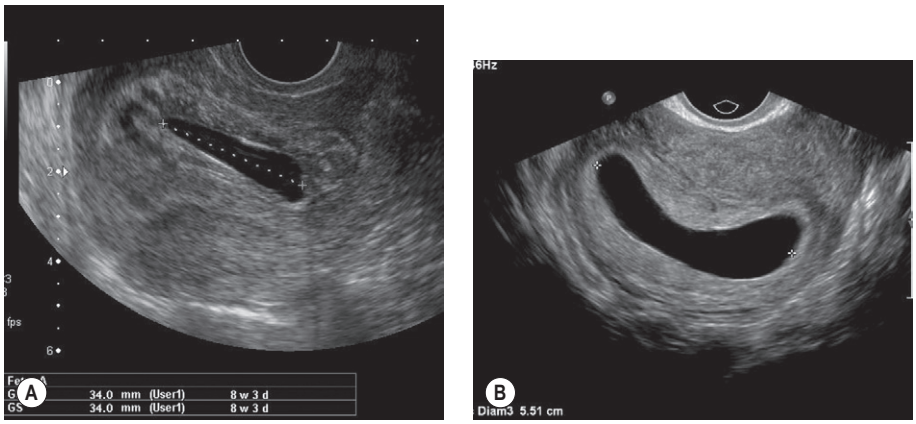


Figure 39.31 A and B: Grossly irregular shapes will also be predictive of an abnormal outcome.

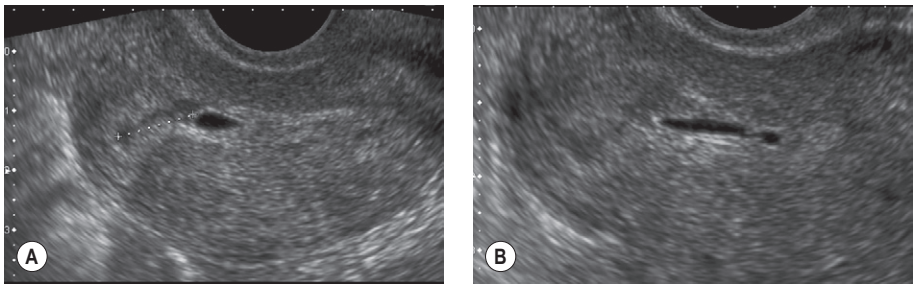


Figure 39.32 A and B: Two sequential images taken 3 minutes apart demonstrating movement of the gestation sac down through the endometrial cavity with a marked change in shape also.

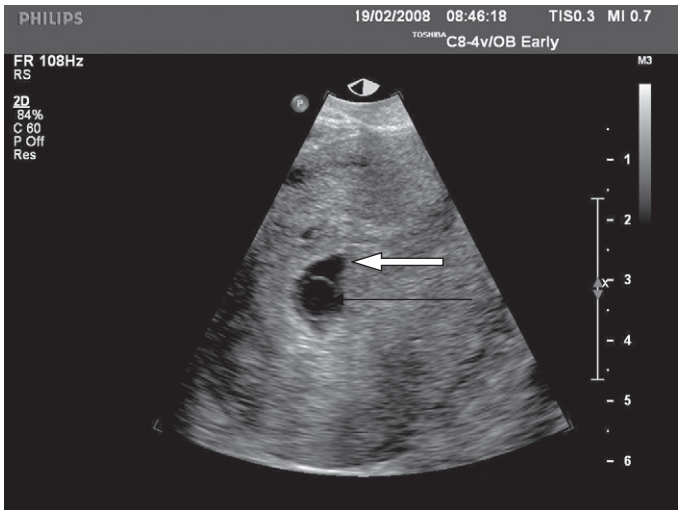


Figure 39.33 A gestation sac (white arrow) containing a yolk sac (black arrow) with virtually no true decidual reaction surrounding the entire gestation sac.

excluded, the low position within the uterine cavity is actually believed to be a stage in the evolution of a miscarriage and not a prognostic feature (Fig. 39.32A and B). Gentle pressure with the probe will often exaggerate this appearance and is referred to as the *sliding sign of probe pressure*.

Thin poorly reflective decidual reaction, weak decidual amplitude, absence of the double decidual sac sign

All of these features relate to an abnormality of the chorionic tissue and the decidual reaction. A very thin or weakly echogenic decidual reaction (Fig. 39.33) is reliably associated with an abnormal outcome. The converse is not true, as a very thick decidual reaction does not guarantee normality. Hydropic degeneration of the placenta and early molar change will produce a thickened chorionic tissue reaction (Fig. 39.34). The major role of the double decidual sign (DDS) is to confirm that the early collection of fluid seen is actually a true sac. In cases of pregnancy failure, the DDS sign may not be seen due to necrosis of the decidua; this is not a sign to be used in isolation.[3]

Early pregnancy failure

- 25% of pregnant women will have spotting or bleeding in early pregnancy.
- 50% of patients presenting with threatened miscarriage will have a normal outcome.
- The diagnostic ultrasound criteria for early pregnancy failure must be reliable.
- Demonstration that an embryo of >6 mm lacks cardiac motion is the most specific evidence of embryonic demise.
- A sac of 25 mm MGSD on transabdominal scan lacking an embryo is a failed pregnancy.
- A sac of 20 mm MGSD on transvaginal scan lacking a yolk sac or an embryo is a failed pregnancy.
- The empty amnion sign is universally predictive of an anembryonic gestation.

EARLY PREGNANCY COMPLICATIONS

First trimester haemorrhage

There are many potential sites for blood accumulation in pregnancy:

1. bleeding behind the placenta which separates the placenta from the endometrium, i.e. abruption
2. subchorionic, the commonest cause of bleeding in the first trimester

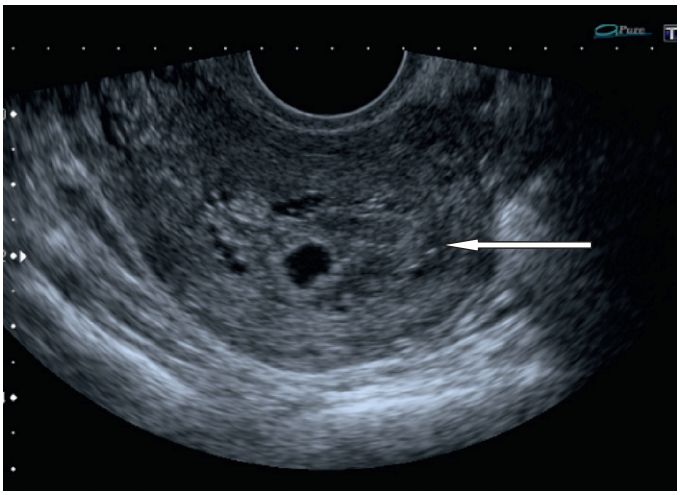


Figure 39.34 A thickened heterogeneous chorionic reaction (white arrow) due to early molar change within the placenta.

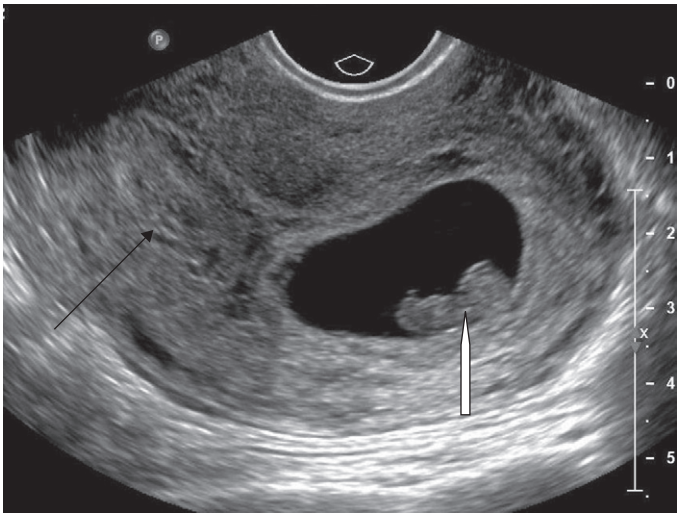


Figure 39.35 Acute echogenic and heterogenous haemorrhage (thin arrow) adjacent to a gestation sac containing a dead embryo (block arrow).

3. chorioamniotic
4. intra-amniotic.

Subchorionic haemorrhage

This type of intrauterine haemorrhage (IUH) is the commonest site of bleeding within the early gestation sac and is a crescent-shaped echo-free area between the chorionic membrane and the myometrium. The appearance of the blood depends on the age of the haematoma. Acute bleeding will be echogenic and particulate (Fig. 39.35). As the haemorrhage evolves it becomes less echogenic (Fig. 39.36). Understanding of the resolution of these haematomas and the prognostic relevance of this ultrasound finding is limited.[40]

The size of a subchorionic haematoma is graded according to the percentage of the chorionic cavity elevated by the haematoma:

- small: < ⅓
- moderate: ⅓ – ⅔ (Fig. 39.37)
- large: > ⅔ (Fig. 39.38).

The overall loss rate with a subchorionic haematoma is 9.3% (7.7–9.5% with a small to moderate haematoma and 18.8% with a

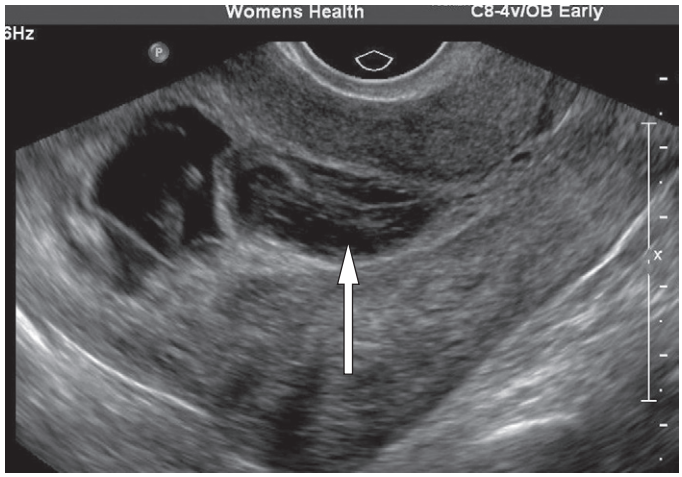


Figure 39.36 Evolving haematoma becoming less echogenic and more fluid-like.

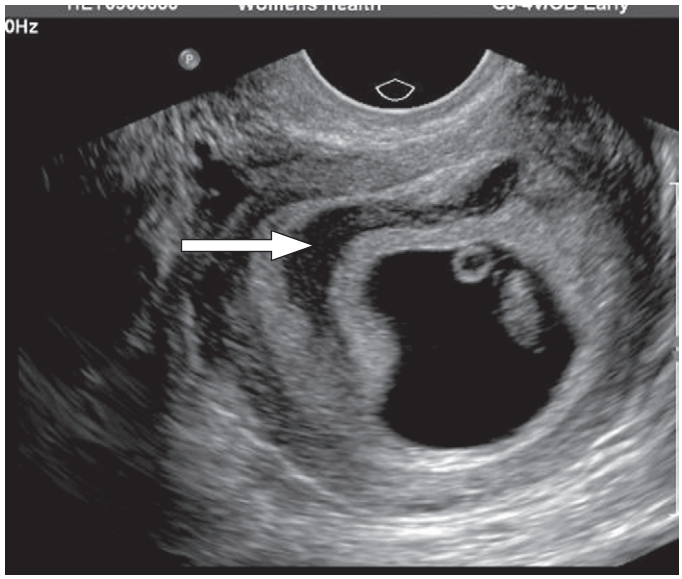


Figure 39.37 A moderate subchorionic haematoma.

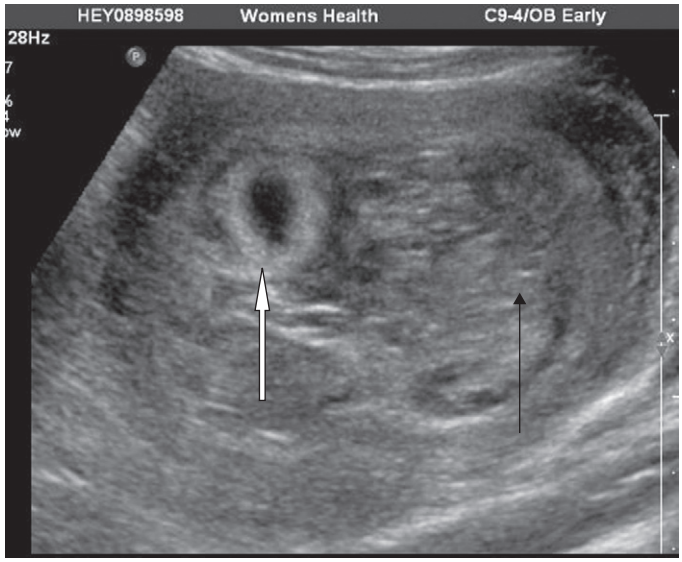


Figure 39.38 A haematoma (black arrow) that is so large that the gestation sac (white arrow) appears to have no attachment to the endometrium.

Table 39.9 Adverse outcome related to maternal age and gestational age at presentation

Maternal age	<35 years: loss rate 7%
Maternal age	>35 years: loss rate 14%
Gestational age	<8 weeks: loss rate 14%
Gestational age	>8 weeks: loss rate 6%

large haematoma) Additional factors will have an impact on the outcome, i.e. maternal age at presentation and gestational age at presentation[41] (Table 39.9). A haematoma cannot be treated nor can the outcome with a haematoma be changed. Moreover what may actually be more important and significant for the patient is not the size of the haematoma but its location and the possible association with intrauterine growth retardation later in pregnancy.[42]

It has been observed that women with bleeding in the second half of the first trimester are at higher risk of preterm premature rupture of fetal membranes and preterm labour. These risks are independent of the presence or absence of an IUH on the initial ultrasound examination. This would suggest that threatened miscarriage in the first trimester is a risk factor for adverse pregnancy outcome regardless of the ultrasound findings.[41]

Crown–rump length

There is conflicting evidence for an association between early growth restriction, as defined by a deficit between the CRL and that predicted by the last menstrual period, and karyotypic abnormalities. A smaller than expected CRL has been associated with subsequent miscarriage but this finding must be used with caution and not as a solitary parameter for pregnancy failure.[43]

Early pregnancy failure due to ectopic implantation

The current incidence of ectopic pregnancy is difficult to estimate from available data, not only because inpatient hospital treatment of ectopic pregnancy has decreased but also because the number of hospital visits for a single ectopic pregnancy has increased.[44] The incidence of ectopic pregnancy in the UK is 11/1000 at present, which is twice that in the period 1973–1999 (4.9/1000).[45] This increase in incidence is strongly associated with the increased incidence of pelvic inflammatory disease that preceded it.[46] However, the rise in incidence is probably also related to greater diagnostic accuracy as a result of transvaginal ultrasound and more sensitive immunoassays for β-hCG.

Even though the incidence is increasing, morbidity and mortality have diminished in inverse proportion. However, it is important to remember that ectopic pregnancy is still the leading cause of pregnancy-related maternal death in the first trimester. In 2003 to 2005 ectopic pregnancy was responsible for 10 maternal deaths despite improved diagnostic methods leading to earlier detection and treatment. In 1985 to 1987 ectopic pregnancy accounted for 11 maternal deaths.[46] Transvaginal ultrasound has been pivotal in the advances in diagnosis. Early diagnosis has altered the clinical presentation from that of a life-threatening condition to a condition that is amenable to medical management in some cases.

Risk factors for ectopic pregnancy

All patients of reproductive age are at risk for ectopic pregnancy. The prevalence of ectopic pregnancy in a clinically suspected group varies according to the patient population and their inherent risk factors. The following factors are associated with an increased incidence of ectopic pregnancy. The common element is prevention or delay of transit of the zygote through the fallopian tube.[47]

Table 39.10 Location of ectopic gestations

95% of all ectopics are tubal in location:
- 70% will be ampullary
- 2% will be in the isthmus of the fallopian tube

5% of ectopics will be non-tubal in location:
- 2–5% will be cornual or interstitial in location
- 0.5–1% of all ectopics will be ovarian
- 0.1% of all ectopics will be cervical

Ectopic pregnancy

- The present incidence of ectopic pregnancy in the UK is approximately 11/1000.
- Ectopic pregnancy is still the leading cause of pregnancy-related maternal death in the first trimester.
- All patients of reproductive age are at risk for ectopic pregnancy.
- Prevention or delay of transit of the zygote through the fallopian tube is the common element to all ectopic risk factors.
- Unusual ectopic locations are increasing in incidence.
- 95% of all ectopics are tubal and 70% of these will be ampullary in location.
- 2–5% of all non-tubal ectopics will be cornual or interstitial in location

1. A past history of salpingitis, pelvic inflammatory disease or tubal surgery.
2. Previous ectopic pregnancy (conservative methotrexate treatment for ectopic pregnancy 8% risk of recurrence, conservative surgery 15%).
4. Use of an intrauterine contraceptive device. (The lowest rates are observed with the copper-containing intrauterine contraceptive devices and the progesterone-releasing IUCD. The latter is, however, associated with a higher absolute rate of ectopic pregnancy than that seen in women not using any contraception.)
5. Advanced maternal age.
6. Infertility.
7. Ovulation induction.
8. In-vitro fertilisation (particularly if the cause of infertility is due to tubal factors).

As well as the increase in overall rate of ectopic gestation, there has also been an increase in unusual ectopics (Table 39.10),[48] namely: heterotopic gestation (the simultaneous occurrence of an ectopic and an intrauterine pregnancy – 1% of artificial reproduction techniques, 1/30 000 in the non-IVF population); interstitial and cervical ectopic gestations; bilateral ectopic pregnancy; 'trophoblast in regression', i.e. an early ectopic pregnancy that is actually in the process of spontaneous resolution. There are undoubtedly ectopic pregnancies that implant, die and resorb spontaneously.

The early diagnosis of ectopic pregnancy provides the patient with choice in terms of often a non-surgical approach to treatment. The sonographic diagnosis is based on a combination of morphological findings in the uterus and the adnexa. The diagnosis of ectopic gestation should be considered at each site within the pelvis.

The uterine findings in ectopic pregnancy

Normal intrauterine pregnancy

The primary role of ultrasound is the identification of an intrauterine pregnancy at the earliest possible stage. This involves visualisation and recognition of the gestation sac when it first appears even as a small 2 to 3 mm hypoechoic collection of fluid surrounded by an echogenic rim. Recognition at this stage is dependent on subtle



Figure 39.39 A trilaminar endometrium as seen in the peri-ovulatory phase of the menstrual cycle. Proven ectopic.

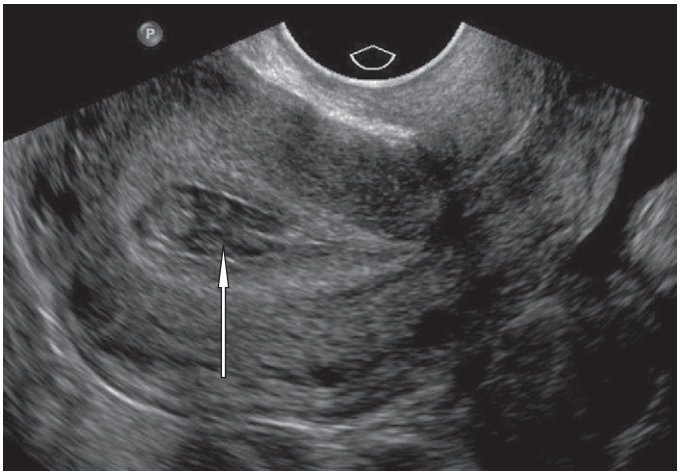


Figure 39.40 Heterogeneous decidual reaction. Proven ectopic.

Table 39.11 The endometrial appearances in ectopic gestation

1. Homogeneously thickened and echogenic: secretory endometrium seen in 22% of cases
2. Thin
3. Trilaminar in appearances: early proliferative endometrium seen in 12% of cases (Fig. 39.39)
4. Demonstrate a pseudo-gestation sac
5. Non-specific thickening often quite heterogeneous: decidual reaction seen in 42% of cases (Fig. 39.40)

findings (Figs 39.6, 39.7 and 39.8). A recent study suggests that 74% of ectopic pregnancies can be visualised at first ultrasound examination.[49]

Endometrial appearances

Failure to diagnose an intrauterine pregnancy means that the assessment of the endometrium itself is of major importance. There are a number of possible endometrial appearances that can occur in an ectopic pregnancy (Table 39.11; Figs 39.39 and 39.40).[50] It would be useful if there was one specific appearance of the endometrium which would diagnose an ectopic gestation but, though there has been much debate, unfortunately this is not the case.[51]

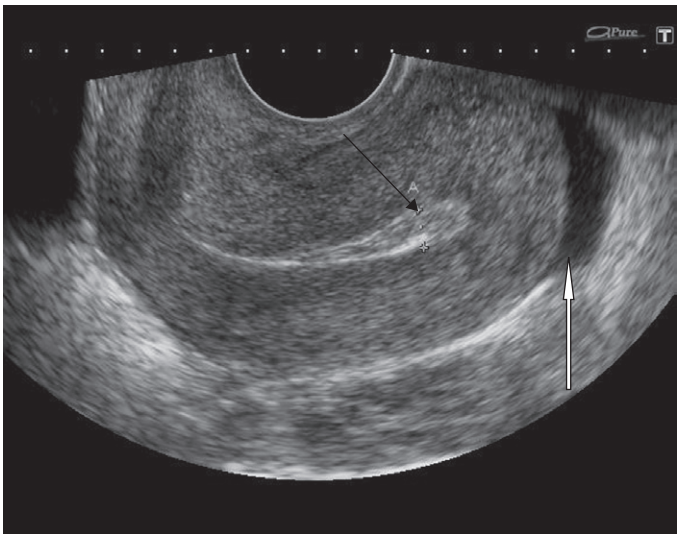


Figure 39.41 Thin endometrium (black arrow) with fluid in the Pouch of Douglas (white arrow) Proven ectopic.

The endometrium during the late proliferative phase/peri-ovulatory stage of the menstrual cycle has a trilaminar appearance consisting of three hyperechoic and two hypoechoic lines. There are conflicting reports on its usefulness but in general it is thought to be unhelpful in the diagnosis of ectopic gestation.[52] Conversely, a thin endometrium is helpful because it is not compatible with a normal ongoing intrauterine pregnancy (Fig. 39.41).[53]

The pseudo-gestation sac

This is seen in approximately 5% of all ectopic pregnancies. It simply consists of fluid within the endometrial cavity (Fig. 39.42). The outline of this 'sac' is elongated and irregular, the decidual reaction is usually less than 2 mm and there may be debris within the fluid. The shape of the pseudo-gestation sac will vary over the course of the scan and can be made to change with probe pressure (sliding sign of probe pressure).

The adnexal findings in ectopic pregnancy

The appearances of the adnexal region (Table 39.12) will depend on the gestational age at which the patient is being examined.

Normal adnexal regions

Adnexal abnormalities are not always observed in ectopic gestations, particularly in patients undergoing IVF due to the very early timing of the scan. In 15–35% of women there will not be an identifiable adnexal lesion. Even in the presence of normal adnexa, there is still a risk of about 5% for the presence of an *unruptured* ectopic pregnancy.[53] Any adnexal finding assumes greater importance if the pregnancy test is positive and there is no evidence of an intrauterine pregnancy, particularly if the risk of ectopic gestation based on the history is high. The negative predictive value of normal adnexa in this situation will be much lower.[54]

Tubal ring with yolk sac/tubal ring with embryo

The presence of an adnexal mass with a yolk sac or an embryo is found in 16–32% of all ectopics (Fig. 39.43). Higher rates are a

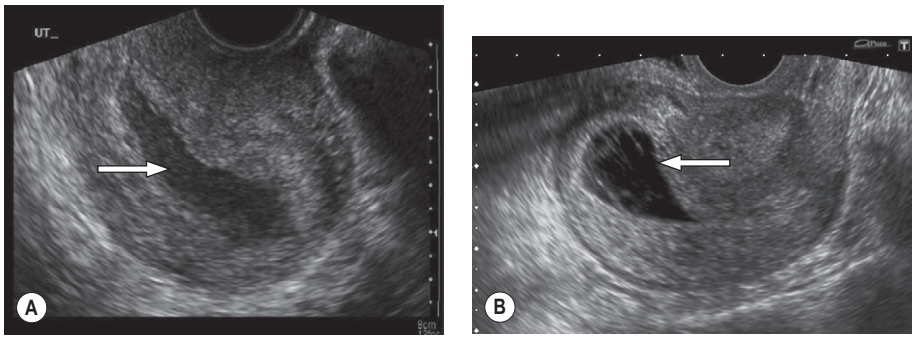


Figure 39.42 A and B: Two very different examples of fluid within the central endometrial cavity echo (white arrow) consistent with a pseudo-sac.

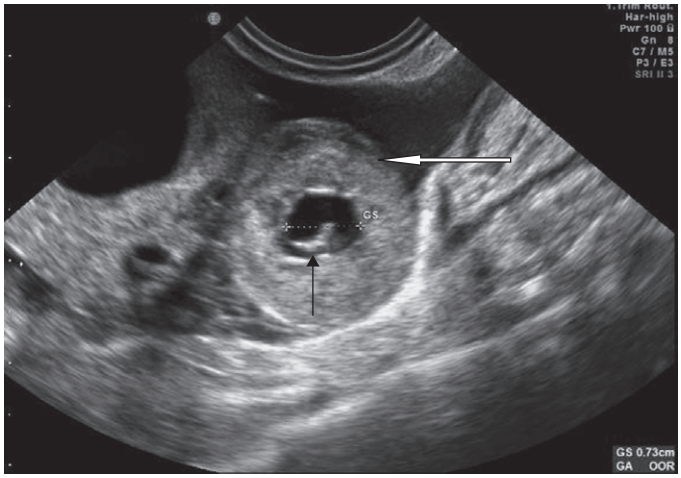


Figure 39.43 An adnexal mass (white arrow) containing a yolk sac and an embryo (black arrow).

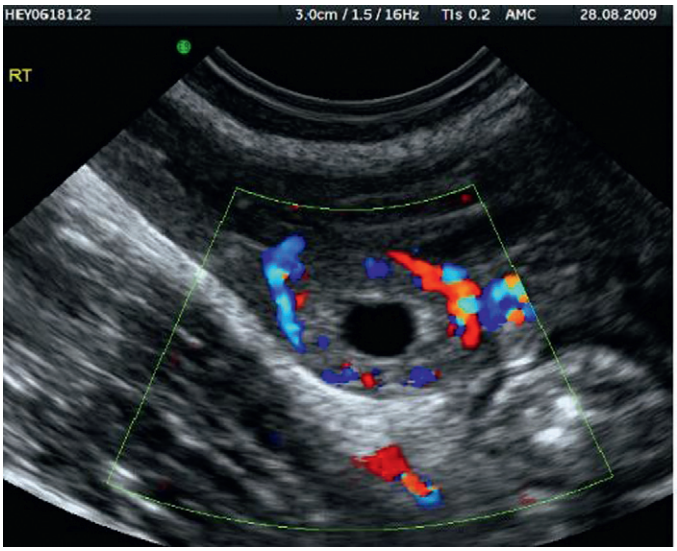


Figure 39.44 The bagel sign: an unruptured right-sided ectopic pregnancy.

Table 39.12 Possible adnexal findings in an ectopic gestation

1. Normal adnexal regions (negative findings)
2. Tubal ring ± yolk sac ± embryo
3. Complex mass
4. Free peritoneal fluid

consequence of early scans and a higher proportion of unruptured ectopic pregnancies (Fig. 39.44). The appearance of the well-defined gestation sac within the unruptured tube is likened to a bagel or doughnut.[55] The corpus luteum is ipsilateral to the tubal pregnancy in about 70% of cases (Fig. 39.45) and contralateral to the ectopic in 25–30% of cases.[56] The two structures can be similar in appearances but they are differentiated by the following factors: the corpus luteum is eccentrically placed within a border of normal ovarian tissue (Fig. 39.46); the tubal ring, in contrast, is a central hypoechoic fluid within a mass of echogenic trophoblastic tissue (Fig. 39.47).[57]

Complex mass

A complex mass within the adnexa is the most frequent sonographic finding seen in 15–20% of ectopics (Fig. 39.48).[58] This complex mass is either a tubal miscarriage or tubal rupture. Transvaginal scanning is expanding its role from simple diagnosis to determining prognosis, with an increasing role in selecting patients who can be managed conservatively or medically rather than surgically.[59]

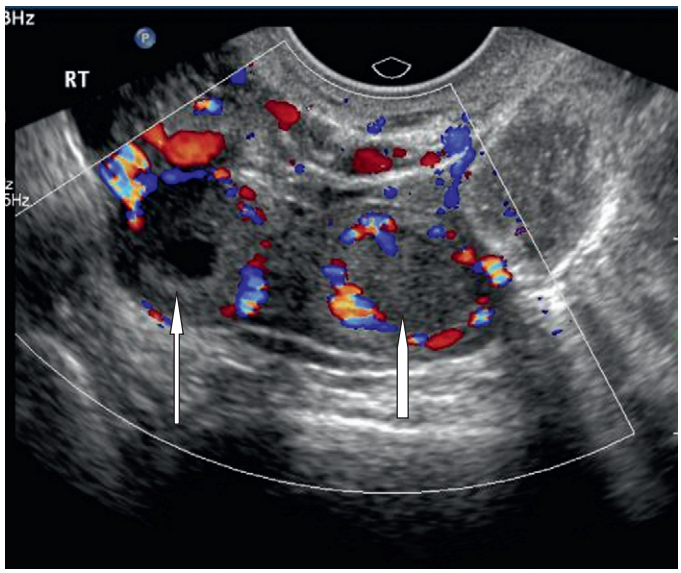


Figure 39.45 An unruptured ectopic 'bagel sign' (thin arrow) ipsilateral to the corpus luteum (thick arrow).

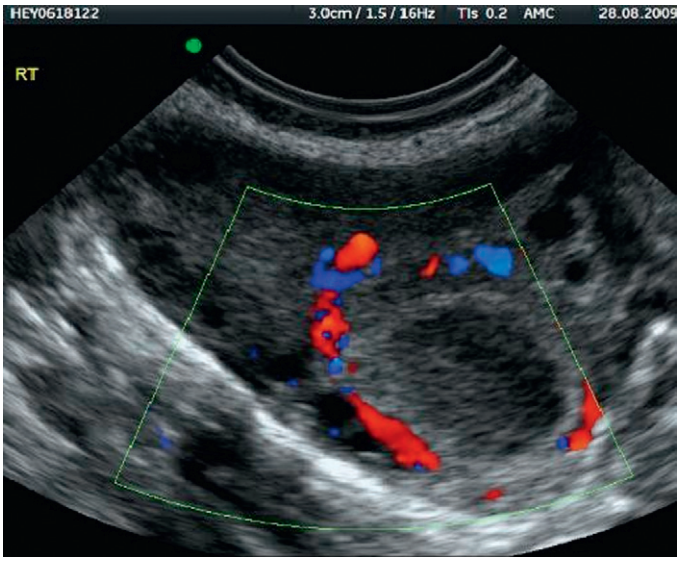


Figure 39.46 The corpus luteum eccentrically placed within normal ovarian tissue. The 'ring of fire' around the corpus luteum is the colour flow appearance of peritrophoblastic flow.

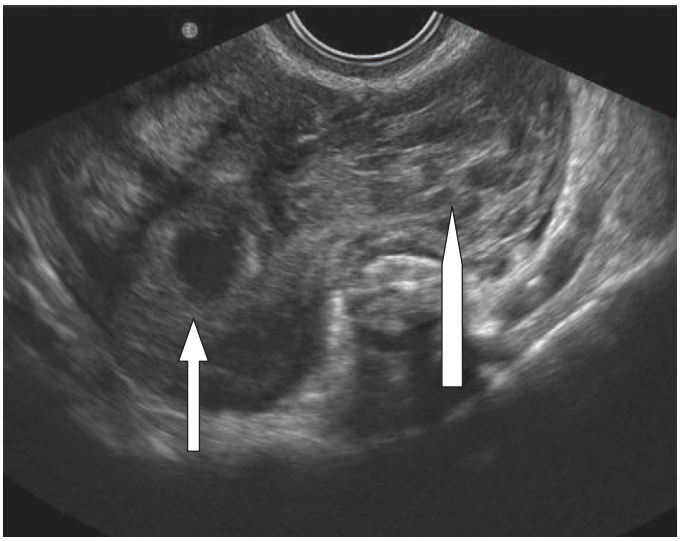


Figure 39.48 An indistinct mass (block arrow) which could be either tubal rupture or tubal miscarriage lateral to the right ovary (thin arrow).

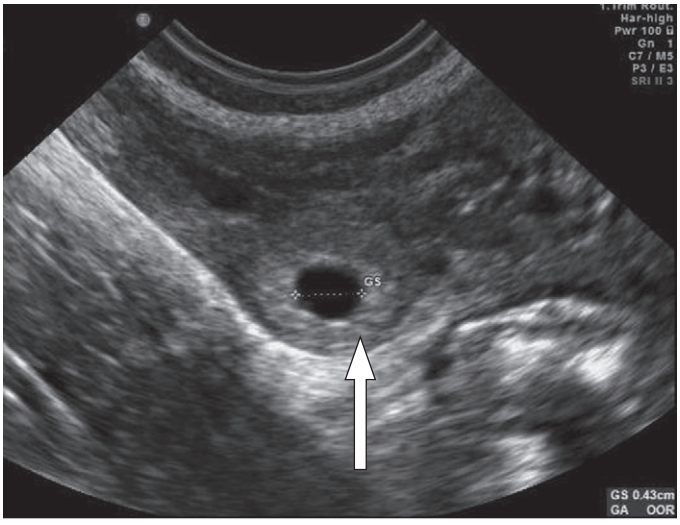


Figure 39.47 The tubal ring consists of centrally placed fluid within an echogenic ring (thin arrow).

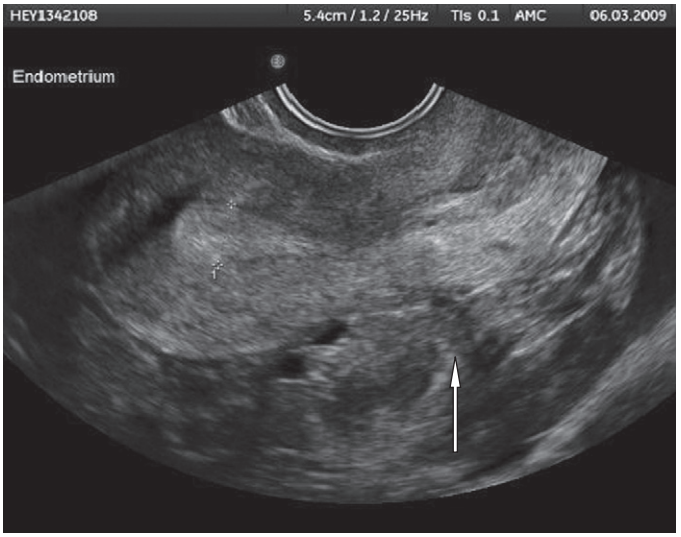


Figure 39.49 An ill-defined heterogeneous mass (thin arrow) conforming to the shape of the pelvis associated with a large amount of particulate free fluid: tubal rupture.

Tubal rupture is a consequence of tubal necrosis with profound haemorrhage. If a complex pelvic mass has poorly defined margins it is probably due to tubal rupture rather than tubal miscarriage (Fig. 39.49). Risk factors are listed in Table 39.13.
Tubal miscarriage occurs due to arrest of development of the ectopic with expulsion of the products of conception through the fimbria. The resulting pelvic mass is therefore usually well defined and localised (Fig. 39.50).

Table 39.13 Risk factors for tubal rupture

1. History of tubal damage
2. History of infertility
3. β-hCG level >10 000 IU/L

Intraperitoneal fluid

Intraperitoneal fluid is found in 10–30% of all ectopics and fluid will be seen in 20% of normal pregnancies due to exudation from the normal corpus luteum. There is no quantitative amount of fluid that is diagnostic but the greater the volume the greater the likelihood of an ectopic gestation (Fig. 39.51). The possibility of finding a ruptured ectopic is extremely low if there is no free intraperitoneal fluid. The nature of the fluid can be useful as echogenic fluid will be found in 25–36% of patients with an ectopic gestation.[60]

The role of Doppler ultrasound in the diagnosis of ectopic pregnancy

There are three areas in the pelvis that can be evaluated with colour Doppler as an adjunct to simple greyscale ultrasound assessment when attempting to diagnose an ectopic pregnancy:[61]

1. An adnexal mass, if it is due to ectopic trophoblastic tissue, will demonstrate peritrophoblastic flow, i.e. intense

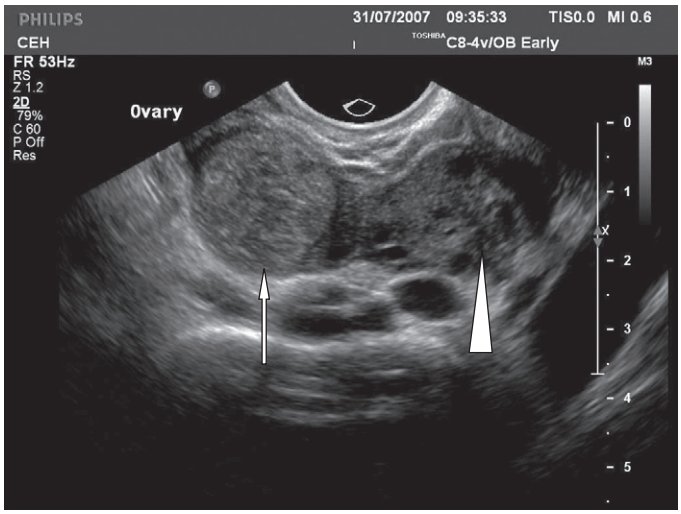


Figure 39.50 **A very well defined mass** (thin arrow) adjacent to the left ovary (block arrow) consistent with a tubal miscarriage.

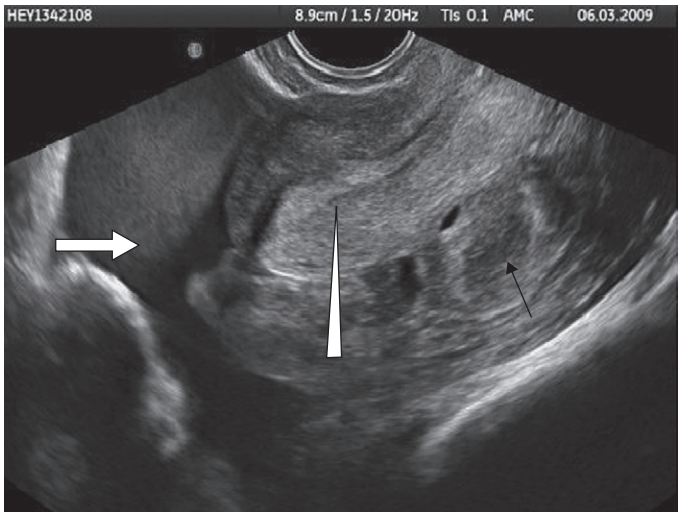


Figure 39.51 **An empty uterus** containing echogenic endometrium only (arrowhead), pelvic clot (thin arrow) and a large amount of particulate free fluid (block arrow) consistent with tubal rupture.

circumferential flow on colour Doppler with the high-velocity, low-resistance Doppler signal associated with developing trophoblast seen on spectral analysis.
2. Confirmation that the mass is actually the corpus luteum within the ovary with the colour flow 'ring of fire' (Fig. 39.46).
3. Demonstration of arterial flow within the endometrium, which lowers the risk of ectopic pregnancy.

Unusual ectopic gestations

Interstitial ectopic gestation

Interstitial or cornual ectopic pregnancy accounts for 2–3% of all ectopic gestations (Fig. 39.52). Two predisposing factors are in-vitro fertilisation (IVF) and a history of an ipsilateral salpingectomy.[62] One third of all interstitial pregnancies are detected in the IVF group of patients. Interstitial ectopics present as larger pregnancies because of the greater degree of myometrial distensibility of the cornual region. As a result of the larger sac size and abundant dual blood supply, the degree of viability is far higher than in tubal

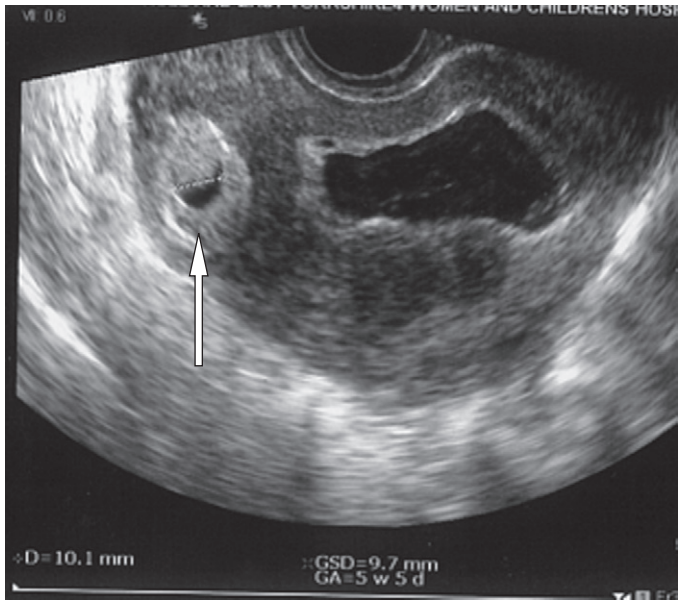


Figure 39.52 **A gestation sac** (thin arrow) in the right interstitial region consistent with an interstitial ectopic.

Table 39.14 **Presentation of interstitial ectopics**

36–44% of interstitial ectopics will be viable and so present with a live embryo compared with 17–21% of tubal ectopics
36% will present with an empty sac
28% will just be a solid heterogeneous mass

ectopics (Table 39.14) and when rupture occurs haemorrhage can be catastrophic and fatal. The diagnosis of an interstitial ectopic is based on the eccentric location of the gestation sac, which can be considered as follows:[63]

1. A distance of at least 10 mm from the lateral margin of the endometrium to the gestation sac/trophoblastic mass.
2. Thinning of the myometrial mantle to less than 5 mm all around the sac. However, rather than assign a rigid measurement, it is more important to visualise a mantel or rim of myometrium (irrespective of actual thickness) all around the gestation sac interrupted only by the interstitial line.
3. Absence of the double decidual sac sign because the pregnancy has not implanted within the endometrium.
4. The presence of the interstitial line sign has improved the diagnostic sensitivity of ultrasound in diagnosing interstitial ectopics. This refers to the interstitial part of the tube joining the endometrium to the trophoblast. The interstitial line has better sensitivity and specificity than either eccentric gestation sac location or myometrial thinning (Figs 39.53 and 39.54).

The delayed diagnosis of interstitial pregnancy is responsible for the high maternal mortality rate of 2–2.5% when compared to 0.14% for tubal ectopics. It is important to remember that an angular pregnancy is not an interstitial pregnancy. An angular implantation is a normal intrauterine pregnancy which just happens to be high and lateral within the uterine cavity. It is of no consequence. The term cornual pregnancy should be restricted to a pregnancy present in the rudimentary horn of a bicornuate uterus.[53]

Cervical ectopic gestation

Cervical ectopics account for 0.1% of all ectopic gestations. The precise aetiology is unknown but is likely due to a combination of

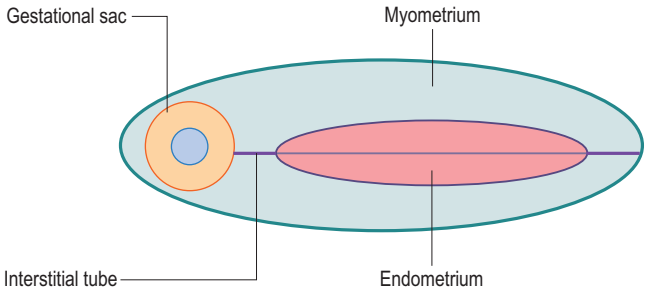


Figure 39.53 Diagrammatic representation of the interstitial line sign. Reproduced with kind permission form Wiley Interscience.

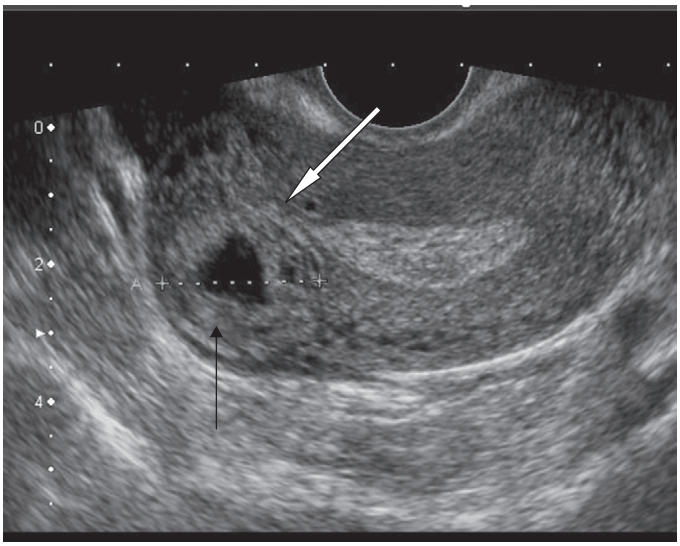


Figure 39.54 **Ultrasound demonstration of an interstitial ectopic;** empty gestation sac (black arrow) and the interstitial line (white arrow).

factors: local cervical pathology of iatrogenic origin such as previous dilatation and curettage, Asherman's syndrome, caesarean section, cervical or uterine surgery and IVF with embryo transfer.[64] The diagnosis requires visualisation of an intracervical ectopic gestation or an intracervical trophoblastic mass. Transabdominal scanning is extremely helpful in this situation and often suggests the diagnosis as it allows visualisation of the uterus, cervix and vagina in a single plane. Indeed it may be preferable to transvaginal scanning in advanced cases (Fig. 39.55). The true cervical pregnancy needs to be differentiated from the cervical stage of normal miscarriage[65] (Tables 39.15 and 39.16; Figs 39.56, 39.57, 39.58 and 39.59).

Caesarean scar ectopic pregnancy (Table 39.17)

A gestation sac in the lower uterus causes great concern and presents a very definite diagnostic difficulty. A true sac low in the uterus could be:

1. evolving miscarriage
2. a caesarean scar ectopic pregnancy
3. implantation of a sac onto a caesarean section scar.

The differentiation of a pregnancy attached to a caesarean section scar and a true scar ectopic is important (Fig. 39.60). Low anterior implantation of the sac onto a scar has been associated with placenta accreta (Fig. 39.61). This sonographic feature of first trimester diagnosis of placenta accreta carries all the attendant complications of not only early pregnancy failure but also accreta complicating delivery.[66]

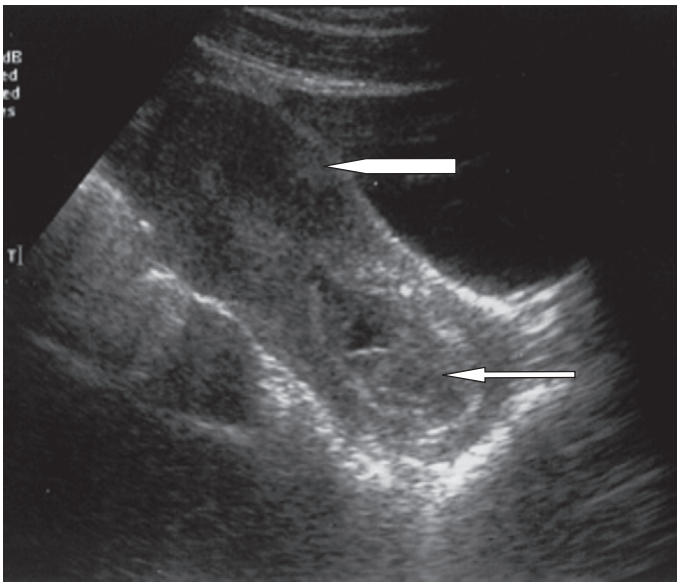


Figure 39.55 **A transabdominal scan** illustrating the uterus (block arrow) and cervix (thin arrow) in a single plane which greatly facilitate the diagnosis of cervical ectopic.

Table 39.15 **Features of a cervical miscarriage**

1. The embryonic heart beat is absent
2. The uterus is enlarged and globular (Fig. 39.56)
3. The endometrium is a mixed echogenic mass and the internal cervical os is open (Fig. 39.57)
4. No intact cervical canal is seen
5. With repeat scanning increased crenellation and distortion of the sac is seen

Table 39.16 **Features of a true cervical ectopic**

1. An embryonic heartbeat is often present and the embryo grows with time
2. The uterine fundus is small and hourglass shaped (Fig. 39.58)
3. The endometrium is a regular echogenic decidual reaction or shows pseudo-gestation sac formation (Fig. 39.58)
4. The internal os is closed
5. Intact cervical canal seen between the endometrium and the sac
6. The sac is round and unchanged on repeat scanning apart from showing an increase in size (Fig. 39.59)

Ovarian ectopic gestation

These ectopics account for 1:3600 to 1:13000 pregnancies. The presence of an intrauterine device is considered a risk factor for ovarian ectopic gestation. The diagnosis is made sonographically on the basis of:

1. There is no evidence of an intrauterine pregnancy.
2. There is an adnexal mass which cannot be separated from the ovary, i.e. the pregnancy will be surrounded by ovarian tissue and it will not be possible to separate the ectopic from the ovary, i.e. the 'sliding organs sign' is negative.
3. There will be progressive enlargement of the ovary.
4. There will be more than a structure resembling the 'corpus luteum' within the ovary.[67]

The negative sliding organs sign will be present in some tubal ectopics when adhesions cause the ectopic to be fixed to the ovary.[68]

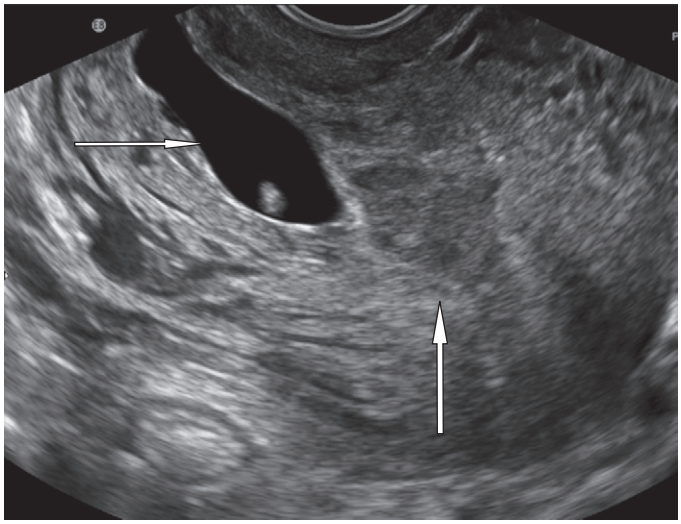


Figure 39.56 A sac can be seen within the cervix (thin arrow) but this uterus is enlarged and globular and the endometrium is heterogenous (block arrow).

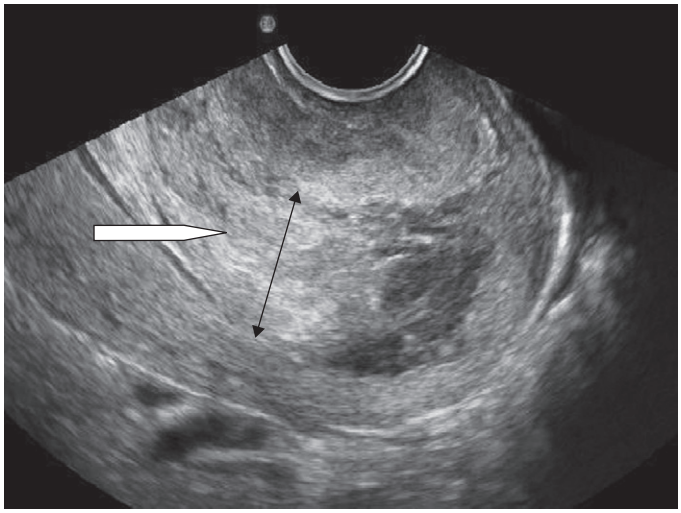


Figure 39.57 In the cervical stage of a miscarriage the endometrium (block arrow) will be heterogenous and ill defined and the internal os (thin arrow) is open.

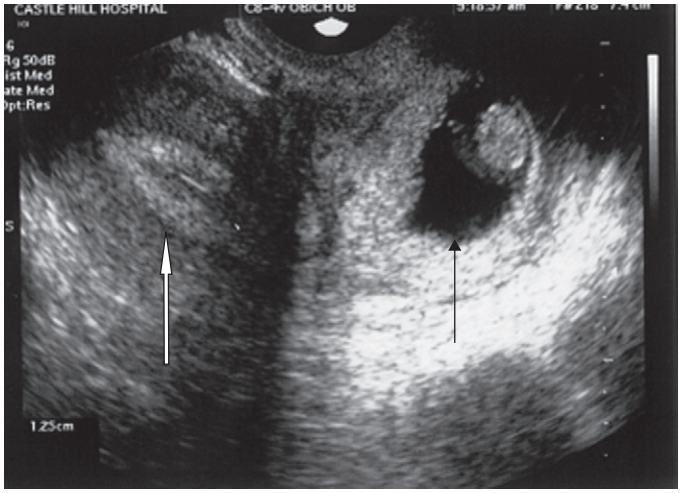


Figure 39.58 In a cervical ectopic (black arrow) the uterus is small. The uterus and cervix produce an hour glass shape. The endometrium is regular and in this case trilaminar (white arrow).

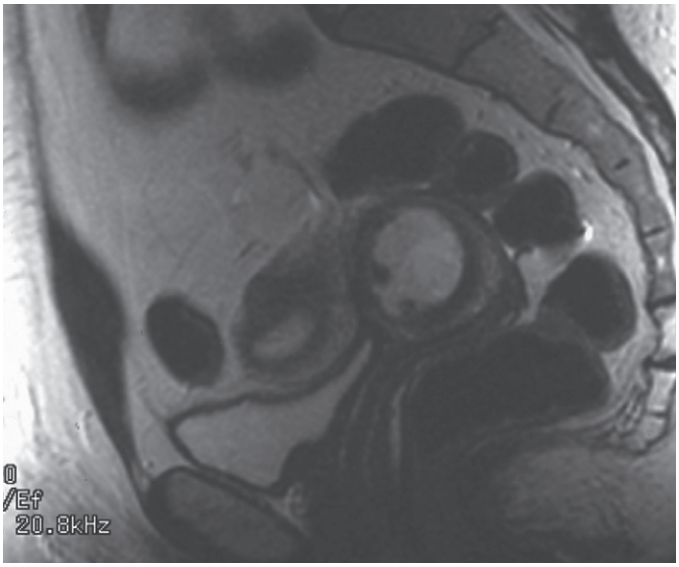


Figure 39.59 MRI demonstration of a true cervical ectopic: hourglass uterus and extreme thinning of the wall of the cervix due to growth of the trophoblast.

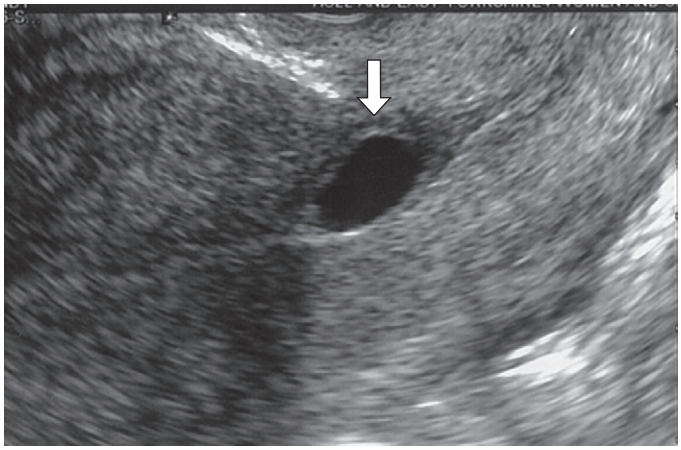


Figure 39.60 A true scar ectopic in which the gestational sac is embedded in the scar tissue within the anterior myometrium (white arrow) eccentric to the central cavity echo (black arrow)

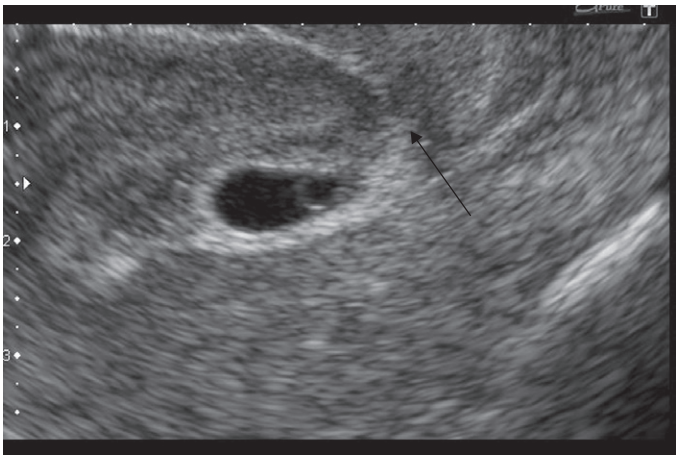


Figure 39.61 Anterior implantation of the gestation sac onto the scar (thin arrow).

Table 39.17 Ultrasound features that facilitate a diagnosis of caesarean scar pregnancy

1. The uterus is empty
2. The endometrium is clearly demonstrated and not distorted by blood or fluid
3. The cervical canal is empty and not ballooned
4. The gestational sac shows a 'double ring' sign in the anterior part of the isthmic portion of the uterus
5. The gestational sac is embedded and surrounded by a diminished myometrial layer
6. A discontinuity in the anterior wall of the uterus
7. The gestation sac is separated from the endometrial cavity
8. Evidence of functional trophoblastic/placental circulation on Doppler examination
9. Negative 'sliding organs sign', which is defined as the inability to displace the gestational sac from its position at the level of the internal os using gentle pressure applied by the transvaginal probe

Table 39.18 Falling β-hCG level

A falling β-hCG level is most likely consistent with a failed pregnancy, which may simply be an:

1. Arrested intrauterine pregnancy (Fig. 39.62) previously called an anembryonic gestation
2. Tubal miscarriage
3. Spontaneously resolving ectopic pregnancy

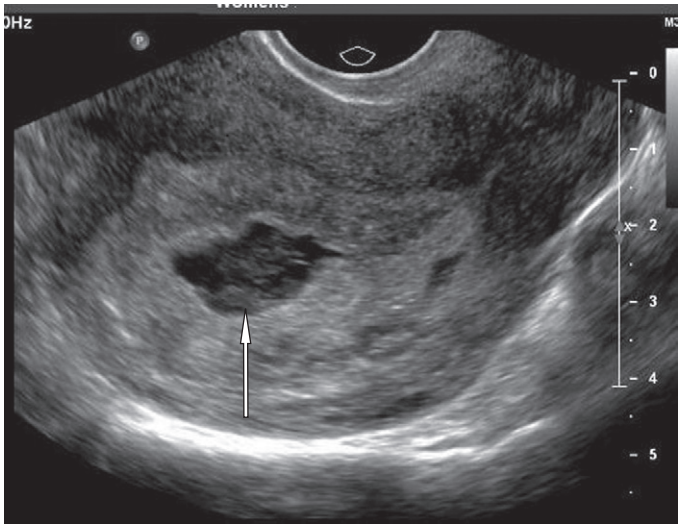


Figure 39.62 A crenellated pseudo gestation sac filled with debris consistent with an ectopic gestation.

Negative ultrasound

Patients are being scanned increasingly early in their pregnancies and some patients may fail to demonstrate either an intrauterine pregnancy or an adnexal abnormality when initially scanned. Some may never demonstrate an abnormality at all. It is essential to acknowledge and understand that ultrasound, no matter how good, must never be used in isolation when evaluating a patient. The clinical presentation and findings as well as the serum β-hCG level are very important.

The role of a discriminatory serum β-hCG level

A viable intrauterine pregnancy will show a 66% rise in β-hCG every 48 hours in the first 40 days of pregnancy.[69] Only 13% of ectopic pregnancies will show such a rise in levels. A β-hCG rise of <50% in 48 hours is almost always associated with a non-viable pregnancy of either intra- or extrauterine origin.

An ectopic pregnancy is considered very likely in the absence of an intrauterine pregnancy on transvaginal scanning when the serum β-hCG level is greater than a certain discriminatory level. There is controversy about the discriminatory level of β-hCG above which a viable intrauterine pregnancy should be seen on the scan (1500–2000 IU/L).[70] The problem with discriminatory levels for biochemical parameters is that there is no known discriminatory level for twin gestations and there is a very great variability in expertise amongst sonographers.[71]

Pregnancy of unknown location

- Pregnancy of unknown location (PUL) means that the location of the pregnancy is not determined at the initial visit.
- The incidence of PUL depends upon gestational age at presentation and operator experience.
- Only a minority of PUL will have an ectopic pregnancy (8–14%).
- Most pregnancies of unknown location may be safely managed expectantly.

Pregnancy of unknown location (PUL)

The term 'pregnancy of unknown location' (PUL) refers to a situation in which the location of the pregnancy cannot be determined at the initial visit. The incidence of this is quoted as 8–10% of cases presenting to an early pregnancy assessment unit. The location may not be known because the scan is performed too early in pregnancy (normal or ectopic), the scan is performed too late in a miscarriage or the scan findings are missed or misinterpreted.[72]

Factors that determine the incidence of PUL are:

1. gestational age of the pregnancy at presentation
2. operator experience
3. resolution of the ultrasound machine.

Within a group of patients with an initial diagnosis of PUL, only a minority will have an ectopic pregnancy. Potentially large numbers of women could be subjected to invasive diagnostic procedures in view of the anxiety associated with missing an ectopic pregnancy. A substantial number of non-visualised pregnancies are failing pregnancies, either intrauterine or ectopic, and these may resolve spontaneously. In these cases active therapeutic intervention can be avoided if the outcome can be accurately predicted.[73]

Management of a PUL usually consists of repeating the β-hCG after an interval of 2 days. A serum β-hCG level that is increasing or that has plateaued without sonographic findings of pregnancy within the uterus implies a high chance of ectopic gestation (Table 39.18; Fig. 39.62). The rate of β-hCG fall also tends to be slower with ectopic pregnancies than with complete miscarriages. Weekly β-hCG level concentrations should be monitored until the result is negative. It is now accepted that pregnancies of unknown location may be safely managed expectantly with a high success rate. Surgical intervention was required in only 23 (29%) pregnancies of unknown location[74] (Table 39.19).

Table 39.19 Range of possible outcomes with an initial diagnosis of PUL

1. 45–50% pregnancies resolve spontaneously and the initial true origin will never be identified
2. 8–14% are due to ectopic gestations
3. 27–47% evolve into normal intrauterine pregnancies

THE ROLE OF ULTRASOUND IN PREDICTING AN ABNORMAL PREGNANCY OUTCOME

Ultrasound bias and loss of reassurance: the ultrasound conundrum

With the increasing use of transvaginal ultrasound the background loss rate of early pregnancies is higher than had been observed using the transabdominal route. This is obviously not causative but due to the fact that earlier pregnancies in which the background loss rate is known to be high are now being scanned.

With the use of transabdominal ultrasound the visualisation of an embryo with cardiac activity was very reassuring due to the size of the viable embryo when visualised (10 mm, i.e. a gestational age of 7 weeks and 2 days). This is not the case with transvaginal ultrasound, when even with the identification of cardiac activity, 30% of pregnancies with symptoms of miscarriage and 15% without symptoms will miscarry.[75]

Ultrasound in the prediction of early pregnancy loss

Many parameters have been investigated both singly and in combination in attempts to predict those pregnancies that will result in miscarriage. First trimester ultrasound has become a means of predicting an abnormal outcome not only in the presence of a live embryo but also before visualisation of the embryo itself. There are findings which can be used to identify a subgroup of embryos at high risk of embryonic demise or subsequent diagnosis of fetal anomaly that require close follow-up.

The embryonic heart rate: embryonic bradycardia

The demonstration of embryonic cardiac activity indicates that the embryo is alive at the time of the examination. An abnormally slow heart rate may predict impending demise. A single observation of an abnormally slow heart rate does not necessarily indicate subsequent embryonic death, but a continuous decline of embryonic heart activity is inevitably associated with miscarriage. A heart rate of 100 bpm or higher is considered normal in embryos less than 5 mm in CRL (Table 39.20).

It is important not to lose the perspective of the presence of cardiac activity as the single most important diagnostic finding indicating that the embryo-fetus is alive at a particular stage. The presence of cardiac activity changes the prognosis in patients presenting with threatened miscarriage from a 50% rate of pregnancy failure to much more favourable odds.[3]

Mean gestational sac diameter in relation to the crown–rump length

The measurement of the MGSD should be 5 mm greater than the CRL. The term 'first trimester oligohydramnios' is a misnomer; the fluid is in the chorionic space. The term refers to the appearance of a small sac relative to the size of the embryo (Fig. 39.63). When the difference between the MGSD and the CRL was less than 5 mm a poor outcome occurred in one study in 94% of patients. This measurement has been used to predict pregnancy outcome with varying degrees of accuracy.[43]

Table 39.20 The risk of demise related to the heart rate in embryos less than 5 mm

A heart rate of less than 80 bpm was universally associated with subsequent embryonic demise
A heart rate of 80–90 bpm was associated with a 64% risk of demise
A heart rate of 90–99 bpm was associated with a 32% risk
A heart rate of 100 bpm or more was associated with an 11% risk

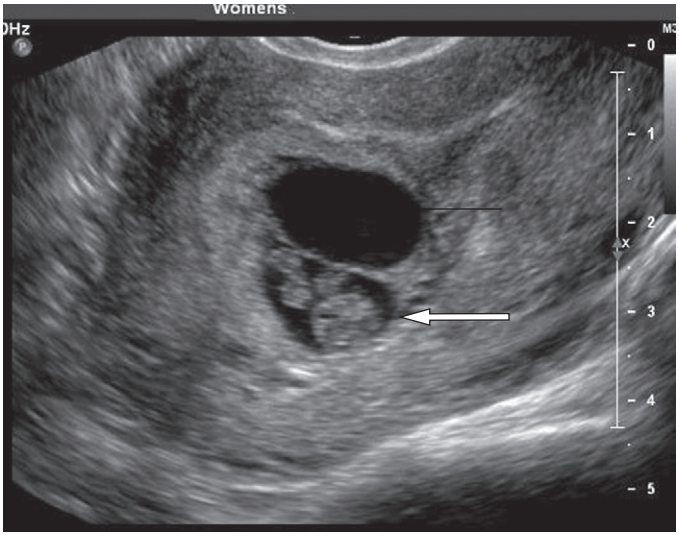


Figure 39.63 A dichorionic twin with vanishing twin in one sac (thin arrow) and first trimester low fluid volume in the second sac (block arrow).

Yolk sac size and shape

Yolk sac abnormalities either in terms of abnormal size or shape may predict an abnormal outcome in pregnancies that are otherwise completely normal.

Yolk sac size

The yolk sac is often demonstrated on transvaginal ultrasound when the MGSD is 5–6 mm and it should always be visualised when the MGSD is at least 8 mm. The yolk sac grows at a rate of 0.1 mm per millimetre of growth of the MGSD before 15 mm MGSD, after which it grows at a rate of 0.03 mm per millimetre of growth of the MGSD. Variations in the yolk sac either too small (<2 mm) or too large (>6 mm) are associated with an increased risk of abnormal outcome (Fig. 39.64).[12,77]

Yolk sac shape

The degeneration of the secondary yolk sac (SYS) coincides with the initial production of urine by the metanephros.[78] Variations in SYS size and sonographic appearance in most abnormal pregnancies are probably the consequence of poor embryonic development or embryonic death rather than being the primary cause of early pregnancy failure (Fig. 39.65). It is usually the yolk sac that is found to persist inside the gestational sac after embryonic demise



Figure 39.64 A yolk sac measuring 7 mm in size, there was no embryo within the gestation sac.

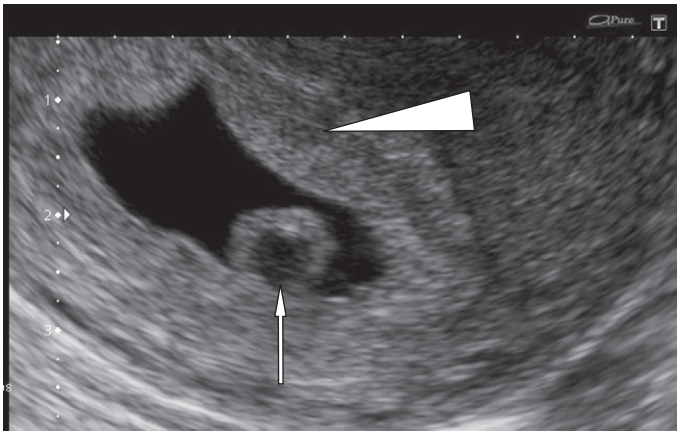


Figure 39.65 A bizarre shaped gestation sac (arrowhead) and an echogenic yolk sac (thin arrow).

– 'nubbin of tissue' (Fig. 39.66).[3] A persistently abnormal yolk sac shape is a predictor of abnormal outcome.[79] However, if the yolk sac is crenated or irregular, caution must be exercised if all other features of the pregnancy are normal. The outcome appears to depend on the appearance of the yolk sac on follow-up examination.[79] When the shape reverts to normal the outcome is nearly always normal. When the yolk sac shape remains abnormal, the embryos are at increased risk of embryonic demise or fetal anomaly.

Care must be taken to avoid being too rigid about predicting a poor outcome on the basis of a single ultrasound feature at a single moment of time. Making a prediction of outcome on very early features in particular is to be avoided and is not a reassuring practice for patients or sonologists. It is far more reassuring to wait and perform a single diagnostic scan at a later stage when a much more robust prognosis can be given (See Table 39.21).

FIRST TRIMESTER MASSES

Ovarian masses

The corpus luteum forms in the secretory phase of the menstrual cycle and increases in size if pregnancy occurs, secreting progesterone to support the pregnancy until the placenta can take over its hormonal function. The normal corpus luteum of pregnancy is a thin-walled, unilocular cyst less than 5 cm in diameter.

The commonest mass seen in the first trimester of pregnancy is the corpus luteal cyst, which may vary considerably in appearances. Corpus luteal cysts may be large, often more than 10 cm in diameter. The cyst may have internal septations and echogenic debris due to haemorrhage (Fig. 39.67).

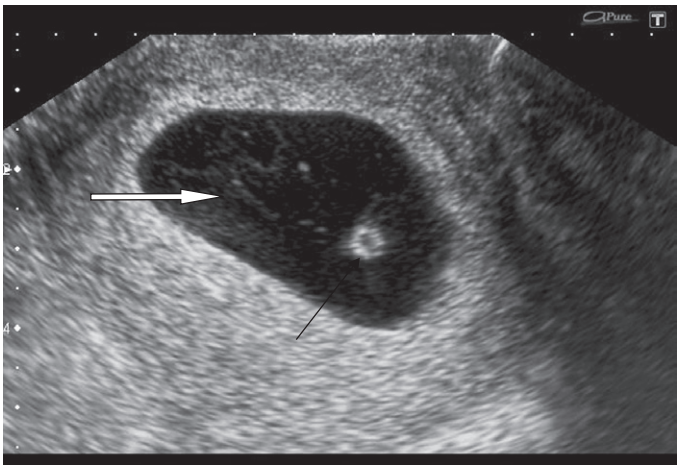


Figure 39.66 An abnormally shaped sac containing remnants of the amnion (thin arrow) and a nubbin of tissue likely to be the contracted yolk sac (black arrow).

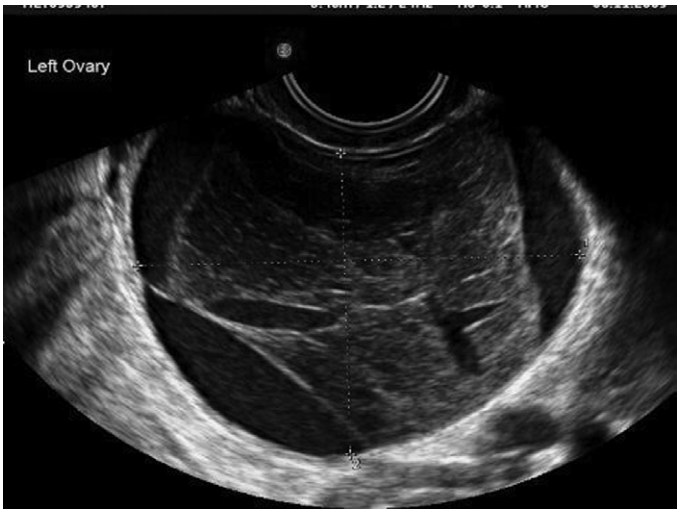


Figure 39.67 A very typical haemorrhagic corpus luteal cyst showing internal 'spiders web reticulation'.

Table 39.21 Prognostic significance of sonographic milestones on transvaginal scanning (TVS)

	Subsequent loss rate
TVS demonstration of gestation sac	11.5%
TVS demonstration of a yolk sac	8.5%
TVS demonstration of an embryo <5 mm in size	7.2%
TVS demonstration of an embryo 6–10 mm in size	3.3%
TVS demonstration of an embryo >10 mm in size	0.5%



Figure 39.68 This rather suspicious looking mass was removed at 16 weeks and was histologically confirmed as a decidualised endometriotic cyst.

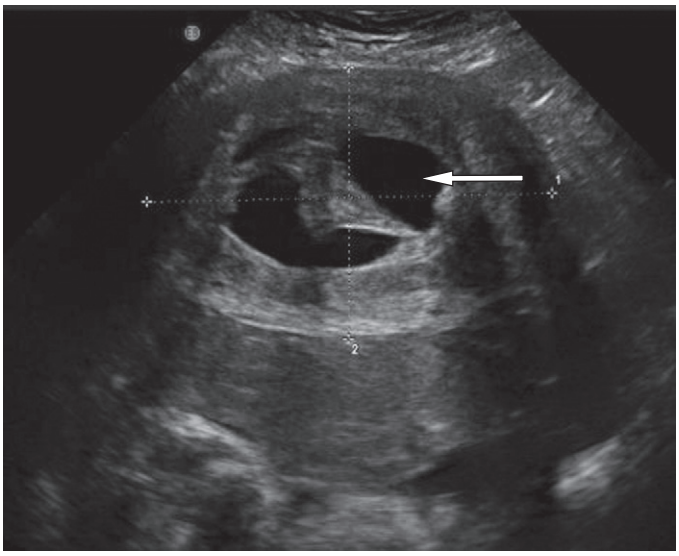


Figure 39.69 A large pedunculated fibroid which became extremely painful at 16 weeks and underwent necrotic cystic change (thin arrow).

Corpus luteal cysts usually regress or decrease in size on follow-up sonographic examination at 16–18 weeks menstrual age.[80] Not all cysts regress, however, and differentiation from a pathological cyst may be impossible. The evaluation of an ovarian cyst in pregnancy should follow the same technique of assessment and diagnosis as a cyst in the non-pregnant pelvis (Fig. 39.68).[80] All cysts should be followed to assess change in size. Malignant ovarian neoplasm associated with pregnancy is rare. Torsion, rupture or dystocia due to cyst size are not. If surgery is indicated then it is usually performed in the second trimester, when the likelihood of inducing premature labour is considered to be lowest.[81]

Fibroids

Approximately one-third of women experience fibroid growth in the first trimester; the remaining women have stable or reduced fibroid size during pregnancy.[82] Changes in the uterine blood supply may render a fibroid ischaemic and produce painful acute necrosis and cystic degeneration (Fig. 39.69). Calcification with acoustic shadowing may be either central in nature or peripheral in location, which is more common after fibroid embolisation. Of great importance is the sonographic differentiation between a fibroid and a myometrial contraction. The echotexture of a fibroid may be hypoechoic, hyperechoic or isoechoic relative to the normal myometrium. A contraction will be of the same echogenicity as the rest of the myometrium and it will resolve/change over the course of the scan.

Fibroids may produce problems in all three trimesters:

1. Spontaneous miscarriage in the first trimester is more common due to abnormal placentation.
2. There is an increased risk of placental abruption, antepartum haemorrhage, retained placenta, postpartum haemorrhage and premature rupture of the membranes. The risk of abruption appears to be related to the size and location of the myoma; it is substantially increased if the myoma is large, e.g. ≥6 cm) or subjacent to the placental site (Fig. 39.70)
3. In the third trimester there may be fetal compression deformities and malpresentation, particularly with cervical fibroids (Fig. 39.71).

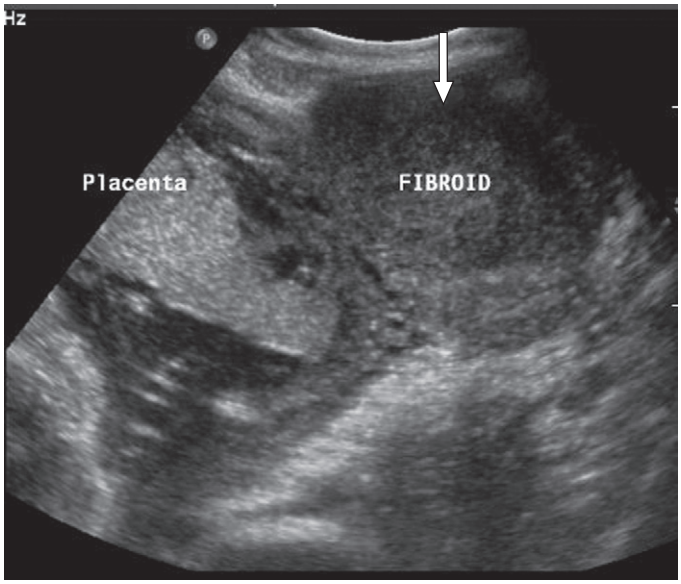


Figure 39.70 A retro placental fibroid (arrow). The echotexture is hypoechoic relative to the normal myometrium.



Figure 39.71 A cervical fibroid which may produce dystocia.

GESTATIONAL TROPHOBLASTIC DISEASE

Gestational trophoblastic disease (GTD) can be a source of confusion. This confusion is due to varied terminology and to the existence of conditions that mimic this pathology.

Histologically there are different disease entities:

1. complete mole
2. partial mole
3. invasive mole
4. placental site trophoblastic tumours
5. choriocarcinoma.

Complete hydatidiform mole

Classically patients with complete hydatidiform mole present with:

1. vaginal bleeding
2. uterine enlargement greater than expected for gestational age
3. an abnormally high level of serum β-hCG.

Medical complications include pregnancy-induced hypertension, hyperthyroidism, hyperemesis, anaemia and the development of ovarian theca lutein cysts.

A classical mole may coexist with a normal fetus and placenta in cases of molar transformation of one ovum in a dizygotic twin pregnancy.[83]

Molar changes can be detected from the second month of pregnancy by ultrasound, which reveals a uterine cavity filled with multiple sonolucent areas of varying size and shape ('snow-storm' appearance) without associated embryonic or fetal structures (Fig. 39.72).[84] This classical sonographic description of complete mole applies to pregnancies between 9 and 12 weeks of amenorrhoea. However, the vast majority of complete and partial moles abort spontaneously during the first trimester of pregnancy. The sonographic appearances are usually non-specific, most often resembling a failed intrauterine pregnancy (Fig. 39.73).[85] The incidence of molar pregnancies has been estimated to be 1 per 41 miscarriages.[86]

Theca lutein cysts secondary to the very high β-hCG levels may be diagnosed in up to 50% of cases, producing either a 'soap bubble' or a 'spoke wheel' appearance of the ovaries (Fig. 39.74). The ovarian hyperstimulation and enlargement of both ovaries may subsequently lead to ovarian torsion or rupture of theca lutein cysts. With earlier diagnosis, the incidence of all complications has decreased.

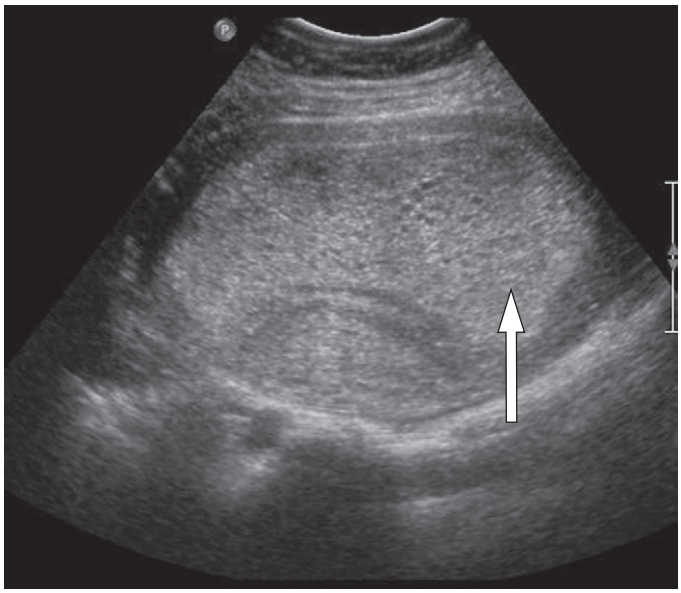


Figure 39.72 A large uterus, endometrial cavity packed with material which is cystic (arrow) in nature.

Partial hydatidiform mole (PHM)

This type of molar pregnancy involves the combination of a fetus with localised placental molar degenerations (Fig. 39.75A and B).

Vaginal bleeding has been reported in both types of triploidy in the first or second trimester with a total incidence of 47%. Diandric triploidies are associated with a higher miscarriage rate than digynic triploidies.

The phenotypic expression of both diandric and digynic triploidy includes growth restriction which will be found in over 70% of cases and in over 80% of these fetuses the growth restriction will be symmetrical. Structural defects are seen in over 90% of triploid fetuses (Table 39.23).

Early molar change must be differentiated from hydropic degeneration of the placenta. Hydropic changes within the placenta may occur in 1–3% of all pregnancies. Histologically the chorionic villi

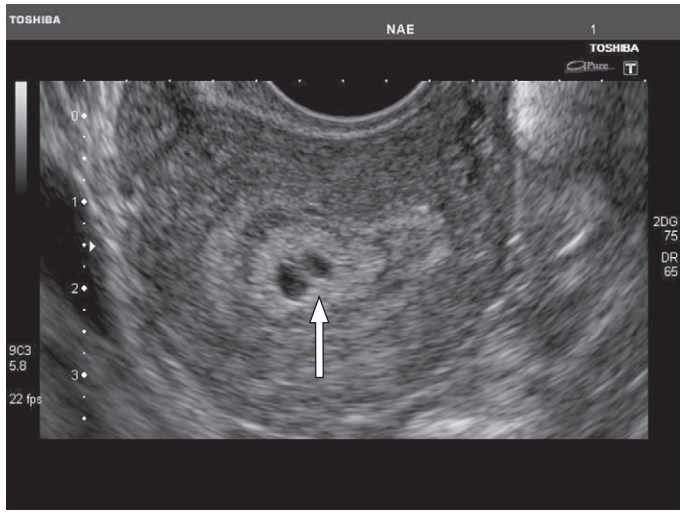


Figure 39.73 Abnormal expansion of the endometrial cavity by heterogenous material some of which is cystic in nature (arrow). Histology confirmed a complete mole.

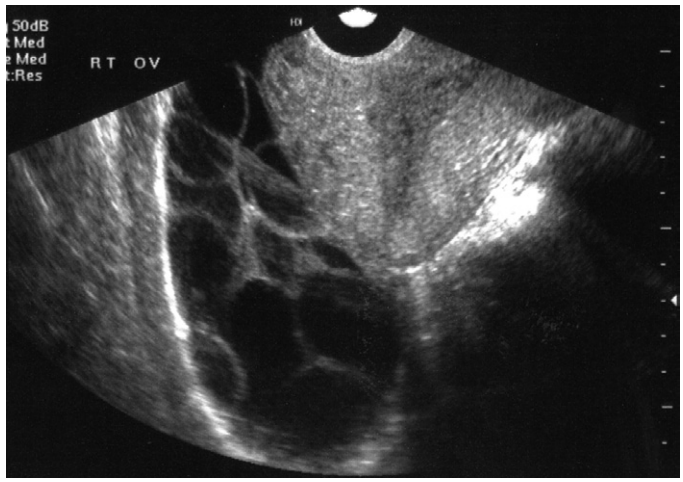


Figure 39.74 The right ovary demonstrates a classic soap bubble appearance typical of theca lutein cyst formation. Note the abnormal uterine cavity.

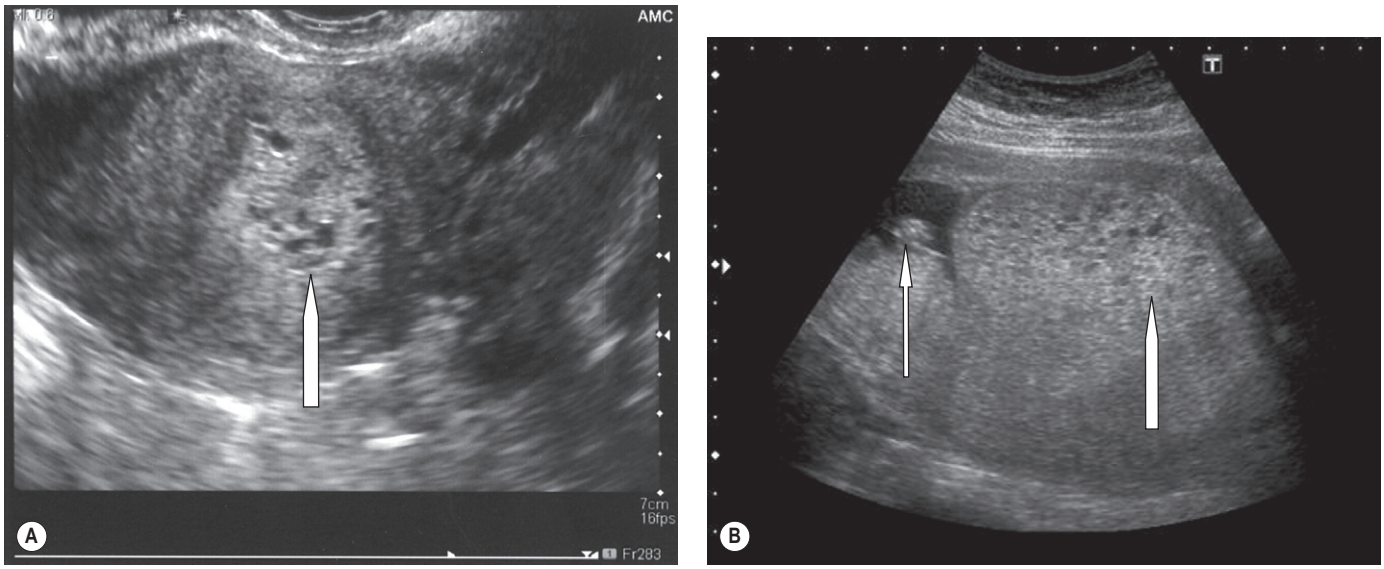


Figure 39.75 A and B The presence of localized placental molar change (block arrows) and an embryo (thin arrow) consistent with the diagnosis of partial molar change.

Table 39.22 The pathological characteristics of complete (CHM) and of partial (PHM) hydatidiform mole

	CHM	PHM
Chromosomal complement	Diploid chromosomal complement	Partial moles are almost always triploid
Origin of chromosomes	Paternal genome as a result of fertilisation of an oocyte by a diploid spermatozoon	Diandric due to two sets of chromosomes of paternal origin (⅔ of all triploidies) Digynic origin due to a double maternal contribution
Chorionic villi	Marked oedema and enlargement	Marked oedema and enlargement
Villous blood vessels	Disappearance of the villous blood vessels	
Trophoblast	Proliferation of the lining trophoblast	Focal trophoblastic hyperplasia
Fetal tissue	Absence of fetal tissue	Presence of fetal tissue

Table 39.23 Structural defects associated with triploidy

1. Central nervous system: agenesis of the corpus callosum, Dandy–Walker malformation, holoprosencephaly, spina bifida
2. Facial: cleft lip, micrognathia, hypertelorism
3. Cardiovascular: ventricular septal defect, atrial septal defect
4. Genitourinary: renal agenesis, multicystic kidneys, and hypospadias
5. Intrauterine growth retardation, cystic hygroma, omphalocele, club foot, syndactyly, sandal gap

may be engorged but proliferation of the lining trophoblast is not seen (Fig. 39.76).[87]

THE ULTRASOUND DIAGNOSIS OF RETAINED PRODUCTS OF CONCEPTION

Scan requests for retained products of conception pose a very significant time and financial burden on ultrasound departments. The management of this problem is compounded by the fact that there is no consensus agreement as to the appearance of the endometrium that is consistent with retained products of conception, either in terms of actual endometrial thickness or abnormal morphology such as an echogenic mass (Fig. 39.77). As a consequence reliance on the use of sonography to diagnose retained products of conception is associated with an unacceptably high false positive rate.

Various studies have suggested endometrial measurements varying from 15 to 25 mm but studies have shown that many of these levels are neither sensitive nor specific enough to be of benefit.[88] Other studies have considered the morphological appearances of the postpartum endometrium (the presence of an echogenic mass) (Fig. 39.79) and yet others have factored the use of Doppler into algorithms for diagnosis (Fig. 39.78).[89] Even if a consensus could be reached in terms of definition of terms there would still be problems with rigid application of limits to ultrasound measurements of endometrial thickness. It has been shown that even in women with endometrial thickness <10 mm on preoperative ultrasound scan, chorionic villi have been detected on histology. This group of women would not have fulfilled any of the sonographic definitions for diagnosis. Conversely, many women have quite thickened endometria but do not consider the blood loss they are experiencing to be significant in terms of amount or duration.

More importantly, women with incomplete miscarriages who present for the first time with a relatively thin endometrium on ultrasound scan are likely to be classified as having pregnancies of unknown location.[90] These women are often perceived as being at risk of having ectopic pregnancy and they are routinely followed by serial blood tests to measure the dynamic of hCG levels.

The diagnosis of retained products is a very pertinent example of the necessity to perform a scan only for a good clinical reason. What is likely to be more important is what the endometrium looks

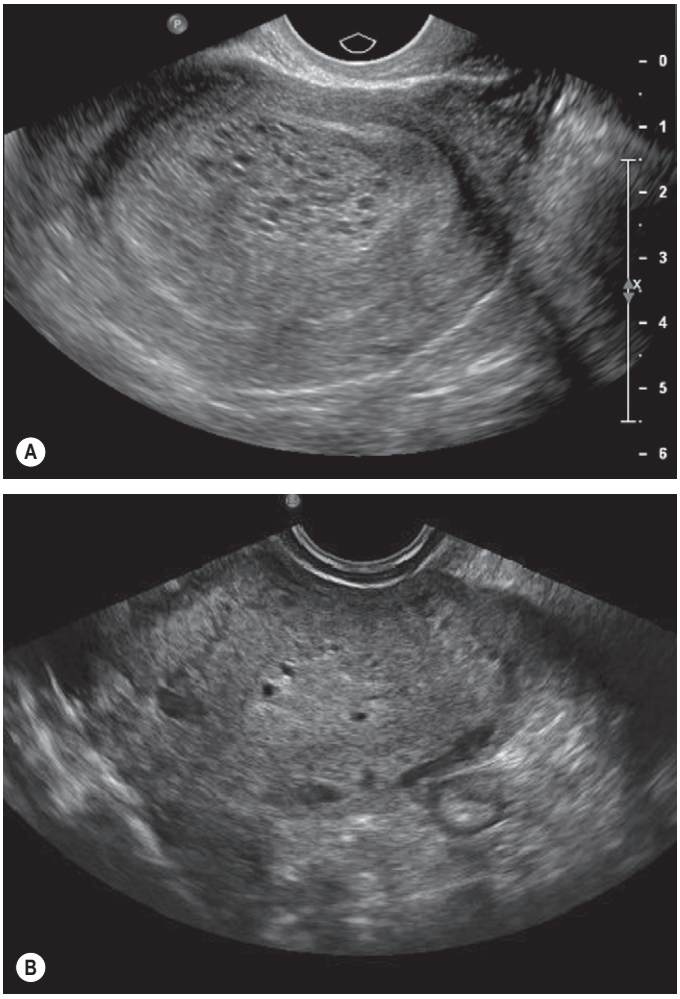


Figure 39.76 **Hydropic degeneration of the placenta** which sonographically may be indistinguishable from molar change.

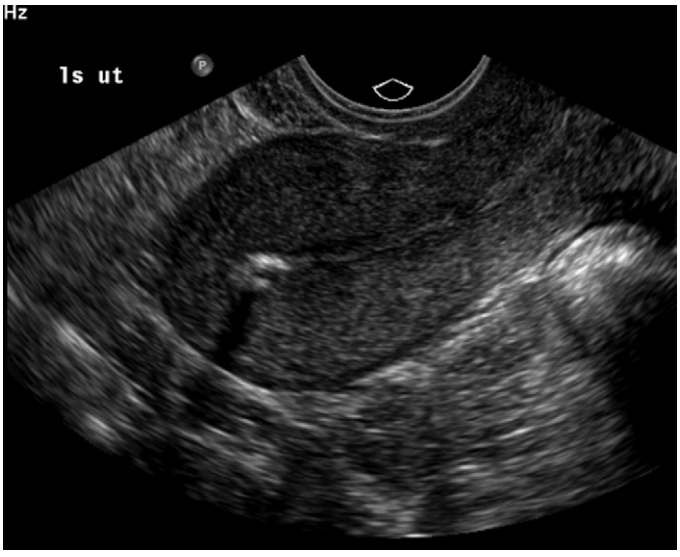


Figure 39.77 **A small but very echogenic mass of tissue** high up in the fundus of the uterus.

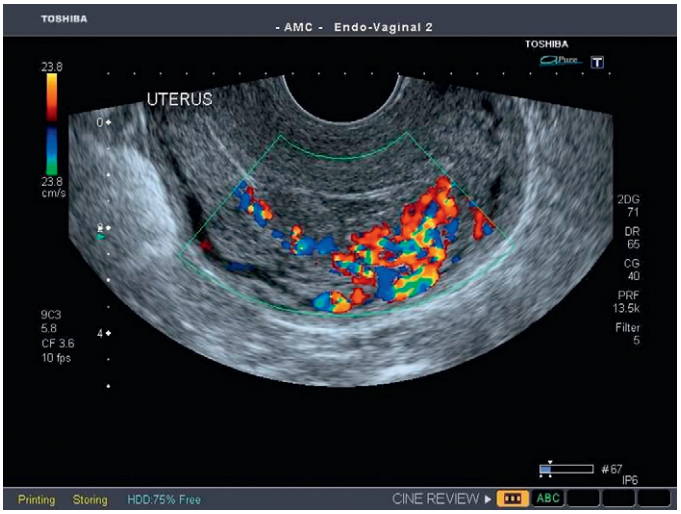


Figure 39.78 **Abnormal flow** persisting in the underlying myometrium extending into the abnormal endometrial tissue.

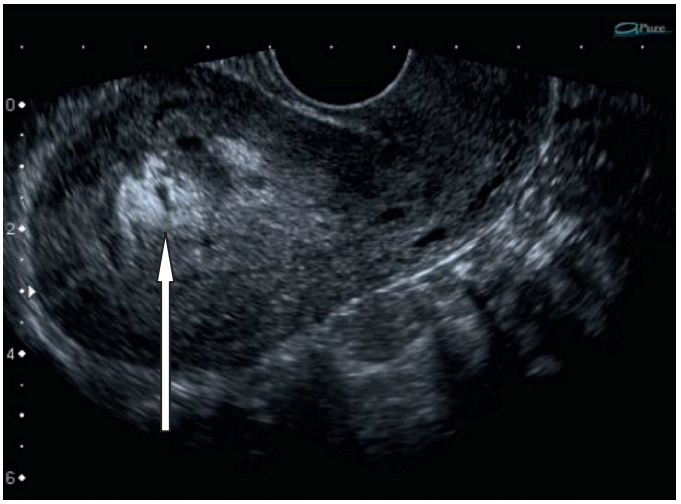


Figure 39.79 **Expanded endometrial cavity** containing blood and an echogenic mass (arrow) consistent with RPOCS.

like in a *symptomatic* woman but the symptomatology will require careful definition. The combination of clinical, ultrasound findings and serum biochemical markers may provide a much more logical approach to establishing the diagnosis of incomplete miscarriage and planning further management.[91]

THE NON-SURGICAL MANAGEMENT OF ECTOPIC PREGNANCY

The success of high quality transvaginal ultrasound and sensitive assays for β-hCG levels has resulted in earlier diagnosis of ectopic pregnancy and facilitated the diagnosis of non-tubal ectopics at a stage in their evolution when surgery is not always the most appropriate treatment.

Methotrexate is an antimetabolite chemotherapeutic agent which interferes with DNA synthesis and disrupts cell multiplication. This drug has long been used in the treatment of gestational trophoblastic disease so extending its role to the treatment of trophoblast problems was a relatively easy step to take. Methotrexate

Table 39.24 Factors that may influence methotrexate therapy

Patient factors to be considered prior to methotrexate therapy:

1. Patient must be haemodynamically stable: no active bleeding, no haemoperitoneum
2. Patient must be reliable, compliant and able to return for follow-up; the importance of this cannot be overemphasised
3. Patient must have no contraindications to the use of methotrexate such as immunodeficiency, liver disease, blood dyscrasias

Sonographic factors that would be considered contraindications to methotrexate therapy:

1. A β-hCG level >5000 IU/L (there is an inverse relationship between the β-hCG level and the successful medical management of ectopic pregnancy
2. Fetal cardiac activity
3. Free fluid in the pouch of Douglas; however, even now this feature may not be as alarming as first thought

has changed the management of non-tubal ectopic pregnancies, i.e. cervical, interstitial and scar ectopics, ectopic pregnancies, in which surgical treatment is notoriously difficult and dangerous (Table 39.24).[92]

Methotrexate regimens

The most popular regimen is the single dose injection. This is an intramuscular injection. The dose of methotrexate used in this protocol is relatively low dose and as a consequence side effects are few and there is no requirement for folinic acid rescue.

Prior to therapy a baseline full blood count, renal and hepatic biochemical profiles as well as baseline β-hCG level are determined.

Monitoring of methotrexate therapy with β-hCG levels has shown that there is a characteristic initial increase at day 3. This usually coincides with an episode of increased abdominal pain which is thought to be due to the separation of the trophoblast from the implantation site, i.e. tubal miscarriage, not tubal rupture.

The level of β-hCG starts to decline from days 4–7. There should be a drop of 15% from the initial baseline. If this drop in level occurs then treatment is deemed to be successful. Success rates reported in the literature range from 65% to 95%. In addition, the tubal patency and subsequent pregnancy rates are very encouraging with pregnancy rates of over 80% recorded. Even more importantly the rate of spontaneous intrauterine pregnancy has been quoted as over 80%.[93]

Failure of therapy is indicated by the following

1. failure of β-hCG level to fall
2. a plateau in β-hCG levels
3. inadequate drop in levels at days 4–7.

A second dose can be given and the reported requirement for further therapy in studies has varied from 3% to 27%.

There have been studies looking at the sonographic features of ectopic pregnancies following methotrexate therapy. Interestingly in the cases in which therapy was successful there was an initial increase in size of the ectopic. This increase is postulated to be due to oedema, necrotic decidua or enlarging haematoma and such changes were not seen in cases in which therapy failed. An increase in pelvic fluid was seen in both successful and unsuccessful cases and was not considered a cause for alarm.[92] The tubal mass may not actually reduce in size until long after the β-hCG level has fallen to zero.

REFERENCES

1. Cacciatore B, Tiitnen A, Stenman UH, Ylostalo P. Normal early pregnancy: serum hCG levels and vaginal ultrasonography findings. Br J Obstet Gynaecol 1990;97:899–903.
2. Robinson HP. The diagnosis of early pregnancy failure by sonar. Br J Obstet Gynaecol 1975;82(11):849–857.
3. Jauniaux E, Johns J, Burton GJ. The role of ultrasound imaging in diagnosing and investigating early pregnancy failure. Ultrasound Obstet Gynecol 2005;25:613–624.
4. Jurkovic D, Gruboeck K, Campbell S. Ultrasound features of normal early pregnancy development. Curr Opin Obstet Gynecol 1995;7:493–504.
5. Nyberg DA, Filly RA. Predicting pregnancy failure in 'empty' gestational sacs. Ultrasound Obstet Gynecol 2003;21:9–12.
6. Yeh HC, Goodman JD, Carr L, Rabinowitz JG. Intradecidual sign: a US criterion of early intrauterine pregnancy. Radiology 1986;161:436–467.
7. de Crespigny LC, Cooper D, McKenna M. Early detection of intrauterine pregnancy with ultrasound. J Ultrasound Med 1988;7(1):7–10.
8. Wagener RK, Calhoun BC. The routine obstetric ultrasound examination. Obstet Gynecol Clin North Am 1998;25(3):451–463.
9. Grubeock K, Zosmer N, Jurkovic D. Ultrasound features of early pregnancy development. In: Jurkovic D, Jauniaux E, editors. Ultrasound and early pregnancy. Carnforth, UK: Parthenon Publishing; 1996.
10. Filly RA. Ultrasound evaluation during the first trimester. In: Callen PW, editor. Ultrasonography in obstetrics and gynecology. Philadelphia: WB Saunders; 1994.
11. Makikallio K, Tekay P, Joupilla P. Yolk sac and umbilicoplacental haemodynamics during early human embryonic development. Ultrasound Obstet Gynecol 1999;14:175–179.
12. Stampone C, Nicotra M, Muttinelli C, Cosmi EV. Transvaginal sonography of the yolk sac in normal and abnormal pregnancy. J Clin Ultrasound 1996;24:3–9.
13. Jauniaux E, Jurkovic D, Henreity Y, et al. Development of the secondary human yolk sac: correlation of sonographic and anatomical features. Hum Reprod 1991;6:1160–1166.
14. Levi CS, Lyons EA, Zheng XH, et al. Endovaginal US: demonstration of cardiac activity in embryos of less than 5 mm in crown rump length. Radiology 1990;176:71–74.
15. Robinson HP. Sonar measurement of fetal crown rump length as means of assessing maturity in the first trimester of pregnancy failure by sonar. BMJ 1973;4:28–31.
16. Doubilet PM, Benson CB. Embryonic heart rate in the first trimester: What rate is normal? J Ultrasound Med 1995;14:431–434.
17. McKenna KM, Feldstein VA, Goldstein RB, Filly RA. The empty amnion: a sign of early pregnancy failure. J Ultrasound Med 1995;14(2):117–121.
18. Souka AP, Nicolaides KH. Diagnosis of fetal abnormalities at the 10–14 week scan. Ultrasound Obstet Gynecol 2002;10(6): 429–442.
19. van Zalen-Spock RM, van Vugt JMG, van Geijn HP. First trimester sonography of physiological midgut herniation and the diagnosis of omphalocoele. Prenat Diagn 1997;17:511–518.
20. Braithwaite JM, Armstrong MA, Economides DL. Assessment of fetal anatomy at 12 to 13 weeks gestation by transabdominal and transvaginal sonography. Br J Obstet Gynaecol 1998;103:82–85.
21. Sebire NJ, Von Kaisenberg C, Rubio C, et al. Fetal megacystis at 10–14 weeks of gestation. Ultrasound Obstet Gynecol 1996;8:387–390.
22. Becker R, Mende B, Stiemer B, Entezami M. Sonographic markers of exencephaly at 9+3 weeks of gestation. Ultrasound Obstet Gynecol 2002;16:582–584.
23. Chatzipapas IK, Whitlow BJ, Economides DL. The 'Mickey Mouse' sign and the diagnosis of anencephaly in early pregnancy. Ultrasound Obstet Gynecol 2002;13:196–199.
24. Carroll SG, Soothill PW, Abdel-Fattah SA, et al. Prediction of chorionicity in twin pregnancies at 10–14 weeks of gestation. Br J Obstet Gynaecol 2002;109(2):182–186.
25. Smith AP. Abnormalities of twin pregnancies. In: Twining P, McHugo JM, Pilling DW, editors. Textbook of fetal abnormalities. 2nd ed. Edinburgh: Churchill Livingstone Elsevier; 2007.
26. Sampson A, de Crespigny LC. Vanishing twins: the frequency of spontaneous fetal reduction of a twin pregnancy. Ultrasound Obstet Gynecol 1992;2:107–109.
27. Landy HJ, Keith LG. The vanishing twin: a review. Hum Reprod Update 1998;4(2):177–183.
28. Sepulveda W, Sebire NJ, Hughes K, et al. Evolution of the lambda or

twin chorionic peak sign in dichorionic pregnancies. Obstet Gynecol 1997;89:439–441.
29. Selpulveda W. Chorionicity determination in twin pregnancies: double trouble? Editorial. Ultrasound Obstet Gynecol 2002;10:79–81.
30. Bora SA, Papageorghiou AT, Bottomly C, et al. Reliability of transvaginal ultrasonography at 7–9 weeks' gestation in the determination of chorionicity and amnionicity in twin pregnancies. Ultrasound Obstet Gynecol 2008;32(5):618–621.
31. Robinson HP, Fleming JE. A critical evaluation of sonar crown rump length measurements. Br J Obstet Gynaecol 1975;82:702–710.
32. Harville EW, Wilcox AJ, Bird DD, Weinberg CR. Vaginal bleeding in very early pregnancy. Obstet Gynecol Surv 2004;59(3):172–173.
33. Silver RM, Ware Branch D. Sporadic and recurrent pregnancy loss. In: Reece AE, Hobbins JC, Gant NF, editors. Handbook of clinical obstetrics: the fetus and mother. Oxford: Blackwell Publishing; 2007.
34. Farquharson RG, Jauniaux E, Exalto N. Updated and revised nomenclature for description of early pregnancy events. Hum Reprod 2005;20(11):3008–3011.
35. Robinson HP. Detection of fetal heart movement in the first trimester of pregnancy using pulsed ultrasound. BMJ 1972;4:466–468.
36. Schouwink MH, Fong BF, Mol BWJ, van der Veen F. Ultrasonographic criteria for non-viability of first trimester intra-uterine pregnancy. Early Pregnancy 2000;4(3):203–213.
37. RCR/RCOG Committee. Guidance on ultrasound procedures in early pregnancy. 1995 reissued without change 2006. Royal College of Radiologists. The Royal College of Obstetricians and Gynaecologists.
38. Exalto N, Christiansen OB, Farquharson RG, Jauniaux E. Early pregnancy failure: a review. Eur Clin Obstet Gynaecol 2006;2(4):171–179.
39. McKenna KM, Feldstein VA, Goldstein RB, Filly RA. The empty amnion sign: a sign of early pregnancy failure. J Ultrasound Med 1995;14(2):117–121.
40. Maso G, D'Ottavio G, De Seta F, et al. First trimester intra uterine hematoma and outcome of pregnancy. Obstet Gynecol 2005;105:339–344.
41. Weiss J, Malone F, Vidaver J, et al. Threatened abortion: a risk factor for poor pregnancy outcome, a population based screening study. Am J Obstet Gynecol 2004;190:745–750.
42. Johns J, Hyett J, Jauniaux E. Obstetric outcome after threatened miscarriage with or without a haematoma on ultrasound. Am J Obstet Gynecol; 2003;102:483–487.
43. Bromley B, Harlow BL, Laboda LA, Benacerraf BR. Small sac size in the first trimester: a predictor of poor fetal outcome. Radiology 1991;178:375–377.
44. Zane SB, Kieke BA, Kendrick JS, Bruce C. Surveillance in a time of changing health care practices: estimating ectopic pregnancy incidence in the United States. Matern Child Health J 2002;6:227.
45. Lewis G, editor. The Confidential Enquiry into Maternal and Child Health. (CEMACH). Saving mothers' lives: reviewing maternal deaths to make motherhood safer – 2003–2005. The Seventh Report on Confidential Enquiries into Maternal Deaths in the United Kingdom. London: CEMACH; 2007.
46. Kamwendo F, Forslin L, Bodin L, Danielsson D. Epidemiology of ectopic pregnancy during a 28 year period and the role of pelvic inflammatory disease. Sex Transm Infect 2000;76:28.
47. Ankum WM, Mol BWJ, Van Der Veen F, et al. Risk factors for ectopic pregnancy: a meta analysis. Fertil Steril 1996;65:1093.
48. Filly RA. Ectopic pregnancy [Figure 32.2, p 642]. In: Callen PW, editor. Ultrasonography in obstetrics and gynecology. Philadelphia: Saunders; 1994. p. 641–659.
49. Kirk E, Papageorghiou AT, Condous G, et al. The diagnostic effectiveness of an initial transvaginal scan in detecting ectopic pregnancy. Hum Reprod 2007;22:1744–1750.
50. Lazarus E. What's new in first trimester ultrasound. Radiol Clin North Am 2003;41(4):663–679.
51. Mehta TS, Levine D, McArdle CR. Lack of sensitivity of endometrial thickness in predicting the presence of an ectopic pregnancy. J Ultrasound Med 1999;18:117–122.
52. Wachsberg RH, Karimi S. Sonographic endometrial three layer pattern in symptomatic first trimester pregnancy: not diagnostic of ectopic pregnancy. J Clin Ultrasound 1998;26:199–201.
53. Jurkovic D, Mavrelos D. Editorial. Catch me if you scan: ultrasound diagnosis of ectopic pregnancy. Ultrasound Obstet Gynecol 2007;30:1–7.
54. Condous G. The management of early pregnancy complications. Best Pract Res Clin Obstet Gynaecol 2004;18(1):37–57.
55. Stein MW, Ricci ZJ, Novak L, et al. Sonographic comparisons of the tubal ring of ectopic pregnancy with the corpus luteum. J Ultrasound Med 2004;23:57–62.
56. Frates MC, Visweswaran A, Laing FC. Comparison of tubal ring and corpus luteum echogenicities: a useful differentiating characteristic. J Ultrasound Med 2001;20:27–31.
57. Bhatt S, Ghazale H, Dogra V. Sonographic evaluation of ectopic pregnancy. Radiol Clin North Am 2007;45(3):549–560.
58. Barnhart K, Esposito M, Coutifaris C. An update on the medical treatment of ectopic pregnancy. Obstet Gynecol Clin North Am 2000;27(3):653–667.
59. Job-Spira N, Fernandez H. Ruptured tubal ectopic pregnancy: risk factors and reproductive outcome: results of a population based study in France. Am J Obstet Gynecol 1999;180:938–944.
60. Wachsberg RH, Levine CD. Echogenic peritoneal fluid as an isolated sonographic finding; significance in patients at risk of ectopic pregnancy. Clin Radiol 1998;53(7):520–522.
61. Dubinsky TJ, Pravey HR, Maklad N. Endometrial color flow/image directed Doppler imaging: negative predictive value for excluding ectopic pregnancy. J Clin Ultrasound 1997;25(3):103–109.
62. Agarwal SK, Wisot AL, Garzo G, Meldrum DR. Cornual pregnancies in patients with prior salpingectomy undergoing in vitro fertilization and embryo transfer. Fertil Steril 1996;65:659–660.
63. Ackerman TE, Levi CS, Dashefsky SM, et al. Interstitial line: sonographic finding in interstitial (cornual) ectopic pregnancy. Radiology 1993;189:83–87.
64. Ushakov FB, Elchalal U, Aceman PJ, Schenker JG. Cervical pregnancy: past and future. Obstet Gynecol Surv 1997;52:45.
65. Gun M, Mavrogiorgis M. Cervical ectopic pregnancy: a case report and literature review. Ultrasound Obstet Gynecol 2002;19:297–301.
66. Comstock CH. Antenatal diagnosis of placenta accreta: a review. Ultrasound Obstet Gynecol 2005;26:89–96.
67. Chang FW, Chen CH, Liu JY. Early diagnosis of ovarian pregnancy by ultrasound. Int J Obstet Gynecol 2004;85:186–187.
68. Comstock CH, Huston K, Lee W. The ultrasonic appearances of ovarian ectopic pregnancies. Obstet Gynecol 2005;105:42–45.
69. Tay JI, Moore J, Walker JJ. Ectopic pregnancy. BMJ 2000;320:916.
70. Seeber BE, Banhart KT. Suspected ectopic pregnancy. Obstet Gynecol 2006;107(2 Pt 1):399–413.
71. Kadar N, DeVore G, Romero R. Discriminatory hCG zone: its use in the sonographic evaluation for ectopic pregnancy. Obstet Gynecol 1981;58:156.
72. Bottomley C, Van Belle V, Mukri F, et al. Ability to make a diagnosis at first early pregnancy ultrasound assessment according to gestational age. Ultrasound Obstet Gynecol 2007;30(4):388.
73. Banerjee S, Aslam N, Zosmer N, et al. The expectant management of women with early pregnancy of unknown location. Ultrasound Obstet Gynecol 1999;14:231–236.
74. Condous G, Okaro E, Bourne T. Pregnancies of unknown location: diagnostic dilemmas and management. Curr Opin Obstet Gynecol 2005;17:568–573.
75. Jauniaux E, Gavriil P, Nicolaides KH. Ultrasonographic assessment of early pregnancy complications. In: Jurkovic D, Jauniaux E, editors. Ultrasound and early pregnancy. Carnforth, UK: Parthenon Publishing; 1996. p. 53.
76. Sawyer E, Jurkovic D. Ultrasonography in the diagnosis and management of abnormal early pregnancy: first trimester pregnancy complications. Clin Obstet Gynecol 2007;50(1):31–54.
77. Chama CM, Marupa JY, Obed JY. The value of the secondary yolk sac in predicting pregnancy outcome. J Obstet Gynecol 2005;25(3): 245–247.
78. Jauniaux E, Jurkovic D, Henriet Y, et al. Development of the secondary human yolk sac: correlation of sonographic and anatomic features. Human Reprod 1991;6:1160–1166.
79. Mara E, Foster GS. Spontaneous regression of a yolk sac associated with embryonic death. J Ultrasound Med 2000;19:655–656.
80. Filly RA: Ovarian masses … what to look for … what to do. In: Callen PW, editor. Ultrasonography in obstetrics and gynecology. Philadelphia: Saunders; 1994. p. 625–639.
81. Giuntoli RL, Vang RS, Bristow RE. Evaluation and management of adnexal masses during pregnancy. The adnexal mass. Clin Obstet Gynecol 2006;49(30):506–516.
82. Salvador E, Penstock J, Blakemore KJ, Pressman E. Leiomyomata uteri, genetic amniocentesis, and the risk of second-trimester spontaneous abortion. Am J Obstet Gynecol 2002;186:913.
83. Callen PW. Ultrasound evaluation of gestational trophoblastic neoplasia. In: Callen PW, editor. Ultrasonography in obstetrics and gynecology. Philadelphia: Saunders; 1994. p. 625–639.
84. Benson CB, Genest DR, Bernstein MR, et al. Sonographic appearance

of first trimester complete hydatidiform moles. Ultrasound Obstet Gynecol 2000;16:188–191.
85. Betel C, Atri M, Arensen AM, et al. Sonographic diagnosis of gestational trophoblastic disease and comparison with retained products of conception. J Ultrasound Med 2006;25:985–993.
86. Fowler DJ, Lindsay I, Seckl MJ, Sebire NJ. Routine pre-evacuation diagnosis of hydatiform mole: experience of more than 1000 cases from a regional referral centre. Ultrasound Obstet Gynecol 2006;27:56–60.
87. Jauniaux E, Nicolaides KH. Early ultrasound diagnosis and follow-up of molar pregnancies. Ultrasound Obstet Gynecol 1997;9:17–21.
88. Sawyer E, Ofuasia E, Ofili-Yebovi D, et al. The value of measuring endometrial thickness and volume on transvaginal ultrasound scan for the diagnosis of incomplete miscarriage. Ultrasound Obstet Gynecol 2007;29:205–209.
89. Leung SW, Pang MW, Chung TKH. Retained products of gestation in miscarriage: an evaluation of transvaginal ultrasound criteria for diagnosing an empty uterus. Am J Obstet Gynecol 2004;191:1133–1137.
90. Luise C, Jermy K, Collins WP, Bourne TH. Expectant management of incomplete, spontaneous first trimester miscarriage: outcome according to initial ultrasound criteria and value of follow-up visits. Ultrasound Obstet Gynecol 2002;19:580–582.
91. Elson J, Tailor A, Salim R, et al. Expectant management of miscarriage-prediction of outcome using ultrasound and novel biochemical markers. Hum Reprod 2005;20(8):2330–2333.
92. Kirk E, Condous G, Bourne T. The non-surgical management of ectopic pregnancy. Ultrasound Obstet Gynecol 2006;27:91–100.
93. Jongeward KL, Kutella ET, Fleischer AC, et al. Sonographic features of ectopic pregnancies following systemic methotrexate therapy: a case series. Ultrasound Obstet Gynecol 2008;32(3):OP12.08:349–350.

INDEX

Note: Page numbers followed by b indicate boxes, f indicate figures and t indicate tables.

A

Abdomen
  interventional techniques, 847–864 (*see also specific techniques*)
  muscles, 1076
  trauma *see* Abdominal trauma
  wall *see* Abdominal wall
Abdominal aorta
  anatomy, 773, 774f
  aneurysms *see* Abdominal aortic aneurysms
  atherosclerosis, 787, 788f
  diameter, 774, 774t
  dissection, 789, 789f
  occlusion, 788–789
  stenosis, 788f
Abdominal aortic aneurysms
  aortic diameter and, 774, 774t
  background, 774–775
  causes of, 774–775
  diagnosis, 1198
  dissecting, 775
  duplex scanning, 777–781
    abnormal appearance, 777–779, 778f–780f
    distance between renal arteries and aneurysm sac, 780
    limitations and pitfalls, 781
    measurement of aneurysm size, 780, 781f
    normal appearance, 777, 778f
    objectives, 777, 777f
    patient preparation, 777, 778f
    variability of measurement between ultrasound and CT, 779
  false, 775
  mycotic, 775, 779
  risk factors, 775, 775b
  saccular, 775
  shapes and types, 775, 776f
  size, 775
  surveillance programmes, 775–776, 777b, 777t, 782–787
  symptoms, 775
  treatment, 781–782
    endovascular repair, 781–787, 783f–787f, 783t–784t, 784b
    open repair, 781
Abdominal trauma, 828–846
  bladder trauma, 841
  bowel trauma, 841, 842f
  computed tomography
    versus contrast-enhanced ultrasound, 832–833, 833f
    versus full potential ultrasound, 832–833, 841b
  contrast-enhanced ultrasound, 832f
    versus computed tomography, 832–833, 833f
  diaphragm trauma, 841
  FAST, 828–829, 829b, 829f–830f
    versus full potential ultrasound, 831–832
  follow-up, 844–845, 844f–845f
  free peritoneal fluid, 833–835, 834f, 835b
  full potential ultrasound, 829–831, 831b, 831f
    versus computed tomography, 832
    versus FAST, 831–832
  gallbladder trauma, 841
  liver trauma, 835–837
    classification, 835–836, 835t
    general considerations, 835
    mechanisms of injury, 835–836
    ultrasound findings, 836–837, 836f–837f
  pancreas trauma, 841
  penetrating, 843
  pitfalls, 841–842, 842f
  renal trauma, 838–841
    classification, 839–840, 839t
    general considerations, 838–841
    mechanisms of injury, 839–840
    ultrasound findings, 840–841, 840f–841f
  scanning methodology, 828–833, 829b
  spleen trauma, 837–838
    classification, 837–838, 838t
    general considerations, 837
    mechanisms of injury, 837–838, 838f
    ultrasound findings, 838, 839f
  unstable patient, 843, 843f
Abdominal wall, 798–807
  abscess, 799–800
  anatomy, 798, 799f–800f, 799t
  cysts, 805–807, 806b
  desmoid tumours, 806, 807f
  divarication of the rectus muscles, 800
  endometriomas, 806, 806f
  fibromatosis, 806
  hernias, 801–805, 1081 (*see also specific types*)
    postoperative, 805, 805f–806f
    types of, 801t, 806b
  infections, 799–800, 801f
  lipoma, 805, 806f
  liposarcoma, 806
  masses, 805–807, 806b
  musculo-cutaneous flaps, 800
  nerve entrapment, 807
  pathological conditions affecting, 798–801
  sarcoma, 806
  trauma, 801
  ultrasound technique, 798
  varices, 805–806
Abductor digiti minimi, accessory, 1160
Abductor pollicis longus (APL), 1055
Ablation
  endovenous, 1246–1248
  tumour see Tumour ablation
  see also specific techniques
Abscesses
  abdominal, 1401
  abdominal wall, 799–800
  adrenal gland, 1464
  appendiceal, 391, 392f, 1397, 1397f
  aspiration/drainage, 1192, 1193f
    breast, 989
    intra-abdominal, 815
    liver, 124, 125f
    pelvic *see* Pelvic abscess drainage
  breast, 989, 989f
  cervical, in children, 1304
  chest wall, 1352f–1353f
  Crohn's disease, 374–375, 375f
  dental, 906, 906f
  epididymal, 615, 615f
  fallopian tubes, 682, 683f
  intra-abdominal, 813–815, 814f–815f, 815b
  liver, 124–127, 145–146, 146f–147f
    amoebic, 126–127, 127f–128f, 1364–1365
    bacterial, 123f–126f, 124–126, 145–146
    brucellar, 126
    in children, 1364–1365, 1364f
  lungs, 1015, 1015f, 1340, 1342f
  muscle, 1156
  neonatal cerebral, 1273, 1275f
  ovarian, 682, 683f
  pancreatic, 299, 300f
  parotid gland, 903, 904f
  pericholecystic, 244–245, 245f–246f
  perirenal, 462
  post-liver transplantation, 212, 215, 215f
  post-renal transplantation, 535
  prostatitis, 582–584, 582f, 583t, 591

psoas muscle, 821, 823, 823f
renal, 462, 462f, 496–497, 496f–497f, 1452f
retroperitoneal, 821, 823, 823f–824f
spleen, 338–340, 339f–340f
testicular, 604, 605f
thyroid, 1310, 1310f
tubo-ovarian, 682, 683f
ultrasound appearances, 1116
Absorption, 11
Acalculous cholecystitis, 1375
Accessory muscles, 1141–1143, 1146t–1147t, 1160
hand/wrist, 1066–1067
Acetabulum, labral abnormalities, 1070–1071, 1072f
Achalasia, oesophageal, 359–360
Achilles bursa injection, 1188, 1188f
Achilles tendon, 1093–1095, 1094f–1095f
injection, 1188–1189, 1188f–1189f
paratenon, 1093–1094
injection, 1189, 1189f
tears, 1102, 1102f
tendinopathy, 1101–1102, 1101f–1102f
xanthomas, 1117, 1118f
Acinic cell carcinoma, parotid gland, 902
Acoustic cavitation, 5, 87
definition, 54–55
experimental work associated with, 55
factors affecting incidence of, 55–56
hazards from, 55
high risk situations, 56
in-vivo animal and human effects, 55
modelling, 55
reducing the risk of, 56b
safety, 54–56
and tissue, 55b
Acoustic energy absorption, 52b
Acoustic impedance, 9
Acoustic output regulation, 51
Acoustic shadowing *see* Shadowing
Acquired cystic disease of the kidney (ACDK), 453–454, 454f, 498, 498b, 499f
Acquired immunodeficiency syndrome (AIDS)
and liver disease, 131–132
renal infections in, 465
spleen in, 343
Acromioclavicular joint, 1039–1040
cyst, 1039–1040, 1040f
injection, 1040, 1173, 1175f
osteoarthritis, 1039–1040
Actin, 1138
Actinomycosis, intrauterine devices, 708
Acute tubular necrosis (ATN), 449, 451, 484, 532, 542
in children, 1443
Adductor brevis, 1075
Adductor longus, 1072–1073, 1075, 1076f–1077f, 1081, 1082f
Adductor magnus, 1075
Adductor muscles, 1081
Adductor origin injection, 1180, 1181f
Adenocarcinomas
appendiceal, 393
bladder, 561–562
colonic, 402
pancreatic, 306–309, 307f–310f, 309b
small bowel, 380, 381f
vaginal, 716
Adenoid cystic carcinoma
parotid gland, 902
submandibular gland, 897
Adenolymphoma, parotid gland, 901, 901f
Adenomas
adrenal, 636, 636f
bile duct, 261
gallbladder, 249, 249f
hepatic, 1363
liver, 143–145, 145f
metanephric, 508
papillary, 508
parathyroid, 886–887, 886f–887f
parotid gland, 899f
pleomorphic, 899f, 900, 901f
renal, 508, 508f
salivary gland, 1308, 1309f
submandibular gland, 897
thyroid, 1310–1312, 1312f
Adenomatoid tumour, epididymis, 610, 610f
Adenomyomatosis, 247, 248f
Adenomyosis, 694–695, 694b
diagnosis, 694–695, 694f–695f
symptoms, 694
Adnexal torsion, 1488–1489
Adolescents, ovarian cysts, 1484, 1485f
Adrenal glands, 632–642
abscess, 1464
adenoma, 636, 636f
agenesis, 634
anatomy, 632–633
calcification, 635
in children, 1464–1466, 1464f
computed tomography role, 642
congenital anomalies, 634, 634f
congenital hyperplasia, 1464
cortical carcinoma, 637, 639f
cysts, 634–635, 634f, 1464, 1465f
discoid, 634, 634f
embryology, 1464
enlargement, 1475–1476, 1479f
haemorrhage, 635, 635f, 1464, 1464f
post-liver transplantation, 213, 213f
hyperplasia, 634–635, 634f
imaging anatomy, 1464
magnetic resonance imaging role, 642
metastases, 640–641, 640f–641f
myelolipoma, 636–637, 637f
neuroblastoma, 637–640, 640f, 1459t, 1464–1466, 1465f, 1465t
normal appearances, 633, 633b, 633f
phaeochromocytoma, 637, 638f–639f
scanning techniques, 632–633
staging, 1465t
tumours, 635–641
Adrenal rest cells, 603, 603f
Adrenarche, 1470
isolated premature, 1481
Adrenocorticotrophic hormone (ACTH), 635
testicular adrenal rest tumours, 603
Adult polycystic liver disease (APLD), 97–98, 98f
Advanced Trauma Life Support (ATLS), 843
Agenesis
adrenal glands, 634
gallbladder, 1375
Müllerian duct, 1473
pancreas, 1378
renal, 1418, 1419f
AIDS *see* Acquired immunodeficiency syndrome (AIDS)
AIDS-related parotid cysts, 905
AIUM/NEMA Output Display Standards (ODS), 51
Alagille's syndrome, 216, 1371–1372, 1374f
Albumin-coated microbubbles, 80
Alcohol
fatty liver, 105
hepatitis, 121–122, 122f
pancreatitis risk, 294, 301
tumour ablation, 859–860
Alcoholic liver disease, 216
Aliasing, 28, 41, 41f, 74–75
α-Fetoprotein (AFP)
cirrhosis screening, 115–116
hepatoblastoma, 1360–1361
hepatocellular carcinoma screening, 154
5-Alpha reductase agents, 581
Amaurosis fugax, 941–942, 965
Amenorrhoea, 1481–1482, 1481t, 1482b
American Association for the Surgery of Trauma (AAST)
liver injury scale, 835–836, 835t
renal trauma, 839, 839t
spleen trauma, 837–838, 838t
American Joint Committee on Cancer (AJCC) classification, 921
Amnion, 745, 745f, 750, 750f
Amoebic colitis, 391–392, 400, 400f
Amoebic liver abscess, 126–127, 127f–128f, 145–146, 1364–1365
Amoebomas, 400
Amplitude, 3, 4f
Amplitude modulation/power modulation (PM/AM), 82, 82f
Ampullary carcinoma, 263
Amyloid
liver, 117
renal, 452, 452f
Amyloidosis, 1134
Anal canal, 405–409
anatomy, 406–407, 406f
anorectal tumours, 407–408, 407f
sepsis, 408, 408f
sphincters *see* Anal sphincters
trauma, 408, 408f
ultrasound technique, 405–406
Anal sphincters, 406–407, 406f
abnormalities, 409, 409b
solitary rectal ulcer syndrome, 409
traumatic injury, 408
Anaplastic carcinomas, thyroid, 879–880, 880b, 880f
Anastrozole, 706
Anconeus epitrochlearis, 1141–1143
Androblastoma, ovarian, 678
Anencephaly, 746–747
Aneurysm Detection and Management (ADAM) Veterans Affairs Cooperative Study Group, 775
Aneurysms
aortic *see* Abdominal aortic aneurysms; Aorta, aneurysms

carotid arteries, 974
in children, 1301–1302
dilatation, 1198
of the extremities, 1117
haemodialysis access, 1222
hand/wrist, 1066–1067
hepatic artery, 192, 192f
iliac artery, 779, 780f
mycotic, 775, 779
peripheral arterial disease, 1211, 1212f
popliteal artery, 1117, 1198, 1211, 1212f
portal vein, 189
posterior communicating arteries, 982f
pulsatile neck masses, 974
renal, 495–496, 496f
renal arteries, 482–483, 483b, 483t
splanchnic arteries, 791–792, 791f
splenic artery, 342, 342f, 791–792, 791f
splenic vein, 342
tibial vessels, 1105
transcranial Doppler ultrasound, 982, 982f
Angiomatosis, 1120–1121
Angiomyoleiomas, 1121
Angiomyolipomas (AML)
in children, 1461–1462
liver, 149
renal, 490, 502, 509–512, 509f–511f, 512b
Angioplasty, 1210
Angiosarcomas, 1121
breast, 997
spleen, 334, 336f
Angiotensin, 473
Anisakiasis, 379
Anisotropy
biceps tendon, 1037–1039, 1039f
shoulder, 1030–1031, 1033f
Ankle
Achilles region, 1093–1095
anatomy, 1093–1101, 1094b, 1094f
anterior, 1094b, 1097–1098, 1097f–1098f, 1105–1106
bone problems, 1105–1106
bursitis, 1102, 1102f
calcific mass lesions, 1103
disease processes, 1101–1107, 1107b
enthesopathy, 1102–1103, 1103f
interventional techniques, 1187–1190
joint problems, 1104–1105
lateral, 1094b, 1098–1100, 1099f–1100f, 1105
medial, 1094b, 1096–1097, 1096f–1097f, 1103–1105
neurovascular bundle, 1105
posterior, 1093–1095, 1094b, 1095f–1096f, 1101–1103
tendon tears, 1102, 1102f
ultrasound technique, 1093–1101, 1101b
xanthomata, 1103
Ankle brachial pressure index (ABPI), 1199
Annular ligament, 1046
Annular pulleys, 1055–1056, 1057f, 1060–1062, 1062f
tears, 1063
Anorectal tumours, 407–408, 407f
Anterior communicating artery
anatomy, 976
transcranial Doppler ultrasound, 976–978
Anterior talofibular ligament, 1099, 1099f, 1105, 1105f
Anticoagulant drugs, 170
Antiplatelet drugs, 170
Antral dyskinesia, 1386
Anus
ectopic, 1399
imperforate, 1399, 1399f
see also Anal canal
Anxiety in biopsy patients, 848
Aorta, 773
abdominal *see* Abdominal aorta
aneurysms, 773 (*see also* Abdominal aortic aneurysms)
dissection, 789
Aortic valve disease, 971f
Aortocaval fistulae, 795
Aperture control, 21, 21f
Apophyseal injuries, 1505
Appendagitis, epiploic, 402–405, 405f
Appendicitis
acute, 389–392, 390f, 392b
in children, 389
differential diagnosis, 391–392
mesenteric lymphadenopathy, 389–390, 391f
occasions, 389
perforation, 391, 391f
pitfalls, 391–392
in children, 389, 1395, 1396f–1397f, 1397–1398, 1399b
diagnostic efficacy, 1398
isolated granulomatous, 394
stump, 394, 394f
Appendicoliths, 389–390, 390f
Appendicular artery, 388
Appendix, 388–394
abscess, 391, 392f, 1397, 1397f
adenocarcinoma, 393
anatomy, 388, 389f–390f
appendicitis *see* Appendicitis
carcinoid tumour, 392–393
in children, 1395–1398
Crohn's disease, 394, 394f
inflammation *see* Appendicitis
lymphoma, 393
mucocele, 392, 393f
phlegmon, 391, 392f
retrocaecal, 1398, 1398f
tumours, 392–393, 393f
ultrasound technique, 388–389, 389f
Appendix testis, 595, 597f, 598
Aqueous humour, 940–941
Arachnoid cyst, 1279–1280, 1284
Arcade of Frohse, 1044
Arm
muscles, 1139, 1140t, 1141f
peripheral arterial disease, 1212–1214
occlusive arterial disease, 1214
Raynaud's disease, 1214, 1219f
Takayasu's arteritis, 1214, 1218f
thoracic outlet syndrome, 1213–1214
ultrasound investigation, 1212–1214, 1216f
Artefacts, 61–76
beam edge, 1126, 1127f
beam width, 72–74, 72f–73f, 73b
Chinese hat, 73, 74f
comet-tail, 68, 69f
contrast imaging, 88, 88f
Doppler, 88
flash, 1126, 1127f
grating lobe, 73, 73f
mirror image, 65–67, 67f
missing echoes, 63, 63f
multiple echoes, 65–68, 67f–68f
noise, 61, 61b
gain-related, 62f
structured, 62f
propagation, 88, 88f
ranging, 74, 75f
refractive, 68–70, 70f–71f
reverberation, 67–68, 68b, 69f
simple renal cysts, 487, 487f
in rheumatological ultrasound, 1126, 1127f
scattering, 61–63, 62f
shadowing, 64f
edge, 65, 66f
and increased sound transmission, 64–65, 64f, 65b
reflective, 65f
refractive, 65, 66f
types of, 64t
specular interfaces, 61–63, 62f, 64b
testis, 595–598
in three-dimensional scanning, 75
time sampling problems, 74–75, 74b
velocity errors, 68–72, 70f, 70t, 71b
Arteriography
hypertension in children, 1455–1456
penis, 625–626
Arteriovenous fistula
acquired, 192
in children, 1301–1302
orbital, 960–961
post-renal biopsy, 457, 457f
post-renal transplantation, 538–539, 541f
renal, 481, 481b, 481f
congenital, 481–482, 482f–483f
post-traumatic, 481f
traumatic, 1212, 1216f
upper limb, 1241
Arteriovenous malformations, 1120
in children, 1301, 1351
congenital, 1284
renal, 481–482, 482f–483f, 495–496, 507
and renal cell carcinoma, 513
transcranial Doppler ultrasound, 982
uterine, 695–696, 696f, 711–712
Artery bypass, vein mapping, 1248–1249
Arthritis
mimics, 1133–1134
monitoring disease progression, 1132–1133, 1132b
ultrasound features of, 1127–1131
see also specific types
Arthrography, magnetic resonance *see* Magnetic resonance arthrography
Arthropathy, inflammatory, 1025
Arthroplasty, hip, 1071–1072, 1072f
A-scan, eye, 941, 942f
Ascariasis
biliary, 266, 266f
gallbladder, 250–251
Ascaris lumbricoides, 250–251, 266
Ascites, 808–812, 808f–809f, 811f
bowel loops in, 810–811, 810f–811f

in children, 1401, 1401f
gallbladder in, 242–243, 242f, 811, 812f
loculated, 811, 811f
malignant, 812, 812f–814f
in ovarian tumours, 678
subtle, 810–811, 811f
Asherman's syndrome, 697, 709
Asphyxia, perinatal, 1265
Aspiration, 1169
abscess, 1192, 1193f
cystic lesions, 1192–1193
diagnostic, versus drainage, 853
ganglion cysts, 1178, 1179f
hip, 1181–1184, 1184b, 1184f
knee, 1185–1186, 1186f–1187f
tibiofibular joint, 1187
see also Drainage techniques
Asplenia, 330, 331f, 1356
Asteroid hyalosis, 949, 949f
Astrocytomas, neonatal, 1333
Asymptomatic Carotid Artery Surgery Trial, 965–966
Atelectasis, 1010–1011, 1011f
in children, 1339–1340
Atheroma, carotid arteries, 966
Atherosclerosis
abdominal aorta, 787, 788f
grading, 788
imaging, 788
peripheral arterial disease, 1198
signs, 788
upper limb, 1214
waveform appearance, 788, 788f
Athletic groin pain, 1081–1082
adductor muscles, 1081, 1082f
anatomy, 1081, 1081f
clinical overview, 1081
normal ultrasound appearances, 1081
role of ultrasound, 1082
symphysis pubis, 1081, 1081f
ultrasound-guided intervention, 1082
Attenuation, 11, 11t, 13b
Attenuation coefficients, 52, 52t
Atypical ductal hyperplasia (ADH), breast, 991
Autoimmune pancreatopathy, 305–306, 305f
Autonephrectomy, 463–464, 465f
Autosomal dominant polycystic kidney disease (ADPKD), 97–98
in children, 1436–1437, 1437f–1438f
and pancreatic cysts, 1378
Autosomal recessive polycystic kidney disease (ARPKD)
in children, 1436, 1436f
Axial resolution, 15
Axillary artery, 1213
Axillary vein, 1241
Axilla staging in breast cancer, 997–999, 998f–999f
Axons, 1158
Azathioprine, 529–530

B

Backscatter, 14
Bacteroides spp., 124
Bagel sign, 754–755, 755f
Baker's cyst, 1089, 1090b, 1090f, 1115
paediatric, 1510, 1510f
Bandwidth, 18
Barbotage, 1037, 1038f
of calcific supraspinatus tendinopathy, 1172, 1172b, 1172f
Barcelona Clinic Liver Cancer (BCLC) classification, 172
Barlow test, 1497–1498, 1498f
Barrett's oesophagus, 356, 358f
Bartonella hensellae, 133–134
Basilar artery, 1259t
anatomy, 976
transcranial Doppler ultrasound, 976
Basilic vein, 1043
bypass grafts, 1207–1208
Basivertebral veins, 1320–1322
Baum's bumps, 940, 941f
Beak sign, simple renal cysts, 487, 487f
Beam edge artefacts, 1126, 1127f
Beam former, 21, 23b
Beams, 6, 17
electronic focusing, 21, 21f
steering, 19f, 20, 42, 43f
width of, 17
Beam width artefacts, 72–74, 72f–73f, 73b
Behçet's syndrome, 379t
Benign lymphoepithelial lesions (BLELs), 904–905, 906b
Benign prostate hyperplasia/hypertrophy (BPH), 579–581, 580t, 581f–582f, 583t
Benign sternomastoid tumour of infancy, 1302, 1303f
Berardinelli-Seip syndrome, 116
β-human chorionic gonadotropin (β-hCG), 758
Bezoars, 1387, 1387f
Biceps femoris, 1075, 1091, 1091f
Biceps tendon
anatomy, 1043, 1044f
dislocation, 1039, 1039f–1040f
injury, 1048, 1048f–1049f
long head of
anatomy, 1030
fatty atrophy, 1039, 1039f
normal, 1032f
pathology, 1037–1039, 1039f
Bicipital groove, 1030–1031, 1032f
Bicipitoradial bursitis, 1050, 1050f
Bifid median nerve, 1159, 1160f
Bile
echogenic, 240–241, 241f–242f
leaks, post-liver transplantation, 212, 221
milk of calcium (limy), 240
volume increase, 256
Bile ducts, 94–95
anastomosis, strictures, 211, 212f
anatomy, 227, 229f, 234f
ascariasis, 266, 266f
biliary epithelial dysplasia of, 150
Caroli's disease, 264–265, 266f
in children, 1356–1375
cholangiocarcinoma, 156–160
choledochal cysts, 263–264, 265f–266f
choledocholithiasis *see* Choledocholithiasis
diameter changes, rapid, 255–258
dilatation, 254–255, 254f–256f, 1372
post-liver transplantation, 211, 220, 221f
ultrasound signs, 254, 255f
without jaundice, 255
gallbladder distension, 256–258, 257f
gas in, 259, 260f
hypoplasia, 216
injury, intraoperative ultrasound, 279
jaundice *see* Jaundice
measuring, 189, 234–236, 235f
neoplasms, 261–263, 261f–265f, 1372–1375
normal anatomical variants, 227–228, 234f–236f
obstruction, 1372
pancreatitis complications, 299
without dilatation, 255
oriental cholangiohepatitis, 265–266
pathology, 253–267
sclerosing cholangitis, 267, 267f
spontaneous perforation, 1370, 1373f
stones *see* Choledocholithiasis
strictures, 212f
Biliary ascariasis, 266, 266f
Biliary atresia
congenital extrahepatic, 216
extrahepatic, 1368–1369, 1369f–1370f
Biliary atresia-splenic malformation syndrome, 1368–1369, 1370f
Biliary cirrhosis, 115, 116f, 154
post-liver transplantation, 216
Biliary epithelial dysplasia of the intrahepatic bile ducts, 150
Biliary sludge, 240–241, 241f–242f, 1375, 1375f
Biliary system
cystadenocarcinoma, 161
cystadenoma, intrahepatic, 149–150
hypoplasia, 1371–1372
rhabdomyosarcoma, 1374f
Biliary tree
anatomy, 228f
endoscopic ultrasound, 236, 236f
intraoperative ultrasound, 279–280, 280f
laparoscopic ultrasound, 236, 273
liver transplantation complications, 211–212, 220–221, 221f
normal anatomy, 227
ultrasound technique and appearance, 228–236
Bilirubin, 1367
Biometry
eye, 958, 958f
first trimester, 748–749
Biomicroscope, ultrasound
eye, 942
Biopsies, 1169
bone lesions, 1191–1193, 1192f
breast, 1000–1002, 1001t, 1002f
cervical lymph nodes, 934–935, 935b
coaxial technique, 850
core *see* Core biopsy
fine-needle aspiration *see* Fine-needle aspiration (FNA)
general principles, 847–853
hepatocellular carcinoma, 154
large-bore vacuum-assisted, 1001–1002, 1001t
liver, 167–170
complications, 170, 170b

image-guided approach, 167–168, 168f
indications, 169, 169b, 169f
patient management, 170, 170b
percussion-palpation approach, 167
quality of specimen, 168–169
technique, 167–169, 168t
type of needle, 168
lungs, 1017–1018
needle guides, 852, 852f
needle tip visualisation, 850–852, 851b, 851f–852f
omental, 720–722, 721b, 721f
complications, 722
method, 720–721
rationale, 720
pancreas, 290, 318–319, 318f, 319b
complications, 318–319
indications, 318
results, 318
techniques, 318
patient selection/preparation, 847–848
post-procedural care, 853
pre-procedural assessment, 848
procedural planning and ergonomics, 852, 852f
prostate, 587–591, 589b
abscess/cyst drainage, 591
post-prostatectomy bed, 590–591, 591f
principles, 587–590, 590f
seminal vesicles/ejaculatory ducts injection, 591
renal, 455–458
complications, 456–457, 457f
contraindications, 455–456
indications, 455–456
renal transplant, 457–458
technique, 456, 456f
safety/complications, 853
small bowel, 385, 386f
soft tissue masses, 1191–1192, 1191b, 1192f
specimen handling, 852–853, 853f
spleen, 345
track seeding, 853
Tru-cut, 318
Birth-related brain injury, 1285, 1289f
Birth weight, epidemiological studies, 56
Bladder, 550–571
adenocarcinoma, 561–562
anatomy, 550–551
cancer, 561, 562t
invasion from adjacent tumours, 565–566, 566f
staging, 563–564, 563b, 564f–565f
tumour detection, 562–563, 563f
tumour follow-up, 564–565, 565f
catheter balloon puncture, 569
in children, 1409, 1413f–1414f, 1422–1428
colour duplex imaging: ureteric jets, 551, 553f
conduits, 568
contrast imaging, 85, 552–553
development, 1407–1409, 1408f
diverticula, 566, 567t, 1425, 1429f
ears, 1425, 1429f
emptying (residue), 553–556
endocavity ultrasound, 551
endometriosis, 568
extrinsic masses, 567–568, 567f
fistulae to the, 566, 567t, 568
flowmetry, 554–555, 555f
flow patterns, 555–556, 555b
foreign bodies, 556–558, 558f–559f
gross anatomy, 550
harmonic imaging, 551–552
infection, 568, 568b
inflammation, 568
leiomyosarcoma, 562
lower urinary tract symptoms, 553, 553b
lumen, 556–559
lymphoma, 562
masses, 561–566
megacystis, 1425
metastases, 562
microscopic anatomy, 550–551
neck, cysts, 581
neurogenic, 1425, 1430f
normal sonographic appearance, 576
outflow obstruction, 560, 562b, 562f
pelvi-ureteric dilatation, 436–438
partial resections, 568
pathology outside the bladder, 566–568
postoperative conditions, 568
pregnancy-related pathology, 568
procedures, 569
rhabdomyosarcoma, 562
squamous cell cancer, 561–562
stones, 556, 557f
suprapubic catheterisation, 569
transabdominal imaging, 551, 552f
transitional cell carcinoma, 431
trauma, 569, 569b, 841
tumours, 561–566
ultrasound technique, 1409, 1413f–1414f
urachus, 559, 561f
ureteroceles, 558–559, 560f–561f
urothelium, 551
volume, 553–556
assessment, 1413f
estimation, 554f
accuracy of, at different volumes and in bladder shapes, 554
calculating, 554b
technology comparisons, 554
wall, 560
thickness, 1414f
Blake's pouch cyst, 1279–1280
Blood clot
pelvi-ureteric dilatation, 434
see also Thrombosis
Blood flow *see specific organs; specific vessels*
Blood supply
ovaries, 648
prostate, 574
seminal vesicles, 574
small bowel, 371
uterus, 649
see also specific organs; specific vessels
B-mode imaging, 17f, 18b
aortic dissection, 789
artefacts in, 61–76
hypoxic ischaemic encephalopathy, 1266
image processing, 23, 23f, 25b
instrumentation, 25b
parameters, 32, 34–40, 39b
adaptive processing, 38–40
depth, 36, 37f
dynamic range, 36, 36f–37f
focus, 36, 38f
frequency, 36
gain, 34, 35f
harmonics, 37, 38f
spatial and frequency compounding, 37–38, 39f
time gain control/depth gain control, 35, 35f
zoom, 36–37, 38f
penis, 623–624
Peyronie's disease, 628
priapism, 627
principles, 17–18
pulse-echo cycle, 17f
scanners, 32, 39b
Bochdalek hernias, 1348–1349, 1350f
Bone-at-focus thermal index (TIB), 54
Bone(s), 1029
erosions *see* Erosions
implications of heating, 53
lesions, biopsy, 1191–1193, 1192f
Bosniak renal cyst classification system, 488, 488t, 489f, 492
Bowel
large *see* Colon
small *see* Small bowel
Boxer's knuckle, 1060–1062
Brachial artery, 1043, 1213, 1216f
Brachialis muscle, 1043
Brachial neuritis, 1037
Brachial plexus, 911–912, 912f
Brachytherapy
ocular melanoma, 952–953
tumour ablation, 860, 860f
Brain
neonatal see Neonatal brain
see also specific anatomical areas
Brain death evaluation, 983, 1290, 1290f
Branchial cleft cyst, 908, 908b, 909f–910f
Branchial cysts, 905, 1296–1297, 1297f–1298f
BRCA1-related tumours, 996
Breast, 987–1004
abscess, 989, 989f
benign pathology, 987–993, 989b
cystic lesions, 987–989, 988f–989f
solid lesions, 989–993, 990f–992f
cancer *see* Breast, malignant pathology
complex sclerosing lesions, 992–993
core biopsy, 1001, 1002f
equipment, 987
fat necrosis, 988, 988f
fibroadenoma, 990–991, 990f
fine-needle aspiration, 1001
galactoceles, 988, 988f
hamartoma, 991
implants, 1000, 1000f
infection, 989
large-bore vacuum-assisted biopsy, 1001–1002
lipoma, 991, 991f
malignant pathology, 993–1000, 993b, 994f
angiosarcoma, 997
assessment of response after chemotherapy, 999
axilla, 997–999, 998f–999f
BRCA1-related tumours, 996
classification, 993–996

contrast imaging, 993
cribriform carcinoma, 995
diagnostic techniques, 993
Doppler imaging, 993
ductal carcinoma in situ, 996, 996f
ductal carcinoma of no special type, 993–995
elastography, 993
focality, 997
impalpable, 1002
intraductal extension, 997, 998f
invasive carcinomas, 994f
lobular cancer, 995
medullary carcinoma, 995
metaplastic carcinoma, 996
metastases to the breast, 997, 997f
mucinous cancer, 995
papillary carcinoma, 995, 995f
screening, 999–1000
size, 997
staging operable cancer, 997–999, 998f–999f
tubular cancer, 995
ultrasound computer-aided classification, 993
oil cysts, 988
papillary lesions, 991–992, 992f
papillomas, 992, 992f
phyllodes tumours, 990–991, 991f
radial scars, 992–993
screening, 999–1000
simple cysts, 987–988, 988f
technique, 987
ultrasound-guided biopsy, 1000–1002, 1001t, 1002f
wire localisations of impalpable lesions, 1002
Breech delivery, 1330
Brenner (transitional cell) tumours, ovarian, 674, 674f
Bridging vascular sign, fibroids, 691
British Medical Ultrasound Society (BMUS) guidelines, 57–58
Broad ligament, 660
Bronchial walls, 1014
Bronchogenic carcinoma, 1007
Bronchogenic cysts, 1299, 1348, 1348f
Bronchopulmonary sequestration, 1342, 1343f
Brucellar liver abscess, 126
Brucellosis, 126
Bruits, 965–966
Bruxism, 906
Buccal fat pad, 907, 907f
Buccal region, 898–907, 900f
lymph nodes, 924, 925f
pathology, 906–907
Buck's fascia, 621
Budd-Chiari syndrome, 193–195, 196f, 202, 202f, 1367
post-liver transplantation, 215
Bulbar artery, 621
Bursae, 1115–1116, 1134, 1134f
adventitial, 1134
synovial, 1134
Bursitis
ankle, 1102, 1102f
bicipitoradial, 1050, 1050f
deep infrapatellar, 1089
elbow, 1050
in enthesitis, 1131
olecranon, 1050, 1051f, 1134, 1134f
perigluteal, 1184
subacromial, 1036–1037, 1036f
Butterfly wings sign, 808, 809f
Bypass graft, cephalic vein, 1207–1208

C

CA125, ovarian cancer, 680
Caecum, 369–370, 394–395
tumours, 391–392
Caesarean scar ectopic pregnancy, 758, 759f, 760t
Caesarean section scars, 697, 698f
Calcaneofibular ligament, 1099, 1100f, 1105
Calcification
adrenal, 635
extra-testicular, 611–612
hepatic, 134, 134t, 135f
kidneys, 451, 451b, 451f
cortex, 446
cysts, 491–492, 491f
shadowing, 64–65
soft tissue masses, 1111–1113, 1113b, 1113f
testicular, 607–608, 608f
thyroid nodules, 870, 871f
tunica albuginea, 611–612, 611f
tunica vaginalis, 611–612, 611f
Calcific myonecrosis, 1115
Calcific tendinitis, 1037, 1037f–1038f
Calculi
bladder, 556, 557f
gallbladder *see* Gallstones
parotid gland, 904, 904f
pelvi-ureteric dilatation, 430
salivary, 1308
staghorn, 430, 431f
submandibular gland, 895–897, 896f
see also specific areas
Calf vein imaging, 1232–1233, 1232f–1233f
deep vein thrombosis, 1236
problems and pitfalls, 1234b
Caliectasis, 1429
Calyceal diverticula, 493, 494f, 1442f
Calyceal system, dilated, 493, 494f
Campylobacter colitis, 401
Candida albicans
neonatal brain infection, 1274, 1276f
spleen, 339, 340f
Candidiasis
hepatosplenic, 339
liver, 127–128, 128f
renal involvement, 464, 1453, 1455f
Capillary haemangioma, 334, 1120
Captopril isotope renography, 474t–475t, 475
Captopril test, 474t–475t, 475
Carcinoid tumours
appendiceal, 392–393, 393f
gastric, 362, 364f
small bowel, 381, 382f
Cardiac shunts, 77
CARDIOsphere, 79t, 80–81
Caroli's disease, 264–265, 266f
Carotid arteries
anatomy, 966–967, 976
aneurysms, 974
atheroma, 941–942
atypical symptoms, 966
bifurcation, 967–968, 967f
carotid body tumours, 909, 911f, 974, 975f
direct measurement, 971–972, 971f
disease, in children, 1301–1302
dissection, 966, 974, 974f
Doppler criteria, 969–971, 970t, 971f
epidemiological studies, 966
indications for ultrasound, 965–966, 966b
ischaemic symptoms, 965–966
neonatal brain, 1258–1259, 1259t
occlusion, 973–974, 973f–974f
plaque characteristics, 972–973, 972b, 972f, 973t
post-endarterectomy follow-up, 966
pulsatile neck masses, 966, 974, 974b, 975f
stenosis, 941–942, 970, 970f, 975t
stents, 974, 975t
in thyroid carcinoma, 873, 873f
transcranial Doppler ultrasound, 976–983
trauma, 966
ultrasound technique, 967–968, 967b–968b, 967f–968f
Carotid body tumours, 909, 911f, 974, 975f
Carpal joint injection, 1178, 1179f
Carpal tunnel injection, 1177–1178
Carpal tunnel syndrome (CTS), 1057, 1064–1065, 1064f–1065f, 1162–1163, 1164f
Cartilaginous lesions in children, 1353–1354
Cataract, 943, 943f
Catheter angiography, 474, 474t
Catheter drainage, 803f, 809–810
Cat scratch disease, 133–134, 1364
Cauda equina, 1318
Caudal regression syndrome, 1327–1328, 1329f
Caudate nucleus, 1255
Caval filters, 794, 794f
Cavernosal arteries, 621, 622f, 623–624
duplication, 624, 624f
erectile dysfunction, 624
Cavernosography, 625–626
Cavernous haemangioma, 1120
liver, 140–142, 141f–142f
spleen, 334
Cavitation *see* Acoustic cavitation
Cavum septum pellucidum, 1257, 1280, 1282f
Cavum vergae, 1257
Cellulitis in children, 1352, 1352f
Central precocious puberty, 1478–1480
Central retinal artery, 942
Central retinal vein, 942
Cephalhaematoma, 1285
Cephalic vein, 1043
bypass grafts, 1207–1208
Cerebellum, 1258
Cerebral aqueduct stenosis, 1276–1277
Cerebral arteries, 1258
anatomy, 976
colour Doppler imaging, 977
neonatal brain, 1259t
power Doppler, 977
transcranial Doppler ultrasound, 976, 978

Cerebral oedema, 1287
Cerebral perfusion reserve, 979
Cerebrospinal fluid (CSF), 1274–1275
  flow, 1315
  hydrocephalus *see* Hydrocephalus
Cervical ectopic gestation, 757–758, 758f–759f, 758t
Cervical lymph nodes, 920–937
  biopsy techniques, 934–935, 935f–936f
  classification, 921, 922b, 922f
  lymphatic circulation, 920–921
  malignancy assessment, 927–933
    angioarchitecture, 931–932, 932b, 932f–934f
    cortex and hilum, 930, 930f
    echotexture, 928–930, 929f–930f
    location, 933
    margins of the node, 931, 931f–932f
    necrosis, 930–931, 931f
    shape, 928, 928f
    size, 927–928, 928f
  miscellaneous conditions involving, 934
  normal, in children, 1303–1304, 1304f
  structure and function, 920, 921f
  ultrasound in seven sweeps, 921–927
    anterior cervical nodes, 926–927, 927f
    deep cervical chain/internal jugular chain, 924–925, 925f–926f
    parotid and buccal region nodes, 924, 924f–925f
    posterior triangle, 926, 926f
    submandibular nodes, 922–923, 924f
    submental nodes, 922, 923f
    supraclavicular fossa/transverse cervical chain, 926
Cervical nerve roots, 912, 912f
Cervix, 712–715, 713f
  cancer, 714–715, 715f
    aetiology, 714
    bladder involvement, 568
    management, 715
    other investigations, 714–715
    staging, 715t
    symptoms, 714
    ultrasound appearances, 714
  clear cell tumours, 1488
  fibroids, 713, 714f
  incompetence, 714
  nabothian cysts, 713, 713f
  obstruction, 710, 711t, 712f
  polyps, 713
  scanning techniques, 687
  stenosis, 710
  symptoms, 688–689
  ultrasound anatomy, 653, 653f
  variation in age, 649, 649t
Charcot-Marie-Tooth disease, 1166
Chemotherapy
  assessment of response after, in breast cancer, 999
  ovarian cancer, 669, 720
Chest
  indications in children, 1339
  normal anatomy, 1338–1339
  paediatric, 1337–1355
  ultrasound technique, 1337–1338, 1338f
  wall *see* Chest wall
Chest wall, 1005–1007
  abscess, 1352f
  bony lesions, 1006–1007
  examination technique, 1005
  haemangioma, 1350–1351, 1352f
  haematoma, 1352
  lesions, 1350–1354
  masses, 1350–1353, 1351b
  paediatric, 1350–1354
  patient position, 1005
  peridiaphragmatic lesions, 1007, 1007f
  soft tissue lesions, 1005–1006, 1006f–1007f
  technical requirements, 1005
  thoracic lymph nodes, 1007
Children *see* Paediatric patients
Chimney phenomenon, 1006–1007
Chinese hat artefacts, 73, 74f
Chlamydia trachomatis
  endometritis, 709
  epididymo-orchitis/epididymitis, 614
  pelvic inflammatory disease, 682
Cholangiocarcinoma, 156–160, 159f
  bile duct, 261–263, 261f–263f
  magnetic resonance cholangiopancreatography, 236
  metastases, 263
  post-liver transplantation, 216
  pre-liver transplantation ultrasound, 201
Cholangitis
  recurrent pyogenic, 265–266
  sclerosing, 267, 267f
Cholecystectomy
  laparoscopic, 237
  in liver transplantation, 1377
Cholecystitis
  acalculous, 1375
  acute, 243–246
    acalculous, 246, 246f
    complications, 244
    emphysematous, 245–246, 246f
    halo sign, 243–244
    pericholecystic collection, 244–245, 245f
    signs, 243–244, 244f, 244t
  chronic, 246–247, 247f
    carcinoma risk, 249–250
  gangrenous, 244, 245f
Cholecystitis glandularis proliferans, 247
Cholecystoses, hyperplastic, 247, 248f
Choledochal cysts, 263–264, 265f, 1369–1370, 1371f–1372f
Choledocholithiasis, 258–261, 258f–261f
  diagnosis, 258–259
  gallbladder distension, 257f
  intraoperative ultrasound, 279–280
  presentation, 258
Cholelithiasis *see* Gallstones
Choleresis, 256
Cholescintigraphy, 237
Cholesterolosis, 247, 248f
Chondroid tumours, thyroid cartilage, 917, 918f
Chondromatosis, synovial, 1123, 1123f
Choriocarcinomas
  testicular, 599–600
  uterine, 696
Chorion, 745, 745f
Choroid, 940
  detachment, 946
  haemangioma, 954, 954f
  melanoma, 951–953, 951f–953f
  metastases, 953
  naevus, 954
  osteoma, 954, 954f
Choroidectomy, 952–953
Choroid plexus, 1255
  cysts, 1255
Chronic exertional compartment syndrome (CECS), 1155–1156
Chronic granulomatous disease, 133
Churg-Strauss syndrome, 379t
Chylothorax, 1344
Ciclosporin
  renal transplantation, 539
  in renal transplantation, 529–530, 536
Ciliary body, 940
  melanoma, 951–953, 953f
Circle of Willis, 977, 1258
Cirrhosis, 111–116, 201f
  aetiology, 111, 112t
  associated findings, 115, 115f
  biliary, 115, 116f, 154
  causes of, 111
  in children, 1358, 1359f
  classification, 111
  definition, 111
  diagnosis, 112
  dysplastic nodules, 115, 115f, 154–156, 156f
  echotexture, 112, 113f
  hepatocellular carcinoma risk, 153–156, 155f–156f
  liver morphology, 112, 112f
  macronodular, 200
  micronodular, 200
  portal hypertension in, 180–181
  portal vein thrombosis in, 188–189
  pre-liver transplantation ultrasound, 200, 200f
  regenerating nodules, 112–114, 114f, 154–156, 155f
  screening in, 115–116
  sonographic features, 115b
  surface nodularity, 112, 113f–114f
Cisterna magna, 1320
  mega, 1279–1280
Citrobacter, 1273, 1275f
Clear cell tumours
  cervix, 1488
  ovarian, 674, 674f
  vagina, 1488
Clefts, spinal, 1328–1330
Clergyman's knee, 1089
Climber's finger, 1060–1062, 1062f
Clinical-Etiology-Anatomy-Pathophysiology (CEAP) classification, 1243, 1243t
Cloaca, 1407–1409, 1408f
  anomalies, 1473, 1478f
  exstrophy, 1428
  malformation, 1428
Clonorchiasis, gallbladder, 251
Clonorchis sinensis, 251, 265–266
Clostridium difficile, 400
Clostridium spp., liver abscess, 124
Clutter, 61
Coagulative necrosis, 930, 931f

Coats' disease, 955, 955f
Coccygeus, 647
Coded excitation, 84
Coeliac artery, 789, 790f
  stenosis, 789–791, 791f
Coeliac disease, 385
Cogwheel sign, pelvic inflammatory disease, 682
Colic veins, 388
Colitis
  amoebic, 391–392, 400, 400f
  in children, 1399, 1400f
  differential diagnosis, 399t
  granulomatous, 1399
  infective, 399–401, 401b, 401f
  inflammatory *see* Crohn's disease; Ulcerative colitis
  ischaemic, 399t, 401, 402f
  neutropenic, 1399, 1400f
  pseudomembranous, 399t, 400–401, 1399, 1400f
  tuberculous, 399–400, 399f, 399t
  typhlitis, 399t, 401, 401f
  ulcerative *see* Ulcerative colitis
  Yersinia enterocolitis, 399t, 401
Collateral ligaments
  elbow, 1045–1046, 1046f, 1051, 1051f
  fingers, 1064b
  knee
    lateral, 1084, 1091
    medial, 1084, 1085f, 1090
  wrist, 1063–1064
Collateral veins, 1235
Collateral vessel formation, 206–207, 206f
Collecting duct carcinoma, 517
Colloid cysts, 1309, 1310f
Colon, 394–405
  adenocarcinoma, 402
  anatomy, 394–395, 395f
  ascending, 394–395
  in children, 1399–1401, 1399b
    colitis, 1399
    imperforate or ectopic anus, 1399
    necrotising enterocolitis, 1400, 1401f
    neoplasms, 1400–1401
    normal anatomy, 1399
  colitis *see* Colitis
  congenital abnormalities, 395–396, 395f
  descending, 394–395
  diverticular disease, 395f–396f, 396–397
    right-sided, 397, 397f
  duplication cyst, 395–396, 395f
  endometriosis, 402, 404f
  epiploic appendagitis, 402–405, 405f
  haustrations, 395, 395f
  intussusception, 402, 405f
  lipoma, 402, 404f
  lymphoma, 402, 404f
  pseudo-kidney appearance, 402, 403f
  scanning technique, 394–395, 395f
  sigmoid, 394–395
  transverse, 394–395
  trauma, 841, 842f
  tumours, 402, 403f–404f
Colorectal cancer, 275–276
Colour blooming, 88
Colour Doppler imaging, 28–29, 29f–30f
  abdominal aorta atherosclerosis, 788
  abdominal trauma, 830
  acute appendicitis, 389–390, 391f
  adenomyosis, 694–695
  adrenal glands, 637
  aortic dissection, 789
  appendix, 1396
  artefacts, 88
  before aspiration, 1192
  biliary tree, 279–280
  carotid arteries, 967, 969
  cerebral arteries, 977
  cervical lymphatic malformations, 1295–1296
  cervical node vascularity, 932
  chronic venous insufficiency, 1244
  colitis, 1399
  colour blooming, 88
  Crohn's disease, 1392
  deep vein thrombosis, 1232, 1232t, 1235–1236
  endoleaks, 785, 787f
  eye, 942, 942f
  gastro-oesophageal reflux, 1384
  gestational trophoblastic disease, 696–697
  hepatic artery pseudo-aneurysm, 208–209
  hepatic veins
    occlusion, 195
    stenosis, 210–211
  hepatocellular carcinoma, 155–156
  image processing, 30b
  instrumentation, 30b
  intussusception, 1390
  kidneys
    arteriovenous fistula, 481
    renal cell carcinoma, 513–517
    renal vein thrombosis, 448
    simple renal cysts, 487
    transplantation, 530–533, 531f
    trauma, 840–841
  knee joint effusion, 1088
  limitations of, 29–30
  liver
    adenoma, 145
    angiomyolipoma, 149f
    fibronodular hyperplasia, 142
    haemangiomas, 140
    transplantation, 199
  lung cancer, 1017
  ocular melanoma, 951–952
  ovaries
    lesions, 670
    torsion, 668, 1489
  pancreas, 288–290, 290f
    transplantation, 320
    tumours, 309
  parameters, 32, 40–44, 44b
    beam steering in linear arrays, 42, 43f
    box/area size, 42, 42f
    filter, 42–44
    flow settings - combination controls, 44, 45f
    focus, 42, 43f
    frequency/patient type, 41, 42f
    gain, 40, 40f
    invert, 41, 41f
    persistence, 42–44
    post-processing, 42–44
    power, 40
    priority, 42–44, 44f
    scale/pulse repetition frequency, 40–41, 40f–41f
    space/time, 42–44, 45f
  penis *see* Penis, stimulated colour Doppler ultrasound
  peripheral veins, 1229–1232, 1230f–1232f
  Peyronie's disease, 628
  portal veins, 179, 180f
    stenosis, 209–210
  priapism, 627
  proliferative haemangiomas, 1300
  prostate, 576
  retained products of conception, 711
  in rheumatological ultrasound, 1132
  scanners, 32, 44b
  soft tissue masses, 1113
  spleen
    abscess, 338–339
    infarction, 340–342
  tendinopathy, 1025
  testicular torsion, 617
  thoracic disease, 1018
  thyroid nodules, 872
  transcranial, 85, 979
  venous reflux, 1245
Colour fluid sign, 1018
Column of Bertin, 505, 506f
  hypertrophied, 1417f
Comedocarcinoma, prostate gland, 589t
Comet-tail artefacts, 68, 69f, 1008, 1008f
  thyroid nodules, 872, 872f
Common extensor origin injection, 1053, 1173–1174, 1176f
Common extensor tendon, 1046, 1046f
Common flexor tendon, 1045, 1046f
Common hepatic duct, 95, 103, 103f
Common peroneal nerve, 1100
Communicating arteries
  anterior
    anatomy, 976
    transcranial Doppler ultrasound, 976–978
  posterior, 1259t
    anatomy, 976
    aneurysm, 982f
    transcranial Doppler ultrasound, 976–977, 979f, 981f
Communicating cavernous ectasia of the intrahepatic ducts *see* Caroli's disease
Compartment syndromes, 1155–1156
  acute, 1155
  chronic exertional, 1155–1156
Complete portal tracts (CPTs), 168
Compression stockings, venous incompetence, 1246
Compression technique, appendix assessment, 388
Computed tomography (CT)
  abdominal aorta, 773
    aneurysm, 779
  adrenal glands, 632, 636, 640, 642
  bladder cancer, 562, 564
  cervical cancer, 714
  cholangiocarcinoma, 158–160

contrast-enhanced *see* Contrast-enhanced computed tomography (CECT)
elbow loose bodies, 1047
endometrial cancer, 705
epithelioid haemangioendothelioma, 160–161
erosions, 1129
versus full potential ultrasound in abdominal trauma, 832
inguinofemoral hernia, 1077
kidneys
abscess, 496
renal cell carcinoma, 513–517, 523
trauma, 840–841, 1458
kidneys, ureter and bladder, 428
liver
focal lesions, 138
metastases, 151–153
radio-frequency ablation, 172
lung biopsy, 1017–1018
oesophageal cancer, 354
ovarian cancer, 669
paediatric chest, 1337
pancreas, 285
biopsy, 318
pancreatitis
acute, 295–296
chronic, 301–302
tumours, 306
peripheral nerves, 1158
small bowel
ischaemia, 379
obstruction, 384
thymus, 1339
thyroid, 867
transitional cell carcinoma, 518–520, 521f
in tumour ablation, 863
unstable trauma patient, 843
uterus, 687
Computed tomography (CT) angiography
peripheral arterial disease, 1197, 1200–1201
pulmonary embolus, 1015
renal artery stenosis, 474, 474t–475t
Computed tomography during arterial portography (CTAP), 277
Congenital anomalies
liver, 97
prostatic, 579
see also specific anomalies
Congenital cystic adenomatoid malformation (CCAM), 1341, 1343, 1344f
Congenital extrahepatic biliary atresia, 216
Congenital generalised lipodystrophy (CGL), 116
Congenital malformations, neonatal brain, 1279–1283
Dandy-Walker complex, 1279–1280, 1281f
destructive lesions, 1283, 1283f
disorders of sulcation and migration, 1280–1282, 1282f
dysgenesis of the corpus callosum, 1279, 1281f
holoprosencephaly, 1280, 1282f
tuberous sclerosis, 1282, 1283f
Conjoined twins, 748, 748f
Connatal cysts, 1257–1258
Connective tissue disorders, kidney involvement, 453
Conn's syndrome, 636
Consolidated lungs, 1339–1340, 1341f
Continuous ambulatory peritoneal dialysis (CAPD), 454–455
in children, 1444
Continuous wave (CW) Doppler, 15, 26, 27f
peripheral arterial disease, 1199–1200, 1203b
transducers, 8
Contrast agents, 77–89
bladder, 552–553
breast cancer diagnosis, 993
British Medical Ultrasound Society (BMUS) guidelines, 58
cavernous haemangioma, 141–142
clinical applications of, 84–86
diffuse parenchymal liver disease, 104
European Federation of Societies of Ultrasound in Medicine and Biology (EFSUMB) guidelines, 58
fallopian tube patency, 734–735
generations, 79
history and development, 77
imaging artefacts, 88
kidneys, 467, 470f
acute tubular necrosis, 484
renal cell carcinoma, 513
liver, 84, 85f, 138–139, 139t
diffuse parenchymal liver disease, 104
metastases, 151–153
microbubbles *see* Gas bubbles
optimisation, 139–140
scanning strategy, 139–140
types of, 78–81, 79t, 81b
World Federation for Ultrasound in Medicine and Biology (WFUMB), 58–59
see also Contrast-enhanced computed tomography (CECT); Contrast-enhanced intraoperative ultrasound (CE-IOUS); Contrast-enhanced ultrasound (CEUS)
Contrast-enhanced computed tomography (CECT)
hepatic artery
pseudo-aneurysm, 208–209
stenosis, 208
thrombosis, 205–207
hepatocellular carcinoma, 200–201
portal venous thrombosis, 201
post-transplant lymphoproliferative disease, 213
Contrast-enhanced intraoperative ultrasound (CE-IOUS), 273
liver metastases, 152–153, 277–278, 277f–278f
Contrast-enhanced ultrasound (CEUS)
abdominal trauma, 829–830, 832–833, 832f–833f
bladder, 553
cholangiocarcinoma, 158–160
versus computed tomography in abdominal trauma, 832–833, 833f
epithelioid haemangioendothelioma, 160–161
gallbladder polyps, 249
hepatic artery thrombosis, 206–207
hepatocellular carcinoma, 155–156, 157f–159f, 200–201
liver
abscess, 124, 125f
lymphoma, 160
radio-frequency ablation, 172, 173f
trauma, 837
neuroendocrine tumours, 314
pancreas, 288, 291f
tumours, 306–309
portal venous thrombosis, 201
renal trauma, 840–841
spleen, 326–327
abscess, 338–339
infarction, 341f
metastases, 334
trauma, 838
tumours, 334–337
in tumour ablation, 863
Contrast resolution, 15
Conus medullaris, 1319
Copper intrauterine devices, 706–707
Coracoacromial ligament, 1030, 1032f
Coracohumeral ligament, 1030, 1032f
Core biopsy, 318
breast, 1001, 1001t
cervical lymph nodes, 935, 935b, 936f
versus fine-needle aspiration, 848
lungs, 1017
needle types, 849–850, 849f, 849t
fully automated sheathed, 850
manual sheathed, 849
Menghini technique, 849
semi-automated sheathed, 849, 850f
Cornea, 938
Coronary artery bypass, vein mapping, 1248–1249
Coronary ligaments, liver, 93
Coronary vein varices, 183, 184f
Coronoid fossa, 1043
Corpora amylacea, 576
Corpora cavernosa, 621, 622f
air in, 623–624, 623f
Corpus callosum, 1257
dysgenesis of the, 1279, 1281f
Corpus luteum, 662–663, 663f
cysts, 663, 762–763, 762f
Corpus spongiosum, 621, 622f
Cortical necrosis
acute, 452, 452f
in children, 1444
Couinaud classification, 93, 95–96, 179, 180f, 193
Courvoisier's law, 256
Cranial bone thermal index (TIC), 54
Cranial sutures, 1254
Cremasteric artery, 594–595
Crescent in doughnut sign, 384, 385f
Cribriform carcinoma, breast, 995
Cricoid cartilage, 914
Crohn's disease, 371–376, 372b
abscess, 374–375, 375f
activity, 375–376
appendiceal, 394, 394f
in children, 1392–1393, 1393f
clinical features, 372
colonic, 397, 397b, 398f

differential diagnosis, 399t
inflammatory phase, 397
versus ulcerative colitis, 397b
differential diagnosis, 379b
fat wrapping, 373
fistula, 375, 376f
local complications, 374–375
locoregional lymphadenopathy, 374
stricture, 374, 375f
ultrasound features, 372–374, 372f–374f
vascular changes, 374
Crossover syndrome, 1059
Crown-rump length (CRL), 745, 745f, 749, 753, 761
Cruciate ganglia, 1186
Cruciate ligaments, 1090
Cruciform bands, 1055–1056
Cryoablation
renal cell carcinoma, 523
tumours, 858–860, 858f–859f
Cryptorchidism, 807, 1491, 1491f
CT *see* Computed tomography (CT)
Cubital tunnel, 1052
Cumulative pregnancy rates, 730, 731f
Currarino's triad, 1334, 1335f
Cushing's syndrome, 636
Cutaneous pits, 1328–1330, 1330f
Cystadenomas
intrahepatic biliary, 149–150
pancreas, 311–312, 311f
Cystic adenoid carcinoma, prostate gland, 589t
Cystic duct, 95, 103f
anatomy, 227
normal anatomical variants, 227–228
Cystic fibrosis (CF)
in children, 1358–1359
liver involvement, 117–118, 117f, 1358–1359
microgallbladder, 251
pancreas in, 1380
Cystic hygroma
cervical, 913
parotid gland, 905, 906f
submandibular region, 898
Cystic necrosis, 930
Cystic renal dysplasia, 1439f
in children, 1437–1438
Cystitis, 568, 568b
in children, 1449–1453
Cyst of Morgagni, 595, 597f, 598
Cystoscopy, bladder cancer, 562–563, 565
Cystosis, 1380
Cysts, 1115–1116
abdominal wall, 806b
ablation, 816
acromioclavicular joint, 1039–1040, 1040f
adrenal, 634–635, 634f, 1464, 1465f
AIDS-related parotid, 905
arachnoid, 1279–1280, 1284
aspiration, 1192–1193
Baker's *see* Baker's cyst
Blake's pouch, 1279–1280
branchial, 905, 1296–1297, 1297f–1298f
branchial cleft, 908, 908b, 909f–910f
breast, 987–988, 988f
bronchogenic, 1299, 1348, 1348f
choledochal, 263–264, 265f, 1369–1370, 1371f–1372f
choroid plexus, 1255
colloid, 1309, 1310f
colonic duplication, 395–396, 395f
corpus luteum, 663, 762–763, 762f
dermoid, 674–676, 674f–677f, 676b, 893–894, 1298, 1298f–1299f
duplication *see* Duplication cysts
echinococcal, 129–130, 130f–131f, 170
endometrium, 742f
epidermal inclusion, 1116
epidermoid, 602, 603f, 893–894, 894f
epididymal, 608, 609f
ganglion *see* Ganglion cysts
Gartner's duct, 716, 716f
hydatid *see* Hydatid disease
juxtaventricular, 1257–1258
labral, 1037, 1038f
liver, 97–98, 98f, 1363–1364, 1364f
lymphoepithelial, 905, 905f
meniscal, 1091, 1091b, 1091f, 1115–1116
mesenteric *see* Lymphangiomas
milk of calcium, 492, 511–512, 511f
Müllerian duct, 716
myometrial, 694–695
nabothian, 713
neonatal brain, 1284
neurenteric, 1348
oesophageal, 358–359, 359f
oil, breast, 988
omental, 1483
ovarian *see* Ovaries, cysts
paediatric, 1510
pancreas
congenital, 1378
neoplasms, 311–313, 311f–314f, 312b
paraovarian, 664, 1485
parathyroid, 887, 1298–1299
parotid gland, 905, 905f
periarticular, 1134, 1134f
pericardial, 1348, 1349f
peripheral nerve compression, 1165–1166, 1166f
peritoneal inclusion, 697–698, 699f
popliteal *see* Baker's cyst
prostate, 579, 580f, 583–584, 583t, 584f–585f, 591
renal *see* Kidneys, cysts
retroperitoneal, 821, 822f
sebaceous, 989, 989f
spleen, 337–340, 338t, 339f, 341f, 344
synovial, 1091, 1115
testicular, 605–606, 606f
theca lutein *see* Theca lutein cysts
thymic, 1298–1299
thyroglossal duct, 893, 1294–1295, 1295f
thyroid, 870, 870f, 1309, 1310f
transvaginal drainage/aspiration, 722–723, 722b, 723f–724f
complications, 723
method, 722–723
rationale, 722
tunica albuginea, 606
tunica vaginalis, 606
urachal, 807
vaginal, 716, 716f
Cytomegalovirus
in HIV/AIDS, 132
neonatal brain infection, 1273

D

Damped waveform
limitations of, 477
renal artery stenosis, 476–477, 476t
Dandy-Walker complex, 1279–1280, 1281f
Dartos fascia, 621
D-dimer testing, 1236
Decibels (dB), 23–24
Deep inguinal ring, 802, 803f, 1077
Deep vein thrombosis (DVT)
acute, 1235–1237, 1238f, 1238t
asymptomatic, 1237
and Baker's cyst, 1089
chronic, 1237–1240, 1238t, 1239f
diagnosis, 1232, 1232f, 1232t
facts, 1228b
lower limb venous imaging, 1227–1228
microbubbles, 1240
monitoring of clot lysis, 1240
and pulmonary embolus, 1015–1016
symptomatic, 1235–1237, 1237f
upper limb venous imaging, 1240, 1240t
Wells clinical score, 1236t
Definity, 79–80, 79t, 80f, 87
Delayed-onset muscle soreness (DOMS), 1151–1152
Deltoid ligament, 1096, 1097f, 1104
Demodulation, 25, 25f
De Morsier's syndrome, 1280
Denonvillier's fascia, 573
Dental abscess, 906, 906f
De Quervain disease, 1060, 1061f
De Quervain's thyroiditis, 883–884, 884f
Dermal sinuses, 1326–1327, 1327f–1328f
Dermatofibrosarcoma protuberans (DFSP), 1123
Dermoid cysts, 675f–677f, 676b, 893–894
in children, 1298, 1298f–1299f
ovarian, 674–676, 674f
spinal, 1327f–1328f
Dermoid mesh, 674–675, 675f
Desmoid tumours, abdominal wall, 806, 807f
Destruction-replenishment, 82–84
Developmental anomalies
implications of heating, 53
prostatic, 579
Developmental dysplasia of the hip, 1497, 1498t
Diabetes mellitus
kidney involvement, 452–453
and peripheral arterial disease, 1198
Dialysis, 454–455
complications, 455, 455f
Diaphragm, 1010
anatomy, 1339, 1339f
crura, 98, 99f, 818
eventration, 1350, 1351f
hernias, 1348–1350, 1350f
inverted, 1010, 1011f
liver transplantation complications, 221
normal, 1007, 1007f
paediatric, 1339, 1339f, 1348–1350, 1349b

paralysis and paresis, 1350, 1351f
rupture, 1007
trauma, 841
Diastematomyelia, 1325, 1326f
Dicrocoelium dendriticum, 251
Diffraction, 5–6, 6f
Digastric muscles, 891
Dilated pelvicalyceal system, 493, 494f, 518
Dimples, spinal, 1328–1330
Disciform lesions, retina, 948, 948f
Disease-modifying anti-rheumatic drugs (DMARDs), 1132
Distal augmentation, peripheral veins, 1231, 1231f, 1234–1235, 1236f
Distal intersection syndrome, 1059
Distortion, non-linear, 12
Diverticular disease
bladder, 566, 567t, 1425, 1429f
calyceal, 493, 494f, 1442f
colonic, 396–397, 396f
right-sided, 397, 397f
renal pelvic, 493, 494f
Doppler imaging, 13–14, 13f–14f, 14b, 26–30
abdominal trauma, 829
aliasing, 28
aortic dissection, 789
artefacts, 88
arteriovenous fistula, 481
autocorrelator, 29
axillary lymph nodes, 998
breast cancer
diagnosis, 993
response to chemotherapy, 999
carotid arteries, 969–971, 970t, 971f, 976–983
carpal tunnel syndrome, 1064–1065
cervical lymph nodes, 932, 933f
colour flow *see* Colour Doppler imaging
continuous wave *see* Continuous wave (CW) Doppler
in ectopic pregnancy, 756–757
endoleaks, 787
eye, 941–942, 942f
frequency estimation and display, 28, 29f
hepatic artery, 189–192
stenosis, 208
thrombosis, 205–207
hepatocellular carcinoma, 155–156
high pass filtering, 28, 28f
hypoxic ischaemic encephalopathy, 1266, 1269
inferior vena cava thrombosis, 792
instrumentation, 28b
kidneys, 467, 469–470, 1409, 1412f
abnormalities in hypertension, 475–476, 478f
acute glomerulonephritis, 484
acute tubular necrosis, 484
arteriovenous fistula, 481
arteriovenous malformations, 482
in children, 1456–1457
chronic renal failure, 484
colour flow map, 469, 469f
disease, 447
haematoma, 495
hepatorenal syndrome, 484
intrarenal vessels, 470–471, 477
main renal trunks, 471–472, 471f–473f, 477
normal pattern, 469–470
parenchymal disease, 483–484, 484b
renal artery occlusion, 478f
renal artery stenosis, 448, 467, 474t–475t, 475–477
renal infarcts, 478, 479f
renal vein thrombosis, 479–480
small vessel disease, 484
spectral (pulsed wave) arterial pattern, 469–470, 470f
technique, 470–472
transplantation, 467–468, 530–533
tubulo-interstitial disease, 484
vasculitis, 484
muscle injury, 1137
ocular melanoma, 952–953
ovaries
endometriosis, 681
haemodynamics, 655
lesions, 670
pancreatic tumours, 309
pelvi-ureteric dilatation, 441
portal hypertension, 181
power *see* Power Doppler
pulsed wave *see* Pulsed wave Doppler
pyelonephritis, 460
resolution, 15
in rheumatological ultrasound, 1126, 1132
shift frequency estimation, 29
transcranial, 85
transducers, 8
transjugular intrahepatic portosystemic shunt, 187–188, 188b
uterus haemodynamics, 655
Dorsal dermal sinuses, 1326–1327, 1327f–1328f
Dorsalis pedis artery, 1207, 1207f
Double-bleb sign, 750, 750f
Double-bubble sign, 1388
Double decidual sign, 751
Double wall sign, 1483
Doughnut sign, 384, 385f, 1390
Drainage techniques, 853–857
abscesses, 1192, 1193f
breast, 989
intra-abdominal, 815
liver, 124, 125f
pelvic *see* Pelvic abscess drainage
cyst ablation, 856–857
diagnostic aspiration versus, 853
drain fixation, 856, 856b, 857f
drain placement, 854–856, 856f–857f
drain types, 854, 856f, 856t
locking drains, 813
nature of the collection, 854, 854t, 855f
post-procedural care, 856
pre-procedural assessment, 854
Seldinger technique, 804f, 816
side holes, 813–815
sump drains, 813
Trocar technique, 815–816
Dromedary hump, renal, 505, 506f
Drug delivery, contrast microbubbles, 87
Drusen (hyaline bodies), 948, 948f
Ductal carcinoma in situ (DCIS)
breast, 991, 996, 996f, 1002
vacuum-assisted biopsy, 1002
Duct ectasia, 583–584, 583t, 584f
Ductus deferens, artery to the, 594–595
Ductus epididymis, 594
Duodenum, 365, 366f
atresia, 1388, 1389f
duplication, 1394, 1394f
haematoma, 1394, 1394f
Duplex scanning
abdominal aortic aneurysms, 777–781
abnormal appearance, 777–779, 778f–780f
distance between renal arteries and aneurysm sac, 780
limitations and pitfalls, 781
measurement of aneurysm size, 780, 781f
normal appearance, 777, 778f
objectives, 777, 777f
patient preparation, 777, 778f
variability of measurement between ultrasound and CT, 779
bladder, 551, 553f
peripheral arterial disease, 1200–1207, 1203b, 1203f–1204f
aorto-iliac and femoropopliteal segments, 1206
below-knee segments, 1206–1207, 1207f
reporting, 1207, 1208f
scanning technique, 1205–1206, 1205f–1206f
peripheral artery bypass grafts, 1209
transcranial, 85
Duplication cysts, 816, 1347b, 1348
duodenal, 1394, 1394f
neonatal, 1483
pancreas, 1378
Dupuytren's contracture, 1122
Dynamic range, 23–24, 24f
Dynamic scanning
carpal tunnel syndrome, 1064–1065
muscle injury, 1137
Dysfunctional uterine bleeding (DUB), 688–689
Dysgerminoma, ovarian, 676
Dyslexia, 56–57
Dysmenorrhoea, 688
Dyspareunia, 688, 691

E

Eagle-Barrett syndrome, 1427–1428
Echinococcal cyst, 129–130, 130f–131f, 170
see also Hydatid disease
Echinococcosis *see* Hydatid disease
Echinococcus granulosus, 129, 339–340
Echinococcus multilocularis, 130
Echo-endoscopes, 351–352, 352f
Echoes
B-mode imaging, 17
definition, 16
dynamic range, 23–24, 24f
liver, 104–105, 106f
multiple, 65–68, 67f
scattered, 61–62

Echogenic bile, 240–241, 241f–242f
Echogenic fluid, 64–65, 65f
Echogenic swirling sign, 1009
Echovist, 79, 734, 735f
Ectopia lentis, 943, 944f
Ectopic pregnancy, 753b
  adnexal findings, 754–756, 755f, 755t
  bagel sign, 755f
  β-hCG level, 760, 760t
  caesarean scar, 758, 759f, 760t
  cervical, 757–758, 758f–759f, 758t
  complex mass, 755–756, 756f–757f
  Doppler ultrasound, 756–757
  endometrial appearances, 754f, 754t
  heterotopic gestation, 753
  incidence, 753
  interstitial, 757, 757f–758f, 757t
  intraperitoneal fluid, 756, 757f
  locations, 753t
  methotrexate, 757, 767, 767t
  negative ultrasound, 760
  non-surgical management, 766–767
  normal adnexal regions, 754
  ovarian, 758
  pregnancy of unknown location, 760, 760b, 760f, 761t
  pseudo-gestation sac, 754, 755f
  risk factors, 753
  tubal miscarriage, 756, 757f
  tubal ring with yolk sac/embryo, 754–755, 755f–756f
  tubal rupture, 756, 756f, 756t
  unusual gestations, 757–758, 757f
  uterine findings, 753–754, 754f, 754t
Egyptian eye, 1244–1245, 1244f
Ejaculation, retrograde, 580t
Ejaculatory ducts, 574
  cysts, 583t, 584f
  injection of contrast, 591
  normal sonographic appearances, 576–579
  obstruction, 584, 585f
Elastofibroma, 1122
Elastography, 12–13
  breast cancer diagnosis, 993
  pancreas, 288
  soft tissue masses, 1113
  thyroid nodules, 872
Elbow, 1043–1054
  anatomy, 1043–1046, 1046b
  anterior compartment, 1043–1044, 1044f
  bursitis, 1050, 1050f–1051f
  effusion, 1047, 1047f
  injection, 1053
  interventional techniques, 1173–1175
  joint aspiration, 1053
  joint injection, 1175, 1177f
  lateral compartment, 1046, 1046f
  lateral epicondylitis (tennis elbow), 1049, 1050f
  ligament injury, 1051, 1051f
  loose bodies, 1047–1048, 1047f–1048f
  medial compartment, 1045, 1046f
  medial epicondylitis (golfer's elbow), 1050
  nerve entrapment, 1052–1053, 1052b, 1052f–1053f
  paediatric bony injury, 1051, 1051b, 1052f
  posterior compartment, 1045, 1045f
  pulled, 1051, 1052f
  synovial osteochondromatosis, 1047–1048, 1048f
  synovitis, 1047, 1047f
  technique, 1043–1046, 1046b
  tendon injury, 1048–1050, 1048f–1049f
Elderly patients, acute appendicitis, 389
Electronic focusing, 21, 21f
Elevation focusing, 21, 22f
Emboli
  counting, 979–980, 980f
  pulmonary, 1015–1016, 1016b, 1016f
Embryo
  appearance in the first trimester, 744–745, 744f–745f, 745t
  heartbeat, 745, 761, 761t
  transfer, 737, 737f
Embryology
  adrenal glands, 1464
  implications of heating, 53
  ovaries, 1468–1470
  parathyroid, 884
  prostate, 572
  renal tract, 1407–1409
  spine, 1322
  testis, 593–594
  thyroid, 868–869
  uterus, 1468–1470
Embryonal cell carcinoma, testicular, 599–600, 600f
Emphysema, congenital lobar, 1343–1344
Emphysematous pyelitis, 460
Empty amnion sign, 745, 750, 750f
Empyema, 1009, 1009f
  in children, 1346f
Encephalopathy, hypoxic ischaemic, 1264–1269, 1266b, 1267t, 1268f–1270f
Endarterectomy, 966
Endoanal ultrasonography, 406
Endocardial border definition (EBD), 79, 85–86
Endocavity ultrasound
  bladder, 551
  transducers, 19f
Endocrine development, female, 1470
Endodermal sinus tumours *see* Yolk sac tumours
Endoleaks, 782, 783t, 784b, 784f, 786f–787f, 787
Endoluminal ultrasound, bladder cancer, 564
Endometrioid tumours, 673, 673f
Endometriomas, 402
  abdominal wall, 806, 806f
  extraperitoneal, 1117
  ovarian, 680–681, 681b, 681f, 730
Endometriosis, 402, 404f
  bladder, 568
  as a cause of subfertility, 730
  ovarian, 680–681, 681b, 681f
Endometritis, 709, 709b, 710f
  pelvic inflammatory disease, 682, 682f
Endometrium, 700–712
  ablation, 697
  anastrozole and, 706
  Asherman's syndrome, 709
  cancer, 702–705, 705b
    aetiology, 702
    diagnosis, 702–705, 702f–705f
    management, 705
    other investigations, 705
    screening, 705
    staging, 704–705, 706f, 706t
    symptoms, 702
  cyst, 742f
  in ectopic pregnancy, 754, 754f, 754t
  endometriosis *see* Endometriosis
  endometritis *see* Endometritis
  haematometrium and related conditions, 709–711, 711f–712f
  hormone replacement therapy and, 705–706
  hyperplasia, 700, 700b, 700f, 700t, 706
  hysteroscopy, 688
  intrauterine devices, 706–708, 707f–709f, 708b
  intrauterine synechiae, 709
  medications and, 705–706
  normal, 699f, 700
  oral contraceptive pill and, 705
  osseous metaplasia, 732–733, 732f
  polyps, 693, 700–702, 701f, 702b, 733, 733f
  postpartum uterus, 711–712, 712f
  retained products of conception, 696, 711–712
  tamoxifen and, 706, 707f
  thickening in early pregnancy, 741, 741f
Endomysium, 1138
Endoneurium, 1158
Endoscopic retrograde cholangiopancreatography (ERCP)
  bile duct calculi, 236
  choledocholithiasis, 280
  pancreatitis, chronic, 302
Endoscopic ultrasound (EUS)
  biliary system, 236, 236f
  equipment, 351–352, 352f
  general principles, 351b
  islet cell tumours, 279
  neuroendocrine tumours, 314–315
  pancreas, 285, 288–291, 291f–292f
    biopsy, 318
    pancreatitis
      acute, 296
      chronic, 302–304
    tumours, 309, 310f
  upper gastrointestinal tract, 353f
    appearance, 352–353
    cancer staging, 353–354, 355t, 356f–357f, 360
    clinical indications, 353
    equipment, 351–352
    oesophagus, 354–360
    present and future, 366
    stomach, 360–365
Endotension, 783t
Endovaginal ultrasound, bladder, 551
Endovascular aneurysm repair (EVAR), abdominal aortic aneurysm, 781–787, 783f–787f, 783t–784t, 784b
Endovascular Aneurysm Repair Trial 1 (EVAR1), 782
Endovenous ablation, 1246–1248
Enhancement, 64, 64f

Entamoeba histolytica, 126, 400, 1364–1365
Entheseal disease, 1131, 1131b, 1132f
Enthesitis, 1131, 1132f
Enthesopathy, ankle, 1102–1103, 1103f
Enuresis, 1462
Ependymomas, 1333
Epicondylar groove, 1052
Epicondylitis
  diagnosis, 1053
  lateral, 1049, 1050f
  medial, 1050
Epidemiology, safety of ultrasound, 56–57
Epidermal inclusion cysts, 1116
Epidermoid cyst, 893–894, 894f
  testicular, 602, 603f
Epididymis
  abscess, 615, 615f
  adenomatoid tumour, 610, 610f
  anatomy, 594
  appendage torsion, 617, 618f
  cysts, 608, 609f
  inflammatory disease, 614–615
  leiomyoma, 610
  normal ultrasound appearance, 595–598, 597f
  tubular ectasia, 608
  vasectomy, 608, 609f
Epididymitis, 614–615, 614f
  chronic, 615
  tuberculous, 615, 615f
Epididymo-orchitis, 612–615, 615b
  paediatric, 1492, 1493f
Epigastric hernia, 804, 804f
Epiglottis, 913, 913f
Epimysium, 1138
Epineurium, 1158
Epiphyses, elbow, 1043
Epiploic appendagitis, 402–405, 405f
Epithelial cell tumours, ovarian, 1487
Epithelioid haemangioendothelioma, 160–161
Erectile dysfunction, 621–623
  arteriogenic, 624
  background, 621–623
  physiology of the erectile process, 623
  priapism, 627, 627b, 627f
  veno-occlusive, 624–625, 626f
Erosions, ultrasound features of, 1129, 1129b, 1130f
Escherichia coli
  epididymo-orchitis/epididymitis, 614
  liver abscess, 124
  renal abscess, 496
  urinary tract infection, 1448
Ethanol ablation, parathyroid lesions, 887
European Carotid Surgery Trial (ECST), 965
European Federation of Societies of Ultrasound in Medicine and Biology (EFSUMB), 58
  contrast agents guidelines, 139
  contrast-enhanced ultrasound for liver metastases, 153
European Society of Hysteroscopy fibroid classification, 691
Ewing's sarcoma, 1110f
Extended field-of-view (EFOV) imaging, 1137
Extensor carpi radialis brevis (ECRB), 1055, 1056f
Extensor carpi radialis longus (ECRL), 1055, 1056f, 1058f
Extensor carpi ulnaris (ECU), 1055, 1056f, 1062
Extensor digiti minimi (EDM), 1055, 1056f
Extensor digitorum brevis (EDB), 1098
Extensor digitorum communis (EDC), 1055, 1056f
Extensor digitorum longus (EDL), 1097–1099
Extensor hallucis longus (EHL), 1097–1098
Extensor indicis proprius (EIP), 1055, 1056f
Extensor pollicis brevis (EPB), 1055, 1056f
Extensor pollicis longus (EPL), 1055, 1056f, 1058, 1058f
Extensor tendons, 1055, 1056f
  tears, 1057, 1058f
External oblique muscle, 1076
Extra-corporeal shock-wave lithotripsy (ESWL), 55
Extradural haematoma, 1285
Extrahepatic biliary atresia (EHBA), 1368–1369, 1369f–1370f
Extrahepatic duct, 95
Extramedullary haematopoiesis, 507
Extrarenal pelvis, 1412, 1417f
Eye, 938–958
  anatomy, 938–941, 939f–941f
  biometry, 958, 958f
  British Medical Ultrasound Society (BMUS) guidelines, 58
  choroid, 940
    detachment, 946
    haemangioma, 954, 954f
    melanoma, 951–953, 951f–953f
    metastases, 953, 954f
    naevus, 954
    osteoma, 954, 954f
  ciliary body, 940
    melanoma, 951–953, 953f
  cornea, 938
  examination technique, 941–943
    A-scan, 941, 942f
    Doppler, 941–942, 942f
    2D scanning, 941
    3D scanning, 943, 943b
    ultrasound biomicroscope, 942, 942f
  eyeball, 938, 959
  foreign bodies, 957–958, 958f
  indications, 943, 943b
  iris, 940
  lens, 943
    cataract, 943, 943f
    ectopia lentis, 943, 944f
    intraocular implant, 943, 943f
    trauma, 956, 956f
  muscles, 959–960
  refracting media, 940–941, 941b
  retina, 940, 941f, 943–948
    acquired retinoschisis, 947–948, 948f
    detachment, 943–947, 944f
      choroidal detachment, 946, 947f
      conditions mimicking, 947b
      exudative, 946
      non-rhegmatogenous, 946
      posterior vitreous detachment, 944–945, 945f
      proliferative vitreoretinopathy, 945–946, 946f
      rhegmatogenous, 944
      traction, 946–947, 947f
      vitreoretinal traction, 944–945, 944f–945f
    disciform lesions, 948, 948f
    drusen (hyaline bodies), 948, 948f
    haemorrhage, 952
    tear, 944–945, 945f
  sclera, 938, 940f
  trauma, 956–958, 956f–958f, 957b
  tumours, 951–955
  ultrasound features, 938–941
  vitreous, 949–950
    asteroid hyalosis, 949, 949f
    haemorrhage, 952, 956, 956f
    persistent hyperplastic primary, 949, 949f, 955
    posterior detachment, 949–950, 949f–950f
      incomplete, 950, 951f
    synchysis scintillans, 949
  see also Orbit

F

Falciform ligament, liver, 93, 205, 205f
Fallopian tubes
  abscess, 682, 683f
  hysterosalpingo-contrast sonography for patency of, 734–735, 735f
  normal development, 1469f
  patency of, 734–735, 735f
  pelvic inflammatory disease, 682, 682f–683f
  rupture in ectopic pregnancy, 756, 756t
  spasm, 735
  torsion, 1488–1489
Fascia bulbi, 938
Fasciculi, 1138
Fasciola hepatica, 131, 251
Fascioliasis
  acute, 131
  gallbladder, 251
FAST *see* Focused assessment with sonography in trauma (FAST)
Fat atrophy, muscle, 1154, 1154f
Fat necrosis, 1115, 1115f
  breast, 988, 988f
Fatty infiltration
  infraspinatus, 1035, 1035f
  liver *see* Fatty liver
Fatty liver, 105–111, 146–148
  causes of, 105
  in children, 1359–1360, 1359f–1360f
  conditions associated with, 107t
  diffuse, 105–106, 108f
  focal fatty change, 107, 109f, 110b, 147
  focal fatty sparing, 108–110, 109f–110f, 110b, 147, 148f
  histology, 105, 106f
  multifocal steatosis, 147–148
  non-alcoholic fatty liver disease, 105, 110–111, 111f
  non-alcoholic steatohepatitis, 110–111, 111f
  temporal changes, 105, 107f
Female pseudohermaphrodites, 1475–1476
Female sexual cycle, 649, 650f

Femoral artery, 1229–1230
occlusion, 1205f
stenosis, 1204f–1206f, 1206
Femoral canal, 1079–1080
Femoral hernias, 803–804, 804f, 1079–1080, 1080f
Femoral neck fracture, 1070
Femoral veins, 1228–1230
duplication, 1234
spontaneous flow, 1230–1231
Femoroacetabular impingement, 1070–1071
Fertility
assessment of, 730–739
and fibroids, 691
hysterosalpingo-contrast sonography for tubal patency, 734–735, 734f–735f, 735b
infertility *see* Infertility
scanning through an IVF cycle, 735–738
downregulation, 735–736
embryo transfer, 737, 737f
follicular development, 736, 736f
oocyte capture, 736–737, 736f
ovarian hyperstimulation syndrome, 738, 738f, 738t
subfertility *see* Subfertility
Fetal anomalies, first trimester, 746–747, 746f
Fetal heart monitoring, British Medical Ultrasound Society (BMUS) guidelines, 58
Fibroadenoma, breast, 990–991, 990f
Fibro-adipose septa, 1026
Fibrohistiocytoma, retroperitoneal, 819–820
Fibroids, 668, 689–694, 693b
bridging vascular sign, 691
calcification, 691–692, 692f
as a cause of subfertility, 731–732, 732b, 732f
cervical, 713, 714f
in early pregnancy, 763, 763f
fertility and, 691
malignant change, 693
necrosis, 692, 693f
nomenclature of site of, 691
pregnancy and, 690, 690f
pyomyoma, 690
risk factors, 689
size and age, 690
subserosal, 691
symptoms, 691
torted pedunculated, 691
treatment, 693–694
ultrasound appearances, 691–693, 691f–692f
vaginal, 716
vascularity, 693
venetian blind pattern, 691–692, 692f
Fibrolamellar hepatocellular carcinoma (FLHCC), 160, 201, 216
Fibrolipoma, filum terminale, 1324
Fibrolipomatous hamartoma, 1166
Fibromas
medullary, 512
ovarian, 678, 679f
plantar fascia, 1106
Fibromatosis, 1122
in children, 1302–1303
congenital generalised, 1302–1303
deep, 1122
infantile (desmoid-type), 1303
palmar, 1122
plantar, 1122
plantar fascia, 1106
superficial, 1122, 1122f
Fibromatosis colli, 1302, 1303f, 1511, 1511f
Fibronodular hyperplasia (FNH), 142–143, 144f–145f
Fibrosarcoma, 1123
Fibrosis
hepatic, 111, 111f
penile, 628
Fibrotic haemangioma, liver, 141–142, 143f
Field, 6
FIGO staging
cervical cancer, 715t
endometrial cancer, 706t
Filum terminale, 1318
lipoma, 1324, 1324f
tight filum terminale syndrome, 1324–1325, 1325f
Fine-needle aspiration (FNA)
breast, 1001, 1001t
cervical lymph nodes, 934–935, 935b, 935f
versus core biopsy, 848
general principles, 847–853
lungs, 1017
needle guides, 852, 852f
needle tip visualisation, 850–852, 851b, 851f–852f
needle types, 848–849, 848b, 849f, 849t
oesophageal cancer, 354
pancreas, 290
biopsy, 318
patient selection/preparation, 847–848
post-procedural care, 853
pre-procedural assessment, 848
procedural planning and ergonomics, 852, 852f
safety/complications, 853
specimen handling, 852–853, 853f
spleen, 345
thyroid nodules, 882
track seeding, 853
Fistulae
aortocaval, 795
arteriovenous *see* Arteriovenous fistula
to the bladder, 566, 567t, 568
Crohn's disease, 375, 376f
dialysis, 455, 455f
haemodialysis access, 1215, 1220t–1221t, 1223, 1224f
inferior vena cava, 795, 795f
trans-sphincteric, 408
Flash artefact, 1126, 1127f
Flash contrast imaging, 82–84, 83f
Flash frames, 82–83, 83f
Flexor carpi radialis (FCR), 1055–1056, 1056f, 1059–1060, 1060f
Flexor carpi ulnaris (FCU), 1055–1056, 1059–1060, 1061f
Flexor digitorum longus, 1096, 1104
Flexor digitorum profundus (FDP), 1055, 1056f
Flexor digitorum superficialis (FDS), 1055, 1056f
Flexor hallucis brevis, 1096
Flexor hallucis longus, 1096, 1104, 1106–1107
Flexor pollicis longus (FPL), 1055, 1056f, 1059f
Flexor retinaculum, 1057
Flexor tendons, 1055, 1056f
tears, 1058–1059, 1059f
Flowmetry, 554–555, 555f
Fluid bronchogram, 1014
Fluid collections
aspiration/drainage, 1192–1193
liver transplantation, 212–213
nature of, in drainage, 801t, 803f, 807–809
peritoneum, 815–816, 816f
retroperitoneum, 821–823, 822t, 823f–825f
Fluid colour sign, 1008, 1009f
Focal nodular hyperplasia (FNH), 1364f
in children, 1363
Focused assessment with sonography in trauma (FAST), 829f
abdominal aortic aneurysm, 775
abdominal trauma, 828–829, 829b, 829f–830f, 831–832, 843
bladder, 569
versus full potential ultrasound, 831–832
unstable trauma patient, 843
Focused ultrasound, tumour ablation, 859
Focusing
electronic, 21
elevation, 21
Foley balloon catheter, 556, 558f, 569
Follicle(s)
development, 736
rupture, 730
Follicle-stimulating hormone (FSH), 649, 661
in in-vitro fertilisation, 736
menarche, 1472–1473
Follicular neoplasm, thyroid, 876–878, 877b, 877f–878f
Fontanelles, 1254, 1254f–1255f
Food and Drug Administration (FDA), 51, 57, 57t
Foot
anatomy, 1098, 1100b
disease processes, 1106–1107, 1107b
interventional techniques, 1187–1190
mass lesions, 1107
pain, 1106–1107
plantar aspect, 1100–1101, 1100f–1101f
short muscles, 1101
technique, 1098, 1098f, 1101b
Footballer's ankle, 1105
Foramen of Winslow, 93
Forearm muscles, 1140t, 1141, 1142f
Forefoot injections, 1189–1190
Foregut
duplication cysts, 1347b, 1348
malformations, congenital, 1299
Foreign bodies
bladder lumen, 556–558, 558f–559f
eye, 957–958, 958f
granulomas, 1117
localisation, 1190–1191
paediatric, 1507–1508, 1508f
vaginal, 715–716, 1490
Fourier components, 7, 7f–8f
Fournier's gangrene, 618, 618f

Fractures
ankle, 1105–1106
greater tuberosity, 1041, 1041f
Frame averaging, 26, 26f
Freiberg's disease, 1107
Frequencies, 3, 8b, 17–18, 29
analysis, 7
application set-ups, 33
Frozen shoulder, 1037, 1038f
Full potential ultrasound
abdominal trauma, 829–832, 831b, 831f
versus computed tomography, 832
versus FAST, 831–832
Fundamental imaging, 81, 81f
Fungal infection
liver, 127–128, 128f
renal, 464, 465b
spleen, 339
Fungus balls, 434

G

Galactoceles, breast, 988, 988f
Gallbladder
adenomas, 249, 249f
agenesis, 1375
anatomy, 227, 230f–231f
in ascites, 242–243, 242f
biliary sludge, 240–241, 241f–242f
bilobed, 1375
carcinoma, 249–250, 250f–252f
in children, 1356, 1375–1376
cholecystitis *see* Cholecystitis
contracted, 238–239, 238f
disease in children, 1375
distension, 251, 253f
in jaundice, 256–258
double-arc shadow sign, 238f, 239
ectopic, 1375
empyema, 245
folding, 228, 232f, 1375
function studies, 236
hydrops, 251, 253f
in children, 1375
hyperplastic cholecystoses, 247, 248f
intrahepatic, 228
metastatic deposits, 250, 252f
microgallbladder, 251–253, 253f
microlithiasis, 240–241, 241f
mucocele, 251, 253f
neck of, 230f–231f
normal anatomical variants, 228, 232f, 1375
parasitic infections, 250–251, 252f
pathology, 236–253
Phrygian cap, 228, 231f
polyps, 247–249, 248f–249f
porcelain, 250, 251f
septa, 228, 232f, 1375
stones *see* Gallstones
strawberry, 247
tenderness, 244
trauma, 841
ultrasound technique and appearance, 228–236, 233f, 1375
wall, 228, 233f–234f
gas in, 245–246
lesions in children, 1375–1376
thickening, 242f–243f, 243–244, 243t
in acute liver disease, 120–121, 122f
in ascites, 811, 812f
in chronic liver disease, 200, 200f
spurious, 234f
worms, 250–251
Gallstones, 228, 237–240
carcinoma risk, 249–250
in children, 1375, 1375f
classic appearances, 237–238, 237f–238f
contracted gallbladder, 238–239, 238f
double-arc shadow sign, 238f, 239
versus gas, 233, 234f
movement/layering/floating of, 239–240, 239f–241f
pancreatitis risk, 294
prevalence, 237
shadowing, 237, 237f–238f
Gamekeeper's thumb, 1063–1064, 1064f
Gamma curve, 26, 26f
Ganglion cysts, 1116, 1116f
ankle, 1104–1105, 1105f
aspiration, 1178, 1179f, 1192
cruciate, 1186
foot, 1107
Hoffa's, 1186, 1187f
nerve compression, 1165–1166, 1166f
paediatric, 1510, 1510f
proximal tibiofibular joint, 1091
wrist, 1066, 1066f
Ganglioneuroblastoma, 1466
Ganglioneuromas, 1312, 1313f
in children, 1466
Gartner's duct cyst, 716, 716f
Gas
bile duct, 259, 260f
gallbladder wall, 245–246
versus gallstones, 233, 234f
portal vein, 189, 191f, 210
vaginal, 716
Gas bubbles
acoustic cavitation *see* Acoustic cavitation
contrast
albumin-coated, 80
dynamics, 78, 78b
imaging of, 81–84
fundamental imaging, 81, 81f
high MI techniques, 82–84, 83f
low MI techniques, 82, 82f
newer techniques, 84
second harmonic imaging, 81–82, 82f
lipid-stabilised, 79–80
other potential uses, 86–87
polymer-coated, 80–81
in renal transplantation, 542–547, 544f–546f, 546b
resonant behaviour of, 78
safety of, 87–88
size, 77–79
targeted, 86–87
deep vein thrombosis, 1240
experimental work associated with, 55
factors affecting incidence of, 55–56
hazards from, 55
high risk situations, 56
in-vivo animal and human effects, 55
modelling, 55
safety, 54–56
shadowing, 64–65
Gastrinomas, 279, 313–314, 316f
Gastrocnemius muscle, 1093
Gastroduodenal artery, 286
Gastrointestinal stromal tumours (GISTs), 358, 358f, 362, 363f
in children, 1388f
small bowel, 381, 383f
Gastrointestinal tract obstruction, 300
Gastro-oesophageal junction in children, 1383–1384, 1384f
gastro-oesophageal reflux, 1383–1384, 1384f
technique and normal anatomy, 1383
Gastro-oesophageal reflux, 1383–1384
Gene delivery, contrast microbubbles, 87
Genioglossus muscle, 913
Geniohyoid muscles, 893
Genitalia, ambiguous, 1473–1478
Genital tract
female
congenital anomalies, 655–659
normal development, 1468–1470, 1469f
see also specific anatomical areas
Germ cell tumours
mixed, 599, 600f
non-seminomatous, 599–600
ovarian, 1485, 1486f–1487f, 1487–1488
regressed/burnt-out, 600, 601f
seminomatous, 599
testicular, 599–600, 600f–601f, 1494
Germinal matrix haemorrhage, 1260–1263, 1262f–1265f, 1262t
Gerota's fascia, 413, 817
Gestational trophoblastic disease (GTD), 696–697, 696f–697f, 764–765
complete hydatidiform mole, 764, 764f, 765t
partial hydatidiform mole, 764–765, 765f, 765t
Gestation sac, 741–743, 742f–743f, 742t, 744t
abnormally low position, 750–751, 751f
pseudo-gestation sac, 754
shape, 750, 751f
size, 750, 750f
Giacomini vein, 1242, 1245
Giant cell tumour of tendon sheath (GCTTS), 1066, 1067f, 1123
Glaucoma, 943
Glenohumeral joint, 1033f, 1040–1041
effusions, 1040, 1040f
osteoarthritis, 1040–1041
rheumatoid arthritis, 1040f
Glenohumeral ligaments, 1030
Gliding sign, 1008, 1338
Glioma, optic nerve, 962–963
Glomerulocystic kidney disease (GCKD), 1439
Glomerulonephritis, 445–447, 446f–447f, 449
acute, Doppler imaging, 484
membranous, 478
Glomus tumours, 909–911, 1066–1067
Gluteal insertion injection, 1184–1185, 1185f
Gluteal muscles, 1072–1073, 1075, 1076f
Glycogen storage diseases (GSDs), 116

Goitre
in children, 1310, 1311f
multinodular, 1310, 1311f
Golfer's elbow, 1050
Gonadal dysgenesis, 1477
Gonadal stromal tumours, 600–601
Gonadarche, 1470
Gonadotrophin-releasing hormone (GnRH)
in in-vitro fertilisation, 735
in puberty, 1470
Gonads
female *see* Ovaries
indifferent, 1468
male *see* Testis
Gout, 1130, 1131f
Gouty tophi, 1117, 1133, 1133f
Gracilis muscle, 1075
Graf technique, hip examination, 1498–1501, 1499f
alpha angle, 1499, 1499f
beta angle, 1499, 1499f
cradle, 1499f
Graf type D, 1501
Graf type I, 1499–1500, 1500f
Graf type IIa, 1500, 1500f
Graf type IIb, 1500, 1500f
Graf type IIc, 1500, 1500f
Graf type III, 1501, 1501f
Graf type IV, 1501
modified, 1501
pitfalls, 1501
Graft-versus-host disease, 215, 401
Granulomas
foreign body, 1117
silicone, 1000, 1000f
sperm, 608–609, 610f
stitch, 799
Granulomatous colitis, 1399
Granulomatous hepatitis, 132–133
Granulosa cell tumours, ovarian, 677, 678f
Grating lobes, 73, 73f
Graves' disease, 960
in children, 1310, 1311f
Gray-white matter differentiation (GWMD), 1266
Greater tuberosity fracture, 1041, 1041f
Grey matter, 1320
injury, 1266
Groin
athletic pain *see* Athletic groin pain
transducer choice, 1069
Guyon tunnel, 1057
Guyon tunnel syndrome, 1065, 1065f, 1164f
Gynaecological intervention techniques, 720–729
see also specific techniques
Gynaefix, 707

H

Haemangioendothelioma, 1121, 1362, 1363f
Haemangiomas, 1120, 1121f–1122f
arteriovenous *see* Arteriovenous malformations
capillary, 334, 1120
cavernous *see* Cavernous haemangioma
chest wall, 1350–1351, 1352f
in children, 1299–1301, 1299f–1300f
choroid, 954, 954f
extra-testicular, 610, 611f
hepatic, 1362, 1363f
infantile/congenital, 901
liver
cavernous, 140–142, 141f–142f
fibrotic, 141–142, 143f
mesenteric, 1403, 1403f
non-involuting congenital, 1301
orbital, 961, 961f
parotid gland, 901, 902f
proliferative, 1299–1301, 1299f–1300f
rapidly involuting congenital, 1301
renal, 512
spleen, 334, 336f–337f
Haemangiopericytomas, 1121
retroperitoneal, 819–820
Haemarthrosis, post-traumatic, 1088
Haematocele, 612, 613f
Haematocolpos, 709, 711
Haematomas
aspiration/drainage, 1192
chest wall, 1005–1006, 1352
duodenal, 1394, 1394f
extradural, 1285
first trimester, 752, 752f
infratentorial, 1285
liver, 148, 149f, 837, 838f
muscle contusion, 1114–1115, 1148
paediatric, 1507, 1507f
paravaginal, 716
peritoneal, 815–816
post-hysterectomy, 697–698, 698f
post-liver transplantation, 212, 221
postoperative, 805
post-renal transplantation, 535, 536f
renal, 495, 496f
retroperitoneal, 821–822, 825f
spleen, 837–838
subchorionic, 752, 752f
subdural, 1285
testicular, 604–605, 605f
Haematometrium, 709–711
post-hysterectomy, 698–700, 699f
Haematometrocolpos, 657, 710–711
Haematopoiesis, extramedullary, 507
Haematosalpinx, 657, 710
Haematospermia, 580t, 584–585, 585f
Haematuria, 838
Haematuria loin pain syndrome, 456
Haemochromatosis, 117
Haemodialysis, 454–455
access, 1214–1223
abnormalities and complications, 1222–1223
aneurysms, 1222
fistulae, 1215, 1220t–1221t, 1223, 1224f
normal characteristics, 1222
permanent
postoperative assessment, 1218–1219, 1220f
pre-assessment, 1218–1219, 1219f, 1220b
pseudo-aneurysms, 1222, 1223f
reporting dialysis fistula examinations, 1223, 1224f
scanning the access circuit, 1221–1222
sites, 1215, 1216t
steal syndromes, 1222, 1223f
stenoses, 1222, 1222f
temporary, 1215–1218
thrombosis, 1222
volume flow, 1220–1221, 1220f–1221f
Haemo-hydronephrosis, 434
Haemolytic uraemic syndrome, 1399, 1400f
in children, 1443–1444, 1444f
Haemoperitoneum, 833–835, 834f, 837, 844
Haemophilus influenzae, 1273
Haemorrhage
adrenal, 635, 635f, 1464, 1464f
first trimester, 751–753, 752f
germinal matrix, 1260–1263, 1262f–1265f, 1262t
intraparenchymal, 1285
intrauterine, 751–753
intraventricular, neonatal, 1260–1263, 1262f–1265f, 1262t
kidneys
cysts, 489f–490f, 490
post-renal biopsy, 456–457, 457f
renal cell carcinoma, 513
transplantation, 535
trauma, 839
and liver biopsy, 170
ovarian cysts, 663–664, 664f–665f, 1485, 1486f
pancreatitis complications, 299
parenchymal, 1270, 1271f
post-liver transplantation, 212–213, 221
retina, 952
retrohyaloid, 949–950, 950f
small bowel, 1393
subarachnoid, 982, 982f
subchorionic, 752–753, 752f
subdural, 1285
subretinal, 956–957
vitreous, 950, 950f, 952, 956, 956f
Haemorrhagic stroke, 982–983
Haemothorax, 1009
in children, 1344, 1346f
Haglund's deformity, 1103
Hamartomas
breast, 991
mesenchymal, 1362–1363
spleen, 337, 338f
Hammer toe, 1106–1107
Hamstrings, 1072–1075, 1075f
Hand, 1055–1068
anatomy, 1055–1057
injection of the small joints of, 1179–1180, 1180f
interventional techniques, 1175–1180
ligament and fibrocartilage disorders, 1063–1064, 1063f–1064f
lipomas, 1066
space-occupying lesions, 1066–1067, 1067b
technique, 1055–1057
tendon tears, 1057–1059
Handedness, epidemiological studies, 57
Harcke technique, 1501–1503, 1502f–1503f
Harmonic imaging, 8, 13b, 24–25, 24f
abdominal trauma, 829
bladder, 551–552
second, 81–82, 82f
Hartmann's pouch, 227

Hashimoto's thyroiditis, 869, 880, 883f
in children, 1310
Head masses in children, 1294–1314
Heart
anatomy, 77
contrast imaging, 85–86, 86f
disease, hepatic venous waveforms in, 195–197, 197f
thrombus, contrast imaging, 86, 86f
Heart block, complete, 197
Heating
due to tissue absorption, 52–53
experimental investigation of, 52–53
implications of, 53–54, 54b
mechanisms, 52, 52t
transducer, 53
Helicobacter pylori, 360
Hemidiaphragm, 1007f–1008f, 1008
Henoch-Schönlein purpura, 379t, 1443, 1444f
in children, 1393–1394, 1393f–1394f
scrotal involvement, 1494
Hepatic alveolar echinococcosis (HAE), 130
Hepatic arteries, 189–192
anatomy, 94, 94f, 102, 189, 232f
aneurysms, 192, 192f
flow changes in portal hypertension, 182
hereditary haemorrhagic telangiectasia, 192, 193f
liver transplantation complications, 205, 209b
normal anatomical variants, 228, 232f–233f
normal findings, 189–192
pre-liver transplantation assessment, 202–203, 203f
pseudo-aneurysm, post-transplantation, 208–209, 209f
scanning techniques, 189
stenosis, post-transplantation, 207–208, 208f, 220
thrombosis, post-transplantation, 205–207, 206f–207f, 219–220, 219f
Hepatic ducts, 227
anatomy, 95, 228f
normal anatomical variants, 227–228
Hepatic pedicle, 93
Hepatic veins, 192–197
anatomy, 94–96, 94f–95f, 102–103, 102f–103f, 192–193, 194f
liver transplant complications, 210–211, 220
normal anatomical variations, 193–194
occlusion, post-transplantation, 210–211
outflow obstruction, 194–195, 196f
peliosis hepatis, 197, 197f
pre-liver transplantation assessment, 202, 202f
scanning technique, 192–193
stenosis, post-transplantation, 210–211, 211f
thrombosis, 194–195, 196f (*see also* Budd-Chiari syndrome)
transit times, 197
veno-occlusive disease, 195, 196f
waveforms, 194, 194f–195f
in cardiac and pulmonary disease, 195–197, 197f
Hepatitis, 120–123, 121f
acute, 120–122, 121t
alcoholic, 121–122, 122f
in children, 1358t
viral, 120–121, 121t, 122f
in children, 1357, 1358t
chronic, 122–123, 123f
in children, 1357
gallbladder wall thickening in, 243, 244f
granulomatous, 132–133
see also Hepatitis B; Hepatitis C
Hepatitis B
hepatocellular carcinoma risk, 153
post-liver transplantation, 215–216
Hepatitis C
hepatocellular carcinoma risk, 153
and non-Hodgkin's lymphoma, 160
post-liver transplantation, 215–216
Hepatoblastomas
in children, 1360–1361, 1361f
liver transplantation complications, 221
Hepatocellular carcinoma (HCC), 153–156, 157f–159f, 201f
arterial neo-angiogenesis, 155–156
basket pattern, 155–156
in children, 222, 1361
and cirrhosis, 153–156, 155f–156f
differentiation from adenomas, 145
diffuse, 155
dysplastic nodules and, 154–156, 156f
fibrolamellar, 160, 201, 216
incidence, 153
intraoperative ultrasound, 278–279, 278f
massive, 155
nodular, 155
percutaneous ethanol injection, 174t
poorly differentiated, 158f
post-liver transplantation, 216, 222
pre-liver transplantation ultrasound, 200–201
presentation, 155–156
pseudo-capsule, 155
radio-frequency ablation, 174–175, 174t–175t
regenerating nodules and, 154–156, 155f
screening and surveillance, 153–154
well-differentiated, 155, 156f, 159f
Hepatogastric ligament, 93
Hepatomegaly, 101
Hepatorenal fossa, 413, 808
Hepatorenal syndrome, 453, 484
Hereditary haemorrhagic telangiectasia (HHT), 192, 193f
Hereditary neuropathy with liability to pressure palsies (HNPP), 1161–1162
Herlyn-Werner-Wunderlich syndrome, 710
Hermaphrodites, 1476–1477
Hernias, 1076–1081, 1080b
abdominal wall, 801–805, 1081
Bochdalek, 1348–1349, 1350f
diaphragmatic, 1348–1350, 1350f
epigastric, 804, 804f
femoral, 803–804, 804f, 1079–1080, 1080f
incisional, 804, 1081
inguinal, 612, 802–803, 802f
direct, 802–803, 804f
indirect, 802, 803f
inguinal-scrotal, 1491
inguinofemoral, 1076–1079
lumbar, 804
Morgagni, 1348–1349
muscle, 1113, 1114f
myofascial, 1154–1155, 1155f
para-umbilical, 804
parts of, 801, 802f
postoperative, 805, 805f–806f
Spigelian, 804, 1081, 1081f
sportsman's, 804–805
types of, 802b
umbilical, 804, 1081
Herniography, 1076–1077
Herpes simplex, 1273, 1274f
Heterotaxy syndrome, 330, 331f
Heterotopic gestation, 753
High pass filtering, 28, 28f
Hill-Sachs deformity, 1041, 1041f
Hindfoot injections, 1188, 1188f
Hip
anatomy, 1498, 1498f
anterior capsular distance, 1503, 1504t
arthroplasty, 1071–1072, 1072f
aspiration, 1069–1070, 1181–1184, 1184b, 1184f
blind aspiration or injection, 1069–1070
capsular thickening, 1070t
clinical examination, 1498
developmental dysplasia of the, 1497, 1498t
direct needle visualisation, 1070
femoroacetabular impingement, 1070–1071
Graf technique *see* Graf technique, hip examination
Harcke technique, 1501–1503, 1502f–1503f
injection, 1069–1070, 1071f, 1181–1182
interventional techniques, 1181–1185, 1182f–1183f
irritable, 1503–1505, 1504f
joint effusion, 1069–1070, 1070f–1071f, 1070t
labral abnormalities, 1070–1071, 1072f
paediatric, 1497–1505, 1505b
Terjesen technique, 1503
transducer choice, 1069
transient synovitis, 1503–1504, 1504f
ultrasound examination, 1498–1503
ultrasound-guided aspiration, 1069–1070
Histiocytic necrotising lymphadenitis, 934
Histiocytomas
extra-testicular, 611
malignant fibrous, 1123
Histocompatibility testing, 529
HIV *see* Human immunodeficiency virus (HIV)
Hodgkin's disease, 263, 263f, 1348f
in children, 1307
liver metastases, 160
spleen in, 331–333
thyroid, 880
Hoffa's ganglia, 1186, 1187f
Holoprosencephaly, 1280, 1282f
Hormone replacement therapy (HRT), 705–706
Horseshoe kidneys, 424–425, 425f, 1419–1420, 1421f
Housemaid's knee, 1089

Human chorionic gonadotrophin (hCG), 667
in in-vitro fertilisation, 736
ovarian hyperstimulation syndrome, 738
Human immunodeficiency virus (HIV)-associated nephropathy, 465
cervical lymph nodes in, 934
and liver disease, 131–132
salivary gland disease in, 1308, 1308f
Human papilloma virus (HPV), 714
Humero-radial articulation, 1043
Humero-ulnar articulation, 1043
Humerus, supracondylar process, 1160
Hürthle cell neoplasms, 878
Hyaline bodies, 948, 948f
HyCoSy *see* Hystero-contrast-sonography (HyCoSy)
Hydatid disease, 129–130, 130f–131f, 170
in children, 1363–1364
hepatic alveolar, 130
presentation, 487
renal, 464, 490–491
renal involvement, 1453–1454
soft tissue involvement, 1117
spleen, 339–340, 341f
Hydranencephaly, 1283, 1283f
Hydroceles, 611–612, 613f
abdominal wall, 805–806
paediatric, 1491, 1491f
Hydrocephalus, 1274–1279, 1277f–1280f
Hydrocolpos, 716, 1473, 1476f
Hydrometrocolpos, 1473, 1476f
Hydromyelia, 1325, 1328
Hydronephrosis, 421, 422f, 1433
in the newborn, 1433
physiological, of pregnancy, 421, 422f
postnatal evaluation of antenatally detected, 1433–1434
renal, 493, 494f
in renal transplantation, 542
Hydrops, gallbladder, 251, 253f
Hydrosalpinx
as a cause of subfertility, 733, 733f
pelvic inflammatory disease, 682, 682f
Hymen, imperforate, 1473, 1476f
Hyoglossus muscle, 891–895
Hyoid bone, 893, 913
Hyperbilirubinaemia
conjugated, 1368
unconjugated, 1367
Hypercalciuria, idiopathic, 1445
Hypereosinophilic syndrome, 134
Hyperoxaluria, 1445
Hyperparathyroidism, 884, 887
in children, 1445
Hyperplastic cholecystoses, 247, 248f
Hyperreactio luteinalis, 667–668
Hypertension
in children, 1455–1457
kidney disease, 449
renal artery stenosis, 448
renovascular *see* Renal arteries, stenosis; Renovascular hypertension
Hypertrophic pyloric stenosis (HPS), 1385–1386, 1385f
Hypoalbuminaemia, 242–243, 243f
Hypoglycaemia, 1283–1284, 1284f
Hypotension, 843
Hypoxic ischaemic encephalopathy, 1264–1269, 1266b, 1267t, 1268f–1270f
Hysterectomy, 697–700
fibroids, 693–694
subtotal, 697–700
Hystero-contrast-sonography (HyCoSy), 653–654, 688, 688f, 734–735, 735f
Hysterography, saline infusion *see* Saline infusion hysterography
Hysterosalpingogram (HSG), 656–657, 658f, 688, 688f
Hysteroscopy, 688

I

Ileitis, 377, 377f
Ileocaecitis, infectious, 377, 377f
Ileocolic veins, 388
Iliac arteries, 773
aneurysm, 779, 780f
in renal transplantation, 532
stenosis, 1201, 1203f, 1206
Iliac fossae, 369–370, 370f
Iliacus, 647
Iliac veins, 792, 1228
assessment, 1233–1234
in renal transplantation, 532
spontaneous flow, 1230–1231
Ilioinguinal nerve, 1081
Iliopsoas bursal injection, 1185, 1186f
Iliopsoas muscle, 1072–1073, 1073f–1074f
Iliotibial band, 1084, 1085f, 1091
Images, 16–17, 16f
B-mode imaging, 17–18
formats, 18–20, 19f
frame averaging, 26, 26f
memory, 25
processing, 23–26
colour Doppler imaging, 30b
demodulation, 25, 25f
dynamic range, 23–24, 24f
field of view, 25–26
harmonic imaging, 24–25, 24f
image memory, 25
post, 26, 26f
pulse coding, 25, 25f
time gain compensation, 23
zoom, 25–26
quality of, 31
Image speckle, 6–7, 7f
Imagify, 79t, 81
Imavist, 79t, 80
Immunosuppression, renal transplantation, 529–530
Imperforate anus, 1399, 1399f
Impingement syndrome, shoulder, 1032–1033, 1033f, 1036b
Inborn errors of metabolism, 1284, 1357–1358
Incidentalomas, thyroid, 881–882
Incisional hernias, 804, 1081
Indifferent gonads, 1468
Inertial (transient) cavitation, 78, 87
Infarcts
neonatal brain, 1269–1272, 1270f, 1272f
omental, 1401–1402, 1402f
prostate, 589t
pulmonary, 1018
renal, 477–478, 478f–479f
splenic, 340–342, 341f, 342t, 838
testicular, 603, 604f, 614–615, 614f
Infections
abdominal aortic aneurysms, 775
abdominal wall, 799–800, 801f
bladder, 568, 568b
breast, 989
colitis, 1399
joint, 1134–1135, 1135b
muscle, 1156, 1156f
neonatal brain, 1273–1274
postnatal causes, 1273–1274, 1275f–1276f
prenatal causes, 1273, 1274f
pancreatic, 299–301, 300f
parotid gland, 903
pelvi-ureteric dilatation, 434
post-liver transplantation, 215, 215f
renal cysts, 490–491, 490f
spleen, 338–340, 340f
splenomegaly, 332t
see also specific infections
Inferior epigastric vessels, 1077
Inferior mesenteric artery (IMA), 773, 789, 790f
Inferior oblique muscle, 959–960
Inferior vena cava (IVC), 792–795
abnormal findings, 792–794
anatomy and flow patterns, 792, 792f, 792t
assessment, 1233–1234
caval filters, 794, 794f
fistulae, 795, 795f
liver, 94–95, 94f–95f
liver transplantation, 220, 794, 794f
membranous obstruction, 195
objectives of the scan, 792
portacaval anastomosis, 795f
renal cell cancer propagation into, 480, 480f
scanning technique, 792, 793f
thrombosis, 792, 793f
tumour obstruction, 793–794, 793f
Infertility
male
evaluation of, 584
obstructive, 580t
see also Fertility; Subfertility
Inflammatory arthritis, 1130
Inflammatory masses
in children, 1303–1307
liver, 1364–1365
Inflammatory pseudo-tumour (IPT), liver, 131, 150
Inflammatory soft tissue masses, 1116–1117
Infrapatellar bursa, 1089
Infrapatellar fat pad impingement, 1186
Infraspinatus, 1030, 1031f
fatty infiltration, 1035, 1035f
Infundibular stricture, 434
Inguinal canal evaluation, 1077
examination technique, 1077
normal anatomy, 1077
normal ultrasound appearances, 1077, 1078f–1079f
Inguinal hernia, 612, 802–803, 802f
direct, 802–803, 804f
indirect, 802, 803f

Inguinofemoral hernias, 1076–1079
bulging, 1079, 1080f
differing imaging modalities, 1076–1077
inguinal canal evaluation, 1077
examination technique, 1077
normal anatomy, 1077
normal ultrasound appearances, 1077, 1078f–1079f
overview, 1076–1077
postoperative evaluation, 1079, 1080f
pre-hernia complex, 1079
ultrasound appearance of, 1077–1078, 1078f–1079f
In-plane resolution, 15
Inspissated bile syndrome, 1370, 1372f
Insulinomas, 279, 313–314, 316f
Intensity, 5, 5f
Intensity spatial average, 15
Intensity spatial peak, 15
Intensity spatial peak pulse average, 15
Intensity spatial peak temporal average, 15
Intercostal artery, 1012, 1012f
bleeding, 1013, 1013f
Interference, 5–6, 6f, 8b
Intermenstrual bleeding, 688
Intermittent claudication, 1198
Internal oblique muscle, 1076
Interosseous ligaments, 1101
Interstitial ectopic gestation, 757, 757f–758f, 757t
Interstitial laser photocoagulation (ILP), 859
Interstitial nephritis, acute, 451, 452f
Interventional techniques
abdomen, 847–864
joints, 1135
musculoskeletal procedures, 1168–1193
elbow, 1173–1175
foot and ankle, 1187–1190
foreign body localisation, 1190–1191
hip, 1181–1185
knee, 1185–1187
masses, 1191–1193
pelvis, 1180–1181
risks of, 1169b
shoulder, 1170–1173
wrist and hand, 1175–1180
see also specific techniques
Intestines
large *see* Colon
small *see* Small bowel
Intracranial pressure, transcranial Doppler ultrasound, 980
Intraductal papillary mucinous neoplasm (IPMN), 312, 313f
Intradural lipoma, 1324
Intrahepatic biliary cystadenoma, 149–150
Intraocular lens implant, 943, 943f
Intraoperative ultrasound (IOUS), 273–281
clinical applications, 275–280
biliary tree, 279–280, 280f
liver, 275–279, 275f–279f
pancreas, 279, 279f, 291–293, 293f
urology, 280, 280f
contrast-enhanced *see* Contrast-enhanced intraoperative ultrasound (CE-IOUS)
equipment, 273–275, 274f
laparoscopic *see* Laparoscopic ultrasound techniques, 273–275, 275f
Intraperitoneal fluid, ectopic pregnancy, 756, 757f
Intrarenal vessels, 470–471, 477
Intrauterine devices (IUDs), 706–708, 707f–709f
Intravenous urography (IVU), transitional cell carcinoma, 518
Intraventricular haemorrhage, neonatal, 1260–1263, 1262f–1265f, 1262t
Intussusception
in children, 1390–1391, 1392f
colonic, 402, 405f
small bowel, 384, 1391
In-vitro fertilisation (IVF), 667
scanning through a cycle, 735–738, 738b
downregulation, 735–736
embryo transfer, 737, 737f
follicular development, 736, 736f
oocyte capture, 736–737, 736f
ovarian hyperstimulation syndrome, 738, 738f, 738t
IPMN (intraductal papillary mucinous neoplasm), 312, 313f
Iris, 940
Ischaemia
acute, peripheral arterial disease, 1211
liver, 206–207, 207f
lower limb, 1198, 1211
small bowel, 379, 379t
symptoms, 965–966
Ischaemic colitis, 399t, 401, 402f
Ischaemic stroke, 982–983
Islet cell tumours
endoscopic ultrasound, 279
intraoperative ultrasound, 279

J

Jaundice, 253–254
causes of, 253
diagnosis, 253–254
gallbladder distension in, 256–258
medical, 253
neonatal, 1367–1372, 1371b
prolonged, 1368
surgical causes of, 1368–1372
obstructive, 253–255, 254f
in older children, 1372–1375, 1374b
surgical, 253–254
Jejuno-ileal atresia, 1388–1389
Jersey finger, 1058
Joint effusion
ankle, 1104, 1106
elbow, 1047, 1047f
glenohumeral joint, 1040, 1040f
hip, 1069–1070, 1070f–1071f, 1070t, 1503, 1504f
knee, 1088, 1088f–1089f, 1089b
monitoring, 1132
ultrasound features of, 1129, 1129b, 1129f
Joint(s), 1029, 1029f
aspiration
elbow, 1053
hip, 1069–1070, 1071f
cysts, 1134, 1134f
effusion *see* Joint effusion
infection, 1134–1135, 1135b
interventional techniques, 1135
masses, 1133–1134
rheumatological ultrasound, 1126
ultrasound-guided techniques, 1135
Jugular varix, 1301, 1302f
Jugular veins, 908
thrombosis, 908–909, 910f–911f, 1304
in thyroid carcinoma, 873
Jugulodigastric node, 908, 925, 925f
Jumper's knee, 1084–1086, 1086f
Juvenile nephronophthisis, 1438
Juvenile recurrent parotitis, 905, 905f
Juxtarenal process, 1448, 1451f
Juxtaventricular cysts, 1257–1258

K

Kager's fat pad, 1093–1094
Kaposi's sarcoma, 1121
Kasabach-Merritt syndrome, 140, 334, 1301
Kasai procedure, 216, 1369
Kidneys, 413–427
abscesses, 462, 462f, 496–497, 496f–497f, 1452f
access sites, 415, 415f
acute tubular necrosis, 484
adenomas, 508, 508f
metanephric, 508
papillary, 508
anatomical relations, 413, 414f
anatomy, 413–414, 414f
aneurysms, 495–496, 496f
angiomyolipoma, 509–512, 509f–511f
arteriolar resistance, 469
arteriovenous fistula, 481, 481b, 481f
arteriovenous malformations, 481–482, 482f–483f, 495–496, 507
atrophy, 425, 426f
autonephrectomy, 463–464, 465f
bifid renal pelvis, 1420, 1422f
biopsy, 455–458
complications, 456–457, 457f
contraindications, 455–456
indications, 455–456
renal transplant, 457–458
technique, 456, 456f
blood flow
changes in pelvi-ureteric dilatation, 440–441
damped waveform, 476
disturbance (turbulence), 476
increased velocity, 475–476, 476t, 478f
calcification, 451, 451b, 451f, 463–464, 465f
candidiasis, 1453, 1455f
in children, 1409, 1411b
abnormalities, 1418–1420, 1418f
cystic disease, 1435b, 1435t
duplex anomalies, 1420–1422, 1423f
end-stage failure, 1444–1445
fetal lobulation, 1412
infectious diseases of, 1453–1454
malignancy, 1458–1462
normal appearances, 1409–1412, 1416f, 1416t

normal sonographic values, 1412–1418
transplantation, 1444–1445
trauma, 1458f
collecting duct carcinoma, 517
collecting system, 413, 421–422, 422f
duplex, 423, 423f
column of Bertin, 505, 506f
congenital solitary, 425–426
congenital variants, 423–426, 426b
contrast imaging, 84–85, 85f, 467, 470f
cortex
calcification, 446
changes in disea25, 446–447
necrosis, 1444
normal ultrasound appearance, 418–419, 419f–420f
thickness, 415–417, 416f
crossed fused ectopia, 1420, 1421f
cystic dysplasia, 1437–1438, 1439f
cysts, 453–454, 454f, 486–504, 502b
acquired, 498, 498b, 499f
calcified, 491–492, 491f
in children, 1434–1440
classification, 488t, 489f
complicated, 488–492
contrast imaging, 85f
differential diagnosis, 493–498, 493f–497f, 498b
haemorrhagic, 489f–490f, 490
hereditary, 1439
infected, 462, 490–491, 490f
localised, 498
lymphatic, 493–495, 495f
malignant, 492, 492f, 493b
medullary, 502
milk of calcium, 492
multicystic dysplastic kidney, 498–499, 499f, 502b
multiple simple, 488, 488f
polycystic kidney disease *see* Polycystic kidney disease
septations, 488
simple, 486–488, 487f–488f, 488b
simple cyst, 1439
syndromal, 1439
tuberous sclerosis, 502, 502b, 502f–503f
Von Hippel-Lindau disease, 500–502, 501f, 502b
development, 1407, 1407f–1408f
diffusely echogenic, 1440–1442, 1440t, 1442t, 1443f
dilated pelvicalyceal system, 493, 494f, 518
discoid, 1419f
disease, 445–459 (*see also specific diseases*)
acquired cystic, 453–454, 454f
acute cortical necrosis, 452, 452f
acute interstitial nephritis, 451, 452f
acute tubular necrosis, 449
amyloid, 452, 452f
autosomal dominant polycystic, 97–98, 98f
connective tissue disorders, 453, 453f
cortical changes, 446
corticomedullary differentiation, 446–447
diabetes mellitus, 452–453
dialysis patients, 454–455, 455f
end-stage, 454f
glomerulonephritis, 449
hepatorenal syndrome, 453
medical, in children, 1442–1444
medullary changes, 446–447
medullary sponge kidney, 450, 450f
nephrocalcinosis, 451, 451f
renal papillary necrosis, 449–450, 450f
renal size, 445
sickle cell disease, 453
ultrasound features, 445–447
vascular disorders, 447–449, 449f
diverticula, 493, 494f
Doppler imaging *see* Doppler imaging, kidneys
dromedary hump, 505, 506f
duplex, 435–436, 437f–438f
anomalies, 1420–1422
collecting system, 423, 423f
dysplasia, 1437–1438, 1439f
ectopic, 418, 418f, 423–424, 424f–425f, 1419, 1419f
examination techniques, 415–418, 415b
extramedullary haematopoiesis, 507
extrarenal pelvis, 1412, 1417f
failure
acute, 446f
in children, 1442–1443
in children, 1442–1443
chronic
in children, 1442–1443
Doppler imaging, 484
end-stage, 1444–1445
fetal lobulation, 414, 420, 420b, 1416f
fungal infections, 464, 465b
glomerulonephritis, acute, 484
granulomatous pseud-tumours, 507
haemangioma, 512
haematoma, 495, 496f
hepatorenal syndrome, 484
hereditary tumours/syndromes, 522
hilum, 413
horseshoe, 424–425, 425f, 1419–1420, 1421f
hydatid disease, 464
hydronephrosis, 493, 494f
hypertension *see* Renovascular hypertension
and hypertensive disease, 449
hypoplasia, 425, 426f
infarction, 477–478, 478f–479f
infectious diseases of, 460–466
intraoperative ultrasound, 280, 280f
intrarenal vessels, 470–471, 477
junctional parenchymal defect, 414, 414f
leiomyoma, 512
leiomyosarcoma, 521, 523f
leukaemia, 521
liver transplantation complications, 214
lobar nephronia, 460–462, 461f
lymphatic cysts, 493–495, 495f
lymphoma, 521, 521b, 522f
main renal trunks, 471–472, 471f–473f
malacoplakia, 463
medulla, 418–419, 420f
carcinoma, 517
changes in disease, 446–447
fibromas, 512
necrosis, 1444
metastases, 521
mixed epithelial and stromal tumour, 492, 497–498
multilocular cystic nephroma, 497–498, 497f
nephropathy, HIV-associated, 465
nephroptosis, 418, 419f, 1419
normal ultrasound appearances, 418–422, 1409–1412, 1410f–1411f, 1416f
number abnormalities, 1418
obstruction, 300
oncocytoma, 508–509, 509b
pancake, 424, 425f
papillary necrosis, 493, 493f
parasitic infections, 464–465, 465b
parenchyma
disease
Doppler studies, 484b
vascular aspects, 483–484
infection, 460
normal ultrasound appearance, 418–421, 419f
thickness, 415–417, 416f
partial duplication, 1420
pelvic, 1419f
perirenal structures, 417
persistent fetal lobulation, 505
position abnormalities, 1419–1420
positioning for examination, 415
post-obstructive cystic dysplasia, 499, 499f
pre-renal failure, 484
pseudo-tumours, 505–507, 506b
pyelonephritis
acute bacterial, 460, 461f
chronic, 462, 464f
xanthogranulomatous, 463, 465f
pyonephrosis, 462, 463f
pyramids, 493, 493f
renal cell carcinoma *see* Renal cell carcinoma
renal sinus, 413, 420b, 421–422, 421f
reninoma, 512
rotational abnormalities, 1419
sarcoma, 521
scarring, 462, 464f, 505, 506f, 1452f
schistosomiasis, 464–465
septa of Bertin, 420–421, 420b, 421f
size, 415, 416f, 416t, 445, 475, 475t
small, 475, 475t
small vessels, 467, 484
splenic humps, 420, 420b, 420f
splenorenal fusion, 505–507
stones, 430, 430b, 430f–431f
supernumerary, 1418
thoracic, 1419, 1420f
transitional cell carcinoma, 517–521
transplantation *see* Renal transplantation
trauma, 838–841, 845, 845f
in children, 1457–1458, 1457f–1458f
classification, 839–840, 839t
general considerations, 838–841
mechanisms of injury, 839–840
ultrasound findings, 840–841, 840f–841f
tuberculosis, 463–464, 465b, 465f, 1453–1454
tuberous sclerosis, 1441f
tubulo-interstitial disease, 484
tumours, 478
ultrasound technique, 1409

unilateral agenesis, 1418, 1419f
vascular anatomy, 468–469, 468f
vascular disorders of, 467–485
in children, 1454–1455
vascular response to disease, 483–484
vasculitis, 484, 1443
vessels, 417–418, 417f, 421–422, 421f, 423f
viral infections, 465b
Kikuchi disease, 934
Kimura disease, 934
Klatskin tumours, 156–157, 261f
Klebsiella pneumoniae
liver abscess, 124
renal abscess, 496
Klippel-Trénaunay syndrome, 334, 336f
Knee, 1084–1092
anatomy, 1084, 1085f–1086f
anterior, 1084–1089
Baker's cyst, 1089, 1090b, 1090f
biceps femoris, 1091, 1091f
cruciate ligaments, 1090
iliotibial band, 1091
interventional techniques, 1185–1187
joint aspiration, 1185–1186, 1186f–1187f
joint effusion, 1088, 1088f–1089f, 1089b
lateral, 1091
lateral collateral ligament, 1091
lateral meniscus, 1091
medial, 1090–1091
medial collateral ligament, 1090
medial meniscus, 1090–1091, 1090f–1091f
Osgood-Schlatter disease, 1088
other bursae, 1089, 1089f
patellar tendinosis, 1084–1087, 1086f–1087f
pes anserinus bursa, 1091
popliteus tendon, 1091
posterior, 1089–1090
proximal tibiofibular joint, 1091
quadriceps and patellar tendons tears, 1087–1088, 1087f–1088f, 1088b
synovial biopsy, 1185–1186
ultrasound examination, 1084
Krukenberg tumour, 678, 680f
Kupffer cells, deficiency/dysfunction, 139
Kuttner tumour, 897, 897f

L

Labral cyst, 1037, 1038f
Lambda sign, 747–748
Laparoscopic ultrasound
biliary tree, 236, 273, 279
equipment, 274, 274f
islet cell tumours, 279
liver, 273
pancreas, 291–293, 293f
radio-frequency ablation, 278–279, 278f
technique, 275
urology, 280
Large-bore vacuum-assisted biopsy, 1001–1002, 1001t
Large bowel *see* Colon
Laryngocele, 917
Larynx, 913, 914b
tumours, 917
Lateral epicondylitis, 1049, 1050f
Lateral humeral condyle fracture, 1051
Lateral ligamentous complex, ankle, 1099
Lateral meniscus, 1091
Lateral rectus muscle, 959–960
Latero-conal ligaments, 816
Left ventricle, apical thrombus, 86, 86f
Left ventricular opacification (LVO), 79, 85–86
Leg *see* Lower limb
Legg-Calvé-Perthes disease, 1504, 1505f
Leiomyomas, 1121
epididymis, 610
renal, 512
Leiomyosarcomas
bladder, 562
extra-testicular, 611
malignant, 1121
renal, 521, 523f
retroperitoneal, 819
uterine, 693, 693f
Lemierre's syndrome, 1304
Lens, 943
cataract, 943, 943f
ectopia lentis, 943, 944f
intraocular implant, 943, 943f
trauma, 956, 956f
Lenses, 10–11, 11f
Lenticulostriate vasculopathy, 1272, 1273f
Lesser omentum, 93, 808
Leukaemia
in children, 1307, 1461
prostate gland, 589t
renal involvement, 521, 1461
testicular involvement, 602, 602f, 1494
Leukocoria, 949, 955
Leukodystrophy, metachromatic, 1375–1376
Levator ani muscles, 576, 647
Levator fascia, 573
Levator palpebrae, 960
Levonorgestrel, 689
Levovist, 81, 140
Leydig cell tumour, testicular, 601, 601f, 1494
Lidocaine, 1169–1170
Ligaments, 1028, 1028f
Ligamentum teres, 93, 98
Ligamentum venosum, 93
Lighthouse phenomenon, 1006–1007
Limy bile, 240
Lipid-stabilised contrast microbubbles, 79–80
Lipohaemarthrosis, knee joint, 1088, 1089f
Lipoleiomyoma, uterine, 695
Lipomas, 1117, 1119f
abdominal wall, 805, 806f
breast, 991, 991f
chest wall, 1005–1006
in children, 1352
colonic, 402, 404f
filum terminale, 1324
gastric, 362, 363f
hand, 1066
inter-/intramuscular, 1117
intradural, 1324
liver, 149
oesophageal, 358, 359f
paediatric, 1511–1512, 1511f–1512f
retroperitoneal, 819–820
size and shape, 1110, 1111f
small bowel, 381
spermatic cord, 609, 610f
spinal, 1322–1324, 1323f
subcutaneous, 1117
submandibular region, 898, 899f
uterine, 695
variants, 1119
Lipomyelomeningocele, 1323
Lipomyeloschisis, 1323, 1323f
Liposarcomas, 1119
abdominal wall, 806
retroperitoneal, 819–820, 821f
spermatic cord, 611
Lippes loop, 707, 708f
Lissencephaly, 1281–1282
Lister tubercle, 1055, 1056f
Liver
abscess, 124–127, 145–146, 146f–147f
amoebic, 126–127, 127f–128f, 1364–1365
bacterial, 123f–126f, 124–126, 145–146
brucellar, 126
in children, 1364–1365, 1364f
acute failure, 199–200, 217
acute fascioliasis, 131
adenoma, 143–145, 145f, 1363
alcoholic disease, 216
amyloid, 117
anatomical variants, 1356–1357
anatomy, 93, 1356
segmental, 95–96, 96b, 179, 180f
variations, 96–98, 96f–98f
angiomyolipoma, 149
attenuation, diffuse parenchymal liver disease, 104, 105f
biliary architecture, 94–95
biliary cystadenocarcinoma, 161
biliary epithelial dysplasia of the intrahepatic bile ducts, 150
biopsy, 167–170
complications, 170, 170b
image-guided approach, 167–168, 168f
indications, 169, 169b, 169f
patient management, 170, 170b
percussion-palpation approach, 167
quality of specimen, 168–169
technique, 167–169, 168t
type of needle, 168
blind area, 99, 99f
blunt trauma, 148
calcification, 134, 134t, 135f
cat scratch fever, 133–134
caudate lobe, 96, 97f
measurement, 101, 101f
in children, 1356–1375, 1357f
abscesses, 1364–1365
anatomical variants, 1356–1357
anatomy, 1356
diffuse parenchymal disease, 1357–1360
focal lesions, 1360–1364
inflammatory masses, 1364–1365
jaundice in older children, 1372–1375
neonatal jaundice, 1367–1372
portal hypertension, 1365–1367
technique, 1356
vascular disorders, 1365–1367
cholangiocarcinoma, 156–160
chronic disease, 200–201, 216–217
chronic granulomatous disease, 133
cirrhosis *see* Cirrhosis
classic lobule, 95

computed tomography
focal lesions, 138
congenital anomalies, 97
congenital fibrosis, 1360
congenital generalised lipodystrophy, 116
contrast imaging, 84, 85f, 138–139, 139t
diffuse parenchymal liver disease, 104
Couinaud classification, 93, 95–96, 179, 180f, 193
cystic fibrosis, 117–118, 117f
cysts, 97–98, 98f
in children, 1363–1364, 1364f
developmental variations, 96–98
diffuse parenchymal disease, 104–119, 1357–1360
disease
adult polycystic, 97–98, 98f
in children, 1357–1358
diffuse parenchymal, 104–119
metabolic causes, 1357–1358, 1358t
ductal morphology, 102–103, 102f–103f
echinococcal infection, 129–130, 130f–131f
echogenic lesions, 1364
echo pattern, 104–105, 106f
enlarged, 101
epithelioid haemangioendothelioma, 160–161
fatty *see* Fatty liver
fetal circulation, 94f
fibrolamellar hepatocellular carcinoma, 160
fibronodular hyperplasia, 142–143, 144f–145f
fibrosis, 111, 111f
focal lesions, 138 (*see also specific lesions*)
benign, 140–150
in children, 1360–1364
contrast imaging, 84
fracture, 835–836
fungal infection, 127–128, 128f
glycogen storage diseases, 116
granulomatous hepatitis, 132–133, 132t, 133f–134f
haemangioma, 1362, 1363f
cavernous, 140–142, 141f–142f
fibrotic, 141–142, 143f
haematoma, 148, 149f, 837, 838f
haemochromatosis, 117
hepatitis *see* Hepatitis
hepatocellular carcinoma *see* Hepatocellular carcinoma (HCC)
histology, 169
HIV/AIDS, 131–132, 132t
hypereosinophilic syndrome, 134
infections and inflammations, 120–137
inflammatory masses, 1364–1365
inflammatory pseudo-tumour, 131, 150
intrahepatic biliary cystadenoma, 149–150
intraoperative ultrasound, 275–279, 275f–279f
metastatic disease, 275–278, 276f–278f
transplantation, 279, 279f
ischaemia, 206–207, 207f
lacerations, 836
laparoscopic ultrasound, 273
lipoma, 149
liver acinus, 95
lobes/segments
anatomy, 93, 95–96, 96b
Couinaud classification, 93, 95–96
scanning techniques, 98–100, 98f–100f
lymphatic system, 95
lymphoma, 160, 161f
magnetic resonance imaging, 138
mesenchymal hamartoma, 1362–1363
metabolic disease, 217
metastases, 150–153, 151f–152f
appearance, 150–151
bile duct cholangiocarcinomas, 263
in children, 1362
from colorectal cancer, 275–276
contrast imaging, 85f
detection with contrast-enhanced intra-operative ultrasound, 152–153
from gastrointestinal tract cancers, 150
hypervascular, 150–151
hypovascular, 150–151, 160
intraoperative ultrasound, 275–278, 276f–278f
from pancreatic tumours, 309, 310f
radio-frequency ablation, 175–176, 175t
and radio-frequency ablation, 172
nodular regenerative hyperplasia, 116, 117f
normal sonographic features, 105b
parenchyma, 100, 100f
assessment, 104
chronic disease, 200, 200f
diffuse disease, 104–119
peliosis hepatitis, 150
peritoneum, 93
portal lobule, 95
radio-frequency ablation, 171–176, 171b
clinical results, 174–176, 174t–175t
complications, 174
indications, 172–174, 172t
technique, 171–172, 172f–173f
rare lesions
benign, 148–150
malignant, 160–161
reduction, 204, 217
reflectivity, 100, 100f
causes of increased, 107t
diffuse parenchymal liver disease, 104, 105f
Riedel's lobe, 96, 97f
rupture, 835–836
sarcoidosis, 150
scanning techniques, 98–103, 1356
liver parenchyma, 100, 100f
liver size, 101–102, 101f
liver surface, 101, 101f
segmental approach, 98–100, 99f–100f
vascular and ductal morphology, 102–103, 102f–103f
schistosomiasis, 128, 129f
sepsis, 206–207, 207f
size, 101–102, 101f
solitary necrotic nodule, 150
steatosis *see* Fatty liver
surface, 93, 101, 101f
texture, 100
toxocariasis, 129
transplantation *see* Liver transplantation
trauma, 835–837, 844–845, 844f
classification, 835–836, 835t
general considerations, 835
mechanisms of injury, 835–836
ultrasound findings, 836–837, 836f–837f
tumours, 217 (*see also specific tumours*)
benign, in children, 1362–1364
contrast agents, 139
malignant, in children, 1360–1362
vascular architecture, 94–95, 94f–95f
vascular disorders, 179–198
in children, 1365–1367, 1367b
vascular morphology, 102–103, 102f–103f
veno-occlusive disease, 1366–1367
volume assessment, 203–204
Wilson's disease, 117
Liver transplantation, 199–224
auxillary, 217
biliary system complications, 211–212
early postoperative ultrasound, 204–213
abnormal, 205–213
complications of split liver transplantation, 213
miscellaneous complications, 213
non-vascular complications, 211–213
normal, 205
vascular complications, 205–211
fluid collections, 212–213
indications for, 199, 200t
inferior vena cava assessment after, 794, 794f
intraoperative ultrasound, 279, 279f
long-term follow-up, 213–216
Budd-Chiari syndrome, 215
disease recurrence, 215–216
graft versus host disease, 215
infection, 215, 215f
non-vascular complications, 213–216
post-transplant lymphoproliferative disease, 213–214, 214f
rejection, 215
renal complications, 214
orthotopic, 204, 204f
paediatric, 216–222, 220b, 1376–1377, 1376f–1377f, 1377b
clinical indications, 216–217
complications, 219–221, 219f
recurrent disease, 221–222
surgical techniques, 217, 218f–219f
ultrasound patient evaluation, 217–219
piggy-back, 204, 204f, 794, 794f
pre-transplant ultrasound, 199–204
acute liver failure, 199–200
assessment of living related donors, 203
chronic liver disease, 200–201
liver volume assessment, 203–204
preoperative vascular assessment, 201–203
reduced, 204, 217
rejection, 211, 215
split, 217
surgical techniques, 204, 204f
Lobar nephronia, 460–462, 461f
Local anaesthesia, 1169–1170
Localised pigmented villonodular synovitis, 1066, 1067f
Locking drains, 810–812
Loeffler syndrome, 134

Long saphenous vein, 1228, 1242
  bypass grafts, 1207–1208
  duplication, 1245
Loose bodies, elbow, 1047–1048, 1047f–1048f
Loss-of-correlation imaging (LOC), 83–84
Lower limb
  artery bypass, vein mapping, 1248–1249
  ischaemia, 1198, 1211
  lengthening, 1509
  muscles, 1141, 1143t, 1144f–1145f
  peripheral veins, 1227–1228
  venous anatomy, 1228, 1228f
Ludwig's angina, 894, 895f
Lumbar hernia, 804
Luminity, 79t, 80f
Lung gliding sign, 1008, 1338
Lung point, 1011
Lungs, 1010–1011
  abscess, 1015, 1015f, 1340, 1342f
  anatomy, 1338, 1339f
  atelectasis, 1010–1011, 1011f
  cancer, 1016–1017, 1017f–1018f
    colour Doppler imaging, 1018
    metastases, 1016–1017, 1017f
  colour Doppler imaging, 1018
  congenital parenchymal masses, 1341–1344, 1343f
  consolidated, 1339–1340, 1341f
  disease, hepatic venous waveforms in, 195–197
  examination technique, 1005
  hepatisation, 1340, 1341f
  necrosis, 1340, 1342f
  neoplasia, 1344, 1345f
  paediatric, 1338–1344, 1339f
  patient position, 1005
  peripheral consolidation, 1014–1018, 1014f, 1015b
  pleura *see* Pleura
  technical requirements, 1005
  tissue damage from diagnostic ultrasound, 55
  ultrasound-guided biopsy, 1017–1018
Lung sliding sign, 1014
Lunotriquetral ligament (LTL), 1056–1057, 1063
Luteinising hormone (LH), 649, 661
  in in-vitro fertilisation, 735
  menarche, 1472–1473
  ovarian hyperstimulation syndrome, 738
  in puberty, 1470
Lymphadenitis
  acute suppurative, 1304, 1305f–1306f
  chronic, 1305
  mycobacterial, 1305–1306
  subacute, 1305
Lymphadenopathy
  in appendicitis, 389–390, 391f
  cervical
    in children, 1303–1304, 1304f
    neoplastic, in children, 1307
    in thyroid carcinoma, 872–873
  Crohn's disease, 374
  in gastric cancer, 360
  pancreatic tumours, 309
  porta hepatis, 263, 263f
  retroperitoneum, 819, 819f
  small bowel, 371, 374
Lymphangiectasia, renal, 495
Lymphangiomas
  in children, 1352f, 1402, 1402f
  neonatal, 1483
  renal, 495
  spleen, 337, 338f
  submandibular region, 898
Lymphatic cysts, renal, 493–495, 495f
Lymphatic drainage
  liver, 95
  prostate, 574
  spleen, 324–325
Lymphatic malformations
  cervical, in children, 1295–1296, 1296f
  in children, 1351–1352, 1352f
  paediatric, 1510
  submandibular region, 898
Lymph nodes
  breast/axillary, 997–999, 998f–999f
  cervical *see* Cervical lymph nodes
  chest wall, 1005–1006, 1006f
  jugulodigastric, 925, 925f
  mastoid, 927
  neck *see* Cervical lymph nodes
  occipital, 927
  paratracheal, 927, 927f
  parotid gland, 900
  prelaryngeal, 927, 927f
  pretracheal, 927, 927f
  small bowel, 371
  submandibular, 922–923, 924f
  submental, 922, 923f
  suppurative, 929, 929f
  supraclavicular, 1006f
  thoracic, 1007
  tuberculous, 929
Lymphoceles
  peritoneal, 815–816, 816f
  post-hysterectomy, 697–698
  post-renal transplantation, 535–536
  retroperitoneal, 823
Lymphoedema, 1121
Lymphoepithelial cyst, 905, 905f
Lymphomas
  appendiceal, 393
  bladder, 562
  cervical lymph nodes in, 928, 929f
  in children, 1307, 1394–1395, 1395f, 1461, 1462f
  collar of disease, 521, 522f
  colonic, 402, 404f
  gastric, 360, 362f
  hepatic, 160, 161f
  mediastinal, 1347, 1348f
  mesenteric, 1403, 1403f
  orbital, 962, 962f
  ovarian, 680
  pancreatic, 315, 317f
  parotid gland, 903
  prostate gland, 589t
  renal, 521, 521b, 522f, 1461, 1462f
  retroperitoneal, 819
  small bowel, 381, 382f–383f, 1394–1395, 1395f
  spleen, 331–334, 333f–334f, 334b
  testicular, 601–602, 602f, 1494
  thyroid, 880–881, 880b, 880f
  uterine, 695

M

Magnetic resonance angiography (MRA)
  peripheral arterial disease, 1197, 1200–1201
  renal artery stenosis, 474t–475t, 475
Magnetic resonance arthrography
  femoroacetabular impingement, 1071
  glenohumeral joint, 1041
  shoulder joint, 1172–1173
Magnetic resonance cholangiopancreatography (MRCP)
  cholangiocarcinoma diagnosis, 236
  choledocholithiasis, 280
  pancreatitis, chronic, 302
Magnetic resonance imaging (MRI)
  abdominal aorta, 773
  adrenal glands, 632, 636, 640, 642
  bladder, 552
    cancer, 564
    metastases, 566
  breast implants, 1000, 1000f
  calcified renal cysts, 491
  cervix, 687
    cancer, 714
  elbow loose bodies, 1047
  endometrial cancer, 705
  epithelioid haemangioendothelioma, 160–161
  erosions, 1129
  fibroids, 692
  gestational trophoblastic disease, 696–697
  head and neck masses in children, 1294
  hypoxic ischaemic encephalopathy, 1265–1266
  infant spine, 1315–1316
  inguinofemoral hernia, 1077
  liver
    focal lesions, 138
    metastases, 152–153, 277
    radio-frequency ablation, 172
  muscle injury, 1137
  neonatal brain, 1253
  ovaries
    endometriosis, 681
    lesions, 669–670
  paediatric chest, 1337
  pancreas, 285
  pelvic masses, 566
  peripheral nerves, 1158
  renal cell carcinoma, 513–517
  rheumatological disease, 1132
  shoulder, 1030
  soft tissue masses, 1109
  synovitis, 1128
  thymus, 1339
  thyroid, 867
  uterus, 687, 688f
Magnetic resonance venography (MRV), portal venous thrombosis, 201
MAG-3 renogram, 442
Malacoplakia, 463
Male pseudohermaphrodites, 1477
Malignant fibrous histiocytoma (MFH), 1123
Malignant melanoma *see* Melanomas
Malignant peripheral nerve sheath tumours (MPNST), 1120

Mammography, 997
Mantoux test, 1306
Marfan's syndrome, 943
Masseteric hypertrophy/bruxism, 906
Mastitis, periductal, 989
Mastoid infection in children, 1304, 1306f
Mastoid lymph nodes, 927
Mayer-Rokitansky-Kuster-Hauser syndrome, 657, 1473
Mean gestational sac diameter (MGSD), 741, 748–749, 761
Mechanical index (MI), 34, 54, 78
  British Medical Ultrasound Society (BMUS) guidelines, 57–58
  in clinical practice, 56
  definition, 56
  reduction during scanning, 56
  surveys of values in clinical practice, 56
Meconium ileus, 1388–1389, 1389f
Meconium peritonitis, 1389, 1389f
Meconium pseudocyst, 1389, 1390f
Medial epicondyle, avulsion fracture, 1051
Medial epicondylitis, 1050
Medial meniscus, 1084, 1090–1091, 1090f–1091f
Medial rectus muscle, 959–960
Median artery, persistent, 1160, 1160f–1161f
Median nerve, 1043, 1057
  bifid, 1159, 1160f
  penetrating injuries, 1065–1066
Mediastinum, 1018–1019, 1019f
  masses, 1347b
    anterior, 1347
    middles, 1348
    posterior, 1348
  paediatric, 1347–1348
Mediastinum testis, 595, 596f
Medulla oblongata, 1320
Medullary carcinomas, 517
  breast, 995
  thyroid, 878–879, 879b, 879f
Medullary cystic disease, 502
  in children, 1438
Medullary necrosis, 1444
Medullary sponge kidney, 450, 450f
  in children, 1439, 1440f
Medulloblastomas, neonatal, 1333
Megacystis, 1425
Megaureter, 1422, 1426f
Meigs' syndrome, 678
Melanomas
  ocular, 942, 951–953, 951f–953f
  vaginal, 716
Menarche, 1470, 1472–1473
Ménétrier's disease, 1386
Menghini technique biopsy needles, 849
Meningiomas
  neonatal, 1333
  optic nerve sheath, 963
Meningitis, 1273, 1275f
Meningocele, 1322
Meniscal cysts, 1091, 1091b, 1091f, 1115–1116
Menorrhagia, 688
Menstruation, 649, 650f
  disorders, 1481–1482
Mesenchymal tumours, small bowel, 381
Mesenteric adenitis, 1395, 1395f–1396f
Mesenteric cysts *see* Lymphangiomas
Mesenteric haemangiomas, 1403, 1403f
Mesenteric lymphoma, 1403, 1403f
Mesenteric pseudocysts, 1402, 1402f
Mesenteric teratomas, 1402–1403
Mesenteric tumours, 1402–1403
Mesonephric ducts, 655–656
Mesonephros, 1407
Mesothelioma, extra-testicular, 611
Metabolic disorders, neonatal, 1283–1284
  hypoglycaemia, 1283–1284, 1284f
  inborn errors of metabolism, 1284
Metacarpophalangeal joint (MCPJ), 1055
  injection, 1180, 1180f
Metachromatic leukodystrophy, 1375–1376
Metanephric adenoma, 508
Metanephros, 1407
Metaplastic carcinoma, breast, 996
Metatarsalgia, 1106
Methotrexate, 757, 767, 767t
Mickey Mouse sign, 439, 440f
Microbubbles *see* Gas bubbles
Microcysts, prepubertal, 1483–1484
Microgallbladder, 251–253, 253f
Microlithiasis
  gallbladder, 240–241, 241f
  testicular, 607–608, 608b, 608f, 1492, 1492f
Microwave ablation, tumours, 859
Microwave therapy, renal cell carcinoma, 523
Milk of calcium cysts, 492–493, 494f, 511–512, 511f
Miller-Dieker syndrome, 1281–1282
Miner's elbow, 1050, 1051f
Mirena intrauterine system, 706–707, 708f
  abnormal vaginal bleeding, 689
  and uterine fibroids, 689
Mirror image artefacts, 65–67, 67f
Mirrors, 10–11, 11f
Miscarriage *see* Pregnancy, failure
Mitral valve echo, 77
Mixed epithelial and stromal tumour (MEST), kidney, 492, 497–498
Molar pregnancy, 696, 696f
Mönckeberg's sclerosis, 1198
Morel-Lavallée lesion, 1074, 1115
Morgagni hernia, 1348–1349
Morison's pouch, 93, 413, 808–810, 810f, 833
Morton's neuroma, 1106, 1107f
  injection, 1189–1190, 1192f
Mouth floor, 892f–893f
MRI *see* Magnetic resonance imaging (MRI)
Mucinous carcinoma, breast, 995
Mucinous cystadenocarcinoma, ovarian, 672, 673f
Mucinous cystadenoma, ovarian, 672, 672f
Mucinous cystic neoplasm, pancreas, 312, 312f
Mucoceles
  appendiceal, 392, 393f
  gallbladder, 251, 253f
Mucoepidermoid carcinoma
  parotid gland, 902
  salivary glands, 1308–1309, 1309f
Mucosa, gastrointestinal tract, 352
Mucosa associated lymphoid tissue (MALT), 360
Müllerian duct
  abnormalities, 579
  agenesis, 1473
  anomalies, 655, 657f
  cysts, 579, 580f, 583t, 585f, 716
  development, 1470
  fusion, 1470
  obstructive anomalies, 1473
  organogenesis, 1469
Müllerian tumours, myometrial, 695
Multicystic dysplastic kidney, 498–499, 499f, 502b, 1434, 1434f–1435f
Multilocular cystic nephroma, 497–498, 497f
  in children, 1439–1440, 1442f
Multinodular thyroid, 882, 882b
Multiple echoes, 65–68, 67f–68f
Multiple endocrine neoplasia (MEN)
  and medullary thyroid carcinoma, 879
  type 1, 313–314
Multiple pregnancy diagnosis, 747–748
  see also Twinning
Murphy's sign, ultrasonic, 244–245
Muscle injury, 1137–1157
  acute, 1143–1152
  avulsion injury, 1150, 1150f
  children, 1507f
  chronic, 1152–1156
  compartment syndromes, 1155–1156
    acute, 1155
    chronic exertional, 1155–1156
  contusion, 1143–1148, 1148f–1149f
  direct, 1143–1148
  fat atrophy, 1154, 1154f
  hernias, 1113, 1114f
  indirect (strain)
    biomechanical aspects, 1149
    clinical features, 1149
    clinical grading system, 1149, 1151b
    clinical-sonographic correlation, 1150–1151, 1150b, 1151f–1153f
    delayed-onset muscle soreness, 1151–1152
    location within the muscle, 1149–1150, 1149f–1150f
    prognostic value of sonography, 1152
    sports-specific, 1149b
  infection, 1156, 1156f
  intramuscular scar/fibrosis, 1152–1153, 1153f
  laceration, 1143, 1148f
  myofascial hernia, 1154–1155, 1155f
  myositis ossificans, 1154, 1154f
  paediatric, 1506–1507
  sonographic technique, 1137, 1138b
  tears, 1114, 1149–1150, 1150f, 1506–1507, 1507f
Muscle(s), 1025–1026, 1025b–1026b, 1026f
  accessory, 1141–1143, 1146t–1147t, 1160
  anatomy, 1138
  compartmental anatomy, 1139–1141, 1140t, 1141f–1142f, 1143t
  contractions, 1149
  fibres, 1138
  fusiform, 1025–1026
  haematoma, 1114–1115
  injury *see* Muscle injury
  lower limb, 1141, 1143t, 1144f–1145f
  microstructure, 1138, 1138f

morphological types, 1139, 1140f
multipennate, 1025–1026
normal sonographic appearance, 1139, 1139f
oblique orientation, 1139
parallel, 1139
pennate, 1139
triangular, 1139
tumours, 1121
unipennate, 1025–1026
upper limb, 1139–1141, 1140t, 1141f–1142f
Muscularis propria, 352
Musculo-cutaneous flaps, 800
Musculoskeletal ultrasound, 1025–1029
paediatric, 1497–1513
see also Bone(s); Muscle(s)
Mycetoma, 464
Mycobacterial lymphadenitis, 1305–1306
Mycobacterium avium complex, 131–132
Mycobacterium tuberculosis infection
in HIV/AIDS, 131–132
splenic involvement, 339, 340f
Mycophenolate, 529–530
Mycotic aneurysms, 775, 779
Myeloceles, 1322
Myelolipomas, adrenal, 636–637, 637f
Myelomeningoceles, 1322
Mylohyoid muscle, 890–891, 892f, 894–895
boutonnière, 897, 898f
Myocardial perfusion, 79, 86
Myofascial hernia, 1154–1155, 1155f
Myofibrils, 1138
Myomectomy, fibroids, 693–694
Myometrium, 689–700
adenomyosis *see* Adenomyosis
arteriovenous malformation, 695–696, 696f
cysts, 694–695
fibroids *see* Fibroids
gestational trophoblastic disease, 696–697, 696f–697f
lipoma, 695
lymphoma, 695
malignant mixed Müllerian tumours, 695
metastases, 695
sarcoma, 695
Myosin, 1138
Myositis, 960
infective, 1156, 1156f
Myositis ossificans, 1115, 1115f, 1154, 1154f
paediatric, 1508
Myxoma, 1121

N

Nabothian cysts, 713, 713f
Naevus, choroid, 954
Nasopharyngeal infection in children, 1304
Neck, 890–919
anterior (infrahyoid), 913–917
normal ultrasound anatomy, 913–914
pathology, 914–917
technique, 913–914
jugulodigastric region and deep cervical chain, 908–911
normal ultrasound anatomy, 908
pathology, 908–911
technique, 908
masses in children, 1294–1314
parotid and buccal region, 898–907
normal ultrasound anatomy, 898–900, 899f–900f
pathology, 900–907
technique, 898–900
posterior triangle, 912–913
normal ultrasound anatomy, 912–913, 912f
pathology, 913
technique, 912–913
pulsatile masses, 966, 974, 974b, 975f
submandibular region, 894–898
normal ultrasound anatomy, 894–895, 895f–896f
pathology, 895–898
technique, 894–895
submental region, 890–894
normal ultrasound anatomy, 890–893, 891f–893f
pathology, 893–894
technique, 890–893, 891f
supraclavicular fossa, 911–912
normal ultrasound anatomy, 911–912, 912f
pathology, 912
technique, 911–912
Necrosis
cervical lymph nodes, 930–931, 931f
coagulative, 930, 931f
cortical, 1444
cystic, 930
lung, 1340, 1342f
medullary, 1444
Necrotising enterocolitis, 1400, 1401f
Necrotising fasciitis, 618
Needle guides, 852, 852f
Needle placement technique, 1170
Needles
core biopsy, 849–850, 849f, 849t
fully automated sheathed, 850
manual sheathed, 849
Menghini technique, 849
semi-automated sheathed, 849, 850f
fine-needle aspiration, 848–849, 848b, 849f, 849t
liver biopsy, 168
visualisation, 1170, 1170b
Needle track seeding, 853
Neisseria gonorrhoeae
endometritis, 709
epididymo-orchitis/epididymitis, 614
pelvic inflammatory disease, 682
Neonatal brain, 1253–1293
anatomy, 1255–1260, 1255f–1257f, 1255t
arterial infarction, 1269–1270, 1270f–1272f
brain death evaluation, 1290, 1290f
cerebrovascular complications, 1260–1272
premature infants, 1260–1264
term infants, 1264–1272
congenital malformations, 1279–1283
Dandy-Walker complex, 1279–1280, 1281f
destructive lesions, 1283, 1283f
disorders of sulcation and migration, 1280–1282, 1282f
dysgenesis of the corpus callosum, 1279, 1281f
holoprosencephaly, 1280, 1282f
tuberous sclerosis, 1282, 1283f
germinal matrix, 1260–1263, 1262f–1265f, 1262t
hydrocephalus, 1274–1279, 1277f–1280f
hypoxic ischaemic encephalopathy, 1264–1269, 1266b, 1267t, 1268f–1270f
infection, 1273–1274
postnatal causes, 1273–1274, 1275f–1276f
prenatal causes, 1273, 1274f
intraventricular haemorrhage, 1260–1263, 1262f–1265f, 1262t
lenticulostriate vasculopathy, 1272, 1273f
metabolic disorders, 1283–1284
hypoglycaemia, 1283–1284, 1284f
inborn errors of metabolism, 1284
periventricular leukomalacia, 1263–1264, 1266f–1267f
space-occupying lesions, 1284
cysts, 1284
neoplasms, 1284, 1285f–1287f
vascular malformations, 1284, 1288f
technique, 1253–1254, 1254f
trauma, 1285–1287
accidental injury, 1285
birth-related injury, 1285, 1289f
non-accidental injury, 1285–1287, 1289f–1290f
variation with gestational age, 1258, 1258f
vascular anatomy, 1258–1260, 1259f–1261f, 1259t
venous thrombosis and infarction, 1255, 1270–1272, 1272f
ventricular system, 1255, 1255t
Neonatal hepatitis syndrome (NHS), 1368
Neonates
adrenal glands, 633
brain *see* Neonatal brain
British Medical Ultrasound Society (BMUS) scanning guidelines, 58
hydronephrosis, 1433
ovarian cysts, 1483, 1483f
pelvic masses, 1483, 1484f
Neopharynx, postoperative, 917, 918f
Nephrectomy, 517, 522–523
Nephroblastomatosis, 1461, 1461f
Nephrocalcinosis, 446–447, 447f, 451, 451f
in children, 1446, 1446t, 1449f
Nephrogenic systemic fibrosis (NSF), 552–553
Nephromas
congenital mesoblastic, 1461
multilocular cystic, 497–498, 497f
Nephropathy, HIV-associated, 465
Nephroptosis, 418, 419f, 1419
Nephrotic syndrome, 446f
Nephroureterectomy, 520–521
Nerve entrapment, 1163f–1164f
abdominal wall, 807
definition, 1161–1162
frequently affected nerves, 1166b
radiography and computed tomography in, 1158
ultrasound nerve changes in, 1163b
Nerve fascicles, 1158
Nerve fibres, 1158

Nerves, 1028, 1029f
Nerve sheath, 1158
tumours, 901–902, 911, 1120
Nerve tumours, 1119–1120
Neurenteric cysts, 1348
Neurilemmoma *see* Schwannomas
Neuroblastomas
adrenal, 637–640, 640f, 1459t, 1464–1466, 1465f, 1465t
in children, 1312, 1362f
mediastinal, 1347b, 1348, 1349f
neonatal, 1333
Neuroendocrine tumours (NETs)
imaging, 314
pancreatic, 313–315, 314b, 315f–317f
ultrasound, 314–315
Neurofibromas, 1066, 1120, 1120f, 1164–1165, 1165f
cervical, 911
focal, 1120
neonatal, 1333
optic nerve, 962–963
parotid gland, 901–902
plexiform, 1120, 1312, 1313f
Neurolemmoma, 1119
Neuroma, tibial nerve, 1105
Neurovascular bundles, prostate, 572
Neutropenic colitis, 1399, 1400f
Neutropenic enterocolitis *see* Typhlitis
Nodular fasciitis, 1122, 1303
Nodular regenerative hyperplasia (NRH), 116, 117f
Noise, 61, 61b
gain-related, 62f
random, 61
structured, 61, 62f
Non-accidental head injury, 1285–1287, 1289f–1290f
Non-accidental injury, 1506
Non-alcoholic fatty liver disease (NAFLD), 105, 110–111, 111f
Non-alcoholic steatohepatitis (NASH), 110–111, 111f
Non-Hodgkin's lymphoma
adrenal involvement, 640–641
in children, 1307, 1347
gastric, 360
and hepatitis C, 160
liver metastases, 160
spleen in, 331–333, 333f–334f
thyroid, 880
Non-involuting congenital haemangioma (NICH), 1301
Norman-Roberts syndrome, 1281–1282
North American Symptomatic Carotid Endarterectomy Trial (NASCET), 965

O

Oarsman's forearm, 1059
Obesity, 689
Oblique orientation muscle fibres, 1139
Obstetric examination
British Medical Ultrasound Society (BMUS) guidelines, 57–58
European Federation of Societies of Ultrasound in Medicine and Biology (EFSUMB) guidelines, 58
see also Pregnancy
Obstructive uropathy, 429, 429b, 441–443
Obturator internus, 647
Occipital lymph nodes, 927
Ocular muscles, 959
Oedema
abdominal wall, 799
orbital, 960, 961f
scrotal wall, 618, 618f
Oesophagus, 914, 916f
achalasia, 359–360
anatomical structure, 352, 353f
Barrett's, 356, 358f
benign posterior mediastinal masses, 358–359, 359f
cancer
endoscopic ultrasound, 354–356
lymph nodes, 354, 356f–357f, 356t
management, 354
staging, 353–354, 357f
in children, 1384b
cysts, 358–359, 359f
dysmotility disorders, 359–360
endoscopic ultrasound, 352–360
lipoma, 358, 359f
submucosal (subepithelial) lesions, 358, 358f–359f
varices, 183, 359, 359f–360f
Oestrogen
deficiency, 700, 705
and uterine fibroids, 689
Oil cysts, breast, 988
Olecranon bursitis, 1050, 1051f, 1134, 1134f
Olecranon fossa, 1045, 1045f
Omentum
biopsy, 720–722, 721b, 721f
complications, 722
method, 720–721
rationale, 720
cysts, 1483
infarction, 1401–1402, 1402f
Omohyoid muscle, 908, 925, 926f
Oncocytic thyroid neoplasms, 878
Oncocytomas, 509b
parotid gland, 901
renal, 508–509
On-table cholangiography (OTC), 279
Oocytes capture in in-vitro fertilisation, 736–737, 736f
Ophthalmic artery, 942, 977–978
Opisthorchis felineus, 251
Opisthorchis viverrini, 251
Optic axis, 938
Optic nerve, 959
tumours, 962–963, 963f
Optison, 79t, 80, 87
Oral contraceptive pill
abnormal vaginal bleeding, 689
adenomas and, 143
and the endometrium, 705
Orbit, 959–963
anatomy, 959–960, 959f–960f
arteriovenous fistula, 960–961
contents, 959
haemangioma, 961, 961f
indications for ultrasound, 959b
inflammatory disease (pseudo-tumour), 960, 961f
lymphoproliferative disorders, 962, 962f
metastases, 962
muscles, 959–960
optic nerve tumours, 962–963, 963f
rhabdomyosarcoma, 962
thyroid ophthalmology, 960, 960f
tumours, 961–962
ultrasound features, 959–960
varices, 960
vascular disease, 941–942
Orchitis, 604, 605f, 615
complicated, 615f
see also Epididymo-orchitis
Organ donors
assessment of living related, 203
supply, 529
Oriental cholangiohepatitis, 265–266
Orthotopic liver transplantation (OLT), 204, 204f
Ortolani test, 1497–1498, 1498f
Osgood-Schlatter disease, 1088, 1506
Osseous choristoma, 954, 954f
Osseous lesions in children, 1353–1354
Osseous tumours, extraskeletal, 1124
Ossification, 1115
Osteoarthritis
acromioclavicular joint, 1039–1040
ankle, 1104–1105
degenerative, 1059–1060
glenohumeral joint, 1040–1041
ultrasound features of, 1130
Osteochondritis dissecans, 1047, 1048f
Osteochondroma, 1353–1354, 1354f
Osteochondromatosis, synovial, 1123, 1123f
Osteoma, choroidal, 954, 954f
Osteomyelitis, 1352, 1353f
paediatric, 1508–1509, 1509f
Osteophytes, ankle, 1105
Out-of-plane resolution, 15
Output, 5, 34
Output Display Standards (ODS), 51
Ovarian artery, 648–649, 655
Ovarian hyperstimulation syndrome, 667–668, 667f
Ovarian hyperstimulation syndrome (OHSS), 738, 738f, 738t
in in-vitro fertilisation, 736
Ovarian remnant syndrome, 666, 666f
Ovarian veins, 648
Ovaries, 660–685
abscess, 682, 683f
adnexal masses, 668–670, 669f
age-related differences in, 655t
anatomy, 647–648
benign versus malignant lesions, 670, 670b
blood supply, 648
Brenner (transitional cell) tumours, 674, 674f
cancer, 670–680
classification, 671, 671t
epithelial neoplasms, 671–674, 673b
germ cell tumours, 674–676
metastatic tumours, 678–679, 680f
omental biopsy, 720
risk factors, 670
screening, 678–679

sex cord stromal tumours, 677–678
symptoms, 671
treatment, 669, 669f
tumour markers, 676b
in children, 1468–1490
clear cell tumours, 674, 674f
cyclical variations, 655b, 661–663, 663f
cysts, 663–668
adolescent, 1484, 1485f
as a cause of subfertility, 733–734, 734b, 734f
corpus luteal, 663
follicular, 663, 663f
haemorrhagic, 663–664, 664f–665f, 681, 1485, 1486f
neonatal, 1483, 1483f–1485f
ovarian hyperstimulation syndrome, 667–668, 667f
ovarian remnant syndrome, 666, 666f
paraovarian, 664, 665f
peritoneal inclusion, 664–666, 666f
polycystic ovaries, 1482–1483, 1482f
polycystic ovary syndrome (PCOS), 666–667, 667f, 1482, 1482f
postmenopausal, 666, 666f
prepubertal, 1483–1484
theca lutein, 667
dysgerminomas, 676
echotexture, 1471–1472
ectopic gestation, 758
embryology, 1468–1470
endometrioid tumours, 673, 673f
endometriosis, 680–681, 681b, 681f
epithelial cell tumours, 1487
fibromas, 678, 679f
follicles, 661
development, 1473
normal appearance, 1471–1472
germ cell tumours, 1485, 1486f–1487f, 1487–1488
granulosa cell tumours, 677, 678f
growth, 1473
haemodynamics by Doppler imaging, 655
inguinal, 1476, 1479f
ligaments, 660, 661f
lymphoma, 680
masses in first trimester, 762–763, 762f–763f
mucinous tumours, 672, 672f–673f
mural nodules, 664
neoplasms, paediatric, 1485–1488, 1486f
non-visualisation, 1471
normal appearances, 660–663, 662f, 1472f
of developing, 1471–1473
normal development, 1468–1469, 1469f
outline, 1471
pelvic inflammatory disease, 682, 682b, 682f–683f
polycystic, 1482–1483, 1482f
position, 660, 661f–662f, 1471
pseudomyxoma peritonei, 672–673, 673f
round ligament of, 660
septa, 664, 665f
serous tumours, 671–672, 671f–672f
Sertoli-Leydig cell tumours (androblastoma), 678
sex cord stromal tumours, 1487, 1487f
size, 660–661
teratomas, 1487–1488
immature, 676
mature (dermoid), 674–676, 674f–677f, 676b
thecomas, 678, 679f
torsion, 668, 668f–669f, 1488–1489, 1490f
transvaginal scanning technique, 654, 654f
ultrasound anatomy, 654, 654f
ultrasound technique, 1471
volume, 660, 661t, 1471, 1472t
yolk sac tumours, 676
Overuse injuries, paediatric, 1506
Overuse tendinopathies
pelvic area, 1072
wrist, 1059–1063, 1060f

P

Paediatric patients
acute appendicitis, 389
adrenal glands, 1464–1466, 1464f
appendix, 1395–1398, 1397f
abscess, 1397, 1397f
appendicitis, 1395, 1396f–1397f, 1397–1398, 1399b
retrocaecal, 1398, 1398f
atypical renal infection, 1453–1454
Baker's cyst, 1510, 1510f
bile ducts, 1356–1375
bladder, 1409, 1413f–1414f, 1422–1428
bony elbow injury, 1051, 1051b
branchial cysts, 1296–1297, 1297f–1298f
cancer, 56
cartilaginous lesions, 1353–1354
cellulitis, 1352, 1352f
cervical lymphadenopathy, 1303–1304, 1304f
cervical lymphatic malformations, 1295–1296, 1296f
chest, 1337–1355
chest wall, 1350–1354
colon, 1399–1401, 1399b
colitis, 1399
imperforate or ectopic anus, 1399
necrotising enterocolitis, 1400, 1401f
neoplasms, 1400–1401
normal anatomy, 1399
congenital cystic lesions, 1294–1299, 1299b
congenital foregut malformations, 1299
Crohn's disease, 1392–1393, 1393f
cysts, 1510
dermoid cysts, 1298, 1298f–1299f
diaphragm, 1339, 1339f, 1348–1350, 1349b
enuresis, 1462
fibromatosis, 1302–1303
foreign bodies, 1507–1508, 1508f
gallbladder, 1356, 1375–1376
gallstones, 1375, 1375f
ganglion cysts, 1510, 1510f
ganglioneuroblastoma, 1466
ganglioneuroma, 1466
gastro-oesophageal junction, 1383–1384, 1384f
gastro-oesophageal reflux, 1383–1384, 1384f
technique and normal anatomy, 1383
goitre, 1310
haemangiomas, 1299–1301, 1299f–1300f
haematoma, 1507, 1507f
head and neck masses, 1294–1314
Henoch-Schönlein purpura, 1393–1394, 1393f–1394f
hepatocellular carcinoma, 222
hip, 1497–1505, 1505b
aspiration, 1183–1184, 1184b, 1184f
hypertension, 1455–1457
inflammatory masses, 1303–1307
intussusception, 1390–1391, 1392f
kidneys, 1409, 1411b
abnormalities, 1418–1420, 1418f
cystic disease, 1434–1440, 1435b, 1435t
duplex anomalies, 1420–1422, 1423f
end-stage failure, 1444–1445
malignancy, 1458–1462
normal appearances, 1409–1412, 1416f, 1416t
normal sonographic values, 1412–1418
renovascular disease, 1454–1455
transplantation, 1444–1445, 1445f
trauma, 1457–1458, 1457f–1458f
leg lengthening, 1509
leukaemia, 1307, 1461
lipomas, 1352, 1511–1512, 1511f–1512f
liver, 1356–1375, 1357f
abscesses, 1364–1365
anatomical variants, 1356–1357
anatomy, 1356
diffuse parenchymal disease, 1357–1360
focal lesions, 1360–1364
inflammatory masses, 1364–1365
jaundice in older children, 1372–1375
neonatal jaundice, 1367–1372
portal hypertension, 1365–1367
technique, 1356
transplantation, 216–222, 220b, 1376–1377, 1376f–1377f, 1377b
clinical indications, 216–217
complications, 219–221, 219f
recurrent disease, 221–222
surgical techniques, 217, 218f
ultrasound patient evaluation, 217–219
vascular disorders, 1365–1367
lungs and pleura, 1338–1347, 1339f
lymphangiomas, 1352f
lymphatic malformations, 1351–1352, 1352f
lymphoma, 1394–1395, 1461, 1462f
mastoid infection, 1304, 1306f
mediastinum, 1347–1348
mesenteric adenitis, 1395, 1395f–1396f
muscle injury, 1506–1507, 1507f
myositis ossificans, 1508
nephrocalcinosis, 1446, 1446t, 1449f
neuroblastoma, 637, 640f, 1312
non-accidental injury, 1506
obstructive uropathy, 1428–1433
oesophagus, 1384b
osseous lesions, 1353–1354
osteomyelitis, 1508–1509, 1509f
ovaries, 1468–1490
neoplasms, 1485–1488, 1486f
overuse injuries, 1506
pancreas, 1377–1381, 1380b
cysts, 1378
pancreatitis, 1378–1380, 1379f

parathyroid cysts, 1298–1299
parotitis, acute, 1307–1308
peritoneal cavity, 1401–1403, 1403b
ascites, 1401, 1401f
inflammatory disease, 1401
omental infarction, 1401–1402, 1402f
tumours, 1402–1403
post-transplant lymphoproliferative disease, 213, 221
prostate gland, 1409, 1415f
pyomyositis, 1508
renal tract ultrasound technique, 1409
renovascular hypertension in, 477
retropharyngeal infection, 1304
rhabdomyosarcoma, 1312, 1353, 1353f
salivary glands, 1307–1309
seminal vesicles, 1409, 1415f
sialolithiasis, 1308
small bowel, 1388–1395
masses, 1394–1395, 1395b
normal anatomy, 1388
obstruction, 1388–1391, 1388f, 1391b
wall thickening, 1392–1394, 1393b
soft tissue infections, 1508–1509, 1509b
spleen, 1356–1357, 1357f, 1357t, 1377–1381, 1380b
splenomegaly, 1380, 1380t
stomach, 1384–1387, 1388b
masses, 1386–1387
obstruction, 1385–1386
technique and normal anatomy, 1384–1385
wall thickening, 1386
thymus, 1338–1339, 1338f, 1340f
cysts, 1298–1299
thyroglossal duct cysts, 1294–1295, 1295f
thyroid, 1309–1312
trauma, 1505–1508, 1506b
ureters, 1409, 1413f, 1422–1428
urethra, 1422–1428
urinary tract infection, 1446b, 1448–1453
urolithiasis, 1445–1446, 1446b, 1446f–1448f
uterus, 1468–1490
vascular lesions, 1299–1302, 1301b
vascular/lymphatic malformations, 1510
vascular malformations, 1301–1302, 1301f, 1351
vesicoureteric reflux in, 553
PAIR (percutaneous aspiration injection and re-aspiration), 130
Palmar plate tear, 1064
Pancake kidneys, 424, 425f
Pancreas, 285–323
adenocarcinoma, 306–309, 307f–310f, 309b
agenesis, 1378
anatomy, 285–286, 286f
annular, 1378
autoimmune pancreatopathy, 305–306, 305f
biopsy, 290, 318–319, 318f, 319b
complications, 318–319
indications, 318
results, 318
techniques, 318
in children, 1377–1381, 1380b
congenital variations, 1377–1378
contrast imaging, 85
in cystic fibrosis, 1380
cysts, congenital, 1378
echogenicity, 293, 294f
embryological development, 286f
fine-needle aspiration, 290
head, 285–286
carcinomas, 263, 264f
enlargement, 263
hyperechoic, 293, 294f–295f
intraoperative ultrasound, 279, 279f
mass, 306
metastases, 306, 315, 317f
neck, 285–286
necrosis, 298, 300–301
normal appearances, 293, 293f, 295b, 1377–1378
pancreatitis *see* Pancreatitis
phlegmon, 299, 299f
pseudocysts, 298f, 299–300
scanning techniques, 286–293
endoscopic ultrasound, 288–291, 291f–292f
intraoperative ultrasound, 291–293, 293f
transabdominal ultrasound, 286–288, 287f–291f
transplantation, 319–320, 319f–320f, 320b
combined with renal transplantation, 541
trauma, 841
tumours, 288, 306–315
adenocarcinoma, 306–309, 307f–310f, 309b
cystic, 311–313, 311f–314f, 312b
differential diagnosis, 306
imaging, 306
miscellaneous, 315, 317f
neuroendocrine, 313–315, 314b, 315f–317f
Pancreas divisum, 293, 295
in children, 1378
Pancreatic ducts, 286, 293, 294f, 303
in children, 1378, 1378f
dilatation, 306, 307f
Pancreatico-biliary malunion, 1375–1376
Pancreatico-duodenal varices, 183
Pancreatitis
acute, 293–301, 296f, 301b
aetiology, 294
appearances on ultrasound, 297, 297f
in children, 1378–1380, 1379f
clinical features, 295
complications, 298–300
arterial bleeding and pseudoaneurysm, 299, 301f
biliary obstruction, 299
gastrointestinal tract/renal obstruction, 300
infection, 299, 300f
pancreatic necrosis, 298
pancreatic phlegmon, 299, 299f
portal venous thrombosis, 299
pseudocysts, 298f, 299
dilated bile duct, 263, 264f
general considerations, 293–295
intervention, 300–301
infected necrosis, 300–301
pseudocyst aspiration/drainage, 300, 302f
thrombin injection of pseudoaneurysm, 301
mild, 296f, 297
mortality rates, 295
pathophysiology, 294–295
role of ultrasound, 295–297
severe, 295, 297, 297f
traumatic, 295
chronic, 301–304, 303f–304f, 306b
in children, 1378–1380, 1379f
diagnosis, 301
dilated bile duct, 263
endoscopic ultrasound, 302–304, 304f
focal, 302, 302f
imaging, 301–302
protein plug, 303, 304f
ultrasound, 302–304
post-liver transplantation, 213, 213f
Papillary adenomas, 508
Papillary carcinomas
breast, 995, 995f
thyroid, 873–876, 874f–877f, 875b, 928, 929f, 933
cystic variant, 876
diffuse sclerosing, 876
follicular variant, 876
Papillary cystadenoma, 610
Papillary lesions, breast, 991–992, 992f
Papillary necrosis
pelvi-ureteric dilatation, 434, 436f
renal, 449–450, 450f
Papillomas
bile duct, 261, 261f
breast, 992, 992f
Paracentesis, 813
Paraepiglottic fat space, 913, 913f–914f
Paragangliomas, 819, 909–911
Paraglottic fat, 913–914, 915f
Parallel muscles, 1139
Paraovarian cysts, 664, 1485
Pararenal space, 816–817
Parasitic infections, 252f
gallbladder, 250–251, 252f
renal, 464–465, 465b
spleen, 339–340
see also specific infections
Paratenon, 1093–1094
Parathyroidectomy, 884
Parathyroid glands, 884–887
accessory/supernumerary, 885
anatomy, 884–885, 885f
cysts, 887, 1298–1299
embryology, 884
ethanol ablation of lesions, 887
scanning techniques, 886, 886f
ultrasound features of lesions, 886–887, 886f–887f
Paratracheal lymph nodes, 927, 927f
Paraumbilical hernia, 804
Paraurethral glands, dilation, 716
Parenchymal haemorrhage, 1270, 1271f
Parotid glands, 907b
abscess, 903, 904f
acinic cell carcinoma, 902
adenoid cystic carcinoma, 902
adenolymphoma, 901, 901f

calculi, 904, 904f
carcinoma ex-pleomorphic adenoma, 902–903
in children, 1307, 1307f
cystic hygroma, 905, 906f
cystic lesions, 905, 905f
enlargement, 1308
haemangioma, 901, 902f
infection, 903
inflammation, 903–905
lymph nodes, 900, 924, 924f
lymphoma, 903
metastases, 903
mucoepidermoid carcinoma, 902
nerve sheath tumours, 901–902
neurofibroma, 901–902
normal appearances, 898–907, 899f
oncocytoma, 901
pathology, 900
pleomorphic adenoma, 899f, 900, 901f
sarcoidosis, 904
schwannoma, 901–902
technique, 898–907
tumours, 897, 900–903, 903f
Parotitis
acute, 903, 903f
in children, 1307–1308, 1308f
recurrent, 1307–1308, 1308f
chronic, in children, 1308
juvenile recurrent, 905, 905f
Parsonage-Turner syndrome, 1037
Parvus tardus waveform *see* Damped waveform
Patella, 1085f
Patellar tendinosis, 1084–1087, 1086f–1087f
Patellar tendon, 1084, 1085b, 1085f
tears, 1087–1088, 1087f–1088f, 1088b
Patent foramen ovale (PFO), 77, 78f
Patient monitoring, transcranial Doppler ultrasound, 980
Peak systolic velocity (PSV), 1202, 1204f
Peliosis hepatis, 197, 197f
Peliosis hepatitis, 150
Peliosis of the spleen, 340
Pelvic abscess drainage, 724–727, 725f–726f, 726b
complications, 727
method, 724–726
rationale, 724
Pelvicalyceal system, dilated, 433–434, 433f, 435f–436f, 493, 494f, 518
see also Pelvi-ureteric dilatation
Pelvic brim, 646
Pelvic floor, 647, 647f
Pelvic inflammatory disease (PID), 682, 682b, 682f–683f
Pelvis
female
anatomy, 646–649
in children, 1470–1471
muscles, 647, 647f–648f
skeleton, 646, 646f
ultrasound anatomy, 652–654
ultrasound scanning technique, 645–646, 649–654, 1470–1471
viscera, 647–649, 648f
interventional techniques, 1180–1181
muscle injury, 1072–1075
musculoskeletal soft tissue masses, 1082
neonatal masses, 1483, 1484f
pain
in children, 1488–1490
gynaecological causes of, 1488
non-gynaecological causes of, 1490
tendon injury, 1072–1075
Pelvi-ureteric dilatation, 428–444
causes of, 428–438
pathological, 429–438
physiological, 428–429, 429f
congenital causes, 435–436
diagnosis, 438–439
Doppler technique, 441, 441f–442f
functional evidence using Doppler, 440–441
iatrogenic, 438
idiopathic, 436
management of obstructive uropathy, 441–443, 442f
trauma, 438
ultrasound appearances, 439–440, 440f
Penile arteries, 621
Penis, 621–631
anatomy, 621, 621b, 622f
appearances, 621, 622f
arterial supply, 621, 622f
erectile dysfunction, 621–623
arteriogenic, 624
background, 621–623
physiology of the erectile process, 623
veno-occlusive, 624–625, 626f
fibrosis, 628
masses, 628–629, 628f–629f
metastases, 628–629
Peyronie's disease, 627–628, 628b, 628f
priapism, 627, 627b
ischaemic, 627, 627b, 627f
non-ischaemic, 627, 627b
prostheses, 629f
squamous cell cancer, 628–629
stimulated colour Doppler ultrasound, 623–626
arteriogenic erectile dysfunction, 624, 625f
false venous leak, 626, 626f
further imaging, 625–626
haemodynamic parameters, 626b
normal response, 624, 624f–625f
pharmacological agents, 623
technique, 623, 623f
veno-occlusive erectile dysfunction, 624–625, 626f
trauma, 629, 629f
urethral ultrasound, 629
venous leak, 623–625
false, 626, 626f
Pennate muscles, 1139
Peptic ulcer disease, 365
Percutaneous aspiration injection and re-aspiration (PAIR), 130
Percutaneous ethanol injection (PEI), 174, 174t
Percutaneous nephrostomy, 442–443, 442f
Perforating veins, 1245, 1245f
Periareolar infection, 989
Pericardial cysts, 1348, 1349f
Pericholecystic varices, 183
Periductal mastitis, 989
Peri-epiglottic fat space, 913
Perimysium, 1138
Perineurium, 1158
Peripheral arterial disease, 1197–1226
acute ischaemia, 1211
aneurysms, 1211, 1212f
angioplasty, 1210
ankle brachial pressure index, 1199
in the arm, 1212–1214
occlusive arterial disease, 1214
Raynaud's disease, 1214, 1219f
Takayasu's arteritis, 1214, 1218f
thoracic outlet syndrome, 1213–1214
ultrasound investigation, 1212–1214, 1216f
arteriovenous fistula, 1212, 1216f
bypass grafts *see* Peripheral artery bypass grafts
clinical problem, 1197–1198
continuous wave Doppler ultrasound, 1199–1200, 1203b
dissection, 1212, 1216f
duplex ultrasound, 1200–1207, 1203b, 1203f–1204f
aorto-iliac and femoropopliteal segments, 1206
below-knee segments, 1206–1207, 1207f
reporting, 1207, 1208f
scanning technique, 1205–1206, 1205f–1206f
equipment, 1198–1199
continuous wave ultrasound, 1198, 1198f
ultrasound scanners, 1198–1199
haemodialysis access *see* Haemodialysis, access
injuries, 1212
popliteal entrapment, 1211
pseudo-aneurysms, 1212, 1213f–1215f
stenosis criteria, 1201–1202
stents, 1210
velocity waveform analysis, 1199–1200, 1200f–1202f, 1202t
Peripheral artery bypass grafts, 1207–1210
failure, 1207, 1207t, 1209
postoperative scanning, 1209–1210, 1209f–1211f, 1210b
preoperative scanning, 1207–1208, 1209f
stenoses in, 1209–1210, 1209f
Peripheral nerves, 1158–1167
anatomical variations, 1159–1160, 1159b, 1160f–1161f
compression, 1162–1163, 1166f
entrapment neuropathies *see* Nerve entrapment
examination technique, 1158–1159
miscellaneous disorders, 1166
normal anatomy, 1158, 1159f
tears, 1161
trauma, 1161–1163, 1162f–1164f, 1163b
tumours and masses, 1164–1166, 1165f–1166f
ultrasound anatomy, 1158, 1159f
Peripheral veins, 1227–1250
anatomical variants, 1234, 1235f
clinical applications for ultrasound, 1235–1240

collateral veins, 1235
dilatation, 1231, 1231f
distal augmentation, 1231, 1231f, 1234–1235, 1236f
lower limb, 1227–1228
pre-arterial bypass vein mapping, 1248–1249
problems and pitfalls, imaging, 1234–1235, 1234b
reflective augmentation, 1231
response to probe compression, 1231
spontaneous flow, 1230–1231, 1230f
suspected pulmonary thromboembolic disease, 1241–1242
technique, 1228–1235
upper limb, 1240–1241
variation of spectral waveform with respiration, 1231, 1234
venous incompetence, 1242–1248
Periprostatic fascia, 573, 573f
Perirenal space, 817
Peristalsis, small bowel, 371
Peritoneal carcinomatosis, 672, 672f, 720
Peritoneal cavity, 807–808, 807f
in children, 1401–1403, 1403b
ascites, 1401, 1401f
inflammatory disease, 1401
omental infarction, 1401–1402, 1402f
tumours, 1402–1403
Peritoneum, 807–816
anatomy, 807–809, 807f, 809f
ascites *see* Ascites
duplication cysts, 816
fluid collections, 808, 815–816, 816f, 829, 830f, 833–835, 834f, 835b
inclusion cysts, 664–666, 666f, 697–698, 699f
intra-abdominal abscess, 813–815, 814f–815f
mesenteric tumours, 816, 816f–817f
metastases, 816, 817f
paracentesis, 813
scanning technique, 809–810, 810f
tumours, 816, 817f, 1402–1403
Peritonitis
appendicitis complications, 1397, 1398f
meconium, 1389, 1389f
pseudomyxoma, 812, 813f
sclerosing, 455, 455f
tuberculous, 812, 813f
Periventricular haemorrhagic infarction, 1261–1262
Periventricular leukomalacia, 1263–1264, 1266f–1267f
Peroneal artery stenosis, 1206–1207
Peroneal veins, 1232
Peroneus brevis, 1098, 1099f, 1105
Peroneus longus, 1098, 1099f, 1105
Peroneus quartus, 1099, 1143
Peroneus tertius, 1099
Persistence, 26
Persistent hyperplastic primary vitreous, 949, 949f, 955
Pes anserinus bursa, 1084, 1091
PESDA, 80
Peutz-Jeghers syndrome, 1375–1376
Peyronie's disease, 627–628, 628b, 628f
Phaeochromocytomas
adrenal, 637, 638f–639f
retroperitoneal, 819
Pharyngeal pouch, 917, 917f
Phase inversion imaging, 82, 82f
Phentolamine, 626, 626f
Phleboliths, 1120
Phlegmons
appendiceal, 391, 392f
pancreatic, 299, 299f
Phosphodiesterase type 5 (PDE-5) inhibitors, 622–623
Phrenocolic ligament, 808, 808f
Phrygian cap, 228, 231f, 1375
Phthisis bulbi, 957
Phyllodes tumours, breast, 990–991, 991f
Physeal fracture, 1505
Physics of ultrasound, 3–15
absorption and attenuation, 11, 11t, 13b
diffraction and interference, 5–6, 6f, 8b
Doppler effect, 13–14, 13f–14f, 14b
Fourier components, 7, 7f–8f
image speckle, 6–7, 7f
intensity and power, 5, 5b, 5f
lenses and mirrors, 10–11, 11f
non-linear propagation, 11–12, 12f, 13b
production, 3–4, 4b, 4f, 4t
reflection, 9, 9f, 9t, 10b
refraction, 10, 10b, 10f, 10t
resolution, 14–15
scattering, 9–10, 10b, 10f, 10t
standing waves and resonance, 7–8, 8b, 8f
tissue characterisation and elastography, 12–13, 12f
Piezoelectric material, 18
Piggy-back liver transplantation, 204, 204f, 794, 794f
Pigmented villonodular synovitis (PVNS), 1123, 1133
Pilomatrixoma, 907
Pipe stem calcification, 1198
Piriformis, 647
Pitcher's elbow, 1050
Placenta percreta, 568
Plantar fascia, 1100, 1101f
injection, 1189, 1189b, 1190f–1191f
Plantar fasciitis, 1106, 1106f
Plantaris, 1095, 1095f
Plaque, carotid arteries, 972–973, 972b, 972f, 973t
Pleomorphic adenoma, parotid gland, 899f, 900, 901f
Pleura, 1007–1014
anatomy, 1338, 1339f
effusion *see* Pleural effusions
examination technique, 1005
masses, 1346, 1347f
normal appearances, 1007–1008, 1008b, 1008f
paediatric, 1338, 1339f, 1344–1347
patient position, 1005
technical requirements, 1005
visceral, 1010–1011
Pleural effusions, 808f, 1006–1010
exudative, 1009
fibrinous attachments, 1012, 1013f
intercostal bleed, 1013, 1013f
malignant, 1010
paediatric, 1344–1345, 1345f–1346f
pleural fluid detection and characteristics, 1008–1010, 1009b, 1009f–1010f
septated, 1013, 1013f
septations, 1009–1010, 1010f
transudative, 1009
ultrasound-guided interventions for, 1012, 1012f–1014f, 1014b
Pleural stripe, 1007, 1008f
Pleurodesis, 1014
Pneumatosis intestinalis, 1400
Pneumocystis carinii, 132
Pneumonia, 1014–1015, 1015f
Pneumothorax, 1011–1012, 1011f, 1012b
in children, 1346–1347
Polyarteritis nodosa, 379t
Polycystic kidney disease, 499–500
autosomal dominant, 500, 501f, 502b
autosomal recessive, 499–500, 502b
calcifications, 491–492, 491f
presentation, 490
Polycystic ovaries, 1482–1483, 1482f
Polycystic ovary syndrome (PCOS), 666–667, 667f, 1482, 1482f
as a cause of subfertility, 733–734, 734b, 734f
and uterine fibroids, 689
Polymer-coated microbubbles, 80–81
Polyorchidism, 598, 598f
Polyps
cervical, 713
colonic, 1400–1401
endometrial, 693, 700–702, 701f, 702b, 733, 733f
gallbladder, 247–249, 248f–249f
gastric, 360–362, 363f
Polysplenia, 330, 331f, 1356
Pons, 1320
Popeye sign, 1039
Popliteal arteries
aneurysm, 1117, 1198, 1211, 1212f
entrapment, 1211
occlusion, 1205f
stenosis, 1206–1207
Popliteal cysts *see* Baker's cyst
Popliteal veins, 1228
duplication, 1234, 1235f
spontaneous flow, 1230–1231
Popliteus tendon, 1091
Porencephaly, 1283
Portacaval anastomosis, 795f
Portacaval end-to-side shunt, 186
Portacaval side-to-side shunt, 795, 795f
Porta hepatis, 102
lymphadenopathy, 263, 263f
varices, 183
Portal cavernoma, 1365–1366, 1366f–1367f
Portal congestion index, 181
Portal hypertension, 180–185
backward flow theory, 180–181
in children, 1365–1367, 1367b
definition, 180
forward flow theory, 180–181
hepatic arterial flow changes, 182
hyperkinetic, 180–181
main causes, 180, 181b
management, 185–188
surgical portosystemic shunt, 185–186

transjugular intrahepatic portosystemic shunt, 186–188, 186f–187f, 188b
paediatric liver transplantation, 217
pathophysiology, 180–181
portal vein calibre change, 182, 182f
portal vein flow changes, 181, 181f–182f
portosystemic collaterals (varices), 181, 183f–185f
pre-liver transplantation assessment, 201
splenic involvement, 342
splenomegaly, 182
ultrasound findings in, 181, 181b
Portal veins, 179–189
anatomy, 94–96, 94f, 98, 99f, 102, 102f, 179, 180f
aneurysm, 189
calibre changes in portal hypertension, 182
cavernous transformation of, 1365–1366
in children, 1365–1366, 1365f–1366f
congenital absence of, 1365
duplication, 1365
flow changes in portal hypertension, 181
gas, 189, 191f, 210
hypoplastic, 1365
mean velocity, 179
normal findings, 179, 180f
occlusion, 188–189, 188b, 188f–191f, 210
periodicity, 179
phasicity, 179
portal hypertension *see* Portal hypertension
preduodenal, 1365
pre-liver transplantation assessment, 201, 202f
pulsatility, 179
scanning techniques, 179, 180f
size, 179
stenosis, post-transplantation, 209–210, 210f, 220, 220f
thrombosis, 188–189, 188b, 188f–191f, 201, 1365–1366, 1366f
pancreatitis complications, 299
post-transplantation, 210, 210f, 220, 220f
varix, 1366
Porto-enterostomy, 216
Portosystemic collaterals (varices), 181, 183f–185f
Portosystemic shunts, surgical
portal hypertension, 185–186
pre-liver transplantation assessment, 203, 203f
Positron emission tomography computed tomography (PET-CT)
cervical cancer, 714
spleen lymphoma, 331–333
Positron emission tomography (PET)
endometrial cancer, 705
pelvic examination, 688
thyroid, 867
Postcoital bleeding (PCB), 688
Posterior communicating arteries, 1259t
anatomy, 976
aneurysm, 982f
transcranial Doppler ultrasound, 976–977, 979f, 981f
Posterior interosseous nerve, 1044
entrapment, 1052–1053, 1053f
Posterior talofibular ligament, 1099
Posterior urethral valve (PUV), 1422–1425, 1427f–1428f
Postmenopausal bleeding, 688
Postmenopausal ovarian cysts, 666, 666f
Post-transplant lymphoproliferative disorder (PTLD), 160, 213–214, 214f
in children, 221, 1362
Pouch of Douglas, 808–810, 810f
fluid in, 834
Power, 5
Power Doppler, 30
abdominal trauma, 829
aortic dissection, 789
carotid arteries, 970
cerebral arteries, 977
cervical node vascularity, 932, 934f
embryo transfer, 737
knee joint effusion, 1088
liver
adenoma, 145
fibronodular hyperplasia, 142
haemangiomas, 140
parameters, 32
patellar tendinosis, 1086–1087, 1087f
renal transplantation, 533
in rheumatological ultrasound, 1126, 1132
scanners, 32
soft tissue masses, 1113
tendinopathy, 1025, 1026f
thyroid nodules, 872
transcranial, 979, 981f
Power-modulated pulse inversion (PIAM), 82
Precocious puberty, 1478, 1480t
Pre-epiglottic fat space, 914f
Pregnancy
abnormal outcome prediction, 761–762
bladder pathology in, 568
cumulative pregnancy rates, 730, 731f
ectopic *see* Ectopic pregnancy
failure, 749–751, 751b
major criteria, 750, 750f–751f
minor criteria, 750–751, 751f–752f
of normal progression, 749
sonographic diagnosis, 749–751, 750f
ultrasound prediction, 761–762
and fibroids, 690, 690f
first trimester, 740–770
abnormal outcome prediction, 761–762, 761f–762f, 761t
amnion appearance, 745, 745f
biometry, 748–749
chorion appearance, 745, 745f
complications, 751–760
ectopic implantation *see* Ectopic pregnancy
haemorrhage, 751–753, 752f
crown-rump length, 749
embryo appearance, 744–745, 744f–745f
embryonic anatomy, 746f, 747b
embryonic heartbeat, 745
endometrium thickening, 741, 741f
failure, 749–751, 749t–750t, 750f–752f
fetal anomalies, 746–747, 747b, 747f
gestational trophoblastic disease, 764–765, 764f–766f, 765t
gestation sac appearance, 741–743, 742f–743f, 742t, 744t
masses, 762–763
fibroids, 763, 763f
ovarian, 762–763, 762f–763f
mean gestational sac diameter, 748–749
multiple pregnancy diagnosis, 747–748, 747f–748f, 747t, 748b
normal sonographic development, 741–747, 741t
retained products of conception, 765–766, 766f
transvaginal scanning, 741
yolk sac appearance, 743–744, 743f–744f, 744b, 744t
heterotopic gestation, 753
hydronephrosis of, 421, 422f
intrauterine devices in, 708, 708f
molar, 696, 696f
pelvi-ureteric dilatation, 428–429, 429f
pregnancy of unknown location, 760, 760b, 760f, 761t
scanning in *see* Obstetric examination
Pregnancy of unknown location (PUL), 760, 760b, 760f, 761t
Prelaryngeal lymph nodes, 927, 927f
Premature infants, cerebrovascular complications, 1260–1264
Prepatellar bursar, 1089
Pretracheal lymph nodes, 927, 927f
Priapism, 627, 627b
ischaemic, 627, 627b, 627f
non-ischaemic, 627, 627b
Primitive neuroectodermal tumour, prostate gland, 589t
Probes
endoscopic ultrasound, 351
intraoperative ultrasound, 274, 274f
laparoscopic ultrasound, 274, 274f
small intestine ultrasound, 369
Profunda femoris vein, 1229–1230
Progesterone, abnormal vaginal bleeding, 689
Proliferative vitreoretinopathy, 945–946, 946f
Pronephros, 1407
Propagation, 13b
non-linear, 11–12, 12f
Prostaglandin E1 (PGE-1), 623, 626
Prostate, 572–592
abscess, 582–584, 582f, 583t, 591
accessory structures, 574–576
acquired abnormalities
benign, 579–585, 588t
malignant, 585–587
benign hyperplasia/hypertrophy, 579–581, 580t, 581f–582f, 583t
biopsy, 587–591, 589b
abscess/cyst drainage, 591
post-prostatectomy bed, 590–591, 591f
principles, 587–590, 590f
seminal vesicles/ejaculatory ducts injection, 591
blood flow, 576
blood supply, 574
cancer, 585–587, 587b, 587f
bladder involvement, 568
cystic, 583–584, 583t, 584f
follow-up, 587
locally advanced, 587f
staging, 585–587
suspected recurrent tumour, 587, 589f

transrectal ultrasound, 566, 585, 586f, 588t
in children, 1409, 1415f
congenital or developmental anomalies, 579
cystic cancer, 583–584, 583t, 584f
cysts, 579, 580f, 583–584, 583t, 585f, 591
dimensions of normal, 572
embryology, 572
gross anatomy of, 572, 573f
infarction, 589t
lobes, 573–574
lymphatic drainage, 574
metastases, 589t
nerve supply, 574
neurovascular bundles, 572
normal sonographic appearances, 576, 577f–578f, 578b
periprostatic fascia, 573
prostatic capsule, 573
size, 572, 576
surface relations of, 572–573
transrectal ultrasound, 574–576, 575f, 576b, 577f, 578b, 581, 582f
-guided intervention, 587–591
unusual abnormalities, 587, 589f, 589t
transurethral resection of (TURP), 581, 582f
ultrasound technique, 1409, 1415f
vascularity, 576, 578f
zonal anatomy of, 573–574
Prostate, Colorectal, Lung and Ovarian Cancer screening trial, 680
Prostatic capsule, 573
Prostatic fascia, 573
Prostatic utricles
abnormalities, 579
cysts, 583–584, 583t, 584f–585f
Prostatitis, 582–583
abscess, 582–584, 582f, 583t
acute, 580t, 582
cavitary, 583t
chronic, 580t, 583, 583f
focal, 582f
granulomatous, 583, 583f
Proteinuria, Tamm-Horsfall, 1443, 1443f
Proteus mirabilis, 614
Proteus spp., 1273, 1448–1449
Proximal intersection syndrome, 1059
Proximal tibiofibular joint, 1091
Prune belly syndrome, 1427–1428
Pseudoaneurysms, 1237f
abdominal wall, 807
haemodialysis access, 1222, 1223f
hand/wrist, 1066–1067
hepatic artery, 208–209, 209f
pancreatitis complications, 299, 301, 301f
peripheral arterial disease, 1212, 1213f–1215f
renal, 481
splenic artery, 342
thrombin injection, 301
Pseudocysts
meconium, 1389, 1390f
mesenteric, 1402, 1402f
pancreas, 298f, 299–300, 1379, 1379f
spleen, 338, 339f
Pseudo-gestation sac, 754
Pseudohermaphrodites
female, 1475–1476
male, 1477
Pseudo-kidney sign, 384, 1390
Pseudomembranous colitis, 399t, 400–401, 1399, 1400f
Pseudomyxoma peritonei, 672–673, 673f
Pseudomyxoma peritonitis, 812, 813f
Pseudoprecocious puberty, 1480–1481, 1480f
Pseudo-tumour, orbital, 960, 961f
Psoas muscle, 647
abscess, 821, 823, 823f
Pubalgia *see* Athletic groin pain
Puberty
central precocious, 1478–1480
delayed, 1481
female, 1470
precocious, 1478, 1480t
pseudoprecocious, 1480–1481, 1480f
Pudendal arteries, 621
Pulled elbow, 1051, 1052f
Pulmonary embolus, 1015–1016, 1016b, 1016f
Pulmonary infarction, 1018
Pulmonary sequestration, 1018
Pulmonary thromboembolism (PTE), 1227, 1242f
imaging suspected, 1241–1242
induction of, 1235
Pulmonary tuberculosis, 1015
Pulsatile neck masses, 966, 974, 974b, 975f
Pulsatility index (PI), 1199–1200
cervical lymph nodes, 932
renal transplantation, 532–533
Pulse coding, 25, 25f
Pulsed wave Doppler, 15, 26–28, 27f
parameters, 32, 50b
scanners, 32, 50b
transcranial, 978–979, 978f
transducers, 8
Pulse inversion imaging, 25, 82, 82f, 155–156, 157f
Pulse repetition frequency (PRF), 28, 40–41
high, 46–48, 48f
Pyelectasis, 1429
Pyelitis, emphysematous, 460
Pyelonephritis
acute
bacterial, 460, 461f
in children, 1448–1449, 1450f–1452f
in children, 1448–1449, 1450f–1452f
chronic, 462
in children, 1449, 1452f
emphysematous, 460
focal, 507, 507f
xanthogranulomatous, 463, 465f, 507, 507b
Pylorospasm, 1386, 1386f
Pyocele, 612, 613f
Pyogenic liver abscess, 123f–126f, 124–126, 145–146
Pyomyoma, 690
Pyomyositis, 1117, 1156, 1156f, 1508
Pyonephrosis, 438f, 462, 463f
in children, 1448, 1451f
pelvi-ureteric dilatation, 442–443
Pyosalpinx, 682, 682f
Pyramids, renal, 493, 493f

Q

Quadriceps, 1073, 1084, 1085f
Quadriceps tendon, 1084, 1085f
tears, 1087–1088, 1087f–1088f, 1088b

R

Radial artery, 1043, 1213
Radial collateral ligament, 1046, 1051
Radial modulation imaging, 84
Radial nerve, 1043, 1057
Radial scars, breast, 992–993
Radiocapitellar joint, 1043, 1044f
Radio-frequency ablation (RFA)
laparoscopic guided, 278–279, 278f
liver, 171–176, 171b
clinical results, 174–176, 174t–175t
complications, 174
indications, 172–174, 172t
technique, 171–172, 172f–173f
renal cell carcinoma, 523–526, 524f–526f, 526b
tumours, 858, 858f, 861f
Radio-isotope scanning, 1227
Radiotherapy
affect on submandibular gland, 897
cervical lymph nodes after, 930
Radioulnar articulation, 1043
Ranula, 893, 893f
diving, 897–898
Rapidly involuting congenital haemangioma (RICH), 1301
Rayl, 9
Raynaud's disease, 1214, 1219f
Real-time compression ultrasound, 1228–1229, 1229f
Rectovesical pouch, 808–809
Rectum, 405–409
anatomy, 407
anorectal tumours, 407–408, 407f
solitary rectal ulcer syndrome, 409
ultrasound technique, 405–406
Rectus abdominis, 798, 1076
divarication of the, 800, 805f
Rectus femoris, 1073, 1084
Reflection, 9, 9f, 9t, 10b
Reflective augmentation, peripheral veins, 1231
Refracting media, 940–941, 941b
Refraction, 10, 10b, 10f, 10t
Refractive artefacts, 68–70, 70f–71f
Renal arteries, 413–414, 414f, 417, 417f, 422
accessory, 468, 469f
anatomy, 468–469, 468f
aneurysm, 482–483, 483b, 483t
angioplasty, 474
branches, 469, 469f
colour flow map, 469
in kidney disease, 447
main trunks, Doppler studies, 471–472, 471f–473f, 477
occlusion, 448, 477–478, 478f, 546, 547f
peak systolic velocity, 448–449
in renal transplantation, 532
stenosis, 448–449, 448f–449f, 449b, 537–538, 538f–539f, 546

abnormalities
on greyscale ultrasound studies, 475
in renal Doppler studies, 475–476
causes of, 474t
in children, 477, 1455
clinical considerations, 473
Doppler imaging, 467, 476–477
in renal transplant patients, 477
screening, 474–475, 474t–475t
simple greyscale ultrasound studies, 474
spectral (duplex) Doppler, 471–472, 471f–473f
thrombosis, 533–534, 534f, 1455, 1457f
view through kidney, 471f
waveform, 469–470, 470f
Renal artery/aorta velocity ratio (RAR), 448–449
Renal cell carcinoma, 480, 480f, 487, 490, 492, 492f, 512–517, 512f
and acquired cystic kidney disease, 498
aetiology, 513b
appearances, 513, 513b, 514f–516f
asymmetric necrosis, 492, 492f
in children, 1462
cryoablation, 523
differential diagnosis, 511–513
incidence, 522–523
microwave therapy, 523
minimally invasive treatment of, 522–526
multilocular cystic, 492
pelvi-ureteric dilatation, 434
presentation, 513, 513b
radio-frequency ablation, 523–526, 524f–526f, 526b
rare presentations, 513, 517f
screening, 513
staging, 513–517, 516t
survival, 516t
treatment, 517
Renal transplantation, 528–549
acute tubular necrosis, 532
arterial thrombosis, 533–534, 534f
arteriovenous fistula, 538–539, 541f
background, 528–529
biopsy, 457–458
ciclosporin toxicity, 536, 539
combined renal and pancreatic transplantation, 541
complications
early, 532–536, 536b
late, 537–541, 540b, 541t
contraindications, 529
delayed function, 532–533, 533f, 533t
development of, 528
donor supply, 529
Doppler imaging, 467–468
haemorrhage, 535
histocompatibility testing, 529
hypertension in, 477
imaging the transplanted kidney, 530–532, 530f–531f
immunosuppression, 529–530
indications, 529
infection, 536
malignancy in, 541, 544f
post-transplant collections, 535–536, 536f–537f
preoperative management, 529
recurrent disease, 540
rejection, 532, 539–540, 542, 542f
renal artery stenosis, 546
renal masses, 546
renal vein thrombosis, 478–479
surgery, 529, 530f
tacrolimus toxicity, 536, 539
transplant artery stenosis, 537–538, 537t, 538f–540f
ureteric obstruction, 535
ureteric stenosis, 537
urinary leak, 535
urinary tract infection, 540, 543f
use of micro-bubble contrast agents, 542–547, 546b
vascular occlusion, 546, 547f
venous thrombosis, 534–535, 535f, 535t
Renal veins, 413–414, 417–418, 417f, 422
anatomy, 469
colour flow map, 469
occlusion, 447–448
renal cell cancer propagation into, 480
in renal transplantation, 532
thrombosis, 447–448, 478–480, 480b, 480f, 534–535, 535f, 535t, 1454–1455, 1456f
acute, 479, 480f
chronic, 478–479
Doppler ultrasound appearances, 479–480
greyscale ultrasound appearances, 479
symptoms, 478–479
Renin, 473
Reninoma, renal, 512
Renovascular hypertension, 473–477
see also Renal arteries, stenosis
Resistance index (RI), 476
cervical lymph nodes, 932
erectile dysfunction, 624–625
hypoxic ischaemic encephalopathy, 1266–1269
pelvi-ureteric dilatation, 441, 441f
peripheral arterial disease, 1199–1200
renal arteries, 422
renal transplantation, 532–533
in rheumatological ultrasound, 1132–1133
Resolution, 14–15
Resonance, 7–8, 8b
Retained products of conception (RPOC), 696, 711–712, 712f
ultrasound diagnosis, 765–766, 766f
Retention cysts, 583t
Rete testis, 595, 597–598, 597f–598f
dilatation, 606–607, 606f
Retina, 940, 941f, 943–948
acquired retinoschisis, 947–948, 948f
detachment, 943–947, 944f
choroidal detachment, 946, 947f
conditions mimicking, 947b
exudative, 946
non-rhegmatogenous, 946
posterior vitreous detachment, 944–945, 945f
proliferative vitreoretinopathy, 945–946, 946f
rhegmatogenous, 944
traction, 946–947, 947f
vitreoretinal traction, 944–945, 944f–945f
disciform lesions, 948, 948f
drusen (hyaline bodies), 948, 948f
haemorrhage, 952
tear, 944–945, 945f
Retinacula-related disorders, wrist, 1059–1063
Retinoblastoma, 954–955, 955f
Retinoschisis, acquired, 947–948, 948f
Retrograde ejaculation, 580t
Retrohyaloid haemorrhage, 949–950, 950f
Retrolental fibroplasia, 955, 955f
Retromandibular vein, 896f, 898–900
Retroperitoneal space, 817, 818f
Retroperitoneum, 816–824
abscesses, 821, 823, 823f–824f
anatomy, 816–818, 818f
cysts, 821, 822f
fat, 818, 819f
fibrosis, 823–824, 825f
fluid collections, 821–823, 822t, 823f–825f
general appearances, 818–819, 819f
haematoma, 821–822, 825f
lymphadenopathy, 819, 819f
scanning techniques, 818–819
tumours, 819–821, 819b, 820f–821f, 820t
Retropharyngeal infection, 1304
Reverberations, 67–68, 68b, 69f
simple renal cysts, 487, 487f
Rhabdoid tumour, 1462
Rhabdomyosarcomas, 1121
biliary, 1374f
bladder, 562
in children, 1312, 1353, 1353f
female lower genital tract, 1488, 1489f
orbital, 962, 962f
prostate gland, 589t
spermatic cord, 611
testicular, 1494
urinary tract, 1462, 1463f
vaginal, 716, 717f
Rheumatoid arthritis, 1040f
Rheumatoid nodules, 1117, 1131, 1133, 1133f
Rheumatoid vasculitis, 379t
Rheumatological disease, 1126–1136
see also specific diseases
Rhombencephalon, fetal, 746, 746f
Ribs
bifid, 1509f–1510f
cartilaginous abnormalities, 1353–1354
dislocation, 1006–1007
fissures, 1006–1007
fracture, 1006–1007, 1006f, 1353–1354, 1354f
metastases, 1005–1006, 1006f
normal appearances, 1006–1007, 1007b
Riedel's lobe, 96, 97f
Riedel's thyroiditis, 884
Right ventricular dysfunction, hepatic venous waveforms in, 195
Rokitansky-Aschoff sinuses, 247
Rokitansky nodule, 674–675
Rotator cuff
anatomy, 1030, 1031f
disease, 1039b
interval, 1030
post-repair, 1035–1036

tears
full thickness, 1033–1035, 1034f–1035f
partial thickness, 1035, 1035f
Rubella, 1273

S

Sacrococcygeal tumours, 1333, 1334f
Safety, 51–60
British Medical Ultrasound Society (BMUS) guidelines, 57–58
cavitation, 54–56
epidemiology, 56–57
European Federation of Societies of Ultrasound in Medicine and Biology (EFSUMB), 58
Food and Drug Administration (FDA), 51, 57, 57t
gas body effects, 54–56
hazard indication, 54
regulations and guidelines, 57–59
thermal effects, 52–54
World Federation for Ultrasound in Medicine and Biology (WFUMB), 58–59
Sagittal band, 1055
rupture, 1062–1063
Sagittal sinus thrombosis, 982–983
Saline
breast implants, 1000
as a contrast agent, 77, 78f
Saline infusion hysterography, 700–702, 701f, 704, 706, 727–728, 727f–728f
complications, 728
method, 727–728
rationale, 727
Salivary glands
in children, 1307–1309
tumours, 1308–1309, 1309f
see also Parotid glands; Sublingual glands; Submandibular gland
Salmonella colitis, 401
Sandwich sign, 384, 385f, 817f
Santorini duct, 286
Saphenofemoral junction, 1242, 1243f
Saphenopopliteal junction, 1242
Sarcoidosis
cervical lymph nodes in, 934
liver involvement, 132, 133f, 150
parotid gland involvement, 904
prostate gland in, 589t
spleen in, 343, 343f
testicular, 604, 604f
Sarcomas
abdominal wall, 806
bony, 1512
in children, 1362, 1362f
clear cell, 1462, 1463f
Ewing's, 1110f
Kaposi's, 1121
prostate gland, 589t
renal, 521
retroperitoneal, 820, 820f
size and shape, 1110
soft tissue, 1512
synovial, 1124
thyroid, 879
undifferentiated embryonal, 1362, 1362f
uterine, 695, 695f
Sartorius, 1073, 1074f
Scalenus anterior muscle, 911–912
Scanners
application set-ups, 33–34
output power, 34
patient type/frequency, 33
controls, 31–32, 32f
general controls, 32
keys, 32
nomenclature, 31–32
variation in, 31–32
see also specific types
Scapholunate ligament (SLL), 1056–1057, 1063, 1063f
Scarpa's fascia, 621
Scattering, 9–10, 10b, 10f, 10t, 61–63, 62f
Schistosoma haematobium, 464–465, 561–562
Schistosoma intercalatum, 128
Schistosoma japonicum, 128
Schistosoma mansoni, 128, 129f
Schistosoma mekongi, 128
Schistosomiasis
liver, 128, 129f
renal, 464–465, 1453–1454
Schizencephaly, 1282, 1282f
Schwann cells, 1158
Schwannomas, 1066, 1119, 1119f, 1164–1165, 1165f
cervical, 911, 911f
extra-testicular, 611
neonatal, 1333
optic nerve, 962, 963f
parotid gland, 901–902
retroperitoneal, 819–820
tibial nerve, 1105
Sclera, 938, 940f
Sclerosing cholangitis, 216, 267, 267f
Sclerosing lesions, complex, 992–993
Sclerosing peritonitis, 455, 455f
Screening
breast cancer, 999–1000
endometrial cancer, 705
renal artery stenosis, 474–475, 474t–475t
renal cell carcinoma, 513
Wilms' tumour, 1459–1461
Scrotal pearl, 611–612, 612f
Scrotal sac
anatomy, 594
normal ultrasound appearance, 595–598
vascular anatomy, 594–595
Scrotal wall abnormalities, 618, 618f
Scrotum
acute, 612–618, 614t
paediatric, 1492–1493
Fournier's gangrene, 618, 618f
involvement in systemic disease, 1494
tumours, 1493–1494, 1494f
Sebaceous cysts, 989, 989f
Second harmonic imaging, 81–82, 82f
Secretin-stimulated ultrasound, pancreas, 304
Seldinger drainage technique, 804f, 816
Semen analysis, subfertility assessment, 735
Semimembranosus tendon, 1084, 1086f
Seminal vesicles, 574
blood supply of, 574
in children, 1409, 1415f
distension, 584, 584f
injection of contrast, 591
normal size, 576–578
normal sonographic appearances, 576–579, 579f
ultrasound technique, 1409, 1415f
Seminiferous tubules, 594
Seminoma, 599, 608f
Semitendinosus tendon, 1084, 1086f
Sentinel node biopsy, 998
Sepsis, anal, 408, 408f
Septa of Bertin, 420–421, 420b, 421f
Septations
gallbladder, 1375
ovarian, 664, 665f
pleural effusion, 1013, 1013f
in pleural fluid, 1009–1010, 1010f
renal cysts, 488
uterine, 657, 659f
vagina, 716, 1473
Seromas, 805
post-traumatic, 1115
Serous cystadenocarcinoma, ovarian, 671–672, 671f
Serous cystadenoma, 311–312, 311f
ovarian, 671–672, 671f
Sertoli cell tumour, 601
Sertoli-Leydig cell tumours (androblastoma), 678
Sesamoid bones, 1096, 1097f, 1106–1107
Sesamoiditis, 1106–1107
Sex cord stromal tumours, 677–678, 1487, 1487f
Sexual cycle, female, 649, 650f
Sexual differentiation, 1468
disorders, 1473–1478, 1478t
Sexual maturation disorders, 1478–1481, 1480b
Shadowing, 64f, 88, 88f
edge, 65, 66f
gallstones, 237, 237f–238f
and increased sound transmission, 64–65, 64f, 65b
reflective, 65f
refractive, 65, 66f
types of, 64t
Shaken baby syndrome, 1287
Shaken impact syndrome, 1330
Shear waves, 13
Short saphenous vein, 1228, 1242, 1243f
bypass grafts, 1207–1208
Shoulder, 1030–1042
acromioclavicular joint, 1039–1040, 1040f
anatomy, 1030, 1031f–1033f
biceps tendon pathology, 1037–1039, 1039f–1040f
bursitis, 1036–1037, 1036f
calcific tendinitis, 1037, 1037f–1038f
degeneration, 1033, 1034f
fracture, 1041, 1041f
frozen, 1037, 1038f
full thickness tears, 1033–1035, 1034f–1035f
glenohumeral joint, 1040–1041, 1040f–1041f
impingement, 1032–1033, 1033f, 1036b
interventional techniques, 1170–1173
joint injection, 1172–1173, 1174f
partial thickness tears, 1035, 1035f

post rotator cuff repair, 1035–1036
suprascapular nerve palsy, 1037, 1038f
technique, 1030–1032
Sialectasis, juvenile, 1308, 1308f
Sialoadenitis, 897, 897f, 904, 905b
Sialolithiasis, 895–897, 1308
Sialosis, 906
Sickle cell disease, 453
Side holes, 813–815
Sigmoid colon, 394–395
Sildenafil, 622–623
Silicone breast implants, 1000
Silicone granulomas, 1000, 1000f
Sinuses, spinal, 1328–1330
Sinus tarsi syndrome, 1105
Sipple's syndrome, 929
Sirolimus, 529–530
Sister Joseph's nodule, 806
Sjögren's syndrome, 904, 904f
Skeletal muscle *see* Muscle(s)
Skier's thumb, 1063–1064
Skin tags, spinal, 1328–1330, 1330f
Slice thickness, 21, 22f
Slipped femoral capital epiphysis, 1504–1505, 1505f
Small bowel, 369–387
abnormal ultrasound appearance, 371, 371b
adenocarcinoma, 380, 381f
altered blood flow, 371
anisakiasis, 379
blood supply, 371
carcinoid tumours, 381, 382f
in children, 1388–1395
masses, 1394–1395, 1395b
normal anatomy, 1388
obstruction, 1388–1391, 1388f, 1391b
wall thickening, 1392–1394, 1393b
coeliac disease, 385
Crohn's disease *see* Crohn's disease
duplication cysts, 816
extramural changes, 371
gastrointestinal stromal tumours, 381, 383f
haemorrhage, 1393
ileocaecitis, 377, 377f
infections, 376–379
intussusception, 384, 385f
ischaemia, 379, 379t
layers, 370
lipoma, 381
liver transplantation complications, 221
lumen, 371
lymph nodes, 371
lymphoma, 381, 382f–383f, 1394–1395, 1395f
malrotation, 1389–1390, 1391f
mesenchymal tumours, 381
mesenteric lymphadenopathy, 371
metastases, 381, 384f
mobility, 371
normal ultrasound appearance, 370–371, 370b, 370f
obstruction, 384, 386f, 1388–1391, 1388f, 1391b
peristalsis, 371
plasticity, 371
secondary malignancies, 381, 384f
technique, 369–370, 370b, 370f
tuberculosis, 377, 377f–378f
tumours, 380–381, 384b
ultrasound-guided biopsy, 385, 386f
vasculitis, 379–380, 379t, 380f
wall
layers, 371–373
thickness, 371–372
Soft tissue infections, paediatric, 1508, 1509b
Soft tissue masses, 1109–1125
benign, in children, 1350–1352
biopsy, 1191–1192, 1191b, 1192f
bursae, 1115–1116
calcification, 1111–1113, 1113b, 1113f
cysts, 1115–1116, 1116f (*see also* Cysts)
echo pattern, 1111
ganglion, 1116, 1116f (*see also* Ganglion cysts)
inflammatory, 1116–1117, 1117f
location, 1110, 1111b
malignant, in children, 1353
margin, 1111, 1111b, 1112f
paediatric, 1509–1512, 1512f
pseudo-masses, 1113–1114, 1114f
size and shape, 1110, 1111f
tissue density/compressibility, 1113, 1113f
of traumatic origin, 1114–1115, 1115f
tumour-like, 1113–1117
tumours, 1117–1124
extraskeletal osseous, 1124
fibrous and fibrohistiocytic, 1121–1123
lipomatous, 1117–1119
muscle, 1121
nerve tumours and tumour-like lesions, 1119–1120
synovial, 1123–1124
vascular, 1120–1121
ultrasound technique, 1109b–1110b, 1110–1113, 1110f–1111f
vascular, 1117, 1118f
vascularity, 1113, 1114f
see also specific masses
Soft tissue thermal index (TIS), 54
Soleus muscle, 1093
accessory, 1143
Solid pseudopapillary neoplasm, 312
Solitary fibrous tumour, prostate gland, 589t
Sonavist, 140
Sonazoid, 79t, 80
Sonication, 77
Sonoporation, 87
SonoVue, 79, 79t, 80f, 288, 291f
Space-occupying lesions, neonatal, 1284
cysts, 1284
neoplasms, 1284, 1285f–1287f
vascular malformations, 1284, 1288f
Specimen handling, 852–853, 853f
Speckle, 6–7, 7f, 75
Spectral broadening, 476
Spectral (duplex) Doppler
abdominal aorta atherosclerosis, 788
aortic dissection, 789
arteriovenous fistula, 481
carotid arteries, 967–968
hepatic vein occlusion, 195
main renal artery trunks, 471–472
ovarian lesions, 670
parameters, 32, 44–49, 50b
angle correction, 45–46, 46f
angle correction errors, 49, 50f
beam/flow angle, 45–46, 46f
gain, 46, 47f
high pulse repetition frequency, 46–48, 48f
invert, 46, 47f
power, 46
sample volume/gate size, 48, 48f
scale, 46–48, 48f
sweep, 49, 49f
velocity, 49, 50f
wall filter, 49, 49f
peripheral veins, 1229, 1230f
portal vein, 179, 201
priapism, 627
renal cell carcinoma, 513
renal transplantation, 530–532
scanners, 32, 50b
Specular interfaces, 61–63, 62f, 64b
Speed of ultrasound, 4, 4t
Spermatic cord, 594–595, 596f
haemangioma, 610, 611f
lipoma, 609, 610f
liposarcoma, 611
rhabdomyosarcoma, 611
spontaneous de-torsion, 617
torsion, 612–614, 616–617, 617b, 617f, 1492–1493
Spermatoceles, 608, 609f
Sperm granuloma, 608–609, 610f
Spigelian hernias, 804, 1081, 1081f
Spina bifida aperta, 1322
Spina bifida cystica, 1322
Spinal arteries, 1320
Spine
infant, 1315–1336
anatomy, 1316–1322
cervical region, 1320
coccygeal region, 1318
conus, 1319–1320
extraspinal, 1316, 1316f
intraspinal, 1318–1320, 1318b
lumbar region, 1318, 1318f–1319f
sacral region, 1318
spinal, 1316–1318, 1316f–1318f
thoracic region, 1319–1320, 1319f–1321f
vascular structures, 1320–1322, 1321f
contraindications for ultrasound, 1316
embryology, 1322
indications for ultrasound, 1316, 1316b
lipoma, 1322–1324, 1323f
spinal dysraphism, 1322–1330
closed, 1322–1330, 1322b
open, 1322, 1322b
technique, 1315–1316
trauma, 1330–1332, 1331f
tumours, 1332–1334, 1333f–1334f
ultrasound versus magnetic resonance imaging, 1316
vascular anomalies, 1332, 1332f–1333f
Splanchnic arteries, 789–792, 790f–791f
aneurysm, 791–792, 791f
stenosis, 789–791, 791f
Spleen, 324–347
abscess, 338–340, 339f–340f
accessory, 328–329, 328f–329f

in AIDS, 343
anatomical variants, 1356–1357
anatomy, 324–325, 325f
angiosarcoma, 334, 336f
biopsy, 345
calcifications, 343, 344f, 344t
in children, 1356–1357, 1357f, 1357t, 1377–1381, 1380b
clefts, 327, 328f
contrast imaging, 85, 86f
contusion, 837–838
cysts, 337–340, 338t, 339f, 341f, 344
contrast imaging, 86f
echogenicity, 326–327
embryology, 324–325
enlarged *see* Splenomegaly
examination technique, 325–326
focal lesions, 331–343
differential diagnosis, 343–344
function, 324
haemangioma, 334, 336f–337f
haematoma, 837–838
hamartoma, 337, 338f
heterotaxy syndrome: polysplenia and asplenia, 330, 331f
infarction, 340–342, 341f, 342t, 838
infection, 338–340, 340f
laceration, 837–838
lymphangioma, 337, 338f
lymphatic drainage, 324–325
lymphoma, 331–334, 334b, 334f
metastases, 334, 335f
microstructure, 324–325
normal ultrasound findings, 326–327, 326f–328f
notches, 327
peliosis, 340
pseudocysts, 338, 339f
red/white pulps, 325
sarcoidosis, 343, 343f
septation, 327, 328f
size, 327, 327b
in children, 1380
splenosis, 328–329, 330f
spontaneous rupture, 343, 344f
trauma, 837–838, 844
classification, 837–838, 838t
general considerations, 837
mechanisms of injury, 837–838, 838f
ultrasound findings, 838, 839f
tumours, 331–337
ultrasound interventions, 345
vascular lesions, 340–342, 342b
wandering, 329, 330f, 1356–1357
Splenectomy, 324
Splenic artery, 324–325
aneurysm, 342, 342f, 791–792, 791f
pseudoaneurysms, 342
splenic infarction, 340–342
Splenic humps, 420, 420b, 420f
Splenic vein, 324–325
aneurysm, 342
thrombosis, 342, 343f
Spleno-gonadal fusion, 603, 603f
Splenomegaly, 331
causes of, 332f, 332t
in children, 1380, 1380t
in portal hypertension, 182
Splenorenal fusion, 505–507
Splenorenal varices, 183, 185f, 342, 343f
Sportsman's hernia, 804–805
Spring ligament, 1097, 1097f, 1104
Squamous cell cancer (SCC)
bladder, 561–562
cervical lymph nodes in, 928, 931f
penile, 628–629
Staghorn calculi, 430, 431f
Standing waves, 7–8, 8f
Staphylococcus aureus
breast abscess, 989
cellulitis, 1352
liver abscess, 124
olecranon bursitis, 1050
parotitis, acute, 1307
renal abscess, 496
Staphylococcus spp., post-renal transplantation, 536
Starry-sky appearance, 120–121, 121b, 122f
Steal syndromes, 1222, 1223f
Steatohepatitis, non-alcoholic (NASH), 110–111, 111f
Steatosis
in children, 1359–1360, 1359f–1360f
hepatic *see* Fatty liver
Stener lesion, 1063–1064, 1064f
Stensen's duct, 900
Stents, peripheral arterial disease, 1210
Step ladder sign, breast implants, 1000, 1000f
Sternocleidomastoid tumour, 1511, 1511f
Sternomastoid tumour of infancy, benign, 1302, 1303f
Steroid injections, 1169–1170
Steroid therapy, 529–530
Stimulated acoustic emission (SAE), 83–84
Stomach
anatomical structure, 352
bezoar, 1387, 1387f
cancer, 360, 362f
early/late diagnosis, 360
staging, 353–354, 360
carcinoid tumours, 362, 364f
in children, 1384–1387, 1388b
masses, 1386–1387
obstruction, 1385–1386
technique and normal anatomy, 1384–1385
wall thickening, 1386
duodenum, 365, 366f
duplications, 1386–1387, 1387f
endoscopic ultrasound, 352–353, 360–365
hypertrophic folds, 362
lipoma, 362, 363f
lymphoma, 360, 362f
peptic ulcer disease, 365
polyps, 360–362, 363f
submucosal lesions, 362
teratomas, 1387
tumours, 1387, 1388f
varices, 183, 363–365, 365f–366f
Stones *see* Calculi; *specific anatomical areas*
Streptococcus milleri, 124
Streptococcus spp., cellulitis, 1352
Stress fractures, ankle, 1105–1106
Stress testing, peripheral arterial disease, 1199
String of beads sign, pelvic inflammatory disease, 682
Stroke, 965
haemorrhagic, 982–983
ischaemic, 982–983
transcranial Doppler ultrasound, 980–982
Student's elbow, 1050, 1051f
Stump appendicitis, 394, 394f
Subacromial/subdeltoid bursa, 1030, 1036–1037, 1036f
effusions, 1040–1041, 1040f
injection, 1170–1172, 1171f
Subarachnoid haemorrhage, 982, 982f
Subclavian artery, 1212–1213
occlusion, 1217f
stenosis, 1214
Subclavian steal syndrome, 1213–1214, 1217f
Subclavian vein, 1241, 1241f
Subdural collection, 1273, 1275f
Subdural effusions, 1273, 1275f
Subdural haematoma, 1285
Subdural haemorrhage, 1285
Subfertility, 731b
causes of, 730–734, 731f
congenital uterine abnormalities, 731, 732f
endometrial polyps, 733, 733f
endometriosis, 730
hydrosalpinges, 733, 733f
osseous metaplasia of the endometrium, 732–733, 732f
polycystic ovaries/PCOS, 733–734, 734b, 734f
uterine fibroids, 731–732, 732b, 732f
Subharmonic imaging, 84
Subhepatic collections, 212, 212f
Sublingual glands, 891–893
Submandibular duct, 891–893, 892f, 895, 895f–896f
obstruction, 896–897, 897f
Submandibular gland, 894–895
calculi, 895–897, 896f
post-radiotherapy changes, 897
tumours, 897, 898f
Submandibular lymph nodes, 894, 922–923, 924f
Submental lymph nodes, 922, 923f
Submucosa, gastrointestinal tract, 352
Subretinal haemorrhage, 956–957
Subscapularis, 1030, 1031f
Subureteric transurethral injection (STING) procedure, 1422, 1427f
Sugiura procedure, 186
Sump drains, 813
Superficial inguinal ring, 802, 802f
Superior mesenteric artery (SMA), 94, 773, 789, 790f
hepatic artery arising from, 189
stenosis, 789–791
Superior oblique muscle, 959–960
Suppurative lymphadenitis, acute, 1304, 1305f–1306f
Suppurative lymph nodes, 929, 929f
Supraclavicular fossa, 911–912
normal ultrasound anatomy, 911–912
pathology, 912
technique, 911–912
Supracondylar process, humerus, 1160
Suprapatellar recess, 1084
Suprapubic catheterisation, 569

Suprascapular nerve palsy, 1037, 1038f
Supraspinatus, 1030, 1031f–1032f
  barbotage of calcific tendinopathy, 1172, 1172b, 1172f
  rupture, 1035, 1035f
Sural nerve, 1095
Suspensory ligament, 941
Sutures, cranial *see* Cranial sutures
Symphysis pubis, 1081–1082, 1081f
  injection, 1082, 1180–1181
Synchysis scintillans, 949
Synchysis senilis, 944–945
Synechiae, intrauterine, 709, 711f
Synovial cysts, 1115
Synovial osteochondromatosis, 1047–1048, 1048f, 1123, 1123f
Synovial sarcoma, 1124
Synovial tumours, 1123–1124
Synovitis
  ankle, 1104, 1104f, 1107
  elbow, 1047, 1047f
  localised pigmented villonodular, 1066, 1067f
  ultrasound features of, 1127–1128, 1128b, 1128f
Syringomyelia, 1328, 1329f
Systemic lupus erythematosus, 379t, 453, 453f
Systolic acceleration time (SAT), 207–208

T

Tacrolimus, 529–530, 536, 539
Takayasu's arteritis, 1214, 1218f
Tamm-Horsfall proteinuria, 1443, 1443f
Tamoxifen, 706, 707f
Tampons, retained, 715–716
Tapeworm, 129
Tardus parvus waveform, hepatic artery, 206–208
Targeted contrast microbubbles, 86–87
Tarsal tunnel syndrome, 1105
Tear, 944–945
Technique, 1253–1254
Temporal resolution, 15
Tendinitis
  biceps, 1039
  calcific, 1037, 1037f–1038f
Tendinopathy, 1025, 1026f
  calcific, 1172, 1172b, 1172f
Tendinosis, 1025, 1026f
  ankle, 1107b
  triceps, 1048–1049, 1049f
Tendons, 1027–1028, 1027f–1028f, 1028b
  disease, ultrasound features of, 1130–1131, 1131b, 1131f
  neovascularity, 1025, 1025b
Tendon sheath injection, 1175–1176, 1177b, 1178f
Tennis elbow, 1049, 1050f
Tennis leg, 1089, 1151, 1151f, 1153, 1153f
Tenon's capsule, 938
Tenosynovitis, 1130, 1131f
Tensor fascia lata, 1072–1074, 1074f
Teratocarcinoma, testicular, 600, 601f
Teratomas
  gastric, 1387
  immature ovarian, 676
  mature ovarian, 674–676, 674f–677f, 676b
  mediastinal, 1347, 1347b
  mesenteric, 1402–1403
  ovarian, 674–676, 674f–677f, 676b, 1487–1488
  retroperitoneal, 819–820
  sacrococcygeal, 1333, 1334f
  testicular, 599–600, 601f
Teres minor, 1030
Terjesen technique, 1503
Terminal ileum, 369–370
  acute, 1393
  in children, 1393
Terson's syndrome, 950
Testicular artery, 594–595, 597f
Testicular veins, 594–595
Testis
  abscess, 604, 605f
  adrenal rest cells, 603, 603f
  anatomy, 593–595, 594f, 595b, 1490–1491
  appendage torsion, 617, 618f, 1493, 1493f
  artefacts, 595–598
  atrophy, 607, 607f
  carcinoma, 598–599
  choriocarcinoma, 600
  congenital anomalies, 1491–1492
  cystic dysplasia, 607, 1492
  cysts, 605–606, 606f
  embryology, 593–594
  embryonal cell carcinoma, 600
  epidermoid cyst, 602, 603f
  focal lesions
    neoplastic, 598–602, 599t
    non-neoplastic, 602–607
  germ cell tumours, 599–600, 600f–601f, 1494
  gonadal stromal tumours, 600–601
  haematoma, 604–605, 605f
  inguinal, 1491, 1491f
  intra-testicular abnormalities, 598–608
  leukaemia, 602, 602f, 1494
  Leydig cell tumour, 601, 601f, 1494
  lymphoma, 601–602, 602f, 1494
  macrocalcification, 607–608, 608f
  metastases, 602, 602f
  microlithiasis, 607–608, 608b, 608f, 1492, 1492f
  normal ultrasound appearance, 595–598
  normal variants, 595–598
  orchitis, 604, 605f
  paediatric, 1490–1494, 1494b
  post-biopsy, 605
  postoperative, 605
  prosthesis, 607, 607f
  rhabdomyosarcoma, 1494
  sarcoidosis, 604, 604f
  segmental infarction, 603, 604f
  Sertoli cell tumour, 601
  size, 595, 596f
  spleno-gonadal fusion, 603, 603f
  spontaneous de-torsion, 617
  teratocarcinoma, 600, 601f
  teratoma, 600, 601f
  torsion, 616–617, 617b, 617f, 1492–1493, 1493f
    congenital, 1491–1492
  trauma, 615–616, 616f, 1493, 1494f
  tumours, 1494, 1494f
  two-tone, 597, 597f
  ultrasound examination technique, 593, 594f, 1490
  vascular anatomy, 594–595, 595f
  venous infarction, 614–615, 614f
  yolk sac tumour, 600, 600f
Tethered cord syndrome, 1324–1325, 1325b, 1325f
Thalamus, 1257
Theca lutein cysts, 667, 764, 764f
Thecoma, ovarian, 678, 679f
Thelarche, 1470
  isolated premature, 1481, 1481f
Thermal effects of ultrasound, 52–54
  experimental investigation of heating, 52–53
  heating mechanisms, 52, 52t
  implications of heating, 53–54
  World Federation for Ultrasound in Medicine and Biology (WFUMB), 58
Thermal index (TI), 34, 52–54, 54b
  bone-at-focus, 54
  British Medical Ultrasound Society (BMUS) guidelines, 57–58
  cranial bone, 54
  hazard indication, 54
  soft tissue, 54
  use of during ultrasound examination, 54
Thermography, 1227
Thigh muscles, 1141, 1143t, 1144f
Thoracic outlet syndrome, 1213–1214
Thoracic ultrasound, 1005–1021
  see also specific anatomical areas
Thoracoscopy, 1013–1014
Three-dimensional scanning
  artefacts, 75
  bladder cancer, 562–563
  cervical cancer, 714
  endometrial cancer, 704
  eye, 943
Thrombin injection
  oesophageal varices, 359, 360f
  pseudoaneurysms, 301
Thrombolysis, 980–982
Thrombolysis in Brain Ischaemia (TIBI) classification, 980
Thrombosis
  calf vein, 1233, 1233f
  haemodialysis access, 1222
  hepatic artery, 205–207, 206f–207f, 219–220, 219f
  hepatic veins, 194–195, 196f (*see also* Budd-Chiari syndrome)
  inferior vena cava, 792, 793f
  internal jugular vein, 1304
  jugular veins, 908–909, 910f–911f
  neonatal brain, 1270–1272, 1272f
  portal vein, 188–189, 188b, 188f–191f, 201, 220, 220f, 1365–1366, 1366f
  renal artery, 533–534, 534f, 1455, 1457f
  in renal cell carcinoma, 513–517
  renal vein, 447–448, 534–535, 535f, 535t, 1454–1455, 1456f
  sagittal sinus, 982–983
  splenic vein, 342, 343f
Thymic cysts, 1298–1299

Thymus, 884, 914, 916f
anatomy, 1338, 1338f
in children, 1338–1339, 1338f, 1340f
ectopic, 1340f
Thyroglossal duct cysts, 893, 914–917, 917f
in children, 1294–1295, 1295f
Thyroid gland, 867–884
abscess, 1310, 1310f
adenoma, 1310–1312, 1312f
anatomy, 867, 868f
carcinoma, 1312
in children, 1309–1312
cysts, 1309, 1310f
diffuse disease, 1310
diffuse parenchymal diseases, 882–884
ectopic, 1309
ectopic tissue, 894, 894f
embryology, 868–869
focal lesions, 1310–1312
goitre *see* Goitre
malignant tumours, 873–882
anaplastic carcinoma, 879–880, 880b, 880f
follicular neoplasm, 876–878, 877b, 877f–878f
incidentalomas, 881–882
lymphoma, 880–881, 880b, 880f
medullary carcinoma, 878–879, 879b, 879f, 929
metastases, 881, 881b, 881f
papillary carcinoma, 873–876, 874f–877f, 875b, 928, 929f, 933
nodular disease, 869–872
colour and power Doppler, 872
comet tail sign, 872, 872f
echogenicity, 870
elastography, 872
generic ultrasound features of nodules, 869
interval growth of nodule, 872
investigative strategies for, 881–882
margins, 870–871
multiple, 882, 882b
nodule size, 869
patterns of calcification, 870, 871f
shape: tall versus wide, 871–872
solid/cystic nodules, 870, 870f
solitary versus multiple nodules, 869–870, 869f
ophthalmology, 960–963, 960f
sarcoma, 879
scanning technique, 867
thyroiditis *see* Thyroiditis
ultrasound features of adjacent structures suggestive of thyroid carcinoma, 872–873, 873f
Thyroiditis, 882–884
acute suppurative, 884, 1310, 1310f
classification, 882, 883t
de Quervain's, 883–884, 884f
general ultrasound appearance, 883
Hashimoto's, 880, 883, 883f
Riedel's, 884
Tibial artery
calcification, 1207f
stenosis, 1205f, 1206–1207
Tibialis anterior, 1097–1098, 1098f
Tibialis posterior, 1096, 1096f, 1103–1104, 1103f–1104f
Tibial nerve
neuroma, 1105
posterior, 1096
schwannoma, 1105
Tibial veins, 1232
Tibiofibular joint
aspiration and injection, 1187
proximal, 1091
Tibiofibular ligaments, 1099, 1099f
Tibionavicular ligament, 1097
Tibiotalar joint injection, 1187
Tibiotalar ligament, 1097
Tight filum terminale syndrome, 1324–1325, 1325f
Time gain compensation (TGC), 23
Time sampling artefacts, 74–75, 74b
Tinel sign, 1119
Tip of the iceberg sign, mature teratomas, 674–675, 675f
Tissue absorption, heating due to, 52–53
Tissue characterisation, 12–13, 12f
TNM staging
bladder cancer, 563, 563b
upper gastrointestinal tract cancer, 353–354, 355t
Tongue, 893f
Topical anaesthesia, paediatric hip aspiration, 1183
Toxocara canis, 129
Toxocara catis, 129
Toxocariasis, 129, 955
Toxoplasmosis, 1273, 1274f
Trachea, 914
Trachelectomy, 697–700
Traction retinal detachment, 946–947, 947f
Tranexamic acid, 689
Transabdominal ultrasound
bladder, 551, 552f, 562
cancer, 563
female pelvis, 645–646, 646b, 649–651, 650f–651f
neuroendocrine tumours, 314
pancreas, 286–288, 287f–291f
uterus, 686–687
Transcranial Doppler ultrasound
anatomy, 976–977
aneurysms, 982
applications, 979–983
arteriovenous malformations, 982
carotid arteries, 976–983
examination technique, 977–978
pulsed, 978, 978f
suboccipital window, 977
transorbital window, 977–978
transtemporal window, 977, 977f–978f
Transcranial imaging
British Medical Ultrasound Society (BMUS) guidelines, 58
contrast agents, 85
see also Transcranial Doppler ultrasound
Transducers, 8, 16, 32–33, 33f
aperture control, 21, 21f
array, 19f, 23b
curved, 19f, 20
curvilinear, 22, 22f
linear, 19f–20f, 20, 42, 43f
square, 22, 22f
steered, 20, 20f
stepped, 20, 20f
B-mode imaging, 17
construction, 18, 18b, 18f
elevation focusing, 21, 22f
endo-cavity, 19f
endoscopic ultrasound, 351
focusing, 21, 21f–22f
heating, 53
intraoperative ultrasound, 273–274, 274f
mechanical, 22–23
paediatric chest, 1337
pelvic region, 1069
3/4D, 21–22, 22f
Transient ischaemic attacks (TIAs), 965
Transient synovitis, hip, 1503–1504, 1504f
Transitional cell carcinoma (TCC)
bladder, 431, 517, 561–562
ovarian, 674, 674f
pelvi-ureteric dilatation, 433–434, 433f–434f
renal, 517–521, 519b
aetiology, 517–518
other tests, 519–520
patterns of spread, 520
staging, 520t
survival, 520t
symptoms, 518
treatment, 520–521
ultrasound findings, 518–519, 519f–521f
Transjugular intrahepatic portosystemic shunt (TIPS)
assessment of function, 186–187
complications, 186
occlusion, 188
portal hypertension, 186–188, 186f
pre-liver transplantation assessment, 203
stenosis, 187–188
Trans-mediastinal artery, 595, 597f
Transperineal scanning, anal canal, 405–406
Transrectal ultrasound (TRUS)
benign prostate hyperplasia/hypertrophy, 581, 582f
bladder, 551
cervical cancer, 714
-guided intervention, 587–591
haematospermia, 584–585
male infertility evaluation, 584
prostate, 574–576, 575f, 576b, 577f, 578b
biopsy *see* Prostate, biopsy
cancer, 566, 585, 586f, 588t
indications for, 576b
TRUS-guided intervention, 587–591
unusual abnormalities, 587, 589f, 589t
Transurethral resection of the prostate (TURP), 581, 582f
Transurethral ultrasound, 563–564
Transvaginal biopsy, 722–723, 722b, 723f–724f
complications, 723
method, 722–723
rationale, 722
Transvaginal scanning (TV)
anal canal, 405–406
bladder, 551, 566
in early pregnancy, 741
endometrial cancer, 704, 705f

female pelvis, 646, 646b, 651–652, 651f–652f
ovarian cancer, 680
transducer heating, 53
uterus, 686–687
Transverse colon, 394–395
Transverse tibiofibular ligament, 1099
Transversus abdominis, 1076
Transvesical ultrasound, 566
Trauma
abdominal *see* Abdominal trauma
abdominal wall, 801
anal, 408, 408f
bladder, 569, 569b
carotid arteries, 966
eye, 956–958, 956f–958f, 957b
foot, 1107
neonatal brain, 1285–1287
accidental injury, 1285
birth-related injury, 1285, 1289f
non-accidental injury, 1285–1287, 1289f–1290f
paediatric, 1505–1508, 1506b
pelvi-ureteric dilatation, 438
penile, 629, 629f
peripheral nerves, 1161–1163, 1162f–1164f, 1163b
renal, 838–841, 845, 845f
in children, 1457–1458, 1457f
classification, 839–840, 839t
general considerations, 838–841
mechanisms of injury, 839–840
ultrasound findings, 840–841, 840f–841f
soft tissue masses, 1114–1115
spinal, 1330–1332, 1331f
testicular, 615–616, 616f, 1493, 1494f
Triangle sign, 945–946, 946f
Triangular fibrocartilage complex (TFC), 1057, 1063
Triangular ligaments, liver, 93
Triceps tendon, 1045
rupture, 1049, 1049f
tendinosis, 1048–1049, 1049f
Tricuspid regurgitation, 195, 197f
Triggered imaging, 82–84
Trigger finger, 1060
Triploidy, 764, 765t
Trocar drainage technique, 815–816
Trochanteric bursal injection, 1184, 1185f
Troisier's sign, 926
Trousseau's syndrome, 909
Tubal ring, ectopic pregnancy, 754–755, 755f–756f
Tuberculosis
intestinal, 399–400, 399f, 399t
liver involvement, 132–133, 133f–134f
lymphadenitis, 1305–1306
Mantoux test, 1306
peritonitis, 812, 813f
prostate gland, 589t
pulmonary, 1015
renal, 463–464, 465b, 465f, 1453–1454
small intestine, 377, 377f–378f
Tuberculous lymph nodes, 929
Tuberous sclerosis, 502, 502b, 502f–503f, 509f
neonatal brain, 1282, 1283f
renal manifestations, 1441f
Tubo-ovarian abscess, 682, 683f
Tubo-ovarian complex, 682, 683f
Tubular necrosis, acute, 449, 451, 532, 542
Tubulo-interstitial disease, 484
Tumour ablation, 816–824
ablative energy, 816–818
brachytherapy, 806f
cryoablation, 803f, 821
focused ultrasound, 823–824
peri-procedural monitoring, 806f–807f
post-procedural imaging, 807f
procedural targeting, 806f
interstitial laser photocoagulation
microwave, 821–823
radio-frequency, 804f, 819–821
techniques, 818–819
tumour pathophysiology and its modification, 808f
Tumours
ablation *see* Tumour ablation
inferior vena cava obstruction, 793–794, 793f
pathophysiology and its modification, 861–862
pelvi-ureteric dilatation, 431–434
see also specific anatomical areas
Tunica albuginea, 594, 621, 661
calcification, 611–612, 611f
cyst, 606
Tunica vaginalis, 594
calcification, 611–612, 611f
cyst, 606
Turner's syndrome, 1477–1478, 1480f
Twinning, 747–748, 747f–748f, 747t, 748b
Twin peak sign, 747–748
Two-tone testis, 597, 597f
Typhlitis, 399t, 401, 401f

U

UK Collaborative Trial of Ovarian Cancer Screening (UKCTOCS), 680
Ulcerative colitis, 397, 399f, 1399
versus Crohn's disease, 397b
differential diagnosis, 399t
Ulnar artery, 1043, 1213
Ulnar collateral ligament, 1045, 1046f, 1063–1064
injury, 1051, 1051f
Ulnar nerve, 1045, 1045f, 1057
compression, 1141–1143
division, 1045
entrapment, 1052, 1052f
Umbilical hernias, 804, 1081
Umbilical vein varices, 183, 184f–185f
Uncinate process, 285–286
United Kingdom Small Aneurysm Trial Participants (UKSAT), 775
Upper limb
muscles, 1139–1141, 1140t, 1141f–1142f
vascular anatomy, 1240, 1240f
venous imaging, 1240–1241
Urachus
abnormalities, 1425–1427, 1431f
bladder, 559, 561f
cyst, 807
Ureteric jets, 441, 442f, 551, 553f
Ureteric JJ stent, 556, 559f
Ureteritis, 1449–1453
Ureteroceles, 436, 499, 558–559, 560f–561f
in children, 1422, 1424f
complications, 1422
ectopic, 559, 1422
orthoptic, 1422
prolapsed, 1425f
sonographic features, 1422
Ureteropelvic junction obstruction, 1428–1430, 1432f
Ureters, 551
calculi, 430
in children, 1409, 1413f, 1422–1428
development, 1407
duplex, 423, 559
megaureter, 1422, 1426f
obstruction, 1430–1433, 1433f
acute, 484
in renal transplantation, 535
stenosis, post-renal transplantation, 537
ultrasound technique, 1409, 1413f
Urethra
cancer, 565–566
in children, 1422–1428
development, 1407–1409, 1408f
normal sonographic appearance, 576
posterior urethral valve, 1422–1425, 1427f–1428f
sphincters, 574, 576
ultrasound, 629
Urethrography, 629
Urinary continence, male, 574
Urinary leak, renal transplantation, 535
Urinary tract dilatation, 1433–1434, 1434f
Urinary tract infection (UTI), 568
in children, 1446b, 1448–1453, 1453f
imaging protocols, 1453
lower, 1449–1453, 1453f
lower, 1449–1453, 1453f
post-renal transplantation, 536, 540, 543f
in pregnancy, 568
upper, 1448–1449
Urine
echogenicity, 556, 557f
flow
high, 555
intermittent, 556
low, 555–556
patterns, 555–556
rates, 555b
flowmetry, 554–555, 555f
Urinomas, 815–816, 823
post-hysterectomy, 697–698
post-renal transplantation, 535
Urogenital sinus, 1475–1476, 1479f
Urolithiasis, 1445–1446, 1446b, 1446f–1448f
Urology, intraoperative ultrasound, 280, 280f
Uropathy, obstructive, 1428–1433
Urothelial cancer *see* Transitional cell carcinoma (TCC)
Uterine artery, 649, 655, 656f
embolisation, 693–694
Uterine bleeding, abnormal *see* Vaginal bleeding, abnormal
Uterine tubes, 649, 653–654
Uterine vein, 649
Uterovesical pouch, 808–809
Uterus, 687f
anatomy, 648–649

arcuate, 657
arteriovenous malformation, 695–696, 696f, 711–712
bicornuate, 657, 658f–659f
blood supply, 649
caesarean section scars, 697, 698f
in children, 1468–1490
congenital abnormalities as a cause of subfertility, 731, 732f
developmental anomalies, 1473, 1475f, 1475t
didelphys, 657, 658f, 1473, 1477f
dilatation and curettage, 697, 697f
dysfunctional uterine bleeding, 688
in ectopic pregnancy, 753–754
embryology, 1468–1470
endometrium, 700–712
ablation, 697
anastrozole and, 706
Asherman's syndrome, 709
cancer, 702–705, 705b
aetiology, 702
diagnosis, 702–705, 702f–705f
management, 705
other investigations, 705
screening, 705
staging, 704–705, 706f, 706t
symptoms, 702
endometritis *see* Endometritis
haematometrium and related conditions, 709–711, 711f–712f
hormone replacement therapy and, 705–706
hyperplasia, 700, 700b, 700f, 700t
hysteroscopy, 688
intrauterine devices, 706–708, 707f–709f, 708b
intrauterine synechiae, 709
medications and, 705–706
normal, 699f, 700
oral contraceptive pill and, 705
polyps, 693, 700–702, 701f, 702b
postpartum uterus, 711–712, 712f
retained products of conception, 696, 711–712, 712f
tamoxifen and, 706, 707f
ultrasound anatomy, 652–653, 653b
fibroids *see* Fibroids
formation, 1470, 1470f
haemodynamics by Doppler imaging, 655
inversion, 691
leiomyosarcoma, 693, 693f
lipoleiomyomas, 695
lipoma, 695
lymphoma, 695
metastases, 695
myometrium, 689–700
adenomyosis *see* Adenomyosis
arteriovenous malformation, 695–696, 696f
fibroids *see* Fibroids
gestational trophoblastic disease, 696–697, 696f–697f
lipoma, 695
lymphoma, 695
malignant mixed Müllerian tumours, 695
metastases, 695
sarcoma, 695
ultrasound anatomy, 652
normal appearances, 1474f of developing, 1473
normal development, 1469f, 1474f, 1475t
in normal pregnancy, 753–754
postoperative, 697–700, 698b
postpartum, 711–712, 712f
retroverted, 694–695, 695f
round ligament of, 660
sarcoma, 695, 695f
scanning techniques, 686–688, 688f
septate, 657, 659f, 731, 732f
symptoms, 688–689
tumours, 1488
ultrasound anatomy, 652–653, 652f–653f
ultrasound technique, 1471
variation in age, 649, 649t
Uterus didelphys, 710, 711f

V

VACTERL syndrome, 1422
Vacuum-assisted biopsy, 1001–1002, 1001t
Vagina, 686–688, 715–716, 716b
abnormal bleeding *see* Vaginal bleeding, abnormal
adenocarcinoma, 716
anatomy, 649
calculi, 716
clear cell tumours, 1488
cysts, 716, 716f
developmental anomalies, 1473, 1475f, 1475t
discharge, 1490
endodermal sinus tumours, 1488
fibroids, 716
fluid-filled lesions, 709, 716f
foreign bodies, 715–716, 1490
formation, 1470, 1470f
gas in, 716
melanomas, 716
neonatal bleeding, 1490
normal development, 1469f
prolapse, 716
rhabdomyosarcoma, 716, 717f
septa, 716, 1473
solid lesions, 716
symptoms, 688–689
tumours, 716, 1488
Vaginal bleeding, abnormal, 688
causes, 689t
dysfunctional uterine bleeding, 688–689
intermenstrual bleeding, 688
management, 688–689
postcoital bleeding, 688
postmenopausal bleeding, 688
Valleculae, 913, 913f
Valsalva manoeuvre
peripheral vein imaging, 1234, 1234f
venous reflux, 1245
Varices
abdominal wall, 805–806
gastric, 183, 363–365, 365f–366f
oesophageal, 183, 359, 359f–360f
orbital, 960
pancreatico-duodenal, 183
pericholecystic, 183
porta hepatis, 183
portosystemic collaterals, 181, 183f–185f
splenorenal, 183, 185f, 342, 343f
umbilical vein, 183, 184f–185f
Varicoceles, 612, 613f
paediatric, 1492, 1492f
and renal cell carcinoma, 513
Varicose veins, 1117, 1118f, 1246
Varicosities, tibial vessels, 1105
Vascular disorders/lesions
in children, 1299–1302, 1301b
renal, 447–449, 467–485
spinal, 1332, 1332f
Vascular malformations
buccal region, 906, 907f
in children, 1301–1302, 1301f, 1351
paediatric, 1510
Vascular soft tissue masses, 1117
Vascular supply *see* Blood supply
Vascular tumours, 1120–1121
intermediate, 1121
malignant, 1121
Vasculitis
renal, 484, 1443
small bowel, 379–380, 380f
Vas deferens, 574, 579f
Vasectomy, 608, 609f
Vastus intermedius, 1084
Vastus lateralis, 1084
Vastus medialis, 1084
Vein mapping, pre-arterial bypass, 1248–1249
Vein of Galen malformations, 1284, 1288f
Velocity error artefacts, 68–72, 70f, 70t, 71b
Velocity waveform analysis, 1199–1200, 1200f–1202f
Venography, 1227–1228
Veno-occlusive disease (VOD), 1366–1367
Venous incompetence, 1242–1248
anatomy, 1242–1243, 1243f
chronic venous insufficiency, 1243–1246, 1243t
treatments for, 1246–1248
Venous insufficiency, chronic, 1243–1246
background, 1243–1244
classification, 1243, 1243t
colour duplex examination, 1244
prevalence, 1243–1244
ultrasound technique, 1244–1246, 1244b, 1244f–1246f
venous reflux investigation, 1244
Venous malformations
buccal region, 906, 907f
in children, 1301, 1301f, 1351
Venous reflux
investigation, 1244
quantifying, 1245, 1247f–1248f
sources of superficial, 1246, 1248f
Ventricular index (VI), 1255, 1255t
Ventricular system, neonatal brain, 1255, 1255t
Ventriculitis, 1273–1274
Venturi effect, 475–476
Vertebral arteries, 966, 1259t
anatomy, 967, 976
indications for ultrasound, 965–966, 966b
normal and abnormal findings, 975, 976f

transcranial Doppler ultrasound, 976
ultrasound technique, 969, 969f
Vertebral bodies, 1316–1318
Vertebral steal, 975
Vesicoureteric reflux (VUR), 1422, 1427f
in children, 553
contrast imaging, 85
Vesico-uterine fistulae, 566
Vesico-vaginal fistulae, 566
Vessel sign, 1015, 1016f
Viral infections
hepatitis, 120–121, 121t, 122f
post-liver transplantation, 215–216
renal, 465b
see also specific infections
Virchow's node, 926
Visceral pleura, 1010–1011
Vitreoretinal traction, 944–945, 944f–945f
Vitreoretinopathy, proliferative, 945–946, 946f
Vitreous, 949–950
asteroid hyalosis, 949, 949f
haemorrhage, 950, 950f, 952, 956, 956f
persistent hyperplastic primary, 949, 949f, 955
posterior detachment, 949–950, 949f–950f
incomplete, 950, 951f
synchysis scintillans, 949
Vitreous body, 941
Vocal cords, 913, 915f
Voiding cystourethrogram (VCUG)
megaureter, 1422
posterior urethral valve, 1425
Volvulus, midgut, 1390
Von Gierke's disease, 116
Von Hippel-Lindau disease, 500–502, 501f, 502b, 512, 512f, 1378

W

Waist sign, pelvic inflammatory disease, 682
Walker-Warburg syndrome, 1281–1282
Wall thump filter, 28, 28f
Warren shunt, 186
Wartenberg syndrome, 1065
Warthin's tumour, 901, 901f
Watershed infarction, 1266, 1269f
Waveform, 3, 4f
damped *see* Damped waveform
hepatic venous, 194–197, 194f
parvus tardus *see* Damped waveform
velocity analysis, 1199–1200, 1200f–1202f
Wavefronts, 3
Wavelength, 3, 4f
Waves, 3
shear, 13
standing, 7–8, 8f
Wells clinical score, 1236t
Wharton's duct *see* Submandibular duct
White matter, 1320
Wilms' tumour, 1458–1461, 1458t–1459t, 1459f–1461f, 1465–1466
Wilson's disease, 117, 1357–1358
Wirsung duct, 286
Wolffian duct, 1469
development, 1470
World Federation for Ultrasound in Medicine and Biology (WFUMB), 58–59, 87–88
Wrist, 1055–1068
anatomy, 1055–1057
interventional techniques, 1175–1180
ligament and fibrocartilage disorders, 1063–1064, 1063f–1064f
neuropathies, 1064–1066, 1064f–1065f, 1066b
overuse tendinopathies, 1059–1063, 1060f–1061f
retinacula-related disorders, 1059–1063
space-occupying lesions, 1066–1067, 1066f, 1067b
technique, 1055–1057
tendon tears, 1057–1059

X

Xanthogranulomatous pyelonephritis, 1453, 1454f
Xanthomas, 1103, 1117, 1118f

Y

Yersinia enterocolitis, 399t, 401
Yolk sac, 743–744, 743f–744f, 744b, 744t, 761–762
shape, 761–762, 762f
size, 761, 762f
tumours *see* Yolk sac tumours
Yolk sac tumours
ovarian, 676
testicular, 600, 600f
vaginal, 1488

Z

Zollinger-Ellison syndrome, 313–314